







FOURTH ANNUAL AIRCRAFT ENGINEERING RESEARCH CONFERENCE
 UNDER THE AUSPICES OF
 THE NATIONAL ADVISORY COMMITTEE FOR AERONAUTICS
 LANGLEY FIELD, VIRGINIA, MAY 14, 1929

Seated, front row, left to right: DR. GEORGE W. LEWIS, Director of Aeronautical Research; *DR. ORVILLE WRIGHT; *DR. D. W. TAYLOR, Vice Chairman; *DR. CHARLES F. MARVIN; *CAPT. E. S. LAND, U. S. N.; *BRIG. GEN. W. E. GILLMORE, U. S. A.; *MAJ. GEN. JAMES E. FECHET, U. S. A.; *DR. JOSEPH S. AMES, Chairman; *REAR ADMIRAL WILLIAM A. MOFFETT, U. S. N.; *Assistant Secretary of Commerce, WILLIAM P. MACCRACKEN; HON. W. H. NEWTON, Secretary to the President; *HON. EDWARD P. WARNER; *HARRY F. GUGGENHEIM; SENATOR HIRAM BINGHAM; Assistant Secretary of the Navy, DAVID S. INGALLS; *DR. GEORGE K. BURGESS

(Those marked with an asterisk are members of the National Advisory Committee for Aeronautics)

AERONAUTICS

FIFTEENTH ANNUAL REPORT

OF THE

NATIONAL ADVISORY COMMITTEE

FOR AERONAUTICS

1929

INCLUDING TECHNICAL
REPORTS NOS. 309 TO 336



UNITED STATES
GOVERNMENT PRINTING OFFICE
WASHINGTON: 1930

LETTER OF SUBMITTAL

To the Congress of the United States:

In compliance with the provisions of the act of March 3, 1915, establishing the National Advisory Committee for Aeronautics, I submit herewith the Fifteenth Annual Report of the committee for the fiscal year ended June 30, 1929.

It is evident from the committee's report that, although material progress has been made in aeronautics during the past year, the best efforts of America are needed to keep pace with other progressive nations in the rapidly developing science of aeronautics. Attention is invited to Part V of the committee's report presenting a summary of the progress in aircraft development, and especially to the conclusion, wherein the committee expresses certain opinions with reference to the relative position of the United States and other nations that are active in the development of aeronautics.

I concur in the committee's opinion that progress on the two outstanding problems of increased safety and decreased costs necessitates continuous scientific research on the fundamental problems of flight. To this end enlarged facilities are being provided at the committee's laboratories at Langley Field, Va.

It is gratifying to note the committee's opinion that the efforts of all agencies, governmental and private, concerned with the technical development of aircraft are effectively coordinated in prosecuting the research programs of the committee.

HERBERT HOOVER.

THE WHITE HOUSE,
December 5, 1929.

LETTER OF TRANSMITTAL

NATIONAL ADVISORY COMMITTEE FOR AERONAUTICS,

Washington, D. C., November 19, 1929.

Mr. PRESIDENT: In compliance with the provisions of the act of Congress approved March 3, 1915 (U. S. C., p. 1698, sec. 153), I have the honor to transmit herewith the Fifteenth Annual Report of the National Advisory Committee for Aeronautics for the fiscal year ended June 30, 1929.

Substantial progress has been made during the past year in the scientific investigation of the fundamental problems of flight. The Army, Navy, and Department of Commerce air organizations, the Weather Bureau, and the Bureau of Standards have continued to cooperate effectively for the general development of American aeronautics. The efforts of governmental agencies, of the aircraft industry, of universities teaching aeronautical engineering, and of individuals active in the field of technical development have been largely coordinated through the technical subcommittees of the National Advisory Committee for Aeronautics, with the result that the aeronautical research programs of the committee have been prosecuted efficiently and without duplication, and existing facilities throughout the country have been utilized to good advantage. The net result has been continuous improvement in the design and performance of aircraft.

Attention is invited to Part V of the committee's report presenting a summary of progress in aircraft development. The committee has taken note of constant improvement in foreign types of aircraft, especially in military aircraft, and believes that our best efforts are necessary to keep pace with foreign progress in this rapidly advancing art. Developments in military aircraft continue to find application in the improvement of commercial aircraft. The most vital problems confronting aeronautics at this time are the needs for greater safety and for lower costs. On these basic problems the committee is concentrating its major effort.

The committee is grateful to the President and to the Congress for the liberal support of scientific research in aeronautics and firmly believes that the continuous prosecution of fundamental research is the most effective guarantee of continuous progress.

Respectfully submitted.

JOSEPH S. AMES,
Chairman.

THE PRESIDENT,
The White House, Washington, D. C.

CONTENTS

Letter of submittal.....	Page
Letter of transmittal.....	III
Fifteenth annual report.....	V
	1

PART I. ORGANIZATION

Functions of the committee.....	4
Organization of the committee.....	5
Meetings of the entire committee.....	6
The executive committee.....	6
Subcommittees.....	7
Quarters for committee.....	8
The Langley Memorial Aeronautical Laboratory.....	9
The Office of Aeronautical Intelligence.....	10
Financial report.....	11

PART II. GENERAL ACTIVITIES

Study of aircraft accidents.....	12
Consideration of aeronautical inventions.....	14
Relations with the aircraft industry.....	14
Rigid airships.....	15
The Daniel Guggenheim Fund for the Promotion of Aeronautics.....	17
Cooperation with State Department abroad.....	18
Cooperation with British Aeronautical Research Committee.....	18
Cooperation of Army and Navy.....	19
Investigations undertaken for the Army and the Navy.....	19
Exhibit at Seville International Exposition.....	20

PART III. REPORTS OF TECHNICAL COMMITTEES

Report of committee on aerodynamics.....	22
Report of committee on power plants for aircraft.....	37
Report of committee on materials for aircraft.....	48
Report of committee on problems of air navigation.....	57

PART IV. TECHNICAL PUBLICATIONS OF THE COMMITTEE

Summaries of Technical Reports.....	61
List of Technical Notes issued during the past year.....	72
List of Technical Memorandums issued during the past year.....	73
List of Aircraft Circulars issued during the past year.....	75
Bibliography of Aeronautics.....	76

PART V. SUMMARY OF PROGRESS IN AIRCRAFT DEVELOPMENT

Aerodynamics.....	77
Airplane structures.....	83
Airships.....	85
Aircraft engines.....	85
Factors that have contributed to the present state of aeronautic progress.....	87
Outlook for the future.....	88
Conclusion.....	89

TECHNICAL REPORTS

	Page
No. 309. Joint Report on Standardization Tests on N. P. L. R. A. F. 15 Airfoil Model. By Walter S. Diehl.....	91
No. 310. Pressure Element of Constant Logarithmic Stiffness for Temperature Compensated Altimeter. By W. G. Brombacher and F. Cordero.....	111
No. 311. Aerodynamic Theory and Test of Strut Forms. By R. H. Smith.....	125
No. 312. The Prediction of Airfoil Characteristics. By George J. Higgins.....	149
No. 313. Drag and Cooling with Various Forms of Cowling for a "Whirlwind" Radial Air-Cooled Engine—I. By Fred E. Weick.....	163
No. 314. Drag and Cooling with Various Forms of Cowling for a "Whirlwind" Radial Air-Cooled Engine—II. By Fred E. Weick.....	189
No. 315. Aerodynamic Characteristics of Airfoils—VI. By National Advisory Committee for Aeronautics.....	211
No. 316. Tables for Pressure of Air on Coming to Rest from Various Speeds. By A. F. Zahm and F. A. Loudon.....	247
No. 317. Wind Tunnel Tests on a Series of Wing Models Through a Large Angle of Attack Range, Part I—Force Tests. By Montgomery Knight and Carl J. Wenzinger.....	255
No. 318. Speed and Deceleration Trials of U. S. S. Los Angeles. By S. J. De France and C. P. Burgess.....	305
No. 319. Aerodynamic Characteristics of Twenty-four Airfoils at High Speeds. By L. J. Briggs and H. L. Dryden.....	325
No. 320. The Measurement of Fluctuations of Air Speed by the Hot-Wire Anemometer. By H. L. Dryden and A. M. Kuethe.....	357
No. 321. Fuel Vapor Pressures and the Relation of Vapor Pressure to the Preparation of Fuel for Combustion in Fuel Injection Engines. By Wm. F. Joachim and A. M. Rothrock.....	383
No. 322. Investigation of Air Flow in Open-Throat Wind Tunnels. By Eastman N. Jacobs.....	397
No. 323. Flow and Force Equations for a Body Revolving in a Fluid. By A. F. Zahm.....	409
No. 324. Flight Tests on U. S. S. Los Angeles, Part I—Full Scale Pressure Distribution Investigation. By S. J. De France.....	449
No. 325. Flight Tests on U. S. S. Los Angeles, Part II—Stress and Strength Determination. By C. P. Burgess.....	483
No. 326. Tests of Five Metal Model Propellers with Various Pitch Distributions in a Free Wind Stream and in Combination with a Model VE-7 Fuselage. By E. P. Lesley and Elliott G. Reid.....	499
No. 327. The Effect of Supercharger Capacity on Engine and Airplane Performance. By O. W. Schey and W. D. Gove.....	517
No. 328. Water Pressure Distribution on a Twin-Float Seaplane. By F. L. Thompson.....	537
No. 329. The Torsional Strength of Wings. By C. P. Burgess.....	555
No. 330. Experimental and Analytical Determination of the Motion of Hydraulically Operated Valve Stems in Oil Engine Injection Systems. By A. G. Gelalles and A. M. Rothrock.....	569
No. 331. Collection of Wind-Tunnel Data on Commonly used Wing Sections. By F. A. Loudon.....	589
No. 332. The Effect of Cowling on Cylinder Temperatures and Performance of a Wright J-5 Engine. By Oscar W. Schey and Arnold E. Biermann.....	635
No. 333. Full-Scale Turning Characteristics of the U. S. S. Los Angeles. By F. L. Thompson.....	657
No. 334. The Torsion of Members Having Sections Common in Aircraft Construction. By George W. Trayer and H. W. March.....	671
No. 335. Aerodynamic Theory and Test of Strut Forms—II. By R. H. Smith.....	721
No. 336. Tests of Large Airfoils in the Propeller Research Tunnel, Including Two with Corrugated Surfaces. By Donald H. Wood.....	761

NATIONAL ADVISORY COMMITTEE FOR AERONAUTICS

3841 NAVY BUILDING, WASHINGTON, D. C.

JOSEPH S. AMES, Ph. D., *Chairman*,
President Johns Hopkins University, Baltimore, Md.
DAVID W. TAYLOR, D. Eng., *Vice Chairman*,
Washington, D. C.
CHARLES G. ABBOT, Sc. D.,
Secretary Smithsonian Institution, Washington, D. C.
GEORGE K. BURGESS, Sc. D.,
Director Bureau of Standards, Washington, D. C.
WILLIAM F. DURAND, Ph. D.,
Professor Emeritus of Mechanical Engineering, Stanford University, California.
JAMES E. FECHET, Major General, United States Army,
Chief of Air Corps, War Department, Washington, D. C.
BENJAMIN D. FOULOIS, Brigadier General, United States Army,
Chief Matériel Division, Air Corps, Wright Field, Dayton, Ohio.
HARRY F. GUGGENHEIM, M. A.,
President Daniel Guggenheim Fund for the Promotion of Aeronautics, New York City.
WILLIAM P. MACCRACKEN, Jr., Ph. B.,
Chicago, Ill.
CHARLES F. MARVIN, M. E.,
Chief United States Weather Bureau, Washington, D. C.
WILLIAM A. MOFFETT, Rear Admiral, United States Navy,
Chief Bureau of Aeronautics, Navy Department, Washington, D. C.
S. W. STRATTON, Sc. D.,
President Massachusetts Institute of Technology, Cambridge, Mass.
JOHN H. TOWERS, Commander, United States Navy,
Assistant Chief Bureau of Aeronautics, Navy Department, Washington, D. C.
EDWARD P. WARNER, M. S.,
Editor Aviation, New York City.
ORVILLE WRIGHT, Sc. D.,
Dayton, Ohio.

GEORGE W. LEWIS, *Director of Aeronautical Research*

JOHN F. VICTORY, *Secretary*

HENRY J. E. REID, *Engineer in Charge Langley Memorial Aeronautical Laboratory, Langley Field, Va.*

JOHN J. IDE, *Technical Assistant in Europe, Paris, France*

EXECUTIVE COMMITTEE

JOSEPH S. AMES, *Chairman*

DAVID W. TAYLOR, *Vice Chairman*

CHARLES G. ABBOT.
GEORGE K. BURGESS.
JAMES E. FECHET.
BENJAMIN D. FOULOIS.
WILLIAM P. MACCRACKEN.
CHARLES F. MARVIN.

WILLIAM A. MOFFETT.
S. W. STRATTON.
JOHN H. TOWERS.
EDWARD P. WARNER.
ORVILLE WRIGHT.

JOHN F. VICTORY, *Secretary*

FIFTEENTH ANNUAL REPORT

OF THE

NATIONAL ADVISORY COMMITTEE FOR AERONAUTICS

WASHINGTON, D. C., *November 12, 1929.*

To the Congress of the United States:

In accordance with the act of Congress approved March 3, 1915, establishing the National Advisory Committee for Aeronautics, the committee submits herewith its fifteenth annual report for the fiscal year 1929.

The most significant fact in the progress of aeronautics during the past year is that the airplane has found a place in the transportation needs of the country. Its accelerated development as a military weapon during the great war gave promise of its ultimate successful use for purposes of business and of pleasure. An ensuing decade of scientific research, of military experimentation, and of earnest study and application of fundamental principles of aerodynamics, and we now witness the airplane used regularly with increasing safety and efficiency, on a growing network of airways, carrying more and more passengers, mail, and merchandise at steadily decreasing costs.

The airplane as an improved means of transportation may be expected not only to bring our own people closer together but to bring the nations of the world closer to us. The peoples of all progressive nations are taking an interest in aeronautics. The present generation of Americans is learning how to see America from the air. The great interest of the youth of our land indicates that the rising generation may use the airplane as naturally, although perhaps not as generally, as we use motor cars to-day.

It is difficult accurately to appraise the significance of the present period of transition through which we are passing. The rapid advancement of technical science and increased economic pressure are bringing results steadily in improving the safety and efficiency of aircraft. The Federal Government has followed a wise constructive policy for the development and encouragement of the civil uses of aircraft upon a sound economic basis. The temporary overexpansion in certain phases of the aircraft industry is but characteristic of new and promising industries in America. The groundwork for commercial aeronautics has been well laid. The important figures that indicate the growth of American aeronautics, according to official estimates of the Department of Commerce obtained November 1, 1929, show, for example: That operating companies in the United States have developed scheduled air transport services which fly approximately 82,000 miles daily; that there are 170 different types of airplanes licensed by the Department of Commerce, including 12 types having two or more engines; that there are approximately 9,300 licensed or identified civil aircraft in the United States; that there are 35,000 miles of airways of which approximately 12,500 miles are lighted for night flying; that mail carried by aircraft has increased tenfold since 1926 to an estimated total for 1929 of 8,000,000 pounds; that paying passengers have increased from 8,000 in 1926 to 85,000 in 1929; that there are now 1,520 airports and landing fields and over 1,200 proposed; that 8,900 civilian pilots' licenses and 28,000 pilot student permits have been issued.

These are evidences of the present growth in the use of aircraft and reflect the progress made in the design, construction, and performance of aircraft. The factor that has contributed the

most to the improvement in the airplane itself has been the direct assistance of the Federal Government during the past 10 years. During most of this time the major stress was laid on improving the characteristics of airplanes for the national defense. The demands upon military aircraft are much more exacting and much more difficult to meet than in the case of commercial aircraft, and hardly a single military improvement has failed to find an application in commercial aircraft. In more recent years the Federal Government, through the activities of the Aeronautics Branch of the Department of Commerce and the extended weather-report service provided by the Weather Bureau, has provided those essential aids to air navigation that are properly the function of the Government. These factors, combined with the fundamental scientific research conducted by the National Advisory Committee for Aeronautics, the results of which are applicable alike to military and commercial aircraft, and the engineering and experimental development work of the Army and Navy, have served largely to pave the way for a greater development in commercial aviation in America, uninfluenced either in nature or extent by direct cash subsidies.

All of the experience with aircraft, governmental and private, emphasizes the need for greater safety and greater efficiency, for despite the wonderful record of progress and accomplishment there are accidents, and aviation is still expensive.

The War, Navy, and Commerce Departments are keeping systematic records of the causes of accidents in accordance with a plan proposed by the committee, and these records are given intensive study by the subcommittee on aircraft accidents. Wherever this study indicates the need for the scientific investigation of any particular problem, the matter is referred to the appropriate technical subcommittee to initiate the necessary item of research. It is the duty of the technical subcommittees to outline the specific problems to be attacked and prepare programs of research, which embody the allocation of the problems recommended to various agencies, public and private, that are best equipped to undertake given investigations. Most of the fundamental investigations conducted by the committee have a bearing alike on the improvement of military and commercial airplanes, and the results are brought to the attention of the governmental agencies concerned, of the manufacturers of aircraft, and of others interested, through the committee's Office of Aeronautical Intelligence. That office serves as the Government depository for scientific and technical data on aeronautics, and collects, analyzes, classifies, and disseminates such data originating both at home and abroad.

The airplane must be made safer and less costly. On these major problems the committee is concentrating most of the efforts of the Langley Memorial Aeronautical Laboratory at Langley Field, Va., the facilities of which are being expanded under appropriations made for the purpose. In this connection the committee wishes to express its appreciation to the President and to the Congress for the liberal support by the Government of scientific research in aeronautics. Money expended in this direction is constantly yielding new knowledge obtainable in no other way. The members of the National Advisory Committee for Aeronautics are enthusiastic over the prospects for the future of aeronautics in America, and, while not making prophecies, nevertheless firmly believe that with the continued support of coordinated scientific research, there will be continued progress in the solution of the basic problems of increased safety and of increased efficiency in aviation. It is primarily in this manner that the airplane will ultimately be enabled to render its fullest service to mankind as an agency of transportation that is destined to contribute much to the advancement of civilization.

This annual report is submitted in five parts. Part I describes the organization of the committee, states its functions, outlines the facilities available under the committee's direction for the conduct of scientific research in aeronautics, explains the activities and growth of the Office of Aeronautical Intelligence in the collection, analysis, and dissemination of scientific and technical data, and presents a financial report of expenditures during the fiscal year ended June 30, 1929.

In Part II of this report the committee describes its miscellaneous activities, including the study of aircraft accidents, the consideration of aeronautical inventions and designs, the relations with the aircraft industry, and the cooperation with other governmental agencies.

In Part III the committee presents reports on the major results of its fundamental work in the form of reports of its standing technical subcommittees on aerodynamics, power plants for aircraft, materials for aircraft, and problems of air navigation, which include statements of the organization and the functions of each and of the progress of investigations conducted under their general cognizance in governmental and private laboratories.

In Part IV the committee presents summaries of the Technical Reports published during the past year, and enumerates by title the Technical Notes, Technical Memorandums, and Aircraft Circulars issued.

In Part V the committee presents a summary of progress in the technical development of aircraft. The report closes with a reference to the factors that have contributed to the advancement of American aeronautics.

PART I

ORGANIZATION

FUNCTIONS OF THE COMMITTEE

The National Advisory Committee for Aeronautics was established by act of Congress approved March 3, 1915. The organic act charged the committee with the supervision and direction of the scientific study of the problems of flight with a view to their practical solution, the determination of problems which should be experimentally attacked, and their investigation and application to practical questions of aeronautics. The act also authorized the committee to direct and conduct research and experimentation in aeronautics in such laboratory or laboratories, in whole or in part, as may be placed under its direction.

Supplementing the prescribed duties of the committee under its organic act, its broad general functions may be stated as follows:

First. Under the law the committee holds itself at the service of any department or agency of the Government interested in aeronautics, for the furnishing of information or assistance in regard to scientific or technical matters relating to aeronautics, and in particular for the investigation and study of fundamental problems submitted by the War and Navy Departments with a view to their practical solution.

Second. The committee may also exercise its functions for any individual, firm, association, or corporation within the United States, provided that such individual, firm, association, or corporation defray the actual cost involved.

Third. The committee institutes research, investigation, and study of problems which, in the judgment of its members or of the members of its various subcommittees, are needful and timely for the advance of the science and art of aeronautics in its various branches.

Fourth. The committee keeps itself advised of the progress made in research and experimental work in aeronautics in all parts of the world, particularly in England, France, Italy, Germany, and Canada.

Fifth. The information thus gathered is brought to the attention of the various subcommittees for consideration in connection with the preparation of programs for research and experimental work in this country. This information is also made available promptly to the military and naval air organizations and other branches of the Government and such as is not confidential is immediately released to university laboratories and aircraft manufacturers interested in the study of specific problems, and also to the public.

Sixth. The committee holds itself at the service of the President, the Congress, and the executive departments of the Government for the consideration of special problems which may be referred to it.

By act of Congress approved July 2, 1926 (Public, No. 446, 69th Cong.), and amended March 3, 1927 (Public, No. 748, 69th Cong.), the committee was given an additional function. This legislation created and specified the functions of an Aeronautical Patents and Design Board, consisting of an Assistant Secretary of War, an Assistant Secretary of the Navy, and an Assistant Secretary of Commerce, and provided that upon favorable recommendation of the National Advisory Committee for Aeronautics the Patents and Design Board shall determine questions as to the use and value to the Government of aeronautical inventions submitted to any branch of the Government. The legislation provided that designs submitted to the board should be referred to the National Advisory Committee for Aeronautics for its recommendation and this has served to impose upon the committee the additional duty of considering on behalf of the Government all aeronautical inventions and designs submitted.

ORGANIZATION OF THE COMMITTEE

The membership of the National Advisory Committee for Aeronautics was increased from 12 to 15 members by the act of Congress approved March 2, 1929 (Public, No. 908, 70th Cong.), which reads as follows:

An Act to increase the membership of the National Advisory Committee for Aeronautics

Be it enacted by the Senate and House of Representatives of the United States of America in Congress assembled, That the membership of the National Advisory Committee for Aeronautics is hereby increased from twelve members to fifteen members: *Provided,* That the three additional members to be appointed by the President shall be acquainted with the needs of aeronautical science, either civil or military, or skilled in aeronautical engineering or its allied sciences, and shall serve as such without compensation.

The qualifications prescribed for the three additional members are identical with the qualifications prescribed for the five members from private life authorized in the organic act.

The organic act of 1915, as amended by the above-quoted act, provides for the appointment by the President of 15 members of the committee, as follows: 2 members from the War Department, from the office in charge of military aeronautics; 2 members from the Navy Department, from the office in charge of naval aeronautics; a representative each of the Smithsonian Institution, the United States Weather Bureau, and the United States Bureau of Standards; and not more than 8 additional persons acquainted with the needs of aeronautical science, either civil or military, or skilled in aeronautical engineering or its allied sciences. The law further provides that all members as such shall serve without compensation.

On April 5, 1929, the President appointed the three additional members authorized by the act approved March 2, 1929, as follows: Hon. Harry F. Guggenheim, president of the Daniel Guggenheim Fund for the Promotion of Aeronautics; Hon. William P. MacCracken, jr., Assistant Secretary of Commerce for Aeronautics; and Hon. Edward P. Warner, editor of Aviation.

On June 13, 1929, Capt. Emory S. Land (C. C.), United States Navy, submitted his resignation as a member of the committee on account of his extended leave of absence from active duty in the Navy, and under date of July 6, the President appointed Commander John H. Towers, United States Navy, Assistant Chief of the Bureau of Aeronautics of the Navy, to succeed Captain Land as a member of the committee. Commander Towers executed the oath of office on July 18, 1929. He had previously served as a naval representative on the committee from January 10, 1917, to August 16, 1919.

Under date of July 2, 1929, Brig. Gen. William E. Gillmore, United States Army, submitted his resignation as a member of the committee on his relief from duty as chief of the matériel division of the Air Corps, and under date of August 5, Brig. Gen. Benjamin D. Foulois, General Gillmore's successor as chief of the matériel division, was appointed to succeed him as a member of the committee. General Foulois executed the oath of office on August 14, 1929.

The entire committee meets twice a year, the annual meeting being held in October and the semiannual meeting in April. The present report includes the activities of the committee between the annual meeting held on October 18, 1928, and that held on October 24, 1929.

The organization of the committee at the close of the past year was as follows:

Joseph S. Ames, Ph. D., chairman, president of Johns Hopkins University, Baltimore, Md.

David W. Taylor, D. Eng., vice chairman, Washington, D. C.

Charles G. Abbot, Sc. D., Secretary of the Smithsonian Institution.

George K. Burgess, Sc. D., Director of the Bureau of Standards.

William F. Durand, Ph. D., professor emeritus of mechanical engineering, Stanford University, California.

Maj. Gen. James E. Fechet, United States Army, Chief of the Air Corps.

Brig. Gen. Benjamin D. Foulois, United States Army, chief of the matériel division, Air Corps.

Harry F. Guggenheim, M. A., president of the Daniel Guggenheim Fund for the Promotion of Aeronautics.

William P. MacCracken, jr., Ph. B., Chicago, Ill.

Charles F. Marvin, M. E., Chief of the Weather Bureau.

Rear Admiral William A. Moffett, United States Navy, Chief of the Bureau of Aeronautics, Navy Department.

S. W. Stratton, Sc. D., president of the Massachusetts Institute of Technology, Cambridge, Mass.

Commander John H. Towers, United States Navy, Assistant Chief of the Bureau of Aeronautics, Navy Department.

Edward P. Warner, M. S., editor of Aviation.

Orville Wright, Sc. D., Dayton, Ohio.

MEETINGS OF THE ENTIRE COMMITTEE

The semiannual meeting of the entire committee was held on April 18, 1929, at the committee's headquarters in Washington, and the annual meeting on October 24, 1929, also at the committee's headquarters. At these meetings the recent progress in aeronautical research was reviewed and some of the principal problems of aeronautics were discussed. Administrative reports were submitted by the secretary, Mr. John F. Victory, and by the Director of the Office of Aeronautical Intelligence, Dr. Joseph S. Ames.

At both the annual and semiannual meetings Doctor Ames, as chairman of the executive committee, presented detailed reports of the research work being conducted by the committee at the Langley Memorial Aeronautical Laboratory, Langley Field, Hampton, Va., and exhibited charts and photographs showing the methods used and the results obtained in the more important investigations.

The election of officers was the concluding feature of the annual meeting. The officers of the committee were reelected for the ensuing year, as follows: Chairman, Dr. Joseph S. Ames; vice chairman, Dr. David W. Taylor; chairman executive committee, Dr. Joseph S. Ames; vice chairman executive committee, Dr. David W. Taylor.

THE EXECUTIVE COMMITTEE

For the purpose of carrying out the work of the Advisory Committee the regulations provide for the election annually of an executive committee, to consist of seven members and to include in addition any member of the Advisory Committee not otherwise a member of the executive committee, but resident in or near Washington, and giving his time wholly or chiefly to the special work of the committee.

As a result of the appointment of three additional members to the Advisory Committee during the past year, the executive committee has been increased from 11 to 13 members. Its present organization is as follows:

Joseph S. Ames, Ph. D., chairman.

David W. Taylor, D. Eng., vice chairman.

Charles G. Abbot, Sc. D.

George K. Burgess, Sc. D.

Maj. Gen. James E. Fechet, United States Army.

Brig. Gen. Benjamin D. Foulois, United States Army.

William P. MacCracken, jr.

Charles F. Marvin, M. E.

Rear Admiral William A. Moffett, United States Navy.

S. W. Stratton, Sc. D.

Commander John H. Towers, United States Navy.

Edward P. Warner, M. S.

Orville Wright, Sc. D.

The executive committee, in accordance with general instructions of the Advisory Committee, performs the functions prescribed by law for the whole committee, administers the affairs of the committee, and exercises general supervision over all its activities.

The executive committee has organized the necessary clerical and technical staffs for handling the work of the committee proper. General responsibility for the execution of the policies and the direction of the activities as approved by the executive committee is vested in the Director of Aeronautical Research, Mr. George W. Lewis. He has immediate charge of the scientific and technical work of the committee, being directly responsible to the chairman of the executive committee, Dr. Joseph S. Ames. The secretary, Mr. John F. Victory, is ex officio secretary of the executive committee, directs the administrative work of the organization, and exercises general supervision over the expenditures of funds and the employment of personnel.

SUBCOMMITTEES

In order to facilitate the conduct of its work the executive committee has organized the following standing committees with subcommittees as indicated:

Aerodynamics—

Subcommittee on airships.

Subcommittee on aeronautical research in universities.

Power plants for aircraft.

Materials for aircraft—

Subcommittee on metals.

Subcommittee on woods and glues.

Subcommittee on coverings, dopes, and protective coatings.

Subcommittee on aircraft structures.

Problems of air navigation—

Subcommittee on problems of communication.

Subcommittee on instruments.

Subcommittee on meteorological problems.

Aircraft accidents.

Aeronautical inventions and designs.

Publications and intelligence.

Personnel, buildings, and equipment.

Governmental relations.

The organization and work of the technical committees on aerodynamics, power plants for aircraft, materials for aircraft, and problems of air navigation are covered in the reports of those committees in Part III of this report, while the activities of the committee on aircraft accidents and the committee on aeronautical inventions and designs are included in Part II under the subjects of the study of aircraft accidents and the consideration of aeronautical inventions, respectively.

Statements of the organization and functions of the administrative committees on publications and intelligence; personnel, buildings, and equipment; and governmental relations, follow:

COMMITTEE ON PUBLICATIONS AND INTELLIGENCE

FUNCTIONS

1. The collection, classification, and diffusion of technical knowledge on the subject of aeronautics, including the results of research and experimental work done in all parts of the world.
2. The encouragement of the study of the subject of aeronautics in institutions of learning.
3. Supervision of the Office of Aeronautical Intelligence.
4. Supervision of the committee's foreign office in Paris.
5. The collection and preparation for publication of the Technical Reports, Technical Notes, Technical Memorandums, and Aircraft Circulars of the committee.

ORGANIZATION

Dr. Joseph S. Ames, chairman.
Prof. Charles F. Marvin, vice chairman.
Miss M. M. Muller, secretary.

COMMITTEE ON PERSONNEL, BUILDINGS, AND EQUIPMENT**FUNCTIONS**

1. To handle all matters relating to personnel, including the employment, promotion, discharge, and duties of all employees.
2. To consider questions referred to it and make recommendations regarding the initiation of projects concerning the erection or alteration of laboratories and offices.
3. To meet from time to time on the call of the chairman and report its actions and recommendations to the executive committee.
4. To supervise such construction and equipment work as may be authorized by the executive committee.

ORGANIZATION

Dr. Joseph S. Ames, chairman.
Dr. David W. Taylor, vice chairman.
Prof. Charles F. Marvin.
John F. Victory, secretary.

COMMITTEE ON GOVERNMENTAL RELATIONS**FUNCTIONS**

1. Relations of the committee with executive departments and other branches of the Government.
2. Governmental relations with civil agencies.

ORGANIZATION

Prof. Charles F. Marvin, chairman.
Dr. David W. Taylor.
John F. Victory, secretary.

QUARTERS FOR COMMITTEE

The headquarters of the National Advisory Committee for Aeronautics are located in the rear of the eighth wing, third floor, of the Navy Building, Eighteenth and B Streets NW., Washington, D. C., in close proximity to the Army and Navy air organizations. This space has been officially assigned for the use of the committee by the Public Buildings Commission. The administrative office is also the headquarters of the various subcommittees and of the Office of Aeronautical Intelligence.

The committee has been seriously handicapped in its ability to discharge its functions most effectively by the lack of sufficient office space. The committee's needs have been presented from time to time to the Public Buildings Commission, and although that commission has appeared fully appreciative of the situation only partial relief could be granted. During the past year the committee has obtained 400 additional square feet of office space, making the total office space in Washington 7,394 square feet. The committee regrets that it has been prevented by lack of quarters from rendering the fullest possible measure of useful service to the public and to the aircraft industry. It appears that substantial relief must await progress in the prosecution of the Federal building program in Washington.

Field stations of the committee are the Langley Memorial Aeronautical Laboratory, at Langley Field, Hampton, Va., and the office of the technical assistant in Europe, located at the American Embassy in Paris.

The scientific investigations authorized by the committee are not all conducted at the Langley Memorial Aeronautical Laboratory, but the facilities of other governmental laboratories are utilized, as well as the laboratories connected with institutions of learning whose cooperation in the scientific study of specific problems in aeronautics has been secured.

THE LANGLEY MEMORIAL AERONAUTICAL LABORATORY

The Langley Memorial Aeronautical Laboratory is operated under the direct control of the committee. It is located at Langley Field, Va., on a plot of ground set aside by the War Department for the committee's use. The laboratory was started in 1916 coincident with the establishment of Langley Field.

The laboratory is organized with six divisions, as follows: Aerodynamics division, power plants division, technical service division, flight operations division, property and clerical division, and a recently created hydrodynamics division. The laboratory is under the immediate direction of an engineer in charge, Mr. Henry J. E. Reid, subject to the general supervision of the officers of the committee.

During the past year authority of law was obtained for the construction of a full-scale wind tunnel at an estimated cost of \$900,000, a seaplane channel at an estimated cost of \$208,000, and a combination heating plant, storehouse, and garage at an estimated cost of \$30,000. The latter structure was erected on plot 16 during the summer of 1929 at a cost of \$27,055. It is a brick structure 102 by 52 feet by 29 feet high, with an outside brick smoke-stack 64 feet high.

The War Department has assigned to the committee additional space on a suitable part of Langley Field for the erection of the full-scale wind tunnel and for the construction of the seaplane channel. It is expected that these structures will be in operation during the fiscal year 1931. In its estimates for the fiscal year 1931 the committee has requested authority for the erection of a permanent new brick hangar to replace the present steel hangar which must be removed to make way for extensive military improvements at Langley Field.

There are nine structures at present comprising the Langley Memorial Aeronautical Laboratory, housing activities as follows:

1. A research laboratory building containing administrative offices, technical library, photographic laboratory, and headquarters of the various divisions.

2. An atmospheric wind tunnel building containing a 5-foot wind tunnel of standard type with a closed throat, and a refrigerated wind tunnel with an open-throat diameter of 6 inches for the investigation of ice formation on aircraft.

3. A variable-density wind tunnel building, housing the variable-density wind tunnel. A research balance of an entirely new design intended to insure greater reliability, accuracy, and adaptability for model tests has been installed and this equipment is again in full operation after the fire which destroyed the mechanism on August 1, 1927. In rebuilding the tunnel after the fire the design was changed to an open-throat type with the same throat diameter of 5 feet. In rebuilding the tunnel features were incorporated which resulted in greater efficiency and ease of operation, better accessibility of apparatus, improved quality of air flow, and the elimination of all combustible material. This building also houses the new jet-type wind tunnel for investigations at approximately the velocity of sound in air, or in excess of 750 miles per hour. Waste air from the variable-density wind tunnel is utilized by means of the injector principle to create a flow of air through a test chamber 12 inches in diameter at speeds up to 800 miles per hour.

4. Two engine dynamometer laboratories of a semipermanent type equipped to carry on investigations in connection with power plants for aircraft.

5. A service building containing an instrument laboratory, drafting room, machine shop, woodworking shop, and storeroom.

6. A propeller research tunnel in which tests may be made in a 20-foot air stream at 100 miles per hour. This equipment permits the full-scale testing of propellers, fuselages, and landing gears.

7. An airplane hangar with a repair shop and facilities for taking care of airplanes used in flight research.

8. A combination heating plant, storehouse, and garage.

Items 1, 2, 3, 4, 5, and 8 above are located on plot 16. Item 6, the propeller research tunnel, is located within 2 blocks of the laboratory headquarters and is near the site of the proposed full-scale wind tunnel and seaplane channel. Item 7, the airplane hangar, is located on the flying field.

Recognition by the Government of the necessity of satisfying the increasing demand for new and accurate knowledge on the fundamental problems of flight has made possible the development of the Langley Memorial Aeronautical Laboratory as an efficient research organization numbering 181 employees at the close of the fiscal year 1929. The work of the laboratory is conducted without interference with military operations at the field. In fact, there is a splendid spirit of cooperation on the part of the military authorities, who by their helpfulness in many ways have aided the committee materially in its work.

THE OFFICE OF AERONAUTICAL INTELLIGENCE

The Office of Aeronautical Intelligence was established in the early part of 1918 as an integral branch of the committee's activities. Its functions are the collection, classification, and diffusion of technical knowledge on the subject of aeronautics to the military and naval air organizations, aircraft manufacturers, educational institutions, and others interested, including the results of research and experimental work conducted in all parts of the world. It is the officially designated Government depository for scientific and technical reports and data on aeronautics.

Promptly upon receipt, all reports are analyzed, classified, and brought to the special attention of the subcommittees having cognizance and to the attention of other interested parties through the medium of public and confidential bulletins. Reports are duplicated where practicable, and distributed upon request. Confidential bulletins and reports are not circulated outside of Government channels.

The records of the committee show that during the past year there has been an increase of 47 per cent over the previous year in the distribution of technical publications. A total of 16,923 written requests for reports were received during the year in addition to innumerable telephone and personal requests and 77,729 reports were distributed upon request, which represents an increase of 28,189 over last year.

The technical publications were distributed as follows:

Committee and subcommittee members.....	1, 739
Langley Memorial Aeronautical Laboratory.....	2, 518
Paris office of the committee.....	5, 222
Army Air Corps.....	2, 352
Naval Air Service, including Marine Corps.....	3, 499
Manufacturers.....	15, 619
Educational institutions.....	9, 515
Bureau of Standards.....	670
Miscellaneous.....	62, 942
Total distribution.....	104, 076

The above figures include the distribution of 33,259 Technical Reports, 17,763 Technical Notes, 29,554 Technical Memorandums, and 14,093 Aircraft Circulars of the National Advisory Committee for Aeronautics. Part IV of this report presents the titles of the publications issued during the past year the distribution of which is included in the foregoing figures.

To handle efficiently the work of securing and exchanging reports in foreign countries, the committee maintains a technical assistant in Europe, with headquarters at the American Embassy in Paris. It is his duty to visit the government and private laboratories, centers of aeronautical information, and private individuals in England, France, Italy, Germany, and other European countries, and endeavor to secure for America not only printed matter which would in the ordinary course of events become available in this country, but more especially

to secure advance information as to work in progress and any technical data not prepared in printed form, which would otherwise not reach this country. John Jay Ide, of New York, has served as the committee's technical assistant in Europe since April, 1921.

FINANCIAL REPORT

The appropriation for the National Advisory Committee for Aeronautics for the fiscal year 1929, as carried in the independent offices appropriation act approved May 16, 1928, was \$615,770, under which the committee reports expenditures and obligations during the year amounting to \$611,633.27, itemized as follows:

Personal services.....	\$448, 771. 16
Supplies and materials.....	32, 714. 07
Communication service.....	1, 267. 63
Travel expenses.....	14, 620. 46
Transportation of things.....	977. 44
Furnishing of electricity.....	7, 511. 30
Rent of office (Paris).....	960. 00
Repairs and alterations.....	3, 779. 51
Special investigations and reports.....	47, 222. 15
Equipment.....	53, 809. 55
<hr/>	
Expenditures.....	611, 633. 27
Personnel reserve.....	3, 300. 00
Unobligated balance.....	836. 73
<hr/>	
Total.....	615, 770. 00

In addition to the above, the committee had a separate appropriation of \$13,000 for printing and binding, of which \$12,925.61 was expended.

The appropriations for the fiscal year 1930 total \$1,300,000, which includes \$525,000 toward the construction of a full-scale wind tunnel at an authorized cost of \$900,000; and \$30,000 for the construction of a combined heating plant, storehouse, and garage. In addition there is an appropriation for the fiscal years 1929 and 1930 of \$208,000 for the construction of a seaplane channel which, in effect, when added to the regular appropriation for 1930, makes the total appropriation for 1930, \$1,508,000.

PART II

GENERAL ACTIVITIES

STUDY OF AIRCRAFT ACCIDENTS

In response to request of the Air Coordination Committee, consisting of the Assistant Secretaries for Aeronautics in the Departments of War, Navy, and Commerce, the National Advisory Committee for Aeronautics organized, in March, 1928, a special committee on the nomenclature, subdivision, and classification of aircraft accidents, to prepare a basis for the classification and comparison of aircraft accidents, both civil and military. This committee made a detailed study of the problem, and as a result drew up a chart for the analysis of accidents, combining consideration of the immediate causes, underlying causes, and results of accidents. This chart, together with a detailed explanation, was published in October, 1928, as Technical Report No. 308 of the National Advisory Committee for Aeronautics, entitled "Aircraft Accidents—Methods of Analysis," and was officially adopted for use by the War, Navy, and Commerce Departments.

On completion of this report, the special committee on the nomenclature, subdivision, and classification of aircraft accidents was discharged, and, as it was thought probable that the introduction of the proposed chart would result in questions as to interpretation and suggestions as to changes, and that a study of the information obtained from the application of the method of analysis would indicate that certain features in aircraft operation or construction should be given more detailed study or consideration, a new standing committee on aircraft accidents was appointed with the same personnel as the special committee, to consider from time to time such new questions regarding aircraft accidents as might appear desirable or as might be brought before it.

The present membership of the committee on aircraft accidents is as follows:

Dr. George K. Burgess, Bureau of Standards, chairman.

Lieut. Harold Brand, United States Army, Air Corps, War Department.

Edward P. Howard, Aeronautics Branch, Department of Commerce.

George W. Lewis, National Advisory Committee for Aeronautics.

Lieut. Commander L. C. Stevens, United States Navy, Bureau of Aeronautics, Navy Department.

Hon. Edward P. Warner, editor of Aviation.

The committee when first organized included in its membership the following Army and Navy officers who have supplied valuable information regarding the study of accidents in their respective services, and who have since been relieved from membership upon their transfer to duty outside of Washington:

Lieut. J. D. Barker, United States Army.

Lieut. Charles R. Brown, United States Navy.

Lieut. D. B. Phillips, United States Army.

Doctor Burgess has expressed a desire to be relieved as chairman of this committee, and it is therefore contemplated that when the revision now being made of the report on methods of accident analysis has been completed, he will be succeeded in the chairmanship by Mr. Warner.

The committee has been aided from time to time in the study of its problems by a number of invited representatives from the Government organizations concerned, among whom were the following:

Dr. L. H. Bauer, Aeronautics Branch, Department of Commerce.

Dr. H. J. Cooper, Aeronautics Branch, Department of Commerce.

Commander R. G. Davis (M. C.), United States Navy.
P. Edgar, Aeronautics Branch, Department of Commerce.
Lieut. Col. L. M. Hathaway (M. C.), United States Army.
F. J. Martel, Aeronautics Branch, Department of Commerce.
Lieut. Commander John R. Poppen (M. C.), United States Navy.
Lieut. Stanhope C. Ring, United States Navy.
E. R. Strong, Aeronautics Branch, Department of Commerce.
Starr Truscott, National Advisory Committee for Aeronautics.

The analysis of aircraft accidents by the Army, Navy, and Department of Commerce in accordance with the standard method confirmed the conclusion previously reached, that a large percentage of aircraft accidents are due to pilots' errors. The need for the study and analysis of the defects or shortcomings of pilots which account for this fact was brought to the attention of the committee on aircraft accidents by Lieutenant Phillips, at that time a member of the committee. The initial meeting of the accidents committee was held on March 16, 1929, to consider this problem, and meetings have been held at frequent intervals since that date. Consideration has been given not only to problems affecting the personnel element in accident causes, but to a number of other aspects of the subject as well.

In the period which has elapsed since the adoption of the chart as a standard method of accident analysis, its value has been definitely demonstrated. The analysis of accidents in accordance with the prescribed standard has enabled the three services to learn important facts as to causes of accidents, and to take appropriate steps toward remedying these causes. It has made it possible for the Aeronautics Branch of the Department of Commerce to reorganize its inspection service on a more effective basis.

Some doubt has been expressed as to the possibility of actually standardizing accident statistics on account of the probable lack of consistency in analyses made by different individuals or groups of individuals. In this connection it is of interest to note that the results obtained in the analysis of a large number of accidents by different individuals and groups showed excellent agreement.

In view of the large percentage of accidents due to pilots' errors, the prompt and thorough study of accident statistics is of great importance, particularly in connection with the issuance of licenses to pilots of civil aircraft by the Department of Commerce. A study has been made by the committee on aircraft accidents of some of the more important influences contributing to pilots' errors. The importance of adequate flight training, especially for pilots in commercial service, including a reasonable amount of actual piloting experience, is evident, and during the past year Congress has authorized the Secretary of Commerce to provide for the examination and rating of civilian schools giving instruction in flying.

Some of the more important mental and physical characteristics of pilots which affect their ability to operate aircraft safely were given consideration by the committee on aircraft accidents. It was found that a large percentage of the pilot's accident responsibility had been ascribed in the accident analysis to "poor reaction." Important information as to this phase of the problem was presented to the committee by medical authorities from the War, Navy, and Commerce Departments, and in these discussions suggestions were presented which were of benefit to the members in connection with the work of their respective departments in the prevention of accidents.

Other physiological factors entering into the accident problem were discussed, including sight, hearing, general health, effect of worry, etc. The influence of these factors on the efficiency of the pilot is evidence of the value of specialized medical supervision over flying personnel.

The accidents committee is now engaged in a revision of Technical Report No. 308, Aircraft Accidents—Methods of Analysis, clarifying the definitions in the light of the experience gained in the analysis of accidents by the three Government services, and including some of the suggestions presented in the discussions in the meetings of the committee. This revision when completed will be published as a Technical Report of the National Advisory Committee for Aeronautics.

CONSIDERATION OF AERONAUTICAL INVENTIONS

By act of Congress approved July 2, 1926, a Patents and Design Board was created, and it was provided that upon recommendation of the National Advisory Committee for Aeronautics the board should determine questions as to the use and value to the Government of aeronautical inventions submitted to the Government. By act of Congress approved March 3, 1927, the act of July 2, 1926, was amended in such a manner as to limit the board to the consideration of such cases as were favorably recommended to it by the National Advisory Committee for Aeronautics. This relieved the board of the burden of considering cases which were unfavorably recommended by the committee, but at the same time it made the National Advisory Committee for Aeronautics responsible for the final disapproval of the large majority of the devices submitted as applications for awards.

In order to discharge the duties devolving upon the committee under this legislation, a committee on aeronautical inventions and designs was created, the present membership of which is as follows:

Dr. D. W. Taylor, chairman.

Dr. George K. Burgess, vice chairman.

Prof. Charles F. Marvin.

Commander John H. Towers, United States Navy.

J. F. Victory, secretary.

Inventions and designs submitted are considered by the Director of Aeronautical Research. The committee on aeronautical inventions and designs considers in committee only such inventions or designs as are presented by the Director of Aeronautical Research or are recommended for committee consideration by any other member of the National Advisory Committee. The Director of Aeronautical Research is authorized to submit his unfavorable recommendations direct to the Aeronautical Patents and Design Board, but any favorable recommendations must be considered and made by the committee on aeronautical inventions and designs.

Under the present procedure careful consideration is given to all inventions and designs submitted. The Aeronautical Patents and Design Board and the National Advisory Committee for Aeronautics are working in harmony and the burden of considering large numbers of inventions is placed so as to reduce the demands on the time of the members of the committee on aeronautical inventions and designs and of the members of the Aeronautical Patents and Design Board to the consideration of submissions which have received competent preliminary examination and are deemed worthy of further consideration.

In the past year, which was the third year of the operation of the Aeronautical Patents and Design Board, the committee received about 2,400 letters relating to inventions. Fifty per cent of these represented wholly new submissions. This number includes 150 inventions and designs submitted to the Aeronautical Patents and Design Board. In each of these cases the committee made a report to the board as to the merits of the device. The remaining cases, being addressed to the committee, were acted on by direct correspondence with the submitters. Two cases were sufficiently meritorious to warrant favorable recommendation.

RELATIONS WITH THE AIRCRAFT INDUSTRY

In 1926 the National Advisory Committee for Aeronautics established the policy of holding at its laboratory at Langley Field, the Langley Memorial Aeronautical Laboratory, annual conferences with representatives of the manufacturers and operators of aircraft. The purpose of these conferences was to give to aircraft manufacturers and operators an opportunity to become acquainted with the facilities for aeronautical research at the committee's laboratory and also to afford them an opportunity to make suggestions to the committee as to aeronautical research problems of interest to the industry which in their opinion the committee is especially equipped to solve.

In accordance with this policy, the Fourth Annual Aircraft Engineering Research Conference was held at the Langley Memorial Aeronautical Laboratory on May 14, 1929. In addition to the representatives of the industry, the conference was attended by representatives

of aeronautical journals and of educational institutions engaged in the teaching of aeronautical engineering. The committee was represented by its officers, members of the main committee, and the members of its committees on aerodynamics and power plants for aircraft. The conference was presided over by Dr. Joseph S. Ames, chairman of the National Advisory Committee for Aeronautics.

At the morning session the principal investigations under way at the laboratory were explained by the engineers in charge of the work, and charts were exhibited showing some of the results obtained. Some of the more important investigations outlined were the study of pressure distribution over the wings and tail surfaces of pursuit airplanes; the study of water pressure distribution on seaplane floats and hulls; the determination of the stresses on the oleo type landing gear in landing; the effect of mass distribution on the spinning characteristics of airplanes; the effect of slots and flaps on the performance of aircraft; the effect on airplane performance of the N. A. C. A. low-drag cowling for radial air-cooled engines; the study of cooling with the N. A. C. A. cowling; interference effects between wing and propeller; the effect of high tip speeds on propellers; the development of the Roots type supercharger; and the development of a high-speed heavy-oil fuel-injection engine. At the close of the session, the representatives of the industry were conducted on a tour of inspection of the committee's laboratories, and the research equipment was shown in operation.

The afternoon session was devoted to the discussion of the problems of commercial aeronautics, and 24 suggestions were made, chiefly by representatives of the industry. A number of these problems were already a part of the committee's research program. Among the problems discussed were the causes of abnormal spins of airplanes; the reduction of airplane resistance and the study of interference effects; the interaction between engine nacelle, propeller, and wing; and the study of take-off and landing characteristics. The need for the thorough study of the characteristics of seaplanes and flying boats was pointed out, and it was announced that the committee had obtained authority from Congress and was proceeding with plans for the construction at Langley Field of a model tank for the testing of models of seaplanes and flying boats.

The 24 suggestions presented at the conference have since been carefully considered by the committee on aerodynamics, and two of them—the determination of load and load distribution on commercial type airplanes, and the wind-tunnel investigation of the placing of nacelles with biplane structures, including the measurement of propeller efficiencies—have been incorporated in the committee's research program.

Following the conference, demonstration flights were made by the Pitcairn Autogiro, through the courtesy of Mr. Harold F. Pitcairn, and by the Stinson Detroiter with the Packard Diesel heavy-oil engine, through the courtesy of Mr. L. M. Woolson and the Packard Motor Car Co.

RIGID AIRSHIPS

The round-the-world flight of the German rigid airship *Graf Zeppelin* in August and September, 1929, was an epochal achievement that challenged the admiration of the world. It served to focus attention on the possibilities of long-distance air navigation by the use of rigid airships and to prompt a review of the American airship development program. In order clearly to grasp the situation in America, the following brief chronology of events is presented:

1917.—Appointment of a joint Army and Navy airship board.

1918.—The sending of a commission abroad by that board to investigate the rigid airship situation.

1918.—Appropriations made by Congress for the construction of one or more rigid airships.

1918.—Decision to build a duplicate of the *L-49*, plans of which were secured from the French (later the *ZR-1*, *Shenandoah*).

1918.—Preliminary work begun on the *Shenandoah*.

1918.—Joint Army and Navy board recommended that the development of rigid airships be assigned to the Navy. Approved by the Secretary of War and the Secretary of the Navy.

- November 11, 1918.*—The armistice. After the armistice work continued on the *Shenandoah*. Plans made for the hangar at Lakehurst, N. J.
- 1919.*—British rigid airship *R-34* made round-trip flight between England and the United States.
- 1919.*—Rigid airships *Bodensee* and *Nordstern* constructed in Germany and flown successfully as passenger carriers for nine months, when they were taken over by the Allies and allotted one to France and one to Italy.
- 1919.*—Airship board recommended purchase of British airship *R-38*, then 80 per cent complete. Contract was executed with British Government and the airship designated by the United States, *ZR-2*.
- 1919-21.*—Diplomatic negotiations under way to secure an airship from Germany as a result of an armistice agreement under which the United States was entitled either to an airship or a cash payment in lieu of an airship destroyed by the Germans at the time of the armistice.
- 1919-21.*—*R-36* was flown in England. Great Britain, except for operating this airship, virtually abandoned airship development.
- August, 1921.*—*R-38 (ZR-2)* destroyed in England on trial flight, with loss of 46 lives.
- October, 1921.*—Council of ambassadors at Paris agreed to permit the United States to have a modern rigid airship constructed in Germany.
- 1921.*—Erection of *ZR-1, Shenandoah*, just getting under way.
- February-June, 1922.*—Contract negotiated with Zeppelin Co. for building the *ZR-3*, later the *Los Angeles*, against the account of the German Government.
- July, 1922.*—Construction of the *ZR-3* started.
- July, 1923.*—The *Shenandoah* made her first flight.
- 1923.*—Great Britain planned for two large rigid airships—*R-100* and *R-101*—ready for flight in 1929.
- October, 1924.*—The *ZR-3, Los Angeles*, delivered in America by Doctor Eckener.
- September, 1925.*—*Shenandoah* was wrecked in a storm over Ohio, with a loss of 14 lives.
- October, 1925.*—Steps taken in Navy Department toward replacement of *Shenandoah* and establishment of a definite rigid airship construction program.
- December, 1925.*—The National Advisory Committee for Aeronautics, after analysis of the situation as developed by the loss of the *Shenandoah*, definitely recommended that the development of rigid airships be continued.
- 1926.*—Restrictions on airship construction in Germany removed. Construction of *Graf Zeppelin* started by the Zeppelin Co. largely under public subscription.
- 1926.*—Contract executed by the Navy for first metal-clad airship, which was successfully flown in the fall of 1929.
- 1926.*—Five-year Navy aircraft building program authorized construction of two rigid airships.
- 1928.*—No appropriation having been made for construction of the two airships, and certain inquiries having been presented to the committee, the National Advisory Committee for Aeronautics adopted the following resolution:
- “*Resolved*, That it is the opinion of the National Advisory Committee for Aeronautics that the present state of the art of constructing and operating large rigid airships has progressed to the point where we are justified in believing that large rigid airships can be constructed and operated successfully.
- “*Resolved further*, That it is the opinion of the National Advisory Committee for Aeronautics that the most practical step to be taken at the present time to encourage the development of an airship industry in the United States is to begin the construction of the airships authorized under the 5-year building program. The construction of these airships will foster the development of an airship industry, and this, with the knowledge to be acquired from experience in the operation of airships, will be necessary in order to enable the United States to meet the needs for commercial airship construction and operation when they arise.”

Funds were appropriated for the construction of two rigid airships of 6,500,000-cubic-foot capacity each, and contracts were entered into with the Goodyear-Zeppelin Corporation of Akron, Ohio. The keel ring of the first of the two airships was laid on November 7, 1929. These airships are at present designated the *ZRS-4* and *ZRS-5*. This step marks the beginning of a rigid airship industry in the United States, as the only rigid airship heretofore built in America was the *Shenandoah*, which was fabricated at the Philadelphia Navy Yard and assembled at Lakehurst. The present American rigid airship program as authorized by law also includes the maintenance of an airship base on the east coast at Lakehurst and the construction of an additional airship base on the west coast.

The present airship program also brings into existence a new helium industry, all helium for airships having heretofore been produced by the Government. Additional helium fields have been located in the United States, and it is the present belief of authorities on the subject that the present known supply of helium is much more than ample to meet any requirements for the next generation. The United States continues to enjoy an apparent monopoly in the possession and production of helium in quantities sufficient for use in airships. As helium is noninflammable and noncombustible, its use contributes materially to the safety of rigid airships, although its lifting capacity is approximately 8 per cent less than hydrogen per unit of volume.

A consideration of the economic possibilities in the use of various types of aircraft for long flights leads the committee to express the belief that the most useful field for rigid airships is for flights of over 1,000 miles over the water; that for flights under 1,000 miles over the water large seaplanes will prove more efficient; and for long flights over the land airplanes of the land type will be used, with stops for refueling every 400 or 500 miles.

Rigid airships have great potential value for military purposes, the present primary military field being that of naval scouts. There are great possibilities in the use of rigid airships for commercial purposes which were strikingly demonstrated by the round-the-world flight of the *Graf Zeppelin*. If the United States is to take full advantage of the possibilities of air transportation, especially in the field of transoceanic air travel, the importance of the development of rigid airships can not be overemphasized, as in transportation by air over long distances, and especially over the water, rigid airships have marked advantages over airplanes. In order to develop their naval uses and in order more especially to assist and hasten the development of rigid airships in America for commercial purposes, the committee recommends firm support by the President and by the Congress of the present Navy rigid airship development program.

THE DANIEL GUGGENHEIM FUND FOR THE PROMOTION OF AERONAUTICS

The cordial relations which already existed between this committee and the Daniel Guggenheim Fund for the Promotion of Aeronautics were strengthened by the appointment, in April of this year, of Mr. Harry F. Guggenheim, president of the fund, as one of the three additional members of the committee as authorized by act of Congress approved March 2, 1929.

During the current year the fund has been able to round out some of its activities, and as a result of a progress in aviation which has exceeded its expectations, its work will terminate about the end of this year. Since the fund was founded in January, 1926, its existence will cover a 4-year period, during which the character of the fund's work has changed as aviation has advanced. By the middle of 1928 public support of aviation was assured, and the fund, therefore, began to concentrate particularly upon the problem of safe flying and landing through fog.

During the present year the Daniel Guggenheim Fund has continued its activities in providing practical and substantial assistance to aeronautics in its commercial, industrial, and scientific aspects. The fund has extended its financial support of educational institutions. It has given appropriations totaling over \$1,200,000 to five engineering universities as follows:

California Institute of Technology.

Massachusetts Institute of Technology.

Stanford University.

University of Michigan.

University of Washington.

It announced this fall it would undertake a survey for the purpose of making a similar grant to some university in the South.

In addition to these appropriations among higher institutions the fund established a committee on elementary and secondary aeronautic education so as to carry this work into the schools as well. The fund has itself published from time to time documents of both a popular and a technical nature on various aeronautical problems.

Among its new projects the fund recently announced an appropriation of \$250,000, made to the city of Akron and the California Institute of Technology for the establishment of an airship institute; an appropriation of \$140,000 for a chair at the Library of Congress for the purpose of organizing a complete aeronautical library for research purposes; and a large number of smaller grants to other institutions.

On September 24, 1929, at Mitchel Field, the Daniel Guggenheim Fund made a demonstration of a method of safe flying and landing through fog. This experiment established the principle of safe fog flying which must, however, be eventually perfected for commercial use. It points the way to the elimination of one of the greatest hazards to the reliability of airplane travel. This demonstration was realized through the aid of only three instruments which are not already the standard equipment of an airplane, and of these three instruments two will replace two instruments now in use.

Another important activity recently undertaken by the Guggenheim Fund is the preparation of an encyclopedia of aerodynamic theory. This work is to be international in character and will present a fairly complete statement of the present condition of aerodynamic theory, the various portions being written by authors who have especial and first-hand knowledge of their subjects. This project is now under way under the direction and supervision of Dr. W. F. Durand.

The safe-airplane competition inaugurated by the fund has been continued. This competition was initiated for the purpose of promoting safety in flying and has led to efforts on the part of manufacturers and designers to make safer airplanes.

The fund has also included in its activities the study of the problem of regulation of civil aeronautics and has called attention to the desirability of uniform State legislation to provide regulations for intrastate flying identical with the Federal regulations for interstate flying.

COOPERATION WITH STATE DEPARTMENT ABROAD

The committee has cooperated with the Department of State by making available the services of its technical assistant in Europe, Mr. John J. Ide, for attendance as unofficial observer or technical adviser on behalf of the United States at several international air conferences abroad. The Department of State accepted the committee's offer. In accordance with action by the State Department Mr. Ide represented the United States unofficially at the following conferences: Meeting in Paris on May 6, 1929, of the International Technical Committee of Aerial Juridical Experts; meeting in Paris beginning on June 10, 1929, of the International Commission for Air Navigation; and the Second International Diplomatic Conference on Private Aeronautical Law, held at Warsaw, Poland, beginning on October 4, 1929.

COOPERATION WITH BRITISH AERONAUTICAL RESEARCH COMMITTEE

It is a great pleasure to this committee to offer its congratulations to the Aeronautical Research Committee of Great Britain on the completion, in April of this year, of 20 years of aeronautical research under the direction of that committee and its predecessor, the Advisory Committee for Aeronautics. Our own committee, established in 1915, was organized along similar lines to those of the British committee. Aeronautics throughout the world owes a debt of gratitude to the British organization for its accomplishments in scientific research during the past two decades.

The officers and members of our committee were most pleased to receive during the past year a visit from Mr. H. E. Wimperis, director of scientific research of the British Air Ministry, and Mr. R. McKinnon Wood, head of the aerodynamics section of the Royal Aircraft Establishment.

This visit presented an opportunity for the informal discussion of a number of problems of aeronautical research and development which are of special interest to the two committees.

Comparative tests by the two committees, initiated several years ago with a view to standardizing the results of wind-tunnel tests, have been continued. These tests have been extended to include the comparison of flight test results obtained in England with results obtained on models of the same airplanes in the variable-density wind tunnel, and have yielded valuable information on the subject of scale effect. Tests are being made in the variable-density tunnel on a British model of a Hawker Hornbill airplane with A. D. 1 wing section, and it is hoped that useful information relating to the problems of stability and control at or near the stalling angle will be obtained from these tests. Tests in the variable-density tunnel of a British model of an R. A. F. airfoil are also contemplated.

An exchange of flight test instruments has been made for comparative study, this committee receiving a force recording rudder bar and a force recording control stick, and lending to the British committee in return a 3-component accelerometer.

COOPERATION OF ARMY AND NAVY

Through the personal contact of the heads of the Army and Navy air organizations serving on the main committee and the frequent personal contact on the subcommittees of their chief subordinates who have to do with technical matters in aeronautics, there has been accomplished in fact not only a coordination of aeronautical research, which is the major function of the committee, but also a coordination of experimental engineering activities of the services and an exchange of first-hand information, comment, and suggestions that have had beneficial effects in both services. The needs of each service in the field of aeronautical research are discussed and agreements invariably reached that promote the public interests. The cordial relations that usually follow from frequent personal contact are supplemented by the technical information service of the committee's Office of Aeronautical Intelligence, which makes available the latest scientific data and technical information secured from all parts of the world. Although there is a healthy rivalry between the Army and Navy air organizations, there is at the same time a spirit of cooperation and a mutual understanding of each other's problems that serve to prevent unnecessary duplication in technical developments in aeronautics.

Much of the fundamental research work of the committee has grown out of requests received from the Army and Navy for the study by the committee of particular problems encountered in the services, and in connection with this work the committee desires to give special recognition to the splendid spirit of cooperation of the two services with the committee. Both services have placed at the disposal of the committee airplanes and engines required for research purposes, and have otherwise aided in every practical way in the conduct of scientific investigations by the committee. Without this cooperation the committee could not have prosecuted successfully many of its investigations that have made for progress in aircraft development. The committee desires especially to acknowledge the many courtesies extended by the Army authorities at Langley Field, where the committee's laboratories are located, and by the naval authorities at the Hampton Roads Naval Air Station.

INVESTIGATIONS UNDERTAKEN FOR THE ARMY AND THE NAVY

As a rule research programs covering fundamental problems demanding solution are prepared by the technical subcommittees and recommended to the executive committee for approval. These programs supply the problems for investigation by the Langley Memorial Aeronautical Laboratory. When, however, the Army Air Corps, the Naval Bureau of Aeronautics, or the Aeronautics Branch of the Department of Commerce desires special investigations to be undertaken by the committee, such investigations, upon approval by the executive committee, are added to the current research programs.

The investigations thus under conduct by the committee during the past year for the Army, the Navy, and the Department of Commerce may be outlined as follows:

FOR THE AIR CORPS OF THE ARMY

Investigation of cowling for protection of gunners and pilots from air currents.
 Wind-tunnel investigation of biplane cellules.
 Investigation of pressure distribution on observation-type airplane.
 Study of comparative performance with various types of superchargers.
 Study of mutual interference of propeller and fuselage, with geared engine.
 Study of ice formation.
 Determination of moment coefficients and hinge moment coefficients for different tail surfaces.
 Determination of aileron hinge moments versus rolling moments for various types of ailerons and wings.
 Investigation of wing flutter.
 Investigation of the flat spin.
 Investigation of pressure distribution and accelerations on pursuit type airplane.
 Acceleration readings on the PW-9 airplane.

FOR THE BUREAU OF AERONAUTICS OF THE NAVY DEPARTMENT

Investigation of flight path characteristics.
 Ice formation on aircraft.
 Comparative tests of rubber and oleo type landing gears.
 Investigation of windshields and fairings for protection from air currents.
 Study of design factors for metal propellers.
 Investigation of autorotation and spinning characteristics of airplanes.
 Determination of radii of gyration of airplanes.
 Investigation of comparative aerodynamic resistance of riveted and bolted construction.
 Investigation of parasite resistance and propeller efficiencies of PB-2.
 Investigation of methods of improving wing characteristics by control of the boundary layer.
 Investigation of the forces on seaplane floats under landing conditions.
 Investigation of water-pressure distribution on seaplane hulls.
 Development of solid-injection type of aeronautical engine.
 Investigation of application of compression ignition to air-cooled engine cylinders.
 Effect of varying the aspect ratio and area of wings on performance of fighter airplane with supercharged air-cooled engine.
 Investigation of aerodynamic loads on the U. S. S. *Los Angeles*.
 Development of aircraft engine supercharger.
 Effect of various forms of cowling on performance and engine operation of fighter airplane with supercharged air-cooled engine.

FOR THE AERONAUTICS BRANCH OF THE DEPARTMENT OF COMMERCE

Study of high-speed cowling as ignition shielding of air-cooled engines to aid radio reception.

EXHIBIT AT SEVILLE INTERNATIONAL EXPOSITION

On invitation of the Commissioner General of the United States for the International Exposition at Seville, Spain, the committee prepared an exhibit and selected Chester W. Hicks, a member of the engineering staff at Langley Field, to install and maintain it. The installation was completed March 18, 1929, and the exhibit was among the first ready for public inspection. The expenses involved were defrayed from the allotment of \$5,000 made by the commission for this purpose. The unexpended balance of \$782.50 was returned to the State Department.

A room of 480 square feet in one of the United States Government buildings was made available for the committee's exhibit. The hexagonal shape of the room is ideally adapted to the arrangement of the models to the best possible advantage. It is the most prominent space in the United States buildings. The exhibit is composed of 5 working models, 1 show case con-

taining airplane models and instruments, 2 tables on which are shown the results of pressure distribution investigations on the surfaces of an airplane and airship, and 18 charts illustrating the facilities and methods employed in the conduct of aeronautical research in the committee's laboratories at Langley Field, Va. The five working models consist of scale models of the propeller research tunnel and of the variable-density wind tunnel; a model showing the operation of the control system of an airplane; a model showing why an airplane flies, which illustrates graphically the dynamic reaction of the air upon an airplane in flight; and a model showing the effect of a rotating cylinder in an air stream and illustrating the principle involved in the Flettner rotor ship. Mr. Hicks has reported that visitors appreciate and praise this method of demonstration.

A band of blue satin with the name of the committee inscribed in gold letters, around the walls near the ceiling, with blue and white streamers symbolic of the national colors, contributes to the appearance of the exhibit.

The daily attendance varies from 800 on week days to 2,000 on Sundays and holidays. The reports made by Mr. Hicks indicate that the Spanish public and visitors to Seville from many nations are interested in aeronautics and that the committee's exhibit is proving popular.

Sufficient data are included to make the exhibit of interest also to the technically trained visitors and particularly to those connected with aeronautical activities. The committee's exhibit is part of a comprehensive exhibit entered by the Government of the United States.

PART III

REPORTS OF TECHNICAL COMMITTEES

REPORT OF COMMITTEE ON AERODYNAMICS

ORGANIZATION

The committee on aerodynamics is at present composed of the following members:

Dr. David W. Taylor, chairman.

Dr. L. J. Briggs, Bureau of Standards.

G. G. Budwig, Aeronautics Branch, Department of Commerce.

Lieut. W. S. Diehl (C. C.), United States Navy.

Lieut. Grandison Gardner, United States Army, matériel division, Air Corps, Wright Field.

Maj. C. W. Howard, United States Army, matériel division, Air Corps, Wright Field.

George W. Lewis, National Advisory Committee for Aeronautics (ex officio member).

Prof. Charles F. Marvin, Weather Bureau.

Lieut. Commander A. C. Miles (C. C.), United States Navy.

Hon. Edward P. Warner, editor, Aviation.

Dr. A. F. Zahm, construction department, Washington Navy Yard.

FUNCTIONS

The functions of the committee on aerodynamics are as follows:

1. To determine what problems in theoretical and experimental aerodynamics are the most important for investigation by governmental and private agencies.

2. To coordinate by counsel and suggestion the research work involved in the investigation of such problems.

3. To act as a medium for the interchange of information regarding aerodynamic investigations and developments, in progress or proposed.

4. To direct and conduct research in experimental aerodynamics in such laboratory or laboratories as may be placed either in whole or in part under its direction.

5. To meet from time to time on call of the chairman and report its actions and recommendations to the executive committee.

The committee on aerodynamics, by reason of the representation of the various organizations interested in aeronautics, is in close contact with all aerodynamical work being carried out in the United States. The current work of each organization is therefore made known to all, duplication of effort being thus prevented. Also all research work is stimulated by the prompt distribution of new ideas and new results, which add greatly to the efficient conduct of aerodynamic research. The committee keeps the research workers in this country supplied with information on European progress in aerodynamics by means of a foreign representative who is in close touch with aeronautical activities in Europe. This direct information is supplemented by the translation and circulation of copies of the more important foreign reports and articles.

The committee on aerodynamics has direct control of the aerodynamical research conducted at Langley Field and of a number of special investigations conducted at the Bureau of Standards. The aerodynamical investigations undertaken at the Washington Navy Yard, the matériel division of the Army Air Corps at Wright Field, and the Bureau of Standards are reported to the committee on aerodynamics.

SUBCOMMITTEE ON AIRSHIPS

In order that the committee on aerodynamics may be kept in close touch with the latest developments in the field of airship design and construction, and that research on lighter-than-air craft may be fostered and encouraged, a subcommittee on airships has been organized under the committee on aerodynamics, the membership of which is as follows:

Hon. Edward P. Warner, editor of Aviation, chairman.

Starr Truscott, National Advisory Committee for Aeronautics, vice chairman.

Dr. Karl Arnstein, Goodyear-Zeppelin Corporation.

Commander Garland Fulton (C. C.), United States Navy.

George W. Lewis, National Advisory Committee for Aeronautics (ex officio member).

Capt. Edgar P. Sorenson, United States Army, matériel division, Air Corps, Wright Field.

Ralph H. Upson, Red Bank, N. J.

During the past year the subcommittee on airships presented recommendations for two investigations on airship models to be conducted in the propeller research tunnel at the Langley Memorial Aeronautical Laboratory, both of which have been added to the committee's program. These two investigations were the study of the effect of appendages on airship hulls, including tests of an airship model about 40 inches in diameter with different protrusions, such as water-recovery apparatus, cars, propeller mountings, fins, and rudders of different contours; and the study of the forces on an airship entering a hangar, including the construction of models of two types of hangars and the measurement of the forces and moments on an airship model in various positions with respect to the hangar and the direction of the wind stream.

The subcommittee has continued the consideration of problems of atmospheric structure as affecting airship operation, particularly vertical air currents and gustiness, and is cooperating with the subcommittee on meteorological problems of the committee on problems of air navigation in the study of this subject.

SUBCOMMITTEE ON AERONAUTICAL RESEARCH IN UNIVERSITIES

In order to coordinate the aerodynamic research work undertaken by the various institutions of learning and to aid in improving the courses in aeronautical engineering and in promoting the study of aeronautics, a subcommittee on aeronautical research in universities has been organized under the committee on aerodynamics.

The membership of this subcommittee is as follows:

Prof. Charles F. Marvin, Weather Bureau, chairman.

Hon. Harry F. Guggenheim, president of Daniel Guggenheim Fund for the Promotion of Aeronautics.

Prof. Alexander Klemin, New York University.

Prof. E. P. Lesley, Stanford University.

George W. Lewis, National Advisory Committee for Aeronautics (ex officio member).

Prof. Clark B. Millikan, California Institute of Technology.

Prof. F. W. Pawlowski, University of Michigan.

The functions of the subcommittee on aeronautical research in universities are as follows:

1. To consider aeronautical problems with a view to the initiation and conduct of aeronautical research by educational institutions; and in connection therewith to prepare programs of suggested lines of research intended to supplement existing research programs and to develop and train personnel for the conduct of scientific research in aeronautics along original lines.

2. To seek through interchange of ideas to improve the courses in aeronautical engineering and to promote the study of aeronautics and aerology in educational institutions.

3. To meet from time to time on call of the chairman and to report its actions and recommendations to the committee on aerodynamics.

The subcommittee on aeronautical research in universities held its initial meeting at the Langley Memorial Aeronautical Laboratory on June 21, 1929. The topics under discussion at this meeting included the equipment for aerodynamics departments at educational institutions, courses of study, and aerodynamic problems suitable for investigation by universities. In connection with the meeting the members of the subcommittee made a tour of inspection of the

facilities and activities of the laboratory. On recommendation of the subcommittee, the standard wind-tunnel models on which comparative tests have been conducted during the past few years in the principal wind tunnels of this country are being made available for test in the wind tunnels of the various educational institutions, and in accordance with this plan the standard airship models are now being tested by the California Institute of Technology.

LANGLEY MEMORIAL AERONAUTICAL LABORATORY

AERODYNAMIC SAFETY.—As commercial aeronautics develops, the problem of safety in flight continues to be one of increasing importance, affecting more and more the general public, as well as the aircraft operators and manufacturers. Improvement in the accuracy of aircraft accident reports has made possible a more detailed analysis of the relative seriousness, as well as the underlying causes, of accidents. The air-accident statistics of the Department of Commerce for 1928 indicate that the pilot was at fault in nearly half the accidents occurring in that year. As analyzed from the standpoint of the nature of each accident, these data show that two-thirds were due to spins and forced or bad landings. Thus, we are brought to the conclusion that the airplane of to-day is too easy to spin and too difficult to land and, consequently, that too much is expected of the pilot and not enough of the designer. In other words, the airplane still possesses certain undesirable aerodynamic characteristics which should be definitely recognized, investigated, and ultimately removed.

The National Advisory Committee for Aeronautics has always recognized the importance of the problem of safety in flight, and a large part of the work of the laboratory has been devoted to its various phases, such as spinning, stability, controllability, maneuverability, ice formation on aircraft, structural safety, landing, and piloting under adverse weather conditions.

Spinning.—Most fatal air accidents are due to the tendency of an airplane when stalled to dive or to roll sharply contrary to the desire and the efforts of the pilot, resulting in a spin and if the airplane is near the ground, in a crash. Since there is no need for the spin as a customary maneuver for civil aircraft, it is desirable that the tendency to spin should be eliminated. If an airplane wing is stalled, it will have, among other things, a tendency to roll about an axis approximately parallel to the direction of flight, and this rolling will in itself produce a torque tending to build up the motion. If at the same time the wing is sideslipping, an additional torque acting in the same direction is produced. The resulting rolling motion is termed autorotation. These two torques are of the same order of magnitude, in general, and appear to be important factors in starting and maintaining the spin.

An investigation of autorotation was inaugurated about three years ago in the atmospheric wind tunnel. The test program included force, pressure distribution, and autorotation torque tests up to 90° angle of attack on models of a wide variety of wing systems. The force and pressure distribution tests have been completed and the results published. The first of the autorotation tests are now being made on an autorotation dynamometer in the wind tunnel. It is proposed to extend these tests at a later date by modifying the dynamometer so that pitching and yawing, as well as rolling moments, may be measured.

The problem involved with military airplanes is somewhat different since the airplane is required to spin as a military maneuver. The problem then is one of safe recovery from a spin.

An important factor in the recovery of airplanes from spins is the effect of the distribution of the mass of the airplane, and the flight research section of the laboratory has concentrated chiefly on this factor. Apparatus of great accuracy for measuring the mass distribution of an airplane has been developed, and the moments of inertia and ellipsoids of inertia of a number of airplanes have been determined. A study has been made of these inertia data, together with such information as is available on the type of spin executed by each airplane, and a definite relation between mass distribution and the type of spin appears to exist. The chief difficulty in this study has been the lack of accurate knowledge of the magnitude of the variables that enter into the dynamics of the spin, such as the radius and rate of rotation. Methods of measuring these variables in flight have been perfected, and complete data on one airplane have been obtained, from which the dynamic forces producing and maintaining these spins have been

determined. The investigation is to be continued on other airplanes, and in particular on one normally spinning airplane in which the mass distribution is to be changed in an attempt to produce a flat spin.

Stability.—Safety depends to a great extent upon stability. Departure from a desired flight direction or attitude should be but momentary and loss of altitude small, whether the controls are being held by the pilot or left free. Many airplanes possess satisfactory stability below the angle of attack of maximum lift, but very few, if any, are as satisfactory in stalled flight. An investigation of stability in stalled flight is being carried on in the atmospheric wind tunnel. Tests have recently been made to determine the effect on stability of twisting a wing, and at the same time the effect of change in profile along the span. Both methods were found to give improved stability, and the report on the work is in preparation.

Controllability.—Safety also depends on controllability. The pilot must have at his command means for changing the path of the airplane with sufficient rapidity to avoid collisions, or to enter and recover from maneuvers, but not so rapidly as to stress unduly the airplane structure. Moreover, it is highly desirable that the change of direction should be smooth and constant without sudden or unexpected accelerations. Most airplanes have satisfactory controllability in normal flight, but when stalled many of them exhibit an anomalous behavior when the controls are operated. This is particularly true of airplanes equipped with the conventional type of ailerons, for in stalled flight operation of these ailerons produces at first a sluggish roll in the desired direction, followed shortly by a reversal of direction, while the ailerons are still held in the initial position. Obviously, this effect is confusing and likely to result in disaster. Considerable interest also centers around the fact that some military and many civil types of airplanes have been found to resist attempts at recovery from the steady spin, particularly when the spin has been allowed to develop for several turns. During such spins, either the controls have been practically ineffective or the force required to operate them has been too great for the pilot to exert.

A study has been made in the atmospheric wind tunnel of the effectiveness of various types of ailerons, particularly from the standpoint of stalled flight and the spin, and it is planned in the near future to conduct flight tests on a special monoplane arranged for convenient changing of the wings, ailerons, and tail surfaces. In these tests, every effort is to be made to obtain accurate information on the rolling and yawing tendencies of the airplane with various methods of control while in stalled flight.

A series of pressure distribution tests recently completed in the variable-density wind tunnel on an R. A. F. 30 airfoil with flaps should also be of considerable assistance in studying the effectiveness of ailerons, and particularly how it varies with scale. The results of these tests are being prepared for publication.

Maneuverability.—The work on the comparative maneuverability of airplanes has been continued. A series of maneuverability tests has now been carried out on two pursuit airplanes. The results have been analyzed and a report prepared covering the tests on one airplane. The results obtained on the second airplane are being studied. The degree of maneuverability is determined basically by the flight path obtainable by an airplane, and considerable attention has been given to improving the methods of determining the flight path in flight. A program of work for a similar research on an airplane of the observation type has been outlined, and preliminary plans for measuring the maneuverability of commercial monoplanes are under consideration. This work has required greater sensitivity on the part of recording instruments, particularly angular-velocity recorders, than has been required for any other flight research activity and has made necessary, among other things, a careful study of damping oils for use in such instruments. It has been sought to obtain an oil which would permit uniform accuracy of the instrument under various conditions of temperature and rate of motion of the airplane.

Ice formation.—The formation of ice on aircraft has been regarded for some time as an element of danger. It appears that ice will form under a variety of atmospheric conditions,

resulting not only in an increase in the weight of the airplane but also in the deformation of the aerodynamic shapes on which the lift and drag depend.

Flight tests have been conducted in order to study the formation of ice under a variety of weather conditions, such as fog, rain, and sleet. Photographs were made of the ice deposits on wings, wires, and struts. In several instances, ice formation was obtained on the propellers. While no means of preventing this hazard was discovered, the formation could often be partially or wholly eliminated by flying at different altitudes, or at temperatures at which the minimum deposit was found. It appears thus far that the only safe procedure in service is for the pilot to land before the deposit assumes such proportions as to interfere with control. It was noted, however, that the ice forms in dangerous amounts only within a small range of temperature below 32° F. A report has been published covering this phase of the work.

A small refrigerated wind tunnel for studying the problems of ice formation has been in operation during the year, considerable time having been devoted to means for controlling the amount of water sprayed into the air stream, the size of the water particles, and the temperatures of the air and the water.

The first phase of the problem undertaken, that of studying the possibility of using a protective coating on the aircraft surfaces to prevent the forming of ice, has yielded mainly negative results. It has been found, however, that glucose, corn sirup, and some similar substances in solid or semisolid form, and certain liquids, as a mixture of glycerin and alcohol, do have some effect in preventing the formation of ice. A report is in preparation covering this phase of the work.

Structural safety.—The determination of the air loads experienced by airplanes under all conditions of flight has constituted a large part of the work of the flight research section. The distribution of load over the wings, tail surfaces, and the fuselage of a pursuit airplane has been measured under all conditions of flight. The results have been studied from the standpoint of the structural designer, and a report covering this entire research is practically completed. The results bring out several points of great importance, one being the torsional deflection of the wing under load and the resulting change of load distribution, and another being the effect of inertia loads on the airplane structure. Under certain conditions of flight the latter loads combine with the aerodynamic loads in such a manner as to give new maxima.

The above investigation has furnished additional data as to the loads on the tail surfaces of a pursuit airplane, supplementing those obtained in an investigation made last year for that specific purpose. As a result, there has been made available knowledge of the tail-surface loading experienced on pursuit airplanes having control surfaces of both thick and thin section. Both investigations show the necessity of increasing the design requirements for the tail surfaces of airplanes which are to be required to execute maneuvers at high speed. The information has already resulted in an arbitrary increase by the military services in the loads for which the tail structure must be designed. The subject has been studied and discussed in conference with representatives of the services to determine a satisfactory basis for the establishment of a permanent set of specifications covering loads on tail surfaces.

The determination of load distribution is being continued in flight, and two airplanes are now being arranged for pressure-distribution tests. One of these, an observation airplane, is being prepared for a complete pressure-distribution investigation over the wings and tail surfaces; the second airplane is being arranged for an investigation of the loads on wing tips of various plan form. This latter investigation is for the express purpose of determining the exactness of the existing arbitrary specifications of wing-tip loading and to determine the possibility of developing a wing tip with a constant location of the center of pressure and a desirable load distribution, in order to reduce the possibility of excessive load on the tip portion of the wing.

The research on the distribution of water pressure over the bottoms of various types of seaplane floats and hulls has been continued throughout the year. An investigation conducted on a twin-float seaplane has been completed and the results published. A similar investigation has been completed on a flying-boat hull, the results of which are now being prepared for publication. As in the former tests, the latter investigation has covered the conditions of landing,

take-off, and taxiing. With the flying boat, it was possible to maneuver on much rougher water, and the pressures were measured under conditions which were as bad as the seaplane could withstand without breaking up. The maximum pressures recorded were about 15 pounds per square inch, as compared with a maximum of approximately 10 pounds per square inch on the floats previously investigated. As a result of the tests on the three seaplanes, there have been derived static load distributions to be recommended as safe practice in design. Apparatus is now being assembled for static tests on one of the seaplane floats.

The work on airships during the past year has consisted chiefly in preparation for publication of reports of researches previously conducted on the U. S. S. *Los Angeles*. One report covering the pressure distribution on the hull and tail surfaces has been prepared for publication. A preliminary study of the velocity of air in gusts has been completed and a report prepared.

Landing and take-off.—Other things being equal, an airplane which can land and take off in a smaller space than another airplane is obviously safer. A series of tests was carried out on a Douglas mail airplane carrying various loads to find the length of landing and take-off runs with and without brakes on the wheels. The brakes were found to be advantageous both from the standpoint of landing and taxiing. The results of this investigation have been published.

Blind flying.—In order to afford some information on the physical reactions of a pilot while flying through fog, or other conditions under which he would have to rely entirely upon his sense of balance or upon his instruments to assume and hold the position of normal flight, experiments were made by a number of service pilots of various ages and experience. The pilots were blindfolded during the tests and the movements of the airplanes were closely followed and recorded by an observer pilot. These tests showed that there is an unmistakable tendency on the part of the pilot to direct the airplane along a spiral path and that normal controlled flight is not possible over any extended period unless the pilot has either some object outside the airplane which he can use to orient himself, or a good set of instruments, including a bank indicator and a turnmeter, in which he has complete confidence.

The pilots varied somewhat in the manner in which they handled the airplane, but as a whole the younger pilots seemed to respond much more quickly to the "feel" of the controls and the various eccentric positions the airplane assumed during their flight. The usual flight lasted about three minutes before the airplane assumed a dangerous high-speed condition beyond the pilot's control.

AERODYNAMIC EFFICIENCY.—A large part of the work of the laboratory may be classified under the general heading of the study of aerodynamic efficiency. Under this heading are included the study of means of reducing the drag of the airplane and the mutual interference of its parts, investigations with reference to propeller efficiency, and tests of airfoils.

The reduction of engine drag by the use of cowling.—The investigation of the effect of cowling on the drag and cooling of a Wright Whirlwind J-5 engine as fitted to the fuselage of a cabin monoplane and of an open-cockpit biplane was continued with interesting results. In the tests carried out in the propeller research tunnel 67 thermocouples were installed over the engine for recording the temperatures, and various degrees of cowling were employed ranging from that in which the engine was completely exposed to that in which the engine was entirely covered. The latter cowling resulted in a large reduction in the drag of the engine-fuselage combination. When subsequently applied to an AT-5 airplane in flight, it resulted in an increase of speed of about 20 miles per hour. The wind-tunnel tests indicated the possibility of still greater savings in the drag of nacelles. The results of the tests in the propeller research tunnel have been published, and that part of the investigation is regarded as finished, but further work on the development of the N. A. C. A. cowling has been carried on through flight tests.

In order to determine the effect of the new cowling on the drag of the nacelles of wing engines, flight tests were carried out on a trimotor Fokker transport airplane. It was thought that this airplane, having three J-5 engines, offered an excellent opportunity for demonstrating the value of the new cowling. All three engines were cowed, the two wing engines being fitted with larger nacelles to suit the larger diameter of the cowling, and the center or nose engine having the cowling somewhat modified to properly fair in with the large fuselage to the rear.

Flight tests with the original installation showed very little increase in speed. A study of the air flow about the nacelles by means of threads attached to their surfaces indicated a bad interference condition between the nacelles and the wing, and it was found that some improvement could be effected by fairing the nacelles into the wing. This question of the interference between the wing and nacelles was then taken up in the variable-density wind tunnel.

Flight tests are still in progress in connection with the development of the N. A. C. A. cowling, on a Navy XF7C-1 pursuit type airplane powered with a Pratt and Whitney Wasp engine. The air flow is being studied, particularly in the vicinity of the slot where the flow leaves the cowling and at the nose of the cowling. The engine is equipped with thermocouples, in order that the temperatures may be carefully watched. The shape of the after portion of the cowling has been changed in various ways, and the shape of that portion which influences the flow from the slot has been found to be rather critical. Tests are being made with a simple ring surrounding the engine, similar to the Townend ring, and with modifications of the same. The tests show favorable results for both the complete N. A. C. A. cowling and the ring type from the standpoint both of performance and cooling.

Interference.—The experiments in cowling the engines of the Fokker trimotor led to a series of tests in the variable-density tunnel to ascertain how the interference between the engine nacelles and the wing might best be reduced. Tests were made of a wing-nacelle combination in which the nacelle was located in various positions with reference to the wing and faired into the wing in various ways. The results, which, however, do not include the effect of the slip stream, indicate the importance of interference effects and the necessity of still further investigation along these lines. They show that a marked improvement in the performance of airplanes with outboard nacelles would result if the nacelles were equipped with the N. A. C. A. cowling and so located that they would be partially inclosed in the wing. A report has been published covering this investigation.

Models and equipment have been constructed for the investigation of the interference between a flat plate and a streamline body. Further interference effects will be studied in the variable-density tunnel in connection with tests of a cabin airplane model now being designed. Valuable information on this question will also be obtained, it is believed, in connection with the wing-nacelle tests soon to be taken up in the propeller research tunnel.

Investigations of propeller efficiency.—The propeller research tunnel has been in successful operation throughout the year, and it has been possible to investigate a number of questions relating to the efficiency of propellers under various conditions of operation, which had not been possible previously. A preliminary investigation of the effect of high tip speeds had indicated no loss in propulsive efficiency as the tip speeds were increased up to 900 feet per second. The airplane engine used in the tests at that time did not have sufficient power to permit tests at higher tip speeds. This investigation has been continued on a Curtiss D-12 engine installed on an open-cockpit fuselage. The larger engine has made it possible to run the same propellers up to speeds of 1,350 feet per second, and in addition to test a series of special propellers of similar plan form, but differing in section and camber. These tests indicate a reduction in efficiency beginning at tip speeds of 950 to 1,000 feet per second and continuing at the rate of about 10 per cent loss in efficiency per 100 feet per second increase in tip speed. In these tests readings were also made of the deflection of the blades and of the velocity and twist of the slip stream back of the propeller. This information will be used in computing the characteristics of a series of airfoils for use in propeller design. A report is now in preparation giving the results of the tests at high tip speeds.

As a contribution to the data available on the interference of a body behind a propeller, tests were made on a series of geometrically similar propellers but of different diameters, operating in front of the same fuselage. The propeller diameters varied from 9 feet to 10.5 feet, and it was found that the propulsive efficiency was about $2\frac{1}{2}$ per cent higher for the largest propeller than for the smallest. A Technical Report has been prepared on the results of this investigation.

In order to ascertain whether any great improvement in propeller efficiency might be expected from changes in plan form, a series of tests was made on propellers varying in this respect.

Only a small difference in efficiency was noted for the series tested, but the form with the thinnest airfoil section had the highest efficiency, and it was shown to be advantageous as regards propulsive efficiency for a propeller operating in front of a body such as a radial engine, to have its pitch reduced toward the hub. The results of this work also have been prepared for publication as a Technical Report.

To gain some preliminary information on the efficiency of geared propellers as compared to directly driven propellers, a series of tests was made using a J-5 geared and ungeared engine on a large and a small fuselage. The results of these tests have also been prepared for publication. The investigation was made in such a manner that the propeller-body interference factors were isolated, and it was found that, considering this interference only, the geared propellers had an appreciable advantage in propulsive efficiency, partially due to the larger diameter of the propellers with respect to the bodies, and partially because the geared propellers were located farther ahead of the engines and bodies.

The question has often been raised as to how the efficiency of a propeller may be affected when the blades are cut down to adjust a given propeller to a particular engine. In order to obtain some information on this question, a 10-foot propeller was cut down in diameter in five successive steps to 8 feet 6 inches. At each diameter the propeller was tested at several pitch settings. It was found that the loss in propulsive efficiency for the greatest decrease in diameter amounted to 5 per cent. This loss is partly chargeable, of course, to the increase in body interference and partly to the less favorable shape of the propeller tips. This information is being prepared for publication as a Technical Report.

Another investigation which should yield results which will be helpful to propeller designers is that of the effect of the wing behind the propeller on the propulsive efficiency. A preliminary test has been made in connection with this problem, and the information prepared for publication. A much more complete investigation of this question is now being made, however. This will include a study of the effect of the wing on the propeller efficiency, the effect of the propeller slip stream on the wing characteristics, and the interference between a wing nacelle and the wing. The investigation is being carried out in the propeller research tunnel by use of a model wing of 16-foot span and an aspect ratio of 5. A nacelle containing an electric motor which drives a 4-foot propeller is to be located in various positions relative to the wing, and measurements made of the lift, drag, and pitching moment of the wing and of the propulsive efficiency of the propeller with all the various combinations.

In order to put all the information obtained on the effect of these various factors on propeller efficiency into a form readily usable by propeller designers, a series of design charts is being prepared for publication.

Airfoil studies.—Studies of airfoil characteristics and particularly of scale effect, are being carried out from time to time in the various wind tunnels by force and pressure-distribution tests. A series of seven airfoils was tested during the year in the propeller research tunnel. They included the Clark Y, the Göttingen 398, the N. A. C. A. M-6, and the N. A. C. A. 84. These airfoils were of 2-foot chord and 12-foot span. The Reynolds Number was about 2,000,000, which is about half the maximum obtainable in the variable-density tunnel. The above series included two airfoils with corrugated surfaces, as well as some other variations in surface conditions. The results were in good agreement with results obtained in the variable-density tunnel at a corresponding Reynolds Number, suitable correction having been made, of course, for the tunnel-wall effect in the variable-density tunnel and the effect of the air-stream boundary in the open-throat propeller research tunnel. The corrugated airfoils gave a slightly greater drag than the smooth, but a marked flattening of the lift curve in the vicinity of maximum lift was found, which is regarded as advantageous from the standpoint of safety.

The question of the effect of scale on investigations of pressure distribution in the wind tunnel as compared with those made in flight has never been satisfactorily answered. In order to throw some light on this matter, a series of pressure-distribution tests was made in the variable-density wind tunnel at 1 and 20 atmospheres pressure. A liquid manometer was used for the 1-atmosphere tests but for the 20-atmosphere tests a manometer of the optically recording

diaphragm type was used. The airfoils tested included the M-6, a symmetrical (R. A. F. 30) airfoil equipped with trailing-edge flaps, an R. A. F. 31 airfoil equipped with a Handley Page leading-edge slot, Clark Y, and others. The results on the Handley Page slotted airfoil have been published. The others are in preparation for publication. It may be stated that, in general, the scale effect shown by these tests is slight.

It has not been possible in the past to secure very satisfactory agreement between the air flow about airfoils as determined by pressure-distribution measurements in the wind tunnel and as computed from theoretical considerations. In order to ascertain whether a better agreement may be obtained between results of tests at high Reynolds Number, as in the variable-density tunnel, and the computed results, there were included in the above program one Joukowski section and two modified Joukowski sections. The agreement with theory was found to be fair, although the scale effect, as stated above, was, in general, not striking. The results of this investigation are in preparation for publication.

Another investigation of interest consisted in testing the variable-density wind tunnel of a group of eight airfoils approximately 20 per cent of the chord in thickness. The purpose was to study, in particular, the effect of scale on discontinuities in the characteristic curves near the region of maximum lift. Six of the eight airfoils exhibited discontinuities at a Reynolds Number of 150,000, and these discontinuities became less pronounced as the Reynolds Number was increased. None of the airfoils showed a discontinuity when the Reynolds Number was increased to 720,000.

In view of the fact that the results of airfoil tests in the variable-density tunnel have, in general, not been corrected for the effect of the tunnel walls, and furthermore, in order to put the data on these airfoils in a form more convenient for ready reference, the data on all airfoils tested in the variable-density tunnel have been recomputed and replotted.

What is believed to be one of the most valuable investigations carried on thus far in the variable-density wind tunnel consists in an investigation of the effect of thickness and of the shape of the mean camber line on airfoil characteristics. It is planned to make tests on a family of about 80 airfoils having the same relative variation in thickness along the chord, but having six values of the maximum thickness, 6, 9, 12, 15, 18, and 21 per cent of the chord. The airfoils are based on five differently shaped mean camber lines, each having 4° of camber.

Aerodynamic efficiency may be increased by applying the principle of boundary-layer control to the wings and possibly also to other parts of an airplane. Certain advantages in this direction have already been obtained by means of the Handley Page type of slotted wing. Still greater improvement seems to be possible by the use of a properly located narrow slot opening into the wing and so arranged that air may be discharged from the wing or sucked into it by suitable means. An investigation of the possibilities of this type of slotted wing has been carried out in the atmospheric wind tunnel during the past year. A model equipped with a slot adjustable both in position and width was used. Arrangements were made for applying either suction or pressure and the power required to produce the flow was measured. Large increases in lift were obtained with moderate pressures, and the minimum drag was reduced.

Airship investigations.—The aerodynamic efficiency of an airship is evidently dependent on careful design, not only of the hull and control car, but also of the control surfaces. Some further work has been done during the year in connection with flight tests previously made on the U. S. S. *Los Angeles*. Data obtained in speed and deceleration tests have been prepared for publication. A report covering the pressure distribution on the hull and tail surfaces, and a report covering the investigations to determine the drag of the airship with and without water-recovery apparatus, have been published. Speed and deceleration tests for the purpose of determining the drag of a small commercial type airship have been carried out in conjunction with the Goodyear-Zeppelin Corporation, and apparatus is now being assembled for similar tests on a TC airship and on a small service type airship.

The variable-density wind tunnel and the propeller research tunnel both offer facilities for making model tests on airships at higher Reynolds Number than can be conducted in other tunnels. This fact has led to a series of tests now in progress in the variable-density wind

tunnel on a model of the *ZRS-4* airship and preparation for tests on a large model in the propeller research tunnel. The tests in the variable-density tunnel have consisted of lift, drag, and pitching-moment measurements of the *ZRS-4* model in comparison with a model of lower fineness ratio. The tests are being made with and without a control car. It is planned in the propeller research tunnel to measure the pressure distribution over the hull of the airship model, its lift and drag at various angles of pitch, and at the same time to measure the forces and moments exerted on the elevator hinge.

Miscellaneous investigations of particular interest in connection with airship work have included some preliminary studies on gusts and also on the use of a Friez type cup anemometer for measuring the velocity of a gusty wind.

DEVELOPMENTS IN EQUIPMENT.—It is constantly necessary to make improvements in the equipment of the laboratory and to add new pieces of equipment, if the work is to keep up with the advancement of the art. In connection with the work of the atmospheric wind tunnel, there has been developed an integrating manometer for use in pressure-distribution measurements. By means of a number of tubes of different cross-sectional area connecting with a common reservoir, the chord load at any particular wing section is integrated automatically and is thus measured by means of a single liquid column. This manometer has saved considerable labor in the working up of the results of pressure-distribution tests.

The balance of the variable-density wind tunnel as rebuilt is similar in principle to the old balance, but differs in some minor details. It consists of a cradle of structural steel which surrounds the lower half of the air stream and which is suspended by rods from balance beams which are visible through peepholes in the outer shell. The model is rigidly fastened to the cradle by vertical struts which are protected from the air stream as far as possible by fairings. The sliding weights on the beams, as well as coarse weights which are carried on bridges, are operated by electric motors with control switches on the outside.

It has been found possible during the past year to improve the operation of the tunnel in a number of ways. An objectionable vibration, which at times resulted in damage to the knife edges, has been greatly reduced by mounting the structure supporting the balance on rubber shock absorbers similar to those used in mounting certain aircraft engines.

A slight twist, which was found to exist in the air stream, was eliminated by installing longitudinal deflectors in the return passage, and the velocity distribution at the test section was improved by introducing resistance at certain parts of the cross section by the attachment of wire mesh to the honeycomb.

The reduction in turbulence in the new tunnel as compared to the old was effectively demonstrated by means of a series of sphere tests, a report of which has been published. There tests also served to substantiate the principle upon which the variable-density tunnel is based, since it was found possible to obtain the same drag at a given Reynolds Number whether obtained by varying the density, velocity, or sphere size.

The only alteration made in the propeller research tunnel has been the installation of a dial type scale for the drag balance in place of the ordinary beam type previously used. This eliminates the delay formerly experienced in getting this scale in balance before each reading.

A small water channel has been found useful for studying the flow along surfaces of various contour and through model entrance and exit cones. The channel is 8 inches wide and the character of flow about a body is made visible by scattering aluminum dust on the surface of the water.

A small water tunnel having a 2½-inch throat diameter in which a speed of 45 feet per second may be obtained has been found useful for studying cavitation on airfoils of various shape. A 5-stage turbine type pump was developed for circulating the water. This has the advantage that the water can be circulated at high speed without the milky appearance which resulted from cavitation when a single driving propeller was used.

Development work on the high-speed tunnel has progressed somewhat slowly as tests are made only when the pressure in the variable-density tunnel is being reduced to 1 atmosphere. Experiments have been made with different designs of open and closed throat and with vanes for preventing twisting of the air stream. It has been possible to obtain an air speed of 1,290 feet

per second in a throat 12 inches in diameter, and it has also been possible, by the use of optically recording diaphragm type manometers similar in principle to those used in flight tests, to record the pressure distribution on an airfoil section and at the same time the dynamic pressure. A balance has been designed for this tunnel, and this is now under construction. It will be possible with this balance to measure the lift, drag, and pitching moment of an airfoil which will be mounted in the stream passing directly through from one side to the other. The balance consists of a forked member which holds the two ends of the airfoil and provides means for changing the angle of attack. The aerodynamic forces are made to deflect steel beams and the deflection is recorded optically on a photographic film. Timing lines will be provided by a timer, which is standard equipment in connection with the instruments used at this laboratory. Another curve on the same film will indicate the dynamic pressure in the air stream.

In connection with the design of the full-scale wind tunnel, mentioned earlier in this report, considerable study has been given to the effect of varying the shape of the entrance and exit cones of open-throat tunnels in order to determine whether it is practical to use an elongated jet, and thus make possible the testing of an airplane of large span without too great a cross-sectional area at the throat. A series of tests was carried out on a number of different shapes of entrance and exit cones in the atmospheric wind tunnel. In each pair of cones three airfoils were tested having dimensions of 3 inches by 15 inches, 4 inches by 20 inches, and 5 inches by 25 inches. Force tests were made in order to determine the effect of the change of shape of the air stream. The series consisted first of a circular cone; second, a rectangular one having a ratio of height to width of 1 to the square root of 2; third, one of the same proportions having semicircular ends; and fourth, one similar to the above having the ratio of height to width of 1 to 2. The Prandtl correction was found to apply to the circular cone, and it was found possible to derive corrections for the other cones to give the same results. A report covering this work is in preparation.

It has been decided to adopt the fourth shape of throat mentioned above, for the full-scale tunnel—that is, one having a ratio of height to width of 1 to 2 and having semicircular ends. The height of the jet will be 30 feet and the width 60 feet. A scale model of the proposed tunnel has been built and tests are in progress to study such questions as energy ratio and air-flow conditions.

The development of flight research methods and the consequent necessity for increased accuracy of measurements have called for greater refinement in the recording instruments used in flight research. Laboratory tests are being conducted almost continuously on the instruments to reduce errors caused by mechanical friction and time lag in the parts, changes in the viscosity of the damping oil, lack of balance of moving parts, etc. This work is particularly necessary for instruments used in accelerated flight, and a considerable portion of this work has been concerned with the angular-velocity recorders and recording accelerometers. For investigations where measurements must be made in a very short period of time, such as when impact loads are measured, it has been necessary to greatly increase the film speed. A new electric motor has been constructed for driving the film in order to obtain more driving torque without increasing the size or weight of the motor, and this, together with a new low-friction dynamically balanced film drum, has given speeds approximately ten times those obtainable with the standard motor and drum. A control force recorder suitable for recording stick forces in accelerated and level flight has been designed and constructed during the year and is now being tested.

BUREAU OF STANDARDS

Wind-tunnel investigations.—Substantial progress has been made in the investigation of wind-tunnel turbulence and its bearing on the problem of standardization of wind tunnels. Technical Report No. 320 of the National Advisory Committee for Aeronautics describes the apparatus used for the measurement of one quantity which is of interest in turbulent motion, namely, the mean amplitude of the fluctuations of the air speed. The primary element is a hot-wire anemometer, the wire being about 0.017 millimeter in diameter. The report contains the theory of the lag of the anemometer, a theory, description, and experimental test of a method of compensating for the lag, and some typical experimental results.

Measurements in the three wind tunnels at the Bureau of Standards at a number of possible working sections showed a large range of values of the turbulence as measured with the hot-wire anemometer. It was possible, therefore, to determine experimentally in a quantitative manner the effect of turbulence in wind-tunnel measurements on spheres and airship models. Direct correlation was established between the forces and the turbulence. For spheres, the relation between the critical Reynolds Number (Reynolds Number at which the drag coefficient is 0.3) and the turbulence was determined in the form of a "calibration" curve by means of which spheres may be used for quantitative measurements of turbulence. Experimental proof was obtained that the discrepancies in the results on the N. P. L. standard airship models are due mainly to differences in the turbulence of the wind tunnels in which the tests were made.

It was found possible to account for the observed effects of turbulence in terms of the boundary-layer theory, by assuming that the flow in the boundary layer may be either laminar or turbulent as determined by the Reynolds Number formed from the speed at the outer edge of the boundary layer and the thickness of the boundary layer. The value of the Reynolds Number at which the change occurs is assumed to depend on the magnitude of the initial turbulence (that of the wind-tunnel air stream), decreasing as the initial turbulence increases. It is found necessary to assume that the body itself sets up turbulence shortly behind the maximum cross section. As a result, airship models in which the maximum cross section is far forward are much less sensitive to the wind-tunnel turbulence than those in which the maximum cross section is well aft.

Apparatus has been designed and is under construction for a study in some detail of the transition from laminar to turbulent flow on a flat plate.

The report on the characteristics of 24 airfoil sections at speeds from 0.5 to 1.08 times the speed of sound has been published as Technical Report No. 319 of the National Advisory Committee. A series of sections with plane lower surfaces and cylindrical upper surfaces has been constructed for test, since one section of this type included in the first series showed better lift-drag ratios than other sections of different shape but of the same thickness.

The measurements of the rolling and yawing moments produced by ailerons of various chords and spans on 10 by 60 inch models of Clark Y and U. S. A. 27 sections have been extended to large angles of attack, in cooperation with the Aeronautics Branch of the Department of Commerce and the National Advisory Committee for Aeronautics. Measurements of hinge moments are in progress.

Aeronautic instrument investigations.—The work on aeronautic instruments has continued to be conducted in cooperation with the Bureau of Aeronautics of the Navy Department and the National Advisory Committee for Aeronautics.

A report has been prepared on the present status of air navigation instruments which is to be submitted by the subcommittee on instruments, after approval and contribution by its members, to the committee on problems of air navigation.

The bureau cooperated with the Bureau of Aeronautics in the preliminary technical work incident to the annual conference of the Army Air Corps and the Bureau of Aeronautics with instrument manufacturers on current purchase specifications. Two important changes, one relating to the size of instrument cases and the other to the standard test temperatures, were adopted in the conference. A uniform size of instrument case, based on a dial $2\frac{3}{4}$ inches in diameter, was adopted as a standard for altimeters, air-speed indicators, and tachometers, and a uniform size, based on a dial $1\frac{7}{8}$ inches in diameter, for engine thermometers and pressure gauges. These new sizes are in considerable favor with aircraft operators and are likely to be adopted as a general standard. The lowest temperature at which the performance of instruments is determined has been changed from -20° to -35° C. The standard temperatures at which instruments are now tested are -35° , $+20^{\circ}$, and $+45^{\circ}$ C.

The development program covered new and improved apparatus for testing aircraft instruments, improvements in service instruments, and the development of aircraft instruments for special purposes. An accelerometer-testing apparatus was constructed in which the accelerations are secured by means of a rotating table and the indications of the instrument under test

photographed. A nonmagnetic vibration rack for use in testing magnetic compasses is now under construction which is similar to previously constructed racks except that it is to be of nonmagnetic materials as far as possible. Two accelerometers, one with a maximum pointer, have been constructed for use in measuring the acceleration of airplanes in the direction perpendicular to the floor of the airplane. An oil-pressure gauge has been modified so as to test the feasibility of using a nonfreezing liquid in the tubing between the engine and the indicator instead of the oil, in order to improve the performance of oil-pressure gauges in aircraft which operate at low temperatures. Work has continued on the further development of the electric resistance thermometer for measuring free air temperatures and, in cooperation with instrument manufacturers, on the development of a satisfactory type electric tachometer for multiengined aircraft.

A report has been prepared on the fundamentals of instrument mechanism design, considering factors such as inertia effects and damping in its relation to the effect of vibration of the aircraft. A report is in preparation on the results thus far obtained on the variation of the torsion modulus of nonferrous and ferrous materials with temperature, and further experimental work is being planned. Revision of the report covering the elastic afterworking of diaphragm metals is in progress based on the study of the data in Technical Note No. 261. An experimental program has been drawn up covering work on the friction of step and shoulder bearing pivots in which particular attention is given to the effect of the finish of the pivots.

The investigation of damping liquids for aircraft instruments has centered during the past year on extending the low-temperature limit of the viscosity data published in Technical Report No. 299 to -50°C . and in finding a suitable liquid for the ball-type inclinometer. In extending the results to lower temperatures an apparatus was constructed in which the liquid bath could be cooled by carbon dioxide "ice." The damping liquid for the inclinometer must be such that its viscosity is not too great at -35°C ., and great enough at $+30^{\circ}\text{C}$. to damp out the rotation of the ball of the inclinometer when the latter is under vibration. This rotation coupled with linear oscillations causes the ball to climb the tube. As a criterion of the usefulness of a liquid at low temperatures the temperature at which its kinematic viscosity is five times that at $+30^{\circ}\text{C}$. has been proposed. The greatest temperature change required to produce the fivefold increase in viscosity of the liquids so far investigated is about 50°C . for liquids having a viscosity of 0.05 poise (25°C .) and about 70°C . for liquids of 0.025 poise. Liquids with these characteristics do not fully meet the requirements of the ball inclinometer.

WASHINGTON NAVY YARD

The wind-tunnel equipment at the Washington Navy Yard consists of an 8 by 8 foot closed-circuit type and a 4 by 4 foot N. P. L. type. The large tunnel is employed continuously in making tests on current airplane design models and on problems connected with current design. The small tunnel is used for miscellaneous investigations, but practically all of the tests are made to answer questions arising in the course of design studies. A limited number of extended investigations are undertaken from time to time, although most of the general problems are now submitted for study to the National Advisory Committee for Aeronautics.

Airplane models.—During the past year 22 model airplanes representing 18 designs were given complete tests in pitch and yaw. Many of these designs were given additional tests covering such items as effect of wing location, effect of nacelle location, effect of changes in control surfaces, etc. In several models serious interference effects were eliminated by patient testing of slight successive modifications. Work of this nature requires considerable time in the wind tunnel but it supplies information of the greatest value.

Airfoils.—No extended series of wing sections has been investigated during the past year, but a group of nine new airfoils is to be tested at the first opportunity. Routine tests have been made on three airfoil sections in connection with the tests on airplane models in which they were used.

A short investigation was made on the effect of the curvature of concave under cambers with particular reference to the burbling that occurs on the bottom surface at low angles of

attack. During this study a few tests were made to investigate the possibility of simple methods of flow control, but the results were not very encouraging.

Floats and fuselages.—Four seaplane floats have been tested for drag at various speeds in continuation of the series previously tested. Additional tests are to be made as the models become available.

Nine fuselage models have been tested, also in continuation of a previous series. This completes the fuselage tests laid out two years ago, but a new series is to be started during the coming year. These models are based on current designs and are selected to cover the various types used in design.

Windshields.—Several tests have been made on windshields of various forms designed to give better protection to the crew or to reduce drag. Part of this work has been done on complete model airplanes, and part on special fuselage models. It is felt that this type of testing is in general rather unsatisfactory. There appears to be a great need, however, for some windshield design data along the lines of protection of the gunner in a rear cockpit. This general problem is now under investigation by the National Advisory Committee for Aeronautics.

Nacelle interference.—Nacelle interference with wings has been determined for a series of models, in order to obtain certain design data. The tests indicate that the best fairing varies with angle of attack and that it must be worked out for each design. Further work along this line at the Washington Navy Yard appears to be unnecessary in view of the proposed research by the National Advisory Committee for Aeronautics.

Struts.—Three extensive series of struts have been tested during the past year. The first series consisted of 11 modifications of the Navy No. 1 strut, the program being so laid out as to include the study of the effects of fineness ratio and trailing-edge radius. A report covering these tests is now being prepared. The second series consisted of five theoretical shapes supplemented by three standard struts. The tests included pressure distributions and drag measurements, which were compared with the calculated values. A report by Dr. R. H. Smith on this work has been published by the National Advisory Committee for Aeronautics as Technical Report No. 335. The third series was less systematic than the other two and consisted chiefly in measurement of the effect on drag of slight modifications in the contour, surface, and size of standard struts.

Slots and flaps.—Four wing models incorporating the Handley Page automatic slot have been given thorough tests for slot operation with reference to the angles of opening and closing for various linkage systems. These tests also included force measurements on the leading airfoil, and velocity explorations in the slot. All the models were tested in connection with the adaptation of the slot to service-type airplanes, rather than as a detached investigation.

Lighter-than-air.—Some calibration tests have been made on the new oscillator which was completed during the past year. The results appear very satisfactory, and further oscillation tests are to be made when the time is available.

A series of power cars for use on rigid airships is being given tests for drag at various speeds. This series includes a group having the N. A. C. A. Venturi cowlings in several forms. The general problem of the interference and drag of power cars on airships is being continued by the National Advisory Committee for Aeronautics both in the variable-density wind tunnel and in the propeller research tunnel.

MATÉRIEL DIVISION, ARMY AIR CORPS

WIND TUNNELS.—The reinstallation of the McCook Field 5-foot and 14-inch wind tunnels at Wright Field was completed in February, 1929. The new installations are practically the same as at McCook Field, with only minor improvements, and the air flow, etc., are essentially the same.

Routine tests.—In addition to the calibration check, only one routine wind-tunnel model test, that of a $\frac{1}{10}$ -scale model of the XO-14 airplane, has been run. The primary purpose of this test was to compare the lift and drag characteristics obtained in the wind tunnel with the characteristics of the complete airplane obtained from glides without thrust.

Wing flutter.—A preliminary wind-tunnel investigation of wing flutter has been made. This investigation covered different types of flutter in several common wing sections at angles near the burble point and near the angle of zero lift. The distribution of the mass, the shape of the tips, and the elastic axis were all variable, and the frequency was further varied by added weight and by adjustment of the support.

Engine cowling.—A series of cowlings for air-cooled engines mounted in wing nacelles was tested for drag and cooling properties, and the data obtained were made available to designers.

Tail surfaces.—An investigation of the characteristics of the horizontal tail surfaces of a $\frac{1}{2}$ -scale model of the AT-4 fuselage with two tail surface arrangements, begun at McCook Field, was completed during the past year.

Pressure distribution.—Pressure distribution on the Clark Y and Göttingen 398 wings has been determined at very close intervals over the leading edge to facilitate the design of automatic slots.

FULL-SCALE EXPERIMENTS—Glide testing.—A “zero thrust” indicator has been devised which makes glide testing practicable for determining the lift and drag characteristics of airplanes in flight. Polar curves have been obtained for the XO-2, the XO-6, and the XO-14 airplanes. The profile drag of the XO-6 was found to be greater with a corrugated wing surface than with a smooth surface. A torque meter adaptable to geared engines has been designed, which, used in combination with data obtained from glide tests, will determine power and propeller efficiency in flight.

Performance reduction.—The performance data obtained both in summer and in winter on four airplanes have been reduced to standard air performances by different methods which were proposed to improve present methods of reduction; no improvement, however, was found, and therefore no changes have been made in the methods.

Slots and flaps.—Controlled leading-edge slots with trailing-edge flaps were tested on the Driggs Dart airplane and found to be of some benefit in taking off and landing, but the reduction of high speed and climb was not measured. Automatic slots were tried on the PT-3 airplane and found to reduce high speed and climb with no improvement in landing or take-off qualities.

OLEO JIG.—A jig for the drop testing of oleo and other shock absorbers has been completed, making it possible to closely approximate actual landings and accurately record accelerations and stresses.

EDUCATIONAL INSTITUTIONS

Massachusetts Institute of Technology.—A new Venturi-type 5-foot wind tunnel has been added to the equipment at the Massachusetts Institute of Technology. This wind tunnel is of the closed-throat and open-return type, and has an air speed of about 100 miles per hour with a 75-horsepower motor. Thesis investigations have been made on the effect of yaw on the autorotation of a monoplane airfoil; the heat transfer from the lower surface of an airfoil at various angles of attack; and the air flow around, and the resistance of, a horizontal opposed engine in a wing, with comparative V and radial engine tests. In a special high-speed tunnel a study of heat transfer from finned surfaces has been made, and wind-tunnel work has also been in progress on the mutual interference effects of airplane propellers and other parts of the airplane.

Stanford University.—An investigation has been completed on the effect of fuselage fineness upon propeller performance, and tests of six 3-bladed adjustable pitch propeller models have been conducted for the Army Air Corps. In the investigation of the profile drag of certain airfoils, a single special-form airfoil of Clark Y section has been given a preliminary test, and the indications are that this airfoil has no induced drag, so that it will be possible to measure the profile drag directly with a balance.

New York University.—At the Daniel Guggenheim School of Aeronautics a number of tests were made, in cooperation with the Goodyear-Zeppelin Corporation, on an airship model suspended in the wind tunnel at various angles to the wind, close to the ground and to the hangar. Three-component measurements of forces were made, and information relating to the forces present in the ground handling of airships was obtained. A cabin fuselage of typical form was tested with various types of forward windshield arrangements, and the results indicated the possibility

of developing a type of windshield combining desirable aerodynamic properties with satisfactory vision. In these tests it was found that a slight modification in the shape of the forward part of the cabin fuselage might increase the resistance of the fuselage to a detrimental extent. A study was made of the fairing between wings and fuselage, in which it was found that a fairing lying in a horizontal plane gave no aerodynamic advantage, but that fairing in a vertical plane would reduce the combined resistance of the fuselage and wings appreciably. By means of a rigid I beam whose deflection, recorded optically on a drum, gave a measure of the loads without the complication of any shock absorption in the apparatus itself, drop tests of oleo struts were made under conditions simulating actual use, and in addition the displacement of the struts was measured by optical methods. Complete load-time and displacement-time curves were thus obtained for a number of oleo struts.

California Institute of Technology.—At the Guggenheim Laboratory of the California Institute of Technology, a new 10-foot wind tunnel has recently been completed and its flow characteristics calibrated. A set of automatic balances was especially designed for the new tunnel and has been calibrated. Theoretical investigations have been under way on the motion of compressible inviscid fluids and of incompressible viscous fluids, and on the forces and moments acting on the individual wings of a biplane cellule. Wind-tunnel tests have been conducted on the drag of a sphere and of replicas of the N. P. L. streamline models tested several years ago in various wind tunnels in this country. Study has been made of the bending strength of tubes with small thickness-diameter ratio, and of the strength of corrugated duralumin sheet under compressive loads parallel to the corrugations.

University of Michigan.—Investigations have been under way at the University of Michigan on boundary-layer removal by suction, and on the lift, drag, and stability, including rolling and yawing moments, of a low-wing monoplane and of an amphibian with outboard engines. Several problems relating to the air resistance of automobiles and of engineering structures have also been investigated.

REPORT OF COMMITTEE ON POWER PLANTS FOR AIRCRAFT

ORGANIZATION

The committee on power plants for aircraft is at present composed of the following members:

- Dr. S. W. Stratton, Massachusetts Institute of Technology, chairman.
- George W. Lewis, National Advisory Committee for Aeronautics, vice chairman.
- Henry M. Crane, Society of Automotive Engineers.
- Prof. Harvey N. Davis, Stevens Institute of Technology.
- Dr. H. C. Dickinson, Bureau of Standards.
- Carlton Kemper, National Advisory Committee for Aeronautics.
- Lieut. E. R. Page, United States Army, Matériel Division, Air Corps, Wright Field.
- Lieut. Commander James M. Shoemaker, United States Navy.
- Prof. C. Fayette Taylor, Massachusetts Institute of Technology.

FUNCTIONS

The functions of the committee on power plants for aircraft are as follows:

1. To determine which problems in the field of aeronautic power-plant research are the most important for investigation by governmental and private agencies.
2. To coordinate by counsel and suggestion the research work involved in the investigation of such problems.
3. To act as a medium for the interchange of information regarding aeronautic power-plant research in progress or proposed.
4. To direct and conduct research on aeronautic power-plant problems in such laboratories as may be placed either in whole or in part under its direction.
5. To meet from time to time on call of the chairman and report its actions and recommendations to the executive committee.

By reason of the representation of the Army, the Navy, the Bureau of Standards, and the industry upon this subcommittee, it is possible to maintain close contact with the research work

being carried on in this country and to exert an influence toward the expenditure of energy on those problems whose solution appears to be of the greatest importance, as well as to avoid waste of effort due to unnecessary duplication of research.

The committee on power plants for aircraft has direct control of the power-plant research conducted at Langley Field and also of special investigations authorized by the committee and conducted at the Bureau of Standards. Other power-plant investigations undertaken by the Army Air Corps or the Bureau of Aeronautics are reported upon at the meetings of the committee on power plants for aircraft.

LANGLEY MEMORIAL AERONAUTICAL LABORATORY

COMPRESSION-IGNITION ENGINES.—The research work in connection with the development of the high-speed, compression-ignition engine for aircraft use has been continued. Particular attention has been given to the problem of improving the processes of combustion by obtaining a more even distribution of the fuel in the combustion chamber. The results have been lower specific fuel consumptions and higher percentages of computed full-load torque with a clear exhaust.

Analysis of theoretical cycle efficiencies.—The theoretical investigation of a number of design factors controlling the actual cycle efficiencies of compression-ignition engines has been continued. A method of calculating cycle efficiencies and mean effective pressures for the dual cycle has been developed in order to determine the effect of compression ratio, maximum cylinder pressure, and excess air on the theoretical cycle efficiency. The calculations show that increasing the compression ratio from 8 to 18 for a constant maximum cylinder pressure of 800 pounds per square inch increases the indicated mean effective pressure 10 per cent. The same percentage increase would also be obtained by raising the maximum cylinder pressure from 700 to 1,200 pounds per square inch for a compression ratio of 14. A report on the investigation to determine the effect of compression ratio and maximum cylinder pressure on the cycle efficiency of compression-ignition engines operating on the dual combustion cycle is being prepared for publication.

In order to determine the error that is made in the cycle calculations by considering the specific heats of the gases of combustion to be constant, two series of calculations have been made; one using constant specific heat values, the other using specific heat values that vary with the temperature. In each series of calculations the working fluid was considered to be actual cylinder gases, the mixture to vary at different points of the dual cycle, and the combustion of the fuel to be complete. The investigation covered a range of compression ratios from 10 to 16 and maximum cylinder pressures from 700 to 1,200 pounds per square inch, full-load fuel, and no excess air. It was found that the cycle efficiency and indicated mean effective pressure were 13 per cent greater when the specific heats of the gases were considered to be constant than when the specific heats were considered to vary with the temperature. Calculations have also been made for excess air quantities at full load from 0 to 72 per cent for the above range of compression ratios and maximum cylinder pressures. Increasing the full load percentage of excess air increases the cycle efficiency and percentage of fuel burned at constant volume, and decreases the indicated mean effective pressure; with increase of the compression ratio and maximum cylinder pressure. The results also show that the quantity of fuel required to raise the pressure of a given volume of mixture from one pressure to another is independent of the quantity of excess air present. The average variation was not over 1 per cent for 26 out of 31 sets of calculations and one-half of these did not vary more than 0.5 per cent.

Of the total amount of energy liberated by the combustion of fuel in an internal-combustion engine, 25 to 37 per cent is obtained for useful work. The remainder is lost in the exhaust gases and in radiation, conduction and convection to the cylinder walls and piston. As these three methods of heat transmission rarely occur singly, an investigation is being made of the available literature to determine the possibility of segregating and reducing these losses by a knowledge of their magnitude and part of the cycle in which they have the greatest effect.

Combustion-chamber investigation—Integral type.—Work has been continued with the cylinder head having a vertical disk-type combustion chamber formed between horizontally arranged inlet and exhaust valves. This combustion chamber has only a slight degree of air turbulence, because of a large rectangular orifice between the cylinder and the combustion chamber. The fuel-injection system used with this engine consists of a cam-operated fuel-injection pump and a spring-loaded automatic injection valve having various combinations of seven small round orifices arranged at different angles, but in the same plane. The injection valve was placed in the top of the combustion chamber and the sprays were directed toward the rectangular orifice. Several nozzles having two additional orifices delivering fuel to the air in the upper portion of the combustion chamber have also been tested. These 9-orifice nozzles give a slight increase in engine performance and a clearer exhaust than the 7-hole nozzles, which indicates that the improvement in combustion efficiency is due to the better fuel spray distribution obtained with the two additional orifices.

At 1,500 r. p. m. with a fuel quantity giving approximately three-fourths full-load torque, which corresponds to engine operation at cruising speeds, and maximum cylinder pressures less than 500 pounds per square inch, the 5-inch bore by 7-inch stroke test engine developed an indicated mean effective pressure of 104 pounds per square inch. The corresponding fuel consumption was 0.36 pound per indicated horsepower per hour. Based on a mechanical efficiency of 85 per cent for multicylinder engine operation, this performance gives a brake mean effective pressure of 82 pounds per square inch and a fuel consumption of 0.45 pound per brake horsepower per hour. A clear exhaust is maintained up to 82 per cent of full-load torque.

A series of tests has been made to determine the friction losses of the component parts of a single-cylinder Universal test engine when operated with a compression ratio of 13.5 and a speed of 1,500 r. p. m. The two major items of friction were the pumping and piston-ring losses, which amounted to 29.4 and 22.3 per cent, respectively, of the total friction. These test results indicate the need for an assembly of compression and oil rings which will maintain the high-compression pressures required for operation of the compression-ignition engine and at the same time will give low piston-ring friction.

Combustion-chamber investigation—Precombustion chamber type.—The investigation to determine the effect of high combustion-air turbulence as influenced by the design of the cylinder head, and of the type of fuel spray, on the performance characteristics of a high-speed compression-ignition engine has been continued with the cylinder head having a pear-shaped precombustion chamber. In determining the performance characteristics of this combustion chamber a centrifugal fuel spray had been previously used which gave good distribution within the precombustion chamber. Operation with this type of fuel spray gave low indicated mean effective pressures and high maximum cylinder pressures. The fuel spray has been changed to a noncentrifugal spray injected from an orifice of 0.050 inch diameter placed flush with the precombustion chamber. The injection duration for full-load fuel quantity with this fuel valve and nozzle and a cam-operated fuel injection pump is 34 crank degrees. At 1,500 r. p. m., full load fuel, i. e., the fuel quantity giving 15 per cent excess air in the cylinder, the single-cylinder test engine developed an indicated mean effective pressure of 133 pounds per square inch. The corresponding fuel consumption was 0.040 pound per indicated horsepower per hour. The maximum cylinder pressure as indicated by the disk-type maximum cylinder pressure indicator was 760 pounds per square inch. The exhaust was colorless and smokeless up to 85 per cent of full load. This full-load indicated mean effective pressure represents an increase in indicated mean effective pressure of 13.7 per cent obtained without an increase in the maximum cylinder pressure.

Fuel-injection systems.—The mathematical analysis of automatic injection valves has been continued. The effects of operating forces and valve design have been investigated for a diaphragm-loaded valve and for a valve in which the loading is given by the extension or compression of a member of the valve. Experimental records of the motion of a helical spring-loaded valve are being obtained to determine the agreement between the mathematical analysis and the actual conditions. The motion of the injection-valve stem is recorded on a film drum moving at a speed of 1,000 inches per second. It has been found that the valve stem opens

fully in approximately 0.003 second and the fuel-spray formation and cut-off follow the opening and closing of the valve within a few hundred-thousandths of a second. Furthermore, it has been learned that unless the valve is fitted with a mechanical stop the stem oscillates, giving in extreme cases a pulsating effect to the fuel spray. The experiments conducted so far indicate that the secondary discharges which have been previously discussed in Technical Report No. 258 of the committee are caused by a bouncing of the moving member of the injection valve. This secondary discharge has been partially eliminated by enlarging the area of the by-pass valve of the injection system under investigation.

The time lag at which the fuel is injected into the cylinder of a compression-ignition engine is an important factor in the combustion efficiency of the engine. To determine the time lag it is necessary to know the time interval required for any given pressure at the fuel pump or the fuel-distributing mechanism to reach the injection valve. The time lag of the fuel-injection system is a function of the valve design, the valve opening pressure, the pressure in the injection system and the length of tube between the fuel pump or distributor and the injection valve. An investigation of the factors affecting injection time lag is being conducted at this laboratory. Photographic records of the motion of the timing valve and the injection-valve stems are obtained by using small mirrors which are rotated by the movement of the stems and reflect two light beams on a revolving film drum. The time lag of the injection system is the time interval which elapses between the start of lift of the timing valve and the start of lift of the injection valve. For an injection pressure of 4,000 pounds per square inch and an injection tube length of 70 inches the time lag is approximately 0.0025 second. At an engine speed of 1,500 r. p. m. this corresponds to approximately 25 crank degrees.

The ratio of the length to the diameter of the orifice of an injection valve for a compression-ignition engine has an effect on the distribution and penetration of the fuel spray delivered from the valve. In order to provide information for the designers of compression-ignition engines, the sprays from single orifices varying in diameter from 0.005 to 0.040 inch are being photographed by means of the N. A. C. A. spray photography equipment. From the photographs both the penetration and distribution of the fuel spray are obtained. The length-diameter ratio of the orifices is being varied from 4.00 to 0.75. The photographs are being taken for injection pressures from 2,000 to 8,000 pounds per square inch, valve-opening pressures from 2,000 to 4,000 pounds per square inch, and for spray-chamber air densities from 4 to 17 atmospheres. The photographs are being taken for both a straight stem and a helical grooved stem in the injection valve.

Considerable work has already been done at the laboratory on the determination of the coefficient of discharge of liquids through small round orifices. This investigation is to be extended to cover the effect of the length-diameter ratio of the orifice and also the effect of the injection valve as a whole. The tests which have been started are being conducted in conjunction with the research on the effects of the length-diameter ratio of the orifice on the spray characteristics. The same range of injection pressures, valve-opening pressures, and chamber densities will be investigated and the same spray nozzles will be employed.

A dual-rate fuel-injection valve has been designed to give a varying rate of injection in accordance with the combustion requirements of the dual-combustion cycle. The first part of the fuel charge is injected through orifices of small diameter and the remainder of the fuel charge through an annular orifice. The primary injection is controlled by a poppet valve loaded by a helical spring and the main injection by the lips of the orifice, loaded through a combination of spring disks. In designing this valve to fulfill theoretical combustion requirements, it was necessary to devise methods by which calculations could be made to determine the desired rate of fuel injection at any point in the injection cycle. A method was also developed for the calculation of instantaneous injection pressures and from these pressures the instantaneous rates of fuel discharge. The effective mass centers of the spray and the combustion air were calculated for the various crank degrees during injection, and the fuel sprays were so directed as to make the two coincide as nearly as possible. Preliminary tests have been made of the fuel valves and the quantity and rate of fuel injected were found to check the design calculations.

An investigation of the problems of fuel distribution and injection encountered in the operation of fuel-injection systems for multicylinder compression-ignition engines of aircraft type has been undertaken. A 6-plunger cam-operated fuel-injection pump has been constructed and subjected to preliminary development tests. The fuel quantities delivered by each individual plunger through the dual-rate fuel-injection valve were measured and the timing of start and duration of spray from each valve determined by means of an oscilloscope. Preliminary engine tests have also been made with this fuel pump.

Indicators for internal-combustion engines.—A large amount of valuable information on the combustion characteristics of various fuel sprays can be obtained from accurate indicator cards of high-speed compression-ignition engines. The great difficulty has been to obtain an indicator which would accurately follow the variation of pressure within the cylinder of the compression-ignition engine. Work has been continued on the design of an optical-type engine indicator which will give the variation of pressure for a single engine cycle. While the necessary design and development work is being done, a commercial balanced-pressure, electric-recording indicator which gives a composite card, has been altered so as to give results of a higher degree of accuracy. These alterations include an 80 per cent reduction in the weight of the moving disk, a decrease in the seat width from 0.031 to 0.004, and the use of a light-weight paper which requires only half the primary voltage.

In order to compare performance data of compression-ignition engines, it is necessary that the maximum cylinder pressures be accurately indicated. The work of improving the various types of maximum cylinder-pressure indicators has been continued. At the present time the maximum cylinder pressures are indicated by means of a modified Bureau of Standards balanced-pressure diaphragm-type indicator. The balance condition of the diaphragm is indicated by the flash of a neon lamp.

TWO-STROKE CYCLE, GASOLINE-INJECTION ENGINE INVESTIGATION.—The design of a single-cylinder, 2-stroke cycle, gasoline-injection, electric-ignition, air-cooled test engine has been continued. This work has for its object the determination of the fundamental factors affecting the operation of such a power plant in order that the inherent advantages of greater power output per unit weight of an engine of this type may be made available for pursuit-type aircraft. A standard Liberty air-cooled engine cylinder has been altered and adapted to the crankcase of an N. A. C. A. Universal test engine. The design of the combustion and scavenging-air system and the propeller-type blower for cooling the cylinder has been completed and construction of the blower unit started. The fuel-injection system will consist of a cam-operated fuel-injection pump and two automatic injection valves. Tests have been made of several injection valves designed to give a well-distributed sheet of fuel spray. A fuel-injection pump is being designed with plunger port, fuel admission, and cut-off which will permit of consistent operation at the higher pump speeds necessary with the 2-stroke cycle engine.

SUPERCHARGER INVESTIGATION—Roots type supercharger.—The analysis of data on geared centrifugal, turbocentrifugal, and Roots type superchargers has been continued. The adiabatic efficiency of these superchargers has been computed from the test data available. The computations and curves on the power required by a geared centrifugal supercharger to compress 1 pound of air per second at various pressure differences are being checked. Computations are also being made on the test data now available and on the data from tests now in progress to determine the effect of various types of superchargers on the net engine power obtained at various altitudes.

A report has been prepared for publication presenting the results of tests to determine the effect of supercharger capacity on engine and airplane performance. The performance in level flight and in climb of a DH-4 M-2 airplane powered with a Liberty engine was determined for four supercharger capacities obtained by varying the drive-gear ratio of the supercharger. The engine power was measured with a calibrated propeller. The results of these tests show that there was very little sacrifice in sea-level performance obtained with the larger gear ratio as compared with that obtained with the smallest.

The steel impellers reported last year as being under construction for the Roots type supercharger have been tested. The dimensions of these impellers and the clearances obtained with the impellers assembled in a supercharger case were satisfactory. Tests have been conducted on these impellers to determine the change in impeller diameter with change in speed. It was found that rotating the steel impellers at 9,000 r. p. m. increased the diameter 0.018 inch as compared with an increase of 0.009 inch for the aluminum and magnesium alloy impellers at the same speed. On account of the method of construction the steel impellers were not satisfactory for laboratory testing in the Roots type supercharger.

The turbo-centrifugal supercharger.—Tests to determine the performance in climb and level flight of a modified DH-4 M-2 airplane equipped with a turbocentrifugal supercharger are in progress. Test data have been obtained which will give the rate of climb, speed, power delivered to the propeller, and the fuel consumption. A worm-gear reduction drive for a tachometer has been constructed and used to obtain the rotational speed of the supercharger impeller at altitude. The flight work for both supercharged and unsupercharged conditions has been completed and the test data obtained on the flights are now being reduced to the conditions of a standard atmosphere. The results obtained have been compared with similar results previously obtained on the same airplane with a Roots type supercharger. This comparison shows the same ceiling and practically the same rate of climb for the two types of superchargers, but the level-flight performance at higher altitudes showed a decided improvement when the turbocentrifugal supercharger was used. A report is being prepared for publication which will present the comparative performance as obtained with the turbocentrifugal supercharger and the Roots type supercharger.

Effect of valve timing on supercharged-engine performance.—For unsupercharged engines a valve timing is usually selected which gives maximum charging efficiency at a given engine speed. This same valve timing is used when the engine is equipped with a supercharger and operated at altitude. With increase in altitude of the supercharged engine, however, the differential pressure available for inducting the charge into the cylinder increases. In order to determine the effect of valve timing on the performance of a supercharged engine, tests are being made with an N. A. C. A. Universal test engine operating under conditions of exhaust and inlet pressures simulating those of a supercharged engine for altitudes up to 20,000 feet. Since the timing of the exhaust and inlet valves can be altered over a wide range while the engine is in operation, the equipment is particularly adaptable to this investigation. The engine tests have been started and the performance determined with normal valve timing for both supercharged and unsupercharged test conditions.

Hub dynamometer.—The determination of the flight performance of airplanes would be greatly simplified if the power delivered to the propeller could be accurately measured at all times. The designing of a hub dynamometer for this purpose and the testing of its component parts have been continued. The dynamometer is of the hydraulic type. Three torque cells filled with liquid are interposed between the propeller and the engine. As the engine power is transmitted through the cells the liquid within the cell is subjected to pressure which is transmitted through small tubes to an optical recording system. The optical recording system produces a continuous photographic record of cell pressures. A torque cell of the type to be used in the dynamometer has successfully passed a fatigue test of 5,000,000 stress reversals. Several methods of driving the film drum have been tested and a compound-wound electric motor was found to give the most satisfactory operation. This motor showed satisfactory speed and torque characteristics when revolved on a dynamometer at speeds at 3,000 r. p. m. An optical system for the dynamometer has been constructed and is now being tested.

COWLING OF AIR-COOLED ENGINES.—Information obtained in tests to determine the effect of different amounts and kinds of cowling on the cylinder temperatures and the performance of a Wright J-5 engine has been prepared for publication. The cowlings investigated varied from the extreme of no cowling on the engine to the other extreme of the engine completely cowed and the cooling air flowing inside the cowling through an opening in the nose and out through an annular opening in the rear of the engine. Air speeds from 60 to 100 miles were investigated.

These tests show that increasing the amount of cowling reduces the drag, but has the disadvantage of increasing the cylinder temperatures. Satisfactory cooling was obtained with the cowling that covered 35 per cent of the cylinder cooling area, but the cowling which covered 73 per cent of the cooling area gave excessive temperatures. The cowling which completely inclosed the engine gave a reduction of 40 per cent in drag at 100 miles per hour as compared with the uncowed engine and did not give excessive cylinder temperatures.

BUREAU OF STANDARDS

Supercharging of aircraft engines.—The altitude laboratory is again in service after extensive alterations and will be used to test a Curtiss D-12 engine equipped with a Roots type supercharger. As the excess air delivered by the supercharger below its critical altitude will be recirculated, steps are being taken to increase further the capacity of the refrigerating system.

Not only have tests of the Curtiss D-12 engine been made under ideal supercharging conditions—that is, with air supplied to the carburetor at sea-level pressure for altitudes from 0 to 27,000 feet—but similar tests have been made with the carburetor air maintained at other constant pressures. The results are being prepared for publication and should be of value in analyzing the performance of exhaust-driven as well as gear-driven superchargers. For example, the normal sea-level power of this engine is 400 horsepower at the test speed (2,000 r. p. m.), the normal power at 15,000 feet is 200, and ideal supercharging at this altitude gives 430 horsepower. Hence, to restore full sea-level power at 15,000 feet requires a supercharger consuming only 30 horsepower or producing not more than 6 pounds exhaust back pressure.

Phenomena of combustion.—The major work with the constant-pressure bomb has been an intensive study of the gaseous explosive reaction with oxygen, of butane and of composite fuels made up of butane and carbon monoxide. Results obtained with these fuels confirm the conclusions stated in Technical Report No. 305 for composite fuels made up of carbon monoxide and methane or hydrogen. The facts that (a) the equivalent reaction order of a composite fuel may be determined from the reaction orders of its components and (b) the velocity constant of the fuel may be determined from the velocity constants of the components, support the assumption that high-order reaction processes consist of many simultaneous simpler ones, each running its course within the reaction zone according to its own order and mechanism, independently of any other reactions occurring at the same time. A report of this work soon to be published by the National Advisory Committee for Aeronautics is entitled "The Gaseous Explosive Reaction at Constant Pressure—The Reaction Order and Reaction Rate."

Data already available on the effect of total pressure are being supplemented by a large number of photographic records obtained at total pressures less than 1 atmosphere.

Combustion in an engine cylinder.—Preliminary runs to determine the "explosion time" (i. e. the interval for the flame to travel from the spark plug to the most distant window) and the "duration of flame" (the interval between the occurrence of the spark and the disappearance of the flame in the cylinder) were made under various operating conditions on a single-cylinder engine equipped with 31 quartz windows in the cylinder head. From these trials, the visual method of estimating flame travel appeared to be sufficiently promising to warrant considerable refinement in the test equipment. Accordingly, the stroboscope drive and phase-changing device were redesigned to reduce backlash to a minimum, and the engine was provided with a heavier flywheel to increase smoothness of operation. When measurements are resumed in the near future the cylinder pressure corresponding to each observation of flame position will be determined with the balanced diaphragm indicator.

Temperatures and pressures in an aircraft engine.—The review of the literature has been continued with particular attention to gas temperatures and pressures and to published information regarding the characteristics and use of available high-speed engine pressure indicators. Methods of analyzing indicator diagrams to show temperatures and heat generation and flow have also been studied. Such methods are of considerable interest in that they constitute the most promising means of estimating the cyclic fluctuation of charge temperature in high-speed engines and also afford a means of comparing in detail the deviations of the actual cycle from the

ideal. The program for experimental work includes (1) the making of indicator diagrams on a single-cylinder variable-compression Liberty engine provided with a balanced diaphragm indicator of the type described in Technical Report No. 107 and equipped to burn gaseous or liquid fuels under a wide range of test conditions, and (2) the development of a method of interpreting these diagrams to show temperature variations, combustion progress, and heat interchange between the working gas and its surroundings. A number of preliminary runs have been made on propane in an effort to eliminate possible sources of error in the test equipment and procedure.

Effect of spark character on ignition ability.—The study of spark ignition was resumed this year at the request of the National Advisory Committee for Aeronautics and the Navy Department. A special laboratory has been fitted up and provided with a single-cylinder test engine equipped for comparing the effectiveness of different sparks under controlled operating conditions. Optical methods have been developed for (a) studying the physical condition of the fuel charge at the time of ignition, (b) estimating the apparent flame temperatures during combustion, and (c) determining the volume of charge affected by sparks of different characteristics. By passing a series of sparks through an explosive mixture of oxygen and hydrogen at low pressure in a discharge tube cooled with liquid air, the region where ignition takes place can be determined from the location of the ice formed and the number of molecules reacting can be determined from the change in pressure. The latter may afford a direct means of comparing the overall effectiveness of different sparks.

Preliminary work has been done on the effect of adding high resistance in the secondary of the ignition system and on the effect of capacitance in shielded ignition systems. Preparations are being made to undertake the routine testing of "shielded harnesses."

Automatic carburetor altitude control.—The 2-cylinder multiplied-pressure pump designed and built to control automatically an altitude adjustment on the carburetor of the Wasp engine has shown excessive variation in delivered pressure at constant speed and altitude. It is expected that the development of a more reliable check valve will overcome this erratic behavior, after which the device will be installed in a Navy pursuit airplane for flight test.

Gaseous fuels for aircraft engines.—The relative engine performance to be expected with a number of pure fuels used either singly or in mixtures has been determined from a theoretical analysis based on an ideal Otto cycle and also from actual engine tests. Considering the great differences between the ideal and actual cycles the results of the two methods agree surprisingly well. The power and efficiency obtainable under similar conditions are found to be nearly the same with the exception of methane, which gives about 10 per cent less power. The antiknock characteristics of the gases are much better than those of the liquid fuels and thus higher compression ratios with their attendant advantages are possible with the gaseous fuels. A limited number of trials with gaseous fuels at compression ratios as high as 9:1 in a variable-compression single-cylinder Liberty engine indicate that the useful compression ratios for such fuels may be limited by their tendency to preignite rather than by their tendency to detonate. Hydrogen and carbon monoxide are not very satisfactory as regards engine performance. This work was done at the request of the Navy and funds for its extension to other gaseous fuels will be made available by an industrial concern through the National Research Council.

Effect of air humidity on engine performance.—It has been shown (N. A. C. A. Technical Note No. 309) that failure to allow for the effect of differences in atmospheric humidity may introduce errors as great as would be occasioned by failure to allow for changes in barometric pressure. Under extreme conditions either correction may amount to nearly 10 per cent of the indicated power. Nomograms for the convenient determination of humidity values from psychromatic data, based on the Ferrel formula, will be found in the above reference. The work on humidity is to be continued at the request of the Navy.

Vapor lock in airplane fuel systems.—Funds were made available through the Society of Automotive Engineers for a study of aviation gasolines in order to develop, if possible, suitable means of distinguishing between fuels which are suitable for use in airplane engines and those which are unsuitable on account of possible difficulty from vapor lock. Measurements on representative

aviation gasolines freed from water and dissolved gases show, as in the case of motor gasolines, that the vapor pressure data can be computed with sufficient accuracy (within 5 mm. Hg) from the 10 per cent American Society for Testing Materials distillation temperatures. The solubility of water, air, and other gases in aviation gasolines and the contribution of these constituents to the total vapor pressure have been studied. Bubble formation and growth with commercial aviation gasolines under typical flow conditions are being studied at present in the laboratory. Data on the temperatures occurring under flight conditions at various points in an airplane fuel system were obtained recently at Langley Field and have been made available to the bureau. Arrangements are being made to secure similar data on other types of airplanes in cooperation with the Army and the Navy. It is expected that the laboratory experiments will indicate the temperature-pressure conditions likely to result in vapor lock with any gasoline and the flight data will show whether the present Federal specifications for aviation gasoline can safely be changed to admit more volatile fuels.

Type testing of commercial engines.—After further conference with representatives of the Army and the Navy, the basis on which commercial aircraft engines are rated was modified slightly in November, 1928. Instead of requiring the engine manufacturer to specify both rated speed and rated power, he is asked to designate only the maximum speed at which the engine should be operated at full throttle. This is taken as the rated speed and the rated power is determined by the average brake horsepower developed in a 5-hour nonstop run at full throttle and rated speed. The remaining nine 5-hour periods of the endurance test are run with the engine throttled sufficiently to reduce the speed about 3 per cent.

The number of engines submitted for test has exceeded all estimates and the torque stand unit at College Park, in service since May, 1928, was recently supplemented by two such units at Arlington Farms, Va. Future work will be concentrated at the Arlington testing laboratory, where an office, shop, and four torque stands will eventually be available. During the year, tests have been undertaken on 26 engines, and of this number 12 failed, 5 were withdrawn, 7 have been approved, and 2 are still under test. Ten of the failures occurred prior to January 1, 1929. Seven more engines have qualified as ready for immediate test. At the end of June, 25 engines had received approved type certificates from the Department of Commerce. Many of these were engines approved on the basis of Army or Navy tests.

NEW ENGINE TYPES

The major effort in the development of aircraft engines during the past year has been centered on the problem of reducing head resistance. The matériel division of the Army Air Corps has concentrated its efforts on the study of high-temperature liquid cooling, especially as applied to the Curtiss D-12 and V-1570 series of engines. The high-temperature liquid cooling investigation with Prestone as a cooling liquid has been successfully carried to the flight stage by the application of this system of cooling in three pursuit type airplanes equipped with reduced tubular core, wing skin, and Heinrich type of radiators. With the different installations a study was made of the reduction in weight, frontal area, fuel consumption, and improvement in performance and maneuverability of the airplane. As a result of this investigation, all Curtiss D-12 and V-1570 engines now on production contract are equipped for either Prestone or water cooling. Paralleling the investigation the matériel division has studied different types of fuels with a view to permitting the use of high compression ratios when operating at the higher temperatures.

The application of the low-drag cowling to air-cooled radial type engines has been investigated by the committee at its laboratories at Langley Field and further investigated by the matériel division, with special reference to the application of this type of cowling to military types of airplanes. Both the Army and the Navy, in the application of the low-drag cowling to radial air-cooled engines, have found that the performance of aircraft has been improved. However, the cowling has not been definitely adopted for any particular type, as the visibility characteristics have not been satisfactory.

During the past year 26 aircraft engines have been submitted to the Department of Commerce for test. The air regulations of the Department of Commerce require that engines used

in interstate air commerce shall be of types which have been approved after suitable tests. Of the 26 engines submitted, only 7 have been approved and 2 are still undergoing tests. At the end of October, 1929, 32 aircraft engines had received their approved type certificates from the Department of Commerce.

It is of interest to note that all of the engines submitted to the Department of Commerce for test are of the air-cooled type, having either radial or in-line type cylinder arrangement. The majority of the engines submitted are of the fixed radial air-cooled type, having either 5, 7, or 9 cylinders.

The Bureau of Aeronautics of the Navy Department and the matériel division of the Army Air Corps have continued the development of the accepted standard types of engines used by the services.

Development work has been continued on the Curtiss V-1570 and D-12 engines, with a view to obtaining satisfactory operation and performance, using higher compression ratios and Prestone cooling.

The Curtiss V-1570 is a 12-cylinder V-type water-cooled engine, which was built for both geared and direct drive. Both types are rated by the Department of Commerce at 600 horsepower at 2,400 r. p. m.

The only other water-cooled aircraft engines which are used in military types of aircraft are the Packard A-1500 and the Packard A-2500. The 3A-1500 is rated at 600 horsepower at 2,500 r. p. m., and the 3A-2500 is rated at 770 horsepower at 2,000 r. p. m.

The Pratt & Whitney Co. has further developed and refined the Wasp 9-cylinder radial engine. This engine is rated at 450 horsepower at 2,100 r. p. m. and is standard equipment for a number of types of service airplanes in the Army and is also extensively used in commercial service.

The Hornet engine, manufactured by the same company, is rated at 525 horsepower at 1,900 r. p. m. and is still one of the most used of the larger-powered air-cooled radial engines both in military and commercial service.

The Curtiss Aeroplane & Motor Co. has continued the development of the Chieftain (H-1640). This is a 12-cylinder 2-row radial engine rated at 600 horsepower at 2,200 r. p. m. The arrangement of providing two rows of cylinders and having a 2-throw crank shaft makes possible the reduction of the over-all diameter and the elimination of providing the counterweight that is required on all single-throw crank shafts for fixed radial engines.

The Curtiss Challenger (R-600) engine, which develops 170 horsepower, is the same design as the Chieftain, having two rows of six cylinders. The engine is largely used in commercial type aircraft. Further development has been continued on both these engines.

Air-cooled engines.—The latest development in the air-cooled engine field is the Wright V-1460 12-cylinder inverted V-type engine. The cylinder dimensions are $4\frac{7}{8}$ -inch bore and $6\frac{1}{2}$ -inch stroke, with a piston displacement of 1,456 cubic inches. This engine has been undergoing tests at Wright Field.

In the new series of radial air-cooled engines developed by the Wright Aeronautical Corporation, known as the J-6 series, there are three engines, a 5-cylinder engine rated at 160 horsepower, a 7-cylinder engine rated at 220 horsepower, and a 9-cylinder engine rated at 300 horsepower, all at 2,000 r. p. m. In the development of the J-6 series the Wright Aeronautical Corporation had in mind the advantages of interchangeability of parts, and in each engine the cylinders and many other parts are the same and are interchangeable.

The Wright Cyclone engine, known as the R-1750, is a 9-cylinder radial engine rated at 525 horsepower at 1,900 r. p. m. Further development has been continued on this particular engine and it is being used by the Navy Department as standard equipment for some of the larger type service airplanes and seaplanes.

Compression-ignition engines.—The Packard Motor Car Co. demonstrated its 9-cylinder air-cooled radial-type compression-ignition engine by a flight from Detroit to the committee's laboratories at Langley Field. The flight was made to the annual aircraft manufacturers' conference and the engine was demonstrated to those attending. The following companies are

now developing compression-ignition oil engines for aircraft purposes: The Allison Engineering Co., the Emsco Aero Engine Co., the Westinghouse Electric & Manufacturing Co., and the Packard Motor Car Co.

On October 30, 1929, 32 different types of aircraft engines had approved-type certificates issued by the Department of Commerce. Following is a list of engines that have received their approved-type certificates:

- Aircraft Comet, 7-cylinder, radial, air-cooled, 130 horsepower at 1,825 r. p. m.
- Aircraft Engine Corporation, L-A1, 7-cylinder, radial, air-cooled, 140 horsepower at 1,800 r. p. m.
- American Cirrus, 4-cylinder, in-line, air-cooled, 90 horsepower at 2,100 r. p. m.
- Alliance, Hess Warrior, 7-cylinder, radial, air-cooled, 115 horsepower at 1,925 r. p. m.
- Arnold Harris, 8-cylinder, "Vee," water-cooled, 90 horsepower at 1,400 r. p. m.
- Axelson Machine Co., 7-cylinder, radial, air-cooled, 115 horsepower at 1,800 r. p. m.
- Continental, A-70, 7-cylinder, radial, air-cooled, 165 horsepower at 2,000 r. p. m.
- Curtiss Challenger, R-600, 6-cylinder, radial, air-cooled, 170 horsepower at 1,800 r. p. m.
- Curtiss Conqueror V-1550, 12-cylinder, "Vee," water-cooled, 600 horsepower at 2,400 r. p. m.
- Curtiss Conqueror GV-1570, geared, 12-cylinder, "Vee," water-cooled, 600 horsepower at 2,400 r. p. m.
- Curtiss Chieftain H-1640, 12-cylinder, radial, air-cooled, 600 horsepower at 2,200 r. p. m.
- Curtiss D-12, 12-cylinder, "Vee," water-cooled, 435 horsepower at 2,300 r. p. m.
- Dayton Bear, 4-cylinder, in-line, air-cooled, 100 horsepower at 1,500 r. p. m.
- Fairchild Caminez 447-C, 4-cylinder, radial, air-cooled, 120 horsepower at 960 r. p. m.
- Kinner K-5, 5-cylinder radial, air-cooled, 90 horsepower at 1,810 r. p. m.
- LeBlond 60, 5-cylinder, radial air-cooled, 65 horsepower at 1,950 r. p. m.
- LeBlond 90, 7-cylinder, radial, air-cooled, 90 horsepower at 1,975 r. p. m.
- Lycoming R-645, 9-cylinder, radial, air-cooled, 185 horsepower at 2,000 r. p. m.
- Michigan Aero Engine Corporation Rover, 4-cylinder, in-line, air-cooled, inverted, 55 horsepower at 1,900 r. p. m.
- Packard 3A-1500 direct, 12-cylinder, "Vee," water-cooled, 525 horsepower at 2,100 r. p. m.
- Packard 3A-2500 direct, 12-cylinder, "Vee," water-cooled, 800 horsepower at 2,000 r. p. m.
- Pratt & Whitney Hornet, 9-cylinder, radial, air-cooled, 500 horsepower at 1,900 r. p. m.
- Pratt & Whitney Hornet, 9-cylinder, radial, air-cooled, 525 horsepower at 1,900 r. p. m.
- Pratt & Whitney Hornet, 9-cylinder, radial, air-cooled, 575 horsepower at 1,950 r. p. m.
- Pratt & Whitney Wasp, 9-cylinder, radial, air-cooled, 450 horsepower at 2,100 r. p. m.
- Velie, 5-cylinder, radial, air-cooled, 55 horsepower at 1,815 r. p. m.
- Warner Scarab, 7-cylinder, radial, air-cooled, 110 horsepower at 1,850 r. p. m.
- Wright J-5 Whirlwind, 9-cylinder, radial, air-cooled, 220 horsepower at 2,000 r. p. m.
- Wright J-6, R-540, 5-cylinder, radial, air-cooled, 165 horsepower at 2,000 r. p. m.
- Wright J-6, R-760, 7-cylinder, radial, air-cooled, 225 horsepower at 2,000 r. p. m.
- Wright J-6, R-975, 9-cylinder, radial, air-cooled, 300 horsepower at 2,000 r. p. m.
- Wright Cyclone R-1750-A, 9-cylinder, radial, air-cooled, 525 horsepower at 1,900 r. p. m.

REPORT OF COMMITTEE ON MATERIALS FOR AIRCRAFT

ORGANIZATION

The present organization of the committee on materials for aircraft is as follows:

Dr. George K. Burgess, Bureau of Standards, chairman.
 H. L. Whittemore, Bureau of Standards, vice chairman and acting secretary.
 Lieut. R. S. Barnby (C. C.), United States Navy.
 S. K. Colby, United States Aluminum Co.
 Warren E. Emley, Bureau of Standards.
 Commander Garland Fulton (C. C.), United States Navy.
 Henry A. Gardner, Institute of Paint and Varnish Research.
 Dr. H. W. Gillett, Battelle Memorial Institute.
 Prof. George B. Haven, Massachusetts Institute of Technology.
 C. H. Helms, National Advisory Committee for Aeronautics.
 Zay Jeffries, Aluminum Co. of America.
 J. B. Johnson, matériel division, Army Air Corps, Wright Field.
 George W. Lewis, National Advisory Committee for Aeronautics (ex officio member).
 Lieut. Alfred J. Lyon, United States Army, matériel division, Air Corps, Wright Field.
 Lieut. Commander H. R. Oster (C. C.), United States Navy.
 H. S. Rawdon, Bureau of Standards.
 E. C. Smith, Central Alloy Steel Corporation.
 G. W. Trayer, Forest Products Laboratory, Forest Service.
 Starr Truscott, National Advisory Committee for Aeronautics.
 Hon. Edward P. Warner, Editor, Aviation.

FUNCTIONS

Following is a statement of the functions of the committee on materials for aircraft:

1. To aid in determining the problems relating to materials for aircraft to be solved experimentally by governmental and private agencies.
2. To endeavor to coordinate, by counsel and suggestion, the research and experimental work involved in the investigation of such problems.
3. To act as a medium for the interchange of information regarding investigation of materials for aircraft in progress or proposed.
4. To direct and conduct research and experiment on materials for aircraft in such laboratory or laboratories, either in whole or in part, as may be placed under its direction.
5. To meet from time to time on call of the chairman and report its actions and recommendations to the executive committee.

The committee on materials for aircraft, through its personnel acting as a medium for the interchange of information regarding investigations on materials for aircraft, is enabled to keep in close touch with research in this field of aircraft development. Much of the research, especially in the development of light alloys, must necessarily be conducted by the manufacturers interested in the particular problems, and both the aluminum and steel industries are represented on the committee. In order to cover effectively the large and varied field of research on materials for aircraft, four subcommittees have been formed, as follows:

Subcommittee on metals:

H. S. Rawdon, Bureau of Standards, chairman.
 Dr. H. W. Gillett, Battelle Memorial Institute.
 Zay Jeffries, Aluminum Co. of America.
 J. B. Johnson, matériel division, Army Air Corps, Wright Field.
 George W. Lewis, National Advisory Committee for Aeronautics (ex officio member).
 E. C. Smith, Central Alloy Steel Corporation.
 Starr Truscott, National Advisory Committee for Aeronautics.
 H. L. Whittemore, Bureau of Standards.

Subcommittee on woods and glues:

G. W. Trayer, Forest Products Laboratory, Forest Service, chairman.
H. S. Betts, Forest Service.
George W. Lewis (ex officio member).
H. L. Whittemore, Bureau of Standards.

Subcommittee on coverings, dopes, and protective coatings:

C. H. Helms, National Advisory Committee for Aeronautics, chairman.
Dr. W. Blum, Bureau of Standards.
Warren E. Emley, Bureau of Standards.
Henry A. Gardner, Institute of Paint and Varnish Research.
Prof. George B. Haven, Massachusetts Institute of Technology.
Isadore M. Jacobsohn, Bureau of Standards.
George W. Lewis (ex officio member).
P. H. Walker, Bureau of Standards.
E. R. Weaver, Bureau of Standards.

Subcommittee on aircraft structures:

Starr Truscott, National Advisory Committee for Aeronautics, chairman.
Lieut. C. E. Archer, United States Army.
Lieut. H. Z. Bogert, United States Army, matériel division, Air Corps, Wright Field.
C. P. Burgess, Bureau of Aeronautics, Navy Department.
Charles Ward Hall, Hall-Aluminum Aircraft Corporation.
Lieut. Lloyd Harrison, United States Navy.
Kenneth M. Lane, Aeronautics Branch, Department of Commerce.
George W. Lewis (ex officio member).
Charles J. McCarthy, Chance Vought Corporation.
Dr. L. B. Tuckerman, Bureau of Standards.

Much of the research in connection with the development of materials for aircraft is financed directly by the Bureau of Aeronautics of the Navy Department, the matériel division of the Army Air Corps, and the National Advisory Committee for Aeronautics.

The Bureau of Aeronautics and the matériel division of the Air Corps, in connection with the operation of tests in their own laboratories, apportion and finance research problems on materials for aircraft to the Bureau of Standards, the Forest Products Laboratory, and the industrial research laboratories.

MEETINGS OF THE COMMITTEE

Meetings of the committee were held several times during the year to consider reports on the work being conducted by the subcommittees. Particular attention was given the continuation of work on the development of methods for protecting light alloys, particularly duralumin, from corrosion. This work was begun some years ago and has always formed a major subject for investigation.

SUBCOMMITTEE ON METALS

The study of the properties of metals as related to their application to aircraft construction has been carried out at the Bureau of Standards, in cooperation with the Bureau of Aeronautics of the Navy Department, the matériel division of the Army Air Corps, and the National Advisory Committee for Aeronautics. Special attention has been given to the subject of the permanence under service conditions of the light alloys which in wrought form are used for structural purposes. The study of the corrosion resistance of the duralumin type of alloy has been continued and marked progress has been made in the development of suitable protective measures to be observed in its use. The study of its endurance under fatigue stresses has also been continued and tentative values for its fatigue resistance have been obtained.

Intercrystalline embrittlement of sheet duralumin.—The National Advisory Committee for Aeronautics issued two Technical Notes during the year dealing with two different phases of this investigation, thus bringing the total number of Technical Notes on this subject to six. These new notes (Nos. 304 and 305) deal with the results of weather-exposure tests of duralumin and the effect of corrosion when accompanied by stress.

Intercrystalline embrittlement of sheet duralumin—Weather-exposure tests.—The exposure tests have been in progress for two years at the Bureau of Standards and the naval air station at Hampton Roads, Va., and 18 months at the naval air station, Coco Solo, Canal Zone. Quite definite conclusions are believed to be warranted on the basis of the results to date, which on the whole are very consistent with the tentative views previously expressed on the basis of the laboratory test results. The test racks at Hampton Roads were damaged in some unknown way during the year and some of the racks knocked into the water. These have been recovered and it is interesting to find that, although the rate of corrosion was altered as a result of the two months' immersion in the sea water, the relative order of corrosion resistance of the various materials, heat-treated and coated in various ways, was practically unchanged by the more severely corrosive conditions.

The tests in general have shown, beyond question, that the lack of permanence observed in sheet duralumin under some conditions is a corrosion phenomenon and not a "spontaneous" phase change within the alloy. A corrosive attack of an intercrystalline nature is very largely responsible for the embrittlement produced. In the exposure tests, like the laboratory tests, the rate of embrittlement was greatly accelerated by a marine atmosphere and by a tropical climate. The tests were carried out upon full-size tension bars, the change in the tensile properties being used as a measure of the effect of corrosion. This method is by far the best in cases like the present, in which the tensile properties of the material undergo material change without corresponding change in surface appearance. In numerous cases of coated specimens, the surface, after exposure, appears still in good condition. The underlying metal, however, may show marked evidence of attack by its changed tensile properties. Variations in composition of duralumin which do not result in wide departure from the ordinary duralumin composition are apparently of almost negligible importance so far as corrosion behavior is concerned. Of the high-strength aluminum alloys which differ materially in composition from duralumin, the alloy containing copper as the principal alloying element was most susceptible to intercrystalline attack.

Variations in the heat-treatment procedure used for duralumin appear to be major factors which determine the susceptibility of heat-treated duralumin sheet to embrittlement during exposure to the weather. The quenching rate, as determined by the use of cold or hot water or oil as quenching media, and the aging treatment (room-temperature aging versus accelerated aging) are most important in this respect. The use of hot water or oil as a quenching medium for sheet duralumin, or the use of an accelerated aging treatment, should be very carefully guarded against for duralumin which must withstand severe climatic conditions, such as marine and tropical service.

Cold working of properly heat-treated sheet duralumin by stretching or cold rolling does not affect very greatly the susceptibility of the material to embrittlement by intercrystalline attack when exposed to the weather. With improperly heat-treated duralumin this factor is of much more importance.

The exposure tests have clearly shown that corrosion of the more familiar or pitting type may occur with any duralumin. The effect upon the tensile properties, although similar in character, is, in most cases, decidedly less than that of the intercrystalline type. So far it has not been possible to correlate definitely the tendency of the alloy toward this form of corrosive attack with any condition of the material resulting from any particular heat treatment or other condition.

The determination of the permanence of coatings on duralumin when exposed to the weather has been successfully made by applying the coating to tension bars of duralumin which had been improperly heat-treated and were hence quite susceptible to attack. The relatively rapid attack of the underlying or basic metal following the breakdown of the coating was shown in the tension tests of such specimens after exposure. In this way it has been very clearly shown that aluminum coatings are by far the most dependable. The useful life of clear varnishes is very short, but the addition of aluminum pigment increases the permanence of the varnish very greatly. On the other hand, the addition of aluminum pigment to rubberlike coatings,

while decidedly successful in the laboratory, has not given satisfactory results under exposure conditions. Surface oxidation by the anodic process and similar coatings have no lasting protective value unless well greased, and even when greased they have not proved to be resistant against severe exposure conditions (Coco Solo), although with milder exposure conditions (Washington) quite satisfactory results have been obtained. Simple grease coatings reinforced with aluminum powder have given satisfactory service under mild exposure conditions but not entirely so for severe (marine) conditions. In general, it is quite evident from all data available that for inland use (mild exposure), the coating need not be scrutinized very closely. For marine service, however, the choice of a suitable coating appears to be very limited.

The above statements apply particularly to fairly thick sheet, such as 14 gage. Exposure tests of thin (0.008 inch) sheet, even under rather mild conditions (Washington), have shown a marked difference in tensile properties after six months, a drop in elongation from 17 to 4 per cent being observed. Under the more severe conditions at Coco Solo a similar change occurred in a much shorter time. Unlike the thicker material, the corrosion resistance of thin sheet apparently can not be greatly improved by modifying the method of heat treatment. Thin sheet duralumin (0.010 inch), aluminum coated, as in the Alclad process was found to be much more resistant, although even here the corrosion resistance was not so high as that shown by the same material in thicker sheets.

Intercrystalline embrittlement of sheet duralumin—Stress-corrosion tests.—In the laboratory, accelerated corrosion tests have been continued throughout the year in order to determine whether the corrosion resistance of duralumin may be influenced by stress acting simultaneously with the corrosive attack. The material, in the form of tension bars, was corroded while stressed (a) in static tension in some cases nearly to and in other cases considerably below the yield point, and (b) while repeatedly stressed in flexure. The tests were carried out as in the previous work; that is, after exposure to the corrosive conditions for a predetermined period the tensile properties of the corroded material were determined. The tests have served particularly well to demonstrate the marked superiority of aluminum-coated duralumin when subject to severely corrosive conditions. This material was in good condition after 60 days' exposure to accelerated corrosion (sodium chloride solution containing hydrogen peroxide) while subjected to 20,000 pounds per square inch tension, which is about one-half its "yield stress" (0.006 in/in extension under load). With a stress of 31,000 pounds per square inch accompanied by corrosion, 40 days' attack did not very materially affect it, nor did rather severe scratching of the surface produce any marked effect during stress corrosion at 20,000 pounds per square inch.

With plain duralumin properly heat-treated, however, 13 days' attack in stress corrosion at 25,500 pounds per square inch tension reduced the ductility from 22 to 4 per cent, although unstressed material likewise was severely attacked, the ductility being reduced to 8 per cent. With material improperly heat-treated the effect on the plain duralumin was still more strongly marked. On the whole, static tensile stress does not appear to increase the corrosive attack very decidedly.

Corrosion accompanied by repeated flexural stress constitutes a severe test. Plain duralumin, properly heat-treated, repeatedly flexed to 10,000 pounds per square inch maximum fiber stress, showed such low tensile properties after 7 days as to render it practically worthless, although some bars remained intact for 30 days. The attack on improperly heat-treated duralumin was much more severe, a life of only 5 days, instead of 30 being attained in this case. Aluminum-coated duralumin exposed to the same conditions showed no deterioration whatsoever after prolonged attack (24 days). Indeed, some specimens after 65 days' attack showed as high tensile properties as in their initial state. It is quite evident that any material showing high resistance to corrosion under stress conditions of this character can be regarded as a dependable one for extremely severe service conditions.

Weather-exposure tests of magnesium and magnesium alloys.—The program of exposure tests was extended this year to include magnesium and magnesium alloys. The same testing procedure is being followed as in the case of duralumin; that is, full-size tension bars are used for the exposure specimens, the tensile properties of which are to be determined after different

exposure periods. The materials used are of commercial quality and represent both the rolled sheet and the cast alloy. They were furnished by the two leading manufacturers of this type of material.

The sheet materials consist of cold-rolled magnesium, an alloy composed of 96 per cent of magnesium and 4 per cent of aluminum, which previous investigators have reported to have a low corrosion resistance, and an alloy containing 95.6 per cent magnesium, 4 per cent aluminum, and 0.4 per cent manganese, which has been reported to have a relatively high corrosion resistance. Likewise, in the case of the cast alloys, two compositions differing markedly in their corrosion resistance were used. The castings were in the form of flat tension bars.

The bars have been exposed to the weather at the Bureau of Standards and at the naval air station, Coco Solo, Canal Zone. A third set to be used as "control" bars, has been stored within sealed glass jars containing a desiccating substance for maintaining a truly dry atmosphere.

The problem of protecting this type of material against corrosion appears to be mainly that of finding a suitable coating together with the proper treatment of the surface prior to the application of the coating. For each of the three exposures and for each of the five materials, the specimens are exposed in the bare state as well as in the coated condition. The coatings used are those which appear most promising according to either the results already obtained with duralumin or by other investigators. As is well known, the adherence of coatings on magnesium is determined in large measure by the surface characteristics, and in order to obtain good adherence, one-half of the number of specimens comprising each set were treated with a phosphate solution whereby a fine matte surface was produced. The remainder were used in the untreated condition, i. e., as rolled or as cast.

The coatings applied included a variety of types: spar varnish with aluminum pigment, rubber base with graphite pigment, lacquers of the nitrocellulose type applied over various undercoats, linseed oil with lampblack as a pigment. One transparent coating, vinyl acetate resin, has been included.

Results are expected from these exposure tests within a shorter period of time than in the case of duralumin.

High-frequency fatigue.—Six high-frequency flexural fatigue machines are now in operation at the Bureau of Standards 14 hours a day. A series of tests on 14 different materials in the aluminum and magnesium light alloy group is in progress. The materials under consideration are:

1. Pure magnesium, as rolled.
2. Pure magnesium, annealed.
3. Magnesium alloy (4 per cent aluminum, 0.4 per cent manganese, remainder magnesium), as rolled.
4. Eleven different aluminum alloys of various compositions and heat treatments.

Tests on the magnesium alloy (4 per cent aluminum, 0.4 per cent manganese, remainder magnesium) have been completed and runs are now in progress on two of the aluminum alloys.

Results of the tests on the magnesium alloy indicate an endurance limit of 5,000 to 6,000 pounds per square inch for the longitudinal specimens, with a maximum of 7,000 pounds per square inch for the transverse specimens tested. The material was found to be so variable that the determination of a more definite endurance limit could only be made by a statistical study of a much larger number of tests than have been made. The results of such an extended series of tests on this material would not repay the extra labor and time. It is believed that the transverse specimens indicated a higher value for the endurance limit only because it happened that those transverse specimens tested were a little better than the longitudinal specimens selected for test.

Generally the specimens were not run much more than 200,000,000 cycles. If failure had not occurred when this stage was reached, "coaxing" was resorted to, i. e., the stress was increased and the test continued at the higher stress. As is generally known, numerous investigators have found that a specimen which is tested at a stress below its endurance limit is actually

strengthened by this process and if retested at a higher stress will last longer than a specimen tested initially at that stress. This fact has been made use of in the determination of the endurance limit. If, from tests already made, a "coaxing" test shows that a specimen lasts longer at the higher of the two stresses of that test than it would have if tested initially at that stress, then the lower or initial stress is considered as being lower than the endurance limit of that material.

Tests on one of the aluminum alloys have progressed far enough to allow the making of the statement that the endurance value is close to 12,000 pounds per square inch. For the other the preliminary results indicate a value in the neighborhood of 10,000 pounds per square inch.

Fatigue of Alclad duralumin.—This investigation has been carried on in cooperation with the Aluminum Co. of America.

Over 118 specimens obtained from corroded and uncorroded Alclad and comparable duralumin sheets have been tested. Some of these specimens have been subjected to over 100,000,000 cycles of stress.

The results from specimens of corroded material indicate that the corroded Alclad specimens have approximately the same life as the uncorroded specimens, while for the corroded duralumin specimens the results lie below the results obtained for those uncorroded. This is added evidence for the greater durability of aluminum-covered duralumin.

SUBCOMMITTEE ON WOODS AND GLUES

With the great reduction in the use of wood in military aircraft, the Bureau of Aeronautics of the Navy Department and the matériel division of the Army Air Corps have practically ceased to initiate activities regarding woods and glues. Wood is still largely used in commercial-airplane structures, but it is quite evident that its use is gradually decreasing. With the development of production methods by large aircraft manufacturers it appears that the use of metal ribs is more economical than the older types of built-up wooden ribs. However, in commercial types of airplanes where large numbers are not in production, the spruce spar, usually routed from the solid, is still more economical than the built-up metal spar and satisfies the requirements.

With the decreased use of wood in aircraft structures there has been also a decrease in interest in the initiation of new investigations as to woods and glues for aircraft structures. The work of this subcommittee has correspondingly decreased and attention is now being directed toward the making available in the most convenient form of the information which has been accumulated. The investigations on the strength of airplane woods, plywood webs for box beams, wing rib design, lateral buckling and twisting of beams, twisting of members under compression, influence of blocks and fillets on wooden beams, and the study of continuous beams, will be reported in publications now in preparation. It is believed that these reports will summarize the information available so completely that very little additional information will be required by manufacturers who desire to use wood in their aircraft structures. The work of preparing these reports is now in progress and they should appear during the coming year.

SUBCOMMITTEE ON COVERINGS, DOPES, AND PROTECTIVE COATINGS

Much of the work on the development of coverings, dopes, and protective coatings is carried out at the Bureau of Standards, and in many cases it involves cooperation with the work of the subcommittee on metals. Investigations are also carried out by the exposure of test panels at the United States naval air stations at Hampton Roads, Va., and Coco Solo, Canal Zone. Exposure tests were also made on the roof of the laboratory of Mr. H. A. Gardner.

Some of the more important investigations in progress during the last year are outlined below.

Gas cell fabrics.—The gas cell made of the substitute for goldbeaters' skin fabric which was constructed last year and installed in the *Los Angeles* has not given as good results as was anticipated. This is another instance of the failure of production materials and processes to show as good performance as was obtained from laboratory materials and processes. It is believed probable that the production material did not completely reproduce the material developed in

the laboratory, and in order to determine whether it is possible by ordinary commercial methods to reproduce the laboratory material, three orders, each for 1,000 yards of fabric of this type, have been placed by the Bureau of Aeronautics of the Navy Department with three different manufacturers. Each of these is to follow his own methods and it is hoped that the laboratory quality may be obtained from at least one of the manufacturers. If this is done, it will be possible to determine how the processes followed differ and to learn how to reproduce the material more perfectly.

The disappointing results obtained from the one type of substitute for goldbeaters' skin fabric have led to continued study of other types, and one manufacturer is attempting to produce a substitute along independent lines.

Protective coatings for duralumin and magnesium.—Exposure tests of coatings for aluminum and magnesium alloys have been continued in cooperation with the subcommittee on metals. The test specimens have been exposed at Coco Solo, Canal Zone, at the naval air station at Hampton Roads, Va., and at the Bureau of Standards. Tension tests are made of the specimens after exposure to determine the change in tensile properties due to corrosive attack.

In the tests on duralumin, coatings of aluminum have been found to be most dependable. The protective value of clear varnishes is of very short duration, but their permanence is greatly increased by the addition of aluminum pigment. Surface oxidation by the anodic process, and other coatings of similar nature, when well greased, and also grease coatings reinforced with aluminum powder, have given satisfactory service under mild exposure conditions, but have not proved resistant under severe conditions. From all the data available it appears that for mild exposure conditions there are a number of satisfactory coatings, but for marine service the choice of a suitable coating is very limited.

A number of types of protective coatings, including some of the same as were used on duralumin specimens, are being tested on magnesium alloys. The most important of these are spar varnish with aluminum pigment, rubber-base coatings with graphite pigment, lacquers of the nitrocellulose type applied over various undercoatings, linseed oil with lampblack as a pigment, and vinyl acetate resin. The results from the exposure tests on magnesium specimens are not yet available.

Substitute for silk parachute cloth.—The feasibility of processing cotton textiles for parachutes on a large scale so that the resulting material would have properties approximating those of silk cloth was discussed with members of several finishing plants. The methods were tested on a large scale and were modified to conform to commercial practice in nonessential details and where necessary. These modified procedures gave satisfactory results with yarn processing. However, large-scale operations on cloth did not give as good results as were to be expected from the smaller scale work.

The prospect of obtaining cotton yarn which is suitable for the making of parachute fabric which may be used as a substitute for silk has improved somewhat as domestic cotton spinning mills have begun to spin cotton yarns which meet the requirements for this use.

The spinning of the cotton yarns at the Bureau of Standards was completed. Some of these yarns were woven into fabrics, which were processed, and the remainder were processed and then woven into experimental fabrics. This work has resulted in considerable valuable data on the effect of the various treatments on the properties of the yarns and fabrics and has pointed the way to the most satisfactory constructions and processes.

Ordinary H H balloon cloth sufficient for three parachutes was processed in three ways. Two commercially available fabrics which may be suitable for parachute construction were processed to improve their strength. All this material has been forwarded to the Naval Aircraft Factory at Philadelphia, Pa., to be manufactured into parachutes for testing purposes.

It has been found possible to increase the tear resistance of the cotton fabric materially by a change in the weave. Preliminary experiments have been completed and fabric for two additional parachutes will be woven from commercial yarn using the modified weave.

SUBCOMMITTEE ON AIRCRAFT STRUCTURES

Practically all the investigations under the cognizance of this subcommittee are conducted at the Bureau of Standards. These investigations are undertaken at the request of the Bureau of Aeronautics of the Navy Department, the matériel division of the Army Air Corps, or the National Advisory Committee for Aeronautics. Some of the more important investigations in progress or completed during the past year are outlined below.

Welded joints in tubing.—This investigation was originally requested by the Aeronautics Branch of the Department of Commerce. It was desired that the various types of joints used in welded fuselage construction should be studied to determine their strengths and to develop improved joints.

The first group of joints tested numbered 165 in all. These joints were designed from data supplied by aircraft manufacturers. They were welded under procedure control, and were tested in special fixtures.

Although no quantitative data are available as yet, several conclusions based on observation may be made. The most serious problem encountered in designing reinforcement in a welded joint is the formation of cracks in gusset plates after cooling. It is evident that the problem is one of design as well as of welding technique. Best results seem to be obtained by making the thickness of gusset plates somewhat greater than the tube thickness and keeping the plan area of the gusset as small as possible. Whenever possible the design should allow for movement of the members as the joint cools.

The results of this first series of tests are being prepared as a progress report for publication as a Technical Note of the National Advisory Committee for Aeronautics.

From data based on the results of these tests more improved joints will be made and finally the best type for each purpose will be determined.

Form factors for tubing of duralumin and steel under combined column and beam loads.—The experimental work on this investigation has been continued. A very careful and time-consuming study of the experimental results which have been obtained led to a satisfactory analysis.

The experimental results were combined on a semitheoretical basis which permitted a direct comparison of columns made of materials of markedly different physical properties.

By using this method it was possible not only to combine in a single chart the tubes of widely different properties and of different dimensions but to obtain also a considerable increase of maximum allowable stresses over the old method of treatment of the experimental results. In the case of certain tubes in the range of high l/r ratios the increase amounted to over 100 per cent.

Although the experimental results were obtained on tubes within a limited range of dimensions, the consistency with which the experimental points fall close to the average curves makes it seem probable that this method will prove to be more generally applicable to tubes of other diameters and of other wall thicknesses.

A report on this work has been published by the National Advisory Committee for Aeronautics as Technical Note No. 307, Strength of Tubing under Combined Axial and Transverse Loading.

A study of the results showed that the strength of tubing depends greatly upon the yield point of the material. Although the test results showed that the ultimate strength of the tubing was probably as high as could be obtained on commercial tubing, the yield point of the tubing used in this investigation was considerably higher than the specified minimum. If the requirements as to yield point were raised, higher stresses could safely be used in design. It seems probable that it will be found possible to alter these specifications so as to take advantage of this increase in reducing the weight of tubular aircraft construction. This investigation is being continued to cover a wider range of dimensions of tubing, and to determine if possible the causes underlying the characteristic differences in the relationship between tensile properties and modulus of rupture of duralumin and chrome-molybdenum tubing.

Airship girders and airship structural members.—During the past year tests on experimental plate girders of the Arnstein type have been continued. Two short girders fabricated by the Naval Aircraft Factory were tested in compression.

In connection with tests of girders of the Arnstein type a new procedure has been worked out for the determination of their minimum cross-section area. Preliminary tests indicate that by means of this procedure it is possible to determine the minimum cross-section area of a girder, fabricated from flanged-sheet material containing lightning holes, within less than 1 per cent of the actual value.

Several girders made by the Goodyear-Zeppelin Corporation for the new 6,500,000 cubic-foot airships of the Navy were tested in compression and under combined bending and axial loading, respectively.

Electrically welded steel tubing.—Tests on low-carbon steel tubing formed from flat strip and welded by the electrical resistance process, which have been carried on in cooperation with the manufacturers, Steel and Tubes (Inc.), have been completed and will be reported shortly in the Bureau of Standards Journal of Research. The tubes tested varied from 0.625 inch to 3 inches outside diameter and from 0.028 to 0.120 inch in wall thickness.

As was to be expected from the method of manufacture this tubing, as produced commercially, shows much less variation in wall thickness than seamless steel tubing.

The tests included tension, compression, torsion, hydrostatic, and flanging tests of the tubes as a whole, tension tests of the weld alone, indentation (hardness) tests on both weld and base metal, and micrographic examination of the weld and adjacent material.

All the tests showed that, except in the case of the swaged-annealed tubing, the properties of the base metal (the metal not affected by the welding operation) can be used in determining the working stresses for different structural uses of tubing made by the process used in the manufacture of this electrically welded tubing. No allowance is necessary for the altered structure in and adjacent to the weld.

So far this tubing has been produced commercially only in carbon steel. Crome-molybdenum tubing has, however, been produced experimentally. If welded alloy tubing showing equivalent results under test can be produced commercially by this process it should add materially to the progress of aircraft construction.

End fixation of struts.—Some degree of end fixation is usually present in compression members, as used in aircraft, but rarely is it sufficient to justify designing on the basis of fixed ends. A quantitative evaluation is needed of the added strength afforded by the degree of fixation actually used. At the request of the Bureau of Aeronautics, the Bureau of Standards has undertaken a study of this problem with the purpose of securing data for the design of aircraft.

As was expected, the problem has not proved simple. It has been studied from the theoretical standpoint and a search has been made in the files of technical and scientific journals for clues to previous work. Only the vaguest suggestions for methods of attacking the problem were found in publications.

The study, however, seemed to indicate fairly definitely the most promising line of attack. This consists in applying elastic restraints to the ends of the members under compression proportional to the transverse stiffness of the members. The study further indicated that useful results were to be expected mainly in the transition range of l/r below the Euler range.

The theoretical studies have further brought out the very useful result that in these end fixation tests it is possible to eliminate the end correction found necessary by Karman in his "round-end" tests. The relationship shows that results obtained with apparatus for a particular fixation factor will be applicable to columns of the same slenderness ratio but with a smaller fixation factor to be calculated directly from the dimensions and the end load found. This relationship is true whether the columns are deflecting elastically or whether the stresses are carried beyond the elastic limit. This relationship simplifies very materially the testing procedure.

Apparatus has been designed and constructed for making the tests, and preliminary testing is now in progress.

The results have been more encouraging than was expected in an investigation in an admittedly difficult field and one about which so little is known.

Technique of testing flat plates under normal pressure.—Work has been completed on a small experimental frame. From the facts brought out by the use of various packing and holding

systems it has been possible to design a larger fixture and measuring device. This larger machine will accommodate plates of square section from 25 square inches area up to 900 square inches and rectangular plates of a 3 to 1 side ratio of areas of 75 square inches up to 2,700 square inches.

Considerable difficulty was encountered in securing the base plate and clamping bars. Efforts along this line were finally successful and the assembling of the apparatus is now nearly completed, so that the actual tests of specimens can be started soon.

REPORT OF COMMITTEE ON PROBLEMS OF AIR NAVIGATION

ORGANIZATION

In response to the need for the coordination of scientific research being conducted by a number of different agencies, both within and without the Government, on the problems of air navigation, particularly in the fields of navigation instruments, aerial communications, and meteorological problems, the National Advisory Committee for Aeronautics in 1928 established a new standing committee on problems of air navigation, with members representing the principal agencies concerned with the development of aids to air navigation.

The committee on problems of air navigation is at present composed of the following members:

Hon. William P. MacCracken, jr., chairman.
Dr. L. J. Briggs, Bureau of Standards.
Lloyd Espenschied, American Telephone & Telegraph Co.
Brig. Gen. B. D. Foulois, United States Army, chief of matériel division, Air Corps, Wright Field.
Paul Henderson, National Air Transport (Inc.).
Capt. S. C. Hooper, Director of Naval Communications, Navy Department.
Dr. J. C. Hunsaker, Goodyear-Zeppelin Corporation.
Capt. E. S. Land, United States Navy, The Daniel Guggenheim Fund for the Promotion of Aeronautics.
George W. Lewis, National Advisory Committee for Aeronautics (ex officio member).
Col. Charles A. Lindbergh.
Prof. Charles F. Marvin, Weather Bureau.
C. M. Young, Assistant Secretary of Commerce for Aeronautics.

FUNCTIONS

The functions of the committee on problems of air navigation are as follows:

1. To determine the problems in the field of air navigation that are most important for investigation by governmental and private agencies.
2. To coordinate by counsel and suggestion the research work involved in the investigation of approved problems.
3. To act as a medium for the interchange of information regarding investigations and developments in air navigation, in progress or proposed.
4. To meet from time to time on call of the chairman and report its actions and recommendations to the executive committee.

In order to cover effectively the large and varied field of research and development on problems of air navigation, subcommittees on problems of communication, on instruments, and on meteorological problems have been organized under the committee on problems of air navigation.

SUBCOMMITTEE ON PROBLEMS OF COMMUNICATION

The membership of the subcommittee on problems of communication is as follows:

Lloyd Espenschied, American Telephone & Telegraph Co., chairman.
Dr. J. C. Hunsaker, Goodyear-Zeppelin Corporation, vice chairman.
C. H. Helms, National Advisory Committee for Aeronautics, secretary.
Maj. William R. Blair, United States Army, Signal Corps, War Department.
Dr. J. H. Dellinger, Bureau of Standards.

George W. Lewis, National Advisory Committee for Aeronautics (ex officio member).
 W. G. Logue, Radiomarine Corporation of America.
 J. L. McQuarrie, International Telephone & Telegraph Co.
 Eugene Sibley, Aeronautics Branch, Department of Commerce.
 Lieut. E. E. Stone, United States Navy, Office of the Director of Naval Communications, Navy Department.

The subcommittee on problems of communication when originally organized had as its chairman Dr. Edward B. Craft, of the Bell Telephone Laboratories, and Doctor Craft's recent death has deprived the subcommittee of the leadership of one particularly well qualified for the work. During his illness and until the appointment of Mr. Espenschied, Doctor Hunsaker, the vice chairman, has served as acting chairman. Appreciation is also due to Commander W. J. Ruble, United States Navy, the first secretary of the subcommittee, for his services in connection with the organization of the subcommittee.

The subcommittee has outlined in a general way some of the important problems in the field of aircraft communications, and each of these phases of the subject has been assigned to an individual member of the subcommittee for the preparation of a statement as to the present status of its development and needs for the future. Among the problems being studied in accordance with this plan are radio goniometry as applied to a network of airways, radio transmission between ground and aircraft, and the standardization of aircraft radio power supply.

Ignition shielding.—The problem of the interference of the engine ignition with radio reception has also been considered. The suppression of ignition interference to radio reception appears to depend upon the complete shielding of the electrical equipment. At a conference of interested manufacturers held at the Bureau of Standards on June 11, 1929, steps were taken to standardize the shields for magnetos, wiring, and spark plugs. Tests made at the Langley Memorial Aeronautical Laboratory to determine the shielding effect of the N. A. C. A. cowling indicated that the cowling would be useful to the extent of eliminating the need for a shield for the spark plug. Since the spark plug offers the most difficult problem with respect to shielding, the cowling may serve an additional useful purpose.

Distribution of weather information.—As a result of cooperation between the Weather Bureau and the Aeronautics Branch of the Department of Commerce reports of weather conditions are now being broadcast every 30 minutes from 24 radio stations located along more than 75,000 miles of airways, to airplanes flying on definite schedules. This information covers a band 100 miles wide on each side of the airways. In conjunction with the weather service, radiobeacons are also established. Fifteen additional radio stations are under construction at this time. A simple radio receiving set aboard the airplane enables the pilot to be constantly advised of changing weather conditions.

SUBCOMMITTEE ON INSTRUMENTS

The subcommittee on instruments is at present organized as follows:

Dr. L. J. Briggs, Bureau of Standards, chairman.
 Marshall S. Boggs, Aeronautics Branch, Department of Commerce.
 Dr. W. G. Brombacher, Bureau of Standards.
 Dr. Samuel Burka, Dayton, Ohio.
 C. H. Colvin, Society of Automotive Engineers.
 Lieut. A. F. Hegenberger, United States Army, matériel division, Air Corps, Wright Field.
 Dr. A. W. Hull, General Electric Co.
 George W. Lewis, National Advisory Committee for Aeronautics (ex officio member).
 Lieut. T. C. Lonnquest, United States Navy, Bureau of Aeronautics, Navy Department.
 H. J. E. Reid, National Advisory Committee for Aeronautics.

A large number of the investigations in connection with the development of instruments for air navigation are conducted by the Bureau of Standards in cooperation with the Bureau of Aeronautics of the Navy, the Army Air Corps, and the National Advisory Committee for Aeronautics. These investigations have been carried out under the cognizance of the committee

on aerodynamics and are outlined in the report of that committee. Among the investigations now under way are a study of the fundamentals of instrument mechanism design, an investigation of damping liquids for aircraft instruments, and a study of the present status of air navigation instruments. In some instances manufacturers of aircraft instruments and engineering societies are cooperating in the investigation of particular problems.

Vibration of aircraft instrument panels in flight.—A survey has been made of the problem of the vibration of instrument panels in an airplane in flight. This problem includes a study of the effect of vibration on the performance of various aircraft instruments; the measurement of the vibration of typical instrument boards in aircraft; and the effecting of a general agreement as to the standard amount of vibration which an instrument should be able to withstand. Laboratory work has been done by the Bureau of Standards on the effect of vibration on instruments, various instruments submitted by the Bureau of Aeronautics for type test having been given vibration tests on a specially designed vibration rack. The Bureau of Standards has also designed an apparatus for investigating the second phase of the problem, namely, the measurement of the vibration of instrument panels in aircraft. The general problem of instrument-board vibration is still under consideration by the subcommittee.

SUBCOMMITTEE ON METEOROLOGICAL PROBLEMS

The membership of the subcommittee on meteorological problems is as follows:

Prof. Charles F. Marvin, Weather Bureau, chairman.

Thomas H. Chapman, Aeronautics Branch, Department of Commerce.

Dr. W. R. Gregg, Weather Bureau.

Dr. W. J. Humphreys, Weather Bureau.

Dr. J. C. Hunsaker, Goodyear-Zeppelin Corporation.

George W. Lewis, National Advisory Committee for Aeronautics (ex officio member).

Lieut. F. W. Reichelderfer, United States Navy, naval air station, Lakehurst.

Dr. C. G. Rossby, Daniel Guggenheim Fund for the Promotion of Aeronautics.

Capt. Bertram J. Sherry, United States Army, Signal Corps, War Department.

One of the principal agencies engaged in the study of meteorological problems as related to air navigation is, of course, the Weather Bureau, but practically every organization concerned with the operation of aircraft is interested in problems of this nature. The chief problems which have received consideration by the subcommittee on meteorological problems during the past year are ice formation on aircraft in flight, fog and fog dispersal, and the structure of the atmosphere.

Ice formation on aircraft.—The subcommittee has kept in touch with the work being conducted at the Langley Memorial Aeronautical Laboratory on the study of ice formation on airplanes. This problem is being investigated both in flight and in a special low-temperature wind tunnel. The results of these tests indicate that ice forms on aircraft in dangerous amounts only within a small range of temperature below 32° F., and the best method so far discovered to prevent ice formation is for the pilot to observe the temperature of the air through which he is passing by means of an accurate strut thermometer and avoid flying through atmosphere at the dangerous temperatures. At the Bureau of Standards a study has been made of possible coatings on aircraft to prevent ice formation, and the coatings suggested as a result of this study are being tested in the low-temperature tunnel at Langley Field.

Fog and fog dispersal.—The problem of fog as a danger to safe flying has been given considerable attention by a number of agencies. One of the most important investigations in connection with this problem has been the work carried on by the Daniel Guggenheim Fund for the Promotion of Aeronautics, in cooperation with other organizations, on the development of instruments for safe flying through fog. The Weather Bureau, with the cooperation of the Guggenheim Fund, has made a study of fog and haze, and an interesting report on the subject, prepared by H. C. Willett, was published in the Monthly Weather Review for November, 1928. Experiments have been conducted at Wright Field, Hadley Field, and the Lakehurst Naval Air Station on the possibility of fog and cloud dispersal by means of sand particles carried aloft,

given a very high electrical charge, and scattered through the air. A summary of experimental work on the problem of fog dispersal is in preparation.

Structure of the atmosphere.—The principal problem considered by the subcommittee on meteorological problems during the past year was the study of the structure of the atmosphere. A digest of the status of this problem was prepared at the Weather Bureau by Mr. Welby R. Stevens, and a request of the airship subcommittee that the problem be given attention with a view to the initiation of research to increase the knowledge of the subject was given careful consideration.

One of the important phases of the study of this subject is the type of instrument to be used, and considerable thought has been given to the requirements of such an instrument. It is believed that it is desirable to study the variation in velocity and direction of air currents in a space approximately the size of a large airship and that the instrument for this purpose should have a minimum moment of inertia and should give an automatic record.

On suggestion of the subcommittee, a 3-cup type anemometer was tested in the variable-density wind tunnel at Langley Field, and as a result of these tests it was found that this particular instrument did not follow closely enough the fluctuations of velocity to be suitable for indicating the rapid changes in the velocity of air as in gusts.

The study of the sensitiveness of anemometers has been given considerable attention at the Weather Bureau during the last few months, and interesting results have been obtained from this investigation.

The possibilities of studying the turbulence of the upper air by motion-picture photographic records of the movements of smoke are also being considered by the subcommittee.

At the Langley Memorial Aeronautical Laboratory a preliminary investigation was made to obtain information on the velocity and acceleration of air in gusts. Recording air-speed apparatus was mounted on a building at an altitude of about 70 feet, and continuous records of the velocity of the air were obtained for periods when the air was particularly gusty or bumpy. In these tests the most violent acceleration measured was one in which the air velocity changed 20.6 miles per hour in 0.25 second (an acceleration of 121.6 feet per second per second). With the exception of one other case the acceleration never exceeded 80 feet per second per second. In these experiments it was found that the velocity of the mean wind had no definite relation to the accelerations measured. A further and more complete investigation is contemplated.

PART IV

TECHNICAL PUBLICATIONS OF THE COMMITTEE

The National Advisory Committee for Aeronautics has issued technical publications during the past year covering a wide range of subjects. There are four series of publications, namely, Technical Reports, Technical Notes, Technical Memorandums, and Aircraft Circulars.

The Technical Reports present the results of fundamental research in aeronautics carried on in different laboratories in this country, including the Langley Memorial Aeronautical Laboratory, the aerodynamical laboratory at the Washington Navy Yard, the Bureau of Standards, the Weather Bureau, Stanford University, and the Massachusetts Institute of Technology. In all cases the reports were recommended for publication by the technical subcommittees having cognizance of the investigations. During the past year 28 Technical Reports were submitted for publication.

Technical Notes present the results of small research investigations and the results of studies of specific detail problems which form parts of long investigations. The committee has issued during the past year, in mimeographed form, 21 Technical Notes.

Technical Memorandums contain translations and reproductions of important foreign aeronautical articles of a miscellaneous character. A total of 51 Technical Memorandums was issued during the past year.

Aircraft Circulars contain translations or reproductions of articles descriptive of new types of foreign aircraft. During the past year 20 Aircraft Circulars were issued.

Summaries of the 28 Technical Reports and lists of the Technical Notes, Technical Memorandums, and Aircraft Circulars follow:

SUMMARIES OF TECHNICAL REPORTS

The first annual report of the National Advisory Committee for Aeronautics for the fiscal year 1915 contained Technical Reports Nos. 1 to 7; the second annual report, Nos. 8 to 12; the third annual report, Nos. 13 to 23; the fourth annual report, Nos. 24 to 50; the fifth annual report, Nos. 51 to 82; the sixth annual report, Nos. 83 to 110; the seventh annual report, Nos. 111 to 132; the eighth annual report, Nos. 133 to 158; the ninth annual report, Nos. 159 to 185; the tenth annual report, Nos. 186 to 209; the eleventh annual report, Nos. 210 to 232; the twelfth annual report, Nos. 233 to 256; the thirteenth annual report, Nos. 257 to 282; the fourteenth annual report, Nos. 283 to 308; and since the preparation of the fourteenth annual report for the year 1928 the committee has authorized the publication of the following Technical Reports, Nos. 309 to 336:

Report No. 309, entitled "Joint Report on Standardization Tests on N. P. L. R. A. F. 15 Airfoil Model," by Walter S. Diehl, Bureau of Aeronautics, Navy Department.

This report contains the wind-tunnel test data obtained in the United States on a 36 by 6 inch R. A. F. 15 airfoil model prepared by the British Aeronautical Research Committee for international trials. Tests were made in cooperation with the National Advisory Committee for Aeronautics at the Bureau of Standards, Langley Memorial Aeronautical Laboratory, Massachusetts Institute of Technology, and McCook Field.

In addition to brief descriptions of the various wind tunnels and methods of testing, the report contains an analysis of the test data. It is shown that while in general the agreement is quite satisfactory there are two cases in which it is unsatisfactory. Since the lack of agreement in the latter is probably explained by errors known to be inherent in the methods of determining and applying corrections in these particular tests, it is concluded that the agreement obtained is more a matter of technique than a wind-tunnel characteristic.

Report No. 310, entitled "Pressure Element of Constant Logarithmic Stiffness for Temperature Compensated Altimeter," by W. G. Brombacher and F. Cordero, Bureau of Standards.

The usual type of altimeter contains a pressure element, the deflections of which are approximately proportional to pressure changes. An evenly divided altitude scale is secured by using a mechanism between the pressure element and pointer which gives the required motion of the pointer. A temperature-compensated altimeter was constructed at the Bureau of Standards for the Bureau of Aeronautics of the Navy Department which contained a manually operated device for controlling the multiplication of the mechanism to the extent necessary for temperature compensation. The introduction of this device made it difficult to adjust the multiplying mechanism to fit an evenly divided altitude scale. To meet this difficulty a pressure element was designed and constructed which gave deflections which were proportional to altitude; that is, to the logarithm of the pressure. Mathematically, the logarithmic stiffness S' of the element equals

$$S' = \frac{d \log_e P}{dy}$$

from which is derived the deflection y for the change in pressure from P_o to P

$$y = \frac{\log_e P - \log_e P_o}{S'}$$

The element consisted of a metal bellows of the sylphon type coupled to an internal helical spring which was designed so as to have a variable number of active coils. This report presents a description of and laboratory data relating to the special pressure element for the altimeter. In addition, equations which apply generally to springs and pressure elements of constant logarithmic stiffness are developed, including the deflection and the spacing between the coils in terms of the constants of the helical spring and pressure element.

Report No. 311, entitled "Aerodynamic Theory and Test of Strut Forms," Part I, by R. H. Smith, aerodynamical laboratory, Bureau of Construction and Repair, Navy Department.

The whole study under this title is in two parts, only the first of which is reported here. In this part the symmetrical inviscid flow about an empirical strut of high service merit is found by both the Rankine and the Joukowski methods. The results can be made to agree as closely as wished. Theoretical stream surfaces as well as surfaces of constant speed and pressure in the fluid about the strut are found. The surface pressure computed from the two theories agrees well with the measured pressure on the fore part of the model but not so well on the after part. From the theoretical flow speed the surface friction is computed by an empirical formula. The drag integrated from the friction and measured pressure closely equals the whole measured drag. As the pressure drag and the whole drag are accurately determined, the friction formula also appears trustworthy for such fair shapes.

Report No. 312, entitled "The Prediction of Airfoil Characteristics," by George J. Higgins, National Advisory Committee for Aeronautics.

This paper describes and develops methods by which the aerodynamic characteristics of an airfoil may be calculated with sufficient accuracy for use in airplane design. These methods for prediction are based on the present aerodynamic theory and on empirical formulas derived from data obtained in the N. A. C. A. variable-density wind tunnel at a Reynolds Number corresponding approximately to full scale.

Report No. 313, entitled "Drag and Cooling with Various Forms of Cowling for a Whirlwind Radial Air-Cooled Engine-I," by Fred E. Weick, National Advisory Committee for Aeronautics.

The National Advisory Committee for Aeronautics has undertaken an investigation in the 20-foot propeller research tunnel at Langley Field on the cowling of radial air-cooled engines. A portion of the investigation has been completed in which several forms and degrees of cowling were

tested on a Wright Whirlwind J-5 engine mounted in the nose of a cabin fuselage. The cowlings varied from the one extreme of an entirely exposed engine to the other in which the engine was entirely inclosed. Cooling tests were made and each cowling modified, if necessary, until the engine cooled approximately as satisfactorily as when it was entirely exposed. Drag tests were then made with each form of cowling, and the effect of the cowling on the propulsive efficiency determined with a metal propeller.

The propulsive efficiency was found to be practically the same with all forms of cowling. The drag of the cabin fuselage with uncowed engine was found to be more than three times as great as the drag of the fuselage with the engine removed and nose rounded. The conventional forms of cowling, in which at least the tops of the cylinder heads and valve gear are exposed, reduce the drag somewhat, but the cowling entirely covering the engine reduces it 2.6 times as much as the best conventional one. The decrease in drag due to the use of spinners proved to be almost negligible.

The use of the cowling completely covering the engine seems entirely practical as regards both cooling and maintenance under service conditions. It must be carefully designed, however, to cool properly. With cabin fuselages its use should result in a substantial increase in high speed over that obtained with present forms of cowling on engines similar in contour to the J-5.

Report No. 314, entitled "Drag and Cooling with Various Forms of Cowling for a Whirlwind Radial Air-Cooled Engine-II," by Fred E. Weick, National Advisory Committee for Aeronautics.

This report gives the results of the second portion of an investigation in the 20-foot propeller research tunnel of the National Advisory Committee for Aeronautics, on the cowling and cooling of a Whirlwind J-5 radial air-cooled engine. The first portion, which is reported in N. A. C. A. Technical Report No. 313, pertains to tests with a cabin fuselage. This report covers tests with several forms of cowling, including conventional types, individual fairings behind the cylinders, individual hoods over the cylinders, and the new N. A. C. A. complete cowling, all on an open cockpit fuselage. Drag tests were also made with a conventional engine nacelle, and with a nacelle having the new complete cowling.

In the second part of the investigation the results found in the first part were substantiated. It was also found that the reduction in drag with the complete cowling over that with conventional cowling is greater with the smaller bodies than with the cabin fuselage; in fact, the gain in the case of the completely cowed nacelle is over twice that with the cabin fuselage. The individual fairings and hoods did not prove effective in reducing the drag. The results of flight tests on an AT-5A airplane (reported in the appendix to N. A. C. A. Technical Report No. 313) have been analyzed and found to agree very well with the results of the wind-tunnel tests.

Report No. 315, entitled "Aerodynamic Characteristics of Airfoils-VI," by the National Advisory Committee for Aeronautics.

This collection of data on airfoils has been made from the published reports of a number of the leading aerodynamic laboratories of this country and Europe. The information which was originally expressed according to the different customs of the several laboratories is here presented in a uniform series of charts and tables suitable for the use of designing engineers and for purposes of general reference.

It is a well-known fact that the results obtained in different laboratories, because of their individual methods of testing, are not strictly comparable, even if proper scale corrections for size of model and speed of test are supplied. It is, therefore, unwise to compare too closely the coefficients of two wing sections tested in different laboratories. Tests of different wing sections from the same source, however, may be relied on to give true relative values.

The absolute system of coefficients has been used, since it is though by the National Advisory Committee for Aeronautics that this system is the one most suited for international use and yet it is one from which a desired transformation can be easily made. For this purpose a set of transformation constants is given.

Each airfoil section is given a reference number, and the test data are presented in the form of curves from which the coefficients can be read with sufficient accuracy for designing purposes. The dimensions of the profile of each section are given at various stations along the chord in per cent of the chord length, the latter also serving as the datum line. The shape of the section is also shown with reasonable accuracy in order to enable one to more clearly visualize the section under consideration, the outside of the heavy line representing the profile.

The authority for the results here presented is given as the name of the laboratory at which the experiments were conducted, as explained under abbreviations, with the size of model, wind velocity, and year of test.

Report No. 316, entitled "Tables for Pressure of Air on Coming to Rest from Various Speeds," by A. F. Zahm and F. A. Loudon, construction department, Washington Navy Yard.

In Technical Report No. 247 of the National Advisory Committee for Aeronautics theoretical formulas are given from which was computed a table for the pressure of air on coming to rest from various speeds, such as those of aircraft and propeller blades. In that report, the table gave incompressible and adiabatic stop pressures of air for even-speed intervals in miles per hour and for some even-speed intervals in knots per hour. Table II of the present report extends the above-mentioned table by including the stop pressures of air for even-speed intervals in miles per hour, feet per second, knots per hour, kilometers per hour, and meters per second. The pressure values in Table II are also more exact than the values given in the previous table.

To furnish the aeronautical engineer with ready numerical formulas for finding the pressure of air on coming to rest, Table I has been derived for the standard values specified below it. This table first presents the theoretical pressure-speed formulas and their working forms in C. G. S. units as given in N. A. C. A. Technical Report No. 247, then furnishes additional working formulas for several special units of speed.

Report No. 317, entitled "Wind Tunnel Tests on a Series of Wing Models through a Large Angle of Attack Range. Part I. Force Tests," by Montgomery Knight and Carl J. Wenzinger, National Advisory Committee for Aeronautics.

This investigation covers force tests through a large range of angle of attack on a series of monoplane and biplane wing models. The tests were conducted in the atmospheric wind tunnel of the National Advisory Committee for Aeronautics. The models were arranged in such a manner as to make possible a determination of the effects of variations in tip shape, aspect ratio, flap setting, stagger, gap, decalage, sweep back, and airfoil profile. The arrangements represented most of the types of wing systems in use on modern airplanes.

The effect of each variable is illustrated by means of groups of curves. In addition, there are included approximate autorotational characteristics in the form of calculated ranges of "rotary instability."

A correction for blocking in this tunnel which applies to monoplanes at large angles of attack has been developed, and is given in an appendix.

Report No. 318, entitled "Speed and Deceleration Trials of U. S. S. *Los Angeles*," by S. J. De France, National Advisory Committee for Aeronautics, and C. P. Burgess, Bureau of Aeronautics, Navy Department.

The trials reported herein were instigated by the Bureau of Aeronautics of the Navy Department for the purpose of determining accurately the speed and resistance of the U. S. S. *Los Angeles* with and without water recovery apparatus, and to clear up the apparent discrepancies between the speeds attained in service and in the original trials in Germany.

The trials proved very conclusively that the water-recovery apparatus increases the resistance about 20 per cent, which is serious, and shows the importance of developing a type of recovery having less resistance.

Between the American and German speed trials without water recovery there remains an unexplained discrepancy of nearly 6 per cent in speed at a given rate of engine revolutions.

Warping of the propeller blades and small cumulative errors of observation seem the most probable causes of the discrepancy.

It was found that the customary resistance coefficients C are 0.0242 and 0.0293 without and with the water-recovery apparatus, respectively. The corresponding values of the propulsive coefficient K are 56.7 and 44.6. If there is any error in these figures, it is probably in a slight overestimate of C and an underestimate of K . The maximum errors are almost certainly less than 5 per cent.

No scale effect was detected indicating variation of C with respect to velocity.

Report No. 319, entitled "Aerodynamic Characteristics of Twenty-Four Airfoils at High Speeds," by L. J. Briggs and H. L. Dryden, Bureau of Standards.

The aerodynamic characteristics of 24 airfoils are given for speeds of 0.5, 0.65, 0.8, 0.95, and 1.08 times the speed of sound, as measured in an open-jet air stream 2 inches in diameter, using models of 1-inch chord. The 24 airfoils belong to four general groups. The first is the standard R. A. F. family in general use by the Army and Navy for propeller design, the members of the family differing only in thickness. This family is represented by nine members ranging in thickness from 0.04 to 0.20 inch. The second group consists of five members of the Clark Y family, the members of the family again differing only in thickness. The third group, comprising six members, is a second R. A. F. family in which the position of the maximum ordinate is varied. Combined with two members of the first R. A. F. family, this group represents a variation of maximum ordinate position from 30 to 60 per cent of the chord in two camber ratios, 0.08 and 0.16. The fourth group consists of three geometrical forms, a flat plate, a wedge, and a segment of a right circular cylinder. In addition one section used in the Reed metal propeller was included. These measurements form a part of a general program outlined at a conference on propeller research organized by the National Advisory Committee for Aeronautics and the work was carried out with the financial assistance of the committee.

Report No. 320, entitled "The Measurement of Fluctuations of Air Speed by the Hot-Wire Anemometer," by H. L. Dryden and A. M. Kuethe, Bureau of Standards.

The hot-wire anemometer suggests itself as a promising method for measuring the fluctuating air velocities found in turbulent air flow. The only obstacle is the presence of a lag due to the limited energy input which makes even a fairly small wire incapable of following rapid fluctuations with accuracy. This paper gives the theory of the lag and describes an experimental arrangement for compensating for the lag for frequencies up to 100 or more per second when the amplitude of the fluctuation is not too great. An experimental test of the accuracy of compensation and some results obtained with the apparatus in a wind-tunnel air stream are described. While the apparatus is very bulky in its present form, it is believed possible to develop a more portable arrangement.

Report No. 321, entitled "Fuel Vapor Pressures and the Relation of Vapor Pressure to the Preparation of Fuel for Combustion in Fuel Injection Engines," by William F. Joachim and A. M. Rothrock, National Advisory Committee for Aeronautics.

This investigation on the vapor pressures of fuels was conducted at the Langley Memorial Aeronautical Laboratory at Langley Field, Va., in connection with the general research on combustion in fuel injection engines. The purpose of the investigation was to study the effects of high temperatures such as exist during the first stages of injection on the vapor pressures of several fuels and certain fuel mixtures, and the relation of these vapor pressures to the preparation of the fuel for combustion in high-speed fuel injection engines.

Report No. 322, entitled "Investigation of Air Flow in Open-Throat Wind Tunnels," by Eastman N. Jacobs, National Advisory Committee for Aeronautics.

Tests were conducted on the 6-inch wind tunnel of the National Advisory Committee for Aeronautics during May and June, 1928, to form a part of a research on open-throat wind

tunnels. The primary object of this part of the research was to study a type of air pulsation which has been encountered in open-throat tunnels, and to find the most satisfactory means of eliminating such pulsations.

In order to do this it was necessary to study the effects of different variables on all of the important characteristics of the tunnel. This paper gives not only the results of the study of air pulsations and methods of eliminating them, but also the effects of changing the exit-cone diameter and flare, and the effects of air leakage from the return passage.

It was found that the air pulsations in the 6-inch wind tunnel could be practically eliminated by using a moderately large flare on the exit cone in conjunction with leakage introduced by cutting holes in the exit cone somewhat aft of its minimum diameter.

Report No. 323, entitled "Flow and Force Equations for a Body Revolving in a Fluid," by A. F. Zahm, construction department, Washington Navy Yard.

This report, submitted to the National Advisory Committee for Aeronautics for publication, is a slightly revised form of United States Navy Aerodynamical Laboratory Report No. 380, completed for the Bureau of Aeronautics in November, 1928. The diagrams and tables were prepared by Mr. F. A. Loudon; the measurements given in Tables IX to XI were made for this paper by Mr. R. H. Smith, both members of the aeronautics staff.

Part I gives a general method for finding the steady-flow velocity relative to a body in plane curvilinear motion, whence the pressure is found by Bernoulli's energy principle. Integration of the pressure supplies basic formulas for the zonal forces and moments on the revolving body.

Part II, applying this steady-flow method, finds the velocity and pressure at all points of the flow inside and outside an ellipsoid and some of its limiting forms, and graphs those quantities for the latter forms. In some useful cases experimental pressures are plotted for comparison with theoretical.

Part III finds the pressure, and thence the zonal force and moment, on hulls in plane curvilinear flight.

Part IV derives general equations for the resultant fluid forces and moments on trisymmetrical bodies moving through a perfect fluid, and in some cases compares the moment values with those found for bodies moving in air.

Part V furnishes ready formulas for potential coefficients and inertia coefficients for an ellipsoid and its limiting forms. Thence are derived tables giving numerical values of those coefficients for a comprehensive range of shapes.

Report No. 324, entitled "Flight Tests on U. S. S. *Los Angeles*. Part I. Full Scale Pressure Distribution Investigation," by S. J. De France, National Advisory Committee for Aeronautics.

The investigation reported herein was conducted by the National Advisory Committee for Aeronautics at the request of and in conjunction with the Bureau of Aeronautics, Navy Department. The purpose was primarily to obtain simultaneous data on the loads and stresses experienced in flight by the U. S. S. *Los Angeles*, which could be used in rigid airship structure design. A secondary object of the investigation was to determine the turning and drag characteristics of the airship. The stress investigation was conducted by the Navy Department.

The aerodynamic loading was obtained by measuring the pressure at 95 locations on the tail surfaces, 54 on the hull, and 5 on the passenger car. These measurements were made during a series of maneuvers consisting of turns and reversals in smooth air and during a cruise in rough air which was just short of squall proportions.

The results of the pressure measurements on the hull indicate that the forces on the forebody of an airship are relatively small. The tail surface measurements show conclusively that the forces caused by gusts are much greater than those caused by horizontal maneuvers. In this investigation the tail surface loadings caused by gusts closely approached the designed loads of the tail structure.

The turning and drag characteristics will be reported in separate papers.

Report No. 325, entitled "Flight Tests on U. S. S. *Los Angeles*. Part II. Stress and Strength Determination," by C. P. Burgess, Bureau of Aeronautics, Navy Department.

The tests described in this report furnished data on the actual aerodynamic forces, and the resulting stresses and bending moments in the hull of the U. S. S. *Los Angeles* during as severe still-air maneuvers as the airship would normally be subjected to, and in straight flight during as rough air as is likely to occur in service, short of squall or storm conditions. The maximum stresses were found to be within the limits provided for in accepted practice in airship design. Normal flight in rough air was shown to produce forces and stresses about twice as great as the most severe still-air maneuvers. No light was thrown upon the forces which might occur in extreme or exceptional conditions, such as the storm which destroyed the *Shenandoah*.

The transverse aerodynamic forces on the hull proper were found to be small and irregular. Owing to the necessity of conserving helium, it was impossible to fly the airship in a condition of large excess of buoyancy or weight in order to determine the air pressure distribution at a fixed angle of pitch. However, there is every reason to believe that in that condition the forces on the actual airship are as close to the wind-tunnel results as can be determined by present type of pressure-measuring apparatus.

It is considered that the most important data obtained are the coefficients of tail-surface forces and hull-bending moments. These are tabulated in this report.

Report No. 326, entitled "Tests of Five Metal Model Propellers with Various Pitch Distributions in a Free Wind Stream and in Combination with a Model VE-7 Fuselage," by E. P. Lesley and Elliott G. Reid, Stanford University.

This report describes the tests of five adjustable blade metal model propellers both in a free wind stream and in combination with a model fuselage with stub wings, which were conducted at Stanford University under research authorization of the National Advisory Committee for Aeronautics. The propellers are of the same form and cross section but have variations in radial distributions of pitch. By making a survey of the radial distribution of air velocity through the propeller plane of the model fuselage it is found that this velocity varies from zero at the hub center to approximately free stream velocity at the blade tip.

The tests show that the efficiency of a propeller when operating in the presence of the airplane is, over the working range, generally less than when operating in a free wind stream, but that a propeller with a radial distribution of pitch of the same nature as the radial distribution of air velocity through the propeller plane suffers the smallest loss in efficiency.

Report No. 327, entitled "The Effect of Supercharger Capacity on Engine and Airplane Performance," by O. W. Schey and W. D. Gove, National Advisory Committee for Aeronautics.

Supercharging has already demonstrated its value as a means of improving the performance of an airplane at moderate and high altitudes. In order to obtain a maximum increase in the performance of an airplane designed to meet definite service requirements, it is necessary that a supercharger of the proper capacity be selected.

The effect of different supercharger capacities on the performance of an airplane and its engine was investigated by the staff of the National Advisory Committee for Aeronautics at Langley Field, Va. The tests were conducted on a DH-4 M-2 airplane powered with a Liberty 12 engine. In this investigation four supercharger capacities, obtained by driving a Roots type supercharger at 1.615, 1.957, 2.4, and 3 times engine speed, were used to maintain sea-level pressure at the carburetor to altitudes of 7,000, 11,500, 17,000, and 22,000 feet, respectively.

The performance of the airplane in climb and in level flight was determined for each of the four supercharger drive ratios and for the unsupercharged condition. The engine power was measured during these tests by means of a calibrated propeller.

Although the results of this investigation are not conducive to general conclusions as to the proper capacity or type of supercharger for use with all types of airplanes, the information collected on the variation with altitude and supercharger capacity of such factors as carburetor air temperatures, power required to drive the supercharger, and the net engine power is of value

as a guide in the selection of the most suitable supercharger capacity for airplanes having different performance characteristics than those of the one tested.

Several interesting conclusions pertaining to the effect of the capacity of a Roots type supercharger on the performance of this particular airplane have been drawn from the results of these tests.

It was found that very little sacrifice in sea-level performance was experienced with the larger supercharger drive ratios as compared with performance obtained when using the smaller drive ratios.

The results indicate that further increase in supercharger capacity over that obtained when using the 3:1 drive ratio would give a slight increase in ceiling and in high-altitude performance, but would considerably impair the performance for an appreciable distance below the critical altitude.

As the supercharger capacity was increased, the height at which sea-level high speeds could be equaled or improved became a larger percentage of the maximum height of operation of the airplane.

Report No. 323, entitled "Water Pressure Distribution on a Twin-Float Seaplane," by F. L. Thompson, National Advisory Committee for Aeronautics.

The investigation reported herein was conducted by the National Advisory Committee for Aeronautics at the request of the Bureau of Aeronautics, Navy Department. This is the second of a series of investigations to determine water-pressure distribution on various types of seaplane floats and hulls, and was conducted on a twin-float seaplane. It consisted of measuring water pressures and accelerations on a TS-1 seaplane during numerous landing and taxiing maneuvers at various speeds and angles.

The results of this investigation show that water pressures as great as 10 pounds per square inch may occur at the step in various maneuvers and that pressures of approximately the same magnitude occur at the stern and near the bow in hard pancake landings with the stern well down. At other parts of the float the pressures are less and are usually zero or slightly negative for some distance abaft the step. A maximum negative pressure of 0.87 pound per square inch was measured immediately abaft the step. The maximum positive pressures have a duration of approximately one-twentieth to one one-hundredth second at any given location and are distributed over a very limited area at any particular instant. The greatest accelerations measured normal to the thrust line at the C. G. occurred in pancake landings, and a maximum of 4.3 *g* was recorded. Approximate load-distribution curves for the worst landing conditions are derived from the data obtained to serve as a guide in static tests.

Report No. 329, entitled "The Torsional Strength of Wings," by C. P. Burgess, Bureau of Aeronautics, Navy Department.

This report is submitted to the National Advisory Committee for Aeronautics by the Bureau of Aeronautics, Navy Department. It describes a simple method for calculating the position of the elastic axis of a wing structure having any number of spars. It is shown that strong drag bracing near the top and bottom of a wing greatly increases the torsional strength. An analytical procedure for finding the contribution of the drag bracing to the torsional strength and stiffness is described, based upon the principle of least work, and involving only one unknown quantity.

The validity of the new method of analysis is tested by applying it to a two-fifths scale model of the large steel tubular 3-spar wing of the Huff-Daland XHB monoplane. The calculated stresses are checked by comparison with the strains observed by means of electric telemeter strain gages secured to the spars during sand load tests in the static testing laboratory of the Army Air Service engineering division at Dayton, Ohio.

The torsional strength of a wing determines very largely the distribution of air forces upon it, and the tendency to flutter. Insufficient torsional strength produces washin or an increasing angle of attack toward the wing tips in the high incidence condition, further increasing the load on the front spar in the condition which is already the most severe. Conversely, torsional yield-

ing in the low incidence and nose-dive conditions produce washout of the wing shape and may exaggerate the critical condition for the rear spar.

The mathematical theory of the forces producing flutter is not yet sufficiently far advanced to determine by direct calculation the critical air speed at which flutter will commence. Comparison with successful practice must still be the principal criterion upon which to judge the adequacy of the torsional strength of a new design of wing. Obviously this comparison will be greatly facilitated by use of a coefficient of torsional rigidity including the principal factors in torsional strengths. A coefficient for comparing the torsional rigidity of different wings is derived in this report.

Report No. 330, entitled "Experimental and Analytical Determination of the Motion of Hydraulically Operated Valve Stems in Oil Engine Injection Systems," by A. G. Gelalles and A. M. Rothrock, National Advisory Committee for Aeronautics.

This research on the pressure variations in the injection system of the N. A. C. A. spray photography equipment and on the effects of these variations on the motion of the timing valve stem was undertaken in connection with the study of fuel injection systems for high-speed oil engines. The spray photography equipment employed for these tests consists of a fuel injection system for producing an oil spray, an electrical spark system for illuminating the spray, and a photographic camera for recording its development. The fuel injection system contains a high-pressure hand pump for producing the injection pressures, an oil reservoir for maintaining the pressures of the fuel during the injection, a timing valve for timing the start of the oil spray, an injection valve for atomizing the oil, and a by-pass valve for controlling the cut-off of the spray. Additions were made to the apparatus in order to record the motion of the timing valve stem photographically.

The timing valve stem was held against its seat by a helical spring so adjusted that the total hydraulic force on the stem actuated it immediately after it had been mechanically lifted from its seat. The lift of the stem was recorded photographically to determine the effects of injection tubes 7 inches and 43 inches long. The pressure variations at the seat and in the injection valve tubes were analyzed and the lifts of the stem for both tubes computed from the analysis and compared with the experimental records.

The calculations indicate that the hydraulic pressure at the timing valve seat was rising at a rate of 350,000,000 pounds per square inch per second when the timing valve stem had been lifted 0.004 inch, and that the hydraulic pressure throughout the tube did not approximate that of the oil in the reservoir until 0.0028 second after the timing valve started to open with the 43-inch tube and 0.003 second with the 7-inch tube. The calculations and experiments indicate that after the by-pass valve started to open the hydraulic pressure in the tube dropped to the closing pressure of the timing valve in 0.0015 second with the 43-inch tube and in 0.0004 second with the 7-inch tube. The photographic records of the stem motion show that the stem reached the maximum lift approximately 0.001 second later with the 43-inch tube than with the 7-inch tube, and that the valve stem seated 0.0005 second later with the 43-inch tube than with the 7-inch tube.

The general equation for the motion of the stem of a spring-loaded valve when the motion is controlled by hydraulic pressure is

$$f = \lambda s + m \frac{d^2 s}{dt^2}$$

where

f = hydraulic force on the stem at any time t seconds after the start of motion plus or minus the friction of the stem in its guide,

λ = scale of spring,

s = compression of the spring at any time t seconds after the start of motion,

m = mass of moving parts.

The methods of analysis of the pressure variations and the general equation for the motion of the spring-loaded stem for the timing valve are applicable to a spring-loaded automatic injec-

tion valve, and in general to all hydraulically operated valves. A sample calculation for a spring-loaded automatic injection valve is included.

Report No. 331, entitled "Collection of Wind-Tunnel Data on Commonly Used Wing Sections," by F. A. Loudon, Bureau of Aeronautics, Navy Department.

This report was prepared at the request of the National Advisory Committee for Aeronautics in the Bureau of Aeronautics of the Navy Department in order to group in a uniform manner the aerodynamic properties of commonly used wing sections as determined from tests in various wind tunnels.

The data have been collected from reports of a number of laboratories. Where necessary, transformation has been made to the absolute system of coefficients and tunnel wall interference corrections have been applied. Tables and graphs present the data in the various forms useful to the engineer in the selection of a wing section.

Report No. 332, entitled "The Effect of Cowling on Cylinder Temperatures and Performance of a Wright J-5 Engine," by Oscar W. Schey and Arnold E. Biermann, National Advisory Committee for Aeronautics.

This report presents the results of tests conducted by the staff of the National Advisory Committee for Aeronautics to determine the effect of different amounts and kinds of cowling on the performance and cylinder temperatures of a standard Wright J-5 engine. These tests were conducted in conjunction with drag and propeller tests in which the same cowlings were used.

The engine was mounted in the nose of a cabin fuselage and placed in the air stream of the committee's 20-foot propeller research tunnel, which is located at the Langley Memorial Aeronautical Laboratory. The power was measured by means of a torque dynamometer placed within the fuselage. Sixty-nine iron-constantan thermocouples and three recording pyrometers were used for obtaining the cylinder temperature measurements.

Four different cowlings were investigated, in tests herein reported, varying from the one extreme of no cowling on the engine to the other extreme of the engine completely cowed and the cooling air flowing inside the cowling through an opening in the nose and out through an annular opening at the rear of the engine. Each cowling was tested at air speeds of approximately 60, 80, and 100 miles per hour.

For the conventional type of engine cowling the results of these tests indicate that increasing the amount of cowling has the advantage of reducing the drag, but the disadvantage of increasing the cylinder barrel temperatures. Satisfactory cooling was obtained with the conventional cowling that covered 35 per cent of the cylinder cooling area. With the conventional cowling that covered 73 per cent of the cooling area the cylinder temperatures were excessive even though a large portion of the cooling air was permitted to flow inside the cowling through slots in the front of the cowling.

For the cabin fuselage with the N. A. C. A. cowling, which completely inclosed the engine and took in all of the cooling air through a 28-inch diameter opening in the nose, the drag was reduced 40 per cent at 100 miles per hour, as compared with the same unit with no cowling on the engine. The mean temperatures of the spark-plug boss and the cylinder head were slightly reduced for the same test conditions, but the barrel temperatures were increased.

The spark-plug boss temperatures, as used by many manufacturers, are a valuable indication of engine performance, but they alone should not be used as a criterion to determine the amount an engine can be cowed, since the barrel temperatures do not vary in parallel with them.

Report No. 333, entitled "Full-Scale Turning Characteristics of the U. S. S. *Los Angeles*," by F. L. Thompson, National Advisory Committee for Aeronautics.

This paper presents a description of the method employed and results obtained in full-scale turning trials on the rigid airship U. S. S. *Los Angeles*. This investigation was requested by the Bureau of Aeronautics, Navy Department, and was carried out in conjunction with pressure distribution and stress investigation. The pressure and turning investigations were

conducted by representatives of the National Advisory Committee for Aeronautics and the stress investigation by the Bureau of Aeronautics.

The results of this investigation are not sufficiently comprehensive to permit definite conclusions as to the variation of turning characteristics with changes in speed and rudder angle. They indicate, however, that the turning radius compares favorably with that for other large airships, that the radius is independent of the speed, that the position of the point of zero yaw is nearly independent of the rudder angle and air speed, and that a theoretical criterion for stability in a turn gives a close approximation to actuality. The method of determining turning characteristics by recording instruments aboard the airship appear to be satisfactory, with the exception that a better method of determining the small angular velocities of airships should be devised.

Report No. 334, entitled "The Torsion of Members Having Sections Common in Aircraft Construction," by George W. Trayer and H. W. March, Forest Products Laboratory.

Structural members designed for pure torsion are usually made with circular, elliptical, rectangular, or other regular cross sections that have already yielded to direct mathematical treatment as regards torsion. However, members designed primarily for thrust or bending and consequently as a usual thing of irregular section are subjected to torsion also, and under certain conditions they may fail by buckling and twisting through lack of sufficient torsional rigidity. In order to design against the possibility of such failure in thin deep beams or in compression members with thin, outstanding parts, we must be able to calculate their torsional rigidity. Such sections as I, T, L, and U have not been brought within the range of mathematical analysis, and up to a few years ago the engineer had practically nothing on which to base an estimate of the torsional strength and rigidity of rods of irregular section. This publication presents the results of investigations of the torsion of structural members undertaken by the Forest Products Laboratory and financed by the Bureau of Aeronautics, Navy Department, under the national defense act.

Within recent years a great variety of approximate torsion formulas and drafting-room processes have been advocated. In some of these, especially where mathematical considerations are involved, the results are extremely complex and are not generally intelligible to engineers. The principal object of the investigation was to determine by experiment and theoretical investigation how accurate the more common of these formulas are and on what assumptions they are founded and, if none of the proposed methods proved to be reasonably accurate in practice, to produce simple, practical formulas from reasonably correct assumptions, backed by experiment. A second object was to collect in readily accessible form the most useful of known results for the more common sections.

This report reviews informally the fundamental theory of torsion and shows how the more common formulas are developed from it. Formulas for all the important solid sections that have yielded to mathematical treatment are listed. Then follows a discussion of the torsion of tubular rods with formulas both rigorous and approximate.

It is shown by a series of tests of prisms of simple section that wood is a suitable material for the experimental investigation of the torsion problem. Accordingly wood was used for the experiments on full-sized members because of the ease with which it can be worked into different shapes and because of its low torsional stiffness. The possible effect of different moduli of rigidity in radial and tangential planes was investigated mathematically, and the effects of rate of loading and of moisture content were determined experimentally. Furthermore, soap films were used in order to take advantage of a mathematical similarity that exists between the torsion problem and the problem of finding the deflection of a thin membrane under pressure. The analogy is discussed in detail in the report.

Our experimental work with beams of irregular sections that have not yielded to mathematical treatment is described. From these experiments and certain mathematical considerations empirical formulas are set up for irregular sections whose component parts are rectangles.

Report No. 335, entitled "Aerodynamic Theory and Test of Strut Forms--Part II," by R. H. Smith, aerodynamical laboratory, Bureau of Construction and Repair, Navy Department.

This report, submitted to the National Advisory Committee for Aeronautics for publication, presents the second of two studies under the same title. In this part five theoretical struts are developed from distributed sources and sinks and constructed for pressure and resistance tests in a wind tunnel. The surface pressures for symmetrical inviscid flow are computed for each strut from theory and compared with those found by experiment. The theoretical and experimental pressures are found to agree quantitatively near the bow, only qualitatively over the suction range, the experimental suction being uniformly a little low and not at all near the stern.

This study is the strut sequel to Fuhrmann's research on airship forms, the one being a study in two dimensions, the other in three. A comparison of results indicates that the agreement between theory and experiment is somewhat better for bodies of revolution than for cylinders when both are shaped for slight resistance. The consistent deficiency of the experimental suction which is found in the case of struts was not found in the case of airships, for which the experimental suction was sometimes above, sometimes below their theoretical values.

Along with these five theoretical struts were made three empirical struts of high repute, the British strut given in Reports and Memoranda No. 183, the German strut No. 53, and the United States Navy No. 2, and all eight tested for total resistance. Of the five theoretical struts, No. I excels as a fairing, No. V as a strut. No. V and the United States Navy No. 2 have about equal merit as struts, with the German No. 53 a close second and the British a poor third, the relative merits being 100, 103, and 112, respectively, of Reynolds Number 12×10^4 .

Report No. 336, entitled "Tests of Large Airfoils in the Propeller Research Tunnel, Including Two with Corrugated Surfaces," by Donald H. Wood, National Advisory Committee for Aeronautics.

This report gives the results of the tests of seven 2 by 12 foot airfoils (Clark Y, smooth and corrugated, Göttingen 398, N. A. C. A. M-6, and N. A. C. A. 84). The tests were made in the propeller research tunnel of the National Advisory Committee for Aeronautics at Reynolds Numbers up to 2,000,000. The Clark Y airfoil was tested with 3° of surface smoothness.

The effect of small variations of smoothness of an airfoil is shown to be negligible. Corrugating the surface causes a flattening of the lift curve at the burble point and an increase in drag at small flying angles.

LIST OF TECHNICAL NOTES ISSUED DURING THE PAST YEAR

- | | |
|------|--|
| No. | |
| 299. | The Effect of Fillets Between Wings and Fuselage on the Drag and Propulsive Efficiency of an Airplane. By Melvin N. Gough. |
| 300. | The Variation in Pressures in the Cockpit of an Airplane in Flight. By Thomas Carroll and William H. McAvoy. |
| 301. | Drag and Cooling with Various Forms of Cowling for a Whirlwind Engine in a Cabin Fuselage. By Fred E. Weick. |
| 302. | A New Method for the Prediction of Airplane Performance. By E. P. Lesley and E. G. Reid. |
| 303. | Condensed Data on the Aircraft Engines of the World. Compiled by C. S. Fliedner. |
| 304. | Corrosion Embrittlement of Duralumin. V. Results of Weather-Exposure Tests. By Henry S. Rawdon. |
| 305. | Corrosion Embrittlement of Duralumin. VI. The Effect of Corrosion, Accompanied by Stress on the Tensile Properties of Sheet Duralumin. By Henry S. Rawdon. |
| 306. | Curves Showing Column Strength of Steel and Duralumin Tubing. By Orrin E. Ross. |
| 307. | Strength of Tubing Under Combined Axial and Transverse Loading. By L. B. Tuckerman, S. N. Petrenko, and C. D. Johnson. |
| 308. | Pressure Distribution on a Slotted R. A. F. 31 Airfoil in the Variable Density Wind Tunnel. By Eastman N. Jacobs. |
| 309. | Correcting Engine Tests for Humidity. By Donald B. Brooks. |

- No.
 310. Wind Tunnel Pressure Distribution Tests on a Series of Biplane Wing Models. Part I: Effects of Changes in Stagger and Gap. By Montgomery Knight and Richard W. Noyes.
 311. The Use of Wheel Brakes on Airplanes. By Thomas Carroll and Smith J. De France.
 312. Sphere Drag Tests in the Variable Density Wind Tunnel. By Eastman N. Jacobs.
 313. The Formation of Ice upon Airplanes in Flight. By Thomas Carroll and William H. McAvoy.
 314. Spiral Tendency in Blind Flying. By Thomas Carroll and William H. McAvoy.
 315. Viscosity of Diesel Engine Fuel Oil Under Pressure. By Mayo D. Hersey.
 316. Wind Tunnel Tests on a Model of a Monoplane Wing with Floating Ailerons. By Montgomery Knight and Millard J. Bamber.
 317. Tests of Four Racing Type Airfoils in the Twenty-Foot Propeller Research Tunnel. By Fred E. Weick.
 318. Full Scale Investigation of the Drag of a Wing Radiator. By Fred E. Weick.
 319. Some Experiments on Autorotation of an Airfoil. By Shatswell Ober.

LIST OF TECHNICAL MEMORANDUMS ISSUED DURING THE PAST YEAR

482. Ignition and Combustion Phenomena in Diesel Engines. By F. Sass. Translation from *Zeitschrift des Vereines deutscher Ingenieure*, September 10, 1927.
 483. Ignition Points and Combustion Reactions in Diesel Engines. Part I. By J. Tausz and F. Schulte. Communication from the Petroleum Research Laboratory of the Institute of Applied Chemistry, Technical High School, Karlsruhe.
 484. Ignition Points and Combustion Reactions in Diesel Engines. Part II. By J. Tausz and F. Schulte. Communication from the Petroleum Research Laboratory of the Institute of Applied Chemistry, Technical High School, Karlsruhe.
 485. Research on the Control of Airplanes. By Melvill Jones. From *Nature*, May 12, 1928. Lecture delivered at the Royal Institution, February 10, 1928.
 486. Tank Tests of Twin Seaplane Floats. By H. Herrmann, G. Kempf, and H. Kloess. Translation from *Luftfahrtforschung*, January 3, 1928.
 487. The Constructional Design of Metal Flying-Boat Hulls, Part I. Workshop Notes on the Building of Metal Hulls, Part II. By M. Langley. From *The Aeroplane*, March 28, and July 25, 1928.
 488. Determination of the Air Forces and Moments Produced by the Ailerons of an Airplane. By C. Wieselsberger and T. Asano. Translation from *Zeitschrift für Flugtechnik und Motorluftschiffahrt*, July 14, 1928.
 489. On the Take-Off of Heavily Loaded Airplanes. By Louis Breguet. Translation from *La Revue Scientifique*, No. 12, 1927.
 490. Structures of Thin Sheet Metal, Their Design and Construction. By Herbert Wagner. Translation of preprint of a paper read at seventeenth meeting of the *Wissenschaftliche Gesellschaft für Luftfahrt*, at Danzig, Germany, June 2-5, 1928.
 491. Propeller Problems. By A. Betz. Translation of reprint from *Zeitschrift für angewandte Mathematik und Mechanik*, November, 1927.
 492. Influence of Fuselage on Propeller Design. By Theodor Troller. Translation from *Zeitschrift für Flugtechnik und Motorluftschiffahrt*, July 28, 1928.
 493. Aerodynamic Characteristics of Thin Empirical Profiles and Their Application to the Tail Surfaces and Ailerons of Airplanes. By A. Toussaint and E. Carafoli. Translation from *L'Aerophile*, June, 1928.
 494. "Safety" Fuels for Aircraft Engines. By A. Grebel. Translation from *Memoires et compte rendu des Travaux de la Societe des Ingenieurs Civils de France*, July-August, 1927.
 495. Device for the Automatic Control of Airplanes. By Alfred Gradenwitz. (Drexler control.) Translation from *Der Motorwagen*, March 31, 1928.
 496. Photogrammetric Take-Off and Landing Measurements. By Bruno Spieweck. Translation from *Yearbook of the Wissenschaftlichen Gesellschaft für Luftfahrt*, December, 1926.

- No.
497. Effect of Oxygen on the Ignition of Liquid Fuels. By H. Pahl. Translation from *Zeitschrift des Vereines deutscher Ingenieure*, June 16, 1928.
498. Fluttering of the Tail Surfaces of an Airplane and the Means for Its Prevention. By F. N. Scheubel. Translation from *Yearbook of the Wissenschaftlichen Gesellschaft für Luftfahrt*, December, 1926.
499. Danger of Ice Formation on Airplanes. By W. Kopp. Translation from reports of the German Aeronautical Weather Service, Volume I, No. 25, Lindenberg Aeronautical Observatory, Berlin.
500. Remarks on Airplane Struts and Girders Under Compressive and Bending Stresses. Index Values. By Herbert Wagner. Translation from *Zeitschrift für Flugtechnik und Motorluftschiffahrt*, June 14, 1928.
501. Effect of Intake Pipe on the Volumetric Efficiency of an Internal Combustion Engine. By Antonio Capetti. Translation from *Anali della R. Scuola d'Ingegneria di Padova*, Volume VI, No. 4, December, 1927. Paper read at the International Motor Congress, Padova, June, 1927.
502. Analysis of Flight and Wind-Tunnel Tests on Udet Airplanes with Reference to Spinning Characteristics. By H. Herrmann. Translation from *Zeitschrift für Flugtechnik und Motorluftschiffahrt*, January 14, 1929.
503. Effect of Stressed Covering on Strength of Internal Girders of a Wing. By H. Tellers. Translation from *Yearbook of the Wissenschaftlichen Gesellschaft für Luftfahrt*, 1927.
504. Mechanical Control of Airplanes. By H. Boykow. Translation from *Yearbook of the Wissenschaftlichen Gesellschaft für Luftfahrt*, 1928.
505. Impact Waves and Detonation. Part I. By R. Becker. Translation from *Zeitschrift für Physik*, Volume VIII, 1922.
506. Impact Waves and Detonation. Part II. By R. Becker. Translation from *Zeitschrift für Physik*, Volume VIII, 1922.
507. Landing and Braking of Airplanes. By Louis Breguet. Translation from *La Chronique des Avions Breguet*, supplements to Nos. 8 and 9, 1928.
508. Aeromechanical Experimentation. (Wind-tunnel Tests.) By R. Katzmayer. Translation from *Luftflotten*, 1928.
509. The Transformation of Heat in an Engine. By Kurt Neumann. Translation from *Geiger and Scheel's Handbuch der Physik*, Chapter 9, Volume XI, 1926.
510. Theoretical Investigation of the Effect of the Ailerons on the Wing of an Airplane. By C. Wieselsberger. Translation from report of the Aeronautical Research Institute, Tokyo Imperial University, No. 30, Volume II, 16, December, 1927.
511. On the Strength of Box Type Fuselages. By J. Mathar. Translation from *Yearbook of the Wissenschaftliche Gesellschaft für Luftfahrt*, 1928.
512. Technical Report of the 1928 Rhön Soaring Flight Contest. By A. Lippisch. Translation from *Zeitschrift für Flugtechnik und Motorluftschiffahrt*, February 14, 1929.
513. Contribution to the Technique of Landing Large Airships. By O. Krell. Part I. Translation from *Zeitschrift für Flugtechnik und Motorluftschiffahrt*, September 28, 1928.
514. Contribution to the Technique of Landing Large Airships. By O. Krell. Part II. Translation from *Zeitschrift für Flugtechnik und Motorluftschiffahrt*, September 28, 1928.
515. Materials and Methods of Construction in Light Structures. By Adolf Rohrbach. Translation from *Yearbook of the Wissenschaftliche Gesellschaft für Luftfahrt*, December, 1926.
516. Crank Case Scavenging of Two-Stroke-Cycle Engines. By Hans List. Translation from *Zeitschrift des Vereines deutscher Ingenieure*, February 16, 1929.
517. Investigation of the Effect of the Fuselage on the Wing of a Low-Wing Monoplane. By H. Muttray. Translation from *Luftfahrtforschung*, June 11, 1928.
518. Investigation of Atomization in Carburetors. By J. Sauter. Translation from *Zeitschrift des Vereines deutscher Ingenieure*, November 3, 1928.
519. Force Measurements on Airplanes. By F. Seewald. Translation from *Zeitschrift für Flugtechnik und Motorluftschiffahrt*, October 7, 1928.

- No.
 520. Torsional Rigidity of Cantilever Wings with Constant Spar and Rib Sections. By Giuseppe Gabrielli. Translation from *Luftfahrtforschung*, June 26, 1928.
 521. Wings with Nozzle-Shaped Slots. By Richard Katzmayer. Translation from *Berichte der Aeromechanischen Versuchsanstalt in Wien*, Volume I, No. 1, 1928.
 522. The Analysis of Aircraft Structures as Space Frameworks. Method Based on the Forces in the Longitudinal Members. By Herbert Wagner. Translation from *Zeitschrift für Flugtechnik und Motorluftschiffahrt*, August 14, 1928.
 523. Autogenous Welding in Airplane Construction. By Ludwig Kuchel. Translation from *Schweissen, Schneiden und Metallspritzen mittels Acetylen*, 1927.
 524. Lualaba as a Material for Airplane Construction. By Paul Brenner. Translation from *Yearbook of the Deutsche Versuchsanstalt für Luftfahrt*, 1928.
 525. Buckling Tests of Light-Metal Tubes. By August Schroeder. Translation from *Yearbook of the Deutsche Versuchsanstalt für Luftfahrt*, 1928.
 526. Metal Construction Development. By H. J. Pollard. Part I: General. Strip Metal Construction—Fuselage. From *Flight*, January 26, and February 23, 1928.
 527. Metal Construction Development. By H. J. Pollard, Part II: Strip Metal Construction—Wing Spars. From *Flight*, March 29 and May 31, 1928.
 528. Metal Construction Development. By H. J. Pollard. Part III: Workshop Practice. Strip Metal Construction—Wing Ribs. From *Flight*, June 21, July 19, October 25, and December 27, 1928.
 529. Metal Construction Development. By H. J. Pollard, Part IV: Moments of Inertia of Thin Corrugated Sections. From *Flight*, April 25, 1929.
 530. Travel of the Center of Pressure of Airfoils Transversely to the Air Stream. By Richard Katzmayer. Translation from *Berichte der Aeromechanischen Versuchsanstalt in Wien*, Volume I, No. 1, 1928.
 531. Welding Rustproof Steels. By W. Hoffman. Translation from *Autogene Metallbearbeitung*, Volume XX, December 15, 1927.
 532. Welding of Stainless Materials. By H. Bull and Lawrence Johnson. From *Industrial Gases*, March and June, 1929.

LIST OF AIRCRAFT CIRCULARS ISSUED DURING THE PAST YEAR

83. The Vickers *Vellore* (British)—A Freight Carrier (Airplane) which Carries a Load Greater than Its Own Weight. From *Flight*, September 6, 1928.
 84. The Caproni Monoplanes *Ca 97* (Italian). Translation from *Bollettino Aeronautico*, May-June, 1928.
 85. The Gloster *Goldfinch* (British)—A Single-Seat Fighter. From *Flight*, October 4, 1928.
 86. Bleriot Combat Monoplane 127 (French). Translation from *Les Ailes*, September 20, 1928.
 87. Villiers 24 Slotted-Wing Airplane (French)—Night Pursuit Sesquiplane. Translation from *L'Aeronautique*, March and April, 1928.
 88. Farman Two-Engine Commercial Biplane *F. 180* (French). Translation from a circular received from Paris office, N. A. C. A., August 3, 1928.
 89. Albessard *Triavion* Airplane (French)—A Two-Seat Tandem Monoplane. By J. Serryer. Translation from *Les Ailes*, September 2, 1926.
 90. The Boulton and Paul *Partridge* (British)—All-Metal Single-Seat Fighter. From *Flight*, December 6, 1928.
 91. The De Havilland D. H. 75 *Hawk Moth* (British)—Cabin Monoplane. From *Flight*, February 7, 1929.
 92. Nieuport-Delage 640 (French)—Commercial High-Wing Monoplane. Translation from manufacturer's circular received from Paris office, N. A. C. A., August 3, 1928.
 93. Morane-Saulnier 180 Light Airplane (French)—A Single-Seat Training Monoplane. By Andre Frachet. Translation from *Les Ailes*, November 22, 1928.
 94. The Blackburn *Bluebird* Mark IV (British)—All-Metal Biplane. From *Flight*, January 17, 1929.

No.

95. The *Westland IV* Commercial Monoplane (British)—Three Cirrus III Engines. From *Flight*, February 28, 1929.
96. The *Potez 33* Military Airplane (French). Translation from *Bulletin Technique des Avions* H. Potez, January, 1929.
97. The *Amiot S. E. C. M. 110 C. 1*—A Single-Seat Pursuit Monoplane. Translation from *Les Ailes*, May 16, 1929.
98. The *Bernard 20 C. 1* (French)—A Single-Seat Pursuit Monoplane. Translation from *L'Aeronautique*, May, 1929.
99. The *Parnall Pipit* (British)—A Single-Seat Ship's Fighter. From *Flight*, June 13, 1929.
100. The *K-47* of the A. B. Flygindustri—An Armored Pursuit Monoplane. By R. Schulz. Translation from *Luftwacht*, May, 1929.
101. The A. B. C. *Robin* (British)—A Single-Seat Cabin Monoplane. From *Flight*, May 30, 1929.
102. The *Fairey III. F* (British)—A General-Purpose Biplane. From a circular issued by The Fairey Aviation Co. (Ltd.), England.

BIBLIOGRAPHY OF AERONAUTICS

During the past year the committee issued bibliographies of aeronautics for the years 1926 and 1927. It has previously issued bibliographies for the years 1909 to 1916, 1917 to 1919, 1920 to 1921, 1922, 1923, 1924, and 1925. A bibliography for the year 1928 is now in the hands of the printer, and should be ready for distribution during the coming year. A bibliography is now being published annually by the committee. All issues of the Bibliography of Aeronautics to date were prepared by Paul Brockett.

Citations of the publications of all nations are included in the language in which the publications originally appeared. The arrangement is in dictionary form, with author and subject entry, and one alphabetical arrangement. Detail in the matter of subject reference has been omitted on account of cost of presentation, but an attempt has been made to give sufficient cross reference to make possible the finding of items in special lines of research.

PART V

SUMMARY OF PROGRESS IN AIRCRAFT DEVELOPMENT

AERODYNAMICS

With an appreciation that the main theoretical foundations of this new science have been laid and that its further advances will be along the lines of extensions of or additions to existing theory, the aeronautical research laboratories in the United States have been largely engaged during the past year with problems relating to aerodynamic safety and efficiency.

In any general survey of the problems studied by the National Advisory Committee for Aeronautics in the past, or the problems to be undertaken in the future, it is highly important that the influence of the immediate technical requirements of air commerce and the military and naval services be recognized. To meet these requirements a large part of the research program of the committee is concerned with problems of immediate technical interest to the services and the industry.

The major problems contemplated or now under investigation are concerned with some phase of the general subject of safety in flight. The most important of these are the studies of spinning, low-speed control, stability, and load distribution under various conditions of flight.

A second group of almost equal importance is concerned with problems of aerodynamic improvement by the reduction of drag. A third group is concerned with problems relating to general design and operation, such as landing and taking off, local loading on wings, propeller characteristics, and the prevention of ice formation.

The problem of spinning is at present considered the most important of all the investigations now being undertaken by the committee. There are two phases of this problem, the prevention of spins from unintentional stalls at low altitude, and the uncontrolled spin generally known as the flat spin. Considerable progress has already been made in the study of this problem and the present research programs call for the intensive study that the importance of this subject justifies.

There follows below a brief summary of the work that has been accomplished during the past year and a reference to future research programs.

Wind tunnels.—The investigation of turbulence undertaken by the Bureau of Standards has yielded information of great value in the interpretation of wind-tunnel data. Many discrepancies formerly observed in tests on the same model in various wind tunnels may now be fully explained. This condition applies particularly to models having a critical Reynolds Number, such as spheres and streamline bodies. Tests have been made in the variable-density wind tunnel in which a given Reynolds Number was obtained from various combinations of model size, wind speed, and air density. These tests show conclusively that within reasonable bounds the Reynolds Number effect is absolutely independent of the values of the component terms. Furthermore, tests on large airfoils made in the propeller research tunnel are found to check very closely with tests at the same Reynolds Number in the variable-density tunnel. It may now be stated with assurance that the validity of the wind tunnel as a method of test is completely proven.

The present wind-tunnel testing program necessarily includes a large amount of work on low-speed control, spinning, interference, and propeller characteristics. Much of this work is now under way in some form or other. However, the main part of the spinning program will be undertaken upon completion of the special vertical wind tunnel, and most of the interference and low-speed control program must await the completion of the full-scale wind tunnel.

Spinning.—The program of wind-tunnel investigations on the problem of spinning included force, pressure distribution, and autorotation torque tests up to 90° angle of attack on models of a wide variety of wing sections. The pressure distribution and force tests have been completed and the results published. During the past year an autorotation dynamometer has been completed and the first of a series of tests is now being made with this equipment. The program provides for the measurement of the pitching and yawing moments as well as the rolling moments.

At the Massachusetts Institute of Technology an investigation was made on the effect of yaw on the autorotation of a monoplane airfoil.

The mass distribution of an airplane is an important factor in its recovery from a spin. The flight research section of the laboratory has completed an apparatus for the accurate measurement of the mass distribution of an airplane, and the moments and ellipsoids of inertia of several military and commercial airplanes have been determined. A study of these inertia data, together with the information as to the type of spin executed by each of these airplanes, indicates that a definite relation exists between the mass distribution and the type of spin. The chief difficulty in definitely determining this relation is the lack of accurate knowledge of the magnitude of the variables that enter into the dynamics of the spin, such as the radius and the rate of rotation. A method for the measurement of these variables in flight has been perfected, and complete data have been obtained on one airplane. From these data the dynamic forces producing and maintaining the spin have been determined. The future program will include the study of a number of types of airplanes, and in particular one airplane which has normal spinning characteristics, and in which the mass distribution will be changed until a flat spin is produced.

Stability.—The stability characteristics of most airplanes are satisfactory below angles of attack of maximum lift, but very few have satisfactory characteristics in stalled flight. In the investigation in the atmospheric wind tunnel of stability in stalled flight, a series of tests has been conducted to determine the effect on stability of twisting a wing and at the same time determine the effect of changing the profile along the span. The investigation showed that both methods gave improved stability characteristics.

Controllability.—A study has been made in the atmospheric wind tunnel of the effectiveness of various types of ailerons, particularly from the standpoint of stalled flight and the spin. It is planned to conduct in the near future a series of flight tests on a special monoplane arranged for the convenient changing of the wings, ailerons, and tail surfaces. In this investigation it is expected that accurate information on the rolling and yawing tendencies of the airplane with various methods of control will be obtained while in stalled flight.

The Bureau of Standards has completed an investigation on the measurement of the rolling and yawing moments produced by ailerons of various chords and spans on 10 by 60 inch models of the Clark Y and U. S. A. 27 airfoil sections. This investigation covers angles of attack up to the stalled position.

In the variable-density wind tunnel a series of pressure-distribution tests on the R.A.F. 30 airfoil with flaps has been completed, and the information obtained in these tests will be of considerable assistance in the study of the effectiveness of ailerons, and also of scale effect.

Maneuverability.—The committee has continued the study of maneuverability, and has carried out a series of tests on two types of pursuit airplanes. The maneuverability of the airplane is determined basically by the flight path obtainable, and during the past year considerable attention has been given to improving the methods for determining the flight path. A report covering the study of the maneuverability of one pursuit airplane has been completed, and a report on the second airplane is in progress.

The future program provides for a study of the maneuverability characteristics of an observation type of airplane and also of a commercial monoplane.

Structural safety.—The major activity of the flight research section of the laboratory has been in connection with the determination of the air loads experienced by airplanes under the various

conditions of flight. The results obtained in the measurement of the load distribution on the wings, tail surfaces, and fuselage of an airplane in all conditions of flight have been studied from the standpoint of the structural designer. This investigation brought out several points of great importance, one of which was the torsional deflection of the wing under load, which results in a change in the load distribution, and another the effect of the inertia loads on the airplane structure. In this investigation accelerometers were placed at the center of gravity, at the wing tips, and in the tail unit. In the measurement of the inertia loads it was found that under certain conditions of flight they combine with the aerodynamic loads to give new maxima.

From this investigation additional information was obtained on the pressure distribution on the tail surfaces of pursuit type airplanes, and on the difference in the loads experienced with control surfaces of thick and thin section. The results obtained on both types of airplanes indicated the necessity for an increase in the design requirements as to tail loads for airplanes which are expected to execute maneuvers at high speeds, and from a study of the results and from conference with the subcommittee on aircraft structures a satisfactory basis has been established for the preparation of design specifications for tail surface loads.

In order to obtain information as to the possible need of modifications in the existing specifications for loading on wing tips, and to develop a wing tip with constant location of the center of pressure, the program for the study of the distribution of air loads on the observation type airplane has been planned so as to include the investigation of the loads on wing tips of various plan forms.

Water-pressure distribution.—The study of the distribution of water pressure on various types of seaplane floats and hulls has been continued. This investigation was first carried out on a single-float and a twin-float seaplane, and has recently been completed on an H-16 flying boat. With the flying boat it was possible to maneuver on rough water, so that the maximum pressures recorded were considerably higher than those obtained on the smaller seaplanes. On the H-16 the maximum pressures were 15 pounds per square inch, as compared with a maximum of approximately 10 pounds per square inch on the floats of lighter seaplanes.

This investigation will be continued during the coming year, and will include the measurement of the deflection of a seaplane float in static test with the loading exactly the same as that obtained in the flight tests.

Aerodynamic efficiency.—A large number of the investigations on the research program of the committee may be classified as problems of aerodynamic efficiency. These include the study of the reduction of the drag of the airplane and engine, the study of the mutual interference of the airplane and its parts, the investigation of propeller efficiency, and the study of airfoil characteristics.

Reduction of drag.—One of the most important investigations undertaken by the committee has been the study of the effect of cowling and cooling a radial air-cooled engine. The importance of this study can readily be appreciated when it is realized that the majority of engines in both military and commercial service are of this type. Only one manufacturer in the United States is now in production on water-cooled engines for military and commercial purposes.

The propeller research tunnel made possible the study of this problem at full scale. The cowling and cooling of a Wright Whirlwind engine were investigated with both a cabin monoplane and an open-cockpit biplane. Various degrees of cowling were included in the investigation, from the uncowed engine to a cowling that entirely inclosed the engine. The latter type, designated as the N. A. C. A. cowling, showed a large reduction in drag, and this cowling, subsequently applied to the AT-5, the Lockheed Vega, and other airplanes, showed a very substantial increase in high speed. The results of the investigation in the propeller research tunnel have been published as Technical Reports Nos. 313 and 314, Drag and Cooling with Various Forms of Cowling for a Whirlwind Radial Air-Cooled Engine, Parts I and II.

The investigation of the drag of engine nacelles with various forms of cowling indicated the possibility of still greater savings in drag than when the engine is mounted in the fuselage of an airplane. To determine the effect on the drag of mounting an engine nacelle in or near

the wing of an airplane flight tests were carried out on a 3-engined transport airplane. This airplane was equipped with three J-5 engines, and the two wing engines and the engine in the fuselage were cowled with the N. A. C. A. cowling. The results obtained were very disappointing, as the flight tests showed only a very slight increase in high speed. An investigation of the problem indicated a large increase in drag due to serious interference between the wings and the engine nacelle.

In order to study this interference effect, tests were conducted in the variable-density wind tunnel at 10 atmospheres on a one-tenth scale model of the Fokker wing. The investigation included the study of the nacelle and interference drag with the engine nacelle mounted in various positions above and below the wing. In the installation of the cowling on the full-sized Fokker airplane, it was believed that the interference drag would be considerably reduced by fairing the cowling into the wing. The tests in the variable-density tunnel with the nacelle faired into the wing showed an appreciable decrease in drag. The mounting of the engine nacelle in or near the leading edge of the wing showed the least interference drag.

The Matériel Division of the Army Air Corps has conducted an investigation in the wind tunnel on models of various forms of complete cowling. Particular attention was given in these tests to the measurement of the air flow through the cowling.

The investigation of the cowling is being continued at the Langley Memorial Aeronautical Laboratory on a pursuit type airplane powered with a Pratt & Whitney Wasp engine. A study is being made of the air flow in the vicinity of the slot where the air leaves the cowling and the air flow entering the slot. The engine cylinders are equipped with thermocouples and a careful study is being made of the variation of cylinder temperatures with change of air flow. Various forms of cowling are being studied in this investigation, including the British Townend ring. The results so far obtained on both the N. A. C. A. cowling and the ring type are favorable as regards both performance and cooling.

Interference.—The successful application of cowling to radial type engines installed in multi-engined airplanes is dependent upon the control or decrease of the interference drag. The results of the investigation of engine nacelles and wings in the variable-density wind tunnel indicated a marked improvement in the performance of an airplane with outboard nacelles. These tests were made without propeller, however, and therefore did not include the effect of the propeller slipstream. To investigate this problem further, there has been constructed a large model of an engine nacelle on which a propeller will be operated by a 20-horsepower electric motor. This nacelle will be tested in combination with the wing in the propeller research tunnel. The program includes the placing of the nacelle in all possible positions with reference to the wing, and the results should yield information which will enable the designer so to place the engine and nacelle with reference to the wing or wing cellule as to obtain the least drag, both of the nacelle itself and from interference effects.

In connection with the further improvement of the aerodynamic efficiency of the airplane, the committee plans an investigation during the coming year to determine the interference drag between different combinations of wing and fuselage forms. The investigation will also include a study of the drag characteristics of various forms of landing gears and windshields.

Propeller efficiency.—An investigation has been conducted in the propeller research tunnel of the effect on propeller efficiency of high tip speeds. Tests with propellers operating at tip speeds above the velocity of sound up to speeds of 1,350 feet per second have been included in the investigation. The results indicate a reduction in propulsive efficiency beginning at tip speeds of 950 to 1,000 feet per second, and a loss of efficiency of about 10 per cent for each 100 feet per second increase in tip speed above 1,000 feet per second. In these tests measurements were made of the deflection of the blades and of the velocity and twist of the slip stream back of the propeller.

In an investigation of the effect on propulsive efficiency of the interference of the body behind the propeller, a series of geometrically similar propellers varying in diameter from 9 to 10½ feet was tested. The results indicated that the propulsive efficiency is about 2½ per cent higher for the largest propeller than for the smallest.

To determine the effect of changes in plan form on propeller efficiency, a series of tests was made on propellers varying in this respect. The results indicated only a slight difference in efficiency, but the form with the thinnest airfoil section showed the highest efficiency, and for propellers operating in front of a body such as the radial engine it was found that the propulsive efficiency is increased if the propeller pitch is reduced toward the hub.

At Stanford University an investigation has been carried out on the effect of fuselage fineness on propeller performance.

A comparative study of the efficiency of geared and direct-drive propellers on the J-5 engine has been made in the propeller research tunnel, with a large and a small fuselage. The investigation was made in such a manner that the propeller-body interference factors were isolated, and it was found that, considering this interference only, the geared propeller had an appreciable advantage in propulsive efficiency. This advantage is partially due to the larger diameter of the geared propellers with respect to the bodies, and partially to the fact that the geared propellers were located farther ahead of the engines and bodies.

The investigation of the general problem of propeller efficiency as affected by various factors is being continued, and will include the effect of the wing on propeller efficiency, the effect of the propeller slip stream on wing characteristics, and interference effects between a wing nacelle and the wing. It is planned to prepare a series of design charts covering all the information obtained on the effect of various factors on propeller efficiency.

Airfoils.—The investigation of airfoil sections at high speeds has been continued at the Bureau of Standards during the year, and a report has been issued on the characteristics of 24 sections at 0.5 to 1.08 times the speed of sound. In this group of airfoils one section having a plane lower surface and a cylindrical upper surface showed better lift-drag ratios than any other section of different shape but of the same thickness, and a series of airfoils of this type will be tested during the coming year.

In order to compare airfoil characteristics as determined in the propeller research tunnel with the results of tests in the variable-density wind tunnel at a corresponding Reynolds Number, a series of seven airfoils was tested, including the Clark Y, the Göttingen 398, the N. A. C. A. M-6, and the N. A. C. A. 84. The models tested had a chord of 2 feet and a span of 12 feet, and the Reynolds Number obtained in the propeller research tunnel was about 2,000,000. The results of the tests were in good agreement with the results obtained in the variable-density tunnel at a corresponding Reynolds Number. Two of the large models tested were made with corrugated surfaces, and showed a slightly greater drag than the airfoils with smooth surfaces. The lift curves of the models with corrugated surfaces showed a marked flattening in the vicinity of maximum lift.

For the purpose of studying the scale effect in investigations of pressure distribution, a series of pressure-distribution tests on wing models was made in the variable-density wind tunnel at 1 to 20 atmospheres. The airfoils tested included the M-6, the R. A. F. 30, the Clark Y, and the R. A. F. 31 equipped with the Handley Page leading-edge slot. The results of this investigation are being prepared for publication.

In order to study the effect of scale on discontinuities in the lift curve near the region of maximum lift, a group of eight airfoils approximately 20 per cent of the chord in thickness were tested in the variable-density wind tunnel. Six of the eight airfoils exhibited discontinuities at a Reynolds Number of 150,000. The discontinuities became less pronounced as the Reynolds Number was increased and disappeared entirely when the Reynolds Number reached 720,000.

An investigation is to be made in the variable-density wind tunnel on a family of about 80 airfoils to determine the effect of thickness and shape of the mean camber line on airfoils characteristics. The airfoils included in the program will have the same relative variation in thickness along the chord, and will have six values of maximum thickness varying from 6 to 21 per cent of the chord. The airfoils are based on five differently shaped mean camber lines, each having 4° of camber.

The investigation in the atmospheric wind tunnel at Langley Field of the problem of boundary-layer control has been continued. The model used in this investigation is provided with a

narrow slot which opens into the wing and is so arranged that air may be discharged from or sucked into the wing. The slot is adjustable, both as to position on the surface of the wing and as to width. The results of these tests show considerable increase in lift with moderate pressures and a reduction in the minimum drag.

Struts.—At the Washington Navy Yard three extensive series of tests on struts have been made in the past year. The first series included 11 modifications of the Navy No. 1 strut, the program being so arranged as to cover the study of the effects of fineness ratio and trailing edge radius. The second series, conducted on five theoretical shapes supplemented by three standard struts, included pressure distribution and drag measurements, and the results of the tests were compared with calculated values. In the third series the effect on drag of slight modifications in standard struts was measured. The results obtained in these investigations have been published as Technical Reports of the National Advisory Committee for Aeronautics.

Ice formation.—The study of ice formation on airplanes in flight has been continued during the year, both in the special low-temperature wind tunnel and in flight. Flight tests have been made under a variety of weather conditions such as fog, rain, and sleet. Photographs have been made for study of the ice deposits on wings, wires, and struts. In several instances ice formed on the propellers. It was found that ice will form under a number of different atmospheric conditions, but forms in dangerous amounts only within a small range of temperature below 32° F. In the low-temperature wind tunnel a study has been made of the possibility of preventing the formation of ice on airplane parts by the use of a protective coating. The results up to the present time have not been of a positive nature, but it has been found that glucose, corn sirup, and a mixture of glycerin and alcohol do have some effect in the prevention of ice formation. A report on this investigation is in preparation for publication.

Airships.—Flight tests on airships during the past year have been confined to speed and deceleration tests, conducted in conjunction with the Goodyear-Zeppelin Corporation, to determine the drag of a small commercial-type airship. Similar investigations will be carried out on a TC-type airship for the Army Air Corps, and on the metal-clad airship *ZMC-2* at Lakehurst for the Bureau of Aeronautics of the Navy.

The results obtained in the investigation previously conducted by the committee for the Bureau of Aeronautics on the U. S. S. *Los Angeles* have been carefully studied, and a report has been prepared on the pressure distribution on the hull and tail surfaces and on the drag of the airship with and without the water-recovery apparatus.

In the variable-density wind tunnel a series of tests is now in progress on a model of the *ZRS-4* airship and a model of lower fineness ratio. The investigation includes the determination of the lift, drag, and pitching moments on both models, with and without control car.

An investigation will be carried on in the propeller research tunnel on a larger model of the *ZRS-4* airship, and will include the measurement of the pressure distribution over the hull and the determination of the lift and drag of the airship at various angles of pitch, and measurements at the same time of the forces and moments exerted on the elevator hinge.

In the wind tunnel at New York University tests are being carried on for the Goodyear-Zeppelin Corporation to obtain information as to the forces involved in the ground handling of airships. The forces are being measured on a model of an airship suspended at various angles to the wind, close to the ground and to a model of a hangar.

Fields for future research.—Previous summaries have pointed out the desirability of progress in aerodynamics along the lines of increase in safety and refinement in design. In the further improvement of the design of aircraft more knowledge is essential regarding maximum air loads and air-load distribution on the airplane structure, more information on methods of reducing drag, and in particular on the proper location of power plants for minimum interference and the greatest improvement in propulsive efficiency. The solution of the problem of increase in safety will come from an intensive study of spinning, low-speed control, and stability characteristics of aircraft. The major problems on the research program of the committee are concerned with some phase of the general subjects of safety in flight and improvement in aerodynamic efficiency.

AIRPLANE STRUCTURES

TREND OF DESIGN—*Standardization of types.*—The tendency toward standardization of types has continued. An increasing appreciation by designers of the importance of large aspect ratio and low parasite drag is reflected in the increase in the number of airplanes of the monoplane type, which now seems firmly established as a preferred type of design for large airplanes for use in regular scheduled commercial service. The monoplane has not been universally accepted, however, since two large biplanes have been constructed during the past year for this type of service. In the smaller classes of airplanes, of the three or four passenger type there has been a large increase in new types of monoplanes. This increase exceeds 300 per cent, yet the biplane still exceeds the monoplane in actual number of types and still holds a dominant position from the standpoint of production. This is particularly true for military service, where maximum maneuverability must be obtained and the span kept as low as practicable.

The demand on the part of the passenger and pilot for comfort is reflected in the great increase in the number of closed-body types, the increase in this type during the past year being nearly 300 per cent. For 2-place and 3-place airplanes, the open-cockpit type appears to be preferred. This is probably not so much a matter of comfort as a question of lower cost.

The military services are taking advantage of the existence of well-proven types of large commercial airplanes to acquire examples for transport service. Development of these types into strictly military types would be very costly and the independent development of parallel military types even more costly. Hence the number of types of very large purely military airplanes must remain very few as a matter of economy.

Number and location of engines.—Operating conditions in the United States, especially over the mountainous parts of the transcontinental air routes, require that the multiengined commercial airplane shall be able to fly at an altitude of 10,000 feet with one engine not running. It is further necessary that an airplane operating over this route shall be able to take off with its full load at altitudes from 5,000 to 7,000 feet. These rather severe requirements have made it necessary to increase the power of the engines of all large passenger airplanes operating over the transcontinental route.

At present nearly all of the large transport airplanes are of the 3-engined type, one engine being placed in the nose of the fuselage.

In the design of the newer types of transport airplanes the tendency is to place all the engines in wing nacelles or in the wing itself. In the designs of this type so far constructed four engines have been used instead of two. This arrangement of engines shows an appreciation of the value of comfort for the passengers and the desire to avoid the disagreeable vibration and noise, which has been very difficult to control when the engine is mounted in the fuselage.

The use of multiengined airplanes has been extended to the light or sport type. The latest designs have provided for two engines of relatively small horsepower, mounted in the wings.

In foreign types of airplanes there is a marked tendency to mount the engines above the wing. This arrangement has been followed in only one or two designs built in this country.

In all multiengined airplanes care is being exercised to provide that the propellers do not overlap and that the propeller wash does not seriously interfere with the structural parts of the airplane, as such interference creates a vibration which is very disagreeable to the passengers. The effect of the propeller slip stream on adjacent structures in the design of any aircraft to carry passengers is most important.

In designing passenger airplanes the designer is being forced to consider the comfort of the passenger as a primary feature in the design. The chief factors involved are noise and vibrations due to the engine and to aerodynamic forces on the structure. These latter may be the result either of the wash from the propeller or from the variations in pressure and velocity of the air over the fuselage, due to the peculiarities in design.

Amphibian airplanes.—The obvious advantages of the amphibian type are being more generally appreciated and the construction of airplanes of this character is being extended to additional commercial and military types, and especially to the smaller types intended for commercial purposes.

Landing gear.—Landing gears of the orthodox type have been more or less standardized by the manufacturers of this type of equipment. Most commercial and military types are now fitted with oleo gears. There is, however, an increased appreciation of the gain in performance which may be obtained by either simplifying the landing gear or retracting the landing gear while in flight. A number of the designs of retractable landing gear which have appeared during the year show promise, and efforts are being made to reduce the drag of the stationary type landing gear.

Shock absorbers.—The hydraulic type of shock absorber is now almost universally used, even on relatively light airplanes. However, the development of a new type of tire having a very large cross-sectional area and operating under low air pressure may make it unnecessary to provide shock absorbing mechanisms other than the tire itself in the lighter types of airplanes.

Wheel tail skids.—The use of a wheel either with a hard or a pneumatic tire to replace the tail skid has been extended, especially to the larger types of airplanes. The use of such wheels, especially in connection with wheel brakes on the main landing wheels, has proved successful in the operation of a number of standard types.

Brakes.—Brakes are now almost universally used on commercial type airplanes. Practically all manufacturers make some provision for the fitting of brakes, either as regular equipment or at the option of the purchaser.

Difference between military and commercial types.—The steady demand for increased performance in military airplanes, and in particular the demand for the ability to perform violent maneuvers at high speeds, has made it necessary to raise the structural strength requirements of many types of military airplanes to a higher standard than ever before. These requirements are now so severe that it may be doubted whether they will ever be applied generally to commercial airplanes. In meeting these requirements by improved design features and by improving methods of construction and materials used, the results will undoubtedly influence commercial airplane design.

In spite of the continued increase in the quality of design, materials, and construction of commercial airplanes, which is resulting from the requirements of the Department of Commerce, the unsuitability of commercial airplanes for military use is increasingly apparent. This does not prevent the use of certain types of transport airplanes for similar purposes by the military services, for here the demands on the airplane are practically the same in both civil and military use.

STRUCTURAL MATERIALS—*Metal construction.*—Although the number of parts in which wood is used continues to decrease, there are still many arguments advanced in favor of it. It is notable, however, that as the demands on the structure are increased there is a tendency to reduce the use of wood, especially in small sections. Many airplanes are now produced in which practically the only wooden members are the wing spars, everything else, except possibly a few fairing strips, being of metal. Metal wing spars of various original designs have been proposed but apparently their general use has been delayed by their relatively greater cost.

Welding is entering more and more largely into the construction of airplanes generally. The reliability of the welded structures appears to be regarded as entirely satisfactory. However, certain designers continue to voice objections to welding, and insist on the use of bolted or riveted joints.

The problem of internal corrosion has always been before the designer who used closed sections, and this has led to the development and use of corrosion-resisting structural materials. When such materials are generally available, designers will be able to do many things at present not approved in this country. Among other things it may be expected that the use of thin steel in sections which derive their strength from the complex character of their curvature will appear. Proposals are already being made for the use of this material in combination with a special system of spot welding.

Steel tubing.—Steel tubing of the corrosion-resisting type is still not available generally, but methods of protecting the steels ordinarily used in aircraft have been developed to a point where they may be said to be standardized.

AIRSHIPS

The placing of a contract for the building of two 6,500,000 cubic foot airships for the Navy Department in October, 1928, was a definite step in the resumption of airship building in the United States and a step toward the creation of an airship industry in the United States. Progress on design has proceeded at a normal rate. Fabrication of parts has begun. The keel ring of the first of these airships was laid on November 7, 1929. The first of these airships is due for completion in 1931, the second in 1932.

The Goodyear-Zeppelin Corporation, of Akron, Ohio, the contractor for the airships *ZRS-4* and *ZRS-5*, has practically completed the airship shed in which the airships are to be erected. The shed is 1,175 feet long, 325 feet wide, and 180 feet high. In the design of the shed the operating experience of the past four years has been carefully considered and the type of design is thought to be much superior to any types that have as yet been built.

Experimental investigation and research on the development of improved materials for airships have been continued.

Experimental flight operations have been continued with the *Los Angeles*. Improvements in water-recovery apparatus have been accomplished. Carrying, launching, and recovering service type airplanes have been accomplished in a more comprehensive manner than heretofore. This work is preliminary to the design of apparatus for use with the Navy Department's new airships.

Development of improved methods of mechanical aid to the handling of rigid airships has been continued. The mobile mooring mast is a reasonably satisfactory piece of equipment and is helpful in the handling of airships. Further improvements in this mast are in contemplation and should increase its utility. No difficulties have been encountered in the use of the stub mooring mast as a riding point for an airship. As yet the problem of making a flying moor to the stub type of mast has not been satisfactorily solved.

The metal-clad airship.—The Aircraft Development Corporation has completed and delivered the metal-clad airship, *ZMC-2*. The airship has successfully completed its flight trials. The Navy Department has placed the airship in service at the naval air station at Lakehurst, where further tests will be made to obtain more comprehensive data as to the performance and general utility of this type of airship construction.

Helium.—The new Government plant near Amarillo, Tex., has been placed in operation, making available increased quantities of helium, and with the increase in production lower costs for the helium are being quoted.

A commercial company which has been producing helium for airships announces the discovery of a new field containing a natural gas with over 6 per cent helium, a very much larger percentage than that in any gas hitherto available in production quantities. This concern has moved the major portion of its plant to this new source of helium-bearing gas.

The Navy Department purchased a new type of helium tank car which carries the helium in 28 seamless drawn pipes instead of three forged cylinders. The cost of this type of car is materially less than the cost of a car carrying forged cylinders.

Progress in Germany.—The around-the-world flight of the *Graf Zeppelin* was an outstanding achievement in airship operation.

Progress in Great Britain.—After many delays the British airship *R-101* has made several flights. The second British airship, *R-100*, is practically complete and ready for flight trials.

AIRCRAFT ENGINES

An important factor influencing aircraft engine development during the past year has been the large number of new designs which have appeared on the market. The influx of a large number of new engines has influenced development along three separate lines: First, designers have attempted to increase the tractive horsepower available by reducing the head resistance; second, their interest has been increased in the possibilities of the compression-ignition engine; and third, they have attempted to reduce the initial and maintenance costs of the engine.

The introduction of the low-drag cowling which reduced the head resistance of the direct air-cooled radial type engine to a point where it approached or was less than the head resistance of the water-cooled engine and its radiator, was the result of investigations conducted at the committee's laboratories at Langley Field.

A study of high-temperature liquid cooling at Wright Field indicated the possibility of further reducing the drag of the liquid-cooled type engine by the use of small radiators.

To meet the reduced drag obtained in liquid-cooled engines by using liquids of high boiling point, designers of radial air-cooled engines are now concerned with reducing the overall diameter of the radial engine.

The compression-ignition engine offers many possibilities for obtaining high fuel economy, and a number of manufacturers are now designing and constructing aircraft engines of this type.

To reduce the initial cost of the engine, many of the smaller manufacturers are concentrating on one model, while one of the large manufacturers has a series of 5, 7, and 9 cylinder engines, which are built with the same bore and stroke, resulting in marked manufacturing and maintenance economies.

The application of the low-drag cowling to the radial engine was investigated in the 20-foot propeller research tunnel at Langley Field under full-scale conditions. The Army, Navy, and commercial services have found that the application of the cowling to different types of airplanes has definitely improved the performance. At the annual air races held in Cleveland this year and in the transcontinental nonstop flights, all previous records were lowered by airplanes equipped with radial engines and using the low-drag cowling.

To improve the visibility and reduce the drag, the side-valve radial engine and the 2-cycle engine are being developed in an attempt to reduce the overall diameter by doing away with the overhead valve gear.

The matériel division of the Army Air Corps has concentrated on the study of high-temperature liquid cooling of aircraft engines. Ethylene glycol has been used for several years experimentally with some success by the Army and the Navy, but it was not until last year that liquid-cooled engines were put in service.

As a result of the high operating temperatures obtained with ethylene glycol, a much more uniform cylinder temperature is maintained, with the absence of hot spots. The experience of both services indicates that higher compression ratios may be used in engines with this type of cooling.

The committee, at the request of the Navy Department, undertook the investigation of the compression-ignition engine using Diesel oil as a fuel. The results of the investigation carried on under the direction of the committee have been widely disseminated. The first experimental aircraft compression-ignition engine, known as the Attendu engine, was constructed and tested at the Naval Aircraft Factory in Philadelphia.

During the past year, interest and activity in the development of this type of engine have increased and have been stimulated by the flights of the Packard 9-cylinder radial compression-ignition engine and the Junkers 6-cylinder in-line water-cooled engine.

The Packard Motor Car Co. has been experimenting for the past two and a half years with the radial air-cooled compression-ignition engine and has made successful flight tests with very good fuel economy. At present, experimental engines are being developed by the Allison Engineering Co., the Emsco Aero Engine Co., and the Packard Motor Car Co.

During the year a large number of aircraft engine manufacturers completed their designs and facilities for manufacturing. The Warner and the Kinner companies have concentrated on one model and are building new facilities for its manufacture. The Curtiss Aeroplane & Motor Co. erected a new factory to produce the Challenger engine, and the Wright Aeronautical Corporation has built a special factory in St. Louis to manufacture the new Gypsy engine.

The concentration on one model of an engine in a single factory will no doubt have an influence on reducing the cost per horsepower of aircraft engines. Nearly all the new engine development has followed the conventional design of the fixed radial air-cooled type, being either 5, 7, or 9 cylinder engines.

In all commercial aircraft operations there has been a demand for higher-powered engines. Air transport service airplanes are now equipped with engines of the highest power obtainable, either of the Wasp, Hornet, or Cyclone type. The Wright Aeronautical Corporation has replaced the well-known J-5 engine with a new series known as the J-6, of 160, 220, and 300 horsepower.

There has been a definite tendency during the year to increase the revolutions per minute of radial type engines by refined design, resulting in the purchaser being benefited by the lower cost per horsepower.

No new types of water-cooled engines were brought out during the past year and only one manufacturer in the United States is in current production on water-cooled engines.

High-powered air-cooled engines for both military and commercial service are being developed with reduction gears. The use of reduction gears promises to become general in large multiengined airplanes, especially in flying boats.

It is interesting to note that all the recent engines submitted for type tests to the Department of Commerce are air-cooled. About one-third of all the engines submitted for test are finally approved. At present there are available for both military and commercial aviation 32 approved type engines manufactured in the United States.

FACTORS THAT HAVE CONTRIBUTED TO THE PRESENT STATE OF AERONAUTIC PROGRESS

Among the major factors that have contributed to the present state of aeronautical development in America are the great expanse of the United States and the distances that can conveniently be covered by aircraft with a material saving of time and without the usual handicaps attendant upon crossing international boundaries. This is one great natural advantage that will continue to promote the use of aircraft in America. The most important active influence upon aeronautics has been the far-sighted constructive policy of the Federal Government, liberally supported by the President and the Congress, in providing for the continuous prosecution of organized scientific research and of fundamental engineering development through the various governmental agencies concerned. Next in importance has been the progress made by the aircraft industry during the past four years or since the adoption of the Army and Navy 5-year aircraft programs. The military services have cooperated effectively with each other, with the industry, and with public-spirited organizations. These factors have had to do with the development of the airplane itself. Foremost among the factors that have promoted the use of aircraft was the development and extension of the air mail service under Government operation until its fundamental purpose had been demonstrated, namely, that it was practicable to carry mails by aircraft on regular schedule and at reasonable costs. This activity when taken over by private contractors led directly to the establishment of air transport lines which are growing steadily.

A major step in the national aviation policy was the enactment in 1926 of the air commerce act, under which national airways and aids to air navigation were established by the Department of Commerce with the cooperation of the Weather Bureau in giving special weather report service, and under which provision was made for the regulation, licensing, and inspection of aircraft and airmen under uniform rules and regulations.

American business men have been both farsighted and patriotic in their willingness to enter into the development of aeronautics on a sound economic basis and without the direct cash subsidies that have been deemed indispensable in other countries. This means that American aeronautics will be developed to meet the needs of the people unhampered and unaffected in nature or extent by a policy of limited cash subsidy.

The most recent major factor promoting the use of aircraft in America has been the development of reliable air transport, largely assisted by air mail contracts which have been the main support of most long-distance air transport companies. The air mail service under private operation of carriers continues to give the best demonstration of the practicability of the use of aircraft for civil purposes. At the annual meeting of the entire committee, held on October 24, 1929, a resolution was adopted reiterating the opinion expressed in 1921 in a special report to the Congress, submitted through the President and published as Senate Document No. 358,

Sixty-sixth Congress, third session. The committee is still of the opinion, as then expressed, that, "The air mail service is in effect an experimental laboratory for the development of the civil uses of aircraft," and viewing it from this angle alone, believes it is worth what it costs over and above the difference between the revenue derived from the excess postage and the cost of carrying, if any.

The Daniel Guggenheim Fund for the Promotion of Aeronautics, which is terminating its activities at the end of the year 1929, has been a helpful factor in many ways. Its major work in establishing schools of aeronautical engineering in various universities will continue indefinitely to exercise a good influence on aeronautics.

The great economic question confronting aeronautics at this time is, Are the people willing in increasing numbers to pay the present costs of air travel? We think not. Costs must be reduced to a competitive basis where after making allowance for time saved and for the inherent attractiveness of air travel the costs will be fairly comparable with other means of transportation. We believe this can be done, but not by governmental regulation of rates and services. The problem of reducing costs, however, is too involved to be accomplished in this manner. It is easy to see that reduction in unit costs can be accomplished by increase in volume, but volume can not be satisfactorily increased with costs as they are. The answer is to improve the airplane; make it lighter and stronger; make it faster and more controllable; make it carry more pay load and consume less fuel and oil; construct it more simply and cheaply and make it easier to maintain and overhaul; make it more reliable by improving methods and facilities of air navigation; improve the landing and take-off characteristics of the airplane so as to enable it to land and take off in small areas—in short, improve its aerodynamic efficiency and make it more controllable, especially at low speeds. All of these problems are included in the current research programs of the committee, and the efforts of all existing agencies, governmental and private, are coordinated in an organized plan to solve them.

OUTLOOK FOR THE FUTURE

Among the factors that make the future of aeronautics particularly bright may be mentioned the following:

Improved radio communication and direction-finding facilities have become a practical reality and will be developed and extended on national airways.

To supplement the national airways certain States, notably New York and Virginia, are taking an interest in the development of State airports and airways, and in the opinion of the committee, it is but proper that the States generally should do this.

Airports are being established in the progressive cities and towns of America.

Larger airplanes are being built with more consideration for the safety, stability, and comfort of passengers.

Business executives and others who value time are using the airplane with increasing confidence.

The youth of the land is interested in aeronautics and is eager to fly. The attendance at flying schools manifests this and the standard of instruction in such schools is improving to meet increasing Federal requirements for approved certificates.

Metal construction is coming gradually into general use. This will make airplanes stronger and safer, and by lengthening their lives and decreasing structural maintenance will operate to decrease flying costs.

The fuel-injection aircraft engine using Diesel oil instead of gasoline gives promise of decreasing the fire hazard, of decreasing costs of operation, and of increasing the fueleconomy and range of operation.

Aerodynamic improvements are being constantly made that decrease the drag and improve the controllability, the general efficiency, and the safety of airplanes.

The governmental agencies concerned with aeronautics are organized on a sound and logical basis and function in cooperation. The Army and Navy air organizations are constantly improving the airplane to meet the needs of national defense and these improvements invariably find an application in commercial aircraft. The education of aeronautical engineers has received

an impetus from the grants to several universities by the Daniel Guggenheim Fund for the Promotion of Aeronautics. Details of the technical progress made in other nations are promptly made available in America through the committee's Office of Aeronautical Intelligence. The results of scientific research on the fundamental problems of flight are made available by the committee and utilized by the industry. The committee's facilities for such research are being materially extended under appropriations from Congress for the construction of a wind tunnel suitable for testing full-sized airplanes, and for the construction of a seaplane channel necessary for the investigation and improvement of the landing and take-off characteristics of seaplanes. The air mail service will no doubt be extended to serve the needs of the country as rapidly as conditions warrant.

The great fundamental problem of how most effectively to increase the use of aircraft by the people can be met in part by increased activity on the part of those private organizations which concern themselves with the civic, national, and scientific development of the country, in promoting the establishment of airports and in educating the people generally as to the service that aircraft can render on a sound economic basis. But withal there remains the necessity of improving the safety and efficiency of the airplane, and in the last analysis the answer is to be found in the continuous prosecution of organized scientific research.

CONCLUSION

The United States leads other nations in the use of aircraft for commercial purposes; in the private ownership and operation of aircraft; in the extent and lighting of airways; in the provision of weather-report service; in the number of airports and intermediate landing fields; in the development of radio communication and directional finding facilities; in the transportation of mail by air; in crop dusting and forest patrol by air; in aerial photographic surveying and mapping; in the development of cowling for air-cooled engines, and of engine starters; in the development of catapult launching and deck arresting devices; and in the development of parachutes. In addition the United States has taken the lead in the analysis and study of causes of aircraft accidents. America is abreast of other nations in the development of military types of airplanes, in its airship development program, in the development and use of metal construction for aircraft, and in the development of air-cooled and fuel-injection engines. America is definitely behind other nations in the development of seaplane floats and in the development and use of seaplanes, water-cooled engines, and large air transports, and also in the development of air passenger traffic. America holds the world's seaplane altitude record but is far behind in maximum speed.

The authorization by the Congress of a seaplane channel for the committee will enable America to improve her position in the matter of seaplane floats, which will permit the building of better seaplanes. The committee has recently recommended a program for the development of liquid-cooled engines, which are deemed essential for the attainment of maximum speeds. It is only a question of time, in the committee's judgment, when America will lead the world in air passenger traffic, for it is producing the requisite technical knowledge so to improve the safety and efficiency of aircraft as to bring this about without direct cash subsidies, and because its great area will make an important factor of the time to be saved by air travel.

We are, however, confronted as are other nations with the serious fundamental problems of increasing the safety and decreasing the costs of aviation. The committee feels that the answer is to be found through scientific research. The committee is grateful to the President and to the Congress for the support that has been given to scientific research in aeronautics. The committee believes that the continuous and systematic study and investigation of the basic problems of flight is the most fundamental activity of the Government in connection with the development of aeronautics, and in the discharge of its responsibility under the law recommends the continued support of its work in the fields of pure and applied research in aeronautics.

Respectfully submitted.

NATIONAL ADVISORY COMMITTEE FOR AERONAUTICS,
JOSEPH S. AMES, *Chairman*.

REPORT No. 309

JOINT REPORT ON STANDARDIZATION TESTS ON N. P. L. R. A. F. 15 AIRFOIL MODEL

By WALTER S. DIEHL
Bureau of Aeronautics

REPORT No. 309

JOINT REPORT ON STANDARDIZATION TESTS ON N. P. L. R. A. F. 15 AIRFOIL MODEL

By WALTER S. DIEHL

SUMMARY

This report contains the wind-tunnel test data obtained in the United States on a 36 by 6 inch R. A. F. 15 airfoil model prepared by the British Aeronautical Research Committee for international trials. Tests were made in cooperation with the National Advisory Committee for Aeronautics at the Bureau of Standards, Langley Memorial Aeronautical Laboratory, Massachusetts Institute of Technology, and McCook Field.

In addition to brief descriptions of the various wind tunnels and methods of testing, the report contains an analysis of the test data. It is shown that while in general the agreement is quite satisfactory there are two cases in which it is unsatisfactory. Since the lack of agreement in the latter is probably explained by errors known to be inherent in the methods of determining and applying corrections in these particular tests, it is concluded that the agreement obtained is more a matter of technique than a wind-tunnel characteristic.

INTRODUCTION

During the early development of experimental aerodynamics it was found that test data on the same wing section from different wind tunnels frequently showed rather large and important lack of agreement that could not be ignored. This condition led many engineers to distrust all wind-tunnel test data and for many years prevented the wind tunnel from receiving the attention and credit it deserves. The situation has been greatly improved in recent years owing to the general adoption of more careful test methods and the application of corrections now known to be necessary. Since it is a matter of some interest, a few of the more important advances will be discussed briefly.

The early attempts which were made to find the cause or causes of lack of agreement in wind-tunnel tests on airfoil models centered chiefly on interference effects from the method of attachment to the balance. One of the first papers on this subject is an appendix to a report by Bairstow, Pannell, Lavender, Fage, and Cowley.¹ It was pointed out in this paper that the so-called "crank-spindle" method of attachment was unreliable. Concerning this, the report says, "We have been unable to find any means of supporting a model airfoil from its center which does not involve disturbance of flow of air round the aerofoil to a considerable extent; with the best of such arrangements we have yet found the residual correction after subtracting the resistance of the spindle alone is of the order of 20 per cent on the minimum drag." The next important paper on the subject is by Pannell and Campbell.² By this time it was generally recognized that unless great precautions were taken, good agreement could not be obtained in tests on the same model with different methods of support in the same wind tunnel, while good agreement between two tunnels using the same method of supporting the model was disappointingly rare. It is to be emphasized that in this phase of wind-tunnel development the chief sources of error may be ascribed to lack of familiarity with the equipment and with the fundamental aerodynamic laws involved. As the technique of testing improved there was a noticeable improvement in test data as shown by better agreement between the results in the various tunnels.

¹ Experiments on the Variation of the Forces and Moments on an Airfoil as the Speed Changes. British Advisory Committee for Aeronautics Reports and Memoranda No. 148, March, 1915.

² Pannell, J. R., and Campbell, N. R., Methods of Support for Models During the Measurement of their Aerodynamic Resistance. Br. A. C. A. R&M No. 244, July, 1916.

Further efforts to improve the quality of test data led to a rather general adoption of the Göttingen wire balance³ with its greatly reduced interference effects from the model supports. This type of balance has been found very satisfactory and although the drag correction is quite large it may be determined with considerable accuracy when proper care is used.

In 1919 ("Tragflugeltheorie" Göttingen Nachrichten) Prandtl⁴ gave the corrections for tunnel-wall interference, but it was not until about 1924 that these corrections were generally known to bring most of the discordant test results into good agreement. Glauert⁵ appears to have given the first experimental verification of the validity of the wall-interference correction. In a subsequent paper⁶ he demonstrated in a very striking manner how effective these corrections are in bringing test data into agreement.

The combination of improved technique and wind-tunnel equipment, with the general application of wall effect corrections, removed practically all doubt concerning the validity of wind-tunnel test data, but it appeared desirable to conduct comparative tests on the same model in different wind tunnels in order to establish some measure or idea of the normal variations encountered. This project was proposed by a number of investigators, but no definite action was taken until the British Aeronautical Research Committee decided to prepare a series of models for international trials. The inception and purpose of the International Trials are fully explained in R. and M. No. 954⁷ from which the following statement is quoted: "Acting on a suggestion made by the Director of Research, the Aeronautical Research Committee decided in March 1920, to institute comparative model tests in as many as possible of the aerodynamic laboratories of the world. It was thought that such tests, in which the same models would be tested successively by all laboratories, would supply valuable information which had not previously been available. The aim of wind-tunnel experimental work is to obtain reliable estimates of the forces which would be experienced by bodies moving at specified speeds through still air of infinite extent; but in practice it is necessary to hold the model stationary and to generate a flow of air past it and measurements made in this way are in some degree open to question, in that the forces imposed upon the model may be affected (1) by the limited extent of the air stream in which they are placed and (2) by the turbulence which can never be entirely eliminated. The results must furthermore depend to some extent upon the methods adopted for connecting the models to the measuring apparatus. Different methods are adopted in different countries, and wind tunnels of varying size and design are employed; thus there is some uncertainty as to the extent to which a comparison can be made—e. g., between different aerofoils tested in different countries—and this uncertainty, it was thought, would be reduced if comparative figures were available from tests upon the same models.

"It was at first intended that the proposed international trials should comprise:

"(1) Determination of lift, drag, and center of pressure for a standard aerofoil model at various angles of incidence.

"(2) Resistance measurements at zero angle of yaw on a very good streamline airship model.

"(3) Tests of a complete aeroplane model, including complete determination of forces and moments, and of the more important stability derivatives.

"At a later date it was decided to delete the third test, and under the second heading to test two models differing by the amount of parallel portion included between head and tail. Invitations to participate in these trials were sent to the authorities in U. S. A., France, Italy, Holland, Canada, and Japan, and were in every case accepted. A model aerofoil and two airship models were constructed at the National Physical Laboratory, and after preliminary tests in Great Britain, these models were sent abroad, the aerofoil in the first instance to France and the airships to U. S. A.

³ For a description see *Ergebnisse der Aerodynamischen Versuchsanstalt zu Göttingen*, 1921.

⁴ See also Prandtl, *Applications of Modern Hydrodynamics to Aeronautics*. N. A. C. A. Technical Report No. 116 (1921).

⁵ H. Glauert, *Experimental tests of the Vortex Theory of Airfoils*. Br. Aeronautical Research Committee Reports and Memoranda No. 889, November, 1923.

⁶ H. Glauert, *An Experimental Test of the Prandtl Correction for Tunnel Wall Interference*. Br. A. R. C. R. and M. No. 898, January, 1924.

⁷ *International Trials—Report of Aerofoil Tests at National Physical Laboratory and Royal Aircraft Establishment*. Br. A. R. C. R. and M. No. 954, May, 1925.

"It was at first contemplated that no report should be published until all the laboratories had completed their measurements, so that an exhaustive comparison of the results could be made. But the length of time involved in these trials, where every refinement which experience can suggest is being employed by the collaborating establishments, suggests that a different procedure is desirable, and it has recently been decided to invite each participating nation to publish an account of its own tests, the intention being that when the whole series is complete some critical summary shall be prepared and published by the A. R. C."

The airfoil model was received by the N. A. C. A. in 1923, and tests were made during the latter part of 1923 and the early part of 1924. Owing to the limited time available it was not feasible to make tests at more than four laboratories, as follows: Bureau of Standards, Langley Memorial Aeronautical Laboratory, Massachusetts Institute of Technology, and McCook Field. This report is a compilation of the data contained in the reports from these laboratories.

There appears to have been some misunderstanding regarding the nature of the tests, which, according to the quotation from the British report given above, were supposed to be made with unusual accuracy, while it was agreed that the tests in this country should be made in the routine manner. The model was supplied to each of the four laboratories without specification as to method of support, wind speed to be used, etc. In other words, no restrictions whatever were imposed. Consequently, there is a lack of uniformity in test speeds, but it is felt that, with one exception to be noted later, the results may be considered as quite fairly representing the average test at each of the four laboratories.

DESCRIPTION OF WIND TUNNELS

Brief descriptions of the four wind tunnels have been compiled from the test reports. It is believed that these descriptions will prove to be of value in any interpretation of the test data.



FIGURE 1.—Bureau of Standards wind tunnel

BUREAU OF STANDARDS: The 10-foot outdoor tunnel was used in these tests. This tunnel is of circular cross section with a total length of 84 feet, divided into a cylindrical section 10 feet in diameter by 50 feet in length and an exit cone which expands to a diameter of 14 feet 2 inches at the exit end. A honeycomb with cells 4 by 4 by 12 inches deep is installed at the entrance to the cylindrical section and a short faired intake is fitted immediately in front of the honeycomb. The axis of the tunnel is 8 feet above the ground and the distance from the honeycomb to the working section is approximately 27 feet. The propeller has 4 blades, 14 feet diameter by 9.8 feet pitch, and it is directly connected to a 200 HP. electric motor. The maximum R. P. M. is about 550, giving a wind speed of about 70 miles per hour. Figure 1 shows the general external appearance.

LANGLEY MEMORIAL AERONAUTICAL LABORATORY: This wind tunnel is fully described in N. A. C. A. Technical Report No. 195,⁸ from which the sectional view (Fig. 2), is taken. The over-all length is approximately 51 feet, divided into a 15 foot 9 inch entrance cone, an 11 foot 2 inch cylindrical test section, and a 24 foot 10 inch exit cone. The cross section is everywhere circular, and the throat diameter is 5 feet. The flow is effectively straightened by three honeycombs and a torque reactor. One of the honeycombs is located at the mouth of the entrance

⁸ Elliott G. Reid, Standardization Tests of N. A. C. A. No. 1 Wind Tunnel (1924).

cone and the other two are at the ends of the cylindrical test section. These devices result in an exceptionally smooth and steady flow.

The 4-bladed 10-foot propeller is directly connected to a 200 HP. D. C. motor.

MASSACHUSETTS INSTITUTE OF TECHNOLOGY: The 7.5-foot wind tunnel which was used in these tests is of the closed Venturi type (fig. 3), consisting of an experimental section 7.5 feet in diameter by 15 feet in length, an elliptically flared entrance 15 feet in diameter at the

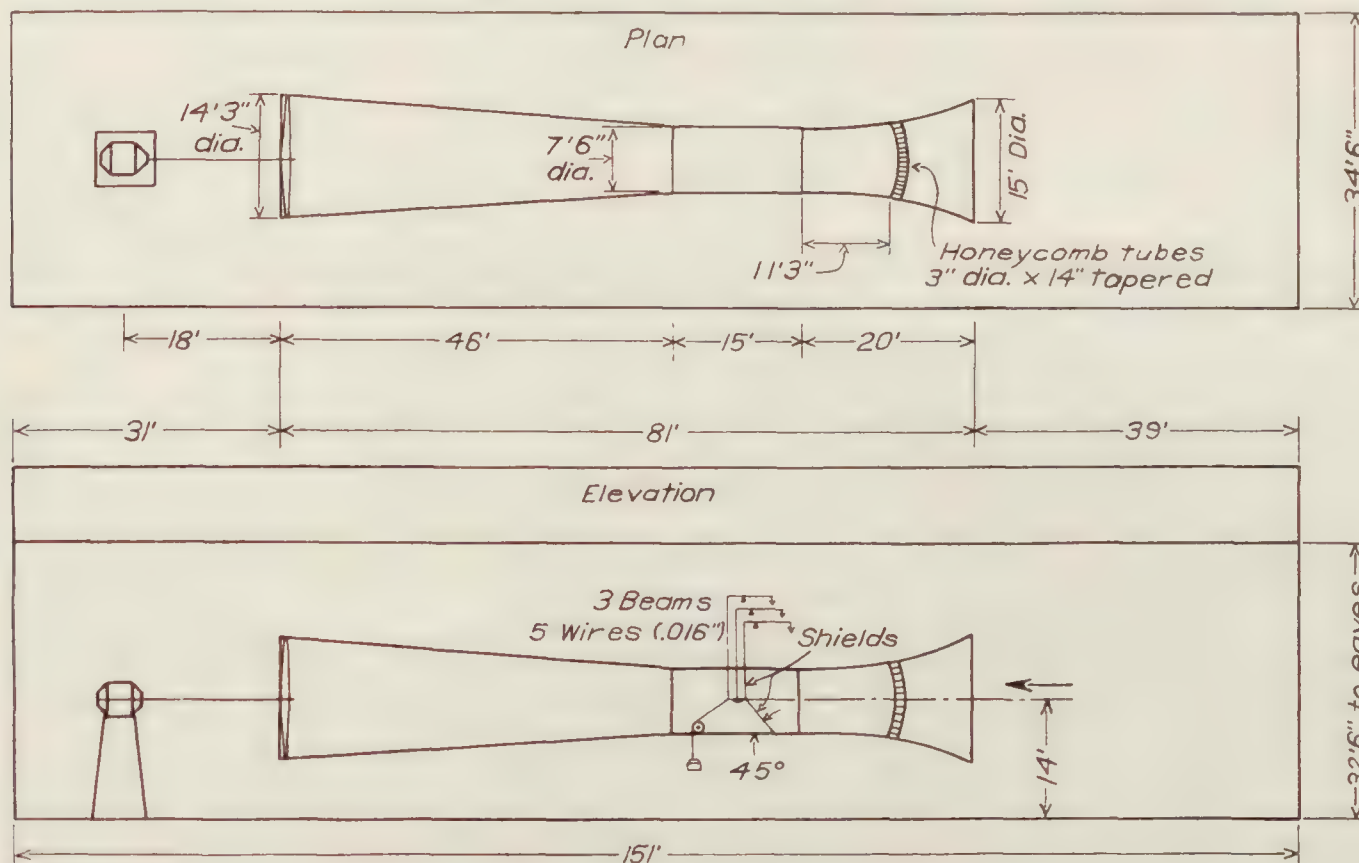


FIGURE 3.—Massachusetts Institute of Technology wind tunnel

mouth by 20 feet in length, and a straight tapered exit cone with a maximum diameter of 14 feet 3 inches and a total length of 46 feet. The honeycomb, which is located approximately midway in the entrance cone, is built up from tapered tubes 3 inches in diameter by 14 inches in length.

A 4-bladed propeller 14 feet 1 inch in diameter is directly connected to a 100 HP. electric motor. A wind speed of 60 feet per sec. is given at 300 R. P. M., using about 12 horsepower.

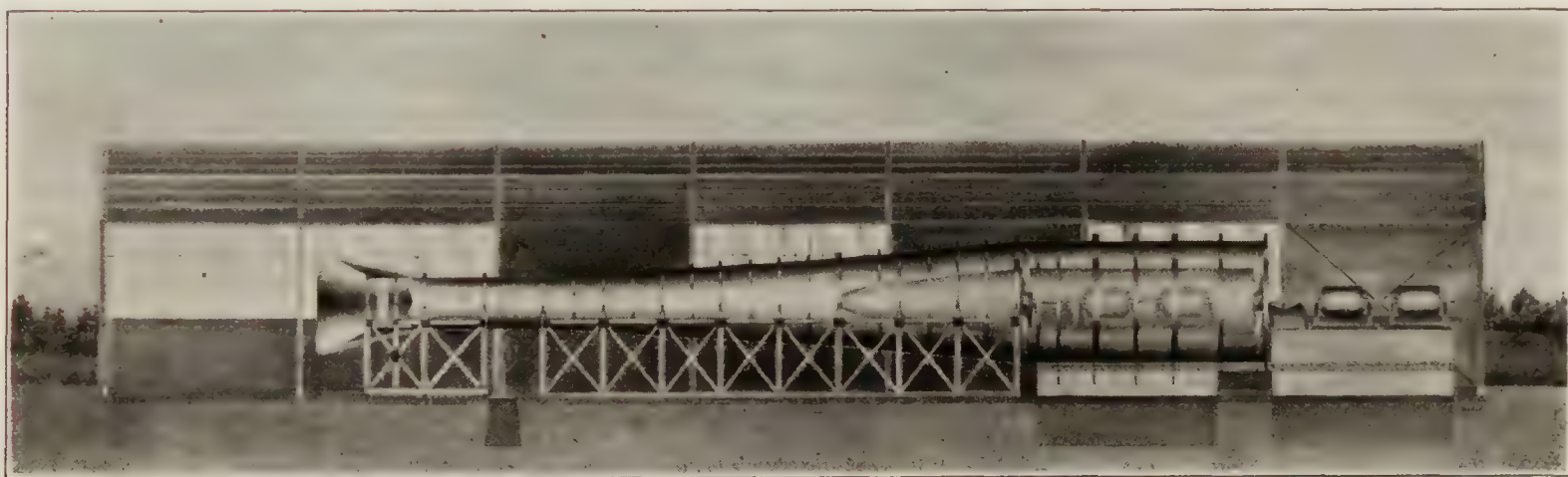


FIGURE 4.—McCook Field wind tunnel

McCOOK FIELD: The 5-foot tunnel used in these tests has a cylindrical test section 18 feet long, a flared intake 10 feet in diameter by 11.25 feet in length, and a 2-piece exit cone 14 feet maximum diameter by 68 feet over-all length. The exit cone has a straight taper from 5 feet to 14 feet diameter in the first 44 feet of its length. The remaining length is cylindrical to accommodate the tandem propeller drive. The center line of the tunnel is 10 feet above the floor. A honeycomb built up of hexagonal tubing 4 inches across the flats and 20 inches long is located near the entrance of the test section and an air-flow straightener, consisting of 16

radical vanes, is mounted at the entrance of the intake cone. The balance is located 11.25 feet from the honeycomb. Two propellers, 11 feet 11 inches diameter, are driven by 600-HP. motors. A wind speed of 150 M. P. H. is obtained at 900 R. P. M. Many of the details are shown in Figure 4.

DESCRIPTION OF MODEL

The international standard R. A. F. 15 airfoil was of rectangular plan form, 6-inch chord by 36-inch span. The material was aluminum or aluminum alloy.

The condition of the model was a cause of some concern at each laboratory. The comments of the Bureau of Standards were as follows: "The model in its journey received rather severe treatment. Fifty-six holes had been drilled in various parts of it by testing laboratories, the condition of the surface was rather poor, and the model as a whole was warped and bent. The contour

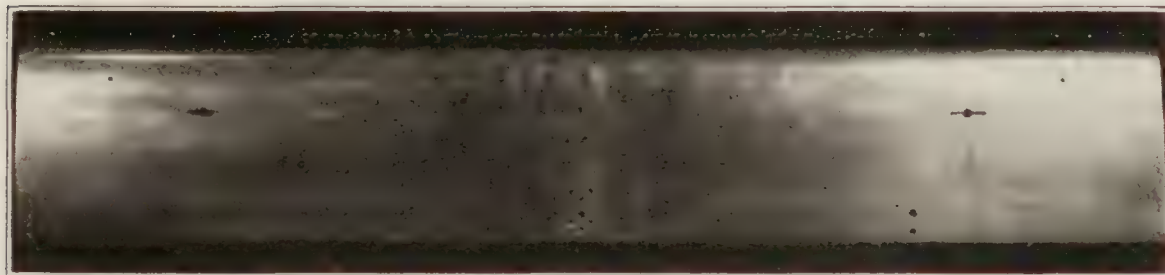


FIGURE 5.—Airfoil plan

of the model as received was determined by the Gauge Section of the bureau. The angle of attack at the right tip was greater than that at the center by 0.35° while the angle at the left tip was greater than that at the center by 0.10° * * *. The value of the comparison of the measurements of lift and drag in different wind tunnels has been greatly reduced by the changes in the shape of the model." The comments from the Langley Memorial Aeronautical Laboratory were similar: "The model had been tested in several laboratories before reaching Langley Field and bore evidences of its travel * * *. While the holes, slots, etc., already in the wing were carefully filled with wax, the surface was considerably rougher than that of a new, carefully made airfoil and, as the ordinates were not measured here, it is possible that some distortion may have passed unnoticed. Comparison of the test results with those from slightly smaller R. A. F. 15 airfoils would indicate, however, that no distortion of major importance existed, and that the surface irregularities may have been responsible for the minimum drag being higher than expected."

The condition of the model which led to the foregoing comments is clearly shown by the photographs made at Langley Field. (Figs. 5 and 6.) The

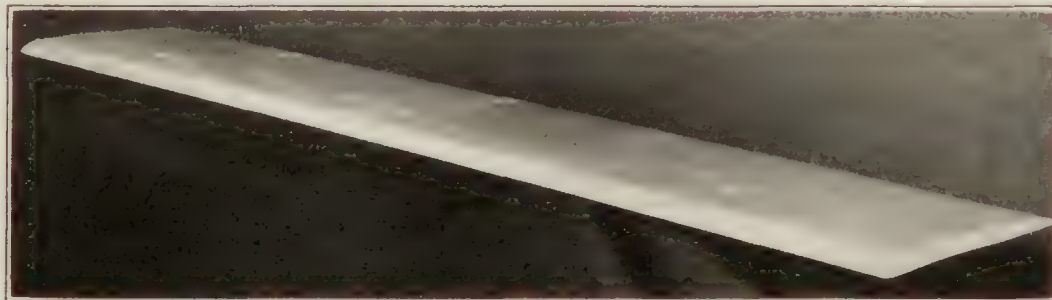


FIGURE 6.—Airfoil $\frac{3}{4}$ front view

ordinates as measured by the Gauge Section of the Bureau of Standards are given in Table I. In addition to the ordinates the Bureau of Standards measured the curvature along the span at the maximum ordinate and found the following distortion:

Distance from right end, inches	0	6	12	18	24	30	36
Height above center, inches	0.161	0.073	0.022	0	0.024	0.083	0.139

Attention is invited to the fact that none of the distortions noted is very serious and that the effect on comparative tests should be negligible so long as no changes occur from one laboratory to the next. The latter condition may be expected to have been substantially met in the tests under discussion.

METHODS OF TESTING

Brief descriptions of the methods of holding the model and applying corrections have been compiled from the test reports.

BUREAU OF STANDARDS: A simple wire balance employing different set-ups for lift and drag measurements was used. For lift measurement the airfoil was suspended by four

parallel wires in the inverted position from a framework mounted on direct reading scales. The pair of wires on each wing tip were 3 inches apart and 20 inches long. The angle of attack was varied by tilting the framework. At ordinary angles the model was very steady, and a moderate yawing motion would give only a very small variation in the balance reading. Drag was taken by the shift link of the balance so that only the vertical component of the force was read. Measurements were not attempted at the angle of maximum lift or higher on account of violent yawing motions, nor were they extended to zero lift in the inverted position because of the danger to the model. A few measurements were made at negative angles with the airfoil right side up.

For drag measurements the wires were spread at the top in a plane perpendicular to the wind direction in order to reduce the yawing motion to a negligible amount. The model was allowed to swing downstream until the moment of the weight plus the vertical component of the air force balanced the moment of the horizontal component. The displacement of the model was measured by a sliding telescope and the total horizontal force computed. The correction due to the drag of the 0.0324-inch diameter wires used in the suspension was computed and amounted to about 75 per cent of the minimum drag.

Angles of attack were determined as follows: A steel straightedge 42 inches long was clamped tightly to the airfoil and the distance from each end to the floor of the tunnel measured.

The angle of the airfoil to the floor with the straightedge attached was thus determined. Subsequent to the force measurements a small mirror was mounted on the surface of the airfoil and the change in angle due to the addition of the straightedge and the change due to air loads were measured by an optical method, thus determining the angle under which the forces were measured. The inclination of the wind stream and the alignment of the balance were determined from readings with the airfoil right side up and inverted.

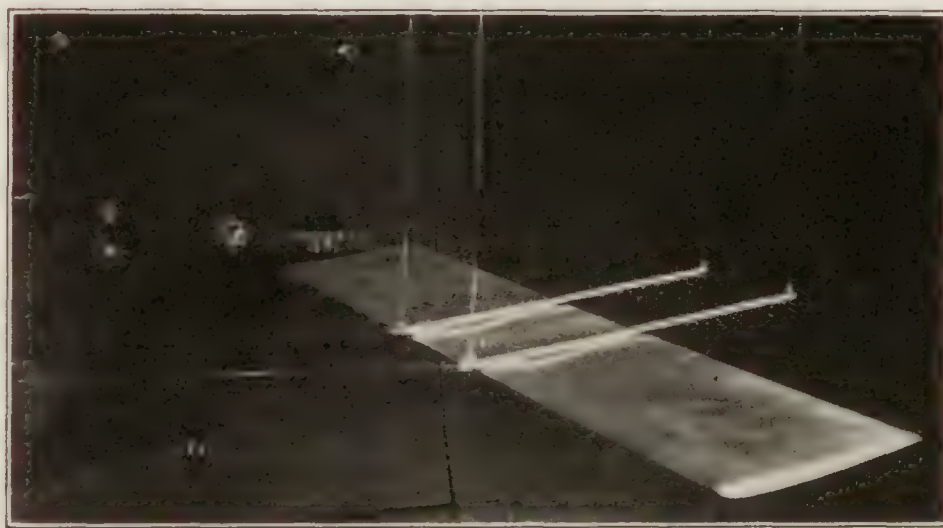


FIGURE 7.—Langley Memorial Aeronautical Laboratory (N. A. C. A.) wire balance

Readings were taken at wind speeds of 40, 57.5, and 100 feet per second.

LANGLEY MEMORIAL AERONAUTICAL LABORATORY: The model was supported on the wire balance shown in the Figure 7. The skids upon which the wing rested were symmetrically disposed, 8 inches apart. The wire sizes were as follows: Front lift 0.023 inch, rear lift 0.013 inch, drag 0.013 inch, counterweight 0.013 inch for erect runs and 0.023 inch for inverted runs.

The wire drag correction was determined by successively replacing the wing with two different lengths of drill rod of the same diameter and subtracting from the drag readings taken on one of these combinations the drag of the rod as calculated from the differences between the two sets of data. Tests were made with a third skid mounted at midspan in an attempt to detect any interference or variation of support drag with angle of attack, but no perceptible change was found. The maximum change in angle of attack caused by the application of air load was measured and found to be less than 3 minutes for angles of attack below 10° . The total drag correction amounted to about 72 per cent of the minimum measured drag at 10 meters per second.

Balance readings are corrected for variation of forces in the static suspension with angle of attack, in addition to the support drag correction. Moments are computed not about the leading edge but about a point one-eighth inch below the leading edge on the skid center line, since this procedure simplified the computations and introduced no appreciable error except in the immediate neighborhood of zero moment.

MASSACHUSETTS INSTITUTE OF TECHNOLOGY: A wire balance having the same general arrangement as the Göttingen balance, but greatly modified in detail, was used. The model is supported by two lift wires and one moment wire and is normally inverted. The lift wires are attached to small fittings 18 inches apart in the leading edge and the moment wire is attached to a sting on the center line of the model at a point 10 inches aft of the plane of the lift wires. The two lift wires lead to a cross arm mounted on a simple balance beam above the tunnel; the moment wire leads direct to another simple balance beam. The sum of the tensions in the lift and moment wires is the total lift on the model while the moment about the leading edge is given directly by the moment leading.

Drag is taken by two horizontal wires attached to the lift wire fittings. These horizontal drag wires are carried forward to a small fitting from which are led two wires, one vertical and the other inclined upstream and downward at 45° . This arrangement gives a load in the vertical wire exactly equal to the drag, while effectively preventing any yawing oscillation. The two vertical wires pass to a cross arm mounted on the third balance beam.

The angle of attack is varied by reeling the moment wire in or out on a drum, and the system is kept in tension by a single counterweight which is attached to a wire running down and back over a pulley. The effective wire drag is found by substituting for the wing a form of known drag, as measured at the same speed in this tunnel on a bell-crank balance. Since the wires are shielded by streamlike guards, the total wire-drag correction is of the order of 65 per cent of the minimum drag of good 36 by 6 inches wing model. Two calibrations are necessary to compensate for the stretch of the wires under load; the first is a direct drag calibration made by applying known drags to the model, and the second is a change in the first calibration caused by known lifts. A small correction for the effect of inclination in the moment wire at large angles of attack is necessary.

McCOOK FIELD: An N. P. L. type of balance was used in the McCook Field tests. This balance is well known and needs no further description here. (See E. P. Warner and F. H. Norton, Wind Tunnel Balances—N. A. C. A. Technical Report No. 72.) Normally the model is supported vertically by a spindle in the lower end, but tests were also made in this case with the model horizontal. In order to eliminate the effect of air-stream inclination the model was inverted in each position and the mean taken of the two readings.

In the vertical position three operators were employed to obtain best results. One operator observes the Wahlen gage, which is sensitive to one-tenth of 1 per cent in velocity head, and controls the speed while the other two operators read lift and drag. Moment readings were not taken simultaneously with lift and drag. Tare tests included spindle drag using the dummy-spindle method and deflection measurements.

TEST RESULTS

Test results are given in Tables II to X, inclusive. These data may be divided into three groups representing test speeds of approximately 35, 60, and 100 ft. per sec. Following this grouping the data are plotted in Figures 8 to 19, inclusive. The data in each group are plotted on polar diagrams with and without wall correction and also against angle of attack, with and without wall correction.

The correction for wall effect is made by the Prandtl⁹ formulas

$$\Delta C_D = \frac{C_L^2 S}{2\pi D^2} = \frac{C_L^2 S}{8A}$$

and

$$\Delta \alpha = \frac{57.3 C_L S}{2\pi D^2} = 7.16 \frac{C_L S}{A}$$

where S is the area of the model, D the diameter of the wind tunnel, and A the cross-sectional area of the wind tunnel. These corrections are added to the drag and angle of attack observed in a wind tunnel having a closed test section.

⁹ L. Prandtl, Applications of Modern Hydrodynamics to Aeronautics. (N. A. C. A. Technical Report No. 116.)

DISCUSSION OF TEST DATA

Consider the first group consisting of tests made at speeds between 29.3 and 40 ft. per sec. The polar plot of drag uncorrected for wall effect is given on Figure 8. The same data corrected for wall effect are plotted on Figure 9. Comparing these two figures it is seen that the wall-

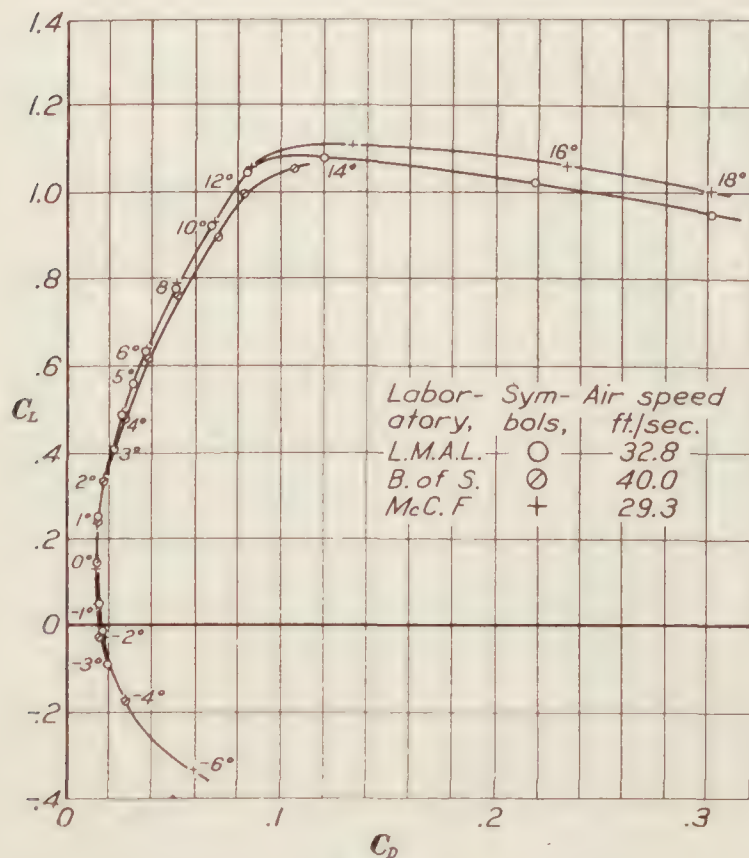


FIGURE 8

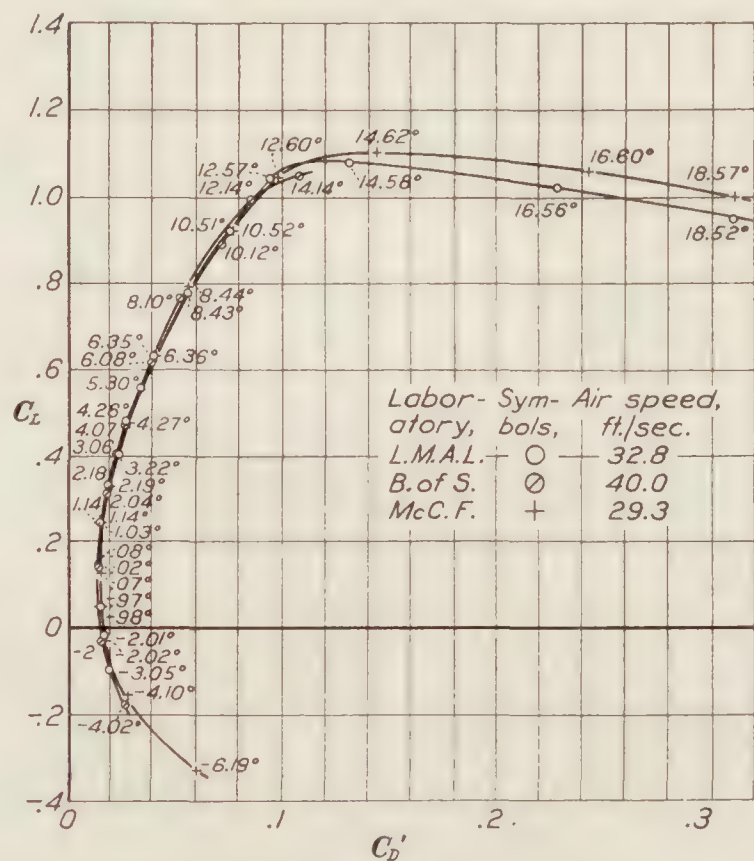


FIGURE 9

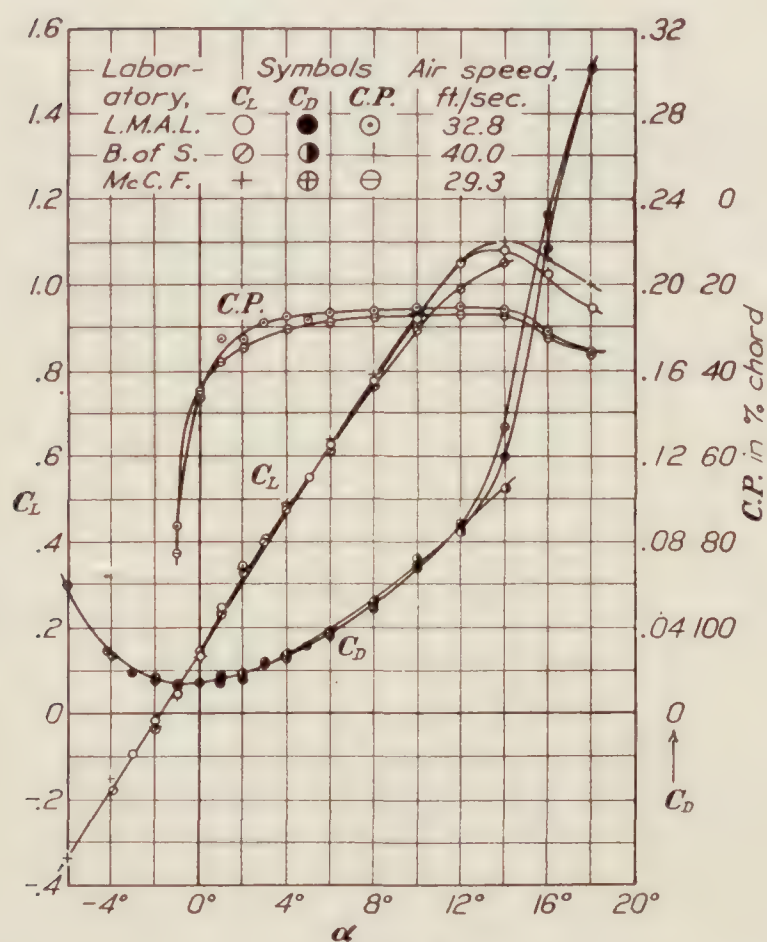


FIGURE 10

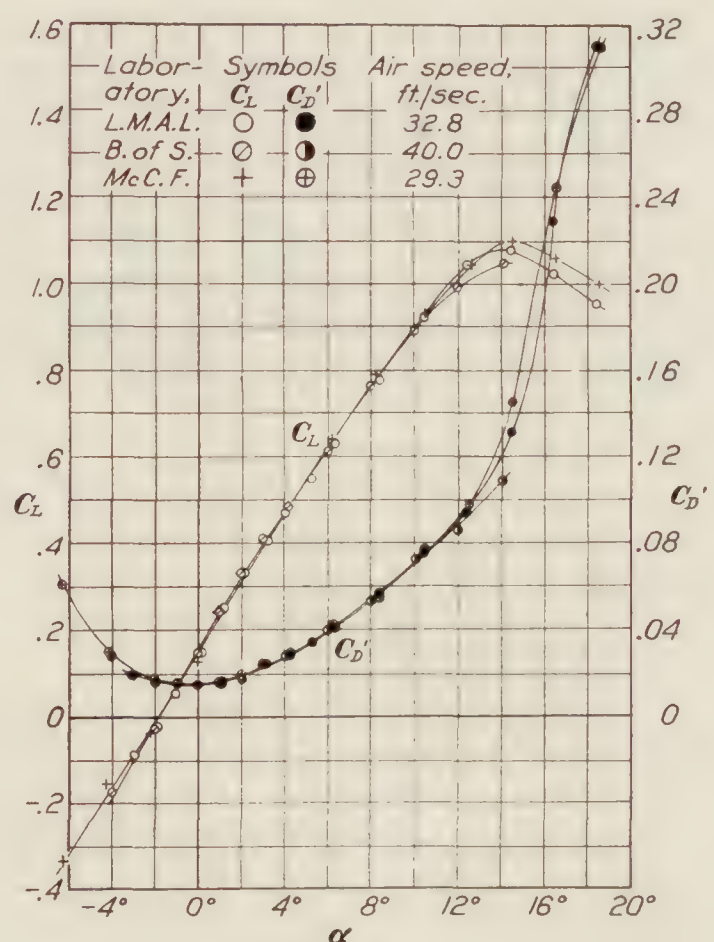


FIGURE 11

effect correction results in better agreement. The same conclusion may be reached from a study of these data plotted against angle of attack as in Figures 10 and 11.

The second group of tests were made at speeds between 57.5 and 65.6 ft. per sec. The polar plot of uncorrected data (fig. 12) shows greater divergencies than does Figure 8, but

most of the discrepancies are ironed out when the wall effect correction is applied, as shown in Figure 13. The two outstanding differences from mean values are the high maximum lift obtained in the McCook Field tests and the low minimum drag obtained in the Massachusetts Institute of Technology tests. These will be discussed later.

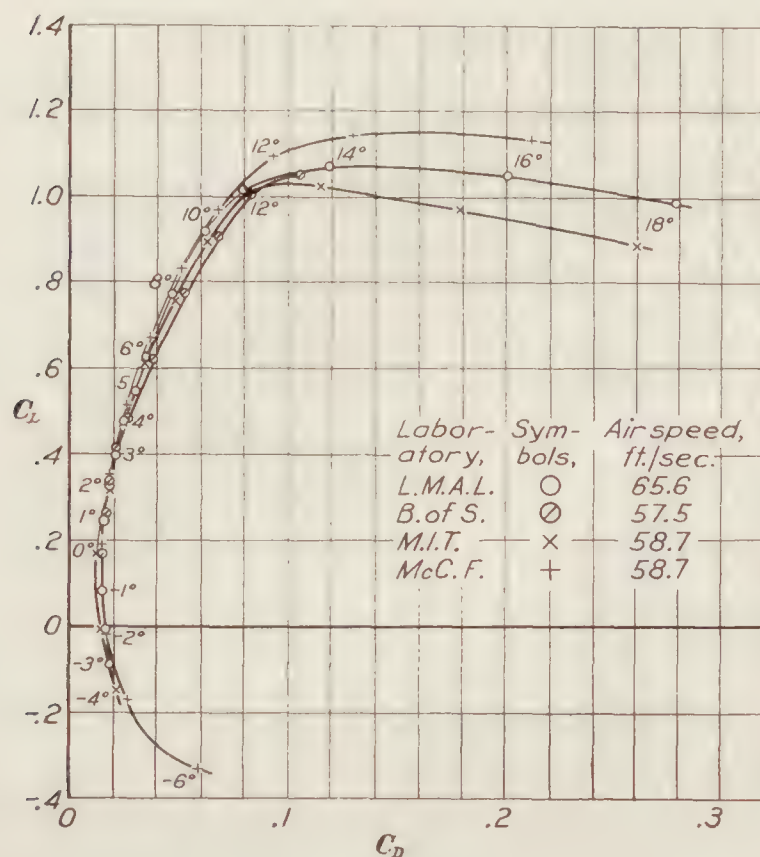


FIGURE 12

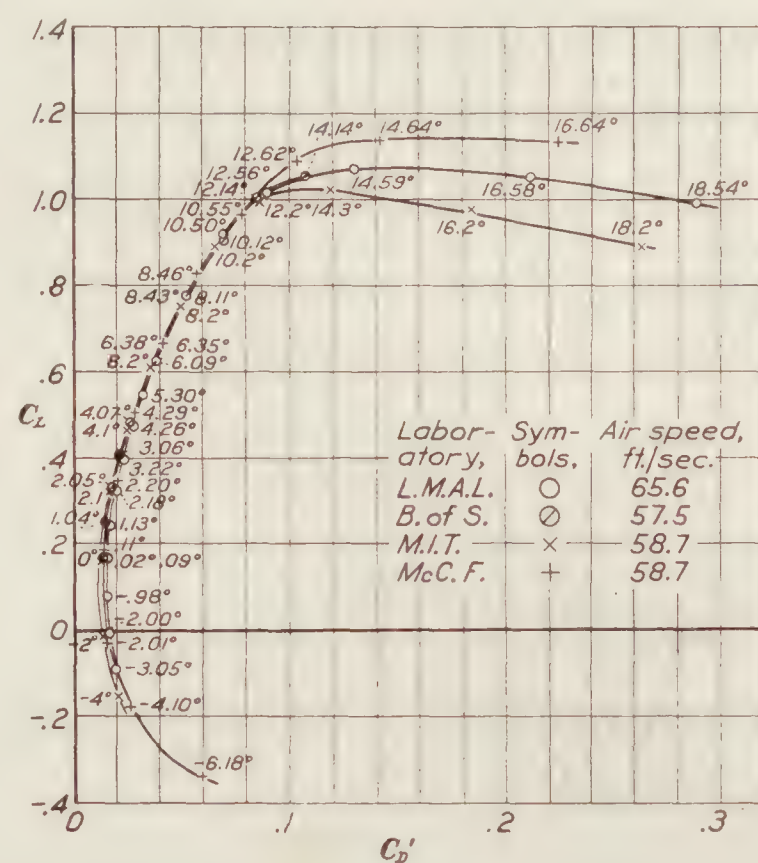


FIGURE 13

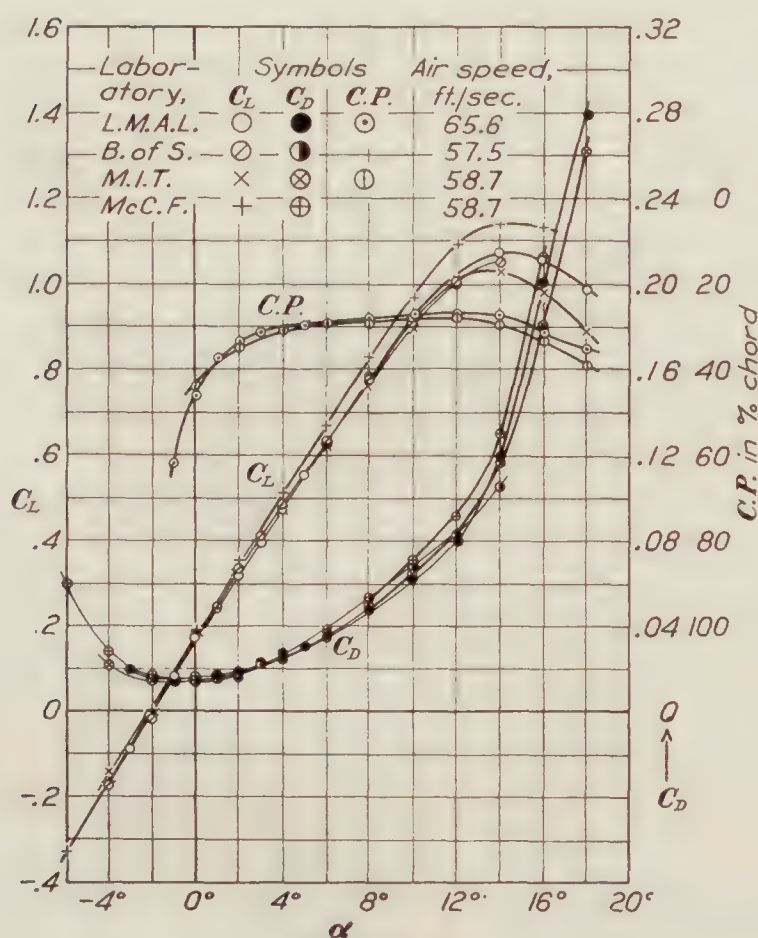


FIGURE 14

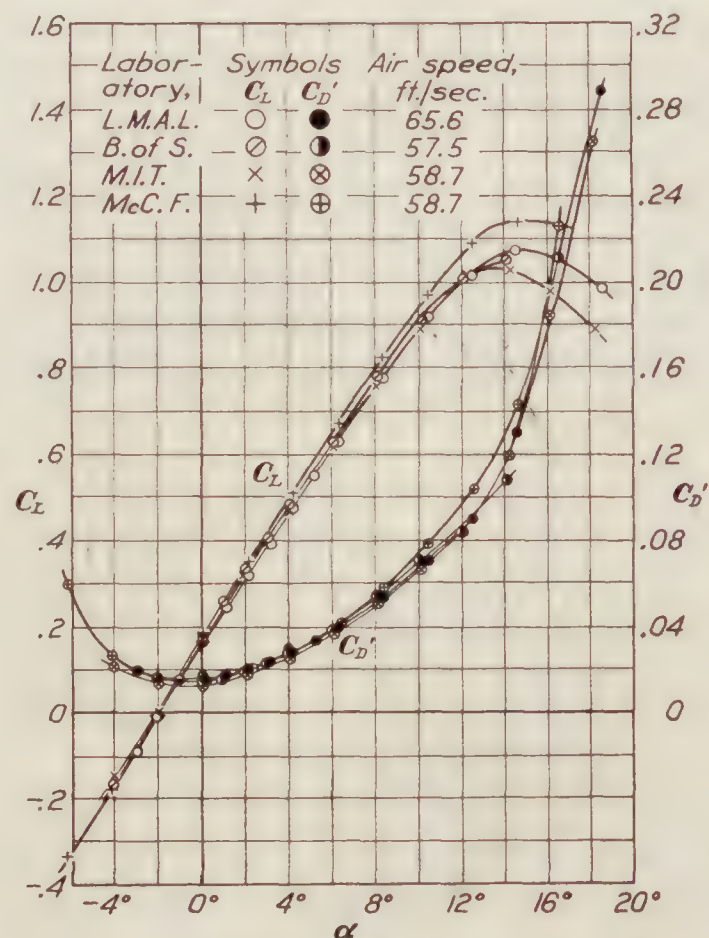


FIGURE 15

The third group consists of only two tests, one at 98.4 ft. per sec., the other at 100 ft. per sec. In this group the polar plots (figs. 16 and 17) show close agreement, but the plot against angle of attack (figs. 18 and 19) show some differences. The agreement is improved, however, by applying the wall interference correction.

A summary of the test data given in Table XI brings out the general points of agreement or divergence. These will now be considered individually, using the corrected test data only.

I. MAXIMUM LIFT.—The values of $C_{L\max}$ range from 1.040 to 1.153, but the McCook Field values of 1.110 and 1.153 look questionable. If these be neglected, the variation is from

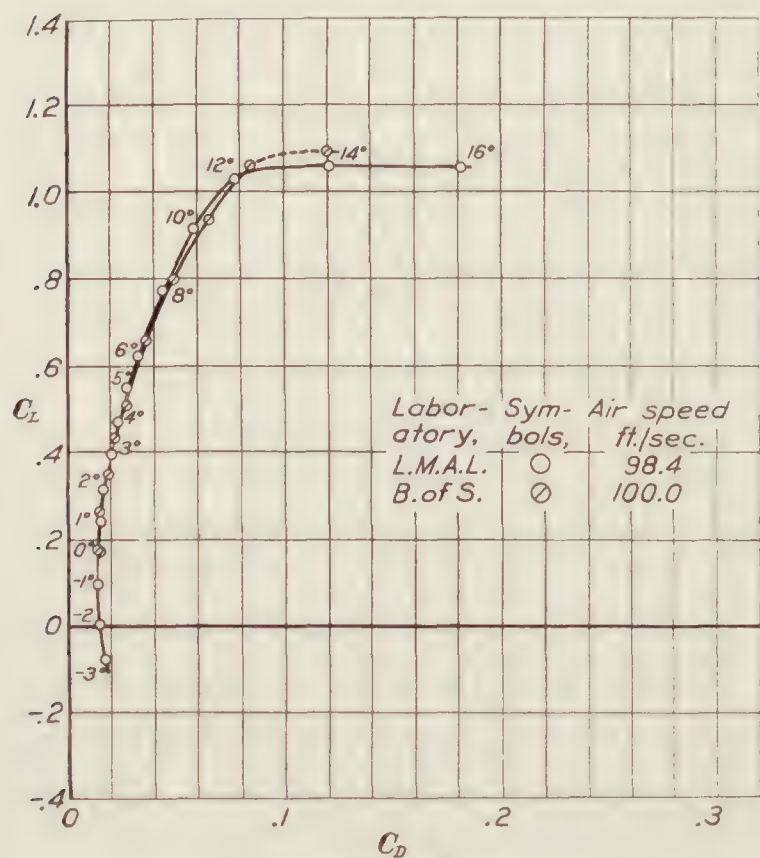


FIGURE 16

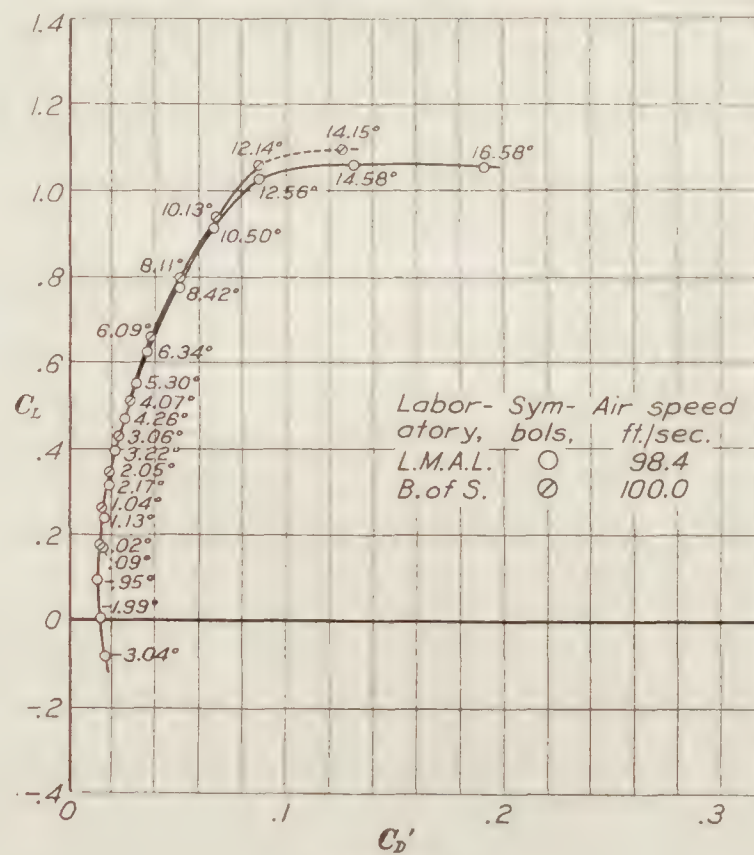


FIGURE 17

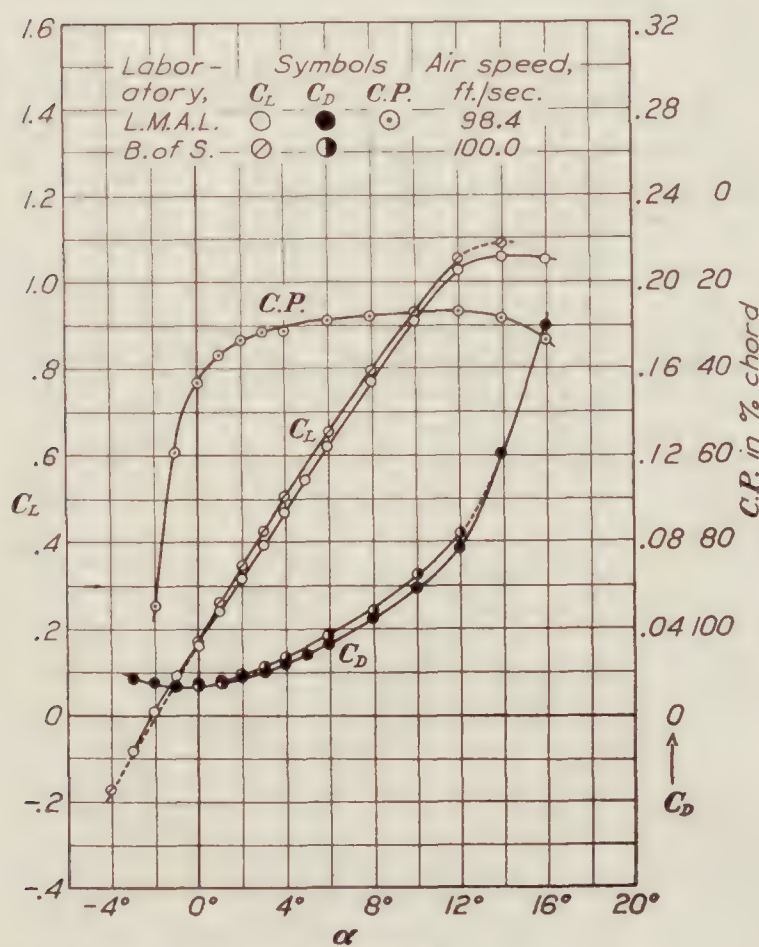


FIGURE 18

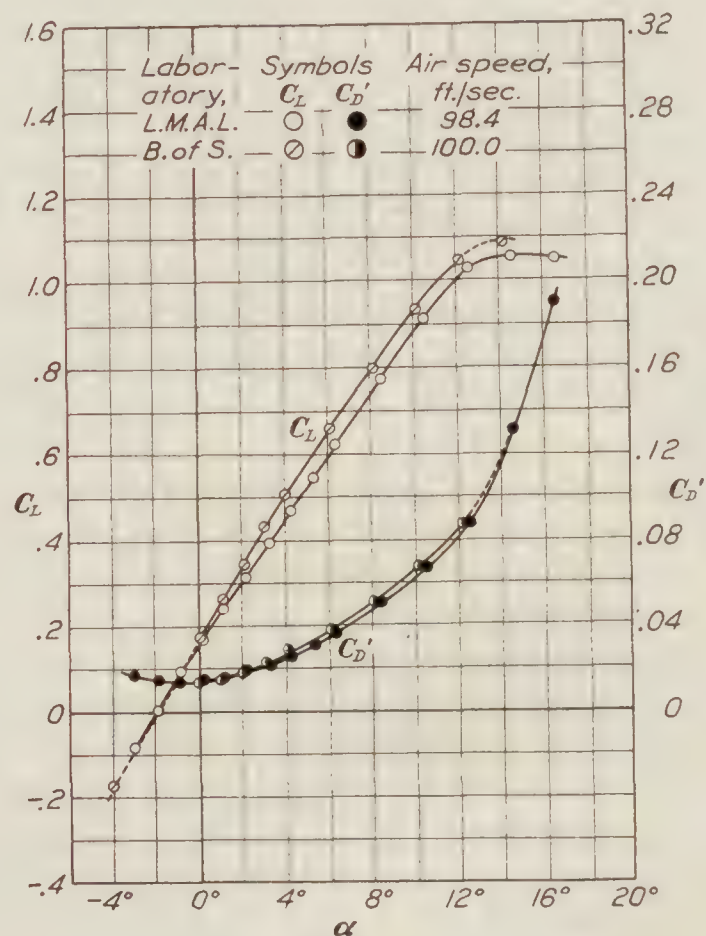


FIGURE 19

1.040 to 1.093. This must be considered reasonable agreement in this quantity which is sensitive to a number of factors, some tending to increase, some tending to decrease the observed value. In this case, the characteristics at high angles of attack in the McCook Field test at 40 miles per hour were determined with the model attached horizontally at its center to the

spindle of the N. P. L. type balance. This type of attachment is known to yield very unreliable results and the agreement obtained, though not close, speaks well for the care used in measuring the corrections in this case. In the tests at 20 miles per hour the model was held vertically by an end spindle and the average of the readings taken at a limited number of angles was used to determine the correction at all angles for spindle drag interference. This procedure is considered inadvisable, since there is no assurance that the correction does not vary erratically. The general practice is to determine the correction at each angle of attack. The report does not mention a correction for spindle lift and it is assumed that none was applied. This may partially explain the high maximum lift since this correction normally reduces the measured lift.

II. MINIMUM DRAG.—With the exception of the M. I. T. value, the agreement in minimum drag is very good. While the values of $C_{D\ min}$ range from 0.0138 to 0.0147, part of the variation is due to scale effect as shown by the plot of $C_{D\ min}$ against test speed on Figure 20. $C_{D\ min}$ would be expected to vary along a curve similar to the dotted line shown on this figure.

In regard to the low value of $C_{D\ min}$ obtained in the M. I. T. tests, the report from this laboratory contains the following statement: "The test on this airfoil was made in a routine manner, no extra preparation being made or precautions beyond those regularly taken being used. It is felt that the proper comparison is between routine tests and not between those of a highly specialized nature." Readings were taken at intervals of 2° over the entire angular

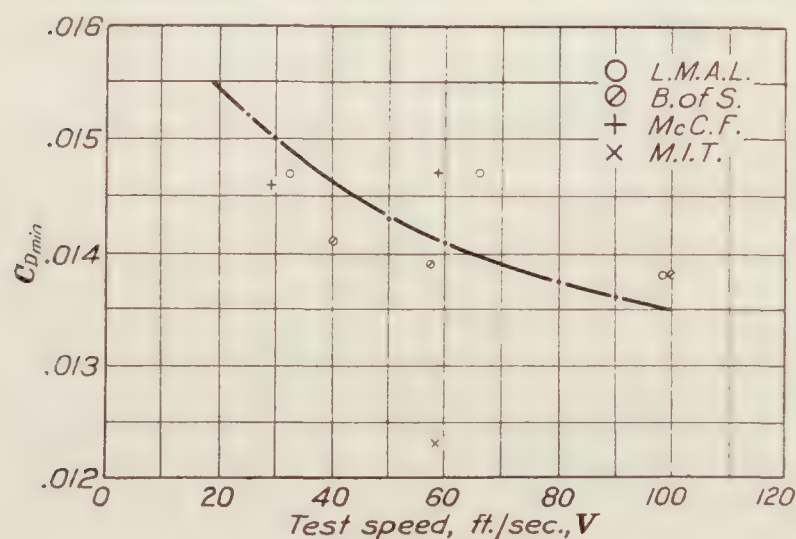


FIGURE 20

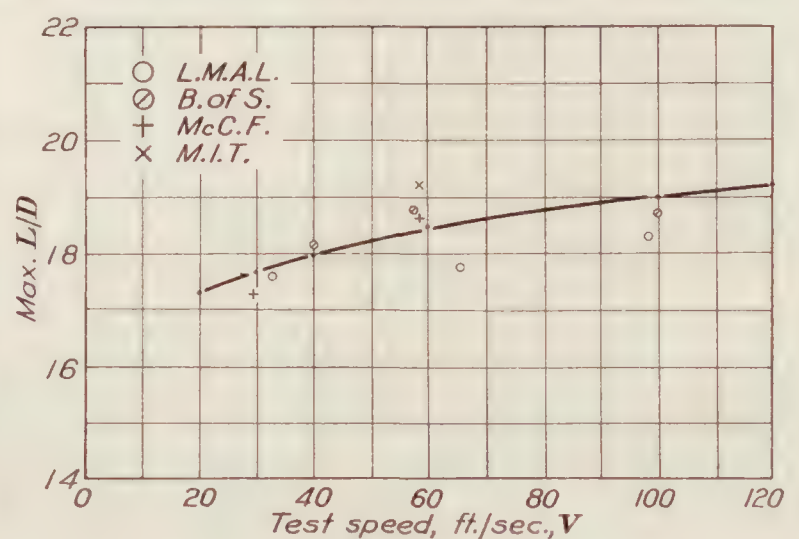


FIGURE 21

range of the tests, and the drag correction of the wire balance was determined by attaching a streamline rod the drag of which had been measured on a bell-crank balance. This at best gives only a close approximation to the wire drag correction, and some doubt naturally exists as to the accuracy in this case. In the Langley Field tests the wire drag correction was determined by testing two lengths of the same size rod on the wire balance, thus eliminating the attachment interference involved in the bell-crank balance.

After allowance has been made for different methods of holding the model and the general difficulty of securing great accuracy in measuring a low minimum drag, it is believed that a variation of more than 5 per cent from the mean should be considered excessive. It is generally agreed that in order to obtain accurate minimum drag data, the drag correction must be very accurately determined and the readings for model in normal and inverted positions averaged in order to eliminate the effects of unsymmetrical air flow. The M. I. T. tests were purely routine, and as such did not include the precautions usually employed in a precision test. While the remaining data are in good agreement, it appears probable that the drag values are low for this reason.

III. MAXIMUM $\frac{L}{D}$.—Using faired values altogether, the agreement in maximum L/D is very satisfactory. The extreme range is from 17.30 to 19.20, but if allowance be made for scale effect the deviation from a mean curve is relatively small, as shown on Figure 21.

IV. RATIO $\frac{C_{L \max}}{C_{D \min}}$.—This ratio is plotted against test speed in Figure 22. The extreme variation is from 73 to 84.6 if the M. I. T. value is included, or from 73 to 79.3 if the M. I. T. value is neglected. Again, part of the variation is due to scale effect as indicated by the dotted curve on Figure 21, which shows the expected trend.

V. CENTER OF PRESSURE.—A large scale plot of center of pressure C_p against angle of attack is given on Figure 23. The Langley Field values at 20 and 30 meters per second and the McCook Field values at 20 miles per hour are in excellent agreement, while the Langley Field values at 10 meters per second are apparently about $1\frac{1}{2}$ per cent too far forward and the M. I. T. values at 40 miles per hour are apparently about $1\frac{1}{2}$ per cent too far aft. Centers of pressure were not measured in the Bureau of Standards tests.

The agreement obtained is really quite satisfactory since a wire balance of the type used at Langley Field is rather unsatisfactory for measuring both forces and moments at low speeds.

CONCLUSIONS

A number of conclusions may be drawn from a study of these tests and while these conclusions are, in general, not new, it is considered desirable to give them as a general summary.

1. The Prandtl wall-effect correction is of great value. This correction should be incorporated in all published wind-tunnel data.

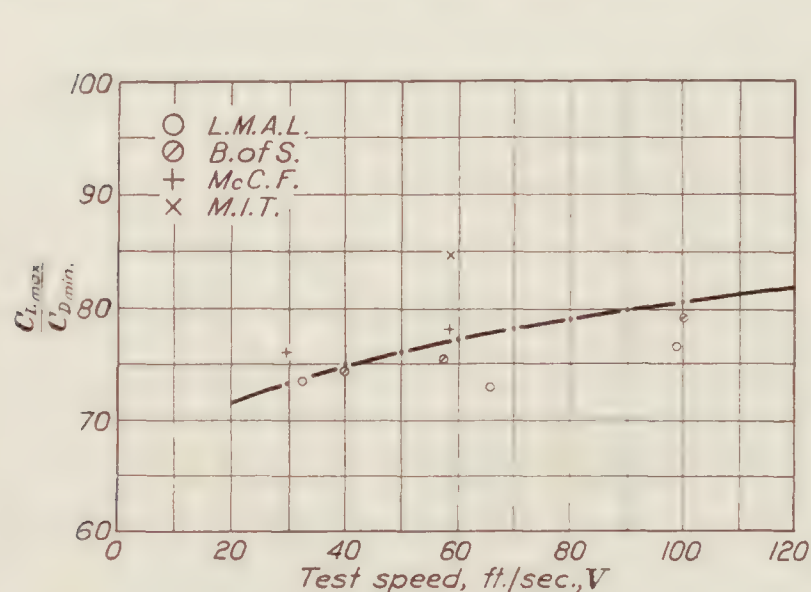


FIGURE 22

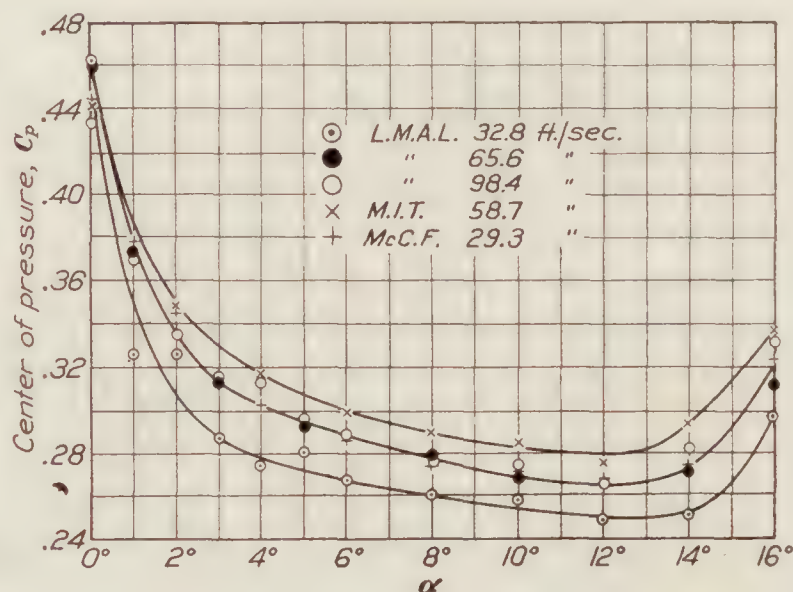


FIGURE 23

2. The agreement between the results from various wind tunnels, obtained in comparative tests of this type depends almost entirely on the care used in making the tests.

3. If accurate results are required, it is essential that all sources of error be investigated at each angle of attack. There is no assurance that a correction measured at one or two angles of attack can be interpolated or extrapolated.

4. The practice of testing an airfoil in both the upright and the inverted attitude and averaging the results should be made general.

5. During the last few years a very marked improvement in the quality of wind-tunnel test data has been made. The average routine test as now made is quite accurate for all design purposes.

6. These standardization tests should be of considerable interest and some value, but it is not likely that any similar additional series of tests would supply any new or valuable information. Such routine tests as are needed for standardization purposes can probably be handled most satisfactorily by agreement between the laboratories concerned.

ACKNOWLEDGMENT

The basic reports from which this analysis has been compiled were issued in various forms by the laboratories concerned. The report designations or descriptions and authors are as follows:

Bureau of Standards: The report from this laboratory entitled "Lift and Drag of Standard R. A. F. 15 Airfoil" was issued without designation of authors, but it is understood that these were Dr. H. L. Dryden and Mr. G. C. Hill.

Langley Memorial Aeronautical Laboratory: The test data from this laboratory are given in a report entitled "Tests of N. P. L. Standard Airfoil Model." The authors are not indicated but it is understood that these were Mr. E. G. Reid, Mr. A. J. Fairbanks, and Mr. E. D. Perkins.

Massachusetts Institute of Technology: The data from this laboratory are given in a report entitled "Report on Test of British International Trials Airfoil," Report Serial No. 204, by Mr. Shatswell Ober.

McCook Field: The data from this laboratory are given in a report entitled "Test in McCook Field Five-Foot Wind Tunnel of R. A. F. 15, 6 by 36 inch Airfoil (N. P. L. Metal Airfoil Circulated by N. A. C. A. for Wind Tunnel Standardization Tests)." This report is also designated as "Wind Tunnel Test No. 104" and is by Mr. E. N. Fales.

TABLES

Table	Air speed	Table	Air speed
I. Ordinates of Model.		VII. L. M. A. L.	98. 4 f. p. s.
II. Bureau of Standards	40 f. p. s.	VIII. M. I. T.	58. 7 f. p. s.
III. Bureau of Standards	57. 5 f. p. s.	IX. McCook Field	29. 3 f. p. s.
IV. Bureau of Standards	100 f. p. s.	X. McCook Field	58. 7 f. p. s.
V. L. M. A. L.	32. 8 f. p. s.	XI. Summary of Test Data.	
VI. L. M. A. L.	65. 6 f. p. s.		

TABLE I

Ordinates of 6 by 36 inch International Standard Airfoil as measured by the Gauge Section of the Bureau of Standards

Distance from L. E.	Section 12 inches from right tip		Section 16¼ inches from right tip		Section 24 inches from right tip		Standard R. A. F. 15	
	Upper	Lower	Upper	Lower	Upper	Lower	Upper	Lower
	Inch	Inch	Inch	Inch	Inch	Inch	Inch	Inch
0. 00								
. 15	0. 238	0. 024	0. 234	0. 023	0. 232	0. 022	0. 2286	0. 0216
. 30	. 305	. 006	. 301	. 006	. 300	. 005	. 2970	. 0072
. 45	. 344	. 002	. 341	. 000	. 340	. 000	. 3360	. 0018
. 60	. 370	. 000	. 367	. 001	. 365	. 001	. 3606	. 0006
. 90	. 398	. 001	. 395	. 011	. 393	. 011	. 3900	. 0114
1. 20	. 410	. 026	. 407	. 026	. 405	. 025	. 4014	. 0258
1. 80	. 408	. 051	. 406	. 052	. 405	. 052	. 4014	. 0504
2. 40	. 394	. 047	. 391	. 048	. 390	. 048	. 3870	. 0480
3. 00	. 370	. 032	. 367	. 033	. 366	. 033	. 3642	. 0336
3. 60	. 337	. 012	. 334	. 012	. 334	. 011	. 3318	. 0126
4. 20	. 292	. 000	. 289	. 000	. 288	. 000	. 2886	. 0012
4. 80	. 238	. 001	. 234	. 003	. 235	. 001	. 2334	. 0018
5. 40	. 172	. 012	. 168	. 014	. 169	. 012	. 1704	. 0138

NOTE.—Ordinates given are the heights above a plane tangent to the lower surface.

TABLE II

International Standard R. A. F. 15 model, Bureau of Standards 10-foot wind tunnel, June, 1924

[Air speed, 40 feet per second]

α	C_L	C_D	L/D	Corrected for wall effect		
				α	C_D	L/D
-4	-0.180	0.0274	-6.56	-4.02	0.0275	-6.54
-2	-0.033	.0167	-1.98	-2.00	.0167	-1.98
0	+.141	.0143	9.85	+.02	.0143	+9.85
1	.240	.0157	15.30	1.03	.0158	15.20
2	.328	.0184	17.82	2.04	.0187	17.54
3	.406	.0221	18.35	3.06	.0225	18.03
4	.475	.0271	17.50	4.07	.0276	17.20
6	.616	.0385	16.00	6.08	.0394	15.62
8	.762	.0513	14.85	8.10	.0527	14.46
10	.891	.0708	12.60	10.12	.0727	12.23
12	.995	.0833	11.93	12.14	.0857	11.61
14	1.051	.1058	9.95	14.14	.1085	9.70

TABLE III

International Standard R. A. F. 15 model, Bureau of Standards, June, 1924

[Air speed, 57.5 feet per second]

α	C_L	C_D	L/D	Corrected for wall effect		
				α	C_D	L/D
-4	-0.173			-4.02		
-2	-.015			-2.00		
0	+.168	0.0141	+11.91	+.02	0.0142	+11.82
1	.257	.0152	16.90	1.04	.0154	16.68
2	.336	.0178	18.86	2.05	.0181	18.55
3	.410	.0216	18.96	3.06	.0220	18.63
4	.481	.0264	18.22	4.07	.0270	17.82
6	.621	.0379	16.38	6.09	.0388	16.00
8	.778	.0522	14.90	8.11	.0537	14.50
10	.907	.0681	13.32	10.12	.0701	12.94
12	1.006	.0828	12.17	12.14	.0852	11.84
14	1.052	.1053	9.99	14.14	.1080	9.74

TABLE IV

International Standard R. A. F. 15 Airfoil model, Bureau of Standards, June, 1924

[Air speed, 100 feet per second]

α	C_L	C_D	L/D	Corrected for wall effect		
				α	C_D	L/D
-4	-0.173			-4.02		
-2	.000	0.0000	0.00	-2.00		0.00
0	+.175	.0140	+12.50	.02	0.0141	+12.41
1	.262	.0154	17.00	1.04	.0156	16.80
2	.346	.0185	18.70	2.05	.0188	18.40
3	.430	.0226	19.00	3.06	.0230	18.70
4	.508	.0277	18.35	4.07	.0283	17.96
6	.658	.0367	17.93	6.09	.0377	17.46
8	.799	.0492	16.23	8.11	.0507	15.80
10	.935	.0655	14.28	10.13	.0676	13.83
12	1.059	.0841	12.60	12.14	.0868	12.20
14	1.093			14.15		

TABLE V

International Standard R. A. F. 15 Airfoil, Langley Memorial Aeronautical Laboratory 5-foot wind tunnel
[Test speed (10 meters per second), 32.8 feet per second]

α	C_L	C_D	L/D	C_p	Corrected for wall effect		
					α	C_D	L/D
-3	-0.092	0.0198	-4.65	-4.56	-3.05	0.0199	-4.62
-2	-.017	.0173	-.98	-.851	-2.01	.0173	-.98
-1	+.052	.0154	+3.38	+.760	-.97	.0154	+3.38
0	.142	.0145	9.79	.462	+.08	.0147	9.66
+1	.248	.0152	16.32	.326	1.14	.0157	15.78
2	.328	.0178	18.43	.324	2.18	.0187	17.54
3	.403	.0215	18.76	.287	3.22	.0230	17.53
4	.480	.0257	18.68	.275	4.26	.0279	17.20
5	.555	.0308	18.00	.281	5.30	.0338	16.42
6	.632	.0368	17.20	.268	6.35	.0406	15.58
8	.781	.0504	15.50	.261	8.43	.0563	13.86
10	.920	.0665	13.83	.258	10.50	.0746	12.33
12	1.042	.0843	12.51	.251	12.57	.0947	11.00
14	1.078	.1199	9.00	.252	14.58	.1310	8.23
16	1.020	.2181	4.68	.308	16.56	.2281	4.47
18	.947	.3008	3.15	.354	18.52	.3095	3.05

TABLE VI

International Standard R. A. F. 15 Airfoil, Langley Memorial Aeronautical Laboratory 5-foot wind tunnel, October, 1923
[Test speed (20 meters per second), 65.6 feet per second]

α	C_L	C_D	L/D	C_p	Corrected for wall effect		
					α	C_D	L/D
-3	-0.088	0.0189	-4.66	-4.04	-3.05	0.0190	-4.63
-2	-.008	.0163	-.49	-2.27	-2.00	.0163	-.49
-1	+.080	.0147	+5.43	+.620	-.96	.0148	+5.41
0	.167	.0149	11.20	.460	+.09	.0152	10.98
1	.246	.0163	15.10	.373	1.13	.0169	14.55
2	.322	.0184	17.50	.336	2.18	.0194	16.60
3	.398	.0211	18.85	.313	3.22	.0226	17.60
4	.472	.0246	19.18	.305	4.26	.0267	17.67
5	.549	.0291	18.86	.294	5.30	.0320	17.16
6	.626	.0345	18.14	.289	6.35	.0382	16.38
8	.777	.0470	16.53	.279	8.43	.0527	14.72
10	.917	.0612	14.96	.269	10.50	.0692	13.24
12	1.014	.0792	12.80	.267	12.56	.0890	11.40
14	1.069	.1186	9.01	.272	14.59	.1295	8.25
16	1.050	.2008	5.22	.311	16.58	.2113	4.97
18	.986	.2788	3.53	.352	18.54	.2881	3.42

TABLE VII

International Standard R. A. F. 15 Airfoil, Langley Memorial Aeronautical Laboratory 5-foot wind tunnel, October, 1923
[Test speed (30 meters per second), 98.4 feet per second]

α	C_L	C_D	L/D	C_p	Corrected for wall effect		
					α	C_D	L/D
-3	-0.081	0.0176	-4.60	-5.79	-3.04	0.0177	-4.57
-2	+.004	.0149	+.27	+9.42	-1.99	.0149	+.27
-1	.096	.0137	7.04	.593	-.95	.0138	6.96
0	.171	.0144	11.92	.433	+.09	.0147	11.60
1	.240	.0159	15.13	.370	1.13	.0165	14.52
2	.316	.0174	18.12	.335	2.17	.0184	17.17
3	.394	.0201	19.57	.315	3.22	.0216	18.24
4	.469	.0238	19.72	.313	4.26	.0259	18.11
5	.547	.0281	19.44	.296	5.30	.0309	17.70
6	.621	.0329	18.91	.289	6.34	.0366	16.97
8	.771	.0446	17.32	.278	8.42	.0503	15.33
10	.912	.0588	15.52	.275	10.50	.0667	13.67
12	1.027	.0779	13.18	.266	12.56	.0880	11.67
14	1.059	.1206	8.75	.282	14.58	.1313	8.07
16	1.055	.1805	5.82	.331	16.58	.1911	5.52

TABLE VIII

International Standard R. A. F. 15 Airfoil model, Massachusettes Institute of Technology 7½-foot wind tunnel
February, 1924

[Air speed, 58.67 feet per second.]

α	C_L	C_D	L/D	C_p	Corrected for wall effect		
					α	C_D	L/D
-4	-0.144	0.0210	-6.85	-----	-4.0	0.0212	-6.79
-2	-.006	.0138	-.43	-----	-2.0	.0138	-.43
0	+.176	.0122	+14.42	0.441	.0	.0124	+14.09
2	.328	.0166	19.76	.348	+2.1	.0172	19.17
4	.472	.0242	19.50	.317	4.1	.0252	18.73
6	.618	.0346	17.88	.299	6.2	.0362	17.07
8	.758	.0478	15.86	.289	8.2	.0502	15.10
10	.894	.0634	14.10	.285	10.2	.0668	13.38
12	1.012	.0810	12.50	.276	12.2	.0852	11.88
14	1.026	.1154	8.88	.294	14.3	.1198	8.56
16	.976	.1792	5.44	.336	16.2	.1840	5.30
18	.888	.2608	3.40	.391	18.2	.2640	3.36

TABLE IX

International Standard R. A. F. 15 Airfoil, McCook Field 5-foot wind tunnel, March, 1924

[Test speed (20 miles per hour), 29.3 feet per second]

α	C_L	C_D	L/D	C_p	Corrected for wall effect		
					α	C_D	L/D
-6	-0.337	0.0598	-5.63	-----	-6.19	0.0608	-5.54
-4	-.152	.0285	-5.33	-5.98	-4.10	.0287	-6.11
-2	-.033	.0168	-1.97	-.463	-2.02	.0168	-1.97
-1	+.042	.0156	+2.68	.822	-.98	.0156	+2.68
0	.131	.0145	9.03	.443	+.07	.0146	8.96
+1	.242	.0149	16.22	.379	1.14	.0154	15.73
2	.331	.0184	18.00	.345	2.19	.0194	17.00
4	.483	.0266	18.16	.303	4.27	.0289	16.70
6	.638	.0371	17.20	.286	6.36	.0412	15.50
8	.785	.0508	15.48	.275	8.44	.0568	13.82
10	.928	.0693	13.40	.272	10.52	.0776	11.97
12	1.057	.0859	12.31	.267	12.60	.0970	10.89
14	1.106	.1329	8.32	.274	14.62	.1446	7.65
16	1.060	.2325	4.56	.323	16.60	.2435	4.35
18	1.004	.3000	3.35	.360	18.57	.3100	3.24

TABLE X

International Standard R. A. F. 15 Airfoil, McCook Field 5-foot wind tunnel, March, 1924

[Test speed (40 miles per hour), 58.7 feet per second]

α	C_L	C_D	L/D	Corrected for wall effect		
				α	C_D	L/D
-6	-0.329	0.0589	-5.58	-6.18	0.0599	-5.50
-4	-.174	.0268	-6.50	-4.10	.0271	-6.42
-2	-.012	.0163	-7.36	-2.01	.0163	-.74
0	+.187	.0144	+12.98	4.11	.0148	+12.62
2	.355	.0188	18.88	2.20	.0201	17.68
4	.510	.0262	19.46	2.29	.0275	18.53
6	.673	.0370	18.20	6.38	.0415	16.20
8	.826	.0512	16.10	8.46	.0577	14.32
10	.971	.0687	14.12	10.55	.0780	12.45
12	1.093	.0921	11.86	12.62	.1038	10.53
14	1.140	.1296	8.78	14.64	.1424	8.00
16	1.133	.2120	5.33	16.64	.2247	5.05

TABLE XI

International Standard R. A. F. 15 Airfoil, summary of test data

Laboratory	Bureau of Standards		
Test speed, f. p. s.-----	40. 0	57. 5	100. 0
$C_{L\ max}$ -----	1. 050	1. 050	1. 093
<i>1. Data uncorrected for wall effect</i>			
$C_{D\ min}$ -----	. 0140	. 0138	. 0137
L/D_{max} -----	18. 40	19. 10	19. 10
$C_{L\ max}/C_{D\ min}$ -----	75. 0	76. 1	79. 8
<i>2. Data corrected for wall effect</i>			
$C_{D\ min}$ -----	. 0141	. 0139	. 0138
L/D_{max} -----	18. 10	18. 75	18. 70
$C_{L\ max}/C_{D\ min}$ -----	74. 5	75. 5	79. 3
α for zero lift-----	-1. 62	-1. 84	-2. 00
Laboratory	Langley Memorial Aeronautical Laboratory		
Test speed, f. p. s.-----	32. 8	65. 6	98. 4
$C_{L\ max}$ -----	1. 083	1. 073	1. 057
<i>1. Data uncorrected for wall effect</i>			
$C_{D\ min}$ -----	. 0145	. 0145	. 0137
L/D_{max} -----	18. 80	19. 20	19. 80
$C_{L\ max}/C_{D\ min}$ -----	74. 7	74. 1	77. 2
<i>2. Data corrected for wall effect</i>			
$C_{D\ min}$ -----	. 0147	. 0147	. 0138
L/D_{max} -----	17. 60	17. 75	18. 30
$C_{L\ max}/C_{D\ min}$ -----	73. 7	73. 0	76. 6
α for zero lift-----	-1. 75	-1. 91	-1. 96
Laboratory	Massachusetts Institute of Technology	McCook Field	
Test speed, f. p. s.-----	58. 7	29. 3	58. 7
$C_{L\ max}$ -----	1. 040	1. 110	1. 153
<i>1. Data uncorrected for wall effect</i>			
$C_{D\ min}$ -----	. 0120	. 0143	. 0143
L/D_{max} -----	20. 20	18. 50	19. 60
$C_{L\ max}/C_{D\ min}$ -----	86. 8	77. 6	80. 5
<i>2. Data corrected for wall effect</i>			
$C_{D\ min}$ -----	. 0123	. 0146	. 0147
L/D_{max} -----	19. 20	17. 30	18. 60
$C_{L\ max}/C_{D\ min}$ -----	84. 6	76. 0	78. 3
α for zero lift-----	-1. 94	-1. 12	-1. 90

BUREAU OF AERONAUTICS,
NAVY DEPARTMENT,
June, 1928.

REPORT No. 310

**PRESSURE ELEMENT
OF CONSTANT LOGARITHMIC STIFFNESS FOR
TEMPERATURE COMPENSATED ALTIMETER**

By W. G. BROMBACHER and F. CORDERO
Bureau of Standards

REPORT No. 310

PRESSURE ELEMENT OF CONSTANT LOGARITHMIC STIFFNESS FOR TEMPERATURE COMPENSATED ALTIMETER

By W. G. BROMBACHER and F. CORDERO

SUMMARY

The usual type of altimeter contains a pressure element, the deflections of which are approximately proportional to pressure changes. An evenly divided altitude scale is secured by using a mechanism between the pressure element and pointer which gives the required motion of the pointer. A temperature-compensated altimeter was constructed at the Bureau of Standards for the Bureau of Aeronautics of the Navy Department which contained a manually operated device for controlling the multiplication of the mechanism to the extent necessary for temperature compensation. The introduction of this device made it difficult to adjust the multiplying mechanism to fit an evenly divided altitude scale. To meet this difficulty a pressure element was designed and constructed which gave deflections which were proportional to altitude; that is, to the logarithm of the pressure. Mathematically, the logarithmic stiffness S' of the element equals

$$S' = \frac{d \log_e P}{dy}$$

from which is derived the deflection y for the change in pressure from P_o to P

$$y = \frac{\log_e P - \log_e P_o}{S'}$$

The element consisted of a metal bellows of the sylphon type coupled to an internal helical spring which was designed so as to have a variable number of active coils. This report presents a description of and laboratory data relating to the special pressure element for the altimeter. In addition equations which apply generally to springs and pressure elements of constant logarithmic stiffness are developed, including the deflection and the spacing between the coils in terms of the constants of the helical spring and pressure element.

INTRODUCTION

An altimeter is a pressure-measuring instrument calibrated in altitude according to the altitude-pressure relation of a standard atmosphere. It consists essentially of two parts, one the pressure element and the other the multiplying mechanism. The latter is that part which connects the pressure element to the pointer. As pressure elements ordinarily have deflections very nearly directly proportional to pressure changes, a scale evenly divided in altitude units requires that the ratio of the linear motion of the pointer to the deflection of the pressure element (multiplying ratio) must vary continuously with the air pressure.

In the course of the development of a temperature-compensated altimeter for the Bureau of Aeronautics of the Navy Department considerable difficulty was experienced in obtaining an evenly divided altitude scale. This was largely due to the restrictions imposed on the multiplying mechanism by the device by which compensation was made for the effect of air temperature, which was secured by suitably controlling the multiplication of the motion of the pressure element. This was manually controlled by a thumb nut by which settings were made to correspond to the observed air temperature at the ground level. The addition of this extra mechanism to the altimeter did not appear to permit the adjustment necessary for an evenly divided scale. It was not considered advisable to change the general design of the mechanism.

Consideration was then given to the possibility of designing a pressure element which would give deflections proportional to changes in altitude (that is, proportional to the logarithm of the pressure) and thus eliminate the need for a mechanism with a variable multiplying ratio. The original pressure-element design consisted of a "sylphon" bellows enclosing a steel helical spring and evacuated in accordance with usual practice. The possibilities narrowed down finally to the modification of the design of the spring. A successful design was finally found which gave approximately the desired straight-line relation between deflection and altitude in the altitude range of the altimeter.

STATEMENT OF THE PROBLEM

The relation between pressure and altitude to which altimeters are calibrated in the United States is that of the standard atmosphere which is for altitudes below 35,332 feet,

$$Z = 63,691.8 \frac{T_m}{288} \log_{10} \frac{760}{p} \quad (1)$$

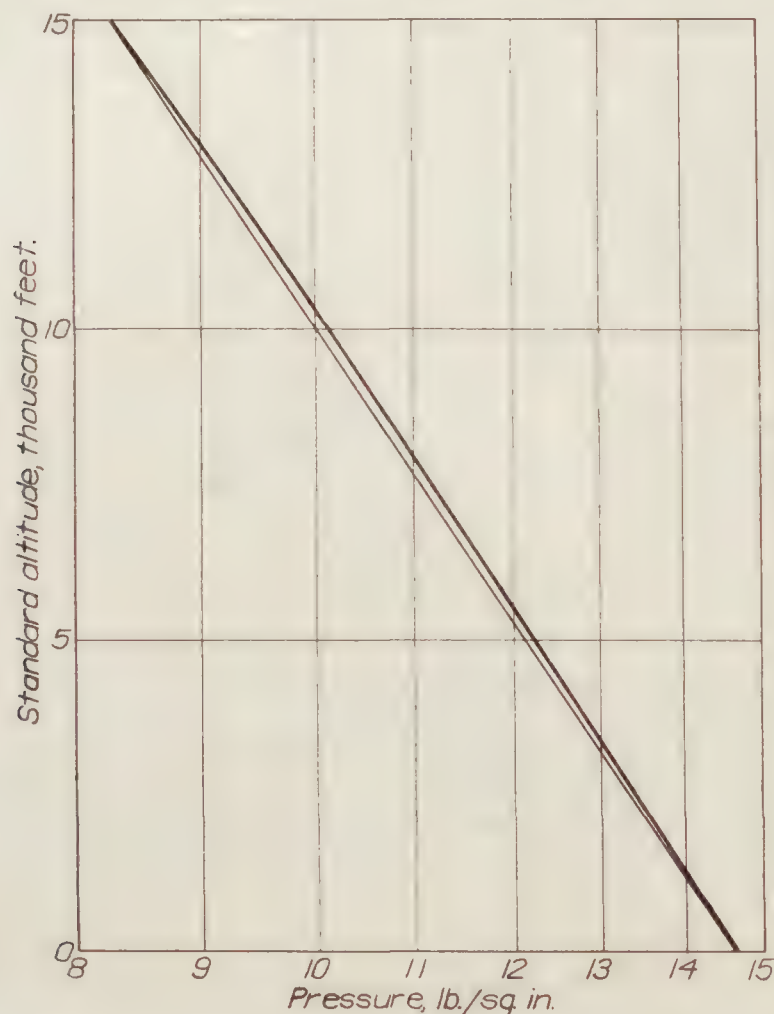


FIGURE 1.—Standard altitude varies approximately as the logarithm of the air pressure

in which Z is the standard altitude in feet, T_m the standard mean temperature for Z , and p the air pressure at altitude Z in millimeters of mercury. (For further details on the standard atmosphere see References 1, 2, and 3. For convenient altitude-pressure tables, see Reference 3.) An inspection of equation (1) will show that variations in the temperature term $T_m/288$ are of the second order compared with those of $\log \frac{760}{p}$. This point is brought out in Figure 1, in which standard

altitude is plotted against the logarithm of the pressure. The deviation of the curve from a straight line is so small that for all practical purposes a pressure element with deflections proportional to altitude is secured if the deflections are proportional to the logarithm of the pressure.

The solution depends entirely on the design of the spring. This was accomplished by adjusting the spacing between the coils so that the number of active coils of the spring gave the desired stiffness. Thus, if the pressure acting externally on a pressure element containing such a spring increased, the number of active coils decreased and vice versa. The inactive coils, being in contact, could not contribute to the deflection.

It is necessary for the purpose of design to obtain a relation between the spacing between the coils of the spring of a "logarithmic pressure element" and the position on the spring. The latter may be best located by giving the distance on the spring wire starting from the bottom of the spring. The following assumptions are fundamental:

1. The unmodified pressure element gives a straight line relation between pressure and deflection for the working pressure range.
2. A helical spring is used.
3. The relation between spring stiffness s and length of active wire l is

$$s = \frac{1}{Kl}$$

where K is a constant.

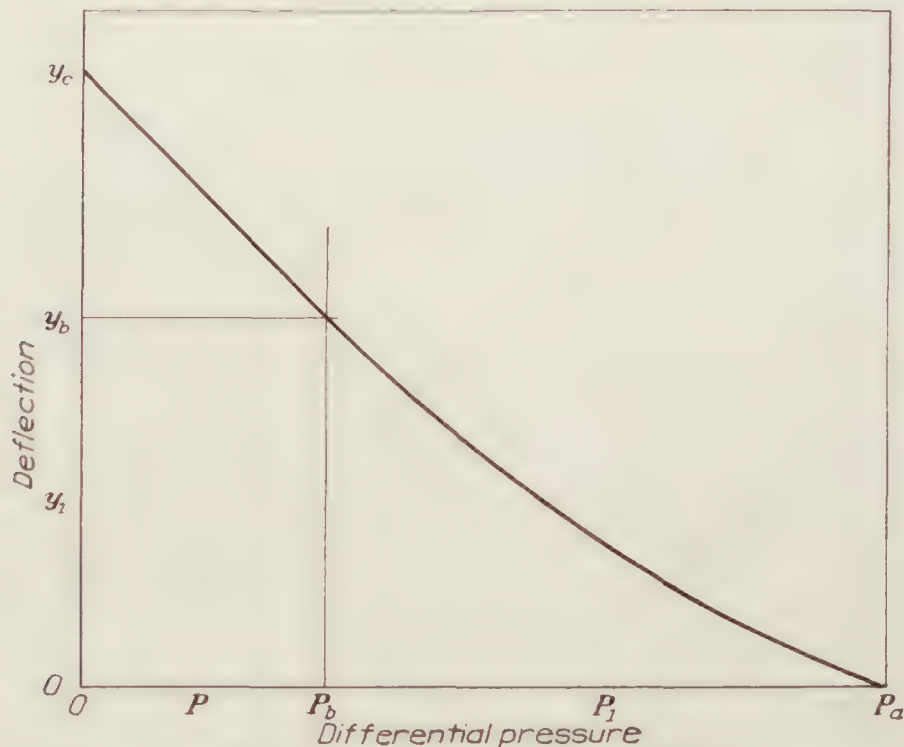


FIGURE 2.—Typical curve for logarithmic element
 $y_1 \propto \log P_1$, $y_c - y_b \propto P$

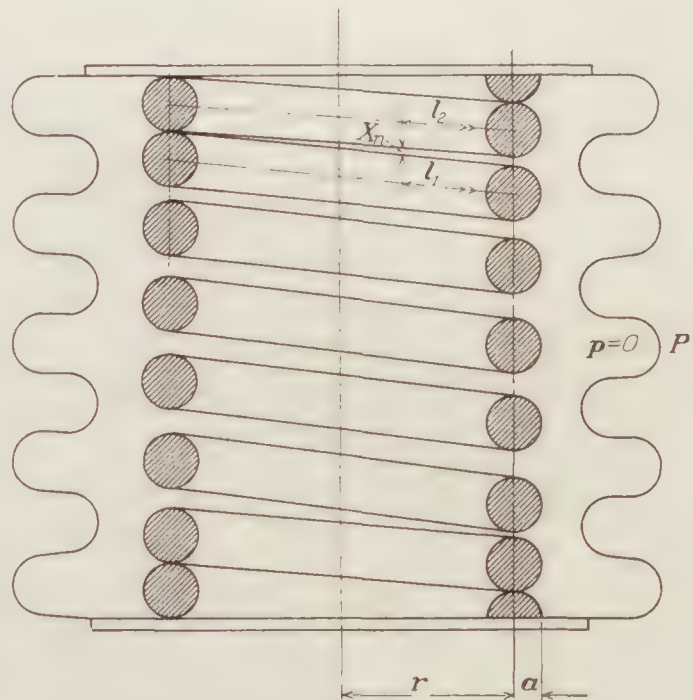


FIGURE 3.—Cross section of pressure element

DESIGN OF SPRING FOR LOGARITHMIC PRESSURE ELEMENT

DEFINITIONS

P = the differential air pressure in pounds per square inch acting on the pressure element.

P_a refers to the value at sea level atmospheric pressure;

P_b to the value below which all of the spring wire will contribute to the deflection;

P_1 to the value in the region P_a to P_b ;

P_o to zero differential pressure.

See Figures 2 and 3.

S = the stiffness of the pressure element in pounds per inch corresponding to values of the pressure P .

y = the deflection of the pressure element in inches corresponding to values of the pressure P .

S' = the logarithmic stiffness of the pressure element.

s = the stiffness of the spring in pounds per inch; the various values correspond to the pressure P .

l = the length of the active portion of the spring wire in inches; the various values correspond to the pressure P . l is measured from the bottom of the spring to the top. It forms a convenient way of locating points on the spring; thus $l=0$ is the bottom of the spring, $l=l_b$ is top, and $l=l_1$ is the length of spring wire which is active when the pressure element is subject to pressure P_1 , and marks the point on the spring below which the spring wire is active, and above which, inactive.

The corresponding values of the various quantities are given in the following table:

P	S	y	s	l
P_a	S_a	0	s_a	l_a
P_1	S_1	y_1	s_1	l_1
P_b	S_b	y_b	s_b	l_b
0	S_b	y_c	s_b	l_b

s_d = the stiffness of the sylphon in pounds per inch.

p = the gas pressure inside of the pressure element. This is zero. See Figure 3.

A_q = the equivalent area of the sylphon in square inches.

d_1 and d_2 = the diameter in inches, respectively, of the circumscribing and inscribing cylinders of the sylphon bellows.

r = the radius of the spring coils in inches.

a = the radius of the spring wire in inches.

G = the modulus in torsion of the spring material in pounds per square inch.

X_m = the sum of the spacings between all of the coils of the spring in inches between points l_b and l_1 , measured on a generatrix of the cylinder passing through the center line of the wire. The spacing is that when the pressure element is subject to the differential pressure P_b .

X_m' = the same as X_m except that it refers to the value of X_m between points on the spring $l_2 = l_1 + 2\pi r$ and l_b .

X_n = the spacing in inches between two adjacent coils measured between points on the spring l_1 and l_2 . See Figures 3 and 4. It equals $X_m - X_m'$ and therefore is the value when the pressure element is subject to a differential pressure P_b .

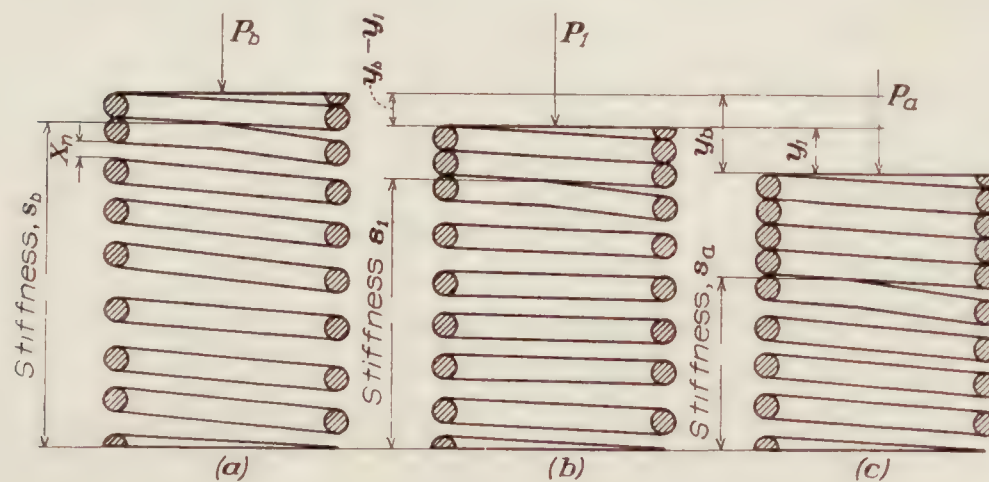


FIGURE 4

THEORY.—The stiffness of a pressure element is the sum of stiffnesses of the elements. (Reference 5.)

$$S = s + s_d \quad (2)$$

The stiffness of the sylphon or diaphragm capsule s_d is usually small in comparison to that of the spring.

The commonly used helical spring formulas given for s :

$$s = \frac{1}{Kl} \quad (3)$$

in which

$$K = \frac{2r^2}{\pi G a^4} \quad (4)$$

In order to meet the conditions, the deflection of the pressure element should be proportional to the standard altitude which, as shown in Figure 1, is very closely proportional to the logarithm of the pressure in the altitude range, 0 to 15,000 feet. That is,

$$\frac{d \log_e A_q P_1}{dy_1} = \text{a constant} \equiv S' \quad (5)$$

in which A_q equals for a sylphon,

$$A_q = \frac{\pi}{8} (d_1^2 + d_2^2) \quad (\text{Reference 4}). \quad (6)$$

Further,

$$S' = \frac{1}{P_1} \frac{dP_1}{dy_1} \quad (7)$$

and by the definition of stiffness,

$$S_1 = \frac{dA_q P_1}{dy_1} = A_q \frac{dP_1}{dy_1} \quad (8)$$

From equations (2), (7), and (8), adding the proper subscripts,

$$\begin{aligned} S_1 &= S' A_q P_1 \\ &= s_1 + s_d \end{aligned} \quad (9)$$

Substituting for s from equation (3) and evaluating for P_1

$$P_1 = \frac{1 + s_d K l_1}{S' A_q K l_1} \quad (10)$$

This gives the relation between l_1 and the pressure P_1 .

In the region P_1 to P_a , it follows directly from equation (5), that

$$y_1 = \frac{\log_e P_a - \log_e P_1}{S'} \quad (11)$$

Noting equations (2) and (9) it follows that

$$s_1 = S_1 - s_d = A_q S' P_1 - s_d \quad (12)$$

The deflection, $y_c - y_b$ is

$$y_c - y_b = \frac{A_q P_b}{s_b + s_d} \quad (13)$$

s_b is here a constant, that for the spring when all of its length is acting.

It is desired to find a relation between the length of the spring wire and the gap or spacing between the coils.

Let the reference point be chosen at the condition when the pressure equals P_b , that is, the evacuated pressure element is subjected to the external pressure at which all the coils of the spring are active, but start to go out of action as the pressure is increased. See Figure 4. As the pressure is increased to a given value P_1 , the resulting deflection may be divided into two parts, that due to the part of the spring active at P_1 , and that due to the part of the spring which has gone out of action in the pressure interval P_b to P_1 . Let the component of the deflection of the element due to the coils which are active at pressure P_1 , that is from $l=0$ to l_1 be designated by y_1' . The other component is X_m . Then

$$y_b - y_1 = y_1' + X_m \quad (14)$$

The component y_1' is

$$y_1' = \frac{A_q (P_1 - P_b)}{s_1 + s_d} \quad (15)$$

The above expression for y_1' is derived as follows: In Figure 4(b) the pressure element is subject to pressure P_1 and the spring has an instantaneous stiffness s_1 and a definite active portion

of length l_1 . Referring now to Figure 4(a), if only the deflection of the portion of the spring l_1 that is y_1' , be considered for the pressure change P_b to P_1 , it is seen that the stiffness of the spring is constant and equal to s_1 . The expression for y_1' then follows from the definition of stiffness, noting that the stiffness of the element is $s_1 + s_d$.

The value of X_m is determined introducing the value of y_1 given in equation (11).

$$X_m = y_1 - y_1' - y_b = -\frac{\log_e P_1 - \log_e P_a}{S'} - \frac{A_d(P_1 - P_b)}{s_1 + s_d} - y_b \quad (16)$$

Substitute in equation (16) for P_1 , the value given in equation (10) and for $\frac{A_d}{s_1 + s_d}$ from equation (9).

$$X_m = \frac{1}{S'} \log_e \frac{l_a(1 + s_d K l_1)}{l_1(1 + s_d K l_a)} - \left[\frac{1}{S'} - \frac{l_1(1 + s_d K l_b)}{S' l_b(1 + s_d K l_1)} \right] - y_b \quad (17)$$

$$\text{Let } l_2 \text{ be defined by } l_2 - l_1 = 2\pi r. \quad (18)$$

Then if l_2 be substituted for l_1 in equation (17) there is obtained

$$X_m' = \frac{1}{S'} \left[\log_e \frac{l_a(1 + s_d K l_2)}{l_2(1 + s_d K l_a)} \right] - \left[\frac{1}{S'} - \frac{l_2(1 + s_d K l_b)}{l_b S' (1 + s_d K l_2)} \right] - y_b \quad (19)$$

It is evident that the difference $X_m - X_m'$ gives the spacing between adjacent coils of the spring in terms of the length of the spring wire. That is

$$X_n = X_m - X_m' \quad (20)$$

It should be noted that l , the length of the wire is always the length of the active wire. The convention is here conveniently adopted of measuring the wire length from the bottom of the spring to the top, the coils at the top going out of action as the pressure increases.

Equation (20) applies to pressure elements containing a diaphragm or sylphon and a helical spring and is based on the following assumptions:

- (a) The sylphon or diaphragm gives a straight line pressure-deflection curve.
- (b) The deflection is zero when the external pressure is equal to the atmospheric pressure and is approximately zero inside of the pressure element.
- (c) The deflection is positive when the external pressure decreases and is proportional to the logarithm of the pressure for all values in the range from atmospheric to P_b . See Figure 2.

DESIGN OF LOGARITHMIC HELICAL SPRING

In view of the relations just developed there is no difficulty in arriving at the design equation for a simple helical compression spring, the deflection of which is directly proportional to the logarithm of the load.

- Let
- $L =$ the load in pounds applied to the spring.
 - L_o and L_m are respectively the lower and upper limits of the loads for which the deflection is logarithmic.
 - L_1 is a load between L_o and L_m .
 - $y =$ the deflection of the spring in inches.
 - $y_o = 0$, y_m and y_1 correspond to the loads L_o , L_m and L_1 .
 - $l =$ the length of the spring wire in inches, the subscripts corresponding to those for L . l is measured from the bottom end of the spring.
 - $X_m =$ the sum of the spacing between all of the coils of the spring in inches from the end l_o of the spring wire to any point l_1 , measured on an element of the cylinder passing through the center line of the wire. It refers to the spacing when the spring is subject to the load L_o .
 - $X_m' =$ the same as X_m except that it refers to the value of X_m between the points on the spring $l_2 = l_1 + 2\pi r$ and the top end of the spring l_o .
 - $X_n =$ the spacing in inches between two adjacent coils measured between points on the spring l_1 and l_2 . The value is that when the spring is subject to load L_o .

The expressions for the load-deflection characteristics of a "logarithmic" helical compression spring are given below. As for the pressure element,

$$\frac{d \log_e L_1}{dy_1} = a \text{ constant} \equiv s' \quad (21)$$

from which

$$y_1 = \frac{1}{s'} \log_e \frac{L_1}{L_o} \quad (22)$$

The following relation is also true, in which $\frac{dL}{dy}$ may be called the instantaneous stiffness.

$$\frac{dL}{dy} = s \quad (23)$$

From relations (21) and (23)

$$s_1 = s' L_1 \quad (24)$$

Similarly as for the pressure element just considered, the sum of the spacing X_m between the coils along an element in the cylinder passing through the axis of the wire is given the difference between the total deflection y_1 and the deflection y_1' due to the coils which remain active after load L_1 is applied. This may be made clearer by assuming that the spring is in two parts, one consisting of the portion of the spring, all the coils of which contribute to the deflection as the load changes from L_o to L_1 and the other of the portion which is fully active for load L_o and entirely inactive for load L_1 . The deflection y_1 can be assumed as the sum of the deflections of the two parts. That is,

$$y_1 = X_m + y_1' \quad (25)$$

It is evident that

$$y_1' = \frac{L_1 - L_o}{s_1} \quad (26)$$

Putting in the values of y_1' given in equation (26) and y_1 from equation (22), equation (25) becomes

$$X_m = y_1 - y_1' = \frac{1}{s'} \log_e \frac{L_1}{L_o} - \frac{L_1 - L_o}{s_1} \quad (27)$$

Noting equations (3) and (24),

$$X_m = \frac{1}{s'} \log_e \frac{l_o}{l_1} - \frac{l_o - l_1}{s' l_o} \quad (28)$$

As before, choose l_2 so that

$$l_2 - l_1 = 2\pi r \quad (29)$$

and substituting l_2 for l_1 in equation (28), X_m' is obtained.

$$X_m' = \frac{1}{s'} \log_e \frac{l_o}{l_2} - \frac{l_o - l_2}{s' l_o} \quad (30)$$

The space X_n between any two coils is then given by

$$X_n = X_m - X_m' = \frac{1}{s'} \log_e \frac{l_2}{l_1} - \frac{l_2 - l_1}{s' l_o} \quad (31)$$

Equation (31) gives the desired relation between the spacing for adjacent coils and the length of the spring wire.

Equation (31) is identical with equation (20) for the pressure element if the stiffness of the sylphon s_d is assumed equal to zero.

DESCRIPTION AND PERFORMANCE OF "LOGARITHMIC" PRESSURE ELEMENTS

In connection with the development of the altimeter, four pressure elements were constructed according to the design which had been previously found to be satisfactory. It was found that the deflection-altitude curve of each element varied with the position of the gauge on the rigid top of the element due to slight tilting or cocking of the spring, which was caused by coils coming into or going out of action. The amount of this effect is shown in Figure 5, which gives deflection curves for four angular positions of the measuring gauge on the top of a pressure element. In each case the angular position at the proper distance from the center was found at which the deflection was most nearly proportional to the standard altitude or the logarithm of the pressure.

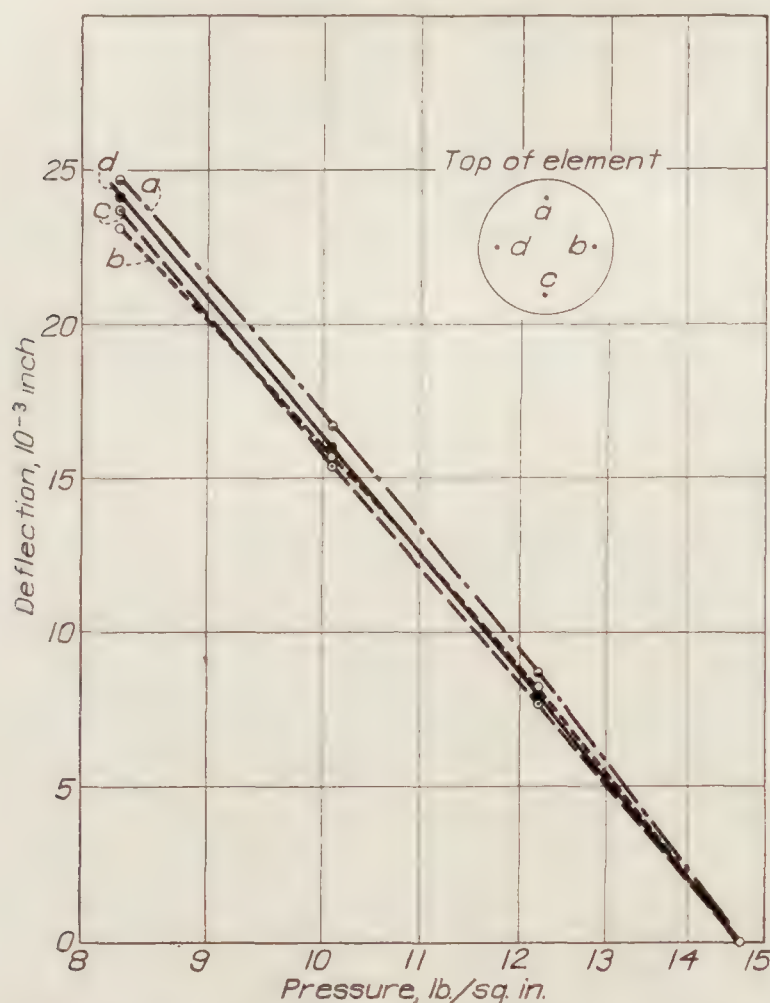


FIGURE 5.—Effect of position on the deflection of pressure element No. 4

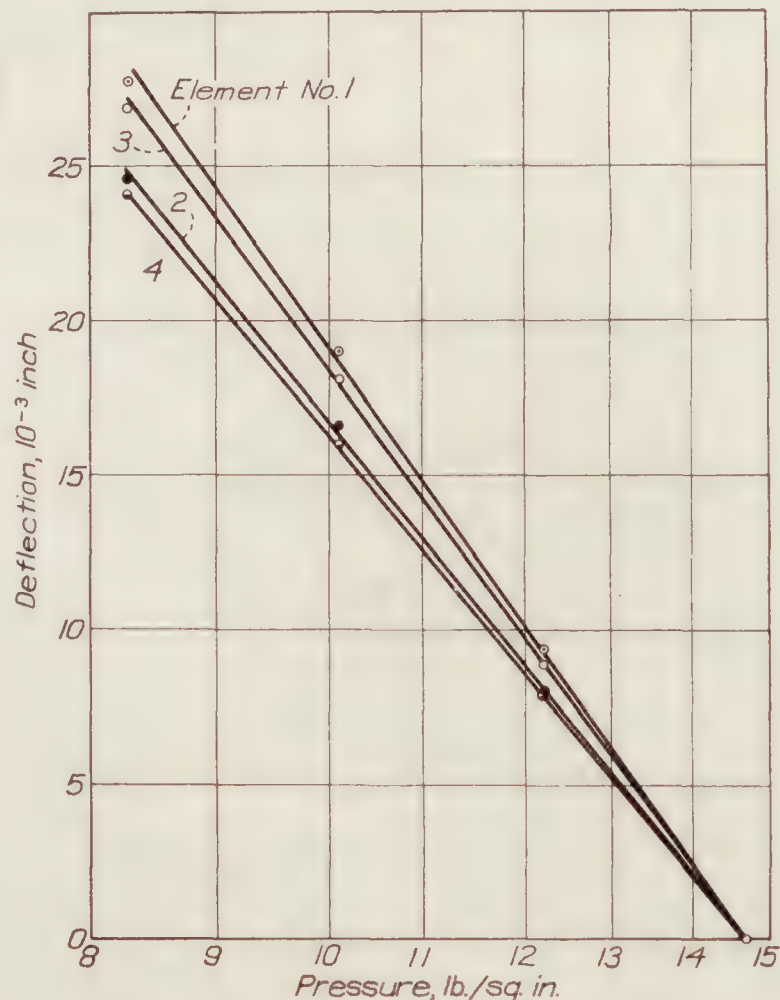


FIGURE 6.—Load-deflection data for four pressure elements

The best curves for the four elements are plotted in Figure 6. The variation in the maximum deflections is somewhat great but offers no difficulty, since the altimeter mechanism can be easily adjusted to give the proper deflection of the pointer. It is essential that the deflection curves be straight lines within close tolerances. The four elements when inserted in the altimeters were each found to give a satisfactory performance of the instrument. The range of the altimeter was 15,000 feet, which corresponds to pressure limits of 760 and 428.8 millimeters of mercury.

The helical springs were made from chrome-vanadium steel S. A. E. 6145 and were heat treated.

The constants of the spring and sylphon of element No. 3 are as follows, the symbols having the same meaning as in the previous sections.

S' logarithmic stiffness of element	20.9
r radius of coils in inches	0.405
a radius of wire in inches	0.062
G modulus in torsion in pounds per square inch	12×10^6
A_q equivalent area of sylphon in square inches	1.27
l_b total length of active wire of spring in inches	12.7
l_a length of active wire at differential pressure of 14.7 pounds per square inch in inches	4.86
P_a differential pressure in pounds per square inch (zero altitude)	14.7
P_b differential pressure in pounds per square inch (25,750 feet altitude)	5.28
s_d the stiffness of the sylphon in pounds per inch, approximately	5
s_a the stiffness of the spring in pounds per inch when the pressure is 14.7 pounds per square inch	385
s_b the stiffness of the spring in pounds per inch when all the wire is active	135
s_1 the stiffness of the spring in pounds per inch when the differential pressure is 8.29 pounds per square inch (15,000 feet)	215

The fundamental constant is the logarithmic stiffness S' defined in equation (5) which is obtained from Figure 6 by determining the slope of the deflection-log pressure line. Then in accordance with the relation

$$S_a = S' A_q P_a \quad (9)$$

the pressure element stiffness S_a was computed, from which the spring stiffness s_a was found by allowing for the sylphon stiffness. It is then possible to compute l_a .

It was assumed that the springs had five turns when all coils were active which, while reasonable, is open to question in view of the end effects which can not be easily calculated. Assuming still further that equation (9) holds in the region P_a to P_b , stiffness S_b was first calculated by use of equation (3) and then P_b determined by means of equation (9), noting that the pressure element stiffness equals the sum of that of the sylphon and spring.

The equivalent area A_q was computed by use of formula (6).

A measure of the differences in the four springs may be found in the variation of the value of S' determined from Figure 6.

Element No.	S'
1	20.0
2	23.0
3	20.9
4	23.6

The maximum fiber stress of the spring material occurs when the sylphon is evacuated and thus subject to a differential pressure equal to atmospheric. It was computed to be approximately 20,000 pounds per square inch.

The spacing between the coils of the helical spring which is required to give the above-described deflection curve will be calculated making use of the constants for element No. 3. As derived, the formulas relate to a spring in which the coils progressively go out of action from one end, while the spring was made so that the coils at each end go out of action as the load is applied. A modification of the latter method may offer the practical advantage of permitting an arrangement whereby the cocking can be eliminated. If the coils are spaced so that the two points of contact are kept 180° apart, no cocking should theoretically occur.

For the design of this pressure element formula (20) can be simplified with little loss in accuracy by neglecting the stiffness of the sylphon since it is small in comparison with that of the spring. The ratio of the two stiffnesses varies from 36 to 74 in the working pressure range. If $s_d = 0$, formula (20) becomes

$$X_n = \frac{1}{S'} \log_e \frac{l_2}{l_1} - \frac{l_2 - l_1}{S' l_b} \quad (32)$$

The spacing X_n between adjacent coils of the spring were computed using the above simplified equation.

CALCULATION OF COIL SPACING

Coil between length of wire, l_2-l_1 inches		Spacing X_n in inches		At zero differential pressure
		At differential pressure of 5.28 pounds per square inch (25,750 feet)	At differential pressure of 14.7 pounds per square inch (zero altitude)	
(l_1)	(l_2)			
0	4.86		All coils active.	
4.86	7.40	0.0106	0	0.0202
6.13	8.68	.0071	0	.0167
7.40	9.95	.0046	0	.0142
8.68	11.22	.0027	0	.0123
9.95	12.49	.0013	0	.0109
10.16	12.70	.0011	0	.0107
12.70	12.70	0	0	.0096

Computed deflection of element for pressure changes
from—

	Inch
0 to 5.28 pounds per square inch.....	0.0479
5.28 to 14.7 pounds per square inch.....	.0473
0 to 14.7 pounds per square inch.....	.0952

The spacing of the constructed spring was such that the active portion of spring changed throughout the pressure interval 0 to 14.7 pounds per square inch, however no effort was made to obtain the logarithmic stiffness outside of the pressure interval 14.7 to 8.30 pounds per square inch. The total deflection for element No. 3 for the pressure change from 0 to 14.7 pounds

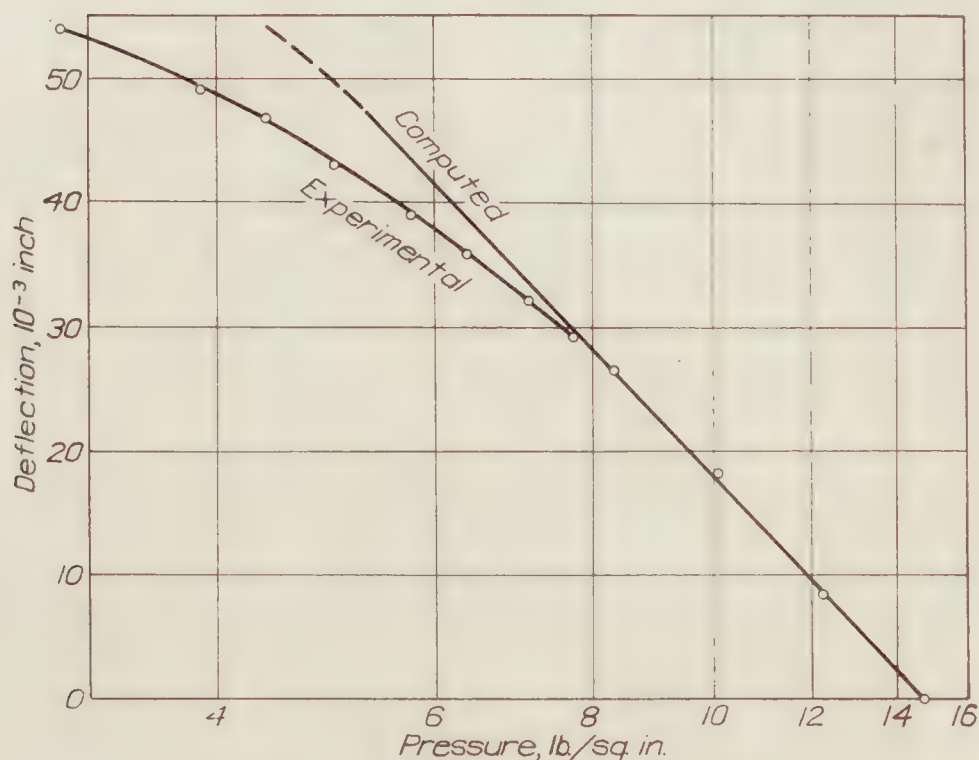


FIGURE 7.—Load-deflection data for element No. 3

per square inch is 0.079 inch, which compares with 0.094 inch given in the previous table. A comparison of the computed and measured deflections is given in Figure 7, which, of course, is significant only for pressures below 8.3 pounds per square inch, since the computation is based on the measured value of S' , the logarithmic stiffness. The difference in the deflection for pressures below 8.3 pounds per square inch is not important, since it is easily accounted for by the difference in the spring as constructed and as assumed for computation. The constructed spring should have the greater stiffness under a given load because part of the coils are always out of action.

A measure of the smoothness of the deflection of the pressure element is given in Figure 8. The corrections to be applied to the altimeter readings are plotted against its readings. It will be noticed that the curves have a discontinuity at a reading in the region 5,000 to 7,000 feet (pressures, 12.2 to 11.4 pounds per square inch) which amounts to approximately 250 feet, or 1.6 per cent of 15,000 feet, and is approximately equivalent to a deflection of 0.0005 inch

of the pressure element. It is probably due to an irregularity in the spacing between the coils or to lack of smoothness in the surface of the spring wire. An idea of the elastic hysteresis of the pressure element is also given in Figure 8. This is the difference in the correction at the same reading for pressures decreasing and increasing. The maximum value for the instrument is about 90 feet, or 0.6 per cent of the maximum range, and is no doubt materially lower for the pressure element. There is remarkably little difference in the corrections for instrument temperatures of $+25^{\circ}$ and -30° C.

The authors desire to acknowledge the interest and encouragement of Lieut. M. F. Schoeffel, United States Navy, during the progress of the work.

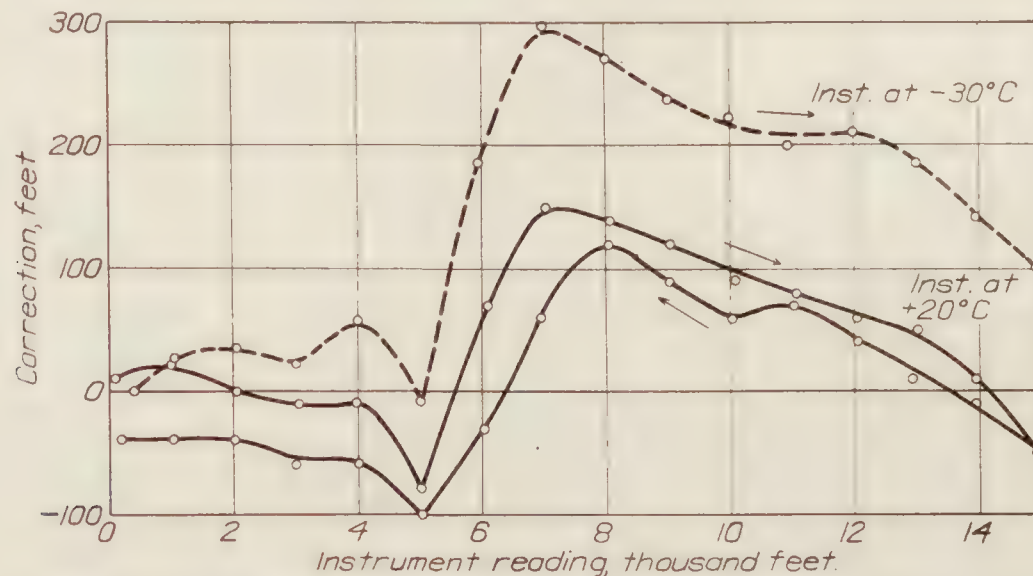


FIGURE 8.—Scale correction of BS-Navy altimeter, corrected for air temperature. (Temperature scale set at $+13^{\circ}$ C.)

CONCLUSION

The possibility of constructing a pressure element for altimeters which will eliminate the necessity for a variable multiplying ratio in order to obtain an evenly divided altitude scale has been demonstrated. Four such pressure elements were constructed. It was found possible to use any of the elements in the altimeter without making more than a routine and simple adjustment in the multiplying mechanism. The smoothness of operation of the pressure elements of logarithmic stiffness requires some improvement. This improvement can be obtained by more experience in the selection of the spacers used for securing the variable pitch of the springs and by investigating in greater detail the effect of surface irregularities in the spring wire due to heat treatment.

Roughly, the required multiplication of the deflection of a pressure element at 20,000 feet is twice, and at 40,000 feet four times that at sea level. It is evident that the difficulty of securing an evenly divided altitude scale increases with the range of altimeters. For high-range instruments of the ordinary type it might be practical to use the logarithmic pressure element and thus eliminate the necessity of adjusting the multiplying mechanism in order to obtain proper motion of the pointer.

REFERENCES

1. Gregg, W. R.: Standard Atmosphere. N. A. C. A. Technical Report No. 147 (1922).
2. Diehl, W. S.: Standard Atmosphere—Tables and Data. N. A. C. A. Technical Report No. 218 (1925).
3. Brombacher, W. G.: Tables for Calibrating Altimeters and Computing Altitudes Based on the Standard Atmosphere. N. A. C. A. Technical Report No. 246 (1926).
4. Eaton, H. N. and Keulegan, G. H.: Sylphon Diaphragms; a Method for Predicting Their Performance for Purposes of Instrument Design. N. A. C. A. Technical Note No. 90 (1922).
5. Hersey, M. D.: Diaphragms for Aeronautic Instruments. N. A. C. A. Technical Report No. 165 (1923).

REPORT No. 311

AERODYNAMIC THEORY AND TEST OF STRUT FORMS

By R. H. SMITH

**Aerodynamical Laboratory, Bureau of Construction
and Repair, U. S. Navy**

REPORT No. 311

AERODYNAMIC THEORY AND TEST OF STRUT FORMS

By R. H. SMITH

PART I¹

SUMMARY

This report, submitted to the National Advisory Committee for Aeronautics for publication, presents the whole study under this title in two parts, only the first of which is reported here. In this part the symmetrical inviscid flow about an empirical strut of high service merit is found by both the Rankine and the Joukowski methods. The results can be made to agree as closely as wished. Theoretical stream surfaces as well as surfaces of constant speed and pressure in the fluid about the strut are found. The surface pressure computed from the two theories agrees well with the measured pressure on the fore part of the model but not so well on the after part. From the theoretical flow speed the surface friction is computed by an empirical formula. The drag integrated from the friction and measured pressure closely equals the whole measured drag. As the pressure drag and the whole drag are accurately determined, the friction formula also appears trustworthy for such fair shapes.

INTRODUCTION

The mathematical treatment of symmetrical flow past symmetrical bodies, which are streamlined for low resistance, is directed toward the solution of one of two general problems. Either one seeks to determine the nonviscous flow past forms whose rooting² is specified but final shape unknown, or about those whose final shape is specified and rooting unknown. The latter, being the inversion of the other, may be called the inverse problem, while the former may be called the direct problem. Almost all of the theoretical investigation on fluid flow past such shapes has been devoted to forms of fixed rooting, although they are, technically at least, the less important of the two. This partiality to the direct problem results from the fact that it naturally runs along with, while the other runs counter to, a mathematical development which is practically irreversible; that is, one which can be followed in the reverse direction only with the greatest difficulty.

Following logically the theory of fluid motion, the direct problem was successfully studied early, in the case of poorer forms of simple origin, in both two and three dimensions. The method was that due to Rankine, in which sources and sinks of equal total strength are imagined created along a streamline of a uniform stream of fluid, and the separate streams, each flowing as if alone, combined by superposition. (References 1, 2, and 3.) The closed surface of separation between the source-sink and the external streams is then made the surface of a solid body. The substitution of this body for the source-sink flow leaves the external stream unchanged since (in a nonviscous fluid) the inner flow and the body produce the same boundary conditions at the surface of separation. Since the external stream is known from the superposition of the flows before the substitution, the flow about the body is known.

Such surfaces of separation for water, suitable as forms for surface ships, have since been derived graphically by Taylor (References 3 and 4) and McEntee (Reference 5) by assuming more complicated source-sink combinations. These forms are made long and narrow with

¹ This part was submitted in May, 1928, to the Johns Hopkins University in conformity with the requirements for the M. A. degree. The second part will be completed and the whole submitted in 1929 in conformity with the requirements for the Ph. D. degree.

² By rooting is meant the premises which fix the form of the body, namely, the arrangement of the sources and sinks in the Rankine theory or of the complex poles in the Joukowski theory.

sharp, or sharply rounded, bows and sterns, in order to reduce the wave-making and inertia forces which together are large compared to the viscous forces. Because of their large surfaces such forms are not suited, however, for deep submersion in either water or air, where the viscous forces predominate.

While the development of deep-sea shapes of least drag has been very little studied because of their lack of utility, the practical need for minimum resistance air forms has led to a large amount of experimentation on empirical and, to a much less extent, on theoretical streamline forms. An important experiment on theoretical airship forms was made by G. Fuhrmann in 1912. (Reference 6.) Using Taylor's graphical method, he derived six beautifully streamlined separation surfaces of revolution, and showed the agreement between the surface pressures about them as computed and as experimentally measured. The 2-dimensional sequel to Fuhrmann's work is the subject of Part II of this general study, and was suggested to me by Dr. A. F. Zahm as suitable for a thesis.

In two dimensions, the direct problem can be treated also by the method of conformal transformation. An extensive literature has been built up during the last few years on the development of Joukowski and kindred airfoils by this method. (References 7, 8, 9, 10, 11, and 12.) The corresponding development of symmetrical shapes suitable for struts, however, has been little studied although the strut derivatives of Joukowski profiles are more easily obtained and are more like successful service forms. A Joukowski strut of high merit is developed in the present study, and the theoretical and experimental flows about it are compared.

The inverse problem, in which the final shape is specified, has been undertaken in only one investigation. (Reference 14.) Von Karman found the flow past arbitrary half bodies of revolution, and then past an airship, whose shape was specified, by forming its bow and stern of two half bodies, cut to the correct length, and joining them. Certain approximations and assumptions incident to the splicing were made and investigated. While they shorten a very long problem until it is practically solvable, these approximations destroy much of the mathematical elegance and exactness of the method.

Since Von Karman's method is an important theoretical and technical advance, it has been thought worth while to carry through, at least once, the laborious task of extending it rigorously to an arbitrary whole body. The body chosen was the United States Navy Number 2 strut, whose form is empirical and whose service merit (Reference 13) is unexcelled. This investigation, together with that of the Joukowski strut referred to, which differs from the Navy Number 2 only at the extreme trailing edge, gives two independent developments of the theoretical flow about this strut. The two theoretical flows are finally compared with the experimental flow found by measuring the pressure over the strut surfaces. The Von Karman and Joukowski strut studies constitute Part I of the whole investigation.

Whether we consider the problem of solving the flow about a strut of fixed final form or of fixed rooting, the mathematical treatment is possible only when viscosity is neglected. Under usual conditions, it is well established that fluids, like air and water, stick without slipping to the surface of the body past which they flow, and that the retardation of the near-by fluid takes place in a thin layer called the boundary layer. In this layer the viscous forces are of the same order of magnitude as the inertia forces and lead to the formation of vortices when the retardation is sufficient to cause a reverse flow. (References 15 and 16.) Such sufficient retardations always occur in the immediate wake of conventional streamline bodies, particularly if their trailing parts are blunt. The surface line dividing the upstream region of nonreverse flow and the downstream region of reverse flow, is called the line of separation. The shifting of this line with change of air speed, in the case of some forms, is one cause for the variation of the resistance coefficient with Reynolds Number. The line of separation for easy shapes is never far from the aftmost point of the body and shifts most for those with rounded tails. For well streamlined bodies with sharp tails or trailing edges, the line of separation is sometimes stationary for a considerable range of Reynolds Number. Such forms produce a stable flow whose pattern is fixed and have a very low resistance, most of which is found to be due to viscous friction. They represent the optimum easy forms and are the most interesting from

the practical, as well as from the theoretical, point of view. The struts considered here are bodies of this class.

THE SOURCE-SINK ENVELOPE APPROXIMATING THE UNITED STATES NAVY NUMBER 2 STRUT

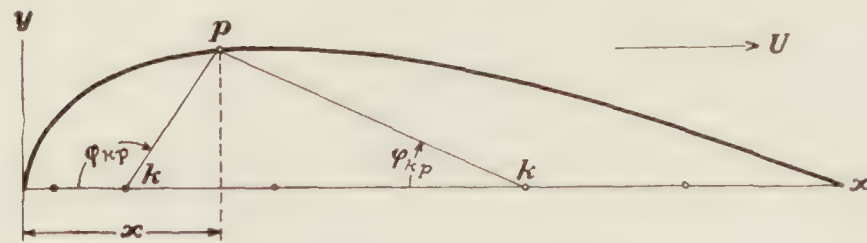


FIGURE 1

At any point p on the separation line (fig. 1) inclosing a source-sink system in a plane stream U , clearly the stream function is

$$\psi_p = 0 = Uy - \sum \frac{\varphi_{kp}}{2\pi} Q \quad (1)$$

where Q is the strength of any source or sink and φ_{kp} the angle as shown. The condition of closure, viz, that the Q flow shall stay inside the line, is

$$\sum Q = 0 \quad (2)$$

Hence, if y , φ are given for enough points p , equations (1), (2) determine the Q 's that condition the given closure line in the given stream. Let the closure line be the section of the United States Navy Number 2 strut in the plane stream U .

Equation (1) is true, in two dimensions, for any type or distribution of sources and sinks. It will be convenient to assume line sources and sinks which run in the strut plane of symmetry parallel to the strut length, and located on the ordinates by which the strut is specified. There will then be n sources and sinks and n equations of type (1), for n ordinates. To meet the condition of closure, equation (2) is added and another source or sink, making in all $n+1$ sources and sinks and $n+1$ equations.

Since its curvature is important, a streamline form can not be specified by fewer than 10 or 12 ordinates judiciously chosen. In this study, 12 coordinates are used to fix the form, and one coordinate added at the stern to fix the position of the thirteenth source or sink. The coordinates for the United States Navy Number 2 strut, multiplied by 2, (fig. 2) are as follows:

p	x	y	p	x	y	p	x	y
0	0	0	5	2.600	2.360	10	16.800	1.700
1	.200	.680	6	4.200	2.751	11	18.400	1.202
2	.600	1.200	7	7.200	3.000	12	20.000	.570
3	1.000	1.551	8	10.400	2.920	13	20.500	.290
4	1.600	1.918	9	13.600	2.418	14	21.000	0

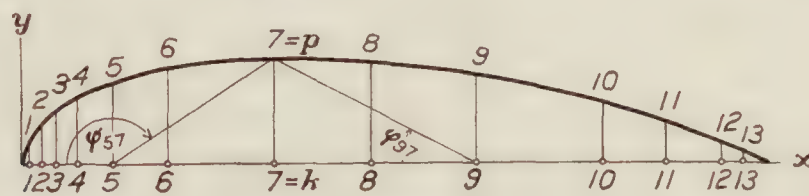


FIGURE 2

Hence, the value of φ_{57} , for example, is $\varphi_{57} = \pi - \tan^{-1} \frac{3.000}{7.20 - 2.60} = \pi - 0.578 = +2.564$. Likewise

the value of φ_{97} is found to be $\varphi_{97} = \tan^{-1} \frac{3.000}{13.60 - 7.20} = +0.438$. After substituting the numerical values for the coefficients and unity for the value of U , the constants of equations (1) and (2) take the form given in Table I.

There is nothing new, and very little of interest, in the way this system of linear equations has been solved. The solution was accomplished in steps, each of which reduced the number

both of equations and of unknowns by one. After each reduction the new equations were rearranged so that the next reduction could be made by using factors of the order of unity. For example, the first reduction was made by eliminating column 2, Table I, by multiplying the second row by -0.9624 , and adding the result to the first row, then by multiplying the third row by -0.6614 and adding to the second row, and so on down the column. The new set, so obtained, contains no Q_2 column, and has only 12 rows. These rows were rearranged for the next reduction in the order 1, 12, 10, 8, 7, 5, 3, 2, 4, 6, 9, 11, and multiplied, as before, by the proper factors to eliminate column 7. Carrying through this process to the end involves almost prohibitive work. Ways to save labor and chance of error by proper tabulation are obvious, however, and success depends principally on how well they are used. Numbers of seven places or more must be carried throughout, which increases considerably the chance of error. Table I is given here reduced from seven places to four places for brevity. The solution of this set of 13 equations was found to be

$Q_1 = + 1.6650$	$Q_5 = + 7.0304$	$Q_9 = - 3.3078$
$Q_2 = - 5.8767$	$Q_6 = - 2.1855$	$Q_{10} = - .1097$
$Q_3 = + 13.0072$	$Q_7 = + .8824$	$Q_{11} = - 3.2608$
$Q_4 = - 5.8817$	$Q_8 = - 1.2550$	$Q_{12} = + 1.0123$
		$Q_{13} = - 1.7202$

Figure 3 shows graphically the distribution and the relative strengths of the sources and sinks along the chord of the strut profile. A positive Q is a source, a negative one a sink, by defini-

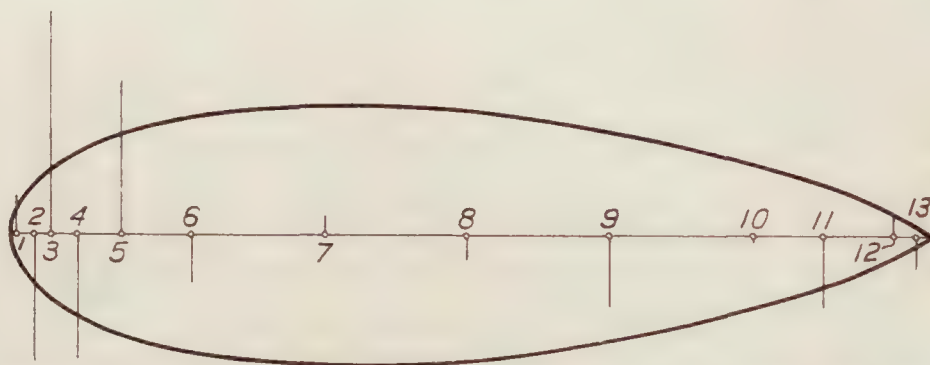


FIGURE 3.—The distribution and relative strengths of sources and sinks whose separation surface in a unit stream is indistinguishable from the United States Navy No. 2 strut

tion, hence there are five sources and eight sinks, the sources predominating at the bow and the sinks at the stern.

It is relatively easy to find the components of velocity and the pressure at each surface point p , from the known strengths and positions of the sources and sinks. The stream function ψ_{kp} , at each point p , due to the k^{th} source or sink, is simply

$$\psi_{kp} = \frac{Q_k}{2\pi} \varphi_{kp}$$

and the radial velocity q_{kp} , simply

$$q_{kp} = \frac{\partial \psi_{kp}}{\partial \varphi_{kp}} = \frac{Q_k}{2\pi r_{kp}}$$

where $r_{kp} = [(x_p - x_k)^2 + y_p^2]^{1/2}$. The cartesian components of q_{kp} are

$$u_{kp} = \frac{Q_k(x_p - x_k)}{2\pi r_{kp}^2}, \quad v_{kp} = \frac{Q_k y_p}{2\pi r_{kp}^2},$$

which become, when summed for all sources and sinks,

$$u_p = \frac{1}{2\pi} \sum_{k=1}^{13} \frac{Q_k(x_p - x_k)}{r_{kp}^2} \quad (3)$$

$$v_p = \frac{1}{2\pi} \sum_{k=1}^{13} \frac{Q_k y_p}{r_{kp}^2} \quad (4)$$

The velocity U_0 of the uniform stream must be added to u_p giving

$$q_p = [(U_0 + u_p)^2 + v_p^2]^{1/2} \quad (5)$$

for the resultant velocity of p . Then the pressure p_p at p , above the stream pressure, is

$$p_p = p_0 \left(1 - \frac{q_p^2}{U_0^2} \right) \quad (6)$$

where p_0 is the dynamic pressure, $\frac{1}{2} \rho U_0^2$, of the distant stream and p_p is in terms of p_0 as a unit.

Table II gives the values of u_p , v_p , q_p , and p_p derived from equations (3), (4), (5), and (6) for the United States Navy Number 2 strut. The values of the point pressure p_p are shown plotted against the strut width in Figure 4 and against its half thickness in Figure 5. The

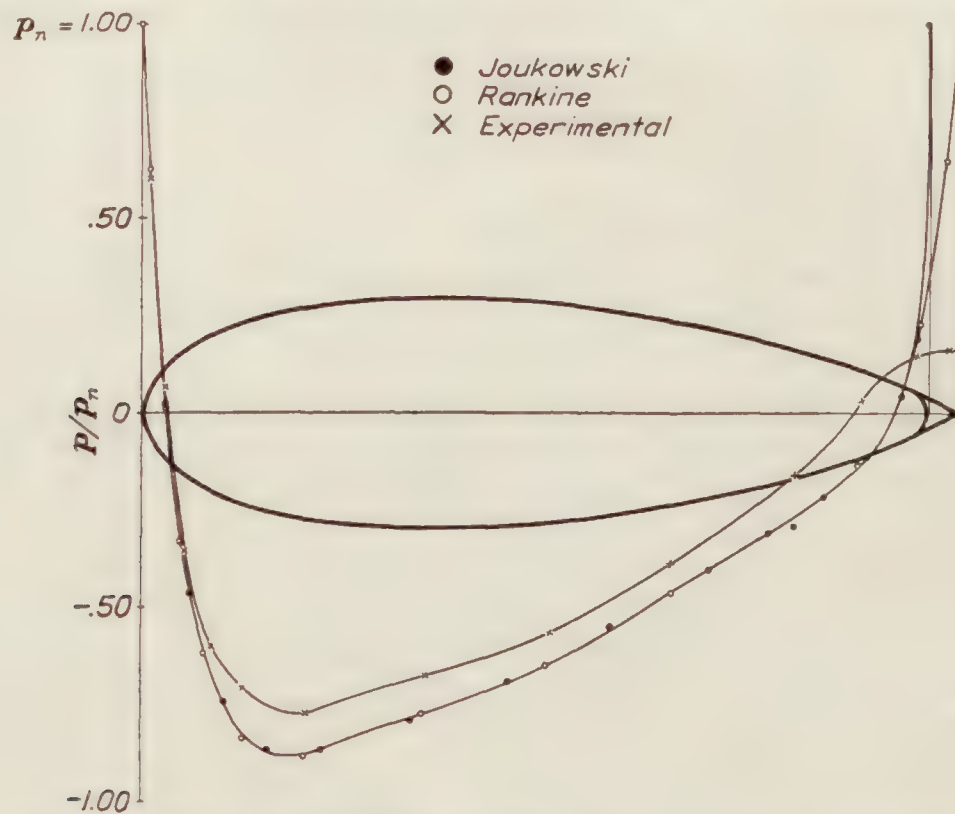


FIGURE 4.—Curves of point pressure, p/p_0 , over surface of Navy No. 2 strut from experiment and from Rankine and Joukowski theories

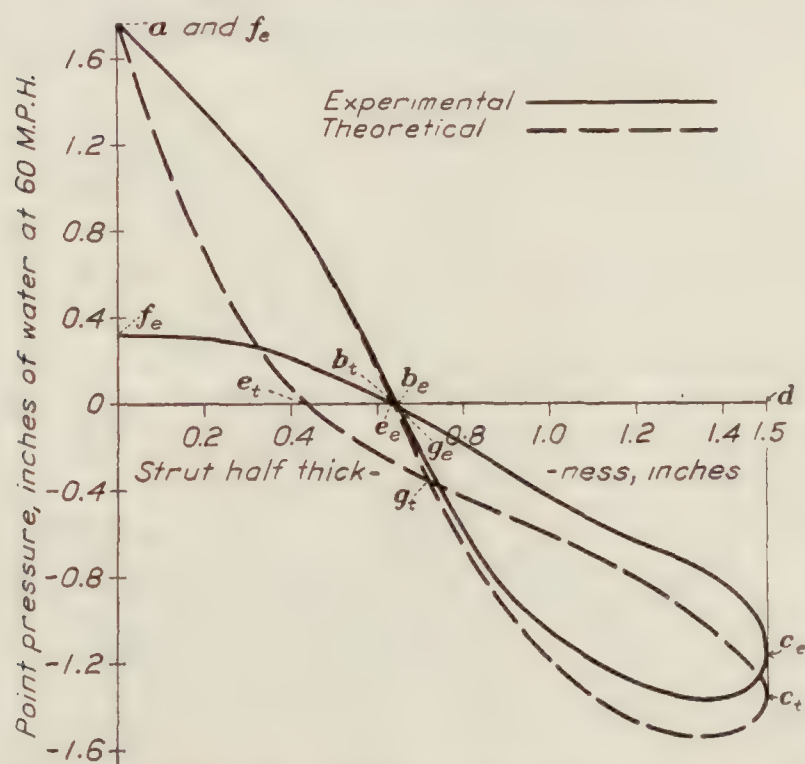


FIGURE 5.—Point pressure versus strut half thickness for experiment and theory. The Joukowski and Rankine theoretical curves coincide

integrated pressural drag is clearly proportional to the difference between the areas $a b g e f$ and $g c g$ of the theoretical curve (fig. 5), which is found to be zero when the two areas are planimetered. The theoretical resistance of this empirical strut is, therefore, zero. Figures 4 and 5 also give the point pressures found by measurement and by the Joukowski theory, which will be explained presently.

The calculation of the streamlines and velocity distribution afield would be long, but not difficult, by use of equations (3) to (6). They are more easily found when the strut is considered as a Joukowski profile. These extensions of the development of the flow about the strut will, therefore, be left for the Joukowski treatment, now to be considered.

THE JOUKOWSKI STRUT WHOSE FORM APPROXIMATES THE UNITED STATES NAVY NO. 2

The method of finding wing and other streamline forms by a conformal transformation of circular and elliptic cylinders is due to Joukowski and later to Mises, Betz, Muller, Witoszynski, and others. (References 7, 8, 9, 10, 11, 12.) Strictly speaking, the Joukowski profiles are those of simple 2-pole origin with upper and lower lines forming a cusp at the trailing edge. These profiles were soon extended by his followers, in an effort to derive more practical wings, to forms of multi-pole origin and to those whose upper and lower surfaces intersect at a small angle at the trailing edge.

The general theory of conformal transformation of plane flow has been well worked out in the wing studies cited, and will not be considered here, except to mention two theorems. The law of Riemann, in the theory of functions, states that there is a circle and surrounding potential field into which one can transform any simple holomorphic contour and surrounding potential field so that the field at infinity remains unchanged. Then, more recently, the theorem of Bieberbach, which states that there is one, and only one, function for this transformation, namely,

$$\zeta = z + \frac{a_1}{z} + \frac{a_2}{z^2} + \frac{a_3}{z^3} + \dots \quad (7)$$

in which $\zeta = \xi + i\eta$ are the coordinates in the ζ plane of the circle and $z = x + iy$ are the coordinates in the z plane of the contour. These theorems apply, naturally, only in two dimensions.

Equation (7) may be written

$$\frac{d\zeta}{dz} = \left(1 - \frac{c_1}{z}\right) \left(1 - \frac{c_2}{z}\right) \left(1 - \frac{c_3}{z}\right) \left(1 - \frac{c_4}{z}\right) \dots \quad (8)$$

where c_n are the complex poles of the transformation, and $\sum c_n = 0$. The Joukowski solution of the inverse problem, viz, of transforming a circle and flow field to a given profile with corresponding field, reduces to the task of finding the c_n or the a_n complex coefficients in these equations. The direct problem, on the other hand, begins with these given in the premises, and has been studied, with some difficulty, up to five poles. (Reference 11.) It would be surprising if fewer than this number were sufficient to fix satisfactorily the transformation of a circle to an arbitrary streamline form. The theory in its present state gives no practical way to determine even five poles which would produce roughly a specified form. The Joukowski method, therefore, gives no solution yet of the inverse problem. One must resort to a fit and try method to find a Joukowski strut that coincides with one arbitrarily chosen and be satisfied with a good approximation. This method will be used to find the Joukowski strut that approximates the United States Navy Number 2.

In carrying out this approximation a modified Joukowski profile will be used, but before considering the profile it may be well to summarize briefly that part of the Joukowski theory which applies to symmetrical flow. The theory begins with the very old transformation by which a circle of radius b is flattened into a straight line whose length is $4b$. The transformation formula is the simple 2-pole equation

$$z = \zeta + \frac{b^2}{\zeta} \quad (9)$$

which decomposes into two equations,

$$\begin{aligned} x &= \xi \left(1 + \frac{b^2}{\xi^2 + \eta^2} \right) \\ y &= \eta \left(1 - \frac{b^2}{\xi^2 + \eta^2} \right) \end{aligned} \quad (10)$$

The same transformation flattens circles, concentric with the map circle $r=b$, into ellipses and distorts their radii into hyperbolas, the ellipses and hyperbolas being focused at the ends of the line $4b$, Figure 6.

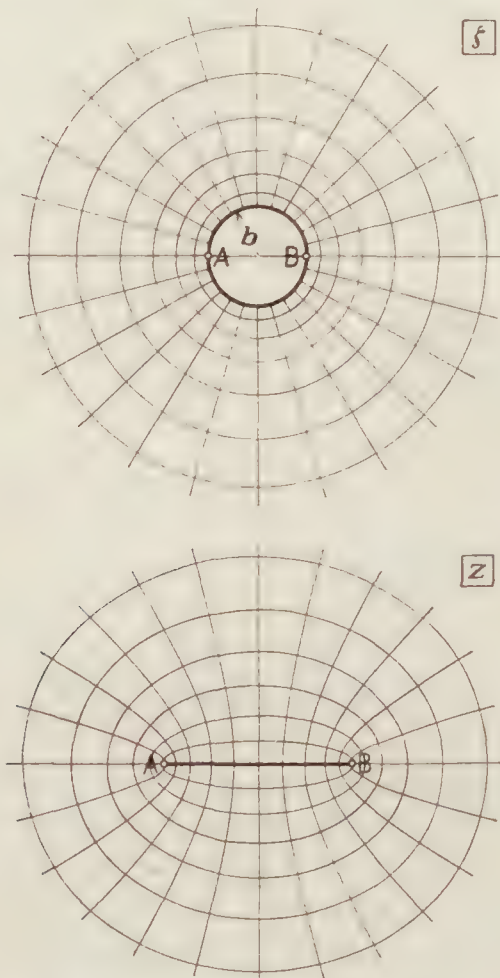


FIGURE 6.—Conformal transformation of map circle, $r=b$, and its potential field into the straight line $4b$ and its potential field

For a uniform stream crossing a solid cylinder $r=b$, the streamlines, $\psi_\xi = \text{const.}$ graded from the circle $r=b$, in the ξ plane, become transformed into straight parallel lines graded from the line $4b$ in the z plane, and the curves $\varphi_\xi = \text{const.}$ become straight lines orthogonal to them, the two sets of lines forming together an ordinary cartesian network. The said flow about the circular cylinder $r=b$, is thus transformed into the flow past a flat plane lying along the general stream.

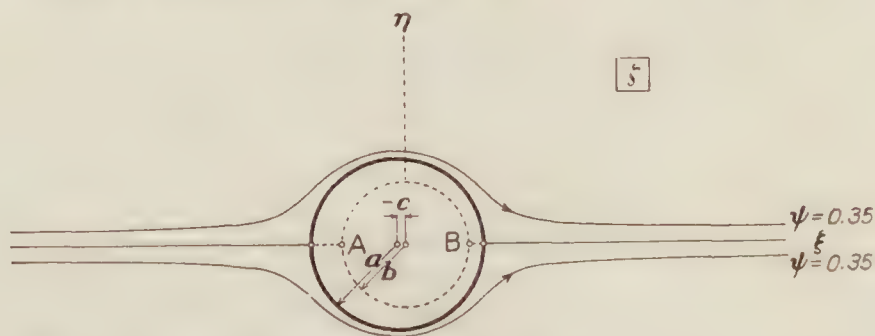


FIGURE 7a.—Round cylinder, $a=2.00$, centered at $c=-0.20$ map cylinder, $b=1.48$, transformed into Joukowski approximation of United States Navy No. 2 strut, Figure 7b

Similarly, for flow across the solid cylinder $a > b$, the curves $\psi_\xi = \text{const.}$ graded from the concentric circle $r=a > b$, in the ξ plane, become curves $\psi_z = \text{const.}$ graded from the corresponding ellipse in the z plane. The flow about the circular cylinder $r=a$ is transformed, in this way, into the flow about an elliptic cylinder, focused at $x = \pm 2b$. When the circle $r=a$ is not concentric with the map circle, $r=b$, but eccentrically centered at $\xi = -c$ (fig. 7a), the curve in the

z plane corresponding to $r=a$, becomes an ellipse distorted into a more or less streamline strut form. (Fig. 7b.) If the shift of the circle $r=a$ along $-\xi$ is sufficient to make $c=b-a$ —that is, to make the circles tangent at $\xi=b$ —the trailing edge of the strut degenerates to a cusp, and one has a symmetrical Joukowski profile.

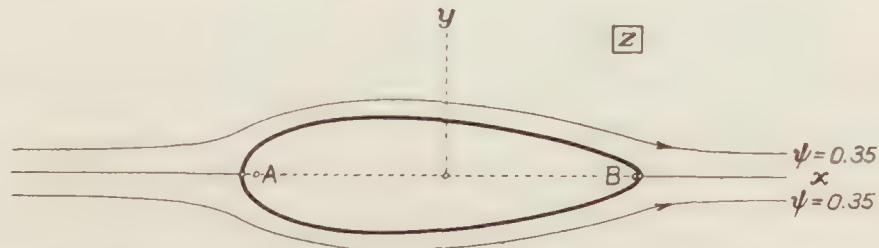


FIGURE 7b.—Joukowski approximation of endless United States Navy No. 2 strut, transformed from endless round cylinder, Figure 7a

By trying a number of sizes and positions for the circle $r=b$, one finds without much difficulty that the map circle $b=1.48$, transforms the circle $a=2.00$, centered at $\xi=-0.20$ into the Navy Number 2 strut accurately to within $1\frac{1}{2}$ per cent of the maximum ordinate everywhere except near the extreme trailing edge. The actual agreement is seen in Table III and Figure 8.



FIGURE 8.—Joukowski approximation to United States Navy No. 2 strut

This agreement is satisfactory, especially since most, if not all, of the objectionable discrepancy near the trailing edge, where the Joukowski strut is rounded while the Navy Number 2 continues to an edge, occurs aft the lines of separation where the form of the surface is largely immaterial.

Having obtained the Joukowski strut, the flow about it is easily found. In general, the flow about a circular cylinder of radius a is given by the equation

$$\phi_{\zeta} + i\psi_{\zeta} = U_0 \left(\zeta + \frac{a^2}{\zeta} \right) \quad (11)$$

whose ψ_{ζ} component is

$$\psi_{\zeta} = U_0 \eta - \frac{U_0 \eta a^2}{\xi^2 + \eta^2} \quad (12)$$

When the cylinder is centered at $\xi=-0.20$, and has a radius $r=a=2.00$, equation (12) becomes

$$\psi_{\zeta} = U_0 \eta - \frac{4 U_0 \eta}{\eta^2 + (\xi + 0.20)^2}, \quad (13)$$

whence the component velocities at any point (ξ, η) about the cylinder are

$$u_{\zeta} = \frac{\partial \psi_{\zeta}}{\partial \eta} = U_0 \left\{ 1 - 4 \frac{(\xi + 0.20)^2 - \eta^2}{[(\xi + 0.20)^2 + \eta^2]^2} \right\} \quad (14)$$

$$v_{\zeta} = -\frac{\partial \psi_{\zeta}}{\partial \xi} = 8 U_0 \eta \frac{\xi + 0.20}{[(\xi + 0.20)^2 + \eta^2]^2} \quad (15)$$

In order to find the corresponding components u_z and v_z about the strut, the lengths of corresponding path segments in the ζ and z planes must be found. That is, the differential quotient of z and ζ must be evaluated. Then

$$\frac{u_{\zeta}}{u_z} = \frac{v_{\zeta}}{v_z} = \left| \frac{dz}{d\zeta} \right| \quad (16)$$

The evaluation of $\left| \frac{dz}{d\zeta} \right|$ is known, and can be easily varied to be

$$\left| \frac{dz}{d\zeta} \right| = \frac{1}{\xi^2 + \eta^2} \{ (\xi^2 + \eta^2 - b^2)^2 + 4b^2\eta^2 \}^{1/2} \quad (17)$$

Finally, the resultant velocity q_ζ , at any point ζ , about the cylinder is given by

$$q_\zeta^2 = u_\zeta^2 + v_\zeta^2 \quad (18)$$

Likewise the resultant velocity q_z , at any point, z , about the strut is given by

$$q_z^2 = u_z^2 + v_z^2 \quad (19)$$

The surfaces of constant speed or pressure near the cylinder are easily found analytically, but those near the strut can not easily be found directly.³ In the latter case, the values of q_z must be found along a number of closely graded streamlines, and the surfaces of constant q_z found by use of an auxiliary plot of q_z for each streamline, first against x and then against y .

The surfaces of constant speed q_ζ , about the cylinder (References (18) and (21)) may be found as follows. If the velocity U_0 of the uniform stream is unity, equation (12), in polar coordinates, takes the form

$$\psi_\zeta = \left(r - \frac{a^2}{r} \right) \sin \theta \quad (20)$$

By differentiation, equation (20) gives the two polar components of velocity,

$$\begin{aligned} q_r &= \frac{\partial \psi_\zeta}{\partial r} = \left(1 + \frac{a^2}{r^2} \right) \sin \theta \\ q_\theta &= \frac{\partial \psi_\zeta}{r \partial \theta} = \left(1 - \frac{a^2}{r^2} \right) \cos \theta \end{aligned} \quad (21)$$

Hence

$$q_\zeta^2 = q_r^2 + q_\theta^2 = \left(1 + \frac{a^2}{r^2} \right)^2 \sin^2 \theta + \left(1 - \frac{a^2}{r^2} \right)^2 \cos^2 \theta$$

or

$$q_\zeta = \frac{1}{r^2} [(a^2 + r^2)^2 - 4a^2 r^2 \cos^2 \theta]^{1/2} \quad (22)$$

From this equation q_ζ clearly has the maximum value 2, at the point where $\theta = \frac{\pi}{2}$ and $r = a$, and the minimum value, zero, at the rest points $\theta = 0, \pi$, $r = a$. Surfaces of constant speed q_ζ , intermediate between 0 and 2 are shown, plotted from Table IV, in Figure 9a, where those above the ξ axis are for even speeds, those below for even pressures.

One surface of constant speed is of special interest—namely, the surface $q_\zeta = 1$ —showing where the speed beyond the cylinder is equal to that of the uniform stream. For this case

$$r^4 = (a^2 + r^2)^2 - 4a^2 r^2 \cos^2 \theta \quad (23)$$

or

$$a^2 + 2r^2 (1 - 2 \cos^2 \theta) = 0.$$

Since $\cos^2 \theta = \frac{\xi^2}{\xi^2 + \eta^2}$, equation (23) becomes

$$a^2 + 2(\eta^2 - \xi^2) = 0,$$

from which

$$\frac{\xi^2}{K} - \frac{\eta^2}{K} = 1, \text{ where } K = \frac{a^2}{2}. \quad (24)$$

³ Surfaces of constant speed and pressure are of practical interest in showing where to place anemometers to indicate, with least correction, the relative speed of the strut and the general air stream.

The surfaces $q_z = U_0$ are therefore two equilateral hyperbolas with foci at the ends of the cylinder diameter which lies along the general stream. (Fig. 9a.)

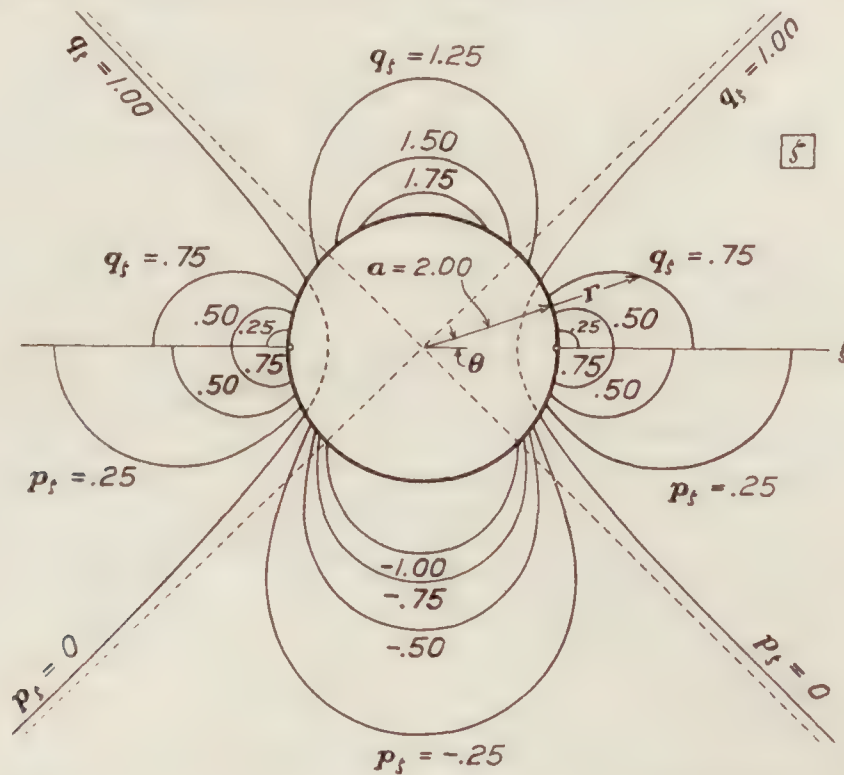


FIGURE 9a.—Lines of constant speed and pressure of perfect flow past end-less round cylinder

To find the corresponding surfaces of constant speed near the strut, one must first determine a number of closely graded streamlines near the cylinder, and the corresponding ones about the strut. Equation (13) must, therefore, be solved for a number of values of ψ_z and the values ξ and η transformed to x and y by equation (10). Since ψ_z is a cubic in η and only a quadratic in ξ , equation (13) is best put in the form,

$$\xi + 0.20 = \eta \left[\frac{1 - \frac{\psi_z}{\eta} - \left(\frac{a}{\eta}\right)^2}{\frac{\psi_z}{\eta} - 1} \right]^{1/2} \quad (25)$$

and solved for ξ . The values ξ, η, x, y of the streamlines useful in finding surfaces of constant speed about the strut, as well as values of $\frac{dz}{d\xi}$ and the velocities q_z and q_x , are illustrated in Table V-b, which is for the streamline $\psi_z = 0.01$ only. The coordinates of the constant speed curves taken, as explained, from auxiliary plots of speed versus x and y for each streamline are given in Table VI, for as many of the even speeds and pressures, used for the cylinder, as exist for the strut. Since the maximum speed about the strut, Table Va, is $q_z = 1.37$, and the minimum pressure $p_z = -0.867$, the curves $q_z = 1.5, 1.75$ and $p_z = -1.00$, given for the cylinder, do not appear for the strut. The curves for constant q_z intermediate between 0 and 1.37 are

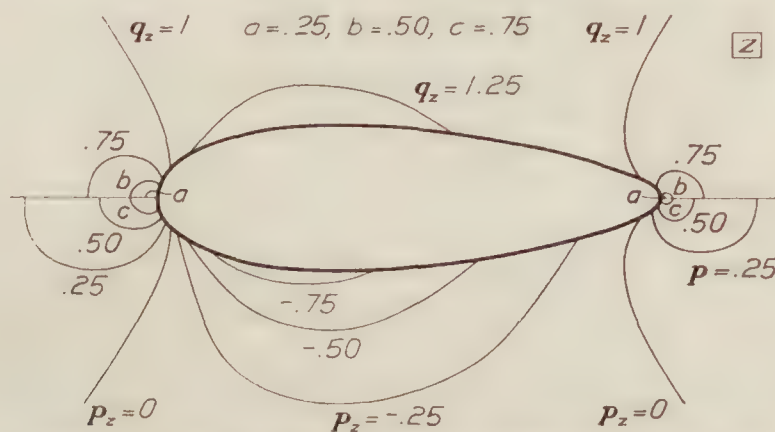


FIGURE 9b.—Lines of constant speed and pressure for perfect flow past United States Navy No. 2 strut (Joukowski approximation) at zero pitch and yaw

shown in Figure 9b, where again those above the x axis are for even speeds, and those below are for even pressures.

The computed point pressures over the surface of the Joukowski strut are given in Table Va, and plotted against strut width in Figure 4, along with the computed pressures for the Rankine strut and those measured by experiment. The plot of pressure against strut half-thickness (fig. 5) coincides with that for the Rankine strut. Hence the theoretical resistance of the Joukowski strut is zero also.

Normally graded streamlines, $\psi = \text{const.}$, are found about the round cylinder, and then transformed to those about the strut, by the equations already used to find the surfaces of constant speed. The values computed for these curves are illustrated in Table Vc, which is for the streamline $\psi = 0.35$ only. A number of evenly graded streamlines are drawn past both the round cylinder and the strut in Figures 10a and 10b.

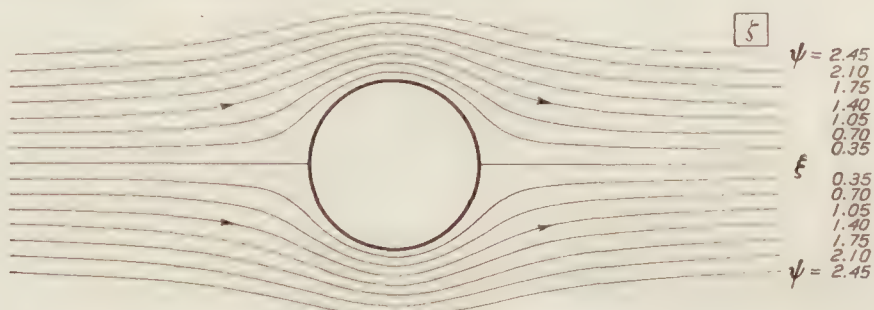


FIGURE 10a.—Round cylinder fixed in a boundless uniform stream of inviscid fluid

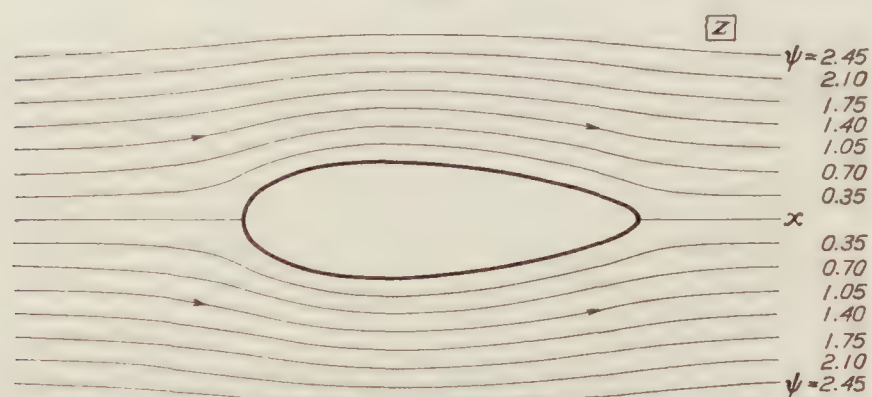


FIGURE 10b.—United States Navy No. 2 strut (Joukowski approximation) fixed in a boundless uniform stream of inviscid fluid

EXPERIMENTAL INVESTIGATION OF THE UNITED STATES NAVY NUMBER 2 STRUT

The precise measurement of the actual drag of bodies shaped for slight resistance is difficult, since the drag is so small compared to the general proportions of the body, and so sensitive to any disturbance or tripping of the surface flow. It is still more difficult to determine experimentally the pressural part of the drag, because it is a small residue of two much larger quantities, viz, the downstream and upstream pressural forces. The frictional part of the drag, being the drag minus its pressural part, is therefore the least precisely determined of the three. For these reasons any experimental measurements of the actual pressure on thick forms of low resistance, however carefully these forms are made and tested, are likely to be more or less unsatisfactory when analyzed.

The basic experimental data for the investigation of the actual flow past the United States Navy Number 2 strut are simply the measurements of the total drag and the point pressures at 14 positions on the strut surface. (Tables VII and VIII.) These data were obtained from a smooth wooden strut model 3 by 10½ by 60 inches faced, where pressures were collected, by a brass plate carefully fitted and perforated by 1-millimeter pressure holes. The ends of the strut were so shielded that the strut was the equivalent of an equal segment of a strut infinitely long. The total drag was measured on the aerodynamic balance, to which the strut was attached by prongs which entered the middle of the strut, as explained in Reference 20. The location of the pressure holes is given in Table VIII. Measurements of drag and pressure were obtained in the large Navy wind tunnel with the air stream held at five different speeds. The laboratory equipment for measuring these quantities and the technique of the experiment will be found clearly discussed in Reference 20, and will not be considered here

Figures 4 and 5, in which the measured pressures are plotted against the strut width and the half thickness, respectively, have already been referred to. In Figure 4 the other four experimental curves are omitted, namely, those for 20, 30, 40, and 50 miles per hour. However, for each speed there is a point of full impact pressure q , at the nose and two points of zero pressure at the side, the first at a distance of 3.3 per cent of the strut width from the front, and the second at a distance of 87.1 per cent. The corresponding theoretical values are 3.1 per cent for the first, and 92.1 per cent for the second. At about one-fifth of the width from the leading edge occurs the maximum suction which equals about four-fifths of the nose pressure q . The maximum theoretical suction occurs at the same place but is larger, being about seven-eighths of the nose pressure. At the trailing edge the experimental pressure is about one-sixth q , while the theoretical pressure there is q . Throughout most of the suction range the experimental suction is uniformly less than the theoretical by about one-tenth q . As may be seen from the data, the pressure at each hole varies nearly as the square of the speed, but with a degree of approximation slightly diminishing aft of the thickest part of the strut and more pronouncedly at the lower speeds. That this is even approximately true near the trailing edge indicates that the line of separation moves only slightly, if at all, throughout the speed range covered. This invariance of flow pattern with air speed is also shown by the fact that the rear zero pressure line does not shift along the surface of the strut as the speed is varied. This contrasts with the results obtained on a 2 by 8 inch elliptical cylinder (Reference 20), which has a shifting rear zero-pressure point and a varying flow pattern near the trailing edge.

One must turn to Figure 5 to find the consequence of the variation of the experimental point pressures from the theoretical. In this figure the integrals of the segments of the pressure graphs give the elements of pressural drag and their sum gives the resultant pressural drag. We have already seen that this sum is zero for the theoretical curve. The elements of pressural drag are given both separately and summed for both theory and experiment in Table IX. The lower part of the table is of special interest as showing the relation of the drag to its pressural and frictional parts, and the relation of the pressural drag to its four upstream and downstream parts.⁴ At 60 miles per hour air speed, the integral experimental pressures exert an upstream force of 0.6383 pound, and a downstream force of 0.7012 pound per foot of strut length. The resultant pressural drag D_p , is therefore 0.0629 pound per foot. Since the measured drag at this speed is 0.1748 pound, the frictional drag is 0.1119 pound, being the drag minus its pressural part. The order of graphic integration, used to find the force $\int p \, dy$ over the various portions of the strut surface, for 1-foot length of strut, is detailed at the bottom of Table IX.

We have just seen that the measured drag exceeds the resultant force of the integrated pressures by 0.1119 pound, and that this is the measured frictional drag. The frictional drag can also be computed from well-known formula for surface friction. Wieselsberger (Reference 19) gives, for example,

$$D_f = C_f O q \quad (26)$$

as the equation for the frictional drag of a plane whose total washed area is O . In this equation

$$C_f = 0.0375 \left(\frac{\nu}{LV} \right)^{0.15}$$

where L is measured along stream, and V is the stream speed. Writing $O = 2L$ for 1-foot length of plane, and $q = \frac{1}{2} \rho V^2$, equation (26) becomes

$$D_f = 0.0375 \rho \nu^{0.15} L^{0.85} V^{1.85}$$

or

$$D_f = K L^{0.85} V^{1.85} \quad (27)$$

where D_f is the frictional drag per foot run and $K = 0.0375 \rho \nu^{0.15}$.

Since one keeps only the downstream component of the tangential friction, the resultant frictional drag over the strut surface is equal, quite approximately, to that over its median plane, when the tangential speeds are the same at equal distances from the leading edge. One

⁴ This method is due to Zahm, Reference 17.

has then to apply equation (27) only to the strut median plane, using for L the distance from the entering edge and for V the surface speed past the element of strut surface, whose projection on the plane is dL . From equation (6) the actual surface speed past the strut is $V = \sqrt{p_o - p_p}$ where p_p is the measured pressure and $U_o = 1$. Let $V = f(L)$ as plotted in Figure 11. Then equation (27) becomes, for L in feet,

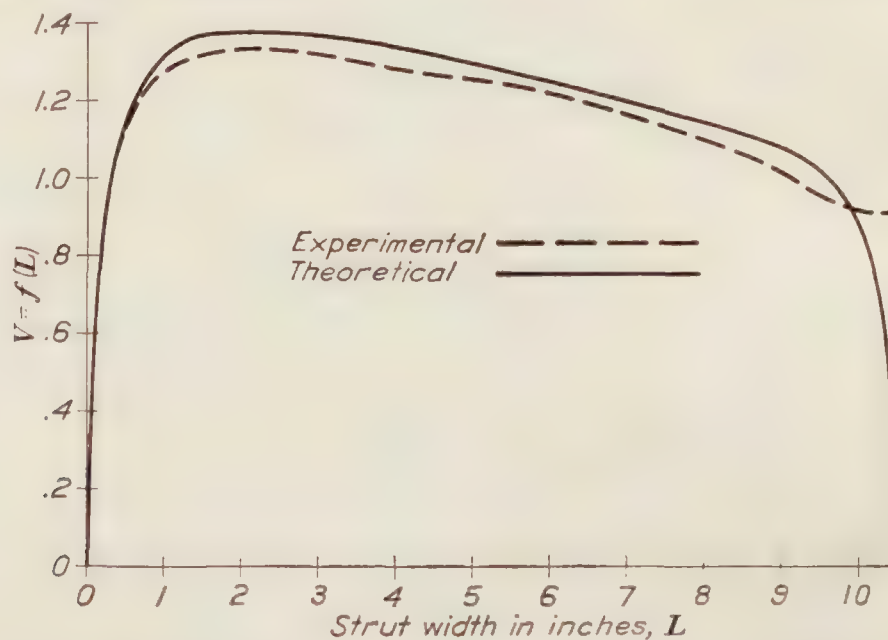


FIGURE 11.—Experimental and theoretical air speeds over surface of United States Navy No. 2 strut for unit stream speed

$$D_f = KL^{0.85}f^{1.85}$$

or

$$dD_f = K[0.85 L^{-0.15}f^{1.85}dL + 1.85L^{0.85}f^{0.85}f'dL] \quad (27)$$

where f' is the slope of the curve $V = f(L)$. Then

$$D_f = K[0.85 \int L^{-0.15}f^{1.85}dL + 1.85 \int L^{0.85}f^{0.85}f'dL]$$

or

$$D_f = K[I_1 + I_2] \quad (28)$$

The integrals I_1 and I_2 were graphically integrated from curves of $L^{-0.15}f^{1.85}$ versus L (fig. 12), the data for which is found in Table X. The value of I_1 and I_2 are found to be $I_1 = 1.343$, $I_2 = -0.2$ and

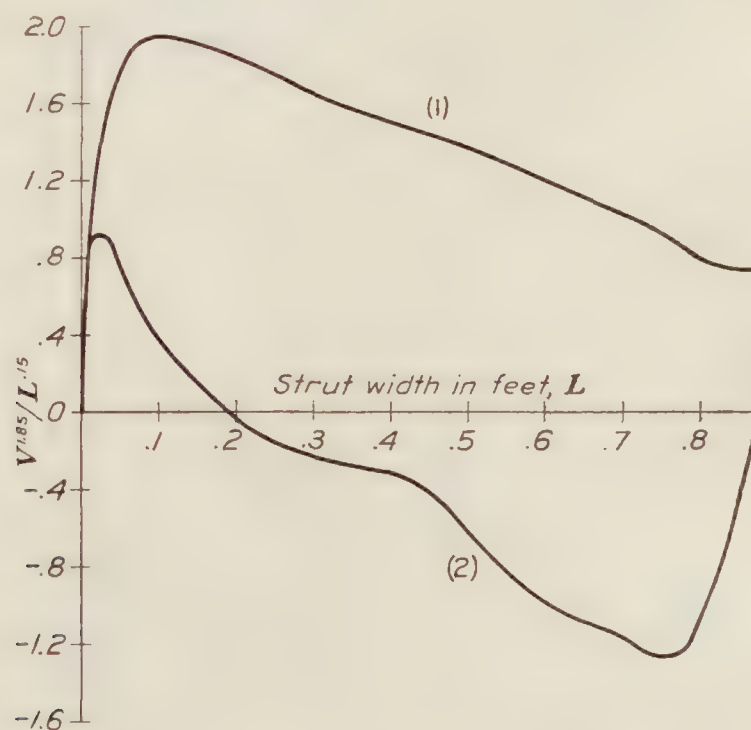


FIGURE 12.—Curves of $V^{1.85}/L^{0.15}$ versus strut width for unit stream speed. Areas under (1) and (2) give I_1 and I_2 in equation 28

$$I_1 + I_2 = 1.055$$

Since the integration was carried through for a unit stream speed, the total frictional drag at 88 feet per second is

$$D_f = K(1.055) (88^{1.85})$$

Using in K the values $\rho = 0.00237$ and $\nu^{0.15} = 0.2711$,

$$D_f = 0.1006.$$

This value compares satisfactorily with

$$D_f = 0.1119$$

found as the excess of total drag over pressural drag, both values being pounds per foot run at 60 miles per hour.

We have found, furthermore, that the measured point pressures and the computed surface friction give, as the value of the total drag of the Navy Number 2 strut, the value

$$D = D_p + D_f = 0.0629 + 0.1006 = 0.1635 \text{ lb./ft.},$$

which is about 6 per cent less than the actual measured drag,

$$D = 0.1748 \text{ lb./ft.}$$

CONCLUSIONS

The theoretical flow past symmetrical forms of predetermined shape can be rigorously solved by use of von Karman's adaptation of Rankine's theory, but not yet by Joukowski's theory or any of its extensions.

Using the empirical United States Navy Number 2 strut as the predetermined shape, the pressures about a very close approximation from the Joukowski theory and about the exact form from the Rankine theory agree within the precision of the computations. While agreement between the theories was to be expected, still it is reassuring to have two theoretical treatments, which are so widely different as these in their mathematical premises and developments, to finally give the same results for an actual body, especially since the body, being empirical, allowed no advantage to either.

The frictional resistance, determined from experiment, agrees, for the strut studied, within 10 per cent with that computed from the experimental surface speeds, and would agree still better with that computed from the theoretical surface speeds. Also the total resistance as measured agrees within 6 per cent with that computed from experimental surface pressure and friction. These agreements are rather better than one should expect, considering the fact that some of the quantities are small-order residues, and probably can not be taken as indicating the accuracy of such analyses in general. They tend to show, however, that the parts of the whole drag experienced by a body moving through a real fluid can be fully accounted for and accurately calculated from surface pressure and friction, granting sufficiently accurate experimental measurements of surface pressure.

REFERENCES

- Reference 1. Rankine, W. J. M.: On Plane Water Lines in Two Dimensions. Philosophical Transactions, 1864, p. 369.
- Reference 2. Rankine, W. J. M.: On the Mathematical Theory of Streamlines, Especially Those with Four Foci and Upwards. Philosophical Transactions, 1871, p. 267.
- Reference 3. Taylor, D. W.: On Ship-Shaped Stream Forms. Transactions of the British Institute of Naval Architects, 1894.
- Reference 4. Taylor, D. W.: On Solid Stream Forms and the Depth of Water Necessary to Avoid Abnormal Resistance of Ships. Transactions of the British Institute of Naval Architects, 1895.
- Reference 5. McEntee, William: On Some Ship-Shaped Stream Forms. Transactions of the Society of Naval Architects and Marine Engineers, 1909.
- Reference 6. Fuhrmann, G.: Theoretische und Experimentelle Untersuchungen an Balloonmodellen, Jahrbuch der Motorluftschiff-Studien-Gesellschaft, Band V, 1911-12.

- Reference 7. Joukowski, N.: *Aerodynamique*, 1916.
- Reference 8. Mises, R. von: *Zur Theorie des Tragflachen-auftriebes*, *Zeitschrift für Flugtechnik und Motorluftschiffahrt*, Vol. 1917, p. 157, et Vol. 1920, p. 68.
- Reference 9. Betz, A.: *Beiträge zur Tragflugeltheorie, mit besonderer Berücksichtigung des einfachen rechteckigen Flugels*. Diss. Gottingen, 1919.
- Reference 10. Kutta, W. M.: *Über ebene Zirkulationströmungen, nebst flugtechnischen Anwendungen*. Sitzungsberichte der Bayer. Akademie der Wissenschaften, 1910 and 1911.
- Reference 11. Nüller, Wilhelm: *Über der Form- und Auftriebsinvarianten für eine besondere Klasse von Flugelprofilen*, p. 389; and *Zur Konstruktion von Tragflachenprofilen*, p. 213. *Zeitschrift für Angewandte Mathematik und Mechanik*, Band 4, 1924.
- Reference 12. Witoszynski, C.: *On the Motion of Cylinders in a Perfect Fluid*. *Przeglad Techniczny* (Technical Review), Warsaw, Poland, 1919.
- Reference 13. Warner, Edward P.: *Aerodynamics: Airplane Design*, 1927, p. 214.
- Reference 14. Karman, Th. v.: *Berechnung der Druckverteilung an Luftschiffkörpern*. *Abhandlungen aus dem Aerodynamischen Institut an der Technischen Hochschule, Aachen*, 1927.
- Reference 15. Prandtl, L.: *Applications of Modern Hydrodynamics to Aeronautics*. N. A. C. A. Technical Report No. 116, Washington, 1921.
- Reference 16. Glauert, H.: *Airfoil and Airscrew Theory*, 1926, pp. 115–116.
- Reference 17. Zahm, A. F., Smith, R. H., and Hill, G. C.: *Point Drag and Total Drag of Navy Struts No. 1 Modified*. N. A. C. A. Technical Report No. 137, Washington, 1922.
- Reference 18. Zahm, A. F.: *Flow and Drag Formulas for Simple Quadrics*. N. A. C. A. Technical Report No. 253, Washington, 1927.
- Reference 19. Wieselsberger, C.: *Ergebnisse der Aerodynamischen Versuchsanstalt zu Gottingen*, 1 Lieferung 1921, p. 120.
- Reference 20. Zahm, A. F., Smith, R. H., and Loudon, F. A.: *Forces on Elliptic Cylinders in Uniform Air Stream*. N. A. C. A. Technical Report No. 289, 1928.
- Reference 21. Wieselsberger, C.: *Linien Konstanter Strömungsgeschwindigkeit*, Report of the Aeronautical Research Institute, Tokyo Imperial University, Vol. II.

AERODYNAMICAL LABORATORY,
BUREAU OF CONSTRUCTION AND REPAIR,
NAVY YARD, *Washington, D. C.*

TABLE I
Constants φ_{kp} in Equations 1 and 2

1		3	4	5	6	7	8	9	10	11	12	13	$2\pi Uy$
+	+	+	+	+	+	+	+	+	+	+	+	+	+
1. 000	1. 000	1. 000	1. 000	1. 000	1. 000	1. 000	1. 000	1. 000	1. 000	1. 000	1. 000	1. 000	0
+	+	+	+	+	+	+	+	+	+	+	+	+	+
1. 571	1. 039	. 7045	. 4520	. 2761	. 1684	. 0969	. 0666	. 0507	. 0409	. 0373	. 0343	. 0335	4. 273
+	+	+	+	+	+	+	+	+	+	+	+	+	+
1. 893	1. 571	1. 249	. 8761	. 5405	. 3217	. 1801	. 1219	. 0921	. 0740	. 0674	. 0619	. 0603	7. 540
+	+	+	+	+	+	+	+	+	+	+	+	+	+
2. 047	1. 823	1. 571	1. 201	. 7703	. 4516	. 2446	. 1635	. 1225	. 0980	. 0891	. 0816	. 0793	9. 739
+	+	+	+	+	+	+	+	+	+	+	+	+	+
2. 201	2. 051	1. 873	1. 571	1. 090	. 6350	. 3302	. 2147	. 1588	. 1257	. 1137	. 1038	. 1012	12. 064
+	+	+	+	+	+	+	+	+	+	+	+	+	+
2. 364	2. 274	2. 167	1. 972	1. 571	. 9750	. 4741	. 2938	. 2113	. 1646	. 1481	. 1347	. 1311	14. 828
+	+	+	+	+	+	+	+	+	+	+	+	+	+
2. 539	2. 489	2. 432	2. 328	2. 098	1. 571	. 7423	. 4177	. 2845	. 2148	. 1914	. 1722	. 1671	17. 279
+	+	+	+	+	+	+	+	+	+	+	+	+	+
2. 737	2. 715	2. 691	2. 649	2. 564	2. 356	1. 571	. 7534	. 4384	. 3031	. 2618	. 2301	. 2218	18. 849
+	+	+	+	+	+	+	+	+	+	+	+	+	+
2. 863	2. 852	2. 840	2. 821	2. 783	2. 701	2. 401	1. 571	. 7400	. 4282	. 3502	. 2955	. 2814	18. 347
+	+	+	+	+	+	+	+	+	+	+	+	+	+
2. 963	2. 957	2. 952	2. 942	2. 925	2. 890	2. 780	2. 494	1. 571	. 6478	. 4672	. 3616	. 3373	15. 205
+	+	+	+	+	+	+	+	+	+	+	+	+	+
3. 039	3. 037	3. 034	3. 030	3. 022	3. 007	2. 967	2. 882	2. 653	1. 571	. 8153	. 4885	. 4307	10. 681
+	+	+	+	+	+	+	+	+	+	+	+	+	+
3. 076	3. 074	3. 072	3. 070	3. 066	3. 057	3. 035	2. 993	2. 897	2. 498	1. 571	. 6434	. 5191	7. 540
+	+	+	+	+	+	+	+	+	+	+	+	+	+
3. 113	3. 112	3. 112	3. 111	3. 109	3. 106	3. 097	3. 082	3. 053	2. 965	2. 799	1. 571	. 8506	3. 581

TABLE II

Pressure and velocity over the separation surface whose form is the Navy No. 2 strut

Point <i>p</i>	<i>x</i>	<i>y</i>	<i>U_p</i>	<i>v_p</i>	(1+ <i>u_p</i>) ²	<i>v_p</i> ²	<i>q_p</i> ²	<i>p</i> =1- <i>q_p</i> ²
0	0	0	-1.000	0	0	0	0	+1.000
1	.200	.680	-.634	+.488	+.134	+.238	+.372	+.628
2	.600	1.200	-.317	+.724	+.466	+.524	+.990	+.010
3	1.000	1.251	-.069	+.680	+.868	+.462	+1.330	-.330
4	1.600	1.918	+.126	+.588	+1.264	+.346	+1.610	-.610
5	2.600	2.360	+.279	+.452	+1.636	+.204	+1.840	-.840
6	4.200	2.751	+.356	+.211	+1.839	+.044	+1.883	-.883
7	7.200	3.000	+.331	+.045	+1.772	+.002	+1.774	-.774
8	10.400	2.920	+.279	-.116	+1.636	+.013	+1.650	-.450
9	13.600	2.418	+.178	-.272	+1.388	+.074	+1.462	-.462
10	16.800	1.700	+.109	-.243	+1.230	+.059	+1.289	-.289
11	18.400	1.202	-.044	-.468	+.913	+.219	+1.132	-.132
12	20.000	.570	-.128	-.098	+.760	+.010	+.770	+.230

TABLE III

The *x* and *y* coordinates of the Joukowski strut, transformed from the circle *a*=2.00 centered at $\xi=-0.20$, by equations 10, when the map circle is *b*=1.48

Point <i>p</i>	Round cylinder		Joukowski strut		Navy No. 2 strut		Per cent of maximum <i>y</i> error in <i>y</i>
	ξ	η	<i>x</i>	<i>y</i>	<i>x</i>	<i>y</i>	
0	-2.200	0	-3.196	0	-3.196	0	0
1	-2.170	+.347	-3.154	+.190	-3.154	+.186	+.4
2	-2.079	+.684	-3.030	+.371	-3.030	+.361	+.9
3	-1.932	+1.000	-2.826	+.535	-2.826	+.529	+.6
4	-1.732	+1.286	-2.547	+.680	-2.547	+.680	0
5	-1.486	+1.532	-2.200	+.795	-2.200	+.793	+.2
6	-1.200	+1.732	-1.792	+.877	-1.792	+.877	0
7	-.719	+1.932	-1.089	+.936	-1.089	+.936	0
8	-.200	+2.000	+.308	+.916	+.308	+.922	-.6
9	+.319	+1.932	+.501	+.827	+.501	+.835	-.9
10	+.800	+1.732	+1.281	+.690	+1.281	+.701	-1.2
11	+1.086	+1.532	+1.760	+.582	+1.760	+.594	-1.4
12	+1.332	+1.286	+2.183	+.464	+2.183	+.476	-1.3
13	+1.532	+1.000	+2.534	+.345	+2.534	+.357	-1.3
14	+1.679	+.684	+2.798	+.228	+2.798	+.258	-3.2
15	+1.800	0	+3.017	0	+3.017	+.175	-18.7

TABLE IV

Values of *q_ξ*, *p_ξ*, *r*, θ from equation 22 giving surfaces of constant speed near the round cylinder, from *q_ξ*=0.250 to *q_ξ*=1.000, omitting *q_ξ*=1.118 to *q_ξ*=1.750

<i>q_ξ</i>	<i>p_ξ</i>	<i>r</i>	θ		<i>q_ξ</i>	<i>p_ξ</i>	<i>r</i>	θ	
0.250	0.937	2.00	7	11	0.707	0.500	2.00	20	50
		2.05	7	15			2.25	23	20
		2.10	6	59			2.50	23	10
		2.15	6	31			2.75	23	20
		2.20	5	43			3.00	19	20
		2.25	4	26			3.25	17	10
		2.30	1	44			3.50	13	50
.250	.937	2.31	0		.707	.500	4.00	0	
.500	.750	2.00	14	29	.866	.250	2.00	25	40
		2.10	15	2			2.25	28	10
		2.20	14	49			2.50	29	30
		2.30	14	31			2.75	31	30
		2.40	13	39			3.00	31	20
		2.50	12	31			3.25	31	20
		2.70	8	23			3.50	35	20
.500	.750	2.83	0		.866	.250	4.00	26	50
.750	.438	2.00	22	2	1.000	0	2.00	30	0
		2.25	23	55			2.50	35	40
		2.50	24	17			3.00	38	35
		2.75	23	41			3.50	40	18
		3.00	22	12			4.00	41	24
		3.25	20	7			5.00	42	42
		3.50	16	46			6.00	43	24
.750	.438	4.00	0		1.000	0	8.00	44	6

TABLE V-a

Contour, velocity, and pressure values for the round cyclinder $a=2.00$ centered at $\xi=-0.20$ and for the corresponding Joukowski strut when map cylinder is $b=1.48$

ψ	Round cylinder					Joukowski strut				
	η	ξ	u_{ζ}	v_{ζ}	q_{ζ}	x	y	$\left \frac{dz}{d\zeta}\right $	q_z	p_z
	Eq. 25		Eq. 14, 15, 18			Eq. 10		Eq. 17	Eq. 16	Eq. 6
0	0	-4.200	+0.750	0	0.750	-4.721	0	0.876	0.856	+0.267
0	0	-3.200	+.556	0	.556	-3.884	0	.786	.707	+.500
0	0	-2.200	0	0	0	-3.196	0	.547	0	+1.000
0	.347	-2.170	+.060	+.342	.347	-3.154	+.190	.586	.592	+.650
0	.684	-2.079	+.234	+.643	.684	-3.030	+.371	.688	.994	+.012
0	1.000	-1.932	+.500	+.860	1.000	-2.826	+.537	.824	1.213	-.472
0	1.286	-1.732	+.826	+.985	1.286	-2.547	+.680	.974	1.320	-.741
0	1.532	-1.486	+1.173	+.985	1.532	-2.200	+.795	1.122	1.366	-.865
0	1.732	-1.200	+1.500	+.877	1.732	-1.792	+.877	1.261	1.374	-.867
0	1.932	-.719	+1.866	+.501	1.932	-1.090	+.936	1.429	1.351	-.719
0	2.000	-.200	+2.000	0	2.000	-.308	+.916	1.535	1.303	-.697
0	1.932	+.319	+1.866	-.501	1.932	+.501	+.827	1.552	1.245	-.549
0	1.732	+.800	+1.500	-.867	1.732	+1.281	+.690	1.464	1.183	-.401
0	1.532	+1.086	+1.173	-.985	1.532	+1.760	+.580	1.341	1.142	-.305
0	1.286	+1.332	+.826	-.985	1.286	+2.183	+.464	1.168	1.101	-.212
0	1.000	+1.532	+.500	-.867	1.000	+2.535	+.346	.949	1.053	-.110
0	.684	+1.679	+.234	-.643	.684	+2.798	+.228	.700	.976	+.046
0	0	+1.800	0	0	0	+3.017	0	.324	0	+1.000
0	0	+2.800	+.556	0	.556	+3.582	0	.721	.771	+.405
0	0	+3.800	+.750	0	.750	+4.376	0	.848	.884	+.218

TABLE V-b

Contour, velocity, and pressure values for closely graded streamlines, $\psi=\text{const.}$ used to find constant speed surfaces near strut. $\psi=0.03, 0.05, 0.10, 0.20, 0.50$ omitted

ψ	Round cylinder					Joukowski strut				
	η	ξ	u_{ζ}	v_{ζ}	q_{ζ}	x	y	$\left \frac{dz}{d\zeta}\right $	q_z	p_z
	Eq. 25		Eq. 14, 15, 18			Eq. 10		Eq. 17	Eq. 16	Eq. 6
0.01	0.05	+2.155	+0.280	+0.031	0.281	+3.171	+0.026	0.530	0.531	+0.718
.01	.05	-2.555	+.280	-.031	.281	-3.412	+.033	.512	.550	+.698
.01	.10	+1.903	+.102	+.086	.133	+3.051	+.040	.405	.329	+.892
.01	.10	-2.303	+.102	-.086	.133	-3.283	+.059	.591	.225	+.949
.01	.15	+1.865	+.076	+.135	.155	+3.032	+.056	.395	.392	+.846
.01	.15	-2.265	+.076	-.135	.155	-3.228	+.086	.581	.267	+.929
.01	.20	+1.821	+.049	+.190	.196	+3.010	+.104	.390	.503	+.746
.01	.20	-2.221	+.049	-.190	.196	-3.199	+.168	.572	.343	+.882
.01	.40	+1.786	+.101	+.377	.390	+2.933	+.143	.498	.784	+.386
.01	.40	-2.186	+.101	-.377	.390	-3.155	+.222	.606	.645	+.584
.01	.70	+1.689	+.253	+.642	.690	+2.796	+.241	.709	.972	+.054
.01	.70	-2.089	+.253	-.642	.690	-3.032	+.384	.695	.992	+.016
.01	1.00	+1.544	+.500	+.844	.971	+2.543	+.352	.943	1.029	-.059
.01	1.00	-1.944	+.500	-.844	.971	-2.835	+.541	.823	1.180	-.392
.01	1.50	+1.133	+1.117	+.986	1.490	+1.835	+.570	1.313	1.135	-.288
.01	1.50	-1.533	+1.117	-.986	1.490	-2.263	+.786	1.098	1.357	-.842
.01	2.00	-.060	+1.985	+1.390	1.982	+.092	+.906	1.546	1.282	-.643
.01	2.00	-.340	+1.985	-1.390	1.982	-.521	+.936	1.493	1.328	-.763

TABLE V-c

Contour, velocity, and pressure values for normally graded streamlines, $\psi = \text{const.}$ $\psi = 0.70, 1.05, 1.40, 1.75, 2.10,$ and 2.45 omitted

ψ	Round cylinder					Joukowski strut				
	η	ξ	u_ξ	v_ξ	q_ξ	x	y	$\frac{dz}{d\xi}$	q_s	p_s
	Eq. 25		Eq. 14, 15, 18			Eq. 10		Eq. 17	Eq. 16	Eq. 6
0.35	0.35	+	1.000	0	1.000	+	+0.350	0	1.000	0
.35	.35	-	1.000	0	1.000	-	+.350	0	1.000	0
.35	.50	+3.417	+.711	+.081	.716	+4.044	+.408	.826	.867	+.248
.35	.50	-3.817	+.711	-.081	.716	-4.381	+.426	.858	.834	+.304
.35	.70	+2.540	+.561	+.240	.610	+3.342	+.479	.732	.834	+.304
.35	.70	-2.940	+.561	-.240	.610	-3.645	+.532	.786	.777	+.397
.35	.80	+2.344	+.539	+.232	.611	+3.181	+.514	.750	.815	+.335
.35	.80	-2.744	+.539	-.232	.611	-3.480	+.585	.787	.777	+.396
.35	1.00	+2.070	+.561	+.479	.731	+2.928	+.586	.810	.903	+.185
.35	1.00	-2.470	+.561	-.479	.731	-3.232	+.692	.807	.906	+.179
.35	1.25	+1.798	+.685	+.647	.937	+2.619	+.679	.933	.993	+.013
.35	1.25	-2.198	+.685	-.647	.937	-2.951	+.823	.876	1.071	-.145
.35	1.50	+1.523	+.894	+.759	1.173	+2.253	+.781	1.102	1.064	-.133
.35	1.50	-1.923	+.894	-.759	1.173	-2.631	+.947	.963	1.218	-.483
.35	1.75	+1.192	+1.180	+.779	1.411	+1.774	+.895	1.263	1.116	-.246
.35	1.75	-1.592	+1.180	-.779	1.411	-2.215	+1.065	1.093	1.290	-.665
.35	2.00	+.721	+1.536	+.627	1.659	+1.070	+1.031	1.407	1.179	-.390
.35	2.00	-1.121	+1.536	-.627	1.659	-1.588	+1.167	1.268	1.308	-.712
.35	2.10	+.424	+1.698	+.455	1.758	+.627	+1.098	1.452	1.211	-.466
.35	2.10	-.824	+1.698	-.455	1.758	-1.179	+1.196	1.347	1.304	-.702

TABLE VI-a

Constant speed contours about the Joukowski strut

<i>q</i>	<i>p</i>	Bow		Stern		<i>q</i>	<i>p</i>	Abreast	
		<i>x</i>	<i>y</i>	<i>x</i>	<i>y</i>			<i>x</i>	<i>y</i>
0. 25	+0. 937	-3. 188	0. 075	+3. 012	0. 013	1. 25	-0. 563	-2. 800	0. 570
. 25	+. 937	-3. 237	. 077	+3. 050	0			-2. 750	. 600
		-3. 315	. 050					-2. 700	. 660
		-3. 330	0					-2. 640	. 730
. 50	+. 75	See Table VI-b						-2. 550	. 830
. 75	+. 438	-3. 125	0. 250	+2. 960	0. 125			-2. 380	1. 015
		-3. 158	. 315	+3. 025	. 300			-2. 152	1. 180
		-3. 200	. 362	+3. 125	. 340			-. 600	1. 330
		-3. 300	. 450	+3. 340	. 300			-. 165	1. 175
		-3. 470	. 520	+3. 520	. 065			+. 050	1. 070
		-3. 670	. 520	+3. 525	0			+. 270	. 935
		-3. 890	. 412					+. 375	. 870
		-4. 000	. 250					+. 412	. 835
		-4. 040	. 140						
		-4. 050	0						
. 75	+. 438					1. 25	-. 563		
1. 00	0	-3. 025	. 380	+2. 750	. 250				
		-3. 025	. 440	+2. 680	. 350				
		-3. 030	. 510	+2. 637	. 440				
		-3. 048	. 610	+2. 600	. 525				
		-3. 080	. 775	+2. 570	. 692				
		-3. 130	. 910	+2. 550	. 845				
		-3. 200	1. 080	+2. 570	1. 048				
		-3. 360	1. 400	+2. 660	1. 375				
		-3. 535	1. 730	+2. 800	1. 720				
		-3. 730	2. 052	+2. 975	2. 030				
1. 00	0								

TABLE VI-b
Constant pressure contours about Joukowski strut

<i>p</i>	<i>q</i>	Bow		Stern		<i>p</i>	<i>q</i>	Abreast	
		<i>x</i>	<i>y</i>	<i>x</i>	<i>y</i>			<i>x</i>	<i>y</i>
+0.75	0.50	-3.175	0.160	+3.008	0.030	-0.25	1.118	-2.940	0.451
		-3.180	.170	+3.033	.060			-2.900	.625
		-3.260	.210	+3.108	.065			-2.730	.880
		-3.470	.130	+3.135	.030			-2.790	1.020
+.75	.50	-3.525	0	+3.150	0			-2.725	1.240
+.50	.707	-3.130	.240	+2.975	.095			-2.600	1.600
		-3.170	.290	+3.000	.170			+1.975	.527
		-3.230	.330	+3.050	.235			+1.830	.750
		-3.330	.375	+3.350	.175			+1.745	.900
		-3.775	.290	+3.395	.075			+1.660	1.030
		-3.880	.140	+3.410	0	-.25	1.118	+1.210	1.635
+.50	.707	-3.900	.050			-.50	1.225	-2.825	.535
		-3.900	0					-2.700	.700
+.25	.866	-3.085	.310	+2.900	.175			-2.480	1.000
		-3.105	.370	+2.913	.250			-2.080	1.370
		-3.130	.425	+2.930	.330			-2.240	1.480
		-3.190	.525	+2.965	.400			+.135	1.260
		-3.295	.652	+3.045	.535			+.330	1.120
		-3.490	.800	+3.375	.670	-.50	1.225	+.750	.790
		-3.950	.900	+3.820	.613	-.75	1.323	-2.500	.696
		-4.310	.851	+4.180	0			-2.320	.830
		-4.700	.580					-2.000	.975
		-4.775	.420					-2.230	1.075
+.25	.866	-4.820	0					-.820	1.025
0	1.00	See Table VI-a				-.75	1.323	-.565	.930

TABLE VII
Resistance values for Navy No. 2, 5-foot strut with shielded ends at various air speeds and zero pitch and yaw

Air-speed, M. P. H. <i>V</i>	Net resist- ance per foot <i>R</i> lb.	<i>V</i> ₁ <i>D</i> ₁ (ft.×ft./sec.)	$C = \frac{2Rg}{\rho L D_1 V_1^2}$
20	0.0240	7.34	0.0940
30	.0472	11.00	.0821
40	.0796	14.67	.0779
50	.1206	18.34	.0755
60	.1748	22.00	.0761

R=resistance per foot length of strut, lb.
D=strut thickness in inches.
*D*₁=strut thickness in feet.
C=shape coefficient.
V=air speed in miles per hour.
*V*₁=air speed in feet per second.
 $\rho/g=0.00237$ slug/feet.

TABLE VIII

Point pressure in terms of nose pressure, p/p_n , at various wind speeds for Navy No. 2 strut—zero of pitch and yaw

Pressure hole			Point pressure p/p_n				
Num- ber	Coordinates		Wind speed in M. P. H.				
	x	y	20	30	40	50	60
1	0	0	+1.000	+0.998	+1.004	+1.000	+1.000
2	.100	.370	+.608	+.602	+.601	+.604	+.600
3	.320	.620	+.066	+.066	+.071	+.068	+.066
4	.540	.830	-.332	-.348	-.345	-.350	-.356
5	.880	1.000	-.612	-.608	-.593	-.604	-.594
6	1.300	1.170	-.704	-.712	-.695	-.706	-.700
7	2.100	1.370	-.780	-.784	-.762	-.768	-.766
8	3.640	1.500	-.688	-.698	-.667	-.668	-.662
9	5.250	1.460	-.586	-.586	-.570	-.566	-.552
10	6.800	1.210	-.414	-.408	-.386	-.386	-.380
11	8.400	.850	-.178	-.176	-.158	-.152	-.146
12	9.220	.590	-.026	-.010	+.016	+.022	+.042
13	9.950	.300	+.142	+.154	+.158	+.150	+.146
14	10.330	.100	+.178	+.172	+.170	+.168	+.162

p = point pressure at any hole.
 p_n = point pressure at nose = $\frac{1}{2}\rho U_0^2$

TABLE IX

Along-stream forces per foot run of Navy No. 2 strut expressed both in pounds and in per cent of total drag for theory and experiment at 60 miles per hour

Air speed M. P. H.	Downstream			Upstream			Pressure drag $D_p=P_1-P_2$	Friction drag D_f	Total drag $D=D_p+D_f$
	Push	Suction	Total P_1	Push	Suction	Total P_2			
Pounds per foot run—theory									
60	0. 4151	0. 4109	0. 8260	0. 2010	0. 6250	0. 8260	0	0	0
Pounds per foot run—experiment									
60	0. 4230	0. 2752	0. 7012	0. 0893	0. 5490	0. 6383	0. 0629	0. 1119	0. 1748
Per cent of total drag—experiment									
60	242	159	401	51	314	365	36	64	100

DIAGRAM I

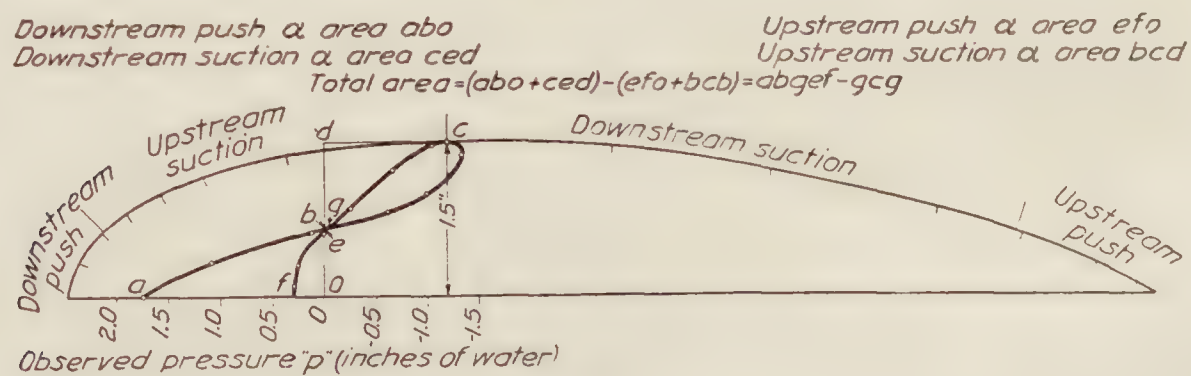


TABLE X

Values of abscissæ, air speeds, and accelerations used in evaluating I_1 and I_2 in Equation 18

Distance aft bow L in feet	Measured tangential speed V_0	$V_0^{0.35} = f^{0.55}$	$V_0^{1.85} = f^{1.55}$	$L^{0.65}$	$L^{0.65}/L =$ $L^{-0.15}$	$\frac{dV_0}{dL} = f'$ (faired)	$\frac{1.85 \times}{f^{0.55} L^{0.55} f' =}$ I_2	$\frac{0.85 \times}{f^{0.85} L^{-0.15} =}$ I_1
0	0	0	0	0				
.0208	.920	.930	.855	.0373	1.793	+14.40	+0.924	+1.303
.0417	1.125	1.105	1.243	.0671	1.609	+6.288	+ .862	+1.700
.0833	1.276	1.233	1.573	.1210	1.453	+1.675	+ .462	+1.943
.1250	1.316	1.262	1.661	.1708	1.366	+ .624	+ .249	+1.930
.1666	1.330	1.274	1.695	.2181	1.309	+ .156	+ .080	+1.886
.2083	1.330	1.274	1.695	.2635	1.263	- .108	- .067	+1.820
.2500	1.318	1.265	1.666	.3079	1.232	- .222	- .160	+1.744
.2916	1.298	1.248	1.621	.3506	1.203	- .270	- .219	+1.657
.3333	1.282	1.235	1.584	.3932	1.179	- .292	- .262	+1.587
.3748	1.268	1.224	1.552	.4345	1.158	- .294	- .289	+1.528
.4166	1.256	1.214	1.524	.4749	1.139	- .320	- .341	+1.475
.4585	1.242	1.203	1.493	.5152	1.123	- .387	- .444	+1.425
.5000	1.220	1.184	1.444	.5546	1.113	- .511	- .621	+1.366
.5415	1.194	1.163	1.388	.5930	1.094	- .622	- .794	+1.291
.5832	1.165	1.139	1.326	.6321	1.084	- .711	- .947	+1.222
.6250	1.135	1.113	1.264	.6693	1.071	- .765	-1.087	+1.151
.6666	1.102	1.086	1.197	.7083	1.062	- .788	-1.122	+1.081
.7082	1.067	1.057	1.127	.7460	1.052	- .826	-1.205	+1.008
.7500	1.016	1.014	1.030	.7828	1.043	- .871	-1.279	+1.913
.7915	.956	.961	.918	.8185	1.034	- .780	-1.133	+ .807
.8333	.920	.930	.855	.8566	1.028	- .474	- .698	+ .747
.8755	.916	.929	.850	.8930	1.020	- .030	- .046	+ .737

REPORT No. 312

THE PREDICTION OF AIRFOIL CHARACTERISTICS

By GEORGE J. HIGGINS

Langley Memorial Aeronautical Laboratory

REPORT No. 312

THE PREDICTION OF AIRFOIL CHARACTERISTICS

By GEORGE J. HIGGINS

SUMMARY

This paper describes and develops methods by which the aerodynamic characteristics of an airfoil may be calculated with sufficient accuracy for use in airplane design. These methods for prediction are based on the present aerodynamic theory and on empirical formulas derived from data obtained in the N. A. C. A. variable density wind tunnel at a Reynolds Number corresponding approximately to full scale.

INTRODUCTION

Since the time that Eiffel first developed the use of the wind tunnel for obtaining the aerodynamic characteristics of airfoils, a great amount of data has been accumulated. Many attempts have been made in the analysis of these data to generalize and thereby develop a method for the prediction of airfoil characteristics. These have been more or less successful. In all cases though, the experimenters have been handicapped by "scale effect." This unknown factor undoubtedly contributed a great deal to the differences found between the models and the full scale wings.

In theoretical aerodynamics, the air is treated as a nonviscous fluid. Consequently, the profile drag of an airfoil can not be accounted for. However, by assuming that the fluid outside of the "boundary layer" is nonviscous and that within the "layer" is viscous, one can combine the pure theory fairly well with the experimental modifications and obtain satisfactory results. Scale effect, also a factor caused by viscosity, can not be determined by theoretical treatment.

Empirical derivations from test data modified in accordance with the above theories lead to certain formulas which may be used for determining airfoil characteristics. Heretofore such expressions have been rather unreliable because of the scale effect mentioned above. Now, however, there are available results of tests made under conditions of full scale on airfoils in the variable density wind tunnel of the National Advisory Committee for Aeronautics. These data then can be used for developing more accurate expressions for prediction.

This paper covers the development of such expressions from experiments in the variable density tunnel and from the present aerodynamic theory. A comparison is made showing the differences between predicted airfoil characteristics and observed data from tests in the wind tunnel at 20 atmospheres density at a Reynolds Number corresponding to full scale.

The author acknowledges the suggestions and aid given in the development of this paper by E. N. Jacobs and M. Knight, of the Langley Memorial Aeronautical Laboratory.

THE PREDICTION OF AIRFOIL CHARACTERISTICS

The main characteristics of an airfoil section are the lift coefficient, profile drag coefficient, and the pitching moment coefficient for any angle of attack within the flying range. When these characteristics are known, any other derived characteristics may be determined and sufficient data is then available for use in airplane design. Heretofore, it has been necessary to use wind-tunnel tests for the particular airfoil to obtain these characteristics. This has been particularly true in regard to the profile drag coefficient because of the lack of theory to cover its computation. Test data from the ordinary wind tunnel have been also subject to correction for scale effect; but there are now available considerable data from tests in the variable density

wind tunnel made at a Reynolds Number equivalent to full scale. Where the term "full scale" is used throughout this report a Reynolds Number of approximately 3,400,000 (a Vl of 534, or a $7\frac{1}{4}$ -foot chord at 50 M. P. H.) is meant.

It is possible to determine the lift and moment coefficients by theoretical computation and the profile drag coefficient by an empirical derivation for any angle of attack up to the burble point. The values of total C_D , L/D , C_p , etc., can then be computed.

The useful angular range in lift from zero lift to the burble point has been found from tests in the variable density tunnel to vary from 18° for thin low cambered sections to 24° for thick high-cambered sections. As a normal airplane is limited to about 15° in its range of angle of attack from the high-speed condition to that of landing, it may be seen that only in special designs does an airplane land or take off at or very near the burble point. Hence, if an airfoil section of normal shape is to be used, the burble point is of secondary importance.

THE LIFT COEFFICIENT

The slope of C_L curve.—Prandtl, Munk, and others, in their development of the theory of lift for an airfoil of infinite span, find the following:

$$C_L = 2\pi \sin \alpha \quad (1)$$

or

$$C_L = 2\pi\alpha \text{ (radians), approx. (Reference 1).}$$

and

$$\frac{dC_L}{d\alpha} = 2\pi \quad (2)$$

For wings of finite span having an elliptical span loading and an aspect ratio of $\frac{b^2}{S}$,

$$\alpha_a = \alpha_e + \alpha_i \quad (3)$$

where α_a = absolute angle of attack measured from the position of zero lift.

α_e = effective angle of attack, i. e., the angle of attack at which an airfoil of infinite span would give the same lift coefficient as the airfoil of finite span under consideration.

From equation (1) above,

$$\alpha_e = \frac{C_L}{2\pi}$$

α_i = induced angle of attack.

Munk gives for the induced angle of attack

$$\alpha_i = \frac{C_L S}{\pi b^2} \quad (4)$$

Substituting for α_e and α_i

$$\alpha_a = \frac{C_L}{2\pi} + \frac{C_L S}{\pi b^2} \quad (5)$$

Solving,

$$C_L = \frac{2\pi\alpha_a}{1 + \frac{S}{b^2}} \quad (\alpha_a \text{ in radians}) \quad (6)$$

$$= 0.10965 \frac{\alpha_a}{1 + \frac{S}{b^2}} \quad (\alpha_a \text{ in degrees}) \quad (7)$$

Because of the general inefficiency of the wing and because the air is not a nonviscous fluid, experiments show that $\frac{dC_L}{d\alpha_e} < 2\pi$

or

$$\frac{dC_L}{d\alpha_e} = k2\pi \quad (8)$$

From this

$$\alpha_e = \frac{C_L}{k2\pi} \quad (9)$$

The value of k as determined from many tests conducted at a high Reynolds Number in the variable-density wind tunnel is approximately 0.875.

The induced angle of attack is affected by the shape of the plan form. Glauert gives the following expression for the induced angle of attack

$$\alpha_i = \frac{C_L S}{\pi b^2} (1 + \tau) \quad (\text{Reference 2}) \quad (10)$$

where τ is a factor for determining the additional angle caused by the change in span loading from that of the elliptical due to the shape of the plan form. For an elliptical plan form τ is zero. Values for rectangular plan forms of different aspect ratios are given in Table I.

TABLE I

Correction factors for rectangular airfoils

Aspect ratio, $\frac{b^2}{S}$	τ	σ
3	0.11	0.022
4	.14	.033
5	.16	.044
6	.18	.054
7	.20	.064
8	.22	.074
9	.23	.083

Substituting these expressions of α_e and α_i in equation (3) and solving for C_L , one obtains

$$C_L = \frac{2\pi k \alpha_a}{1 + \frac{2kS}{b^2}(1 + \tau)} \quad (\alpha_a \text{ in radians}) \quad (11)$$

or

$$C_L = \frac{0.0960 \alpha_a}{1 + \frac{1.75S}{b^2}(1 + \tau)} \quad (\alpha_a \text{ in degrees}) \quad (12)$$

The slope of the curve of C_L plotted against α then becomes

$$\frac{dC_L}{d\alpha} = \frac{0.0960}{1 + \frac{1.75S}{b^2}(1 + \tau)} \quad (13)$$

For an elliptical wing, or a wing having elliptical span loading, of aspect ratio 6.00, where τ is zero,

$$\frac{dC_L}{d\alpha} = 0.0743,$$

and for a rectangular wing of the same aspect ratio

$$\frac{dC_L}{d\alpha} = 0.0714.$$

Angle of zero lift.—

Munk has developed (Reference 3) a method by which the angle of zero lift α_{L_0} may be found. He gives

$$-\alpha_{L_0} = F_1 \frac{\xi_1}{c} + F_2 \frac{\xi_2}{c} + \dots + F_n \frac{\xi_n}{c} \quad (\text{in degrees}) \quad (14)$$

where

α_{L_0} = angle of attack where the lift is zero, measured from the chord line.

F = a factor.

ξ = ordinates of the mean camber line at a point (X) on the chord line minus the ordinate of the mean camber line at the trailing edge.

c = chord of the airfoil.

For ordinary use, the 5-point method given is sufficiently accurate. This gives

$$-\alpha_{L0} = 1,252.24 \frac{\xi_1}{c} + 109.05 \frac{\xi_2}{c} + 32.596 \frac{\xi_3}{c} + 15.684 \frac{\xi_4}{c} + 5.978 \frac{\xi_5}{c}, \text{ in degrees} \quad (15)$$

where ξ_1, ξ_2 , etc., are the ordinates of the mean camber line at the points

$$X_1 = 99.458\% c$$

$$X_2 = 87.426\% c$$

$$X_3 = 50.000\% c$$

$$X_4 = 12.574\% c$$

$$X_5 = 0.542\% c,$$

respectively.

By substituting the correct values in the above equation, the angle of zero lift can be evaluated. Then, knowing that the lift varies very nearly as a linear function of the angle of attack and after determining the slope from equation (13), the curve of C_L vs. α may be readily drawn for the section under consideration. (See fig. 1.) As stated before, the burble

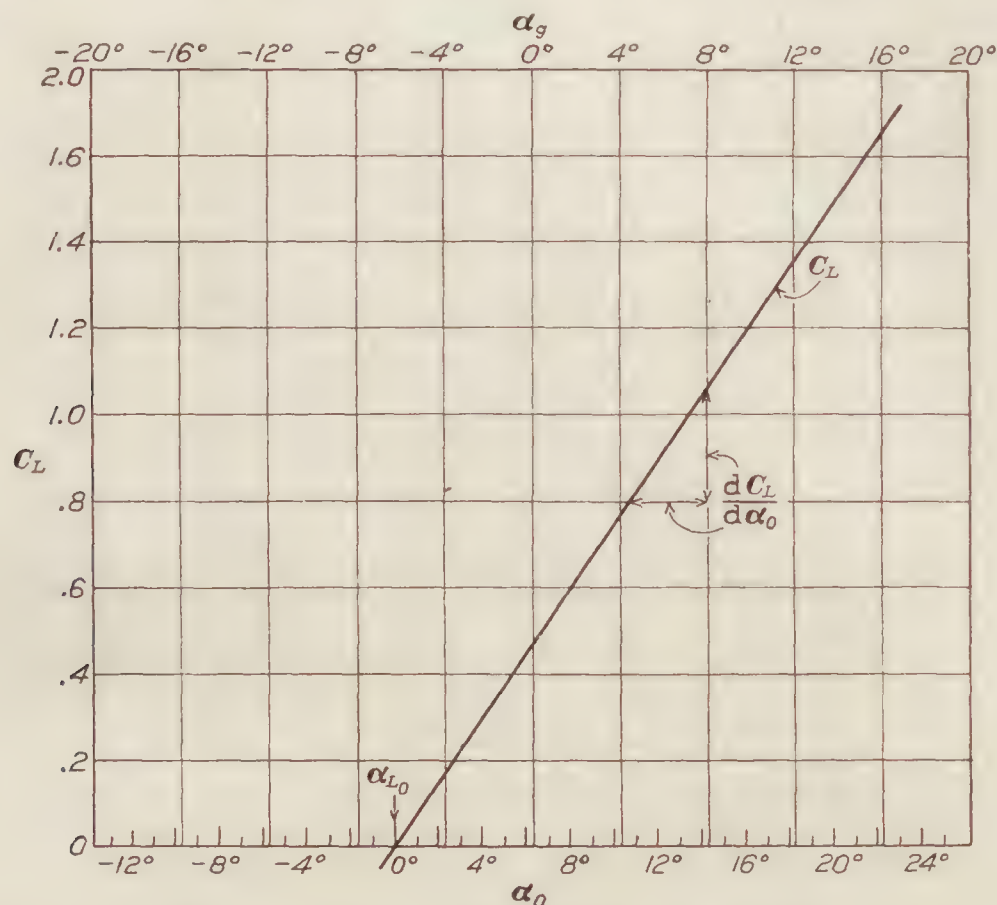


FIGURE 1.— C_L vs. α , α_{L0} must be determined for each airfoil

point is not known, but this is only of secondary importance. However, it is of interest to note that the highest maximum C_L ever recorded in the variable density wind tunnel on a normal airfoil, i. e., without flaps, slots, etc., at a Reynolds Number equivalent to full scale, is 1.50.

THE DRAG COEFFICIENT

The total drag of a wing may be divided into two parts, the profile drag and the induced drag, or

$$C_D = C_{D_0} + C_{D_i} \quad (16)$$

Theory gives

$$C_{D_i} = \frac{C_L^2 S}{\pi b^2} \quad (\text{for elliptically loaded wings, Reference 1}) \quad (17)$$

then

$$C_D = C_{D_o} + \frac{C_L^2 S}{\pi b^2} \quad (18)$$

It has been usually assumed that C_{D_o} is constant for all values of C_L ; but from tests on many airfoils at a high Reynolds Number in the variable density tunnel, it appears that this is not the case. Mr. Knight, of the laboratory staff, pointed out that the variation in profile drag for these airfoils was similar and seemed to follow a power law. Let

$$C_{D_o} = C_{D_{L_0}} + \Delta C_{D_o} \quad (19)$$

where $C_{D_{L_0}}$ is the profile drag coefficient when the lift is zero and when there are no disturbances or burbling effects from the lower surface (fig. 2), and where ΔC_{D_o} is the additional profile drag

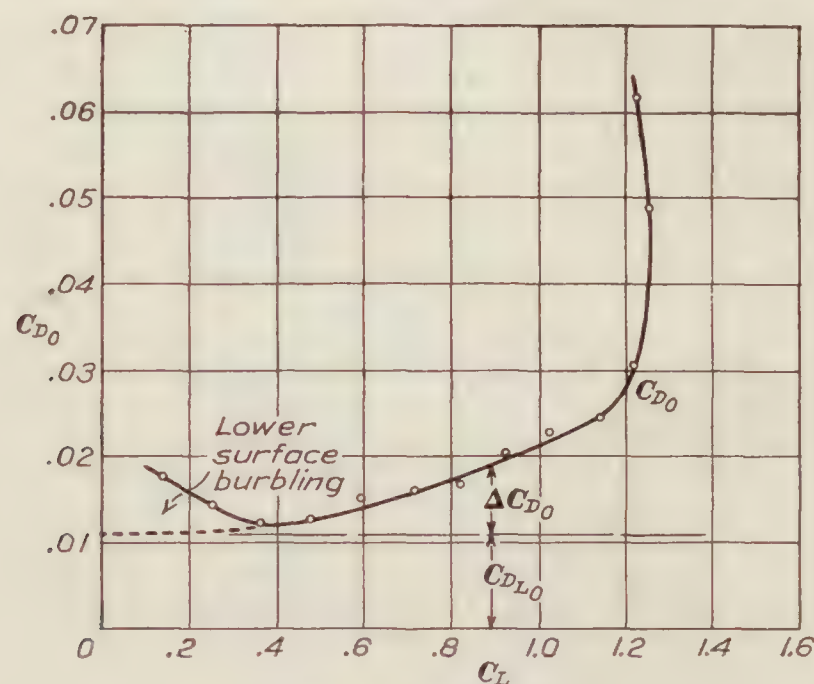


FIGURE 2.— C_{D_o} vs. C_L

coefficient, increasing as the lift increases.

For airfoils that are not extreme in shape and design, values of $C_{D_{L_0}}$ may be found from the charts in Figures 3, 4, and 5. These curves of $C_{D_{L_0}}$ against thickness and against camber

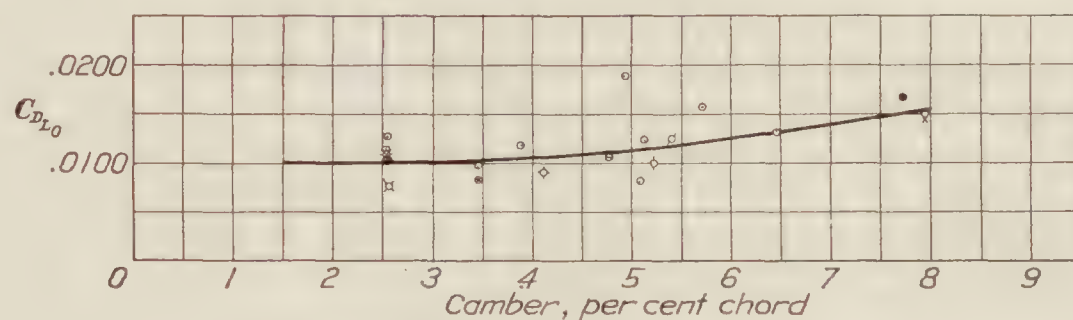


FIGURE 3.—Variation of $C_{D_{L_0}}$ with camber

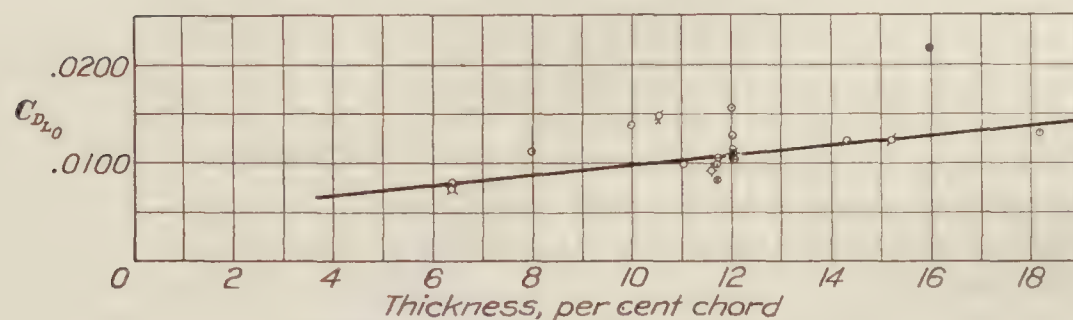
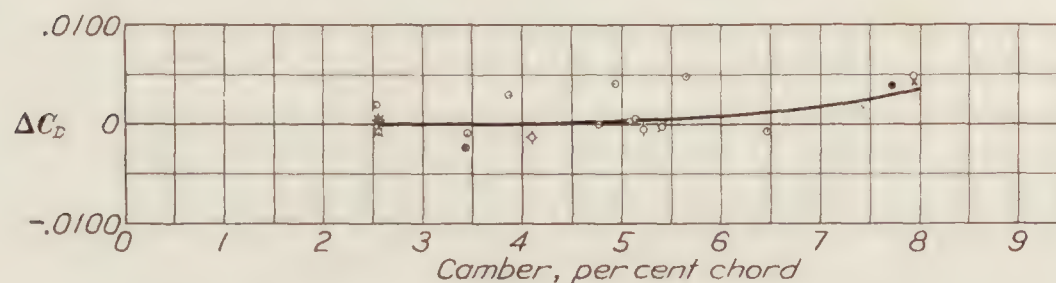
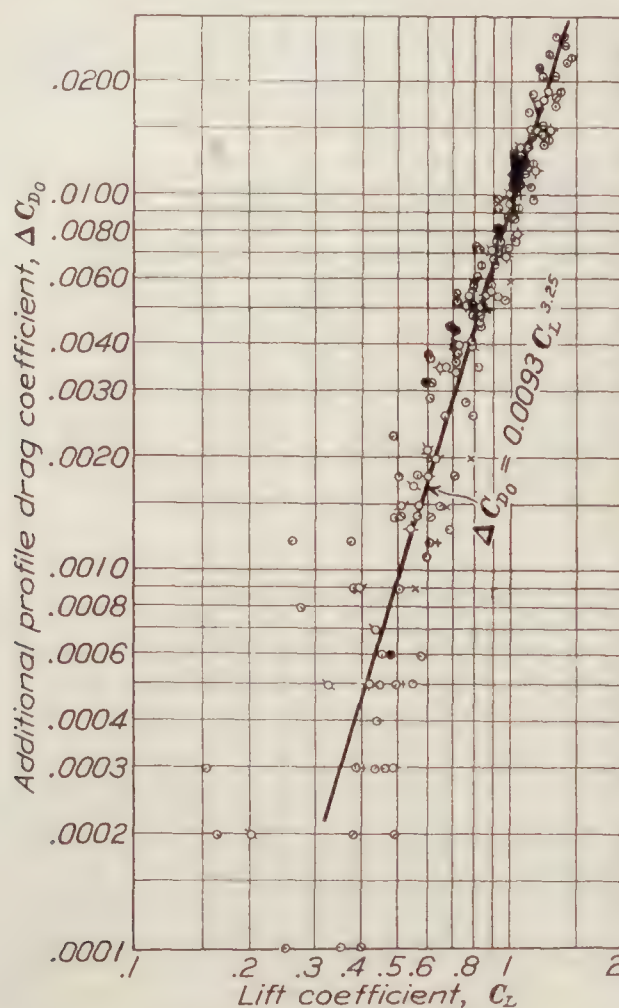


FIGURE 4.—Variation of $C_{D_{L_0}}$ with thickness

FIGURE 5.—Additional ΔC_D due to the effect of camber

were plotted from data obtained in the variable density tunnel. The accuracy of these curves can be surmised by the scattering of points plotted; the error, however, is only a small per cent of the total wing drag and still a smaller per cent of the total airplane drag.

From Figure 6, where ΔC_{D_0} has been plotted against C_L from 22 tests on different airfoils

FIGURE 6.— ΔC_{D_0} vs. C_L

at high Reynolds Numbers, one finds in support of Mr. Knight's suggestion that, as a simple approximation

$$\Delta C_{D_0} = 0.0093 C_L^{3.25} \quad (20)$$

This holds true approximately for all normal-shaped sections. Hence,

$$C_{D_0} = C_{D_{L_0}} + 0.0093 C_L^{3.25} \quad (21)$$

and

$$\text{Total } C_D = C_{D_{L_0}} + 0.0093 C_L^{3.25} + \frac{C_L^2 S}{\pi b^2} \quad (\text{elliptical wings}) \quad (22)$$

$$\text{Total } C_D = C_{D_{L_0}} + 0.0093 C_L^{3.25} + \frac{C_L^2 S}{\pi b^2} (1 + \sigma) \quad (\text{rectangular wings, Reference 2}) \quad (23)$$

where σ is the factor for the additional induced drag caused by the change in span loading from the elliptical. (See Table I.)

From the above expressions the polar curves can now be determined up to the burble point.

Figure 7 is a chart showing the relationship of the different drag components of a wing or airfoil and of an airplane. The different curves in the upper half of the chart show the effect of aspect ratio and represent the part of the drag that varies with a change in the lift; this portion of the drag is independent of the choice of the section and is equal to the sum of the induced drag and the additional profile drag. The lower part shows the drag dependent on the airfoil section and the other parts of the airplane. This chart is convenient for use for determining rapidly the characteristics of any airfoil section or any airplane.

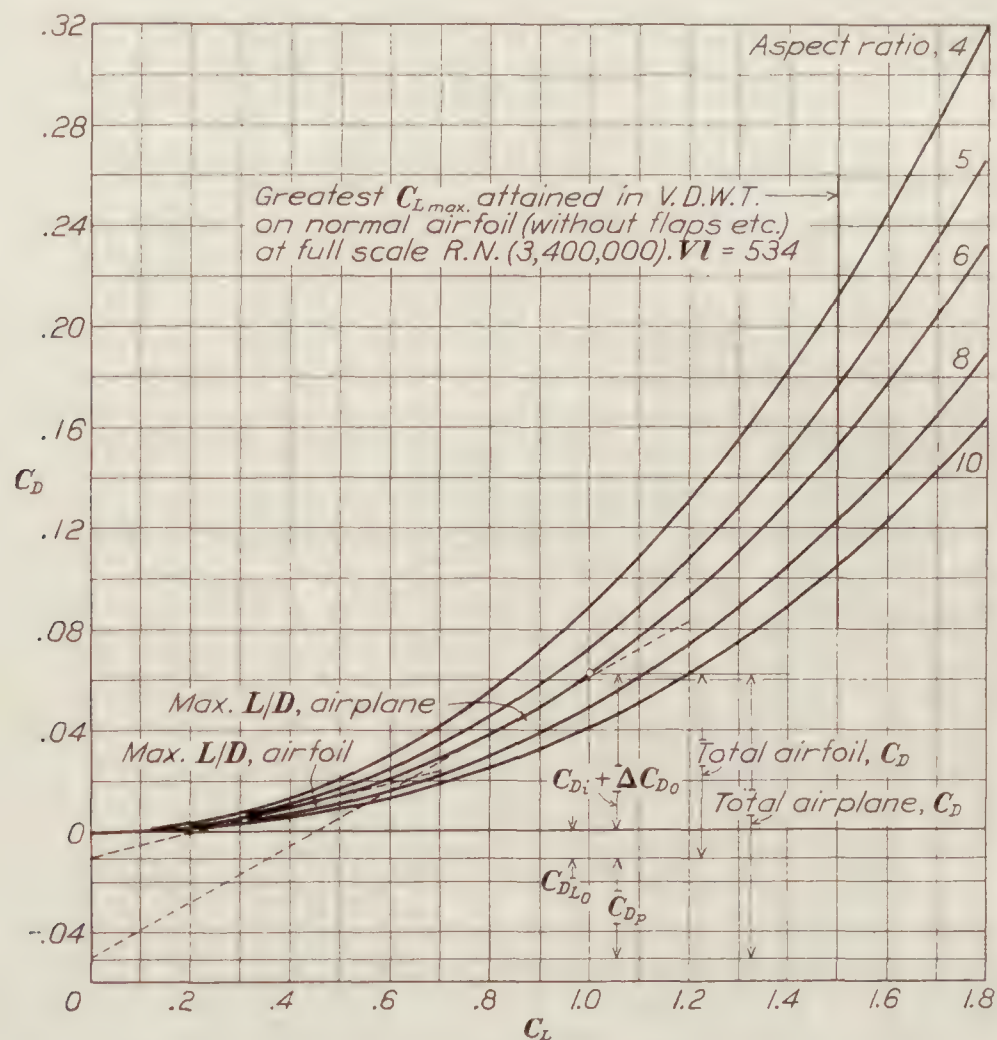


FIGURE 7.—Airplane characteristics showing the relation of the different drag components

LIFT-DRAG RATIO

Values of L/D can be obtained as usual by dividing the C_L by C_D and may be plotted against the angle of attack or the lift coefficient as desired. Values of α , of course, are determined from the curve of C_L vs. α .

THE MOMENT COEFFICIENT

Reference 3 also gives a method for evaluating the angle of attack when the pitching moment about the 50 per cent chord point is zero, α_{M_0}

$$\alpha_{M_0} = 62.634 \left(\frac{\xi_A}{c} - \frac{\xi_B}{c} \right), \text{ in degrees} \quad (24)$$

where

ξ = ordinate of the mean camber line at a point (X) on the chord minus the ordinate of the mean camber line at the trailing edge.

$$X_A = 95.74\% c.$$

$$X_B = 4.26\% c.$$

When the airfoil is in such a position that the moment about the 50 per cent point of the chord is zero, the resultant force will obviously pass through this point. Neglecting the moment due to the drag force which is very small, the moment about any other point on the chord can be computed by obtaining the product of the lift force and its lever arm (l) about the point.

(See fig. 8.) By this method, the moment about a point at 25 per cent of the chord is determined. Munk shows theoretically (Reference 1) that the moment about this point is constant for all angles of attack and values of lift. The moment about the quarter chord point becomes

$$M_{c/4} = L(\alpha_{M_o}) \times l = L \times \frac{c}{4} \cos \alpha_{M_o} = L \times \frac{c}{4} \text{ approximately} \quad (25)$$

and the moment coefficient is

$$C_{M_{c/4}} = \frac{M}{qcS} = \frac{L}{qcS} \times \frac{c}{4} = \frac{C_L(\alpha_{M_o})}{4} \quad \text{or} \quad C_{M_{c/4}} = \frac{C_L(\alpha_{M_o})}{4} = \frac{1}{4} \times 0.0960\alpha' = 0.0240\alpha'. \quad (26)$$

where α' is the angle $\alpha_{L_o} - \alpha_{M_o}$. $C_{M_{c/4}}$ is negative (diving moment) when $C_L(\alpha_{M_o})$ is positive.

The $C_{M_{c/4}}$ curve may be then plotted by drawing a straight line parallel to the C_L axis and with a $C_{M_{c/4}}$ value as found above.

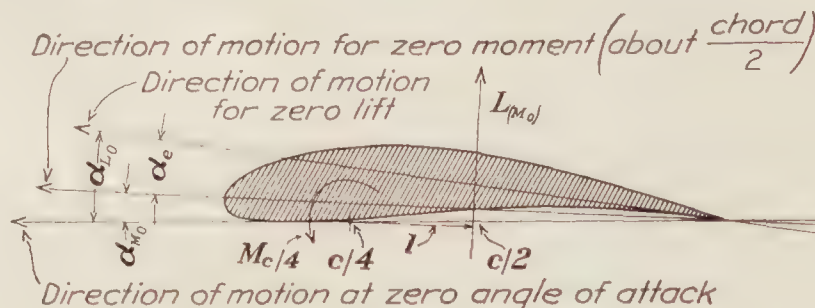


FIGURE 8

CENTER OF PRESSURE COEFFICIENT

The center of pressure coefficient can be readily determined from the other characteristics already computed by the expression

$$C_p = 0.25 - \frac{C_{M_{c/4}}}{C_L \cos \alpha - C_D \sin \alpha} \quad \text{or} \quad C_p = 0.25 - \frac{C_{M_{c/4}}}{C_L}, \text{ approx.} \quad (27)$$

The latter expression is sufficiently accurate for all general purposes. The graph of C_p vs. C_L can be plotted in the usual manner. It is sometimes convenient to know the C_p in per cent chord aft of the quarter chord point. For this

$$C. P. = -100 \frac{C_{M_{c/4}}}{C_L}, \text{ per cent chord.} \quad (28)$$

COMPARISON OF PREDICTED AND OBSERVED CHARACTERISTICS

Figures 9, 10, and 11 show the characteristics of an N. A. C. A. M6 airfoil, a Clark Y airfoil, and an R. A. F. 15 airfoil, all of aspect ratio 6.85 and with a rectangular plan form. There are given on these charts graphs of C_L , C_D , L/D , and $C_{M_{c/4}}$ vs. α , and C_D and C_p vs. C_L . The calculated curves are shown as solid lines and the observed data are shown by points and dashed lines. These latter data are from tests at 20 atmospheres density in the variable density wind tunnel, a Reynolds Number corresponding to full scale. It is interesting to note the close agreement that is obtained between the computed and the observed curves for each of the different characteristics. The greatest difference occurs with the Clark Y section when the characteristics are plotted against the angle of attack. This seems to be mainly as the angle approaches the critical burbling condition. Since the C_D is computed from the C_L , it also is at variance with the observed values in this region. These discrepancies seem to offset each other in the polar curve for there the agreement is good. The predicted L/D curve is slightly low mainly because the observed drag of the Clark Y is low for a section of its thickness.

Figures 12, 13, 14, 15, 16, and 17 show the profile drag coefficients for six common sections, the U. S. A. 35A, N. A. C. A. M6, U. S. A. 27, R. A. F. 15, Clark Y, and the U. S. N. P. S. 4, plotted against C_L . Predicted and observed values are shown here in the same manner. In these charts the C_{D_o} scale is twice the usual one to show the differences more clearly.

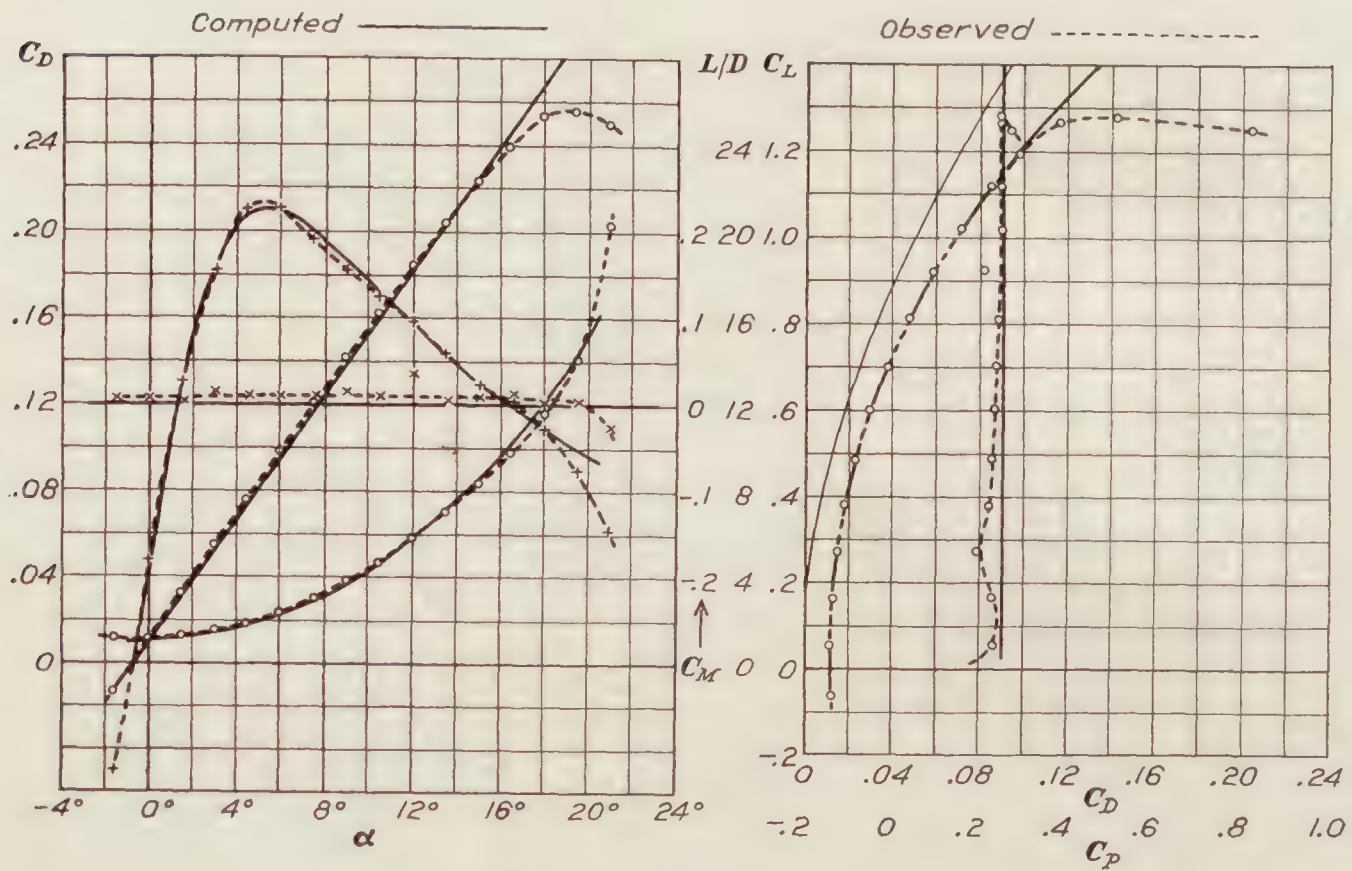


FIGURE 9.—Characteristics of M6 airfoil

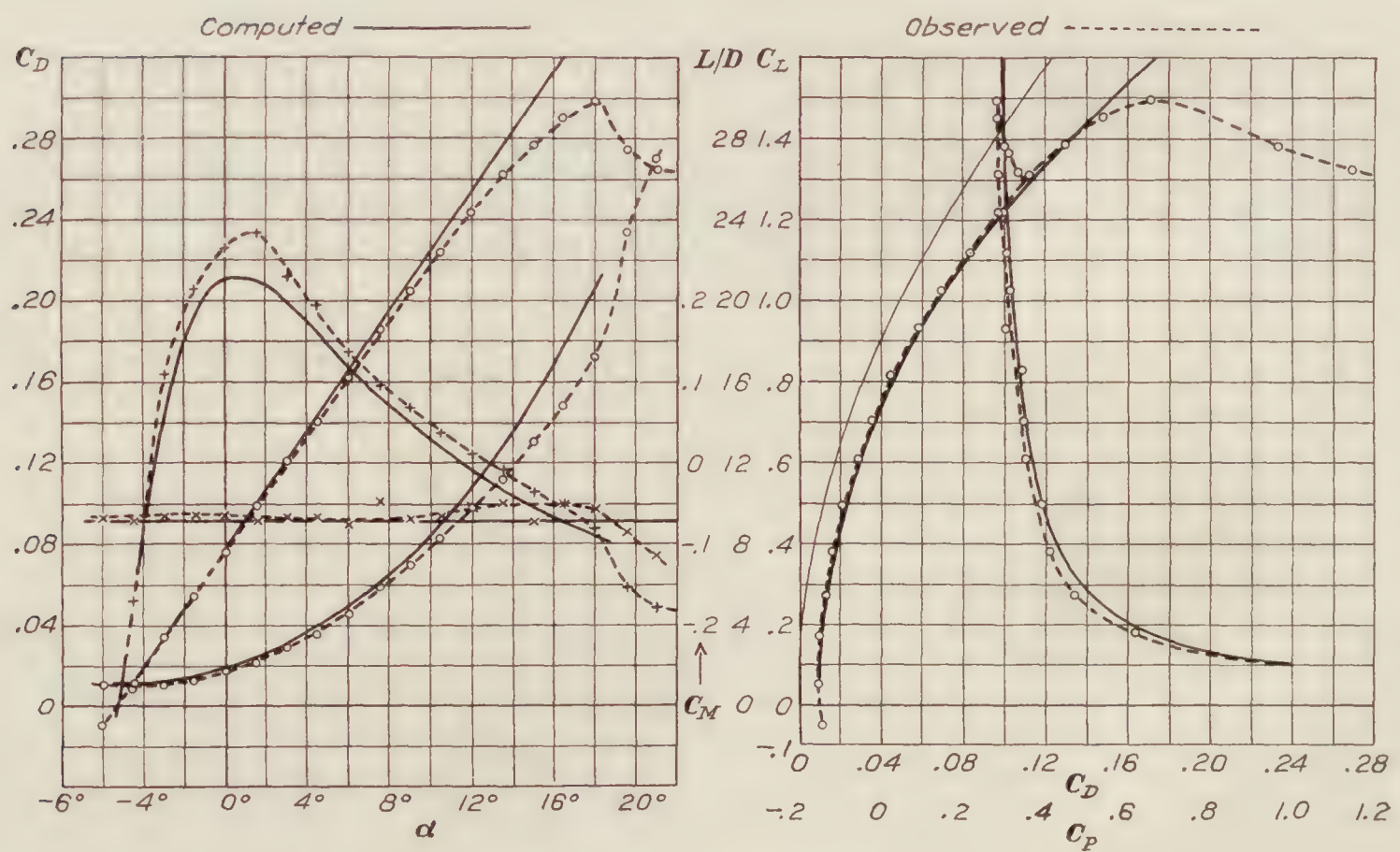


FIGURE 10.—Characteristics of Clark Y airfoil

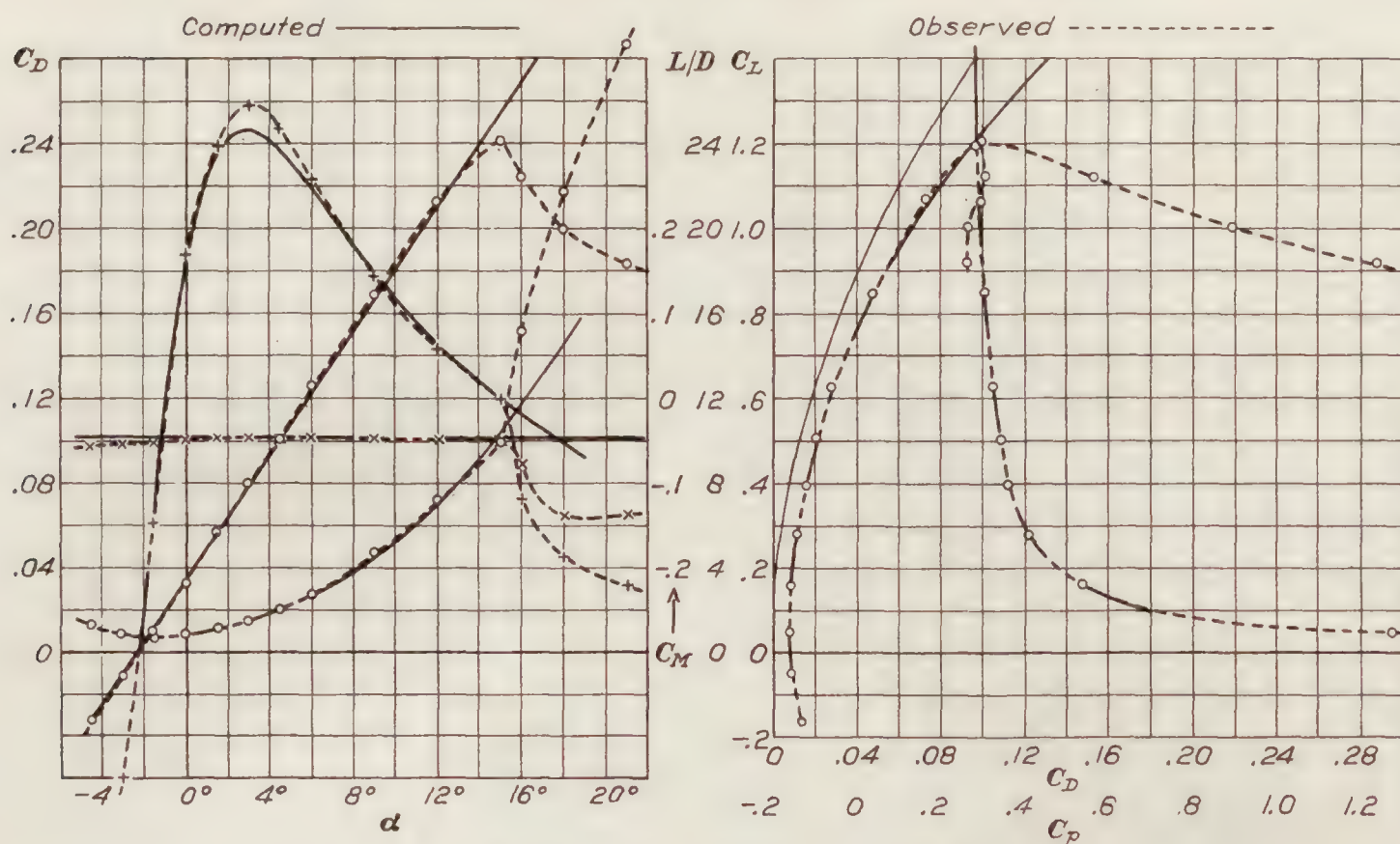


FIGURE 11.—Characteristics of R. A. F. 15 airfoil

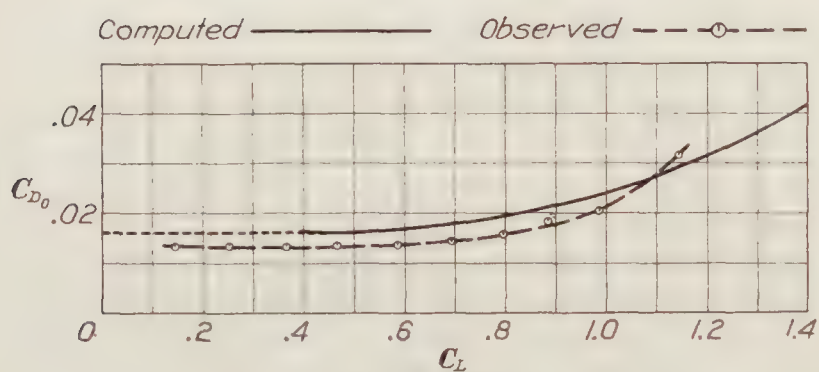


FIG. 12 U.S.A. 35A

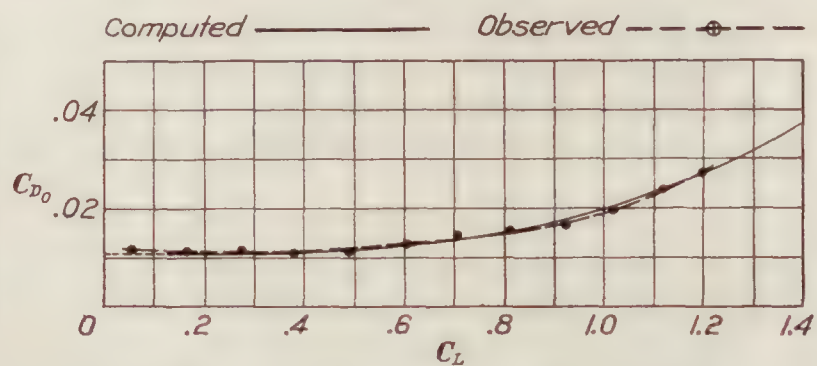


FIG. 13 M 6

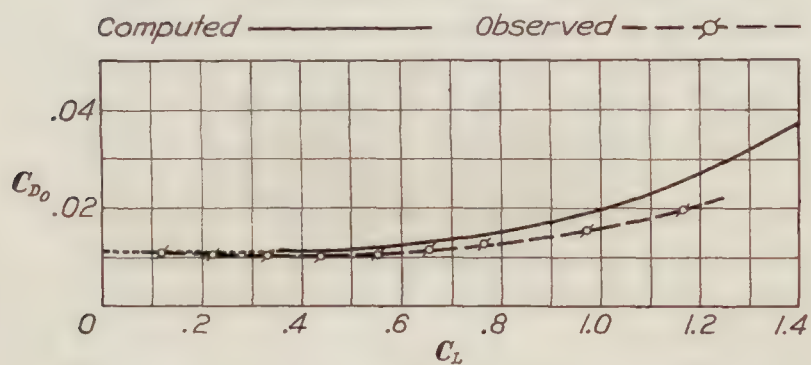


FIG. 14 U.S.A. 27

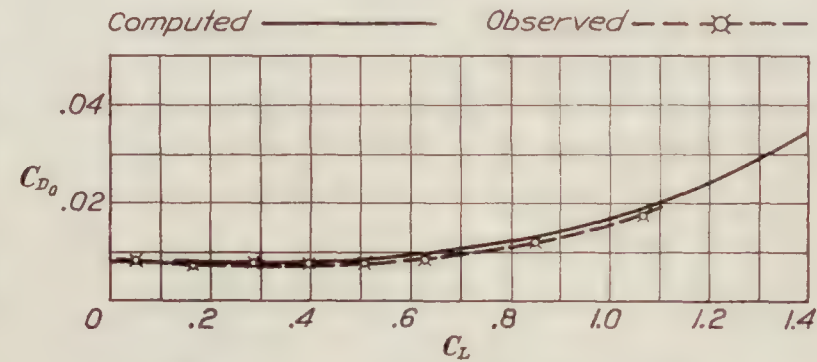


FIG. 15 R.A.F. 15

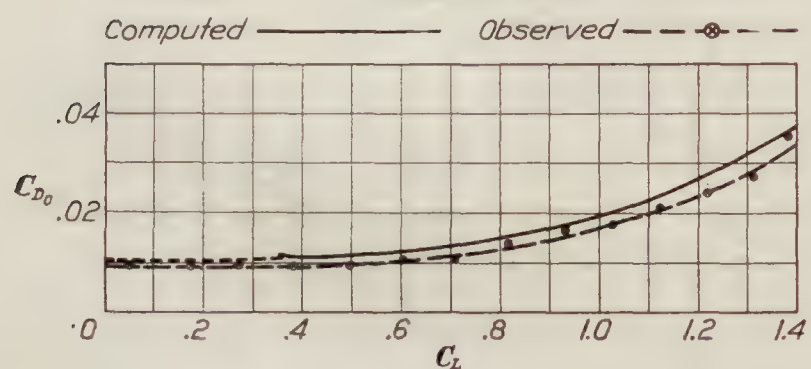


FIG. 16 Clark Y

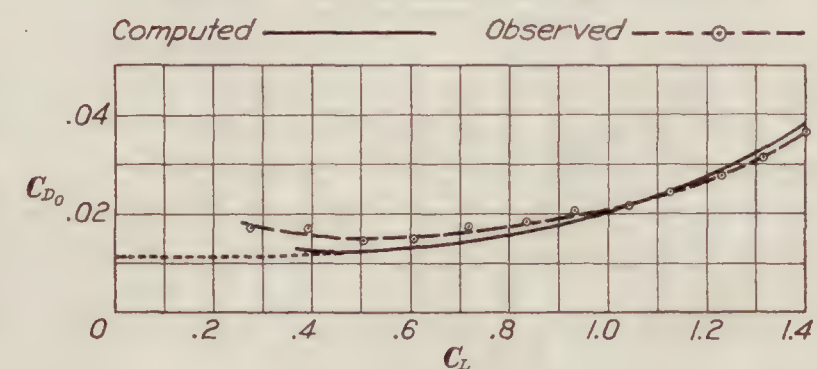


FIG. 17 P.S. 4

FIGURES 12, 13, 14, 15, 16, 17.—Profile drag characteristics

CONCLUSION

The aerodynamic characteristics of an airfoil can be predicted by the above methods with sufficient accuracy for use in airplane design. From comparison with observed wind tunnel test data at "full scale" it is found that very close agreement is obtained between the predicted and the actual characteristics from tests.

LANGLEY MEMORIAL AERONAUTICAL LABORATORY,
NATIONAL ADVISORY COMMITTEE FOR AERONAUTICS,
March 14, 1928.

REFERENCES

1. Munk, Max M.: Elements of the Wing Section Theory and of the Wing Theory. N. A. C. A. Technical Report No. 191, 1924.
2. Glauert, H.: The Elements of Airfoil and Airscrew Theory. Chap. XI. Cambridge University Press, 1926.
3. Munk, Max M.: The Determination of the Angles of Attack of Zero Lift and Zero Moment, Based on Munk's Integrals. N. A. C. A. Technical Note No. 122, 1923.

TABLE OF SYMBOLS

C_L	Absolute lift coefficient, L/qS .
$C_L(\alpha_{M_o})$	Lift coefficient at the angle α_{M_o} .
C_D	Absolute drag coefficient, D/qS .
C_{D_i}	Induced drag coefficient.
C_{D_o}	Profile drag coefficient.
$C_{D_{L_o}}$	Profile drag coefficient when the lift is zero.
ΔC_{D_o}	Additional profile drag coefficient or $C_{D_o} = C_{D_{L_o}} + \Delta C_{D_o}$.
C_{D_P}	Parasite drag coefficient.
$C_{M_{c/4}}$	Pitching moment coefficient, $\frac{M_{c/4}}{cqS}$.
C_p	Center of pressure coefficient as a fraction of the chord.
$C. P.$	Center of pressure.
L	Lift.
D	Drag.
$M_{c/4}$	Pitching moment about the quarter chord point.
L/D	Lift-drag ratio.
α_a	Absolute angle of attack, measured from the position where the lift is zero. (See fig. 1.)
α_i	Induced angle of attack.
α_e	Effective angle of attack.
α_{L_o}	Angle of attack when the lift is zero, measured from the chord line.
α_{M_o}	Effective angle of attack when the moment about the half chord point is zero.
α'	Angle of attack equal to $\alpha_{L_o} - \alpha_{M_o}$.
b	Span of airfoil.
c	Chord of airfoil.
S	Plan form area of airfoil.
q	Dynamic pressure, $\frac{1}{2}\rho V^2$.
ρ	Density of air.
V	Velocity.
k	Correction factor for inefficiency of airfoil. (See text.)
τ	Correction for additional induced angle of attack for rectangular wing.
σ	Correction for additional induced drag coefficient for rectangular wing.
$\xi_1, \xi_2, \text{etc.}$	Ordinates of mean camber line of airfoil at points (X) on chord; for use in determining α_{L_o} .
ξ_A, ξ_B	Ordinates of mean camber line of airfoil at points (X) on chord; for use in determining α_{M_o} .
$X_1, X_2, \text{etc.}$	Points on the airfoil chord. (See text.)
X_A, X_B	Points on the airfoil chord. (See text.)
$f_1, f_2, \text{etc.}$	Multiplying factors. (See text.)

REPORT No. 313

**DRAG AND COOLING WITH
VARIOUS FORMS OF COWLING FOR A “WHIRLWIND”
RADIAL AIR-COOLED ENGINE—I**

**By FRED E. WEICK
Langley Memorial Aeronautical Laboratory**

TECHNICAL REPORT No. 313

DRAG AND COOLING WITH VARIOUS FORMS OF COWLING FOR A "WHIRLWIND" RADIAL AIR-COOLED ENGINE—I¹

By Fred E. Weick

SUMMARY

The National Advisory Committee for Aeronautics has undertaken an investigation in the 20-foot Propeller Research Tunnel at Langley Field on the cowling of radial air-cooled engines. A portion of the investigation has been completed, in which several forms and degrees of cowling were tested on a Wright "Whirlwind" J-5 engine mounted in the nose of a cabin fuselage. The cowlings varied from the one extreme of an entirely exposed engine to the other in which the engine was entirely inclosed. Cooling tests were made and each cowling modified, if necessary, until the engine cooled approximately as satisfactorily as when it was entirely exposed. Drag tests were then made with each form of cowling, and the effect of the cowling on the propulsive efficiency determined with a metal propeller.

The propulsive efficiency was found to be practically the same with all forms of cowling. The drag of the cabin fuselage with uncowed engine was found to be more than three times as great as the drag of the fuselage with the engine removed and nose rounded. The conventional forms of cowling, in which at least the tops of the cylinder heads and valve gear are exposed, reduce the drag somewhat, but the cowling entirely covering the engine reduces it 2.6 times as much as the best conventional one. The decrease in drag due to the use of spinners proved to be almost negligible.

The use of the cowling completely covering the engine seems entirely practical as regards both cooling and maintenance under service conditions. It must be carefully designed, however, to cool properly. With cabin fuselages its use should result in a substantial increase in high speed over that obtained with present forms of cowling on engines similar in contour to the J-5.

INTRODUCTION

The problem of cowling radial air-cooled engines has puzzled aircraft designers since the adoption of the static radial engine. The cowling has an important effect on both the cooling of the engine and the drag of the airplane, and no reliable data on either have been available.

At the conference of aircraft manufacturers held at Langley Field on May 24, 1927, several requests were made that an investigation of the cowling and cooling problem in regard to radial air-cooled engines be undertaken in the new full-scale Propeller Research Tunnel which was then just being completed. A program for a series of tests was drawn up and submitted to the manufacturers for criticisms and suggestions, several of which were adopted.

The program as finally arranged includes 10 main forms of cowling to be tested on a J-5 engine in connection with 2 fuselages, 3 on an open cockpit fuselage and 7 on a closed cabin type. The seven forms of cowling on the cabin fuselage range from the one extreme of an engine entirely exposed except for the rear crank case, to the other extreme of a totally inclosed engine. One of the cowlings with the open cockpit fuselage includes individual fairings behind each cylinder. Three forms of cowling, two of which are on the cabin fuselage, afford direct comparisons with and without a propeller spinner. The program involves the measurement of the engine cylinder temperatures, each cowling being modified, if necessary, until the cooling is satisfactory. The cowling is then tested for its effect on drag and propulsive efficiency.

¹ This report was originally published as N. A. C. A. Technical Note No. 301.

The portion of the investigation involving the cabin fuselage is covered in this report, and the rest of the investigation will be given in another report called part 2 (reference 2).

Although the tests are being made in the Propeller Research Tunnel, a great deal of help has been received from other sections of the laboratory, especially the Flight Operations Section, which made a beautiful job of the cowling and also contributed many helpful suggestions, and the Power Plants Division, which conducted the measurement of the cylinder temperatures.

METHODS AND APPARATUS

The Propeller Research Tunnel is of the open throat type with an air stream 20 feet in diameter, in which velocities up to 110 M. P. H. can be obtained. A complete description of the tunnel, balances, and other measuring devices is given in Reference 1.

A standard Wright "Whirlwind" J-5 engine delivering 200 HP. at 1,800 R. P. M. was used for these tests. It was mounted on a dynamometer inclosed within the fuselage so that the engine torque could be measured directly. The torque as measured included the torque on the engine cylinders due to the twist of the slip stream. In order to correct for this effect a special test was made in which three J-5 cylinders complete with valve housings were mounted under the front portion of a water-cooled Wright E-2 engine on a VE-7 fuselage in the Propeller Research Tunnel (Fig. 11). The cylinders were in the same position relative to the propeller as on a J-5 engine. The middle cylinder only was supported in such a manner that its torque about the engine axis could be measured, and the same propeller used in the cowling tests was driven by the E-2 engine. The torque on the middle cylinder was then found for various engine and air speeds with different amounts of cowling, and the results have been used to apply a correction, amounting to as much as 3 per cent in some cases, to the engine torque and power.

The cabin fuselage was designed to have a shape and size approximating the average of the fuselages of several commercial "Whirlwind" engined cabin monoplanes. The fuselage was of rectangular cross section from the maximum section to the tail, and the forward portion was gradually faired to a circular section at the engine. This whole forward portion was rebuilt for the various cowlings.

In order to make certain that the tests would be directly applicable to the present-day high-wing cabin monoplanes, a stub wing and pilot's extension cabin and windshield were mounted on the fuselage and tested with three different cowlings. The wing, which was constructed of flat sheet aluminum over a wooden frame, had the Göttingen 398 section, with a 7-foot chord and 16-foot span.

The open cockpit fuselage is similar in shape to that of a Vought UO-1 airplane, and a UO-1 type landing gear is being used with both the open and cabin fuselages in this investigation in order to keep the landing gear factor constant.

The cylinder temperatures of the J-5 engine were measured at 69 different points, 47 being on the top (Number 1) cylinder and the rest distributed at two or three representative points on each of the other cylinders. A mass of other engine data such as the manifold depression, fuel consumption, and carburetor air temperature, were also obtained. Only a small portion of the engine data is necessary to the present investigation, and most of it, along with a complete description of the thermocouples, pyrometers, and other instruments, will be published in a separate report by the Power Plants Division of the laboratory.

The entire program includes ten main sets of cowling. Numbers 1, 2, and 3 are to be used with the open cockpit fuselage and have not yet been tested. The cowlings tested on the cabin fuselage may be outlined as follows:

Number 4. No cowling over cylinders or crank case. Tested with and without wing. (Fig. 1.)

Number 5. Cowling covering slightly less than one-half of each cylinder and over crank case. Tested with and without wing. (Fig. 2.)

Number 6. Same as Number 5, but with spinner. Tested with and without wing. (Fig. 3.)

Number 7. Cowling over nearly all of each cylinder and over crank case. (Fig. 4.)

Number 8. Same as Number 7, but with spinner. (Fig. 5.)

Number 9. Single cowling completely covering cylinders, but no cowling over crank case. (Fig. 6.)

Number 10. Same as Number 9, but with internal cowling similar to Number 5 over lower portion of cylinders and crank case. (Fig. 7.)

All of the cowlings were constructed in a practical manner with fire walls and louvers.

The first test made with each cowling was on the cooling properties, the cylinder temperatures with the uncowed engine (Number 4) being used as a criterion. In the first few series of cooling tests the engine was run at full throttle at air speeds of 60, 80, and 100 M. P. H. At each speed the run was maintained until the temperature conditions had become constant. It was found that in each case the engine ran slightly warmer at 80 M. P. H. than at either 60 or 100, so the remainder of the tests were run at 80 M. P. H. as representing the worst flight conditions for cooling. The conditions were therefore similar to those in an extended full throttle climb in flight. If the cooling with any cowling was not as satisfactory as that with the uncowed engine, the cowling was modified until satisfactory.

Drag tests were run with the various cowlings, both as they were originally constructed and as they were finally modified to cool properly.

After a cowling cooled properly, propeller tests were made to determine the effect of the cowling on the propulsive efficiency. The propeller, which had adjustable aluminum alloy blades (Fig. 31), was tested at both a low and a high pitch setting with each cowling. The hub to which the blades were fitted was of steel, and in order to save weight, had been made 1 inch shorter than the hub for which the blades had been designed, so that while the drawing shows a 9-foot propeller, the diameter in these tests was actually 8 feet 11 inches. The propulsive efficiency found from these propeller tests includes the increase in drag of all parts of the body affected by the slip stream and also the effect of the body interference on the propeller thrust and power.

COOLING TESTS

The cylinder temperatures obtained with cowling Number 4 (engine uncowed, Figs. 1, 12, and 13) at full throttle and 80 M. P. H. were used as a criterion by which to judge the cooling with the other forms of cowling. The particular temperatures used for comparison are tabulated in Table I. The hottest part of each cylinder was the rear spark-plug boss, and it was at first thought that the average of the rear spark-plug boss temperatures for all nine cylinders would be used as a measure for comparison. In some runs, however, one or two cylinders had very low temperatures, probably because they were not developing full power, so the average of the five hottest cylinders has been taken as a better criterion of the cooling. The highest temperature recorded on any cylinder was also used as a criterion, and also three representative points on cylinder Number 1 (top cylinder). One of these was at the rear spark-plug boss, one at the rear central portion of the barrel, and the third at the rear lower portion of the barrel. The rear points were chosen because they represented the highest temperatures around the cylinders. In addition to the above cylinder temperatures, the lubricating oil temperature and the temperature of the air in the tunnel were considered.

The temperature conditions under which these tests were made in the wind tunnel were more severe than the conditions found in flight in a temperate climate, and probably correspond to those of a sustained full throttle climb in a tropical climate. The cylinder temperatures recorded were therefore in the neighborhood of 100° higher than have been found in flight tests.

The cooling with cowling Number 5 (Figs. 2 and 14), in which the cowling covered the crank case and nearly half of each cylinder, was better than with no cowling whatever over the engine. The hottest five cylinder head temperatures averaged nearly 70° F. lower than with cowling Number 4, while the cylinder barrel and oil temperatures were the same. With cowling Number 6 (Figs. 3 and 15), which was the same as Number 5 excepting for the spinner, the cooling effect would be obviously about the same as with Number 5, so no cooling tests were considered necessary. (Since the full throttle running seemed unusually severe, and since it was necessary to run the engine with thermocouples attached for over 100 hours in all no full throttle running was done which was not necessary.)

Number 7 cowling (Figs. 4 and 16) as originally constructed inclosed the whole engine except for the tops of the cylinder heads and the valve gear. At the front of the cylinder the cowling came just under the spark plug, and at the rear it came just over the cylinder head proper, inclosing the rear spark plug. The cooling with this cowling was not satisfactory, for the oil and cylinder barrel temperatures were excessive, although the head temperatures, even those of the inclosed rear spark-plug boss, were considerably lower than with no cowling over the engine.

Apparently with cowling Numbers 5, 6, 7, and 8, the air flows past the cylinder heads at greater speed than with no cowling over the engine. In order to improve the oil and cylinder barrel cooling with cowling Number 7, four slots were cut in the nose as shown in Figure 17. These were effective in reducing the oil and barrel temperatures somewhat, but the temperatures were still too high, and on this run the piston in cylinder Number 9 failed, due apparently to excessive temperature. The high piston temperature was probably due to the fact that with the high oil and cylinder wall temperatures with cowling Number 7, the heat was not conducted away from the piston skirt rapidly enough. The engine was repaired, and six larger slots were put in the nose cowling over the crank case as shown in Figure 18. Enough louvers were already in the cowling behind the engine to permit the escape of the air passing through the nose slots. With this arrangement the cooling was considered satisfactory as compared with that of the uncowed engine (Number 4). The cylinder head temperatures were a little lower than for the uncowed engine, the oil temperature was practically the same, and the barrel temperatures were a little higher.

Incidentally, a series of tests with different sized carburetor jets was run with cowling Number 7. It was found that the cylinder temperatures could be reduced materially by increasing the jet size.

Cowling Number 8, which was the same as Number 7 except that it had a spinner, is shown as originally constructed in Figures 5, 19, and 20. On account of the large spinner, nose slots similar to those in cowling Number 7 could not be used. Instead, the cowling was cut away immediately in front of each cylinder, as shown in Figure 21, to make the engine cool properly.

Cowling Number 9 completely covered the engine (Figs. 6 and 22). The air was taken in at the nose and allowed to flow past the engine, which was entirely uncowed inside of the outer hood, and out of an annular slot similar in section to some wing slots which have been tested. This type of nose and slot were designed to offer as little disturbance to the flow of air over the fuselage as possible, separating the air for cooling the engine from the general flow and then feeding it back smoothly through the slot. No information was available when this cowling was designed regarding the necessary size of the hole in the nose or the slot. In the cooling test with the original Number 9 cowling the cylinder head temperatures became excessive in a very short time.

Number 10 cowling was the same as Number 9 except that it had Number 5 cowling inside also (Figs. 7 and 23), so that the air was directed more particularly at the cylinder heads, and at the same time had a smoother path past the engine. This improved the cooling of the cylinder heads slightly, but they still ran much too hot. During the test the head of Number 3 cylinder developed a small hole about one-eighth inch in diameter, apparently caused by a defective spot in the aluminum alloy becoming too hot to withstand the cylinder pressures. This cylinder was therefore replaced. It is interesting to note that the two cylinders which gave trouble due to cooling—Numbers 3 and 9—were deprived of their full share of cooling air by the magnetos, which on the J-5 engine are placed in front of the cylinders.

The outlet area at the slot had originally been made smaller than the inlet area, and the cowling was then modified by cutting 3 inches off of the skirt of the hood or nose piece, which increased the area of the slot to that of the opening at the nose. With this modification the cooling was fairly satisfactory except for the cylinders located behind the magnetos (Numbers 2, 3, 8, and 9). The magnetos effectively blocked most of the air from those cylinders.

Next, deflectors, as shown in Figure 9, were installed between the cylinders to direct the air to the hottest portions at the rear. These also reduced the temperatures slightly and were retained. The next modification was to enlarge the hole in the nose from 24 inches to 28 inches

in diameter. It was thought that this would not only allow more air to flow past the engine, but also enable some air to pass over the magnetos. With the 28-inch opening the cooling was much better, but the cylinders behind the magnetos, especially Number 9, still ran too hot.

Next a cut-out was made in the nose piece over each magneto. This improved the conditions somewhat, but not sufficiently, so the cut-outs over the magnetos were enlarged, the cowling as it then appeared being as shown in Figures 8, 24, and 25. With this arrangement, the cooling was fairly satisfactory, but the temperatures were still a little higher than for the uncowed engine, especially at the lower portion of the cylinder barrels.

In the original design the slot had been placed as far forward as possible in the hope that it would help remove the boundary layer near the region of rather sharp curvature at the nose, and thereby help reduce the drag. This necessitated a sharp rise in the internal cowling immediately behind the cylinders, which hindered the flow of the cooling air. In an effort to reduce mainly the barrel, but also the head temperatures, still further, the rise behind the cylinders was made gradual and the slot moved farther back as shown in Figures 8 and 26. The inside deflectors were retained as before. With this arrangement the cooling was very nearly as good as with the uncowed engine, and for the first time with the cowling completely covering the engine, the test was continued until the temperature conditions became constant (about 10 minutes). The five highest head temperatures averaged about 30° F. higher than for the uncowed engine, the barrel temperatures averaged about 60° F. higher, and the oil temperature was only 5° F. higher. The oil temperature could, of course, be reduced by reducing the cowling covering the crank case. One thermocouple had consistently recorded the highest temperatures with Number 10 cowling, and this one was still somewhat high.

A run was made next without the deflectors which directed the air around the cylinders. All of the cylinder temperatures became rather high in a short time, and the run was stopped.

Since the above deflectors were evidently very helpful in cooling the engine, another run was made with improved ones. The original deflectors directed the air around both sides of the cylinders, but the second set turned the air in one direction only, as shown in Figures 10 and 27. They were larger than the first ones, and directed about two-thirds of the air between each two cylinders around the exhaust valve and rear spark plug. The cooling with this arrangement was considered approximately as satisfactory as with the uncowed engine. The cylinder head temperatures were about the same, and the cylinder barrel temperatures, which still averaged about 60° F. higher, were considered permissible.

In order to determine whether inclosing the propeller hub in a spinner would help the air flow, and consequently the cooling and drag, the above cowling was tested with Number 6 nose inside as shown in Figure 28. After a few minutes of running it was apparent that the cooling and drag were about the same as without the spinner, so the run was discontinued.

RESULTS OF DRAG TESTS

The observed drag-test data are given in Table II and the results are plotted in Figure 30. The drag of the bare fuselage (without supports or landing gear) with the various cowlings is given for an air speed of 100 M. P. H. in the following table:

Cowling		Fuselage and engine drag, pounds at 100 M. P. H.	Reduction from uncowed engine, pounds at 100 M. P. H.
Number 4.	Engine uncowed.....	125	0
Number 5.	No spinner; original.....	119	6
Number 6.	Spinner; original.....	116	9
Number 7.	No spinner; original.....	103	22
Number 7.	Modified to cool.....	111	14
Number 8.	Spinner; original.....	100	25
Number 8.	Modified to cool.....	106	19
Number 10.	Combination of 9 and 5; original.....	64	61
Number 10.	Modified to cool.....	75	50
Number 10.	Modified to cool; with spinner.....	75	50
Number 4.	Engine removed, nose rounded.....	40	85

The last item listed, Number 4 cowling with the engine removed and the nose rounded as shown in Figure 29, has been included as an ideal with which to compare the effect of the various cowlings. Using this as a basis, the uncowed engine is responsible for an increase in drag of 85 pounds at 100 M. P. H.

The outstanding feature of the drag tests is the large reduction in drag obtained with the cowling which completely covers the engine. Considering only the cowlings which cool properly the reduction of drag with Number 10 cowling is about 60 per cent of the total possible reduction, and is 2.6 times as great as with the next best, Number 8.

The drag of the bare fuselage without engine is only 40 pounds at 100 M. P. H. When the uncowed engine is placed on the nose the drag is increased to 125 pounds, or 3.13 times that of the bare fuselage without engine. With the best conventional cowling (Number 8) the drag is 106 pounds, or 2.65 times that of the fuselage alone, and with the cowling totally inclosing the engine (Number 10) the drag is 75 pounds, or 1.87 times that of the fuselage without engine.

The forms of cowling most used in service are similar to Numbers 5 and 6, and these have a very slight effect on the drag, and consequently an almost insignificant effect on the performance of an airplane. The reduction of drag is small even when practically the whole of the cylinders are cowed in, as in Number 8. Apparently, if even a small portion of the engine is exposed, it is sufficient to disturb the smooth flow over the body, and the turbulent flow is associated with high drag. When the entire engine is covered and the cooling air is separated from and returned to the outside air smoothly, as with cowling Number 10, the smoother flow is evidently accompanied by a substantial decrease in drag.

It is interesting to note that with cowling Numbers 7, 8, and 10, it cost, respectively, 8, 6, and 11 pounds in drag at 100 M. P. H. to make the original designs cool properly. Apparently, the method used with Number 8, which was to cut away the cowling immediately in front of the cylinders, costs slightly less in drag than the slots of Number 7.

The value of spinners in reducing the drag, when used in front of radial air-cooled engines, is shown by a comparison of cowling Numbers 5, 6, 7, and 8 as originally designed. In each case the drag with spinner was 3 pounds less at 100 M. P. H. than the drag without spinner. This would represent a difference in speed of a small fraction (about one-third) of a mile per hour on an average airplane with a J-5 engine.

It is interesting that the stub wing with windshield increased the drag only 57 pounds at 100 M. P. H. with cowling Number 4 and 50 pounds with Numbers 5 and 6 (Number 4 had slightly more pilot's windshield exposed), although the drag of the wing alone would be about 75 pounds as computed from model tests.

RESULTS OF PROPELLER TESTS

A large mass of propeller test data has been obtained during these cowling tests, only a small portion of which is necessary to show the effect of the various cowlings on propulsive efficiency. The rest will be used in another report dealing with body interference. The propulsive efficiencies obtained with the various cowlings are shown in Figure 32 for a propeller blade angle of 15° at the 42-inch radius, and in Figure 33 for 23° at the 42-inch radius. (These angle settings correspond to pitch-diameter ratios of 0.66 and 1.02, the pitch being taken at 75 per cent of the radius. The pitch of this propeller is approximately uniform for all working sections when the pitch-diameter ratio is about 0.5.) The curves of propulsive efficiency are very nearly the same for all cowlings, although for both pitch settings the efficiencies with cowling Number 10 are the highest. The power and thrust coefficients were also practically the same for all cowlings.

DISCUSSION

Effect on Airplane Performance.

It is interesting to compare the various forms of cowling with regard to their effect on the performance of a typical "Whirlwind" engined cabin monoplane. Suppose such an airplane with an uncowed engine similar to Number 4 required 200 HP. to fly horizontally at 125 M. P. H. If the airplane were equipped with the usual amount of cowling, similar to Numbers

5 and 6, the power required would be reduced to 196 or 194 HP., respectively, at 125 M. P. H. If a cowling similar to Number 8, which is the best of the conventional forms, were used, the airplane would require only 187 HP., and with a cowling covering the entire engine similar to Number 10, 167 HP. The airplane with the latter cowling could therefore fly at 125 M. P. H. with the engine throttled more than 100 R. P. M. from the revolution speed required with the uncowed engine. If the full 200 HP. were to be used, a cowling similar to Number 6 (with spinner) would increase the speed less than 1 M. P. H., one similar to Number 8, about 3 M. P. H., and one similar to Number 10, about 8 M. P. H.

Considering all types of cabin airplanes having the same engine, the higher the speed attained with ordinary forms of cowling, the greater will be the improvement possible. This is, of course, due to the fact that in the faster airplanes the fuselage-engine drag is a larger portion of the total.

Practicability.

All of the forms of cowling tested have been used on airplanes in service excepting the one entirely covering the engine. The forms inclosing a large portion of the engine have been found rather poor from a maintenance standpoint because of the large number of small parts which must be removed when it is necessary to work on the engine. This difficulty is accentuated where metal spinners are used, but, fortunately, as these tests have shown, spinners have an almost negligible effect on the performance of airplanes.

The Number 10 cowling is similar to Number 5 in construction, except for the nose piece. When this is removed, most parts of the engine requiring frequent attention are accessible. As made for the tests, the nose piece for Number 10 cowling was a 1-piece ring which was easily constructed and easily handled, its shape being such that it was stiff and strong without bracing. It had the disadvantage, however, that in order to remove it, it was first necessary to take off the propeller. To avoid this in practice it would probably be desirable to make the nose piece in two or three quick-detachable sections.

With the J-5 engine it was necessary to have a rather sharp curvature at the nose of the Number 10 cowling. A better shape, and therefore still better performance, could be obtained with an engine having (1) a greater distance between the cylinders and the propeller, (2) smaller over-all diameter, (3) the valve gear at the rear of the cylinders instead of projecting in front, and (4) magnetos at the rear of the cylinders.

CONCLUSIONS

1. The drag of an average sized cabin fuselage with the engine removed and the nose rounded is tripled by placing an uncowed J-5 engine on the nose.

2. With the conventional forms of cowling, in which a portion of the cylinders and valve gear is exposed, the drag becomes less as the cowling is increased, but even in the most extreme case the reduction amounts to only about 23 per cent of the increase in drag due to an uncowed engine.

3. A spinner, if used in front of a radial engine, decreases the drag but a very small amount and has an almost negligible effect on the performance of an airplane.

4. With a cowling similar to Number 10, which covers the entire engine and separates the cooling air from the general flow about the body, the reduction in drag is about 60 per cent of the increase due to an uncowed engine. This is about 2.6 times as great as with the best conventional form of cowling.

5. The use of cowling similar to Number 10 seems entirely practical as regards both cooling and maintenance under service conditions. It must be carefully designed, however, to cool properly.

REFERENCE

1. Weick, Fred E., and Wood, Donald H.: The Twenty-Foot Propeller Research Tunnel of the National Advisory Committee for Aeronautics. N. A. C. A. Technical Report No. 300. (1928.)
2. Weick, Fred E.: Drag and Cooling with Various Forms of Cowling for a "Whirlwind" Radial Air-Cooled Engine, II. N. A. C. A. Technical Report No. 314. (1929.)

TABLE I.—COOLING TEST DATA

Cowling	Average temperature 5 hottest cylinder heads, rear plug boss	Highest temperature on any cylinder	Cylinder Number 1, rear plug boss	Cylinder Number 1 barrel, middle rear	Cylinder Number 1 barrel, bottom rear	Oil temperature	Air temperature
	° F.	° F.	° F.	° F.	° F.	° F.	° F.
Number 4.....	673	728	583	353	378	140	84
Number 5.....	605	666	585	361	379	138	86
Number 7.....	626	681	618	476	557	167	88
Number 7, 4 holes in nose ¹	638	702	612	397	458	144	88
Number 7, 6 large holes.....	664	750	653	432	447	146	82
Number 9 ¹	731	800+	673	377	438	127	93
Number 10 ¹	755	800+	682	403	430	133	97
Number 10, larger slot ¹	740	800+	654	335	355	126	91
Number 10, 28-inch hole in nose, cylinder deflection ¹	695	768	635	428	467	133	75
Number 10, cut-outs over magnetos ¹	705	760	658	452	477	132	77
Number 10, larger cut-outs ¹	697	778	670	460	498	140	82
Number 10, slot moved back.....	701	772	668	396	428	145	86
Number 10, cylinder deflectors removed ¹	704	778	670	460	498	145	86
Number 10, single cylinder deflectors.....	683	753	662	430	432	149	86

¹ Run stopped because of high temperatures before constant conditions were reached.

TABLE II.—OBSERVED GROSS DRAG DATA, INCLUDING LANDING GEAR AND SUPPORTS

Number 4 (without wing)		Number 5 (without wing)		Number 6 (without wing)		Number 7-O (without wing)		Number 4 (with wing)		Number 5 (with wing)		Number 6 (with wing)		Number 4 (with wing, without engine)	
q lb. per sq. ft.	Drag lb.	q lb. per sq. ft.	Drag lb.	q lb. per sq. ft.	Drag lb.	q lb. per sq. ft.	Drag lb.	q lb. per sq. ft.	Drag lb.	q lb. per sq. ft.	Drag lb.	q lb. per sq. ft.	Drag lb.	q lb. per sq. ft.	Drag lb.
18.25	169	16.50	149	17.99	161	16.92	143	17.78	202	16.31	182	17.07	186	18.40	147
18.32	169	16.50	149	18.01	161	16.97	143	17.78	202	16.49	182	16.94	185	18.39	147
20.95	193	17.92	161	18.90	169	19.06	160	25.05	279	18.14	198	18.21	199	20.43	161
20.73	191	17.92	162	18.96	169	19.08	160	25.05	281	18.02	198	18.21	199	20.62	161
25.40	231	20.00	179	20.18	181	20.30	169	25.85	290	19.42	212	20.35	221	25.40	202
25.05	230	20.00	179	19.11	170	20.15	170	26.26	295	19.35	212	20.23	220	25.70	202
25.96	235	24.82	221	25.00	220	26.18	215	20.06	228	22.70	247	24.48	265	16.72	135
25.76	236	24.58	219	24.95	220	26.28	217	20.60	232	22.61	247	24.82	265	16.72	134
16.82	156	14.76	135	14.88	134	13.92	118	18.15	207	15.13	168	14.98	164	15.25	124
16.87	157	14.83	135	15.14	137	13.58	116	18.38	208	15.13	168	15.03	166	15.05	124
15.32	143	13.29	123	12.59	115	11.25	98	15.03	172	14.04	155	13.35	147	13.30	109
15.20	143	13.08	119	13.18	121	11.28	97	14.95	172	13.89	155	13.39	150	13.30	110
15.39	129	11.59	108	10.58	97	9.43	81	13.03	150	11.42	130	10.22	118	11.58	96
13.50	128	11.50	106	10.89	99	9.88	85	13.12	153	11.42	129	10.17	114	11.24	94
11.98	114	9.05	85	8.34	78			11.00	128	10.01	114	8.64	95	9.40	79
11.53	110	8.97	84	8.85	81			11.14	129	10.12	115	8.86	100	9.41	79
9.27	90							9.08	107	8.95	102			8.24	69
9.95	96							8.72	102	8.80	100			8.37	72
7.94	79							7.84	93						
8.04	78							7.84	93						

NOTE.—O denotes original.

TABLE II.—OBSERVED GROSS DRAG DATA, INCLUDING LANDING GEAR AND SUPPORTS—Continued

No. 8-O (without wing)		No. 7-M (without wing)		No. 8-M (without wing)		No. 10-O (without wing)		No. 10-M (without wing)		No. 10-M (with spinner, without wing)		Landing gear and supports only	
q lb. per sq. ft.	Drag lb.	q lb. per sq. ft.	Drag lb.	q lb. per sq. ft.	Drag lb.	q lb. per sq. ft.	Drag lb.	q lb. per sq. ft.	Drag lb.	q lb. per sq. ft.	Drag lb.	q lb. per sq. ft.	Drag lb.
16.71	140	16.63	146	16.42	141	16.58	115	15.96	117	16.60	122	16.44	72
16.70	140	16.58	145	16.46	141	16.56	115	15.96	117	16.62	122	16.56	72
19.09	157	18.70	163	18.33	156	18.34	127	17.32	127	18.10	131	17.05	74
18.86	157	18.70	163	18.60	156	18.42	127	17.38	127	18.09	131	17.07	75
20.25	168	20.00	174	19.95	169	20.43	140	18.12	131	19.29	139	17.01	74
20.35	167	20.00	174	19.91	169	20.08	138	18.00	131	19.30	140	18.71	80
24.95	203	25.48	219	24.45	206	24.60	167	19.30	142	20.42	148	18.60	80
24.95	205	25.38	218	24.90	209	24.67	167	19.30	140	20.44	149	19.76	85
15.45	130	17.07	150	14.40	123	14.98	106	19.35	141	24.50	175	19.66	85
15.14	127	17.13	150	14.92	129	15.18	106	14.52	109	24.95	179	20.91	89
14.04	117	14.64	130	13.01	113	13.43	94	14.45	107	14.88	110	25.82	110
14.14	119	14.64	130	13.02	113	13.37	94	12.70	92	14.68	108	15.40	68
12.98	111	12.30	110	11.24	97	11.83	84	12.60	94	13.41	100	15.30	67
12.69	107	12.52	111	11.15	98	11.90	85	20.50	148	13.10	97	13.95	62
11.84	101	11.00	99	9.66	84	9.60	68	20.55	149	11.82	89	14.14	62
11.92	101	11.25	101	9.69	85	9.48	69	25.00	180	11.96	90	12.63	56
9.92	85	8.65	79	9.07	80	8.67	61	24.35	174	10.31	77	12.60	57
10.19	87	8.84	79	9.00	80	8.65	61	24.95	180	10.42	78	10.94	50
9.00	77							10.97	83	9.79	73	10.94	50
8.41	73							11.11	84			9.86	45
								10.00	73			9.81	45
								10.09	77			8.24	39
												8.24	38

NOTE.—O denotes original. M denotes modified to cool.

APPENDIX

FLIGHT TESTS OF NUMBER 10 COWLING

By THOMAS CARROLL

In order that the practical value of the information in the foregoing report might be demonstrated, simple flight tests have been made of the Number 10 cowling.

Through the courtesy of the Army Air Corps at Langley Field, Va., a Curtiss AT-5A airplane was obtained on which an adaptation of the Number 10 cowling was installed as shown in Figures 34 and 35. A series of flights was made by the three pilots of the laboratory.

The maximum speed of this type airplane as in use at Langley Field had been reported at 118 miles per hour. This was checked by making a series of level runs with a Curtiss AT-5A airplane at low altitude over the water at full power. The maximum speed was found to be 118 miles per hour at 1,900 R. P. M., both air speed and R. P. M. being measured on calibrated instruments. Similar high speed runs made with the modified AT-5A showed a performance of 137 miles per hour at 1,900 R. P. M., an increase of 19 miles per hour. The original speed of 118 miles per hour was attained at 1,720 R. P. M. on the modified airplane.

While the type of cowling as normally installed on an AT-5 is not particularly adaptable to speed, the increase is considered remarkable. Furthermore, the improvement of flying qualities in smoothness of operation was also very favorably commented upon by all pilots who have flown it. The air flow over the fuselage and over the tail surfaces is very obviously improved.

The cooling of the engine was found to be normal in these tests. The oil temperature reached 58° and was fairly constant, and there was no other indication of overheating. Likewise, there was no interference to the pilot's vision in any useful field.

LANGLEY MEMORIAL AERONAUTICAL LABORATORY,
NATIONAL ADVISORY COMMITTEE FOR AERONAUTICS,
LANGLEY FIELD, VA., *October 13, 1928.*

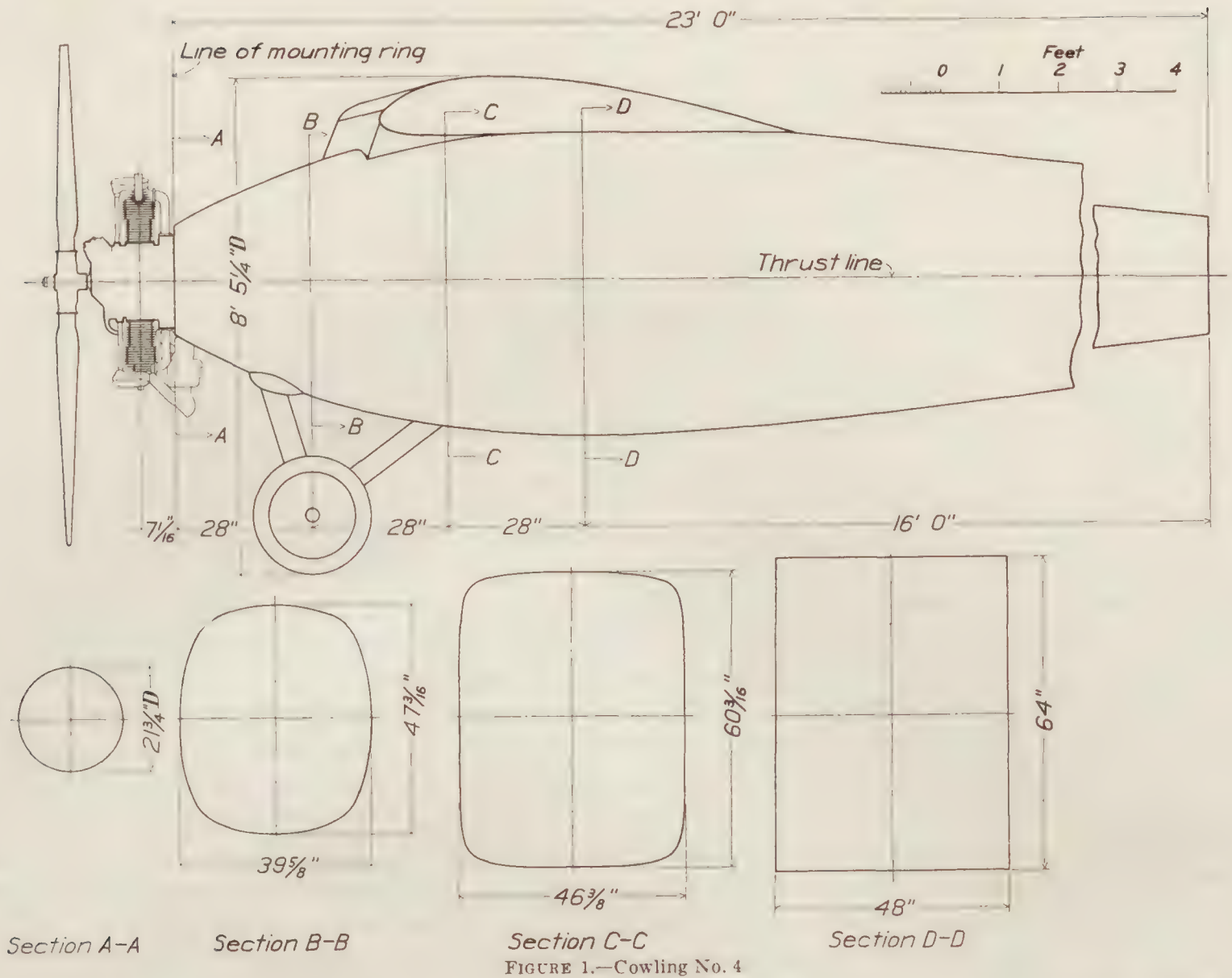


FIGURE 1.—Cowling No. 4

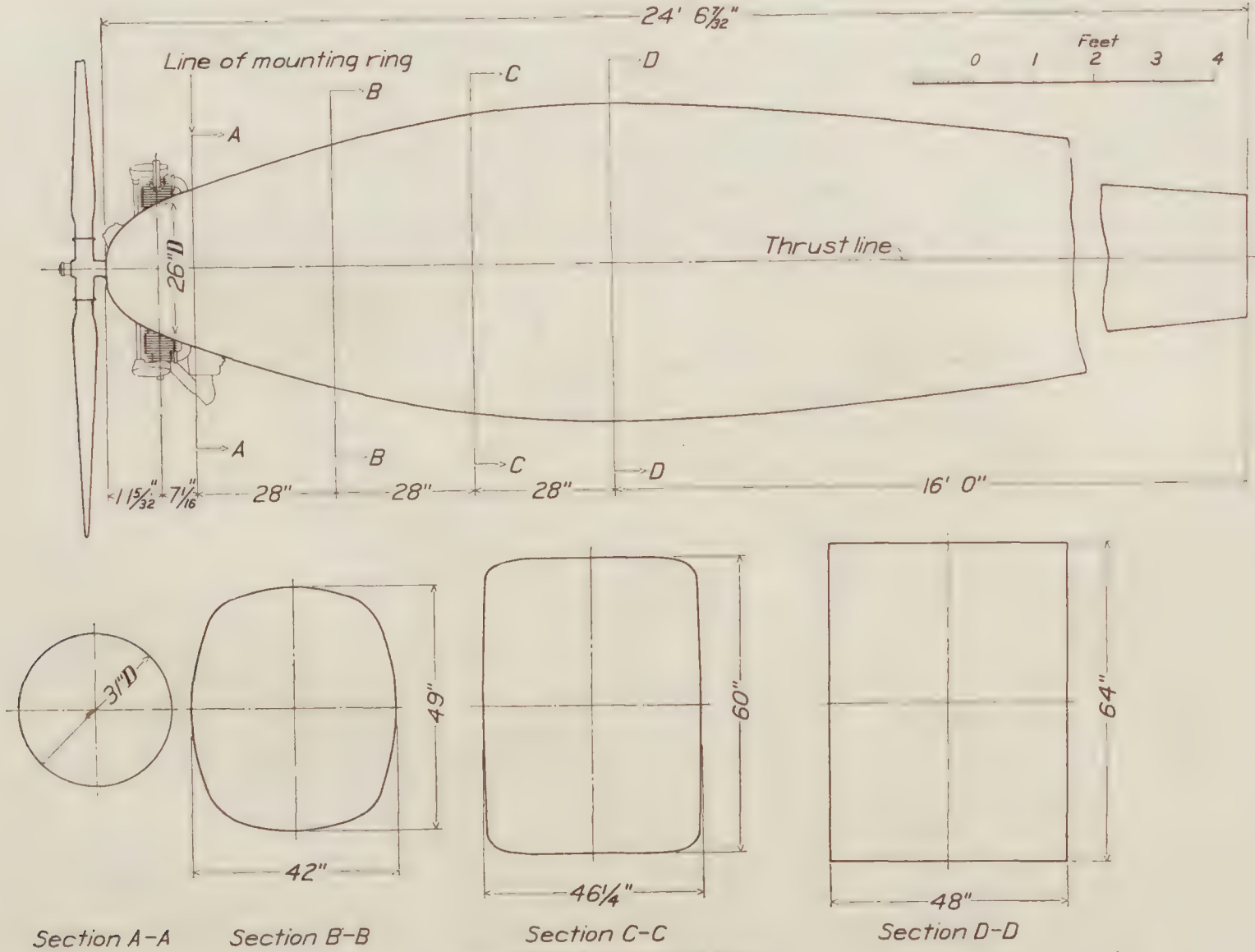


FIGURE 2.—Cowling No. 5

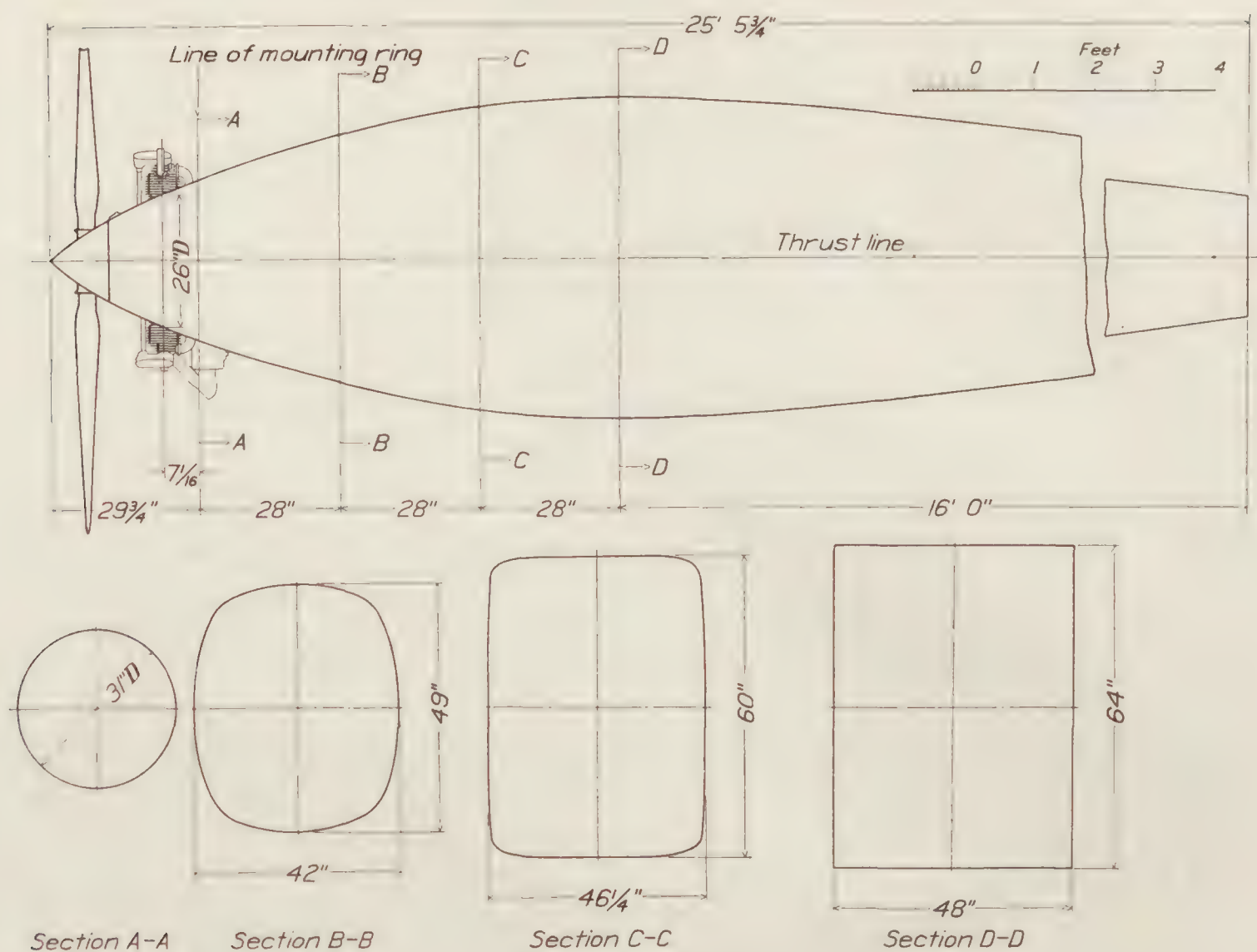


FIGURE 3.—Cowling No. 6

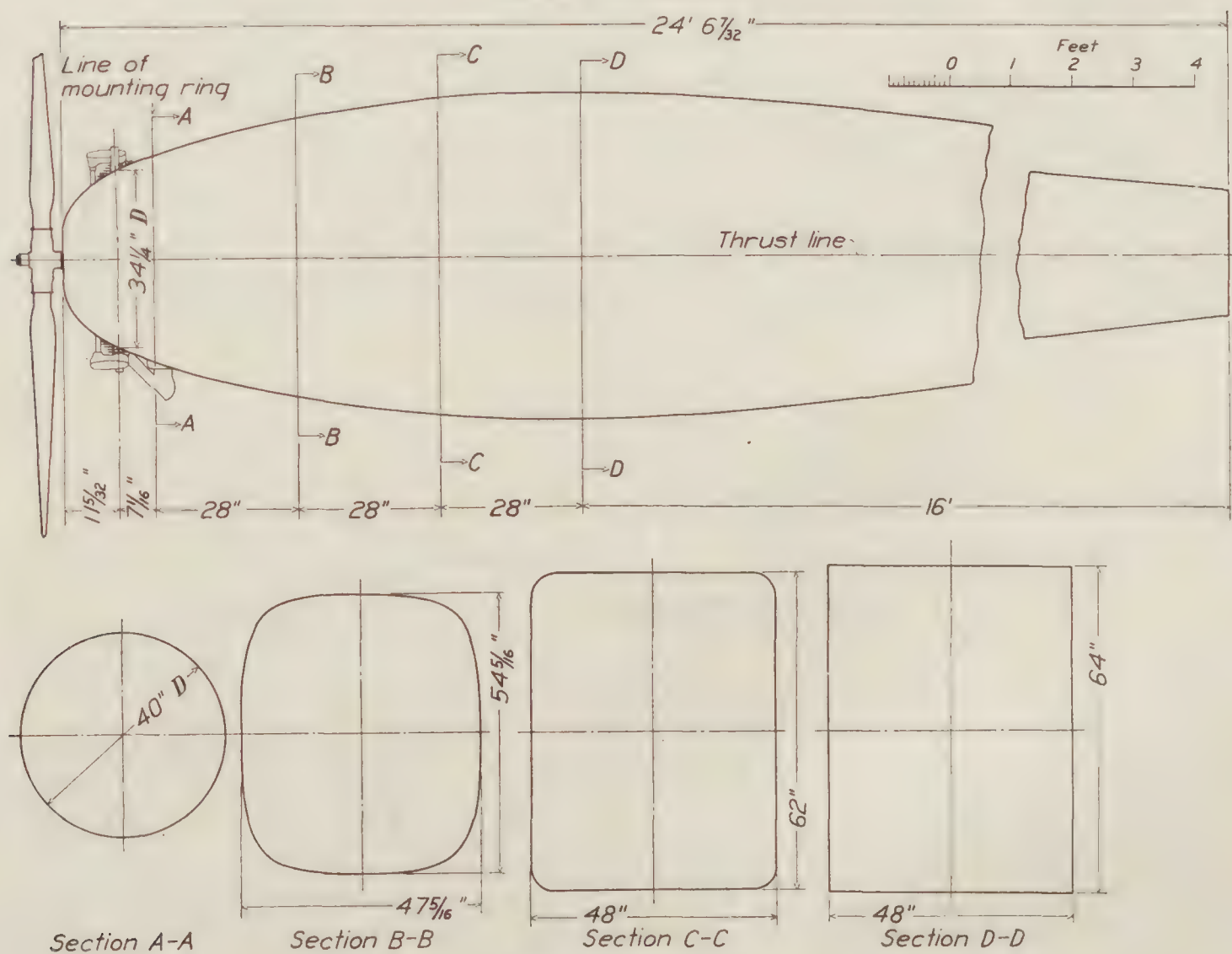


FIGURE 4.—Cowling No. 7

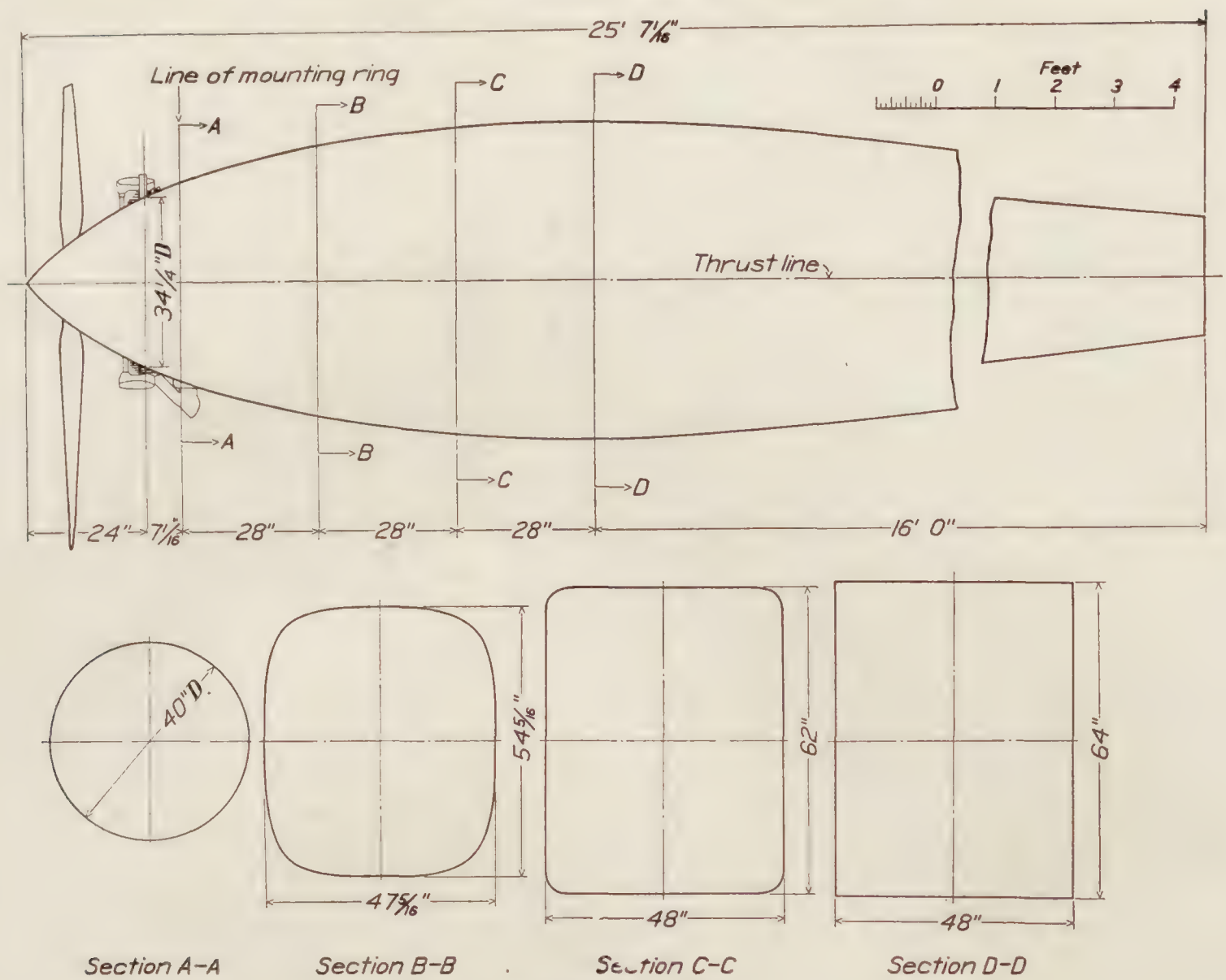


FIGURE 5.—Cowling No. 8

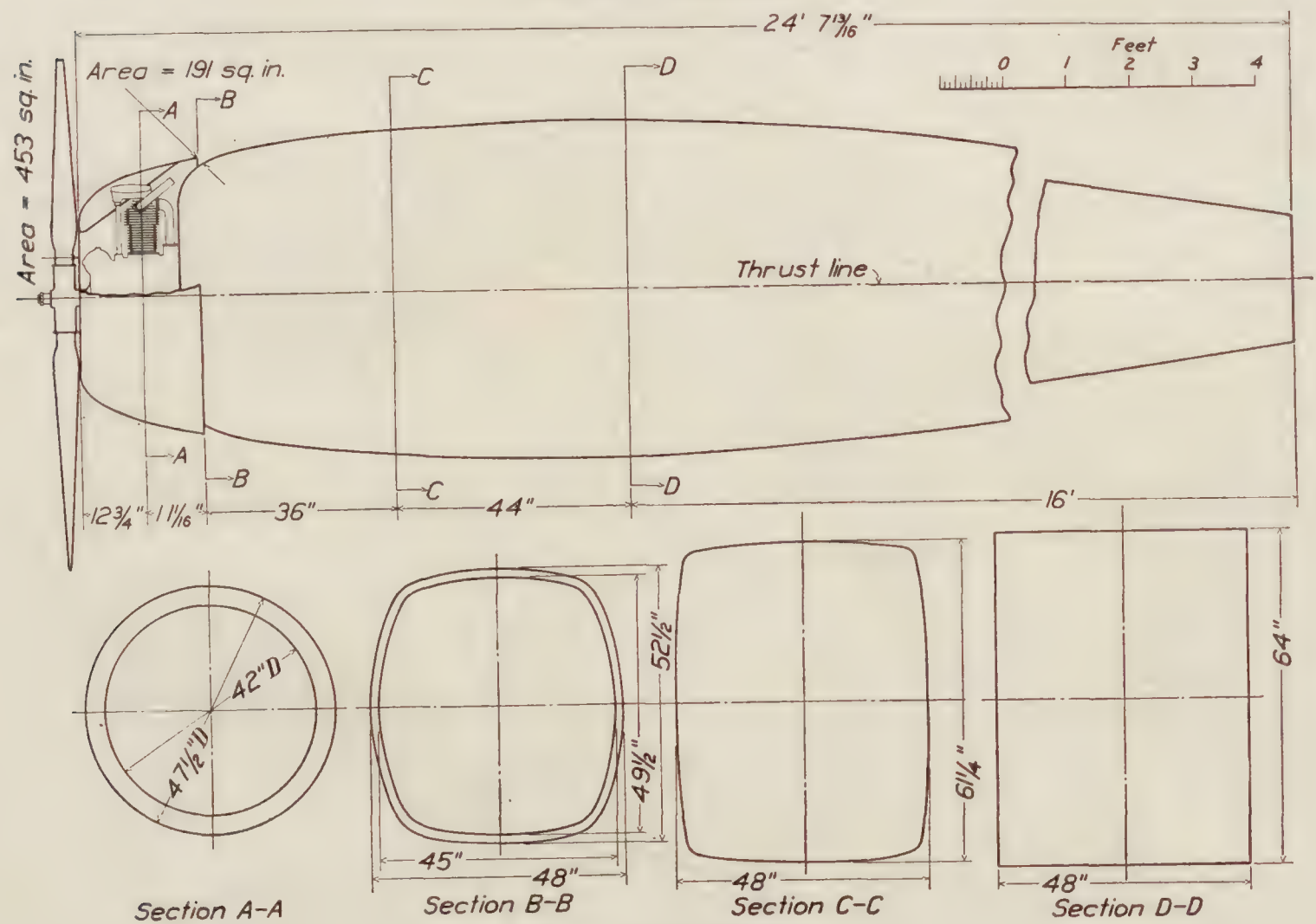


FIGURE 6.—Cowling No. 9

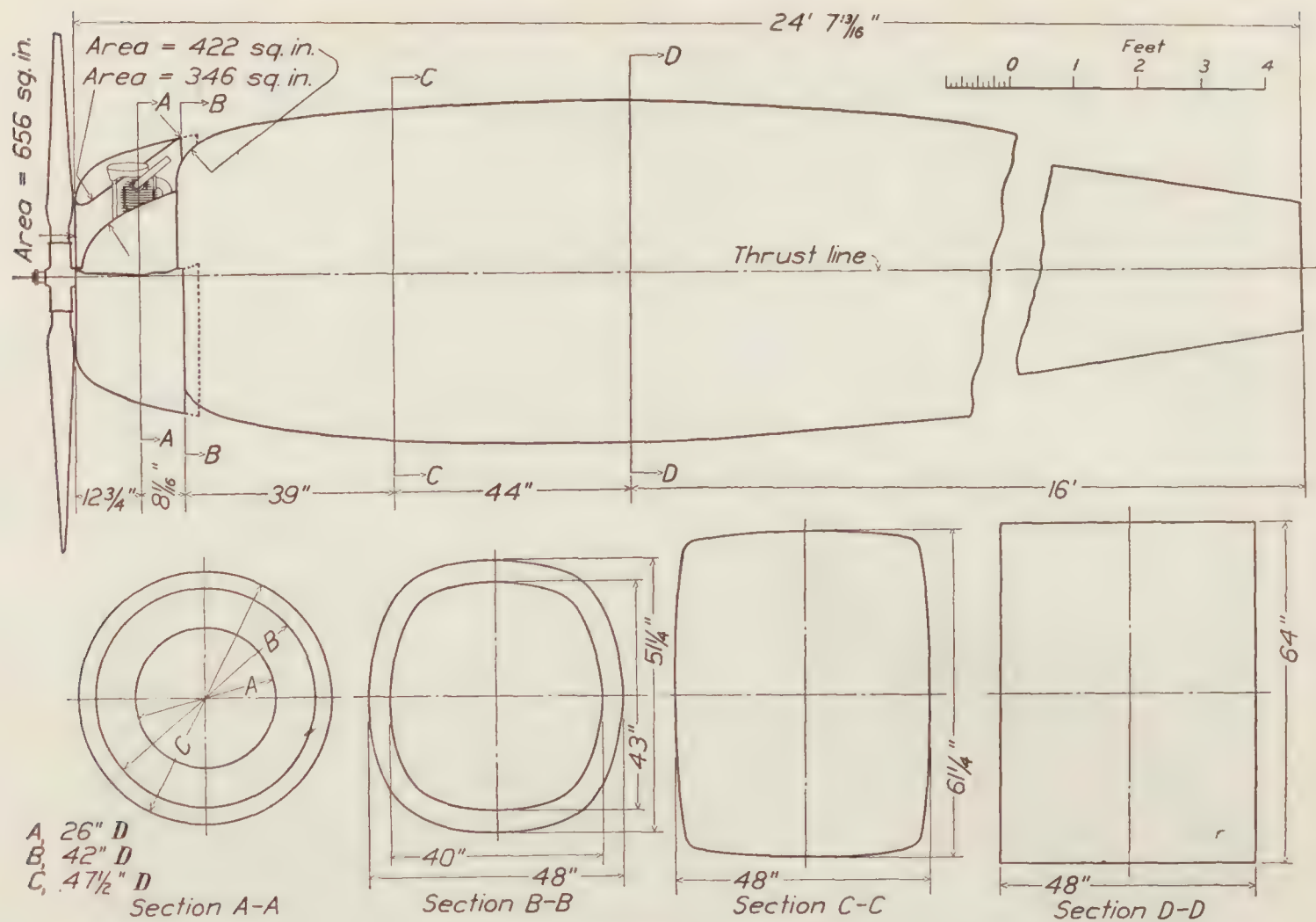


FIGURE 7.—Cowling No. 10 modified

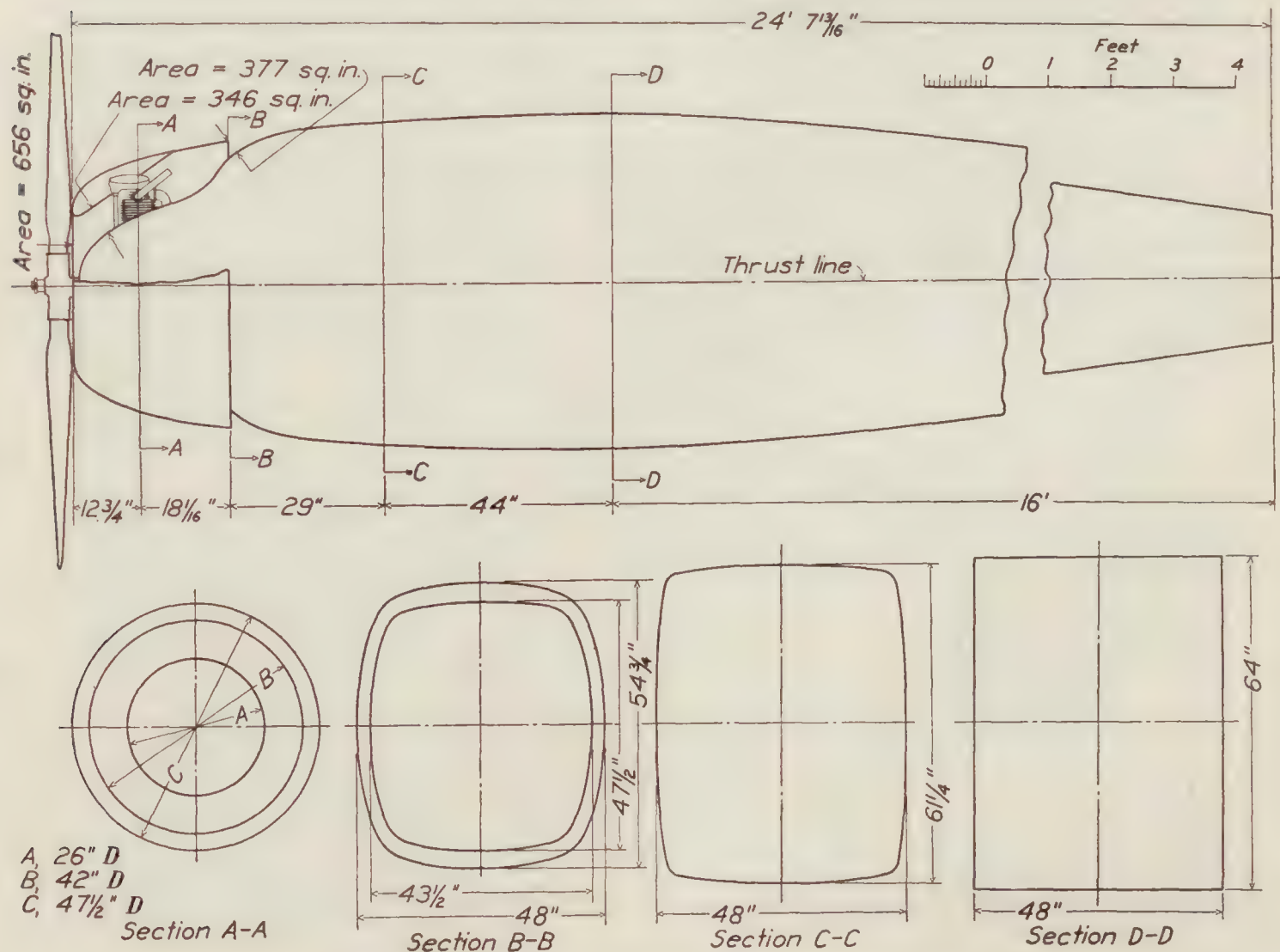


FIGURE 8.—Cowling No. 10 modified. Slot in nose moved back

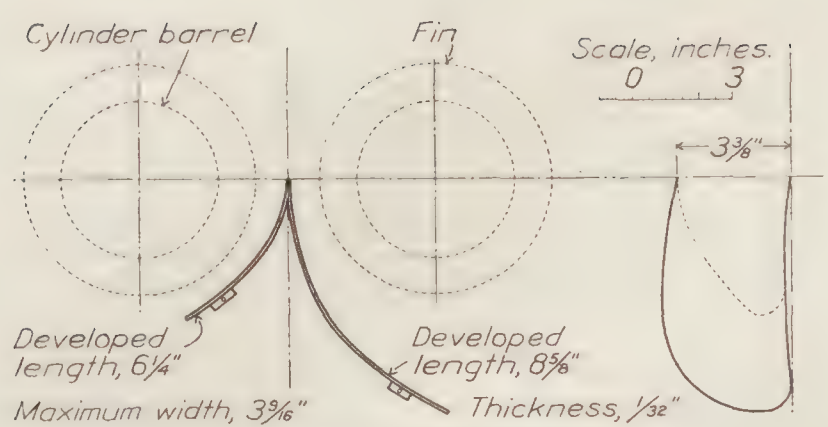


FIGURE 9.—Double deflectors

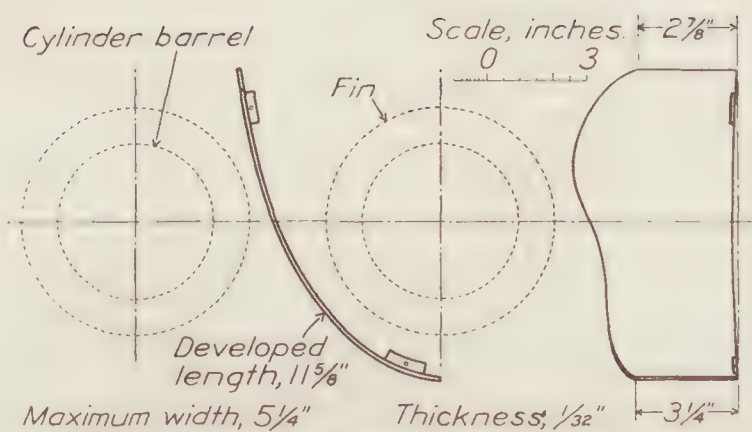


FIGURE 10.—Single deflector

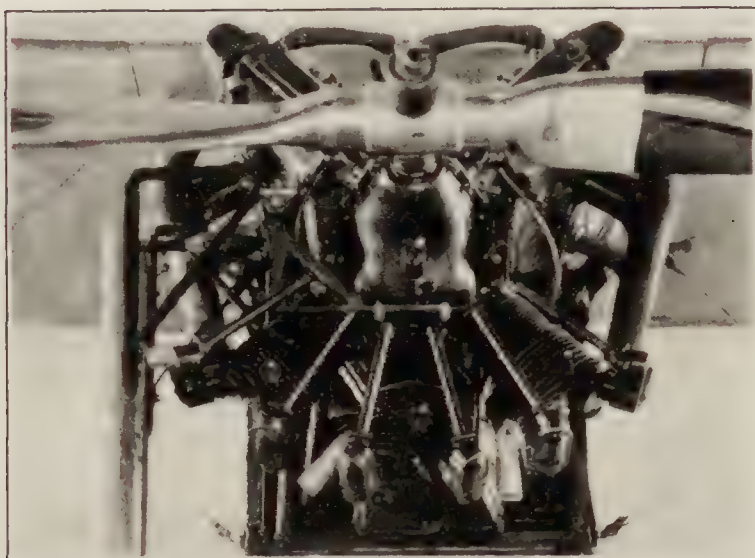


FIGURE 11.—J-5 cylinders mounted on E-2 engine for slip-stream torque tests



FIGURE 12.—Cowling No. 4, engine exposed



FIGURE 13.—Cowling No. 4 on fuselage with stub wing and landing gear mounted in the propeller research tunnel

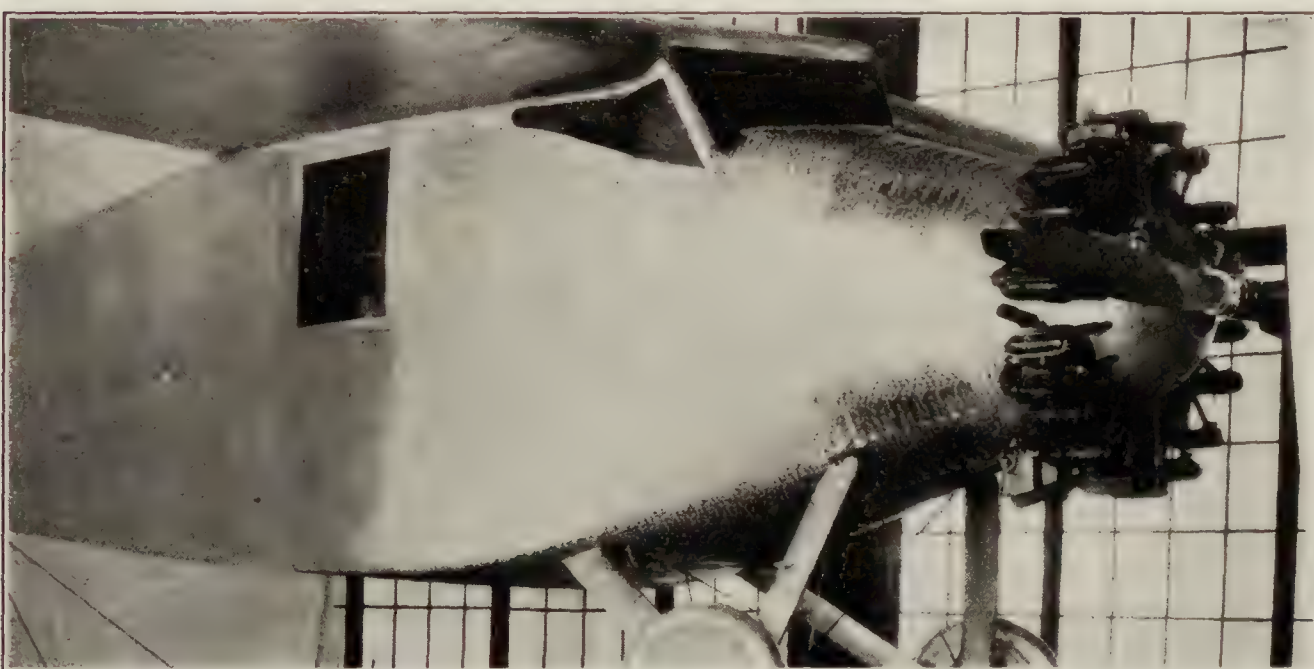


FIGURE 14.—Cowling No. 5

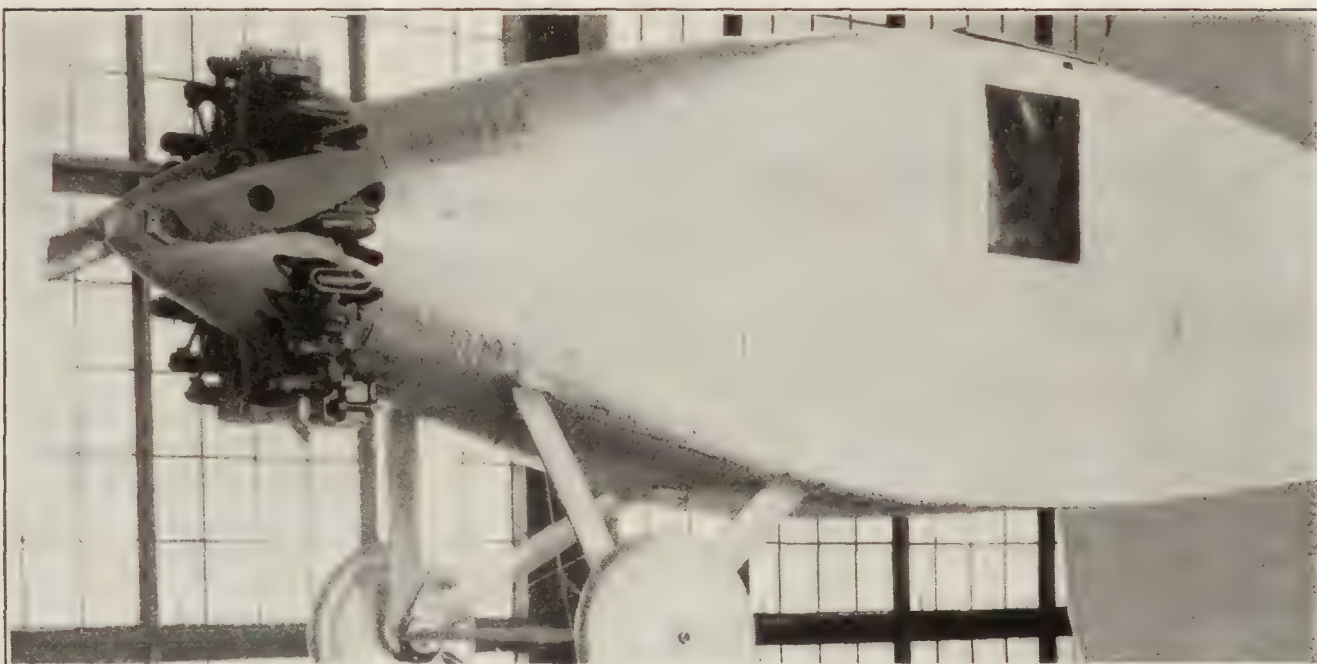


FIGURE 15.—Cowling No. 6



FIGURE 16.—Cowling No. 7, original

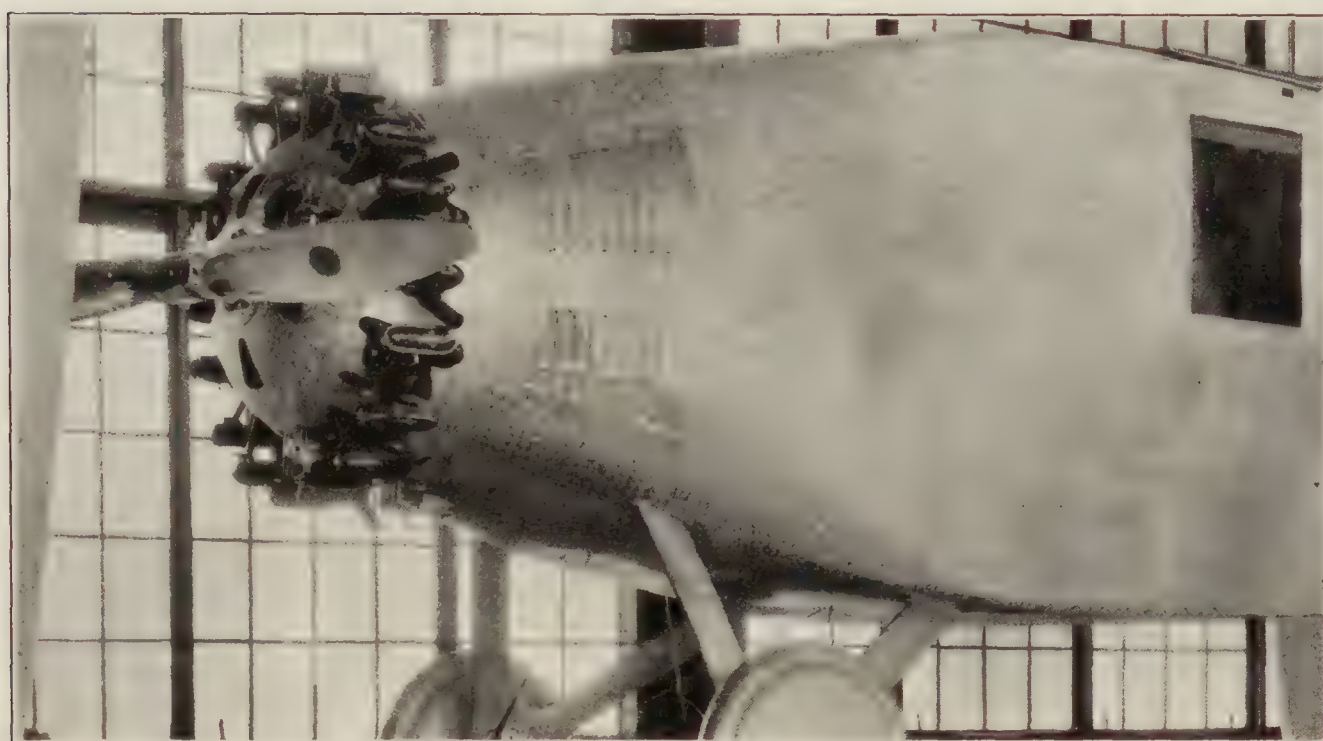


FIGURE 17.—Cowling No. 7, four slots

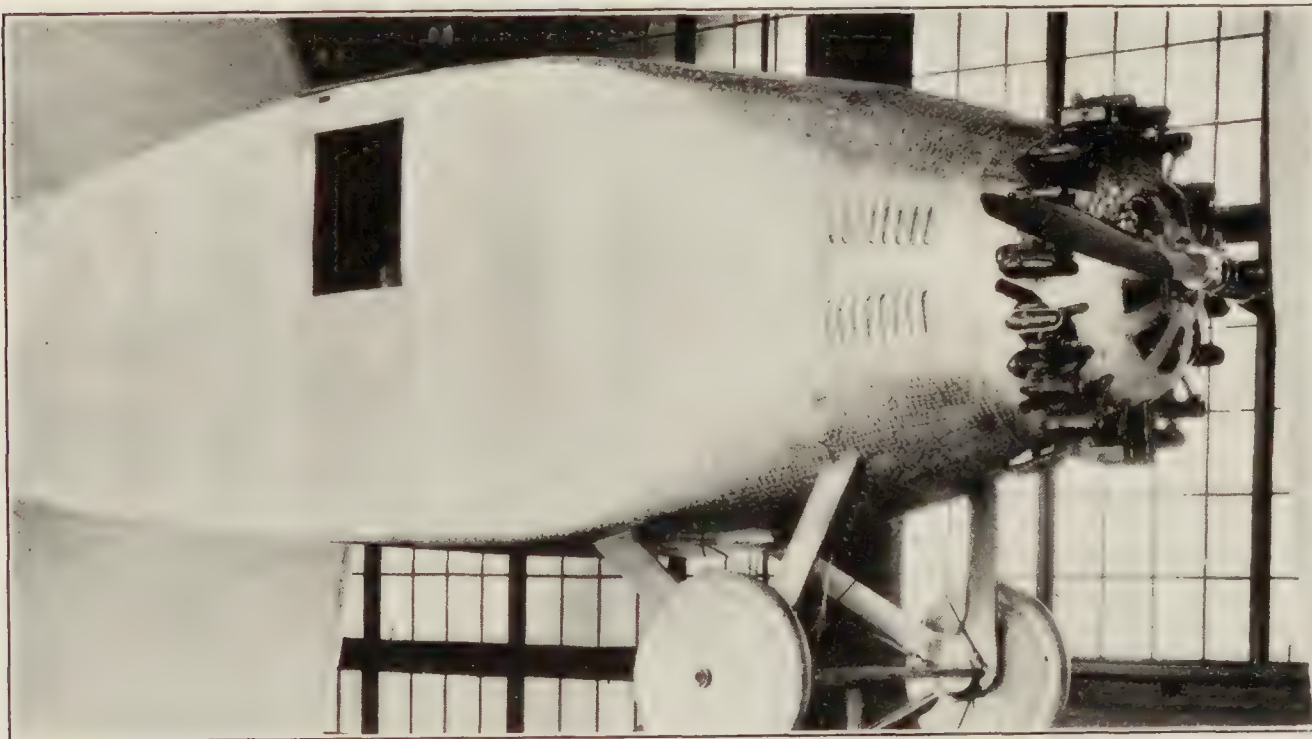


FIGURE 18 —Cowling No. 7, six large slots

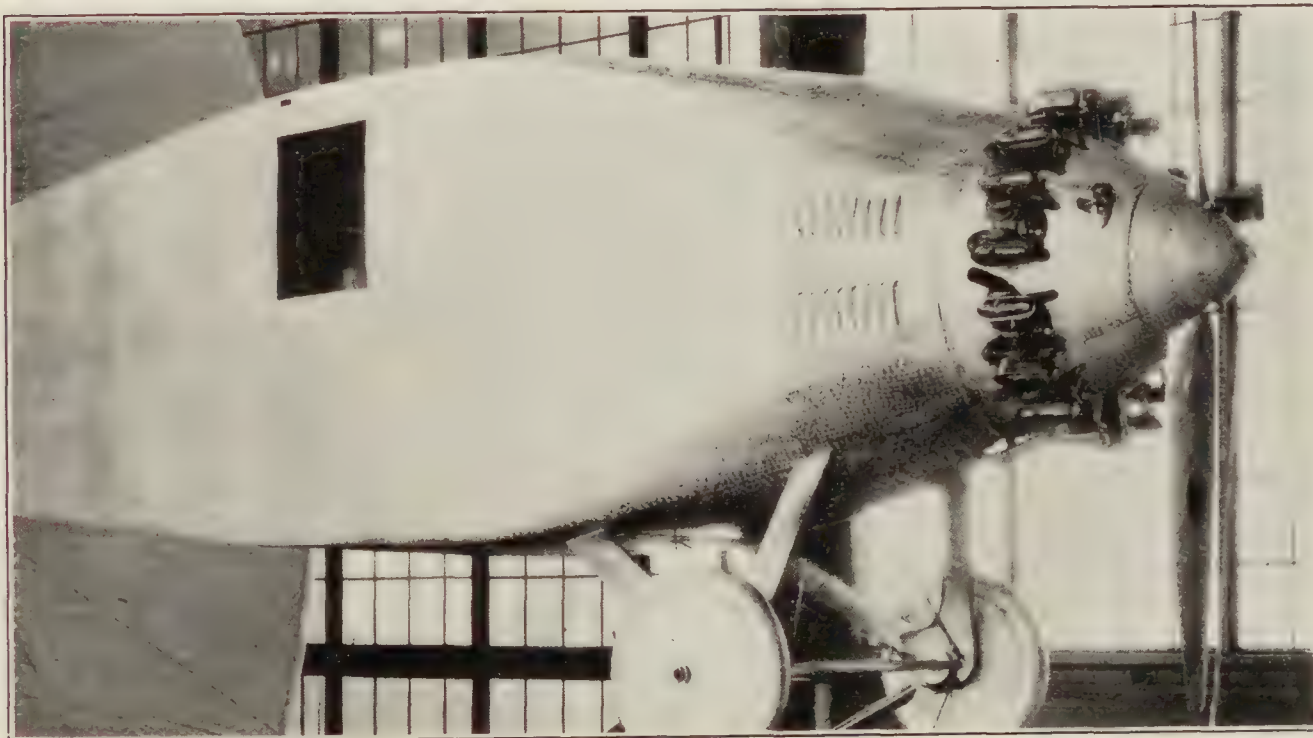


FIGURE 19.—Cowling No. 8, original

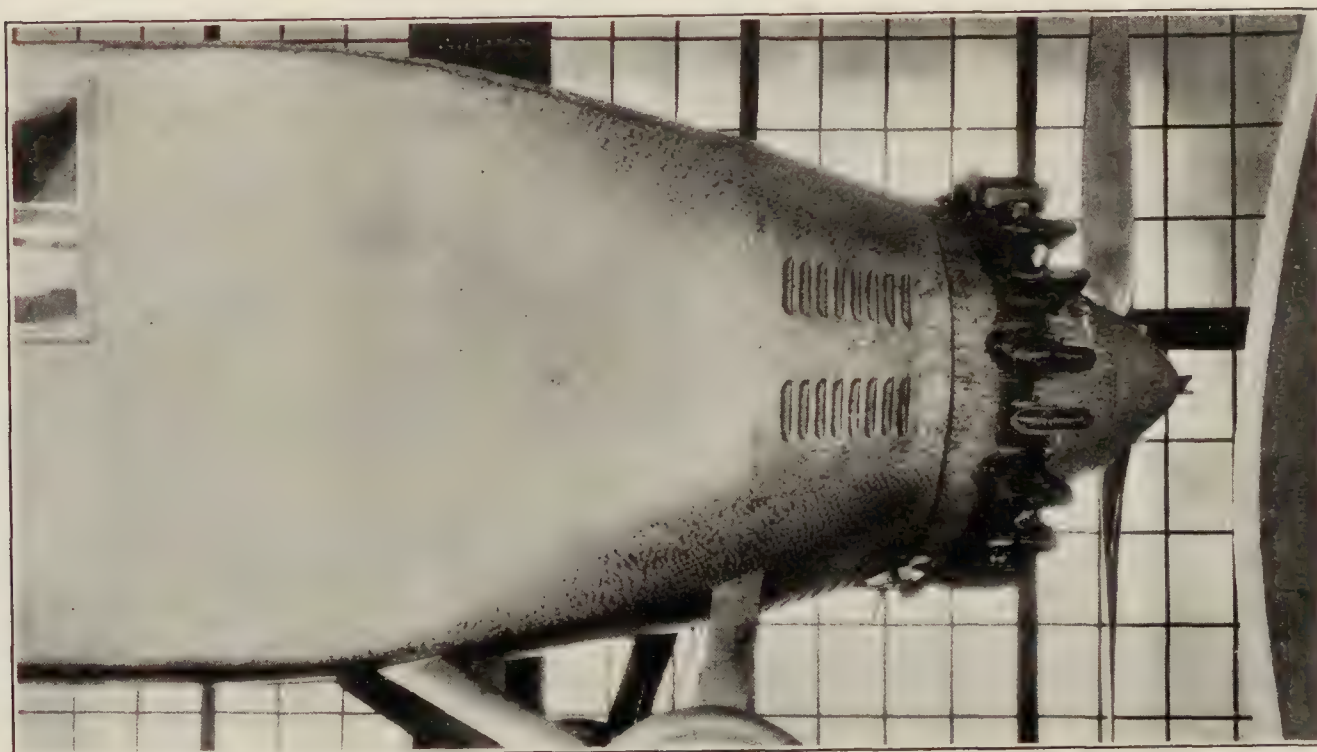


FIGURE 20.—Cowling No. 8, original

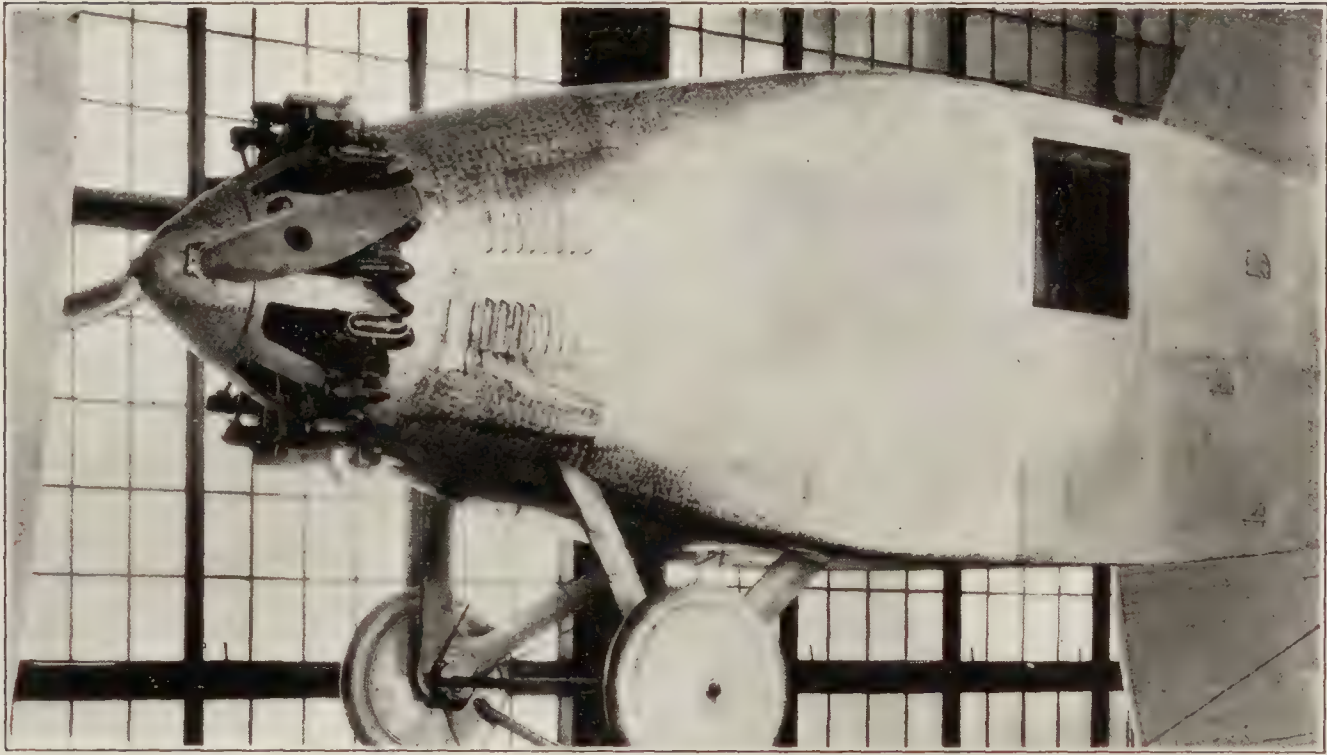


FIGURE 21.—Cowling No. 8, with cut-outs

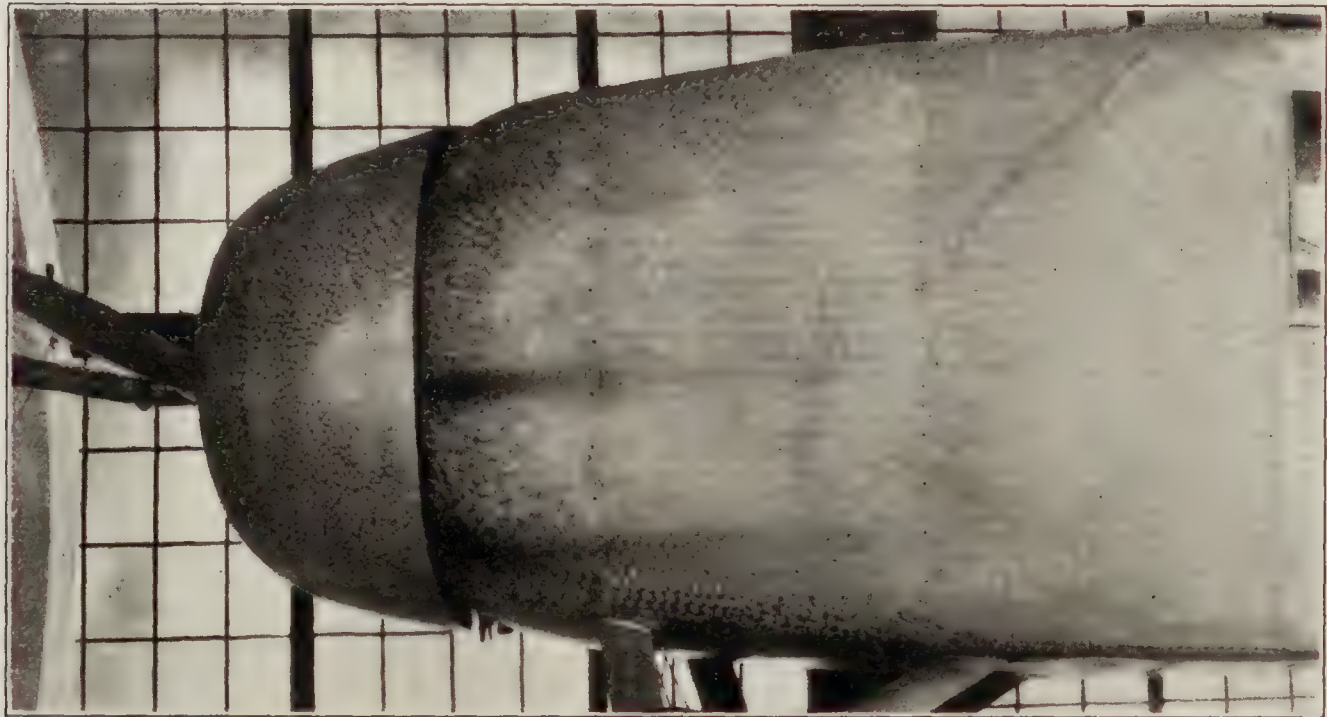


FIGURE 22.—Cowling No. 9

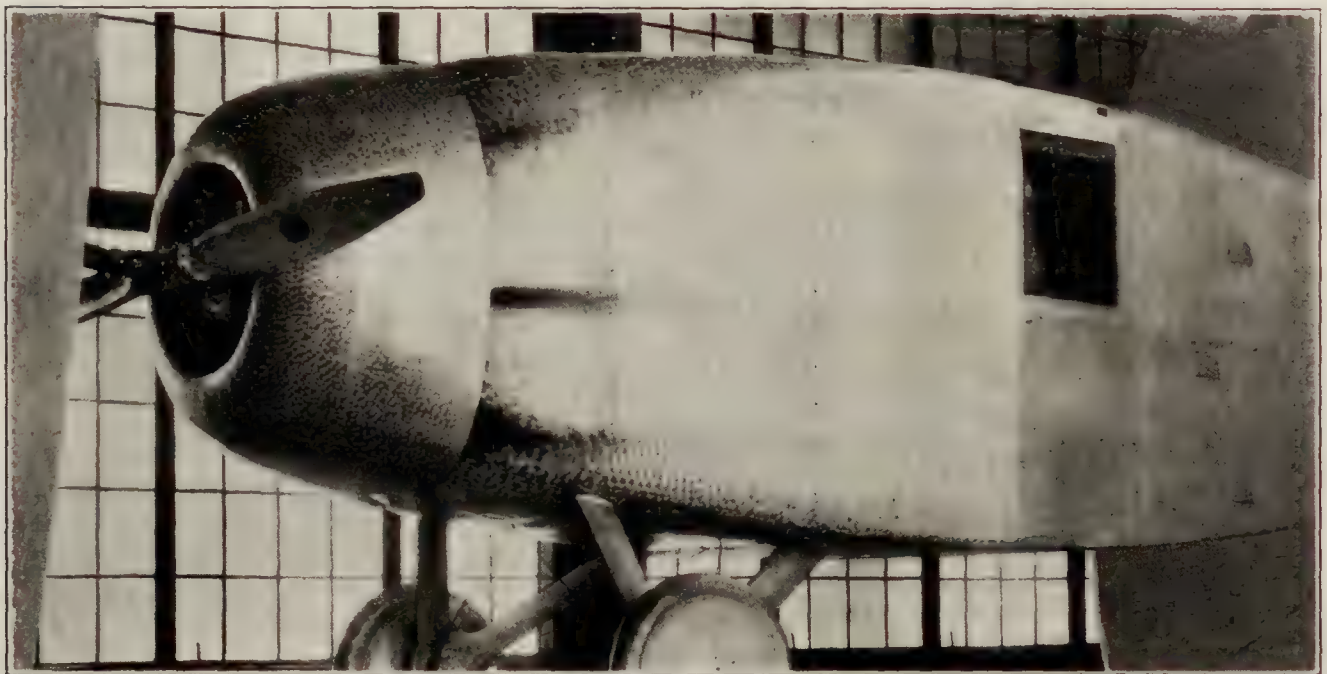


FIGURE 23.—Cowling No. 10

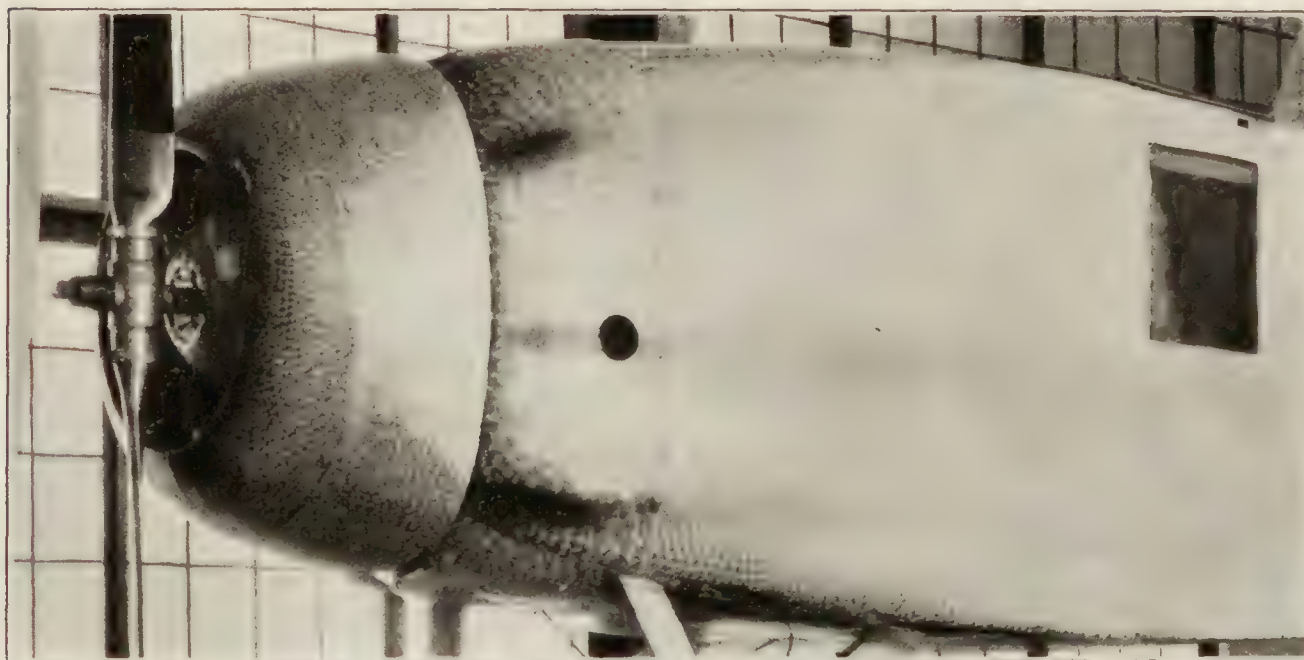


FIGURE 24.—Cowling No. 10, enlarged slot and nose hole and cut-outs over magnetos

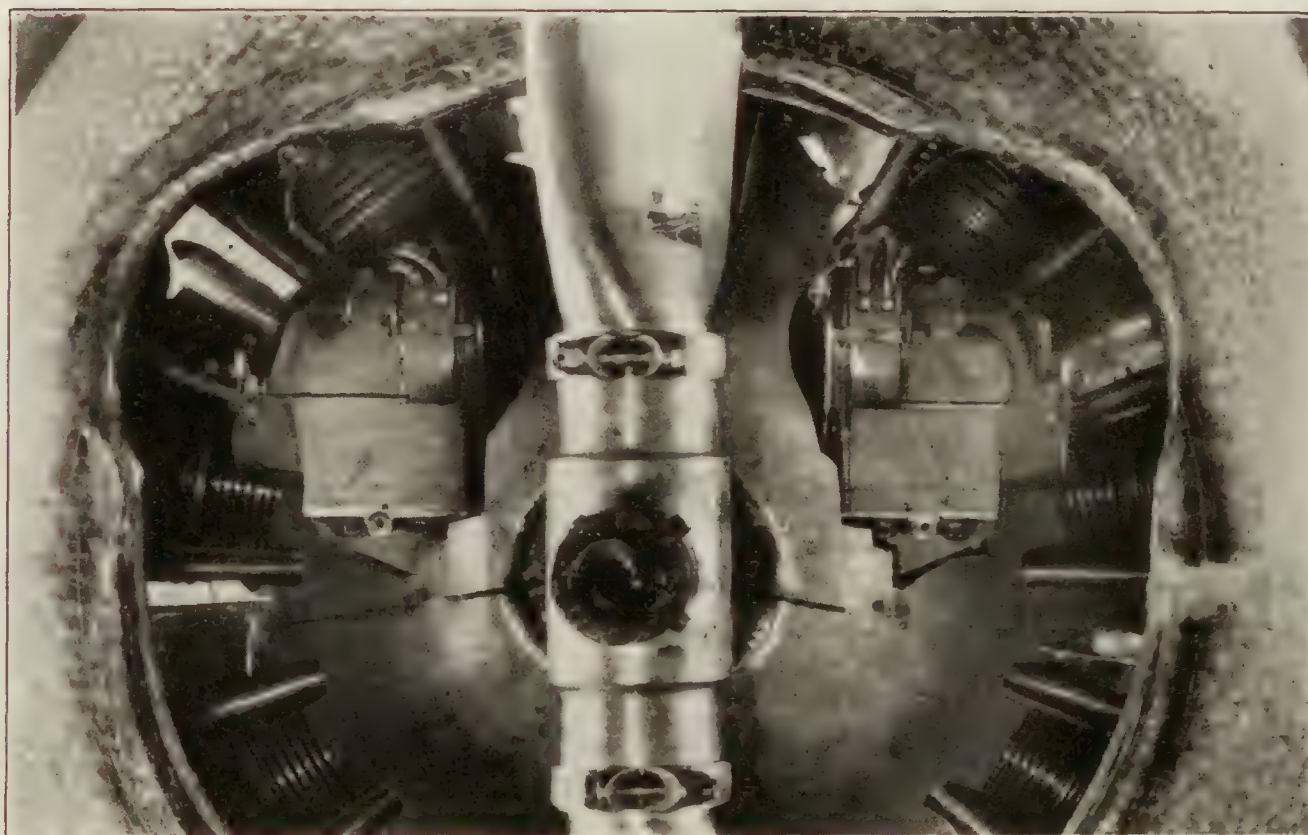


FIGURE 25.—Detail view of cut-outs over magnetos

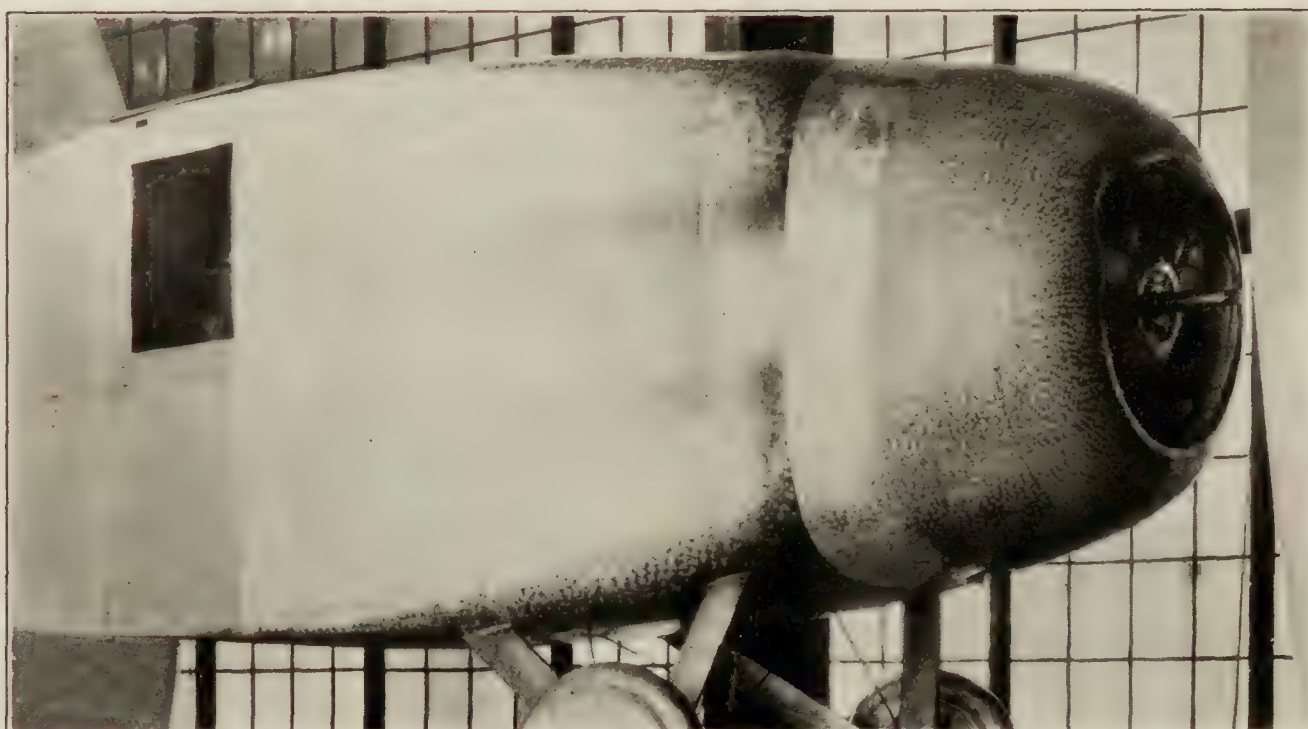


FIGURE 26.—Cowling No. 10 with slot moved back

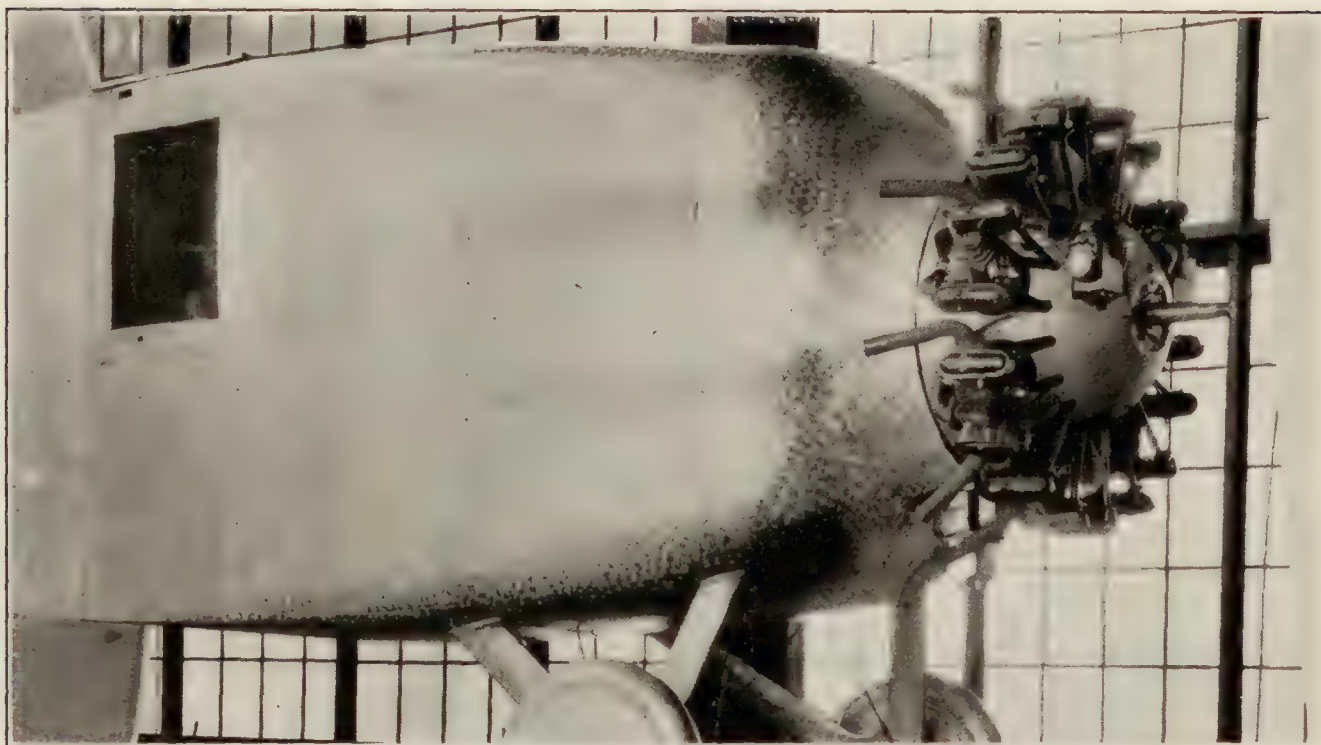


FIGURE 27.—Modified cowling No. 10 with nose piece removed showing deflectors between cylinders

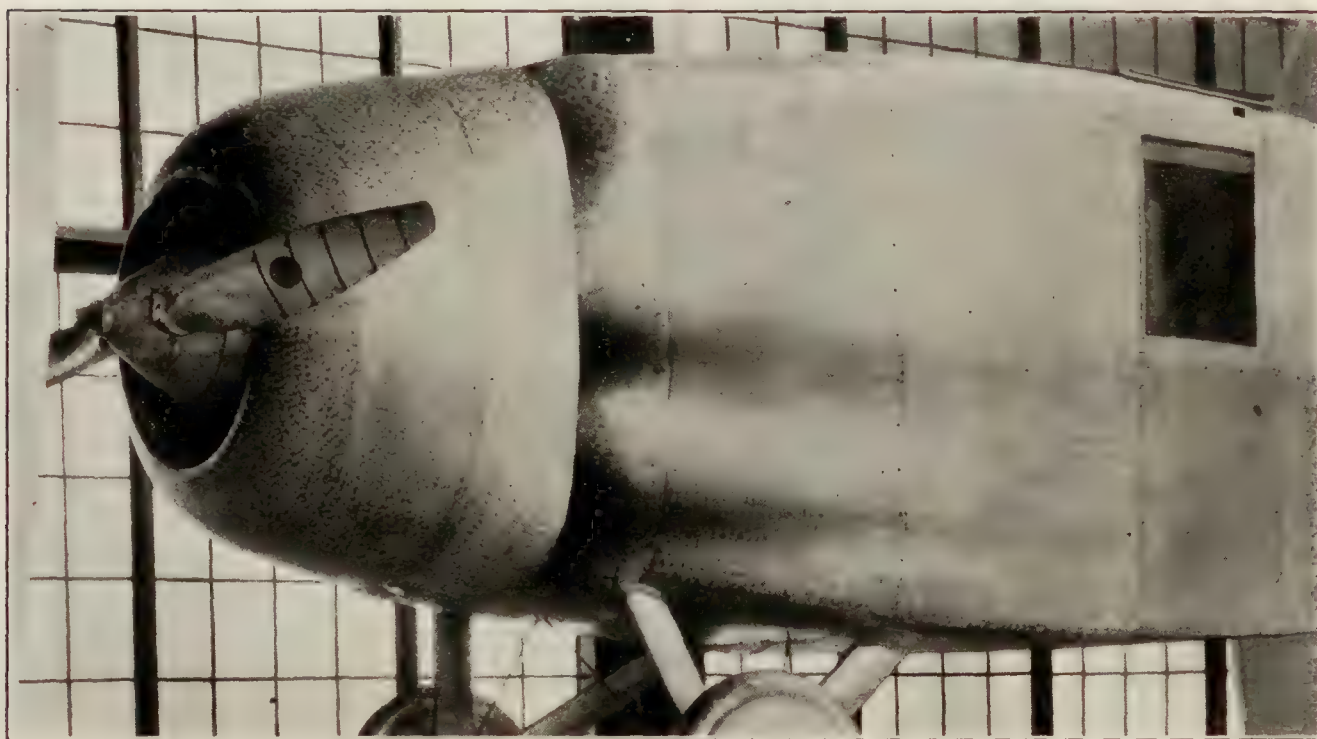


FIGURE 28.—Cowling No. 10 with No. 6 nose with spinner

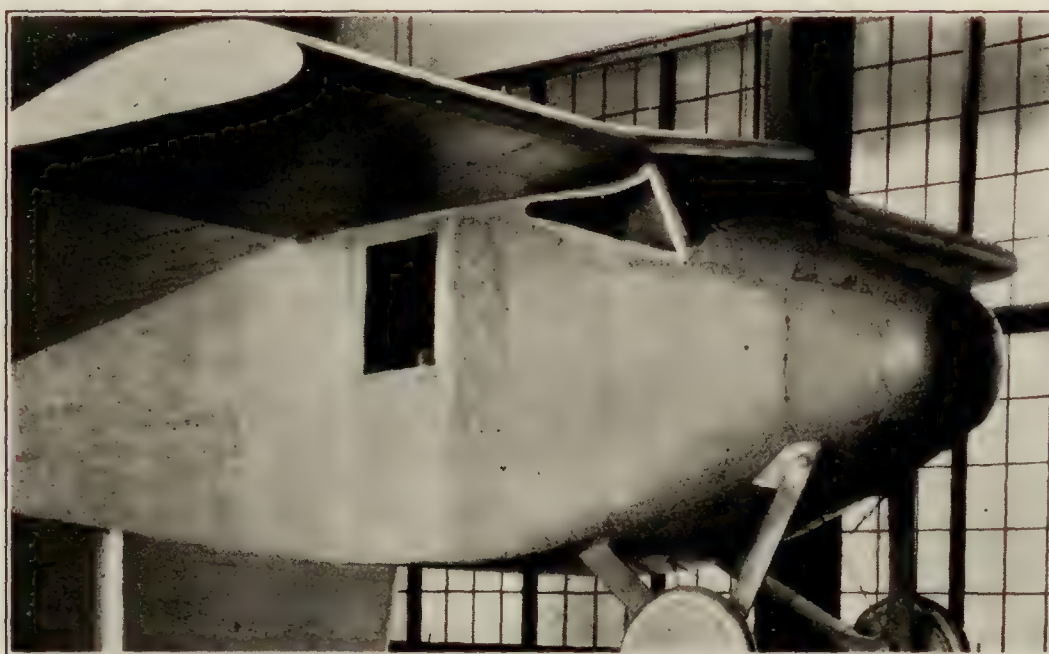


FIGURE 29.—No. 4 with engine removed and nose rounded

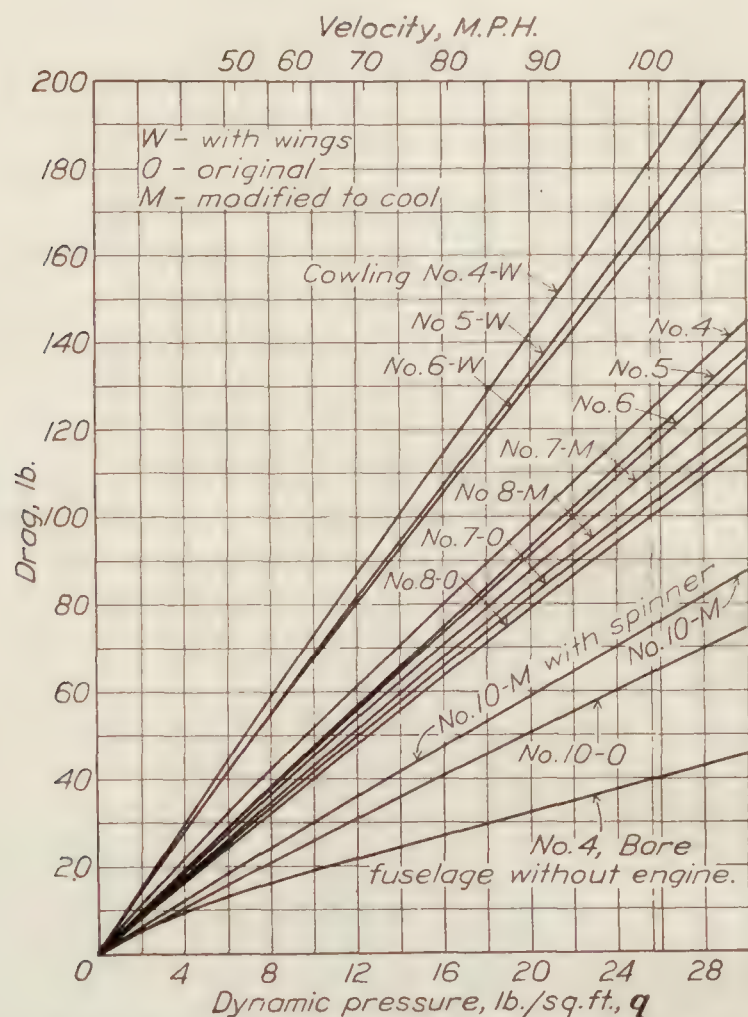


FIGURE 30.—Drag of fuselage and engine with various cowlings

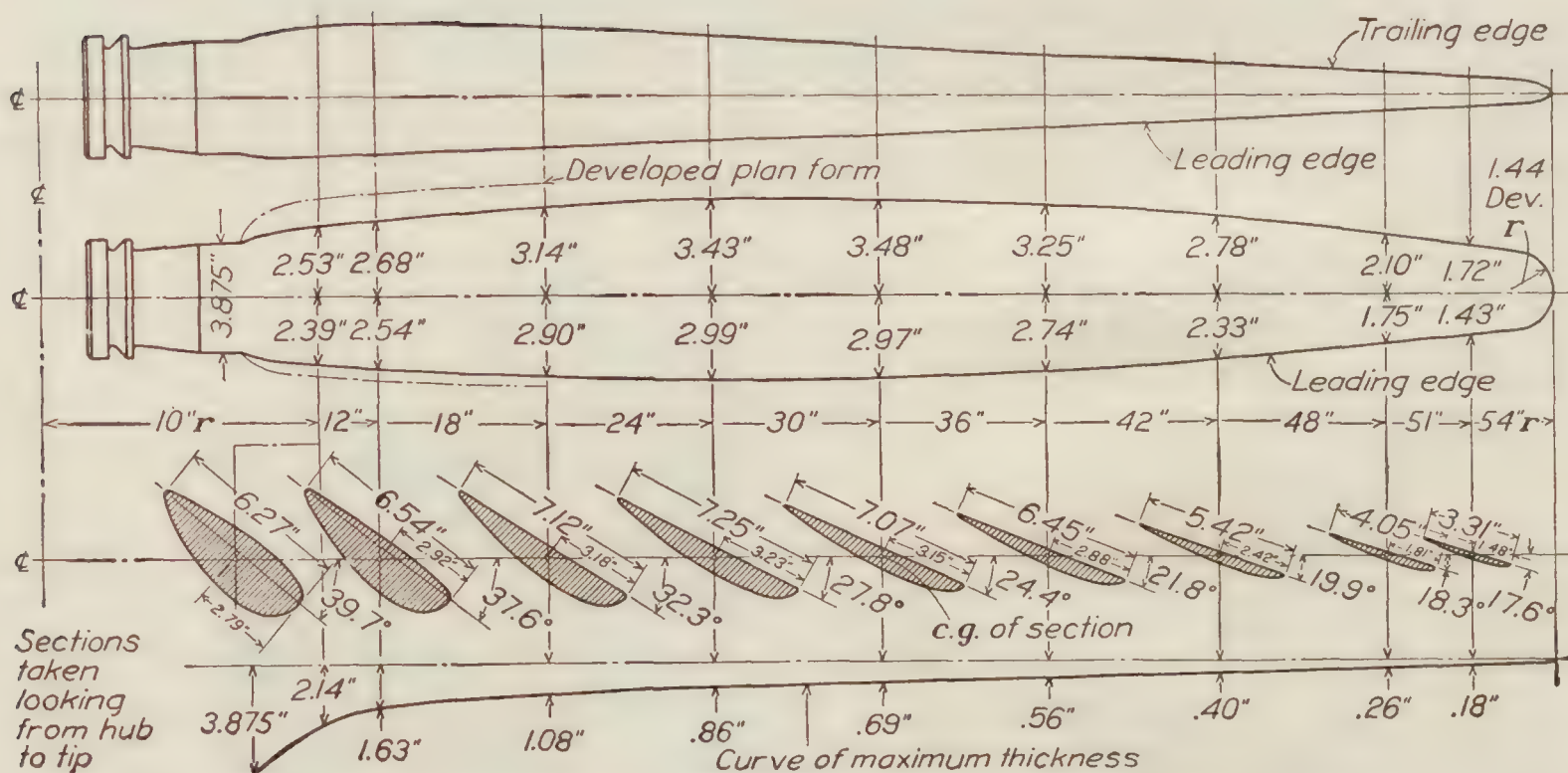


FIGURE 31.—Metal propeller blade, 9 feet diameter, right hand. Navy Department, Bureau of Aeronautics

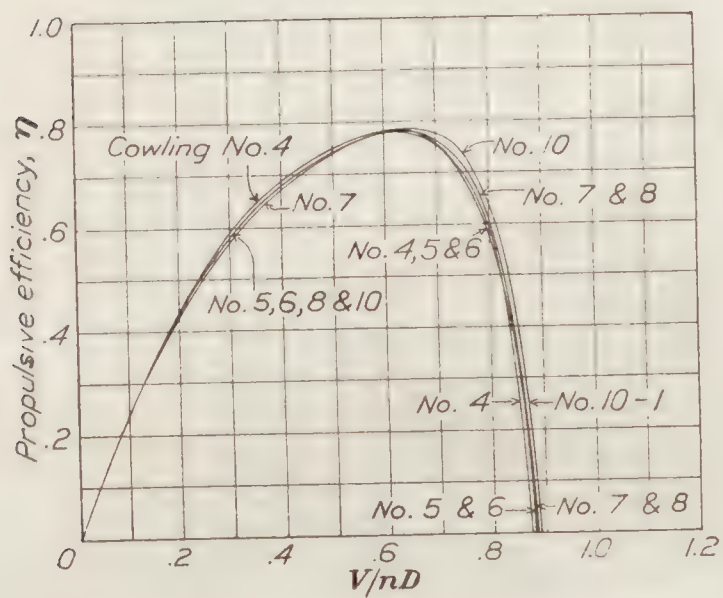


FIGURE 32.—Propeller No. 4412 (15° at 42 inches) on various cowlings without wing and with J-5 engine

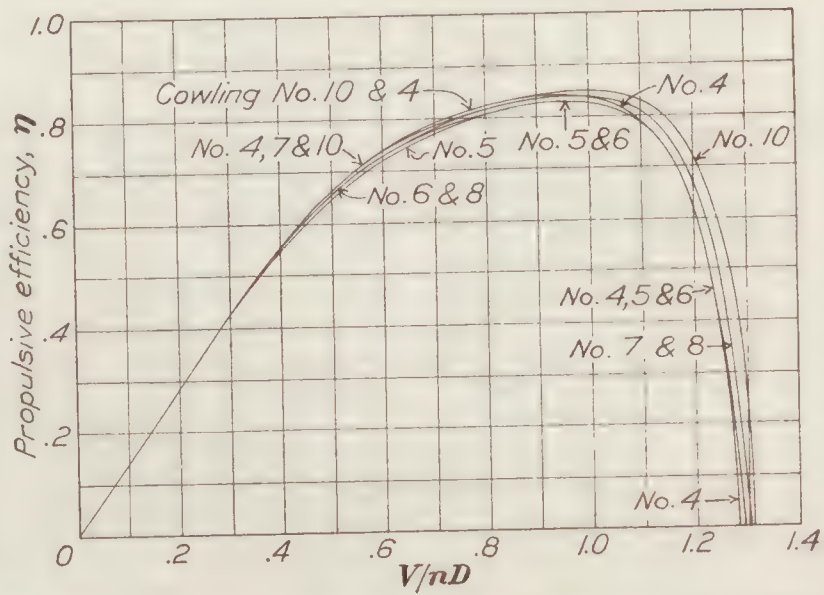
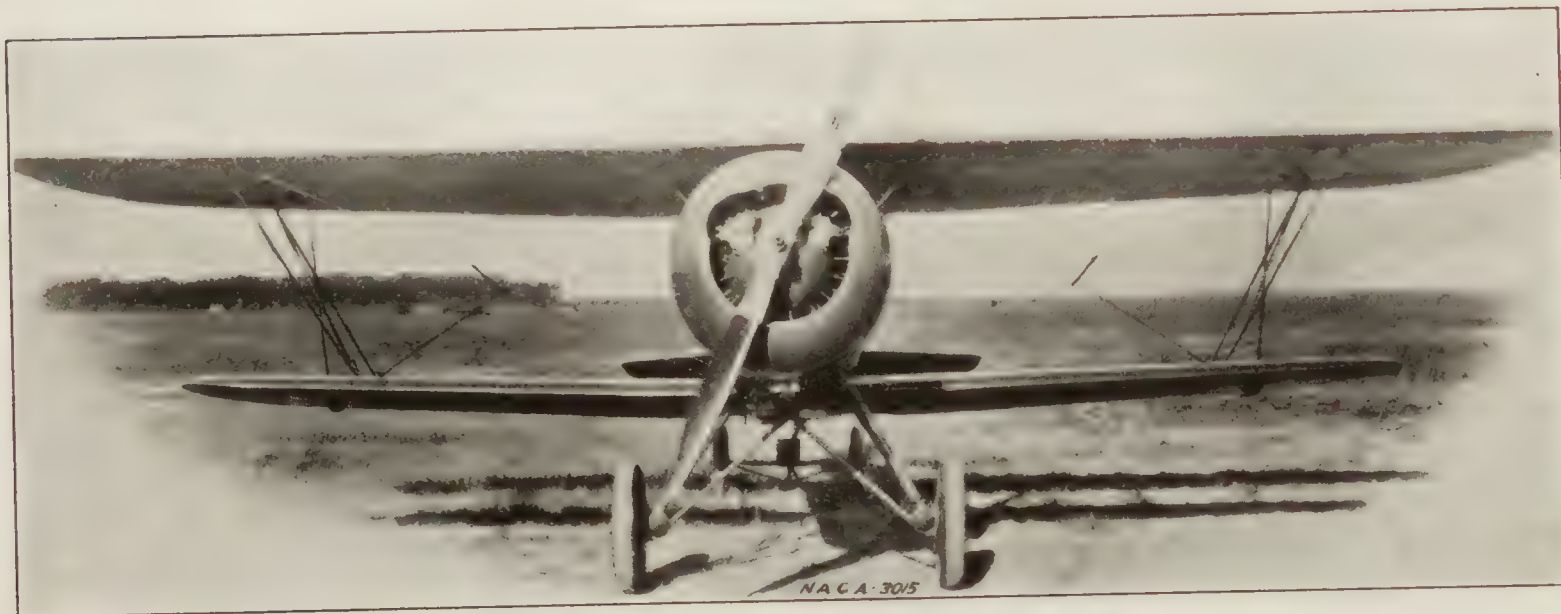


FIGURE 33.—Propeller No. 4412 (23° at 42 inches) on various cowlings without wings and with J-5 engine



FIGURES 34, 35.—Curtiss' A T-5 airplane with No. 10 cowling

REPORT No. 314

**DRAG AND COOLING WITH
VARIOUS FORMS OF COWLING FOR A "WHIRLWIND"
RADIAL AIR-COOLED ENGINE—II**

By FRED E. WEICK
Langley Memorial Aeronautical Laboratory

REPORT No. 314

DRAG AND COOLING WITH VARIOUS FORMS OF COWLING FOR A "WHIRLWIND" RADIAL AIR-COOLED ENGINE—II

By Fred E. Weick

REPRINT OF REPORT No. 314, ORIGINALLY PUBLISHED FEBRUARY, 1929

SUMMARY

This report gives the results of the second portion of an investigation in the Twenty-Foot Propeller Research Tunnel of the National Advisory Committee for Aeronautics, on the cowling and cooling of a "Whirlwind" J-5 radial air-cooled engine. The first portion, which is reported in N. A. C. A. Technical Report No. 313, pertains to tests with a cabin fuselage. This report covers tests with several forms of cowling, including conventional types, individual fairings behind the cylinders, individual hoods over the cylinders, and the new N. A. C. A. complete cowling, all on an open cockpit fuselage. Drag tests were also made with a conventional engine nacelle, and with a nacelle having the new complete cowling.

In the second part of the investigation the results found in the first part were substantiated. It was also found that the reduction in drag with the complete cowling over that with conventional cowling is greater with the smaller bodies than with the cabin fuselage; in fact, the gain in the case of the completely cowled nacelle is over twice that with the cabin fuselage. The individual fairings and hoods did not prove effective in reducing the drag. The results of flight tests on an AT-5A airplane (reported in the appendix to N. A. C. A. Technical Report No. 313) have been analyzed and found to agree very well with the results of the wind tunnel tests.

INTRODUCTION

This report covers the second and final portion of an investigation of the cowling and cooling of radial air-cooled engines. The first portion, which dealt with the cowling of a "Whirlwind" engine in a cabin fuselage, has been reported in N. A. C. A. Technical Report No. 313 (Reference 1).

The original program included 10 main forms of cowling for a "Whirlwind" J-5 engine, Nos. 1 to 3, on an open cockpit fuselage and Nos. 4 to 10 on a cabin fuselage. The seven forms of cowling on the cabin fuselage ranged from the one extreme of an entirely exposed engine to the other extreme of a totally inclosed engine. Only the first three degrees of cowling were to have been tested on the open cockpit fuselage, and one of these included individual fairings behind each cylinder. During the progress of the tests the following additions were made to the program:

(a) The complete cowling (No. 10 on the cabin fuselage) was tested on the open cockpit fuselage also and called cowling No. 11.

(b) Tests were made with individual hoods over the cylinders on the open cockpit fuselage.

(c) Two nacelles were tested for drag, one with the complete cowling and one with a conventional cowling. A drag test was also made on the uncowed engine by itself.

METHODS AND APPARATUS

The tests were made in the Twenty-Foot Propeller Research Tunnel, which is of the open-throat type with an air stream in which velocities up to 110 M. P. H. can be obtained. The tunnel with its balances and other equipment is described more completely in Reference 2.

A standard 9-cylinder Wright "Whirlwind" engine developing 200 HP. at 1,800 R. P. M. was used for the tests. The open cockpit fuselage was similar in shape to that of a Vought UO-1 except that the usual break in the bottom contour at the back of the cowling was filled

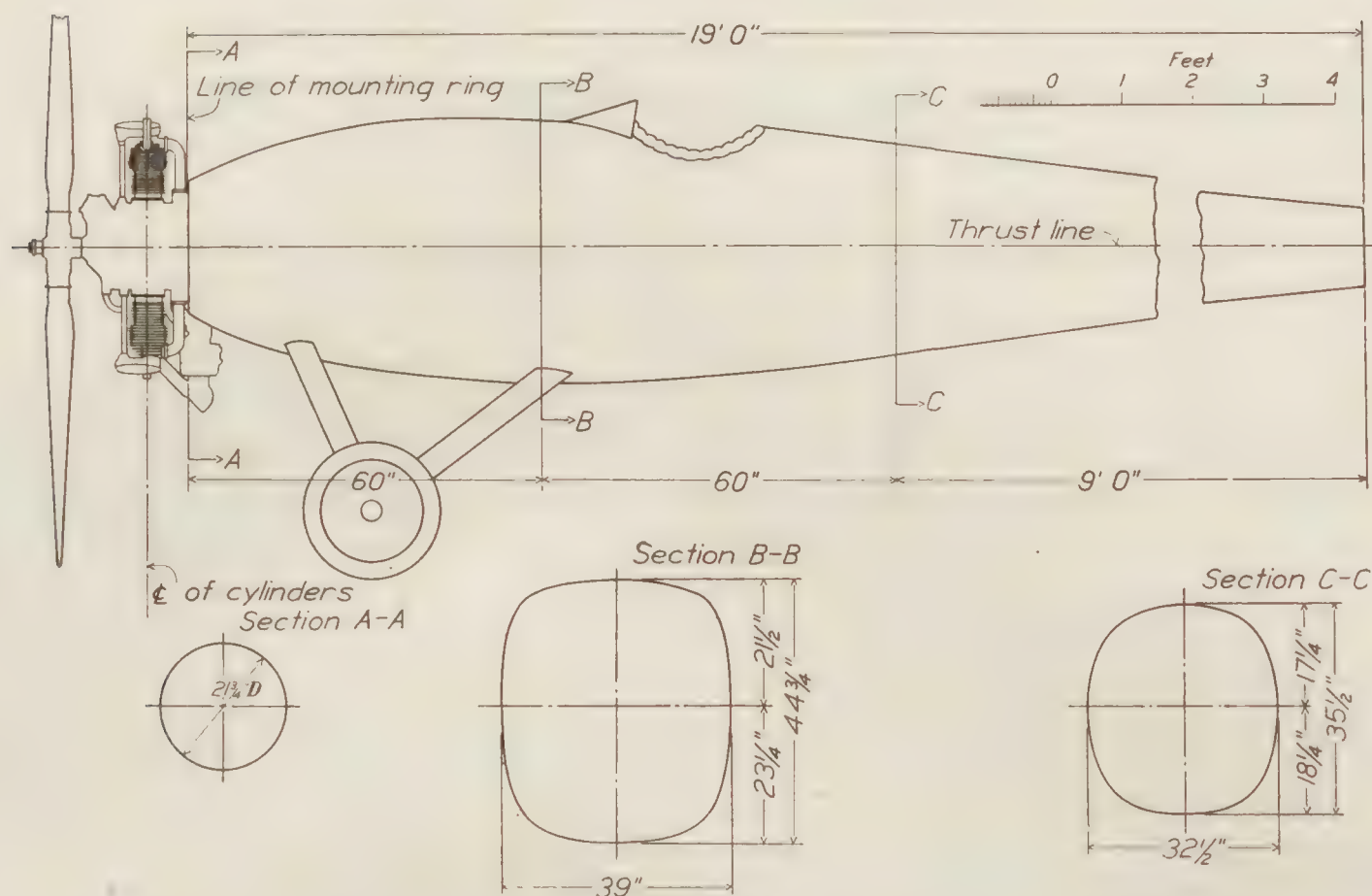


FIG. 1.—Cowling No. 1

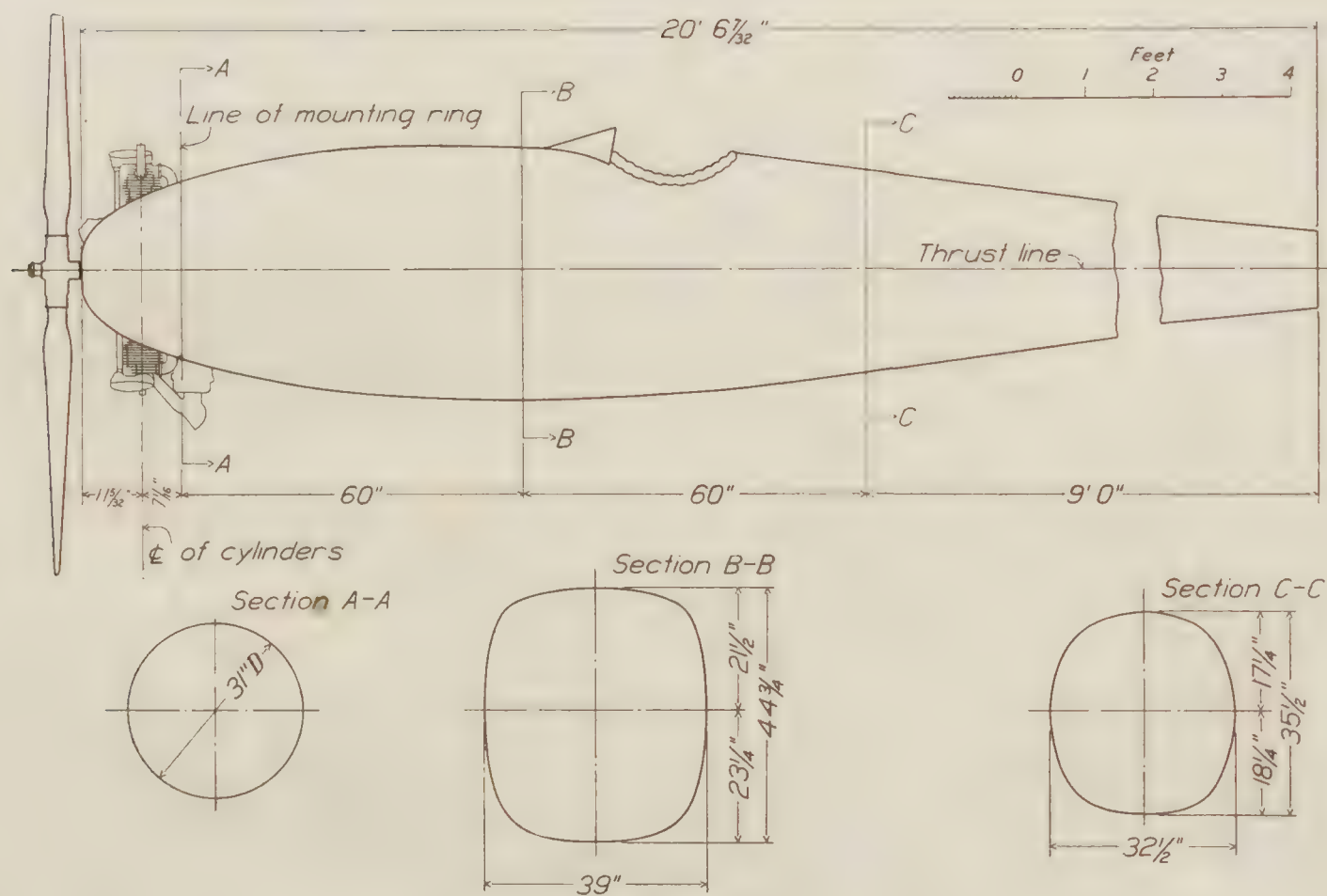


FIG. 2.—Cowling No. 2

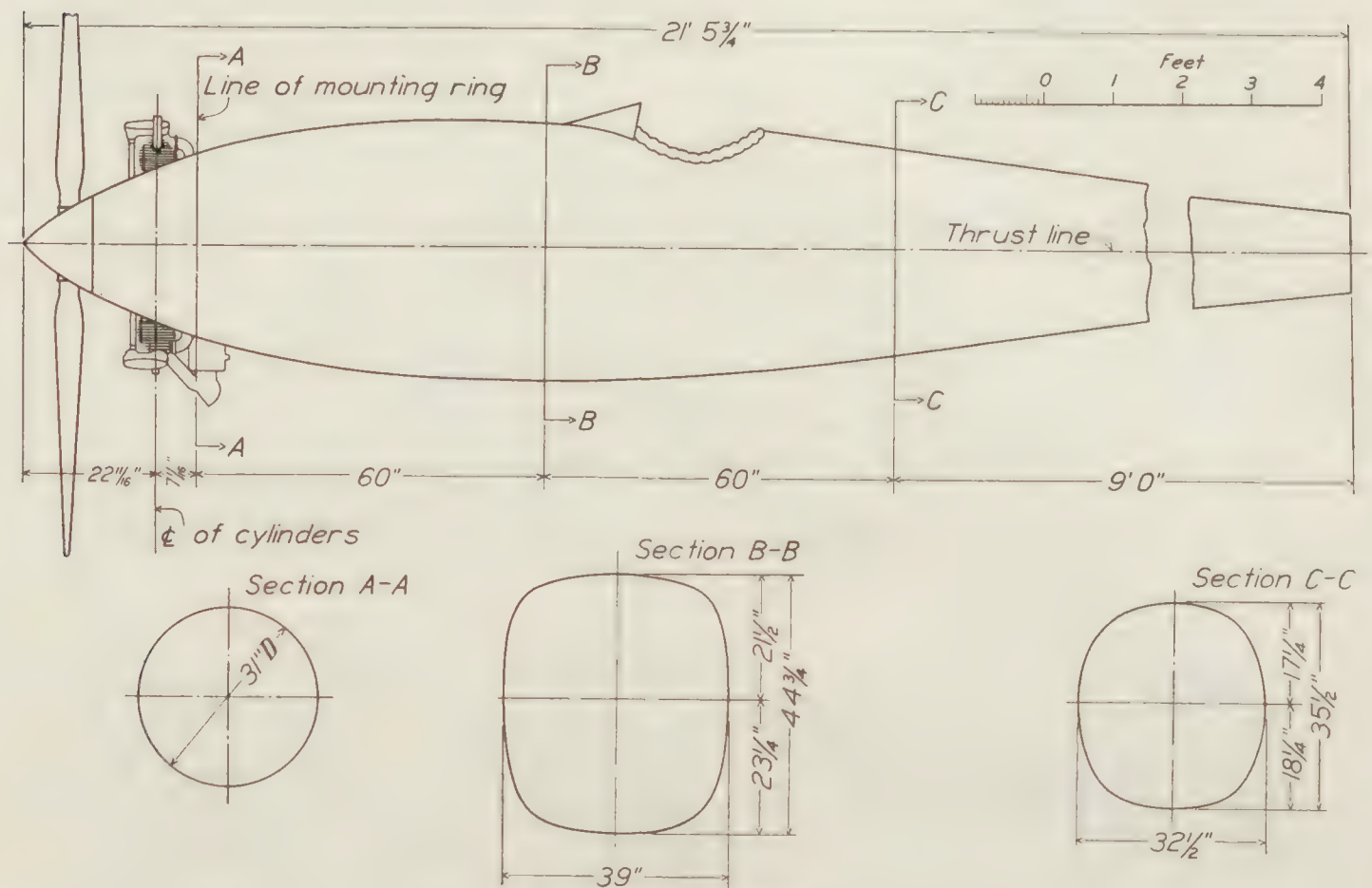


FIG. 3.—Cowling No. 3

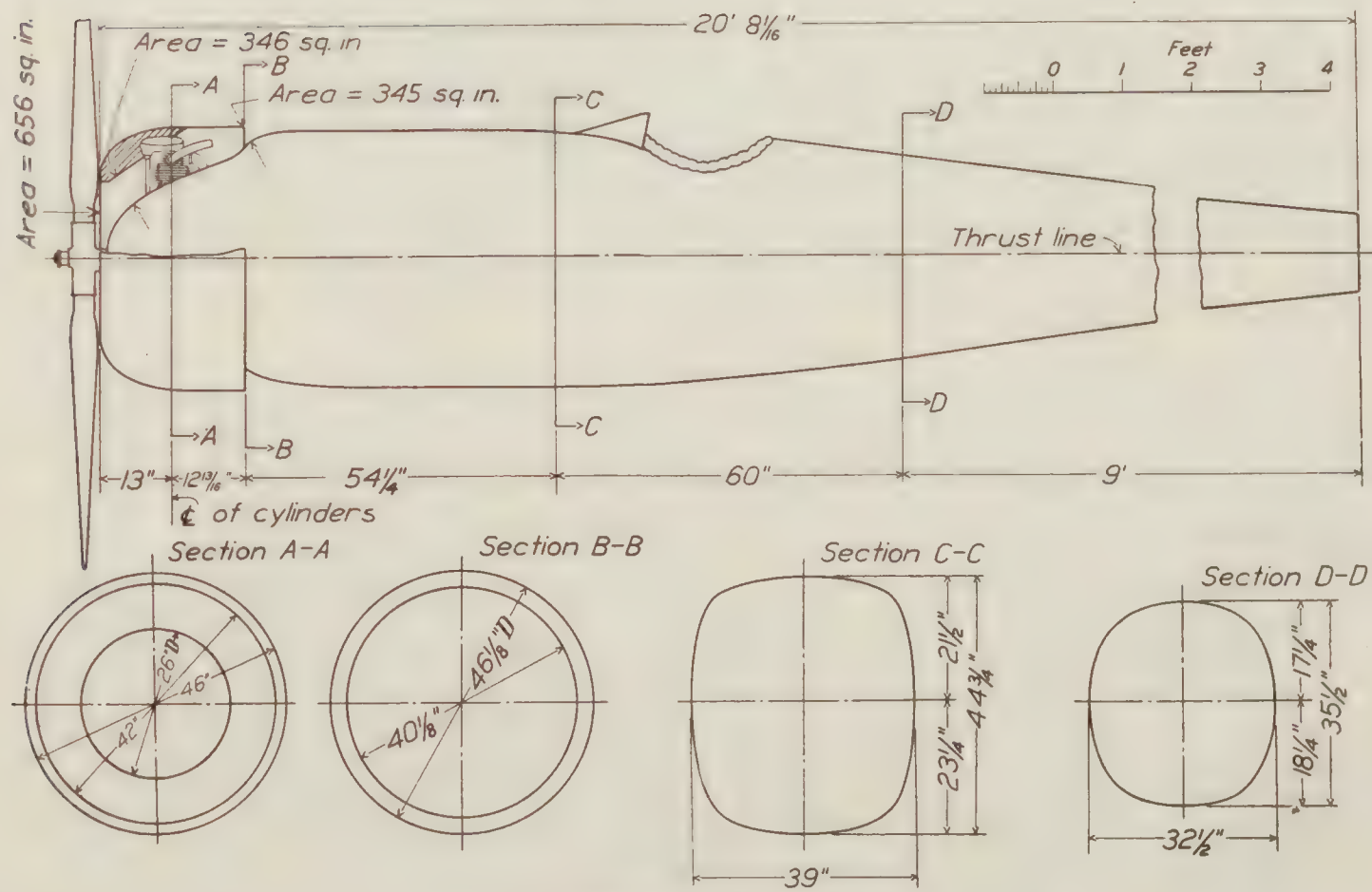


FIG. 4.—Cowling No. 11
NOTE.—Cross hatch section of cowling is not solid

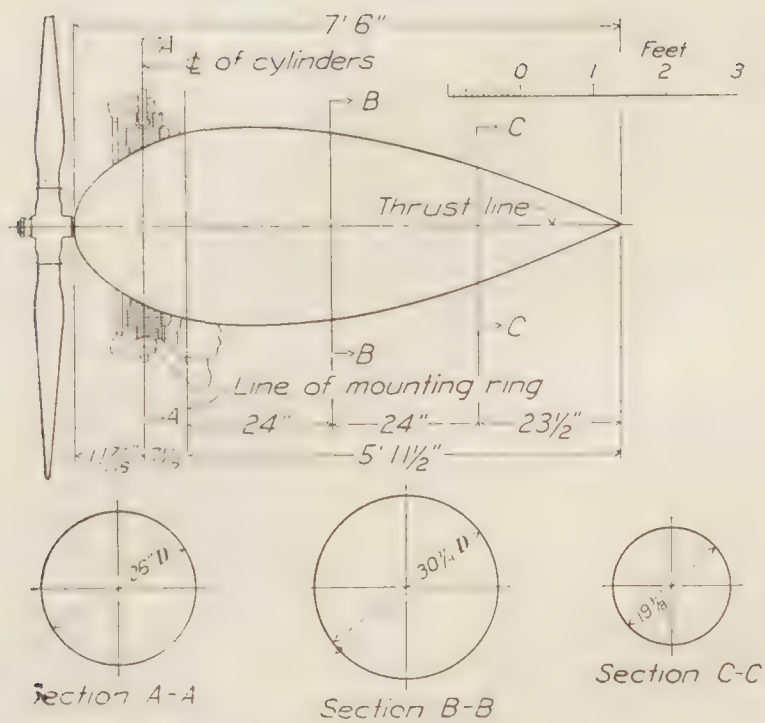


FIG. 5.—Nacelle No. 13

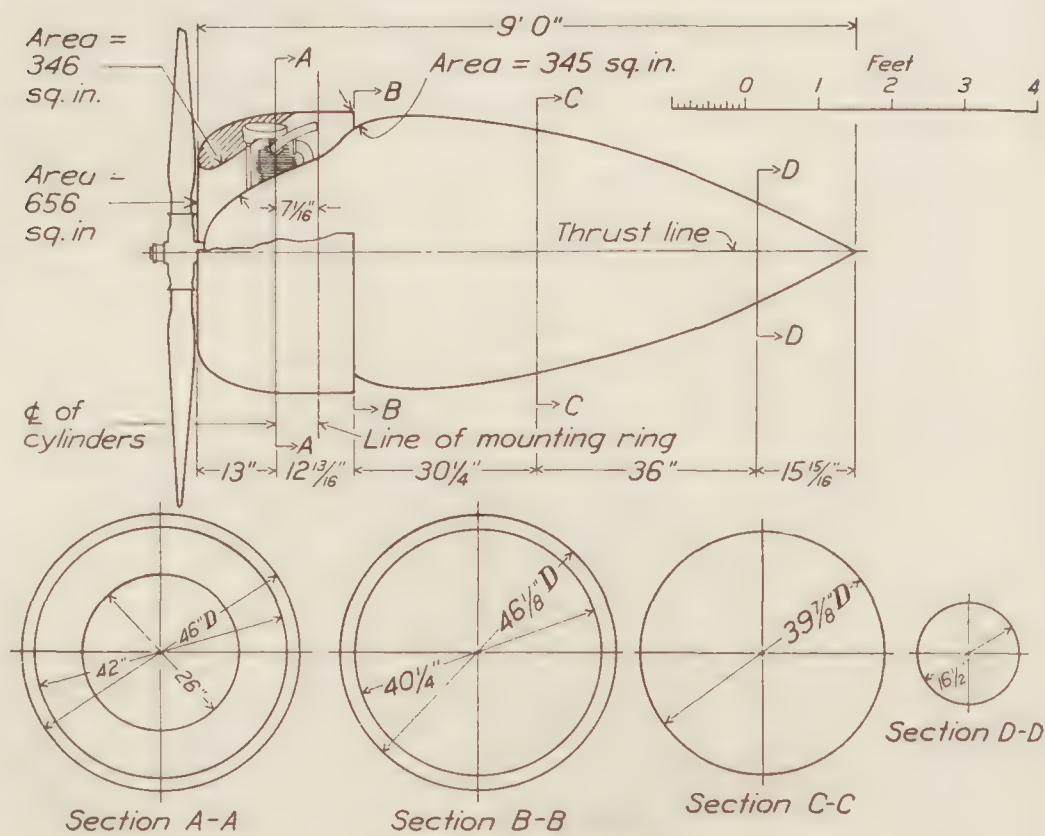


FIG. 6.—Nacelle No. 14

NOTE.—Cross hatch section of cowling is not solid

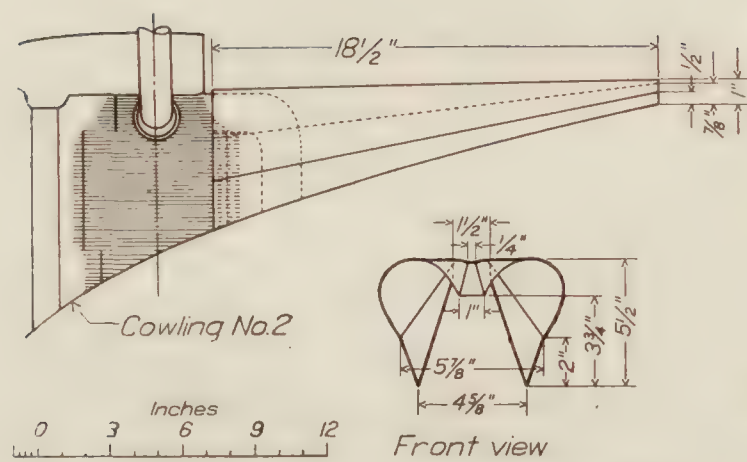


FIG. 7.—Fairing behind cylinder. Cowling No. 2a

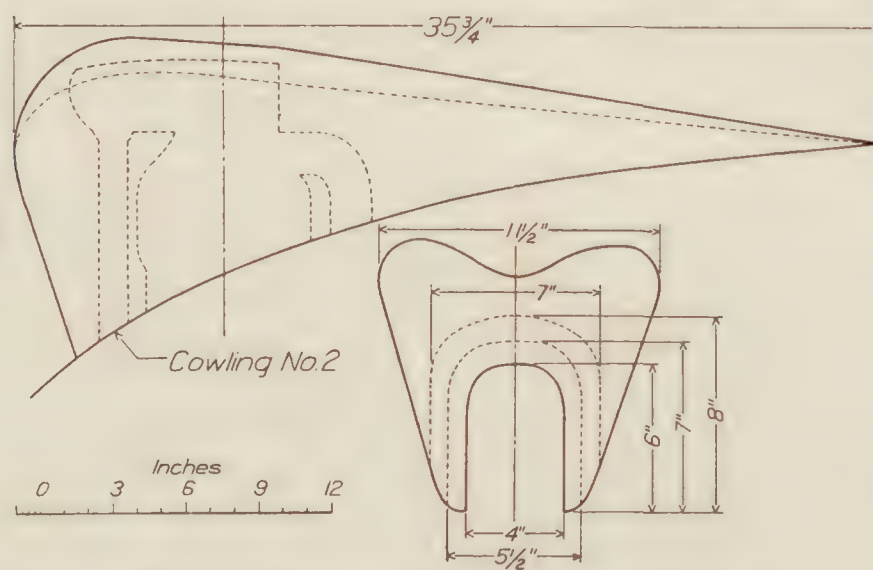


FIG. 8.—Hood over individual cylinders. Cowling No. 2c

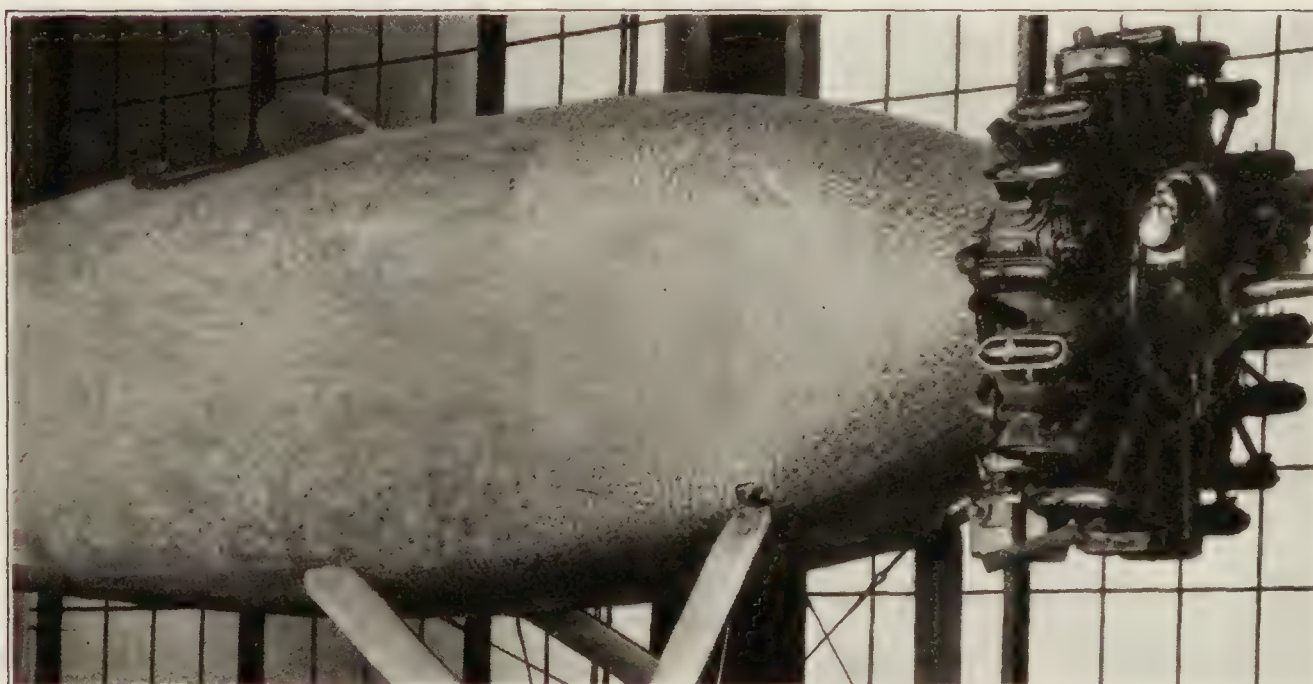


FIG. 9.—Cowling No. 1

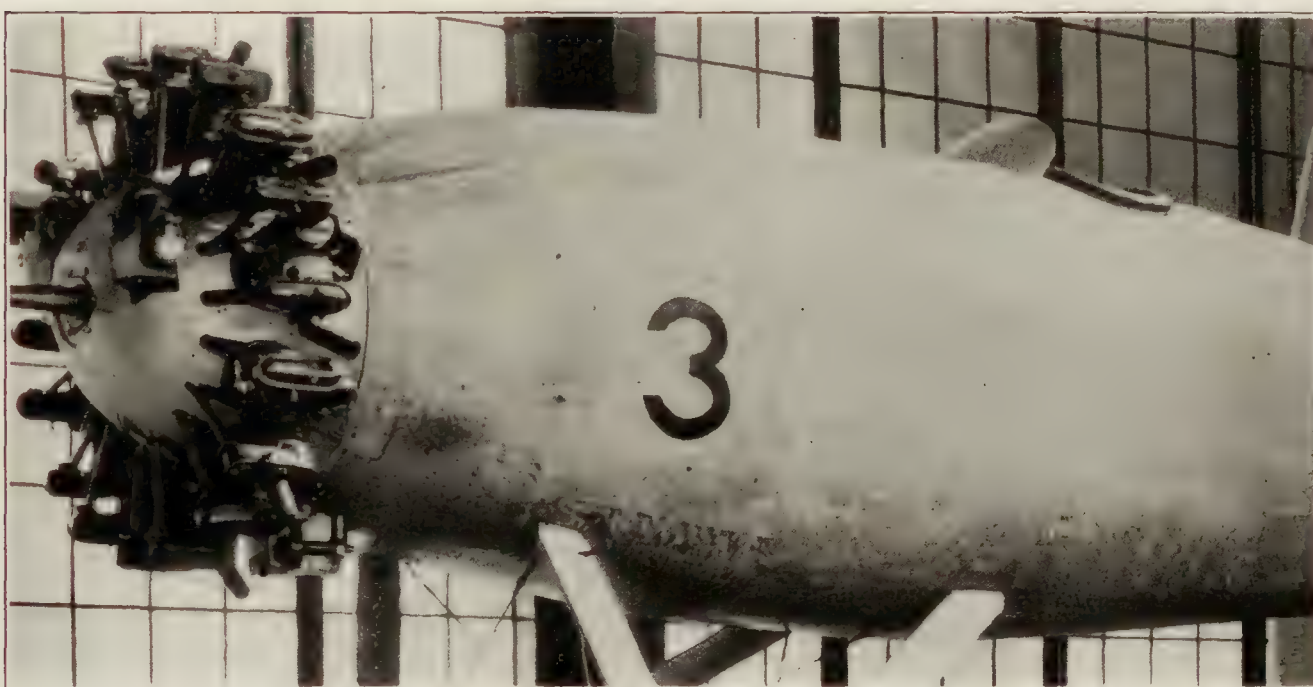


FIG. 10.—Cowling No. 2

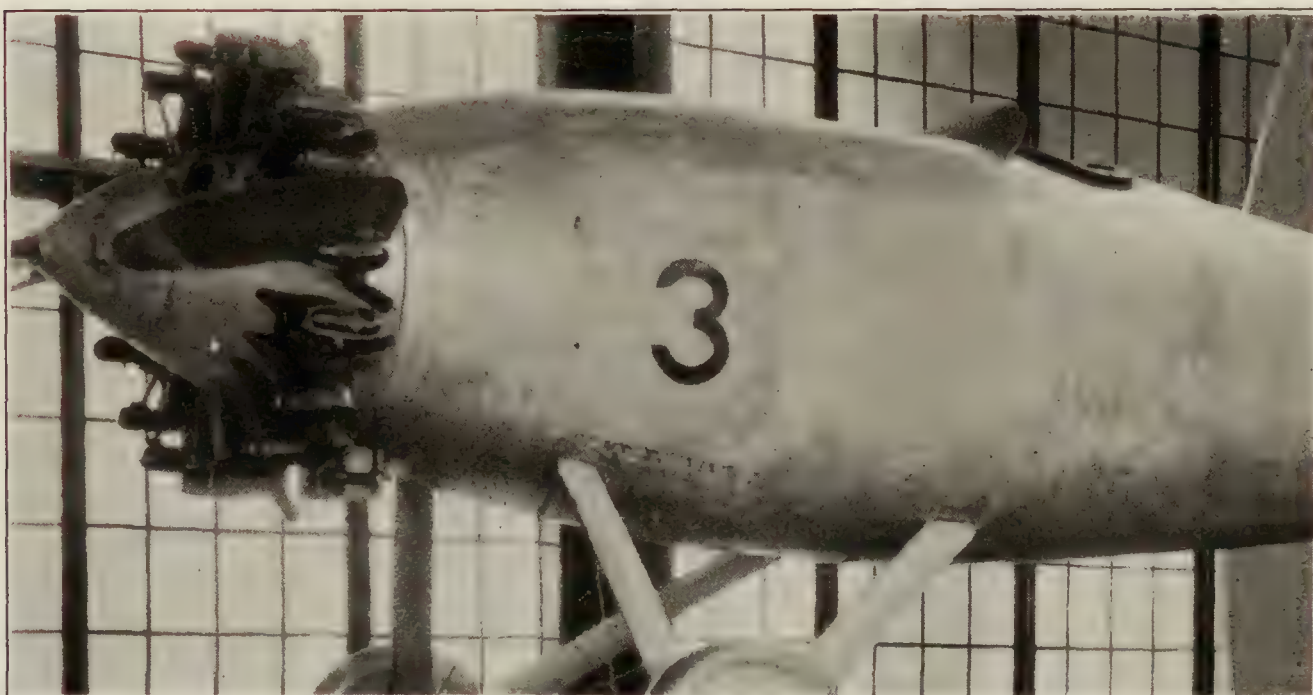


FIG. 11.—Cowling No. 3

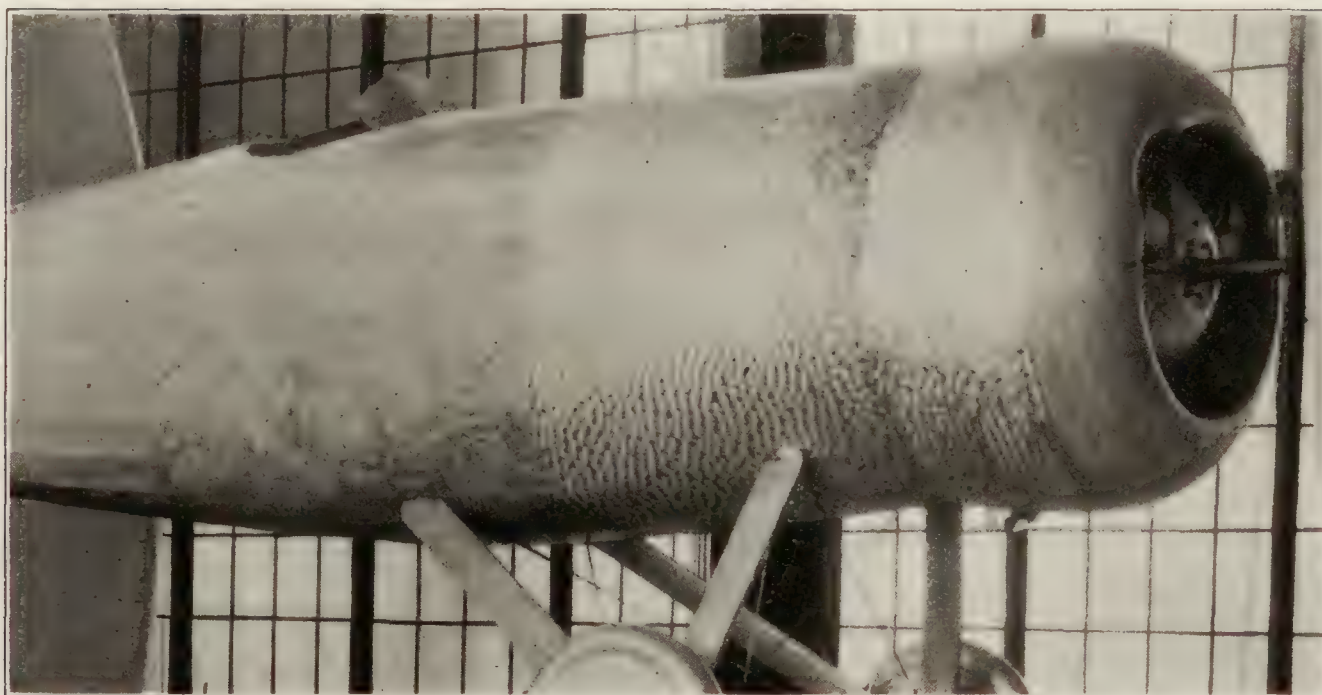


FIG. 12.—Cowling No. 11



FIG. 13.—No. 1, engine removed



FIG. 14.—No. 2, engine removed

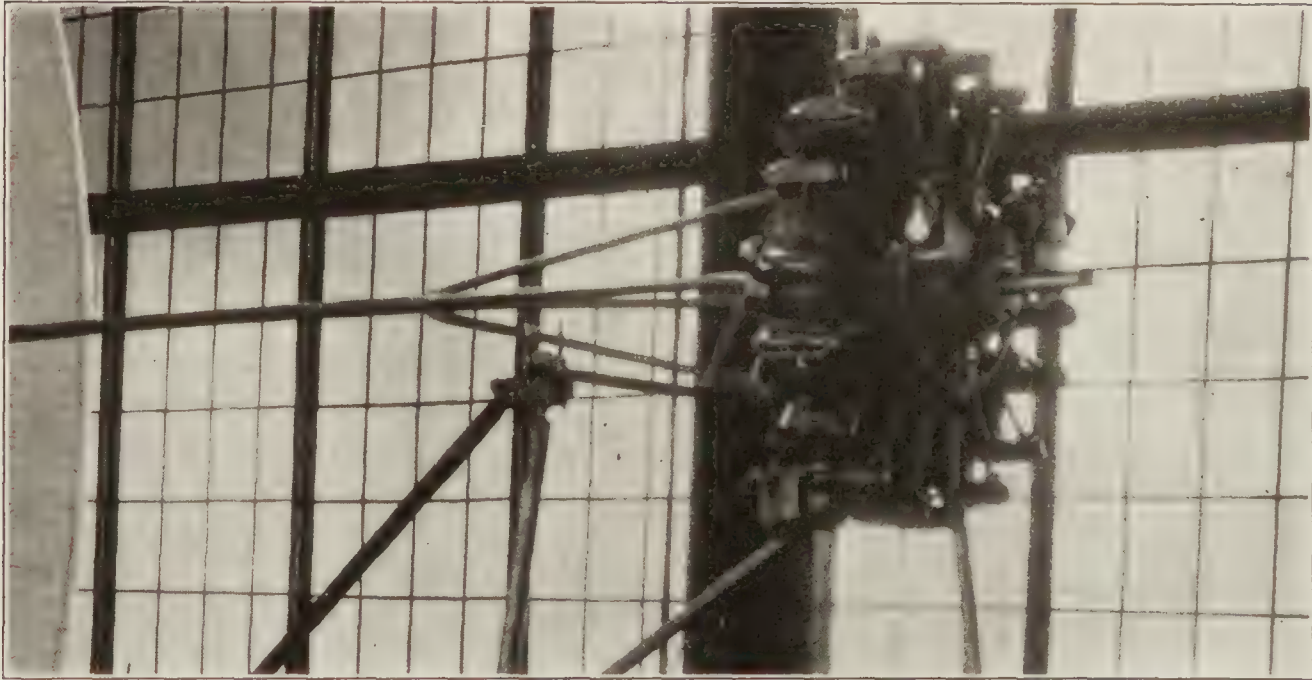


FIG. 15.—No. 12, engine alone

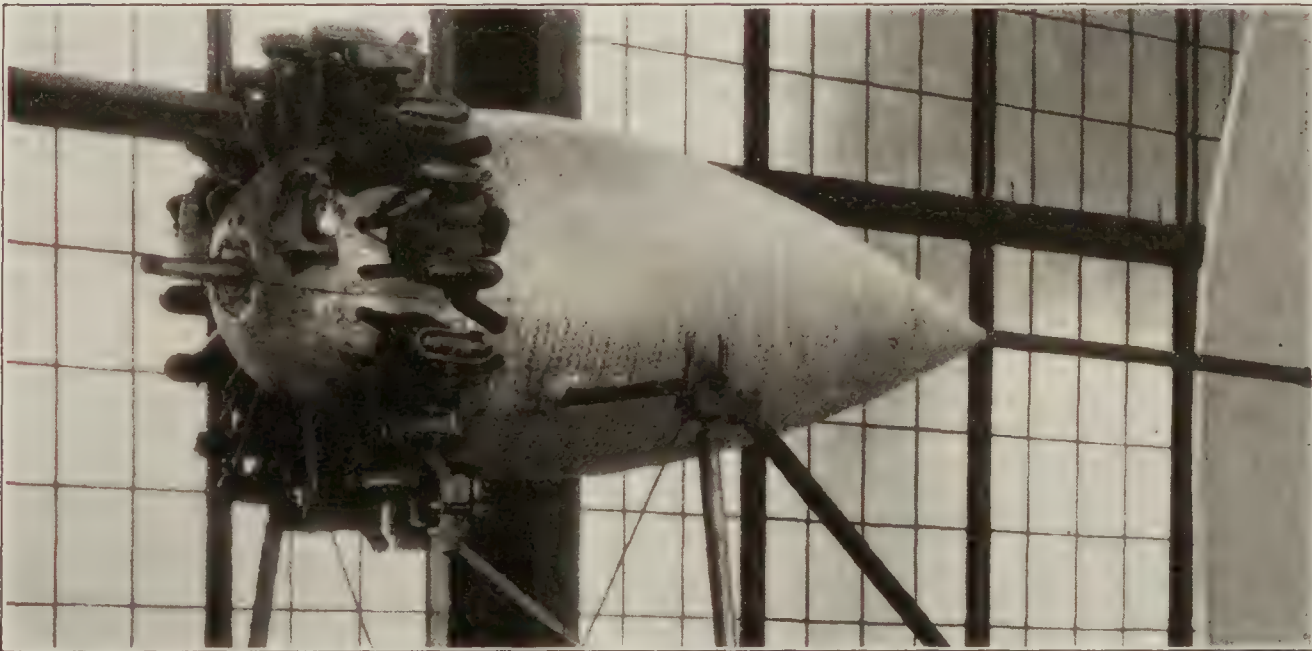


FIG. 16.—No 13 conventional nacelle

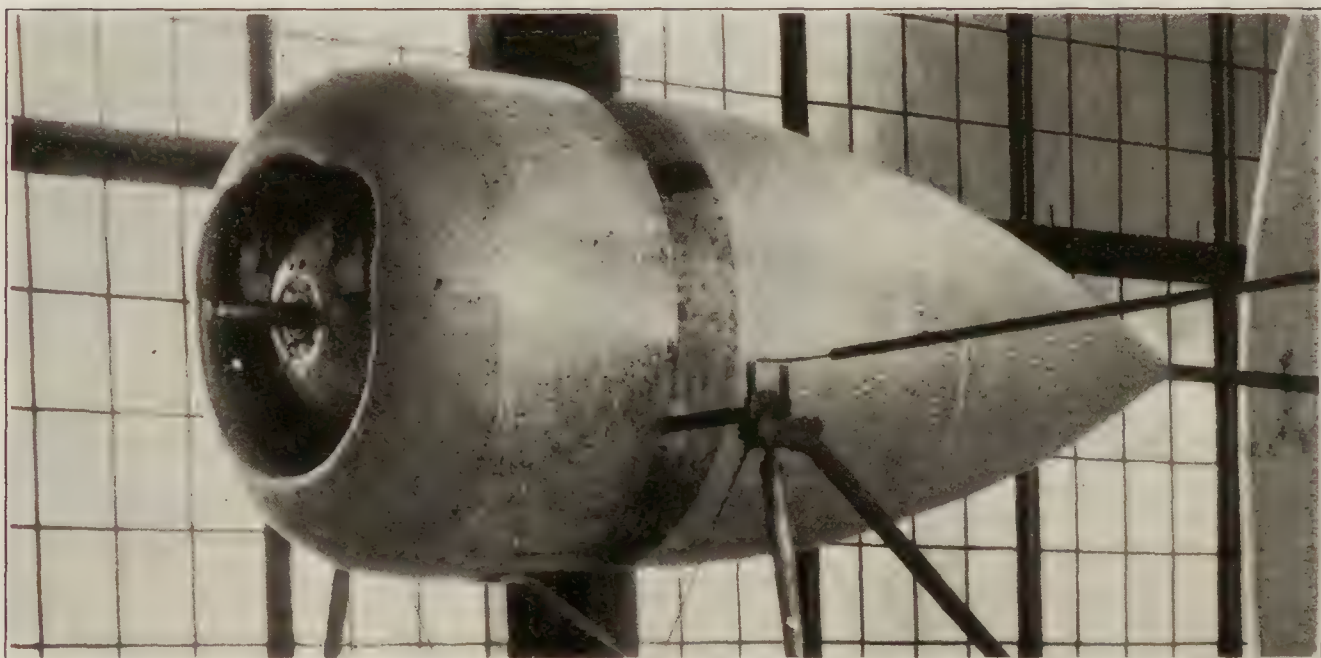


FIG. 17.—No. 14 completely cowled nacelle

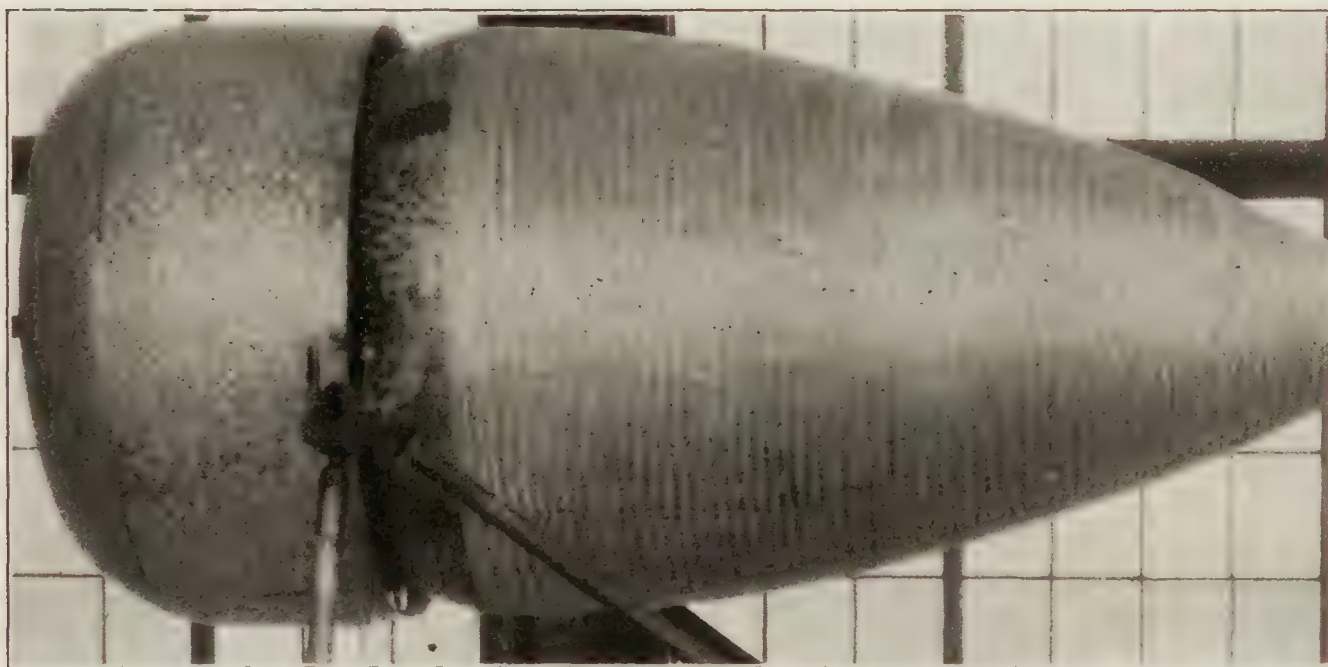


FIG. 18.—No. 14

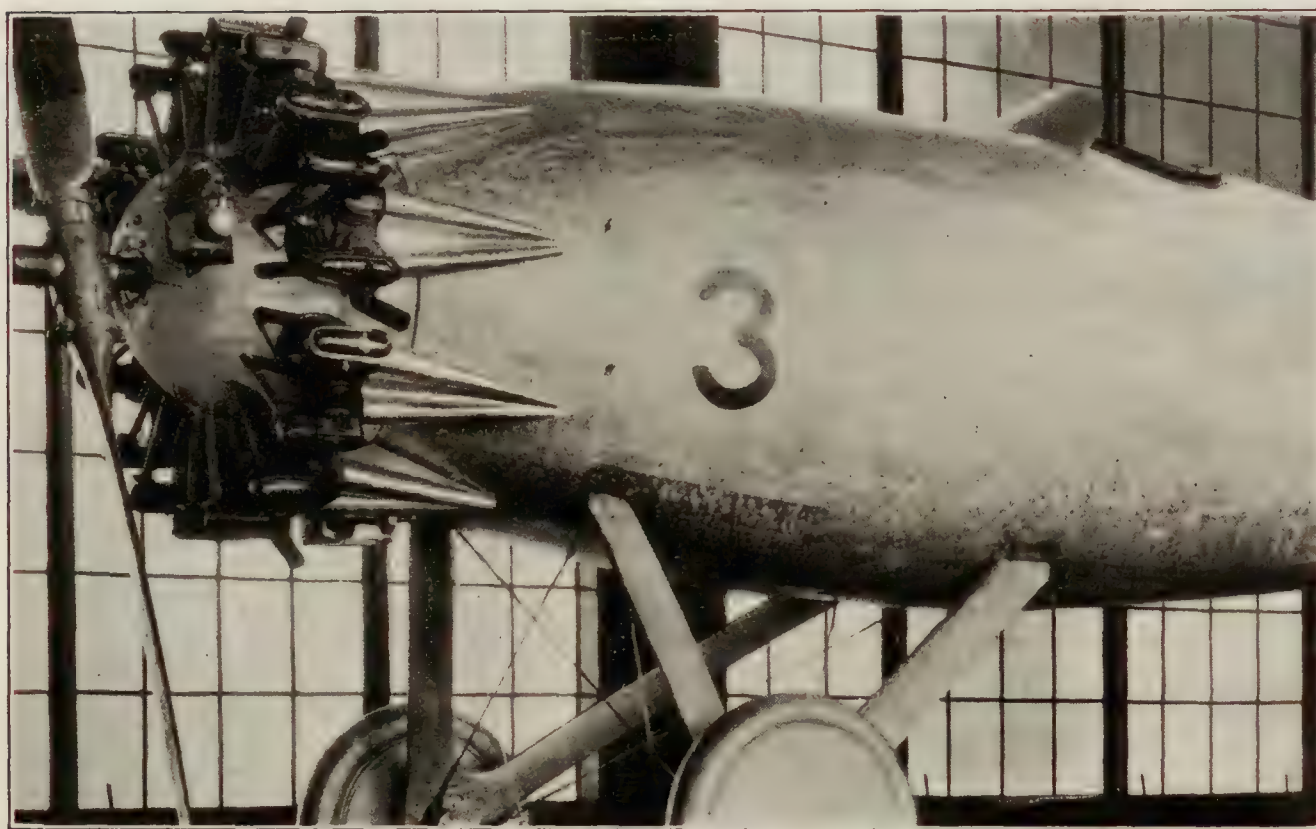


FIG. 19.—Cowling No. 2a fairings behind cylinders

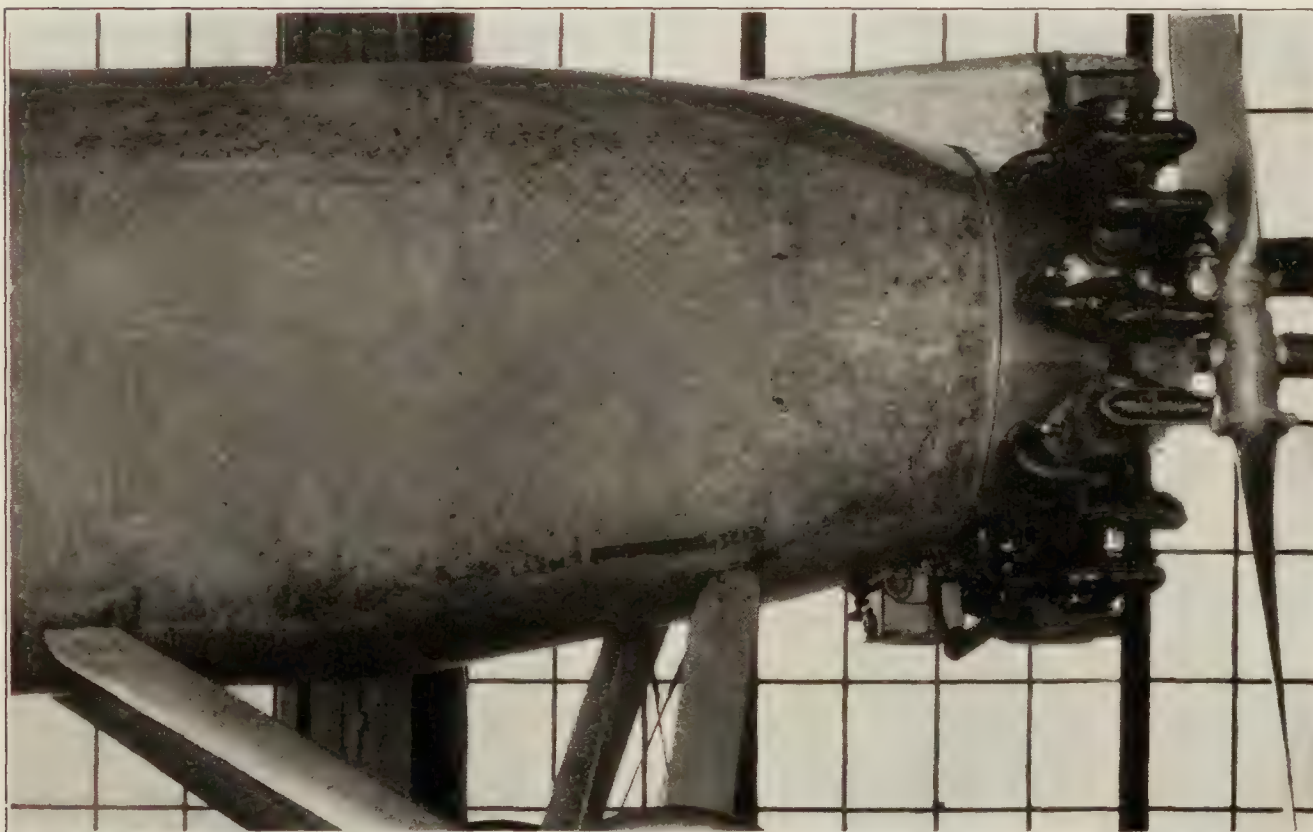


FIG. 20.—Hood over top cylinder for cooling test

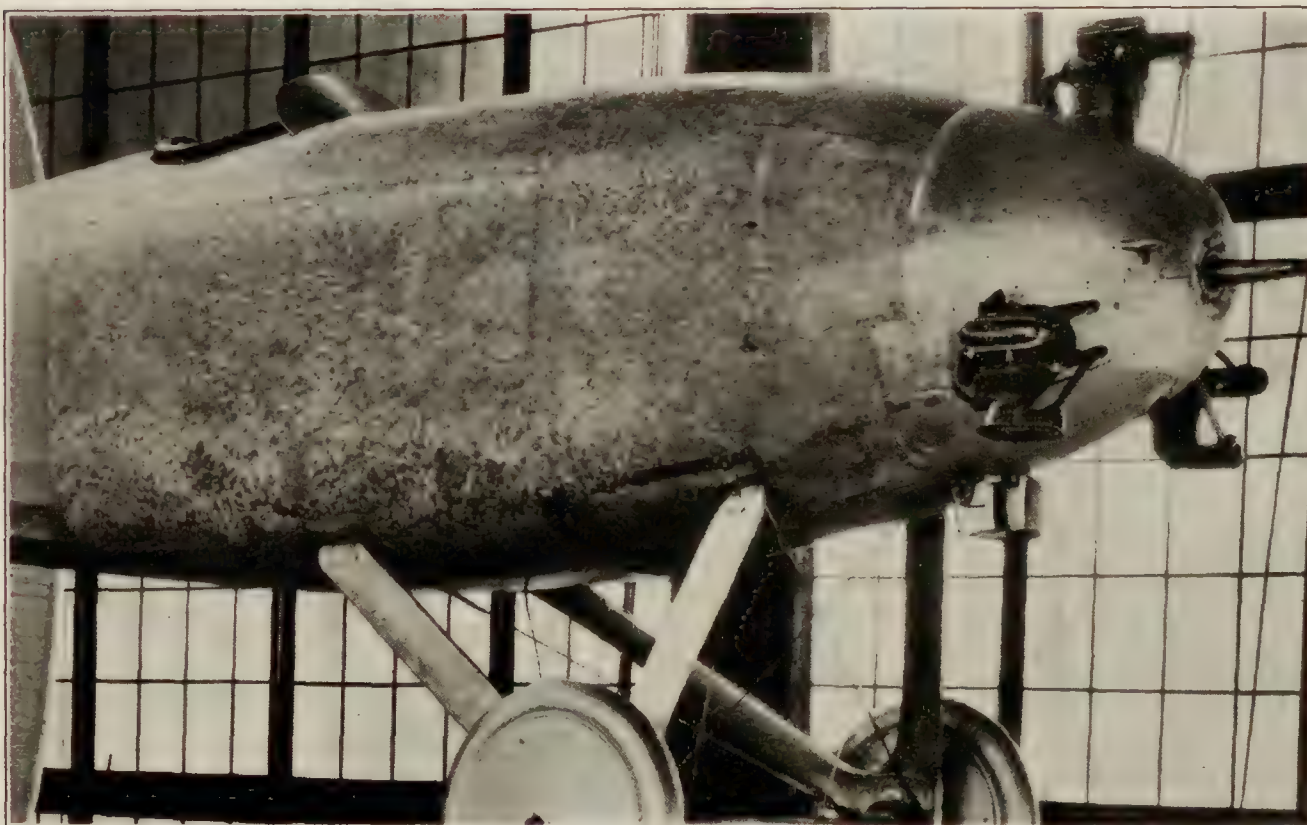


FIG. 21.—Cowling No. 2b, six cylinders removed

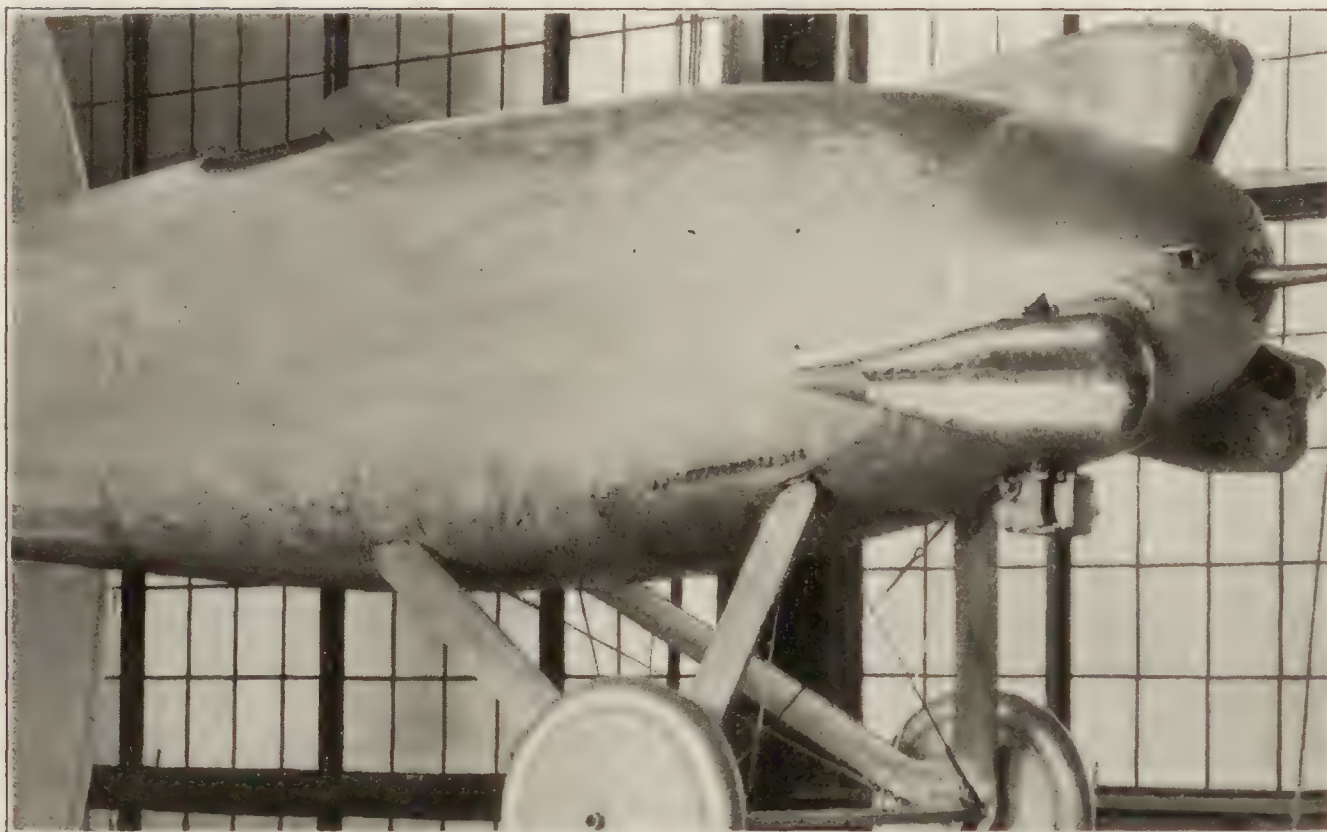


FIG. 22.—Cowling No. 2c, individual hoods with smallest holes

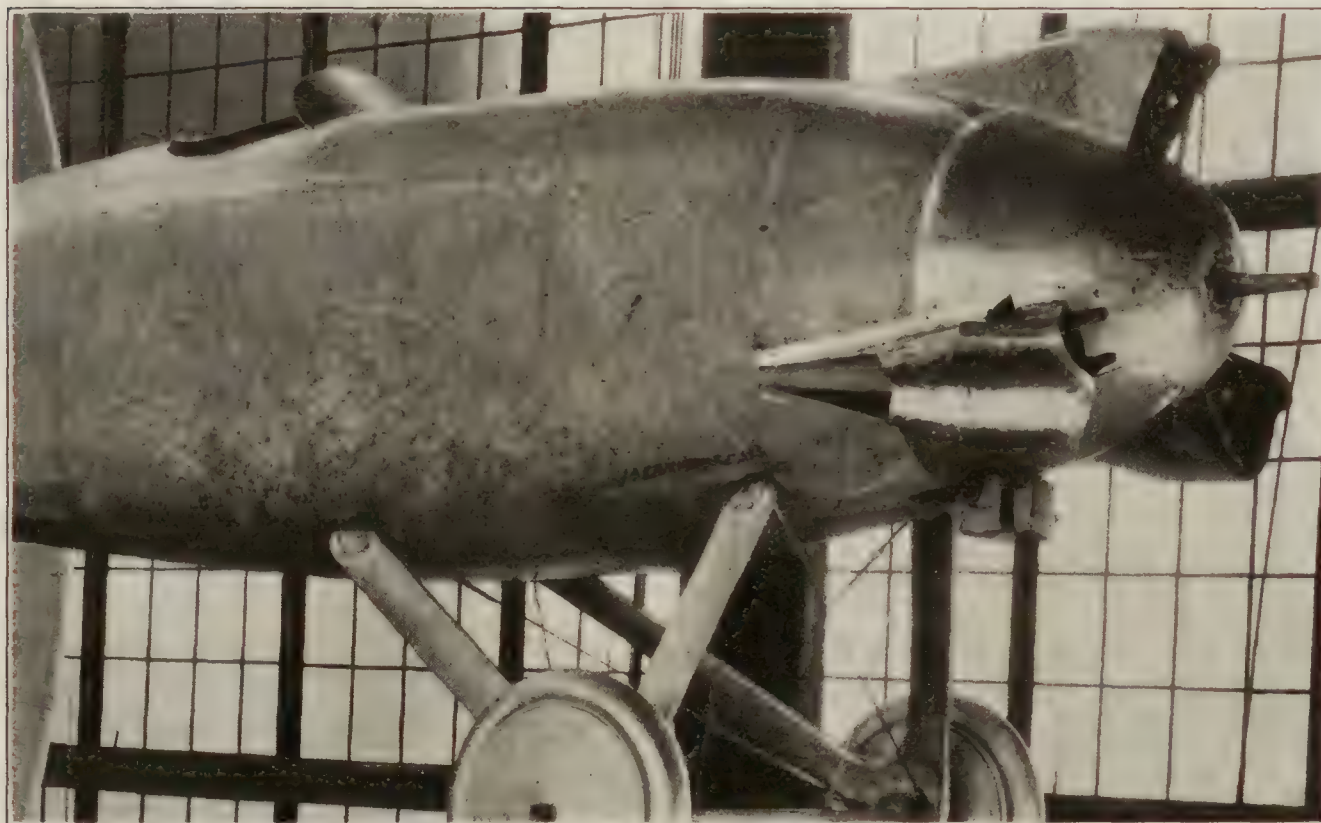


FIG. 23.—No. 2c with front section of hoods removed



FIG. 24.—Cowling No. 5 with round section exhaust collector ring



FIG. 25.—Cowling No. 4 with streamline exhaust ring

in and the bottom was rounded throughout the entire length. Also, the front cockpit was eliminated, giving the fuselage unbroken lines from the engine to the tail, except for the rear cockpit. The forward portion of the fuselage was rebuilt to fair with the various cowlings. A UO-1 type landing gear was used to support the fuselage for the tests, but the landing gear drag is not included in the results.

In the tests with the cabin fuselage the cylinder temperatures were thoroughly investigated by means of 69 thermocouples, 47 of which were on the top of No. 1 cylinder. Since with the open cockpit fuselage each form of cowling was the same back to the engine mount as the corresponding cowling with the cabin fuselage, it was not considered necessary to repeat all of the cooling tests. The 47 thermocouples on No. 1 cylinder were retained, however, for checking the previous tests and for further cooling tests with fairings behind and over the individual cylinders.

The general procedure of testing was the same for the open cockpit as for the cabin fuselage, except for the case of the individual hoods or helmets over each cylinder. It was not practical



FIG. 23.—Cowling No. 2 with individual tapered exhaust stacks

to put individual hoods over each cylinder of the 9-cylinder "Whirlwind" engine, for with the particular design of this engine there is insufficient room between the cylinders. The drag tests with hoods were therefore made with what was in effect a 3-cylinder "Whirlwind" engine, six of the cylinders having been removed and the cowling faired over as shown in Figure 21. With only the three cylinders, it is thought that the aerodynamic interference between them was negligible. It was not possible, of course, to run the engine with six cylinders removed, so the cooling tests were made with the complete engine, but with only one hood, which was placed over the cylinder fitted with thermocouples. (Cylinder No. 1.)

The cowlings tested in the portion of the investigation covered in this report may be outlined as follows:

OPEN COCKPIT FUSELAGE

- No. 1. No cowling over cylinders or crank case. (Figs. 1 and 9.)
- No. 2. Cowling over slightly less than one-half of each cylinder and over crank case. (Figs. 2 and 10.)
- No. 3. Same as No. 2 but with spinner. (Figs. 3 and 11.)
- No. 11. Single cowling completely covering entire engine with internal cowling similar to No. 2 over lower portion of cylinders and crank case. (Figs. 4 and 12.)

NACELLES

- No. 12. Engine alone. No cowling. (Fig. 15.)
No. 13. Conventional cowling, nose same as Nos. 2 and 5. (Figs. 5 and 16.)
No. 14. Complete cowling, nose same as No. 11. (Figs. 6 and 17.)

INDIVIDUAL CYLINDER FAIRINGS

- No. 2a. Same as No. 2 but with individual fairings behind each cylinder. (Figs. 7 and 19.)
No. 2b. Same as No. 2 but with only three cylinders. (Figs. 2 and 21.)
No. 2c. Same as No. 2b but with hoods completely covering the cylinders. (Figs. 8, 22, and 23.)

In the cooling tests the engine was run with wide open throttle at an air speed of 80 M. P. H. until the temperatures became substantially constant, which usually required about 10 minutes. If the cooling with any cowling was not approximately the same as for the uncowed engine, an attempt was made to modify the cowling until it was so.

Drag tests were run with all of the original and modified cowlings; with the open cockpit fuselage with the engine removed and the nose rounded; and with the windshield removed and the cockpit covered. Special tests were also made on the engine drag with various exhaust stacks and on the completely cowed nacelle with the slot covered.

The propulsive efficiency was found with an adjustable pitch metal propeller (fig. 31 of Reference 1) at two pitch settings, with cowling Nos. 1, 2, 3, and 11. This propulsive efficiency includes the increase in drag of all parts of the body affected by the slip stream and also the effect of the body interference on the propeller characteristics.

COOLING TESTS

It was not thought necessary to run cooling tests with cowling Nos. 1, 2, 3, and 11 on the open cockpit fuselage, because the same forms had all been tested on the cabin fuselage and No. 11 had proven satisfactory in flight tests also. (Appendix of Reference 1.) However, check tests were made on the temperatures of cylinder No. 1 with cowling Nos. 2 and 3. The temperatures, which are recorded in Table I, were somewhat higher than in the cabin fuselage tests, probably because the cylinder was developing greater power.

Since the engine cowlings on the nacelles were also the same as the corresponding forms on both fuselages, no cooling tests were necessary and the engine was not run, the drag tests only being made. This simplified the nacelle installations greatly.

With the No. 2 cowling equipped with an individual fairing behind each cylinder (figs. 7 and 19), the cooling, as shown in Table I, was about the same as with the regular No. 2 cowling without the fairings.

With the individual hood, as originally constructed, on cylinder No. 1 (figs. 8 and 22), the temperatures became excessive in less than three minutes of full throttle running at an air speed of 80 M. P. H. The entire front section was then removed (fig. 23) and an equivalent area cut in the rear, after which the temperatures still became somewhat higher than without the hoods, but were not considered excessive. It is no doubt possible that an improved hood could be designed with which the cooling would be considerably better, but the results of the drag tests did not indicate that the effort would be worth while.

RESULTS OF DRAG TESTS

The observed drag test data are given in Table II and the results are plotted in Figures 27, 28, and 29.

Open cockpit fuselage.

The drag of the open cockpit fuselage (without supports or landing gear) with the various cowlings is given for an air speed of 100 M. P. H. in the following table:

Cowling	Fuselage and engine drag, pounds at 100 M. P. H.	Reduction from uncowed engine, pounds at 100 M. P. H.
No. 1. Engine uncowed.....	141	0
No. 2. No spinner.....	136	5
No. 3. Spinner.....	132	9
No. 11. Complete cowling.....	73	68
No. 1. Engine removed and nose rounded.....	42	99
No. 2. Engine removed and cylinder holes closed.....	42	99
No. 1. Engine and windshield removed and cockpit covered.....	28	113

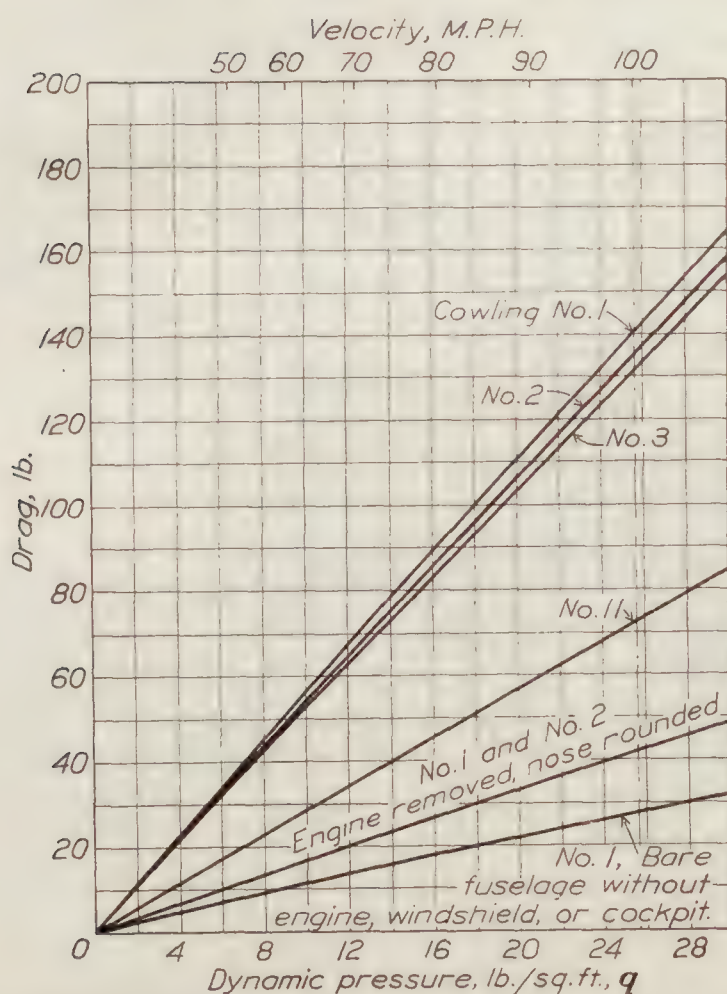


FIG. 27.—Drag of open cockpit fuselage and engine with various cowlings

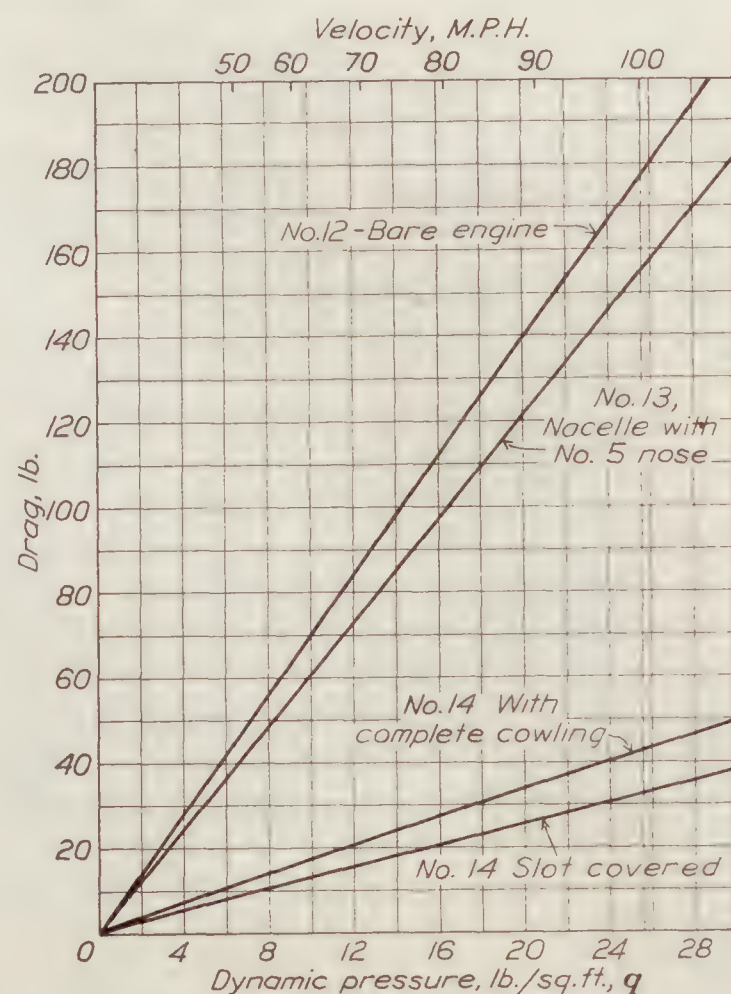


FIG. 28.—Drag of J-5 engine with various nacelles

The last three items have been included in order to show the additional drag due to the engine on this fuselage, and the last item, in which the windshield and cockpit are eliminated as well as the engine, also affords a direct comparison with the nacelles. It is interesting that both No. 1 and No. 2, which had decidedly different nose shapes, had the same drag when the engine was removed. Using either of these as a basis, therefore, the uncowed engine is responsible for an increase in drag of 99 pounds at 100 M. P. H. on the open cockpit fuselage.

As in the case of the cabin fuselage, the outstanding feature of these drag tests is the low drag of the complete cowling, No. 11. The conventional forms of cowling, Nos. 2 and 3, have but a very slight effect on the drag.

The windshield and cockpit are responsible for a drag of 14 pounds at 100 M. P. H., which is 50 per cent of the drag of the bare closed fuselage.

The drag of the fuselage with uncowed engine but without cockpit is about 127 pounds at 100 M. P. H., which is over four and one-half times that of the bare closed fuselage without the engine.

Nacelles.

The drags of the three nacelles at 100 M. P. H. are as follows:

Nacelle	Drag in pounds at 100 M. P. H.	Reduction from uncowed engine, pounds at 100 M. P. H.
No. 12. Engine alone, uncowed.....	178	0
No. 13. Conventional cowling.....	155	23
No. 14. Complete cowling.....	43	135

The nacelles represent the extremes of the features found in the open and cabin fuselage tests. The drag of the bare engine by itself is just over half that of a flat disk having the same outside diameter—45 inches. The conventional nacelle has 23 pounds less drag at 100 M. P. H. than the engine alone, but with the nacelle having the new complete cowling the reduction is 135 pounds. Thus, the drag with the completely cowled nacelle is 112 pounds less at 100 M. P. H. than that with the conventional nacelle.

Individual fairings behind cylinders.

The drag of No. 2a (No. 2 cowling with an individual fairing behind each cylinder, figs. 7 and 19) was found to be 134 pounds at 100 M. P. H., or just 2 pounds less than that of the standard No. 2 cowling without the fairings. It may, therefore, be said that fairings of this type behind cylinders similar in shape to those of the "Whirlwind" J-5 engine, decrease the drag to a practically negligible extent.

Hoods inclosing each cylinder.

As stated previously, due to the small space between the cylinders of the J-5 engine, for the tests with individual hoods six cylinders were removed, leaving in effect a 3-cylinder engine as shown in Figure 21. In the cooling tests the cylinder temperatures became excessive at 80 M. P. H. with the original hood, which had openings in the front and rear of the same area per cylinder as the successful complete cowling, No. 11. It was thought, however, that this type of cowling might have some use on airplanes having a high enough speed to give proper cooling. The drag was, therefore, measured for the hooded 3-cylinder engine with four different sized openings in the front and rear of the hoods, including the original one of 4 by 6 inches, one 5 by 7 inches, one 6 by 8 inches, and one with the entire front section removed. (Figs. 8, 22, and 23.)

In each case the outlet area was made equal to the inlet area. The values of the drag are as follows:

Cowling	Drag in pounds at 100 M. P. H.	Reduction from 3 cylinders on No. 2 nose, pounds at 100 M. P. H.
No. 2b. No. 2 nose with 3 cylinders projecting.....	70	0
No. 2c. Hoods with 4 by 6 inch openings.....	59	11
No. 2c. Hoods with 5 by 6 inch openings.....	62	8
No. 2c. Hoods with 6-by 8 inch openings.....	66	4
No. 2c. Hoods with front section removed.....	82	-12
No. 2. Engine removed and cylinder holes covered.....	42	28

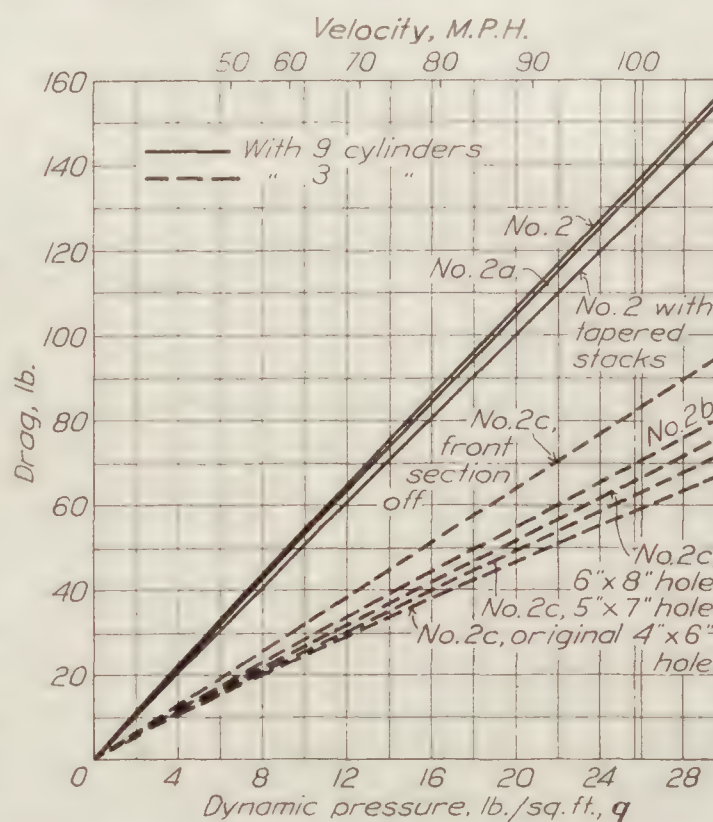


FIG. 20.—Drag of cowling No. 2 with individual fairings and hoods

The three cylinders add 28 pounds, or 9.3 pounds per cylinder, to the drag of the bare No. 2 fuselage, as compared with 94 pounds, or 10.4 pounds per cylinder, for the nine cylinders. Thus, the additional interference with the 9-cylinder engine makes the drag per cylinder 12 per cent higher.

With the hoods having the smallest openings and the lowest drag, the drag is 11 pounds less than with the three exposed cylinders. This represents a saving of only 3.7 pounds per cylinder, whereas the saving over No. 2 with the complete No. 11 cowling is 7 pounds per cylinder. With the larger holes the reduction in drag is even less, and in fact with the largest opening the drag was increased 12 pounds over that for the exposed cylinders. While it is possible that hoods with considerably improved drag and cooling properties could be developed, the results with those tested indicate that, for cylinders having a shape similar to those of the J-5 engine, the effort would not be warranted.

Effect of various exhaust stacks on drag.

In order to make the investigation of the drag of the "Whirlwind" engine complete, the engine was tested with four different types of exhaust stacks as follows (see also Reference 3):

(1) Original individual stacks, $1\frac{3}{4}$ inches in diameter and approximately 5 inches long, projecting outward and somewhat to the rear, as shown in Figure 9. (These stacks were used throughout the cowling tests.)

(2) Round collector ring 36 inches in mean diameter, having a circular cross section 3 inches in diameter, the exhaust from all nine cylinders coming out on the left side. (Fig. 24.)

(3) Stream-line collector ring similar to the above except that it had a stream-line cross section 2 inches wide and 5 inches long with the same cross-sectional area as that of a 3-inch circle. (Fig. 25.)

(4) Individual tapered stacks which projected rearward and allowed the exhaust to escape through a longitudinal slot. (Fig. 26.)

The original short stacks had the greatest drag. The reduction in drag from that with the original stacks is given for the various stacks in the following table:

Type of exhaust stack	Reduction in drag from that with original short stacks, pounds at 100 M. P. H.	
	No cowl- ing over en- gine Nos. 1 or 4	Conven- tional cowling Nos. 2 or 5
Original, short individual stacks-----	0	0
Round section collector ring-----	2	0
Stream-line section collector ring-----	2	2
Individual tapered slotted stacks-----		8

It is notable that there is very little difference in drag with the first three types of stacks, but that an appreciable reduction is obtained with the individual tapered stacks.

RESULTS OF PROPELLER TESTS

Propeller tests were made with cowling Nos. 1, 2, 3, and 11 on the open cockpit fuselage. The engine could not, of course, be run with the cowling having individual hoods, for which six cylinders had been removed, and the power could not have been measured with the nacelles without reconstructing the test fuselage with its special dynamometer. Moreover, it was thought that the effect of the nacelles on the propulsive efficiency would be similar to that of the open cockpit fuselage with the corresponding cowling.

The propulsive efficiencies obtained are shown in Figure 30 for a propeller blade angle setting of 15° at the 42-inch radius, and in Figure 31, for a setting of 23° at the 42-inch radius.

(These angle settings correspond to pitch-diameter ratios of 0.66 and 1.02, the pitch being taken at 75 per cent of the radius. The pitch of this propeller is approximately uniform for all working sections when the pitch-diameter ratio is about 0.5.)

The curves of propulsive efficiency with the conventional cowlings are all very nearly the same, and they are also about the same as the corresponding curves with the cabin fuselage. The propulsive efficiency with the new complete cowling on the open cockpit fuselage, however, is about 2.5 per cent greater than with any of the others.

DISCUSSION

The drag tests afford several interesting comparisons, a few of which will be discussed here.

The drag of the engine alone is 178 pounds at 100 M. P. H., but it caused an increase of only 99 pounds when entirely exposed on the nose of the open cockpit fuselage, and only 85 pounds on the cabin fuselage. Thus, it is evident that the larger the body behind the engine the less is the drag due to the engine. In this connection it should be mentioned that the open cockpit fuselage used in these tests was larger in cross section than the fuselages of most single-

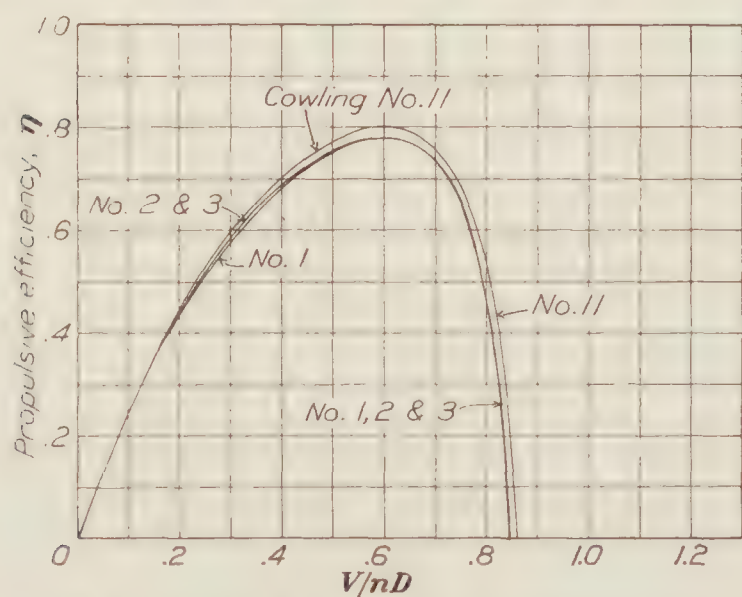


FIG. 30.—Propeller No. 4412 (15° at 42'') on various cowlings with open cockpit fuselage and J-5 engine

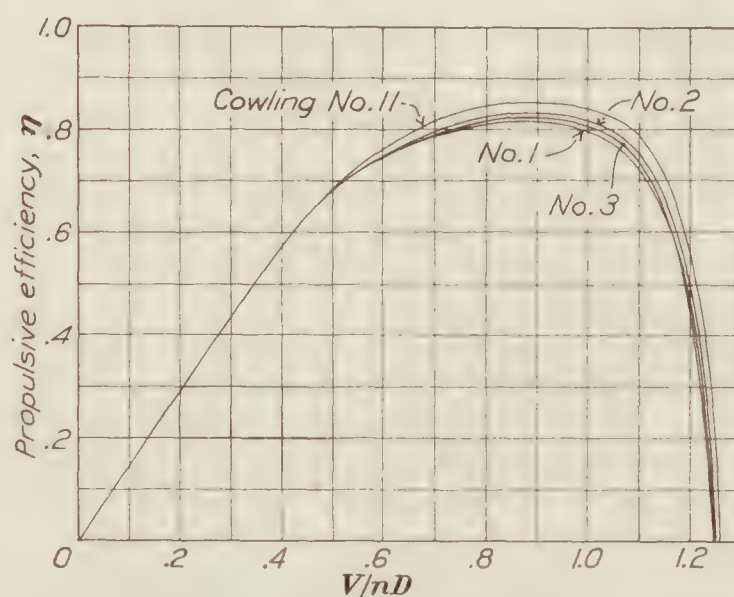


FIG. 31.—Propeller No. 4412 (23° at 42'') on various cowlings with open cockpit fuselage and J-5 engine

place airplanes, and that the drag due to the engine with most airplanes of that type will ordinarily be greater. This effect is so pronounced that even though the drag of the larger body is proportionately greater, the total drag of the body and engine is larger with the smaller body, as shown by the following table:

Body and cowling number	Fuselage and engine drag, pounds at 100 M. P. H.
Cabin fuselage, No. 5.....	119
Open cockpit fuselage, No. 2, cockpit covered.....	122
Nacelle, No. 13.....	155

The drag of the open fuselage without cockpit was obtained by subtracting from the actual drag the 14 pounds found for the windshield and cockpit when the engine was removed and the nose rounded. The windshield would probably have less drag in the turbulent air behind the engine, so that the drag given in the above table for the open fuselage is probably a little low. It should be noted that all of these drag values are for a moderate degree of conventional cowling.

The drags of the three closed bodies with the N. A. C. A. complete cowling are as follows:

Body and cowling number	Drag, pounds at 100 M. P. H.	Reduction from uncowed engine, pounds at 100 M. P. H.	Percentage reduction of drag of uncowed engine
Cabin fuselage, No. 10.....	75	50	59
Open cockpit fuselage, No. 11, cockpit covered.....	59	68	69
Nacelle, No. 14.....	43	135	76

It is seen from this table that the smaller the body behind the engine the larger is the reduction in drag with the complete cowling. In fact, even the percentage reduction of the drag due to the uncowed engine is greater with the smaller bodies.

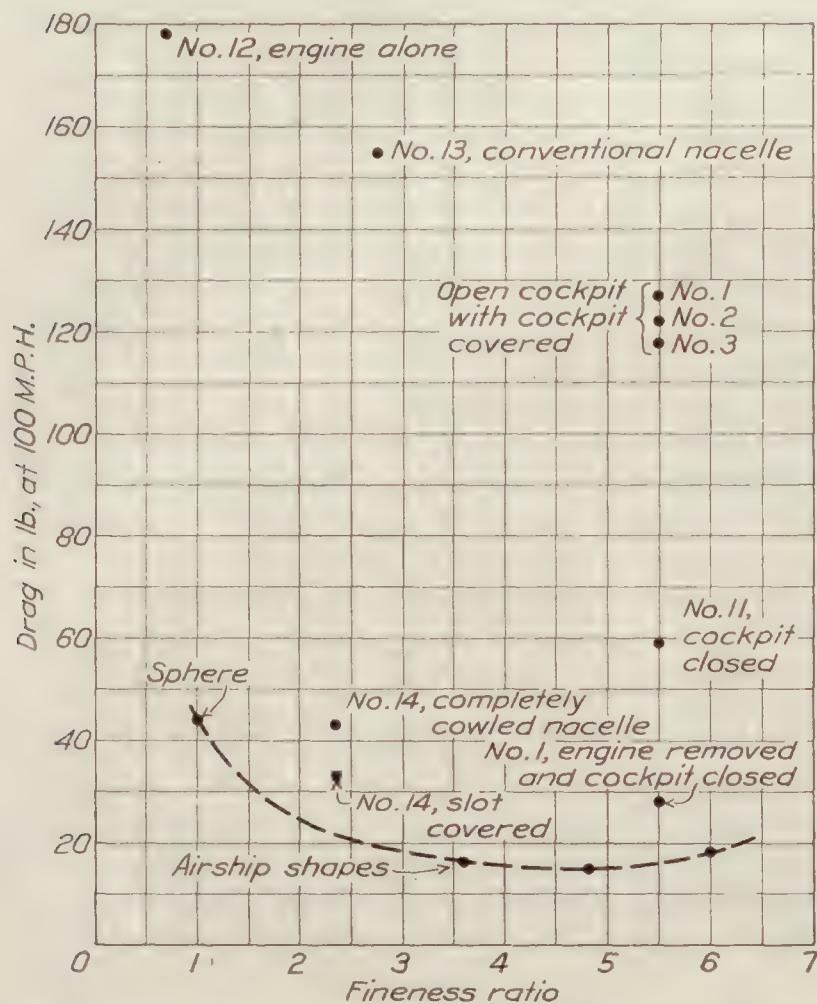


FIG. 32.—The expression "open cockpit with cockpit covered" means that the drag of the cockpit and windshield has been deducted so that the tests are comparable with the nacelle tests

The drag of the open cockpit fuselage with the complete cowling and the cockpit covered, it will be noticed, is 59 pounds, as compared with only 43 pounds for the nacelle with the complete cowling. Since both have the same identical forward portion and the same maximum cross section, the difference seems rather large. It may be partially explained by the fact that the rear half of the open cockpit fuselage was covered with fabric and was not very smooth.

The drags of several streamline airship bodies of various fineness ratios are plotted in Figure 32, the data being obtained from high Reynolds number tests in the variable density wind tunnel. The drag values are all for bodies of the same maximum diameter as the completely cowled nacelle and open fuselage (46 inches), and for an air speed of 100 M. P. H. The drag at any fineness ratio may be considered an ideal with which to compare the drag of a fuselage or nacelle of the same fineness ratio, and with this in view, the drags for the various nacelles and open fuselages with cockpit covered have also been plotted on Figure 32.

The drag of the completely cowled nacelle is only about 22 pounds greater than that of a good airship shape having the same maximum diameter and fineness ratio. The further possible improvement is therefore slight compared with the 112 pounds improvement over a good conventional nacelle, especially considering the fact that the engine must be cooled. The 22 pounds may be looked upon as the cost of cooling the engine with the present completely cowled nacelle. Based on the difference in drag between the completely cowled fuselages and the fuselages without the engine, the cost in drag to cool the engine with the open cockpit fuselage is 31 pounds, and that with the cabin fuselage is 35 pounds all at an air speed of 100 M. P. H.

Effect of slot.

When the slot was originally designed for the complete cowling it was hoped that it would tend to reduce the drag because of its effect on the boundary layer. A test made on the nacelle with the slot covered, however, showed that the drag is 10 pounds less at 100 M. P. H. without the slot. The nacelle with the slot covered had only about 60 per cent more drag than the airship body, which seems remarkably low considering the blunt nose with the open pocket in the center.

During one of the drag runs with the completely cowled nacelle with the slot open, a rough survey was made of the air flow coming out of the slot and also of that just outside the slot. It was found that the velocity of the air coming out was fairly constant across the slot and had a value of 9 per cent lower than the velocity of the tunnel air stream. Outside the body but close to it, the velocity of the air was also constant for a distance of several inches and had a value of 11 per cent greater than the tunnel velocity. The velocity of the air immediately outside of the slot was, therefore, 22 per cent higher than that coming out of the slot, and the change from the low to the high velocity took place within one-half an inch or less. The boundary layer of the outside air at the slot is apparently small on a body of this form, and no great reduction in drag could be expected from the slot, even if it were of the best possible proportions. It is likely that the cooling air could be collected after it had passed the cylinders, and directed out to the outside flow through one or two openings, say at the bottom or both sides, with no increase in drag over that with the annular slot. The annular slot is, however, a very convenient means for getting the used cooling air back to the general outside flow.

Check between wind tunnel and flight tests.

The appendix to the report on the first part of this investigation (Reference 1) describes flight tests on a Curtiss AT-5A airplane with the N. A. C. A. complete cowl. The original cowl was similar to No. 1, with the engine entirely exposed, but the fuselage was smaller in cross section than that of No. 1. The airplane had a 200 HP. Wright "Whirlwind" J-5 engine similar to the one used for the cowl tests in the 20-foot wind tunnel.

The maximum sea-level speed of this airplane was increased from 118 M. P. H. with the original cowl to 137 M. P. H. with the complete cowl, an increase of 19 M. P. H.

It is interesting to compute from the flight tests the difference in drag required to cause this increase in speed, and to compare this with the results of the wind-tunnel tests. Part of the increase in speed is due to the lower induced drag at the higher speed, and part is due to higher propulsive efficiency. According to full scale wind-tunnel tests on the identical propeller used in the flight tests, the propulsive efficiency would be 2.8 per cent greater at 137 M. P. H. than at 118 due to the higher pitch, and as shown by the tests in this report, a further increase of 2.5 per cent would be obtained due to the complete cowl. The propulsive efficiencies (including body interference and slip-stream effect) are given below along with calculations of the drag with each cowl:

	AT-5A with original cowl	AT-5A with complete cowl
Maximum speed, M. P. H.	118	137
Horsepower (approximate)	200	200
Propulsive efficiency	0.760	0.801
Thrust horsepower	152	160.2
$\text{Drag} = \frac{T \text{ HP.} \times 550}{\text{Velocity in feet per second}}$	1 484	1 439
Drag at same angle of attack at 100 M. P. H.	1 348	1 234
$C_L = \frac{L}{qS} = \frac{2471}{q \times 250}$	0.2780	0.2058
$C_{Di} = \frac{C_L^2 S}{\pi b^2} = \frac{C_L^2 \times 250}{\pi \times 33.4^2}$	0.00551	0.00302

¹ Pounds.

The difference in induced drag due to the two different angles of attack, when reduced to a speed of 100 M. P. H., becomes

$$\Delta C_{Di} q S = (0.00551 - 0.00302) \times 25.57 \times 250 = 16 \text{ pounds.}$$

There are other differences in drag due to the fact that the complete cowl covered certain fittings and a portion of the landing gear struts, which were exposed with the original cowl, but in a comparison of the AT-5A results with the wind-tunnel results these differences approximately balance the difference between the tapered exhaust stacks used on the AT-5A and the cylindrical stacks used in the wind-tunnel tests.

The reduction in drag at 100 M. P. H. due to the complete cowling is then
 $(348 - 234) - 16 = 98$ pounds.

In Figure 33 the corresponding reduction in drag at 100 M. P. H. is plotted for three of the wind-tunnel tests, on the basis of the cross-sectional area of the bodies behind the exposed engine.

The point calculated from the flight tests, it will be noticed, falls on the curve through the wind-tunnel points. The fact that the flight-test point falls exactly on the curve is merely fortuitous, for the calculated drag reduction can not be expected to be more than approximately correct. Within the limitations of the calculations, however, the agreement between the flight and wind tunnel tests is excellent, and the increase in maximum speed of 19 M. P. H. is substantiated by the results of the wind-tunnel tests.

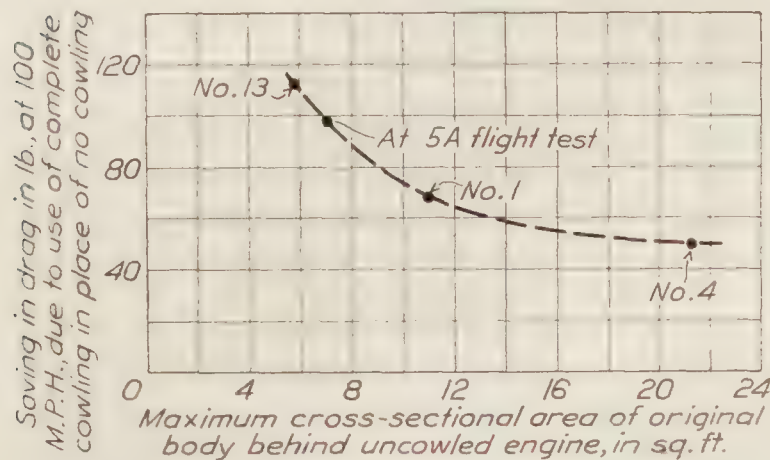


FIG. 33.—Comparison of flight and wind tunnel tests

CONCLUSIONS

1. The results and conclusions given in the report covering the first part of this investigation including the tests with a cabin fuselage (Reference 1) are substantiated.
2. Individual fairings behind cylinders having a form similar to those of the J-5 engine have no appreciable effect on the drag.
3. Individual hoods over each cylinder result in but a slight reduction in drag when used on cylinders similar in shape to those of the J-5 engine.
4. The only large reductions in drag were obtained with the new complete cowling on Nos. 11 and 14. The reduction in drag with the complete cowling on the nacelle was remarkable, being more than twice as great as that found with the cabin fuselage, and being 76 per cent of the drag of the totally exposed engine alone.
5. The reduction in drag obtained with the complete cowling is greater for the smaller original bodies behind the exposed or partially exposed engine.
6. The reduction of drag as computed from flight tests with the complete cowling on an AT-5A airplane is in excellent agreement with that found by the wind-tunnel tests.

LANGLEY MEMORIAL AERONAUTICAL LABORATORY,
 NATIONAL ADVISORY COMMITTEE FOR AERONAUTICS,
 December 17, 1928.

REFERENCES

1. Weick, Fred E.: Drag and Cooling with Various Forms of Cowling for a "Whirlwind" Engine in a Cabin Fuselage. N. A. C. A. Technical Note No. 301 (1928), later published as "Drag and Cooling with Various Forms of Cowling for a 'Whirlwind' Radial Air-cooled Engine-I." N. A. C. A. Technical Report No. 313. (1929.)
2. Weick, Fred E. and Wood, Donald H.: The Twenty-foot Propeller Research Tunnel of the National Advisory Committee for Aeronautics. N. A. C. A. Technical Report No. 300. (1928.)
3. Weick, Fred E.: The Drag of a J-5 Radial Air-cooled Engine. N. A. C. A. Technical Note No. 292. (1928.)

REPORT No. 315

AERODYNAMIC CHARACTERISTICS OF AIRFOILS—VI

CONTINUATION OF REPORTS Nos. 93, 124, 182, 244, and 286

By

**NATIONAL ADVISORY COMMITTEE
FOR AERONAUTICS**

TABLE OF CONTENTS

	Page
Introduction.....	213
Transformation constants.....	213
Chart index.....	215
Index of abbreviations.....	215
Group index.....	216
Alphabetical index.....	217
Airfoil sections.....	218-242
United States sections.....	218-220
German sections.....	220-227
French sections.....	227-232
Belgium sections.....	233-235
Italian sections.....	235-242
Charts Nos. 21, 22, 23, 24.....	243-246

REPORT No. 315

AERODYNAMIC CHARACTERISTICS OF AIRFOILS—VI

CONTINUATION OF REPORTS NOS. 93, 124, 182, 244, AND 286

By NATIONAL ADVISORY COMMITTEE FOR AERONAUTICS

INTRODUCTION

This collection of data on airfoils has been made from the published reports of a number of the leading aerodynamic laboratories of this country and Europe.¹ The information which was originally expressed according to the different customs of the several laboratories is here presented in a uniform series of charts and tables suitable for the use of designing engineers and for purposes of general reference.

It is a well-known fact that the results obtained in different laboratories, because of their individual methods of testing, are not strictly comparable even if proper scale corrections for size of model and speed of test are supplied. It is, therefore, unwise to compare too closely the coefficients of two wing sections tested in different laboratories. Tests of different wing sections from the same source, however, may be relied on to give true relative values.

The absolute system of coefficients has been used, since it is thought by the National Advisory Committee for Aeronautics that this system is the one most suited for international use and yet it is one from which a desired transformation can be easily made. For this purpose a set of transformation constants is given.

Each airfoil section is given a reference number, and the test data are presented in the form of curves from which the coefficients can be read with sufficient accuracy for designing purposes. The dimensions of the profile of each section are given at various stations along the chord in per cent of the chord length, the latter also serving as the datum line. The shape of the section is also shown with reasonable accuracy in order to enable one to more clearly visualize the section under consideration, the outside of the heavy line representing the profile.

The authority for the results here presented is given as the name of the laboratory at which the experiments were conducted, as explained under abbreviations, with the size of model, wind velocity, and year of test.

TRANSFORMATION CONSTANTS

For the convenience of those who prefer to use a system of units other than the absolute system, there is given below a table of transformation constants based on the standard condition adopted by the National Advisory Committee for Aeronautics of—

Temperature	= 15° C	= 59° F.
Pressure	= 760 mm Hg	= 29.92 in. Hg.
Humidity	= 0	
Gravity	= 9.80665 m/s ²	= 32.1740 ft./sec. ²

thus giving values of specific weight of air

$$W = 1.2255 \text{ kg/m}^3 = 0.07651 \text{ lb./cu. ft.}$$

¹ A previous collection of airfoil sections numbered 1 to 759 and Charts 1 to 20 may be found in N. A. C. A. Reports Nos. 93, 124, 182, 244, and 286.

and of density

$\rho = 0.12497 \text{ kg-m}^{-3}$ in the French engineering or kilogram, meter, second system.

Or

$\rho = 0.002378 \text{ lb.-ft.}^{-3}$ in the English or pound, foot, second system.

In absolute units	$P = CV^2 \rho / 2$
In kg/m^2 (m/s)	$P = .0625 CV^2$
In kg/m^2 (km/h)	$P = .004822 CV^2$
In lb./sq. ft. (ft./sec.)	$P = .001189 CV^2$
In lb./sq. ft. (mi./hr.)	$P = .002558 CV^2$

(Note that these constants are half as large as those used in Reports Nos. 93 and 124 and that the absolute coefficients used in this report are twice as large as the old coefficients. See Report No. 240 regarding change in absolute coefficients.)

INDEX

Four separate types of indexes are given—chart indexes which make it possible for a designer to select the wing section most suitable for the particular design in which he is interested; a group index which is arranged by countries and laboratories at which tests were conducted, each section also being designated by a reference number; an index of abbreviations, used on the characteristic sheets, to indicate the laboratories at which the tests were made; and an alphabetical index.

CHART INDEX

In order that the designer may easily pick out a wing section which is suited to the type of airplane on which he is working, four index charts are given which classify the wings according to their aerodynamic and structural properties. In the charts of this report a lower-case letter is placed adjacent to the reference number giving VL values, so that a comparison can be made without referring to the individual drawings. In this value V represents the wind velocity in feet per second and l a linear dimension, the chord length in feet.

In chart No. 21 the minimum drag C_D , is plotted against the L/D at one-fourth the maximum lift C_L . This chart should be used in choosing a wing section for a high-speed airplane, the wing sections being more suited for this use the farther they are from the lower left-hand corner.

In chart No. 22 the mean spar depth is plotted against the maximum lift C_L , in order to show the possible strength and lightness of the wing structure. The higher the maximum lift coefficient is, the smaller will be the wing area and the lighter the structural weight, and in the same way the greater the depth of the spars the lighter will be their weight, so that the sections the greatest distance from the lower left-hand corner will give the lightest and strongest wings. The "mean spar depth" is obtained by assuming the spars to be located, respectively, at 15 and 60 per cent of the chord, and by dividing the sum of their thicknesses, in per cent of chord length at these points, by 2.

In chart No. 23 the maximum L/D is plotted against the maximum lift C_L , which is of use in choosing the wing section for a slow and efficient airplane. In the same way as before the sections farthest from the lower left-hand corner are the best for this purpose.

In chart No. 24 the L/D at two-thirds the maximum lift C_L , is plotted against the maximum lift C_L . This chart can be used for choosing a section that will give an efficient climb or a long range at cruising speed. The best sections for this purpose will be farthest from the lower left-hand corner of the chart.

CHART INDEX

	Page
Chart No. 21. Minimum drag C_D , plotted against L/D at one-fourth the maximum lift C_L -----	243
Chart No. 22. Mean spar depth plotted against the maximum lift C_L -----	244
Chart No. 23. Maximum L/D plotted against maximum lift C_L -----	245
Chart No. 24. L/D at two-thirds the maximum lift C_L , plotted against the maximum lift C_L -----	246

INDEX OF ABBREVIATIONS

Name of laboratory at which tests were made	Abbreviations used on figures
Langley Memorial Aeronautical Laboratory of the National Advisory Committee for Aeronautics, U. S. A.	L. M. A. L.
Washington Navy Yard, U. S. A.-----	W. N. Y.
Engineering Division, McCook Field, U. S. A.-----	McC. F.
Ergebnisse der Aerodynamischen Versuchsanstalt zu Göttingen, Germany-----	Göttingen.
Service Technique de l'Aéronautique, France-----	S. T. Aé.
Laboratoire Aerotechnique de Rhode St. Genese-Bruxelles, Belgium-----	Rhode St. Genese.
Istituto Sperimentale Aeronautico, Italy-----	I. S. A.

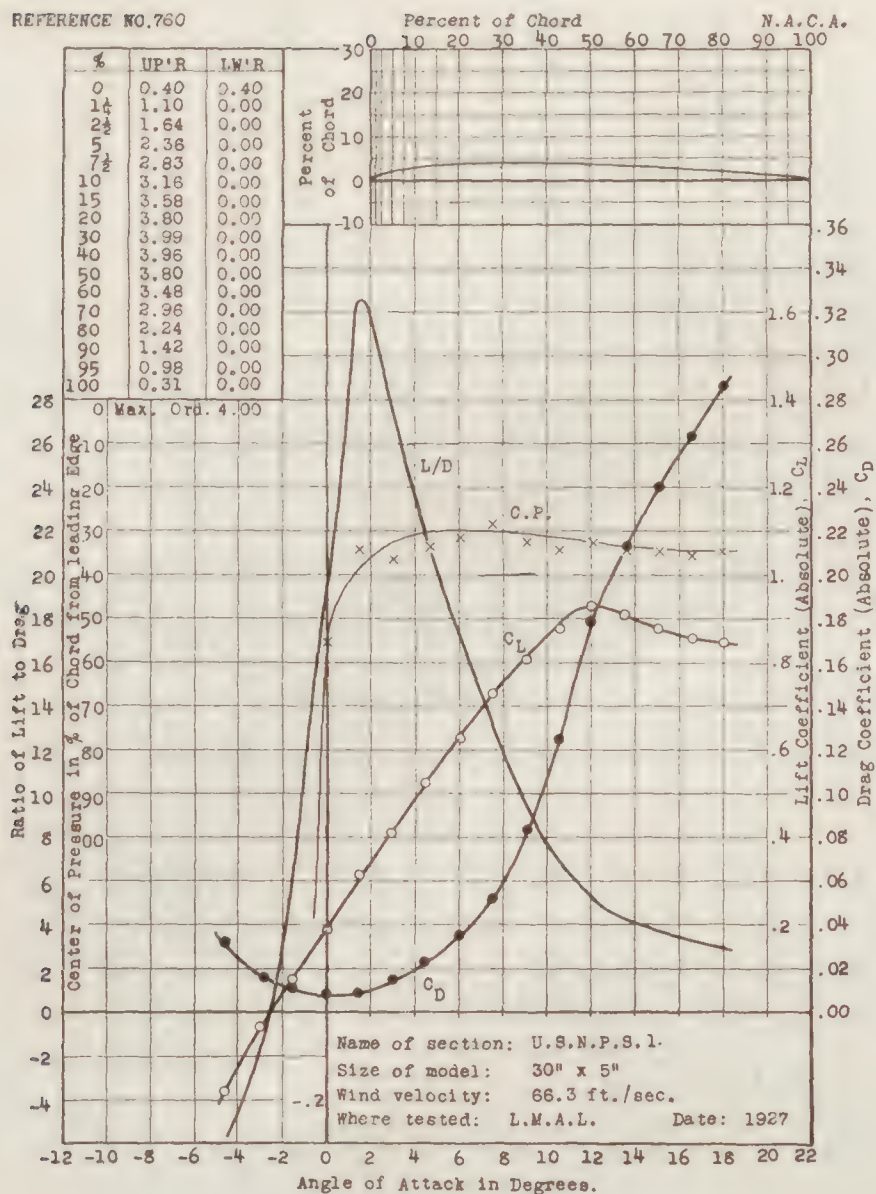
GROUP INDEX

Airfoil	Wind tunnel where tested	Report reference number	Airfoil	Wind tunnel where tested	Report reference number
UNITED STATES			FRANCE—continued		
U. S. N. P. S. 1	L. M. A. L.	760	St. Cyr 162 (Royer)	S. T. Aé. Lab.	810
U. S. N. P. S. 2	do	761	St. Cyr 170 (Royer)	do	811
U. S. N. P. S. 3	do	762	St. Cyr 174 (Royer)	do	812
U. S. N. P. S. 4	do	763	St. Cyr 233 (Bartel 37-Ib)	do	813
U. S. N. P. S. 5	do	764	St. Cyr 235 (Bartel 37-Ic)	do	814
U. S. N. P. S. 6	do	765	St. Cyr 237 (Bartel 15-Ic)	do	815
Martin M-I	W. N. Y.	766	St. Cyr 239 (Bartel 37-IIa)	do	816
Martin M-II	do	767	St. Cyr 240 (Bartel 37-IIb)	do	817
Martin M-III	do	768	St. Cyr 242 (Bartel 57-IIc)	do	818
R-3 (Root section)	McC. F.	769	St. Cyr 243 (Bartel 37-IIc)	do	819
U. S. A. 45M	do	770			
GERMANY			BELGIUM		
Göttingen 359	Göttingen	771	Rhode St. Genese 1	Rhode St. Genese	820
Göttingen 361	do	772	Rhode St. Genese 2	do	821
Göttingen 362	do	773	Rhode St. Genese 16	do	822
Göttingen 368	do	774	Rhode St. Genese 17	do	823
Göttingen 369	do	775	Rhode St. Genese 19	do	824
Göttingen 371	do	776	Rhode St. Genese 26	do	825
Göttingen 372	do	777	Rhode St. Genese 29	do	826
Göttingen 373	do	778	Rhode St. Genese 31	do	827
Göttingen 374	do	779	Rhode St. Genese 33	do	828
Göttingen 375	do	780	Rhode St. Genese 35	do	829
Göttingen 377	do	781	Rhode St. Genese 37	do	830
Göttingen 392	do	782			
Göttingen 397	do	783	ITALY		
Göttingen 399	do	784	I. S. A. 334	I. S. A.	831
Göttingen 401	do	785	I. S. A. 390	do	832
Göttingen 402	do	786	I. S. A. 472	do	833
Göttingen 403	do	787	I. S. A. 500	do	834
Göttingen 408	do	788	I. S. A. 501	do	835
Göttingen 417	do	789	I. S. A. 502	do	836
Göttingen 428	do	790	I. S. A. 507	do	837
Göttingen 437	do	791	I. S. A. 605	do	838
Göttingen 438	do	792	I. S. A. 663	do	839
Göttingen 439	do	793	I. S. A. 693	do	840
Göttingen 442	do	794	I. S. A. 695	do	841
Göttingen 443	do	795	I. S. A. 768	do	842
Göttingen 444	do	796	I. S. A. 776	do	843
Göttingen 445	do	797	I. S. A. 801	do	844
			I. S. A. 803	do	845
			I. S. A. 804	do	846
			I. S. A. 805	do	847
			I. S. A. 806	do	848
			I. S. A. 807	do	849
			I. S. A. 809	do	850
			I. S. A. 812	do	851
			I. S. A. 820	do	852
			I. S. A. 821	do	853
			I. S. A. 829	do	854
			I. S. A. 858	do	855
			I. S. A. 881a	do	856
			I. S. A. 881b	do	857
			I. S. A. 881c	do	858
			I. S. A. 911	do	859
FRANCE					
Eiffel 359 (Nieuport Astra)	S. T. Aé. Lab.	798			
Eiffel 386 (S. T. Aé.)	do	799			
Eiffel 387 (S. T. Aé.)	do	800			
Eiffel 402 (Pescara)	do	801			
Eiffel 429 (Lachassagne)	do	802			
Eiffel 432 (Lachassagne)	do	803			
Eiffel 433a (Chalambel)	do	804			
Eiffel 438 (Lachassagne)	do	805			
St. Cyr 152 (Royer)	do	806			
St. Cyr 153 (Royer)	do	807			
St. Cyr 156 (Royer)	do	808			
St. Cyr 157 (Royer)	do	809			

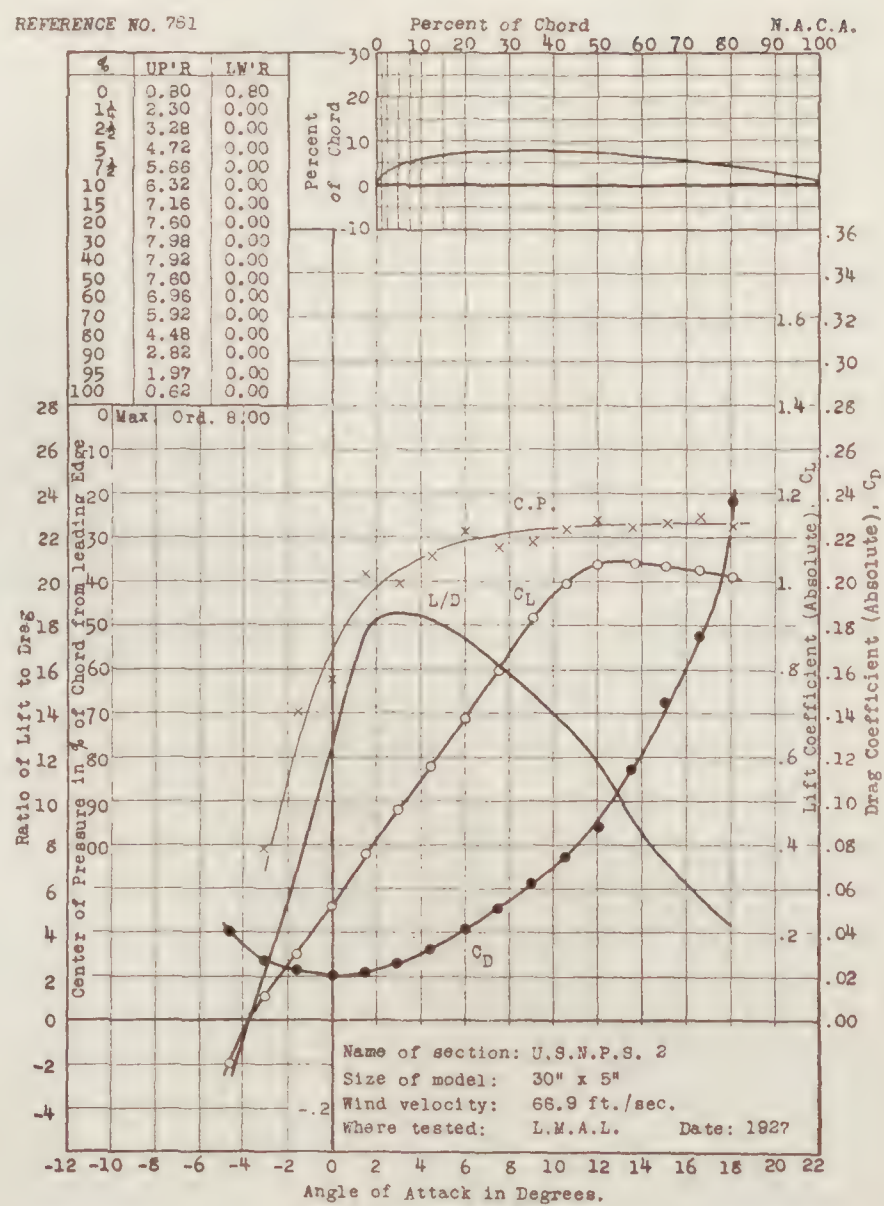
ALPHABETICAL INDEX

Airfoil	Report reference number	Airfoil	Report reference number
Eiffel 359 (Nieuport Astra)	798	I. S. A. 804	846
Eiffel 386 (S. T. Aé.)	799	I. S. A. 805	847
Eiffel 387 (S. T. Aé.)	800	I. S. A. 806	848
Eiffel 402 (Pescara)	801	I. S. A. 807	849
Eiffel 429 (Lachassagne)	802	I. S. A. 809	850
Eiffel 432 (Lachassagne)	803	I. S. A. 812	851
Eiffel 433a (Chalambel)	804	I. S. A. 820	852
Eiffel 438 (Lachassagne)	805	I. S. A. 821	853
Göttingen 359	771	I. S. A. 829	854
Göttingen 361	772	I. S. A. 858	855
Göttingen 362	773	I. S. A. 881a	856
Göttingen 368	774	I. S. A. 881b	857
Göttingen 369	775	I. S. A. 881c	858
Göttingen 371	776	I. S. A. 911	859
Göttingen 372	777	Martin M-I	766
Göttingen 373	778	Martin M-II	767
Göttingen 374	779	Martin M-III	768
Göttingen 375	780	R-3 (Root Section)	769
Göttingen 377	781	Rhode St. Genese 1	820
Göttingen 392	782	Rhode St. Genese 2	821
Göttingen 397	783	Rhode St. Genese 16	822
Göttingen 399	784	Rhode St. Genese 17	823
Göttingen 401	785	Rhode St. Genese 19	824
Göttingen 402	786	Rhode St. Genese 26	825
Göttingen 403	787	Rhode St. Genese 29	826
Göttingen 408	788	Rhode St. Genese 31	827
Göttingen 417	789	Rhode St. Genese 33	828
Göttingen 428	790	Rhode St. Genese 35	829
Göttingen 437	791	Rhode St. Genese 37	830
Göttingen 438	792	St. Cyr 152 (Royer)	806
Göttingen 439	793	St. Cyr 153 (Royer)	807
Göttingen 442	794	St. Cyr 156 (Royer)	808
Göttingen 443	795	St. Cyr 157 (Royer)	809
Göttingen 444	796	St. Cyr 162 (Royer)	810
Göttingen 445	797	St. Cyr 170 (Royer)	811
I. S. A. 334	831	St. Cyr 174 (Royer)	812
I. S. A. 390	832	St. Cyr 233 (Bartel 37-Ib)	813
I. S. A. 472	833	St. Cyr 235 (Bartel 37-Ic)	814
I. S. A. 500	834	St. Cyr 237 (Bartel 15-Ic)	815
I. S. A. 501	835	St. Cyr 239 (Bartel 37-IIa)	816
I. S. A. 502	836	St. Cyr 240 (Bartel 37-IIb)	817
I. S. A. 507	837	St. Cyr 242 (Bartel 57-IIc)	818
I. S. A. 605	838	St. Cyr 243 (Bartel 37-IIIc)	819
I. S. A. 663	839	U. S. A. 45M	770
I. S. A. 693	840	U. S. N. P. S. 1	760
I. S. A. 695	841	U. S. N. P. S. 2	761
I. S. A. 768	842	U. S. N. P. S. 3	762
I. S. A. 776	843	U. S. N. P. S. 4	763
I. S. A. 801	844	U. S. N. P. S. 5	764
I. S. A. 803	845	U. S. N. P. S. 6	765

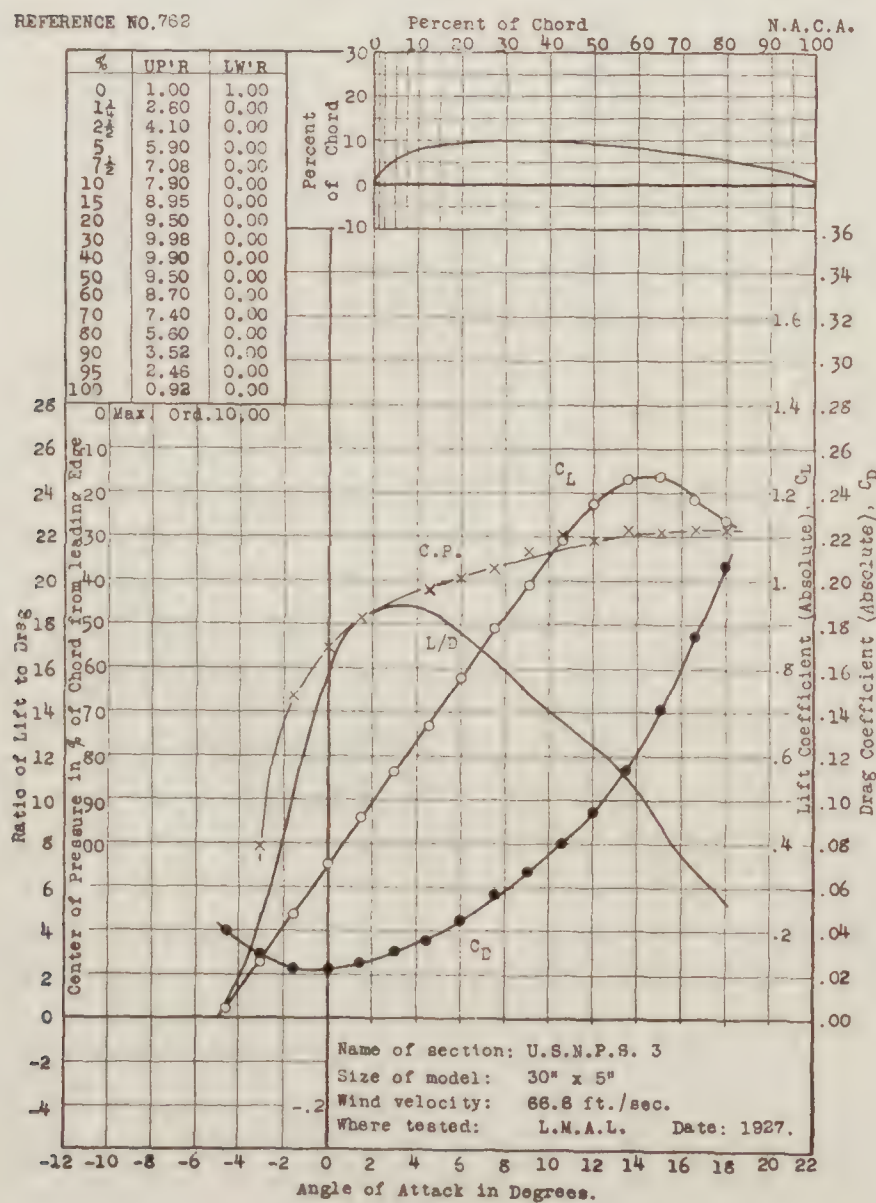
REFERENCE NO. 760



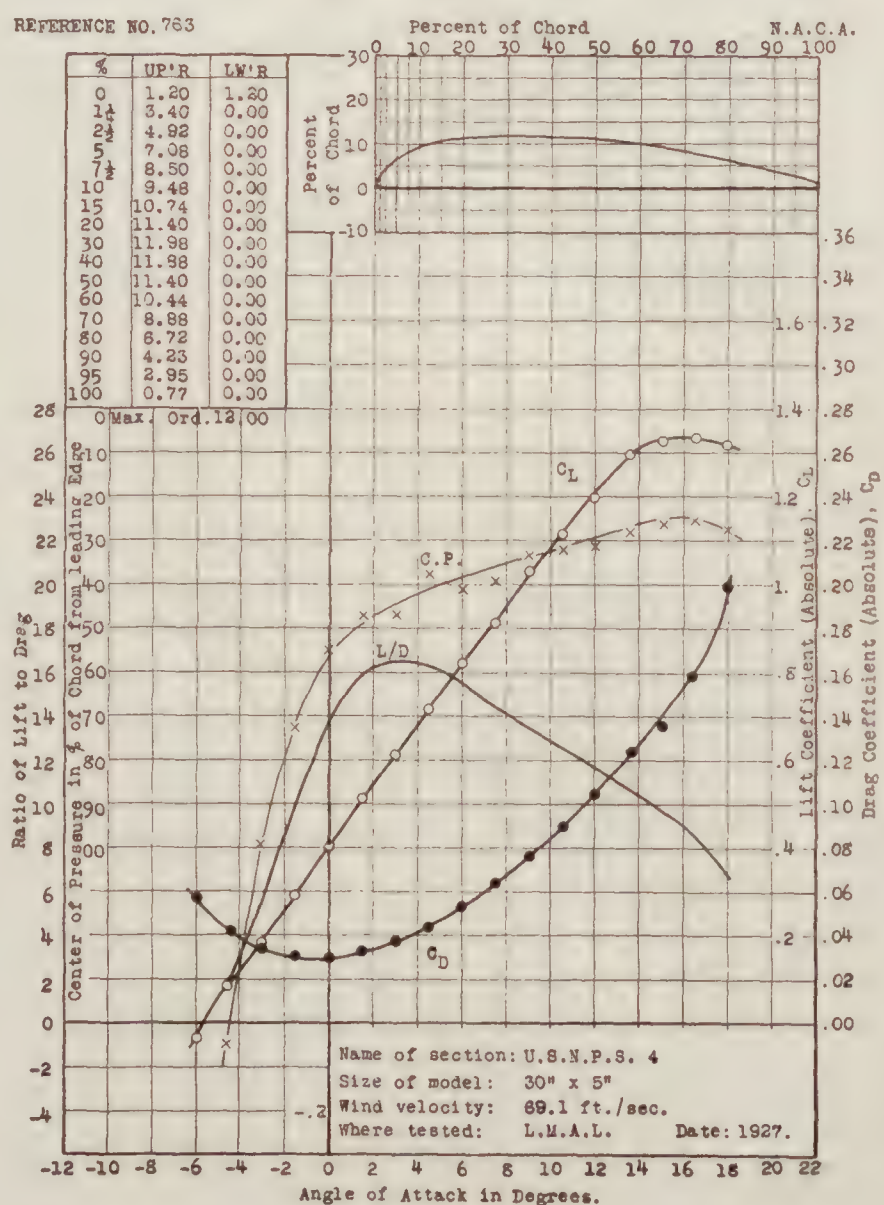
REFERENCE NO. 781



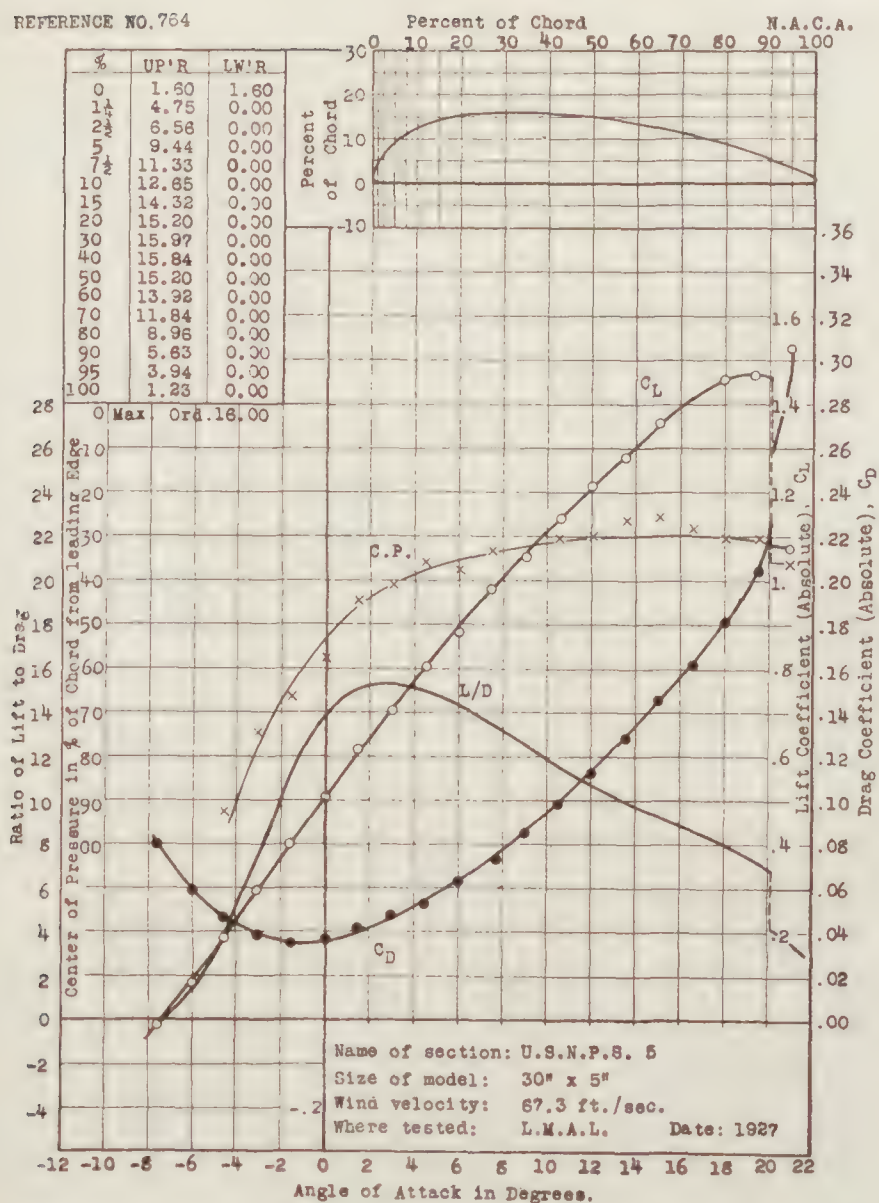
REFERENCE NO. 762



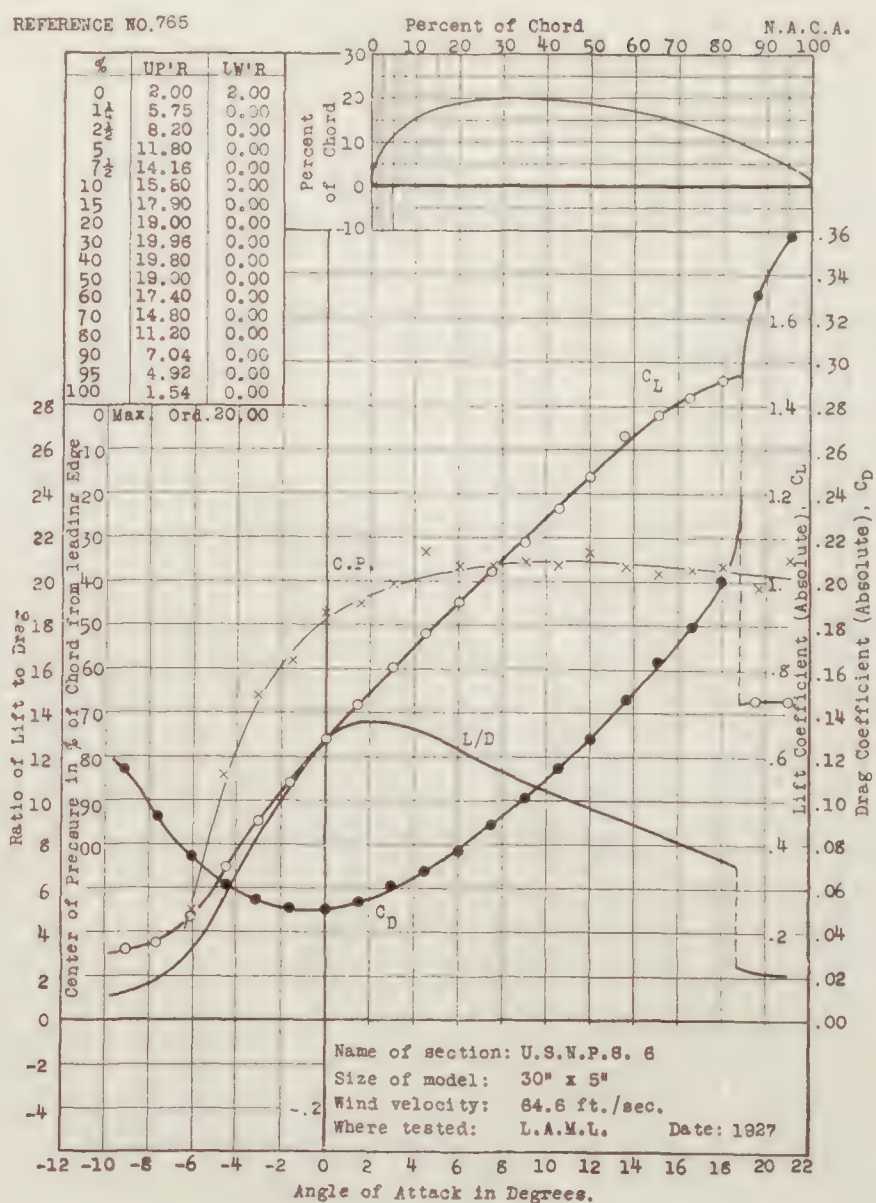
REFERENCE NO. 763



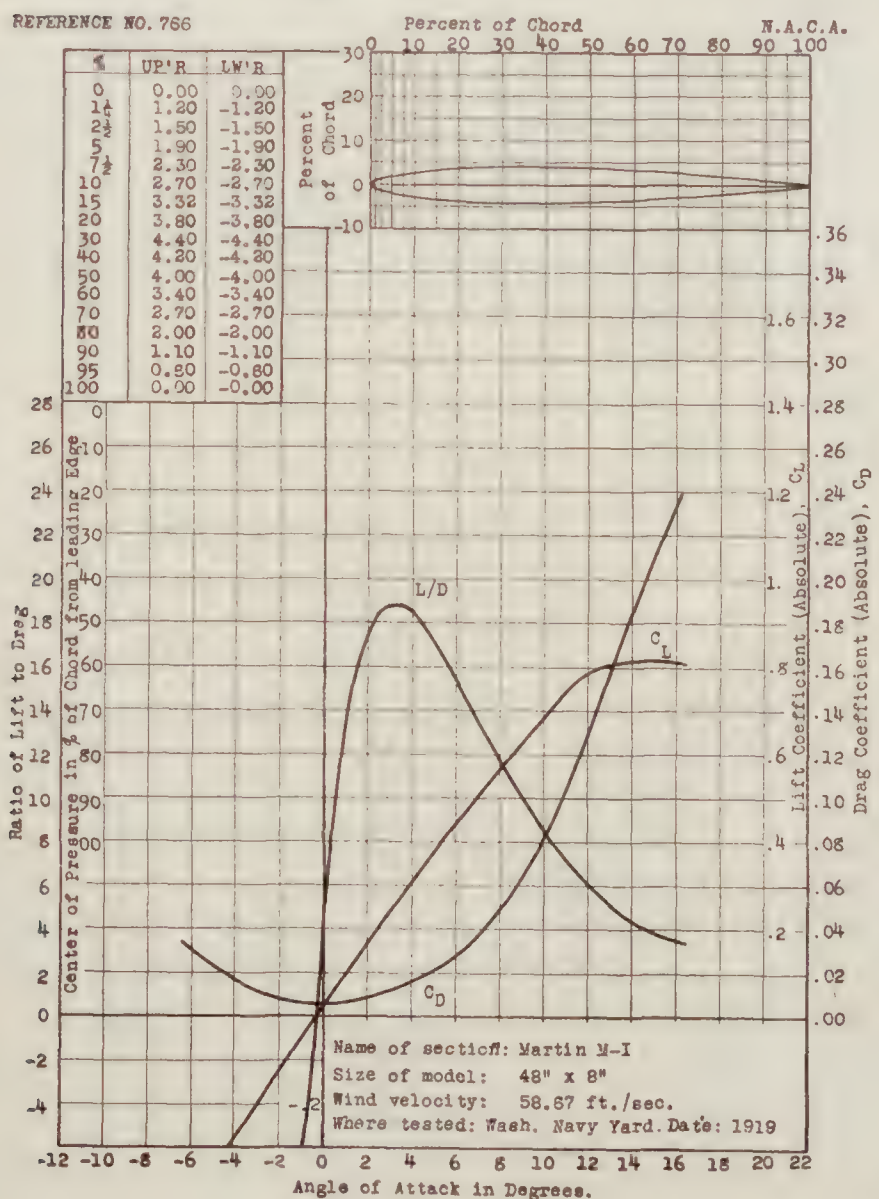
REFERENCE NO. 764



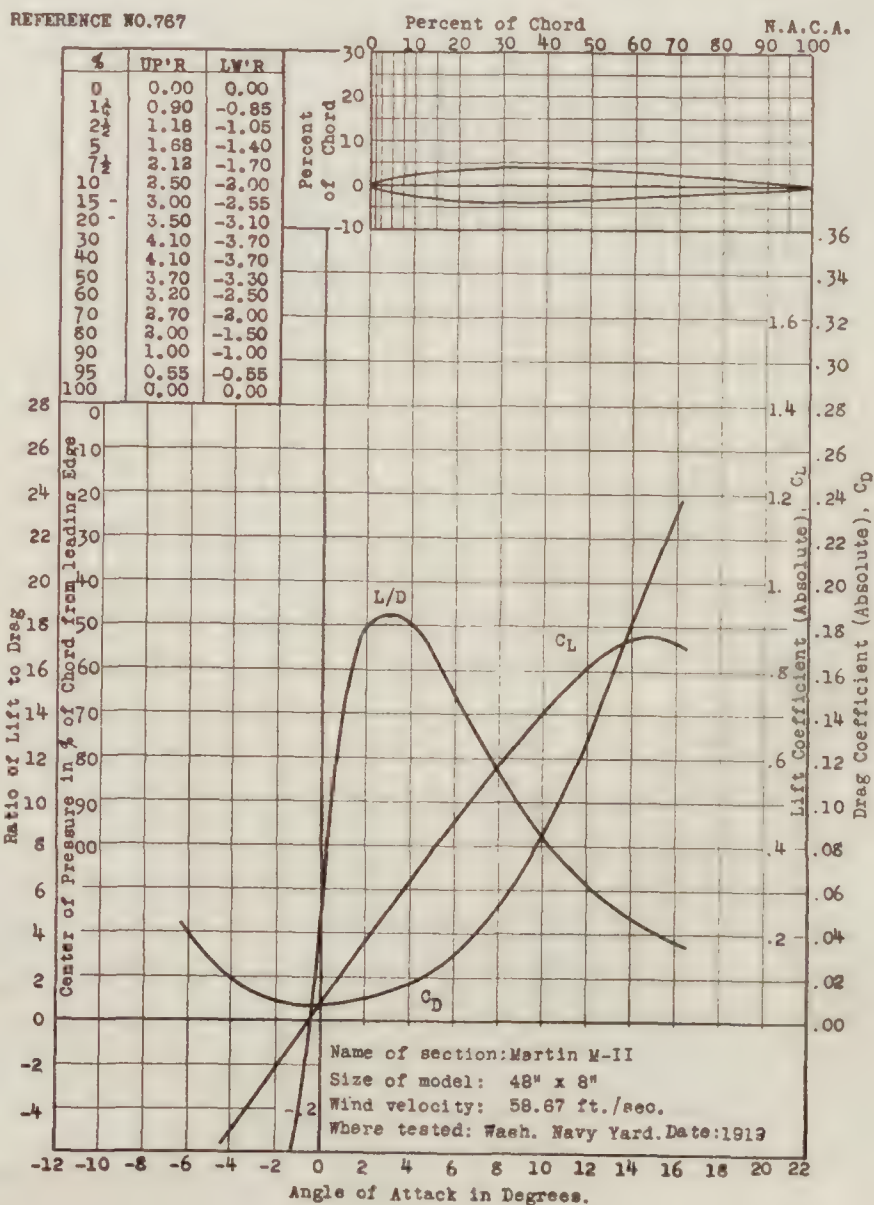
REFERENCE NO. 765



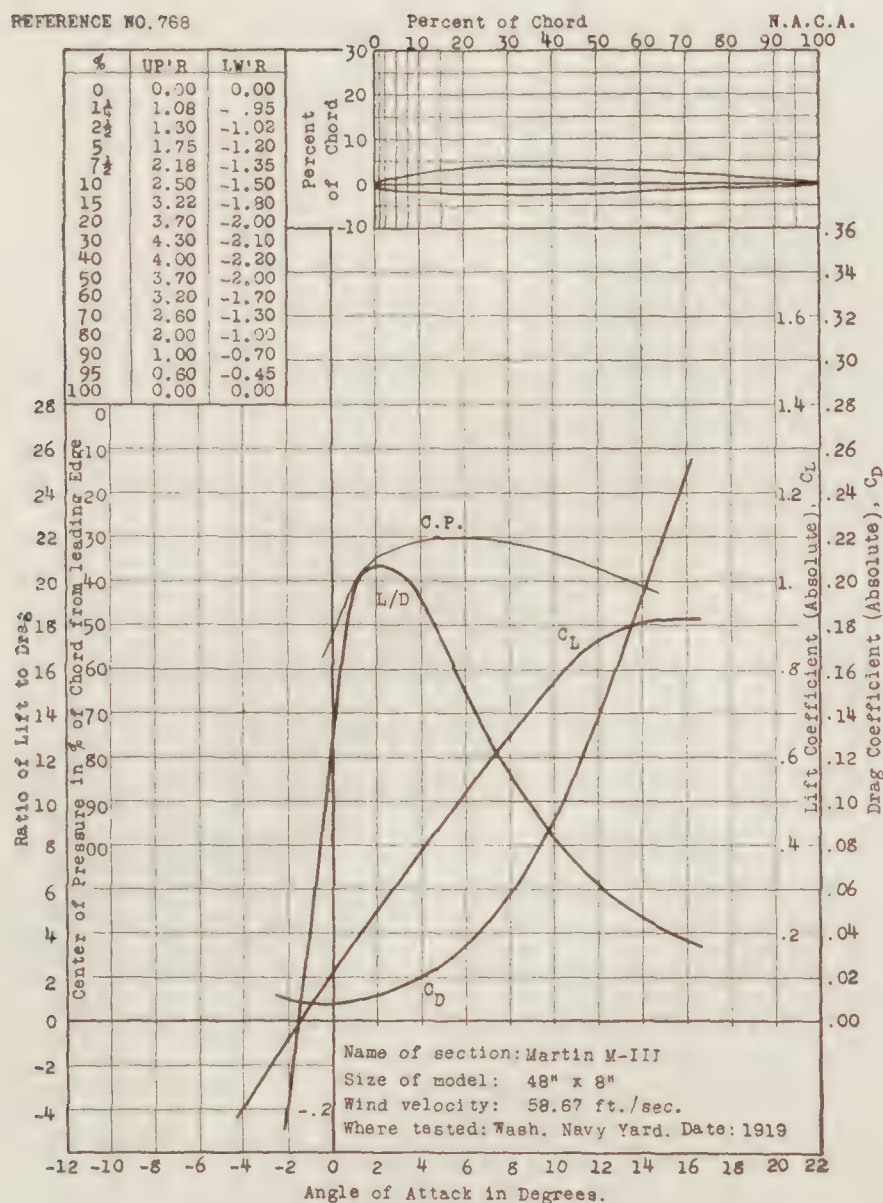
REFERENCE NO. 766



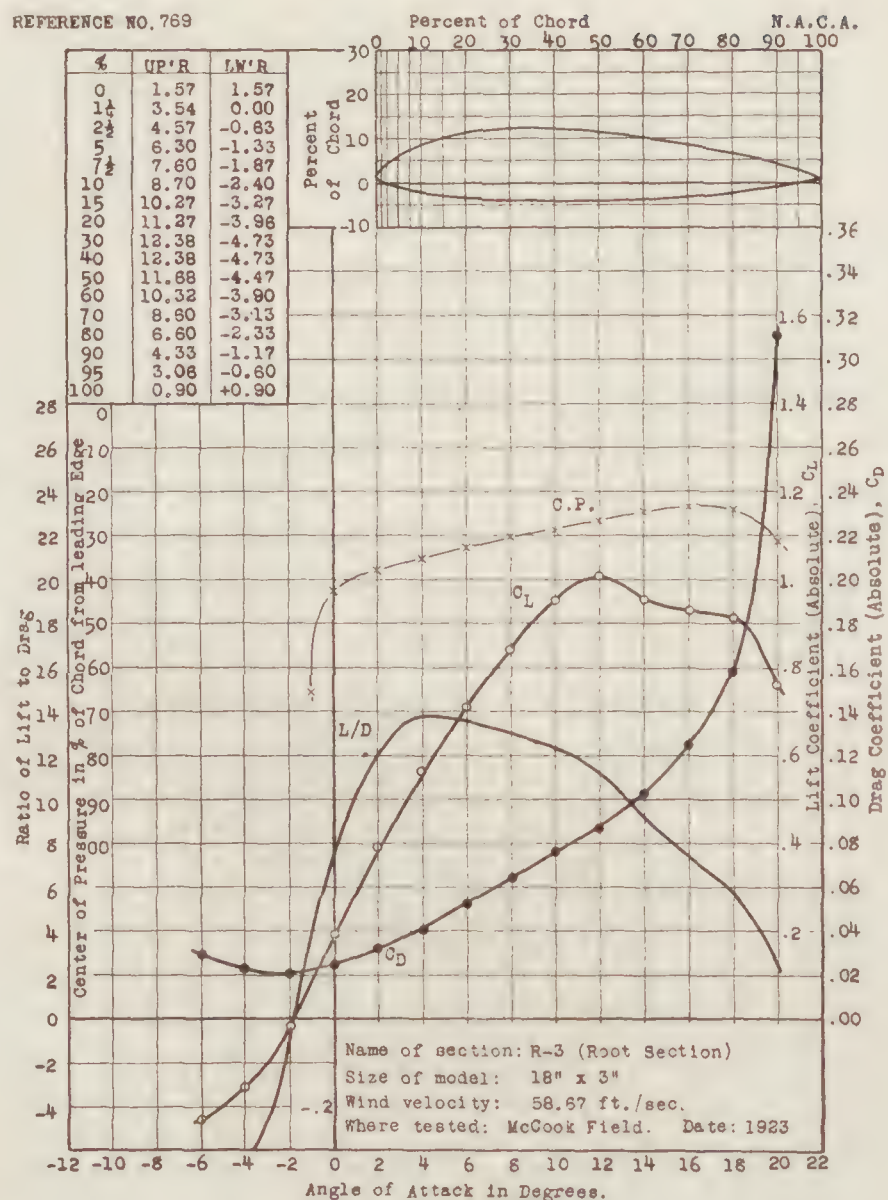
REFERENCE NO. 767



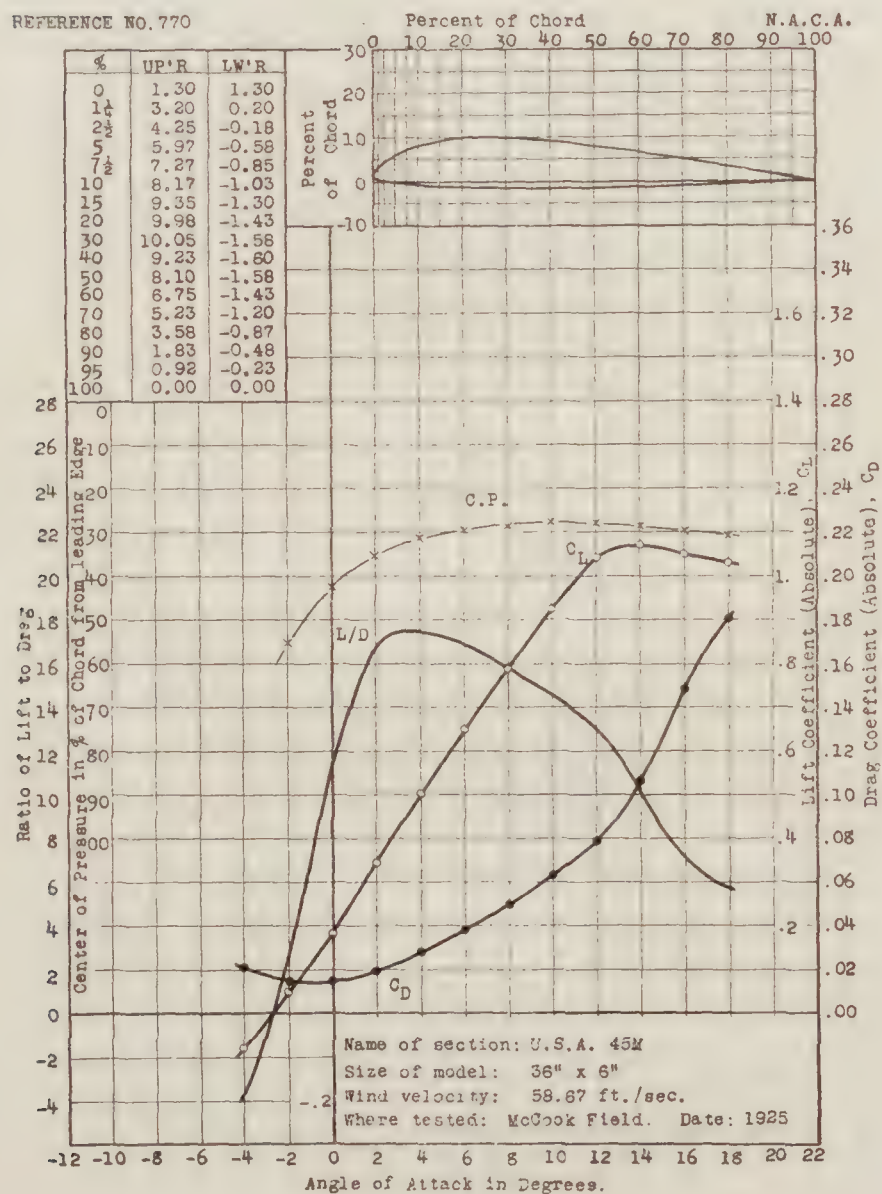
REFERENCE NO. 768



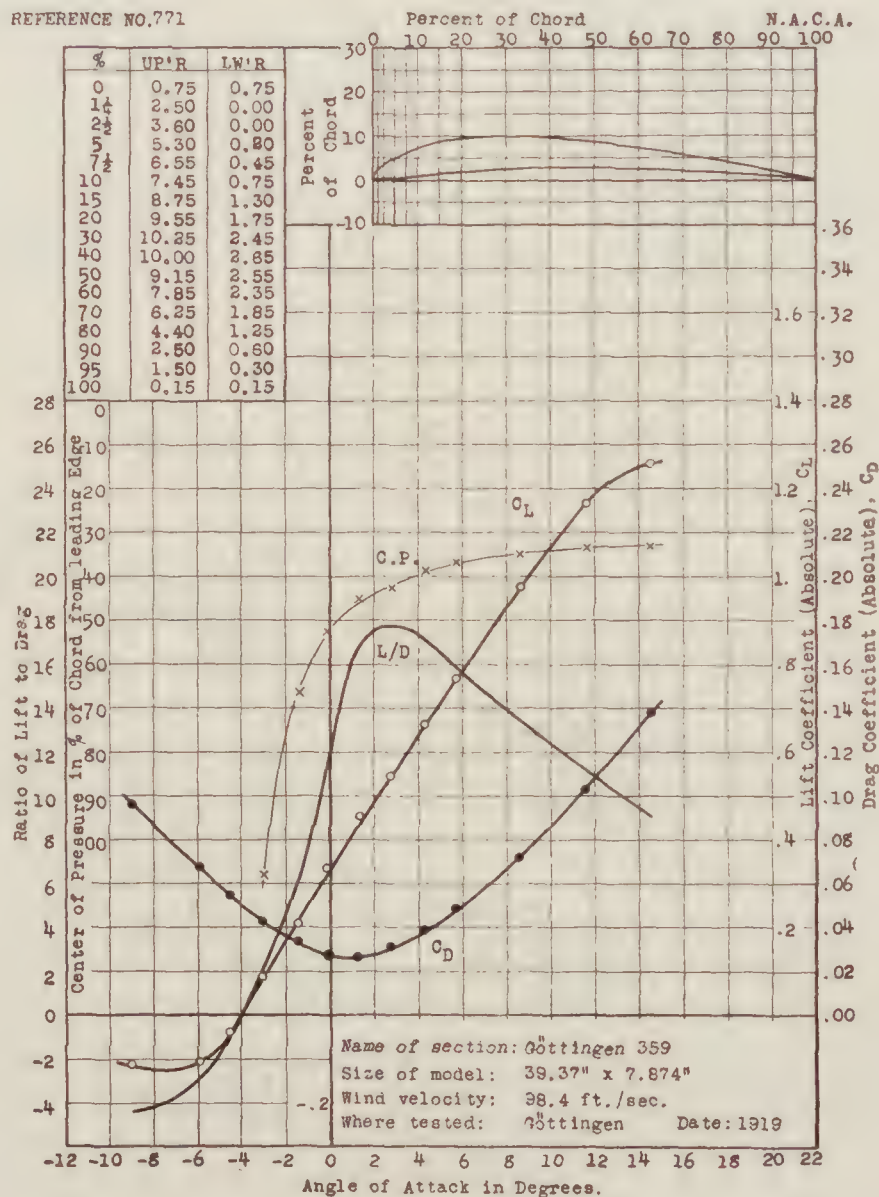
REFERENCE NO. 769



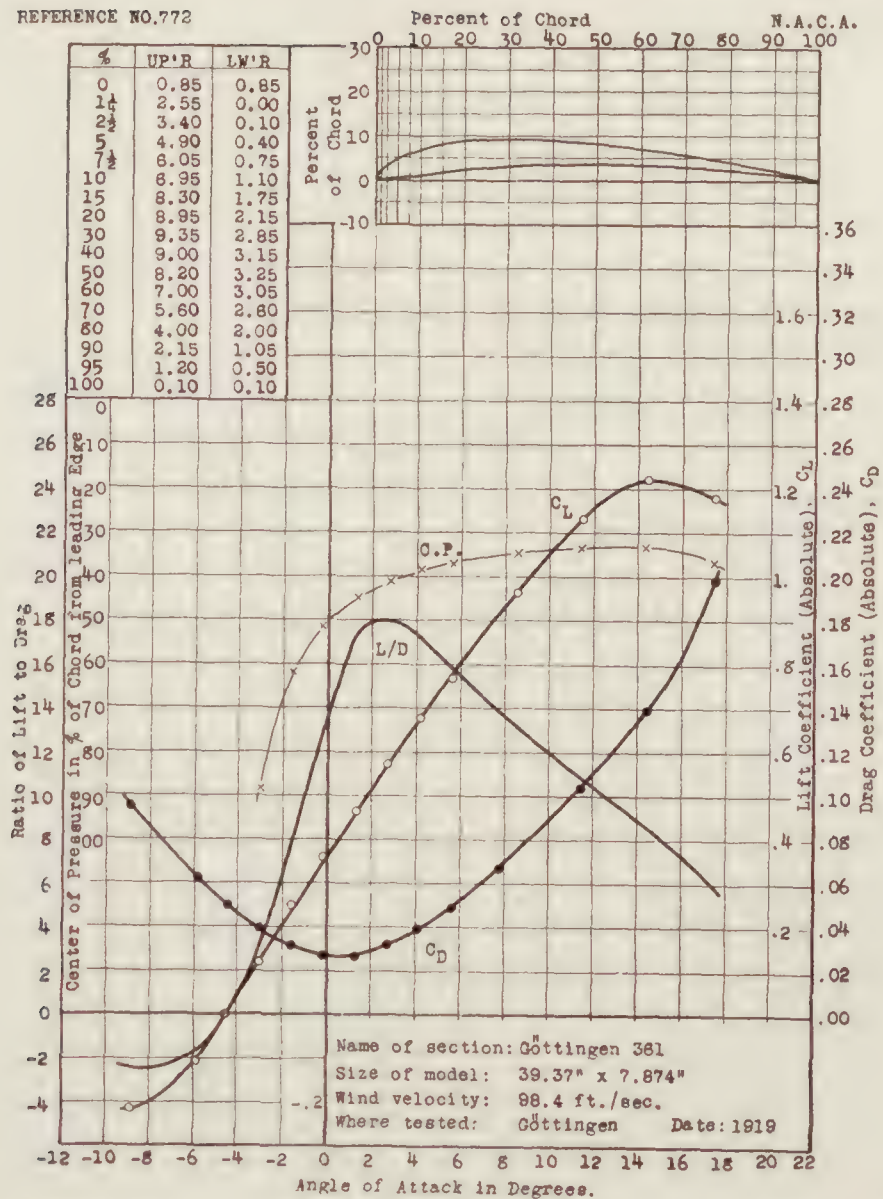
REFERENCE NO. 770



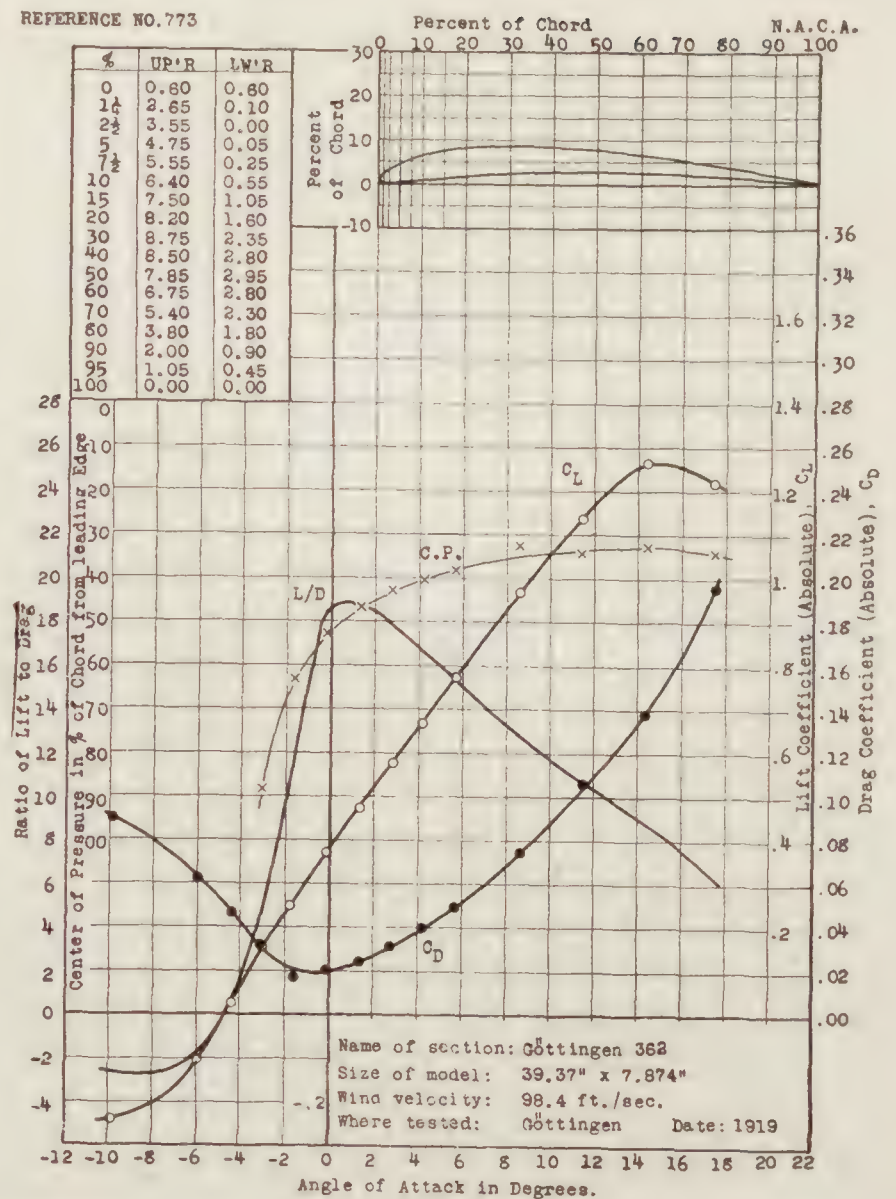
REFERENCE NO. 771



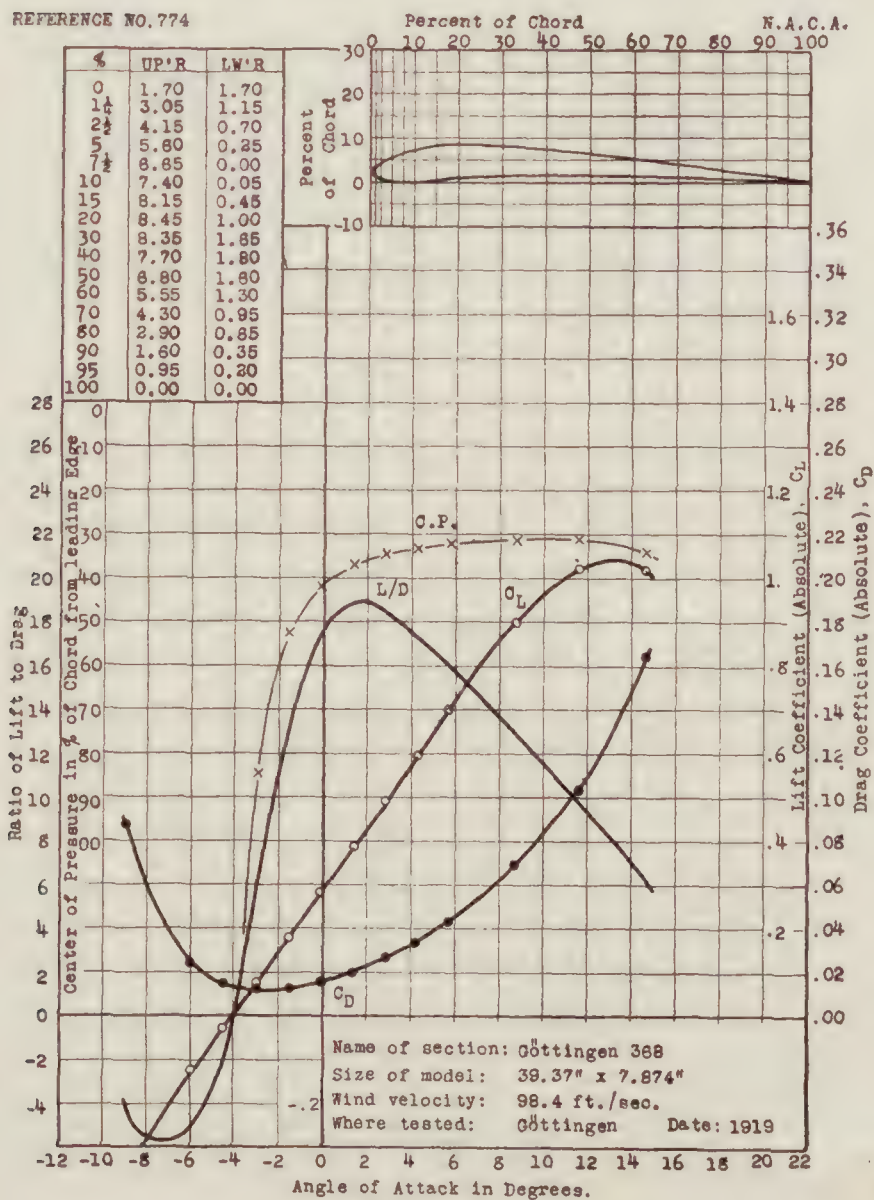
REFERENCE NO. 772



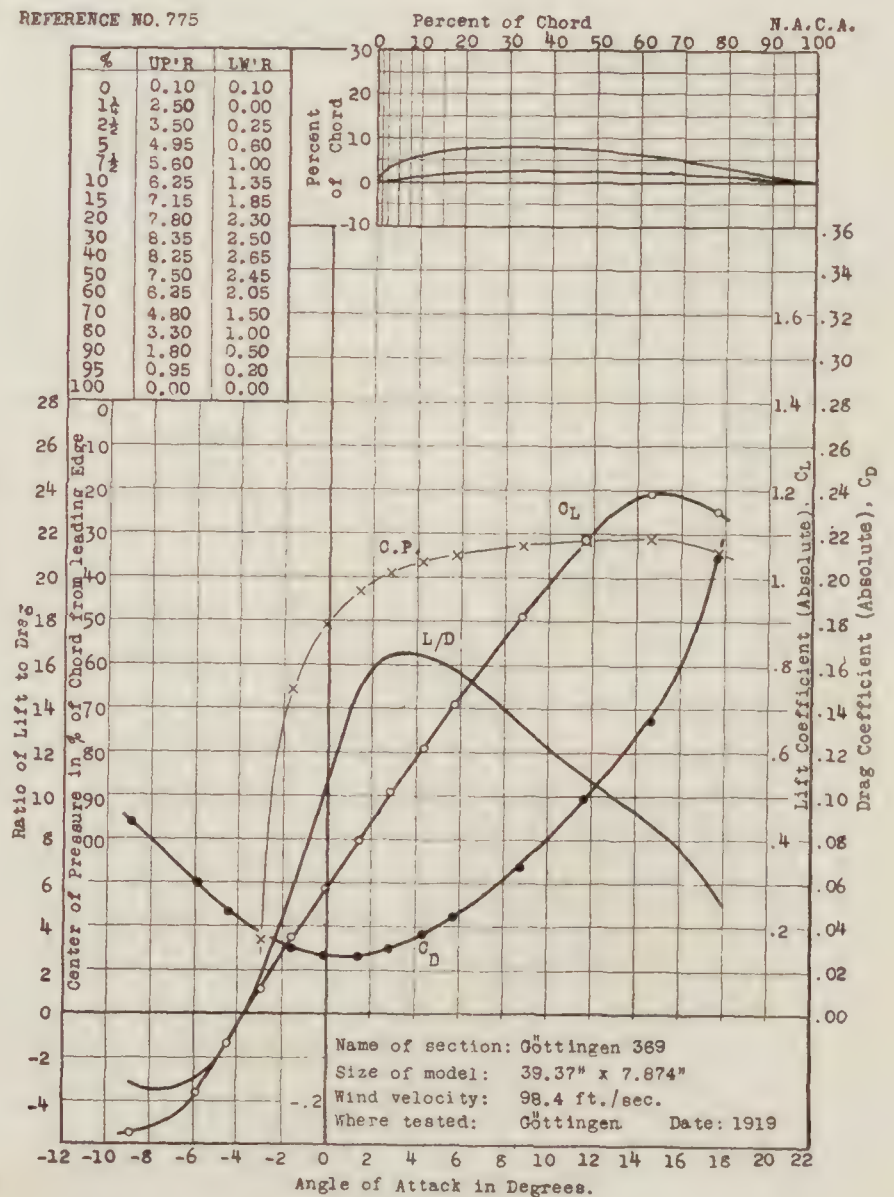
REFERENCE NO. 773



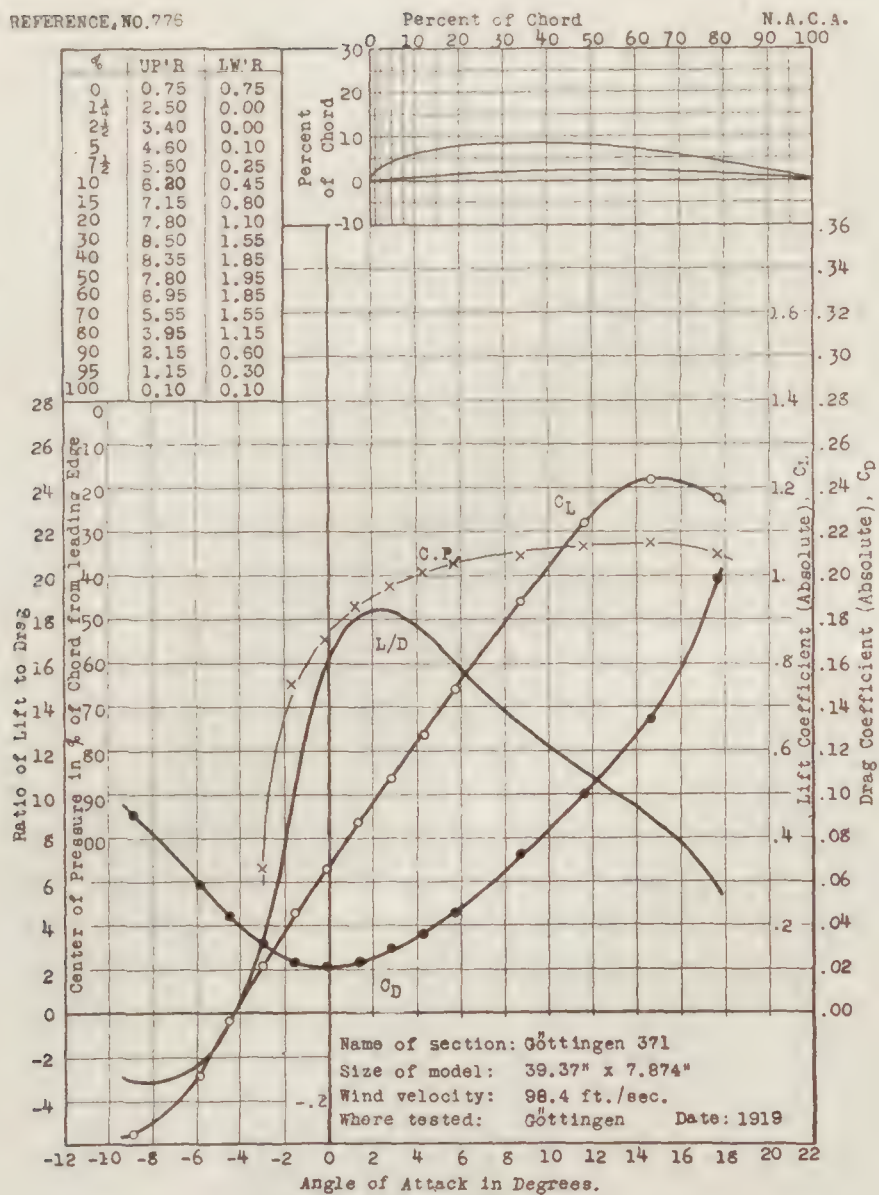
REFERENCE NO. 774



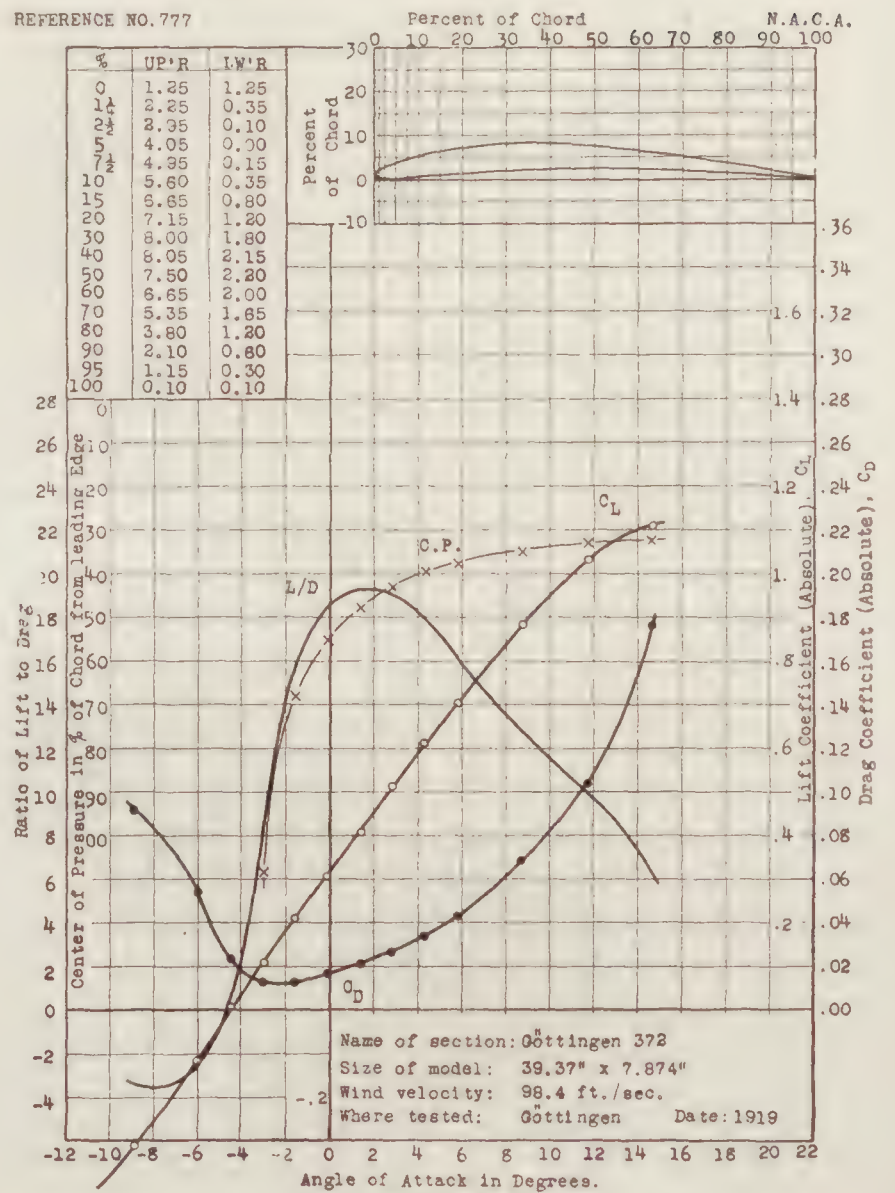
REFERENCE NO. 775



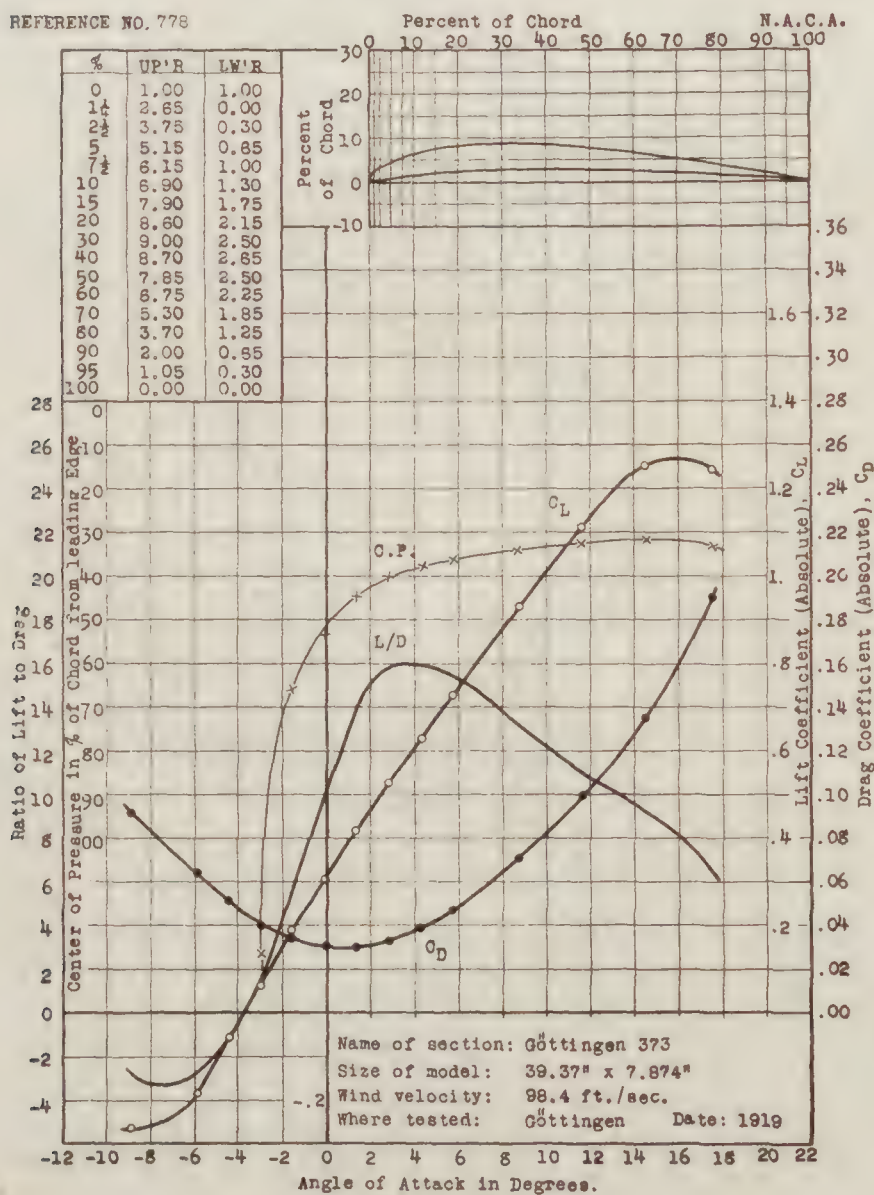
REFERENCE NO. 775



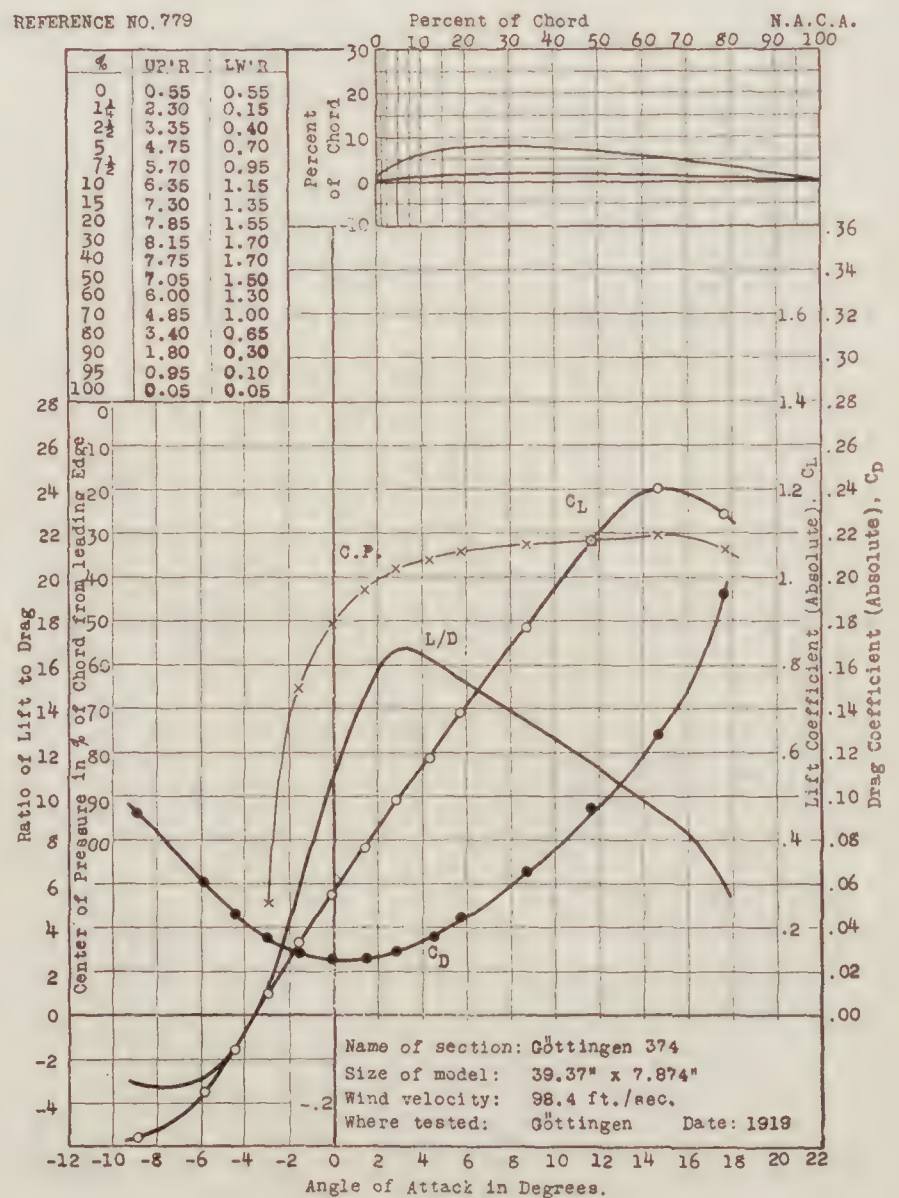
REFERENCE NO. 777



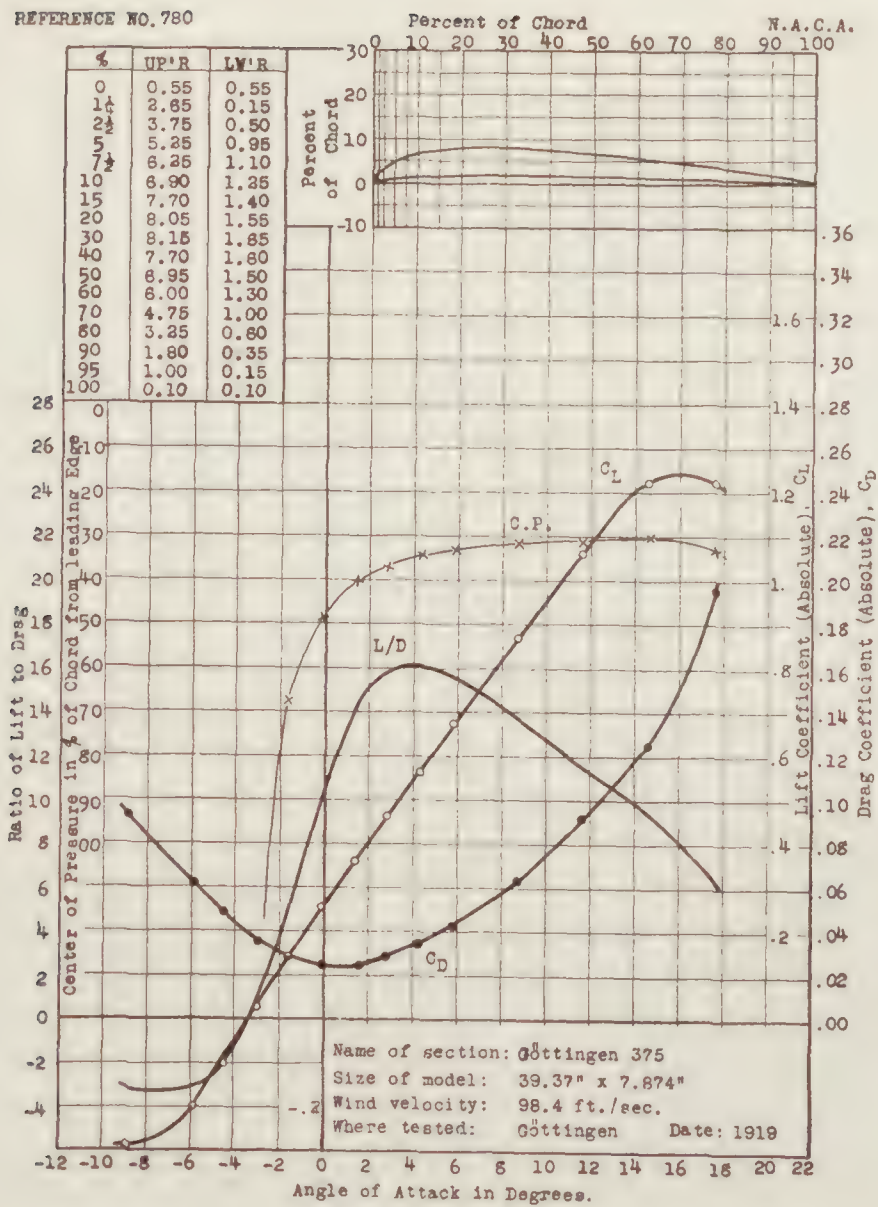
REFERENCE NO. 778



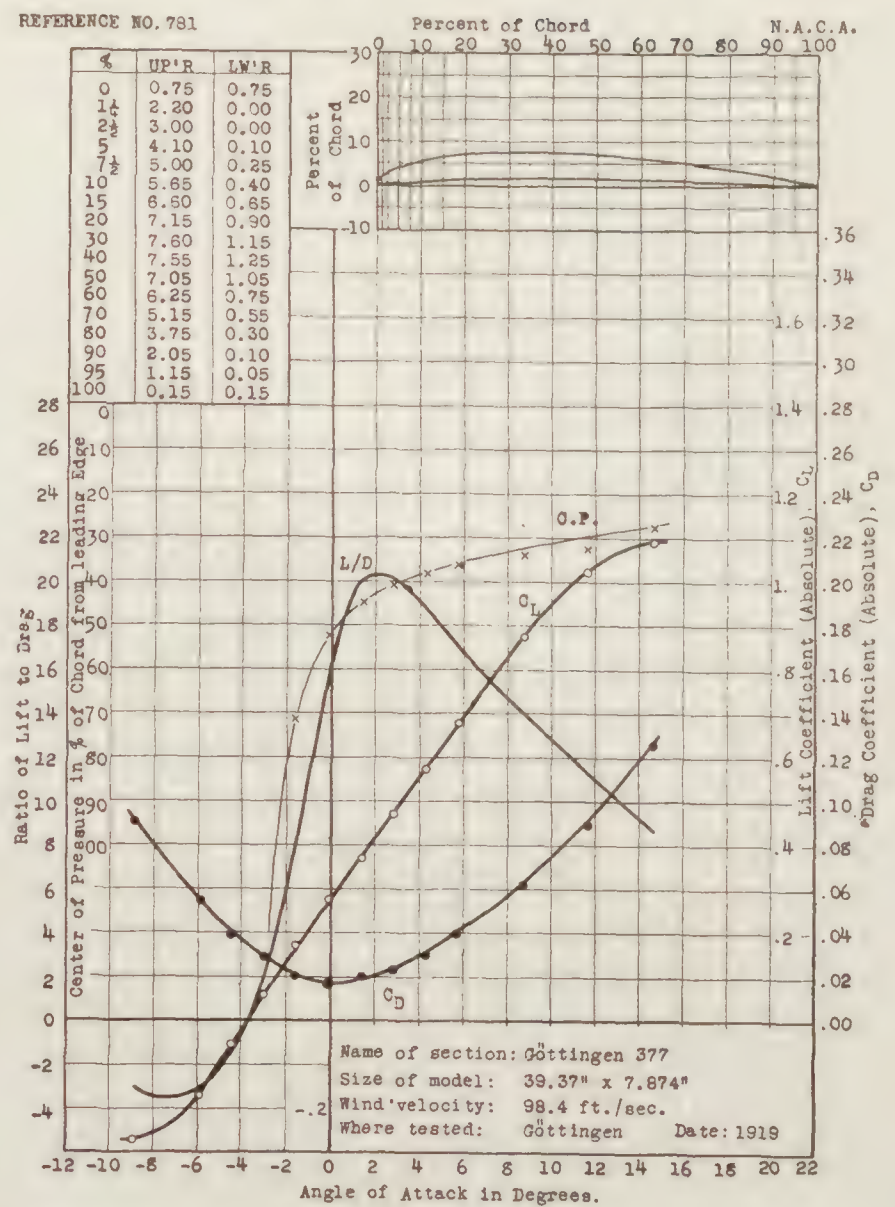
REFERENCE NO. 779



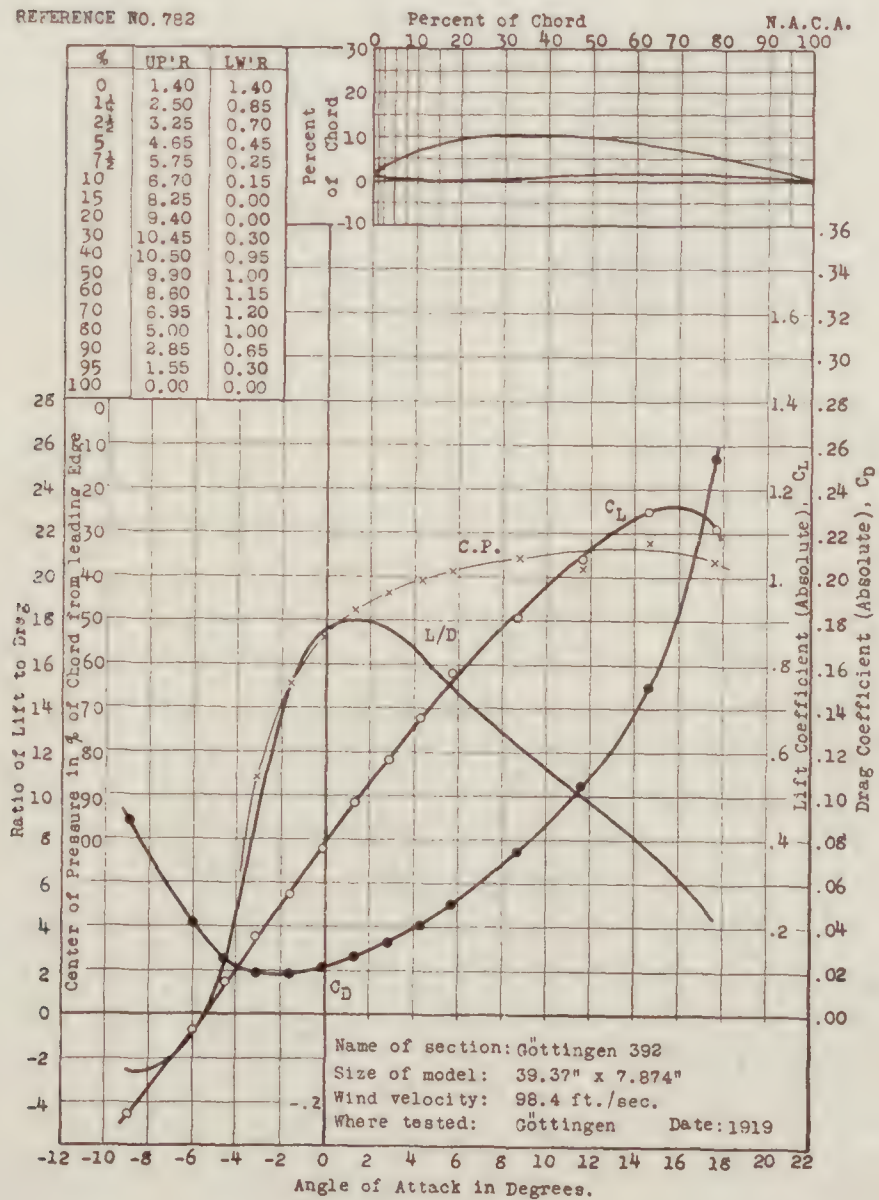
REFERENCE NO. 780



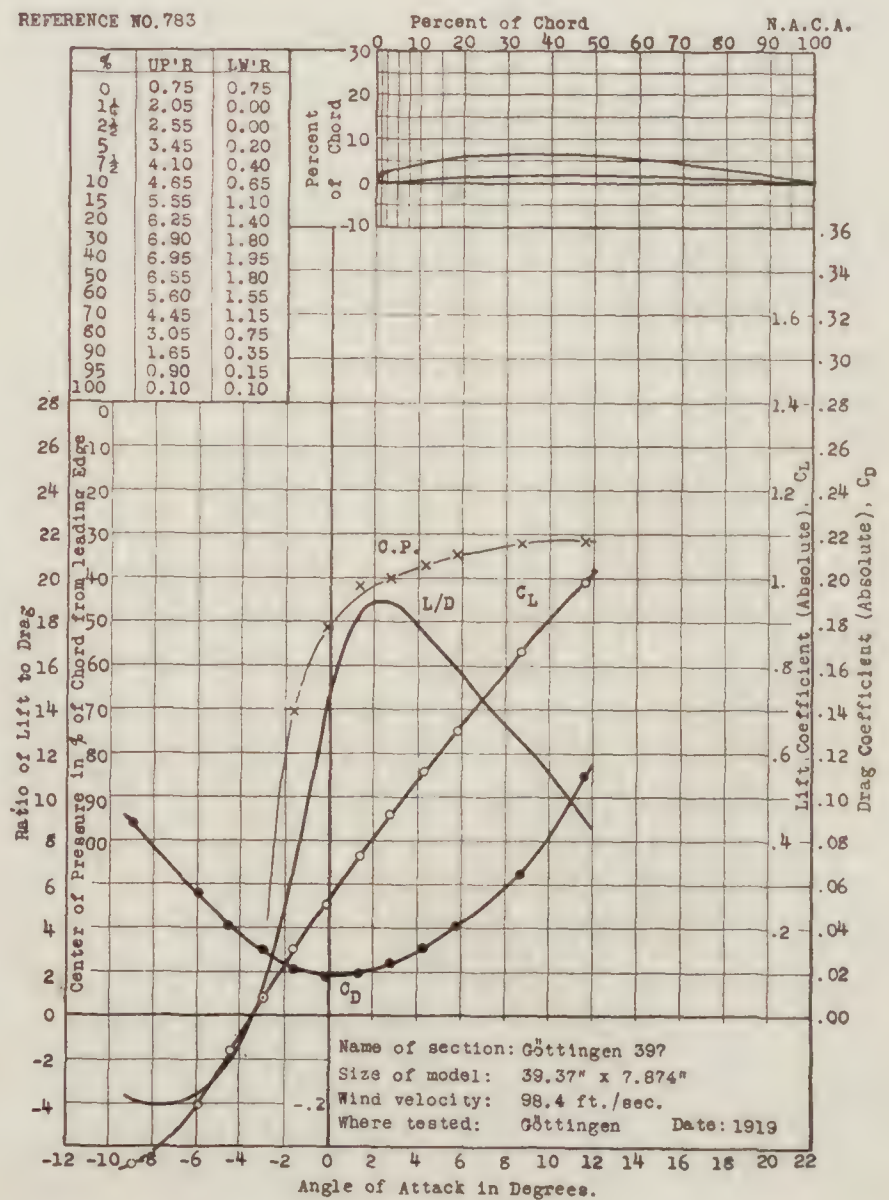
REFERENCE NO. 781



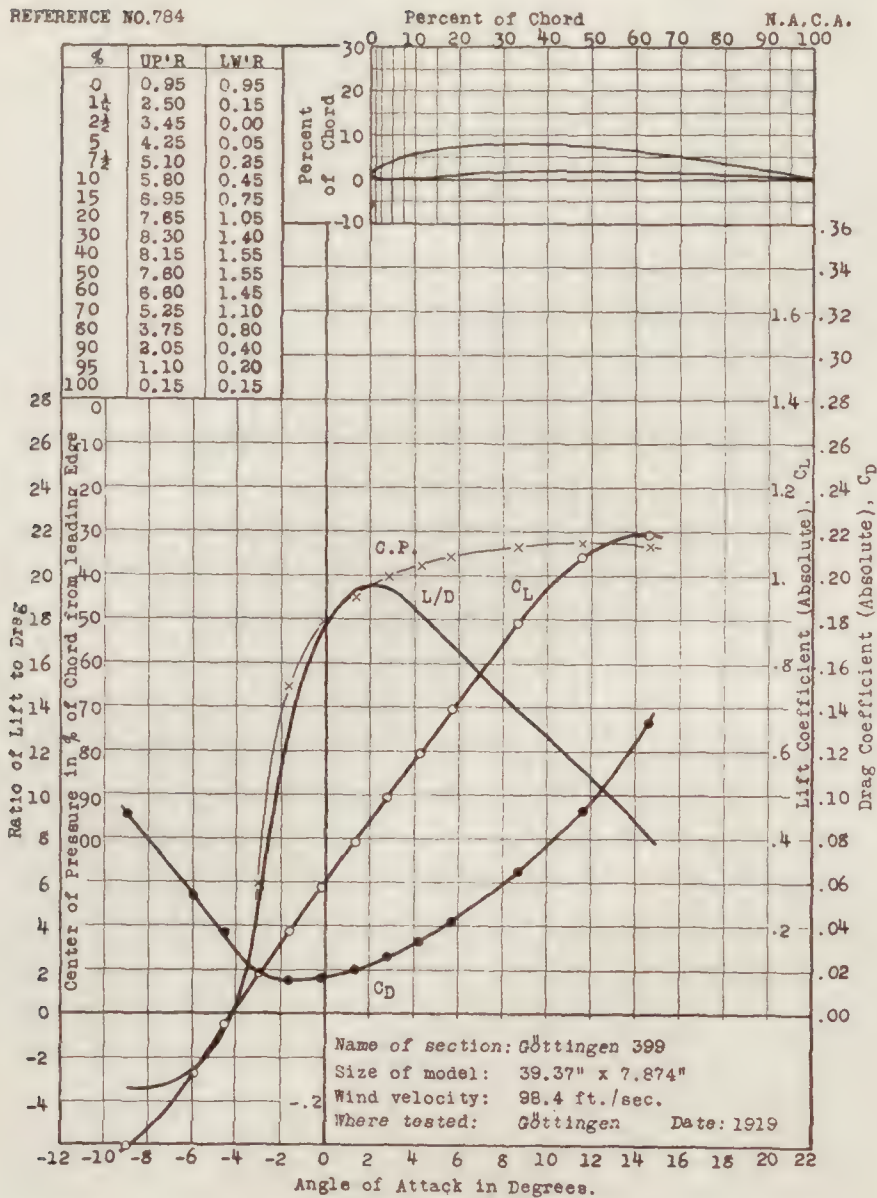
REFERENCE NO. 782



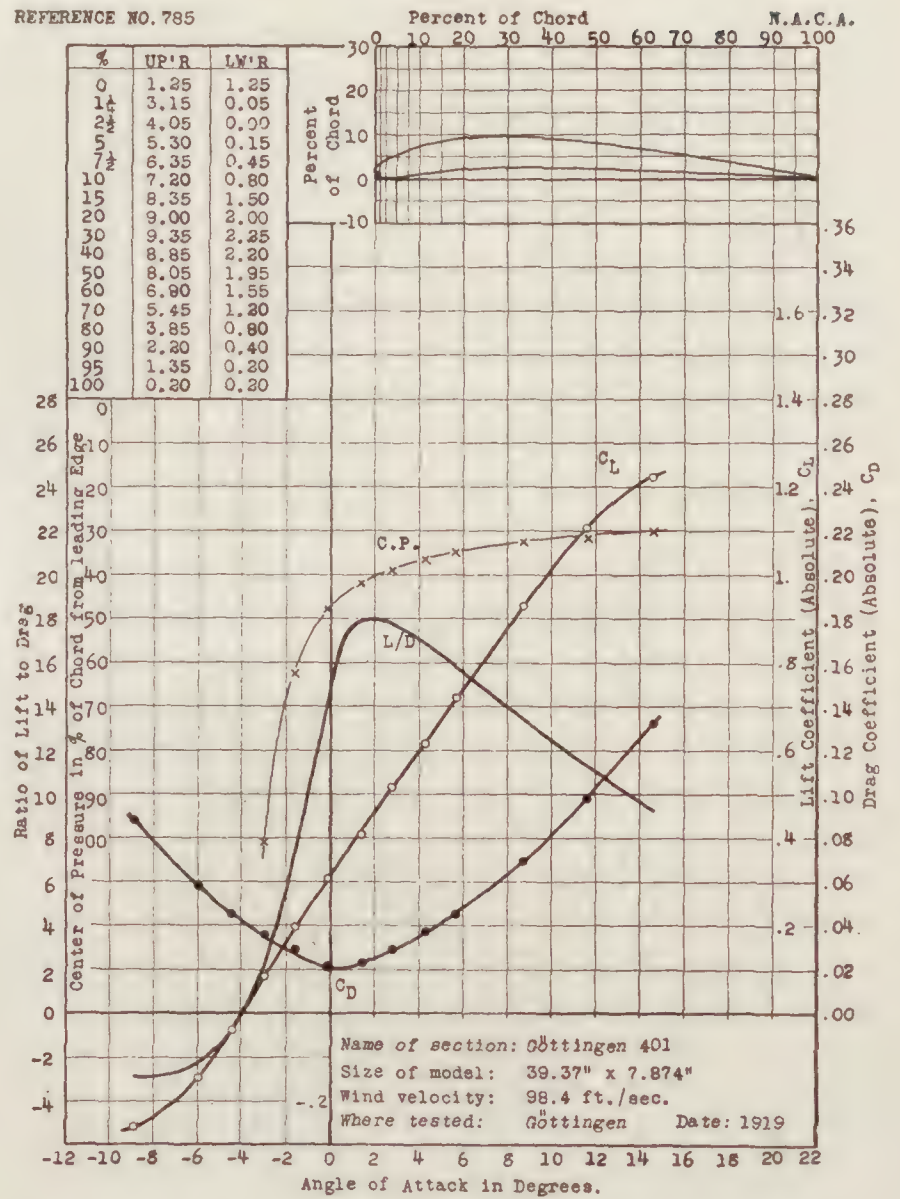
REFERENCE NO. 783



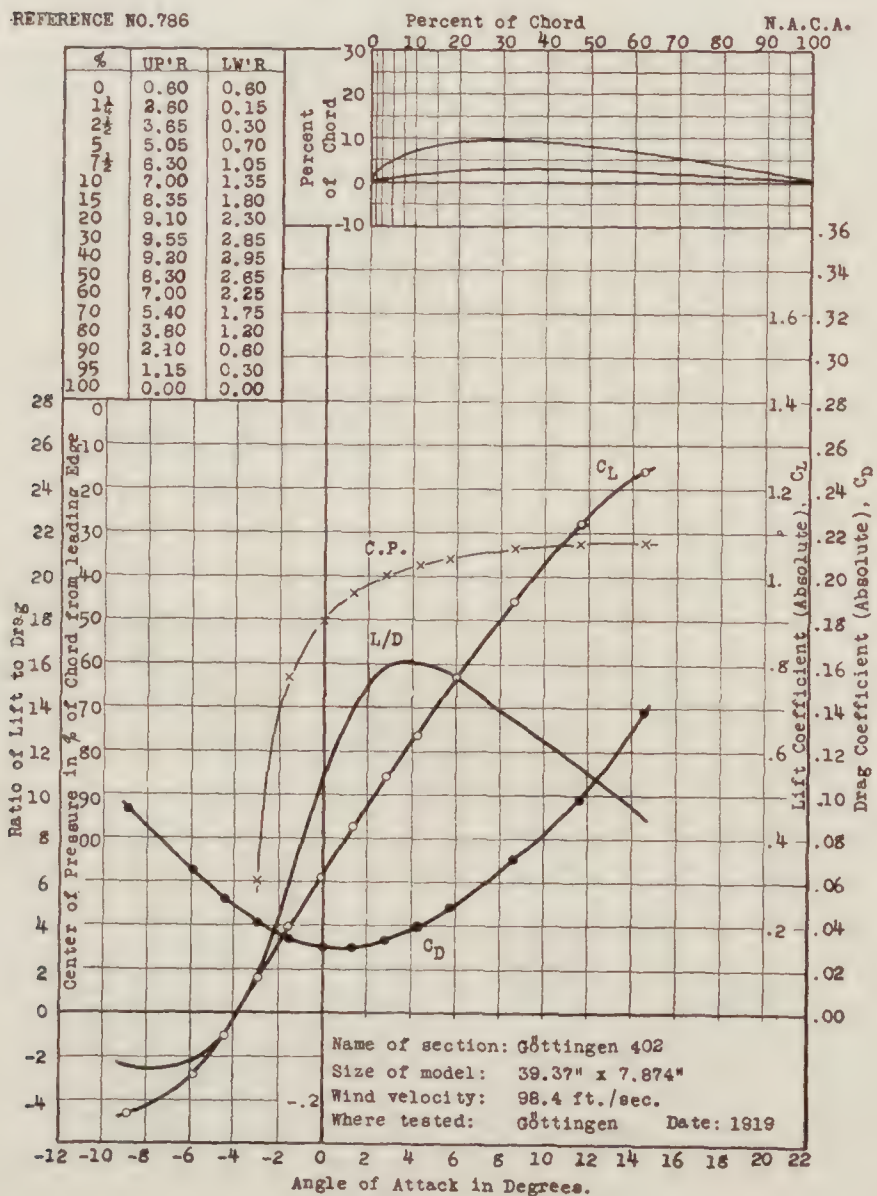
REFERENCE NO. 784



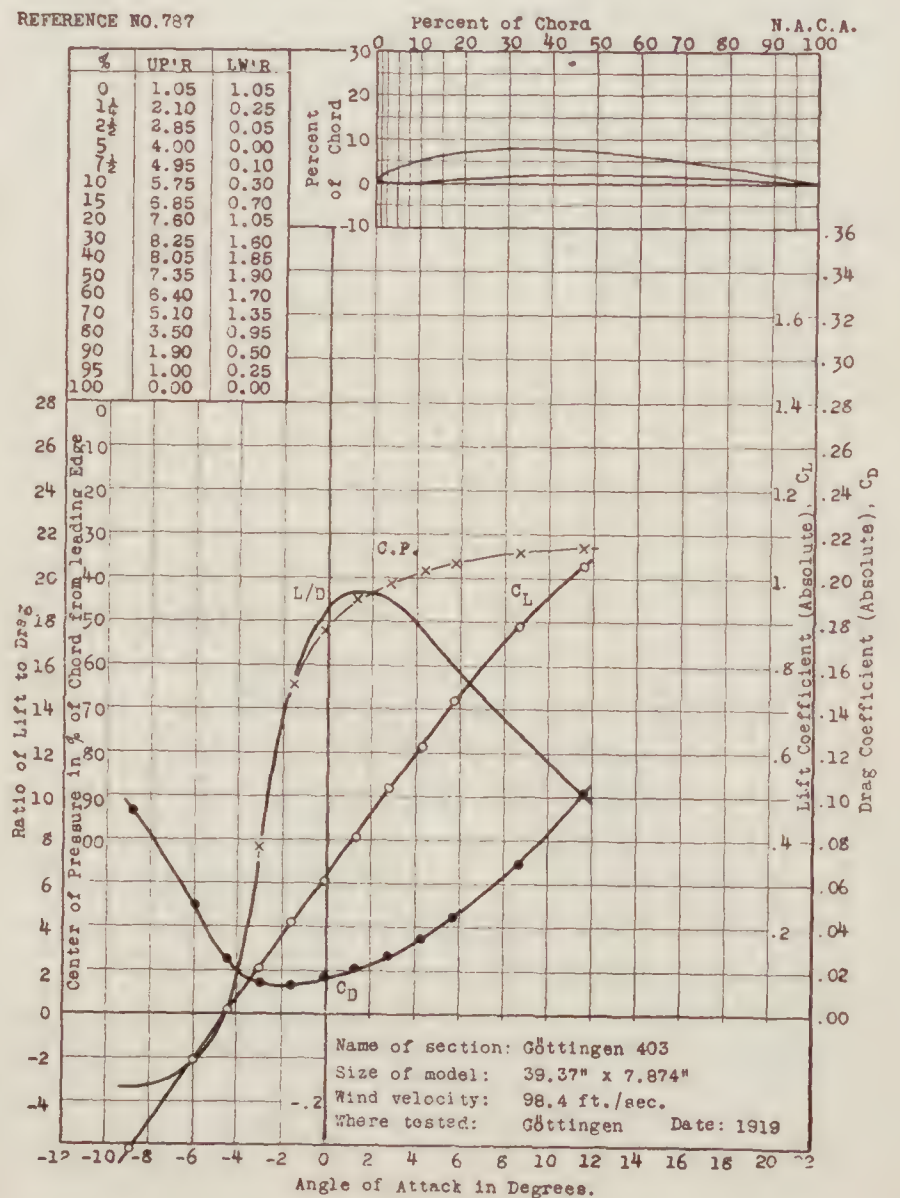
REFERENCE NO. 785



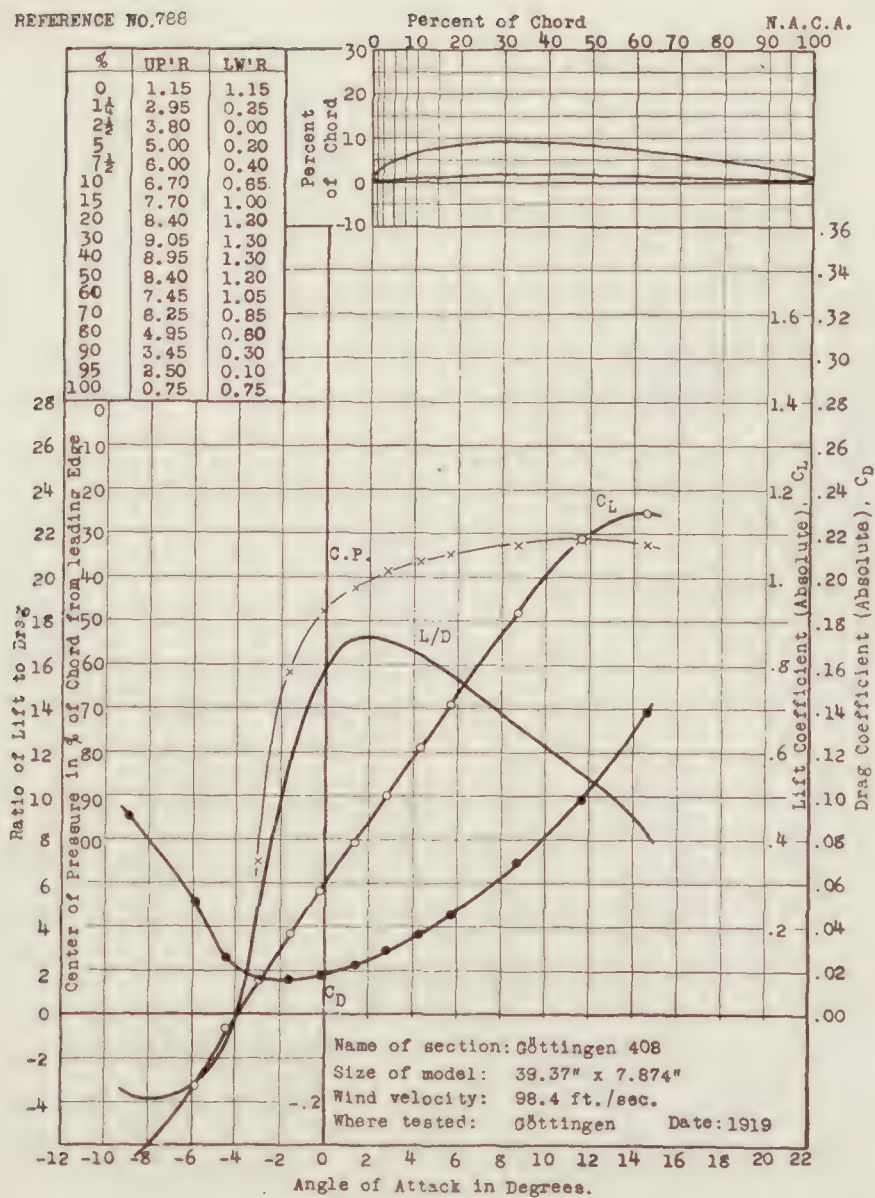
REFERENCE NO. 786



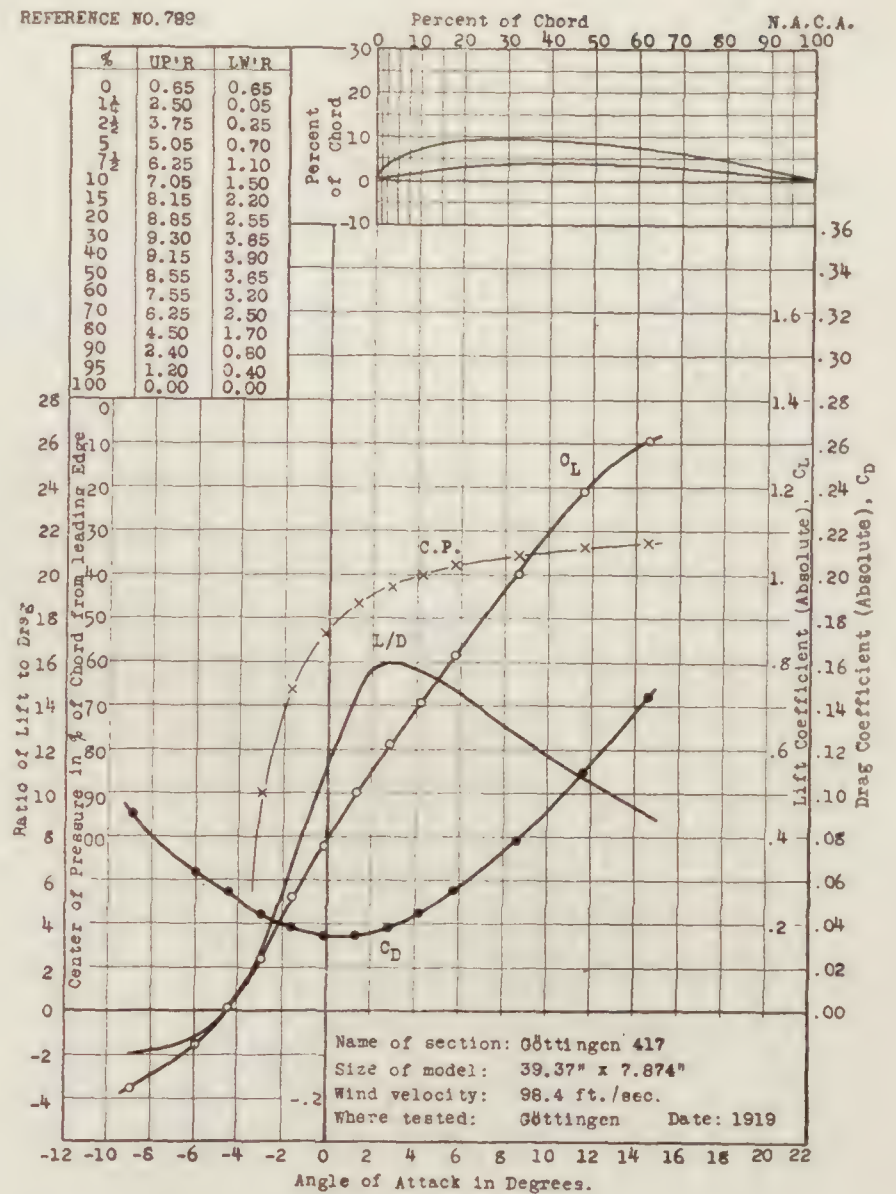
REFERENCE NO. 787



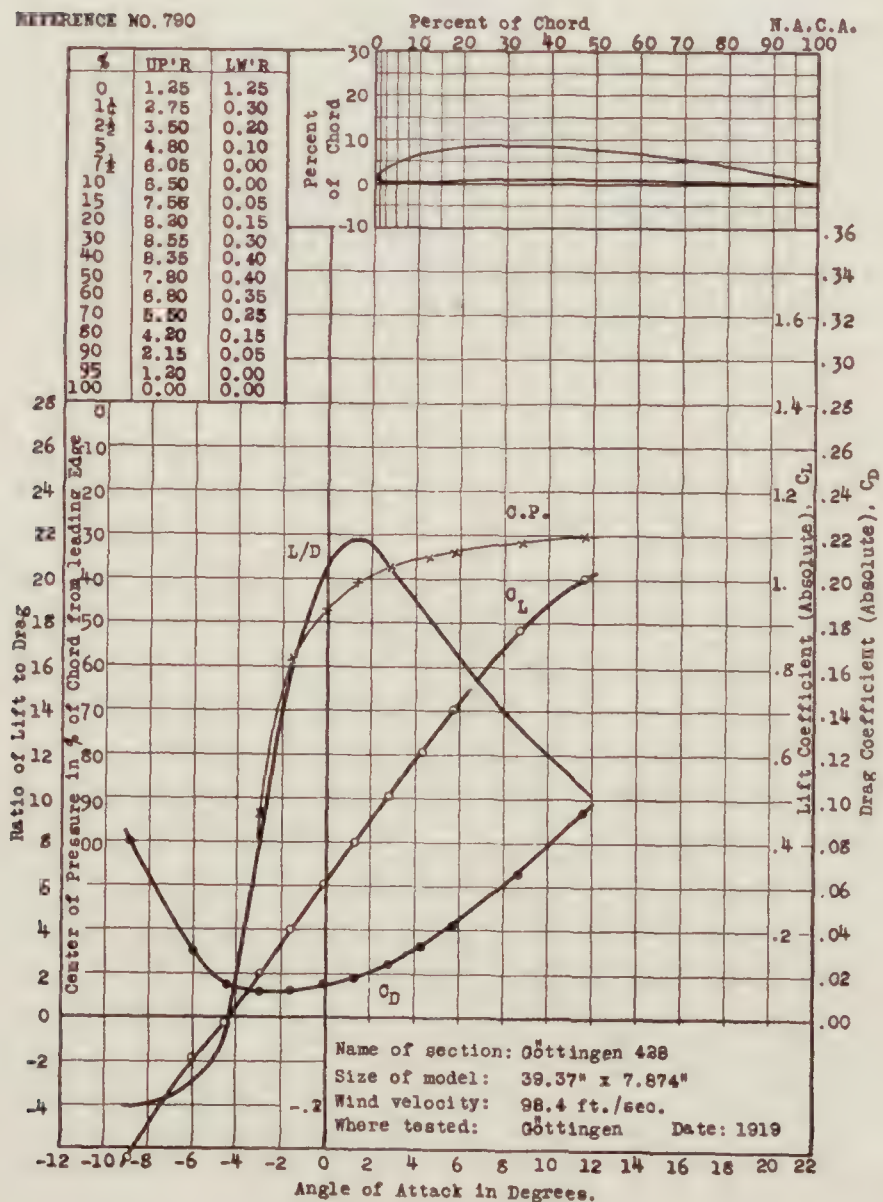
REFERENCE NO. 788



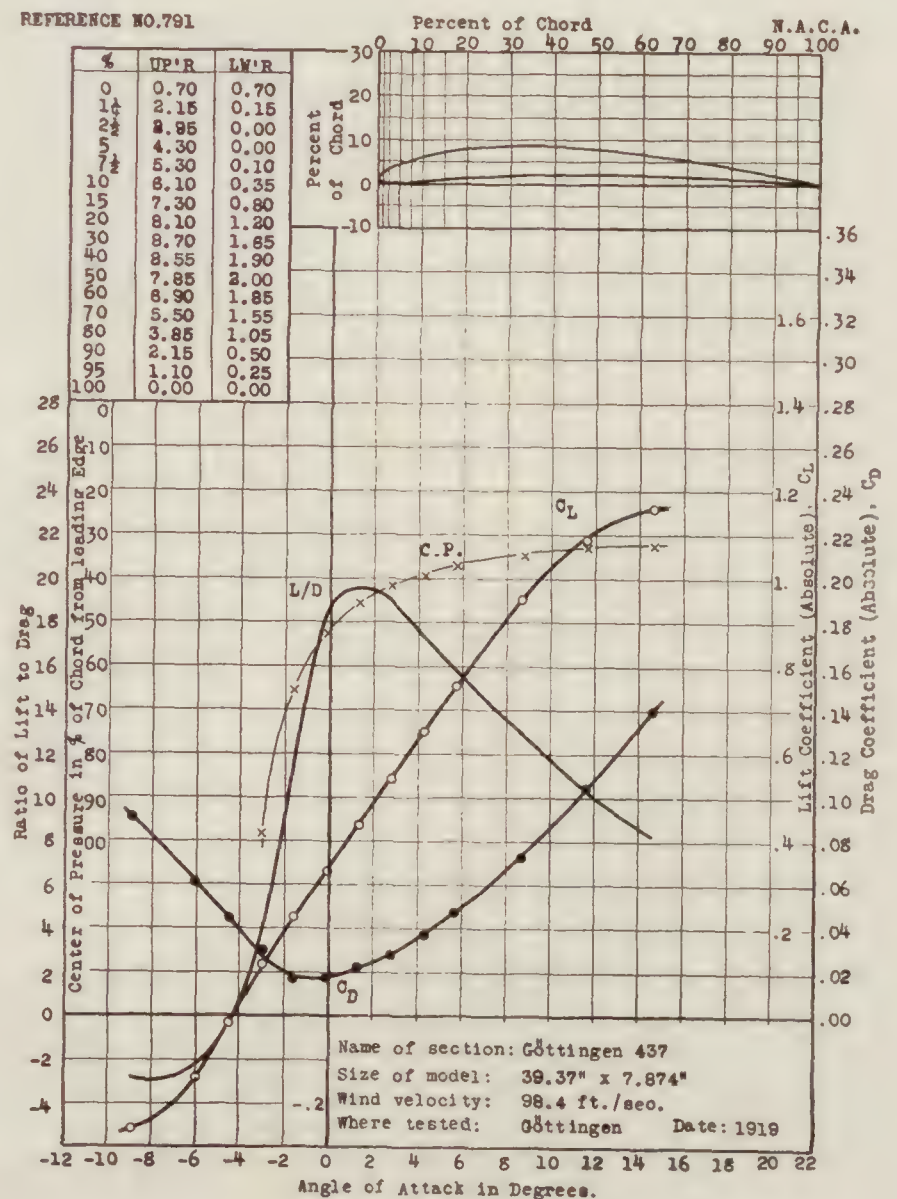
REFERENCE NO. 789



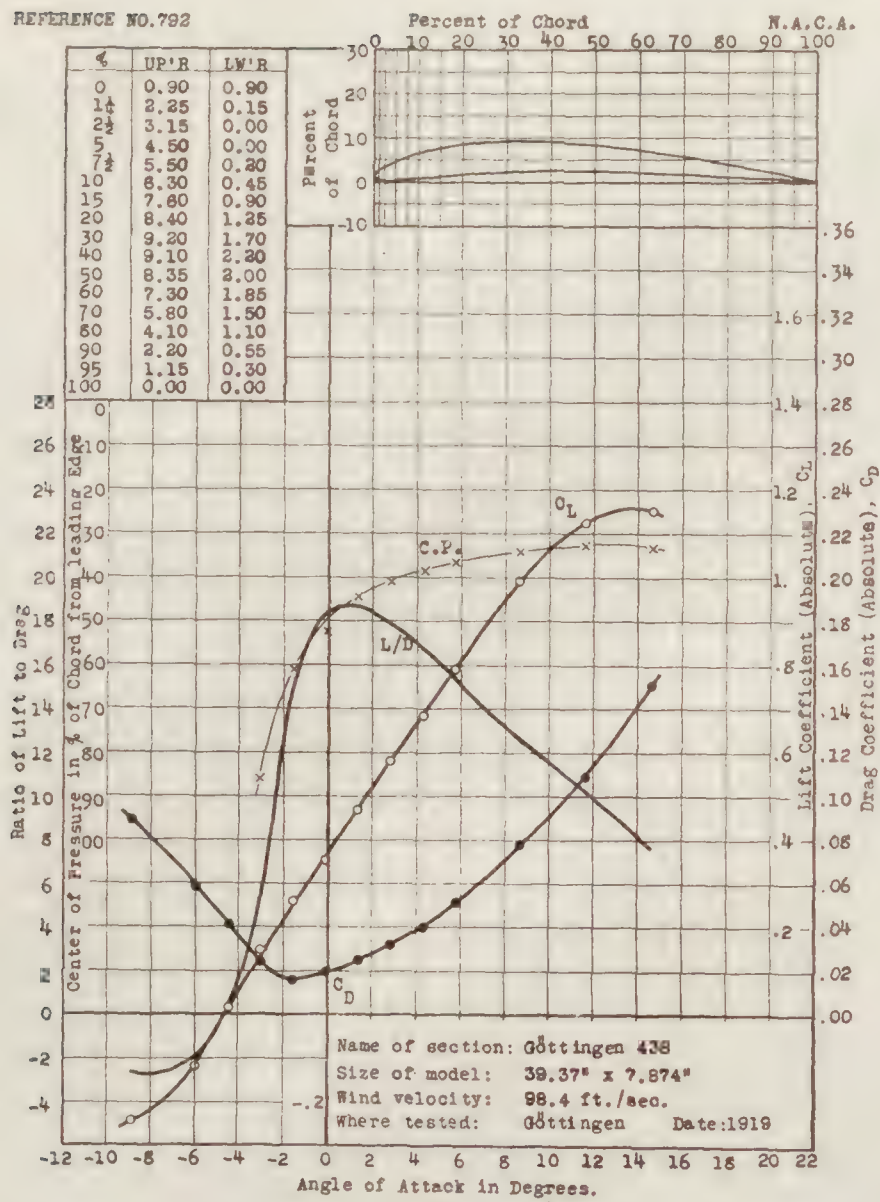
REFERENCE NO. 790



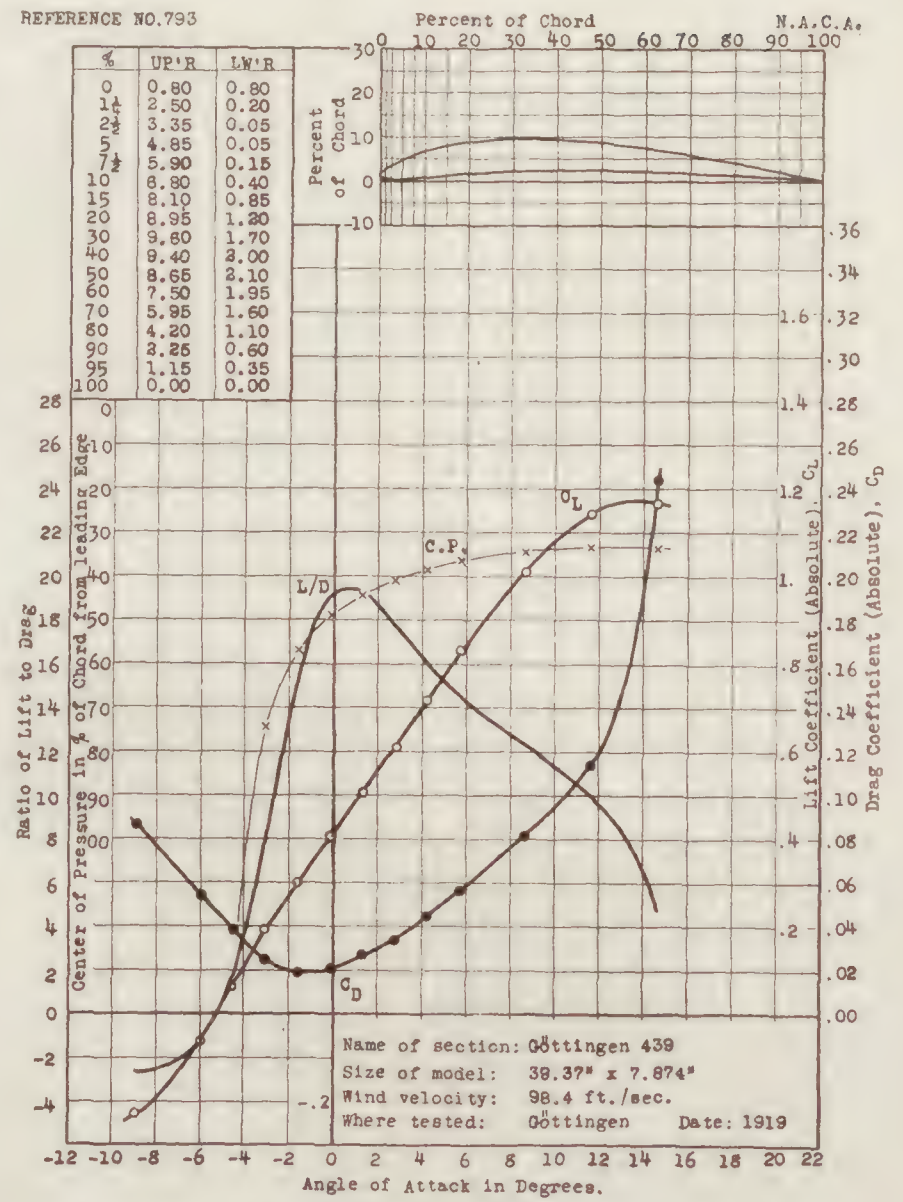
REFERENCE NO. 791



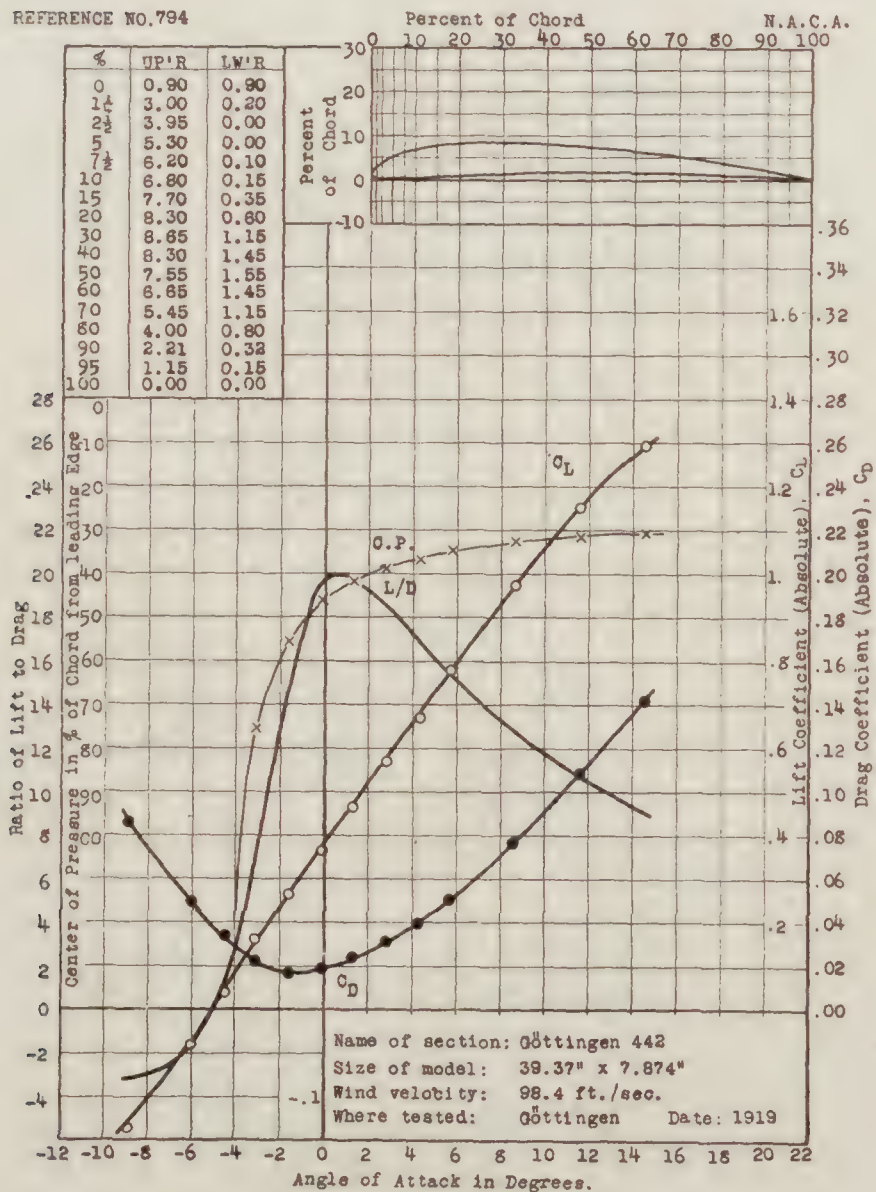
REFERENCE NO. 792



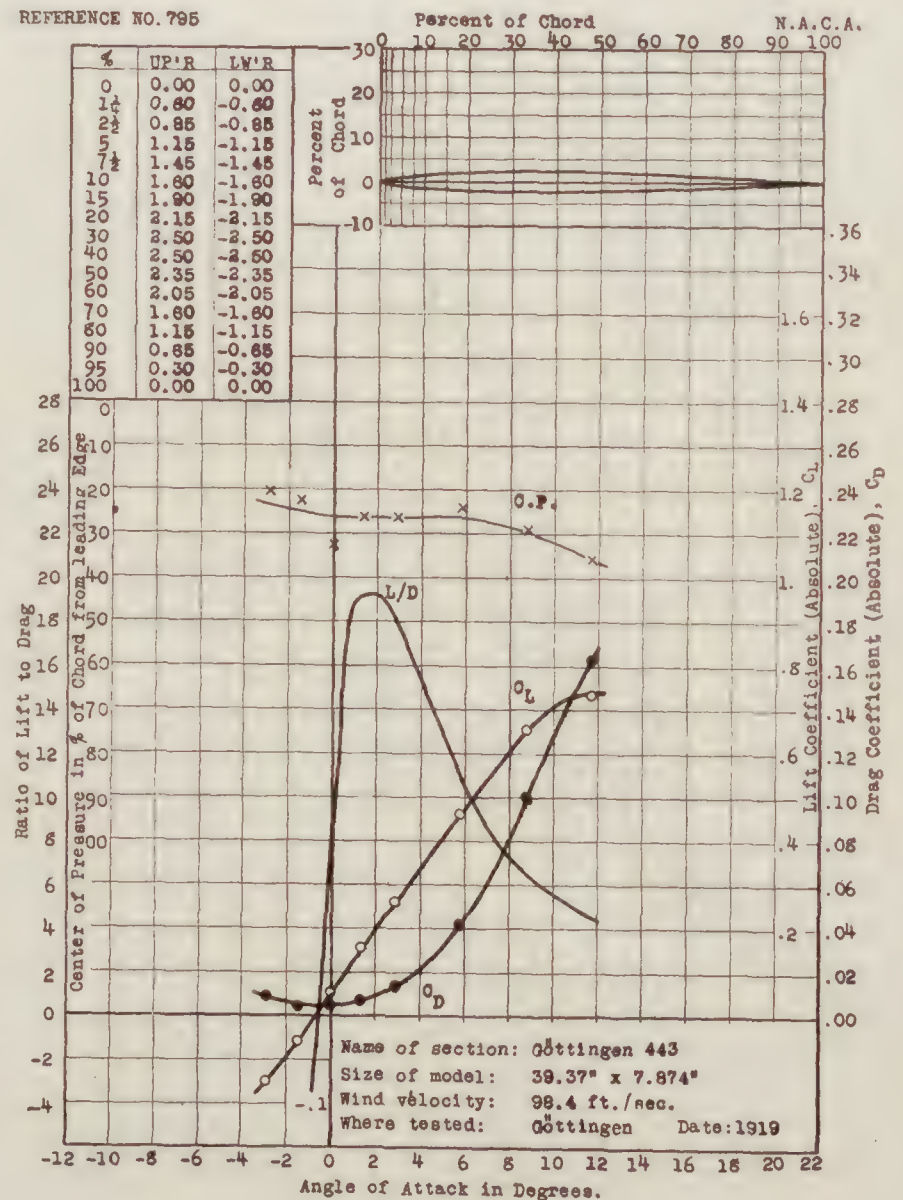
REFERENCE NO. 793



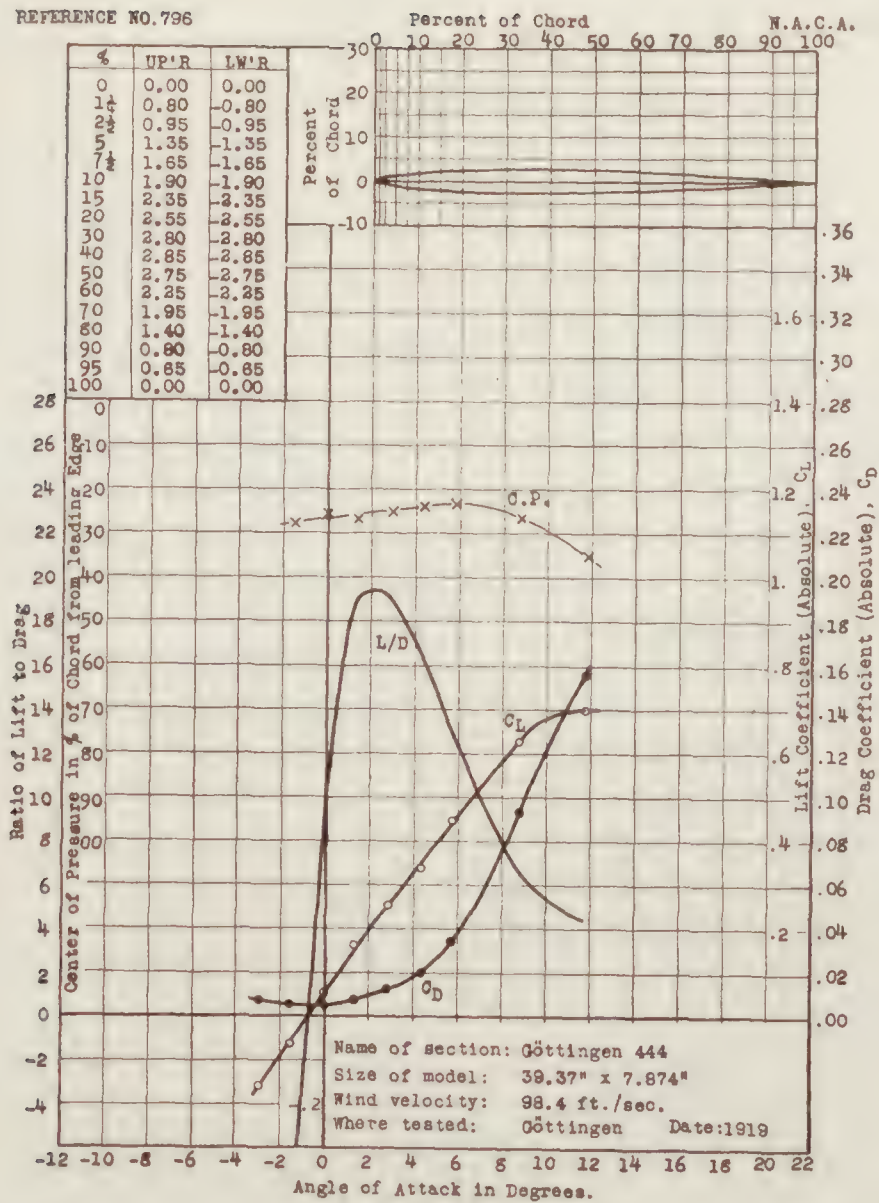
REFERENCE NO. 794



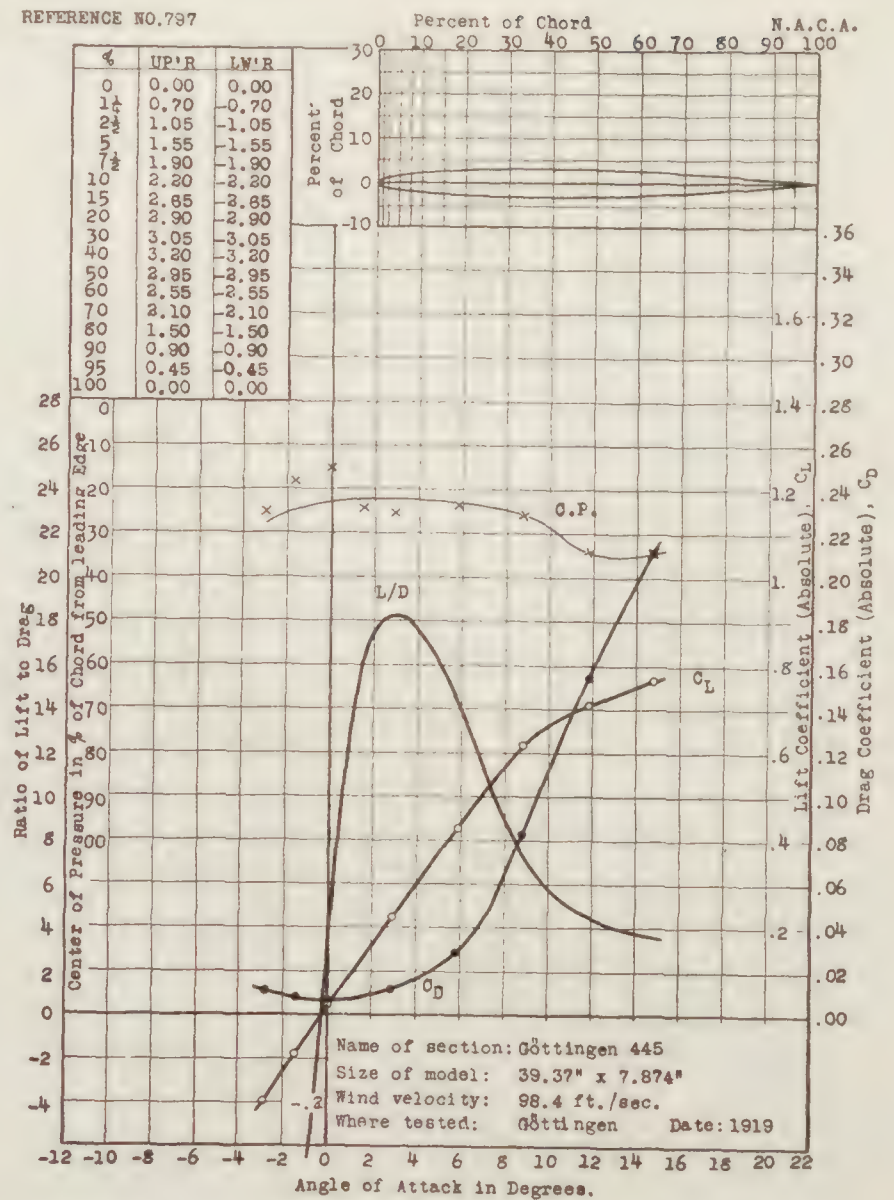
REFERENCE NO. 795



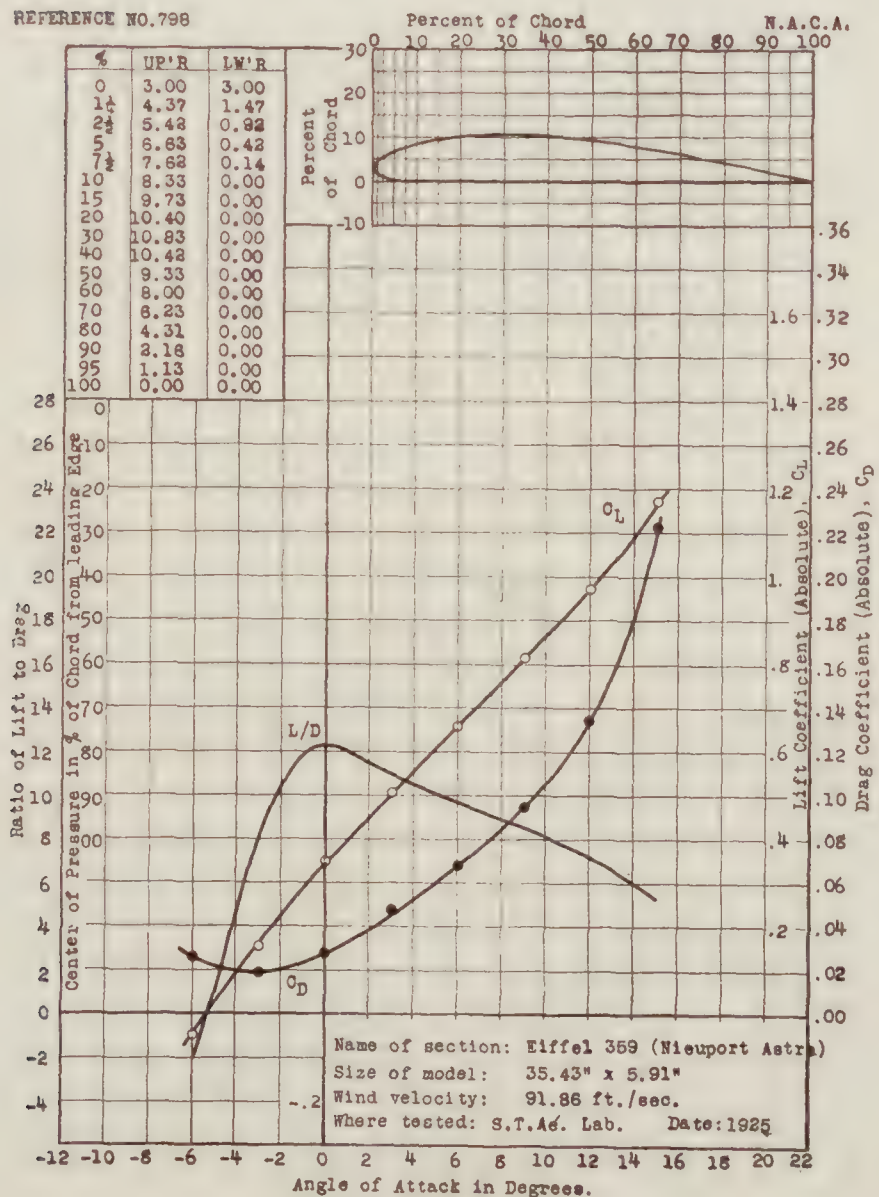
REFERENCE NO. 796



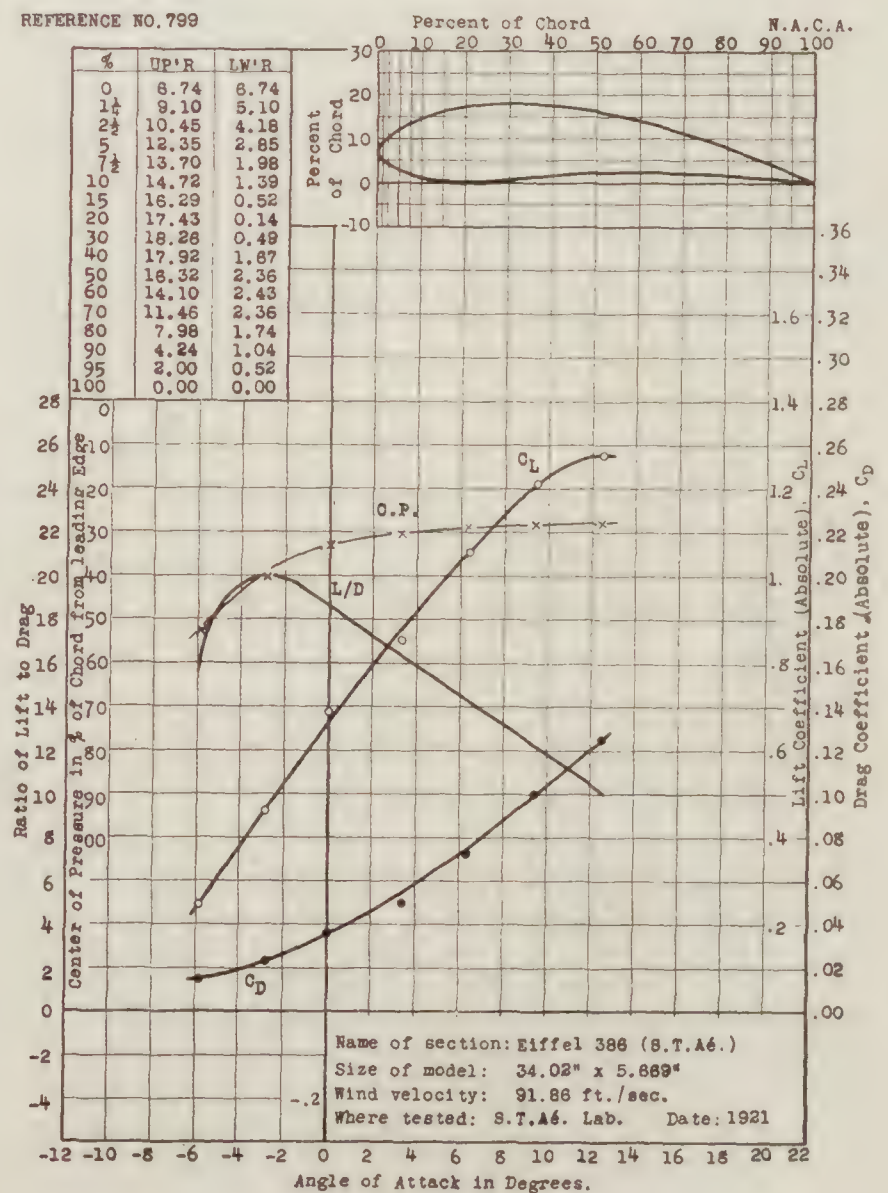
REFERENCE NO. 797



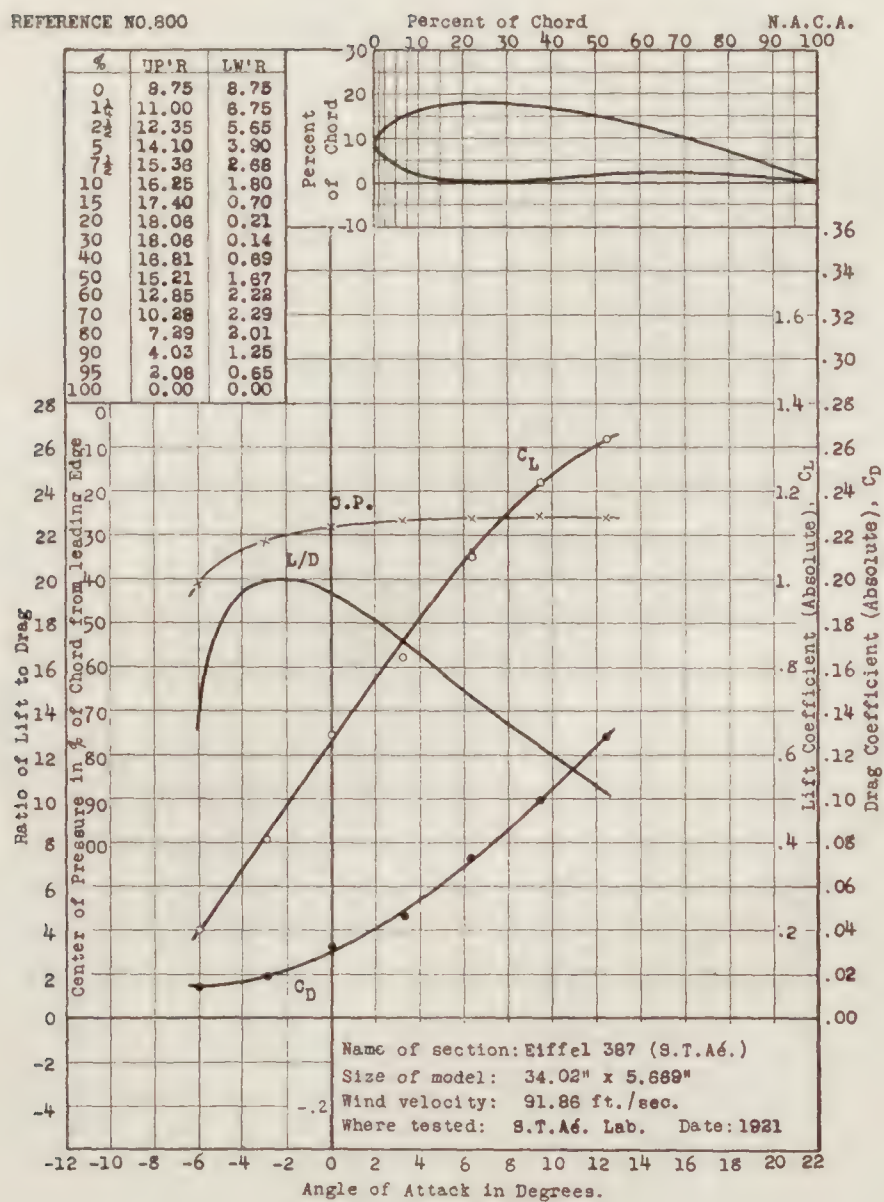
REFERENCE NO. 798



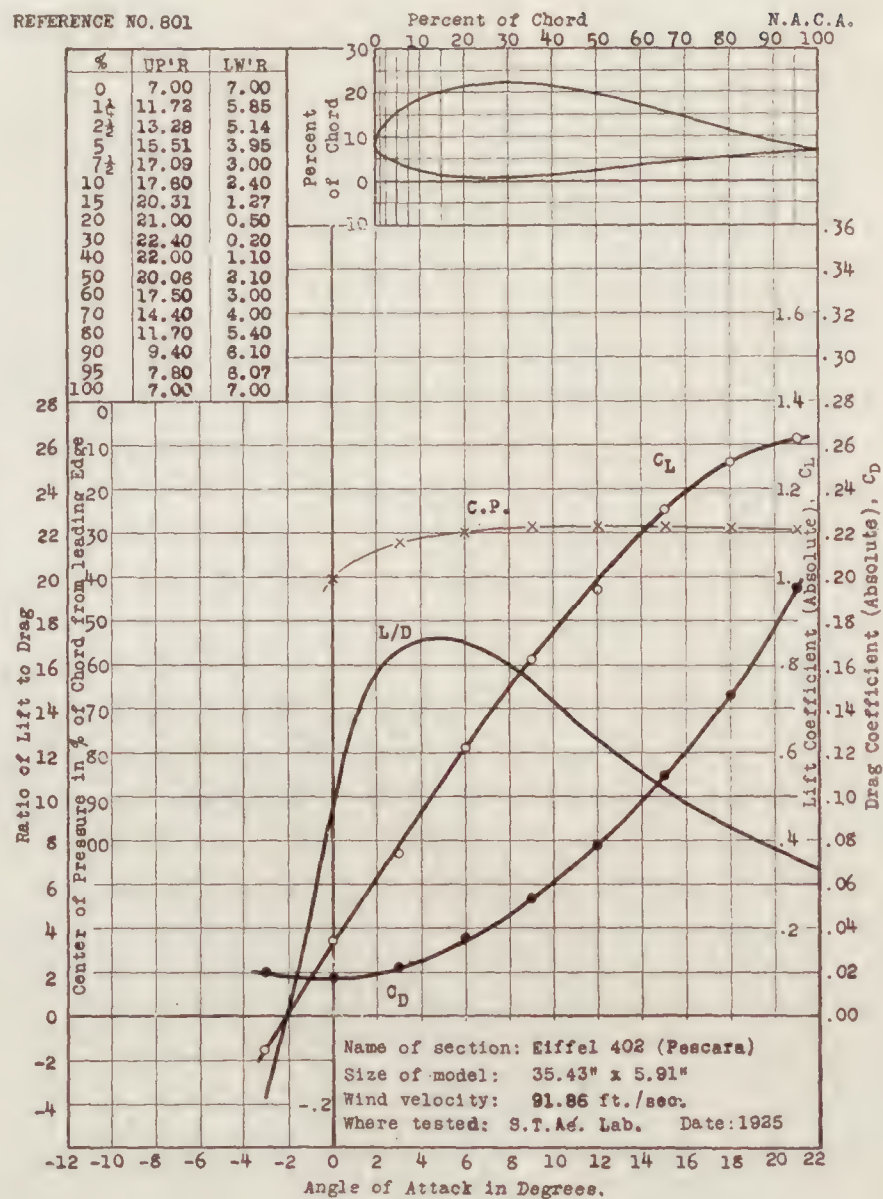
REFERENCE NO. 799



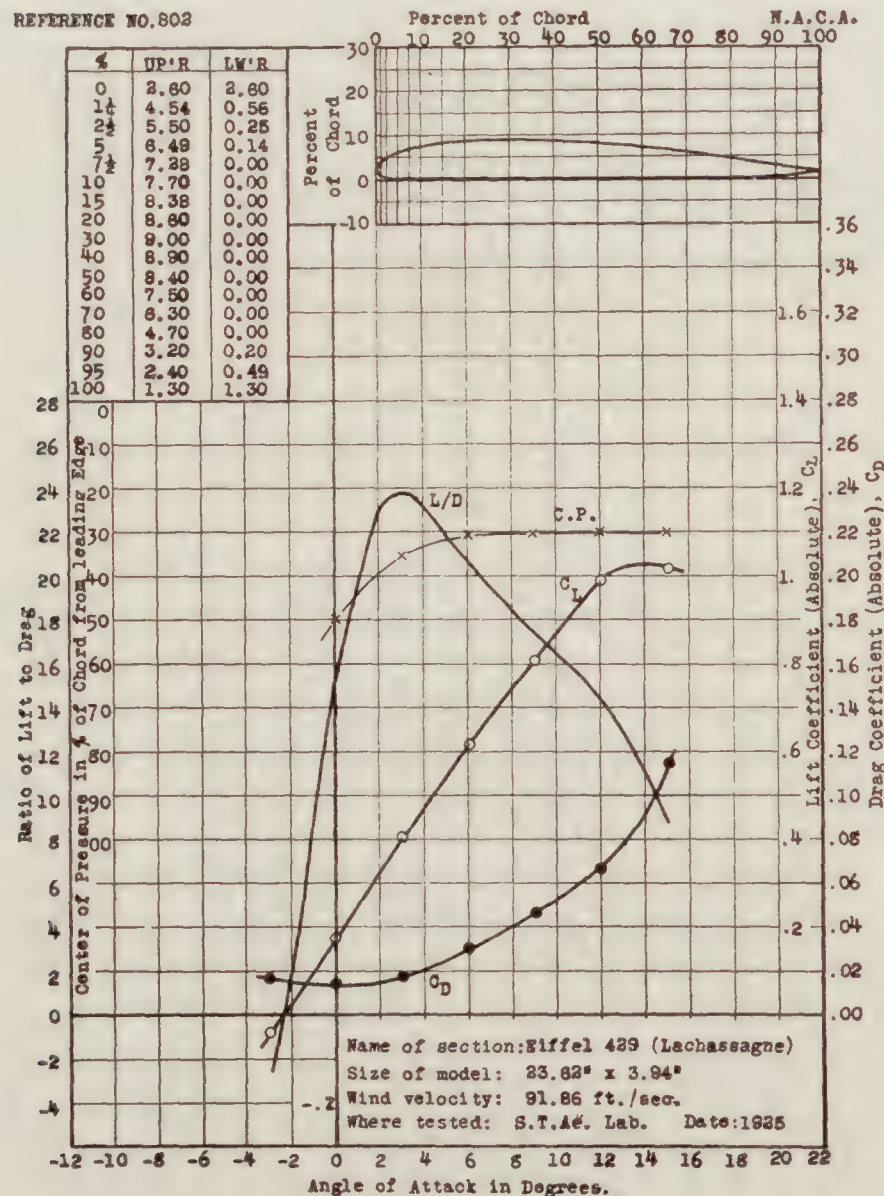
REFERENCE NO. 800



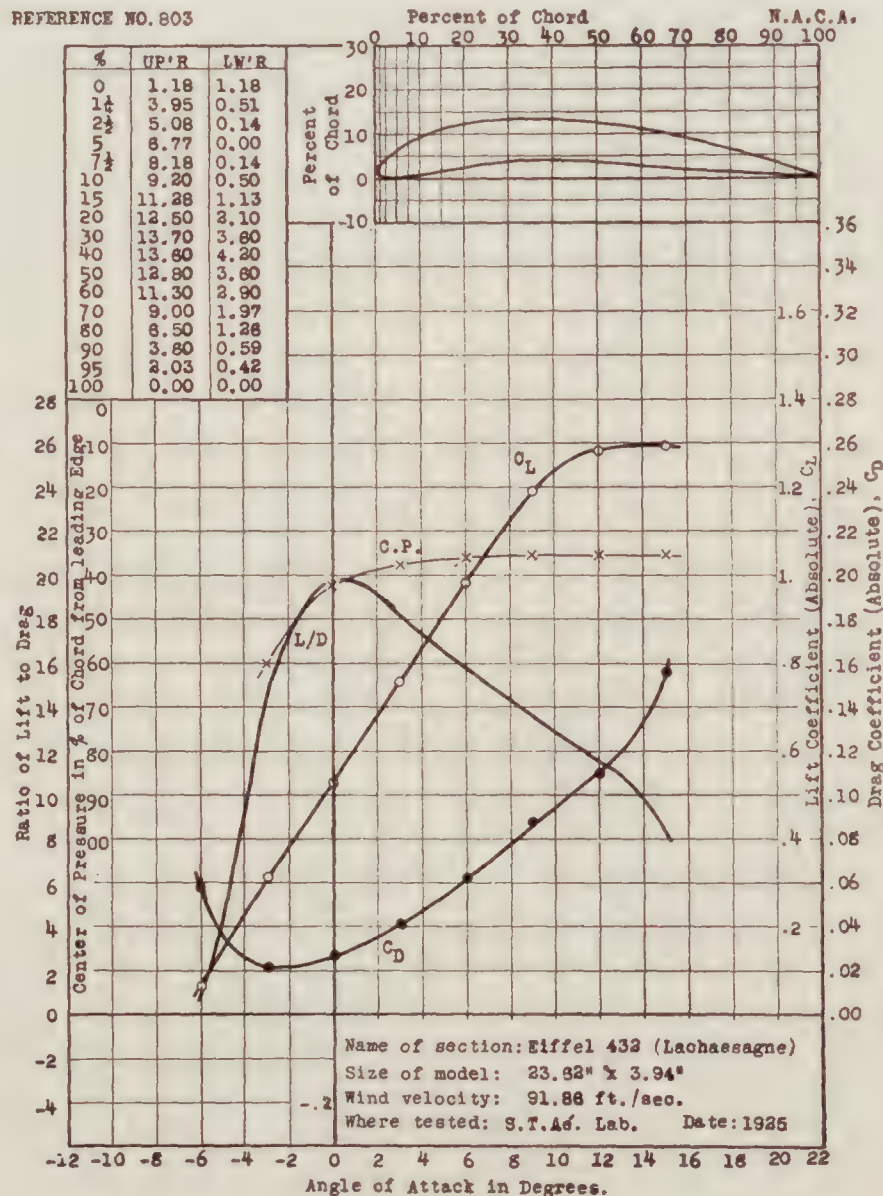
REFERENCE NO. 801



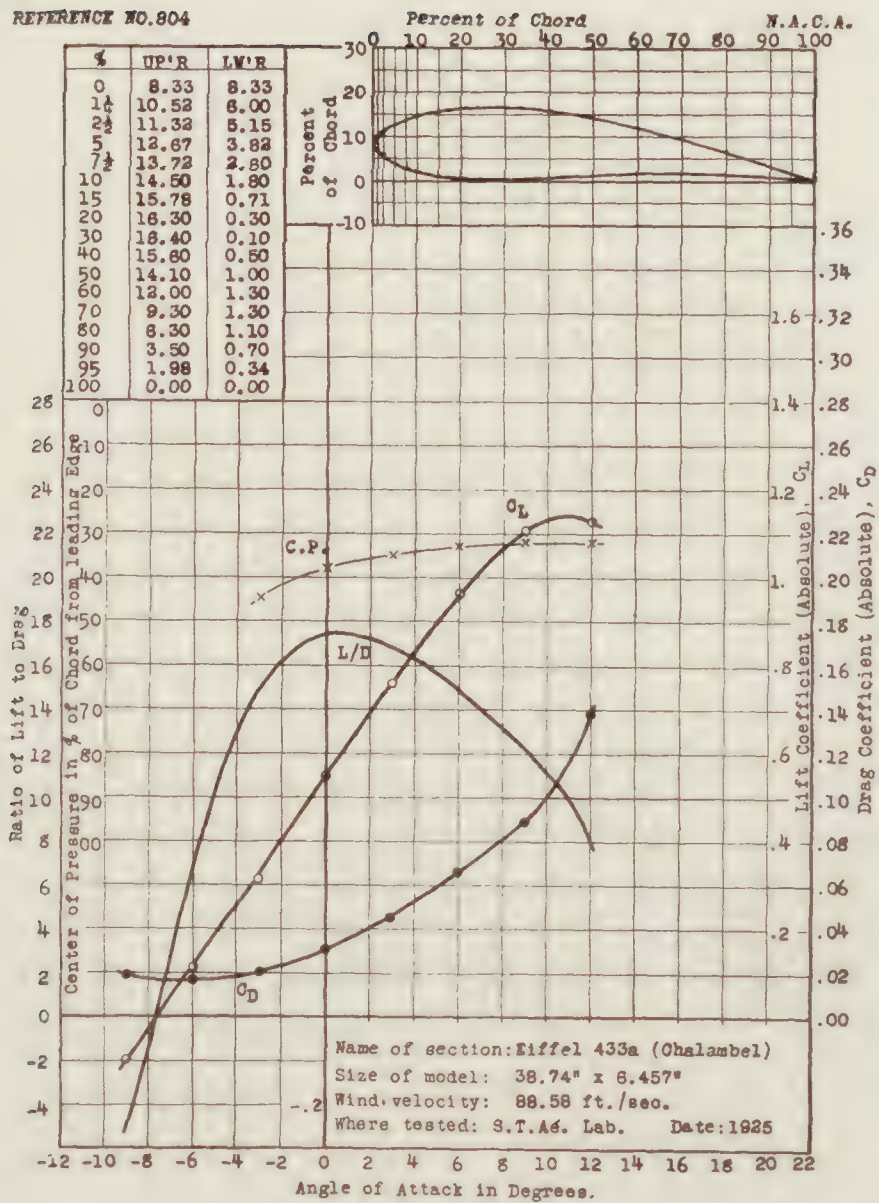
REFERENCE NO. 802



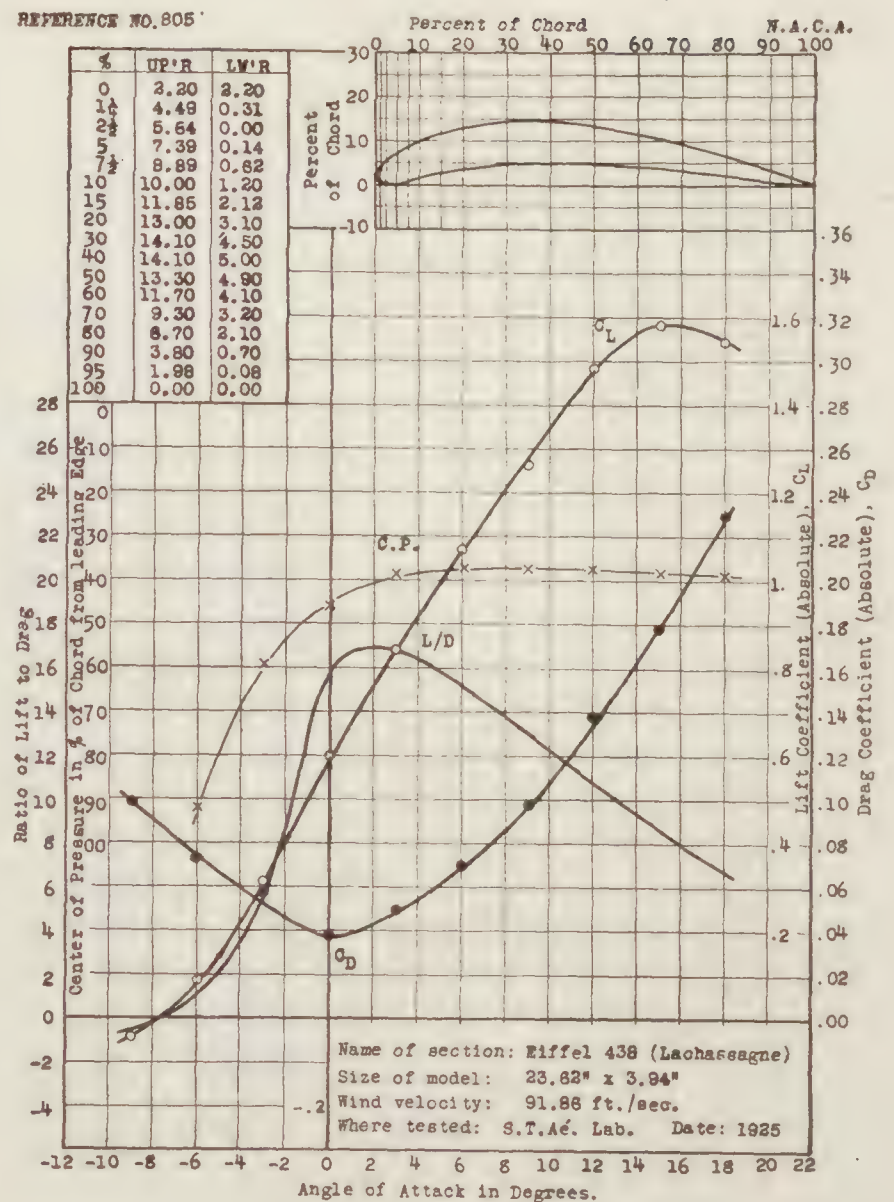
REFERENCE NO. 803



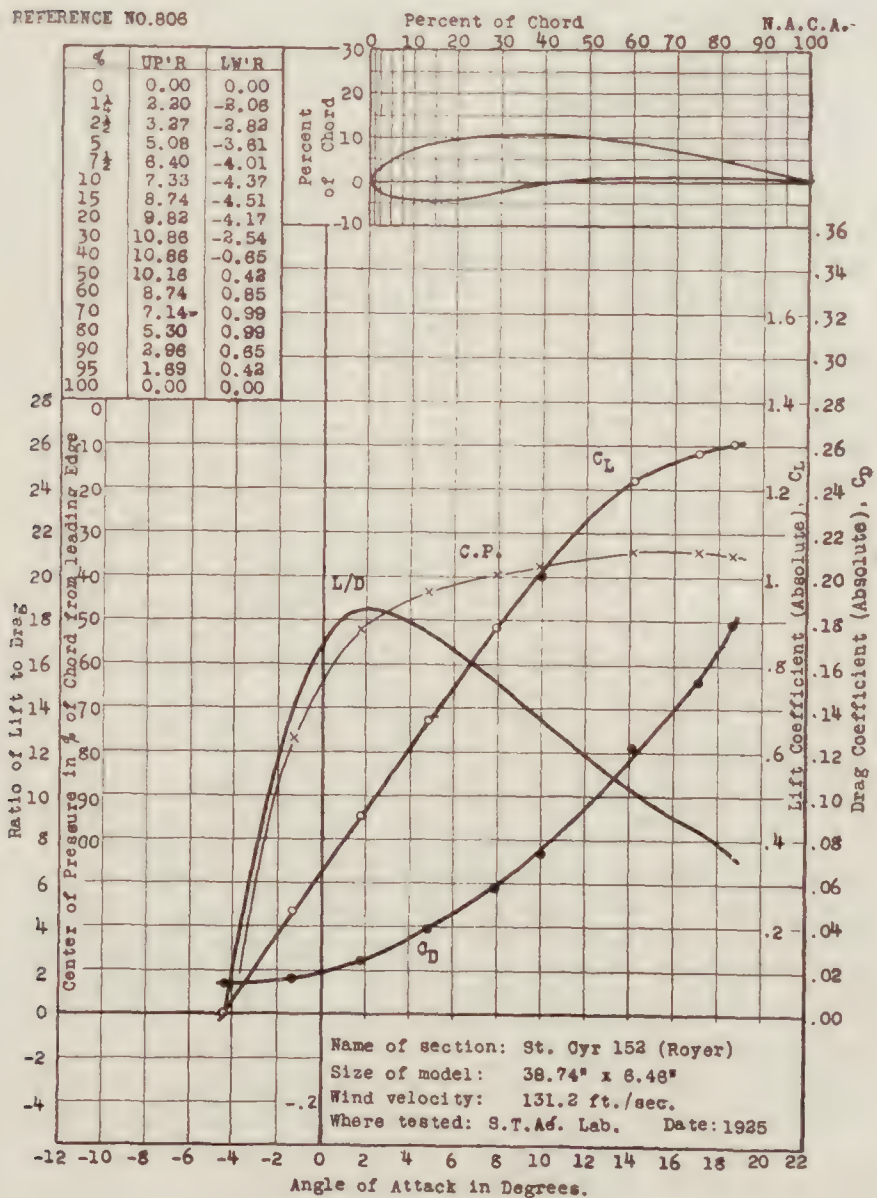
REFERENCE NO. 804



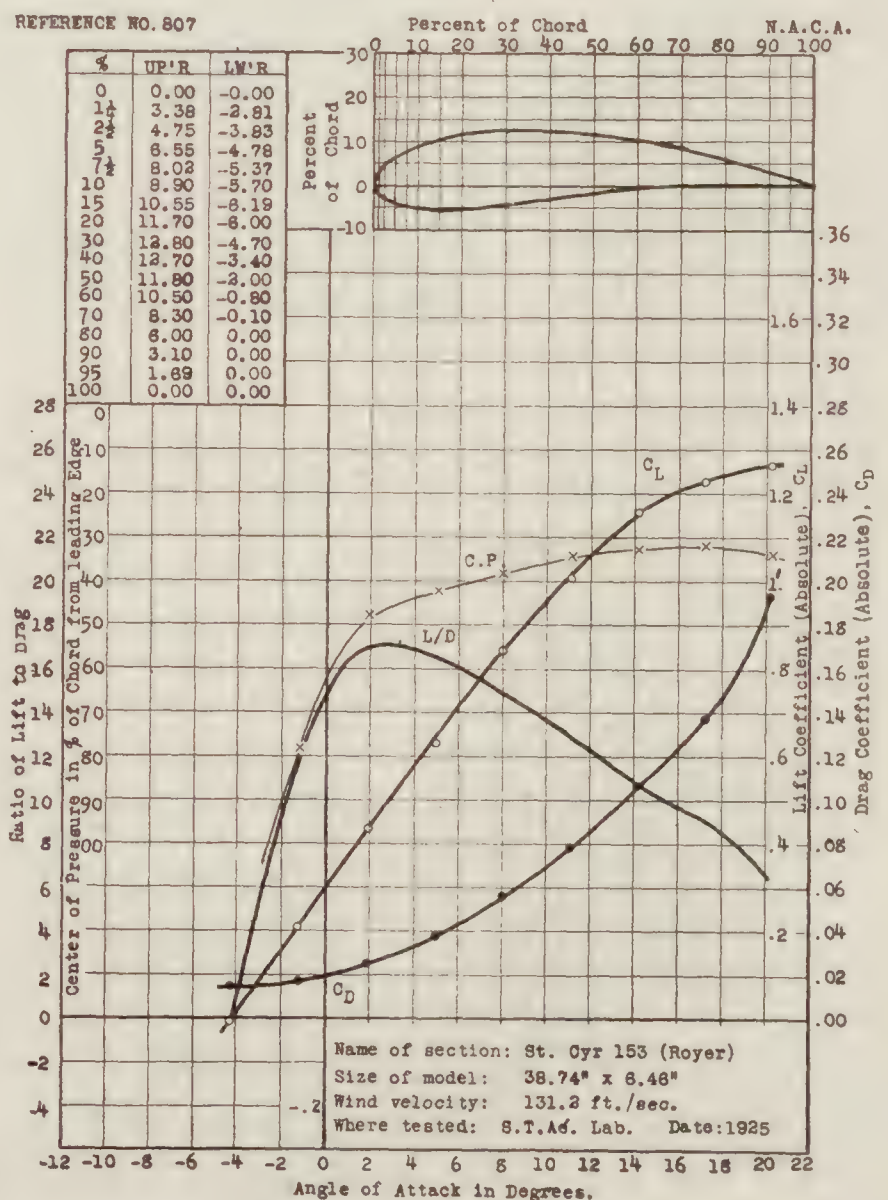
REFERENCE NO. 805



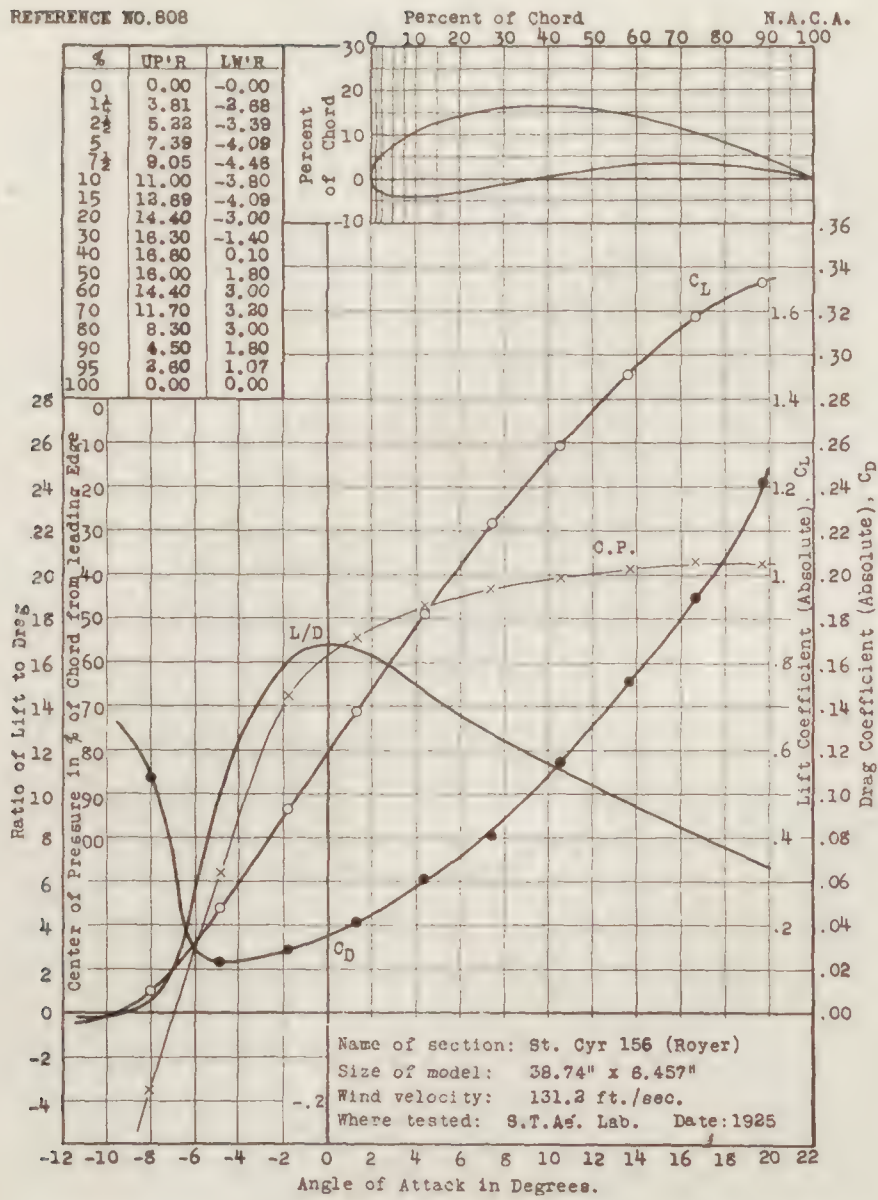
REFERENCE NO. 808



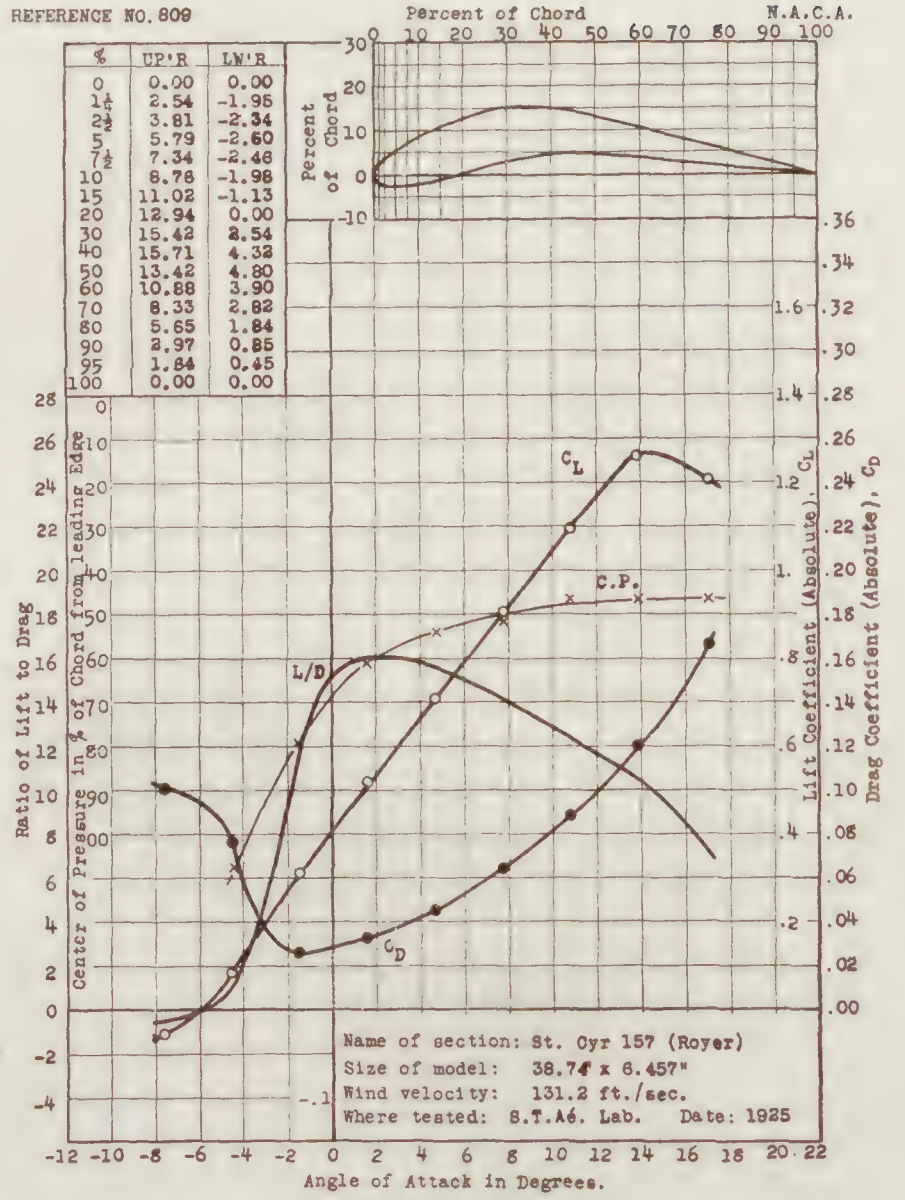
REFERENCE NO. 807



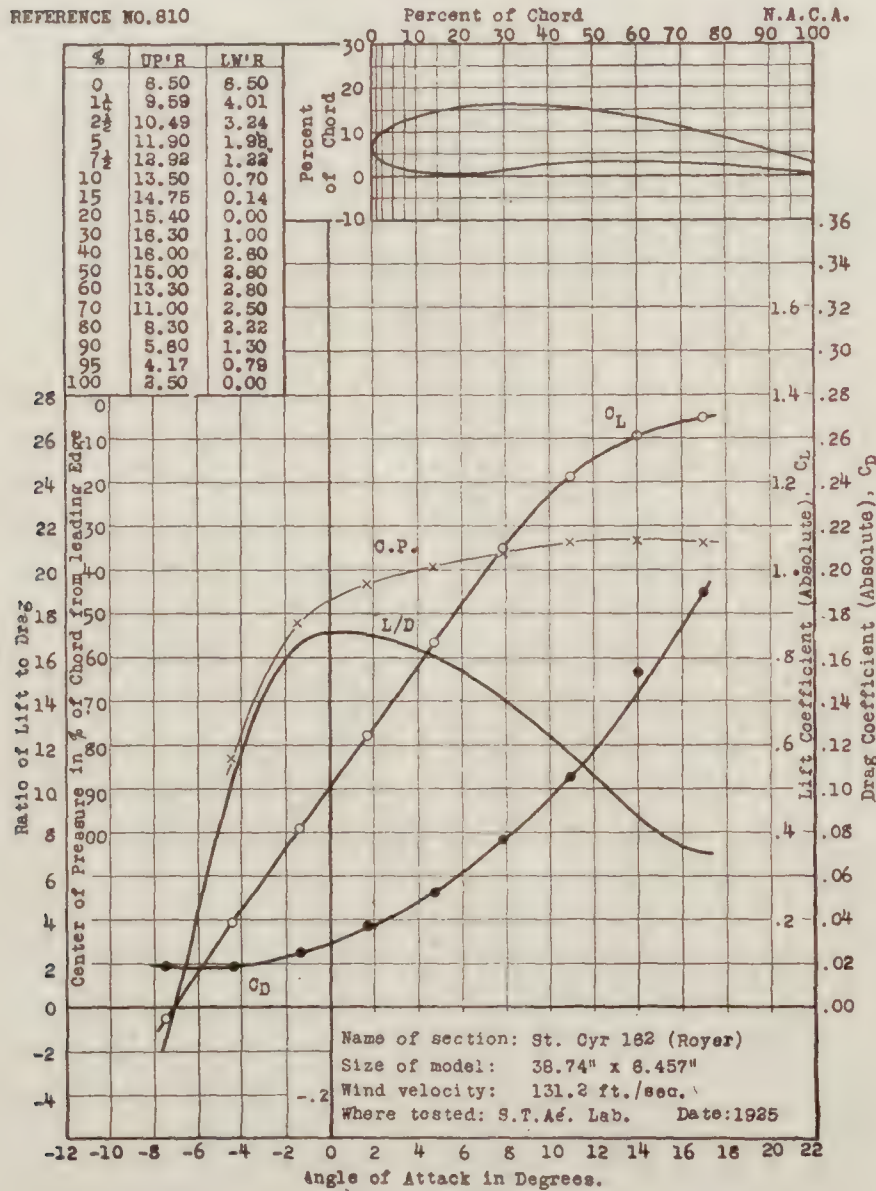
REFERENCE NO. 808



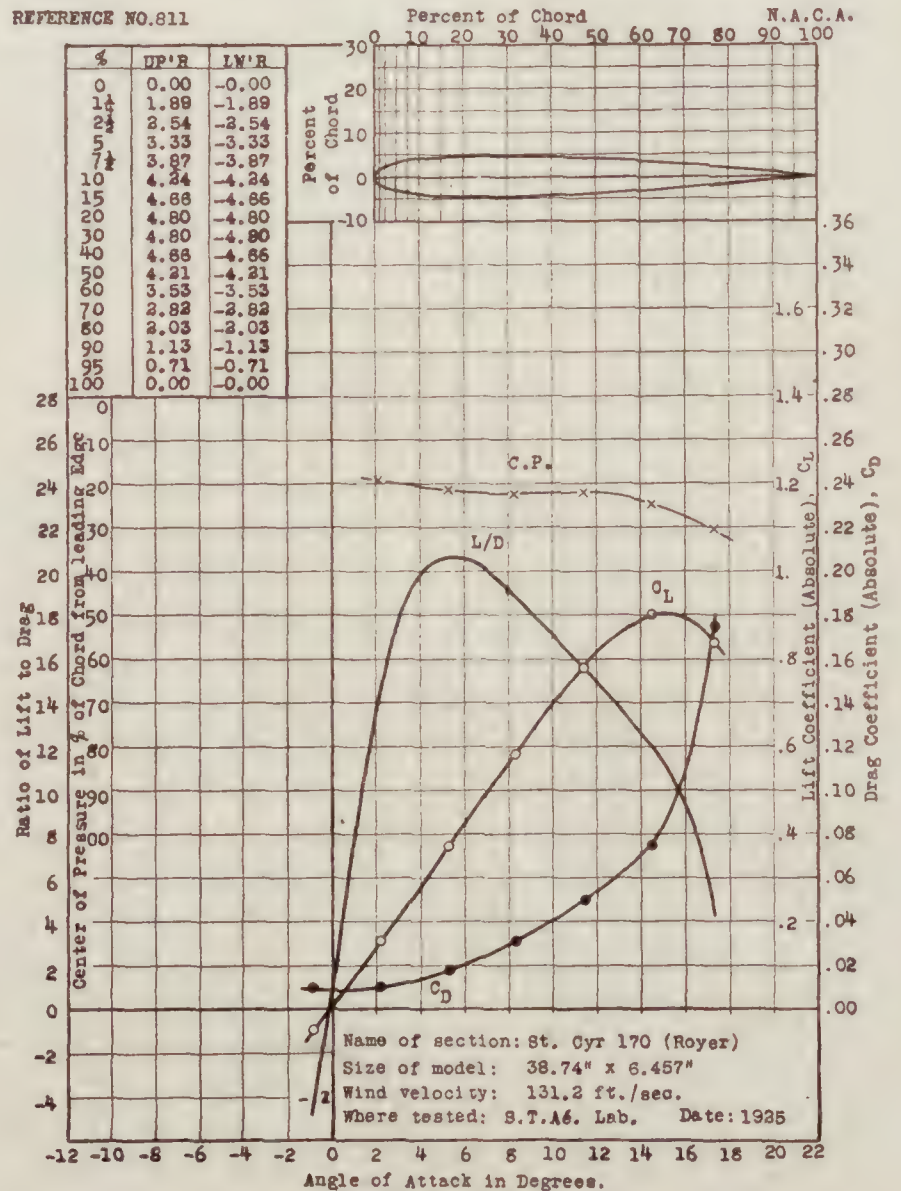
REFERENCE NO. 809



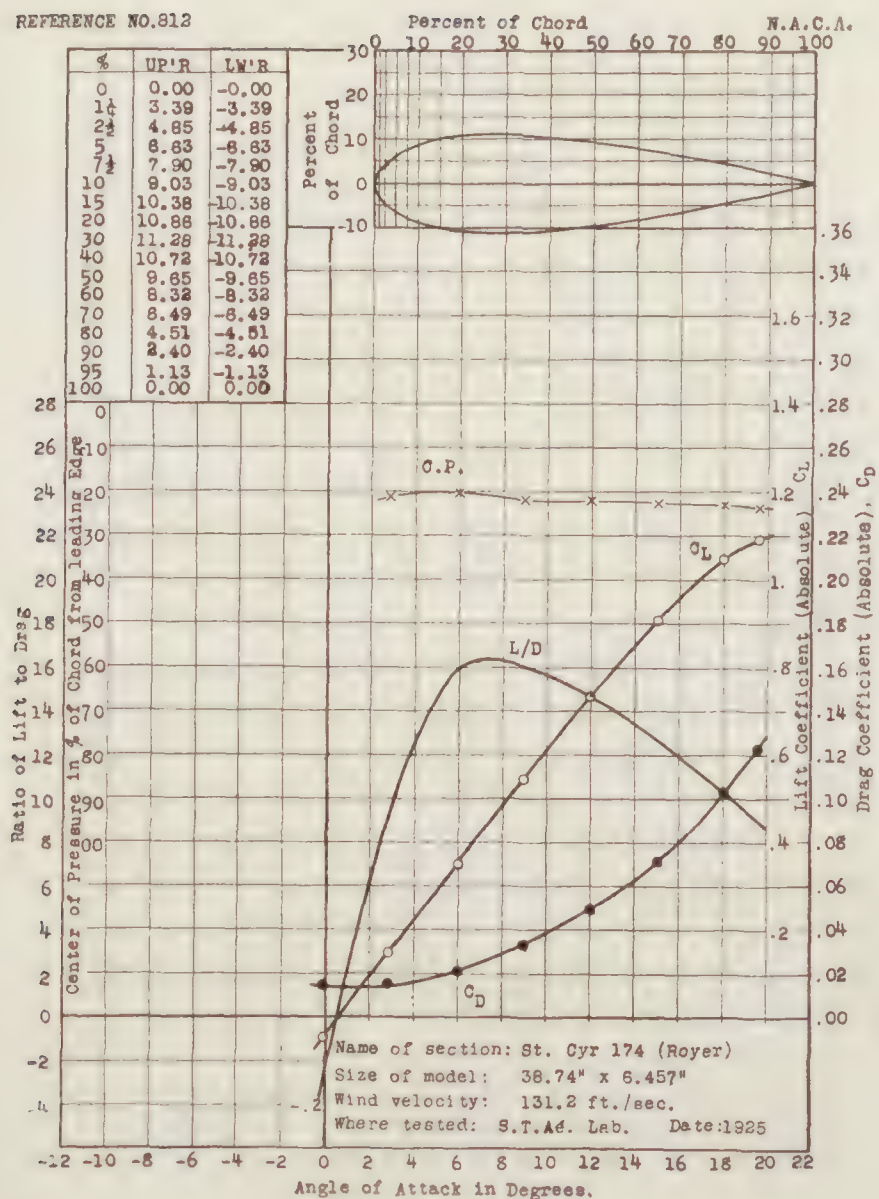
REFERENCE NO. 810



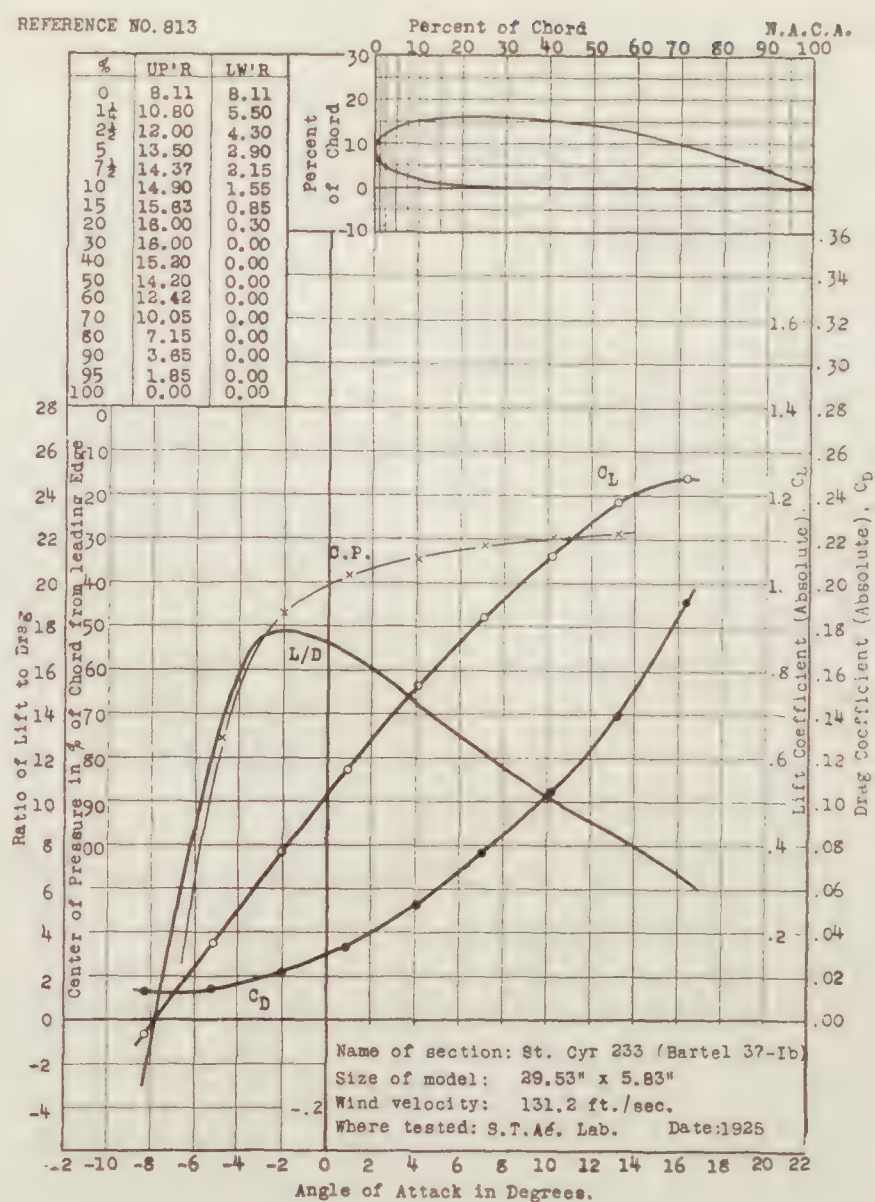
REFERENCE NO. 811



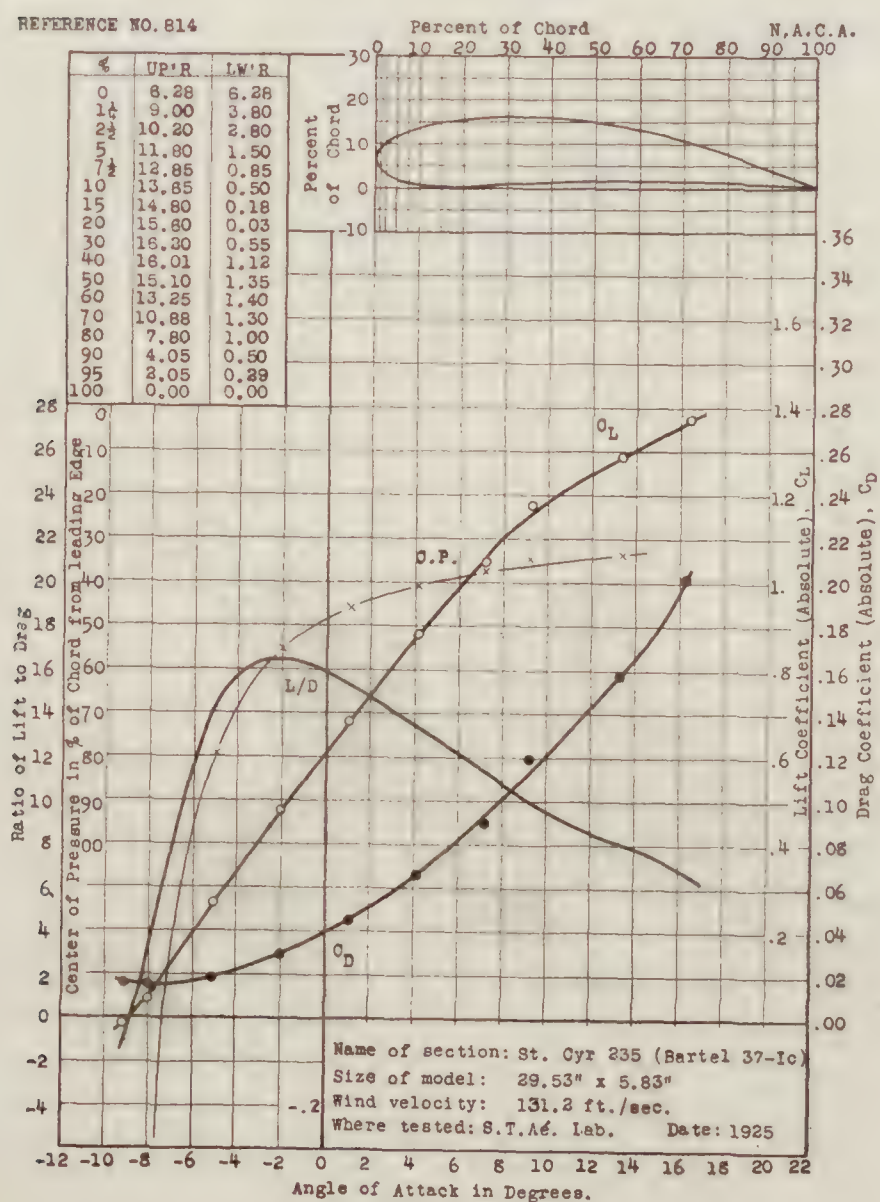
REFERENCE NO. 812



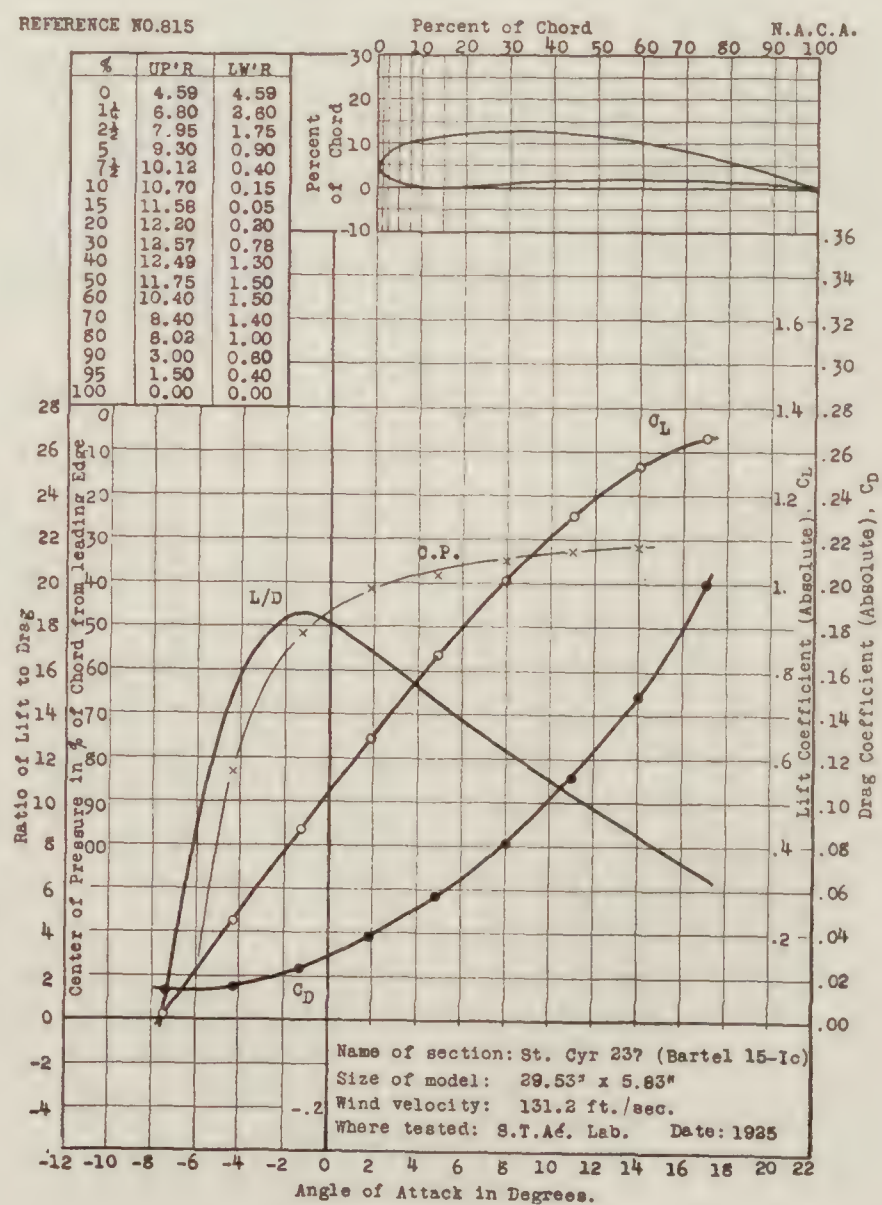
REFERENCE NO. 813



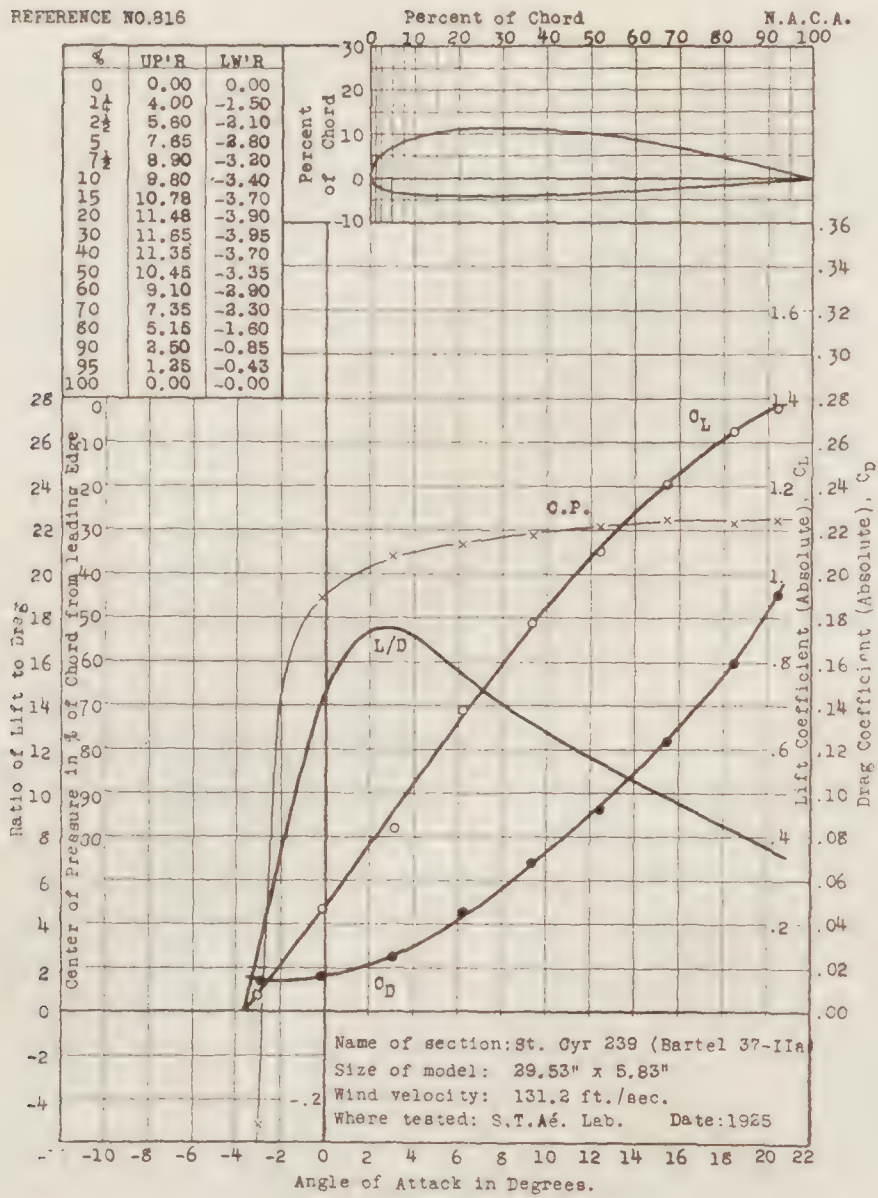
REFERENCE NO. 814



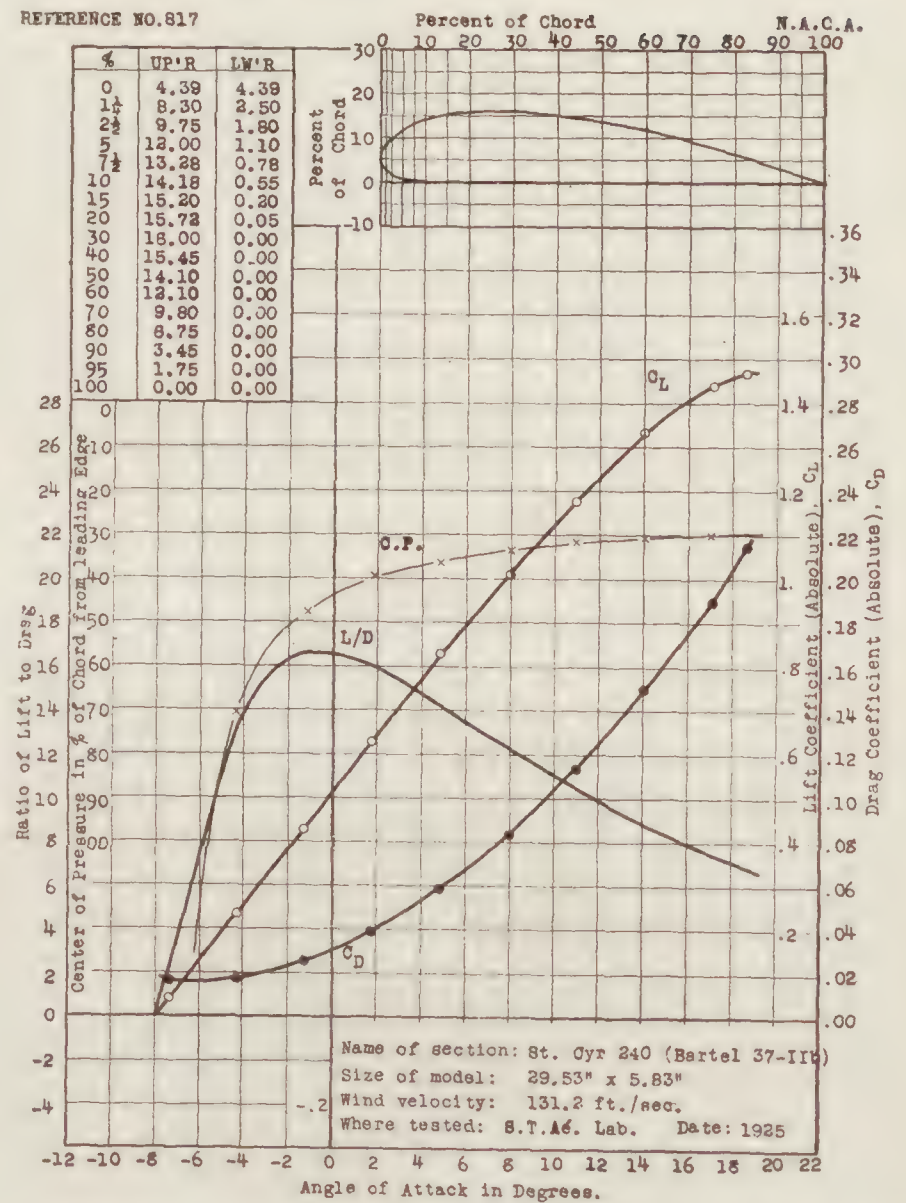
REFERENCE NO. 815



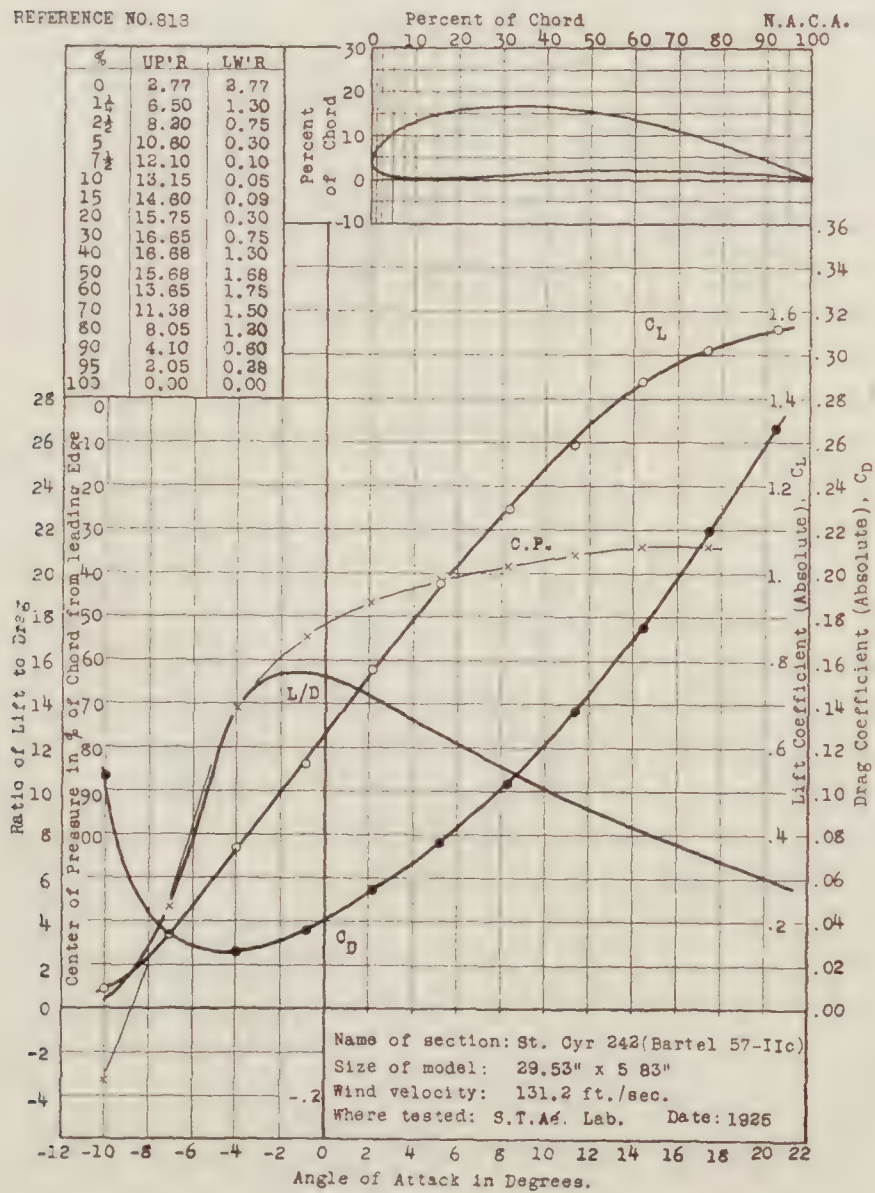
REFERENCE NO.816



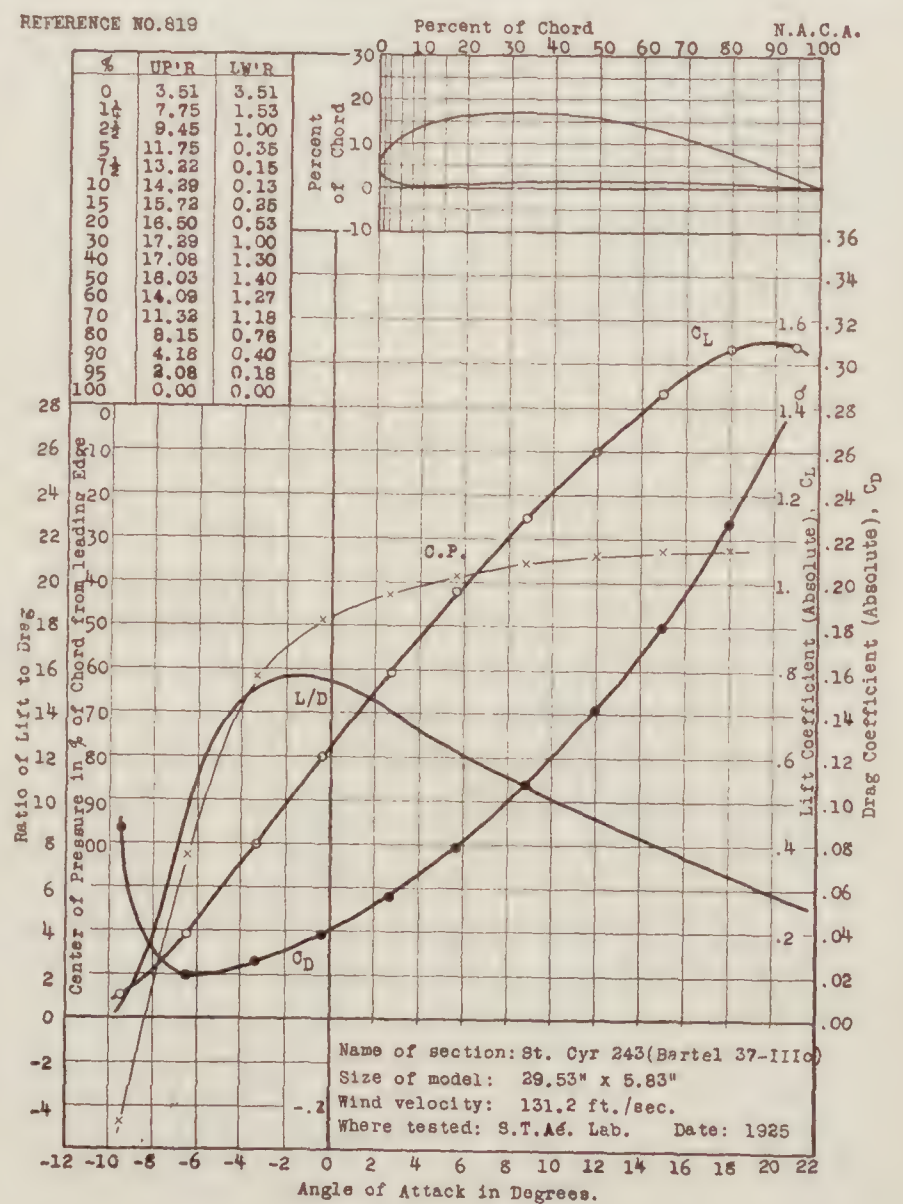
REFERENCE NO.817



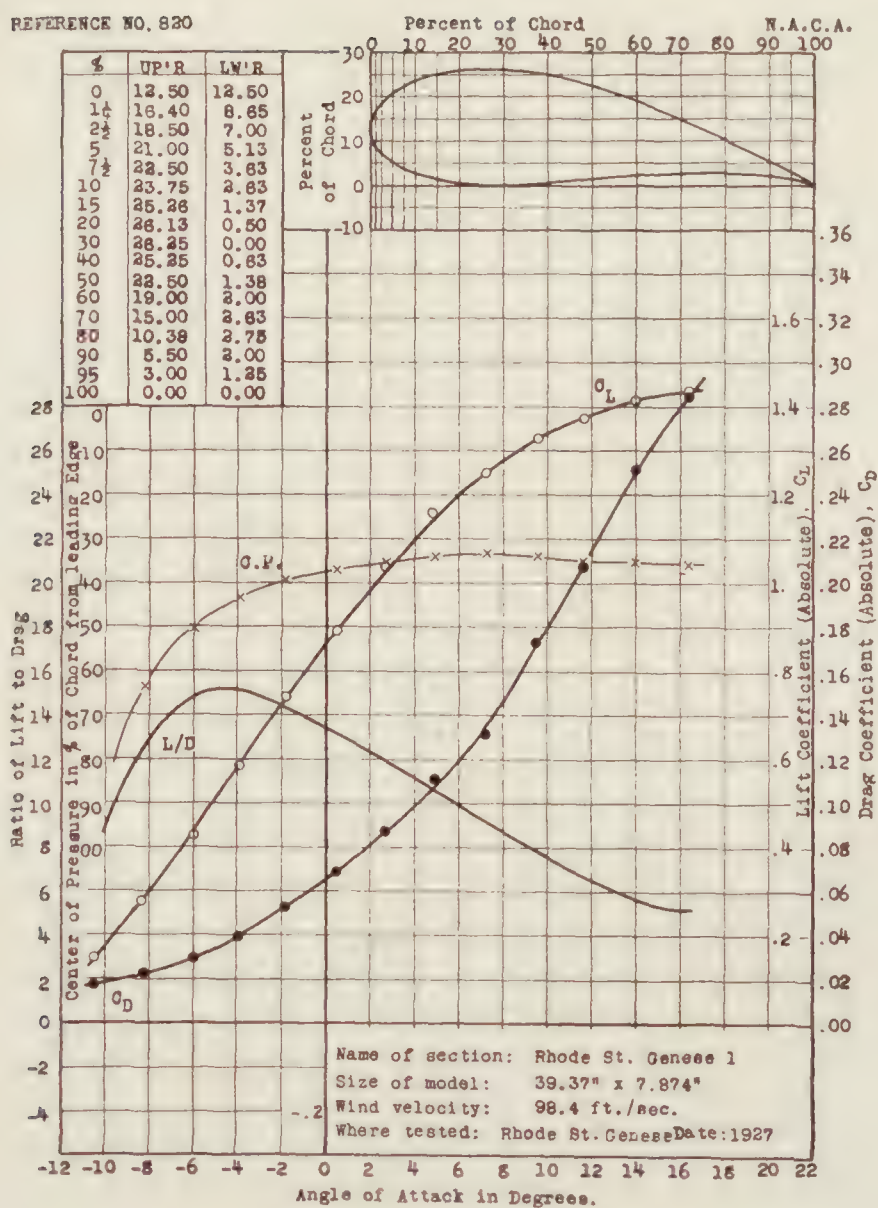
REFERENCE NO.818



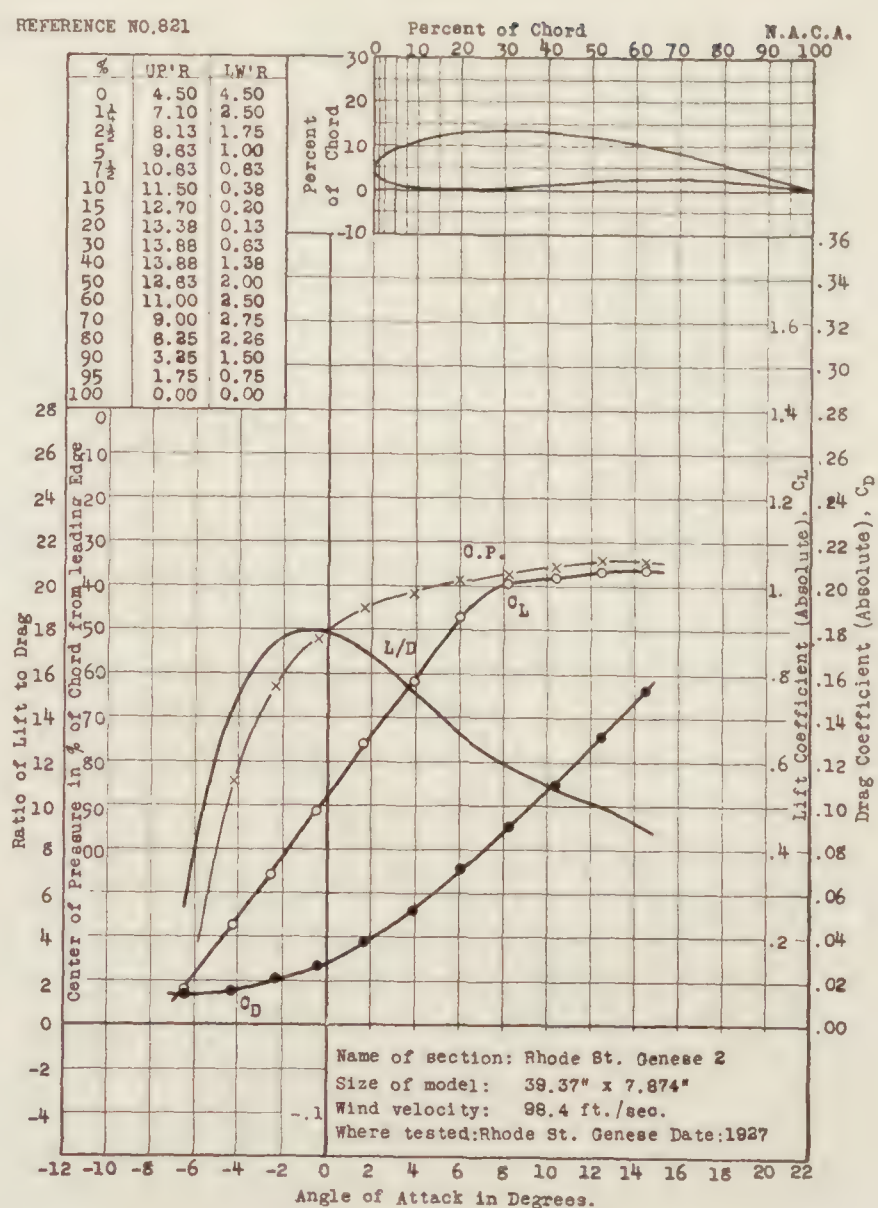
REFERENCE NO.819



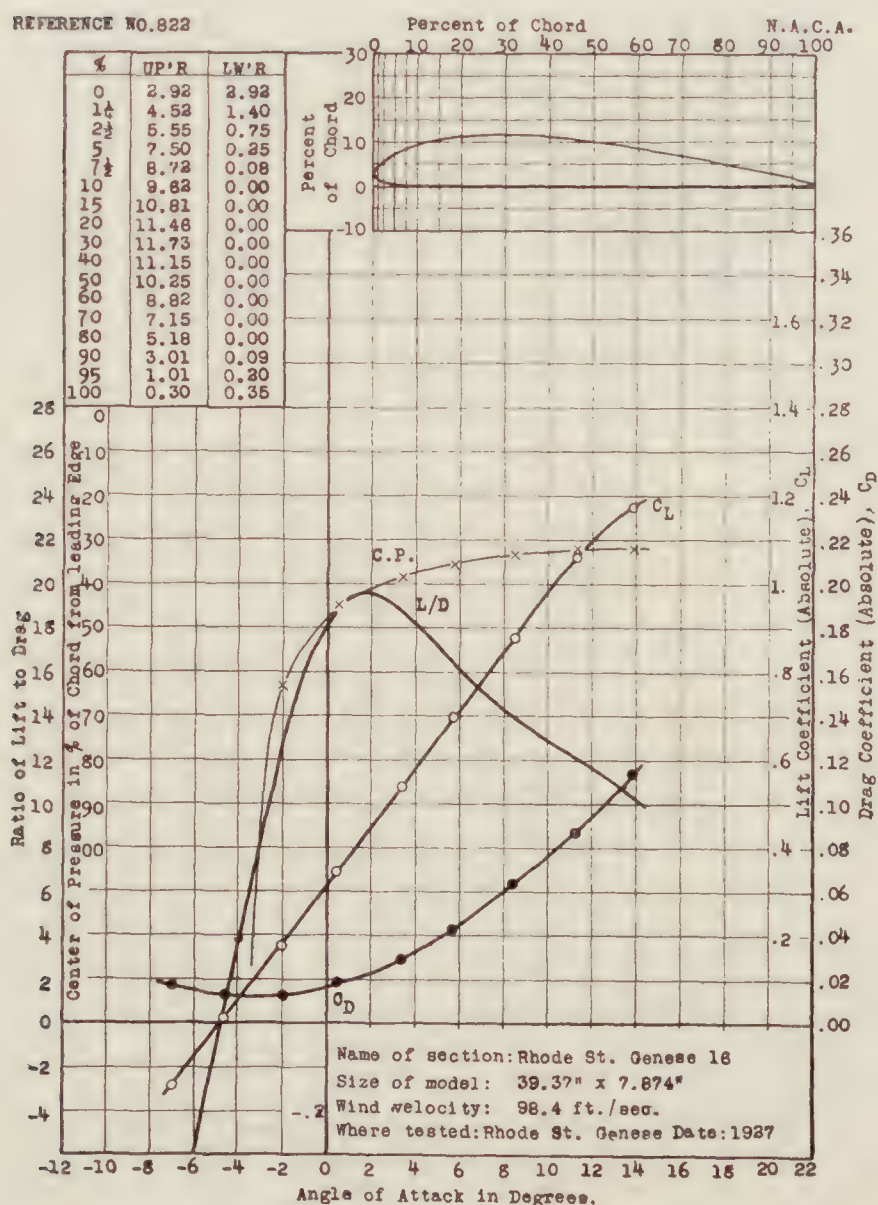
REFERENCE NO. 820



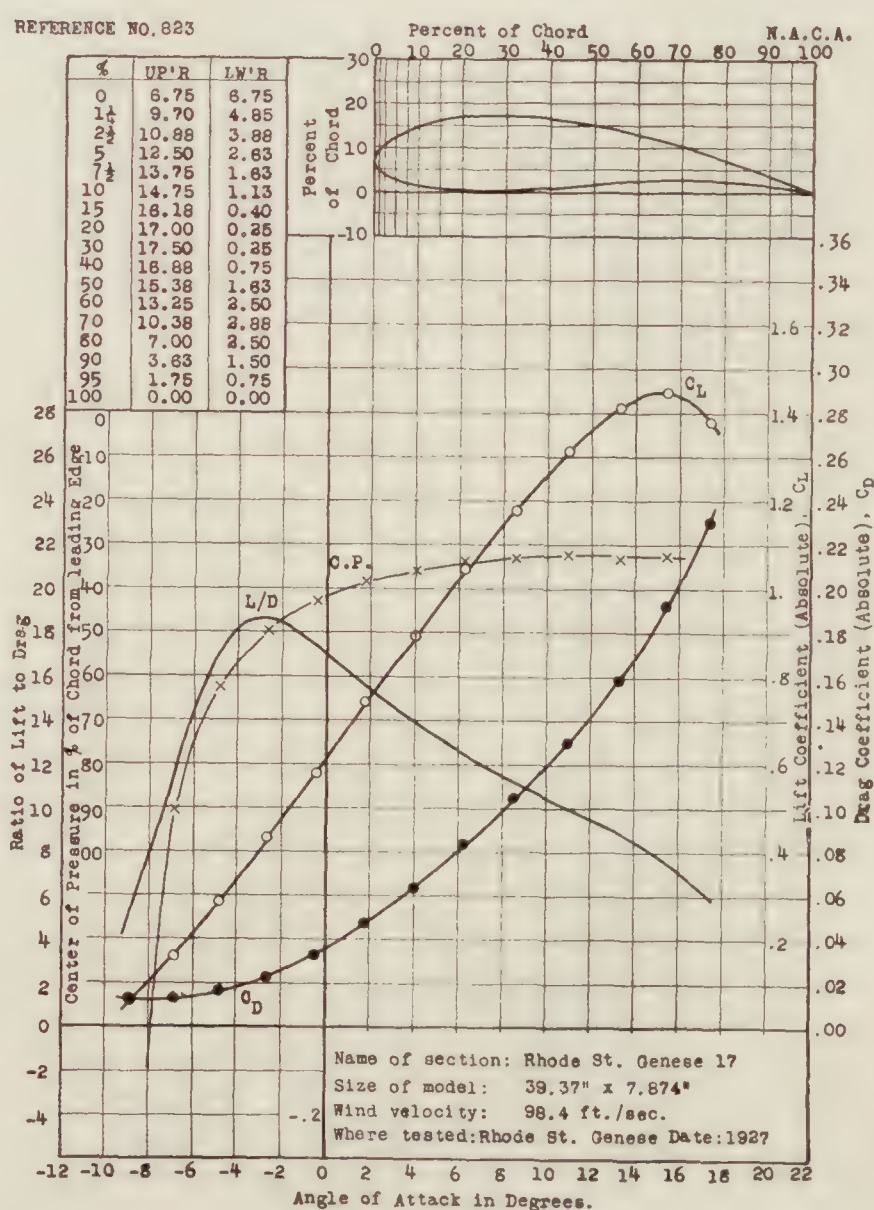
REFERENCE NO. 821



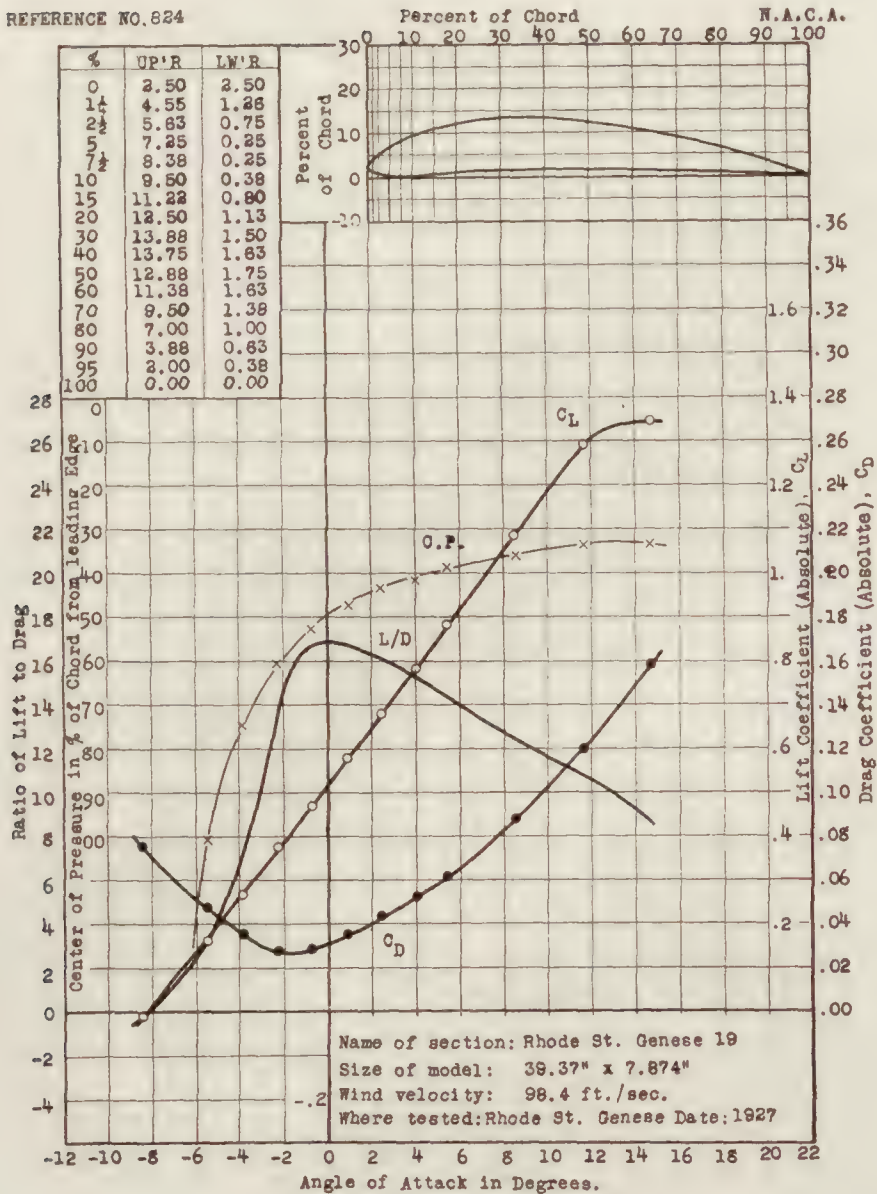
REFERENCE NO. 822



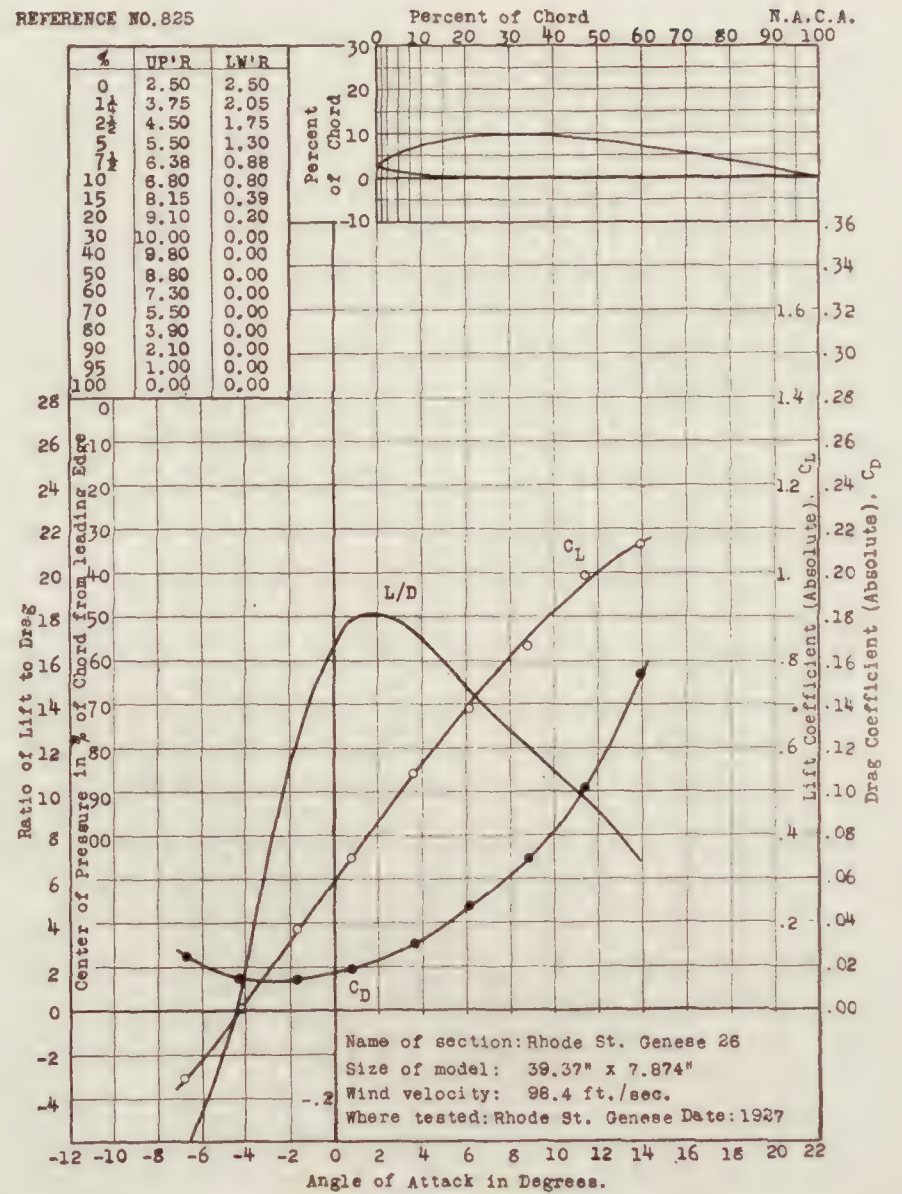
REFERENCE NO. 823



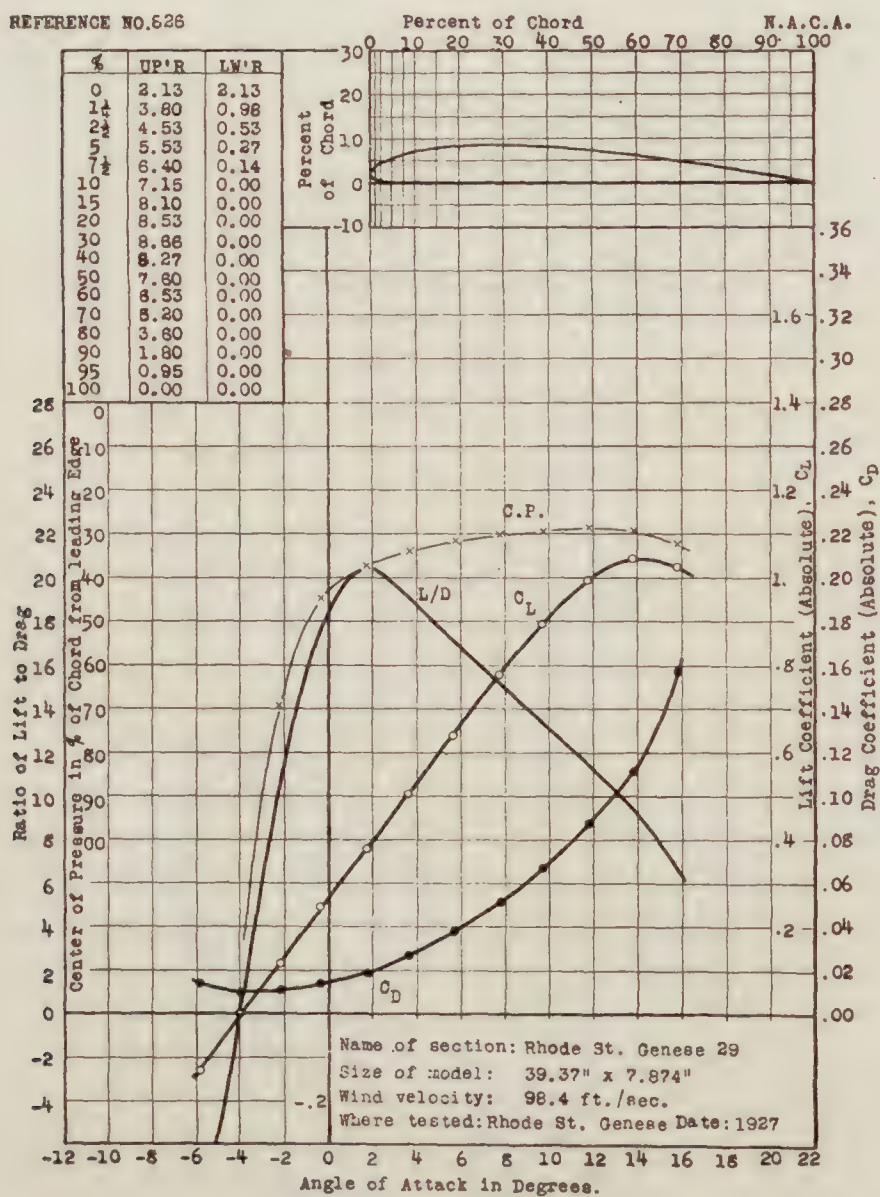
REFERENCE NO. 824



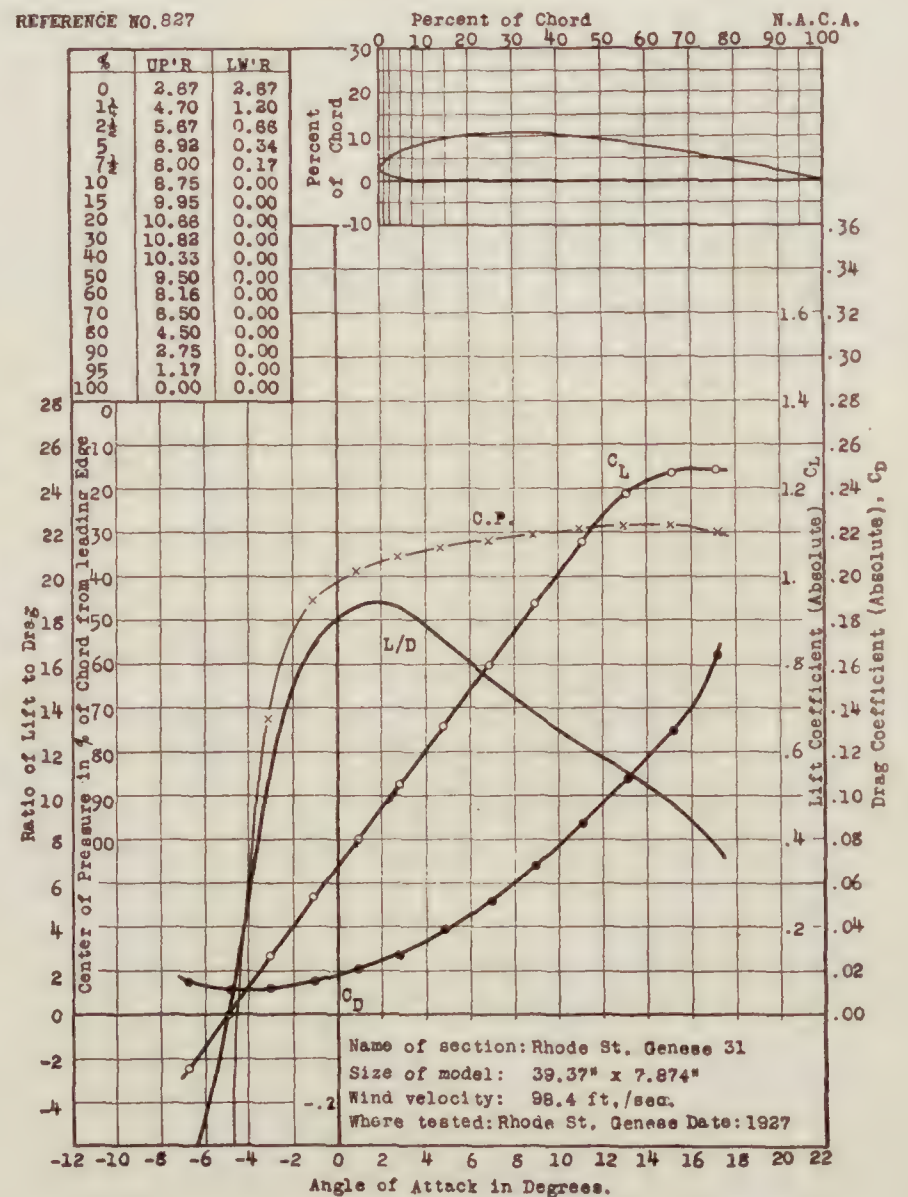
REFERENCE NO. 825



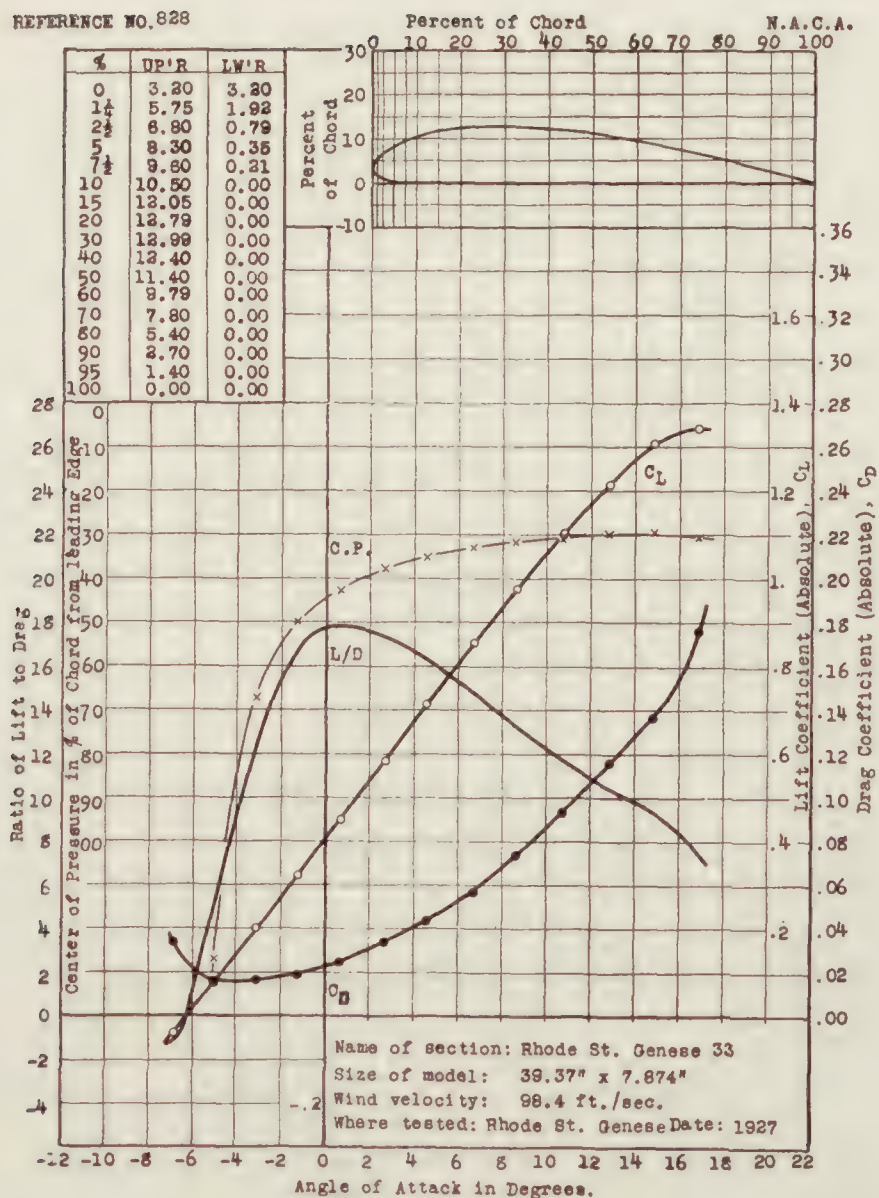
REFERENCE NO. 826



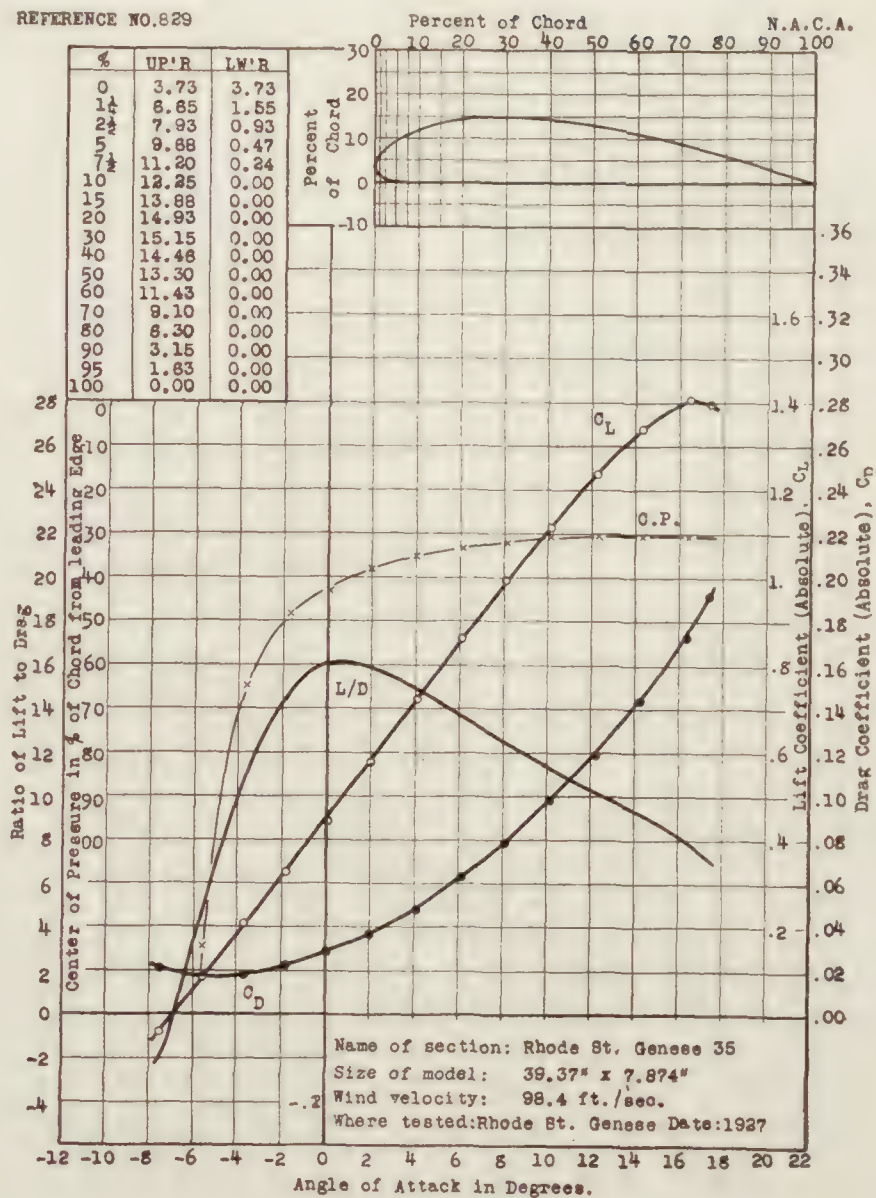
REFERENCE NO. 827



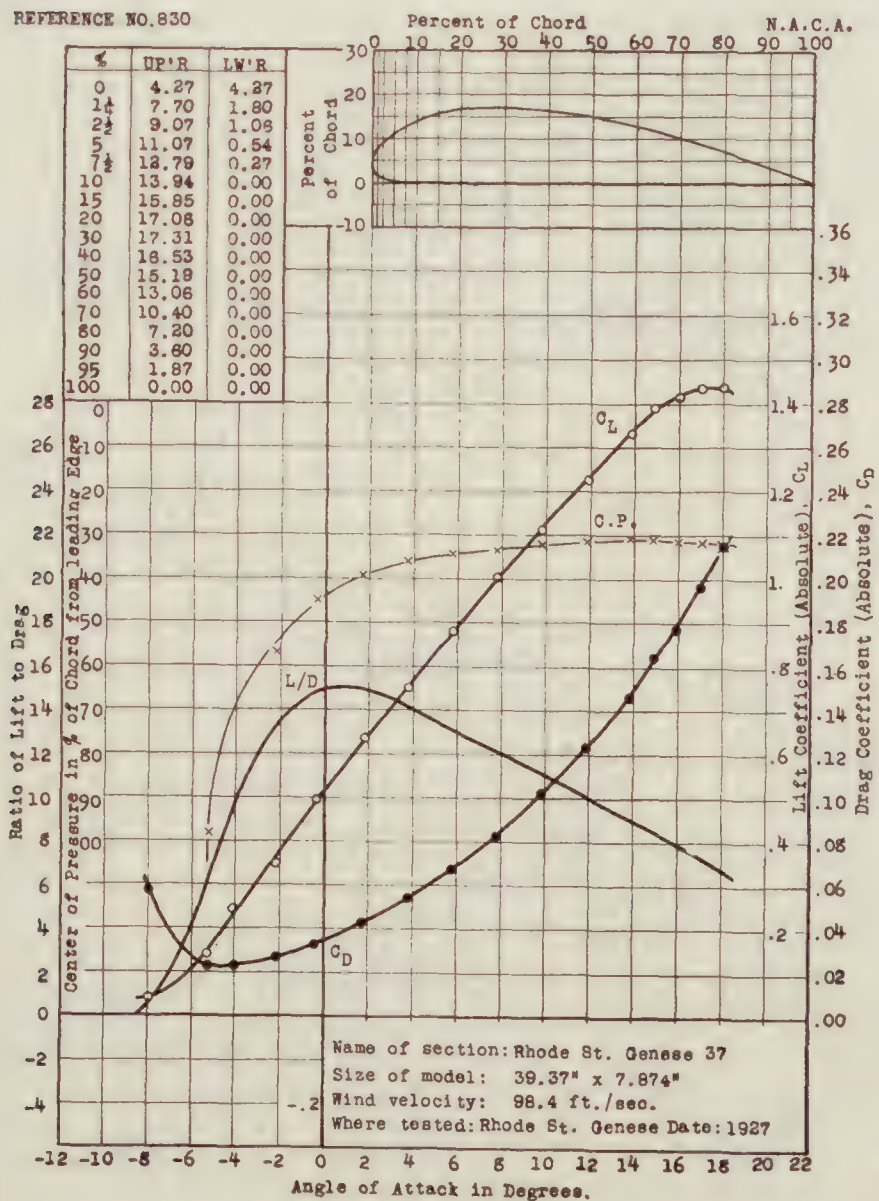
REFERENCE NO. 828



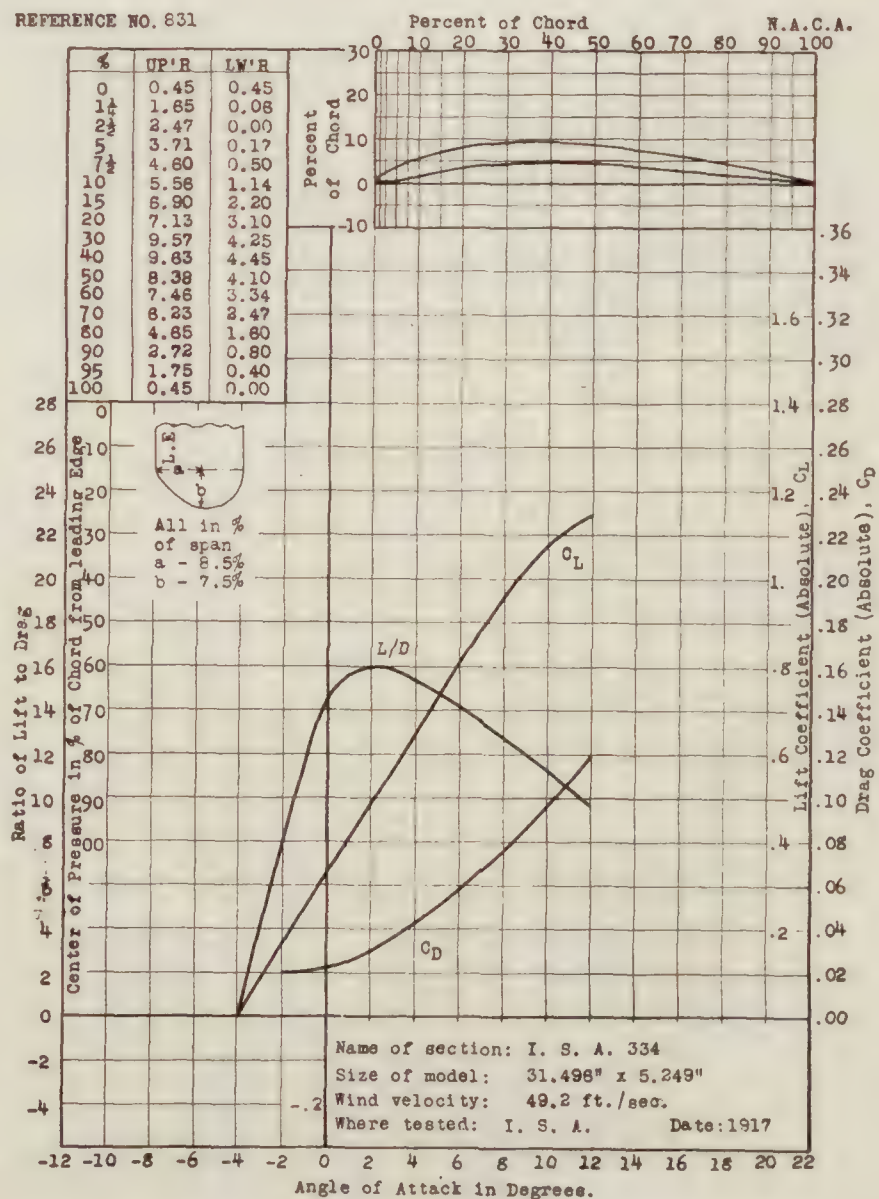
REFERENCE NO. 829



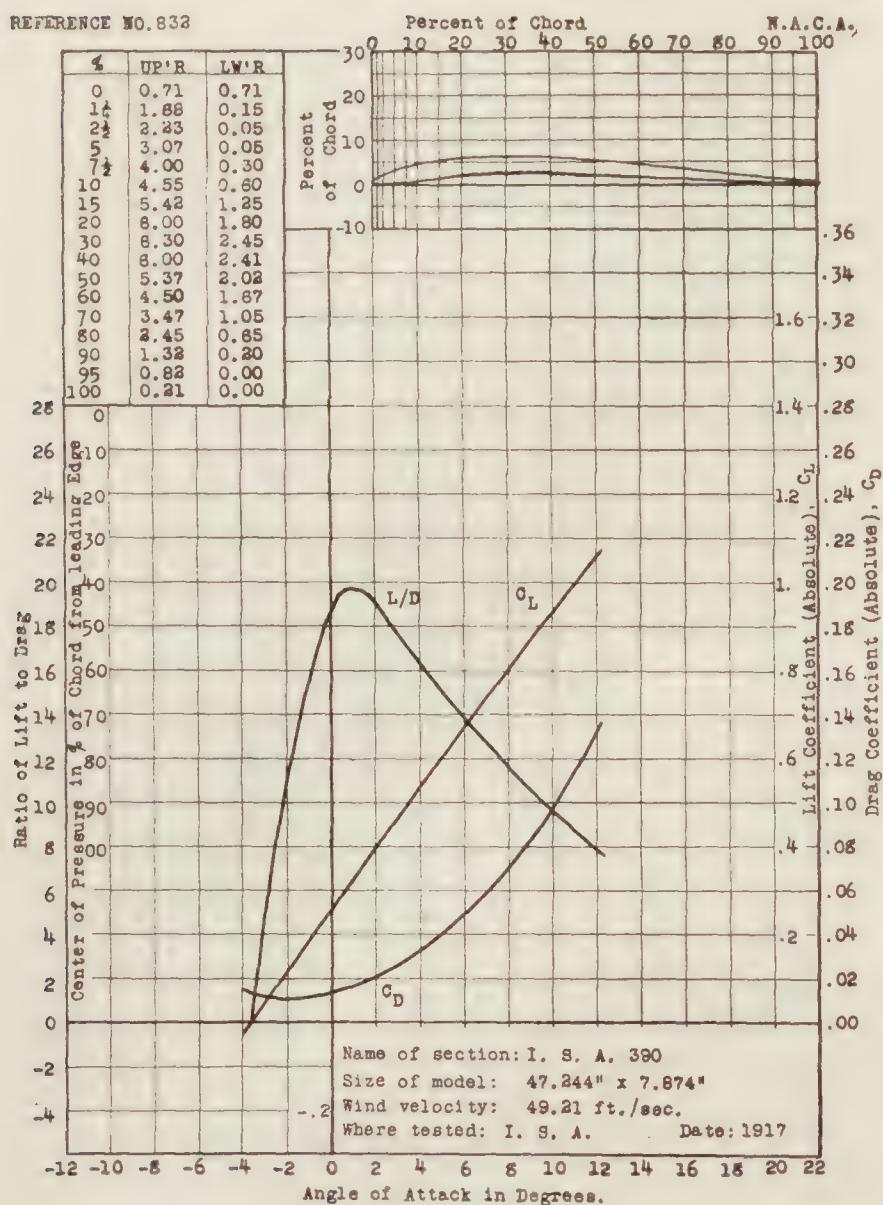
REFERENCE NO. 830



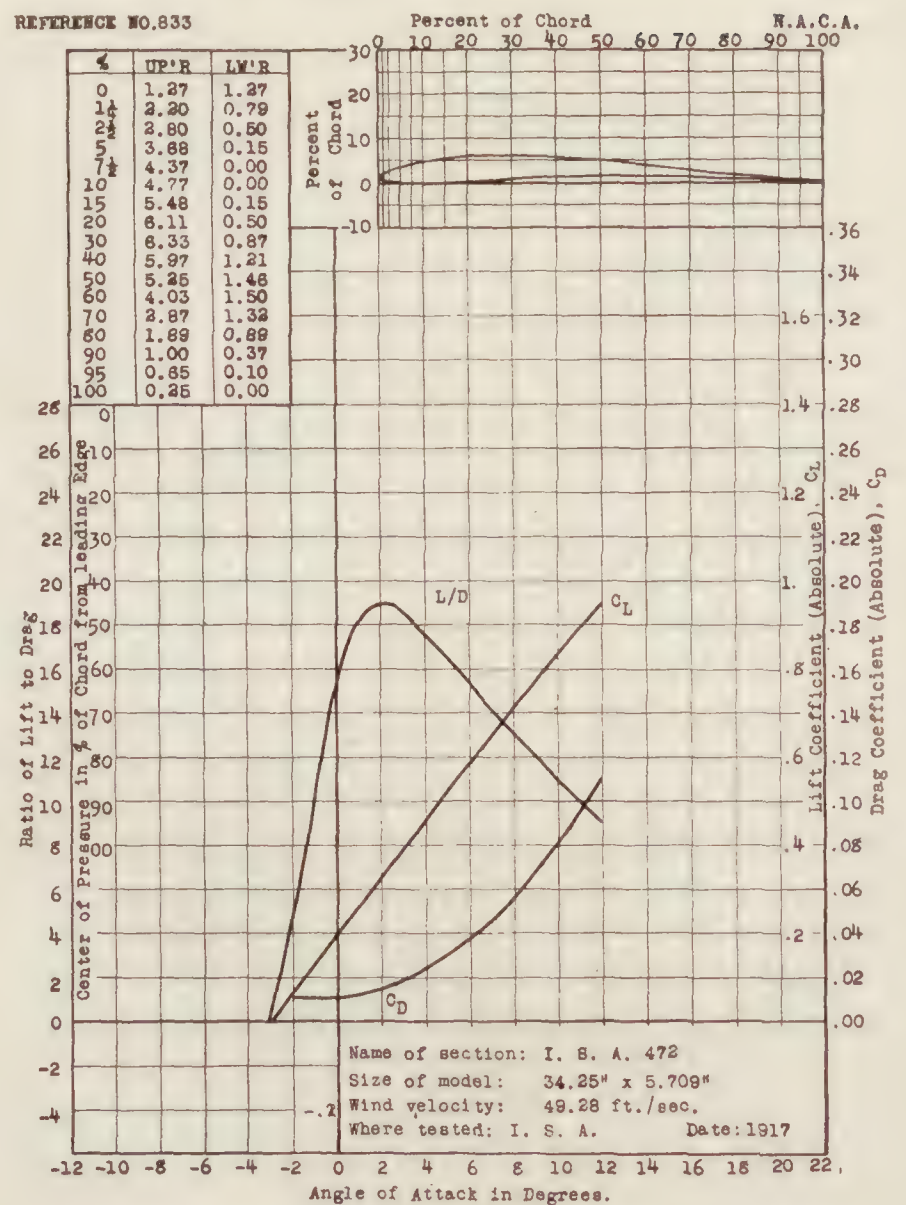
REFERENCE NO. 831



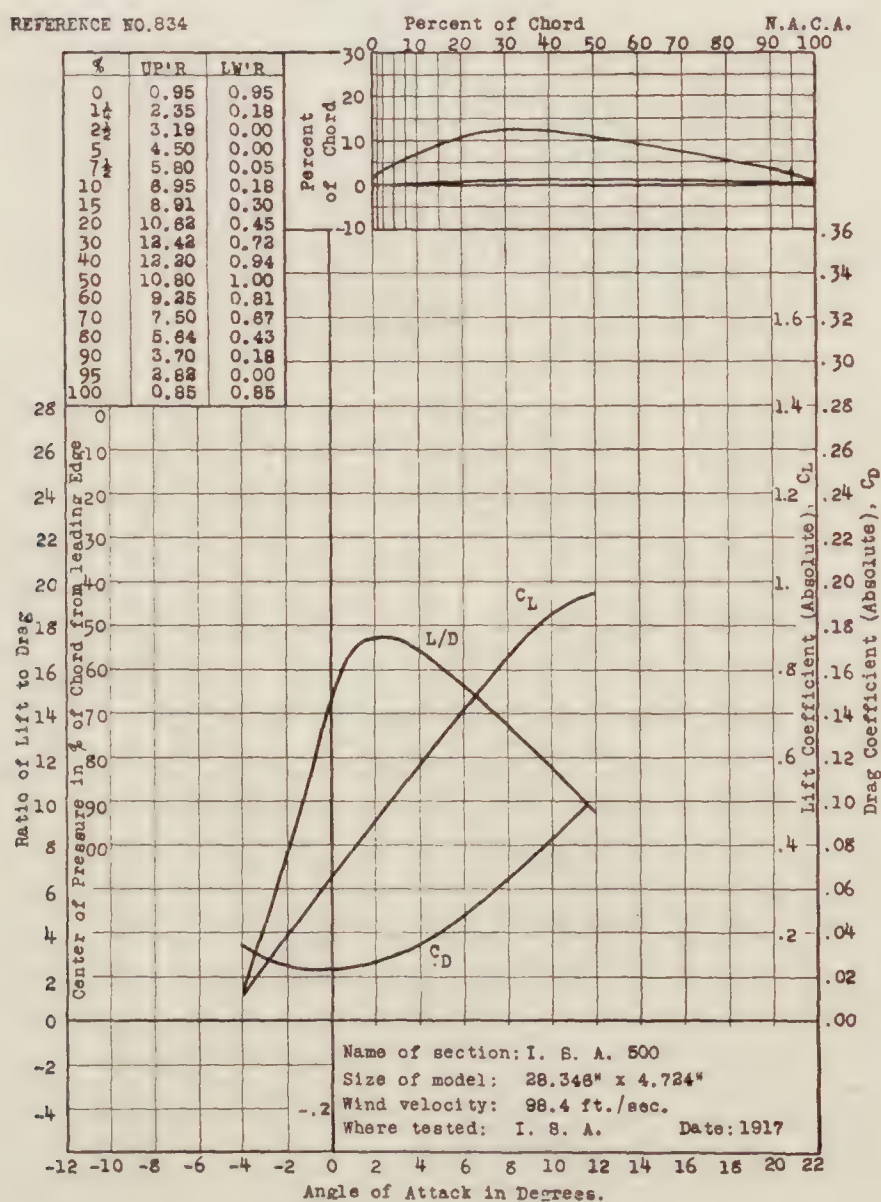
REFERENCE NO. 832



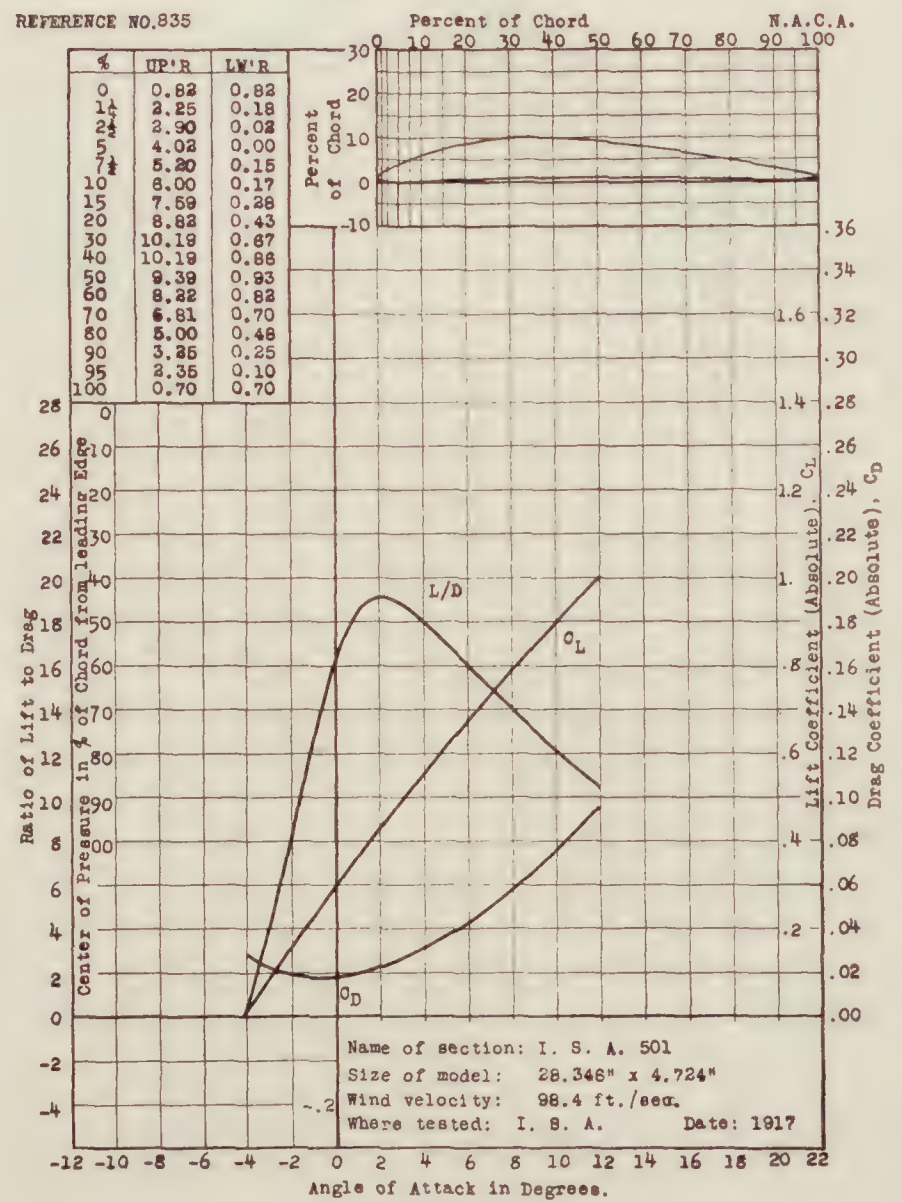
REFERENCE NO. 833



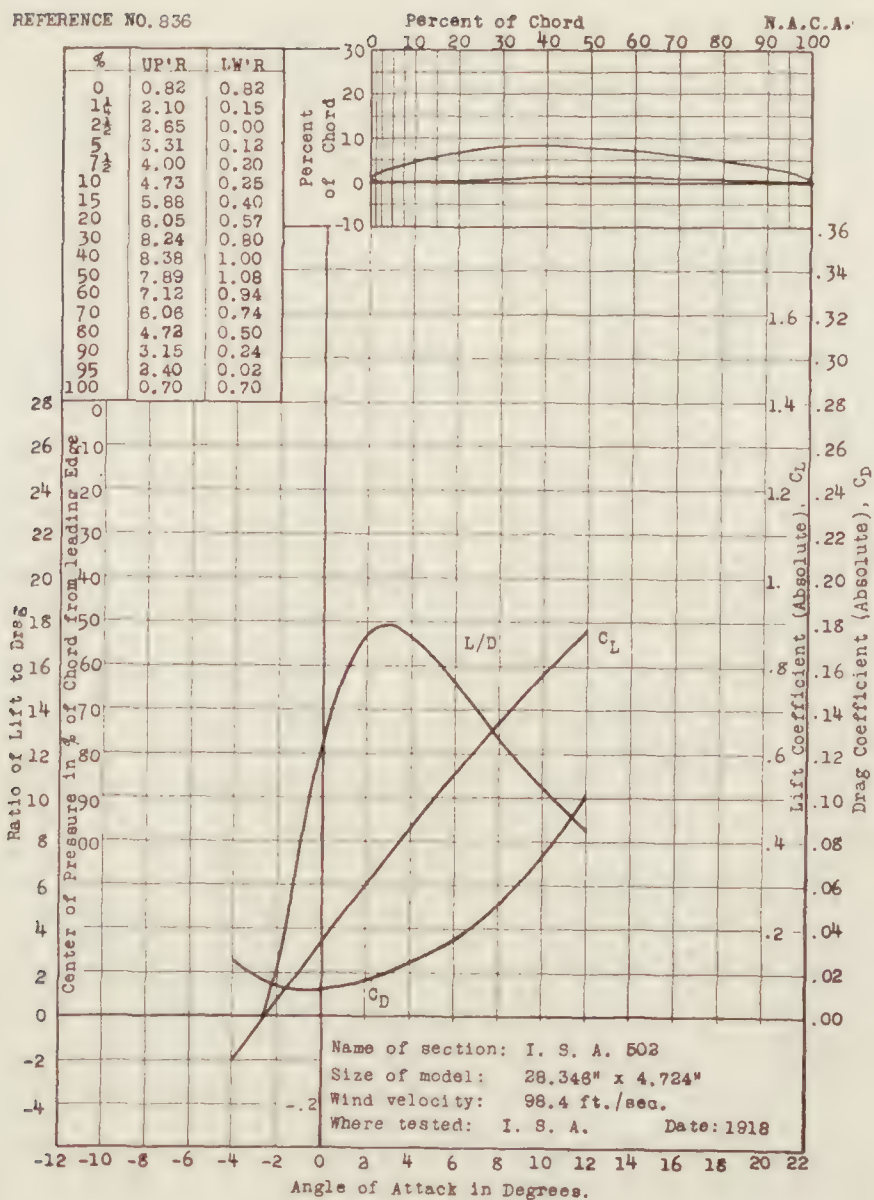
REFERENCE NO. 834



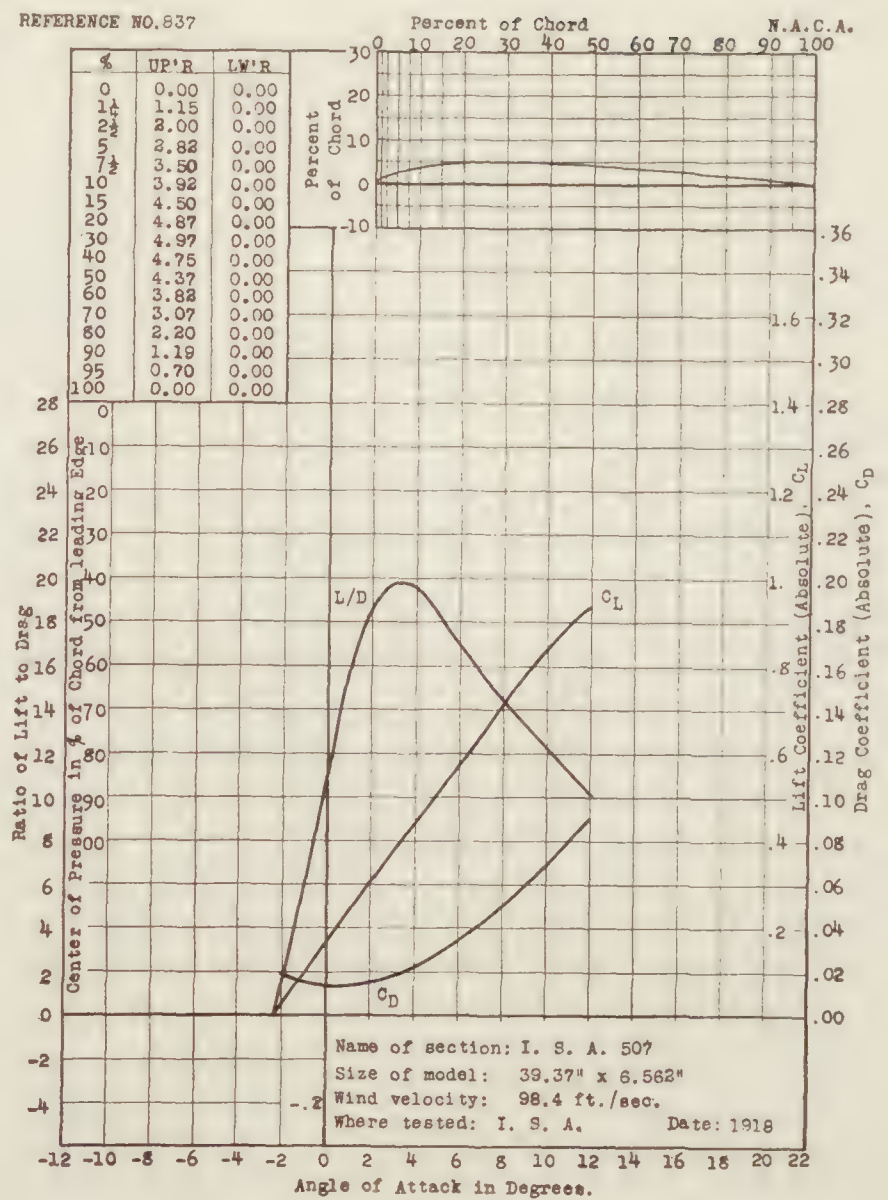
REFERENCE NO. 835



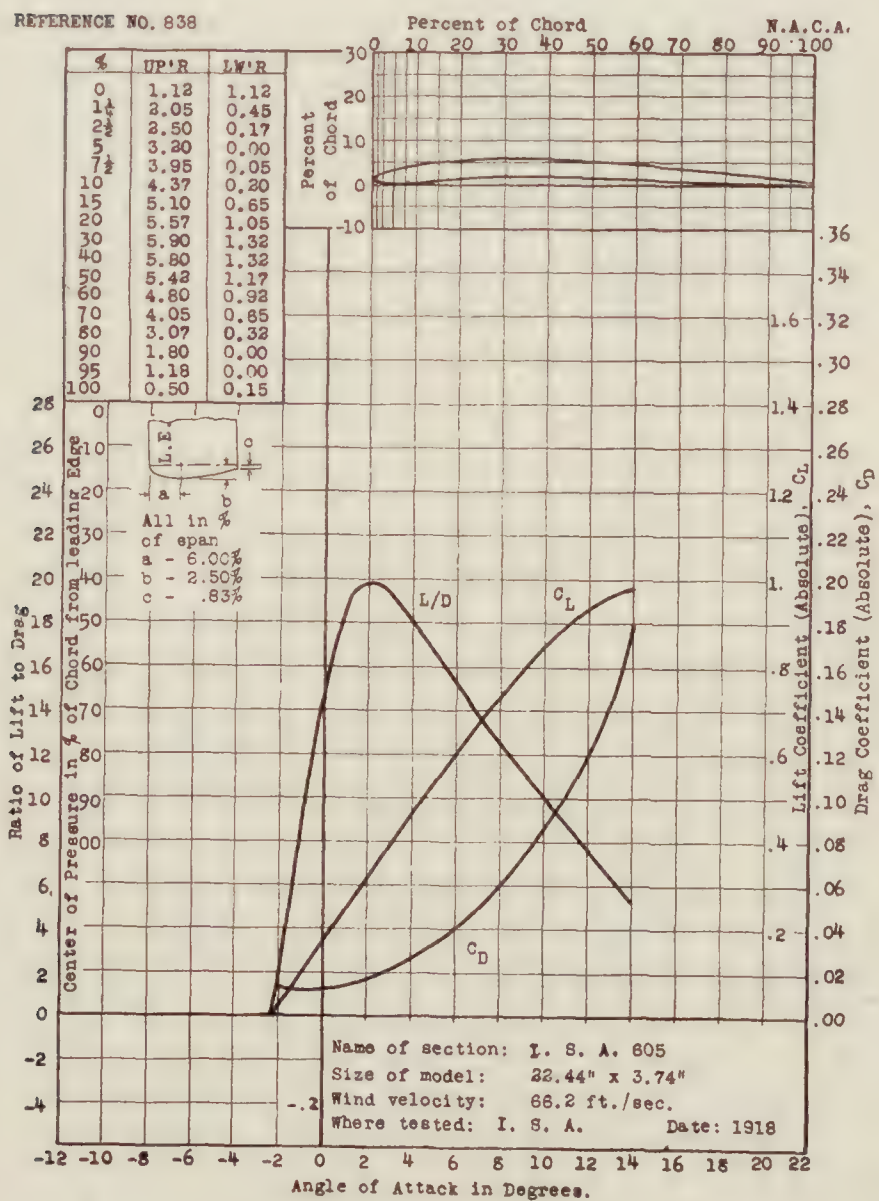
REFERENCE NO. 836



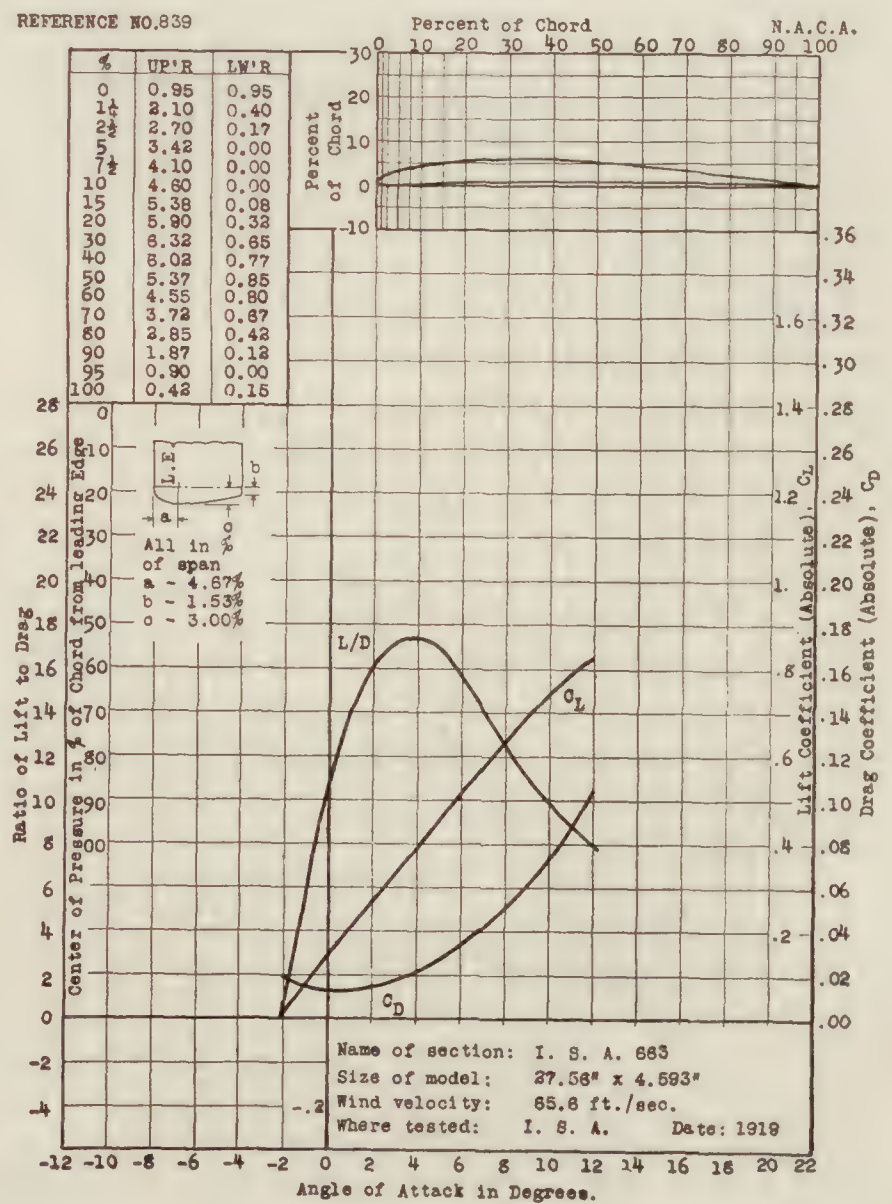
REFERENCE NO. 837



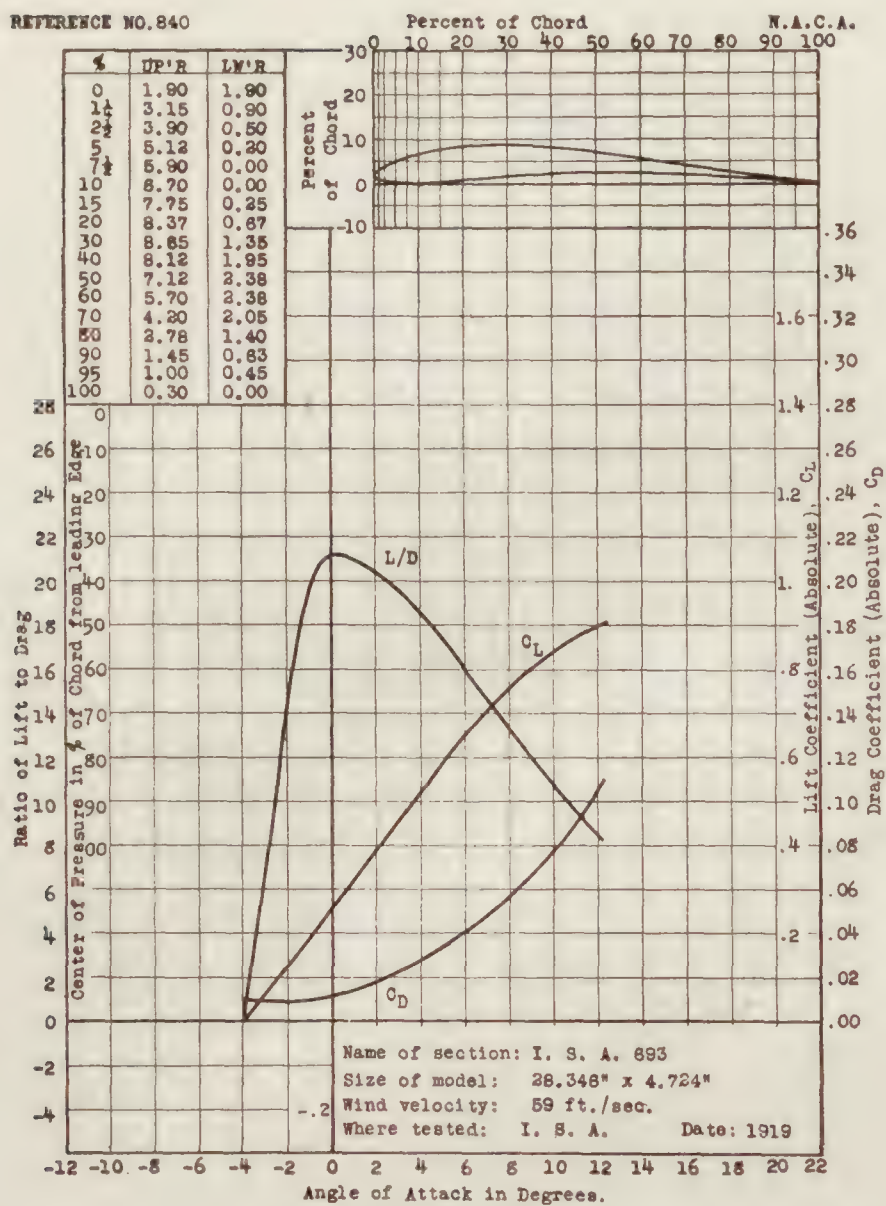
REFERENCE NO. 838



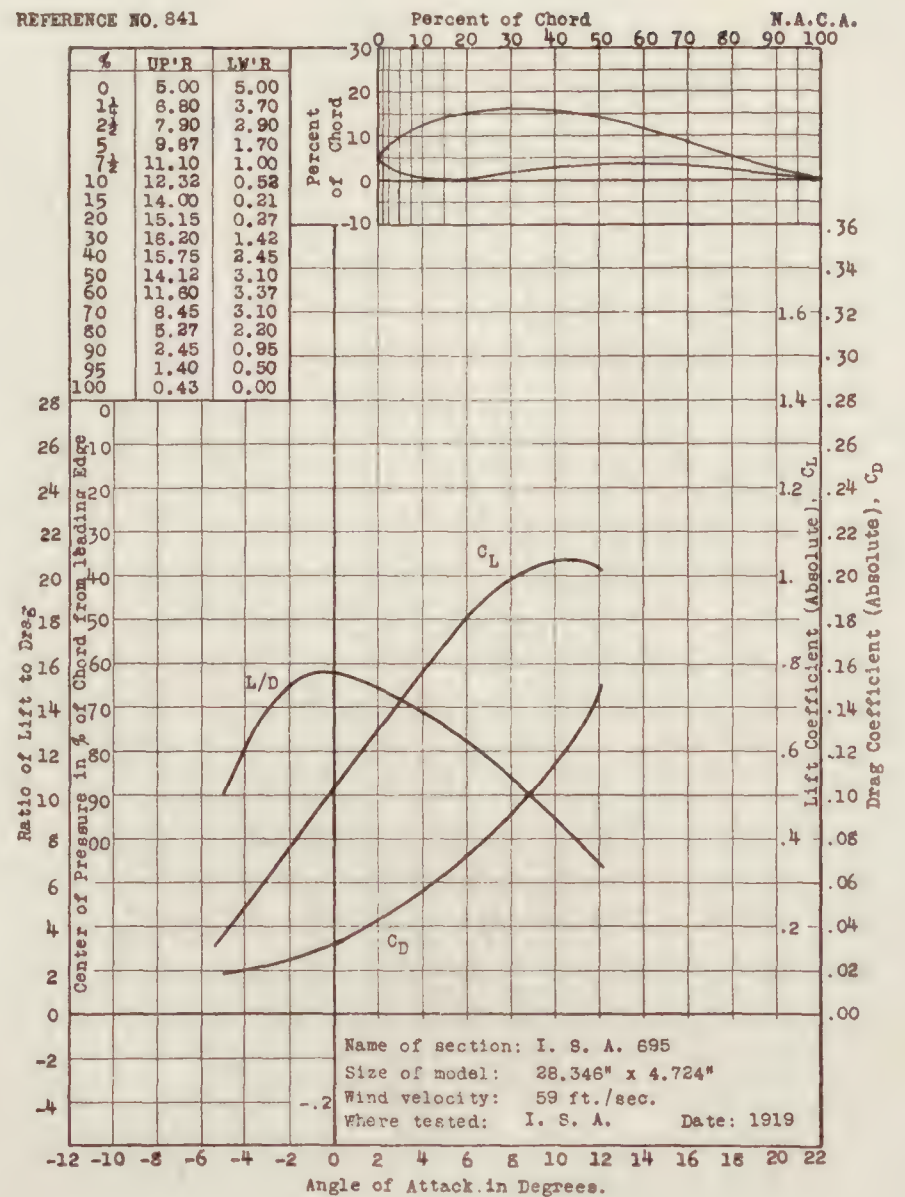
REFERENCE NO. 839



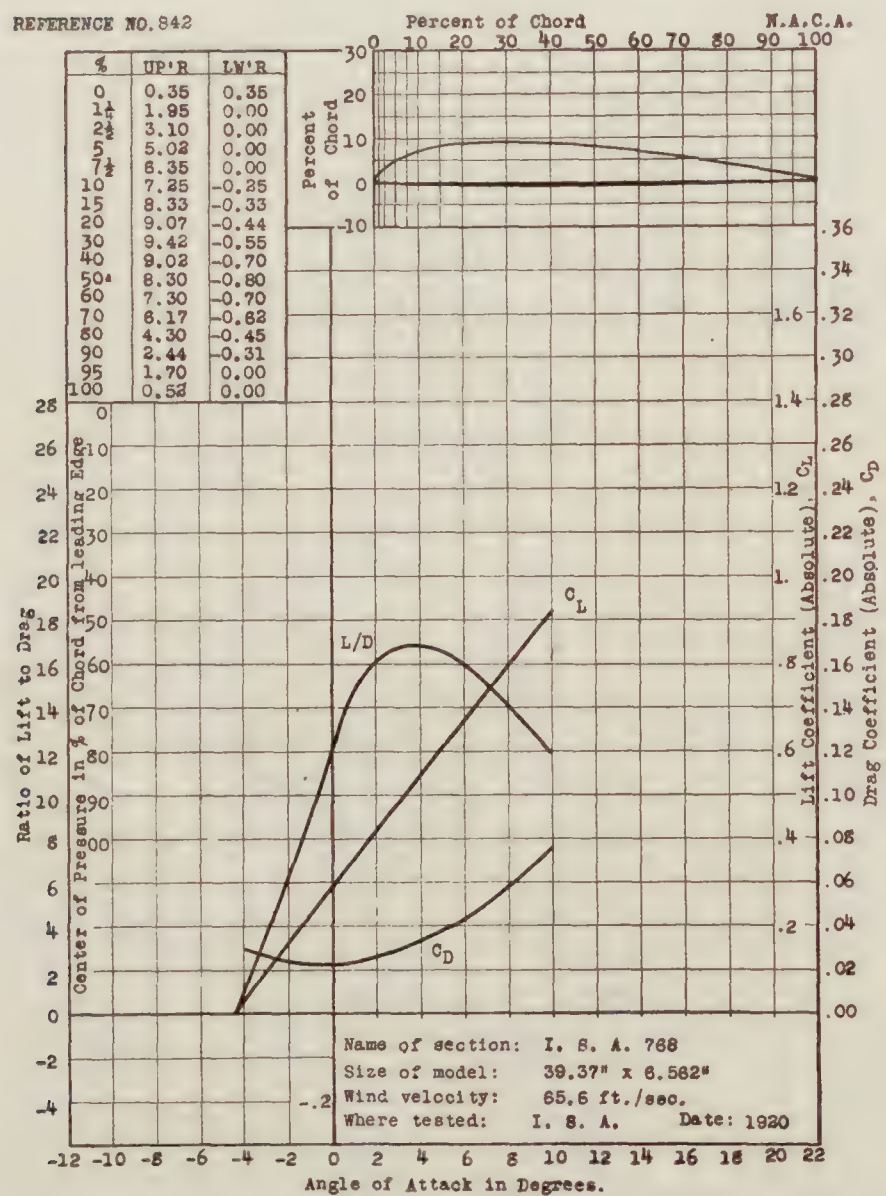
REFERENCE NO. 840



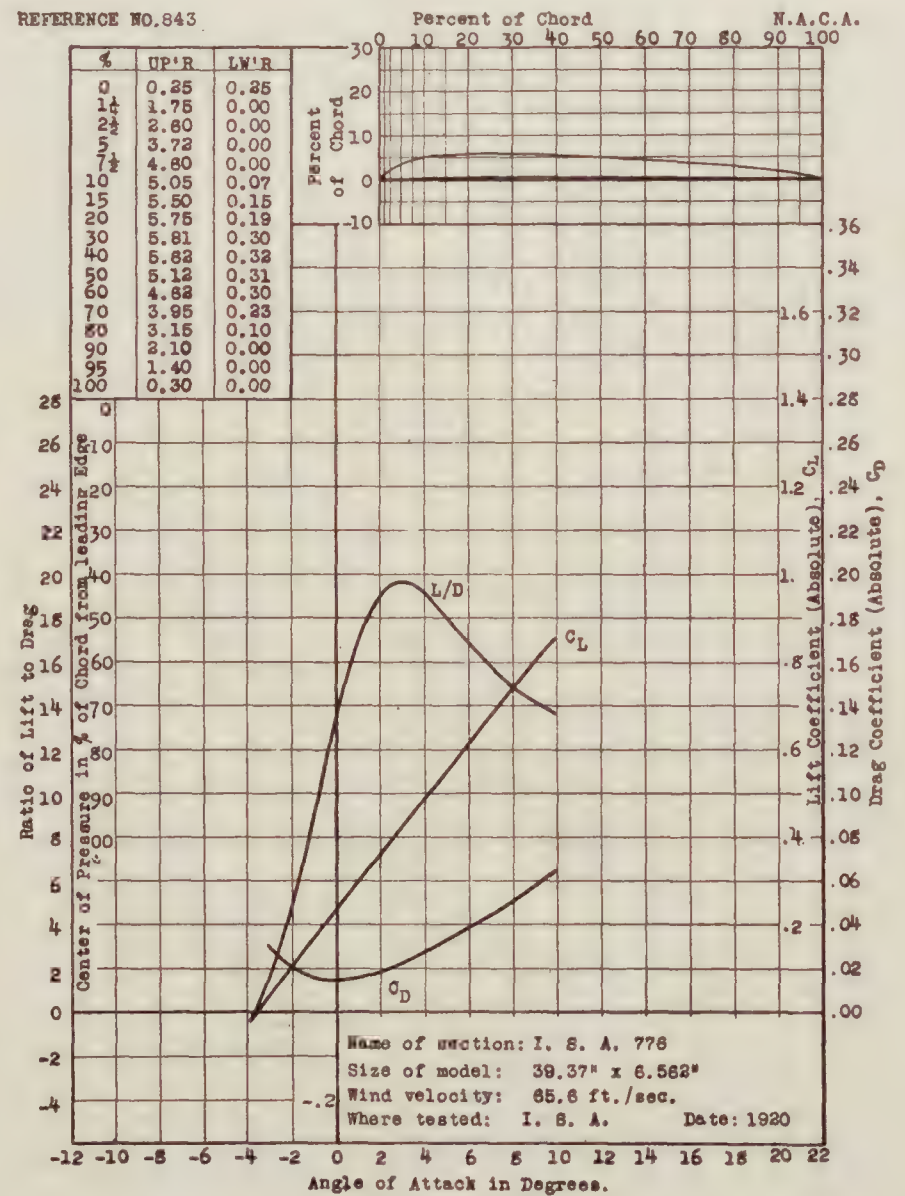
REFERENCE NO. 841



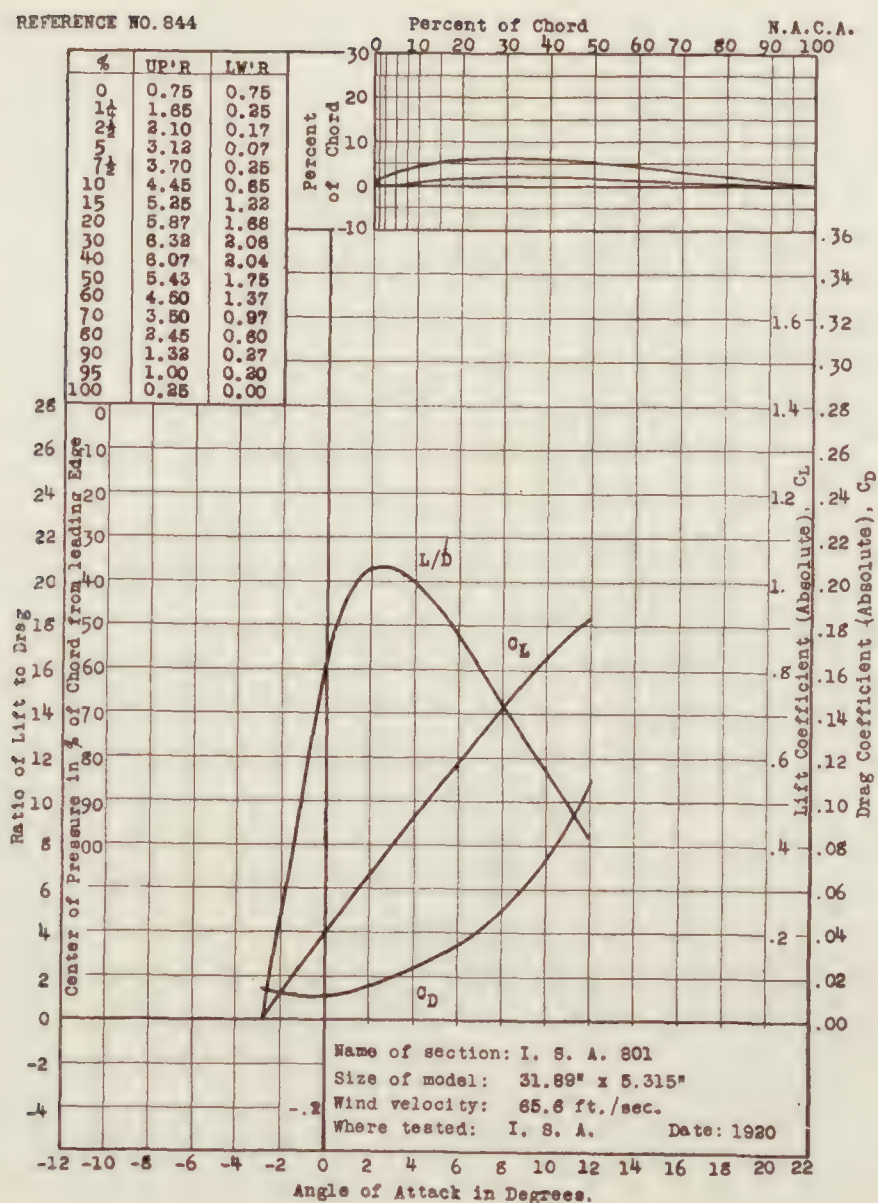
REFERENCE NO. 842



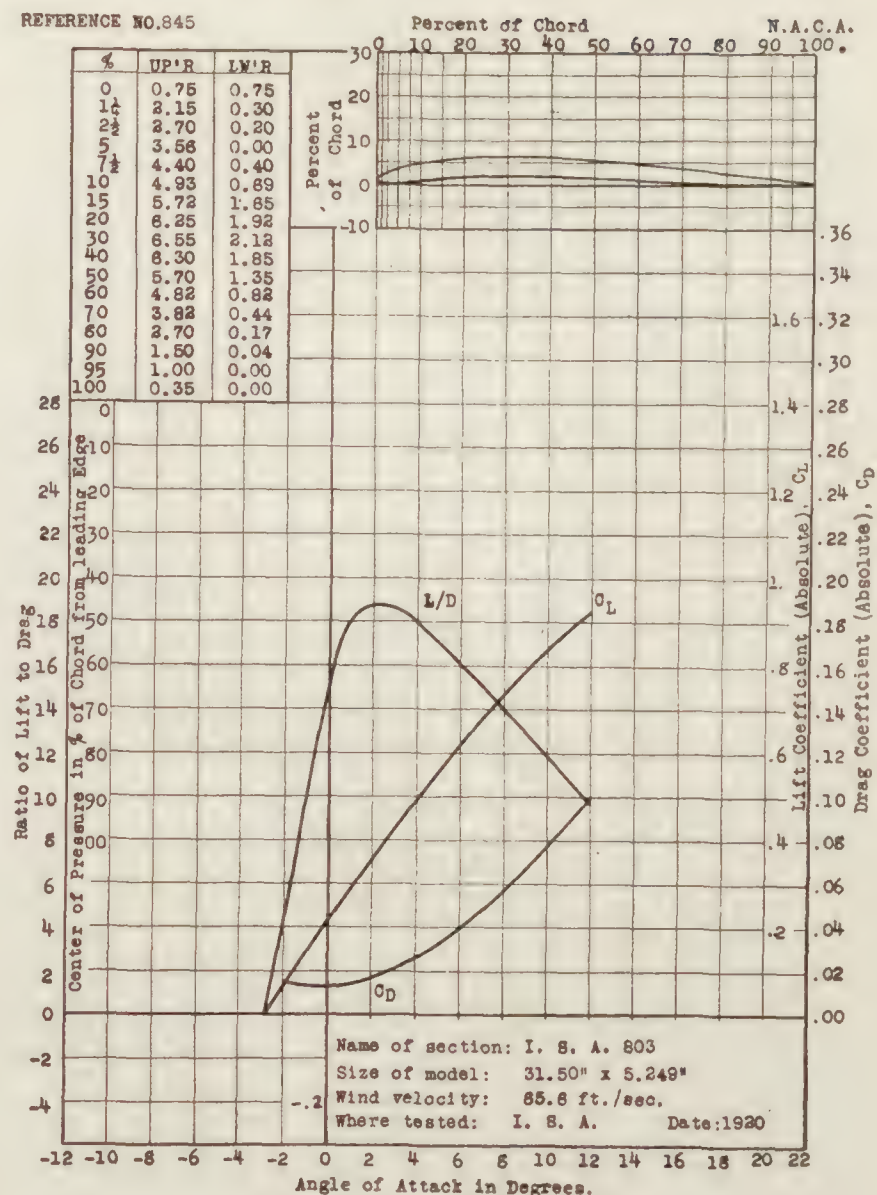
REFERENCE NO. 843



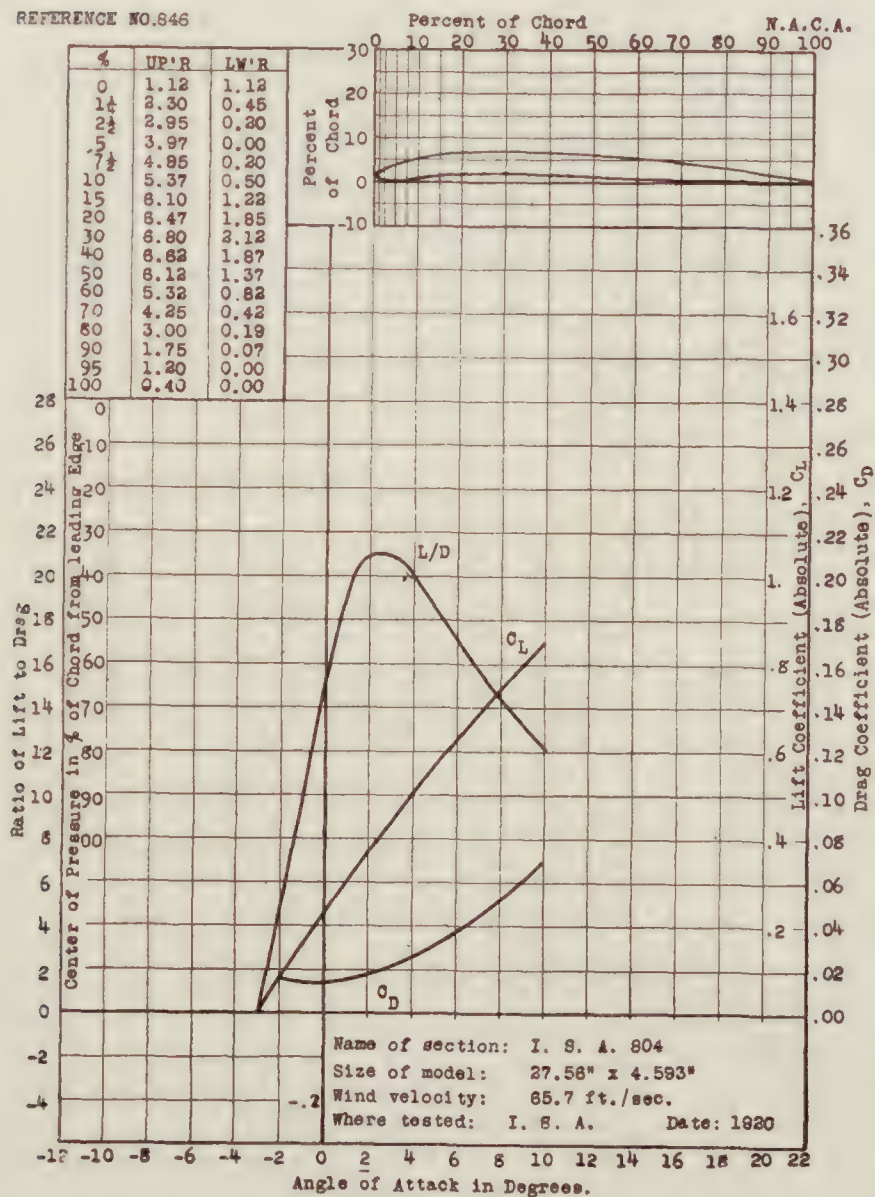
REFERENCE NO. 844



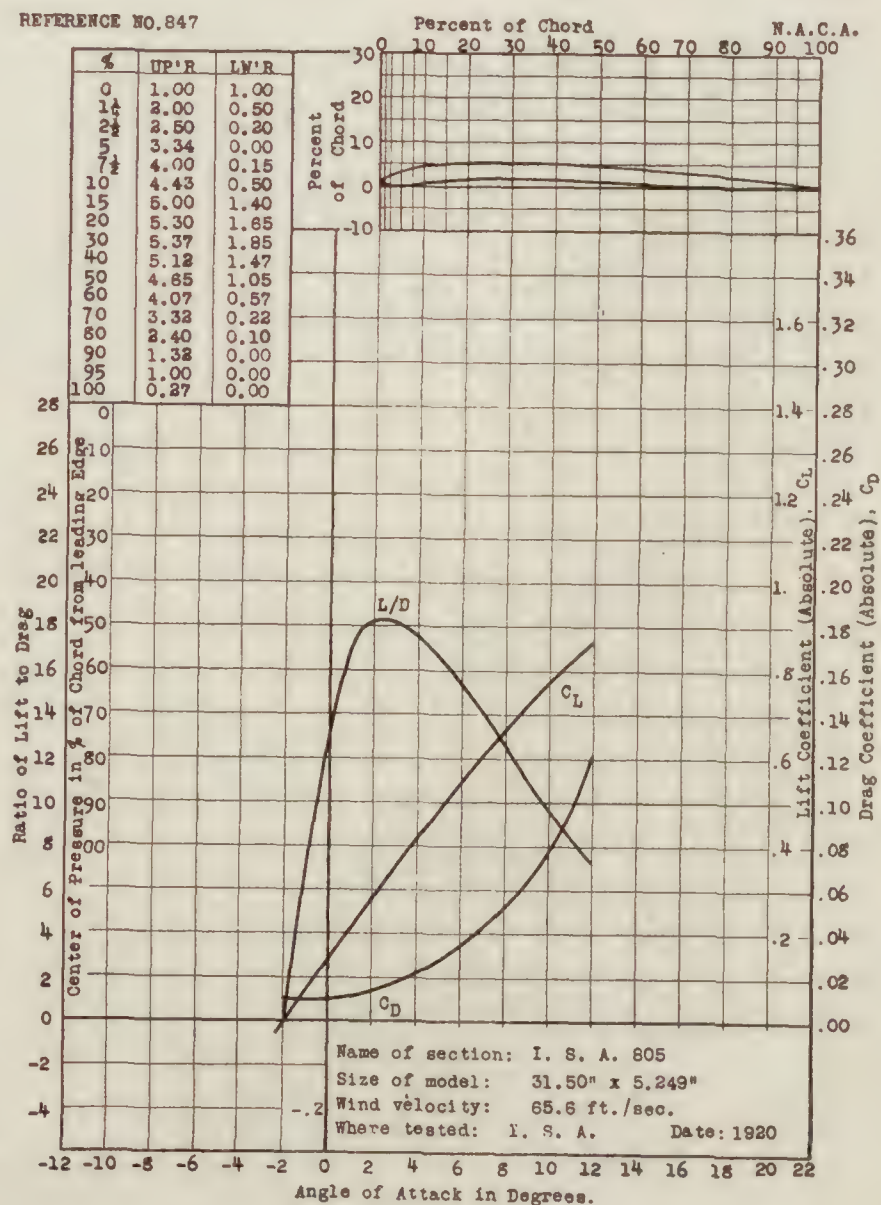
REFERENCE NO. 845



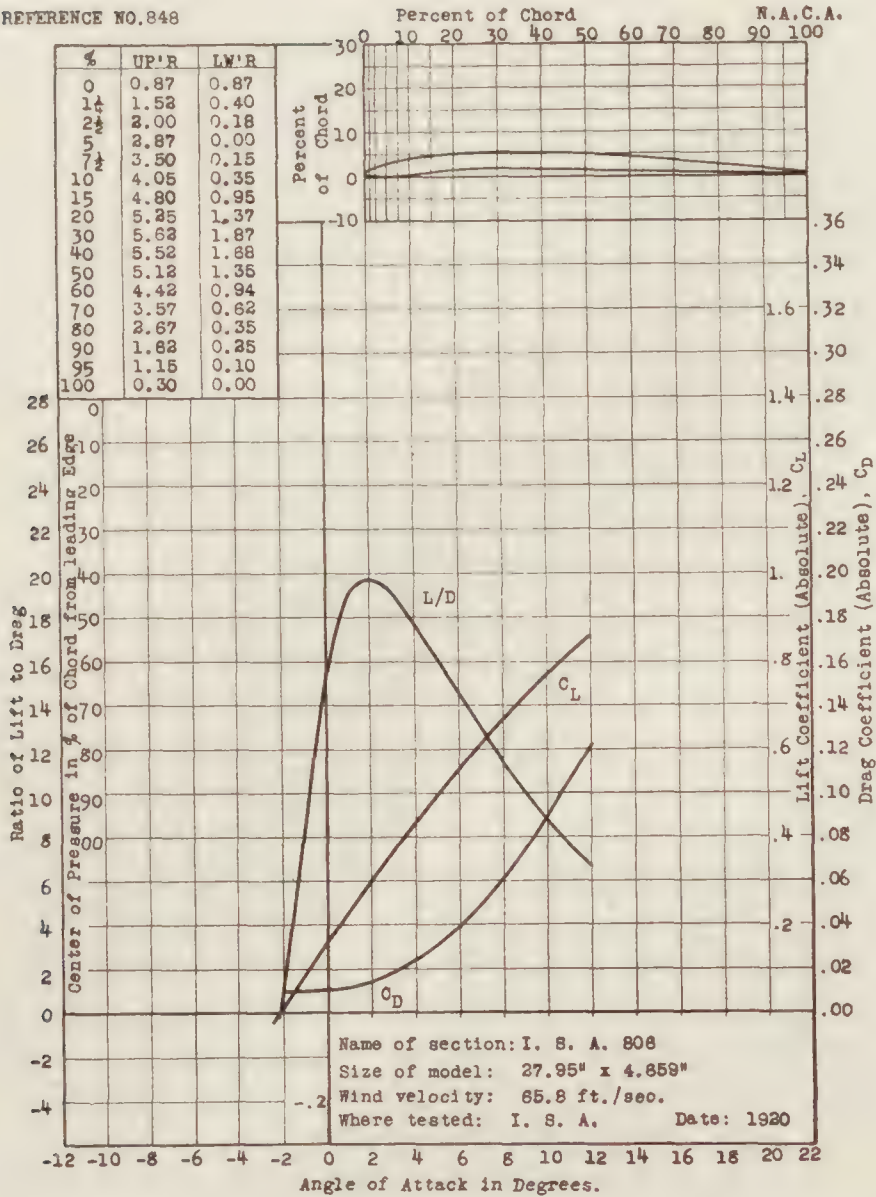
REFERENCE NO. 846



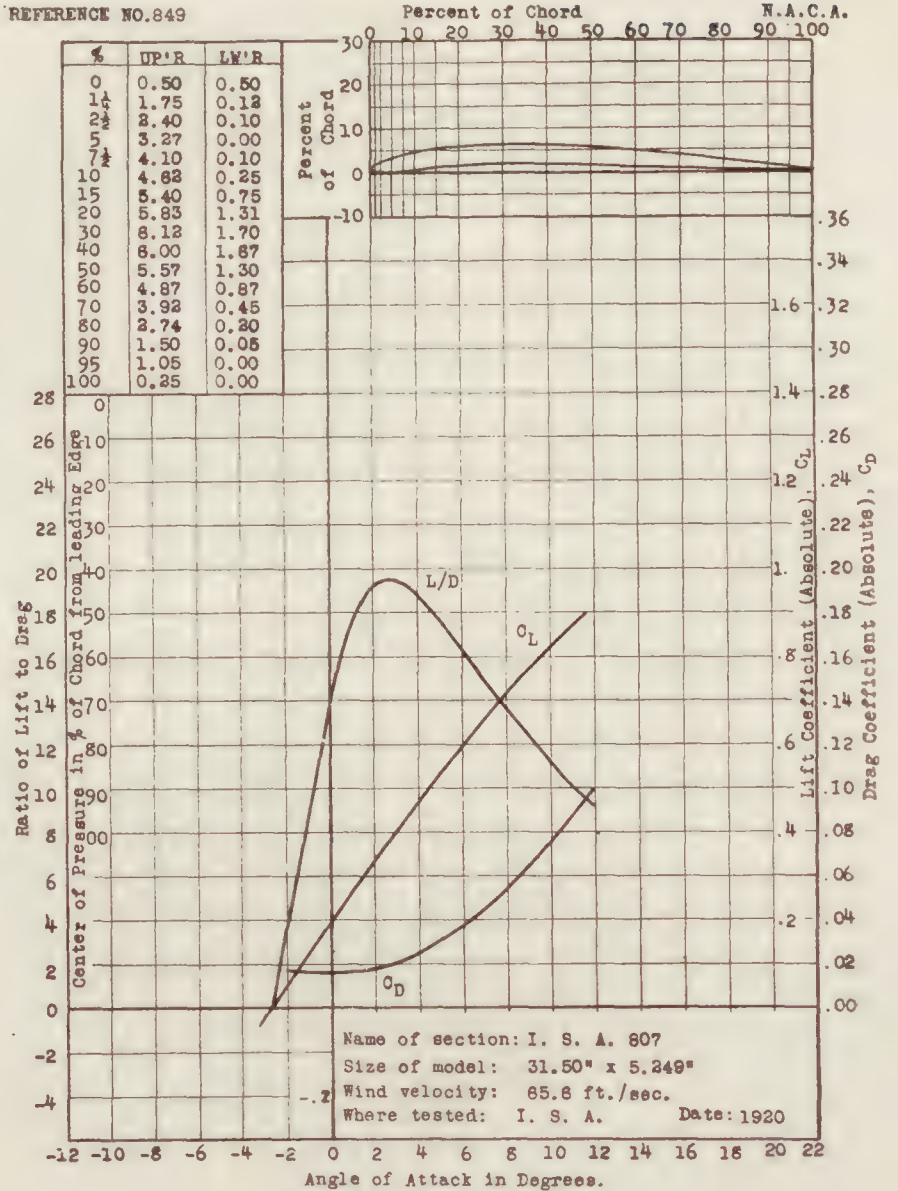
REFERENCE NO. 847



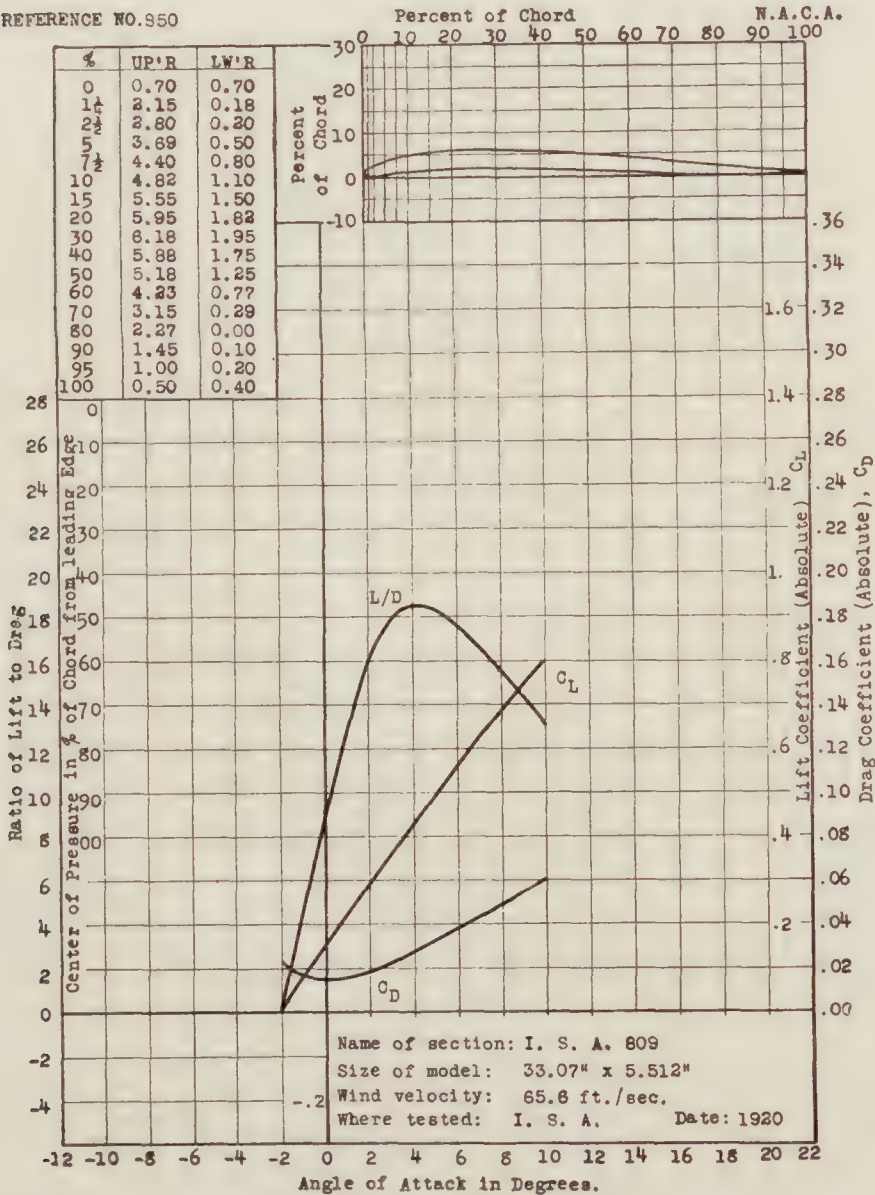
REFERENCE NO. 848



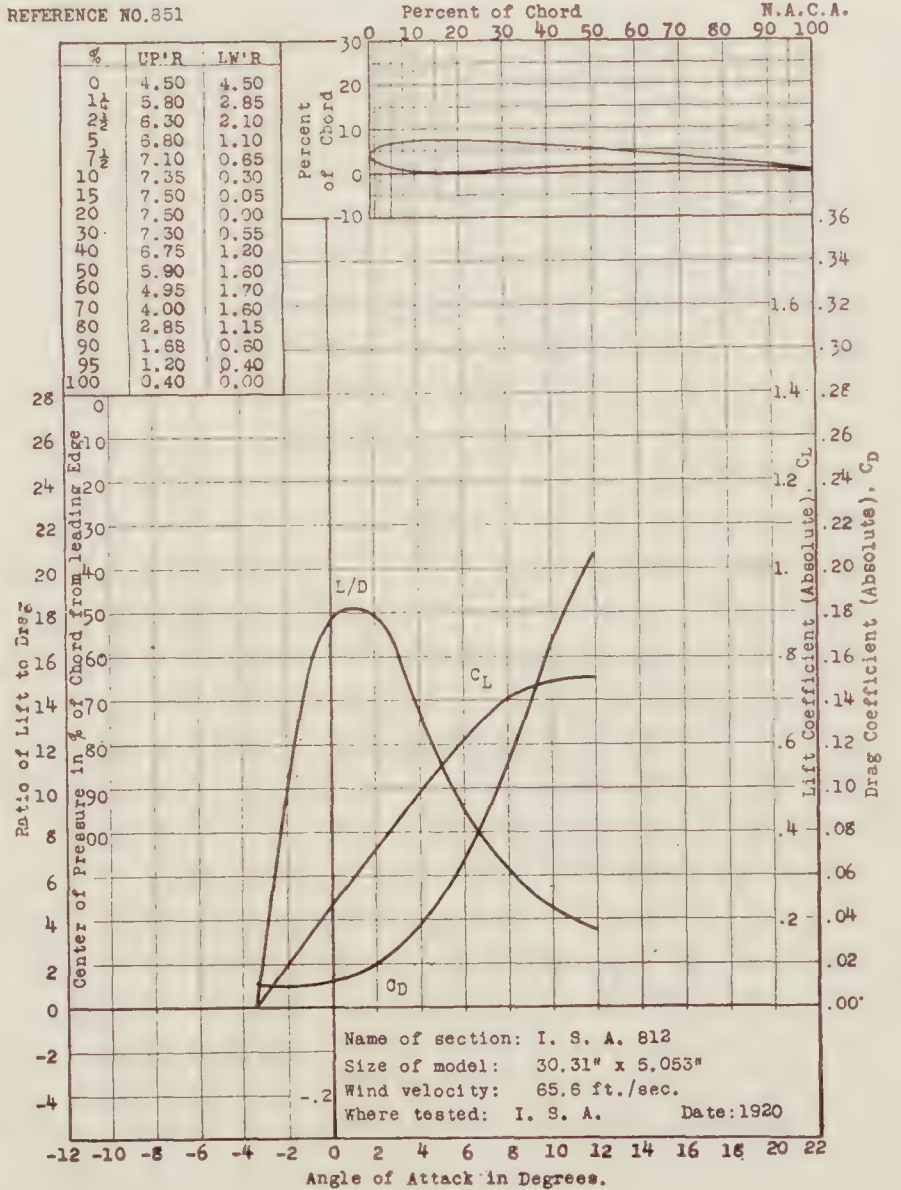
REFERENCE NO. 849



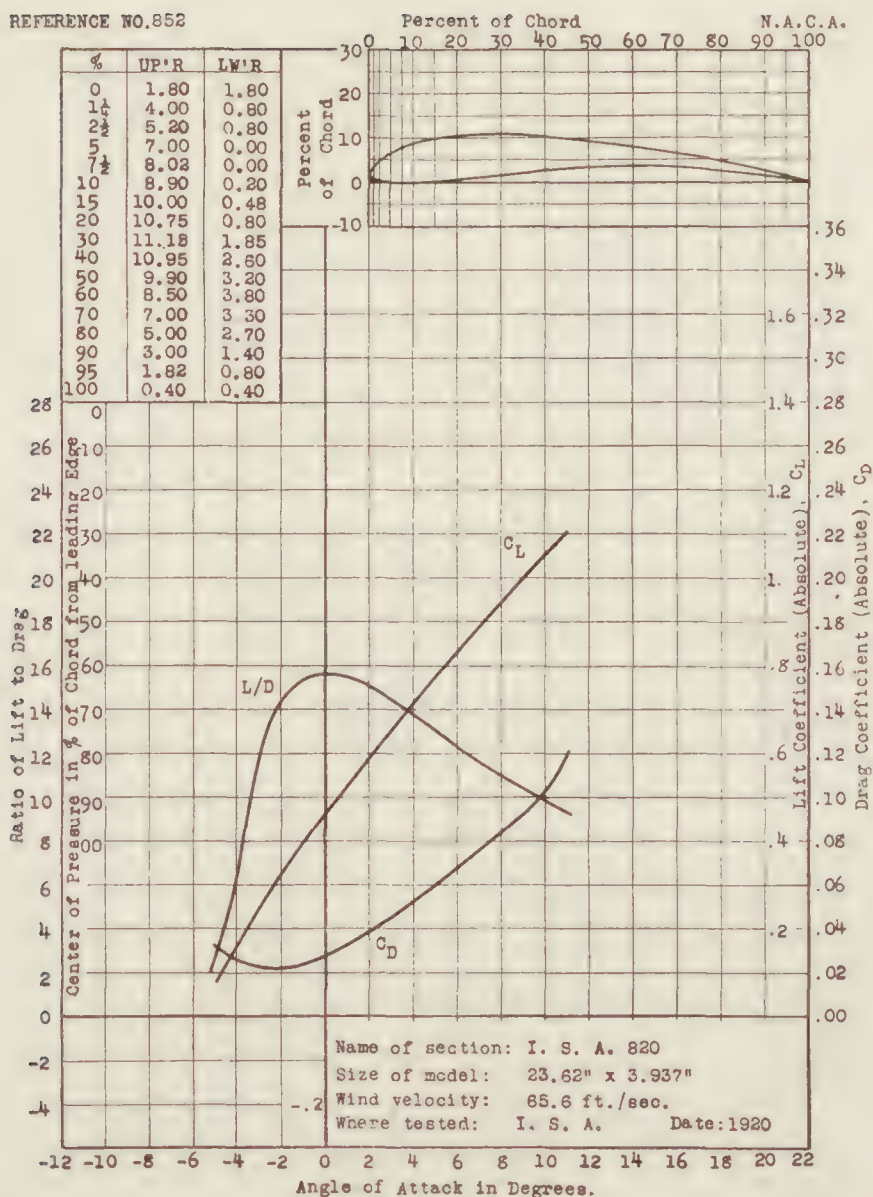
REFERENCE NO. 850



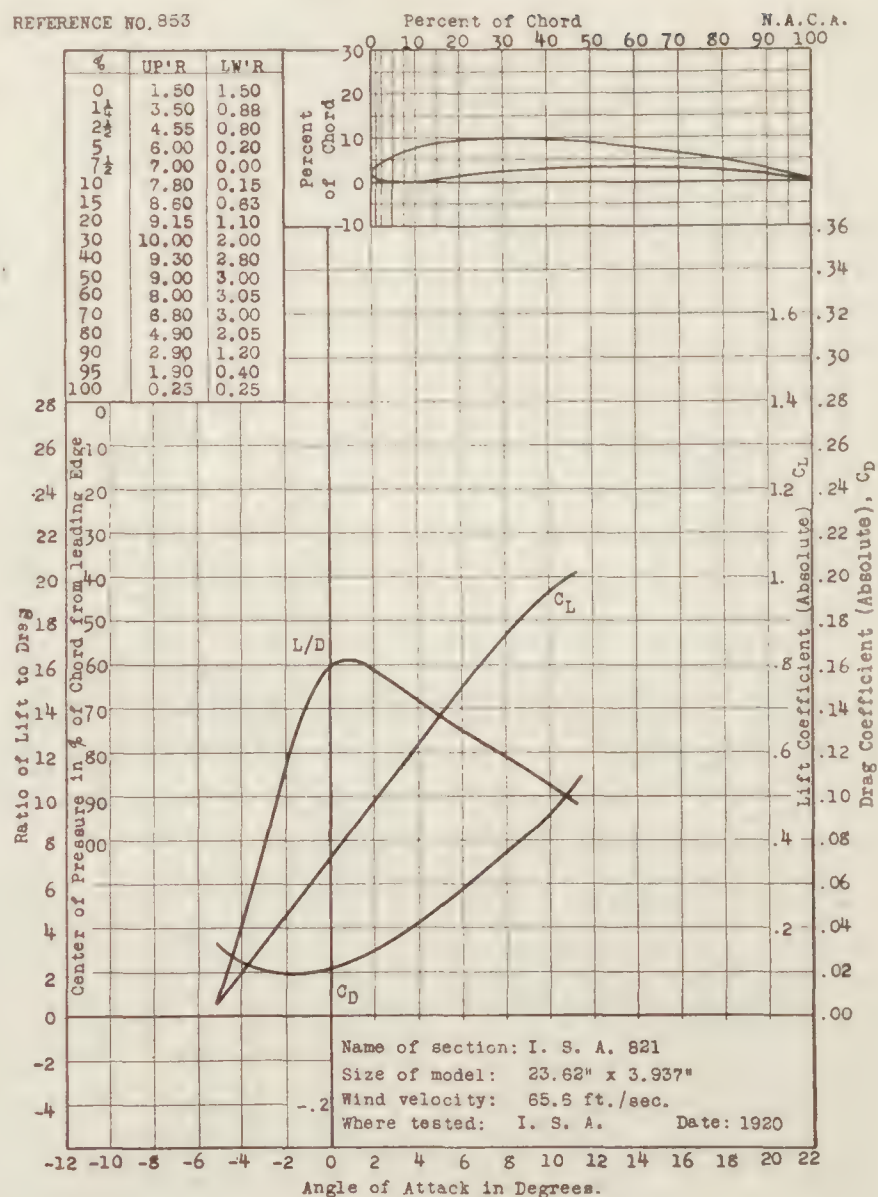
REFERENCE NO. 851



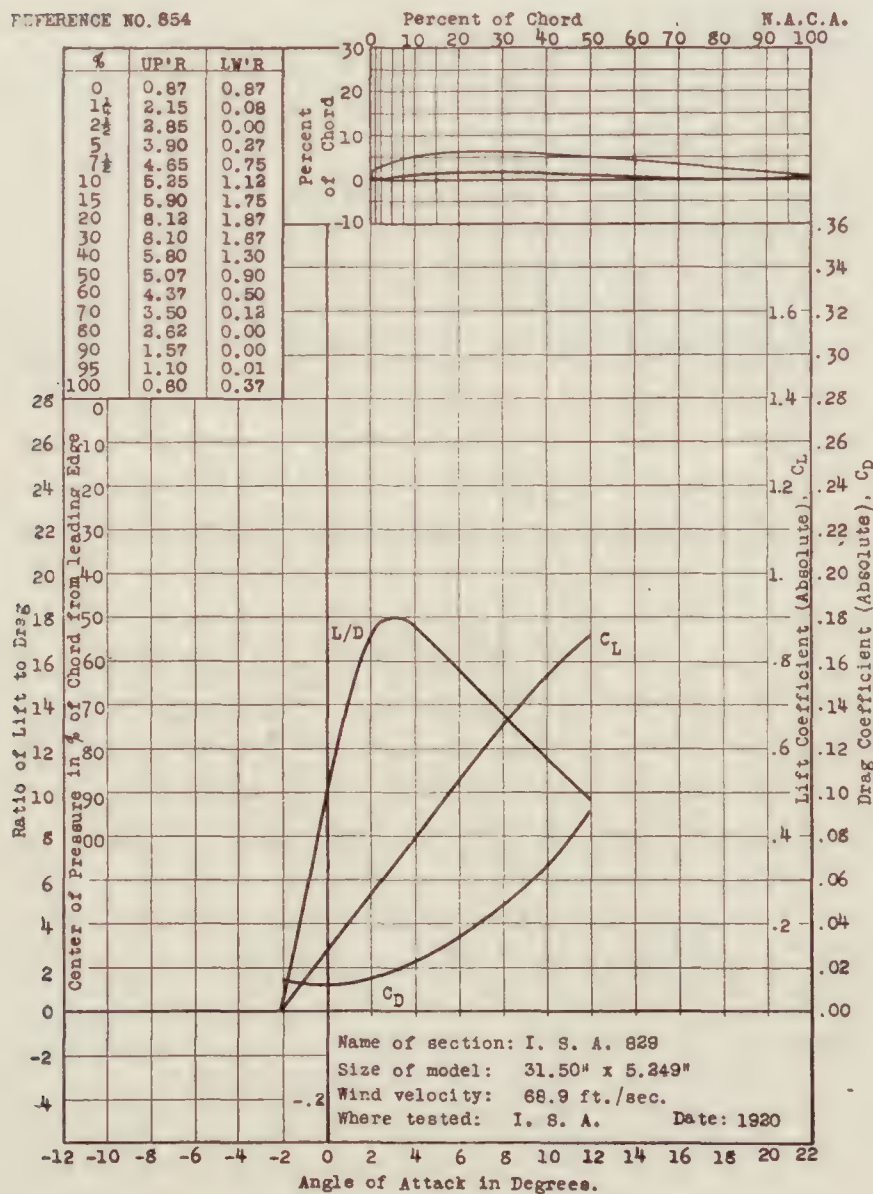
REFERENCE NO. 852



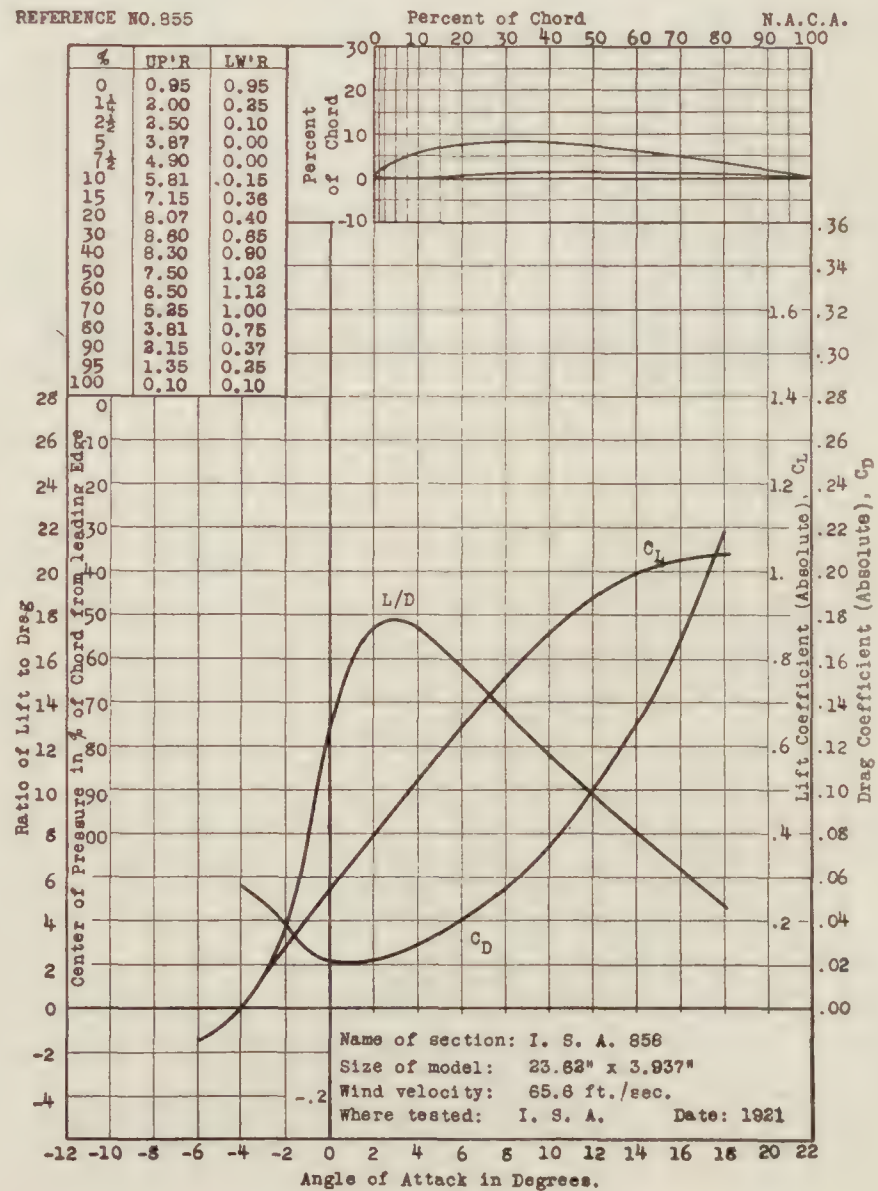
REFERENCE NO. 853



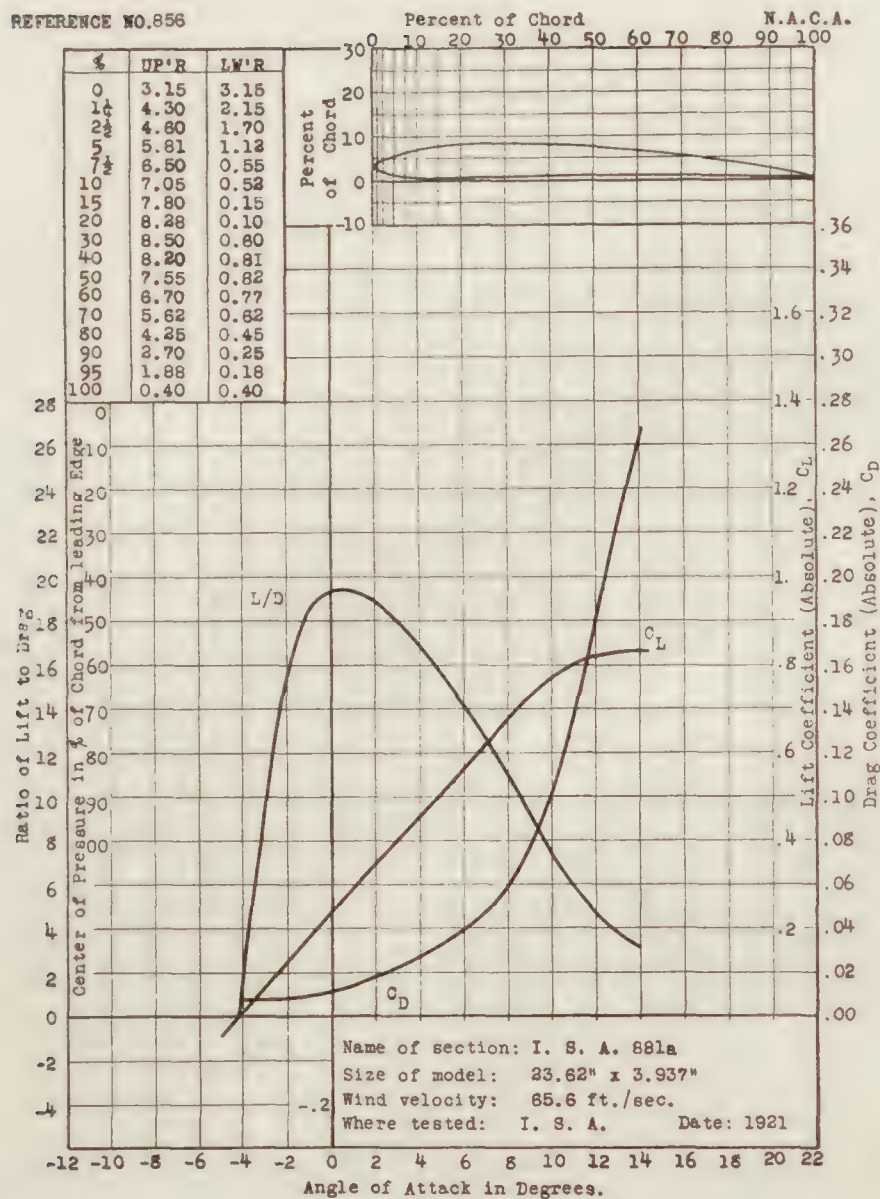
REFERENCE NO. 854



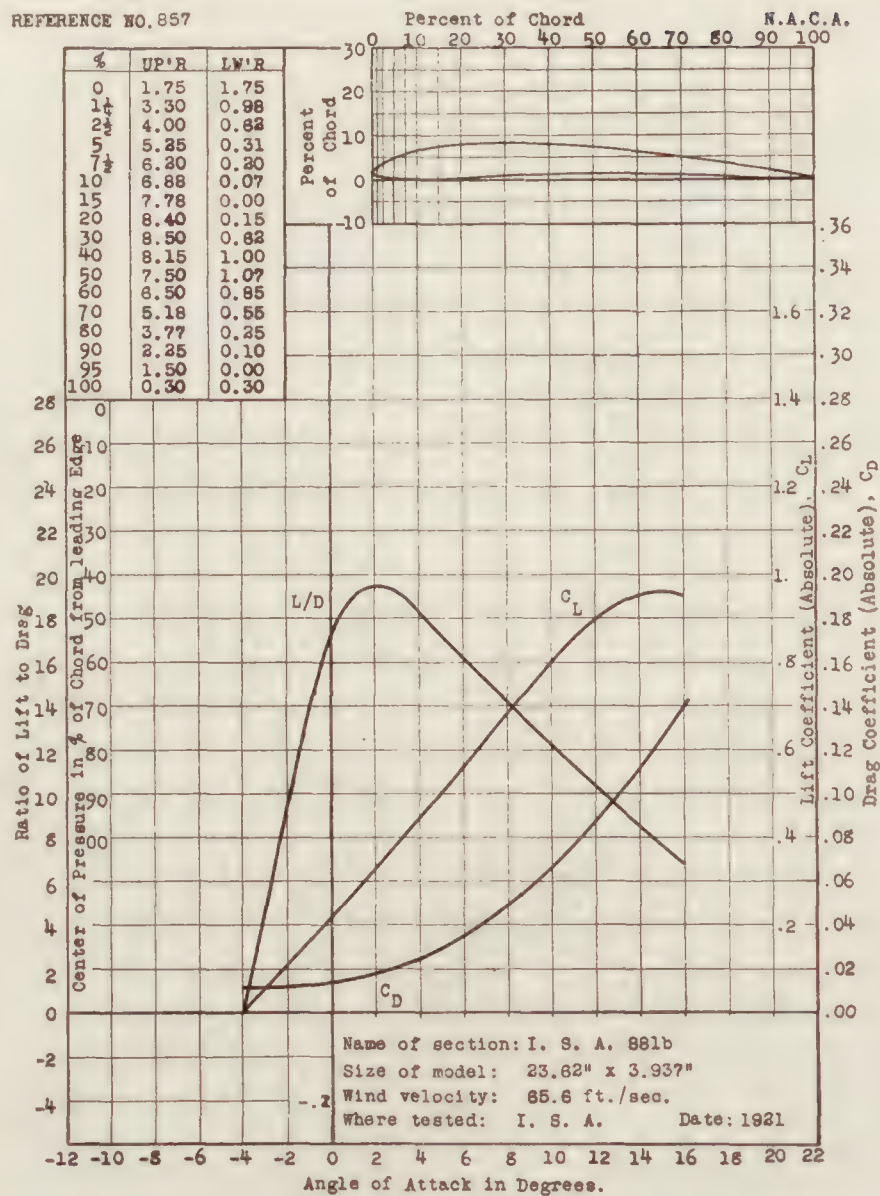
REFERENCE NO. 855



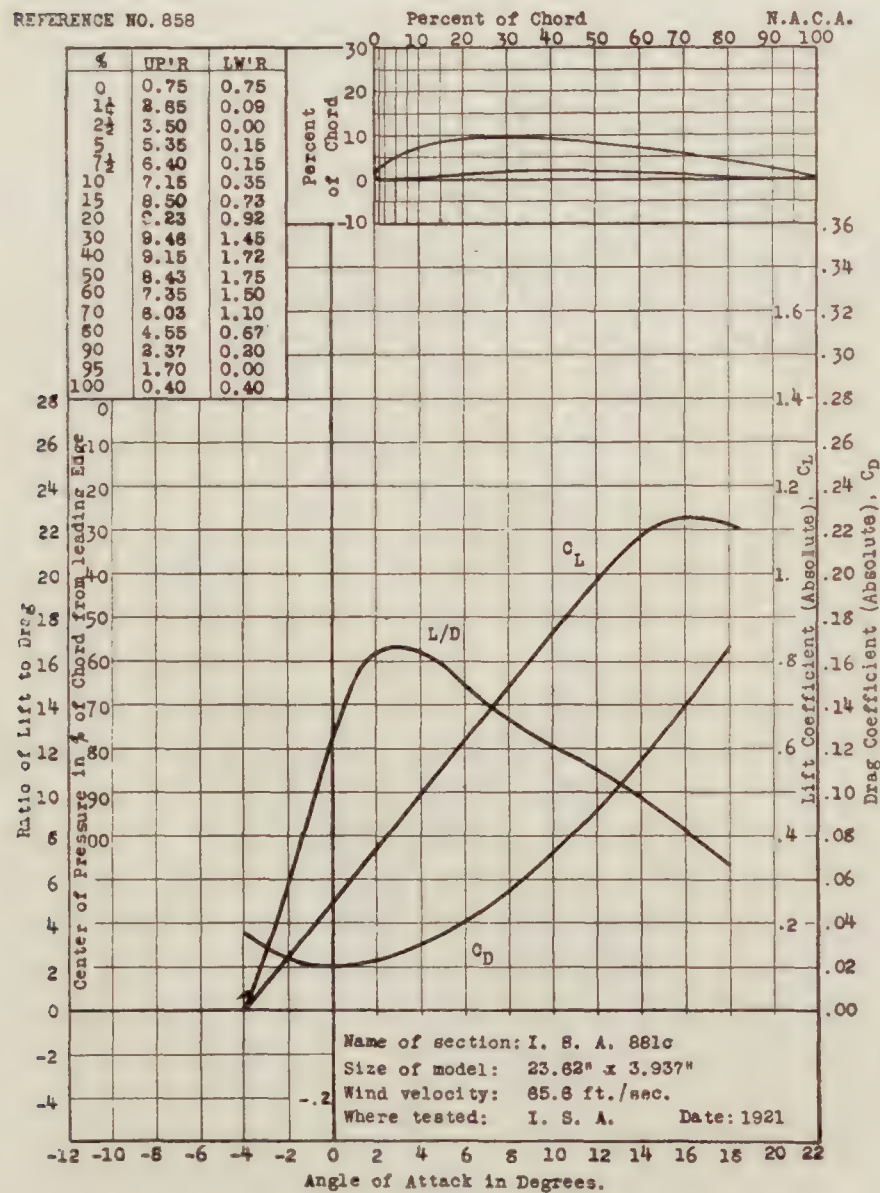
REFERENCE NO. 856



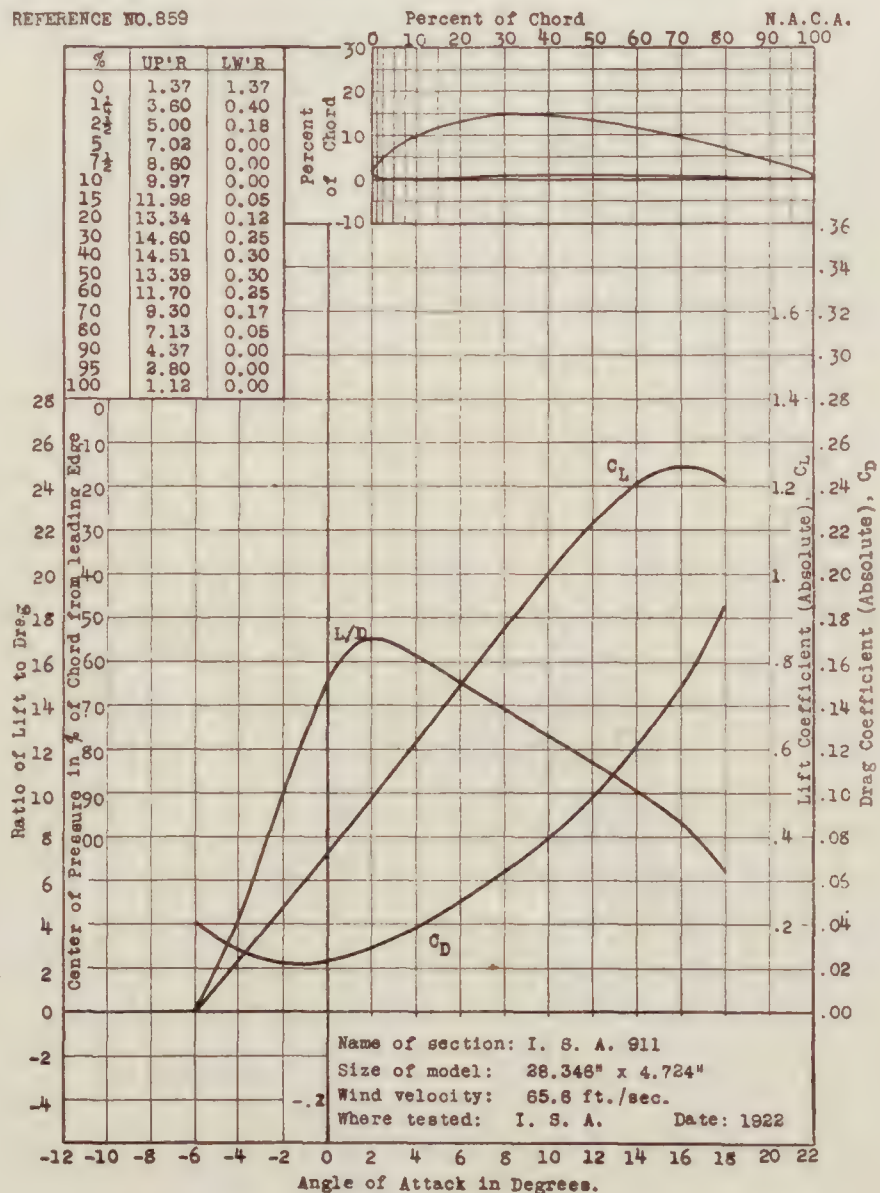
REFERENCE NO. 857

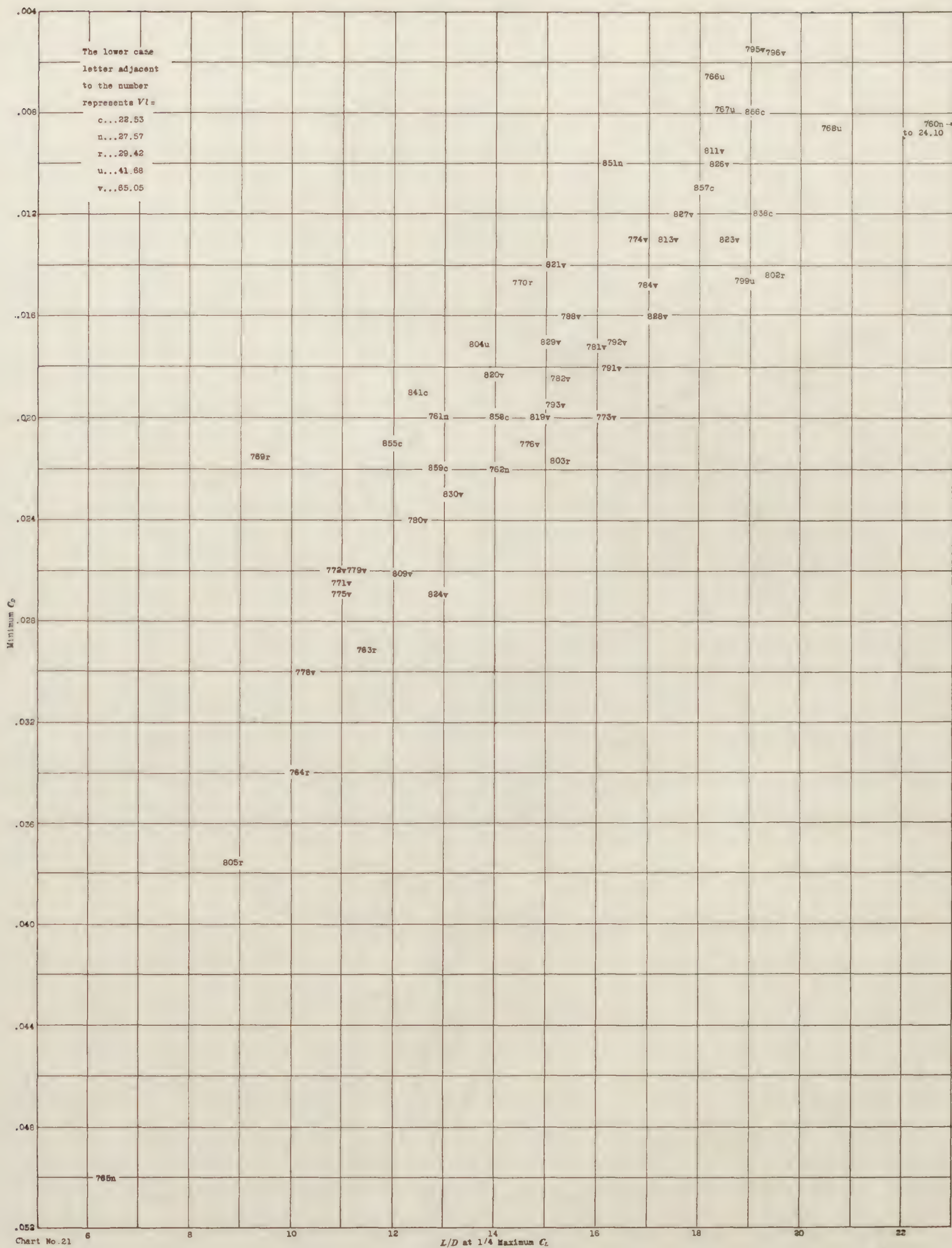


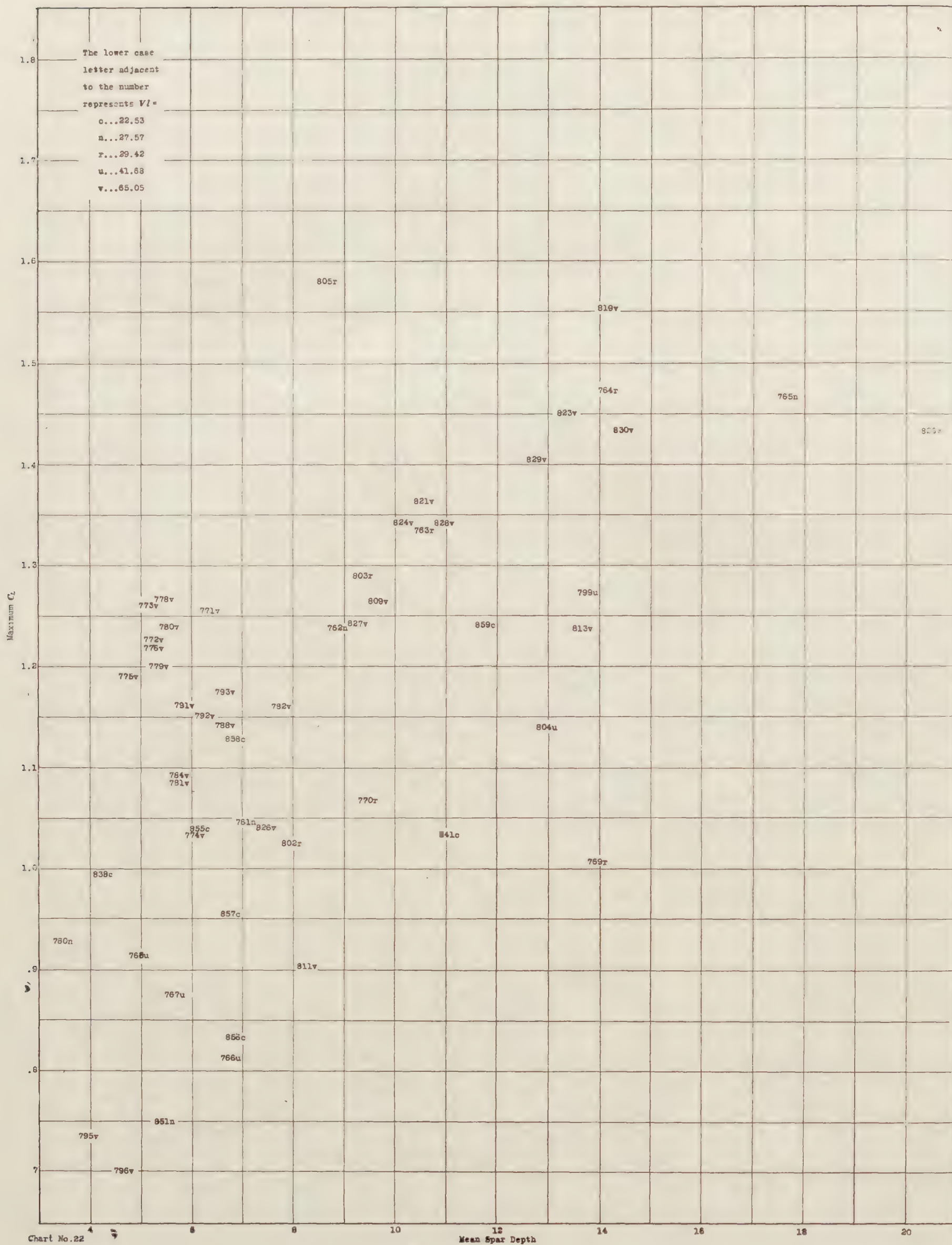
REFERENCE NO. 858

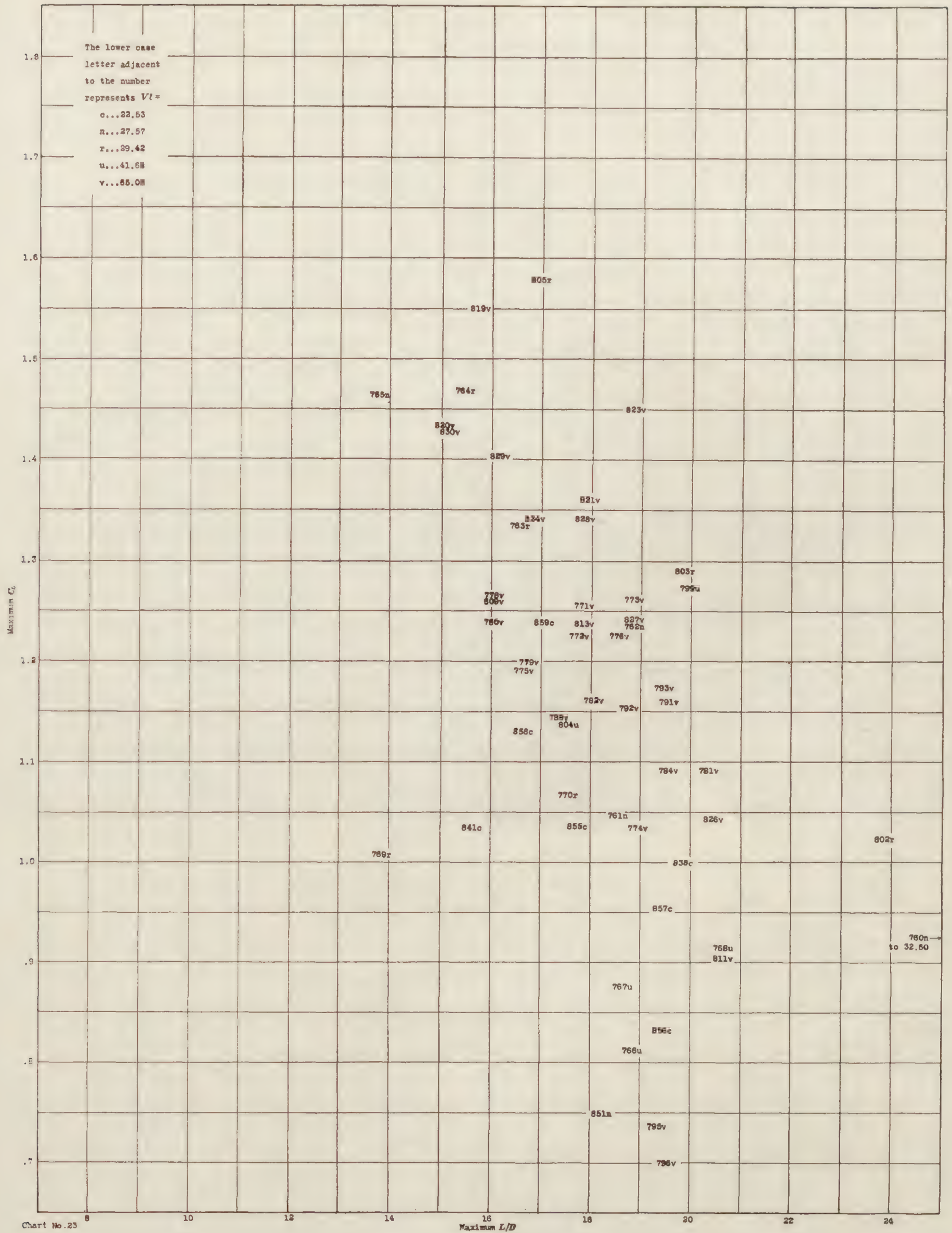


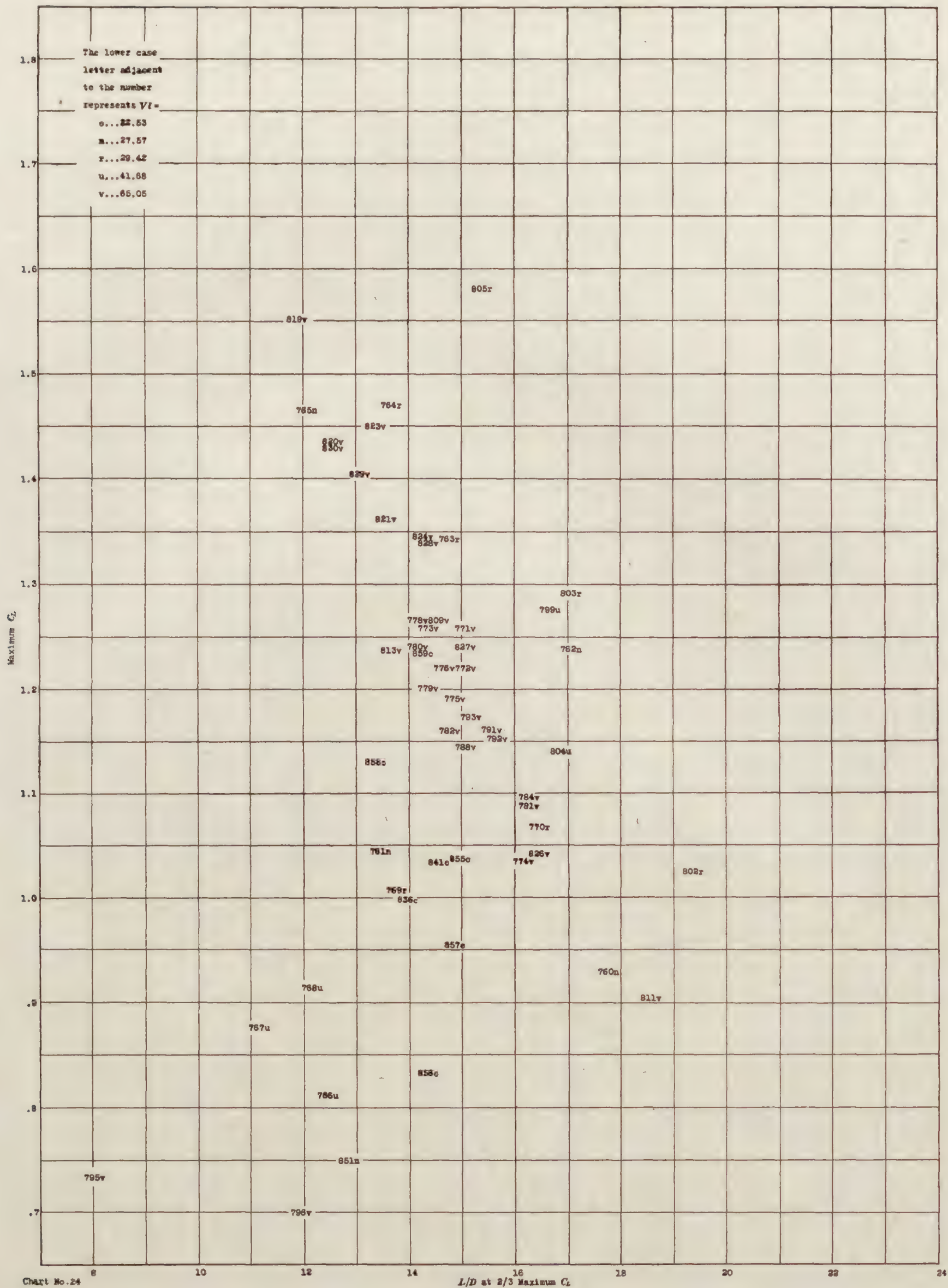
REFERENCE NO. 859











REPORT No. 316

TABLES FOR PRESSURE OF AIR ON COMING TO REST FROM VARIOUS SPEEDS

By A. F. ZAHM and F. A. LOUDEN

Aerodynamical Laboratory, Bureau of Construction and Repair, U. S. Navy

REPORT No. 316

TABLES FOR PRESSURE OF AIR ON COMING TO REST FROM VARIOUS SPEEDS

By A. F. ZAHM and F. A. LOUDEN

In Technical Report No. 247 of the National Advisory Committee for Aeronautics theoretical formulas are given from which was computed a table for the pressure of air on coming to rest from various speeds, such as those of aircraft and propeller blades. In that report, the table gave incompressible and adiabatic stop pressures of air for even-speed intervals in miles per hour and for some even-speed intervals in knots per hour. Table II of the present report extends the above-mentioned table by including the stop pressures of air for even-speed intervals in miles per hour, feet per second, knots per hour, kilometers per hour, and meters per second. The pressure values in Table II are also more exact than the values given in the previous table.

To furnish the aeronautical engineer with ready numerical formulas for finding the pressure of air on coming to rest, Table I has been derived for the standard values specified below in C. G. S. units as given in N. A. C. A. Technical Report No. 247, then furnishes additional working formulas for several special units of speed.

TABLE I.—FORMULAS FOR PRESSURE OF AIR ON COMING TO REST FROM MODERATE SPEEDS
viz, for $V_0 < 1000$ mi./hr.

		Formulas for barometric plus impact pressure in standard atmospheres	
		Incompressible p_1/p_0	Adiabatic p_2/p_0
General formula-----		$p_1/p_0 = 1 + \rho_0 V_0^2 / 2p_0$	$p_2/p_0 = [1 + (\gamma - 1) \rho_0 V_0^2 / 2\gamma p_0]^{\gamma / \gamma - 1}$
Specific working formula, $V_0 = \text{cm/s.}$		$p_1/p_0 = 1 + .60471 \times 10^{-9} V_0^2$	$p_2/p_0 = (1 + 1.727735 \times 10^{-10} V_0^2)^{3.50}$
Additional working formulas	$V_0 = \text{mi./hr}$	$p_1/p_0 = 1 + 1.20841 \times 10^{-6} V_0^2$	$p_2/p_0 = (1 + .345259 \times 10^{-6} V_0^2)^{3.50}$
	$V_0 = \text{ft./s}$	$p_1/p_0 = 1 + .56180 \times 10^{-6} V_0^2$	$p_2/p_0 = (1 + 1.60513 \times 10^{-7} V_0^2)^{3.50}$
	$V_0 = \text{knots/hr}$	$p_1/p_0 = 1 + 1.60260 \times 10^{-6} V_0^2$	$p_2/p_0 = (1 + .457884 \times 10^{-6} V_0^2)^{3.50}$
	$V_0 = \text{km/h}$	$p_1/p_0 = 1 + .46660 \times 10^{-6} V_0^2$	$p_2/p_0 = (1 + 1.33313 \times 10^{-7} V_0^2)^{3.50}$
	$V_0 = \text{m/s}$	$p_1/p_0 = 1 + .60471 \times 10^{-5} V_0^2$	$p_2/p_0 = (1 + 1.727735 \times 10^{-6} V_0^2)^{3.50}$

$p_0 = 1.0133 \times 10^6$ dynes/cm² = 1 std. atmo. } U. S. std. values. (See N. A. C. A. Technical Report No. 218.)
 $\rho_0 = .0012255$ g/cm³ ----- }
 $\gamma = 1.40$
 $V_0 =$ Air speed
 $p_1, p_2 =$ Incompressible and adiabatic stop pressures above vacuo.

TABLE II.—PRESSURE OF AIR ON COMING TO REST FROM VARIOUS SPEEDS

[Symbols defined at bottom of table]

Air speed miles per hour	Barometric plus impact pressure in standard atmos- pheres: 1 std. atmo. = 1.0133×10^6 dynes/cm ² = p_0		Impact pressure in pounds per square foot: 1 std. atmo. = 2,116.8 lb./sq. ft.		Impact pressure in inches of water: 1 std. atmo. = 407.2 in. of water		Percentage difference
	Incompressible	Adiabatic	Incompress- ible	Adiabatic	Incompress- ible	Adiabatic	
0	1. 00000000	1. 00000000	0. 000	0. 000	0. 000	0. 000	0. 00
10	1. 00012084	1. 00012084	. 256	. 256	. 049	. 049	. 00
20	1. 00048336	1. 00048343	1. 023	1. 023	. 197	. 197	. 01
30	1. 0010876	1. 0010880	2. 302	2. 303	. 443	. 443	. 04
40	1. 0019335	1. 0019348	4. 093	4. 096	. 787	. 788	. 07
50	1. 0030210	1. 0030243	6. 395	6. 402	1. 230	1. 231	. 11
60	1. 0043503	1. 0043569	9. 209	9. 223	1. 771	1. 774	. 15
70	1. 0059212	1. 0059338	12. 534	12. 561	2. 411	2. 416	. 21
80	1. 0077338	1. 0077553	16. 371	16. 416	3. 149	3. 158	. 28
90	1. 0097881	1. 0098223	20. 719	20. 792	3. 986	4. 000	. 35
100	1. 012084	1. 012136	25. 579	25. 689	4. 921	4. 942	. 43
110	1. 014622	1. 014698	30. 952	31. 113	5. 954	5. 985	. 52
120	1. 017401	1. 017509	36. 834	37. 063	7. 086	7. 130	. 62
130	1. 020422	1. 020572	43. 229	43. 547	8. 316	8. 377	. 73
140	1. 023685	1. 023886	50. 136	50. 562	9. 645	9. 726	. 85
150	1. 027189	1. 027454	57. 554	58. 115	11. 071	11. 179	. 97
160	1. 030935	1. 031278	65. 483	66. 209	12. 597	12. 736	1. 11
170	1. 034923	1. 035361	73. 925	74. 852	14. 221	14. 399	1. 25
180	1. 039152	1. 039702	82. 877	84. 041	15. 943	16. 167	1. 40
190	1. 043624	1. 044308	92. 343	93. 791	17. 764	18. 042	1. 57
200	1. 048336	1. 049175	102. 32	104. 09	19. 682	20. 024	1. 74
210	1. 053291	1. 054313	112. 81	114. 97	21. 700	22. 116	1. 92
220	1. 058487	1. 059721	123. 81	126. 42	23. 816	24. 318	2. 11
230	1. 063925	1. 065397	135. 32	138. 43	26. 030	26. 630	2. 30
240	1. 069604	1. 071352	147. 34	151. 04	28. 343	29. 055	2. 51
250	1. 075526	1. 077586	159. 87	164. 23	30. 754	31. 593	2. 73
260	1. 081689	1. 084101	172. 92	178. 02	33. 264	34. 246	2. 96
270	1. 088093	1. 090898	186. 48	192. 41	35. 871	37. 014	3. 18
280	1. 094739	1. 097987	200. 54	207. 42	38. 578	39. 900	3. 43
290	1. 10163	1. 10537	215. 13	223. 05	41. 384	42. 907	3. 68
300	1. 10876	1. 11305	230. 22	239. 30	44. 287	46. 034	3. 94
310	1. 11613	1. 12102	245. 82	256. 18	47. 288	49. 279	4. 21
320	1. 12374	1. 12931	261. 93	273. 72	50. 387	52. 655	4. 50
330	1. 13160	1. 13790	278. 57	291. 91	53. 588	56. 153	4. 79
340	1. 13969	1. 14680	295. 70	310. 75	56. 882	59. 777	5. 09
350	1. 14803	1. 15602	313. 35	330. 26	60. 278	63. 531	5. 40
400	1. 19335	1. 20707	409. 28	438. 33	78. 732	84. 319	7. 10
500	1. 30210	1. 33612	639. 49	711. 50	123. 02	136. 87	11. 26
600	1. 43503	1. 50688	920. 87	1, 073. 0	177. 14	206. 40	16. 52
700	1. 59212	1. 72815	1, 253. 4	1, 541. 3	241. 11	296. 50	22. 97
800	1. 77338	2. 01124	1, 637. 1	2, 140. 6	314. 92	411. 78	30. 76
900	1. 97881	2. 37045	2, 071. 9	2, 901. 0	398. 57	558. 05	40. 01
1, 000	2. 20841	2. 82371	2, 558. 0	3, 860. 4	492. 06	742. 61	50. 92

TABLE II.—PRESSURE OF AIR ON COMING TO REST FROM VARIOUS SPEEDS—Continued

Air speed feet per second	Barometric plus impact pressure in standard atmos- pheres: 1 std. atmo.=1.0133×10 ⁶ dynes/cm ² =p ₀		Impact pressure in pounds per square foot: 1 std. atmo.=2,116.8 lb./sq. ft.		Impact pressure in inches of water: 1 std. atmo.=407.2 in. of water		Percentage difference
	Incompressible	Adiabatic	Incompress- ible	Adiabatic	Incompress- ible	Adiabatic	
0	1. 000000000	1. 000000000	0. 000	0. 000	0. 000	0. 000	0. 00
10	1. 000056180	1. 000056180	. 119	. 119	. 023	. 023	. 00
20	1. 00022472	1. 00022473	. 476	. 476	. 092	. 092	. 00
30	1. 00050562	1. 00050570	1. 070	1. 070	. 206	. 206	. 02
40	1. 00089888	1. 00089915	1. 903	1. 903	. 366	. 366	. 03
50	1. 0014045	1. 0014052	2. 973	2. 975	. 572	. 572	. 05
60	1. 0020225	1. 0020241	4. 281	4. 285	. 824	. 824	. 08
70	1. 0027528	1. 0027556	5. 827	5. 833	1. 121	1. 122	. 10
80	1. 0035955	1. 0036002	7. 611	7. 621	1. 464	1. 467	. 13
90	1. 0045506	1. 0045582	9. 633	9. 649	1. 853	1. 856	. 17
100	1. 0056180	1. 0056292	11. 892	11. 916	2. 288	2. 292	. 20
110	1. 0067978	1. 0068142	14. 390	14. 424	2. 768	2. 775	. 24
120	1. 0080899	1. 0081133	17. 125	17. 174	3. 294	3. 304	. 29
130	1. 0094944	1. 0095267	20. 098	20. 166	3. 866	3. 879	. 34
140	1. 011011	1. 011055	23. 308	23. 401	4. 484	4. 502	. 40
150	1. 012641	1. 012697	26. 758	26. 877	5. 147	5. 170	. 44
160	1. 014382	1. 014456	30. 444	30. 600	5. 856	5. 886	. 51
170	1. 016236	1. 016330	34. 368	34. 567	6. 611	6. 650	. 58
180	1. 018202	1. 018322	38. 530	38. 784	7. 412	7. 461	. 66
190	1. 020281	1. 020428	42. 931	43. 242	8. 258	8. 318	. 72
200	1. 022472	1. 022653	47. 569	47. 952	9. 151	9. 224	. 81
210	1. 024775	1. 024995	52. 444	52. 909	10. 088	10. 178	. 89
220	1. 027191	1. 027456	57. 558	58. 119	11. 072	11. 180	. 97
230	1. 029719	1. 030036	62. 909	63. 580	12. 102	12. 231	1. 07
240	1. 032360	1. 032735	68. 500	69. 293	13. 177	13. 330	1. 16
250	1. 035113	1. 035555	74. 327	75. 263	14. 298	14. 478	1. 26
260	1. 037978	1. 038496	80. 392	81. 488	15. 465	15. 676	1. 36
270	1. 040955	1. 041556	86. 694	87. 966	16. 677	16. 922	1. 47
280	1. 044045	1. 044741	93. 234	94. 708	17. 935	18. 219	1. 58
290	1. 047247	1. 048049	100. 01	101. 71	19. 239	19. 566	1. 70
300	1. 050562	1. 051481	107. 03	108. 97	20. 589	20. 963	1. 82
310	1. 053989	1. 055037	114. 28	116. 50	21. 984	22. 411	1. 94
320	1. 057528	1. 058721	121. 78	124. 30	23. 425	23. 911	2. 07
330	1. 061180	1. 062528	129. 51	132. 36	24. 912	25. 461	2. 20
340	1. 064944	1. 066463	137. 47	140. 69	26. 445	27. 064	2. 34
350	1. 068821	1. 070529	145. 68	149. 30	28. 024	28. 719	2. 48
360	1. 072809	1. 074720	154. 12	158. 17	29. 648	30. 426	2. 62
370	1. 076910	1. 079045	162. 80	167. 32	31. 318	32. 187	2. 78
380	1. 081124	1. 083501	171. 72	176. 75	33. 034	34. 002	2. 93
390	1. 085450	1. 088089	180. 88	186. 47	34. 795	35. 870	3. 09
400	1. 089888	1. 092810	190. 27	196. 46	36. 602	37. 792	3. 25
410	1. 094439	1. 097665	199. 91	206. 74	38. 456	39. 769	3. 42
420	1. 099102	1. 10266	209. 78	217. 31	40. 354	41. 803	3. 59
430	1. 10388	1. 10779	219. 89	228. 17	42. 300	43. 892	3. 76
440	1. 10876	1. 11305	230. 22	239. 30	44. 287	46. 034	3. 94
450	1. 11376	1. 11846	240. 81	250. 76	46. 323	48. 237	4. 13
460	1. 11888	1. 12401	251. 65	262. 50	48. 408	50. 497	4. 32
470	1. 12410	1. 12970	262. 69	274. 55	50. 534	52. 814	4. 51
480	1. 12944	1. 13553	274. 00	286. 89	52. 708	55. 188	4. 70
490	1. 13489	1. 14151	285. 54	299. 55	54. 927	57. 623	4. 91
500	1. 14045	1. 14763	297. 30	312. 50	57. 191	60. 115	5. 11
550	1. 16994	1. 18051	359. 73	382. 10	69. 200	73. 504	6. 22
600	1. 20225	1. 21728	428. 12	459. 94	82. 356	88. 476	7. 43
700	1. 27528	1. 30342	582. 71	642. 28	112. 09	123. 55	10. 22
800	1. 35955	1. 40813	761. 10	863. 93	146. 41	166. 19	13. 51
900	1. 45506	1. 53392	963. 27	1, 130. 2	185. 30	217. 41	17. 33
1, 000	1. 56180	1. 68372	1, 189. 2	1, 447. 3	228. 76	278. 41	21. 70
1, 100	1. 67978	1. 86121	1, 439. 0	1, 823. 0	276. 81	350. 68	26. 69
1, 200	1. 80899	2. 07050	1, 712. 5	2, 266. 0	329. 42	435. 91	32. 33
1, 300	1. 94944	2. 31650	2, 009. 8	2, 786. 8	386. 61	536. 08	38. 66
1, 400	2. 10113	2. 60489	2, 330. 9	3, 397. 2	448. 38	653. 51	45. 75
1, 500	2. 26405	2. 94219	2, 675. 7	4, 111. 2	514. 72	790. 86	53. 65

TABLE II.—PRESSURE OF AIR ON COMING TO REST FROM VARIOUS SPEEDS—Continued

Air speed knots per hour	Barometric plus impact pressure in standard atmos- pheres: 1 std. atmo. = 1.0133×10^6 dynes/cm ² = p_0		Impact pressure in pounds per square foot: 1 std. atmo. = 2,116.8 lb./sq. ft.		Impact pressure in inches of water: 1 std. atmo. = 407.2 in. of water		Percentage difference
	Incompressible	Adiabatic	Incompressible	Adiabatic	Incompressible	Adiabatic	
0	1. 00000000	1. 00000000	0. 000	0. 000	0. 000	0. 000	0. 00
10	1. 00016026	1. 00016026	. 339	. 339	. 065	. 065	. 00
20	1. 00064104	1. 00064117	1. 357	1. 357	. 261	. 261	. 02
30	1. 0014423	1. 0014431	3. 053	3. 055	. 587	. 588	. 06
40	1. 0025642	1. 0025665	5. 428	5. 433	1. 044	1. 045	. 09
50	1. 0040065	1. 0040122	8. 481	8. 493	1. 631	1. 634	. 14
60	1. 0057694	1. 0057814	12. 213	12. 238	2. 349	2. 354	. 21
70	1. 0078527	1. 0078746	16. 623	16. 669	3. 198	3. 207	. 28
80	1. 010257	1. 010294	21. 712	21. 790	4. 177	4. 192	. 36
90	1. 012981	1. 013041	27. 478	27. 605	5. 286	5. 310	. 46
100	1. 016026	1. 016118	33. 924	34. 119	6. 526	6. 563	. 57
110	1. 019391	1. 019526	41. 047	41. 333	7. 896	7. 951	. 70
120	1. 023077	1. 023268	48. 849	49. 254	9. 397	9. 475	. 83
130	1. 027084	1. 027347	57. 331	57. 888	11. 029	11. 136	. 97
140	1. 031411	1. 031765	66. 491	67. 240	12. 791	12. 935	1. 13
150	1. 036059	1. 036524	76. 330	77. 314	14. 683	14. 873	1. 29
160	1. 041027	1. 041632	86. 846	88. 127	16. 706	16. 953	1. 47
170	1. 046315	1. 047087	98. 040	99. 674	18. 859	19. 174	1. 67
180	1. 051924	1. 052893	109. 91	111. 96	21. 143	21. 538	1. 87
190	1. 057854	1. 059060	122. 47	125. 02	23. 558	24. 049	2. 08
200	1. 064104	1. 065584	135. 70	138. 83	26. 103	26. 706	2. 31
210	1. 070675	1. 072478	149. 60	153. 42	28. 779	29. 513	2. 55
220	1. 077566	1. 079740	164. 19	168. 79	31. 585	32. 470	2. 80
230	1. 084778	1. 087375	179. 46	184. 96	34. 522	35. 579	3. 06
240	1. 092310	1. 095393	195. 40	201. 93	37. 589	38. 844	3. 34
250	1. 10016	1. 10380	212. 02	219. 72	40. 785	42. 267	3. 63
260	1. 10834	1. 11259	229. 33	238. 33	44. 116	45. 847	3. 92
270	1. 11683	1. 12179	247. 31	257. 81	47. 573	49. 593	4. 25
280	1. 12567	1. 13138	266. 02	278. 11	51. 173	53. 498	4. 57
290	1. 13478	1. 14139	285. 30	299. 29	54. 882	57. 574	4. 90
300	1. 14423	1. 15182	305. 31	321. 37	58. 730	61. 821	5. 26
350	1. 19632	1. 21047	415. 57	445. 52	79. 942	85. 703	7. 21
400	1. 25642	1. 28076	542. 79	594. 31	104. 41	114. 33	9. 49
500	1. 40065	1. 46130	848. 10	976. 48	163. 14	187. 84	15. 14
600	1. 57694	1. 70582	1221. 3	1494. 1	234. 93	287. 41	22. 34
700	1. 78527	2. 03087	1662. 3	2182. 1	319. 76	419. 77	31. 28
800	2. 02566	2. 45841	2171. 1	3087. 2	417. 65	593. 86	42. 19
900	2. 29811	3. 01654	2747. 8	4268. 6	528. 59	821. 14	55. 34

TABLE II.—PRESSURE OF AIR ON COMING TO REST FROM VARIOUS SPEEDS—Continued

Air speed kilometers per hour	Barometric plus impact pressure in standard atmos- pheres: 1 std. atmo. = 1.0133×10^6 dynes/cm ² = p_0		Impact pressure in kilograms per square meter: 1 std. atmo. = 10332 kg/m ²		Impact pressure in millime- ters of water: 1 std. atmo. = 10343 mm of water		Percentage difference
	Incompressible	Adiabatic	Incompressible	Adiabatic	Incompressible	Adiabatic	
0	1. 000000000	1. 000000000	0. 000	0. 000	0. 000	0. 000	0. 00
10	1. 000046660	1. 000046660	. 482	. 482	. 483	. 483	. 00
20	1. 00018664	1. 00018664	1. 928	1. 928	1. 930	1. 930	. 00
30	1. 00041994	1. 00041999	4. 339	4. 339	4. 343	4. 344	. 01
40	1. 00074656	1. 00074675	7. 713	7. 715	7. 722	7. 724	. 03
50	1. 0011665	1. 0011670	12. 052	12. 057	12. 065	12. 070	. 04
60	1. 0016798	1. 0016808	17. 356	17. 366	17. 374	17. 385	. 06
70	1. 0022863	1. 0022882	23. 622	23. 642	23. 647	23. 667	. 08
80	1. 0029862	1. 0029894	30. 853	30. 886	30. 886	30. 919	. 11
90	1. 0037795	1. 0037843	39. 050	39. 099	39. 091	39. 141	. 13
100	1. 0046660	1. 0046737	48. 209	48. 289	48. 260	48. 340	. 17
110	1. 0056459	1. 0056573	58. 333	58. 451	58. 396	58. 513	. 20
120	1. 0067190	1. 0067351	69. 421	69. 587	69. 495	69. 661	. 24
130	1. 0078855	1. 0079077	81. 473	81. 702	81. 560	81. 789	. 28
140	1. 0091454	1. 0091751	94. 490	94. 797	94. 591	98. 049	. 33
150	1. 010499	1. 010538	108. 48	108. 88	108. 59	108. 99	. 37
160	1. 011945	1. 011996	123. 42	123. 94	123. 55	124. 07	. 43
170	1. 013485	1. 013550	139. 33	140. 00	139. 48	140. 15	. 48
180	1. 015118	1. 015199	156. 20	157. 04	156. 37	157. 20	. 54
190	1. 016844	1. 016946	174. 03	175. 09	174. 22	175. 27	. 61
200	1. 018664	1. 018788	192. 84	194. 12	193. 04	194. 32	. 66
210	1. 020577	1. 020728	212. 60	214. 16	212. 83	221. 51	. 73
220	1. 022583	1. 022766	233. 33	235. 22	233. 58	235. 47	. 81
230	1. 024683	1. 024901	255. 02	257. 28	255. 30	257. 55	. 88
240	1. 026876	1. 027135	277. 68	280. 36	277. 98	280. 66	. 96
250	1. 029163	1. 029467	301. 31	304. 45	301. 63	304. 78	1. 04
260	1. 031542	1. 031899	325. 89	329. 58	326. 24	329. 93	1. 13
270	1. 034015	1. 034430	351. 44	355. 73	351. 82	356. 11	1. 22
280	1. 036581	1. 037062	377. 95	382. 92	378. 36	383. 33	1. 32
290	1. 039241	1. 039795	405. 44	411. 16	405. 87	411. 60	1. 41
300	1. 041994	1. 042627	433. 88	440. 42	434. 34	440. 89	1. 51
310	1. 044840	1. 045561	463. 29	470. 74	463. 78	471. 24	1. 61
320	1. 047780	1. 048599	493. 66	502. 12	494. 19	502. 66	1. 71
330	1. 050813	1. 051742	525. 00	534. 60	525. 56	535. 17	1. 83
340	1. 053939	1. 054986	557. 30	568. 12	557. 89	568. 72	1. 94
350	1. 057159	1. 058335	590. 57	602. 72	591. 20	603. 36	2. 06
360	1. 060471	1. 061787	624. 79	638. 38	625. 45	639. 06	2. 18
370	1. 063878	1. 065349	659. 99	675. 19	660. 69	675. 90	2. 30
380	1. 067377	1. 069012	696. 14	713. 03	696. 88	713. 79	2. 43
390	1. 070970	1. 072787	733. 26	752. 04	734. 04	752. 84	2. 56
400	1. 074656	1. 076667	771. 35	792. 12	772. 17	792. 97	2. 69
410	1. 078435	1. 080657	810. 39	833. 35	811. 25	834. 24	2. 83
420	1. 082308	1. 084754	850. 41	875. 68	851. 31	876. 61	2. 97
430	1. 086274	1. 088966	891. 38	919. 20	892. 33	920. 11	3. 12
440	1. 090334	1. 093284	933. 33	963. 81	934. 32	964. 84	3. 27
450	1. 094487	1. 097718	976. 24	1, 009. 6	977. 28	1, 010. 7	3. 42
460	1. 098733	1. 10226	1, 020. 1	1, 056. 6	1, 021. 2	1, 057. 7	3. 57
470	1. 10307	1. 10692	1, 064. 9	1, 104. 7	1, 066. 1	1, 105. 9	3. 74
480	1. 10750	1. 11169	1, 110. 7	1, 154. 0	1, 111. 9	1, 155. 2	3. 90
490	1. 11203	1. 11658	1, 157. 5	1, 204. 5	1, 158. 7	1, 205. 8	4. 06
500	1. 11665	1. 12159	1, 205. 2	1, 256. 3	1, 206. 5	1, 257. 6	4. 24
510	1. 12136	1. 12671	1, 253. 9	1, 309. 2	1, 255. 2	1, 310. 6	4. 41
520	1. 12617	1. 13196	1, 303. 6	1, 363. 4	1, 305. 0	1, 364. 9	4. 59
530	1. 13107	1. 13732	1, 354. 2	1, 418. 8	1, 355. 7	1, 467. 5	4. 77
540	1. 13606	1. 14280	1, 405. 8	1, 475. 4	1, 407. 3	1, 477. 0	4. 95
550	1. 14115	1. 14840	1, 458. 4	1, 533. 3	1, 459. 9	1, 534. 9	5. 14
600	1. 16798	1. 17830	1, 735. 6	1, 842. 2	1, 737. 4	1, 844. 2	6. 14
700	1. 22863	1. 24791	2, 362. 2	2, 561. 4	2, 364. 7	2, 564. 1	8. 43
800	1. 29862	1. 33184	3, 085. 3	3, 428. 6	3, 088. 6	3, 432. 2	11. 12
900	1. 37795	1. 43173	3, 905. 0	4, 460. 6	3, 909. 1	4, 465. 4	14. 23
1, 000	1. 46660	1. 54960	4, 820. 9	5, 678. 5	4, 826. 0	5, 684. 5	17. 79
1, 100	1. 56459	1. 68779	5, 833. 3	7, 106. 2	5, 839. 6	7, 113. 8	21. 82
1, 200	1. 67190	1. 84896	6, 942. 1	8, 771. 5	6, 949. 5	8, 780. 8	26. 35
1, 300	1. 78855	2. 03633	8, 147. 3	10, 707	8, 156. 0	10, 719	31. 42
1, 400	1. 91454	2. 25347	9, 449. 0	12, 951	9, 459. 1	12, 965	37. 06
1, 500	2. 04985	2. 50463	10, 847	15, 546	10, 859	15, 562	43. 32

TABLE II.—PRESSURE OF AIR ON COMING TO REST FROM VARIOUS SPEEDS—Continued

Air speed meters per second	Barometric plus impact pressure in standard atmos- pheres: 1 std. atmo.=1.0133×10 ⁶ dynes/cm ² =p ₀		Impact pressure in kilograms per square meter: 1 std. atmo.=10332 kg/m ²		Impact pressure in millime- ters of water: 1 std. atmo. =10343 mm of water		Percentage difference
	Incompressible	Adiabatic	Incompres- sible	Adiabatic	Incompres- sible	Adiabatic	
0	1. 00000000	1. 00000000	0. 000	0. 000	0. 000	0. 000	0. 00
5	1. 00015118	1. 00015118	1. 562	1. 562	1. 571	1. 571	. 00
10	1. 00060471	1. 00060482	6. 248	6. 249	6. 255	6. 256	. 02
15	1. 0013606	1. 0013612	14. 058	14. 064	14. 073	14. 079	. 04
20	1. 0024188	1. 0024209	24. 991	25. 013	25. 018	25. 039	. 09
25	1. 0037794	1. 0037844	39. 049	39. 100	39. 090	39. 142	. 13
30	1. 0054424	1. 0054531	56. 231	56. 341	56. 291	56. 401	. 20
35	1. 0074077	1. 0074274	76. 536	76. 740	76. 618	76. 822	. 27
40	1. 0096754	1. 0097089	99. 966	100. 31	100. 07	100. 42	. 35
45	1. 012245	1. 012299	126. 52	127. 07	126. 65	127. 21	. 44
50	1. 015118	1. 015199	156. 20	157. 04	156. 37	157. 20	. 54
55	1. 018292	1. 018412	188. 99	190. 23	189. 19	190. 44	. 66
60	1. 021770	1. 021939	224. 93	226. 67	225. 17	226. 92	. 78
65	1. 025549	1. 025783	263. 97	266. 39	264. 25	266. 67	. 92
70	1. 029631	1. 029946	306. 15	309. 40	306. 47	309. 73	1. 06
75	1. 034015	1. 034430	351. 44	355. 73	351. 82	356. 11	1. 22
80	1. 038701	1. 039241	399. 86	405. 44	400. 28	405. 87	1. 40
85	1. 043690	1. 044376	451. 41	458. 49	451. 89	458. 98	1. 57
90	1. 048982	1. 049845	506. 08	515. 00	506. 62	515. 55	1. 76
95	1. 054575	1. 055648	563. 87	574. 96	564. 47	575. 57	1. 97
100	1. 060471	1. 061787	624. 79	638. 38	625. 45	639. 06	2. 18
105	1. 066669	1. 068271	688. 82	705. 38	689. 56	706. 13	2. 40
110	1. 073170	1. 075103	755. 99	775. 96	756. 80	776. 79	2. 64
115	1. 079973	1. 082282	826. 28	850. 14	827. 16	851. 04	2. 89
120	1. 087078	1. 089818	899. 69	928. 00	900. 65	928. 99	3. 15
125	1. 094486	1. 097717	976. 23	1009. 6	977. 27	1010. 7	3. 42
130	1. 10220	1. 10598	1055. 9	1095. 0	1057. 1	1096. 2	3. 70
135	1. 11021	1. 11461	1138. 7	1184. 2	1139. 9	1185. 4	3. 99
140	1. 11852	1. 12363	1224. 5	1277. 3	1225. 9	1278. 7	4. 31
145	1. 12714	1. 13302	1313. 6	1374. 4	1315. 0	1375. 8	4. 62
150	1. 13606	1. 14280	1405. 8	1475. 4	1407. 3	1477. 0	4. 95
155	1. 14528	1. 15298	1501. 0	1580. 6	1502. 6	1582. 3	5. 30
160	1. 15481	1. 16355	1599. 5	1689. 8	1601. 2	1691. 6	5. 65
200	1. 24188	1. 26351	2499. 1	2722. 6	2501. 8	2725. 5	8. 94
250	1. 37794	1. 43173	3904. 9	4460. 6	3909. 0	4465. 4	14. 23
300	1. 54424	1. 65842	5623. 1	6802. 8	5629. 1	6810. 0	20. 98
350	1. 74077	1. 95803	7653. 6	9898. 4	7661. 8	9908. 9	29. 33
400	1. 96754	2. 34964	9996. 6	13944.	10007.	13959.	39. 49
450	2. 22454	2. 85774	12652.	19194.	12665.	19215.	51. 71

$p_0=1.0133\times10^6$ dynes/cm²=1 std. atmo. } U. S. std. values. (See N. A. C. A. Technical Report No. 218.)
 $\rho_0=.0012255$ g/cm³ }
 $\gamma=1.40$.
 V_0 =Air speed in cm/s.
 p_1/p_0 (incompress.)= $1+\rho_0 V_0^2/2p_0=1+.60471\times10^{-6} V_0^2$ atmo.
 p_2/p_0 (adiabatic)=[$1+(\gamma-1)\rho_0 V_0^2/2\gamma p_0$] ^{$\gamma/\gamma-1$} =($1+1.727735\times10^{-10} V_0^2$)^{3.50}
Using $\gamma=1.404$ would lower the values in columns 5 and 7 less than 0.02 per cent for speeds less than 350 miles per hour.

AERODYNAMICAL LABORATORY,
BUREAU OF CONSTRUCTION AND REPAIR, UNITED STATES NAVY,
WASHINGTON, D. C., December 17, 1928.

REPORT No. 317

**WIND TUNNEL TESTS ON A SERIES OF WING MODELS
THROUGH A LARGE ANGLE OF ATTACK RANGE
PART I—FORCE TESTS**

**By MONTGOMERY KNIGHT and CARL J. WENZINGER
Langley Memorial Aeronautical Laboratory**

REPORT No. 317

WIND TUNNEL TESTS ON A SERIES OF WING MODELS THROUGH A LARGE ANGLE OF ATTACK RANGE

PART I. FORCE TESTS

By MONTGOMERY KNIGHT and CARL J. WENZINGER

SUMMARY

This investigation covers force tests through a large range of angle of attack on a series of monoplane and biplane wing models. The tests were conducted in the atmospheric wind tunnel of the National Advisory Committee for Aeronautics. The models were arranged in such a manner as to make possible a determination of the effects of variations in tip shape, aspect ratio, flap setting, stagger, gap, decalage, sweep back, and airfoil profile. The arrangements represented most of the types of wing systems in use on modern airplanes.

The effect of each variable is illustrated by means of groups of curves. In addition, there are included approximate autorotational characteristics in the form of calculated ranges of "rotary instability."

A correction for blocking in this tunnel which applies to monoplanes at large angles of attack has been developed, and is given in an appendix.

INTRODUCTION

The need of greater safety in airplane flight leads to a consideration of the characteristics of wing systems at low speeds or large angles of attack. In general, the region of danger lies above the angle of maximum lift, and comparatively little information has been published relating to the landing, spinning, stability, and controllability of airplanes in this region.

In order to augment the information on this subject, a comprehensive test program is being carried out in the atmospheric wind tunnel at the Langley Memorial Aeronautical Laboratory. This program includes force, pressure distribution, and autorotation tests on a series of models representing most of the wing systems in use on modern airplanes. The angle of attack range of the tests is sufficiently large to cover practically all attitudes attainable by an airplane in flight.

The force test part of the program has been completed, and the results have already been published in part. (Reference 1.) The present report gives the complete information as to lift, drag, and resultant force, and also includes the calculated probable ranges of "rotary instability," an important phase of autorotation. With reference to rotation about a fixed axis in the plane of symmetry, and parallel to the wind direction, certain terms relating to autorotation are of importance, and may be defined as follows:

1. "Rotary instability" signifies a state of equilibrium in rectilinear motion such that rotations caused by small disturbances will increase in rate until a uniform angular velocity has been attained.

2. "Rotary stability" signifies a state of equilibrium in rectilinear motion such that rotations caused by small disturbances will decrease in rate until the angular velocity becomes zero.

3. "Neutral rotary equilibrium" signifies that state of equilibrium existing between the conditions of rotary stability and instability.

MODELS AND TESTS

The wing models which were constructed of laminated mahogany had a 5-inch chord and an aspect ratio of 6, except as noted in Tables I and II. The Clark Y profile was employed in all but a few of the tests in which the N. A. C. A. M-1 profile was used. With the exception of those tested to show tip effects, circular tipped models were used throughout.

The upper and lower wings of the biplane models were connected by means of two streamlined struts spaced 0.6 chord length apart, located along the span, 0.45 chord length from the leading edge and equidistant from the midspan. These struts fitted into sockets built into the wings. The sockets were designed so that the struts could be inclined in a fore and aft direction, and clamped rigidly in position. This arrangement, used in combination with struts of different lengths, made it possible to vary gap, stagger, and decalage as desired.

All of the force tests were conducted in the 5-foot atmospheric wind tunnel (Reference 2), which has a circular, closed-throat test section. The models were mounted in the wind tunnel on the usual wire balance as shown in Figure 1.

The tests were arranged to enable the determination of the effects produced by the variations in the wing models shown in Tables I and II. Lift, drag, and pitching moment were

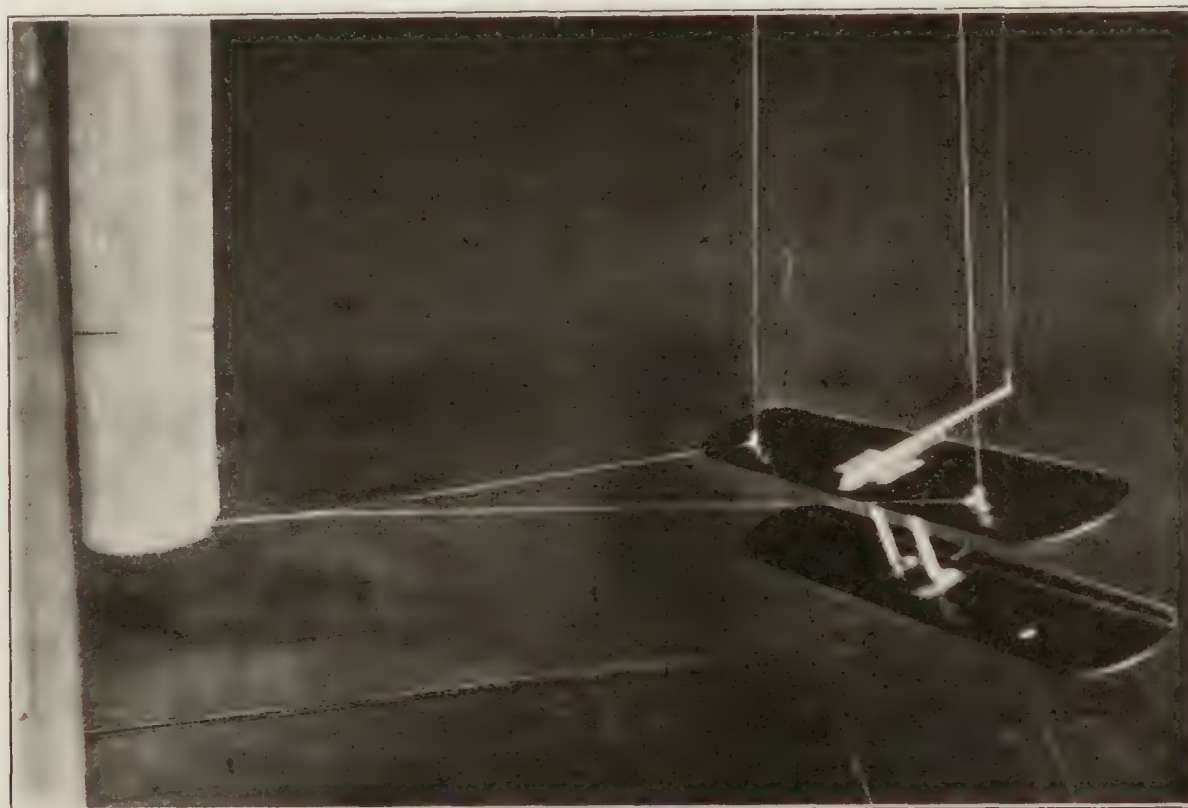


FIGURE 1.—Biplane set up in wind tunnel

measured for angles of attack ranging from -45° to $+90^\circ$. Due to the nature of the set-up, it was necessary for the complete test on each model to be made in three parts, the angle of attack range of one part overlapping by a few degrees that of the next.

The tests were conducted at an average dynamic pressure of 19.93 kg. per m^2 corresponding to an average air speed of 17.9 meters per second (40.0 M. P. H.), and an average Reynolds Number of 153,000.

All drag readings were corrected for the drag of the supporting system. The biplane strut drag was found to be negligible, and was therefore disregarded.

The test results are not corrected for tunnel wall interference for the following reasons:

a. The Prandtl correction for tunnel wall interference effects on the wing-tip vortices is known to be accurate only up to maximum lift. In general, it appears that at about 25° angle of attack this correction becomes negligible. However, between the angle of maximum lift and 25° the amount of the correction is not known, and in consequence it has been omitted.

b. At approximately 25° the blocking of the air flow by the model causes an increase in effective dynamic pressure in the region of the model. This effect reaches a maximum at an

TABLE I
MONOPLANE WING TESTS

Variable	Tip	Aspect ratio	Flap	Profile	Figure No.
Tip	Rectangular	6	0	Clark Y	2, 3, 4, 5, 6, 7.
	Negative rake	6	0	do	
	Circular	6	0	do	
Aspect ratio	do	4	0	do	7, 8, 9, 10, 11, 12.
	do	6	0	do	
	do	8	0	do	
Flap (20 per cent chord)	do	6	15° up	do	7, 13, 14, 15, 16, 17, 18, 19.
	do	6	0°	do	
	do	6	15° down	do	
	do	6	25° down	do	
	do	6	30° down	do	
	do	6	0	do	
Profile	do	6	0	N. A. C. A.-M1	7, 20, 21, 22, 23.
	do	6	0	do	

TABLE II
BIPLANE WING TESTS

Variable	Stagger	Gap/ chord	Deca- lage	10° Sweep back		Profile		Figure No.
				Upper wing	Lower wing	Upper wing	Lower wing	
Stagger	<i>Per cent</i>		<i>Degrees</i>					
	-25	1.0	0	0	0	Clark Y	Clark Y	24, 25, 26, 27, 28, 29, 30.
	0	1.0	0	0	0	do	do	
	+25	1.0	0	0	0	do	do	
Gap	+50	1.0	0	0	0	do	do	28, 31, 32, 33, 34, 35.
	0	1.5	0	0	0	do	do	
	0	1.0	0	0	0	do	do	
Decalage	0	0.5	0	0	0	do	do	28, 36, 37, 38, 39, 40.
	0	1.0	+3	0	0	do	do	
	0	1.0	0	0	0	do	do	
Sweep back ¹	0	1.0	-3	0	0	do	do	41, 42, 43, 44, 45, 46, 47.
	0	1.0	0	Straight	Sweep back	do	do	
	0	1.0	0	Sweep back	Straight	do	do	
	+50	1.0	0	do	do	do	do	
Profile	-50	1.0	0	Straight	Sweep back	do	do	28, 48, 49, 50, 51, 52.
	0	1.0	0	0	0	do	do	
	0	1.0	0	0	0	do	N. A. C. A.-M1	
	0	1.0	0	0	0	N. A. C. A.-M1	Clark Y	

¹ Stagger measured at midspan.

angle of attack of about 90° for a given wing. Tests have been made from which a correction for blocking has been derived, and the results are given in the appendix. This correction, however, applies to monoplanes only, and hence it has not been used in this report, which covers biplanes as well as monoplanes. The determination of the blocking corrections for biplane wings is a problem which requires further research.

The lift, drag, and pitching moment were measured in general to within an accuracy of ± 1.5 per cent. In the construction of the wing models the tolerance with reference to the airfoil ordinates was ± 0.003 inch.

RESULTS

For purposes of direct comparison, the test results are presented in groups of curves and diagrams, each group showing the effects of one of the variables as listed in Tables I and II. These groups, given in Figures 2 to 52, are arranged for each variable in four consecutive sections as follows:

- (a) Absolute lift and drag coefficients vs. angle of attack (C_L and C_D vs. α).
- (b) Polars (C_L vs. C_D).
- (c) Center of pressure coefficients vs. angle of attack (C_p vs. α).
- (d) Vector diagrams.

In the center of pressure curves for the monoplanes, the plotted points represent the intersection of the resultant force vectors with the wing chord line. Similarly, the "mean chord" (halfway between the chords of the upper and lower wings as indicated on the vector diagrams) of the biplane models was used in obtaining the C_p values. It should be borne in mind that the C_p curves illustrated hold good only for the base lines assumed, and that any other reference lines would give different results.

Lift and drag coefficients and angle of attack for each complete force test are given in Tables IV to XXVII, inclusive.

The calculated probable ranges of "rotary instability" for each model tested are indicated in Table III. These ranges were obtained by noting the points on the polar curves at which radial lines through the origin were perpendicular to the curves. Each point of intersection signifies a state of "neutral rotary equilibrium," as previously defined, and is shown as such on the comparative polar curve groups. Then where the slope of the curve is negative between these points with respect to the radial lines, the wing model will be capable of autorotation, i. e., will be in a state of "rotary instability." The negative slope indicates a decreasing resultant force with increasing angle of attack, and this is the criterion for "rotary instability," which may be expressed as—

$$\frac{d(C_R)}{d\alpha} < 0$$

(See Reference 3 for derivation), where C_R is the absolute coefficient of resultant force, and α is the angle of attack of the wing. This criterion, however, is an approximation, subject to the limitations of the "strip method" of autorotation calculation, which assumes a uniform distribution of the resultant force along the span, for the wing in rectilinear motion.

DISCUSSION OF RESULTS

A general survey of the curves and diagrams demonstrates the appreciable effects which changes in the geometry of wing systems have on lift, drag, and center of pressure, particularly at large angles of attack. It will be noted that the effect on drag is the most marked, and the influence of stagger is greater than that of gap or decalage. The effects of variations in stagger, gap, and sweep back, at the large angles of attack, are largely due to the partial shielding of the biplane upper wing by the lower. (Reference 4.)

Referring now to the curves in greater detail, the effects of the variables on the aerodynamic characteristics of the wing models may be listed as follows:

MONOPLANES

1. TIPS

LIFT (figs. 2, 3):

Maximum C_L is highest for rectangular tips, next for negative raked tips, and lowest for the circular tips, although the difference is small.

DRAG (figs. 2, 3):

Minimum C_D shows little difference, and in general C_D is much the same for the three models with different tip shapes.

CENTER OF PRESSURE (figs. 4, 5, 6, 7):

The C_p curves show little variation for the three different tips, and the differences may be explained as due to the different dispositions of the wing area.

2. ASPECT RATIO

LIFT (figs. 8, 9):

Maximum C_L increases with increase of aspect ratio. The slope of the lift curve below maximum C_L becomes greater due to the decrease in the induced angle of attack. This decrease is also partly due to tunnel wall interference.

DRAG (figs. 8, 9):

Minimum C_D is practically the same for the aspect ratios investigated. The effects of aspect ratio and the tunnel walls on induced drag are apparent below maximum lift. Above 20° angle of attack, C_D increases in the order of the aspect ratio and the differences are due in great measure to blocking effects at large angles.

CENTER OF PRESSURE (figs. 7, 10, 11, 12):

The C_p curves for the different aspect ratios covered in the tests are practically the same.

3. FLAP

LIFT (figs. 13, 14):

Maximum C_L increases with increasing flap angle in the downward direction, and occurs at slightly lower angles of attack. Moving the flap downward through a given angle increases the lift by an amount approximately equal to the decrease produced by moving it up through the same angle. It will be noted that in Figure 13, just beyond each of the primary and secondary lift peaks the changes in lift are small.

DRAG (figs. 13, 14):

Above zero angle of attack the drag increases in a regular manner, both with increasing angle of attack and with flap moving from up to down positions.

CENTER OF PRESSURE (figs. 7, 15, 16, 17, 18, 19):

For angles of attack above zero lift the $C. P.$ travel becomes smaller with decreasing flap angle, due to the decrease of the effective camber of the wing. With the flap displaced upward 15° , the travel is backward above zero lift. For flap settings of from 15° to 30° down, the C_p curves are much the same above zero lift, but are displaced to the rear with respect to the neutral flap curve. Attention is called to the marked difference in the shape of the curves for the 15° upward and downward flap displacements below zero lift.

4. PROFILE

LIFT (figs. 20, 21):

Maximum C_L is much higher for the Clark Y than for the symmetrical N. A. C. A.-M1. The angle of zero lift is higher for the N. A. C. A.-M1, due to its straight mean camber line.

DRAG (figs. 20, 21):

From -3° to $+8^\circ$, the drag of the N. A. C. A.-M1 is less than that for the Clark Y, and is greater from $+8^\circ$ to 18° . Above 18° , and below -3° , C_D for the N. A. C. A.-M1 is the lower.

CENTER OF PRESSURE (figs. 7, 22, 23):

The *C. P.* travel for the N. A. C. A.-M1 is practically negligible from -6° to $+6^\circ$ angle of attack, and then moves rearward. The Clark Y, however, has a forward motion of *C. P.* up to 12° angle of attack, and rearward beyond this angle.

BIPLANES

5. STAGGER

LIFT (figs. 24, 25):

Maximum C_L increases with increase of stagger up to +25 per cent and then remains the same for 50 per cent stagger, although occurring at a slightly smaller angle of attack.

DRAG (figs. 24, 25):

Minimum C_D is highest for the zero stagger. Above the angle of maximum C_L , however, C_D increases greatly with increase in stagger. These effects on drag at the large angles of attack are due mainly to the partial shielding of the upper wing of the biplanes by the lower.

CENTER OF PRESSURE (figs. 26, 27, 28, 29, 30):

The distance traveled back by the *C. P.* above maximum C_L becomes greater with increasing stagger. The peculiar behavior of negative stagger at large angles of attack should be noted.

6. GAP

LIFT (figs. 31, 32):

Maximum C_L increases up to G/c ratio of 1.0 where it appears to remain constant for G/c ratio increase, although the slope of the lift curve becomes greater with higher G/c ratios. This is due to the decrease in induced angle of attack with increasing gap.

DRAG (figs. 31, 32):

Minimum C_D is approximately the same for the G/c ratios tested. For the large angles of attack, C_D increases with increasing G/c ratios.

CENTER OF PRESSURE (figs. 28, 33, 34, 35):

As the G/c ratio is increased, the *C. P.* above maximum lift recedes farther with increase of angle of attack up to 50° , although not as far as for the staggered biplanes.

7. DECALAGE

LIFT (figs. 36, 37):

Positive and negative decalage cause a lower maximum C_L than zero decalage, but the magnitude is about the same for the same values of decalage, plus or minus. For positive decalage, maximum C_L occurs at a smaller angle of attack, and that of negative decalage at a larger angle than that for zero decalage.

It can also be seen that the lift and drag curves for positive or negative decalage are shifted by an approximately constant angle to one or the other side of those for zero decalage. Since the lower wing of the biplane was set at $\pm 3^\circ$ with respect to the upper wing at zero lift, the "effective" angle of attack becomes respectively 1.5° minus or plus the angle of attack of zero lift for no decalage.

DRAG (figs. 36, 37):

Maximum C_D shows little difference for the angles of decalage investigated, but C_D increases with increase of decalage.

CENTER OF PRESSURE (figs. 28, 38, 39, 40):

Negative decalage causes a more rapid recession of the *C. P.* above maximum C_L , with increase of angle of attack, than does either zero or positive decalage. The sharp peak on the -3° curve is remarkable.

The effects of decalage are not as great as those produced by stagger, but they are greater than those due to changes in gap.

8. SWEEP BACK

LIFT (figs. 41, 42):

Maximum C_L occurs at about the same angle of attack for all conditions tested. C_L is highest for +50 per cent stagger at midspan with the upper wing swept back, and lowest for the same combination with zero stagger.

The similarity is very striking between the lift curves of the two combinations with upper wing swept back, +50 per cent midspan stagger, and lower wing swept back, zero stagger. The other two combinations tested are also very similar, and this indicates that sweep back in one wing is, effectively, stagger. No appreciable difference is shown whether the stagger used with the swept-back wing is at the tips or at midspan.

DRAG (figs. 41, 42):

The similarity between the drag curves of the same pairs of combinations as noted in the case of lift, is very noticeable, and also indicates that sweep back in one wing is, in effect, stagger.

CENTER OF PRESSURE (figs. 43, 44, 45, 46, 47):

The most noticeable effect brought out by the C_p curves is the fairly close resemblance between the results for the biplane with upper wing swept back, zero midspan stagger, and that with the lower wing swept back, -50 per cent midspan stagger.

9. PROFILE

LIFT (figs. 49, 50):

The N. A. C. A.-M 1 in combination with the Clark Y gives a lower maximum C_L than with both wings Clark Y, and the lift curves have more rounded peaks.

DRAG (figs. 49, 50):

Minimum C_D is slightly lower for the combination of N. A. C. A.-M1 wing lower and Clark Y upper. In general, with both wings Clark Y, the drag is slightly higher at large angles of attack.

CENTER OF PRESSURE (figs. 28, 48, 51, 52):

The C_p curves for the three combinations tested do not show any great variations. The combination of the N. A. C. A.-M1 lower wing and Clark Y upper wing is probably the most desirable from the standpoint of safety, due to the smaller slope of the curve in the region of the angle of maximum C_L , which means less instability longitudinally.

10. ROTARY INSTABILITY

From a consideration of the calculated ranges of rotary instability (Table III), the following points may be noted:

None of the monoplanes show any tendency toward autorotation above 26° , but the biplanes indicate additional autorotational tendencies above this angle.

Positive stagger is seen to reduce the tendency of the biplanes to autorotate at the large angles, while increase in gap within practical limits has a similar effect, only to a smaller degree.

Sweep back arranged so as to give positive stagger at the tips appears to reduce the range of rotary instability at large angles of attack. Geometrically, sweep back in one wing of a biplane is merely a progressive change in stagger along the span. The criterion for rotary instability is based on the assumption of uniform span loading, and for this reason the points of neutral rotary equilibrium are only roughly approximate for the swept-back wing combinations.

Decalage seems to have no appreciable effect in reducing the rotary instability ranges of the biplanes.

CONCLUSIONS

Since these force tests have been made at the low Reynolds Number of 153,000, any conclusions as to the effects of the variable factors should be drawn with that in mind. As the effects at angles of attack below maximum lift have already been fully investigated, the conclusions given here apply to the results at maximum C_L and above.

MONOPLANES

1. TIPS.—Different shaped tips produce only small effects.
2. ASPECT RATIO.—Increase of aspect ratio slightly increases maximum C_L , and C_D also increases at large angles.
3. FLAP.—Moving the flap down increases maximum C_L which occurs at slightly lower angles of attack. C_D also increases with downward movement of the flap.
4. PROFILE.—The Clark Y has a much higher maximum C_L than the N. A. C. A.-M1.

BIPLANES

5. STAGGER.—Increase in stagger raises the maximum C_L , and greatly increases C_D above the angle of maximum lift.
6. GAP.—Larger gap slightly increases the maximum C_L , and causes an increase in C_D , although the effects are not as great as those of stagger.
7. DECALAGE.—Positive and negative decalage have very little effect except to shift the lift and drag curves as a whole to one side or the other of those for zero decalage.
8. SWEEP BACK.—Sweep back may be considered as a form of stagger, since the result of combining a swept-back wing with a straight wing in a biplane is similar to staggering a straight wing biplane.
9. PROFILE.—The N. A. C. A.-M1 wing in combination with the Clark Y gives lower maximum C_L than with both wings Clark Y, and the lift curve peaks are more rounded.
10. ROTARY INSTABILITY.—The autorotational characteristics of wing systems are greatly affected by changes in profile and in the geometrical arrangement of the wings.

BIBLIOGRAPHY

Reference 1

Wenzinger, C. J., and Harris, T. A.: Wind Tunnel Force Tests on Wing Systems through Large Angles of Attack. N. A. C. A. Technical Note No. 294 (1928).

Reference 2.

Reid, Elliott G.: Standardization Tests of N. A. C. A. No. 1 Wind Tunnel. N. A. C. A. Technical Report No. 195 (1924.)

Reference 3.

Knight Montgomery: Wind Tunnel Tests on Autorotation and the Flat Spin. N. A. C. A. Technical Report No. 273 (1927).

Reference 4.

Loeser, jr., Oscar E.: Pressure Distribution Tests on PW-9 Wing Models from -18° through 90° Angle of Attack. N. A. C. A. Technical Report No. 296 (1928).

Glauert, H.: The Rotation of an Aerofoil about a Fixed Axis. B. A. C. A. Reports and Memoranda No. 68 (1919).

Irving, H. B., and Batson, A. S.: The Effects of Stagger and Gap on the Aerodynamic Properties of Biplanes at Large Angles of Incidence. B. A. C. A. Reports and Memoranda No. 1064 (1927).

Gates, S. B., and Bryant, L. W.: The Spinning of Aeroplanes. B. A. C. A. Reports and Memoranda No. 1001 (1926).

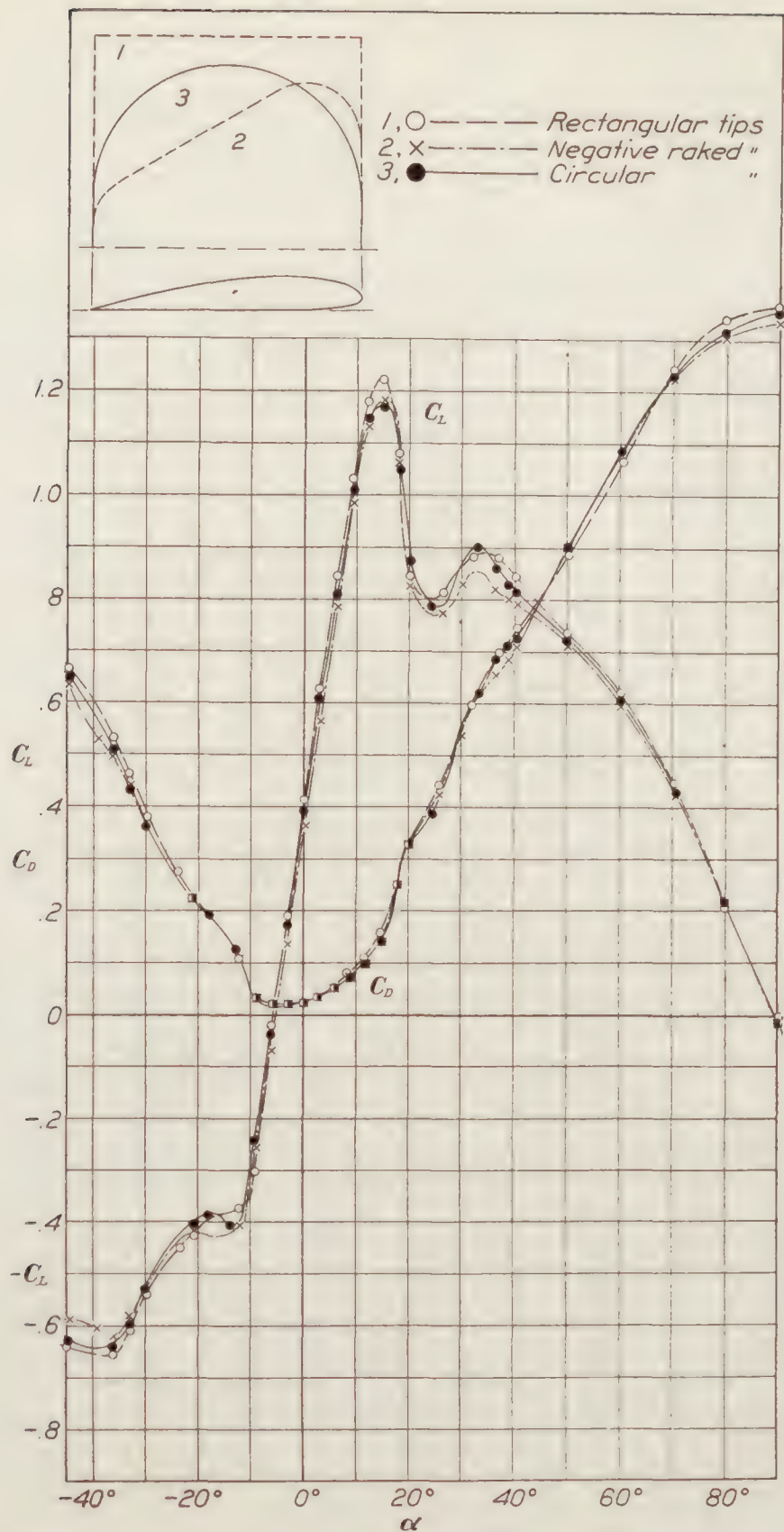


FIGURE 2.—Monoplane wing. Tip shape effect. Clark Y. 5-inch chord. A. R. 6

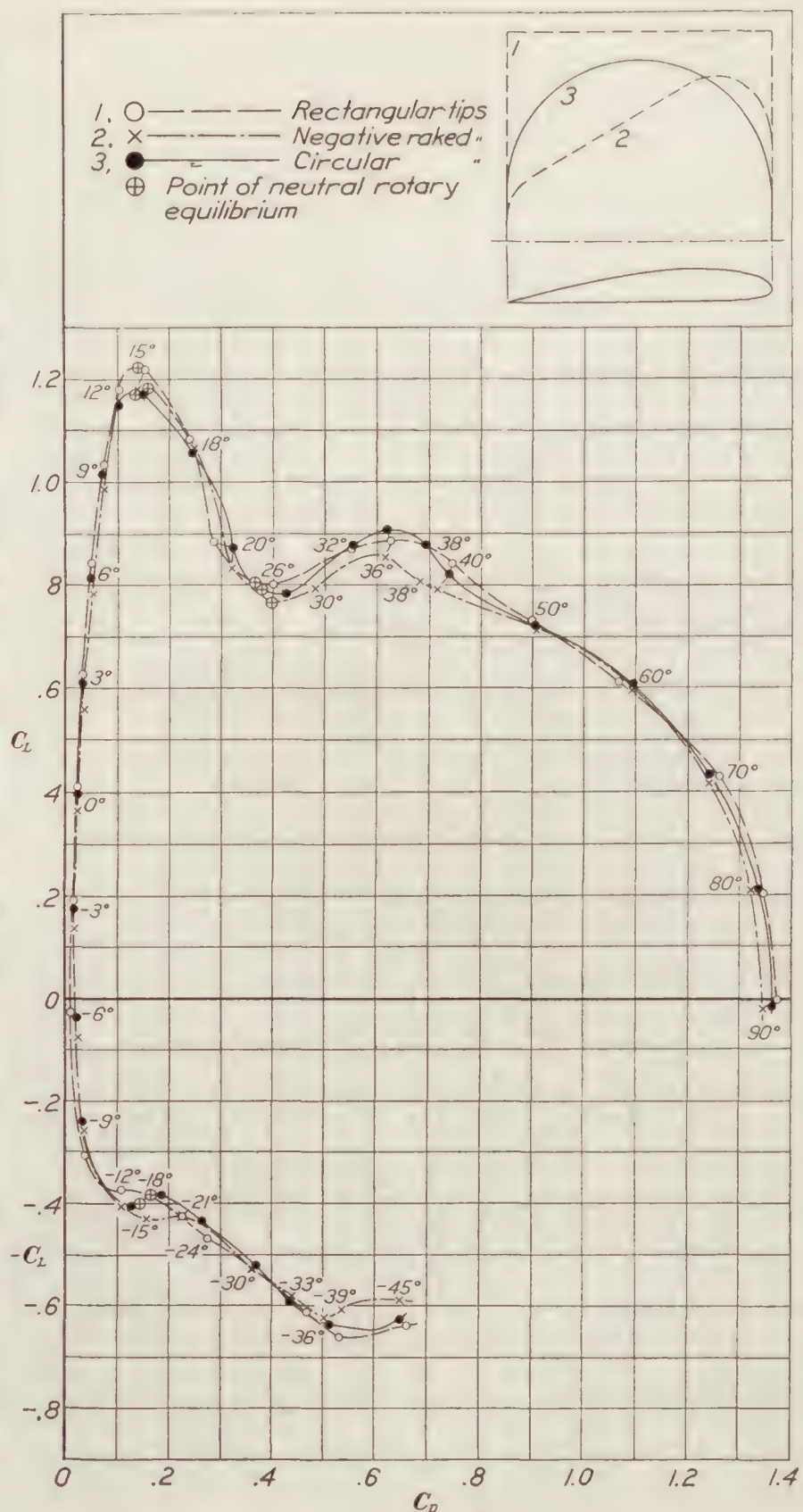


FIGURE 3.—Monoplane wings. Tip shape effect. Polars. Clark Y. 5-inch chord. A. R. 6

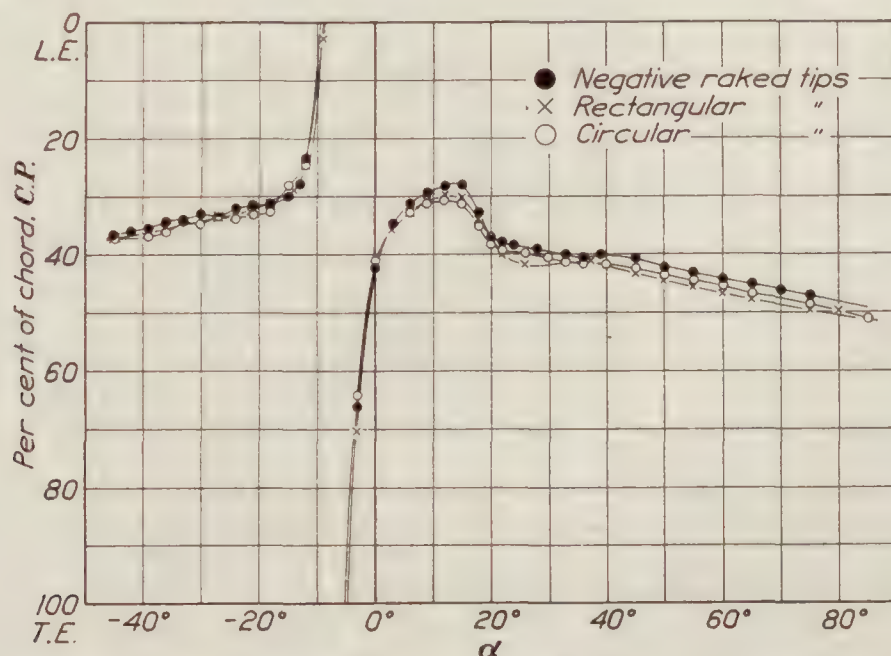


FIGURE 4.—Monoplane wings. Tip shape effect. Clark Y. 5-inch chord. A. R. 6

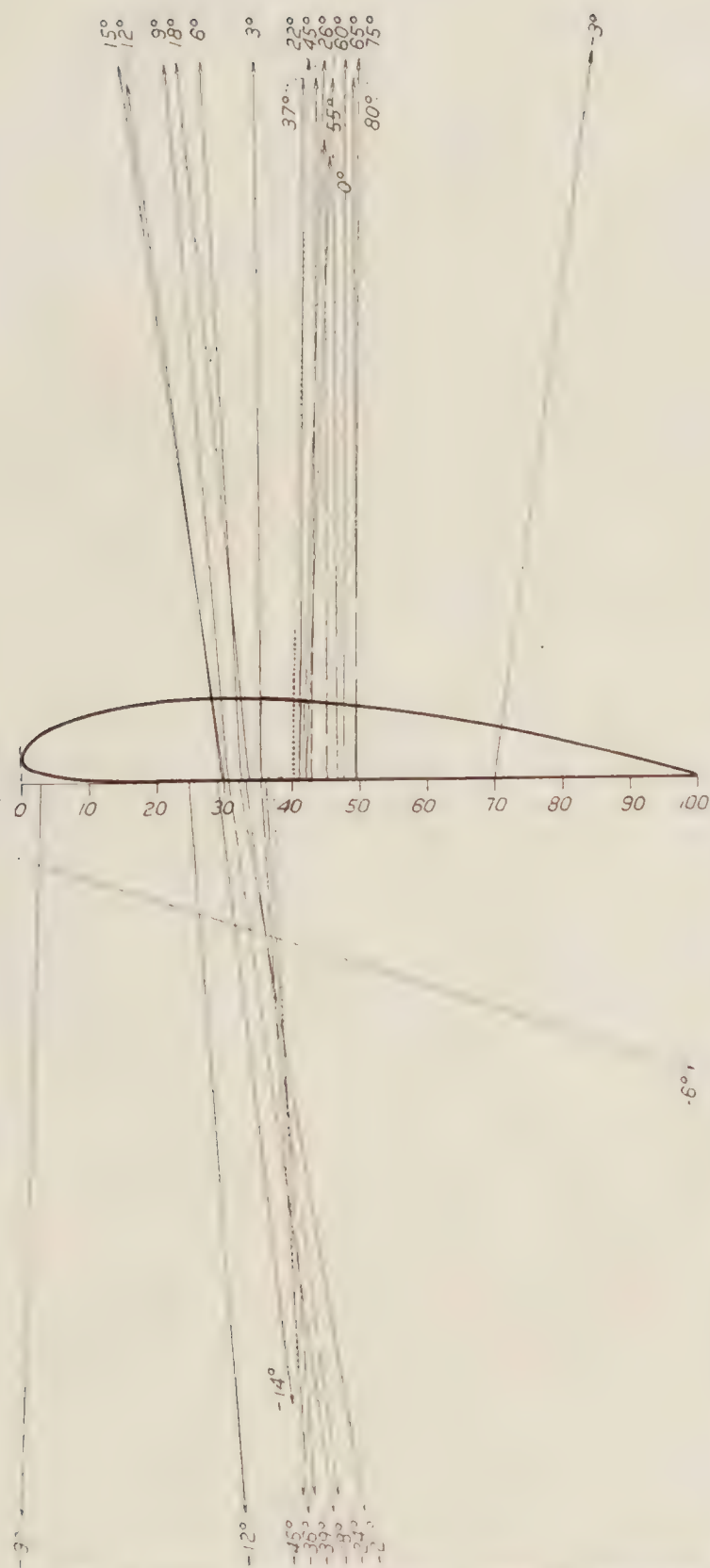


FIGURE 5.—Monoplane vector diagram. Clark Y. Rectangular tips. 5-inch chord. A. R. 6



FIGURE 6.—Monoplane vector diagram. Clark Y. Negative raked tips. 5-inch chord. A. R. 6

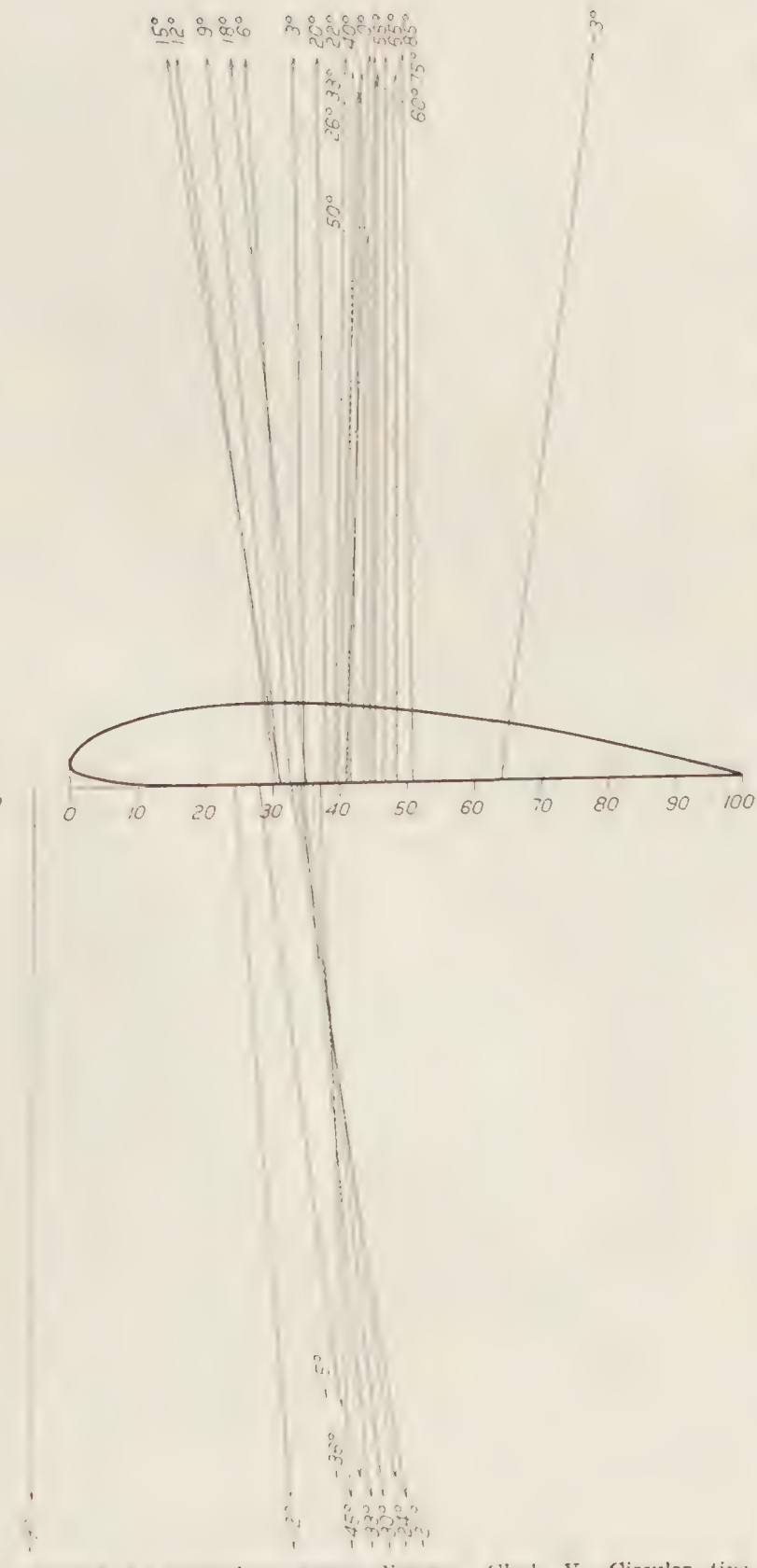


FIGURE 7.—Monoplane vector diagram. Clark Y. Circular tips. 5-inch chord. A. R. 6

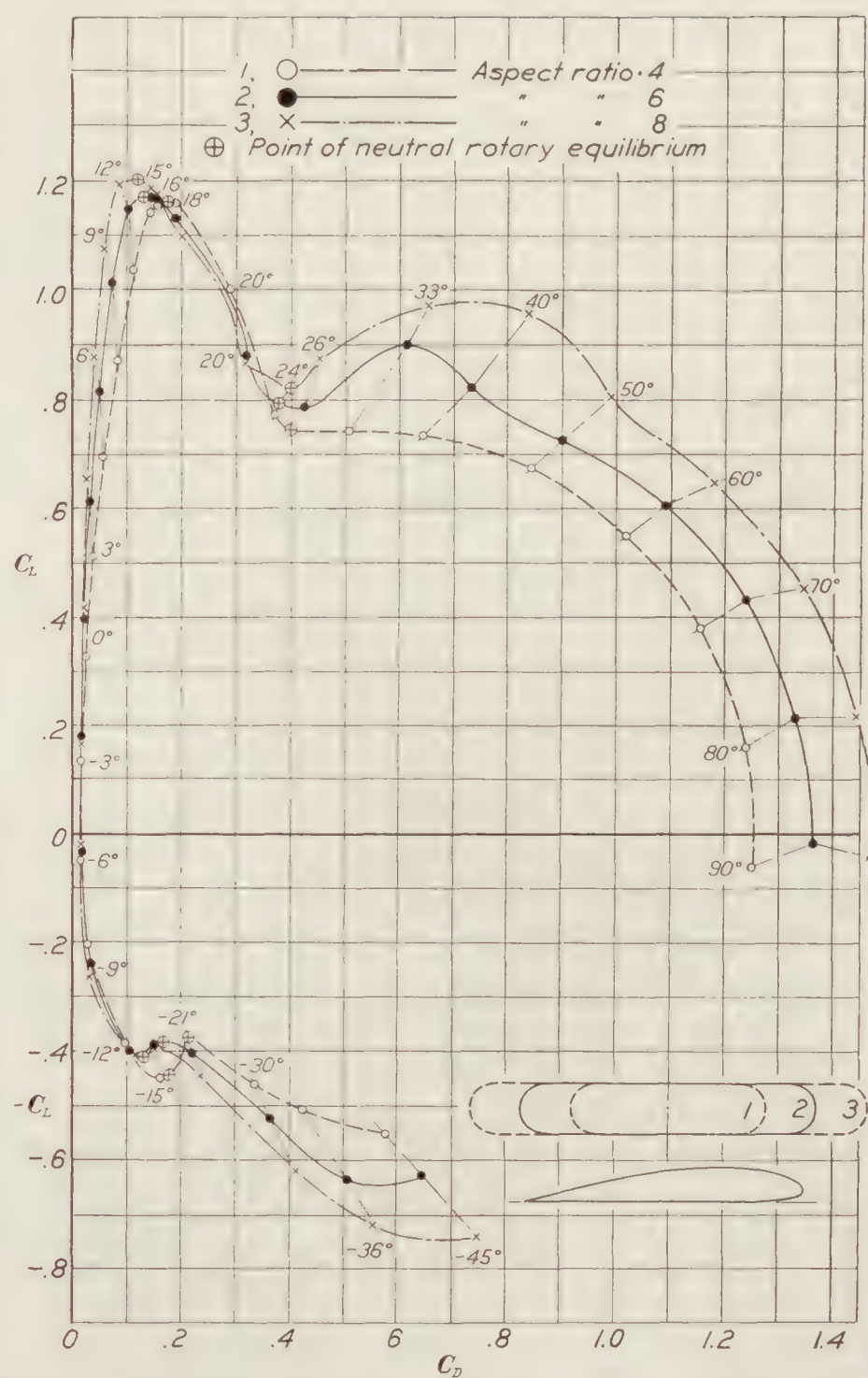
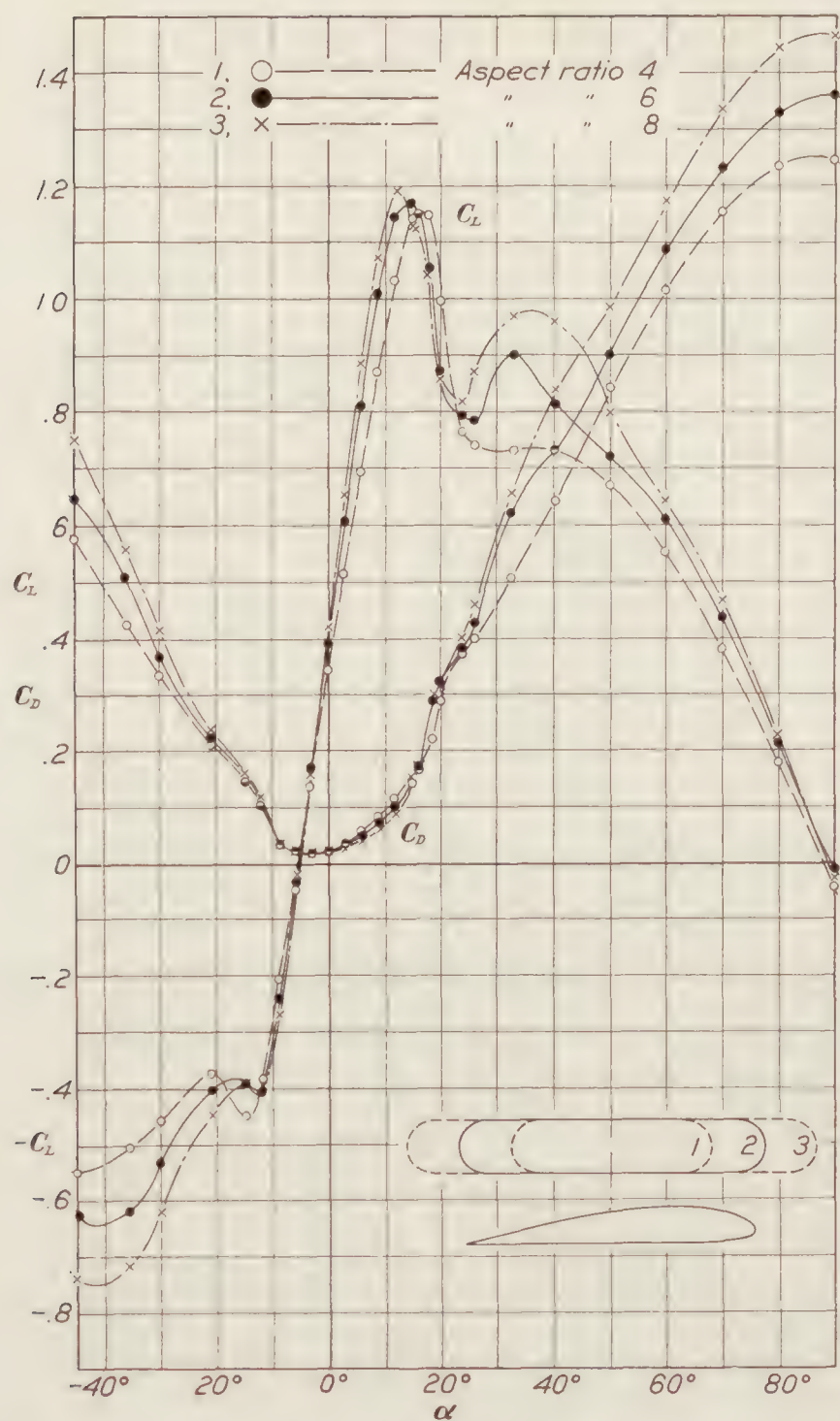


FIGURE 8.—Monoplane wings. Aspect ratio effect. Clark Y. Circular tips. 5-inch chord

FIGURE 9.—Monoplane wings. Aspect ratio effect. Polars. Clark Y. Circular tips. 5-inch chord

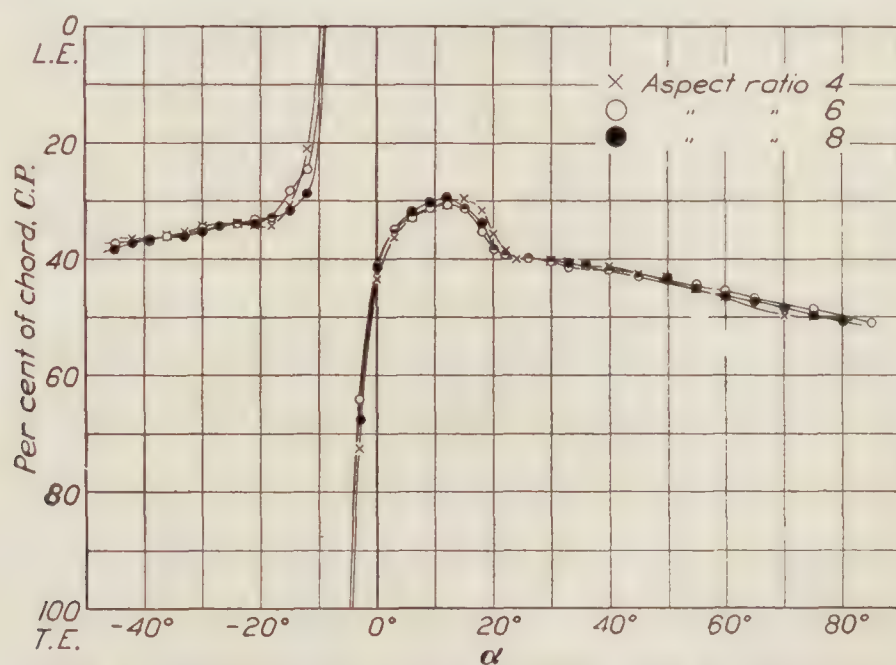


FIGURE 10.—Monoplane wings. Aspect ratio effect. Clark Y. Circular tips. 5-inch chord

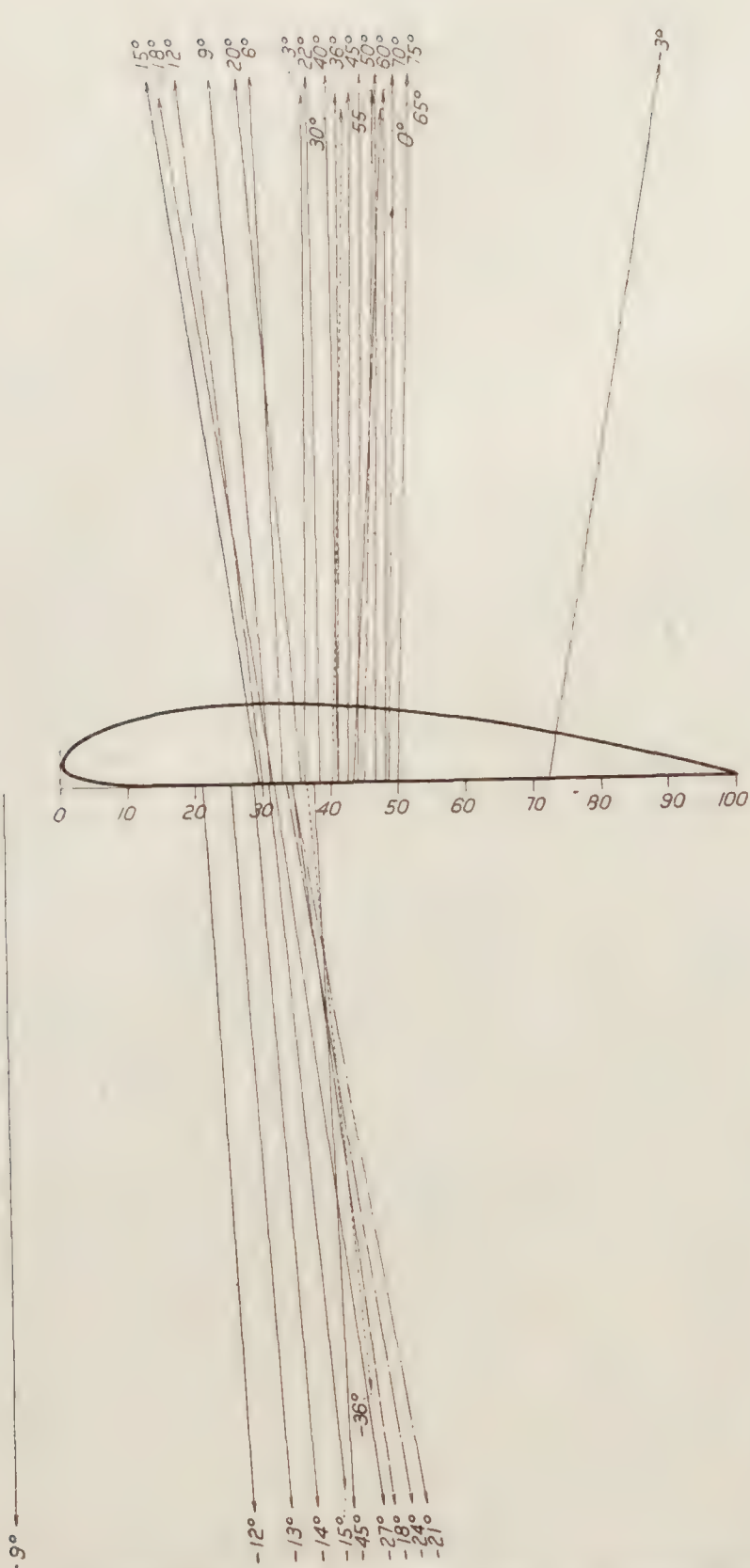


FIGURE 11.—Monoplane vector diagram. Clark Y. Circular tips. 5-inch chord. A. R. 4

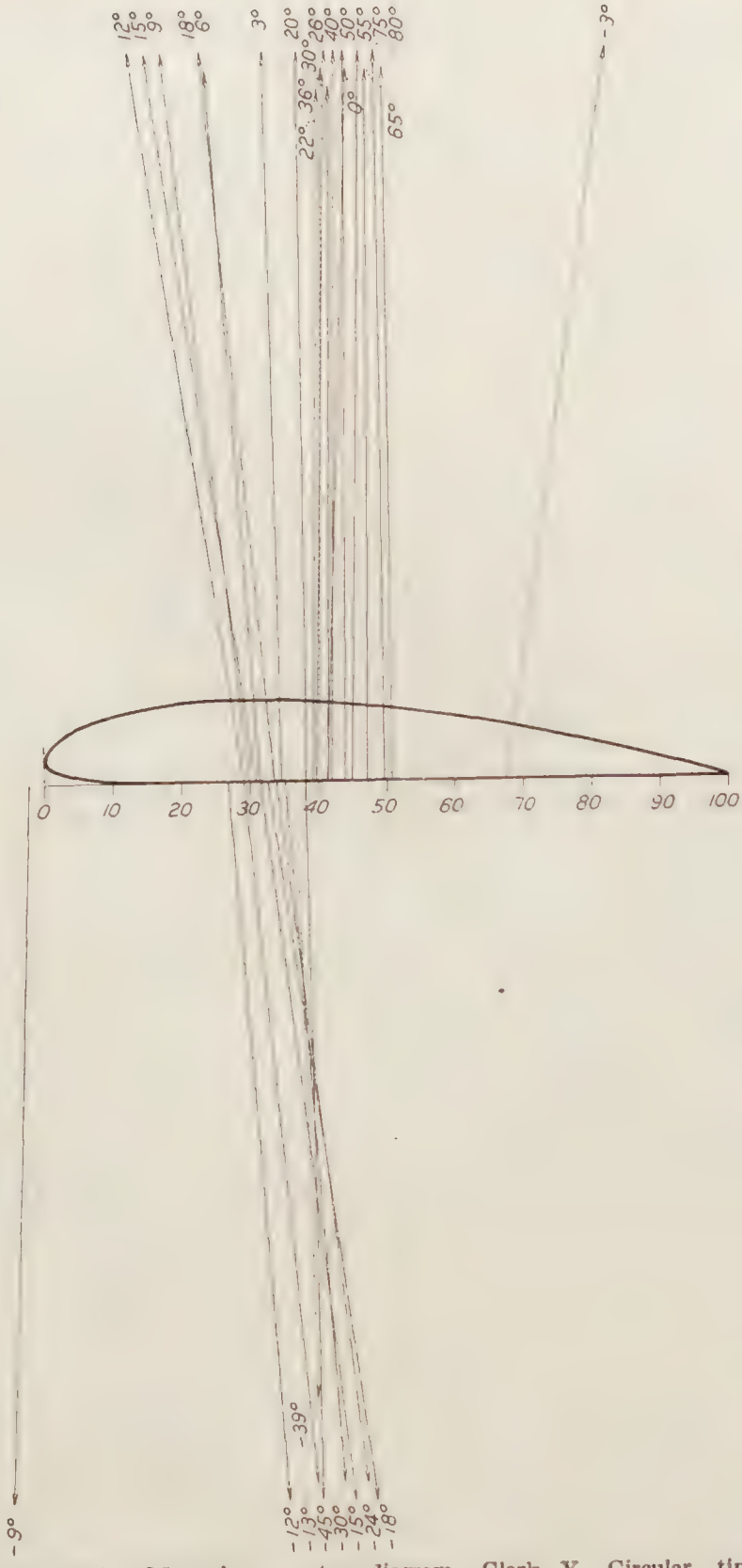


FIGURE 12.—Monoplane vector diagram. Clark Y. Circular tips. 5-inch chord. A. R. 8

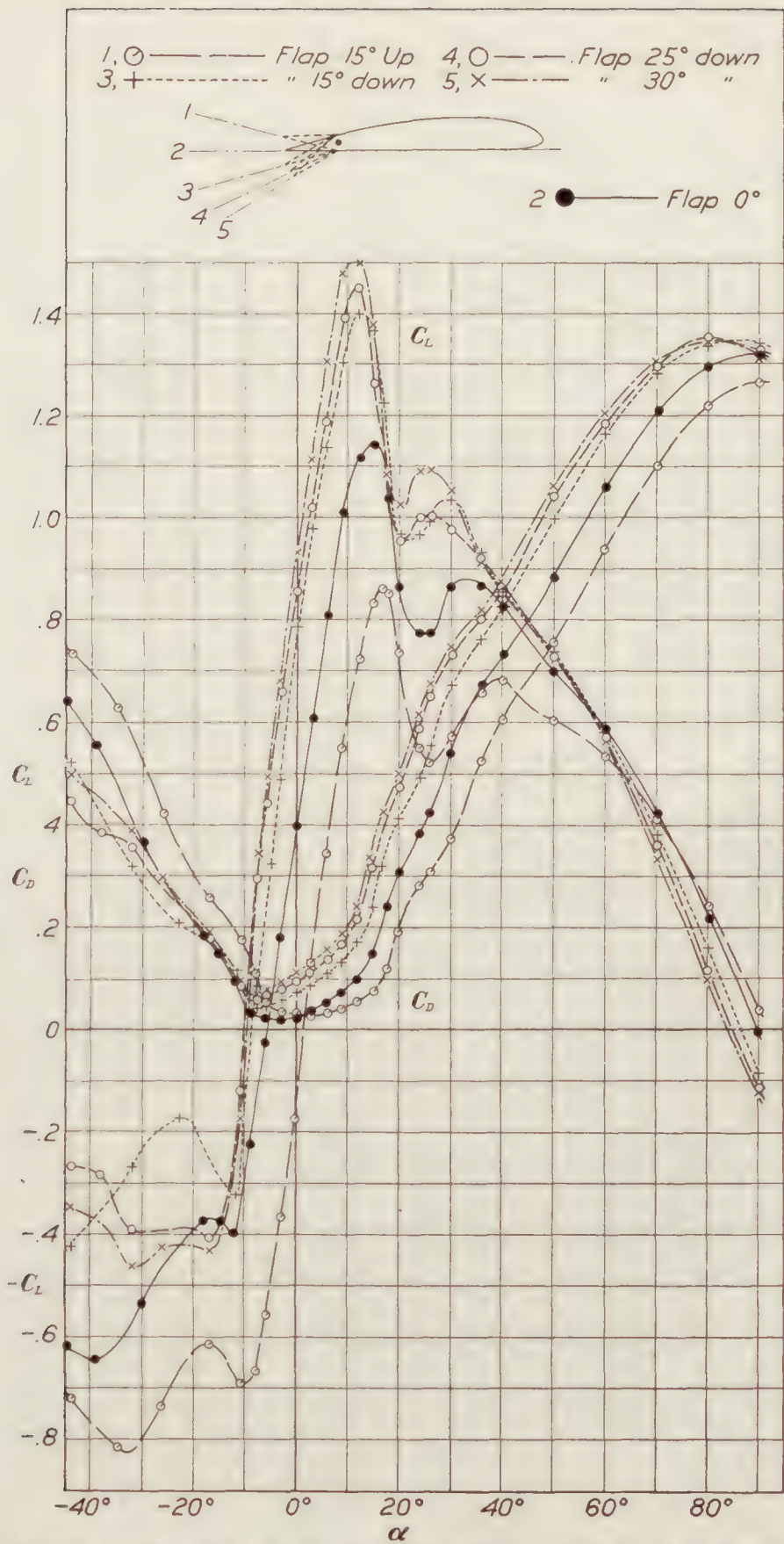


FIGURE 13.—Monoplane wings. Flap-setting effect. Clark Y. Flaps 20 per cent chord. Circular tips. 5-inch chord. A. R. 6

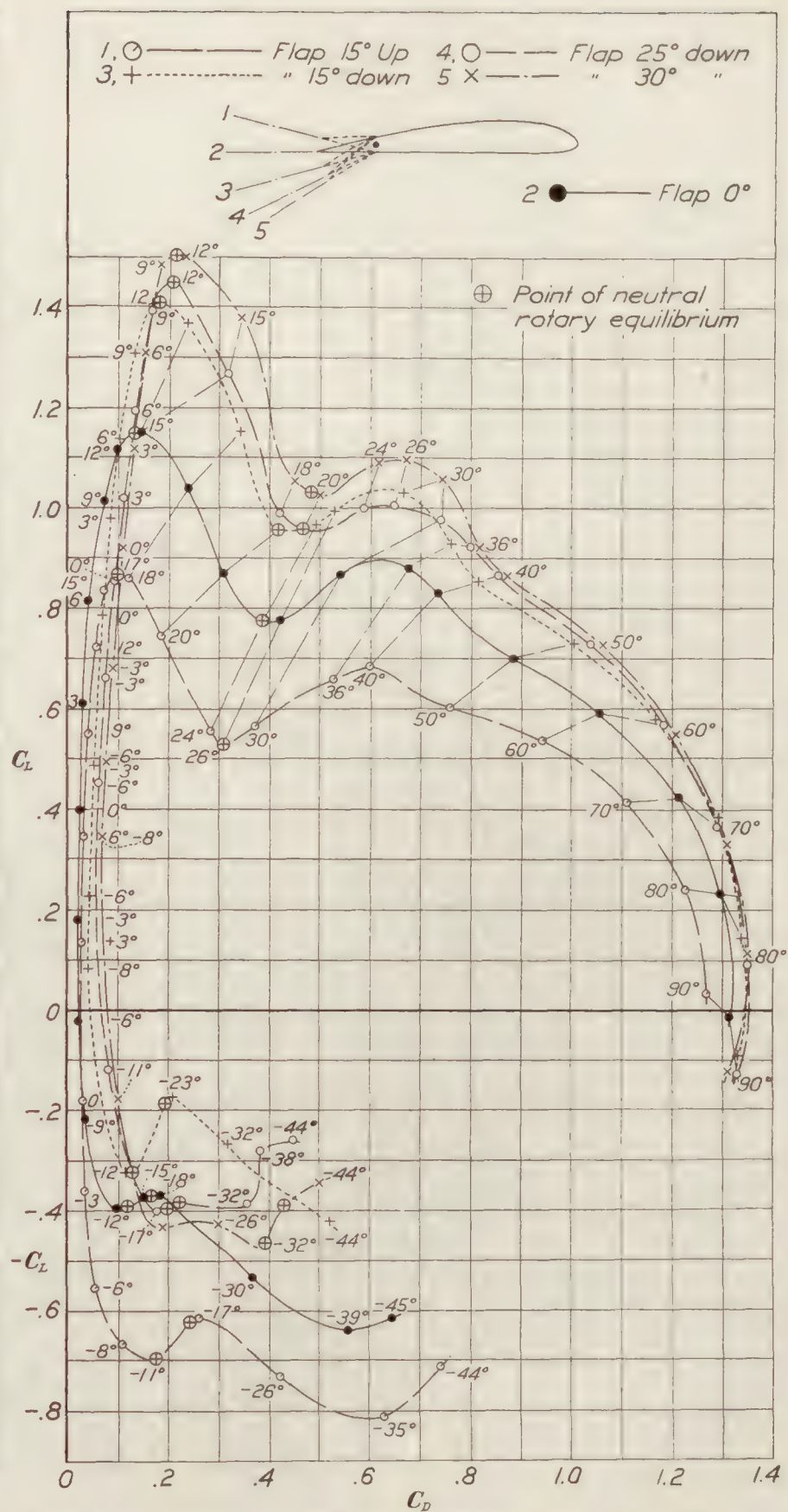


FIGURE 14.—Monoplane wings. Flap-setting effect. Polars. Clark Y. Flaps 20 per cent chord. Circular tips. 5-inch chord. A. R. 6

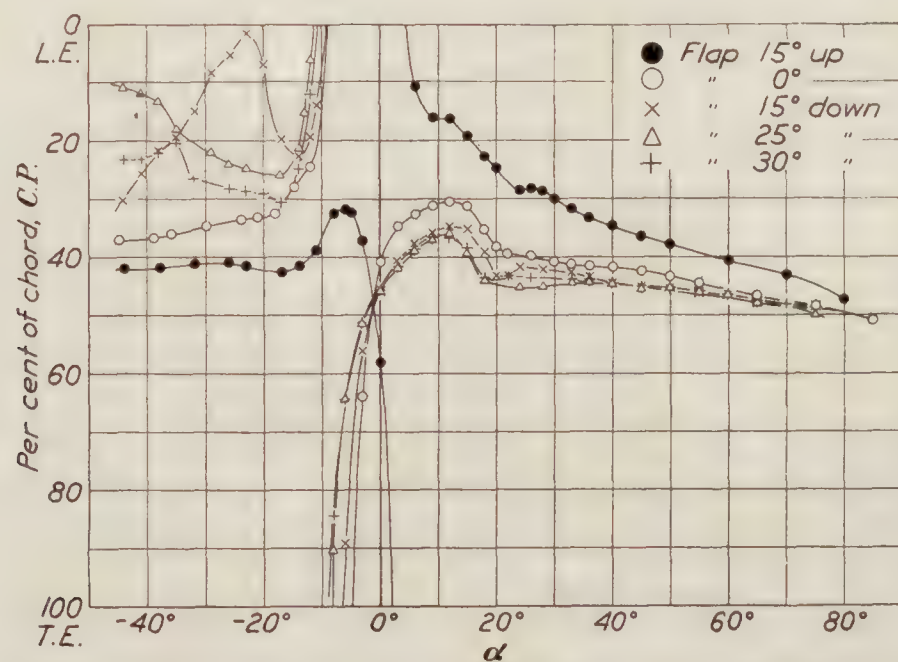


FIGURE 15.—Monoplane wings. Flap-setting effect. Clark Y. Flaps 20 per cent chord. Circular tips 5-inch chord. A. R. 6

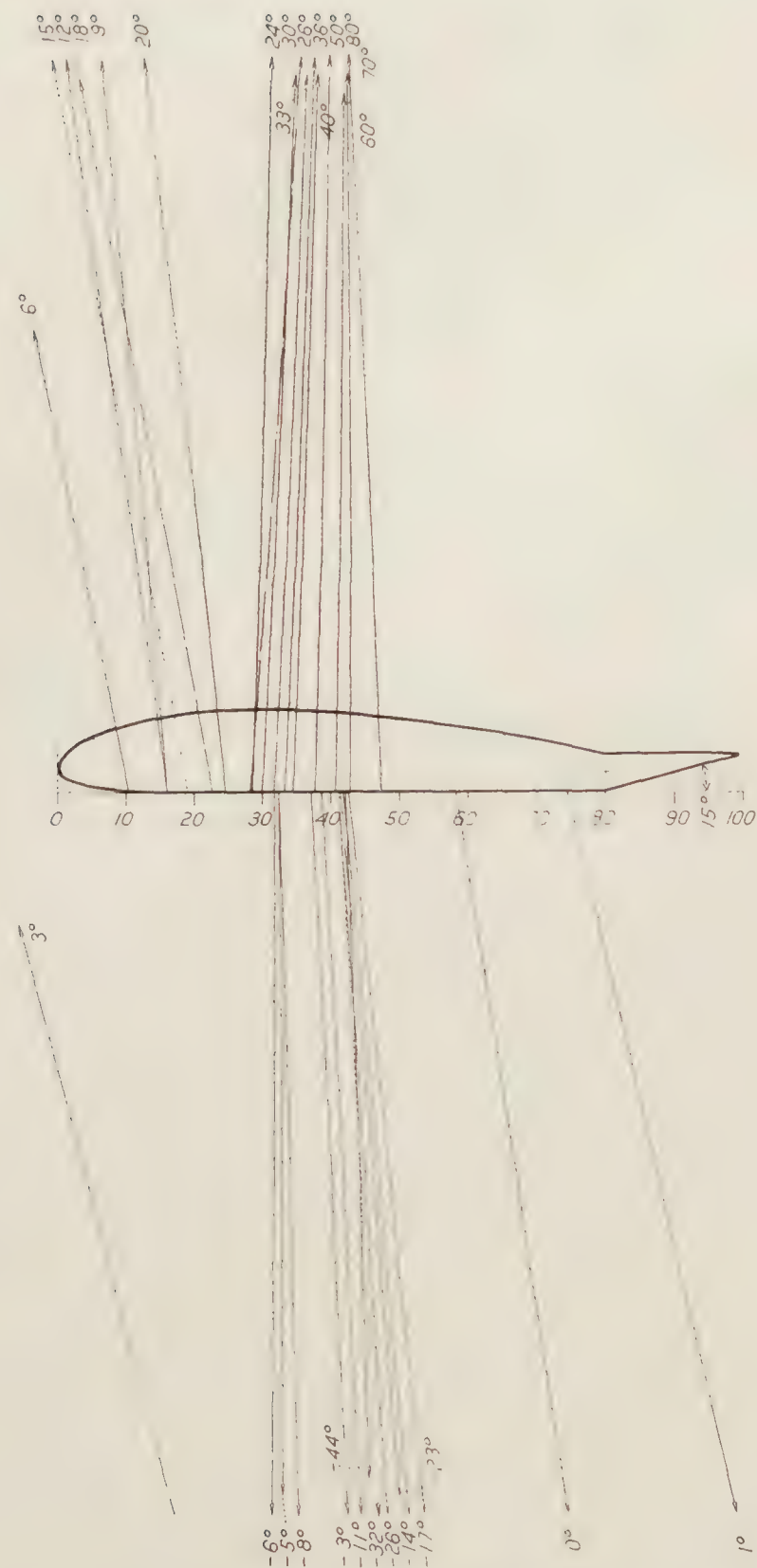


FIGURE 16.—Monoplane vector diagram. Clark Y. Circular tips. 5-inch chord. A. R. 6. Flap up 15°

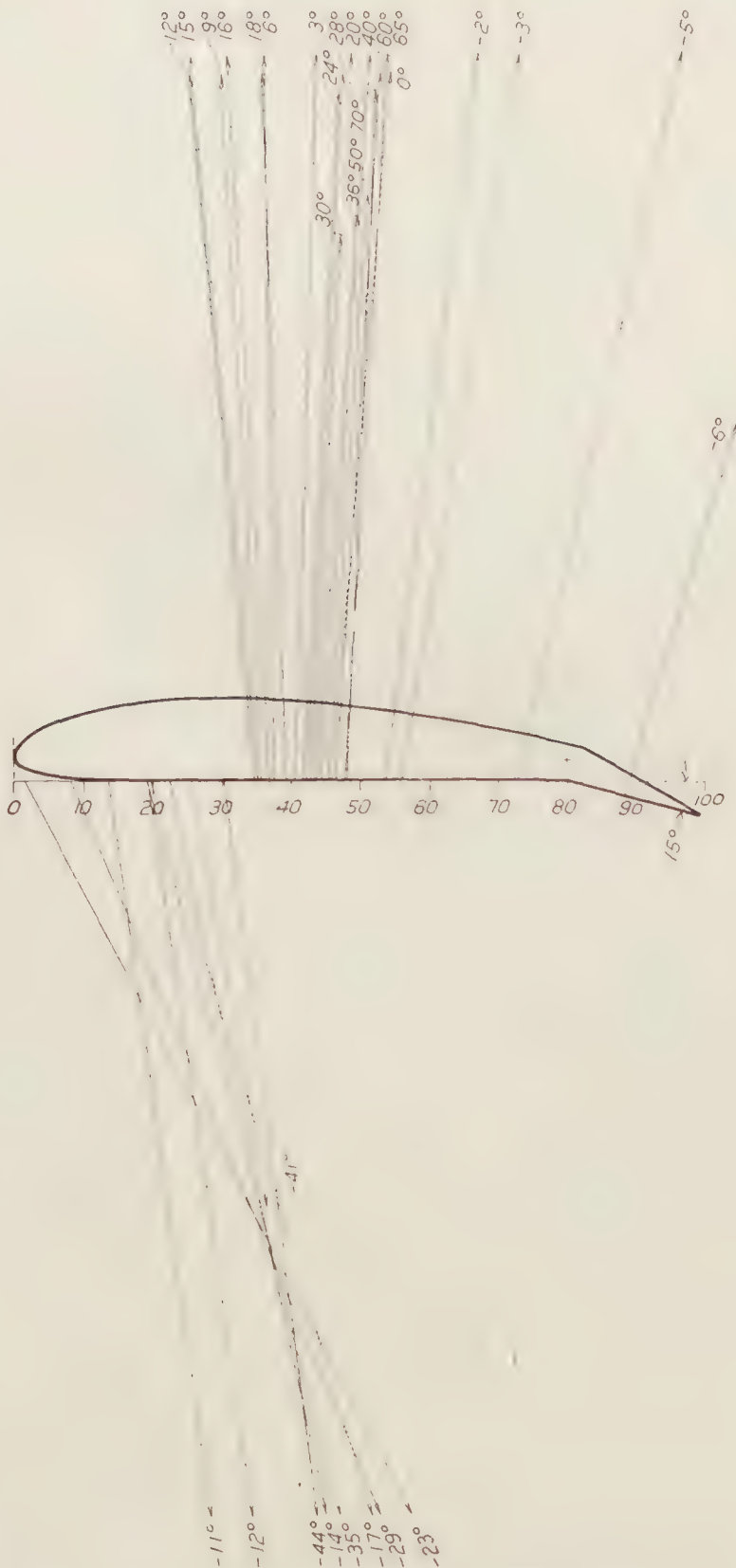


FIGURE 17.—Monoplane vector diagram. Clark Y. Circular tips. 5-inch chord. A. R. 6. Flap down 15°



FIGURE 18.—Monoplane vector diagram. Clark Y. Circular tips.
5-inch chord. A. R. 6. Flap down 25°



FIGURE 19.—Monoplane vector diagram. Clark Y. Circular tips.
5-inch chord. A. R. 6. Flap down 30°

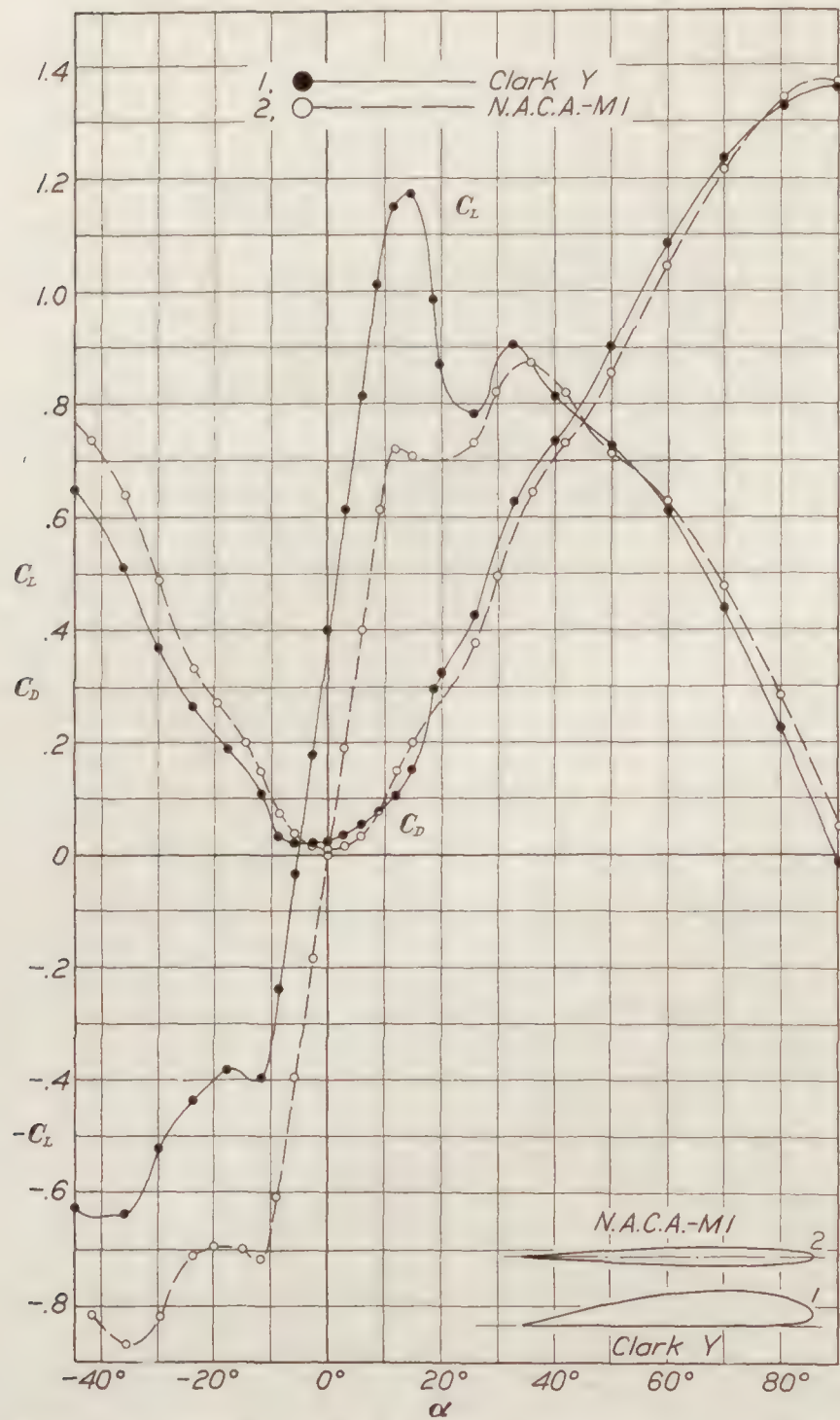


FIGURE 20.—Monoplane wings. Profile effect. Clark Y. and N. A. C. A.-M1. Circular tips. 5-inch chord. A. R. 6

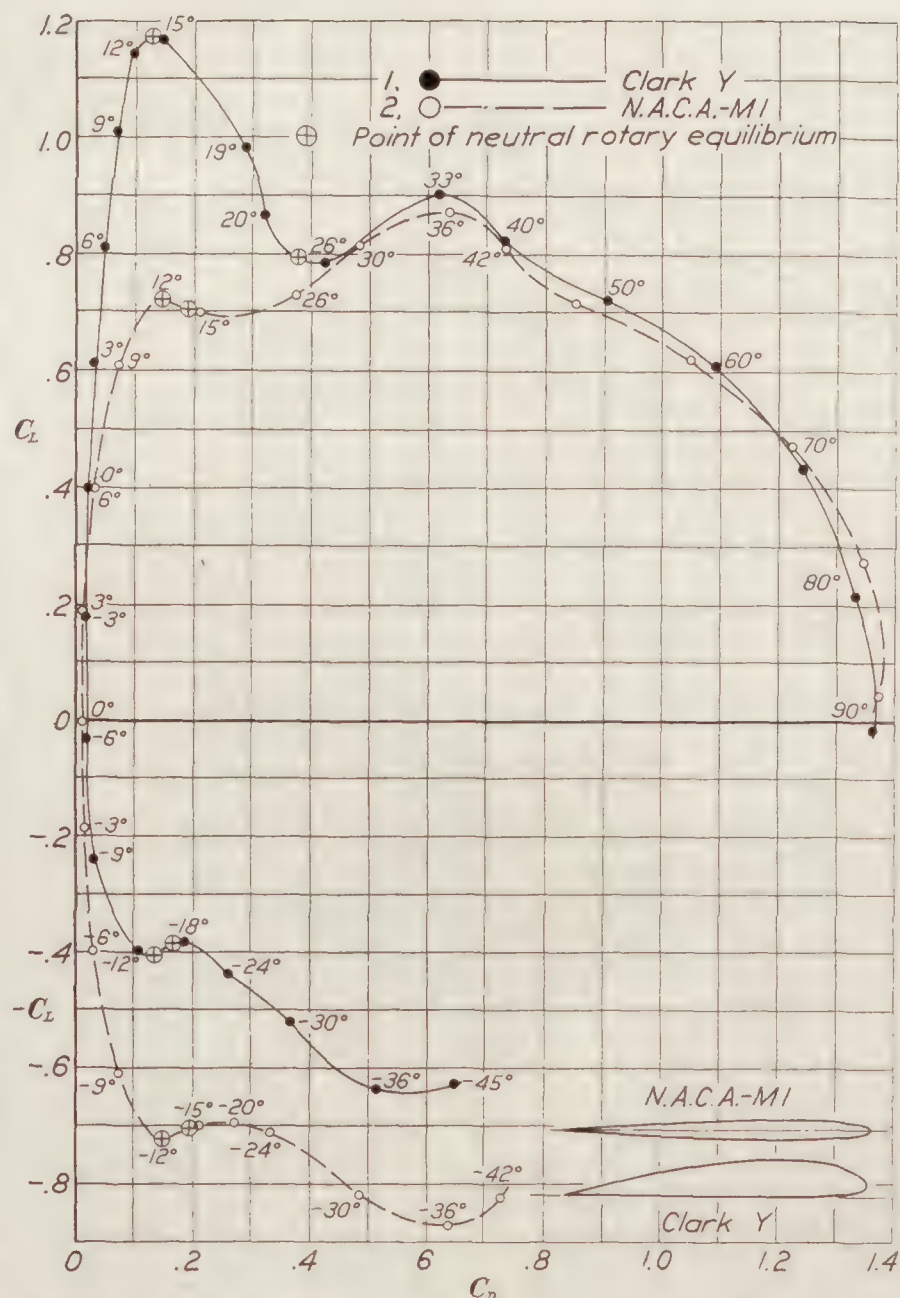


FIGURE 21.—Monoplane wings. Profile effect. Polars. Clark Y. and N. A. C. A.-M1. Circular tips. 5-inch chord. A. R. 6

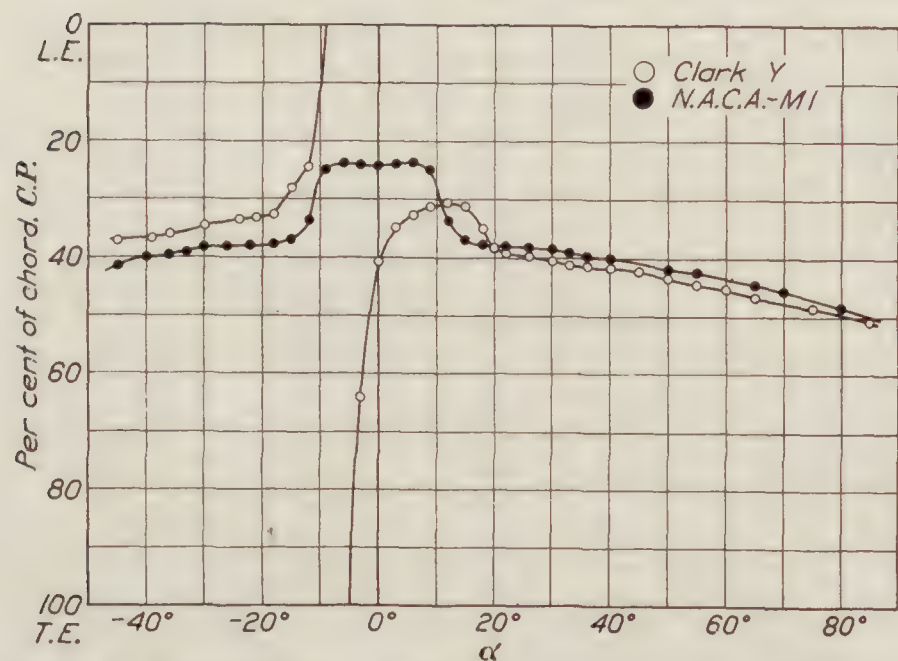


FIGURE 22.—Monoplane wings. Profile effect. Clark Y. and N. A. C. A.-M1. Circular tips. 5-inch chord. A. R. 6

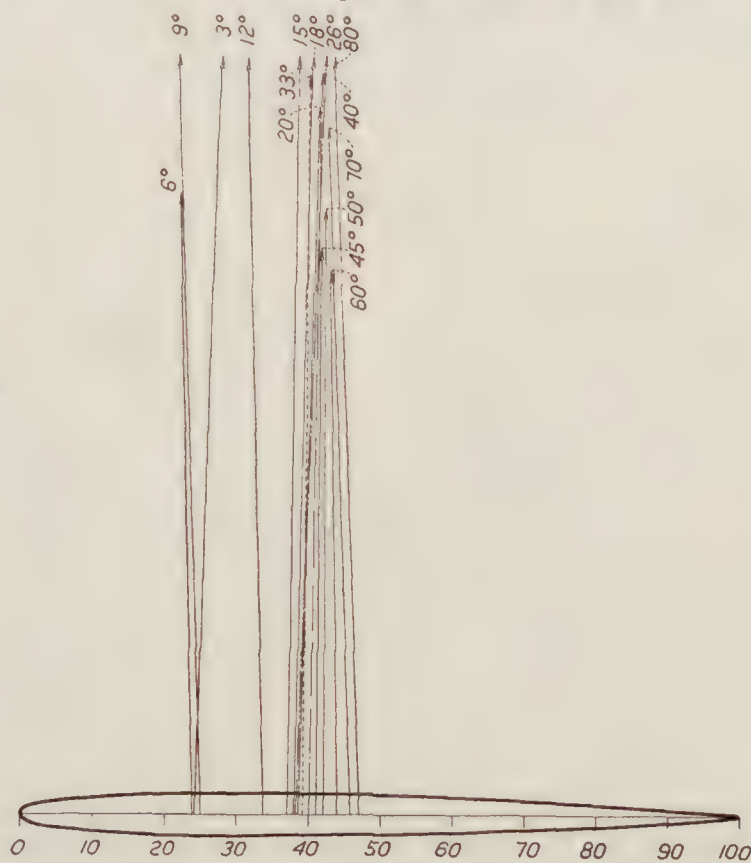


FIGURE 23.—Monoplane vector diagram. N. A. C. A.-M1. Circular tips. 5-inch chord. A. R. 6

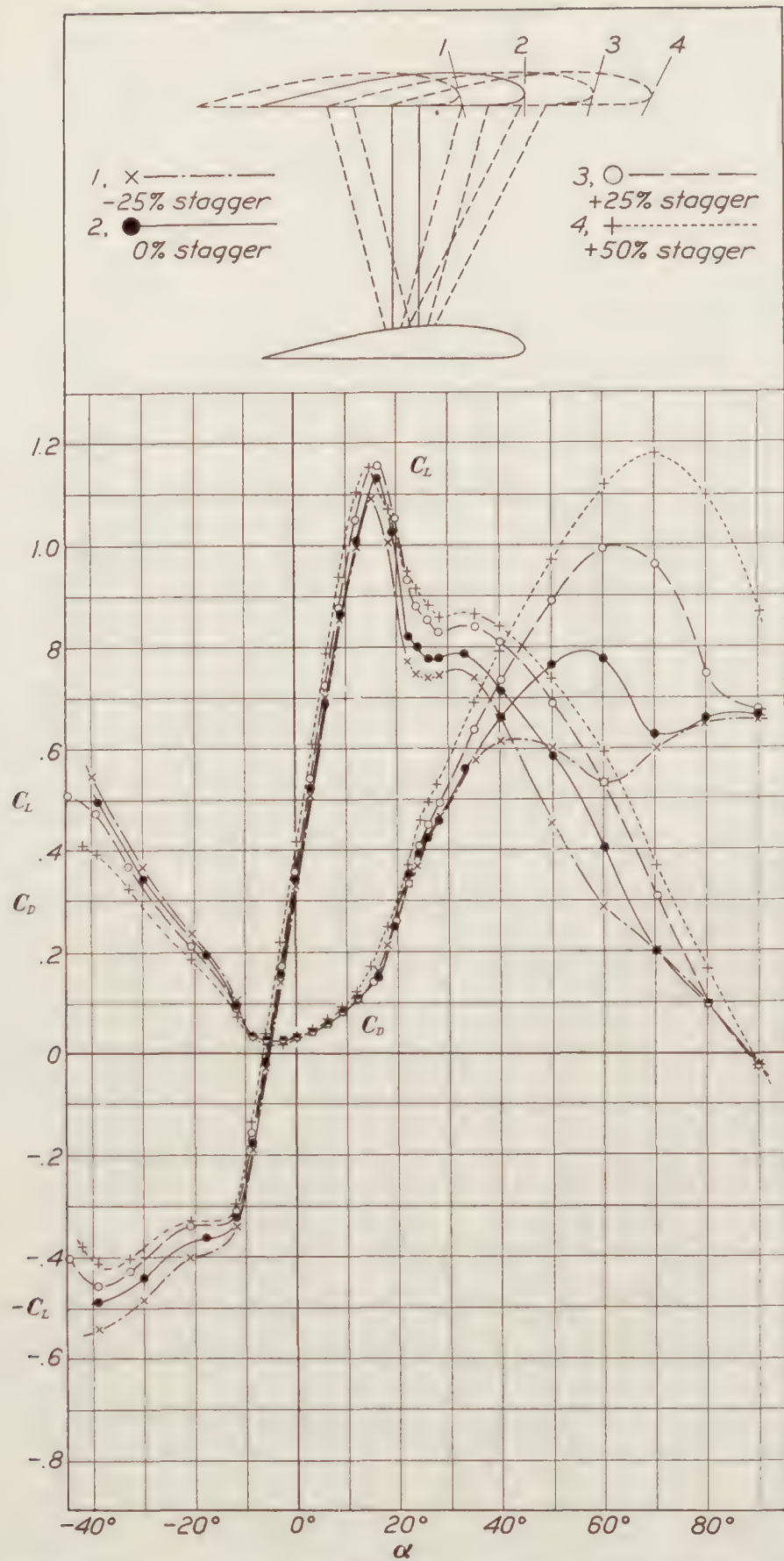


FIGURE 24.—Biplane wings. Stagger effect. Clark Y. Circular tips. 5-inch chord. A. R. 6. Gap/chord=1. Decalage, 0°

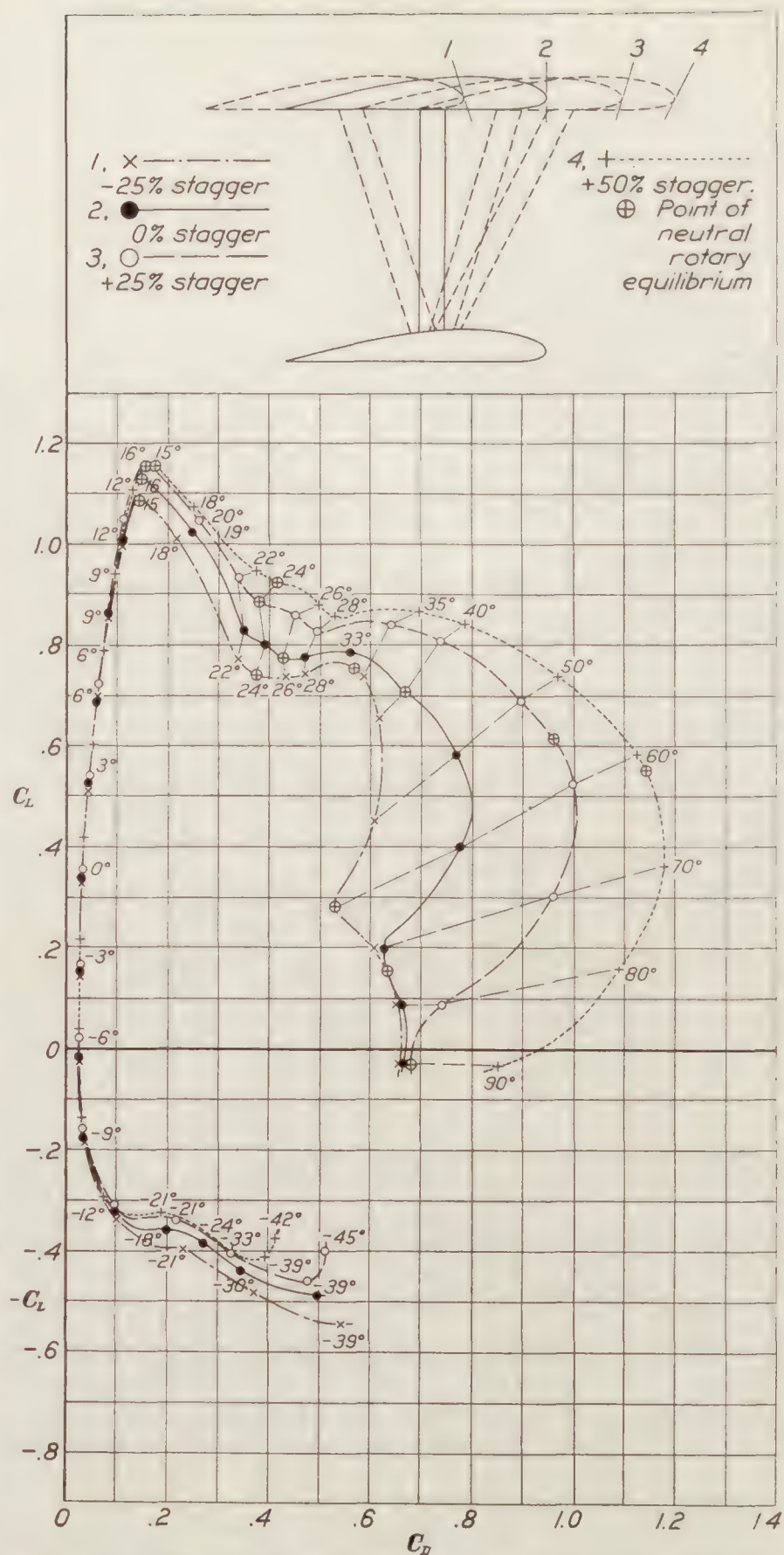


FIGURE 25.—Biplane wings. Stagger effect. Polars. Clark Y. Circular tips. 5-inch chord. A. R. 6. Gap/chord=1. Decalage, 0°

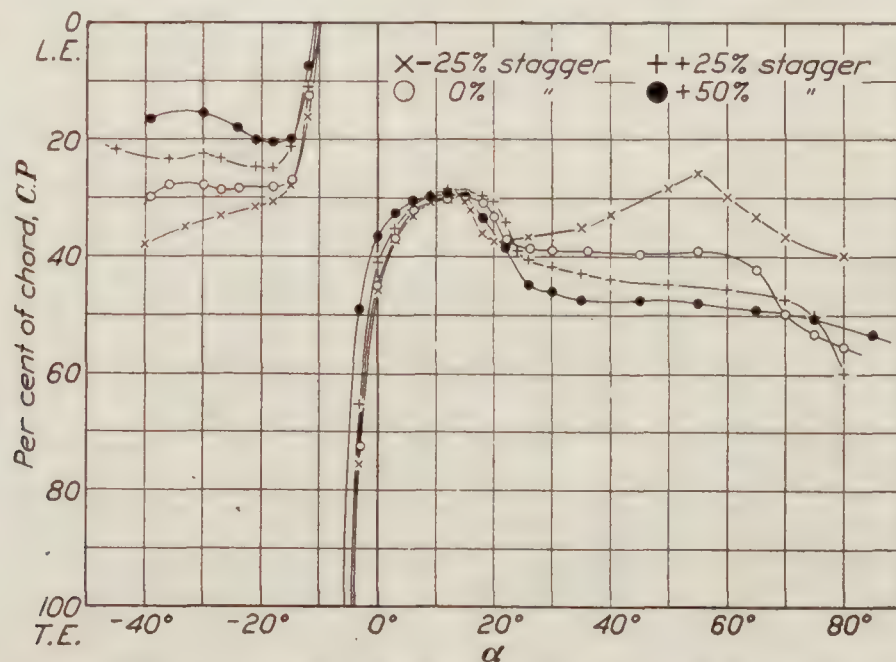


FIGURE 26.—Biplane wings. Stagger effect. Clark Y. Circular tips. 5-inch chord. A. R. 6. Gap/chord=1. Decalage, 0°

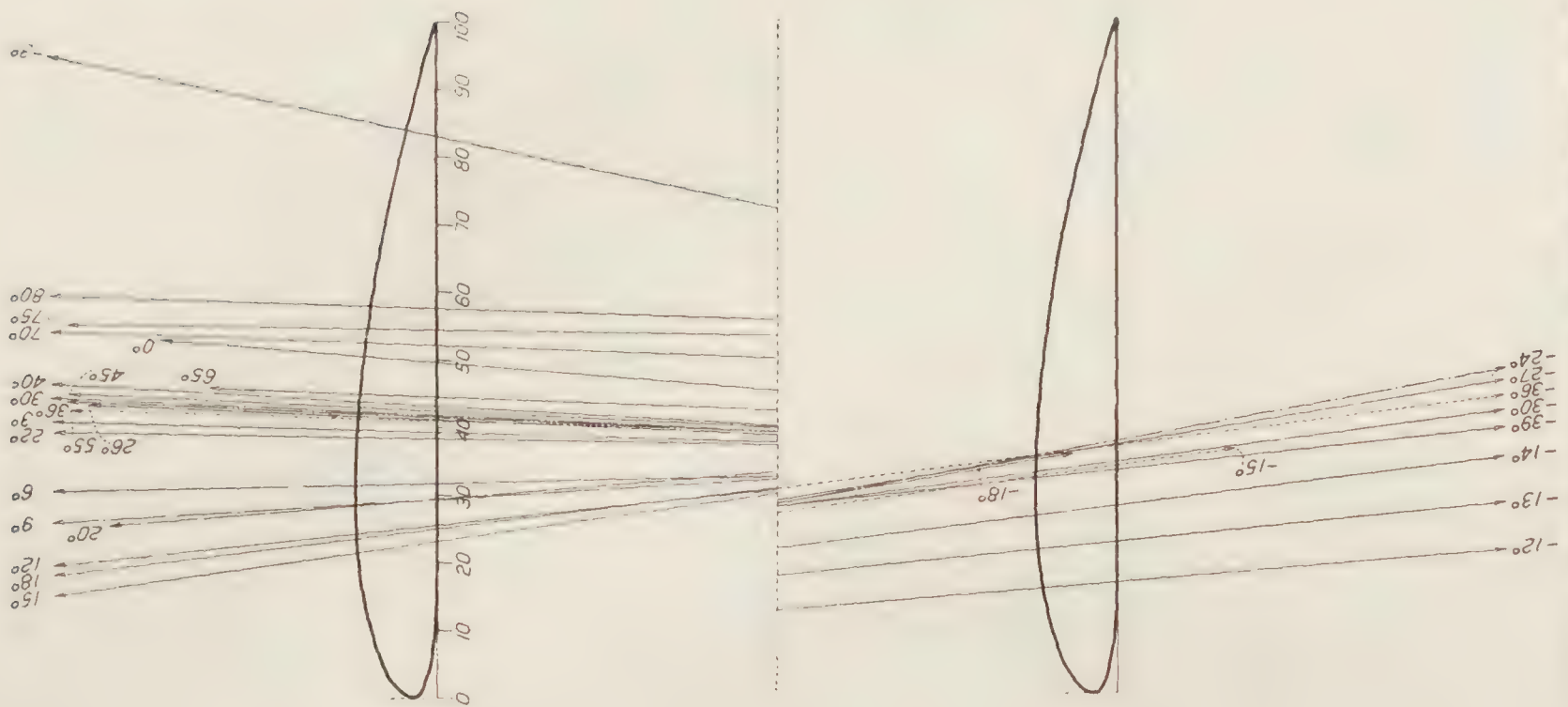


FIGURE 27.—Biplane vector diagram. Clark Y. Circular tips. 5-inch chord. A. R. 6. Gap/chord = 1. Decalage, 0°. Stagger, 0.

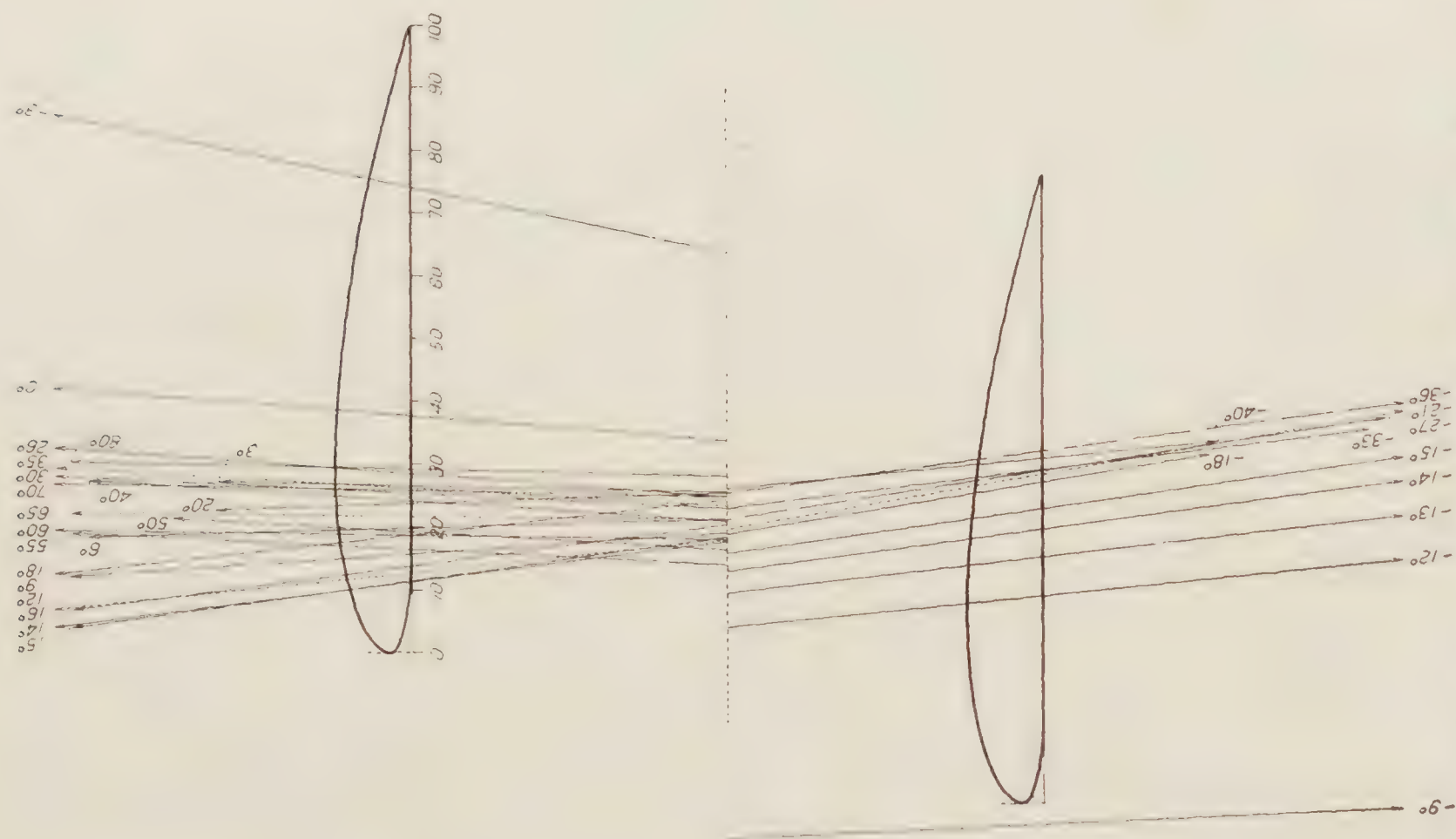


FIGURE 28.—Biplane vector diagram. Clark Y. Circular tips. 5-inch chord. A. R. 6. Gap/chord = 1. Decalage, 0°. Stagger, 0.

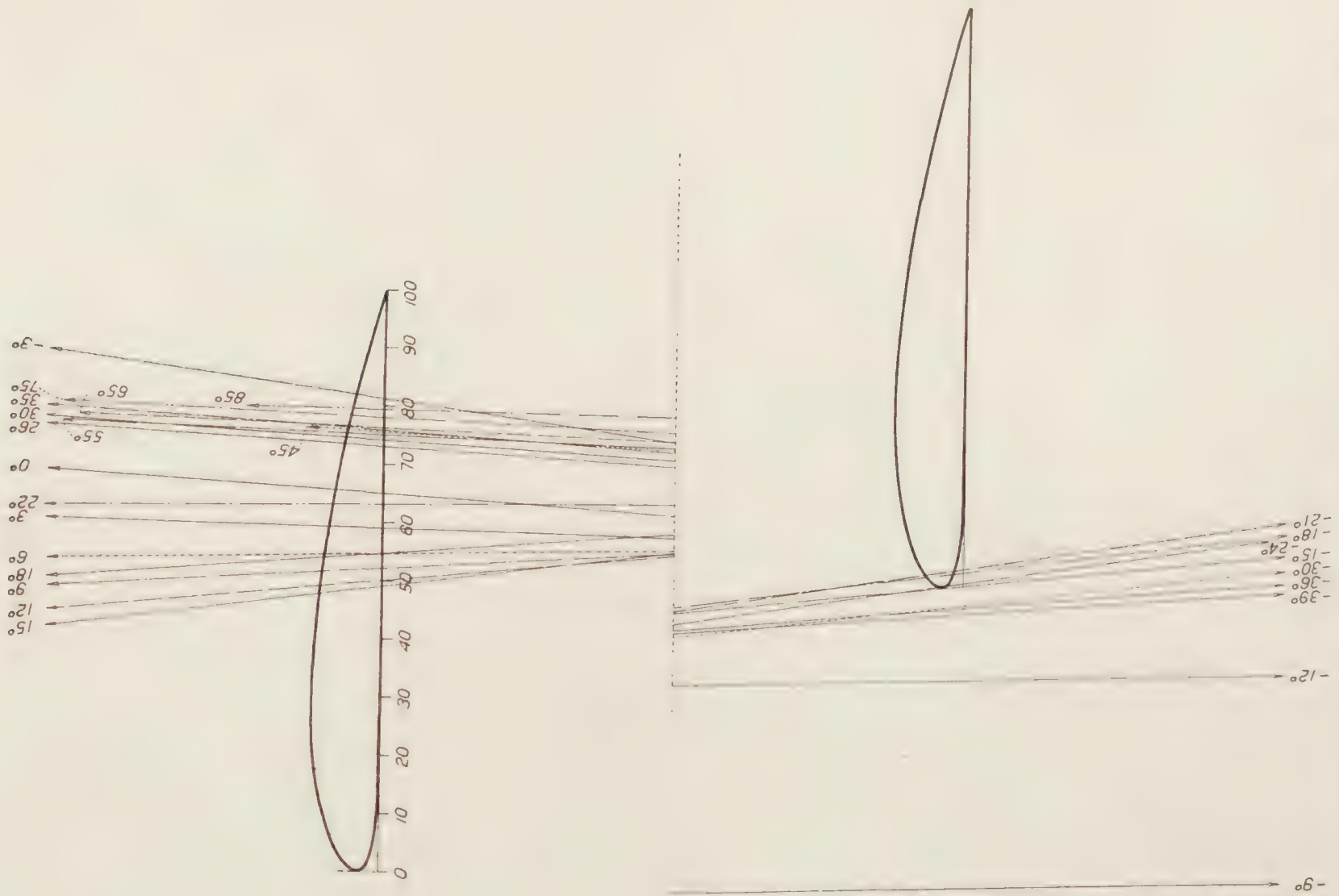


FIGURE 29.—Biplane vector diagram. Clark Y. Circular tips. 5-inch chord. A. R. 6.
Gap/chord=1. Decalage, 0°. Stagger, +25 per cent chord

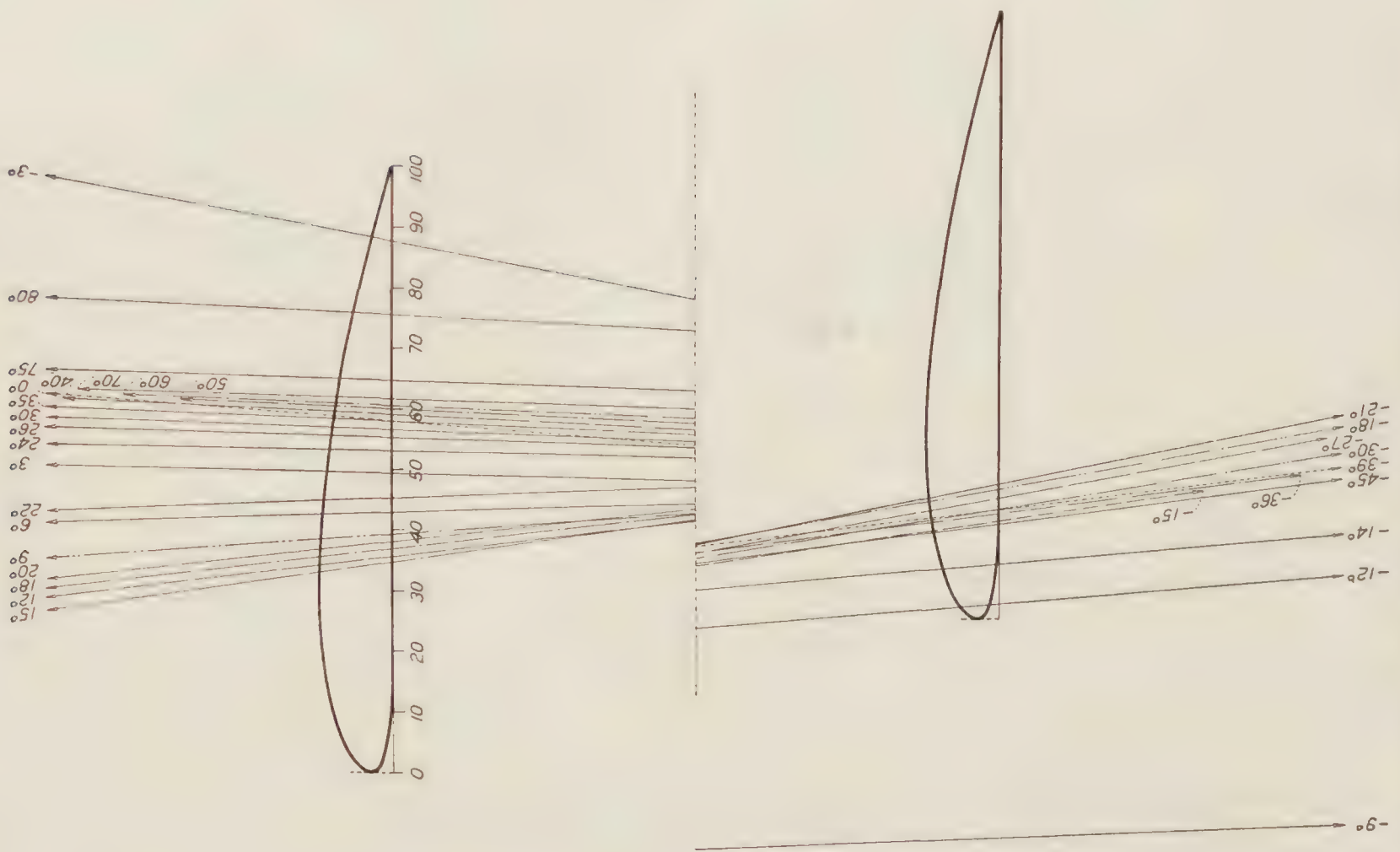


FIGURE 30.—Biplane vector diagram. Clark Y. Circular tips. 5-inch chord. A. R. 6.
Gap/chord=1. Decalage, 0°. Stagger, +50 per cent chord

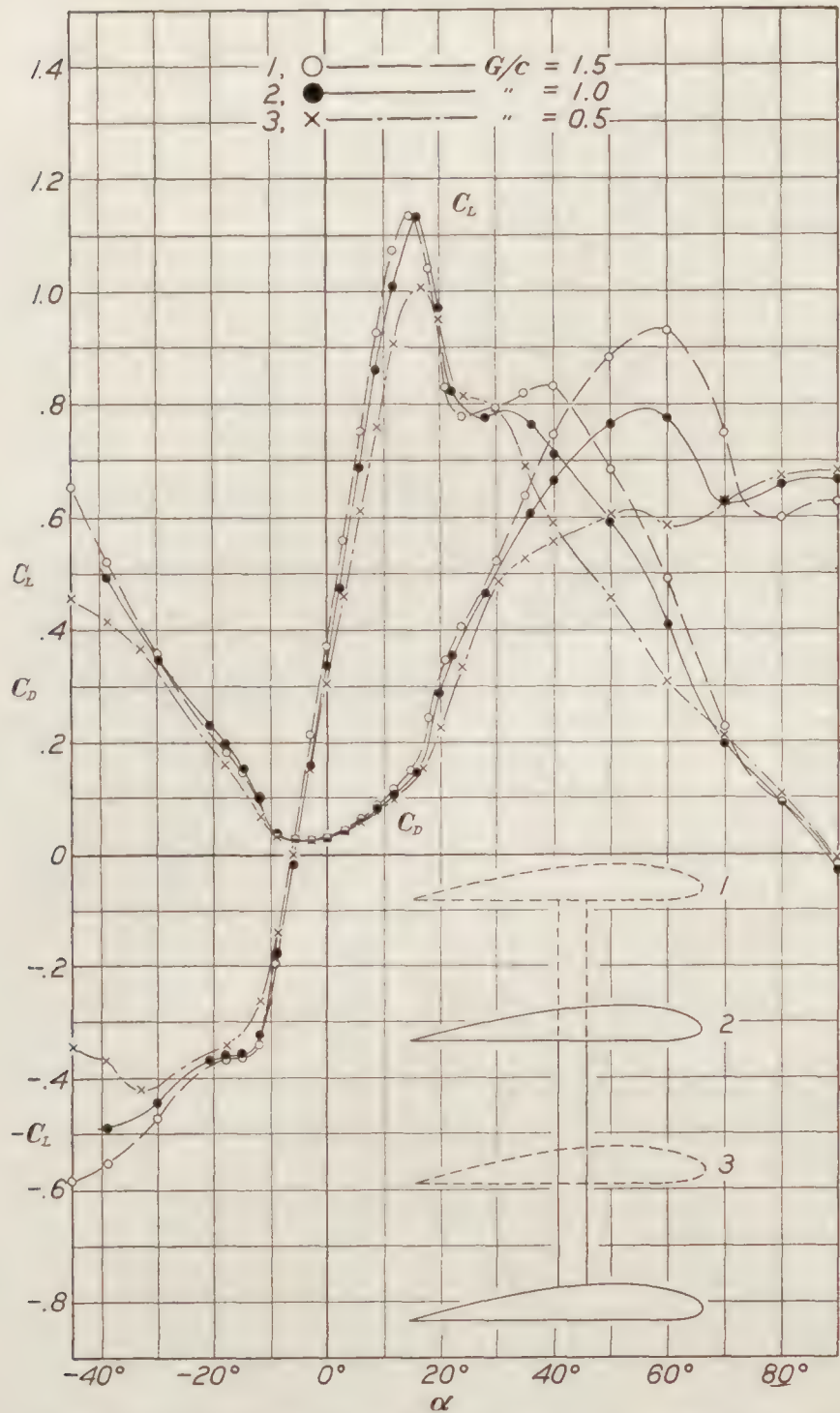


FIGURE 31.—Biplane wings. Gap effect. Clark Y. Circular tips. 5-inch chord. A. R. 6. Decalage, 0°. Stagger, 0

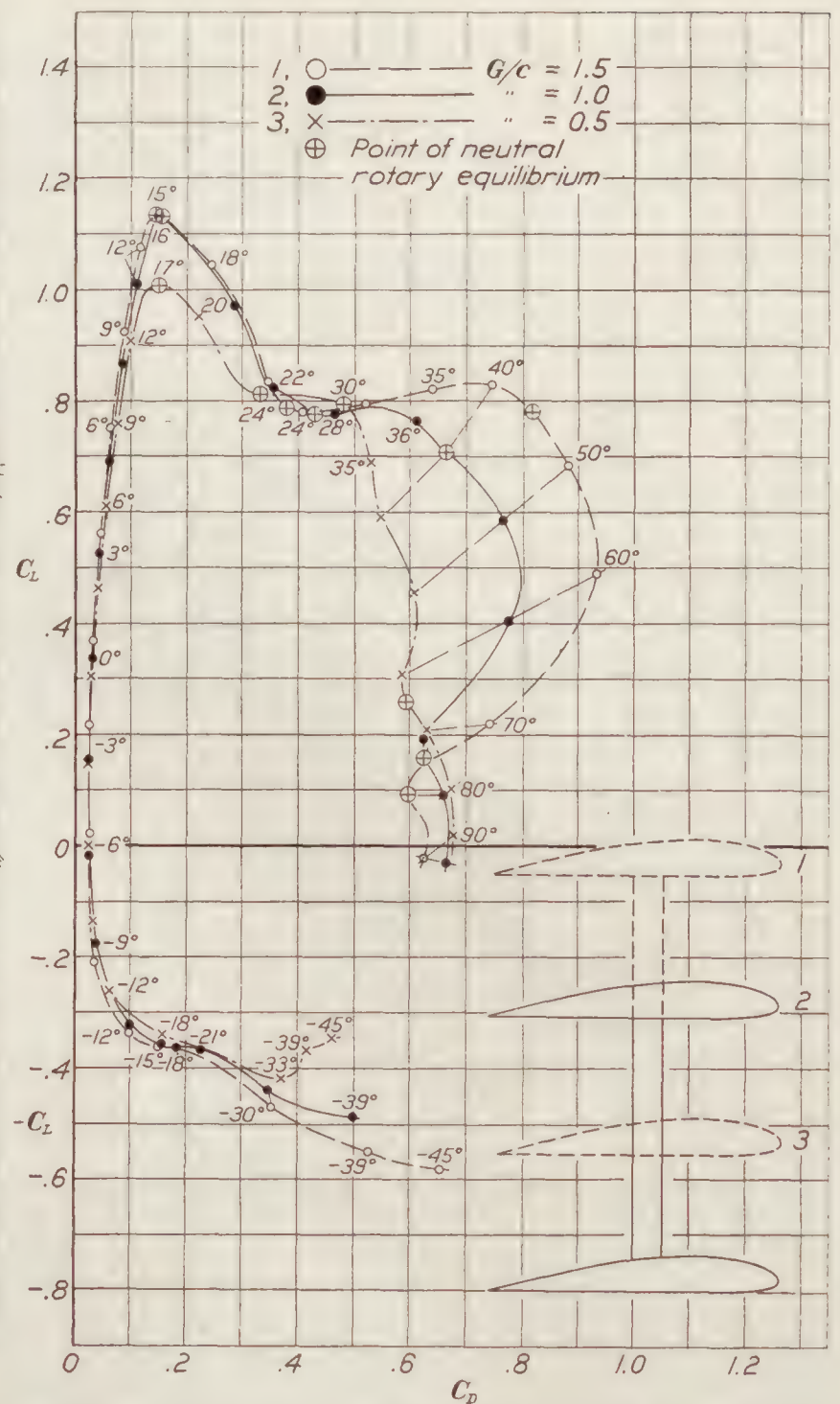


FIGURE 32.—Biplane wings. Gap effect. Polars. Clark Y. Circular tips. 5-inch chord. A. R. 6. Decalage, 0°. Stagger, 0

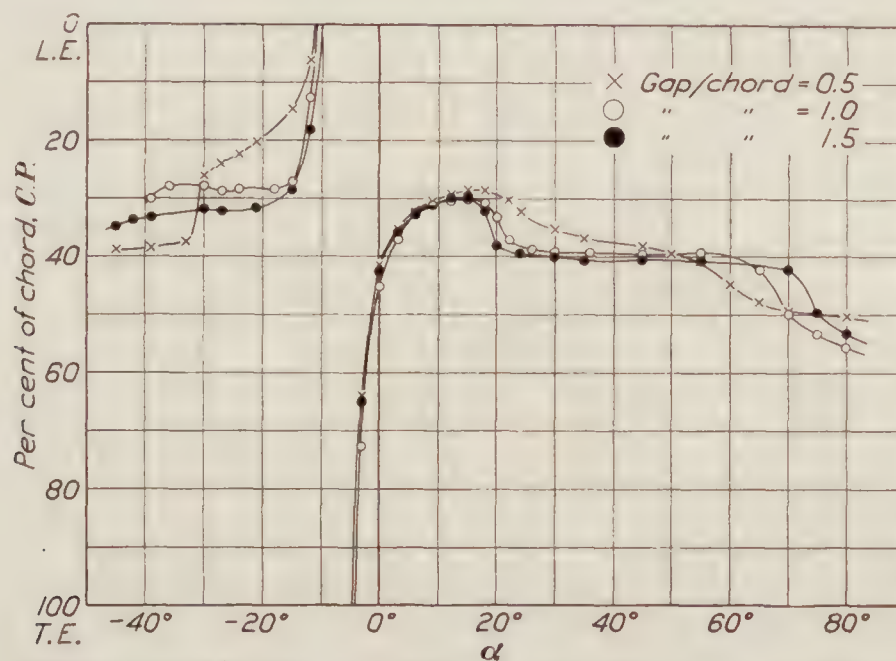


FIGURE 33.—Biplane wings. Gap effect. Clark Y. Circular tips. 5-inch chord. A. R. 6. Decalage, 0°. Stagger, 0



FIGURE 34.—Biplane vector diagram. Clark Y. Circular tips. 5-inch chord. A. R. 6. Gap/chord=1.5. Decalage, 0° . Stagger, 0

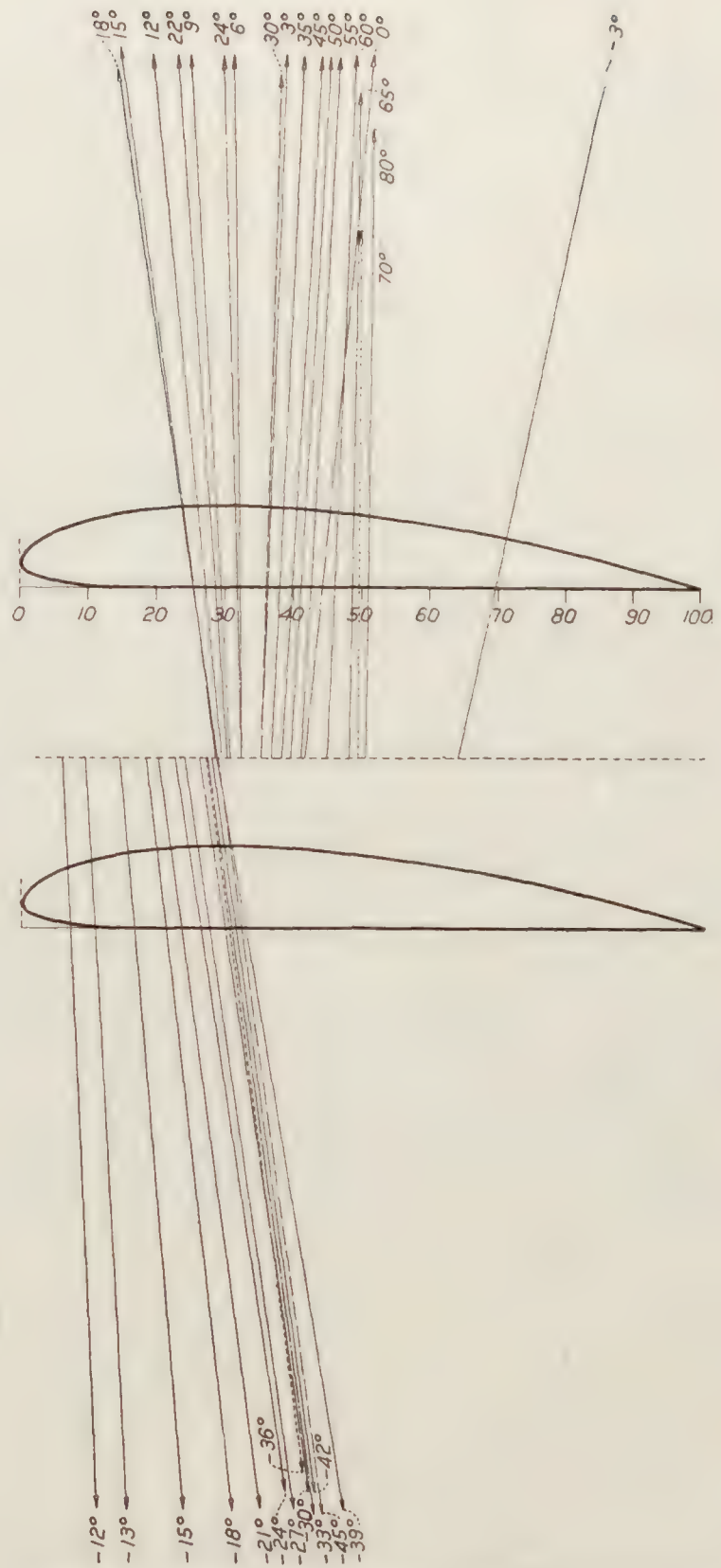


FIGURE 35.—Biplane vector diagram. Clark Y. Circular tips. 5-inch chord. A. R. 6. Gap/chord=0.5. Decalage, 0° . Stagger, 0

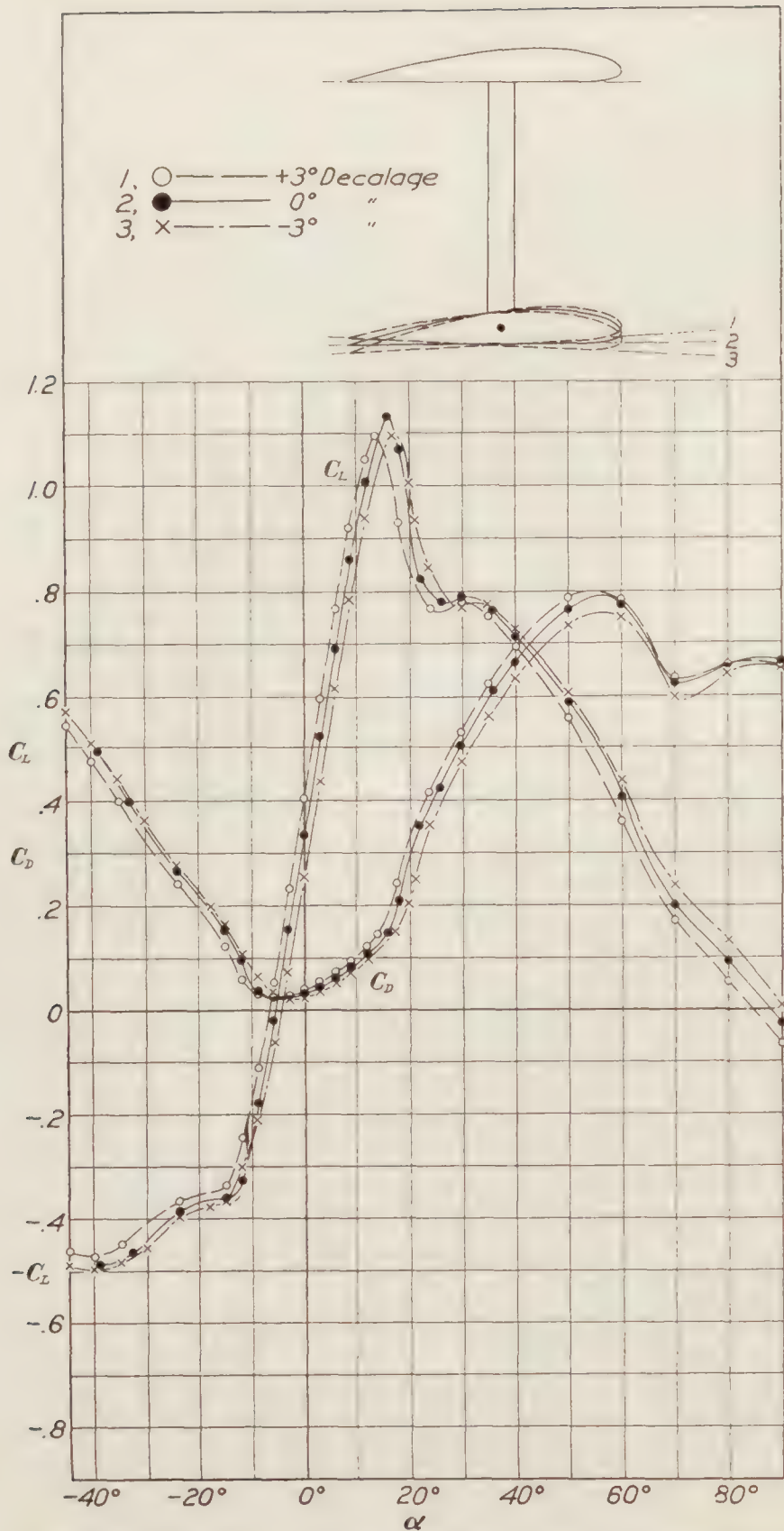


FIGURE 36.—Biplane wings. Decalage effect. Clark Y. Circular tips. 5-inch chord. A. R. 6. Gap/chord=1. Stagger, 0

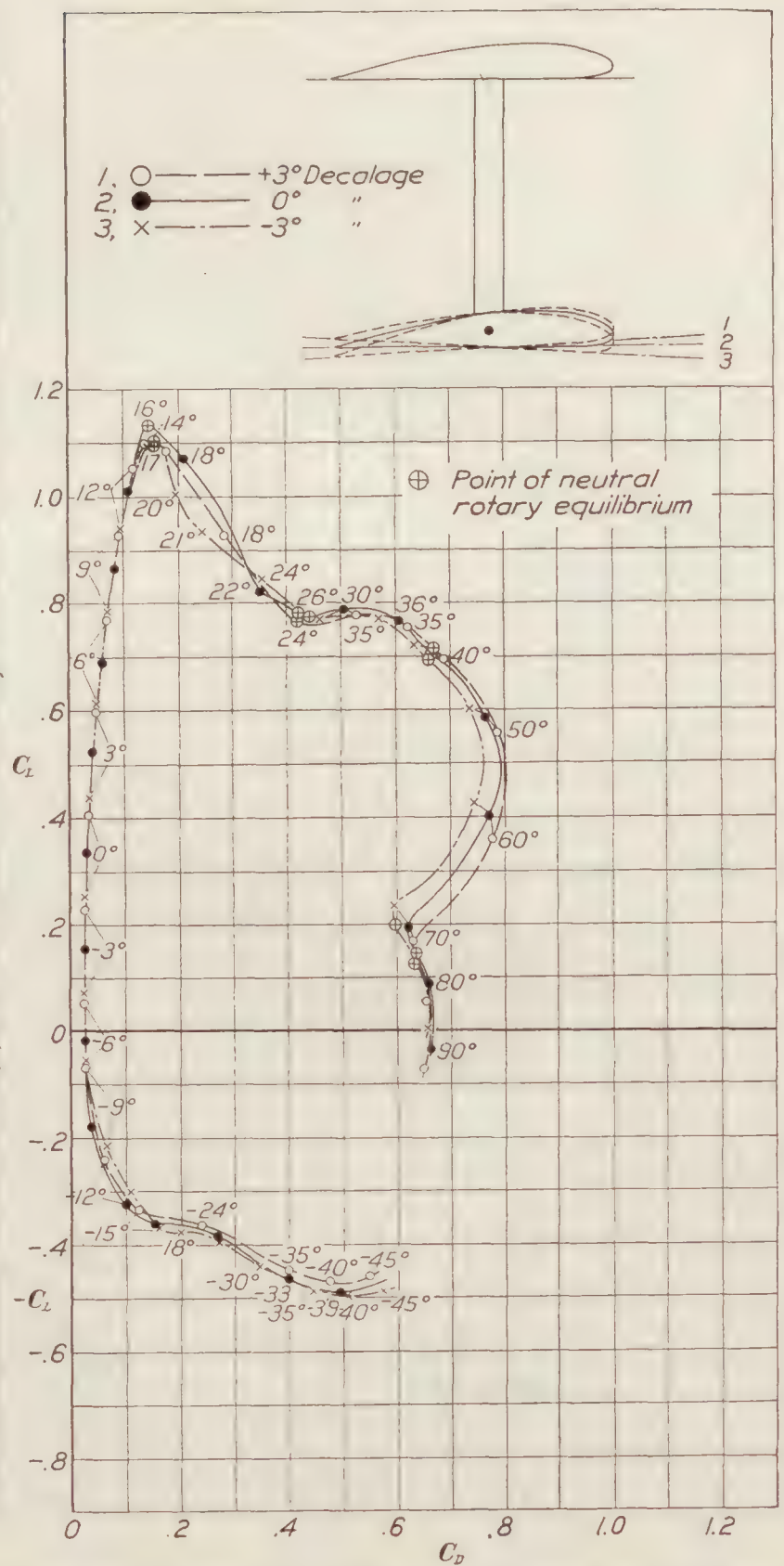


FIGURE 37.—Biplane wings. Decalage effect. Polars. Clark Y. Circular tips. 5-inch chord. A. R. 6. Gap/chord=1. Stagger, 0

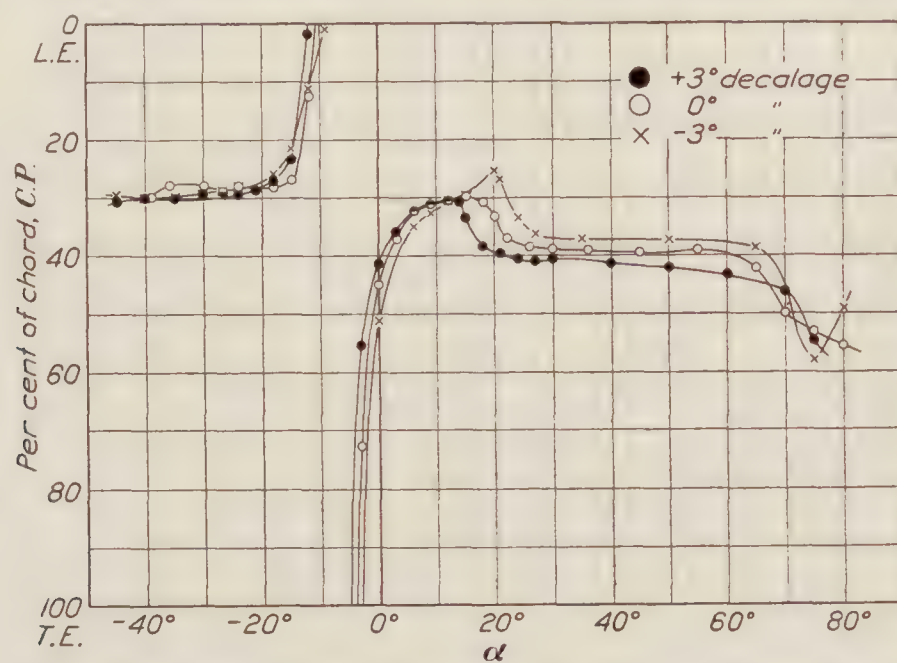


FIGURE 38.—Biplane wings. Decalage effect. Clark Y. Circular tips. 5-inch chord. A. R. 6. Gap/chord=1. Stagger, 0

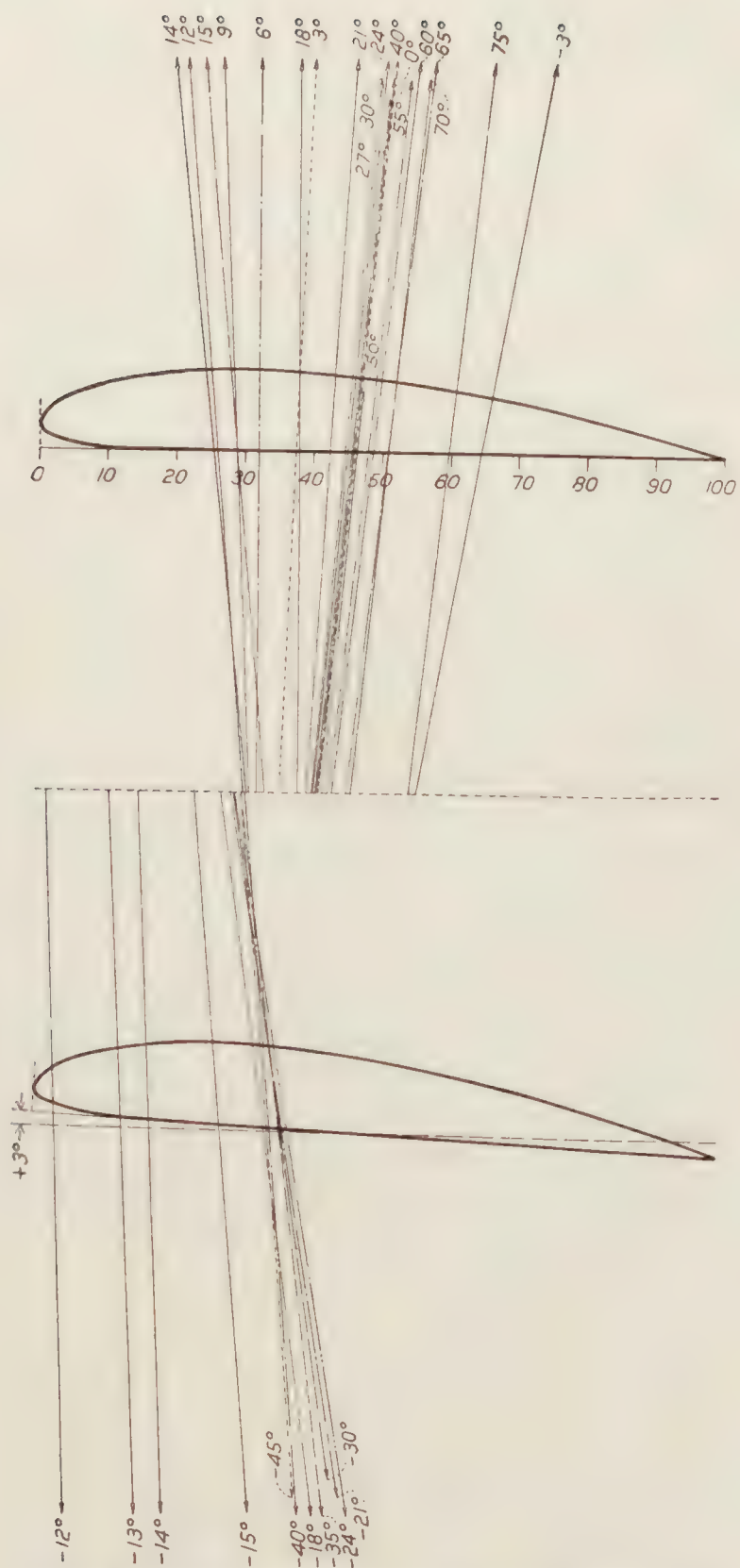


FIGURE 39.—Biplane vector diagram. Clark Y. Circular tips. 5-inch chord. A. R. 6. Gap/chord=1. Decalage, $+3^\circ$. Stagger, 0

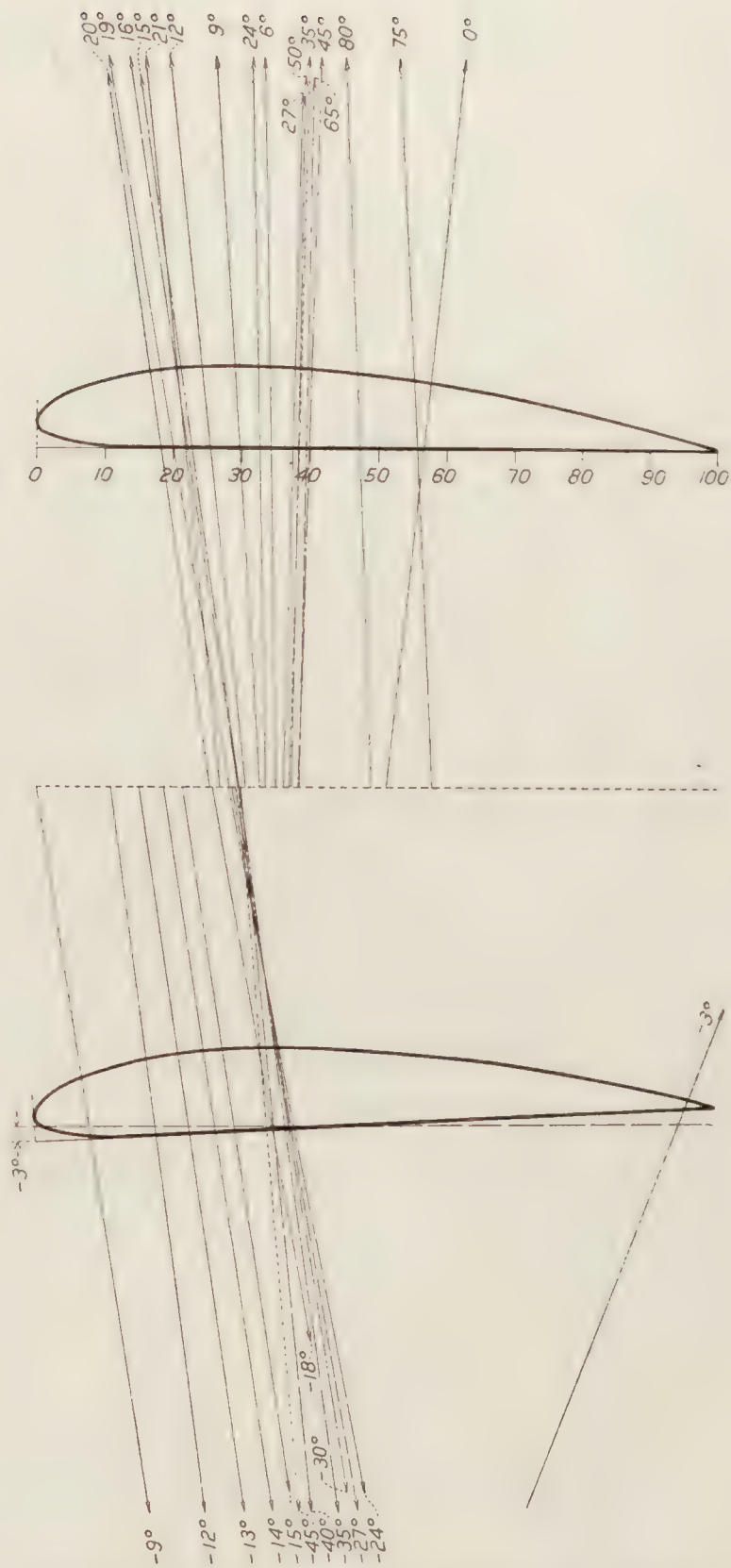


FIGURE 40.—Biplane vector diagram. Clark Y. Circular tips. 5-inch chord. A. R. 6. Gap/chord=1. Decalage, -3° . Stagger, 0

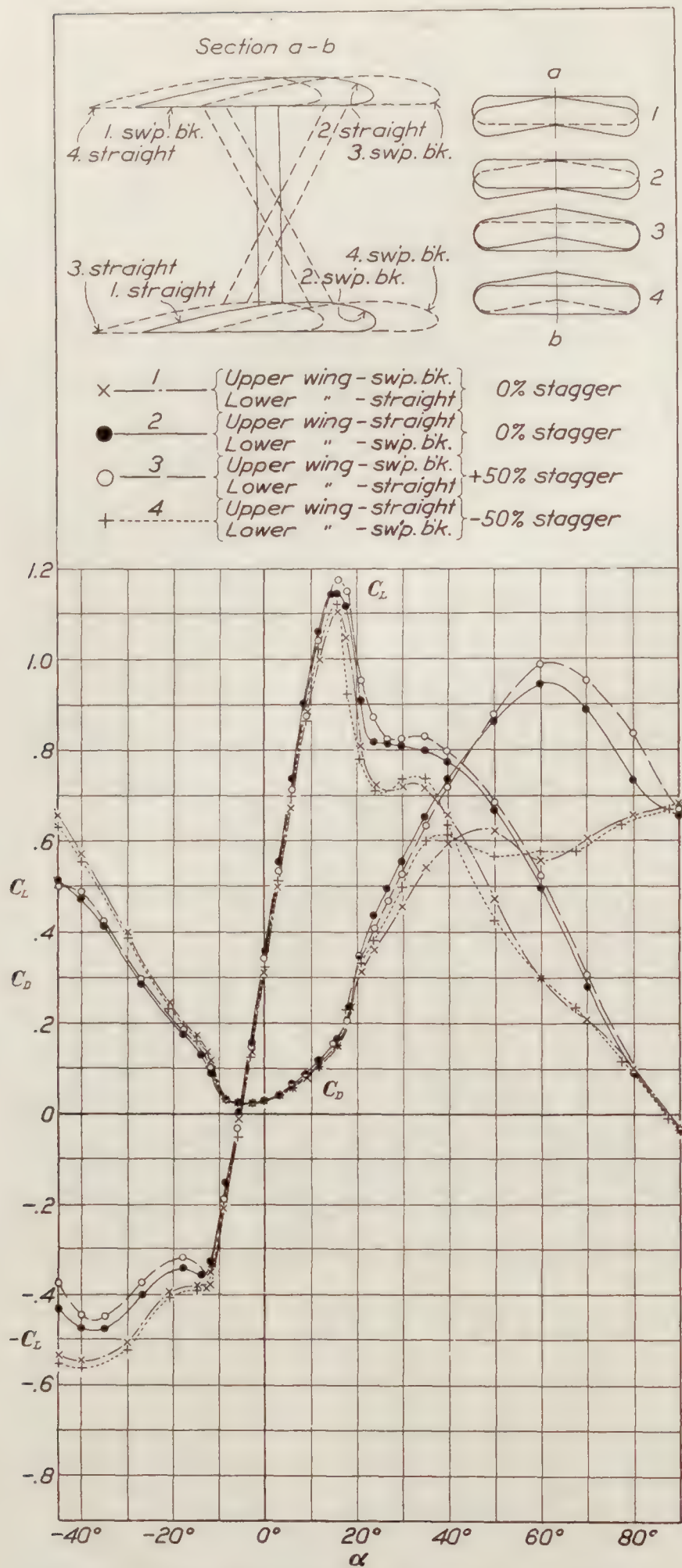


FIGURE 41.—Biplane wings. Sweep-back effect. Clark Y. Circular tips. 5-inch chord. A. R. 6. Gap/chord=1. Decalage, 0°

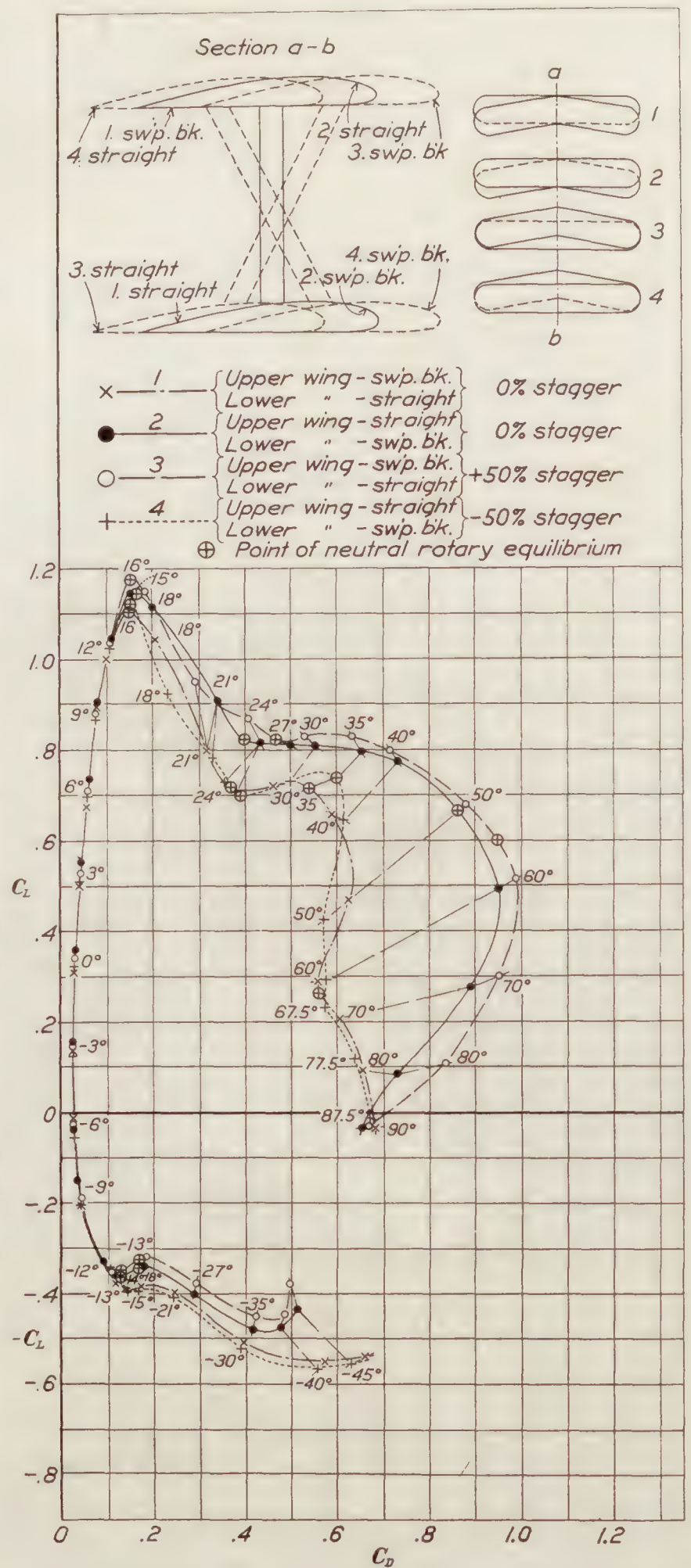


FIGURE 42.—Biplane wings. Sweep-back effect. Polars. Clark Y. Circular tips. 5-inch chord. A. R. 6. Gap/chord=1. Decalage 0°

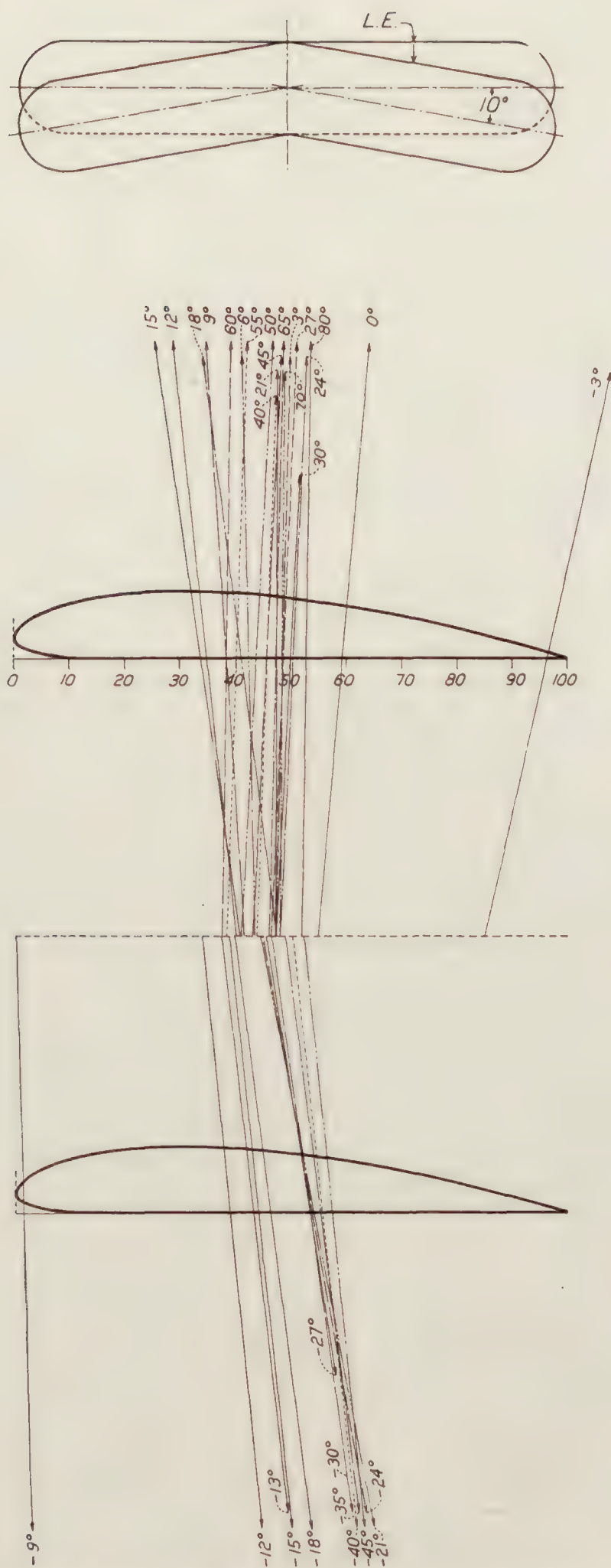


FIGURE 43.—Biplane vector diagram. Clark Y. Upper wing, swept back. Lower wing, straight. Circular tips. 5-inch chord. A. R. 6. Gap/chord=1. Decalage, 0°. Stagger, 0

104397—30—19

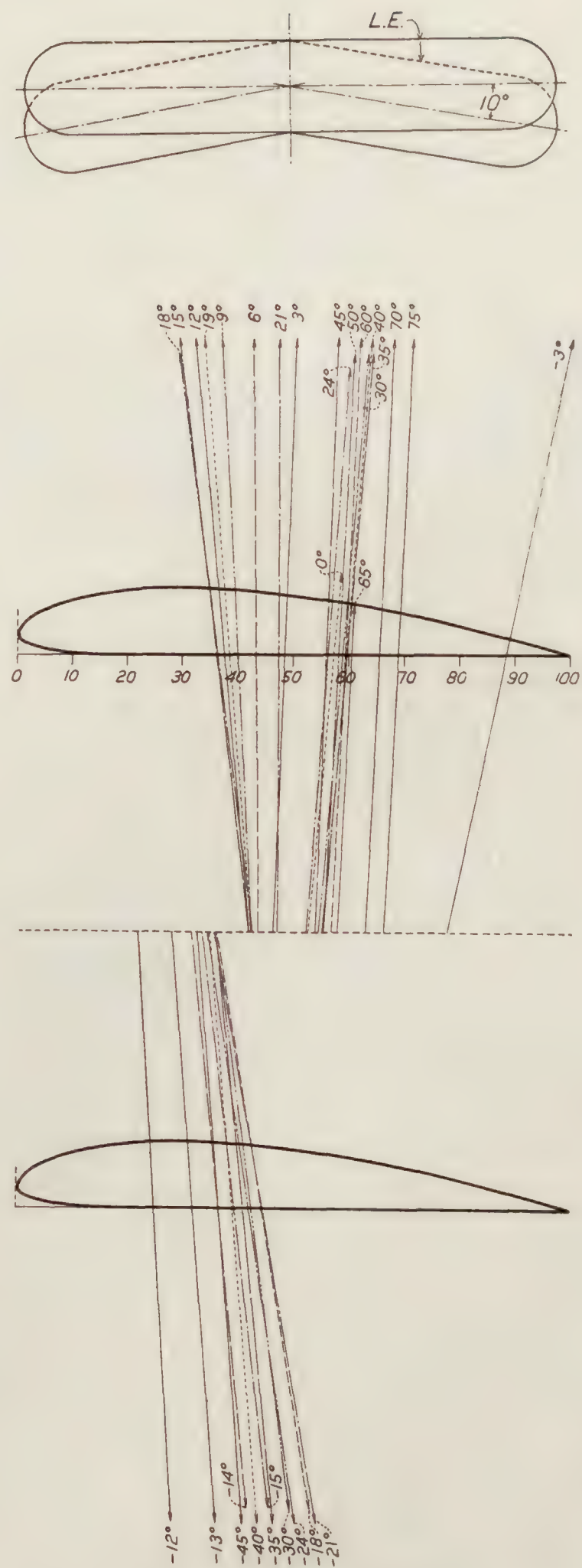


FIGURE 44.—Biplane vector diagram. Clark Y. Upper wing, straight. Lower wing, swept back. Circular tips. 5-inch chord. A. R. 6. Gap/chord=1. Decalage, 0°. Stagger, 0

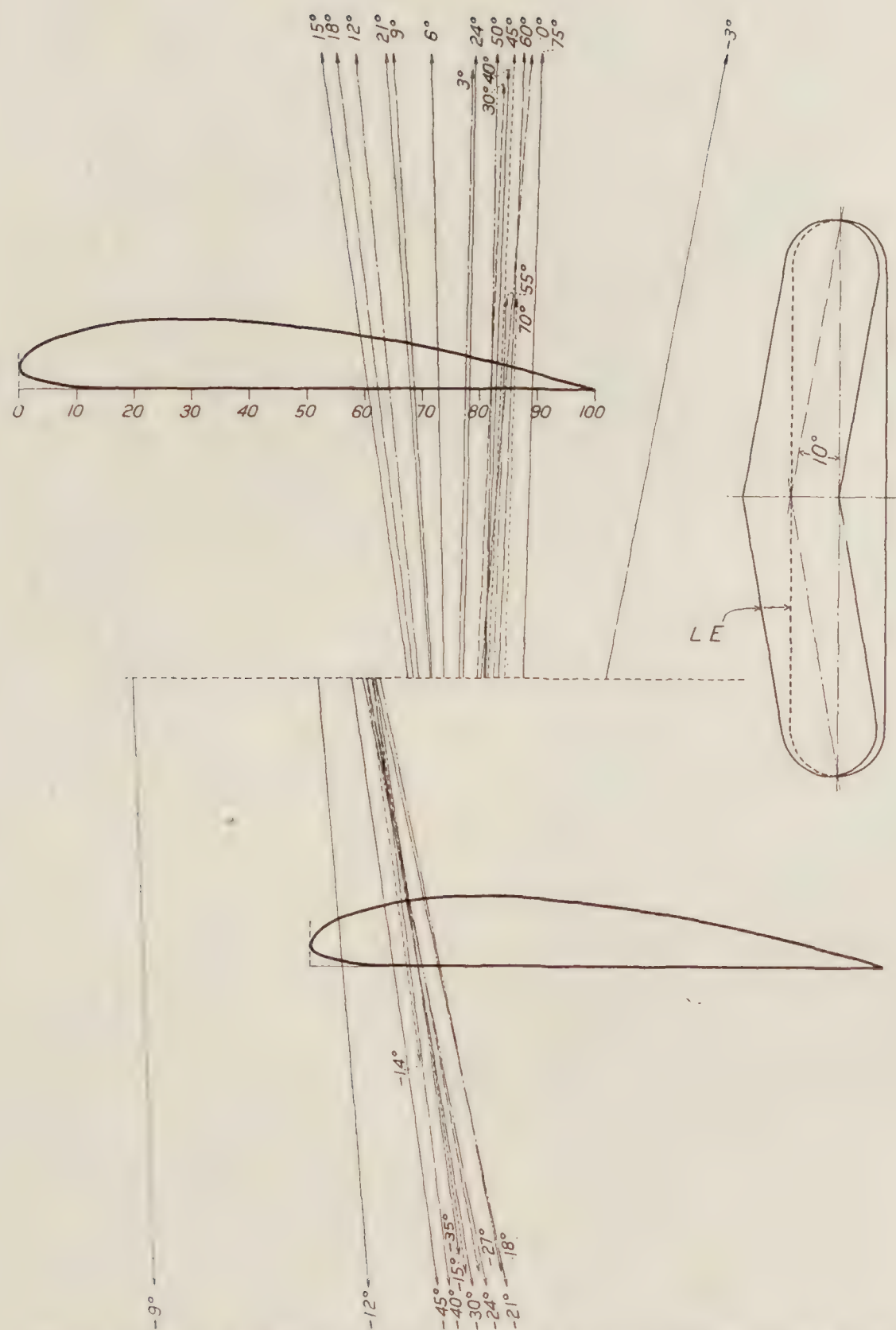


FIGURE 45.—Biplane vector diagram. Clark Y. Upper wing, swept back. Lower wing, straight. Circular tips. 5-inch chord. A. R. 6. Gap/chord=1. Decalage, 0°. Stagger, +50 per cent chord

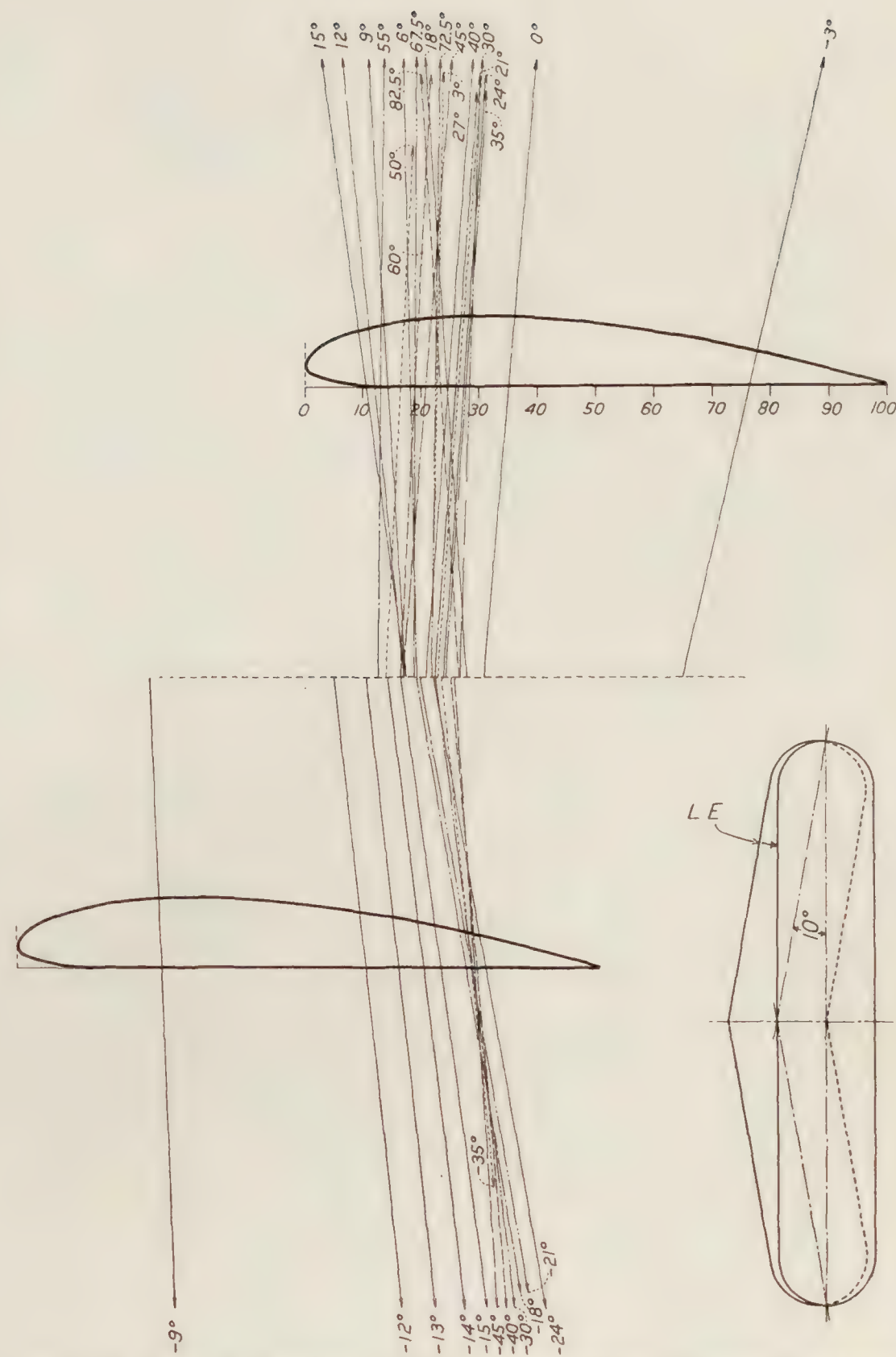


FIGURE 46.—Biplane vector diagram. Clark Y. Upper wing, straight. Lower wing, swept back. Circular tips. 5-inch chord. A. R. 6. Gap/chord=1. Decalage, 0°. Stagger, -50 per cent chord

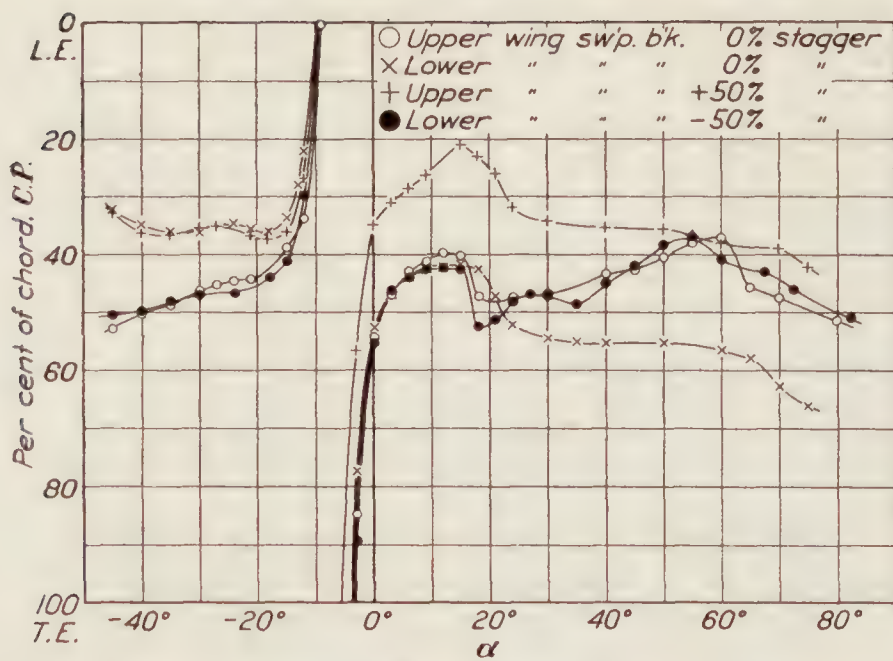


FIGURE 47.—Biplane wings. Sweep-back effect. Clark Y. Circular tips. 5-inch chord. A. R. 6. Gap/chord=1. Decalage, 0°

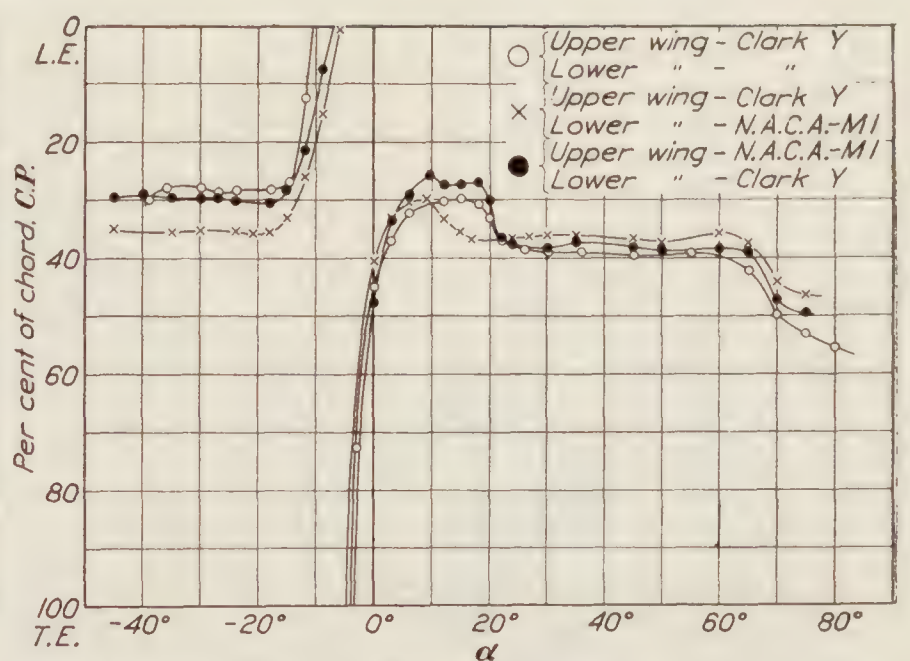


FIGURE 48.—Biplane wings. Profile effect. Clark Y. and N. A. C. A.-M1. Circular tips. 5-inch chord. A. R. 6. Gap/chord=1. Decalage, 0°. Stagger, 0

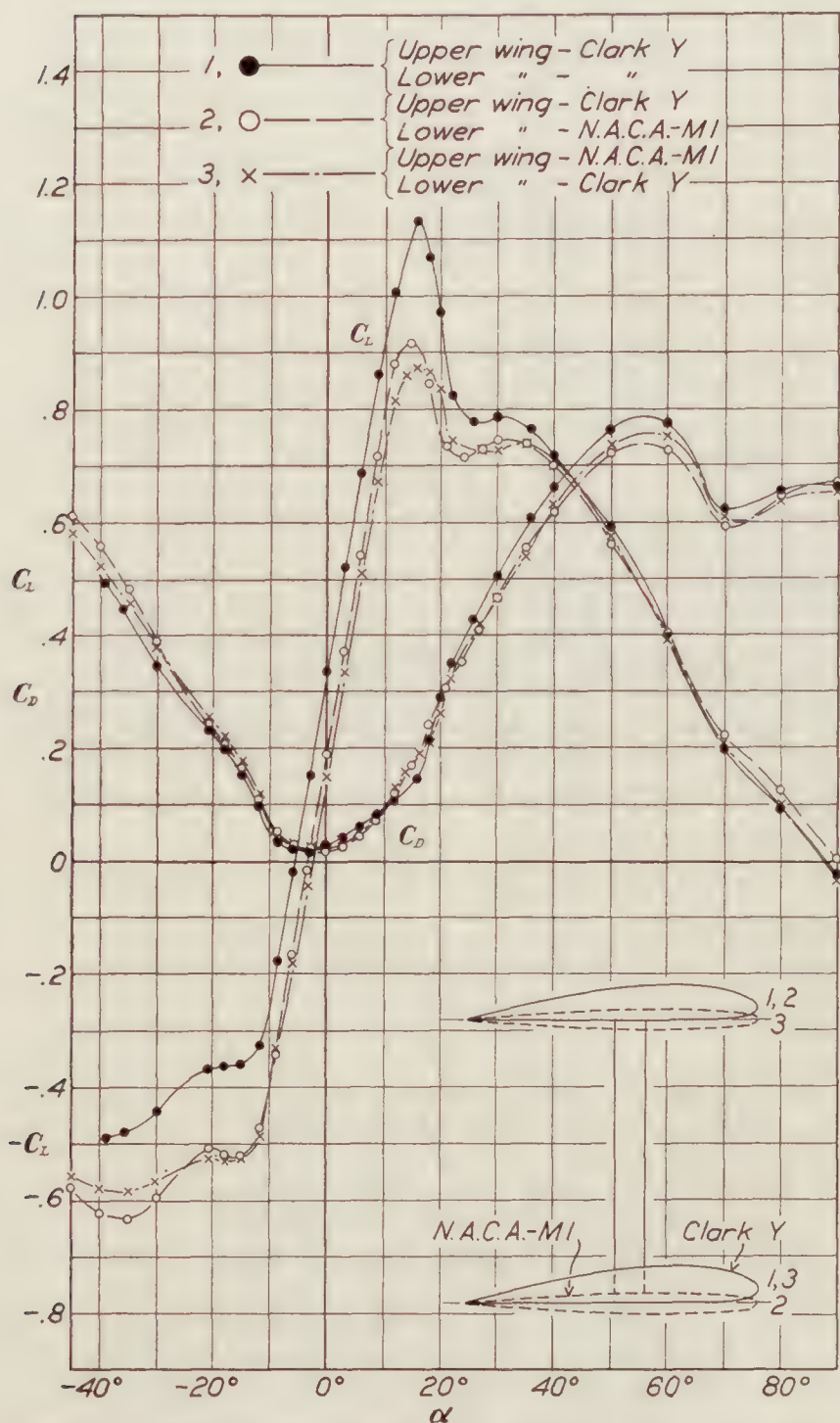


FIGURE 49.—Biplane wings. Profile effect. Clark Y. N. A. C. A.-M1. Circular tips. 5-inch chord. A. R. 6. Gap/chord=1. Decalage, 0°. Stagger, 0

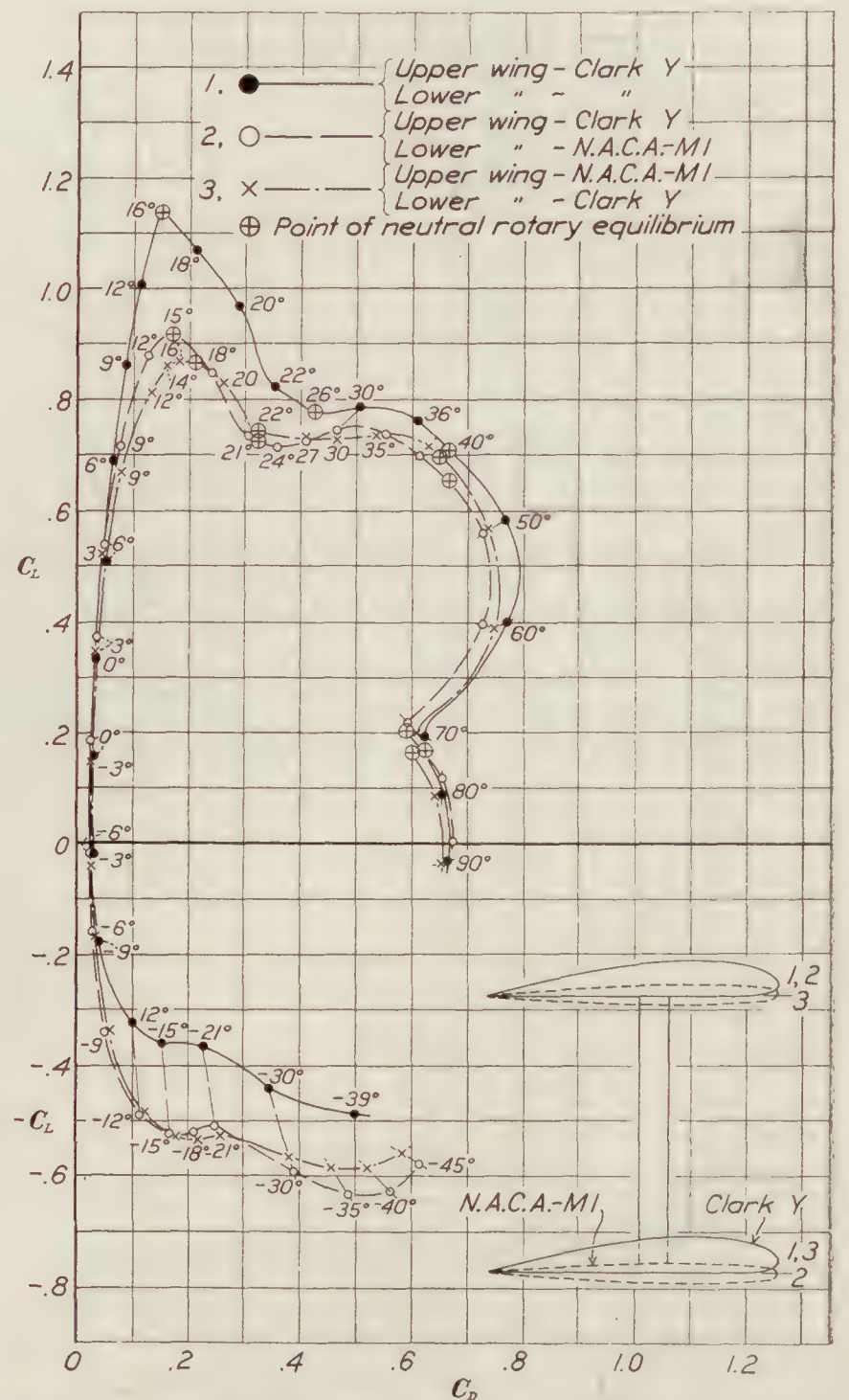


FIGURE 50.—Biplane wings. Profile effect. Polars. Clark Y. N. A. C. A.-M1. Circular tips. 5-inch chord. A. R. 6. Gap/chord=1. Decalage, 0°. Stagger, 0

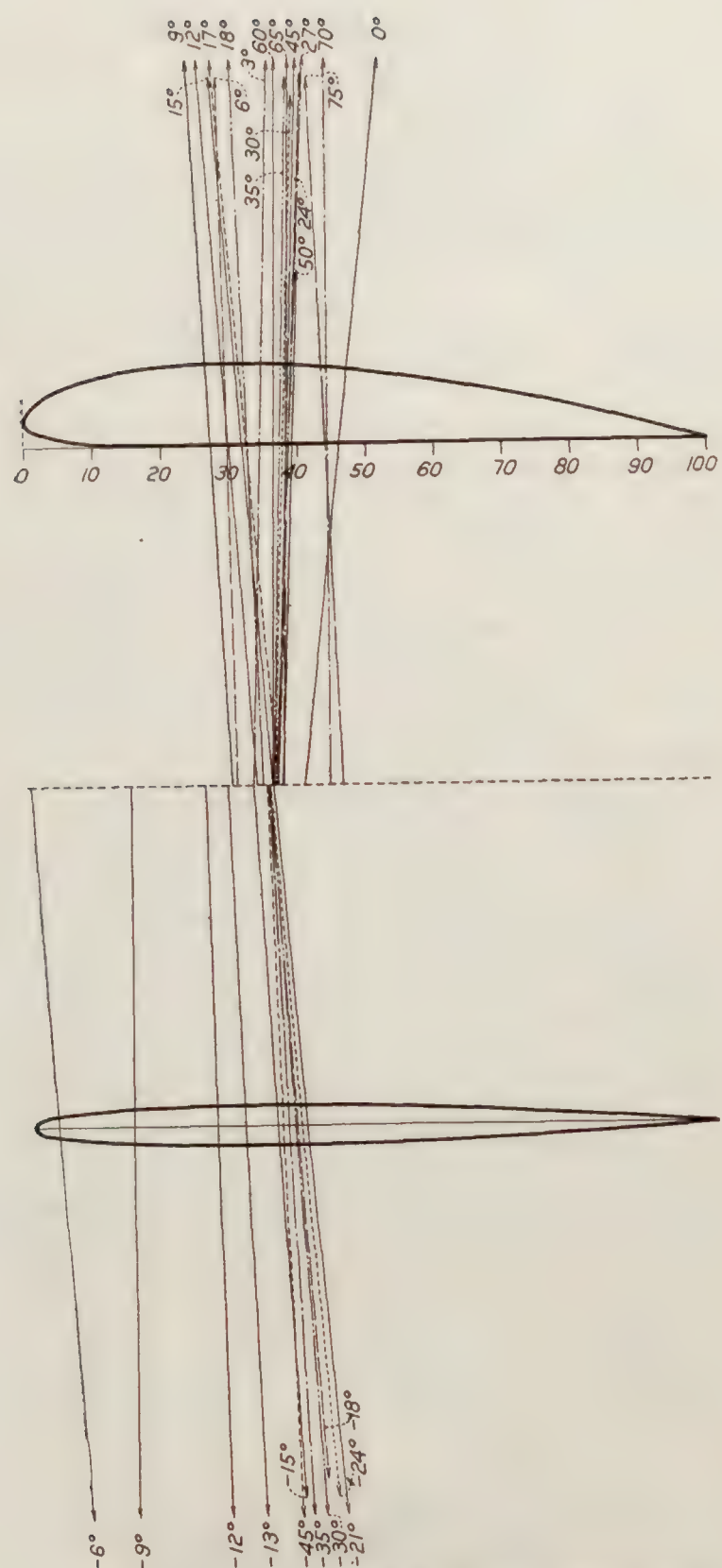


FIGURE 51.—Biplane vector diagram. Upper wing, Clark Y. Lower wing, N. A. C. A.-M1. Circular tips. 5-inch chord. A. R. 6. Gap/chord=1. Decalage, 0° . Stagger, 0

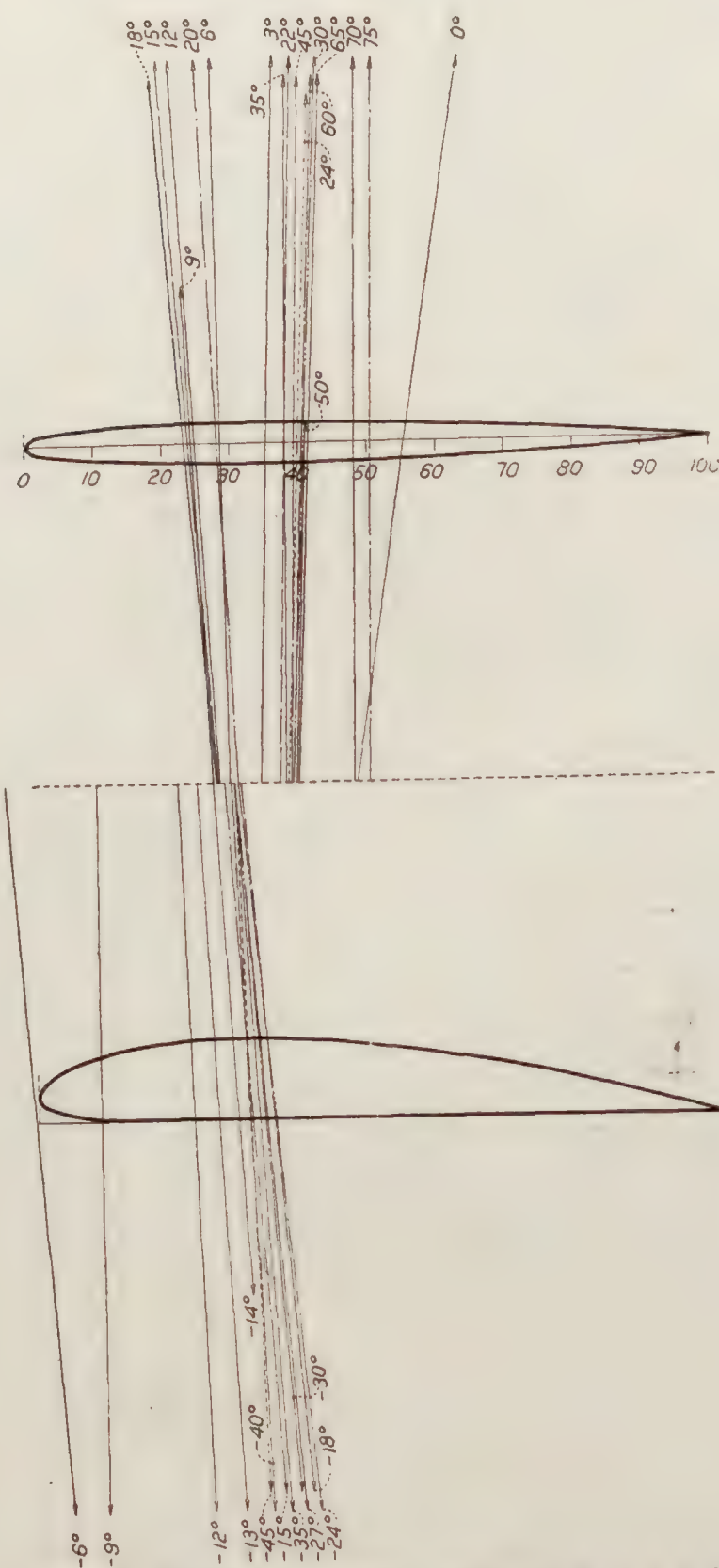


FIGURE 52.—Biplane vector diagram. Upper wing, N. A. C. A.-M1. Lower wing, Clark Y. Circular tips. 5-inch chord. A. R. 6. Gap/chord=1. Decalage, 0° . Stagger, 0

APPENDIX

By Thomas A. Harris

In the force tests described in the foregoing report, the dynamic pressure was maintained constant at the position of the "service Pitot." (Fig. 53.) This dynamic pressure q' , is a certain fraction of the dynamic pressure q , at the position of the model (with model removed from the tunnel), several feet downstream with the honeycomb between it and the "service Pitot." (Fig. 53.) In order to determine the relation between q' and q , a Pitot-static survey was conducted at the position of the model, and the "service Pitot" was then calibrated against this survey.

Since this wind tunnel is of the closed throat test section type, if part of the test section is blocked by a model, the same amount of air must pass through the restricted area that formerly passed through the unobstructed section. With the model at small angles of attack, the blocked area is small, but at large angles the blocking causes the dynamic pressure q'' , at the position of the model, to increase appreciably, while it does not affect the dynamic pressure q' , at the "service Pitot." The variable dynamic pressure q'' , is the value from which the absolute coefficients should be calculated. In the tests described in the foregoing report, however, the absolute coefficients C_D and C_L (uncorrected for blocking), were calculated from values of q . Since q is less than q'' , these coefficients are higher than C_D' and C_L' (corrected for blocking).

TESTS

To determine the blocking correction, force tests were made on a series of rectangular "flat" plates, with 3, 4, 5, 6, and 7 inch chords, and of aspect ratio 6. The upstream surface of each plate was flat, while the downstream surface was pyramidal in form, beveled 15° from all edges. These flat plates were used instead of airfoils because they were more easily constructed, and answered the same purpose.

The force tests on these plates were made on the regular wire balance of the wind tunnel. (Reference 2.) Lift and drag data were obtained for angles of attack ranging from 20° to 90° , and the absolute coefficients (C_D and C_L) were then calculated. All tests were run at an average Reynolds Number of 153,000, the chord length being taken as the characteristic dimension.

RESULTS

The results of the force tests on the flat plates are given in Table XXIX, and as curves in Figures 57a and 58a. C_D was also plotted against the areas of the flat plates for the various angles of attack (Figure 54). These curves were extrapolated to zero area (as shown by the broken lines), to obtain C_D' the absolute free air coefficient.

From the curves (fig. 54) it can readily be seen that:

$$C_D' = KC_D \quad (1)$$

from which it follows that

$$K = \frac{C_D'}{C_D} \quad (2)$$

Values of K were calculated for the several plates at the various angles of attack by means of equation (2), and by data obtained from the curves. (Fig. 54.) It is apparent that K is a function of the area ratio (a/A), where a is the projected area of the model perpendicular to the air stream, and A is the cross-sectional area of the tunnel at the test section. Values of (a/A)

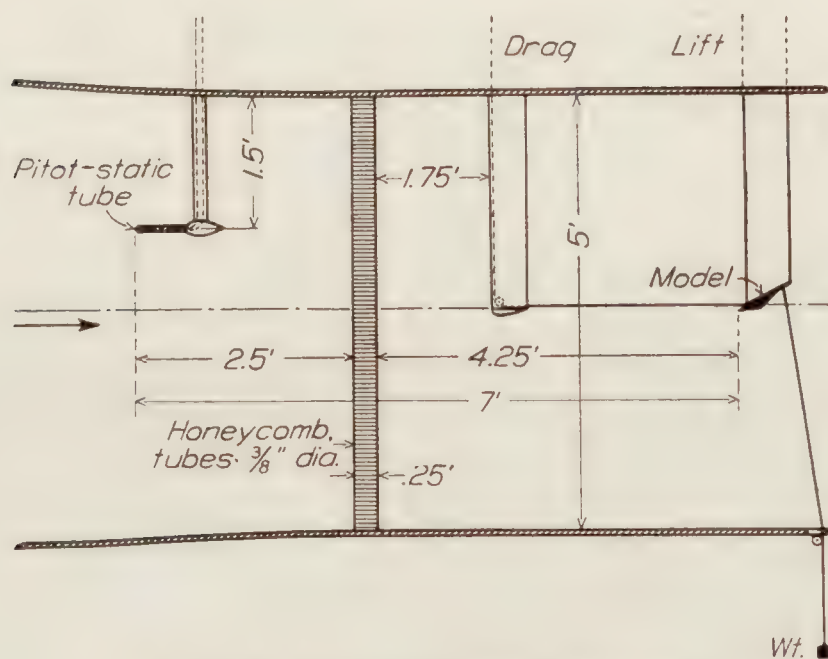


FIGURE 53.—Blocking tests. Wind tunnel set-up

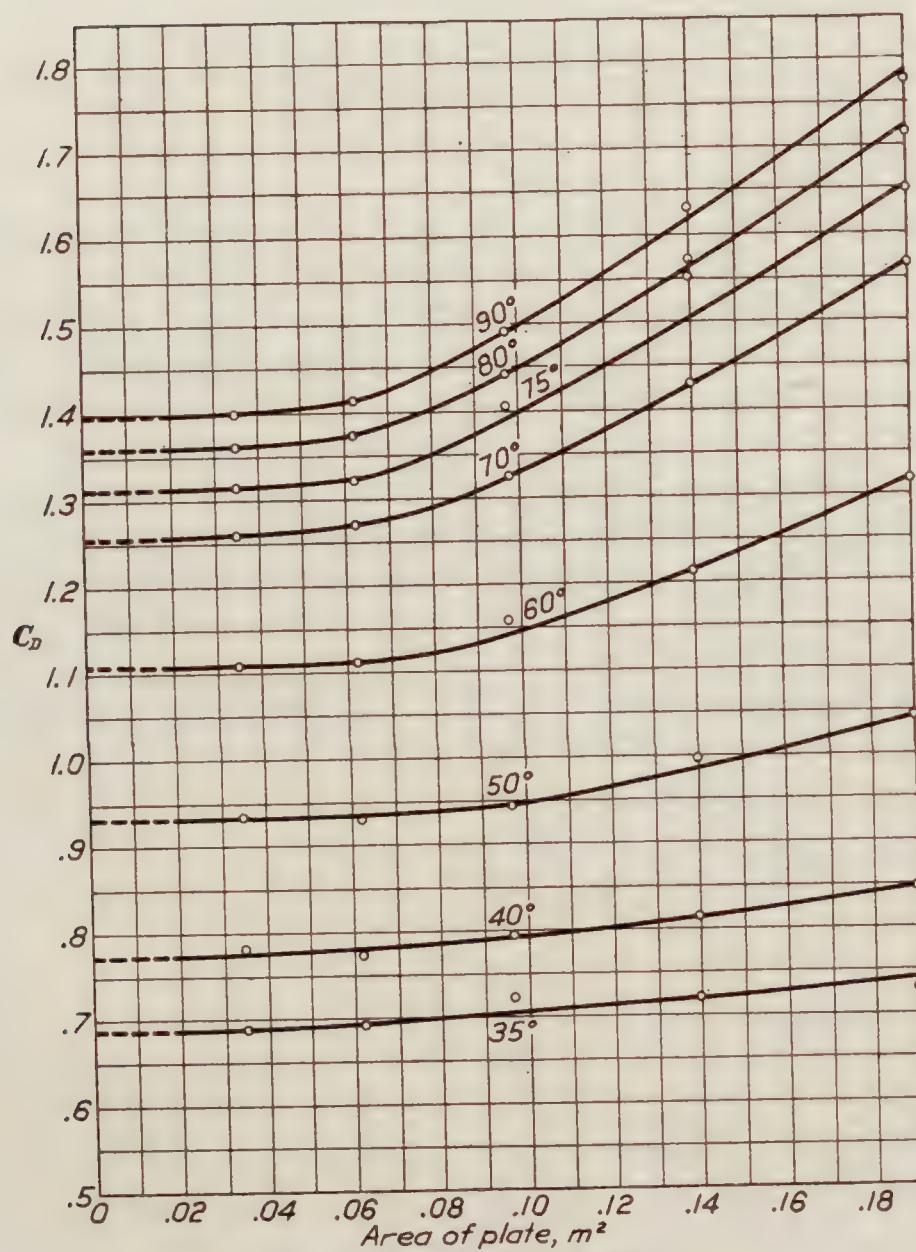


FIGURE 54.—Drag versus area of plate

with the corresponding values of K are given in Table XXVIII, and are plotted in logarithmic form in Figure 55. It was found that a straight line could be drawn through these points, with a maximum deviation of about 2 per cent.

From an analysis of this line it was found that:

$$K = 1 - 6.75 (a/A)^{2.4} \quad (3)$$

This equation was plotted on regular cross-section paper (Figure 56) to be used in finding corrections for C_D and C_L for any value of area ratio up to about 0.08. The area ratios of the 7-inch chord flat plate exceeded this value and the curve of the equation would not pass through these points. A broken line is, however, faired through them.

As (a/A) increases, q'' also increases while q' is kept constant. Therefore the lift and drag are both affected and the same correction applies to each. C_D was used for determining the blocking correction because as the angle of attack increases, C_D increases, while C_L decreases,

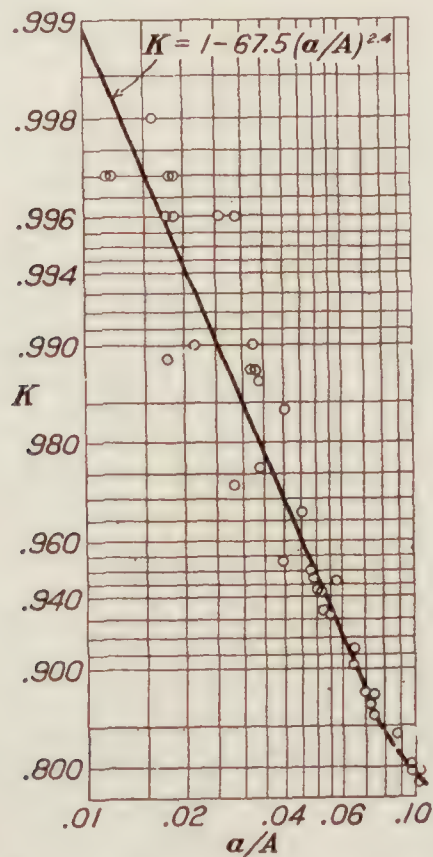


FIGURE 55.—Blocking correction versus area ratio (logarithmic)

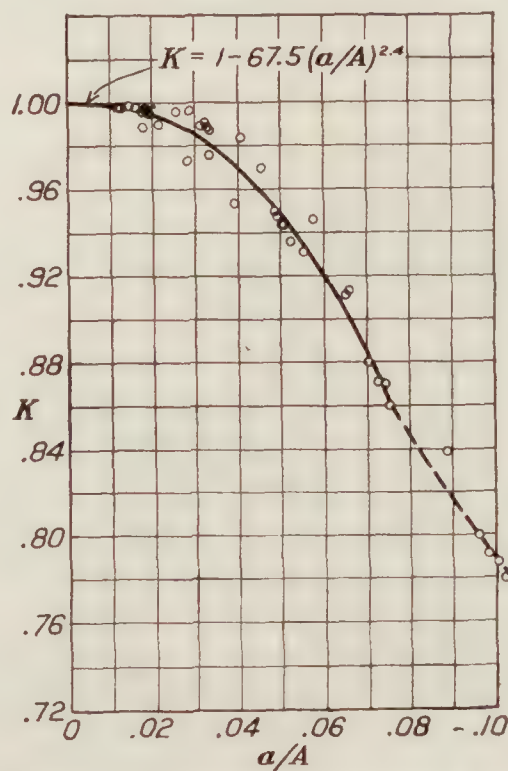


FIGURE 56.—Blocking correction versus area ratio

and for large angles of attack the experimental error becomes a larger percentage of the C_L results.

By use of equation (3) the flat plate data for chord lengths 3, 4, 5, and 6 inches were corrected. The values of C_D , C_L , C_D' , and C_L' are given in Table XXIX, and are plotted in Figures 57 a and b, and 58 a and b, as absolute coefficients vs. angle of attack, and as polars. The corrected points are within the experimental error of the force test results for the flat plates. The limit of (a/A) for the flat plate tests was about 0.10. This value is safely beyond any value of (a/A) used in the series of wing model tests.

To verify formula (3), the correction was applied to the data obtained from force tests on two circular tipped Clark Y airfoils, of aspect ratio 8, with 3 and 5 inch chords. These data are given in Table XXX and are plotted in Figures 59 a and b, and 60 a and b, as absolute coefficients vs. angle of attack, and as polars. The corrected values of C_D and C_L for the airfoils are, in general, within 1 per cent of the faired curves, which is within the experimental error of the force tests.

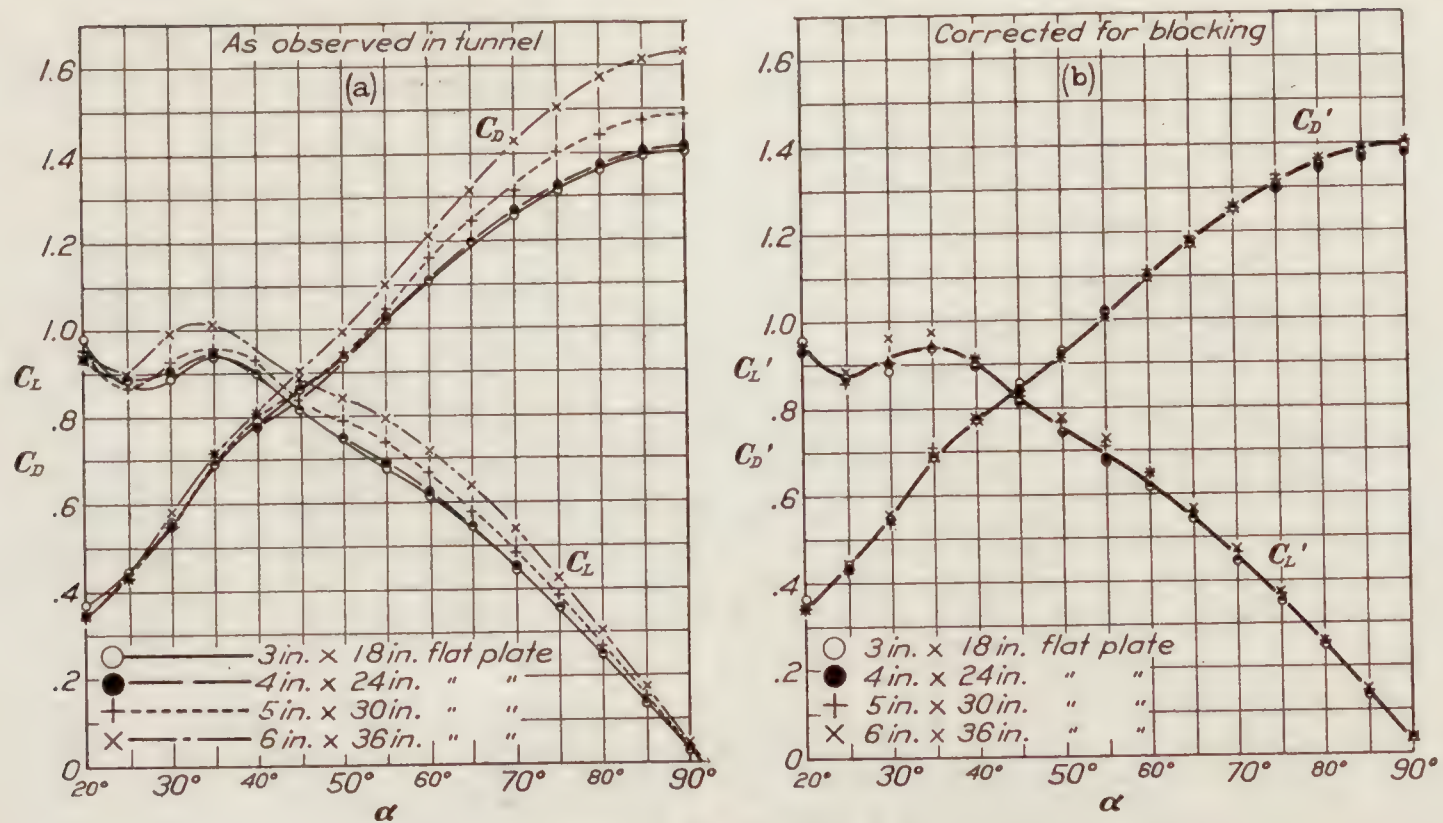


FIGURE 57.—Flat plates. A. R. 6

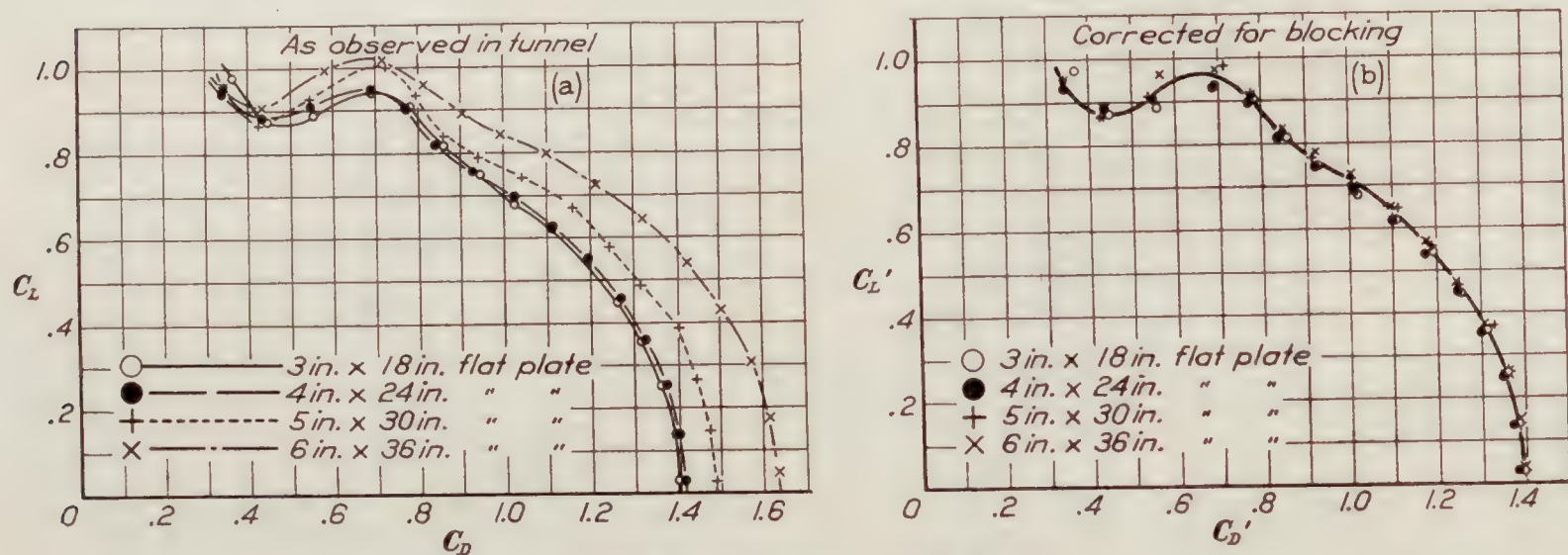


FIGURE 58.—Flat plates. A. R. 6. Polars

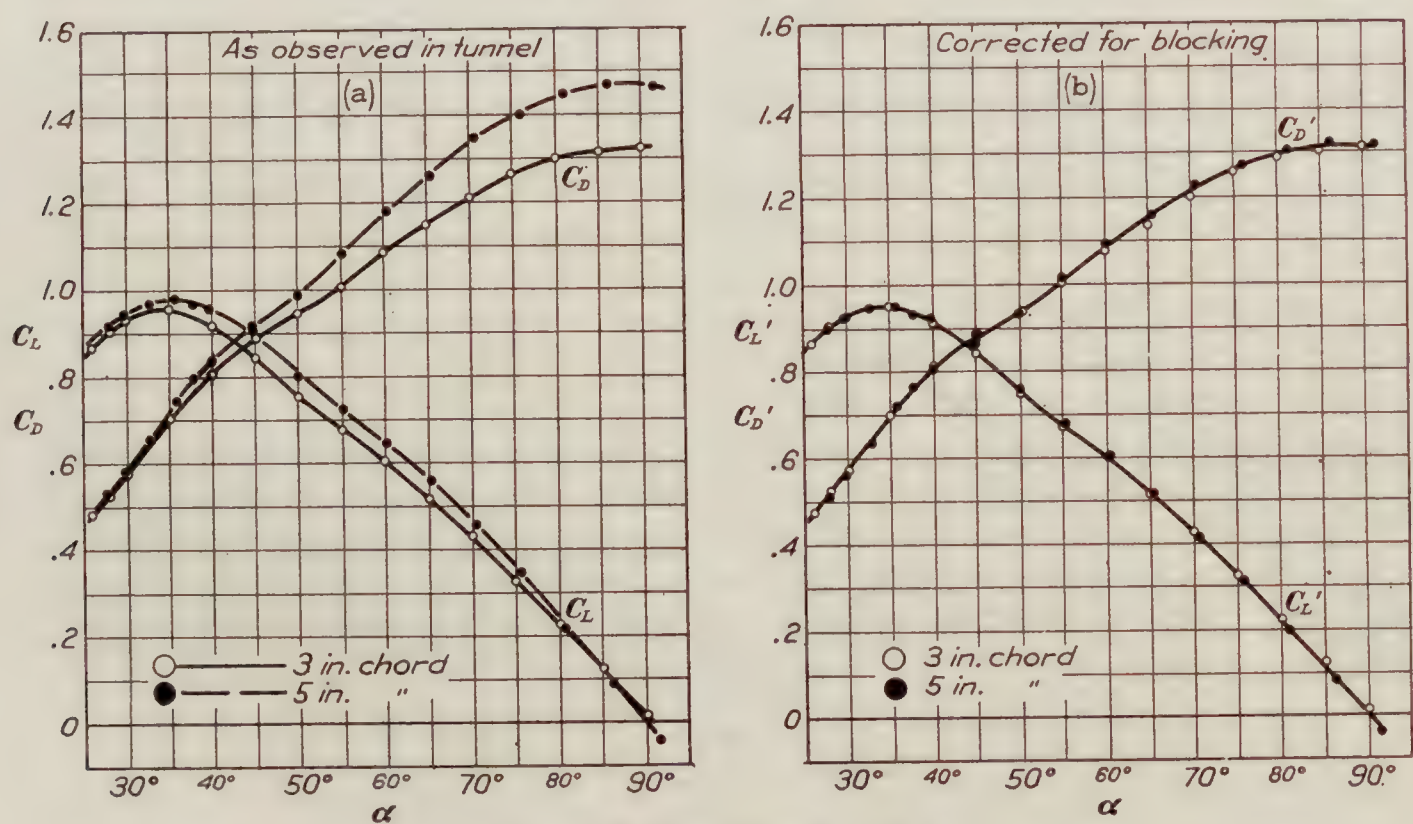


FIGURE 59.—Clark Y wings. A. R. 8

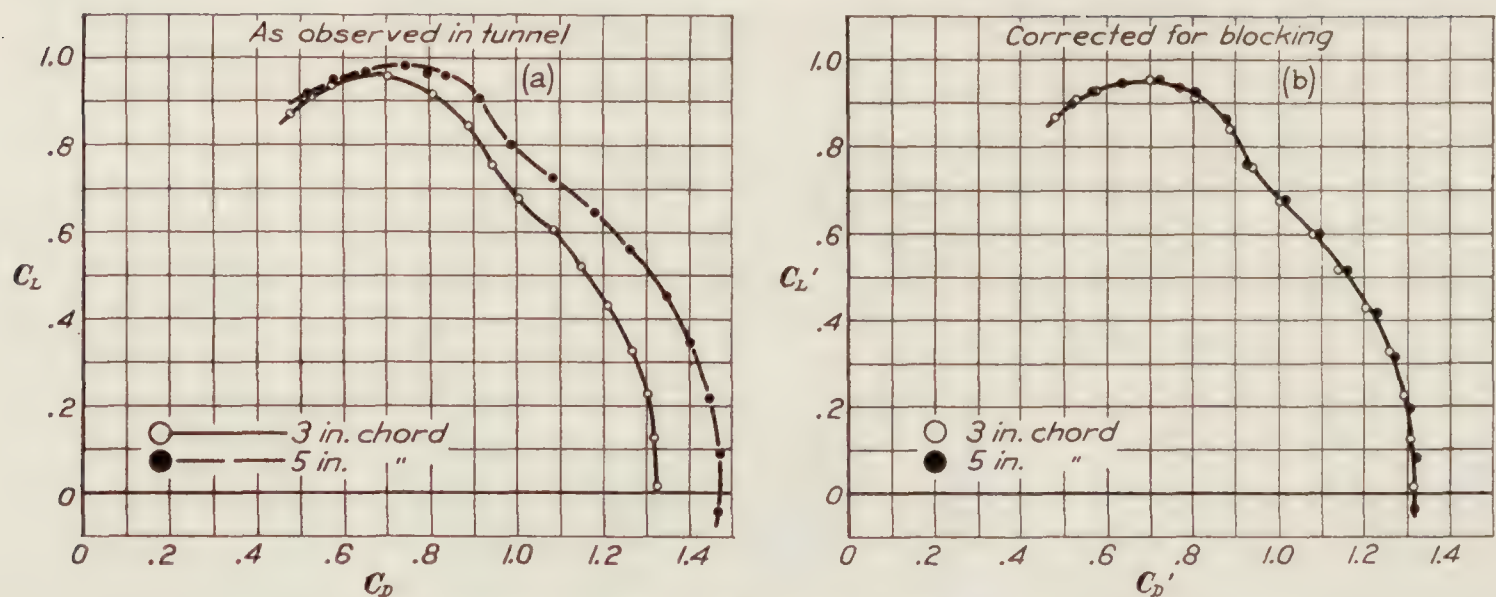


FIGURE 60.—Clark Y wings. A. R. 8. Polars

CONCLUSIONS

1. A blocking correction curve for monoplane test results has been obtained which applies to this wind tunnel for ratios of projected area of the model to cross-sectional area of the tunnel up to about 0.10.
2. Further research is necessary to obtain a similar correction for biplane test results at large angles of attack.
3. It is highly desirable that some means be devised for maintaining the dynamic pressure constant in the vicinity of the model, regardless of the change in angle of attack, above maximum lift.

TABLE III
CALCULATED PROBABLE RANGES OF ROTARY INSTABILITY

Model	Rotary instability								
	Normal spinning range			Flat spinning range			Inverted spinning range		
	α° limits		Range	α° limits		Range	α° limits		Range
	Lower	Upper		Lower	Upper		Lower	Upper	
<i>Monoplane</i>									
Rectangular tip	Degrees	Degrees	Degrees	Degrees	Degrees	Degrees	Degrees	Degrees	Degrees
Negative rake tip	14.5	24.5	10.0			0			0
Circular tip A. R.=6	15.0	26.0	11.0			0			0
Circular tip A. R.=4	14.5	24.0	9.5			0	-13.0	-16.0	3.0
Circular tip A. R.=8	17.5	26.0	8.5			0	-15.5	-21.0	5.5
Flap 15° up	13.5	24.0	10.5			0	0	0	0
Flap 15° down	17.0	26.0	9.0			0	-11.0	-16.5	5.5
Flap 25° down	13.0	20.0	7.0			0	-12.5	-22.0	9.5
Flap 30° down	12.0	20.0	8.0			0	-18.0	-20.0	2.0
N. A. C. A. M-1 A. R.=6	11.0	19.5	8.5			0	-32.0	-37.0	5.0
	12.0	14.5	2.5			0	-12.0	-14.5	2.5
<i>Biplane</i>									
Stagger-25%	15.0	24.0	9.0	33.5	60.0	26.5			0
Stagger 0%	16.0	26.0	10.0	40.0	74.0	34.0			0
Stagger +25%	16.0	24.0	8.0	55.0	90.0	35.0			0
Stagger +50%	15.0	24.0	9.0	62.0					0
Gap/chord 1.5	15.0	23.0	8.0	44.0	80.0	36.0			0
Gap/chord 0.5	17.0	24.0	7.0	30.0	64.0	34.0			0
Decalage +3°	14.5	24.0	9.5	37.0	75.0	38.0			0
Decalage -3°	18.0	29.0	11.0	42.0	73.0	31.0			0
Sweep back U. W. } 0% stagger ¹	16.0	24.5	8.5	35.0	62.5	27.5			0
Straight L. W. }									
Straight U. W. } 0% stagger ¹	16.0	23.5	7.5	50.0			-14.0	-17.0	3.0
Sweep back L. W. }									
Sweep back U. W. } +50% stagger ¹	16.0	27.0	11.0	55.0			-14.0	-17.0	3.0
Straight L. W. }									
Straight U. W. } -50% stagger ¹	16.0	24.5	8.5	35.0	67.5	32.5			0
Sweep back L. W. }									
Clark Y. U. W. }	15.0	22.0	7.0	45.0	71.0	26.0			0
N. A. C. A. M-1 L. W. }									
N. A. C. A. M-1 U. W. }	18.0	22.0	4.0	42.0	73.0	31.0			0
Clark Y. L. W. }									

¹ Stagger measured at midspan.

TABLE IV
FORCE TEST

Clark Y monoplane. 5-inch chord.
Aspect ratio=6. Rectangular tips.
 $q=19.86 \text{ kg/m}^2$
Reynolds No.=149,000.

α°	C_D	C_L	α°	C_D	C_L
-45	0.665	-0.638	17	0.218	1.130
-42	.618	-.651	18	.245	1.080
-39	.584	-.654	19	.286	.885
-36	.532	-.659	20	.321	.844
-33	.461	-.610	22	.362	.805
-30	.380	-.542	24	.397	.805
-27	.323	-.493	26	.441	.812
-24	.275	-.467	28	.485	.844
-21	.232	-.426	30	.552	.870
-18	.186	-.392	32	.600	.880
-15	.153	-.384	34	.630	.886
-14	.139	-.378	37	.693	.880
-13	.126	-.371	40	.749	.842
-12	.110	-.371	45	.811	.780
-9	.037	-.301	50	.894	.733
-6	.019	-.018	55	.983	.681
-3	.018	+.188	60	1.065	.614
0	.022	.412	65	1.170	.525
+3	.035	.630	70	1.260	.431
6	.052	.844	75	1.310	.322
9	.081	1.030	80	1.345	.203
12	.105	1.180	85	1.357	.078
15	.156	1.220	90	1.367	.000
16	.198	1.160			

TABLE V
FORCE TEST

Clark Y monoplane. 5-inch chord.
Aspect ratio=6. Negative rake tips.
 $q=19.92 \text{ kg/m}^2$
Reynolds No.=149,000.

α°	C_D	C_L	α°	C_D	C_L
-45	0.643	-0.589	16	0.159	1.184
-42	.574	-.593	17	.216	1.118
-39	.531	-.604	18	.254	1.067
-36	.496	-.628	19	.306	.893
-33	.436	-.577	20	.319	.838
-30	.362	-.526	22	.362	.800
-27	.311	-.479	24	.391	.769
-24	.265	-.441	26	.428	.775
-21	.227	-.423	28	.477	.794
-18	.195	-.429	30	.531	.833
-15	.157	-.426	33	.615	.857
-14	.145	-.421	36	.658	.818
-13	.130	-.415	40	.716	.796
-12	.110	-.403	45	.808	.753
-9	.032	-.254	50	.908	.715
-6	.018	-.047	55	1.005	.670
-3	.019	+.139	60	1.092	.597
0	.023	.366	65	1.172	.515
+3	.035	.566	70	1.237	.422
6	.051	.785	75	1.283	.322
9	.073	.988	80	1.315	.214
12	.099	1.130	85	1.332	+.091
15	.142	1.181	90	1.340	-.018

TABLE VI
FORCE TEST

Clark Y monoplane. 5-inch chord.
Aspect ratio=6. Circular tips.
 $q=19.90 \text{ kg/m}^2$
Reynolds No.=151,000.

α°	C_D	C_L	α°	C_D	C_L
-45	0.646	-0.626	17	0.188	1.130
-42	.611	-.648	18	.246	1.053
-39	.564	-.639	19	.291	.985
-36	.511	-.637	20	.322	.869
-33	.434	-.593	22	.356	.803
-30	.369	-.522	24	.376	.794
-27	.307	-.466	26	.426	.781
-24	.262	-.438	28	.482	.823
-21	.224	-.402	30	.552	.874
-18	.187	-.383	33	.619	.906
-15	.153	-.391	36	.688	.872
-14	.141	-.402	38	.711	.841
-13	.125	-.408	40	.733	.815
-12	.108	-.397	45	.808	.769
-9	.032	-.240	50	.904	.722
-6	.021	-.019	55	1.000	.675
-3	.017	+.176	60	1.090	.608
0	.021	.398	65	1.170	.524
+3	.034	.614	70	1.240	.435
6	.050	.813	75	1.290	.321
9	.073	1.012	80	1.330	.215
12	.101	1.148	85	1.360	+.098
15	.149	1.172	90	1.360	-.017
16	.169	1.154			

TABLE VII
FORCE TEST

Clark Y monoplane. 5-inch chord.
Aspect ratio=4. Circular tips.
 $q=19.94 \text{ kg/m}^2$
Reynolds No.=151,000.

α°	C_D	C_L	α°	C_D	C_L
-45	0.576	-0.549	16	0.166	1.157
-42	.523	-.541	17	.189	1.157
-39	.475	-.523	18	.203	1.149
-36	.427	-.506	19	.222	1.117
-33	.381	-.479	20	.287	1.000
-30	.336	-.458	22	.345	.852
-27	.288	-.427	24	.373	.769
-24	.248	-.392	26	.396	.743
-21	.214	-.371	28	.426	.743
-18	.202	-.410	30	.458	.735
-15	.160	-.449	33	.509	.735
-14	.142	-.445	36	.561	.739
-13	.123	-.422	40	.642	.733
-12	.099	-.384	45	.744	.712
-9	.031	-.204	50	.846	.673
-6	.019	-.048	55	.933	.611
-3	.017	+.135	60	1.020	.551
0	.021	.328	65	1.096	.473
+3	.037	.513	70	1.155	.378
6	.056	.696	75	1.201	.279
9	.082	.870	80	1.240	.161
12	.112	1.035	85	1.249	+.061
15	.144	1.142	90	1.246	-.057

TABLE VIII
FORCE TEST

Clark Y monoplane. 5-inch chord.
Aspect ratio=8. Circular tips.
 $q=19.94 \text{ kg/m}^2$
Reynolds No. =153,000.

α°	C_D	C_L	α°	C_D	C_L
-45	0.750	-0.740	17	0.205	1.098
-42	.681	-.752	18	.245	1.050
-39	.620	-.737	19	.300	.935
-36	.558	-.719	20	.321	.866
-33	.487	-.678	22	.365	.840
-30	.414	-.616	24	.400	.816
-27	.339	-.542	26	.457	.875
-24	.287	-.491	28	.528	.914
-21	.238	-.448	30	.578	.946
-18	.195	-.407	33	.654	.968
-15	.155	-.394	36	.742	.980
-14	.145	-.400	38	.795	.965
-13	.130	-.405	40	.838	.959
-12	.114	-.405	45	.916	.906
-9	.032	-.269	50	.986	.800
-6	.018	-.029	55	1.081	.723
-3	.017	+.171	60	1.180	.646
0	.019	.420	65	1.260	.560
+3	.028	.655	70	1.348	.453
6	.041	.883	75	1.400	.344
9	.061	1.075	80	1.446	.216
12	.086	1.192	85	1.470	+.089
15	.148	1.137	90	1.465	-.043
16	.172	1.128			

TABLE IX
FORCE TEST

Clark Y monoplane. 5-inch chord.
Aspect ratio=6. Circular tips.
Flap 20 per cent chord. 15° up.
 $q=19.87 \text{ kg/m}^2$
Reynolds No.=151,000.

α°	C_D	C_L	α°	C_D	C_L
-44	0.738	-0.716	16	0.084	0.854
-41	.706	-.759	17	.101	.866
-38	.672	-.784	18	.118	.859
-35	.627	-.815	19	.164	.782
-32	.574	-.824	20	.187	.742
-29	.501	-.778	22	.252	.605
-26	.422	-.736	24	.284	.555
-23	.355	-.672	26	.305	.524
-20	.301	-.629	28	.336	.538
-17	.260	-.615	30	.369	.568
-14	.221	-.646	33	.450	.622
-13	.208	-.660	36	.525	.658
-12	.193	-.677	40	.617	.679
-11	.174	-.694	45	.686	.631
-8	.110	-.666	50	.756	.606
-5	.045	-.497	55	.842	.578
-3	.035	-.364	60	.939	.533
0	.028	-.182	65	1.033	.485
+3	.027	+.132	70	1.108	.413
6	.029	.345	75	1.171	.326
9	.041	.549	80	1.228	.242
12	.056	.723	85	1.257	.138
15	.072	.835	90	1.265	.037

TABLE X
FORCE TEST

Clark Y monoplane. 5-inch chord.
Aspect ratio=6. Circular tips.
Flap 20% chord. 15° down.
 $q=19.86 \text{ kg/m}^2$
Reynolds No.=153,000.

α°	C_D	C_L	α°	C_D	C_L
-44	0.520	-0.427	16	0.288	1.280
-41	.471	-.385	17	.321	1.218
-38	.418	-.354	18	.343	1.150
-35	.366	-.320	19	.389	.977
-32	.317	-.267	20	.407	.959
-29	.270	-.216	22	.446	.954
-26	.234	-.197	24	.491	.965
-23	.206	-.171	26	.554	.993
-20	.187	-.194	28	.616	1.032
-17	.170	-.258	30	.666	1.032
-14	.142	-.295	33	.718	.988
-13	.132	-.317	36	.761	.932
-12	.117	-.329	40	.823	.855
-11	.101	-.302	45	.912	.793
-8	.039	+.076	50	.998	.732
-5	.044	.323	55	1.082	.670
-3	.053	.488	60	1.169	.580
0	.067	.783	65	1.231	.476
+3	.081	.977	70	1.289	.383
6	.106	1.136	75	1.320	.273
9	.131	1.305	80	1.336	.146
12	.168	1.400	85	1.350	+.031
15	.235	1.370	90	1.334	-.090

TABLE XI
FORCE TEST

Clark Y monoplane. 5-inch chord.
Aspect ratio=6. Circular tips.
Flap 20% chord. 25° down.
 $q=19.85 \text{ kg/m}^2$
Reynolds No.=153,000.

α°	C_D	C_L	α°	C_D	C_L
-44	0.448	-0.266	17	0.371	1.160
-41	.404	-.268	18	.422	.986
-38	.383	-.282	19	.446	.973
-35	.378	-.352	20	.466	.955
-32	.357	-.391	22	.529	.966
-29	.312	-.394	24	.586	1.000
-26	.279	-.391	26	.649	1.005
-23	.243	-.386	28	.695	.995
-20	.211	-.386	30	.734	.977
-17	.178	-.405	33	.773	.950
-14	.139	-.358	36	.800	.921
-13	.121	-.316	38	.829	.899
-12	.107	-.260	40	.845	.874
-11	.083	-.120	45	.945	.800
-8	.056	+.299	50	1.042	.727
-5	.066	.515	55	1.122	.655
-3	.078	.664	60	1.183	.565
0	.091	.855	65	1.245	.461
+3	.111	1.018	70	1.289	.360
6	.137	1.190	75	1.341	.236
9	.166	1.396	80	1.352	+.112
12	.212	1.450	85	1.342	-.008
15	.320	1.264	90	1.329	-.129
16	.354	1.190			

TABLE XII
FORCE TEST

Clark, Y monoplane. 5-inch chord.
Aspect ratio=6. Circular tips.
Flap 20% chord. 30° down.
 $q=19.85 \text{ kg/m}^2$
Reynolds No.=152,000.

α°	C_D	C_L	α°	C_D	C_L
-44	0.500	-0.348	16	0.384	1.301
-41	.471	-.362	17	.425	1.095
-38	.450	-.376	18	.450	1.049
-35	.411	-.416	19	.475	1.040
-32	.394	-.466	20	.496	1.022
-29	.342	-.455	22	.548	1.049
-26	.296	-.429	24	.614	1.090
-23	.255	-.421	26	.673	1.096
-20	.223	-.426	28	.713	1.079
-17	.190	-.432	30	.741	1.057
-14	.142	-.381	33	.793	.983
-13	.130	-.328	36	.817	.916
-12	.113	-.278	40	.884	.853
-11	.101	-.177	45	.979	.795
-8	.067	+.345	50	1.063	.721
-5	.075	.553	55	1.139	.651
-3	.092	.680	60	1.210	.545
0	.110	.919	65	1.262	.444
+3	.129	1.112	70	1.310	.329
6	.159	1.307	75	1.330	.213
9	.189	1.483	80	1.351	+.093
12	.237	1.498	85	1.338	-.031
15	.346	1.377	90	1.313	-.124

TABLE XIII
FORCE TEST

N. A. C. A.-M1 monoplane. 5-inch chord.
Aspect ratio=6. Circular tips.
 $q=19.95 \text{ kg/m}^2$
Reynolds No.=153,000.

α°	C_D	C_L	α°	C_D	C_L
-42	0.727	-0.820	16	0.212	0.699
-36	.636	-.871	17	.229	.702
-33	.570	-.863	18	.245	.705
-30	.485	-.820	19	.260	.699
-28	.428	-.774	20	.271	.693
-26	.374	-.729	22	.300	.702
-24	.332	-.713	24	.332	.713
-22	.300	-.702	26	.374	.729
-20	.271	-.693	28	.428	.774
-19	.260	-.699	30	.485	.820
-18	.245	-.705	33	.570	.863
-17	.229	-.702	36	.636	.871
-16	.212	-.699	42	.727	.820
-15	.196	-.704	45	.770	.765
-12	.149	-.721	50	.854	.716
-9	.074	-.610	55	.950	.675
-6	.032	-.398	60	1.049	.622
-3	.015	-.189	65	1.129	.551
0	.012	-.003	70	1.218	.474
+3	.015	+.189	75	1.289	.371
6	.032	.398	80	1.340	.273
9	.074	.610	85	1.378	.156
12	.149	.721	90	1.367	.045
15	.196	.704			

TABLE XIV

FORCE TEST

Clark Y biplane. 5-inch chord.
 Aspect ratio=6. Circular tips.
 Stagger=-25 per cent chord. $G/c=1.0$
 Decalage= 0° . $q=19.92 \text{ kg/m}^2$
 Reynolds No.=152,000.

α°	C_D	C_L	α°	C_D	C_L
-40	0.542	-0.542	15	0.138	1.090
-36	.470	-.529	16	.164	1.075
-33	.417	-.509	18	.211	1.006
-30	.367	-.484	20	.288	.879
-27	.318	-.453	22	.336	.771
-24	.272	-.425	24	.369	.743
-21	.231	-.398	26	.433	.742
-18	.199	-.395	28	.470	.745
-15	.157	-.381	30	.484	.757
-14	.142	-.372	35	.581	.740
-13	.123	-.357	40	.615	.655
-12	.103	-.338	45	.610	.550
-9	.036	-.184	50	.603	.450
-6	.024	-.022	55	.561	.350
-3	.023	+.150	60	.527	.286
0	.028	.333	65	.555	.247
+3	.040	.514	70	.606	.199
6	.058	.695	75	.633	.145
9	.079	.860	80	.652	.086
12	.106	.999	85	.658	+.029
14	.128	1.083	90	.657	-.035

TABLE XV

FORCE TEST

Clark Y biplane. 5-inch chord.
 Aspect ratio=6. Circular tips.
 Stagger=0. $G/c=1.0$.
 Decalage= 0° . $q=19.94 \text{ kg/m}^2$
 Reynolds No.=151,000.

α°	C_D	C_L	α°	C_D	C_L
-39	0.495	-0.489	18	0.210	1.068
-36	.449	-.482	19	.249	1.027
-33	.400	-.465	20	.286	.971
-30	.343	-.441	22	.352	.821
-27	.302	-.409	24	.393	.801
-24	.270	-.384	26	.424	.776
-21	.226	-.369	28	.463	.777
-18	.196	-.362	30	.505	.786
-15	.152	-.359	33	.559	.785
-14	.137	-.356	36	.610	.765
-13	.116	-.341	38	.633	.736
-12	.098	-.324	40	.664	.709
-9	.035	-.176	45	.726	.657
-6	.025	-.017	50	.764	.584
-3	.025	+.154	55	.791	.521
0	.029	.335	60	.773	.400
+3	.042	.523	65	.704	.287
6	.059	.689	70	.624	.193
9	.082	.863	75	.634	.145
12	.108	1.009	80	.660	.090
15	.135	1.103	85	.668	+.031
16	.145	1.135	90	.664	-.032
17	.163	1.121			

TABLE XVI
FORCE TEST

Clark Y biplane. 5-inch chord.
Aspect ratio=6. Circular tips.
Stagger=+25 per cent chord. $G/c=1.0$.
Decalage=0°. $q=19.88 \text{ kg/m}^2$
Reynolds No.=151,000.

α°	C_D	C_L	α°	C_D	C_L
-45	0.509	-0.402	16	0.157	1.156
-42	.500	-.440	17	.172	1.153
-39	.474	-.460	18	.219	1.091
-36	.424	-.454	19	.238	1.078
-33	.369	-.428	20	.256	1.048
-30	.325	-.404	22	.335	.934
-27	.284	-.377	24	.411	.875
-24	.244	-.348	26	.456	.857
-21	.215	-.338	28	.491	.829
-18	.180	-.336	30	.526	.837
-15	.145	-.336	35	.640	.842
-14	.124	-.337	40	.735	.809
-13	.112	-.329	45	.819	.764
-12	.091	-.310	50	.890	.689
-9	.031	-.157	55	.962	.616
-6	.021	+.027	60	.995	.525
-3	.023	.167	65	.999	.419
0	.028	.356	70	.958	.306
+3	.047	.542	75	.877	.190
6	.059	.725	80	.736	.086
9	.082	.862	85	.686	+.025
12	.109	1.050	90	.677	-.031
15	.143	1.153			

TABLE XVII
FORCE TEST

Clark Y biplane. 5-inch chord.
Aspect ratio=6. Circular tips.
Stagger=+50 per cent chord. $G/c=1.0$.
Decalage=0°. $q=19.94 \text{ kg/m}^2$
Reynolds No.=153,000.

α°	C_D	C_L	α°	C_D	C_L
-42	0.408	-0.377	15	0.169	1.156
-39	.394	-.413	16	.215	1.104
-36	.365	-.420	17	.234	1.094
-33	.325	-.404	18	.250	1.076
-30	.285	-.380	20	.304	1.008
-27	.252	-.355	22	.372	.947
-24	.219	-.341	24	.458	.914
-21	.188	-.328	26	.495	.879
-18	.156	-.327	28	.527	.857
-17	.141	-.330	30	.571	.862
-16	.136	-.331	35	.692	.865
-15	.126	-.327	40	.786	.841
-12	.071	-.299	45	.882	.791
-9	.033	-.134	50	.966	.737
-6	.021	+.039	55	1.048	.670
-3	.019	.220	60	1.122	.586
0	.027	.420	65	1.165	.477
+3	.047	.608	70	1.176	.364
6	.068	.790	75	1.146	.247
9	.094	.936	80	1.087	.158
12	.125	1.104	85	1.007	+.052
13	.138	1.131	90	.846	-.035
14	.155	1.150			

TABLE XVIII

FORCE TEST

Clark Y biplane. 5-inch chord.
 Aspect ratio=6. Circular tips.
 Stagger=0. $G/c=1.5$.
 Decalage=0°. $q=19.94 \text{ kg/m}^2$
 Reynolds No.=152,000.

α°	C_D	C_L	α°	C_D	C_L
-45	0.651	-0.582	13	0.122	1.106
-42	.586	-.574	14	.135	1.130
-39	.523	-.551	15	.149	1.135
-36	.467	-.529	16	.167	1.116
-33	.407	-.504	17	.184	1.107
-30	.351	-.473	18	.243	1.044
-27	.303	-.430	21	.342	.832
-24	.259	-.400	24	.403	.778
-21	.219	-.377	27	.460	.790
-18	.184	-.362	30	.516	.792
-15	.147	-.361	35	.636	.818
-14	.133	-.359	40	.741	.831
-13	.110	-.354	45	.826	.764
-12	.097	-.338	50	.879	.684
-9	.032	-.212	55	.924	.596
-6	.024	-.022	60	.930	.488
-3	.024	+.217	65	.866	.346
0	.030	.370	70	.741	.218
+3	.044	.559	75	.609	.134
6	.063	.750	80	.597	.089
9	.088	.924	85	.628	+.038
12	.116	1.073	90	.624	-.021

TABLE XIX

FORCE TEST

Clark Y biplane. 5-inch chord.
 Aspect ratio=6. Circular tips.
 Stagger=0. $G/c=0.5$.
 Decalage=0°. $q=19.95 \text{ kg/m}^2$
 Reynolds No.=153,000.

α°	C_D	C_L	α°	C_D	C_L
-45	0.456	-0.345	16	0.135	1.004
-42	.435	-.363	17	.153	1.010
-39	.413	-.366	18	.172	.999
-36	.393	-.408	19	.199	.971
-33	.367	-.422	20	.221	.951
-30	.328	-.410	22	.273	.851
-27	.277	-.390	24	.330	.811
-24	.236	-.370	26	.386	.811
-21	.194	-.353	28	.443	.802
-18	.157	-.342	30	.483	.794
-15	.113	-.311	35	.528	.688
-14	.099	-.304	40	.548	.587
-13	.085	-.289	45	.582	.516
-12	.069	-.263	50	.604	.453
-9	.031	-.136	55	.610	.379
-6	.024	+.003	60	.583	.303
-3	.024	.148	65	.594	.259
0	.029	.303	70	.629	.209
+3	.040	.460	75	.654	.156
6	.055	.610	80	.673	.102
9	.075	.760	85	.676	.049
12	.099	.903	90	.679	.020
15	.124	.995			

TABLE XX

FORCE TEST

Clark Y biplane. 5-inch chord.
 Aspect ratio=6. Circular tips.
 Stagger=0. $G/c=1.0$.
 Decalage=+3°. $q=19.94 \text{ kg/m}^2$
 Reynolds No.=153,000.

α°	C_D	C_L	α°	C_D	C_L
-45	0.547	-0.463	14	0.142	1.096
-40	.474	-.472	15	.177	1.082
-35	.398	-.446	18	.287	.926
-30	.319	-.402	21	.365	.823
-27	.276	-.380	24	.417	.766
-24	.240	-.363	27	.475	.763
-21	.202	-.356	30	.530	.776
-18	.167	-.345	35	.626	.754
-15	.122	-.335	40	.690	.692
-14	.102	-.315	45	.746	.630
-13	.079	-.282	50	.786	.555
-12	.062	-.244	55	.800	.458
-9	.028	-.067	60	.780	.357
-6	.026	+.054	65	.701	.241
-3	.027	.233	70	.629	.169
0	.036	.405	75	.638	.107
+3	.050	.594	80	.660	+.053
6	.071	.767	85	.664	-.013
9	.095	.920	90	.652	-.074
12	0.122	1.051			

TABLE XXI

FORCE TEST

Clark Y biplane. 5-inch chord.
 Aspect ratio=6. Circular tips.
 Stagger=0. $G/c=1.0$.
 Decalage=-3°. $q=20.03 \text{ kg/m}^2$
 Reynolds No.=154,000.

α°	C_D	C_L	α°	C_D	C_L
-45	0.574	-0.485	16	0.136	1.077
-40	.506	-.496	17	.150	1.096
-35	.440	-.479	18	.164	1.100
-30	.361	-.449	19	.177	1.089
-27	.314	-.424	20	.199	1.002
-24	.271	-.390	21	.248	.936
-21	.233	-.378	24	.352	.847
-18	.199	-.375	27	.422	.787
-15	.158	-.365	30	.464	.772
-14	.143	-.345	35	.562	.775
-13	.125	-.323	40	.630	.721
-12	.106	-.302	45	.693	.669
-9	.067	-.212	50	.735	.603
-6	.029	-.059	55	.756	.521
-3	.024	+.072	60	.745	.426
0	.026	.252	65	.692	.318
+3	.036	.437	70	.595	.236
6	.051	.613	75	.606	.185
9	.072	.782	80	.642	.126
12	.096	.937	85	.660	.067
15	.124	1.054	90	.658	.006

TABLE XXII

FORCE TEST

Clark Y biplane. 5-inch chord.
 Upper wing—swept back. Circular tips.
 Lower wing—straight. Aspect ratio=6.
 Midspan stagger=0. $G/c=1.0$.
 Decalage=0°. $q=20.02 \text{ kg/m}^2$
 Reynolds No.=154,000.

α°	C_D	C_L	α°	C_D	C_L
-45	0. 657	-0. 538	15	0. 135	1. 095
-40	. 569	-. 549	16	. 148	1. 108
-35	. 482	-. 536	17	. 167	1. 091
-30	. 395	-. 508	18	. 205	1. 048
-27	. 340	-. 469	21	. 316	. 804
-24	. 285	-. 422	24	. 361	. 723
-21	. 242	-. 395	27	. 400	. 709
-18	. 206	-. 383	30	. 459	. 719
-15	. 170	-. 384	35	. 540	. 716
-14	. 154	-. 388	40	. 592	. 658
-13	. 137	-. 388	45	. 623	. 568
-12	. 119	-. 377	50	. 624	. 470
-9	. 038	-. 207	55	. 588	. 376
-6	. 024	-. 008	60	. 558	. 292
-3	. 023	+. 135	65	. 571	. 247
0	. 028	. 312	70	. 606	. 208
+3	. 040	. 500	75	. 636	. 161
6	. 057	. 673	80	. 655	. 093
9	. 079	. 892	85	. 669	+. 030
12	. 105	. 998	90	. 684	-. 032
14	. 123	1. 067			

TABLE XXIII

FORCE TEST

Clark Y biplane. 5-inch chord.
 Upper wing—straight. Circular tips.
 Lower wing—swept back. Aspect ratio=6.
 Midspan stagger=0. $G/c=1.0$.
 Decalage=0°. $q=19.93 \text{ kg/m}^2$.
 Reynolds No.=152,000.

α°	C_D	C_L	α°	C_D	C_L
-45	0. 510	-0. 434	15	0. 154	1. 141
-40	. 473	-. 476	16	. 168	1. 145
-35	. 413	-. 478	17	. 184	1. 133
-30	. 333	-. 433	18	. 201	1. 116
-27	. 287	-. 402	19	. 258	1. 041
-24	. 246	-. 372	21	. 343	. 908
-21	. 209	-. 347	24	. 435	. 816
-18	. 177	-. 341	27	. 496	. 813
-15	. 142	-. 354	30	. 554	. 810
-14	. 129	-. 359	35	. 654	. 799
-13	. 113	-. 358	40	. 742	. 770
-12	. 090	-. 327	45	. 804	. 738
-9	. 031	-. 146	50	. 864	. 667
-6	. 023	+. 004	55	. 913	. 589
-3	. 023	. 155	60	. 948	. 495
0	. 030	. 360	65	. 942	. 387
+3	. 043	. 552	70	. 886	. 275
6	. 069	. 735	75	. 816	. 176
9	. 089	. 905	80	. 727	. 088
12	. 118	1. 061	85	. 677	+. 022
13	. 128	1. 108	90	. 653	-. 036
14	. 140	1. 133			

TABLE XXIV

FORCE TEST

Clark Y biplane. 5-inch chord.
 Upper wing—swept back. Circular tips.
 Lower wing—straight. Aspect ratio=6.
 Midspan stagger=+50 per cent chord $G/c=1.0$
 Decalage= 0° . $q=20.00$ kg/m²
 Reynolds No.=155,000.

α°	C_D	C_L	α°	C_D	C_L
-45	0.497	-0.377	15	0.143	1.162
-40	.486	-.448	16	.153	1.177
-35	.420	-.450	17	.168	1.171
-30	.337	-.406	18	.184	1.152
-27	.293	-.377	19	.239	1.046
-24	.250	-.349	21	.290	.952
-21	.215	-.328	24	.409	.873
-18	.181	-.317	27	.468	.820
-15	.150	-.335	30	.526	.825
-14	.138	-.343	35	.631	.831
-13	.123	-.355	40	.713	.796
-12	.104	-.345	45	.808	.741
-9	.037	-.192	50	.880	.680
-6	.024	-.033	55	.945	.608
-3	.023	+.150	60	.988	.515
0	.028	.343	65	.988	.411
+3	.040	.532	70	.951	.303
6	.060	.709	75	.896	.195
9	.084	.876	80	.837	.109
12	.111	1.042	85	.733	+.022
14	.133	1.135	90	.667	-.032

TABLE XXV

FORCE TEST

Clark Y biplane. 5-inch chord.
 Upper wing—straight. Circular tips.
 Lower wing—swept back. Aspect ratio=6.
 Midspan stagger=-50% chord $G/c=1.0$
 Decalage= 0° . $q=20.00$ kg/m²
 Reynolds No.=154,000.

α°	C_D	C_L	α°	C_D	C_L
-45	0.629	-0.552	15	0.140	1.113
-40	.555	-.564	16	.155	1.124
-35	.473	-.554	17	.196	1.010
-30	.388	-.520	18	.233	.924
-27	.330	-.474	21	.332	.782
-24	.279	-.432	24	.379	.709
-21	.238	-.405	27	.428	.706
-18	.201	-.391	30	.498	.731
-15	.161	-.391	35	.600	.738
-14	.145	-.386	40	.614	.644
-13	.129	-.381	45	.583	.501
-12	.108	-.343	50	.569	.427
-9	.038	-.196	55	.571	.389
-6	.024	-.060	60	.576	.292
-3	.023	+.129	67.5	.576	.231
0	.028	.314	72.5	.612	.176
+3	.038	.507	77.5	.638	.118
6	.059	.700	82.5	.654	+.058
9	.083	.866	87.5	.670	-.007
12	.110	1.021	92.5	.729	-.072
14	.130	1.099			

TABLE XXVI

FORCE TEST

Biplane. 5-inch chord.
 Upper wing—Clark Y. Circular tips.
 Lower wing—N. A. C. A.-M1. Aspect ratio=6.
 Stagger=0. $G/c=1.0$.
 Decalage=0°. $q=19.92 \text{ kg/m}^2$
 Reynolds No.=152,000.

α°	C_D	C_L	α°	C_D	C_L
-45	0.612	-0.579	15	0.168	0.917
-40	.560	-.625	16	.181	.914
-35	.481	-.634	17	.193	.899
-30	.388	-.593	18	.242	.847
-27	.330	-.559	21	.305	.734
-24	.284	-.529	24	.354	.714
-21	.244	-.509	27	.410	.727
-18	.207	-.522	30	.462	.744
-15	.169	-.522	35	.551	.738
-14	.151	-.518	40	.614	.700
-13	.134	-.506	45	.682	.639
-12	.112	-.488	50	.726	.558
-9	.050	-.339	55	.738	.488
-6	.027	-.163	60	.728	.393
-3	.020	-.017	65	.670	.294
0	.020	+.185	70	.593	.218
+3	.030	.371	75	.611	.178
6	.045	.539	80	.654	.119
9	.073	.715	85	.666	.059
12	.121	.880	90	.674	.004
14	.153	.914			

TABLE XXVII

FORCE TEST

Biplane. 5-inch chord.
 Upper wing—N. A. C. A. M-1. Circular tips.
 Lower wing—Clark Y. Aspect ratio=6.
 Stagger=0. $G/c=1.0$.
 Decalage=0°. $q=19.99 \text{ kg/m}^2$
 Reynolds No.=154,000.

α°	C_D	C_L	α°	C_D	C_L
-45	0.581	-0.560	15	0.169	0.866
-40	.521	-.582	16	.182	.869
-35	.456	-.585	17	.196	.869
-30	.379	-.563	18	.210	.866
-27	.335	-.554	20	.264	.833
-24	.293	-.531	22	.324	.742
-21	.255	-.525	24	.369	.736
-18	.218	-.531	27	.412	.729
-15	.175	-.527	30	.465	.728
-14	.157	-.514	35	.534	.736
-13	.137	-.500	40	.630	.714
-12	.116	-.486	45	.699	.651
-9	.050	-.336	50	.734	.569
-6	.029	-.167	55	.756	.485
-3	.023	-.042	60	.750	.387
0	.023	+.150	65	.696	.281
+3	.031	.338	70	.609	.199
6	.049	.510	75	.608	.149
9	.075	.670	80	.644	.088
12	.127	.814	85	.652	+.025
14	.156	.858	90	.654	-.038

TABLE XXVIII
FLAT PLATES

Area ratio (a/A) and blocking correction (K) as determined from tests

α°	3 by 18 inches		4 by 24 inches		5 by 30 inches		6 by 36 inches		7 by 42 inches	
	a/A	K	a/A	K	a/A	K	a/A	K	a/A	K
35°	0. 0116	0. 997	0. 0179	0. 989	0. 0281	0. 973	0. 0392	0. 953	0. 0551	0. 931
40°	. 0121	. 997	. 0215	. 990	. 0336	. 976	. 0485	. 950	. 0658	. 913
50°	. 0144	. 999	. 0256	. 996	. 0405	. 984	. 0576	. 946		
60°	. 0163	. 998	. 0289	. 996	. 0453	. 969	. 0651	. 911	. 0888	. 839
70°	. 0177	. 996	. 0315	. 988	. 0492	. 947	. 0707	. 880	. 0962	. 800
75°	. 0181	. 997	. 0323	. 990	. 0505	. 943	. 0726	. 871	. 0988	. 791
80°	. 0187	. 997	. 0329	. 988	. 0515	. 942	. 0741	. 870	. 1008	. 788
90°	. 0188	. 996	. 0335	. 987	. 0522	. 936	. 0752	. 860	. 1023	. 780

TABLE XXIX
FORCE TESTS—FLAT PLATES

C_L and C_D uncorrected for blocking.
 C_L' and C_D' corrected for blocking.
Reynolds No. = 153,000.
(For 3 by 18 inch plate $q = 55.20$ kg/m²)
(For 4 by 24 inch plate $q = 31.05$ kg/m²)
(For 5 by 30 inch plate $q = 20.00$ kg/m²)
(For 6 by 36 inch plate $q = 13.79$ kg/m²)

α°	3 by 18 inch plate				4 by 24 inch plate			
	C_D	C_D'	C_L	C_L'	C_D	C_D'	C_L	C_L'
20°	0. 366	0. 366	0. 976	0. 976	0. 340	0. 340	0. 933	0. 931
25°	. 444	. 444	. 872	. 872	. 432	. 432	. 886	. 884
30°	. 556	. 556	. 887	. 886	. 549	. 549	. 907	. 905
35°	. 689	. 688	. 939	. 937	. 691	. 687	. 944	. 938
40°	. 781	. 780	. 905	. 903	. 772	. 767	. 900	. 894
45°	. 859	. 857	. 816	. 814	. 839	. 833	. 816	. 810
50°	. 932	. 930	. 749	. 747	. 928	. 918	. 751	. 743
55°	1. 022	1. 020	. 676	. 675	1. 022	1. 011	. 691	. 683
60°	1. 110	1. 108	. 618	. 617	1. 111	1. 097	. 624	. 616
65°	1. 193	1. 191	. 543	. 542	1. 191	1. 173	. 546	. 537
70°	1. 260	1. 256	. 443	. 441	1. 270	1. 249	. 455	. 447
75°	1. 315	1. 311	. 355	. 354	1. 321	1. 299	. 356	. 350
80°	1. 361	1. 357	. 250	. 249	1. 374	1. 350	. 250	. 246
85°	1. 394	1. 388	. 136	. 136	1. 400	1. 372	. 135	. 132
90°	1. 399	1. 390	. 029	. 029	1. 413	1. 385	. 028	. 027
α°	5 by 30 inch plate				6 by 36 inch plate			
	C_D	C_D'	C_L	C_L'	C_D	C_D'	C_L	C_L'
20°	0. 342	0. 341	0. 957	0. 954	0. 344	0. 341	0. 950	0. 940
25°	. 426	. 423	. 867	. 861	. 436	. 428	. 903	. 887
30°	. 546	. 540	. 925	. 915	. 581	. 566	. 992	. 966
35°	. 723	. 713	. 952	. 937	. 719	. 693	1. 014	. 978
40°	. 794	. 778	. 932	. 914	. 811	. 772	. 958	. 912
45°	. 861	. 841	. 839	. 819	. 904	. 848	. 800	. 835
50°	. 942	. 913	. 789	. 765	. 995	. 921	. 841	. 779
55°	1. 042	1. 006	. 740	. 714	1. 100	1. 006	. 796	. 728
60°	1. 160	1. 113	. 670	. 643	1. 215	1. 095	. 721	. 650
65°	1. 244	1. 188	. 577	. 551	1. 322	1. 178	. 640	. 570
70°	1. 315	1. 250	. 484	. 460	1. 428	1. 257	. 939	. 474
75°	1. 405	1. 331	. 386	. 366	1. 501	1. 310	. 427	. 372
80°	1. 441	1. 361	. 269	. 254	1. 572	1. 363	. 304	. 262
85°	1. 473	1. 389	. 145	. 137	1. 614	1. 392	. 174	. 150
90°	1. 488	1. 400	. 026	. 024	1. 613	1. 400	. 044	. 038

TABLE XXIX—Continued

FORCE TESTS—FLAT PLATES

C_L and C_D uncorrected for blocking.
 Reynolds No. = 153,000.
 (For 7 by 42 inch plate $q = 10.17 \text{ kg/m}^2$)

α°	7 by 42 inch plate		α°	7 by 42 inch plate	
	C_D	C_L		C_D	C_L
20°	0.338	0.982	60°	1.318	0.775
25°	.420	.914	65°	1.445	.689
30°	.584	.989	70°	1.567	.579
35°	.727	1.036	75°	1.650	.467
40°	.843	1.000	80°	1.716	.339
45°	.926	.921	85°	1.761	.198
50°	1.042	.888	90°	1.777	.055
55°	1.195	.848			

TABLE XXX

FORCE TESTS—CLARK Y WINGS

Aspect ratio = 8. Circular tips.
 C_L and C_D uncorrected for blocking.
 C_L' and C_D' corrected for blocking.
 Reynolds No. = 153,000.

(For 3-inch chord $q = 55.10 \text{ kg/m}^2$) (For 5-inch chord $q = 20.05 \text{ kg/m}^2$)

α°	3-inch chord				α°	5-inch chord			
	C_D	C_D'	C_L	C_L'		C_D	C_D'	C_L	C_L'
26°	0.479	0.479	0.868	0.868	27.75°	0.528	0.519	0.914	0.898
28°	.527	.527	.908	.907	29.70°	.578	.567	.946	.928
30°	.572	.571	.932	.930	32.70°	.654	.638	.968	.945
35°	.701	.700	.954	.952	35.70°	.742	.721	.980	.952
40°	.807	.805	.915	.912	37.70°	.795	.769	.965	.934
45°	.888	.885	.843	.840	39.75°	.838	.808	.959	.925
50°	.942	.939	.752	.750	44.85°	.916	.876	.906	.866
55°	1.005	1.002	.675	.675	50.00°	.986	.934	.800	.757
60°	1.084	1.080	.602	.599	55.15°	1.081	1.015	.723	.676
65°	1.146	1.139	.519	.515	60.25°	1.180	1.095	.646	.599
70°	1.210	1.202	.430	.427	65.45°	1.260	1.160	.560	.515
75°	1.266	1.258	.326	.324	70.65°	1.348	1.230	.453	.413
80°	1.300	1.290	.226	.224	75.85°	1.400	1.270	.344	.312
85°	1.314	1.305	.123	.122	81.05°	1.446	1.304	.216	.195
90°	1.322	1.312	.013	.013	86.25°	1.470	1.322	.089	.080
					91.50°	1.465	1.317	-.043	-.039

LANGLEY MEMORIAL AERONAUTICAL LABORATORY,
 NATIONAL ADVISORY COMMITTEE FOR AERONAUTICS,
 LANGLEY FIELD, VA., July 31, 1928.

REPORT No. 318

SPEED AND DECELERATION TRIALS OF U. S. S. LOS ANGELES

S. J. De FRANCE
Langley Memorial Aeronautical Laboratory
and
C. P. BURGESS
Bureau of Aeronautics

REPORT No. 318

SPEED AND DECELERATION TRIALS OF U. S. S. LOS ANGELES

By S. J. DE FRANCE and C. P. BURGESS

SUMMARY

The trials reported herein were instigated by the Bureau of Aeronautics of the Navy Department for the purpose of determining accurately the speed and resistance of the U. S. S. "Los Angeles" with and without water recovery apparatus, and to clear up the apparent discrepancies between the speeds attained in service and in the original trials in Germany.

The trials proved very conclusively that the water recovery apparatus increases the resistance about 20 per cent, which is serious, and shows the importance of developing a type of recovery having less resistance.

Between the American and German speed trials without water recovery there remains an unexplained discrepancy of nearly 6 per cent in speed at a given rate of engine revolutions. Warping of the propeller blades and small cumulative errors of observation seem the most probable causes of the discrepancy.

It was found that the customary resistance coefficients C , are 0.0242 and 0.0293 without and with the water recovery apparatus, respectively. The corresponding values of the propulsive coefficient K , are 56.7 and 44.6. If there is any error in these figures, it is probably in a slight overestimate of C , and an underestimate of K . The maximum errors are almost certainly less than 5 per cent.

No scale effect was detected indicating variation of C with respect to velocity.

INTRODUCTION

Less careful deceleration trials in 1925 and 1926 showed the extreme delicacy of such tests, and the necessity for special precautions to attain trustworthy results. The Bureau of Aeronautics accordingly requested the National Advisory Committee for Aeronautics and the Goodyear-Zeppelin Corporation to lend their personnel and apparatus to assist in the proposed trials. Four different instruments for measuring air speed were provided, and were checked by running the airship over a measured triangular course, approximately 10 miles to a leg, in Lower New York Bay.

APPARATUS

The four instruments used for measuring the air speed were: (a) The ship's electric air-speed meter of the suspended windmill type, having a wooden windmill about 8 inches in diameter turning a commutator by which a condenser is alternately charged from the ship's electric system and discharged through a galvanometer graduated in knots.

(b) The ship's Venturi air-speed meter consisting of a double Venturi tube located about 2 feet from the hull of the ship, abreast of the control car. The manometer with indicating dial graduated in meters per second is mounted in the control car.

(c) A Pitot-static tube belonging to the National Advisory Committee for Aeronautics, suspended below the control car by 75 feet of $\frac{1}{2}$ -inch flexible metal hose housing two small rubber tubes for transmitting the static and dynamic pressures to the recording apparatus.

(d) An apparatus belonging to the Goodyear-Zeppelin Corporation having separate static and impact orifices. The static pressure was obtained by orifices on a light "fish" suspended by a single rubber tube about 40 feet below the control car. In the trials without the water recovery apparatus, the impact head was obtained by a hook tube extending only a few feet

from the hull. In the later trials with the water recovery installed, a Pitot-static head was mounted on a V-shaped frame about 19 feet below the bottom of the control car.

Both the National Advisory Committee for Aeronautics and the Goodyear-Zeppelin Pitot-static apparatus were hooked up to the N. A. C. A. recording instrument. The principal elements of the recorder are pressure capsules, each containing a steel diaphragm of high natural period, in which the opposite sides are acted upon by the static and dynamic pressures. The movements of the diaphragm are recorded by a beam of light reflected upon a moving photographic film. This instrument is described in detail in N. A. C. A. Technical Note No. 64. (Reference 1.)

The engine speeds were observed and recorded by the mechanics in the power cars, using the centrifugal tachometers which are parts of the ship's equipment. These tachometers were calibrated during the trials by a portable stroboscope designed and furnished by the Goodyear-Zeppelin Corporation. This instrument is described by Doctor Klemperer of the Goodyear-Zeppelin Corporation as follows: "It consisted of a small electric motor taken from an automobile horn, equipped with a 2-slot shutter disc and centrifugal tachometer of fairly wide dial divisions in the range of the R. P. M. of the tests. Ten R. P. M. differences could be easily recognized by watching the apparent motion of the propeller through the prism and shutter of the stroboscope and adjusting a rheostat so as to prevent the propeller image from rotating in either direction. A 6-volt dry battery furnished the current."

SPEED TRIALS WITHOUT WATER RECOVERY APPARATUS

The speed trials without water recovery apparatus were held on September 2, 1927, over a triangular course between Sandy Hook, Staten Island, and Rockaway. The lengths and compass courses of the three legs of the triangle are as follows:

Leg	Direction, degrees	Length	
		Feet	Nautical miles
AC	343	59,500	9.79
CB	100	60,800	10.00
BA	222.5	63,200	10.40

Two complete runs were made around this course, in opposite directions, passing directly over the marks at the beginning and end of each leg, with a wide outward turn between successive legs. The observed ground speeds are recorded in Table I. The wind velocity was calculated and compensated by the geometrical construction shown in Figure 4.

The ground speeds are determined from the distance and time on each leg of the course, and plotted as vectors from a single point as in Figure 1; a circle is drawn through the ends of the vectors representing the ground speeds on three successive runs. If the ship's air speed and the wind velocity are constant during these runs, the radius of the circle represents the air speed, and the line from the origin of the vectors to the center of the circle represents the direction and velocity of the wind to the same scale as the ground speed vectors. It is found that one circle can be passed very nearly through the ends of all six vectors, showing that the wind was nearly constant at 10.2 knots from the southwest, and the ship's air speed was 58.4 knots.

The speeds indicated by the four air-speed meters on the ship are summarized in Table II; the agreement between them is quite good. Most reliance is placed upon the N. A. C. A. Pitot-static instrument, which was calibrated in the wind tunnel and in flight just before these trials, and found to be correct to within ± 0.5 M. P. H. at speeds up to 70 M. P. H. It is, therefore, believed that the ship's true air speed was 59.7 ± 0.5 kts. The discrepancy between this figure and the 58.4 kts. calculated from the ground speed is no more than might be expected from irregularities in steering, and lengthening of the course through errors in allowing for drift.

The records of the engine revolutions show that 1,230 R. P. M. was maintained with great constancy during the trial. This was the highest engine speed which it was considered safe to maintain. The runs on the measured course were made at only one speed.

SPEED TRIALS WITH WATER RECOVERY

A series of speed trials with the water recovery apparatus installed in the ship were conducted while returning from Harrisburg to Lakehurst on the night of September 6-7, 1927. Each trial was of four minutes duration. The air speed was observed or recorded by the four instruments used in the previous trials. Since these instruments had already been checked against ground-speed, it was considered unnecessary to attempt to measure the ground speed and wind velocity in these trials.

Runs were made at four different rates of engine revolutions as recorded in Table III. In all speed and deceleration trials except one, the precaution was taken to close all hatches, windows

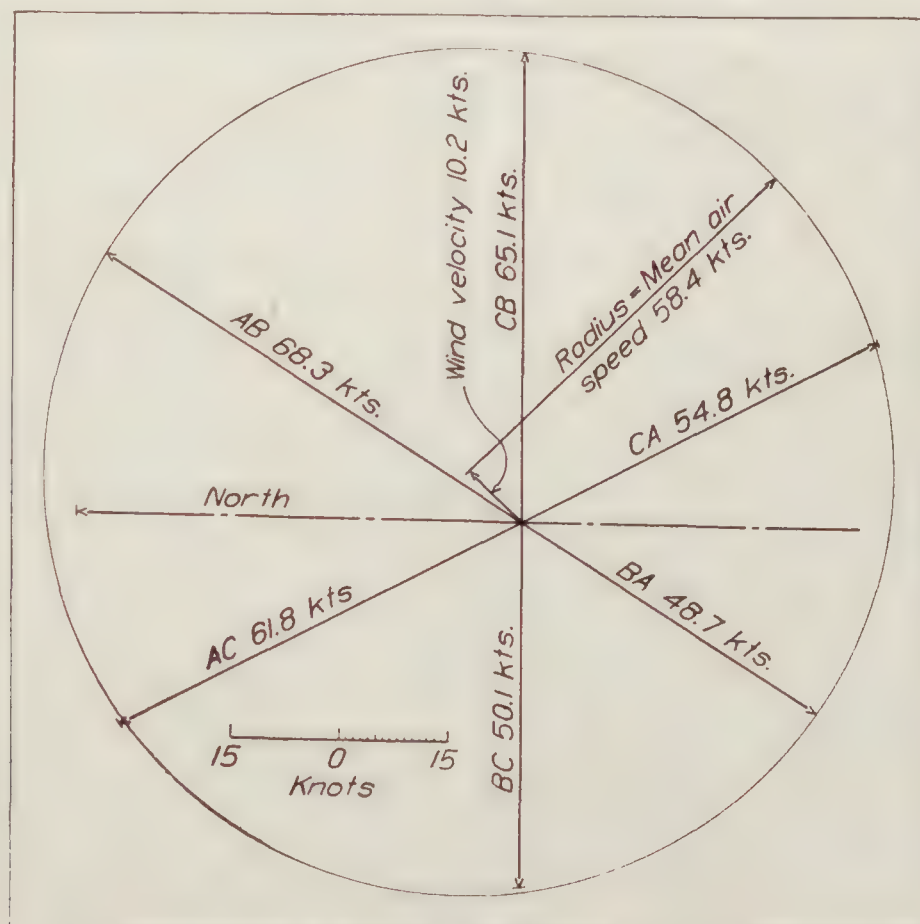


FIGURE 1

and other openings, and to house within the ship the various windmills used for driving the pumps and generators. In the fifth speed run on September 7, at 1,150 R. P. M., the hatches were opened. Table III shows that this reduced the speed by only about half a knot in comparison with the second run at the same R. P. M. In general service, it has several times been observed that the speed at 1,150 R. P. M. is only about 48 to 49 knots, and indeed, this observation was made on this very night of September 6-7, before commencing the speed trials. Since opening the hatches apparently accounts for only about half a knot speed, the remaining 2 knots discrepancy between service and speed trial conditions must be due to other causes. The ship was practically in equilibrium in the service conditions, so that the only explanation appears to be the difference between ordinary steering, and the specially careful steering in the smooth air of the speed trials. It was noted that the air was so ideally smooth in the trials on September 7 that the ship held her course during each of the 4-minute runs with practically no movements of either rudders or elevators.

DECELERATION TRIALS

Four deceleration runs were carried out on September 2, 1927, without the water recovery apparatus; and four on the night of September 6-7, with that apparatus installed. In each series of four runs, the propellers were blocked in the first two runs, and idling in the second two.

The theory of the deceleration test is that when an airship in static equilibrium is moving without power through air at rest or in uniform motion, the resistance is given by:

$$R = m \frac{dv}{dt} = \rho V_m \frac{dv}{dt} \quad (1)$$

where

R = the resistance

V_m = the virtual volume

$\frac{dv}{dt}$ = the deceleration.

The virtual volume V_m is the actual air volume inclosed by the ship, plus the additional volume of air carried along externally by the motion of the ship. Lamb has calculated the additional volume coefficients for ellipsoids of various fineness ratios moving in the ideal, non-viscous, incompressible fluid of hydrodynamic theory. Munk has suggested that the additional volume be assumed equal to $\frac{\pi r^3}{3}$ where r is the radius of the largest cross section of the airship. By Lamb's coefficients or Munk's approximation, the virtual volume of conventional airships, such as the *Los Angeles*, is about 4 per cent more than the actual volume. The practice of the Goodyear-Zeppelin Corporation, based upon Karman's theory of frictional resistance is to allow 8 per cent instead of 4 per cent for the additional volume in order to include the air carried along by the frictional wake and the parasite parts. The larger allowance for additional volume seems reasonable, and is adopted in this report.

A customary expression for the resistance of bodies moving in air is

$$R = A \rho v^2 / 2 \quad (2)$$

where A is an area defined as the area of drag.

Combining expressions (1) and (2),

$$dt/dv = S/v^2 \quad (3)$$

where S is a length equal to $2 V_m/A$.

By integration of (3),

$$t = -S/v + B.$$

In a deceleration test starting at $v = v_0$ when $t = 0$ $B = S/v_0$, whence at time t and speed v ,

$$S = \frac{t}{1/v - 1/v_0}.$$

In other words, S is the reciprocal of the slope of $1/v$ plotted against t .

From the definition of S ,

$$A = 2 V_m / S \quad (4)$$

The area of drag found in this way includes the drag of the propellers, for which a correction must be made. The propellers of the *Los Angeles* have a diameter of 11.83 feet, a mean blade width of 0.073 times the diameter, and a pitch/diameter ratio of 0.46. They closely resemble Durand's propeller No. 11, for which the experimentally determined drag coefficients are 0.028 when stopped, and 0.048 when spinning freely; whence the areas of drag for the propellers of the *Los Angeles* are:

$$A = 2 \times 0.028 \times \overline{11.83}^2 = 7.84 \text{ sq. ft. for each stopped propeller,}$$

and

$$A = 2 \times 0.048 \times \overline{11.83}^2 = 13.44 \text{ sq. ft. for each idling propeller.}$$

Five times these areas, according to whether the propellers were stopped or idling, are subtracted from the overall drag area to obtain the net drag area of the airship.

The shape coefficient is given by:

$$C = \frac{A}{V^{2/3}}$$

where

C = shape coefficient

A = net area of drag

V = actual air volume.

It is assumed in the calculations in this report that $V = 2,840,000$ cubic feet and $V_m = 1.08 \times V = 3,070,000$ cubic feet.

The reciprocals of the speeds, and the characteristic lengths S , calculated from the readings or records of the air-speed meters are plotted in Figures 2 to 26. The corresponding values of S , A , and C are summarized in Tables IV to VII.

Inspection of the values of C in Tables IV and V shows that the two recording instruments agreed fairly well. Much less accurate results are to be expected from the readings of the indicating instruments during deceleration tests; and it is obvious from the large discrepancy between the readings of the Venturi meter and the other instruments that there was a lag in the action of the Venturi indicator.

Both recording instruments showed an exceptionally high mean rate of deceleration on the fourth run, and it is probable that there was some disturbance producing erroneous results. Neglecting the fourth run, the mean C without water recovery is 0.0244 according to the N. A. C. A. instrument, and 0.0240 according to the Goodyear-Zeppelin one, or 0.0242 average for both instruments together. The maximum departure of either instrument from this average figure is 2.5 per cent, and the mean departure is 0.9 per cent. This is considered very good for a test of this nature.

In the four runs with water recovery, both recording instruments showed a little more net resistance (after allowing for the propellers) with the propellers blocked than with them idling. This may have been due to some slight delay in blocking the propellers after cutting the ignition. The mean values of C are 0.0288 by the National Advisory Committee for Aeronautics, and 0.0298 by the Goodyear-Zeppelin instrument, or 0.0293 average of both. For some unknown reason, the agreement between the two air-speed meters is not quite so good as in the trials without water recovery. The maximum variation of C according to either instrument from the average of both is 3.75 per cent, and the mean departure is 2.30 per cent.

An interesting point in regard to the motion of the ship during deceleration tests was brought out by Doctor Klemperer after the trials. The elevator man was instructed to keep the ship in horizontal trim during each test, regardless of rise or fall. Stopping the engines appeared to cause a sudden drop of the ship's bow, felt by the personnel, and indicated by the inclinometer. This was thought to be due to removal of the nosing-up couple produced by the thrust of the propellers at a considerable distance below the center of resistance; and it was checked by applying up-elevator. Doctor Klemperer has suggested that the apparent drop of the bow was mainly an illusion due to the initial inertia force of about one-thirtieth of the weight of the ship acting forward, combining with gravity to produce a resultant indistinguishable from the true gravitational force, but actually inclined at about 2° forward of the vertical. According to this theory, the lifting of the elevator turns the ship upward, and probably an oscillating movement follows with some increase in the resistance. The altimeter and variometer readings taken at 1-minute intervals (see Tables VIII and IX) do not show any appreciable vertical movements; but it is possible that there was some such motion during the first 30 seconds, which is the most important part of the deceleration test. It is estimated that 2° pitch would not increase the resistance more than 3 per cent. The lesson for future deceleration trials is to instruct the elevator man to ignore his own sensations and the indications of the inclinometer, but to keep the ship level by observation of some distant object.

SCALE EFFECT

For practical design purposes, it is important to learn as much as possible about scale effect, or the variation of the resistance coefficient with Reynolds Number. It is the practice of some designers to assume that the resistance varies as $(vL)^{1.87}$ instead of as $(vL)^2$. This is equivalent to assuming that C is proportional to $(vL)^{-0.13}$ instead of constant. If this is true, then in a deceleration trial, S should vary inversely as $(1/v)^{0.13}$, or when $1/v$ has twice its initial value, S should be diminished in the ratio of 1 to $2^{0.13}$ or 1/1.094. This change in S can not be detected in the curves of $1/v$ against t ; but on the other hand, it is true that at the higher values of $1/v$, the points are rather scattered, and there is so much uncertainty about the exact slope of the line that it is impossible to affirm definitely that there is no appreciable increase in the resistance.

The speed trials are also inconclusive in regard to scale effect. In an airship in steady conditions the propeller thrust is almost exactly proportional to the square of the R. P. M. Figure 26 shows the speed increasing slightly faster than the R. P. M. in the trials without water recovery apparatus, indicating that the resistance varied a little less rapidly than as the square of the speed; or in other words, there was some positive scale effect. On the other hand, in the trials with the water recovery apparatus installed, the speed was observed at several R. P. M. and found to vary slightly less rapidly than the R. P. M., indicating some negative scale effect.

On the whole, it does not seem unduly conservative in the design of larger and faster ships than the *Los Angeles* to assume that there is no scale effect tending to reduce the value of the drag coefficient C .

COORDINATION OF SPEED AND DECELERATION TRIALS

The customary propulsive coefficient K is defined by:

$$K = \frac{\rho v^3 V^{2/3}}{550 \text{ HP.}}$$

$$= \frac{\rho V^{2/3} \left(\frac{v}{n}\right)^3 n^3}{550 \left(\frac{v}{n}\right)^3 \text{ HP.}}$$

where n is the engine revolutions per second, and the other symbols have their usual significance. The horsepower is proportional to ρ and to n^3 when driving a propeller at air speeds proportional to n , as in an airship. It follows that $\rho n^3/\text{HP.}$ is constant. According to information furnished by Doctor Klemperer, tests of the engines of the *Los Angeles* in Germany showed that 1,970 HP. is developed at full throttle at 1,360 R. P. M. when $\rho = 0.0022$ slugs/cubic feet, whence

$$\frac{\rho V^{2/3} n^3}{550 \text{ HP.}} = \frac{0.0022 \times 20,000 \times 1,360^3}{550 \times 1,970 \times 60^3} = 0.473/\text{cu. ft.}$$

From the curves of speed vs. R. P. M. in Figure 26 of this report, at 1,230 R. P. M., $v/n = 4.55$ feet and 4.93 feet, with and without water recovery, respectively. Whence without water recovery,

$$K = 0.473 \times 4.93^3 = 56.7$$

and with water recovery,

$$K = 0.473 \times 4.55^3 = 44.6$$

The propulsive efficiency is given by

$$E = \frac{Rv}{550 \text{ HP.}} \quad (5)$$

where E = the propulsive efficiency, and R = the resistance of the airship.

Also

$$R = \frac{C \rho v^2 V^{2/3}}{2} \quad (6)$$

Combining (5) and (6)

$$E = \frac{C_p v^3 V^{2\beta}}{2 \times 550 \text{ HP.}} = \frac{CK}{2} \quad (7)$$

Whence, without water recovery,

$$E = \frac{.0242 \times 56.7}{2} = 68.6 \text{ per cent}$$

and with water recovery,

$$E = \frac{.0293 \times 44.6}{2} = 65.3 \text{ per cent}$$

The propellers were designed to have an efficiency of 67.5 per cent without water recovery, which agrees well with the 68.6 per cent calculated from these trials in the same condition. The

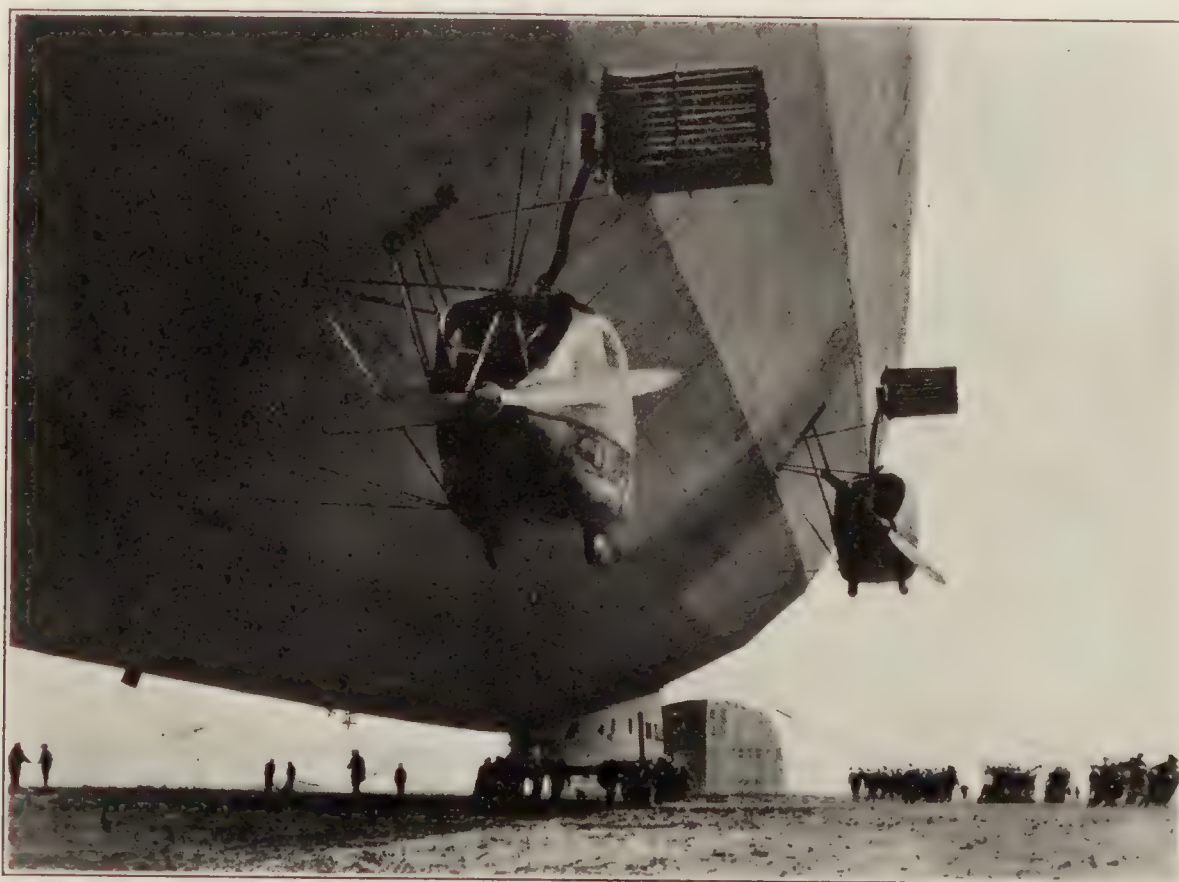


FIGURE 27.—Side power cars and water recovery apparatus of U. S. S. *Los Angeles*

water recovery apparatus increases the slip by reducing the speed, and interferes to some extent with the flow of air to the propellers. Both effects reduce the propulsive efficiency, so that the difference in the efficiencies with and without water recovery is not surprising.

RESISTANCE OF WATER RECOVERY APPARATUS

The deceleration trials showed that the water recovery increased the area of drag 20 per cent, from 488 square feet to 586 square feet. Two of the five units are shown in Figure 27. The actual projected frontal area of the 1-inch diameter tubes constituting the principal cooling elements of the apparatus is only 16 square feet. The headers, water separators, piping, special struts and fittings add approximately 37 square feet to the projected frontal area. A large frictional drag is to be expected from the long headers with their axes parallel to the air flow, and the 45 rows of tubes so placed that they present the frontal area of only one row. Furthermore, the angular arrangement of the tubes in elevation, and their spacing in plan view produces much turbulence, so that the large excess of drag area over frontal area is not surprising.

The increase of drag coupled with the diminished propulsive efficiency with the water recovery involves a loss of 21 per cent in the endurance, or almost as much as the change from

hydrogen to helium. Looking at the problem from another point of view, the size would have to be increased about 50 per cent to obtain a ship with the present type of water recovery apparatus capable of the same endurance at a given speed as the *Los Angeles* without that apparatus. This shows the enormous importance of developing a condenser that will use the skin of the ship for cooling area, instead of a system of external tubes as at present.

COMPARISON OF GERMAN AND AMERICAN SPEED AND DECELERATION TRIALS

Speed and deceleration trials of the *Los Angeles* were carried out in Germany when the ship was new and in the hands of her builders, the Luftschiffbau-Zeppelin. At that time there was no water-recovery equipment on the ship. An air speed of 32.5 m/sec. (106.7 ft./sec.) was observed at 1,250 R. P. M. on 4 engines and 1,150 R. P. M. on 1 engine, or a mean of 1,230 R. P. M. for all engines, whence $v/n = 5.20$ feet.

From the German deceleration trials the net area of drag was calculated to be 377 square feet at high speeds and 441 square feet at low speeds. The change from the smaller to the larger area of drag appeared to occur at a critical speed of about 22 m/s, which agrees with the results found by Munk in an analysis of the speed trials of earlier Zeppelin airships. (See N. A. C. A. Technical Report No. 117—Reference 2.) The speeds were measured by Venturi and Pitot tubes suspended 30 feet below the hull. The rates of deceleration indicated by the instruments were much the same as by the Venturi air-speed meter in the American trials without water recovery; and it is suspected that there were errors due to lag of the instruments such as were proved to occur in the Venturi meter in the American trials. If the German figures on speed and deceleration are accepted,

$$C = \frac{A}{V^{2/3}} = \frac{377}{20,000} = .01885$$

$$K = .473 \times 5.20^3 = 66.5$$

$$E = \frac{CK}{2} = 62.7 \text{ per cent}$$

This is an improbably low value of E , and confirms the suspicion that C is too small.

Since lag of the instruments affords a very probable explanation of the low rate of deceleration observed in the German trials, the real discrepancy to be cleared up between the German and American trials is the relation of ship's speed to engine revolutions, without water recovery, i. e., it should be explained why $v/n = 5.20$ feet in Germany and $v/n = 4.93$ feet in America.

The difference is less than 6 per cent, but it leads to 17 per cent discrepancy in the apparent value of K , and also of C calculated from K and a known value of E . Some change of v/n might result from slackening of the outer cover, although there appeared to be very little slackness during the American trials. A more probable explanation is warping of the propeller blades, and some difference in a propeller of American manufacture supposed to be copied from the German propeller for which it was substituted, but actually having slightly greater pitch.

Finally, it must be remembered that the discrepancy of 6 per cent in question would result if in the German trials the observations of ship's speed and engine revolution were in error by only 1.5 per cent on the plus and minus sides, respectively, and the opposite errors were made in the American trials. The fact that such small errors involve 18 per cent discrepancy in the apparent value of K shows the great difficulty in determining this coefficient accurately.

Of the three quantities C , K , and E the last is the most definite and certain. For the *Los Angeles* without water recovery, E is undoubtedly close to 67.5 per cent. The calculation of E by the expression $E = CK/2$, using the values of C and K determined by the American trials, gave $E = 68.6$ per cent. Although this is a good agreement, it is not proof of the accuracy of the trial results because it is possible that C and K are in error in equal percentages in opposite directions. If the use of the elevators in the deceleration trials produced an increase in C over the actual value, the true value of K is probably slightly greater than calculated from the observations of speed and engine revolutions in the speed trials.

CONCLUSIONS

The water-recovery apparatus increases the resistance of the *Los Angeles* about 20 per cent, and reduces the propulsive efficiency about 7 per cent. Most of this added resistance could be eliminated by adopting a type of water-recovery apparatus using the surface of the hull for cooling area. Such an apparatus would probably weigh considerably more than the present type, and would have the further disadvantages of less simple and rugged construction and less facility of temperature control.

During deceleration trials, the ship should be kept in level trim by observing a distant object instead of by watching the inclinometer which gives erroneous indications because of the superposition of the longitudinal deceleration upon the acceleration of gravity. Too much use of the elevators in the deceleration trials may have increased the resistance of the ship by about 3 per cent.

REFERENCES

1. Norton, F. H.: N. A. C. A. Recording Air-Speed Meter. N. A. C. A. Technical Note No. 64, 1921.
2. Munk, Max M.: The Drag of Zeppelin Airships. N. A. C. A. Technical Report No. 117, 1921.

NATIONAL ADVISORY COMMITTEE FOR AERONAUTICS,
WASHINGTON, D. C., June 12, 1928.

TABLE I.—GROUND SPEEDS OF U. S. S. "LOS ANGELES" ON SPEED TRIALS SEPTEMBER 2, 1927

Leg	Course	Length	Time	Speed	Speed
	<i>Degrees</i>	<i>Feet</i>	<i>Seconds</i>	<i>Ft./sec.</i>	<i>Knots</i>
AC	332	59,500	570	104.3	61.8
CB	89	60,800	552	110.0	65.1
BA	211.5	63,200	769	82.3	48.7
AB	31.5	63,200	548	115.3	68.3
BC	269	60,800	718	84.7	50.1
CA	152	59,500	642	92.6	54.8

TABLE II.—AIR SPEEDS SHOWN BY FOUR AIR-SPEED METERS IN THE SPEED TRIALS OF SEPTEMBER 2, 1927, WITHOUT WATER-RECOVERY APPARATUS

Run	Leg	Air speed, knots			
		N. A. C. A. instrument	Goodyear- Zeppelin	Electric meter	Venturi meter
1	1	59.5	60.5	59.0	59.5
1	2	60.0	61.0	59.0	60.0
1	3	59.5	60.7	58.8	59.5
2	3	59.5	60.5	58.0	59.5
2	2	60.0	61.2	60.0	60.0
2	1	59.5	60.3	59.5	59.0
Mean	-----	59.7	60.7	59.1	59.6

The mean ground speeds were 59.0 knots for run 1, and 57.7 knots for run 2.

TABLE III.—AIR SPEEDS SHOWN BY FOUR AIR-SPEED METERS IN THE SPEED TRIALS OF U. S. S. "LOS ANGELES," SEPTEMBER 6-7, 1927, WITH WATER RECOVERY APPARATUS INSTALLED

Run No.	Time run began		R. P. M.	Air speed, knots			
				N. A. C. A. meter	Goodyear-Zeppelin	Electric meter	Venturi meter
	Hours	Minutes					
1	23	21	1, 250	56. 0	56. 5	57. 5	55. 5
2	23	30	1, 150	51. 3	51. 5	52. 5	50. 5
3	23	38	1, 050	46. 5	47. 0	49. 0	47. 0
4	23	47	950	41. 0	42. 0	43. 0	42. 0
5	23	59	1, 150	-----	-----	52. 5	50. 0

TABLE IV.—SUMMARY OF DECELERATION TRIALS OF U. S. S. "LOS ANGELES," SEPTEMBER 2 AND 7, 1927, BASED ON N. A. C. A. AIR-SPEED METER RECORDS

Run No.	Condition	Propellers	<i>S</i>	<i>A</i> (total)	<i>A</i> (net)	<i>C</i>
			<i>Feet</i>	<i>Square feet</i>	<i>Square feet</i>	
1	Without water recovery.	Blocked-----	11, 600	529	490	0. 0245
2		---do-----	11, 760	522	483	. 0242
3		Idling-----	11, 050	556	489	. 0244
4		---do-----	10, 520	584	517	. 0259
5	With water recovery.	Blocked-----	9, 820	625	586	. 0293
6		---do-----	9, 840	624	585	. 0292
7		Idling-----	9, 730	631	564	. 0282
8		---do-----	9, 650	636	569	. 0285

TABLE V.—SUMMARY OF DECELERATION TRIALS OF U. S. S. "LOS ANGELES," SEPTEMBER 2 AND 7, 1927, BASED ON GOODYEAR-ZEPPELIN AIR-SPEED METER RECORDS

Run No.	Condition	Propellers	<i>S</i>	<i>A</i> (total)	<i>A</i> (net)	<i>C</i>
			<i>Feet</i>	<i>Feet</i>	<i>Feet</i>	
1	Without water recovery	Blocked-----	11, 700	525	486	0. 0243
2		---do-----	11, 810	520	481	. 0240
3		Idling-----	11, 390	539	472	. 0236
4		---do-----	10, 520	584	517	. 0258
5	With water recovery.	Blocked-----	9, 500	646	607	. 0303
6		---do-----	9, 500	646	607	. 0303
7		Idling-----	9, 220	666	599	. 0299
8		---do-----	9, 650	636	569	. 0285

TABLE VI.—SUMMARY OF DECELERATION TRIALS OF U. S. S. "LOS ANGELES," SEPTEMBER 2 AND 7, 1927, BASED ON ELECTRIC AIR-SPEED METER READINGS

Run No.	Condition	Propellers	<i>S</i>	<i>A</i> (total)	<i>A</i> (net)	<i>C</i>
			<i>Feet</i>	<i>Square feet</i>	<i>Square feet</i>	
1	Without water recovery.	Blocked-----	11, 600	529	490	0. 0245
2		---do-----	10, 900	563	524	. 0262
3		Idling-----	9, 530	644	577	. 0288
4		---do-----	10, 400	590	523	. 0262
5	With water recovery.	Blocked-----	8, 400	731	692	. 0346
6		---do-----	8, 850	694	655	. 0327
7		Idling-----	9, 150	671	604	. 0302
8		---do-----	8, 820	696	629	. 0315

TABLE VII.—SUMMARY OF DECELERATION TRIALS OF U. S. S. "LOS ANGELES," SEPTEMBER 2 AND 7, 1927, BASED ON VENTURI AIR-SPEED METER READINGS

Run No.	Condition	Propellers	<i>S</i>	<i>A</i> (total)	<i>A</i> (net)	<i>C</i>
			<i>Feet</i>	<i>Square feet</i>	<i>Square feet</i>	
1	Without water recovery.	{Blocked----	12, 800	480	441	0. 0220
2		{--do-----	13, 300	462	423	. 0212
3		{Idling-----	13, 400	458	391	. 0195
4		{--do-----	13, 700	448	381	. 0191
5	With water recovery.	{Blocked----	13, 400	458	419	. 0209
6		{--do-----	12, 220	502	463	. 0232
7		{Idling-----	12, 500	491	424	. 0212
8		{--do-----	13, 600	451	384	. 0192

TABLE VIII.—GENERAL DATA

Taken on deceleration trials, September 2, 1927, without water recovery]

FIRST RUN

Time	Tempera- ture	Humidity	Altitude	Elevator angle	Pitch angle	Vari- ometer fifth of meter/ second
<i>Minutes</i>	<i>° F.</i>	<i>Per cent</i>	<i>Feet</i>	<i>Degrees</i>	<i>Degrees</i>	
0	68	88	1, 675	0	0	R1
1	68	88	1, 725	U3	D½	R1
2	68	88	1, 740	U5	U½	R1
3	68	88	1, 840	U5	0	R2

SECOND RUN

0	69	90	1, 710	U4	D½	0
1	69	90	1, 790	U4	0	R1
2	69	90	1, 825	U3	0	R2
3	69	90	1, 900	U6	0	R2

THIRD RUN

0	70	90	1, 750	0	0	R1
1	70	90	1, 850	U5	0	R3
2	70	90	1, 900	U7	0	R1½

FOURTH RUN

0	71	89	1, 700	0	D½	R1
1	71	89	1, 775	U5	0	R2
2	71	89	1, 875	U8	0	R3

TABLE IX.—GENERAL DATA

[Taken on deceleration trials, September 7, 1927, with water recovery]

FIFTH RUN

Time		Tempera- ture	Altitude	Elevator angle	Pitch angle	Vari- ometer fifth of meter/ second
<i>Min.</i>	<i>Sec.</i>	<i>° F.</i>	<i>Feet</i>	<i>Degrees</i>	<i>Degrees</i>	
0		64	3, 100	2½D	0	R1
1		64	3, 150	5U	0	R1
2		64	3, 150	2U	0	0
3		64	3, 150	0	0	0

SIXTH RUN

0	0	64	3, 000	4D	0	F1
	20	64	3, 010	4U	0	R2
	40	64	3, 050	0	0	R1
1	00	64	3, 050	3U	0	0
1	20	64	3, 050	5U	0	0
1	40	64	3, 050	4U	0	0
2	00	64	3, 050	0	0	0

SEVENTH RUN

0	0	64	3, 040	5D	2D	F1
	20	64	3, 025	0	0	0
	40	64	3, 025	5U	0	0
1	00	64	3, 025	5U	0	0
1	20	64	3, 040	5U	0	0
1	40	64	3, 040	0	0	0
2	00	64	3, 040	4U	0	0

EIGHTH RUN

0	0	64	3, 040	1D	0	0
	20	64	3, 040	0	0	R1
	40	64	3, 040	1D	0	R1
1	00	64	3, 075	5U	0	0
1	20	64	3, 070	0	0	R1
1	40	64	3, 070	7U	0	0
2	00	64	3, 070	4U	0	0
2	20	64	3, 100	10U	1D	0

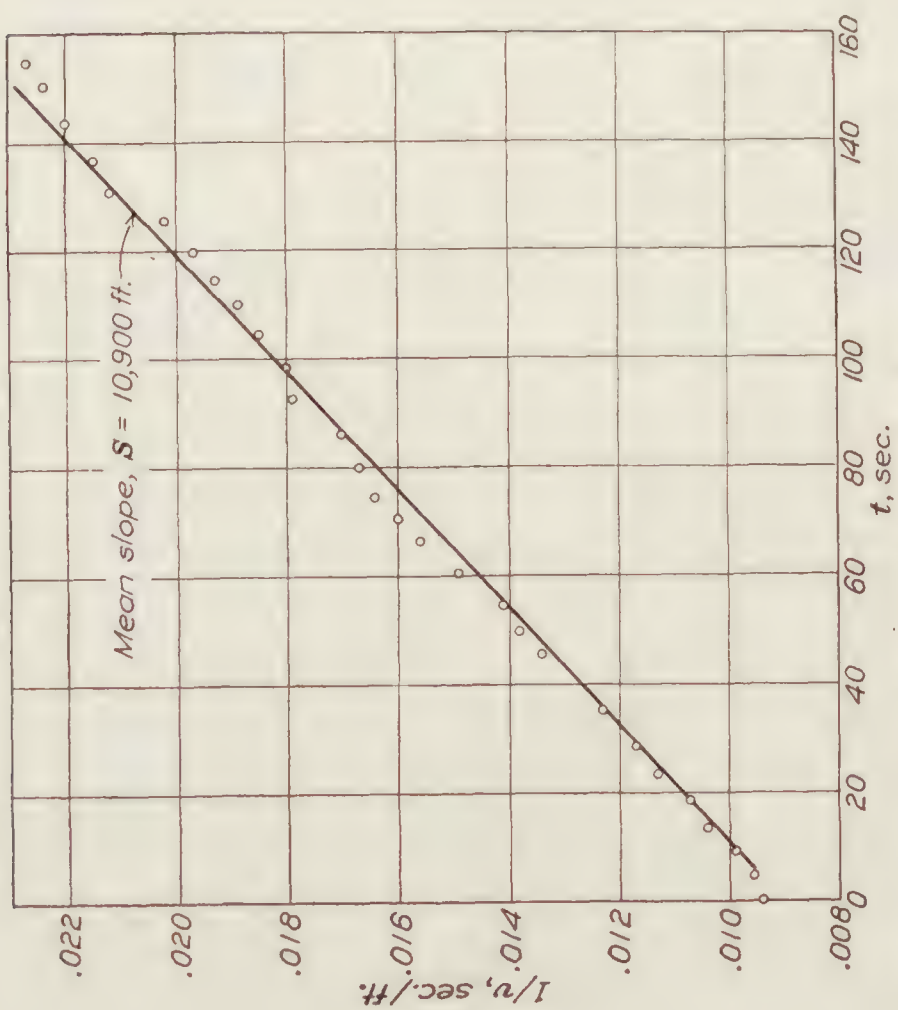


FIGURE 3.—Run No. 2. Deceleration without water recovery. Propellers stopped. Speeds by electric meter

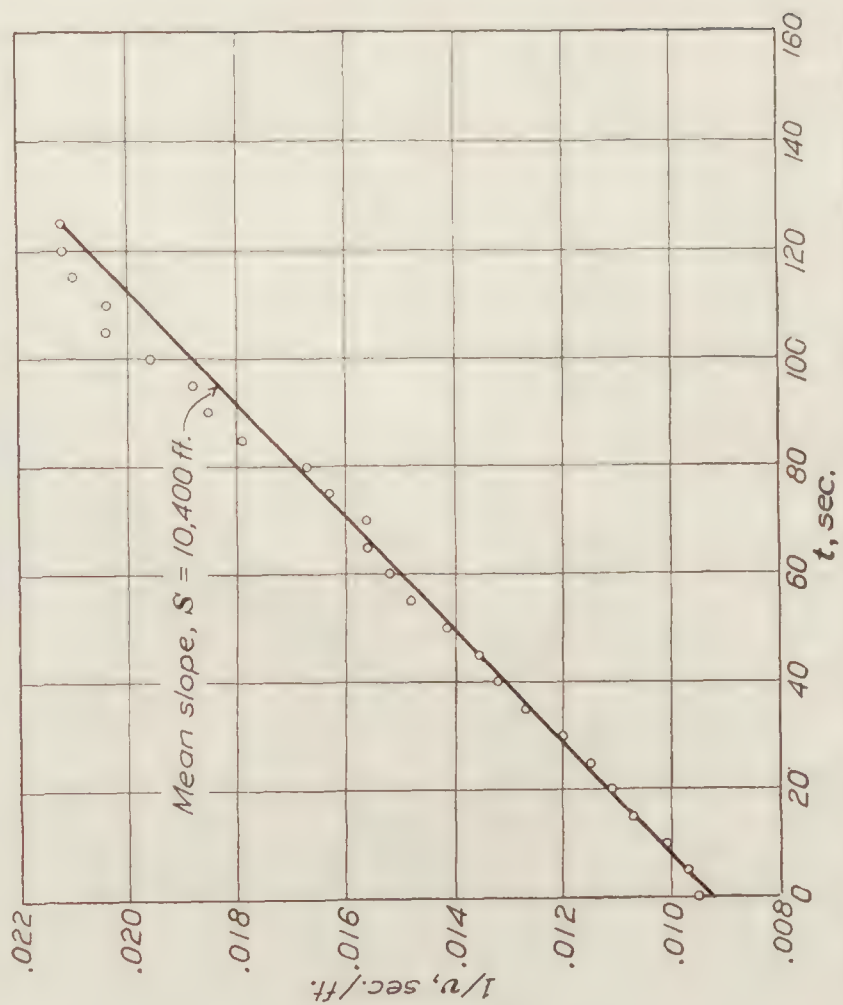


FIGURE 5.—Run No. 4. Deceleration without water recovery. Propellers idling. Speeds by electric meter

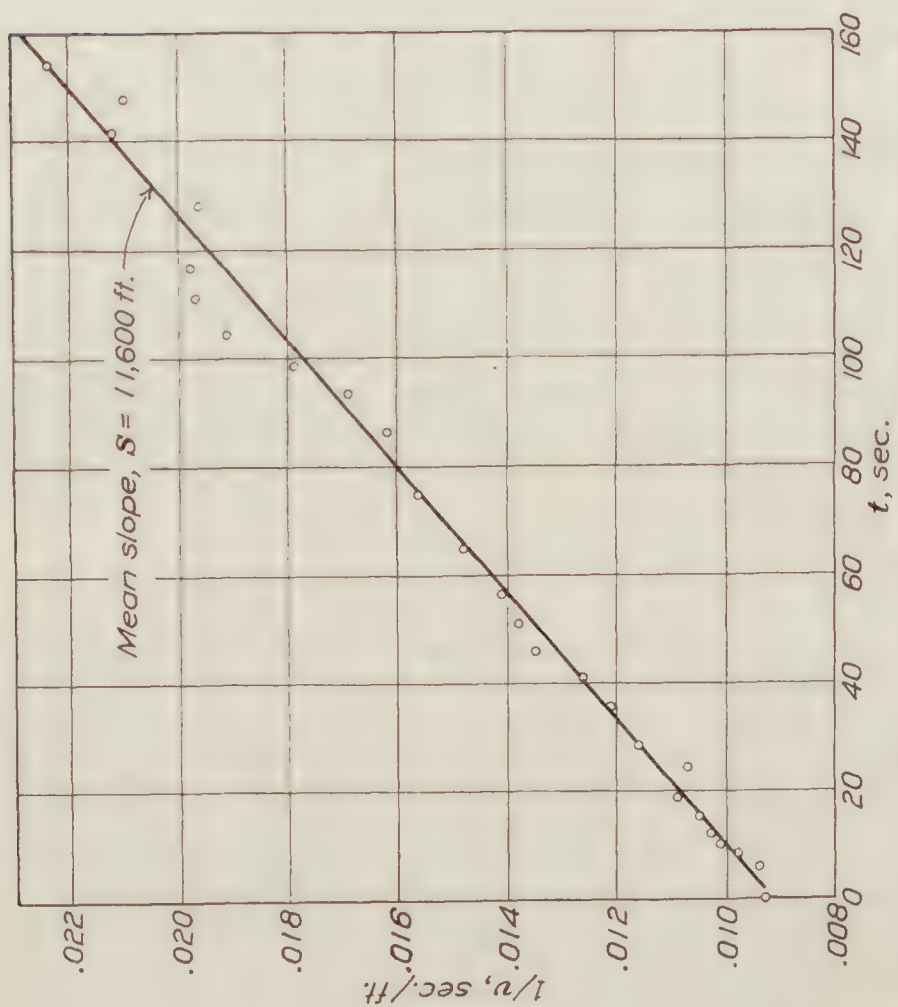


FIGURE 2.—Run No. 1. Deceleration without water recovery. Propellers stopped. Speeds by electric meter

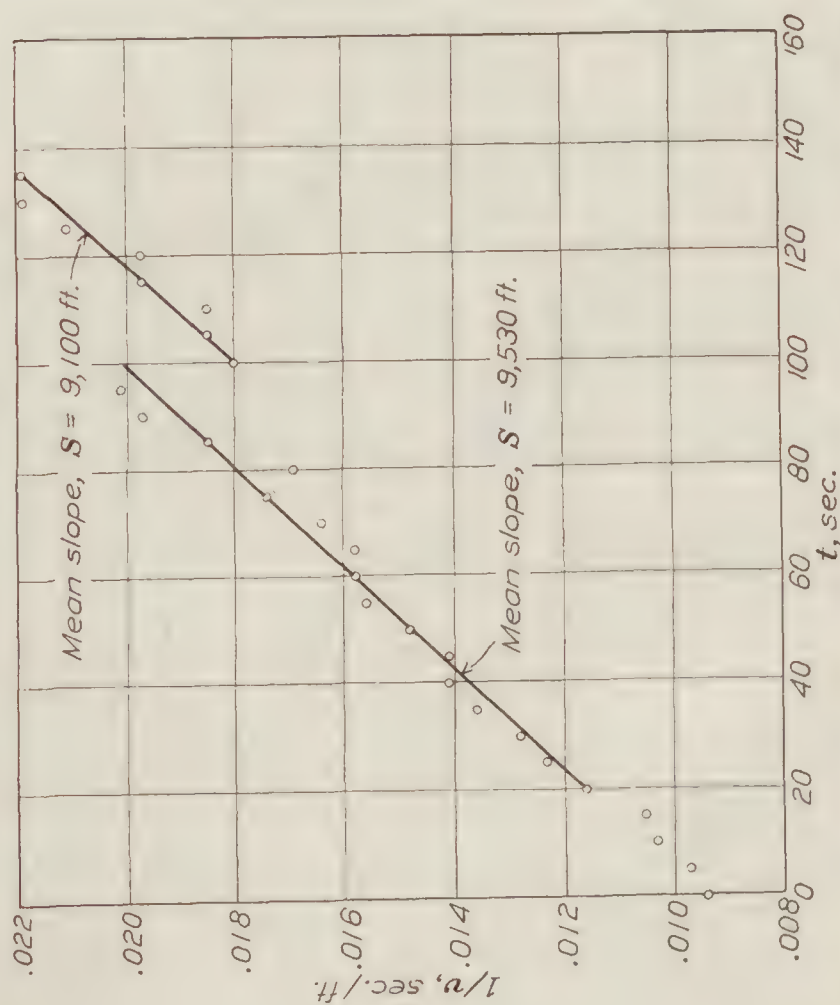


FIGURE 4.—Run No. 3. Deceleration without water recovery. Propellers idling. Speeds by electric meter

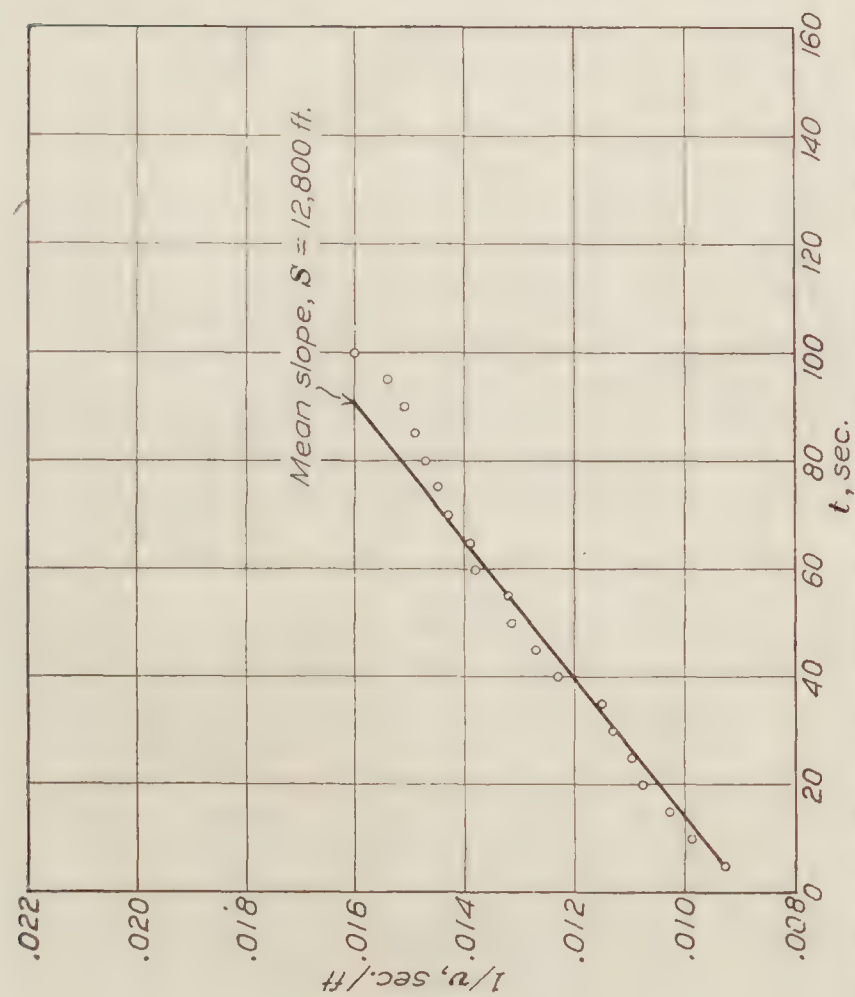


FIGURE 6.—Run No. 1. Deceleration without water recovery. Propellers stopped. Speeds by Venturi meter

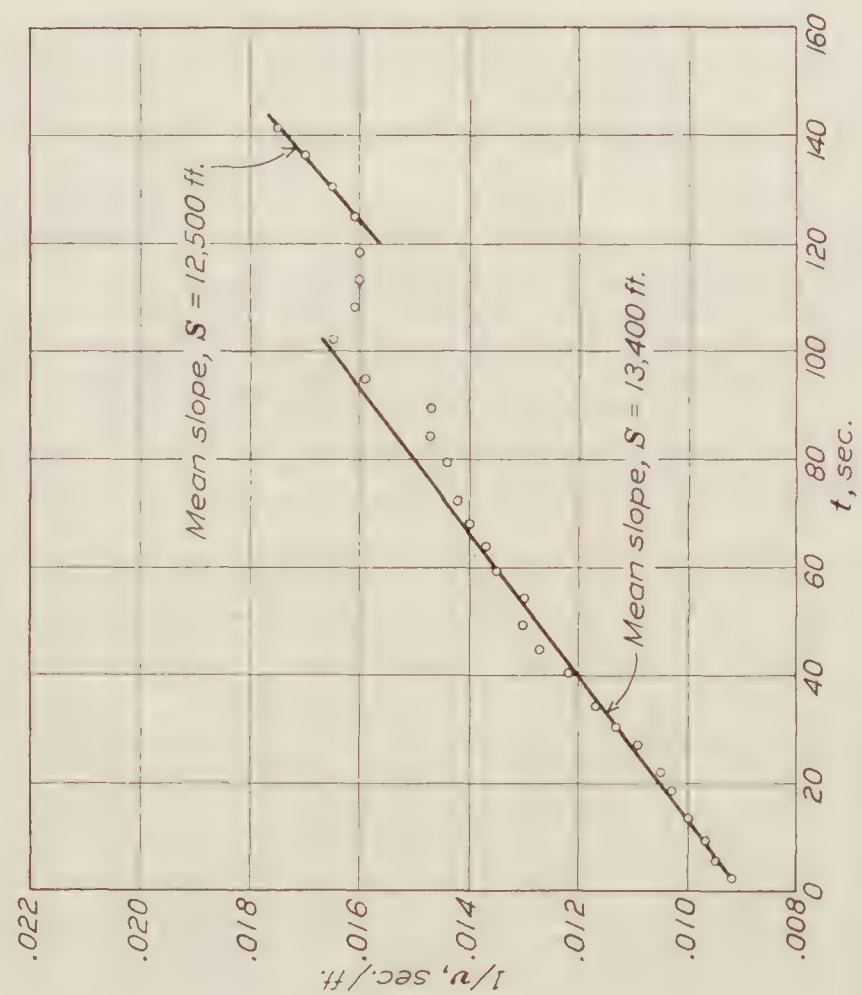


FIGURE 8.—Run No. 3. Deceleration without water recovery. Propellers idling. Speeds by Venturi meter

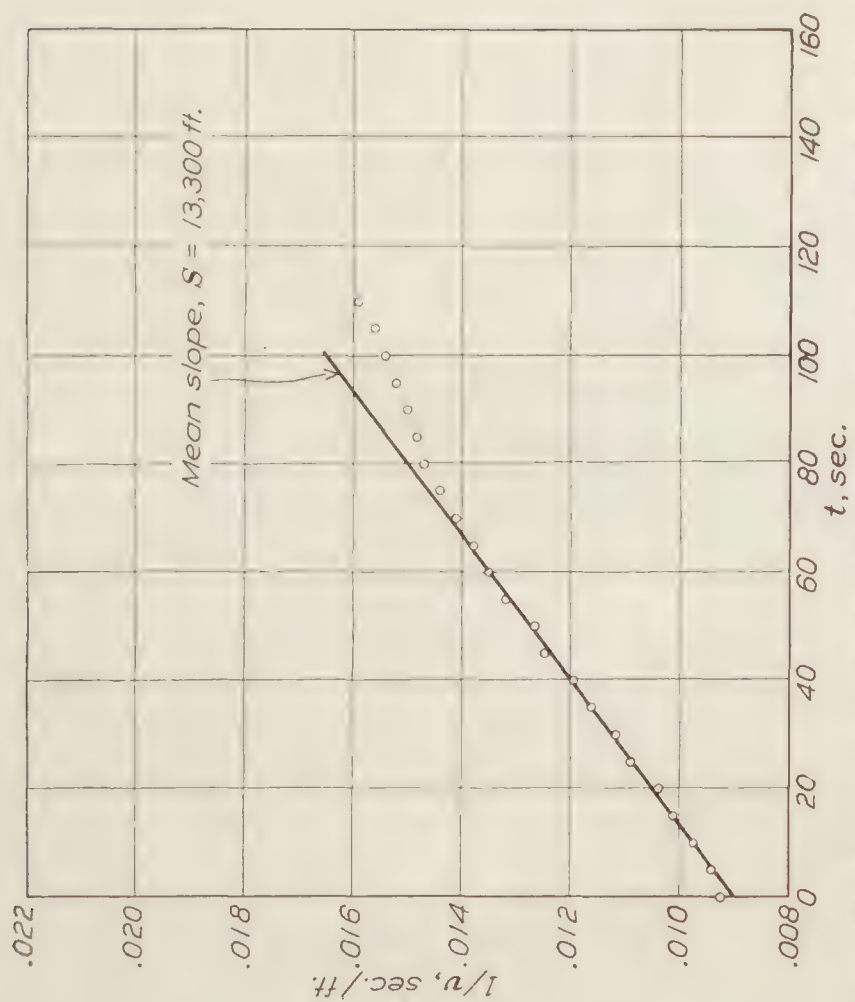


FIGURE 7.—Run No. 2. Deceleration without water recovery. Propellers stopped. Speeds by Venturi meter

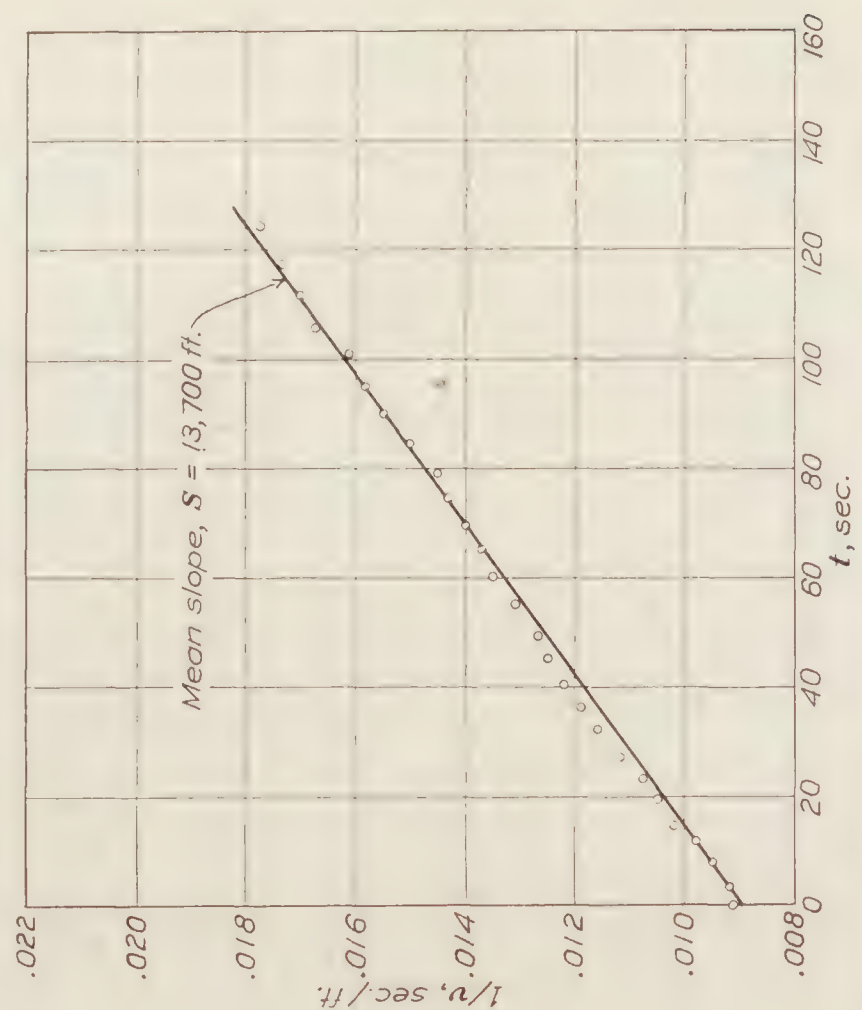


FIGURE 9.—Run No. 4. Deceleration without water recovery. Propellers idling. Speeds by Venturi meter

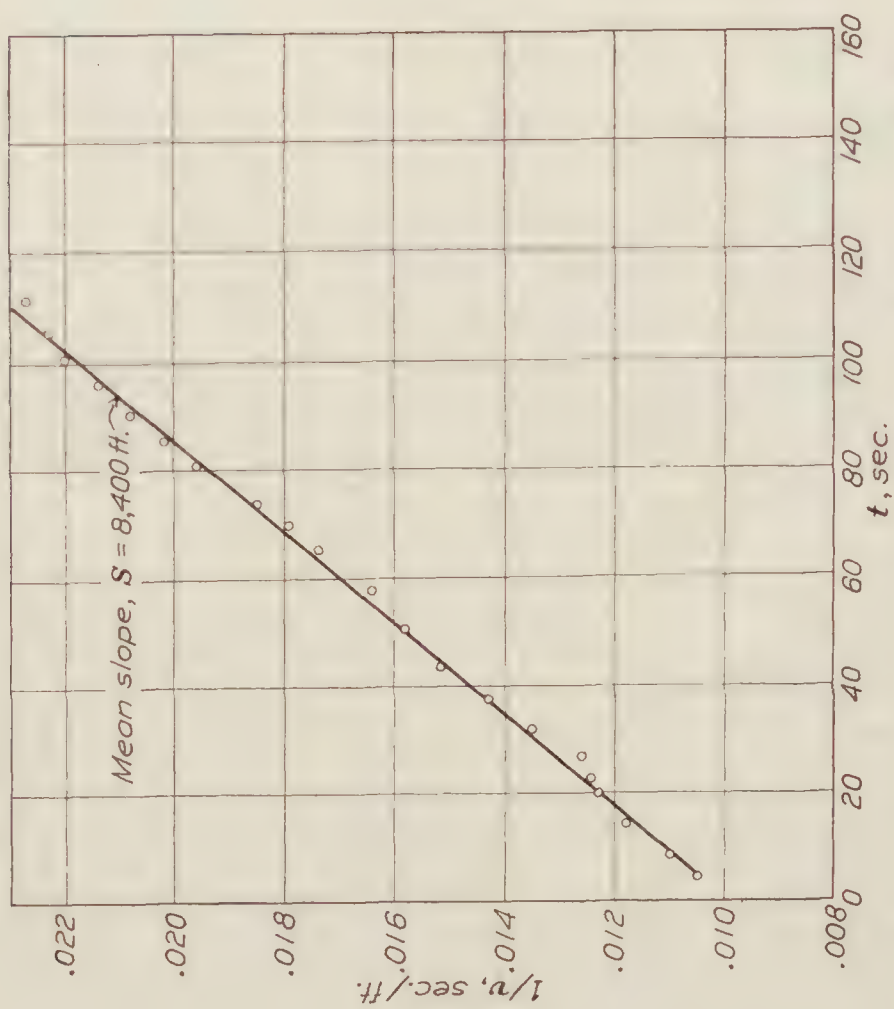


FIGURE 10.—Run No. 5. Deceleration with water recovery. Propellers stopped. Speed by electric meter

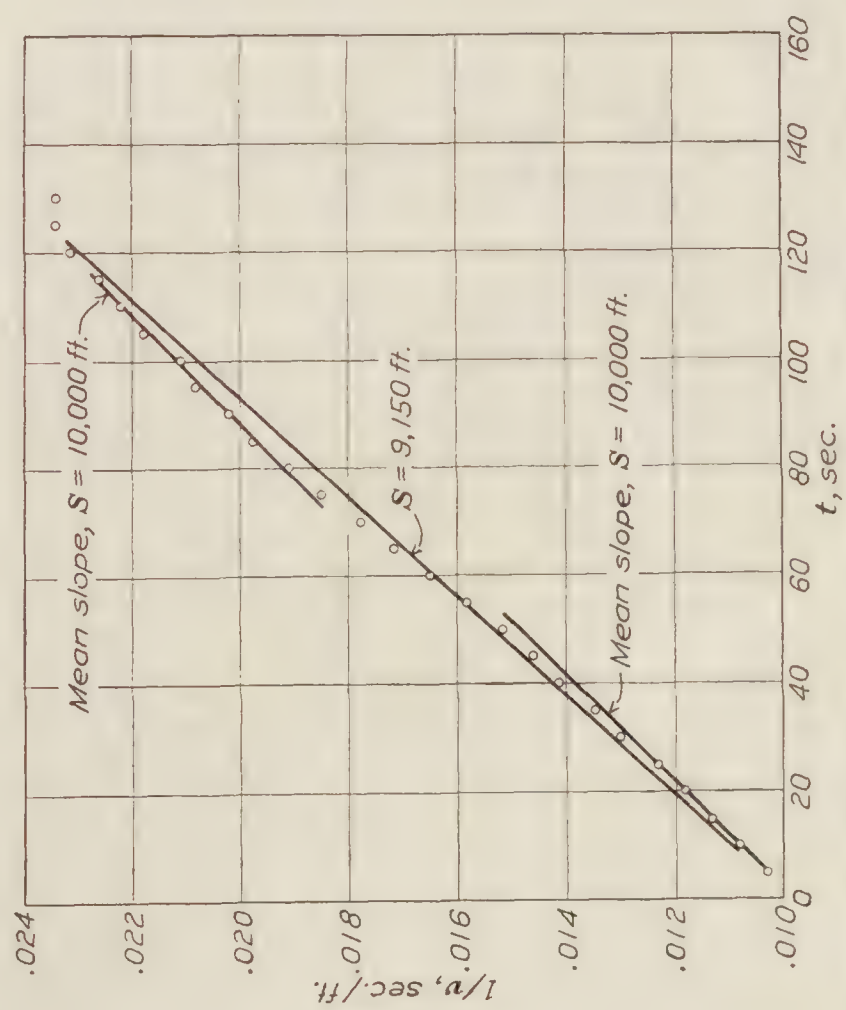


FIGURE 12.—Run No. 7. Deceleration with water recovery. Propellers idling. Speeds by electric meter

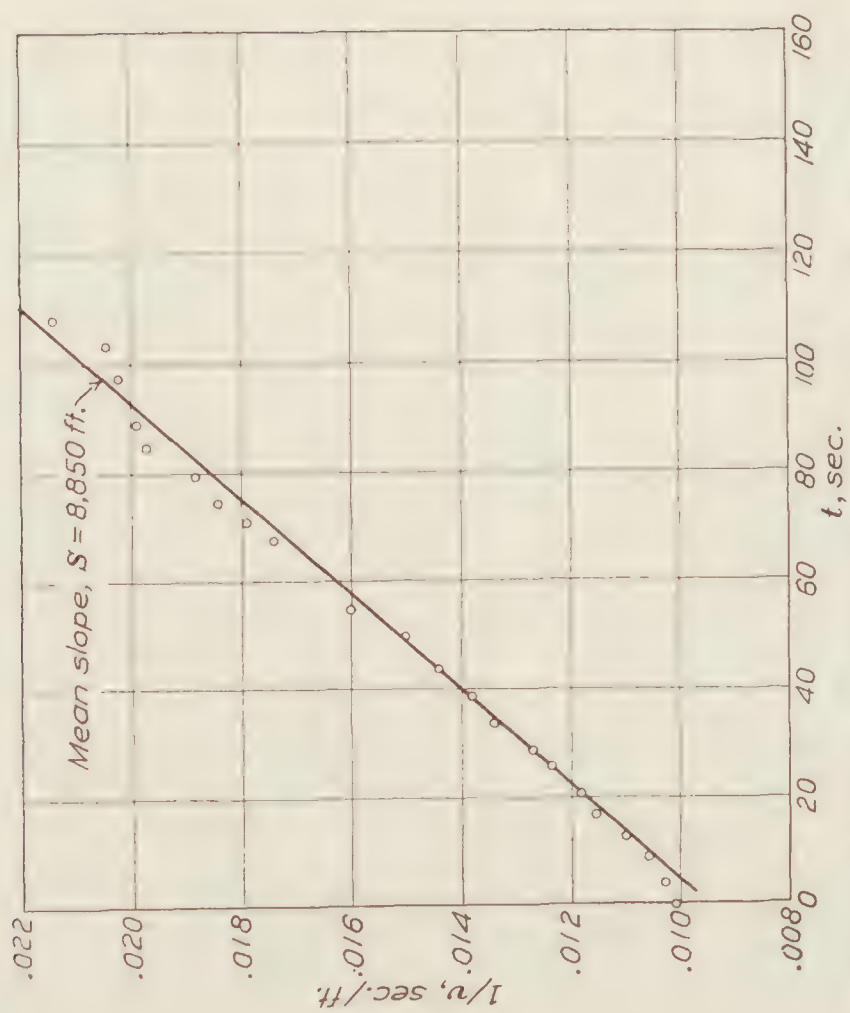


FIGURE 11.—Run No. 6. Deceleration with water recovery. Propellers stopped. Speeds by electric meter

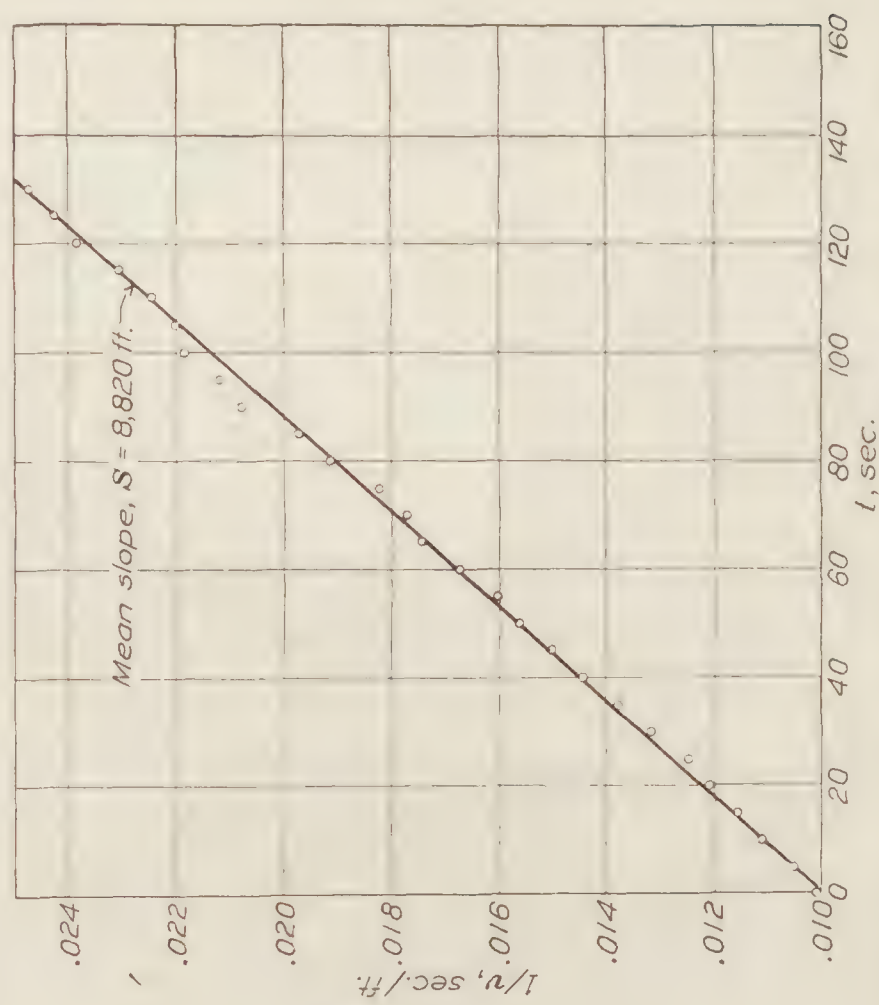


FIGURE 13.—Run No. 8. Deceleration with water recovery. Propellers idling. Speeds by electric meter

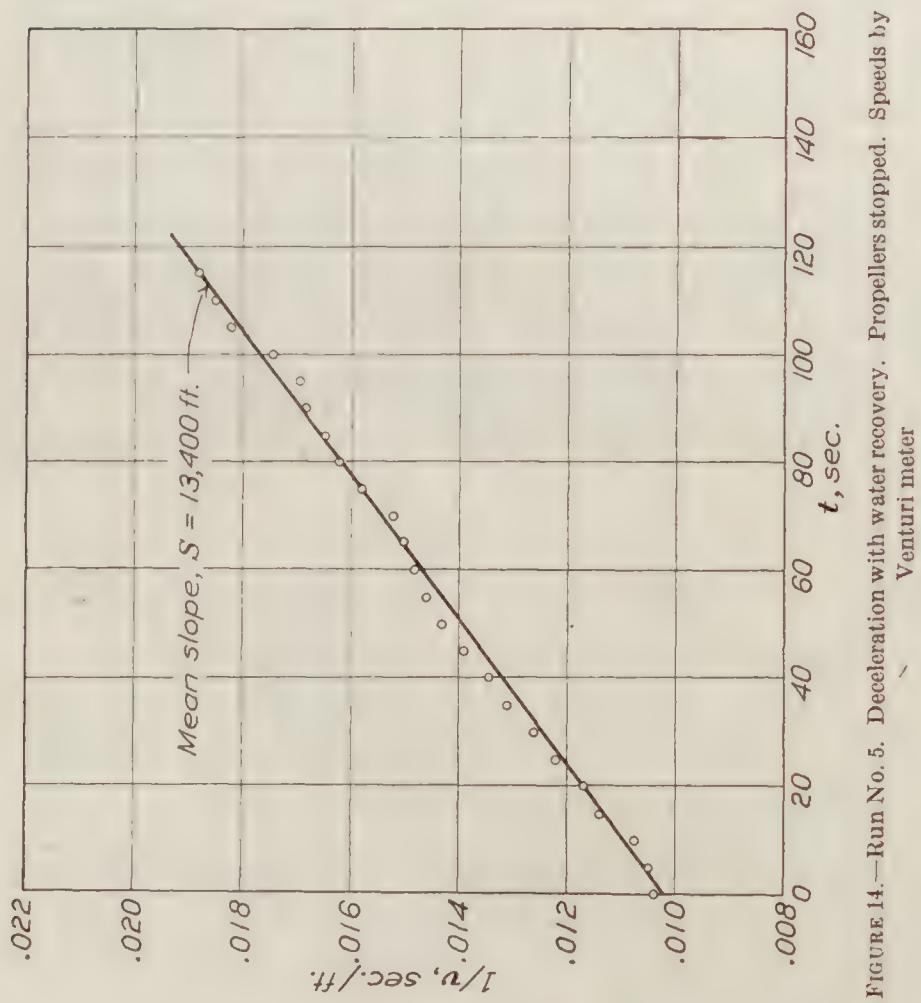


FIGURE 14.—Run No. 5. Deceleration with water recovery. Propellers stopped. Speeds by Venturi meter

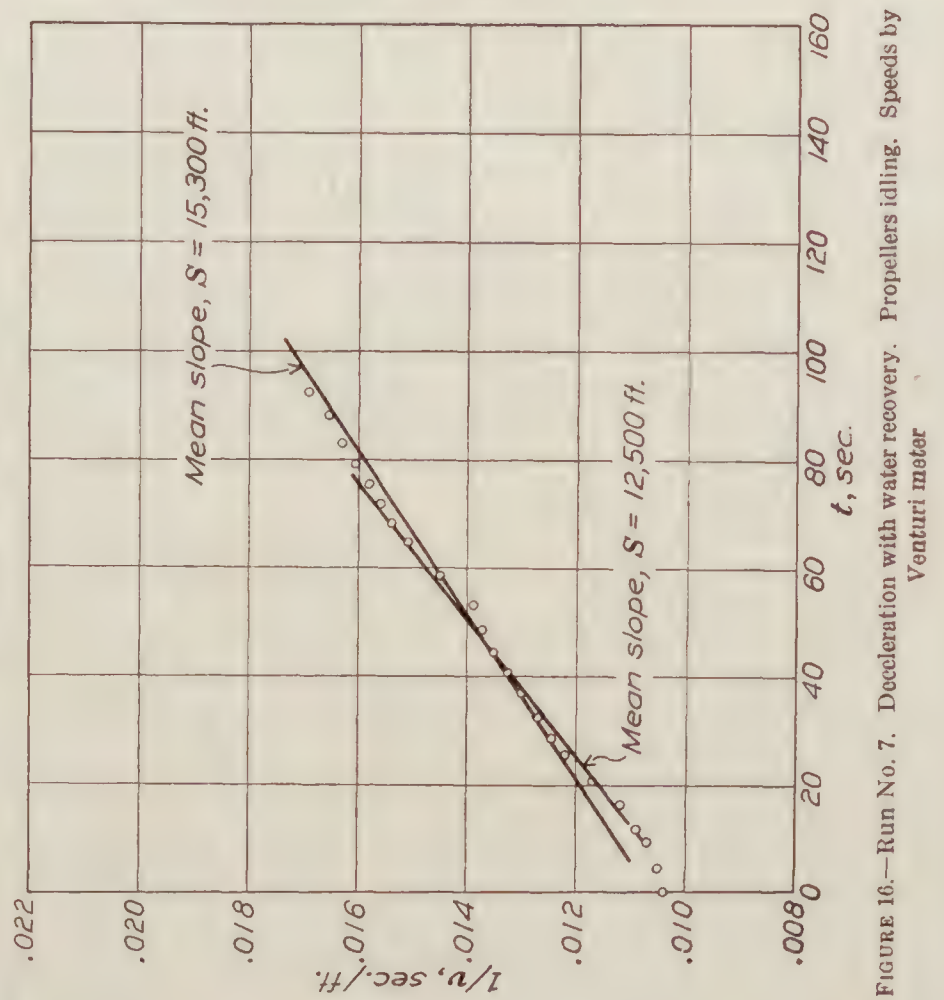


FIGURE 16.—Run No. 7. Deceleration with water recovery. Propellers idling. Speeds by Venturi meter

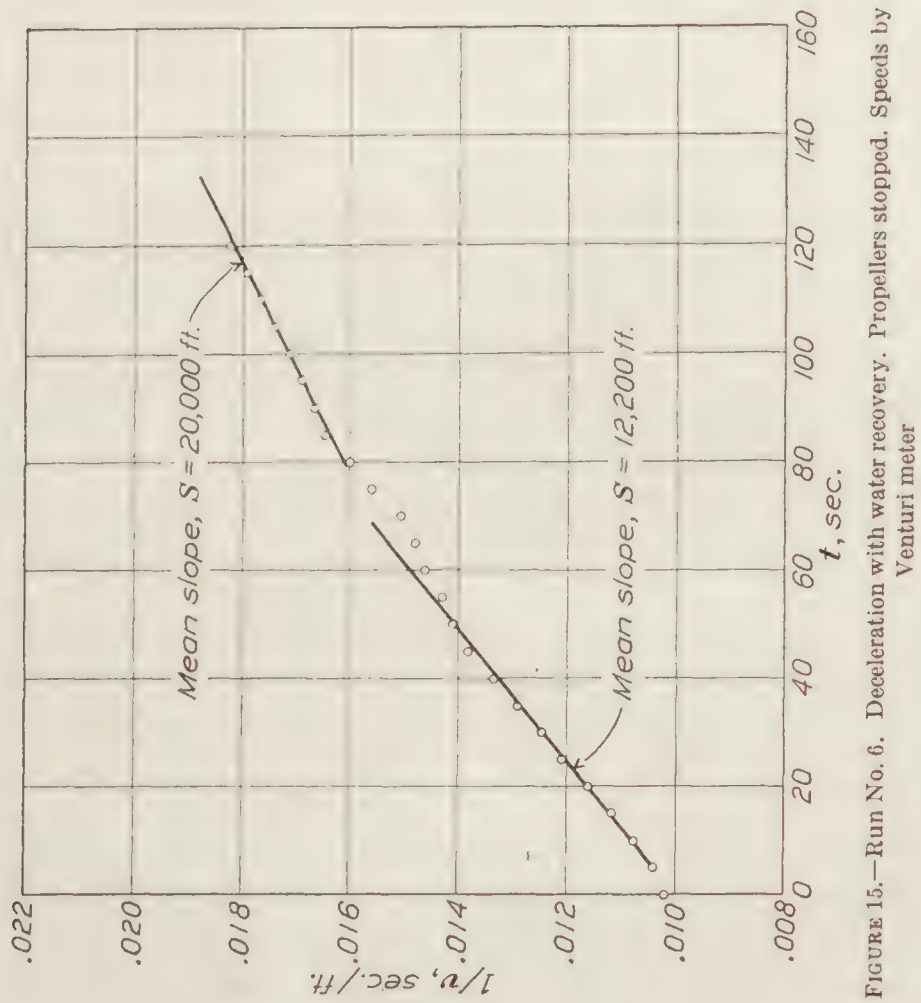


FIGURE 15.—Run No. 6. Deceleration with water recovery. Propellers stopped. Speeds by Venturi meter

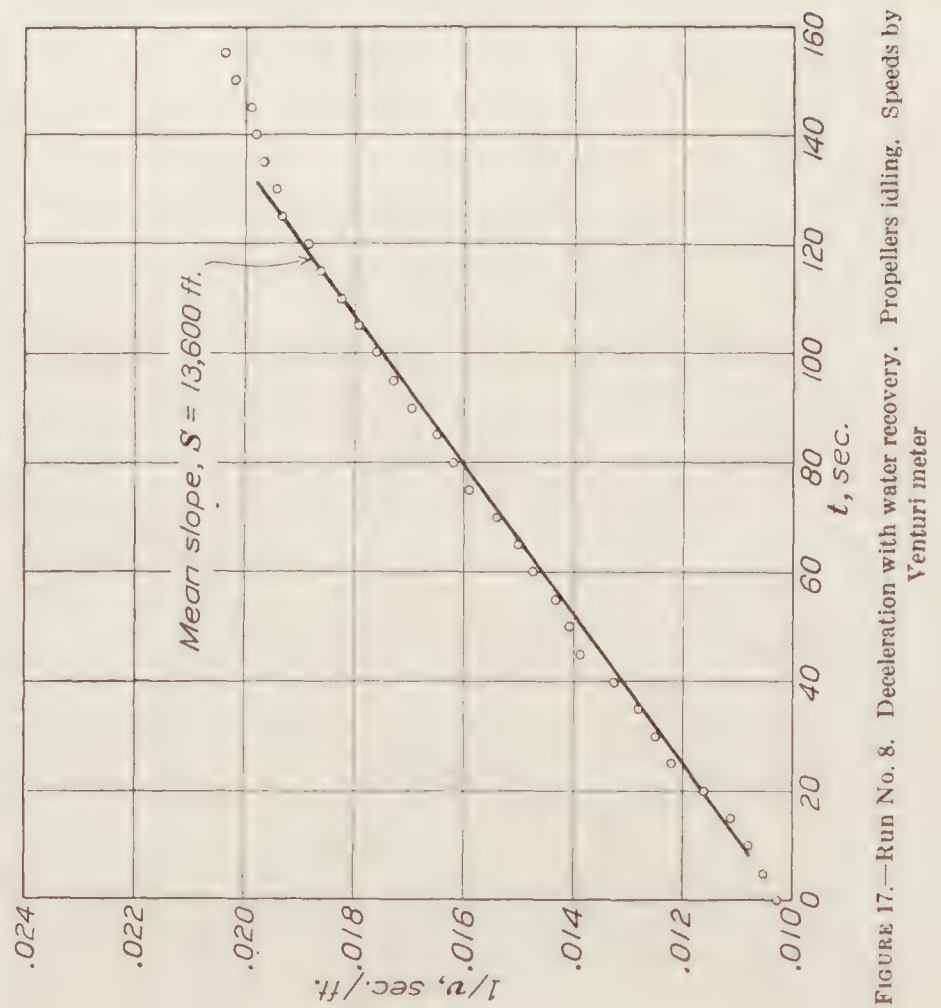


FIGURE 17.—Run No. 8. Deceleration with water recovery. Propellers idling. Speeds by Venturi meter

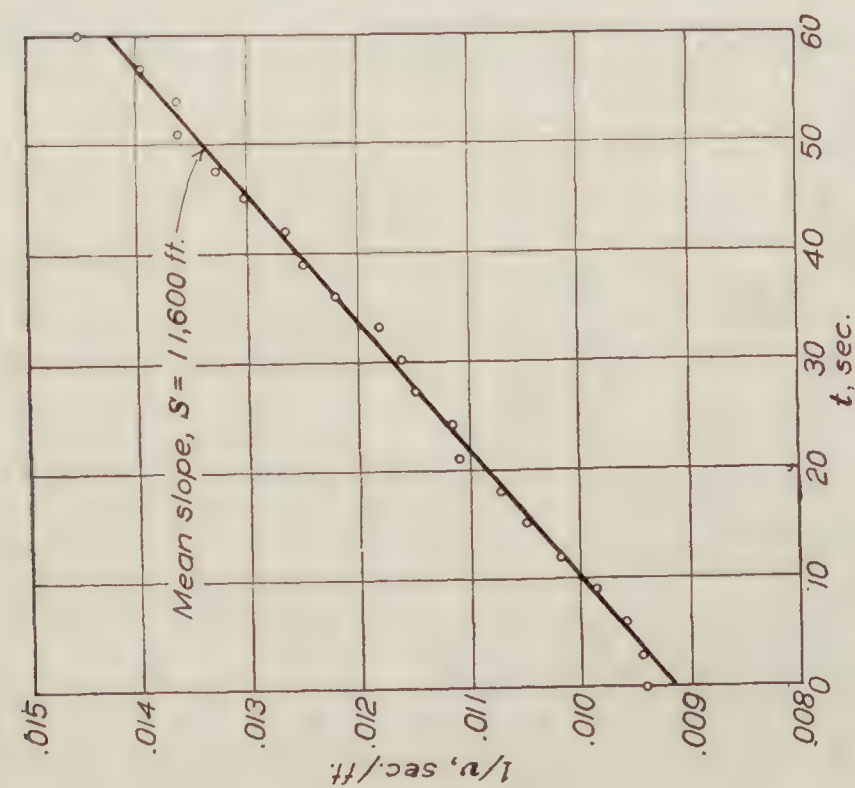


FIGURE 18.—Run No. 1. Deceleration without water recovery. Propellers stopped. Speeds by N. A. C. A. recording instrument

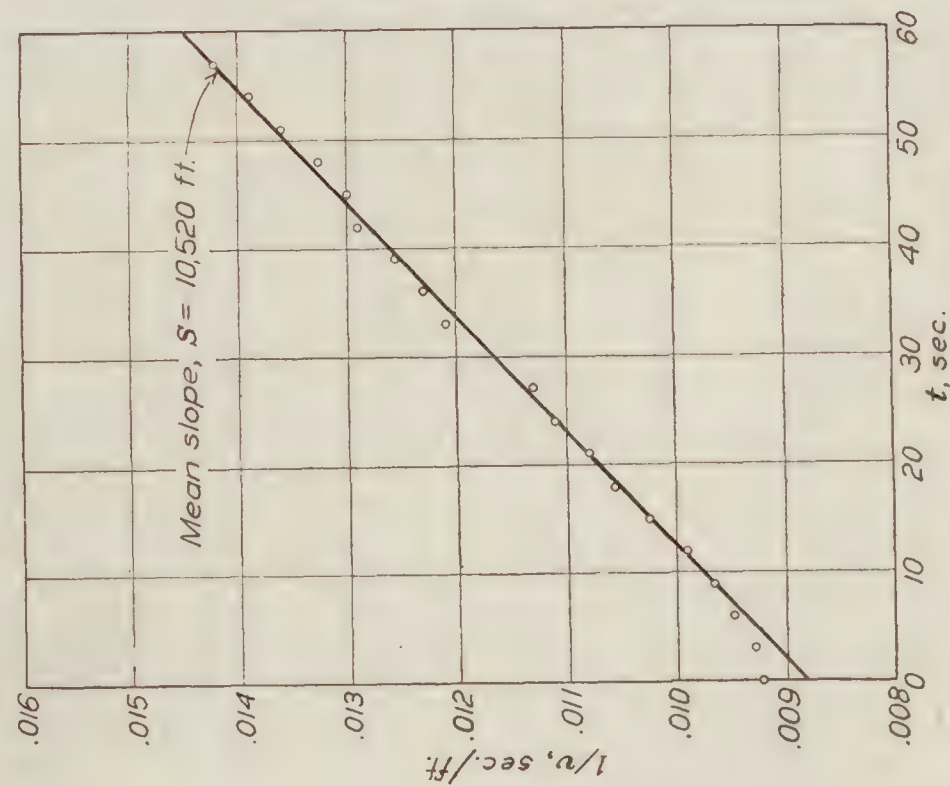


FIGURE 21.—Run No. 4. Deceleration without water recovery. Propellers idling. Speeds by N. A. C. A. recording instrument

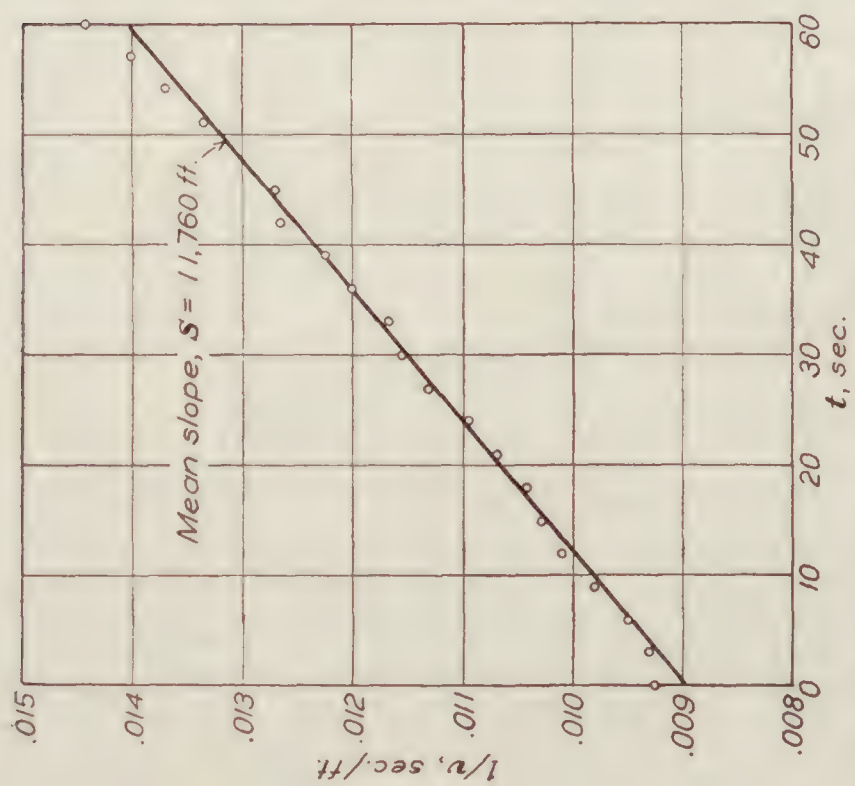


FIGURE 19.—Run No. 2. Deceleration without water recovery. Propellers stopped. Speeds by N. A. C. A. recording instrument

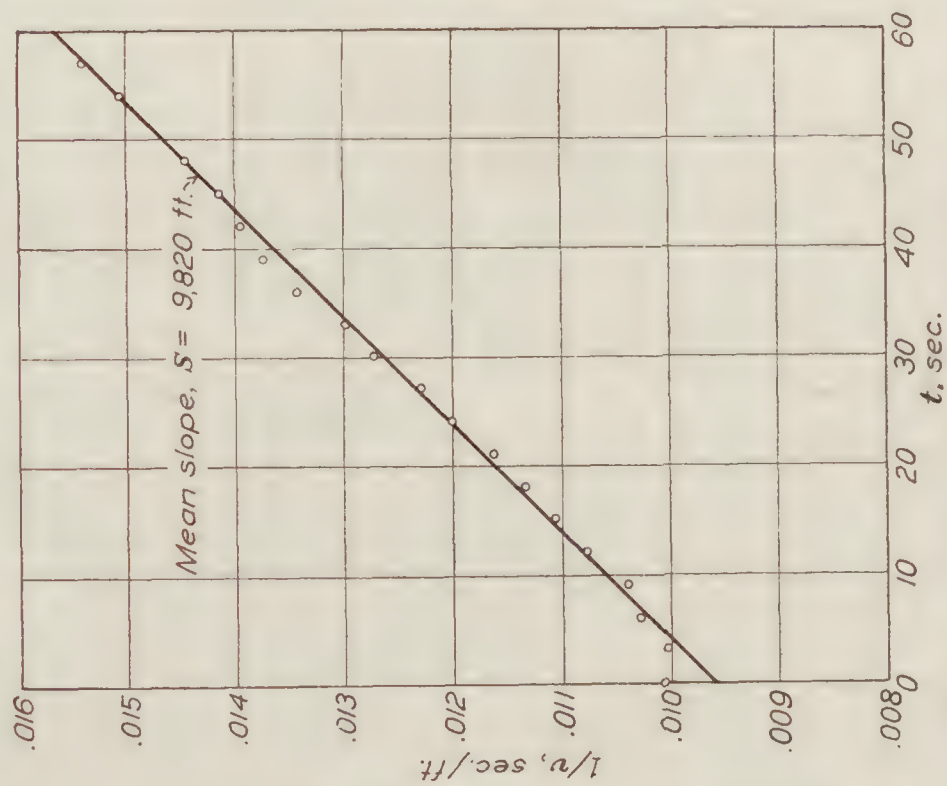


FIGURE 22.—Run No. 5. Deceleration with water recovery. Propellers stopped. Speeds by N. A. C. A. recording instrument

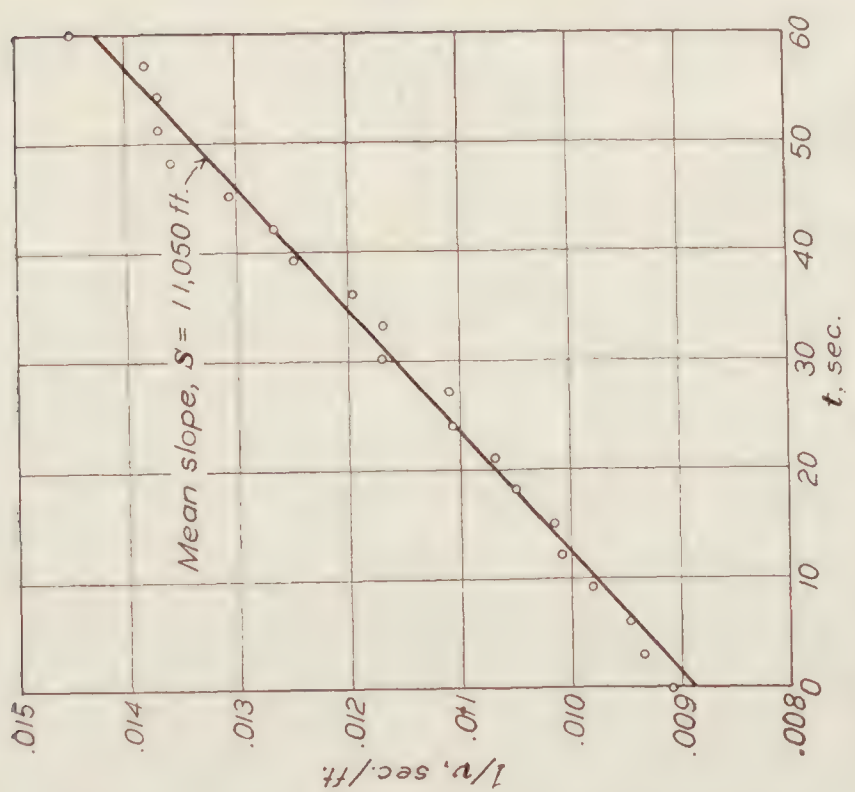


FIGURE 20.—Run No. 3. Deceleration without water recovery. Propellers idling. Speeds by N. A. C. A. recording instrument

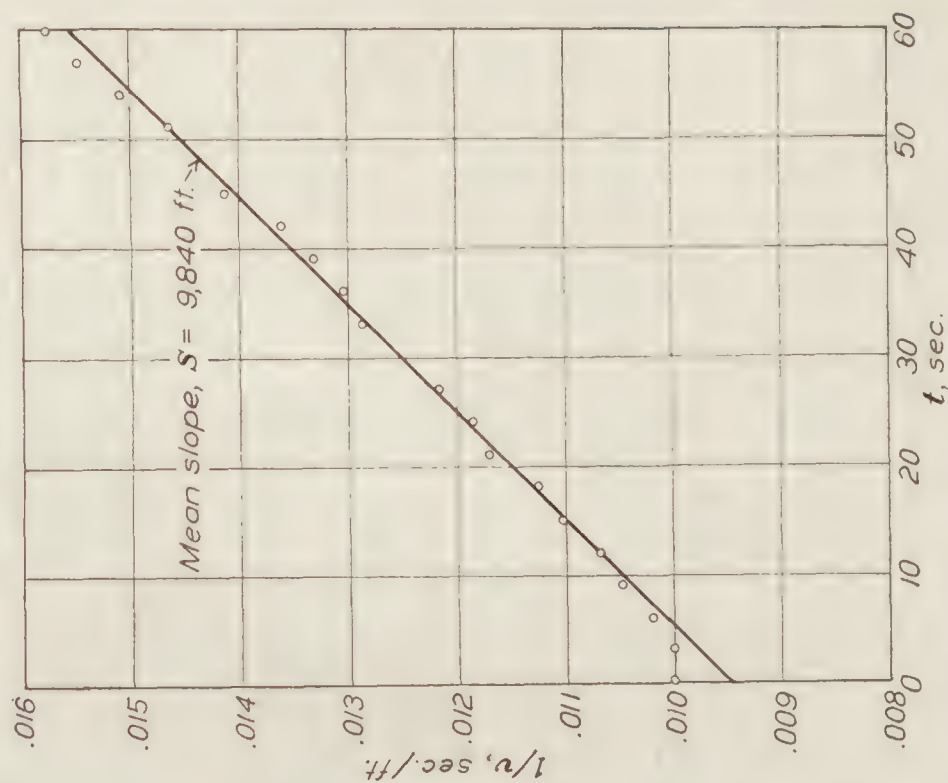


FIGURE 23.—Run No. 6. Deceleration with water recovery. Propellers stopped. Speeds by N. A. C. A. recording instrument

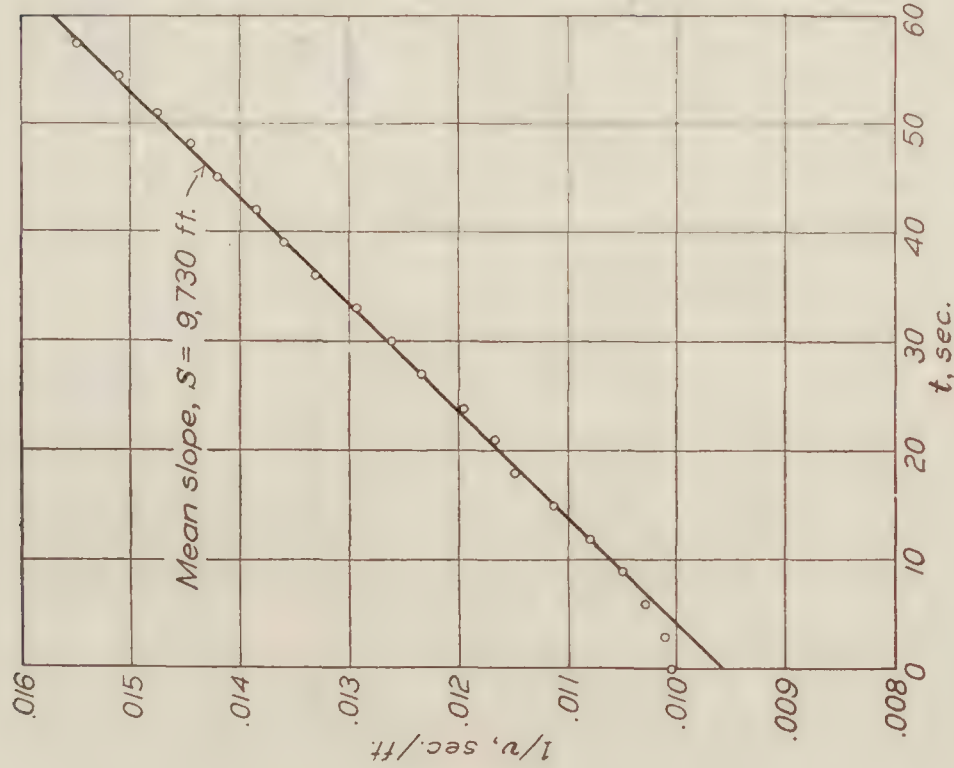


FIGURE 24.—Run No. 7. Deceleration with water recovery. Propellers idling. Speeds by N. A. C. A. recording instrument

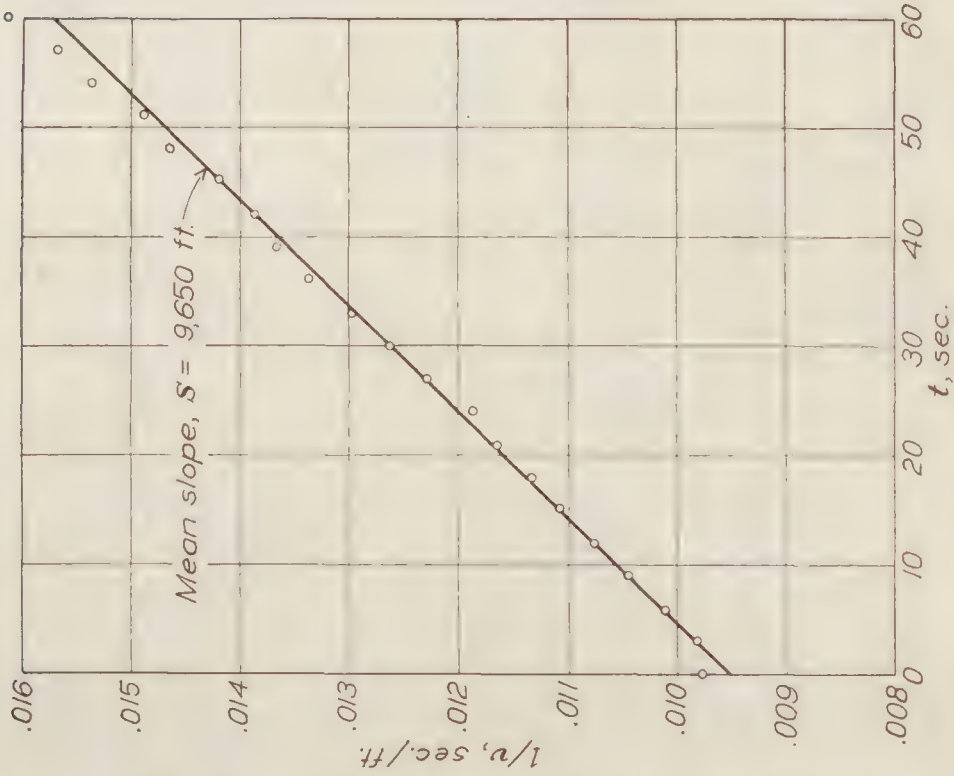


FIGURE 25.—Run No. 8. Deceleration with water recovery. Propellers idling. Speeds by N. A. C. A. recording instrument

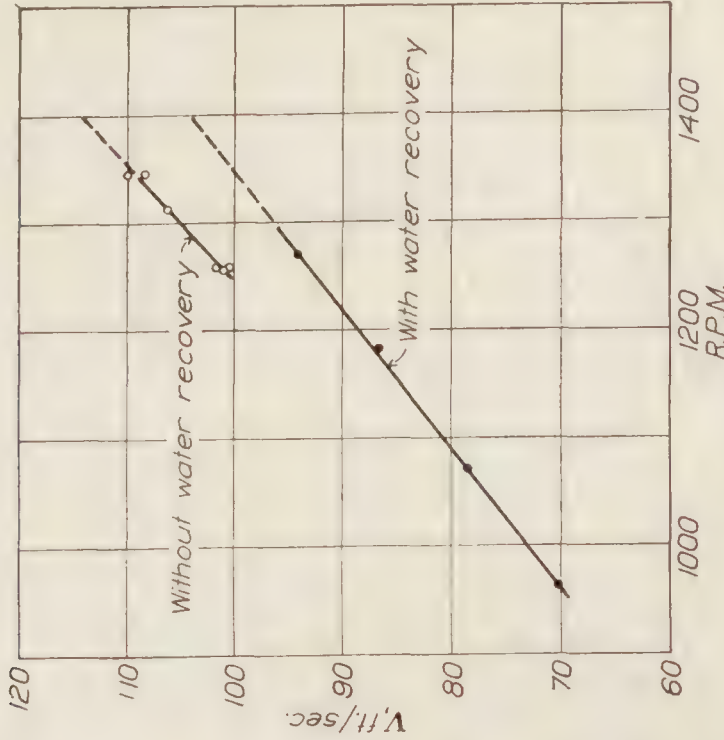


FIGURE 26. U. S. S. *Los Angeles* true air speed versus R. P. M. September 2 and 6, 1927

REPORT No. 319

**AERODYNAMIC CHARACTERISTICS OF TWENTY-FOUR
AIRFOILS AT HIGH SPEEDS**

By L. J. BRIGGS and H. L. DRYDEN
Bureau of Standards

REPORT No. 319

AERODYNAMIC CHARACTERISTICS OF TWENTY-FOUR AIRFOILS AT HIGH SPEEDS

By L. J. BRIGGS and H. L. DRYDEN

SUMMARY

The aerodynamic characteristics of 24 airfoils are given for speeds of 0.5, 0.65, 0.8, 0.95, and 1.08 times the speed of sound, as measured in an open-jet air stream 2 inches in diameter, using models of 1-inch chord. The 24 airfoils belong to four general groups. The first is the standard R. A. F. family in general use by the Army and Navy for propeller design, the members of the family differing only in thickness. This family is represented by nine members ranging in thickness from 0.04 to 0.20 inch. The second group consists of five members of the Clark Y family, the members of the family again differing only in thickness. The third group, comprising six members, is a second R. A. F. family in which the position of the maximum ordinate is varied. Combined with two members of the first R. A. F. family, this group represents a variation of maximum ordinate position from 30 to 60 per cent of the chord in two camber ratios, 0.08 and 0.16. The fourth group consists of three geometrical forms, a flat plate, a wedge, and a segment of a right circular cylinder. In addition one section used in the Reed metal propeller was included. These measurements form a part of a general program outlined at a conference on propeller research organized by the National Advisory Committee for Aeronautics and the work was carried out with the financial assistance of the committee.

INTRODUCTION

In Technical Report No. 207 of the National Advisory Committee for Aeronautics (Reference 1) an account is given of the results of some measurements by G. F. Hull and the authors of the aerodynamic characteristics of six airfoils of 3-inch chord in an open-jet air stream 12 inches in diameter at speeds from about 0.5 the speed of sound, to speeds in some instances approaching the speed of sound. The measurements supplemented those made by Caldwell and Fales at McCook Field (Reference 2), at speeds up to about 0.5 the speed of sound, confirmed the important influence of speed on the lift and drag coefficients, and established the following general relations:

1. The lift coefficient for a fixed angle of attack decreases rapidly as the speed increases.
2. The drag coefficient under the same conditions increases rapidly.
3. The center of pressure moves back toward the trailing edge.
4. The speed at which the rapid change in coefficients begins is decreased by (a) increasing the angle of attack and by (b) increasing the camber ratio.
5. The angle of zero lift shifts to higher negative angles up to the "critical" speed and then moves rapidly toward 0° .

These phenomena were further studied by measurements of the pressure distribution on models of 1-inch chord in a 2-inch air stream as described by the writers in Technical Report No. 255 (Reference 3) of the National Advisory Committee for Aeronautics. Speeds up to 1.08 times the speed of sound were obtained and it was shown that the large changes in the force coefficients were associated with a breaking away of the air flow from the upper surface, similar to that which occurs at the burble point at ordinary wind-tunnel speeds.

If a propeller is mounted directly on the shaft of a modern high-speed airplane engine, the outer airfoil sections of the propeller travel at speeds approaching the speed of sound. It is

possible by the use of gearing and a somewhat larger propeller to reduce the speed of the propeller sections, but only at the expense of additional weight and some frictional loss of power.¹ In order to determine whether gearing is desirable, it is necessary to know the loss of efficiency due to high tip speeds and to compare this loss with that due to the use of gearing. The problem is of increasing importance and at a conference on propeller research called by the National Advisory Committee for Aeronautics the Bureau of Standards was asked to determine the characteristics of the families of sections used by the Army and Navy in propeller design and such other sections as might be expected to lead to more efficient performance. This report presents the results of this work.

APPARATUS

AIR STREAM.—The air stream was furnished by a duplex reciprocating compressor having a capacity of 1,800 cubic feet of free air per minute at gauge pressures up to 30 pounds per square inch. The air passed through three stabilizing tanks into a vertical pipe 8 inches in diameter, with a flow nozzle mounted at the upper end for forming the high-speed jet. The speed of the air stream was controlled and maintained constant by wasting air through blow-off valves on the stabilizing tanks. The values of the air speed were computed from the pressure observed on a manometer connected to a small hole in the 8-inch pipe about 1 foot ahead of the nozzle. Observations were taken at speeds of 0.5, 0.65, 0.8, 0.95, and 1.08 times the speed of sound at the temperature of the jet, corresponding to 563, 732, 902, 1,071, and 1,218 feet per second at 20° C.

NOZZLES.—The two nozzles described in N. A. C. A. Technical Report No. 255 (Reference 3) were again used. A 2-inch cylindrical nozzle was employed for speeds below the speed of sound and a slightly expanding nozzle with a throat diameter of 1.9 inches and taper of 1 in 21 was used for the highest speed (1.08 times the speed of sound).

AIRFOILS.—The airfoils were 1 inch in chord and 6 inches long, and were mounted so as to span the air stream. The sections, Figures 6 to 45, may conveniently be considered as belonging to four groups. The first group may be termed the R. A. F. family and is based on one of the British R. A. F. sections (R. A. F. 6a). The members of the family differ only in thickness, all ordinates being increased in the same ratio, and are designated by a combination of numbers and letters such as 3R12. The R denotes that the family is derived from the R. A. F. section; the first number 3 denotes the position of the maximum ordinate in tenths of the chord length, and the second number denotes the camber ratio (or thickness ratio since the lower surface is plane) in hundredths of the chord length. Six members of the family, namely, 3R10, 3R12, 3R14, 3R16, 3R18, and 3R20 are the sections used in the tests described in N. A. C. A. Technical Reports Nos. 207 and 255 (References 1 and 3), referred to there as airfoils 1, 2, 3, 4, 5, and 6.² In the present work 3R4, 3R6, and 3R8 were included with the six already referred to, making a total of nine members in the family.²

The second group was of the same type except that a Clark Y section was used as the basic section. Five members of the family were represented in the tests, namely, C4, C8, C12, C16, and C20. The maximum ordinate designation is omitted since no additional C sections were tested.

The third group consisted of two subgroups, both derived from the R section. The primary variable was the position of the maximum ordinate and the subgroups correspond to two camber ratios. In the above designation the additional sections were 4R8, 5R8, 6R8, 4R16, 5R16, and 6R16. Two members of the first family, namely, 3R8 and 3R16, may also be considered in this third family.

The fourth group consisted of four sections belonging to none of the preceding families. A flat plate with the ratio of thickness to chord equal to 0.04, a wedge with the base thickness equal to 0.08 times the chord, a circular arc of camber ratio equal to 0.08, and a section repre-

¹ It is common practice to increase propeller efficiency by using reduction gear to secure aerodynamic advantage.

² The same sections are designated as U. S. N. P. S. sections in Technical Report No. 259 of the National Advisory Committee for Aeronautics (Reference 4), and carry different numbers, 3R10 or 1 corresponding to U. S. N. P. S. 3, 3R12 or 2 to U. S. N. P. S. 4, 3R16 or 4 to U. S. N. P. S. 5, and 3R20 or 6 to U. S. N. P. S. 6. U. S. N. P. S. 1 and U. S. N. P. S. 2 correspond to 3R4 and 3R8 in our new designation.

sentative of those used in the Reed metal propeller were included. All of these special sections had a chord of 1 inch.

The nominal ordinates of the sections are shown in Table I. The airfoils were made by W. H. Nichols, of Waltham, Mass., and check measurements showed that the departures from the nominal ordinates did not exceed 0.001 inch and were usually much less.

BALANCE.—The balance used for the force measurements is shown in Figure 1 and the airfoil mounting alone in Figure 2. The diagrammatic sketch in Figure 3 gives a somewhat better illustration of the operation. The airfoil is held in a fork **A**, which is rotatable (about a longitudinal axis in the airfoil) by means of a worm and gear with respect to a second fork **B**, which is rigidly attached to a post **C** hung from the beam of the drag balance **D**. The lift force is transmitted by the parallel linkage **E** to the drag balance support **F**, the joints of the linkage being made by thin flexible strips **G**. The drag force is balanced by means of weights on a scalepan **H**, a rider **I**, and finally by a chain **J** hung from the end of the beam and from a graduated wheel **K**. The zero position of the drag beam is indicated by a level **L** on the lower member of the linkage **E**.

The drag balance is supported by one member **M** of the lift linkage, which is in the form of a parallelogram with ball bearings **N** at the four corners. One arm of the linkage carries a lever **O** which transmits the lift force to the platform of the lift balance **P**. Suitable counterweights and damping devices are provided, and the whole mechanism is mounted on sliding ways so that the airfoil can be removed from the stream and be replaced by another without stopping the air stream. Lift and drag measurements may be made independently and simultaneously.

REDUCTION OF OBSERVATIONS.—In N. A. C. A. Technical Report No. 255 (Reference 3) we have given at some length the method of computing the air speed and the velocity pressure, $\frac{1}{2} \rho V^2$. Consequently, we repeat only the notation and the final equations.

NOTATION

- p_i = absolute static pressure inside pipe (velocity pressure negligible).
- p_o = absolute static pressure in jet (equal to barometric pressure).
- $p_i - p_o$ = impact pressure.
- V = speed of air in jet.
- c = speed of sound at temperature of jet.
- c_o = speed of sound at 0° C.
- ρ = density of air in jet.
- $q = \frac{1}{2} \rho V^2$ = velocity pressure.
- J = mechanical equivalent of heat.
- C_p = specific heat of air at constant pressure.
- k = ratio of specific heats.
- C_L = lift coefficient.
- C_D = drag coefficient.
- A = area of airfoil taken as chord times exit diameter of nozzle.
- L = lift.
- D = drag.

The following relations are derived in N. A. C. A. Technical Report No. 255 (Reference 3):

$$\frac{V^2}{c^2} = \frac{546 J C_p}{c_o^2} \left\{ \left(\frac{p_i}{p_o} \right)^{\frac{k-1}{k}} - 1 \right\}$$

$$\frac{1}{2} \rho V^2 = \frac{288 \times 0.0012255}{1013300} J C_p p_o \left\{ \left(\frac{p_i}{p_o} \right)^{\frac{k-1}{k}} - 1 \right\}$$

$$\frac{p_i - p_o}{\frac{1}{2} \rho V^2} = \frac{(1 + 0.19991 V^2/c^2)^{7/2} - 1}{3.5088 \times 0.19991 V^2/c^2}$$

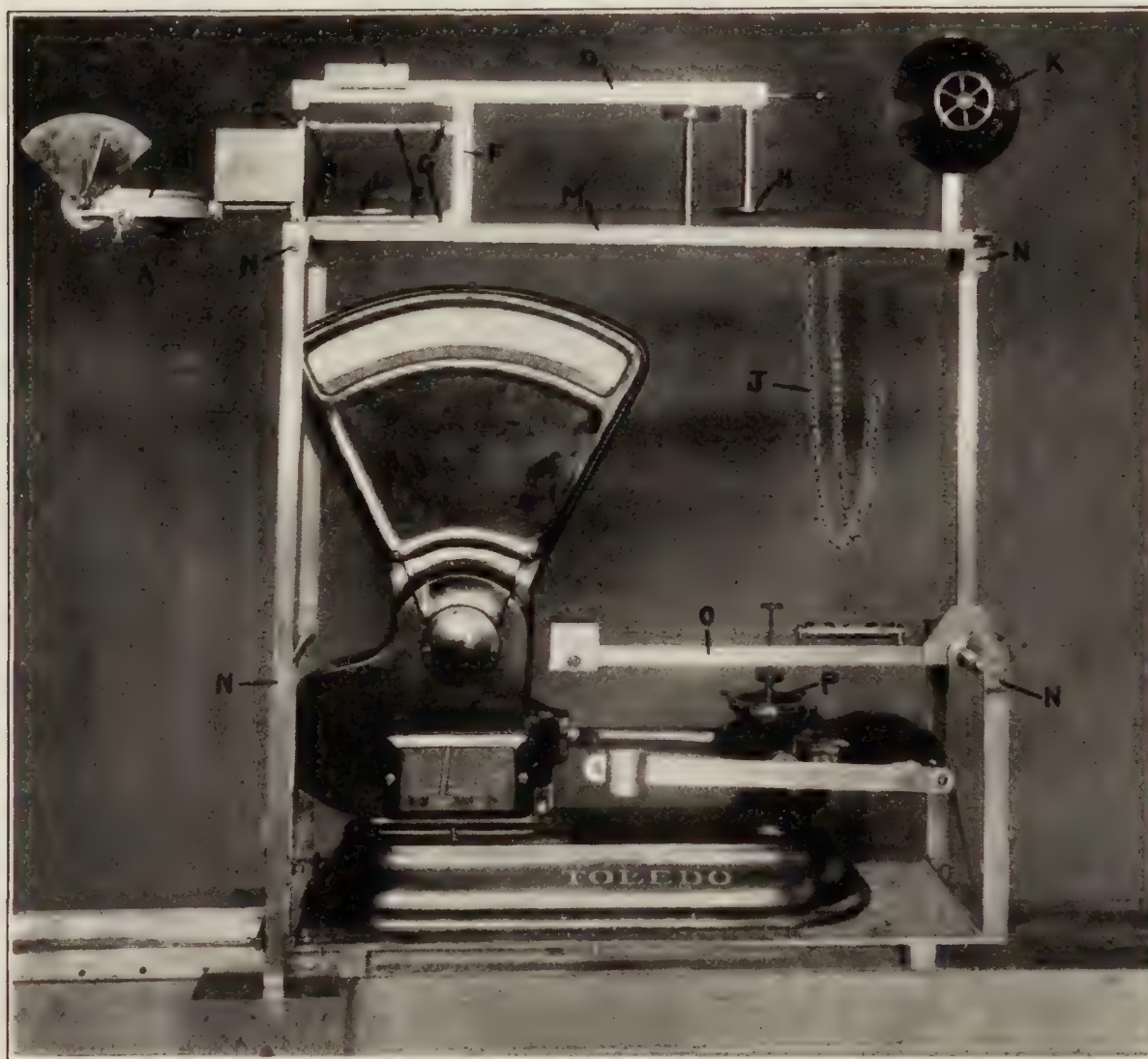


FIGURE 1.—The balance



FIGURE 2.—The airfoil mounting

The lift and drag coefficients are defined by the equations:

$$C_L = \frac{L}{\frac{1}{2} \rho V^2 A}$$

$$C_D = \frac{D}{\frac{1}{2} \rho V^2 A}$$

The quantities V/c , C_L , and C_D were computed from the observed lift, drag, pressure inside the pipe, and the barometric pressure by means of these equations.

RESULTS.—The results are given in the form of polar diagrams in Figures 6 to 14, 21 to 25, 31 to 36, and 42 to 45, inclusive, and comparison between members of the same family is facilitated by the cross-plots of drag coefficient against camber ratio for various lift coefficients given

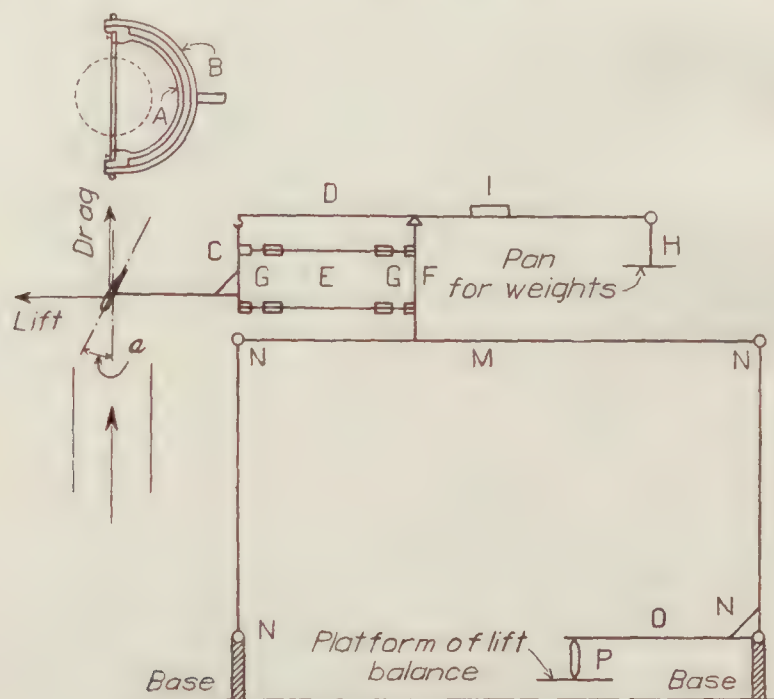


FIGURE 3.—Diagrammatic sketch of airfoil balance

in Figures 16 to 20 and 26 to 30. The data for the most useful range of angles from -4° to $+20^\circ$ are also given in tabular form in Table II.

As an experiment in visual representation, Figures 4 and 5 are photographs of a three-dimensional model giving the results for one airfoil. One pair of axes correspond to the usual C_L and C_D axes of the polar diagram, and sections parallel to the plane of these axes are polar diagrams. The third axis is that of V/c . The main characteristic of the surface is a hillside slope running diagonally across the model connecting two fairly level plateaus. The higher plateau (to the right in the photographs) represents the region of smooth flow and the lower (to the left) the high-speed burbling type of flow. The diagonal trend of the slope shows that at the higher lift coefficients, the change of flow begins at a lower speed.

EFFECT OF POSITION OF AIRFOIL IN AIR STREAM

The measurements given in this report were made with the center of the airfoils at a distance of 5 centimeters from the plane of the mouth of the nozzle. A number of measurements were made at other positions, namely, 2.7 centimeters above and 10 centimeters above. It was found that so long as the flow was smooth no appreciable effect of position was found. When, however, the flow breaks away from the surface as at high speeds or with thick sections, systematic effects are present. The greater part of the effect can be described by saying that the forces behave as if the absolute pressure in the "dead water" region decreased as the distance of the airfoil from the plane of the nozzle mouth was increased. The changes amounted to 0.04 in the lift coefficient and to 0.008 in the drag coefficient at a given angle of attack for the thickest sections at the two higher speeds; that is, in the worst cases.

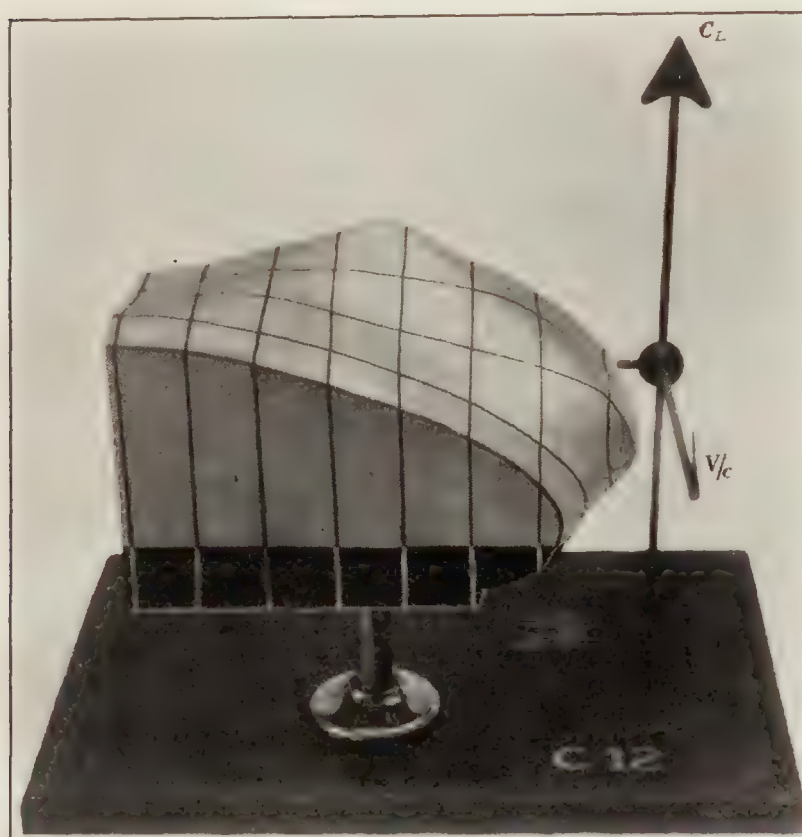


FIGURE 4.—Solid model illustrating relationship between C_L , C_D , and V/c

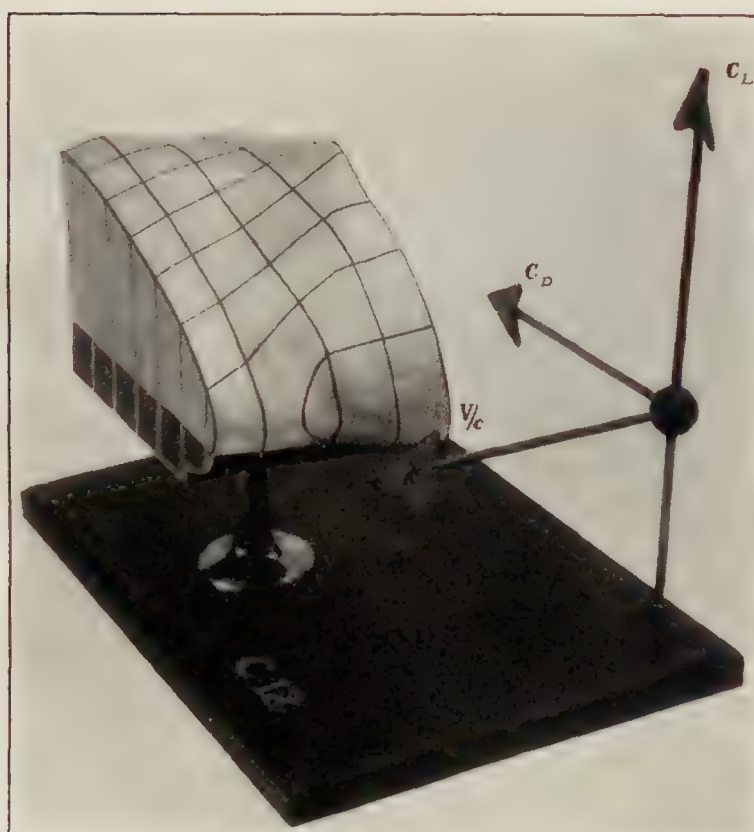
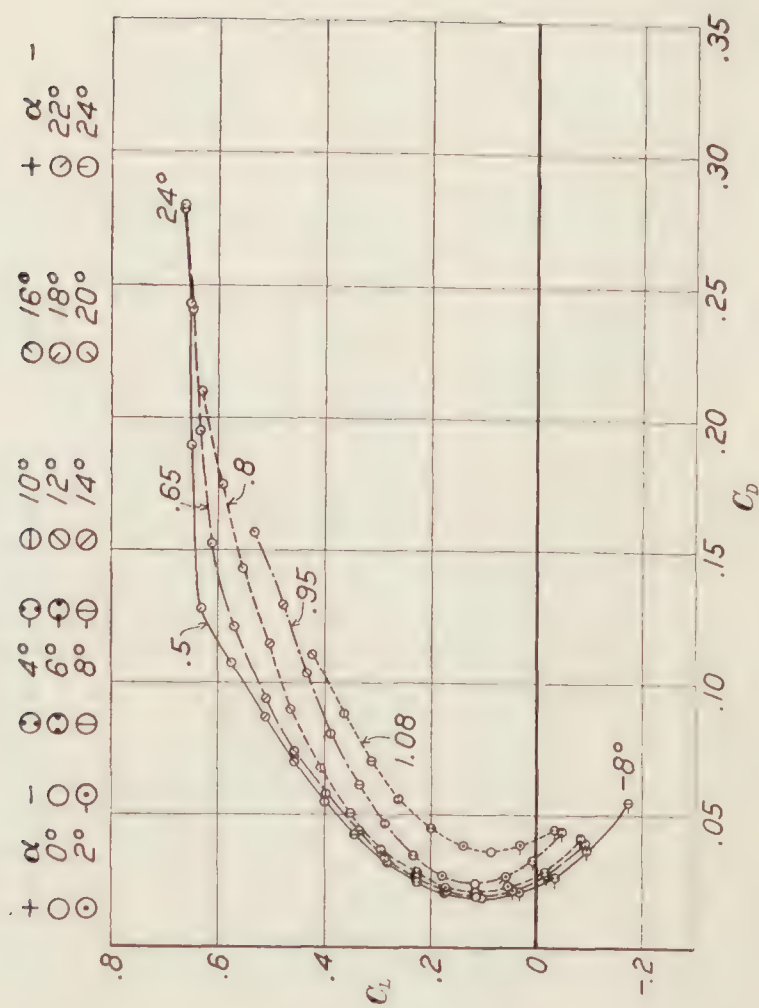
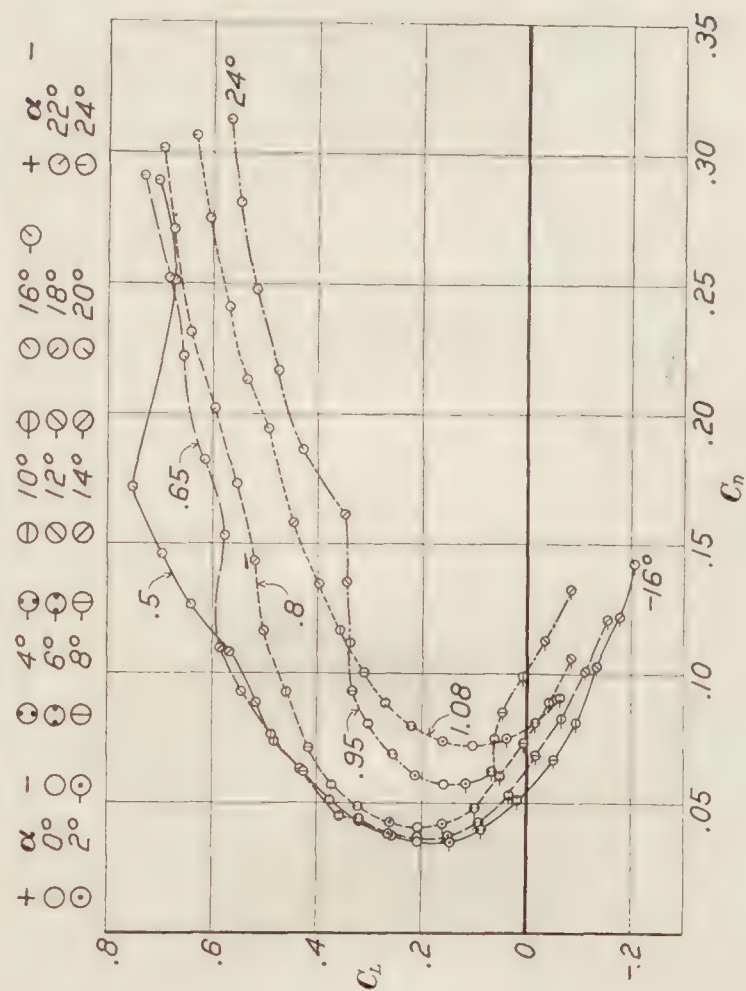
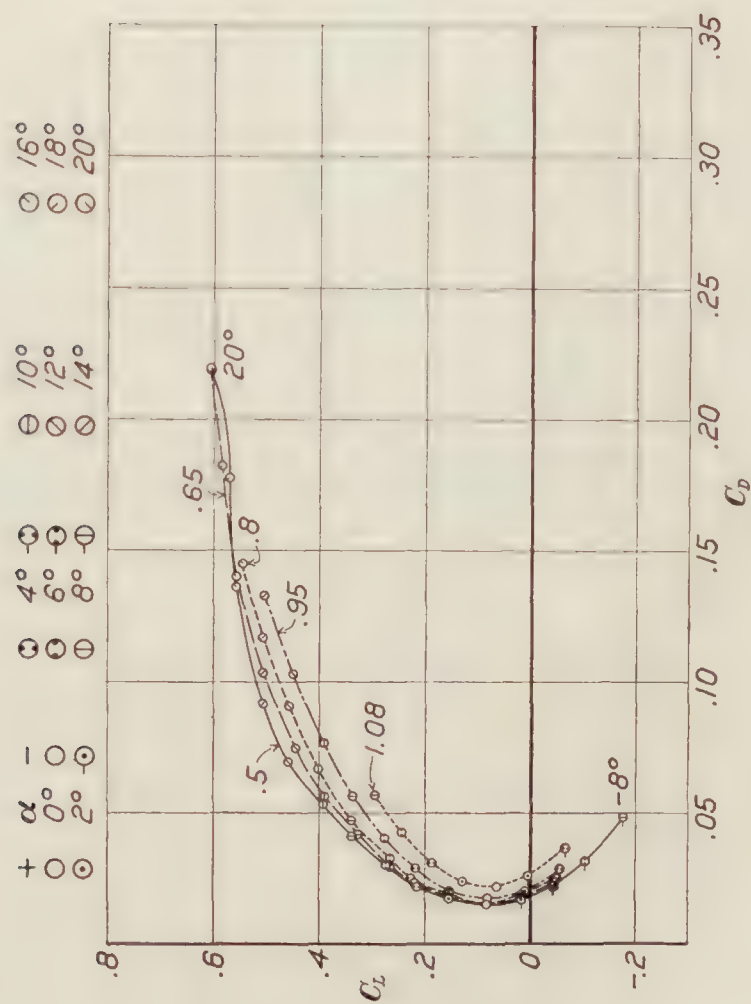
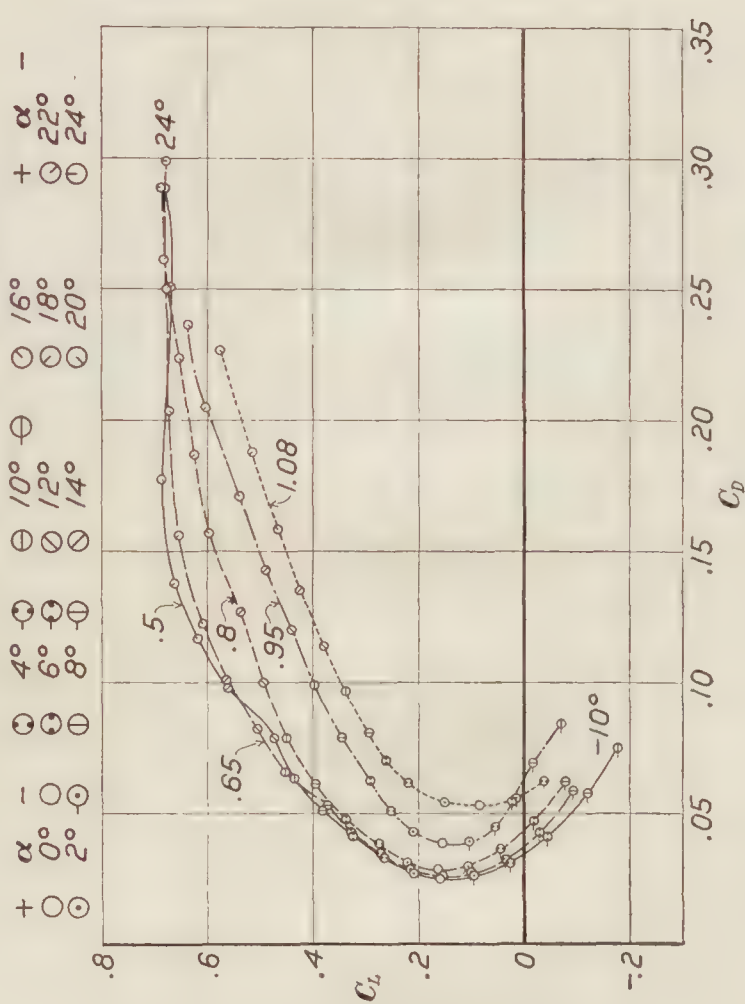
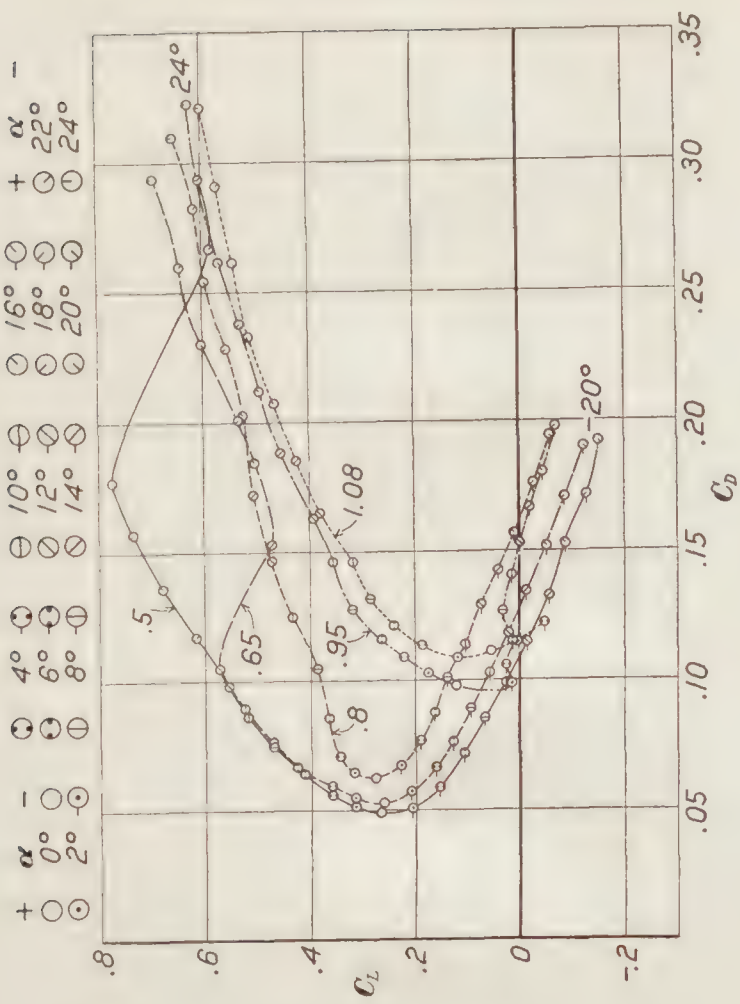
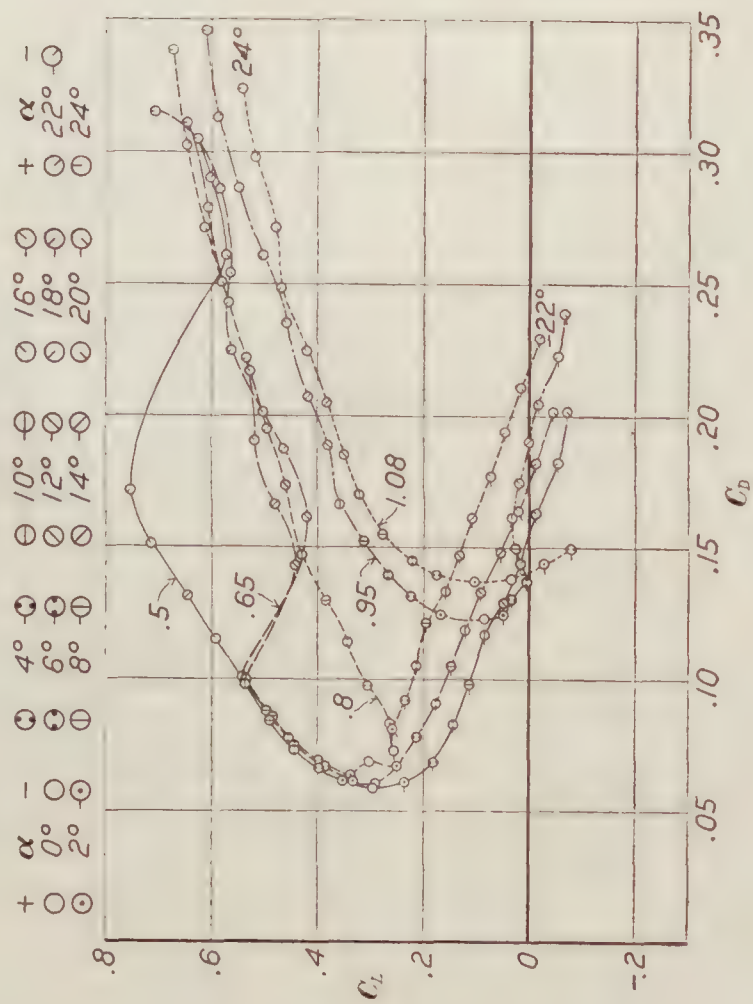
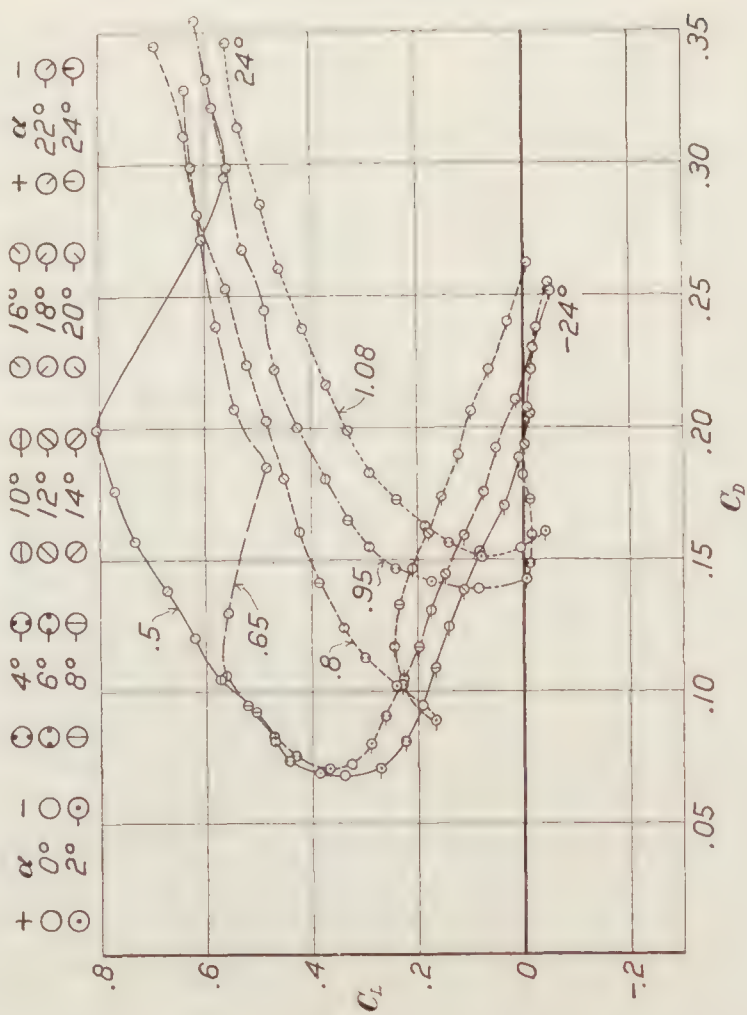


FIGURE 5.—Solid model illustrating relationship between C_L , C_D , and V/c

FIGURE 7.—Polar diagrams for airfoil 3R6 for five values of V/c FIGURE 9.—Polar diagrams for airfoil 3R10 for five values of V/c FIGURE 6.—Polar diagrams for airfoil 3R4 for five values of V/c FIGURE 8.—Polar diagrams for airfoil 3R8 for five values of V/c

FIGURE 10.—Polar diagrams for airfoil 3R12 for five values of V/c FIGURE 11.—Polar diagrams for airfoil 3R14 for five values of V/c FIGURE 12.—Polar diagrams for airfoil 3R16 for five values of V/c FIGURE 13.—Polar diagrams for airfoil 3R18 for five values of V/c

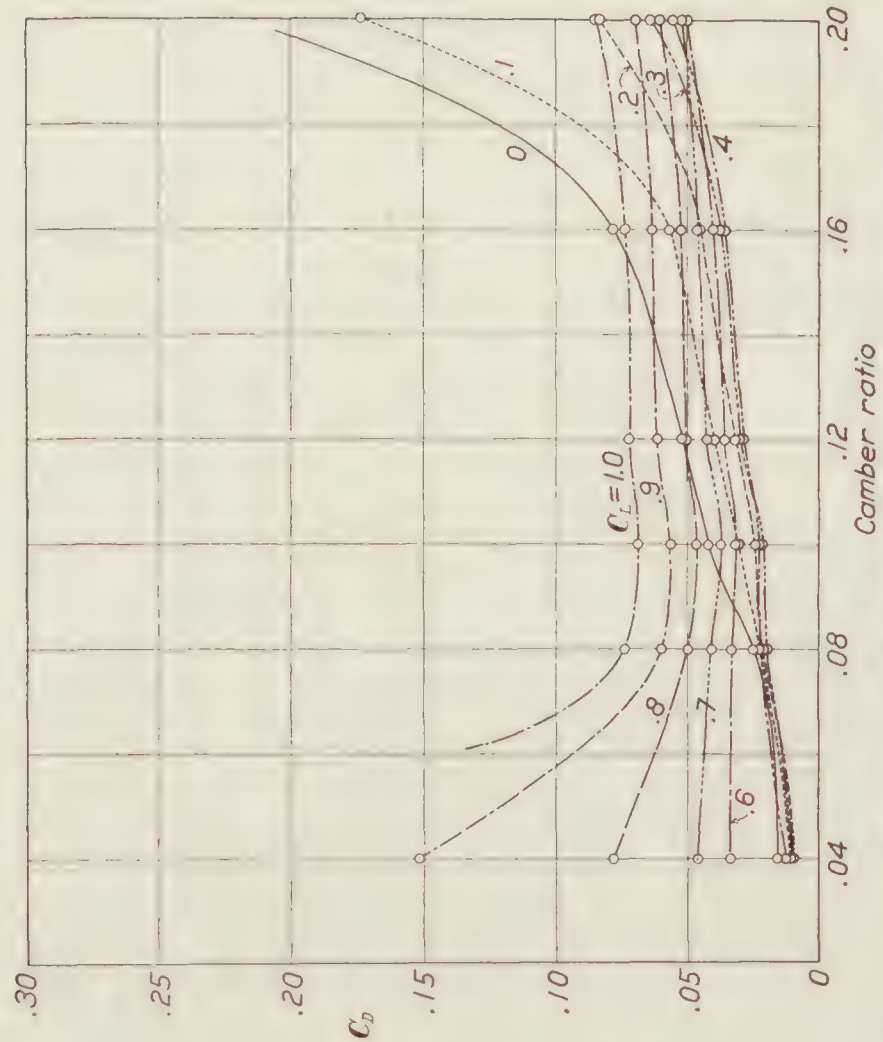


FIGURE 15.—Drag coefficient, C_D vs. camber ratio for various lift coefficients, C_L , at $V/c=0.05$, for 3R family

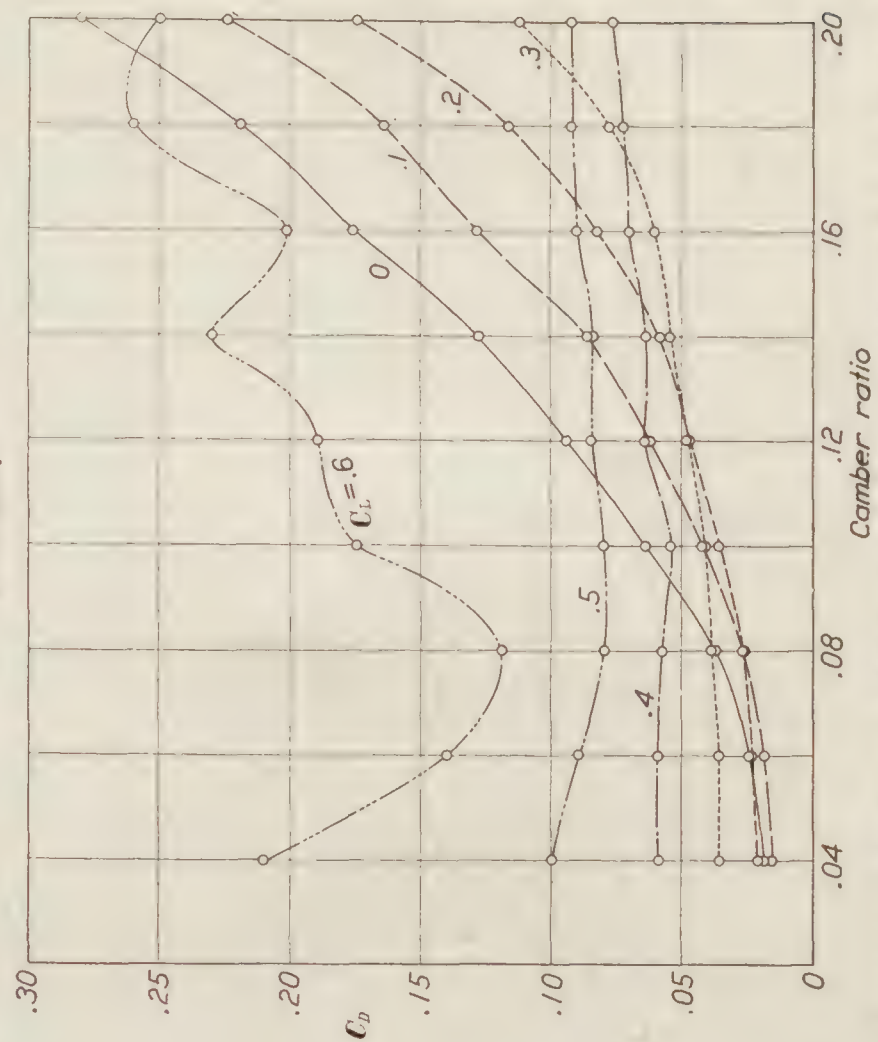


FIGURE 17.—Drag coefficient, C_D vs. camber ratio for various lift coefficients, C_L , at $V/c=0.05$, for 3R family

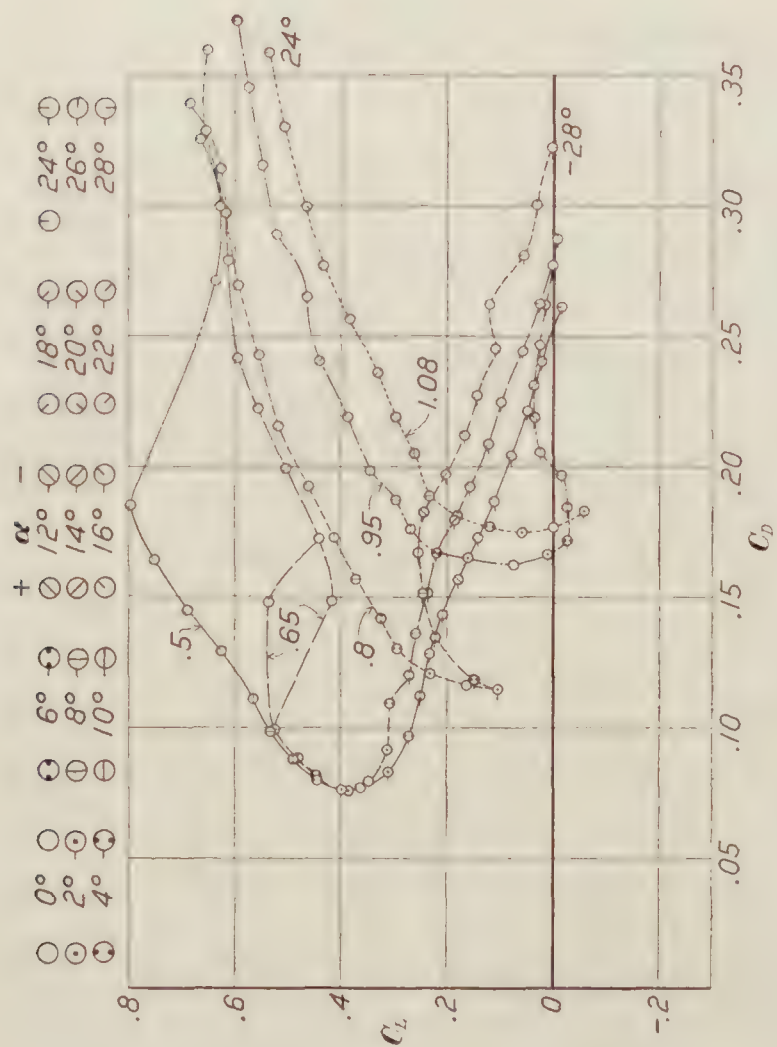


FIGURE 14.—Polar diagrams for airfoil 3R20 for five values of V/c

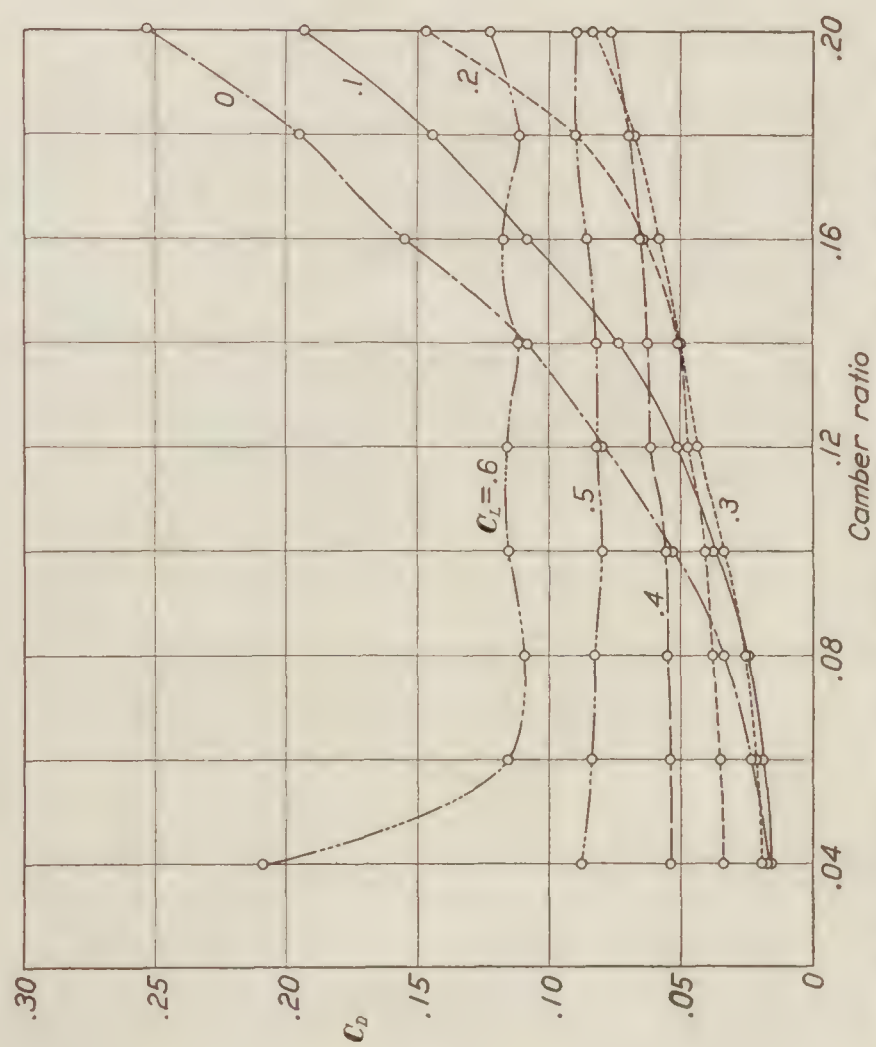


FIGURE 16.—Drag coefficient, C_D vs. camber ratio for various lift coefficients, C_L , at $V/c=0.50$, for 3R family

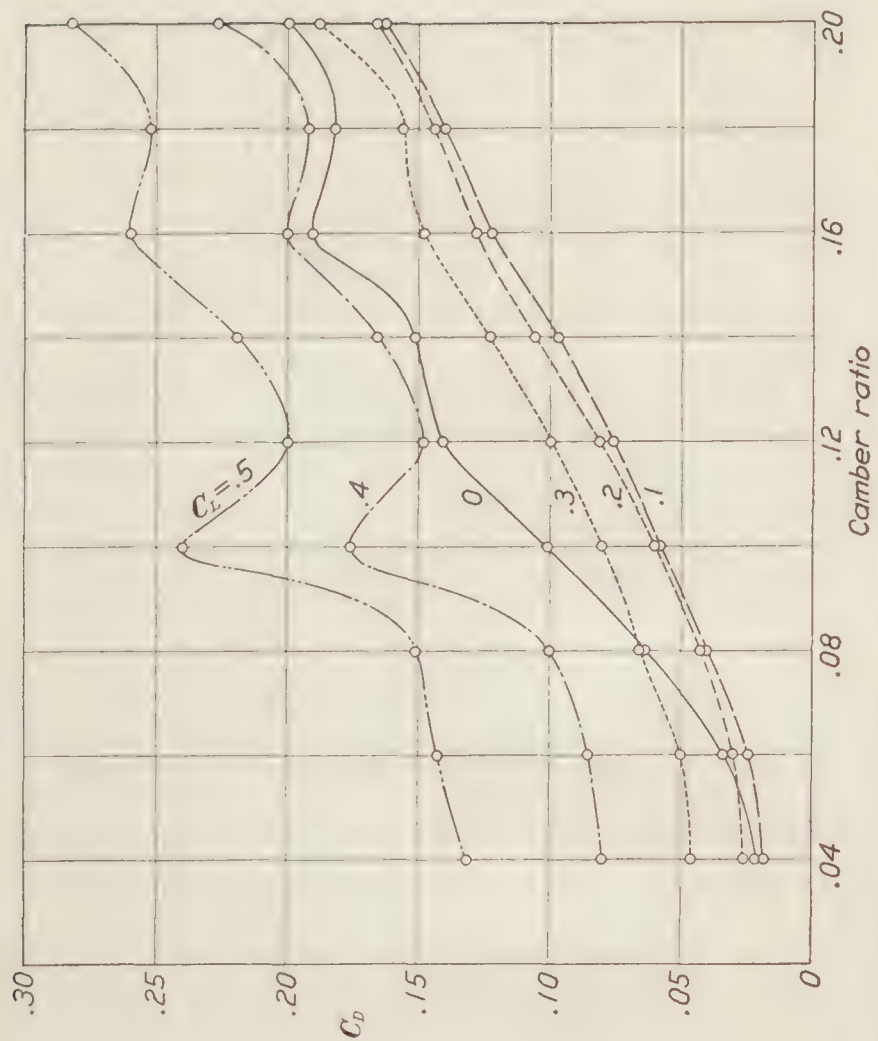


FIGURE 19.—Drag coefficient, C_D vs. camber ratio for various lift coefficients, C_L , at $V/c=0.95$, for 3R family



FIGURE 18.—Drag coefficient, C_D vs. camber ratio for various lift coefficients, C_L , at $V/c=0.80$, for 3R family

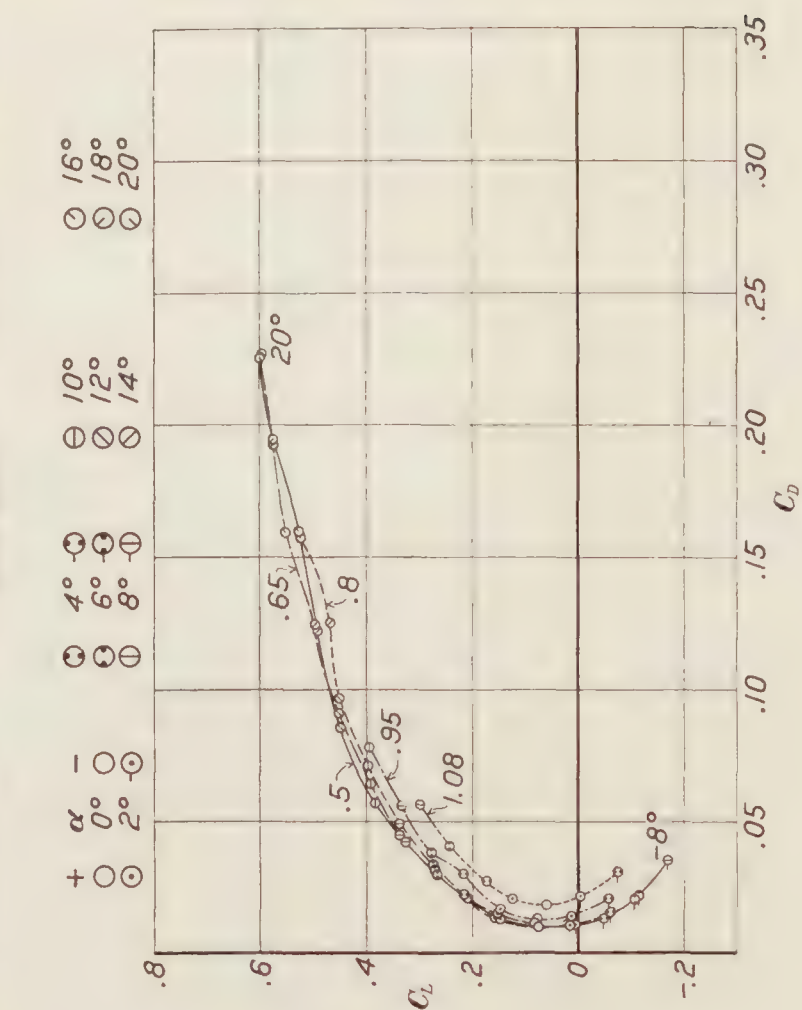


FIGURE 21.—Polar diagrams for airfoil C4 for five values of V/c

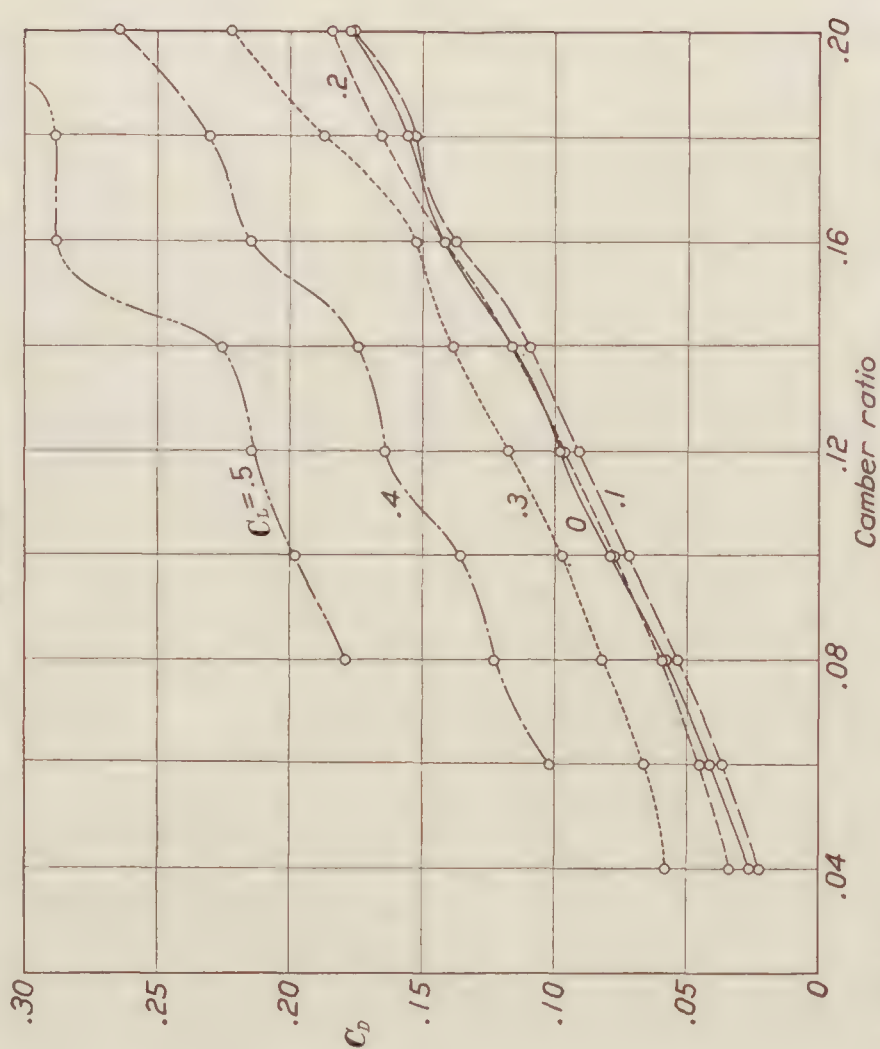


FIGURE 20.—Drag coefficient, C_D vs. camber ratio for various lift coefficients, C_L , at $V/c=1.08$, for 3R family



FIGURE 23.—Polar diagrams for airfoil C12 for five values of V/c

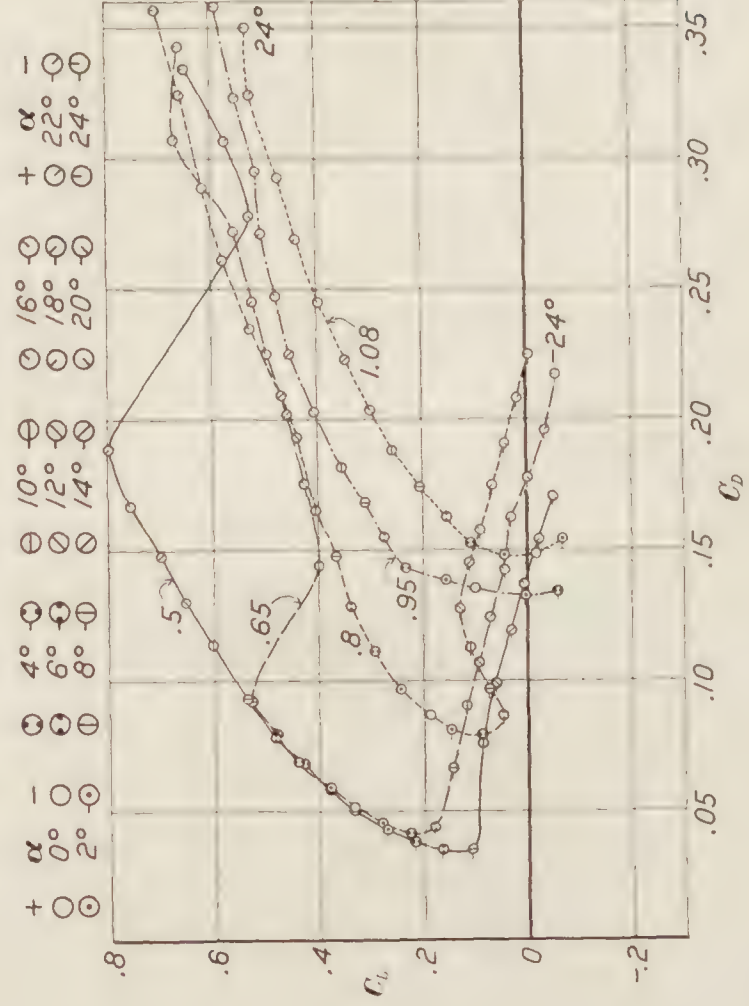


FIGURE 25.—Polar diagrams for airfoil C20 for five values of V/c

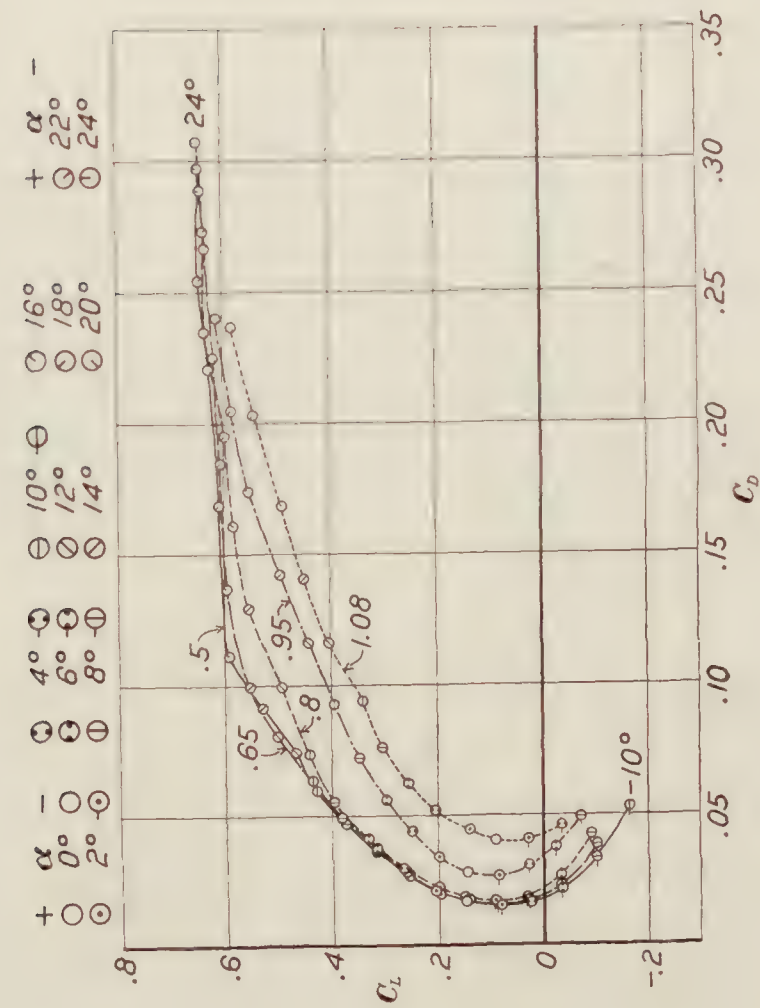


FIGURE 22.—Polar diagrams for airfoil C8 for five values of V/c

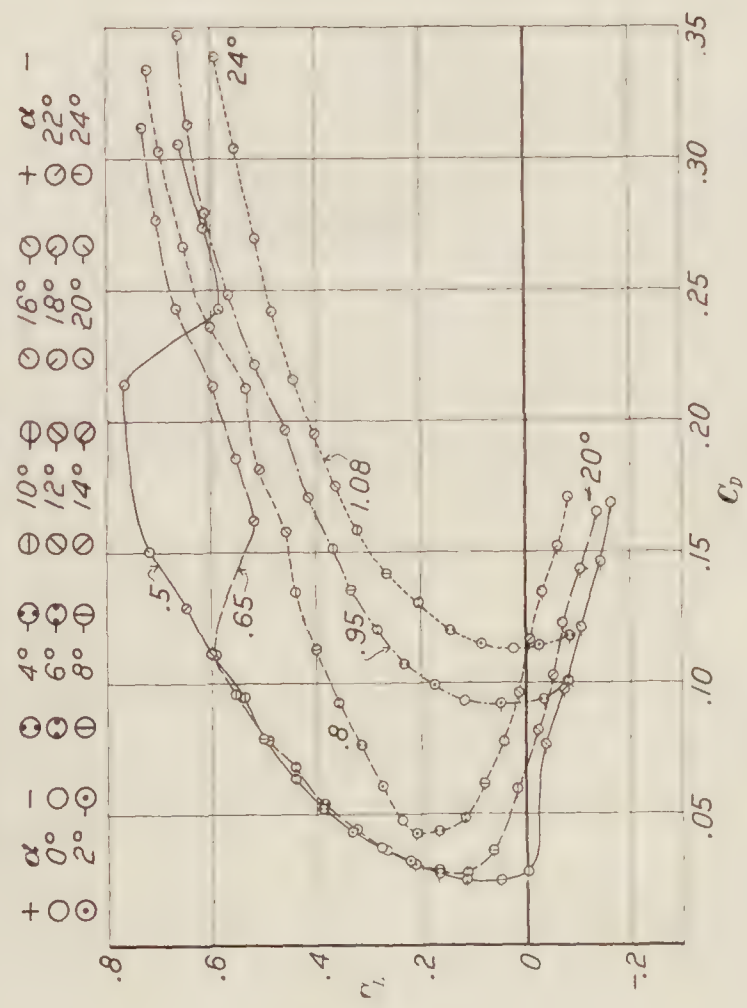


FIGURE 24.—Polar diagrams for airfoil C16 for five values of V/c

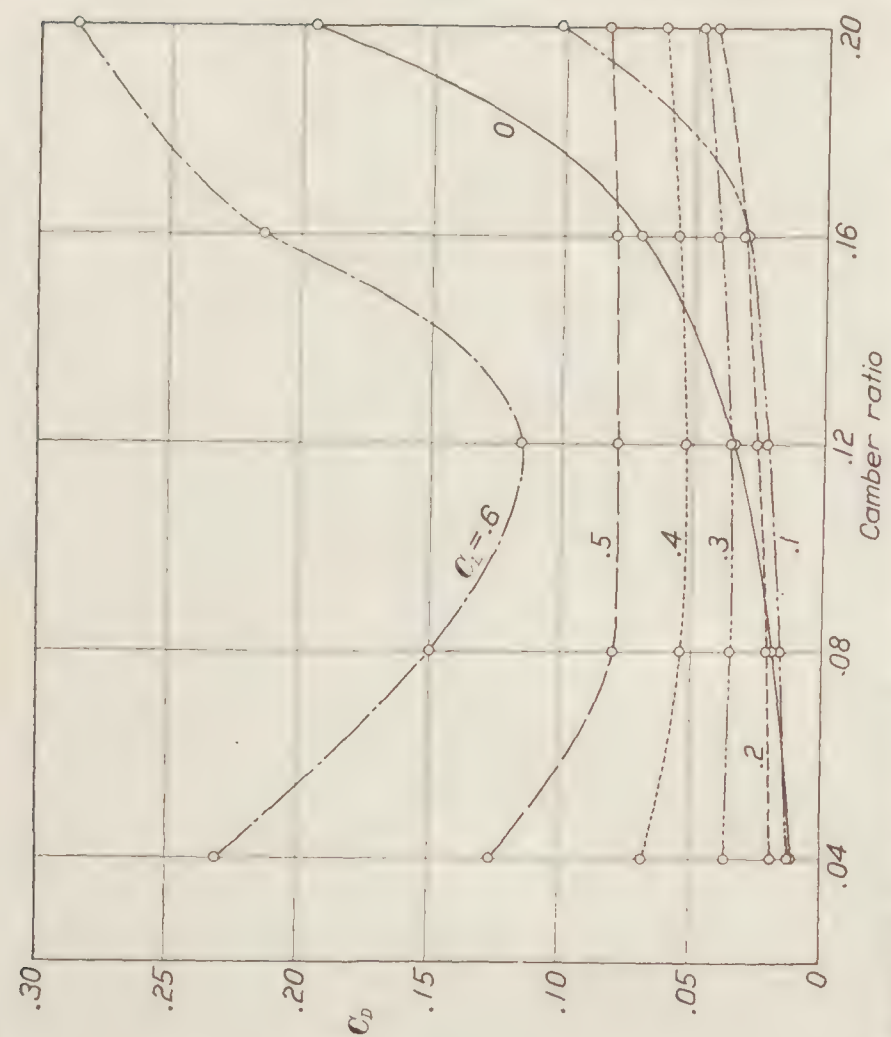


FIGURE 27.—Drag coefficient, C_D vs. camber ratio for various lift coefficients, C_L , at $V/c=0.65$, for C family

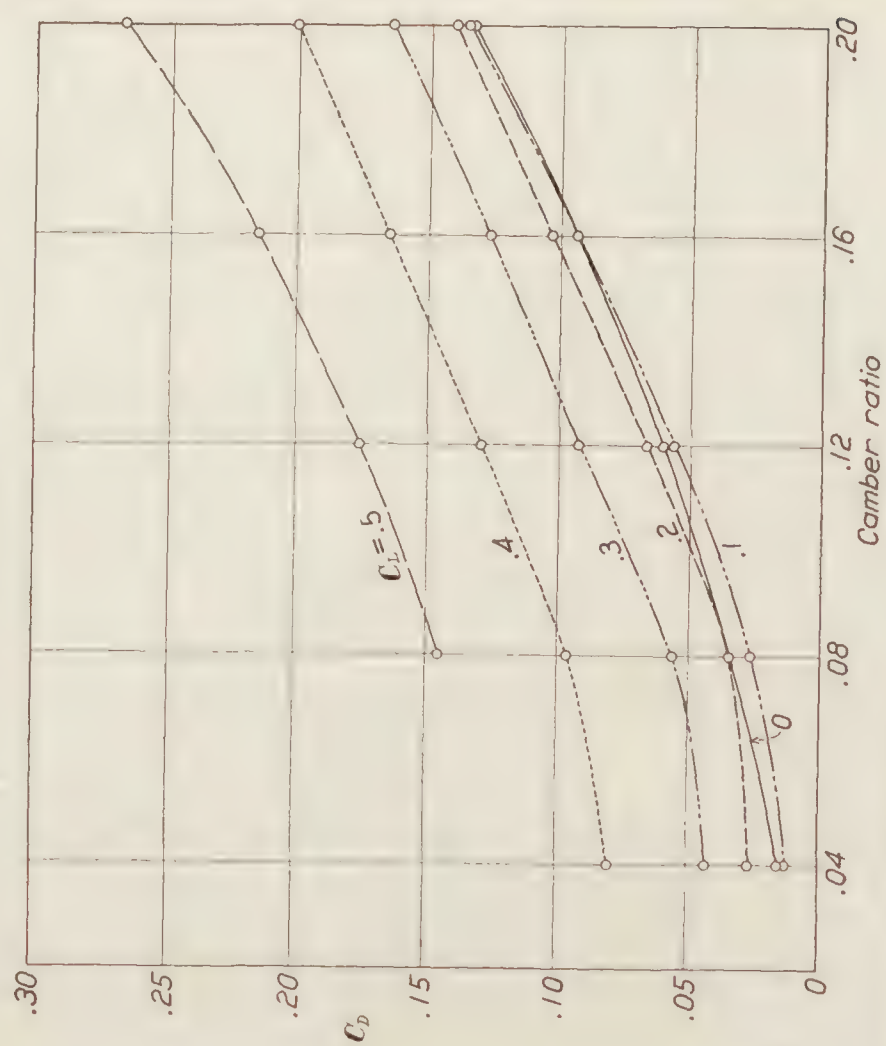


FIGURE 29.—Drag coefficient, C_D vs. camber ratio for various lift coefficients, C_L , at $V/c=0.95$, for C family

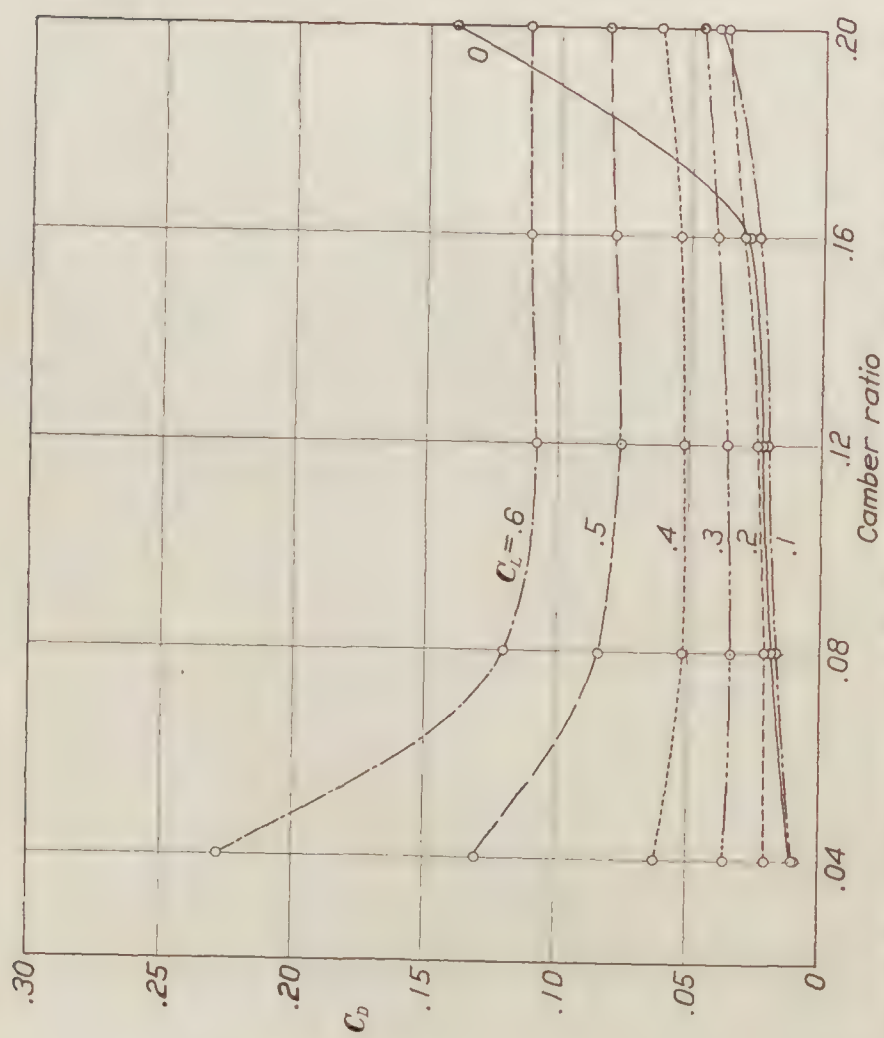


FIGURE 26.—Drag coefficient, C_D vs. camber ratio for various lift coefficients, C_L , at $V/c=0.50$, for C family

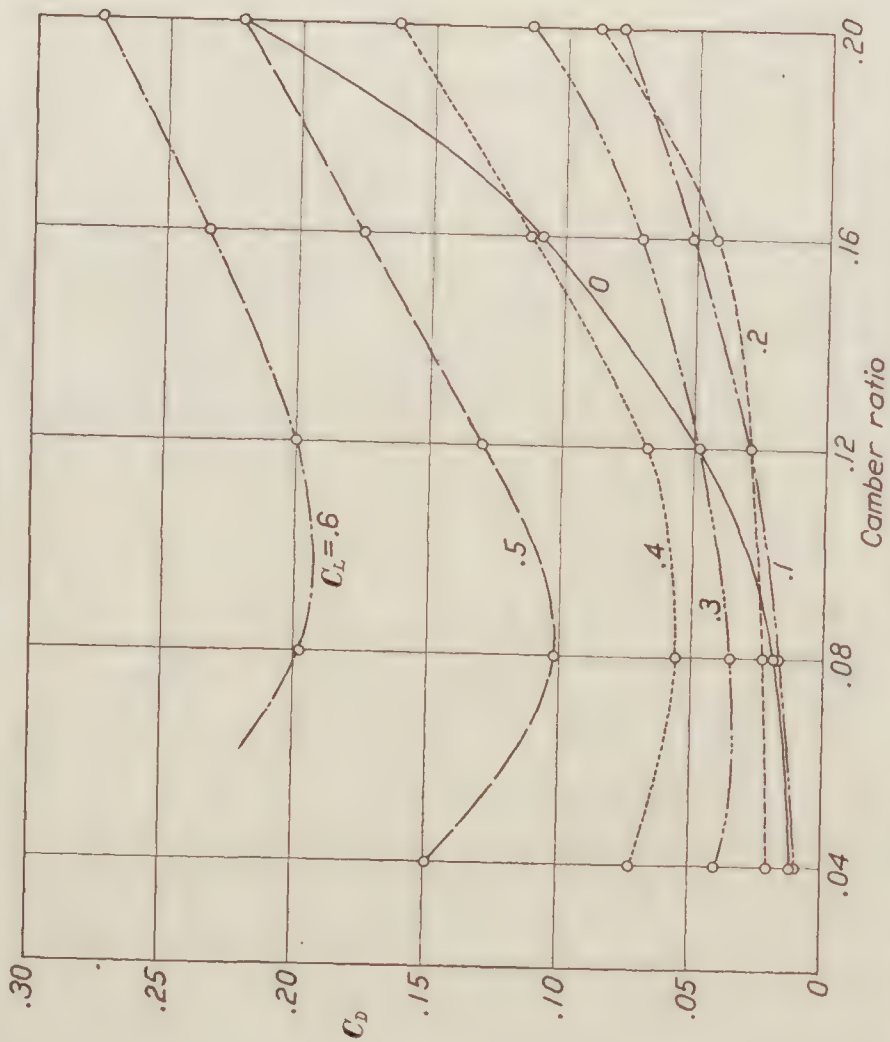


FIGURE 28.—Drag coefficient, C_D vs. camber ratio for various lift coefficients, C_L , at $V/c=0.80$, for C family

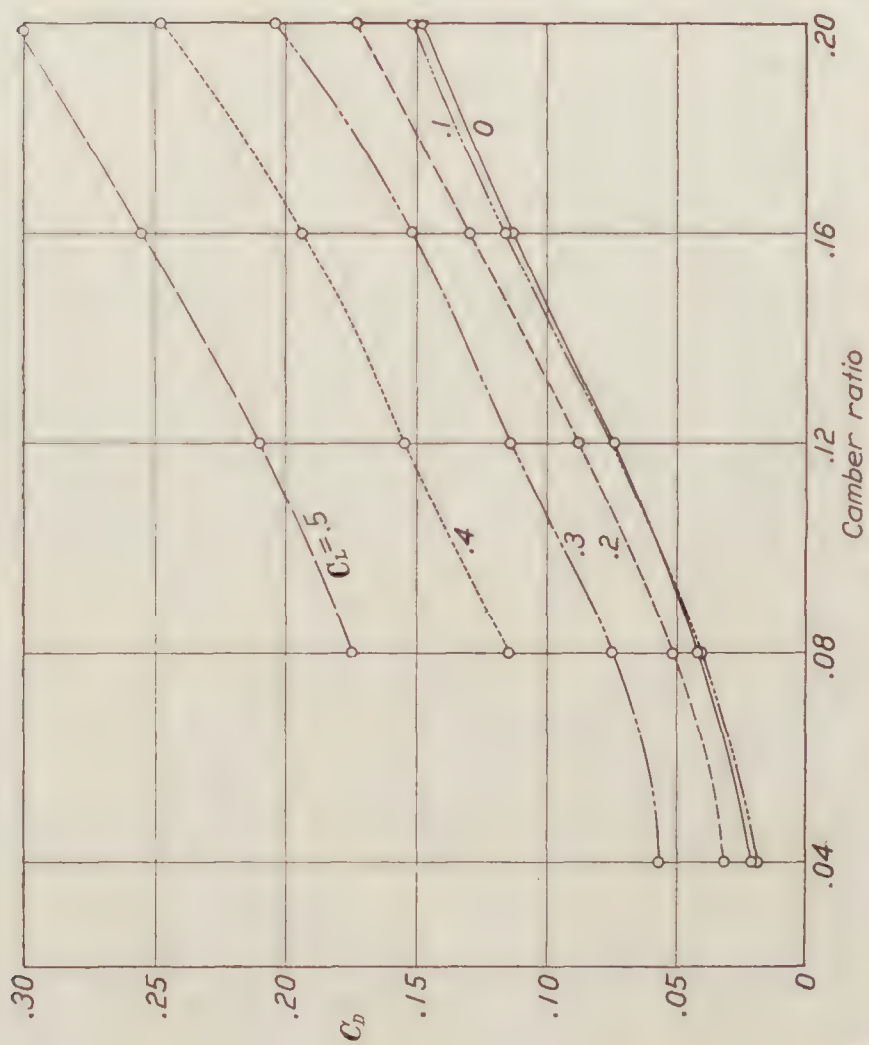


FIGURE 30.—Drag coefficient, C_D vs. camber ratio for various lift coefficients, C_L , at $V/c = 1.08$, for C family

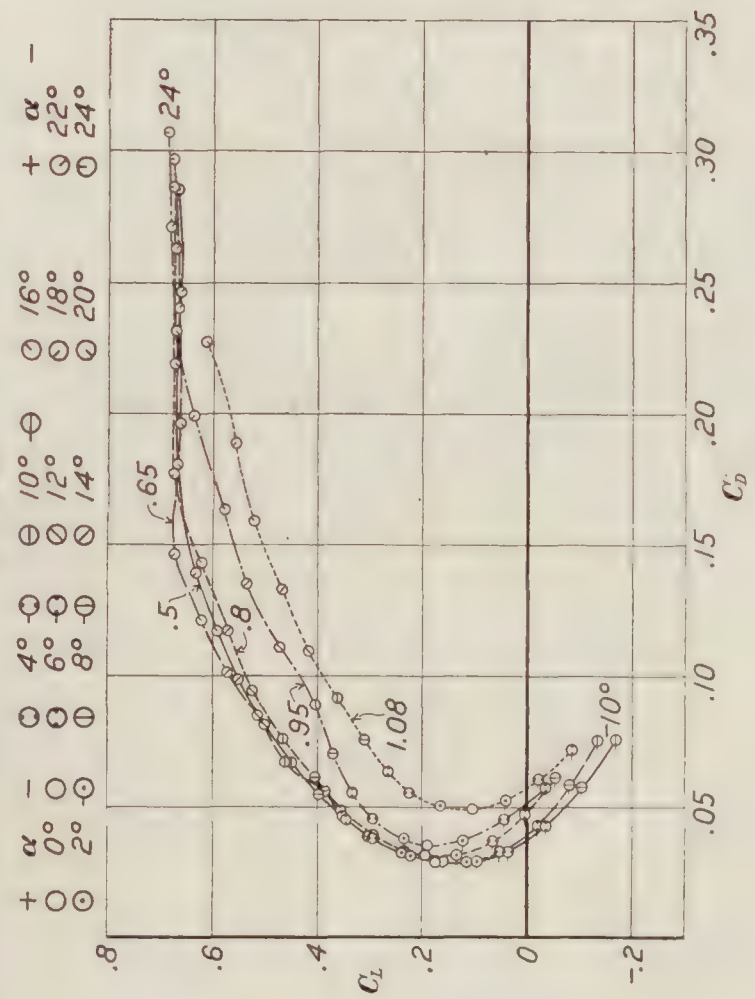


FIGURE 32.—Polar diagrams for airfoil 5R8 for five values of V/c

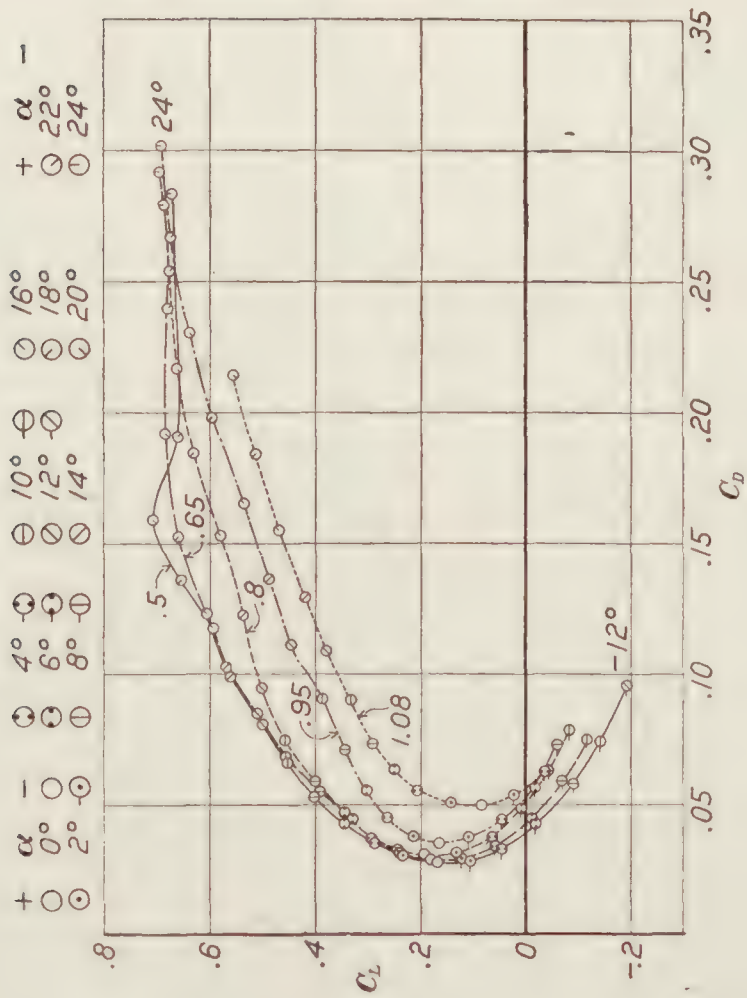


FIGURE 31.—Polar diagrams for airfoil 4R8 for five values of V/c

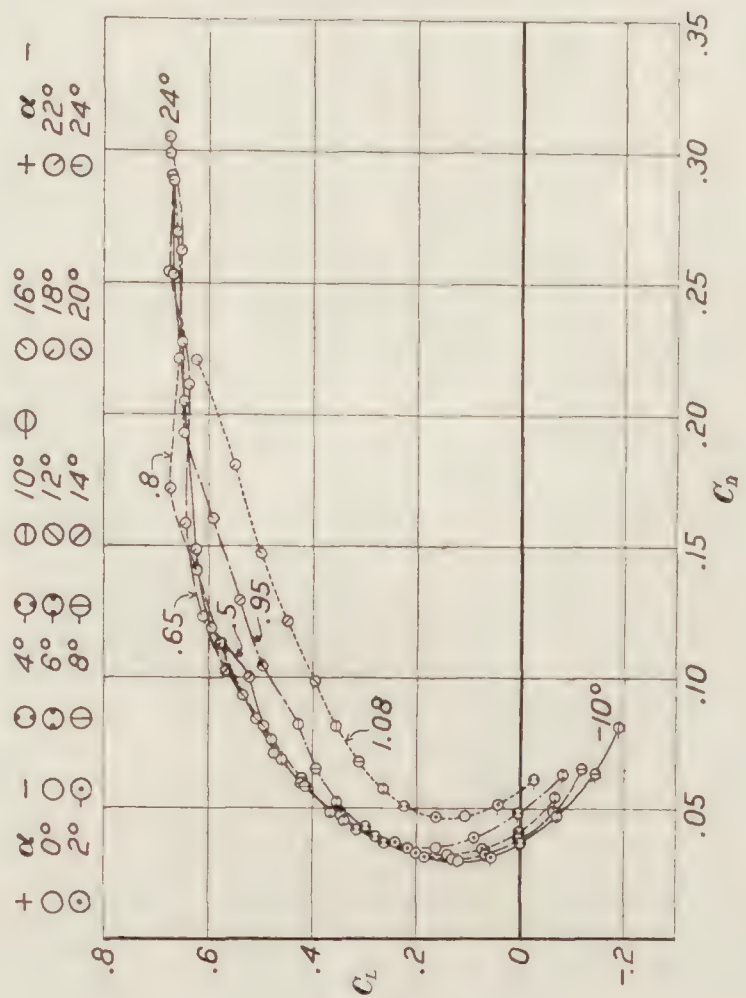
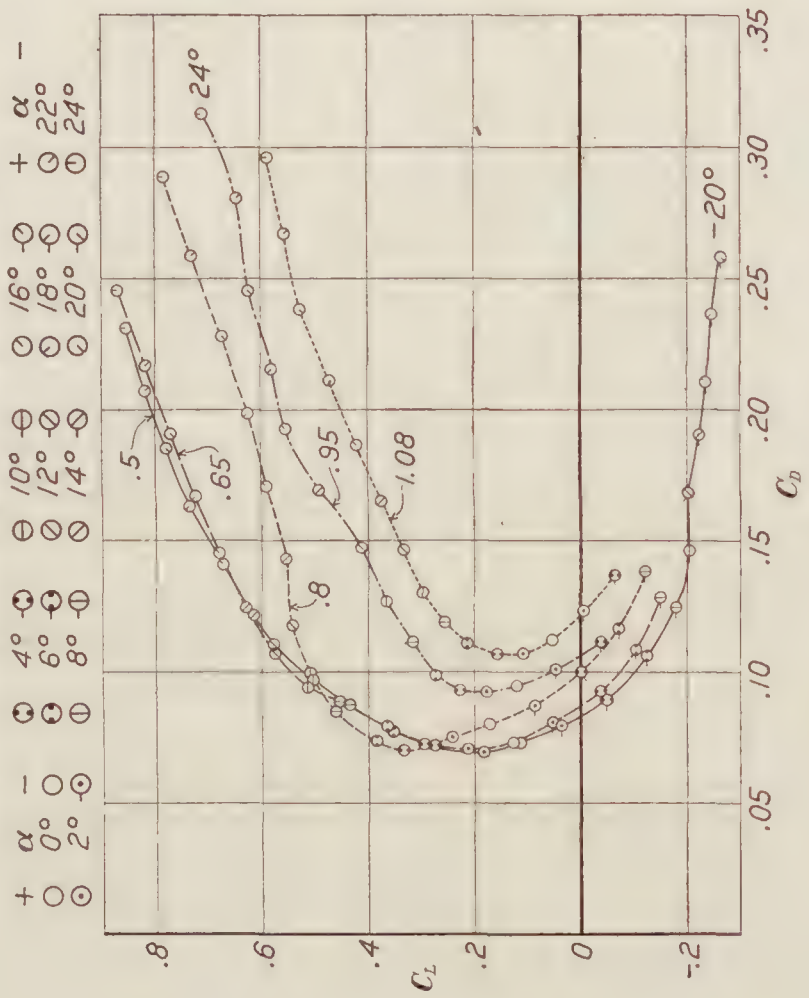
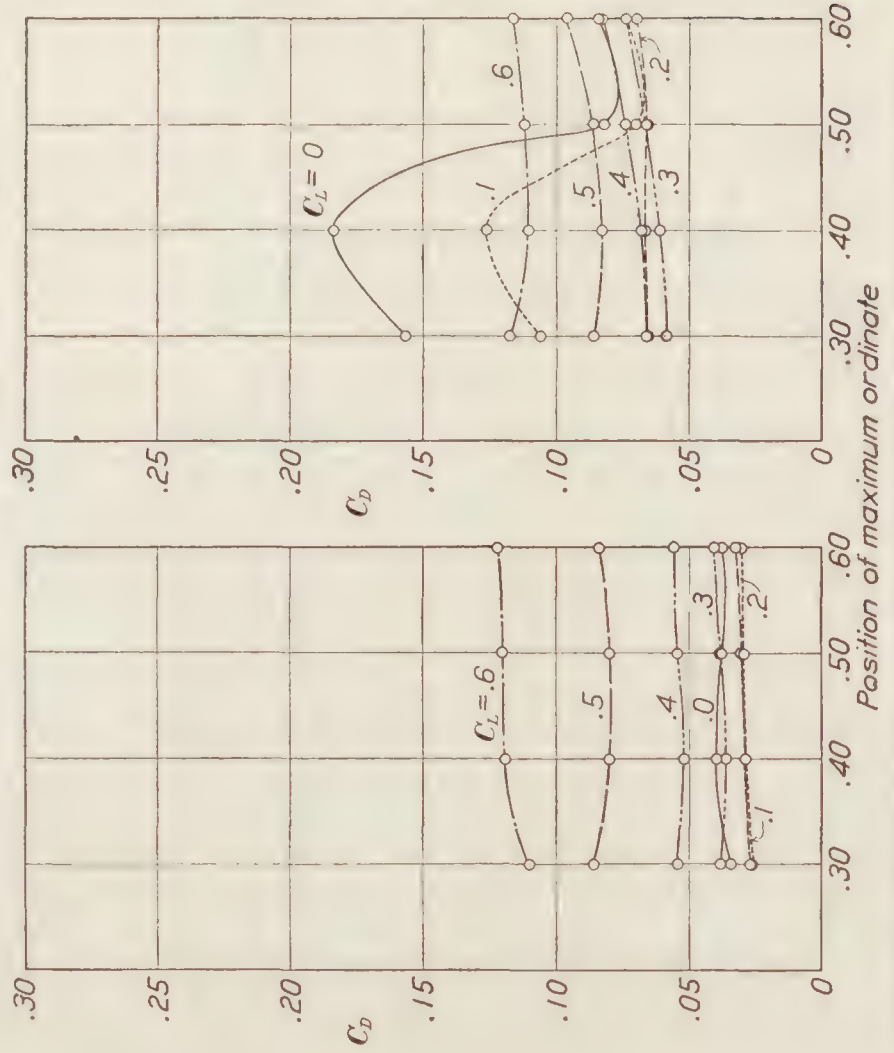


FIGURE 33.—Polar diagrams for airfoil 6R8 for five values of V/c

FIGURE 34.—Polar diagrams for airfoil 4R16 for five values of V/c FIGURE 36.—Polar diagrams for airfoil 6R16 for five values of V/c FIGURE 35.—Polar diagrams for airfoil 5R16 for five values of V/c FIGURE 37.—Drag coefficient, C_D vs. position of maximum ordinate for various lift coefficients, C_L , at $V/c=0.50$ for R family. R8 group at left, R16 group at right

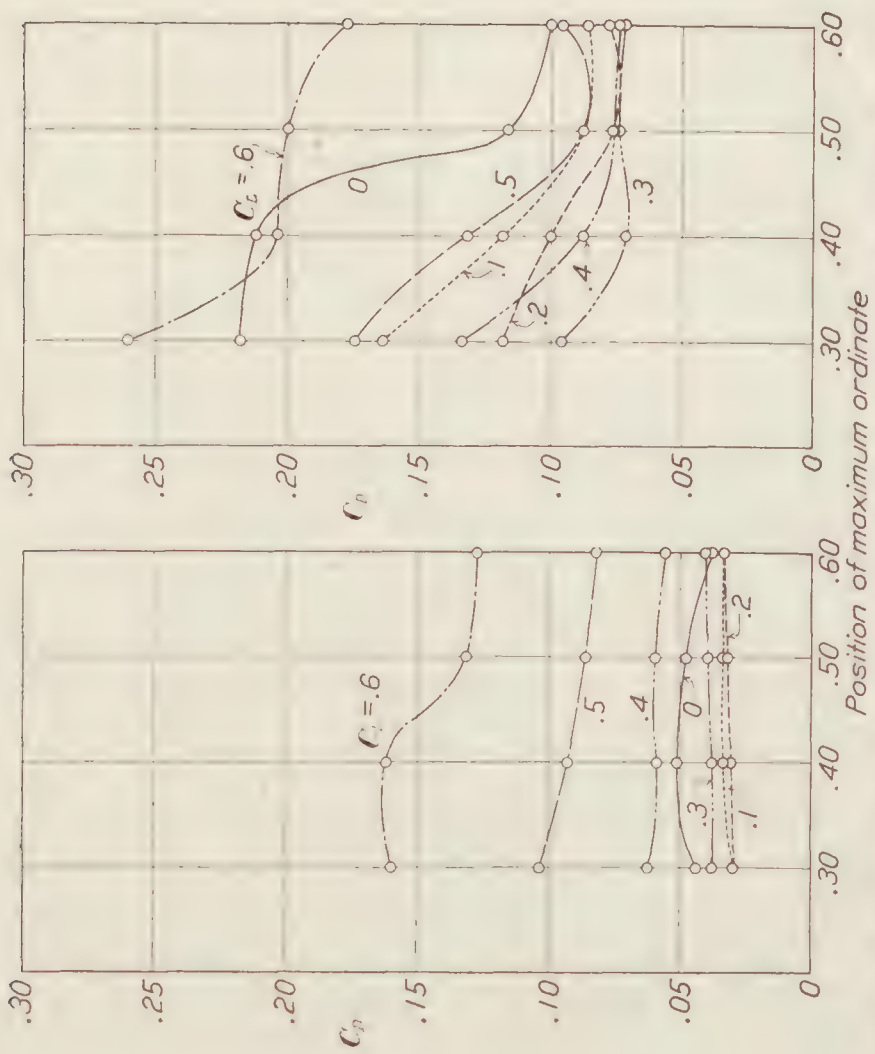


FIGURE 39.—Drag coefficient, C_D vs. position of maximum ordinate for various lift coefficients, C_L , at $V/c=0.80$ for R family. R8 group at left, R16 group at right

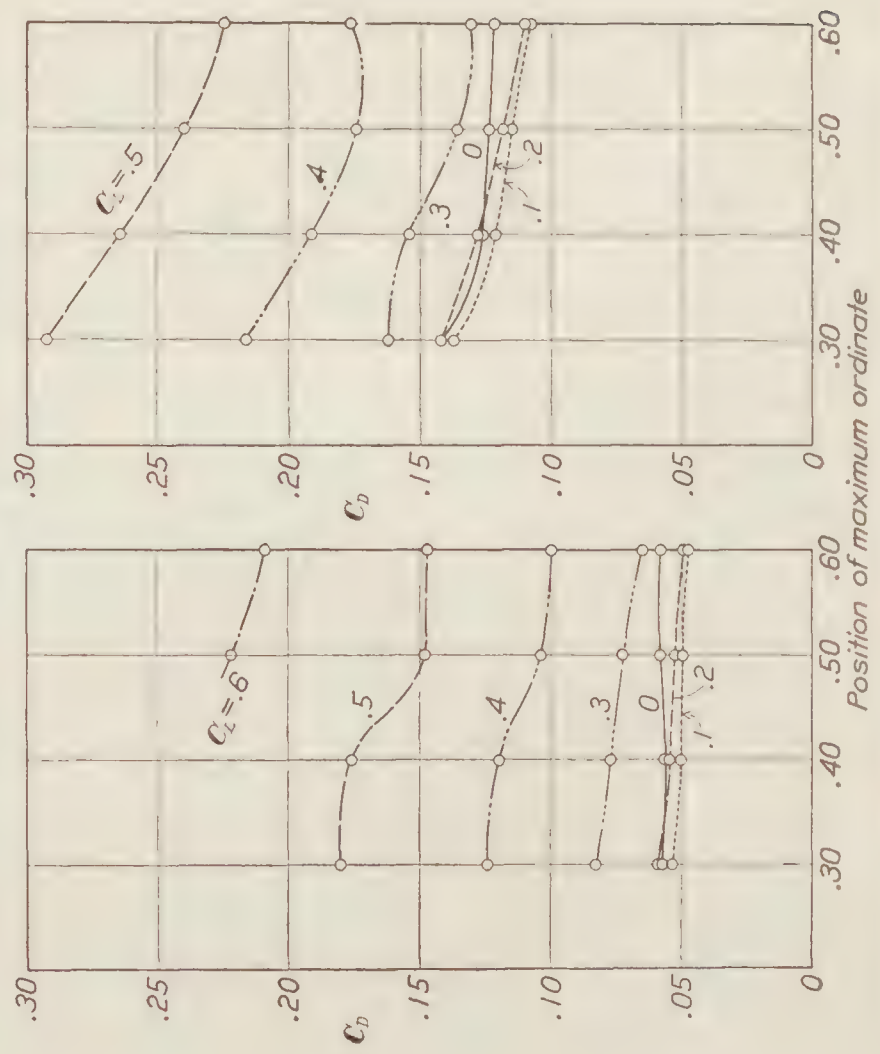


FIGURE 41.—Drag coefficient, C_D vs. position of maximum ordinate for various lift coefficients, C_L , at $V/c=1.08$ for R family. R8 group at left, R16 group at right

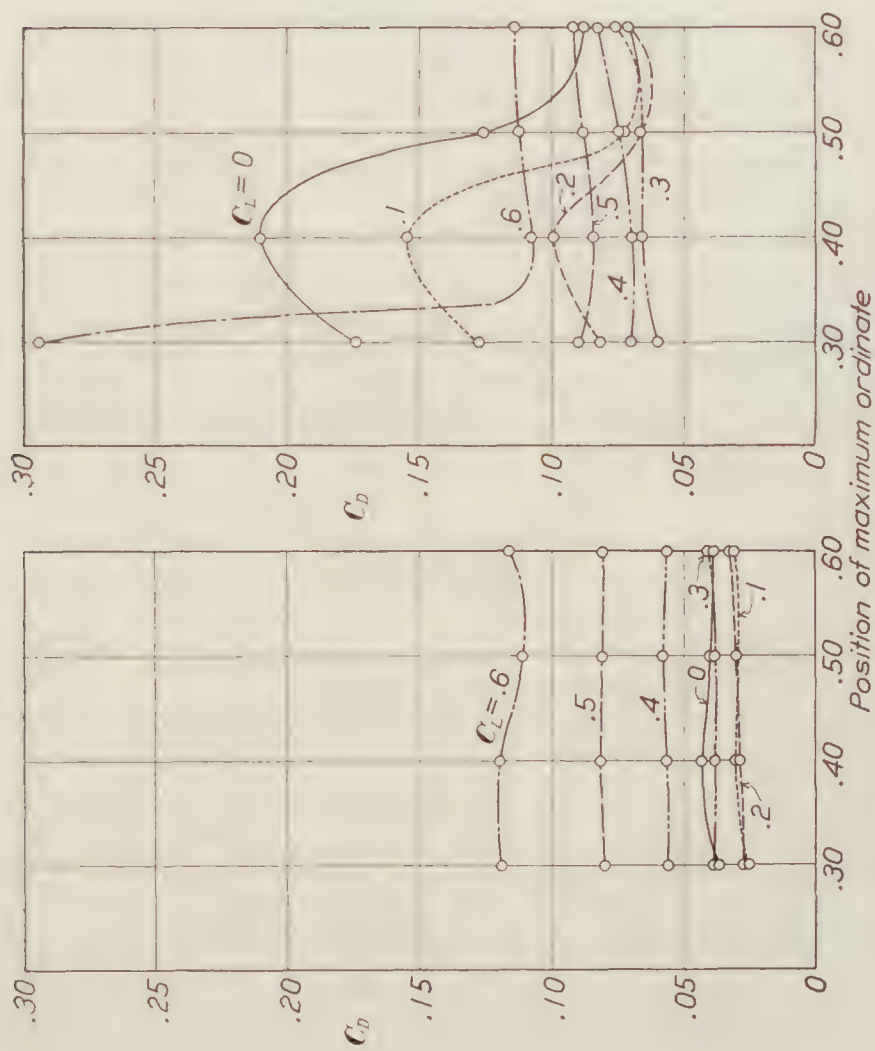


FIGURE 38.—Drag coefficient, C_D vs. position of maximum ordinate for various lift coefficients, C_L , at $V/c=0.65$ for R family. R8 group at left, R16 group at right

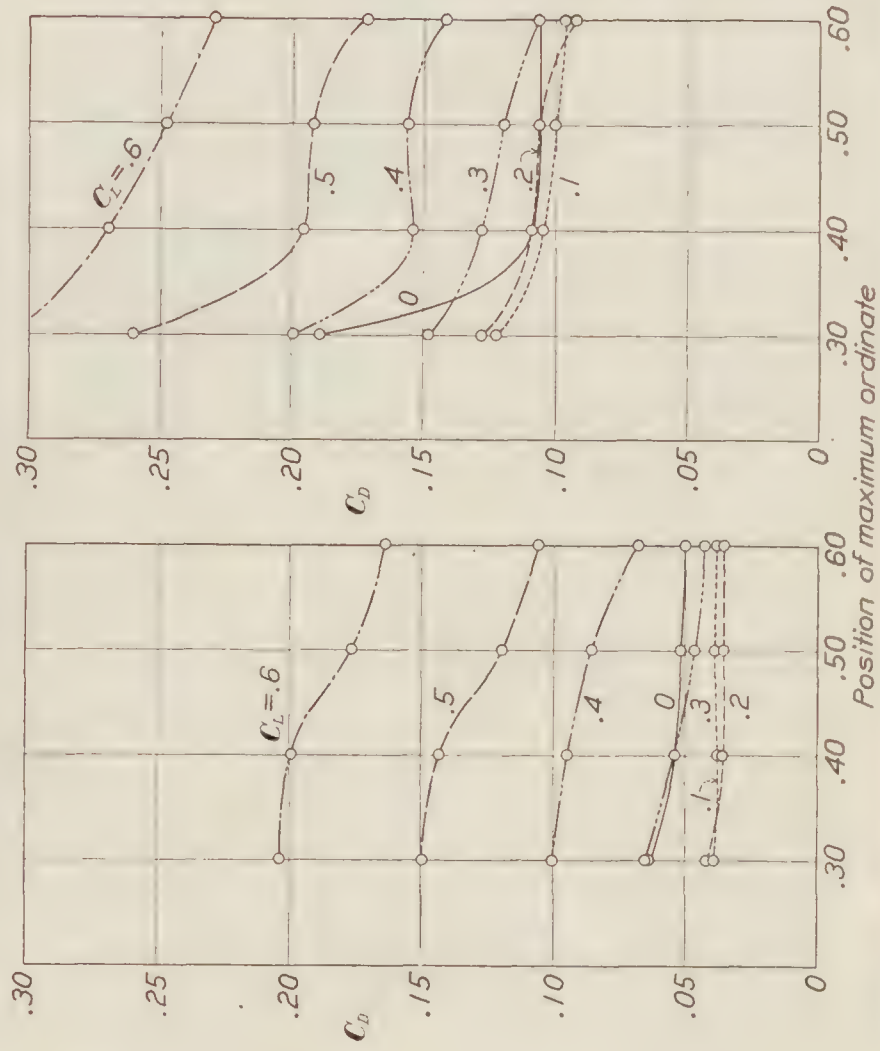


FIGURE 40.—Drag coefficient, C_D vs. position of maximum ordinate for various lift coefficients, C_L , at $V/c=0.95$ for R family. R8 group at left, R16 group at right

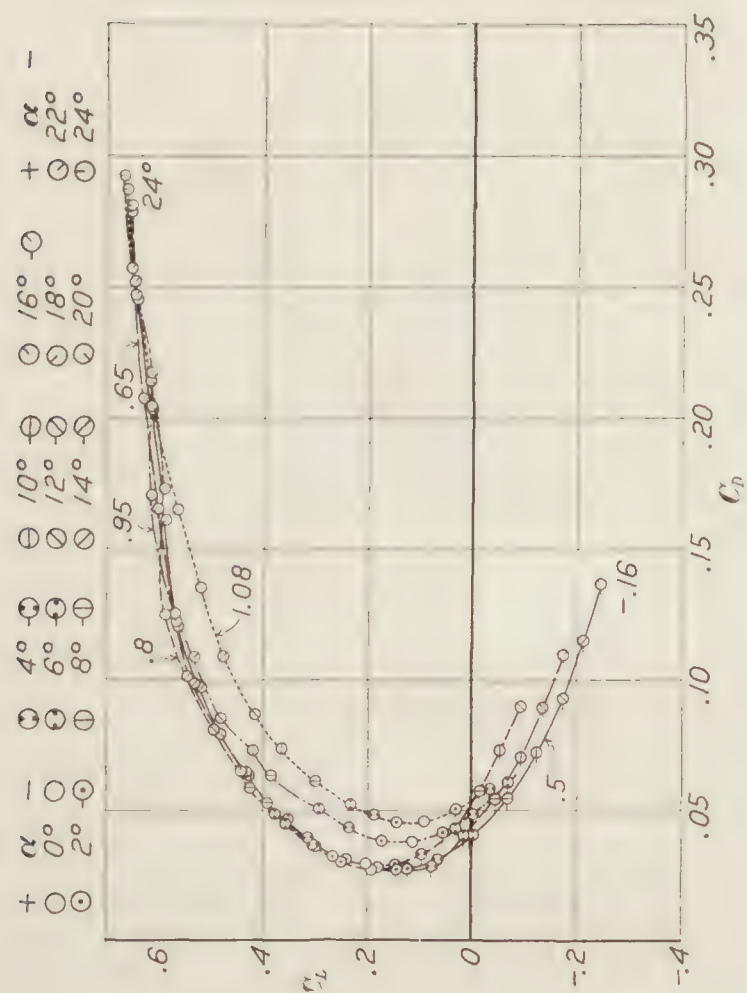


FIGURE 42. Polar diagram for Reed airfoil for five values of V/c

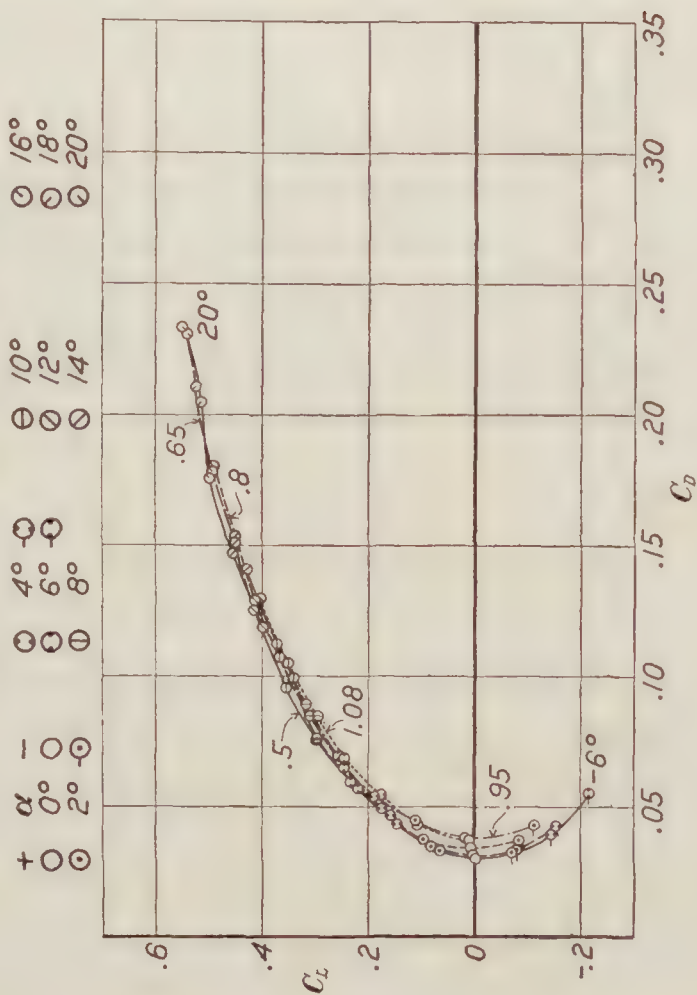


FIGURE 43. Polar diagram for circular arc airfoil for five values of V/c

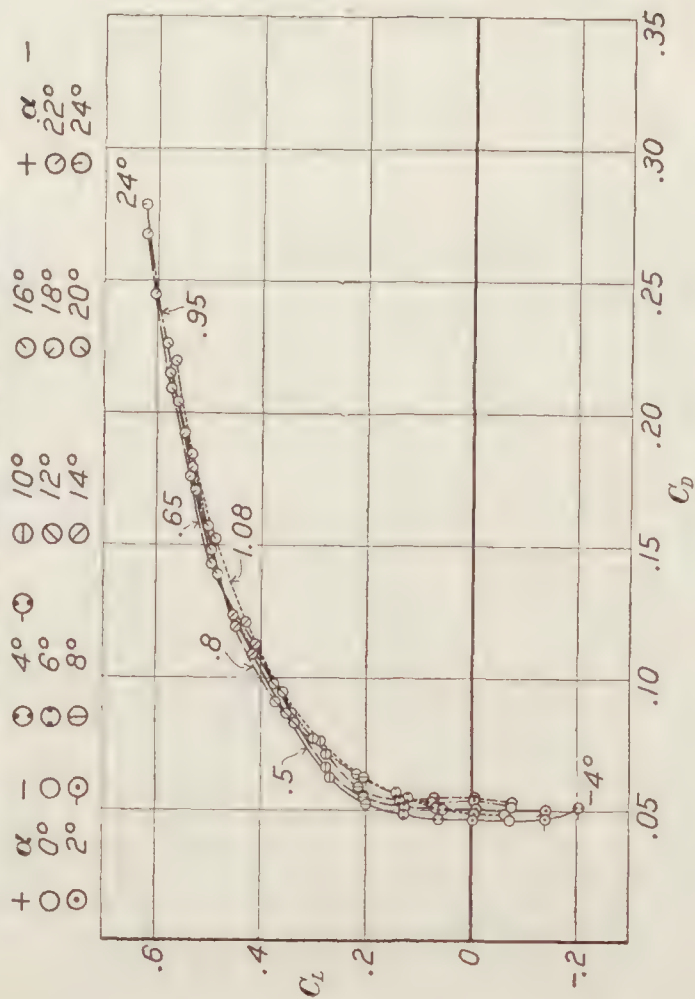


FIGURE 44. Polar diagram for flat plate for five values of V/c

FIGURE 45. Polar diagram for wedge for five values of V/c

The alignment of the air stream was checked as in our earlier work by moving the balance to the opposite side of the stream so that the lift direction was reversed with respect to the air stream. Good agreement was obtained between the normal runs and the runs with airfoil reversed.

We may say, therefore, that it is possible to repeat measurements under given conditions with satisfactory precision, but the characteristics of flow over thick sections are such that small changes in the end conditions at the edge of the jet produce noticeable systematic effects. The speed effect is, however, much greater so that the position effect does not at all obscure the main changes. Moreover, the position effect is of the same general nature for all airfoils so that the results from a comparative standpoint are believed to be reliable.

COMPARISON OF FORCE MEASUREMENTS WITH PRESSURE DISTRIBUTION MEASUREMENTS

Airfoil sections 3R10, 3R12, 3R14, 3R16, 3R18, and 3R20 were used in the pressure distribution measurements described in N. A. C. A. Technical Report No. 255 (Reference 3). Consequently, a comparison may be made between the integration of the pressure distribution at the central section and the average force on the whole airfoil. No general relation applicable to all airfoil sections and to all speeds appears to exist, and a detailed comparison of each section and speed does not seem advisable. In the ideal elliptical distribution of lift, the lift coefficient for the central section is greater than the average lift coefficient for the whole airfoil, in the ratio of 1 to $\pi/4$, and the induced drag is distributed in the same manner. Now even at low speeds the distribution of lift over an airfoil of rectangular plan form is not exactly elliptical but under conditions of smooth flow the lift at the central section is greater than the lift for the whole section. This same qualitative relation is found to hold in the high-speed tests where the flow is smooth; that is, for thin sections, small angles of attack, and at the lower speeds.

At the higher speeds the situation is quite different, for the breaking away of the flow from the surface occurs first at the center of the airfoil and consequently the lift is lowest at the central section and the drag is greatest. This fact was not adequately appreciated in N. A. C. A. Technical Report No. 255 (Reference 3) and the conclusions regarding the influence of Reynolds Number on the drag coefficient are not supported by the force measurements. The drag coefficient in the pressure distribution measurements was high as compared with the Lynn measurements, not because of the smaller model but because the inefficient type of flow occurs first at the center where the pressure distribution measurements were made.

As a result of this fact the pressure distribution measurements show the decrease in lift and increase in drag occurring at a somewhat lower speed and the differences in the curves for $V/c=0.5$ and $V/c=1.08$ are somewhat greater than for the force measurements. The force measurements average the inefficient flow at the center with the more efficient flow near the ends.

It should be emphasized here that the flow at high speeds is of the same general appearance as burbling flow at low speeds and just as no theory has been worked out for burbling flow, so no theory is available for the high-speed type of flow. Corrections for aspect ratio can not be computed and the estimation of interference between blade elements of propellers can not be based on the theory of induced drag. We hope to carry out later some experiments on the effects of aspect ratio.

For the present no method is known of using the coefficients of this report quantitatively for full-scale propeller computations due largely to our ignorance of methods of treating burbling flow. The curves are, however, self-consistent and are believed trustworthy for the comparison of airfoil sections as to their efficiency at high speeds.

COMPARISON OF R. A. F. AND CLARK Y FAMILIES.—An inspection of the table and curves shows that the Clark Y sections are more efficient than the R. A. F. sections (comparing sections of equal thickness) under all conditions except for very thin sections at high lift coefficients (Figs. 6, 8, 21, and 22). The Clark Y thin sections do not attain as high a maximum lift as the R. A. F. thin sections so that the polar curves cross at high lift coefficients, and under these conditions the R. A. F. sections give lower drag coefficients.

The ratio of the efficiencies of Clark Y and R. A. F. sections varies greatly with the thickness of section and with the speed. To illustrate the diversity of relationship of the two families, a detailed study is given of the variations of the minimum drag coefficient. Values taken from the tabulated values are summarized in the following table and the ratios for the two families are shown in the last column.

Thickness ratio	V/c	Minimum drag coefficient		Ratio $\frac{\text{R. A. F.}}{\text{Clark}}$
		R. A. F. family	Clark Y family	
0.04	0.50	0.016	0.010	1.60
	.65	.016	.011	1.45
	.80	.016	.011	1.45
	.95	.018	.013	1.38
	1.08	.022	.019	1.16
.08	.50	.025	.016	1.56
	.65	.026	.016	1.62
	.80	.029	.017	1.71
	.95	.039	.027	1.45
	1.08	.053	.040	1.32
.12	.50	.045	.020	2.25
	.65	.046	.021	2.19
	.80	.052	.026	2.00
	.95	.076	.056	1.36
	1.08	.090	.073	1.23
.16	.50	.059	.025	2.36
	.65	.068	.028	2.43
	.80	.073	.043	1.70
	.95	.123	.092	1.34
	1.08	.138	.112	1.23
.20	.50	.076	.035	2.17
	.65	.078	.042	1.86
	.80	.115	.079	1.46
	.95	.163	.131	1.24
	1.08	.175	.148	1.18

It will be noted that at the two low speeds, the ratio is approximately 1.6 for thickness ratios of 0.04 and 0.08, while for thickness ratios of 0.12, 0.16, and 0.20 the ratio is over 2. A curve of the ratio plotted against thickness-ratio is seen to rise rapidly between 0.08 and 0.12, reach a maximum near 0.16, and then fall off a little. In other words, the ratio of the minimum drag of the R. A. F. sections to that of the Clark Y sections is much greater for thick sections than for thin sections and a rapid increase occurs between a thickness-ratio of 0.08 and 0.12 when the speed is below 0.65 the speed of sound. The single value obtainable from ordinary wind tunnel tests N. A. C. A. Technical Reports Nos. 233 and 259 (References 5 and 4, respectively) at the same Reynolds Number is 2.3 for a thickness-ratio of approximately 0.12 and is in good agreement with the above values.

At the higher speeds, on the other hand, the ratio is nearly independent of thickness ratio and is much lower, namely, about 1.25. Hence the relative advantage of Clark Y sections is less at the higher speeds.

The effect of speed may be shown most readily by means of a separate table.

Thickness ratio	Ratio of minimum drag at $V/c=1.08$ to $V/c=0.50$	
	R. A. F. family	Clark Y family
0.04	1.38	1.90
.08	2.12	2.56
.12	2.00	3.65
.16	2.34	4.48
.20	2.30	4.23

The increase in the minimum drag coefficient with speed is much greater for the Clark Y family than for the R. A. F. family. Also, the increase with speed reaches a nearly constant value in the R. A. F. family for a thickness ratio of 0.08, whereas in the Clark Y family the maximum is not reached until a thickness ratio of 0.16 is attained.

Propeller sections are practically never run at the low lift coefficients corresponding to minimum drag, the lift coefficient usually being greater than 0.4. The above comparison can not therefore be considered as representing the relative merits of the two families for use in the design of propellers. So long as the thickness of the section is one-tenth the chord or greater, the Clark Y family shows an advantage in all cases. For thinner sections the two families give approximately the same results. Our experiments on thin sections do not cover the full range because at high angles and speeds the thin airfoils were deformed by the air-stream.

The curves of Figures 15 to 20 and 26 to 30 give an opportunity for comparison under a great variety of conditions. Figure 15 is plotted from the data given by E. N. Jacobs in N. A. C. A. Technical Report No. 259. (Reference 4.) It shows that for low and moderate lift coefficients thin sections are the most efficient. Thick sections give greatly increased drag for very low lift coefficients due to the fact that the angle of attack is negative and a burbling type of flow results. Figure 16 shows results for a speed of one-half the speed of sound. The curves are similar in nature to the low-speed tests except that the lift coefficients obtained are much lower due to the small aspect ratio. The increased drag for thick sections at low lift coefficients also covers a wider field of thickness ratio and lift coefficient. This region spreads as the speed is increased (Figs. 17 and 18) until for a speed of 0.95 the speed of sound (Fig. 19), thin sections are best for all lift coefficients. For a speed of 1.08 times the speed of sound (Fig. 20) an approximately linear variation of the drag (for a given lift) with thickness ratio is found.

Figure 26 for the Clark Y family at a speed of one-half the speed of sound shows that over a wide range of thickness ratio the drag for a given lift is roughly constant. However, the same changes occur and for $V/c=0.8$ (Fig. 28) we have already a suggestion of the character finally developed in Figures 29 and 30 for the higher speeds. Comparison of Figures 20 and 30 show the greater slope and hence the greater speed effect for the Clark Y family.

These examples serve to illustrate the complexity of the relationships found. Perhaps the best general statement that can be made is that when the flow is no longer smooth, all sections are brought more nearly to the same level irrespective of their efficiencies when the flow is smooth. The efficient sections therefore suffer most.

When the thickness is 0.10 the chord or greater, the use of the Clark Y type of section at high speeds is, however, most desirable on account of a 25 per cent decrease in minimum drag. The great advantage of using as thin a section as possible is also clearly apparent.

The present experiments do not indicate any advantage for the Clark Y family when sections thinner than 0.10 the chord are used in modern thin blade metal propellers.

EFFECT OF POSITION OF MAXIMUM ORDINATE

Figures 37 to 41, inclusive, show the effect of the position of the maximum ordinate, which is of less magnitude than the effect of thickness or of speed. At a speed of 0.5 the speed of sound the 30 per cent position of the maximum ordinate is best except for the thick sections at very low lift coefficients. As the speed increases it is advantageous to move the maximum ordinate further back, especially in the case of the thick sections. As the effect is relatively small for thin sections and at low speeds it is recommended that no change be made except for sections of thickness ratio greater than 0.12 for use at speeds greater than 0.9 the speed of sound.

CONCLUSIONS.—The more important general conclusions are as follows:

1. The Clark Y family is more efficient than the R. A. F. family (sections of equal thickness being compared) when the thickness is greater than 0.10 the chord. The Clark Y thin sections do not attain as high a maximum lift as the R. A. F. thin sections, so that the polar curves cross at high lift coefficients and the R. A. F. sections under these conditions give less drag.

2. At high speeds, the maximum ordinate on thick sections should be moved back to secure the best results. The minimum drag is often increased but the drag at high lift coefficients is decreased and at very high speeds the minimum drag is also decreased.

3. In most cases the flow leaves the rear part of the upper surface at all positive angles of attack at speeds above approximately 0.8 the speed of sound.

4. The thinner sections maintain their lift coefficients very well to the highest speeds, but the thicker sections show a marked decrease in lift coefficient. The total lift actually decreases as the speed increases over a certain range.

5. All sections show a marked increase in drag coefficient with increasing speed, the rate of increase rising rather abruptly at a speed well below the speed of sound. At large angles of attack the drag coefficient reaches a maximum approximately at the speed of sound.

6. Airfoil sections are more efficient at high speeds than a flat plate or wedge. A cylindrical segment in the single test made was found to be somewhat more efficient than the airfoil sections.

7. Aspect ratio effects are large. A theory of these effects is available only for the lower speeds where the type of flow is relatively smooth. In this case the theoretical minimum induced drag is the same as for aspect ratio 2. Since, however, no theoretical laws for aspect-ratio effects have been developed for the types of flow observed at high speeds, the measurements in the 2-inch air stream must be considered as qualitative in character until the correction for aspect ratio is known. (References 1 and 6.)

BUREAU OF STANDARDS,

WASHINGTON, D. C., *August 7, 1928.*

REFERENCES

1. Briggs, L. J., Hull, G. F., and Dryden, H. L.: Aerodynamic Characteristics of Airfoils at High Speeds. N. A. C. A. Technical Report No. 207. (1925.)
2. Caldwell, F. W., and Fales, E. N.: Wind Studies in Aerodynamic Phenomena at High Speed. Part I. Model Wind Tunnel Experiments. Part II. The McCook Field Wind Tunnel. Part III. Model Tests on Propeller Aerofoils. N. A. C. A. Technical Report No. 83. (1920.)
3. Briggs, L. J., and Dryden, H. L.: Pressure Distribution Over Airfoils at High Speeds. N. A. C. A. Technical Report No. 255. (1927.)
4. Jacobs, Eastman N.: Characteristics of Propeller Sections Tested in the Variable Density Wind Tunnel. N. A. C. A. Technical Report No. 259. (1927.)
5. Munk, Max M., and Miller, Elton W.: The Aerodynamic Characteristics of Seven Frequently Used Wing Sections at Full Reynolds Number. N. A. C. A. Technical Report No. 233. (1926.)
6. Kumbach, H.: Zeitschrift für Flugtechnik und Motorluftschiffahrt, Vol. X, Nos. 9 and 10.

TABLE I.—ORDINATES OF AIRFOILS

RAF FAMILY

ORDINATES OF UPPER SURFACE

Distance from nose	3R4	3R6	3R8	3R10	3R12	3R14	3R16	3R18	3R20
0. 025	0. 016	0. 024	0. 032	0. 041	0. 049	0. 057	0. 065	0. 073	0. 082
. 050	. 024	. 035	. 047	. 059	. 070	. 082	. 094	. 106	. 118
. 100	. 032	. 047	. 063	. 079	. 094	. 110	. 126	. 142	. 158
. 200	. 038	. 057	. 076	. 095	. 114	. 133	. 152	. 171	. 190
. 300	. 040	. 060	. 080	. 100	. 120	. 140	. 160	. 180	. 200
. 400	. 040	. 059	. 079	. 099	. 118	. 138	. 158	. 178	. 198
. 500	. 038	. 057	. 076	. 095	. 114	. 133	. 152	. 171	. 190
. 600	. 035	. 052	. 069	. 087	. 104	. 121	. 139	. 156	. 174
. 700	. 030	. 044	. 059	. 094	. 088	. 103	. 118	. 133	. 148
. 800	. 022	. 033	. 044	. 056	. 067	. 078	. 089	. 100	. 112
. 900	. 014	. 021	. 028	. 035	. 042	. 049	. 056	. 063	. 070

NOTE.—Lower surface is plane.

Distance from nose	4R8	5R8	6R8	4R16	5R16	6R16
0. 050	0. 042	0. 037	0. 032	0. 084	0. 075	0. 065
. 100	. 057	. 052	. 047	. 113	. 104	. 094
. 200	. 070	. 067	. 063	. 141	. 134	. 126
. 300	. 078	. 074	. 071	. 156	. 149	. 142
. 400	. 080	. 078	. 076	. 160	. 157	. 152
. 500	. 079	. 080	. 079	. 158	. 160	. 158
. 600	. 074	. 078	. 080	. 148	. 156	. 160
. 700	. 065	. 071	. 077	. 130	. 142	. 154
. 800	. 050	. 056	. 064	. 100	. 112	. 129
. 900	. 030	. 039	. 040	. 061	. 079	. 081

NOTE.—Lower surface is plane.

CLARK Y FAMILY

ORDINATES OF UPPER AND LOWER SURFACES

Dis- tance from nose	C 4		C 8		C 12		C 16		C 20	
	Upper	Lower	Upper	Lower	Upper	Lower	Upper	Lower	Upper	Lower
0. 000	0. 012	0. 012	0. 024	0. 024	0. 037	0. 037	0. 048	0. 048	0. 061	0. 061
. 025	. 022	. 005	. 044	. 010	. 066	. 015	. 088	. 020	. 110	. 025
. 050	. 027	. 003	. 054	. 006	. 080	. 009	. 107	. 012	. 134	. 016
. 075	. 031	. 002	. 061	. 004	. 092	. 006	. 122	. 008	. 153	. 010
. 100	. 033	. 001	. 065	. 003	. 098	. 004	. 131	. 005	. 164	. 006
. 150	. 036	. 000	. 073	. 001	. 109	. 001	. 146	. 002	. 182	. 003
. 200	. 039	. 000	. 078	. 000	. 116	. 000	. 155	. 000	. 193	. 000
. 300	. 040	. 000	. 080	. 000	. 120	. 000	. 160	. 000	. 200	. 000
. 400	. 039	. 000	. 078	. 000	. 117	. 000	. 156	. 000	. 195	. 000
. 500	. 036	. 000	. 072	. 000	. 108	. 000	. 144	. 000	. 180	. 000
. 600	. 031	. 000	. 062	. 000	. 094	. 000	. 125	. 000	. 156	. 000
. 700	. 025	. 000	. 050	. 000	. 075	. 000	. 100	. 000	. 126	. 000
. 800	. 018	. 000	. 036	. 000	. 053	. 000	. 071	. 000	. 089	. 000
. 900	. 010	. 000	. 019	. 000	. 029	. 000	. 037	. 000	. 048	. 000

Reed section	
Distance from nose	Ordinate of upper surface
0.100	0.056
.200	.080
.300	.094
.400	.094
.500	.091
.600	.084
.700	.074
.800	.058
.900	.039

Flat plate is 0.04 inch by 1 inch.
Wedge is 0.08 inch at base by 1 inch.
Circular arc airfoil has a plane lower surface and a maximum ordinate of 0.08 inch.
The chord is 1 inch in all cases.

NOTE.—Lower surface plane.

TABLE II.—LIFT AND DRAG COEFFICIENTS OF AIRFOILS AT VARYING ANGLES OF ATTACK FOR DIFFERENT VALUES OF V/c

AIRFOIL 3R4

LIFT COEFFICIENTS C_L

V/c	Angle of attack											
	−4	−2	0	2	4	6	8	10	12	14	16	20
0.50	−0.043	0.017	0.085	0.154	0.214	0.273	0.340	0.394	0.461	0.506	0.558	0.604
.65	−.047	.017	.086	.156	.217	.271	.326	.394	.462	.508	.558	.610
.80	−.052	.017	.087	.151	.217	.266	.339	.402	.458	.508	.544	-----
.95	−.056	.010	.081	.151	.218	.277	.336	.392	.451	.506	-----	-----
1.08	−.067	.003	.068	.130	.188	.245	.296	-----	-----	-----	-----	-----

DRAG COEFFICIENTS C_D

0.50	0.023	0.017	0.016	0.018	0.022	0.030	0.041	0.054	0.070	0.092	0.136	0.219
.65	.024	.018	.016	.018	.024	.030	.042	.056	.075	.104	.140	.220
.80	.026	.019	.016	.019	.025	.033	.047	.067	.091	.117	.149	-----
.95	.029	.021	.018	.021	.029	.041	.056	.077	.103	.133	-----	-----
1.08	.037	.026	.022	.024	.031	.043	.057	-----	-----	-----	-----	-----

AIRFOIL 3R6

LIFT COEFFICIENTS C_L

V/c	Angle of attack											
	−4	−2	0	2	4	6	8	10	12	14	16	20
0.50	−0.033	0.033	0.104	0.174	0.229	0.281	0.344	0.401	0.458	0.510	0.575	0.649
.65	−.018	.044	.112	.170	.229	.287	.335	.397	.459	.510	.572	.635
.80	−.017	.054	.116	.172	.225	.294	.351	.408	.464	.503	.555	.631
.95	.007	.060	.119	.179	.234	.286	.335	.389	.436	.480	.532	-----
1.08	−.033	.030	.096	.139	.200	.261	.310	.364	.423	-----	-----	-----

DRAG COEFFICIENTS C_D

0.50	0.027	0.021	0.018	0.020	0.025	0.032	0.043	0.055	0.070	0.088	0.108	0.190
.65	.028	.021	.020	.021	.026	.034	.044	.058	.074	.094	.121	.195
.80	.029	.023	.021	.023	.029	.037	.051	.068	.090	.115	.144	.210
.95	.033	.027	.025	.027	.035	.047	.062	.081	.104	.128	.157	-----
1.08	.045	.039	.037	.039	.045	.056	.071	.088	.111	-----	-----	-----

AIRFOIL 3R8
LIFT COEFFICIENTS C_L

V/c	Angle of attack											
	-4	-2	0	2	4	6	8	10	12	14	16	20
0.50	0.023	0.094	0.155	0.209	0.264	0.324	0.381	0.433	0.473	0.561	0.618	0.686
.65	.033	.099	.157	.216	.272	.328	.374	.452	.502	.563	.608	.672
.80	.045	.105	.165	.221	.276	.337	.394	.450	.495	.537	.597	.654
.95	.054	.103	.158	.211	.254	.293	.346	.398	.440	.490	.540	.638
1.08	-.039	.016	.086	.150	.219	.262	.293	.339	.369	.424	.466	.576

DRAG COEFFICIENTS C_D

0.50	0.031	0.026	0.025	0.027	0.033	0.042	0.051	0.064	0.079	0.098	0.117	0.178
.65	.032	.027	.026	.028	.035	.043	.053	.066	.082	.101	.122	.204
.80	.036	.030	.029	.032	.038	.048	.061	.079	.100	.128	.157	.224
.95	.045	.040	.039	.043	.051	.063	.079	.099	.120	.143	.171	.236
1.08	.063	.056	.053	.055	.062	.070	.081	.097	.114	.135	.159	.226

AIRFOIL 3R10
LIFT COEFFICIENTS C_L

V/c	Angle of attack											
	-4	-2	0	2	4	6	8	10	12	14	16	20
0.50	0.086	0.144	0.206	0.257	0.322	0.378	0.427	0.481	0.517	0.569	0.642	0.753
.65	.092	.150	.208	.265	.321	.358	.430	.487	.546	.586	.579	.656
.80	.099	.160	.205	.261	.321	.371	.414	.459	.502	.520	.552	.642
.95	.068	.115	.160	.213	.254	.301	.343	.393	.437	.472	.528	.618
1.08	-.017	.038	.103	.160	.218	.270	.310	.356	.396	.446	.493	.569

DRAG COEFFICIENTS C_D

0.50	0.040	0.036	0.035	0.037	0.043	0.051	0.062	0.074	0.089	0.108	0.126	0.172
.65	.043	.038	.036	.038	.044	.045	.063	.077	.093	.110	.153	.220
.80	.048	.042	.040	.043	.049	.057	.072	.093	.116	.144	.174	.232
.95	.062	.058	.058	.061	.068	.080	.094	.112	.135	.160	.186	.248
1.08	.082	.075	.072	.074	.080	.089	.100	.116	.135	.158	.184	.241

AIRFOIL 3R12
LIFT COEFFICIENTS C_L

V/c	Angle of attack											
	-4	-2	0	2	4	6	8	10	12	14	16	20
0.50	0.113	0.176	0.240	0.292	0.340	0.382	0.445	0.499	0.558	0.597	0.656	0.750
.65	.129	.179	.237	.287	.349	.385	.456	.499	.554	.591	.593	.642
.80	.140	.188	.234	.296	.339	.381	.419	.453	.490	.523	.548	.642
.95	.063	.086	.145	.198	.243	.290	.343	.365	.407	.452	.496	.579
1.08	-.025	.027	.081	.136	.202	.247	.297	.331	.369	.414	.471	.538

DRAG COEFFICIENTS C_D

0.50	0.049	0.045	0.045	0.047	0.052	0.060	0.071	0.083	0.098	0.115	0.133	0.177
.65	.054	.048	.046	.047	.053	.061	.071	.084	.099	.118	.162	.233
.80	.064	.054	.052	.053	.059	.069	.086	.108	.131	.159	.185	.247
.95	.083	.077	.076	.081	.088	.097	.112	.128	.150	.174	.197	.255
1.08	.103	.094	.090	.090	.095	.103	.116	.131	.150	.170	.194	.247

AIRFOIL 3R14
LIFT COEFFICIENTS C_L

V/c	Angle of attack											
	-4	-2	0	2	4	6	8	10	12	14	16	20
0.50	0.142	0.204	0.266	0.315	0.360	0.412	0.468	0.521	0.547	0.616	0.680	0.775
.65	.160	.208	.261	.313	.360	.426	.470	.523	.572	.472	.505	.604
.80	.190	.229	.278	.316	.347	.365	.387	.434	.473	.506	.524	.596
.95	.026	.014	.124	.176	.221	.263	.318	.365	.394	.454	.493	.568
1.08	-.049	.003	.057	.120	.187	.242	.284	.319	.381	.425	.464	.542

DRAG COEFFICIENTS C_D

0.50	0.059	0.052	0.050	0.052	0.056	0.064	0.075	0.087	0.098	0.117	0.136	0.178
.65	.067	.057	.053	.055	.060	.067	.077	.090	.105	.153	.185	.230
.80	.077	.067	.062	.065	.071	.086	.105	.125	.147	.173	.203	.254
.95	.106	.099	.099	.103	.109	.116	.128	.146	.163	.188	.212	.261
1.08	.122	.115	.111	.109	.114	.121	.132	.147	.165	.185	.207	.262

AIRFOIL 3R16
LIFT COEFFICIENTS C_L

V/c	Angle of attack											
	-4	-2	0	2	4	6	8	10	12	14	16	20
0.50	0.181	0.236	0.298	0.354	0.399	0.445	0.490	0.539	0.592	0.648	0.716	0.574
.65	.215	.252	.282	.335	.392	.450	.492	.540	.421	.462	.501	.580
			.308						.445	.483	.552	.635
.80	.231	.259	.247	.259	.307	.344	.386	.430	.461	.496	.528	.614
.95	.032	.048	.086	.167	.223	.267	.311	.359	.380	.421	.457	.549
1.08	-.079	-.027	.034	.103	.176	.222	.278	.320	.349	.382	.420	.479

DRAG COEFFICIENTS C_D

0.50	0.069	0.061	0.059	0.061	0.066	0.073	0.084	0.098	0.115	0.132	0.151	0.261
.65	.078	.067	.068	.062	.068	.076	.087	.100	.143	.167	.190	.253
			.060						.162	.190	.216	
.80	.092	.081	.073	.083	.098	.114	.130	.148	.174	.195	.217	.271
.95	.130	.125	.123	.124	.132	.140	.152	.166	.189	.208	.236	.287
1.08	.150	.144	.138	.138	.140	.145	.155	.170	.185	.205	.225	.272

AIRFOIL 3R18
LIFT COEFFICIENTS C_L

V/c	Angle of attack											
	-4	-2	0	2	4	6	8	10	12	14	16	20
0.50	0.224	0.271	0.340	0.388	0.433	0.469	0.505	0.575	0.620	0.674	0.735	0.810
.65	.260	.289	.322	.369	.430	.473	.522	.563	.558	.485	.546	.606
.80	.229	.168	.185	.242	.299	.339	.388	.425	.452	.485	.522	.613
.95	-.012	-.008	.087	.175	.242	.291	.334	.373	.424	.459	.489	.561
1.08	-----	-.041	.007	.080	.142	.187	.239	.291	.329	.371	.415	.495

DRAG COEFFICIENTS C_D

0.50	0.081	0.072	0.069	0.070	0.074	0.081	0.093	0.105	0.120	0.139	0.157	0.198
.65	.091	.080	.072	.071	.076	.083	.095	.106	.130	.186	.207	.272
.80	.103	.089	.094	.102	.113	.125	.142	.161	.181	.203	.224	.281
.95	.149	.143	.139	.142	.147	.155	.165	.181	.201	.221	.245	.299
1.08	-----	.160	.155	.152	.156	.164	.173	.183	.199	.217	.238	.285

AIRFOIL 3R20
LIFT COEFFICIENTS C_L

V/c	Angle of attack											
	-4	-2	0	2	4	6	8	10	12	14	16	20
0.50	0.275	0.309	0.363	0.399	0.442	0.489	0.534	0.564	0.624	0.687	0.749	0.635
.65	.309	.313	.343	.388	.444	.481	.523	.417	.443	.503	.566	.811
.80	.147	.103	.168	.230	.292	.327	.373	.536	.462	.518	.552	.612
.95	-.026	.010	.076	.160	.220	.269	.297	.411	.386	.428	.464	.627
1.08	-----	-.057	.000	.059	.121	.179	.233	.344	.297	.452	.382	.547
								.260	.332	.332	.464	

DRAG COEFFICIENTS C_D

0.50	0.097	0.083	0.078	0.076	0.080	0.088	0.099	0.112	0.129	0.145	0.164	0.271
.65	.109	.092	.080	.078	.081	.089	.099	.148	.173	.200	.223	.279
.80	.118	.115	.115	.120	.131	.142	.157	.174	.192	.216	.243	.297
.95	.172	.167	.163	.165	.167	.177	.188	.199	.219	.240	.265	.316
1.08	-----	.183	.177	.175	.177	.181	.190	.205	.219	.236	.257	.300

AIRFOIL 4R8
LIFT COEFFICIENTS C_L

V/c	Angle of attack											
	-4	-2	0	2	4	6	8	10	12	14	16	20
0.50	0.047	0.105	0.171	0.234	0.290	0.345	0.403	0.453	0.500	0.562	0.594	0.704
.65	.059	.123	.184	.240	.295	.330	.395	.459	.511	.569	.606	.685
.80	.067	.134	.196	.242	.293	.347	.401	.459	.504	.538	.580	.664
.95	.048	.110	.166	.215	.265	.304	.346	.389	.446	.490	.537	.640
1.08	-.038	.024	.087	.145	.209	.250	.292	.333	.381	.421	.469	.556

DRAG COEFFICIENTS C_D

0.50	0.033	0.028	0.028	0.031	0.036	0.043	0.053	0.066	0.081	0.099	0.118	0.160
.65	.034	.029	.029	.031	.037	.044	.055	.068	.084	.103	.123	.192
.80	.038	.032	.031	.033	.037	.047	.059	.075	.095	.123	.153	.217
.95	.045	.038	.035	.038	.045	.056	.071	.091	.111	.137	.166	.230
1.08	.062	.054	.050	.051	.056	.064	.075	.090	.109	.130	.155	.214

AIRFOIL 5R8
LIFT COEFFICIENTS C_L

V/c	Angle of attack											
	-4	-2	0	2	4	6	8	10	12	14	16	20
0.50	0.037	0.095	0.157	0.225	0.294	0.346	0.400	0.450	0.502	0.552	0.593	0.671
.65	.051	.115	.175	.240	.303	.351	.385	.461	.514	.572	.622	.661
.80	.068	.133	.193	.241	.296	.356	.408	.467	.524	.571	.622	.674
.95	.044	.123	.191	.235	.296	.333	.371	.404	.473	.536	.578	.672
1.08	-.020	.042	.106	.165	.225	.267	.311	.361	.417	.466	.522	.614

DRAG COEFFICIENTS C_D

0.50	0.033	0.029	0.029	0.031	0.038	0.045	0.055	0.067	0.081	0.099	0.117	0.181
.65	.034	.029	.029	.032	.039	.046	.056	.069	.085	.102	.121	.196
.80	.037	.032	.031	.034	.040	.049	.061	.076	.094	.117	.143	.219
.95	.046	.037	.036	.038	.046	.056	.070	.089	.111	.135	.164	.231
1.08	.061	.053	.050	.050	.056	.064	.076	.092	.110	.133	.159	.227

AIRFOIL 6R8
LIFT COEFFICIENTS C_L

V/c	Angle of attack											
	-4	-2	0	2	4	6	8	10	12	14	16	20
0.50	0.000	0.056	0.119	0.185	0.262	0.339	0.412	0.459	0.496	0.524	0.596	0.647
.65	.003	.065	.129	.202	.280	.347	.429	.473	.509	.566	.611	.639
.80	.003	.074	.139	.218	.315	.366	.421	.479	.535	.579	.624	.657
.95	.004	.090	.163	.239	.300	.353	.394	.427	.498	.542	.592	.653
1.08	-.026	.044	.108	.162	.225	.265	.311	.356	.396	.450	.500	.623

DRAG COEFFICIENTS C_D

0.50	0.037	0.031	0.030	0.032	0.037	0.046	0.059	0.069	0.082	0.100	0.119	0.205
.65	.038	.032	.031	.033	.039	.048	.060	.071	.084	.103	.123	.212
.80	.042	.035	.032	.035	.042	.049	.061	.076	.093	.113	.140	.221
.95	.049	.039	.035	.037	.044	.053	.066	.082	.104	.130	.160	.228
1.08	.062	.052	.047	.047	.051	.058	.068	.081	.099	.121	.147	.220

AIRFOIL 4R16
LIFT COEFFICIENTS C_L

V/c	Angle of attack											
	-4	-2	0	2	4	6	8	10	12	14	16	20
0.50	0.176	0.232	0.302	0.358	0.416	0.481	0.524	0.575	0.635	0.674	0.721	0.790
.65	.220	.249	.317	.374	.440	.486	.541	.582	.623	.667	.702	.636
.80	.149	.186	.245	.310	.348	.381	.418	.462	.506	.547	.577	.650
.95	-.064	-.021	.068	.135	.187	.244	.297	.360	.429	.476	.519	.594
1.08	-----	-.036	.020	.080	.130	.190	.240	.283	.324	.377	.428	.470

DRAG COEFFICIENTS C_D

0.50	0.071	0.063	0.062	0.064	0.069	0.078	0.090	0.102	0.121	0.133	0.150	0.188
.65	.079	.069	.066	.067	.072	.080	.091	.103	.117	.131	.149	.222
.80	.088	.075	.070	.071	.074	.082	.095	.114	.135	.162	.188	.247
.95	.123	.111	.106	.105	.107	.116	.128	.143	.163	.184	.207	.263
1.08	-----	.132	.124	.121	.122	.127	.136	.148	.163	.181	.202	.242

AIRFOIL 5R16
LIFT COEFFICIENTS C_L

V/c	Angle of attack											
	-4	-2	0	2	4	6	8	10	12	14	16	20
0.50	0.017	0.098	0.186	0.271	0.354	0.426	0.508	0.571	0.622	0.650	0.701	0.791
.65	.056	.131	.212	.297	.365	.457	.533	.579	.602	.652	.700	.670
.80	.076	.149	.222	.317	.397	.467	.510	.504	.525	.556	.582	.662
.95	-.052	.013	.107	.164	.221	.263	.310	.361	.400	.467	.526	.574
1.08	-.072	-.012	.047	.108	.169	.224	.278	.320	.362	.413	.449	.514

DRAG COEFFICIENTS C_D

0.50	0.079	0.070	0.066	0.066	0.070	0.078	0.090	0.106	0.118	0.128	0.145	0.190
.65	.080	.070	.066	.066	.071	.080	.094	.104	.113	.130	.150	.219
.80	.093	.081	.075	.074	.076	.081	.091	.107	.132	.159	.184	.242
.95	.117	.104	.100	.098	.102	.109	.122	.139	.158	.180	.204	.259
1.08	.138	.127	.118	.115	.116	.121	.130	.142	.158	.179	.199	.250

AIRFOIL 6R16
LIFT COEFFICIENTS C_L

V/c	Angle of attack											
	-4	-2	0	2	4	6	8	10	12	14	16	20
0.50	-0.049	0.036	0.112	0.182	.0275	0.354	0.431	0.502	0.579	0.616	0.672	0.777
.65	-.038	.052	.126	.211	.293	.366	.455	.515	.575	.629	.680	.771
.80	.000	.086	.172	.242	.334	.386	.462	.510	.543	.554	.590	.675
.95	-.039	.048	.121	.178	.228	.272	.318	.365	.413	.493	.558	.625
1.08	-.064	-.005	.052	.109	.158	.215	.256	.298	.334	.377	.421	.529

DRAG COEFFICIENTS C_D

0.50	0.090	0.080	0.073	0.069	0.072	0.078	0.088	0.097	0.110	0.122	0.141	0.185
.65	.093	.081	.073	.070	.073	.079	.089	.094	.108	.124	.145	.191
.80	.100	.087	.080	.075	.070	.074	.085	.100	.118	.143	.171	.228
.95	.112	.101	.095	.092	.093	.099	.112	.127	.148	.169	.193	.246
1.08	.137	.124	.113	.107	.107	.111	.119	.130	.147	.166	.187	.239

AIRFOIL C4
LIFT COEFFICIENTS C_L

V/c	Angle of attack											
	-4	-2	0	2	4	6	8	10	12	14	16	20
0.50	-0.048	0.017	0.075	0.146	0.209	0.268	0.327	0.383	0.440	0.492	0.527	0.599
.65	-.048	.014	.082	.151	.210	.271	.338	.390	.452	.496	.548	.599
.80	-.060	.006	.077	.147	.216	.272	.338	.398	.449	.478	.524	-----
.95	-.057	.012	.077	.147	.217	.278	.333	.392	-----	-----	-----	-----
1.08	-.075	-.001	.060	.126	.173	.243	.300	-----	-----	-----	-----	-----

DRAG COEFFICIENTS C_D

0.50	0.013	0.011	0.010	0.014	0.021	0.030	0.042	0.057	0.086	0.122	0.160	0.227
.65	.014	.011	.011	.015	.022	.032	.045	.065	.091	.125	.160	.226
.80	.015	.011	.011	.014	.022	.034	.050	.071	.097	.126	.158	-----
.95	.021	.014	.013	.017	.025	.038	.056	.078	-----	-----	-----	-----
1.08	.031	.022	.019	.021	.028	.040	.057	-----	-----	-----	-----	-----

AIRFOIL C8
LIFT COEFFICIENTS C_L

V/c	Angle of attack											
	-4	-2	0	2	4	6	8	10	12	14	16	20
0.50	0.026	0.084	0.148	0.197	0.255	0.315	0.373	0.429	0.466	0.530	0.594	0.629
.65	.027	.083	.143	.206	.261	.316	.382	.437	.503	.552	.594	.616
.80	.032	.090	.149	.199	.268	.333	.398	.442	.494	.552	.583	.635
.95	.029	.086	.144	.198	.249	.298	.349	.396	.444	.494	.550	.614
1.08	-.035	.030	.087	.140	.205	.255	.303	.340	.403	.450	.490	.585

DRAG COEFFICIENTS C_D

0.50	0.017	0.016	0.017	0.020	0.027	0.036	0.047	0.060	0.074	0.092	0.111	0.220
.65	.017	.016	.018	.021	.028	.037	.049	.064	.081	.100	.137	.225
.80	.018	.017	.019	.022	.030	.041	.056	.074	.100	.130	.161	.235
.95	.031	.027	.028	.034	.044	.056	.073	.093	.116	.142	.174	.240
1.08	.046	.041	.040	.044	.052	.063	.076	.094	.116	.141	.169	.237

AIRFOIL C12

LIFT COEFFICIENTS C_L

V/c	Angle of attack											
	-4	-2	0	2	4	6	8	10	12	14	16	20
0.50	0.099	0.146	.210	0.264	0.328	0.386	0.446	0.504	0.554	0.612	0.656	0.770
.65	.097	.152	.212	.272	.329	.389	.450	.502	.561	.598	.625	.684
.80	.108	.162	.224	.281	.330	.381	.419	.458	.498	.537	.574	.659
.95	.014	.074	.128	.180	.234	.289	.338	.388	.442	.482	.532	.620
1.08	-.058	-.004	.053	.118	.167	.227	.283	.324	.376	.425	.467	.564

DRAG COEFFICIENTS C_D

0.50	0.020	0.022	0.026	0.031	0.039	0.050	0.063	0.078	0.094	0.112	0.132	0.176
.65	.021	.023	.026	.032	.039	.051	.065	.079	.096	.115	.151	.223
.80	.028	.026	.029	.036	.045	.059	.080	.104	.129	.158	.186	.247
.95	.059	.056	.058	.064	.074	.088	.102	.124	.145	.167	.194	.258
1.08	.080	.074	.073	.076	.082	.094	.109	.126	.145	.167	.192	.252

AIRFOIL C16

LIFT COEFFICIENTS C_L

V/c	Angle of attack											
	-4	-2	0	2	4	6	8	10	12	14	16	20
0.50	0.165	0.212	0.271	0.333	0.388	0.440	0.502	0.539	0.603	0.648	0.719	0.816
.65	.169	.225	.278	.325	.387	.442	.497	.555	.596	.519	.552	.588
.80	.169	.211	.238	.275	.316	.359	.401	.440	.459	.510	.534	.654
.95	-.035	.048	.117	.175	.233	.284	.334	.366	.418	.460	.518	.614
1.08	-.083	-.026	.025	.087	.145	.205	.267	.321	.360	.405	.443	.516

DRAG COEFFICIENTS C_D

0.50	0.027	0.031	0.037	0.044	0.053	0.064	0.079	0.095	0.112	0.130	0.150	0.243
.65	.029	.032	.038	.045	.054	.064	.078	.096	.111	.162	.186	.243
.80	.044	.043	.048	.061	.076	.093	.113	.135	.158	.182	.213	.267
.95	.094	.092	.093	.099	.108	.120	.136	.152	.172	.197	.222	.280
1.08	.118	.114	.113	.115	.120	.131	.142	.158	.176	.195	.216	.270

AIRFOIL C20

LIFT COEFFICIENTS C_L

V/c	Angle of attack											
	-4	-2	0	2	4	6	8	10	12	14	16	20
0.50	0.217	0.271	0.333	0.379	0.430	0.484	0.537	0.603	0.654	0.699	0.756	0.528
.65	.226	.279	.331	.380	.439	.483	.528	.398	.426	.457	.494	.555
.80	.090	.148	.188	.244	.294	.338	.379	.405	.438	.479	.527	.615
.95	-.059	.002	.098	.156	.236	.277	.312	.357	.405	.453	.478	.515
1.08	-----	-.066	-.017	.045	.109	.154	.203	.256	.300	.345	.395	.471

DRAG COEFFICIENTS C_D

0.50	0.038	0.043	0.050	0.058	0.068	0.078	0.093	0.114	0.130	0.148	0.167	0.278
.65	.042	.046	.051	.058	.069	.079	.092	.144	.175	.202	.225	.272
.80	.079	.081	.086	.097	.111	.129	.148	.165	.194	.210	.235	.289
.95	.134	.133	.133	.134	.143	.155	.168	.182	.203	.225	.249	.295
1.08	-----	.154	.150	.148	.152	.162	.174	.189	.204	.223	.245	.293

REED AIRFOIL
LIFT COEFFICIENTS C_L

V/c	Angle of attack											
	-4	-2	0	2	4	6	8	10	12	14	16	20
0.50	0.071	0.135	0.194	0.257	0.305	0.363	0.421	0.468	0.528	0.575	0.618	0.687
.65	.081	.144	.200	.254	.313	.365	.424	.482	.544	.590	.638	.720
.80	.087	.150	.206	.266	.321	.378	.432	.480	.528	.568	.628	.738
.95	.038	.091	.139	.193	.240	.288	.337	.392	.436	.498	.564	.686
1.08	-.033	.028	.092	.145	.201	.241	.277	.323	.374	.429	.478	.581

DRAG COEFFICIENTS C_D

0.50	0.035	0.031	0.031	0.034	0.040	0.048	0.058	0.071	0.087	0.104	0.120	0.161
.65	.036	.032	.032	.035	.040	.049	.061	.074	.090	.107	.124	.170
.80	.041	.035	.035	.038	.044	.053	.066	.079	.096	.119	.143	.206
.95	.059	.053	.051	.053	.060	.068	.080	.096	.113	.137	.164	.229
1.08	.076	.068	.064	.063	.067	.074	.083	.098	.112	.133	.156	.216

FLAT PLATE AIRFOIL
LIFT COEFFICIENTS C_L

V/c	Angle of attack											
	-4	-2	0	2	4	6	8	10	12	14	16	20
0.50	-0.146	-0.071	-0.001	0.064	0.146	0.219	0.298	0.356	0.399	0.455	0.498	0.550
.65	-.155	-.080	.000	.080	.159	.231	.298	.341	.415	.450	.493	.540
.80	-----	-.084	.006	.095	.173	.245	.312	.369	.415	.449	.491	-----
.95	-----	-.112	.013	.110	.187	.257	.319	.373	.430	-----	-----	-----
1.08	-----	-----	.012	.105	.175	.244	.295	.351	.406	-----	-----	-----

DRAG COEFFICIENTS C_D

0.50	0.039	0.032	0.030	0.033	0.043	0.057	0.075	0.095	0.119	0.146	0.175	0.233
.65	.042	.033	.031	.034	.046	.059	.078	.099	.125	.150	.178	.230
.80	-----	.038	.034	.037	.050	.065	.085	.108	.128	.152	.180	-----
.95	-----	.043	.038	.044	.054	.069	.089	.112	.140	-----	-----	-----
1.08	-----	-----	.037	.044	.055	.069	.084	.105	.130	-----	-----	-----

WEDGE AIRFOIL
LIFT COEFFICIENTS C_L

V/c	Angle of attack											
	-4	-2	0	2	4	6	8	10	12	14	16	20
0.50	-0.204	-0.140	-0.071	-0.004	0.064	0.129	0.200	0.272	0.339	0.416	0.487	0.562
.65	-----	-.142	-.073	-.008	.067	.129	.205	.279	.349	.412	.499	.574
.80	-----	-----	-.077	-.004	.072	.137	.216	.278	.373	.449	.496	.575
.95	-----	-----	-.078	-.003	.075	.146	.218	.302	.374	.456	.505	.581
1.08	-----	-----	-.063	-.004	.056	.120	.208	.288	.359	.431	.488	.564

DRAG COEFFICIENTS C_D

0.50	0.052	0.047	0.047	0.046	0.047	0.048	0.053	0.063	0.083	0.109	0.140	0.205
.65	-----	.050	.050	.051	.052	.052	.055	.066	.087	.113	.144	.209
.80	-----	-----	.053	.055	.055	.054	.059	.071	.091	.120	.148	.215
.95	-----	-----	.052	.054	.054	.057	.064	.077	.098	.124	.158	.227
1.08	-----	-----	.050	.049	.051	.056	.063	.076	.095	.121	.153	.220

CIRCULAR ARC AIRFOIL

LIFT COEFFICIENTS C_L

V/c	Angle of attack											
	-4	-2	0	2	4	6	8	10	12	14	16	20
0.50	0.064	0.124	0.179	0.240	0.300	0.358	0.397	0.429	0.483	0.519	0.564	0.618
.65	.078	.142	.191	.252	.304	.353	.394	.435	.479	.533	.568	.632
.80	.096	.148	.205	.264	.314	.378	.427	.442	.497	.548	.590	.618
.95	-.002	.057	.115	.173	.238	.295	.388	.421	.483	.532	.572	.616
1.08	-.034	.031	.094	.144	.189	.233	.301	.368	.418	.476	.521	.615

DRAG COEFFICIENTS C_D

0.50	0.031	0.028	0.028	0.031	0.036	0.045	0.053	0.064	0.079	0.097	0.120	0.204
.65	.028	.028	.028	.031	.037	.046	.053	.064	.080	.098	.122	.208
.80	.033	.029	.029	.032	.039	.049	.058	.065	.081	.101	.125	.214
.95	.049	.041	.038	.039	.043	.051	.064	.073	.086	.109	.136	.218
1.08	.058	.050	.046	.045	.048	.053	.061	.074	.087	.109	.136	.203

REPORT No. 320

**THE MEASUREMENT OF
FLUCTUATIONS OF AIR SPEED BY THE
HOT-WIRE ANEMOMETER**

By H. L. DRYDEN and A. M. KUETHE
Bureau of Standards

REPORT No. 320

THE MEASUREMENT OF FLUCTUATIONS OF AIR SPEED BY THE HOT-WIRE ANEMOMETER

By H. L. DRYDEN and A. M. KUETHE

SUMMARY

The hot-wire anemometer suggests itself as a promising method for measuring the fluctuating air velocities found in turbulent air flow. The only obstacle is the presence of a lag due to the limited energy input which makes even a fairly small wire incapable of following rapid fluctuations with accuracy. This paper gives the theory of the lag and describes an experimental arrangement for compensating for the lag for frequencies up to 100 or more per second when the amplitude of the fluctuation is not too great. An experimental test of the accuracy of compensation and some results obtained with the apparatus in a wind-tunnel air stream are described. While the apparatus is very bulky in its present form, it is believed possible to develop a more portable arrangement.

INTRODUCTION

In a historic paper (reference 1) Osborne Reynolds distinguished experimentally two types of fluid motion in pipes which are to-day termed laminar and turbulent. In the laminar motion the fluid particles follow each other in paths parallel to the axis of the pipe and the flow is steady—i. e., the speed at any point is not a function of the time. In the turbulent motion the fluid is filled with a mass of eddies, and while on the average the flow is parallel to the axis of the pipe there is a rapid fluctuation of the velocity at any point about a mean value. A stream of smoke or colored fluid introduced into a laminar flow retains its identity for a considerable time, whereas in a turbulent flow the stream is very rapidly diffused throughout the fluid. In laminar flow the stresses are transferred from layer to layer of the fluid solely by the action of molecular diffusion, whereas in turbulent flow there is in addition a molar diffusion or the transfer of momentum by extensive groups of molecules. The velocity distribution in laminar flow may be computed from the equations of motion of an incompressible viscous fluid on the assumption that a steady state of flow exists in which the lines of flow are parallel to the axis of the pipe. The speed is found to be a parabolic function of the radial distance from the axis of the pipe. In turbulent flow the speed is found to vary as a power of the distance from the wall of the pipe over most of the cross section, but it can not as yet be shown how this result may be derived from the equations of motion nor can a physical meaning be attributed to the exponent of the power law.

It was shown experimentally by Reynolds that turbulent motion could not exist if the value of the ratio $VD\rho/\mu$, now known as the Reynolds Number, was less than 2,000. V denotes the mean speed of flow, D the diameter of the pipe, ρ the density, and μ the viscosity of the fluid. At Reynolds Numbers much larger than 2,000 laminar motion is not possible, while in a certain intermediate range laminar motion is unstable, the degree of stability being dependent on the magnitude of the disturbances present.

These conceptions of laminar and turbulent motions and of the Reynolds Number as a criterion determining the type of flow have been extended to fluid motion in general. In the extension the designation "turbulent motion" has sometimes been restricted to those cases in which the fluctuations of velocity are more or less random in nature. In general, however,

the periodic motions which occur behind many bodies as, for example, behind cylinders, and which may be approximately represented as the effect of a limited number of moving singularities (vortices), are also classed as turbulent motions.

In wind tunnels it is desired to reproduce as closely as possible the same relative flow as if the model were moving forward in still air. To obtain this result, it is necessary to secure an air stream of large cross section as compared to the cross section of the model and of uniform and steady speed throughout. It is at once apparent that the ideal condition can not be secured. In the first place the Reynolds Numbers required for even moderate speeds and cross-sectional areas are far above 2,000, so that the flow is of necessity turbulent. In the second place, the distribution of average speed in fully developed laminar or turbulent flow (i. e., far from the entrance of a tube) is not uniform across the section and therefore unsatisfactory. The compromise usually made is to work near enough to the entrance of a large tube that the effect of the walls does not have time to reach the center. Conditions are therefore not steady, and turbulence is always present.

Turbulence in wind tunnels does not seem to produce any large effects as judged by a comparison of results obtained on similar models in different wind tunnels except for cylinders, spheres, spheroids, ellipsoids, and airship hulls. In these instances very large effects are produced. (References 2 and 7.) The desire to make some direct measurement of the turbulence in wind tunnels was the incentive for the work here described, but before proceeding further it is desirable to specify in more detail what is meant by the word "turbulence."

In 1895 Reynolds (reference 3) gave a mathematical formulation of turbulent flow. He began by a consideration of the meaning of the velocities entering into the general equations of motion. The equations are obtained on the assumption of a continuous medium whereas we know in fact that the medium is discontinuous, consisting of individual molecules. We think of the velocity at any point at a given instant not as the velocity of a single molecule at that point but as the velocity of a fictitious fluid particle. We imagine a small volume around the point, for example, a small sphere of radius r , and define the velocity at the point V , as the average velocity of all the molecules within the sphere. To satisfy the conditions of continuity, the sphere must be so small that the variation of average velocity taken about other points within the sphere is small. Thus if we consider the variation in any direction s , $r \frac{d^2 V}{ds^2}$ must be negligible in comparison with $\frac{dV}{ds}$. On the other hand, the sphere must be large compared with the mean free path of the molecules. After an infinitesimal interval of time dt , we assume that the "particle" has reached the point Vdt . The fluid particle may thus be given a definite mathematical meaning, but it has no physical existence and in particular it does not consist always of the same molecules.

It is possible to define the velocity at a point in a manner not involving the conception of a fluid particle by taking the vectorial average velocity of all molecules passing through a small volume around the point in a certain time dt , which is long enough to include a large number of molecules.

The effect of the motion of the molecules is taken care of in the theory by a system of stresses, which are explained as due to the transfer of momentum by the molecular motions. In terms of the kinetic theory of gases for the simple case of two-dimensional parallel flow, the transfer of momentum per unit area per unit time is proportional to the density, the mean molecular speed, the mean free path, and the velocity gradient. In terms of hydrodynamical theory, the stress is equal to the product of the coefficient of viscosity, which is a constant for a given fluid at a given temperature, and the velocity gradient.

Reynolds proposed to treat the problem of turbulence in somewhat the same way. He proposed to substitute for the real motion an average or mean motion on which fluctuations were superposed and to take account of the effect of the fluctuations by a system of stresses. In the simple case of two-dimensional parallel flow the additional shearing stress turns out to be $\rho \overline{uv}$ times the velocity gradient where ρ is the density and \overline{uv} is the mean value of the product

of the superposed fluctuating components parallel and at right angles to the mean flow. Reynolds was also able to set up equations giving the relations which must exist between the variables in the steady state (in the kinetic sense)—namely, the condition that the rate at which the energy of the mean motion is converted to energy of the fluctuations is equal to the rate at which the energy of the fluctuations is dissipated by viscosity or in terms of the kinetic theory converted into the energy of the molecular fluctuations or heat motion.

H. A. Lorentz (reference 4) and J. M. Burgers (reference 5) have stated the equations of Reynolds in a somewhat different form and have shown that the knowledge of three mean values is sufficient to permit the computation of the resistance. These are the mean value of the product \overline{uv} , the mean value of $\overline{uv^2}$, and the mean value of the square of the vorticity.

Th. von Karman (reference 6) has given an excellent summary of the theory of turbulence developed along these lines to which the reader is referred for a summary of the mathematical treatment of the subject. It is clear from this summary that the treatment outlined by Reynolds has not as yet led to anything conclusive, principally because there is no method of computing the required mean values and because there is not sufficient experimental data on the fluctuations to give a clue to fruitful hypotheses. The great need at the present time in the further development of the theory of turbulence is more experiments on the actual fluctuations to supplement the data already available on the distribution of mean velocity.

It has been pointed out that the ordinary theory of laminar flow is based on certain average velocities which could be defined in terms of space averages or in terms of time averages. The averages taken for turbulent flow to obtain the mean or fundamental motion may also be based on either space or time averages, and it is usually assumed that the same result will be obtained in all cases provided the spaces and times over which the averages are taken are suitably chosen. It is clear that this method of procedure can be applied to a given flow in a great many ways by using space and time intervals of different orders of magnitude. The result obtained depends on what we wish to consider as the basic or fundamental flow. The process is an artificial one based on convenience, and some of the confusion as to the meaning of turbulence arises from the failure to appreciate this fact. For example, in the case of the natural wind we might consider averages over 5-minute intervals, 5-second intervals, or 0.05-second intervals, depending on the purpose in question. In no case would the fundamental motion be an absolutely stationary one, and in every case the conception of turbulence would be different. In most practical cases we define the fundamental flow as the one indicated by the instruments at our disposal which give mean values over a period ranging from, say, one second to one minute. Every physical instrument gives some kind of an average over a certain volume determined by its size and over a certain interval of time determined by its inertia or other lag characteristics. With the above definition of the fundamental motion we may have as many definitions of turbulence as we have instruments at our disposal.

The particular conception of turbulence adopted in this paper is based on a fundamental motion defined by time averages taken over several seconds. Any variation with frequency greater than one per two or three seconds is included in the superposed turbulence. For the present we have no means of taking averages over any extensive volume and no means of obtaining the particular average values used in the present form of the theory. It is the object of this paper to outline a method by means of which the fluctuations of the air speed at a given point may be measured and to give typical results obtained in the turbulent flow in a wind tunnel.

PREVIOUS WORK AT THE BUREAU OF STANDARDS

In Technical Report No. 231 of the National Advisory Committee for Aeronautics (reference 7), the first work carried out at the Bureau of Standards on the problem of turbulence in wind tunnels is described. One section of that report deals with measurements of the air resistance of cylinders in the turbulent flow behind wire screens of varying mesh, and another section deals with attempts to measure fluctuations of static and impact pressures by means of a diaphragm pressure gauge connected to the pressure nozzle by rubber tubing.

In practical wind-tunnel measurements we are interested in the effects of turbulence on the air forces on the models under investigation, but experiment shows that the results obtained for one model can not be applied to another. This seemingly direct method of attack also suffers from the difficulty that no numerical value can be assigned to the turbulence produced by the wire screens commonly used and that there is no method of extrapolation to obtain the result for an air stream free from turbulence.

Attention has therefore been turned to the more fundamental problem of measuring directly the variation of static pressure, speed, and direction of the air stream. Since the publication of National Advisory Committee for Aeronautics Technical Report No. 231 (reference 7), much attention has been given to the development of methods involving the transmission of pressure and to the possible study of directional changes by means of small, light, freely pivoted vanes. All of these mechanical methods have been unsuccessful, primarily due to the large inertia or the low natural frequency of the mechanical system. All such systems seem to oscillate with their natural frequency, abstracting the required small energy from the air stream.

In February, 1926, we began an investigation of the possibility of using a hot-wire anemometer for the measurement of speed fluctuations. After several months' work with a wire about 0.075 mm in diameter, it was concluded that the lag in the heating and cooling of the wire was so great that the method was not very promising. At about this time a paper by Prof. J. M. Burgers, of Delft, on Experiments on the Fluctuations of the Velocity in a Current of Air (reference 10) was called to our attention, in which experiments with wires of much smaller diameter than we had used gave very promising results. We were, however, unable to resume work on the problem until July, 1927. During the summer of 1927 we were fortunate in having associated with our staff Dr. Arthur E. Ruark for a period of two and one-half months. Doctor Ruark assembled a great deal of the necessary electrical apparatus, instructed other members of the section in its use, and made a number of experiments with several suggested arrangements. While Doctor Ruark was not associated with us in the design of the circuits finally used, it is a pleasure to acknowledge his contribution.

INVESTIGATIONS WITH THE HOT-WIRE ANEMOMETER

The classical work on the hot-wire anemometer as an instrument for measuring air speed is that by L. V. King. (Reference 8.) Many additional papers on the subject have appeared since that paper was published, many of them dealing with various modifications of the electrical circuits and of the form of the wire mounting. It is not proposed to give any complete bibliography, and we shall, in fact, refer only to those experiments in which measurements of fluctuations were attempted. The first work of this kind with which we are familiar is that by E. Huguenard, A. Magnan, and A. Planiol (reference 9) on the measurement of gusts in natural winds. These investigators give a brief theoretical treatment of the problem of the lag of the hot-wire anemometer and a method of computing corrections for lag.

Two years later the paper of Professor Burgers (reference 10), which has already been referred to, was published. Burgers also gave a brief computation of the lag, and by the use of wires about 0.015 mm in diameter he was able to reduce the lag considerably. He showed by the use of two instruments that the wire should not be longer than about 1 cm, since this was the maximum spacing for which the two wires gave the same indications at a given instant. Burgers described a method of recording directional variations.

In 1927 A. Fage and F. C. Johansen (reference 11), of the National Physical Laboratory, described some measurements of fluctuations behind plates in connection with measurements of average speed and direction. A wire 0.025 mm in diameter was used in conjunction with a string galvanometer and the measurements were made at low wind speeds to minimize the effect of lag.

The papers of Anrep, Downing, and their coworkers (reference 12) deserve mention in this connection, since the method of computing the correction for lag given by Huguenard and his coworkers was independently derived.

COMPUTATION OF THE LAG OF A HOT-WIRE ANEMOMETER

Since the theoretical treatment of the lag of the hot-wire anemometer given in the papers referred to above does not lend itself readily to the computation of the response of the instrument to an irregular or even to a periodic fluctuation of speed, we wish to give a more comprehensive computation:

The following symbols will be used:

$\frac{dH}{dt}$ = rate of increase of heat energy in the wire.

i = heating current (maintained constant).

R = instantaneous resistance of the wire.

T = instantaneous temperature of the wire.

\bar{R} = average resistance of the wire.

\bar{T} = average temperature of the wire.

T_o = air temperature (room temperature).

R_o = resistance of the wire at temperature T_o .

V = instantaneous air speed.

R_e = resistance of the wire in an air stream of constant speed V .

T_e = temperature of the wire in an air stream of constant speed V .

m = mass of the wire.

s = specific heat of the wire.

α = temperature coefficient of resistance of the wire.

\bar{V} = average wind speed.

$p = 2\pi$ times frequency of air speed variation.

$K(T - T_o)$ = rate of heat loss from wire by radiation and free convection.

$C(T - T_o)$ = rate of heat loss from wire by forced convection of air stream of speed V .

We assume that the rate of heat loss from the hot wire in an air stream of speed V is given by King's equation (reference 13), rate of heat loss equals $K(T - T_o) + C(T - T_o)\sqrt{V}$, in other words, that the rate of heat loss does not depend on the rate of variation of the air speed. We assume further that the heating current i , is maintained at a constant value and we understand by T the mean temperature at any instant as determined by the instantaneous resistance of the wire. By expressing the fact that the rate at which heat energy accumulates in the wire is equal to the rate at which electrical energy enters, less the rate at which heat energy leaves, we obtain the fundamental equation

$$\frac{dH}{dt} = i^2 R - (K + C\sqrt{V})(T - T_o) \quad (1)$$

Now $\frac{dH}{dt} = 4.2 \text{ ms} \frac{dT}{dt}$ since the increase in heat energy produces an increase in the temperature of the wire. Likewise $T - T_o = \frac{R - R_o}{R_o \alpha}$ and thus $\frac{dT}{dt} = \frac{1}{R_o \alpha} \frac{dR}{dt}$. On substitution of these values, we obtain

$$\frac{4.2 \text{ ms}}{R_o \alpha} \frac{dR}{dt} = i^2 R - (K + C\sqrt{V}) \frac{(R - R_o)}{R_o \alpha} \quad (2)$$

from which R is to be determined. If the cycle is performed very slowly so that $\frac{dR}{dt} = 0$, the equilibrium value R_e , would be determined by

$$i^2 R_e - (K + C\sqrt{V}) \frac{(R_e - R_o)}{R_o \alpha} = 0 \quad (3)$$

Equation (3) is the equation of the usual calibration curve of the wire and is found to be in accordance with the experimental results as to the dependence of R_e on i and V as shown in

Figures 1 and 2. The following discussion requires only that the heat loss be proportional to $f(V)(T - T_o)$ whether the wire be in temperature equilibrium or not. Solving equation (3) for $K + C\sqrt{V}$ and substituting in equation (2) we obtain

$$\frac{4.2ms}{R_o\alpha} \frac{dR}{dt} = \frac{i^2 R_o (R_e - R)}{R_e - R_o} \quad (4)$$

and then by adding and subtracting R_o within the parenthesis on the right and some simple transformations

$$R_e - R_o = \frac{R - R_o}{1 - \frac{4.2ms}{i^2 R_o^2 \alpha} \frac{dR}{dt}} \quad (5)$$

For simplicity in further discussion we rewrite this equation in the form

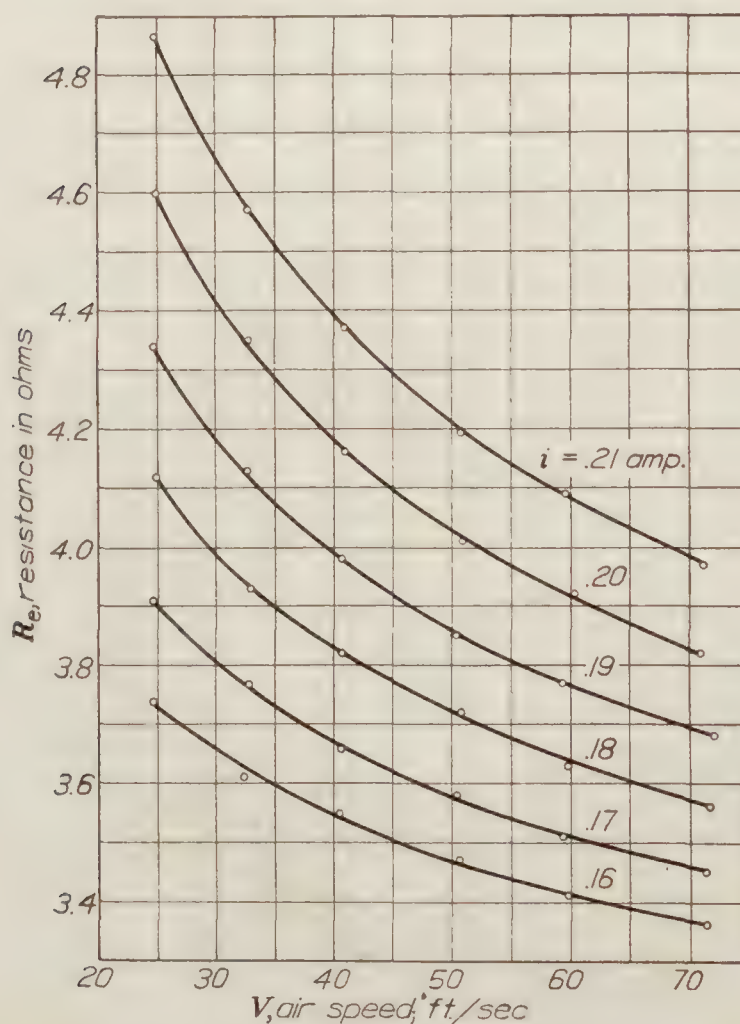


FIGURE 1.—Calibration curves for a hot wire (diameter, 17μ) at different heating currents

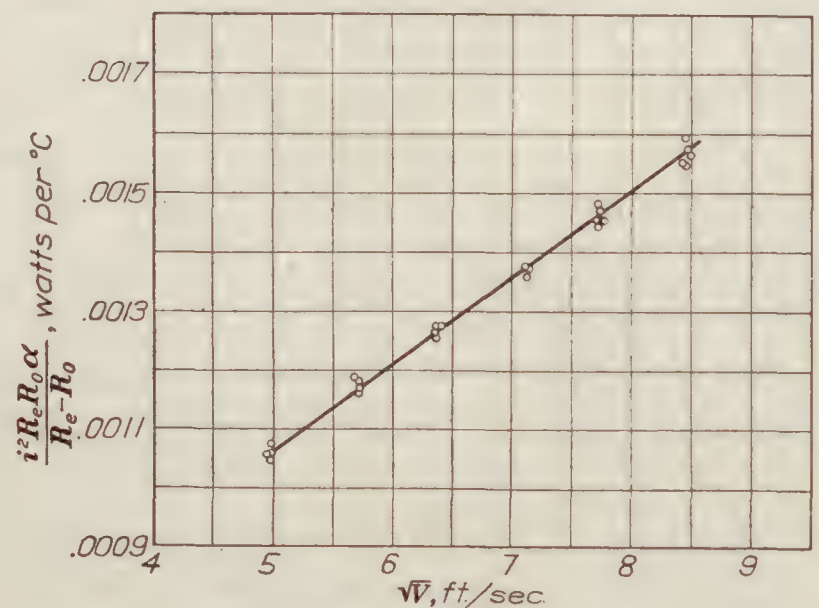


FIGURE 2.—The data on Figure 1 plotted to show the concordance with King's equation

$$\frac{R_e - R_o}{\bar{R} - R_o} = \frac{\frac{R - R_o}{\bar{R} - R_o}}{1 - M \frac{d}{dt} \left(\frac{R - R_o}{\bar{R} - R_o} \right)} \quad (6)$$

where

$$M = \frac{4.2ms(\bar{R} - R_o)}{i^2 R_o^2 \alpha} = \frac{4.2ms(\bar{T} - T_o)}{i^2 R_o} \quad (7)$$

M has the dimensions of time and is the single constant¹ necessary to characterize the behavior of the wire for a given heating current and operating temperature.

The physical meaning of M may be seen by supposing that the air speed is suddenly changed, so that R_e changes from a constant value of, say, R_i to the value of \bar{R} , and investigating the change

¹ The variations of s and α with temperature are negligible under the conditions of operation.

of R . We find rather simply that $R - \bar{R} = (R_i - \bar{R})e^{-t/M}$. M is therefore the time required for $R - \bar{R}$ to become equal to $\frac{1}{e}$ times the original difference $R_i - \bar{R}$.²

It should be noted that the occurrence of the lag is not dependent on a thermal lag. When the speed decreases rapidly, the electric current is not able to supply sufficient energy to raise the temperature of the wire fast enough to correspond to the equilibrium temperature, and when the speed increases rapidly the supply of energy reduces the rate of cooling. The apparently unsymmetrical response obtained by Richardson (reference 14) was produced by oscillating the wire in its own convection current with approximately the same maximum speed as that of the convection current. The phenomena involved in a hot wire oscillated in still air are so complicated by the presence of the convection current and by the air motions set up by the wire and its mounting that this special case is understood to be excluded from the treatment given in this paper.

Equation (6) may be written

$$\frac{d}{dt} \left(\frac{R - R_o}{\bar{R} - R_o} \right) + \frac{\frac{R - R_o}{\bar{R} - R_o}}{M \left(\frac{R_e - R_o}{\bar{R} - R_o} \right)} = \frac{1}{M} \quad (8)$$

The formal solution of this linear equation when M may be regarded as constant is

$$\frac{R - R_o}{\bar{R} - R_o} e^{\int \frac{dt}{M \left(\frac{R_e - R_o}{\bar{R} - R_o} \right)}} = \int \frac{dt}{M \left(\frac{R_e - R_o}{\bar{R} - R_o} \right)} + \text{const.} \quad (9)$$

in which, of course, R_e is a function of t determined from the velocity variation by means of equation (3). Unfortunately the integrations involved under any reasonable assumption as to the variation of velocity with time are very troublesome. Their evaluation in any useful form is beyond the skill of the authors. We therefore turn to simpler methods of attack.

It is obvious that it is always possible to reverse the problem, that is, knowing R and $\frac{dR}{dt}$, to determine R_e . This is the usual experimental problem. Let us suppose that we obtain on the record a sinusoidal curve represented by

$$R - R_o = (\bar{R} - R_o) (1 + a \sin pt) \quad (10)$$

By substitution in (6) and simple transformations we obtain

$$\frac{R_e - R_o}{\bar{R} - R_o} = 1 + \frac{a \sqrt{1 + M^2 p^2} \sin (pt + \tan^{-1} Mp)}{1 - apM \cos pt} \quad (11)$$

If apM is small compared to unity, $R_e - R_o$ also undergoes a sinusoidal variation. We shall see later that in many cases apM is small, which means physically that the variations of resistance are small as compared to $\bar{R} - R_o$, hence the variations of temperature small as compared to the temperature head $\bar{T} - T_o$, and hence the speed variations small as compared to the mean speed. It is of interest therefore to investigate the second approximation and to see how large the speed variations may be. Expanding $\frac{1}{1 - apM \cos pt}$ and performing the multiplication, we get

$$\frac{R_e - R_o}{\bar{R} - R_o} = 1 + a \sin pt + apM \cos pt + a^2 p M \sin pt \cos pt + a^2 p^2 M^2 \cos^2 pt + \dots \quad (12)$$

² This computation was made by Huguenard and his coworkers, by Burgers, and by Anrep and his coworkers in the papers previously referred to.

Hence the average value of

$$\frac{R_e - R_o}{\bar{R} - R_o} \text{ is } 1 + \frac{1}{2} a^2 p^2 M^2 + \dots \quad (13)$$

A more complete calculation gives $\frac{1}{\sqrt{1 - a^2 p^2 M^2}}$ for the average value of $\frac{R_e - R_o}{\bar{R} - R_o}$. Therefore if the

resistance variations are large, the observed mean resistance is too low and the corresponding mean speed too high. This error in the mean speed is offset to some extent by the curvature of the resistance-speed curve which causes the mean resistance to correspond to a speed lower than the mean speed. apM may be as large as 0.14 without introducing an error in the mean

$\frac{R - R_o}{\bar{R} - R_o}$ larger than 1 per cent, which means that the speed may vary by ± 15 to ± 20 per cent

without introducing serious error in the mean speed on account of lag. The effect of curvature of the resistance-speed curve must, however, be considered for such large speed changes.

Similarly, by computing the maximum and minimum value of $R_e - R_o$ we find for the approximate amplitude of the fluctuation in $\frac{R_e - R_o}{\bar{R} - R_o}$

$$\frac{a\sqrt{1 + M^2 p^2 - a^2 p^2 M^2}}{1 - a^2 p^2 M^2} \quad (14)$$

and the error in using $a\sqrt{1 + M^2 p^2}$ is less than 2 per cent for $apM = 0.14$.

We now return to the case in which apM is neglected for more detailed consideration. Returning to equation (4) we suppose that $R_e - R_o$ in the denominator on the right may be replaced by $\bar{R} - R_o$ without sensible error—i. e., that $R_e - \bar{R}$ is negligible compared to $\bar{R} - R_o$. We then obtain

$$M \frac{dR}{dt} = R_e - R \quad (15)$$

The solution of this linear equation consists of a transient term containing the factor $e^{-\frac{t}{M}}$ and a periodic term, if R_e is periodic. The transient term soon becomes negligible and will not be considered further. To obtain the periodic term, we suppose that R_e is expanded in a Fourier series such that

$$R_e - \bar{R} = a_1 \sin pt + a_2 \sin 2pt + \dots + a_n \sin npt + \dots + b_1 \cos pt + b_2 \cos 2pt + \dots + b_n \cos npt + \dots \quad (16)$$

We then assume that

$$R - \bar{R} = c_1 \sin pt + c_2 \sin 2pt + \dots + c_n \sin npt + \dots + d_1 \cos pt + d_2 \cos 2pt + \dots + d_n \cos npt + \dots \quad (17)$$

whence

$$\begin{aligned} \frac{dR}{dt} &= c_1 p \cos pt + 2c_2 p \cos 2pt + \dots + nc_n p \cos npt + \dots \\ &\quad - d_1 p \sin pt - 2d_2 p \sin 2pt - \dots - nd_n p \sin npt - \dots \end{aligned} \quad (18)$$

We then have on substituting in (15)

$$\begin{aligned} Mnc_n p \cos npt &= b_n \cos npt - d_n \cos npt \\ -Mnd_n p \sin npt &= a_n \sin npt - c_n \sin npt \end{aligned} \quad (19)$$

whence

$$d_n = \frac{b_n - a_n Mnp}{1 + M^2 n^2 p^2}, \quad c_n = \frac{a_n + Mnp b_n}{1 + M^2 n^2 p^2} \quad (20)$$

Thus

$$R - \bar{R} = \Sigma \left\{ \frac{a_n}{1 + M^2 n^2 p^2} \sin npt - \frac{a_n Mnp}{1 + M^2 n^2 p^2} \cos npt + \frac{b_n}{1 + M^2 n^2 p^2} \cos npt + \frac{Mnp b_n}{1 + M^2 n^2 p^2} \sin npt \right\} \quad (21)$$

$$= \Sigma \left\{ \frac{a_n}{\sqrt{1 + M^2 n^2 p^2}} \sin (npt - \tan^{-1} Mnp) + \frac{b_n}{\sqrt{1 + M^2 n^2 p^2}} \cos (npt - \tan^{-1} Mnp) \right\} \quad (22)$$

Hence the general result is that the term of frequency $\frac{np}{2\pi}$ has its amplitude diminished in the ratio $\frac{1}{\sqrt{1 + M^2 p^2 n^2}}$ and suffers a phase retardation of $\tan^{-1} Mnp$. This is the generalization of equation (11) when apM is small.

We may state this important result as follows: If the equilibrium value of the resistance is expanded in a Fourier series, the actual value of the resistance will be such that the n th harmonic is reduced in amplitude in the ratio $\frac{1}{\sqrt{1 + n^2 p^2 M^2}}$ and is retarded in phase by an amount $\tan^{-1} npM$ where p is equal to 2π times the fundamental frequency and M equals $\frac{4.2 \text{ ms} (\bar{T} - T_o)}{i^2 R_o}$

Consider the case of platinum wire and let r be the resistivity at temperature T_o , l the length of the wire, A the area of cross section, and ρ the density. Then

$$M = \frac{4.2 \rho l A s (\bar{T} - T_o)}{i^2 r \frac{l}{A}} = \frac{4.2 \rho A^2 s (T - T_o)}{i^2 r}$$

For platinum, $r = 0.000012$, $\rho = 21.37$, $s = 0.035$ approximately, and if operated at say 500°C. , $M = 1.31 \times 10^8 \frac{A^2}{i^2}$. For wire 0.017 mm. in diameter, $A = 2.265 \times 10^{-6}$ and taking i as 0.2 ampere, $M = 0.0168$ second. For this time constant the values of the amplitude reduction factor and the phase shift are as follows:

Frequency	p	$\frac{1}{\sqrt{1 + p^2 M^2}}$	$\tan^{-1} Mp$
1-----	6.3	0.995	6°
5-----	31.4	.884	28°
10-----	62.8	.687	47°
20-----	135.7	.402	66°
50-----	314.2	.186	79°
75-----	471.2	.125	83°
100-----	628.3	.094	85°
200-----	1,256.6	.043	89°

The limitation of the hot wire for high frequencies is apparent. We see that while Burgers, for example, was able to obtain records of variations of reasonable frequency, the amplitudes were not properly reproduced. The value of M is found to vary roughly as the area of the wire (not as A^2 since i must be varied roughly as \sqrt{A}), and for a given wire and fixed temperature head to decrease as the wind speed increases (since i can be increased). It is advantageous to use as low a temperature as the sensitivity of the apparatus permits and we have in most cases used temperatures only 100°C. above the air temperature.

Returning to equation (15) the correction for lag may be made graphically by a simple construction. At a point P on the curve of the observed resistance R (fig. 3), draw the tangent and the perpendicular to the time axis. The value of R_e is given by the point on the perpendicular which is distant by an amount M measured parallel to the time axis from the tangent. A correction similar to this is given by Anrep and Downing (reference 15) as based on a method

given by G. J. Burch (reference 16) for correcting for the lag of a capillary electrometer. It should be noted that the method is valid only if the speed variations are small. If the speed variations are large, a method along similar but not simple lines may be derived from equation (6).

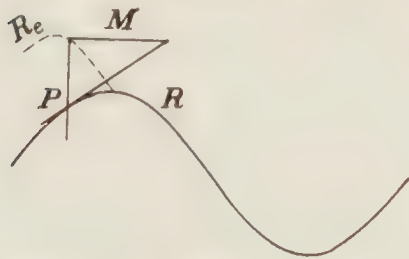


FIGURE 3.—Graphical method of correcting for lag

The form of equation (22) suggests that it might be possible to restore the amplitude and compensate for the lag of the hot wire by an electrical method. The equation is of the same form as that for the current in a circuit containing resistance R and inductance L , provided $\frac{L}{R} = M$, the time constant of the hot wire. If in an amplifier we can pass on to the succeeding stage the voltage variation in a circuit with this time constant, the amplitude can be restored, and an advancement of phase made to compensate for the lag of the wire. The development of such an arrangement is not as simple as might appear and we shall reserve until a later section a description of the compensating circuit, the theory of its action, and a description of the experi-

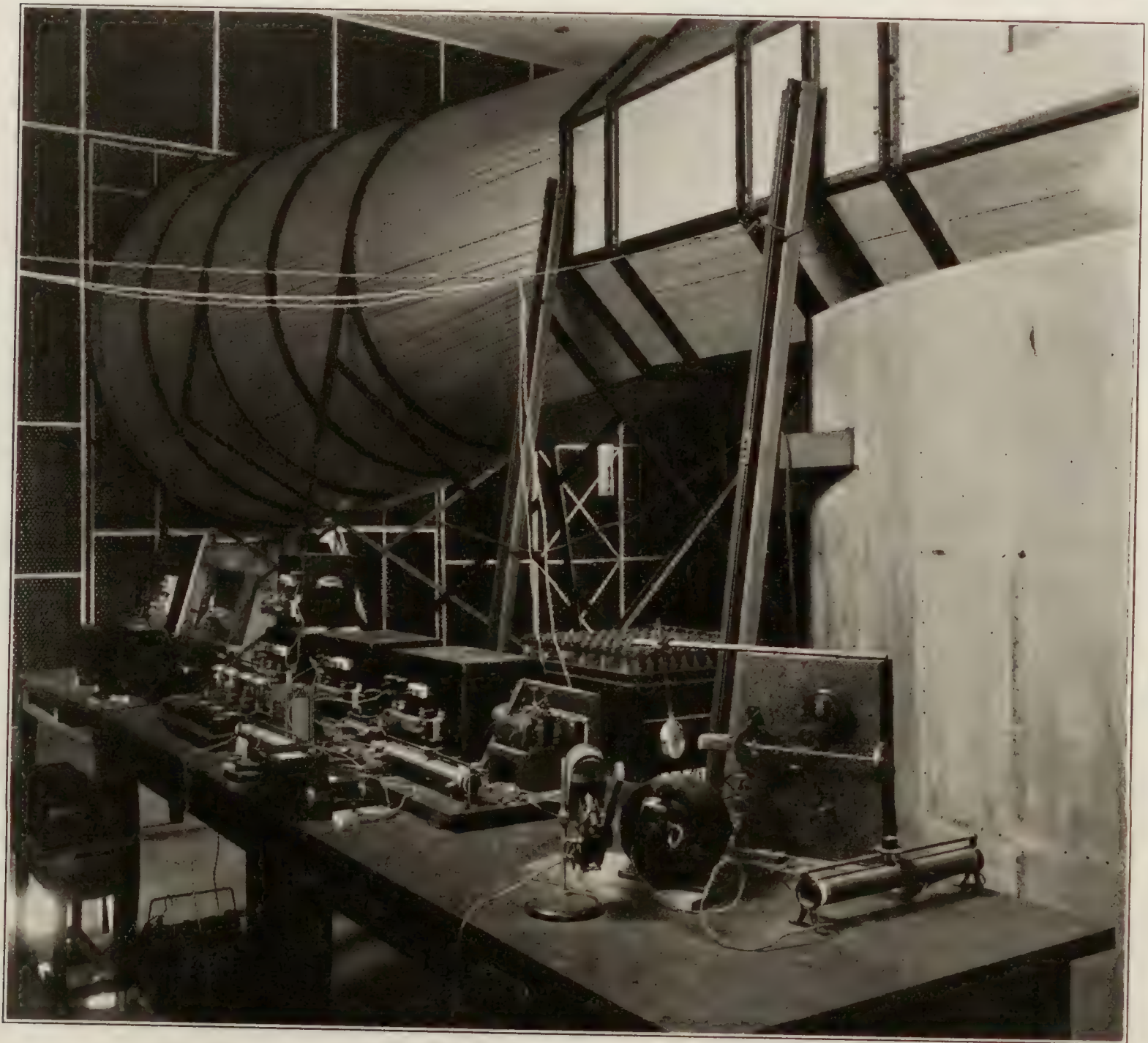


FIGURE 4.—General view of apparatus

mental test of its action. The compensation can not be made perfect as is obvious from the limiting case of high-frequency variations of air speed where the change of resistance of the wire approaches zero. We can not expect to get a positive result from a zero effect and the compensation is therefore confined to frequencies less than a certain upper limit.

GENERAL ARRANGEMENT OF APPARATUS

In the apparatus developed at the Bureau of Standards, the wire, of platinum about 0.017 mm in diameter, is heated from a 120-volt storage-battery line through a large swamping resistance so as to keep the heating current very nearly constant. Potential leads are provided for the measurement of the voltage drop across the wire, from which the resistance is readily computed. The resistance of the wire is a function of the air speed. Variations of air speed produce variations of resistance and hence of the voltage drop across the wire. The voltage

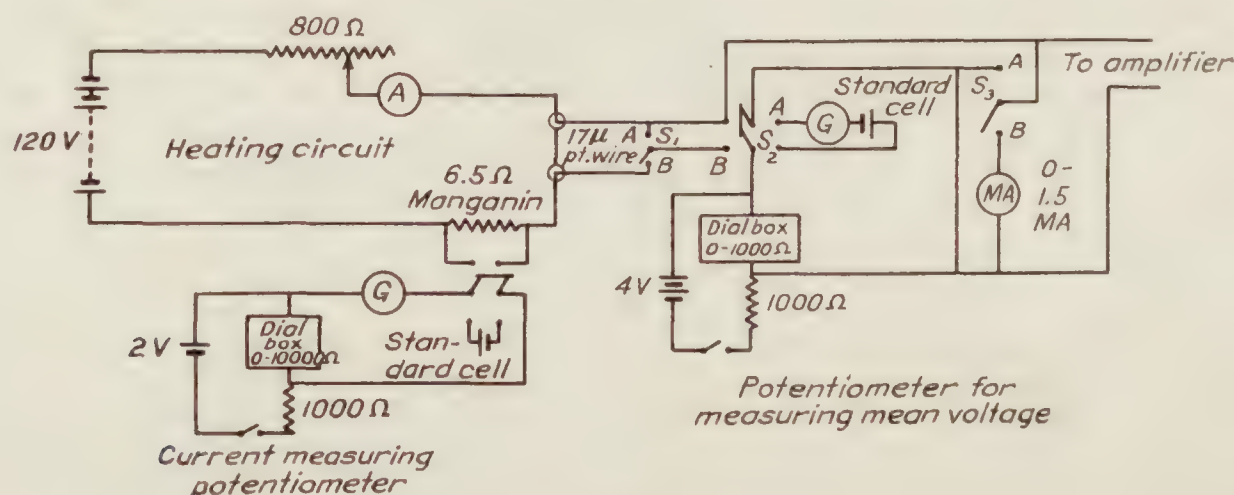


FIGURE 5A.—Wiring diagram of heating circuit and circuit for measurement of mean speed

variations are amplified by means of a direct current resistance coupled amplifier. In the amplifier is incorporated the compensating circuit already referred to, which compensates for the lag of the wire over a certain range of frequencies. The plate current of the last stage of the amplifier is passed through a fixed resistance and the voltage drop across this resistance is balanced by a voltage divider. In the balancing circuit there is placed, in addition to the direct-current milliammeter which serves as the indicating instrument of the voltage divider, an alternating-current milliammeter for measuring the alternating current produced by the fluctuations. If desired, an oscillograph element may be substituted for the alternating-current

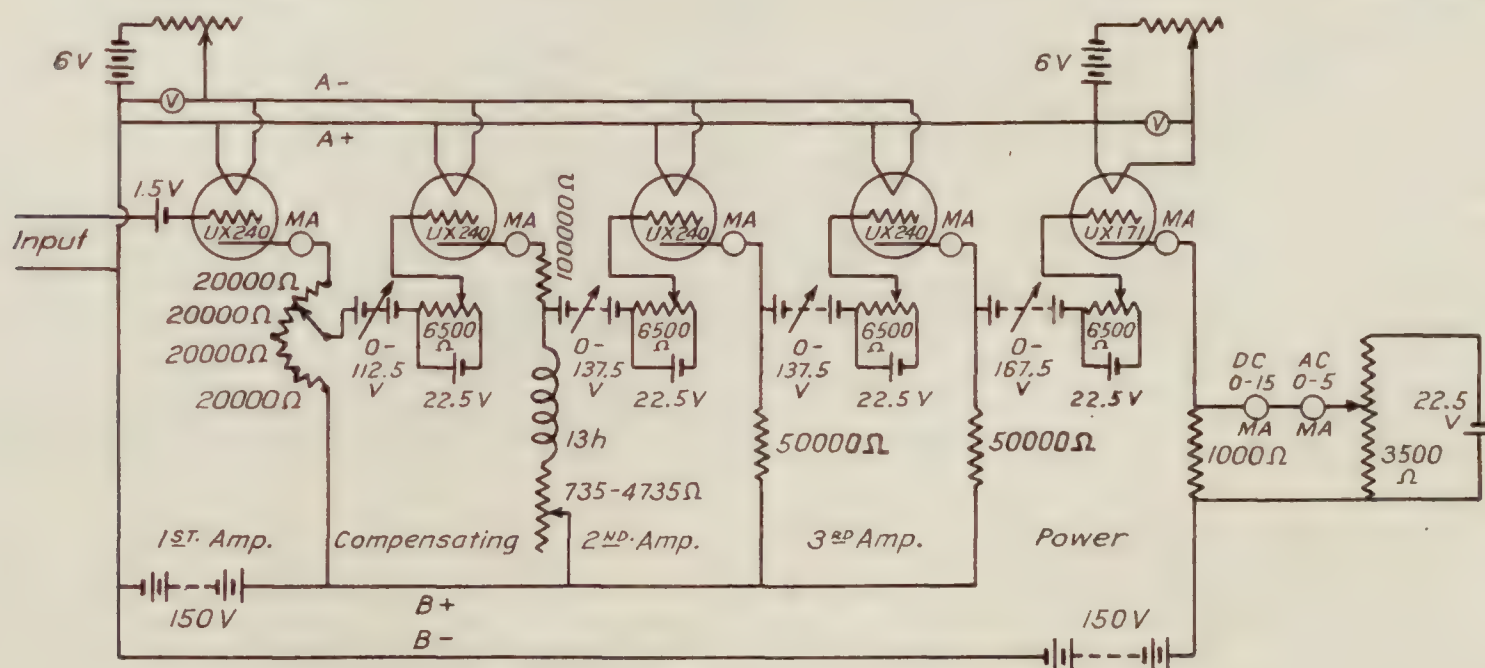


FIGURE 5B.—Wiring diagram of amplifier, compensator, and output circuit

milliammeter and the wave form photographed. A photograph of the apparatus is shown in Figure 4 and a wiring diagram in Figures 5a and 5b. For simplicity, certain protective switches and the oscillograph circuit are omitted in the wiring diagram.

THE HEATING CIRCUIT

It is essential to maintain the heating current reasonably constant. The electron tube used in the amplifier is essentially an electrostatic device and is operated by voltage changes. If one connects a hot wire directly to a battery, the voltage across the wire will remain approxi-

mately constant and equal to the battery voltage (absolutely equal except for the drop in the leads and in the battery) irrespective of changes in the resistance of the wire. Hence, to secure the greatest sensitivity it is desirable to maintain the current constant. The resistance of the wire when hot was usually about 4 ohms and the heating current was usually 0.2 ampere. The maximum variations of resistance in which we are interested do not usually exceed ± 0.25 ohm. Thus by using the laboratory 120-volt storage-battery line with 596 ohms in series with the wire, the maximum change in the heating current during the fluctuation was about 1 part in 2,500, and a voltage fluctuation equal to 0.2, the value of the current, times the resistance fluctuations was impressed on the amplifier.

To measure the current accurately and to maintain it at a constant value as the mean resistance of the wire varied with changing mean speeds, a 6.5-ohm manganin resistance was placed in series with the wire, and the potential drop across this resistance was measured by an improvised potentiometer consisting of a 2-volt storage cell, a 10,000-ohm dial box, a standard 1,000-ohm resistance, a portable galvanometer, and a standard cell.

THE CIRCUIT FOR MEASURING MEAN RESISTANCE

The mean voltage drop across the wire was measured by a similar potentiometer except that a 4-volt storage cell, a 1,000-ohm dial box, and a milliammeter (range 0–1.5 milliamperes) were used. Switch S_2 in the diagram (fig. 5a) permits a check of the potentiometer by a standard cell. Switch S_1 enables the wire to be removed from the amplifier circuit, still retaining a closed circuit when the switch is closed in position **A**. Switch S_3 enables the removal of the indicating milliammeter from the circuit, retaining a closed circuit on the grid of the first amplifying tube when closed in position **A**. The procedure is as follows: S_2 is closed in position **A** and the potentiometer checked against the standard cell, S_2 is then thrown to position **B** and remains there subsequently. S_1 and S_3 are closed in position **B** and the potentiometer adjusted until the milliammeter fluctuates equally about the zero mark. By opening S_3 the fluctuations are passed on to the amplifier. After a reading has been taken, S_3 is closed in position **A**, S_1 thrown to position **A**, the dial box set to zero, and S_3 opened, the object of this procedure being to avoid disturbance to the amplifier by keeping the same average voltage on the grid of the first tube. After these adjustments, known voltages can be applied to the amplifier by turning the dial box, and the amplification can be measured.

THE AMPLIFIER

The amplifying circuit is one given by R. W. King (reference 17) as suitable for direct current amplification. No condensers or transformers are used and there is therefore no selective amplification. The coupling condensers of the more common resistance condenser coupled amplifier are replaced by large C batteries in series with a voltage divider for fine adjustment of the bias voltage. Since the reduction of the wiring diagram given by King to a workable amplifier was attended by some difficulties, it is desired to make a record of the more important ones for the benefit of others intending to use this type of direct-current amplifier. The wiring diagram given in Figure 5b gives the type of tubes used, the values of the battery voltages, and the coupling resistances.

The first difficulty encountered was that due to rapid drifting of the current in the last stage, caused partly by leakage currents from the C batteries, which are at high potential, and partly by small changes in voltage of the various batteries. The measures taken to reduce the drift to a workable value of about 1 milliamperes in the plate current of the power tube in 5 to 10 seconds, corresponding to a voltage change of about 0.001 volt in 5 to 10 seconds at the first grid, were as follows:

- (a) To insulate all C batteries by means of paraffin blocks.
- (b) To use a somewhat smaller plate voltage on the tubes than recommended for ordinary radio use.³

³ It should be noted that the so-called plate voltage specified by some manufacturers really denotes the B-battery voltage to be applied to a plate circuit in which a specified external resistance is placed.

- (c) To use storage cells for B batteries.
- (d) To use 50,000-ohm coupling resistances.

In spite of these precautions it occasionally happens on days of high humidity that the amplifier is unworkable because of a large drift. Trouble from this source is greatly reduced when the amplification is reduced.

A second serious difficulty arose in the attempt to use a common B battery for all stages. It will be seen that the B battery is common to the input circuits in this type of amplifier and forms a coupling between the stages. If the B battery remained of constant voltage, this coupling would cause no trouble, but unfortunately the voltage depends on the current drain. The variation is especially large for the ordinary light-duty dry cells which we attempted to use at first, and many peculiar effects were found. This difficulty was removed by the use of storage B batteries and by using a separate battery for the power tube.

It is found that the amplification changes with time. It is necessary to run the amplifier about 15 minutes before beginning observations and to measure the amplification frequently. To insure that the tubes are always worked on the linear portion of the characteristic curve milliammeters are included in each stage. The characteristics of the amplifier are such that blocking does not occur if the limits of the power tube are not exceeded. It is necessary occasionally to check the characteristics of each tube.

Since in various applications it was desired to measure variations from 0.005 volt to 0.10 volt, or even 0.2 volt, it was desirable to be able to vary the amplification in reasonably close steps. Each stage amplifies about 12 to 15 times, and to secure finer adjustment than was possible by varying the number of stages arrangements were made in the first stage to pass on one-fourth, one-half, three-fourths, or all of the drop across the coupling resistance.

A direct check was made of the nonselectivity of the amplifier (compensating circuit omitted) by observing the amplification of a known alternating current and comparing with the direct current amplification. Frequencies up to 120 cycles per second were tried and no selectivity was observed.

OUTPUT CIRCUIT

In the output circuit the potential difference across a fixed resistance is balanced by a voltage divider. The tap on the voltage divider resistance is set once for all, so that no current flows in the balancing circuit when the plate current of the power tube is at the value corresponding to the midpoint of the linear part of the characteristic curve. Balancing is subsequently made by the C bias voltage divider of one of the stages of the amplifier. Under these conditions the relation between the unbalanced current shown on the milliammeter and the voltage applied to the grid of the first tube is linear over a considerable range (± 10 milliamperes). The alternating current still remaining is measured by an alternating current milliammeter of range 0 to 5 milliamperes. If the alternating current does not exceed 5 milliammeters, and the mean values of the plate currents of the various stages are at the proper values, the tubes are known to be working within the linear range of the characteristic curves and are not blocking.

COMPENSATING CIRCUIT

It has been shown that compensation can be made for the lag of the wire by passing on at some stage the voltage variation in a circuit containing inductance L , and resistance R , such that L/R equals the time constant M , of the wire. We may compute the performance of circuits containing a vacuum tube by assuming (reference 18) that the tube impresses a voltage μe , μ being the amplification factor, and e the grid voltage, in a circuit consisting of the external impedance and the plate resistance of the tube R_o . The distortion term is negligible if the tube is operated in the linear range of the characteristic curve. Since the grid-filament resistance of the succeeding tube is very high and the grid current negligibly small, we need only to compute the voltage variations passed on to the next tube.

The compensating circuit (fig. 5b) consists of a tube of plate resistance R_o , a resistance R_1 , and an inductance L of resistance R_2 . The voltage drop across the inductance L and resistance R_2 is passed on to the next stage. As is customary in similar calculations we consider only the

variable part of the plate current which we call J_o , and the variable part of the grid voltage, which we call e . We have then

$$\mu e = J_o (R_o + R_1 + R_2 + ipL)$$

and the voltage passed on to the next tube as

$$J_o (R_2 + ipL)$$

or

$$\frac{\mu e (R_2 + ipL)}{R_o + R_1 + R_2 + ipL}$$

After some reduction, we find this expression equivalent to

$$\frac{\mu e \sqrt{1 + \frac{p^2 L^2}{R_2^2}}}{\sqrt{\left(\frac{R_o + R_1}{R_2} + 1\right)^2 + \frac{p^2 L^2}{R_2^2}}} \exp. \left[i \tan^{-1} \frac{\frac{pL}{R_2}}{1 + \frac{R_2}{R_o + R_1} + \frac{p^2 L^2}{R_2(R_o + R_1)}} \right]$$

If we can meet the three conditions, that $\frac{R_o + R_1}{R_2} + 1$ is large as compared with $\frac{pL}{R_2}$, that $\frac{R_2}{R_o + R_1} + \frac{p^2 L^2}{R_2(R_o + R_1)}$ is small compared to unity, and that $\frac{L}{R_2}$ is equal to the time constant of the wire, we have the compensation desired.

In the actual circuit, $R_o = 50,000$ ohms, $R_1 = 100,000$ ohms, R_2 varies from 700 to 5,000 ohms (by means of adjustable rheostat) and $L = 13$ henries. Carrying through the limiting cases for a frequency of 100 cycles—i. e., $p = 628$ —we have the following table:

R_2	$\frac{R_o + R_1}{R_2}$	$\frac{pL}{R_2}$	$\left(\frac{R_o + R_1}{R_2} + 1\right)^2$	$\frac{p^2 L^2}{R_2^2}$	$\frac{\frac{p^2 L^2}{R_2^2}}{\left(\frac{R_o + R_1}{R_2} + 1\right)^2}$	$\frac{R_2}{R_o + R_1} + \frac{p^2 L^2}{R_2(R_o + R_1)}$
700	215	11.65	46,700	136	0.0029	0.69
5,000	30	1.63	961	2.66	.0027	.12

The error in compensation for amplitude is only 0.15 per cent, but the errors in phase are apparently much greater. We find from the preceding equations that the phase errors could be made smaller by using 1 megohm for R_1 , but this procedure would reduce the amplification, and since the mean square value does not depend on the relative phases of the various components into which the complex wave shape may be resolved, we have actually used 100,000 ohms. Furthermore, the errors are in reality not as great as they seem. Thus for $R_2 = 700$, the phase is advanced by an amount $\tan^{-1} \frac{11.65}{1.69} = 6.89$ instead of the correct amount $\tan^{-1} 11.65$, i. e., 81.7° instead of 85.1° , and for $R_2 = 5,000$, by 55.4° instead of the correct 58.5° . In other words, the error in phase is only 3° . The compensation is therefore regarded as satisfactory for frequencies up to 100 cycles. The error at 500 cycles is only 4 per cent in amplitude and about 15° to 19° in phase.

The compensation is secured at the expense of the voltage amplification of this stage which is

$$\frac{\mu \sqrt{1 + \frac{p^2 L^2}{R_2^2}}}{1 + \frac{R_o + R_1}{R_2}}$$

For the tube used ($\mu=30$) and the values given above, we find that this stage does not amplify at all but actually reduces the voltage under some conditions. Thus the direct-current amplification is 0.14 for $R_2=700$ and 0.59 for $R_2=5,000$ and the amplification at 100 cycles 16.4 for $R_2=700$ and 1.1 for $R_2=5,000$. The compensation is therefore secured by reducing the low-frequency amplification and an additional stage of amplification is required to make up for this loss.

To secure the computed performance it is very necessary that the inductance L be independent of the frequency and of the current, which means that no iron can be used. The resistance must also be reasonably low. M. Brooks and H. M. Turner (reference 19) have shown that to secure a given value of L/R , a definite weight of wire is required, and in the present case it was only necessary to wind No. 26 wire (about 14 pounds) on a spool until the desired L/R was obtained, in this case about 0.018 second, L being 13 henries and R 735 ohms. Smaller values of L/R could then be secured by introducing additional resistance in series with the coil.

EXPERIMENTAL TEST OF COMPENSATING CIRCUIT

Because of the importance of this feature of our apparatus, we made special tests to obtain a check on the accuracy of compensation. The experimental arrangement for this purpose (shown in fig. 6) consisted of a motor-driven crank, connecting rod, and lever system for imparting an approximately harmonic motion to a slide operating on the outside of a brass pipe $1\frac{1}{4}$ inches in diameter. The pipe was provided with a

bell-mouth entrance at one end, and the other end was inserted in the wall of the 54-inch wind tunnel. A hot wire could be mounted within the pipe on the slide through a narrow slot.

The object of this arrangement was to be able to maintain a reasonably steady air stream past the wire and to superpose on this steady relative motion a harmonic motion by oscillating the wire. The experiment was made in a tube rather than in the wind tunnel itself, so as to be able to eliminate all interference from the motor, crank, connecting rod, and lever systems.

The procedure was as follows: The hot-wire mounting was removed from the pipe and a relation found between the speed at the center of the pipe and the speed indicated by the wind-tunnel gauge. The wire was then replaced and calibrated—i. e., the voltage drop across the wire was measured at several wind speeds. The wire was then oscillated at several frequencies and amplitude so chosen that the product of frequency and amplitude, and therefore the maximum speed produced by the oscillation, was constant, and the reading of the alternating-current milli-

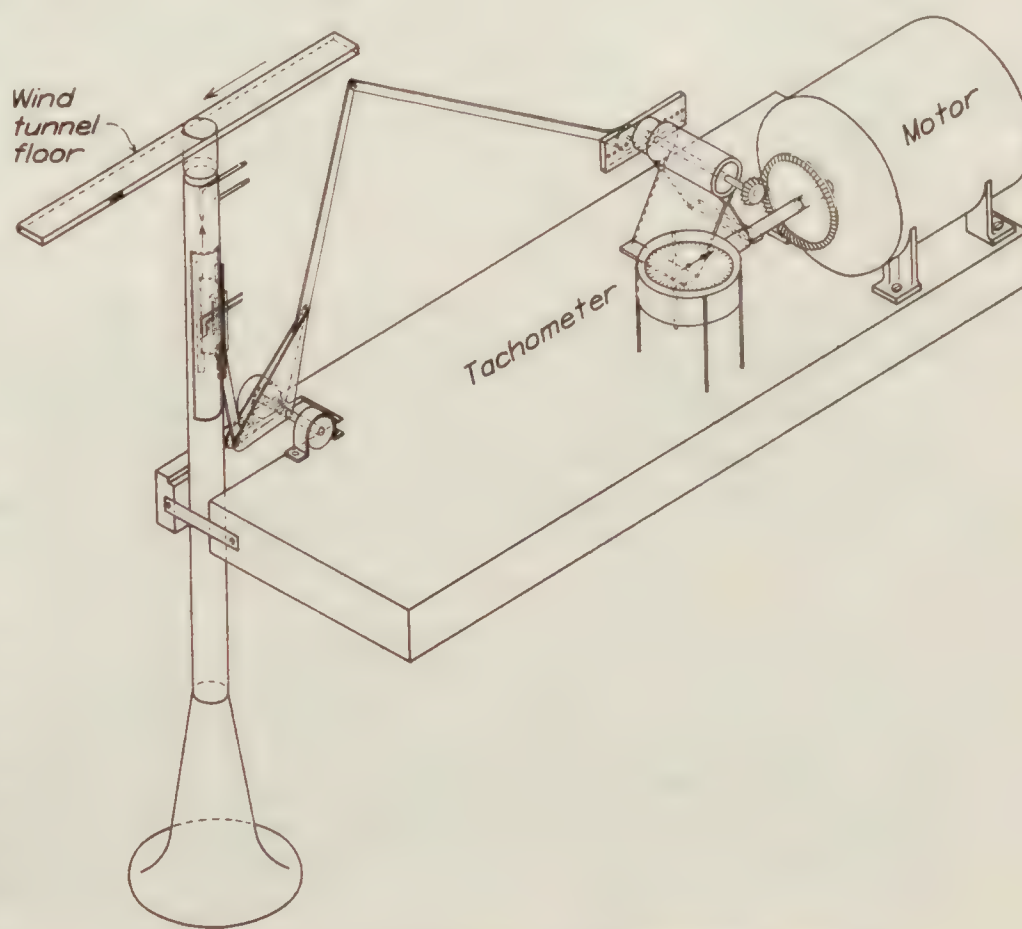


FIGURE 6.—Apparatus for experimental test of compensation

ammeter in the output circuit noted. A typical experiment of this kind gave the following results, the compensating circuit operating:

Mean speed	Double amplitude of motion of wire	Frequency cycles per second	Voltage variation ¹	Corresponding speed variation
<i>Ft./sec.</i>	<i>mm</i>			<i>Ft./sec.</i>
46.9	12.71	20	0.0171	6.3
45.1	6.36	40	.0173	6.1
45.1	4.23	60	.0176	6.3
44.0	0	0	.0056	2.0*
				(*Due to turbulence of stream in the pipe).

¹ The voltage variations are derived from the milliammeter readings by assuming a sinusoidal wave form, hence multiplying by $2\sqrt{2}$ to get the double amplitude and then multiplying by the amplification ratio. Since the mean speed varies a little from one reading to another, a given voltage variation does not correspond always to exactly the same speed variation.

We may attempt to correct for the unavoidable turbulence in the pipe by assuming that the value for a stream free from turbulence is $\sqrt{6.2^2 - 2^2} = 5.9$ ft./sec. The value computed from the amplitude and frequency, assuming sinusoidal motion, is $2\pi \times 20 \times \frac{12.71}{305}$, or 5.2 ft./sec. Considering the several sources of error and the difficulties introduced by the turbulence of the stream, the difference between the two values may not be considered excessive.

Further experiments were made by the use of the oscillograph instead of the milliammeter with the hope of being able to average out the effects of turbulence in the pipe. Sample records are given in Figure 7, and a typical set of results in the table. The wire used was not the same as the one used with the milliammeter and the mean air speed was somewhat different, so that the relation between voltage variations and speed variations is not the same as for the preceding table. The value of the time constant was computed as 0.00415 second.

[Uncompensated, 3.25 mm on film = 0.004 volt]

Double amplitude of motion of wire	Frequency cycles per second	Mean double amplitude on film	$\sqrt{1+p^2M^2}$ times observed amplitude
12.71	20	<i>mm</i> 9.6	<i>mm</i> 10.8
6.36	40	6.8	9.8
4.23	60	5.5	10.2
			Mean 10.3 or 0.0127 volt or a speed variation of 5.5 ft./sec.

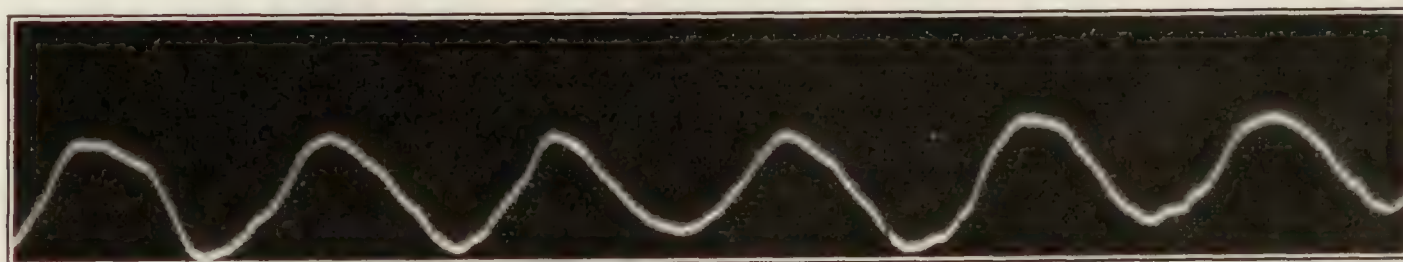
[Compensated, 1 mm on film = 0.004 volt]

Double amplitude of motion of wire	Frequency	Mean double amplitude on film
<i>mm</i>	<i>Cycles/sec.</i>	<i>mm</i>
12.71	20	3.1
6.36	40	3.0
4.23	60	3.0
		Mean 3.03 or 0.0121 volt or 5.3 ft./sec.

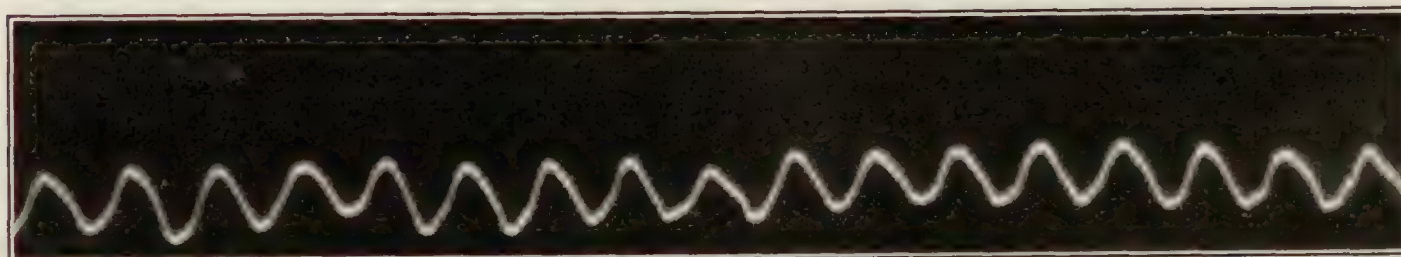
These values show better agreement with the computed value of 5.2 ft./sec. and illustrate the marked difference in response when uncompensated as compared with compensated.

As a result of these and other measurements, we believe that the net effect of the many sources of error, including the errors in determining the time constant of the wire, do not on the average exceed 10 per cent, and since we are attempting to measure variations of air speed which do not remain of constant amplitude this error is not excessive.

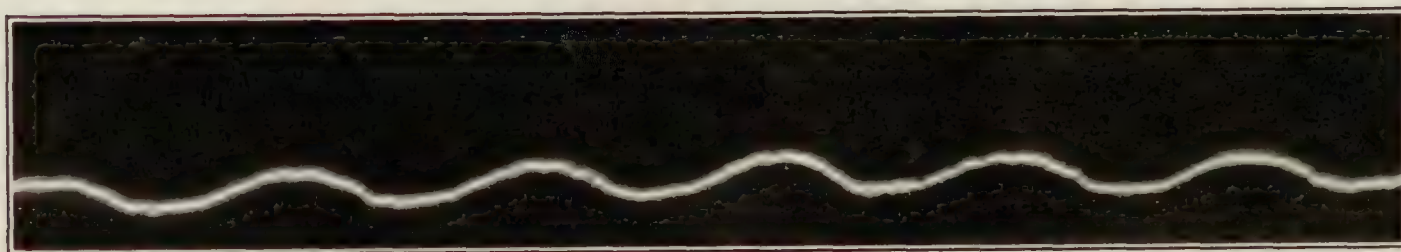
We appreciate full well the errors involved in using a wire 7 mm long in a pipe 32 mm in diameter because of the variation of air speed over different parts of the wire, but we feel that a direct mounting in the wind tunnel involves very much larger errors due to interference effects.



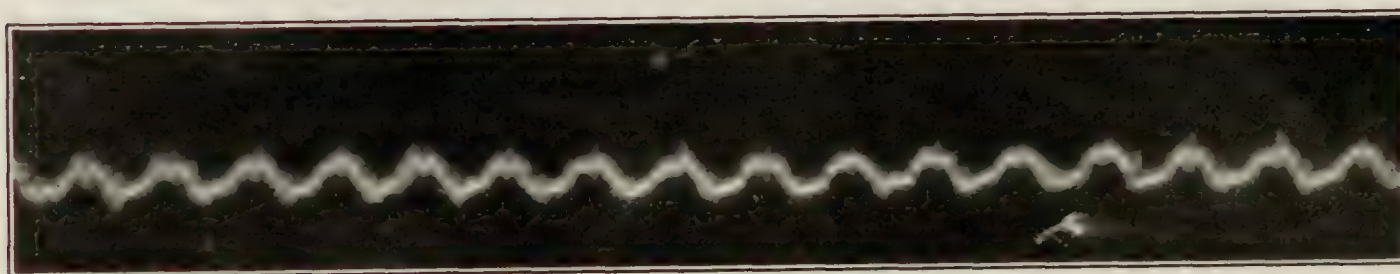
Uncompensated 20 cycles per second



Uncompensated 60 cycles per second



Compensated 20 cycles per second



Compensated 60 cycles per second

FIGURE 7.—Oscillograph records of test of compensation

The impossibility of obtaining a stream free from turbulence and the necessity of keeping the superimposed speed fluctuation reasonably small offer insuperable obstacles to an extremely accurate check, but we may accept these experiments as evidence that no large factor has been overlooked in the theory of the compensator.

The determination of the correct value of M under given conditions requires a knowledge of the diameter, density, temperature coefficient of resistance, resistance at room temperature, specific heat, and mean temperature of the wire. Of these quantities, the wire diameter is most sensitive and is the most difficult to determine accurately. We have used a value obtained by the interferometry section by using the wire to form a wedge between two optical flats and counting the number of fringes. The value is probably correct to ± 2 per cent. A check on

this value was obtained by measuring the resistance of a known length of wire. The resistance at room temperature was measured by a sensitive bridge method so that the current through the wire was very small. The density was taken as 21.37 g/cm^3 , the temperature coefficient as 0.0037, and the specific heat as 0.032. These values should, strictly speaking, be modified according to the wire temperature, but with the accuracy attainable it does not seem worth while to do so at present. At high frequencies the percentage error in the amplitude of the speed fluctuation is equal to the percentage error in M , while at low frequencies it is somewhat less.

A word should perhaps be said about the influence of the temperature distribution along the wire. The distribution may be calculated approximately from the known heat conductivity of the material, the rate at which heat is generated by the electric current, and the heat loss to the air stream. It is found that the arithmetic mean temperature differs from the maximum temperature by $2\frac{1}{2}$ per cent for a maximum temperature of 150° and by $4\frac{1}{2}$ per cent for a maximum temperature of 500° . The errors introduced in taking various types of mean values do not therefore exceed 2 or 3 per cent. After all, the wire is about 350 diameters long and is not at all short as compared to the diameter.



FIGURE 8.—Wire mounting for central part of air stream

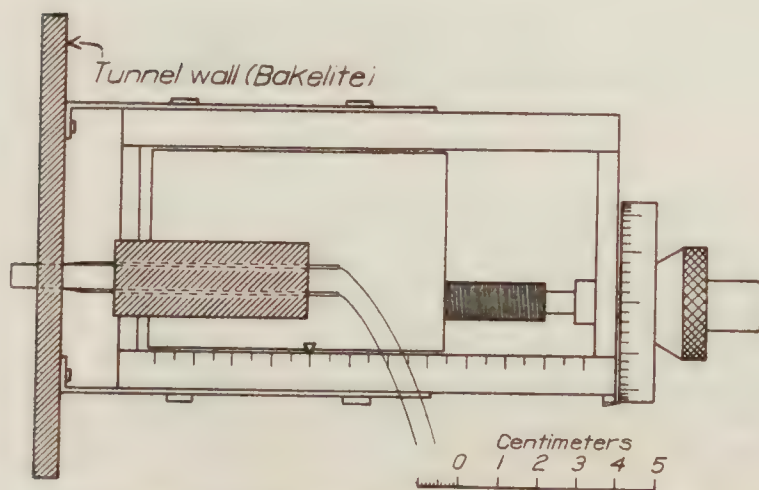


FIGURE 9.—Wire mounting for use near the tunnel wall

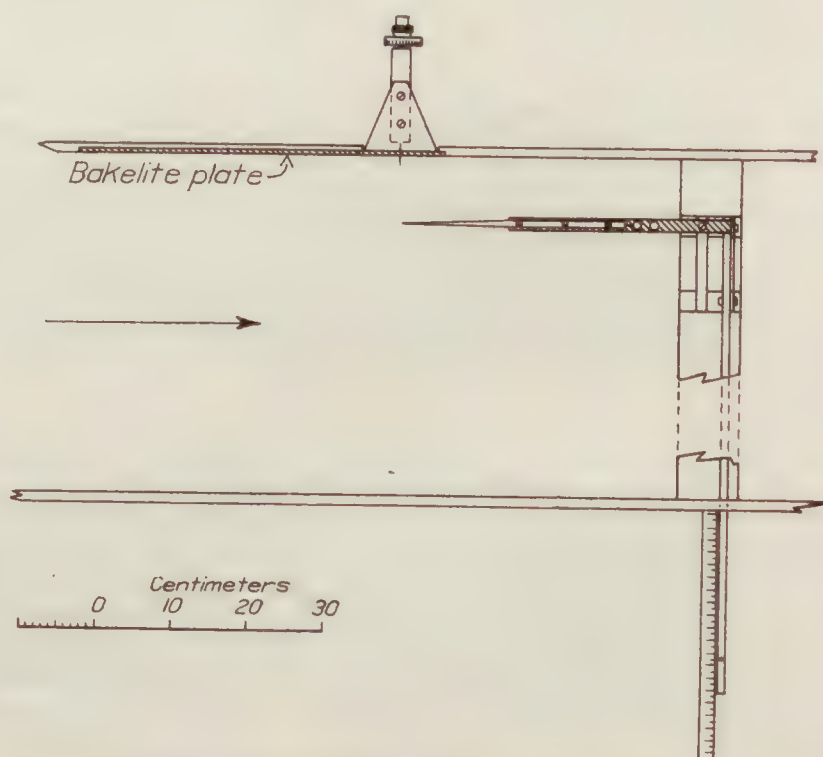


FIGURE 10.—General relation of the two wire mountings

MEASUREMENTS OF WIND TUNNEL TURBULENCE

To illustrate the use of the apparatus described in this paper and the general nature of the results obtainable, we will describe some measurements made in connection with the problem of turbulence in wind tunnels. The methods of mounting the wire and of traversing across the tunnel at a given section are illustrated in Figures 8, 9, and 10, showing the mountings used in the main body of the stream and near the wall. Every effort was made to eliminate interference effects from the supports and to secure reproducible conditions near the wall. A bakelite plate 7.5 cm wide was set into the wall extending about 43 cm upstream and 7 cm downstream from the section at which the traverse was taken. The wire, about $6\frac{1}{2}$ mm. long, was supported by two stiff prongs extending through small holes in the bakelite to a block traveling on a micrometer screw. The zero position of the screw was obtained by observing the reflection of the wire in the smooth bakelite surface. This wire mounting could be used for distances from the wall up to 5 mm. The remainder of the cross section was explored by a wire mounted on two prongs parallel to the wind stream attached to a carriage sliding on a strut about 37 cm downstream. (Figs. 8 and 10.)

The wire was placed in every case at right angles to the wind direction and to the line of traverse. In this position it is least sensitive to directional changes and responds to any change in the resultant speed.

A brief description of the 54-inch wind tunnel in which this work was carried out has been given elsewhere. (Reference 20.) The only change of importance since that description was published has been the removal of the diffuser and the installation of a room honeycomb. Figure 11 shows a sketch of the tunnel with the sections indicated at which traverses were made. Traverses were made only along a single horizontal line toward one wall of the tunnel.

The procedure was as follows: The wire was placed at the center of the tunnel and calibrated against a static plate, which in turn had been calibrated against a Pitot tube placed at the point subsequently occupied by the wire. For the traverse near the wall the wall instrument was calibrated against the center instrument. The tunnel was then operated at the

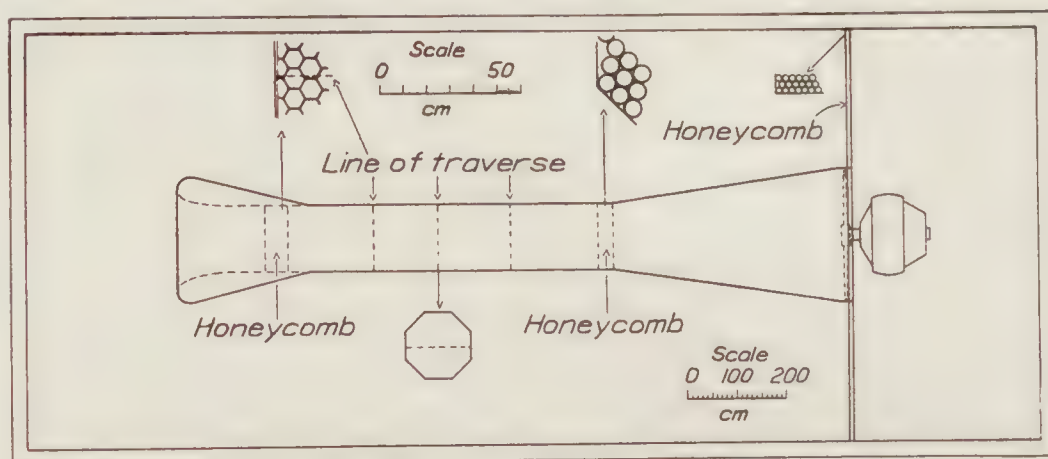


FIGURE 11.—Sketch of 54-inch wind tunnel with traverse positions

speed at which it was desired to make the traverse and the mean voltage drop across the wire balanced with the wire in the desired traverse position. The time constant of the wire was then computed and the compensating resistance set so that the ratio of the inductance to the resistance was equal to the time constant. The fluctuations were then impressed on the amplifier, the direct-current milliammeter reading of the output balancing circuit reduced to as near zero as possible, and the reading of the alternating-current milliammeter noted. In this process two observers cooperated, and an attempt was made to obtain the best average reading of the alternating-current milliammeter when the direct-current instrument was fluctuating equally about the zero mark. In other words, an effort was made to confine attention to disturbances

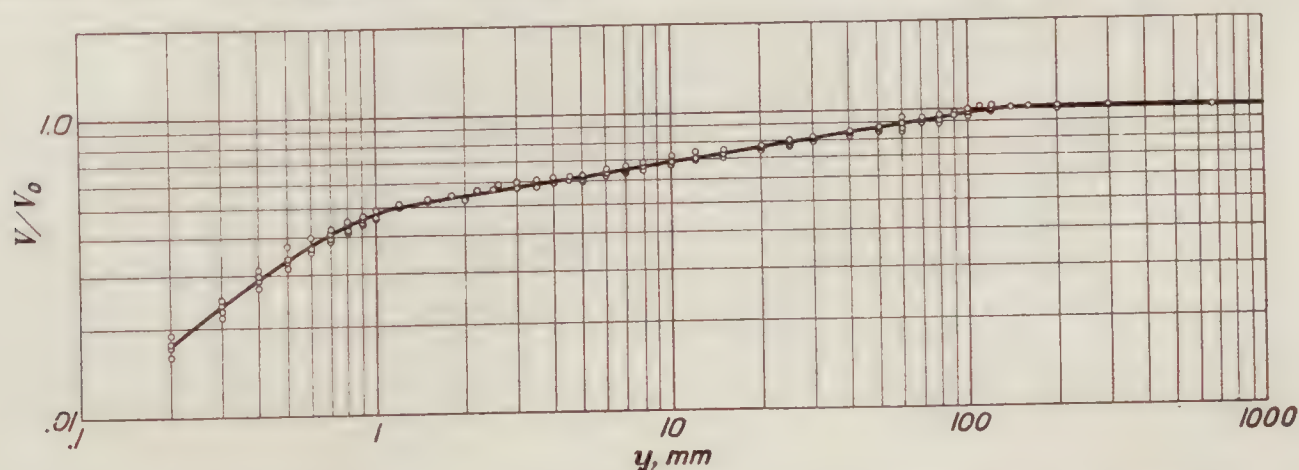


FIGURE 12.—Logarithmic plot of the distribution of mean speed, 5 feet downstream from the working section.
 y = distance from wall, mm. V = mean speed at distance y . V_0 = mean speed at center of working section

of frequency greater than one cycle in one or two seconds. After the reading was obtained the wire was switched out as explained in a previous section and the change in current in the balancing circuit for a known change of voltage determined. The wire was then moved to a new position and the process repeated, the amplification being adjusted if necessary to give a reading in the neighborhood of 2 to 4 milliamperes.

The variations in speed were computed in the following way: We know that the reading of the alternating-current milliammeter is proportional to the square root of the mean square deviation of the resistance from its mean value. We therefore computed the amplitude of the sine curve, giving the same square root of the mean square value and read off from the calibration curve the speeds corresponding to the mean resistance plus this amplitude and the mean

resistance minus this amplitude. We called the mean of the two speeds, the mean speed, and their difference the double amplitude of the speed variation.

If the resistance-speed curve were linear, the above procedure would give accurately the speed variation giving the correct square root of the mean square value, irrespective of the actual wave form. The curvature of the resistance-speed curve introduces an error which we see no way of eliminating at present. For small variations the calibration curve may be considered approximately linear, and the errors from this cause are probably not very great.

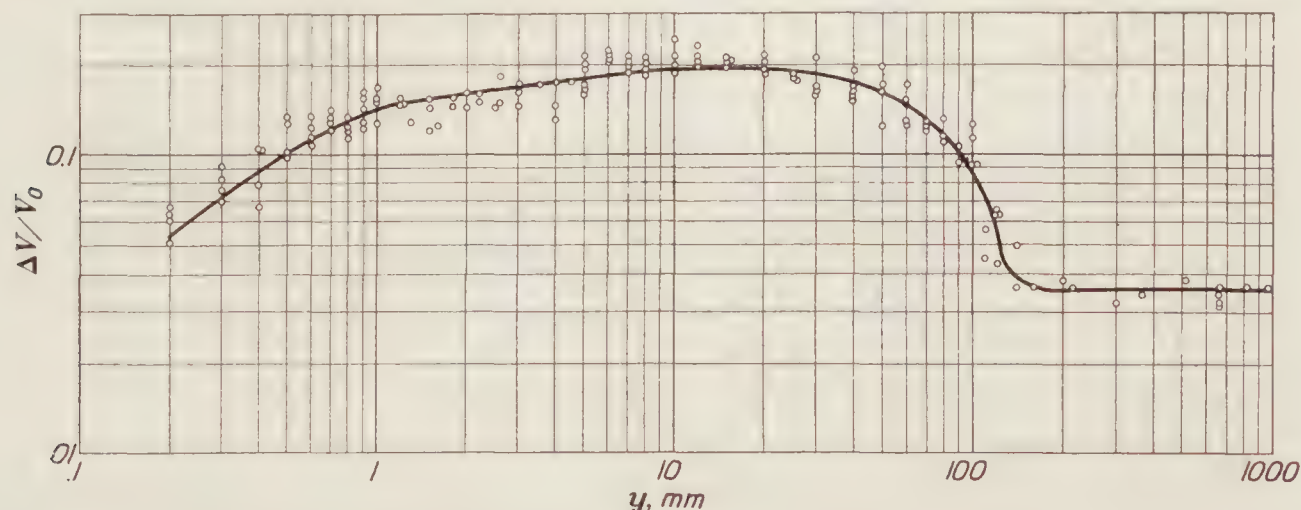


FIGURE 13.—Logarithmic plot of the distribution of the double amplitude of the speed fluctuations, expressed as ratios to the mean speed at the center of the working section. y =distance from wall, mm. ΔV =double amplitude of speed fluctuation. V_0 =mean speed at center of working section

Figure 12 shows the distribution of mean speed along a line from the center of the tunnel to the east wall 5 feet downstream from the working section, plotted with logarithmic scales to show the power law variation. The break in the curve at a distance less than 1 mm is not due to the presence of the wall, since the presence of the wall causes a greater heat loss, cools the wire, and hence gives too high a value for the speed. A method of correction for the effect of the wall has been given by B. J. Van der Hegge Zijnen (reference 21), in which it is assumed that the heat loss to the wall is independent of the wind velocity. This correction has been applied to our values. The correction was negligible for distances greater than 1.2 mm. Van der Hegge

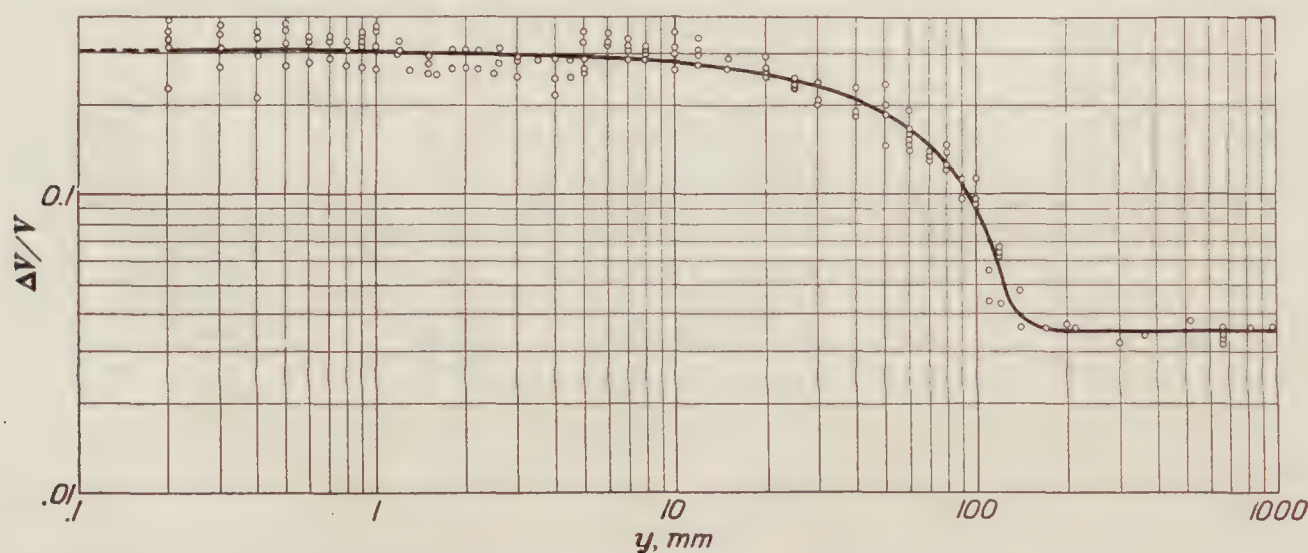


FIGURE 14.—Logarithmic plot of the distribution of the double amplitude of the speed fluctuations, expressed as ratios to the local mean speed. y =distance from wall, mm. ΔV =double amplitude of speed fluctuation. V =mean speed at distance y

Zijnen gives an interpretation of this peculiarity of the distribution curve, for which reference may be made to the original paper.

It is seen that the air stream consists of a core of approximately uniform speed surrounded by a region near the wall in which the speed decreases. The equation of the curve of mean speed in this "boundary layer" is $\frac{V}{V_0} = \left(\frac{y}{\delta}\right)^n$ where V is the local mean speed, V_0 the speed of the core at the working section, y the distance from the wall, δ , the thickness of the boundary layer, in this case 135 mm, and n a constant, in this case 0.15.

The accuracy of measurement of the mean speed is not as great as one might secure by the use of a wire of greater diameter. The wire used, 0.017 mm in diameter, was extremely fragile and broke very frequently. The calibration curve was subject to erratic changes of the same type as those described by Bailey and Simmons (reference 22) for a wire 0.025 mm in diameter

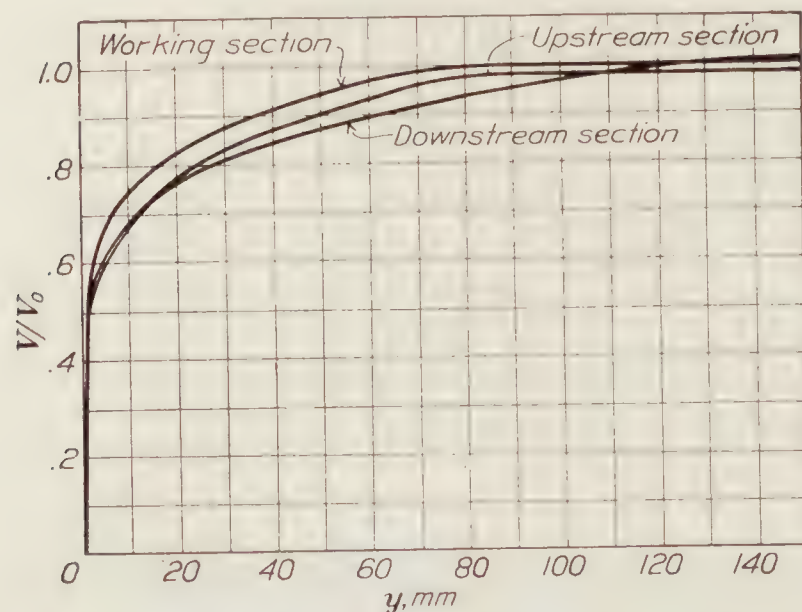


FIGURE 15.—Distribution of mean speed at three sections. y =distance from wall, mm. V =mean speed at distance y . V_0 =mean speed at center of working section

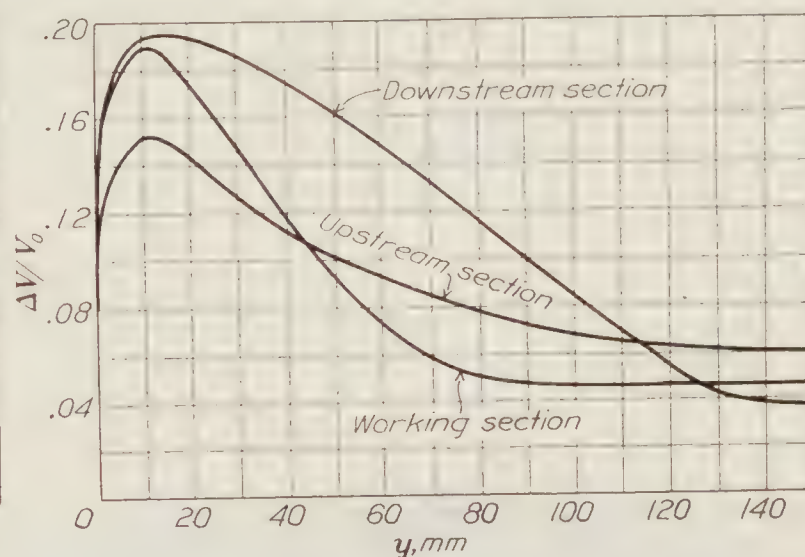


FIGURE 16.—Distribution of the double amplitude of the speed fluctuations at three sections, expressed as ratios to the mean speed at the center of the working section. y =distance from wall, mm. ΔV =double amplitude of speed fluctuation. V_0 =mean speed at center of working section

but even more troublesome. In spite of calibrations two and four times per day and of numerous returns to a reference point during a traverse, it was difficult to secure an accuracy of better than ± 1.5 per cent in the mean speed. Some of the difficulty arose from the ability to see fluctuations on the balancing instrument. To measure fluctuations, the wire must be small, and judg-

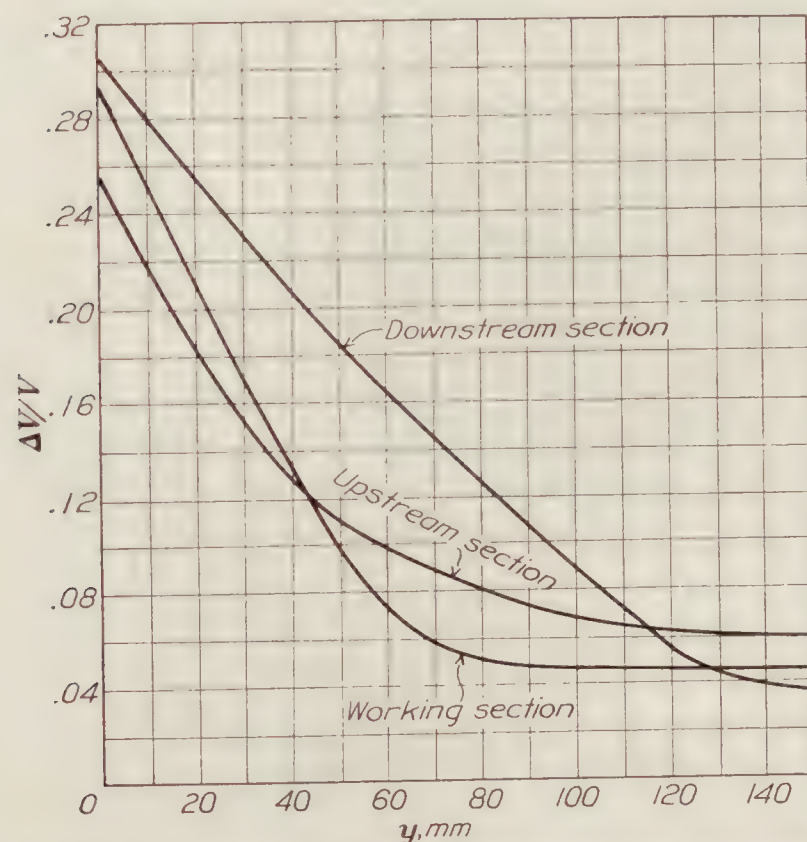


FIGURE 17.—Distribution of the double amplitude of the speed fluctuations at three sections, expressed as ratios to the local mean speed. y =distance from wall, mm. ΔV =double amplitude of speed fluctuation. V =mean speed at distance y

In Figure 14 the speed fluctuations are expressed as ratios to the mean *local speed* instead of to the speed of the central core as in Figure 13. It is probably only a coincidence that the limiting value of the amplitude (i. e., half the double amplitude) of the speed fluctuation at the wall expressed in this way (0.15) is nearly equal to the exponent occurring in the law of distribution of the mean speed (0.15).

ing by the frequency of failure the diameter used is close to the lower limit of mechanical strength for use at speeds up to 60 foot-seconds. The traverses were made at a mean tunnel speed of approximately 55 foot-seconds.

Figure 13 shows the distribution of speed fluctuations, also on a logarithmic scale. The ordinates of the curve are equal to the double amplitudes of the speed fluctuations expressed as a ratio to the mean speed of the central core of the air stream at the working section, derived from the square root of the mean square values on the assumption of a sinusoidal wave form as previously explained. The abscissas are distances from the wall. There is a definite correlation between the variation of the speed fluctuations and the variation of mean speed. Over the central core the double amplitude of the fluctuations of speed is reasonably constant, as is the mean speed. In the boundary layer the fluctuations increase to a flat maximum at about 15 mm from the wall and then decrease as the wall is approached.

In Figures 15, 16, and 17 we have plotted on a linear scale the average curves for the working section, a section 150 cm downstream, and a section 131 cm upstream, the locations being shown on Figure 11. Comparison of the working section and the downstream section shows the expected course of events. The boundary layer increases in thickness, and consequently the speed of the core increases a little. The large variations of speed extend to the limit of the new boundary layer, while the variations of speed in the core are somewhat reduced.

The upstream traverse shows anomalous results, repeatedly checked, which we believe to be due to the fact that the honeycomb axis is at a small angle to the tunnel axis. The traverses shown cover a comparatively limited region and can not be considered as representative of conditions over the entire cross section. Since we do not have sufficient data to make a comprehensive report on the speed variations in our 54-inch wind tunnel and the values given are intended as illustrative of the kind of results obtainable, we shall omit any further discussion.

The precision or perhaps lack of precision is indicated clearly in Figure 13. We believe that the chief difficulty lies in the fact that there are actual changes in the mean values for the time intervals used—i. e., the turbulence as defined by our method of measurement is not constant.



FIGURE 18.—Oscillograph record of speed fluctuation near the wall

We have, of course, been most interested in the turbulence in the core of the air stream. A typical set of values of the double amplitude of the speed variation taken in the core at the working section is shown below.

Distance from center (cm)	First run	Second run
46 west.....	0. 043	0. 041
30 west.....	. 045	. 040
15 west.....	. 041	. 041
0.....	. 043	. 041
15 east.....	. 045	. 041
30 east.....	. 047	. 043
46 east.....	. 045	. 043
Mean.....	. 044	. 041

The mean of a number of readings at the three sections gave the following results:

131 cm upstream.....	0. 060
Working section.....	. 043
150 cm downstream.....	. 035

As a matter of interest, an oscillograph record of the wave form near the wall is shown in Figure 18. The light ray is interrupted at intervals of approximately 0.15 second.

MEASUREMENTS BEHIND CYLINDERS

In the development of the apparatus we made a few measurements of the fluctuations present behind a cylinder 3 inches (7.5 cm) in diameter and extending completely across the tunnel at the working section. We wish to use these measurements (figs. 19 and 20) to illustrate another application of the apparatus. While the accuracy of these measurements is not very great and the cylinder was much too large for the tunnel, blocking about 7 per cent of the cross-

sectional area, the qualitative information as to the rapidity with which the Karman vortex system is dissipated is of some interest. The diagrams are self-explanatory.

CONCLUSION

The apparatus described is very bulky, far from portable, and in many respects inconvenient to use. We believe, however, that a great improvement is possible, and we are now engaged in redesigning the amplifier, using very large coupling condensers in place of the large C batteries. By sacrificing a little in sensitivity and accuracy the wire may be heated from a 6 or 12 volt storage battery.⁴ With several changes of this nature we hope to produce a more portable apparatus. The extension to measurements of directional variations using the 2-wire arrangement of Burgers is relatively easy.

In conclusion we wish to acknowledge with appreciation the assistance of our associates, Dr. Arthur E. Ruark, Messrs. K. H. Simpson, P. S. Balliff, B. H. Monish, and W. H. Boyd.

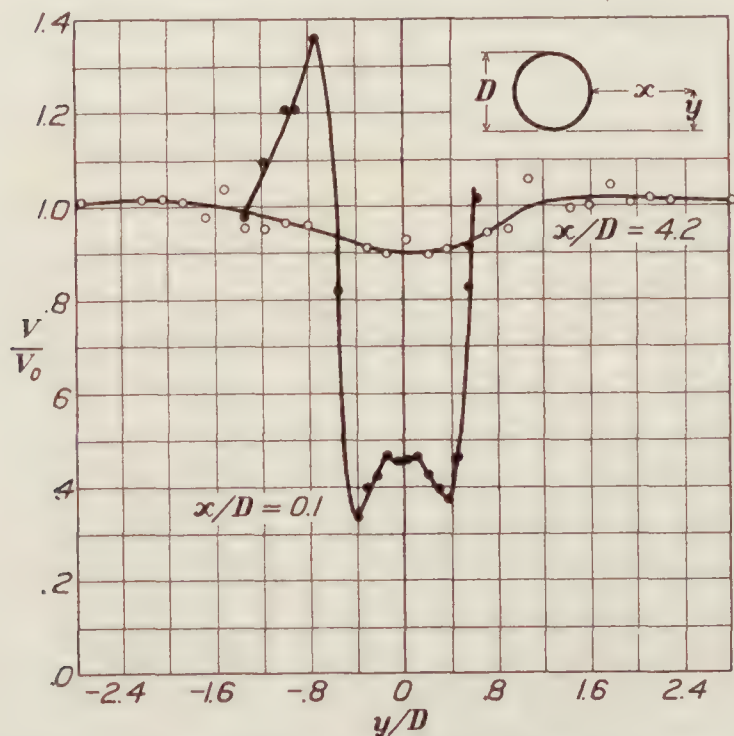


FIGURE 19.—Distribution of mean speed behind a cylinder 3 inches in diameter. V =mean speed at point (x, y) . V_0 =mean speed of undisturbed stream

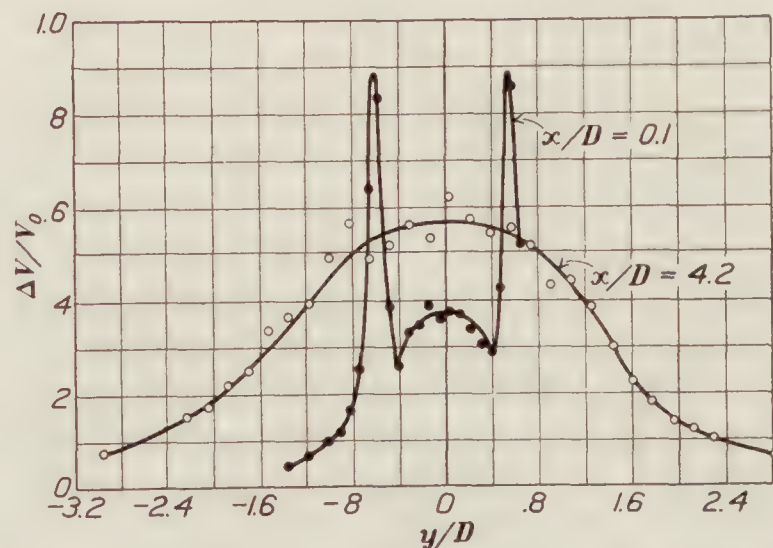


FIGURE 20.—Distribution of double amplitude of speed fluctuations behind a cylinder 3 inches in diameter. ΔV =double amplitude of speed fluctuations at point (x, y) . V_0 =mean speed of undisturbed air stream. Cf. Figure 19 for coordinates (x, y)

REFERENCES

1. Reynolds, Osborne: An Experimental Investigation of the Circumstances Which Determine Whether the Motion of Water Shall be Direct or Sinuous and of the Law of Resistance in Parallel Channels. Phil. Trans. Royal Society, 1883, vol. 174, p. 935.
2. Bacon, D. L., and Reid, E. G.: The Resistance of Spheres in Wind Tunnels and in Air. (1924) N. A. C. A. Technical Report No. 185.
3. Reynolds, Osborne: On the Dynamical Theory of Incompressible Viscous Fluids and the Determination of the Criterion. Phil. Trans. Royal Society, 1895, vol. 186, Part I.
4. Lorentz, H. A.: Abhandlungen uber theoretische Physik, Leipzig, 1907, p. 43.
5. Burgers, J. M.: Verslagen der Kon. Akad. v. Wetensch, Amsterdam, 1923, vol. 26, p. 582.
6. Von Karman, Th.: Abhandlungen aus dem Aerodyn. Inst. Aachen, vol. 4, p. 27.
7. Dryden, H. L., and Heald, R. H.: Investigation of Turbulence in Wind Tunnels by a Study of the Flow about Cylinders. (1926) N. A. C. A. Technical Report No. 231.
8. King, L. V.: Phil. Trans. Royal Society, London A 214, p. 373, 1914.
9. Huguenard, E., Magnan, A., and Planiol, A.: La Technique Aeronautique, 1923, Nov. 15 and Dec. 15; 1924, Jan. 15 and Feb. 15. (For translation, see N. A. C. A. Technical Memorandum No. 264: A Method for the Instantaneous Determination of the Velocity and Direction of the Wind (1924).
10. Burgers, J. M.: Kon. Akad. v. Wetensch. Amsterdam, vol. 29, p. 547, 1926 proceedings.
11. Fage, A., and Johansen, F. C.: Proc. Roy. Soc., London, vol. 116, 1927, p. 170.

⁴ As this paper goes to press, the redesigned equipment has been in use for several months and direct correlation has been obtained between measurements of forces on spheres and streamline models and measurements of speed fluctuations.

12. Anrep, Downing, and coworkers: *Journal Sci. Instruments*, 3, 1925-26, p. 221. *Heart*, Vol. XIV, No. 2, 1927.
13. King, L. V.: *Phil. Trans. Royal Soc., London A* 214, p. 373, 1914.
14. Richardson: *Journal Scientific Instruments*, vol. 3, 1925-26, p. 323.
15. Anrep and Downing: *Journal Sci. Instruments*, 3, 1925-26, pp. 221 and 385.
16. Burch, G. J.: *Proc. Roy. Soc.* 48 (1890), p. 89.
17. King, R. W.: *Journal Opt. Soc.*, vol. 8, January, 1924, p. 98.
18. Carson, J. R.: *Proc. Inst. Radio Engineers*, 7, 1919, p. 187.
19. Brooks, M., and Turner, H. M.: *Univ. of Ill. Eng. Exp. Station, Bull.* 53, 1912.
20. U. S. Bureau of Standards: *Scientific Paper No.* 394.
21. Zijnen, B. J. Van der Hegge: *Doctors Dissertation*, Technical High School, at Delft, 1924, p. 11
22. Simmons, L. F. G., and Bailey, A.: *Note on a Hot-Wire Speed and Direction Meter.* *Brit. Aeron. Research Committee Reports and Memoranda No.* 1019, 1926.

BUREAU OF STANDARDS,
WASHINGTON, D. C., *January 8, 1929.*

REPORT No. 321

FUEL VAPOR PRESSURES AND THE RELATION OF VAPOR PRESSURE TO THE PREPARATION OF FUEL FOR COMBUSTION IN FUEL INJECTION ENGINES

By WM. F. JOACHIM and A. M. ROTHROCK
Langley Memorial Aeronautical Laboratory

REPORT No. 321

FUEL VAPOR PRESSURES AND THE RELATION OF VAPOR PRESSURE TO THE PREPARATION OF FUEL FOR COMBUSTION IN FUEL INJECTION ENGINES

By WM. F. JOACHIM and A. M. ROTHROCK

SUMMARY

This investigation on the vapor pressures of fuels was conducted at the Langley Memorial Aeronautical Laboratory at Langley Field, Va., in connection with the general research on combustion in fuel injection engines. The purpose of the investigation was to study the effects of high temperatures such as exist during the first stages of injection on the vapor pressures of several fuels and certain fuel mixtures, and the relation of these vapor pressures to the preparation of the fuel for combustion in high-speed fuel injection engines.

The apparatus employed in the tests consisted of a gas-tight steel bomb, a Bourdon spring pressure gauge, an electric furnace, a thermocouple, and a potentiometer. The bomb was partially filled with the fuel to be tested, the space above the fuel filled with nitrogen to prevent combustion, and the bomb heated in an electric furnace. Pressure and temperature readings were taken simultaneously during the heating and cooling periods over a temperature range from 175° to approximately 900° F. Vapor and gas pressures up to 5,000 pounds per square inch were measured. The fuels tested were gasoline, kerosene, Diesel engine fuel oil, ethyl alcohol, methyl alcohol, benzol, mixtures of methyl alcohol and gasoline, and mixtures of benzol and gasoline. An aircraft engine lubricating oil was also tested. Water was tested as a standard in order to compare these results with those of other investigators. The conditions of the tests were similar to those met in the combustion chamber of a fuel injection engine and consequently the data apply to those conditions.

It was found that the vapor pressures of the fuels increased rapidly at high temperatures, the rate of pressure increase becoming greater as the temperatures approached the critical value. Beyond the critical temperature, the rate of pressure increase was constant except at one or more temperatures in the case of certain fuels and their vapors in which chemical changes took place. The chemical changes in some of the fuels were such that the cooling curves were materially different from those obtained during the heating periods. Permanent gases were generated during the heating and cooling periods in the case of the alcohols, gasoline, kerosene, and Diesel engine fuel oil so that the fuels removed from the bomb were materially different from those placed in it. The vapor pressures of the fuels differed from each other considerably, methyl alcohol having the highest vapor pressure, 4,370 pounds per square inch, and Diesel engine fuel oil the lowest, 140 pounds per square inch, for the maximum temperature investigated, approximately 850° F.

The data for the vapor pressures of the fuels at high temperatures indicate the compression temperatures required to produce rapid vaporization of the injected fuel for combustion.

INTRODUCTION

In order to control and minimize the maximum cylinder pressures developed in high-speed fuel injection engines, particularly in engines designed for aircraft service, it is desirable to have the combustion proceed in accordance with the dual cycle, which requires the first and smaller part of the injected fuel charge to burn at constant volume and the remainder to burn at con-

stant pressure. The constant volume combustion usually determines the maximum pressure developed in the engine cylinder. It is necessary, therefore, to investigate and control the injection and engine factors that affect the amount of constant volume combustion, in accordance with the spray formation, vaporization, ignition, and combustion requirements of the fuel.

Recent progress in the performance of high-speed fuel injection engines has emphasized the time lag of auto-ignition of the injected fuel as one of the major factors that affect the amount of constant volume combustion. In order to minimize the amount of constant volume combustion in engine operation, it is necessary to distribute the small fuel particles properly in the combustion chamber and raise them to their auto-ignition temperature during injection of the first part of the fuel charge. The maximum cylinder pressure developed is proportional to the fraction of the fuel charge that is injected and prepared for combustion at the instant that auto-ignition occurs. Thus, the earlier that auto-ignition takes place, the start and rate of injection remaining the same, the less will be the amount of constant volume combustion. The cylinder pressures of the constant pressure phase of the dual cycle may be controlled, therefore, by varying the rate of injection of the remainder of the fuel charge. (Reference 1.)

The injected fuel in an aircraft oil engine must be prepared for ignition in less than 10° of crank-shaft rotation for uniform rates of injection if the time lag of auto-ignition is to be short enough for operation with low cylinder pressures. This time lag is dependent upon the type of injection system used; the timing and rate of injection; the fuel spray velocity and penetration; the degree of atomization obtained; the distribution of the spray in the combustion chamber and of the oil particles within the spray; the compression ratio used in the engine and the dependent cylinder pressures and temperatures; the timing, direction, and amount of turbulence employed; the amount of radiation from hot surfaces in the combustion chamber; the initial temperature of the injected fuel; and the chemical and physical properties of the fuel. It is probable that in the past sufficient consideration has not been given to the physical and chemical properties, which is due in part to the lack of experimental data in the range of high temperatures occurring during the first stages of injection in fuel injection engines. This research was conducted at the Langley Memorial Aeronautical Laboratory at Langley Field, Va., to obtain data on the effect of high temperatures on the vapor pressures of several fuels under conditions approximating those in fuel injection engines. In addition the data afford opportunity for analysis of the relation of this fuel property to the preparation of the fuel for combustion.

The principal investigations made heretofore on the effect of temperature on the vapor pressures of liquids have been on water, methyl alcohol, and ethyl alcohol. (Reference 2.) The temperature range investigated has been from room temperature to the critical temperature of the liquid, approximately 500° F. The United States Bureau of Mines in 1922 (reference 3) conducted some experiments on gasoline and kerosene over a similar temperature range. Several of the tar and paraffin oils have been investigated in Germany up to 800° F. (Reference 4.) However, as far as is known, complete data on the effects of high temperatures on the vapor pressures of such fuels as are used in fuel injection engines have not been reported, particularly in the range above the critical temperatures, and data for those fuel mixtures that are used to suppress detonation in gasoline engines are entirely lacking.

The tests reported herein were conducted on gasoline, kerosene, Diesel engine fuel oil, ethyl alcohol, methyl alcohol, benzol, mixtures of ethyl alcohol and gasoline, mixtures of benzol and gasoline, and an aircraft engine lubricating oil. Water was tested as a standard to compare these results with those of other investigators. Temperatures from 175° to approximately 900° F. were investigated and vapor pressures up to 5,000 pounds per square inch were recorded.

METHODS AND APPARATUS

The method employed in the determination of the vapor pressure of a fuel consisted of partially filling a steel bomb with the fuel to be tested and heating it in an electric furnace through the desired temperature range. The bomb was made of steel instead of some inactive substance so that the test conditions in this respect would approach those met in an engine cylinder. The space above the fuel was filled with nitrogen since it would prevent combustion and because the

gas in the combustion chamber of the fuel injection engine preceding injection of the fuel consists of approximately 77 per cent by weight of nitrogen. Temperature and pressure readings were taken simultaneously at regular intervals during both the heating and cooling of the bomb and fuel. The bomb was not held at each recorded temperature until equilibrium conditions were reached, since such a condition does not exist in the combustion chamber.

A photograph of the apparatus is shown in Figure 1 and a diagrammatic sketch of it in Figure 2. The apparatus consisted of a gas-tight steel bomb, a cooling pan, a valve block, a pressure gauge, connecting tubes, an electric furnace, a thermocouple, and a potentiometer.

The steel bomb was made from a piece of $1\frac{3}{4}$ -inch diameter chrome-nickel steel $5\frac{1}{2}$ inches long. A well for holding the fuel and its vapor was drilled in the bomb slightly off center to a depth of $4\frac{1}{2}$ inches. Two small holes were drilled into this well from the other end of the bomb, one to serve as a filling hole connection and the other as an outlet connection to the pressure gauge. Two drilled hexagonal steel bars approximately 8 inches long were screwed and shrunk into these holes. The upper ends of the bars were provided with union fittings, thus providing a separable joint above the cooling pan. Steel tubes with union fittings were fastened to the drilled bars, a gooseneck bend being made in one of the tubes to provide for unequal expansion of the hexagonal bars and tubes. The lower end of the bomb was closed by a plug which was also screwed and shrunk into place. The volume of the well was approximately 22 cm^3 .

It was necessary to have both an inlet and an exhaust opening in the apparatus for the efficient cleaning of the bomb, for filling the bomb with the fuel to be tested, and for displacing the air above

the fuel with nitrogen before the start of each test. These openings were placed in the valve block where they could be closed by needle valves and were connected by drilled holes in the valve block to the two tubes from the bomb. In addition, the tube connected to the inlet opening was also connected by a drilled hole through the valve block to the tube for transmitting the vapor pressures to the pressure gauge.

Several Bourdon spring pressure gauges were used for measuring the pressures exerted by the vapors, their ranges varying from 0 to 200 pounds per square inch to 0 to 5,000 pounds per square inch, depending on the maximum pressure to be obtained with the fuel under test. The gauges were altered by making the entrances to them very small so that the oil placed in the Bourdon spring could not easily escape. In addition a gooseneck bend was made in the steel tube connecting the gauge to the valve block. This tube was also filled with oil and its position arranged so as to maintain oil in the gauge and tube in all the tests. The gauges were calibrated by means of a dead-weight gauge tester.

The cooling pan was placed midway between the valve block and the bomb to cool and condense the hot vapors before they reached the valve block. Cold water was kept flowing through this pan during the tests. Steel wires were inserted in the hexagonal bars in order to prevent the condensed vapors from dropping back into the bomb, the liquid being retained in

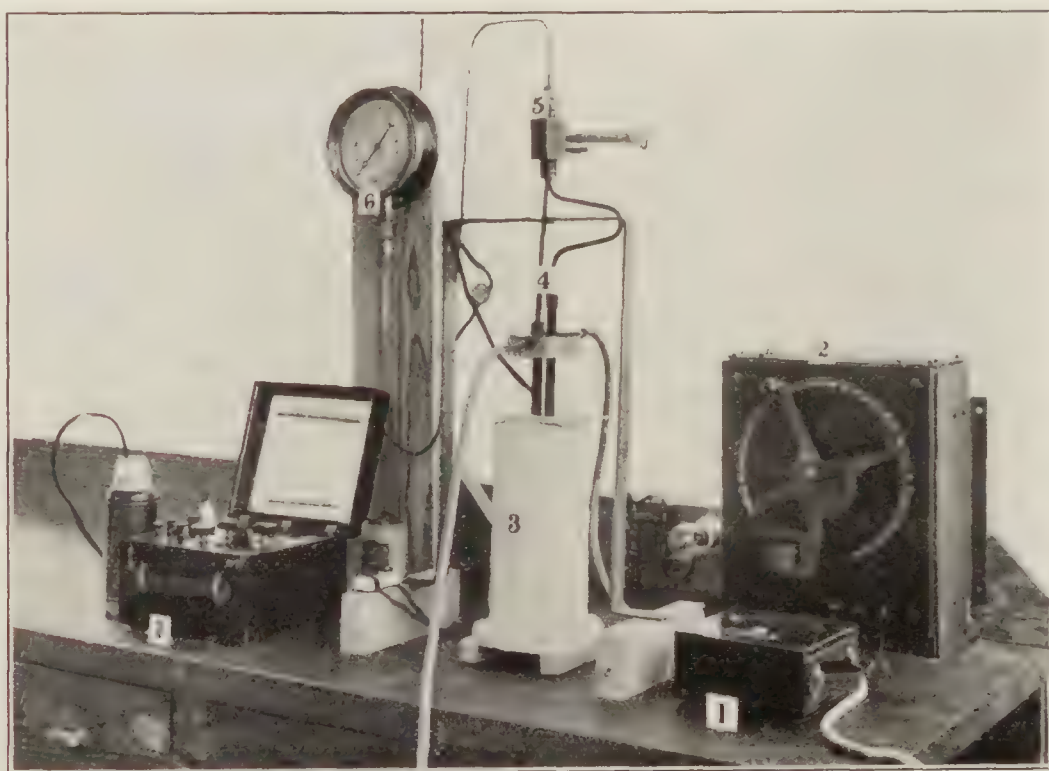


FIGURE 1.—Vapor pressure apparatus. 1. Voltmeter for measuring potential across electric furnace. 2. Rheostat for regulating potential across electric furnace. 3. Electric furnace containing bomb. 4. Cooling pan. 5. Valve block. 6. Bourdon pressure gauge. 7. Potentiometer for indicating temperature of bomb. The thermos bottle holding the cold junction of the thermocouple can be seen immediately to the left of the potentiometer

the bars by surface tension and capillarity, aided by the small annular space between the wire and the drilled hole.

Heat was supplied by a cylindrical electric furnace of slightly larger diameter than the bomb. The heat energy in the furnace was sufficient to heat the bomb considerably above the maximum test temperature. This relation, in addition to the fact that the heat capacity of the bomb was considerably in excess of that of the fuel placed in it, assured a steady though slightly decreasing rate of temperature rise. A hole was drilled in the thickest part of the bomb wall from the bottom of the bomb to a depth of $3\frac{1}{2}$ inches, and the hot junction of the thermocouple placed approximately 1 inch from the top of this hole in order to locate the hot junction near the dividing line of the fuel and the vapor. The cold junction of the thermocouple was surrounded by melting ice in a thermos bottle. The electrical potential generated in the thermocouple

which was indicated by the potentiometer was converted into degrees Fahrenheit from a calibration of the thermocouple made by means of a certified thermometer.

The test procedure followed was the same for all the fuels. The bomb was first washed thoroughly with the fuel to be tested. It was then placed in the electric furnace with opened needle valves and heated to a temperature in excess of that to be used in the test. This was done to complete any chemical reaction that might take place between the metal of the bomb and the fuel and to vaporize any impurities that might be present. When the bomb had again cooled to room temperature, approximately 13 cm³ of the fuel to be tested were placed in it. A tank containing nitrogen was connected to the inlet opening and nitrogen passed through the bomb and connecting tubes for a definite time interval at a slow, steady rate interrupted with occasional intervals of slightly increased flow. Following this replacement of the air in the apparatus by nitrogen, the pressure in the bomb was adjusted to atmospheric pressure, the inlet and exhaust valves closed, and the electric current turned on in the furnace. When a temperature of approximately 175° F. was indicated, the observer began recording the readings

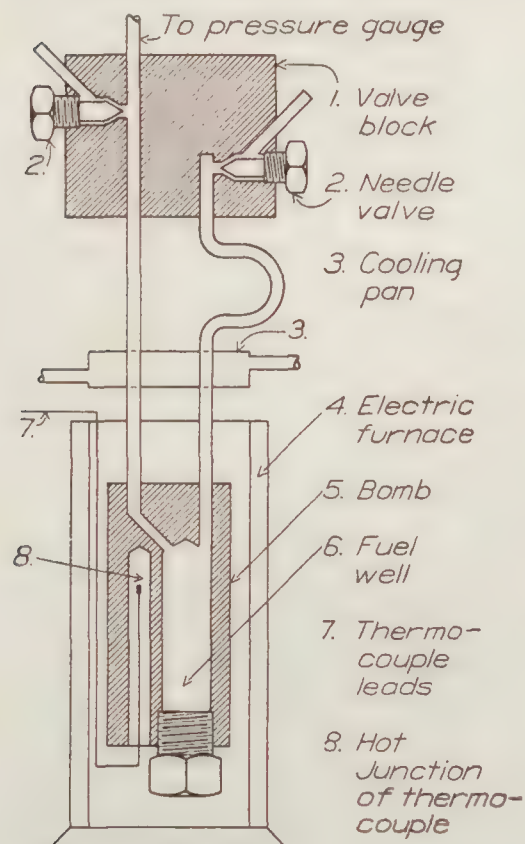


FIGURE 2.—Diagrammatic sketch of vapor pressure temperature apparatus

of the potentiometer and of the pressure gauge simultaneously. Readings were taken at intervals of pressure of from 1 to 50 pounds per square inch, depending on the range of pressures to be covered during the test. When the maximum temperature desired was reached, the electric current in the furnace was turned off and readings were taken during the cooling period in the same manner. The time for a complete test was approximately three hours. Specimens of the fuel and of the gas remaining in the bomb were collected at the completion of each test. The tests were repeated several times with varying amounts of fuel, the bomb being completely prepared previous to each test by washing, heating, and cooling as described above.

Several series of computations and corrections in addition to the temperature and pressure calibrations were made to the recorded data in order to obtain the true temperatures and pressures of the vapor under test. These computations and corrections related chiefly to the nitrogen pressure which was calculated for each temperature, assuming a constant volume relationship to exist in the bomb. The nitrogen pressure was then subtracted from the corrected recorded pressure and the atmospheric pressure added to obtain the vapor pressure of the fuel being tested.

TEST RESULTS

The experimental data from these tests are plotted in Figures 3 to 12. It may be noted that critical points were recorded for most fuels and that pressure fluctuations or other physical-chemical phenomena have taken place. The data for all curves on any fuel were reproducible

with a satisfactory degree of accuracy up to the critical point. Beyond the critical point the data for each fuel were reproducible in their general characteristics, but the vapor pressure for any given temperature increased with the amount of the fuel originally placed in the bomb. The phenomena that were most evident follow.

1. **CRITICAL POINTS.**—The critical point is the point at which the curve changes from one of increasing slope to one of constant slope. It is clearly defined in the curves for gasoline (fig. 3), methyl alcohol (fig. 7), ethyl alcohol (fig. 8), benzol (fig. 9), and the mixtures of gasoline with ethyl alcohol (fig. 11), and with benzol (fig. 12). The temperature indicated at this point is known as the critical temperature of the liquid. At this temperature physical distinctions between the liquid and its vapor disappear.

2. **PRESSURE FLUCTUATIONS.**—These phenomena occurred during the cooling of the kerosene (fig. 4) and of the Diesel oil (fig. 5). During the pressure fluctuations the indicating hand of the pressure gauge, turned at about the speed of the second hand of a watch, stopped, and then traveled back to within a few pounds of the starting pressure, and then repeated the cycle with gradually increasing and later decreasing maximum pressures. These reactions for the Diesel oil continued until the temperature had dropped from about 825° to about 575° F. The reactions for kerosene were considerably more restricted, taking place between 725° and 680° F.

3. **GENERATION OF ONE OR MORE PERMANENT GASES FROM ALL THE FUELS TESTED WITH THE EXCEPTION OF BENZOL.**—The generation of these permanent gases was indicated by the high residual pressures exerted by the vapors after the bomb had been allowed to cool to room temperatures as shown for gasoline, kerosene, Diesel engine fuel oil, methyl alcohol, and ethyl alcohol. (Figs. 3, 4, 5, 7, and 8.)

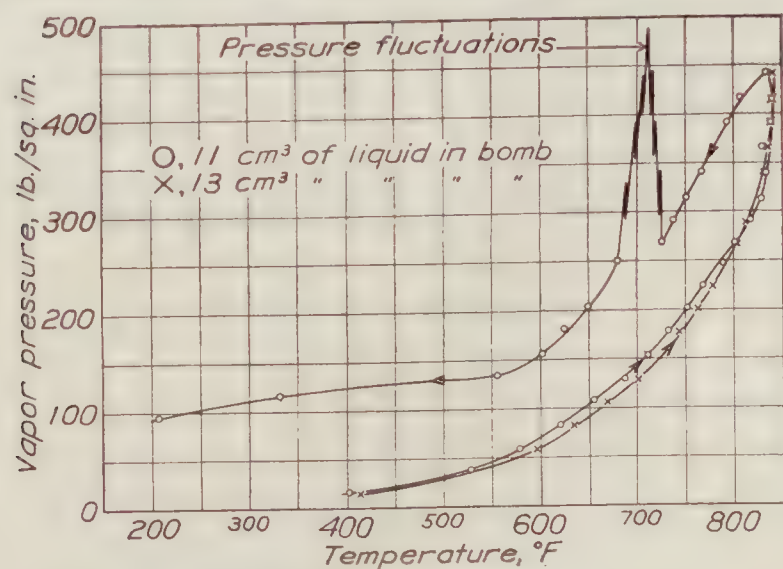


FIGURE 4.—The effect of temperature on the vapor pressure of kerosene

THE CRITICAL TEMPERATURE.—These phenomena are indicated in the curves for the alcohols (figs. 7 and 8) and the benzol (fig. 9). In these curves the straight line temperature-pressure relations above the critical point are made up of two or more straight lines that join but that have different slopes.

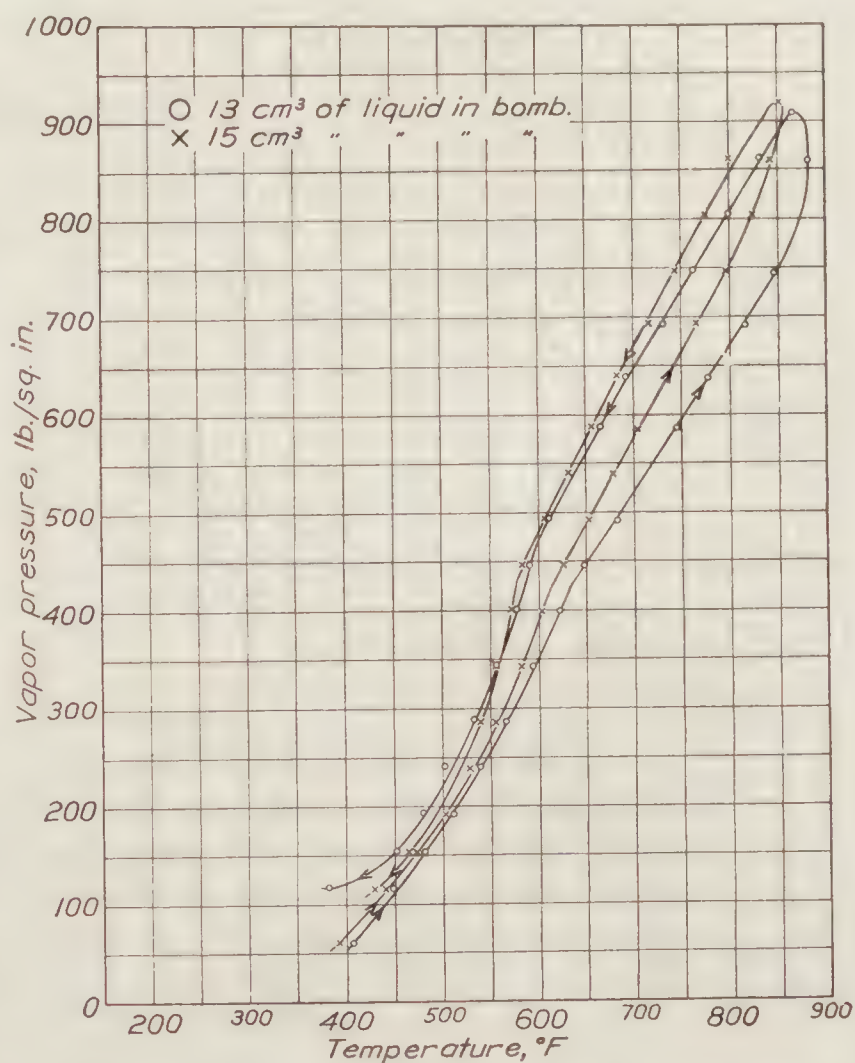


FIGURE 3.—Effect of temperature on the vapor pressure of gasoline

4. **PERMANENT DECOMPOSITION.**—Permanent decomposition or cracking was indicated by the fact that the fuel removed from the bomb following the test was different from that put into it. The alcohols, kerosene, and gasoline were changed from clear white thin liquids to liquids that resembled fuel oil or a very light lubricating oil.

5. **GENERATION OF TWO OR MORE SEPARATE AND DISTINCT VAPORS AT OR ABOVE**

6. RAPID INCREASE IN VAPOR PRESSURES.—The vapor pressure of the aircraft engine lubricating oil (fig. 6) increased at such a rate after it had reached approximately 800° F. that it was necessary to open the exhaust needle valve in order to prevent damage to the pressure gauge. The rate of pressure increase was so much greater than that of the temperature increase as to indicate a physical or chemical change in the oil, such as cracking at a higher temperature than used in manufacture.

7. VARIATION OF THE VAPOR PRESSURES.—A comparison of the vapor pressures of the fuels tested is shown in Figure 10. These curves are the same as those appearing in Figures

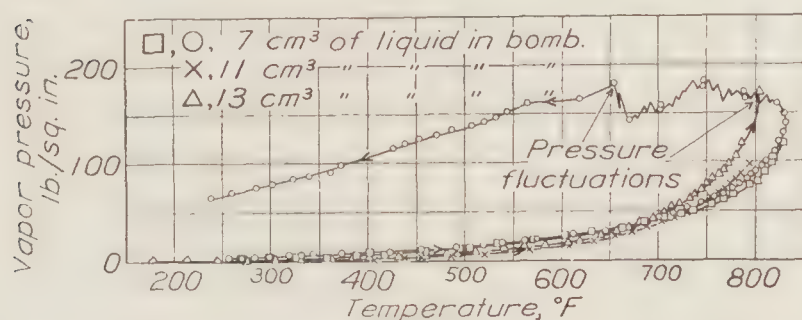


FIGURE 5.—Effect of temperature on the vapor pressure of Diesel engine fuel oil

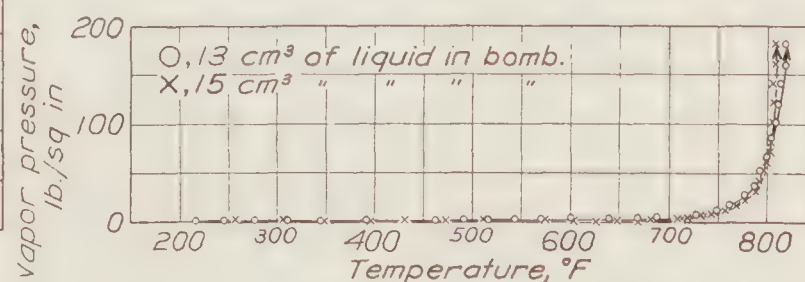


FIGURE 6.—Effect of temperature on the vapor pressure on aircraft engine lubricating oil

3 to 9 for the tests with 13 cm³ of the fuel in the bomb. The wide variation of the vapor pressures of the six fuels and of the lubricating oil is clearly illustrated.

8. DEVIATION FROM DALTON'S LAW OF PARTIAL PRESSURES.—The values for the vapor pressures of the mixtures of ethyl alcohol and of benzol with the gasoline (figs. 11 and 12), are not the sums of the vapor pressures of the individual liquids as would be expected from Dalton's law. This is probably due to the fact that chemical reactions took place between the two fuels or between the gases existing and generated in the bomb at the high temperatures of the tests.

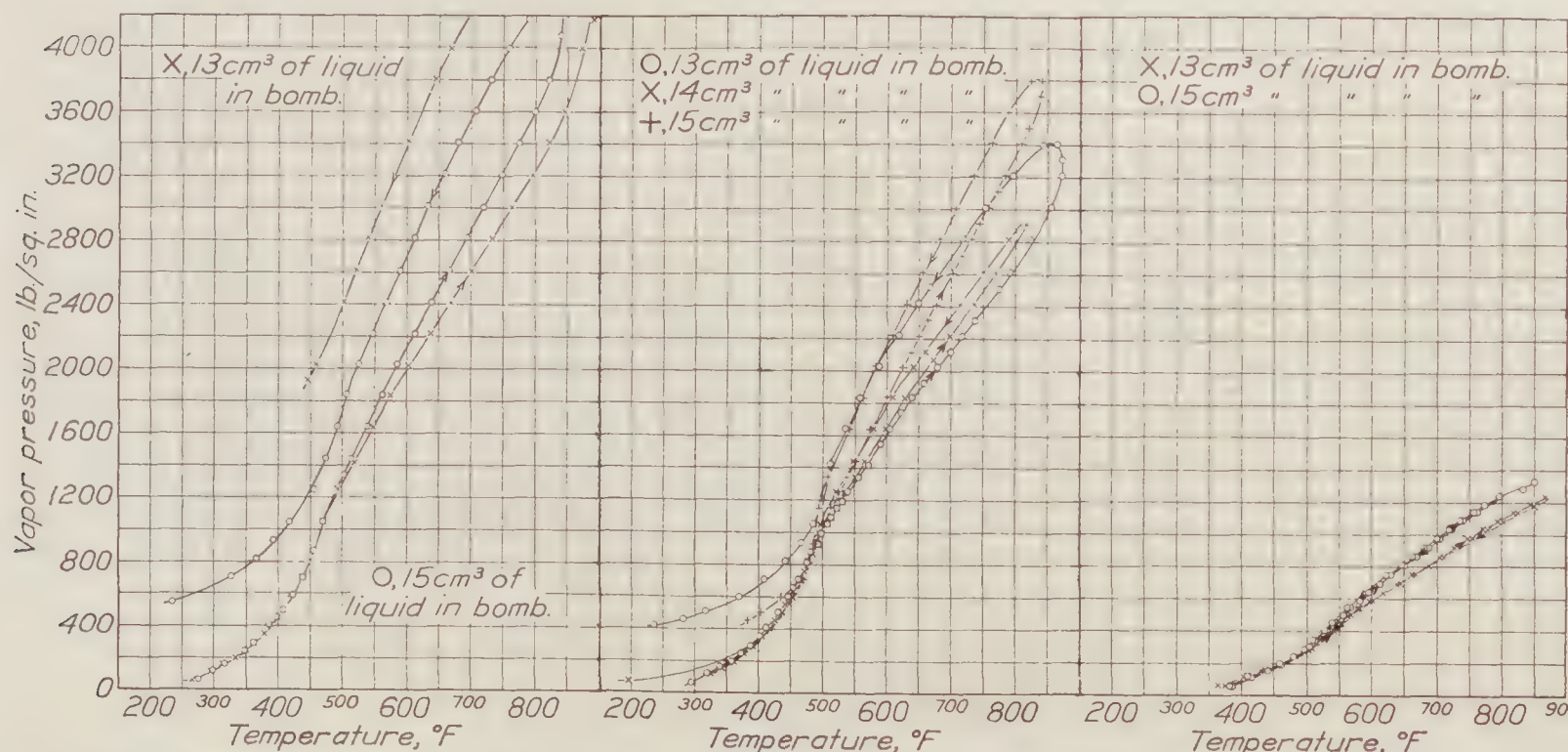


FIGURE 7.—Effect of temperature on the vapor pressure of methyl alcohol

FIGURE 8.—Effect of temperature on the vapor pressure of ethyl alcohol

FIGURE 9.—Effect of temperature on the vapor pressure of benzol

It is particularly interesting to note that in the case of the benzol-gasoline mixtures, at the higher temperatures, the vapor pressures of the mixtures with the exception of the 80 per cent benzol 20 per cent gasoline mixture are less than those of either of the fuels. The curves for these mixtures form a family of curves which has materially different characteristics and trends from the curves for either fuel. This family is further illustrated in Figure 13, which is a cross plot from Figure 12.

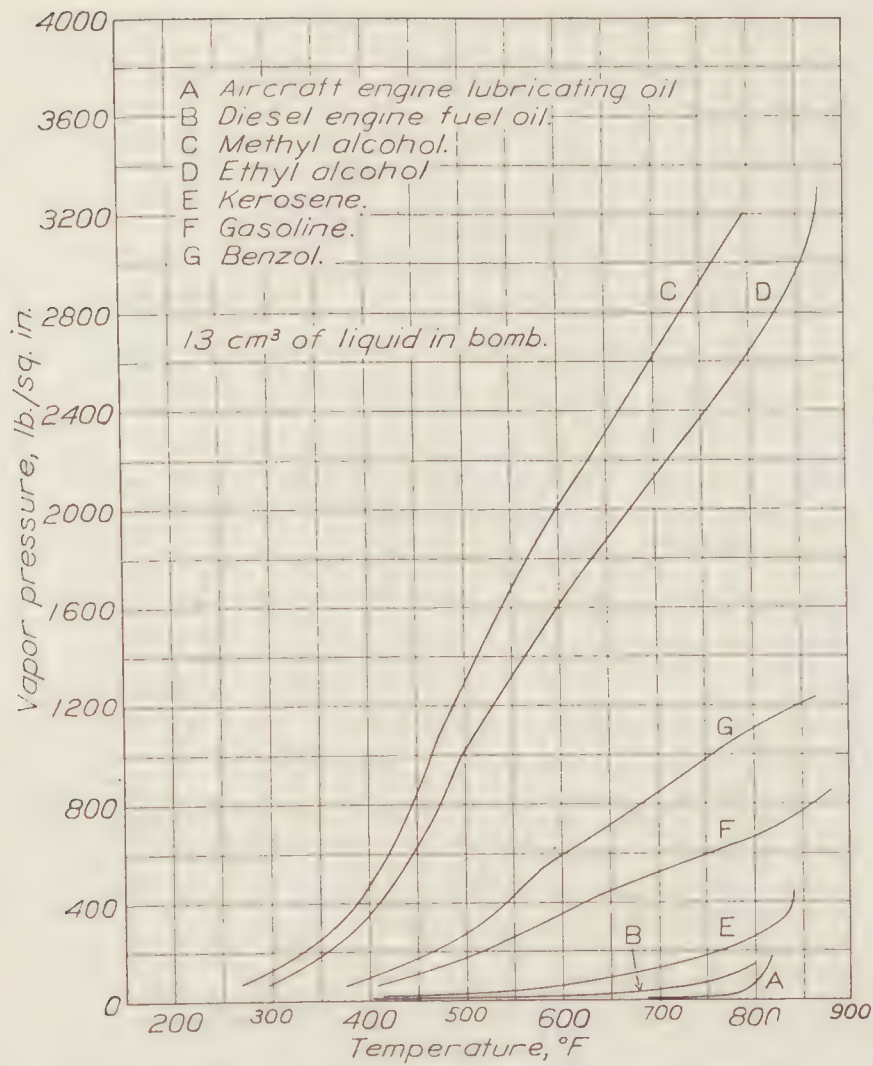


FIGURE 10.—Effect of temperature on the vapor pressure of several fuels and of lubricating oil

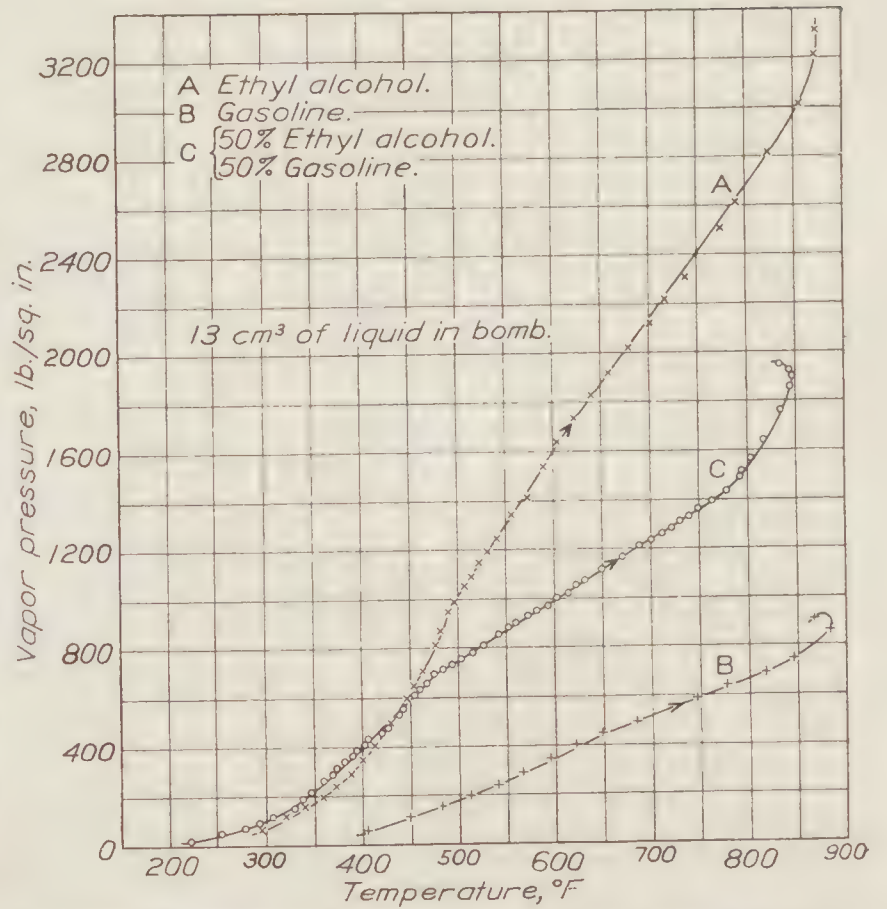


FIGURE 11.—The effect of temperature on the vapor pressure of ethyl alcohol, gasoline, and mixtures of ethyl alcohol and gasoline

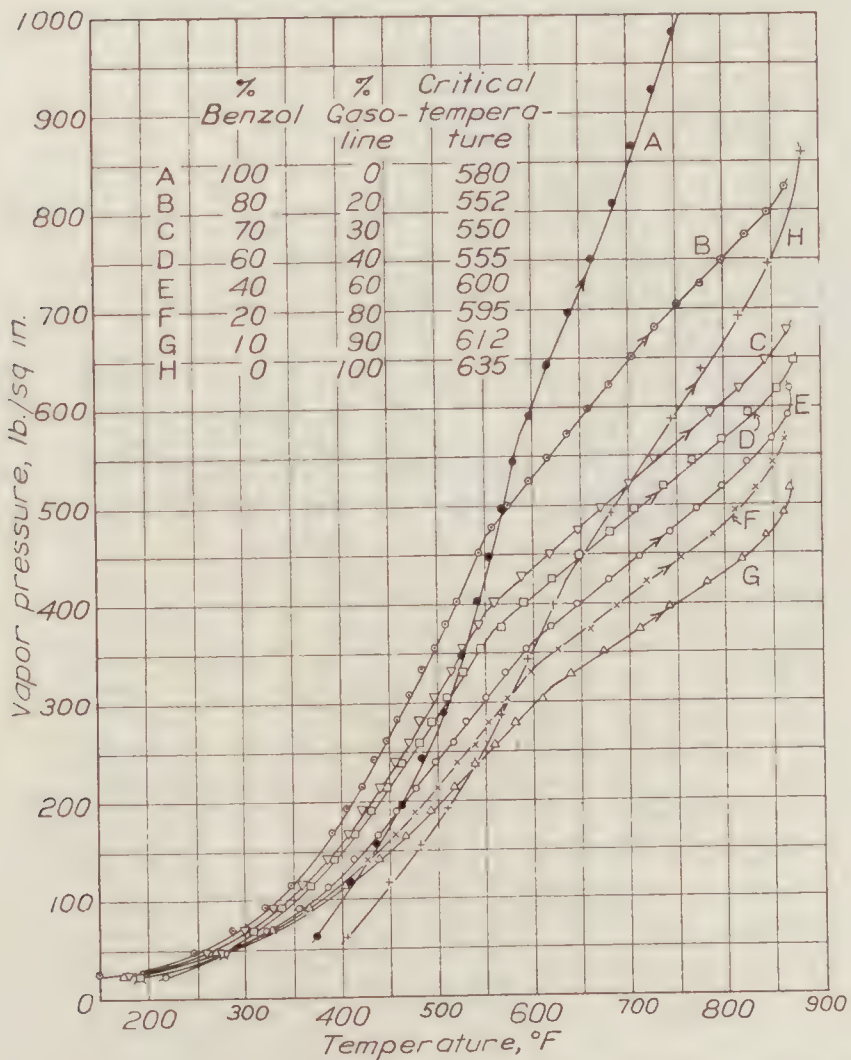


FIGURE 12.—Effect of temperature on the vapor pressure of benzol, gasoline, and benzol-gasoline mixtures

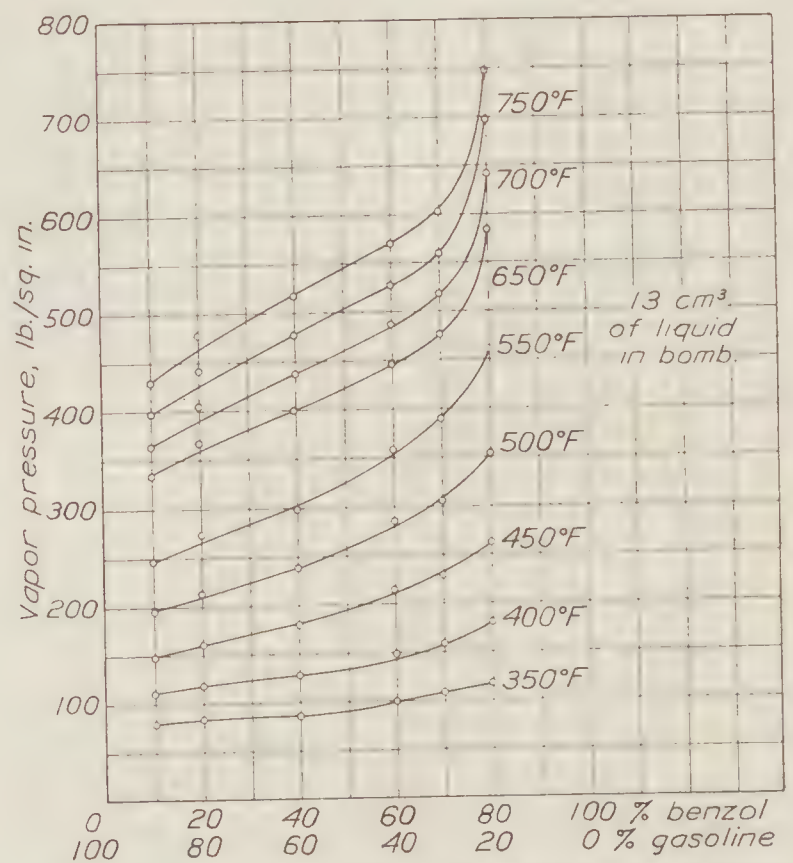


FIGURE 13.—Effect of composition on the vapor pressure of benzol-gasoline mixtures at constant temperatures

ACCURACY OF TEST RESULTS

VAPOR PRESSURES.—The accuracy of the computed vapor pressures depended on the error of observation in the vapor pressure readings, the gauge calibrations, and the computed nitrogen pressures. The error of observation in the pressure gauge readings was 0.5 per cent to 1.0 per cent of the maximum reading of the gauge. The accuracy of the gauge calibration depended upon the accuracy of the standard used. The possible error in this standard, the dead-weight gauge tester, was so small in comparison with that of the Bourdon gauge as to be negligible. However, there was an error in the computation of the nitrogen pressure because its volume did not remain constant as was assumed. The volume occupied by the vapors changed during the test due to the thermal expansion of the bomb and the liquid, the pressure expansion of the bomb and compression of the liquid, and the vaporization of the liquid. The following method was used to determine the magnitude of the error introduced by assuming that the volume of the vapor remained constant.

The change in the volume of the bomb due to the increase in the temperature and the pressure was computed. The volume of the liquid at the temperature and pressure under considera-

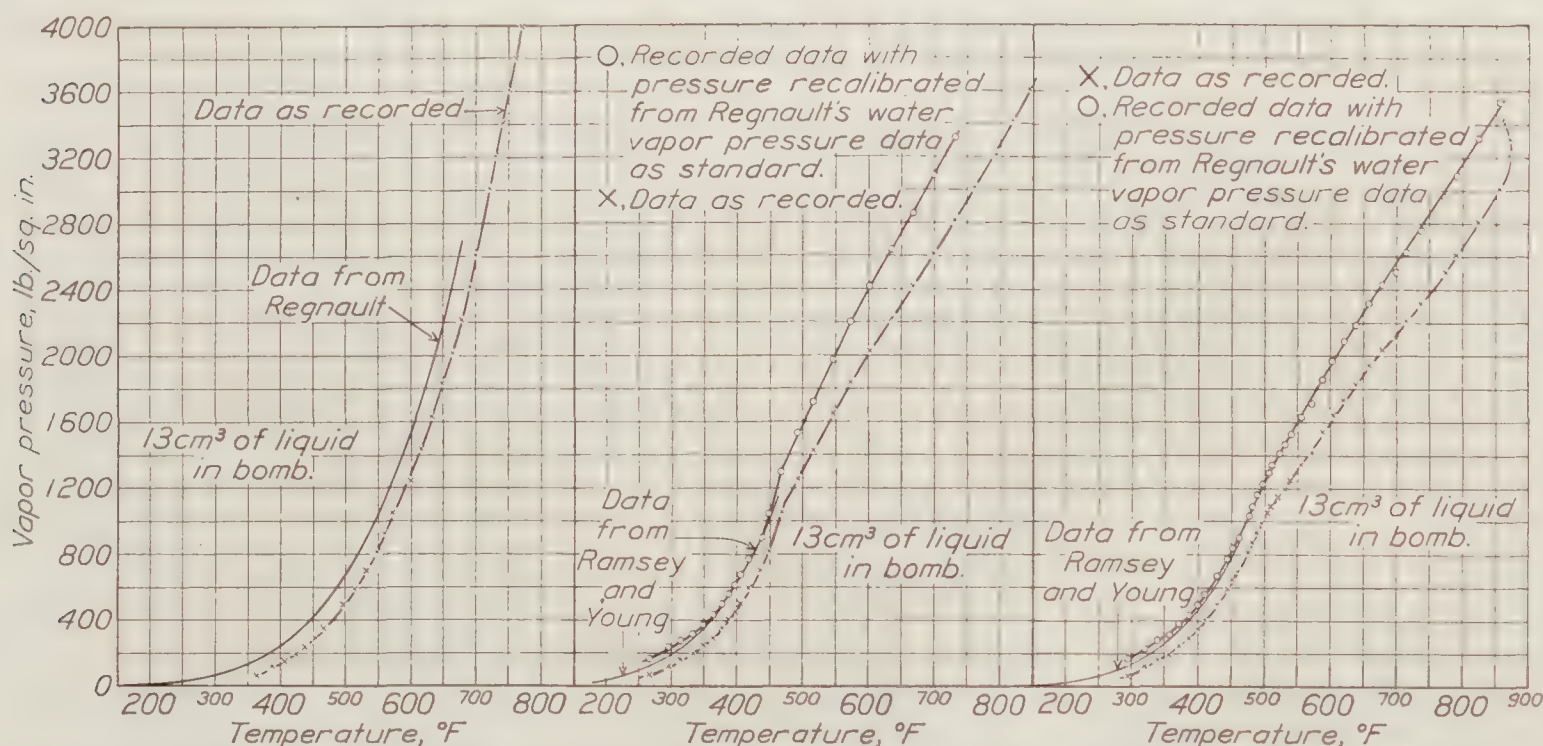


FIGURE 14.—Effect of the conditions of test on the vapor pressure of water

FIGURE 15.—Effect of the conditions of test on the vapor pressure of methyl alcohol

FIGURE 16.—Effect of the conditions of test on the vapor pressure of ethyl alcohol

tion was derived. The volume of the liquid was subtracted from the total volume to obtain the volume occupied by the vapor. The weight of the vapor was computed and subtracted from the total weight of the liquid under test. The volume occupied by the remaining liquid was again computed and these calculations repeated until the true volume of the vapor was found within the accuracy desired. For methyl alcohol at the critical temperature, 473° F., and the corresponding critical pressure, 1,100 pounds per square inch, the true nitrogen pressure was 3.6 pounds per square inch greater than the value obtained by assuming that the vapor volume remained constant. Consequently the vapor pressure computed with this assumption was in error by only 0.33 per cent.

TEMPERATURE.—The accuracy of the temperatures depended on the potentiometer and thermocouple calibration, the error of observation in the potentiometer readings, the temperature gradient between the hot junction of the thermocouple and the vapor, and the conduction losses along the thermocouple wires. The thermocouple and the potentiometer were calibrated by means of a 680° F. thermometer that had previously been calibrated and certified by the United States Bureau of Standards. The maximum variation from the mean of any one reading was 2° F. The error of observation in the potentiometer reading was 0.5° F. The temperature gradient between the hot junction of the thermocouple and the inside wall of the bomb was

computed to be 0.1° F . The wire of the thermocouple was wrapped around the bomb several times to prevent conduction losses from the hot junction along the thermocouple wires. The maximum error of the temperature readings was therefore approximately 2.6° F .

COMPARISON OF DATA WITH THAT OF OTHER INVESTIGATIONS.—Water was tested as a standard for comparison of the data presented with that given by other investigators. This comparison was made to determine whether other factors than those considered affected the experiments. The experimental results from these tests on water are shown in comparison with the values given by Regnault (reference 2) in Figure 14. If the discrepancy in the water data was caused by some factor inherent in the apparatus, the same discrepancy should appear in the data for all the liquids tested which were affected in the same manner by this factor. In order to determine whether or not the same error did appear in the data for the alcohols, the difference in pressures from Figure 14 were added to the vapor pressures as computed from the tests and plotted together with the results obtained by Ramsey and Young for these two liquids (reference 2) in Figures 15 and 16. The conclusion is drawn from an examination of these curves that at any given temperature the effect on the vapor pressure is approximately the same for water and the alcohols. The discrepancy is probably due in part to the different catalytic effects of the materials of the bomb on the liquids. The data presented in this report can only be applied therefore to these fuels when heated under conditions similar to those existing in the tests.

ANALYSIS

Several changes take place in fuels for oil engines when they are injected into the combustion chamber of the engine. The high temperature of the air in the combustion chamber heats the fuel particles, begins to vaporize them, and in some cases decomposes them into new hydrocarbons. The processes continue until some of the fuel reaches its auto-ignition temperature and combustion is initiated. The combustion spreads through the combustion chamber at a rate depending on the degree with which the fuel is mixed with the air and on the rapidity with which the fuel is raised to the auto-ignition temperature. The endeavor to decrease the time lag of auto-ignition is an effort to speed up the processes of preparing the comparatively cold, liquid fuel chemically and physically for auto-ignition. The physical properties of the fuel partially control the time necessary to carry out these processes. Among these properties may be mentioned the specific heat, the heat of vaporization and the saturated vapor pressure of the fuel, and the specific heats of the fuel vapors.

The vapor pressures presented in this report are not in every case the vapor pressures of the fuels originally placed in the bomb. With the exception of the alcohols and benzol, the fuels were a combination of saturated and unsaturated hydrocarbons, and the increasing temperature caused chemical as well as physical changes. The vapor above the fuel formed hydrocarbons which did not appear in the fuel.

The pressure of a vapor is caused by the impact of the swiftly moving molecules on the walls of the retaining vessel. The pressure is proportional to both the number and the magnitude of these impacts. The magnitude is determined by the mean kinetic energy of the molecules.

This is equivalent to $\frac{1}{2} m v^2$ in which m is the mass of the molecule and v is its mean velocity.

The vaporization process consists of energizing the molecules by heating them until they possess sufficient kinetic energy to overcome the surface tension of the liquid and enter the vapor. A decrease of the surface tension of the liquid or an increase in the mean kinetic energy of the molecules in the liquid will result in a greater number of the molecules entering the vapor. When a liquid is subjected to an increasing temperature the surface tension is lowered (reference 5) and the mean kinetic energy of the molecules is raised. As a result the vaporization and consequently the vapor pressure increases at a more rapid rate than the temperature. This is illustrated in all the experimental results.

According to the kinetic theory of gases, for equal volumes and temperatures the number of molecules in any two vapors is proportional to the pressures exerted by the vapors. The total amount of vaporization—that is, total number of free molecules—for equal vapor volumes of any two liquids at a given temperature is, therefore, proportional to their vapor pressures.

An examination of experimental data (fig. 10) indicates that the order of the preparation of the several fuels for combustion in the range of temperatures between 200° and 800° F. is ethyl alcohol, benzol, gasoline, kerosene, and Diesel engine fuel oil. The vapor pressures of these fuels at 450° F. are given in Table I. They are in the ratios 120:35:22:4:1, respectively. The specific heats of the fuels at 104° F., and the latent heats of vaporization at the boiling temperatures are also given in Table I.

TABLE I

Fuel	Vapor pressures, pounds per square inch at 450° F.	Specific heat at 104° F.	Latent heat of vaporization, B. t. u. per pound
Ethyl alcohol.....	600	¹ 0. 648	369 at 173° F. ¹
Benzol.....	175	¹ . 423	166 at 176° F. ¹
Gasoline.....	115	² . 501	137 at 194° F. ³
Kerosene.....	20	² . 482	135 at 244° F. ³
Diesel engine fuel oil.....	5	² . 472	115 at 338° F. ³

¹ Reference 2.² Reference 7.³ Reference 6.

Actual practice indicates that in carburetor engines burning ethyl alcohol or gasoline the alcohol is the more difficult to ignite. This variance from the vapor-pressure data which shows there are a lesser number of free molecules produced in the easily ignited gasoline is due to the comparatively high specific heat and latent heat of evaporation of the alcohol. Ethyl alcohol therefore requires some form of preheating, such as hot spots, high inlet air temperatures, or high compression ratios to supply this heat energy in order to obtain sufficient vaporization for the production of an ignitable and rapidly combustible mixture.

Above 800° F. the vapor pressures of the Diesel engine fuel oil increase at such a rapid rate that a comparatively small change in the temperature, and consequently in the compression ratio of an engine, will result in a considerable decrease in the lag of auto-ignition.

The rapid increase in the vapor pressure of the lubricating oil indicates the maximum temperature at which this oil may be used for lubricating or cooling purposes.

The rate of the increase of vapor pressure with temperature increases rapidly with the temperature. For this reason a small increase in the compression temperature of an engine will result in a marked increase in the vapor pressure of the fuel. The data for the vapor pressures of the fuels, therefore, indicate the compression temperature required to produce the rapid vaporization of the injected fuel for combustion.

CONCLUSIONS

Several conclusions are drawn from the experimental results. The vapor pressures of the fuels tested, which are measures of the number of free molecules produced by the vaporization processes, vary over a wide range of pressure at any given temperature. The rate of change of vapor pressure with temperature for any one fuel increases rapidly until the critical temperature is reached. Above this temperature the rate of increase of the vapor pressure remains at a constant value, which depends on the ratio of the mass of the vapor and liquid per unit volume. At high temperatures the fuel vapors form new hydrocarbons which in some cases on condensation form a fuel of different composition from that originally placed in the bomb. The vapor pressures of the fuel mixtures investigated do not follow Dalton's law of partial pressures, the vapor pressures of the mixtures being either greater or less than the vapor pressures of either of the unmixed fuels. The data for the vapor pressures of the fuels at high temperatures indicate the compression temperatures required to produce rapid vaporization of the fuel for combustion.

LANGLEY MEMORIAL AERONAUTICAL LABORATORY,
NATIONAL ADVISORY COMMITTEE FOR AERONAUTICS,
LANGLEY FIELD, VA., October 16, 1928.

REFERENCES

1. Joachim, W. F.: Research on Oil Engines for Aircraft. *Mechanical Engineering*, Nov., 1926. Vol. 48, No. 11, pp. 1123-1128, figs. 1-11.
2. Fowle, E. F.: *Smithsonian Physical Tables*, 1927. 7th ed., revised, xlvii, 458 pp., 585 tables. Washington, Smithsonian Institution, pp. 178, 228, and 231.
3. Cooke, M. B.: Temperature-Pressure Curves of Petroleum Products. Report of Investigation Bureau of Mines, Department of the Interior, serial No. 2368, 1922.
4. Sass, F.: Ignition and Combustion Phenomena in Diesel Engines. N. A. C. A. Technical Memorandum No. 482, Oct., 1928.
5. Eucken, A., Jetten, E., and Lamer, K.: *Fundamentals of Physical Chemistry*, 1925, 1st ed., 700 pp., figs. New York, McGraw-Hill Book Co. (Inc.), p. 148.
6. Heinlein, Fritz: Experimental Investigation of the Physical Properties of Medium and Heavy Oils, Their Vaporization and Use in Explosion Engines. Part III: Experimental Apparatus. N. A. C. A. Technical Memorandum No. 384, Oct., 1926, p. 7.
7. Washburn, E. W.: *International Critical Tables*, Vol. II, 1927. 616 pp., tables and figs. New York, McGraw-Hill Book Co. (Inc.), pp. 140-144 and 151.

BIBLIOGRAPHY

- Alt, Otto: Combustion of Liquid Fuels in Diesel Engines. N. A. C. A. Technical Memorandum No. 281, Oct., 1924.
- Hubendick, E.: Researches on the Alcohol Internal Combustion Engine Problem. International Air Congress, 1923, Report, London. pp. 498-520.
- Neumann, Kurt: Experiments on Self-Ignition of Liquid Fuels. N. A. C. A. Technical Memorandum No. 391, Dec., 1926.
- Tausz, J. and Schulte, F.: Determination of Ignition Points of Liquid Fuels Under Pressure. N. A. C. A. Technical Memorandum No. 299, Jan., 1925.

REPORT No. 322

**INVESTIGATION OF AIR FLOW IN OPEN-THROAT
WIND TUNNELS**

By EASTMAN N. JACOBS
Langley Memorial Aeronautical Laboratory

REPORT No. 322

INVESTIGATION OF AIR FLOW IN OPEN-THROAT WIND TUNNELS

By EASTMAN N. JACOBS

SUMMARY

Tests were conducted on the 6-inch wind tunnel of the National Advisory Committee for Aeronautics during May and June, 1928, to form a part of a research on open-throat wind tunnels. The primary object of this part of the research was to study a type of air pulsation which has been encountered in open-throat tunnels, and to find the most satisfactory means of eliminating such pulsations.

In order to do this it was necessary to study the effects of different variables on all of the important characteristics of the tunnel. This paper gives not only the results of the study of air pulsations and methods of eliminating them, but also the effects of changing the exit-cone diameter and flare and the effects of air leakage from the return passage.

It was found that the air pulsations in the 6-inch wind tunnel could be practically eliminated by using a moderately large flare on the exit cone in conjunction with leakage introduced by cutting holes in the exit cone somewhat aft of its minimum diameter.

INTRODUCTION

The wind tunnels which have been designed and built within the last few years, both at the Langley Memorial Aeronautical Laboratory and elsewhere, have been, to an increasing extent, of the open-throat type. This is due primarily to the greater ease of mounting and observing the models in this type of tunnel. The earlier experiments on wind tunnels in this country were made on tunnels of the Venturi type, so that there is little information available on which to base the design of open-throat tunnels of the Göttingen type. The need for such data is becoming more apparent as new tunnels are built in which it has been found difficult to secure the desired velocity and to satisfactorily control the air stream passing across the test section. In several open-throat tunnels violent pressure pulsations have been encountered. The exact cause of such pulsations is not yet definitely understood; however, the conditions under which pulsations are set up indicate that the phenomenon is very similar to the generation of pulsations in an organ pipe. Apparently the air in the jet alternately flows in and spills out around the mouth of the exit cone, causing alternate regions of compression and rarefaction in the exit cone and return passage traveling around the tunnel at the speed of sound. This action is regenerative, each compression wave in the exit cone causing more spilling, and vice versa, so that the pulsations may become very violent.

Experiments on the air flow in an open-jet tunnel to study the effect of various sizes, shapes, and spacing of cones were recently made by the National Advisory Committee for Aeronautics. (Reference 1.) The application of these results is somewhat limited because certain variables were not changed and because certain characteristics of the tunnel were not measured. Most important among the variables which remained constant throughout the previous investigation was the amount of air leakage from the return passage back to the test section. Since a considerable portion of the air which was taken in by the exit cone came from this source rather than from the entrance cone, the optimum size of exit cone and exit-cone flare there given

would not be expected to apply to a tunnel having a different amount of leakage. During those tests no tendency toward pulsating flow was observed, probably because of the large amount of leakage.

Since the above-mentioned tests were made, the variable density wind tunnel of the National Advisory Committee for Aeronautics has been redesigned and rebuilt as an open-throat tunnel. It was possible to so design the tunnel that there would be practically no leakage. The exit cone was made small in view of the fact that no space would be required to provide for the reentrance of the leakage air, and also because it was thought that a large exit cone would tend to reduce the velocity downstream in the test section, thus causing an objectionable downstream pressure gradient. Very severe vibrations were encountered when the tunnel was in operation which at first were attributed to the elasticity of the steel structure. During a visit to the laboratory Professor Lesley of Stanford University became interested in the vibrations because of a similar effect which had been encountered in the Stanford tunnel. There it was discovered accidentally that objects protruding into the stream from the edge of the entrance cone reduced the pulsations. A similar experiment was made in the variable density tunnel by simply having four men hold their hands so that they projected into the air stream about 5 inches at the mouth of the entrance cone. This practically eliminated the most severe pulsations. Later eight metal tabs, 3 by 5½ inches, were installed in the tunnel. These were found to be very satisfactory in reducing the vibrations.

With the object of comparing this method of reducing the pulsations with other possible methods, the present investigation was started. Dealing primarily with air pulsations, it forms a part of a larger research now in progress on the design of open-throat wind tunnels. The investigation was conducted in the 6-inch wind tunnel of the National Advisory Committee for Aeronautics because of the comparative ease of constructing new parts for and making modifications to a small tunnel. The effect of the variables on the tendency toward pulsating flow could not be studied without regard to their effect on the other important characteristics of the tunnel. The investigation was therefore extended to include the effects of variables which were not covered in the previous investigations on all of the important characteristics of a wind tunnel. The following are the important variables considered:

1. Flare of exit cone.
2. Diameter of exit cone.
3. Obstructions at mouth of entrance cone.
4. Leakage from diffuser or return passage.

The effects of the above variables were studied with reference to the following characteristics of the tunnel:

1. Tendency toward pulsating flow.
2. Energy ratio.
3. Downstream pressure gradient.
4. Velocity distribution across the stream at the test section.
5. Velocity outside of the stream at the test section.
6. Velocity outside of the stream at the mouth of the exit cone.

APPARATUS

The tunnel used in this investigation, known as the 6-inch wind tunnel, is shown diagrammatically in Figure 1, and described in detail in references 1 and 2. During the present series of tests the diameter of the jet was $6\frac{13}{16}$ inches and the distance between the entrance cone and exit-cone flare was one diameter ($6\frac{13}{16}$ inches). The exit cone consisted of a steel cone slightly over 3 feet long tapering from the variable minimum diameter to the propeller diameter, $12\frac{1}{4}$ inches. The air was returned to the entrance cone through a single rectangular return passage having guide vanes in the corners. Various shapes of exit-cone flares of wood could be slipped on over the mouth of the metal exit cone. (Fig. 1.)

To study the effect of the exit-cone flare two types were used, designated F_1 and F_2 . These, together with a third type designated F_3 and later tested, are shown in Figure 2. F_1 was modeled after the flare in the variable-density tunnel and F_2 and F_3 were larger.

To study the effect of exit-cone diameter, exit cones with the various amounts of flare were constructed having three different minimum diameters. The smallest one, designated E_1 , was modeled after the variable-density tunnel cone. E_2 was three-sixteenth inch larger in diameter and E_3 , the largest, was chosen to give the same divergence angle from the mouth of the entrance cone to the throat of the exit cone as that in the propeller research tunnel of the National Advisory Committee for Aeronautics. Figure 2 is a scale drawing of these cones giving the important dimensions.

Small rectangular metal tabs projecting into the stream from the mouth of the entrance cone were also included among the variables because such obstructions in the mouth of the variable-density tunnel had a tendency to reduce the air pulsations. The effect of eight tabs 3 inches wide and $5\frac{1}{2}$ inches long had been verified in the variable density tunnel; consequently, scale models of these tabs were used in connection with these tests.

The fact that previous experiments which had been conducted on the same tunnel before it was made air-tight, indicated no pressure pulsations led to the belief that a small leakage of air

between the return passage and the test section would have a stabilizing effect on the flow. Preliminary runs were made to study qualitatively the effects of leaks and to determine what leaks should be included in the systematic investigation. As a result, two sets of holes were drilled in the exit cone between the test section and the propeller and one set of holes behind the propeller in the center of the return passage. The investigation included tests with different combinations of these holes opened, together with the various flares and exit-cone diameters. These leaks have been designated L_0, L_1, L_2, L_3 , etc. The location and size of each set of leaks is shown diagrammatically in Figure 1.

TESTS

With each set of conditions a set of runs was made to determine the characteristics of the tunnel. The tendency toward pulsating flow was measured, after adjusting the air speed in the tunnel until the audible pulsations became loudest, by taking a pressure-time record on a recording photomanometer connected to the return passage by means of a 4-inch length of $\frac{1}{4}$ -inch tubing. The energy ratio was obtained by measuring the power input to the driving motor corresponding to a given pressure head as measured on a manometer which was connected to a static plate in the large part of the entrance cone. The velocity distribution across the stream and the static pressure gradient downstream were determined by means of a small Pitot-static tube and alcohol manometer.

A comparative figure indicating in a rough way the magnitude of the balance windage corresponding to each set of conditions was obtained by means of a hot-wire anemometer. The hot wire was held in position corresponding to the balance in the variable density tunnel; that is, 1 inch and 2 inches from the edge of the jet, 0.3 diameter from the entrance cone edge.

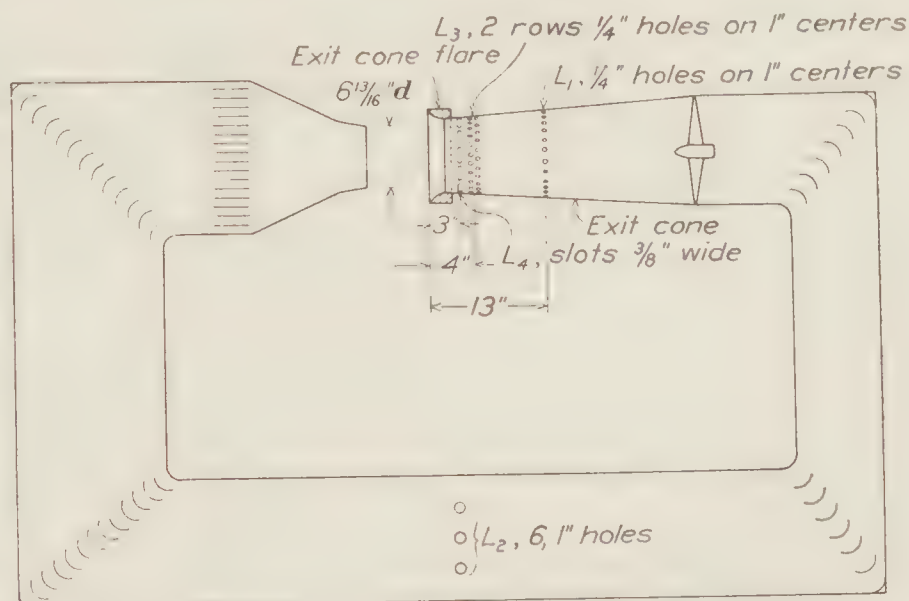


FIGURE 1.—Diagrammatic sectional elevation of the 6-inch wind tunnel

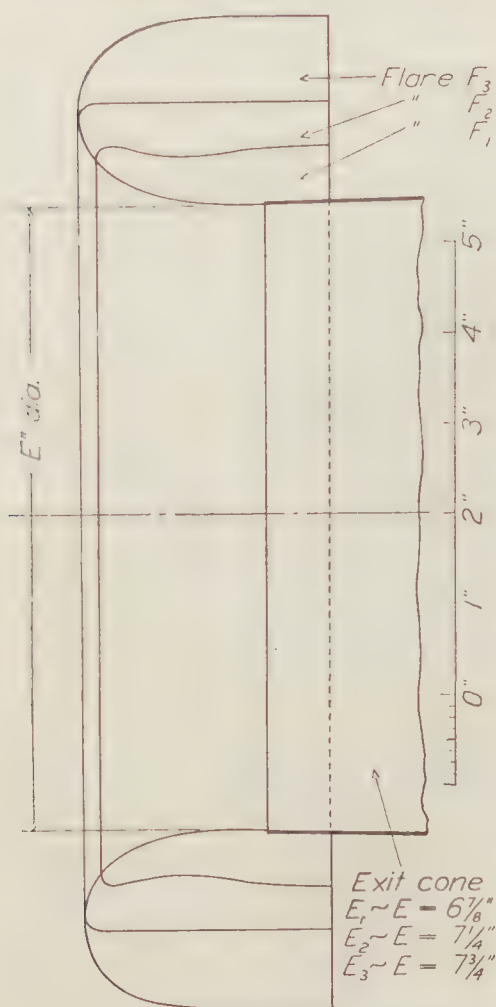


FIGURE 2.—Superimposed diagram of flares. The entrance cone shown on Figure 1 is $6\frac{13}{16}$ inches diameter

Readings to determine spilling velocity were also taken with the hot wire held one-fourth inch and 1 inch away from the edge of the exit cone flare.

RESULTS

The results of the investigation are presented in the form of groups of curves so arranged on one sheet that the curves in the vertical columns represent constant leakage and variable exit cone diameter and flare. The diameter and flare of the exit cone increase from the top of the sheet to the bottom. The curves in the horizontal columns represent different degrees of leakage beginning with minimum leakage at the left. The last vertical column in Figures 3 and 4 gives the results of the test with tabs on the mouth of the entrance cone.

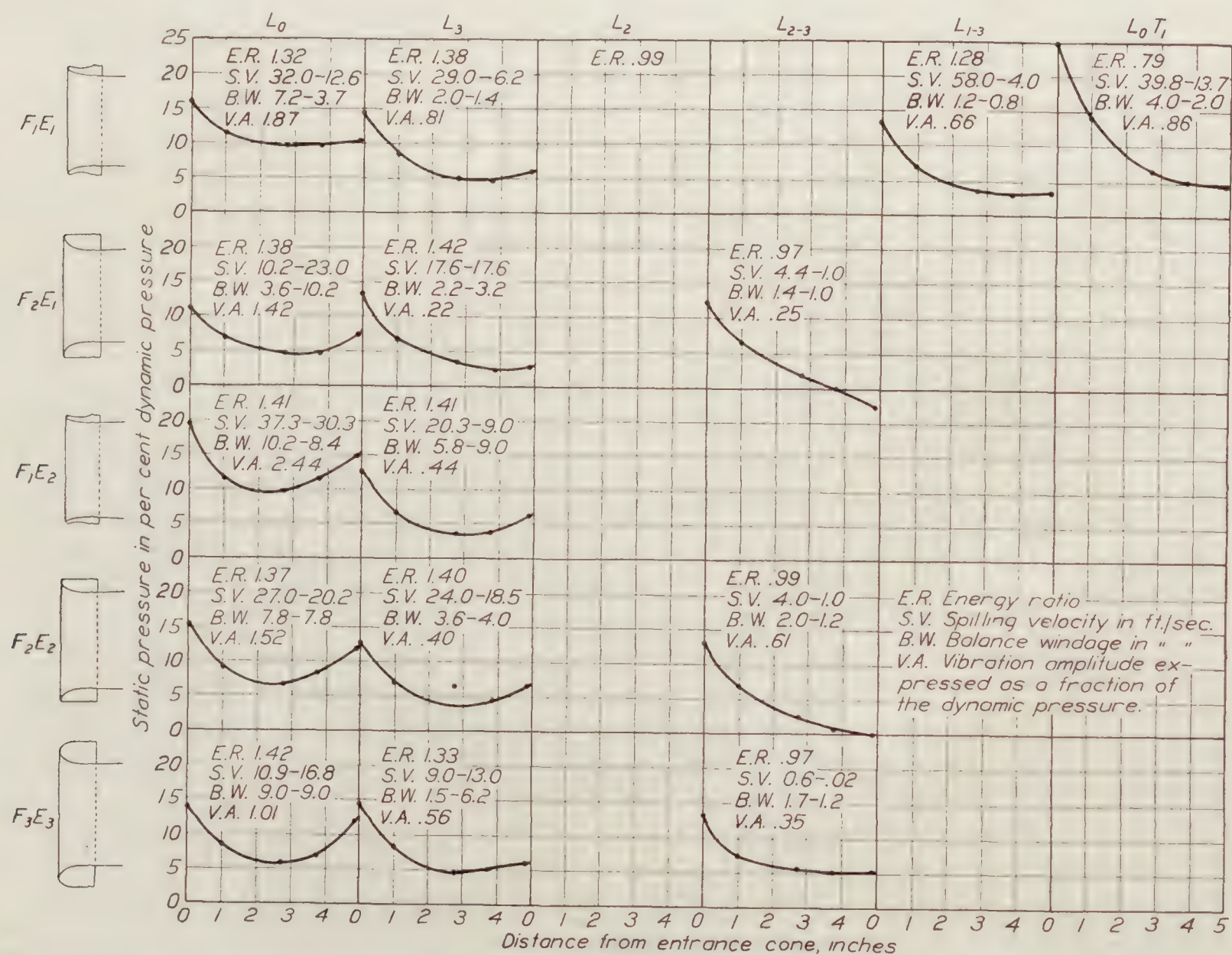


FIGURE 3.—Curves of static pressure in per cent of dynamic pressure measured at test section in the center of the jet plotted versus distance from entrance cone in inches

In this manner, in Figure 3, the curves of static pressure in the center of the jet are plotted against the distance from the mouth of the entrance cone in inches. The static pressure is given in per cent of the dynamic pressure at the test section so that the curves indicate the variation in velocity along the stream as well as the buoyancy which may be expected on a model. On each plot are also given numbers which represent the other characteristics of the tunnel. Opposite E. R. is given the energy ratio of the tunnel; that is, the ratio of kinetic energy of the air passing through the test section in one second to the electrical input power to the driving motor. Opposite S. V. two figures are given which measure roughly the spilling velocity around the mouth of the exit cone in feet per second. The first is the velocity one-fourth inch outside of the outer lip of the exit cone and the second, 1 inch outside. The figures opposite B. W. are indicative of the balance windage. The figures indicate the air velocity in feet per

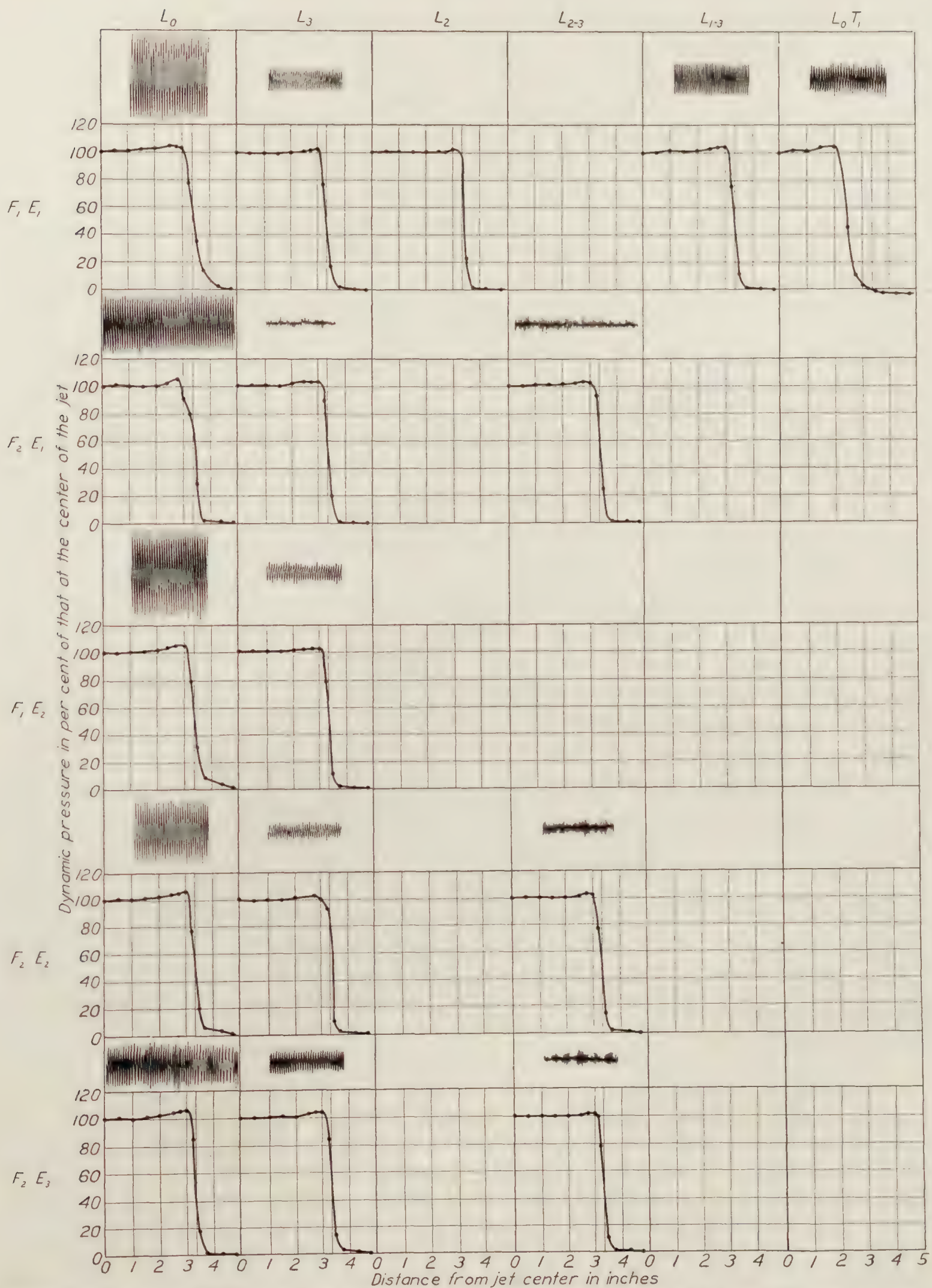


FIGURE 4.—Curves of dynamic pressure across air stream at test section versus distance from jet center in inches. Vertical line indicates entrance cone edge. Pressure records taken in return passage to show air pulsations

second as measured at points 1 inch and 2 inches, respectively, from the edge of the jet, 0.3 diameter aft of the edge of the entrance cone. Opposite V. A. is given the average vibration amplitude as measured on the photomanometer connected to read the static pressure in the return passage. The amplitude is expressed as a fraction of the dynamic pressure in the test section.

In Figure 4, arranged in the same order, are given the results of the dynamic pressure surveys across the air stream at the test section. The dynamic pressure as read from a Pitot-static tube in per cent of the dynamic pressure at the center of the air stream is plotted against the distance from the center of the stream in inches. The vertical lines on the graphs represent the position of the edge of the entrance cones. On each plot is also given a part of the photomanometer record of the static pressure in the return passage.

Figure 5 gives the results of further investigations confined to the smallest diameter exit cone. The results produced by other leaks and by a larger flare, investigated with a view to

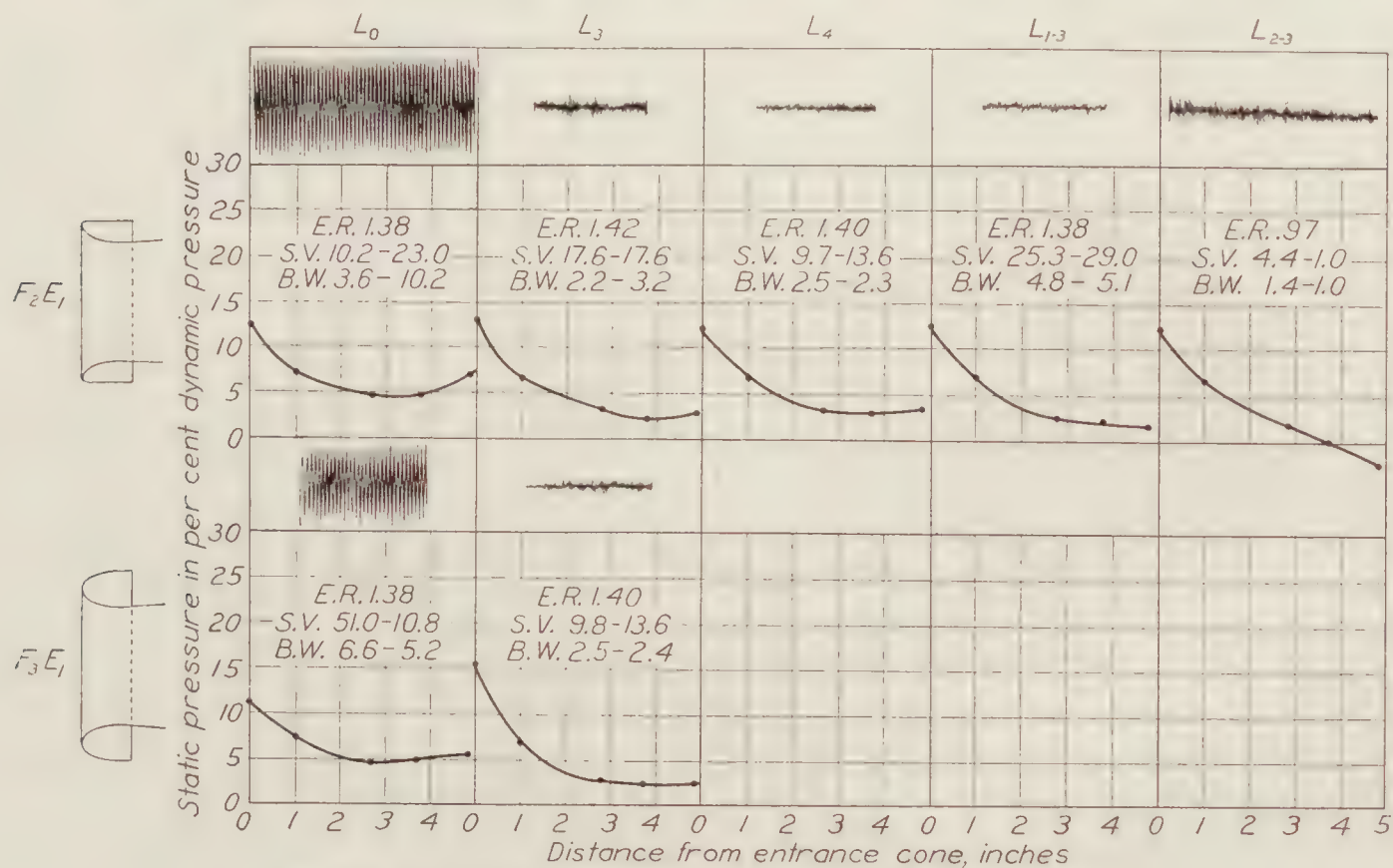


FIGURE 5.—Curves of static pressure and return passage pressure records

solving the problem of pulsations in the variable density wind tunnel, are included, together with other data already given, to complete the figure.

DISCUSSION

Exit-cone diameter.—The effect of exit-cone diameter on the characteristics of the tunnel, as expected, depends to a great extent on the leakage of air from the return passage. An examination of the first vertical row of Figures 3 and 4 shows that from the standpoint of downstream static pressure gradient a small exit cone is desirable when the leakage is small, because the large cones tend to reduce the velocity and increase the static pressure downstream. With a large amount of leakage the opposite is true, the increasing static pressure from the larger cones tending to offset the head lost in accelerating the leakage air as it is picked up by the jet. Enlarging the exit cone has no other marked effect on the characteristics of the tunnel except to reduce the pulsations slightly when little leakage is present and to reduce the spilling velocity in some cases.

Exit-cone flare.—The effect of increasing the exit-cone flare is much the same as the effect of increasing the exit-cone diameter except that, with a small amount of leakage, increasing the flare is much more effective in reducing pulsations.

Leakage from the return passage.—Leakage has a very marked effect on all of the characteristics except on the velocity distribution across the air stream. Leakage from any part of the return passage between the propeller and the entrance cone, while having some beneficial effects in some respects, produces, in all cases, a large reduction in energy ratio. In Figure 6 are given curves of the energy ratio before and after the tunnel was made air-tight. Previously the tunnel was constructed of wood and although it was as air-tight as might be expected, a velocity survey in the exit cone ahead of the propeller indicated that appreciably more air passed into the propeller than came out of the entrance cone. After lining the inside of the tunnel with doped fabric the other curve of energy ratio in Figure 6 was obtained. The latter condition of the tunnel is that designated as L_0 throughout this report and represents a very small amount of leakage.

Three possible reasons are advanced for the effect of leakage on the air pulsations. First, the leakage air forms a sort of cushion surrounding the jet, directing it uniformly into the center of the exit cone. Second, the natural inflow of air around the jet, with leakage, is continuous, whereas without leakage the inflow is apt to continue after the tunnel has become sufficiently filled, resulting in later spilling from the exit cone. Air pulsations would result from a continuous repetition of these events. Third, if violent pressure pulsations should be set up in a leaking return passage, a considerable amount of energy would be dissipated by the air flowing back and forth through the leaks. They would, therefore, have a damping action on the pulsations.

The results of these tests indicate that the beneficial effects of leakage may be realized without sacrificing the energy ratio by placing the leaks where the pressure difference across them is low so that the energy loss will be small. Introducing leaks in the exit cone ahead of the propeller probably has another effect which may partially compensate for the energy dissipated in them. Such leaks tend to remove the boundary layer along the sides of the exit cone, thus stabilizing the flow and increasing the efficiency of the exit cone as a diffuser. (Reference 3.) Figure 3 indicates this effect, the leaks L_3 which consist of two rows of one-fourth inch holes spaced 1 inch apart near the mouth of the exit cone, when used with the smaller diameter exit cone and the large flare, practically eliminated the pulsations and at the same time improved the energy ratio slightly. The same leakage with the larger exit cone diameters was not so effective in reducing the pulsations, because a smaller amount of air was discharged through the holes.

Entrance-cone tabs.—Tabs or obstructions at the mouth of the entrance cone, such as those used in the variable density tunnel, need not be considered as a practical means of reducing pulsations. Not only are the other characteristics of the tunnel impaired, as shown in the upper right-hand plot of Figures 3 and 4, but the pulsations are not sufficiently reduced.

Tendency toward pulsating flow.—The pulsating flow may sometimes be eliminated or reduced by changing the air speed in the tunnel. During these tests it was found that the pulsations existed over a considerable portion of the speed range. Above the speed at which the records were taken the pulsations practically ceased and then came in again at a higher speed with twice the original frequency. The frequency of the pulsations apparently depends on the size of the tunnel and not on the speed of the tunnel propeller. The records given in Figure 4 show a pulsation frequency of 79 cycles per second, whereas the propeller speed varied from one test to another between 48 and 58 r. p. s. Should the tunnel air speed be variable or should the pulsating flow not come at the speed at which tests are made, it is still desirable to design new tunnels so that this difficulty will not be encountered. This may be accomplished by simply providing a rather large exit cone and flare if the return passage leaks considerably, the size of the exit cone

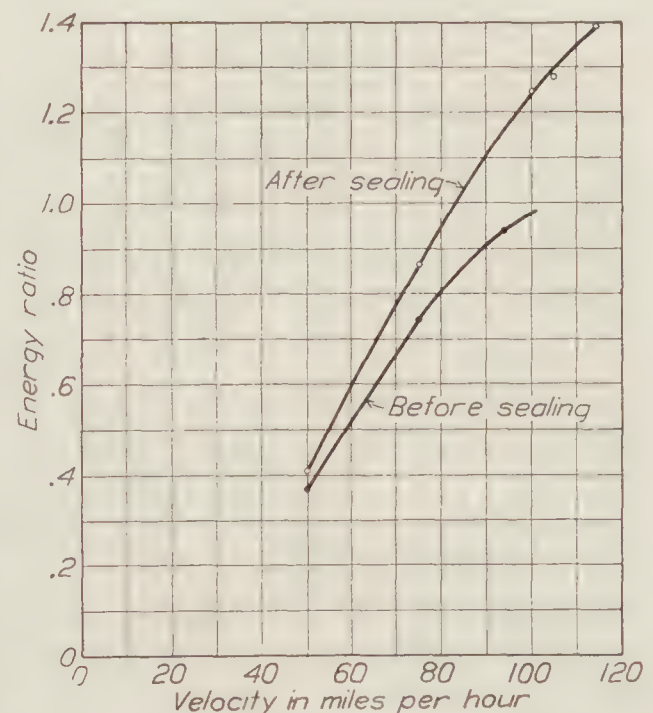


FIGURE 6.—Energy ratio before and after sealing

depending on the amount of leakage present. If the tunnel passages are air-tight the tendency toward pulsating flow may best be avoided by providing holes in the exit cone slightly behind its mouth or bell L_4 , fig. 1) and using an exit cone having a large flare and an only slightly larger diameter than the entrance cone.

Downstream pressure gradient.—This characteristic of a tunnel, while not always of great importance, is here considered because of its effect on testing airships and because it indicates the uniformity of the velocity downstream. The static pressure in the center of the jet at the mouth of the entrance cone was in all cases higher than the pressure of the air surrounding the jet by more than 10 per cent of the dynamic pressure. From this point aft the pressure in the stream dropped at a rate which increased with the amount of leakage. The larger flares and exit cone diameters caused the pressure to rise again as the air approached the exit cone. Therefore, if the amount of leakage is very small, the most uniform static pressure may be secured by using a small exit cone and small flare. If a large amount of leakage is present, it is necessary to use a large exit cone and flare to secure a reasonably uniform static pressure. The large static pressure near the mouth of the entrance cone and the resulting high gradient is probably characteristic of the rather short entrance cone.

Velocity distribution across the air stream.—The dynamic pressure surveys given in Figure 4 were taken across the stream at the position at which models are usually placed, i. e., 30 per cent of the opening behind the mouth of the entrance cone. The results show that at this diameter the velocity distribution is little changed by any of the variables considered except by the tabs which were placed on the entrance cone. The velocity distribution is undoubtedly determined primarily by the shape of the entrance cone, form of the return passage, and position of the honeycomb. All of the surveys show a peculiar high velocity region just inside of the edge of the jet. Otherwise the dynamic pressure is reasonably uniform across the test section under all conditions.

Energy ratio.—The energy ratios based on electrical power input to the motor varied between 1.42 and 0.79. The lowest energy ratio was obtained when the tabs were used on the entrance cone. When leaks were introduced in the return passage the energy ratio was reduced about 40 per cent; otherwise variations in the energy ratio were small.

Spilling velocity.—The figures (opposite S. V. in figs. 3 and 5) representing velocity in feet per second outside of the exit-cone flare, show the difference between the various arrangements in regard to air disturbances around the exit cone. The air flow in this region was found to be very unsteady and difficult to measure so that these figures should be taken only as a rough comparison between different conditions. They show, however, a definite tendency toward lower spilling velocities as the exit cone diameter and flare are increased and an even more marked reduction as the amount of leakage is increased.

Balance windage.—The balance windage, like the spilling velocity, is expressed by figures indicating roughly the velocity in feet per second, which may be expected in the region of the balance. These measurements were difficult to make and appear to be somewhat erratic. In general, it appears that the balance windage will be considerably reduced by the introduction of leakage. In any particular tunnel the balance windage depends on other factors, such as the position of the balance and the shape of the test chamber, so that these results should not be taken as applying to all open-throat tunnels.

CONCLUSIONS

Throughout this series of tests only those variables were investigated which were believed to have an immediate effect on pulsations in the air flow. All of the results may not be applicable to other types of open-throat tunnels, but the following conclusions will probably always be true:

1. Air pulsation in open-throat tunnels may be practically eliminated by introducing leaks between the return passage, or exit cone, and the test section if a large flare is used on the exit cone

2. Leakage from the return passage may cause a large reduction in the energy ratio. However, if the leakage is from a point near the mouth of the exit cone, where the pressure difference is small, the loss in energy is negligible.

3. The velocity distribution across the stream at the test section is little affected by either leakage or shape and size of the exit cone.

LANGLEY MEMORIAL AERONAUTICAL LABORATORY,
NATIONAL ADVISORY COMMITTEE FOR AERONAUTICS,
LANGLEY FIELD, VA., *September 26, 1928.*

REFERENCES

- Reference 1. Weick, Fred E.: Study of Open Jet Wind Tunnel Cones. N. A. C. A. Technical Note No. 260, 1927.
- Reference 2. Weick Fred E.: A Comparison of Propeller and Centrifugal Fans for Circulating the Air in a Wind Tunnel. N. A. C. A. Technical Note No. 281, 1928.
- Reference 3. Ackeret, J.: Removing the Boundary Layer by Suction. N. A. C. A. Technical Memorandum No. 395, 1927.

REPORT No. 323

FLOW AND FORCE EQUATIONS FOR A BODY REVOLVING IN A FLUID

By A. F. ZAHM
Aerodynamical Laboratory
Bureau of Construction and Repair, U. S. Navy

CONTENTS

	Page		Page
SUMMARY.....	411	PART III. ZONAL FORCE AND MOMENT	
PART I. INTRODUCTION.....	412	ON HULL FORMS.....	427
Steady-flow method.....	412	Pressure loading.....	427
General formulas for velocity com- ponents.....	413	Zonal force.....	428
Surface velocity.....	413	Zonal moment.....	428
Zonal forces and moments.....	413	Correction factors.....	428
Geometrical formulas.....	414	PART IV. RESULTANT FORCE AND MO- MENT.....	429
Conventions.....	415	Body in free space.....	429
PART II. VELOCITY AND PRESSURE.....	416	Reactions of fluid.....	429
(A) Bodies in Simple Rotation.....	416	Combination of applied forces.....	431
Elliptic cylinder.....	416	Hydrokinetically symmetric forms..	432
Prolate spheroid.....	418	Examples.....	432
Ellipsoid.....	422	Theory <i>vs.</i> experiment.....	433
(B) Bodies in Combined Translation and Rotation.....	422	Correction factors.....	435
Most general motion.....	422	PART V. POTENTIAL COEFFICIENTS—IN- ERTIA COEFFICIENTS.....	436
Yawing flight.....	422	Green's integrals.....	436
Flow inside ellipsoid.....	424	Potential coefficients.....	436
Potential coefficients.....	426	Inertia coefficients.....	436
Relative velocity and kinetic pres- sure.....	426	Limiting conditions.....	437
		Physical meaning of the coefficients..	437
		SYMBOLS USED IN THE TEXT.....	438
		REFERENCES.....	438
		TABLES AND DIAGRAMS.....	439

REPORT No. 323

FLOW AND FORCE EQUATIONS FOR A BODY REVOLVING IN A FLUID

IN FIVE PARTS

By A. F. ZAHM

SUMMARY

This report, submitted to the National Advisory Committee for Aeronautics for publication, is a slightly revised form of U. S. Navy Aerodynamical Laboratory Report No. 380, completed for the Bureau of Aeronautics in November, 1928. The diagrams and tables were prepared by Mr. F. A. Loudon; the measurements given in Tables 9 to 11 were made for this paper by Mr. R. H. Smith, both members of the Aeronautics Staff.

Part I gives a general method for finding the steady-flow velocity relative to a body in plane curvilinear motion, whence the pressure is found by Bernoulli's energy principle. Integration of the pressure supplies basic formulas for the zonal forces and moments on the revolving body.

Part II, applying this steady-flow method, finds the velocity and pressure at all points of the flow inside and outside an ellipsoid and some of its limiting forms, and graphs those quantities for the latter forms. In some useful cases experimental pressures are plotted for comparison with theoretical.

Part III finds the pressure, and thence the zonal force and moment, on hulls in plane curvilinear flight.

Part IV derives general equations for the resultant fluid forces and moments on trisymmetrical bodies moving through a perfect fluid, and in some cases compares the moment values with those found for bodies moving in air.

Part V furnishes ready formulas for potential coefficients and inertia coefficients for an ellipsoid and its limiting forms. Thence are derived tables giving numerical values of those coefficients for a comprehensive range of shapes.

REPORT No. 323

FLOW AND FORCE EQUATIONS FOR A BODY REVOLVING IN A FLUID

PART I

INTRODUCTION

STEADY-FLOW METHOD.—In some few known cases one can compute the absolute particle velocity q' at any point (x, y, z) of the flow caused by the rotation of a body, say with uniform angular speed Ω , in an infinite inviscid liquid otherwise still. Thence, since q' is unsteady at (x, y, z) , the instantaneous pressure there is found by Kelvin's formula $p_v/\rho = -\partial\varphi/\partial t - q'^2/2$, p_v being the supervacuo pressure there, and φ the velocity potential.

Otherwise superposing upon said body and flow field the reverse speed $-\Omega$, about the same axis, gives the same relative velocity q but which now is everywhere a steady space velocity. In the body's absence the circular flow speed at the radial distance R would be $q_0 = -\Omega R$.¹ If the fixed body's presence lowers the speed at (x, y, z) from q_0 to q , it obviously begets there the superstream pressure

$$p = \frac{1}{2}\rho(q_0^2 - q^2) \text{-----} (1)$$

or in dimensionless form, a being some fixed length in the body,

$$\frac{p}{\frac{1}{2}\rho a^2 \Omega^2} = \frac{R^2}{a^2}(1 - q^2/q_0^2) \text{-----} (1_1)^2$$

The present text finds p by this steady-flow method only, and applies it to streams about various forms of the ellipsoid and its derivatives.

The superposed circular flow, $q_0 = -\Omega R = -\partial\psi/\partial R$, has the stream-function

$$\psi = \frac{1}{2}\Omega R^2 \text{-----} (2)$$

which, for rotation about the z axis, plots as in Figure 4. This flow has no velocity potential, since $\partial\psi/\partial R \neq 0$.

GENERAL FORMULAS FOR VELOCITY COMPONENTS.—In plane flow,² as is known, a particle at any point (x, y) of a line s drawn in the fluid has the tangential and normal velocity components

$$q_t = \frac{\partial\varphi}{\partial s} = -\frac{\partial\psi}{\partial n} \qquad q_n = \frac{\partial\varphi}{\partial n} = \frac{\partial\psi}{\partial s} \text{-----} (3)$$

¹ This velocity entails the centrifugal pressure $p_c = \rho\Omega^2 R^2/2$ at all distances, $R = \sqrt{x^2 + y^2}$ from the rotation axis of the circular stream, here assumed to be constrained by a coaxial closed cylinder infinitely large. To the dynamic pressure $p_c + p$ may also be added any arbitrary static pressure such as that due to weight or other impressed force.

² At any surface point of the body q is the velocity of wash or slip, whether the body moves or not; it is $q'_t - q''_t$, the difference of the tangential space velocities of the fluid and surface point. If the body is fixed $q''_t = 0$, $q = q'_t$.

³ Plane flow, viz two-dimensional flow, literally means flow in a plane; the term applies also to space flow that is the same in all parallel planes.

where δs , δn are elements along the line and its normal. As usual, q_t , q_n are reckoned positive respectively along δs , δn positive; e. g. Figure 2. The components along x , y are

$$u = \frac{\partial \phi}{\partial x} = \frac{\partial \psi}{\partial y} \quad v = \frac{\partial \phi}{\partial y} = -\frac{\partial \psi}{\partial x} \quad (4)$$

In solid flow (3), (4) still hold for ϕ , and further $w = \partial \phi / \partial z$. In general, $q^2 = u^2 + v^2 + w^2 = q_t^2 + q_n^2$. At any point of a surface drawn in the fluid q_t is taken in the plane of q and q_n . All these velocities are referred to fixed space.

SURFACE VELOCITY.—A fixed body in any stream, since $q_n = 0$, has the surface flow velocity $q = q_t$, which put in (1) determines the surface pressure.

At any surface point of an immersed moving body q_n is the same for body and fluid, hence is known from solid kinematics. Thus, if the body is any cylinder rotating as in Figure 1,

$$q_n = -\Omega R \, dR/ds = \Omega R \sin(\theta - \beta) = \Omega h_1 = \Omega(mx - ly) \quad (5)$$

where the symbols are as defined in Figures 1, 2.

More generally, for any surface with velocities Ω_x , Ω_y , Ω_z about the axes x , y , z ,

$$q_n = (ny - mz)\Omega_x + (lz - nx)\Omega_y + (mx - ly)\Omega_z \quad (6)$$

where l , m , n are the direction cosines of the surface normal, as in (13₁).

If at the same time the body has translation components, U , V , W along x , y , z , (6) must be increased by $lU + mV + nW$, giving

$$q_n = l(U + z\Omega_y - y\Omega_z) + m(V + x\Omega_z - z\Omega_x) + n(W + y\Omega_x - x\Omega_y) \quad (7)$$

But (5), (6), (7) express q_n only at the model's surface.

Equations (1) to (7) obtain whether the fluid is inside or outside the body.

ZONAL FORCES AND MOMENTS.—For any cylinder spinning about z , as in Figure 1 or 5, surface integration of p gives, per unit of z -wise length, the zonal⁴ forces and moment, respectively,

$$X = \int p \, dy \quad Y = \int p \, dx \quad N = \int p \, r \, dr \quad (8)$$

where $p \, dy$, $p \, dx$ are the x , y components of the elementary surface force $p \, ds$, and r is the radius vector of (x, y) . To derive N we note that $p \, ds$ has components $p \, r \, d\beta$, $p \, dr$ along and across r . Having no moment, $p \, r \, d\beta$ can be ignored, leaving only $p \, dr$ with arm r . Thus, $2N = \int p \, d(r^2)$, which varies as the area of the graph of p versus r^2 .

A surface of rotation about x , spinning about its z axis, has zonal forces

$$X = \iint p \, dy \, dz \quad Y = \iint p \, dx \, dz \quad (9)$$

⁴ A zone is any part of the surface bounded by two parallel planes; in this text they are assumed normal to x , and the zone has the bounding planes $x=0$, $x=\pm x_1$; in Part III other planes are used; e. g. $x=x_1$, $x=a$.

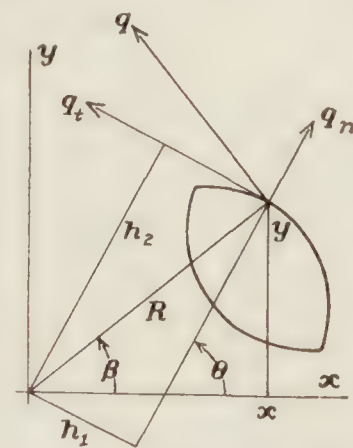


FIGURE 1.—Component velocities q_n , q_t of surface point of any rigid cylinder having angular speed Ω about any axis parallel to its length. $q_n = \Omega h_1$; $q_t = \Omega h_2$. $h_1 = R \sin(\theta - \beta) = -R \, dR/ds = mx - ly$, 1, m being direction cosines of the normal to the contour element ds at (x, y) . If the body rotates in a fluid, $q_n = \partial \psi / \partial s = \partial \phi / \partial n$. At any surface point q_n is the same for body and fluid; q_t different except at points of no slippage

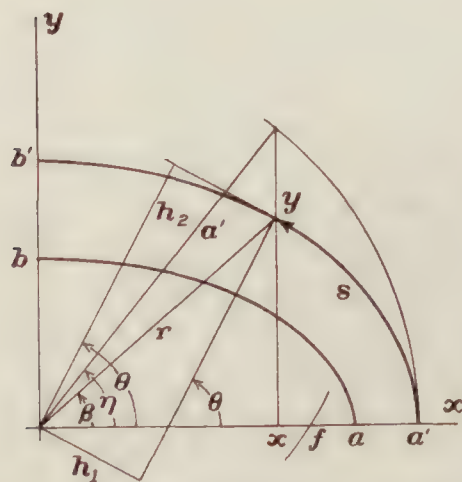


FIGURE 2.—Geometric data for confocal ellipses. $x = a' \cos \eta = r \cos \beta$; $y = b' \sin \eta = r \sin \beta$; $\frac{b'}{a'} \tan \theta = \tan \eta = \frac{a'}{b'} \tan \beta = \frac{a'}{b'} \frac{y}{x}$; $h_1 = r \sin(\theta - \beta)$; $h_2 = r \cos(\theta - \beta)$. $f = ae = a' e'$, $e = \sqrt{1 - b^2/a^2}$ being eccentricity of ab

The partial derivatives of λ are

$$\frac{\partial \lambda}{\partial x} = 2lh_2 \quad \frac{\partial \lambda}{\partial y} = 2mh_2 \quad \frac{\partial \lambda}{\partial z} = 2nh_2 \quad \frac{\partial \lambda}{\partial n} = 2h_2 \quad \dots \quad (14)$$

More generally for any surface $f(x, y, z) = 0$, one knows

$$l = j \frac{\partial f}{\partial x} \quad m = j \frac{\partial f}{\partial y} \quad n = j \frac{\partial f}{\partial z} \quad j = \left[\left(\frac{\partial f}{\partial x} \right)^2 + \left(\frac{\partial f}{\partial y} \right)^2 + \left(\frac{\partial f}{\partial z} \right)^2 \right]^{-\frac{1}{2}} \quad \dots \quad (13_1)$$

and the distance from the origin to the tangent plane at (x, y, z) is

$$h_2 = lx + my + nz = r \cos \gamma \quad \dots \quad (12)$$

γ being the angle between the radius vector r and the normal.

CONVENTIONS.—In all the text x, y, z have the positive directions shown in Figure 3, as also have the x, y, z components of velocity, acceleration, force, linear momentum. The angular components about x, y, z of velocity, acceleration, moment, momentum are positive in the respective directions y to z, z to x, x to y . The positive direction of a plane closed contour s is that followed by one going round it with the inclosure on his left, as in Figure 2; the positive direction of the normal n is from left to right across s ; and $\delta s, \delta n$ determine the positive directions of the tangential and normal flow velocities q_t, q_n , as previously stated. For a closed surface δn is positive outward and δs is positive in the direction of one walking on the outer surface with n on his left.

The word "displaced fluid," used in treating the motion of a submerged body, usually means fluid that would just replace the body if the latter were removed.

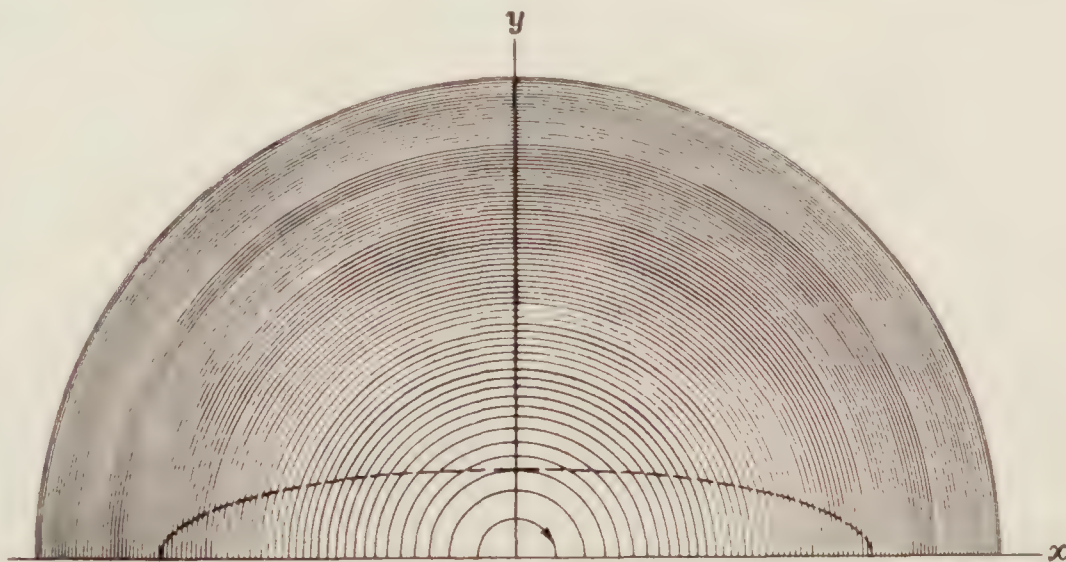


FIGURE 4.—Streamlines for $\psi = \frac{1}{2} \Omega R^2$, with increments $\Delta \psi = .2$, for fluid rotating with uniform angular velocity $\Omega = -1$

REPORT No. 323

FLOW AND FORCE EQUATIONS FOR A BODY REVOLVING IN A FLUID

PART II VELOCITY AND PRESSURE

(A) BODIES IN SIMPLE ROTATION

ELLIPTIC CYLINDER.—For an endless elliptic cylinder, of semiaxes a, b, c ($= \infty$), rotating about c with angular speed Ω_c in an infinite inviscid liquid, otherwise still, one knows ¹

$$\varphi = -m'_c \Omega_c xy = -\frac{1}{2} m'_c \Omega_c a' b' \sin 2\eta \quad \psi = -\frac{1}{2} m'_c \Omega_c a' b' \cos 2\eta \quad (15)$$

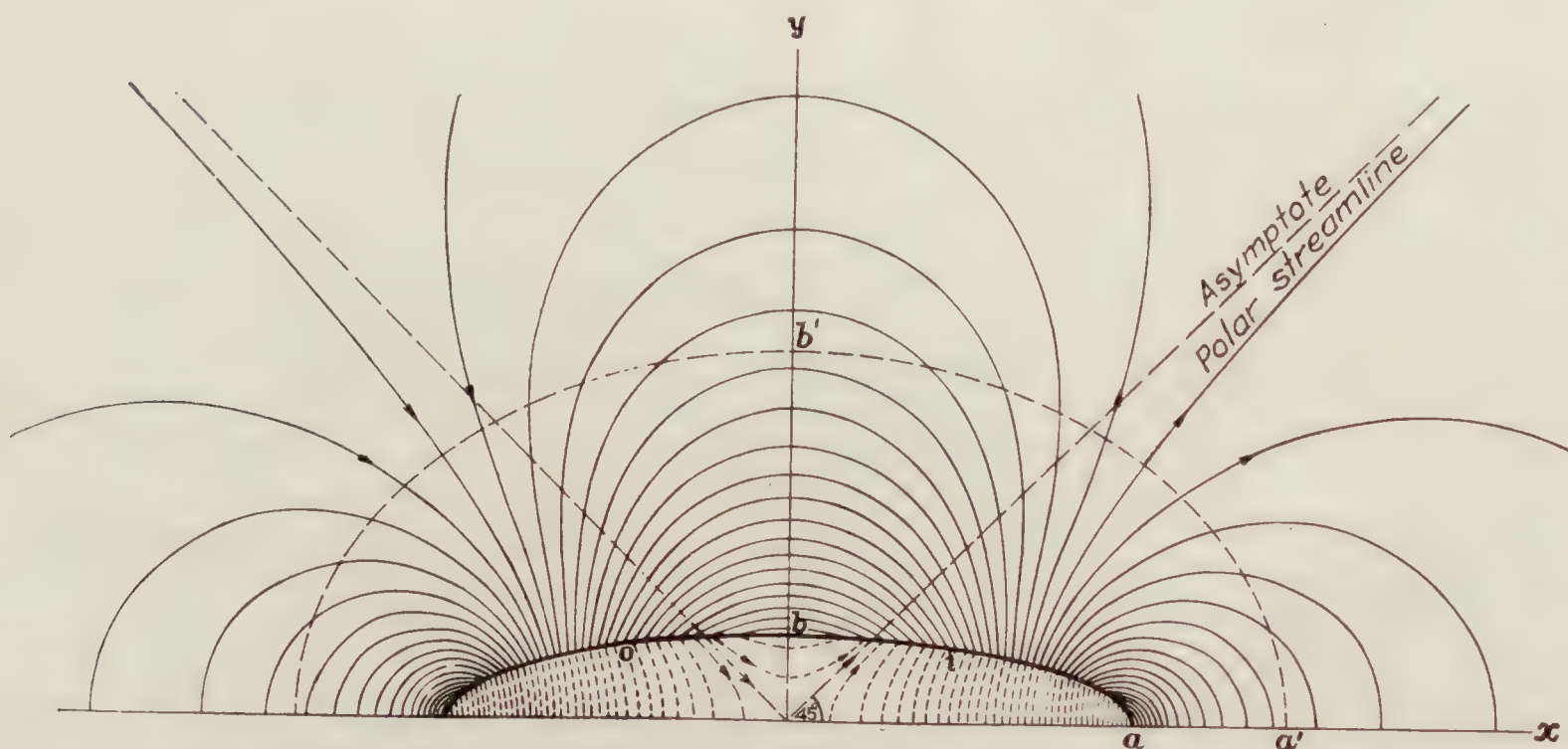


FIGURE 5.—Streamlines for endless elliptic cylinder rotating about its long axis with uniform angular velocity Ω ; shows $\psi = -\frac{1}{2} m'_c \Omega a' b' \cos 2\eta$ with increments $\Delta \psi = .2, \Omega = 1$. For inside fluid, $\psi = -\frac{1}{2} \frac{a^2 - b^2}{a^2 + b^2} \Omega (x^2 - y^2)$

the geometric symbols being as in Figure 2. For any outer confocal $a'b'$ the potential coefficient has the constant value

$$m'_c = (a + b)^2 (a' - b') / 2a'b' (a' + b') \quad (16)^2$$

On the model's surface $a' = a, b' = b$; $m'_c = (a^2 - b^2) / 2ab$.

The equipotential lines on either surface ab or $a'b'$ are its intersections with the corresponding family of hyperbolic cylinders $xy = -\varphi / m'_c \Omega = \text{const.}$ Normal to the equipotentials are the streamlines $\psi = \text{const.}$ Graphs for $\psi = 0, 0.2, 0.4$, etc., are shown in Figure 5 for a model having $a/b = 4$. They are instantaneous streamlines, and form with the model a constant pattern in uniform rotation about c in said infinite liquid.

At any outer confocal $a'b'$ the velocity components are, if $\kappa = m'_c a' b' \Omega_c$,

$$q'_t = \frac{\partial \varphi}{\partial s} = -\kappa \cos 2\eta \frac{d\eta}{ds} \quad q'_n = \frac{\partial \psi}{\partial s} = \kappa \sin 2\eta \frac{d\eta}{ds} = -q'_t \tan 2\eta \quad (17)$$

¹ Proofs of (15), (23), (29), (40) are found in books; e. g., Lamb §§ 72, 106, 110, 115, 5th ed., except that Lamb reverses the sign of φ, ψ .

² Equivalent to (16) is $m'_c = \left(\frac{e'}{e} \frac{e' + \sqrt{1-e^2}}{e + \sqrt{1-e'^2}} \right)^2 \frac{e'^2}{2\sqrt{1-e^2}}$, e, e' being the eccentricities of $ab, a'b'$. On ab this becomes $m'_c = e^2 / \sqrt{1-e^2}$. See (49) for the six potential coefficients $m_a, m_b, m_c, m'_a, m'_b, m'_c$, in the value of φ for more general motion.

where $d\eta/ds = 1/a' \sqrt{1 - e'^2 \cos^2 \eta}$, as one easily finds. Alternative to (17) are

$$q'_t = -m'_c \Omega_c \frac{d}{ds} xy = -m'_c \Omega_c r \cos (\theta + \beta) \quad q'_n = -q'_t \tan 2\eta \quad (17_1)$$

Thus for $\eta = 0, 45^\circ, 90^\circ$ (17) and (17₁) give $q'_t/\Omega_c = -m'_c a', 0, m'_c b'$. At the model's surface, where $m'_c = (a^2 - b^2)/2ab$, (17₁) become

$$q'_t = -\frac{a^2 - b^2}{2ab} \Omega_c r \cos (\theta + \beta) \quad q'_n = \Omega_c r \sin (\theta - \beta) \quad (17_2)$$

the latter being $h_1 \Omega_c$, as in (5).

Where $q'_t = 0$, or $\cos \eta = 1/\sqrt{2}$, viz, at the stream poles, clearly $x = a'/\sqrt{2}$, $y = b'/\sqrt{2}$,

$$x^2 - y^2 = a^2 e^2 / 2 \quad (18)$$

a rectangular hyperbola. (18) is the instantaneous polar streamline, e. g., Figure 5, orthogonal to all the confocal ellipses. Its asymptotes are $y = \pm x$; its vertices are at $x = \pm ae/\sqrt{2}$; it cuts each ellipse where $x/y = a'/b'$, viz, on the diagonals of the circumscribed rectangle. For an endless thin plate of width $2a$, the poles are at $y = 0$, $x = \pm a/\sqrt{2}$.

Superposing $-\Omega_c$ on the body and fluid, and using (2), changes (15) to

$$\psi = \frac{1}{2} (r^2 - m'_c a' b' \cos 2\eta) \Omega_c \quad (19)$$

Its graph, with $\Delta\psi = 0.2$, gives the streamlines in Figure 6 for the flow $\Omega_c = -1$ round a fixed cylinder having $a/b = 4$. About the point (0, 1.45) in Figure 6, is a whirl separated from the outer flow by the streamline $\psi = 4.25$. This line abuts on the model at the inflow points i, i ; spreads round it and emerges at the outflow points o, o .³ The streamlines for an endless thin rectangle having $b = 0$, $e = 1$, are similar to those of Figure 6, but infinitely crowded at the edges.

The superposed particle velocity $-\Omega_c r$ contributes to (17₁)

$$q''_t = -\Omega_c r \cos (\theta - \beta) = -h_2 \Omega_c \quad q''_n = -\Omega_c r \sin (\theta - \beta) = -h_1 \Omega_c \quad (20)$$

also $q''_n = q''_t \tan (\theta - \beta)$. Adding (17₁) and (20) gives the components $q_t = q'_t + q''_t$, $q_n = q'_n + q''_n$, of the resultant flow velocity at any field point. One notes that (20) are the reverse of q_t, q_n in Figure 1.

In particular $q_n = 0$ on the fixed model and x, y axes; hence there

$$q/a\Omega_c = -\frac{r}{a} [m'_c \cos (\theta + \beta) + \cos (\theta - \beta)] \quad q/q_o = m'_c \cos (\theta + \beta) + \cos (\theta - \beta) \quad (21)$$

Thus $q/q_o = 1 + m'_c$ on the x axis; $1 - m'_c$ on the y axis; and 1 at ∞ where $m'_c = 0$. The dashed line in Figure 6 gives $q/a\Omega_c = -(1 - m'_c)y/a$ for points on the y axis; it crosses y at the whirl center where $q = 0$, viz, where $m'_c = 1$. By (16) $m'_c \geq 1$ for the surface of any model having $a/b \geq 1 + \sqrt{2}$; and there is no whirl if $a/b < 1 + \sqrt{2}$. Figure 7 shows $q/a\Omega_c$ for the surface of a model having $a/b = 4$, $m'_c = (a^2 - b^2)/2ab = 15/8$.

Putting q^2/q_o^2 of (21) in (1₁), where $r^2/a^2 = \cos^2 \eta / \cos^2 \beta$, gives

$$p/\frac{1}{2} \rho a^2 \Omega_c^2 = (1 - [m'_c \cos (\theta + \beta) + \cos (\theta - \beta)]^2) \cos^2 \eta / \cos^2 \beta \quad (22)$$

which is graphed in Figure 7 for a model having $a/b = 4$.

Integrating $p/\frac{1}{2} \rho a^2 \Omega_c^2$, as in (8), gives for an inviscid liquid $Y = 0 = N$; $X \neq 0$. Figure 7 delineates X for this case.

³ The points i, o are identical with those in Figure 5; viz, where the slip speed q in (21) is zero; they are called stop points, stagnation points, etc.

For the surface of an endless flat plate ($b=0$, $c=\infty$) fixed in the stream $-\Omega_c$, clearly $m'_c=a/2b$ and generally $r \cos (\theta-\beta)=0$; hence (21) gives

$$q/a\Omega_c = -\frac{r}{2b} \cos (\theta+\beta) = -\sin \theta \cos \eta \cot 2\eta \dots \dots \dots (21_1)$$

which equals $-\infty$, 0 , $1/2$ for $\eta=0^\circ$, 45° , 90° . The flow resembles that in Figure 6; it has twin whirls abreast its middle, stop points at $x=\pm a/\sqrt{2}$, and infinite velocity at the edges.

Putting in (1₁) $r=x$ and $q_0=-x\Omega_c$ gives the plate's surface pressure

$$p/\frac{1}{2}\rho a^2\Omega_c^2 = \frac{x^2}{a^2} - \frac{q^2}{a^2\Omega_c^2} = (1 - \cot^2 2\eta) \cos^2 \eta \dots \dots \dots (22_1)$$

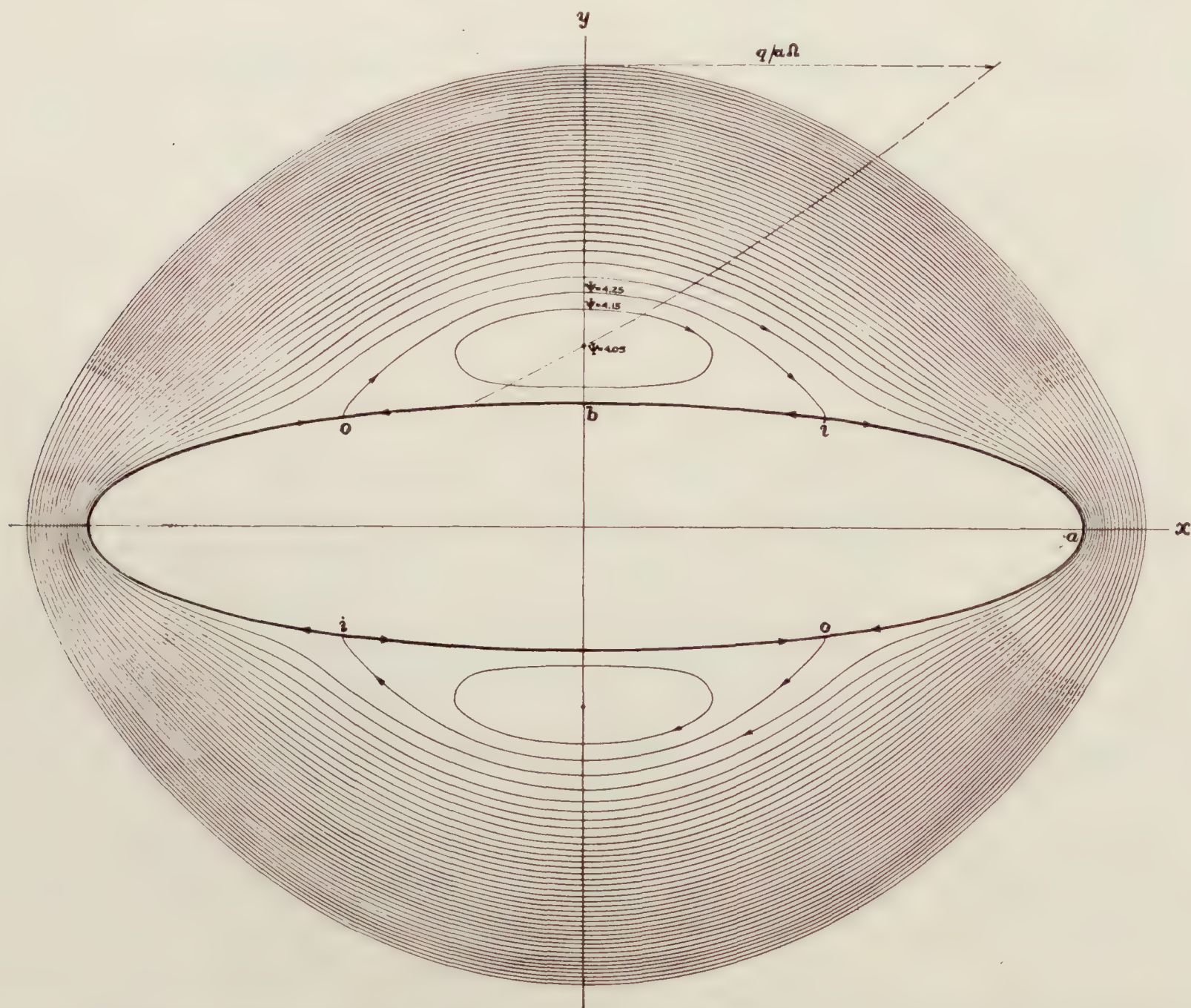


FIGURE 6.—Streamlines about endless elliptic cylinder fixed in infinite inviscid liquid rotating about its long axis with uniform angular speed $-\Omega$; shows $\psi = \frac{1}{2} \Omega (r^2 - m'_c a' b' \cos 2\eta)$ with increments $\Delta \psi = .1$, $\Omega = -1$. Dotted line portrays x -wise speed on y axis

which equals $-1/4$, $1/2$, $-\infty$ for $x=0$, $\pm a/\sqrt{2}$, $\pm a$; viz, for $\eta=90^\circ$, 45° , 0 , etc.

PROLATE SPHEROID.—For a prolate spheroid, of semiaxes a , b , c , rotating about c with speed Ω_c in an infinite inviscid liquid,

$$\varphi = -m'_c \Omega_c xy = -\frac{1}{2} m'_c \Omega_c a' b' \sin 2\eta \cos \omega \dots \dots \dots (23)$$

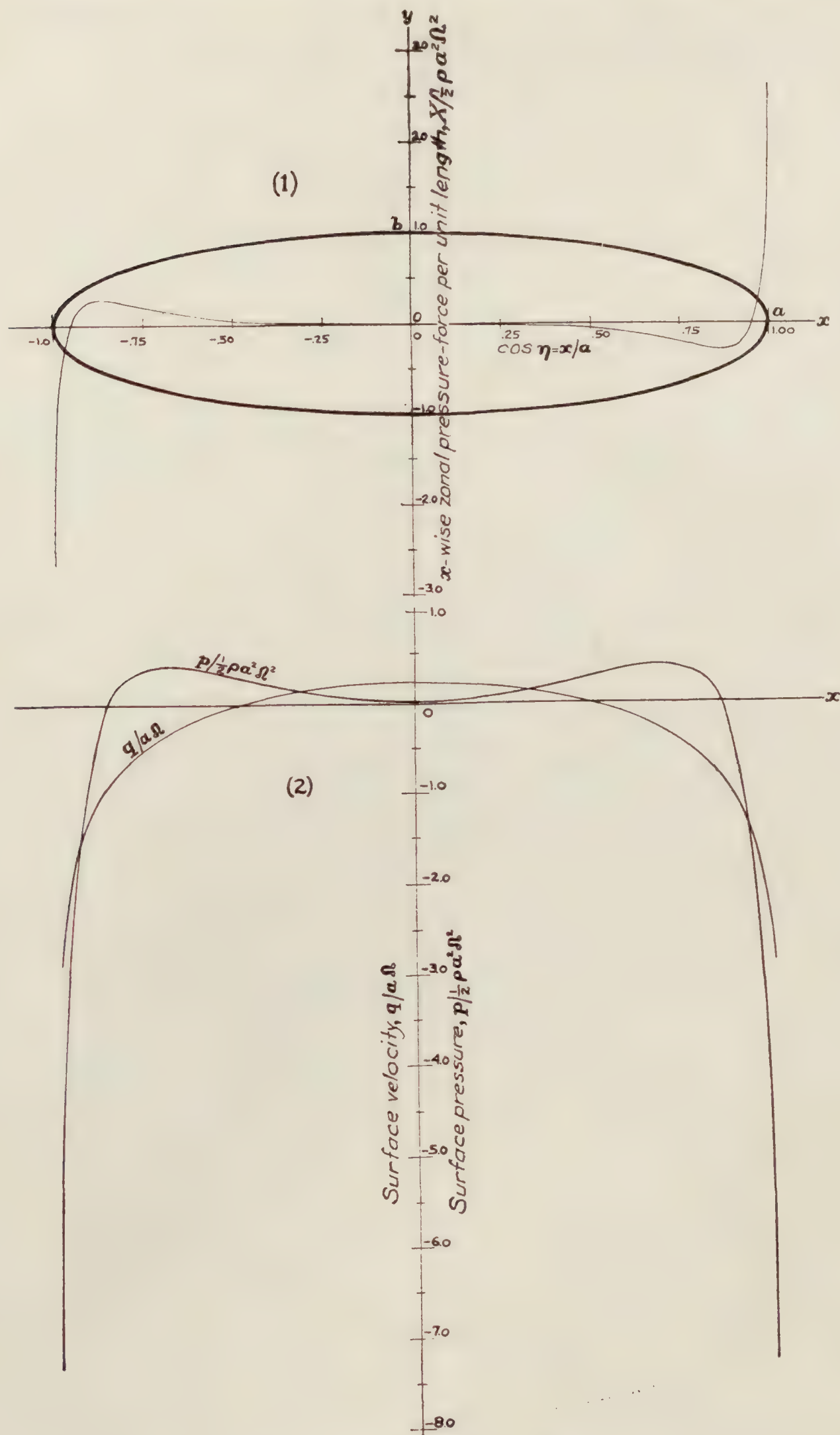


FIGURE 7.—Endless elliptic cylinder fixed in infinite inviscid liquid uniformly rotating about it; shows (1) x -wise zonal pressure-force, $X/2 \rho a^2 \Omega^2$; (2) surface velocity $q/a \Omega$ and surface pressure, $p/2 \rho a^2 \Omega^2$, above or below undisturbed local pressure in uniform stream, $-\Omega$

the geometric symbols being as in Figure 3. For any outer confocal spheroid $a'b'c'$ (23) has the known constant potential coefficient

$$m'_c = \frac{\frac{3}{2e'} \log \frac{1+e'}{1-e'} - 3 - \frac{e'^2}{1-e'^2}}{\frac{3}{2e} (2-e^2) \log \frac{1+e}{1-e} - 6 + \frac{e^2}{1-e^2}} ee' \dots \dots \dots (24)$$

e, e' being the eccentricities of $ab, a'b'$. Table IV gives surface values of m'_c for various shapes of prolate spheroid.

In the yz, zx planes $\varphi=0$; in the xy plane, where $\cos \omega=1$

$$\varphi = -\frac{1}{2} m'_c \Omega_c a' b' \sin 2\eta \quad \psi = -\frac{1}{2} m'_c \Omega_c a' b' \cos 2\eta \dots \dots \dots (23_1)$$

which, except for m'_c , have the same values as (15), entailing the same polar streamlines (18). The equipotentials on $a'b'c'$ are its intersections with the family $xy = -\varphi/m'_c \Omega_c = \text{const.}$

At any point (x, y, z) on $a'b'c'$ the orthogonal velocity components are by (23)

$$q'_n = \frac{\partial \varphi}{\partial e'} \frac{de'}{dn} \quad q'_\eta = \frac{\partial \varphi}{\partial \eta} \frac{d\eta}{ds_\eta} \quad q'_\omega = \frac{\partial \varphi}{\partial \omega} \frac{d\omega}{ds_\omega} \dots \dots \dots (25)$$

$\delta n, \delta s_\eta, \delta s_\omega$ denoting line elements along the normal, meridian, and circle of latitude, as in Figure 3. Since q'_n is absent from (1), we shall not need it; we merely note that on the model's surface it is $r\Omega_c \sin(\theta-\beta) \cos \omega$. By geometry $d\eta/ds_\eta = r \cos(\theta+\beta)/a'b' \cos 2\eta$,⁴ $d\omega/ds_\omega = 1/b' \sin \eta$; hence

$$q'_\eta = -m'_c \Omega_c r \cos(\theta+\beta) \cos \omega \quad q'_\omega = m'_c \Omega_c r \cos \beta \sin \omega \dots \dots \dots (25_1)$$

For $\omega=0$, $q'_\omega (=q'_\eta)$ differs only by m'_c from (17₁) for an elliptic cylinder; also $r \cos \beta = x \therefore q'_\omega = m'_c x \Omega_c \sin \omega = 0$, $m'_c x \Omega_c$ for $\omega=0, \pi/2$.

Superposing $-\Omega_c$ on the above system adds to (25₁), as easily appears

$$q''_n = -\Omega_c r \sin(\theta-\beta) \cos \omega \quad q''_\eta = -\Omega_c r \cos(\theta-\beta) \cos \omega \quad q''_\omega = \Omega_c r \cos \beta \sin \omega \dots \dots (26)$$

At the now fixed surface and on the x, y axes $q_n=0=q'_n+q''_n$; hence summing (25₁), (26) gives there

$$\left. \begin{aligned} q_\eta &= -[m'_c \cos(\theta+\beta) + \cos(\theta-\beta)] \Omega_c r \cos \omega \equiv \bar{q}_\eta \cos \omega \\ q_\omega &= (1+m'_c) \Omega_c r \cos \beta \sin \omega \equiv \bar{q}_\omega \sin \omega \end{aligned} \right\} \dots \dots \dots 27$$

Thus for $\omega=0$ clearly $q/q_0 = m'_c \cos(\theta+\beta) + \cos(\theta-\beta)$, differing from (21) only by m'_c ; for $\omega=\pi/2$, $q/q_0 = -(1+m'_c)$, a formula like that for a negative flow q_0 across a cylinder; for $\omega=0^\circ, 90^\circ, 45^\circ$, $q = \bar{q}_\eta, \bar{q}_\omega, \sqrt{\frac{1}{2}(\bar{q}_\eta^2 + \bar{q}_\omega^2)}$. On the x axis $q/q_0 = 1+m'_c$; on the y axis $q/q_0 = 1-m'_c > 0$ everywhere, hence no whirl centers on y .

Figure 8 shows $|q/a\Omega_c|$ on the meridians $\omega=0, \pm 45^\circ, \pm 90^\circ$ of a fixed spheroid with $a/b=4$. Distributions symmetrical with these occur on the opposite half of the surface. Noteworthy is q for $\omega=\pm 90^\circ$. By (27) it is $q = \pm (1+m'_c) \Omega_c x$; hence the straight-line graph in Figure 8.

Figure 8 shows also, for these meridians, the pressure computed with the working formula, derived from (1₁), (27).

$$\frac{p}{\frac{1}{2} \rho a^2 \Omega_c^2} = A \cos^2 \omega + B \sin^2 \omega \dots \dots \dots (28)$$

⁴ E. g., by (23) $\frac{d}{ds_\eta} xy = \frac{d}{ds_\eta} \cdot \frac{1}{2} a'b' \sin 2\eta \cos \omega$; viz, $r \cos(\theta+\beta) = a'b' \cos 2\eta \frac{d\eta}{ds_\eta}$, which gives $\frac{d\eta}{ds_\eta}$ in (25). Also directly $q'_\eta = \frac{\partial \phi}{\partial s_\eta} = -m'_c \Omega_c \frac{d}{ds_\eta} xy = -m'_c \Omega_c r \cos(\theta+\beta) \cos \omega$.

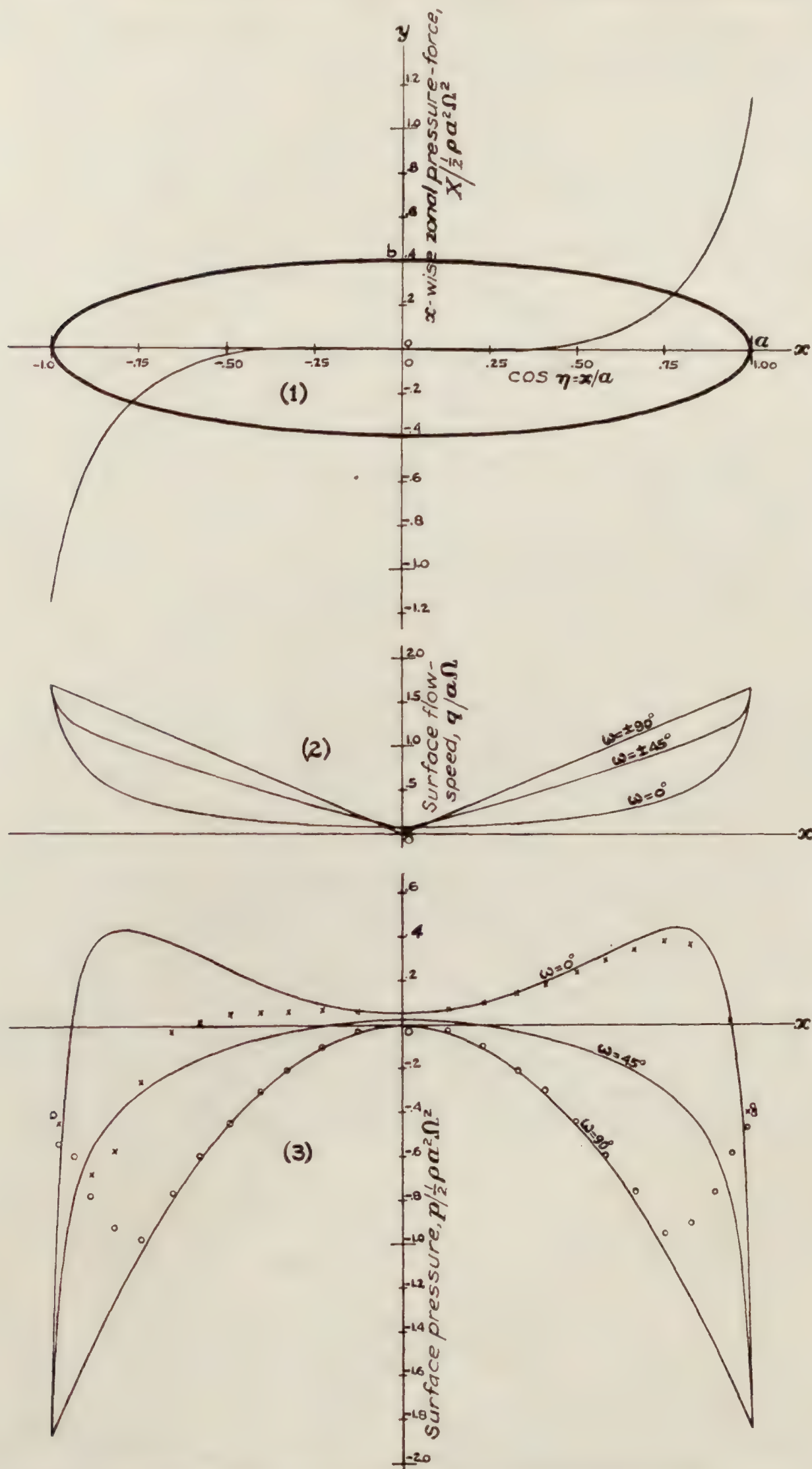


FIGURE 8.—Prolate spheroid fixed in infinite inviscid liquid uniformly rotating about it; shows (1) x -wise zonal pressure-force, $X/\frac{1}{2}\rho a^2\Omega^2$; (2) surface flow-speed, $q/a\Omega$; (3) surface pressure, $p/\frac{1}{2}\rho a^2\Omega^2$, above or below undisturbed local pressure in uniform stream, $-\Omega$. Crosses and circles give measured air pressures for $\Omega = -39.5$ radians per second given in reference 3

where $A = (1 - [m'_c \cos(\theta + \beta) + \cos(\theta - \beta)]^2) \cos^2 \eta / \cos^2 \beta$, $B = -m'_c(2 + m'_c) \cos^2 \eta$. Here $m'_c = .689$ by Table IV. The crosses and circles, giving experimental values taken from Reference 3, show good agreement with (28) for a considerable part of the surface. For $\cos \omega = 0$, $p \propto B \propto x^2$; or the graph is parabolic.

Integrating p , as in (9), (10), gives for an inviscid liquid $Y = 0 = N$, $X \neq 0$. Figure 8 portrays X computed from theory and experiment.

ELLIPSOID.—For an ellipsoid, of semiaxes a, b, c along x, y, z , rotating about c with speed Ω_c in an infinite inviscid liquid, otherwise still,

$$\varphi = -m'_c \Omega_c xy \text{-----} (29)$$

which for any outer confocal ellipsoid $a'b'c'$, has the constant potential coefficient

$$m'_c = C(\beta - \alpha) \quad C = \frac{a^2 - b^2}{2(a^2 - b^2) - (a^2 + b^2)(\beta_0 - \alpha_0)} \text{-----} (30)$$

the Greek letters being as in Part V. Surface values of m'_c are listed in Table IV.

By (29) the equipotential lines on $a'b'c'$ are its intersections with the hyperbolic cylinder family $xy = -\varphi/m'_c \Omega_c = \text{const.}$ The orthogonals to $\varphi = \text{const.}$ at the surface $a'b'c'$ are the streamlines there. These by (31) are parallel to x where $x = 0$; parallel to y where $y = 0$; normal to z where $z = 0$. The same obviously holds for spheroids and other ellipsoidal forms.

In the xy plane the flow has the polar streamlines (18); also it has there

$$\varphi = -\frac{1}{2} m'_c \Omega_c a' b' \sin 2\eta \quad \psi = -\frac{1}{2} m'_c \Omega_c a' b' \cos 2\eta \text{-----} (29_1)$$

whence the streamlines in that plane are plotted. The form of (29₁) is like those of (15) and (23₁), for the elliptic cylinder and prolate spheroid, entailing similar expressions for the velocity and pressure in the plane-flow field $z = 0$.

For the general flow the velocity components at $a'b'c'$ are by (29)

$$u' = -\left(x \frac{\partial m'_c}{\partial x} + m'_c\right) \Omega_c y \quad v' = -\left(y \frac{\partial m'_c}{\partial y} + m'_c\right) \Omega_c x \quad w' = -\Omega_c xy \frac{\partial m'_c}{\partial z} \text{-----} (31)$$

and those due to the superposed velocity $-\Omega_c R = q_0$, are

$$u'' = \Omega_c y \quad v'' = -\Omega_c x \quad w'' = 0 \text{-----} (32)$$

whence the resultant velocity and pressure may be derived for all points of the flow field about the ellipsoid fixed in the steady stream $-\Omega_c R$. In forming the x, y, z derivatives of m'_c one may use the relations (14) and (72).

Everywhere in the planes $x = 0$, $y = 0$, the resultant velocities are respectively, by (31) and (32),

$$q = u = (1 - m'_c) \Omega_c y \quad q = v = -(1 + m'_c) \Omega_c x \text{-----} (33)$$

while in the plane $z = 0$, q can be found as indicated for an elliptic cylinder. (33) apply also to the elliptic cylinder and prolate spheroid previously treated, and to all other forms of the ellipsoid fixed in the flow $-\Omega_c$.

(B) BODIES IN COMBINED TRANSLATION AND ROTATION

MOST GENERAL MOTION.—The most general motion of any body through a fluid may have the components U, V, W along, and $\Omega_a, \Omega_b, \Omega_c$ about, three axes, say a, b, c . The entailed resultant particle velocity q' at any flow point is found by compounding there the individual velocities severally due to $U, V, W, \Omega_a, \Omega_b, \Omega_c$, and computable for an ellipsoid by formulas in Reference 2 and the foregoing text.

YAWING FLIGHT.—In airship study the flow velocity q' caused by a prolate spheroid in steady circular flight is specially interesting. Let the spheroid's center describe about 0,

Figure 9, a circle of radius na , with path speed $na\Omega$. Then if α is the constant yaw angle of attack, the component centroid velocities along a , b , and the steady angular speed about c are, respectively,

$$U = na\Omega \cos \alpha \quad V = na\Omega \sin \alpha \quad \Omega_c = \Omega \text{-----} (34)$$

If, now, velocities the reverse of (34) are imposed on the body and fluid, $q_n = 0$, and the surface velocity q on the fixed spheroid has in longitude and latitude the respective components

$$\begin{aligned} q_\eta &= (1 + k_a) U \sin \theta - (1 + k_b) V \cos \theta \cos \omega - [m'_c \cos (\theta + \beta) + \cos (\theta - \beta)] \Omega_c r \cos \omega \\ q_\omega &= (1 + k_b) V \sin \omega + (1 + m'_c) \Omega_c r \cos \beta \sin \omega \end{aligned} \text{-----} (35)$$

where positive flows along ds are, respectively, in the directions of increasing η , ω , as in Figure 3. The terms in U , V , are known formulas for translational flow, e. g., Reference 2; the others are from (27). Hence q^2 then p is found for any point (β, ω) on the spheroid.⁵ If Ω_c is negligible, $q = \bar{q} \sin \epsilon$, where $\bar{q}^2 = (1 + k_a)^2 U^2 + (1 + k_b)^2 V^2$, and ϵ is the angle between the local and polar normals, as proved in Reference 2.

Figure 9₂ portrays, for specified conditions, theoretical values of $p/\frac{1}{2}\rho Q^2$, Q being the path speed $\sqrt{U^2 + V^2}$ of the spheroid's center; it also portrays $p/\frac{1}{2}\rho Q^2$ for the model in rectilinear motion, with $Q = U$. The difference of $p/\frac{1}{2}\rho Q^2$ for straight and curved paths, though material, is less than experiment gives, as shown by 9₃. Fuller treatment and data are given in Reference 3.

The forces X , Y and moment N , for any zone, may be computed as before; but for the whole model they are more readily found by the method of Part IV. Zonal Y and N for a hull form are found in Part III.

The first of (35) applies also to an elliptic cylinder, with $\cos \omega = 1$, $m'_c = (a^2 - b^2)/2ab$. Fixed in a flow $-U$, $-V$, $-\Omega_c$, it has the surface velocity

$$q = (1 + b/a) U \sin \theta - (1 + a/b) V \cos \theta - \left[\frac{a^2 - b^2}{2ab} \cos (\theta + \beta) + \cos (\theta - \beta) \right] \Omega_c r \text{-----} (36)$$

For an endless flat plate $b = 0$, $\cos \theta = b/a$, $\sin \theta \cot \eta$; and the last term of (36) may be rewritten by (21₁); thus (36) becomes

$$q = (U - V \cot \eta - a\Omega_c \cos \eta \cot 2\eta) \sin \theta \text{-----} (37)$$

These two values of q with (1₁) give the pressure distribution over an elliptic cylinder or flat plate revolving about an axis parallel to its length or fixed in a fluid rotating about that axis.

Thus an endless plate of width $2a$, revolving with angular speed Ω , path radius na , and incidence α , as in Figure 10₁, has by (37) the relative surface velocity, viz, slip velocity

$$q/a\Omega = (n \cos \alpha - n \sin \alpha \cot \eta - \cos \eta \cot 2\eta) \sin \theta \text{-----} (38)$$

and since $\sin^2 \theta = 1$, $q_0^2 = U^2 + (V + x\Omega)^2 = a^2\Omega^2(n^2 + 2n \sin \alpha \cos \eta + \cos^2 \eta)$, (1) gives

$$p/\frac{1}{2}\rho a^2\Omega^2 = \eta^2 + 2n \sin \alpha \cos \eta + \cos^2 \eta - n^2 (\cos \alpha - \sin \alpha \cot \eta - \frac{1}{n} \cos \eta \cot 2\eta)^2 \text{-----} (39)$$

For $n = 3$, $\alpha = 30^\circ$, Figure 10₂ delineates the distribution of slip velocity $q/a\Omega$ on both sides of the plate; 10₃ that of the pressure $p/\frac{1}{2}\rho a^2\Omega^2$ on its two faces. This pressure integrated over the plate's double surface gives $Y = 0$, as may be shown. The dashed line in Figure 10₃ is the pressure-difference graph whose integral for $\eta = 0$ to π is also zero. The resultant forces X , Y and moment N for such a plate are found in Part IV by a method simpler than surface integration of the pressure.

⁵ Here again q is the slip speed of the flow at any point of the body's surface, and depends only on the relative motion of body and fluid.

FLOW INSIDE ELLIPSOID.—At any point inside an ellipsoid with speeds U , V , W , Ω_a , Ω_b , Ω_c , along and about a , b , c , filled with inviscid liquid otherwise still,

$$\varphi = Ux + Vy + Wz + \frac{b^2 - c^2}{b^2 + c^2} \Omega_a yz + \frac{c^2 - a^2}{c^2 + a^2} \Omega_b zx + \frac{a^2 - b^2}{a^2 + b^2} \Omega_c xy \quad (40)$$

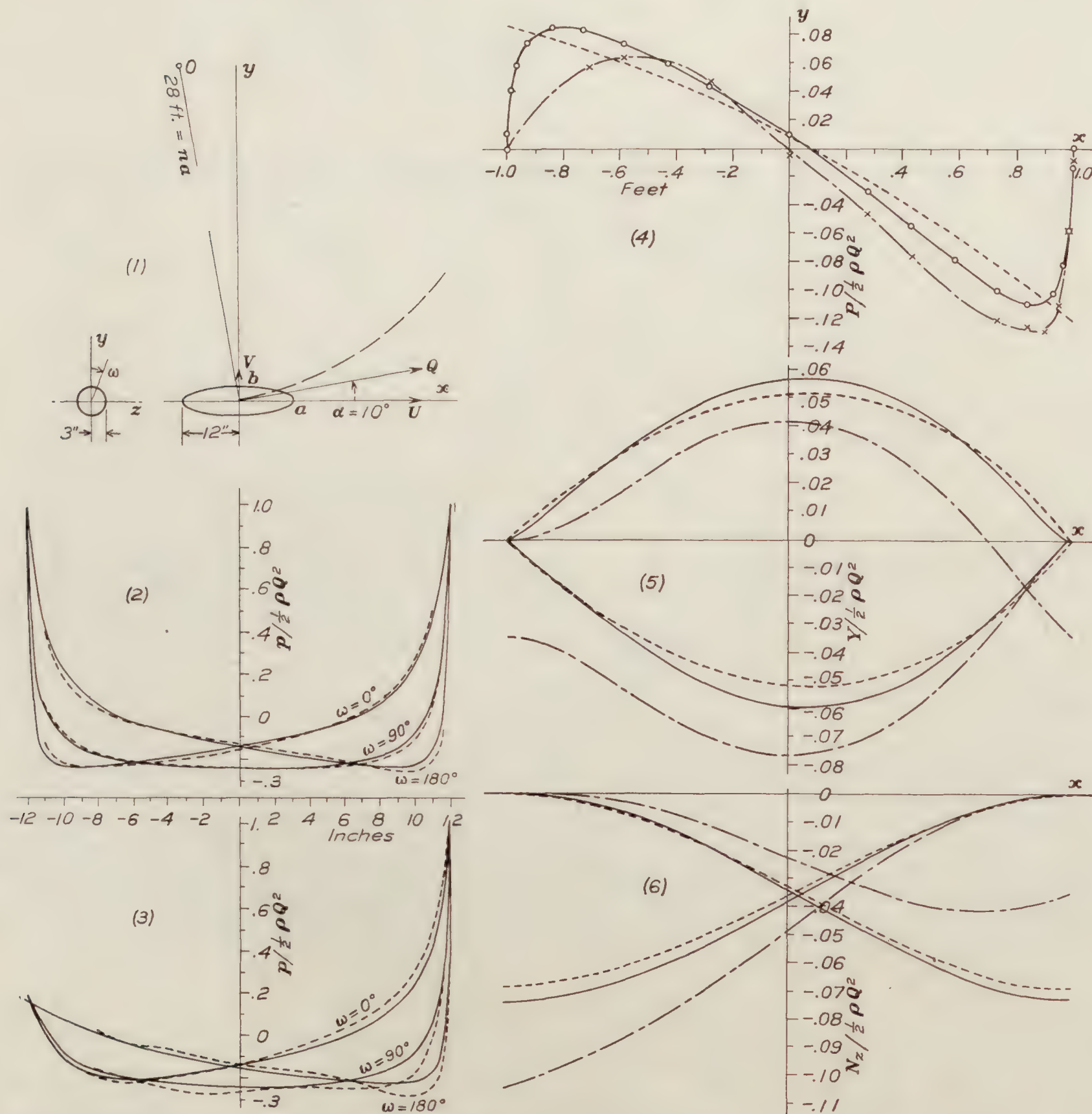


FIGURE 9.—Prolate spheroid in steady yawing flight. (1) Defines velocity conditions; (2) delineates theoretical pressure distribution; (3) experimental pressure distribution for $Q = 40$ feet per second. In (2) and (3), full lines indicate rectilinear, dashed lines curvilinear motion

FIGURE 9 (continued).—For conditions (1), (4) delineates pressure load per unit length; (5) the zonal force; (6) the zonal moment. In (4) the full and dotted lines give theoretical values from equations (a1), (b1); the dashed line, experimental values from reference 3. (5) is obtained by planimetry (4); (6) by planimetry (5)

whose coefficients are constant for the whole interior. Hence the components of the particle velocity q are

$$\frac{\partial \varphi}{\partial x} = u = U + \frac{c^2 - a^2}{c^2 + a^2} \Omega_b z + \frac{a^2 - b^2}{a^2 + b^2} \Omega_c y \quad (41)$$

and like values for v , w found by permuting the symbols. If the fluid were solidified any particle would have

$$u = U + \Omega_b z - \Omega_c y, \text{ etc., etc.} \quad (42)$$

Thus when an ellipsoid full of inviscid still fluid is given any pure translation its content moves as a solid; but when given pure rotation each particle moves with less speed than if the fluid were solidified, since the fractions in (41) are less than unity.

For velocities U , V , Ω_c of the ellipsoid

$$\varphi = Ux + Vy + \frac{a^2 - b^2}{a^2 + b^2} \Omega_c xy \quad (43)$$

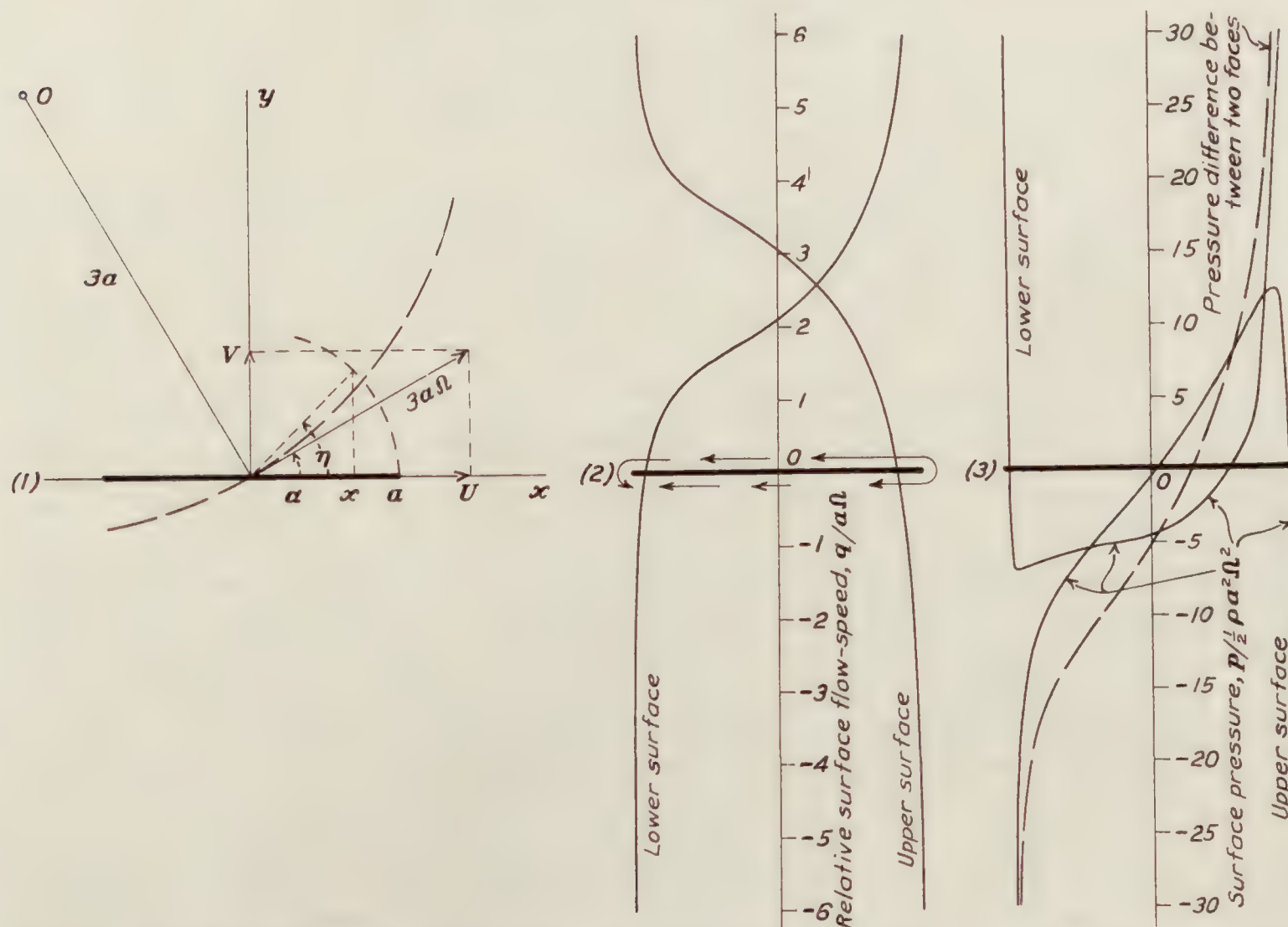


FIGURE 10.—Endless flat plate revolving about axis parallel to its length, in infinite inviscid fluid. (1) Defines conditions; (2) delineates relative velocity $q/a \Omega$ of fluid; (3) pressure $p/\frac{1}{2} \rho a^2 \Omega^2$, and pressure difference $\Delta p/\frac{1}{2} \rho a^2 \Omega^2$ on two faces of plate

for which $w = \partial \varphi / \partial z = 0$. For this plane flow (4) with (43) gives

$$\psi = Uy - Vx - \frac{1}{2} \Omega_c \frac{a^2 - b^2}{a^2 + b^2} (x^2 - y^2) \quad (44)$$

whence the streamlines may be plotted. In particular if the model has simple rotation Ω_c ,

$$x^2 - y^2 = -2 \frac{a^2 + b^2}{a^2 - b^2} \psi / \Omega_c = \text{const.} \quad (45)$$

and the interior streamlines are hyperbolas, as in Figure 5.

Adding (2) to ψ in (45) gives the steady flow

$$\psi = \frac{\Omega_c}{a^2 + b^2} (a^2 y^2 + b^2 x^2) \quad (46)$$

hence the streamlines lie on the elliptic cylinders

$$a^2 y^2 + b^2 x^2 = (a^2 + b^2) / \Omega_c \psi = \text{const.} \quad (47)$$

By (46) $q = 2\Omega_c(a^4y^2 + b^4x^2)^{1/2}/(a^2 + b^2)$, which put in (1) gives at (x, y) , since $q_0 = -\Omega_c R$,

$$p_n - p = \frac{4(a^4y^2 + b^4x^2)}{(a^2 + b^2)^2(x^2 + y^2)} p_n \dots \dots \dots (48)$$

where $p_n = \rho q_0^2/2$. Here p_n is the centrifugal pressure due to the fluid's peripheral velocity q_0 , and p is the pressure change due to $q_0 - q$, q being the relative velocity of fluid and container. In a like balloon hull q would quickly damp out, leaving only p_n as the dynamic pressure. At the ends of a, b, c , respectively, (48) gives

$$\frac{p_n - p}{p_n} = \frac{4b^4}{(a^2 + b^2)^2}, \frac{4a^4}{(a^2 + b^2)^2}, 0.$$

For large a/b the first is negligible, the second approaches 4, giving $p = -3p_n = -1.5\rho\Omega_c^2b^2$ as the temporary dynamic pressure drop inside the hull at the end of b . Experimental proof would be interesting.

POTENTIAL COEFFICIENTS.—An ellipsoid of semiaxes a, b, c along x, y, z , when moving through an infinite inviscid liquid, otherwise still, with velocities $U, V, W, \Omega_a, \Omega_b, \Omega_c$ along and about the instantaneous lines of a, b, c , begets the known velocity potential

$$\varphi = -m_a Ux - m_b Vy - m_c Wz - m'_a \Omega_a yz - m'_b \Omega_b zx - m'_c \Omega_c xy \dots \dots \dots (49)$$

the six potential coefficients m being constant over any outer confocal ellipsoid $a'b'c'$. Their values for abc are given in Tables III, IV. Alternatively (49) can be written for this surface

$$\varphi = -k_a Ux - k_b Vy - k_c Wz - \frac{b^2 + c^2}{b^2 - c^2} k'_a \Omega_a yz - \frac{c^2 + a^2}{c^2 - a^2} k'_b \Omega_b zx - \frac{a^2 + b^2}{a^2 - b^2} k'_c \Omega_c xy \dots \dots \dots (50)$$

the k s being the more familiar inertia coefficients defined and tabulated in Part V. Of the six potential coefficients in (50) the first three are the same as the inertia coefficients k_a, k_b, k_c ; the last three are greater except when c/b or a/c or b/a is zero. Thus, if $b/a = 0$ the last term of (50) is $-k'_c \Omega_c xy$, which is the potential on the outer surface of an elliptic cylinder ($a = \infty$) rotating about c . Everywhere inside of it the potential is $\Omega_c xy$, as (40) shows.

For the flow (40) textbooks give the inertia coefficients

$$k_a, k_b, k_c = 1 \quad k'_a = \left(\frac{b^2 - c^2}{b^2 + c^2} \right)^2 \quad k'_b = \left(\frac{c^2 - a^2}{c^2 + a^2} \right)^2, \text{ etc.} \dots \dots \dots (51)$$

which are the squares of the potential coefficients. One notes too that the ratios of like terms in (40), (50) equal the ratios of like potential coefficients and like inertia coefficients, which latter in turn are known to equal the ratios of like kinetic energies of the whole outer and inner fluids, if the inner moves as a solid.

RELATIVE VELOCITY AND KINETIC PRESSURE.—When a body moves steadily through a perfect fluid, otherwise still, the absolute flow velocity it begets at any point (x, y, z) , being unsteady, is not a measure of the pressure change there. The relative velocity is such a measure. To find it we superposed on the moving body and its flow field an equal counter velocity, thus reducing the body to rest and making the flow about it steady. The same result would follow from geometrically adding to said absolute flow velocity the reversed velocity of (x, y, z) assumed fixed to the body. In particular this process gives for any point of the body's surface the wash velocity, or slip speed, which with Bernoulli's principle determines the entailed change of surface pressure. Conversely, if the pressure change at a point is known or measured, it determines the relative velocity there. In hydrodynamic books the above reversal is used commonly enough for bodies in translation. In this text it is employed as well for rotation; also for combined translation and rotation. However general its steady motion, the body is steadily accompanied by a flow pattern whose every point, fixed relatively to the body, has constant relative velocity and constant magnitude of instantaneous absolute velocity and pressure.

REPORT No. 323

FLOW AND FORCE EQUATIONS FOR A BODY REVOLVING IN A FLUID

PART III

ZONAL FORCES ON HULL FORMS¹

PRESSURE LOADING.—For a prolate spheroid abc with speeds U , V , Ω_c , Figure 9₁, or fixed in a stream $-U$, $-V$, $-\Omega_c$, (35) gives at (x, y, z) on abc the relative velocity

$$q^2 = q_\eta^2 + q_\omega^2 = A - B \cos \omega + C \cos^2 \omega$$

A , B , C being constant for any latitude circle. In forming this equation one finds

$$B = 2(1 + k_a) U \sin \theta \{ (1 + k_b) V \cos \theta + [m'_c \cos (\theta + \beta) + \cos (\theta - \beta)] r \Omega_c \},$$

etc., for A , C . In the body's absence said stream has, at said point (x, y, z) ,

$$q_0^2 = (-U + y\Omega_c)^2 + (-V - x\Omega_c)^2 \equiv A_1 - B_1 \cos \omega + C_1 \cos^2 \omega,$$

where ω alone varies on the latitude circle. Its radius being $y_0 = z_0$, makes $y = y_0 \cos \omega$,

$$B_1 = 2 U z_0 \Omega_c,$$

etc., for A_1 , C_1 . Putting q , q_0 in (1) gives the surface pressure

$$p/.5\rho = q_0^2 - q^2 = (A_1 - A) + (B - B_1) \cos \omega + (C_1 - C) \cos^2 \omega.$$

By (10₁) the loading per unit length of x is, since $\int_0^{2\pi} \cos \omega = 0 = \int_0^{2\pi} \cos^3 \omega$,

$$P/.5\rho = -\frac{z_0}{.5\rho} \int_0^{2\pi} p \cos \omega d\omega = -(B - B_1) z_0 \int_0^{2\pi} \cos^2 \omega d\omega = -\pi(B - B_1) z_0 \text{-----} (a)$$

A , A_1 , C , C_1 vanishing on integration of p . Thus, finally,

$$P/.5\rho Q^2 = -\pi(B - B_1) z_0 / Q^2 \text{-----} (a_1)$$

P having the direction of the cross-hull component of p at $\omega = 0$.

One notes that $q_\omega^2 (\propto \sin^2 \omega)$ contributes nothing to B or the integral in (a); viz, the loading P is unaffected by q_ω , and depends solely on q_η , the meridian component of the wash velocity. Also for $\beta = 0$ and π , $B - B_1 = 0 = P$.

In Figure 9₄ the full line depicts (a₁) for the spheroid shown in 9₁, circling steadily at 40 feet per second. The theoretical dots closely agreeing with it are from Jones, Reference 3, as is also the experimental graph. Beside them is a second theoretical graph plotted from Doctor Munk's approximate formula derived in Reference 8 and given in the next paragraph. But that Professor Jones omitted some minor terms in his value of p , his theoretical $P/.5\rho Q^2$ should exactly equal (a₁). His formula, derived by use of Kelvin's $p_v/\rho = \dot{\varphi} - q^2/2$, can best be studied in the detailed treatment of Reference 3.

In Reference 8 Professor Ames derives Munk's airship hull formula

$$\frac{P}{.5\rho Q^2} = \sin 2\alpha \frac{dS}{dx} + \frac{2}{R} \frac{d}{dx} (xS),$$

¹ This part was added after Parts I, II, IV, V were typed; hence the special numbering of the equations.

S being the area of a cross-section; R the radius of the path of the ship's center. This was assumed valid for a quite longish solid of revolution; for a short one it was hypothetically changed to

$$\frac{P}{.5\rho Q^2} = (k_b - k_a) \sin 2\alpha \frac{dS}{dx} + 2 \frac{k'_c}{R} \frac{d}{dx} (xS) \text{-----} (b)$$

Applying this to a prolate spheroid we derive the working formula

$$\frac{P}{.5\rho Q^2} = -Lx - Mx^2 + N \text{-----} (b_1)$$

where the constants for a fixed angle of attack are ²

$$L = 2(k_b - k_a) \frac{b^2}{a^2} \cdot \pi \sin 2\alpha, \quad M = 3k'_c \frac{b^2}{a^2} \cdot \frac{2\pi}{R} \cos \alpha, \quad N = k'_c b^2 \cdot \frac{2\pi}{R} \cos \alpha.$$

Plotting (b₁) for the conditions in 9₁ gives the dotted curve in 9₄. It shows large values of $P/.5\rho Q^2$ for the ends of the spheroid, where (a₁) gives zero. To that extent it fails, though with little consequent error in the zonal force and moment at the hull extremities. It has the merit of being convenient and applicable to any round hull whose equation may be unknown or difficult to use.

ZONAL FORCE.—An end segment of the prolate spheroid, say beyond the section $x = x_1$, bears the resultant cross pressure

$$Y = \int_{x_1}^a P \, dx \text{-----} (c)$$

which with the resisting shear at x_1 must balance the cross-hull acceleration force on the segment in yawing flight. For the whole model (b₁) with (c) gives $Y = 0$, which is not strictly true for curvilinear motion; but (a₁) with (c) gives the correct theoretical value of Y , and agrees with (67).

In Figure 9₅ graphs of $Y/.5\rho Q^2$, for the values (a₁) and (b₁) of P , are shown beside those derived from Jones' experimental pressure curve. Since Y is proportional to the area of a segment of the graph of P , it can be found by planimetering the segment or by integrating Pdx .

ZONAL MOMENT.—The loading P exerts on any end segment, say of length $a - x$, the moment about its base diameter z

$$N_z = \int_x^a Y \, dx$$

which can be found by planimetering the graph of Y . Figure 9₆ delineates N_z so derived from the three graphs of Y . They show the moment on the right hand segment varying in length from 0 to $2a$; also on the left segment of length from 0 to $2a$. The resisting moment of the cross section must balance N_z and the acceleration moment of the segment.

CORRECTION FACTORS.—No attempt is here made to deduce theoretically a correction factor to reconcile the computed and measured p . In Reference 3 Jones shows that the theoretical and experimental graphs of $P/.5\rho Q^2$ have, for any given latitude $x_1 > a/2$, the same difference of ordinate whatever the incidence $0 < \alpha < 20^\circ$. Thus the ordinate difference found for the zero-incidence graphs, when applied to the theoretical graph for any fixed $0 < \alpha < 20^\circ$, determines the experimental one with good accuracy. Such established agreement in loading favorably affects, in turn, the graphs of Y , N_z the transverse force and moment on any end segment of the spheroid.

² From the meridian curve $\frac{x^2}{a^2} + \frac{y_0^2}{b^2} = 1$, $\frac{dy_0}{dx} = -\frac{b^2}{a^2} \frac{x}{y_0}$, $S = \pi y_0^2$; hence $\frac{dS}{dx} = 2\pi y_0 \frac{dy_0}{dx} = -2\pi \frac{b^2}{a^2} x$, which put in (b) leads to (b₁).

REPORT No. 323

FLOW AND FORCE EQUATIONS FOR A BODY REVOLVING IN A FLUID

PART IV

RESULTANT FORCE AND MOMENT

BODY IN FREE SPACE.—Let a homogeneous ellipsoid of semiaxes a, b, c move freely with component velocities u, v, w, p, q, r ¹ respectively along and about instantaneous fixed space axes x, y, z coinciding at the instant with a, b, c . Then the linear and angular momenta referred to x, y, z are

$$m_1u \quad m_1v \quad m_1w \quad A_1p \quad B_1q \quad C_1r \text{-----} (52)$$

m_1 being the body's mass, A_1, B_1, C_1 its moments of inertia about a, b, c . If, now, forces X_1, Y_1, Z_1 and moments L_1, M_1, N_1 are applied to the body along and about x, y, z , they cause in the vectors (52) the well-known change rates

$$\left. \begin{aligned} m_1(\dot{u} - rv + qw) &= X_1 & A_1\dot{p} - (B_1 - C_1)qr &= L_1 \\ m_1(\dot{v} - pw + ru) &= Y_1 & B_1\dot{q} - (C_1 - A_1)rp &= M_1 \\ m_1(\dot{w} - qu + pv) &= Z_1 & C_1\dot{r} - (A_1 - B_1)pq &= N_1 \end{aligned} \right\} \text{-----} (53)$$

which apply to any homogeneous solid symmetrical about the planes ab, bc, ca .

For motion in the ab plane; viz, for $w, p, q = 0$; (53) give

$$X_1 = m_1(\dot{u} - rv) \quad Y_1 = m_1(\dot{v} + ru) \quad N_1 = C_1\dot{r} \text{-----} (54)$$

and for uniform revolution about an axis parallel to z , as in Figure 11, viz, for $\dot{u}, \dot{v}, \dot{r} = 0$, (54) become

$$X_1 = -m_1rv \quad Y_1 = m_1ru \quad N_1 = 0 \text{-----} (55)$$

where now X_1, Y_1 are merely components of the centripetal force $m_1r\sqrt{u^2 + v^2}$, whose slope is $Y_1/X_1 = -u/v$. Also if $Q = \sqrt{u^2 + v^2}$ is the path velocity of the body's centroid, h its path radius, $r = Q/h$ is the angular velocity of h and of vector m_1Q .

REACTIONS OF FLUID.—If external forces impel the ellipsoid from rest in a quiescent frictionless infinite liquid, with said velocities u, v, w, p, q, r , they beget in the fluid the corresponding linear and angular momenta

$$k_a mu \quad k_b mv \quad k_c mw \quad k'_a Ap \quad k'_b Bq \quad k'_c Cr \text{-----} (56)$$

where m is the mass of the displaced fluid, and A, B, C its moments of inertia about a, b, c .

One calls $k_a m, k_b m, k_c m$ the "apparent additional masses"; $k'_a A, k'_b B, k'_c C$ the "apparent additional moments of inertia," of the body for its axial directions; because the fluid's resistance to its linear and angular acceleration gives the appearance of such added inertia in the body. The six k 's are called "inertia coefficients," and are shape constants. Values of them are given in Tables III, VI, VIII for various simple quadrics.

The component flow momenta (56), like (52), are vectors along the instantaneous directions of a, b, c ; viz, along x, y, z ; hence their time rates of change must equal the forces and moments which the body exerts on the fluid; viz,

$$\left. \begin{aligned} X &= m(k_a \dot{u} - k_b rv + k_c qw) & L &= k'_a A \dot{p} - (k'_b B - k'_c C)qr - (k_b - k_c)mvw \\ Y &= m(k_b \dot{v} - k_c pw + k_a ru) & M &= k'_b B \dot{q} - (k'_c C - k'_a A)rp - (k_c - k_a)mwu \\ Z &= m(k_c \dot{w} - k_a qu + k_b pv) & N &= k'_c C \dot{r} - (k'_a A - k'_b B)pq - (k_a - k_b)muw \end{aligned} \right\} \text{----} (57)$$

¹ These new meanings of u, v, w, p, q, r are assigned for convention's sake and for convenience.

As shown in Figure 12 (60) give the resultant force and slope

$$R^2 = mr \sqrt{k_a^2 u^2 + k_b^2 v^2} \quad Y/X = -\frac{k_a}{k_b} \cot \alpha = -\cot \beta \quad (62)$$

also R and N at the origin are equivalent to a parallel force R through the path center O , along a line (called the central axis of the force system) whose arm and intercepts are

$$l = N/R = h \sin (\beta - \alpha) \quad x = l \sec \beta \quad y = l \operatorname{cosec} \beta \text{-----} (63)$$

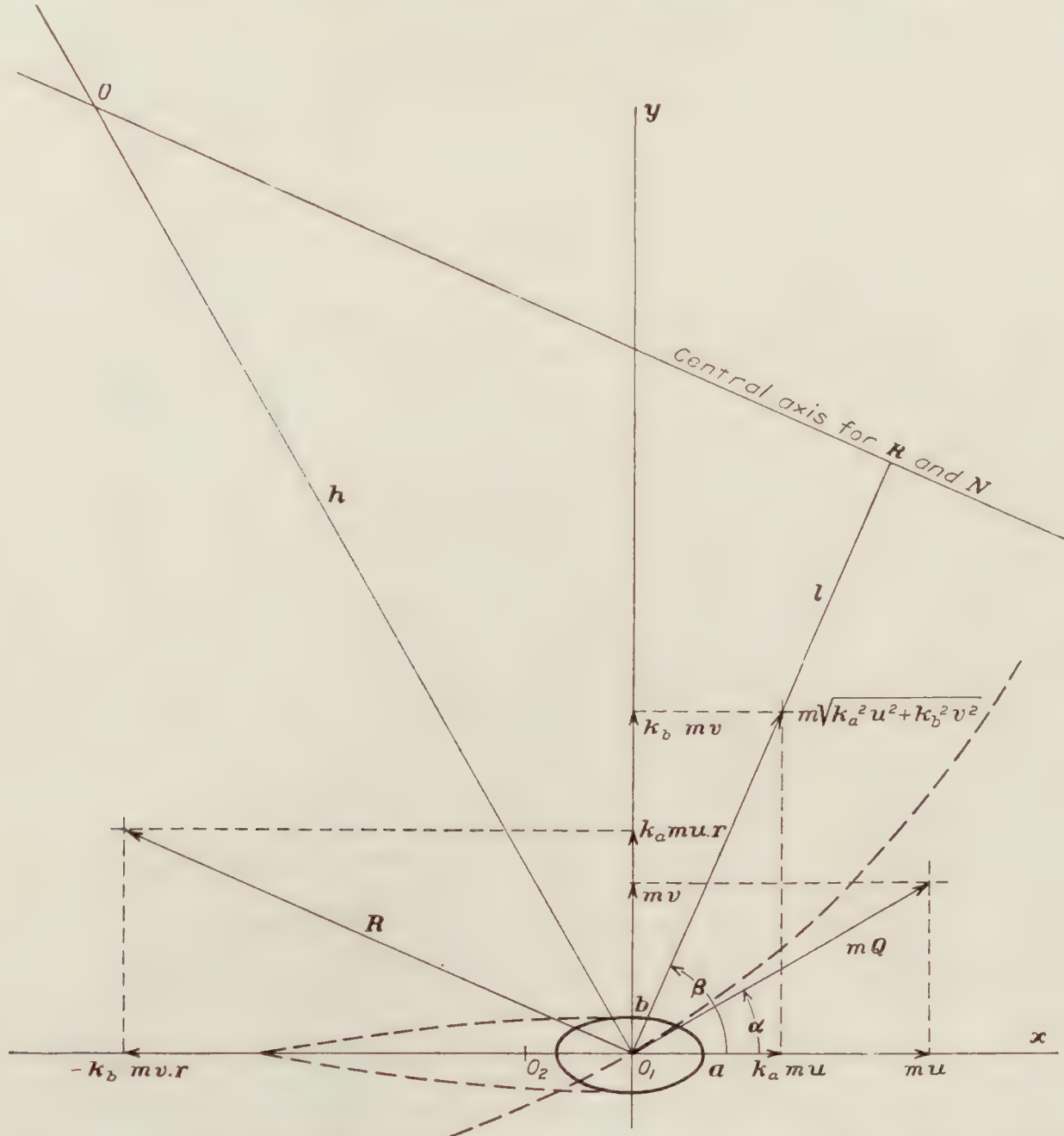


FIGURE 12.—Momenta and forces for symmetrical body in uniform circular motion through frictionless infinite liquid otherwise at rest. Whole hydrodynamic force, $R = m\tau \sqrt{k_a^2 u^2 + k_b^2 v^2}$, has slope $-k_a u/k_b v$. Yaw moment $N = (k_b - k_a) m u v = (k_b - k_a) \tau \frac{\rho Q^2}{2} \sin 2\alpha$, τ being volume

For steady motion (60) show that the body sustains no force in pure translation ($r=0$); no force nor moment in pure rotation ($u, v=0$); no moment in revolution about a point on x or y ; viz, for $u=0$, or $v=0$. For given u, v the moment is the same for revolution as for pure translation. The forces result from combined translation and rotation; the moment from translation oblique to the axes a, b , irrespective of rotational speed.

COMBINATION OF APPLIED FORCES.—To find the whole applied force constraining a body to uniform circular motion in a perfect fluid (55), (60) may be added, or graphs like those of Figures 11, 12, may be superposed. For an airship having $m_1 = m$, (55), (60) give

$$\bar{X} = -(1+k_b)mvr \quad \bar{Y} = (1+k_a)mur \quad \bar{N} = (k_b-k_a)muv \quad (64)$$

* Writing $R = rQ.m\sqrt{k_a^2 \cos^2 \alpha + k_b^2 \sin^2 \alpha}$ we may call it the centripetal force of the apparent mass $m\sqrt{k_a^2 \cos^2 \alpha + k_b^2 \sin^2 \alpha}$ for the body direction of Q .

$$X = -\pi a^2 \rho r v \quad Y = \pi b^2 \rho r u \quad N = \pi(a^2 - b^2) \rho u v = \pi(a^2 - b^2) \frac{\rho Q^2}{2} \sin 2\alpha \quad (65)$$

The resultant force $\pi \rho r \sqrt{a^4 v^2 + b^4 u^2}$ has the slope $-b^2 u/a^2 v = -b^2/a^2 \cot \alpha$; the central axis is through the path center; X is the same as for a round cylinder of radius a ; Y the same as for one of radius b . For a good elliptic aircraft strut $a/b=3$; hence $X/Y = -9v/u = -9 \tan \alpha$; $N = 8\pi b^2 \rho u v = 8\pi b^2 \frac{\rho Q^2}{2} \sin 2\alpha$. By (65) N is the same for all confocal elliptic cylinders, since $a^2 - b^2$ is so.

If $a=b$, as for a round strut, $N=0$, $R = \pi a^2 \rho r Q^2$ and coincides with the body's previously found centripetal force to which it bears the ratio m/m_1 .

If $b=0$, as for a flat plate, (65) become

$$X = -\pi a^2 \rho r v \quad Y = 0 \quad N = \pi a^2 \rho u v = \pi a^2 \frac{\rho Q^2}{2} \sin 2\alpha \quad (66)^5$$

The equivalent resultant force $\pi a^2 \rho r v$, with slope $Y/X = -0$, runs through the path center parallel to x . If $r=0$, the plate has pure translation, with forces X , $Y=0$, and moment $N = \pi a^2 \rho u v$, a well known result. X in (66), being the same as in (65), is independent of the strut thickness b .

(2) For a prolate spheroid, of semiaxes a, b, b , in uniform yawing flight, $m = 4/3 \cdot \pi \rho a b^2$, and k_a, k_b are as given in Table III. Thus for $a/b=4$, $k_a, k_b = 0.082, 0.860$; hence by (60)

$$X = -3.6ab^2 \rho r v \quad Y = 0.3434ab^2 \rho r u \quad N = 3.26ab^2 \rho u v \quad (67)$$

(3) For an elliptic disk of semiaxes a, b, c , moving as in Figure 14, Table VIII gives $k_c m = \frac{4}{3} \pi \rho a b^2 / E$; hence by (57) the forces and moment are

$$Y = -k_c m p w = -\frac{4a}{3E} \pi \rho b^2 p w \quad Z = 0$$

$$L = k_c m v w = \frac{4a}{3E} \pi \rho b^2 v w \quad (68)$$

the other pertinent terms in (57) vanishing, as appears on numerical substitution. Here $E = E\left(\theta, \frac{\pi}{2}\right)$, $\sin^2 \theta = (a^2 - b^2)/a^2$; also $L = \frac{4a}{3E} \pi b^2 \frac{\rho Q^2}{2} \sin 2\alpha$. Compare (68) with (66), calling b the width in both.

THEORY VERSUS EXPERIMENT.—In favorable cases the moment formulas of Part IV accord fairly well with experiment, as the following instances show. For lack of available data the force formulas for curvilinear motion are not compared with experiment.

(1) By (65) an endless elliptic strut with $a=1/3$ foot, $b=1/12$ foot, $c=5$ feet, held at α degrees incidence in a uniform stream of standard air at 40 miles an hour, for which $\rho Q^2/2 = 4.093$ pounds per square foot, sustains the yawing moment per foot length

$$N = \pi(a^2 - b^2) \cdot \frac{\rho Q^2}{2} \cdot \sin 2\alpha = 1.3392 \sin 2\alpha \text{ lb. ft.} \quad (69)$$

This compares with the values found in the Navy 8 by 8 foot tunnel, as shown in Table IX faired from Figure 15. The agreement is approximate for small angles of attack. The model was of varnished mahogany, and during test was held with its long axis c level across stream, and with two closely adjacent sheet metal end plates, 2 feet square, to give the effect of plane flow.

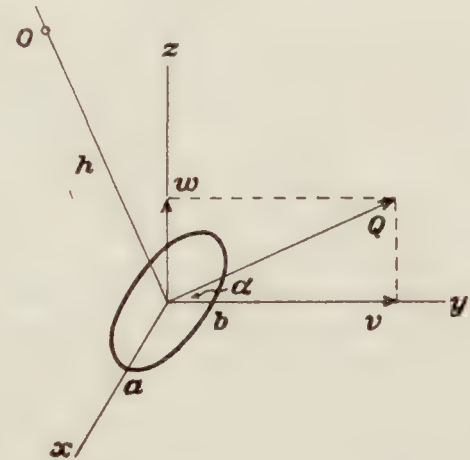


FIGURE 14.—Thin elliptic wing moving parallel to its plane of symmetry through a perfect fluid

⁵ Equations (66) were published in Reference 5 as the result of a special research to determine the fluid forces and moment on a revolving plate. In the present text they follow as corollaries from more general formulas.

(2) By (66) an endless thin flat plate of width $2a=5/12$ feet, similarly held in the same air stream, has per unit length the moment

$$N = \pi a^2 \frac{\rho Q^2}{2} \sin 2\alpha = 0.5581 \sin 2\alpha \text{ lb. ft.} \dots \dots \dots (70)$$

This is compared in Table X and Figure 16 with the values found in the Navy 8 by 8 foot tunnel. The flat plate was of polished sheet aluminum $3/32$ inch thick, with half round edges front and rear.

Again for an endless flat steel plate 5.95 inches wide by 0.178 inch thick at the center, with its front face flat and back face V-tapered to sharp edges, Fage and Johansen, Reference 6,

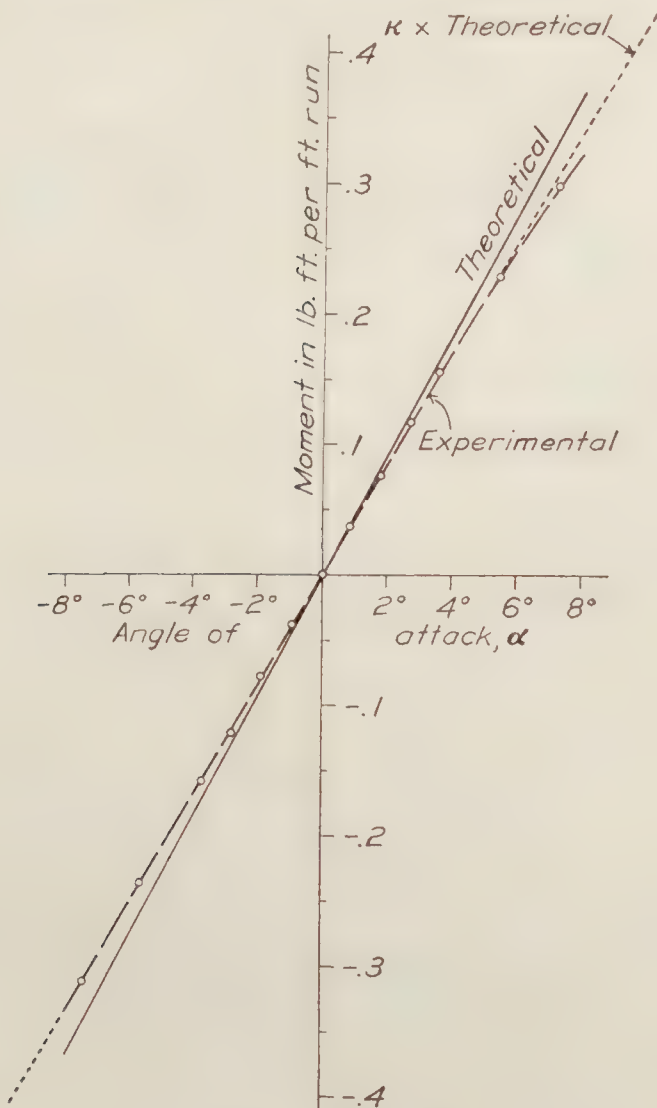


FIGURE 15.—Theoretical and experimental moment about long axis of endless elliptic cylinder. Width 8 inches, thickness 2 inches, air speed 40 miles per hour. Correction factor $\kappa=0.912$

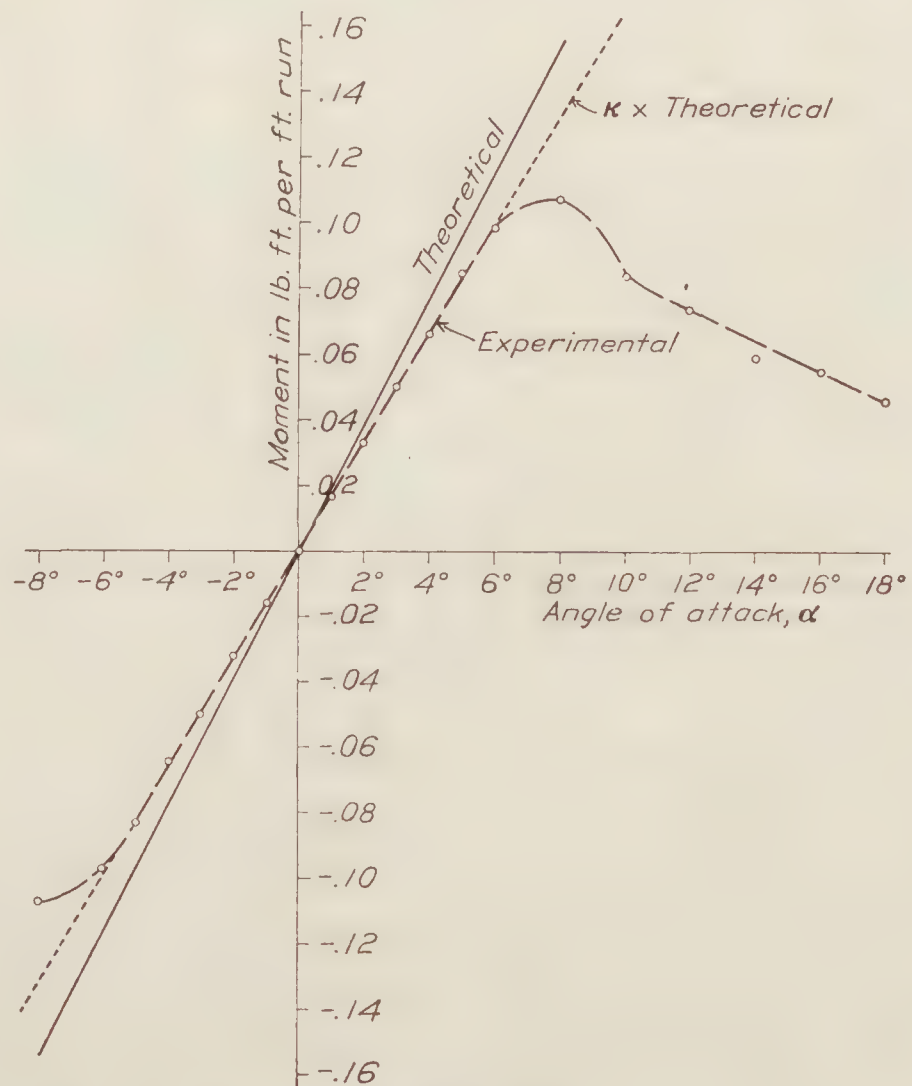


FIGURE 16.—Theoretical and experimental moment about long axis of endless rectangular plate. Width 5 inches, air speed 40 miles per hour. Correction factor $\kappa=0.860$

found, at 50 feet per second and 5.85° angle of attack, $N=0.125$ pound foot as the moment per foot run about the long axis, computed from the measured pressure over the median section. By (66), a thin flat plate would have

$$N = \pi a^2 \cdot \frac{\rho Q^2}{2} \cdot \sin 2\alpha = 0.1931 \times 2.9725 \times 0.2028 = 0.116 \text{ lb. ft.}$$

which is 7 per cent less than 0.125 found with their slightly cambered plate.

(3) An elliptic disk $3/32$ inch thick with $a, b=15, 2.5$ inches, when held as a wing in the Navy 40-mile-an-hour stream, had the moment L versus angle of attack α shown in Figure 17 and Table XI. For this case

$$\sin^2 \theta = (a^2 - b^2)/a^2 = 875/900, \quad \theta = 80^\circ - 24', \quad E = 1.03758.$$

Also in (68) $a=5/4$ feet, $b=5/24$ feet, $Q^2=4.093$; hence

$$L = \frac{4}{3} E \cdot \pi b^2 \cdot \frac{\rho Q^2}{2} \cdot \sin 2\alpha = 0.8963 \sin 2\alpha \text{ lb. ft.} \dots \dots \dots (71)$$

which gives the theoretical values in Figure 17 and Table XI. The agreement is fair at small incidences. The disk as tested was of sheet aluminum cut square at the edges without any rounding or sharpening.

(4) For a wooden prolate spheroid 24 inches long by 6 inches thick, carried as in Figure 12 round a circle of radius $h = 27.96$ feet to the model's center, Jones, Reference 3, found at 40 feet per second the values of N listed in Table XII. For this case Table III gives $k_b - k_a = 0.778$, and (61) gives

$$N = (k_b - k_a)\tau \cdot \frac{\rho Q^2}{2} \cdot \sin 2\alpha = 0.388 \sin 2\alpha.$$

These values appear from Table XII not to accord closely with the experimental ones.

CORRECTION FACTORS.—Figures 15, 16, 17 portray experimental moments, at small angles, as accurately equal to the theoretical times an empirical correction factor κ . Thus amended (61) gives for the experimental moment

$$N_e = \kappa N = \kappa(k_b - k_a)\tau \cdot \frac{\rho Q^2}{2} \cdot \sin 2\alpha.$$

For the given elliptical cylinder $\kappa = 0.912$ with $-8^\circ < \alpha < 6^\circ$; for the endless plate $\kappa = 0.860$ with $-6^\circ < \alpha < 6^\circ$; for the elliptic disk $\kappa = 0.887$ with $-5^\circ < \alpha < 4^\circ$. In such cases one should expect to find the actual air pressure nearly equal to the theoretical over the model's forward part, but so deficient along the rear upper surface as to cause a defect of resultant moment. No effort is made here to estimate it theoretically, nor to determine it empirically for a wide range of conditions.

The measurements shown in Table X, for the flat plate, were repeated at 50 and 60 miles an hour without perceptible scale effect.

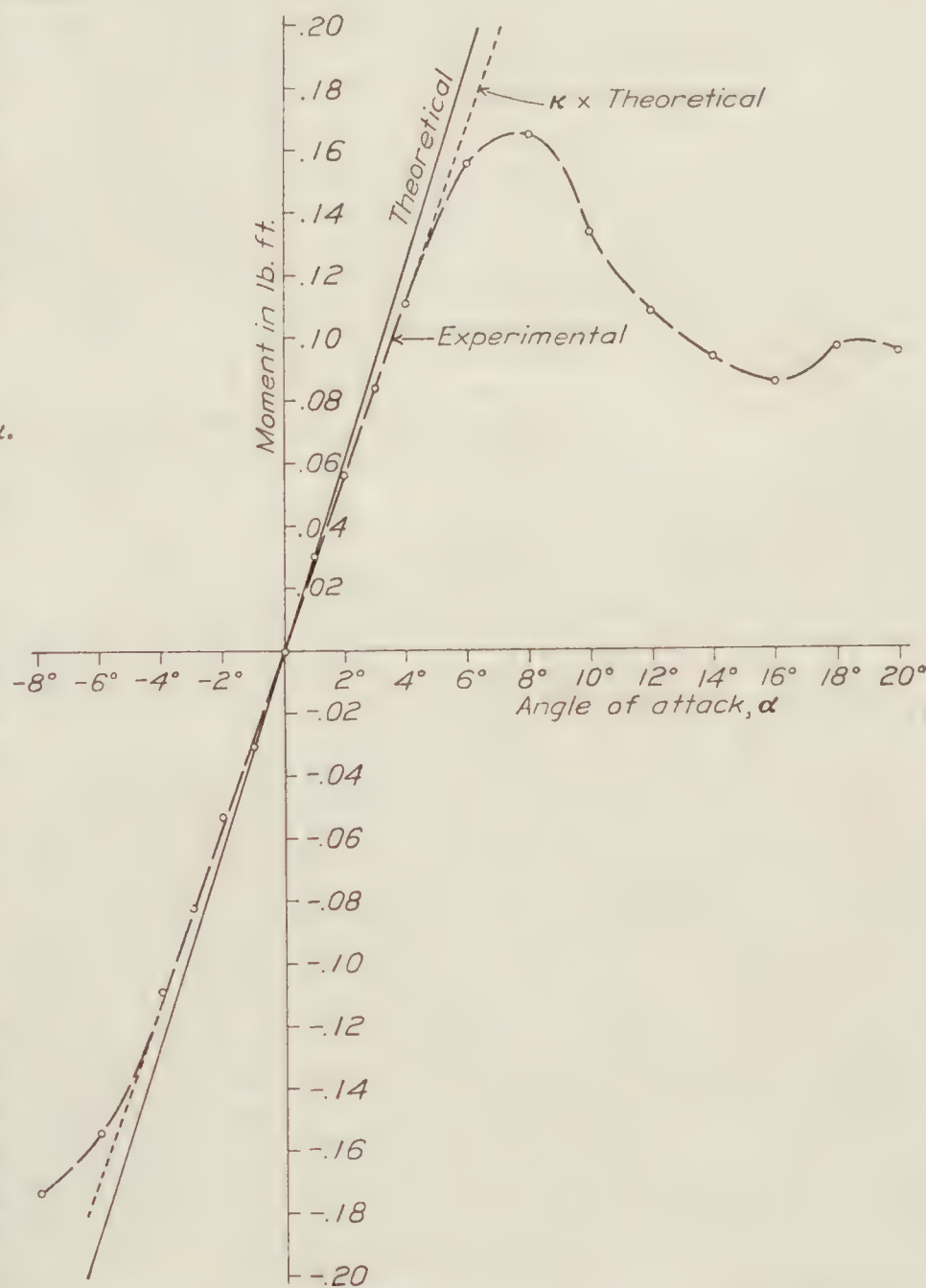


FIGURE 17.—Theoretical and experimental moment about long axis of elliptic disk. Length 30 inches, width 5 inches, air speed 40 miles per hour. Correction factor $\kappa = 0.887$

REPORT No. 323

FLOW AND FORCE EQUATIONS FOR A BODY REVOLVING IN A FLUID

PART V

POTENTIAL COEFFICIENTS, INERTIA COEFFICIENTS

GREEN'S INTEGRALS.—The foregoing text employs Green's well-known integrals, which for the ellipsoid abc may be symbolized thus:

$$\alpha = abc \int_{\lambda}^{\infty} \frac{d\lambda}{a'^3 b' c'}, \quad \beta = abc \int_{\lambda}^{\infty} \frac{d\lambda}{a' b'^3 c'}, \quad \gamma = abc \int_{\lambda}^{\infty} \frac{d\lambda}{a' b' c'^3} \quad (72)$$

where $a' = \sqrt{a^2 + \lambda}$, $b' = \sqrt{b^2 + \lambda}$, etc., are semiaxes of the confocal ellipsoid $a'b'c'$. The integrals have the following values, Reference 4:

$$\left. \begin{aligned} \alpha &= A(b^2 - c^2)[F(\theta, \varphi) - E(\theta, \varphi)] \\ \beta &= A(c^2 - a^2) \left[\frac{b^2 - c^2}{a^2 - c^2} F(\theta, \varphi) + \frac{a^2 - b^2}{\sqrt{a^2 - c^2}} \frac{c'}{a' b'} - E(\theta, \varphi) \right] \\ \gamma &= A(a^2 - b^2) \left[\sqrt{a^2 - c^2} \frac{b'}{a' c'} - E(\theta, \varphi) \right] \end{aligned} \right\} \quad (73)^1$$

where

$$A = \frac{2abc}{(a^2 - b^2)(b^2 - c^2)\sqrt{a^2 - c^2}}, \quad \sin^2 \theta = \frac{a^2 - b^2}{a^2 - c^2}, \quad \sin^2 \varphi = \frac{a^2 - c^2}{a^2 + \lambda} \quad (74)$$

and the elliptic integrals are

$$F(\theta, \varphi) = \int (1 - \sin^2 \theta \sin^2 \varphi)^{-1/2} d\varphi, \quad E(\theta, \varphi) = \int (1 - \sin^2 \theta \sin^2 \varphi)^{1/2} d\varphi \quad (75)$$

Numerical values of $F(\theta, \varphi)$, $E(\theta, \varphi)$, α , β , γ are given in Tables I, II for $\lambda=0$ and various ratios a/b , b/c ; viz, for various shapes of the ellipsoid abc . For $\varphi = \pi/2$ one writes $F(\theta, \varphi) = K$, $E(\theta, \varphi) = E$, by convention.

POTENTIAL COEFFICIENTS.—For motion (49) the ellipsoid abc has the potential coefficients known from textbooks.

$$\left. \begin{aligned} m_a &= \frac{\alpha}{2 - \alpha_0} & m'_a &= \frac{G(\gamma - \beta)}{2G - (\gamma_0 - \beta_0)} \text{ where } G = \frac{b^2 - c^2}{b^2 + c^2} \\ m_b &= \frac{\beta}{2 - \beta_0} & m'_b &= \frac{H(\alpha - \gamma)}{2H - (\alpha_0 - \gamma_0)} \text{ where } H = \frac{c^2 - a^2}{c^2 + a^2} \\ m_c &= \frac{\gamma}{2 - \gamma_0} & m'_c &= \frac{I(\beta - \alpha)}{2I - (\beta_0 - \alpha_0)} \text{ where } I = \frac{a^2 - b^2}{a^2 + b^2} \end{aligned} \right\} \quad (76)$$

m_a , m_b , m_c being for translation along a , b , c and m'_a , m'_b , m'_c for rotation about them, and α_0 , β_0 , γ_0 being (73) for $\lambda=0$; viz, for a' , b' , $c'=a$, b , c . Surface values of (76), viz, for α , β , $\gamma = \alpha_0$, β_0 , γ_0 are given in Tables III, IV. For fluid inside the ellipsoid the potential coefficients are as in (40) and given numerically in Table V.

INERTIA COEFFICIENTS.—From (76) are derived the conventional linear and angular inertia coefficients

$$k_a, k_b, k_c = m_a, m_b, m_c \quad k'_a, k'_b, k'_c = Gm'_a, Hm'_b, Im'_c \quad (77)$$

for the ellipsoid moving through or containing liquid, as in (40), (49). Surface values are given in Tables III, VI, VII.

¹ (73) satisfy the known relation $\alpha + \beta + \gamma = 2abc/a'b'c'$, as appears on adding.

LIMITING CONDITIONS.—In some limiting cases, as for $c=0$, or $a=b$, etc., (73) may become indeterminate and require evaluation, as in Reference 4. In such cases the formulas in Table VIII may be used. For $c=0$, entailing zero mass and infinite k_c , k'_a , k'_b , one may use in (57) the values of k_cm , k'_aA , k'_bB given at the bottom of Table VIII.

PHYSICAL MEANING OF THE COEFFICIENTS.—The tabulated potential coefficients, put in (40) or (49), serve to find the numerical value of the potential φ , or impulse $-\rho\varphi$ per unit area, at any point (x, y, z) of an ellipsoid surface.² Integration of $\rho\varphi$ over any surface, as explained for p in Part I, gives the component linear and angular zonal impulses. So, too, integration of $-\rho\varphi q_n/2$, where q_n is the normal surface velocity at (x, y, z) , gives the kinetic energy imparted to the fluid; and integration of the impulsive pressure $-\rho\partial\varphi/\partial t$ gives the impulsive zonal forces and moments. One finds $\rho\partial\varphi/\partial t$ for (40), (49) by using with them the specified density ρ , accelerations \dot{U} , \dot{V} , \dot{W} , $\dot{\Omega}_a$, $\dot{\Omega}_b$, $\dot{\Omega}_c$, and tabulated potential coefficients for the given semiaxes a , b , c .

Thus putting $-\rho\varphi_c$, $-\rho\varphi'_c$ for p in (9), (10₁), and integrating over the whole ellipsoid surface, easily gives the fluid's linear and angular momenta

$$k_cmW \quad k'_cC\Omega_c \text{-----} \quad (78)$$

where mW , $C\Omega_c$ are respectively the linear and angular momenta of the displaced fluid moving as a solid with velocities W , Ω_c . The like surface integration of $-\rho\varphi_c q_n/2$ gives, as is well known,

$$k_cmW^2/2 \quad k'_cC\Omega_c^2/2 \text{-----} \quad (79)$$

where $mW^2/2$, $C\Omega_c^2/2$ are the kinetic energies of the displaced fluid so moving. Each inertia coefficient therefore is a ratio of the body's apparent inertia, due to the field fluid, to the like inertia of the displaced fluid moving as a solid.

By (49) the potential coefficients due to velocities W , Ω_c are

$$m_c = -\varphi_c/Wz \quad m'_c = -\varphi'_c/\Omega_c xy$$

The first is the ratio of the outer and inner surface potentials due to W at any point z on the ellipsoid abc ; the second is the ratio of the potentials due to Ω_c at (x, y) , respectively on the outer surface of that ellipsoid and inside the cylinder of semiaxes ∞ , b , c .

One notes that the momenta (78) times half the velocities give (79); also that the time derivatives of (78) are the force and moment Z , $N=k_cm\dot{W}$, $k'_cC\dot{\Omega}_c$, as in (57) for the simple z -wise motions, \dot{W} , $\dot{\Omega}$.

For any axial surface, say of torpedo form, moving as in Figure 12, the ratio $-k'_cC\Omega_c/k_cmV$ is the distance from the arbitrary origin O_1 to the impulse center O_2 , or center of virtual mass. This may be taken as origin, and if the body's center of mass also is there Figures 11, 12 can still be superposed as in Figure 13. In the same way are related the acceleration force and moment $k_cm\dot{V}$, $k'_cC\dot{\Omega}_c$, thus illustrating the doctrine that the motion of a hydrokinetically symmetric form in a boundless perfect fluid, without circulation, obeys the ordinary dynamic equations for a rigid body.

AERODYNAMICAL LABORATORY,
BUREAU OF CONSTRUCTION AND REPAIR, U. S. NAVY,
WASHINGTON, D. C., December 17, 1928.

² This impulse is imparted by the moving surface to the fluid, otherwise still; the fluid in turn tends to impart to the body the impulse $\rho\varphi$ per unit area at (x, y, z) .

CHIEF SYMBOLS USED IN THE TEXT

GEOMETRICAL

a, b, c -----	Semiaxes of ellipsoid abc .
a', b', c' -----	Semiaxes of confocal ellipsoid $a'b'c'$.
e, e' -----	Eccentricities of ellipse ab and its confocal $a'b'$; $ae=a'e'=\sqrt{a^2-b^2}$.
$n; h_1, h_2$ -----	Normal to ellipse ab ; distances from origin to normal and tangent.
l, m, n -----	Direction cosines of normal n to any surface.
$s; s_\eta, s_\omega$ -----	Length along any line; lengths along meridian and circle of latitude.
x, y, z -----	Cartesian coordinates; also coordinate axes.
r, β, ω -----	Polar coordinates of prolate spheroid abc .
η, θ -----	Eccentric angle of ab , inclination to x of normal to ab .

KINEMATICAL

u, v, w -----	Component velocities of fluid parallel to x, y, z axes.
q_t, q_n -----	Component velocities of fluid parallel to tangent and normal.
q_o, q -----	Resultant velocity of fluid before and after disturbance.
u, v, w -----	Component translation velocities of abc parallel to a, b, c
U, V, W -----	Component translation velocities of abc parallel to a, b, c
p, q, r -----	Component rotation velocities of abc about a, b, c -----
$\Omega_a, \Omega_b, \Omega_c$ -----	Component rotation velocities of abc about a, b, c -----
φ, ψ -----	Velocity potential, stream function.
m_a, m_b, m_c -----	Potential coefficients for abc with velocities u, v, w or U, V, W .
m'_a, m'_b, m'_c -----	Potential coefficients for abc with velocities p, q, r or $\Omega_a, \Omega_b, \Omega_c$.
$Q=\sqrt{U^2+V^2+W^2}$ -----	Resultant velocity of abc .

Alternative symbols.

DYNAMICAL

A_1, B_1, C_1 -----	Moments of inertia of rigid body about its axes a, b, c .
A, B, C -----	Moments of inertia of displaced fluid moving as a solid.
m_1, m -----	Mass of body, mass of displaced fluid.
ρ, τ -----	Density of fluid, volume of model or displaced fluid.
p, p_n -----	Pressure of fluid moving, pressure on coming to rest.
$X_1, Y_1, Z_1; R_1$ -----	Component forces applied to free rigid body; resultant force.
$X, Y, Z; R$ -----	Component forces exerted by body on fluid; resultant force.
L_1, M_1, N_1 -----	Component moments about a, b, c applied to rigid body.
L, M, N -----	Component moments about a, b, c exerted by body on fluid.
k_a, k_b, k_c -----	Inertia coefficients for abc moving parallel to a, b, c in fluid.
k'_a, k'_b, k'_c -----	Inertia coefficients for abc rotating about a, b, c in fluid.

REFERENCES

- Reference 1. Lamb, H.: Hydrodynamics, 5th ed., 1924. On the Forces Experienced by a Solid Moving Through a Liquid. Quart. Journ. Math. t. XIX (1883).
- Reference 2. Zahm, A. F.: Flow and Drag Formulas for Simple Quadrics. Report No. 253, National Advisory Committee for Aeronautics, 1927.
- Reference 3. Jones, R.: The Distribution of Normal Pressures on a Prolate Spheroid. R. & M. No. 1061, British Aeronautical Research Committee, 1925.
- Reference 4. Tuckerman, L. B.: Inertia Factors of Ellipsoids for Use in Airship Design. Report No. 210, National Advisory Committee for Aeronautics, 1925.
- Reference 5. Cardonazzo, B.: Über die gleichförmige Rotation eines festen Körpers in einer unbegrenzten Flüssigkeit. In Vorträge, etc., edited by Karman & Levi-Civita, 1924.
- Reference 6. Fage and Johansen: On the Flow of Air Behind an Inclined Flat Plate of Infinite Span. R. & M. No. 1104, British Aeronautical Research Committee, 1927.
- Reference 7. Larmor, J.: On Hydrokinetic Symmetry. Quart. Journ. Math. t. XX (1920).
- Reference 8. Ames, J. S.: A Résumé of the Advance in Theoretical Aeronautics made by Max M. Munk. Report No. 213, National Advisory Committee for Aeronautics, 1925.

TABLE I
ELLIPTIC INTEGRALS $F(\theta, \varphi)$, $E(\theta, \varphi)$ ¹
[Defined in eq. (75), Part V]

a/c	b/c										
	1	2	3	4	5	6	7	8	9	10	∞
$F(\theta, \varphi)$											
1	0.00000										
2	1.31696	1.04720									
3	1.76305	1.43870	1.23095								
4	2.06412	1.71374	1.48399	1.31814							
5	2.29319	1.92798	1.68471	1.50687	1.36940						
6	2.47903	2.10413	1.85188	1.66560	1.52053	1.40332					
7	2.63508	2.25400	1.99520	1.80281	1.65204	1.52959	1.42745				
8	2.77024	2.38432	2.12075	1.92379	1.76856	1.64194	1.53595	1.44550			
9	2.89035	2.49971	2.23255	2.03191	1.87318	1.74321	1.63405	1.54065	1.45948		
10	2.99638	2.60288	2.33303	2.12855	1.96804	1.83534	1.72357	1.62768	1.54419	1.47063	
∞	∞	∞	∞	∞	∞	∞	∞	∞	∞	∞	
$E(\theta, \varphi)$											
1	0.00000										
2	.86603	1.04720									
3	.94277	1.07024	1.23095								
4	.96822	1.06091	1.18103	1.31814							
5	.97975	1.05019	1.14337	1.25126	1.36940						
6	.98597	1.04146	1.11604	1.20294	1.29996	1.40332					
7	.98972	1.03472	1.09589	1.16833	1.24893	1.33574	1.42745				
8	.99214	1.02946	1.08071	1.14185	1.21035	1.28451	1.36317	1.44550			
9	.99378	1.02529	1.06894	1.12136	1.18040	1.24464	1.31304	1.38483	1.45948		
10	.99496	1.02195	1.05966	1.10516	1.15669	1.21297	1.27310	1.33642	1.40240	1.47063	
∞	1.00000	1.00000	1.00000	1.00000	1.00000	1.00000	1.00000	1.00000	1.00000	1.00000	

¹ The integrals in this table are culled from L. Potin's Formules et Tables Numerique.

TABLE II
GREEN'S INTEGRALS $\alpha_0, \beta_0, \gamma_0$
[Defined in eq. (73), Part V]

a/c	b/c										
	1	2	3	4	5	6	7	8	9	10	∞
α_0											
1	0.66667										
2	.34713	0.47280									
3	.21751	.31265	0.36460								
4	.15092	.22474	.26820	0.29636							
5	.11171	.17064	.20719	.23189	0.24951						
6	.086527	.13471	.16584	.18769	.20336	0.21541					
7	.069266	.10950	.13629	.15541	.16970	.18079	0.18950				
8	.056894	.091037	.11435	.13135	.14426	.15440	.16254	0.16914			
9	.047710	.077071	.097571	.11276	.12448	.13378	.14132	.14757	0.15271		
10	.040637	.066203	.084381	.097957	.10872	.11728	.12428	.13010	.13500	0.13920	
∞	0	0	0	0	0	0	0	0	0	0	0
β_0											
1	0.66667										
2	.82643	0.47280									
3	.89127	.53423	0.36460								
4	.92459	.56964	.39662	0.29636							
5	.94418	.59182	.41804	.31587	0.24951						
6	.95678	.60693	.43307	.32965	.26265	0.21541					
7	.96538	.61775	.44413	.34083	.27275	.22477	0.18950				
8	.97154	.62577	.45260	.34912	.28071	.23234	.19654	0.16914			
9	.97619	.63184	.45913	.35569	.28709	.23847	.20237	.17458	0.15271		
10	.97972	.63659	.46437	.36109	.29233	.24354	.20725	.17927	.15712	0.13920	
∞	1.00000	.66667	.50000	.40000	.33333	.28572	.25000	.22222	.20000	.18182	0
γ_0											
1	0.66667										
2	.82643	1.05440									
3	.89127	1.15312	1.27078								
4	.92459	1.20572	1.33518	1.40726							
5	.94418	1.23752	1.37478	1.45223	1.50098						
6	.95678	1.25835	1.40110	1.48267	1.53401	1.56918					
7	.96538	1.27273	1.41956	1.50377	1.55754	1.59443	1.62100				
8	.97154	1.28320	1.43306	1.51953	1.57504	1.61325	1.64091	1.66172			
9	.97619	1.29109	1.44329	1.53154	1.58844	1.62775	1.65630	1.67784	1.69457		
10	.97972	1.29720	1.45125	1.54094	1.59895	1.63917	1.66846	1.69062	1.70787	1.72160	
∞	1.00000	1.33333	1.50000	1.60000	1.66667	1.71429	1.75000	1.77778	1.80000	1.81818	2.00000

TABLE III
POTENTIAL COEFFICIENTS m_a, m_b, m_c^* FOR ELLIPSOIDS IN TRANSLATION
(For outer surface of $a b c$)
[Defined in eq. (76)]

a/c	b/c										
	1	2	3	4	5	6	7	8	9	10	∞
	m_a										
1	0.5000										
2	.2100	0.3096									
3	.1220	.1853	0.2229								
4	.08162	.1266	.1549	0.1740							
5	.05916	.09328	.1156	.1312	0.1425						
6	.04522	.07222	.09042	.1036	.1132	0.1207					
7	.03588	.05792	.07313	.08425	.09272	.09938	0.1047				
8	.02928	.04769	.06064	.07029	.07774	.08366	.08846	0.09238			
9	.02444	.04008	.05129	.05975	.06637	.07169	.07603	.07966	0.08267		
10	.02074	.03423	.04405	.05150	.05748	.06229	.06626	.06958	.07239	0.07481	
∞	0	0	0	0	0	0	0	0	0	0	0
	m_b										
	1	2	3	4	5	6	7	8	9	10	∞
	m_c										
1	0.5000										
2	.7042	0.3096									
3	.8039	.3645	0.2229								
4	.8598	.3983	.2474	0.1740							
5	.8943	.4203	.2643	.1876	0.1425						
6	.9171	.4357	.2764	.1974	.1512	0.1207					
7	.9331	.4469	.2855	.2054	.1579	.1266	0.1047				
8	.9447	.4554	.2925	.2115	.1633	.1314	.1090	0.09238			
9	.9535	.4618	.2980	.2163	.1676	.1354	.1126	.09564	0.08267		
10	.9603	.4669	.3024	.2203	.1712	.1387	.1156	.09846	.08526	0.07481	
∞	1.0000	.5000	.3333	.2500	.2000	.1667	.1429	.12500	.11111	.10000	0
	m_c										
	1	2	3	4	5	6	7	8	9	10	∞
	m_c										
1	0.5000										
2	.7042	1.115									
3	.8039	1.362	1.743								
4	.8598	1.518	2.008	2.374							
5	.8943	1.623	2.199	2.651	3.008						
6	.9171	1.697	2.339	2.866	3.292	3.642					
7	.9331	1.750	2.446	3.030	3.520	3.931	4.277				
8	.9447	1.790	2.528	3.163	3.706	4.171	4.570	4.912			
9	.9535	1.821	2.593	3.269	3.860	4.373	4.819	5.208	5.548		
10	.9603	1.846	2.645	3.357	3.987	4.543	5.032	5.465	5.846	6.184	
∞	1.0000	2.000	3.000	4.000	5.000	6.000	7.000	8.000	9.000	10.000	∞

* These have the same values as the inertia coefficients k_a, k_b, k_c .

TABLE IV
POTENTIAL COEFFICIENTS m'_a , m'_b , m'_c FOR ELLIPSOIDS IN ROTATION
(For outer surface of $a\ b\ c$)

[Defined in eq. (76)]

a/c	b/c										
	1	2	3	4	5	6	7	8	9	10	∞
	m'_a										
1	0										
2	0	0.5643									
3	0	.6390	1.045								
4	0	.6768	1.135	1.499							
5	0	.6989	1.190	1.596	1.943						
6	0	.7125	1.225	1.663	2.042	2.380					
7	0	.7211	1.249	1.705	2.113	2.481	2.813				
8	0	.7270	1.266	1.738	2.165	2.556	2.915	3.245			
9	0	.7315	1.278	1.762	2.205	2.615	2.995	3.348	3.675		
10	0	.7348	1.288	1.780	2.235	2.660	3.058	3.430	3.778	4.103	
∞	0	.7500	1.333	1.875	2.400	2.917	3.429	3.937	4.444	4.950	∞
	m'_b										
	1	2	3	4	5	6	7	8	9	10	∞
	0										
1	0										
2	-0.3990	-0.5643									
3	-.5819	-.8853	-1.045								
4	-.6888	-1.104	-1.349	-1.499							
5	-.7581	-1.264	-1.588	-1.800	-1.943						
6	-.8058	-1.384	-1.780	-2.052	-2.243	-2.380					
7	-.8402	-1.476	-1.935	-2.264	-2.504	-2.680	-2.813				
8	-.8659	-1.548	-2.062	-2.445	-2.732	-2.948	-3.114	-3.245			
9	-.8857	-1.607	-2.168	-2.600	-2.931	-3.188	-3.388	-3.547	-3.675		
10	-.9013	-1.654	-2.257	-2.734	-3.107	-3.402	-3.637	-3.825	-3.978	-4.103	
∞	-1.0000	-2.000	-3.000	-4.000	-5.000	-6.000	-7.000	-8.000	-9.000	-10.000	-∞
	m'_c										
	1	2	3	4	5	6	7	8	9	10	∞
	0	0	0	0	0	0	0	0	0	0	0
1	0										
2	0.3990	0									
3	.5819	0.1556	0								
4	.6888	.2420	0.08332	0							
5	.7581	.2969	.1359	0.05193	0						
6	.8058	.3350	.1719	.08705	0.03549	0					
7	.8402	.3627	.1981	.1134	.06127	0.02569	0				
8	.8659	.3836	.2181	.1330	.08081	.04529	0.01951	0			
9	.8857	.3998	.2336	.1484	.09610	.06058	.03486	0.01527	0		
10	.9013	.4127	.2460	.1608	.1084	.07291	.04721	.02770	0.01238	0	
∞	1.0000	.5000	.3333	.2500	.2000	.16667	.14286	.12500	.11111	0.10000	0

TABLE VI
INERTIA COEFFICIENTS ¹ k'_a, k'_b, k'_c FOR ELLIPSOIDS IN ROTATION

(For outer surface of $a\ b\ c$)

[Defined in eq. (77)]

a/c	b/c										
	1	2	3	4	5	6	7	8	9	10	∞
	$k'_a = Gm'_a$										
1	0										
2	0	0.3386									
3	0	.3834	0.8359								
4	0	.4061	.9081	1.323							
5	0	.4194	.9519	1.408	1.793						
6	0	.4275	.9803	1.468	1.885	2.251					
7	0	.4326	.9995	1.505	1.950	2.347	2.701				
8	0	.4362	1.013	1.533	1.999	2.418	2.799	3.145			
9	0	.4389	1.023	1.555	2.035	2.473	2.875	3.245	3.585		
10	0	.4409	1.030	1.571	2.064	2.516	2.935	3.324	3.686	4.022	
∞	0	.4500	1.067	1.654	2.215	2.759	3.291	3.816	4.336	4.852	∞
	$k'_b = Hm'_b$										
	1	2	3	4	5	6	7	8	9	10	∞
	0										
1	0										
2	0.2394	0.3386									
3	.4655	.7082	0.8359								
4	.6078	.9745	1.191	1.323							
5	.6998	1.167	1.466	1.662	1.793						
6	.7622	1.309	1.683	1.941	2.122	2.251					
7	.8066	1.417	1.857	2.174	2.403	2.573	2.701				
8	.8393	1.501	1.999	2.370	2.648	2.857	3.019	3.145			
9	.8641	1.567	2.115	2.536	2.860	3.110	3.305	3.460	3.585		
10	.8834	1.622	2.213	2.679	3.045	3.335	3.565	3.749	3.900	4.022	
∞	1.0000	2.000	3.000	4.000	5.000	6.000	7.000	8.000	9.000	10.000	∞
	$k'_c = Im'_c$										
	1	2	3	4	5	6	7	8	9	10	∞
	0										
1	0										
2	0.2394	0									
3	.4655	0.05985	0								
4	.6078	.1452	0.02333	0							
5	.6998	.2150	.06393	0.01140	0						
6	.7622	.2680	.1031	.03348	0.00640	0					
7	.8066	.3079	.1367	.05758	.01987	0.00393	0				
8	.8393	.3385	.1643	.07982	.03541	.01268	0.00259	0			
9	.8641	.3622	.1869	.09941	.05077	.02330	.00858	0.00179	0		
10	.8834	.3810	.2054	.1164	.06503	.03431	.01616	.00608	0.00130	0	
∞	1.0000	.5000	.3333	.2500	.20000	.16667	.14286	.12500	.11111	0.10000	0

¹ For translation k_a, k_b, k_c are given in Table III.

TABLE VIII
INERTIA VALUES FOR LIMITING FORMS OF ELLIPSOIDS $a > b > c$

INERTIA COEFFICIENTS FOR TRANSLATION AND ROTATION							
a/b	Shape	k_a	k_b	k_c	k'_a	k'_b	k'_c
$c=0$							
1	Circular disk.....	0	0	0	∞	∞	0
1+	Elliptical disk.....	0	0	∞	∞	∞	0
∞	Long rectangle.....	0	0	∞	∞	∞	0
$b > c > 0$							
1	Oblate spheroid $e^2=1-c^2/a^2$	$-\frac{c}{a} \frac{ce-a \sin^{-1}e}{ae(e^2+1)-c \sin^{-1}e}$		$-\frac{a}{c} \frac{ae-c \sin^{-1}e}{ce-a \sin^{-1}e}$	$\frac{e^4(\gamma_0-\beta_0)\dagger}{(2-e^2)[2e^2-(2-e^2)(\gamma_0-\beta_0)]}$		0
1+	Ellipsoid.....						
∞	Elliptical cylinder.....	0	c/b	b/c	$\frac{1}{2bc} \frac{b^2-c^2}{b^2+c^2}$	b/c	c/b
$c=b$							
1	Sphere.....	$\frac{1}{2}$	$\frac{1}{2}$	$\frac{1}{2}$	0	0	0
1+	Prolate spheroid $e^2=1-c^2/a^2$	$\frac{\log_e \frac{1+e}{1-e} - 2e}{\log_e \frac{1+e}{1-e} - 2e}$	$\frac{\log_e \frac{1+e}{1-e} - 2e}{\log_e \frac{1+e}{1-e} - 2e}$	$\frac{\log_e \frac{1+e}{1-e} - 2e}{\log_e \frac{1+e}{1-e} - 2e}$	0	$\frac{e^4(\beta_0-\alpha_0)\dagger}{(2-e^2)[2e^2-(2-e^2)(\beta_0-\alpha_0)]}$	
∞	Round cylinder.....	0	1	1	0	1	1
APPARENT MASSES AND MOMENTS OF INERTIA WHEN $c=0$							
a/b	Shape	$k_a m$	$k_b m$	$k_c m$	$k'_a A$	$k'_b B$	$k'_c C$
1	Circular disk.....	0	0	$\frac{8}{3}\rho a^3$	$\frac{16}{45}\rho a^3$		0
1+	Elliptical disk.....	0	0	$\frac{4}{3}\pi\rho ab^2 E$	$\frac{4\pi\rho}{15} \frac{ab^4(a^2-b^2)}{(2a^2-b^2)E-b^2K}$	$\frac{4\pi\rho}{15} \frac{a^3b^2(a^2-b^2)}{(a^2-2b^2)E+b^2K}$	0
∞	Long rectangle $a=\infty$	0	0	$\pi\rho b^3$	$\frac{1}{3}\pi\rho b^4$	$\pi\rho b^3$	0

$\dagger \gamma_0-\beta_0=-1+\frac{3}{e^2}-\frac{3}{e^3}\sqrt{1-e^2}\sin^{-1}e.$ $\beta_0-\alpha_0=-2+\frac{3}{e^2}-\frac{3}{2}\frac{1-e^2}{e^3}\log_e\frac{1+e}{1-e}.$
* Per unit length of model.

TABLE IX
LIFT, DRAG, AND MOMENT ON ENDLESS ELLIPTIC CYLINDER

[Width 8 inches, thickness 2 inches, air speed 40 miles per hour]

Angle of at- tack α , degrees	Lift	Drag	Moment about long axis pound foot per foot run	
	Pound per foot run		Experi- mental	Theoreti- cal $N=1.3392$ $\sin 2\alpha$
-8	-2.30	0.160	-0.335	-0.3691
-6	-1.94	.139	-.254	-.2784
-4	-1.42	.122	-.170	-.1864
-3	-1.11	.116	-.127	-.1400
-2	-.76	.111	-.084	-.0934
-1	-.40	.108	-.042	-.0467
0	0	.106	0	0
+1	+.41	.108	+.044	+.0467
2	.80	.111	.085	.0934
3	1.13	.116	.129	.1400
4	1.44	.123	.171	.1864
6	1.90	.140	.249	.2784
+8	+2.16	.165	+.325	+.3691

*As the test angles α were in part fractional, all measurements in Table IX are faired from the original graphs of lift, drag, and moment versus α , in fig. 15.

TABLE X
LIFT, DRAG, AND MOMENT ON ENDLESS THIN FLAT PLATE

[Width 5 inches, air speed 40 miles per hour]

Angle of at- tack α , degrees	Lift	Drag	Moment about long axis pound foot per foot run	
	Pound per foot run		Experi- mental	Theoreti- cal $N=0.5581$ $\sin 2\alpha$
-8	-1.345	0.190	-0.107	-0.1538
-6	-.980	.112	-.097	-.1160
-5	-.827	.0816	-.083	-.0984
-4	-.614	.0596	-.064	-.0777
-3	-.471	.0464	-.050	-.0583
-2	-.315	.0360	-.032	-.0389
-1	-.157	.0324	-.016	-.0195
0	0	.0312	0	0
+1	+.155	.0328	+.017	+.0195
2	.311	.0360	.033	.0389
3	.471	.0472	.050	.0583
4	.639	.0648	.066	.0777
5	.831	.0900	.085	.0984
6	1.018	.124	.098	.1160
8	1.346	.206	.107	.1538
10	1.538	.291	.084	+.1909
12	1.594	.360	.074	
14	1.582	.422	.059	
16	1.581	.480	.055	
+18	+1.530	.542	+.046	

TABLE XI
LIFT, DRAG, AND MOMENT ON THIN ELLIPTIC WING

[Length 30 inches, width 5 inches, air speed 40 miles per hour]

Angle of attack α degrees	Lift	Drag	Moment about long axis, pound foot	
	Pounds		Experimental	Theoretical $L=0.8963 \sin 2\alpha$
-8	-2.415	0.426	-0.173	-0.2471
-6	-1.835	.265	-.154	-.1863
-4	-1.186	.169	-.109	-.1247
-3	-.886	.138	-.082	-.0937
-2	-.567	.116	-.053	-.0625
-1	-.294	.105	-.031	-.0313
0	+.005	.103	0	0
+1	.306	.106	+.030	+.0313
2	.590	.118	.056	.0625
3	.890	.136	.084	.0937
4	1.195	.168	.111	.1247
6	1.861	.265	.156	.1863
8	2.474	.422	.185	.2471
10	2.865	.567	.134	+.3066
12	2.958	.696	.109	
14	2.892	.798	.094	
16	2.859	.897	.086	
18	2.769	.974	.097	
+20	+2.725	1.065	+.095	

TABLE XII
MOMENT ON PROLATE SPHEROID ¹

[Length 24 inches, diameter 6 inches, through-air speed 40 feet per second]

Angle of attack α , degrees	Moment about minor axis, pound foot			
	Measured on balance	Found by pressure integration		Theoretical $N=0.388 \sin 2\alpha$
		Rectilinear motion	Curvilinear motion	
-20	-0.179	-0.207	-0.157	-0.249
-10	-.106	-.122	-.078	-.133
-4	-.045	-.052	-.018	-.054
0	0	0	+.021	0
+10	+.106	+.122	.127	+.133
+20	+.179	+.207	+.177	+.249

¹ Data taken from Reference 3.

REPORT No. 324

FLIGHT TESTS ON U. S. S. LOS ANGELES

PART I—FULL SCALE PRESSURE DISTRIBUTION INVESTIGATION

By S. J. DE FRANCE
Langley Memorial Aeronautical Laboratory

REPORT No. 324

FLIGHT TESTS ON U. S. S. LOS ANGELES

PART I—FULL SCALE PRESSURE DISTRIBUTION INVESTIGATION

By S. J. DE FRANCE

SUMMARY

The investigation reported herein was conducted by the National Advisory Committee for Aeronautics at the request of and in conjunction with the Bureau of Aeronautics, Navy Department. The purpose was primarily to obtain simultaneous data on the loads and stresses experienced in flight by the U. S. S. Los Angeles, which could be used in rigid airship structure design. A secondary object of the investigation was to determine the turning and drag characteristics of the airship. The stress investigation was conducted by the Navy Department.

The aerodynamic loading was obtained by measuring the pressure at 95 locations on the tail surfaces, 54 on the hull, and 5 on the passenger car. These measurements were made during a series of maneuvers consisting of turns and reversals in smooth air and during a cruise in rough air which was just short of squall proportions.

The results of the pressure measurements on the hull indicate that the forces on the forebody of an airship are relatively small. The tail surface measurements show conclusively that the forces caused by gusts are much greater than those caused by horizontal maneuvers. In this investigation the tail surface loadings caused by gusts closely approached the designed loads of the tail structure.

The turning and drag characteristics will be reported in separate papers.

INTRODUCTION

Since the design data for rigid airships is still largely empirical, it is obvious that as much additional information as is possible should be obtained from each new design. One of the greatest deficiencies in design data is that concerning the forces imposed upon an airship by various maneuvers and by gusts, especially the latter. With this in mind, the Bureau of Aeronautics, Navy Department, instituted an elaborate series of tests on the U. S. S. *Los Angeles* for the purpose of determining the aerodynamic loads, their distribution, and the resulting stresses in certain structural members of the airship. As a secondary object of this investigation, data were to be obtained from which the turning characteristics of the ship could be determined.

The work was divided into two parts. The Bureau of Aeronautics, Navy Department, conducted the stress investigation and the National Advisory Committee for Aeronautics obtained the aerodynamic load distribution and turning data. All of the data obtained by both agencies were taken simultaneously and the records were synchronized. It is the purpose of this report to present the results of that part of the investigation which was conducted by the National Advisory Committee for Aeronautics.

Probably the best way of obtaining the aerodynamic forces acting on an airship is by the determination of full-scale pressure distribution. Such investigations on rigid airships to date have been limited to the British tests on the *R-32* (reference 1), *R-33* (reference 2), and the *R-38* (reference 3), and to an investigation made in Germany on the *LZ-126* (the present U. S. S. *Los Angeles*), the results of which have not been published. In this country previous airship pressure distribution investigations have been confined to the research on a nonrigid type, the *C-7* (reference 4).

With the exception of the tests on the *R-33* and *C-7*, all of these investigations have consisted of measuring the pressures at comparatively few points. In the investigation herein described the pressures were measured at 95 points on the tail surfaces, 54 on the forward portion of the hull, and 5 on the passenger car. The pressures at these locations were recorded during turning maneuvers and while the ship was encountering gusts.

APPARATUS AND INSTALLATION

In order to measure the pressures, orifices of the type illustrated in Figure 1 were secured to the outer cover, flush with the surface, at the location shown in Figure 2. On the hull, as

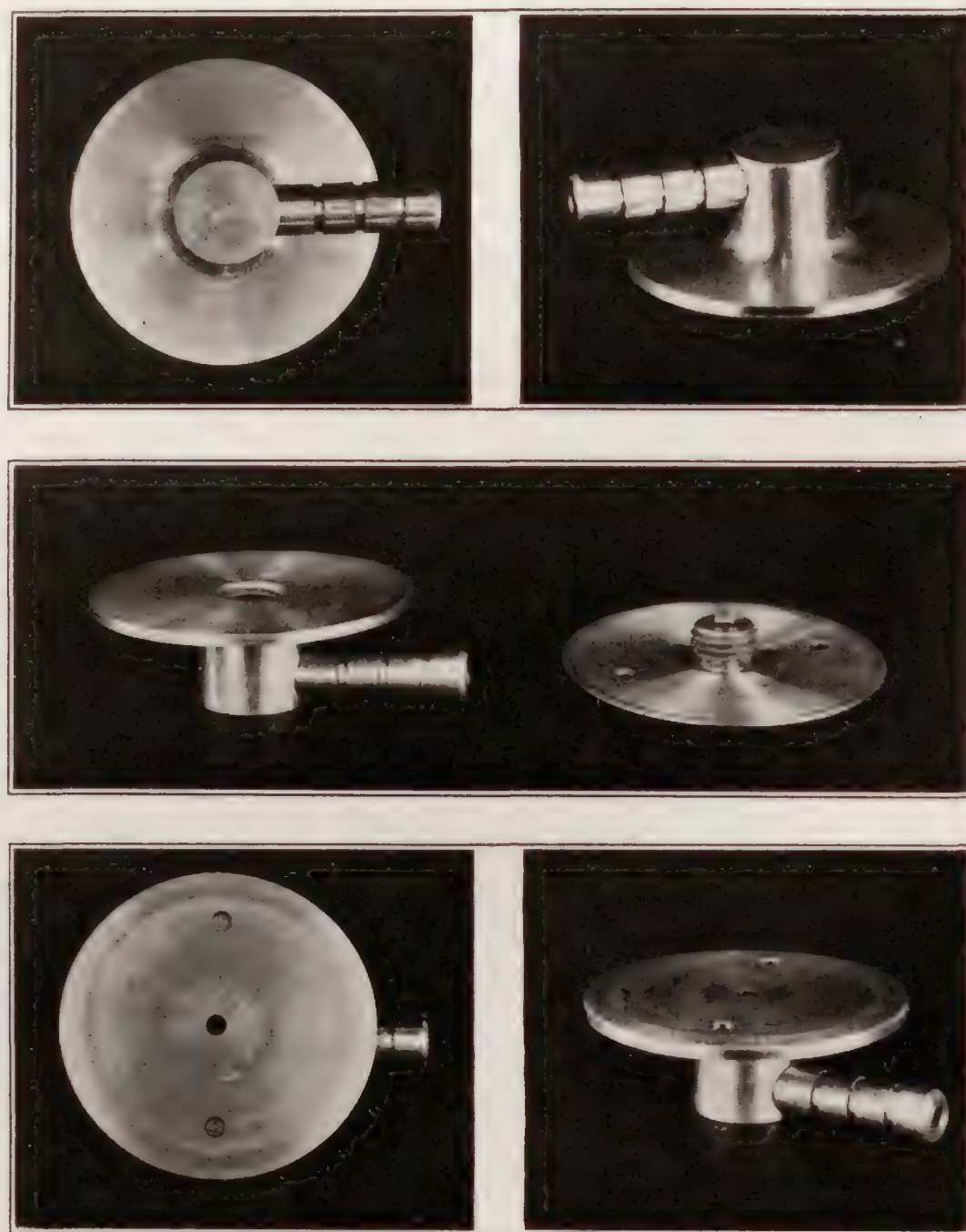


FIGURE 1.—Pressure orifice

shown in Figure 2, a row of orifices was installed along longitudinal 2 from the nose back to frame 145, and two circular rows girdled the hull at frames 175 and 145. In each of the circular rows, four orifices were located between longitudinals 2 and $2\frac{1}{2}$ to determine the effect of the polygonal shape upon the pressure distribution. Orifices were also located inside of the hull, at the points indicated by arrows in Figure 2, for the purpose of determining the fabric loading.

The installation of orifices on the tail assembly (fig. 2) was concentrated on the lower fin and rudder, and on the starboard fin and elevator. The orifices were secured to the opposite sides of the lower fin and rudder at 41 stations and to the opposite sides of the starboard fin and elevator at 42 stations. In addition, orifices were fastened to both sides of the upper and port fins at six stations on each. These were used to obtain pressures for checking purposes.

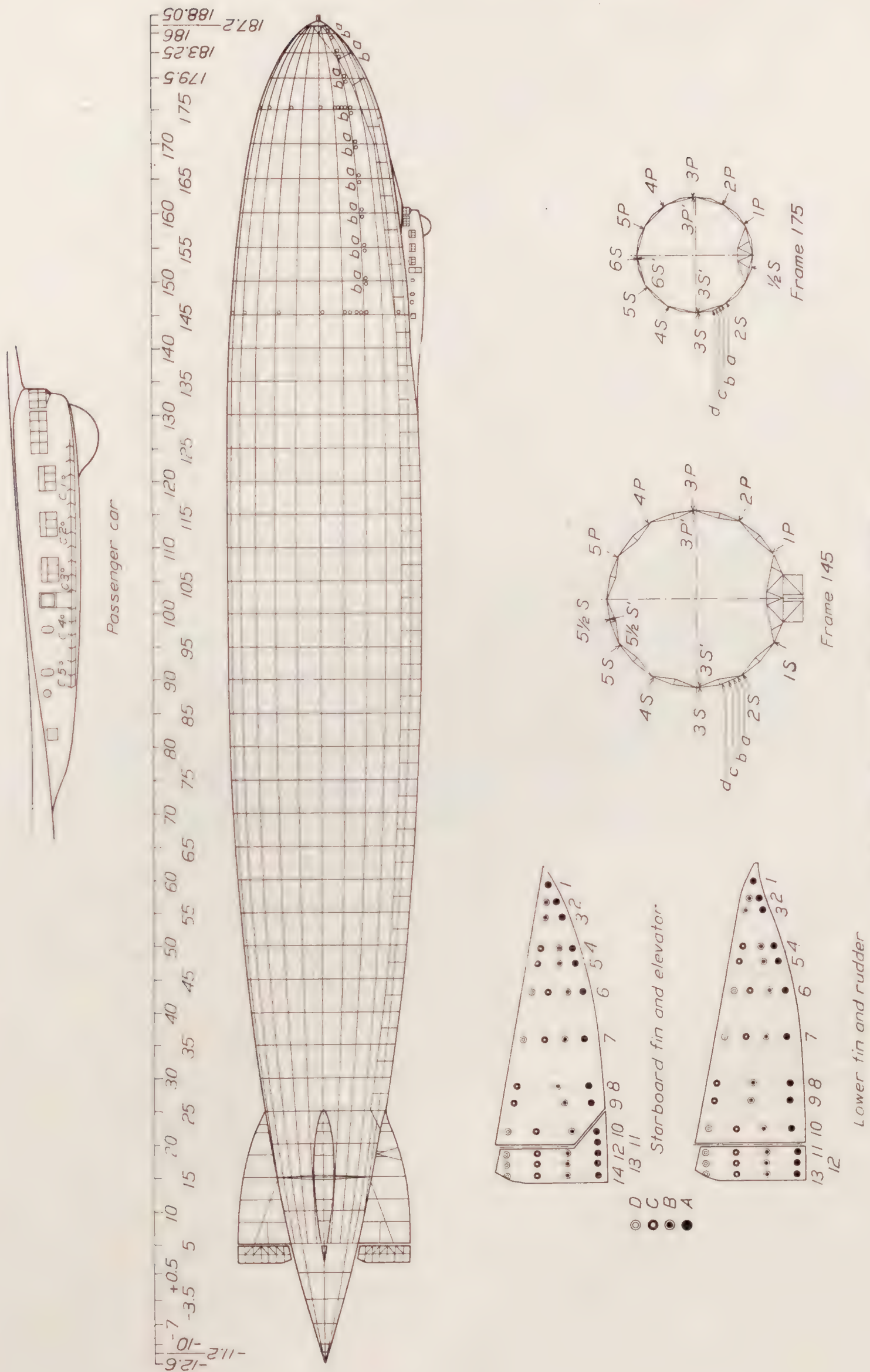


FIGURE 2.—Location of orifices on the U. S. S. Los Angeles

To determine the fin effect of the passenger car, five orifices were secured to each side of this body at the locations shown in Figure 2.

The pressures were transmitted from the orifices to multiple recording manometers by means of $\frac{1}{4}$ -inch aluminum tubing. The manometers (fig. 3) were developed by the National Advisory Committee for Aeronautics for these tests. Each consists essentially of a light-tight aluminum box on which are mounted 60 pressure cells (reference 5), a light source, and a constant-speed electric motor which draws photographic film past the pressure cells at a speed which can be varied by a gear shift. Each manometer records 60 pressures simultaneously and continuous records can be obtained for periods of time varying from 1 to 4 minutes, depending upon the film speed used.

The system used for the hull pressure measurements is shown schematically in Figure 4. As shown, the external pressures normal to the surface were measured relative to that within the keel, which in turn was measured relative to the static pressure as obtained by a static head suspended 30 feet below the ship at frame 165. If the readings of static pressure had been satisfactory, the true aerodynamic pressures acting on the hull could have been determined by adding the two values algebraically. However, the suspended static head was in a disturbed area caused by the passenger car, and the static pressure readings therefore were erratic. Consequently, the pressures acting on the hull could be accurately measured only with respect to the keel pressure.



FIGURE 3.—Type 60 recording multiple manometer

A diagram of the pressure system used on the tail surfaces is given in Figure 5. Orifices on opposite sides of the tail surfaces at the same station are represented by X and Y. By connecting these to the opposite sides of the same pressure cell, the resultant normal pressure was recorded for that station. The internal fin pressure is denoted by Z. By connecting X and Z to another pressure cell, the fabric loading was obtained.

In addition to the multiple manometers employed for recording the pressures, the following instruments were used on board the ship:

(1) *N. A. C. A. Recording Altimeter and Air-Speed Meter*.—This instrument is a standard recording air-speed meter (reference 6) with a sensitive aneroid unit incorporated in it. The air-speed unit was connected by rubber tubing, through a flexible metal hose, to a Pitot-static head (fig. 6), which was suspended 35 feet below the ship at frame 110. Since the Pitot-static head was in a region where the disturbance caused by the ship was negligible, and since the flexible hose permitted the head to turn and assume the true flight path, the true dynamic pressure was recorded.

(2) *N. A. C. A. Recording Turnmeter* (reference 7).—This instrument was mounted so that it could be employed to give a continuous record of the angular velocity in either pitch or yaw.

(3) *N. A. C. A. Control Position Recorder* (reference 8).—This instrument was located in the lower fin so as to have the shortest possible connections to the control surfaces and thereby reduce the error in movement caused by the slackness of the control cables.

(4) *N. A. C. A. Recording Yawmeter*.—This instrument consists of a motion-picture camera, which is operated by a constant speed electric motor (fig. 7) and a streamlined “fish” which is stabilized by tail surfaces and attached to the end of a cable by a swivel. In operation the “fish” was suspended below the airship, where it was free to take up the true flight path. The camera was aligned with the axis of the ship at frame 80, so that the angle between the axis of the “fish” and the edge of the film gave the angle of yaw for this station on the ship’s axis.

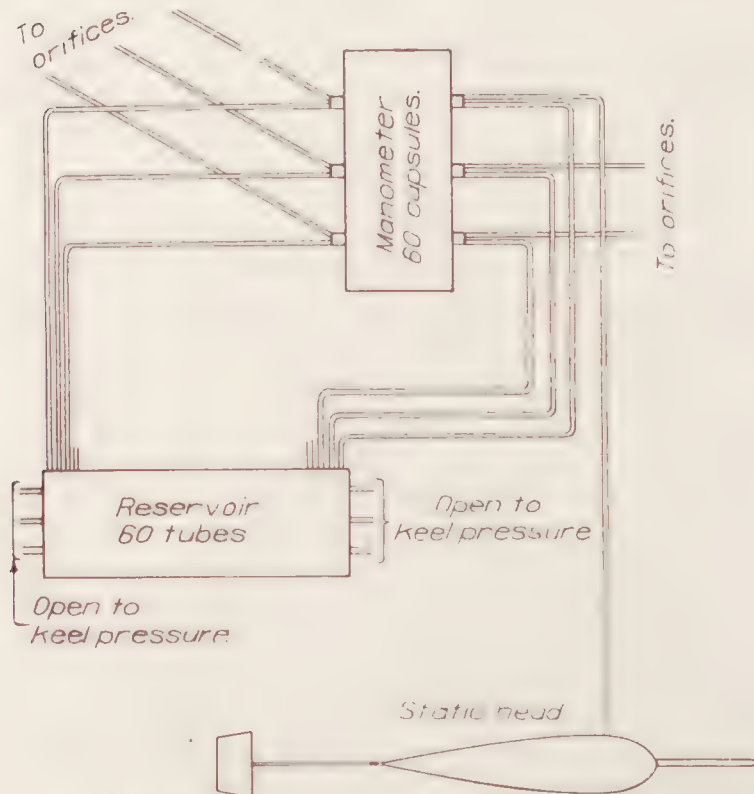


FIGURE 4.—Diagram of tube connections on hull

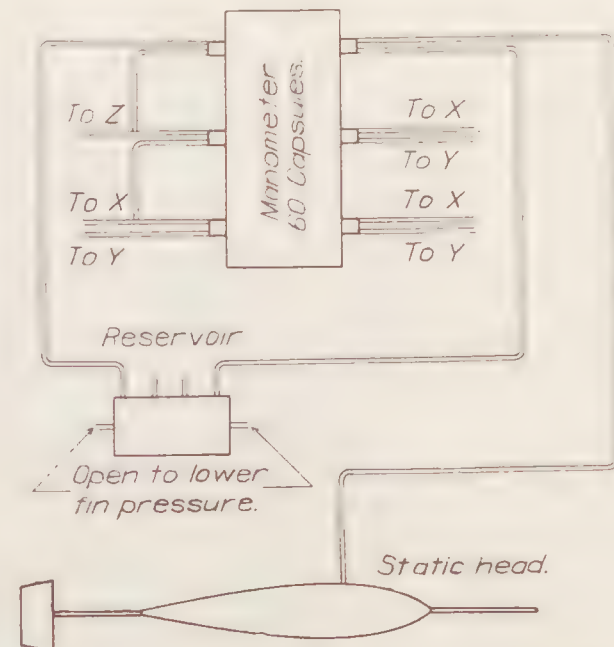


FIGURE 5.—Diagram of tube connections on tail surfaces

(5) *N. A. C. A. Recording Inclinator*.—This instrument consists essentially of an oil-damped pendulum mounted in the standard photographic recording type of instrument used by the National Advisory Committee for Aeronautics. It was used to record the angle of the airship’s axis to the horizontal. Knowing the rate of descent obtained from the sensitive altimeter record, and the air speed, the sine of the angle of the flight path was determined. The algebraic sum of this angle and the angle of inclination gave the angle of pitch.

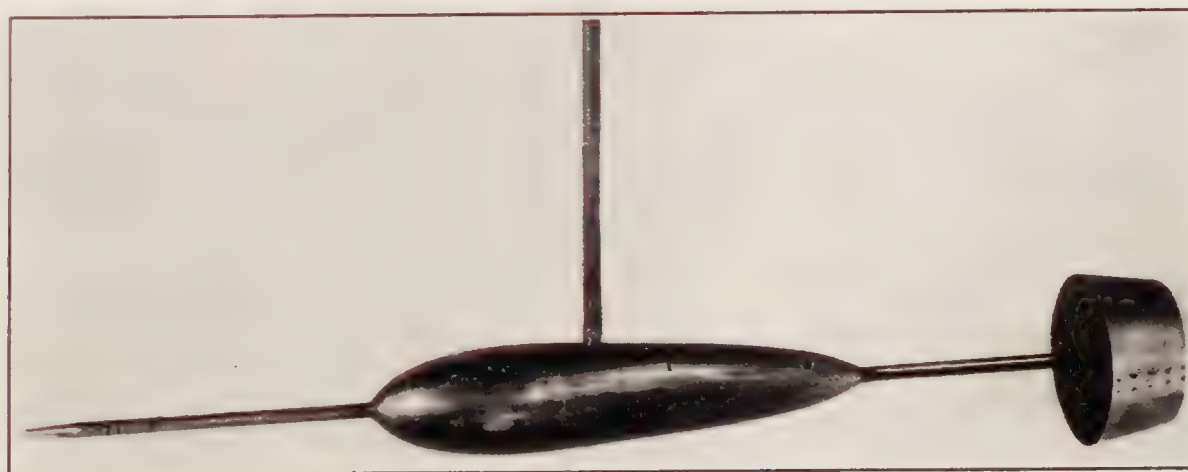


FIGURE 6.—Suspended Pitot static head

(6) *N. A. C. A. Chronometric Timer* (reference 9).—All of the above instrument records were synchronized by means of this instrument.

In addition to the instruments mounted on board the airship, a camera obscura (reference 10) was located on top of the hangar to determine the turning characteristics independently of the data taken on the ship.

FLIGHT TESTS

The test program was divided into two parts—(a) maneuvers in smooth air and (b) flights in rough air to determine the effect of gusts. Because of the condition of the gas cells at the time of the tests and the necessity of conserving helium, it was considered undesirable to make vertical maneuvers. Consequently, all of the smooth-air maneuvers were confined to the horizontal plane. When the air in the vicinity of Lakehurst was smooth enough, these maneuvers were carried out over the camera obscura; but when the local conditions were rough, the tests were conducted well out to sea, where smooth air prevailed. Consequently, camera obscura measurements were not obtained during all of the tests. The second part of the program consisted of taking a series of continuous records while the ship was cruising in rough air.

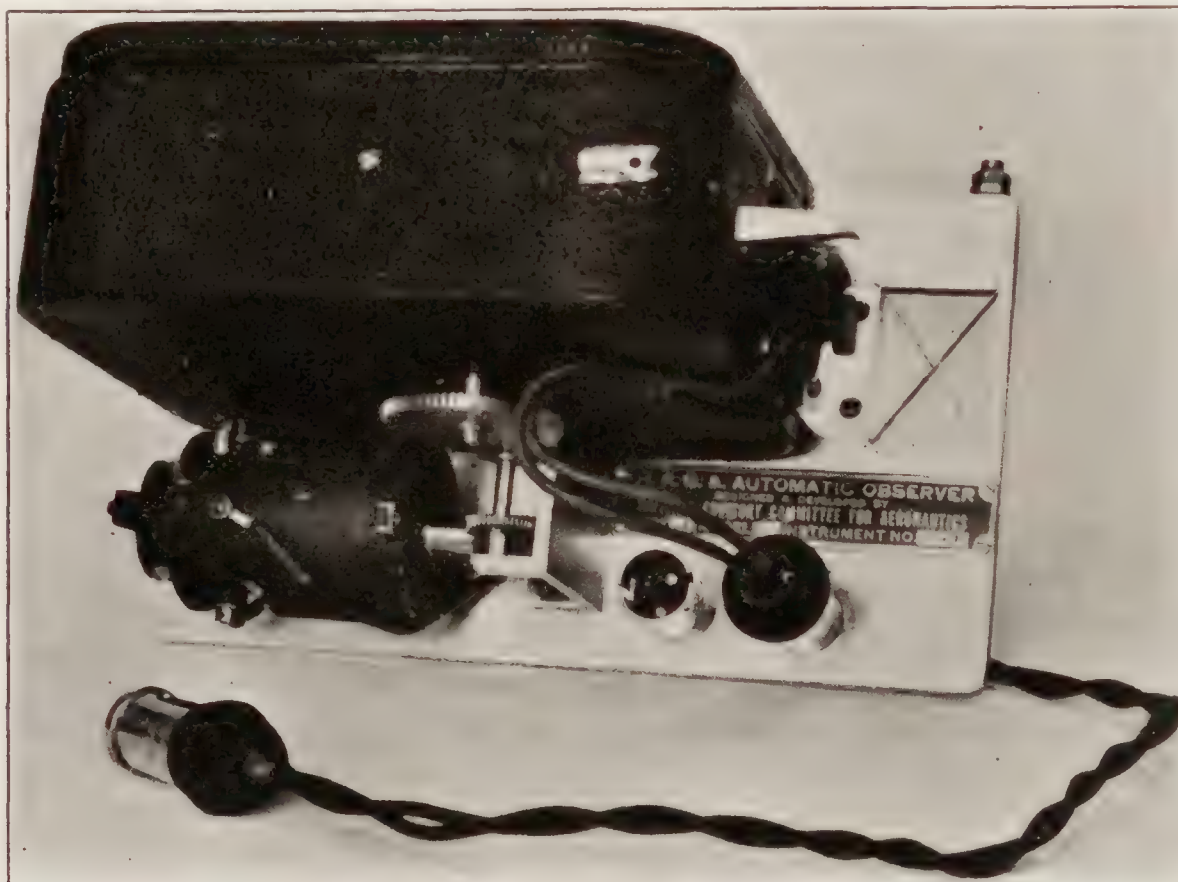


FIGURE 7.—Automatic angle of yaw recorder

A list of the maneuvers performed during the tests is given in the following table:

TABLE I

FLIGHT TEST PROGRAM—U. S. S. "LOS ANGELES" PRESSURE DISTRIBUTION

Maneuver	Requested rudder angle	Requested engine R. P. M.
Steady turn.....	8° R.....	1,050
Do.....	8° R.....	1,230
Do.....	8° L.....	1,050
Do.....	12° R.....	1,050
Do.....	12° R.....	1,230
Reversal.....	8° R. to 8° L.....	1,050
Do.....	8° R. to 8° L.....	1,230
Do.....	12° R. to 12° L.....	1,050
Do.....	12° R. to 12° L.....	1,230
Deceleration.....	0.....	0
Do.....	0.....	Idling.
Cruising in rough air.....

Of the above maneuvers the steady turns need no additional comment. The reversals, deceleration runs, and rough-air tests, however, might be further described. In the reversals, the airship was put into a right turn and when the turn had reached a steady condition, the rudders were rapidly reversed to the corresponding position for left turn. Records were obtained on all instruments from an instant before the rudders were reversed until the airship had reached a condition of steady left turn.

The deceleration tests, which were made to determine the drag characteristics of the airship, were carried out in two ways—(a) with the propellers stopped and (b) with the propellers disengaged and idling. The procedure in these tests was to stop all of the engines simultaneously while the ship was in steady horizontal flight and then to take a record of the air speed against time while the ship was decelerating.

The rough-air measurements were made while the airship was cruising in gusty air. There was, of course, no way of determining when the airship was about to encounter a gust. However, the air was particularly rough, with frequent gusts, while the data were being obtained, so that by taking a series of continuous records, each of four minutes' duration, the effects of several gusts of varying intensity were recorded.

During all of the tests an observer was placed at each instrument station in the ship to see that the instruments were working properly and to load them as it became necessary. Communication was established between the stations by means of a buzzer system and between the master station and the control car by word of mouth. As each maneuver was about to be performed, the master observer signaled a warning to the instrument stations. Then, at the proper moment, he indicated the start of the test and threw the control switch, thus starting all of the instruments at the same time. A similar procedure was carried out at the end of each maneuver. Consequently, the observers knew when the instruments were supposed to be operating. At the start of each flight over the camera obscura, a radio signal was sent to the operator, who started a stop watch and synchronized his records with those on the ship. All runs, with the exception of the decelerations, were of four minutes' duration.

COMPUTATION OF RESULTS

The pressures obtained on the tail surfaces were plotted upon drawings of the surfaces (figs. 8 to 27), and the resulting curves drawn through the points were integrated to determine the load per running foot of surface. These loads in turn were plotted against the length of the surfaces and the curves drawn through the points were integrated to obtain the total loads. The total loads were converted into coefficient form by the following equation

$$C_{NF} = \frac{2F}{S\rho v^2}$$

where

C_{NF} = normal force coefficient.
 F = total load.
 ρ = air density at time of tests.
 S = area of the surface.
 v = true velocity.

The pressures on the hull could not be expressed in coefficient form because of the erratic readings of static pressure previously mentioned, which prevented the determination of the true aerodynamic pressures. Therefore, the values which are given in Table V and plotted in Figures 28 to 36, are with reference to the keel pressure.

The transverse forces acting at frames 145 and 175, Table VI, were determined by plotting the values of pressure, obtained around the ship at these frames, upon base lines representing the horizontal and vertical diameters and integrating the resulting curves.

The resultant transverse pressures on the passenger car were determined in the same manner as the resultant pressures acting upon the tail surfaces. These results are given in Table VII.

PRECISION

The possible sources of error in the pressure measurements are:

- (a) Irregularity in the airship's surface in the vicinity of the orifice location.
- (b) Tube stopped or leaking.
- (c) Change of calibration of pressure cell.
- (d) Effect of acceleration of air in tubes.
- (e) Time lag due to length of tube.

The error due to (a) was negligible, since all of the orifices were located within 18 inches from a girder where the true shape of the ship was maintained and the fabric was taut. The possibility of error due to (b) was removed, since the tubing was inspected after each flight and the data which were obtained from defective tubes were deleted. A clamping device was attached to each manometer which permitted the clamping off of all of the tubes leading to the orifices and the opening of tubes leading from a reservoir to the pressure cells. With the aid of a U-tube manometer which was connected to the reservoir, calibrations were made of all of the multiple recording manometers after each flight. There was a slight change (c) in the calibration of the pressure cells during the tests, and this could account for a maximum error of ± 2 per cent in the pressures.

The effect of acceleration of the air in the tubes (d) was eliminated in the tail surface pressures, since only resultant pressures were measured and the tubes from the orifices on each side of the surface ran parallel to each other from the surface to the manometer. In the hull pressure installation, where the normal hull pressures were measured with respect to the keel pressures, there is a possibility of some error being introduced in the longer tubes. However, the manometer was centrally located so that the average length of tube was about 50 feet and the only appreciable error would be in the measurements from the nose orifices where the tube length reached 100 feet. The probable error in the measurements from these long tubes is ± 1 per cent. The error due to time lag in tubing (e) is negligible, since it has been proven by tests (reference 11) that lag in $\frac{1}{4}$ -inch tubing for 100-foot lengths is too small to measure, and in no part of the installation did the length of an individual tube exceed this value. Consequently, it is safe to say that the tail surface pressure measurements are not in error by more than ± 2 per cent and the hull pressures by not more than ± 3 per cent.

The greatest error in the results is due to the fairing of the curves through the points of plotted pressures. The fairing of these curves could cause a maximum error in the total loads of ± 5 per cent.

DISCUSSION OF RESULTS

TAIL SURFACE RESULTS

The results are presented in tabular and curve form. The maximum pressures recorded for the vertical tail surfaces during turning maneuvers are given in Table II and are presented graphically in Figures 8 to 23. It will be observed that during all of the maneuvers there was a concentration of pressure in a vortex area along the leading edge of the fin. In several cases these local resultant pressures, which were the average of the vortex fluctuations, exceeded 100 per cent q at points 4A and 5A on the lower fin, and in one case, run Number 13D, a value of 1.42 q was reached. These pressures were large but localized, so that the total loads on each surface were never excessive.

The maximum fin load encountered during the turning maneuvers in smooth air was 2,139 pounds. In Table IV this load is reported as having been encountered by the surface during a reversal. Actually, it occurred while the airship was in a right turn, since the rudders had not been reversed at the time that the record was obtained. Unfortunately, the normal force coefficient could not be positively determined for this load, because the air-speed recorder failed and only an approximate value of the dynamic head could be obtained. The approximate head was 1.53 inches of water and the corresponding normal force coefficient was 0.253. This value was exceeded in two of the steady turns at slower speed. The maximum normal force coefficient for a fin alone during the smooth-air maneuvers was 0.320. This occurred during a steady turn at a speed of 64.4 feet per second with rudder 8.3° to starboard and resulted from a load of only 1,482 pounds.

The maximum normal force coefficient for the rudder alone and also the maximum over-all normal force coefficient for the fin and rudder combined, resulting from the turning maneuvers, occurred during a reversal of the helm. In this maneuver, run Number 3C, the rudders were reversed from 12.35° right to 11.55° left in 9 seconds, while the airship was making a speed of 71 feet per second. The resulting coefficients were 0.323 for the rudder and 0.268 for the rudder and fin together.

While flying through gusts, the local pressures and the total loads encountered by the tail surfaces greatly exceeded the values obtained during horizontal maneuvers in smooth air. The pressures caused by two gusts are given in Table III and graphically represented in Figures 24 to 27. Only the results of two gusts are given, but these represent the largest loads encountered during 10 runs of approximately four minutes each, which were made during an elapsed time of four hours. Considering that all of these runs were made in rough air which was just short of squall proportions, the results of these two runs indicate the dangerous loadings that might be expected in a storm.

Considering the total loads and normal force coefficients in Table IV, it can be seen that the greatest effect of the gusts was in a vertical direction. The *Los Angeles* was designed to withstand a force equivalent to a normal force coefficient of 0.34 simultaneously on each set of tail surfaces. In run Number 4A, the normal force coefficient for the horizontal surfaces was 0.349, but that for the vertical surfaces at the same instant was only 0.126. Consequently, the design loading was approached but not exceeded even though the vertical loading was large. In run Number 5A, the design limit for the tail surface loading was more closely approached. Unfortunately the air-speed recorder failed during this run, so that only an approximate value of the dynamic head could be determined. Consequently the normal force coefficients may be in error, but by not more than 10 per cent. Allowing for this possible error, the normal force coefficient for the starboard fin and elevator is still large, and combining this with the normal force coefficient for the vertical surfaces, the resultant closely approaches the design value.

HULL AND PASSENGER CAR RESULTS

The investigation of the hull pressures was not as successful as that of the tail surfaces. The trailing head, from which the static pressure reference for all of the hull pressures was obtained, was not suspended far enough from the keel at frame 165 to be outside of the disturbance caused by the passenger car. Consequently the pressures given in Table V and represented graphically in Figures 28 to 36 are given with respect to the keel pressure. It might be mentioned, though, that by checking the nose pressure, obtained in this manner, against the air speed head it was found that there was never a discrepancy of more than 8 per cent, and therefore it is probable that the values of pressure given with respect to the keel pressure are within 8 per cent of the true aerodynamic pressure.

The error in the true aerodynamic pressure data did not affect the determination of the transverse forces at frames 145 and 175, since these forces were obtained by integrating the resultant pressure curves and, consequently, the effect of the static pressure was eliminated. The transverse forces for these two rings are recorded in Table VI. As can be seen, there was only one smooth-air maneuver that caused a sizable force. This was a steady turn, run Number 5C, and even in this case the force at frame 175 was small. The force at frame 145 might have been caused by a localized lateral gust. The forces obtained during the rough-air flights were somewhat larger, but indications are that for no condition were the forces on the forward portion of the hull excessive.

From the investigation of the pressures on the passenger car, it was found that the fin effect of that body was practically negligible. The resultant pressures are given in Table VII. The maximum pressure obtained was 0.78 lb. per sq. ft. and the majority of the values were practically zero. Therefore the total transverse force, and consequently the fin effect, of the passenger car, were small.

The orifices for measuring the fabric loads were located in the region of maximum pressure on the fin, close to the leading edge, and at three points each on transverse frames 145 and 175. At each location, one orifice was mounted on each side of the cover. The resultant pressures from these orifices are presented in Table VIII. The fabric loading of the hull cover never reached a value as large as 1 lb. per sq. ft., and on the fin cover, a maximum value of only 6.60 lb. per sq. ft. was obtained. Consequently, no excessive stresses were set up in the fabric.

TURNING AND DRAG CHARACTERISTICS

The turning characteristics could not be determined from the records taken on board the airship because of the inconsistent readings from the turnmeter. This instrument was of the airplane type and did not maintain the sensitive adjustment necessary for airship use. However, this information has been obtained from the camera obscura data. The results from these data will be given in a subsequent report.

The deceleration tests were not entirely satisfactory. During these tests the air speed fluctuated so much that consistent data could not be obtained. Consequently, the shape coefficients which were determined were only an indication of the drag characteristics. Another series of deceleration tests has been made on the U. S. S. *Los Angeles* at a more recent date and the data were very consistent. The results of this investigation will be given in a separate report.

CONCLUSION

The results of this investigation show that no excessive aerodynamic loads are imposed upon an airship by normal horizontal maneuvering in smooth air, but that gusts encountered while cruising in rough air can cause forces which closely approach the design limits of the structure.

As a recommendation for future investigation, apparatus should be developed to carefully study the structure of the air with especial reference to gusts.

LANGLEY MEMORIAL AERONAUTICAL LABORATORY,
NATIONAL ADVISORY COMMITTEE FOR AERONAUTICS,
LANGLEY FIELD, VA., August 14, 1928.

REFERENCES

- Reference 1. Pannell, J. B., Frazer, R. A., and Bateman, H.: Experiments on Rigid Airship *R-32*. Part I: Pressures on Upper Fin and Rudder. British A. R. C. Reports and Memoranda No. 811, 1921.
- Reference 2. Richmond, Lieut. Col. V. C.: Full Scale Pressure Plotting Experiments on Hull and Fins of *H. M. A. R.-33*. British A. R. C. Reports and Memoranda No. 1044, 1927.
- Reference 3. Frazer, R. A., and Bateman, H.: Experiments on Rigid Airship *R-38*. British A. R. C. Reports and Memoranda No. 764, 1921.
- Reference 4. Crowley, J. W., jr., and De France, S. J.: Pressure Distribution on the *C-7* Airship. N. A. C. A. Technical Report No. 223, 1926.
- Reference 5. Coleman, Donald G.: Flight Path Angle and Air-Speed Recorder. N. A. C. A. Technical Note No. 233, 1926.
- Reference 6. Norton, F. H.: N. A. C. A. Recording Air-Speed Meter. N. A. C. A. Technical Note No. 64, 1921.
- Reference 7. Reid, H. J. E.: A Study of Airplanes with Special Reference to Angular Velocities. N. A. C. A. Technical Report No. 155, 1922.
- Reference 8. Ronan, K. M.: An Instrument for Recording the Position of Airplane Control Surfaces. N. A. C. A. Technical Note No. 154, 1923.
- Reference 9. Brown, W. G.: Synchronization of N. A. C. A. Flight Records. N. A. C. A. Technical Note No. 117, 1922.
- Reference 10. Crowley, J. W., jr., and Freeman, R. G.: Determination of Turning Characteristics of an Airship by Means of a Camera Obscura. N. A. C. A. Technical Report No. 208, 1925.
- Reference 11. Hemke, Paul E.: The Measurement of Pressure through Tubes in Pressure Distribution Tests. N. A. C. A. Technical Report No. 270, 1927.

TABLE II
RESULTANT PRESSURES ON TAIL SURFACES—TURNING

Run number.....	4B	4C	5C	2B	13D	6C	5D
Timing interval.....	2	7	9	5	13	5th from end	1
Rudder position.....	9.70° L.	8.30° R.	7.85° R.	12.75° R.	12.95° R.	13.25° R.	9.05° R.
Velocity, ft./sec.....	74.2	64.4	75.0	64.0	61.1	74.5	73.4
Angular velocity, rad./sec.....	{ 0.0043 count. clock.	0.0189 clock.	0.0217 clock.	0.0149 clock.	0.0191 clock.	{-----	{ 0.0153 clock.
Yaw at frame 80.....	7.1° L.	7.6° R.	6.8° R.	7.4° R.	7.4° R.	-----	2.7° R.
q in lb./sq. ft.....	6.19	4.37	5.93	4.47	3.95	5.98	5.82
Pressure.....	% q #/sq.ft.	% q #/sq.ft.	% q #/sq.ft.	% q #/sq.ft.	% q #/sq.ft.	% q #/sq.ft.	% q #/sq.ft.

LOWER FIN AND RUDDER

Orifice No.—														
1A.....	36.1	1.88	-6.7	-0.26	-8.8	-0.52	0.0	0.00	10.5	0.42	-10.0	-0.60	-6.2	-0.36
1A'.....	0.0	0.00	0.0	0.00	0.0	0.00	0.0	0.00	0.0	0.00	0.0	0.00	0.0	0.00
2A.....	-67.2	-3.50	108.2	4.74	95.4	5.72	76.8	3.43	98.8	3.90	104.4	6.24	53.3	3.12
2A'.....	-16.8	-0.87	56.0	2.44	52.6	3.12	47.7	2.13	59.2	2.34	53.0	3.17	43.8	2.55
2B.....	-42.0	-2.18	40.5	1.77	39.4	2.34	52.3	1.87	59.2	2.34	34.8	2.08	35.7	2.08
3A.....	-57.1	-2.97	50.0	2.18	52.6	3.12	39.5	1.77	43.4	1.72	55.6	3.32	29.5	1.72
3A'.....	-33.6	-1.75	41.6	1.82	35.1	2.08	23.2	1.04	46.1	1.82	42.5	2.54	10.7	0.62
3B.....	-33.6	-1.75	40.5	1.77	35.1	2.08	32.5	1.46	52.6	2.08	45.2	2.70	17.8	1.04
4A.....	-46.2	-2.40	89.3	3.90	70.1	4.16	113.9	5.10	131.6	5.20	108.6	6.50	38.5	2.24
4A'.....	-21.0	-1.09	34.5	1.51	35.1	2.08	33.7	1.51	26.3	1.04	34.8	2.08	25.9	1.51
4B.....	-39.5	-2.05	29.8	1.30	26.6	1.56	30.2	1.35	32.9	1.30	34.8	2.08	17.8	1.04
4C.....	-29.4	-1.53	23.8	1.04	17.6	1.04	23.2	1.04	22.4	0.88	25.2	1.51	13.5	0.73
5A.....	-69.7	-3.67	130.0	5.67	78.9	4.68	133.7	5.97	142.0	5.62	130.4	8.01	59.0	3.43
5A'.....	-60.5	-3.14	26.2	1.14	21.9	1.30	17.4	0.78	19.8	0.78	26.1	1.56	14.0	0.83
5B.....	-16.8	-0.87	61.8	2.71	52.6	3.12	44.2	1.95	52.7	2.08	53.0	3.17	35.7	2.08
5C.....	-19.3	-1.00	30.9	1.35	26.6	1.56	25.6	1.15	30.3	1.20	29.6	1.77	17.8	1.04
6A.....	-65.5	-3.40	138.3	6.03	100.9	5.98	107.0	4.78	131.5	5.20	140.0	8.37	62.6	3.64
6A'.....	-75.6	-3.93	23.8	1.04	17.5	1.04	9.3	0.42	0.0	0.00	11.3	0.68	13.0	0.73
6B.....	-35.3	-1.83	48.9	2.14	35.1	2.08	24.4	1.09	32.9	1.30	35.6	2.13	25.1	1.46
6C.....	-28.6	-1.49	45.3	1.95	19.4	1.15	22.1	0.99	17.1	0.68	26.9	1.61	8.9	0.52
6D.....	-10.1	-0.53	51.2	2.24	17.5	1.04	24.4	1.09	17.1	0.68	21.7	1.30	7.2	0.42
7A.....	-68.9	-3.58	87.1	3.80	78.9	4.68	65.2	2.91	79.0	3.12	76.5	4.57	29.5	1.72
7B.....	-14.3	-0.74	32.2	1.40	30.7	1.82	23.2	1.04	22.4	0.88	28.7	1.72	15.1	0.88
7C.....	-10.1	-0.53	19.1	0.83	21.9	1.30	17.4	0.78	15.8	0.62	26.9	1.61	8.9	0.52
7D.....	-5.9	-0.31	7.1	0.31	8.7	0.52	4.6	0.28	9.2	0.36	37.4	2.24	2.7	0.16
8A.....	-52.1	-2.71	90.6	3.95	65.8	3.90	73.2	3.28	73.7	2.91	73.9	4.42	32.1	1.87
8B.....	-7.6	-0.40	14.3	0.62	8.7	0.52	-2.3	-0.10	7.9	0.31	12.2	0.73	1.7	0.10
8C.....	-3.4	-0.18	-11.9	-0.52	-8.7	-0.52	-8.1	-0.36	-13.2	-0.52	-11.3	-0.68	-8.9	-0.52
9A.....	-54.6	-2.84	93.0	4.06	68.4	4.06	58.1	2.60	72.4	2.86	65.2	3.90	40.2	2.34
9B.....	-8.4	-0.44	-6.0	-0.26	0.0	0.00	-5.8	-0.26	-7.9	-0.31	-4.3	-0.26	-8.9	-0.52
9C.....	2.5	0.13	0.0	0.00	-4.3	-0.26	-5.8	-0.26	-7.9	-0.31	-5.2	-0.31	-9.8	-0.57
10A.....	-21.0	-1.09	52.4	2.29	35.1	2.08	8.6	0.38	23.7	0.94	38.2	2.28	16.8	0.99
10B.....	0.0	0.00	-11.9	-0.52	-8.7	-0.52	-17.4	-0.78	-19.8	-0.78	-8.7	-0.52	-17.8	-1.04
10C.....	0.0	0.00	0.0	0.00	0.0	0.00	-34.9	-1.56	-20.4	-0.83	13.0	0.78	-14.0	-0.83
10D.....	16.8	0.87	19.1	0.83	8.7	0.52	0.0	0.00	0.0	0.00	0.0	0.00	4.7	0.26
11A.....	-10.9	-0.57	-15.5	0.68	0.0	0.00	-34.9	-1.56	-19.8	-0.78	-34.8	-2.08	-11.0	-0.62
11B.....	-26.0	-1.35	-29.8	-1.30	-21.9	-1.30	-8.6	-0.52	-19.8	-0.78	-21.7	-1.30	-15.0	-0.88
11B'.....	30.5	1.58	-70.3	-3.07	-61.2	-3.64	-69.8	-3.12	-85.6	-3.38	-69.6	-4.16	-47.4	-2.76
11C.....	26.0	1.35	-57.0	-2.50	-53.4	-3.17	-55.8	-2.50	-53.0	-2.08	-60.0	-3.59	-46.4	-2.70
11D.....	8.4	0.44	-26.2	-1.14	-35.1	-2.08	-37.2	-1.63	-39.5	-1.56	-34.8	-2.08	-35.7	-2.08
12A.....	-24.4	-1.27	9.5	0.42	17.5	1.04	2.3	0.10	-6.6	-0.26	0.0	0.00	8.8	0.47
12B.....	5.0	0.26	-33.3	-1.46	-26.6	-1.56	-34.9	-1.56	-46.1	-1.82	-29.6	-1.77	-20.6	-1.20
12C.....	10.1	0.53	-17.9	-0.78	-17.5	-1.04	-25.6	-1.15	0.0	0.00	-18.3	-1.09	-14.0	-0.83
12D.....	10.9	0.57	-9.5	-0.42	-4.4	-0.26	0.0	0.00	-9.2	-0.36	-13.0	-0.78	-6.1	-0.36
13A.....	-8.4	0.44	9.5	0.42	26.6	1.56	8.6	0.52	17.1	0.68	12.2	-0.73	17.8	1.04
13B.....	4.2	0.22	4.8	0.21	0.0	0.00	-8.6	-0.52	0.0	0.00	0.0	0.00	4.4	0.26
13C.....	0.0	0.00	-7.1	-0.31	-8.8	-0.52	-5.8	-0.26	-13.2	-0.52	-11.3	-0.68	-8.9	-0.52

UPPER FIN

1A.....	-62.2	-3.84	89.4	3.90	57.0	3.38	87.2	3.90	56.6	2.23	78.3	4.68	25.9	1.50
2A.....	-5.9	-0.36	65.5	2.86	61.4	3.64	55.8	2.45	72.4	2.86	67.8	4.05	43.7	2.55
2B.....	-37.0	-2.28	33.4	1.43	35.1	2.08	34.9	1.56	32.9	1.30	39.1	2.34	19.7	1.14
3A.....	-82.4	-5.10	85.8	3.74	96.5	5.71	17.5	0.78	105.1	4.16	110.5	6.51	24.1	1.40
4A.....	-65.6	-4.05	60.8	2.65	70.2	4.16	58.1	2.60	65.8	2.60	63.5	3.80	26.8	1.56
4B.....	-4.2	-0.26	11.9	0.52	8.8	0.52	0.0	0.00	6.6	0.26	4.4	0.26	4.5	0.26

* Approximate.
NOTE.—Positive pressures act from port to starboard.

TABLE II

MANEUVERS U. S. S. "LOS ANGELES"

5D		5D		3C		3C		3C		17D		17D		17D		17D	
2¼		6		2		3¼		6		4		6		7		8	
4. 50° L.		7.70° L.		12.35° R.		6.50° L.		11.55° L.		12.50° R.		11.65° L.		12.15° L.		12.15° L.	
72.0		71.7		71.0		70.6		66.4		* 86.8		* 78.4		* 77.2		* 80.3	
0.0180 clock.		0.0096 count. clock.		0.0190 clock.		0.0205 clock.		0.0180 count. clock.		0.0226 clock.		0.0167 clock.		0.0035 clock.		0.0025 count. clock.	
5.1° R.		5.1° L.		6.6° R.		5.2° R.		5.8° L.		8.5° R.		3.6° R.		2.0° L.		5.2° L.	
5.62		5.56		5.41		5.36		4.73		* 7.96		* 6.50		* 6.30		* 6.81	
% q	#/sq.ft.	% q	#/sq.ft.	% q	#/sq.ft.	% q	#/sq.ft.	% q	#/sq.ft.	% q	#/sq.ft.	% q	#/sq.ft.	% q	#/sq.ft.	% q	#/sq.ft.

LOWER FIN AND RUDDER

0.0	0.00	52.2	2.91	-11.5	-0.62	0.0	0.00	-47.2	-2.24		-0.62		0.85		2.24		2.91
0.0	0.00	2.6	0.16	1.9	0.10	1.9	0.10	-2.2	-0.10		0.00		0.10		-0.16		-0.21
55.6	3.12	-59.9	-3.33	94.3	5.09	58.2	3.12	-55.0	-2.60		5.82		0.85		-2.60		-4.58
44.5	2.50	-17.8	-0.99	52.0	2.81	34.0	1.82	-20.9	-0.99		3.43		1.04		-1.04		-1.66
30.7	1.72	-54.1	-3.02	38.5	2.08	26.2	1.40	-14.3	-0.68		4.16		0.16		-3.59		-3.85
30.7	1.72	-42.1	-2.34	48.1	2.60	33.0	1.77	-73.7	-3.48		2.96		0.52		-2.24		-3.95
31.5	1.77	-29.8	-1.66	40.4	2.18	26.2	1.40	-34.1	-1.61		2.96		1.04		-1.30		-2.50
26.0	1.46	-35.6	-1.98	39.4	2.13	27.2	1.46	-40.7	-1.92		3.12		0.10		-1.92		-3.07
36.4	2.03	-46.8	-2.60	66.4	3.59	32.0	1.72	-52.8	-2.50		8.37		0.73		-2.24		-4.32
18.6	1.04	-7.2	-0.42	32.7	1.77	20.2	1.09	-13.2	-0.62		2.44		0.78		-1.30		-1.66
18.6	1.04	-39.3	-2.18	28.9	1.56	15.5	0.83	-46.2	-2.18		2.44		-0.21		-2.18		-3.02
7.5	0.42	-36.5	-2.03	18.3	0.99	4.8	0.26	-46.2	-2.18		1.56		-0.52		-2.86		-1.70
55.3	3.12	-45.0	-2.50	104.0	5.62	49.5	2.68	-67.0	-3.18		9.41		1.14		-1.35		-6.24
16.0	0.88	-46.8	-2.60	15.4	0.83	7.8	0.42	-63.7	-3.02		1.56		0.00		-2.29		-5.36
39.9	2.24	-16.9	-0.94	46.2	2.50	42.7	2.28	-23.1	-1.09		3.38		1.56		-0.88		-1.82
15.7	0.88	-14.0	-0.78	29.8	1.61	19.4	1.04	-18.7	-0.88		2.03		0.26		-0.94		-1.40
71.3	4.06	-65.5	-3.64	134.5	7.28	60.1	3.22	-68.2	-3.22		9.88		0.42		-2.86		-6.60
7.5	0.42	-77.8	-4.32	14.4	0.78	12.6	0.68	-92.3	-4.37		0.78		0.00		-2.13		-6.55
25.3	1.41	-29.9	-1.66	39.4	2.13	25.2	1.35	-30.8	-1.46		2.44		0.36		-1.72		-2.50
4.6	0.26	-31.8	-1.77	18.3	0.99	9.7	0.52	-37.4	-1.77		1.72		-0.26		-1.77		-2.08
7.5	0.42	-14.0	-0.78	21.1	1.14	10.7	0.57	-22.0	-1.04		1.61		0.00		-1.04		-1.04
68.6	3.85	-59.0	-3.28	75.0	4.06	32.0	1.72	-74.8	-3.54		5.20		0.26		-3.12		-5.93
21.4	1.20	-15.8	-0.88	28.9	1.56	25.2	1.35	-18.7	-0.88		2.18		0.52		-0.26		-1.25
11.0	0.62	-14.0	-0.78	15.4	0.83	8.7	0.47	-16.5	-0.78		1.25		0.26		-0.78		-2.50
5.5	0.31	-6.4	-0.36	6.7	0.36	6.8	0.31	-9.9	-0.47		0.52		0.00		-0.26		-0.99
55.6	3.12	-56.6	-3.17	68.2	3.69	51.4	2.76	-61.5	-2.91		5.20		0.31		-2.91		-3.95
13.0	0.73	-5.5	-0.31	5.8	0.31	17.5	0.94	-6.6	-0.31		1.72		0.52		0.52		-0.62
1.8	0.10	2.8	0.16	-11.5	-0.62	-4.0	-0.21	-7.7	-0.36		-0.36		0.16		0.26		-0.05
67.8	3.80	-57.9	-3.22	61.5	3.33	79.5	4.26	-68.2	-3.22		5.20		0.94		-4.11		-4.94
4.6	0.26	-4.6	-0.26	-11.5	-0.62	12.6	0.68	-4.4	-0.21		-0.36		0.21		0.10		-0.10
8.4	0.47	4.6	0.26	-4.8	-0.26	16.5	0.88	9.9	0.47		-0.42		0.62		0.88		0.42
64.8	3.64	-24.3	-1.35	32.7	1.77	83.5	4.47	-9.9	-0.47		2.08		1.77		-1.66		-1.61
25.1	1.41	9.4	0.52	-13.5	-0.73	34.9	1.87	12.1	0.57		-0.52		1.61		1.87		1.09
21.4	1.20	13.1	0.73	-5.8	-0.31	42.7	2.28	26.4	1.25		-0.83		1.82		2.08		1.82
20.3	1.14	18.7	1.04	2.9	0.16	33.0	1.77	29.7	1.41		-0.16		2.03		1.77		1.56
82.6	4.63	-12.2	-0.68	-28.9	-1.56	116.5	6.24	-6.6	-0.31		-1.56		5.36		0.99		0.52
12.1	0.68	-22.5	-1.25	-24.0	-1.30	21.4	1.14	-9.9	-0.47		-1.66		-1.56		-0.83		0.52
42.6	2.39	44.1	2.45	-76.0	-4.11	57.2	3.07	69.3	3.28		-4.68		3.85		5.10		-4.57
36.2	2.03	36.5	2.03	-66.0	-3.59	38.0	2.03	43.0	2.03		-2.81		2.03		3.54		3.54
9.3	0.52	23.4	1.30	-38.5	-2.08	16.5	0.88	27.5	1.30		-2.08		0.85		1.66		2.18
46.4	2.60	-19.6	-1.09	8.7	0.47	59.2	3.17	-17.6	-0.83		0.16		2.24		-0.16		-1.04
5.5	0.31	9.4	0.52	-32.7	-1.77	17.5	0.94	24.2	1.14		-1.92		0.94		0.88		1.20
11.0	0.62	18.7	1.04	-20.2	-1.09	27.0	1.46	13.2	0.62		0.26		1.66		1.66		2.08
0.0	0.00	11.1	0.62	-12.5	-0.68	5.8	0.31	6.6	0.31		-0.78		0.62		0.94		0.62
37.1	2.08	-12.2	-0.68	23.1	1.25	38.8	2.08	-8.8	-0.42		1.04		2.45		-0.26		-0.52
1.8	0.10	9.4	0.52	-3.8	-0.21	16.5	0.88	18.7	0.88		-0.52		0.47		0.47		0.88
-1.8	-0.10	0.0	0.00	-17.3	-0.94	1.9	0.10	0.0	0.00		3.22		0.10		0.10		0.10

UPPER FIN

35.2	1.97	-61.6	3.43	42.3	2.29	19.4	1.04	-90.2	-4.26		4.99		-0.21		-2.60		-5.68
50.9	2.86	-10.7	-0.52	67.3	3.64	27.2	1.45	-5.5	-0.25		3.22		1.30		-1.04		-3.65
23.1	1.30	-32.7	-1.82	32.7	1.77	16.5	0.88	-44.0	-2.08		2.65		0.10		-1.66		-2.92
51.9	2.91	-88.8	-4.94	82.7	4.47	33.0	1.77	-132.0	-6.24		7.49		0.16		-6.14		-9.39
47.2	2.65	-56.1	-3.12	49.0	2.65	43.6	2.39	-79.2	-3.74		4.32		0.21		-1.14		-5.52
12.0	0.67	10.7	0.52	4.8	0.26	19.4	1.04	14.3	0.67		0.00		0.73		0.52		0.26

TABLE III
RESULTANT PRESSURES ON TAIL SURFACES U. S. S. "LOS ANGELES" DUE TO GUSTS

[Pressures in lb./sq. ft.]

Orifice No.	Run No. 4A	Run No. 5A	Orifice No.	Run No. 4A	Run No. 5A	Orifice No.	Run No. 4A	Run No. 5A
STARBOARD FIN AND ELEVATOR								
1A	7.29	6.25	6A	13.02	8.95	10C	0.26	2.86
1A'	3.13	3.12	6B	3.13	1.82	11D	-1.30	1.04
2A	7.29	6.25	6C	3.39	2.08	11A	10.93	12.20
2A'	2.86	2.60	6D	1.82	0.94	11A'	-0.78	2.60
2B	4.69	3.12	7A	8.07	6.25	12A	8.85	11.45
3A	5.22	4.15	7B	1.30	0.78	12B	-1.04	9.35
3A'	2.08	1.82	7C	1.30	0.67	12C	-3.65	4.42
3B	2.87	1.56	7D	0.62	0.36	12D	-1.30	2.86
4A	10.68	7.80	8A	7.81	6.25	13A	1.82	8.58
4A'	1.30	1.04	8B	1.56	1.56	13B	0.52	3.12
4B	4.17	2.60	8C	0.52	0.83	13C	0.52	2.08
4C	2.61	0.94	9A	7.81	7.30	13D	-0.78	0.52
5A	10.68	7.80	9B	1.82	2.08	14A	-0.78	0.00
5A'	1.56	1.56	9C	0.00	0.00	14B	-0.26	1.56
5B	3.13	2.08	10A	13.02	16.10	14C	-0.78	0.52
5C	2.19	1.04	10B	0.52	2.60	14D	0.00	0.00
LOWER FIN AND RUDDER								
1A	2.08	2.18	6A	-3.12	-3.12	10B	-1.00	-2.08
1A'			6A'			10C	-1.30	-2.08
2A	-2.08	-3.02	6B	-2.08	-2.65	10D	0.00	-0.10
2A'	-0.00	0.00	6C	-1.30	-1.82	11A	-4.69	-7.28
2B	-1.56	-2.18	6D	-0.78	-1.04	11B	-2.35	-3.90
3A	-2.35	-3.12	7A	-1.82	-1.56	11B'	-3.38	-5.72
3A'	-1.30	-1.30	7B	-0.78	-1.09	11C	-1.04	-2.08
3B	-1.30	-1.56	7C	-0.52	-0.78	11D	0.00	-0.68
4A	-2.08	-2.08	7D	-0.52	-1.14	12A	-4.17	-6.24
4A'	0.00	-1.04	8A	-1.30	-2.86	12B	-1.30	-1.56
4B	-2.08	-2.08	8B	0.63	-1.04	12C	-0.78	-1.04
4C	-1.30	-1.82	8C	-0.63	-1.19	12D	0.00	-0.26
5A	-0.78	-1.46	9A	-1.30	-5.10	13A	-2.08	-4.58
5A'	0.00	-1.56	9B	-0.52	-0.42	13B		-0.26
5B	-0.52	-0.94	9C	-0.26	-1.04	13C		-5.30
5C	-0.62	-1.30	10A	-2.08	-2.50	13D		

NOTE.—Run 4A, $q=8.01$ lb./sq. ft. Run 5A, $q=7.02$ lb./sq. ft. (approximate).
Positive pressures act from port to starboard and bottom to top.

TABLE IV
FORCES AND NORMAL FORCE COEFFICIENTS TAIL SURFACES U. S. S. "LOS ANGELES"

Maneuvers	Run No.	Timing interval	Rudder position	q lb./ft. ²	Fin load, lbs.	Rudder load, lbs.	Total load, lbs.	C_{NF} Fin	C_{NF} Rudder	C_{NF} Total
LOWER FIN AND RUDDER										
Turn	4B	2	9.70° L.	6.19	-1,255	87	-1,168	-0.191	0.068	-0.149
Do	4C	7	8.30° R.	4.37	1,482	-182	1,300	.320	-.201	.235
Do	5C	9	7.85° R.	5.93	1,533	-229	1,304	.244	-.187	.173
Do	2B	5	12.75° R.	4.47	968	-212	756	.204	-.229	.133
Do	13D	13	12.95° R.	3.95	1,184	-200	984	.282	-.244	.196
Do	6C	5 F. E. ¹	13.25° R.	5.98	1,936	-297	1,639	.305	-.240	.216
Reversal	5D	1	9.05° R.	5.82	728	-182	546	.118	-.151	.074
Do	5D	2¼	4.50° L.	5.62	1,460	219	1,679	.245	.188	.236
Do	5D	6	7.70° L.	5.56	-1,045	120	-925	-.177	.104	-.131
Do	3C	2	12.35° R.	5.41	1,466	-278	1,188	.256	-.248	.173
Do	3C	3¼	6.50° L.	5.36	1,459	358	1,817	.257	.323	.268
Do	3C	6	11.55° L.	4.73	-1,141	168	-973	-.227	.172	-.162
Do	17D	4	12.50° R.	* 7.96	2,139	-217	1,922	* .253	* -.132	* .190
Do	17D	6	11.65° L.	* 6.50	589	329	918	* .085	* .245	* .111
Do	17D	7	12.15° L.	* 6.30	-205	315	110	* .031	* .242	* .014
Do	17D	8	12.15° L.	* 6.81	-1,612	281	-1,331	* .223	* .199	* .154
Rough Air	4A	8¼	3.05° R.	8.01	-1,031	-246	-1,277	-.121	-.149	-.126
Do	5A	9¼	6.90° R.	* 7.02	-1,689	-323	-2,012	* -.227	* -.222	* -.226
STARBOARD FIN AND ELEVATOR										
Rough air	4A	8¼	15.60° D.	8.01	3,227	274	3,501	0.396	0.146	0.349
Do	5A	9¼	18.40° D.	* 7.02	2,533	986	3,519	* .355	* .1598	* .1,400

* Approximate.

NOTE.—Positive pressures act from port to starboard and from bottom to top.

Lower fin area=1,061 sq. ft.
Lower rudder area=207 sq. ft.
Starboard fin area=1,018 sq. ft.
Starboard elevator area=235 sq. ft.

TABLE V
PRESSURES ON HULL OF U. S. S. "LOS ANGELES"

Run No.	4A	5A	4B	4C	5C	6C	3C	3C	3C
Timing interval.....	8 $\frac{1}{4}$	9 $\frac{1}{4}$	2	7	9	5th F. E.	2	3 $\frac{1}{4}$	6
Rudder position.....	3° R.	7° R.	9.70° L.	8.30° R.	7.85° R.	13.25° R.	12.35° R.	6.50° L.	11.55° L.
Velocity ft./sec.....	83.2	* 79.2	74.2	64.4	75.0	74.5	71.0	70.6	66.4
Angular velocity rad./sec.....			{ 0.0043 Count. clock.	{ 0.0189 Clock.	{ 0.0217 Clock.		{ 0.0190 Clock.	{ 0.0205 Clock.	{ 0.0180 Count. clock.
Yaw at frame 80.....			7.1° L.	7.6° R.	6.8° R.		6.6° R.	5.2° R.	5.8° L.
q in lb./ft. ²	8.01	* 7.02	6.19	4.37	5.93	5.98	5.41	5.36	4.73

PRESSURES IN POUNDS PER SQUARE FOOT									
Orifice No.	Longitudinal row								
Nose.....	6.19	7.49	5.73	4.16	5.98	6.14	5.46	5.04	4.73
186A.....	4.94	4.58	3.44	2.71	4.01	4.03	3.28	2.76	3.12
186B.....		1.98	2.16	2.13	2.86	2.86	2.34	2.08	2.34
183- $\frac{1}{4}$ A.....	1.87	1.20	0.99	1.46	1.66	1.74	1.46	1.71	1.46
183- $\frac{1}{4}$ B.....	1.46	1.61	0.83	0.93	1.46	1.09	0.99	0.68	0.83
179- $\frac{1}{2}$ A.....			-0.21						
179- $\frac{1}{2}$ B.....	1.20	0.21		0.21	0.26	0.36	0.21	0.00	0.21
175B.....	0.00	-0.42		0.47	0.52	0.62	0.36	0.26	0.42
170A.....		-0.26		0.00	0.00	0.15	-0.15		0.00
170B.....	-0.10	-0.42	-0.05	-0.21	0.00	0.00	-0.36	-0.31	-0.36
165A.....	-0.62	-0.47	-0.31	-0.21	-0.26	-0.21	-0.36	-0.21	-0.26
165B.....									
160A.....			-0.26	-0.05	0.00	0.00	0.00	0.00	-0.05
160B.....	0.00	+0.10	0.15	0.31	0.26	-0.26	0.10	0.05	0.10
155A.....									
155B.....	-0.42	-0.31	0.00	-0.10	0.00	0.00	0.10	-0.05	-0.10
150A.....	-0.50	-0.68	-0.10	0.42	0.21	0.21	0.00	-0.10	0.21
150B.....	-0.31	-0.52	-0.15	0.15	0.31	0.15	0.15	-0.26	0.15
175-2S.....	-0.68	-0.78	-0.52	-0.26	-0.36	0.15	-0.42	-0.10	-0.36
145-2S.....		-0.26	0.00	0.10	0.00	0.31	0.00	-0.05	0.00
Frame 175									
14S.....	0.42	0.00	0.10	0.42	0.26	0.42	0.10	0.10	0.36
2S.....	-0.68	-0.78	-0.52	-0.26	-0.36	-0.15	-0.42	-0.10	-0.36
2Sa.....	-0.16	-0.36	-0.21	0.15	0.00	0.10	0.00	0.00	0.15
2Sb.....	-0.13	-0.42	0.15	0.31	0.36	0.42	0.15	0.15	0.31
2Sc.....	-0.13	-0.42	0.00	0.15	0.26	0.21	0.05	0.00	0.05
2Sd.....									
3S.....	-0.31	-0.42	-0.10	-0.10	-0.26	0.00	0.31	-0.21	-0.10
3S'.....	-0.16	-0.31	-0.15	0.00	0.00	0.00	0.00	0.00	0.00
4S.....	-0.62	-0.78	-0.10	-0.26	0.00	0.00	-0.36	-0.36	-0.26
5S.....	-0.10	-0.10	-0.36	0.36	0.52	0.68	0.31	0.31	0.36
6S.....	-0.10	-0.21	-0.15	0.00	0.00	0.15	0.00	-0.05	0.00
6S'.....	0.00	-0.05	0.00	0.00	0.00	0.15	0.00	-0.15	0.00
5P.....		-0.78	-0.31	-0.31	-0.52	-0.52	-0.31	-0.31	-0.05
4P.....	-0.68	-0.68	-0.31	0.00	0.00	0.00	-0.31	0.05	-0.10
3P.....		-0.26	0.10	0.00	0.00	0.26	-0.21	0.10	-0.10
3P'.....	-0.39	+0.26	-0.10	0.21	0.21	0.21	0.31	-0.36	0.26
2P.....	-0.42	+0.36	-0.15	0.42	0.36	0.36	0.10	0.36	0.10
1P.....	0.26	0.21	0.21	0.00	0.00	0.15		-0.05	-0.10
Frame 145									
1S.....	-0.68	-0.31	-0.31	-0.31	0.00	0.00	0.00	-0.31	0.00
2S.....		-0.26	0.00	0.10	0.00	0.31	0.00	-0.05	0.00
2Sa.....	-0.42	-0.26	0.00	0.05	0.00	0.00	0.10	0.10	0.10
2Sb.....	-0.42	-0.42	-0.15	0.00	0.00	0.00	0.00	0.00	0.00
2Sc.....	-0.10	-0.10	-0.10	-0.05	0.00	0.00	0.00	0.21	0.00
2Sd.....	-0.31	-0.36	0.00	0.00	0.00	0.00	-0.15	-0.05	-0.10
3S.....	-0.36	-0.52	-0.15	0.00	0.00	0.00	0.00	0.00	-0.36
3S'.....	-0.36	-0.16	-0.15	0.00	0.00	-0.10	0.00	0.00	0.00
4S.....	-0.21	-0.42	-0.21	-0.26	-0.36	-0.52	-0.21	-0.21	-0.21
5S.....	-0.26	-0.36	0.10	0.00	0.26	0.26	0.26	0.05	0.26
5 $\frac{1}{2}$ S.....	-0.68	-0.94	0.57	-0.36	-0.52	-0.52	-0.15	-0.36	-0.21
5 $\frac{1}{2}$ S'.....	-0.10	-0.47	0.62	0.00	0.00	-0.10	-0.10	0.00	-0.10
5P.....	-0.42	-0.31	-0.26	-0.10	0.00	0.00	0.00	-0.05	-0.26
4P.....	-0.36	-0.47	-0.15	-0.21	-1.04	0.00	-0.15	-0.36	-0.15
3P.....	-0.78	-0.94	-0.62	-0.15	0.00	-0.15	-0.15	0.00	-0.15
3P'.....	-0.26	-0.21	0.26	0.00	0.00	0.00	0.15	0.10	0.00
2P.....	-0.62	-0.42	-0.31	-0.10	0.00	-0.10	0.15	-0.10	0.15
1P.....	-0.57	-0.42	-0.15	0.00	0.00	0.00	0.00	-0.15	0.00

* Approximate.

TABLE VI
TRANSVERSE FORCES AT TWO FRAMES U. S. S. "LOS ANGELES" HULL

Run No.	Timing interval	Frame 145		Frame 175	
		Vertical lbs.	Horizontal lbs.	Vertical lbs.	Horizontal lbs.
4A-----	8¼-----	14.40	-12.2	6.70	22.00
5A-----	9¾-----	11.61	11.8	2.50	17.50
4B-----	2-----	19.87	-19.47	-4.60	12.87
4C-----	7-----	2.67	5.73	-4.40	9.33
5C-----	9-----	13.73	25.53	-1.00	5.60
6C-----	5th from end--	0.13	13.93	3.33	8.20
3C-----	2-----	1.33	5.20	6.33	7.67
3C-----	3¼-----	1.80	10.00	-8.40	5.23
3C-----	6-----	-3.07	12.33	1.27	2.87

NOTE.—Positive forces act up and to starboard.

TABLE VII
TURNING MANEUVERS U. S. S. "LOS ANGELES"—RESULTANT PRESSURES ON PASSENGER CAR

Run No.-----		4B	4C	5C	6C	3C	3C	3C
Timing interval-----		2	7	9	(1)	2	3¼	6
q in lb./ft. ² -----		6.19	4.37	5.93	5.98	5.41	5.36	4.73
Orifice No.	Dist. to nose of car, ft.	Resultant pressures in lb./sq. ft.						
C1-----	15.0	-.26	0	.78	0	.10	0	.31
C2-----	22.7	-.21	-.42	.26	-.42	-.21	-.21	-.21
C3-----	30.3	-.73	-.73	0	-.62	-.73	-.62	-.73
C4-----	38.0	0	-.31	.52	-.62	-.31	0	-.31
C5-----	45.6	-.10	0	.78	0	0	0	0

¹ Fifth from end of record.

TABLE VIII
RESULTANT PRESSURES ON FABRIC OF TAIL SURFACES AND HULL DURING MANEUVERS IN SMOOTH AIR

Run No.-----	4A	5A	4B	4C	5C	2B	13D	6C	5D	5D	5D	3C	3C	3C	17D	17D	17D	17D
Timing interval.-----	8¼	9¾	2	7	9	5	13	(1)	1	2¼	6	2	3¼	6	4	6	7	8
Orifice No.	Lower fin and rudder pressure in lb./sq. ft.																	
1A-1A'-----			0.00	0.00	0.00	0.00	0.00	0.00	0.00	0.16	0.10	0.10	0.10	0.00	0.10	0.16	0.21	
2A-2A'-----	0.00	0.00	1.04	2.44	3.12	2.13	2.34	3.17	2.55	2.50	.99	2.81	1.82	.52	3.43	1.04	1.04	1.66
3A-3A'-----	1.30	1.30	2.08	1.82	2.08	1.04	1.82	2.60	.62	1.77	1.67	2.18	1.40	1.61	2.96	1.04	1.30	2.50
4A-4A'-----	0.00	1.04	1.30	1.51	2.08	1.51	1.04	2.08	1.51	1.04	.42	1.77	1.09	.62	2.44	.78	1.30	1.66
5A-5A'-----	0.00	1.56	3.74	1.14	1.30	.78	.78	1.56	.83	.88	2.60	.83	.42	3.02	1.56	.00	2.29	5.36
6A-6A'-----	1.82	1.66	4.68	1.04	1.04	.42	.00	.68	.73	.42	4.31	.78	.68	4.36	.78	.00	2.13	6.60
11B-11B'-----	3.38	5.72	1.61	.88	1.30	.52	.78	1.30	.88	.68	1.25	1.30	1.14	.47	1.66	1.56	.83	.52
	Hull pressure in lb./sq. ft.																	
145-3S-3S'-----	.36	.16	.00	.00	.00			0.10				0.00	.00	.36				
145-5½S-5½S'-----	.10	.47	.05	.36	.52			.42				.05	.36	.10				
145-3P-3P'-3P'-----	.26	.21	.88	.16	.00			.16				.31	.10	.16				
175-3S-3S'-----	.16	.31	.05	.10	.26			.00				.31	.21	.10				
175-6S-6S'-----	.00	.47	.16	.00	.00			.00				.00	.10	.00				
175-3P-3P'-----	.39	.42	.21	.21	.21			.05				.52	.47	.36				

¹ Indicates fifth from end.

NOTE.—Manometer for recording hull pressures was not on board during all runs, causing the lack of hull data.

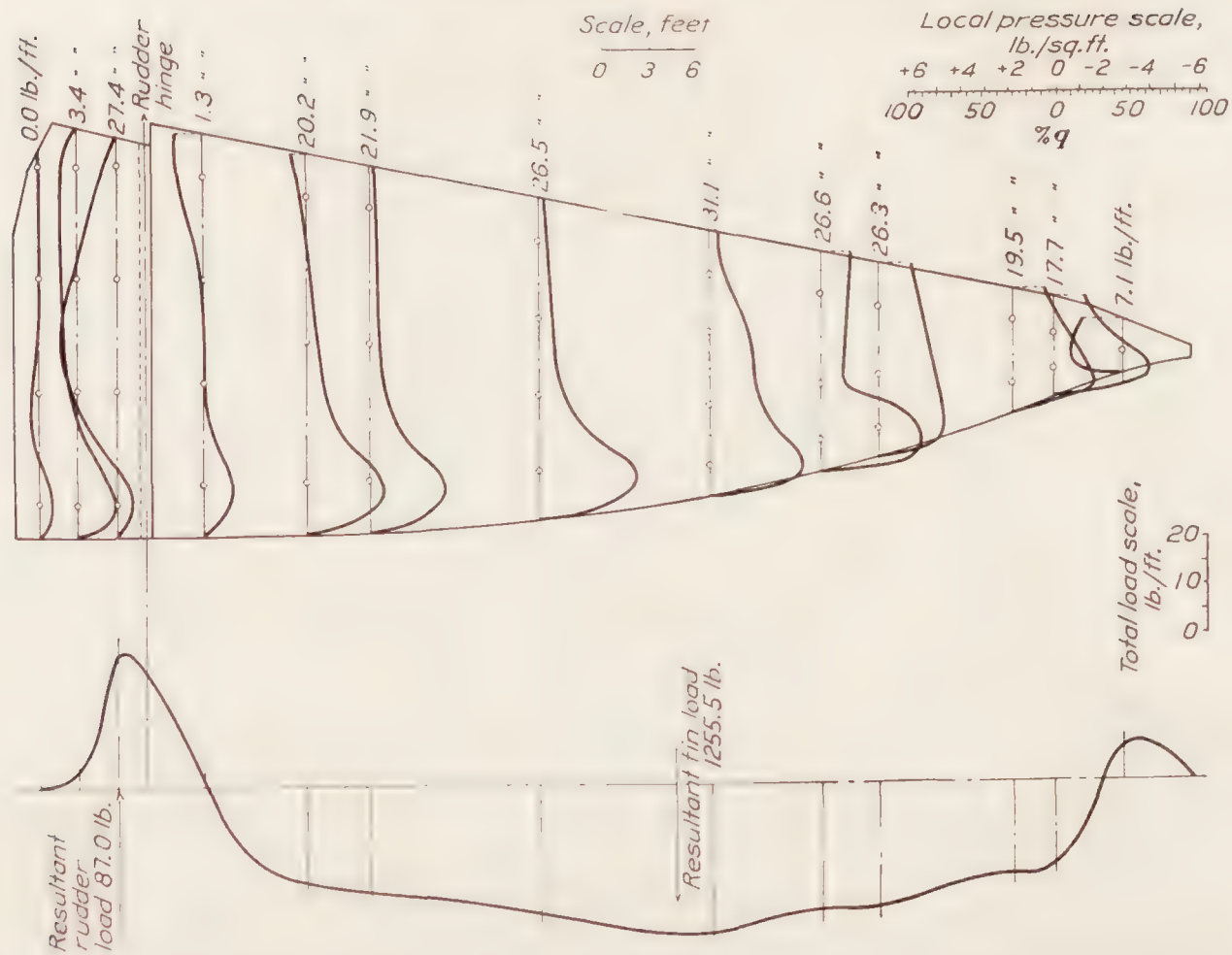


FIGURE 8.—Pressure distribution on lower fin and rudder. Steady turn. Run No. 4B—timing interval 2. Rudder position 9° 15' port. Air speed 50.6 M. P. H.

NOTE.—Positive pressures acting from port to starboard

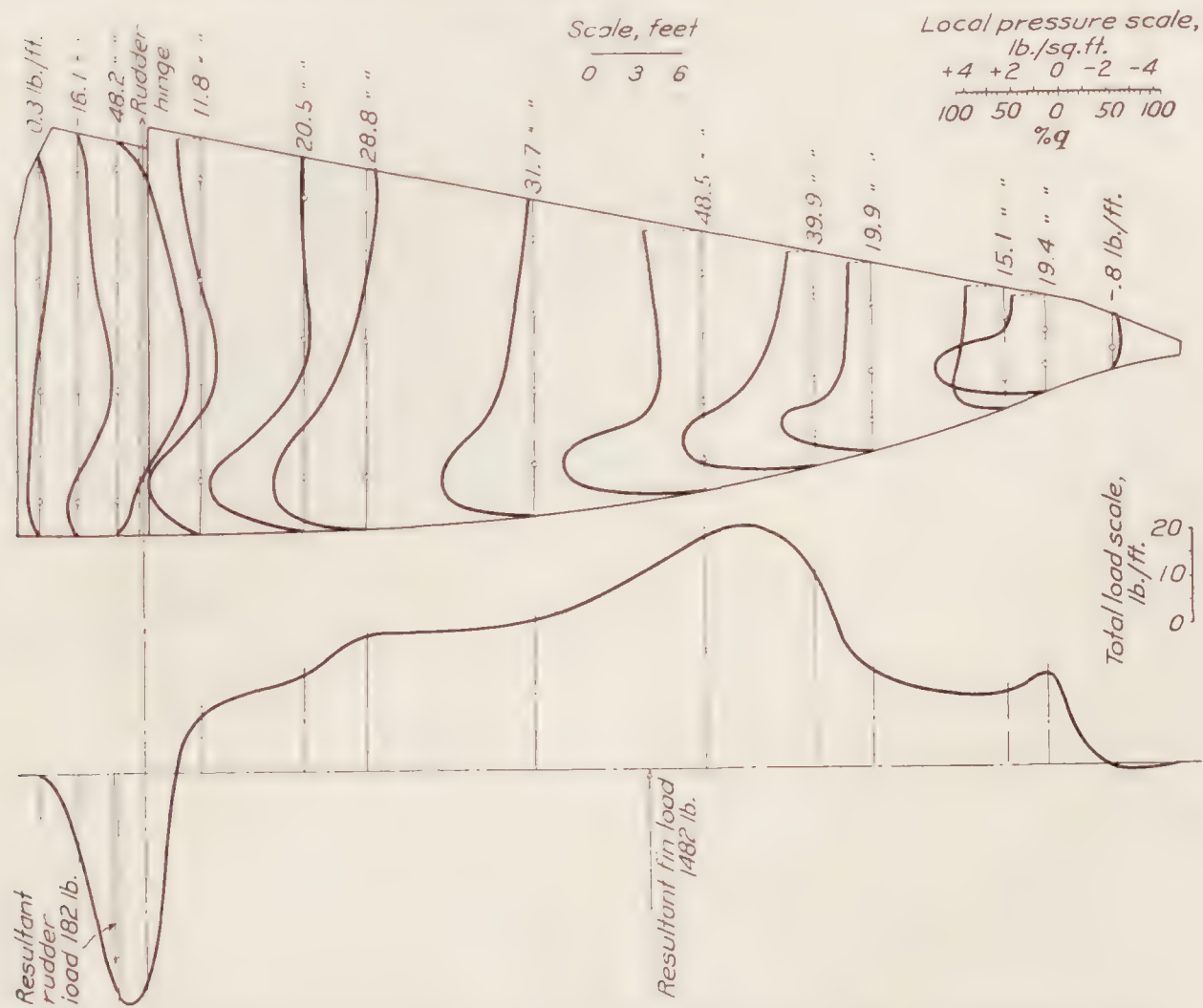


FIGURE 9.—Pressure distribution on lower fin and rudder. Steady turn. Run No. 4C—timing interval 7. Rudder position 8° 15' starboard. Air speed 43.9 M. P. H.

NOTE.—Positive pressures acting from port to starboard

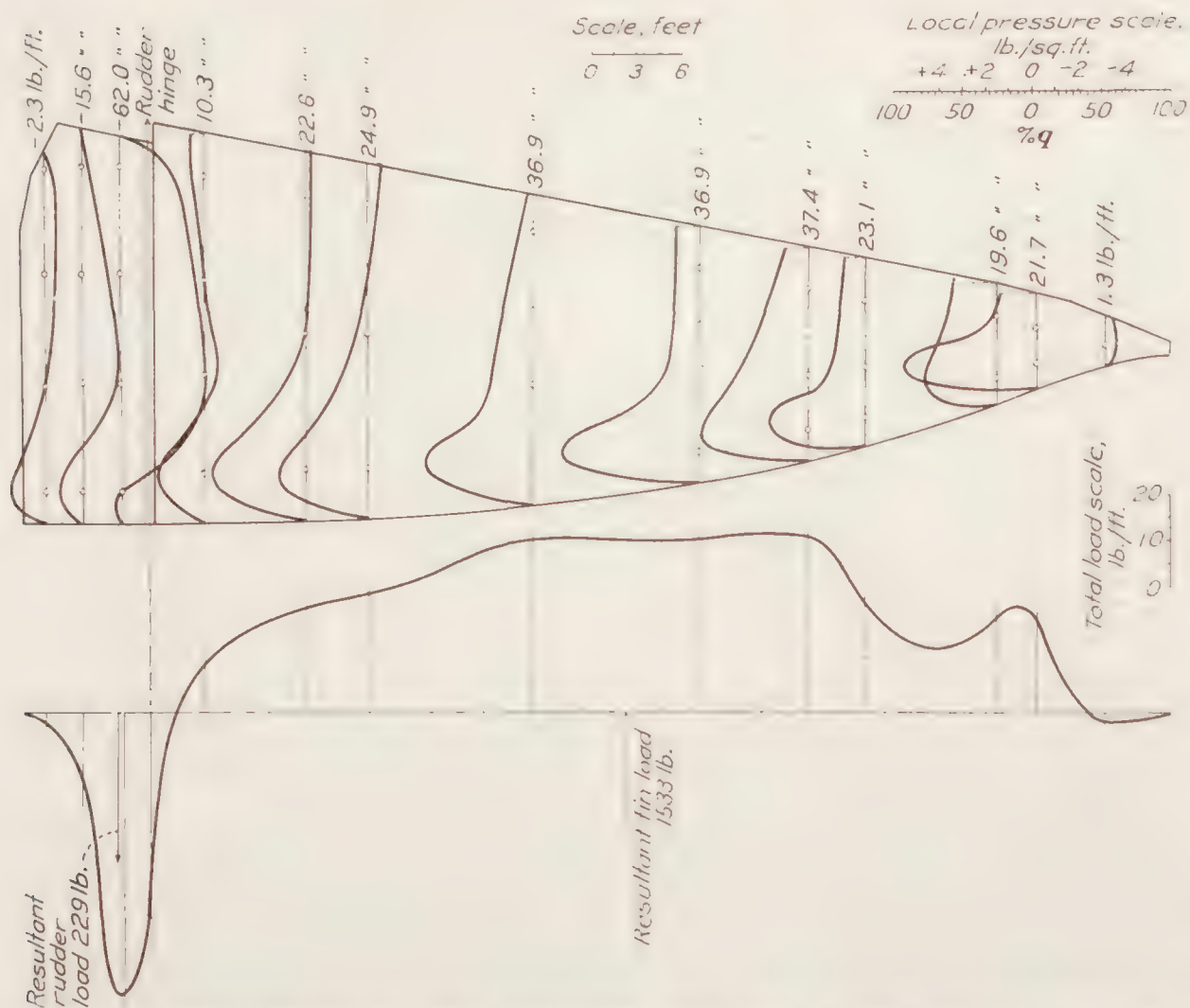


FIGURE 10.—Pressure distribution on lower fin and rudder. Steady turn. Run No. 5C—timing interval 9. Rudder position $7^{\circ} 30'$ starboard. Air speed 51.2 M. P. H.

NOTE.—Positive pressures acting from port to starboard.

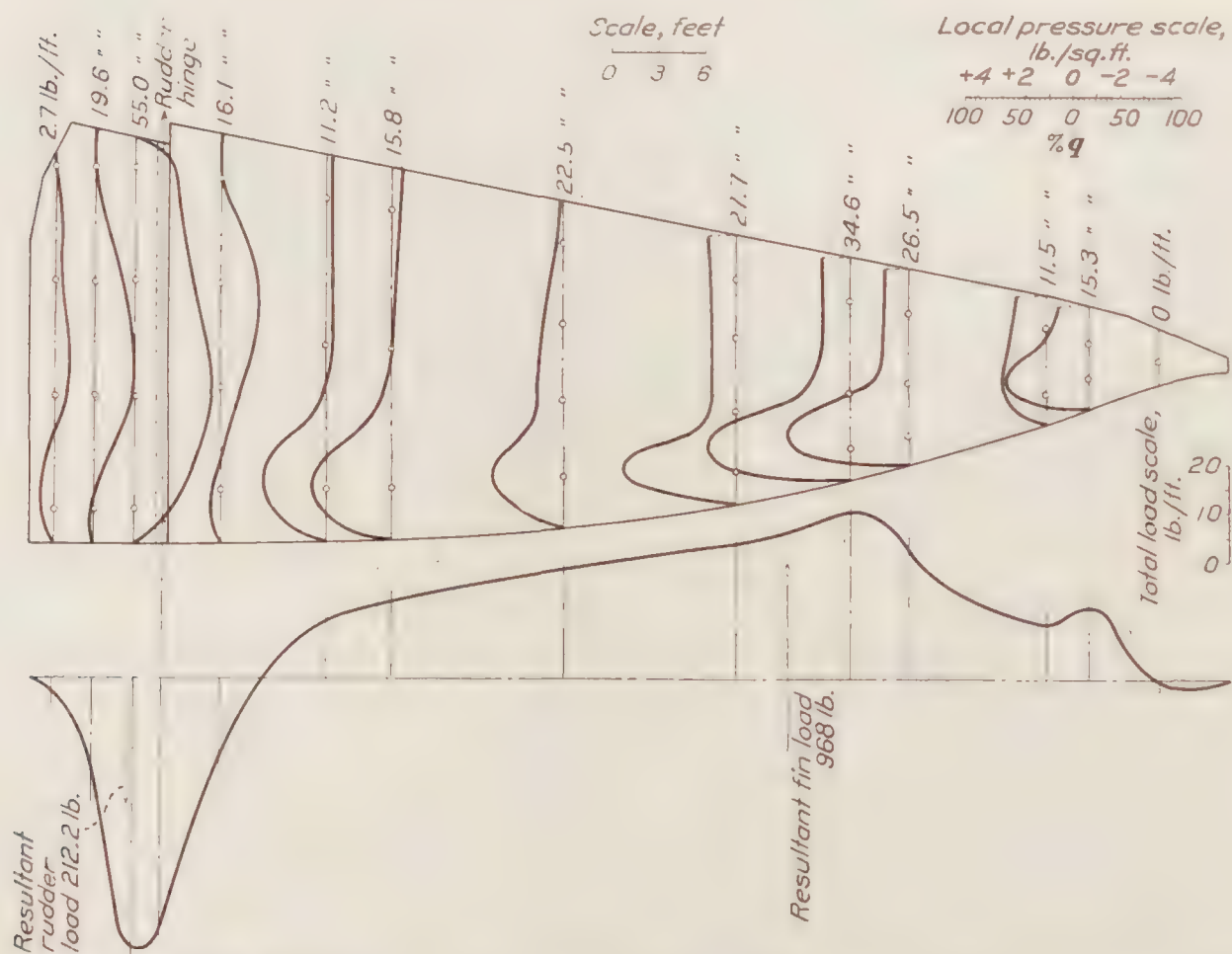


FIGURE 11.—Pressure distribution on lower fin and rudder. Steady turn. Run No. 2B—timing interval 5. Rudder position $12^{\circ} 45'$ starboard. Air speed 43.6 M. P. H.

NOTE.—Positive pressures acting from port to starboard.

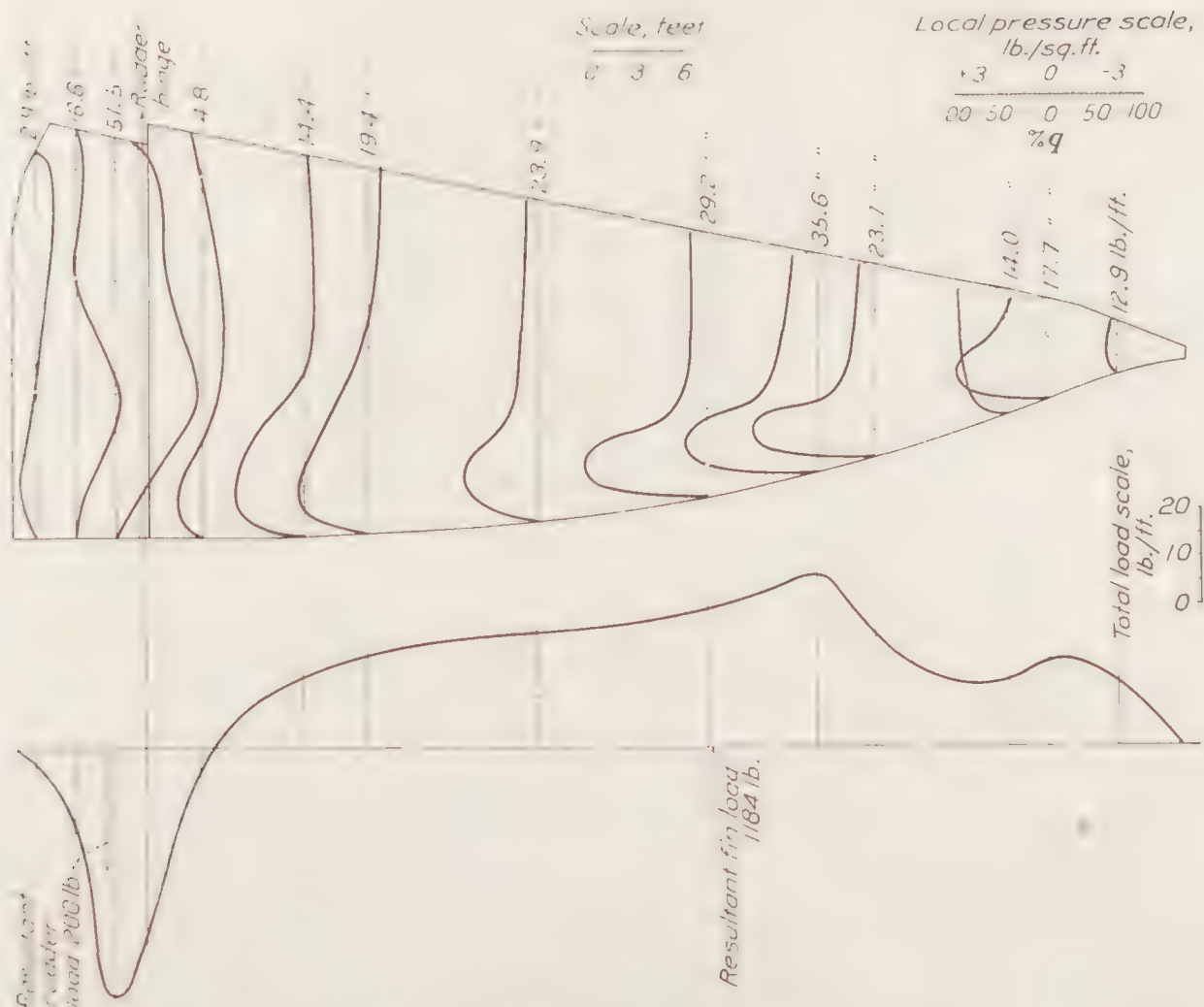


FIGURE 12.—Pressure distribution on lower fin and rudder. Steady turn. Run No. 13D—timing interval 13. Rudder position $12^{\circ} 30'$ starboard. Air speed 41.7 M. P. H.

NOTE.—Positive pressures acting from port to starboard.

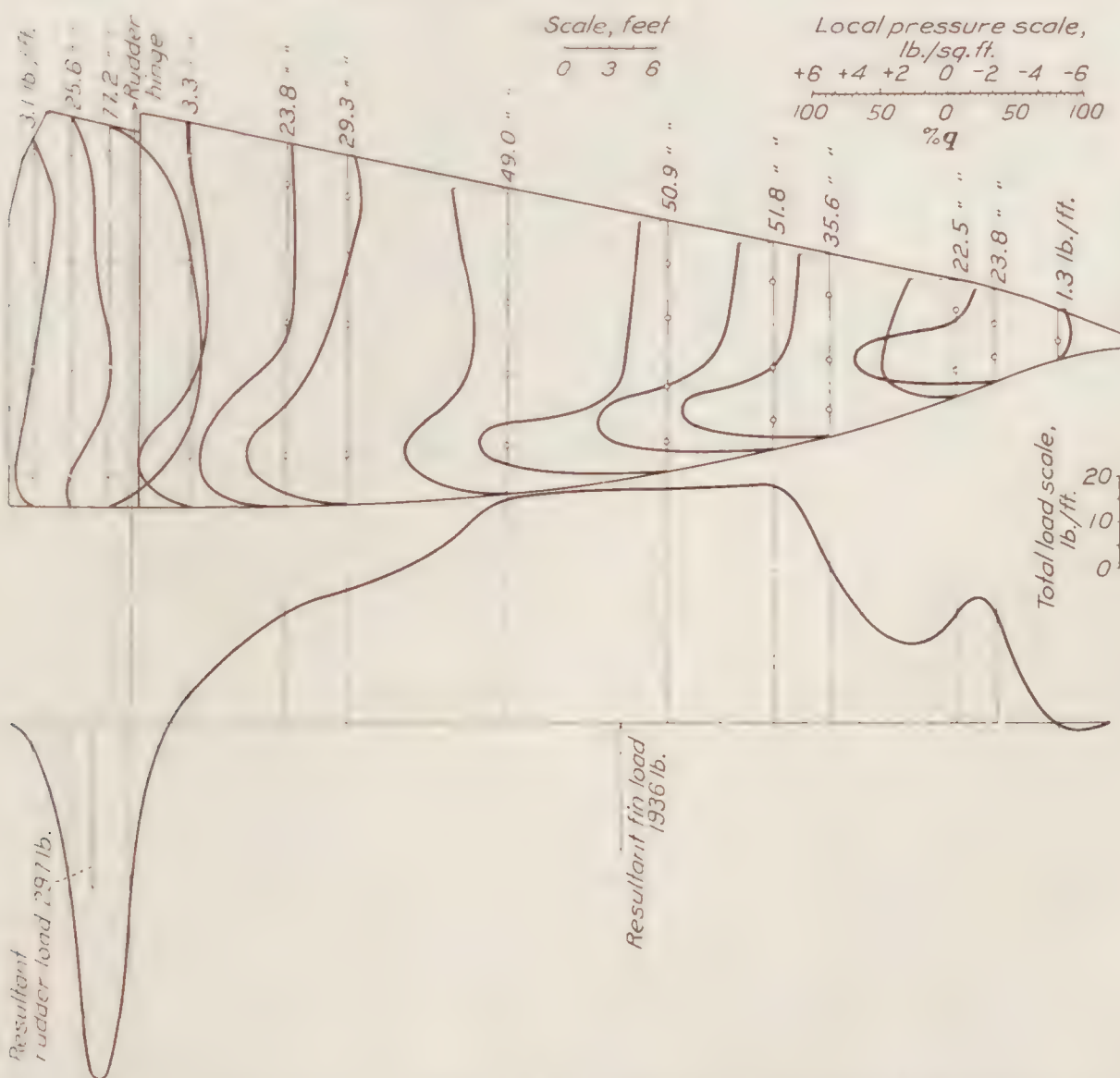


FIGURE 13.—Pressure distribution on lower fin and rudder. Steady turn. Run No. 6C—timing interval 5th from end. Rudder position $12^{\circ} 45'$ starboard. Air speed 50.8 M. P. H.

NOTE.—Positive pressures acting from port to starboard.

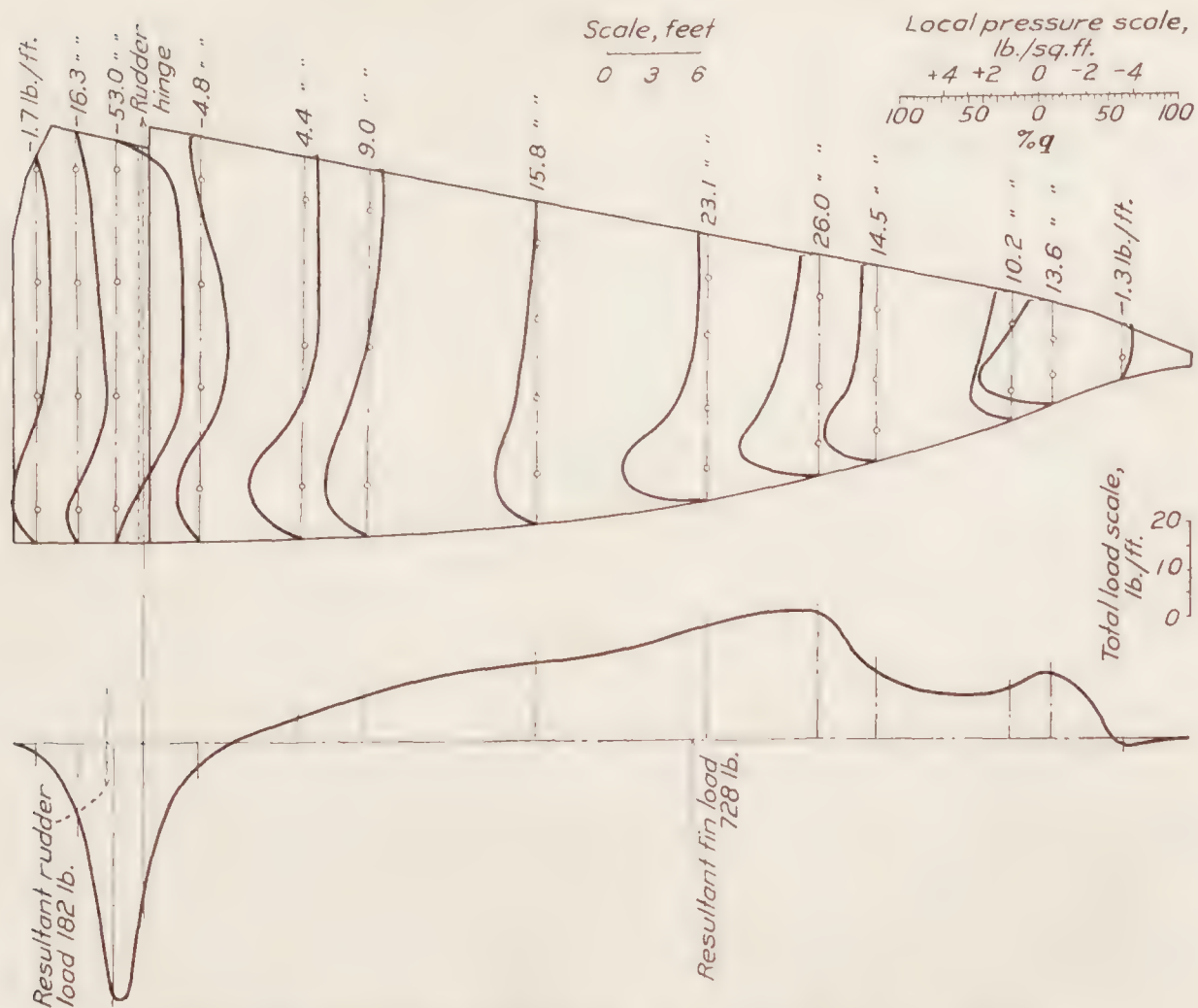


FIGURE 14.—Pressure distribution on lower fin and rudder. Steady turn. Run No. 5D—timing interval 1. Rudder position 9° starboard. Air speed 50.1 M. P. H.

NOTE.—Positive pressures acting from port to starboard.

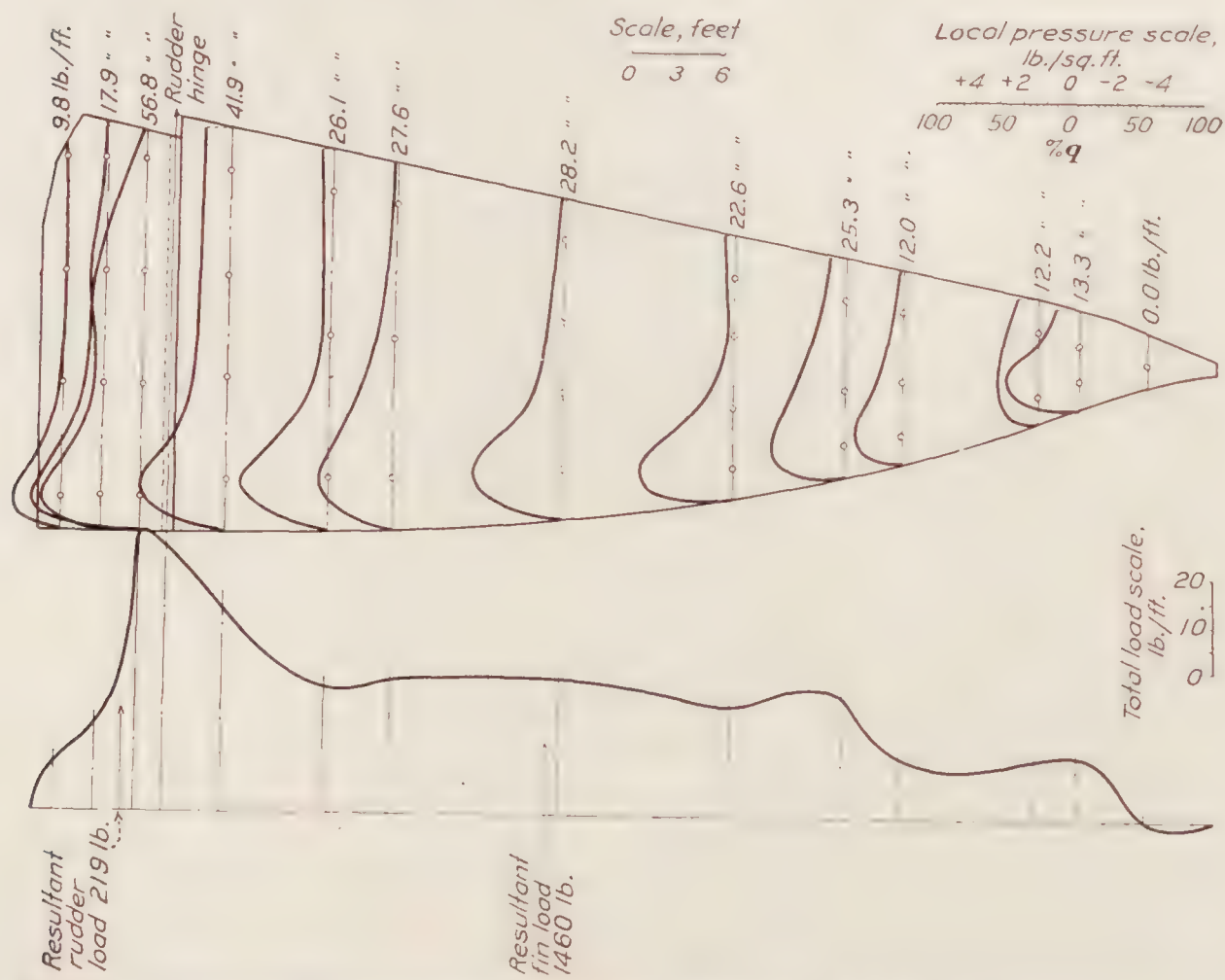


FIGURE 15.—Pressure distribution on lower fin and rudder. Steady turn. Run No. 5D—timing interval $2\frac{1}{4}$. Rudder position $6^\circ 45'$ port. Air speed 49.1 M. P. H.

NOTE.—Positive pressures acting from port to starboard.

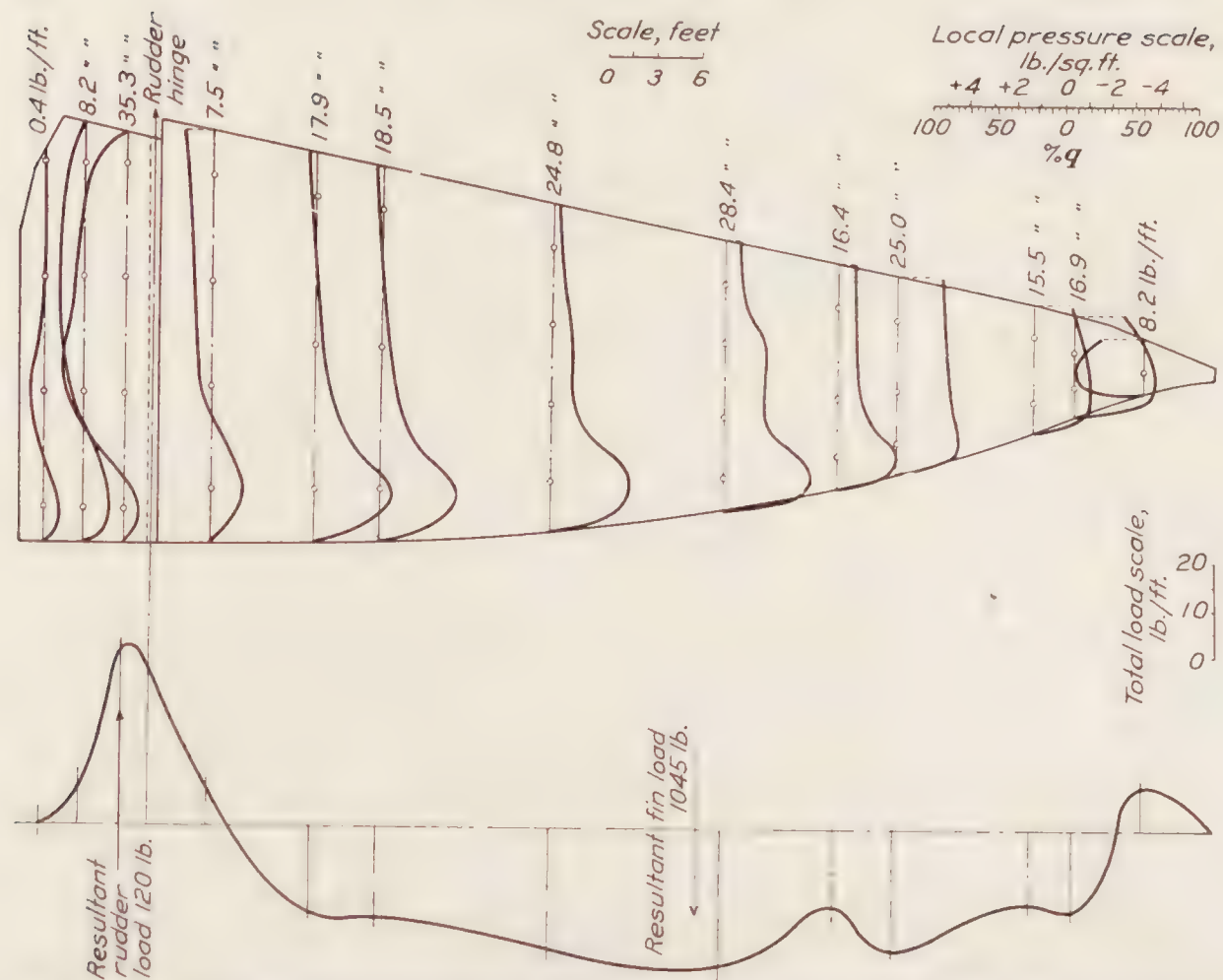


FIGURE 16.—Pressure distribution on lower fin and rudder. Steady turn. Run No. 5D—timing interval 6. Rudder position 7° 45' port. Air speed 48.9 M. P. H.

NOTE.—Positive pressures acting from port to starboard.

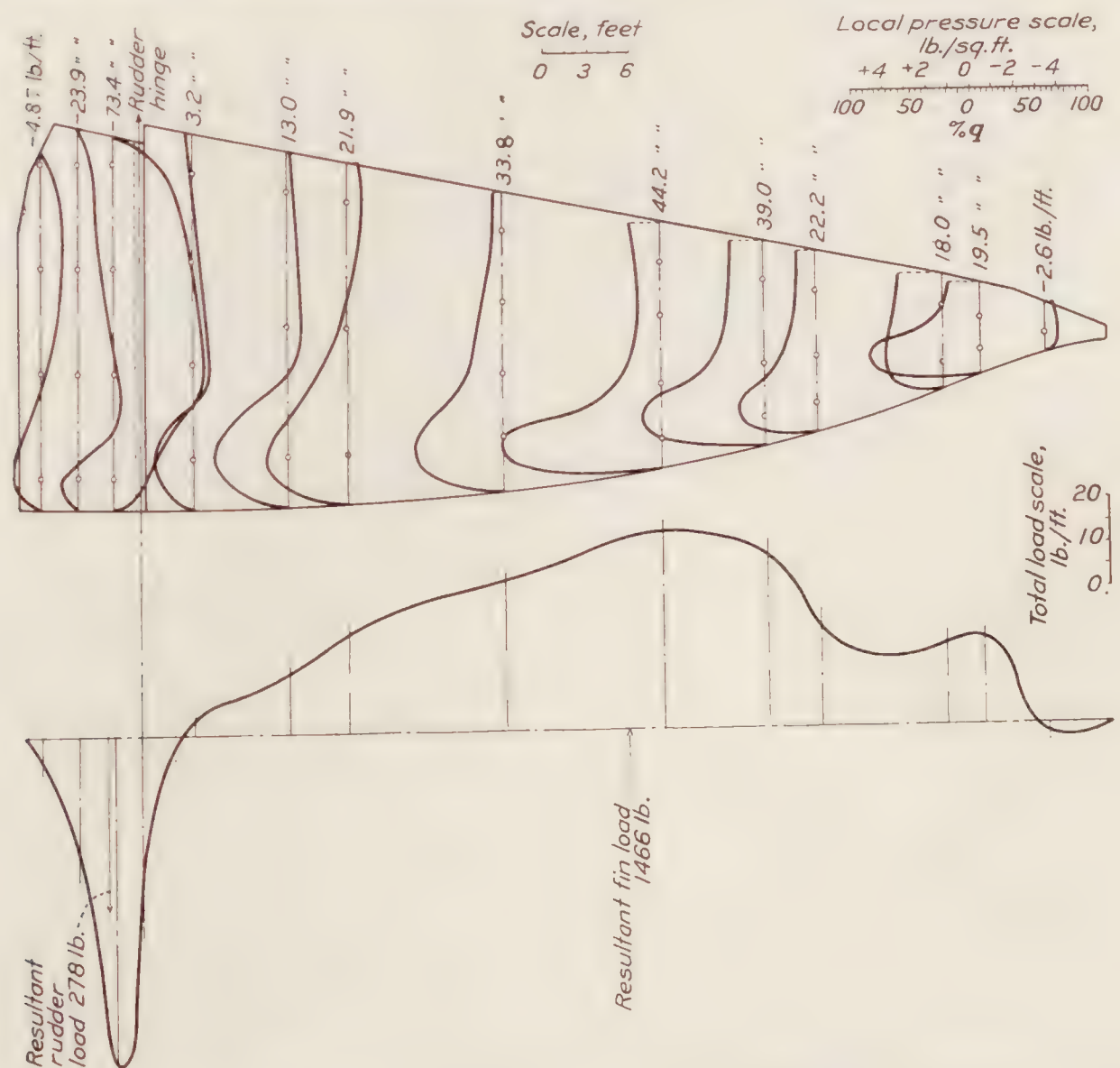


FIGURE 17.—Pressure distribution on lower fin and rudder. Reversal of helm—starboard to port. Run No. 3C—timing interval 2. Rudder position 12° 15' starboard. Air speed 48.4 M. P. H.

NOTE.—Positive pressures acting from port to starboard.



FIGURE 18.—Pressure distribution on lower fin and rudder. Reversal of helm—starboard to port. Run No. 3C—timing interval $3\frac{1}{4}$. Rudder position 3° port. Air speed 48.1 M. P. H.

NOTE.—Positive pressures acting from port to starboard.

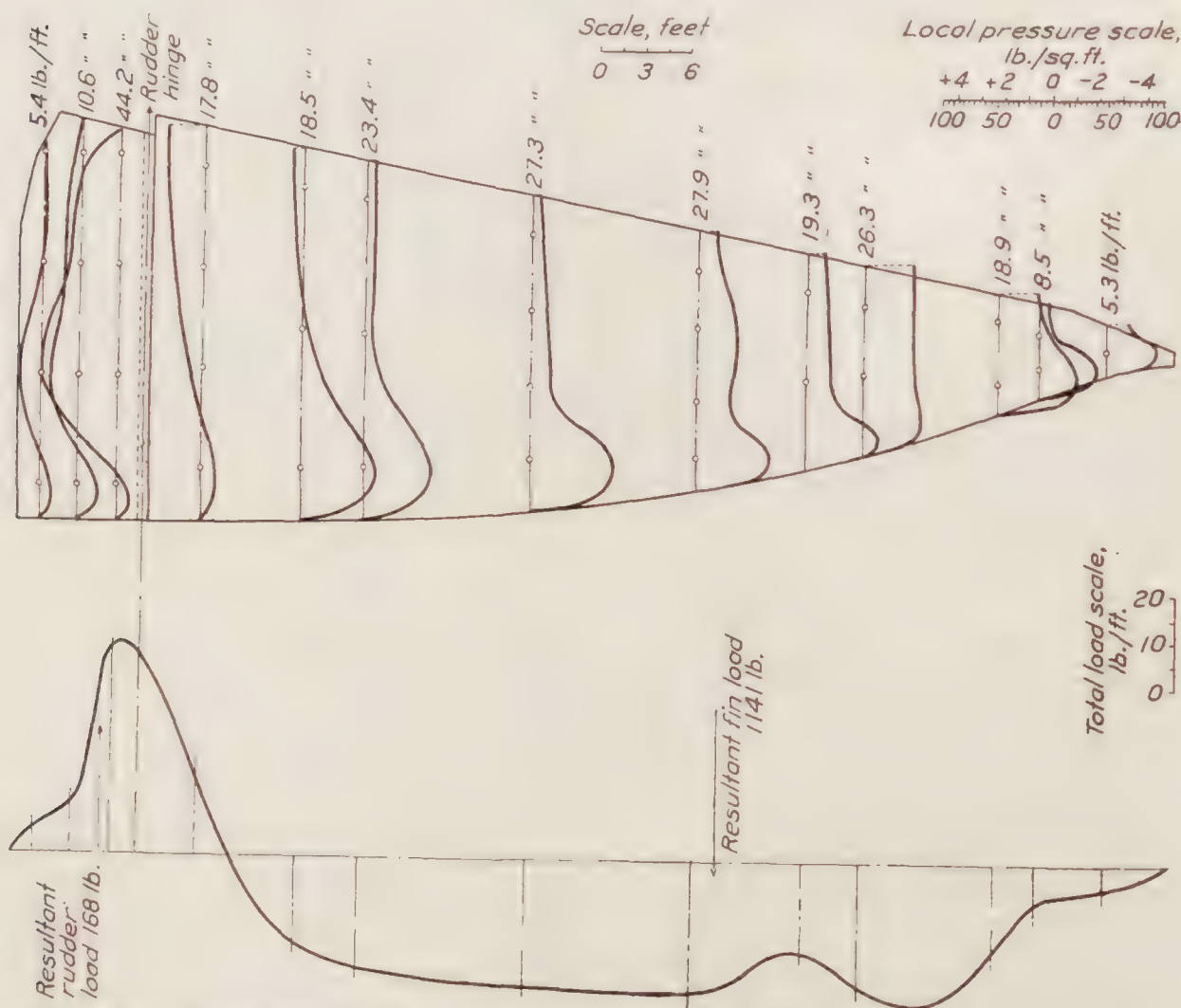


FIGURE 19.—Pressure distribution on lower fin and rudder. Reversal of helm—starboard to port. Run No. 3C—timing interval 6. Rudder position $12^\circ 05'$ port. Air speed 45.3 M. P. H.

NOTE.—Positive pressures acting from port to starboard.

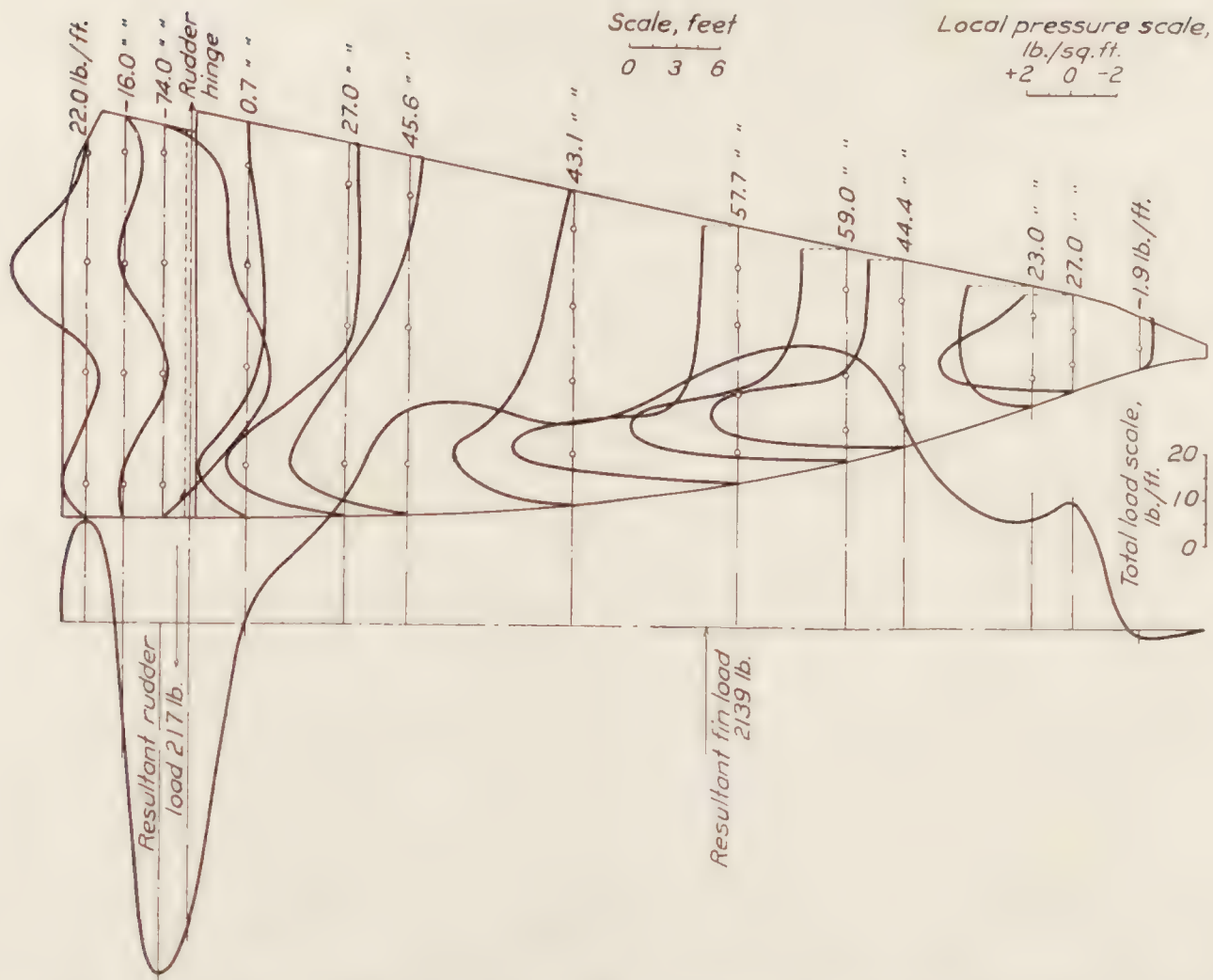


FIGURE 20.—Pressure distribution on lower fin and rudder. Reversal of helm—starboard to port. Run No. 17D—timing interval 4. Rudder position $12^{\circ} 30'$ starboard. Air speed 59.2 M. P. H. (approximate)

NOTE.—Positive pressures acting from port to starboard.

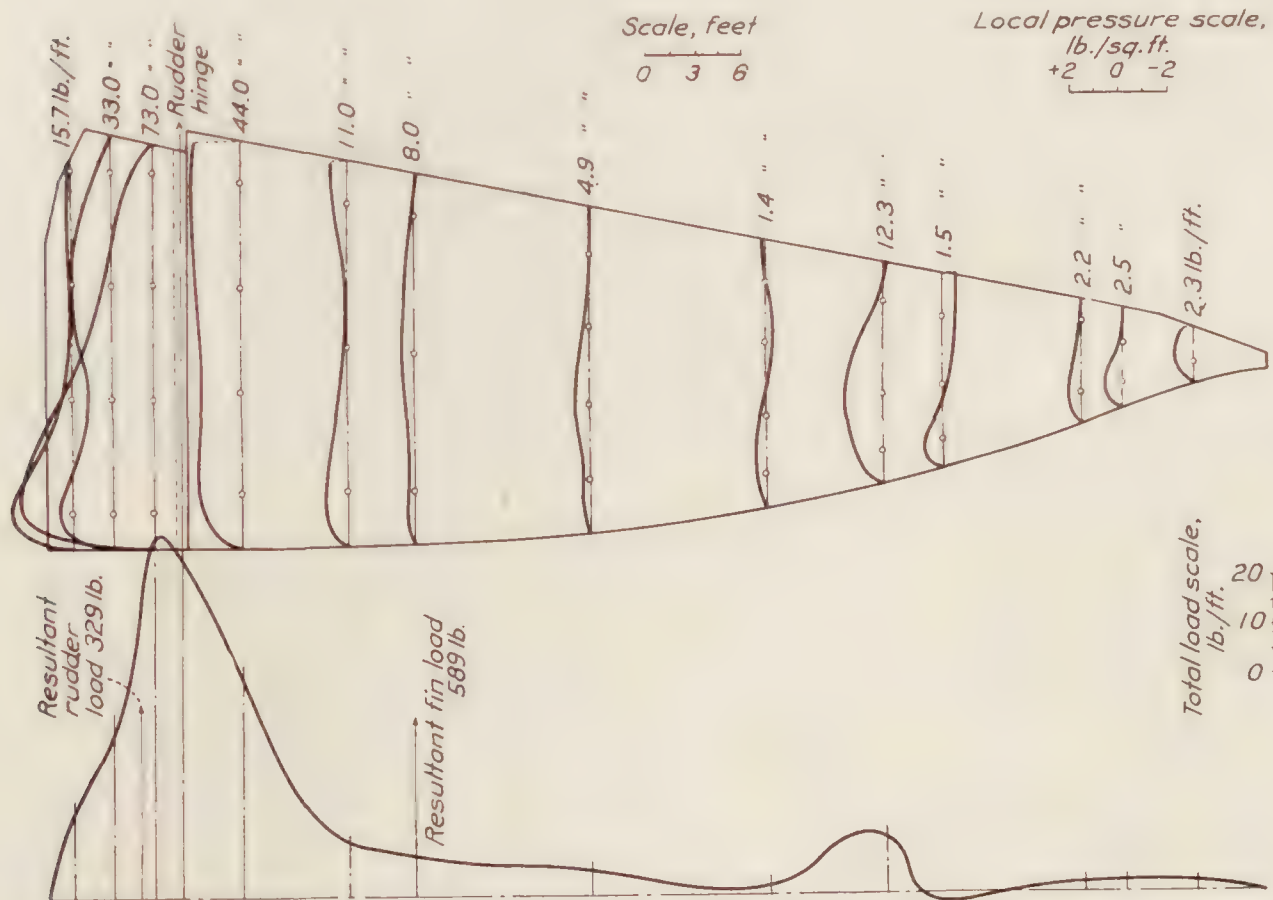


FIGURE 21.—Pressure distribution on lower fin and rudder. Reversal of helm—starboard to port. Run No. 17D—timing intervals. Rudder position $12^{\circ} 30'$ port. Air speed 53.4 M. P. H. (approximate)

NOTE.—Positive pressures acting from port to starboard.

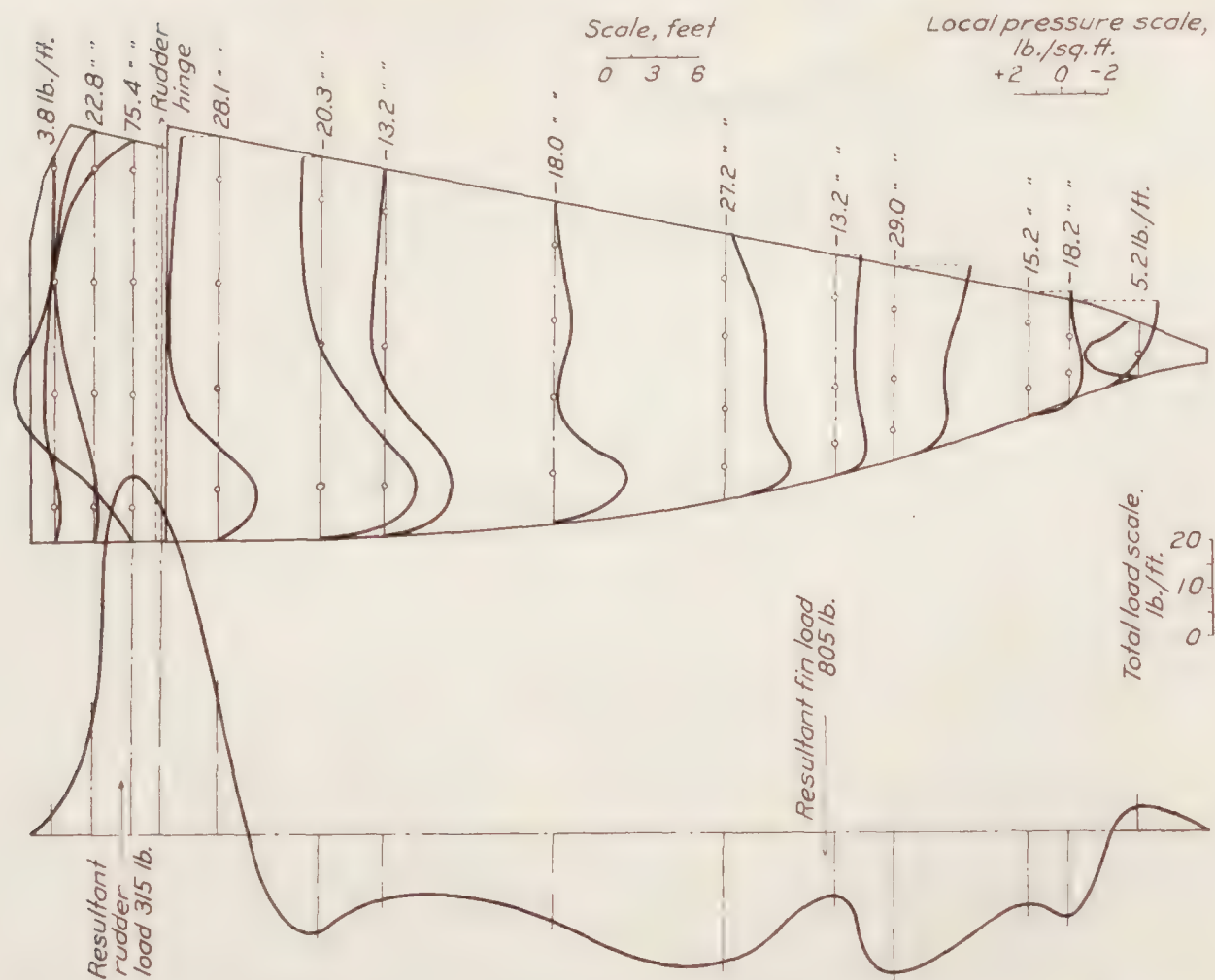


FIGURE 22.—Pressure distribution on lower fin and rudder. Reversal of helm—starboard to port. Run No. 17D—timing interval 7. Rudder position $12^{\circ} 30'$ port. Air speed 52.6 M. P. H. (approximate)

NOTE.—Positive pressures acting from port to starboard.

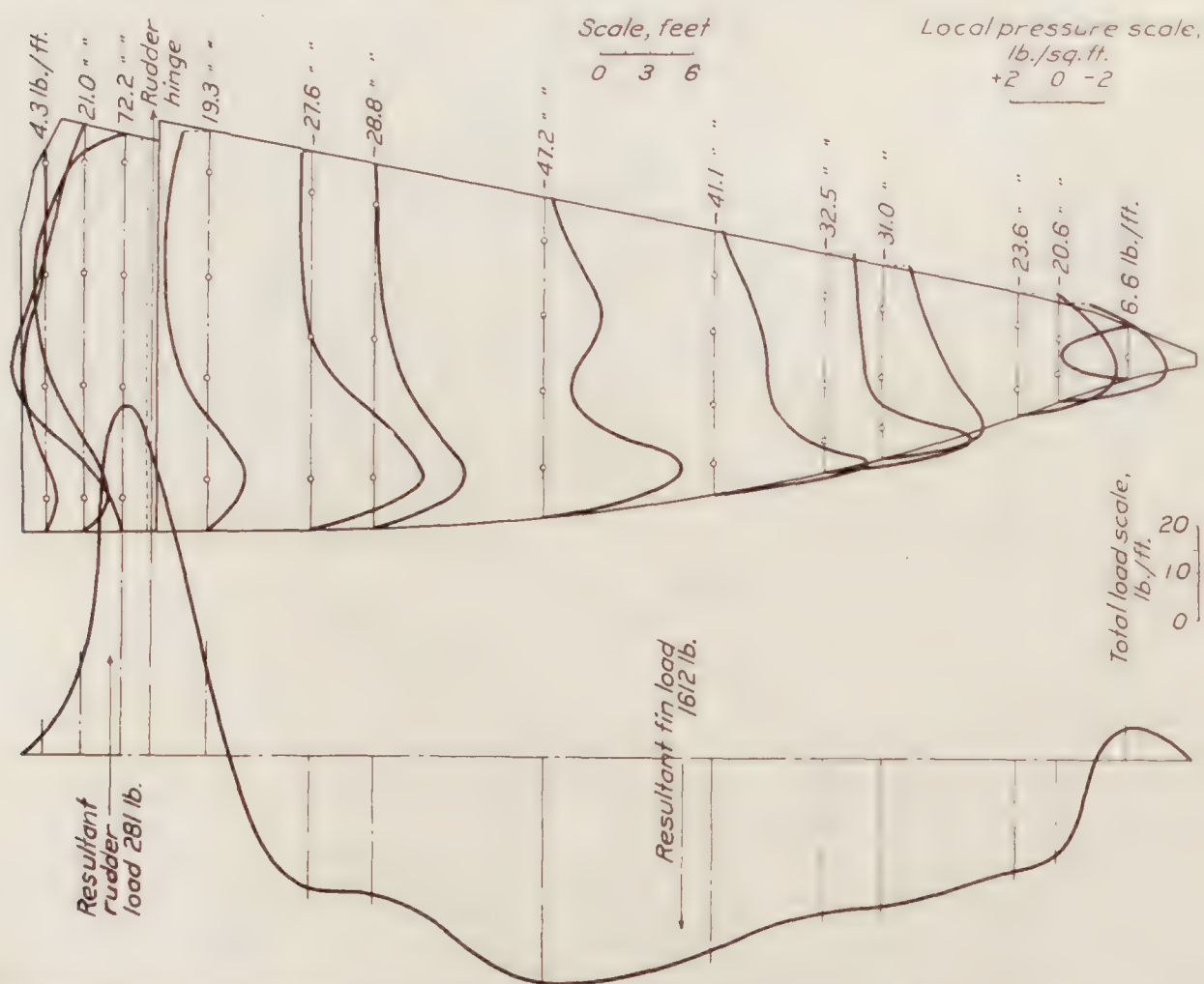


FIGURE 23.—Pressure distribution on lower fin and rudder. Reversal of helm—port to starboard to port. Run No. 17D—timing interval 8. Rudder position $12^{\circ} 30'$ port. Air speed 54.8 M. P. H. (approximate)

NOTE.—Positive pressures acting from port to starboard.

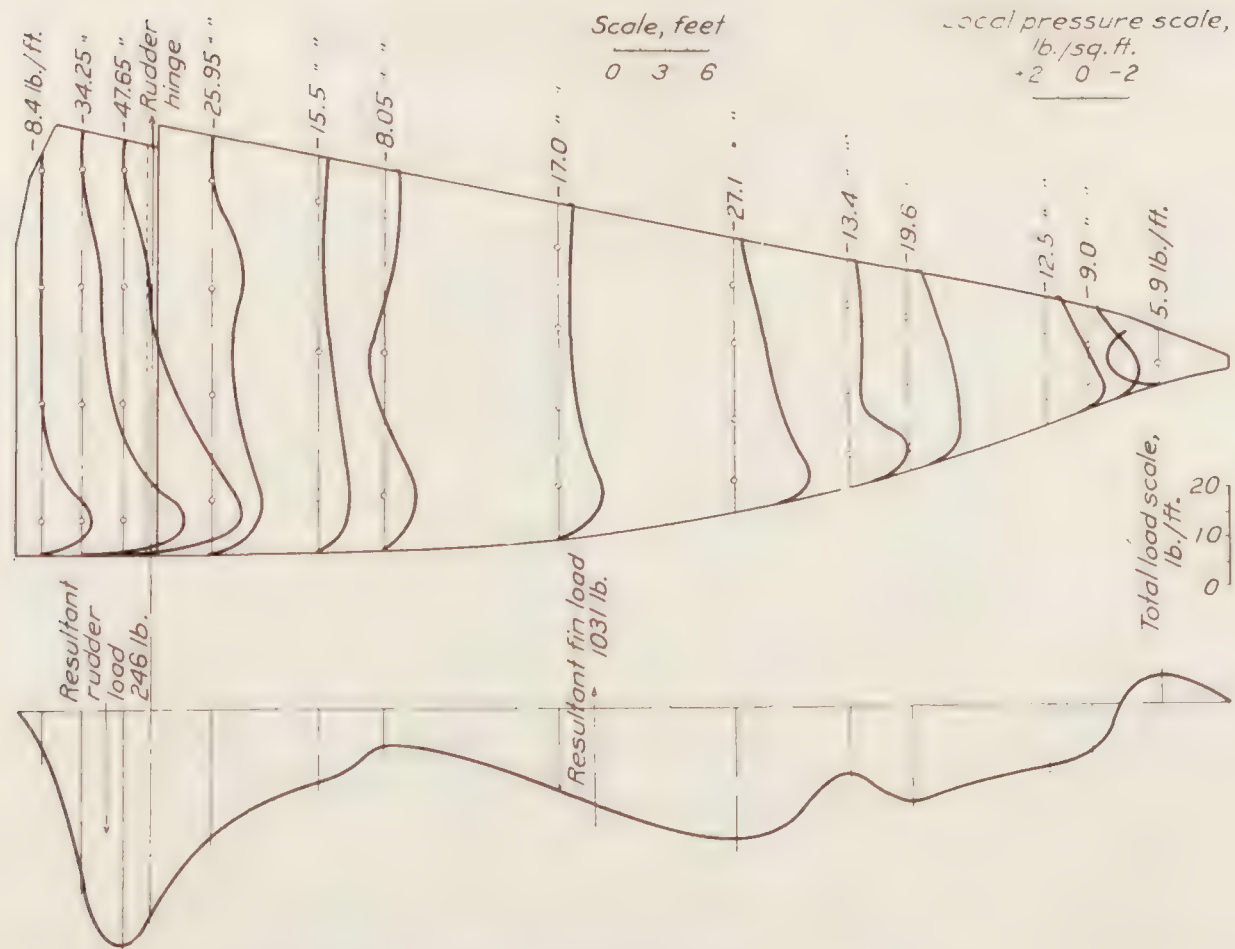


FIGURE 24.—Pressure distribution on lower fin and rudder. Flying through gusts. Run No. 4A—125 seconds from start. Rudder position $2^{\circ} 36'$ starboard. Air speed 56.7 M. P. H.

NOTE.—Positive pressures acting from port to starboard.

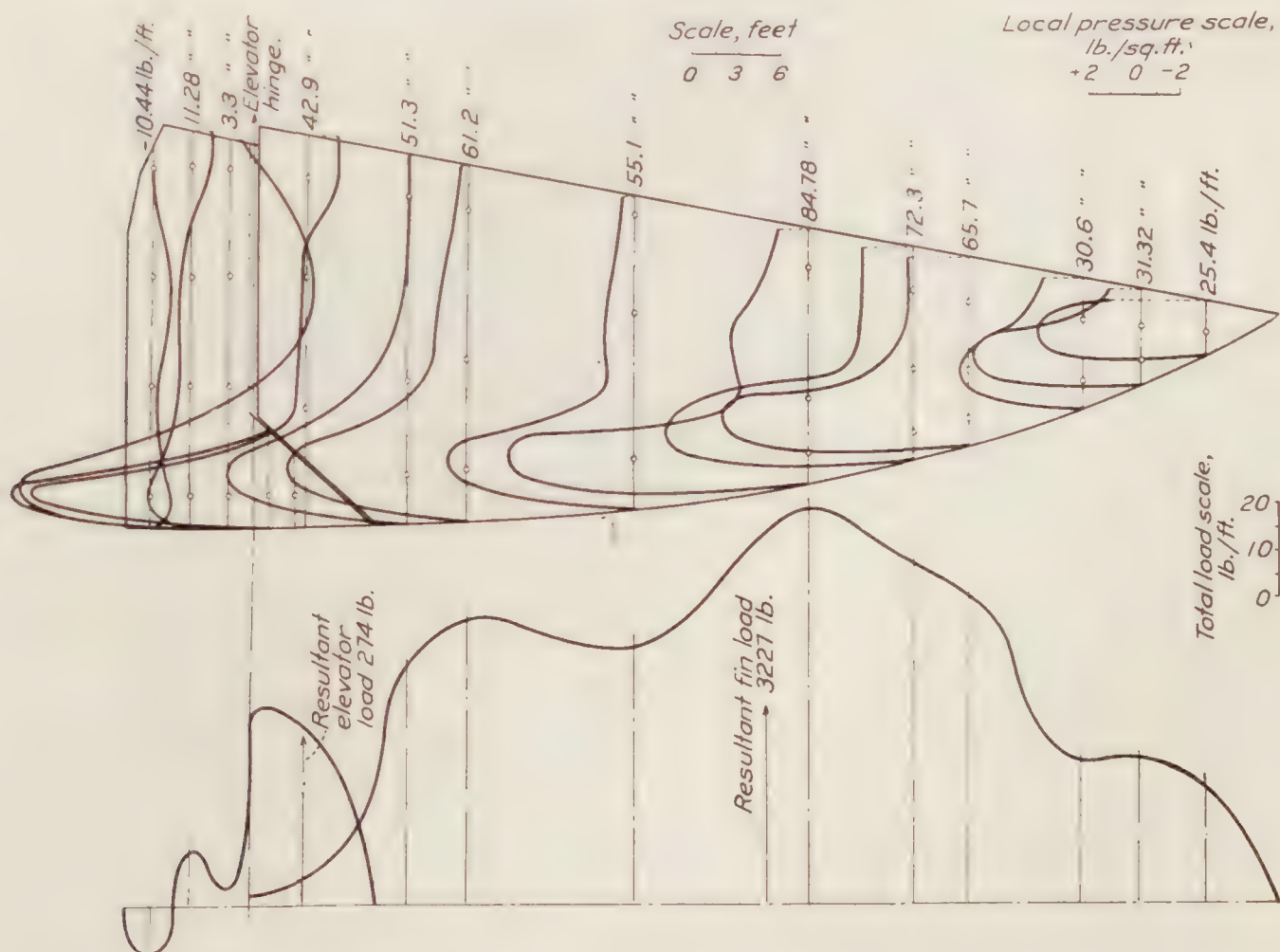


FIGURE 25.—Pressure distribution on starboard fin and elevator. Flying through gusts. Run No. 4A—125 seconds from start. Elevator position 16° down. Air speed 56.7 M. P. H.

NOTE.—Positive pressures acting from lower to upper side of surface.

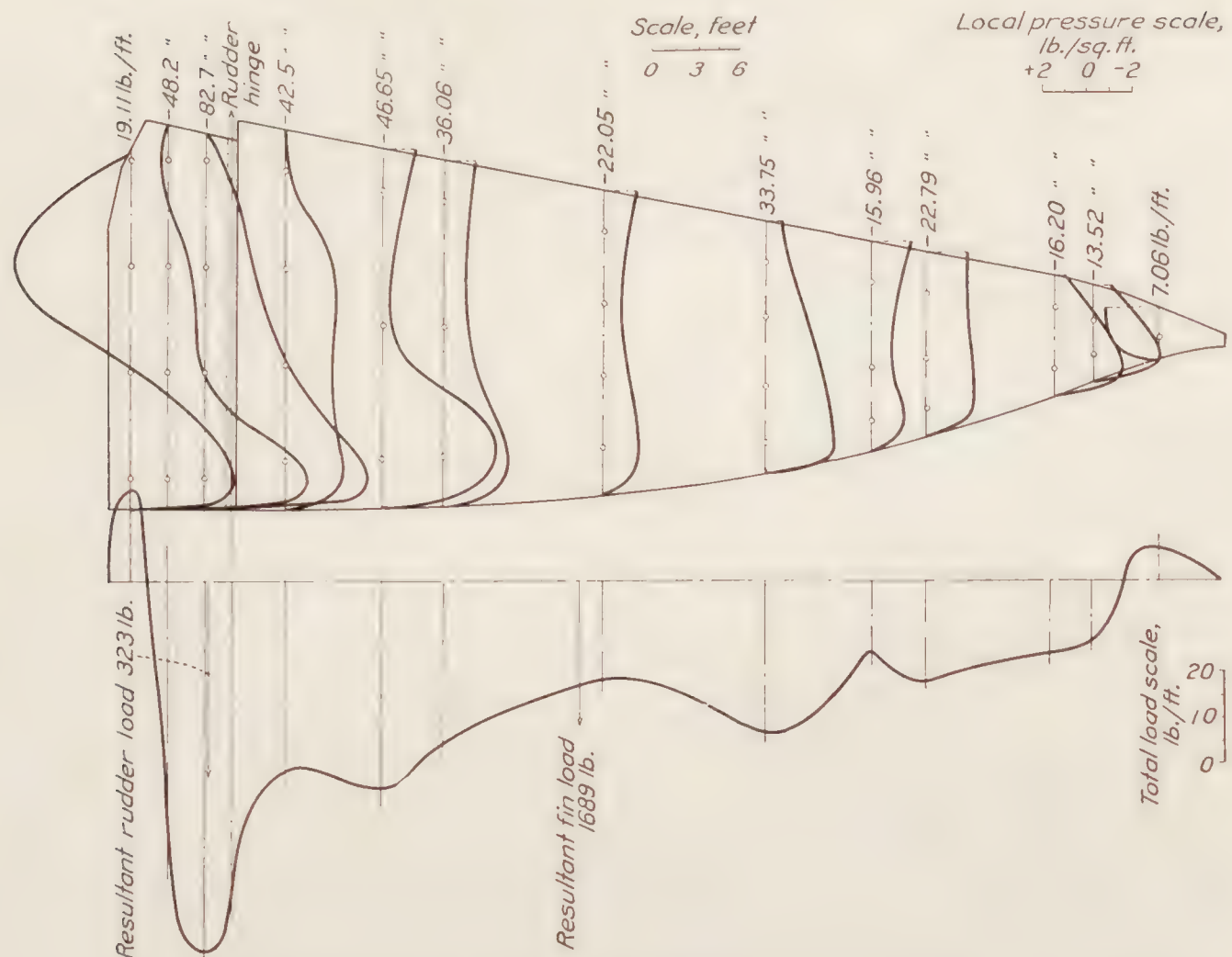


FIGURE 26.—Pressure distribution on lower fin and rudder. Flying through gusts. Run No. 5A—145 seconds from start. Rudder position $6^{\circ} 0''$ starboard. Air speed 54 M. P. H. (approximate)

NOTE.—Positive pressures acting from port to starboard.

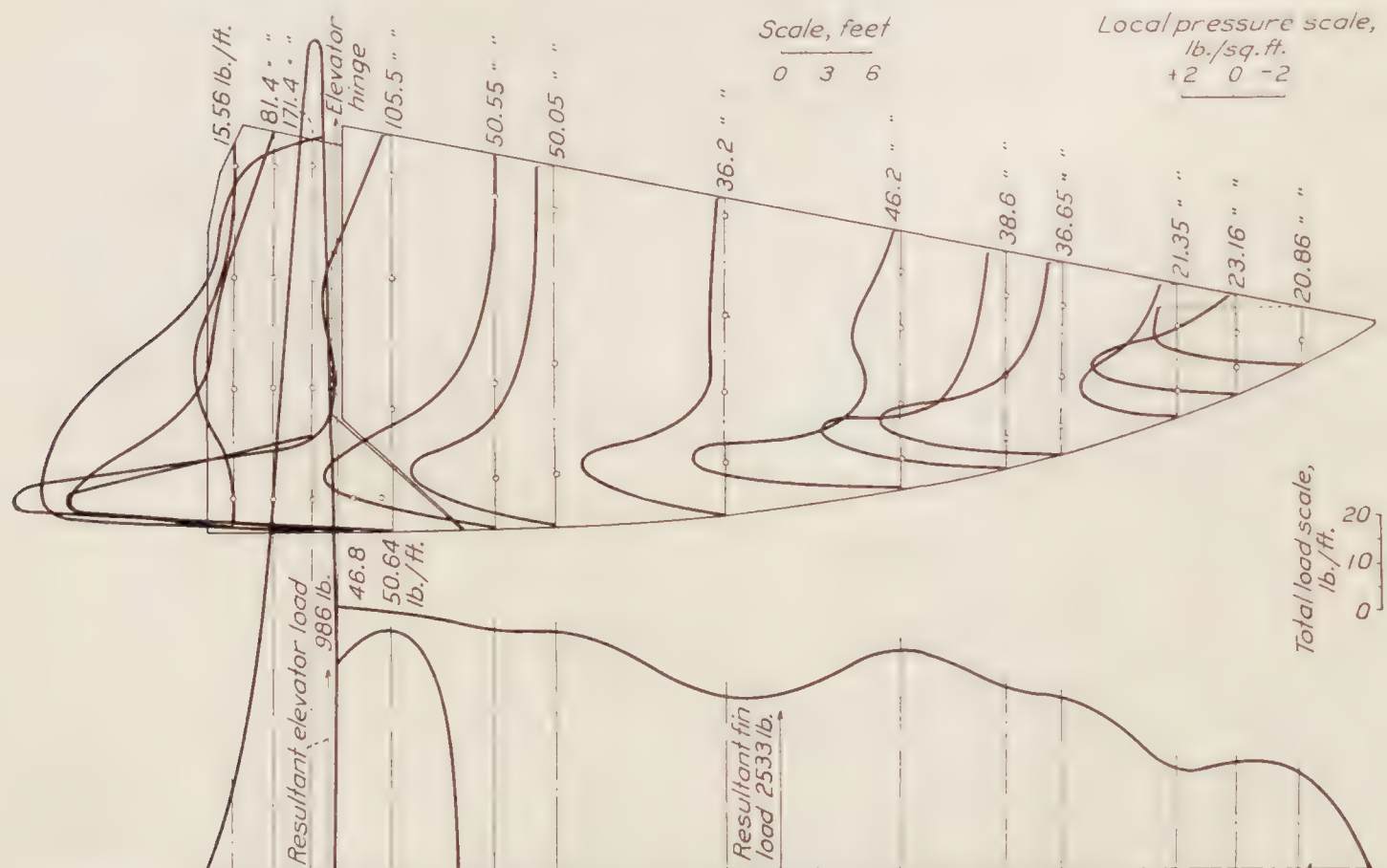


FIGURE 27.—Pressure distribution on starboard fin and elevator. Flying through gusts. Run No. 5A—145 seconds from start. Elevator position $19^{\circ} 15'$ down. Air speed 54 M. P. H. (approximate)

NOTE.—Positive pressures acting from lower to upper side of surface.

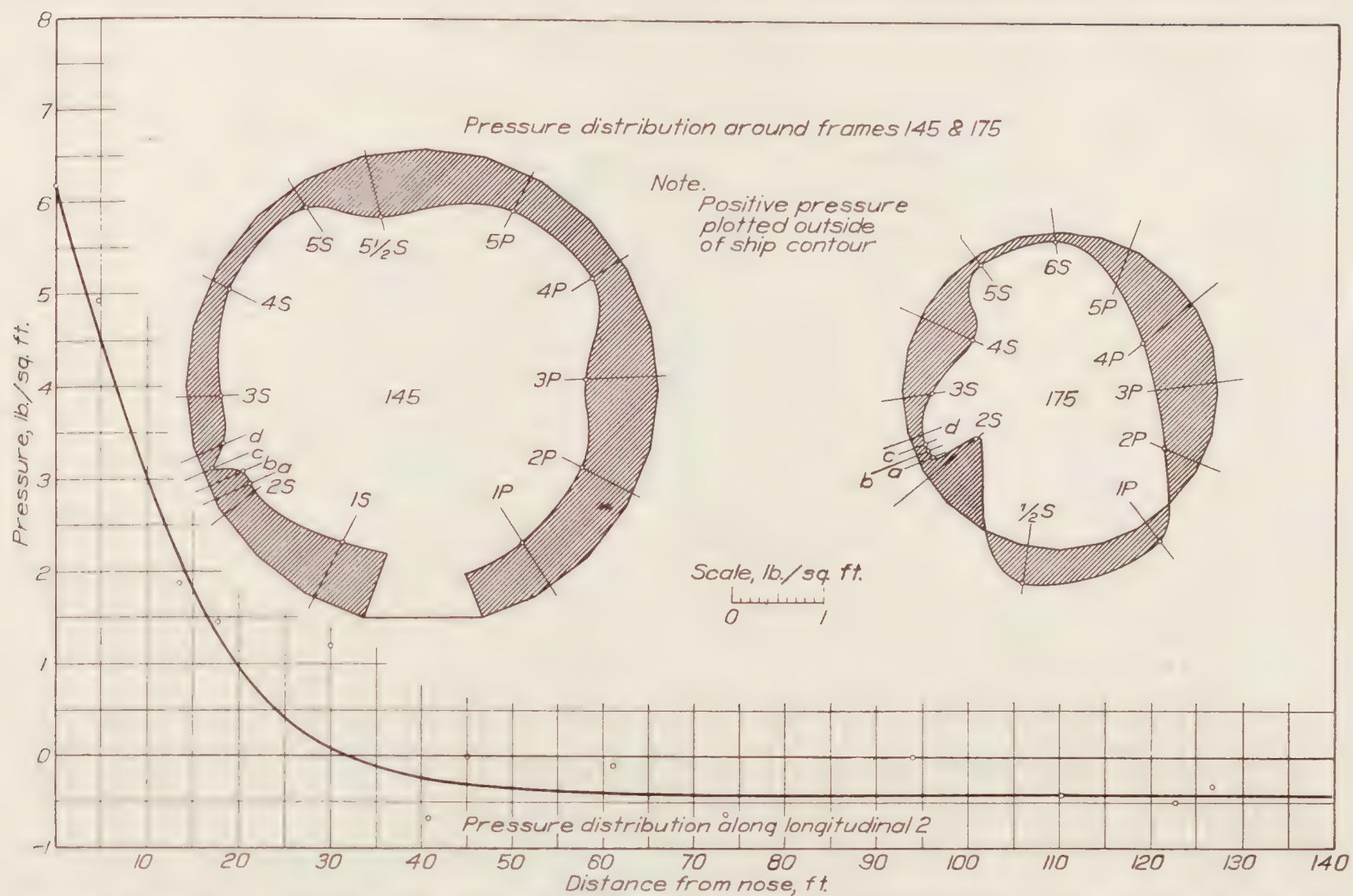


FIGURE 28.—Pressure distribution on hull. Flying through gusts. Rudder 3° 00' starboard; elevator 15° 36' down. Run No. 4A—timing line No. 8 1/4

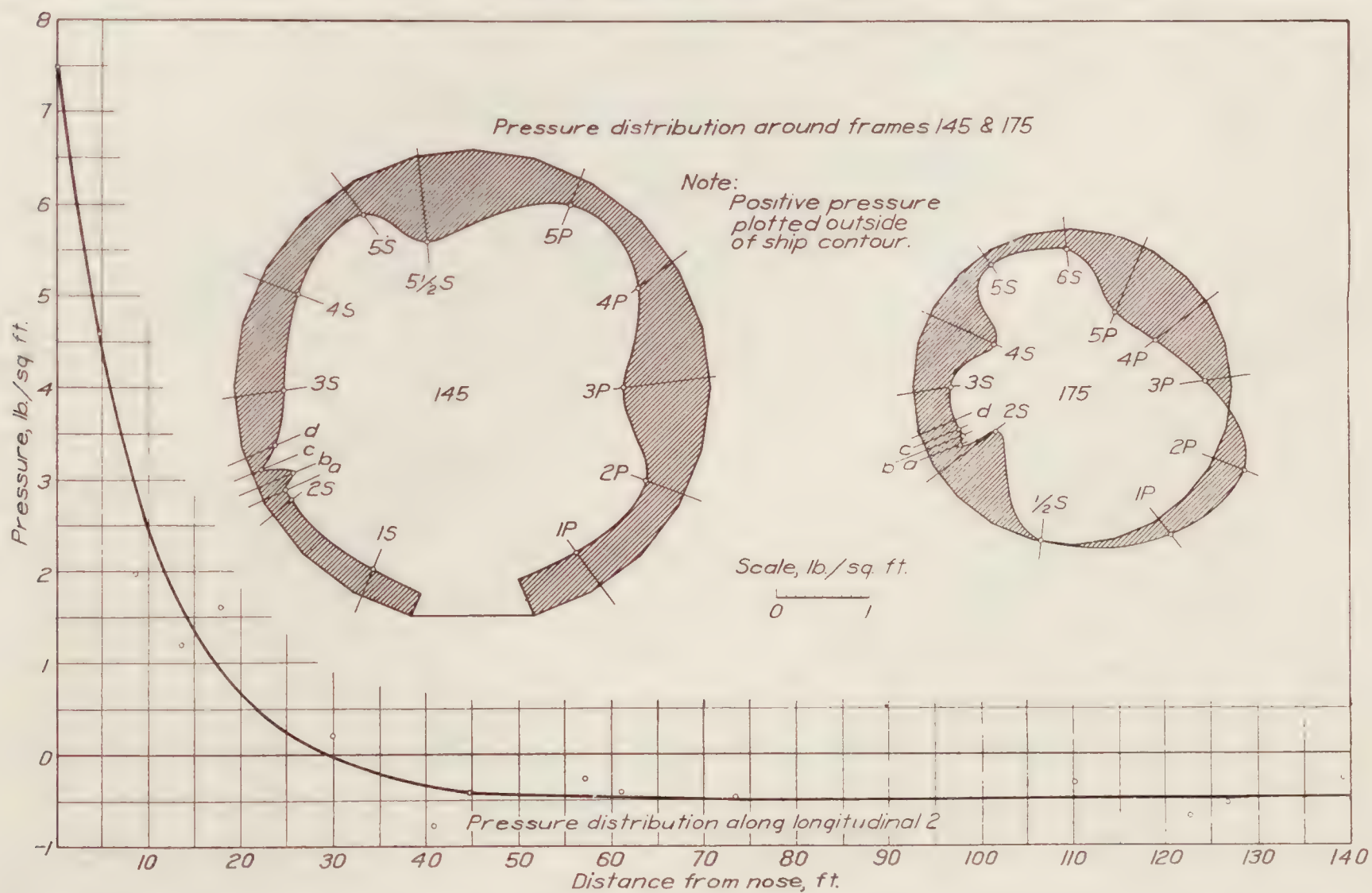


FIGURE 29.—Pressure distribution on hull. Flying through gusts. Rudder 7° 00' starboard; elevator 18° 24' down. Run No. 5A—timing line No. 9 1/4

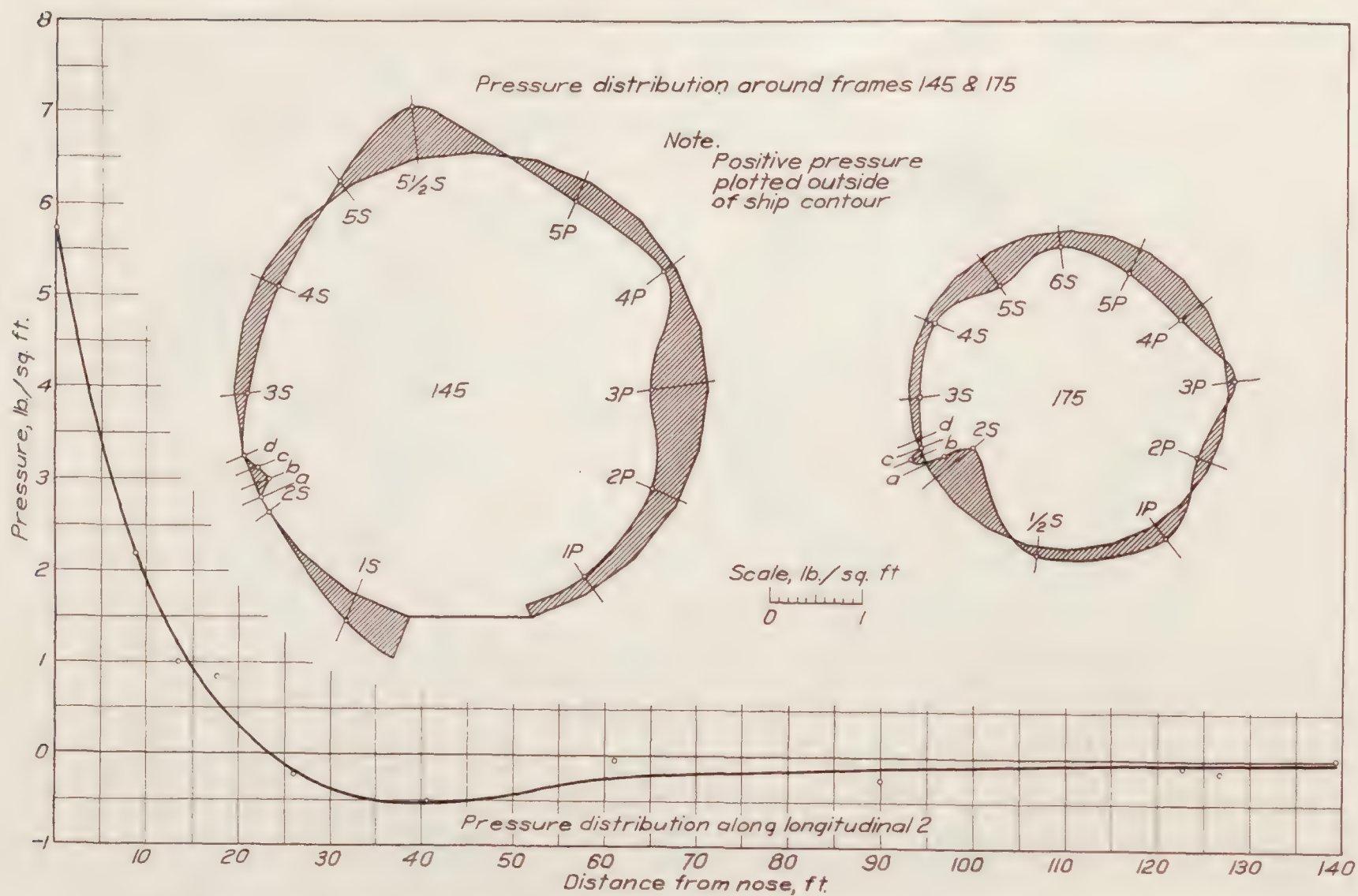


FIGURE 30.—Pressure distribution on hull. Steady turn—rudder 9° 42' port. Run No. 4B—timing line 2

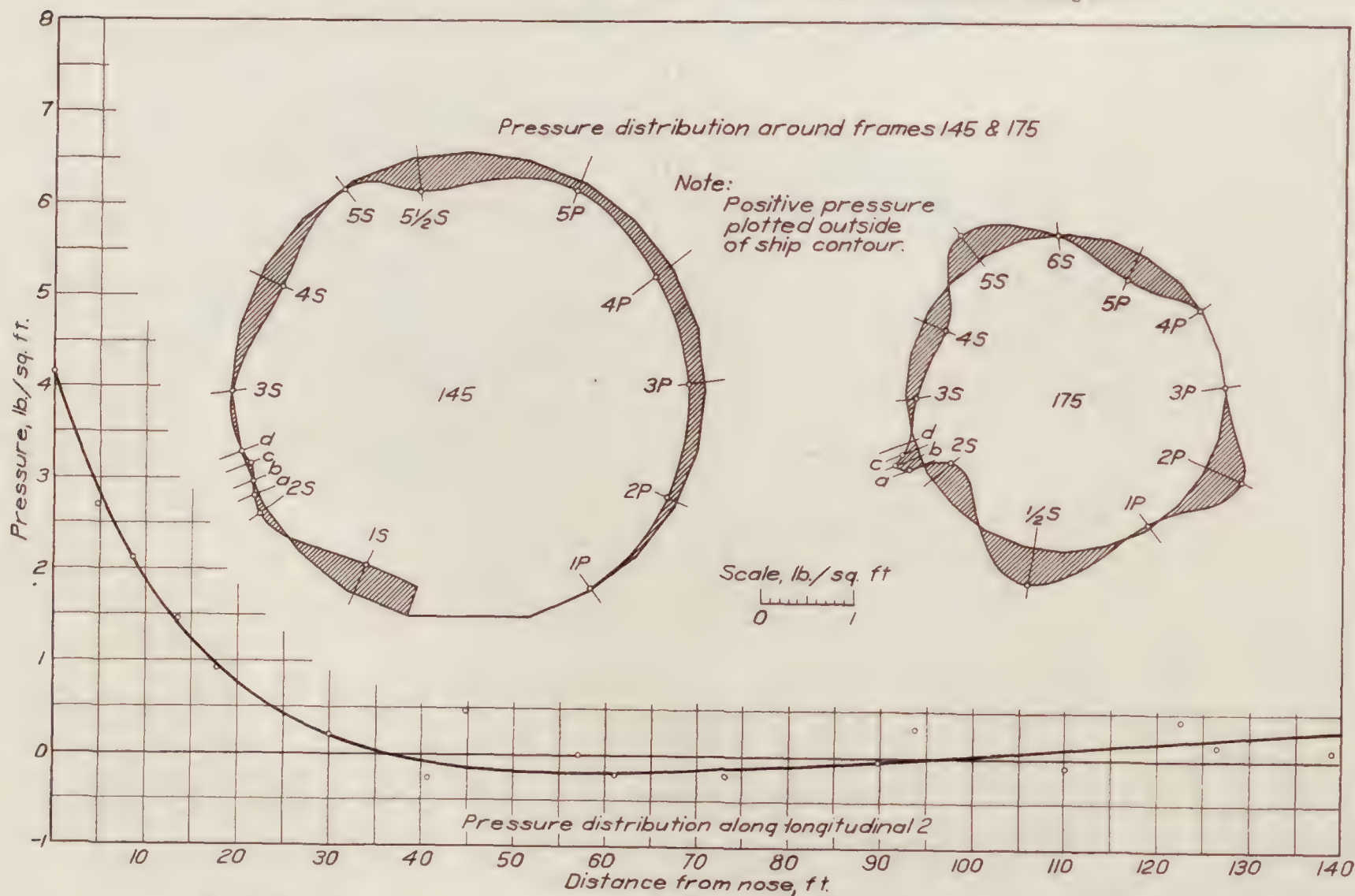


FIGURE 31.—Pressure distribution on hull. Steady turn—rudder 8° 18' starboard. Run No. 4C—timing line 7

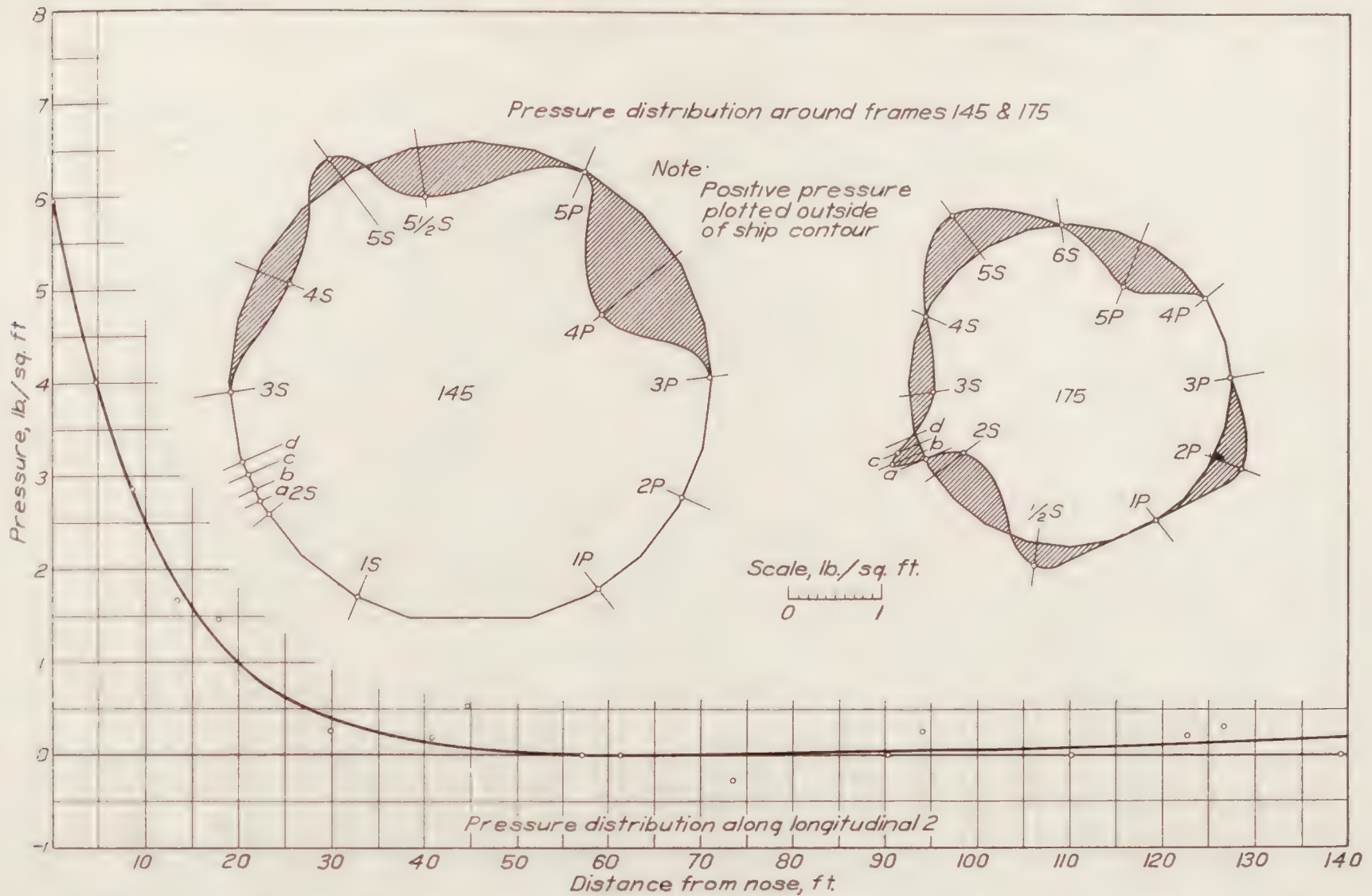


FIGURE 32.—Pressure distribution on hull. Steady turn—rudder 7° 51' starboard. Run No. 5C—timing line 9

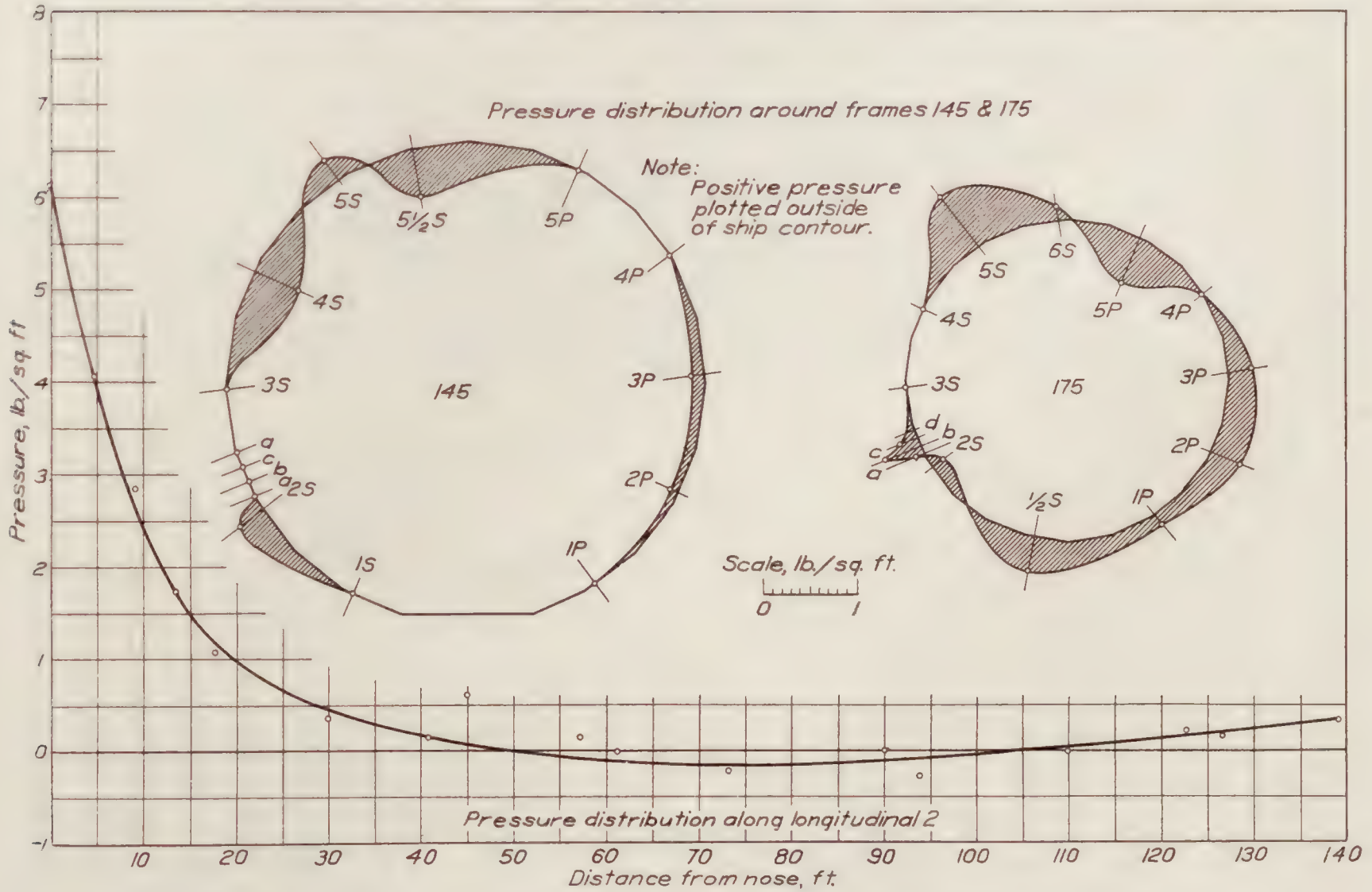


FIGURE 33.—Pressure distribution on hull. Steady turn—rudder 13° 15' starboard. Run No. 6C—timing line 5th from end

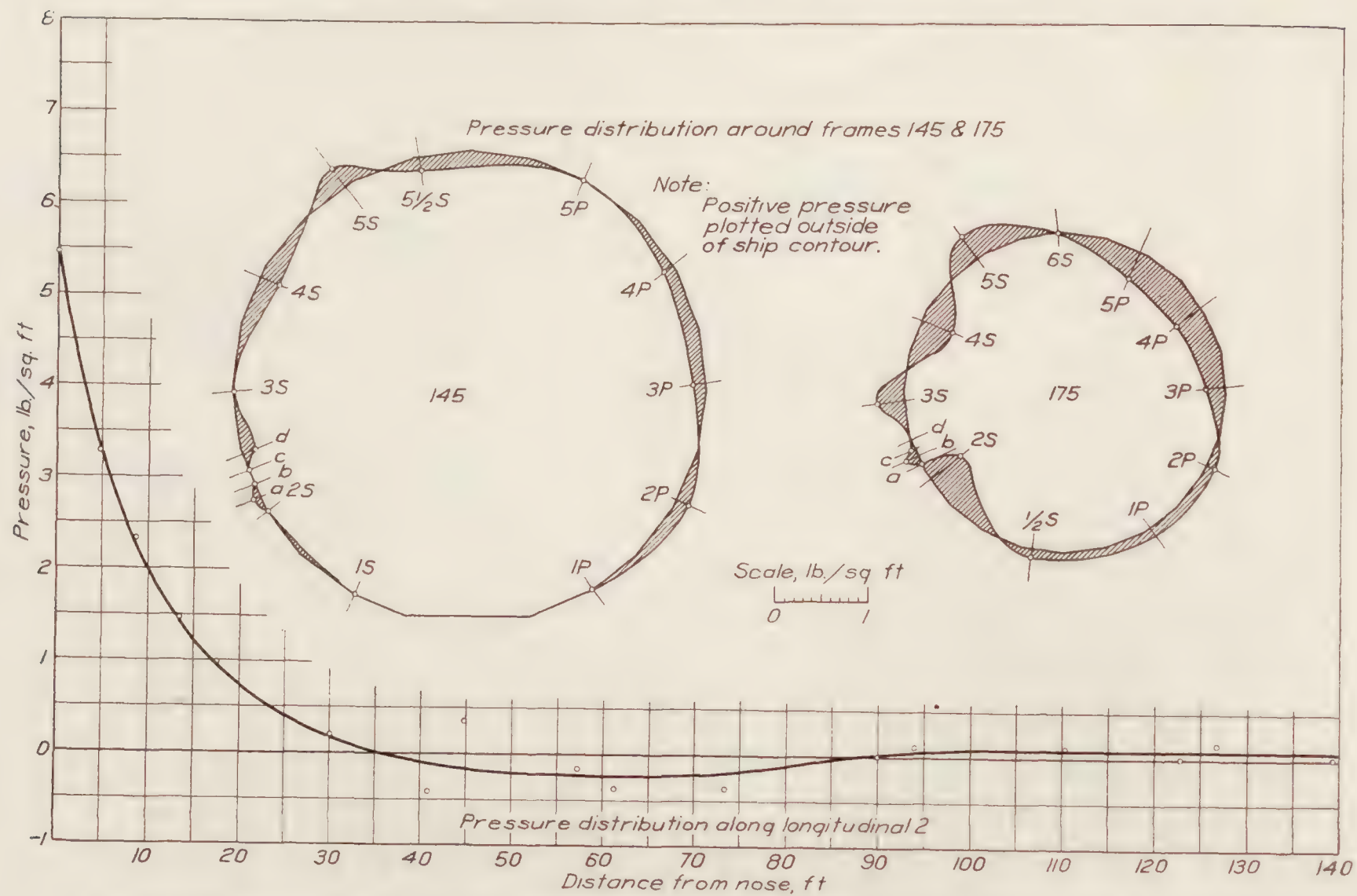


FIGURE 34.—Pressure distribution on hull. Reversal of helm—starboard to port. Rudder 12° 21' starboard. Run No. 3C—timing line 2

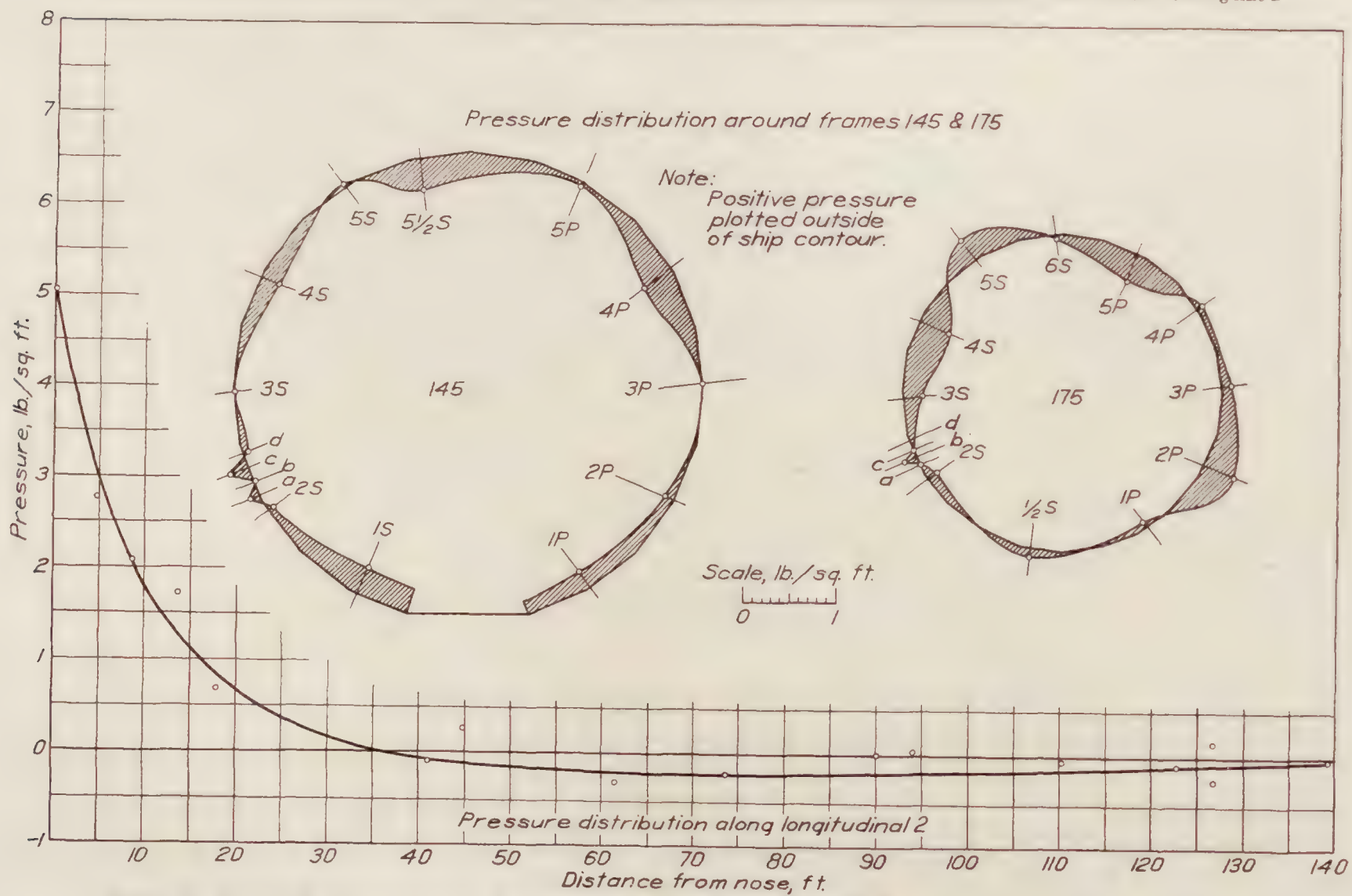


FIGURE 35.—Pressure distribution on hull. Reversal of helm—starboard to port. Rudder 6° 30' port. Run No. 3C—timing line 3¼

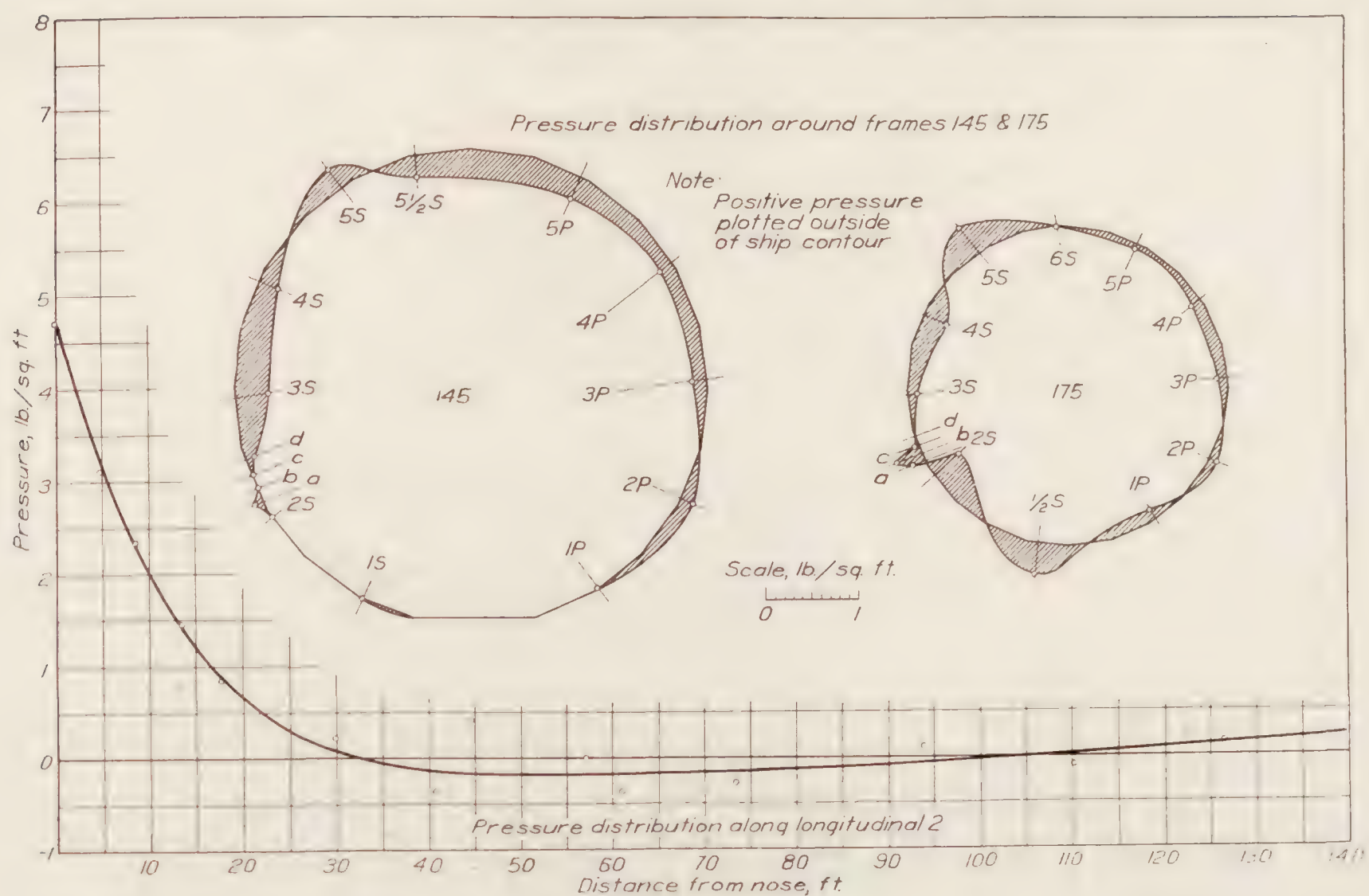


FIGURE 36.—Pressure distribution on hull. Reversal of helm—starboard to port. Rudder $11^{\circ} 33'$ port. Run No. 3C—timing line 6

REPORT No. 325

FLIGHT TESTS ON U. S. S. LOS ANGELES PART II—STRESS AND STRENGTH DETERMINATION

**By C. P. BURGESS ,
Bureau of Aeronautics, Navy Department**

REPORT No. 325

FLIGHT TESTS ON U. S. S. LOS ANGELES

PART II: STRESS AND STRENGTH DETERMINATION

By C. P. BURGESS

SUMMARY

The tests described in this report furnished data on the actual aerodynamic forces, and the resulting stresses and bending moments in the hull of the U. S. S. "Los Angeles" during as severe still-air maneuvers as the airship would normally be subjected to, and in straight flight during as rough air as is likely to occur in service, short of squall or storm conditions. The maximum stresses were found to be within the limits provided for in accepted practice in airship design. Normal flight in rough air was shown to produce forces and stresses about twice as great as the most severe still-air maneuvers. No light was thrown upon the forces which might occur in extreme or exceptional conditions, such as the storm which destroyed the "Shenandoah."

The transverse aerodynamic forces on the hull proper were found to be small and irregular. Owing to the necessity of conserving helium, it was impossible to fly the airship in a condition of large excess of buoyancy or weight in order to determine the air pressure distribution at a fixed angle of pitch. However, there is every reason to believe that in that condition the forces on the actual airship are as close to the wind-tunnel results as can be determined by present type of pressure measuring apparatus.

It is considered that the most important data obtained are the coefficients of tail-surface forces and hull-bending moments. These are tabulated in this report.

INTRODUCTION

The only known experimental determinations of the stresses in the girders of rigid airships in actual flight, previously to the investigations described in this report, were carried out upon the U. S. S. *Shenandoah* in 1923 and 1924, and upon the U. S. S. *Los Angeles* in 1925. The previous experiments were carried out by the Bureau of Aeronautics, using the Bureau of Standards type of electric telemeter strain gage. At the time of the *Shenandoah* experiments suitable recording apparatus had not yet been developed for these instruments, and the investigations were limited by the inability of the observer to watch the simultaneous movements of more than a very few millimeter needles. The experiments on the *Los Angeles* in 1925 were carried out with the strain gages and recording apparatus described in the report; but the program of experiments was short, owing to a projected long-distance flight of the airship; and there was no coordination with external air pressure determinations.

The series of flight tests forming the subject of this report were undertaken with the U. S. S. *Los Angeles* in April and May, 1926, after careful planning to avoid the shortcomings of previous experimental work. The assistance of the National Advisory Committee for Aeronautics was requested, and the pressure distribution investigation was placed in their hands. Part I of this report deals with the work of the National Advisory Committee for Aeronautics. In this, the second and concluding part of the report, the stress determinations are described and coordinated with the other data of the experiments.

It was realized that the roughest air which the ship might encounter in service was not likely to be experienced in these tests, but it was hoped to overcome this difficulty by correlating

the pressures and stresses with the angular accelerations shown by a recording turn indicator, which could be carried regularly as part of the airship's service equipment for recording the angular accelerations occurring in the worst conditions in continued service. Unfortunately, the turn indicator proved to be unsatisfactory, and that part of the experiment was unsuccessful.

APPARATUS AND INSTALLATION

The strain gages were developed by the Bureau of Standards for the Bureau of Aeronautics, Navy Department. The principle of operation of these gages is that the electrical resistance of a stack of carbon piles or disks mounted under pressure in a frame varies rapidly with small changes of the length of the frame. In the stacks used in these gages, the electrical resistance varies about 46 per cent for a change of length of only 0.00217 inch. With a single stack, the change of resistance is not linear with the change of length, but if two stacks are incorporated in a strain gage designed to increase the length of one stack and decrease the length of the other stack equally, they may be arranged in a Wheatstone bridge circuit in which the deflection of a milliammeter or oscillograph will be directly proportional to the change of strain. Such an arrangement is shown diagrammatically in Figure 1.

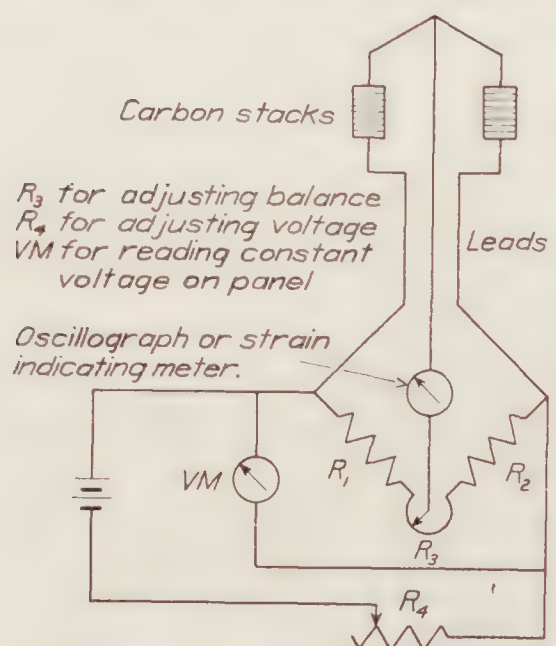


FIGURE 1.—Diagram of circuit of strain gage

The two branches of the bridge circuit consist of the carbon stacks and leads in series on the one hand and the resistances R_1 , R_2 , and R_3 on the other hand. R_1 and R_2 are fixed resistances, and R_3 a slide wire resistance by means of which a fine degree of balance of the bridge is obtainable. The bridging instruments are a milliammeter in the visible indicating element, and a mirror galvanometer reflecting a beam of light in the photographic recorder; they are connected between the mid-point of the carbon stacks and the movable contact on R_3 . The bridge is energized from the battery shown at the left of the diagram; the current is kept at the proper constant value by means of the variable resistance R_4 .

The gage which carries the carbon stacks and is clamped to the member to be investigated is shown in Figure 2. The gage length is approximately 7.8 inches; the length of the leads to the indicating and recording apparatus is 100 feet.

Figure 3 shows the indicating instrument. The left-hand milliammeter and the series rheostat are for controlling the constant bridge current. The right-hand milliammeter is for reading the relative flow of current through the stacks, and hence their changes of length and resistance. It may be arranged to read one milliamperere per 0.001-inch or per 0.0005-inch change of strain. By means of the keys across the middle of the instrument and the transfer switch in the center front, 12 different gages may be cut into the circuit. The leads from the 12 gages are secured to the binding posts shown at the back. The leads at the right go to an aluminum recorder box (fig. 4), which contains 12 mirror galvanometer elements, one for each strain gage. The beams of light reflected from the galvanometers make traces on a roll of sensitized bromide paper contained in the camera (fig. 5) and driven by an electric motor.

The precision of the strain gages is not particularly good. Owing to backlash and hysteresis and a tendency of the carbon piles to a gradual change in their calibration, errors approaching 25 per cent may occur.

The strain gages were installed in three groups, each group having its own recorder. The positions of the gages are given in Tables I and II. Gages 1 to 12, recording on camera No. 3, were placed forward on the longitudinals between frames 115 to 160.

Gages 13 to 24 were strung along longitudinals 1S and 1P, which are the second rows of longitudinals up from the bottom of the airship (see Fig. 2 in Part I of this report) and on the

upper longitudinals of the keel, designated KS and KP, between frames 40 and 85. These gages recorded on camera No. 2.

Gages 25 to 35, recording on camera No. 1, gave much the most interesting and important records. They were secured to the longitudinals in the lower half of the hull, just forward of frame 70, in the region of maximum bending moments from rudder and elevator action.

FLIGHT TESTS

The program of flight tests was explained in Part I. For convenience, it is again summarized in Table III of this part of the report.

Four flights were made during the series of tests. The time, air temperature, altitude, and corrected sea-level barometer of each test run are recorded in Table IV.

DETERMINATION OF THE AERODYNAMIC BENDING MOMENTS

In the strain gage records, a vertical deflection of 1 cm in the record line corresponds to a change of strain in the girder equal to 0.001 inch in the gage length of 7.8 inches. Assuming

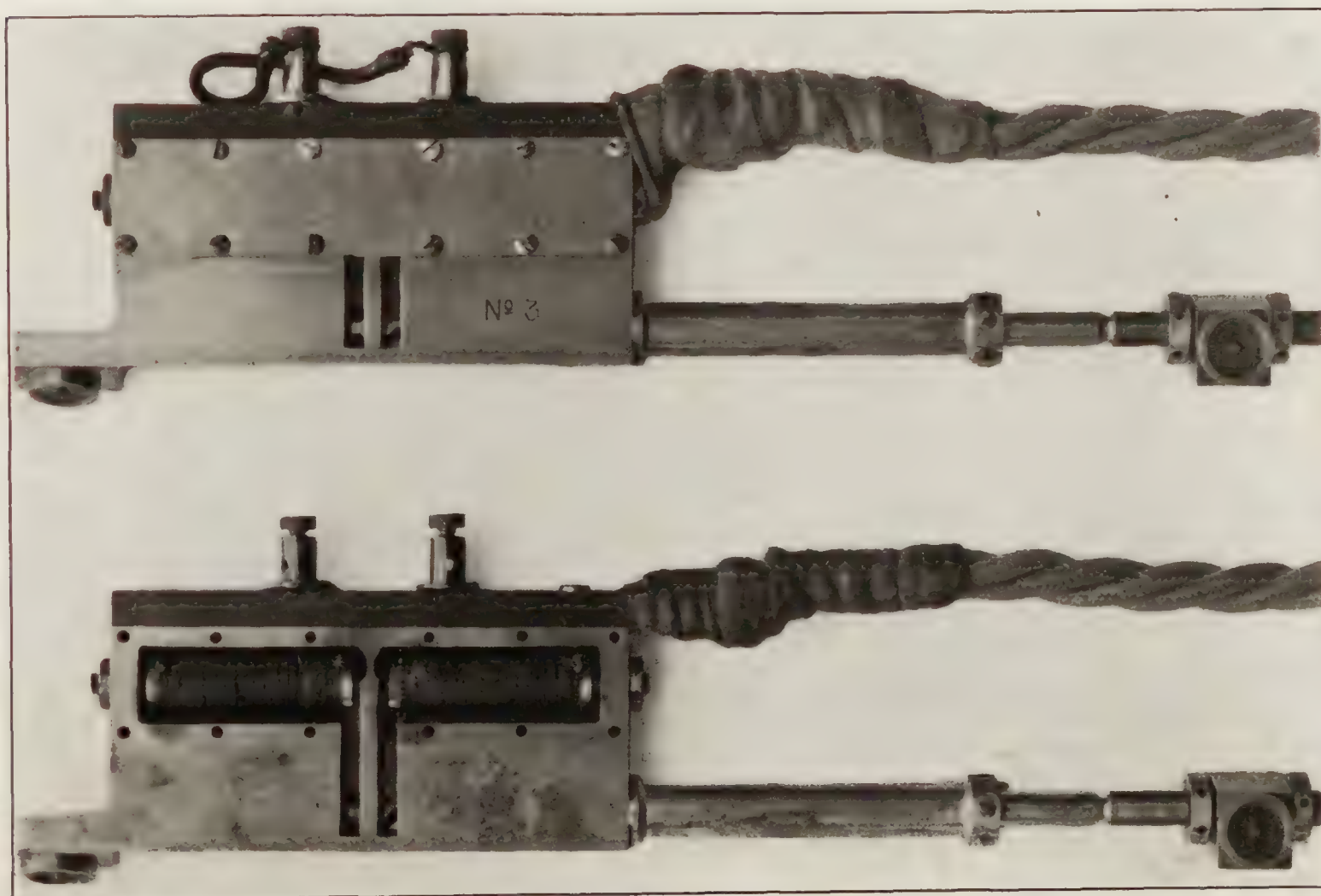


FIGURE 2.—Strain-gage elements for clamping to girders

that the modulus of elasticity of duralumin is $E = 10,500,000$ lb./sq. in., the stress in the girder per centimeter deflection of the record is equal to $10,500,000 \times 0.001 / 7.8 = 1,350$ lb./sq. in. If the section modulus of the cross section of the hull is known, and if the distribution of longitudinal stress is in accordance with the ordinary theory of bending, the bending moment in the hull at any cross section is the product of the section modulus and the maximum longitudinal fiber stress.

The maximum bending moments from forces on the tail surfaces are to be expected between frames 70 and 85. At frame 70, the strain gages were distributed nearly half way around the hull, so that the records include an approximation to the extreme fiber stress for all longitudinal planes of bending. The theoretical mean section modulus at frame 70 is 66 meters \times square inches. Theory and experiments have indicated that the distribution of stress is not in direct

linear proportion to the distance of the members from the neutral axis, but more nearly resembles a parabolic relation in which the stress in the extreme fiber is only about seven-eighths as great as if the linear stress distribution of the ordinary bending theory occurred. The theoretical section modulus is therefore multiplied by $\frac{7}{8}$, making its effective value 75.5 m sq. in. (The combination of meters and square inches may appear curious, but it is very convenient because the even 5-meter spacing of the frames makes the meter-pound a handy unit for measuring the bending moment, and the division of the bending moment in meter-pounds by

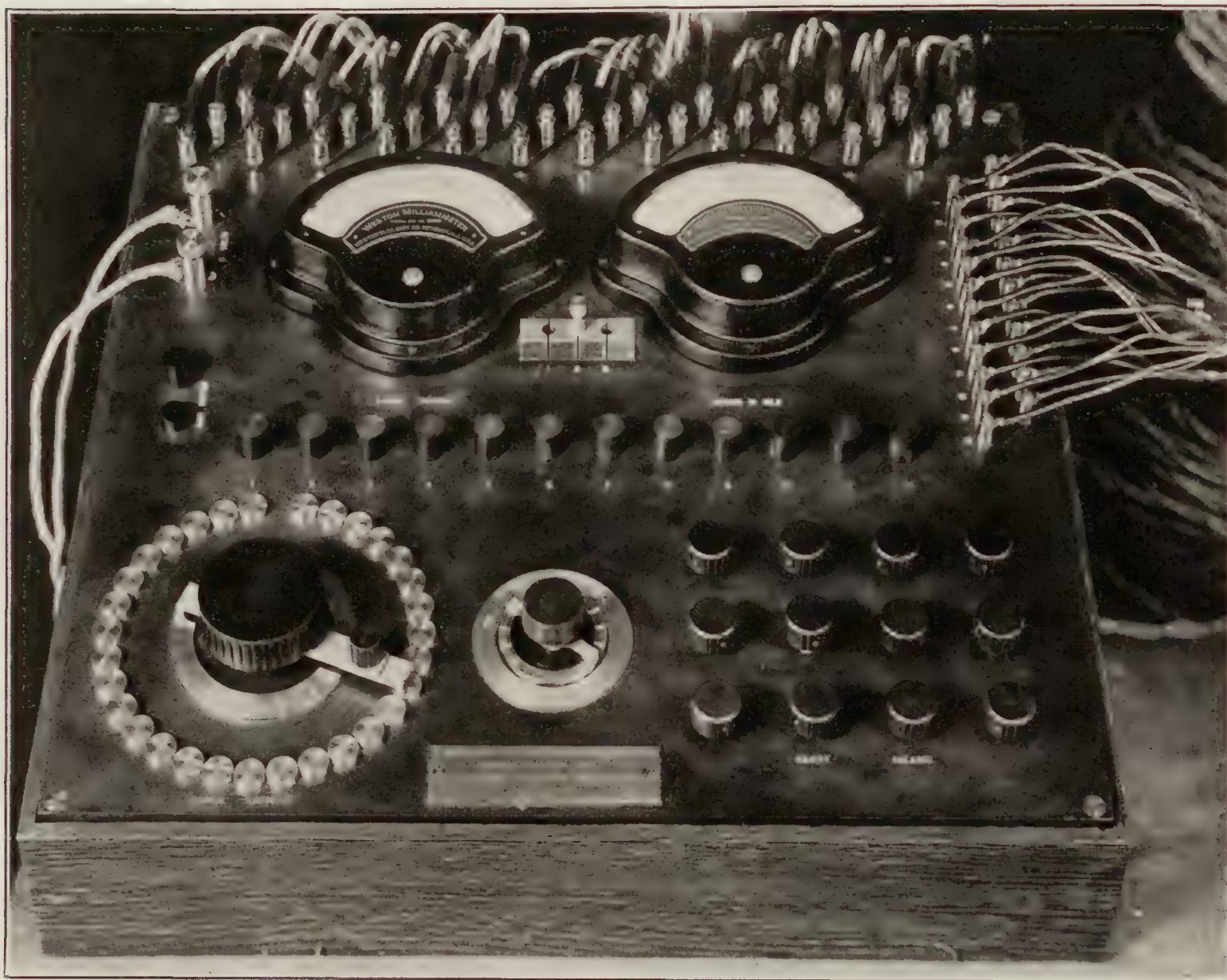


FIGURE 3.—Strain-gage indicating apparatus

the section modulus in meter-square inches gives the stress in the customary engineering units of pounds per square inch.)

Converting the deflections of the strain gage record into stress, and thence into bending moment, 1 centimeter deflection represents $1,350 \times 75.5 = 102,000$ m lb. bending moment.

The sensitized paper was moved through the camera at a mean rate of about 4.5 inches per minute. In tests in which the strain gage recorders were synchronized with the N. A. C. A. instruments, timing lines at 16 seconds intervals were thrown upon the paper by momentarily cutting off the lights.

DISCUSSION OF THE STRAIN GAGE RECORDS

Some typical strain gage records are shown in Figures 6 to 16. Since the strain gages show only changes of stresses in flight, and there are no clearly defined lines or levels of stress which may be regarded as representing either the normal static condition or straight flight in still air, the analysis of the aerodynamic bending moments is based upon the amplitude of stress, or half the total range of stress recorded during any particular maneuver or test run. It might

be thought that in a steady turn, the stresses in any one member would vary in only one direction from the normal; but, in reality, there is a reversal of stress even in maneuvers not involving a reversal of the helm. The reason for this is that when the helm is first put over, a transverse air force is created on the rudders, opposed by the inertia of the airship against angular accelera-

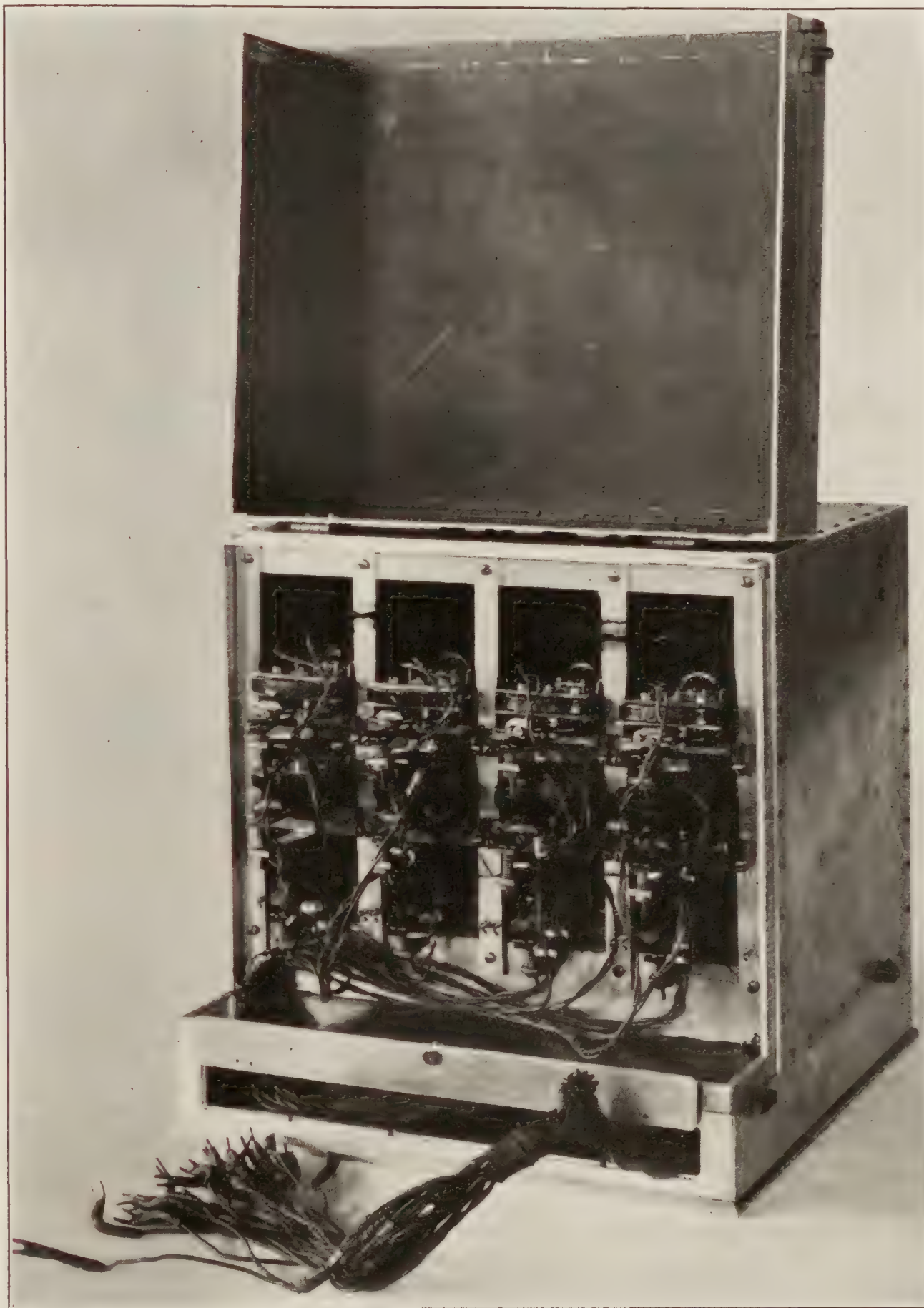


FIGURE 4.—Recording apparatus, interior seen from behind

tion. This produces a moment to bend the airship in the opposite sense to the direction of the coming turn. In other words, during the initial period of angular acceleration, the forces on the bow and stern act outwardly from the center of the turning circle. Later, when the airship has settled to the condition of steady turning without angular acceleration, the direction of the bending moment is reversed by the diminished force on the rudders and the creation of aero-

dynamic forces on the bow and fins, acting inwardly toward the center of the turning circle, opposed by the outwardly acting centrifugal forces distributed along the hull.

Gages 1 to 12 installed in the forward part of the airship, were the old original gages which had been used in the *Shenandoah* three years previously. Their records were not sufficiently satisfactory for quantitative measurements. They agreed with the air-pressure measurements in indicating that the transverse forces on the airship's forebody were small and irregular. Undoubtedly much greater forces and strains would have been recorded on the forebody if

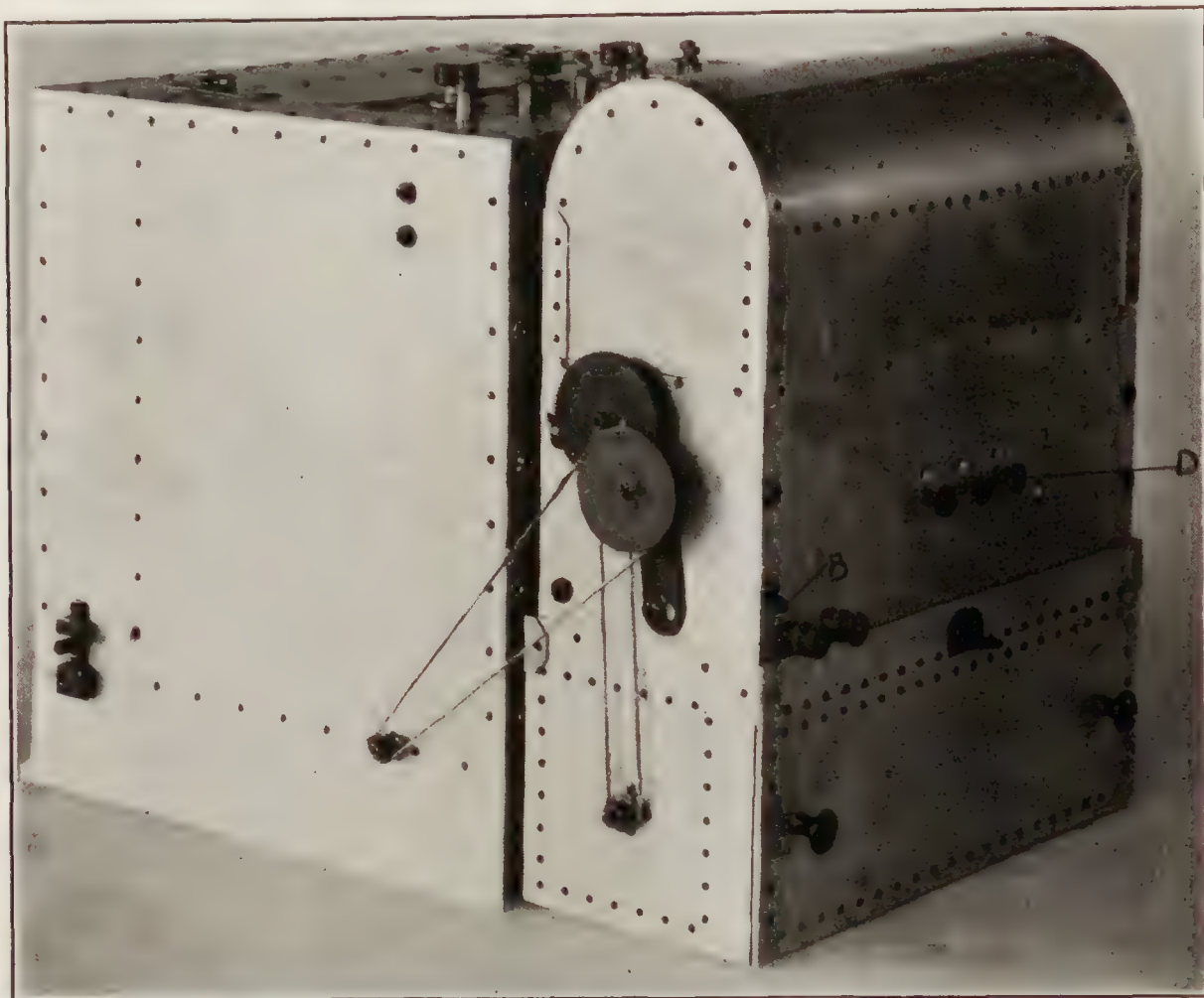


FIGURE 5.—Exterior view of recorder and camera

the airship had been flown at the angles of pitch required to offset large inequalities of weight and buoyancy.

Figures 6 to 11 and Figure 16 are typical records from the strain gages grouped on the longitudinals around frame 70, as listed in Table II.

Figure 6 is the record obtained in run No. 4B. The maneuver was a steady turn with 9.7° left rudder. The stresses were small and fluctuating, indicating that they were primarily the result of disturbances in the air rather than of bending moments imposed by the maneuver.

Figure 7 is an interesting record showing well-defined stresses varying continuously from one side of the airship to the other, as would be expected from a lateral bending moment.

Figure 8 is principally of interest in showing the reversal of stress resulting from reversal of the helm when the airship executes an S curve.

Figure 9 shows the strongly fluctuating stresses which are characteristic of the period just after leaving the mooring mast. An important feature of this record is that bending moments in the vertical plane are indicated by large stresses of the same signs and approximately equal magnitudes in the longitudinals at the top of the keel and the lower part of the hull, showing that the keel behaved as an integral part of the hull, and not as a separate beam. According to the shear theory, and some other theories of stress distribution, the top member of the keel should show stresses of opposite sign to the bottom member when the hull is subjected to vertical bending.

Figure 10 shows a rather gradual reversal of stresses during an S turn.

Figure 11 is a record of an S turn in which the stresses due to the maneuver were overlaid by fluctuating stresses resulting from disturbed air.

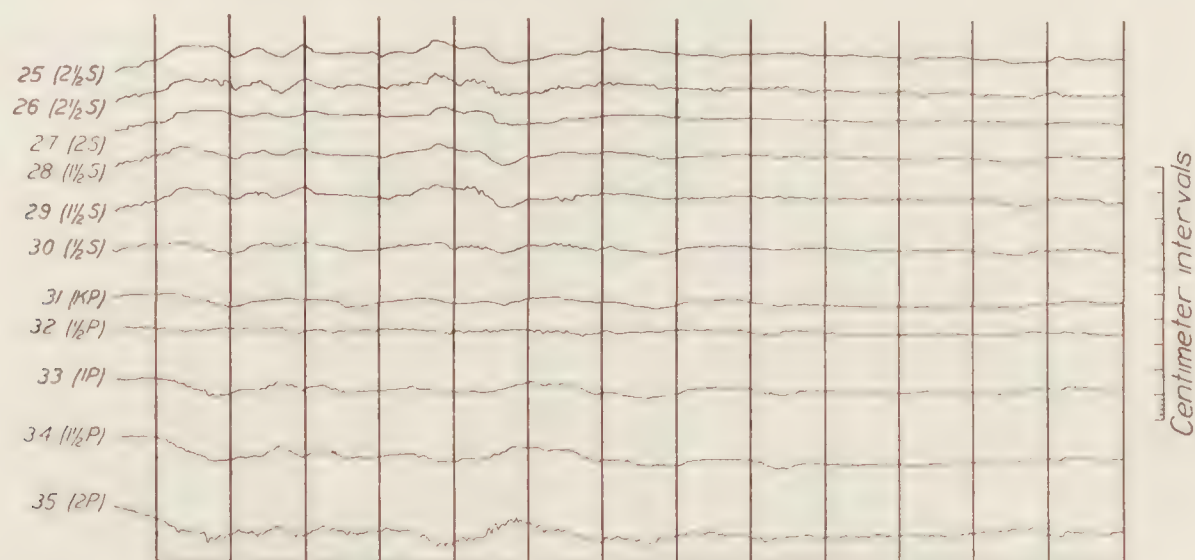


FIGURE 6.—Camera No. 1. Run No. 4

Figures 12 to 15, inclusive, are the records of the gages extended longitudinally along the bottom of the airship as recorded in Table II. Only Figure 15 of this group is of much sig-

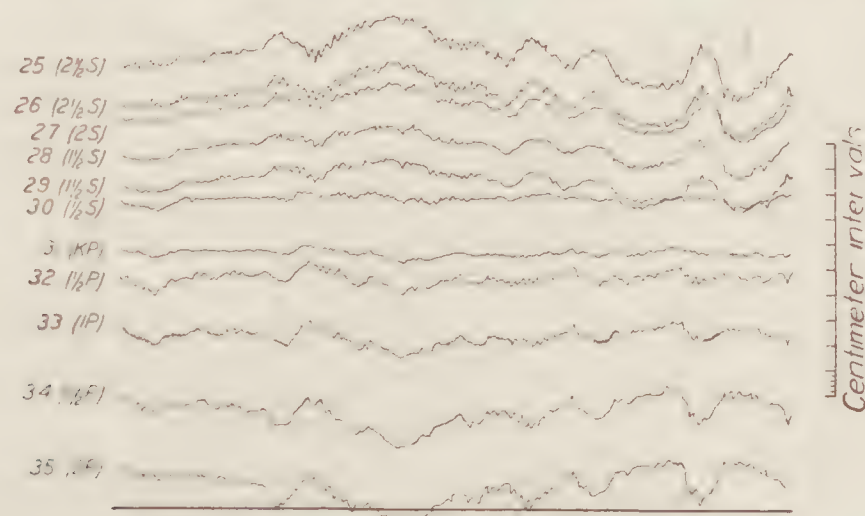


FIGURE 7.—Camera No. 1. Take-off from mast

nificance. It was taken during the critical period after leaving the mast. The fluctuations of stress are large, rapid, and irregular.

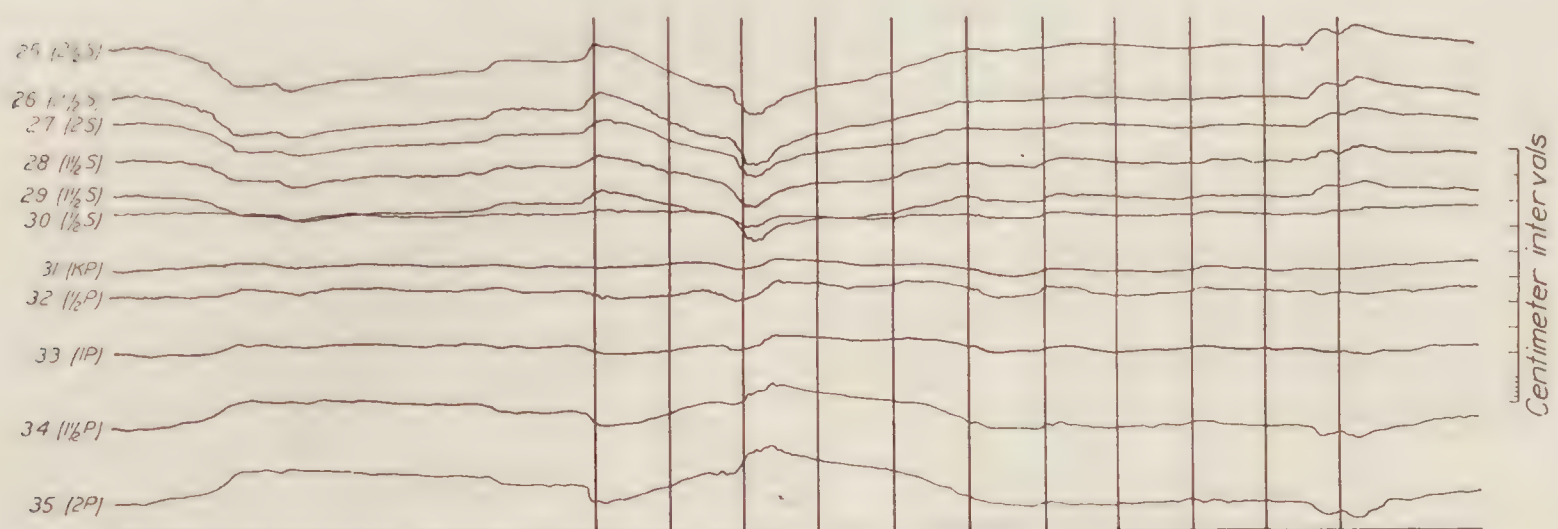


FIGURE 8.—Camera No. 1. Run No. 3

Figure 16 is typical of the large stresses during the rough air of the first day of the trials. This record was not synchronized with the N. A. C. A. normal force measurements, but it is

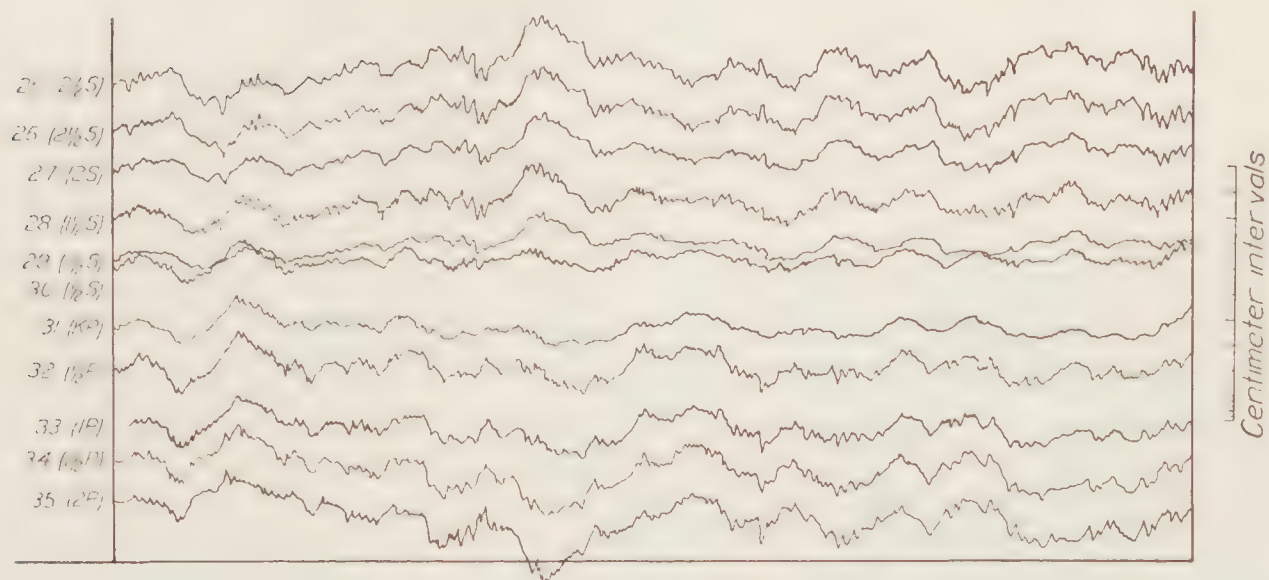


FIGURE 9.—Camera No. 1. Take-off from mast

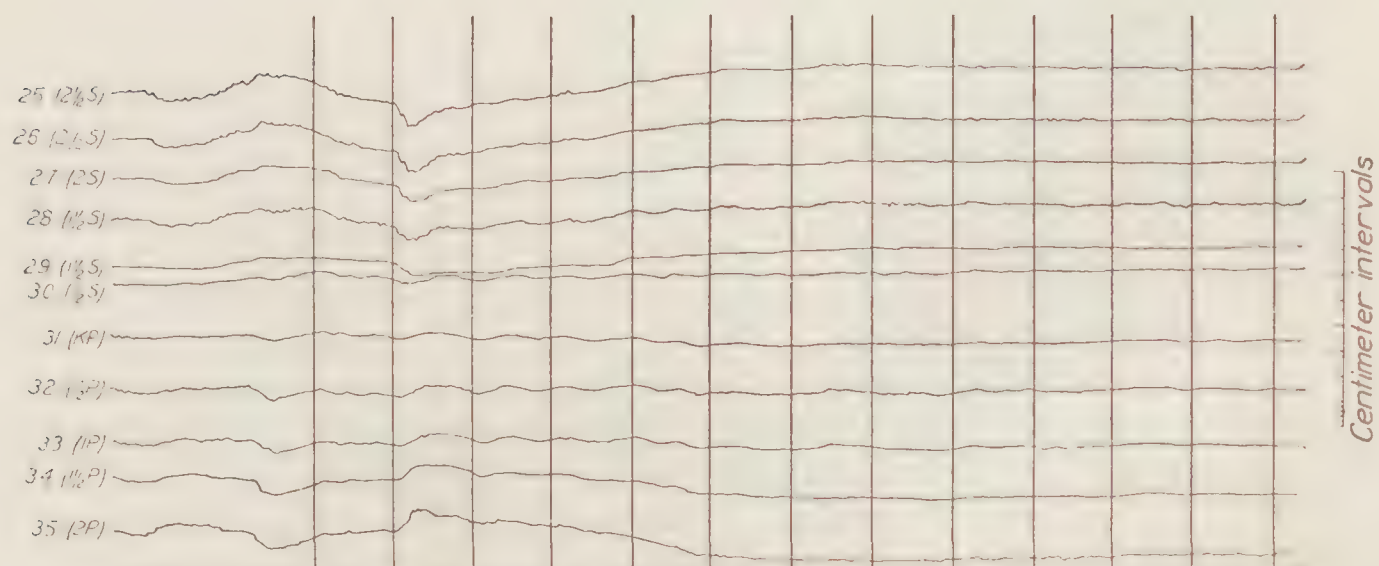


FIGURE 10.—Camera No. 1. Run No. 5

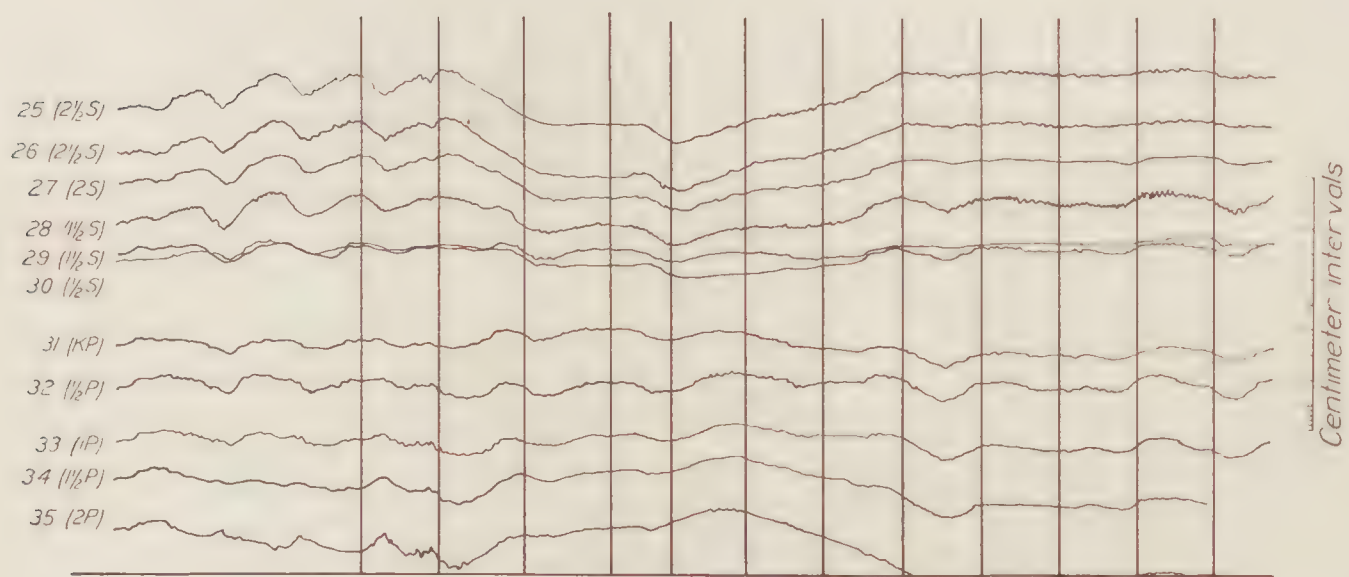


FIGURE 11.—Camera No. 1. Run No. 17

believed to be nearly coincident with run No. 4A. Some of the gages were not working satisfactorily at that time, and consequently, there are gaps in the record.

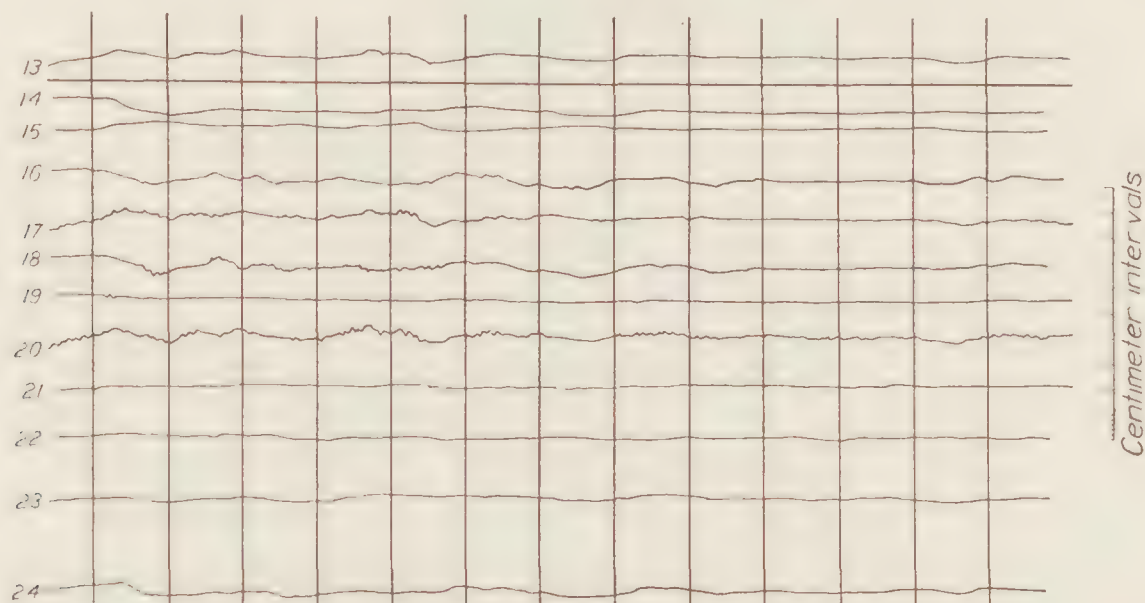


FIGURE 12.—Camera No. 1. Run No. 4

It is a curious fact that the most severe stresses were always recorded immediately after taking off from the mooring mast. A possible explanation is that during the first few minutes

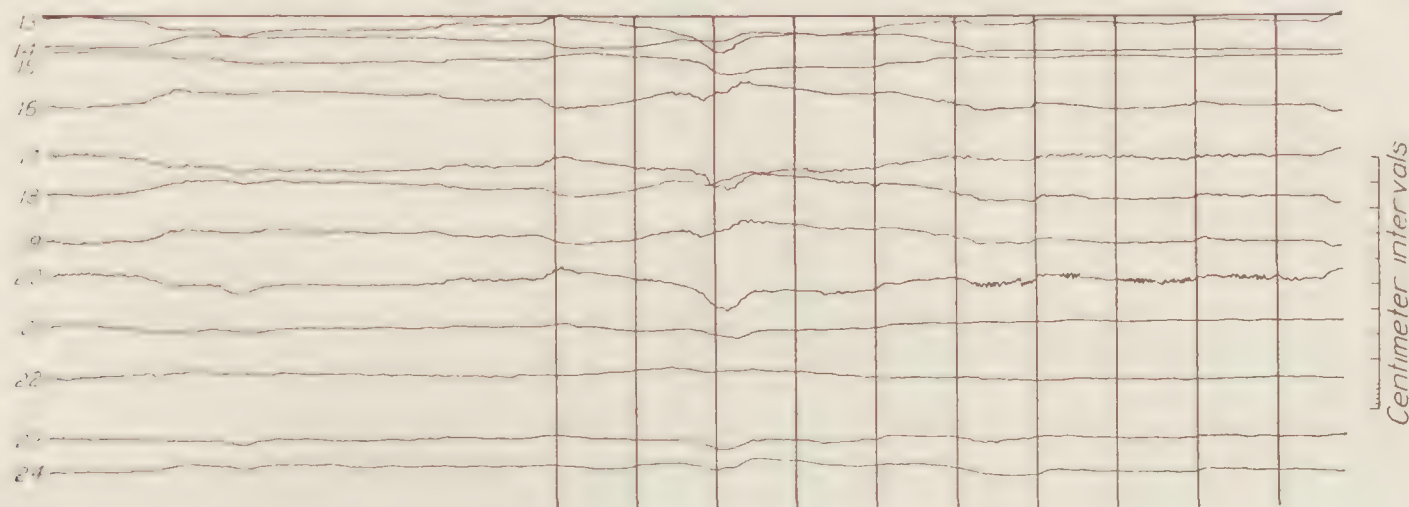


FIGURE 13.—Camera No. 2. Run No. 3

of flight, the airship lost superheat, causing a progressive change of trim that made the airship unsteady on the controls, with consequent rapid fluctuations in the bending moments.

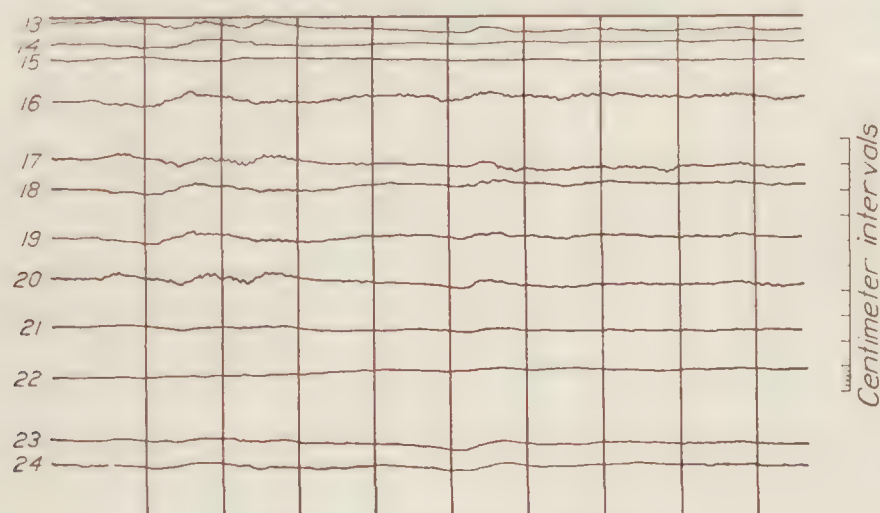


FIGURE 14.—Camera No. 2. Run No. 4

COEFFICIENTS OF AERODYNAMIC BENDING MOMENT

In order to understand the significance of the strains recorded by the strain gages, two steps are necessary—first, to convert the recorded strains into bending moments according to

the relation already derived; second, to express the bending moments in coefficient form for comparison with the tail surface forces and theoretically derived bending moment coefficients. A nondimensional coefficient is derived as follows:

For geometrically similar distributions of air pressure over airship hulls the resulting forces are proportional to the aerodynamic head $\rho v^2/2$, and to the surface area of the hull, or to the volume to the two-thirds power for similar shapes. The aerodynamic bending moment

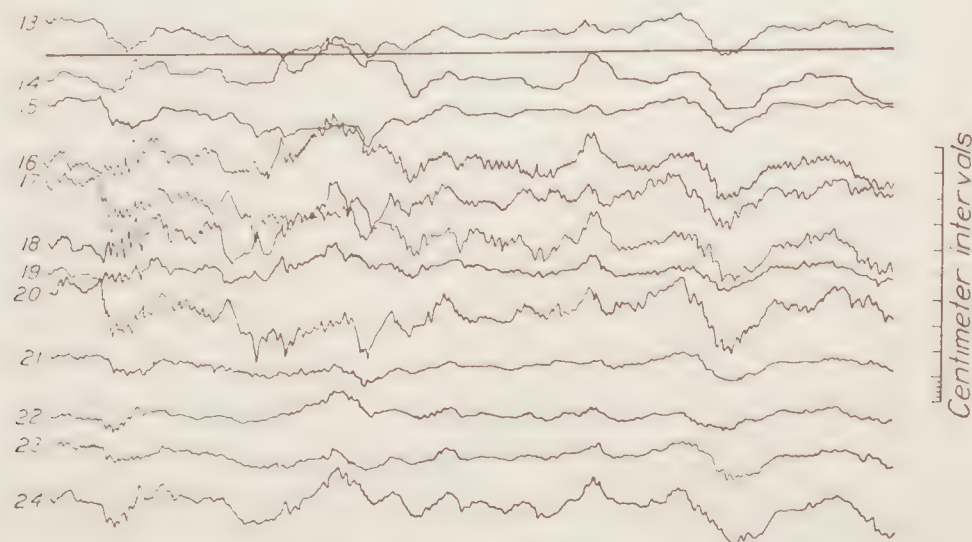


FIGURE 15.—Camera No. 2. Take-off from mast

is proportional to the total force and the length of the hull. Using these relations, the bending moment coefficient is defined by

$$C_M = \frac{M}{q V^{2/3} L}$$

where

C_M = the coefficient of aerodynamic bending moment.

M = the aerodynamic bending moment.

q = the aerodynamic head $\rho v^2/2$.

V = the air volume of the airship.

L = the over-all length of the airship.

For the *Los Angeles*, $V^{2/3} = 20,000$ sq. ft., and $L = 200$ m. Therefore, if M is expressed in m lb., and q in lb./sq. ft.,

$$C_M = \frac{M}{4,000,000 q}$$

Some values of C_M calculated from the observed values of q and the amplitudes of the strains are given in Table V. It is of great significance that flight in the rough air of the first day (run No. 4A) without maneuvers produced stresses corresponding to values of C_M approximately twice as great as were recorded in the maneuvers in the comparatively still air of the succeeding days of the trials.

CORRELATION OF BENDING MOMENTS AND TAIL SURFACE FORCES

Since the pressure distribution measurements showed the transverse forces on the hull to be small, it is to be inferred that the aerodynamic bending moments were mainly the result of tail surface forces opposed by the inertia of the hull against angular acceleration. This conclusion is confirmed by the insignificant strains shown by the strain gage records when the airship had settled to the condition of steady turning. It is unfortunate that satisfactory measurements of the angular accelerations could not be obtained. Lacking data on this subject, the best that can be done is to compare the relation between the observed values of the bending moment and tail surface force coefficients with their theoretical relation when the tail surface force is opposed only by angular acceleration.

In Part I of this report, the tail surface force coefficient C_{NF} is defined by

$$C_{NF} = \frac{2F}{S \rho v^2} = \frac{F}{Sq}$$

where

F = the total force on the tail surface.

S = the total area of the vertical or horizontal tail surface = 2,540 sq. ft.

q = the aerodynamic head.

It may be shown that when a force on the tail surfaces is opposed only by angular acceleration of the airship, a bending moment of about 31 m lb. is produced at frame 70 for every 1-pound force on the surfaces. It follows that in that condition

$$\frac{C_{NF}}{C_M} = \frac{F}{Sq} \times \frac{V^{2/3} L q}{M} = \frac{V^{2/3} L}{31 S} = 50.8$$

It may be seen from Table V that the ratio C_{NF}/C_M varied from 20 to 64, indicating that although the transverse forces were small and irregular, as indicated by the pressure measure-

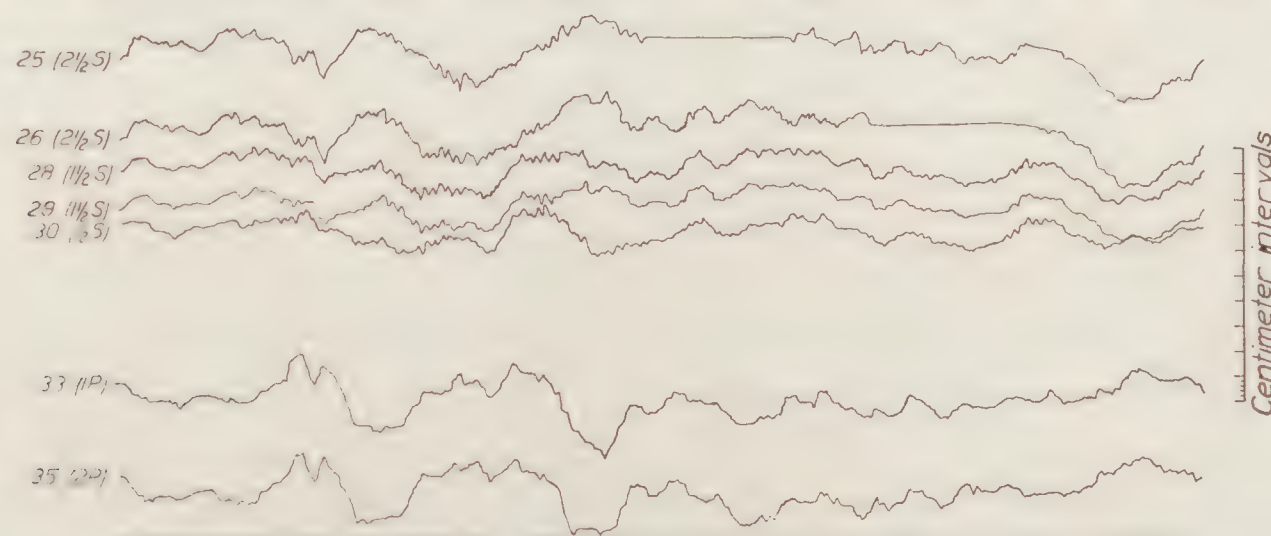


FIGURE 16.—Camera No. 1

ments, their resultant was sufficient to have a very considerable effect on the bending moments, sometimes adding to and at other times subtracting from the effect of the tail surface force. In the rough air run, No. 4A, C_{NF}/C_M is only 27, showing that in rough air the forces on the hull are of relatively greater importance than in most still air maneuvers.

APPLICATION TO DESIGN

In comparing the comparatively moderate forces recorded in still air maneuvers with the much greater forces in rough air flight, it should be borne in mind that the trials were made at rather moderate speed. It is to be expected that in still air maneuvers with any given helm angles, the aerodynamic forces will vary as the square of the speed, and the coefficients C_{NF} and C_M will be constant. On the other hand, when flying in rough air, the angles of attack resulting from sudden changes in the wind velocity will diminish with increasing speed of the airship. Consequently, the forces in rough air vary more nearly as the ship's speed, and the coefficients inversely as the speed.

The high value of 0.0128 calculated for C_M in run No. 4A occurred at only 50 knots speed. Assuming C_M for rough air to be inversely proportional to the speed, its magnitude at 64 knots in the same air conditions would have been only 0.01. It has been accepted practice to design rigid airships, including the *Los Angeles*, for a maximum aerodynamic C_M of about 0.01 at the airship's full speed, plus a material factor of safety of 2.0 to 2.5. The observations in the extremely rough air of the first day of the flight trials indicated that the strength of the *Los Angeles* is sufficient for these conditions, but there is not much margin for hitting a violent and sharply defined wind squall at high speed.

The most recent practice in large airship design has tended toward provision of sufficient strength for a maximum C_M of about 0.02, which theoretical calculations show to be sufficient to withstand a sharply defined squall having a velocity of 60 ft./sec. transversely to the airship's longitudinal axis. This was the squall condition specified in the Navy Department's Airship Design Competition, 1928. It provides a large margin of strength beyond the most severe conditions encountered in the flight trials of the *Los Angeles*.

CONCLUSIONS

The largest aerodynamic forces and bending moments observed in the trials corresponded to coefficients astonishingly close to the design assumptions of the Zeppelin Company. The large airships of the future must be designed to encounter thunderstorm conditions which in the past have been regarded as avoidable hazards, and greater strength than that of the *Los Angeles* is therefore required.

Experiments should be continued to determine the angular and linear accelerations of airships in rough air. For such experiments there is great need to improve the sensitivity and reliability of the instruments at present available.

The risks attendant upon deliberately flying aircraft into thunder squalls are too great to be accepted, but every effort should be made to determine the structure of the air in squalls by means of wind-recording instruments mounted on lofty towers or by sensitive recording accelerometers carried in pilot balloons. Such researches would necessarily be expensive but of inestimable value to the science of air navigation.

BUREAU OF AERONAUTICS,
NAVY DEPARTMENT,
December 3, 1928.

TABLE I
POSITIONS OF FORWARD GROUP OF STRAIN GAGES IN U. S. S. LOS ANGELES APRIL
AND MAY, 1926

Gage No.	Position
1	Longitudinal $\frac{1}{2}$ S low base, forward of frame 115.
2	Longitudinal KS apex, forward of frame 115.
3	Longitudinal 1S low base, forward of frame 130.
4	Longitudinal 2S low base, forward of frame 145.
5	Longitudinal 1S low base, forward of frame 145.
6	Longitudinal 1S low base, forward of frame 160.
7	Longitudinal O apex, forward of frame 160.
8	Longitudinal 1P low base, forward of frame 145.
9	Longitudinal 2S low base, forward of frame 130.
10	Longitudinal 1P low base, forward of frame 130.
11	Longitudinal 2P low base, forward of frame 130.
12	Longitudinal KS apex, forward of frame 130.

NOTE.—Longitudinals are numbered 0, $\frac{1}{2}$, 1, $1\frac{1}{2}$, 2, etc., to 6 from the bottom to the top of the airship. S and P denote starboard and port sides, respectively. The longitudinals along the top of the keel are designated KS and KP. The terms low base, high base, and apex refer to the three channels or booms of the longitudinals.

TABLE II

POSITIONS OF REAR GROUP OF STRAIN GAGES IN U. S. S. LOS ANGELES, APRIL AND MAY, 1926

Gage No.	Position
13	Longitudinal 1S low base, forward of frame 40.
14	Longitudinal 1P low base, forward of frame 40.
15	Longitudinal 1S low base, forward of frame 55.
16	Longitudinal 1P low base, forward of frame 55.
17	Longitudinal 1S low base, forward of frame 85.
18	Longitudinal 1P low base, forward of frame 85.
19	Longitudinal 1P low base, forward of frame 70.
20	Longitudinal 1S low base, forward of frame 70.
21	Longitudinal KS out base, forward of frame 40.
22	Longitudinal KP out base, forward of frame 40.
23	Longitudinal KS apex base, forward of frame 85.
24	Longitudinal KP apex base, forward of frame 85.
25	Longitudinal 2½S high base, forward of frame 70.
26	Longitudinal 2½S low base, forward of frame 70.
27	Longitudinal 2S low base, forward of frame 70.
28	Longitudinal 1½S low base, forward of frame 70.
29	Longitudinal 1½S high base, forward of frame 70.
30	Longitudinal ½S low base, forward of frame 70.
31	Longitudinal KP apex, forward of frame 70.
32	Longitudinal ½P low base, forward of frame 70.
33	Longitudinal 1P low base, forward of frame 70.
34	Longitudinal 1½P low base, forward of frame 70.
35	Longitudinal 2P low base, forward of frame 70.

(See note to Table I.)

TABLE III

RECORD OF TESTS ON U. S. S. LOS ANGELES, APRIL AND MAY, 1926

Date	Run No.	Maneuver
Apr. 27	1	Rough air flying on course.
	2	Do.
	3	Do.
	4	Do.
	5	Do.
	6	Do.
	7	Do.
	8	Do.
	9	Do.
	10	Do.
Apr. 30	1	Turn with 12° R. rudder at 1,050 R. P. M.
	2	Do.
	3	Turn with 8° R. rudder at 1,050 R. P. M.
	4	Turn with 12° L. rudder at 1,050 R. P. M.
	5	Turn with 8° R. rudder at 1,230 R. P. M.
	6	Turn with 12° R. rudder at 1,230 R. P. M.
	7	Running through squall.
	8	Do.
May 7	1	Reversal, 8° R. and L. rudder at 1,050 R. P. M.
	2	Do.
	3	Reversal, 12° R. and L. rudder at 1,050 R. P. M.
	4	Turn, 8° R. rudder at 1,050 R. P. M.
	5	Turn, 8° R. rudder at 1,230 R. P. M.
	6	Turn, 12° R. rudder at 1,230 R. P. M.
May 13	1	Rough air after leaving mast.
	2	Turn, 12° R. rudder at 1,230 R. P. M.
	3	Turn, 8° L. rudder at 1,050 R. P. M.
	4	Turn, 12° R. rudder at 1,050 R. P. M.
	5	Reversal, 8° R. and L. rudder at 1,050 R. P. M.
	6	Reversal, 12° R. and L. rudder at 1,050 R. P. M.
	7	Missed.
	8-12	Deceleration tests.
	13	Turn, 12° R. rudder at 1,050 R. P. M.
	14	Reversal, 12° R. and L. rudder at 1,050 R. P. M.
	15, 16	Deceleration tests.
	17	Reversal, 12° R. and L. rudder at 1,230 R. P. M.

TABLE IV

U. S. S. LOS ANGELES TESTS—TABLE OF DATA (AS TAKEN FROM AIRSHIP'S LOG AND AEROLOGICAL STATION)

Date	Run No.	Time of starting (eastern standard)	Air temperature	Altitude	Corrected sea level barometer
Apr. 27	1	11:38:23	42	1,630	30.092
	2	12:56:23	42	1,800	30.076
	3	13:16:58	42	1,800	-----
	4	13:34:50	42	1,800	-----
	5	13:53:54	42	1,800	30.04
	6	14:17:42	42	2,200	-----
	7	14:29:16	42	2,500	-----
	8	14:43:02	-----	2,500	-----
	9	14:55:28	41	2,500	30.03
	10	15:06:00	41	2,500	-----
Apr. 30	1	11:39:50	51	2,700	-----
	2	12:01:35	51	2,700	29.896
	3	13:00:24	58	1,500	29.885
	4	13:10:57	-----	1,530	-----
	5	13:20:25	58	1,500	-----
	6	14:12:51	-----	1,400	29.87
	7	14:42:33	58	2,000	-----
	8	14:53:13	57	2,000	29.86
May 7	1	17:28:33	63	2,500	29.83
	2	17:43:03	-----	2,500	-----
	3	18:03:12	62	2,500	29.82
	4	18:21:44	61	3,000	-----
	5	18:45:27	-----	-----	-----
	6	Stopped.	-----	-----	-----
May 13	1	19:10:15	61	2,500	29.83
	1	10:32:54	57	2,500	29.78
	2	10:46:25	-----	-----	-----
	3	10:56:11	57	2,500	-----
	4	10:06:03	-----	2,500	29.78
	5	11:15:25	-----	2,500	-----
	6	11:41:36	59	2,100	29.76
	7	-----	-----	-----	-----
	8	14:00:40	60	2,500	29.73
	9	14:08:24	-----	2,500	-----
	10	14:22:32	61	2,500	-----
	11	14:33:14	-----	2,500	-----
	12	14:40:20	61	2,500	29.70
	13	16:38:40	61	2,900	29.70
	14	16:57:22	60	2,900	29.71
	15	17:19:37	60	2,900	-----
	16	17:30:43	61	2,900	-----
	17	17:47:20	-----	2,900	29.72

TABLE V

TAIL SURFACE FORCE AND HULL BENDING MOMENT COEFFICIENTS

Run maneuver	Rudder position	q lb./sq. ft.	F lb.	M m lb.	C_{NP}	C_M	$\frac{C_{NP}}{C_M}$
Lower fin and rudder							
4B (turn).....	9.70° L.....	6.19	1,168	74,000	0.149	0.0030	50
4C (turn).....	8.30° R.....	4.37	1,300	64,000	.235	.0037	64
5C (turn).....	7.85° R.....	5.93	1,304	112,000	.173	.0047	37
2B (turn).....	12.75° R.....	4.47	756	118,000	.133	.0066	20
13D (turn).....	12.95° R.....	3.95	984	94,000	.196	.0059	33
5D (reversal).....	4.50° L.....	5.62	1,679	105,000	.236	.0047	50
3C (reversal).....	6.50° L.....	5.36	1,817	143,000	.268	.0067	40
17D (reversal).....	12.50° R.....	7.96	1,922	144,000	.190	.0045	42
Starboard fin and elevator							
4A (rough air).....	-----	8.01	3,501	410,000	0.349	0.0128	27

REPORT No. 326

TESTS OF FIVE METAL MODEL PROPELLERS WITH VARIOUS PITCH DISTRIBUTIONS IN A FREE WIND STREAM AND IN COMBINATION WITH A MODEL VE-7 FUSELAGE

By E. P. LESLEY and ELLIOTT G. REID
Stanford University

TECHNICAL REPORT No. 326

TESTS OF FIVE METAL MODEL PROPELLERS WITH VARIOUS PITCH DISTRIBUTIONS IN A FREE WIND STREAM AND IN COMBINATION WITH A MODEL VE-7 FUSELAGE

By E. P. LESLEY and ELLIOTT G. REID

SUMMARY

This report describes the tests of five adjustable blade metal model propellers both in a free wind stream and in combination with a model fuselage with stub wings, which were conducted at Stanford University under research authorization of the National Advisory Committee for Aeronautics. The propellers are of the same form and cross section but have variations in radial distributions of pitch. By making a survey of the radial distribution of air velocity through the propeller plane of the model fuselage it was found that this velocity varies from zero at the hub center to approximately free stream velocity at the blade tip.

The tests show that the efficiency of a propeller when operating in the presence of the airplane is, over the working range, generally less than when operating in a free wind stream, but that a propeller with a radial distribution of pitch of the same nature as the radial distribution of air velocity through the propeller plane suffers the smallest loss in efficiency.

INTRODUCTION

In the design of propellers it is generally customary to assume that the axial velocity through the propeller disk is uniform. It has recently been demonstrated (reference 1), however, that such is not the case; the velocity through the propeller plane of a fuselage of conventional form is relatively small in the immediate vicinity of the fuselage. The purpose of the present investigation was to determine the importance of considering this feature in the design of propellers. To this end, the performance characteristics of five model propellers, alike in plan form and blade sections and having approximately the same mean pitch, but with various radial distributions of pitch, have been determined both in the free stream and in the presence of a model fuselage.

A model VE-7 fuselage with stub wings was chosen as a typical slip stream obstruction. The form of the model fuselage is shown in Figure 1. The scale ratio between the model and full size is 0.3674, thus giving a diameter of 3 feet for the model propeller, and a chord of 20.39 inches for the model wing. The model propellers are shown in Figure 2. The blades of all models are adjustable and all fit a single hub. Propeller A is, at the blade angles shown, of uniform geometric pitch and has a geometric pitch/diameter ratio of 7/10. Propellers B and C are of the same form and pitch as A from hub to 10.8-inch radius; from this point to the tip B is gradually increased in pitch and C is gradually decreased. Propellers D and E are the same as propeller A from the 10.8-inch radius outward; from this point toward the hub the blade angles of D are increased and those of E are decreased.

Reference 1. The Effect of the Sperry Messenger Fuselage on the Air Flow at the Propeller Plane. By Fred E. Weick. N. A. C. A. Technical Note No. 274.

PROGRAM OF TESTS

The program for tests was as follows:

1. Tests in an unobstructed wind stream.

(a) Tests of propeller A with blades set at the designed angles.

Reduction of observed data to the usual coefficients

$$C_P = \frac{\text{Power}}{\rho n^3 D^5}, \quad C_T = \frac{\text{Thrust}}{\rho n^2 D^4}$$

and η = efficiency, and plotting of same on abscissa of V/nD .

Calculation of speed power coefficient

$$C_{P_1} = \sqrt{\frac{\rho V^5}{\text{Power } n^2}}$$

and plotting same against V/nD and efficiency, thus determining value of such coefficient for maximum efficiency.

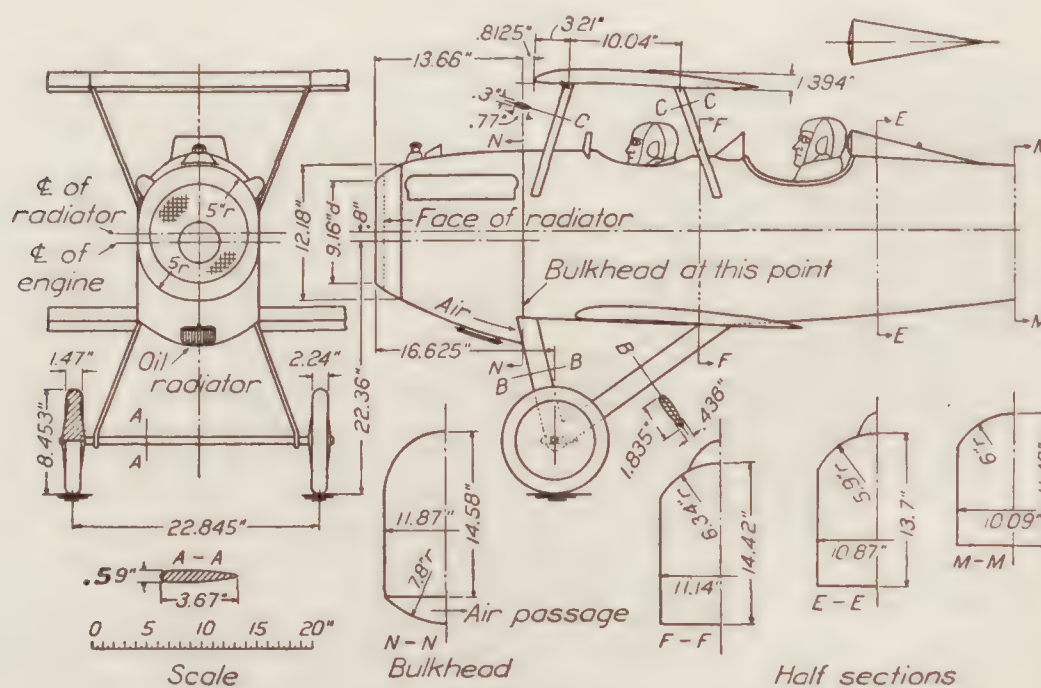


FIGURE 1.—Wind tunnel model of VE-7 airplane

Chord, 20.36 inches; gap, 20.55 inches; stagger, 4.13 inches; angle of wing setting (upper wing) $1^\circ 45'$; lower, $2^\circ 15'$.

(b) Preliminary tests of propellers B, C, D, and E at various blade settings and at values of V/nD in the neighborhood of that for maximum efficiency, to determine the setting giving maximum efficiency for the same value of the speed-power coefficient

$$\sqrt{\frac{\rho V^5}{P n^2}}$$

as that determined for propeller A at maximum efficiency.

(c) Complete tests of propellers B, C, D, and E at the settings determined by (b).

2. Tests of model propellers in combination with the VE-7 model fuselage and stub wings.

(a) Tests similar to 1 (a).

(b) Tests similar to 1 (b).

(c) Tests similar to 1 (c).

3. Survey of the velocity distribution at the propeller plane of the VE-7 model.

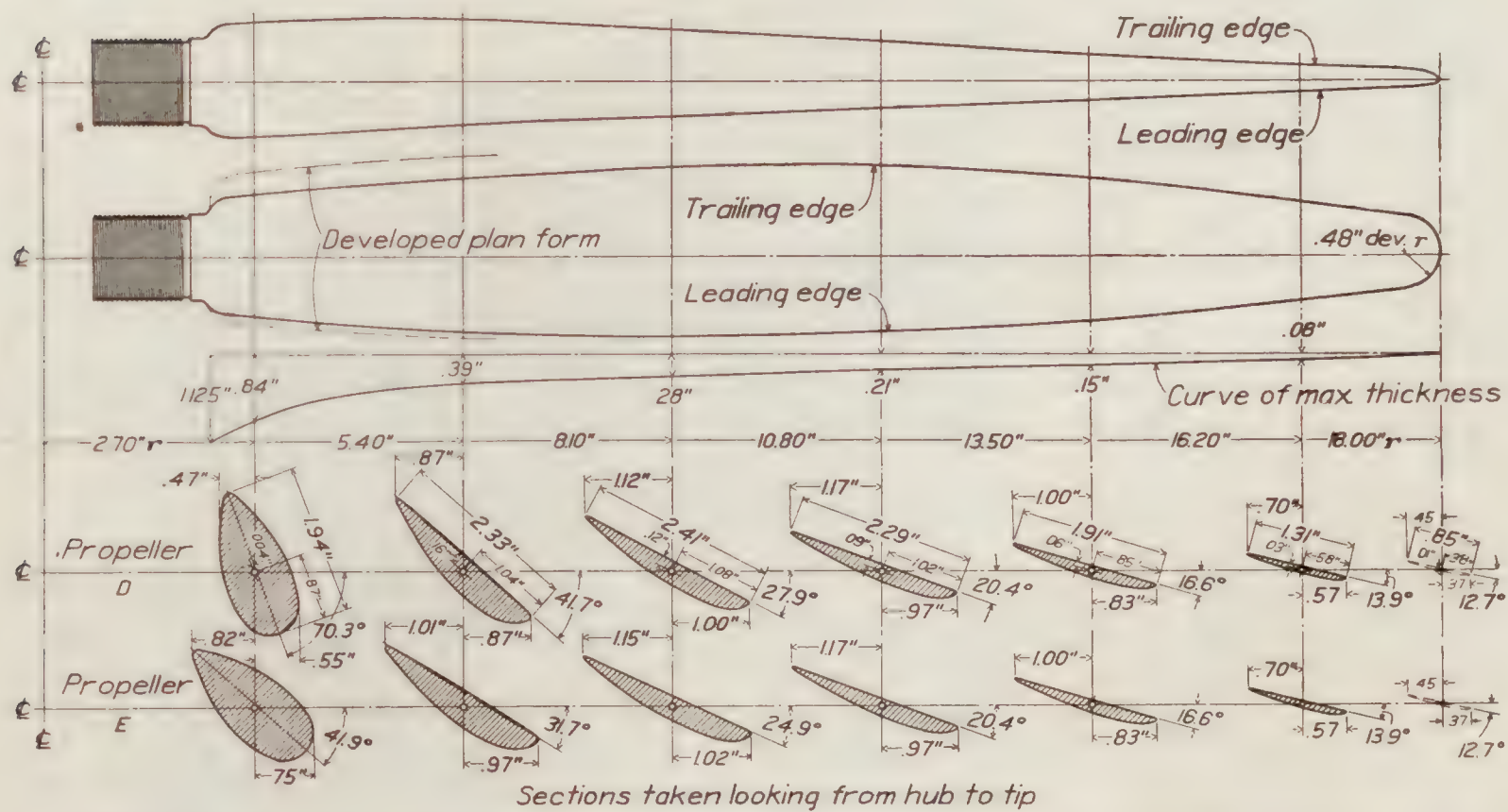
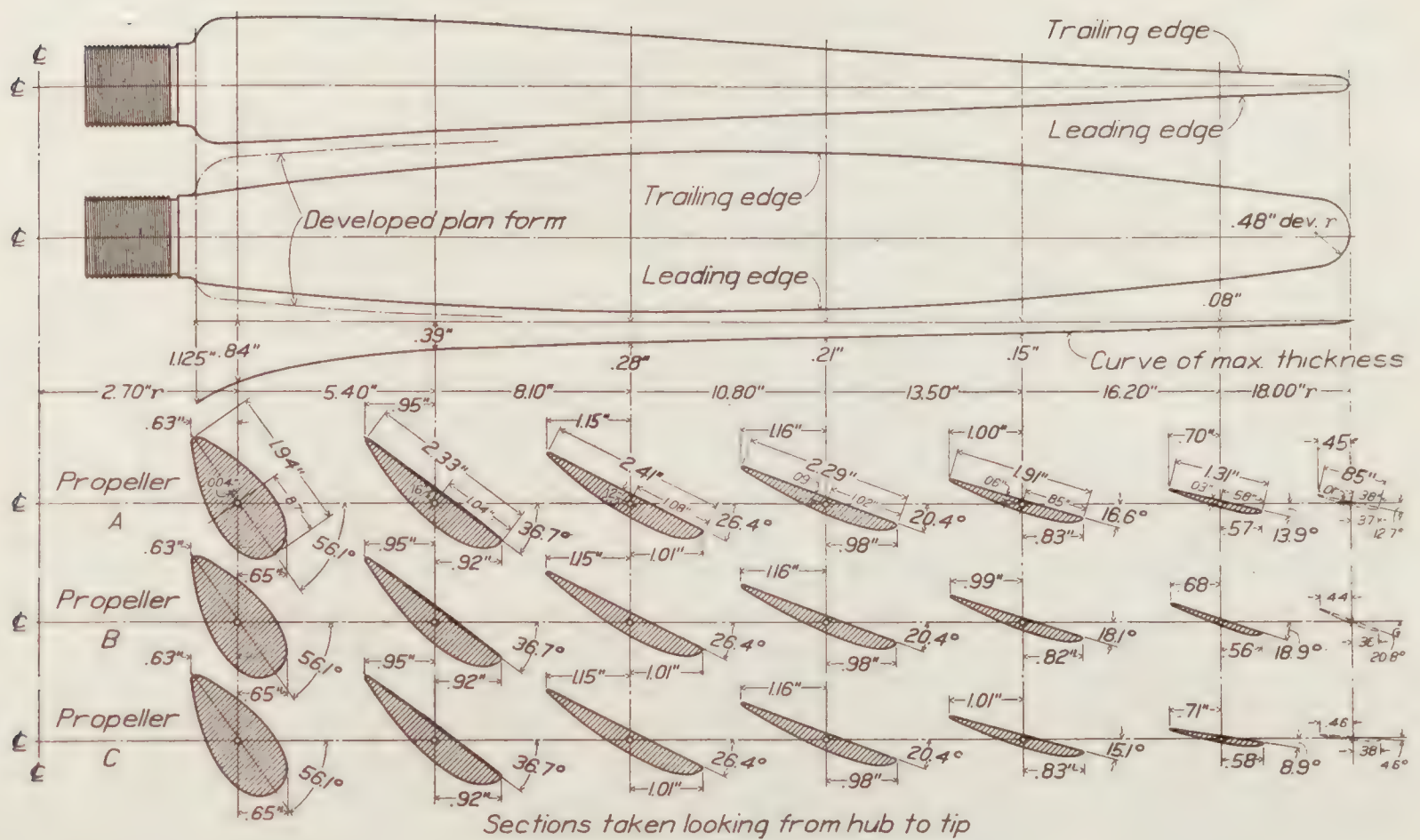


FIGURE 2.—Model propellers A, B, C, D, and E, with varying pitch distribution, but with no change in blade section dimensions

SET-UP OF APPARATUS AND METHOD OF TESTS

The apparatus for the free wind stream tests is shown in Figure 3. The model propellers are mounted on the shaft of a cradle type dynamometer placed at the axis of the wind tunnel.

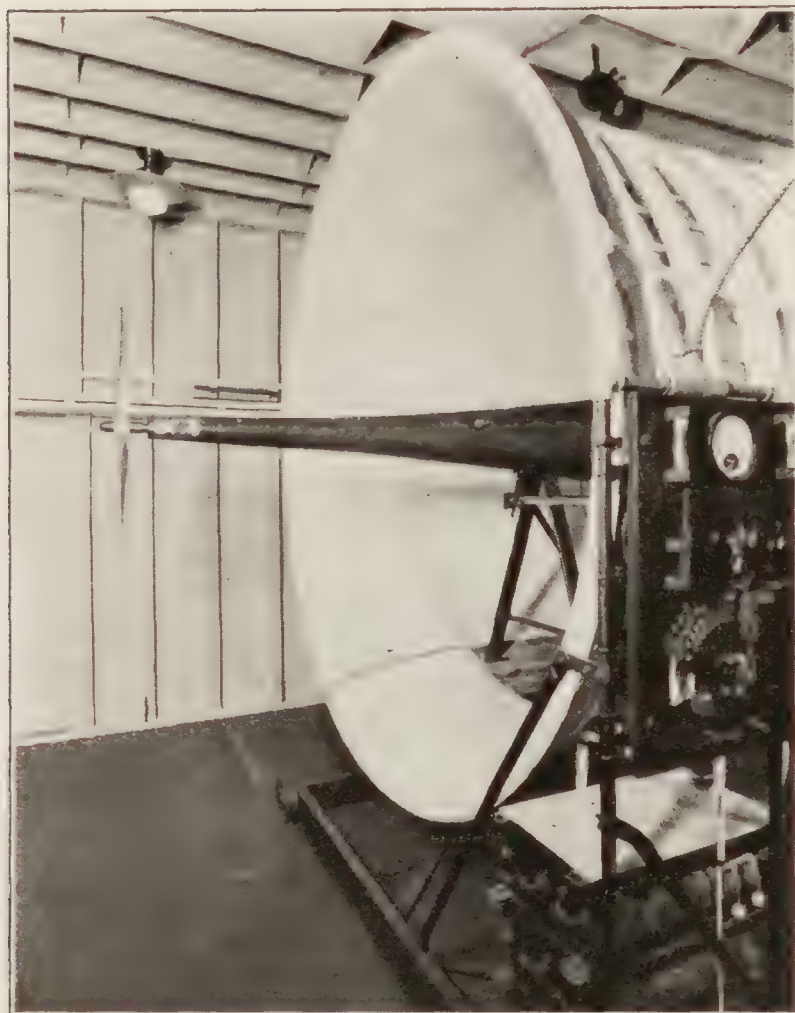


FIGURE 3.—Arrangement of apparatus for free stream tests

The dynamometer barrel, containing the driving motor at the rear end, is long and tapering, the test propeller being $5\frac{1}{2}$ feet in front of any appreciable obstruction and thus in a wind stream of sensibly uniform velocity.

Torque and thrust are measured directly. Revolutions are recorded upon a chronograph and wind speed is determined from the pressure reduction in the experiment chamber and the air density, the relation between experiment chamber pressure reduction and dynamic pressure having been previously determined from a survey with a pitot tube. Air density is determined from observed dry and wet bulb temperature and barometric pressure by reference to tables of General Specifications—Appendix 8, Instructions for Calculating and Testing Ventilating Systems, Bureau of Construction and Repair, United States Navy Department. The usual test procedure is as follows:

1. Check torque and thrust zeros.
2. With wind speed of about 66 feet per second, adjust angular velocity of propeller to give zero thrust and make simultaneous observations for thrust, torque, angular velocity and wind velocity.

3. Increase thrust in suitable increments to give well distributed spots on graphs by increasing angular velocity and make similar observations. This process is continued (with 3-foot models) until a thrust of 30 pounds is reached. The slip is increased for additional observations by reduction of wind velocity until the tunnel fan is shut down entirely, the velocity for the last observation being only that induced in the tunnel by the action of the model propeller itself.

The set-up for tests of the propellers in combination with the VE-7 model fuselage is shown in Figure 4.

In former tests of this kind the model airplane was suspended by wires as shown and the drag was measured by means of a balance forward of the experiment chamber, the connection to the balance



FIGURE 4.—Arrangement of apparatus for test with model fuselage

being a wire with suitable bridle around the propeller. Preliminary tests were made to determine the drag of the model without the propeller. The drag of the model was also measured

with the propeller in operation. The thrust of the propeller was measured as in the free wind stream tests. For determining the propeller characteristics when operating in combination with the model, the propeller was credited with a thrust equal to $T - (R_1 - R_0)$ in which T is the pull upon the propeller shaft as indicated by the thrust balance, R_0 the resistance of the model in a free wind stream and R_1 the resistance of the model when influenced by the propeller.

In the present tests a method simpler for experimental observations, but giving the same final result, was employed. The model airplane was suspended by wires as before. A drag yoke connecting the model to the thrust bearing of the dynamometer was provided. This yoke insured no interference with or effect upon the torque balance. The drag of the model was thus indicated as a negative thrust by the thrust balance beam.

A preliminary test was made to determine the drag or resistance of the model alone.

The procedure for tests of model propellers in combination with the model fuselage was the same as that for the tests in a free wind stream, except that the observations were started at a negative value of the total force upon the propeller shaft about equal to the drag of the model fuselage alone so that the propeller was delivering under this condition approximately zero effective thrust.

With the drag of the model communicated to the thrust balance, it is evident that the force measured by the thrust balance is $T - R_1$, T being as in previous tests the pull exerted by the propeller and R_1 the resistance of the model under the action of wind and slip stream. If to $T - R_1$ is added the resistance of the model in a free wind stream, R_0 , the result is $T - R_1 + R_0$ or $T - (R_1 - R_0)$ the quantity which was determined in previous tests when the drag of the model as influenced by the slip stream was measured independently.

The velocity survey of the propeller plane was confined to three radii, the upward and downward verticals and one horizontal. Observations were made at 2-inch intervals out to the 24-inch radius. The arrangement of the survey apparatus is illustrated by Figure 5. The small pitot tube, built to meet space limitations, was calibrated, while attached to its supporting bar, by comparative tests with a standard National Advisory Committee for Aeronautics pitot tube.



FIGURE 5.—Apparatus for velocity survey

RESULTS OF TESTS

The results of free wind stream tests on propeller A are given in Table Ia and are shown in Figure 6. From the figure it is seen that the maximum efficiency is somewhat above 81 per cent and that the corresponding value of the speed-power coefficient is 1.75. Preliminary tests near the point of maximum efficiency for propellers B, C, D, and E gave the following results:

Propeller	Blade setting at 10.8-inch radius	Speed power coefficient for maximum efficiency	Propeller	Blade setting at 10.8-inch radius	Speed power coefficient for maximum efficiency
B	20-25	2.00	D	20-25	1.90
B	17-25	1.60	D	19-00	1.60
B	18-15	1.75	D	19-30	1.65
C	20-25	1.24	D	19-55	1.75
C	21-55	1.60	E	20-25	1.65
C	22-15	1.65	E	20-40	1.75
C	23-05	1.75			

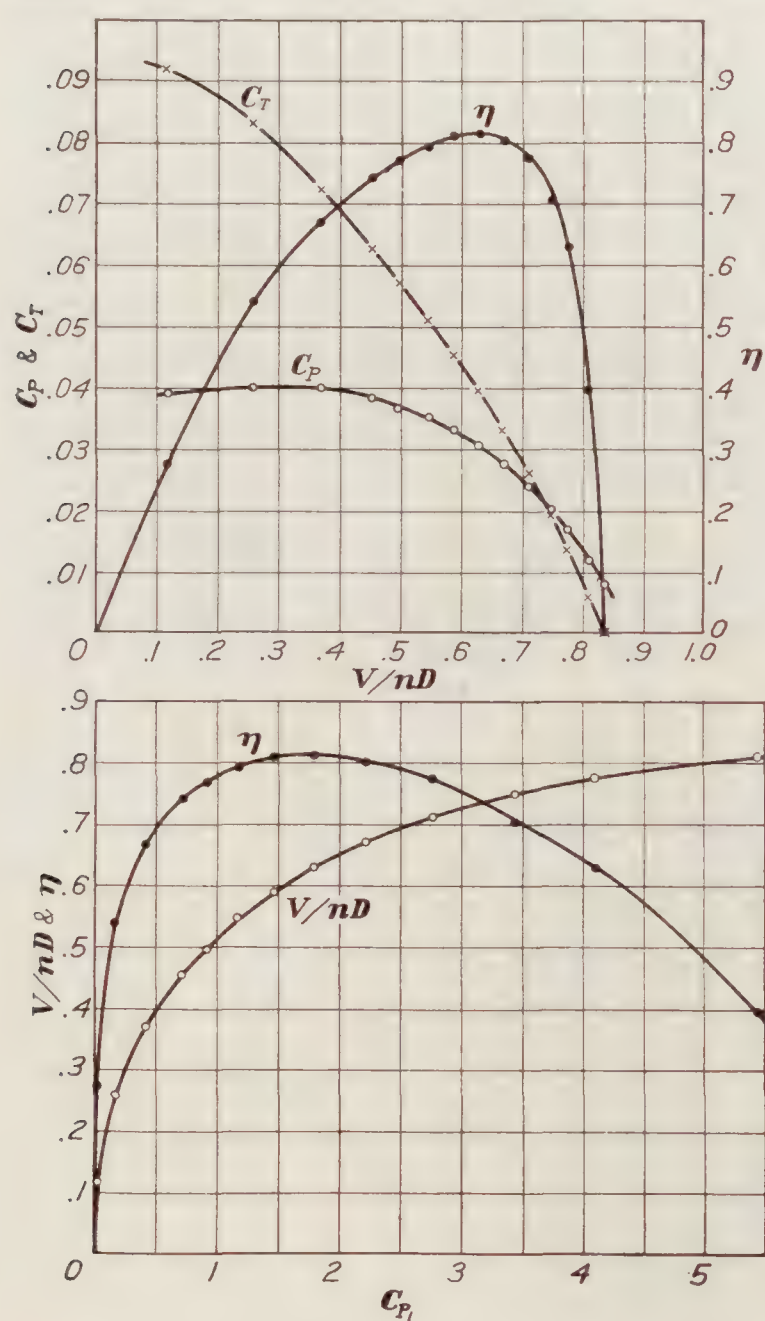


FIGURE 6.—Propeller A in free wind stream

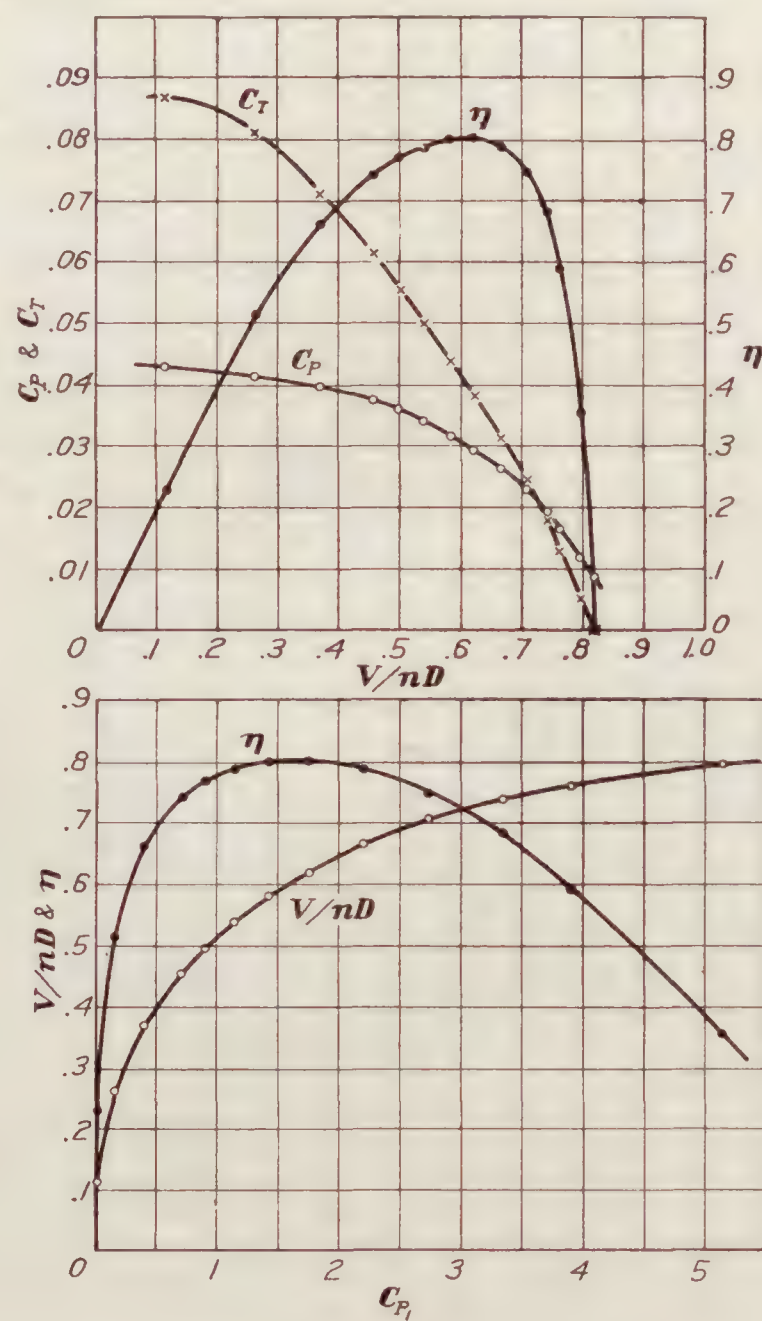


FIGURE 7.—Propeller B in free wind stream

From the above it was determined that the settings for B, C, D, and E at the 10.8-inch radius to give a speed-power coefficient of 1.75 at maximum efficiency were as follows:

Propeller	B	C	D	E
Setting at 10.8-inch radius	18.2°	23.1°	19.9°	20.7°

It may be noted that the angles of B are decreased 2.2° and those of C are increased 2.7°. Likewise the angles of D are decreased 0.5° while those of E are increased 0.3°.

Some apparent inconsistency in the changes required led to the measurement of the angles on all propellers from the 10.8-inch radius outward. No attempt was made to measure the angles inside of the 10.8-inch radius, since the sections are cambered on the driving face and no accurate method for measuring was available. The angles of corresponding sections for two blades of a single propeller were found to differ, in some cases, by 0.1° . The mean angles (for two blades) showed no differences from those of Figure 2 greater than 0.2° .

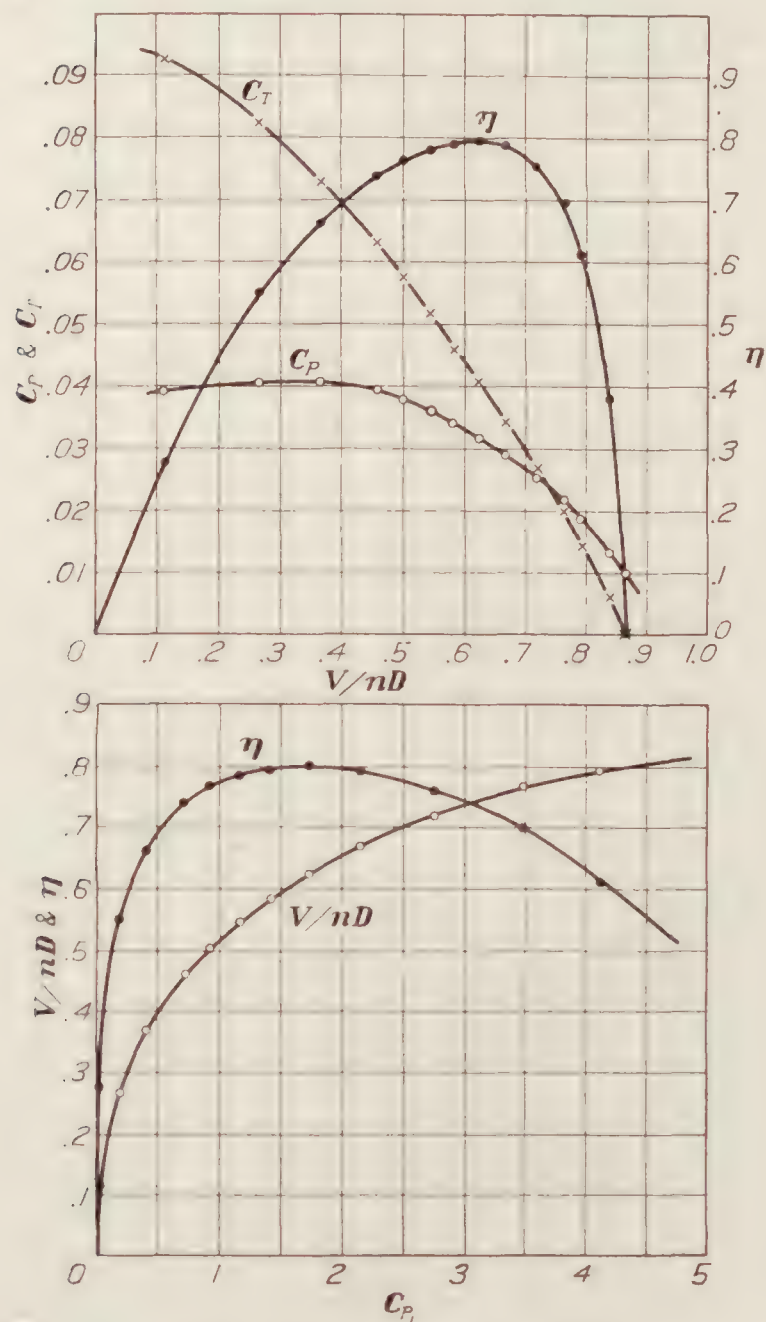


FIGURE 8.—Propeller C in free wind stream

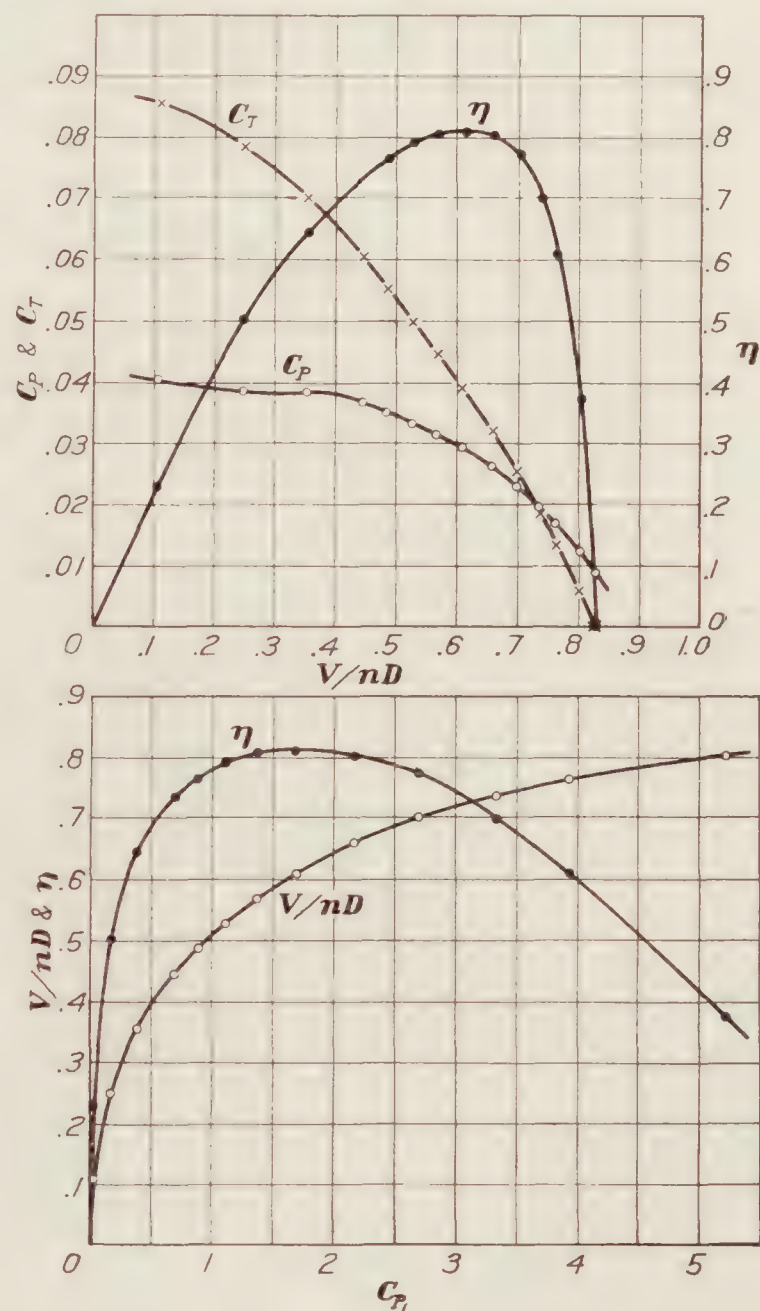


FIGURE 9.—Propeller D in free wind stream

Assuming that the angles of the sections inside of the 10.8-inch radius were, in relation to angle at the 10.8-inch section, as shown by Figure 2, the angles of all sections were, for the settings used, as follows:

Angle of section—	Radius					
	2.7-inch	5.4-inch	8.1-inch	10.8-inch	13.5-inch	16.2-inch
A	56.1	36.7	26.4	20.4	16.5	14.0
B	53.9	34.5	24.2	18.2	16.0	16.7
C	58.8	39.4	29.1	23.1	17.9	11.8
D	69.8	41.2	27.4	19.9	16.0	13.2
E	42.2	32.0	25.2	20.7	17.1	14.3

The results of complete tests in a free wind stream for propellers B, C, D, and E are given in Tables Ib, Ic, Id, and Ie and are shown in Figures 7, 8, 9, and 10.

The observed data from the preliminary tests of the model VE-7 for drag without slip stream are shown in Table II and Figure 11.

The results of tests of propeller A in combination with the model VE-7 are given in Table IIIa and are shown in Figure 12. As stated previously the thrust credited to the propeller is the observed total force on the shaft as shown by the thrust balance plus the resistance, R_0 , corresponding to the observed dynamic pressure and read from the graph Figure 11. For this reason the initial value of thrust is not zero as in the case of the unobstructed wind stream

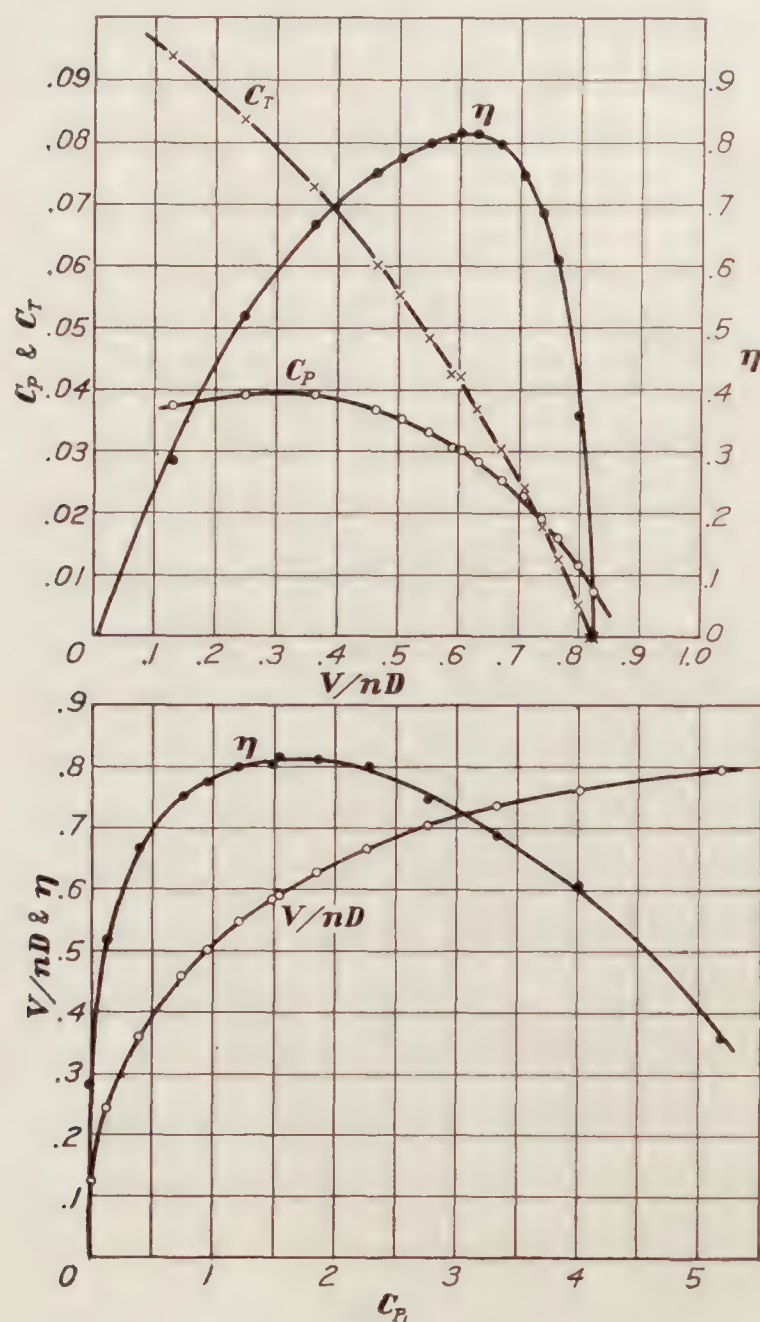


FIGURE 10.—Propeller E in free wind stream

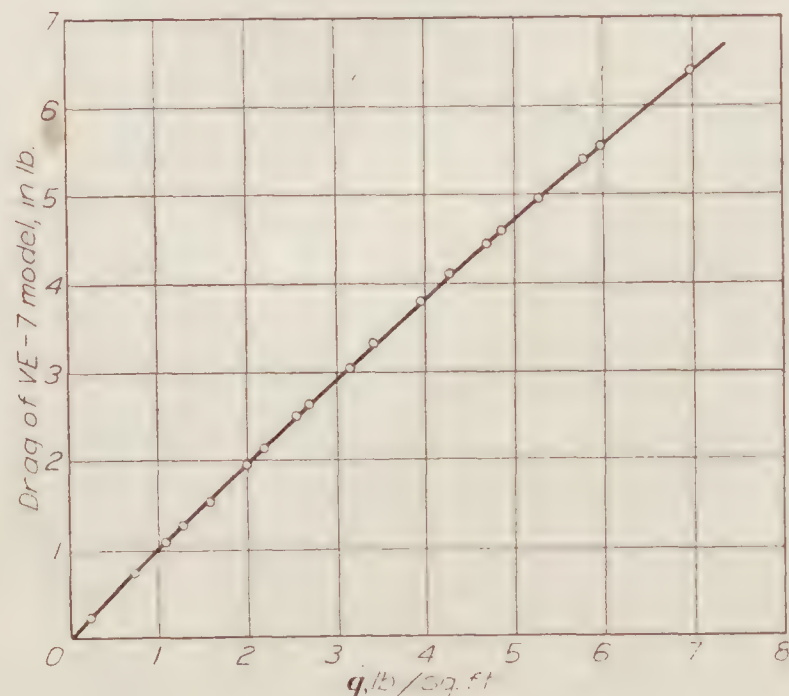


FIGURE 11.—Drag on the VE-7 model

tests, it being impracticable to determine in advance the exact value of dynamic pressure that would be encountered and thus adjust the propeller speed to give a total reaction upon the shaft equal in amount to the resistance of the model without slip stream effect.

Figure 12 shows that the maximum efficiency of propeller A, when operating in front of the model, is slightly over 76 per cent and that this efficiency occurs at a speed power coefficient of 1.85.

Preliminary tests of propellers B, C, D, and E in combination with the VE-7 model showed that no changes of the settings derived in the free stream preliminary tests were required, the value of the speed-power coefficient being, at these settings, 1.85 for maximum efficiency.

The results of complete tests of propellers B, C, D, and E in combination with the model plane are given in Tables IIIb, IIIc, III d, and III e and are shown in Figures 13, 14, 15, and 16.

Table IV and Figure 17 show the results of the velocity survey at the propeller plane. In this survey preliminary tests showed that the ratio of velocity at any point to free stream velocity was practically independent of the velocity employed. Figure 18 shows the ratio of mean velocity in the propeller plane to free stream velocity. This figure is determined by taking the mean

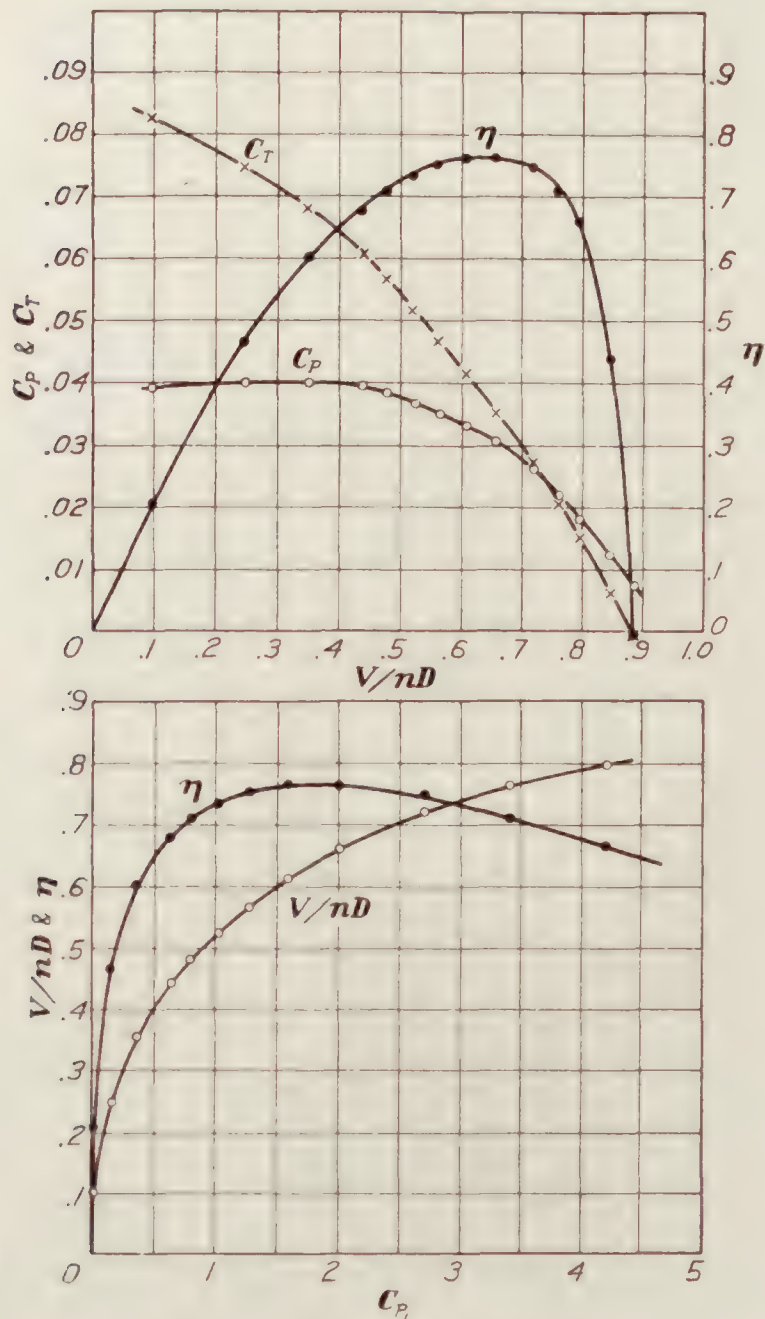


FIGURE 12.—Propeller A with model fuselage

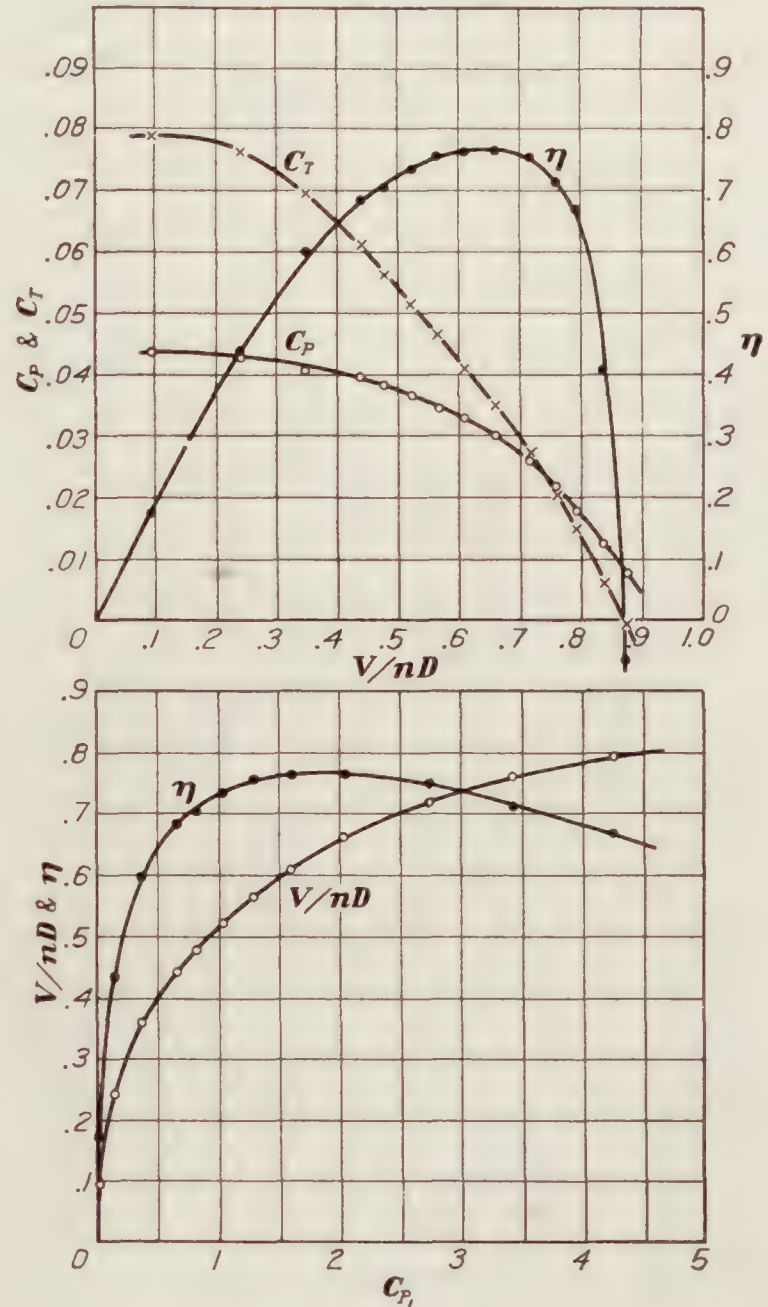


FIGURE 13.—Propeller B with model fuselage

of the ordinates of Figure 17, but including the ordinate for left side twice, it being assumed that the velocity distribution is symmetrical in a horizontal plane.

DISCUSSION

Inspection of Figures 6, 7, 8, 9, and 10 reveals that, so far as can be judged from free stream performance, no one of these propellers has a striking advantage over any other. With possibly a slight advantage in favor of A, propellers A, D, and E are about equal with a peak efficiency of somewhat over 81 per cent. For B and C the peak efficiency is close to 80 per cent, B appearing to be slightly the better.

Neglecting inflow velocity, the angles of attack of the various sections of the five propellers, when operating in a wind stream of uniform velocity and at V/nD for maximum efficiency, are as follows:

ANGLES OF ATTACK OF SECTIONS AT V/nD FOR MAXIMUM EFFICIENCY FOR PROPELLERS IN FREE WIND STREAM

	Radius						
	Angles of attack of section—						
	2.7-inch	5.4-inch	8.1-inch	10.8-inch	13.5-inch	16.2-inch	18-inch
A	3.1	3.2	2.6	2.1	1.7	1.5	1.5
B	1.2	1.2	0.5	0.0	1.3	4.4	7.5
C	5.7	5.8	5.2	4.7	3.0	-0.7	-4.0
D	17.2	8.0	3.9	1.6	1.3	0.9	1.1
E	-10.4	-1.2	1.6	2.6	2.4	2.1	1.9

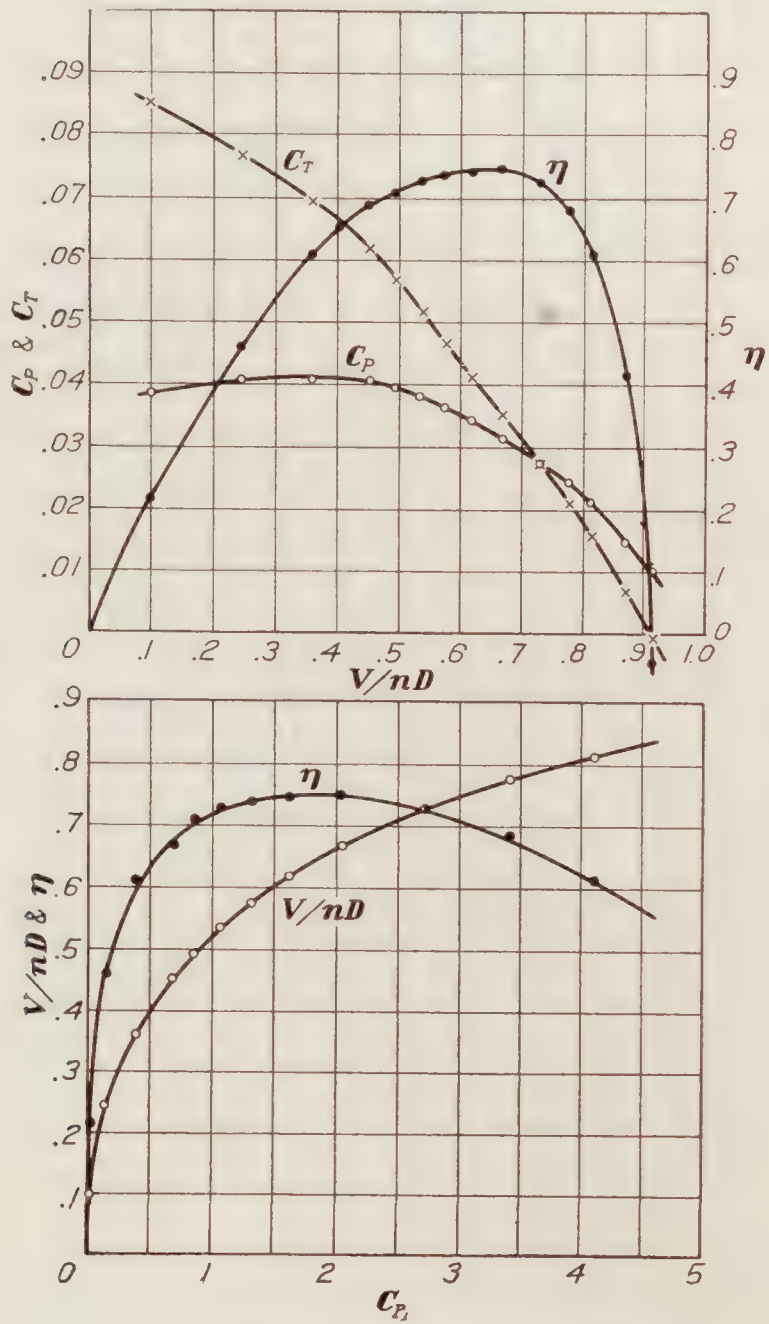


FIGURE 14.—Propeller C with model fuselage

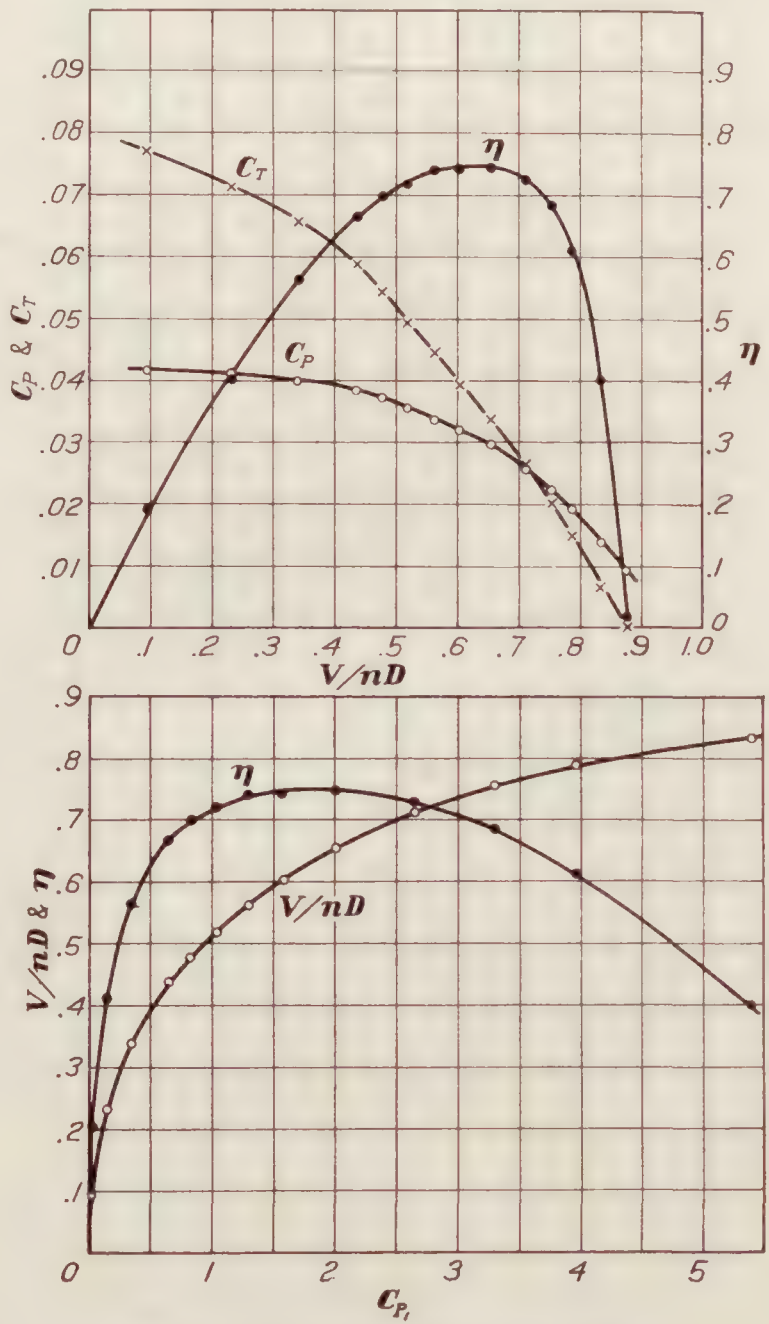


FIGURE 15.—Propeller D with model fuselage

These angles are shown graphically in Figure 19. Without knowing the aerodynamic characteristics of the sections, it is of course impossible to say what the optimum angles of attack are, but assuming that they are moderate and approximately uniform, it would appear from Figure 19 that propeller A should be the best. It would seem, too, that D and E should be next, because of the relative importance of the outer sections, and that B and C should be poorest. It might be expected that D and E would be appreciably inferior to A, but, in view of the fact that there is only a little more than 1 per cent difference in the peak efficiencies of

the best and worst propellers (A and C) the slight differences found in A, D, and E are not surprising.

For the tests in combination with the model fuselage it is seen from Figures 12 to 16 that all propellers show a decrease in peak efficiency from that determined by the free stream tests and an increase in V/nD for zero thrust. This is in agreement with previous tests of a similar nature. (Reference 2.)

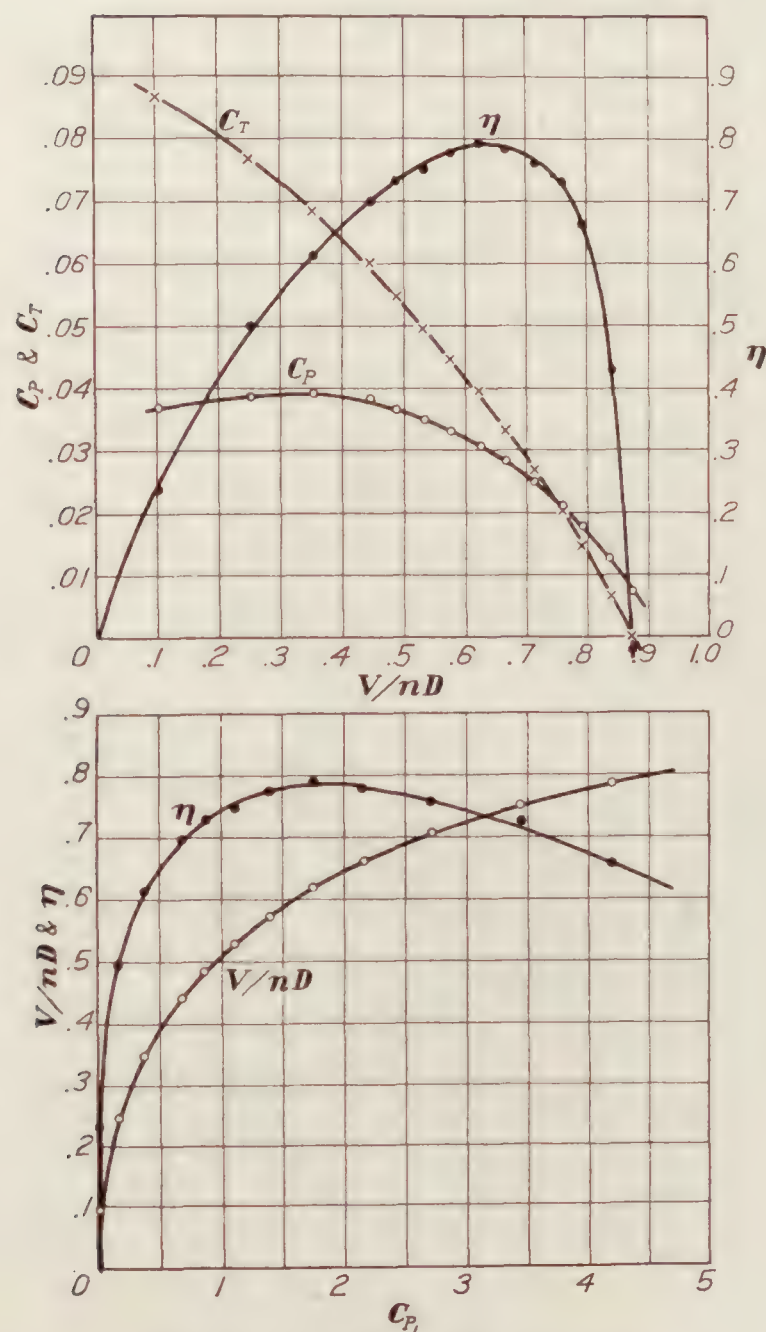


FIGURE 16.—Propeller E with model fuselage

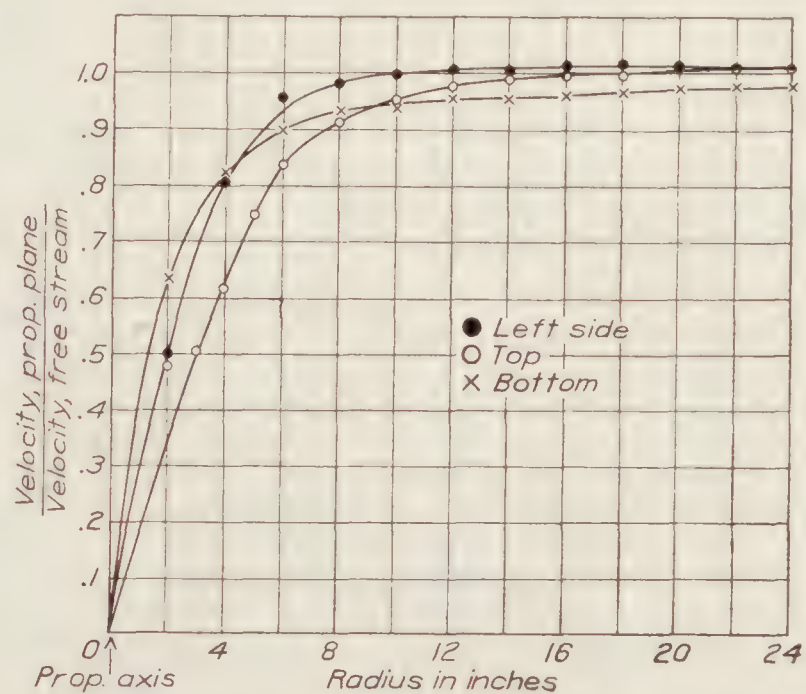


FIGURE 17.—Survey of velocity in propeller plane. VE-7 model

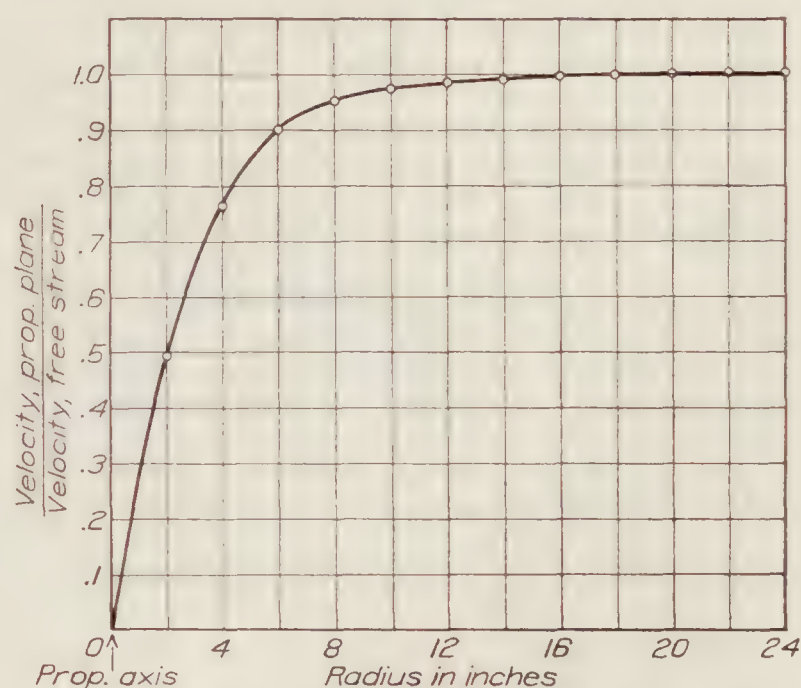


FIGURE 18.—Velocity in propeller plane, average. VE-7 model

The decrease in peak efficiency is, however, not the same for all propellers, so that the peak efficiencies attained are as follows:

Propeller	A	B	C	D	E
Peak efficiency with model fuselage, per cent	76 $\frac{1}{4}$	76 $\frac{3}{4}$	75	75	79

Reference 2. Interaction between Air Propellers and Airplane Structures, by W. F. Durand. N. A. C. A. Technical Report No. 235.

Again, neglecting inflow velocity and assuming a radial velocity distribution as shown by Figure 18, the angles of attack for the various sections of the five propellers when operating in front of the model fuselage at V/nD for maximum efficiency are as follows:

ANGLES OF ATTACK OF SECTIONS AT V/nD FOR MAXIMUM EFFICIENCY FOR PROPELLERS IN COMBINATION WITH MODEL FUSELAGE

Angles of attack of section—	Radius						
	2.7-inch	5.4-inch	8.1-inch	10.8-inch	13.5-inch	16.2-inch	18-inch
A	16.5	6.1	3.0	2.1	1.5	1.3	1.2
B	14.3	4.4	0.8	-0.1	1.0	4.0	7.1
C	19.0	8.6	5.6	4.7	2.8	-1.0	-4.3
D	30.4	10.8	4.2	1.7	1.1	0.6	0.8
E	2.8	1.6	2.0	2.5	2.2	1.7	1.6

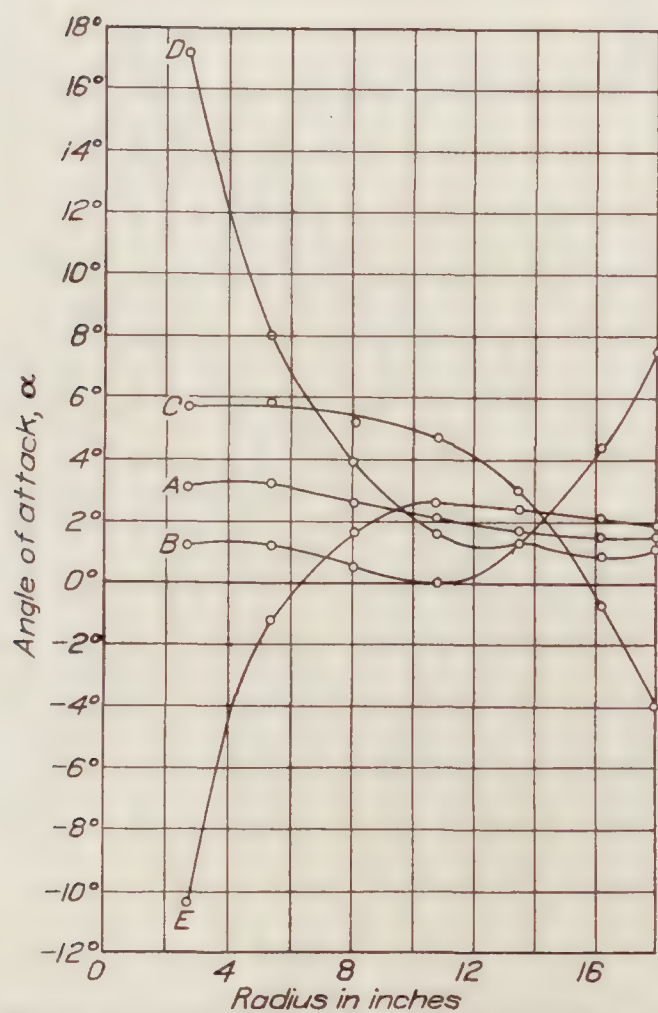


FIGURE 19.—Angles of attack of sections at V/nD for maximum efficiency. Free wind stream

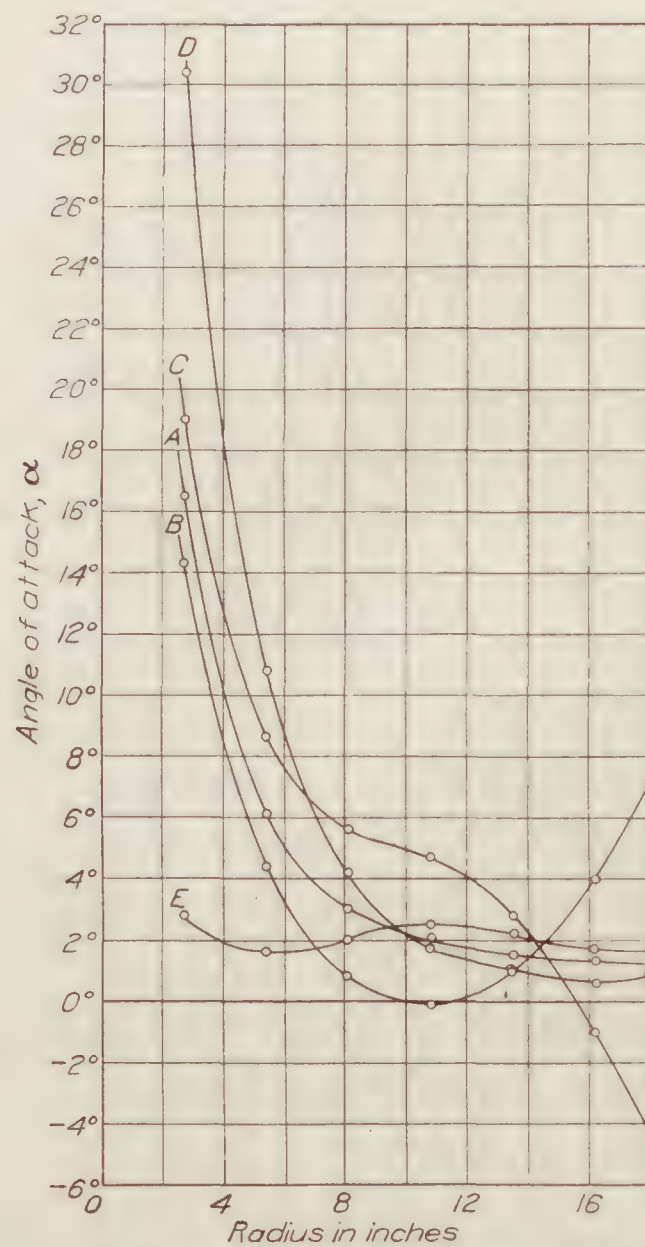


FIGURE 20.—Angles of attack of sections at V/nD for maximum efficiency with model fuselage

These angles are shown graphically in Figure 20. The angles for propeller E are small and nearly uniform and have probably somewhere near the optimum values. The angles for A and B are without doubt distinctly less favorable for high efficiency and those for C and D may be even worse.

CONCLUSIONS

It has been demonstrated by these tests that the reduction of propeller efficiency caused by the presence of an obstruction in the slip stream is minimized by giving the propeller a radial distribution of pitch similar to the radial distribution of velocity through the propeller plane

which exists under the conditions of operation. In other words, a propeller so designed that all its blade sections actually attain their optimum angles of attack at the condition of maximum efficiency is appreciably superior to the conventional constant pitch propeller for use in the presence of a slip stream obstruction.

STANFORD UNIVERSITY,
December, 1928.

TABLE Ia.—PROPELLER A

[Free wind stream]

$\frac{1}{2}\rho V^2$	ρ spec. wt. slugs/cu. ft.	V , veloc- ity, ft./sec.	r. p. s. n	n^2	Thrust, lb.	Torque, lb.-ft.	V/nD	$C_T = \frac{\text{Thrust}}{\rho n^2 D^4}$	$C_P = \frac{\text{Power}}{\rho n^3 D^5}$	Efficiency η	$C_{P_1} = \sqrt{\frac{\rho V^3}{P n^2}}$
4.760	0.002264	64.85	25.83	667.2	0	0.4579	0.8366	0	0.007838	0	7.235
4.857	.002262	65.55	27.00	729.0	.7592	.7440	.8092	.005684	.01167	.3940	5.453
4.996	.002240	66.80	28.72	824.8	2.025	1.193	.7751	.01353	.01669	.6283	4.095
5.013	.002234	66.98	29.78	886.8	3.037	1.528	.7494	.01892	.01994	.7034	3.443
4.936	.002234	66.45	31.16	970.9	4.555	1.999	.7106	.02594	.02382	.7738	2.761
4.993	.002234	66.87	33.28	1,108.0	6.580	2.626	.6698	.03283	.02743	.8015	2.218
5.097	.002231	67.62	35.82	1,283.0	9.111	3.370	.6290	.03930	.03044	.8120	1.789
5.144	.002232	67.92	38.50	1,482.0	12.15	4.209	.5878	.04533	.03290	.8098	1.459
5.244	.002234	68.54	41.90	1,756.0	16.20	5.320	.5452	.05100	.03507	.7928	1.171
5.375	.002234	69.35	46.60	2,172.0	22.27	6.860	.4960	.05670	.03654	.7693	.9063
5.542	.002235	70.41	51.76	2,679.0	30.37	8.859	.4533	.06264	.03825	.7420	.7080
3.192	.002238	53.40	48.20	2,323.0	30.37	8.008	.3691	.07208	.03981	.6684	.4146
1.354	.002241	34.77	44.85	2,016.0	30.37	6.958	.2584	.08300	.03982	.5386	.1704
.2525	.002242	15.01	42.70	1,823.0	30.37	6.162	.1171	.09174	.03900	.2754	.02376

TABLE Ib.—PROPELLER B

[Free wind stream]

$\frac{1}{2}\rho V^2$	ρ spec. wt. slugs/cu. ft.	V , veloc- ity, ft./sec.	r. p. s. n	n^2	Thrust, lb.	Torque, lb.-ft.	V/nD	$C_T = \frac{\text{Thrust}}{\rho n^2 D^4}$	$C_P = \frac{\text{Power}}{\rho n^3 D^5}$	Efficiency η	$C_{P_1} = \sqrt{\frac{\rho V^3}{P n^2}}$
4.919	0.002259	66.00	26.85	721.0	0	0.5624	0.8194	0	0.008934	0	6.425
4.980	.002254	66.50	27.90	778.4	.7592	.8092	.7946	.005343	.01193	.3559	5.150
5.028	.002252	66.81	29.30	858.5	2.025	1.244	.7601	.01294	.01665	.5906	3.903
5.072	.002250	67.15	30.31	918.7	3.037	1.563	.7385	.01813	.01955	.6848	3.350
5.104	.002246	67.40	31.82	1,013.0	4.555	2.056	.7061	.02472	.02336	.7472	2.737
5.139	.002243	67.66	33.93	1,151.0	6.580	2.648	.6646	.03149	.02652	.7891	2.210
5.095	.002246	67.32	36.23	1,313.0	9.111	3.362	.6193	.03816	.02950	.8007	1.756
5.176	.002245	67.92	38.96	1,518.0	12.15	4.204	.5811	.04400	.03192	.8004	1.442
5.223	.002243	68.23	42.20	1,781.0	16.20	5.295	.5390	.05006	.03428	.7870	1.153
5.408	.002243	69.40	46.73	2,184.0	22.27	6.856	.4952	.05612	.03620	.7678	.907
5.674	.002242	71.12	52.07	2,711.0	30.37	8.894	.4553	.06167	.03784	.7420	.717
3.226	.002246	53.56	48.50	2,352.0	30.37	8.076	.3681	.07096	.03956	.6606	.414
1.422	.002249	35.55	45.33	2,055.0	30.37	7.369	.2614	.08112	.04125	.5140	.171
.2493	.002250	14.89	43.80	1,918.0	30.37	7.170	.1133	.08688	.04298	.2290	.021

TABLE Ic.—PROPELLER C

[Free wind stream]

$\frac{1}{2}\rho V^2$	ρ spec. wt. slugs/cu. ft.	V , veloc- ity, ft./sec.	r. p. s. n	n^2	Thrust, lb.	Torque, lb.-ft.	V/nD	$C_T = \frac{\text{Thrust}}{\rho n^2 D^4}$	$C_P = \frac{\text{Power}}{\rho n^3 D^5}$	Efficiency η	$C_{P_1} = \sqrt{\frac{\rho V^3}{P n^2}}$
4.796	0.002242	65.41	25.20	635.0	0	0.5500	0.8652	0	0.009992	0	6.965
4.894	.002239	66.14	26.29	691.2	.7592	.7988	.8386	.006058	.01335	.3806	5.569
4.919	.002236	66.30	27.87	776.7	2.025	1.246	.7930	.01439	.01857	.6145	4.106
4.969	.002234	66.68	28.98	839.8	3.037	1.588	.7670	.01998	.02188	.7004	3.479
4.882	.002233	66.14	30.57	934.5	4.555	2.065	.7212	.02696	.02561	.7592	2.758
4.770	.002233	65.38	32.52	1,058.0	6.580	2.658	.6702	.03439	.02911	.7918	2.154
4.850	.002233	65.93	35.16	1,236.0	9.111	3.394	.6251	.04077	.03182	.8007	1.732
4.984	.002234	66.82	38.09	1,451.0	12.15	4.295	.5848	.04626	.03429	.7940	1.412
5.194	.002233	68.23	41.59	1,730.0	16.20	5.395	.5468	.05176	.03612	.7836	1.164
5.399	.002232	69.55	46.14	2,129.0	22.27	6.958	.5025	.05790	.03789	.7680	.919
5.626	.002232	71.00	51.43	2,645.0	30.37	9.014	.4602	.06354	.03952	.7400	.721
3.121	.002235	52.85	47.85	2,290.0	30.37	8.060	.3682	.07325	.04075	.6618	.408
1.479	.002240	36.34	45.01	2,026.0	30.37	7.100	.2692	.08265	.04046	.5499	.186
.2462	.002241	14.82	42.48	1,805.0	30.37	6.107	.1163	.09271	.03907	.2760	.023

TABLE Id.—PROPELLER D

[Free wind stream]

$\frac{1}{2}\rho V^2$	ρ spec. wt. slugs/cu. ft.	V, veloc- ity, ft./sec.	r. p. s. n	n^2	Thrust, lb.	Torque, lb.-ft.	V/nD	$C_T = \frac{\text{Thrust}}{\rho n^2 D^4}$	$C_P = \frac{\text{Power}}{\rho n^3 D^5}$	Efficiency η	$C_{P_1} = \sqrt{\frac{\rho V^3}{P n^2}}$
4.715	0.002284	64.27	25.82	666.7	0	0.5201	0.8298	0	0.00883	0	6.667
4.802	.002280	64.92	26.93	725.2	0.7592	.7814	.8033	.00567	.012225	.3726	5.228
4.912	.002276	65.65	28.64	820.2	2.025	1.209	.7640	.01339	.01676	.6104	3.940
4.934	.002275	65.82	29.72	883.3	3.037	1.528	.7383	.01866	.01967	.7003	3.335
4.875	.002270	65.53	31.15	970.3	4.555	1.969	.7012	.02553	.02312	.7743	2.704
4.957	.002269	66.08	33.42	1,117.0	6.580	2.576	.6591	.03204	.02629	.8032	2.173
4.802	.002270	65.06	35.58	1,266.0	9.111	3.273	.6095	.03913	.02946	.8095	1.690
4.878	.002270	65.55	38.47	1,480.0	12.15	4.083	.5680	.04464	.03143	.8066	1.370
5.036	.002270	66.60	42.12	1,774.0	16.20	5.154	.5271	.04966	.03309	.7910	1.110
5.293	.002267	68.34	46.91	2,201.0	22.27	6.767	.4856	.05514	.03509	.7630	.878
5.526	.002264	69.90	52.37	2,743.0	30.37	8.786	.4450	.06040	.03660	.7343	.692
3.019	.002267	51.60	48.62	2,364.0	30.37	7.947	.3538	.06994	.03835	.6453	.380
1.322	.002269	34.13	45.92	2,109.0	30.37	7.168	.2477	.07832	.03874	.5007	.155
.232	.002272	14.29	43.93	1,930.0	30.37	6.819	.1084	.08552	.04023	.2304	.019

TABLE Ie.—PROPELLER E

[Free wind stream]

$\frac{1}{2}\rho V^2$	ρ spec. wt. slugs/cu. ft.	V, veloc- ity, ft./sec.	r. p. s. n	n^2	Thrust, lb.	Torque, lb.-ft.	V/nD	$C_T = \frac{\text{Thrust}}{\rho n^2 D^4}$	$C_P = \frac{\text{Power}}{\rho n^3 D^5}$	Efficiency η	$C_{P_1} = \sqrt{\frac{\rho V^3}{P n^2}}$
4.986	0.002337	65.32	26.52	703.3	0	0.5421	0.8214	0	0.008536	0	6.620
4.994	.002337	65.36	27.37	749.1	.7592	.8007	.7960	.005354	.011836	.3598	5.190
5.105	.002333	66.20	28.98	839.8	2.025	1.209	.7614	.01277	.01596	.6090	4.002
5.100	.002333	66.18	29.98	898.8	3.037	1.552	.7359	.01788	.01914	.6870	3.355
5.201	.002332	66.80	31.58	997.3	4.555	2.049	.7052	.02418	.02278	.7482	2.763
5.323	.002329	67.58	33.85	1,146.0	6.580	2.616	.6655	.03046	.02534	.7994	2.273
5.425	.002328	68.26	36.26	1,315.0	9.111	3.362	.6276	.03675	.02840	.8120	1.853
5.425	.002328	68.26	38.98	1,519.0	12.15	4.202	.5838	.04244	.03072	.8063	1.485
5.594	.002349	69.01	39.03	1,523.0	12.15	4.197	.5895	.04195	.03033	.8152	1.533
5.542	.002328	68.99	42.12	1,774.0	16.20	5.282	.5460	.04845	.03308	.7996	1.212
5.703	.002328	69.98	46.64	2,175.0	22.27	6.868	.5002	.05430	.03510	.7738	.945
5.906	.002328	71.20	51.70	2,673.0	30.37	8.871	.4590	.06025	.03686	.7504	.744
2.972	.002331	50.50	47.01	2,210.0	30.37	7.778	.3581	.07280	.03904	.6676	.389
1.190	.002334	31.95	43.81	1,919.0	30.37	6.794	.2431	.08370	.03920	.5190	.1468
.2278	.002335	13.96	41.38	1,712.0	30.37	5.769	.1125	.09380	.03733	.2826	.0189

TABLE II.—DRAG OF THE VE-7 MODEL

$\frac{1}{2}\rho V^2$	Drag, lb.	$\frac{1}{2}\rho V^2$	Drag, lb.
0.2258	0.23	3.428	3.28
.7280	.72	3.960	3.75
1.0665	1.05	4.276	4.05
1.2780	1.25	4.698	4.39
1.5695	1.53	4.857	4.54
1.9920	1.93	5.288	4.91
2.200	2.12	5.793	5.35
2.557	2.46	5.976	5.50
2.698	2.60	6.997	6.35
3.147	3.00		

TABLE IIIa.—PROPELLER A

[With model fuselage]

$\frac{1}{2}\rho V^2$	ρ spec. wt. slugs/cu. ft.	V, veloc- ity, ft./sec.	r. p. s. n	n^2	Thrust, lb.	Torque, lb.-ft.	V/nD	$C_T = \frac{\text{Thrust}}{\rho n^2 D^4}$	$C_P = \frac{\text{Power}}{\rho n^3 D^5}$	Efficiency η	$C_{P_1} = \sqrt{\frac{\rho V^3}{P n^2}}$
4.764	0.002271	64.80	24.40	595.4	-0.05568	0.3808	0.8850	-0.0005083	0.00728	-0.0618	8.639
4.800	.002268	65.07	25.63	656.9	+.7541	.7092	.8459	+.006248	.01231	.4295	5.933
4.850	.002268	65.40	27.36	748.6	2.055	1.180	.7966	.01495	.01798	.6624	4.223
4.878	.002264	65.66	28.69	823.1	3.093	1.588	.7625	.02049	.02202	.7094	3.423
4.936	.002262	66.07	30.54	932.7	4.657	2.148	.7208	.02726	.02632	.7466	2.720
4.483	.002263	62.93	31.81	1,012.0	6.535	2.700	.6592	.03522	.03048	.7615	2.020
4.533	.002262	63.32	34.57	1,195.0	9.106	3.476	.6105	.04160	.03323	.7640	1.599
4.641	.002262	64.07	37.82	1,430.0	12.27	4.410	.5646	.04683	.03510	.7530	1.278
4.820	.002261	65.34	41.67	1,736.0	16.46	5.592	.5226	.05175	.03685	.7338	1.028
5.111	.002260	67.26	46.68	2,179.0	22.66	7.328	.4801	.05678	.03847	.7086	.8133
5.422	.002258	69.32	52.54	2,760.0	30.78	9.542	.4397	.06096	.03958	.6770	.6453
3.119	.002261	52.54	49.41	2,441.0	30.54	8.561	.3543	.06832	.04012	.6034	.3730
1.384	.002266	34.97	46.88	2,198.0	30.17	7.684	.2486	.07480	.03991	.4659	.1545
.1981	.002267	13.22	44.70	1,998.0	30.37	6.898	.0986	.08280	.03939	.2072	.0154

TABLE IIIb.—PROPELLER B

[With model fuselage]

$\frac{1}{2}\rho V^2$	ρ spec. wt. slugs/cu. ft.	V , veloc- ity, ft./sec.	r. p. s. n	n^2	Thrust, lb.	Torque, lb.-ft.	V/nD	$C_T = \frac{\text{Thrust}}{\rho n^2 D^4}$	$C_P = \frac{\text{Power}}{\rho n^3 D^5}$	Efficiency η	$C_{P1} = \sqrt{\frac{\rho V^3}{P n^2}}$
4.742	0.002261	64.78	24.72	611.1	-0.06074	0.3982	0.8733	-0.000543	0.00746	-0.0636	8.427
4.802	.002256	65.25	26.00	676.0	+.7521	.7386	.8362	+.00609	.01252	+.4068	5.796
4.817	.002254	65.40	27.47	754.6	2.025	1.148	.7940	.01472	.01749	.6685	4.248
4.849	.002252	65.66	28.79	828.9	3.068	1.563	.7599	.02029	.02165	.7123	3.421
4.947	.002256	66.22	30.705	942.8	4.677	2.140	.7190	.02716	.02602	.7506	2.716
4.683	.002248	64.53	32.54	1,059.0	6.721	2.770	.6606	.03487	.03009	.7654	2.044
4.600	.002249	63.97	35.00	1,225.0	9.175	3.501	.6092	.04114	.03287	.7622	1.596
4.713	.002250	64.74	38.20	1,459.0	12.32	4.397	.5650	.04635	.03462	.7562	1.290
4.907	.002235	66.24	42.225	1,784.0	16.53	5.629	.5230	.05120	.03651	.7332	1.036
5.152	.002247	67.71	47.18	2,226.0	22.82	7.401	.4782	.05632	.03823	.7040	.8093
5.523	.002245	70.18	52.99	2,808.0	31.24	9.630	.4415	.06120	.03951	.6835	.6515
2.960	.002248	51.32	49.02	2,403.0	30.37	8.454	.3488	.06940	.04045	.5984	.3571
1.295	.002252	33.92	46.57	2,169.0	30.22	8.082	.2427	.07636	.04278	.4332	.1405
.1926	.002253	13.08	45.94	2,110.0	30.36	8.013	.0949	.07882	.04358	.1716	.0133

TABLE IIIc.—PROPELLER C

[With model fuselage]

$\frac{1}{2}\rho V^2$	ρ spec. wt. slugs/cu. ft.	V , veloc- ity, ft./sec.	r. p. s. n	n^2	Thrust, lb.	Torque, lb.-ft.	V/nD	$C_T = \frac{\text{Thrust}}{\rho n^2 D^4}$	$C_P = \frac{\text{Power}}{\rho n^3 D^5}$	Efficiency η	$C_{P1} = \sqrt{\frac{\rho V^3}{P n^2}}$
4.775	0.002242	65.26	23.81	566.9	-0.05366	0.4997	0.9136	-0.000521	0.01016	-0.4686	7.913
4.881	.002240	66.02	25.31	640.6	.823	.8212	.8692	+.007082	.01480	+.4159	5.791
4.940	.002237	66.46	27.19	739.3	2.133	1.354	.8145	.01593	.02118	.6124	4.113
4.966	.002236	66.66	28.61	818.5	3.170	1.717	.7766	.02139	.02428	.6844	3.410
4.988	.002235	66.82	30.58	935.1	4.708	2.248	.7280	.02782	.02781	.7283	2.711
4.640	.002235	64.43	32.24	1,039.0	6.681	2.827	.6656	.03551	.03147	.7511	2.035
4.753	.002231	65.28	35.23	1,241.0	9.315	3.685	.6173	.04154	.03442	.7452	1.614
4.861	.002232	66.00	38.30	1,467.0	12.45	4.623	.5743	.04694	.03650	.7386	1.309
5.067	.002232	67.42	42.09	1,772.0	16.68	5.831	.5337	.05207	.03811	.7294	1.066
5.413	.002231	69.68	47.24	2,232.0	23.05	7.620	.4916	.05712	.03958	.7091	.8519
5.730	.002230	71.67	52.95	2,804.0	31.42	9.620	.4510	.06203	.04060	.6890	.6781
3.126	.002232	52.94	49.24	2,425.0	30.46	8.556	.3583	.06947	.04088	.6090	.3801
1.307	.002237	34.17	46.79	2,189.0	30.41	7.714	.2433	.07667	.04073	.4582	.1449
.1847	.002238	12.85	44.36	1,968.0	30.36	6.520	.0966	.08512	.03827	.2148	.01482

TABLE IIId.—PROPELLER D

[With model fuselage]

$\frac{1}{2}\rho V^2$	ρ spec. wt. slugs/cu. ft.	V , veloc- ity, ft./sec.	r. p. s. n	n^2	Thrust, lb.	Torque, lb.-ft.	V/nD	$C_T = \frac{\text{Thrust}}{\rho n^2 D^4}$	$C_P = \frac{\text{Power}}{\rho n^3 D^5}$	Efficiency η	$C_{P1} = \sqrt{\frac{\rho V^3}{P n^2}}$
4.892	0.002260	65.80	25.040	627.0	0.02025	0.5101	0.8758	0.0001765	0.00931	0.01660	7.440
4.911	.002255	66.00	26.365	695.1	.8453	.8411	.8344	.006657	.01388	.4002	5.392
4.965	.002253	66.42	28.125	791.0	2.156	1.329	.7873	.01494	.01928	.6100	3.959
5.007	.002251	66.70	29.510	870.8	3.212	1.690	.7535	.02024	.02229	.6842	3.300
5.055	.002246	67.10	31.475	990.7	4.768	2.227	.7107	.02647	.02588	.7269	2.646
4.709	.002249	64.70	32.965	1,087.0	6.742	2.819	.6543	.03404	.02981	.7471	2.006
4.789	.002249	65.25	36.090	1,302.0	9.349	3.618	.6027	.03943	.03195	.7438	1.578
4.895	.002249	66.00	39.150	1,533.0	12.47	4.509	.5620	.04467	.03381	.7425	1.288
5.061	.002247	67.12	43.100	1,858.0	16.67	5.741	.5192	.04933	.03556	.7202	1.028
5.343	.002246	69.00	48.160	2,319.0	22.99	7.503	.4776	.05450	.03724	.6990	.817
5.654	.002244	71.00	54.120	2,929.0	31.35	9.815	.4373	.05890	.03863	.6666	.644
2.972	.002247	51.40	50.315	2,532.0	30.34	8.760	.3405	.06590	.03981	.5636	.339
1.274	.002249	33.67	48.305	2,334.0	30.38	8.182	.2323	.07144	.04037	.4111	.129
.1934	.002256	13.09	46.408	2,154.0	30.37	7.859	.09403	.07713	.04180	.1735	.013

TABLE IIIe.—PROPELLER E

[With model fuselage]

$\frac{1}{2}\rho V^2$	ρ spec. wt. slugs/cu. ft.	V , veloc- ity, ft./sec.	r. p. s. n	n^2	Thrust, lb.	Torque, lb.-ft.	V/nD	$C_T = \frac{\text{Thrust}}{\rho n^2 D^4}$	$C_P = \frac{\text{Power}}{\rho n^3 D^5}$	Efficiency η	$C_{P_1} = \sqrt{\frac{\rho V^3}{P n^2}}$
4.794	0.002315	64.35	24.57	603.5	-0.02024	0.3957	0.8732	-0.000179	0.00732	-0.02135	8.325
4.846	.002310	64.78	25.78	664.9	+.7844	.7340	.8574	+.00631	.01235	+.4278	5.773
4.862	.002310	64.90	27.34	747.5	2.065	1.1800	.7913	.01477	.01767	+.6614	4.190
4.906	.002309	65.22	28.70	823.4	3.118	1.5430	.7576	.02026	.02098	.7314	3.446
4.950	.002309	65.48	30.58	935.4	4.672	2.0975	.7137	.02670	.02511	.7610	2.713
4.986	.002309	65.72	32.90	1,082.0	6.720	2.7325	.6660	.03322	.02827	.7828	2.153
5.000	.002309	65.80	35.20	1,239.0	9.115	3.414	.6232	.03936	.03085	.7944	1.746
5.072	.002309	66.28	38.36	1,471.0	12.22	4.330	.5762	.04443	.03296	.7768	1.388
5.200	.002308	67.11	42.00	1,764.0	16.28	5.505	.5327	.04938	.03497	.7522	1.109
5.375	.002310	68.22	46.62	2,173.0	22.28	7.095	.4879	.05480	.03652	.7321	.871
5.600	.002310	69.62	52.11	2,715.0	30.54	9.290	.4454	.06014	.03827	.6999	.675
3.070	.002313	51.53	48.73	2,375.0	30.45	8.3075	.3525	.06847	.03908	.6175	.374
1.378	.002315	34.50	45.86	2,103.0	30.30	7.280	.2508	.07690	.03867	.4988	.159
.194	.002319	12.94	43.10	1,858.0	30.25	6.061	.1001	.08672	.03638	.2386	.017

TABLE IV

SURVEY OF VELOCITY THROUGH PROPELLER PLANE, VE-7 MODEL

Left side				Top				Bottom			
Radius, in.	Free stream velocity, ft./sec.	Velocity through propeller plane, ft./sec.	Ratio	Radius, in.	Free stream velocity, ft./sec.	Velocity through propeller plane, ft./sec.	Ratio	Radius, in.	Free stream velocity, ft./sec.	Velocity through propeller plane, ft./sec.	Ratio
2	71.0	35.5	0.500	2	72.0	34.4	0.478	2	70.2	44.3	0.632
4	71.3	57.4	.806	4	70.2	43.2	.615	4	70.3	57.7	.820
6	71.7	68.5	.956	6	71.4	59.8	.838	6	69.5	62.4	.897
8	71.0	69.8	.982	8	72.0	65.8	.913	8	69.3	64.7	.934
10	70.7	70.5	.997	10	71.2	67.8	.952	10	69.5	65.2	.938
12	71.1	71.4	1.005	12	71.3	69.7	.978	12	69.3	66.2	.955
14	70.8	71.3	1.007	14	70.0	69.4	.991	14	71.7	68.4	.954
16	70.8	71.7	1.013	16	70.0	69.8	.997	16	69.6	66.8	.960
18	70.7	71.9	1.017	18	71.6	71.4	.996	18	69.6	67.4	.968
20	70.6	71.6	1.014	20	71.3	72.3	1.014	20	71.3	69.3	.972
22	70.3	71.1	1.012	22	71.4	72.2	1.011	22	71.4	69.7	.976
24	70.6	71.6	1.014	24	71.7	72.6	1.012	24	71.6	69.9	.977
				3	72.4	36.5	.504				
				5	70.1	52.4	.747				

ORDINATES FOR SECTIONS OF PROPELLERS A, B, C, D, AND E

[See fig. 2]

Radius.....	2.70''		5.40''		8.10''	10.80''	13.50''	16.20''	18''
Chamber.....	Upper	Lower	Upper	Lower	Upper	Upper	Upper	Upper	Upper
Radius L. E..	0.39''		0.05''		0.03''	0.02''	0.02''	0.01''	
2.5	0.18	-0.17	0.16		0.12	0.09	0.06	0.03	0.01
5	.25	-.25	.23		.17	.13	.09	.05	.02
10	.34	-.33	.30	-0.01	.22	.17	.12	.06	.03
20	.41	-.40	.36	-.01	.27	.20	.14	.08	.03
30	.43	-.42	.38	-.01	.28	.21	.15	.08	.03
40	.42	-.41	.38	-.01	.28	.21	.15	.08	.03
50	.41	-.40	.36	-.01	.27	.20	.14	.08	.03
60	.37	-.36	.33	-.01	.25	.19	.13	.07	.03
70	.32	-.31	.28	-.01	.21	.16	.11	.06	.03
80	.24	-.23	.22		.16	.12	.08	.05	.02
90	.15	-.15	.13		.10	.07	.05	.03	.01
Radius T. E..	0.07''		0.03''		0.02''	0.02''	0.01''	0.01''	

Stations in per cent of chord. All ordinates in inches.

REPORT No. 327

**THE EFFECT OF SUPERCHARGER CAPACITY ON
ENGINE AND AIRPLANE PERFORMANCE**

**By O. W. SCHEY and W. D. GOVE
Langley Memorial Aeronautical Laboratory**

REPORT No. 327

THE EFFECT OF SUPERCHARGER CAPACITY ON ENGINE AND AIRPLANE PERFORMANCE.

By O. W. SCHEY and W. D. GOVE

SUMMARY

Supercharging has already demonstrated its value as a means of improving the performance of an airplane at moderate and high altitudes. In order to obtain a maximum increase in the performance of an airplane designed to meet definite service requirements, it is necessary that a supercharger of the proper capacity be selected.

The effect of different supercharger capacities on the performance of an airplane and its engine was investigated by the staff of the National Advisory Committee for Aeronautics at Langley Field, Va. The tests were conducted on a DH4-M2 airplane powered with a Liberty 12 engine. In this investigation four supercharger capacities, obtained by driving a Roots type supercharger at 1.615, 1.957, 2.4, and 3 times engine speed, were used to maintain sea level pressure at the carburetor to altitudes of 7,000, 11,500, 17,000, and 22,000 feet, respectively.

The performance of the airplane in climb and in level flight was determined for each of the four supercharger drive ratios and for the unsupercharged condition. The engine power was measured during these tests by means of a calibrated propeller.

Although the results of this investigation are not conducive to general conclusions as to the proper capacity or type of supercharger for use with all types of airplanes, the information collected on the variation with altitude and supercharger capacity of such factors as carburetor air temperatures, power required to drive the supercharger, and the net engine power is of value as a guide in the selection of the most suitable supercharger capacity for airplanes having different performance characteristics than those of the one tested.

Several interesting conclusions pertaining to the effect of the capacity of a Roots type supercharger on the performance of this particular airplane have been drawn from the results of these tests.

It was found that very little sacrifice in sea-level performance was experienced with the larger supercharger drive ratios as compared with performance obtained when using the smaller drive ratios.

The results indicate that further increase in supercharger capacity over that obtained when using the 3 : 1 drive ratio would give a slight increase in ceiling and in high altitude performance, but would considerably impair the performance for an appreciable distance below the critical altitude.

As the supercharger capacity was increased, the height at which sea-level high speeds could be equaled or improved became a larger percentage of the maximum height of operation of the airplane.

INTRODUCTION

Supercharging has, in the past few years, established its value as a means of improving the performance of airplanes, and, as a result, superchargers are now being used on a number of military and on a few commercial airplanes. Supplying the engine with sufficient air to maintain sea-level carburetor pressure at altitude, and thus increasing the weight of the charge, results in a large increase in power of the supercharged engine over that of the unsupercharged engine. This increase in engine power gives improved climb and level flight performance and an increase in the maximum altitude at which the airplane may be operated.

In the selection of a supercharger for use on an airplane designed to meet definite performance requirements, the question arises as to whether it is advisable to choose a supercharger of sufficient capacity to maintain sea-level pressure to the maximum useful altitude or to choose one of smaller capacity requiring less power. The selection of the best supercharger capacity depends largely upon the manner in which the type of supercharger in question affects the engine power and on the percentage of the engine power that is used in driving the supercharger.

A small amount of information on this subject is found in reports on experimental investigations conducted by the National Advisory Committee for Aeronautics and on a theoretical investigation made by the Matériel Division, Air Corps, United States Army. During the preliminary investigation made to determine the suitability of the Roots type supercharger for airplane service, the performance of an airplane was determined with two supercharger capacities. (Reference 1.) Further information was obtained during an investigation of the supercharging of an air-cooled engine. (Reference 2.) Chenoweth gives theoretical curves of engine power versus altitude when using gear-driven centrifugal superchargers of three different capacities. (Reference 3.)

This investigation was undertaken by the staff of the National Advisory Committee for Aeronautics at the Langley Memorial Aeronautical Laboratory to determine experimentally the effect of the capacity of a Roots type supercharger on the performance of an airplane and its engine. Flight tests were conducted on a DH4-M2 airplane powered with a Liberty 12 engine. The performance of the airplane in climb and in level flight was determined without supercharging and with four supercharger capacities which gave critical altitudes of 7,000, 11,500, 17,000, and 22,000 feet.

DESCRIPTION OF AIRPLANE AND EQUIPMENT

The airplane used in this investigation was designated as a DH4-M2. The fuselage, which was of welded steel tube construction, was so arranged that the space normally used for the rear cockpit was entirely inclosed and available for the instrument installation. The weight of the airplane with all equipment and fully serviced at the start of each flight was 4,300 pounds.

The Liberty 12 engine used on all these tests was equipped with two inverted Stromberg NA-L5A carburetors having $1\frac{5}{8}$ -inch diameter chokes and No. 42 drill size metering jets.

A Roots type supercharger, N. A. C. A. Model II, of 0.382 cubic foot displacement per revolution, was mounted at the rear of the engine and driven through a flexible coupling from the engine crank shaft. Descriptions and performance characteristics of Roots type superchargers are given in references 4 and 5. Four supercharger capacities, obtained by driving the supercharger at 1.615, 1.957, 2.4, and 3 times engine speed, enabled the maintenance of sea-level pressure at the carburetor to altitudes of 7,000, 11,500, 17,000, and 22,000 feet, respectively. The inlet passages to the supercharger were extended slightly beyond the fuselage on both sides to form air scoops. The duct from the supercharger to the carburetors was built from a flexible metal tube. A general view of this installation is shown in Figure 1.

A Martin bomber supercharger propeller, Air Service part No. 065323, diameter 10.67 feet, pitch 6.33 feet, was used on all flights. This propeller had previously been calibrated on the same airplane, by means of a hub dynamometer, and a curve of the variation in its torque coefficient with $\frac{V}{nD}$ obtained.

The cooling system was augmented by a booster radiator, having a 9-inch core with a frontal area of 2.25 square feet, connected in series with the nose radiator as shown in Figure 1. This booster radiator was made sufficiently large so that ample cooling would be obtained during full supercharged continuous climbs in the hottest summer weather. A pressure relief valve set at 3 pounds per square inch was used to increase the boiling point of the water at high altitudes.

All readings taken during this investigation were recorded automatically. The readings of the indicating instrument were recorded by an "automatic observer," which consisted essentially of a light-tight box and a motor-driven motion-picture camera focused on the dials of

the instruments. These indicating instruments were: A sealed altimeter for the measurement of carburetor inlet air pressure; four electric resistance thermometers for measurement of (1) atmospheric temperature at a point under the lower wing, (2) air temperature at the inlet of the supercharger, (3) air temperature at the outlet of the supercharger, and (4) air temperature at the inlet of the carburetor; a chronometric tachometer for measurement of engine speeds; an experimental Venturi type fuel flow meter; and a distance type vapor pressure thermometer for the measurement of fuel temperatures at the flow meter. In addition to the instruments in the automatic observer an N. A. C. A. type recording altimeter air-speed meter unit and a recording pressure instrument were used. The altimeter recorded atmospheric pressure. The air-speed meter was connected to a swivel type Pitot head mounted on a strut. The recording pressure instrument measured the pressure difference between the carburetor inlet and the point of attachment of the priming lines on the inlet manifold. All records were synchronized during flight by an electric motor-driven N. A. C. A. chronometric timer which made regular timing dots on the film records.

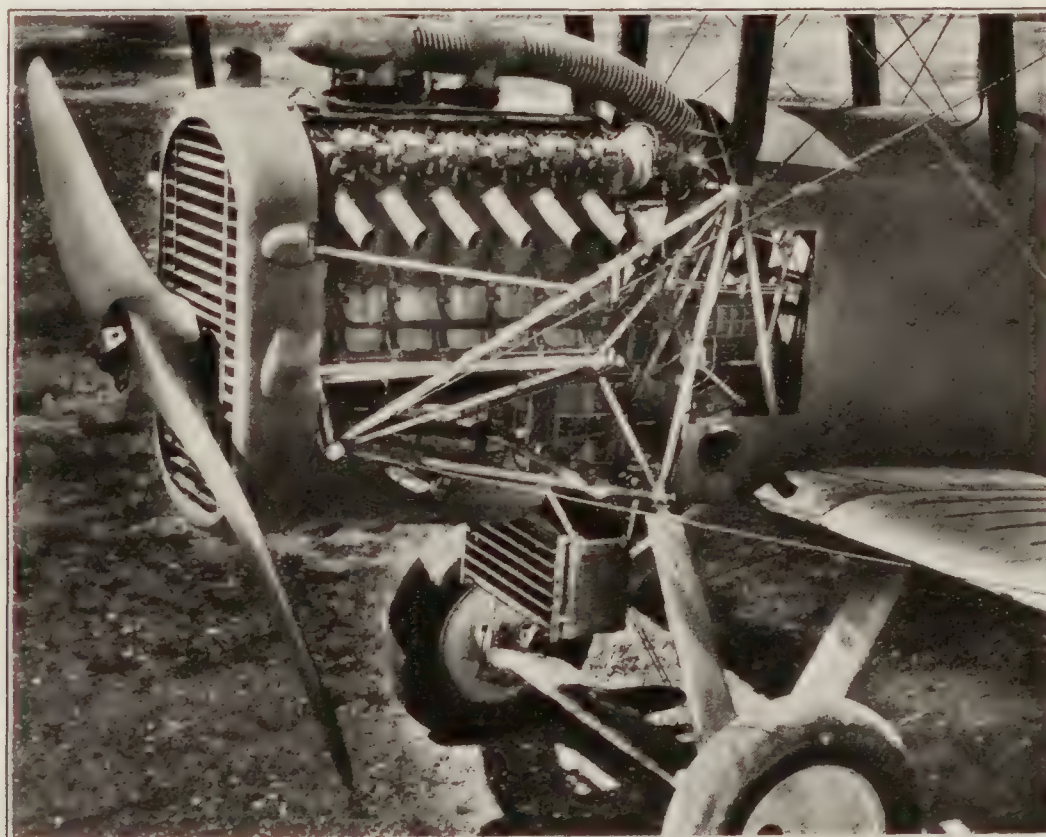


FIGURE 1.—DH4-M2 airplane showing installation of supercharger and booster radiator

METHODS

For an investigation of this nature, the best criteria of comparative performance are rate of climb and speed in level flight. In order that a comparison of climb performance could be obtained, it was necessary to determine the best rate of climb without supercharging and for each of the four supercharging conditions. The rate of climb with full engine power being dependent on air speed, the air speeds for the best rate of climb for each condition of supercharging and without supercharging were determined as follows: A continuous climb was first made at the air speeds estimated to give the best rate of climb, a second climb was made at air speeds 5 M. P. H. higher than in the first flight and a third climb made at air speeds 5 M. P. H. lower than in the first flight. From these three climbs, the air speeds for the best rate of climb were determined, and a final continuous climb was made at the selected air speeds. On all supercharged climbs the pilot first attained full throttle conditions and then, by regulation of the supercharger by-pass valve, maintained as nearly as possible a pressure of 29.92 inches of mercury at the carburetor inlet. These pressures, which were indicated by a sealed altimeter in the cockpit, were maintained constant until the by-pass valve was completely closed. The desired air speed was obtained by varying the attitude of the airplane.

To obtain high-speed performance, level runs of approximately six minutes duration were made at increments of 5,000 feet altitude for each supercharging condition.

During all of these tests the following readings were taken: Atmospheric pressure, atmospheric temperature, supercharger inlet air temperature, supercharger outlet air temperature, carburetor inlet air temperature, carburetor inlet air pressure, pressure drop from the carburetor inlet to the inlet manifolds, volume rate of fuel flow, fuel temperature at the flow meter, air speed, engine speed, and time.

The climb performance of the airplane was reduced to the conditions of operation in standard atmosphere by the method described in N. A. C. A. Technical Report No. 216. (Reference 6.) The rates of climb were determined graphically by drawing tangents to the time-altitude curves plotted on a large scale.

In order that engine power could be measured during this investigation, the propeller used was first calibrated on this airplane by means of a hub dynamometer. To calibrate the propeller, a series of runs was made at various angles of attack covering the useful range of $\frac{V}{nD}$ for the propeller. The values of a nondimensional torque coefficient were computed from measurements of engine torque, air speed, and density. This torque coefficient, commonly used in propeller work, is $C_Q = \frac{Q}{\rho V^2 D^3}$, where Q is torque, ρ is mass density of the air, V is velocity of the airplane, and D is propeller diameter. The values of the coefficient $\frac{V}{nD}$ were computed from air speeds, engine speeds, and propeller diameter. A curve of $\frac{V}{nD}$ versus C_Q was thus obtained for the propeller. This coefficient being nondimensional, is applicable at any altitude provided that there is no blade deflection or twist. For this propeller, no change in coefficient for the same value of $\frac{V}{nD}$ was obtained at 5,000 and at 14,000 feet altitude. The power delivered to the propeller was determined for the flight tests by computing $\frac{V}{nD}$ and then obtaining C_Q from the propeller calibration curve. All quantities in the equation for torque coefficient are known except the torque Q which can then be calculated.

To obtain an accurate comparison between flights, some of which were made in winter and some in summer, the brake horsepower measurements were corrected to standard atmospheric conditions. In applying this correction it was first necessary to establish, from the experimental information available, the variation in carburetor air temperature and pressure with altitude for each supercharging condition. The critical altitude or maximum altitude to which sea-level pressure was maintained was first determined from the experimental data. This critical altitude for each supercharger capacity was corrected for the effect of seasonal temperature changes so as to obtain the critical altitude for standard atmospheric conditions. Below the critical altitudes, the carburetor air pressure was assumed to be 29.92 inches of mercury. Above the critical altitudes the experimental data indicate that there was a gradual increase in the ratio of atmospheric to carburetor air pressure. Using these same rates of increase, the carburetor air pressures were computed from standard atmospheric pressures and the experimental pressure ratios. The temperatures of the supercharger outlet air were determined from the standard atmospheric temperatures and pressures and the established standard carburetor air pressures using the thermodynamic relation for polytropic changes of state $\left(\frac{P_1}{P_2}\right)^{\frac{n-1}{n}} = \frac{T_1}{T_2}$. Mean values of n , determined experimentally for each drive ratio, were used in this equation. The temperature drop from the supercharger outlet to carburetor inlet was found from experimental data to have a direct relation to the temperature difference between the inside and outside of the duct at the supercharger outlet. This relation was used to obtain the carburetor air temperatures from the supercharger outlet temperatures for standard conditions.

The observed values of brake horsepower, for the best flight of each supercharged condition and for the best flight of the unsupercharged condition, were corrected to the established standard

carburetor air temperatures and pressures. Brake horsepower was corrected by direct ratio for the pressure change and by the inverse square-root relation for the temperature change. These changes in pressure and temperature from observed to standard conditions were so small that the error in correcting the brake horsepower rather than the indicated horsepower was negligible. (Reference 7.)

The power required to drive the supercharger at altitude for each capacity was calculated from the relation

$$\text{HP.} = \frac{dn(P_2 - P_1)}{33,000} + \text{power losses}$$

where d is supercharger displacement, n is supercharger speed, and $(P_2 - P_1)$ is the pressure difference at the supercharger outlet and inlet. The power losses for each speed and pressure difference were obtained from the curve of horsepower versus supercharger power losses given in reference 5.

RESULTS

Data from the flight tests are shown in Tables I to XV, inclusive. Calibrations have been applied to all quantities used in computation and designated in tables as "observed." Tables I, IV, VII, X, and XIII give data from the flights considered to be representative of optimum

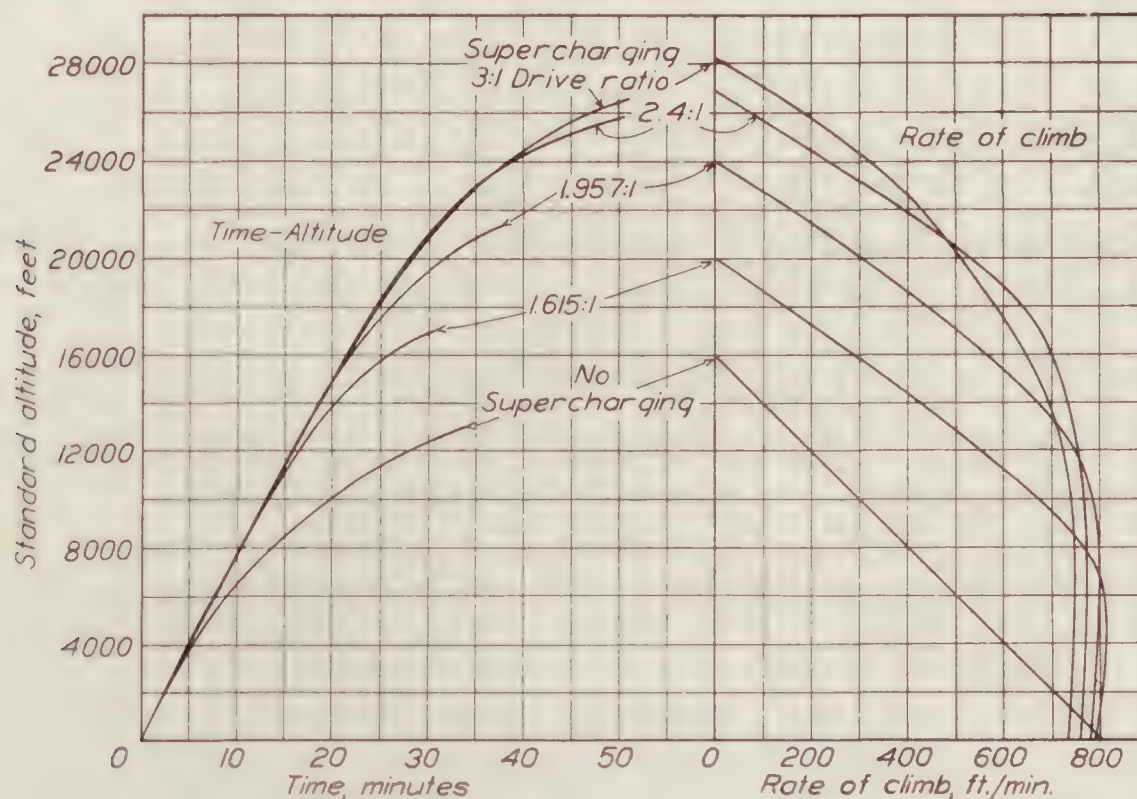


FIGURE 2.—Climb performance of DH4-M2 airplane with no supercharging and with four supercharging capacities

performance without supercharging and with supercharging using the 1.615:1, 1.957:1, 2.4:1, and 3:1 drive ratios, respectively.

Figure 2 shows the time to climb and the rate of climb for the five supercharging conditions plotted against standard altitude. These curves conform closely to the data from the optimum climbs given in the tables but have been faired slightly to form a family of curves. It is of interest to note that there is very little difference in the time to climb to 10,000 feet with the different supercharging conditions.

The air speeds in climb and in level flight for the five conditions are shown in Figure 3. The curves for the climbing conditions show the air speeds giving the best rates of climb as determined from cross plotting of all the data obtained with each supercharging condition. The curves for level flight were drawn from actual test data, but were faired to give a consistent family.

The curves in Figure 4 show the power delivered by the engine to the propeller during climb. These power values were obtained from the optimum climb data by using the propeller

calibration and have been corrected to standard atmosphere. Data at the low altitudes were somewhat scattered and the curves have been faired in this range. The curves of power to

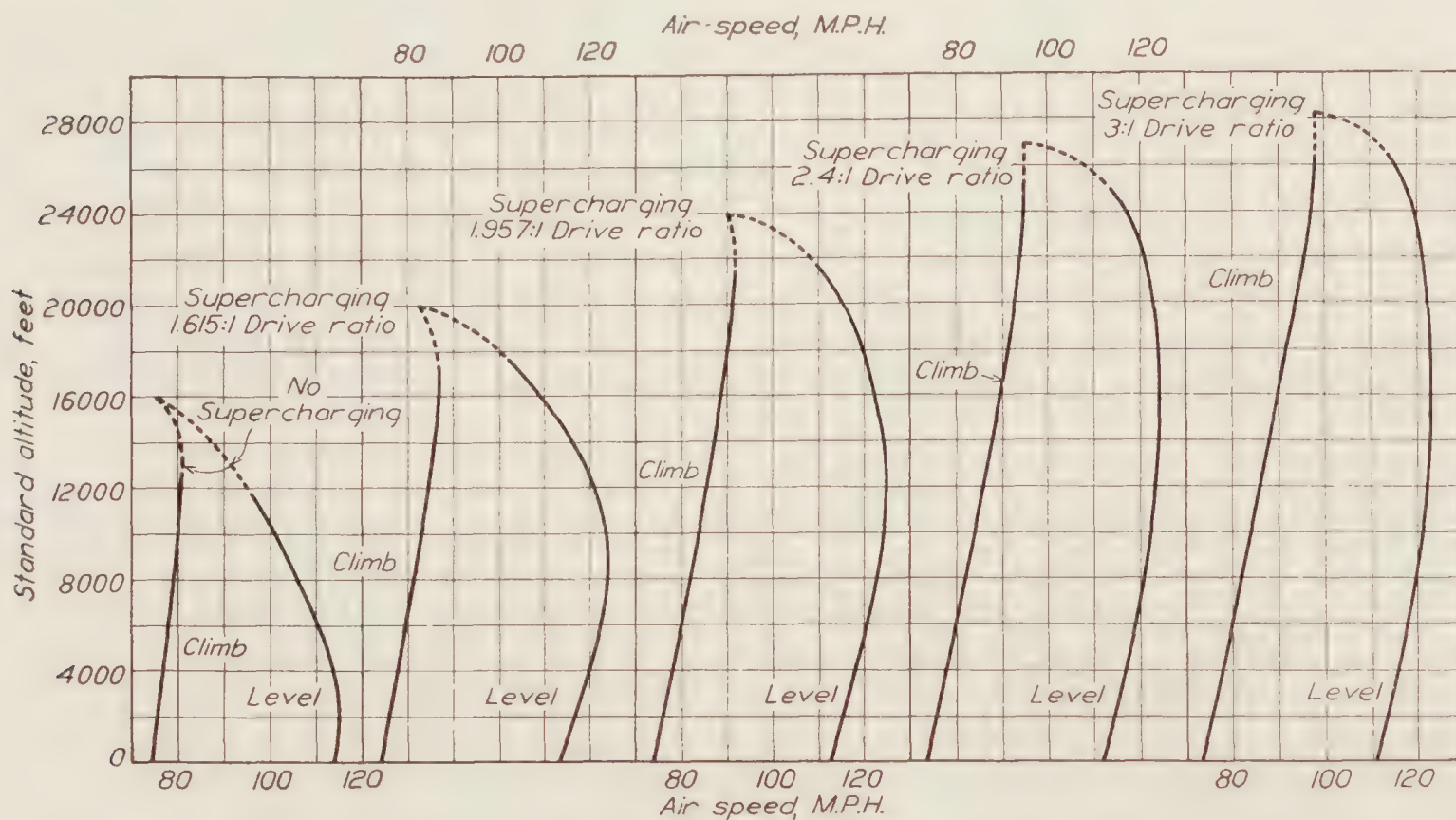


FIGURE 3.—Air speeds of DH4-M2 airplane in climb and in level flight with no supercharging and with four supercharging capacities

drive the supercharger during climb, shown on the same sheet, were drawn from data obtained during previous laboratory tests of the Roots type supercharger. (Reference 5.)

Figure 5 shows the engine speed in climb and in level flight for the different supercharging conditions. The engine speeds for the climbs were determined by fairing curves from all the

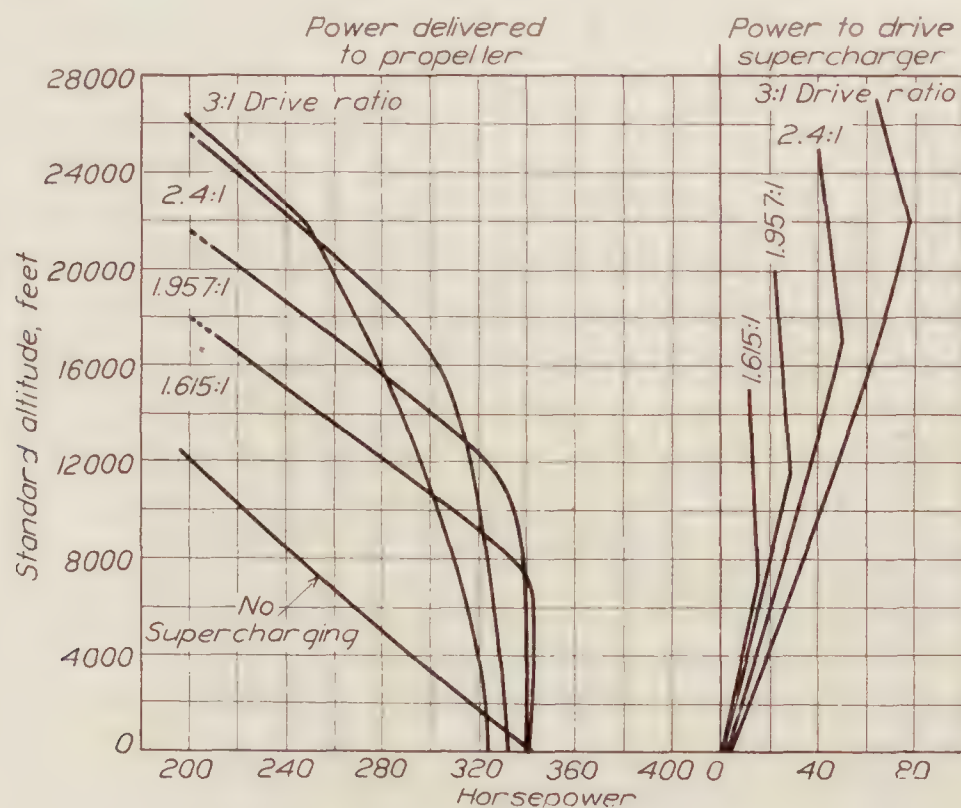


FIGURE 4.—Power delivered by the engine to the propeller and power required to drive the supercharger during climb

test data in a manner similar to that used for determining the air speeds in climb. The engine speed curves for level flight were drawn from actual test data.

Temperatures of the atmospheric air, supercharger outlet air, and carburetor inlet air for the four supercharged climbs are shown in Figure 6. These data were taken from the optimum

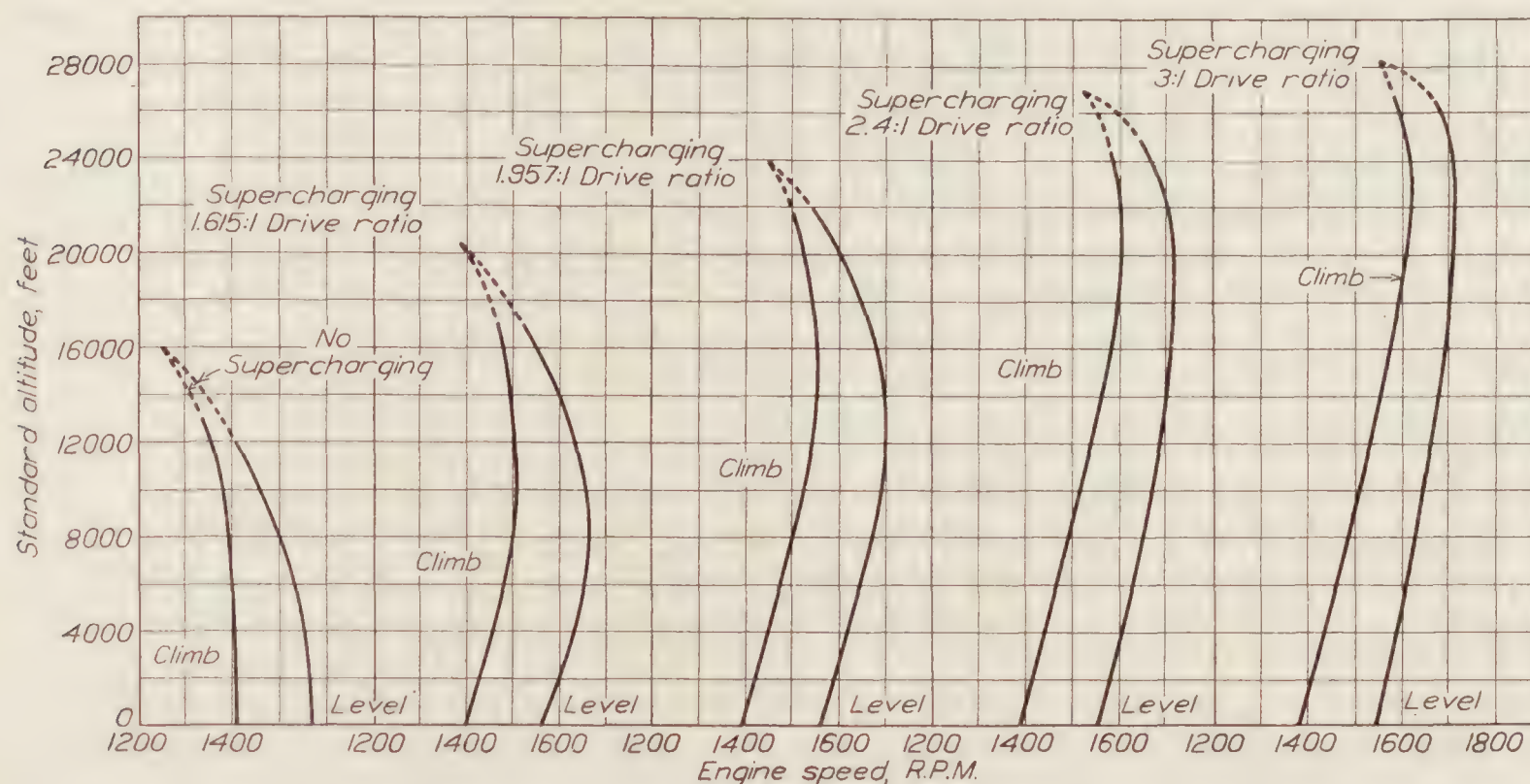


FIGURE 5.—Engine speeds of DH4-M2 airplane in climb and in level flight with no supercharging and with four supercharging capacities

climbs given in Tables IV, VII, X, and XIII. The atmospheric and carburetor air pressures for the same conditions are shown in Figure 7. The abrupt decrease in pressure shown by the carburetor pressure curves indicates that the by-pass valve had been completely closed and that the engine used all of the air delivered by the supercharger at higher altitudes.

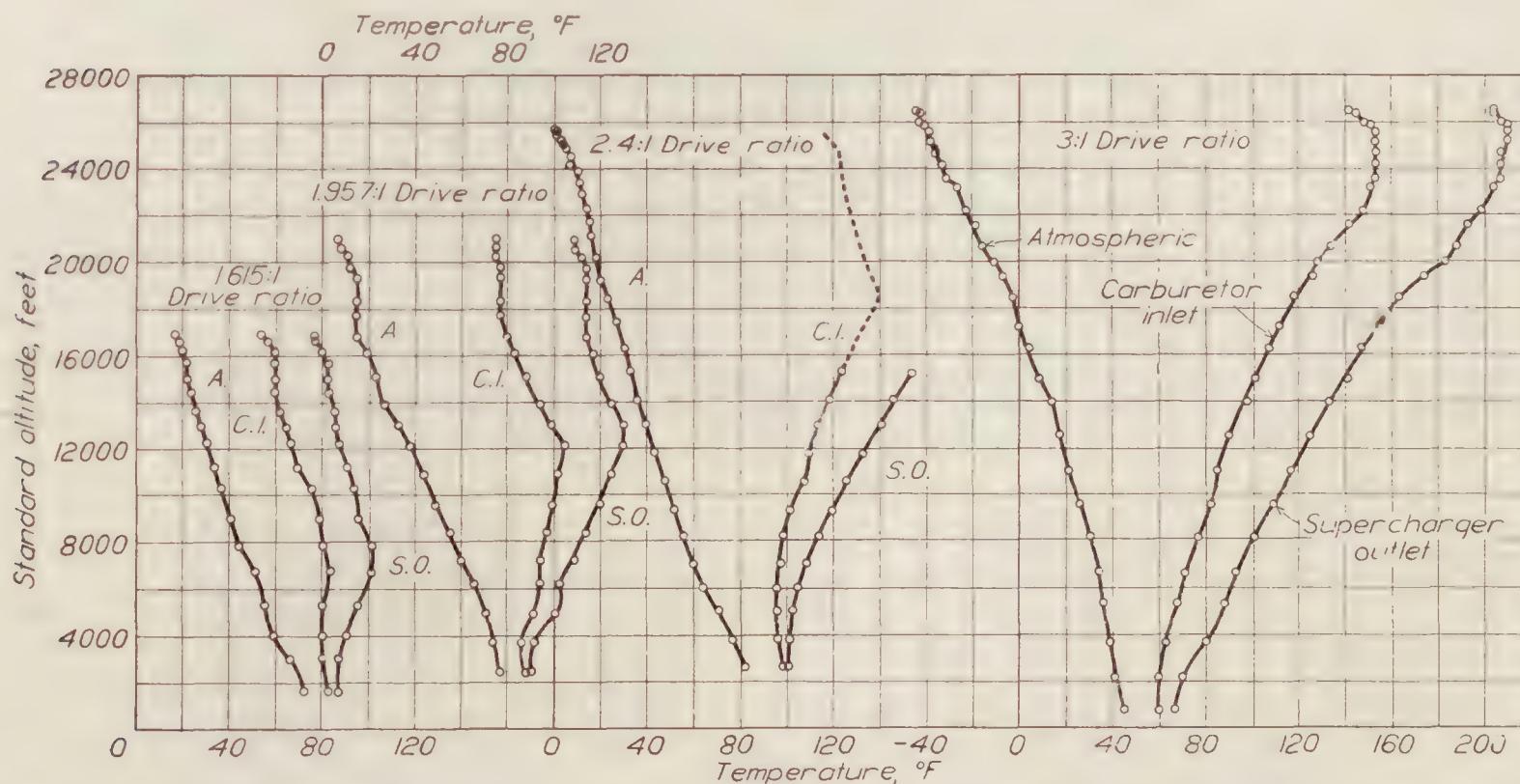


FIGURE 6.—Atmospheric, supercharger outlet and carburetor inlet air temperatures during climb for the four supercharging conditions. Data given in Tables IV, VII, X, and XIII

Figure 8 shows the atmospheric and carburetor air temperatures and pressures for the five test conditions in climb on the basis of operation in standard atmosphere. These curves show a rapid increase in maximum discharge temperature with an increase in supercharger capacity.

The pressure drop from the carburetor inlet to the inlet manifold is shown in the third group of curves of this figure.

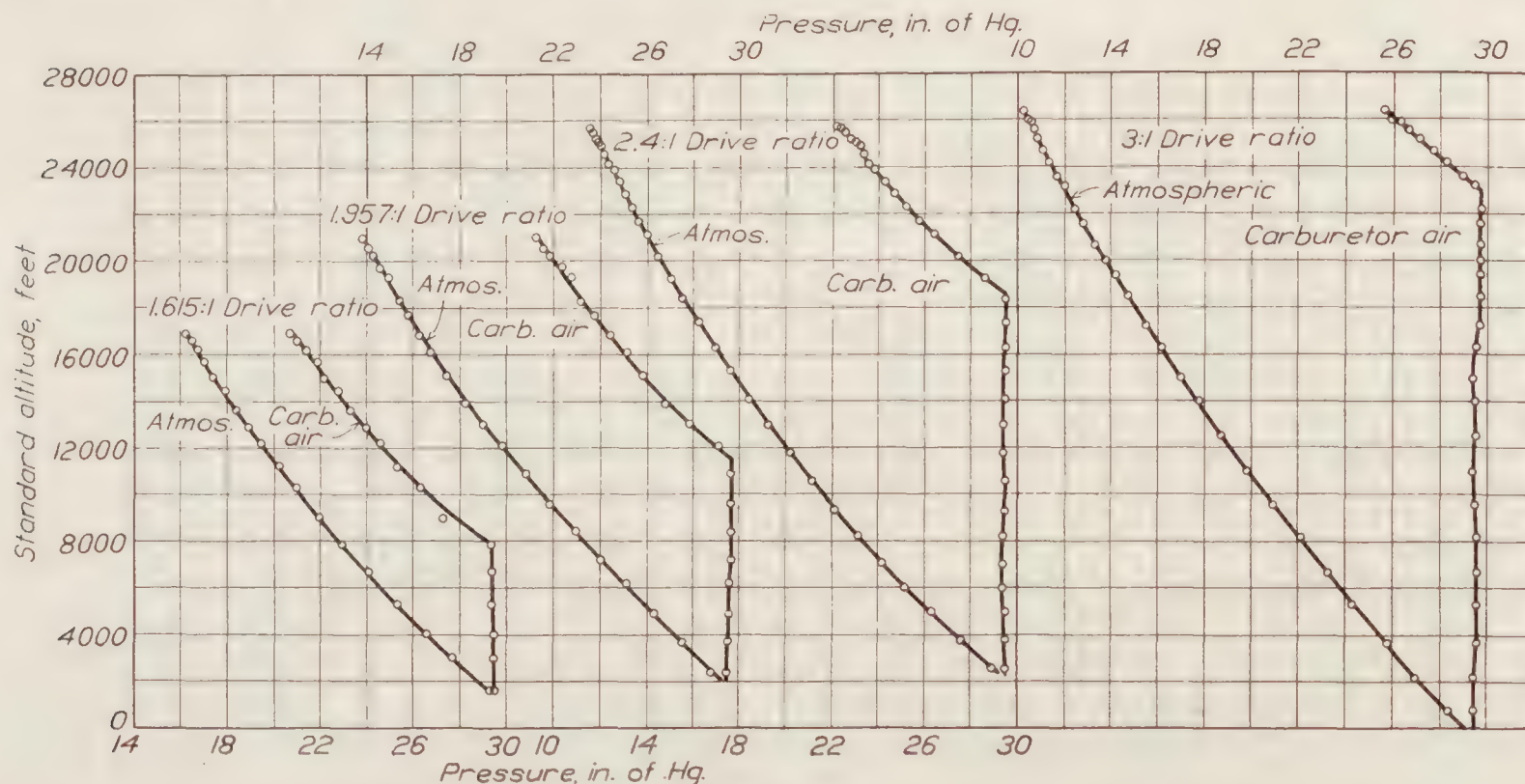


FIGURE 7.—Atmospheric and carburetor air pressures during climb for the four supercharged conditions. Data given in Tables IV, VII, X, and XIII

The slip speed, which is the speed necessary to maintain a definite pressure difference with no delivery, was determined by laboratory tests. The slip speed curve for the supercharger used is shown in Figure 9.

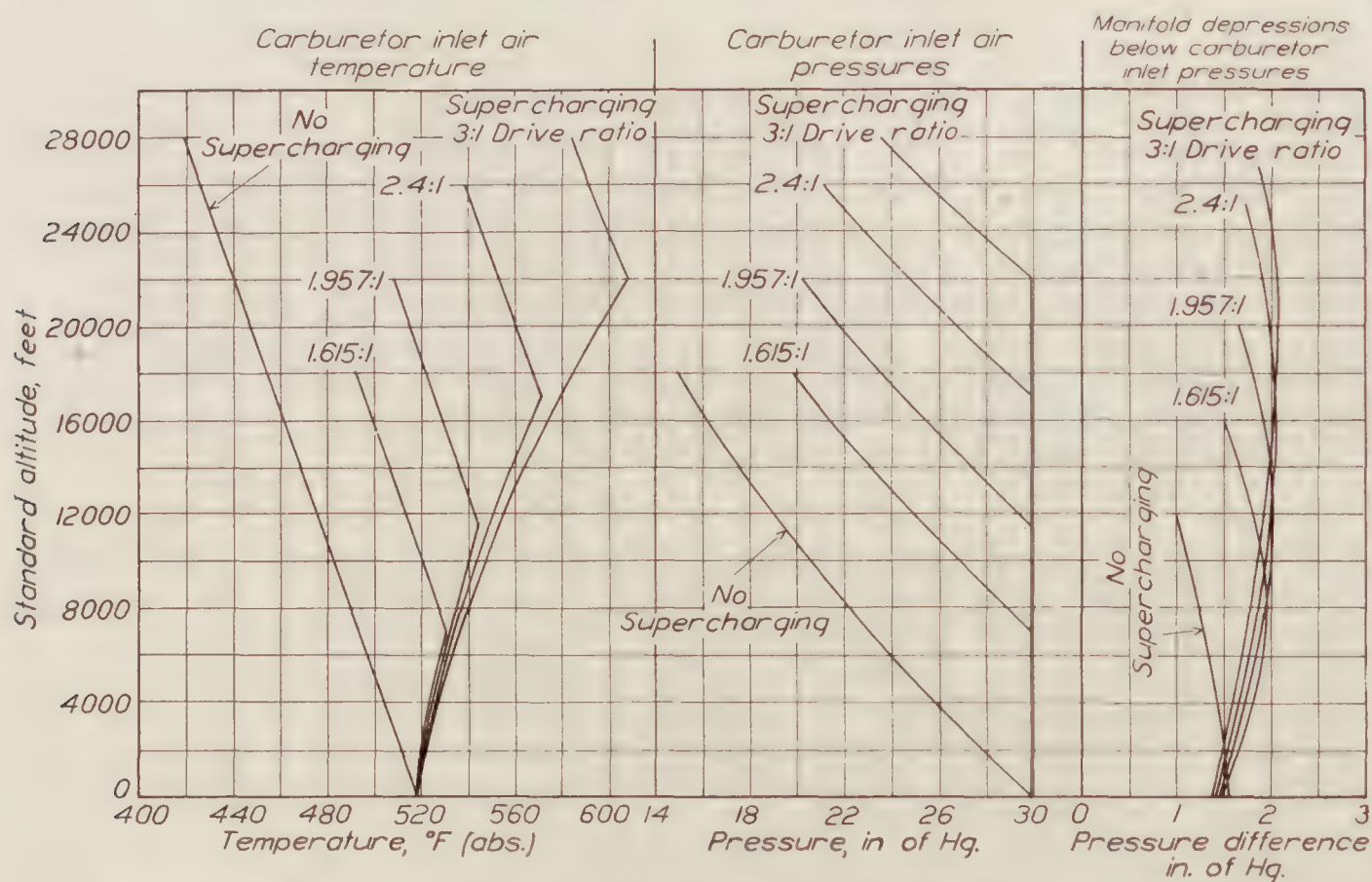


FIGURE 8.—Comparative air temperatures, pressures, and manifold depressions below carburetor inlet pressures for optimum climbs in standard atmosphere

The propeller calibration curve from which engine power was determined is shown in Figure 10.

DISCUSSION OF RESULTS

The airplane performance curves shown in Figures 2 and 3 indicate that there would be very little increase in ceiling and in high altitude performance if the drive ratio were increased beyond 3:1. The trend of the rate of climb curves shows that further increase in supercharger capacity would considerably impair the airplane performance near the critical altitude.

A loss in performance at sea level was expected with the larger capacities, due to the increased power required to drive the supercharger of larger capacity over that required for one

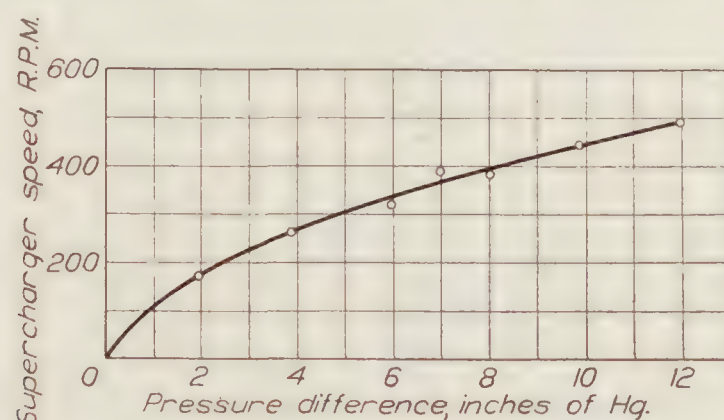


FIGURE 9.—Slip speeds of supercharger used during flight tests

of smaller capacity. This loss in sea-level performance, however, was actually found to be very small, as the curves in Figure 2 indicate. This difference in performance, while hardly noticeable from the time to climb curves, is easily seen from the rate of climb curves.

It is interesting to note, in Figure 3, that as the gear ratio was increased, the height to which sea-level high speed was maintained or bettered became a larger percentage of the maximum height of operation of the airplane. The air-speed curves indicate that up to the critical altitudes the maximum speeds in level flight were very nearly the same for each supercharger capacity.

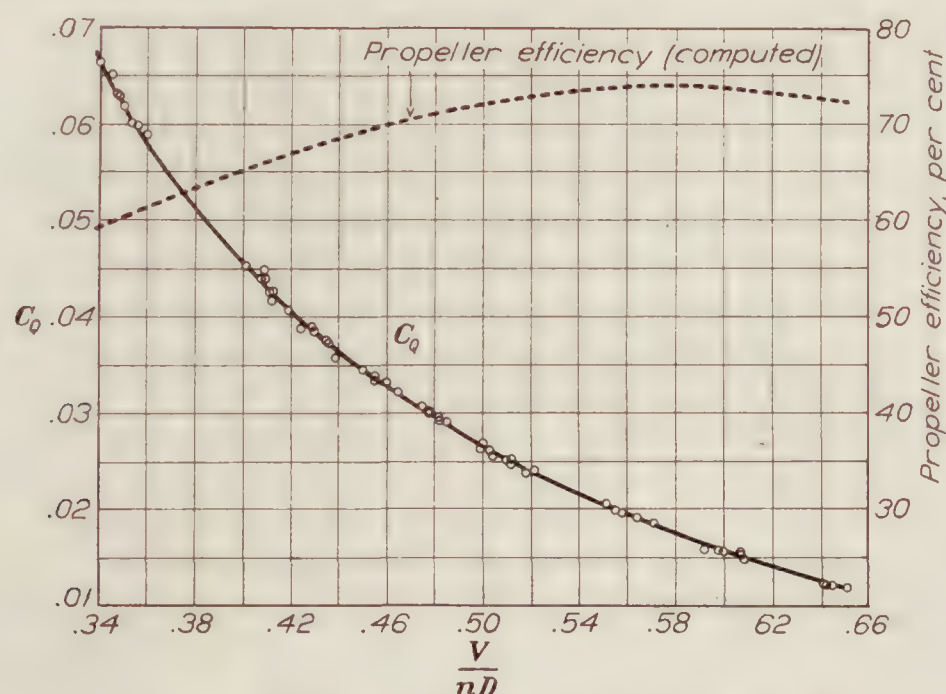


FIGURE 10.—Calibration curves for propeller used during flight tests

A considerable falling off in power below the critical altitude was experienced with the two higher supercharger capacities, as shown in Figure 4. This loss in power is partially accounted for by the increased power required to drive the supercharger, as the second group of curves in Figure 4 indicates. At the critical altitude with the 3:1 drive ratio the sum of net engine power and supercharger power is the same as the engine power at sea level. In all other cases the total engine power at the critical altitudes is slightly higher than at sea level. The net engine power curves represent actual flight conditions for a fixed pitch propeller and are

considered to be of greater value for use in making analyses than power curves at constant engine speed. These power curves substantiate the conclusion made in connection with the airplane performance curves, that the supercharger drive ratio should not be increased beyond 3:1. A striking similarity is found between these power curves and the rate of climb curves of Figure 2.

The supercharger power curves show that, for the higher gear ratios, the power required to drive the supercharger increases very rapidly with altitude and that, for the highest gear ratio, the supercharger power is 24 per cent of the engine power at the critical altitude.

The engine speeds (fig. 5) are of interest only in connection with the manner in which they affect engine power. These engine speeds are influenced by the density of the air and the characteristics of the propeller used. Although it would have been better from the standpoint of performance to have used a series of propellers, each allowing the engine speed in level flight to reach the maximum allowable value for each supercharging condition, it was thought that the experimental work involved in first determining the propellers suitable for each condition and then calibrating the series of propellers would be unwarranted. On these tests a wooden propeller was used primarily because it was the most suitable propeller available for use with supercharged engines and because it could be calibrated on this same airplane. For calibrating the propeller, a hub dynamometer suitable for use at low altitudes and only applicable to wooden propellers was available at this time. The propeller efficiency curve (fig. 10) shows that at the values of $\frac{V}{nD}$ given in the tables the propeller used was operating near its maximum efficiency during climbs. In comparing the performance with the different capacities it should be borne in mind that the performance with the smaller capacities would have been improved somewhat had more suitable propellers been used.

The temperature curves of Figure 6 show the large temperature rise caused by the compression of the air in the supercharger at the higher altitudes. A measure of the cooling that took place while the air flowed from the supercharger to the carburetor is also shown on these curves.

Readings of manifold pressures were taken on several flights for each drive ratio. These data were plotted against altitude and cross plotted against engine speed. The curves in Figure 8 were taken from the constant altitude curves at values of engine speed given in Figure 5.

Although trouble was experienced with the fuel flow meter, measurements of fuel flow were obtained for several flights. These data will be checked on further flight tests and reported upon later.

Because some trouble had previously been experienced from contacting of the impellers with the end of the case, and it was desired to eliminate any possibility of repetition of this trouble during the flight tests, the impeller end clearance was adjusted to 0.015 inch, which was about 0.005 inch more than had been used for laboratory tests. This increase in clearance at the ends of the impellers caused an increased amount of slip over that obtained with smaller clearances. This caused the temperature of the discharged air to be further increased and, therefore, an increase in the polytropic exponent of compression.

The compression exponents for each supercharger capacity were computed from the measurements of temperatures and pressures of the supercharger inlet and outlet. The computations showed that average compression exponents of 1.740, 1.776, 1.838, and 1.915 were obtained for the 1.615:1, 1.957:1, 2.4:1, and 3:1 drive ratios, respectively. Previous laboratory tests with smaller impeller end clearances gave an average value for the compression exponent of 1.48 for this model supercharger. (Reference 5.) Although it was realized that increasing the impeller clearances would lower the volumetric efficiency, it was not expected that the additional heat added to the air slipping back through the clearance spaces would result in such a marked increase in the compression exponent.

Precision type ball bearings were installed in the supercharger for these tests and their successful maintenance of constant impeller end clearance indicates that no mechanical troubles would be expected with clearance reduced to that used in laboratory tests. No mechanical

troubles of any kind were experienced during these tests, which extended over 50 hours of full-power flying.

Considerable cooling of the air delivered to the engine by the supercharger was obtained with the long air duct used on these tests. (See figs. 1 and 6.) The influence of this cooling on the comparative performance of the airplane is of interest. If no cooling were obtained, the carburetor air temperatures would be higher, the engine would use less weight of air, the critical altitude would be raised, and the engine would deliver less power below the critical altitude. If an air intercooler had been used the reverse condition would be true. Above the critical altitude the use of an intercooler is a detriment to performance, for the reason that the engine uses all of the air that the supercharger will deliver regardless of the temperature, while the intercooler creates additional drag. It is evident that the use of an intercooler would improve performance below the critical altitude with the higher supercharger capacities. It is also believed that less cooling of the inlet air would be experienced in most service installations than was obtained in this experimental case unless an intercooler were used. An improvement of the adiabatic efficiency of a supercharger would obviously be of greater value than the use of an intercooler and there would be no increase in drag. For this particular supercharger the efficiency could be considerably improved by reducing the impeller end clearances.

The temperatures recorded by the thermometer at the supercharger inlet were from 10° to 20° F. higher than the atmospheric temperature as measured under the lower wing. It is believed that heat was conducted from the supercharger case to this thermometer, so that in calculating the temperature rise in the supercharger the atmospheric temperature values were used instead of those given by the thermometer in the inlet passage.

CONCLUSIONS

From the results of these tests several interesting conclusions pertaining to the effect of the capacity of a Roots supercharger on the performance of this particular airplane are drawn.

It was found that an increase in supercharger drive ratio resulted in only a very small reduction in sea-level performance from that obtained with the lower gear ratios.

These results indicate that a further increase in supercharger capacity over that when using the 3 : 1 drive ratio would result in but slight increase in ceiling and in high altitude performance. This further increase in capacity would considerably impair the performance for the range of altitudes immediately below the critical altitude.

As the supercharger capacity was increased, the height to which sea level high speed could be equaled or improved became a larger percentage of the maximum height of operation of the airplane.

Although the results of this investigation are not conducive to drawing general conclusions as to the proper capacity or type of supercharger for use with all types of airplanes, the information collected on the variation with altitude and supercharger capacity of such factors as carburetor air temperatures, power required to drive the supercharger, and the net engine power is of considerable value as a guide in the selection of the proper supercharger capacity for airplanes of different performance characteristics than those of the one tested.

LANGLEY MEMORIAL AERONAUTICAL LABORATORY,
NATIONAL ADVISORY COMMITTEE FOR AERONAUTICS,
LANGLEY FIELD, VA., *March 13, 1929.*

REFERENCES

- Reference 1. Gardiner, Arthur W., and Reid, Elliot G.: Preliminary Flight Tests of the N. A. C. A. Roots Type Aircraft Engine Supercharger. N. A. C. A. Technical Report No. 263, 1927.
- Reference 2. Ware, Marsden, and Schey, Oscar W.: A Preliminary Investigation of Supercharging an Air-Cooled Engine in Flight. N. A. C. A. Technical Report No. 283, 1928.
- Reference 3. Chenoweth, Opie: Supercharged Engine Performance, Calculated and Actual. S. A. E. Journal, November, 1927, xxi, 5, 508-515.
- Reference 4. Ware, Marsden: Description and Laboratory Tests of a Roots Type Aircraft Engine Supercharger. N. A. C. A. Technical Report No. 230, 1926.
- Reference 5. Ware, Marsden, and Wilson, Ernest E.: The Comparative Performance of Roots Type Aircraft Engine Superchargers as Affected by Change in Impeller Speed and Displacement. N. A. C. A. Technical Report No. 284, 1928.
- Reference 6. Diehl, Walter S. and Lesley, E. P.: The Reduction of Airplane Flight Test Data to Standard Atmosphere Conditions. N. A. C. A. Technical Report No. 216, 1925.
- Reference 7. Gove, W. D.: The Variation in Engine Power with Altitude Determined from Measurements in Flight with a Hub Dynamometer. N. A. C. A. Technical Report No. 295, 1928.

TABLE I.—OPTIMUM, FULL THROTTLE CLIMB WITH NO SUPERCHARGING

Reading No.	Corrected time, minutes	Observed atmospheric temperature, ° F.	Observed atmospheric pressure, in. Hg.	Atmospheric density, lb. per cu. ft.	Standard altitude, feet	Observed engine speed, R. P. M.	Air speed, M. P. H.	$\frac{V}{nD}$	Brake horsepower	Temperature at supercharger outlet, ° F.	Temperature at carburetor inlet ° F. (abs.)	Pressure at carburetor inlet in. Hg.	Brake horsepower corrected to standard pressure and temperature
1	1.85	71	29.35	0.0733	1,500	1,415	74.0	0.432	319	82	539	29.50	314
2	2.11	64	28.15	.0713	2,400	1,405	75.5	.441	318	78	534	28.20	317
3	4.68	60	26.90	.0687	3,600	1,400	76.5	.451	298	75	531	27.20	295
4	6.06	55	26.10	.0673	4,300	1,395	77.0	.456	287	71	526	26.30	285
5	7.60	50	25.10	.0654	5,300	1,395	77.5	.459	279	65	520	25.40	276
6	9.11	46	24.40	.0640	6,000	1,395	78.0	.462	271	63	515	24.50	269
7	10.77	44	23.60	.0622	6,900	1,385	78.0	.465	259	60	512	23.85	256
8	12.80	44	23.00	.0606	7,750	1,385	79.0	.471	250	60	511	23.20	247
9	15.46	46	22.50	.0590	8,600	1,385	80.5	.480	242	60	512	22.70	237
10	17.35	46	22.00	.0577	9,300	1,375	81.0	.486	230	60	512	22.15	226
11	19.13	45	21.70	.0571	9,700	1,375	81.0	.486	227	60	512	21.80	223
12	20.88	44	21.25	.0560	10,300	1,375	82.0	.492	221	60	512	21.50	215
13	22.18	41	20.90	.0553	10,650	1,375	81.0	.486	220	60	511	21.10	215
14	23.99	40	20.55	.0545	11,150	1,375	81.0	.486	217	60	509	20.80	211
15	25.88	40	20.35	.0539	11,450	1,375	80.5	.483	216	60	508	20.50	211
16	27.53	38	20.05	.0533	11,850	1,365	80.5	.487	208	60	508	20.20	203
17	29.11	37	19.70	.0526	12,300	1,365	80.0	.484	206	59	508	19.90	201
18	29.92	36	19.55	.0523	12,400	1,365	80.0	.484	204	59	508	19.75	200
19	31.13	34	19.35	.0520	12,600	1,365	79.5	.478	204	58	506	19.50	202
20	32.33	33	19.15	.0517	12,800	1,365	79.0	.478	203	55	506	19.40	200

TABLE II.—FULL THROTTLE CLIMB WITH NO SUPERCHARGING

Reading No.	Corrected time, minutes	Observed atmospheric temperature, ° F.	Observed atmospheric pressure, in. Hg.	Atmospheric density, lb. per cu. ft.	Standard altitude, feet	Observed engine speed, R. P. M.	Air speed, M. P. H.	$\frac{V}{nD}$	Brake horsepower	Temperature at supercharger outlet, ° F.	Temperature at carburetor inlet ° F. (abs.)	Pressure at carburetor inlet in. Hg.
1	1.96	66	28.95	0.0730	1,600	1,425	80.0	0.463	330	77	534	29.25
2	3.43	59	27.55	.0704	2,800	1,415	81.0	.472	311	74	528	28.00
3	5.00	55	26.70	.0688	3,600	1,415	81.0	.472	304	68	523	27.10
4	6.26	50	25.80	.0673	4,300	1,415	81.5	.475	295	66	517	26.15
5	7.85	46	25.00	.0657	5,100	1,395	81.5	.482	275	63	515	25.30
6	9.53	42	24.35	.0644	5,800	1,395	82.0	.485	269	58	509	24.60
7	11.05	39	23.75	.0632	6,400	1,395	82.5	.488	263	55	506	24.05
8	12.79	38	23.15	.0618	7,100	1,395	83.5	.494	256			23.55
9	14.98	37	22.70	.0606	7,750	1,395	83.5	.494	251			23.10
10	16.41	35	22.35	.0599	8,100	1,395	84.0	.497	246			22.70
11	18.57	34	21.95	.0589	8,650	1,395	85.0	.503	239			22.30
12	19.56	31	21.60	.0584	8,900	1,395	86.0	.509	235			21.95
13	21.16	30	21.30	.0578	9,250	1,395	86.5	.512	232			21.70
14	23.34	30	21.05	.0571	9,650	1,395	87.0	.515	229			21.40
15	25.49	30	20.80	.0564	10,050	1,395	87.0	.515	226			21.10
16	28.48	31	20.60	.0556	10,500	1,395	87.0	.515	223			20.85
17	30.32	30	20.35	.0550	10,850	1,395	86.0	.509	221			20.65
18	32.13	30	20.10	.0544	11,200	1,385	86.5	.510	220			20.50
19	33.85	30	19.95	.0540	11,400	1,385	86.5	.510	218			20.35

TABLE III.—FULL THROTTLE CLIMB WITH NO SUPERCHARGING

Reading No.	Corrected time, minutes	Observed atmospheric temperature, ° F.	Observed atmospheric pressure, in. Hg.	Atmospheric density, lb. per cu. ft.	Standard altitude, feet	Observed engine speed, R. P. M.	Air speed, M. P. H.	$\frac{V}{nD}$	Brake horsepower	Temperature at supercharger outlet, ° F.	Temperature at carburetor inlet, ° F. (abs.)	Pressure at carburetor inlet, in. Hg.
1	3.39	75	28.90	0.0717	2,200	1,395	74.0	0.438	311	91	546	29.10
2	4.93	71	27.85	.0696	3,200	1,395	74.5	.441	300	89	543	28.10
3	6.35	67	26.85	.0677	4,100	1,395	75.0	.450	291	85	539	27.20
4	7.80	63	26.00	.0661	4,900	1,395	76.0	.450	284	82	535	26.20
5	9.52	60	25.05	.0640	6,000	1,395	77.0	.455	274	78	531	25.35
6	10.98	57	24.55	.0630	6,500	1,395	78.0	.461	269	74	527	24.70
7	12.40	55	23.90	.0617	7,150	1,395	78.5	.464	263	71	524	24.10
8	14.02	52	23.30	.0604	7,850	1,395	79.5	.470	255	70	523	23.60
9	15.97	51	22.95	.0595	8,350	1,395	80.0	.473	251	68	520	23.20
10	16.87	49	22.65	.0591	8,550	1,385	80.0	.477	242	67	517	22.85
11	18.42	48	22.35	.0584	8,900	1,375	78.5	.471	236	66	516	22.60
12	20.62	48	22.20	.0580	9,150	1,370	77.0	.464	233	63	515	22.40
13	22.15	47	21.90	.0574	9,500	1,370	76.0	.458	232	60	515	22.15
14	23.89	47	21.60	.0566	9,900	1,370	77.0	.464	228	-----	513	21.85
15	25.41	45	21.35	.0562	10,200	1,365	76.5	.463	223	-----	512	21.65
16	26.26	44	21.20	.0559	10,300	1,365	76.5	.463	222	-----	512	21.40
17	28.16	43	21.00	.0554	10,600	1,365	77.0	.466	220	-----	512	21.25
18	29.84	42	20.85	.0551	10,800	1,355	76.0	.463	214	-----	512	21.05
19	31.10	41	20.65	.0547	11,000	1,345	75.0	.460	209	-----	510	20.85
20	33.28	41	20.45	.0541	11,350	1,345	75.5	.463	206	-----	510	20.60
21	35.34	41	20.30	.0537	11,600	1,345	76.0	.466	204	-----	510	20.50
22	35.95	40	20.20	.0536	11,650	1,345	76.0	.466	204	-----	510	20.35
23	38.13	40	19.95	.0529	12,100	1,345	76.5	.469	201	-----	512	20.20
24	38.54	38	19.80	.0528	12,150	1,345	76.5	.469	201	-----	512	20.10
25	40.92	38	19.75	.0526	12,250	1,340	76.5	.471	197	-----	510	20.00
26	42.71	38	19.55	.0521	12,550	1,335	77.0	.476	192	-----	509	19.85
27	43.89	37	19.50	.0520	12,600	1,335	76.5	.473	193	-----	-----	19.80
28	45.05	37	19.45	.0519	12,650	1,335	76.5	.473	192	-----	-----	19.75
29	46.21	37	19.40	.0519	12,700	1,335	76.5	.473	192	-----	-----	19.70

TABLE IV.—OPTIMUM, SUPERCHARGED CLIMB USING THE 1.615:1 DRIVE RATIO

Reading No.	Corrected time, minutes	Observed atmospheric temperature, ° F.	Observed atmospheric pressure, in. Hg.	Atmospheric density, lb. per cu. ft.	Standard altitude, feet	Observed engine speed, R. P. M.	Air speed, M. P. H.	$\frac{V}{nD}$	Brake horsepower	Temperature at supercharger outlet, ° F.	Temperature at carburetor inlet, ° F. (abs.)	Pressure at carburetor inlet, in. Hg.	Brake horsepower corrected to standard pressure and temperature
1	2.07	72	29.25	0.0730	1,600	1,425	75.0	0.434	339	87	542	29.50	352
2	3.59	66	27.70	.0699	3,000	1,435	75.5	.434	330	87	539	29.50	341
3	5.01	59	26.55	.0679	4,000	1,445	75.5	.431	330	90	539	29.50	340
4	6.66	55	25.30	.0654	5,300	1,455	76.0	.431	324	95	539	29.40	334
5	8.42	51	24.05	.0625	6,750	1,475	76.5	.428	324	101	542	29.40	334
6	9.87	44	22.95	.0604	7,850	1,485	77.5	.431	316	101	539	28.40	326
7	11.48	40	21.95	.0582	9,000	1,495	79.0	.436	310	95	537	27.30	320
8	13.23	36	20.95	.0560	10,300	1,495	80.5	.444	298	93	534	26.30	306
9	14.80	33	20.20	.0543	11,200	1,495	80.5	.444	290	90	528	25.30	298
10	16.49	30	19.45	.0527	12,200	1,495	82.0	.453	279	87	525	24.60	284
11	18.06	27	18.90	.0516	12,900	1,495	83.0	.458	272	85	523	24.00	276
12	19.59	25	18.35	.0503	13,600	1,495	84.0	.464	263	85	520	23.30	268
13	21.59	23	17.85	.0491	14,450	1,495	83.5	.461	257	82	518	22.80	259
14	22.99	21	17.40	.0481	15,000	1,485	83.0	.461	248	82	518	22.20	252
15	24.95	21	17.00	.0470	15,700	1,475	82.5	.462	235	82	518	21.90	237
16	26.79	19	16.70	.0463	16,200	1,455	82.0	.465	223	79	518	21.40	225
17	28.53	18	16.45	.0457	16,600	1,445	82.5	.471	215	76	515	21.00	218
18	29.81	16	16.20	.0452	16,900	1,435	83.0	.477	207	76	512	20.70	210

TABLE V.—SUPERCHARGED CLIMB USING THE 1.615:1 DRIVE RATIO

Reading No.	Corrected time, minutes	Observed atmospheric temperature, ° F.	Observed atmospheric pressure, in. Hg.	Atmospheric density, lb. per cu. ft.	Standard altitude, feet	Observed engine speed, R. P. M.	Air speed, M. P. H.	V nD	Brake horsepower	Temperature at supercharger outlet, ° F.	Temperature at carburetor inlet, ° F. (abs.)	Pressure at carburetor inlet, in. Hg.
1	3.66	74	28.30	0.0704	2,800	1,445	80.0	0.457	332	85	537	29.50
2	5.36	72	27.10	.0677	4,100	1,475	81.0	.453	342	95	548	29.50
3	6.87	67	25.90	.0654	5,300	1,485	82.0	.456	336	101	550	29.40
4	8.33	61	24.70	.0630	6,500	1,495	82.0	.453	332	103	550	29.40
5	9.54	53	23.65	.0613	7,400	1,515	82.0	.450	332	106	550	29.40
6	11.15	49	22.55	.0588	8,700	1,505	84.0	.461	315	106	548	28.25
7	12.72	45	21.55	.0566	9,900	1,515	85.5	.466	308	101	542	27.20
8	14.08	40	20.80	.0552	10,700	1,515	86.5	.471	300	95	537	26.35
9	15.79	37	20.15	.0537	11,600	1,515	88.0	.479	288	92	534	25.60
10	17.00	33	19.60	.0528	12,150	1,505	87.0	.477	278	90	528	24.85
11	18.31	29	19.10	.0519	12,700	1,505	88.0	.483	271	87	526	24.35
12	19.63	27	18.70	.0511	13,150	1,505	89.0	.487	269	82	523	23.80
13	21.50	26	18.30	.0501	13,800	1,495	90.0	.497	253	82	523	23.40
14	23.43	26	17.95	.0491	14,400	1,495	90.5	.500	246	82	523	23.10
15	25.20	25	17.70	.0485	14,800	1,495	92.0	.508	241	82	520	22.75
16	26.30	22	17.40	.0480	15,100	1,495	90.0	.497	243	79	518	22.50
17	28.28	22	17.05	.0470	15,800	1,485	90.0	.500	232	79	518	22.10
18	29.68	20	16.75	.0463	16,200	1,475	89.0	.498	225	79	515	21.80
19	31.25	19	16.55	.0459	16,500	1,455	87.0	.493	215	76	515	21.50
20	32.63	19	16.40	.0455	16,700	1,445	85.0	.485	211	76	515	21.25

TABLE VI.—SUPERCHARGED CLIMB USING THE 1.615:1 DRIVE RATIO

Reading No.	Corrected time, minutes	Observed atmospheric temperature, ° F.	Observed atmospheric pressure, in. Hg.	Atmospheric density, lb. per cu. ft.	Standard altitude, feet	Observed engine speed, R. P. M.	Air speed, M. P. H.	V nD	Brake horsepower	Temperature at supercharger outlet, ° F.	Temperature at carburetor inlet, ° F. (abs.)	Pressure at carburetor inlet, in. Hg.
1	1.88	75	29.40	0.0729	1,500	1,415	81.0	0.473	320	87	542	29.60
2	3.39	67	28.05	.0707	2,700	1,435	82.0	.472	325	87	539	29.60
3	5.06	63	26.70	.0678	4,100	1,455	83.0	.471	324	87	539	29.50
4	6.86	62	25.65	.0653	5,300	1,475	84.5	.473	325	92	542	29.50
5	8.50	58	24.55	.0629	6,500	1,495	86.0	.475	324	98	545	29.50
6	10.24	55	23.30	.0601	8,000	1,515	88.0	.480	323	103	550	29.30
7	11.96	51	22.25	.0578	9,300	1,525	90.0	.487	315	106	550	28.40
8	13.54	48	21.40	.0560	10,300	1,535	91.5	.492	306	103	547	27.40
9	15.19	44	20.65	.0543	11,250	1,525	93.0	.504	285	101	542	26.55
10	16.65	41	19.95	.0529	12,100	1,525	93.0	.504	277	98	539	25.60
11	18.23	38	19.25	.0514	13,000	1,525	94.0	.509	270	95	535	24.80
12	20.07	36	18.60	.0498	14,000	1,515	94.5	.515	255	92	531	24.15
13	21.47	33	18.10	.0488	14,600	1,515	94.0	.512	251	90	528	23.50
14	22.84	30	17.60	.0478	15,200	1,505	95.0	.521	239	87	527	22.95
15	24.18	27	17.35	.0473	15,500	1,495	95.5	.528	229	87	526	22.45
16	25.62	26	17.00	.0464	16,000	1,495	96.5	.533	224	85	524	22.10
17	27.79	26	16.75	.0458	16,500	1,495	96.0	.530	222	83	523	21.85
18	29.10	26	16.65	.0455	16,700	1,495	96.0	.530	220	82	520	21.65

TABLE VII.—OPTIMUM, SUPERCHARGED CLIMB USING THE 1.957:1 DRIVE RATIO

Reading No.	Corrected time, minutes	Observed atmospheric temperature, ° F.	Observed atmospheric pressure, in. Hg.	Atmospheric density, lb. per cu. ft.	Standard altitude, feet	Observed engine speed, R. P. M.	Air speed, M. P. H.	V nD	Brake horsepower	Temperature at supercharger outlet, ° F.	Temperature at carburetor inlet, ° F. (abs.)	Pressure at carburetor inlet, in. Hg.	Brake horsepower corrected to standard pressure and temperature
1	3.16	77	28.85	0.0713	2,400	1,415	79.5	0.464	316	90	547	29.50	329
2	4.87	74	27.60	.0686	3,700	1,445	80.0	.456	327	92	545	29.60	338
3	6.44	71	26.40	.0661	4,900	1,475	81.5	.456	334	101	550	29.60	345
4	8.09	66	25.20	.0636	6,200	1,495	82.0	.453	336	103	553	29.60	347
5	9.43	60	24.10	.0616	7,200	1,505	83.5	.458	330	109	553	29.70	340
6	11.05	55	23.05	.0594	8,400	1,525	84.0	.455	332	114	556	29.70	341
7	12.48	49	21.90	.0572	9,600	1,535	84.0	.451	328	120	558	29.70	337
8	14.11	44	20.85	.0549	10,900	1,545	86.0	.454	325	125	561	29.70	333
9	15.63	38	19.85	.0529	12,100	1,555	87.0	.461	305	130	564	29.20	312
10	17.21	33	19.00	.0513	13,000	1,555	87.0	.461	304	130	558	27.90	314
11	18.63	27	18.25	.0499	13,900	1,555	88.0	.466	294	125	553	26.90	304
12	20.35	23	17.45	.0480	15,100	1,555	89.0	.472	281	120	547	25.90	289
13	21.93	19	16.75	.0464	16,100	1,545	90.0	.480	265	117	542	25.20	270
14	23.44	15	16.25	.0454	16,800	1,545	90.0	.480	260	114	539	24.50	265
15	25.33	15	15.75	.0440	17,700	1,535	91.0	.489	243	114	536	23.80	246
16	27.08	15	15.40	.0431	18,300	1,535	91.0	.489	239	114	536	23.20	244
17	29.29	15	14.95	.0417	19,300	1,535	92.0	.495	229	114	536	22.80	229
18	30.55	12	14.60	.0411	19,750	1,535	93.0	.505	217	114	536	22.40	219
19	32.15	11	14.30	.0404	20,250	1,525	94.0	.509	212	112	534	21.90	214
20	33.47	8	14.05	.0399	20,600	1,525	94.0	.509	210	109	534	21.60	211
21	35.34	7	13.85	.0394	21,000	1,525	95.0	.514	206	109	534	21.30	208

TABLE VIII.—SUPERCHARGED CLIMB USING THE 1.957 : 1 DRIVE RATIO

Reading No.	Corrected time, minutes	Observed atmospheric temperature, ° F.	Observed atmospheric pressure, in. Hg.	Atmospheric density, lb. per cu. ft.	Standard altitude, feet	Observed engine speed R. P. M.	Air speed, M. P. H.	$\frac{V}{nD}$	Brake horsepower	Temperature at supercharger outlet, ° F.	Temperature at carburetor inlet, ° F. (abs.)	Pressure at carburetor inlet, in. Hg.
1	0.25	47	29.10	0.0760	200	1,415	75.0	0.437	346	66	515	29.60
2	2.00	43	27.65	.0730	1,600	1,425	76.0	.440	338	68	515	29.40
3	3.76	38	26.30	.0701	2,950	1,445	76.0	.434	340	71	515	29.50
4	6.01	39	25.00	.0666	4,650	1,475	77.0	.430	344	82	523	29.50
5	8.06	38	23.80	.0635	6,200	1,495	79.0	.436	340	87	528	29.40
6	9.81	31	22.60	.0611	7,500	1,495	80.0	.441	328	95	528	29.40
7	11.35	26	21.35	.0584	8,900	1,525	82.0	.444	330	101	534	29.40
8	13.26	21	20.25	.0558	10,400	1,535	83.0	.446	321	109	537	29.40
9	14.91	16	19.20	.0536	11,700	1,535	82.0	.440	312	112	537	28.40
10	17.09	18	18.35	.0511	13,150	1,535	83.0	.446	295	112	539	27.30
11	18.97	15	17.60	.0492	14,300	1,545	85.0	.454	286	112	537	26.40
12	20.72	11	16.85	.0475	15,400	1,535	86.5	.465	269	109	531	25.50
13	22.26	7	16.40	.0466	16,000	1,535	86.0	.462	264	103	528	24.90
14	23.76	4	15.95	.0457	16,600	1,535	85.5	.460	258	98	526	24.20
15	25.86	3	15.50	.0444	17,450	1,535	85.0	.457	252	95	523	23.70
16	27.36	1	15.25	.0439	17,800	1,525	86.0	.465	245	95	520	23.40
17	24.13	0	14.95	.0432	18,300	1,525	86.5	.468	240	95	517	23.10
18	29.97	-3	14.70	.0428	18,500	1,525	88.5	.479	235	95	515	22.80
19	32.05	-4	14.45	.0421	19,000	1,525	89.0	.481	232	92	515	22.50
20	33.12	-7	14.30	.0420	19,150	1,505	86.5	.474	222	92	515	22.20
21	35.16	-8	14.20	.0417	19,350	1,495	82.5	.455	220	90	512	21.90
22	37.18	-8	14.00	.0411	19,750	1,495	81.5	.450	218	90	512	21.70
23	38.18	-10	13.80	.0408	19,950	1,495	82.0	.452	216	87	509	21.40

TABLE IX.—SUPERCHARGED CLIMB USING THE 1.957 : 1 DRIVE RATIO

Reading No.	Corrected time, minutes	Observed atmospheric temperature, ° F.	Observed atmospheric pressure, in. Hg.	Atmospheric density, lb. per cu. ft.	Standard altitude, feet	Observed engine speed, R. P. M.	Air speed, M. P. H.	$\frac{V}{nD}$	Brake horsepower	Temperature at supercharger outlet, ° F.	Temperature at carburetor inlet, ° F. (abs.)	Pressure at carburetor inlet, in. Hg.
1	1.02	54	29.05	0.0750	700	1,415	79.0	0.460	334	68	526	29.50
2	2.62	50	27.80	.0725	1,800	1,435	81.0	.465	336	71	523	29.50
3	4.31	45	26.70	.0702	2,900	1,465	82.5	.465	346	74	523	29.60
4	6.07	40	25.30	.0672	4,400	1,495	84.0	.463	353	82	528	29.70
5	7.70	34	23.95	.0644	5,800	1,525	86.0	.465	357	92	534	29.80
6	9.40	30	22.80	.0618	7,100	1,555	87.0	.461	366	98	537	29.70
7	11.14	25	21.55	.0590	8,600	1,565	89.0	.469	352	106	542	29.60
8	13.08	22	20.35	.0560	10,300	1,575	91.0	.476	340	114	545	28.75
9	14.78	18	19.35	.0537	11,600	1,565	92.0	.484	317	111	542	27.30
10	16.51	15	18.55	.0519	12,700	1,555	94.0	.498	296	109	537	26.25
11	18.22	12	17.80	.0501	13,750	1,555	94.0	.498	287	106	534	25.40
12	19.86	9	17.15	.0486	14,700	1,555	94.0	.498	278	106	531	24.35
13	21.52	7	16.60	.0473	15,500	1,535	94.0	.505	254	103	528	23.80
14	23.43	5	16.25	.0464	16,100	1,525	95.0	.514	242	98	526	23.30
15	25.19	4	16.00	.0458	16,500	1,515	96.0	.523	232	98	523	23.00
16	26.89	3	15.75	.0452	16,900	1,515	96.5	.525	231	95	523	22.80
17	28.60	1	15.50	.0446	17,300	1,515	97.0	.528	226	95	520	22.50
18	30.18	0	15.30	.0442	17,600	1,505	96.0	.526	221	93	518	22.15
19	32.28	0	15.10	.0436	18,000	1,505	97.0	.531	215	93	518	21.95
20	34.34	0	14.95	.0432	18,300	1,525	98.5	.532	223	93	518	21.80
21	36.09	-1	14.60	.0423	18,900	1,535	98.0	.526	224	95	520	21.65
22	37.43	-4	14.30	.0417	19,300	1,545	99.0	.529	224	95	518	21.20
23	38.91	-7	14.00	.0411	19,750	1,545	94.0	.502	226	93	515	20.80
24	40.99	-8	13.65	.0401	20,500	1,535	94.0	.504	216	93	512	20.45
25	42.13	-11	13.40	.0397	20,800	1,535	96.0	.516	213	93	512	20.10
26	43.07	-13	13.20	.0393	21,050	1,535	98.0	.526	208	90	512	19.80
27	45.25	-14	13.05	.0389	21,400	1,535	101.0	.543	199	87	512	19.50

TABLE X.—OPTIMUM SUPERCHARGED CLIMB USING THE 2.4:1 DRIVE RATIO

Reading No.	Corrected time, minutes	Observed atmospheric temperature, °F.	Observed atmospheric pressure, in. Hg.	Atmospheric density, lb. per cu. ft.	Standard altitude, feet	Observed engine speed, R. P. M.	Airspeed, M. P. H.	$\frac{V}{nD}$	Brake horsepower	Temperature at supercharger outlet, °F.	Temperature at carburetor inlet, °F. (abs.)	Pressure at carburetor inlet, in. Hg.	Brake horsepower corrected to standard pressure and temperature
1	3.40	82	28.95	0.0708	2,600	1,405	74.5	0.437	316	101	558	29.50	332
2	4.83	77	27.60	.0683	3,800	1,425	74.5	.431	315	101	555	29.50	329
3	6.30	71	26.35	.0659	5,000	1,435	74.0	.425	314	103	555	29.50	326
4	7.60	64	25.20	.0639	6,000	1,455	75.0	.425	317	105	555	29.40	330
5	9.12	60	24.20	.0619	7,050	1,465	75.5	.425	314	109	557	29.40	326
6	10.79	56	23.20	.0597	8,250	1,475	77.0	.430	309	114	558	29.40	320
7	12.27	52	22.20	.0576	9,350	1,495	78.0	.430	312	120	561	29.50	322
8	13.89	48	21.20	.0554	10,600	1,515	79.0	.430	310	126	567	29.50	320
9	15.48	44	20.25	.0533	11,800	1,525	80.0	.433	304	133	569	29.40	315
10	17.00	40	19.30	.0513	13,000	1,545	81.5	.435	303	141	573	29.40	314
11	18.62	36	18.50	.0496	14,100	1,565	82.5	.435	302	146	578	29.50	312
12	20.32	33	17.70	.0477	15,300	1,575	84.0	.440	298	154	583	29.50	307
13	21.90	30	17.00	.0461	16,300	1,585	84.5	.440	294	-----	586	29.50	303
14	23.58	27	16.30	.0445	17,400	1,595	86.0	.445	289	-----	-----	29.50	295
15	25.05	23	15.60	.0430	18,400	1,605	87.5	.450	288	-----	-----	29.50	285
16	26.65	20	15.10	.0418	19,250	1,605	89.0	.457	272	-----	-----	28.60	269
17	28.32	18	14.55	.0405	20,200	1,615	89.5	.457	269	-----	-----	27.45	267
18	30.08	16	14.05	.0392	21,150	1,615	91.0	.465	258	-----	-----	26.45	257
19	31.65	15	13.70	.0384	21,750	1,615	92.0	.470	252	-----	-----	25.80	251
20	33.29	14	13.40	.0376	22,300	1,605	92.5	.475	242	-----	-----	25.20	242
21	35.05	12	13.10	.0369	22,900	1,605	93.0	.478	236	-----	-----	24.70	235
22	36.77	11	12.85	.0362	23,400	1,595	93.5	.483	227	-----	-----	24.25	226
23	38.47	10	12.60	.0356	23,900	1,595	94.5	.489	222	-----	-----	23.85	221
24	39.51	7	12.40	.0353	24,150	1,595	95.0	.491	219	-----	-----	23.60	217
25	41.16	7	12.20	.0348	24,550	1,595	95.5	.494	214	-----	-----	23.40	212
26	43.06	5	12.05	.0344	24,900	1,595	95.0	.491	213	-----	-----	23.20	210
27	44.28	4	11.95	.0342	25,050	1,595	95.0	.491	213	-----	-----	23.00	210
28	45.50	3	11.85	.0340	25,200	1,595	95.5	.494	210	-----	-----	22.80	208
29	47.10	1	11.70	.0337	25,500	1,595	96.0	.496	206	-----	-----	22.55	203
30	49.46	1	11.65	.0335	25,650	1,585	96.0	.494	207	-----	-----	22.40	204
31	50.64	0	11.60	.0334	25,725	1,585	96.0	.494	207	-----	-----	22.25	205

TABLE XI.—SUPERCHARGED CLIMB USING THE 2.4:1 DRIVE RATIO

Reading No.	Corrected time, minutes	Observed atmospheric temperature, °F.	Observed atmospheric pressure, in. Hg.	Atmospheric density, lb. per cu. ft.	Standard altitude, feet	Observed engine speed, R. P. M.	Air speed, M. P. H.	$\frac{V}{nD}$	Brake horsepower	Temperature at supercharger outlet, °F.	Temperature at carburetor inlet, °F. (abs.)	Pressure at carburetor inlet, in. Hg.
1	0.95	47	28.65	0.0749	700	1,390	77.0	0.457	317	64	517	29.40
2	2.43	41	27.45	.0728	1,700	1,420	78.5	.456	329	67	517	29.50
3	4.42	39	26.20	.0697	3,150	1,450	80.0	.455	335	70	519	29.70
4	6.26	36	24.95	.0668	4,550	1,480	81.0	.451	343	75	524	29.50
5	8.37	36	23.80	.0638	6,100	1,500	83.0	.456	340	85	527	29.50
6	10.37	35	22.75	.0610	7,500	1,510	84.5	.462	328	95	535	29.50
7	12.31	34	21.65	.0582	9,000	1,530	86.4	.464	326	106	544	29.50
8	14.14	30	20.60	.0558	10,400	1,550	88.0	.469	324	115	552	29.60
9	15.85	26	19.60	.0535	11,700	1,560	90.0	.476	314	120	554	29.60
10	17.51	23	18.65	.0514	12,950	1,580	91.5	.478	312	130	560	29.60
11	19.44	21	17.80	.0492	14,300	1,600	92.5	.477	313	141	566	29.50
12	20.88	15	17.15	.0480	15,100	1,600	93.0	.480	303	147	571	29.60
13	22.62	12	16.50	.0464	16,100	1,600	94.0	.485	292	152	574	29.50
14	24.09	8	15.90	.0452	16,900	1,610	95.0	.487	290	160	579	29.10
15	25.85	5	15.35	.0438	17,800	1,620	97.0	.494	284	160	579	28.35
16	27.24	1	14.90	.0430	18,400	1,630	98.0	.496	283	160	576	27.55
17	28.67	-2	14.65	.0425	18,750	1,620	97.5	.497	270	155	571	27.05
18	30.54	-3	14.30	.0416	19,400	1,610	97.0	.497	264	152	568	26.50
19	32.12	-5	14.05	.0410	19,800	1,600	96.0	.495	255	149	566	26.05
20	33.88	-6	13.80	.0404	20,250	1,590	96.5	.500	246	149	563	25.70
21	35.64	-8	13.50	.0397	20,800	1,590	98.0	.509	238	147	563	25.20
22	36.90	-10	13.35	.0394	21,000	1,590	99.0	.514	234	144	563	25.00
23	38.32	-11	13.25	.0392	21,150	1,590	100.5	.522	231	144	560	24.80
24	39.95	-12	13.05	.0387	21,500	1,590	100.5	.522	228	144	560	24.45

TABLE XII.—SUPERCHARGED CLIMB USING THE 2.4:1 DRIVE RATIO

Reading No.	Corrected time, minutes	Observed atmospheric temperature, °F.	Observed atmospheric pressure, in. Hg.	Atmospheric density, lb. per cu. ft.	Standard altitude, feet	Observed engine speed, R. P. M.	Air speed, M. P. H.	$\frac{V}{nD}$	Brake horsepower	Temperature at supercharger outlet, °F.	Temperature at carburetor inlet, °F. (abs.)	Pressure at carburetor inlet, in. Hg.
1	1.88	64	29.10	0.0737	1,300	1,420	78.5	0.456	334	75	533	29.40
2	3.47	59	27.85	.0713	2,400	1,430	79.0	.456	329	80	533	29.50
3	5.67	59	26.55	.0679	4,050	1,450	80.0	.455	327	85	536	29.60
4	7.70	59	25.45	.0651	5,400	1,480	81.0	.452	333	96	541	29.60
5	9.22	52	24.35	.0631	6,450	1,490	82.5	.457	328	101	544	29.60
6	10.97	48	23.25	.0607	7,700	1,500	83.5	.460	321	104	546	29.60
7	12.65	43	22.10	.0583	9,000	1,520	84.0	.456	323	107	549	29.40
8	14.45	39	21.00	.0558	10,400	1,530	86.0	.464	313	114	552	29.40
9	16.06	34	19.90	.0535	11,700	1,540	87.0	.466	306	122	557	29.50
10	18.23	36	18.80	.0504	13,550	1,550	88.5	.471	294	136	566	29.50
11	20.43	37	17.85	.0477	15,250	1,570	89.5	.470	290	149	576	29.60
12	22.29	35	17.00	.0457	16,600	1,580	89.5	.468	281	157	584	29.60
13	24.03	32	16.30	.0440	17,700	1,590	89.0	.462	278	169	590	29.50
14	25.87	30	15.60	.0423	18,900	1,590	91.0	.472	265	169	587	28.70
15	27.09	22	15.00	.0413	19,600	1,590	91.5	.475	255	163	582	27.75
16	28.22	17	14.55	.0406	20,100	1,580	91.0	.475	249	163	577	26.90
17	29.82	14	14.30	.0401	20,500	1,580	91.0	.475	246	155	571	26.05
18	32.04	15	13.90	.0389	21,400	1,570	92.0	.484	232	152	568	25.50
19	34.22	17	13.55	.0378	22,200	1,570	93.0	.490	220	152	568	25.00
20	36.07	17	13.30	.0371	22,700	1,560	92.0	.487	216	152	568	24.30
21	38.19	17	13.00	.0362	23,400	1,550	92.0	.490	206	152	566	23.70

TABLE XIII.—OPTIMUM SUPERCHARGED CLIMB USING THE 3:1 DRIVE RATIO

Reading No.	Corrected time, minutes	Observed atmospheric temperature, °F.	Observed atmospheric pressure, in. Hg.	Atmospheric density, lb. per cu. ft.	Standard altitude, feet	Observed engine speed, R. P. M.	Air speed, M. P. H.	$\frac{V}{nD}$	Brake horsepower	Temperature at supercharger outlet, °F.	Temperature at carburetor inlet, °F. (abs.)	Pressure at carburetor inlet, in. Hg.	Brake horsepower corrected to standard pressure and temperature
1	1.22	45	28.40	0.0748	800	1,400	79.5	0.469	319	67	519	29.50	323
2	3.04	41	27.00	.0716	2,200	1,430	81.0	.467	326	70	519	29.50	329
3	5.23	39	25.80	.0687	3,700	1,440	81.5	.467	320	80	522	29.60	322
4	7.12	36	24.35	.0652	5,350	1,450	83.5	.475	317	88	527	29.60	319
5	9.19	34	23.30	.0626	6,700	1,470	83.5	.469	309	93	530	29.60	310
6	11.11	30	22.10	.0598	8,200	1,500	84.0	.462	314	101	536	29.60	316
7	12.90	26	20.95	.0572	9,600	1,500	85.0	.468	301	109	541	29.50	304
8	14.67	21	19.80	.0547	11,050	1,520	85.5	.464	301	117	544	29.40	304
9	16.50	17	18.70	.0521	12,550	1,530	87.5	.472	290	125	549	29.50	292
10	18.45	14	17.75	.0497	14,000	1,550	88.0	.469	288	133	557	29.50	290
11	20.08	9	17.00	.0482	15,000	1,560	89.0	.471	285	141	560	29.40	287
12	21.90	4	16.15	.0461	16,300	1,570	91.0	.478	276	147	566	29.50	278
13	23.57	0	15.50	.0447	17,250	1,580	92.0	.481	272	155	571	29.70	272
14	25.41	-3	14.75	.0429	18,500	1,600	94.5	.488	268	163	577	29.70	267
15	27.16	-7	14.20	.0416	19,400	1,600	94.5	.488	260	174	585	29.70	260
16	28.54	-11	13.75	.0407	20,000	1,600	94.5	.488	254	183	587	29.70	254
17	30.11	-16	13.30	.0398	20,700	1,610	95.5	.490	253	188	593	29.70	254
18	31.89	-19	12.80	.0386	21,600	1,620	96.5	.491	251	193	601	29.70	252
19	33.33	-23	12.40	.0378	22,200	1,620	96.0	.489	244	199	607	29.70	244
20	35.41	-26	11.95	.0365	23,200	1,620	96.0	.489	236	204	610	29.40	230
21	36.63	-31	11.65	.0360	23,600	1,620	96.0	.489	233	207	612	28.90	228
22	38.17	-33	11.30	.0352	24,200	1,610	97.0	.497	223	207	612	28.20	219
23	40.93	-36	11.05	.0346	24,700	1,610	97.0	.497	219	207	612	27.65	215
24	42.66	-38	10.80	.0340	25,200	1,610	97.0	.497	215	210	612	27.05	213
25	44.92	-39	10.65	.0335	25,600	1,600	98.0	.505	204	210	612	26.60	202
26	45.60	-41	10.50	.0332	25,900	1,600	98.5	.508	203	210	610	26.25	201
27	46.43	-43	10.40	.0331	26,000	1,590	93.5	.485	204	207	607	25.90	204
28	48.63	-43	10.25	.0326	26,400	1,570	93.0	.489	192	204	604	25.60	190

TABLE XIV.—SUPERCHARGED CLIMB USING THE 3:1 DRIVE RATIO

Reading No.	Corrected time, minutes	Observed atmospheric temperature, °F.	Observed atmospheric pressure, in. Hg.	Atmospheric density, lb. per cu. ft.	Standard altitude, feet	Observed engine speed, R. P. M.	Air speed, M. P. H.	V nD	Brake horsepower	Temperature at supercharger outlet, °F.	Temperature at carburetor inlet, °F. (abs.)	Pressure at carburetor inlet, in. Hg.
1	2.21	52	28.10	0.0729	1,650	1,420	75.0	0.436	329	75	527	29.70
2	4.12	49	26.70	.0697	3,150	1,440	76.0	.436	330	85	533	29.70
3	5.84	44	25.40	.0670	4,450	1,460	76.0	.429	334	96	538	29.70
4	7.80	40	24.10	.0640	6,000	1,480	77.5	.432	332	104	544	29.70
5	9.91	40	22.95	.0610	7,550	1,500	80.5	.443	326	117	549	29.70
6	11.56	34	21.95	.0589	8,650	1,510	82.0	.488	321	125	555	29.80
7	13.16	30	21.00	.0570	8,700	1,510	81.5	.446	308	133	560	29.80
8	14.95	25	20.10	.0550	10,850	1,520	80.0	.434	305	141	566	29.90
9	16.89	23	19.30	.0530	12,000	1,530	80.0	.431	304	149	574	29.90
10	18.49	19	18.35	.0512	13,100	1,540	80.5	.431	300	160	579	30.00
11	20.55	17	17.55	.0489	14,500	1,540	82.0	.439	286	169	587	30.15
12	22.09	13	17.00	.0478	15,200	1,540	83.5	.447	278	180	596	30.15
13	23.91	8	16.35	.0463	16,200	1,540	83.5	.447	269	188	601	30.30
14	25.37	5	15.80	.0452	16,900	1,550	84.5	.450	268	191	610	30.30
15	27.60	4	15.40	.0440	17,700	1,560	85.0	.449	264	201	612	30.30
16	28.90	0	14.90	.0431	18,300	1,560	85.5	.452	259	207	618	30.30
17	30.73	-3	14.55	.0423	18,900	1,560	85.5	.452	253	212	621	30.30

TABLE XV.—SUPERCHARGED CLIMB USING THE 3:1 DRIVE RATIO

Reading No.	Corrected time, minutes	Observed atmospheric temperature, °F.	Observed atmospheric pressure, in. Hg.	Atmospheric density, lb. per cu. ft.	Standard altitude, feet	Observed engine speed, R. P. M.	Air speed, M. P. H.	V nD	Brake horsepower	Temperature at supercharger outlet, °F.	Temperature at carburetor inlet, °F. (abs.)	Pressure at carburetor inlet, in. Hg.
1	0.74	48	28.90	0.0756	400	1,410	78.0	0.456	333	62	511	29.60
2	2.76	45	27.50	.0724	1,900	1,440	79.0	.453	342	70	522	29.50
3	4.59	41	26.20	.0695	3,250	1,460	81.5	.460	340	78	524	29.50
4	6.33	36	24.80	.0665	4,700	1,480	82.0	.457	339	83	527	29.50
5	8.21	31	23.75	.0642	5,900	1,490	83.0	.460	332	88	530	29.40
6	9.90	26	22.55	.0616	7,200	1,510	84.0	.459	334	93	533	29.50
7	11.58	20	21.30	.0590	8,600	1,520	85.0	.461	326	101	533	29.50
8	13.38	14	20.15	.0564	10,050	1,530	86.5	.467	314	109	536	29.50
9	15.21	10	19.25	.0543	11,250	1,560	87.5	.463	322	114	541	29.50
10	17.18	10	18.30	.0519	12,700	1,570	90.0	.473	311	125	546	29.50
11	19.29	9	17.30	.0491	14,400	1,580	93.5	.488	296	139	560	29.50
12	21.07	5	16.50	.0472	15,600	1,600	95.0	.490	295	144	566	29.50
13	22.76	0	15.75	.0455	16,700	1,610	95.5	.490	290	155	571	29.60
14	24.58	-4	15.20	.0442	17,600	1,620	96.0	.489	287	166	576	29.60
15	26.07	-8	14.55	.0428	18,500	1,630	97.0	.491	283	174	582	29.70
16	27.93	-12	14.10	.0418	19,300	1,630	97.0	.491	277	182	587	29.70
17	29.29	-16	13.65	.0409	19,900	1,640	97.0	.488	276	188	593	29.70
18	31.28	-18	13.25	.0398	20,700	1,640	98.5	.495	276	196	598	29.70
19	32.78	-21	12.80	.0388	21,400	1,640	99.5	.500	258	201	607	29.70
20	34.44	-24	12.40	.0379	22,100	1,640	99.5	.500	252	209	612	29.50
21	36.03	-29	12.05	.0371	22,700	1,640	101.0	.504	248	209	612	28.80
22	37.76	-32	11.70	.0363	23,350	1,630	101.0	.511	234	201	604	27.40
23	39.90	-32	11.45	.0355	24,000	1,630	101.5	.512	229	196	598	27.00
24	41.51	-33	11.25	.0350	24,400	1,625	102.0	.514	224	193	596	26.50
25	42.77	-36	11.00	.0345	24,800	1,625	103.5	.523	218	193	593	26.10
26	44.85	-36	10.85	.0340	25,200	1,620	106.0	.540	207	193	593	25.90
27	46.77	-37	10.75	.0337	25,450	1,610	106.5	.546	199	193	590	25.60
28	48.30	-37	10.70	.0336	25,550	1,610	105.0	.538	200	190	587	25.40
29	50.56	-37	10.55	.0331	26,000	1,610	106.5	.546	195	190	587	25.20
30	52.80	-37	10.50	.0329	26,150	1,610	106.0	.543	195	190	587	25.00

REPORT No. 328

WATER PRESSURE DISTRIBUTION ON A TWIN-FLOAT SEAPLANE

By F. L. THOMPSON

Langley Memorial Aeronautical Laboratory

REPORT No. 328

WATER PRESSURE DISTRIBUTION ON A TWIN-FLOAT SEAPLANE

BY F. L. THOMPSON

SUMMARY

The investigation reported herein was conducted by the National Advisory Committee for Aeronautics at the request of the Bureau of Aeronautics, Navy Department. This is the second of a series of investigations to determine water pressure distribution on various types of seaplane floats and hulls, and was conducted on a twin-float seaplane. It consisted of measuring water pressures and accelerations on a TS-1 seaplane during numerous landing and taxiing maneuvers at various speeds and angles.

The results of this investigation show that water pressures as great as 10 lbs. per sq. in. may occur at the step in various maneuvers and that pressures of approximately the same magnitude occur at the stern and near the bow in hard pancake landings with the stern well down. At other parts of the float the pressures are less and are usually zero or slightly negative for some distance abaft the step. A maximum negative pressure of 0.87 lb. per sq. in. was measured immediately abaft the step. The maximum positive pressures have a duration of approximately one-twentieth to one-hundredth second at any given location and are distributed over a very limited area at any particular instant. The greatest accelerations measured normal to the thrust line at the c. g. occurred in pancake landings, and a maximum of 4.3 g. was recorded. Approximate load distribution curves for the worst landing conditions are derived from the data obtained to serve as a guide in static tests.

INTRODUCTION

There is but little known concerning the magnitude and distribution of water pressures on seaplanes when landing or taxiing on either smooth or rough water. Consequently, the size and arrangement of structural members that make up a seaplane float are based on experience with previous successful designs rather than on definite information as to the forces to be encountered. Floats that are undamaged in operation are sufficiently strong, but knowledge of the actual water pressures encountered is needed before structural weight can be safely reduced to a minimum.

At the request of the Bureau of Aeronautics, Navy Department, a series of investigations to determine water pressures on various types of seaplane floats are being made. The investigation reported herein is the second in this series and was conducted on a twin-float seaplane. The first investigation was conducted on the UO-1 single-float seaplane and has been previously reported. The third investigation is to be conducted on a boat-type seaplane.

A TS-1 twin-float seaplane was used, and positive water pressures were measured at 15 stations on the outboard half of one float bottom. Subsequent to the positive pressure measurements, negative pressures were determined at five points abaft the step and one forward. The apparatus used for measuring positive pressures was the same as that used in the previous investigation (reference 1), with some minor changes. Additional instruments were used to record accelerations normal to the thrust line at the c. g. of the seaplane and to measure, approximately, accelerations of the float bottom.

The tests included numerous taxiing and landing runs at various speeds and attitudes except that negative pressure measurements were confined to take-off runs. Simultaneous records of the water pressures at all stations, the air speed, float angle, and acceleration were

obtained. The average wind velocity was also determined with an anemometer while testing was in progress so that the water speed could be computed.

This report includes a brief description of the instruments and apparatus used in the tests, a description of the test procedure, the results obtained and conclusions reached. The complete data are presented in tables and are summarized by a table and curve showing the distribution of maximum pressures over the float bottom. In addition, there are curves showing the manner in which water pressures act on the float bottom and approximate load distributions for hard pancake landings.

APPARATUS AND METHOD

APPARATUS

These tests were conducted on a TS-1 twin-float seaplane. (Fig. 1.) It is a single-place biplane that may be equipped with either floats or wheels. As a seaplane it has a specified gross



FIGURE 1.—TS-1 seaplane on which the tests were conducted

weight of 2,123 pounds. The weight of the research equipment used in the tests was such that it was necessary to reduce the fuel load one-half to keep the gross weight as specified. It was found that the landing speed was from 60 to 65 M. P. H. for a normal landing.

The floats are of wooden construction and are shaped as shown in Figure 2. The step is 2 inches high at the keel; the angle of the after keel is $5\frac{1}{2}^\circ$; and a line from the bottom of the step to the stern makes an angle of 7° with respect to the deck line. The deck line is parallel to the

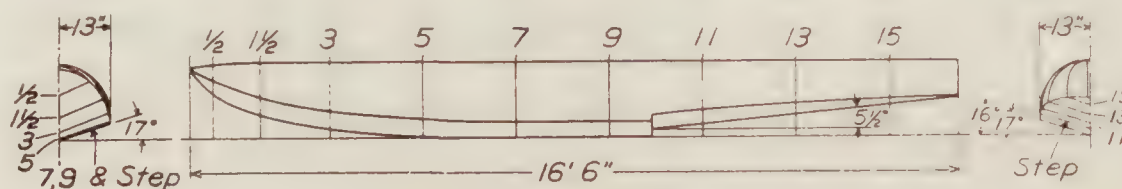


FIGURE 2.—TS-1 float lines

thrust axis and wing chords. The angle of V is 17° at the bottom of the step and increases slightly toward the bow giving a fairly flat entry. Aft the step the angle of V is 16° . Negative pressures were measured on a float of slightly modified shape. The principal differences are in the step which is three inches high, and the after keel angle, which is 4° .

The research equipment included the following instruments and apparatus:

1. A single-component recording accelerometer.
2. A float angle observer.
3. Two recording manometers.
4. A swiveling Pitot-static air-speed head.
5. A motor-type electric timer.
6. A 4-element plunger-type accelerometer.
7. Water-pressure apparatus, positive and negative.

1. A description of the N. A. C. A. single-component recording accelerometer is given in reference 2. This instrument records optically the deflection of a weighted cantilever spring. The component of acceleration normal to the thrust line was measured with this instrument during each run of the positive pressure tests.

2. Longitudinal float angles were recorded by photographing the shore line parallel to the path of the seaplane with a small, motor-driven motion-picture camera rigidly mounted in the fuselage. Five images per second were obtained.

3. Two recording manometers with two pressure cells each were used. An instrument of this sort with one pressure cell is described in reference 3 as the recording element of an N. A. C. A. recording air-speed meter. It records optically the deflections of a diaphragm actuated by the pressure to be measured. One of the four pressure cells thus provided was used to record air speed in these tests. The other three were used to record pneumatic pressures used with the water pressure apparatus.

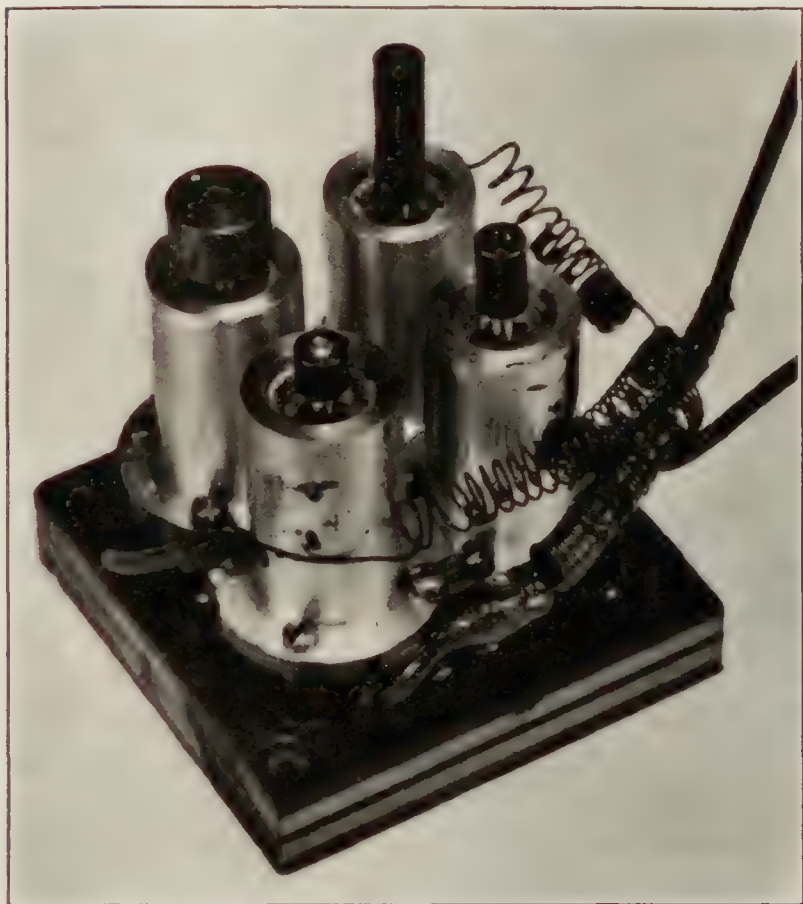


FIGURE 3.—Plunger-type accelerometer

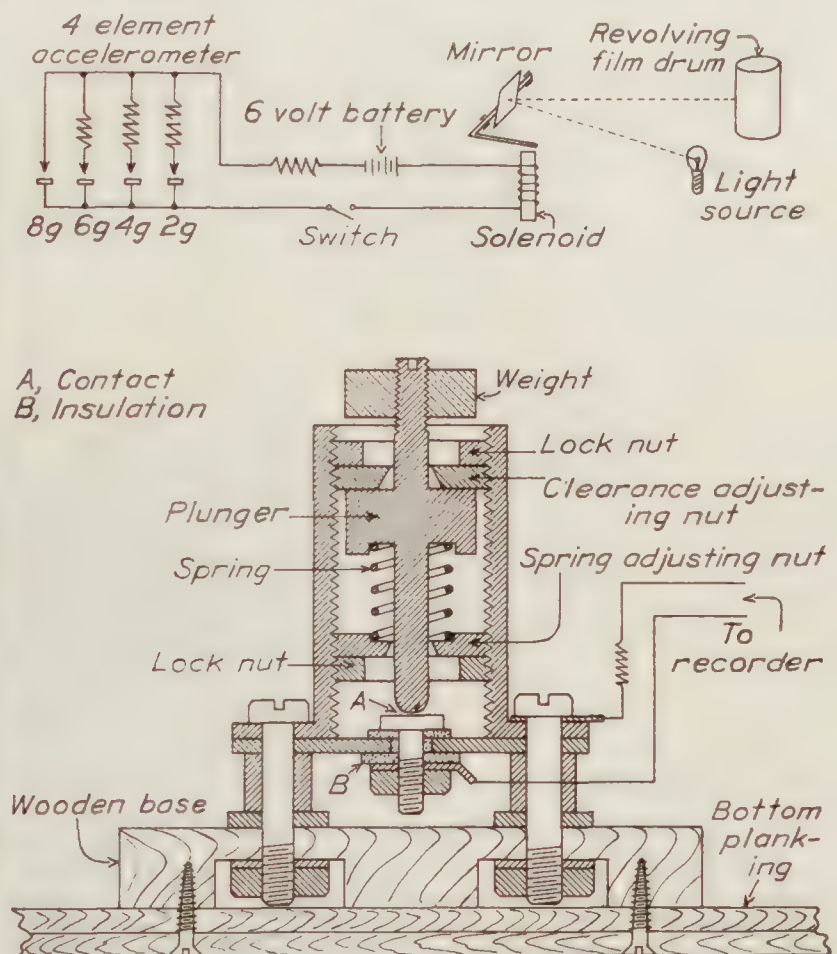


FIGURE 4.—Cross section of one element of accelerometer and diagram of recording circuit

4. The swiveling Pitot-static air-speed head was located on a forward wing strut and was connected to the air-speed recording pressure cell mentioned above.

5. Records were synchronized by timing lines at 1-second intervals with an N. A. C. A. motor-type electric timer. An N. A. C. A. chronometric timer and the method of using it are described in reference 4. The difference in these two instruments is only in the means employed to obtain periodic electrical contacts.

6. A plunger-type accelerometer with four elements was used to measure, approximately, the acceleration of the float bottom planking. This was primarily for the purpose of determining the proper correction to apply to recorded water pressures for the effect of acceleration of the water-pressure units. A photograph of this instrument is shown in Figure 3. It is similar in principle to the accelerometer designed by Doctor Zahm. (Reference 5.) A cross section drawing of one element and a diagram of the recording circuit and mechanism are given in Figure 4. The four elements are similar but respond to different accelerations. The variation in sensitivity is obtained by varying the plunger weight and spring pressure. The elements

were calibrated centrifugally, on a whirling table, and were adjusted to respond to accelerations of $2g$, $4g$, $6g$, and $8g$, respectively. The record obtained is a line broken in steps which indicate the number of plungers making contact. To insure proper accuracy in recording short-period accelerations, the contact clearance was set at 0.003 inch. The instruments was made as small and light as practicable and weighed but 0.6 pound when ready for installation. It was mounted on the right side of the bottom of the left float about 15 inches forward of the step and in the center of an unsupported bottom planking area.

7. A detailed description of a water-pressure unit and the complete apparatus used in recording water pressures is given in reference 1. The water-pressure units operate on a principle of opposing the force due to water pressure on one end of a piston by a force due to a known pneumatic pressure on the other end. When the water force exceeds the pneumatic force the piston makes an electric contact which is indicated in an optical record by deflection of the record line. Four such pistons in each unit respond to different water pressures and cause different deflections. The range of pressures recordable depends on the pneumatic pressure which can be varied as desired. Fifteen of these pressure units were installed in the left side and seven in the right side of the bottom of the left float, as shown in Figure 5. As the water-pressure recorder accommodates but 15 pressure units, all those on the left side were first connected. The remaining seven units were to be connected later to determine if an appreciable difference in pressure existed between the two sides of the float bottom. This was not done, however, since the floats were in very bad condition at the completion of the tests with the first 15 units.

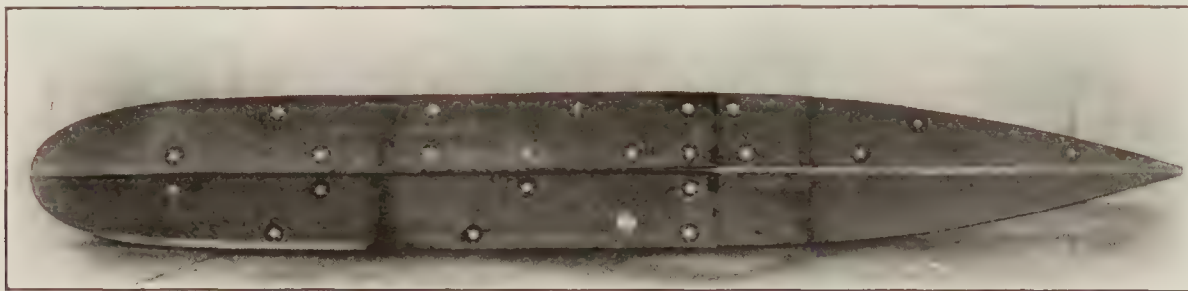


FIGURE 5.—TS-1 float bottom with pressure units installed

The only essential difference between the installation used in these tests and that used formerly, as described in reference 1, is in the connection of all pressure unit recording circuits in parallel to a 6-volt storage battery instead of using independent circuits with a 1.5-volt dry cell for each one. The electrical circuit for each pressure unit is similar to that of the plunger-type accelerometer shown in Figure 4. When this accelerometer was used it was connected to the water pressure recorder in place of one of the water-pressure units.

Negative water pressures were recorded with two 2-pressure-cell recording manometers as described above. They were connected to one-eighth inch diameter orifices in the float bottom by metal tubing. Five orifices were located abaft the step and one immediately forward, all on the same side of the float bottom. Each manometer accommodated two orifices, so that only four orifices at a time could be connected.

The general arrangement of the instrument installation is shown in Figures 6, 7, and 8. The water-pressure recorder is conspicuous in Figure 6. Two storage batteries are carried in the forward compartment over the group of recording instruments which are shown more clearly in Figure 7. Figure 8 shows the pilot's cockpit. The gauges, dial, and hand pump are parts of the apparatus used in adjusting the pneumatic pressure applied to the water-pressure units. One switch on the instrument board and one by the throttle control were operated when making a run. The latter switch could not be left on more than three seconds, which made it necessary to judge accurately the exact time to operate it when landing.

With instruments and installation as thus described, continuous records, synchronized at 1-second intervals, were obtained during each run. The length of the run, when measuring positive water pressures, was limited to three seconds or less by the nature of the recording

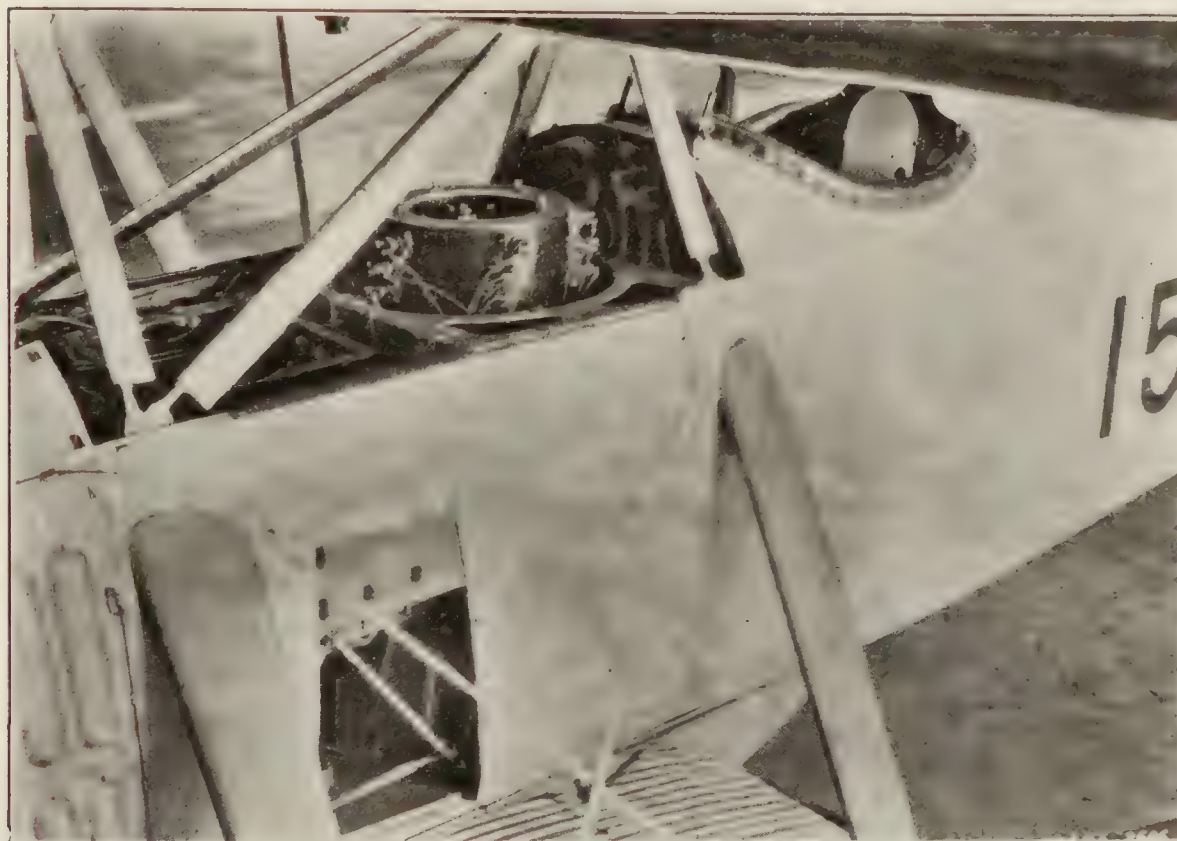


FIGURE 6.—General view of the instrument installation in the TS-1 seaplane



FIGURE 7.—Group of recording instruments in the lower part of the fuselage

arrangement. In the negative pressure tests the length of the records was not limited to so short a period and continuous records of complete take-off runs were obtained. Air speed, longitudinal float angle, acceleration, and water pressures were measured simultaneously during each run, with the exception that during negative pressure tests, acceleration records were not obtained. Positive water pressures were measured at all 15 stations simultaneously, and negative pressures were recorded at six orifices in all, with only four connected at any one time.

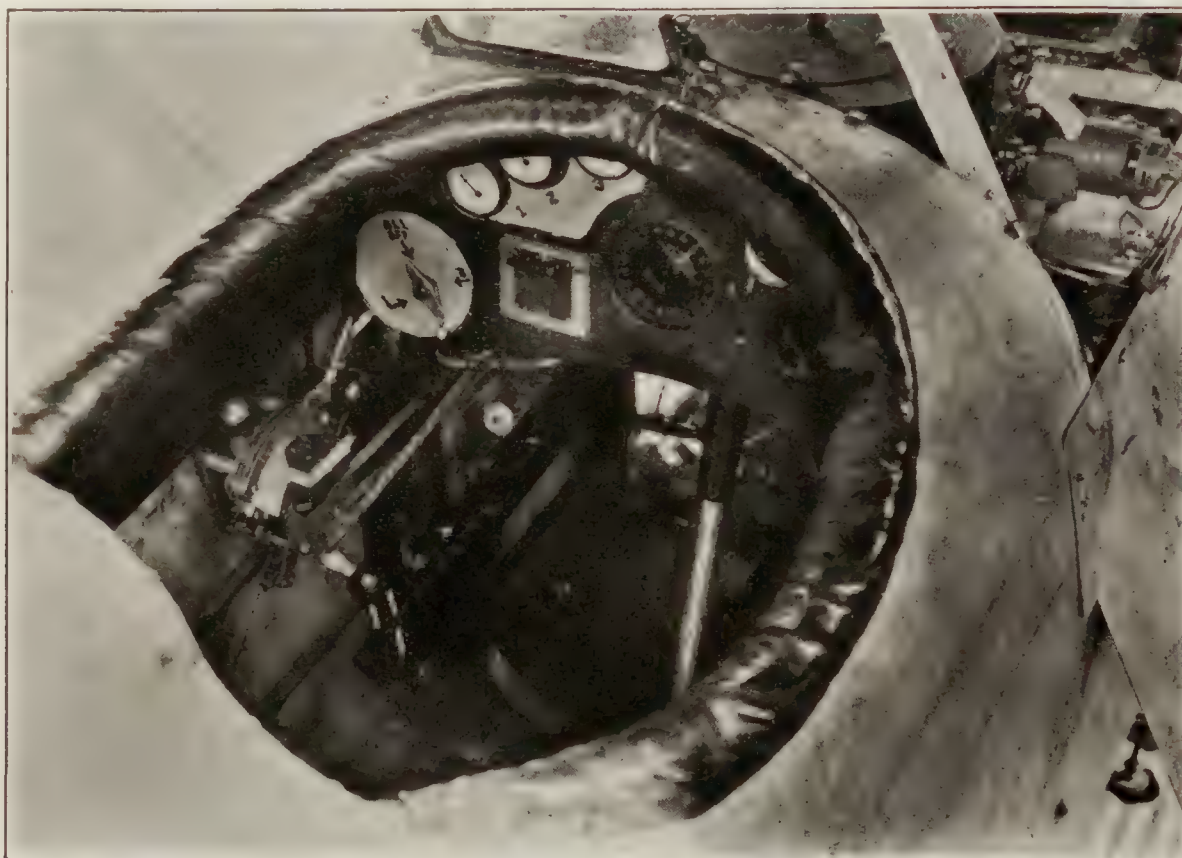


FIGURE 8.—Interior of the cockpit

METHOD

The maneuvers included taxiing at various attitudes and speeds up to get-away, stalled landings with power off and power on, fast landings, pancake landings, and porpoising. Negative pressures were measured during take-offs with the control back, neutral, and forward, respectively. Each negative pressure run was continuous from opening of the throttle to get-away. The actual get-away when taking off with the control neutral or forward was accomplished by pulling the control back. The pancake landings were made by stalling at a very high angle several feet above the water. The seaplane showed a pronounced tendency to porpoise, particularly when decelerating after landing, and water pressures were therefore measured during this maneuver.

The wind velocity was determined with an anemometer while making tests so that the approximate water speed could be obtained from the air-speed record. The tests were all made in sheltered water where the maximum waves encountered were not more than 15 inches high. The pancake and fast landings developed pressures which damaged the float bottom so maneuvers in rough water were not attempted. The pancake landings caused high local pressures to occur over nearly the entire length of the float and also large total loads with the maximum resultant force applied well forward of the *c. g.* This is probably similar to the effect of encountering large waves, although the direction or magnitude of the resultant force caused by waves might be such as to cause greater stresses in the structure, particularly if the waves were not met head-on.

Both floats were cracked at the step during the tests. The right one was in poor condition at the start and was damaged in a fast landing. The left float cracked in a pancake landing. A landing made while making negative pressure trials was unintentionally hard and ruined both floats, making it necessary to replace them both for the negative pressure tests.

PRECISION OF RESULTS

The accuracy with which water pressures are recorded is discussed thoroughly in reference 1. The two chief sources of error, as shown therein, lie in the effect of acceleration on the movable pistons of the pressure units, and in the method of bracketing the true pressure between limits of a pressure exceeded and one not exceeded. The error caused by acceleration may be corrected if the acceleration is known. The error due to bracketing is dependent on the closeness of the pressure limits which varies for different pressure units. The true pressure should be considered as the mean of the limits. For a representative case, the difference between the mean and the limits was found to be about 9 per cent of the mean, but the accuracy of the mean for any particular case must be found from the actual limiting pressures determined. A maximum correction for acceleration should be based on an acceleration of approximately 4 *g*, as determined with an accelerometer in the float bottom. The computed maximum correction to be added to the recorded pressure limits is then approximately one-fourth pound per square inch.

The maximum pressures corrected as above are probably correct within less than ± 10 per cent.

The air-speed measurement is estimated to be accurate within ± 1 M. P. H.

The accuracy of the water-speed measurement depends on the accuracy of the air speed and the accuracy with which the average wind velocity represents the actual wind velocity when a run is made. The accuracy is estimated to be within ± 4 M. P. H.

The float-angle values are correct within $\pm \frac{1}{2}^\circ$.

The accuracy of the negative pressure measurements is within ± 2 per cent.

The accelerations at the *c. g.* are considered to be accurate within ± 0.1 *g*.

The acceleration of the float bottom can only be approximated since it was determined by limiting accelerations between values 2 *g* apart. The limits themselves have negligible errors.

RESULTS

POSITIVE PRESSURES

The maximum pressures recorded during each run are given in Table I, accompanied by a description of the maneuver, the air speed, longitudinal float angle, maximum acceleration, condition of the water surface, and the approximate water speed. The locations of the pressure stations are shown in a figure accompanying the table. For some stations the highest pressure exceeded is not accompanied by an upper limit of pressure not exceeded. Where both limits are given the true maximum pressure is considered to be the mean of the limits plus a correction of one-fourth pound per square inch for acceleration of the pressure unit, as mentioned in the discussion of precision. Where only the lower limit is given the true maximum is considered to exceed this limit by three-fourths pound per square inch, which includes the correction for acceleration and an assumed value of one-half pound per square inch based on a study of the complete data and the limits that were established at other stations. The five highest true pressures at each station are given in Table II with each pressure corrected as above, although it is probable that the correction for acceleration is slightly excessive in some cases, which would make the tabulated pressures a little greater than the actual pressures experienced for such cases. The maximum pressure for each station as given by this table was used in plotting the curve of Figure 9, which shows the distribution of maximum pressures over the float bottom.

The highest pressures occurred in pancake landings, very fast landings, and in fast taxiing runs. The highest vertical accelerations, 4.3 *g* and 3.8 *g*, occurred in pancake landings. Accelerations in excess of 3 *g* also occurred in fast landings, and in one porpoising run in 12 to 15 inch waves. In the latter run the acceleration was 3.4 *g*; the water pressures, however, were not obtained. The worst distribution of pressures occurred in the pancake landings. In these maneuvers the float angle was large and the rate of descent was high. The result was high pressure at the stern followed by high pressure at the step and later at the bow. The reason for

this wide distribution of high pressures was the rotation of the seaplane caused by the force abaft the *c. g.* and subsequently retarded by a force forward of the *c. g.* The shape of the float and the location of the *c. g.* were such that the retarding force was developed suddenly by a high pressure near the bow. During other maneuvers very high pressures were confined to a region extending forward from the step a short distance. The distribution of maximum pressures given by the curve of Figure 9 therefore closely represents the distribution in a severe pancake landing.

The maximum pressures which have been discussed do not occur simultaneously over the entire float bottom, but are confined to a small portion of the bottom at any particular instant, and last only one-twentieth to one one-hundredth second. In a few cases it has been possible to determine accurately the duration and to trace the progress of pressure in excess of a certain value as it travels over the float bottom. The duration and travel of the high pressure can then be shown by curves as described below.

The operation of the first piston of a water-pressure unit indicates that the water pressure has exceeded the minimum pressure which the pressure unit will record with the particular internal pneumatic pressure used. The elapsed time during which this piston remains against

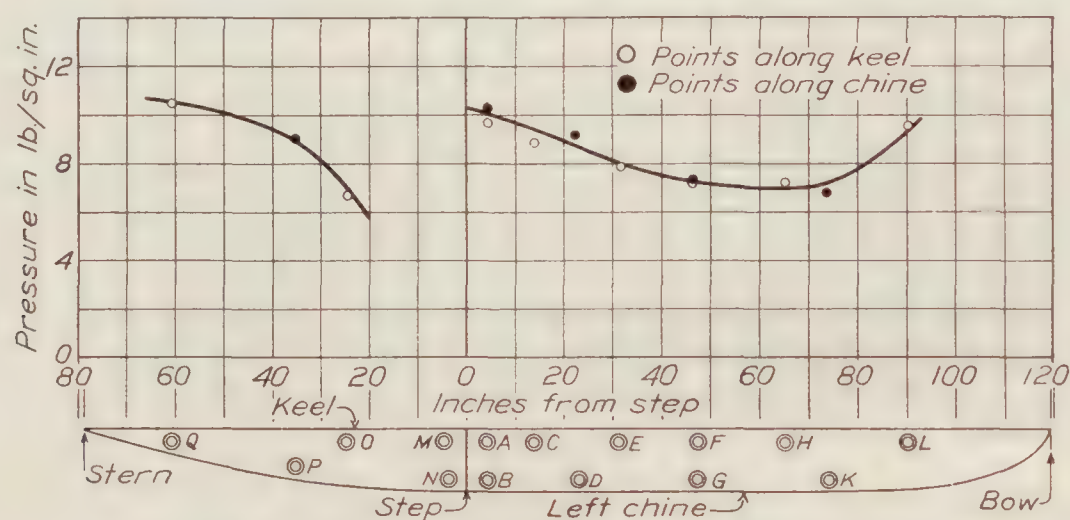


FIGURE 9.—Distribution of maximum water pressures on the float bottom

its contact represents the duration of the water pressure in excess of that minimum. The relative time at which the first piston of each pressure unit operates is determined from the water-pressure record. These values are used as ordinates in plotting a curve with distance of the stations from the step as abscissas. Separate curves are drawn for stations along the keel and along the chine. To these ordinates increments are added which represent the duration of the pressure in excess of the minimum which each unit will record. Two pairs of curves are thus obtained; one represents the travel and duration of pressure in excess of a certain minimum along the keel, and the other does the same for stations along the chine. The difference in time between the start of high pressure at the keel and chine at a given abscissa represents the lag in transverse distribution of pressure due to the V bottom.

The procedure, as described above, was followed for two severe pancake landings, runs 55 and 56. The resulting curves are shown in (A) and (B) of Figures 10 and 11. The lag in transverse distribution of pressure is noticeable in these curves. The minimum pressure recordable was approximately 5 to 6 pounds per square inch for all stations during both of these runs, and the curves therefore represent the travel and duration of pressure exceeding 5 to 6 pounds per square inch. At some stations this minimum pressure was not exceeded and the pressure travel curves, therefore, could not be drawn for the portion of the bottom represented by these stations.

In addition to the high pressure concentrated on a small area at a particular instant, there is also a smaller sustained pressure over a large area to consider. The fluctuations in pressure in a small fraction of a second are usually much greater than the range of pressures that the pressure units will record at one setting of the internal pneumatic pressure. It is therefore

necessary to determine the highest pressures for a maneuver in one run with the internal pressure set for a high pressure range, and the low sustained pressures in a repetition of the maneuver with the internal pressure set for a lower recording range. A study of the records on which low pressures are recorded gives a basis for an assumption as to the sustained pressure to expect over a large area while a concentrated high pressure exists at any given location.

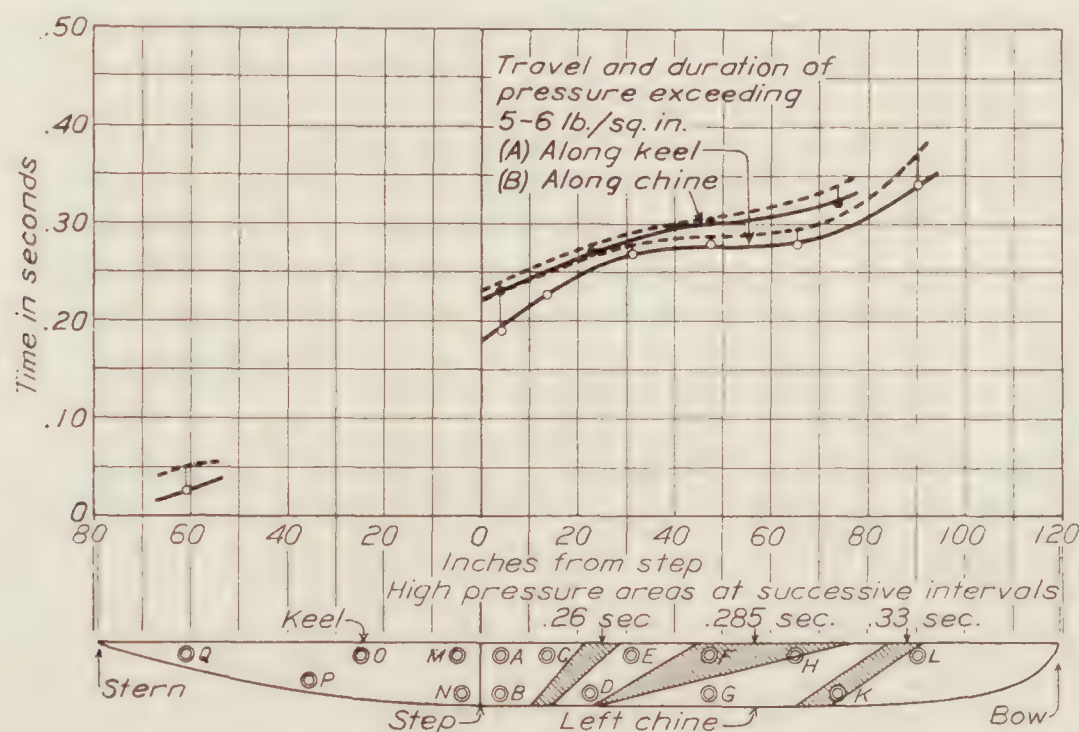


FIGURE 10.—Travel of high local pressure over the float bottom in pancake landing, run 55.
Water speed 48 M. P. H., smooth water

A sustained pressure which continued for at least one-fourth second after the high pressure had passed the stations was recorded at stations C, D, and H during pancake landing run 44. This landing was similar to the pancake landings, runs 55 and 56, for which the pressure travel curves are given, with the exception that it was made on water with 10 to 12 inch waves and

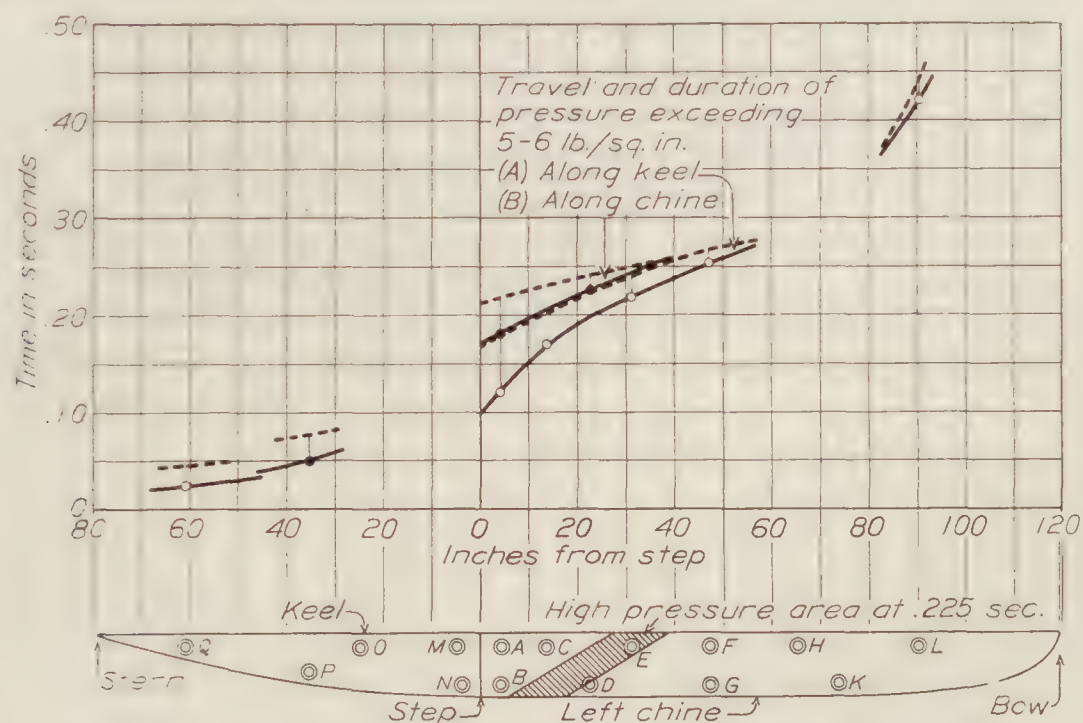


FIGURE 11.—Travel of high local pressure over the float bottom in pancake landing, run 56.
Water speed 47 to 42 M. P. H., smooth water

at 10 M. P. H. less water speed. The highest recorded acceleration at the *c. g.* (4.3 *g*) was obtained in this run and the float bottom was damaged at station B. The sustained pressure was 4.3 to 5.7 pounds per square inch at C, in excess of 4 pounds per square inch at D, and 2.8 to 4.1 pounds per square inch at H. At the same time it was less than 3.1 pounds per square inch at A, 4.5 pounds per square inch at B, 4.3 pounds per square inch at E, and 2.5 pounds per square

inch at stations F, G, K, and L. During other maneuvers large sustained pressures were recorded at some other stations. At station A, 5.3 pounds per square inch was almost continuously exceeded, and at B 5.4 pounds per square inch was intermittently exceeded during taxiing run 24. During taxiing run 20 a sustained pressure of 2.4 to 3.1 pounds per square inch was recorded at station F, and in taxiing run 21 a sustained pressure of 3 to 3.9 pounds per square inch existed at E. Station O, abaft the step, indicated a sustained pressure of 2.1 to 3.5 pounds per square inch during taxiing run 15 while at P during the same run 2.1 pounds per square inch was only exceeded intermittently. In each of these taxiing runs the location of the sustained pressure was dependent on the attitude of the float. The pancake landing is particularly important by reason of the high local pressure which travels from the stern to the bow and the large total load indicated by the acceleration at the *c. g.* It appears permissible to assume for this maneuver that a sustained pressure of 3 pounds per square inch exists over the bottom from the step forward to the position of the high-pressure area at any instant. From results obtained in the negative pressure tests, discussed later, it is considered that the pressure abaft the step is negligible when the high pressure is forward.

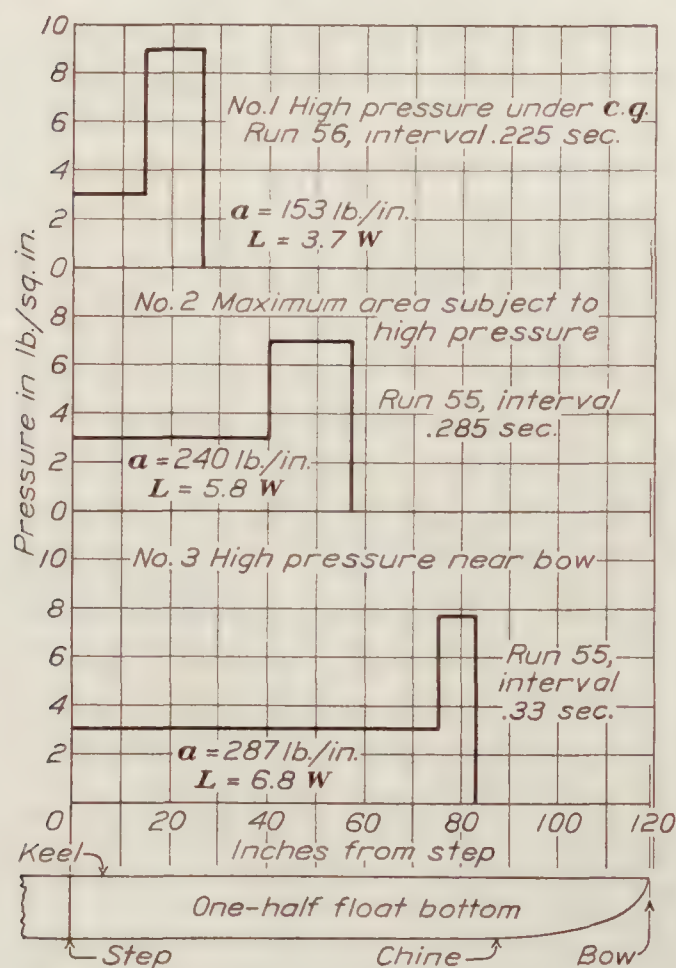


FIGURE 12.—Approximate loads at three intervals for a severe pancake landing

distribution curve of Figure 9. The areas subject to high pressure, as thus determined, are shown by the shaded areas in Figures 10 and 11 on one-half the projected float area. The intervals are chosen to show the areas when the high pressure is under the *c. g.*, in the middle of the forebody, and near the bow. In the middle of the forebody the high pressure area is a maximum, although the pressure is not. The projected area is used because only vertical loads are considered. The boundary lines of the areas are not perpendicular to the keel because of the lag in transverse distribution of pressure.

A rectangular representation of the load distributions at three successive intervals during a pancake landing is given in Figure 12. The high pressure at a given instant is represented by a rectangle with a height equal to the pressure on the area in pounds per square inch. The width is that of an area equivalent to the actual area subject to high pressure as given in Figures 10 and 11, but with sides perpendicular to the keel. It is found by dividing the actual high-pressure area by the width of one-half the float. The lower sustained pressure is represented by another rectangle with a height representing a pressure of 3 pounds per square inch and a

Without records which show the exact simultaneous pressures over the entire float bottom it is impossible to determine an actual load distribution accurately. It is possible, however, to arrive at a probable load distribution from a study of the high local pressures and the low sustained pressures measured for the same maneuvers but on different runs. The sustained pressures likely to prevail in a severe pancake landing have been discussed above. The area subject to high pressure at a given instant in a pancake landing is determined from the pressure-travel curves.

The intersections of a time ordinate with the pressure-travel curves (A) and (B) of Figures 10 and 11 determine four abscissas which are projected down to their respective positions on the lines of the keel and chine stations. These four points determine two sides of the area subject to pressure in excess of 5 to 6 pounds per square inch, which is bounded by the keel and chine on the other two sides. The actual magnitude of the pressure in this area is determined from the pressures given by the maximum pressure

width extending forward from the step to the high-pressure area. The combined areas of these two rectangles multiplied by the width of both floats is the total vertical water load. Thus,

$$L = \frac{a \times 2b}{W} \times W.$$

when

a = combined area of load rectangles.

b = width of one float = 26 inches.

W = gross weight of seaplane = 2,150 pounds.

L = total vertical water load.

The actual weight is substituted only in the denominator so that L is given in terms of W .

The three load distributions of Figure 12 represent the worst conditions of the two pancake landing runs 55 and 56. Case 1 represents the distribution with the high-pressure area under the *c. g.* and was taken from run 56. Cases 2 and 3 were taken from run 55 and represent the distributions when the high pressure is extended over a maximum area in the forebody and when it is near the bow, respectively. The distribution forward in this landing was unusually bad.

The maximum total load thus derived is 6.8 W , where W is the weight of the seaplane. The maximum load indicated by the accelerations measured at the *c. g.* is 4.3 W . The maximum acceleration was not obtained for run 55 and it is possible that it was slightly greater than the 4.3 g determined in a similar landing. It is likely, however, that the chief cause for the discrepancy is inaccuracy in the assumed load distribution, particularly in the sustained pressure extending from the step to the high-pressure area. A small difference due to flexibility of the structure is also to be considered, and there is a possibility that the load is unequally distributed between the floats. The time at which the maximum accelerations occurred in the pancake landings is in fair agreement with the load distributions shown, as the maxima occurred when the high pressures were well forward. The load distributions are, therefore, probably representative of actual conditions with the exception that the magnitude of the computed total load is possibly somewhat greater than that actually experienced.

The point of application of the resultant force may be determined from the load distributions given, but the direction of the resultant is unknown. It does not pass through the *c. g.* when the resultant is forward as there is considerable angular acceleration. The magnitude of this angular acceleration can not be determined accurately from the float angle records, but the record for pancake landing run 44 shows that it may be as great as 10 radians per second per second. This shows that the resultant must pass considerably forward of the *c. g.*

The load distribution abaft the step can not be determined by the method used for the forebody since no continuous pressure travel curves were obtained. However, the accelerometer at the *c. g.* recorded 1.8 g when the high pressure was abaft the step in pancake landing run 56, and at the same time the float bottom accelerometer exceeded 2 g . Stations Q and P both recorded very high pressure in this landing and the resultant load is, therefore, probably applied between these two stations or about 4 feet abaft the step, and is of considerable importance.

NEGATIVE PRESSURES

Simultaneous values of the negative pressures at intervals during take-off are given in Table III with the corresponding air speed, float angle, and approximate water speed; and in a figure accompanying the table the locations of the pressure orifices are shown. The pressures were read at several intervals from continuous records taken from opening of the throttle to get-away. The intervals were chosen so as to include high pressures throughout the runs and are timed in seconds from the start of the take-off.

At low speeds negative pressures were sustained and existed over a small area extending a few inches abaft the step. At high speeds this area extended back along the keel more than 2 feet, but not along the chine, and the pressures were sharply fluctuating as shown in Figure 13. At intermediate speeds the pressures abaft the step were nearly zero but in some cases there were

small peak pressures at regular intervals corresponding to the period of oscillation of the sea-plane. These variations were most noticeable at stations 1, 3, and 4, at which they occurred simultaneously, but the peaks were usually positive at station 3 instead of negative as at 1 and 4. At station 5 the pressure was unusual in that it showed no sharp fluctuations. Forward of the step the pressure was always positive.

The largest negative pressures were recorded at stations 1 and 2 immediately abaft the step and occurred with the control neutral at water speeds of from 9 to 15 M. P. H. The highest value obtained was 0.87 pound per square inch, which is of small structural importance. At high speeds the pressures fluctuated rapidly and there is a possibility that this might cause considerable vibration of the bottom skin.

The negative pressures were influenced by the speed and float angle. One of the forces determining the float angle is the force on the elevators. It was found that with the control held back the sustained negative pressure abaft the step at low speeds was largely eliminated, and that the longitudinal acceleration during take-off was steady. With the control neutral or forward the negative pressure at low speeds was high and sustained for a period of several seconds, during which the acceleration was very slight.

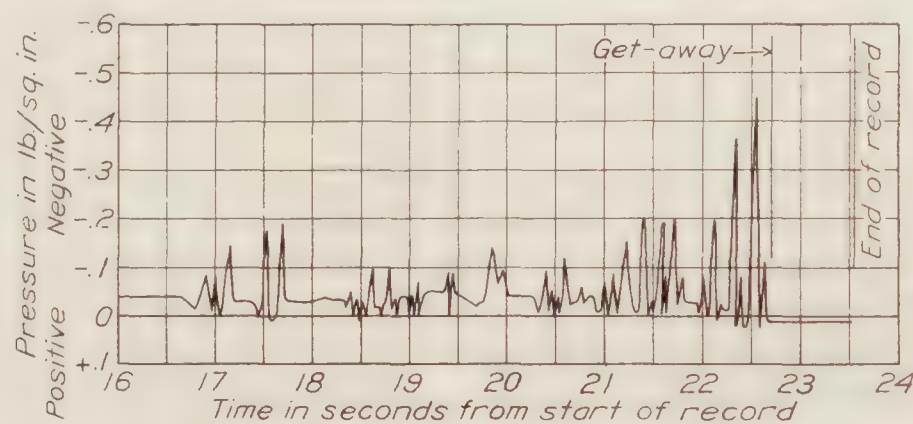


FIGURE 13.—Reproduction of a typical negative pressure record showing rapid fluctuations of pressure near get-away

DISCUSSION OF RESULTS

It is considered that the maximum pressures obtained were excessive for the TS-1 float, since both floats were damaged during tests and eventually ruined in a landing apparently no worse than others for which records were obtained. The complete failure was probably caused by the repetition of hard landings on floats which had had considerable service. The final failure was in the planking, stringers, and stringer bracing a short distance forward of the step. This indicates a failure due to local pressure which is not necessarily coincident with maximum moment or total vertical load.

Large total loads as well as high local pressures result from pancake landings with large float angle. In addition, the maximum resultant force is well forward of the *c. g.* which imposes a large moment. The direction of this resultant force was not determined because no measurements of the longitudinal components of either force or acceleration were made, but the existence of considerable angular acceleration shows that it does not pass through the *c. g.*

The maximum pressure on the TS-1 was about 10 pounds per square inch and on the UO-1, 6.5 pounds per square inch. High pressures were experienced near the bow of the TS-1 and not on the UO-1. The higher pressures on the TS-1 are probably due to unequal distribution of the load between floats, the generally higher speed, and the smaller angle of V . The speed of the TS-1 for comparative maneuvers is 5 to 10 M. P. H. higher than for the UO-1; and the angle of V is 3° less at the step and 10° less at corresponding positions near the bow. The peak pressure near the bow is probably due to the small angle of V and the gradually rising keel line. It is probably influenced also by the location of the *c. g.*, which is 6 inches farther forward on the TS-1 than on the UO-1 float.

The negative pressures are of small magnitude, and the investigation shows that it is reasonable to neglect pressures abaft the step when considering total loads with a pressure

peak forward of the step. The results indicate a relation between negative pressure and float resistance which is possibly of sufficient importance to warrant a more complete investigation of this relation.

CONCLUSIONS

The results of this investigation apply only to the TS-1 seaplane as used in these tests. The effect of variations in speed, float shape, and other characteristics likely to be different in other designs is probably considerable on both the magnitude and distribution of pressures.

Maximum pressures as high as 10 pounds per square inch are most likely to occur at the step, but under some conditions of landing, pressures of practically the same magnitude may also occur at the stern and near the bow.

The only part of the float on which no large pressure occurs is a limited area immediately abaft the step in which a maximum negative pressure of 0.87 pound per square inch was measured.

Maximum pressures are always confined to a small area at any instant and last approximately one-twentieth to one-hundredth second at any given location.

Sustained pressures are always small compared to the maximum pressures and are greatest near the step.

The worst distribution of pressures and the greatest accelerations at the *c. g.* occurred in pancake landings and were principally due to the development of a high pressure near the bow.

The negative pressures which exist abaft the step appear to be of small consequence structurally, but may be of sufficient interest in a study of float resistance and trim to warrant a more complete investigation.

A vertical component of acceleration of 4.5 *g* at the *c. g.* is not likely to be exceeded in a safe landing.

Acceleration of the float bottom is probably 1 to 2 *g* greater than that at the *c. g.* in hard landings.

In future investigations of this sort the longitudinal component of acceleration at the *c. g.* should be measured.

LANGLEY MEMORIAL AERONAUTICAL LABORATORY,
NATIONAL ADVISORY COMMITTEE FOR AERONAUTICS,
LANGLEY FIELD, VA., *December 28, 1928.*

REFERENCES AND BIBLIOGRAPHY

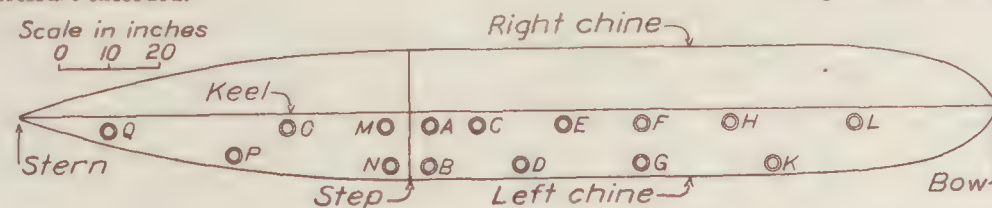
- Reference 1. Thompson, F. L.: Water Pressure Distribution on a Seaplane Float. N. A. C. A. Technical Report No. 290, 1928.
- Reference 2. Norton, F. H. and Warner, E. P.: Accelerometer Design. N. A. C. A. Technical Report No. 100, 1921.
- Reference 3. Norton, F. H.: N. A. C. A. Recording Air-Speed Meter. N. A. C. A. Technical Note No. 64, 1921.
- Reference 4. Brown, W. G.: The Synchronization of N. A. C. A. Flight Records. N. A. C. A. Technical Note No. 117, 1922.
- Baker, G. S. and Keary, E. M.:
Experiments with Full-Sized Machines (2d series). Local Water Pressures on Flying-Boat Hulls. British A. R. C. Reports and Memoranda No. 683, September, 1920.
P-5 Flying Boat N-86, Impact Tests. (Experiments with Full-Sized Machines, 3d series.) British A. R. C. Reports and Memoranda No. 926, April, 1924.
- Bottomley, G. H.: The Impact of a Model Seaplane, Float on Water. British A. R. C. Reports and Memoranda No. 583, March, 1919.
- Richardson, H. C.: Airplane and Seaplane Engineering. Bureau of Aeronautics, Navy Department Technical Note No. 59, 1923.
- Reference 5. Zahm, A. F.: Development of an Airplane Shock Recorder. Journal of the Franklin Institute, August, 1919.

TABLE I.
WATER-PRESSURE DISTRIBUTION ON THE TS-1 SEAPLANE FLOAT
[Recorded water pressures in pounds per square inch]

Run No.	Maneuver	Condition of water	Air speed in M.P.H.	Approximate water speed in M.P.H.	Longitudinal float angle in degrees	Maximum acceleration in terms of <i>g</i>		Pressure stations																								Remarks																					
						c.g.	Float bottom	A		B		C		D		E		F		G		H		K		L		M		N			O		P		Q																
								a	b	a	b	a	b	a	b	a	b	a	b	a	b	a	b	a	b	a	b	a	b	a	b		a	b	a	b	a	b															
15	Taxiing—tail down.	Smooth	47-53	34-40	10-9	1.9		4.3		5.6		5.3		4.4		3.0		2.0		1.9		1.9		1.8		1.8		2.3		2.5		2.1		3.5		2.1		2.3		2.7													
18	do	do				1.9		6.0		9.2		6.6		5.4		5.3				3.7		3.6		3.6		3.4		5.4				5.6		5.6		6.1		6.4															
23	do	do	45-46	45-46	8	1.6		8.7		9.1		8.8		10.5		8.2		8.6		6.4		6.2		5.7		6.3		6.1		6.2		5.8		5.2				5.5		6.4													
24	do	do	43-47	43-47	9-8	1.6		6.7		8.0		8.0				4.7		4.6		3.3		3.5		3.4		3.4		3.2		3.7				5.2				4.7															
51	do	Very smooth	32-33	26-27		1.6	0-2	7.9		5.7				4.2		2.8		1.1		7.0		6.5		6.3		6.1		6.4		4.8				5.0		4.5		5.6															
19	Taxiing—normal.	Smooth			5-2	1.7		4.7		5.4		5.7		5.9		4.9		4.7		3.9		3.1		5.8		3.1		3.1		5.8				6.1		6.1		7.1															
20	do	do			4-2	1.5		2.8		3.5		4.8		5.5		3.9		3.4		4.0		3.9		3.0		2.7		3.2		5.1		2.4		2.3		2.7		2.9		3.4													
21	do	8 to 10 inch waves	62-64	51-53	7-5	2.6		7.2		8.9		8.8		10.5		7.7		6.2		7.2		6.2		7.4		5.6		6.9		6.1		6.0		5.9		5.6		5.2		5.6		6.6											
22	do	do	51-55	40-44	3-2	1.7		4.2		5.0		5.3		5.5		4.5		4.3		3.5		4.3		3.8		4.2		4.9		6.6		4.0		5.1		3.6		4.1		3.8		4.5											
31	do	Smooth	58	47				5.6		7.1		7.1		6.4		7.0				6.7		7.6		7.2		6.5		5.7						6.0		6.0		6.0		6.0													
48	do	12 to 15 inch waves	58-59	41-42		2.4	2-4	5.0		5.1		5.5		5.6		5.6		5.9		6.1		5.9		7.3		5.6		6.0		6.0		4.6				5.0		4.8		5.2													
3	Landing, stalled, power off.	10 to 12 inch waves	65-58	55-48	13-1	2.2		7.3		8.4		7.9		9.8		7.5		10.0		6.1		5.9		6.8		3.9		4.2		4.8		7.0		6.0		6.0		4.5		4.7		4.6		5.0									
5	do	Very smooth	65-60	60-55				5.7		6.3		6.8		8.1		6.8		7.5		5.9		5.7		6.8		4.7		5.2		5.0		5.8		5.1		5.6		6.9				5.2		6.0		5.6		5.5		6.3		7.2	
6	do	do	64-58	59-53		2.3		4.8		6.1		5.9		5.9		3.4		3.7		4.0		4.5		2.2		2.5		1.8		2.3		3.8				1.6		1.6		2.3		2.6		2.0		2.3		2.7		3.3			
30	do	Smooth	53-50	42-39		2.4		6.1		6.6		7.7		6.7		7.7		4.5		4.5		4.7		5.3		6.5		5.1		4.7		5.6				5.7		5.8		5.7		8.3											
43	do	10 to 12 inch waves	55-49	42-36	16-4	2.8		7.4		9.2		9.7		10.4		7.2		9.5		6.4		7.0		7.1		8.2		6.8		6.4		7.7		6.9		6.2		4.8		5.3		5.3		6.1									
47	do	12 to 15 inch waves	56-44	39-27		2.9	4-6	4.9		6.0		6.0		6.7		7.1		8.0		6.6		7.6				5.8		6.0		5.8		6.7		5.5		5.8		4.9		5.3		5.2		5.6		8.4		Unusually high float angle.					
7	Landing, stalled, power on.	Very smooth	60-54	55-49	12-2	2.9		8.9		8.4		10.1		7.9		8.4		6.1		6.0		7.1		4.7		5.2		5.0		5.8		5.2		4.8		5.2		6.0		5.6		5.5		6.3									
8	do	do	56	47		2.4		5.0		5.1		6.2		4.2		4.9		3.5		3.8		3.4		4.0		3.3		3.8		2.6		2.6		3.5		2.5		2.5		2.7		3.2		2.6		2.9		3.3					
13	do	Smooth	66-65	53-52	11-3	1.9		6.1		6.2		7.4		5.7		6.0		4.3		4.2		5.2		2.8		3.4		2.8		3.1		5.5		2.8		2.7		3.0		3.5		2.9		3.1		3.6							
17	do	do			13-2	2.0		7.0		8.4		7.1		8.6		7.5		6.2		6.1		7.3		5.6		6.0		5.9		6.0		5.7		5.2		5.3		5.3		5.3		6.1											
9	Landing, fast	Very smooth	78-75	78-75		3.2		8.4		8.0		7.5		8.0		5.9		5.7		6.8		6.4		7.0		5.6		6.4		5.8		4.9		5.1		5.8		5.5		5.3		6.0		Cracked bottom of right float at step.									
10	do	12 to 15 inch waves	71	49	9-2	2.3		4.2		4.5		4.1		5.2		3.9		2.9		3.6		2.0		2.5		1.9		1.9		1.8		1.8		2.0		2.3		1.7		2.0		2.4											
11	do	do	73-72	51-50	9-3			5.7		6.9		6.0		7.2		5.7		6.9		5.2		5.8		6.4		5.1		4.4		5.3		4.5		4.2		4.6		5.3		4.8		4.7		5.4									
12	do	do	75-72	73-70	9-3	3.0		6.0		6.9		7.1		8.5		5.7		5.6		3.7		2.2		6.1		5.2		5.6		5.5		6.4		5.2		4.9		5.0		5.6		5.2		5.0		5.8							
44	Landing, pancake	10 to 12 inch waves	50-48	37-35	16-3	4.3		5.7		7.1		5.7				4.2		5.0		5.4				2.4		3.0		4.1				3.0						2.3		2.7		3.5		Cracked bottom at station B in this or a similar landing following it. Landing similar to run 44.									
55	do	Very smooth	50-45	47-42				4.6		7.9		9.2		5.7		8.1				8.2		9.7		7.0		6.3		6.2		7.9		6.0		7.5		5.8		6.6		8.8		4.6		4.9		4.9		8.4		Do.			
56	do	do	51	48		3.8	2-4	8.9		7.7				7.9		6.7		6.4				6.4		6.2		5.9		6.3		7.2		5.0				5.9		8.2		9.7													
41	Porpoising	Smooth	44-36	31-23	5-14	2.1				5.3		6.9		7.0		6.4		7.0		6.8		6.4		7.7		6.9		6.2								5.0		5.6															
42	do	do	39-40	26-27	2-10	2.1		3.5		5.1		3.5		2.5		2.8		3.1		1.9		2.1		2.9		3.5		2.3		2.4						2.5		2.8															
53	do	Very smooth				2.1	2-4	6.5		4.6		6.4				3.5		6.8		5.5		9.5		3.8		6.8		3.8		4.9		3.4		4.2		3.7		4.2		3.5		3.6		4.1									
54	do	do				1.6	0-2	4.7		5.1		4.0				5.2		6.4		3.4		6.8		2.2		4.6		2.3		3.4		2.3		3.0		2.5		3.1		2.2													

a=pressure exceeded.

b=pressure not exceeded



Location of pressure stations in the TS-1 float

TABLE II
SUMMARY OF FIVE HIGHEST PRESSURES AT ALL STATIONS

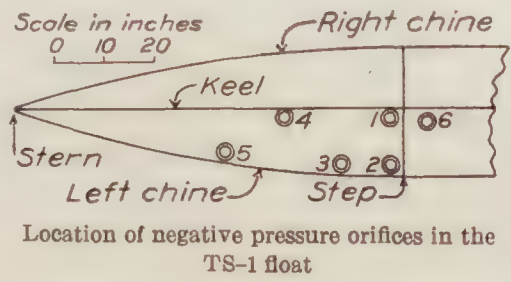
Pressure stations																													
A		B		C		D		E		F		G		H		K		L		M		N		O		P		Q	
Run No.	p	Run No.	p	Run No.	p	Run No.	p	Run No.	p	Run No.	p	Run No.	p	Run No.	p	Run No.	p	Run No.	p	Run No.	p	Run No.	p	Run No.	p	Run No.	p	Run No.	p
7	9.7	43	10.3	3	8.9	55	9.2	43	7.9	56	7.2	55	7.3	30	7.3	3	6.8	55	9.6					56	6.7	56	9.0	56	10.5
6	9.7	18	10.0	24	8.8	56	8.7	55	7.8	55	7.1	30	5.3	9	7.2	55	6.5	5	7.7					15	2.9	24	6.0	55	9.2
3	9.2	21	9.9	23	8.7	30	8.5	56	7.5	9	7.0	11	5.0	55	7.0	5	5.6	56	7.0							44	3.4	5	7.2
9	9.2	23	9.9	43	8.6	47	7.4	21	7.1	21	6.5	53	4.6	48	6.9	11	5.3	3	6.8							15	2.4	30	6.8
5	8.8	7	9.5	7	8.4	43	7.0	17	7.0	11	5.7	22	4.3	47	6.5	22	4.8	11	5.0									47	6.7

p=mean pressure corrected for acceleration in pounds per square inch. Acceleration correction is $+\frac{1}{4}$ pound per square inch, as explained in text. Spaces left blank indicate that no pressure was recorded.

TABLE III
NEGATIVE WATER PRESSURES ON THE TS-1 SEAPLANE FLOAT

Maneuver	Run No.	Time in seconds	Pressure in pounds per square inch. Orifice Nos.						Air speed in M. P. H.	Approximate water speed in M. P. H.	Float angle in degrees	Remarks
			1	2	3	4	5	6				
Take-off, control back	69	6	0.01	-----	0.02	0.01	0	-----	36	36	9	Get-away at 15½ seconds.
		7¾	.11	-----	+	.21	+	-----	42	42	10-6	
		10⅞	.28	-----	+	.32	+	-----	50	50	10-7	
		12⅞	.26	-----	+	.39	+	-----	53	53	8-5	
		14½	.01	-----	.32	.01	+	-----	55	55	7-5	
Do.	74	3	.13	0.42	+	-----	-----	+	20	6	7	Get away at 14 seconds.
		3¾	.16	.19	+	-----	-----	+	22	8	9	
		3¾	.01	.06	.08	-----	-----	+	23	9	10	
		8⅞	.31	.14	.03	-----	-----	+	38	24	10-8	
		13½	.34	.34	0	-----	-----	+	53	39	10-6	
Do.	75	2⅞	.11	.44	+	-----	-----	+	22	8	6	Do.
		2½	.23	.25	+	-----	-----	+	23	9	7	
		2¾	+	.06	+	-----	-----	+	23	9	7	
		3	0	.10	0	-----	-----	+	23	9	8	
		7¾	.19	.16	+	-----	-----	+	37	23	9-7	
		8½	.31	.16	0	-----	-----	+	37	23	9-7	Get-away at 24 seconds.
		10⅞	.39	.34	.02	-----	-----	+	46	32	10-6	
		12¼	.39	.42	+	-----	-----	+	51	37	9-7	
Take-off, control neutral	70	4	.35	-----	+	+	+	-----	20	9	5	
		4¾	.14	-----	.13	+	+	-----	22	11	6	
		5	.01	-----	.04	.01	+	-----	22	11	6	Get-away at 23½ seconds.
		16	.03	-----	.14	.01	0	-----	53	42	3	
		20¼	.46	-----	+	.58	+	-----	55	44	7-5	
Do.	71	3⅞	0.57	-----	+	+	+	-----	23	12	4	
		4⅞	.39	-----	0.28	+	+	-----	23	12	4	
		5½	.05	-----	.04	0.03	+	-----	23	12	5	Get-away at 22½ seconds.
		13	-----	-----	.04	0	-----	46	35	2-4		
		19½	-----	-----	.36	.01	-----	54	43	2-4		
Do.	76	3⅞	.87	.70	+	-----	-----	+	23	9	3	
		4⅞	.39	.83	+	-----	-----	+	27	13	5	
		5¾	.26	.24	.16	-----	-----	+	27	13	5	Get-away at 26½ seconds.
		6	.18	.18	.12	-----	-----	+	28	14	5	
		6¼	.05	.08	.01	-----	-----	+	28	14	6	
		17¾	.19	.16	.16	-----	-----	+	57	43	3	
Do.	77	2⅞	.53	.77	+	-----	-----	+	24	10	4	
		5¼	.27	.77	+	-----	-----	+	28	14	3	
		5½	.53	.64	+	-----	-----	+	29	15	3	
		9½	.27	.32	.16	-----	-----	+	30	16	4	
		11¾	.23	.28	.20	-----	-----	+	30	16	4	
		12½	.05	.07	.05	-----	-----	+	30	16	5	
		14	.03	.07	.03	-----	-----	+	30	16	5	Get-away at 26½ seconds.
		22½	.37	.32	.01	-----	-----	+	52	38	3-6	
Take off, control forward	72	5	.50	-----	+	+	+	-----	23	12	5	
		5⅞	.25	-----	.22	+	+	-----	24	13	3	
		7½	.05	-----	.09	.03	+	-----	25	14	4	
		16¼	.05	-----	.11	.05	0	-----	42	31	5-1	
		24½	.37	-----	+	.55	+	-----	54	43	-----	

+ = positive pressure.



REPORT No. 329

THE TORSIONAL STRENGTH OF WINGS

By C. P. BURGESS

Bureau of Aeronautics, Navy Department

REPORT No. 329

THE TORSIONAL STRENGTH OF WINGS

By C. P. BURGESS

SUMMARY

This report is submitted to the National Advisory Committee for Aeronautics by the Bureau of Aeronautics, Navy Department. It describes a simple method for calculating the position of the elastic axis of a wing structure having any number of spars. It is shown that strong drag bracing near the top and bottom of a wing greatly increases the torsional strength. An analytical procedure for finding the contribution of the drag bracing to the torsional strength and stiffness is described, based upon the principle of least work, and involving only one unknown quantity.

The validity of the new method of analysis is tested by applying it to a two-fifths scale model of the large steel tubular 3-spar wing of the Huff-Daland XHB monoplane. The calculated stresses are checked by comparison with the strains observed by means of electric telemeter strain gauges secured to the spars during sand load tests in the static testing laboratory of the Army Air Service Engineering Division at Dayton, Ohio.

The torsional strength of a wing determines very largely the distribution of air forces upon it, and the tendency to flutter. Insufficient torsional strength produces wash-in or an increasing angle of attack toward the wing tips in the high incidence condition, further increasing the load on the front spar in the condition which is already the most severe. Conversely, torsional yielding in the low incidence and nose dive conditions produce washout of the wing shape and may exaggerate the critical condition for the rear spar.

The mathematical theory of the forces producing flutter is not yet sufficiently far advanced to determine by direct calculation the critical air speed at which flutter will commence. Comparison with successful practice must still be the principal criterion upon which to judge the adequacy of the torsional strength of a new design of wing. Obviously this comparison will be greatly facilitated by use of a coefficient of torsional rigidity including the principal factors in torsional strengths. A coefficient for comparing the torsional rigidity of different wings is derived in this report.

INTRODUCTION

The tendency of modern airplane design is largely toward monoplanes in which the wings are either full cantilevers, or more frequently, are cantilevered beyond a single pair of external struts. In either case, the cantilever portion of the wing must have sufficient torsional strength to prevent wing flutter at all flying speeds.

In the methods commonly prescribed and used for the structural analysis of 2-spar wings, it is assumed that the ribs act in a manner analogous to bridges resting upon the spars as abutments. It is further assumed that the torsional strength of the cantilever portion of the wing is derived solely from the spars acting independently without the assistance of drag bracing to resist torsion. Such a wing is not only inefficient in torsion, but it must have spars designed for two extreme positions of the center of pressure, so that when the front spar is carrying its maximum load, the rear spar is partially idle, and vice versa. The wing is therefore required to carry excess structural weight.

The advantages of strong drag bracing near the top and bottom surfaces of the wing are now generally conceded; but reasonably simple methods of calculating the contribution of the drag bracing to the torsional strength of the wing have not hitherto been presented. It is the

purpose of this paper to describe an improved method for calculating the torsional strength of wings having efficient drag bracing. Moreover, the method is not confined to 2-spar wings, but is equally applicable to multispar construction.

CONTRIBUTION OF THE DRAG BRACING TO TORSIONAL STRENGTH

Figure 1 represents a cross section through a wing having two spars, each consisting of two longitudinal members with diagonal bracing in the plane of each spar only. The arrows represent a torsional moment about the elastic axis or centroid. Without drag bracing, the torsion is resisted only by the strength of the spars in the vertical plane. The addition of drag bracing



FIGURE 1.—Torsion in two spars without drag bracing

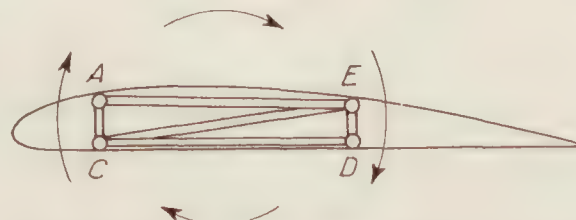


FIGURE 2.—Spars reinforced by drag bracing against torsion

in the top and bottom horizontal planes not only adds two more trusses to resist torque, but may be designed to eliminate entirely all forces in the longitudinal members due to torsion. For example, the longitudinal tubes A and D, in Figure 2, are in compression as members of the front and rear spars, but are in tension as members of the top and bottom drag trusses; and conversely for members C and E. By proper proportioning of the members, these tensile and compressive forces in the longitudinals can be made to cancel each other, with the result that the torsion is resisted entirely by the shear members in the spars and drag trusses. The nearness of the drag trusses to the centroid is largely compensated by their great depth in proportion to the spars.

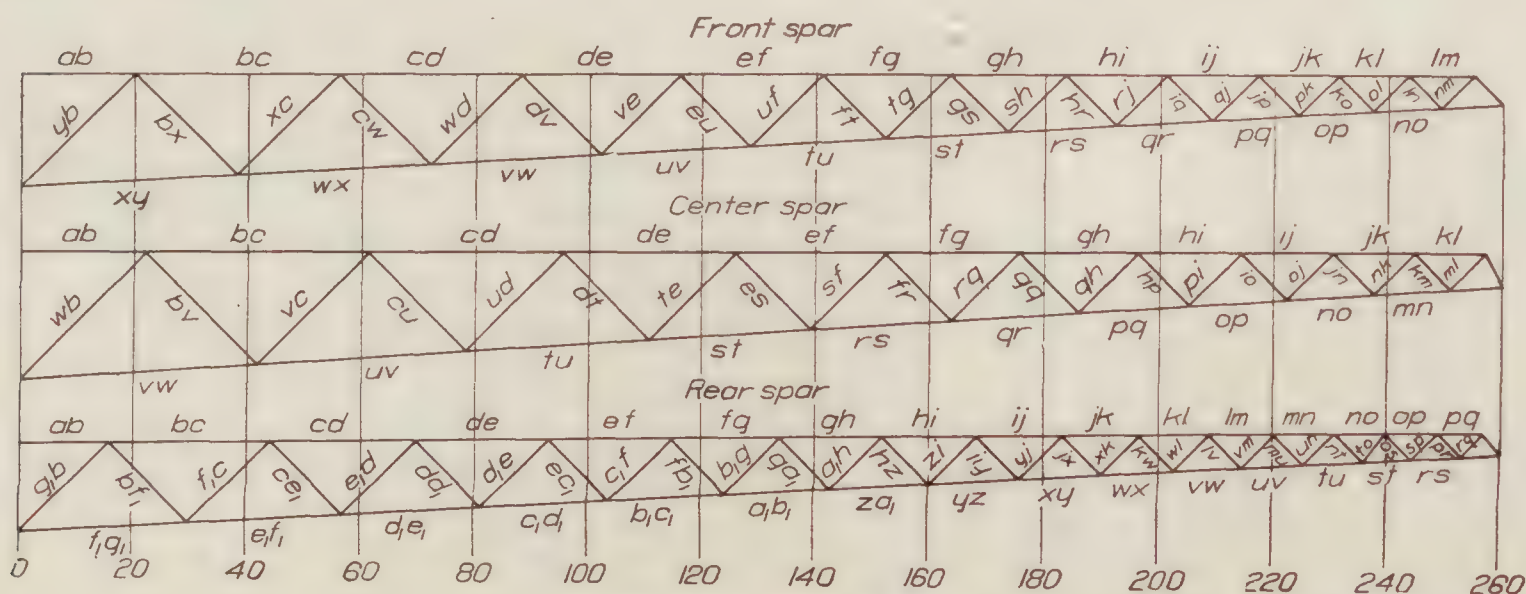


FIGURE 3.—Spar trussing in XHB wing

THE ELASTIC AXIS OR CENTROID

The elastic axis or centroid of the wing is the line across which a transverse force may be applied without causing any rotation of the wing sections. In structural analysis of a wing having more than two spars, or drag bracing resisting torsion, it is convenient to divide the resultant force of the air pressure into forces acting through the elastic axis, and a pure torsional couple.

The distance of the centroid from the leading edge is calculated by taking moments of the factors which determine the rigidity of the wing spars. For example, in spars in which the shearing deflection is negligible, the rigidity, or resistance of the spars to deflection is directly proportional to the moment of inertia of their cross sections. In spars having very flexible shear bracing, an appreciable part of the deflection may be due to shear, and the rigidities of

the spars may be calculated from the internal work under a given load, on the principle that the rigidity is inversely proportional to the work. This follows directly from the well-known fact that with a given load, the work is proportional to the deflection, provided the stresses nowhere exceed the proportional limit.

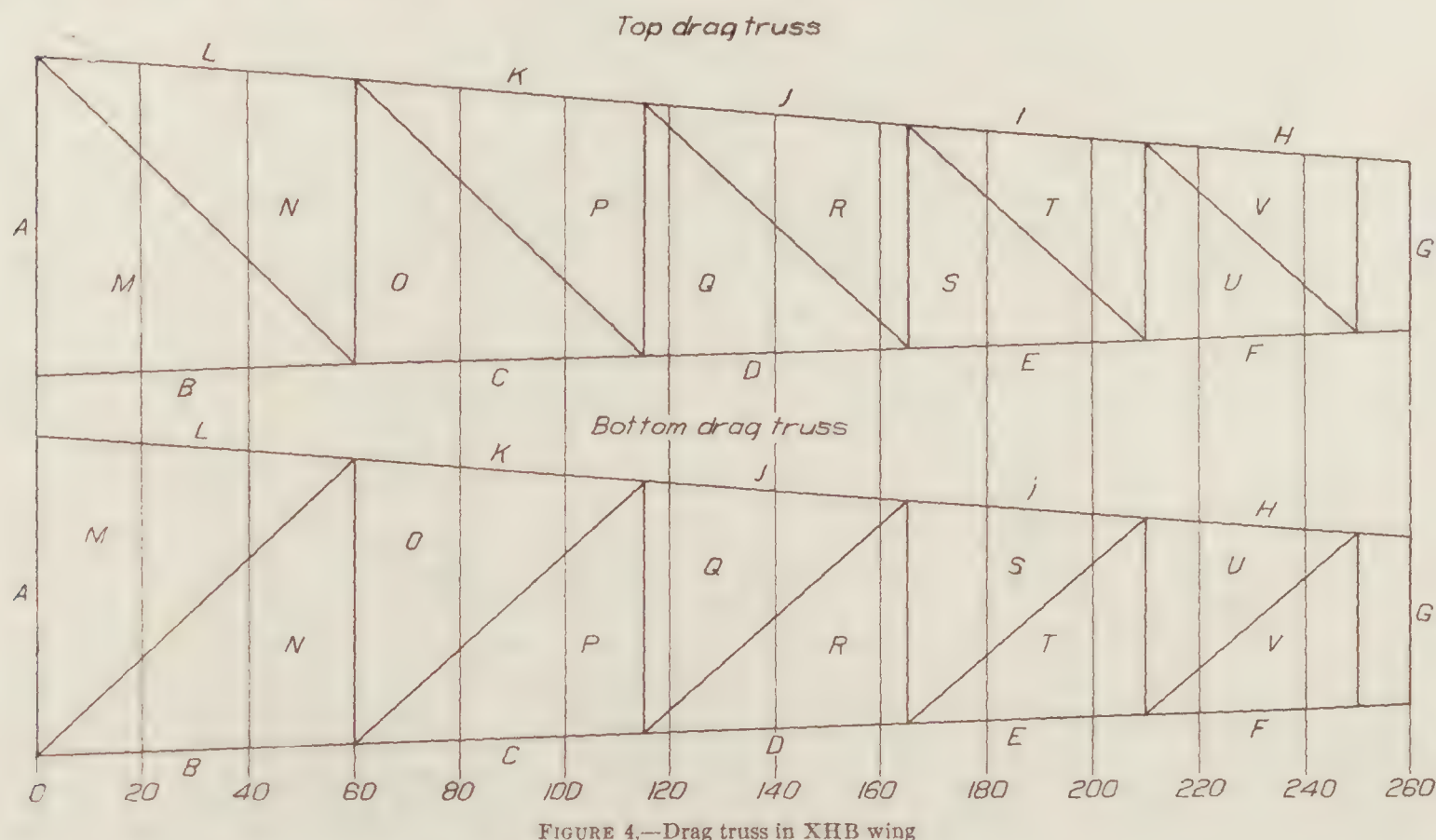


FIGURE 4.—Drag truss in XHB wing

The moment of inertia of the cross section, or the reciprocal of the internal work under a given load may be taken as rigidity factors of the spars. The sum of the moments of the rigidity factors about the leading edge of the wing, divided by the sum of these factors, gives the distance of the elastic axis from the leading edge. This principle is not confined to 2-spar wings, provided that as is usually the case, the ribs and rib bracing between the spars are sufficiently rigid to make the distortions of the wing sections negligible in comparison with the translational and rotational movement of the sections.

As an example, the position of the elastic centroid at Station 22 of the XHB wing, shown in Figures 3, 4, and 5, is calculated. This is a 3-spar, tapered wing in which the distances of the spars from the leading edge remain constant fractions of the tapering chord. It is therefore convenient to express the moment arms about the leading edge as fractions of the chord, rather than as definite lengths. The calculation is made in tabular form as follows:

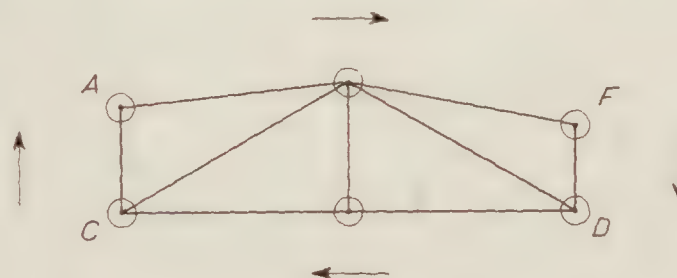


FIGURE 5.—Diagrammatic section through 3-spar wing

TABLE I

Spar	I in. ⁴	% chord from leading edge	Moment
Front.....	44.4	15	666
Center.....	32.8	40	1,312
Rear.....	21.6	65	1,404
	98.8		3,382

The centroid is at $3,382/98.8 = 34.23\%$ of the chord from the leading edge at Station 22.

DIVISION OF THE LOAD BETWEEN THE SPARS

When the resultant of the load normal to the wing chord passes through the elastic axis, there is no rotation of the wing sections, and if the ribs are rigid, all spars have equal deflections, and are loaded in direct proportions to their moments of inertia, I , provided the shearing deflection is negligible. It follows that the running load, w , on each spar due to a total running load, W , acting through the elastic centroid is given by:

$$w = WI/\Sigma I$$

The summation, ΣI , is taken over all spars at the station under investigation. In the XHB wing at Station 22, the division of load between the spars is as follows:

TABLE II

Spar	I	$I/\Sigma I =$ fraction of normal load taken by spar
Front.....	44.4	0.450
Center.....	32.8	.332
Rear.....	21.6	.218
	98.8	1.000

If there were no drag bracing in the top and bottom planes of the wing, a torsional couple about the centroid would be opposed only by the rigidity of the spars, which would be loaded by the torsion in direct proportion to their moments of inertia and their distance from the centroid, i. e. in proportion to Is , where s is the distance of the spar from the centroid. The moments of the resistances of the spars to a torsional couple are equal to Is^2 ; and the loads w due to a torsional moment M are therefore given by:

$$w = MIs/\Sigma Is^2$$

The values of $Is/\Sigma Is^2$ for the present problem are given in the following table, where s is expressed as a percentage of the chord length.

TABLE III

Spar	I	s	Is	Is^2	$Is/\Sigma Is^2$
Front.....	44.4	-19.2	-852.5	16,368	-0.0225
Center.....	32.8	5.8	190.2	1,103	.0050
Rear.....	21.6	30.8	665.3	20,491	.0175
				37,962	

STRESSES IN THE MEMBERS AT STATION 22 DUE TO UNIT LOAD ON EACH SPAR

The unit load on each spar or drag truss is assumed to be 1,514 lb., distributed as shown in Table IV and Figure 6. Table V gives the abbreviations used for the various members in the subsequent analysis, and the stresses in the members at Station 22 due to the unit load being applied to each spar and drag truss in turn. The stresses have been determined by the ordinary analytical solution of determinate structures; it is not considered necessary to give the calculations here.

UNIT TORSIONAL MOMENT

The unit torsional moment is assumed to be the couple produced by 1,514 lb. distributed along the elastic axis in the same way as the unit spar load, acting downwards, and an equal force acting upwards at 1 per cent of the chord length forward of the elastic axis. The loads on the spars due to the unit torsional moment when there is no drag bracing are therefore 1,514 times the values of $Is/\Sigma Is^2$ calculated in Table III.

The depth of the wing at Station 22 is 18.6 per cent of the chord length. The loads on the drag trusses when they alone oppose the unit torsional couple are $\pm 1,514/18.6 = \pm 81.4$ lb.

LEAST WORK CALCULATION OF THE DISTRIBUTION OF TORSIONAL STRESSES

The diagonals of the top and bottom drag trusses are considered to be the redundant members in resisting torsional couples applied to the wing structure. In a pure couple, there can be no resultant drag force, and the forces in the two drag trusses must therefore be equal and opposite, so that there is only a single unknown force to be determined.

The least work analysis is applied to 1 inch length of the wing structure at Station 22. For mathematical exactitude, the least work calculations should be applied to the whole wing structure simultaneously, instead of only to the cross section at which the stresses are desired. It is believed, however, that the proposed method of procedure is not seriously in error provided there are no abrupt changes in the position of the elastic axis, and the sizes of the members in the spars and drag trusses taper out gradually. This limitation is also found in the ordinary

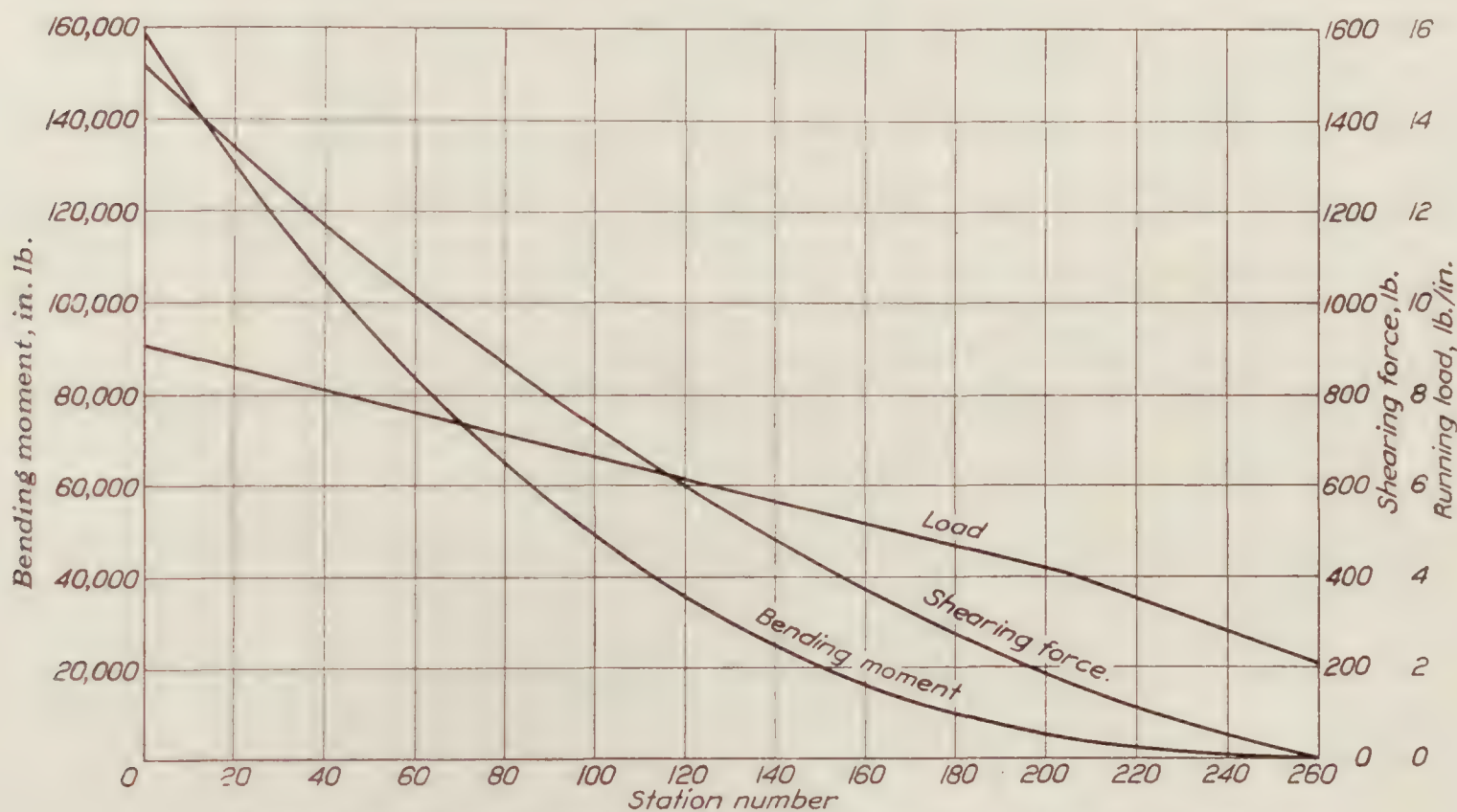


FIGURE 6.—Load, shearing force and bending moment with total distributed load of 1,514 pounds

beam bending theory which, as is well known, does not give the bending stresses correctly in the neighborhood of abrupt changes in the shape of the cross section of a beam.

In applying the principle of least work to the stress calculations the spars without the drag bracing are taken as the basic determinate structure, and the drag bracing as the redundant part. The stress, S , in any member of the structure, due to the unit torsional couple M , is regarded as consisting of two parts. One part, designated S_0 , is the stress resulting from the couple M , opposed only by the spars of the determinate structure. The other part, XS_1 , results from the forces in the redundant drag bracing. The stress, XS_1 , is the product of X , the fraction of M resisted by the drag bracing; and S_1 , the stress resulting from an imaginary condition of internal forces in which the spars and the drag bracing act against each other in torsion with an intensity equal to $-M$ in the spars, and $+M$ in the drag bracing. It follows that in any member, S_1 equals $-S_0$ plus the stress due to M applied to the drag bracing; and $S = S_0 + XS_1$.

In Table VI, the S_0 stresses (column 9) are the same as the stresses due to the unit torsion opposed only by the spars (column 7); and the S_1 stresses (column 10) are equal to $-S_0$ plus the stresses due to the unit torsion opposed only by the drag bracing (column 8).

The total internal work in the portion of the structure under consideration is designated by W , and is given by:

$$W = \sum \frac{S^2 L}{2AE} = \sum \frac{(S_0 + XS_1)^2 L}{2AE}$$

W has its minimum value when $dW/dX = 0$. By differentiating the above expression with respect to X , and equating to zero, the following equation for the solution of X is obtained:

$$X \sum S_1^2 L / EA + \sum S_0 S_1 L / EA = 0.$$

The summation is taken over all that part of the wing structure intercepted between two parallel planes 1 inch apart, perpendicular to the axis of the wing at Stations 22 and 23. The modulus E is the same for all members, and cancels out. Let $U = L/A$. Then

$$X = - \frac{\sum U S_0 S_1}{\sum U S_1^2}$$

The least work calculations are detailed in Table VI. The stresses due to the unit load of 1,514 lb. on each spar and drag truss are taken from Table V. The stresses, S_0 , are the effect of the unit torsional moment opposed by the spars alone, without assistance from the drag bracing. These stresses are obtained by multiplying the stresses in each spar due to 1,514 lb. load by the values of $I_s / \sum I_s^2$ calculated in Table III. The S_1 stresses are equal and opposite to the S_0 stresses, plus the stresses in the drag trusses when they alone resist the unit torsion. The latter stresses, as shown on page 7, are the result of loads of 81.4 lb., acting forward in the upper drag truss, and in the reverse direction in the lower drag truss.

It is found by the computations in Table VI that $X = 0.4919$. The stresses in all members at Station 22, due to the unit torsional moment of 1,514 lb. at 1 per cent of the wing chord aft of the elastic axis, are given in the column headed S in Table VI.

STRESSES AT STATION 22 DUE TO UNIT LOADS IN THREE FLIGHT CONDITIONS

The stresses at Station 22 are calculated for the unit load in the following three conditions of flight:

(a) High Incidence, normal load, 1,514 lb.; antidrag load, 210 lb.; center of pressure at 31 per cent of the chord length from the leading edge, or 3.23 per cent of the chord forward of the elastic axis.

(b) Low Incidence, normal load, 1,514 lb.; drag, 224 lb., center of pressure at 51 per cent of the chord from the leading edge, or 16.77 per cent aft of the elastic axis.

(c) Inverted Flight, normal load, -1,514 lb.; zero drag, center of pressure at 3.23 per cent of the chord forward of the elastic axis.

The drag force is assumed to act through the elastic axis, producing no torsion.

In calculating the stresses in each condition, the effects of the normal force, drag, and torsion are each found by proportionality from the stresses due to the unit loads as already computed. The normal load is distributed between the front, center, and rear spars in the ratios, 0.452, 0.332, and 0.218, respectively, as determined in Table II. The drag is divided equally between the two drag trusses; and the torsional stresses are equal to the final S stresses in Table VI multiplied by the distance of the center of pressure from the elastic axis in terms of per cent of the chord.

COMPARISON OF CALCULATED AND MEASURED STRESSES

The welded steel tubular wing truss, to which the foregoing stress calculations apply, was tested by sand loading at the static testing laboratory at McCook Field. Electric telemeter strain gauges, of the carbon pile resistance type developed by the Bureau of Standards, were clamped to the longitudinal members cut by Station 22.

The readings of the strain gauges, and the corresponding stresses are shown in Tables X, XI, and XII. The locations of the gauges, and the increments of stress per unit load are shown

in Tables XII, XIII, and XIV. The calculated stresses are also given in these tables for comparison with observation. The test at low incidence was the most illuminating because the largest amount of data was obtained, and the torsion of the wing was greatest, giving the best opportunity to check the theory. Inspection of Table XIII shows that the average stresses agreed fairly well with the theory. In fact, the stresses indicated by the gauges for different increments of load varied between themselves more than their averages differed from the theoretical stresses. It is therefore apparent that the theory is as good as the method of measuring stresses in this test, or else that the stresses were not proportional to the applied loads. It should be remembered that the strain gauges are not particularly accurate because of the tendency of the carbon piles to change their sensitivity to pressure and hence disturb their calibration. Moreover, the gauges were at considerable distances from the axes of the tubular members to which they were secured, and the steel was so hard that the points of the gauges could not be pressed into it. To overcome this difficulty, it was necessary to interpose pieces of aluminum, bored to fit the tubes, with flat exterior faces to receive the gauge points. A certain amount of lost motion was inevitable with this arrangement. In the case of compression members, the gauges were placed in pairs, one on each side of the tube. The two units of a pair often indicated quite different stresses, showing that there was buckling of the members. However, the outside radii of the tubes were only about one-third to one-half as great as the distances of the lines of action of the gauges from the neutral axes of the tubes, so that the buckling stresses were not nearly so great as indicated by the differences between the strains shown by the two gauges of a pair.

THE COEFFICIENT OF TORSIONAL RIGIDITY

The angular twist θ , of a wing in a given length of span, L , due to a given torsional bending moment, M , is inversely proportional to the absolute rigidity of the wing. When investigating the torsional rigidity of short lengths of span, it is convenient to replace θ by $Ld\theta/dL$. It is to be expected that the torsional moment acting upon wings of similar sections, with homologous positions of the elastic axis, will vary as qFb , where q is the aerodynamic head, F the area of the wing, and b the chord length. It follows that for equal comparative torsional rigidities of different wings, $\frac{M}{Ld\theta/dL}$ should be proportional to qFb . Hence a measure of comparative rigidity is the nondimensional coefficient, C_t , defined by:

$$\frac{M}{Ld\theta/dL} = C_t q F b, \text{ or}$$

$$C_t = \frac{M \cdot dL}{L \cdot q \cdot F \cdot b \cdot d\theta}$$

The work done by a torsional moment M within the length L is given by

$$W = \frac{ML \cdot d\theta}{2 \cdot dL}$$

And also:

$$W = \sum \frac{S^2 L}{2EA}$$

where the summation is taken over all members of the structure within the length L .

Whence:

$$C_t = \frac{M^2}{2WqFb} = \frac{M^2}{2Fb} \sum \frac{EA}{S^2 L}$$

Other things being equal, C_t is inversely proportional to W . The summations of the last two columns of Table VI show the comparative rigidities of the XHB wing at station 22, with

and without the drag bracing. The work in 1 inch length due to the unit torsion without drag bracing is given by:

$$W = \Sigma \frac{USo^2}{2E} = \frac{445,868}{58,000,000} = 0.0077 \text{ in. lb.}$$

With the drag bracing in action,

$$W = \Sigma \frac{US^2}{2E} = \frac{73,284}{58,000,000} = 0.00126 \text{ in. lb.}$$

That is to say, the torsional rigidity is six and one-tenth times greater with the drag bracing than without it.

CONCLUSIONS AND RECOMMENDATIONS

The structural analysis of a cantilever wing shows that the inclusion of strong drag bracing in the top and bottom of the wing enormously increases the torsional rigidity. It is recommended that the use of drag bracing to improve torsional rigidity be extended to other types of wing. Increasing the torsional stiffness improves the aerodynamic qualities of a wing, and raises the critical speed at which flutter commences. It also improves the structural efficiency by diminishing the shifting of the load between the front and rear spars due to movements of the center of pressure.

The customary procedure of assuming that the air load is divided between the front and rear spars of a 2-spar wing in inverse ratio to their distances from the line of the resultant air load is no longer valid when the drag bracing contributes to the torsional strength. For such wings, the position of the elastic axis should be computed, and if the resultant of the air load does not pass through the elastic axis, it should be resolved into normal and drag forces acting through and perpendicular to the elastic axis, plus a torsional moment about the axis. The stresses due to the bending of the elastic axis, and the twisting of the wing about it, should be computed separately and added together.

BUREAU OF AERONAUTICS,
NAVY DEPARTMENT, *December, 1928.*

TABLE IV

SHEAR AND BENDING IN WING WITH DISTRIBUTED LOAD OF 1,514 LB.

Station, in.	Load, lb.	Shear, lb.	Moment, in. lb.	Station, in.	Load, lb.	Shear, lb.	Moment, in. lb.
260		0	0	130		540.3	29,882
	23.0				60.1		
250		23	115	120		600.4	35,585
	26.2				62.6		
240		49.2	476	110		663.0	41,902
	29.5				65.0		
230		78.7	1,116	100		728.0	48,857
	33.0				67.6		
220		111.7	2,068	90		795.5	56,475
	36.8				70.0		
210		148.5	3,369	80		865.5	64,780
	40.8				72.4		
200		188.8	5,055	70		937.9	73,797
	42.8				74.9		
190		231.6	7,157	60		1,012.8	83,550
	45.3				77.4		
180		276.9	9,700	50		1,090.2	94,065
	47.7				79.9		
170		324.6	12,707	40		1,170.1	105,367
	50.2				82.3		
160		374.8	16,204	30		1,252.4	117,479
	52.7				84.8		
150		427.5	20,216	20		1,337.2	130,427
	55.2				87.3		
140		482.7	24,767	10		1,424.5	144,236
	57.6				89.7		
				0		1,514.2	158,929

TABLE V

Spar or drag truss	Member	Abbrevi- ation	Stress, lb.
Front spar.....	Upper front longitudinal.....	U. F.	-6,010
	Lower front longitudinal.....	L. F.	6,932
	Front spar diagonal.....	F. D.	-1,305
Center spar.....	Upper center longitudinal.....	U. C.	-5,221
	Lower center longitudinal.....	L. C.	6,124
	Center spar diagonal.....	C. D.	-1,280
Rear spar.....	Upper rear longitudinal.....	U. R.	-8,424
	Lower rear longitudinal.....	L. R.	9,290
	Rear spar diagonal.....	R. D.	-1,225
Top drag truss.....	Upper front longitudinal.....	U. F.	2,702
	Upper rear longitudinal.....	U. R.	-1,591
	Upper diagonal.....	U. D.	-1,570
Bottom drag truss.....	Lower front longitudinal.....	L. F.	1,591
	Lower rear longitudinal.....	L. R.	-2,702
	Lower diagonal.....	L. D.	1,570

TABLE VI

CALCULATION OF TORSIONAL STRESSES BY THE METHOD OF LEAST WORK

Member	L	A	U= L/A	Stress due to 1,514 lb. load on each spar or drag truss		Stress due to unit torsion opposed only by—		S ₀	S ₁	$\frac{S_0 S_1}{1,000}$	$\frac{S_1^2}{1,000}$	$\frac{U S_0 S_1}{1,000}$	$\frac{U S_1^2}{1,000}$	0.4919 S ₁	S = S ₀ + 0.4919 S ₁	U S ²	U S ₀ ²
				Spars	Drag trusses	Spars	Drag trusses										
	In.	In. ²	I/In.	Lb.	Lb.	Lb.	Lb.										
U. F-----	1.0	0.3312	3.02	-6,010	2,702	135.2	-145.3	135.2	-280.5	-37.92	78.68	-114.52	237.61	-138.0	-2.8	24	55,203
L. F-----	1.0	.2041	4.90	6,932	1,591	-156.0	85.5	-156.0	241.5	-37.67	58.32	-184.58	285.77	118.8	-37.2	6,781	119,246
F. D-----	1.414	.0786	17.99	-1,305		29.4		29.4	-29.4	-0.86	0.86	-15.47	15.47	-14.5	14.9	3,994	15,551
U. C-----	1.0	.2041	4.90	-5,221		-26.1		-26.1	26.1	-0.68	0.68	-3.33	3.33	12.8	-13.3	867	3,338
L. C-----	1.0	.1198	8.35	6,124		30.6		30.6	-30.6	-0.94	0.94	-7.85	7.85	-15.1	15.5	2,006	7,819
C. D-----	1.414	.0786	17.99	-1,280		-6.4		-6.4	6.4	-0.04	0.04	-0.72	0.72	3.1	-3.3	196	737
U. R-----	1.0	.2855	3.50	-8,424	-1,591	-147.4	85.5	-147.4	232.9	-34.33	54.24	-120.16	189.84	114.6	-32.8	3,765	76,044
L. R-----	1.0	.1656	6.04	9,290	-2,702	162.6	-145.3	162.6	-307.9	-50.06	94.80	-302.36	572.59	-151.5	11.1	744	159,691
R. D-----	1.414	.0786	17.99	-1,225		-21.4		-21.4	21.4	-0.46	0.46	-8.28	8.28	10.5	-10.9	2,137	8,239
U. D-----	1.414	.0923	15.32		-1,570		84.4		84.4		7.12		109.08	41.5	41.5	26,385	
L. D-----	1.414	.0923	15.32		1,570		84.4		84.4		7.12		109.08	41.5	41.5	26,385	
													-757.27	1,539.62		73,284	445,868

$X = -\Sigma US^2 S_1 / \Sigma US_1^2 = 757.27 / 1,539.62 = 0.4919.$

TABLE VII

STRESSES AT STATION 22 DUE TO UNIT LOAD AT HIGH INCIDENCE

Member	Normal forces, lb.	Drag force lb.	Torsional force lb.	Total force, lb.	Unit stress lb./in. ²
U. F.....	-2,705	-188	9	-2,884	-8,708
L. F.....	3,119	-111	119	3,127	15,321
F. D.....	-587		-48	-635	-8,079
U. C.....	-1,733		43	-1,690	-8,280
L. C.....	2,033		-50	1,983	16,553
C. D.....	-425		11	-414	-5,267
U. R.....	-1,836	111	105	-1,619	-5,671
L. R.....	2,025	188	-36	2,177	13,146
R. D.....	-267		35	-232	-2,952
U. D.....		109	-133	-24	-260
L. D.....		-109	-133	-242	-2,622

TABLE VIII

STRESSES AT STATION 22 DUE TO UNIT LOAD AT LOW INCIDENCE

Member	Normal forces, lb.	Drag force lb.	Torsional force lb.	Total force, lb.	Unit stress lb./in. ²
U. F.....	-2,705	200	-47	-2,552	-7,705
L. F.....	3,119	118	-625	2,612	12,798
F. D.....	-587		250	337	4,288
U. C.....	-1,733		-223	-1,956	-9,584
L. C.....	2,033		260	2,293	19,140
C. D.....	-425		-55	-480	-6,107
U. R.....	-1,836	-118	-551	-2,505	-8,774
L. R.....	2,025	-200	186	2,011	12,144
R. D.....	-267		-183	-450	-5,725
U. D.....		-116	697	581	6,295
L. D.....		116	697	813	8,808

TABLE IX

STRESSES AT STATION 22 DUE TO UNIT LOAD IN INVERTED FLIGHT

Member	Normal forces, lb.	Drag force, lb.	Torsional force, lb.	Total force, lb.	Unit stress, lb./in. ²
U. F.....	2,705		-9	2,696	8,140
L. F.....	-3,119		-119	-3,000	-14,699
F. D.....	587		48	635	8,079
U. C.....	1,733		-43	1,690	8,280
L. C.....	-2,033		50	-1,983	-16,553
C. D.....	425		-11	414	5,267
U. R.....	1,836		-105	1,731	6,063
L. R.....	-2,025		36	-1,989	-12,011
R. D.....	267		-35	232	2,952
U. D.....			133	133	1,441
L. D.....			133	133	1,441

TABLE X

TEST OF THREE-SPAR WING, INVERTED FLIGHT

Load factor..... Total load, lb.....	1.0 1,190		2.0 2,700		2.5 3,455		Load removed	
Gauge No.	Gauge reading	Stress lb./in. ²	Gauge reading	Stress lb./in. ²	Gauge reading	Stress, lb./in. ²	Gauge reading	Stress, lb./in. ²
4.....	+2.6	+4,840	+3.3	+12,300	+4.3	+16,000	+0.5	+930
5.....	-5.4	-10,050	-6.6	-24,600	-8.9	-33,100	-0.6	-1,115
6.....	-6.0	-11,170	-7.4	-27,550	-9.3	-34,600	-1.2	-2,230
7.....	+4.1	+7,630	+5.0	+18,600	+6.4	+23,800	+0.7	+1,300
8.....	-6.4	-11,900	-7.7	-28,650	-9.9	-36,800	+0.4	+745
9.....	-6.7	-12,480	-7.8	-29,000	-10.0	-37,200	-0.8	-1,490
10.....	+2.4	+4,460	+2.7	+10,050	+3.3	+12,300	-0.1	-186
11.....	-6.4	-11,900	-7.5	-27,900	-9.8	-36,500	-1.3	-2,420
12.....	-4.1	-7,630	-4.7	-17,500	-6.0	-22,340	-0.6	-1,115

TABLE XI
TEST OF 3-SPAR WING, LOW INCIDENCE

Load factor.....	2.0		2.5		3.0	
Total load, lb.....	2,700		3,455		4,210	
Gauge No.	Gauge reading	Stress lb./in. ²	Gauge reading	Stress lb./in. ²	Gauge reading	Stress lb./in. ²
4.....	+6.8	+25,300	+9.1	+33,830		
5.....	-4.3	-16,000	-5.3	-19,700	-6.5	-24,200
6.....	-4.5	-16,750	-5.9	-22,000	-6.9	-25,700
7.....	+9.9	+36,800				
8.....	-4.8	-17,860	-5.3	-19,700	-6.5	-24,200
9.....	-6.5	-24,200	-7.7	-28,650	-9.2	-34,200
10.....	+5.4	+20,100	+6.3	+23,450	+7.5	+27,900
11.....	-2.9	-10,800	-3.6	-13,400	-4.2	-15,620
12.....	-4.5	-16,750	-5.6	-20,840	-6.6	-24,550
Load factor.....	2.5		2.0		Load removed	
Total load, lb.....	3,455		2,700			
Gauge No.	Gauge reading	Stress lb./in. ²	Gauge reading	Stress lb./in. ²	Gauge reading	Stress lb./in. ²
4.....						
5.....	-5.8	-21,600	-4.6	-17,110	-0.8	-1,490
6.....	-6.0	-22,350	-4.9	-18,240	-1.3	-2,420
7.....						
8.....	-5.3	-19,730	-4.1	-15,270	+1.0	+1,860
9.....	-7.5	-27,900	-5.9	-22,000	+0.8	+1,490
10.....	+6.2	+23,100	+5.0	+18,600	-0.6	-1,116
11.....	-3.6	-13,400	-3.0	-11,160	-0.2	-372
12.....	-5.6	-20,840	-4.6	-17,110	-0.6	-1,116

TABLE XII
TEST OF 3-SPAR WING, HIGH INCIDENCE. LOAD FACTOR 2; TOTAL LOAD, 2,700 LB.

Gauge No.	Position of gauge		Gauge reading	Stress, lb./in. ²	Increment of stress per unit load, lb./in. ²	Calculated increment, lb./in. ²
	Spar tube	Distance from root in.				
11	Upper front.....	38	-3.9	-14,500	-8,100	-8,708
12	do.....	38	-4.6	-17,110	-9,560	-8,708
10	Lower front.....	25.4	+8.1	+30,150	+16,850	15,321
8	Upper center.....	48.5	-5.7	-21,200	-11,850	-8,280
9	do.....	48.5	-5.6	-20,840	-11,650	-8,280
7	Lower center.....	20.8	+8.3	+30,860	+17,250	16,553
5	Upper rear.....	26.9	-1.8	-6,700	-3,740	-5,671
6	do.....	26.9	-2.4	-8,940	-5,000	-5,671
4	Lower rear.....	17.4	+4.8	+17,860	+9,980	13,146

TABLE XIII
TEST OF 3-SPAR WING, LOW INCIDENCE

Load range.....			0 to 2	2 to 2.5	2.5 to 3	3 to 2.5	2.5 to 2	2 to 0	Mean increment lb./in. ²	Calculated increment lb./in. ²	
Gauge No.	Position of gauge		Increment of stress per unit load, lb./in. ²			Increment of stress per unit load, lb./in. ²					
	Spar tube	Inches from root									
11	Upper front.....	38	-6,030	-5,200	-4,440	-4,440	-4,480	-6,010	} -6,600	{ -7,705	
12	do.....	38	-9,350	-8,180	-7,420	-7,220	-7,460	-8,930			{ -7,705
10	Lower front.....	25.4	+11,200	+6,700	+8,900	+9,600	+9,000	+11,000			
8	Upper center.....	48.5	-9,980	-3,680	-9,000	-8,940	-8,920	-9,600	} -10,100	{ -9,584	
9	do.....	48.5	-13,500	-8,900	-11,100	-12,600	-11,800	-13,100			{ -9,584
7	Lower center.....	20.8	+20,600								
5	Upper rear.....	26.9	-8,940	-7,400	-9,000	-5,200	-8,960	-8,730	} -8,280	{ -8,774	
6	do.....	26.9	-9,350	-10,500	-7,400	-6,700	-8,220	-8,840			{ -8,774
4	Lower rear.....	17.4	+14,150	+17,060							

TABLE XIV

TEST OF 3-SPAR WING, INVERTED FLIGHT

Load range.....			0 to 1.0	1 to 2	2 to 2.5	Calculated increment, lb./in. ³
Gauge No.	Position of gauge		Increment of stress per unit load, lb./in. ³			
	Spar tube	Inches from root				
4	Upper front.....	37	+6,150	+7,460	+7,400	8,140
5	Lower front.....	25.4	-12,800	-14,550	-17,000	-14,699
6	do.....	25.4	-14,200	-16,380	-14,100	-14,699
7	Upper center.....	49.4	+9,700	+10,970	+10,400	8,280
8	Lower center.....	19.5	-15,100	-16,750	-16,300	-16,553
9	do.....	19.5	-15,840	-16,520	-16,400	-16,553
10	Upper rear.....	27.5	+5,660	+5,590	+4,500	6,063
11	Lower rear.....	17.3	-15,100	-16,000	-17,200	-12,011
12	do.....	17.3	-9,700	-9,870	-9,680	-12,011

REPORT No. 330

EXPERIMENTAL AND ANALYTICAL DETERMINATION OF THE MOTION OF HYDRAULICALLY OPERATED VALVE STEMS IN OIL ENGINE INJECTION SYSTEMS

By A. G. GELALLES and A. M. ROTHROCK
Langley Memorial Aeronautical Laboratory

REPORT No. 330

EXPERIMENTAL AND ANALYTICAL DETERMINATION OF THE MOTION OF HYDRAULICALLY OPERATED VALVE STEMS IN OIL ENGINE INJECTION SYSTEMS

By A. G. GELALLES and A. M. ROTHROCK

SUMMARY

This research on the pressure variations in the injection system of the N. A. C. A. Spray Photography Equipment and on the effects of these variations on the motion of the timing valve stem was undertaken in connection with the study of fuel injection systems for high-speed oil engines. The Spray Photography Equipment employed for these tests consists of a fuel injection system for producing an oil spray, an electrical spark system for illuminating the spray, and a photographic camera for recording its development. The fuel injection system contains a high-pressure hand pump for producing the injection pressures, an oil reservoir for maintaining the pressures of the fuel during the injection, a timing valve for timing the start of the oil spray, an injection valve for atomizing the oil, and a by-pass valve for controlling the cut-off of the spray. Additions were made to the apparatus in order to record the motion of the timing valve stem photographically.

The timing valve stem was held against its seat by a helical spring so adjusted that the total hydraulic force on the stem actuated it immediately after it had been mechanically lifted from its seat. The lift of the stem was recorded photographically to determine the effects of injection tubes 7 inches and 43 inches long. The pressure variations at the seat and in the injection valve tubes were analyzed and the lifts of the stem for both tubes computed from the analysis and compared with the experimental records.

The calculations indicate that the hydraulic pressure at the timing valve seat was rising at a rate of 350,000,000 pounds per square inch per second when the timing valve stem had been lifted 0.004 inch, and that the hydraulic pressure throughout the tube did not approximate that of the oil in the reservoir until 0.0028 second after the timing valve started to open with the 43-inch tube and 0.0003 second with the 7-inch tube. The calculations and experiments indicate that after the by-pass valve started to open the hydraulic pressure in the tube dropped to the closing pressure of the timing valve in 0.0015 second with the 43-inch tube and in 0.0004 second with the 7-inch tube. The photographic records of the stem motion show that the stem reached the maximum lift approximately 0.001 second later with the 43-inch tube than with the 7-inch tube, and that the valve stem seated 0.0005 second later with the 43-inch tube than with the 7-inch tube.

The general equation for the motion of the stem of a spring-loaded valve when the motion is controlled by hydraulic pressure is

$$f = \lambda s + m \frac{d^2 s}{dt^2}$$

where f = hydraulic force on the stem at any time t seconds after the start of motion plus or minus the friction of the stem in its guide,

λ = scale of spring,

s = compression of the spring at any time t seconds after the start of motion,

m = mass of moving parts.

The methods of analysis of the pressure variations and the general equation for the motion of the spring-loaded stem for the timing valve are applicable to a spring-loaded automatic injection valve, and in general to all hydraulically operated valves. A sample calculation for a spring-loaded automatic injection valve is included.

INTRODUCTION

The design of an efficient, smooth-running, high-speed oil engine requires careful study of the operation of its fuel injection system. Of the two types of injection systems generally used—air injection and hydraulic pressure injection—the hydraulic pressure system is particularly adaptable to the high-speed oil engine. There are two types of hydraulic pressure injection systems, one using a mechanically operated injection valve, and the other a hydraulically operated or automatic injection valve. Most fuel injection systems using automatic injection valves are fitted with an injection tube a foot or more in length between the injection valve and the fuel pump. The oil in this tube, with few exceptions, is subjected to high pressures only during the injection period. The instantaneous pressures at the injection valve are not the same as those in the fuel pump because of the compressibility of the oil within the injection tube, the elasticity of the injection tube walls, and the inertia of the oil.

The form and penetration of a fuel spray from an injection valve depend largely on the hydraulic pressure variations in the injection valve during the injection period. The pressures under which the injection valve operates are affected to a large extent by the compressibility of the oil within the injection tube, the elasticity of the tube walls, and such pressure

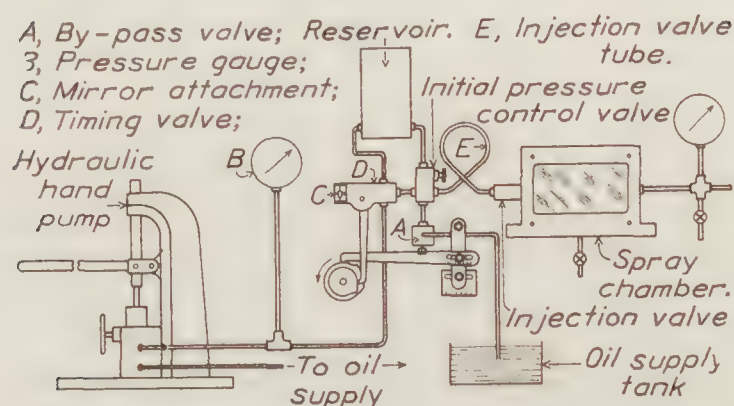


FIGURE 1.—Diagrammatic arrangement of apparatus for production and control of spray

waves as may occur in the injection system. These pressure variations can be approximately determined by analyzing the effects of injection tube length and bore, residual pressure in the injection tube, injection pressure, and different rates of pump displacement. No experimental or theoretical data, so far as is known, have been published on these variations of pressure during the period of injection.

Investigations have been started at the Langley Memorial Aeronautical Laboratory at Langley Field, Va., for the purpose of studying these pressure variations in the injection system of the N. A. C. A. Spray Photography Equipment. (Reference 1.) This injection system consists of an oil reservoir into which the fuel oil is pumped under hydraulic pressures up to 8,000 pounds per square inch, a timing valve to release the oil under pressure from the reservoir to the injection valve, an injection-valve tube connecting the timing valve to the injection valve, and the injection valve from which the oil is sprayed into the spray chamber.

This report covers an investigation of the pressure variations in this injection system in which the motion of the timing valve was determined experimentally when its lift was controlled by the hydraulic pressure of the oil in the reservoir. The purpose of this investigation was, first, to determine how closely the actual motion of the timing-valve stem approached the motion of the stem as it was computed from an analysis of the pressure causing the stem to lift, and, second, to determine the effect of the length of the injection-valve tube on the pressure variations at the timing valve. The timing-valve stem was held against its seat by a helical spring so adjusted that the stem was actuated by the oil pressure after it had been lifted approximately 0.001 inch from the seat by a cam-operated rocker arm. Thus the operation of the timing valve under this spring load was similar to that of a spring-loaded automatic injection valve.

APPARATUS AND METHODS

The N. A. C. A. Spray Photography Equipment (reference 1) consists of a fuel-injection system for producing the oil spray, an electrical-spark system for illuminating the spray, and a photographic camera for recording its development. The fuel injection system (fig. 1) contains a high-pressure hydraulic hand pump for producing the injection pressures, an oil reservoir for maintaining the pressure during injection, a timing valve for timing the start of injection, an injection valve for atomizing the oil, and a by-pass valve for controlling the cut-off of the injection.

The timing valve (fig. 2) is a spring-loaded needle valve operated by a cam and a rocker arm. One half of a clutch similar to the type used in punch presses is rigidly attached to a shaft that is driven by an electric motor at 950 r. p. m. The other half of the clutch is mounted on the cam shaft and engages the first half when a trip lever is struck. The two halves of the clutch remain engaged for one revolution of the cam shaft causing a complete cycle of the operation of the injection system to take place.

Additional apparatus was installed (fig. 3) in order to record the motion of the timing valve stem photographically. A pivoted mirror was connected to the outer end of the timing valve stem by a lever arm. A beam of light from a point source was focused on this mirror by a lens and was reflected onto a photographic film mounted on a drum which was rotated by an electric motor at a speed of 3,400 r. p. m. Any motion of the stem changed the angle of the mirror and the position of the reflected beam of light on the film. The motion of the stem during the operation of the valve was thus recorded on the film as a continuous line.

It was desired in this research to investigate the pressure variations at the timing-valve seat and in the injection tube as well as the motion of the timing valve stem. Consequently, the spring force on the stem was adjusted so that it was less than the hydraulic force on the stem when the valve was opened, but still held the stem against the seat with sufficient force to prevent leakage of the fuel when the valve was closed. The hydraulic force on the stem from the injection pressure used in these tests was 153 pounds when the valve was opened and 67 pounds when the valve was closed. A spring force of 132 pounds was found sufficient to prevent leakage. Under these conditions the hydraulic force actuated the stem after the cam had lifted it sufficiently to permit the oil pressure to build up around the seat and end of the stem. The rocker arm (fig. 2) was adjusted with a clearance of 0.001 inch between it and the spring follower when the valve was closed so that the entire spring force acted upon the seat.

The test procedure was similar to that used in the tests on injection valves with this apparatus. (Reference 1.) The pressure was

raised by means of the hydraulic hand pump to 1,000 pounds per square inch in the injection valve tube and to 8,000 pounds per square inch in the oil reservoir. The rotating half of the clutch and the film drum were brought to the test speeds. The beam of light was focused on the mirror. The clutch trip lever was struck, the clutch engaged, and the cam shaft made one revolution. Oil passed through the opening between the stem and the

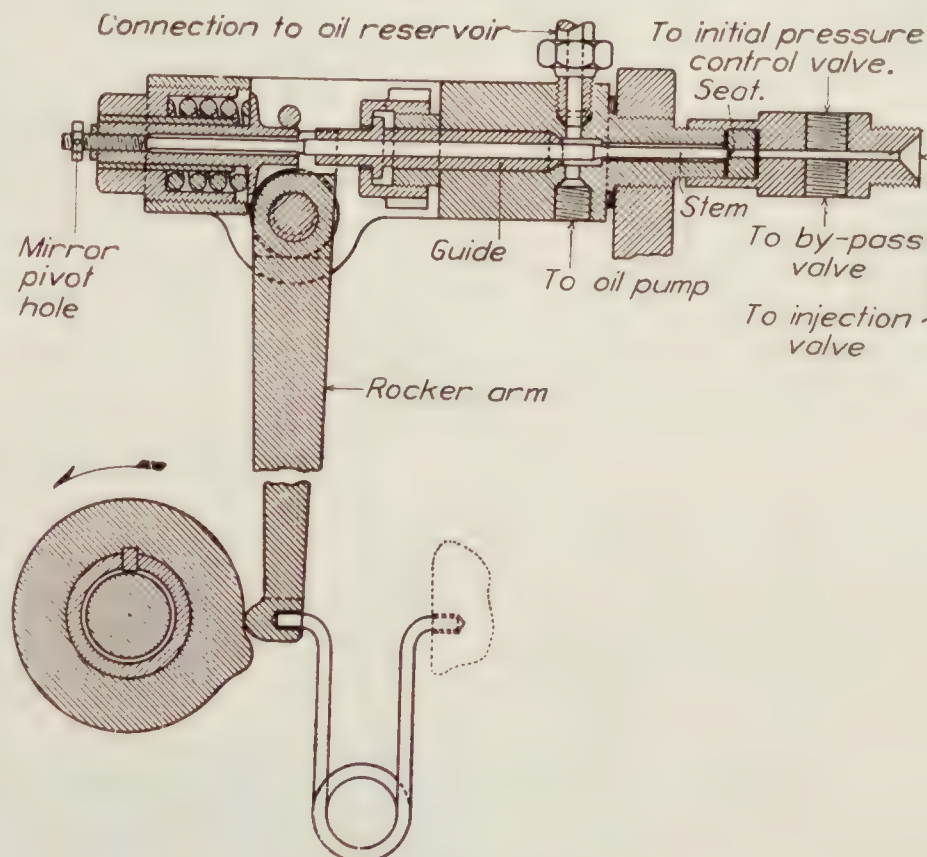


FIGURE 2.—Timing valve mechanism

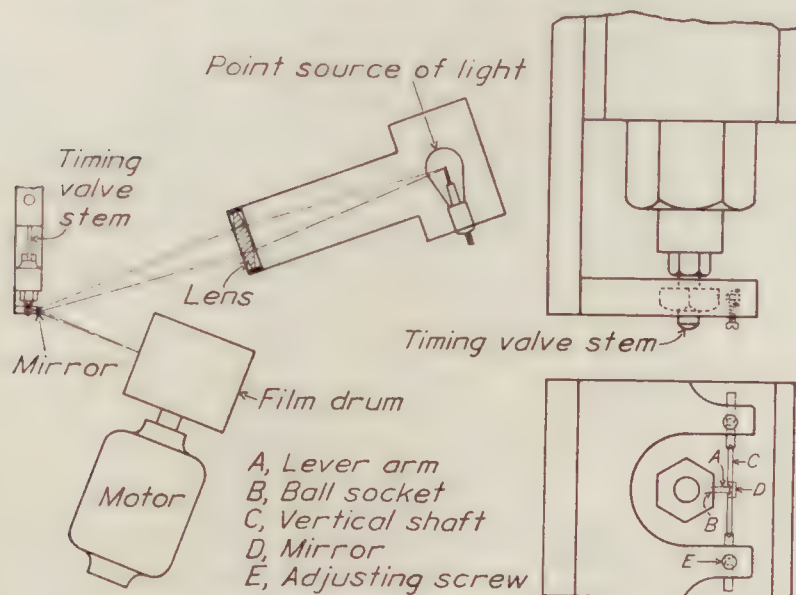


FIGURE 3.—Apparatus for recording the motion of the timing valve stem. Enlarged views of end of timing valve, showing mirror attachment on end of stem, given at right of figure

nozzle seat of the timing valve as the rocker arm lifted the stem and the oil pressure built up around the seat and end of the stem. As soon as the hydraulic force exceeded the spring force, the stem lifted at a faster rate than that produced by the cam. The oil passed through the timing valve into the injection valve tube, forced the injection valve open and sprayed into the spray chamber. A second cam opened the by-pass valve 0.0043 second after the timing valve stem was put in motion, the pressure dropped in the injection tube, and the injection valve closed.

A record was taken of the motion of the timing valve stem as produced by the cam alone with no oil in the system, so that the start of the motion produced by the hydraulic pressure might be obtained. The force acting on the rocker arm at the start of the motion was increased 67 pounds when no hydraulic pressure was used in the system. The effect of the rocker arm deflection on the lift of the stem due to this difference of force was found by both computations and experiment to be 0.0006 inch. Corrections were made for the rocker arm deflection in order to compare this record with those produced by the hydraulic pressure.

EXPERIMENTAL RESULTS

A photographic record of the motion of the timing valve stem with the 7-inch injection tube is shown in Figure 4. The time is recorded horizontally and the lift vertically. The horizontal line represents zero lift. The velocity with which the stem was lifted is seen to have increased during the first part of the opening of the valve and then to have remained practically constant until the maximum lift was reached. This maximum lift, due to the inertia of the

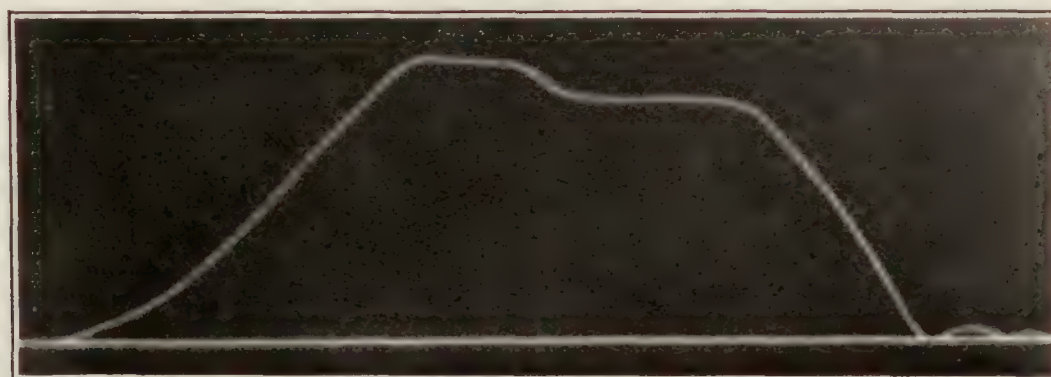


FIGURE 4.—Record of the timing valve stem motion. Tube length 7 inches. Injection pressure 8,000 lb./sq. in. Initial injection tube pressure 1,000 lb./sq. in.

moving parts of the valve, was greater than the lift at which the restoring force of the spring was in equilibrium with the hydraulic force. The resulting harmonic motion produced by this effect was damped out by the reversal of the friction of the stem in its guide and by the inertia of the oil. The stem then remained in the position at which the spring force, hydraulic force, and friction were in equilibrium. This part of the curve has a slight downward slope because of the discharge of the oil from the reservoir. The pressure in the system was released after an interval of 0.0043 second by the opening of the by-pass valve. As the pressure across the timing valve seat dropped the stem was forced back by the valve spring to the closed position. The rate of closing of the valve was controlled by the spring force, the rate of pressure drop, the inertia of the moving parts of the valve, and the friction of the stem in its guide. The stem rebounded after the impact against its seat since the excess of spring force over the hydraulic force at this time was small.

The record shown in Figure 4 is reproduced in curve (a) (fig. 5), with the coordinates of time and lift. Curve (b) (fig. 5) is a reproduction of a photographic record of the stem motion with the 43-inch injection tube. Curve (c) (fig. 5) is a reproduction of a record of the stem motion produced by the cam alone. The variations between curves (a) and (b) are caused by the effects of the injection tube lengths on the volumes of the oil in the tubes and the distance of pressure wave travel, since all other test conditions were maintained constant. The difference between the rates of opening of the valve for the two injection tubes indicates that with the shorter tube and smaller oil volume the pressure at the timing valve seat and across the end of the timing valve stem increased faster than with the longer tube. The maximum lift is greater

with the 7-inch tube because of the higher velocity of the stem as indicated in Figure 5. The rate of closing of the timing valve is approximately the same for both tubes. However, with the 7-inch tube the valve closed about 0.0005 second earlier than with the 43-inch injection tube, although the by-pass valve opened at the same time for both tubes. The curves show that the velocities with which the stem came in contact with the seat, points A and A', were comparatively high and that the valve stem rebounded from the seat.

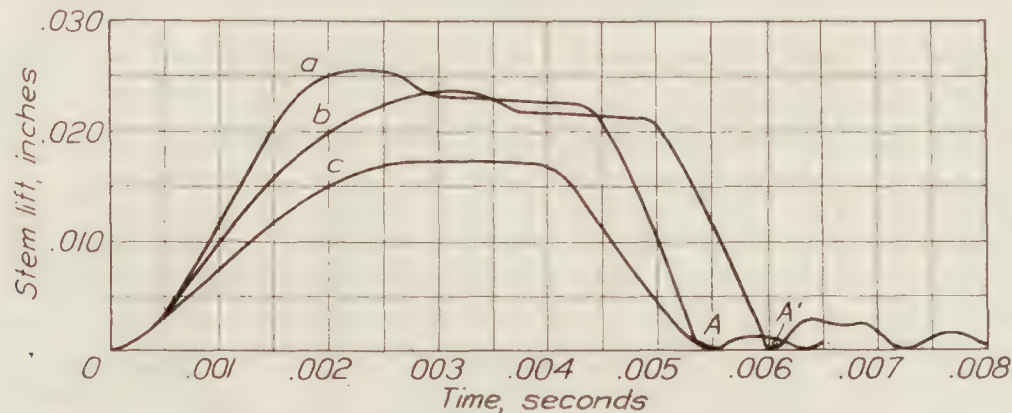


FIGURE 5.—Effect of injection valve tube length on the lift of the timing valve stem. Injection pressure, 8,000 lb./sq. in. Initial pressure in the injection valve tube, 1,000 lb./sq. in. Curve a—tube length 7 inches, inside diameter $\frac{1}{8}$ inch; curve b—tube length 43 inches, inside diameter $\frac{1}{8}$ inch; curve c—stem motion imparted by the cam

The experimental records do not give exact measures of the pressures existing at the timing valve seat and end of the stem while the stem was in motion because of the friction and inertia of the moving parts. They do, however, give a direct comparison between the different test conditions. The straight-line portion of each curve is a measure of the maximum pressure and the friction, since the maximum pressure at the valve seat was maintained for a short time.

ANALYSIS OF PRESSURE VARIATIONS—COMPUTATIONS OF THE VALVE-STEM MOTION

A mathematical analysis can be made of the pressure variations in the timing valve and in the injection valve tube from which the motion of the timing valve stem for given test conditions can be approximately computed. The motion of the stem may be divided into two parts—first, the motion imparted by the cam, and, second, the motion imparted by the hydraulic pressure. The motion is imparted by the cam until the hydraulic force exceeds the spring force by an amount sufficient to give the stem a faster rate of lift than that given by the cam. The time required for the hydraulic force to reach this value can be computed from the test conditions and from a consideration of the flow of a liquid between two parallel planes moving away from each other. These computations will be greatly simplified if it be considered that the seat and the end of the stem are extended to form complete cones, that the oil in the injection tube does not affect the rate of pressure rise between the seat and stem, and that the pressure rises across the end of the stem at the same rate as at the smallest circumference of the seat. The hydraulic pressure p at any point on the conical surface of the seat at a distance l from the apex of the cone, under these conditions, is given by the equation

$$p = P - \frac{3 \mu V (l_2^2 - l^2)}{h^3 \cos^2 \alpha} \quad (A)$$

where P = pressure at the larger circumference of the seat,
 μ = viscosity of the fuel oil,
 V = velocity at which the stem is lifted from its seat,
 h = stem lift or opening measured parallel to the stem axis,
 α = angle the conical surfaces of the seat make with a plane perpendicular to the stem axis, and
 l_2 = distance from apex of cone to its base measured along the conical surface.

Consider the flow of a liquid between two fixed parallel planes, separated by a distance h (fig. 6), with the pressure gradient extending in the directions X and Y . The flow per unit

width in the directions X and Y , respectively, when h is small, is given by equations (1) and (2) (reference 2),

$$U = \frac{h^3}{12\mu} \frac{\partial p}{\partial x} \quad (1)$$

$$T = \frac{h^3}{12\mu} \frac{\partial p}{\partial y} \quad (2)$$

in which U and T are the respective rates of flow, μ the viscosity of the fluid, and p the unit pressure. At the timing valve seats (fig. 7) there are two conical surfaces moving away from each other. Consequently, there is an excess of inflow over outflow to supply the increase of volume between the surfaces. The pressure p between the seat and stem for any lift of the stem h varies from a maximum at r_2 to a minimum at the apex of the cone formed by extending the seat. Consider a differential volume (fig. 7) extending between the seat and stem and contained between two planes normal to the conical surfaces at distances l and $l + \delta l$ from the apex of the cone, and between two planes that intersect along the axis of the stem making a small angle $\delta\theta$ radians on the surfaces. When the stem moves from the seat at a velocity V_1 , measured normal

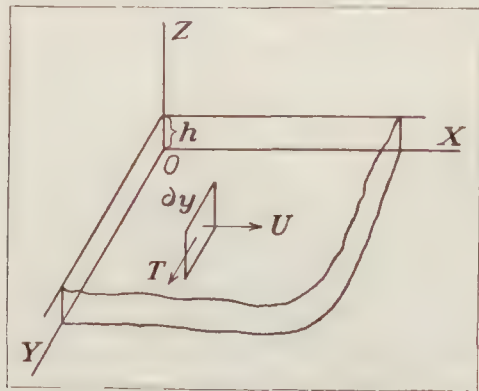


FIGURE 6

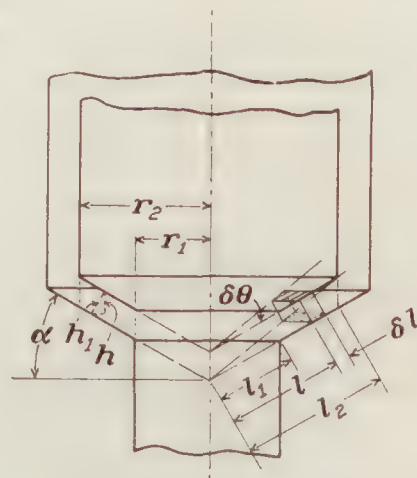


FIGURE 7.—Timing valve seat

to the seat, the rate of increase of volume is $V_1 \delta l \delta \theta$. This rate of increase in volume is also equal to the rate of increase in inflow. Equating the rate of increase of volume to the rate of increase of inflow obtained from equation (1),

$$V_1 \delta l \delta \theta = \frac{\partial}{\partial l} \left[\frac{h_1^3}{12\mu} \frac{\partial p}{\partial l} l \delta \theta \right] \delta l \quad (3)$$

This reduces to

$$\frac{12 V_1 l \mu}{h_1^3} = \frac{\partial}{\partial l} \left[l \frac{\partial p}{\partial l} \right] \quad (3a)$$

Integrating (3a),

$$\frac{6 V_1 l^2 \mu}{h_1^3} = l \frac{\partial p}{\partial l} + C_1 \quad (4)$$

when $l = 0$, $\frac{\partial p}{\partial l} = 0$. Substituting these values in equation (4) it is found that

$$C_1 = 0,$$

so that equation (4) becomes

$$\frac{\partial p}{\partial l} = \frac{6\mu V_1}{h_1^3} \quad (4a)$$

Integrating again,

$$p = \frac{3\mu V_1 l^2}{h_1^3} + C_2 \quad (5)$$

when $l = l_2$, $p = P$. Substituting

$$C_2 = P - \frac{3\mu V_1 l_2^2}{h_1^3}$$

and

$$p = P - \frac{3\mu V_1}{h_1^3} (l_2^2 - l^2) \quad (5a)$$

If V is the rate at which the stem is lifted from the seat, measured parallel to the stem axis, then

$$V_1 = V \cos \alpha,$$

and from Figure 7,

$$h_1 = h \cos \alpha.$$

Equation (5a) then becomes

$$p = P - \frac{3\mu V}{h^3 \cos^2 \alpha} (l_2^2 - l^2). \quad (5b), (A)$$

The pressure p_1 at r_1 for any lift h is

$$p = P - \frac{3\mu V}{h^3 \cos^2 \alpha} (l_2^2 - l_1^2). \quad (5c)$$

For the timing valve stem α is 30° , l_1 is 0.054 inch, l_2 is 0.072 inch, and the pressure P at r_2 is the injection pressure of 8,000 pounds per square inch. Experiments in this laboratory showed that at atmospheric pressure and 60° F., the viscosity of the Diesel oil used was 45 Saybolt seconds, corresponding to 0.000106 pound-second per square foot. (Reference 3.) The viscosities of oils of similar properties to the Diesel oil employed in this investigation (reference 4) are, for the average pressure of these calculations, between three and four times their viscosities at atmospheric pressure and temperature. The value of three times the viscosity of the Diesel oil at 60° F. and atmospheric pressure was used for μ . Substituting these values in (5c),

$$p_1 = 1,152,000 - 0.00127 \frac{V}{h^3} \frac{(0.072)^2 - (0.054)^2}{144} \quad (6)$$

where p_1 is in pounds per square foot, V in feet per second, and h in feet.

The values of V and h are obtained for any instant from an enlargement of a record of the cam-imparted motion of the stem. The spring end of the stem, because of the compression of the stem by the spring, was lifted 0.00157 inch before there was any actual opening between the seat and stem. The time required for this lift was 0.00028 second. Consequently, the exact values of

V and h for the tip end of the stem at the start of its lift could not be determined. It was assumed, however, that these values were the same as those of the spring end of the stem when V and h , as taken from the motion of the spring end of the stem, gave p greater than zero.

The pressure rise at l_1 as the stem lifted from the seat, obtained from equation (6), is plotted in Figure 8. The curve shows that the pressure at the smallest circumference of the stem was 97.5 per cent of the reservoir pressure 0.00011 second after the stem left the seat. The corresponding lift between the seat and stem was 0.00085 inch.

The viscosity of the fluid has been treated as a constant in the derivation of equation (5c); actually the viscosity varies with the pressure. (Reference 5.) Since equation (5c) is intended to give only the order of magnitude of the pressure variations and since the value chosen for the viscosity of the Diesel oil may be in error by as much as 100 per cent, it is believed that the further complications introduced by considering μ as a function of p are not justified.

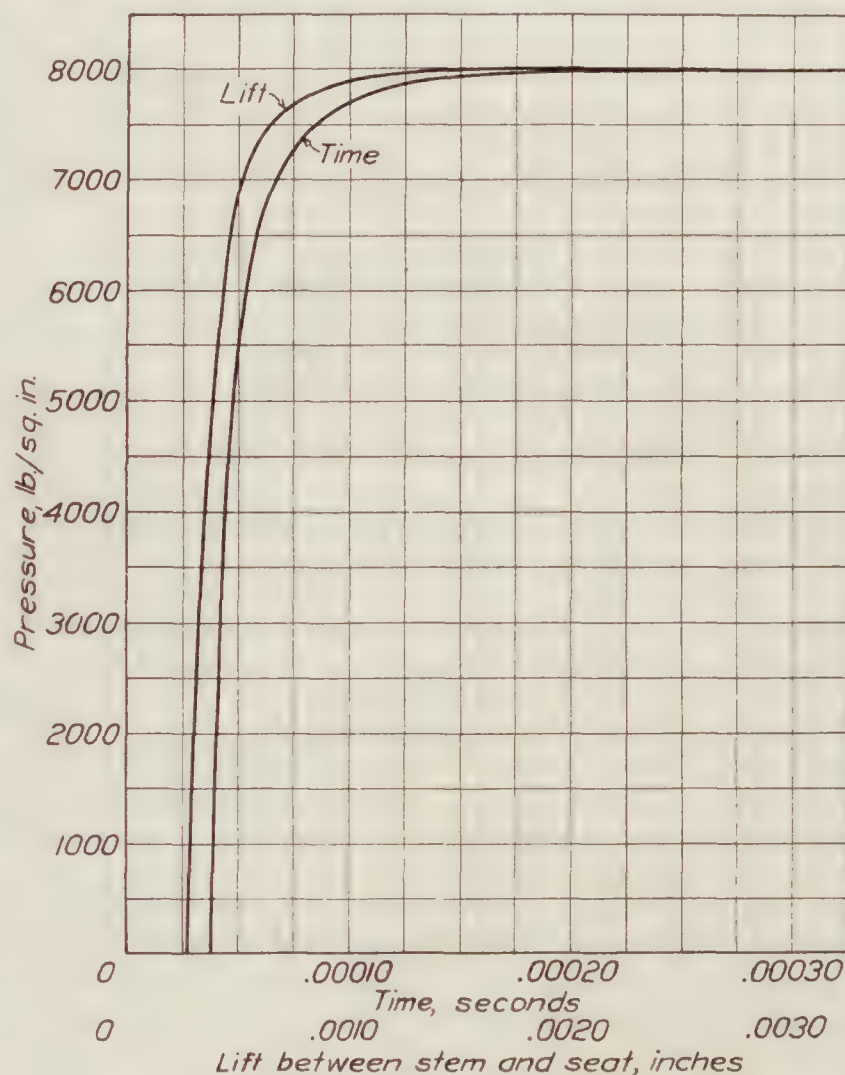


FIGURE 8.—Pressure variation at seat

The hydraulic force on the stem was of sufficient magnitude 0.00011 second after the stem was lifted from the seat to lift the stem at a faster rate than that caused by the cam. The conditions under which the stem was actuated at this time were:

Hydraulic force on stem = 153 pounds.

Spring force on stem, 132 pounds + (0.00085 inch + 0.0157 inch) 1,000 pounds per inch = 135 pounds.

Friction between stem and guide (obtained with spring balance with no pressure in valve) = 5 pounds.

Weight of moving parts = 0.130 pound.

Velocity of stem = 8.4 inches per second.

Lift of spring end of stem, 0.00085 inch + 0.00157 inch = 0.0024 inch.

Time spring end of stem had been in motion (0.00011 second + 0.00028 second) = 0.00039 second.

Spring scale: Compression (by test) = 1,150 pounds per inch; expansion (by test) = 1,125 pounds per inch.

Compression of spring, 0.115 inch + 0.00085 inch + 0.00157 inch = 0.1174 inch.

The equation for the motion of the stem when actuated by the hydraulic force is

$$t = t_1 + \sqrt{\frac{m}{\lambda}} \left[\sin^{-1} \frac{(\lambda s - f)}{k} - \sin^{-1} \frac{(\lambda s_1 - f)}{k} \right] \quad (B)$$

in which

$$k = \sqrt{f^2 + \lambda (mv_1^2 - 2fs_1 + \lambda s_1^2)}$$

where

s_1 = compression of spring at beginning of oil imparted motion,

s = any distance spring is compressed greater than s_1 ,

t_1 = time of travel to s_1 ,

t = time of travel to s ,

m = mass of moving parts,

λ = scale of spring,

f = hydraulic force on the stem minus friction of the stem in its guide, and

v_1 = velocity at s_1 .

Equation (B) is obtained from the general relation between force, mass, and acceleration,

$$F = m\alpha \quad (7)$$

in which F is the resultant force acting at the stem at the time t , and α is the acceleration of the stem. The force F is equal to the difference between the force f and the restoring force of the spring,

$$m\alpha = f - \lambda s, \quad (7a)$$

and

$$\alpha = \frac{f - \lambda s}{m} \quad (7b)$$

Since

$$\alpha = \frac{dv}{dt}, \text{ and } v = \frac{ds}{dt},$$

$$v dv = a ds \quad (8)$$

in which v is the velocity at s .

Substituting (7b) in (8)

$$v dv = \frac{f - \lambda s}{m} ds \quad (8a)$$

Integrating between the limits of v and v_1

$$\frac{v^2 - v_1^2}{2} = \frac{f}{m} (s - s_1) - \frac{(s^2 - s_1^2)}{2} \frac{\lambda}{m} \quad (9)$$

Solving (9) for v and equating to ds/dt ,

$$\frac{ds}{dt} = \sqrt{v_1^2 - \frac{2fs_1}{m} + \frac{\lambda s_1^2}{m} + \frac{2fs}{m} - \frac{\lambda s^2}{m}} \quad (9a)$$

Integrating again between the limits of s and s_1 ,

$$t = t_1 + \sqrt{\frac{m}{\lambda}} \left[\sin^{-1} \frac{(\lambda s - f)}{k} - \sin^{-1} \frac{(\lambda s_1 - f)}{k} \right] \quad (10), (B)$$

Equation (10) becomes, on substituting numerical values:

$$t = 0.00039 + \frac{1}{1849} [\sin^{-1}(78.6s - 10.1) - 1.65\pi] \quad (10a)$$

where t is in seconds and s in inches. Equation (10a) represents the time of motion of the timing valve stem in terms of compression of the spring. The lift of the stem S , is at all times 0.115 in. less than the compression of the spring. Solving for S ,

$$S = 0.0135 + 0.0127 \sin(4.46 + 1849t) \quad (11)$$

The curve for the variation of stem lift with time from equation (11) is plotted in Figure 9, curve e, and Figure 10, curve f,

for the 43-inch and 7-inch tubes, respectively. The curves show that the stem reached its maximum lift of 0.026 inch after the stem had been in motion 0.0018 second. The stem traveled to a higher maximum lift than would have been obtained from the hydraulic force alone, because of the inertia of the moving parts. The stem then returned to the position at which the hydraulic force plus the friction of the stem in its guide were in equilibrium

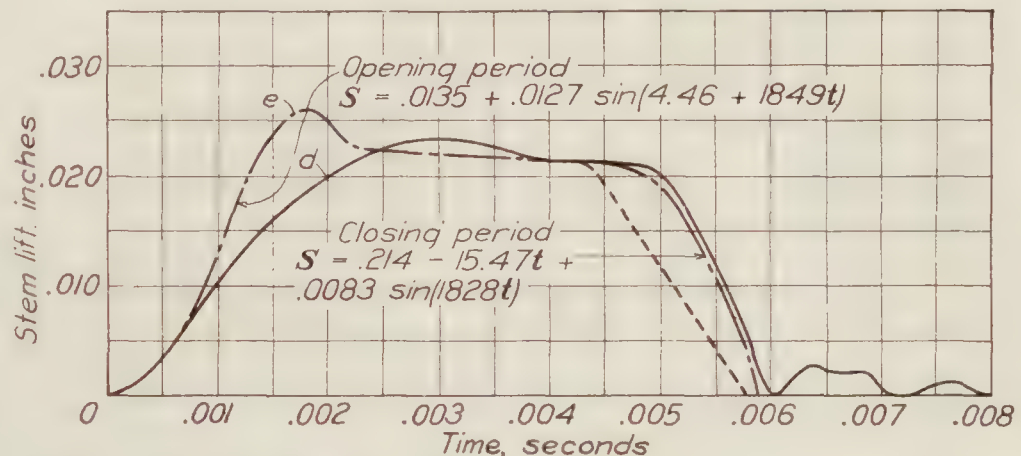


FIGURE 9.—Computed and actual motion of the timing valve stem with the 43-inch tube. Initial spring compression, 130 pounds. Injection pressure, 8,000 lb./sq. in. Initial pressure in the injection valve tube, 1,000 lb./sq. in. Curve e—computed motion; curved—actual motion

with the spring force. The static pressure in the oil reservoir and consequently the hydraulic force on the valve stem was continually reduced by the flow of oil through the timing valve. This flow supplied the oil for the compression of the oil in the injection valve tube, for the expansion of the tube walls, and for the discharge through the injection valve.

Computations for the 43-inch injection tube (appendix) show that the compression of the oil in the tube was completed in 0.0032 second and that the pressure in the oil reservoir was 7,830 pounds per square inch at that time. The forces on the stem with this pressure were in equilibrium at a lift of 0.022 inch. Consequently, the computed curves passed through the point whose coordinates were 0.0032 second and 0.022 inch. The discharge of oil through the injection valve for both tubes caused a drop of static pressure which gave the computed curves a downward slope of 0.0005 inch for each 0.001 second. Therefore, a line was drawn for the 43-inch tube (fig. 9) through the point (0.0032 second, 0.022 inch) with this slope and extended upward to the left until it intersected the curve from equation (11), and downward to the right until it intersected the abscissa 0.0043 second, at which time the by-pass valve was opened.

Similar computations for the 7-inch injection tube show that the compression of the oil column was completed in 0.0006 second and that the pressure in the oil reservoir when the maximum lift was reached was 7,940 pounds per square inch. The forces with this pressure were in equilibrium at a lift of 0.024 inch. Consequently a line was drawn starting at the second

intersection of the curve from equation (11) with the ordinate 0.024 inch and extended downward to the right with the same slope as used for the 43-inch injection tube until it intersected the abscissa 0.0043 second.

The oil force on the seat and end of the stem diminished as the oil flowed through the by-pass valve, so that the spring forced the stem back to the seat. The stem motion for the closing of the timing valve can be computed if the rate of pressure drop in the timing valve is known. The approximate rate of pressure drop at the stem was obtained as follows, assuming the static oil pressure throughout the tube was affected instantaneously by the discharge through the by-pass valve:

The motion of the by-pass valve was determined from the cam contour and linkage. An increment of lift was taken and the average pressure difference was determined for this lift by the method used for the opening of the timing valve. The amount of oil passed through the by-pass valve was calculated by the method used in the Appendix for the timing valve. The average pressure in the injection tube was obtained from the amount of oil discharged through the by-pass valve and the amount of oil passed through the timing valve and through the injection valve, the average rate of flow through the injection valve being determined experimentally (Appendix). The procedure was repeated until the computed pressure in the injection tube was reduced sufficiently to permit the closing of the timing and injection valves.

The pressure in the oil reservoir at the end of injection determined by this method was

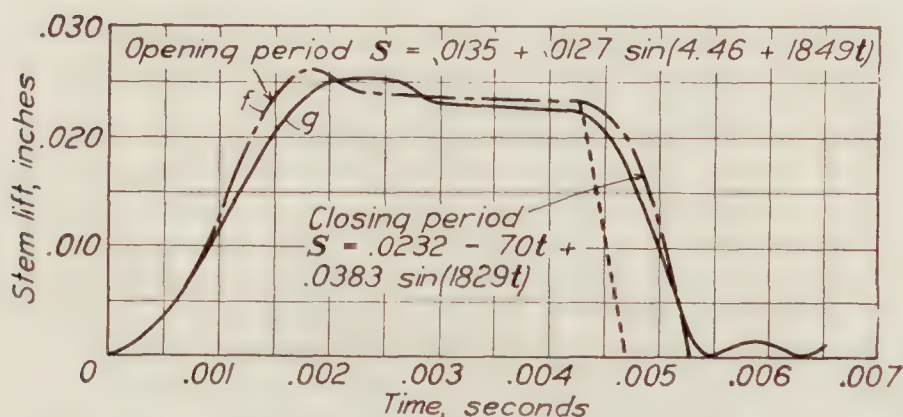


FIGURE 10.—Computed and actual motion of the stem for the 7-inch tube. Initial spring compression, 130 pounds. Injection pressure, 8,000 lb./sq. in. Initial pressure in the injection valve tube, 1,000 lb./sq. in. Curve *f*—computed motion; curve *g*—actual motion

found to be within 1 per cent of the observed pressure in the reservoir at the end of injection. The results of these calculations are represented by the short dashed lines in Figure 9 and Figure 10. These sections of the curves would have represented the travel of the timing valve stem were it not for the inertia of the moving parts and the inertia of the oil to be displaced. They represent the rate of pressure decrease in the tube.

The inertia of the oil can be disregarded since it is negligible in comparison with the other forces. The

instantaneous lag due to the inertia of the moving parts can be derived from the conditions at the start of the closing motion and the rate at which the pressure dropped at the end of the stem. The forces acting on the stem at the start of the closing motion were the hydraulic force and the friction of the stem in its guide, both tending to hold the stem in the open position, and the spring force tending to move the stem to the closed position. Using the same symbols as before, with the exception that *f* is now the sum of the hydraulic force and the friction, the equation of the closing motion is

$$f = \lambda s + ma \quad (12)$$

For any instant, *f* is equal to $C + Kt$, in which *C* is the hydraulic force at the beginning of pressure drop plus the friction, *K* is the rate of decrease of hydraulic force, and *t* the time measured from the beginning of opening of the by-pass valve. Then

$$C + Kt = \lambda s + m \frac{d^2s}{dt^2} \quad (13)$$

The complete integral of (13) is

$$s = A \sin\left(\sqrt{\frac{\lambda}{m}}t\right) + B \cos\left(\sqrt{\frac{\lambda}{m}}t\right) + \frac{C + Kt}{\lambda} \quad (14)$$

when

$$t = 0, s = \frac{C}{\lambda}, \text{ and } \frac{ds}{dt} = 0.$$

Then

$$B = 0$$

Differentiating equation (14),

$$\frac{ds}{dt} = A \sqrt{\frac{\lambda}{m}} \cos \left(\sqrt{\frac{\lambda}{m}} t \right) + \frac{K}{\lambda}$$

Substituting and solving for A ,

$$A = -\frac{K}{\lambda} \sqrt{\frac{m}{\lambda}}$$

Substituting in (14)

$$s = \frac{C}{\lambda} + \frac{Kt}{\lambda} - \frac{K}{\lambda} \sqrt{\frac{m}{\lambda}} \sin \left(\sqrt{\frac{\lambda}{m}} t \right) \quad (15), (C)$$

Substituting numerical values and solving for S , the equation of the closing motion of the timing valve stem with the 43-inch injection tube is

$$S = 0.0214 - 15.47t + 0.0083 \sin (1828t) \quad (16)$$

and with the 7-inch injection tube is

$$S = 0.0232 - 70t + 0.0383 \sin (1828t) \quad (17)$$

The curves from these equations are plotted as continuations from the abscissa 0.0043 second of curve (e) (fig. 9), and of curve (f) (fig. 10).

The experimental curves (fig. 5) are reproduced in Figures 9 and 10 for comparison with the computed curves. The curves indicate that the motion imparted by the oil pressure started at the same time for both the experimental and computed curves. The variation between the computed and experimental curves for the opening of the valve indicates that the pressure across the seat and end of the stem increased at a slower rate than was computed. The curves agree closely for the maximum pressures on the stem and for the times and the rates of closing of the valve.

APPLICATION OF THE RESULTS OF ANALYSIS TO AN AUTOMATIC FUEL-INJECTION VALVE

The opening and closing motion of the spring-loaded stem of an automatic fuel-injection valve can be obtained from the foregoing analysis if the variations of the hydraulic force acting on the stem are known. Consider an injection valve (fig. 11) of a fuel-injection system for an oil engine, the pressure in the system being built up directly by a cam-operated fuel pump and released by a by-pass valve. Assume the following operating conditions:

Helical spring force, 40.9 pounds.

Helical spring scale, 1,000 pounds per inch deflection.

Area of A normal to stem axis, 0.0153 square inch.

Area at stem seat normal to stem, 0.0123 square inch.

Friction of stem in its guide, 5 pounds.

Hydraulic opening pressure of injection valve, 3,000 pounds per square inch.

Maximum hydraulic pressure, 8,000 pounds per square inch.

Engine speed, 1,000 R. P. M.

Fuel-injection period at full load on the engine, 36° crank-shaft travel, 0.006 second.

Time for pressure to increase from opening pressure of the injection valve to maximum, 0.006 second.

Rate of pressure rise throughout the injection-tube length during the period of injection, constant (5,000/0.006 pounds per square inch per second), 833,000 pounds per square inch per second.

Weight of moving parts, 0.04 pounds.

Maximum allowable lift of injection-valve stem, 0.015 inch.

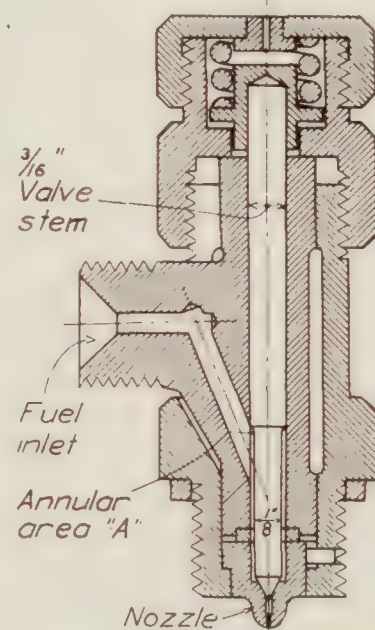


FIGURE 11.—Spring-loaded automatic fuel injection valve

The hydraulic opening pressure of 3,000 pounds per square inch in the injection valve, acting on the annular area A , is sufficient to overcome the spring force and the friction force of the stem in its guide. The hydraulic force does not act at the end of the stem until the stem has lifted sufficiently for a pressure to build up between the seat and stem. It was shown in this report, for approximately the same conditions, that the stem rises from the seat about 0.001 inch before the pressure between the seat and stem rises to that in the injection tube. An equation, therefore, is developed which will give this early part of the stem motion to a lift of 0.001 inch. For this motion, only the hydraulic force acting at the annular area A is considered; the increasing hydraulic force at the end of the stem during the interval may be neglected without appreciable error. Equation (15) may be used, since the hydraulic force varies directly with time and the stem starts from rest.

$$s = \frac{C}{\lambda} + \frac{Kt}{\lambda} - \frac{K}{\lambda} \sqrt{\frac{m}{\lambda}} \sin \left(\sqrt{\frac{\lambda}{m}} t \right) \quad (15)$$

When s is in inches, C is in pounds, λ is in pounds per inch, K is in pounds per second, and t is in seconds, m is w/g , where w is the weight of moving parts of the valve in pounds, and g is the gravitational acceleration in inches per second per second. For this valve, C is the

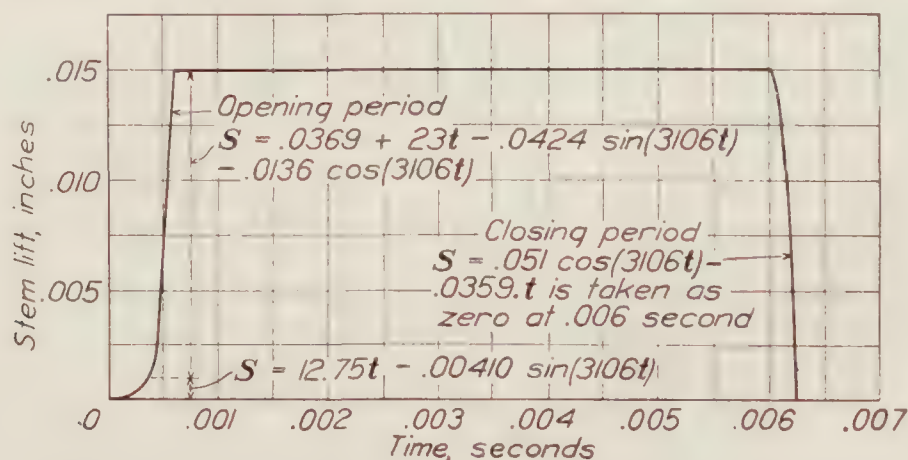


FIGURE 12.—Computed motion of a spring-loaded automatic injection valve stem. Spring scale, 1,000 lb./inch. Weight of moving parts, 0.04 lb. Opening pressure of injection valve, 3,000 lb./sq. in. Maximum pressure in injection tube when by-pass valve opened, 8,000 lb./sq. in. Time for static pressure in injection tube to rise from 5,000 to 8,000 lb./sq. in., 0.006 second. Maximum stem lift allowable, 0.015 inch

hydraulic force on the area A at the beginning of the motion of the stem minus the friction of the stem in its guide,

$$C = 0.0153 \text{ square inch} \times 3,000 \text{ pounds per square inch} - 5 \text{ pounds} = 40.9 \text{ pounds},$$

K is the rate at which the hydraulic force acting on the stem is increasing.

$$K = 833,000 \text{ pounds per square inch per second} \times 0.0153 \text{ square inch} = 12,750 \text{ pounds per second}$$

Substituting numerical values in equation (15),

$$s = \frac{40.9}{1000} + \frac{12750t}{1000} - \frac{12750}{1000} \sqrt{\frac{0.040}{1000 \times 386}} \sin \left(\sqrt{\frac{1000 \times 386}{0.040}} t \right) \quad (15a)$$

$$s = 0.0409 + 12.75t - 0.00410 \sin(3106t), \quad (15b)$$

where s is the compression of the spring in inches. The stem lift S is s minus the initial compression of the spring or $s - 0.0409$ inch. Then,

$$S = 12.75t - 0.00410 \sin(3106t) \quad (18)$$

The curve of this equation (fig. 12) shows that the lift of 0.001 inch is reached in 0.00037 second. The increase of pressure in the system for this interval of time is 308 pounds per square inch.

The hydraulic force acting on the stem during the remainder of the motion is that acting at the annular area A and at the end of the stem. Equation (14) is applicable to this part of the motion,

$$s = \frac{C}{\lambda} + \frac{Kt_1}{\lambda} + A \sin \left(\sqrt{\frac{\lambda}{m}} t_1 \right) + B \cos \left(\sqrt{\frac{\lambda}{m}} t_1 \right) \quad (14)$$

in which t_1 is 0 when $t = 0.00037$ second. The hydraulic pressure is now acting on the entire area of the stem.

Therefore,

$$C = 3,308 \text{ pounds per square inch } (0.0153 + 0.0123) \text{ square inch} - 5 \text{ pounds} = 86.3 \text{ pounds.}$$

$$K = 833,000 \text{ pounds per square inch per second } (0.0153 + 0.0123) \text{ square inch} = 23,000 \text{ pounds per second}$$

The constants of integration in equation (14) are determined from the known initial conditions of this part of the motion. When $t_1 = 0$, $s = 0.042$ inch. Substituting these values in equation (14) and solving for the constant B ,

$$0.042 = \frac{86.3}{1000} + 0 + A \sin (0) + B \cos (0)$$

$$B = -0.0443$$

Further, when $t = 0$, $\frac{ds}{dt_1}$, the velocity, is that which is obtained by differentiating equation (15b) with respect to t ,

$$\frac{ds}{dt} = \frac{d}{dt} [0.0409 + 12.75t - 0.00410 \sin (3106t)] \quad (19)$$

$$\frac{ds}{dt} = 12.75 - 0.00410 \times 3106 \cos (3106t) \quad (19a)$$

When $t = 0.00037$ second, $\frac{ds}{dt} = 7.56$ inches per second $= \frac{ds}{dt_1}$ for $t_1 = 0$. Differentiating equation (14) to determine the other constant of integration,

$$\frac{ds}{dt_1} = \sqrt{\frac{\lambda}{m}} \times A \cos \left(\sqrt{\frac{\lambda}{m}} t_1 \right) - \sqrt{\frac{\lambda}{m}} B \sin \left(\sqrt{\frac{\lambda}{m}} t_1 \right) + \frac{K}{\lambda} \quad (20)$$

Substituting numerical values and solving for the constant A , when $t_1 = 0$,

$$7.56 = 3106 \times A \cos (0) - 3106 \times 0.0443 \sin (0) + \frac{23000}{1000} \quad (20a)$$

$$A = -0.00497$$

The equation for this part of the motion becomes,

$$s = 0.0863 + 23t_1 - 0.00497 \sin (3106t_1) - 0.0443 \cos (3106t_1) \quad (21)$$

$t_1 = 0$ when $t = 0.00037$ second, or $t_1 = (t - 0.00037)$ second.

Substituting in equation (21),

$$s = 0.0863 + 23(t - 0.00037) - 0.00497 \sin [3106(t - 0.00037)] - 0.0443 \cos [3106(t - 0.00037)] \quad (22)$$

$$s = 0.0778 + 23t - 0.0424 \sin (3106t) - 0.0136 \cos (3106t) \quad (22a)$$

The stem motion S is $(s - 0.0409)$.

$$S = 0.0369 + 23t - 0.0424 \sin (3106t) - 0.0136 \cos (3106t) \quad (23)$$

The curve (fig. 12) of this equation shows that the maximum lift of 0.015 inch was reached in 0.0006 second and that the time of opening for this valve is 10 per cent of the injection period at full load on the engine. The bouncing of the stem against the stop is neglected.

The by-pass valves ordinarily employed in the fuel injection systems for oil engines open so rapidly that little error is introduced in the computations for the closing motion of the automatic injection valve stem if it is assumed that the pressure at the valve drops to zero instantaneously. The only force resisting the spring during the closing motion of the stem is the friction of the stem in its guide. Consequently equation (12) represents this part of the motion. The complete integral of equation (12) is

$$s = A \sin \left(\sqrt{\frac{\lambda}{m}} t_2 \right) + B \cos \left(\sqrt{\frac{\lambda}{m}} t_2 \right) + \frac{f}{\lambda} \quad (24)$$

For convenience in the computations, t_2 is taken as zero at the start of the closing motion. Then, when $t_2 = 0$, $s = 0.056$ inch. Substituting in equation (24),

$$0.056 = A \sin(0) + B \cos(0) + \frac{5}{1000}$$

$$B = 0.051$$

Also, when $t_2 = 0$, $\frac{ds}{dt_2} = 0$. Differentiating equation (24) with respect to t_2 ,

$$\frac{ds}{dt_2} = \sqrt{\frac{\lambda}{m}} A \cos \left(\sqrt{\frac{\lambda}{m}} t_2 \right) - \sqrt{\frac{\lambda}{m}} B \sin \left(\sqrt{\frac{\lambda}{m}} t_2 \right) \quad (25)$$

Substituting numerical values,

$$0 = 3106 \times A \cos(0) - 3106 \times B \sin(0)$$

$$A = 0$$

Substituting in equation (24)

$$s = 0.051 \cos(3106 t_2) + 0.005 \quad (26)$$

The equation for the movement of the stem is

$$S = 0.051 \cos(3106 t_2) - 0.0359 \quad (27)$$

The curve of equation (27) (fig. 12) shows that the injection valve stem returned to its seat in 0.00025 second. The velocity with which the stem came against its nozzle seat is found by differentiating equation (26) with respect to t_2 and solving for $\frac{ds}{dt_2}$ for $t_2 = 0.00025$ second. The value obtained is 9.3 feet per second.

CONCLUSIONS

Experiment and analysis indicate that during the operation of an injection system employing an automatic injection valve the rate of oil pressure variations in the injection tube and valve differ considerably for different lengths of tubes. For the injection system and the pressure conditions investigated in this work, the analysis, substantiated by experimental results, shows that when a 43-inch injection tube with a one-eighth-inch bore was used the compression of the oil column in the tube was not completed until 0.0028 second after the timing valve started to open, while when a 7-inch injection tube of the same bore was used the time to complete the compression was 0.0003 second. After the opening of the by-pass valve, the pressure in the injection tube was reduced to the closing pressure of the timing valve 0.001 second earlier, and the timing valve closed 0.0005 second earlier with the 7-inch tube than with the 43-inch tube, although the by-pass valve opened at the same time for both tubes.

The results of an analysis based on the flow of a liquid between two parallel planes show that the hydraulic-pressure variation between the seat and stem of a fuel needle valve for very small lifts is given by the equation:

$$p = P - \frac{3\mu V(l_2^2 - l^2)}{h^3 \cos^2 \alpha}$$

where p = hydraulic pressure on the conical surface of the seat for any lift h at distance l from the apex of the cone which is formed by extending the conical surfaces.

P = pressure at the large circumference of the seat.

μ = viscosity of the fuel oil.

V = velocity at which the stem is lifted from its seat.

h = stem lift or opening between the seats, measured along the stem axis.

α = angle the conical surfaces of the seat make with a plane perpendicular to the stem axis.

l_2 = distance from apex of cone to its base, measured along the conical surfaces.

For the conditions of operation of the timing valve employed in these tests the pressure p at the smallest circumference of the timing valve stem reached 97.5 per cent of the pressure P when the stem had lifted approximately 0.001 inch.

The results of an analysis of the forces acting on the timing valve stem when its motion is controlled by the hydraulic force of the fuel oil show that the motion of the stem is given by the equation:

$$f = \lambda s + m \frac{d^2 s}{dt^2}$$

where f = hydraulic force on the stem at any time t seconds after the motion started plus or minus the friction of the stem in its guide.

λ = scale of the spring.

s = distance spring is compressed in t seconds after motion started.

m = mass of moving parts.

Relations for the lift of stem with time may be obtained from this equation for any particular hydraulic pressure variations.

The results of the analysis of the pressure variations and the equations of motion presented in this report for the timing valve are applicable to spring-loaded automatic injection valves, and in general to all hydraulically operated valves.

LANGLEY MEMORIAL AERONAUTICAL LABORATORY,
NATIONAL ADVISORY COMMITTEE FOR AERONAUTICS,
LANGLEY FIELD, VA., *December 26, 1928.*

APPENDIX

COMPUTATIONS OF THE PRESSURE IN THE INJECTION VALVE TUBE AT COMPLETION OF COMPRESSION OF THE OIL IN THE INJECTION TUBE AND OF THE TIME TO COMPLETE THIS COMPRESSION

Before the pressure in the injection tube approximates that of the oil reservoir, sufficient oil flowed through the timing valve for the compression of the oil column in the injection valve tube, the expansion of the tube walls, and the discharge through the injection valve. The compression of the Diesel oil in the 43-inch injection tube was computed to be 0.0132 cubic inch for the increase in pressure of 7,000 pounds per square inch. These computations were based on data given in reference 4. The volume supplied for the expansion of the tube walls was computed to be 0.0006 cubic inch. The volume discharged through the injection valve during the interval of compression was the product of the average rate of discharge and the interval of time the injection valve was opened. The average rate of discharge from this valve under the test conditions was found by experiment to be 1.99 cubic inches per second. Experiments made in this laboratory showed that with the 43-inch tube and the conditions assumed here the injection valve opened 0.0015 second after the timing valve started to open. The volume discharged through the injection valve was $(t - 0.0015)$ 1.99 cubic inches, where t is the time required to raise the pressure in the injection tube to the maximum value.

The time t can be obtained from the equation

$$\bar{v}tA = C \quad (1)$$

where \bar{v} = average velocity through the timing valve.

t = time required to raise the pressure in the injection tube to that of the oil reservoir.

A = average area of opening of timing valve, 0.004 square inches for a lift of 0.026 inch.

C = volume discharged through timing valve during completion of compression in the injection valve tube.

$$\bar{v}t0.004 = 0.0132 + 0.0006 + 1.99(t - 0.0015) \quad (1a)$$

The average velocity of flow is obtained by equating the loss of strain or resilient energy per unit weight of the oil in the oil reservoir to the kinetic energy per unit weight into which it was transformed as it flowed into the tube. The resilient energy per unit weight which is stored in a liquid, and which is transformed into kinetic energy as the pressure is released, can be found by considering a liquid volume of a unit weight that is subject to a pressure which decreases by an amount p . From the unit strain and unit stress relation $\frac{\beta}{B} = \frac{p}{K}$,

$$\beta = \frac{Bp}{K} \quad (2)$$

where β = change in volume for the change in stress p ,

B = original volume or $1/\rho$ for unit weight, ρ being the density of the fluid,

K = bulk modulus of the fluid, which varies but little for the pressure range considered.

The change of volume is —,

$$\beta = \frac{p}{K\rho} \quad (2a)$$

The differential energy released per unit weight for a differential pressure change is

$$dE = \frac{1}{K\rho} p dp \quad (3)$$

Integrating equation (3) between the limits p_2 and p_1 the total energy released is

$$E = \frac{p_2^2 - p_1^2}{2K\rho} \quad (4)$$

Equating the loss in resilient energy per unit weight to the kinetic energy per unit weight,

$$\frac{p_2^2 - p_1^2}{2K\rho} = \frac{v^2}{2g} \quad (5)$$

where p_2 is the pressure in the oil reservoir, p_1 is the pressure in the injection tube, and v is the velocity through the timing valve at any time during the flow. The dissipation of energy due to the viscosity of the oil has been neglected since little is known of internal losses in the oil at the high pressures considered. The small deviation between the computed curve for the closing of the valve and the experimental curve indicates that the effect of the viscous dissipation of energy is small. Solving (5) for

$$v = \sqrt{\frac{g(p_2^2 - p_1^2)}{K\rho}} \quad (5a)$$

The average velocity is

$$\bar{v} = \frac{1}{(p_2 - p_1)} \int_{p_1}^{p_2} p dv \quad (6)$$

Differentiating equation (5a), substituting in equation (6), and integrating between the limits $p_2 = 8,000$ pounds per square inch and $p_1 = 1,000$ pounds per square inch, the average velocity is found to be 121 feet per second. Substituting in equation (1a).

$$t = 0.0028 \text{ second}$$

The compression of the oil in the injection tube was completed 0.0028 second after the timing valve stem left the seat. The total time from the beginning of the stem motion was 0.0028 second plus 0.00039 second, or 0.0032 second. The total oil volume that left the oil reservoir during this time was $0.0132 + 0.0006 + 1.99(0.0028 - 0.0015) = 0.0164$ cubic inch. This reduced the pressure in the oil reservoir to 7,830 pounds per square inch.

REFERENCES

1. Beardsley, E. G.: "N. A. C. A. Spray Photography Apparatus for Studying Fuel Sprays from Oil Engine Injection Valves and Test Results from Several Researches." N. A. C. A. Technical Report No. 274. (1927.)
2. Michel, A. G. M.: "The Mechanical Properties of Fluids," a collective work, Applied Physics Series, 1923. xiv 362 pp., tables and figures. Glasgow, Blackie & Sons (Ltd.), pp. 116-118.
3. Herschel, Winslow H.: "Standardization of the Saybolt Universal Viscosimeter." Technologic Paper of the Bureau of Standards. No. 112, June, 1918.
4. Fowle, E. F.: Smithsonian Physical Tables, 1927. 7th edition, revised, xlvii 458 pp. 579 tables. Washington, Smithsonian Institution, pp. 155-157.
5. Hersey, M. D.: The Theory of the Torsion and the Rolling Ball Viscosimeters and Their Use in Measuring the Effect of Pressure on Viscosity. Journal of Washington Academy of Sciences, vol. 6, 1916, pp. 525-530.

Report No. 331

COLLECTION OF WIND-TUNNEL DATA ON COMMONLY USED WING SECTIONS

By F. A. LOUDEN
Bureau of Aeronautics
Navy Department

REPORT No. 331

COLLECTION OF WIND-TUNNEL DATA ON COMMONLY USED WING SECTIONS

By F. A. LOUDEN

SUMMARY

This report was prepared at the request of the National Advisory Committee for Aeronautics in the Bureau of Aeronautics of the Navy Department in order to group in a uniform manner the aerodynamic properties of commonly used wing sections as determined from tests in various wind tunnels.

The data have been collected from reports of a number of laboratories. Where necessary, transformation has been made to the absolute system of coefficients and tunnel wall interference corrections have been applied. Tables and graphs present the data in the various forms useful to the engineer in the selection of a wing section.

INTRODUCTION

The wing sections most commonly used in this country are the Clark Y, Clark Y-15, Gottingen G-387, G-398, G-436, N. A. C. A. M-6, M-12, Navy N-9, N-10, N-22, R. A. F.-15, Sloane, U. S. A.-27, U. S. A.-35A, U. S. A.-35B. Data were obtained from References 1 to 14 on all of these airfoils that had been tested in the following wind tunnels:

Large wind tunnel, Göttingen Laboratory.

Variable density wind tunnel, Langley Memorial Aeronautical Laboratory.

7½-foot wind tunnel, Massachusetts Institute of Technology.

5-foot wind tunnel, McCook Field.

8-by-8-foot wind tunnel, Washington Navy Yard.

Some of the airfoils selected had been tested in as many as four of the five tunnels, others in only one of the tunnels.

The results obtained in the different laboratories are not directly comparable, because of the differences in the methods of testing; in the ordinates, size, and aspect ratio of the models tested and in the test speed. The purpose of this report is not to compare results from different laboratories but to present the data in a uniform manner and to compare different wing sections tested in the same laboratory at the same Reynolds Number.

In the individual laboratory reports, the data in some cases were presented in engineering rather than absolute coefficients; in most cases, the tunnel wall interference corrections had not been applied; for some tests the center of pressure had not been determined; the moment coefficient was given with respect to various axes; the data were presented by some laboratories in polar diagrams and by others in angle-of-attack graphs.

In the present report the collected data have been corrected for tunnel wall interference, the absolute system of coefficients is used, and the data are plotted and tabulated in various forms for the convenience of the engineer.

ABSOLUTE SYSTEM OF COEFFICIENTS

The absolute lift and drag coefficients C_L and C_D are defined by dividing the lift L and the drag D by the dynamic pressure $q = \frac{1}{2} \rho V^2$ and the wing area S .

$$C_L = L/qS \qquad C_D = D/qS.$$

The absolute moment coefficient C_M is the moment M about the leading edge divided by qS times the chord length c and is positive when the moment tends to make the leading edge rise.

$$C_M = M/qSc.$$

The center of pressure coefficient C_p is the fraction of the chord length along the chord from the leading edge to the line of action of the resultant force. This distance is equal to the moment coefficient divided by the normal force coefficient C_N .

$$C_p = C.P./c = C_M/C_N$$

where $C_N = C_L \cos \alpha + C_D \sin \alpha$.

The induced drag coefficient C_{Di} is equal to C_L^2 divided by π times the aspect ratio.

$$C_{Di} = C_L^2/\pi \cdot A.R. = C_L^2 S/\pi b^2$$

where b is the span.

The profile drag coefficient C_{D0} is the difference between the coefficients of total drag and induced drag

$$C_{D0} = C_D - C_{Di}$$

TUNNEL WALL INTERFERENCE CORRECTIONS

A large share of the data taken from References 1 to 14 had not been corrected for tunnel wall interference. The following Prandtl corrections have been applied where necessary:

$$\Delta \alpha = \delta \frac{C_L S}{A} \text{ radians} \quad \Delta C_D = \delta \frac{C_L^2 S}{A}$$

A is the cross-sectional tunnel area and δ is equal to 0.125 for a tunnel having a circular cross section. For a tunnel of square cross section, Glauert has shown that δ increases to 0.137.

ORDINATES OF THE AIRFOILS

Table I gives the general shape of the various wing sections. The faired ordinates used by the Bureau of Aeronautics have been given and are called the specified ordinates. These ordinates may be slightly different from those in general use as exact specifications for the various sections do not exist. For this reason, a wing section at one laboratory might be expected to vary to some extent from the same section at another laboratory. The variation becomes greater in the measured ordinates due to the different materials used in airfoil construction and different methods of measuring the ordinates.

The maximum thickness of the airfoils and their thickness for front and rear spar depths are given in Table II. Since the spar depths for a wing to be selected are approximately known, a glance at this table will limit the number of wings for further consideration.

TEST CONDITIONS

No attempt will be made in this report to describe the various wind tunnels or their methods of testing. Only the conditions for the tests selected will be given.

The Göttingen Laboratory tests were made on 20 by 100 centimeter (7.874×39.37 inches) models at a test speed of 30 meters (98.4 feet) per second. This gives a test Vl of 64.58 square feet per second, where l is taken as the chord length. Since the elements of air density and viscosity were not determined, the exact Reynolds Number of the tests is not known. Assuming air of standard density ρ and the coefficient of viscosity μ at standard temperature, $\rho/\mu = 6,378$ sq.ft./sec., and the approximate Reynolds Number $\rho Vl/\mu$ is 412,000.

The Langley Memorial Aeronautical Laboratory (L. M. A. L.) tests were made on 5 by 30 inch models at a test speed of approximately 76 feet per second. Tests on most of the models were made at several pressures, but only the tests at a pressure of about 20 atmospheres are considered here. The average Reynolds Number for each test was determined and is in the neighborhood of 3,600,000 corresponding to full-scale conditions.

The Massachusetts Institute of Technology (M. I. T.) tests were made on 6 by 36 inch models at a test speed of 40 miles an hour. The test V_l is 29.33 sq. ft./sec.; approximate Reynolds Number, 187,000.

The McCook Field (McC. F.) tests were made on 6 by 36 inch models at various air speeds. Only the tests at 80 miles an hour are considered here, giving a test V_l of 58.67 sq. ft./sec.; approximate Reynolds Number, 374,000.

The Washington Navy Yard (W. N. Y.) tests were made on 5 by 30 inch models at a test speed of 40 miles an hour; test V_l , 24.44 sq. ft./sec.; approximate Reynolds Number, 156,000.

With the exception of the Göttingen airfoils of aspect ratio 5, all of the models had the normal aspect ratio of 6. The experimental results of the Göttingen tests could be corrected to an aspect ratio of 6, but since the results from the different laboratories are not directly comparable, it was thought best to leave the data in the original form.

PRESENTATION OF DATA

The data from the Göttingen tests are given separately for each airfoil in Tables III to VI; L. M. A. L. tests, Tables VII to XIV; M. I. T. tests, Tables XV to XXII; McC. F. tests, Tables XXIII to XXV; W. N. Y. tests, Tables XXVI to XXXVII.

The usual C_L , C_D , and C_L/C_D versus angle of attack curves for the 15 wing sections are presented in Figures 1 to 15, and a table is inserted on each figure giving the test conditions. It might have been preferable to have plotted the data from each laboratory in one figure but this was not practical on account of the interference in the numerous curves.

In Figures 16 to 30 are plotted the Lilienthal polar diagrams, C_D and C_M versus C_L , together with the induced drag polar curves.

C_L/C_D is replotted against speed ratio V/V_s in Figures 31 to 45. The center of pressure is also plotted against speed ratio as the curves are approximately straight lines and are easier to read than the usual plots of center of pressure against angle of attack.

Graphs of the profile drag coefficient C_{D0} versus lift coefficient are presented in Figures 46 to 50. For these graphs it was possible to plot the data from each laboratory in one diagram and therefore the curves in each group are comparable. This same method is followed in Figures 51 to 55 which give the ratio of the faired profile drag coefficient to the maximum lift coefficient plotted against speed ratio.

AIRFOIL CHARACTERISTICS AND CRITERIA

Various characteristic values and criteria for the wing sections derivable from the data and graphs are tabulated in Tables XXXVIII to XLIX. When convenient, the tabulation of the criteria are made with respect to the merit of the wing section and a note to that effect is under the heading to the table.

The above-mentioned tables are self-explanatory and derivations of the criteria can be found elsewhere, but a few brief remarks regarding the meaning of some of the criteria appears desirable.

C_L maximum, Table XLI, is the criterion for minimum speed with a given wing loading or if the minimum speed is given, it is the criterion for the load which can be carried per unit area of wing.

The maximum ratio C_L/C_D , Table XLIII, is well known as a criterion for airfoil efficiency, greatest weight carried for a given thrust. It being also a criterion for maximum speed regardless of minimum, flattest glide, and maximum range. The value of C_L at maximum C_L/C_D is also tabulated and should be considered along with the maximum ratio of lift to drag. The ratio of lift to drag is given for various fractions of C_L maximum in Table XLIV. These data show the effectiveness for speed and climb.

The ratio of C_L maximum to C_D minimum, Table XLV, is the criterion for maximum speed with a given minimum. With constant loading, (C_L^3/C_D^2) maximum, Table XLVI, is an index of minimum power, maximum rate of climb, maximum ceiling, maximum duration; the ratio of C_L^3 maximum to C_D^2 minimum, Table XLVII, is the criterion for maximum speed range. For additional detail on the above-mentioned criteria, the reader is referred to Reference 15.

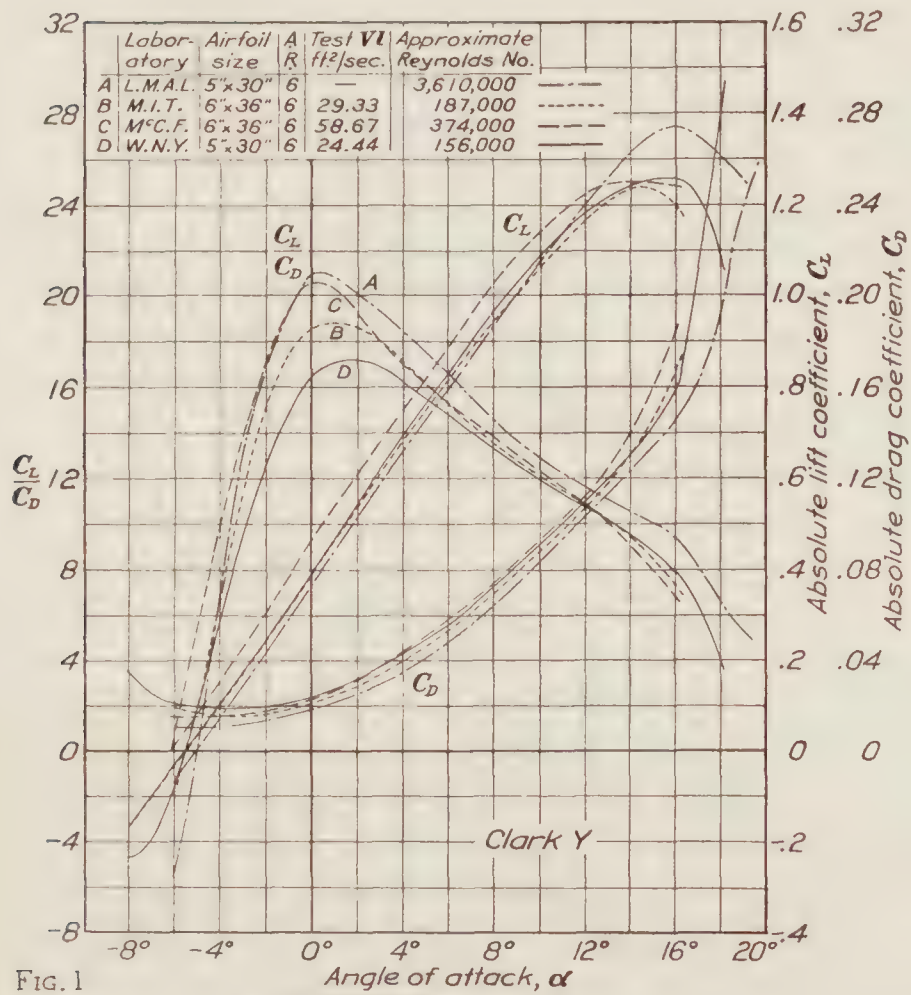


FIG. 1

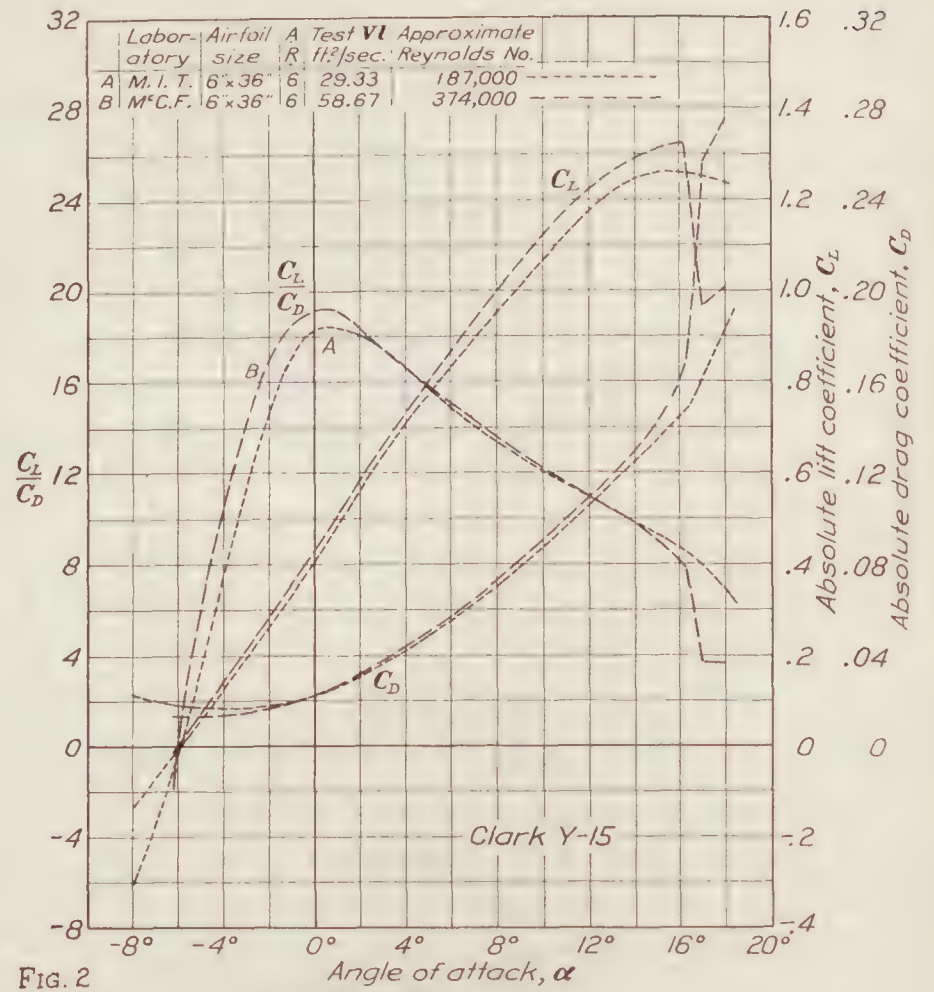


FIG. 2

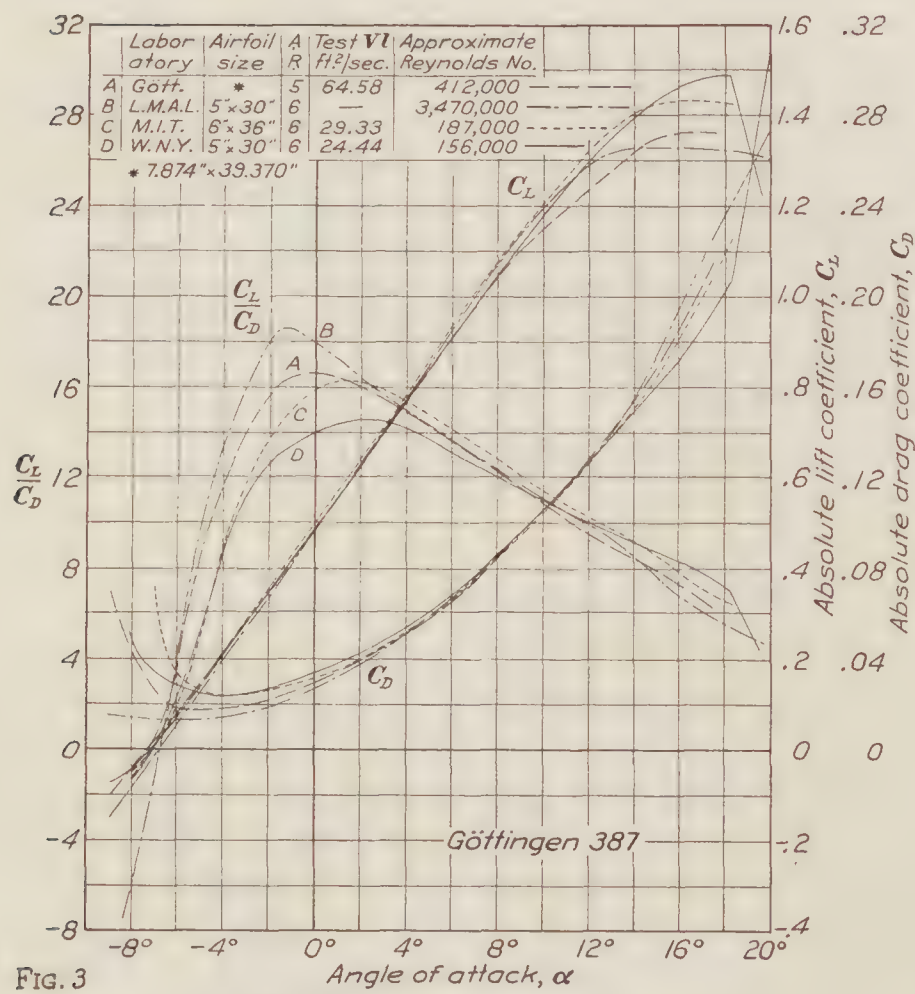


FIG. 3

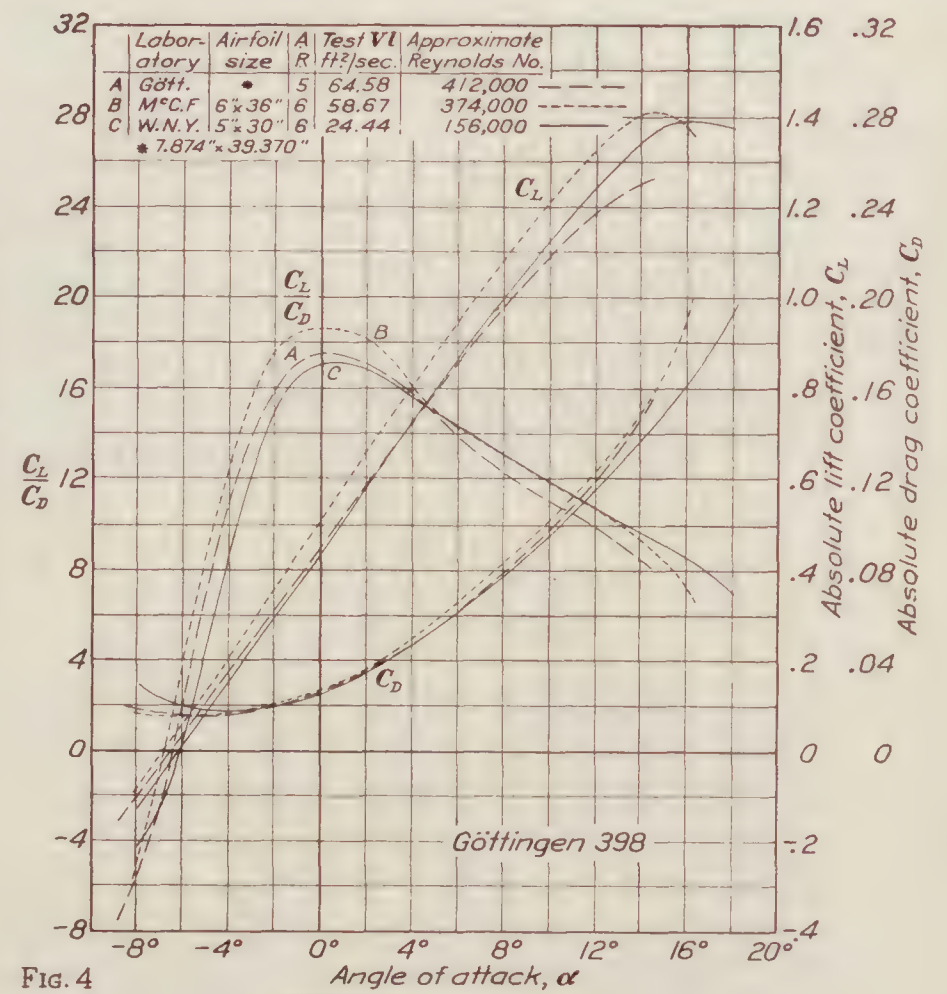
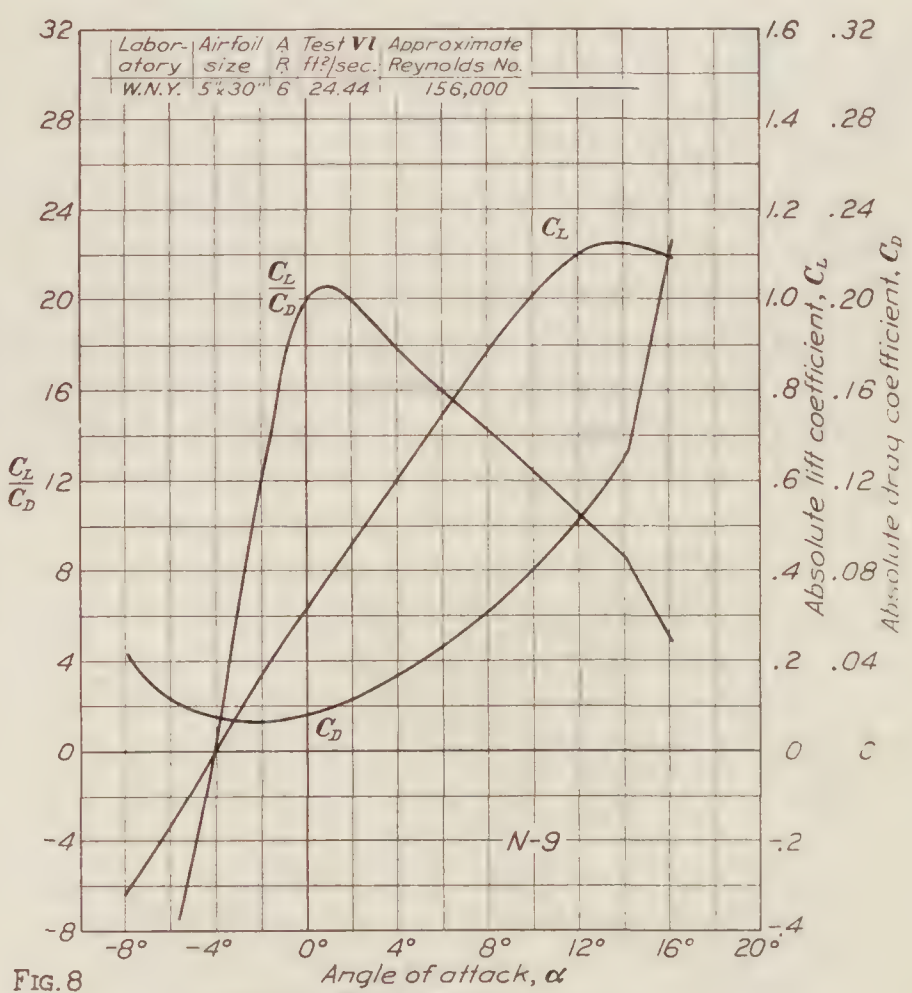
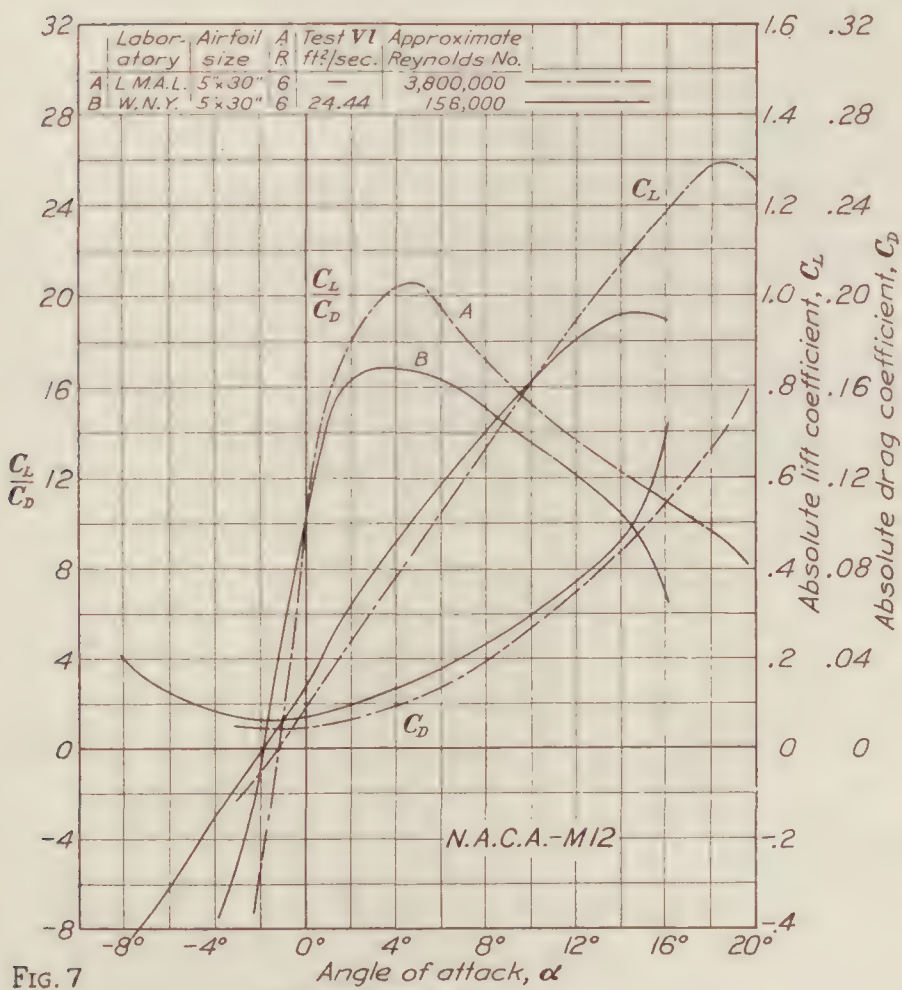
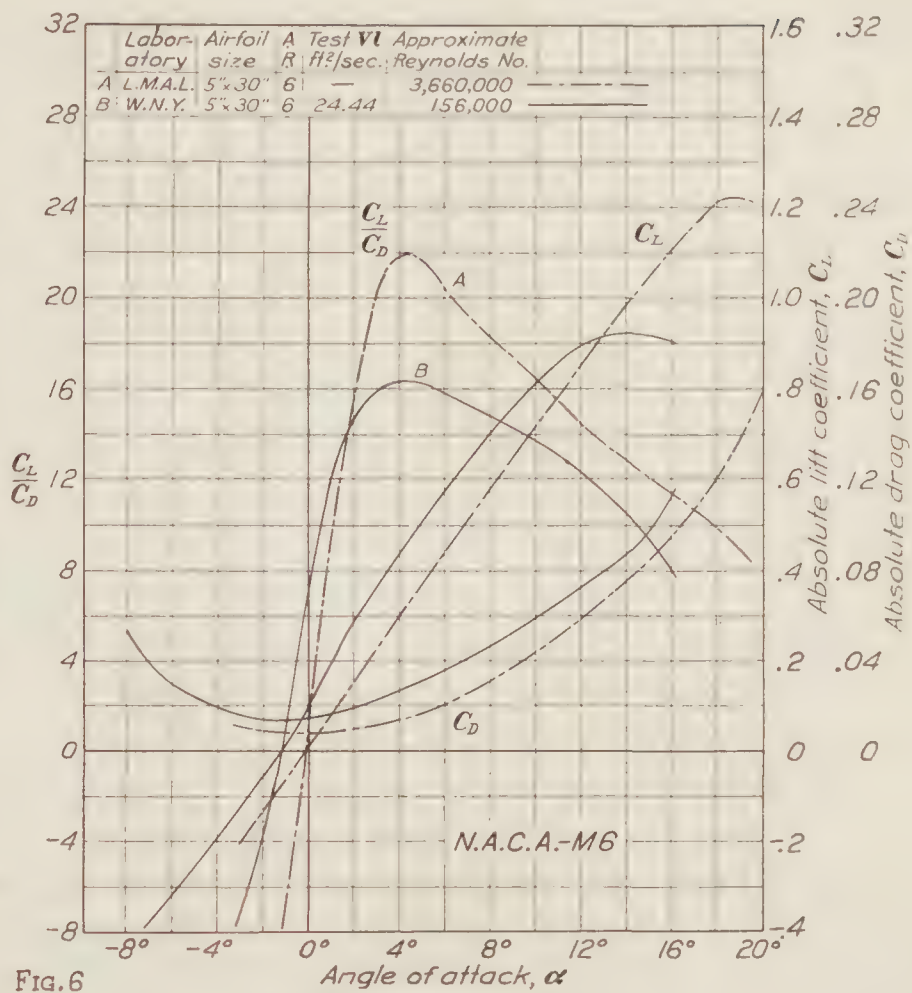
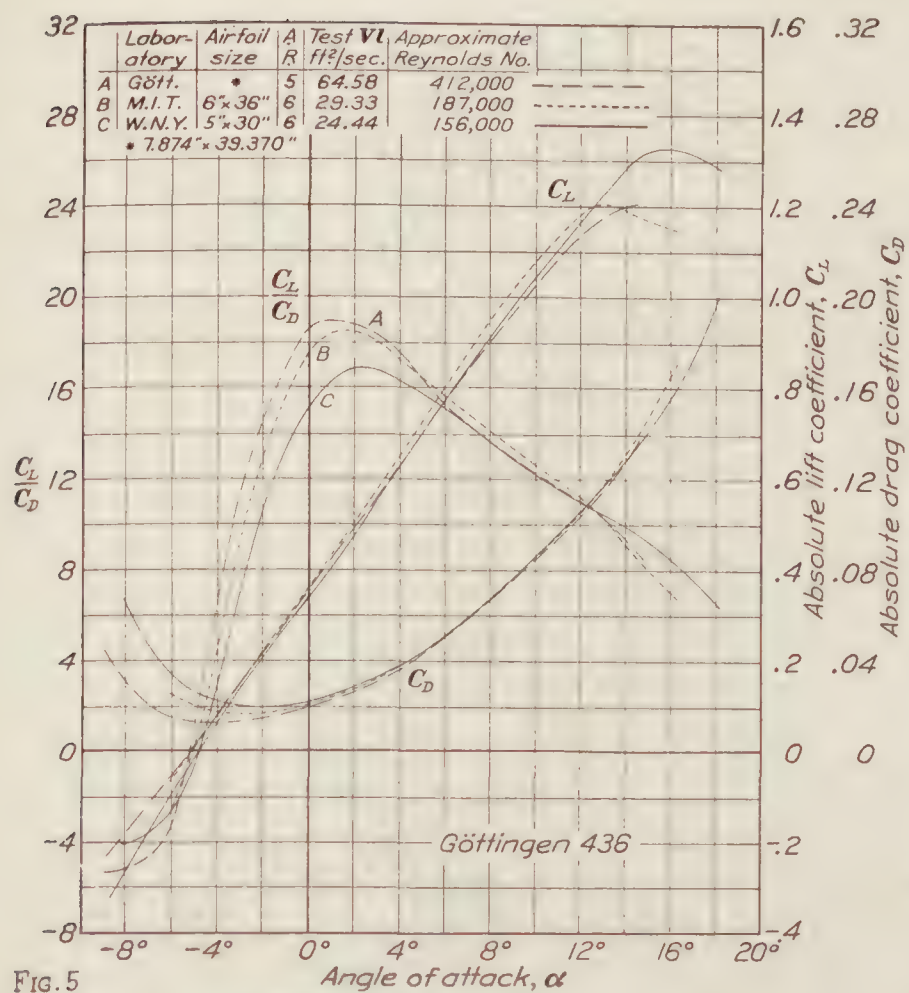
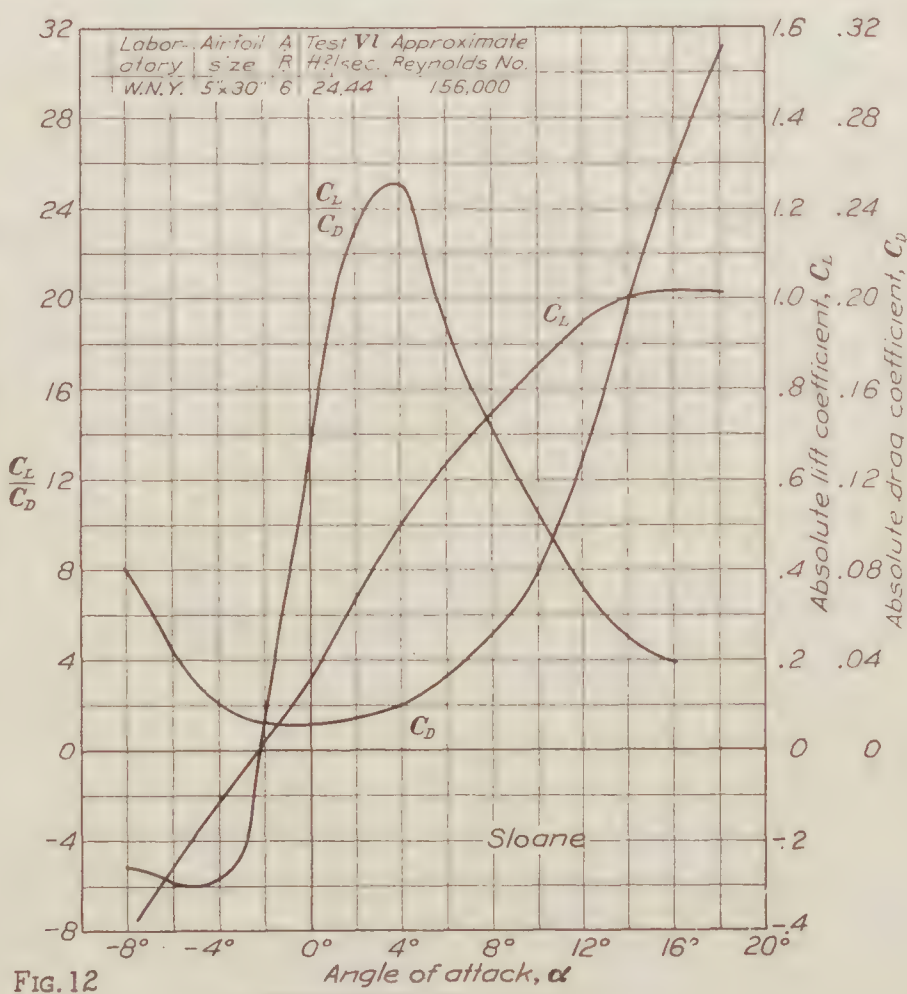
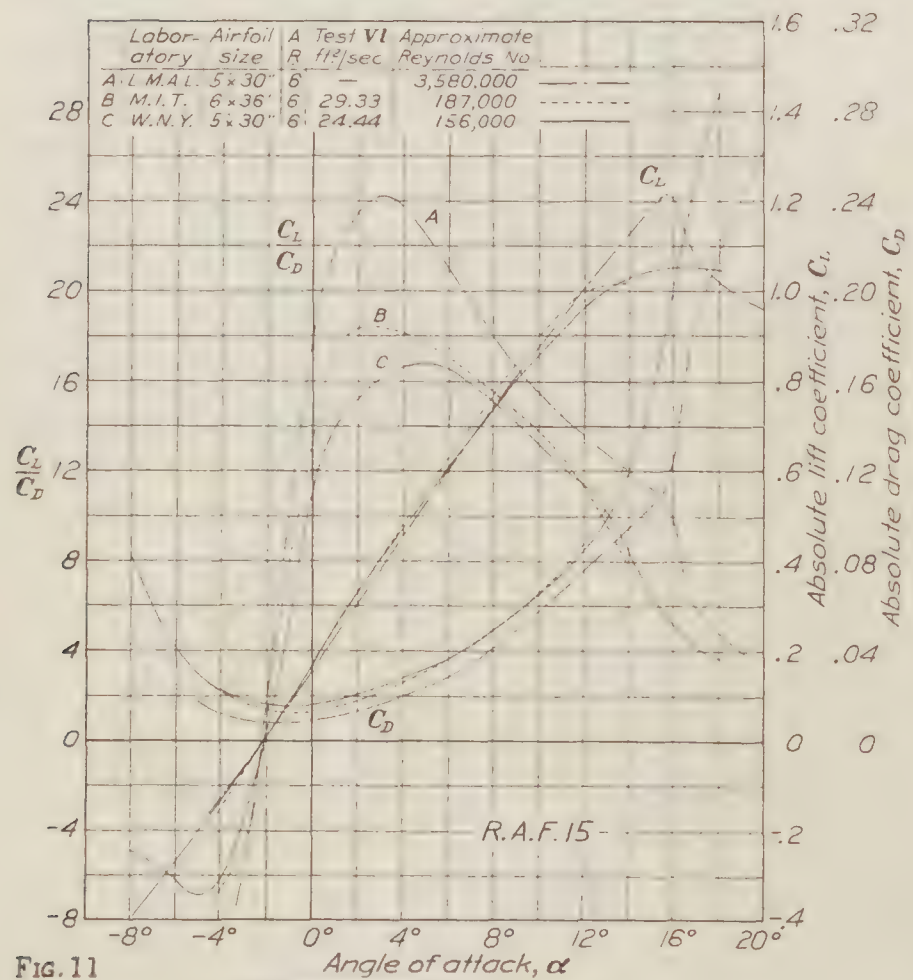
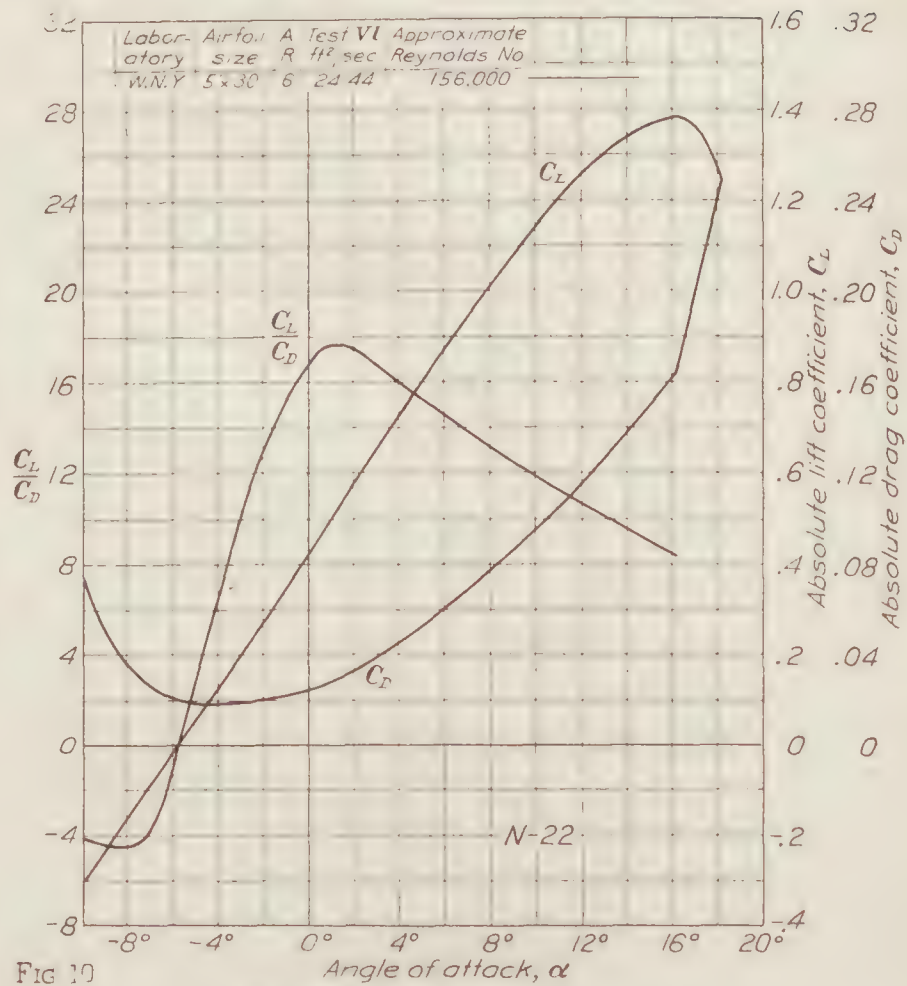
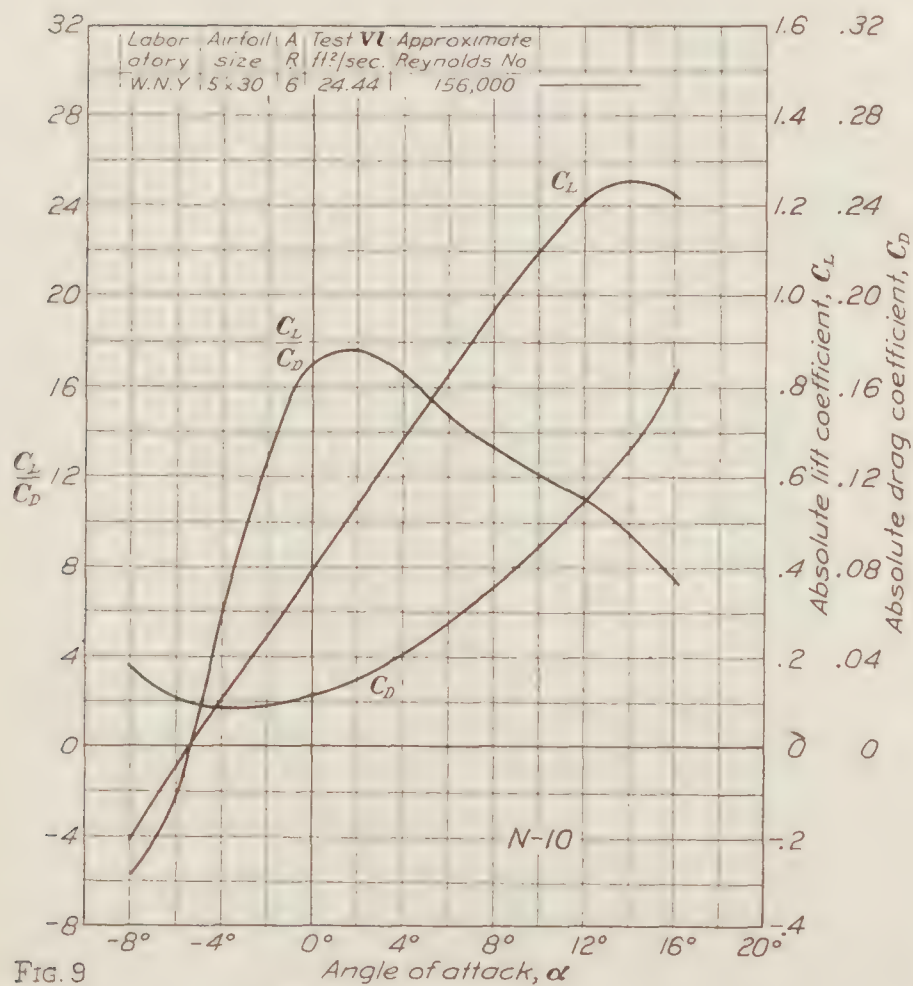


FIG. 4







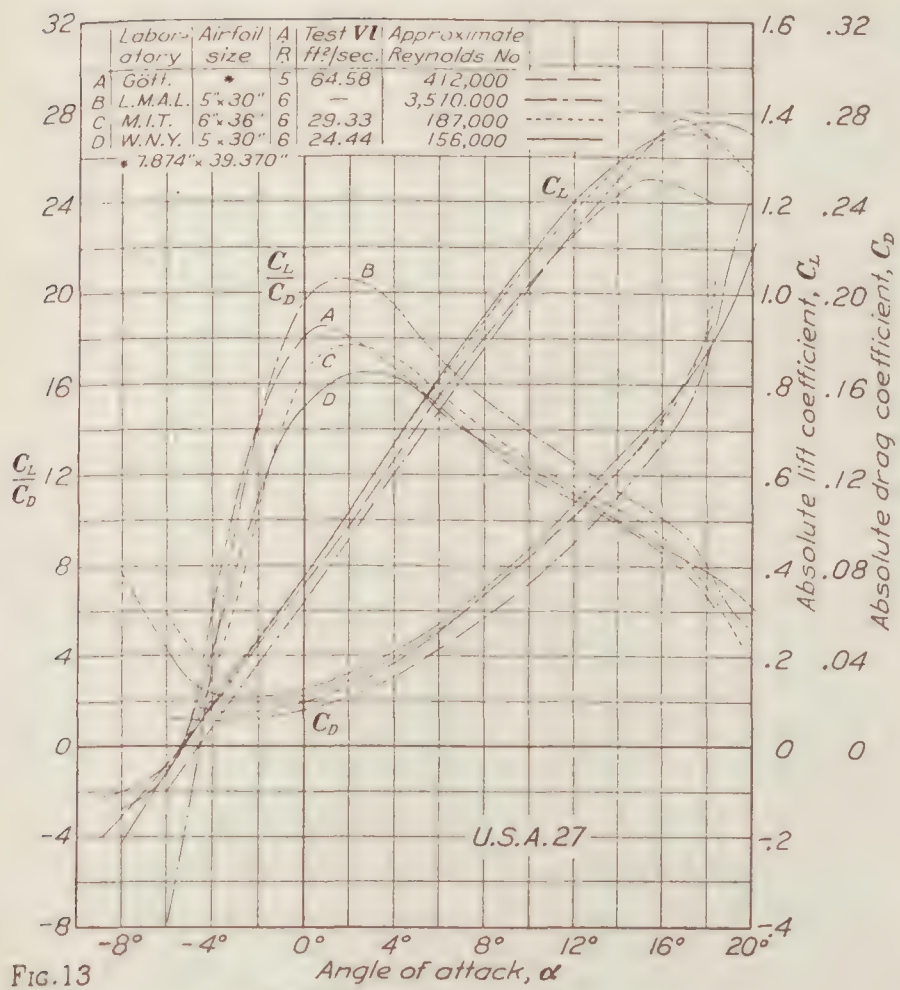


FIG. 13

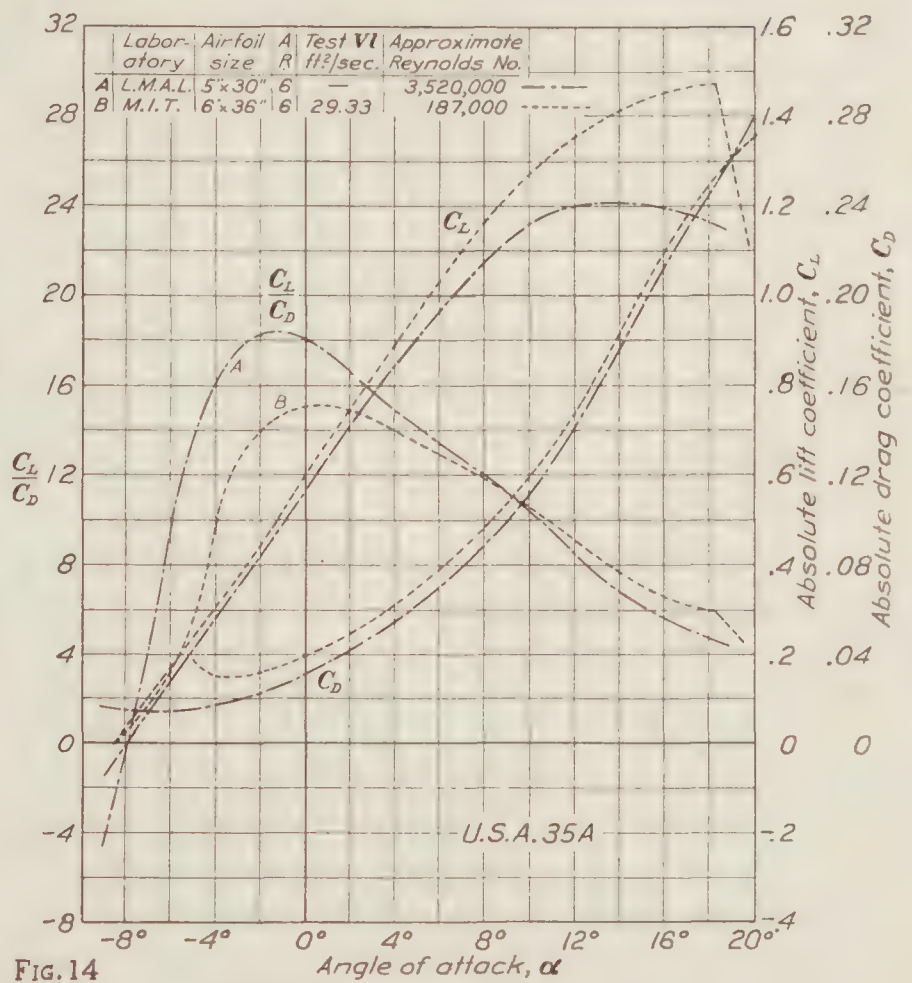


FIG. 14

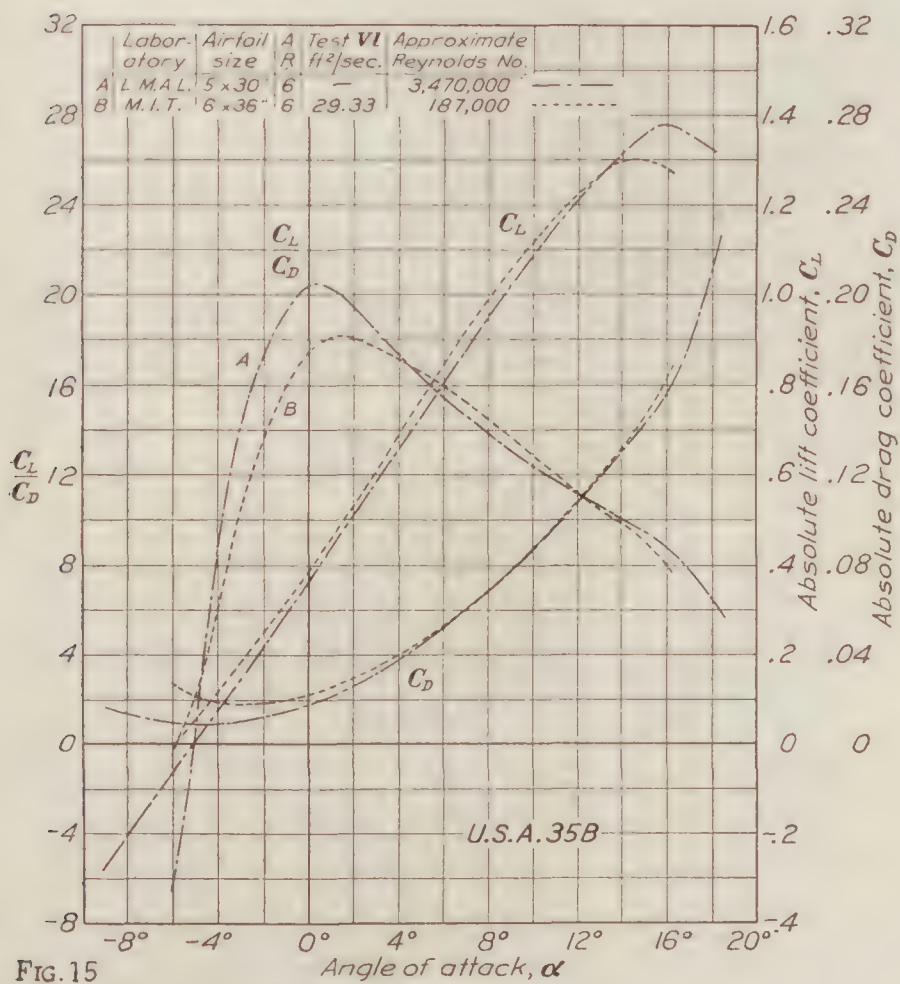


FIG. 15

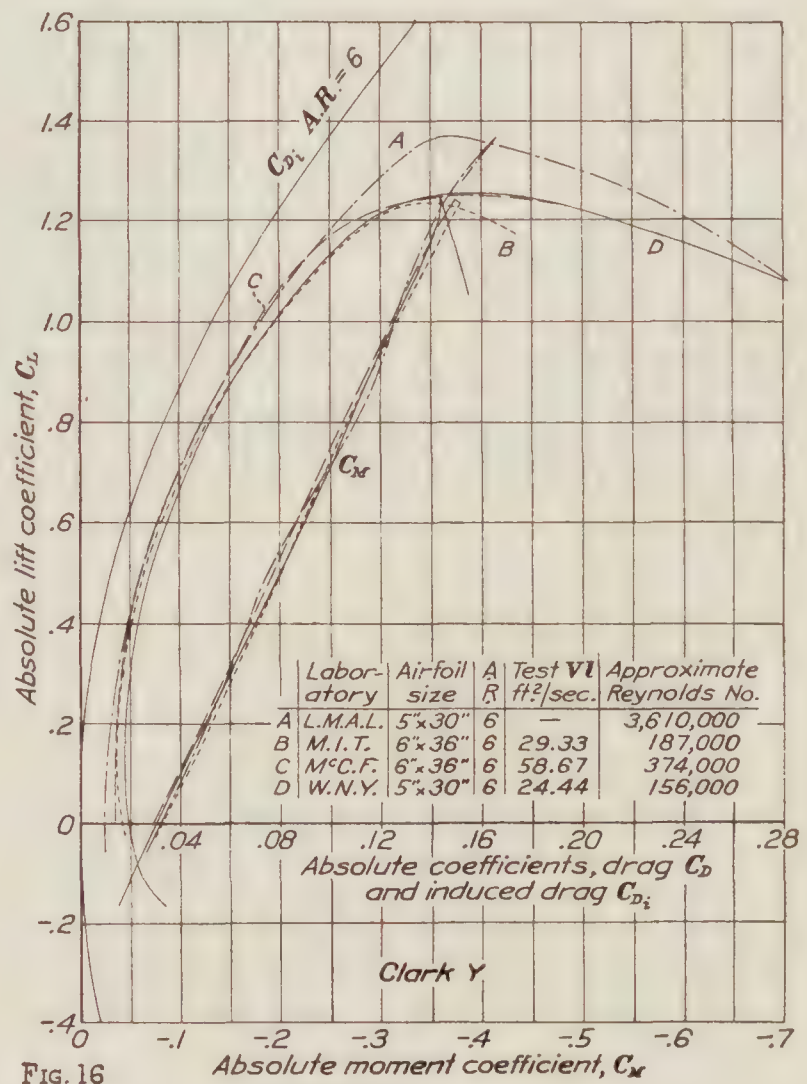


FIG. 16



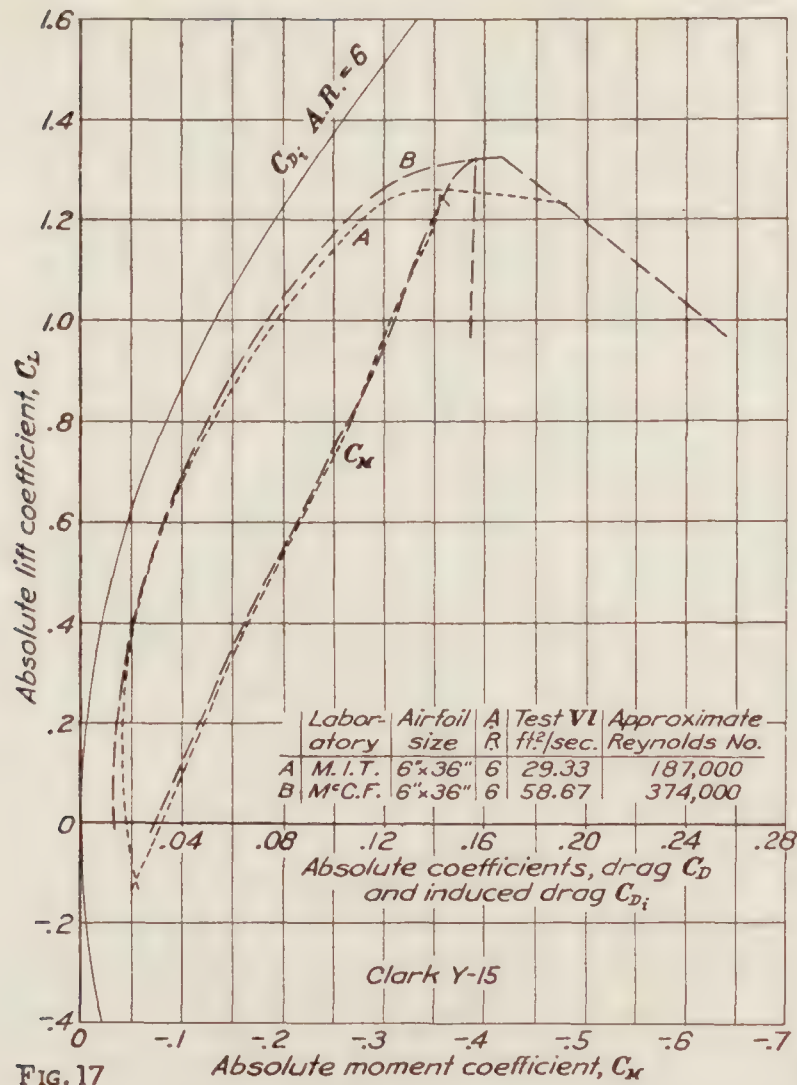


FIG. 17

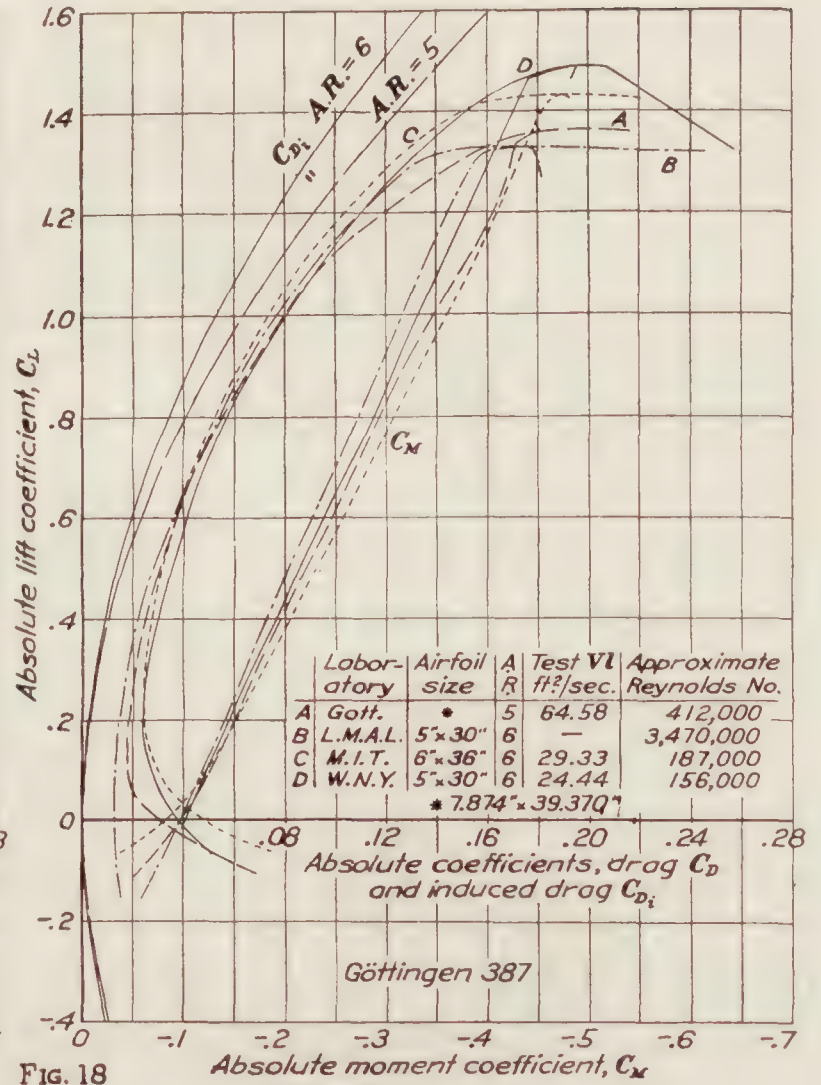


FIG. 18

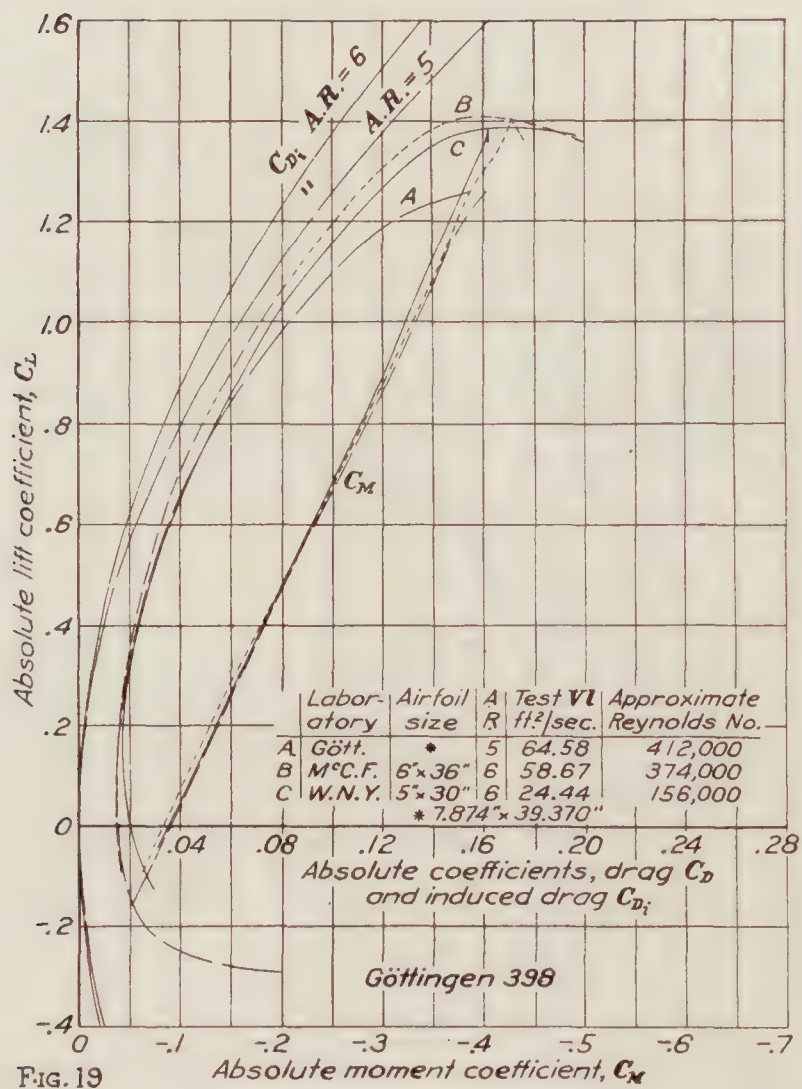


FIG. 19

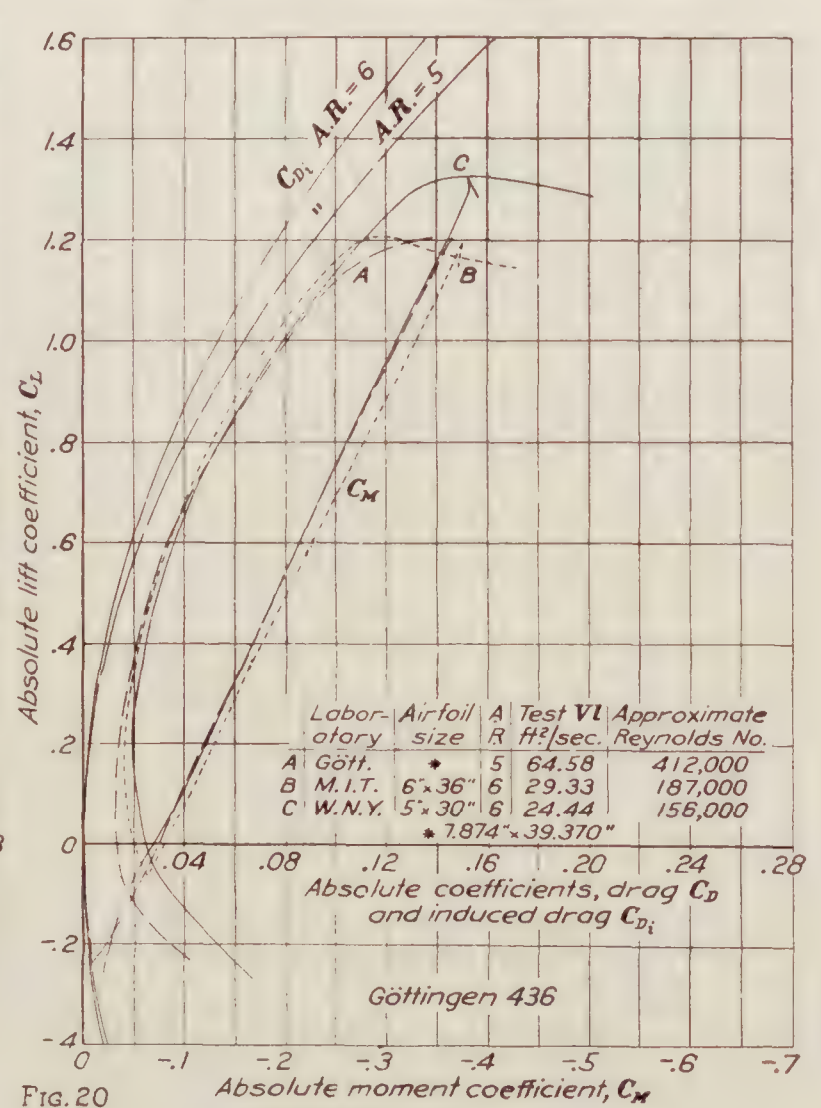


FIG. 20

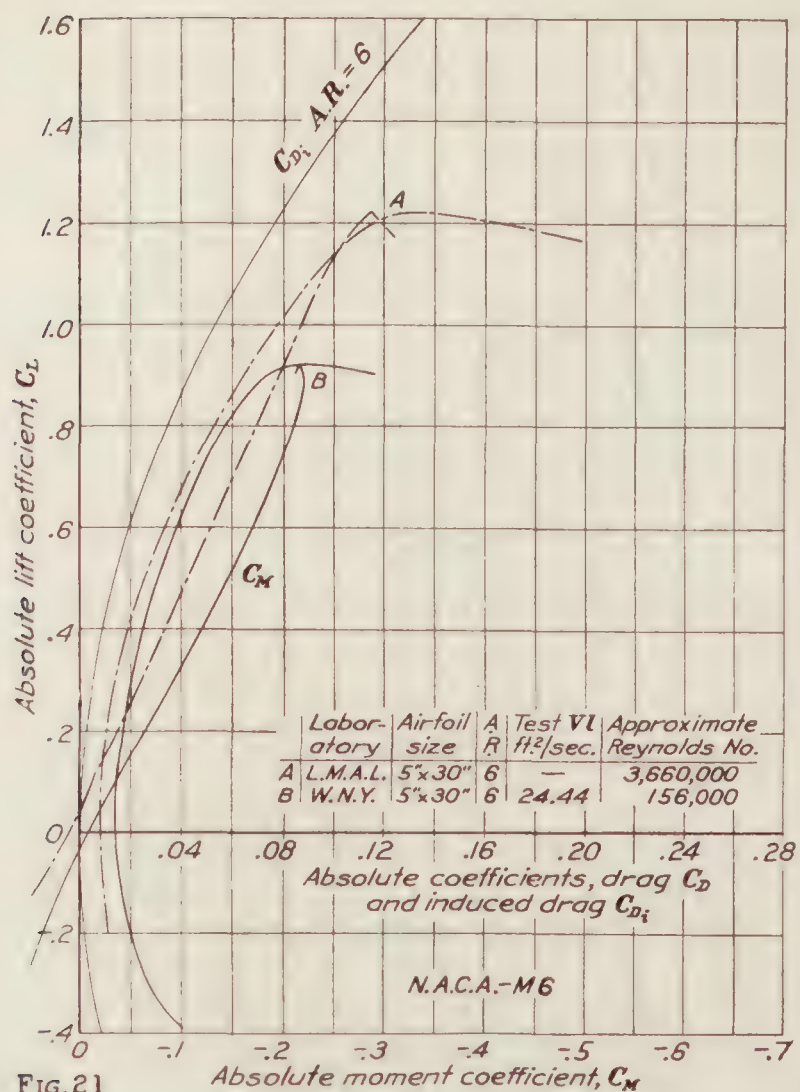


FIG. 21

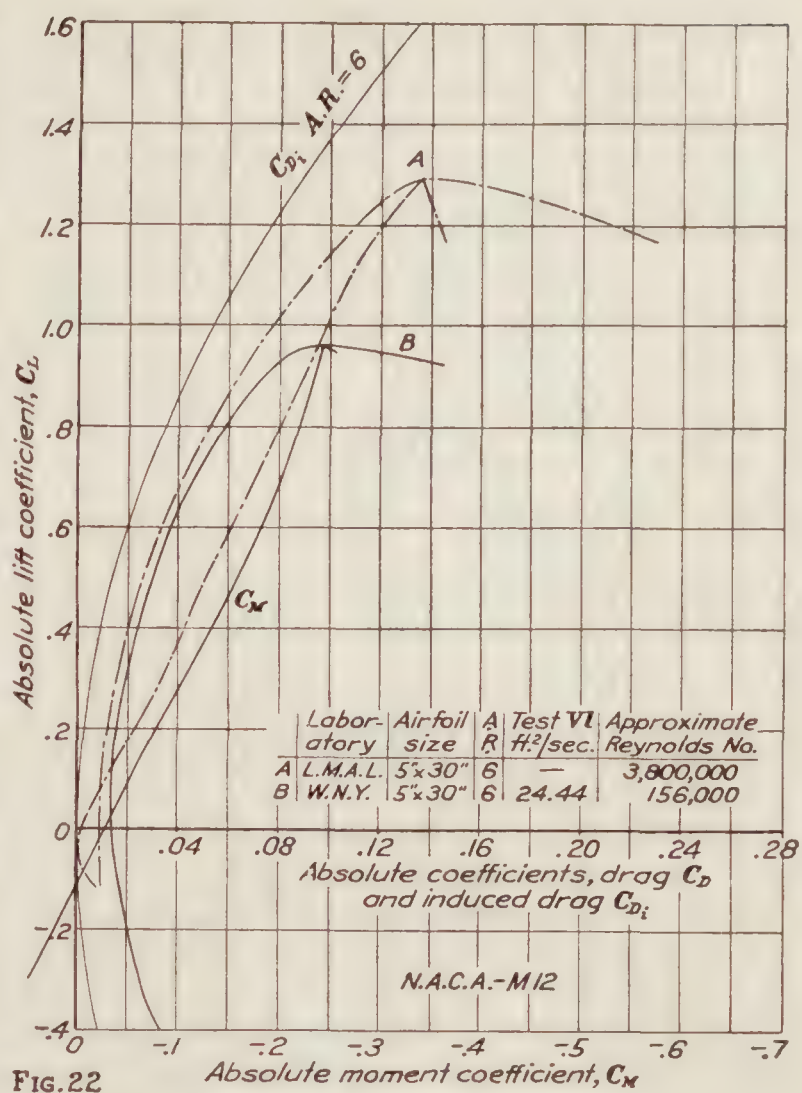


FIG. 22

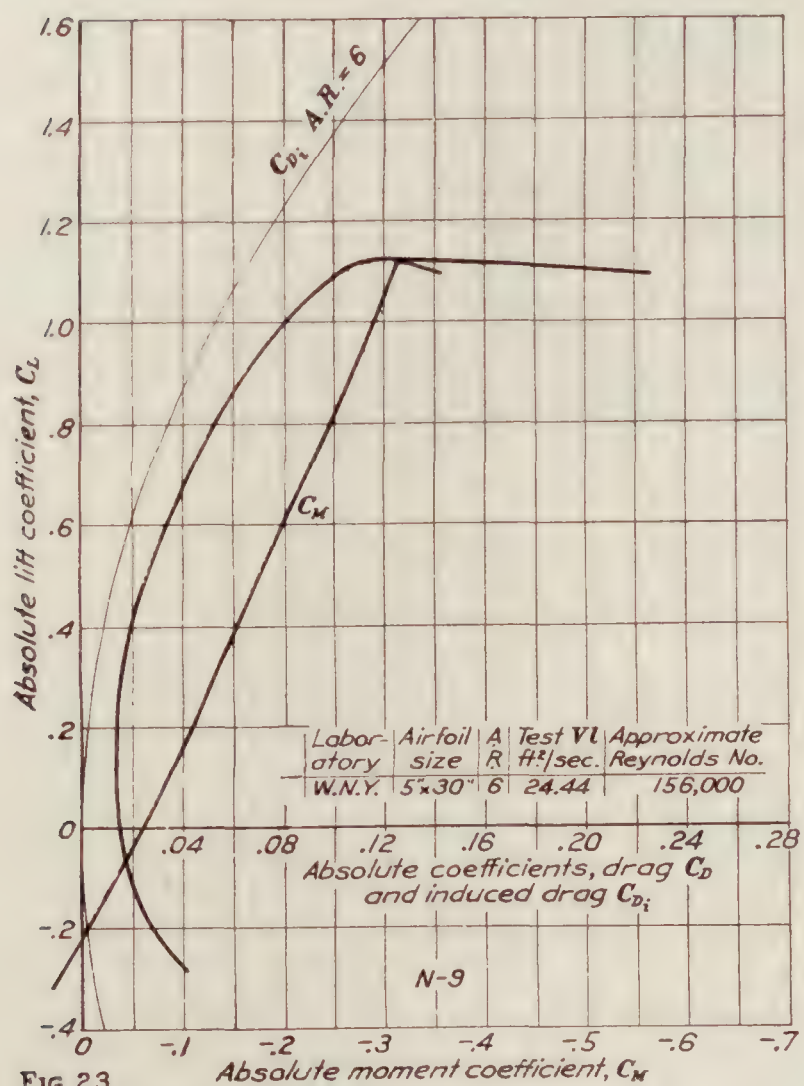


FIG. 23

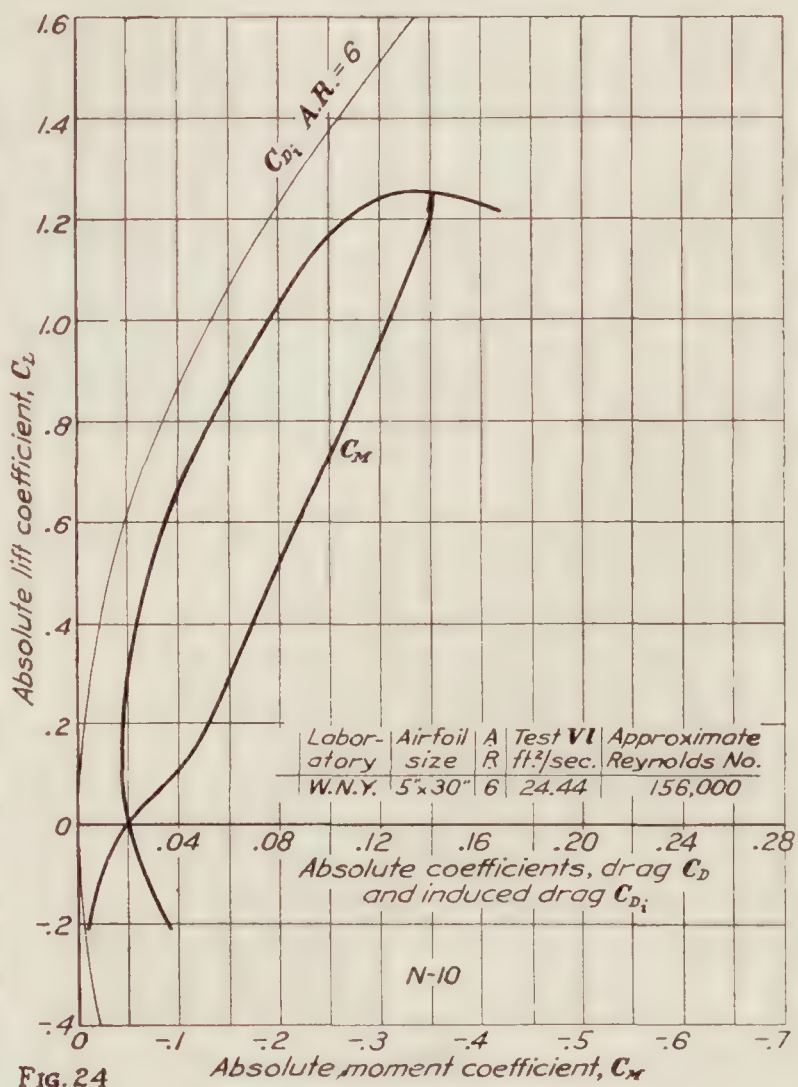
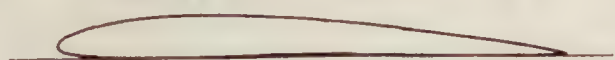


FIG. 24



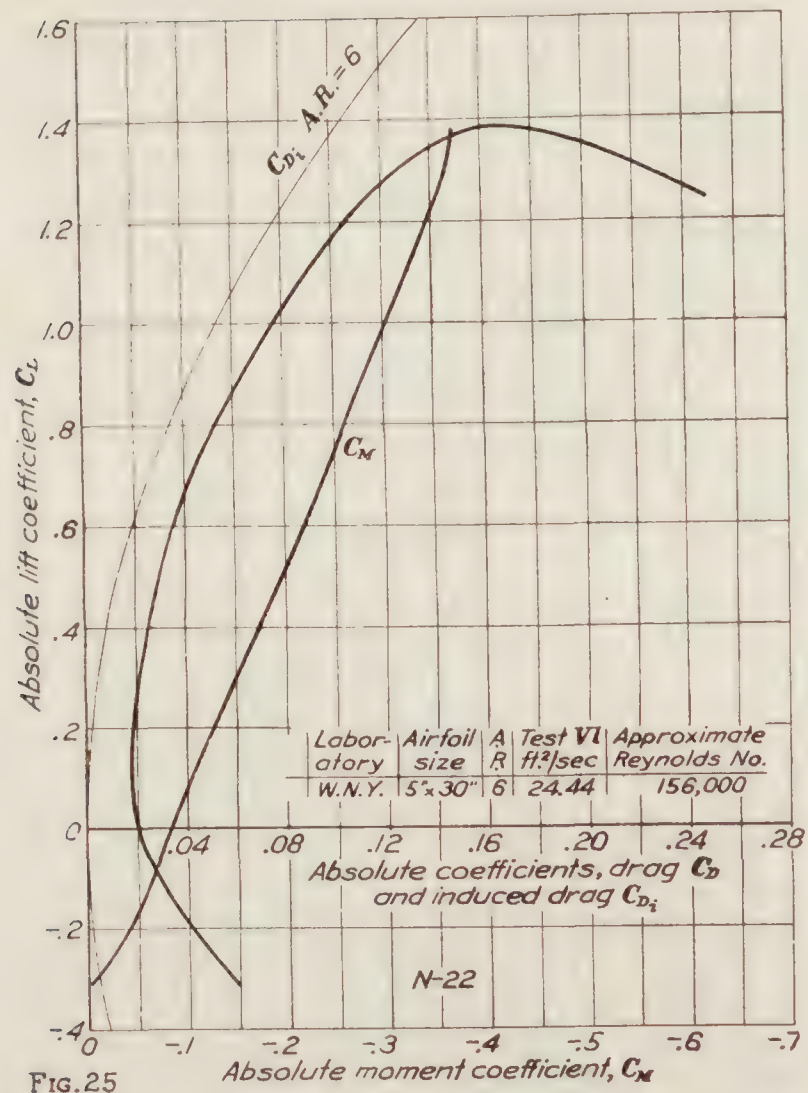


FIG. 25

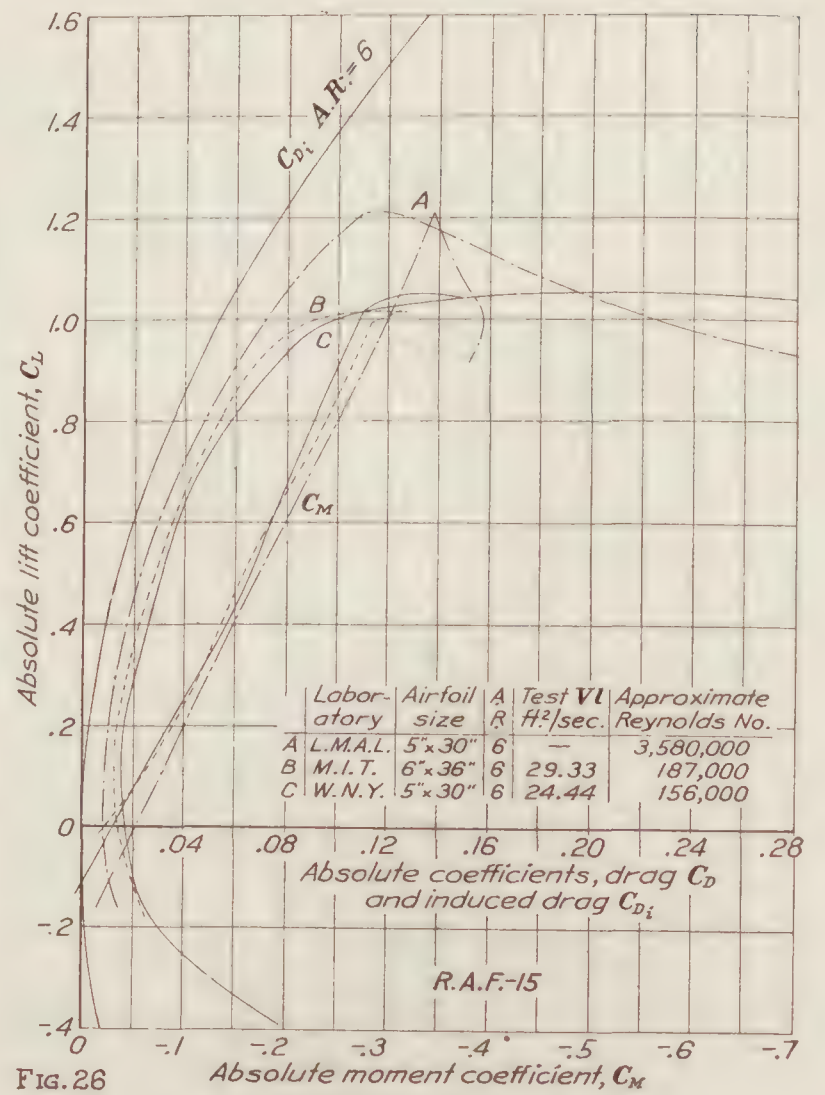


FIG. 26

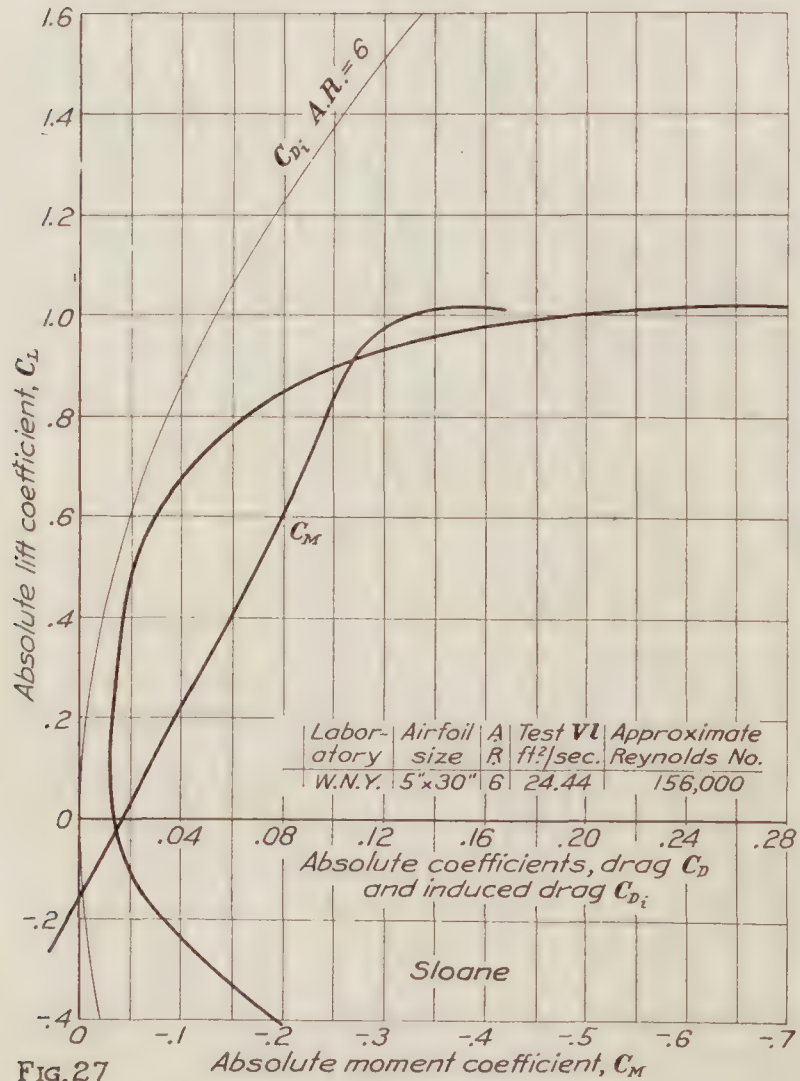


FIG. 27

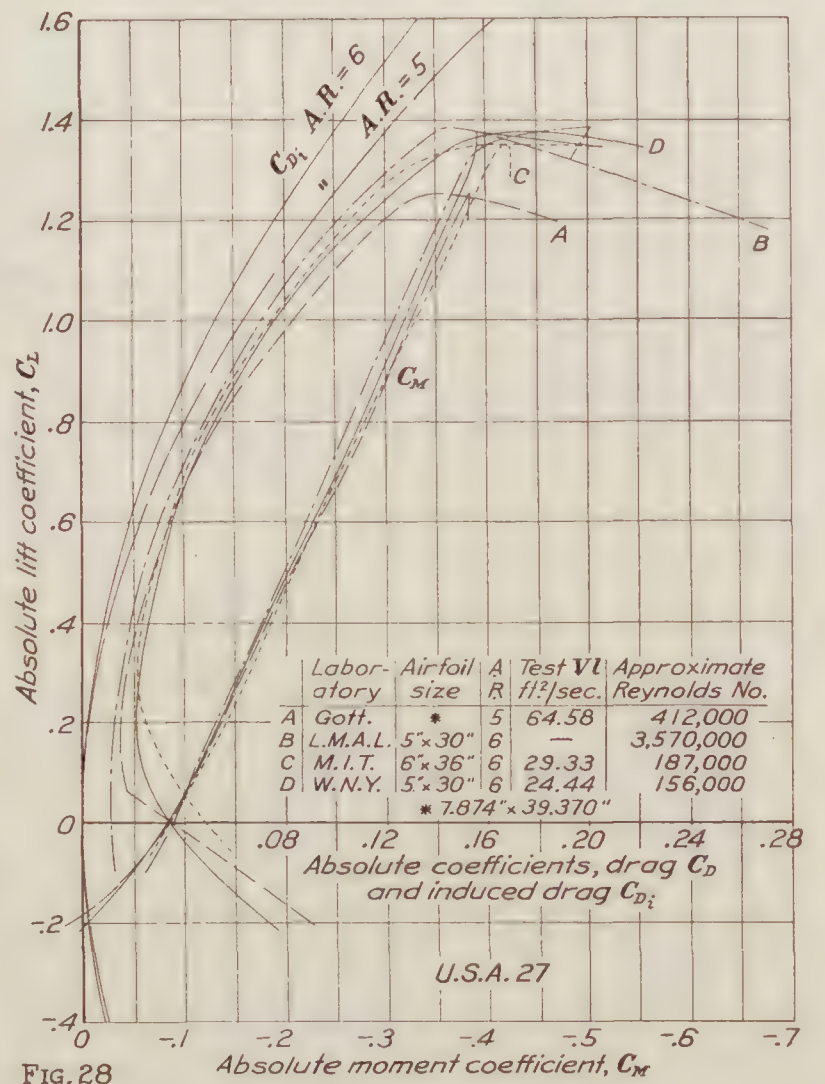


FIG. 28



Table XLIX and Figures 51 to 55 compare the data on the basis of total profile drag for constant load and stalling speed. It is shown in Reference 16 that the section selected will vary with major requirements as follows:

Maximum speed.—Section having least value of C_{D0}/C_L maximum at high speed ratios, $V/V_s > 2.5$.

Maximum climb and ceiling.—Section having least value of C_{D0}/C_L maximum between $V/V_s = 1.10$ and $V/V_s = 1.5$.

Maximum endurance.—Section having least value of C_{D0}/C_L maximum at $V/V_s = 1.10$.

General performance.—Section having least average value of C_{D0}/C_L maximum at all values of V/V_s .

SCALE EFFECT

The same conclusions regarding scale effect can be drawn from Figures 1 to 30 as have been drawn from previous test data. The following conclusions are quoted from Reference 17:

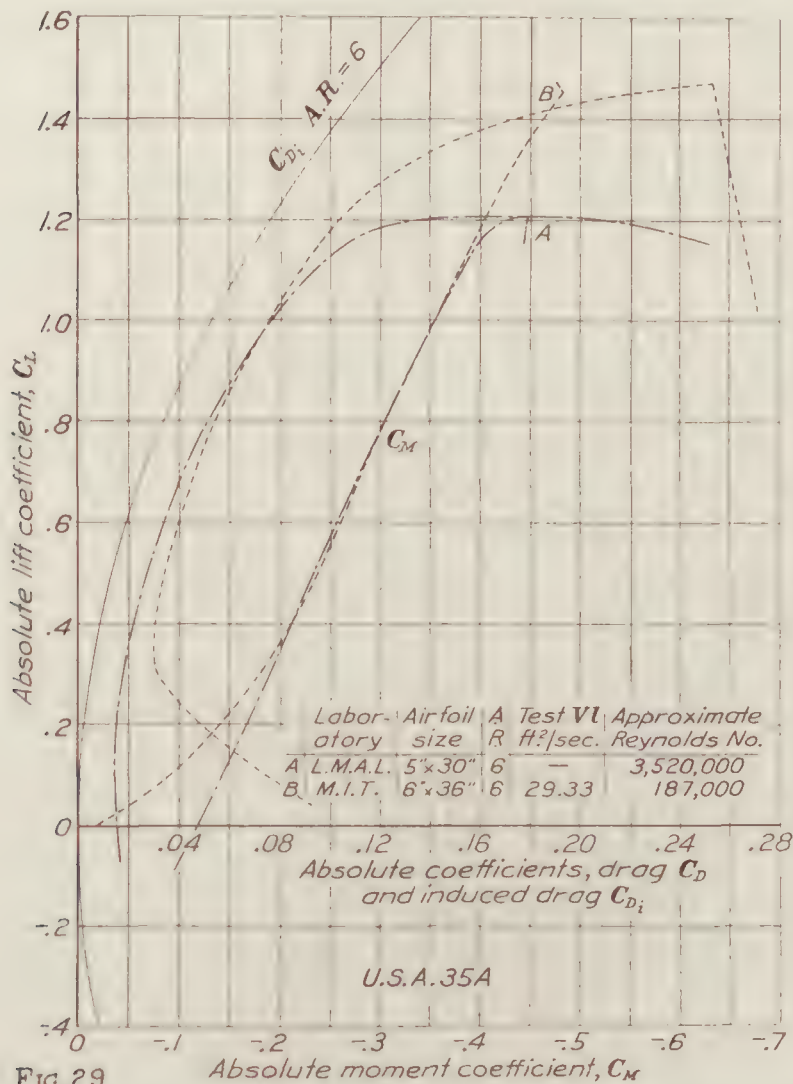


FIG. 29

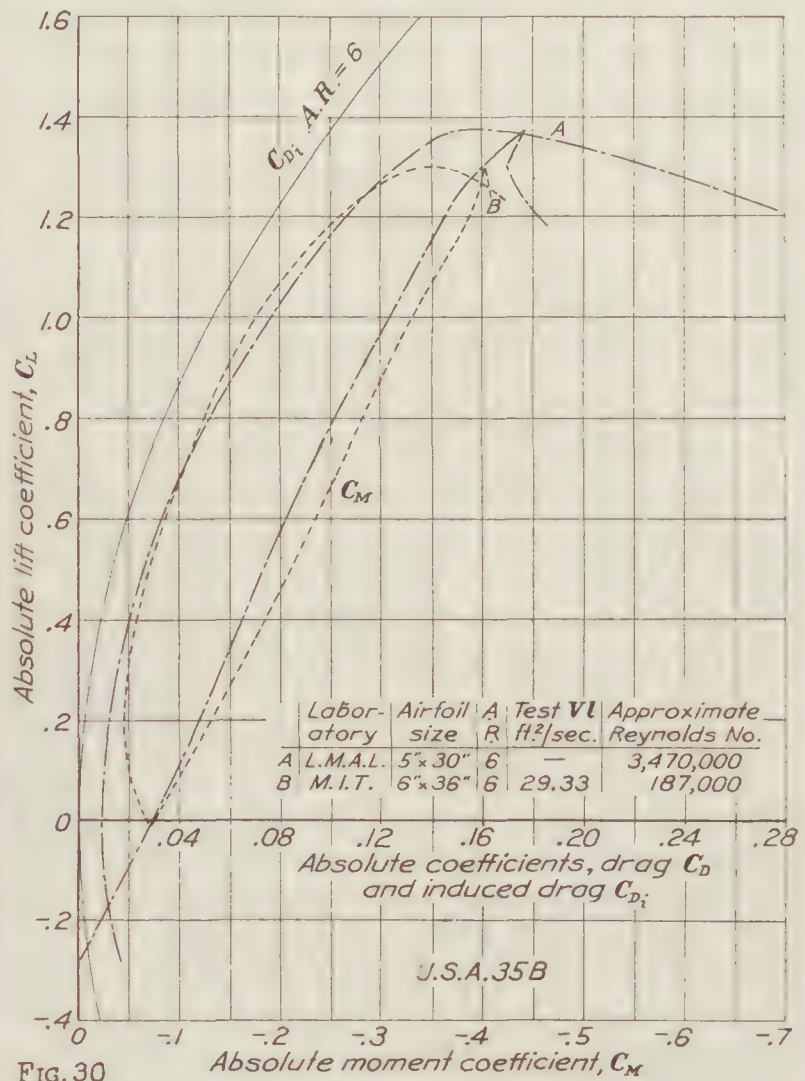
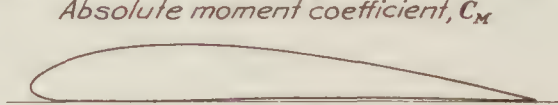


FIG. 30



The scale effects depend on the airfoil section and are in general similar for similar sections.

All airfoil sections may be roughly divided into three general classes as follows:

(a) The highly cambered or very thick section having a very high lift at Reynolds Numbers within the testing range of the average wind tunnel. This class usually shows a decrease in C_L maximum with increase in Reynolds Number.

(b) The moderately cambered, medium lift section. This class usually has a moderate, and favorable scale effect on C_L with a fairly low and favorable scale effect on C_D .

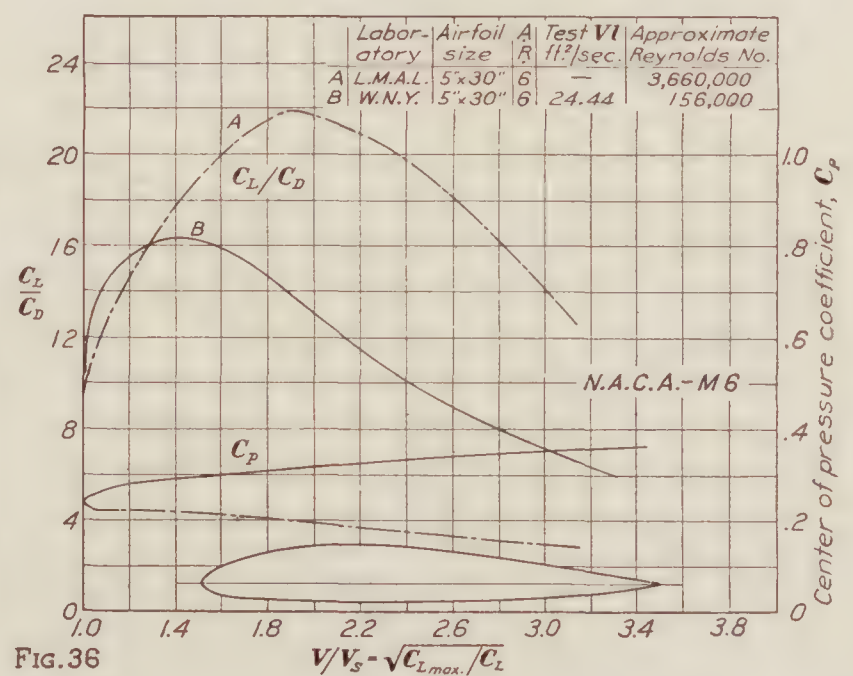
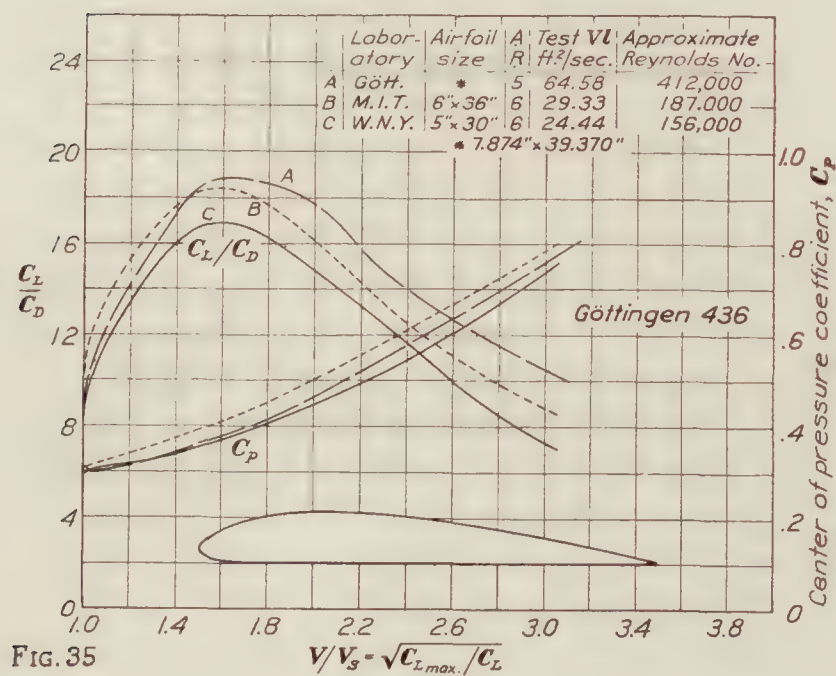
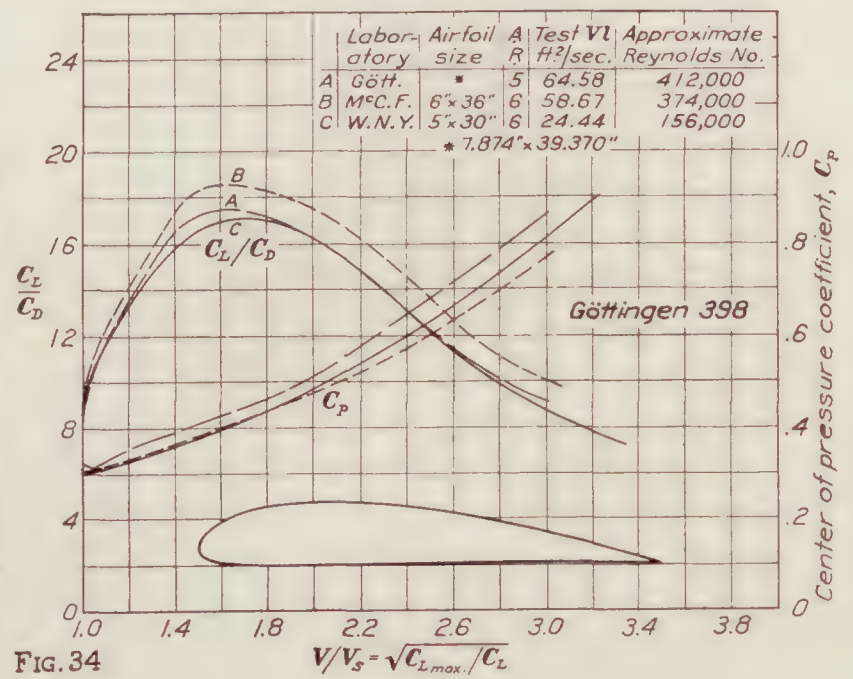
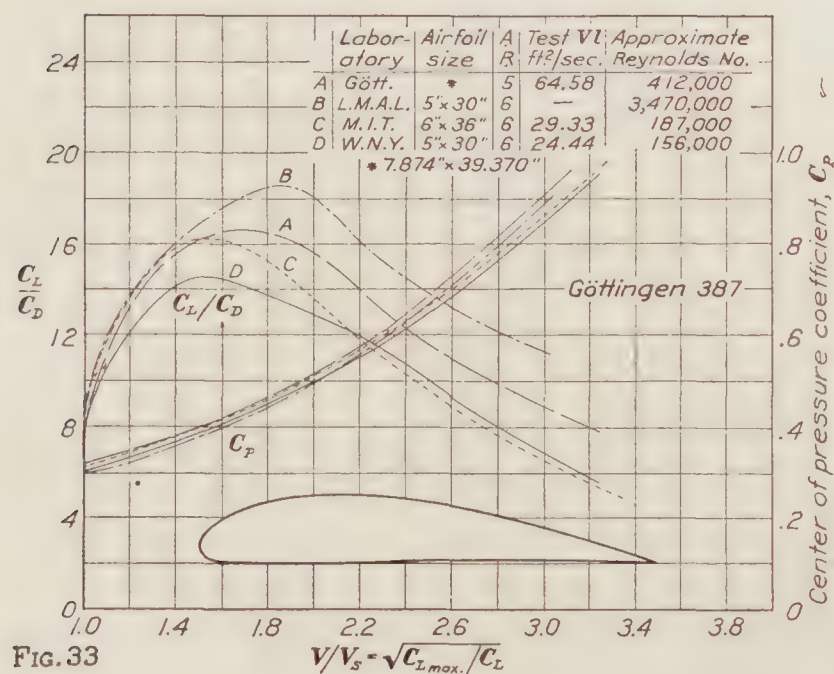
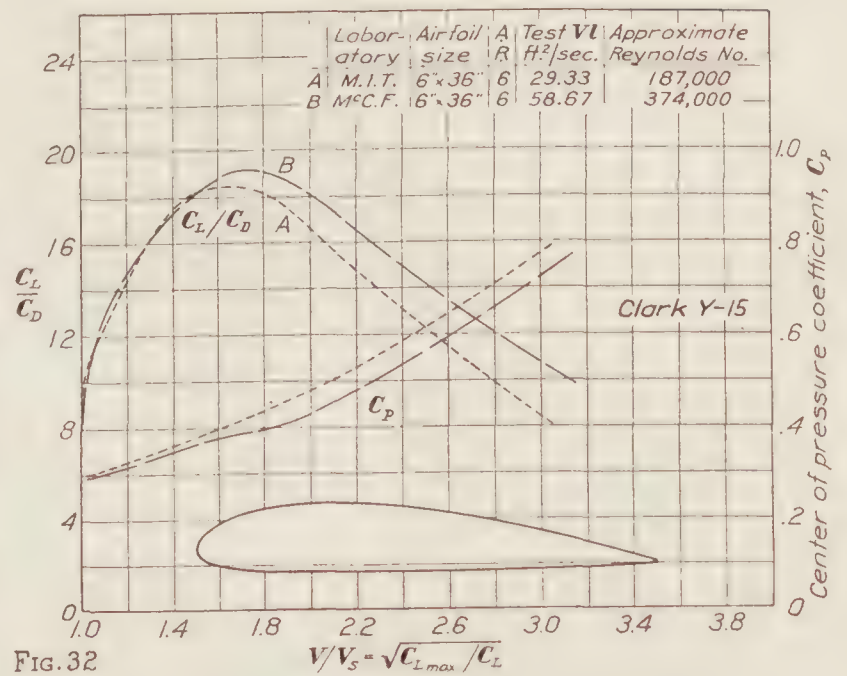
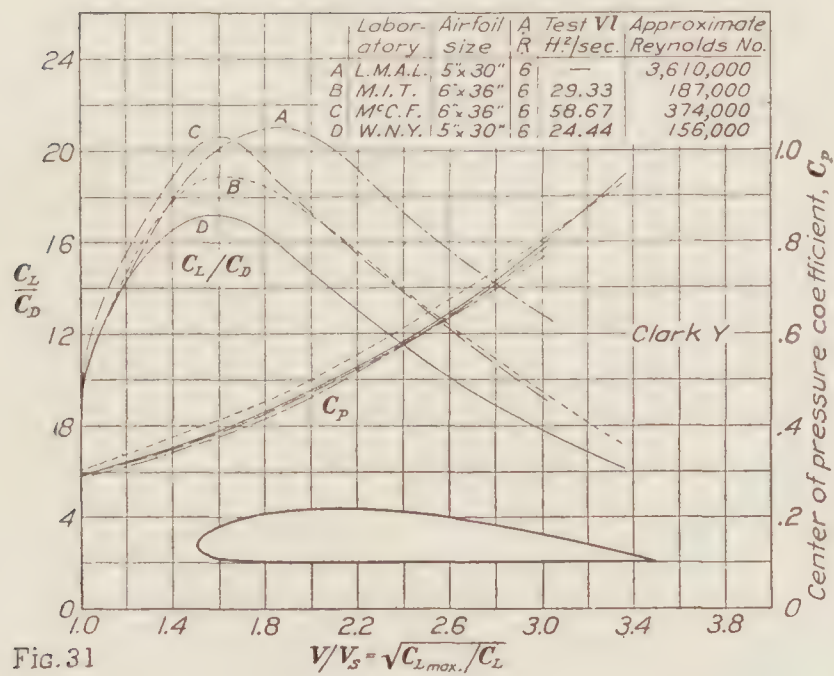
(c) The thin, to moderately thick, double cambered section of low lift at normal test Reynolds Numbers. This class usually shows a large increase in C_L maximum and a moderate decrease in C_D minimum with increase in Reynolds Number.

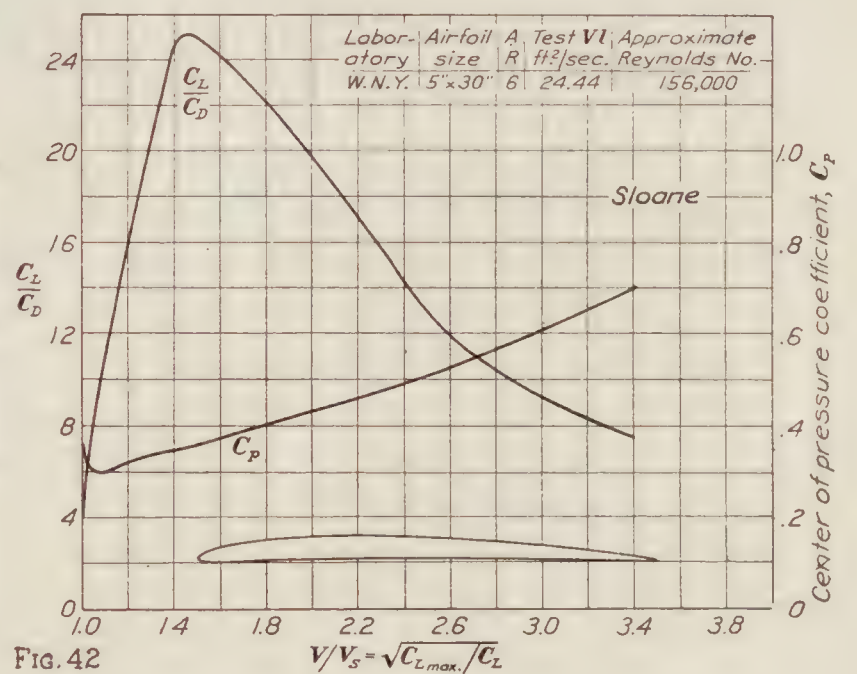
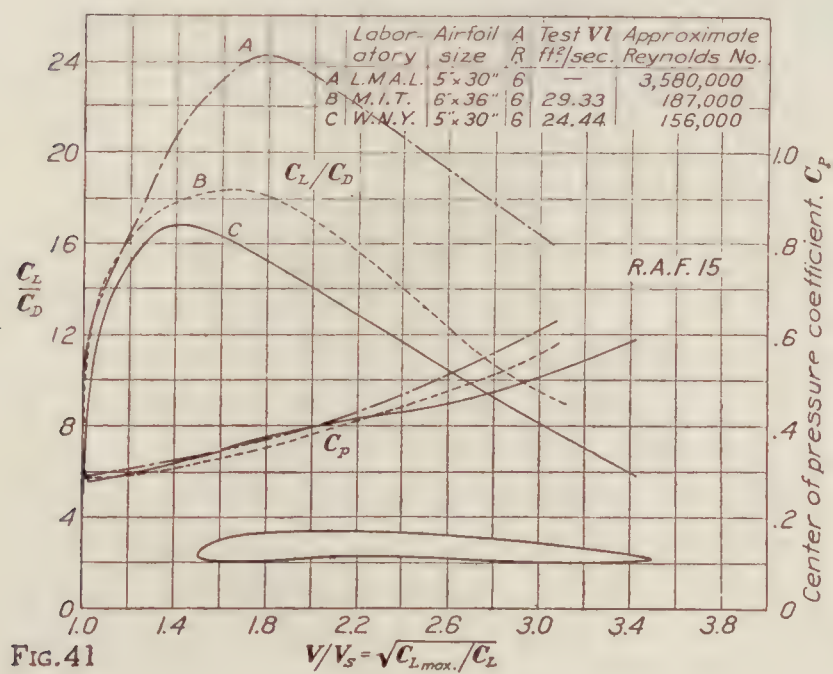
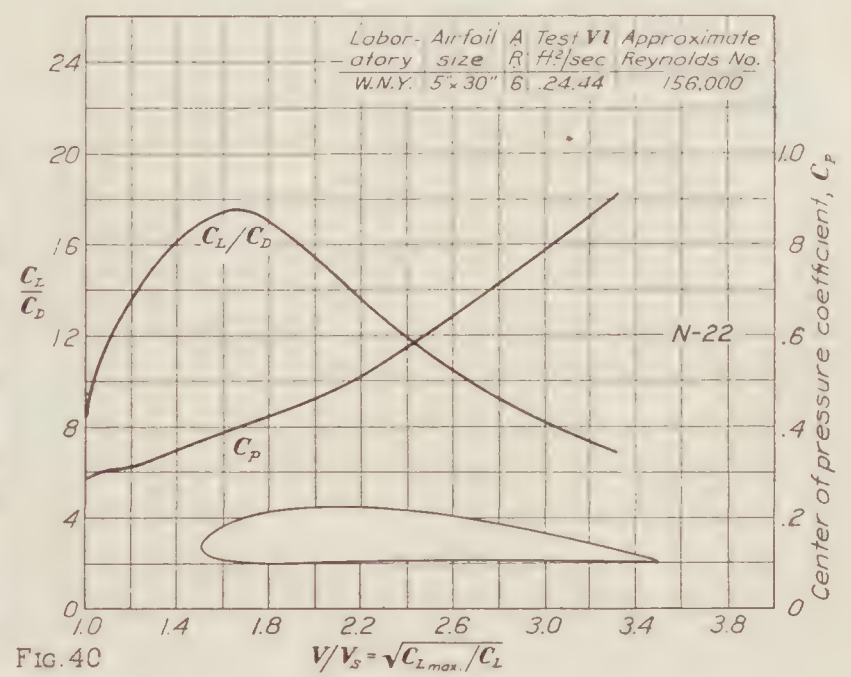
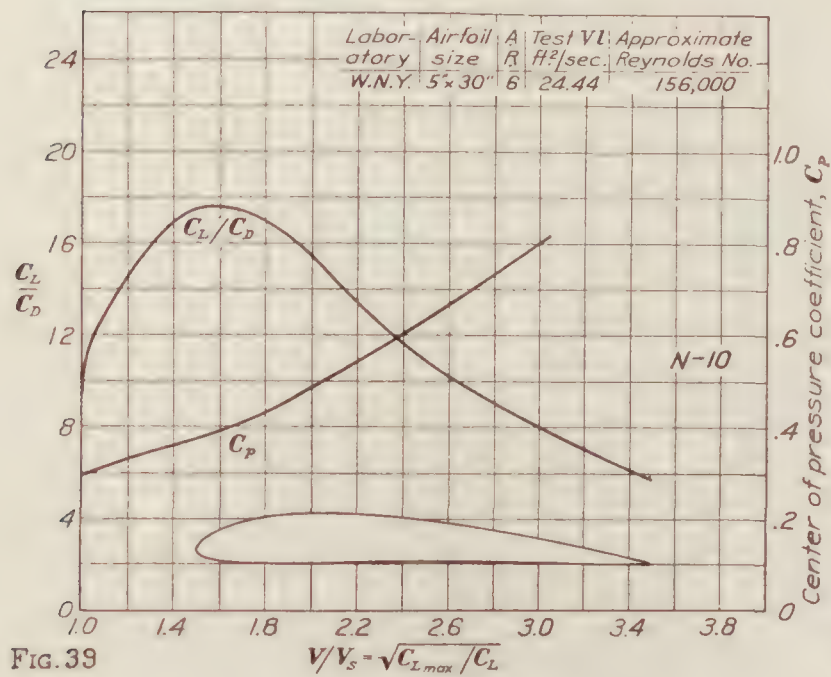
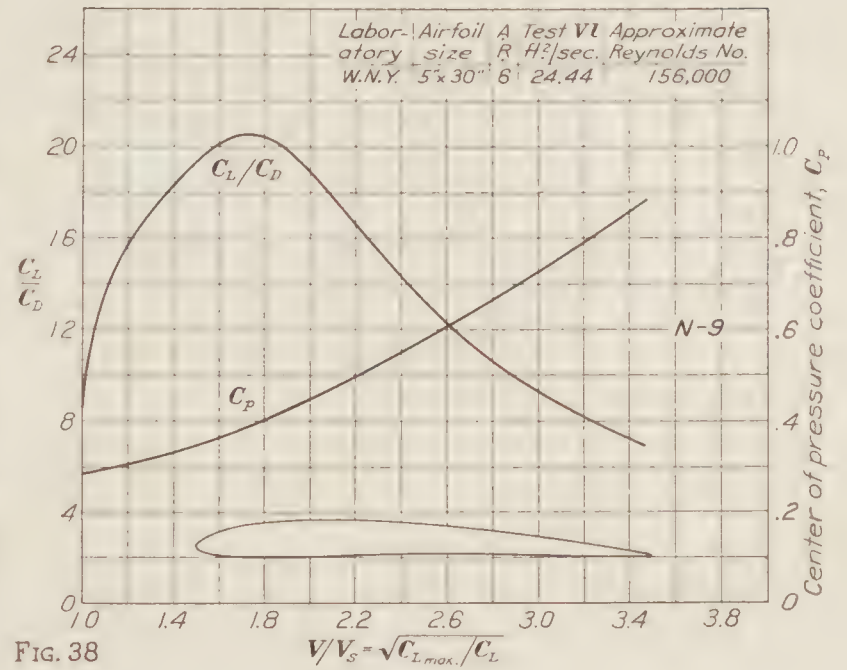
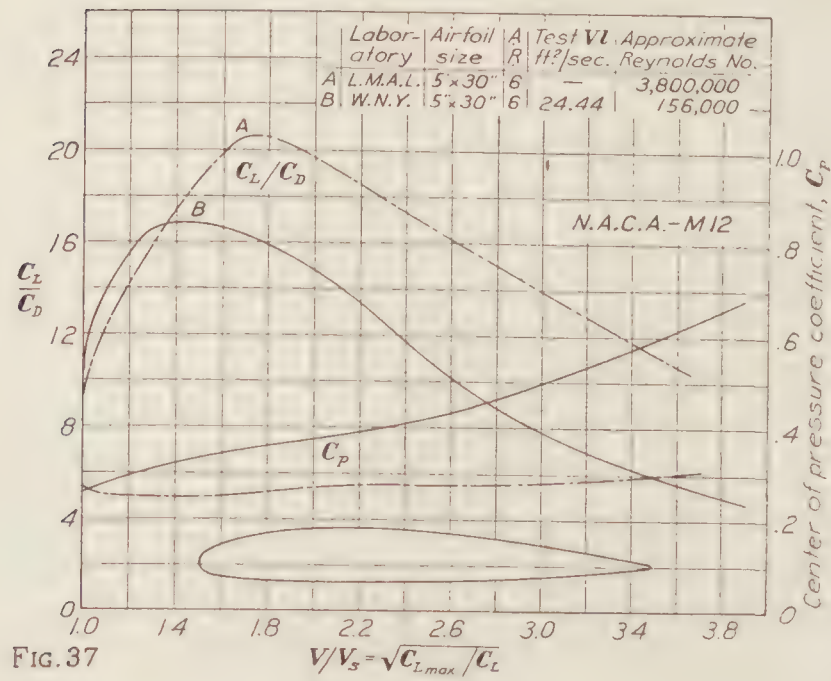
Airfoils such as the G-387 and U. S. A.-35A come in class (a); the R. A. F.-15 and Clark Y in class (b); the M-6 and M-12 in class (c).

USE OF THE DATA

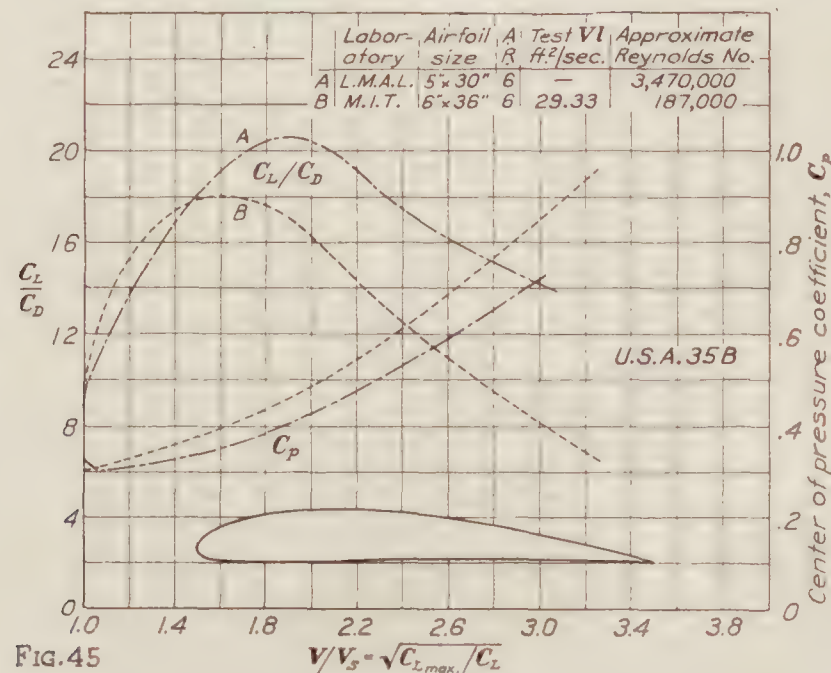
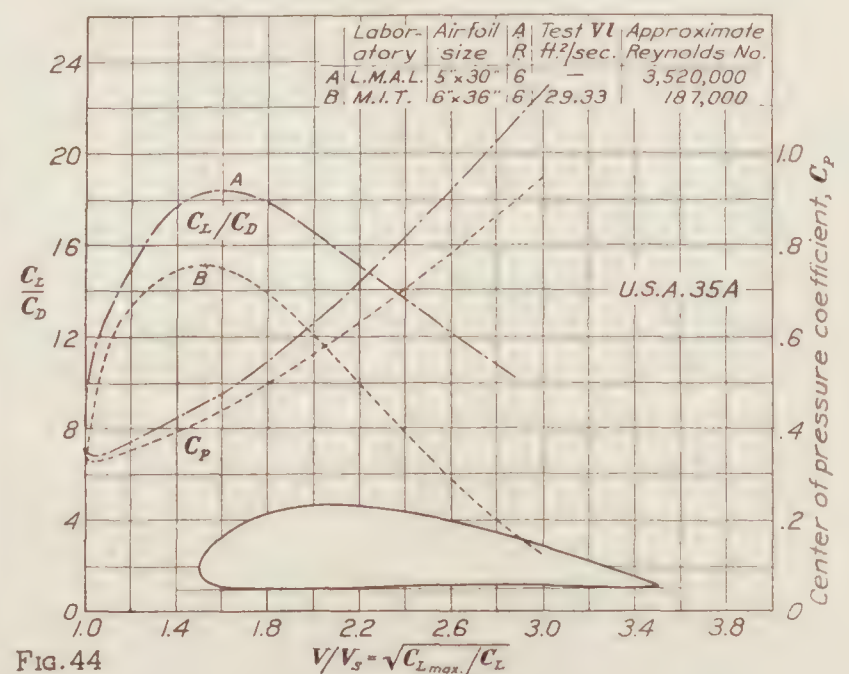
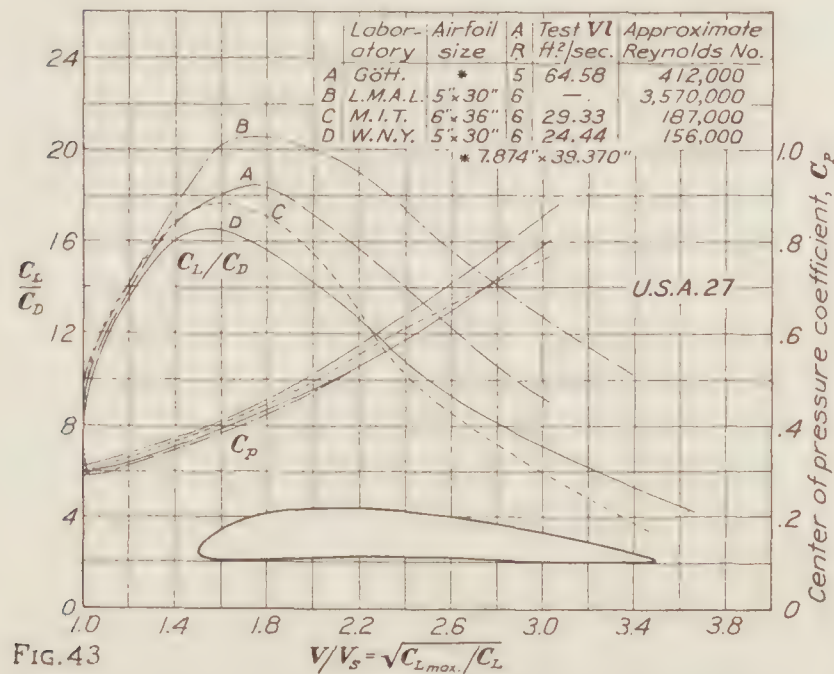
The diagrams and tables enable an engineer to make a logical selection of a wing section.

The full-scale data from the L. M. A. L. tests should be used whenever possible since free-flight tests have verified the validity of these data.





Since the scale effect is in general similar for similar sections, it is to be expected that certain wing sections such as the G-398 and N-22 which show up well in an atmospheric tunnel would have good characteristics at full Reynolds Number. This has been verified by the flight test data on airplanes with these wing sections.



CONCLUSIONS

The following conclusions can be drawn from this collection of airfoil data:

Direct comparison of the data should be made only when the Reynolds Numbers of the tests are the same. True relative values are then obtained at that Reynolds Number.

Allowance for the scale effect should be made when the tests are at different Reynolds Numbers.

The scale effect is in general similar for similar airfoil sections.

Test data at high Reynolds Numbers show better accord with free-flight data. Preference should therefore be given to data from the variable density tunnel.

More wings which show up well in an atmospheric tunnel should be tested at full scale. It is understood that this is now being done for a group of sections including the G-398.

BUREAU OF AERONAUTICS,
NAVY DEPARTMENT, April 18, 1929.

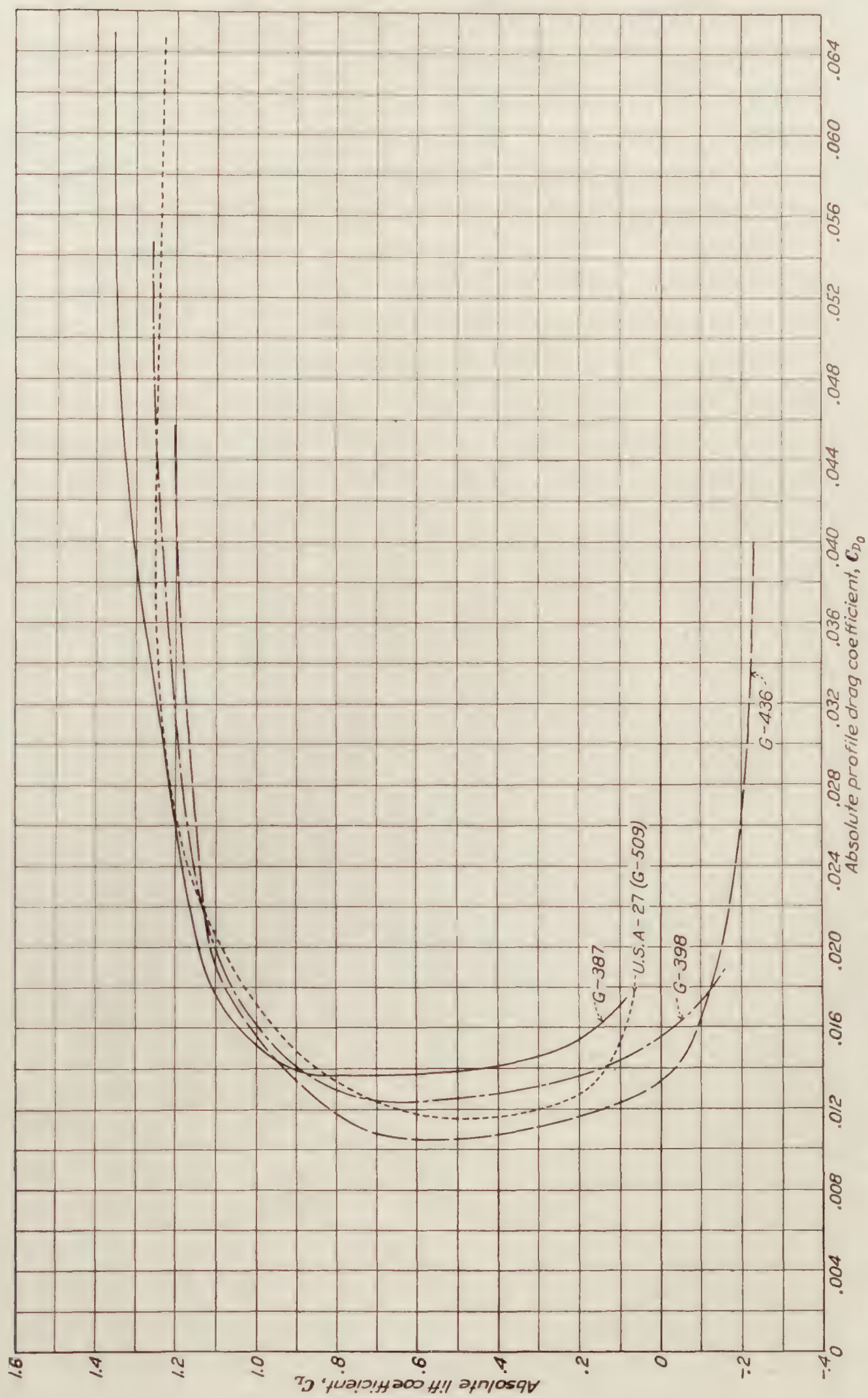


FIGURE 46.—Göttingen Laboratory tests. Airfoil size, 7.874×39.370 inches; aspect ratio, 5; test, $Vl=64.58$ square feet per second; approximate Reynolds Number, 412,000

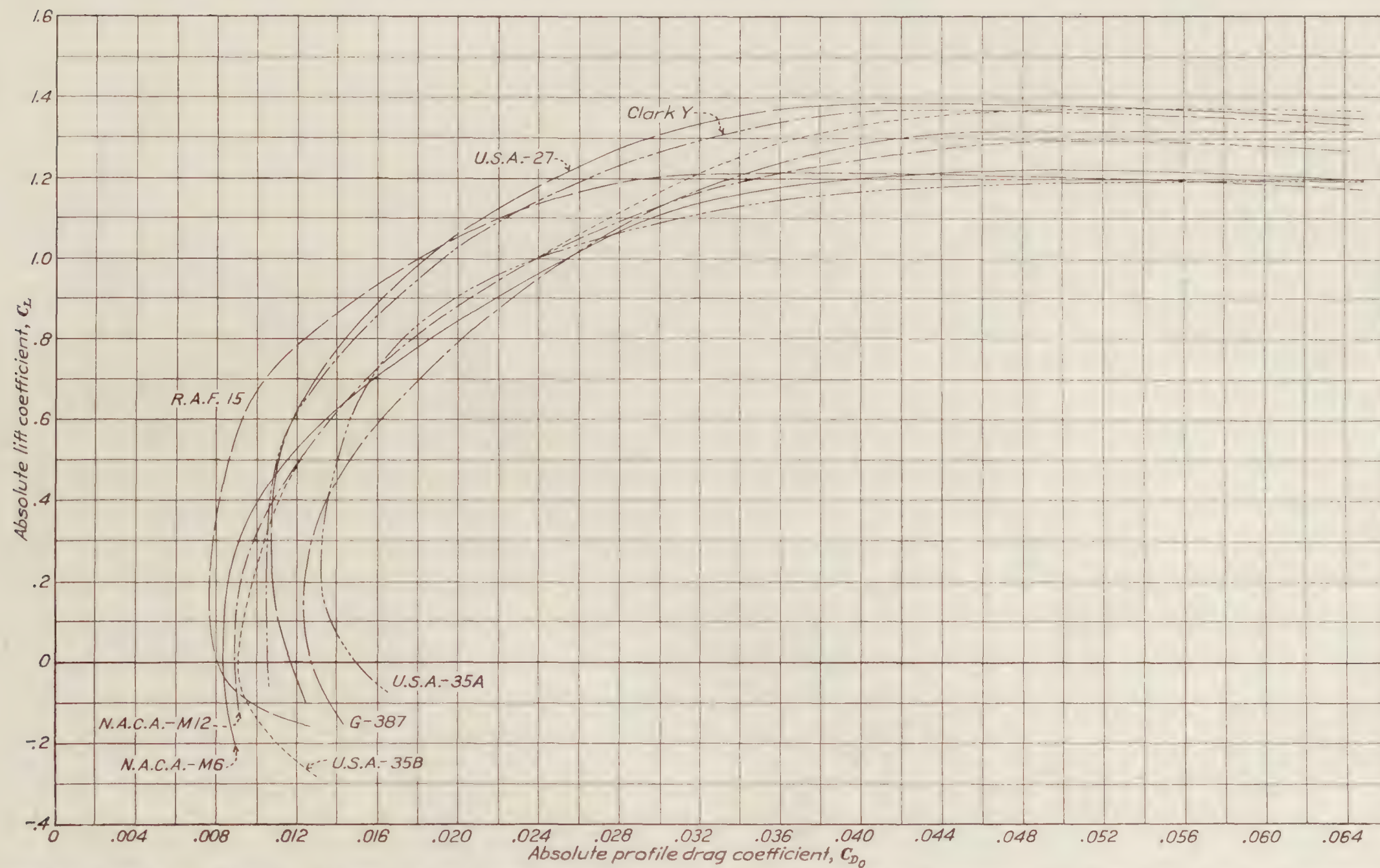


FIGURE 47.—Langley Memorial Aeronautical Laboratory tests. Airfoil size 5×30 inches; aspect ratio, 6. Airfoil, Clark Y, average Reynolds Number, 3,610,000; G-387, average Reynolds Number, 3,470,000; M-6, average Reynolds Number, 3,600,000; M-12, average Reynolds Number, 3,800,000; R. A. F.-15, average Reynolds Number, 3,580,000; U. S. A.-27, average Reynolds Number, 3,570,000; U. S. A.-35A, average Reynolds Number, 3,520,000; U. S. A.-35B, average Reynolds Number, 3,470,000

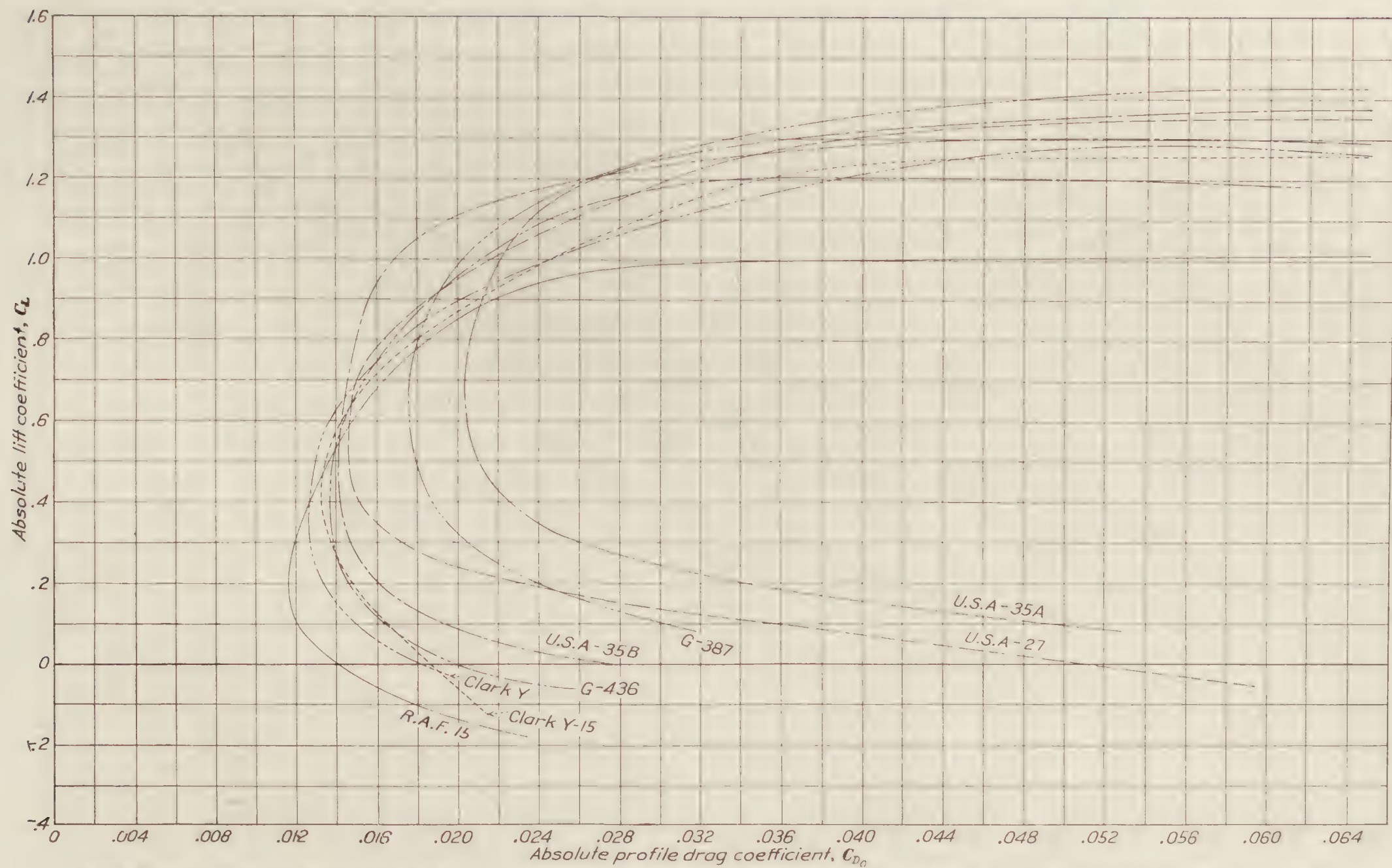


FIGURE 48.—Massachusetts Institute of Technology tests. Airfoil size 6×36 inches; aspect ratio, 6; test $Vl=29.33$ square feet per second; approximate Reynolds Number, 187,000

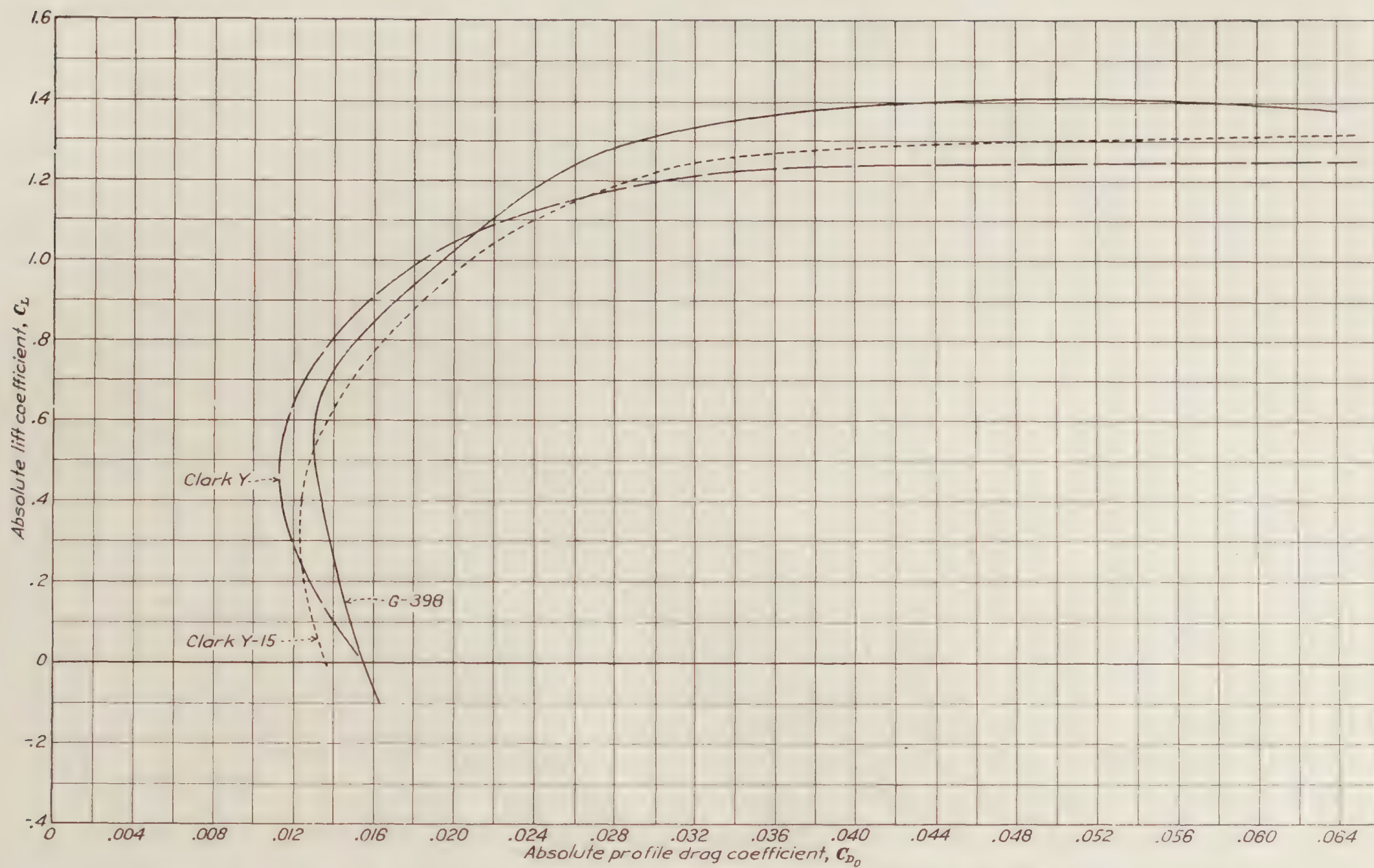


FIGURE 49.—McCook Field tests. Airfoil size, 6×36 inches; aspect ratio, 6; test $V_l=58.67$ square feet per second; approximate Reynolds Number, 374,000

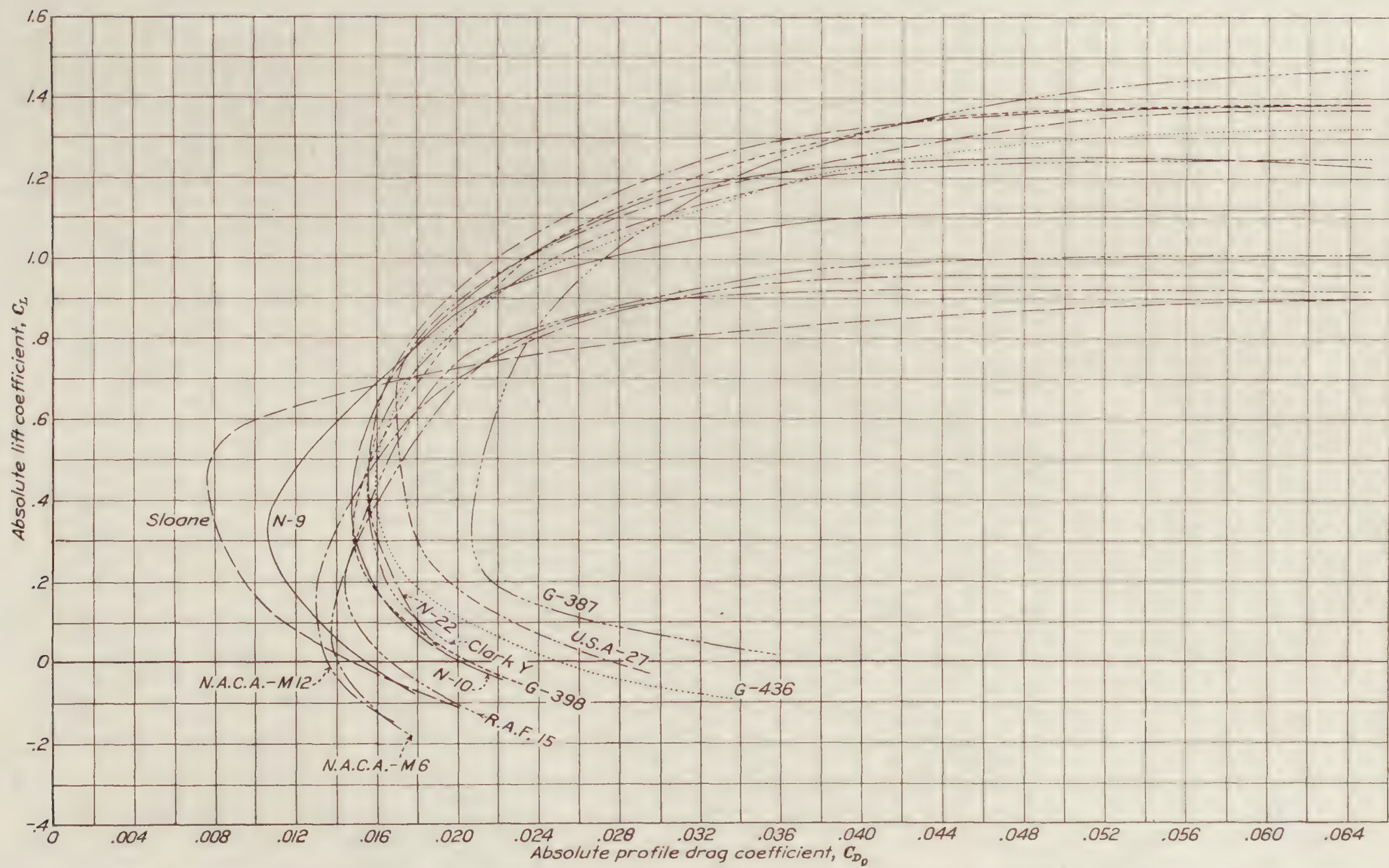


FIGURE 50.—Washington Navy Yard tests. Airfoil size, 5×30 inches; aspect ratio, 6; test, $V_l=24.44$ square feet per second; approximate Reynolds Number, 156,000

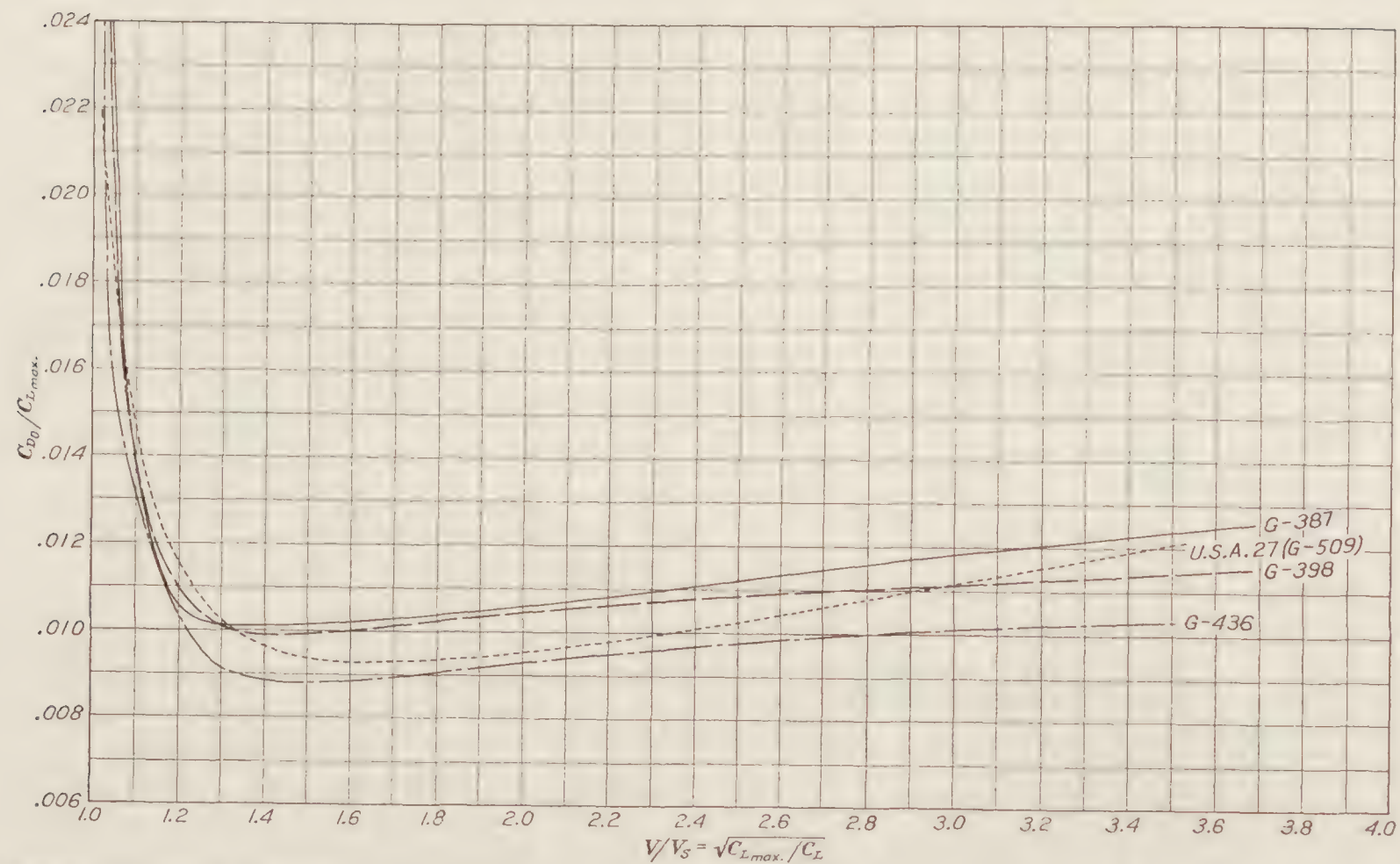


FIGURE 51.—Gottingen Laboratory tests. Airfoil size, 7.874×39.370 inches; aspect ratio, 5; test $Vl=64.58$ square feet per second; approximate Reynolds Number, 412,000

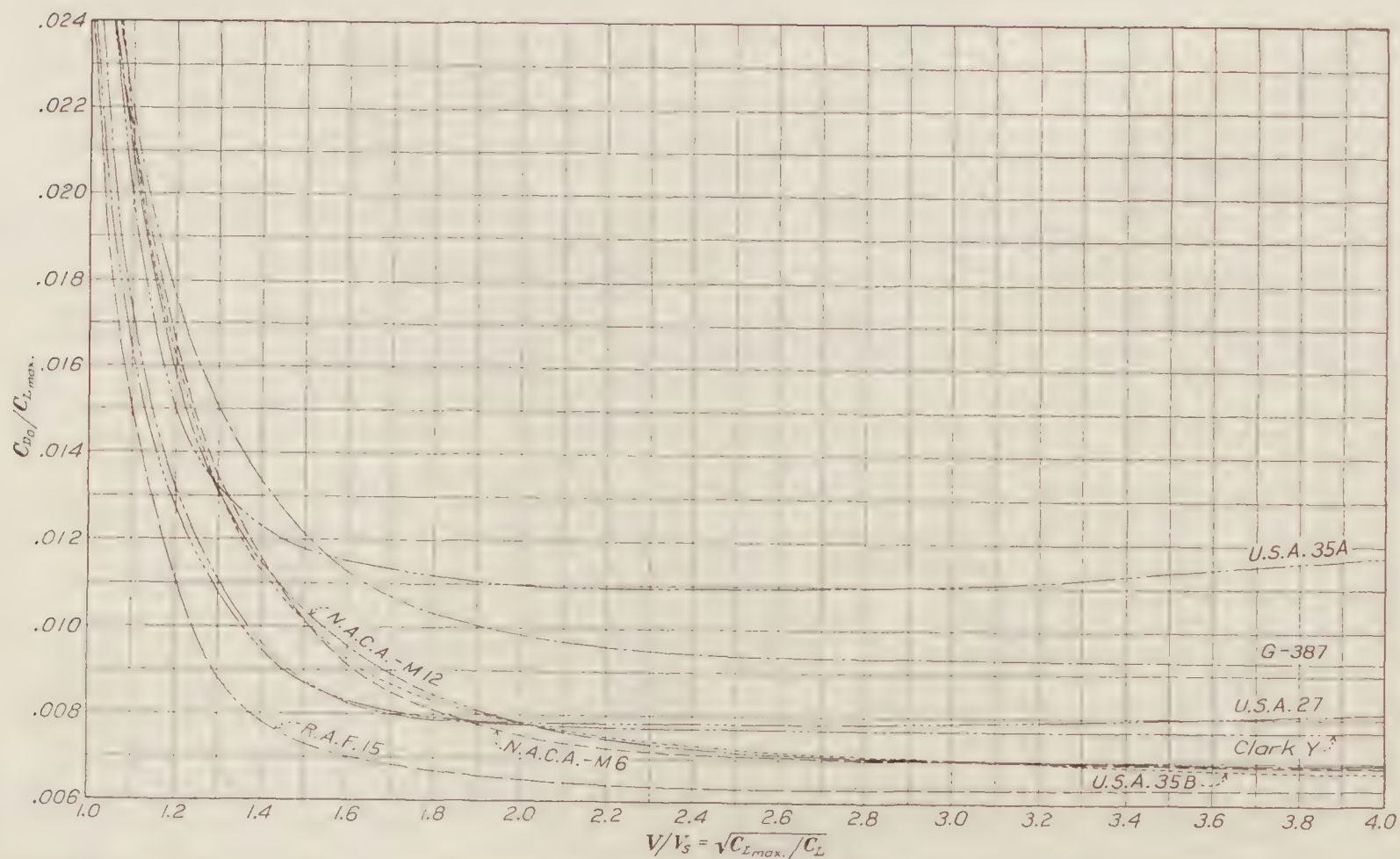


FIGURE 52.—Langley Memorial Aeronautical Laboratory tests. Airfoil size, 5×30 inches; aspect ratio, 6; approximate Reynolds Number, 3,600,000

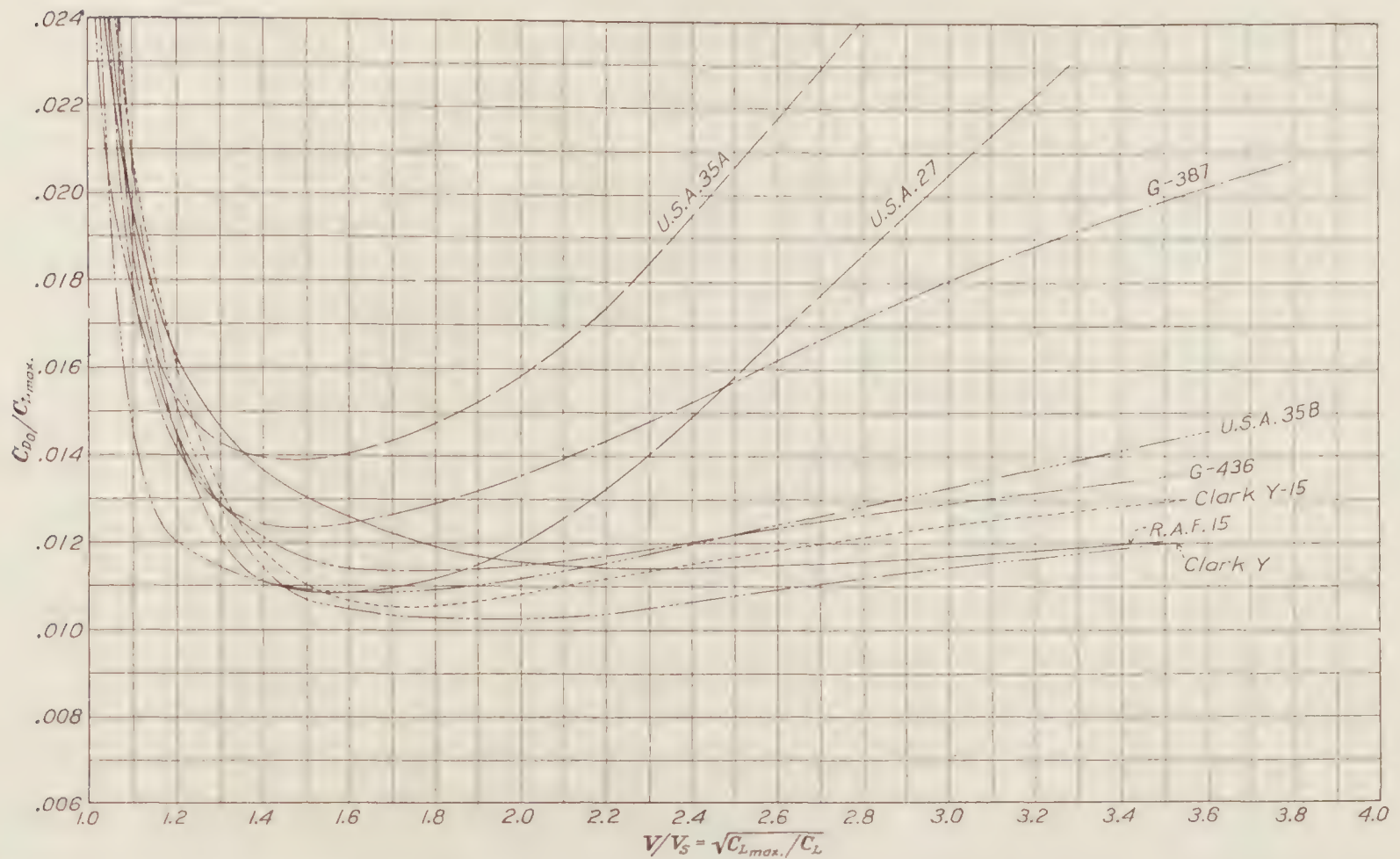


FIGURE 53.—Massachusetts Institute of Technology tests. Airfoil size, 6×36 inches; aspect ratio, 6; test $Vl \times 29.33$ square feet per second; approximate Reynolds Number, 187,000

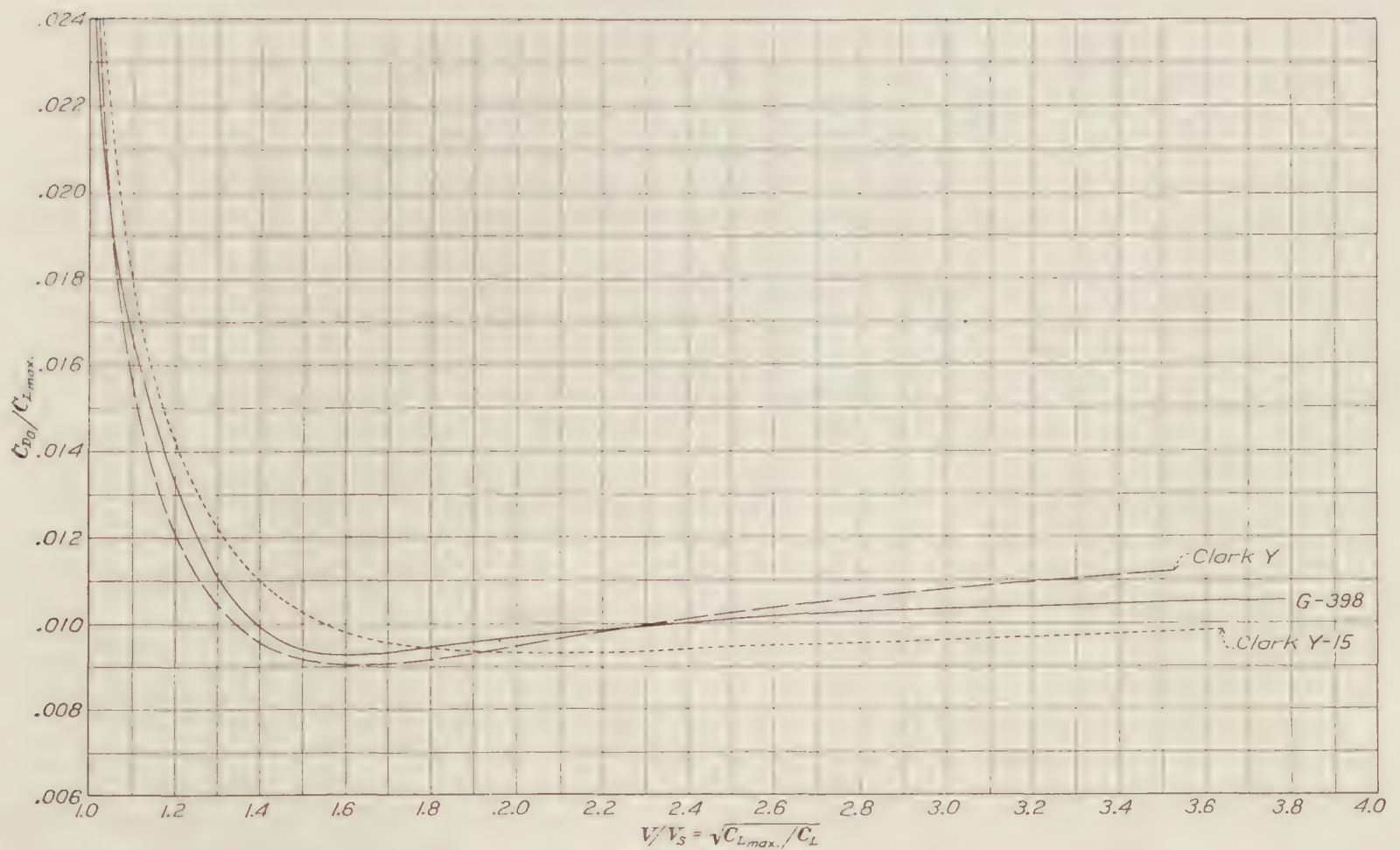


FIGURE 54.—McCook Field tests. Airfoil size, 6×36 inches; aspect ratio, 6; test $Vl = 58.67$ square feet per second; approximate Reynolds Number, 374,000

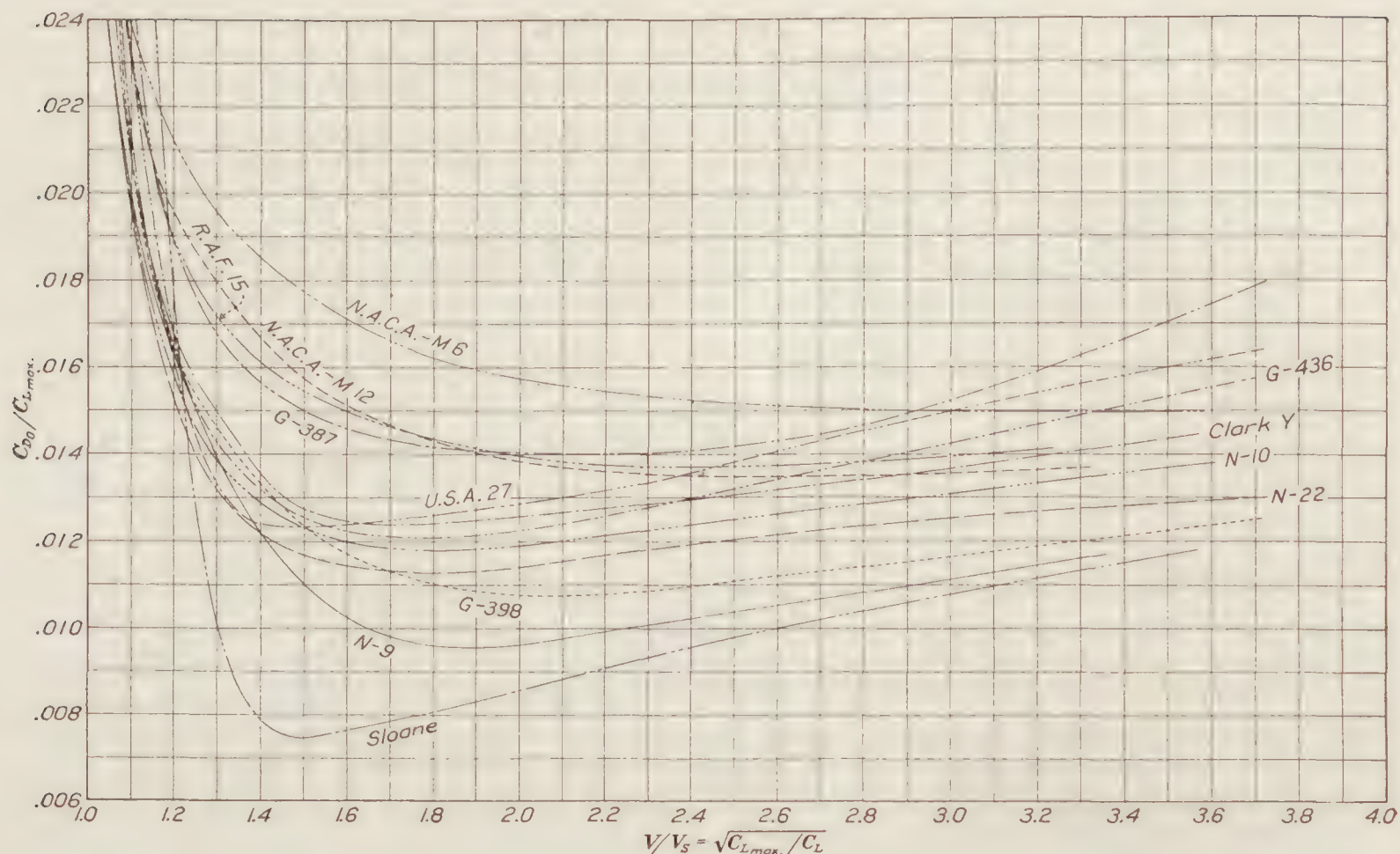


FIGURE 55.—Washington Navy Yard tests. Airfoil size, 5×30 inches; aspect ratio, 6; test, $V_l=24.44$ square feet per second; approximate Reynolds Number, 156,000

REFERENCES

- Reference 1. Munk, Max M., and Miller, Elton W.: Model Tests with a Systematic Series of 27 Wing Sections at Full Reynolds Number. N. A. C. A. Technical Report No. 221. (1925.)
- Reference 2. Munk, Max M., and Miller, Elton W.: The Aerodynamic Characteristics of Seven Frequently Used Wing Sections at Full Reynolds Number. N. A. C. A. Technical Report No. 233. (1926.)
- Reference 3. Ergebnisse der Aerodynamischen Versuchsanstalt zu Göttingen. I. Lieferung. (1921.)
- Reference 4. Ergebnisse der Aerodynamischen Versuchsanstalt zu Göttingen. III. Lieferung. (1927.)
- Reference 5. Morse, A. L.: Wind Tunnel Test of 36"×6" Airfoils. McCook Field Report, Serial No. 2340. (June 28, 1924.)
- Reference 6. Morse, A. L.: Wind Tunnel Test of 36"×6" Airfoils. McCook Field Report, Serial No. 2485. (Mar. 10, 1925.)
- Reference 7. Aerodynamics Branch: Wind Tunnel Test of Clark Y, Clark Y-15, Clark Y-18, Clark Y-21, Göttingen 398, and S. T. Aé.-27a, 6"×36" Airfoils. McCook Field Report, Serial No. 2700. (July 21, 1926.)
- Reference 8. Aeronautics Staff: Air Forces and Moments for Göttingen Airfoils, Nos. 387, 398, 414, 436, 449. Washington Navy Yard Aeronautical Report No. 236. (Sept. 21, 1923.)
- Reference 9. Aeronautics Staff: Air Force and Moment for R. A. F.-15 and Sloane Airfoils. Washington Navy Yard Aeronautical Report No. 237. (Sept. 27, 1923.)
- Reference 10. Aeronautics Staff: Air Force and Moment for Navy Airfoils: N-9, N-10, N-11. Washington Navy Yard Aeronautical Report No. 248. (Dec. 1, 1923.)
- Reference 11. Aeronautics Staff: Air Force and Moments for Navy N-16 to 19, Clark Y, and U. S. A.-27 Airfoils. Washington Navy Yard Aeronautical Report No. 269. (Jan. 6, 1925.)
- Reference 12. Aeronautics Staff: Air Forces and Moments for Navy N-22 to 24 and Boeing 103 Airfoils. Washington Navy Yard Aeronautical Report No. 301. (Jan. 22, 1926.)
- Reference 13. Aeronautics Staff: Air Force and Moment for Navy N-34 to 37 and M-12 Airfoils. Washington Navy Yard Aeronautical Report No. 364. (Apr. 18, 1928.)
- Reference 14. Aeronautics Staff: Air Force and Moment for Navy N-29, 30, 33, and N. A. C. A. M-6 Airfoils. Washington Navy Yard Aeronautical Report No. 365. (Apr. 23, 1928.)
- Reference 15. Warner, Edward P.: The Choice of Wing Sections for Airplanes. N. A. C. A. Technical Note No. 73. (Nov., 1921.)
- Reference 16. Diehl, Walter S.: Engineering Aerodynamics. The Ronald Press. (1928.)
- Reference 17. Higgins, George J., Diehl, Walter S., and DeFoe, George L.: Tests on Models of Three British Airplanes. N. A. C. A. Technical Report No. 279. (1928.)

TABLE I
SPECIFIED ORDINATES OF AIRFOIL SECTIONS
All dimensions are given in per cent of chord length

Distance from leading edge in percentage of chord	Clark Y		Clark Y-15		G-387		G-398	
	Upper camber	Lower camber	Upper camber	Lower camber	Upper camber	Lower camber	Upper camber	Lower camber
0	3.49	3.49	3.50	3.50	3.78	3.78	3.74	3.74
1.25	5.53	1.94	5.98	1.43	6.53	1.43	6.20	1.89
2.5	6.50	1.46	7.21	.76	7.91	.93	7.40	1.28
5	7.87	.94	8.86	-.05	9.89	.40	9.17	.69
7.5	8.86	.61	10.01	-.50	11.32	.15	10.37	.35
10	9.63	.40	10.89	-.87	12.40	.03	11.25	.18
15	10.74	.15	12.17	-1.38	13.84	0	12.53	.03
20	11.35	.04	12.96	-1.57	14.71	.05	13.34	0
30	11.73	0	13.35	-1.65	15.34	.23	13.80	.05
40	11.40	0	13.00	-1.60	14.85	.38	13.34	.17
50	10.52	0	11.99	-1.48	13.47	.50	12.27	.27
60	9.18	0	10.44	-1.29	11.54	.57	10.63	.33
70	7.52	0	8.39	-1.04	9.21	.58	8.53	.35
80	5.54	0	5.95	-.73	6.58	.49	6.12	.27
90	3.22	0	3.19	-.39	3.61	.28	3.40	.13
95	1.88	0	1.75	-.25	2.02	.16	1.92	.06
100	.25	.25	.14	-.01	.25	.25	.25	.25

Distance from leading edge in percentage of chord	G-436		M-6		M-12		N-9	
	Upper camber	Lower camber	Upper camber	Lower camber	Upper camber	Lower camber	Upper camber	Lower camber
0	2.66	2.66	0	0	0	0	2.25	2.25
1.25	4.53	1.21	1.97	-1.76	2.03	-1.65	3.72	1.14
2.5	5.54	.79	2.81	-2.20	2.86	-2.14	4.50	.77
5	7.00	.37	4.03	-2.73	4.01	-2.72	5.51	.39
7.5	8.11	.15	4.94	-3.03	4.89	-3.07	6.22	.21
10	8.98	.05	5.71	-3.24	5.59	-3.31	6.75	.11
15	10.16	0	6.82	-3.47	6.61	-3.62	7.52	.01
20	10.82	0	7.55	-3.62	7.30	-3.80	8.00	0
30	11.08	0	8.22	-3.79	7.95	-3.98	8.26	.03
40	10.55	0	8.05	-3.90	7.86	-3.96	8.00	.10
50	9.60	0	7.26	-3.94	7.25	-3.82	7.38	.16
60	8.28	0	6.03	-3.82	6.27	-3.50	6.38	.20
70	6.60	0	4.58	-3.48	4.98	-3.00	5.13	.21
80	4.70	0	3.06	-2.83	3.50	-2.31	3.67	.16
90	2.64	0	1.55	-1.77	1.89	-1.37	2.07	.08
95	1.54	0	.88	-1.08	1.07	-.81	1.26	.04
100	.25	.25	0	0	0	0	.25	0

Distance from leading edge in percentage of chord	N-10		N-22		R. A. F.-15		Sloane	
	Upper camber	Lower camber	Upper camber	Lower camber	Upper camber	Lower camber	Upper camber	Lower camber
0	2.99	2.99	3.37	3.37	1.50	1.50	0.82	0.82
1.25	4.96	1.51	5.58	1.70	3.14	.76	1.89	.24
2.5	5.92	1.02	6.66	1.15	3.94	.50	2.56	.08
5	7.33	.55	8.25	.62	5.00	.18	3.37	.01
7.5	8.28	.28	9.33	.32	5.67	.02	3.95	.05
10	8.99	.14	10.13	.16	6.09	.02	4.38	.12
15	10.04	.01	11.28	.03	6.67	.18	4.95	.32
20	10.67	.00	12.01	0	6.96	.53	5.29	.50
30	11.01	.04	12.42	.05	6.94	1.02	5.62	.63
40	10.73	.14	12.01	.15	6.63	1.02	5.63	.57
50	9.85	.22	11.04	.24	6.13	.71	5.39	.48
60	8.50	.27	9.57	.30	5.52	.33	4.88	.38
70	6.83	.28	7.68	.32	4.79	.06	4.11	.30
80	4.90	.22	5.51	.24	3.91	.04	3.16	.21
90	2.74	.10	3.06	.12	2.81	.21	2.00	.10
95	1.60	.05	1.73	.05	2.17	.32	1.32	.04
100	.25	.25	.25	.25	.94	.94	.25	.25

TABLE I—Continued

SPECIFIED ORDINATES OF AIRFOIL SECTIONS—Continued

Distance from leading edge in percentage of chord	U. S. A.-27		U. S. A.-35A		U. S. A.-35B	
	Upper camber	Lower camber	Upper camber	Lower camber	Upper camber	Lower camber
0	1.77	1.77	4.33	4.33	2.84	2.84
1.25	3.89	.61	8.09	1.62	5.15	1.03
2.5	5.15	.35	9.58	.96	6.21	.63
5	6.95	.10	11.83	.42	7.62	.28
7.5	8.23	.01	13.58	.22	8.65	.14
10	9.19	0	14.88	.10	9.45	.07
15	10.52	.13	16.60	0	10.56	0
20	11.32	.37	17.72	.08	11.28	.05
30	11.87	.91	18.43	.25	11.76	.15
40	11.59	1.08	17.86	.44	11.41	.28
50	10.78	.78	16.16	.60	10.34	.39
60	9.57	.35	13.91	.67	8.91	.45
70	7.97	.07	11.12	.65	7.05	.42
80	5.92	.01	7.88	.55	5.02	.35
90	3.65	.19	4.33	.32	2.72	.20
95	2.33	.33	2.39	.19	1.52	.12
100	.74	.74	.43	0	.25	.25

TABLE II

SPECIFIED THICKNESS OF AIRFOIL SECTIONS

All dimensions are given in per cent of chord length

Airfoil section	Maximum thickness	Thickness at—			
		10 per cent from leading edge	15 per cent from leading edge	60 per cent from leading edge	70 per cent from leading edge
Clark Y.....	11.73	9.23	10.59	9.18	7.52
Clark Y-15.....	15.00	11.76	13.55	11.73	9.43
G-387.....	15.11	12.37	13.84	10.97	8.63
G-398.....	13.75	11.07	12.50	10.30	8.18
G-436.....	11.08	8.93	10.16	8.28	6.60
M-6.....	12.01	8.95	10.29	9.85	8.06
M-12.....	11.93	8.90	10.23	9.77	7.98
N-9.....	8.23	6.64	7.51	6.18	4.92
N-10.....	10.97	8.85	10.03	8.23	6.55
N-22.....	12.37	9.97	11.25	9.27	7.36
R. A. F.-15.....	6.49	6.07	6.49	5.19	4.73
Sloane.....	5.06	4.26	4.63	4.50	3.81
U. S. A.-27.....	10.96	9.19	10.39	9.22	7.90
U. S. A.-35A.....	18.18	14.78	16.60	13.24	10.37
U. S. A.-35B.....	11.61	9.38	10.56	8.46	6.63

TABLE III

G-387 AIRFOIL

GÖTTINGEN TEST

Airfoil size, 7.874 x 39.370 inches.
Aspect ratio, 5.

Test speed, 98.42 ft./sec.
Test V_L , 64.58 sq. ft./sec.

Data with tunnel wall interference corrections applied are taken from Reference 3

Angle of attack α degrees	Lift coefficient C_L	Drag coefficient C_D	Moment coefficient C_M	Center of pressure coefficient C_p	$\frac{C_L}{C_D}$	Speed ratio $\frac{V}{V_s}$	Profile drag coefficient C_{D_0}
-9.0	-0.104	0.0690	-0.053	-----	-1.51	-----	0.0683
-6.0	.082	.0180	-.123	-----	4.55	-----	.0175
-4.6	.182	.0179	-.146	0.79	10.2	2.74	.0157
-3.1	.280	.0201	-.167	.60	13.9	2.21	.0151
-1.6	.380	.0235	-.192	.50	16.2	1.89	.0143
-0.2	.468	.0291	-.218	.45	16.1	1.71	.0151
1.3	.581	.0357	-.242	.41	16.3	1.53	.0141
2.7	.681	.0438	-.265	.38	15.6	1.41	.0142
4.2	.789	.0531	-.288	.37	14.8	1.32	.0135
5.7	.872	.0631	-.310	.36	12.4	1.25	.0146
8.6	1.085	.0921	-.375	.34	11.8	1.12	.0171
11.6	1.218	.124	-.410	.33	9.81	1.06	.0294
14.5	1.340	.162	-.429	.32	8.27	1.01	.0476
17.5	1.360	.217	-.452	.34	6.27	1.00	.0992

TABLE IV

G-398 AIRFOIL

GÖTTINGEN TEST

Airfoil sizes, 7.874x39.370 inches.
Aspect ratio, 5.

Test speed, 98.42 ft./sec.
Test V_l 64.58 sq. ft./sec.

Data with tunnel wall interference corrections applied are taken from Reference 3

Angle of attack α degrees	Lift coeffi- cient C_L	Drag coeffi- cient C_D	Moment coeffi- cient C_M	Center of pressure coeffi- cient C_p	$\frac{C_L}{C_D}$	Speed ratio $\frac{V}{V_s}$	Profile drag coeffi- cient C_{D_0}
-11.9	-0.297	0.101	0.031	-----	-2.94	-----	0.0954
-8.9	-.159	.0205	-.054	-----	-7.76	-----	.0188
-6.0	.037	.0152	-.100	-----	2.43	-----	.0151
-4.6	.138	.0152	-.122	0.87	9.08	3.02	.0140
-3.1	.232	.0170	-.143	.63	13.7	2.33	.0135
-1.6	.340	.0205	-.170	.49	16.6	1.93	.0132
-0.2	.435	.0249	-.192	.45	17.5	1.70	.0128
2.8	.640	.0386	-.245	.39	16.6	1.40	.0124
5.7	.840	.0597	-.295	.36	14.1	1.23	.0147
8.6	1.015	.0851	-.337	.34	11.9	1.12	.0193
11.6	1.170	.1150	-.371	.31	10.2	1.04	.0278
14.5	1.260	.1560	-.403	.32	8.08	1.00	.0547

TABLE V

G-436 AIRFOIL

GÖTTINGEN TEST

Airfoil size, 7.874x39.370 inches.
Aspect ratio, 5.

Test speed, 98.42 ft./sec.
Test V_l 64.58 sq. ft./sec.

Data with tunnel wall interference corrections applied is taken from Reference 3

Angle of attack α degrees	Lift coeffi- cient C_L	Drag coeffi- cient C_D	Moment coeffi- cient C_M	Center of pressure coeffi- cient C_p	$\frac{C_L}{C_D}$	Speed ratio $\frac{V}{V_s}$	Profile drag coeffi- cient C_{D_0}
-8.9	-0.236	0.0437	-0.009	-----	-5.40	-----	0.0401
-6.0	-.050	.0144	-.063	-----	-3.47	-----	.0142
-4.5	.050	.0130	-.084	-----	3.84	-----	.0128
-3.0	.150	.0133	-.107	0.71	11.3	2.84	.0119
-1.6	.246	.0159	-.130	.53	15.5	2.22	.0121
-0.1	.349	.0189	-.154	.44	18.5	1.86	.0111
1.3	.451	.0247	-.182	.39	18.3	1.64	.0117
2.8	.548	.0294	-.202	.36	18.6	1.49	.0101
4.3	.647	.0382	-.226	.34	16.9	1.37	.0092
5.7	.751	.0488	-.248	.32	15.4	1.27	.0129
8.7	.945	.0728	-.301	.31	13.0	1.13	.0159
11.6	1.120	.0999	-.343	.30	11.2	1.04	.0209
14.6	1.204	.138	-.365	.31	8.73	1.00	.0457

TABLE VI

USA-27 AIRFOIL

GÖTTINGEN TEST

Airfoil size, 7.874x39.370 inches.
Aspect ratio, 5.

Test speed, 98.42 ft./sec.
Test V_l 64.58 sq. ft./sec.

Data with tunnel wall interference corrections applied is taken from Reference 4.(G-509)

Angle of attack α degrees	Lift coeffi- cient C_L	Drag coeffi- cient C_D	Moment coeffi- cient C_M	Center of pressure coeffi- cient C_p	$\frac{C_L}{C_D}$	Speed ratio $\frac{V}{V_s}$	Profile drag coeffi- cient C_{D_0}
-9.0	-0.203	0.0919	0.019	-----	-2.21	-----	0.0893
-6.0	-.037	.0468	-.072	-----	-.79	-----	.0467
-4.5	.063	.0179	-.106	-----	3.52	-----	.0177
-3.0	.164	.0150	-.126	0.77	10.9	2.76	.0133
-1.4	.264	.0166	-.149	.57	15.9	2.18	.0122
0.0	.364	.0201	-.171	.47	18.1	1.85	.0116
1.6	.457	.0251	-.193	.42	18.2	1.65	.0117
3.1	.559	.0317	-.214	.39	17.6	1.50	.0117
4.7	.695	.0432	-.258	.36	16.1	1.34	.0124
6.2	.794	.0536	-.280	.35	14.8	1.25	.0134
9.2	.967	.0781	-.319	.33	12.4	1.14	.0185
12.2	1.140	.1050	-.356	.32	10.9	1.05	.0221
15.3	1.253	.1380	-.384	.31	9.09	1.00	.0379
18.2	1.200	.1890	-.380	.32	6.35	1.02	.0973

TABLE VII

CLARK Y AIRFOIL L. M. A. L. TEST

Airfoil size, 5×30 inches. Average Reynolds Number, 3,610,000.
Aspect ratio, 6.

Data from Reference 2 corrected for tunnel-wall interference

Angle of attack α degrees	Lift coeffi- cient C_L	Drag coeffi- cient C_D	Moment coeffi- cient C_M	Center of pressure coeffi- cient C_p	$\frac{C_L}{C_D}$	Speed ratio $\frac{V}{V_s}$	Profile drag coeffi- cient C_{D_0}
-6.02	-0.000	0.0108	-0.008	-----	-5.55	-----	0.0106
-4.48	.045	.0107	-.091	-----	4.21	-----	.0106
-2.94	.167	.0121	-.120	0.720	13.8	2.86	.0106
-1.40	.268	.0144	-.145	.541	18.6	2.26	.0106
.15	.384	.0182	-.166	.432	21.1	1.89	.0103
1.69	.501	.0245	-.185	.368	20.4	1.65	.0111
3.23	.602	.0312	-.224	.371	19.3	1.51	.0119
6.31	.819	.0508	-.284	.346	16.1	1.29	.0152
9.39	1.034	.0770	-.312	.302	13.4	1.15	.0201
12.47	1.231	.1085	-.360	.294	11.4	1.05	.0280
15.52	1.367	.1395	-.415	.305	9.80	1.00	.0403
18.49	1.283	.2217	-.378	.294	5.80	1.03	.1342
21.41	1.081	.3023	-.328	.293	3.58	1.12	.2402

TABLE VIII

G-387 AIRFOIL L. M. A. L. TEST

Airfoil size, 5×30 inches. Average Reynolds Number, 3,470,000.
Aspect ratio, 6.

Data from Reference 2 corrected for tunnel-wall interference

Angle of attack α degrees	Lift coeffi- cient C_L	Drag coeffi- cient C_D	Moment coeffi- cient C_M	Center of pressure coeffi- cient C_p	$\frac{C_L}{C_D}$	Speed ratio $\frac{V}{V_s}$	Profile drag coeffi- cient C_{D_0}
-9.06	-0.156	0.0156	-0.058	-----	-10.0	-----	0.0143
-5.98	.031	.0126	-.106	-----	4.85	-----	.0124
-4.44	.168	.0139	-.135	0.807	12.1	2.82	.0124
-2.89	.280	.0172	-.168	.602	16.3	2.18	.0130
-1.35	.390	.0210	-.176	.452	18.6	1.85	.0129
.19	.504	.0283	-.202	.401	17.8	1.62	.0148
1.73	.612	.0368	-.234	.381	16.6	1.47	.0168
3.28	.725	.0438	-.255	.351	15.5	1.35	.0188
6.36	.900	.0712	-.285	.296	13.5	1.18	.0222
9.44	1.146	.1004	-.348	.304	11.4	1.08	.0307
12.50	1.308	.1340	-.392	.301	9.75	1.01	.0431
15.50	1.328	.1848	-.441	.332	7.18	1.00	.0911
18.50	1.320	.2462	-.448	.337	5.36	1.01	.1537
21.49	1.276	.3002	-.453	.350	4.25	1.02	.2138

TABLE IX

N. A. C. A.-M6 AIRFOIL L. M. A. L. TEST

Airfoil size, 5×30 inches. Average Reynolds number, 3,660,000.
Aspect ratio, 6.

Data from Reference 1 corrected for tunnel-wall interference

Angle of attack α degrees	Lift coeffi- cient C_L	Drag coeffi- cient C_D	Moment coeffi- cient C_M	Center of pressure coeffi- cient C_p	$\frac{C_L}{C_D}$	Speed ratio $\frac{V}{V_s}$	Profile drag coeffi- cient C_{D_0}
-3.08	-0.202	0.0111	0.084	-----	-18.2	-----	0.0089
-1.54	-.097	.0094	.035	-----	-10.3	-----	.0089
.01	.016	.0080	.008	-----	2.0	-----	.0080
1.55	.126	.0098	-.017	0.141	12.9	3.12	.0090
3.09	.237	.0115	-.045	.187	20.6	2.27	.0085
4.63	.340	.0155	-.064	.187	21.9	1.90	.0093
6.17	.456	.0226	-.096	.211	20.2	1.64	.0115
9.25	.665	.0385	-.145	.218	17.3	1.36	.0150
12.33	.875	.0616	-.192	.221	14.2	1.18	.0209
15.41	1.073	.0892	-.232	.219	12.0	1.07	.0281
18.46	1.222	.1287	-.286	.238	9.52	1.00	.0494
21.44	1.169	.1981	-.312	.269	5.89	1.02	.1256

TABLE X

N. A. C. A.-M12 AIRFOIL

L. M. A. L. TEST

Airfoil size, 5×30 inches.
Aspect ratio, 6.

Average Reynolds number, 3,800,000.

Data from Reference 1 corrected for tunnel-wall interference

Angle of attack α degrees	Lift coeffi- cient C_L	Drag coeffi- cient C_D	Moment coeffi- cient C_M	Center of pressure coeffi- cient C_p	C_L C_D	Speed ratio V V_s	Profile drag coeffi- cient C_{D_0}
-3.05	-0.118	0.0098	-0.019	-----	-12.0	-----	0.0091
-1.51	-.017	.0089	-.001	-----	-1.91	-----	.0089
.04	.096	.0092	-.029	0.302	10.4	3.66	.0087
1.58	.207	.0123	-.057	.274	16.8	2.50	.0100
3.12	.318	.0163	-.088	.275	19.5	2.02	.0109
4.66	.417	.0203	-.107	.257	20.6	1.76	.0110
6.20	.537	.0280	-.131	.244	19.2	1.55	.0126
9.29	.760	.0479	-.192	.253	15.9	1.30	.0172
12.37	.971	.0724	-.241	.250	13.4	1.15	.0223
15.44	1.155	.1022	-.287	.251	11.3	1.06	.0313
18.49	1.293	.1388	-.342	.269	9.32	1.00	.0501
21.44	1.165	.2293	-.364	.312	5.09	1.05	.1572

TABLE XI

R. A. F.-15 AIRFOIL

L. M. A. L. TEST

Airfoil size, 5×30 inches.
Aspect ratio, 6.

Average Reynolds number, 3,580,000.

Data from Reference 2 corrected for tunnel-wall interference.

Angle of attack α degrees	Lift coeffi- cient C_L	Drag coeffi- cient C_D	Moment coeffi- cient C_M	Center of pressure coeffi- cient C_p	C_L C_D	Speed ratio V V_s	Profile drag coeffi- cient C_{D_0}
-4.56	-0.162	0.0141	-0.013	-----	-11.5	-----	0.0127
-3.02	-.052	.0087	-.039	-----	-5.98	-----	.0085
-1.48	.052	.0083	-.066	1.270	6.27	4.82	.0081
0.06	.166	.0090	-.090	0.539	18.5	2.70	.0075
1.61	.285	.0124	-.116	.408	23.0	2.06	.0081
3.15	.398	.0164	-.158	.360	24.3	1.74	.0079
4.69	.507	.0222	-.176	.347	22.8	1.55	.0085
6.24	.629	.0306	-.202	.322	20.6	1.39	.0095
9.32	.850	.0525	-.260	.307	16.2	1.19	.0141
12.41	1.068	.0809	-.313	.296	13.2	1.06	.0203
15.46	1.209	.1093	-.344	.289	11.0	1.00	.0317
16.43	1.127	.1611	-.358	.318	6.98	1.04	.0937
18.38	1.004	.2248	-.394	.385	4.46	1.10	.1712
21.35	0.924	.2928	-.379	.392	3.15	1.14	.2474

TABLE XII

U. S. A.-27 AIRFOIL

L. M. A. L. TEST

Airfoil size, 5×30 inches.
Aspect ratio, 6.

Average Reynolds number, 3,570,000.

Data from Reference 2 corrected for tunnel-wall interference

Angle of attack α degrees	Lift coeffi- cient C_L	Drag coeffi- cient C_D	Moment coeffi- cient C_M	Center of pressure coeffi- cient C_p	C_L C_D	Speed ratio V V_s	Profile drag coeffi- cient C_{D_0}
-6.04	-0.100	0.0128	-0.061	-----	-7.82	-----	0.0123
-4.50	.007	.0117	-.090	-----	.60	-----	.0117
-2.95	.120	.0118	-.112	0.940	10.2	3.40	.0110
-1.42	.221	.0134	-.137	.621	16.5	2.50	.0108
0.13	.332	.0167	-.164	.494	19.9	2.04	.0108
1.67	.439	.0211	-.183	.416	20.6	1.78	.0108
3.21	.553	.0275	-.199	.360	20.1	1.58	.0112
4.75	.654	.0353	-.238	.363	18.5	1.46	.0125
6.29	.768	.0456	-.256	.333	16.8	1.35	.0143
9.37	.972	.0678	-.307	.316	14.3	1.20	.0175
12.44	1.165	.0953	-.342	.295	12.2	1.09	.0232
15.50	1.326	.1285	-.385	.293	10.3	1.02	.0352
16.53	1.386	.1417	-.504	.368	9.79	1.00	.0397
18.50	1.324	.1931	-.482	.367	6.87	1.02	.1001
21.45	1.181	.2712	-.491	.411	4.36	1.03	.1972

TABLE XIII

U. S. A.-35A AIRFOIL

L. M. A. L. TEST

Airfoil size, 5×30 inches.
Aspect ratio, 6.

Average Reynolds number, 3,520,000.

Data from Reference 2 corrected for tunnel-wall interference

Angle of attack α degrees	Lift coeffi- cient C_L	Drag coeffi- cient C_D	Moment coeffi- cient C_M	Center of pressure coeffi- cient C_p	$\frac{C_L}{C_D}$	Speed ratio $\frac{V}{V_s}$	Profile drag coeffi- cient C_{D_0}
-9.03	-0.075	0.0168	-0.098	-----	-4.46	-----	0.0165
-5.94	.146	.0143	-.154	-----	10.2	2.88	.0132
-4.40	.252	.0166	-.178	0.714	15.2	2.19	.0132
-2.86	.365	.0205	-.203	.558	17.8	1.82	.0134
-1.32	.468	.0255	-.224	.479	18.4	1.61	.0138
.22	.586	.0327	-.254	.434	18.0	1.44	.0144
1.76	.692	.0410	-.280	.404	16.9	1.32	.0155
3.30	.798	.0510	-.304	.380	15.6	1.23	.0172
4.84	.884	.0616	-.322	.364	14.3	1.17	.0201
6.37	.984	.0741	-.356	.361	13.3	1.11	.0226
9.43	1.142	.1042	-.392	.342	11.0	1.03	.0350
12.46	1.203	.1495	-.430	.355	8.05	1.00	.0727
15.46	1.201	.2029	-.447	.368	5.93	1.00	.1263
18.44	1.152	.2512	-.443	.378	4.59	1.03	.1808
21.42	1.097	.2956	-.405	.359	3.72	1.05	.2316

TABLE XIV

U. S. A.-35B AIRFOIL

L. M. A. L. TEST

Airfoil size, 5×30 inches.
Aspect ratio, 6.

Average Reynolds number, 3,470,000.

Data from Reference 2 corrected for tunnel-wall interference

Angle of attack α degrees	Lift coeffi- cient C_L	Drag coeffi- cient C_D	Moment coeffi- cient C_M	Center of pressure coeffi- cient C_p	$\frac{C_L}{C_D}$	Speed ratio $\frac{V}{V_s}$	Profile drag coeffi- cient C_{D_0}
-9.11	-0.285	0.0173	-0.001	-----	-16.5	-----	0.0130
-6.02	-.062	.0094	-.058	-----	-6.60	-----	.0092
-4.48	.044	.0093	-.082	-----	4.73	-----	.0092
-2.94	.157	.0109	-.109	0.699	14.4	2.96	.0096
-1.40	.263	.0143	-.136	.516	18.4	2.28	.0106
.14	.378	.0183	-.147	.388	20.6	1.91	.0107
1.69	.488	.0247	-.176	.361	19.8	1.68	.0120
3.23	.603	.0332	-.212	.351	18.1	1.51	.0138
6.31	.823	.0542	-.259	.314	15.2	1.29	.0182
9.40	1.045	.0818	-.320	.307	12.8	1.15	.0265
12.47	1.235	.1131	-.372	.302	10.9	1.06	.0321
15.52	1.374	.1490	-.440	.323	9.23	1.00	.0488
18.50	1.304	.2261	-.423	.323	5.77	1.03	.1359
21.45	1.181	.3057	-.465	.375	3.87	1.08	.2317

TABLE XV

CLARK Y AIRFOIL

M. I. T. TEST

Airfoil size, 6×36 inches.
Aspect ratio, 6.

Test speed, 40 M. P. H.
Test V_l , 29.33 sq. ft./sec.

Faired data from Reference 6 changed to absolute coefficients and corrected for tunnel-wall interference

Angle of attack α degrees	Lift coeffi- cient C_L	Drag coeffi- cient C_D	Moment coeffi- cient C_M	Center of pressure coeffi- cient C_p	$\frac{C_L}{C_D}$	Speed ratio $\frac{V}{V_s}$	Profile drag coeffi- cient C_{D_0}
-6.01	-0.031	0.0196	-0.075	-----	-1.58	-----	0.0195
-3.97	.110	.0154	-.110	0.930	7.15	3.36	.0147
-1.94	.252	.0163	-.144	.562	15.5	2.22	.0129
.10	.401	.0214	-.177	.448	18.7	1.76	.0129
2.13	.553	.0295	-.211	.397	18.7	1.50	.0132
4.17	.696	.0409	-.243	.364	17.0	1.33	.0152
6.20	.835	.0550	-.274	.343	15.2	1.22	.0179
8.23	.960	.0720	-.306	.329	13.3	1.14	.0229
10.26	1.077	.0905	-.337	.316	11.9	1.07	.0289
12.29	1.179	.1103	-.363	.309	10.7	1.03	.0365
14.30	1.239	.1347	-.380	.308	9.21	1.00	.0531
16.29	1.177	.1740	-.401	.340	6.90	1.03	.1005

TABLE XVI

CLARK Y-15 AIRFOIL

M. I. T. TEST

Airfoil size, 6×36 inches.
Aspect ratio, 6.

Test speed, 40 M. P. H.
Test V_l , 29.33 sq. ft./sec.

Faired data from Reference 6 changed to absolute coefficients and corrected for tunnel-wall interference

Angle of attack α degrees	Lift coeffi- cient C_L	Drag coeffi- cient C_D	Moment coeffi- cient C_M	Center of pressure coeffi- cient C_p	C_L C_D	Speed ratio $\frac{V}{V_s}$	Profile drag coeffi- cient C_{D_0}
-7.96	-0.135	0.0224	-0.051	-----	-6.02	-----	0.0214
-5.93	.000	.0180	-.079	-----	0	-----	.0180
-3.90	.135	.0169	-.108	0.790	7.99	3.05	.0159
-1.86	.272	.0179	-.137	.517	15.2	2.15	.0139
.17	.416	.0226	-.170	.411	18.4	1.74	.0133
2.21	.591	.0328	-.216	.371	18.0	1.46	.0142
4.25	.727	.0444	-.249	.346	16.4	1.32	.0163
6.28	.852	.0582	-.276	.327	14.6	1.22	.0196
8.31	.970	.0736	-.300	.314	13.2	1.14	.0235
10.33	1.087	.0910	-.325	.302	11.9	1.08	.0283
12.36	1.191	.1092	-.350	.296	10.9	1.03	.0340
14.37	1.251	.1282	-.356	.291	9.75	1.00	.0451
16.38	1.259	.1482	-.356	.290	8.49	1.00	.0639
18.37	1.230	.1921	-.364	.300	6.40	1.01	.1117

TABLE XVII

G-387 AIRFOIL

M. I. T. TEST

Airfoil size, 6×36 inches.
Aspect ratio, 6.

Test Speed, 40 M. P. H.
Test V_l , 29.33 sq. ft./sec.

Faired data from Reference 6 changed to absolute coefficients and corrected for tunnel-wall interference

Angle of attack α degrees	Lift coeffi- cient C_L	Drag coeffi- cient C_D	Moment coeffi- cient C_M	Center of pressure coeffi- cient C_p	C_L C_D	Speed ratio $\frac{V}{V_s}$	Profile drag coeffi- cient C_{D_0}
-8.02	-0.065	0.0715	-0.035	-----	-0.91	-----	0.0713
-5.98	.076	.0321	-.117	-----	2.37	4.33	.0318
-3.95	.221	.0237	-.156	0.678	9.32	2.54	.0211
-1.91	.368	.0264	-.195	.507	13.9	1.97	.0192
.12	.512	.0320	-.234	.431	16.0	1.67	.0181
2.16	.657	.0405	-.270	.395	16.2	1.48	.0175
4.20	.805	.0527	-.308	.370	15.3	1.33	.0182
6.23	.962	.0689	-.351	.349	14.0	1.22	.0197
8.27	1.103	.0876	-.386	.336	12.6	1.14	.0229
10.30	1.228	.1088	-.417	.325	11.3	1.08	.0287
12.30	1.339	.1315	-.440	.317	10.2	1.03	.0363
14.34	1.414	.1567	-.458	.310	9.06	1.01	.0506
16.35	1.431	.1890	-.473	.312	7.57	1.00	.0804
18.35	1.423	.2217	-.481	.323	6.44	1.00	.1142

TABLE XVIII

G-436 AIRFOIL

M. I. T. TEST

Airfoil size, 6×36 inches.
Aspect ratio, 6.

Test speed, 40 M. P. H.
Test V_l , 29.32 sq. ft./sec.

Faired data from Reference 6 changed to absolute coefficients and corrected for tunnel-wall interference

Angle of attack α degrees	Lift coeffi- cient C_L	Drag coeffi- cient C_D	Moment coeffi- cient C_M	Center of pressure coeffi- cient C_p	C_L C_D	Speed ratio $\frac{V}{V_s}$	Profile drag coeffi- cient C_{D_0}
-6.02	-0.065	0.0258	-0.063	-----	2.52	-----	0.0256
-3.98	.080	.0172	-.099	1.020	4.65	3.88	.0169
-1.95	.225	.0170	-.134	.593	13.2	2.32	.0143
.09	.372	.0219	-.169	.452	17.7	1.80	.0136
2.13	.516	.0281	-.207	.400	18.4	1.53	.0139
4.16	.665	.0387	-.243	.366	17.2	1.35	.0151
6.20	.821	.0529	-.282	.342	15.5	1.21	.0171
8.24	.973	.0701	-.320	.329	13.9	1.11	.0198
10.27	1.097	.0884	-.356	.319	12.4	1.05	.0244
12.29	1.198	.1085	-.375	.310	11.0	1.00	.0324
14.29	1.183	.1361	-.371	.313	8.70	1.01	.0619
16.28	1.146	.1717	-.371	.322	6.69	1.03	.1020

TABLE XIX

Airfoil size, 6 × 36 inches.
Aspect ratio, 6.

R. A. F.-15 AIRFOIL

Test speed, 40 M. P. H.
Test *V* *l*, 29.33 sq. ft./sec.

M. I. T. TEST

Faired data from Reference 5 changed to absolute coefficients and corrected for tunnel-wall interference

Angle of attack α degrees	Lift coeffi- cient <i>C</i> _{<i>L</i>}	Drag coeffi- cient <i>C</i> _{<i>D</i>}	Moment coeffi- cient <i>C</i> _{<i>M</i>}	Center of pressure coeffi- cient <i>C</i> _{<i>p</i>}	<i>C</i> _{<i>L</i>} <i>C</i> _{<i>D</i>}	Speed ratio <i>V</i> <i>V</i> _{<i>S</i>}	Profile drag coeffi- cient <i>C</i> _{<i>D</i>0}
−4.44	−0.184	0.0251			−7.23		0.0233
−2.40	−.018	.0145	−0.015		−1.21		.0145
−0.37	.143	.0122	−.072	0.490	11.7	2.67	.0111
1.67	.303	.0168	−.115	.359	18.0	1.83	.0119
3.71	.460	.0254	−.147	.320	18.1	1.49	.0141
5.75	.610	.0348	−.184	.300	17.5	1.29	.0149
7.78	.755	.0481	−.226	.290	15.7	1.16	.0175
9.82	.895	.0640	−.259	.287	14.0	1.07	.0214
11.84	.995	.0867	−.282	.289	11.5	1.01	.0339
13.85	1.017	.1264	−.310	.299	8.04	1.00	.0713

TABLE XX

Airfoil size 6 × 36 inches.
Aspect ratio, 6.

U. S. A.-27 AIRFOIL

Test speed, 40 M. P. H.
Test *V* *l*, 29.33 sq. ft./sec.

M. I. T. TEST

Faired data from Reference 5 changed to absolute coefficients and corrected for tunnel-wall interference

Angle of attack α degrees	Lift coeffi- cient <i>C</i> _{<i>L</i>}	Drag coeffi- cient <i>C</i> _{<i>D</i>}	Moment coeffi- cient <i>C</i> _{<i>M</i>}	Center of pressure coeffi- cient <i>C</i> _{<i>p</i>}	<i>C</i> _{<i>L</i>} <i>C</i> _{<i>D</i>}	Speed ratio <i>V</i> <i>V</i> _{<i>S</i>}	Profile drag coeffi- cient <i>C</i> _{<i>D</i>0}
−6.01	−0.059	0.0594	−0.065		−0.99		0.0592
−3.97	.112	.0333	−.117	0.860	3.38	3.47	.0326
−1.94	.244	.0226	−.154	.603	10.8	2.35	.0194
.09	.386	.0231	−.182	.465	16.7	1.87	.0151
2.13	.534	.0301	−.215	.402	17.7	1.59	.0149
4.17	.685	.0400	−.253	.369	17.1	1.40	.0150
6.20	.825	.0534	−.286	.345	15.4	1.28	.0172
8.23	.958	.0693	−.320	.329	13.8	1.19	.0204
10.26	1.081	.0871	−.350	.314	12.4	1.08	.0250
12.29	1.198	.1059	−.376	.300	11.3	1.06	.0296
14.31	1.294	.1254	−.399	.295	10.3	1.02	.0368
16.33	1.347	.1491	−.415	.295	9.02	1.00	.0526
18.33	1.347	.2069	−.425	.307	6.50	1.00	.1104
20.31	1.290	.3725	−.426	.311	3.46	1.02	.2841

TABLE XXI

Airfoil size, 6×36 inches.
Aspect ratio, 6.

U. S. A.-35A AIRFOIL

Test speed, 40 M. P. H.
Test *V* *l*, 29.33 sq. ft./sec.

M. I. T. TEST

Faired data from Reference 5, changed to absolute coefficients and corrected for tunnel-wall interference

Angle of attack α degrees	Lift coeffi- cient <i>C</i> _{<i>L</i>}	Drag coeffi- cient <i>C</i> _{<i>D</i>}	Moment coeffi- cient <i>C</i> _{<i>M</i>}	Center of pressure coeffi- cient <i>C</i> _{<i>p</i>}	<i>C</i> _{<i>L</i>} <i>C</i> _{<i>D</i>}	Speed ratio <i>V</i> <i>V</i> _{<i>S</i>}	Profile drag coeffi- cient <i>C</i> _{<i>D</i>0}
−7.99	0.041	0.0931	−0.059		0.44		0.0930
−5.96	.176	.0545	−.131	0.900	3.23	2.89	.0529
−3.92	.315	.0302	−.186	.619	10.4	2.16	.0249
−1.89	.457	.0326	−.227	.495	14.0	1.79	.0215
.15	.608	.0404	−.261	.429	15.1	1.56	.0207
2.18	.759	.0509	−.294	.391	14.9	1.39	.0203
4.22	.905	.0649	−.331	.367	13.9	1.28	.0213
6.26	1.050	.0810	−.367	.350	13.0	1.18	.0225
8.29	1.183	.1001	−.399	.340	11.8	1.11	.0259
10.31	1.286	.1231	−.426	.333	10.4	1.07	.0352
12.33	1.363	.1534	−.450	.330	8.90	1.04	.0548
14.35	1.421	.1896	−.470	.330	7.50	1.02	.0824
16.35	1.453	.2230	−.484	.331	6.52	1.01	.1109
18.36	1.470	.2527	−.477	.351	5.82	1.00	.1378
20.25	1.017	.2709		.390	3.75	1.20	.2158

TABLE XXII

U. S. A.-35B AIRFOIL

M. I. T. TEST

Airfoil size, 6×36 inches.
Aspect ratio, 6.

Test speed, 40 M. P. H.
Test V_l , 29.33 sq. ft./sec.

Faired data from Reference 6 changed to absolute coefficients and corrected for tunnel-wall interference

Angle of attack α degrees	Lift coeffi- cient C_L	Drag coeffi- cient C_D	Moment coeffi- cient C_M	Center of pressure coeffi- cient C_p	C_L C_D	Speed ratio $\frac{V}{V_s}$	Profile drag coeffi- cient C_{D_0}
-6.00	-0.006	0.0278	-0.073	-----	-0.21	-----	0.0278
-3.97	.123	.0189	-.109	0.960	6.50	3.26	.0181
-1.94	.258	.0187	-.147	.560	13.8	2.25	.0151
.10	.397	.0226	-.183	.438	17.6	1.81	.0142
2.13	.542	.0301	-.220	.387	18.0	1.55	.0144
4.17	.698	.0408	-.257	.353	17.1	1.37	.0149
6.21	.860	.0543	-.294	.332	15.8	1.23	.0146
8.24	1.003	.0704	-.331	.321	14.3	1.14	.0169
10.27	1.129	.0895	-.368	.312	12.6	1.07	.0218
12.30	1.238	.1125	-.394	.309	11.0	1.03	.0311
14.32	1.300	.1357	-.402	.305	9.60	1.00	.0460
16.31	1.275	.1684	-.407	.307	7.58	1.01	.0821

TABLE XXIII

CLARK Y AIRFOIL

McC. F. TEST

Airfoil size, 6 × 36 inches.
Aspect ratio, 6.

Test speed, 80 M. P. H.
Test V_l , 58.67 sq. ft./sec.

Data with tunnel-wall interference corrections applied are taken from Reference 7 and changed to absolute coefficients

Angle of attack α degrees	Lift coeffi- cient C_L	Drag coeffi- cient C_D	Moment coeffi- cient C_M	Center of pressure coeffi- cient C_p	C_L C_D	Speed ratio $\frac{V}{V_s}$	Profile drag coeffi- cient C_{D_0}
-6.22	0	0.0152	-0.074	-----	0	-----	0.0152
-4.17	.144	.0149	-.109	0.760	9.71	2.94	.0138
-0.04	.468	.0227	-.183	.392	20.6	1.63	.0110
4.07	.760	.0450	-.253	.332	16.9	1.28	.0144
8.16	1.040	.0759	-.319	.307	13.7	1.10	.0184
12.20	1.232	.1150	-.367	.300	10.7	1.01	.0344
14.18	1.248	.1443	-.374	.302	8.93	1.00	.0615
16.17	1.239	.1892	-.379	.312	6.54	1.01	.1077

TABLE XXIV

CLARK Y-15 AIRFOIL

McC. F. TEST

Airfoil size, 6 × 36 inches.
Aspect ratio, 6.

Test speed, 80 M. P. H.
Test V_l , 58.67 sq. ft./sec.

Data with tunnel-wall interference corrections applied are taken from Reference 7 and changed to absolute coefficients

Angle of attack α degrees	Lift coeffi- cient C_L	Drag coeffi- cient C_D	Moment coeffi- cient C_M	Center of pressure coeffi- cient C_p	C_L C_D	Speed ratio $\frac{V}{V_s}$	Profile drag coeffi- cient C_{D_0}
-6.23	-0.013	0.0137	-0.070	-----	-0.97	-----	0.0137
-4.17	.136	.0137	-.103	0.765	9.98	3.12	.0127
-2.12	.281	.0168	-.133	.475	16.71	2.18	.0126
-0.06	.422	.0219	-.163	.390	19.29	1.78	.0124
2.00	.593	.0328	-.215	.362	18.06	1.50	.0141
4.06	.741	.0446	-.248	.333	16.63	1.34	.0155
6.10	.873	.0579	-.293	.335	15.09	1.23	.0174
8.14	1.009	.0751	-.310	.307	13.43	1.14	.0209
10.18	1.132	.0931	-.333	.295	12.16	1.09	.0251
12.21	1.235	.1118	-.357	.292	11.04	1.04	.0308
14.21	1.294	.1333	-.373	.288	9.71	1.02	.0444
16.20	1.322	.1677	-.392	.298	7.89	1.00	.0750
16.96	.966	.2561	-.346	.347	3.77	1.17	.2065
17.99	1.009	.2757	-.357	.348	3.66	1.14	.2215

TABLE XXV

G-398 AIRFOIL

McC. F. TEST

Airfoil size, 6×36 inches.
Aspect ratio, 6.

Test speed, 80 M. P. H.
Test V_l , 58.67 sq. ft./sec.

Data with tunnel-wall interference corrections applied are taken from Reference 7 and changed to absolute coefficients

Angle of attack α degrees	Lift coeffi- cient C_L	Drag coeffi- cient C_D	Moment coeffi- cient C_M	Center of pressure coeffi- cient C_p	$\frac{C_L}{C_D}$	Speed ratio $\frac{V}{V_s}$	Profile drag coeffi- cient C_{D_0}
-8.23	-0.097	0.0168	-0.062	-----	-5.79	-----	0.0163
-6.20	.044	.0152	-.093	-----	2.87	-----	.0152
-4.14	.198	.0164	-.129	0.657	12.1	2.67	.0143
-2.08	.353	.0199	-.168	.478	17.7	2.00	.0133
-.01	.508	.0274	-.211	.415	18.6	1.67	.0136
2.04	.661	.0360	-.246	.373	18.4	1.46	.0128
4.10	.811	.0516	-.282	.348	15.7	1.32	.0167
6.15	.961	.0676	-.322	.335	14.2	1.21	.0185
8.19	1.098	.0856	-.355	.322	12.8	1.13	.0215
10.23	1.224	.1048	-.379	.310	11.7	1.07	.0253
12.26	1.337	.1271	-.417	.312	10.5	1.03	.0323
14.28	1.408	.1544	-.429	.307	9.12	1.00	.0492
16.22	1.358	.2002	-.442	.327	6.78	1.02	.1023

TABLE XXVI

CLARK Y AIRFOIL

W. N. Y. TEST

Airfoil size 5×30 inches.
Aspect ratio, 6.

Test speed, 40 M. P. H.
Test V_l , 24.44 sq. ft./sec.

Data from Reference 11 corrected for tunnel-wall interference

Angle of attack α degrees	Lift coeffi- cient C_L	Drag coeffi- cient C_D	Moment coeffi- cient C_M	Center of pressure coeffi- cient C_p	$\frac{C_L}{C_D}$	Speed ratio $\frac{V}{V_s}$	Profile drag coeffi- cient C_{D_0}
-8.02	-0.167	0.0356	-0.040	-----	-4.69	-----	-----
-7.01	-.096	.0249	-----	-----	-3.86	-----	-----
-6.00	-.029	.0214	-----	-----	-1.36	-----	-----
-4.99	.041	.0198	-----	-----	2.07	-----	0.0197
-3.99	.111	.0183	-.105	0.950	6.06	3.37	.0176
-2.98	.181	.0184	-.121	.660	9.84	2.64	.0166
-1.97	.254	.0199	-.138	.540	12.8	2.23	.0165
-.96	.325	.0216	-.156	.474	15.0	1.97	.0160
.05	.400	.0241	-.174	.428	16.6	1.77	.0156
2.07	.551	.0320	-.212	.380	17.2	1.55	.0159
4.09	.704	.0437	-.247	.344	16.1	1.34	.0173
6.11	.840	.0573	-.277	.328	14.7	1.22	.0198
8.13	.980	.0743	-.308	.314	13.2	1.14	.0233
10.14	1.093	.0925	-.340	.308	11.8	1.07	.0291
12.15	1.190	.1115	-.355	.300	10.7	1.03	.0364
14.16	1.242	.1322	-.361	.296	9.39	1.00	.0503
16.16	1.257	.1622	-.360	.294	7.74	1.00	.0782
18.13	1.053	.2938	-.388	.354	3.58	1.09	.2349

TABLE XXVII

G-387 AIRFOIL

W. N. Y. TEST

Airfoil size, 5×30 inches.
Aspect ratio, 6.

Test speed, 40 M. P. H.
Test V_l , 24.44 sq. ft./sec

Data from Reference 8 corrected for tunnel-wall interference

Angle of attack α degrees	Lift coeffi- cient C_L	Drag coeffi- cient C_D	Moment coeffi- cient C_M	Center of pressure coeffi- cient C_p	$\frac{C_L}{C_D}$	Speed ratio $\frac{V}{V_s}$	Profile drag coeffi- cient C_{D_0}
-8.01	-0.065	0.0513	-----	-----	-1.27	-----	-----
-7.00	.014	.0357	-----	-----	.39	-----	0.0357
-5.99	.075	.0287	-0.118	-----	2.61	4.46	.0283
-4.98	.141	.0254	-----	0.954	5.55	3.25	.0243
-3.97	.213	.0236	-.147	.702	9.03	2.64	.0212
-2.96	.279	.0247	-.161	.584	11.3	2.31	.0206
-1.95	.352	.0278	-.179	.514	12.7	2.06	.0212
.06	.493	.0353	-.214	.438	14.0	1.74	.0224
2.08	.639	.0439	-.248	.492	14.6	1.53	.0222
4.10	.785	.0555	-.283	.364	14.1	1.38	.0228
6.12	.922	.0708	-.314	.346	13.0	1.27	.0256
8.14	1.057	.0883	-.348	.332	12.0	1.19	.0289
10.15	1.192	.1083	-.378	.322	11.0	1.12	.0329
12.17	1.309	.1306	-.405	.312	10.0	1.07	.0396
14.18	1.404	.1530	-.428	.308	9.18	1.03	.0484
16.19	1.467	.1753	-.441	.306	8.37	1.01	.0610
18.19	1.488	.2074	-.490	.334	7.17	1.00	.0898
20.14	1.105	.3263	-.406	.356	3.38	1.16	.2614

TABLE XXVIII

G-393 AIRFOIL

W. N. Y. TEST

Airfoil size, 5×30 inches.
Aspect ratio, 6.

Test speed, 40 M. P. H.
Test *V*₁, 24.44 sq. ft./sec.

Data from Reference 8 corrected for tunnel-wall interference

Angle of attack α degrees	Lift coeffi- cient C_L	Drag coeffi- cient C_D	Moment coeffi- cient C_M	Center of pressure coeffi- cient C_p	C_L C_D	Speed ratio $\frac{V}{V_s}$	Profile drag coeffi- cient C_{D_0}
-8.02	-0.130	0.0301			-4.32		
-7.01	-.059	.0235			-2.51		0.0232
-6.00	.013	.0200			.65		.0200
-4.99	.083	.0183	-0.108		4.54	4.20	.0179
-3.98	.157	.0175	-.125	0.796	8.97	2.96	.0162
-2.97	.227	.0182	-.141	.620	12.5	2.47	.0155
-1.96	.300	.0197	-.158	.525	15.2	2.15	.0149
.06	.439	.0256	-.189	.432	17.1	1.78	.0153
2.08	.593	.0354	-.230	.388	16.8	1.53	.0167
4.09	.736	.0475	-.262	.356	15.5	1.37	.0188
6.11	.878	.0619	-.297	.340	14.2	1.26	.0210
8.13	1.011	.0780	-.324	.324	13.0	1.18	.0237
10.15	1.137	.0970	-.353	.314	11.7	1.11	.0283
12.16	1.252	.1178	-.379	.308	10.6	1.05	.0345
14.17	1.350	.1396	-.400	.302	9.67	1.01	.0429
16.18	1.387	.1638	-.406	.300	8.47	1.00	.0617
18.17	1.370	.1973	-.403	.306	6.94	1.01	.0977

TABLE XXIX

G-436 AIRFOIL

W. N. Y. TEST

Airfoil size, 5×30 inches.
Aspect ratio, 6.

Test speed, 40 M. P. H.
Test *V*₁, 24.44 sq. ft./sec.

Data from Reference 8 corrected for tunnel-wall interference

Angle of attack α degrees	Lift coeffi- cient C_L	Drag coeffi- cient C_D	Moment coeffi- cient C_M	Center of pressure coeffi- cient C_p	C_L C_D	Speed ratio $\frac{V}{V_s}$	Profile drag coeffi- cient C_{D_0}
-8.03	-0.270	0.0674	-0.021		-4.01		
-6.01	-.094	.0341	-.044		-2.76		0.0336
-5.00	-.017	.0254			-.67		.0254
-3.99	.066	.0223	-.089		2.96	4.49	.0221
-2.98	.142	.0202	-.079	0.760	7.03	3.06	.0191
-1.97	.211	.0196	-.123	.580	10.8	2.51	.0172
-.96	.280	.0207	-.134	.492	13.5	2.18	.0165
.05	.348	.0229	-.154	.436	15.2	1.95	.0165
2.06	.488	.0287	-.187	.380	17.0	1.65	.0160
4.08	.638	.0388	-.222	.350	16.4	1.44	.0171
6.10	.788	.0527	-.257	.328	15.0	1.30	.0198
8.12	.924	.0687	-.292	.322	13.5	1.20	.0233
10.14	1.059	.0879	-.322	.316	12.1	1.12	.0284
12.15	1.177	.1087	-.354	.310	10.8	1.06	.0352
14.17	1.296	.1300	-.382	.302	9.97	1.01	.0409
16.17	1.325	.1580	-.380	.296	8.38	1.00	.0648
18.16	1.285	.2013	-.391	.314	6.38	1.02	.1136

TABLE XXX

N-9 AIRFOIL

W. N. Y. TEST

Airfoil size, 5×30 inches.
Aspect ratio, 6.

Test speed, 40 M. P. H.
Test *V*₁, 24.44 sq. ft./sec.

Data from reference 10 corrected for tunnel-wall interference

Angle of attack α degrees	Lift coeffi- cient C_L	Drag coeffi- cient C_D	Moment coeffi- cient C_M	Center of pressure coeffi- cient C_p	C_L C_D	Speed ratio $\frac{V}{V_s}$	Profile drag coeffi- cient C_{D_0}
-8.04	-0.318	0.0500	0.031		-6.36		
-6.02	-.165	.0236	-.013		-6.99		
-5.01	-.081	.0183	-.036		-4.43		0.0179
-4.00	.008	.0150			.53		.0150
-2.99	.094	.0136	-.083	0.888	6.91	3.47	.0131
-1.98	.167	.0137	-.101	.604	12.2	2.60	.0122
-.97	.246	.0142	-.120	.486	17.3	2.14	.0110
.04	.320	.0160	-.130	.422	20.0	1.88	.0106
2.06	.460	.0231	-.166	.358	19.9	1.57	.0118
4.08	.608	.0342	-.199	.326	17.8	1.36	.0145
6.10	.752	.0474	-.234	.312	15.9	1.23	.0174
8.11	.895	.0632	-.266	.298	14.2	1.12	.0207
10.13	1.011	.0827	-.292	.292	12.2	1.06	.0284
12.14	1.107	.1047	-.310	.288	10.6	1.01	.0396
14.14	1.124	.1328	-.315	.286	8.46	1.00	.0657
16.14	1.094	.2265	-.359	.328	4.83	1.02	.1629

TABLE XXXI

N-10 AIRFOIL

W. N. Y. TEST

Airfoil size, 5×30 inches.
Aspect ratio 6.

Test speed 40 M. P. H.
Test V_l , 24.44 sq. ft./sec.

Data from Reference 10 corrected for tunnel-wall interference

Angle of attack α degrees	Lift coeffi- cient C_L	Drag coeffi- cient C_D	Moment coeffi- cient C_M	Center of pressure coeffi- cient C_p	C_L C_D	Speed ratio V V_s	Profile drag coeffi- cient C_{D_0}
-8.03	-0.209	0.0372	-0.010	-----	-5.62	-----	-----
-6.01	-.047	.0223	-.034	-----	-2.11	-----	0.0222
-5.00	.031	.0193	-.060	-----	1.61	-----	.0192
-3.99	.103	.0179	-.106	-----	5.75	3.50	.0173
-2.98	.173	.0177	-.122	0.700	9.77	2.69	.0161
-1.97	.251	.0191	-.139	.554	13.1	2.24	.0157
-0.96	.321	.0204	-.155	.480	15.7	1.98	.0149
.05	.397	.0232	-.172	.432	17.1	1.78	.0148
2.07	.545	.0310	-.206	.376	17.6	1.52	.0152
4.09	.693	.0422	-.239	.346	16.4	1.35	.0167
6.11	.836	.0573	-.275	.332	14.6	1.23	.0202
8.12	.976	.0729	-.303	.316	13.4	1.13	.0222
10.14	1.110	.0901	-.332	.304	12.3	1.07	.0246
12.16	1.218	.1117	-.354	.298	10.9	1.02	.0329
14.16	1.257	.1347	-.352	.292	9.32	1.00	.0508
16.16	1.215	.1679	-.350	.288	7.24	1.02	.0896

TABLE XXXII

N-22-AIRFOIL

W. N. Y. TEST

Airfoil size, 5×30 inches.
Aspect ratio, 6.

Test speed, 40 M. P. H.
Test V_l , 24.44 sq. ft./sec.

Data from Reference 12 corrected for tunnel-wall interference.

Angle of attack α degrees	Lift coeffi- cient C_L	Drag coeffi- cient C_D	Moment coeffi- cient C_M	Center of pressure coeffi- cient C_p	C_L C_D	Speed ratio V V_s	Profile drag coeffi- cient C_{D_0}
-10.04	-0.309	0.0745	-0.003	-----	-4.15	-----	-----
-8.02	-.165	.0365	-.050	-----	-4.52	-----	-----
-7.01	-.090	.0235	-.064	-----	-3.83	-----	-----
-6.00	-.020	.0210	-----	-----	-0.95	-----	0.0210
-4.99	.053	.0186	-----	-----	2.85	-----	.0184
-3.98	.125	.0183	-.109	0.912	6.83	3.32	.0175
-2.97	.200	.0194	-.126	.654	10.3	2.63	.0173
-1.96	.275	.0207	-.143	.538	13.3	2.24	.0167
-0.96	.330	.0219	-.150	.472	15.1	2.05	.0161
.05	.426	.0251	-.176	.426	17.0	1.80	.0155
2.08	.591	.0345	-.217	.376	17.1	1.53	.0159
4.09	.740	.0462	-.247	.348	16.0	1.37	.0171
6.11	.880	.0627	-.275	.326	14.0	1.26	.0216
8.13	1.024	.0779	-.304	.310	13.1	1.16	.0221
10.15	1.152	.0978	-.334	.304	11.8	1.10	.0273
12.16	1.267	.1184	-.357	.298	10.7	1.05	.0331
14.17	1.347	.1396	-.368	.292	9.65	1.02	.0433
16.18	1.384	.1648	-.369	.286	8.40	1.00	.0631
18.16	1.241	.2490	-----	-----	4.98	-----	.1672

TABLE XXXIII

N. A. C. A.-M6 AIRFOIL

W. N. Y. TEST

Airfoil size, 5×30 inches.
Aspect ratio, 6.

Test speed, 40 M. P. H.
Test V_l , 24.44 sq. ft./sec.

Data from Reference 14, corrected for tunnel-wall interference

Angle of attack α degrees	Lift coeffi- cient C_L	Drag coeffi- cient C_D	Moment coeffi- cient C_M	Center of pressure coeffi- cient C_p	C_L C_D	Speed ratio V V_s	Profile drag coeffi- cient C_{D_0}
-8.06	-0.438	0.0527	0.084	-----	-8.31	-----	-----
-6.04	-.316	.0284	.058	-----	-11.1	-----	-----
-4.02	-.186	.0193	.034	-----	-9.63	-----	0.0175
-3.02	-.122	.0169	.018	-----	-7.22	-----	.0162
-2.01	-.056	.0155	.006	-----	-3.61	-----	.0153
-1.00	.018	.0138	-.013	0.726	1.30	-----	.0138
.01	.108	.0145	-.038	.350	7.45	2.93	.0139
1.03	.207	.0170	-.068	.326	12.2	2.11	.0147
2.04	.296	.0199	-.091	.308	14.9	1.76	.0152
4.06	.442	.0269	-.130	.294	16.4	1.44	.0165
6.07	.577	.0368	-.164	.284	15.7	1.26	.0191
8.09	.709	.0468	-.193	.274	15.1	1.14	.0200
10.10	.821	.0599	-.213	.260	13.7	1.06	.0241
12.12	.900	.0738	-.221	.248	12.2	1.01	.0308
14.12	.922	.0889	-.216	.238	10.4	1.00	.0438
16.12	.904	.1163	-.212	.238	7.77	1.01	.0729

TABLE XXXIV

N. A. C. A.-M12 AIRFOIL

W. N. Y. TEST

Airfoil size, 5×30 inches.
Aspect ratio, 6.

Test speed, 40 M. P. H.
Test V_l , 24.44 sq. ft./sec.

Data from Reference 13, corrected for tunnel-wall interference

Angle of attack α degrees	Lift coeffi- cient C_L	Drag coeffi- cient C_D	Moment coeffi- cient C_M	Center of pressure coeffi- cient C_p	$\frac{C_L}{C_D}$	Speed ratio $\frac{V}{V_s}$	Profile drag coeffi- cient C_{D_0}
-8.06	-0.446	0.0419	0.086	-----	-10.6	-----	-----
-6.04	-.317	.0253	.055	-----	-12.5	-----	-----
-4.02	-.142	.0178	.057	-----	-7.97	-----	0.0167
-3.01	-.080	.0150	-.007	-----	-5.33	-----	.0147
-2.00	-.013	.0136	-----	-----	-.96	-----	.0136
-.99	.063	.0134	-.043	0.682	4.70	3.91	.0132
.02	.147	.0141	-.063	.428	10.4	2.56	.0130
1.03	.241	.0163	-.090	.372	14.8	2.00	.0131
2.04	.325	.0201	-.116	.358	16.2	1.72	.0145
4.06	.466	.0277	-.152	.326	16.8	1.44	.0161
6.08	.591	.0360	-.180	.304	16.4	1.27	.0174
8.09	.710	.0475	-.203	.286	15.0	1.16	.0206
10.10	.817	.0601	-.222	.274	13.6	1.08	.0246
12.12	.909	.0752	-.236	.262	12.1	1.03	.0313
14.12	.960	.0931	-.244	.254	10.3	1.00	.0441
16.12	.944	.1442	-.253	.268	6.54	1.01	.0969

TABLE XXXV

R. A. F.-15 AIRFOIL

W. N. Y. TEST

Airfoil size, 5×30 inches.
Aspect ratio, 6.

Test speed, 40 M. P. H.
Test V_l , 24.44 sq. ft./sec.

Data from Reference 9 corrected for tunnel-wall interference

Angle of attack α degrees	Lift coeffi- cient C_L	Drag coeffi- cient C_D	Moment coeffi- cient C_M	Center of pressure coeffi- cient C_p	$\frac{C_L}{C_D}$	Speed ratio $\frac{V}{V_s}$	Profile drag coeffi- cient C_{D_0}
-8.05	-0.406	0.0829	-----	-----	-4.90	-----	-----
-6.03	-.263	.0423	0.035	-----	-6.21	-----	-----
-4.02	-.135	.0221	.006	-----	-6.11	-----	0.0211
-3.01	-.064	.0181	-.013	-----	-3.54	-----	.0179
-2.00	.009	.0165	-.030	-----	.55	-----	.0165
-0.99	.094	.0160	-.055	0.592	5.88	3.43	.0155
.02	.081	.0156	-.077	.434	11.6	2.41	.0138
1.03	.260	.0185	-----	.402	14.1	2.02	.0149
2.04	.335	.0217	-.124	.374	15.4	1.78	.0157
4.06	.477	.0285	-.156	.334	16.7	1.49	.0164
6.08	.614	.0372	-.184	.304	16.5	1.31	.0171
8.10	.752	.0504	-.214	.292	14.9	1.18	.0204
10.11	.865	.0663	-.238	.284	13.0	1.10	.0265
12.12	.971	.0865	-.262	.278	11.2	1.04	.0364
14.13	1.014	.1238	-.274	.278	8.19	1.02	.0691
16.13	1.054	.2120	-.334	.318	4.97	1.00	.1530
18.13	1.043	.2880	-.372	.354	3.62	1.01	.2301

TABLE XXXVI

SLOANE AIRFOIL

W. N. Y. TEST

Airfoil size, 5×30 inches.
Aspect ratio, 6.

Test speed, 40 M. P. H.
Test V_l , 24.44 sq. ft./sec.

Data from Reference 9 corrected for tunnel-wall interference

Angle of attack α degrees	Lift coeffi- cient C_L	Drag coeffi- cient C_D	Moment coeffi- cient C_M	Center of pressure coeffi- cient C_p	$\frac{C_L}{C_D}$	Speed ratio $\frac{V}{V_s}$	Profile drag coeffi- cient C_{D_0}
-8.05	-0.416	0.0801	-----	-----	-5.19	-----	-----
-7.04	-.340	.0631	-----	-----	-5.39	-----	-----
-6.03	-.265	.0451	0.031	-----	-5.87	-----	-----
-5.02	-.192	.0314	-----	-----	-6.11	-----	-----
-4.02	-.119	.0209	-.010	-----	-5.69	-----	0.0201
-3.01	-.050	.0169	-.029	-----	-2.96	-----	.0168
-2.00	.018	.0118	-.043	-----	1.53	-----	.0118
-.99	.088	.0118	-.061	0.702	7.46	3.41	.0114
.02	.164	.0126	-.082	.508	13.0	2.50	.0112
2.05	.344	.0149	-.133	.394	23.1	1.72	.0086
4.07	.505	.0201	-.171	.348	25.1	1.42	.0065
6.08	.639	.0345	-.207	.330	18.5	1.26	.0128
8.10	.752	.0530	-.231	.312	14.2	1.16	.0230
10.11	.853	.0811	-.250	.300	10.5	1.09	.0424
12.12	.957	.1344	-.285	.304	7.12	1.03	.0857
14.13	1.002	.2008	-.334	.335	4.99	1.01	.1474
16.13	1.019	.2621	-.372	.360	3.88	1.00	.2068
18.13	1.011	.3103	-.396	.380	3.26	1.00	.2560

TABLE XXXVII

U. S. A.-27 AIRFOIL

W. N. Y. TEST

Airfoil size, 5×30 inches.
Aspect ratio, 6.

Test speed, 40 M. P. H.
Test V_l , 24.44 sq. ft./sec.

Data from Reference 11 corrected for tunnel-wall interference

Angle of attack α degrees	Lift coeffi- cient C_L	Drag coeffi- cient C_D	Moment coeffi- cient C_M	Center of pressure coeffi- cient C_p	C_L C_D	Speed ratio V V_s	Profile drag coeffi- cient C_{D_0}
-8.03	-0.217	0.0777	0.003		-2.79		
-7.02	-.131	.0588	-.036		-2.23		
-6.01	-.046	.0440			-1.04		
-5.00	.030	.0296			1.01		0.0295
-3.99	.102	.0242	-.113		4.22	3.67	.0236
-2.98	.174	.0217	-.127	0.728	8.02	2.82	.0201
-1.97	.245	.0220	-.143	.580	11.1	2.37	.0188
-.96	.316	.0232	-.160	.500	13.6	2.09	.0179
.05	.387	.0257	-.178	.452	15.1	1.89	.0177
2.07	.531	.0321	-.211	.388	16.5	1.61	.0171
4.09	.688	.0422	-.249	.360	16.3	1.42	.0170
6.11	.825	.0560	-.281	.336	14.7	1.29	.0198
8.12	.966	.0719	-.311	.320	13.4	1.19	.0222
10.14	1.086	.0896	-.340	.310	12.1	1.13	.0269
12.14	1.211	.1086	-.366	.304	11.1	1.07	.0308
14.16	1.289	.1311	-.382	.298	9.83	1.03	.0429
16.17	1.356	.1498	-.391	.288	9.05	1.01	.0523
18.17	1.378	.1769	-.392	.286	7.70	1.00	.0782
20.17	1.347	.2229	-.512		6.04	1.01	.1266

TABLE XXXVIII

MAIN SLOPE OF LIFT CURVE, $dC_L/d\alpha$

Laboratory and test conditions	Airfoil section	$dC_L/d\alpha$
Göttingen tests.....	G-387.....	0.070
Aspect ratio, 6.	G-398.....	.069
Approximate Reynolds Number, 412,000.	G-436.....	.069
L. M. A. L. tests.....	U. S. A.-27.....	.069
	Clark Y.....	.071
Aspect ratio, 6.	G-387.....	.072
	M-6.....	.070
Approximate Reynolds Number, 3,600,000.	M-12.....	.071
	R. A. F.-15.....	.072
	U. S. A.-27.....	.070
	U. S. A.-35A.....	.071
	U. S. A.-35B.....	.072
M. I. T. tests.....	Clark Y.....	.071
Aspect ratio, 6.	Clark Y-15.....	.070
Approximate Reynolds Number, 187,000.	G-387.....	.071
	G-436.....	.073
	R. A. F.-15.....	.075
	U. S. A.-27.....	.070
	U. S. A.-35A.....	.071
	U. S. A.-35B.....	.070
McC. F. tests.....	Clark Y.....	.072
Aspect ratio, 6.	Clark Y-15.....	.070
Approximate Reynolds Number, 374,000.	G-398.....	.073
W. N. Y. tests.....	Clark Y.....	.071
Aspect ratio, 6.	G-387.....	.070
Approximate Reynolds Number, 156,000.	G-398.....	.072
	G-436.....	.072
	M-6.....	.069
	M-12.....	.068
	N-9.....	.072
	N-10.....	.073
	N-22.....	.075
	R. A. F.-15.....	.073
	Sloane.....	.075
	U. S. A.-27.....	.071

TABLE XXXIX

ANGLE AND MOMENT COEFFICIENT FOR ZERO LIFT

Laboratory and test conditions	Airfoil section	Angle of attack for zero lift (degrees)	C_M at zero C_L
Göttingen tests.....	G-387.....	-7.3	-0.096
Aspect ratio, 5.....	G-398.....	-6.4	-.091
Approximate Reynolds Number, 412,000.	G-436.....	-5.2	-.075
L. M. A. L. tests.....	U. S. A.-27.....	-5.4	-.083
Aspect ratio, 6.....	Clark Y.....	-5.1	-.081
Approximate Reynolds Number, 3,600,000.	G-387.....	-6.8	-.096
	M-6.....	-0.2	.010
	M-12.....	-1.2	-.005
	R. A. F.-15.....	-2.2	-.052
	U. S. A.-27.....	-4.6	-.090
	U. S. A.-35A.....	-7.9	-.119
	U. S. A.-35B.....	-5.1	-.072
M. I. T. tests.....	Clark Y.....	-5.6	-.084
Aspect ratio, 6.....	Clark Y-15.....	-5.9	-.079
Approximate Reynolds Number, 187,000.	G-387.....	-7.1	-.082
	G-436.....	-5.1	-.071
	R. A. F.-15.....	-2.1	-.023
	U. S. A.-27.....	-5.3	-.087
	U. S. A.-35A.....	-8.5	-.020
	U. S. A.-35B.....	-5.9	-.075
McC. F. tests.....	Clark Y.....	-6.2	-.074
Aspect ratio, 6.....	Clark Y-15.....	-6.0	-.073
Approximate Reynolds Number, 374,000.	G-398.....	-6.8	-.084
W. N. Y. tests.....	Clark Y.....	-5.6	-.077
Aspect ratio, 6.....	G-387.....	-7.1	-.101
Approximate Reynolds Number, 156,000.	G-398.....	-6.2	-.089
	G-436.....	-4.8	-.070
	M-6.....	-1.2	-.009
	M-12.....	-1.8	-.028
	N-9.....	-4.0	-.059
	N-10.....	-5.4	-.049
	N-22.....	-5.8	-.082
	R. A. F.-15.....	-2.1	-.030
	Sloane.....	-2.2	-.042
	U. S. A.-27.....	-5.4	-.084

TABLE XL

CENTER OF PRESSURE CHARACTERISTICS

Laboratory and test conditions	Airfoil section	C_p most forward	C_p at $\frac{V}{V_\infty} = 2.0$	C_p at $\frac{V}{V_\infty} = 3.0$
Göttingen tests.....	G-387.....	0.32	0.51	0.91
Aspect ratio, 5.....	G-398.....	.31	.51	.86
Approximate Reynolds Number, 412,000.	G-436.....	.30	.47	.76
L. M. A. L. tests.....	U. S. A.-27.....	.31	.51	.86
Aspect ratio, 6.....	Clark Y.....	.294	.463	.766
Approximate Reynolds Number, 3,600,000.	G-387.....	.301	.494	.889
	M-6.....195	.148
	M-12.....	.246	.269	.280
	R. A. F.-15.....	.289	.400	.610
	U. S. A.-27.....	.293	.473	.792
	U. S. A.-35A.....	.342	.628	1.132
	U. S. A.-35B.....	.302	.425	.718
M. I. T. tests.....	Clark Y.....	.308	.501	.805
Aspect ratio, 6.....	Clark Y-15.....	.290	.478	.773
Approximate Reynolds Number, 187,000.	G-387.....	.310	.511	.859
	G-436.....	.310	.502	.784
	R. A. F.-15.....	.285	.381	.558
	U. S. A.-27.....	.292	.495	.761
	U. S. A.-35A.....	.330	.560	.943
	U. S. A.-35B.....	.305	.485	.850
McC. F. tests.....	Clark Y.....	.300	.475	.783
Aspect ratio, 6.....	Clark Y-15.....	.288	.428	.722
Approximate Reynolds Number, 374,000.	G-398.....	.307	.478	.769
W. N. Y. tests.....	Clark Y.....	.294	.480	.794
Aspect ratio, 6.....	G-387.....	.306	.500	.845
Approximate Reynolds Number, 156,000.	G-398.....	.300	.484	.810
	G-436.....	.296	.448	.739
	M-6.....	.238	.318	.352
	M-12.....	.254	.371	.497
	N-9.....	.286	.449	.728
	N-10.....	.288	.483	.801
	N-22.....	.286	.461	.789
	R. A. F.-15.....	.278	.400	.508
	Sloane.....	.300	.431	.608
	U. S. A.-27.....	.286	.480	.792

TABLE XLI
MAXIMUM LIFT COEFFICIENT, $C_{L_{max}}$
Airfoils listed according to merit

Laboratory and test conditions	Airfoil section	$C_{L_{max}}$	α for $C_{L_{max}}$ degrees
Göttingen tests..... Aspect ratio, 5. Approximate Reynolds Number, 412,000.	G-387.....	1.362	16.5
	G-398.....	1.260	14.5
	U. S. A.-27.....	1.253	15.5
	G-436.....	1.204	14.6
L. M. A. L. tests..... Aspect ratio, 6. Approximate Reynolds Number, 3,600,000.	U. S. A.-27.....	1.386	16.7
	U. S. A.-35B.....	1.377	16.0
	Clark Y.....	1.370	16.0
	G-387.....	1.329	14.6
	M-12.....	1.293	18.6
	M-6.....	1.222	18.6
	R. A. F.-15.....	1.211	15.7
	U. S. A.-35A.....	1.208	13.5
	U. S. A. 35A.....	1.470	18.3
	G-387.....	1.431	16.3
M. I. T. tests..... Aspect ratio, 6. Approximate Reynolds Number, 187,000.	U. S. A.-27.....	1.351	17.3
	U. S. A.-35B.....	1.301	14.6
	Clark Y-15.....	1.260	15.6
	Clark Y.....	1.239	14.4
	G-436.....	1.204	13.0
	R. A. F.-15.....	1.017	13.9
McC. F. tests..... Aspect ratio, 6. Approximate Reynolds Number, 374,000.	G-398.....	1.408	14.5
	Clark Y-15.....	1.322	16.2
	Clark Y.....	1.250	13.8
W. N. Y. tests..... Aspect ratio, 6. Approximate Reynolds Number, 156,000.	G-387.....	1.488	18.2
	G-398.....	1.387	16.2
	N-22.....	1.384	16.2
	U. S. A.-27.....	1.378	18.2
	G-436.....	1.325	15.9
	Clark Y.....	1.258	15.6
	N-10.....	1.257	14.2
	N-9.....	1.125	13.6
	R. A. F.-15.....	1.053	16.4
	Sloane.....	1.019	16.1
	M-12.....	.962	14.6
	M-6.....	.922	14.1

TABLE XLII
MINIMUM DRAG COEFFICIENT, $C_{D_{min}}$
Airfoils listed according to merit

Laboratory and test conditions	Airfoil section	$C_{D_{min}}$	α for $C_{D_{min}}$ degrees
Göttingen tests..... Aspect ratio, 5. Approximate Reynolds Number, 412,000.	G-436.....	0.0130	-4.0
	G-398.....	.0150	-5.4
	U. S. A.-27.....	.0150	-3.0
	G-387.....	.0178	-5.0
L. M. A. L. tests..... Aspect ratio, 6. Approximate Reynolds Number, 3,600,000.	M-6.....	.0080	0.0
	R. A. F.-15.....	.0083	-1.5
	M-12.....	.0089	-1.5
	U. S. A.-35B.....	.0093	-4.8
	Clark Y.....	.0106	-5.5
	U. S. A.-27.....	.0116	-4.0
	G-387.....	.0126	-6.0
	U. S. A.-35A.....	.0142	-6.7
	R. A. F.-15.....	.0123	-0.7
	Clark Y.....	.0153	-3.5
M. I. T. tests..... Aspect ratio, 6 Approximate Reynolds Number, 187,000.	G-436.....	.0165	-3.0
	Clark Y-15.....	.0168	-4.5
	U. S. A.-35B.....	.0185	-2.7
	U. S. A.-27.....	.0220	-1.0
	G-387.....	.0237	-3.9
	U. S. A.-35A.....	.0302	-3.6
McC. F. tests..... Aspect ratio, 6. Approximate Reynolds Number, 374,000.	Clark Y-15.....	.0133	-5.0
	Clark Y.....	.0149	-4.5
	G-398.....	.0152	-6.2
W. N. Y. tests..... Aspect ratio, 6. Approximate Reynolds Number, 156,000.	Sloane.....	.0118	-1.0
	M-12.....	.0134	-1.5
	N-9.....	.0135	-2.5
	M-6.....	.0138	-1.0
	R. A. F.-15.....	.0156	-0.6
	G-398.....	.0175	-4.0
	N-10.....	.0177	-3.5
	N-22.....	.0183	-4.0
	Clark Y.....	.0183	-4.0
	G-436.....	.0196	-2.0
	U. S. A.-27.....	.0217	-2.9
	G-387.....	.0236	-4.0

TABLE XLIII

MAXIMUM RATIO C_L/C_D AND LIFT COEFFICIENT AT MAXIMUM C_L/C_D Airfoils listed according to maximum C_L/C_D merit

Laboratory and test conditions	Airfoil section	Maximum C_L/C_D	α for maximum C_L/C_D degrees
Göttingen tests.....	G-436.....	18.9	1.0
Aspect ratio, 5.	U. S. A.-27.....	18.5	.8
Approximate Reynolds Number, 412,000.	G-398.....	17.5	0
L. M. A. L. tests.....	G-387.....	16.6	0
Aspect ratio, 6.	R. A. F.-15.....	24.3	3.2
Approximate Reynolds Number, 3,600,000.	M-6.....	21.9	4.4
	Clark Y.....	21.1	.3
	M-12.....	20.6	4.8
	U. S. A.-27.....	20.6	1.7
	U. S. A.-35B.....	20.5	.3
	G-387.....	18.6	-1.3
	U. S. A.-35A.....	18.4	-1.3
M. I. T. tests.....	Clark Y.....	18.8	1.0
Aspect ratio, 6.	G-436.....	18.5	1.6
Approximate Reynolds Number, 187,000.	Clark Y-15.....	18.4	.5
	R. A. F.-15.....	18.4	2.5
	U. S. A.-35B.....	18.1	1.5
	U. S. A.-27.....	17.7	2.0
	G-387.....	16.2	1.5
	U. S. A.-35A.....	15.1	.4
McC. F. tests.....	Clark Y.....	20.6	0
Aspect ratio, 6.	Clark Y-15.....	19.2	.5
Approximate Reynolds Number, 374,000.	G-398.....	18.6	0
W. N. Y. tests.....	Sloane.....	25.1	3.8
Aspect ratio, 6.	N-9.....	20.6	1.0
Approximate Reynolds Number, 156,000.	N-10.....	17.6	1.7
	N-22.....	17.6	1.0
	Clark Y.....	17.2	1.8
	G-398.....	17.1	.5
	M-12.....	16.8	4.0
	R. A. F.-15.....	16.8	4.8
	G-436.....	16.8	2.3
	U. S. A.-27.....	16.5	2.8
	M-6.....	16.4	4.1
	G-387.....	14.6	2.1

Laboratory and test conditions	Airfoil section	C_L at maximum C_L/C_D	C_L at max. C_L/C_D $C_{L_{max}}$
Göttingen tests.....	G-436.....	0.430	0.355
Aspect ratio, 5.	U. S. A.-27.....	.410	.327
Approximate Reynolds Number, 412,000.	G-398.....	.448	.355
L. M. A. L. tests.....	G-387.....	.487	.358
Aspect ratio, 6.	R. A. F.-15.....	.401	.331
Approximate Reynolds Number, 3,600,000.	M-6.....	.330	.270
	Clark Y.....	.391	.286
	M-12.....	.439	.348
	U. S. A.-27.....	.440	.318
	U. S. A.-35B.....	.390	.284
	G-387.....	.390	.294
	U. S. A.-35A.....	.470	.389
M. I. T. tests.....	Clark Y.....	.462	.373
Aspect ratio, 6.	G-436.....	.478	.396
Approximate Reynolds Number, 187,000.	Clark Y-15.....	.445	.353
	R. A. F.-15.....	.370	.364
	U. S. A.-35B.....	.495	.370
	U. S. A.-27.....	.520	.385
	G-387.....	.610	.426
	U. S. A.-35A.....	.628	.427
McC. F. tests.....	Clark Y.....	.510	.408
Aspect ratio, 6.	Clark Y-15.....	.470	.355
Approximate Reynolds Number, 374,000.	G-398.....	.470	.334
W. N. Y. tests.....	Sloane.....	.482	.473
Aspect ratio, 6.	N-9.....	.389	.346
Approximate Reynolds Number, 156,000.	N-10.....	.515	.410
	N-22.....	.499	.360
	Clark Y.....	.531	.422
	G-398.....	.471	.340
	M-12.....	.457	.475
	R. A. F.-15.....	.528	.501
	G-436.....	.500	.378
	U. S. A.-27.....	.583	.423
	M-6.....	.445	.483
	G-387.....	.639	.429

TABLE XLIV

RATIO C_L/C_D FOR VARIOUS FRACTIONS OF MAXIMUM C_L .

Laboratory and test conditions	Airfoil section	C_L/C_D at—	
		$\frac{2}{3}$ maximum C_L	$\frac{1}{2}$ maximum C_L
Göttingen tests.....	G-387.....	13.6	15.6
Aspect ratio, 5.....	G-398.....	14.1	16.6
Approximate Reynolds Number 412,000.	G-436.....	14.6	17.8
L. M. A. L. tests.....	U. S. A.-27.....	14.2	16.7
Aspect ratio, 6.....	Clark Y.....	14.8	18.7
Approximate Reynolds Number 3,600,000.	G-387.....	14.0	16.0
M. I. T. tests.....	M-6.....	15.0	17.8
Aspect ratio, 6.....	M-12.....	14.6	17.4
Approximate Reynolds Number 187,000.	R. A. F.-15.....	16.7	20.9
McC. F. tests.....	U. S. A.-27.....	14.8	17.8
Aspect ratio, 6.....	U. S. A.-35A.....	15.4	17.8
Approximate Reynolds Number 374,000.	U. S. A.-35B.....	14.2	17.0
W. N. Y. tests.....	Clark Y.....	15.2	18.0
Aspect ratio, 6.....	Clark Y-15.....	14.8	17.5
Approximate Reynolds Number 156,000.	G-387.....	14.0	15.8
	G-436.....	15.6	17.8
	R. A. F.-15.....	16.6	18.0
	U. S. A.-27.....	14.5	17.1
	U. S. A.-35A.....	13.3	15.0
	U. S. A.-35B.....	15.8	17.4
	Clark Y.....	15.9	19.0
	Clark Y-15.....	15.0	17.5
	G-398.....	14.4	17.7
	Clark Y.....	14.7	16.9
	G-387.....	12.4	14.3
	G-398.....	13.7	15.9
	G-436.....	14.0	16.0
	N-9.....	15.9	18.4
	N-10.....	14.6	17.0
	N-22.....	14.1	16.4
	M-6.....	15.4	16.3
	M-12.....	16.1	16.8
	R. A. F.-15.....	15.6	16.8
	Sloane.....	16.9	25.0
	U. S. A.-27.....	13.8	16.2

Laboratory and test conditions	Airfoil section	C_L/C_D at—		
		$\frac{1}{4}$ maxi- mum C_L	$\frac{1}{6}$ maxi- mum C_L	$\frac{1}{8}$ maxi- mum C_L
Göttingen tests.....	G-387.....	15.5	12.2	9.9
Aspect ratio 5.....	G-398.....	16.1	12.8	10.3
Approximate Reynolds Number, 412,000.	G-436.....	17.4	13.9	11.3
L. M. A. L. tests.....	U. S. A.-27.....	17.2	13.7	10.8
Aspect ratio, 6.....	Clark Y.....	20.6	17.3	14.8
Approximate Reynolds Number, 3,600,000.	G-387.....	17.9	14.5	12.1
M. I. T. tests.....	M-6.....	21.8	19.0	15.4
Aspect ratio, 6.....	M-12.....	19.6	17.2	15.6
Approximate Reynolds Number, 187,000.	R. A. F.-15.....	23.4	20.6	17.4
Mc. C. F. tests.....	U. S. A.-27.....	20.0	16.8	13.8
Aspect ratio, 6.....	U. S. A.-35A.....	16.7	13.3	10.6
Approximate Reynolds Number, 374,000.	U. S. A.-35B.....	20.2	17.6	15.7
W. N. Y. tests.....	Clark Y.....	17.2	13.4	10.2
Aspect ratio, 6.....	Clark Y-15.....	16.6	12.2	9.3
Approximate Reynolds Number, 156,000.	G-387.....	13.8	10.2	7.0
	G-436.....	15.9	11.9	9.4
	R. A. F.-15.....	17.4	13.3	10.8
	U. S. A.-27.....	15.2	9.5	5.9
	U. S. A.-35A.....	12.5	5.8	3.7
	U. S. A.-35B.....	16.0	12.0	9.3
	Clark Y.....	17.3	13.1	10.1
	Clark Y-15.....	18.1	14.6	12.0
	G-398.....	17.5	14.0	11.2
	Clark Y.....	14.8	11.2	8.5
	G-387.....	13.0	10.2	7.7
	G-398.....	16.3	12.6	9.8
	G-436.....	14.9	11.2	8.3
	N-9.....	19.0	13.0	10.2
	N-10.....	15.4	11.3	8.8
	N-22.....	15.2	11.7	9.1
	M-6.....	13.1	10.1	8.2
	M-12.....	14.9	11.1	8.9
	R. A. F.-15.....	14.2	11.6	8.9
	Sloane.....	20.1	14.2	10.3
	U. S. A.-27.....	14.4	10.6	8.0

TABLE XLV

RATIO OF MAXIMUM C_L TO MINIMUM C_D

Airfoils listed according to merit

Laboratory and test conditions	Airfoil section	$\frac{C_{Lmax}}{C_{Dmax}}$
Göttingen tests.....	G-436.....	92.5
Aspect ratio, 5.	G-398.....	84.0
Approximate Reynolds Number, 412,000.	U. S. A.-27.....	83.5
L. M. A. L. tests.....	G-387.....	76.5
Aspect ratio, 6.	M-6.....	153
Approximate Reynolds Number, 3,600,000.	U. S. A.-35B.....	148
	R. A. F.-15.....	146
	M-12.....	145
	Clark Y.....	129
	U. S. A.-27.....	120
	G-387.....	106
M. I. T. tests.....	U. S. A.-35A.....	85.1
Aspect ratio, 6.	R. A. F.-15.....	82.7
Approximate Reynolds Number, 187,000.	Clark Y.....	80.9
	Clark Y-15.....	75.0
	G-436.....	73.0
	U. S. A.-35B.....	70.3
	U. S. A.-27.....	61.4
	G-387.....	60.4
	U. S. A.-35A.....	48.7
McC. F. tests.....	Clark Y-15.....	99.4
Aspect ratio, 6.	G-398.....	92.5
Approximate Reynolds Number, 374,000.	Clark Y.....	83.9
W. N. Y. tests.....	Sloane.....	86.3
Aspect ratio, 6.	N-9.....	83.3
Approximate Reynolds Number, 156,000.	G-398.....	79.1
	N-22.....	75.6
	M-12.....	71.8
	N-10.....	71.0
	Clark Y.....	68.7
	G-436.....	67.6
	R. A. F. 15.....	67.5
	M-6.....	66.8
	U. S. A.-27.....	63.5
	G-387.....	63.0

TABLE XLVI

MAXIMUM RATIO OF C_L^3 TO C_D^3

Airfoils listed according to merit

Laboratory and test conditions	Airfoil section	$(C_L^3/C_D^3)_{max}$
Göttingen tests.....	G-436.....	189
Aspect ratio, 5.	U. S. A.-27.....	188
Approximate Reynolds Number, 412,000.	G-387.....	180
L. M. A. L. tests.....	G-398.....	174
Aspect ratio, 6.	R. A. F.-15.....	265
Approximate Reynolds Number, 3,600,000.	Clark Y.....	237
	U. S. A.-27.....	229
	M-6.....	204
	M-12.....	202
	U. S. A.-35A.....	202
	U. S. A.-35B.....	197
	G-387.....	179
M. I. T. tests.....	U. S. A.-35B.....	215
Aspect ratio, 6.	Clark Y.....	203
Approximate Reynolds Number, 187,000.	U. S. A.-27.....	203
	G-436.....	202
	Clark Y-15.....	201
	R. A. F.-15.....	193
	G-387.....	188
	U. S. A.-35A.....	181
McC. F. tests.....	G-398.....	227
Aspect ratio, 6.	Clark Y.....	226
Approximate Reynolds Number, 374,000.	Clark Y-15.....	204
W. N. Y. tests.....	Sloane.....	326
Aspect ratio, 6.	N-9.....	194
Approximate Reynolds Number, 156,000.	N-10.....	190
	Clark Y.....	188
	N-22.....	185
	U. S. A.-27.....	183
	G-436.....	181
	G-398.....	176
	R. A. F.-15.....	171
	M-12.....	166
	M-6.....	162
	G-387.....	162

TABLE XLVII
RATIO OF MAXIMUM C_L^3 TO MINIMUM C_D^3
Airfoils listed according to merit

Laboratory and test conditions	Airfoil section	$\frac{C_L^3_{max}}{C_D^3_{max}}$
Göttingen tests.....	G-436.....	10,300
Aspect ratio, 5.	G-398.....	8,890
Approximate Reynolds Number, 412,000.	U. S. A.-27.....	8,736
L. M. A. L. tests.....	G-387.....	7,970
Aspect ratio, 6.	U. S. A.-35B.....	30,200
Approximate Reynolds Number, 3,600,000.	M-6.....	28,500
	M-12.....	27,300
	R. A. F.-15.....	25,800
	Clark Y.....	22,900
	U. S. A.-27.....	19,800
	G-387.....	14,800
	U. S. A.-35A.....	8,750
M. I. T. tests.....	Clark Y.....	8,100
Aspect ratio, 6.	Clark Y-15.....	7,090
Approximate Reynolds Number, 187,000.	R. A. F.-15.....	6,960
	U. S. A.-35B.....	6,430
	G-436.....	6,410
	G-387.....	5,220
	U. S. A.-27.....	5,090
	U. S. A.-35A.....	3,490
McC. F. tests.....	Clark Y-15.....	13,100
Aspect ratio, 6.	G-398.....	12,000
Approximate Reynolds Number, 374,000.	Clark Y.....	8,800
W. N. Y. tests.....	G-398.....	8,680
Aspect ratio, 6.	N-22.....	7,910
Approximate Reynolds Number, 156,000.	N-9.....	7,800
	Sloane.....	7,580
	N-10.....	6,320
	G-436.....	6,050
	Clark Y.....	5,930
	G-387.....	5,900
	U. S. A.-27.....	5,550
	M-12.....	4,960
	R. A. F.-15.....	4,800
	M-6.....	4,110

TABLE XLVIII
MINIMUM PROFILE DRAG COEFFICIENT C_{D0} (FAIRED)
Airfoils listed according to merit

Laboratory and test conditions	Airfoil section	$C_{D0\ max}$
Göttingen tests.....	G-436.....	0.0106
Aspect ratio, 5.	U. S. A.-27.....	.0116
Approximate Reynolds Number, 412,000.	G-398.....	.0124
L. M. A. L. tests.....	G-387.....	.0147
Aspect ratio, 6.	R. A. F.-15.....	.0076
Approximate Reynolds Number, 3,600,000.	M-6.....	.0083
	M-12.....	.0089
	U. S. A.-35B.....	.0091
	Clark Y.....	.0105
	U. S. A.-27.....	.0108
	G-387.....	.0123
	U. S. A.-35A.....	.0132
M. I. T. tests.....	R. A. F.-15.....	.0116
Aspect ratio, 6.	Clark Y.....	.0127
Approximate Reynolds Number, 187,000.	Clark Y-15.....	.0132
	G-436.....	.0137
	U. S. A.-35B.....	.0142
	U. S. A.-27.....	.0147
	G-387.....	.0176
	U. S. A.-35A.....	.0204
McC. F. tests.....	Clark Y.....	.0113
Aspect ratio, 6.	Clark Y-15.....	.0124
Approximate Reynolds Number, 374,000.	G-398.....	.0131
W. N. Y. tests.....	Sloane.....	.0076
Aspect ratio, 6.	N-9.....	.0106
Approximate Reynolds Number, 156,000.	M-12.....	.0130
	M-6.....	.0138
	R. A. F.-15.....	.0145
	G-398.....	.0148
	N-10.....	.0148
	N-22.....	.0156
	Clark Y.....	.0156
	G-436.....	.0160
	U. S. A.-27.....	.0170
	G-387.....	.0207

TABLE XLIX

FAIRED RATIO $C_{D0}/C_{L_{max}}$ FOR VARIOUS SPEED RATIOS

Laboratory and test conditions	Airfoil section	$C_{D0}/C_{L_{max}}$ (faired) at—		
		$V/V_s=1.10$	$V/V_s=1.50$	$V/V_s=2.50$
Göttingen tests..... Aspect ratio, 5. Approximate Reynolds Number, 412,000.	G-387.....	0.0140	0.0101	0.0112
	G-398.....	.0140	.0099	.0108
	G-436.....	.0130	.0088	.0098
	U. S. A.-27.....	.0147	.0093	.0102
	Clark Y.....	.0171	.0088	.0077
L. M. A. L. tests..... Aspect ratio, 6. Approximate Reynolds Number, 3,600,000.	G-387.....	.0217	.0121	.0094
	M-6.....	.0212	.0101	.0070
	M-12.....	.0208	.0104	.0071
	R. A. F.-15.....	.0149	.0073	.0063
	U. S. A.-27.....	.0164	.0087	.0078
	U. S. A.-35A.....	.0199	.0117	.0109
	U. S. A.-35B.....	.0211	.0101	.0072
	Clark Y.....	.0208	.0107	.0108
	Clark Y-15.....	.0210	.0110	.0117
	G-387.....	.0180	.0123	.0157
M. I. T. tests..... Aspect ratio, 6. Approximate Reynolds Number, 187,000.	G-436.....	.0177	.0116	.0122
	R. A. F.-15.....	.0195	.0130	.0114
	U. S. A.-27.....	.0193	.0108	.0158
	U. S. A.-35A.....	.0188	.0139	.0207
	U. S. A.-35B.....	.0145	.0109	.0122
	Clark Y.....	.0155	.0092	.0102
	Clark Y-15.....	.0181	.0103	.0094
	G-398.....	.0168	.0094	.0101
	Clark Y.....	.0209	.0127	.0131
	G-387.....	.0235	.0150	.0142
McC. F. tests..... Aspect ratio, 6. Approximate Reynolds Number, 374,000. W. N. Y. tests..... Aspect ratio, 6. Approximate Reynolds Number, 156,000.	G-398.....	.0210	.0123	.0110
	G-436.....	.0232	.0125	.0132
	N-9.....	.0201	.0110	.0108
	N-10.....	.0196	.0123	.0125
	N-22.....	.0196	.0117	.0120
	M-6.....	.0242	.0177	.0152
	M-12.....	.0234	.0157	.0135
	R. A. F.-15.....	.0256	.0154	.0137
	Sloane.....	.0385	.0075	.0096
	U. S. A.-27.....	.0214	.0123	.0138

REPORT No. 332

THE EFFECT OF COWLING ON CYLINDER TEMPERATURES AND PERFORMANCE OF A WRIGHT J-5 ENGINE

By OSCAR W. SCHEY and ARNOLD E. BIERMANN

Langley Memorial Aeronautical Laboratory

REPORT No. 332

THE EFFECT OF COWLING ON CYLINDER TEMPERATURES AND PERFORMANCE OF A WRIGHT J-5 ENGINE

By OSCAR W. SCHEY and ARNOLD E. BIERMANN

SUMMARY

This report presents the results of tests conducted by the staff of the National Advisory Committee for Aeronautics to determine the effect of different amounts and kinds of cowling on the performance and cylinder temperatures of a standard Wright J-5 engine. These tests were conducted in conjunction with drag and propeller tests in which the same cowlings were used.

The engine was mounted in the nose of a cabin fuselage and placed in the air stream of the Committee's Twenty-Foot Propeller Research Tunnel, which is located at the Langley Memorial Aeronautical Laboratory. The power was measured by means of a torque dynamometer placed within the fuselage. Sixty-nine iron-constantan thermocouples and three recording pyrometers were used for obtaining the cylinder temperature measurements.

Four different cowlings were investigated, in tests herein reported, varying from the one extreme of no cowling on the engine to the other extreme of the engine completely cowled and the cooling air flowing inside the cowling through an opening in the nose and out through an annular opening at the rear of the engine. Each cowling was tested at air speeds of approximately 60, 80, and 100 miles per hour.

For the conventional type of engine cowling the results of these tests indicate that increasing the amount of cowling has the advantage of reducing the drag, but the disadvantage of increasing the cylinder barrel temperatures. Satisfactory cooling was obtained with the conventional cowling that covered 35 per cent of the cylinder cooling area. With the conventional cowling that covered 73 per cent of the cooling area the cylinder temperatures were excessive even though a large portion of the cooling air was permitted to flow inside the cowling through slots in the front of the cowling.

For the cabin fuselage with the N. A. C. A. cowling, which completely inclosed the engine and took in all of the cooling air through a 28-inch diameter opening in the nose, the drag was reduced 40 per cent at 100 miles per hour, as compared with the same unit with no cowling on the engine. The mean temperatures of the spark-plug boss and the cylinder head were slightly reduced for the same test conditions, but the barrel temperatures were increased.

The spark-plug boss temperatures, as used by many manufacturers, are a valuable indication of engine performance, but they alone should not be used as a criterion to determine the amount an engine can be cowled, since the barrel temperatures do not vary in parallel with them.

INTRODUCTION

Research on the air-cooled engine has been confined principally to the development of a reliable engine having adequate cooling and high power output per unit of weight. The problem of cowling has been a secondary consideration. Some interesting work, however, has been done, even though no systematic investigation has been conducted. In 1921 Colonel Clark designed an airplane powered with a Wright J-1 engine, having a cowling which completely inclosed the engine. (Reference 1.) The cooling air was taken inside the cowling through an opening in the front and was discharged through an annular opening in the rear of the engine. The Italian engineer, Piero Magni, also conducted tests on a similar cowling which he referred to

as an "aerodynamic cowling." (Reference 2.) As far as the authors are aware, neither of these investigators made temperature measurements nor did they experience any cooling difficulties.

At the request of a large number of aircraft manufacturers the National Advisory Committee for Aeronautics decided to conduct a systematic investigation of the effect of different amounts and kinds of cowling on the drag, propulsive efficiency, cylinder temperatures, and performance of radial air-cooled engines.

The results of the drag and propulsive efficiency tests have been published in N. A. C. A. Technical Reports Nos. 313 and 314. (References 3 and 4.) The cylinder temperature and performance measurements, herein reported, were made on four different cowlings. These cowlings varied from the one extreme of no cowling on the engine cylinders to the other extreme of the engine completely cowed and the cooling air flowing in through an opening in the nose of the cowling and out through an annular opening at the rear of the engine. The tests for each cowling were conducted at air speeds of approximately 60, 80, and 100 miles per hour.

DESCRIPTION OF APPARATUS AND METHODS

The tests herein reported were conducted on a standard Wright "Whirlwind" engine of the J-5 series. The engine, mounted in the nose of a cabin fuselage, was placed in the air stream of the Committee's Twenty-Foot Propeller Research Tunnel. A complete description of this tunnel and test methods may be found in N. A. C. A. Technical Report No. 300. (Reference 5.)

This engine is of the 9-cylinder static-radial air-cooled type, having a $4\frac{1}{2}$ -inch bore, a $5\frac{1}{2}$ -inch stroke, and a 5.4 compression ratio. The engine is rated at 220 horsepower at 2,000 r. p. m. A Stromberg "NA-T4" carburetor was used, having three venturi chokes of $1\frac{7}{16}$ inches diameter and three Number 51 drill size main metering jets. The cylinders on this engine are of composite construction, having an aluminum head screwed and shrunk on a steel barrel. The walls of the steel cylinder barrel are $\frac{5}{64}$ inch thick. The cross-section of this cylinder (fig. 1) shows the finning and construction.

Sixty-nine iron-constantan thermocouples and three multiple duplex recording pyrometers were used for measuring and recording the temperatures of cylinder head, barrel, and fin temperatures. Forty-seven thermocouples were attached to Cylinder Number 1 to obtain information on the distribution of temperatures over this cylinder. The remaining 22 thermocouples were distributed among the other eight cylinders so that information could be obtained on which to compare the operating temperatures of all cylinders and the engine performance. The

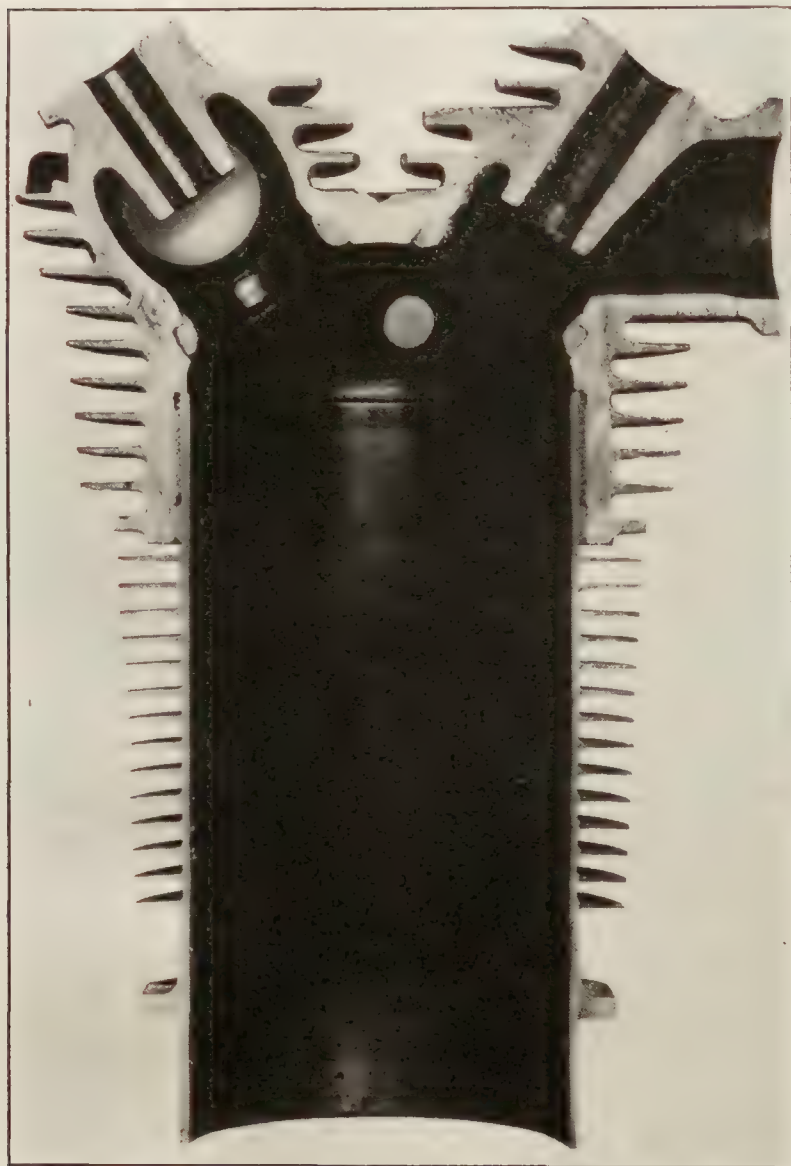


FIGURE 1.—Cross section of a Wright J-5 cylinder

thermocouples were made of 0.020-inch enameled wire and were electrically welded. An automatic electrically operated switch doubled the number of thermocouples that could be connected to each pyrometer. A reading was obtained on each thermocouple every three minutes.

The thermocouples on the head and fins were inserted into small holes and held in place by peening around the wires. Good thermal contact was obtained with this method. The thermocouples on the cylinder barrel were held firmly against the metal surface by means of clamp rings of narrow metal tape. For measuring the spark-plug-boss temperatures the thermocouples were embedded one-eighth inch below the metal surface at the root of the spark-plug bosses.

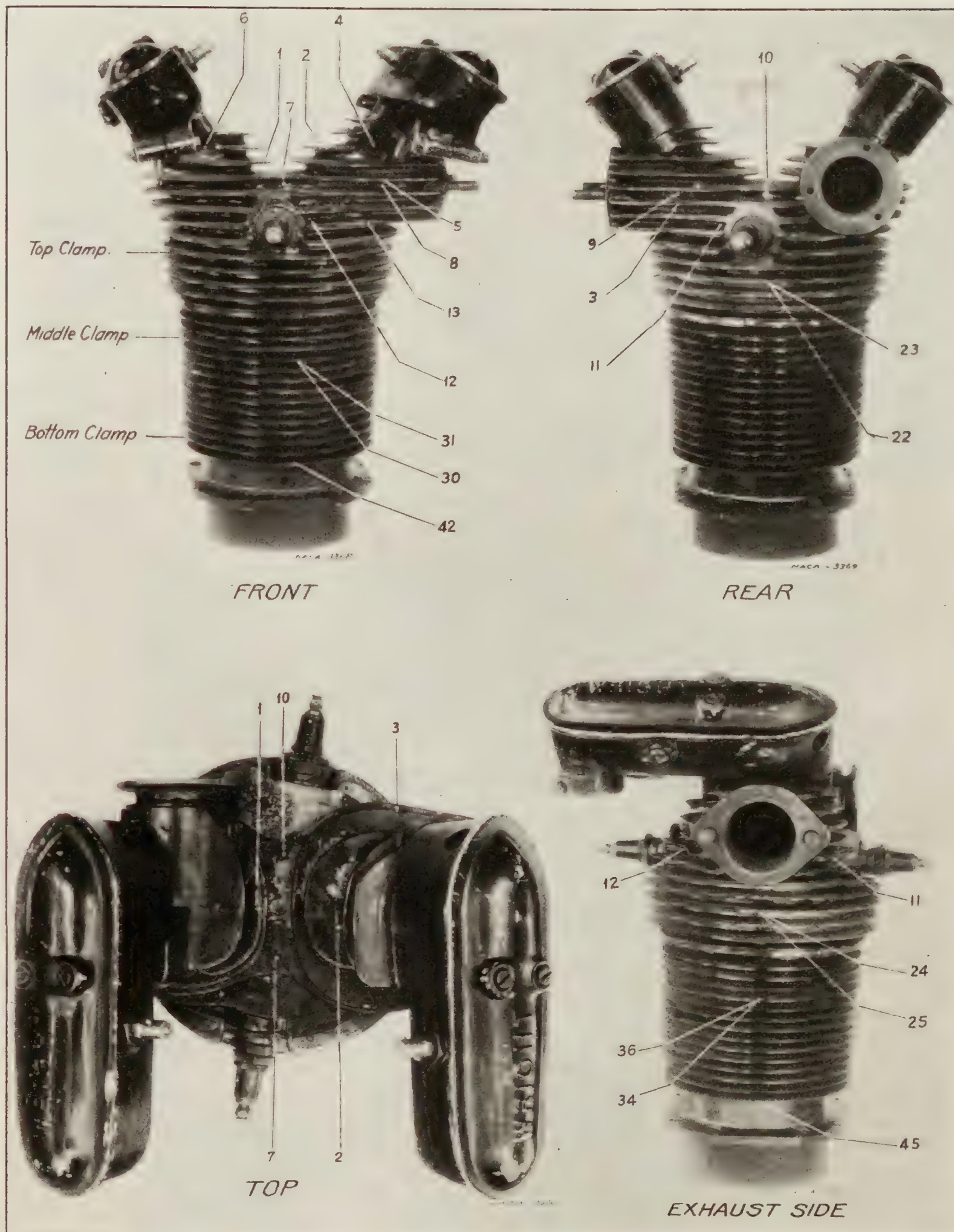


FIGURE 2.—Location of thermocouples on head and fins of cylinder No.

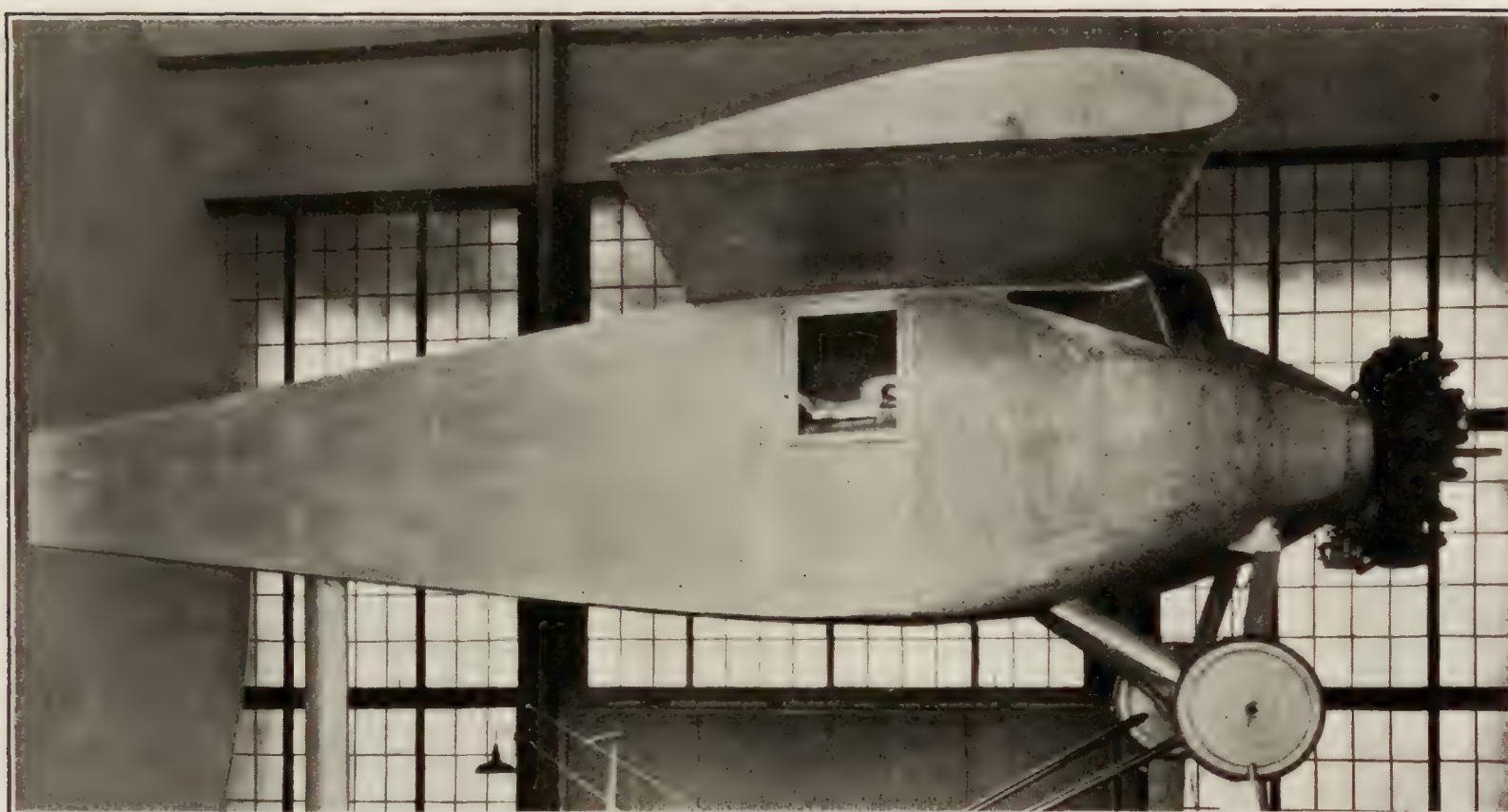


FIGURE 3.—View of fuselage and engine with cowling No. 4



FIGURE 4.—Cowling No. 5

The general location of each thermocouple is given in Table I. The exact location of 23 of the 47 thermocouples on Cylinder Number 1 may be obtained from Figure 2, and the location of the other 24 may be obtained from any of the curves showing the temperatures measured under each clamp ring. Three clamp rings were used, located as follows: the bottom clamp ring between fins 1 and 2, the middle clamp ring between fins 11 and 12, and the top clamp ring between fins 18 and 19. Rear and front spark-plug-boss temperatures were measured on the other eight cylinders in the same location as shown for Thermocouples Numbers 11 and 12 on Cylinder Number 1 in Figure 2.



FIGURE 5.—Front view of cowling No. 7

In addition to the measurements of cylinder temperatures, the oil inlet, oil outlet, carburetor air, and cold junction temperatures were measured with electrical resistance thermometers. The fuel consumption was obtained from measurement of the time required to consume 2 pounds of fuel. Measurements were also obtained of the air speed, engine speed, and torque at full throttle. The engine torque was measured by means of a torque dynamometer placed within the fuselage. (References 3 and 5.) The same pitch setting was used on the propeller for all runs.

The total cooling area of each fin and surface above the mounting flange was carefully determined. By noting the number of fins below the cowling and where the cowling crossed the fins, the percentage of the total cooling area which was cowled could be computed.

The four cowlings for which cylinder temperature and performance measurements were obtained were selected from a series of 10 cowlings that had been constructed for drag tests. The first of these cowlings tested, designated as Number 4, did not cover any of the cylinder cooling area. Figure 3 shows this cowling with engine and fuselage as mounted ready for the test. The second cowling tested, designated as Number 5, covered 35 per cent of the cooling area of the cylinders (fig. 4). This cowling is similar to the conventional cowling used on commercial planes powered with radial engines. The third cowling tested, designated as

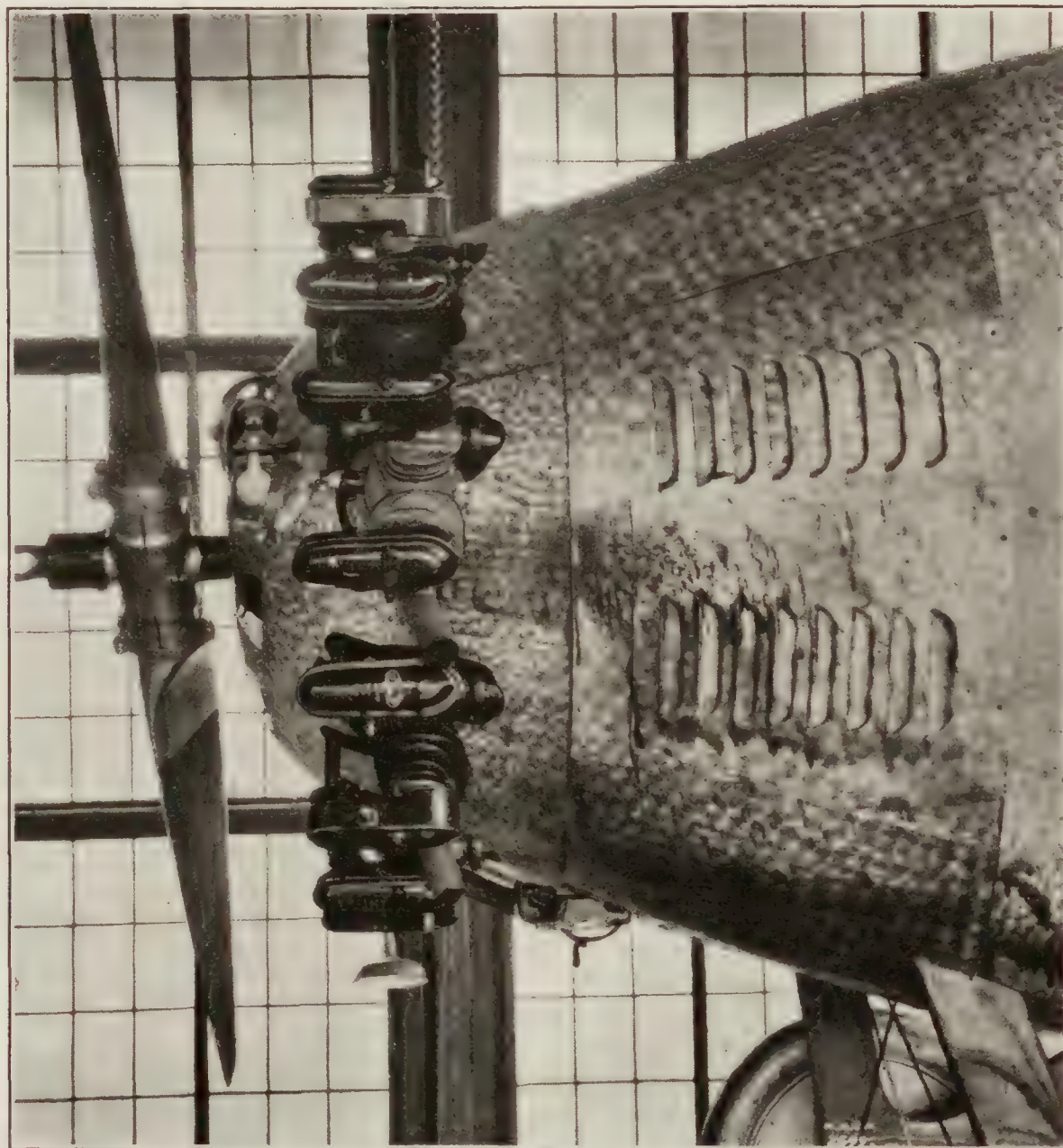


FIGURE 6.—Side view of cowling No. 7

Number 7, covered 73 per cent of the cooling area of each cylinder (figs. 5 and 6). This cowling probably covered a larger percentage of the total cooling area than any of the commercial cowlings now used. It had six slots cut in the nose to permit part of the cooling air to flow inside the cowling. The fourth cowling tested, designated as Number 10, inclosed the entire cooling area, the cowling being faired over the top of the cylinders and so designed as to permit the cooling air to flow inside the cowling and around the cylinders and cylinder heads (figs. 7 and 8). Cowling Number 10 was tested with deflectors between cylinders as shown in Figure 9. Each of these cowlings was tested at air speeds of 60, 80, and 100 miles per hour.

RESULTS

The results of tests on cylinder temperatures and engine performance with the four different cowlings tested are presented in Tables I and II and in Figures 10 to 16, inclusive.

Table I gives the location of each of the 69 thermocouples used. The maximum temperatures obtained at each point during tests on the four cowlings, at air speeds of approximately 60, 80, and 100 miles per hour, are also given in this table.

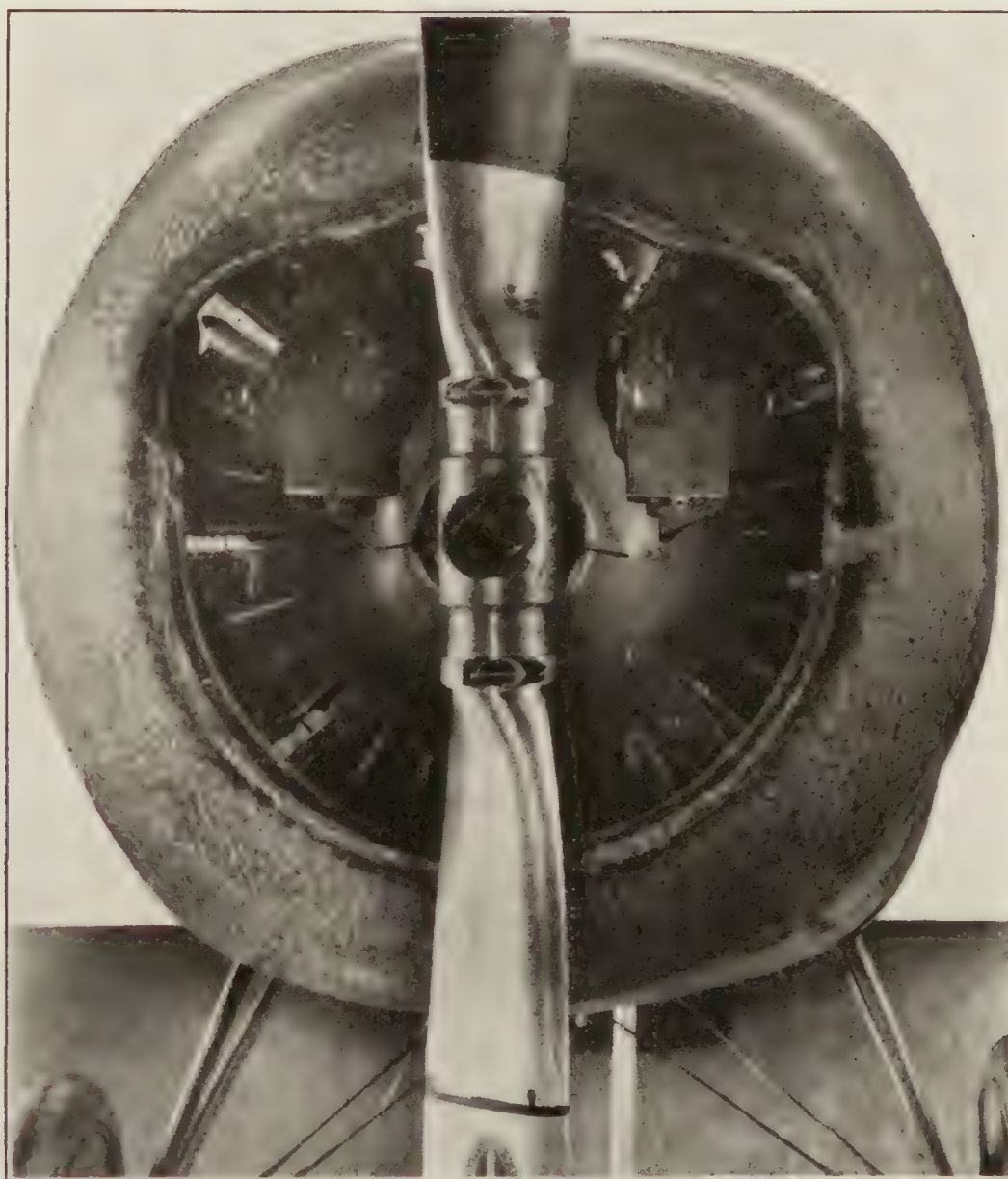


FIGURE 7.—Front view of cowling No. 10

Table II presents test data on engine speed, brake horsepower, fuel consumption, carburetor air temperature, oil-in temperature, and oil-out temperature. Data on air velocity, barometer, and room temperature are also included in this table.

The curves in Figure 10 present information on the variation of barrel temperatures on Cylinder Number 1 with changes in air speed. This information is given for the top, middle, and bottom clamps for each of the four cowlings tested.

A comparison of the barrel temperatures obtained with each cowling is shown in Figure 11. This information is given for the top, middle, and bottom clamps for air speeds of approximately 60, 80, and 100 miles per hour.

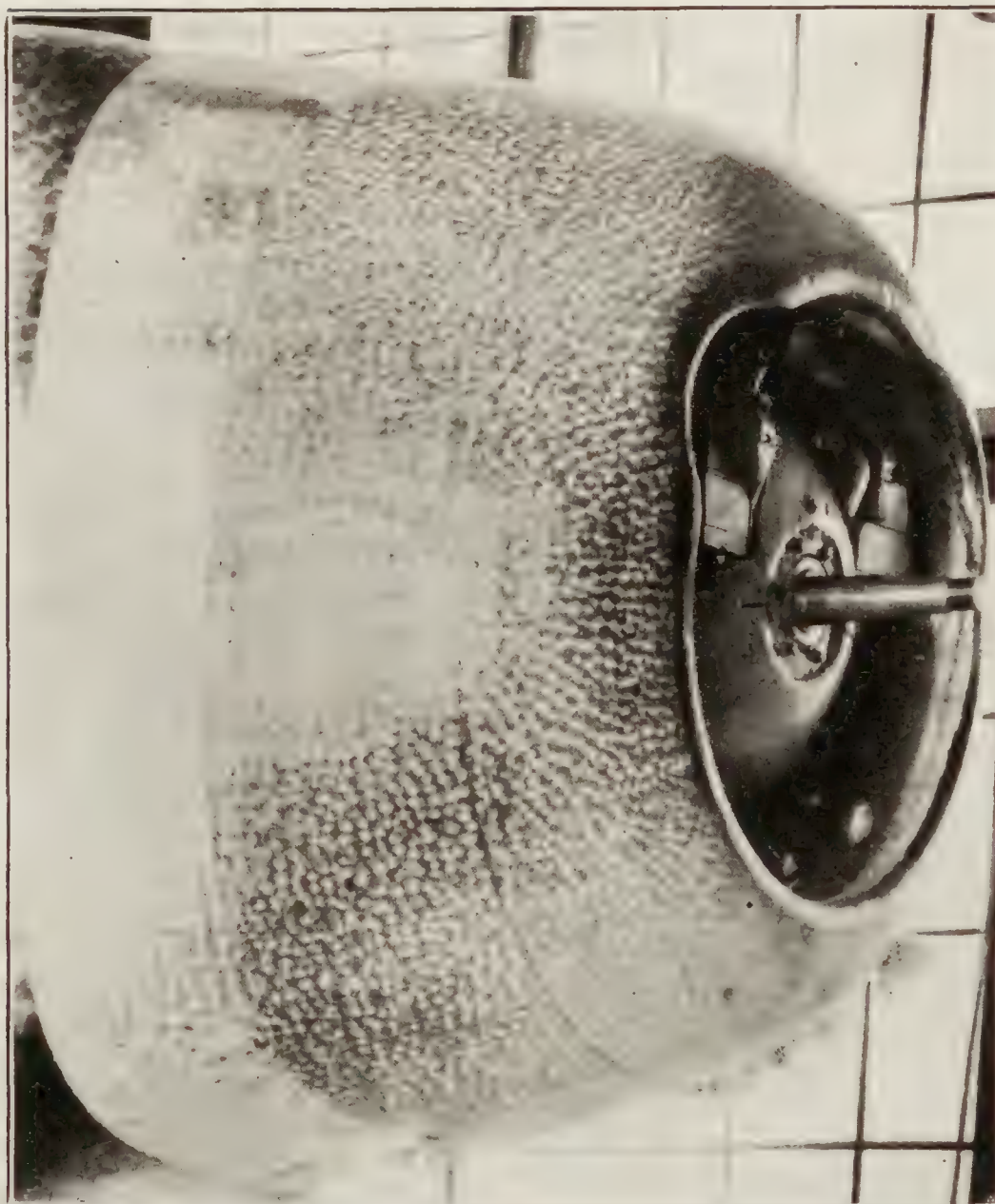


FIGURE 8.—Three-quarter side view of cowling No. 10

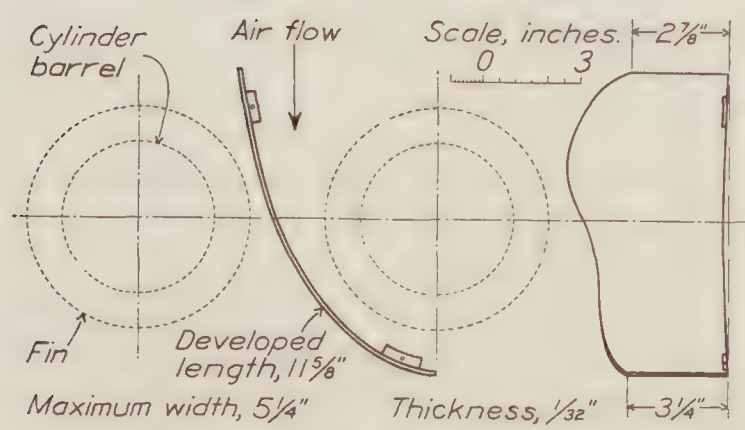


FIGURE 9.—Deflector used with cowling No. 10

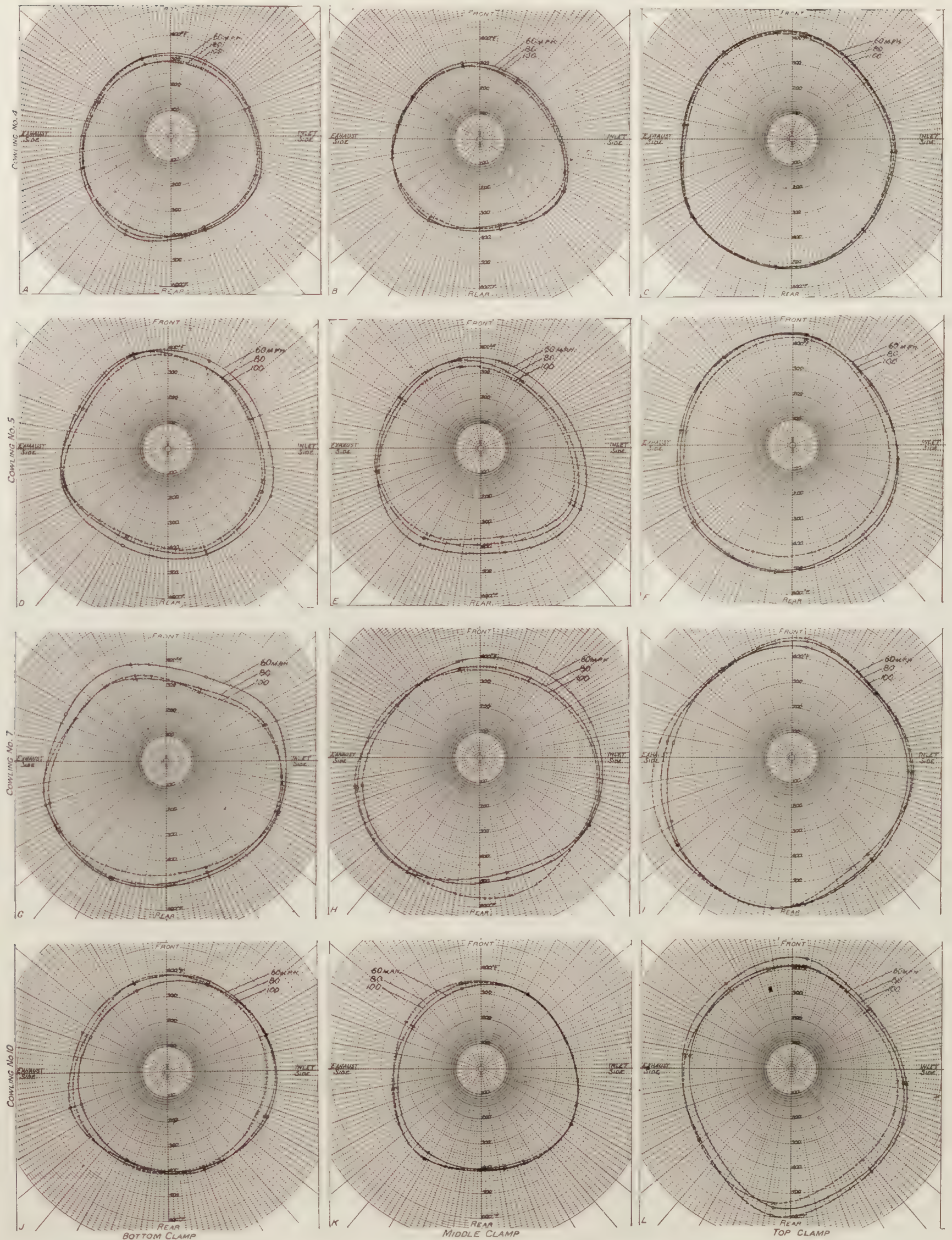


FIGURE 10.—Effect of air speed on cylinder barrel temperatures

In Figure 12 are presented the temperature measurements obtained on the front and rear spark-plug bosses. These temperatures are shown for each of the four cowlings tested at air speeds of approximately 60, 80, and 100 miles per hour. As these readings were taken on each cylinder, they are a good indication of engine performance.

The effect on cylinder barrel temperatures of slots in the nose of the cowling, so as to permit part of the cooling air to flow inside the cowling, is shown in Figure 13. These results are shown without slots and with four and six slots at air speeds of approximately 80 miles per hour. The tests without slots and with four slots were discontinued because of high temperatures.

Figure 14 shows the temperature variation obtained on Cylinder Number 1 for each of the four cowlings tested. These results are given for the front and rear spark-plug bosses and the top, middle, and bottom clamps, for air speeds of approximately 80 miles per hour.

Figure 15 presents information on the variation of power delivered to the propeller for each of the four cowlings for air speeds from approximately 60 to 100 miles per hour.

The distribution of temperatures over Cylinder Number 1 at an air speed of approximately 80 miles per hour is shown in Figure 16. The maximum and minimum temperatures for each clamp ring are also given in this figure.

DISCUSSION OF RESULTS—EFFECT OF COWLING ON CYLINDER TEMPERATURES

The manner in which an air-cooled engine is cowed greatly affects the cylinder temperatures. This effect is so large that a cylinder of indifferent design may, by a careful selection of cowling, operate more satisfactorily than a well-designed cylinder which is improperly cowed. The selection of a satisfactory cowling, however, is not dependent upon cooling alone, but also upon other factors, such as the drag, the propulsive efficiency, the service or type of airplane in which the engine is used, and whether it will be operating in a hot or cold climate.

The results of these tests indicate that if more than 35 per cent of the cooling area of a well-designed cylinder is cowed, the temperatures on the lower part of the cylinder barrel will be high. With Cowling Number 5, which covered 35 per cent of the cooling area of the cylinders, temperatures of 450° F. were obtained on the lower part of the barrel.

The curves in Figure 13 show the effect on cylinder barrel temperatures of increasing the amount of air flowing inside the cowling. These tests were conducted with Cowling Number 7. Temperatures greater than 600° F. were obtained on the lower part of the cylinders with this cowling, but by cutting six slots in the nose of the cowling these temperatures were reduced 270° F. in the front-lower part of the cylinder and 140° F. in the rear-lower part of the cylinder. The effect of these slots in reducing the barrel temperatures was greatest on the bottom of the barrel, but they also reduced the temperatures over 100° F. on the upper part of the barrel. Although these barrel temperatures were reduced considerably by the use of slots they are, nevertheless, excessive. The lowest barrel temperatures were obtained with Cowling Number 4. Cowlings Numbers 5 and 10 gave approximately the same barrel temperatures.

It is interesting to note that increasing the amount of cowling up to a certain limit reduces the spark-plug-boss temperatures. The curves in Figure 12 show that the rear-spark-plug-boss temperatures for Cowling Number 5, which covered 35 per cent of the cooling area, were lower than for Cowling Number 4, which did not cover any of the cooling area. This is due to the fact that with Cowling Number 5 more of the air is forced out to the head and past the upper part of the cylinders. The average temperatures for the rear spark-plug bosses on the seven hottest cylinders, at approximately 100 miles per hour, are 682, 675, 654, and 586° F. for Cowlings Numbers 4, 7, 10, and 5, respectively. From this it must be concluded that the degree to which an engine can be cowed is determined, not from spark-plug-boss temperatures, but from barrel temperatures; and, furthermore, that spark-plug-boss temperatures alone do not offer sufficient information on which to base any reliable conclusions.

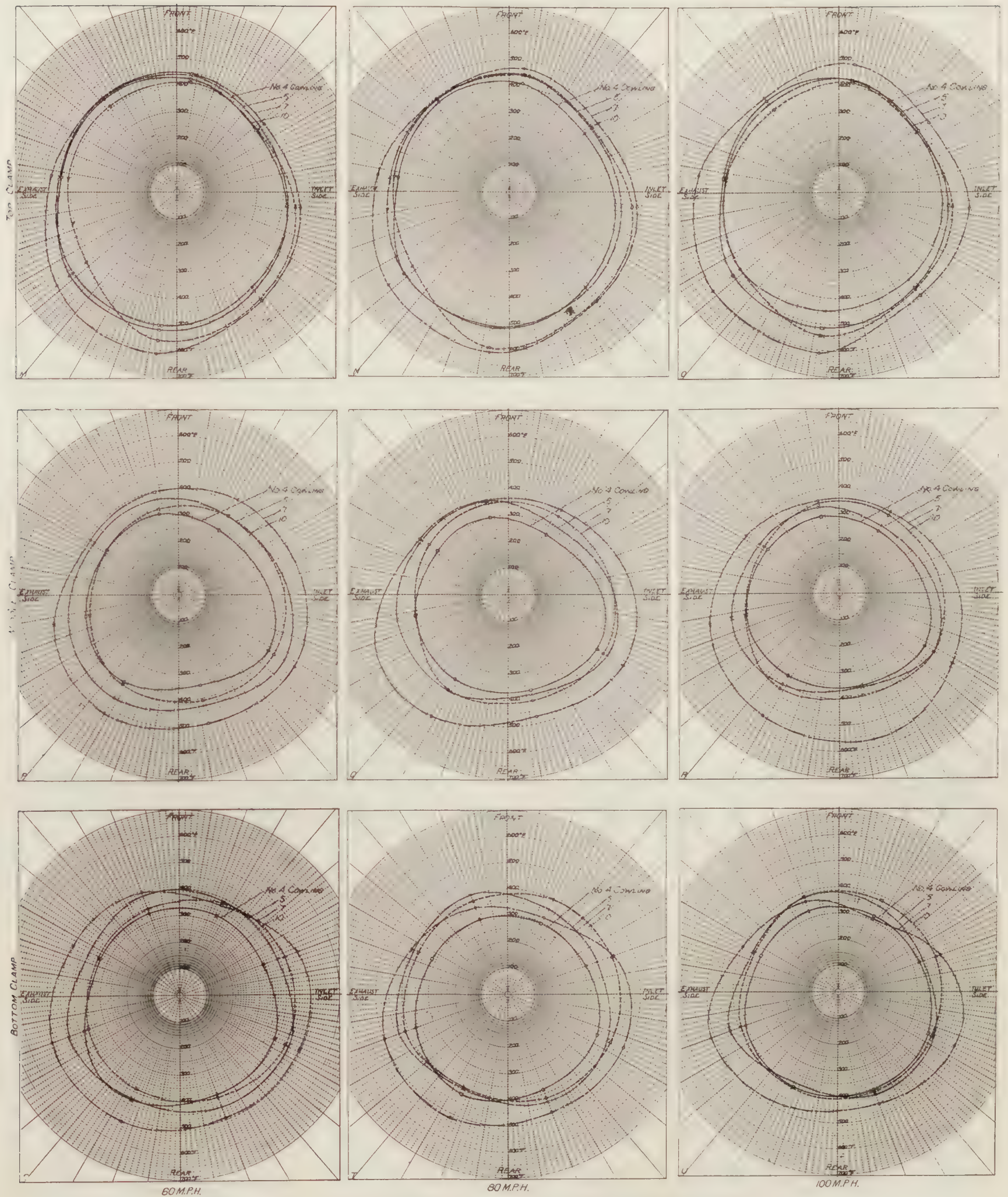


FIGURE 11.—Cylinder barrel temperatures obtained with four different cowlings

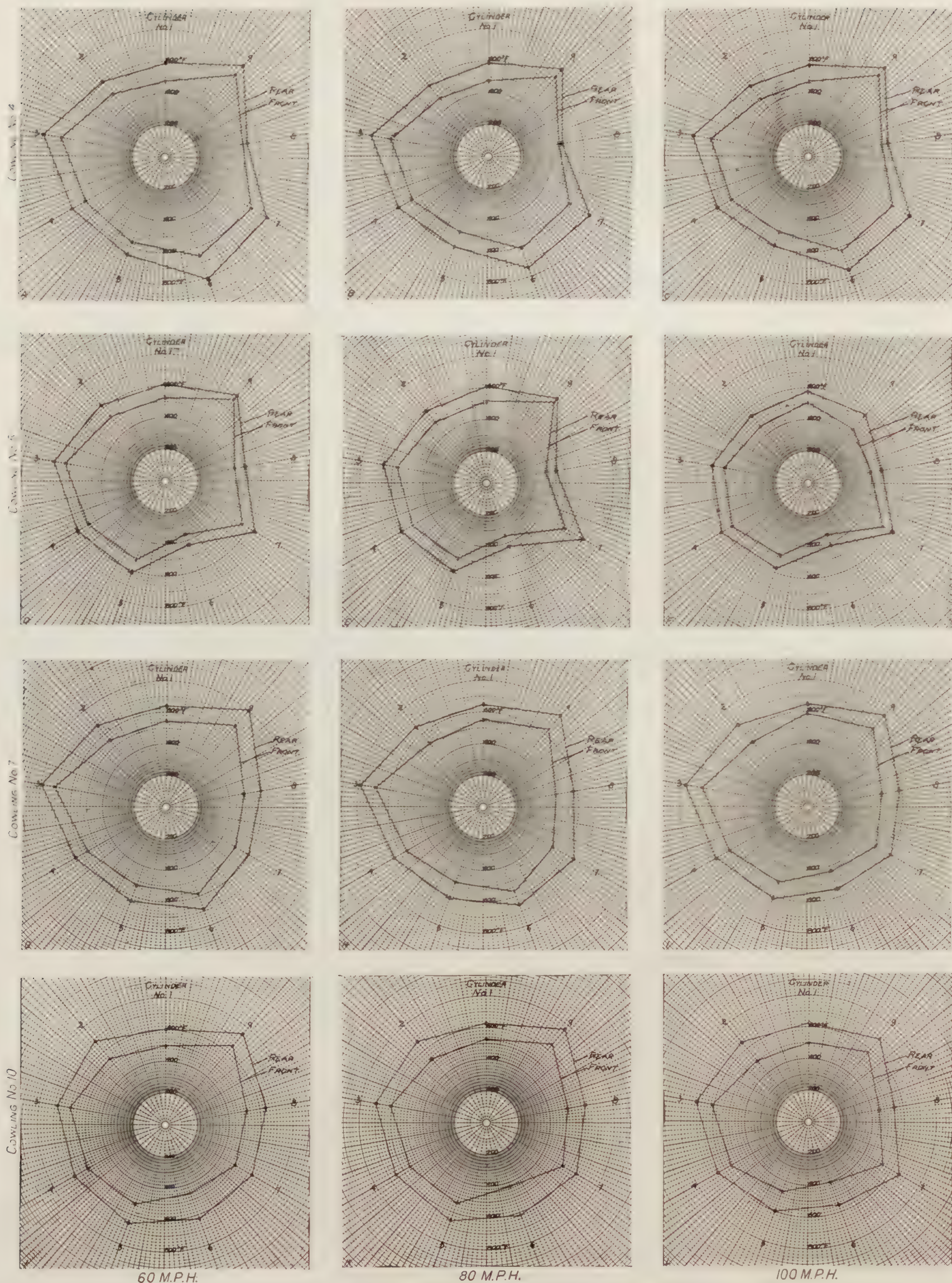
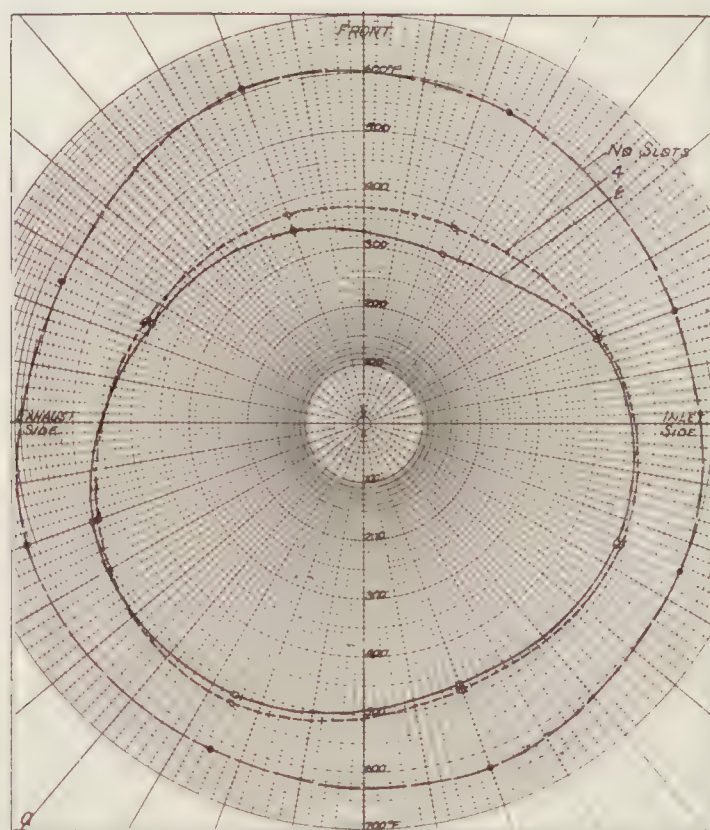
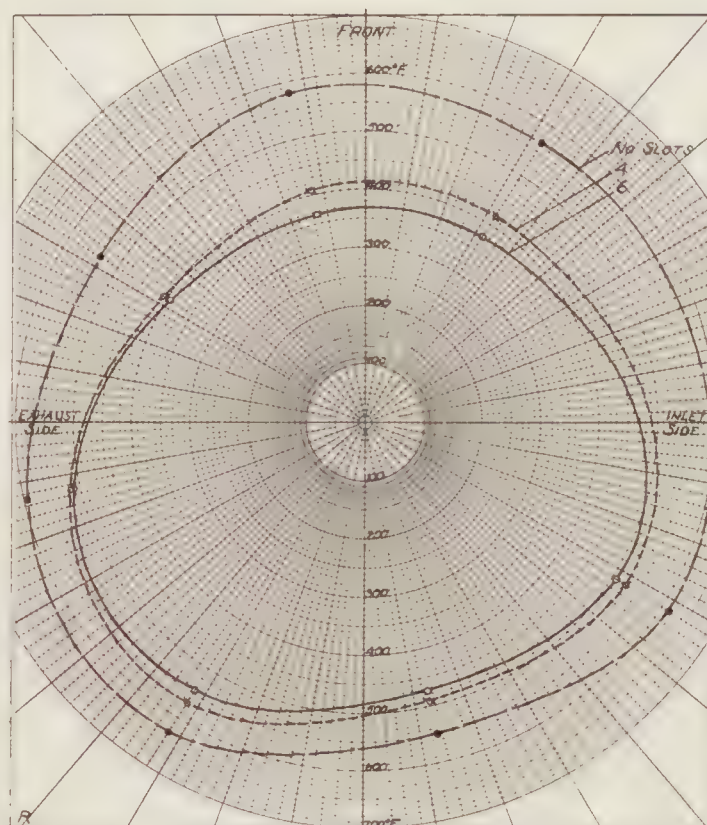


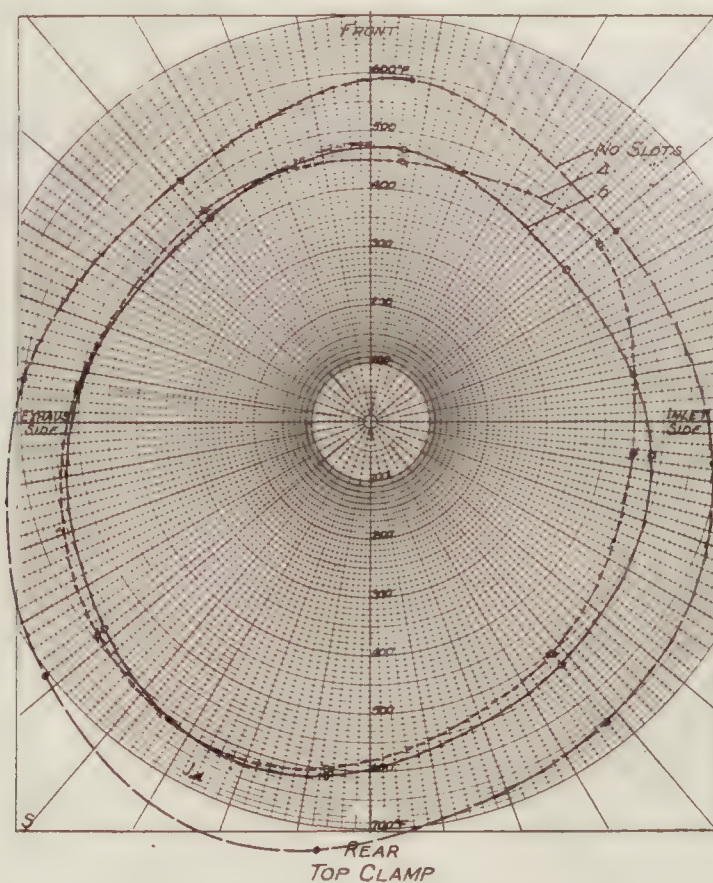
FIGURE 12.—Effect of cowling and air speed on spark-plug-boss temperatures



REAR
BOTTOM CLAMP



REAR
MIDDLE CLAMP



REAR
TOP CLAMP

FIGURE 13.—Effect of slots in nose of cowling No. 7 on cylinder-barrel temperatures at 80 miles per hour
104397—30—42

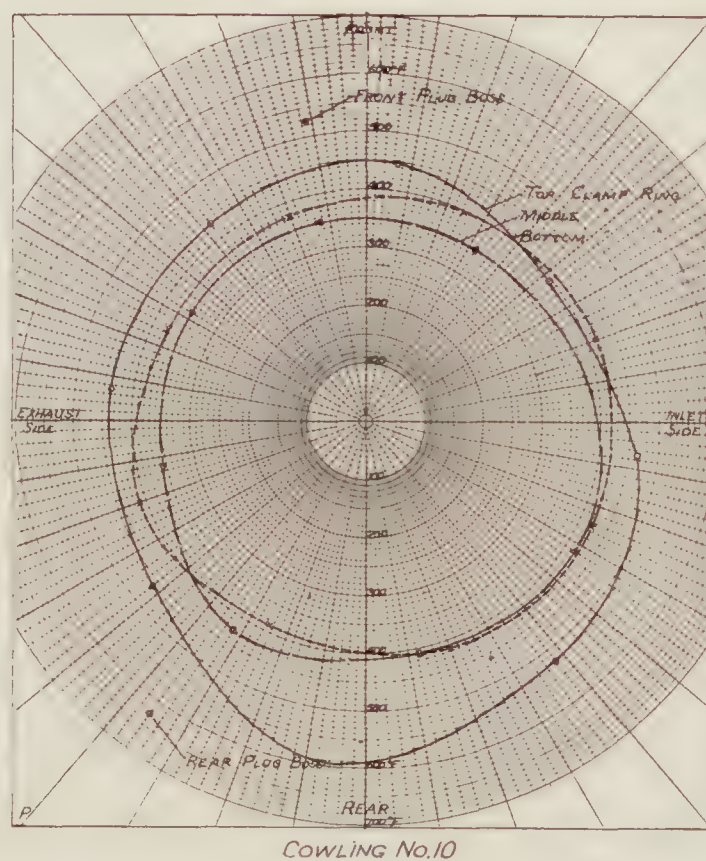
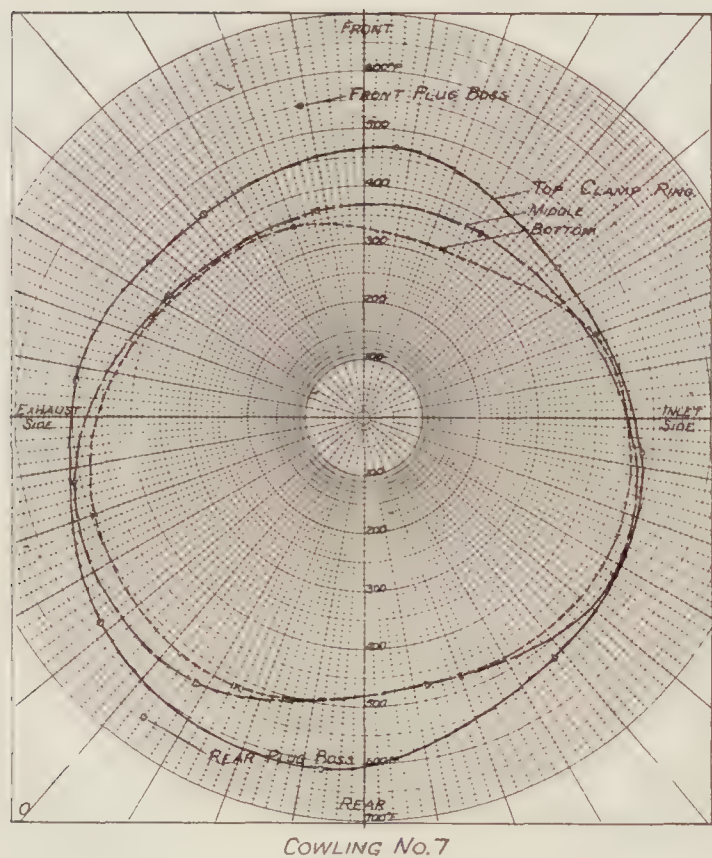
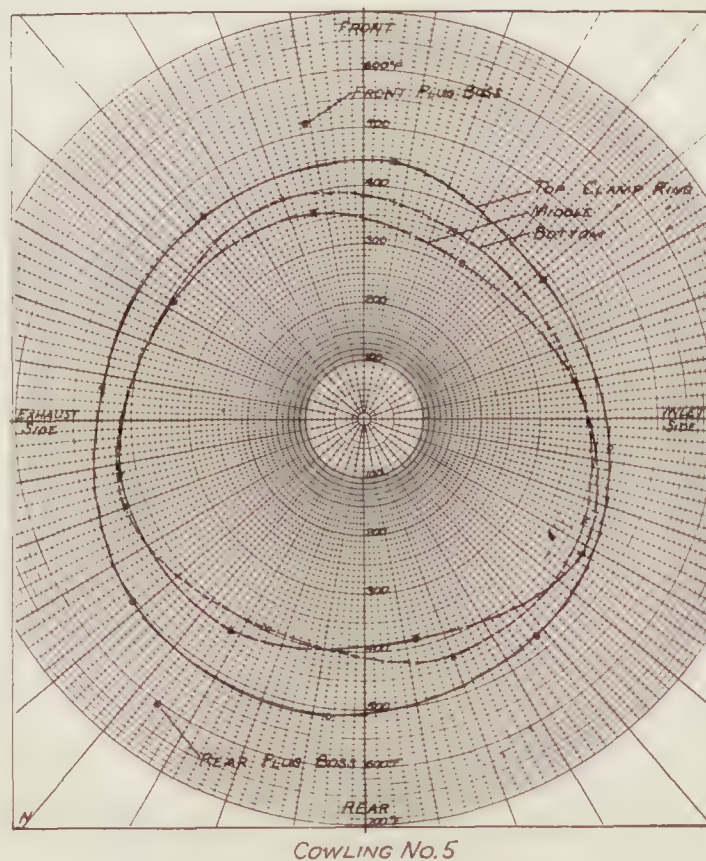
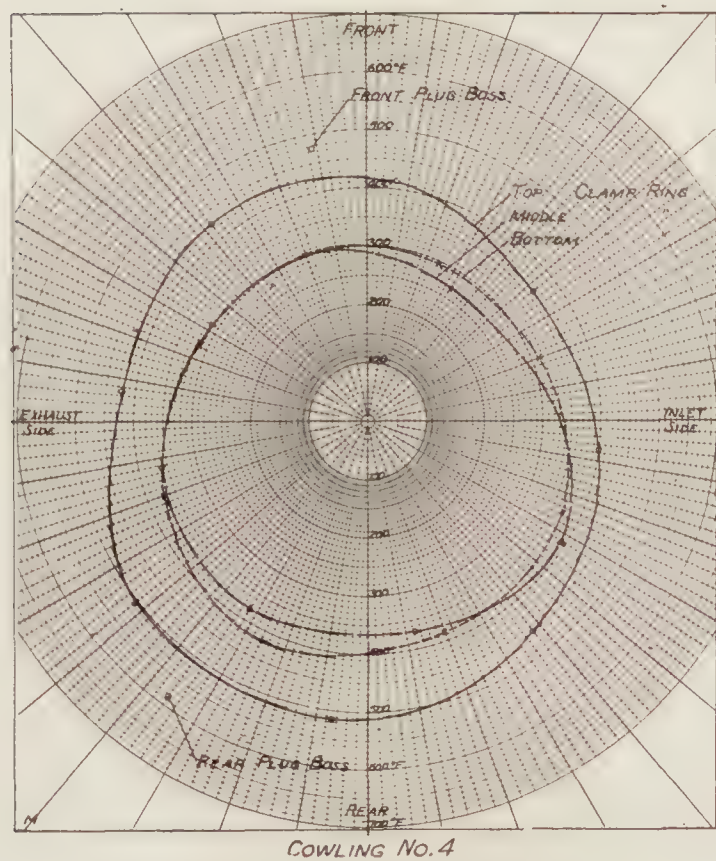


FIGURE 14.—Temperature distribution obtained on cylinder No. 1 at 80 miles per hour

The mean cylinder-head temperatures on the five hottest cylinders, at approximately 100 miles per hour, are 608, 604, 581, and 533° F. for Cowlings Numbers 7, 4, 10, and 5. These head temperatures, like spark-plug-boss temperatures, are no indication as to the amount an engine can be cowled, because the head temperatures decrease with increase in cowling, more of the cooling air being forced out to the head. If the amount of cowling on the lower part of the cylinder barrel is increased, the temperatures on this part of the cylinder will have exceeded the permissible limit long before the cylinder-head temperatures are as high as for an engine with no cowling. If the amount of cowling on the upper part of the cylinder is increased, the head temperatures will increase unless the cowling, like Number 10, is shaped so that the air can flow around the cylinder head.

The results of drag tests with a cabin fuselage, as reported in N. A. C. A. Technical Report Number 313, showed that Cowlings Numbers 5, 7, and 10 gave a reduction in drag of 4.8, 11.2, and 40 per cent, respectively, as compared with Cowling Number 4.

Information on the temperature distribution obtained with each cowling on Cylinder Number 1 at air speeds of 80 miles per hour is presented in Figures 14 and 16. These curves show that for all but Cowling Number 7 lower temperatures were obtained on the middle part of the cylinder than on the bottom. The temperature difference between the top and bottom of the cylinder varies from approximately 50° F. with Cowling Number 5 to over 150° F. with Cowlings Numbers 4 and 10. The circumferential temperature difference is surprisingly large, varying from about 75° F. on the bottom clamp with Cowlings Numbers 5 and 10 to about 200° F. on the top clamp with Cowlings Numbers 7 and 10. The high temperatures obtained in the rear of Cylinder Number 1 with Cowling Number 10 as shown in Figure 14 might be reduced by slight modification in the cowling.

It is interesting to note that for all cowlings except Number 10, in which air deflectors were used, the temperatures on the inlet side of the cylinder were lower than on the exhaust side. Considerably higher temperatures were obtained in tests without these deflectors. The flight tests that have been conducted with this cowling have also shown that the deflectors improve the cooling.

EFFECT OF AIR SPEED ON CYLINDER TEMPERATURES AND PERFORMANCE

The amount of cooling obtained with a given design of air-cooled engine is dependent principally upon the mass flow of air past the cylinders. In flight the amount of cooling air past the cylinders may be increased by increasing the speed of the airplane. However, this does not always result in reduced temperatures, because the power will have to be increased, except in a dive, to effect the increase in air speed. With an increase in power there is a proportional increase in the quantity of heat to be dissipated.

The relation between the air speed and the power developed at full throttle for each cowling is shown by the curves in Figure 15. It may be noted that an increase in air speed of 40 miles per hour results in an increase of approximately 30 horsepower in the power developed for each cowling, because of the higher engine speed.

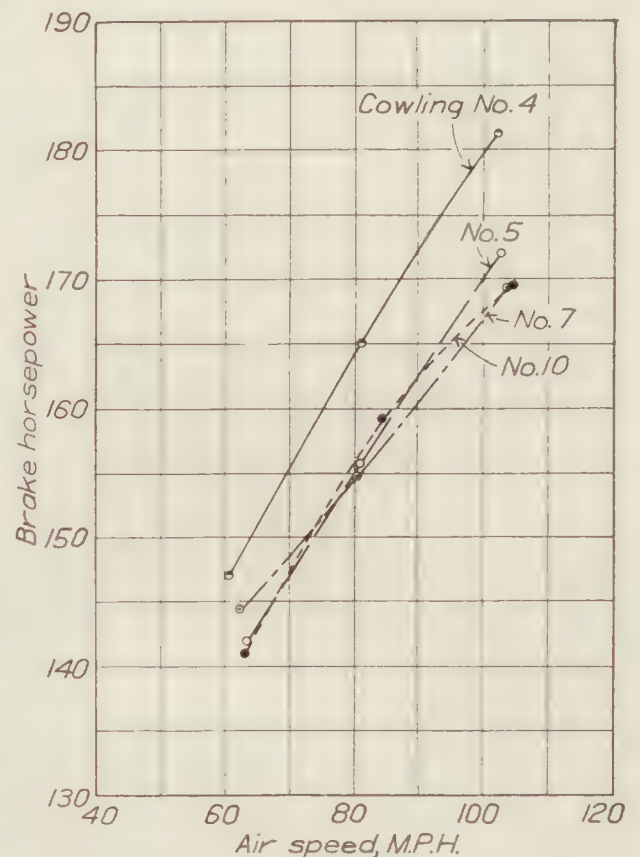


FIGURE 15.—The effect of cowling on the brake horsepower developed

Even though Cylinder Number 8 was not functioning properly, as the curves in Figure 12 indicate, considerably more power was developed with Cowling Number 4 than with any of the other cowlings. A cracked rocker-arm housing, discovered on Cylinder Number 8 at the end of the run with Cowling Number 4, was replaced at this time. The curves in Figure 12 for Cowling Number 5 show that Cylinders Numbers 6 and 8 were not developing their full power, or the temperatures would have been higher. The high temperatures obtained on Cylinder Number 6 during tests on Cowling Number 4 may have warped the valves, and it is possible that the valves in Cylinder Number 8 may also have been warped. As the engine had been completely overhauled between the tests on Cowlings Numbers 5 and 7, and since the cylinder temperatures indicate that all cylinders were functioning properly, the low powers with Cowlings Numbers 7 and 10 are probably due to high temperatures and detonation.

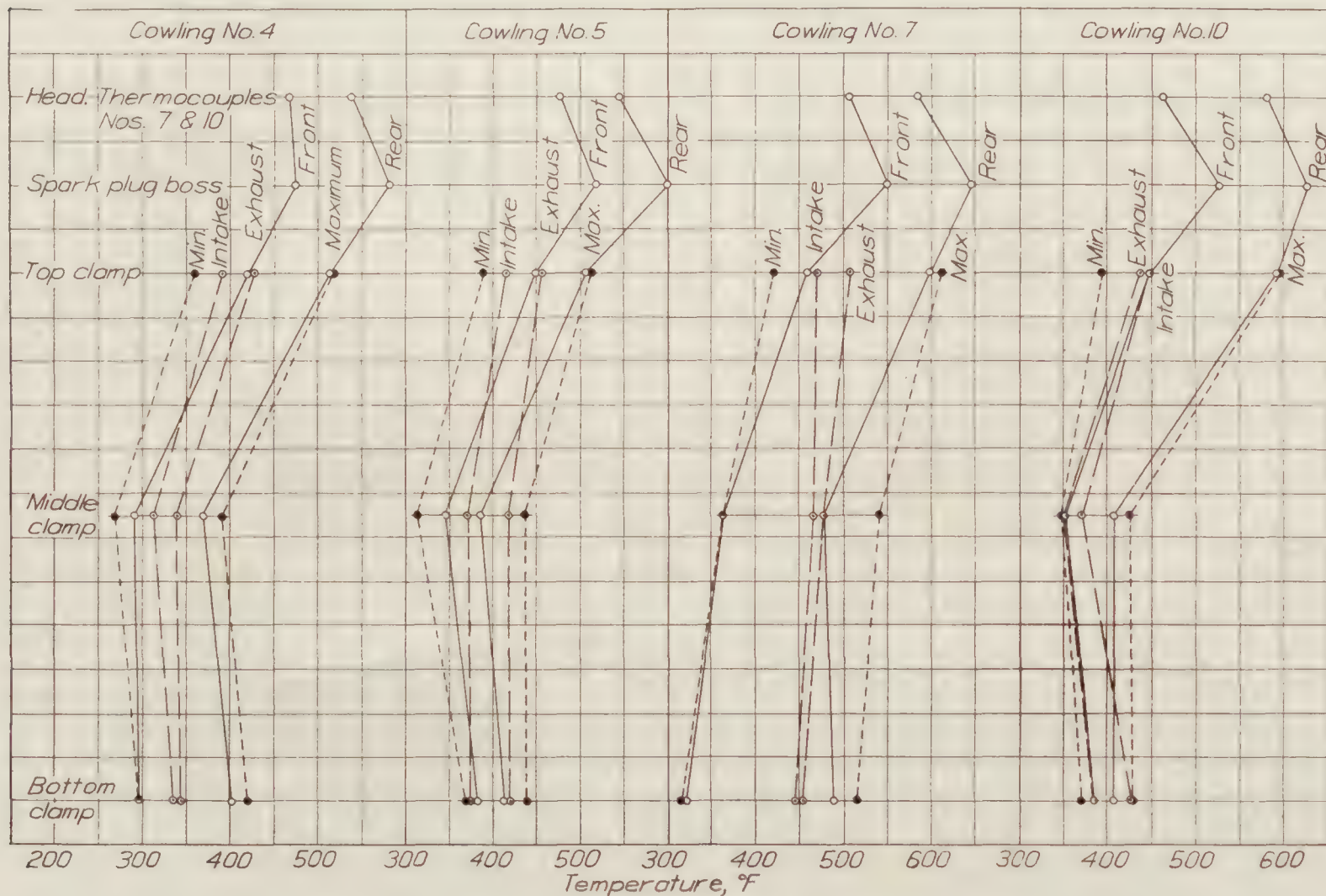


FIGURE 16.—Temperature distribution on cylinder No. 1 at 80 miles per hour

As the range of air speeds investigated in these full throttle tests was small compared to the range of air speeds obtained in climb and level flight even on a transport-type airplane, and since to effect an increase in air speed would require an increase in power, it is reasonable to expect that for these tests the one would very nearly offset the other and the temperature variation with change in air speed would be small. This is substantiated by the experimental evidence presented in the curves in Figures 10 and 12. The conditions for these tests were the same as a full throttle climb, the most severe conditions under which an air-cooled engine can operate.

Although the cylinder-barrel temperatures for Cowlings Numbers 4 and 5 (fig. 10) show very little effect, due to change in air speed, there is, however, sufficient variation to show that at approximately 60 miles per hour the temperatures are higher than for 80 or 100 miles per hour. The results obtained for Cowlings Numbers 7 and 10 do not show such consistent variation in barrel temperature with change in air speed.

By increasing the air speed from approximately 60 to 100 miles per hour the average rear-spark-plug-boss temperatures were reduced 25° to 50° F. for each cowlings.

The cylinder-head temperatures for Cowlings Numbers 4 and 7 do not show a consistent variation with change in air speed. These temperatures show a reduction with increase in air speed for Cowlings Numbers 5 and 10. That this is true for Cowling Number 10 has been further verified by the fact that all airplanes of reasonably high speed have experienced no difficulty in cooling with this type of cowling.

That there is no change in the shape of these curves with change in air speed indicates that the directional flow of air is very nearly the same for each speed.

DISCUSSION OF TEST CONDITIONS

The maximum cylinder temperatures obtained during these full-throttle tests are higher than the maximum of 550° F. recommended by Heron for satisfactory operation. (Reference 6.) As these tests were conducted at full throttle on an engine of 5.4 compression ratio, using domestic aviation gasoline, and at high air stream temperatures, it is reasonable to believe that all cylinder temperatures were aggravated by detonation. Tests have shown that increasing the compression ratio up to the point where detonation starts reduces the temperatures, but that further increase so as to obtain detonation may cause a rise in cylinder-head temperatures of over 100° F. (Reference 6.) Recent tests completed by the Navy on an air-cooled engine of 5.16 compression ratio showed that when the amount of ethyl fluid in the fuel was decreased to 1½ cubic centimeters per gallon lower power and higher cylinder temperatures resulted because of detonation. (Reference 7.)

The error involved in making cylinder temperature measurements was small. Accurate measurements of these temperatures were obtained by assuring good thermal contact and by using small thermocouple wire and fairing it along the cylinder for some distance from the hot junction so that no heat would be conducted from the hot junction. High resistance pyrometers were used so as to reduce to a minimum the effect that any change in resistance of long leads might have on the readings. The pyrometers were calibrated with the same leads used in the tests, and the cold junction correction was applied to all readings.

CONCLUSIONS

The results of these tests indicate that not over 35 per cent of the cooling area of the cylinders of a Wright series J-5 engine should be cowled without permitting part of the cooling air to flow inside the cowling. With 73 per cent of the cooling area cowled barrel temperatures will be excessive, even though large slots are provided so that part of the cooling air may flow inside the cowling.

An increase in air speed from approximately 60 to 100 miles per hour, at full-throttle propeller loads, resulted in only a slight decrease in cylinder temperatures.

The spark-plug-boss temperatures alone should not be used as a criterion of engine cowling, but, instead, readings should be taken on several points on the barrel if the lower part of the cylinder is cowled and on several points on the head if the cowling completely incloses the engine.

Cowling Number 10, at 100 miles per hour, effects a 40 per cent reduction in drag as compared with the uncowled engine. The mean cylinder-head temperatures obtained with this cowling were less than those obtained with no cowling, but the barrel temperatures were slightly higher. It is believed that the cylinder-head temperatures could be further reduced by slight modifications in this cowling, and it is also believed that the power loss of approximately 7 per cent indicated with Cowling Number 10 would not be present at the higher air speeds obtained in flight.

LANGLEY MEMORIAL AERONAUTICAL LABORATORY,
NATIONAL ADVISORY COMMITTEE FOR AERONAUTICS,
LANGLEY FIELD, VA., *May 2, 1929.*

REFERENCES AND BIBLIOGRAPHY

- Reference 1. Aviation, March 23, 1929, xxvi, 12, 898.
- Reference 2. Cooling of air-cooled engines by forced circulation of air. N. A. C. A. Technical Memorandum No. 385, 1926.
- Reference 3. Weick, Fred E.: Drag and cooling with various forms of cowling for a "Whirlwind" radial air-cooled engine. N. A. C. A. Technical Report No. 313, Part I, 1928.
- Reference 4. Weick, Fred E.: Drag and cooling with various forms of cowling for a "Whirlwind" radial air-cooled engine. N. A. C. A. Technical Report No. 314, Part II, 1928.
- Reference 5. Weick, Fred E., and Donald H. Wood: The 20-foot propeller research tunnel of the National Advisory Committee for Aeronautics. N. A. C. A. Technical Report No. 300, 1928.
- Reference 6. Heron, S. D.: Air-cooled cylinder design and development. Trans. Soc. Auto. Eng., 1922, xvii, Part I, 347-430.
- Reference 7. Ballard, J. D.: Test of Pratt and Whitney Model R-1300 engine and investigation of relation between exhaust flame temperatures and air fuel mixture ratios on aircraft engines. Report by Bureau of Aeronautics, U. S. Navy Department, 1928, Serial No. AEL-207.
- Gibson, A. H.: Exhaust and cylinder head temperatures in high-speed petrol engines. Proc. Inst. Mech. Eng., 1923, ii, 4-6, 1045-1091.
- Eade, W. F.: Investigation of heat distribution on J-5 cylinders. Report by Bureau of Aeronautics, U. S. Navy Department, 1927, Serial No. AEL-195.

TABLE I

CYLINDER HEAD, BARREL, AND FIN TEMPERATURES (DEGREES FAHRENHEIT) OBTAINED
IN COWLING TESTS ON A WRIGHT J-5 ENGINE

No.	Location of thermocouple [NOTE.—Right and left are looking front from the cockpit]	Cowling No. 4				Cowling No. 5			Cowling No. 7				Cowling No. 10		
		Air speeds, M. P. H.				Air speeds, M. P. H.			Air speeds, M. P. H.				Air speeds, M. P. H.		
		22	60	80	100	60	80	100	180	60	80	100	60	80	100
1	Cylinder No. 1, fin tip, left side of inlet passage.....	360	346	330	335	346	462	315	430	371	368	353	367	365	353
2	Cylinder No. 1, center of head, top of exhaust passage.....	532	512	507	500	502	494	478	530	510	511	507	535	542	541
3	Cylinder No. 1, fin tip, rear of exhaust passage.....	500	495	480	483	481	447	450	498	469	461	458	522	536	518
4	Cylinder No. 1, on front side of exhaust valve guide.....	450	445	432	438	420	405	402	431	425	414	422	442	458	443
5	Cylinder No. 1, near fin tip, front of exhaust passage.....	420	390	363	372	369	343	325	388	382	370	368	395	400	382
6	Cylinder No. 1, front side of inlet valve guide.....	242	236	218	220	233	210	201	275	248	229	225	232	233	214
7	Cylinder No. 1, in center of head over front spark plug.....	489	475	468	454	487	478	460	588	492	509	488	475	463	473
8	Cylinder No. 1, front of head, side of exhaust passage.....	475	459	447	441	458	440	425	481	461	462	458	470	475	470
9	Cylinder No. 1, rear of head in side of exhaust passage.....	532	522	512	510	520	508	490	563	527	525	520	556	578	570
10	Cylinder No. 1, in center of head over rear spark plug.....	565	538	538	527	555	545	519	660	579	585	573	562	580	563
11	Cylinder No. 1, in left side of rear spark-plug boss.....	600	588	583	573	608	602	575	739	637	646	644	600	628	622
12	Cylinder No. 1, in left side of front spark-plug boss.....	514	475	475	470	522	519	507	638	541	550	585	497	528	498
13	Cylinder No. 1, fin tip, left of front spark-plug boss.....	422	408	398	408	428	444	425	566	440	470	489	394	430	418
14	Cylinder No. 1, under top clamp ring, right, rear.....	490	471	460	459	455	473	420	655	519	528	493	510	523	463
15	Cylinder No. 1, under top clamp ring, right.....	442	418	400	411	420	423	390	590	469	482	490	450	464	428
16	Cylinder No. 1, under top clamp ring, right, front.....	400	379	360	377	397	390	370	531	415	422	425	381	395	368
17	Cylinder No. 1, under top clamp ring, front.....	442	428	413	422	441	444	427	591	448	470	484	414	448	417
18	Cylinder No. 1, under top clamp ring, left, front.....	464	443	430	439	449	443	422	538	450	445	452	409	431	396
19	Cylinder No. 1, under top clamp ring, left.....	440	438	422	435	442	453	429	600	477	500	530	410	438	428
20	Cylinder No. 1, under top clamp ring, left, rear.....	528	510	504	505	495	505	469	708	572	578	601	430	462	470
21	Cylinder No. 1, under top clamp ring, rear.....	547	522	517	515	507	512	450	741	612	612	610	561	595	544
22	Cylinder No. 1, center of fin 18, in the rear.....	498	477	472	473	450	443	392	683	558	558	530	498	529	475
23	Cylinder No. 1, tip of fin 18, in the rear.....	477	461	460	453	449	428	388	660	538	548	518	469	485	432
24	Cylinder No. 1, tip of fin 18, on left side.....	412	411	400	395	401	416	370	518	393	433	450	367	401	361
25	Cylinder No. 1, center of fin 18, on left side.....	455	450	440	429	482	480	450	609	502	531	563	457	475	476
26	Cylinder No. 1, under middle clamp, rear.....	370	350	370	359	429	388	365	550	498	473	569	409	410	397
27	Cylinder No. 1, under middle clamp, right, rear.....	398	399	391	378	468	438	420	614	513	508	500	422	420	419
28	Cylinder No. 1, under middle clamp, right.....								550	335	245	310			
29	Cylinder No. 1, under middle clamp, right, front.....	280	289	269	279	350	314	300	567	421	376	362	351	350	348
30	Cylinder No. 1, center of fin 11, front.....	233	258	241	230	291	283	260	520	325	291	273	265	281	273
31	Cylinder No. 1, tip of fin 11, front.....	174	205	185	180	232	216	200	440	279	227	208	207	218	210
32	Cylinder No. 1, under middle clamp, front.....	302	312	300	298	368	361	335	580	397	366	358	330	353	349
33	Cylinder No. 1, under middle clamp, left, front.....	298	318	312	317	372	385	353	535	390	394	412	318	352	333
34	Cylinder No. 1, center of fin 11, on left side.....	233	252	241	249	310	310	293	488	375	404	362	449	251	244
35	Cylinder No. 1, under middle clamp, left.....	338	360	360	360	428	430	419	595	482	511	502	342	357	362
36	Cylinder No. 1, tip of fin 11, on left side.....	181	206	195	207	240	250	242	403	330	335	297	203	228	209
37	Cylinder No. 1, under middle clamp, left, rear.....	401	387	379	368	458	428	408	630	528	543	545	398	427	425
38	Cylinder No. 1, under bottom clamp, rear, to right.....	382	399	385	396	449	434	418	630	493	477	453	410	418	405
39	Cylinder No. 1, under bottom clamp, right, to rear.....	393	391	370	379	451	414	402	600	494	480	488	439	426	394
40	Cylinder No. 1, under bottom clamp, right, to front.....	330	333	313	328	390	359	343	568	470	425	411	420	419	393
41	Cylinder No. 1, under bottom clamp, front, to right.....	322	330	296	318	389	358	360	590	373	320	305	381	399	383
42	Cylinder No. 1, tip of fin 1, front.....	232	255	224	242	323	314	303	556	315	248	242	289	319	330
43	Cylinder No. 1, under bottom clamp, front, to left.....	309	330	302	328	398	403	383	608	412	350	365	347	377	383
44	Cylinder No. 1, under bottom clamp, left, to front.....	303	330	315	324	378	391	360	572	443	400	401	337	372	353
45	Cylinder No. 1, tip of fin 1, left.....	249	268	250	262	320	318	306	514	435	380	363	264	318	280
46	Cylinder No. 1, under bottom clamp, left, to rear.....	368	382	370	371	447	438	437	618	512	496	512	367	412	392
47	Cylinder No. 1, under bottom clamp, rear, to left.....	412	433	418	398	428	395	382	620	523	517	479	388	390	403
48	Cylinder No. 2, in left side of front spark-plug boss.....	531	512	477	468	529	496	461	568	549	521	532	540	528	500
49	Cylinder No. 2, in left side of rear spark-plug boss.....	613	610	580	572	620	587	551	695	671	657	673	681	668	650
50	Cylinder No. 2, in center of head, over rear spark plug.....	568	550	521	519	555	525	496	603	578	549	558	640	650	617
51	Cylinder No. 3, in left side of front spark-plug boss.....	641	659	620	617	630	579	531	665	708	687	665	600	608	610
52	Cylinder No. 3, in left side of rear spark-plug boss.....	750	777	742	733	701	660	611	770	790	788	779	682	701	710
53	Cylinder No. 3, in center of head, over rear spark plug.....	631	737	692	661	638	614	549	717	733	725	682			
54	Cylinder No. 4, in left side of front spark-plug boss.....	598	568	549	550	551	538	548	627	566	558	560	556	554	553
55	Cylinder No. 4, in left side of rear spark-plug boss.....	682	662	643	650	627	615	623	700	651	647	659	650	658	649
56	Cylinder No. 4, in center of head, over rear spark plug.....	632	607	589	590	578	560	569	645	583	572	570			569
57	Cylinder No. 5, in left side of front spark-plug boss.....	571	571	502	502	528	508	487	520	528	507	509	530	539	468
58	Cylinder No. 5, in left side of rear spark-plug boss.....	665	656	603	595	616	590	570	625	633	612	618	659	653	599
59	Cylinder No. 5, in center of head, over rear spark plug.....	599	598	545	550	560	542	530	565	588	552	565	612	610	558
60	Cylinder No. 6, in left side of front spark-plug boss.....	639	655	612	622	360	351	347	378	582	563	431	455	428	404
61	Cylinder No. 6, in left side of rear spark-plug boss.....	759	812	742	757	426	421	418	465	685	658	548	625	616	558
62	Cylinder No. 6, in center of head, over rear spark plug.....	704	731	674	693	399	390	382	424	703	682	576	662	657	590
63	Cylinder No. 7, in left side of front spark-plug boss.....	610	628	588	607	551	572	541	587	500	502	496	502	549	535
64	Cylinder No. 7, in left side of rear spark-plug boss.....	732	743	733	735	641	702	615	728	597	655	601	626	642	657
65	Cylinder No. 8, in left side of front spark-plug boss.....	492	497	448	463	440	383	400	465	496	465	471	517	517	449
66	Cylinder No. 8, in left side of rear spark-plug boss.....	481	525	466	503	508	447	468	550	602	579	583	637	628	545
67	Cylinder No. 8, in center of head over rear spark plug.....	393	458	371	435	438	393	402	481	473	483	472	428	438	488
68	Cylinder No. 9, in left side of front spark-plug boss.....	668	680	651	668	669	661	440	673	673	640	640	650	644	577
69	Cylinder No. 9, in left side of rear spark-plug boss.....	750	758	718	730	700	695	560	756	801	759	750	750	768	688

¹ Cowling No. 7 without vents.

TABLE II

PERFORMANCE MEASUREMENTS ON A WRIGHT J-5 ENGINE WITH DIFFERENT COWLINGS

	Read- ing No.	Air speed, m. p. h.	Engine speed, r. p. m.	Brake horse- power	Fuel con- sump- tion, pounds per brake horse- power per hour	Barome- ter, inches of Hg.	Carbu- retor air tempera- ture, °F.	Oil-in tempera- ture, °F.	Oil-out tempera- ture, °F.	Air- stream tempera- ture, °F.
Cowling No. 4-----	1	81.4	1,705	170.5	0.677	29.90	76	129	129	82.2
	2	81.7	1,700	169.0	.696	29.90	75	133	133	82.8
	3	81.2	1,690	166.2	.681	29.90	76	139	138	83.5
	4	81.0	1,685	164.9	.720	29.91	76	145	143	84.2
	5	101.8	1,815	183.4	.648	29.80	88	151	149	86.0
	6	102.2	1,810	182.7	.651	29.80	88	151	151	87.0
	7	102.2	1,810	183.8	.650	29.80	90	153	152	87.8
	8	102.3	1,800	181.3	.669	29.80	94	158	156	88.2
	9	63.8	1,605	150.0	.748	30.00	78	158	156	88.0
	10	59.8	1,590	148.3	.749	30.00	77	158	157	87.8
	11	60.6	1,580	147.0	.749	30.00	77	161	160	87.8
	12	60.7	1,580	147.0	.749	30.00	77	166	163	87.8
Cowling No. 5-----	1	79.8	1,690	173.2	.686	30.25	-----	126	124	80.6
	2	80.6	1,645	158.8	.733	30.05	-----	134	132	80.6
	3	81.0	1,640	155.7	.727	30.05	-----	139	138	84.2
	4	81.0	1,640	155.7	-----	30.05	-----	144	143	84.2
	5	103.1	1,795	179.5	.661	29.97	-----	150	146	86.0
	6	103.0	1,790	176.3	.674	29.97	-----	153	151	86.0
	7	102.6	1,790	175.7	.644	29.97	-----	-----	-----	87.8
	8	102.6	1,780	172.3	-----	29.97	-----	-----	-----	87.8
	9	65.5	1,625	159.7	-----	30.13	-----	153	153	87.8
	10	61.8	1,560	141.8	-----	30.17	-----	163	158	87.8
	11	63.8	1,560	141.8	-----	30.17	-----	155	153	87.8
Cowling No. 7-----	1	80.6	1,700	175.7	.690	30.13	74	118	122	80.6
	2	80.7	1,650	159.4	.710	30.13	74	135	136	82.4
	3	80.3	1,625	154.8	-----	30.13	74	144	145	82.4
	4	104.0	1,805	186.4	.650	30.01	84	150	151	84.2
	5	104.3	1,790	177.3	.646	30.01	85	150	152	86.0
	6	103.7	1,760	169.4	-----	30.01	87	154	155	86.0
	7	64.0	1,680	181.5	.635	30.20	80	150	148	86.0
	8	62.0	1,590	153.5	.730	30.20	77	150	150	86.0
	9	62.5	1,560	144.4	-----	30.20	77	156	158	86.0
Cowling No. 10-----	1	85.1	1,730	183.9	-----	29.92	84	123	125	87.8
	2	84.3	1,675	159.2	.704	29.92	82	132	133	87.8
	3	63.6	1,700	187.0	.635	29.80	72	-----	142	78.8
	4	66.5	1,620	158.9	.699	29.80	69	-----	145	78.8
	5	63.2	1,580	141.0	-----	29.80	69	-----	148	78.8
	6	105.4	1,840	197.0	.616	29.60	80	-----	153	80.6
	7	104.6	1,790	177.9	.655	29.60	78	-----	153	80.6
	8	104.5	1,760	169.0	.665	29.61	77	-----	157	82.4

REPORT No. 333

**FULL-SCALE TURNING CHARACTERISTICS OF
THE U. S. S. LOS ANGELES**

By F. L. THOMPSON
Langley Memorial Aeronautical Laboratory

REPORT No. 333

FULL-SCALE TURNING CHARACTERISTICS OF THE U. S. S. LOS ANGELES

By F. L. THOMPSON

SUMMARY

This paper presents a description of the method employed and results obtained in full-scale turning trials on the rigid airship U. S. S. "Los Angeles." This investigation was requested by the Bureau of Aeronautics, Navy Department, and was carried out in conjunction with pressure distribution and stress investigations. The pressure and turning investigations were conducted by representatives of the National Advisory Committee for Aeronautics and the stress investigation by the Bureau of Aeronautics.

The results of this investigation are not sufficiently comprehensive to permit definite conclusions as to the variation of turning characteristics with changes in speed and rudder angle. They indicate, however, that the turning radius compares favorably with that for other large airships, that the radius is independent of the speed, that the position of the point of zero yaw is nearly independent of the rudder angle and air speed, and that a theoretical relation between radius and angle of yaw in a turn gives a close approximation to actuality. The method of determining turning characteristics by recording instruments aboard the airship appears to be satisfactory, with the exception that a better method of determining the small angular velocities of airships should be devised.

INTRODUCTION

The turning characteristics of a number of full-size airships have been determined at various times and places, by divers methods, and with varying degrees of success. The data obtained in such trials are of interest because they are a measure of maneuverability and forces active in a turn, neither of which can be measured in wind-tunnel tests on airship models. Accurate and consistent data, however, are scarce, and any new information is therefore of considerable interest.

This paper presents the results of turning trials on the rigid airship U. S. S. *Los Angeles*. These trials constitute one phase of a joint investigation requested by the Bureau of Aeronautics, Navy Department, to determine structural stress, distribution of pressures over the hull and tail surfaces, and turning characteristics of the airship. The stress investigation was conducted by the Bureau of Aeronautics, and the pressure and turning investigations were conducted by the National Advisory Committee for Aeronautics, all during the same flights from the hangar at Lakehurst, N. J. The stress and pressure investigations have been previously reported. (Reference 1.) Pressures were measured during some of the turning trials, and simultaneous pressure and turning data were obtained in a few cases.

The results obtained and a description of the method employed are contained in this paper. In addition, there are included a comparison of the results with a theoretical relation between radius and angle of yaw in a turn and suggestions regarding a method for future investigations of this sort. The observed data are shown by curves of air speed, yaw, rudder angle, angular displacement, and angular velocity, plotted on a time base. The turning characteristics computed from values taken from these curves are given in tabular form. Complete data were obtained during only a few runs and are therefore insufficient to fully define the turning characteristics with respect to their variation with speed and rudder angle.

METHOD AND APPARATUS

An attempt was made to determine the turning characteristics of the *Los Angeles* by two independent methods simultaneously. In accordance with this plan, air speed, yaw, angular velocity, and rudder position were recorded by instruments aboard the airship during each turn, while a record of the flight path was obtained with a camera obscura on the ground. Satisfactory data from either source are sufficient to define the turning characteristics, providing the camera-obscura records of the flight paths are corrected by the proper wind vectors. It was necessary, therefore, to obtain measurements of the wind velocity and direction at the time of each turn.

All the necessary data were obtained during the flights, but it was found impossible to obtain consistent values for the turning characteristics from the data given by either one of these methods alone. The angular velocities given by the turnmeter records and the wind vectors given by aerological observations were found to be unsatisfactory. The turnmeter, originally designed to record the comparatively high angular velocities of airplanes, failed to give sufficiently accurate records of the small angular velocities of the airship, and the wind vectors were either too inaccurate or inadequate to be used in finding the true flight path.

The angular displacement of the airship, however, is not affected by the wind, and it was possible, therefore, to determine the angular displacements accurately from the camera-obscura records. These data, combined with air speed, yaw, and rudder position records obtained aboard the airship, were used to define the turning characteristics.

The *Los Angeles* is a rigid airship, having the following characteristics: Length, 656 feet; maximum diameter, 90.7 feet; air volume, 2,760,000 cubic feet; horsepower, 2,000; number of engines, 5.

The complete instrument installation aboard the airship has been previously described in the report on the pressure distribution investigation. (Reference 1.) The only parts of this installation of interest in the turning investigation are the yaw observer, air-speed recorder, control position recorder, and the inclinometer. A description of these instruments is repeated.

The yaw observer consists of a motor-driven motion-picture camera focused on a "yaw bomb" suspended on a cable from the airship. The "yaw bomb" is a streamlined body fitted with fins that align it with the direction of the relative wind. The camera was mounted so that it could be rotated about the lateral and longitudinal axes, but not about the vertical axis. One edge of the rectangular picture frame of the camera was used as a reference line and was aligned parallel to the longitudinal axis of the airship. Since the camera could not be rotated about its vertical axis, this reference line always lay in a plane parallel to the airship's longitudinal axis. This alignment was later checked in flight by photographs of the airship's shadow obtained while flying over water with the sun nearly overhead, and was found to be in error by approximately 1° . With the camera pointing directly downward the angle of yaw is given directly by the angle between the "yaw bomb" image and the reference edge of the picture, subject to the correction for misalignment. When the camera is tilted, however, the apparent angle is greater than the true angle by an amount which depends on the angle of tilt and the location of the image in the picture. During the tests the yaw camera was sighted directly on the "yaw bomb" so that its image would always appear in the center of the picture. Consequently, the camera was tilted in pitch by amounts which varied with the air speed. These angles of tilt ranged from $7\frac{1}{2}^\circ$ to $10\frac{1}{4}^\circ$, and the corresponding corrections to the apparent yaw angles varied from 4.5 to 6.5 per cent. A sample record is shown in Figure 1. The camera was driven at a speed of 18 images per minute. The "yaw bomb" was suspended 360 feet abaft the nose of the airship by a 75-foot cable. This distance includes an estimate of 12 feet to allow for rearward displacement due to the resistance of the "yaw bomb" and suspension cable.

An N. A. C. A. recording air-speed meter (Reference 2) connected to a Pitot-static tube suspended from the airship by a cable 35 feet long was used to measure air speed. The resistance of the necessarily large cable was considerable and accounts for an estimated rearward displacement of 15 feet. The total distance of the Pitot-static tube abaft the nose of the airship

was 265 feet. True air speed was obtained by correcting the records for the density at which the flights were made.

An N. A. C. A. control-position recorder (Reference 3) was used to record rudder and elevator positions. In this instrument a mirror is mechanically connected to the control cable through a suitable reduction mechanism, and motion of the mirror is recorded photographically. The recorder was placed inside the lower fin and was connected to the control cables as near to the controls as possible to avoid inaccuracies due to stretch or slack in the cables.

An N. A. C. A. recording inclinometer, which records on photographic film the movement of an oil-damped pendulum, was used to record inclination of the longitudinal axis of the airship. The records obtained with this instrument and also the elevator position records were of use in determining whether or not the airship was reasonably level and steady during turns.

An N. A. C. A. chronometric timer (Reference 4) was used to synchronize the above records at 16-second intervals.

A camera obscura was used to record the path of the airship during turns. (Reference 5.) It is essentially a large camera, which permits a person to remain in the darkened chamber and to observe the image of an external object which is projected on a suitable surface within the



FIGURE 1.—Portion of a yaw-observer record

chamber by a lens in the camera aperture. In these tests a wide-angle lens was used to project the airship's image on a 30 by 30 inch photographic film. The film was completely covered by a movable light-proof screen in which a small motor-driven shutter was mounted, as described in Reference 5. The shutter opened at regular intervals and exposed a film area just large enough to contain the airship's image. By following the moving image with the shutter a photographic record of the position and attitude of the airship at 8-second intervals was obtained during such part of each turn as was made in the camera field. A sample record is shown in Figure 2.

In connection with the camera-obscura records it was necessary to determine the direction and magnitude of the wind at the altitude of flight. These data were obtained from observations made at the local Naval Aerological Station at $\frac{1}{2}$ -hour intervals. The usual pilot-balloon method of observation was used.

Synchronization of the camera-obscura records with those taken aboard the airship was obtained by the use of radio signals and two stop watches which were synchronized before the airship left the ground. One watch was kept at the camera and the other was carried aboard the airship. Communication between the airship and camera-obscura station was established by radio before making a run, and a signal was given when records were started in the airship. The start and stop times for the records at both places were recorded and were used later to determine what part of each turn was recorded simultaneously by instruments and camera obscura.

The method of determining the true flight path and turning characteristics from camera-obscure records is fully described in Reference 5. The true path is found by adding the proper wind vectors to the recorded path. The center of the corrected flight path, the radius of turn, and the angle of yaw at any point along the airship's axis are found by geometrical methods and measurements.

When the wind has an appreciable magnitude the accuracy of the determination of the true flight path is chiefly dependent upon the accuracy with which the wind vectors are determined. Not only is the magnitude important, but the direction also is extremely important. Both of these items must be accurately measured if the yaw and radius of turn are to be accurately determined. The wind vectors given by the aerological data for the days on which turning trials were made showed wide variations both in direction and magnitude at different

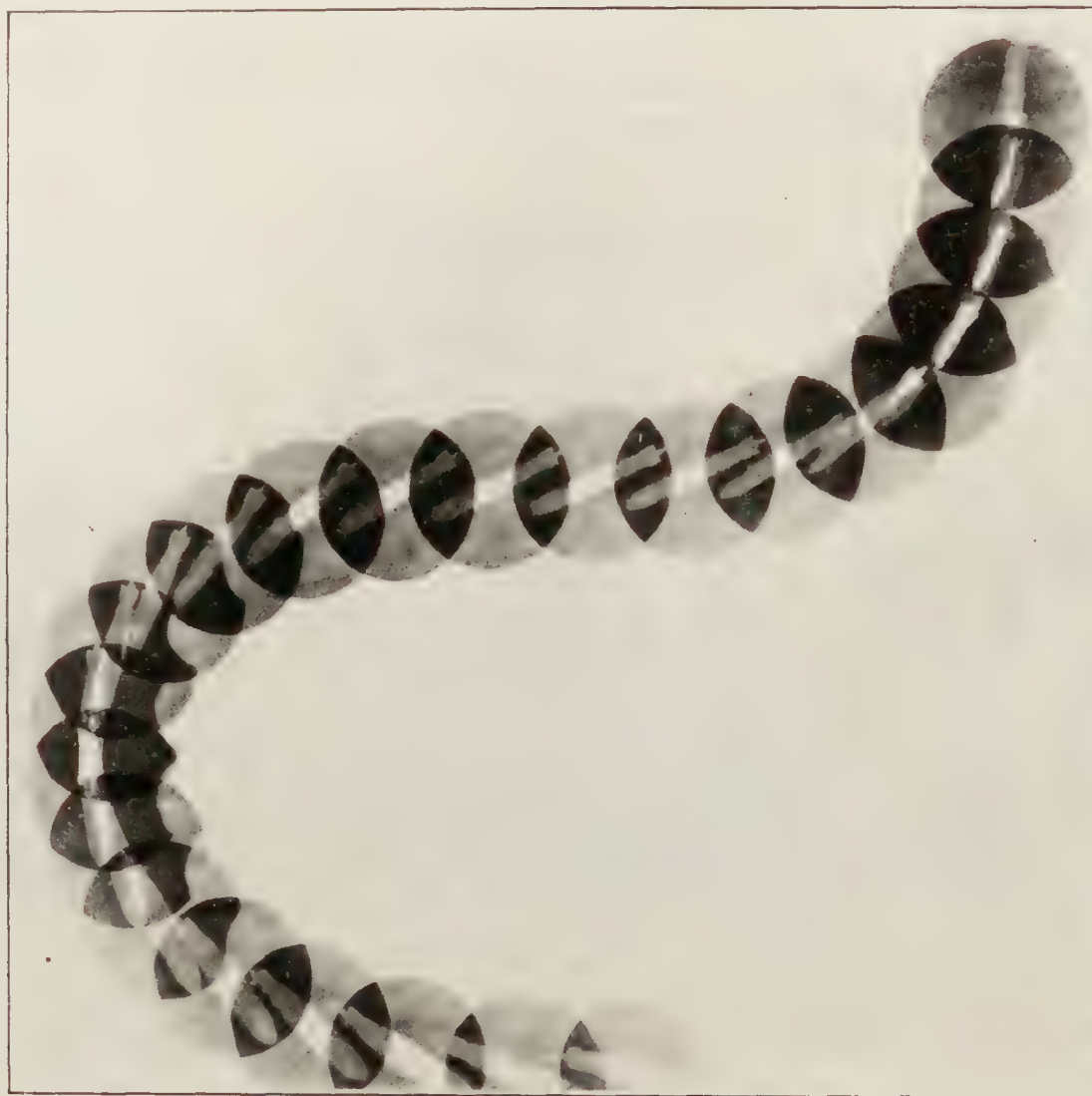


FIGURE 2.—Camera obscure record of a reversal

times and altitudes. In attempting to use these vectors it was found that no consistent results could be obtained, and this method of determining the turning characteristics had to be abandoned. However, the attitude of the airship is not affected by the wind, and it was found possible to measure the angular displacements with good accuracy and to derive angular velocities in steady turns with satisfactory accuracy.

By combining the angular velocities determined by the camera-obscure method with the yaw, air speed, and rudder angle records taken aboard the airship the turning characteristics were determined. Complete data were obtained during only a few turns, so that the available information is insufficient to definitely establish the effect of variations in rudder angles and air speed. The synchronization of camera-obscure records with those taken aboard the airship showed some obvious inconsistencies, which were corrected by judgment based on a proper consideration of the factors affecting the angular displacement and velocity. The resulting synchronization is satisfactory for conditions of steady turning.

PRECISION OF RESULTS

The air-speed records show some variations that were apparently caused by oscillations of the air-speed head, or, in a few cases, to errors in plotting. The possibility of errors in plotting is due to difficulty in properly locating the time intervals in a few cases where the records were crowded due to slippage of the film-drive mechanism. The air speeds are represented by faired curves drawn to avoid these variations. The accuracy of the air-speed recorder is within ± 1 per cent. The accuracy with which the true air speed of the airship is represented by the faired curves is also considered to be within ± 1 per cent, with the exception that in run 5C, the error may be ± 2 per cent.

The individual yaw readings are subject to an error of $\pm \frac{1}{4}^\circ$ in the measurements of the photographed angles. In some cases they are also subject to a larger error, which is indicated by the rapid fluctuation of observed angles and is attributed to oscillations of the "yaw bomb." It is believed, however, that the mean curves drawn through the observed points eliminate the possibility of error from these causes to within $\pm 0.2^\circ$ for conditions of steady turning. There also exists the possibility of a slight constant error of $\pm 0.1^\circ$, due to error in determining the small angle between the yaw camera reference line and the longitudinal axis of the airship. The accuracy of the curves and tabulated values of observed yaw for conditions of steady turning is therefore considered to be within $\pm 0.3^\circ$.

Angular velocities were determined by the graphical differentiation of angular displacement curves. The angular displacement curves were drawn through points obtained from measurements of the attitude of the ship at 8-second intervals, as recorded by the camera obscura. These curves are considered to be accurate within ± 1 per cent. They were drawn to a large scale and differentiated with respect to time. For steady turns the changes in slope are slight and the angular velocities obtained are probably accurate to within ± 2 per cent.

The rudder position record is considered to be accurate to within $\pm \frac{1}{4}^\circ$.

From a consideration of the accuracies stated above it follows that calculations of R and $R\beta$, discussed later, may be in error by ± 3 per cent and ± 7 per cent, respectively. The average values for each run, however, are more accurate.

RESULTS

The observed data are shown by curves, Figures 3 to 7, in which air speed, yaw, rudder angle, angular displacement, and derived angular velocity are plotted against time. The camera-obscura records of angular displacements are noticeably shorter than the instrument records obtained aboard the airship, because the airship was always out of the camera-obscura field at the start and end of each maneuver. Consequently, the angular displacements represented by the curve for each run are measured from the start of the camera-obscura record and not from the start of the maneuver. This does not affect the determination of angular velocity, however, since the slope is not changed by shifting the zero reference.

Time intervals are indicated on the time scales of the curves, so that pressure data which are given in Reference 1 for certain time intervals may be referred to these curves. It should be remembered, however, that the synchronization of camera-obscura records with the records of air speed, yaw, and rudder angle may be slightly in error. Therefore it is likely that a particular value of angular velocity does not correspond to the instant indicated by the time scale within possibly two or three seconds. This has no serious effect on the accuracy of values taken from the curves during steady maneuvers, but would lead to questionable values of angular velocities where the slope of this curve is large. For this reason simultaneous values should not be taken from the curves during periods of pronounced angular acceleration. The curves of Figure 7 can not be used, therefore, except to show the approximate relation between the variations in air speed, yaw, and angular velocity in a hard reversal at high speed, since it does not include a record of the angular velocity during steady turning, either right or left.

The geometry of a turn is illustrated by Figure 8.

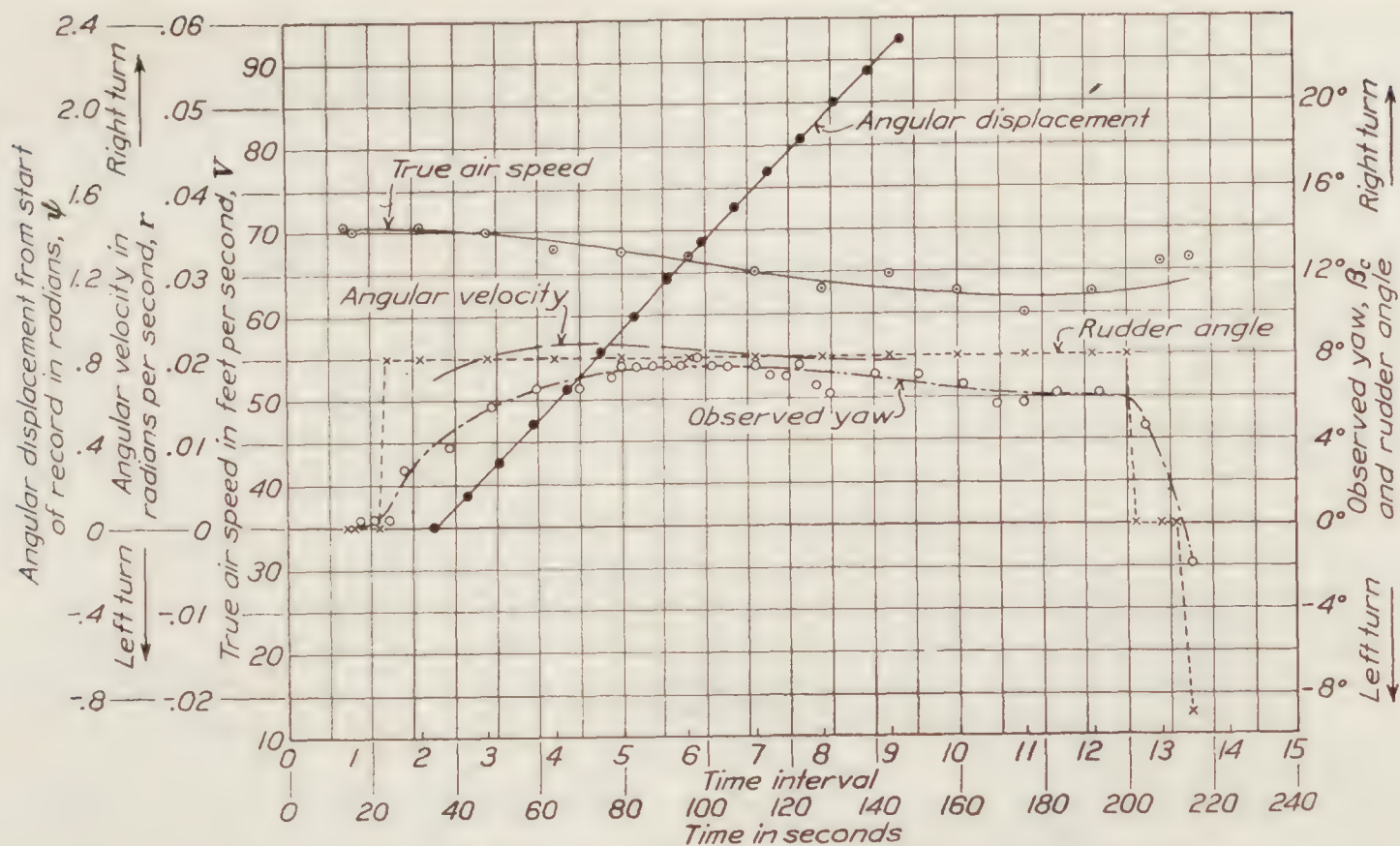


FIGURE 3.—Run No. 4C. Right turn. Altitude referred to standard atmosphere=3,080 feet

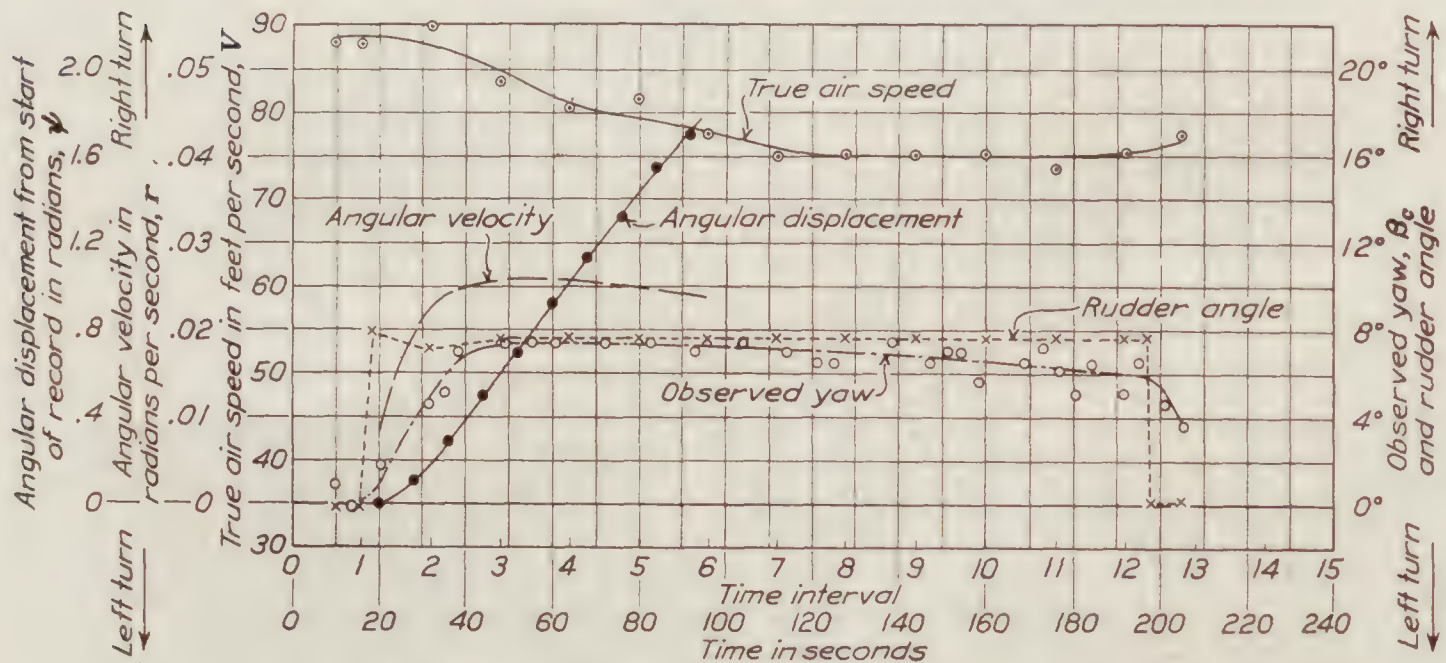


FIGURE 4.—Run No. 5C. Right turn. Altitude referred to standard atmosphere=3,080 feet

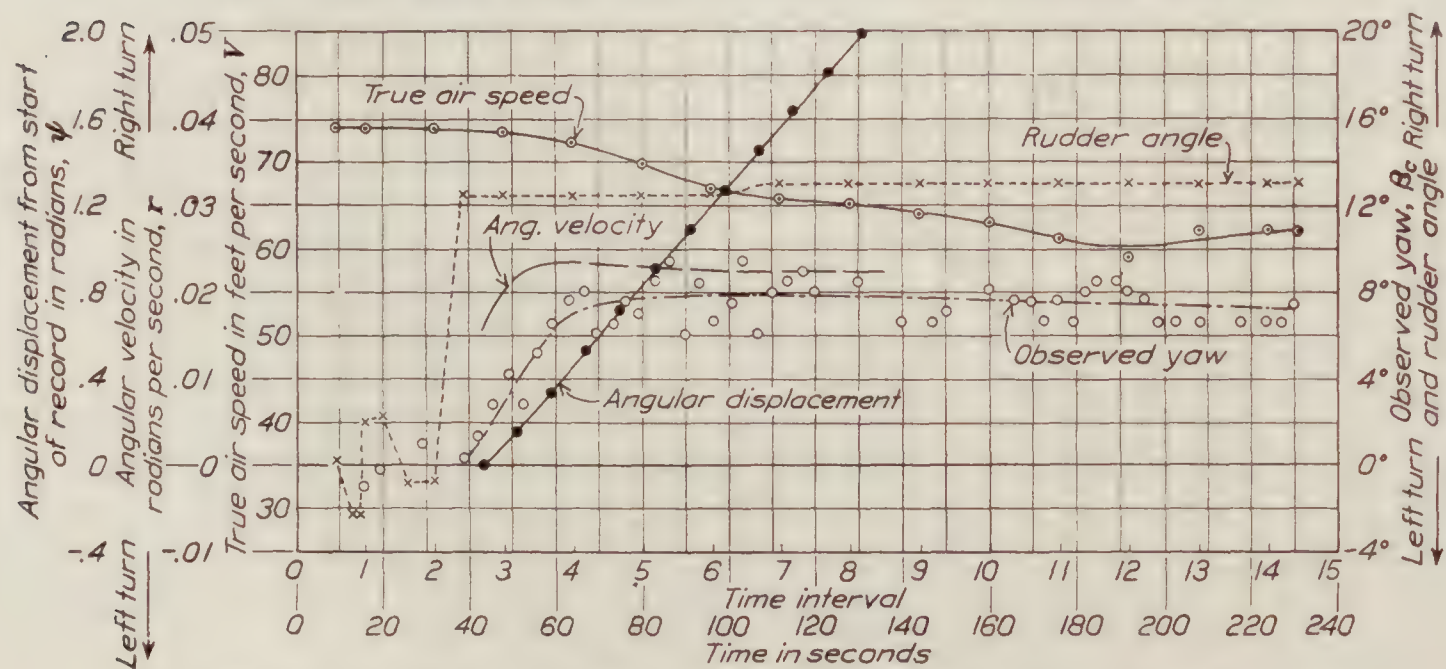


FIGURE 5.—Run No. 13D. Right turn. Altitude referred to standard atmosphere=3,030 feet

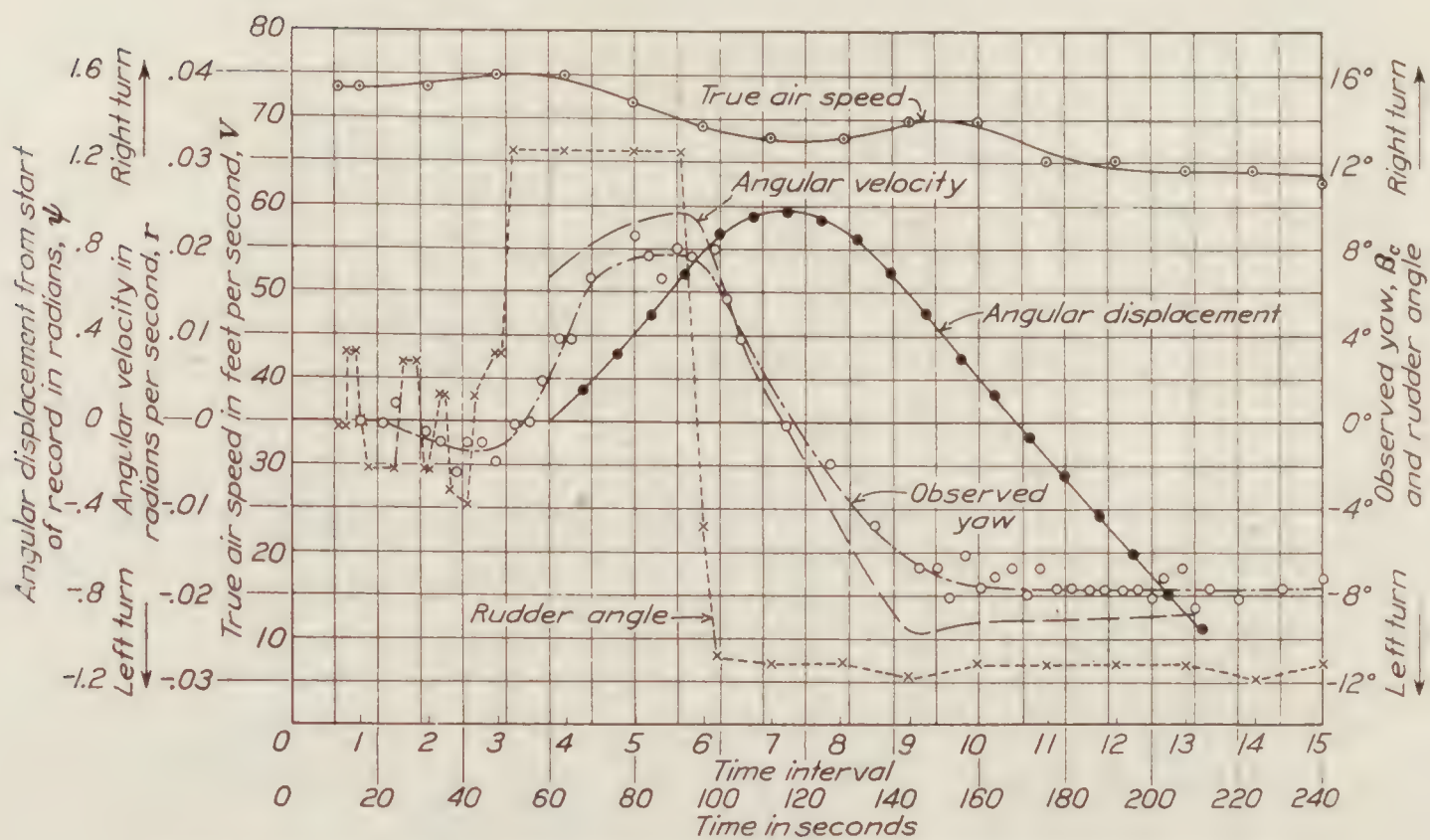


FIGURE 6.—Run No. 14D. Reversal—right to left. Altitude referred to standard atmosphere=3,030 feet

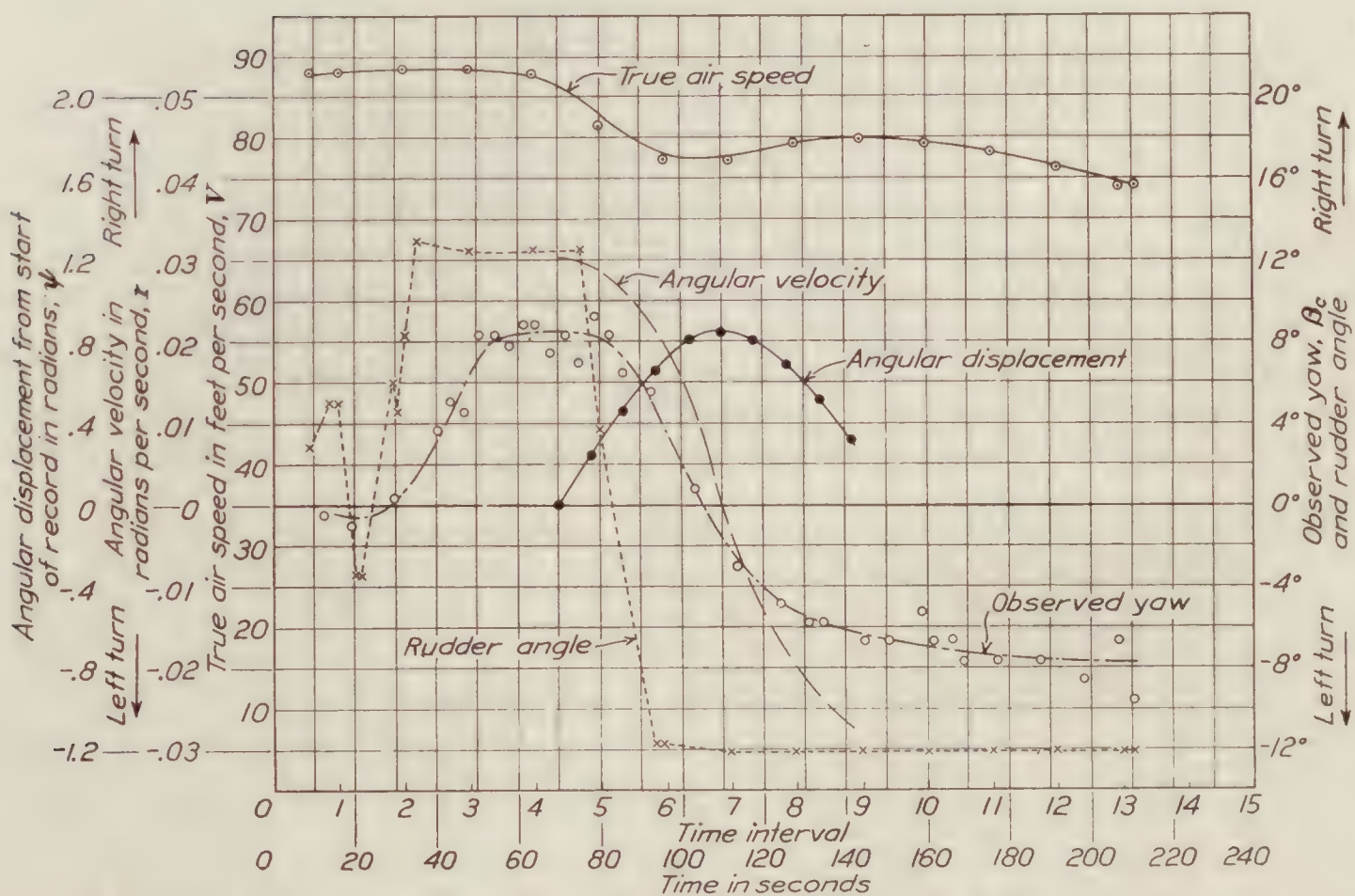


FIGURE 7.—Run No. 17D. Reversal—right to left. Altitude referred to standard atmosphere=3,030 feet

The symbols used are as follows:

A —Location of the point of zero yaw.

B —Location of the air-speed recorder.

C —Location of the yaw observer.

G —Location of the $c. g.$ of the airship.

N —Location of the nose of the airship.

V —True air speed tangential to the path of the $c. g.$

V_B and V_C —True air speed tangential to the paths of the points indicated by the subscripts.

r —Angular velocity of the airship about the center of turn.

β —Angle of yaw at the $c. g.$

β_C —Angle of yaw observed at C .

R —Radius of the path of the $c. g.$

R_A , R_B , and R_C —Radii of the paths of the points indicated by the subscripts.

L —Length of the airship.

$R\beta$ —A linear quantity equal to length GA of Figure 8, which is the distance from the $c. g.$ to the point of zero yaw.

K —Turning coefficient defined as $\frac{2R}{L}$.

a —Distance from the $c. g.$ to the center of pressure on the vertical tail surfaces.

k_2 —Transverse coefficient of additional mass of the airship.

k_1 —Longitudinal coefficient of additional mass of the airship.

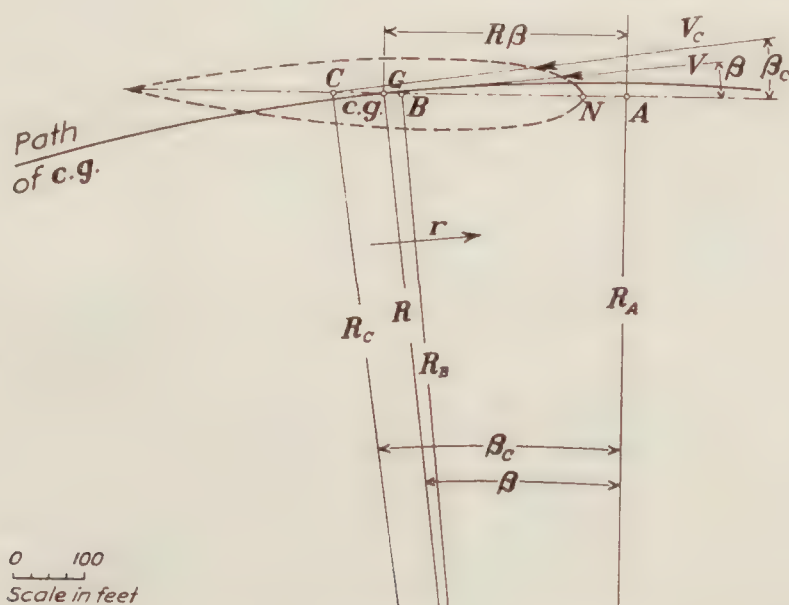


FIGURE 8.—Diagram of the *Los Angeles* in a turn

The turning characteristics were computed from values taken from the curves of Figures 3 to 6 at 10-second intervals during conditions of steady turning. The observed and computed values are given in Table I. An explanation of the method of computing referred to Figure 8 follows.

The observed data give the air speed at point B (V_B), the yaw at point C (β_C), and the angular velocity (r). From these data the air speed at the $c. g.$ (V), the yaw at the $c. g.$ (β), the radius of the path of the $c. g.$ (R), the distance from the $c. g.$ to the point of zero yaw ($R\beta$), and the distance from the nose of the airship to the point of zero yaw (AN) are obtained.

There is a slight difference between the radii R_A and R_C , but the difference between R_B and R_C is only 10 or 15 feet, and therefore may be neglected, since $R \cong 3,000$ feet.

It follows, therefore, that

$$V = V_B$$

and

$$R = \frac{V_B}{r}$$

For angles less than 10° it may be considered that

$$\sin \beta = \beta$$

and, therefore, the distance $R \sin \beta_c = R\beta_c$.

From this it follows that

$$R\beta = R\beta_c - GC$$

and

$$\beta = \frac{R\beta_c - GC}{R} \text{ (in radians)}$$

also

$$AN = R\beta - GN$$

which gives positive values of AN when A is forward of the nose of the airship.

The distances from B , G , and C to the nose (N), Figure 8, are as follows:

$$\begin{aligned} BN &= 265 \text{ feet} \\ GN &= 289 \text{ feet} \\ CN &= 360 \text{ feet and} \\ GC &= 71 \text{ feet.} \end{aligned}$$

The data show the order of magnitude of the turning characteristics, but are too meager to be used in determining definitely the variations of these characteristics with changes in speed and rudder angle. The turning coefficients agree roughly with those given for the British airships *R. 33* and *R. 38* (References 6 and 7) and indicate much better maneuverability than those given for the *R. 29* (Reference 8). The radius of turn shows no variation for two similar turns made at different speeds, which agrees with the results given in Reference 8. The length, $R\beta$, appears to be independent of the rudder angle and nearly independent of the speed, which tends to substantiate the constancy of $R\beta$ indicated by previous tests. (Reference 9.)

A comparison of the results is made with a relation between radius and angle of yaw given by Burgess in Reference 10, derived from the first term of Munk's equation for forces in a turn, Reference 11. The reasoning used in the derivation of this formula is that the transverse fin force equals the centrifugal force in a turn, and the moment of this force about the *c. g.* equals the yawing moment on the hull, expressed by the first term of Munk's equation.

Burgess's equation is

$$\sin 2\beta = \frac{2a}{R(k_2 - k_1)}$$

where a is the distance from the *c. g.* to the center of pressure on the tail, k_2 is the transverse coefficient of additional mass of the airship, and k_1 is the longitudinal coefficient of additional mass.

Lamb's coefficients of additional mass for ellipsoids of various length-diameter ratios are given in References 10 and 11. The equivalent ellipsoid of the airship is given by

$$\frac{\text{length}}{\text{diameter}} \text{ (of ellipsoid)} = \sqrt{\frac{\pi(\text{length})^3}{6 \text{ volume}}} \text{ (of airship)} \quad \text{(Reference 10)}$$

For the *Los Angeles* $k_2 - k_1 = 0.9$, and $a = 275$ feet. (Reference 1.)

A comparison of the experimental angles of yaw at the *c. g.* with the values computed from Burgess's formula is as follows:

Run No.	β experimental in degrees	β computed in degrees	Difference	
			In degrees	In per cent of β experimental
4C.....	5.89	5.57	0.32	5.4
5C.....	6.08	5.56	.52	8.5
13D.....	6.45	6.10	.35	5.4
14D.....	-6.27	-6.07	-.20	3.2
Average.....				5.6

This comparison shows that the agreement between the theoretical expression and the experimental data is within 6 per cent.

Another comparison of the observed data and theoretical calculations may be made when the equation $\sin 2\beta = \frac{2a}{R(k_2 - k_1)}$ is reduced to an expression which defines the point of zero yaw. This expression is

$$\cot \theta = \frac{R}{\frac{a}{k_2 - k_1} - b} \quad (\text{derived in Reference 12})$$

in which θ is the angle of yaw at any point forward of the *c. g.*, b is the distance from the *c. g.* to this point, and the other quantities are as previously defined. It follows that $\cot \theta = \infty$ defines the point of zero yaw. Therefore, when $b = \frac{a}{k_2 - k_1}$, b is the distance from the *c. g.* to the point of zero yaw, $R\beta$ of Figure 8.

For the *Los Angeles* $a = 275$ feet and $k_2 - k_1 = 0.9$. Therefore, $b = 305$ feet or 46.5 per cent L as compared with 50.5 per cent L , the average experimental value of $R\beta$ from Table I.

The disagreement between the above values is about 8 per cent, which is slightly greater than in the former comparison of the experimental and theoretical yaw. Both of these comparisons, however, show an agreement between purely theoretical and observed characteristics that is nearly as close as the accuracy of the experimental data.

The results of these tests point out some objectionable features in the method used to determine turning characteristics which can probably be eliminated in future tests. The camera-obscure method of determining the true flight path is objectionable because it depends so much upon the accuracy of the wind-vector determination; and, furthermore, its usefulness is limited by the difficulty of making more than a small part of a turn, with a large airship, in the camera field. The recording-instrument method would be the more satisfactory means of determining the turning characteristics, providing a sufficiently sensitive and accurate turn-meter were available. The method of determining the yaw appears to be satisfactory, but should be made more accurate by refinements in the method, particularly with regard to the stabilizing and suspension of the "yaw bomb." It would also be advisable to avoid tilting the yaw camera, so that corrections for perspective would be unnecessary. Pointing the camera directly downward, however, would limit its field to a position forward of the swept-back "yaw bomb." This could be remedied by holding the "yaw bomb" forward with a drag-brace wire or by moving the camera back so that its field would include the "yaw bomb" in its swept-back positions.

The suggestion is made that in future work of this nature the air speed, yaw, and rudder angle be recorded as in these tests, and that the angular displacement be recorded by some device aboard the airship. A record of the angular velocity would be preferable, but as yet there appears to be no instrument which will record these small angular velocities accurately. The angular displacement could be recorded by the camera used to record yaw if the flights were

made over ground marked with a number of visible straight lines, such as the streets of a city, for instance. Another suggestion that has been offered is to obtain angular displacement records from a device indicating the attitude of the airship relative to the direction of the sun. This latter method would have the advantage of not limiting the field of operation to any given locality.

CONCLUSIONS

The results of this investigation indicate the following with regard to the turning characteristics of the *Los Angeles* and the method of determining them:

1. The radius of turn is independent of the air speed.
2. The turning coefficients compare favorably with those for other large airships.
3. The position of the point of zero yaw is independent of the rudder angle, is possibly independent of the air speed, and lies forward of the nose an average distance equal to about 6 per cent of the length of the airship.
4. The relation between radius and angle of yaw in a turn derived from Munk's airship formula is in fair agreement with the actual conditions.
5. The method of determining the turning characteristics with instruments aboard the airship is satisfactory, with the exception that a better method of determining angular velocity should be devised.

LANGLEY MEMORIAL AERONAUTICAL LABORATORY,
NATIONAL ADVISORY COMMITTEE FOR AERONAUTICS,
LANGLEY FIELD, VA., *April 17, 1929.*

REFERENCES AND BIBLIOGRAPHY

- Reference 1. DeFrance, S. J.: Flight Tests on the U. S. S. Los Angeles. I. Full Scale Pressure Distribution Investigation. N. A. C. A. Technical Report No. 324. Burgess, C. P.: Flight Tests on the U. S. S. Los Angeles. II. Full Scale Stress Measurements. N. A. C. A. Technical Report No. 325.
- Reference 2. Norton, F. H.: N. A. C. A. Recording Air-speed Meter. N. A. C. A. Technical Note No. 64, 1921.
- Reference 3. Ronan, K. M.: An Instrument for Recording the Position of Airplane Control Surfaces. N. A. C. A. Technical Note No. 154, 1923.
- Reference 4. Brown, W. G.: Synchronization of N. A. C. A. Flight Records. N. A. C. A. Technical Note No. 117, 1922.
- Reference 5. Crowley, J. W., jr., and Freeman, R. G.: Determination of the Turning Characteristics of an Airship by Means of a Camera Obscura. N. A. C. A. Technical Report No. 208, 1925.
- Reference 6. Pannell, J. R., and Frazer, R. A.: Experiments on Rigid Airship R. 33. Reports and Memoranda No. 668, 1919.
- Reference 7. Frazer, R. A., and Bateman, H.: Experiments on Rigid Airship R. 38 (ZR-2). Reports and Memoranda No. 764, 1921.
- Reference 8. Pannell, J. R., and Bell, A. H.: Experiments on Rigid Airship R. 29. Reports and Memoranda No. 675, 1920.
- Reference 9. Jones, R.: The Application of the Results of Experiments on Model Airships to Full-Scale Turning. Reports and Memoranda No. 716, 1920.
- Reference 10. Burgess, C. P.: Airship Design. Ronald Aeronautical Library. Ronald Press Co., New York, 1927.
- Reference 11. Munk, Max M.: The Aerodynamic Forces on Airship Hulls. N. A. C. A. Technical Report No. 184, 1924.
- Reference 12. Fairbanks, Karl J.: Pressure Distribution on the Nose of an Airship in Circling Flight. N. A. C. A. Technical Note No. 224, 1925.

TABLE I.—FULL-SCALE TURNING CHARACTERISTICS OF THE U. S. S. LOS ANGELES

Run No.	Time		Rudder angle in degrees	True air speed V in ft./sec.	Angular velocity r in rad./sec.	Turning radius R in feet	Observed yaw β_c in degrees	Computed yaw at $c. g. \beta$ in degrees	$R\beta$		Turning coefficient K	Length AN in % L
	In seconds	Interval No.							In feet	In % L		
4C-----	60	3 $\frac{3}{8}$	8	69.2	0.0214	3,235	6.5	5.2	296	45.2	9.86	1.1
	70	4 $\frac{3}{8}$	8	68.5	.0218	3,145	7.1	5.8	319	48.7	9.59	4.6
	80	5	8	67.7	.0216	3,135	7.4	6.1	334	51.0	9.56	6.9
	90	5 $\frac{5}{8}$	8	66.9	.0213	3,140	7.5	6.2	340	51.9	9.57	7.8
	100	6 $\frac{3}{8}$	8	66.1	.0208	3,180	7.6	6.3	351	53.5	9.70	9.4
	110	6 $\frac{7}{8}$	8	65.2	.0204	3,195	7.5	6.2	347	53.0	9.74	8.9
	120	7 $\frac{1}{8}$	8	64.3	.0200	3,215	7.4	6.1	344	52.5	9.80	8.4
	130	8 $\frac{1}{8}$	8	63.7	.0198	3,215	7.2	5.9	333	50.8	9.80	6.7
	140	8 $\frac{5}{8}$	8	63.2	.0196	3,225	7.0	5.7	323	49.3	9.83	5.2
	150	9 $\frac{3}{8}$	8	62.8	.0195	3,220	6.7	5.4	306	46.7	9.82	2.6
	Average-----					3,190		5.89		50.3	9.73	6.2
5C-----	50	3 $\frac{1}{8}$	7.6	84.3	.0259	3,255	7.4	6.1	349	53.3	9.84	9.1
	60	3 $\frac{3}{8}$	7.6	81.8	.0260	3,145	7.4	6.1	335	51.1	9.59	7.0
	70	4 $\frac{3}{8}$	7.6	80.3	.0255	3,150	7.4	6.1	336	51.3	9.60	7.2
	80	5	7.6	79.3	.0249	3,185	7.4	6.1	341	52.0	9.71	7.9
	90	5 $\frac{3}{8}$	7.6	78.5	.0242	3,240	7.3	6.0	342	52.2	9.88	8.1
	Average-----					3,195		6.08		52.0	9.72	7.9
13D-----	80	5	12.5	69.7	.0230	3,060	7.7	6.4	340	51.9	9.33	7.8
	90	5 $\frac{5}{8}$	12.5	68.2	.0227	3,005	7.8	6.4	338	51.6	9.16	7.5
	100	6 $\frac{3}{8}$	12.6	66.8	.0226	2,955	7.9	6.5	336	51.3	9.01	7.2
	110	6 $\frac{7}{8}$	13	65.9	.0225	2,930	7.9	6.5	333	50.8	8.93	6.7
	120	7 $\frac{1}{8}$	13	65.5	.0223	2,940	7.9	6.5	335	51.1	8.96	7.0
	130	8 $\frac{1}{8}$	13	65.2	.0222	2,940	7.8	6.4	329	50.2	8.96	6.1
	Average-----					2,972		6.45		51.3	9.06	7.1
14D-----	160	10	-11.2	69.7	-.0232	3,005	-7.5	-6.1	322	49.1	9.16	5.0
	170	10 $\frac{5}{8}$	-11.2	67.5	-.0228	2,960	-7.7	-6.3	327	49.9	9.02	5.8
	180	11 $\frac{3}{8}$	-11.2	65.5	-.0228	2,875	-7.7	-6.3	315	48.0	8.76	4.0
	190	11 $\frac{7}{8}$	-11.2	64.5	-.0227	2,840	-7.7	-6.3	311	47.4	8.66	3.3
	200	12 $\frac{3}{8}$	-11.2	64.2	-.0224	2,870	-7.7	-6.3	315	48.0	8.75	4.0
	210	13 $\frac{1}{8}$	-11.2	64.1	-.0220	2,915	-7.7	-6.3	321	49.0	8.89	4.9
	Average-----					2,911		-6.27		48.6	8.87	4.5

NOTE.—Rudder angle, angular velocity, and yaw are considered positive in a right turn and negative in a left turn. AN is the distance from the point of zero yaw to the nose, considered positive when A is forward of the nose.

REPORT No. 334

THE TORSION OF MEMBERS HAVING SECTIONS COMMON IN AIRCRAFT CONSTRUCTION

By GEORGE W. TRAYER and H. W. MARCH
Forest Products Laboratory

TABLE OF CONTENTS

	Page
Foreword.....	673
Introduction and purpose.....	675
Test material and procedure.....	676
Direct torsion tests of beams.....	676
Soap-film tests.....	676
Discussion.....	680
The torsion problem.....	680
Formulas for simple sections.....	684
Formulas for hollow prisms or tubes.....	687
Solid sections of irregular shape.....	690
Moduli of rigidity of spruce.....	691
Effect of moisture content.....	691
Effect of rate of loading.....	692
Torsion tests of simple sections.....	693
Torsion tests of irregular sections.....	694
The use of soap films in solving the torsion problem for irregular sections.....	694
Formulas for irregular solid sections.....	696
Conclusions.....	703
Summary.....	703
References.....	704
Bibliography.....	704
Appendix A—Prisms of nonisotropic material.....	707
References.....	714
Appendix B—The Griffith and Taylor formulas for torque and stress.....	715
Appendix C—Design values for airplane material.....	719

FOREWORD

An important limitation upon the development of aircraft structures of minimum weight and maximum efficiency is the fact that the results of the basic mathematical theory of elasticity have in general not been so presented that they can be used by the average American engineer. Further, the mathematical solutions of many important specific problems are not known and our knowledge of the physical constants of the materials used is incomplete. As a contribution toward the improvement of this situation, the Bureau of Aeronautics of the Navy Department has from time to time financed work along these lines for presentation primarily from the viewpoint of the engineer. This report, submitted to the National Advisory Committee for Aeronautics for publication, covers an investigation of the torsion problem by the Forest Products Laboratory, Forest Service, Department of Agriculture, undertaken through arrangements between the Navy Department and the Department of Agriculture. The discussion and the findings, while checked largely by tests of wooden specimens, apply equally to wood and to metal, due consideration being given to the elastic properties of the materials used.

The data and the formulas presented apply strictly to the torsion phenomenon. A beam may fail either in a normal type of bending or by lateral buckling resulting from normal loading, or by twisting or wrinkling of an outstanding flange under stresses having their origin in the normal loading. Likewise, a member such as a very thin tube subjected to torsion may fail at a load less than the theoretical load calculated by the torsion formulas because of other phenomena, such as wrinkling, which have their origin in the twisting load. It is necessary either to develop criteria for freedom from such secondary failures or to apply coefficients to the calculated strength values to take care of secondary failure. Technical Note No. 189 of the National Advisory Committee for Aeronautics, which gives formulas for the variation of allowable shearing stress with change in the ratio of diameter to thickness, indicates one method of approach to this problem. The Army and Navy Standards for sizes of tubing permit a range in the ratio of diameter to thickness for seamless tubing of about 5 to 43, and tubes of higher ratio can of course be fabricated.

It should be noted that the polar moment of inertia and the polar moment of inertia divided by the distance to the extreme fiber have no significance in comparing the rigidity and the strength of sections of different form; in this respect they are not analogous to the use of the moment of inertia and the section modulus in comparing the bending of beams. It so happens that the rigorous stress formulas for circular rods and tubes as given in the report reduce to the common form $q = \frac{Tc}{J}$, which is

analogous to the stress formula $S = \frac{MC}{I}$ for beams. The beam formula, however, is general, while the common torsion formula is true only for circular rods and tubes. For members of other shapes an additional factor must be introduced into the formula when reduction is made to the common form.

The results of the actual torsion tests of simple sections in Table III show large variations in observed physical properties, which may cause doubt as to the soundness of design values deduced from the results. Actually part of the material reported on, while acceptable for making tests, is outside the specified acceptable range for aircraft stock—the test material represented the entire tree. Later recommendations for design values are based on the specification range and are conservative for reasonable variations outside that range. For metals these variations (in the ratio of “G” to “E” values) are much less in amount.

Recommended design stresses as furnished by the Bureau of Aeronautics are given in Appendix C.

J. H. TOWERS,
Acting Chief of Bureau.

REPORT No. 334

THE TORSION OF MEMBERS HAVING SECTIONS COMMON IN AIRCRAFT CONSTRUCTION¹

By GEORGE W. TRAYER and H. W. MARCH²

INTRODUCTION AND PURPOSE

Structural members designed for pure torsion are usually made with circular, elliptical, rectangular, or other regular cross sections that have already yielded to direct mathematical treatment as regards torsion. However, members designed primarily for thrust or bending and consequently as a usual thing of irregular section are subjected to torsion also, and under certain conditions they may fail by buckling and twisting through lack of sufficient torsional rigidity. In order to design against the possibility of such failure in thin deep beams or in compression members with thin, outstanding parts, we must be able to calculate their torsional rigidity. Such sections as **I**, **T**, **L**, and **U** have not been brought within the range of mathematical analysis and up to a few years ago the engineer had practically nothing on which to base an estimate of the torsional strength and rigidity of rods of irregular section. This publication presents the results of investigations of the torsion of structural members undertaken by the Forest Products Laboratory and financed by the Bureau of Aeronautics, Navy Department, under the national defense act.

Within recent years a great variety of approximate torsion formulas and drafting-room processes have been advocated. In some of these, especially where mathematical considerations are involved, the results are extremely complex and are not generally intelligible to engineers. The principal object of the investigation was to determine by experiment and theoretical investigation how accurate the more common of these formulas are and on what assumptions they are founded, and, if none of the proposed methods proved to be reasonably accurate in practice, to produce simple, practical formulas from reasonably correct assumptions, backed by experiment. A second object was to collect in readily accessible form the most useful of known results for the more common sections.

This report reviews informally the fundamental theory of torsion and shows how the more common formulas are developed from it. Formulas for all the important solid sections that have yielded to mathematical treatment are listed. Then follows a discussion of the torsion of tubular rods with formulas both rigorous and approximate.

It is shown by a series of tests of prisms of simple section that wood is a suitable material for the experimental investigation of the torsion problem. Accordingly, wood was used for the experiments on full-sized members because of the ease with which it can be worked into different shapes and because of its low torsional stiffness. The possible effect of different moduli of rigidity in radial and tangential planes was investigated mathematically, and the effects of rate of loading and of moisture content were determined experimentally. Furthermore, soap films were used in order to take advantage of a mathematical similarity that exists between the torsion problem and the problem of finding the deflection of a thin membrane under pressure. The analogy is discussed in detail in the report.

¹ Originally submitted as "The Torsion of Cylinders and Prisms."

² Professor of mathematics, University of Wisconsin.

NOTE.—R. J. Roark, associate professor of mechanics, University of Wisconsin, collaborated with the authors in certain phases of this investigation, giving especial attention to the soap-film method.

Our experimental work with beams of irregular sections that have not yielded to mathematical treatment is described. From these experiments and certain mathematical considerations, empirical formulas are set up for irregular sections whose component parts are rectangles.

TEST MATERIAL AND PROCEDURE

DIRECT TORSION TESTS OF BEAMS

The first series of direct torsion tests was confined to rods of simple section, such as the circle, the square, the ellipse, and the equilateral triangle. The test specimens were made of carefully selected Sitka spruce and when several were to be compared directly they were cut from the same plank. The elastic properties of the material in any plank were obtained by testing small minor specimens cut from the plank and so located as to be representative. These specimens usually consisted of two bending, two compression parallel to the grain, two specific gravity, eight shear, and three torsion specimens. The three minor torsion specimens consisted of one piece approximately $1\frac{1}{4}$ inches square, one piece 1 by 3 inches quarter-sawn, and one piece 1 by 3 inches flat-sawn. Four of the shear specimens were tested radially and four tangentially. All major torsion specimens for this first series of tests were 45 inches long and the area of cross section was usually less than 2 square inches.

The second series of tests was made on beams of irregular section, such as **I**, **T**, **L**, and **U**. These beams were 96 inches long, were cut from clear Sitka spruce planks, and were matched as described for the first series.

The apparatus for the first two series of tests, which was constructed expressly for these tests, consisted essentially of an attachment for holding one end of the beam fixed against rotation and a disk for applying torque at the other end. (Fig. 1.) Rollers at the fixed end provided for longitudinal movement. The disk, which was 10 inches in radius, turned on ball bearings. It was rotated by a metal strap attached to and passing around its periphery and thence up to a yoke attached to the weighing platform of a scale, which was accurate to one one-hundredth of a pound. The entire scale was bolted to the movable head of a testing machine and load was applied by raising the head. The usual length over which distortion was read, called the "gage length" in this report, was 24 inches for the short specimens and 36 inches for the long specimens. At one end of the gage length a circular metal frame with a 20-inch radius was clamped to the specimen. On the periphery of this circular frame was attached a steel tape graduated to tenths of an inch. At the other end of the gage length a rectangular frame was also clamped to the specimen, and welded to this frame was a pointer that extended to the scale on the circular frame. As the beam was twisted the scale rotated more than the pointer. Determining the excess movement of the scale by reading the position of the pointer on it thus yielded the angle of twist over a given gage length directly, the total angle in radians being the scale reading divided by the radius, 20 inches. The angle of twist per unit length, in radians, is then this quotient divided by the gage length. Except for tests made specifically to determine the effect of rate of loading, the rate was varied with the type of specimen, in order to obtain approximately the same rate of strain in all tests. Such variation necessitated raising the movable head of the testing machine at rates of from 0.674 inch per minute to 1.40 inches per minute. For tests made to determine the effect of rate of loading, the speed of the movable head was varied from 0.023 inch per minute to 2.25 inches per minute.

SOAP-FILM TESTS

The value of soap films in determining the torsional rigidity of a twisted rod and the stresses in it depends upon an analogy between the torsion problem and that of finding the deflection of a thin membrane under the action of a uniform load. The mathematical similarity is discussed later in this report, where it is shown that if a soap film is stretched over a hole in a flat plate, the hole being the same shape as the cross section of the bar and the film being displaced from the plane of the plate by a slight difference in pressure on the two sides, the following relations hold:

1. The shear stress at any point of the cross section is proportional to the slope of the film at the corresponding point with respect to the plane of its boundary.
2. The contour lines of the film represent the direction of the resultant shear stress at every point.
3. The torsional rigidity of the section is proportional to the volume between the soap film and the plane of the plate.

In order to make use of the analogy it was necessary to design apparatus with which the slope of the film, its contour lines, and the volume of displacement could be determined. The

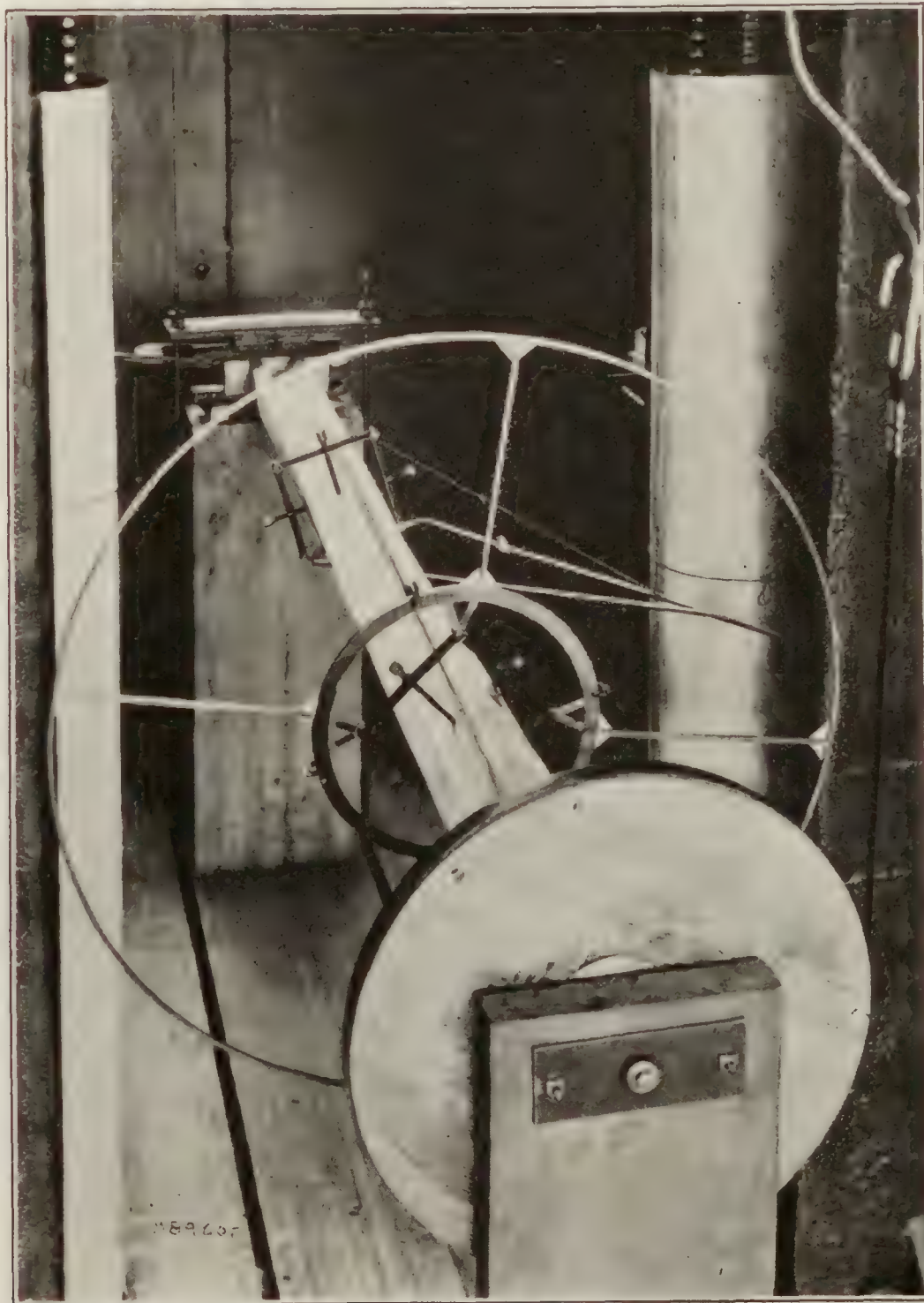


FIGURE 1.—Apparatus for applying torque to structural shapes and measuring the angle of twist

apparatus was patterned after that used by Griffith and Taylor and described by them in Advisory Committee for Aeronautics (British) Reports and Memoranda No. 333, June, 1917. As pointed out, the stresses in the bar are proportional to the inclination of the film and the stiffness of the bar is proportional to the volume generated by the film displacement. The relations hold for any number of films provided the difference in pressure on the sides of a film is the same for all. This condition is readily attainable by making more than one hole in the same test plate; it is evident that the easiest way of obtaining actual stress or rigidity values is to have a circular hole in each plate in addition to the hole that represents the section being

studied. The rigidity of a circular shaft and its stresses are easily calculated, and having the two films in the same plate makes it possible to compare torsional rigidities directly by comparing volumes and to compare stresses directly by comparing slopes.

In assembling the apparatus, a plate with the experimental hole and a circular hole cut in it (fig. 2) was clamped between the bottom and the sides of a cast-iron box (fig. 3). The box bottom, which was $11\frac{3}{4}$ inches square outside and 2 inches thick, was supported on leveling

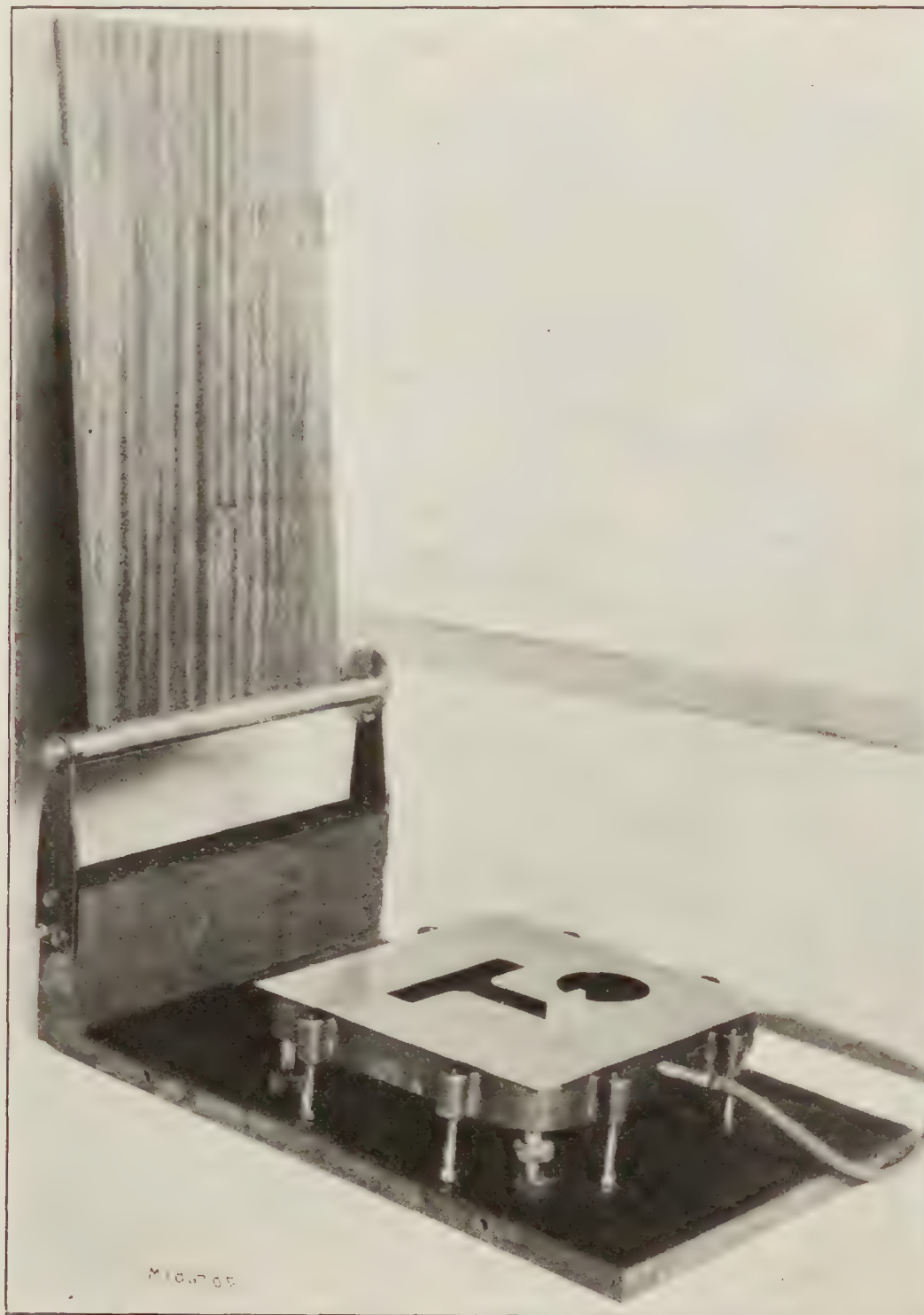


FIGURE 2.—The soap-film apparatus with the upper part of the box removed to show the perforated plate

screws. It was recessed $\frac{1}{4}$ inch inside of the $\frac{3}{4}$ -inch bearing surface on which the plate rested. A square frame $\frac{3}{4}$ inch thick and 2 inches deep formed the sides of the box; both bottom and frame were provided with lugs for clamping screws. Over the frame was placed a piece of plate glass through the center of which a hole had been cut for a micrometer height gage, reading to one one-thousandth of an inch, that carried at its lower end a hardened steel needle point. Fixed axially above the needle point, extending upward from the frame supporting the gage, was a steel recording point. The position of the gage, at each reading, was recorded by pressing against it a sheet of paper attached to a board that could be swung down to the horizontal for this purpose; the board was hinged to the heavy cast-iron base on which the bubble box was

leveled. Provision was made for increasing the air pressure below the soap films or decreasing it above them.

With this apparatus contour lines and hence displacement volumes could be determined. Stress could also be determined, since it is inversely proportional to the distance between con-

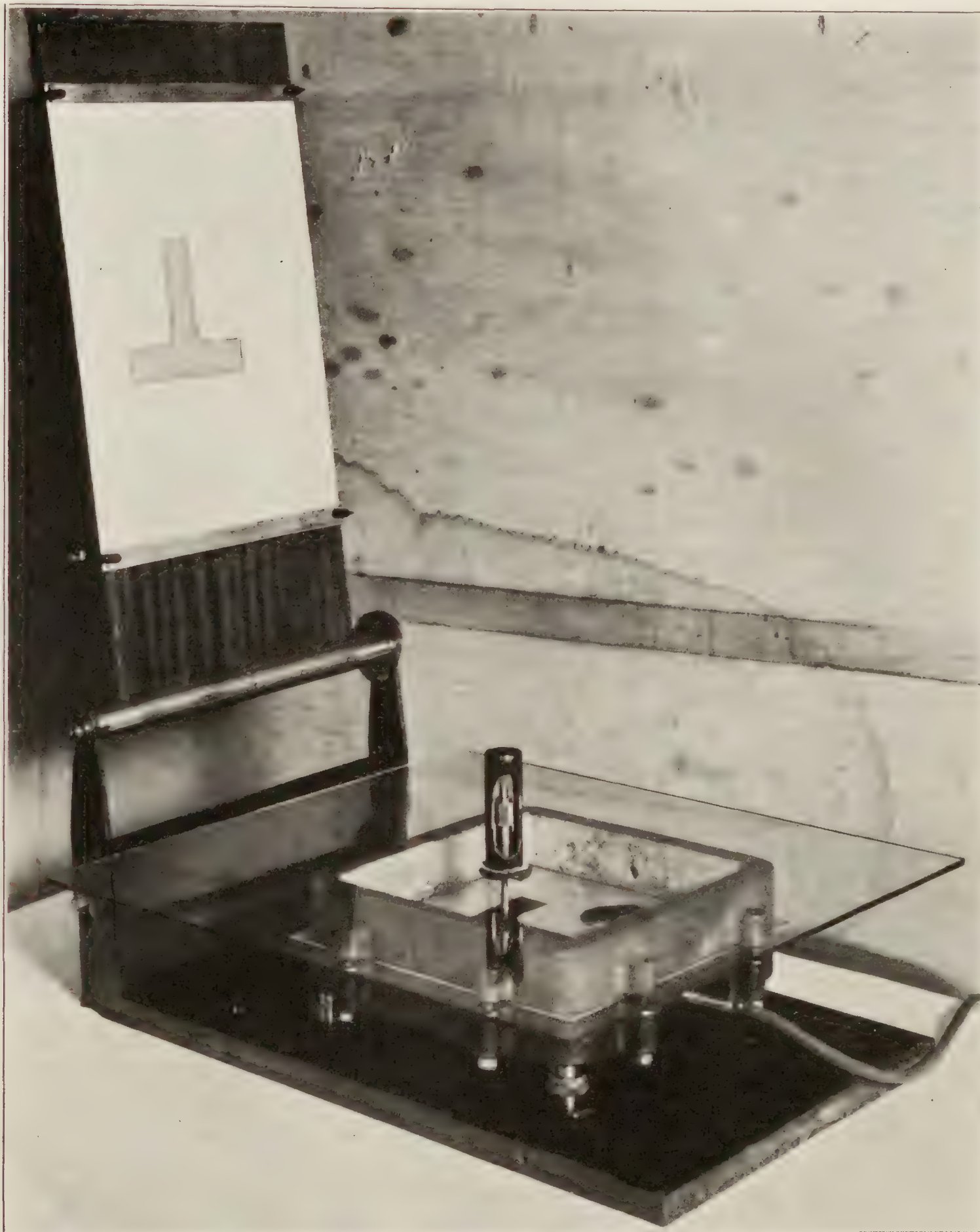


FIGURE 3.—The complete assembly of the soap-film apparatus

secutive contours. A collimator for measuring slope directly was made but time and funds allotted to the study were exhausted before it was put in use.

The test plates were cut from sheet aluminum approximately 0.05 inch thick. The edges around the test holes were beveled; the sharp edge was placed upward in the apparatus and

great care was taken to keep the plates perfectly flat. When divergences from a plane were found they were corrected by propping up the plate from below or by putting small weights on top of it.

With symmetrical sections a complete boundary sometimes was not used. Griffith and Taylor found that the shape of a symmetrical film was unaltered if the film was divided by a vertical septum passing through its axis of symmetry. In our work a septum was carried down about one-eighth inch below the under side of the plate. Figure 2 shows a septum in place.

Best results were obtained with a circular hole about 3 inches in diameter and with the dimensions of the experimental hole such that the ratios of the heights of the bubbles over the two holes were between 2 and 1.

In carrying out the experimental work, a film was drawn across the holes with a strip of celluloid wet with soap solution. The blowing up was done through a burette, the bottom of which was connected to the lower end of a column of water, through a stopcock, and the top to the chamber below the test plate. As water was passed into the bottom of the burette, air was forced out of the top into the apparatus. This method was employed instead of blowing up the bubbles with air from the lungs because the carbon dioxide introduced by that method was harmful to the bubbles.

The success of the method depends largely on obtaining a soap film that will permit the taking of a great number of readings. Some difficulty was at first encountered in obtaining a suitable soap solution. All formulas investigated produced films that would last but a few minutes until a solution used by Dewar was tried. With this solution we were able to obtain films that would often last throughout a whole working day. It was made by adding a very small quantity of triethylamine oleate to a 50 per cent solution of glycerine in distilled water. The triethylamine oleate was prepared as follows, using 2 grams of triethylamine to 5 grams of oleic acid:

The amine was dissolved in warm water and the oleic acid was slowly stirred in. Excess amine in the emulsion was expelled by distillation and the water was expelled by subsequent evaporation on a steam bath. In the preparation an excess of oleic acid should be avoided, since it is not volatile.

Other oleates, such as ammonium, sodium, and potassium, were found by Dewar to be very successful, but the triethylamine solutions are by far the most resistant to atmospheric impurities.

DISCUSSION

THE TORSION PROBLEM

If a right cylinder or prism is twisted and held in equilibrium by means of couples applied at its ends, the portion of the cylinder or prism between any cross section and one end is in equilibrium under two equivalent couples, one in the plane of the cross section and the other the applied couple at the end. The couple in the plane of the cross section will be regarded as the resultant of a suitable distribution of shearing stress, which consists of tangential tractions in the plane of the section combined with equal tangential tractions along appropriate longitudinal sections. Since the cylinder or prism is in equilibrium under the action of the couples that are applied at its ends, the cylindrical surface must be free from traction.

Corresponding to the shearing stresses just referred to, there will be shearing strains of two types, one consisting of the sliding of the elements of one cross section over those of an adjoining section, the other of the relative sliding of different longitudinal elements in the direction of the length of the cylinder. The first type of strain will be expressed in terms of the angle through which the plane of the section has been rotated, the angle being assumed proportional to the distance from one end. The second type of strain, which implies that, in general, the plane cross sections are distorted into curved surfaces, will be expressed in terms of the displacement of the elements of a section in the direction of the length of the cylinder. This displacement is taken to be the same for all sections of a given cylinder or prism.

If the axis of Z be taken in the direction of the length of the prism and the components of the displacement of a point parallel to the X , Y , and Z axes be denoted by u , v , and w , respectively, the state of strain just described is a consequence of the following displacement:

$$u = -\tau y z, \quad v = \tau z x, \quad w = \tau \phi(x, y) \quad (1)$$

where τ is the angle of twist per unit length and ϕ is a function of x and y only, which is to be determined.

The u and v components of the displacement together express a rotation about the Z axis through an angle $z\tau$ of a section at a distance z from one end, while the w component expresses the distortion of each given section from its plane.

From the components of the displacement, the components of strain follow and from these follow the components of stress. (References 1 and 2.) It is found that the X and Y components, X_z and Y_z , respectively, of the shearing stress at a point (x, y) in any cross section, are expressed by the equations:

$$X_z = G\tau \left(\frac{\partial \phi}{\partial x} - y \right), \quad Y_z = G\tau \left(\frac{\partial \phi}{\partial y} + x \right) \quad (2)$$

where G is the modulus of rigidity.

Associated with the stress components X_z and Y_z , which act in the plane of the cross section, are the stress components Z_x and Z_y , which are equal to X_z and Y_z , respectively, and which act in longitudinal planes parallel to the ZX and YZ planes, respectively. All other stress components are zero as a consequence of the assumed displacements (1). Thus the displacements taken in (1) lead to a system of stresses of the type described in the first paragraph of this section.

From the equations of equilibrium of the prism under the state of stress just considered, it follows that the function ϕ satisfies the differential equation

$$\frac{\partial^2 \phi}{\partial x^2} + \frac{\partial^2 \phi}{\partial y^2} = 0 \quad (3)$$

over the area of the cross section of the prism.

The requirement that the lateral surface of the cylinder or prism shall be free from traction leads to the following equation, which must be satisfied by the function ϕ on the curve bounding the cross section of the prism; namely,

$$\frac{\partial \phi}{\partial v} = y \cos(x, v) - x \cos(y, v). \quad (4)$$

In this equation, v denotes the exterior normal to the bounding curve.

The moment T of the couple in the plane of any cross section is expressed in terms of the function ϕ by the equation

$$T = C\tau, \quad (5)$$

where

$$C = G \iint \left(x^2 + y^2 + x \frac{\partial \phi}{\partial y} - y \frac{\partial \phi}{\partial x} \right) dx dy, \quad (6)$$

the integral being extended over the area of the cross section of the prism. It is often convenient to replace C in equation (5) by GK where K is the integral by which G is multiplied in (6). Thus:

$$T = GK\tau. \quad (5')$$

The problem of determining the torsion function ϕ subject to the differential equation (3) and the boundary condition (4) may be replaced by that of finding a function ψ conjugate to ϕ which satisfies the differential equation

$$\frac{\partial^2 \psi}{\partial x^2} + \frac{\partial^2 \psi}{\partial y^2} = 0 \quad (7)$$

and the boundary condition

$$\psi - \frac{1}{2} (x^2 + y^2) = \text{constant.} \quad (8)$$

The following relations connect ϕ and ψ :

$$\frac{\partial \phi}{\partial x} = \frac{\partial \psi}{\partial y}, \quad \frac{\partial \phi}{\partial y} = -\frac{\partial \psi}{\partial x}. \quad (9)$$

If we replace ψ by the function Ψ defined in the following way:

$$\Psi = \psi - \frac{1}{2} (x^2 + y^2), \quad (10)$$

we find from (7) and (8) that Ψ satisfies the differential equation

$$\frac{\partial^2 \Psi}{\partial x^2} + \frac{\partial^2 \Psi}{\partial y^2} + 2 = 0 \quad (11)$$

subject to the condition

$$\Psi = 0 \quad (12)$$

on the boundary of the section, the constant in equation (8) having been chosen to be zero.

From equations (2), (9), and (10), we find that the components of the shearing stress are simply expressed in terms of the function Ψ ; namely,

$$Y_z = -G\tau \frac{\partial \Psi}{\partial x}, \quad X_z = G\tau \frac{\partial \Psi}{\partial y}. \quad (13)$$

Hence the tangential traction at a point in any cross section of the prism has the direction of the tangent to that curve of the family

$$\Psi(x, y) = \text{constant}$$

which passes through this point. The curves, $\Psi = \text{constant}$, are therefore lines of shearing stress.

Further, the resultant shearing stress at a point in a cross section is equal to

$$\sqrt{X_z^2 + Y_z^2} = G\tau \sqrt{\left(\frac{\partial \Psi}{\partial x}\right)^2 + \left(\frac{\partial \Psi}{\partial y}\right)^2} = G\tau \frac{\partial \Psi}{\partial v}, \quad (14)$$

where v denotes the exterior normal to the curve $\Psi = \text{a constant}$ that passes through the point in question. The resultant shearing stress at a point is therefore proportional to the gradient of the function Ψ at that point.

Further, when written in terms of the function Ψ , the expression (6) for the torsional rigidity becomes—

$$C = 2G \iint \Psi \, dx \, dy. \quad (15)$$

(Reference 3.) That is, the torsional rigidity of the prism is equal to twice the product of the modulus of rigidity and the volume inclosed between the surface

$$z = \Psi(x, y)$$

and the plane

$$z = 0.$$

The solution of the torsion problem for a prism of a given section consists in determining the torsion function ϕ to satisfy the differential equation (3) and the boundary condition (4).

The torsion problem may be solved equally well by determining one of the functions ψ or Ψ from the equations (7) or (11), respectively, each subject to its appropriate boundary condition.

This is the complete theory of the torsion of thin rods. An interpretation of the displacements assumed is that all points on the Z axis remain on that axis and that every cross section of the rod except the fixed one is twisted about the Z axis. By our assumptions, cross sections do not usually remain plane but become warped. Figure 4 shows how elliptical, square, rectangular, and triangular sections become elevated in some parts and depressed in others. All originally plane sections become distorted in the same way since w , the longitudinal displacement, is not a function of z . It is clear, therefore, that the theory does not apply to sections near a fixed end nor to sections near the point where the torque is applied. That all cross sections should remain plane would require that w be constant and the only section for which this can

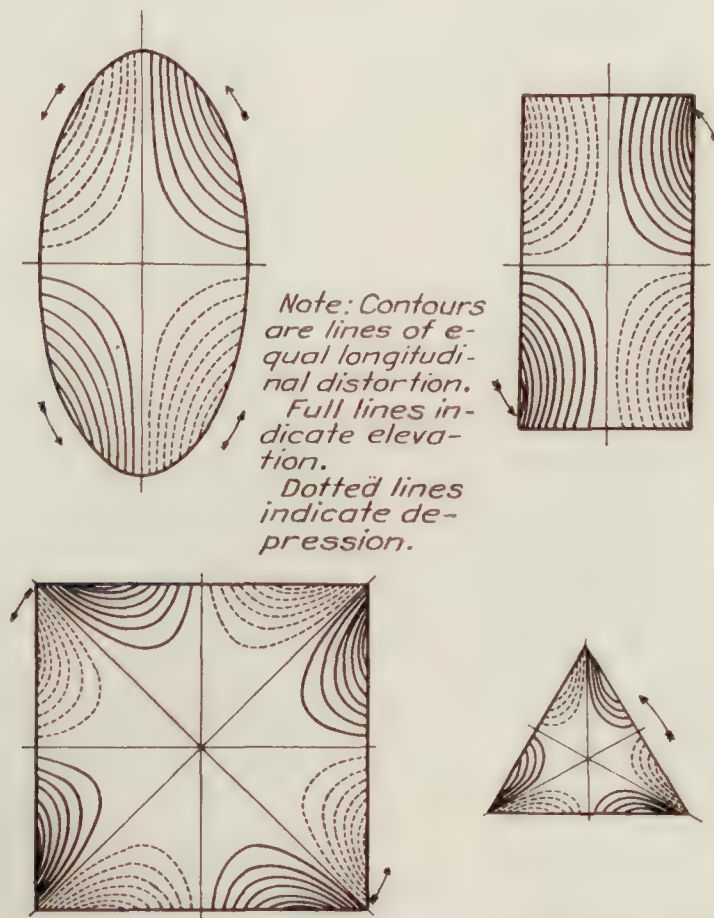


FIGURE 4.—Plane sections of noncircular rods warped in torsion

be true is the circular section. Figure 5, which is taken from Bach's "Elastizität und Festigkeit," shows the distortion in an elliptical cylinder and the lack of it in a circular cylinder.

It has been possible to solve the torsion problem rigorously for only a limited number of sections. The expressions for the torsion function ϕ or the associated function ψ for the more common sections are listed below:

(a) THE CIRCLE:

$$\phi = 0.$$

(b) THE ELLIPSE:

Major and minor axes $2a$ and $2b$ —

$$\phi = -\frac{a^2 - b^2}{a^2 + b^2} xy.$$

(c) THE RECTANGLE:

Sides $2a$ and $2b$ —

$$\phi = -xy + 4b^2 \left(\frac{2}{\pi}\right)^3 \sum_{n=0}^{\infty} \frac{(-1)^n}{(2n+1)^3} \frac{\sinh \frac{(2n+1)\pi x}{2b}}{\cosh \frac{(2n+1)\pi a}{2b}} \sin \frac{(2n+1)\pi y}{2b}.$$

(d) THE EQUILATERAL TRIANGLE:

Origin at centroid. Side a —

$$\psi = \frac{\sqrt{3}}{3a} (3xy^2 - x^3).$$

Corresponding solutions are known for a sector of a circle, a curvilinear rectangle bounded by two concentric circular arcs and two radii, figures bounded by confocal ellipses and hyperbolas,

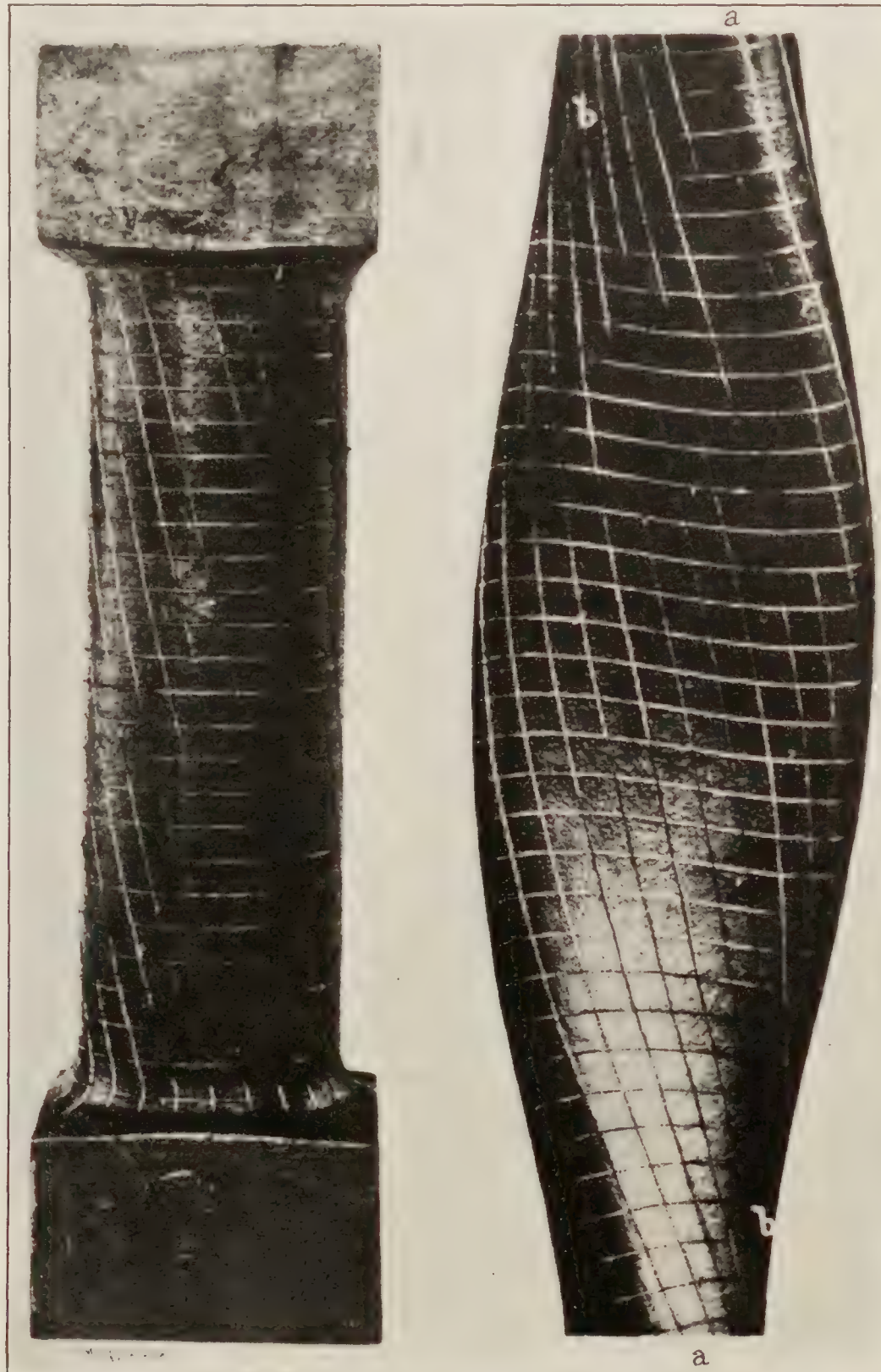


FIGURE 5.—The distortion of plane sections in an elliptical rod and the absence of such distortion in a circular rod

figures shaped like a square but with concave sides and either rounded or sharp corners, and a section somewhat resembling the section of a railway rail. (References 4, 5, and 6.)

Formulas for simple sections.

From the preceding expressions for the torsion functions, the following well-known formulas for torque and maximum stress have been derived:

Let

T = torque.

θ = total angle of twist in radians.

L = length.

G = modulus of rigidity.

q = greatest intensity of stress.

CIRCLE

$$T = \frac{\pi r^4 G \theta}{2L}, \quad q = \frac{2T}{\pi r^3}.$$

r = radius.

ELLIPSE

$$T = \frac{\pi a^3 b^3 G \theta}{(a^2 + b^2)L}, \quad q = \frac{2T}{\pi a b^2}.$$

$2a$ = major axis.

$2b$ = minor axis.

EQUILATERAL TRIANGLE

$$T = \frac{a^4 \sqrt{3} G \theta}{80L}, \quad q = \frac{20T}{a^3}.$$

a = side of triangle.

SQUARE

$$T = \frac{s^4 G \theta}{7.11L}, \quad q = \frac{4.808T}{s^3}.$$

s = side of square.

RECTANGLE

$$T = ab^3 \mu G \frac{\theta}{L}, \quad q = \frac{\gamma T}{\mu a b^2},$$

or

$$T = ab^3 \left(\frac{16}{3} - \lambda \frac{b}{a} \right) G \frac{\theta}{L}.$$

$2a$ = long side of rectangle.

$2b$ = short side of rectangle.

The factors μ , λ , and γ are dependent upon the ratio of the sides. Their values given in Table I are from St. Venant. (Reference 5.) The maximum stress q occurs at the middle of the long side. The stress at the middle of the short side is given by

$$q_1 = \frac{\gamma_1 T}{\mu b^3}$$

in which γ_1 is a factor dependent upon the ratio of the sides. Its values are also given in Table I.

TABLE I.—Factors for calculating torsional rigidity and stress of rectangular prisms

Ratio of sides	λ	μ	γ	γ_1	Ratio of sides	λ	μ	γ	γ_1
1. 00	3. 08410	2. 24923	1. 35063	1. 35063	2. 50	3. 35873	3. 98984	1. 93614	0. 59347
1. 05	3. 12256	2. 35908	1. 39651	-----	2. 75	3. 36023	4. 11143	1. 95687	-----
1. 10	3. 15653	2. 46374	1. 43956	-----	3. 00	3. 36079	4. 21307	1. 97087	-----
1. 15	3. 18554	2. 56330	1. 47990	-----	3. 33	-----	-----	-----	. 44545
1. 20	3. 21040	2. 65788	1. 51753	-----	3. 50	3. 36121	4. 37299	1. 98672	-----
1. 25	3. 23196	2. 74772	1. 55268	1. 13782	4. 00	3. 36132	4. 49300	1. 99395	. 37121
1. 30	3. 25035	2. 83306	1. 58544	-----	4. 50	3. 36133	4. 58639	1. 99724	-----
1. 35	3. 26632	2. 91379	1. 61594	-----	5. 00	3. 36133	4. 66162	1. 99874	. 29700
1. 40	3. 28002	2. 99046	1. 64430	-----	6. 00	3. 36133	4. 77311	1. 99974	-----
1. 45	3. 29171	3. 06319	1. 67265	-----	6. 67	3. 36133	-----	-----	. 22275
1. 50	3. 30174	3. 13217	1. 69512	. 97075	7. 00	3. 36133	4. 85314	1. 99995	-----
1. 60	3. 31770	3. 25977	1. 73889	. 91489	8. 00	3. 36133	4. 91317	1. 99999	. 18564
1. 70	3. 32941	3. 37486	1. 77649	-----	9. 00	3. 36133	4. 95985	2. 00000	-----
1. 75	3. 33402	3. 42843	1. 79325	. 84098	10. 00	3. 36133	4. 99720	2. 00000	. 14858
1. 80	3. 33798	3. 47890	1. 80877	-----	20. 00	3. 36133	5. 16527	2. 00000	. 07341
1. 90	3. 34426	3. 57320	1. 83643	-----	50. 00	3. 36133	5. 26611	2. 00000	-----
2. 00	3. 34885	3. 65891	1. 86012	. 73945	100. 00	3. 36133	5. 29972	2. 00000	-----
2. 25	3. 35564	3. 84194	1. 90546	-----	∞	3. 36133	5. 33333	2. 00000	. 00000

When letters are used for the full sides and not the half sides, letting c represent the long side and d the short side, the formulas become

$$T = cd^3 \beta G \frac{\theta}{L}, \quad q = \frac{8\gamma T}{\mu cd^2},$$

or

$$T = \frac{cd^3}{3} \left(1 - \frac{3\lambda}{16} \frac{d}{c} \right) G \frac{\theta}{L}$$

in which $\beta = \mu/16$, and λ has the same values as before. It can be seen that if $\frac{d}{c}$ is small, we arrive at the common approximate formula:

$$T = \frac{cd^3}{3} G \frac{\theta}{L}.$$

As the ratio $\frac{c}{d}$ varies from 1 to ∞ the expression $\frac{3\lambda}{16}$ varies from 0.578 to 0.630.

St. Venant gives the following approximate formulas for the constants, which agree with exact values within 4 per cent:

$$\gamma = \frac{3}{8} \left(1 + 0.6 \frac{b}{a} \right) \mu,$$

$$\mu = \frac{16}{3} - 3.36 \frac{b}{a} \left(1 - \frac{b^4}{12a^4} \right).$$

Using this value of γ

$$q = \frac{(3a + 1.8b) T}{8a^2 b^2}, \text{ or } q = \frac{(3c + 1.8d) T}{c^2 d^2}.$$

Both are common approximate expressions for the stress at the middle of the long side.

ST. VENANT'S APPROXIMATE FORMULA FOR COMPACT SECTIONS

For fairly compact sections without any reentrant angles St. Venant gives the following approximate formula for the torque:

$$T = \frac{A^4}{40J} G \frac{\theta}{L},$$

in which A is the area of the section, J the polar moment of inertia of the section, G the modulus of rigidity, and $\frac{\theta}{L}$ the angle of twist per unit of length.

Although St. Venant clearly stated that this formula applies only to fairly compact sections with no reentrant angles, it is often applied to other sections, for example, to sections made up of component rectangles. Resulting errors may amount to several hundred per cent in extreme cases. However, when restricted to sections for which it was intended the formula is fairly accurate.

Formulas for hollow prisms or tubes.

The cross section of a hollow prism or cylinder is bounded by two closed curves upon which, in accordance with equation (8), the function Ψ must take constant but, in general, different values. Denoting by Ψ_o and Ψ_i the values of Ψ on the outer and inner boundaries, respectively, and by A_o and A_i the entire areas inclosed by the respective bounding curves, the analysis that led

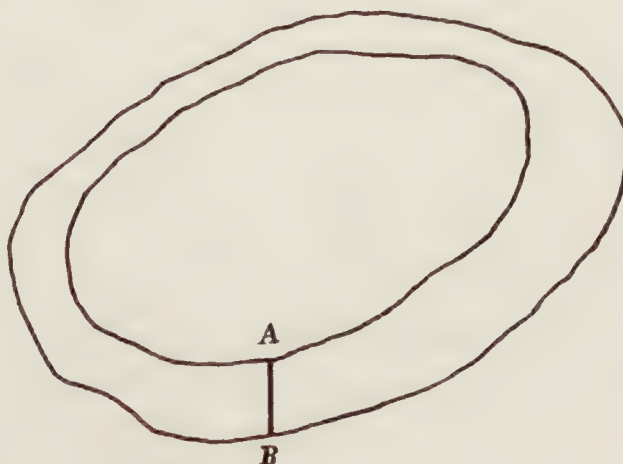


FIGURE 6

to equation (15) for a solid prism or cylinder will now lead to the following expression for the torque:

$$T = -2G\tau\Psi_o A_o + 2G\tau\Psi_i A_i + 2G\tau \iint \Psi(x, y) dx dy. \quad (16)$$

(References 3 and 7.) The integration is extended over the ring-shaped section. If the ring is narrow we can replace Ψ under the integral sign by the constant

$$\Psi_m = \frac{1}{2}(\Psi_o + \Psi_i). \quad (17)$$

The last term in equation (16) then becomes

$$2G\tau\Psi_m(A_o - A_i) = G\tau(\Psi_o + \Psi_i)(A_o - A_i).$$

The expression for T in (16) then reduces to

$$T = 2G\tau A_m(\Psi_i - \Psi_o) = 2G\tau A_m \Delta\Psi \quad (18)$$

where

$$A_m = \frac{A_o + A_i}{2}, \quad \Delta\Psi = \Psi_i - \Psi_o. \quad (19)$$

If we denote by t the width of the ring at any place AB (fig. 6), we obtain (equation 14) as an approximate expression for the average shearing stress at points in AB

$$q = G\tau \frac{\Delta\Psi}{t}. \quad (20)$$

Hence

$$tq = G\tau \Delta\Psi, \quad (21)$$

and (18) becomes

$$T = 2tq A_m. \quad (22)$$

If we form the integral of qds around the curve $\Psi = \Psi_m$ which may, if t is not too large, be taken to be the curve lying half way between the inner and outer boundaries, we find after some reduction

$$\oint qds = 2G\tau A_m. \quad (23)$$

(Reference 8.) Replacing q under the integral in (23) by its value from (22) we obtain

$$\frac{T}{2A_m} \int \frac{ds}{t} = 2A_m G\tau,$$

or

$$T = \frac{4A_m^2 G\tau}{\int \frac{ds}{t}} \quad (24)$$

We find from (22) as the approximate expression for the stress

$$q = \frac{T}{2tA_m}. \quad (25)$$

CIRCULAR TUBES

RIGOROUS METHOD:

When the inner boundary of the tube is a line of shearing stress of a solid section that has the same outer boundary as the tube the rigidity of the tubular section may be obtained directly by subtraction.

$$\begin{aligned} T &= \frac{\pi}{2} \left[\left(r + \frac{t}{2} \right)^4 - \left(r - \frac{t}{2} \right)^4 \right] G \frac{\theta}{L}, \\ &= 2\pi tr \left(r^2 + \frac{t^2}{4} \right) G \frac{\theta}{L}, \quad q = \frac{\left(r + \frac{t}{2} \right) T}{2\pi tr \left(r^2 + \frac{t^2}{4} \right)}. \end{aligned}$$

r = mean radius.

t = thickness of wall.

APPROXIMATE METHOD:

$$\begin{aligned} \frac{T}{A} \int \frac{ds}{t} &= 4AG \frac{\theta}{L}, \quad q = \frac{T}{2tA}, \\ A &= \frac{\pi \left(r + \frac{t}{2} \right)^2 + \pi \left(r - \frac{t}{2} \right)^2}{2}, \\ \int \frac{ds}{t} &= \frac{2\pi r}{t}, \\ T &= 2\pi tr \left(r^2 + \frac{t^2}{2} + \frac{t^4}{16r^2} \right) G \frac{\theta}{L}, \quad q = \frac{T}{2\pi t \left(r^2 + \frac{t^2}{4} \right)}. \end{aligned}$$

Dropping the square and higher powers of t , we have the common approximate formulas

$$T = 2\pi r^3 t G \frac{\theta}{L}, \quad q = \frac{T}{2\pi r^2 t}.$$

ELLIPTICAL TUBES

RIGOROUS METHOD:

The rigorous formulas apply only when the inner and the outer ellipses are similar, that is, when the inner ellipse is a line of shearing stress for a solid shaft having the same outer

boundary as the tube. The semirigorous formulas, of course, apply whether the ellipses are similar or not. Let the inner and outer boundaries be the similar ellipses:

$$\frac{x^2}{a^2} + \frac{y^2}{b^2} = 1,$$

$$\frac{x^2}{a^2} + \frac{y^2}{b^2} = (1+k)^2.$$

Then the inner semimajor axis is a and the outer $a(1+k)$ and the inner semiminor axis b and the outer $b(1+k)$.

$$T = \frac{\pi a^3 b^3}{a^2 + b^2} [(1+k)^4 - 1] G \frac{\theta}{L}, \quad q = \frac{2T}{\pi a b^2 [(1+k)^4 - 1]}.$$

APPROXIMATE METHOD:

Neglecting the square and higher powers of k , the approximate formula (24) gives

$$T = \left[\frac{4\pi k a^3 b^3}{a^2 + b^2} \right] G \frac{\theta}{L}, \quad q = \frac{T}{2\pi k a b^2 (1+k)}.$$

ACCURACY OF APPROXIMATE METHOD

It is apparent from a comparison of the preceding formulas for circular and elliptical tubes that the results from

$$\frac{T}{A} \int \frac{ds}{t} = 4AG \frac{\theta}{L},$$

and

$$q = \frac{T}{2tA}$$

are quite accurate for small values of t . Usually a commercial tube is made with the thickness of metal constant, in which case t in $\int \frac{ds}{t}$ becomes constant. While A had best be regarded as

the mean of the areas inclosed by the inner and the outer boundaries of the section, good results are obtained by drawing a curve midway between the two boundaries of the tube and taking A as the area inclosed by this curve. The quantity ds is an element of length along this curve. Further examples follow.

HOLLOW RECTANGLE

Let the outer boundaries be a and b and let a be the greater side. If t_1 is the thickness of the greater side and t the thickness of the smaller side, the sides of the mean rectangle are $(a-t)$ and $(b-t_1)$ and

$$A = (a-t)(b-t_1),$$

$$\int \frac{ds}{t} = \frac{2(a-t)}{t_1} + \frac{2(b-t_1)}{t},$$

$$T = \frac{2t t_1 (a-t)^2 (b-t_1)^2}{a t + b t_1 - t^2 - t_1^2} G \frac{\theta}{L}, \quad q = \frac{T}{2t(a-t)(b-t_1)}.$$

The equation for stress is true only along the sides of the rectangle where the shear lines are parallel curves. To avoid high stresses at the reentrant angles, the inner corners should be rounded.

CIRCULAR TUBE SPLIT LONGITUDINALLY

A tube of mean radius r and uniform thickness t , split longitudinally, may be regarded as a flat sheet, although this fact is not so well known as it should be. If the ratio of r to t is great, the approximate formula for a rectangle may be applied and

$$\begin{aligned} T &= \frac{1}{3} (2\pi r t^3) G \frac{\theta}{L}, \\ &= \frac{2}{3} \pi r t^3 G \frac{\theta}{L}, \end{aligned}$$

For the closed tube, the approximate formula is

$$T = 2\pi r^3 t G \frac{\theta}{L},$$

and the ratio of the torques for the same $\frac{\theta}{L}$ is

$$\frac{t^2}{3r^2}.$$

It can also be shown that for the same maximum stress the ratio of the torques is approximately equal to

$$\frac{t}{3r}.$$

The split tube, therefore, is much weaker under torsion and very much less rigid.

Solid sections of irregular shape.

We have now discussed substantially all of the sections for which practical formulas have been obtained by direct mathematical treatment. There remain such sections as the **I**, **T**, **U**, and **L** that have not yet been brought within the range of mathematical analysis. These sections normally occur in beams or in compression members and not in members designed primarily to take a torsional couple. Nevertheless, such members are all subject to torsion and the loads that they will sustain may be dependent upon their torsional rigidity. Because of its importance in this connection, our investigation has dealt largely with torsional rigidity rather than with stress.

We will first consider the calculation of the rigidity and later touch upon the matter of stress. For any section we can write

$$T = KG \frac{\theta}{L}.$$

in which K is a constant that depends solely on the shape and dimensions of the cross section and involves the fourth power of a dimension (see the preceding formulas for regular sections). This constant K is usually spoken of as the "torsion constant" of the section and will be so referred to in this report. Our problem is to determine a suitable method of calculating K for various irregular shapes.

Before embarking upon an extended series of tests, it was necessary to make some preliminary tests of wooden members of simple section in order to determine to what extent certain factors governed the torsional properties of wood. As a usual thing, the modulus of rigidity associated with a traction in a radial plane is not equal to the modulus associated with the traction in a tangential plane. In other words, the elastic constant for a shearing stress acting in a plane at right angles to the growth rings is not the same as for a shearing stress acting in a plane tangential to the growth rings. This fact introduces two moduli of rigidity into the problem. There is a third modulus of rigidity for wood which has to do with the stresses that tend to roll contiguous fibers past each other, but when a member is twisted about an axis parallel to the grain of the

wood this elastic constant does not come into play. Our first problem then was to determine what difference, if any, there was between the radial modulus of rigidity and the tangential modulus. Other factors pertinent to our test procedure were the effect of moisture content and the effect of rate of strain. Each of these three factors was studied and a brief discussion of each follows.

Moduli of rigidity of spruce.

It is shown in Appendix A that a rectangular prism, two of whose axes of elastic symmetry lie in the plane of the cross section, behaves as a prism with a parallelogrammatic cross section when these axes are not parallel to the sides and as a prism with a transformed rectangular section when the axes are parallel to the sides. The modulus for the transformed section in either case is computed from the two moduli involved. It is also shown that if G_t is the modulus associated with the plane tangential to the annual rings and G_r the modulus associated with the plane perpendicular to the rings, the relations of Table II hold.

TABLE II

Sides $2a, 2b$	Sides of transformed rectangle	Modulus
Plain-sawn board.....	$2a\sqrt{\frac{G_r}{G_t}}, 2b$	$G_t\sqrt{\frac{G_t}{G_r}}$
Quarter-sawn board.....	$2a\sqrt{\frac{G_t}{G_r}}, 2b$	$G_r\sqrt{\frac{G_r}{G_t}}$

It was possible from these relations to determine the value of G_t and G_r for any plank by testing a quarter-sawn and a plain-sawn piece cut from that plank. This was done for practically every piece used. These minor specimens were 1 by 3 inches in cross section. Occasionally slight season checks, which run radially, caused the quarter-sawn pieces to be less rigid than their corresponding plain-sawn pieces, whereas with sound material the quarter-sawn piece should be the more rigid, since G_r is greater than G_t . It was found that for Sitka spruce G_t was about 90 per cent of G_r . This means that quarter-sawn rectangular beams of Sitka spruce with a large ratio of long side to short side will average about 10 per cent more rigid in torsion than similar plain-sawn beams. Ordinarily no great error will result if the mean modulus as obtained through the test of a circular section is used in calculating the rigidity of beams. It may, of course, introduce on the average about half of the difference between the plain and the quarter-sawn values, or an error of about 5 per cent. It is much easier to make square sections than circular sections and the difference in mean modulus obtained is practically nil. Square minor specimens, therefore, were tested as a check against the values obtained from the 1 by 3 inch minor specimens.

As a check against the mathematical analysis given in Appendix A, a few series of tests were run on beams of rectangular and of elliptical sections with the annual growth rings at various angles to the axes of the sections. The results are shown in Figure 7. The curve for the ellipse was calculated by means of the relations given in Appendix A; the circles along the curve are test values. The curves for the rectangles represent the observations; they agree in form with a curve calculated for a different ratio of the two moduli.

Effect of moisture content.

In order to obviate the necessity of making moisture adjustments, the major and the minor test specimens were always kept in the same condition. They were never separated after fabrication and the time between the testing of the majors and the minors was reduced to a minimum.

A series of tests was made, however, to learn enough about the effect of moisture content on torsional properties to permit the recommendation of permissible stress values for spruce at a

definite moisture content. Twelve matched square pieces were tested, 3 green, 3 at about 21½ per cent, and 3 at about 7 per cent moisture content. The results are given in Figure 8, which shows the variation with moisture content of three properties; namely, modulus of rigidity, fiber stress at elastic limit, and ultimate fiber stress. The results from this small number of tests were in agreement with relations previously established at this laboratory.

Effect of rate of loading.

As tests were run on members of various sizes, the rate of strain was kept fairly uniform in order not to introduce this factor into the results. The ordinary test, however, took several

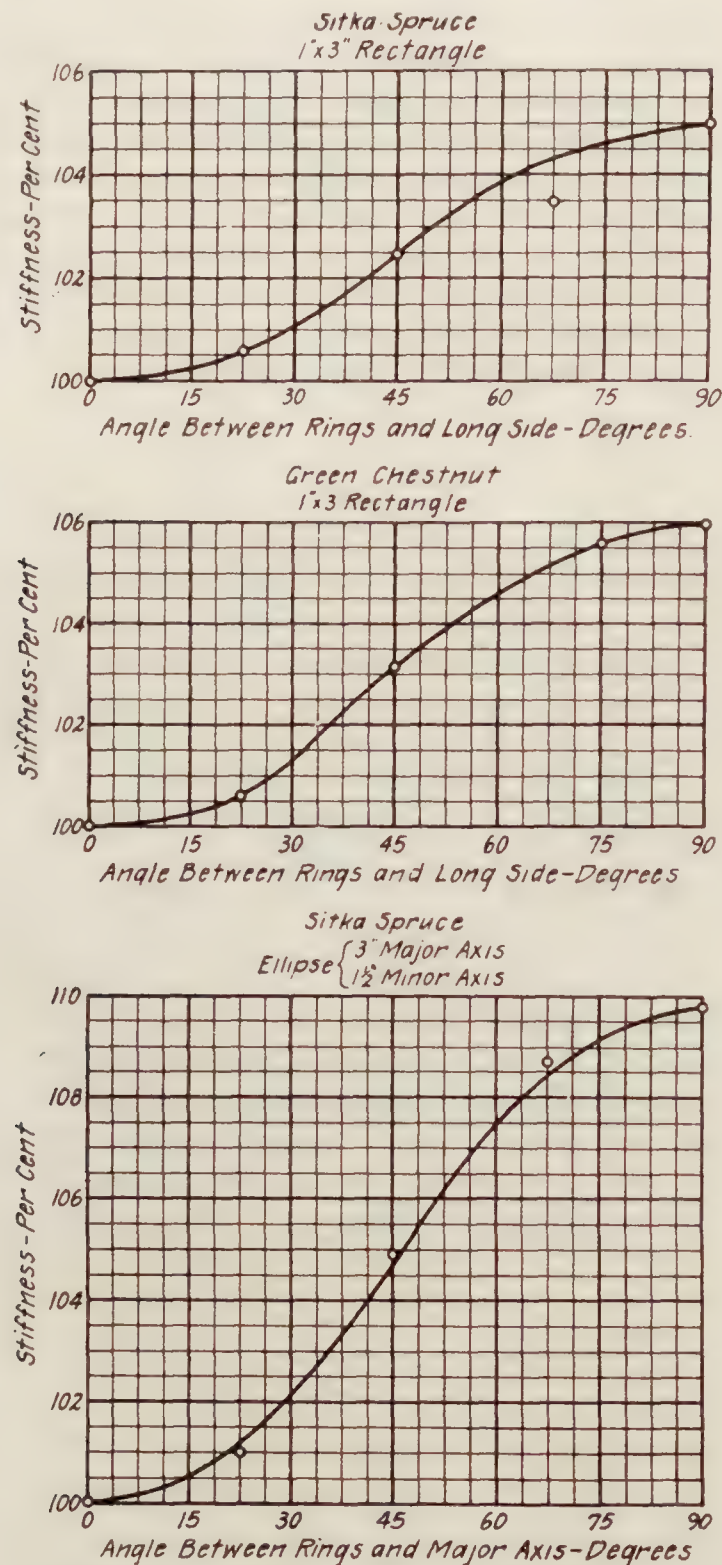


FIGURE 7.—Variation in torsional stiffness with direction of annual rings on the cross section

minutes, whereas the duration of stress assumed for aircraft stresses is three seconds. Consequently, in order to recommend torsional properties of spruce from test, it was necessary to know something about the variation in these properties with rate of strain. A matched set of cylindrical specimens was made and equal numbers of them were tested, respectively, at each of three rates; these rates were in the proportion 1 to 10 to 100. It was found that accompanying a 10 to 1 change in rate there was a 5 per cent increase in modulus of rigidity, a 10 per cent

increase in ultimate fiber stress, and a 20 per cent increase in fiber stress at elastic limit. The exponential increase of stress with increased rate of fiber strain has been previously observed at this laboratory.

Torsion tests of simple sections.

As the next preliminary step before testing wooden beams of irregular section, several series of tests were made on spruce beams of simple section. Beams with the circle, the square, the ellipse, and the equilateral triangle as bounding curves of the cross sections were cut from the same plank. The dimensions and the angle of twist for a given torque as determined by test were substituted in the rigorous formula previously given for the corresponding sections and an apparent modulus of rigidity calculated thereby. Four of each type of beam were cut from each plank. The results are given in Table III. The planks were chosen so as to obtain

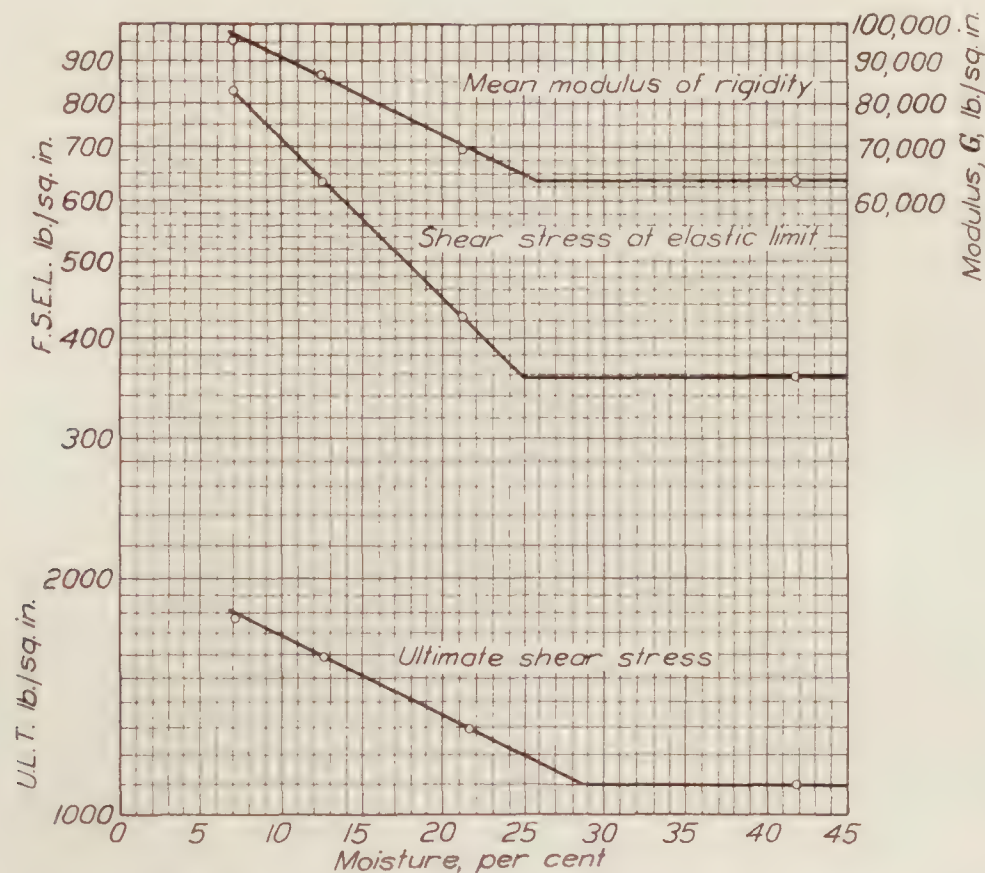


FIGURE 8.—Relation between torsional properties and moisture content of Sitka spruce

a wide range in specific-gravity values. Consequently the first two (Table III) are below the minimum specific gravity (0.36) allowable in aircraft construction.

TABLE III

Plank	Specific gravity	Moduli of rigidity				M. of E. bending
		Circle	Square	Ellipse	Equilateral triangle	
6-1-58	0.322	78,300	72,500	75,800	80,600	1,347,000
6-1-25	.344	82,500	81,600	-----	84,000	1,358,000
5-1-49	.426	116,500	119,200	122,600	121,800	1,520,000

All specimens were 45 inches long and the angle of twist was measured over a 24-inch gage length. The nominal diameter of the circular specimens and the width of the square specimens were each $1\frac{1}{4}$ inches. The major and the minor axes of the elliptical specimens were $1\frac{1}{2}$ inches and 1 inch, respectively, for plank 6-1-58 and $1\frac{1}{4}$ inches and 1 inch for plank 5-1-49. The triangular specimens were 2 inches on each side. An error in grinding the shaper knives for the set with elliptical section from plank 6-1-25 necessitated the culling of that set. Aver-

aging the results from the first and the last sets in Table III, we find that the apparent modulus of rigidity for the square is 1.6 per cent lower than for the circle, for the ellipse 1.8 per cent higher, and for the equilateral triangle 3.8 per cent higher. As pointed out in Appendix A, the direction of the annual rings with respect to the axes of the section has little effect on the rigidity of sections whose bounding curve is a square or an equilateral triangle. For the elliptical section, however, there is some difference. Consequently, the first set in the table was cut with the rings parallel to the major axis and the second set with the rings perpendicular to that axis. Had the specimens been longer, it is thought that the results for the triangular sections would have been somewhat lower. The ends of these specimens were enlarged for the application of torque. With the circular section such enlargement would make little difference as long as the points at which measurements were taken were three or four diameters away from the enlargement. This is because in the circular rod plane sections remain plane. In the triangular rod the tendency of the sections to warp is hindered by the enlargement of the ends with a consequent increase in stiffness. The same fact is true, although to a less extent, of the ellipse. The rods with square sections did not have built-up ends. Taking all these factors into consideration, the agreement as to torsional rigidity as calculated by the rigorous formulas is considered quite suitable.

Table III yields another interesting relation. If the moduli of elasticity in the last column, which were obtained from minor bending tests, are divided by the corresponding moduli of rigidity for the circular section given in the third column, the quotients will average 15.6. This relation for the average of 12 rods checks the relation obtained in 1921 for 20 rods of circular section that were tested in torsion in connection with another investigation. The mean modulus of rigidity for the 20 specimens was 100,200 p. s. i., and the average modulus of elasticity 1,569,000 p. s. i., or a ratio of 1 to 15.6. Hence the ratio for spruce is evidently between one-fifteenth and one-sixteenth, whereas for most metals it is in the neighborhood of two-fifths.

As a further check, four rods of elliptical section were made with a major axis of 2 inches and a minor axis of $1\frac{1}{2}$ inches and were tested within the elastic limit, and then were cut down to a $1\frac{3}{4}$ -inch major axis and $1\frac{1}{4}$ -inch minor axis and retested. The apparent modulus of rigidity in the first case averaged 77,325 p. s. i., and in the second 78,162, a difference of only 1 per cent. A repetition of this series resulted in a difference of slightly over 1 per cent but with the results reversed. Sections with equilateral triangles as bounding curves were cut down in the same way, though in three steps, first with a 2-inch side, then a $1\frac{3}{4}$ -inch side, and finally a $1\frac{1}{2}$ -inch side. The average apparent moduli for four beams were 73,350 p. s. i. for the 2-inch side, 72,250 for the $1\frac{3}{4}$ -inch side, and 72,650 for the $1\frac{1}{2}$ -inch side. The maximum difference is about 1 per cent.

From these tests it appears that dependable results can be obtained by using wood as a test material.

Torsion tests of irregular sections.

Following these preliminary tests, additional tests were made on beams of irregular section. Such sections as I, T, L, U, and Z were used with and without fillets at the reentrant angles. In addition to varying the radius of fillet, the ratio of the thickness of the web to that of the flange or of one leg to that of the other was varied through a considerable range.

The beams were 8 feet long and the angle of twist was read for a gage length of 36 inches at the center. The results of these tests will be discussed later in connection with the coordination of the mathematical and the experimental work in the form of empirical formulas.

The use of soap films in solving the torsion problem for irregular sections.

The value of soap films in determining the torsional rigidity and the stress in twisted beams depends upon the mathematical analogy between the torsion problem and that of a membrane, such as a soap film, under a uniform excess of pressure on one side. Attention was first called to this analogy by Prandtl and very extensive use of it was made by Griffith and Taylor. (References 9 and 10.) The method is extremely useful in that it offers a means of determining the torsional rigidity and the stress of important irregular sections that have not

yielded to mathematical treatment. An apparatus was built and, after it was found to give results for simple sections that agreed closely with calculated values, tests were made on irregular sections. The construction of the apparatus and the method of using it have already been described under the heading "Test Material and Procedure." The mathematical basis of the method and a brief discussion of the technic follow. The test results will be dealt with later in connection with proposed formulas for irregular sections whose component parts are rectangles.

In presenting the mathematical basis of the soap-film method of test, let a very thin homogeneous membrane be stretched under uniform tension T over an opening cut in a plane sheet of rigid material and let the membrane be fixed at the edge of the opening. If a uniform excess of pressure p per unit area acts upon one face of the membrane, the small displacement z of points of the membrane will satisfy the differential equation:

$$T \left(\frac{\partial^2 z}{\partial x^2} + \frac{\partial^2 z}{\partial y^2} \right) + p = 0, \quad (26)$$

and the condition that

$$z = 0 \quad (27)$$

at the edge of the opening.

Let the opening and the section of the prism under consideration be identical in size and shape. If we let

$$z = \frac{p}{2T} \Psi \quad (28)$$

in equations (26) and (27), we obtain equations (11) and (12) for the function Ψ . Hence the function Ψ appropriate to the torsion problem for a section of given shape is proportional to the displacement z of a homogeneous membrane stretched over an opening of the same shape as the section. The proportionality factor in (28) is determined by means of a film stretched over a circular opening and under the same pressure as the test film. It follows from equation (15) that the torsional rigidity of a prism of the given section is proportional to the volume inclosed by the soap film and the plane of the opening. Further, the contour lines, $z = \text{constant}$, of the soap film correspond, in accordance with equations (13), to the lines of shearing stress $\Psi = \text{constant}$ in the torsion problem. And the slope of the film at any point, as a consequence of equation (14), is proportional to the magnitude of the shearing stress at the corresponding point of the section.

In employing the soap-film method, an opening that represents the section of the prism to either a reduced or an enlarged scale may be used. It is necessary only to observe that the ratio of the torsional rigidities of two geometrically similar sections is equal to the fourth power of the ratio of corresponding linear dimensions.

To obtain well-defined edges coinciding with the boundary of the cross section, the edges of the openings were beveled at an angle of 45 degrees. Our experience has been that this does not entirely eliminate the errors at the edges. The film is not always attached at the upper side of the beveled edge but frequently hangs at an intermediate point. Even when great care is used to avoid a surplus of solution, there usually is a layer of solution along the edge of the film that tends to lower the level in its neighborhood and to make uncertain the actual position of the boundary. Further, at points where the stress is great and the film consequently is steep, there is a tendency for the film to run out over the plate.

Errors resulting from edge effects can be avoided by using as boundaries of the cross sections contour lines other than the actual outline of the opening in the plate. These contour lines, if taken near the edge of the opening, approximate the shape of the section with sufficient accuracy. The dimensions of the section bounded by the contour line in question can be measured. In the tables giving the results of our experiments with soap films, we have included, in general, data from one or more inner contour lines as well as from the actual outline of the opening. We have thus increased the number of sections studied. It is our feeling that the results from the inner contours are more reliable than those from the outlines of the openings. In every case

an inner contour line of the spherical bubble over the circular opening was used as the boundary of the comparison cylinder.

There are various ways of finding the volume inclosed by the test bubble. A satisfactory procedure is to take contour lines at frequent intervals, planimeter the areas inclosed by these lines, and obtain the volume between the planes at different levels by the average-end-area method.

For further details in regard to the technic of the soap-film method, the reader should consult the papers by Griffith and Taylor. In our judgment, the high degree of accuracy that they attained in certain cases is not always to be expected.

Formulas for irregular solid sections.

Combining results obtained by soap-film tests with known mathematical facts, Griffith and Taylor developed an empirical method of dealing with solid rods of any section, which is explained in Appendix B of this report. The method gives results for the torsional rigidity of fairly compact sections with errors of only a few per cent. For certain sections, however, the errors are considerable. In their report on the method, they attribute a discrepancy between their results and those of published experimental work to a want of homogeneity in rolled **I** and **U** sections. Some of our soap-film experimental work on **I** and **U** beams, however, fails to check their formula by as much as 25 per cent and the discrepancy is in the same direction as that mentioned in their reports, the formula giving results that are too high.

In an extensive investigation of the torsion problem, Constantin Weber developed, on the basis of the usual mathematical theory, approximate formulas for the torsional rigidity of a large number of sections and for the maximum stress in these sections. (Reference 11.) Torsional rigidities calculated by his formulas are low in comparison with our test results.

In dealing with such sections as the **L**, **U**, **Z**, **T**, and **I**, Weber replaced the given section by an equivalent rectangular section. To represent the situation at the junction of two rectangles, he chose the length of the equivalent rectangle to secure a certain desired area. Now changing the length of a rectangular section in a certain ratio does not alter its stiffness nearly so much as a corresponding change in the breadth. There is essentially an increase in breadth of section at the junction of two rectangles, for instance, at the corner of an **L**. This can not be compensated for by merely increasing the length of the equivalent rectangle in the manner chosen by Weber. Accordingly, his formulas give values of the torsional rigidity considerably below those that we have found by means of direct torsion tests and tests made by the soap-film method. It should be noted that Weber assumed that fillets were always present, their radii being equal to the width of the narrower of the component rectangles of the sections.

For sections such as **I**, **U**, and **T**, whose component parts are rectangles, the following approximate method for calculating stiffness is proposed as a result of our study; we shall first show its derivation.

The problem is to find K in

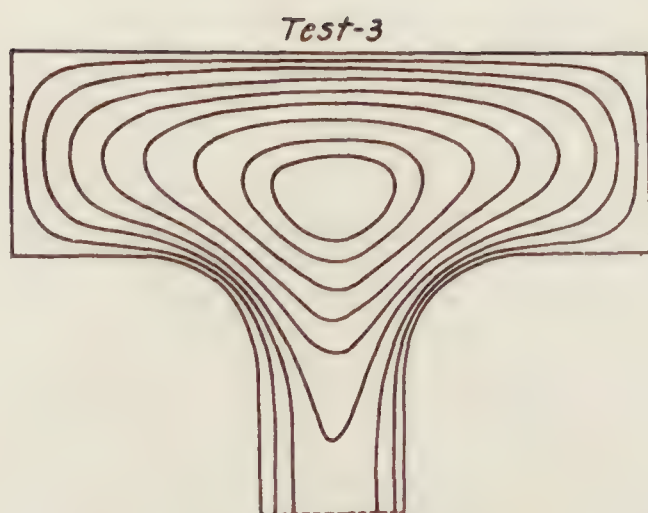
$$T = KG \frac{\theta}{L}.$$

Now K is a constant that depends solely on the shape and the dimensions of the cross section, and involves the fourth power of a dimension. Figures 9 and 10 show that at the junction of two component rectangles there occurs a hump or hill on the soap film. This hump shows that the rigidity of the complete bar is greater than the sum of the rigidities of the separate rectangular parts. The volume of the soap bubble, of course, represents the rigidity of the entire bar and the increased volume at the hump in the bubble represents the amount by which the rigidity of the bar exceeds the sum of the rigidities of its separate rectangular parts.

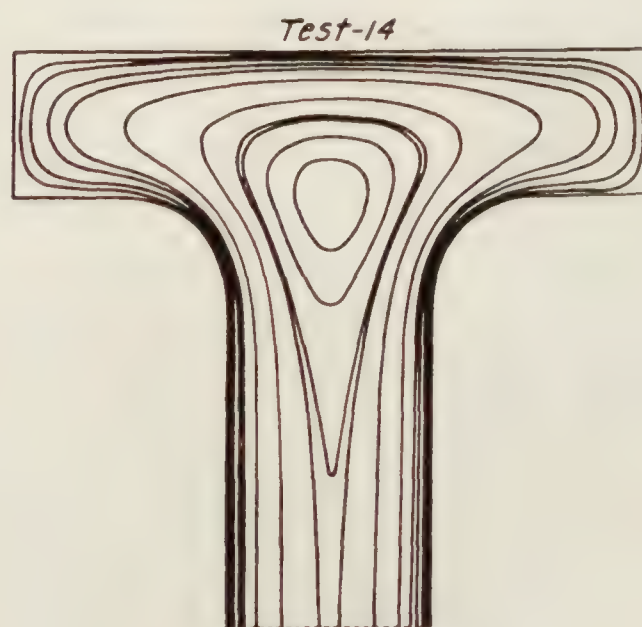
For an **I** beam, we write

$$K = 2K_1 + K_2 + C$$

in which K_1 is the torsion constant of one flange and K_2 that of the web, while C is the term that is to express the additional stiffness caused by the two junctions of the flanges and the web. In place of C we write $2 \alpha D^4$ in which D is the diameter of the largest circle that can be inscribed

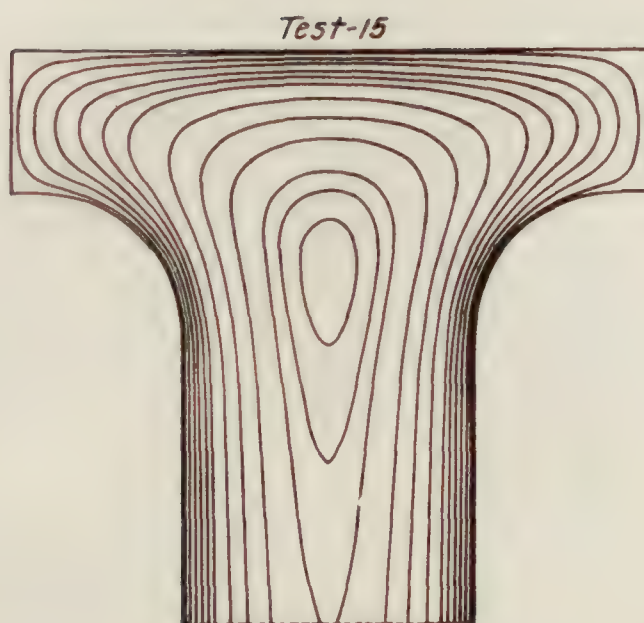


Contour Elevations
 .054-.104-.154-.204
 .254-.304-.354-.379
 Top of Bubble .404

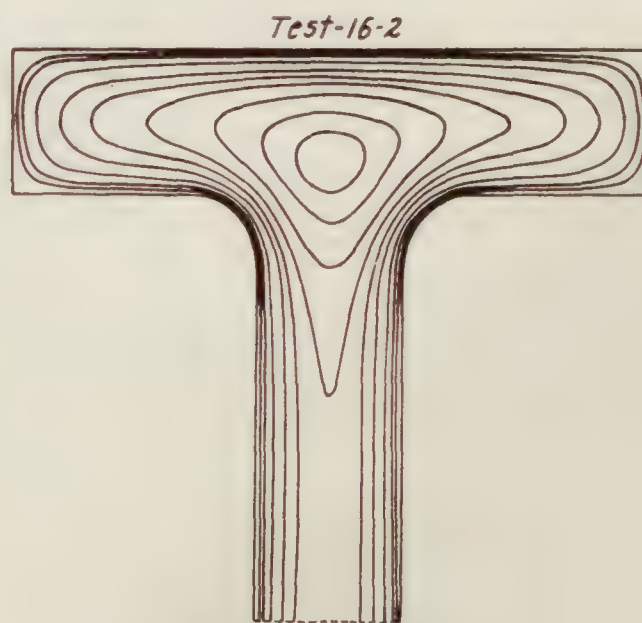


Contour Elevations
 .004-.018-.038-.053-.068
 .138-.173-.178-.203-.228
 Top of Bubble .238

Note:- All Dimensions are in Inches

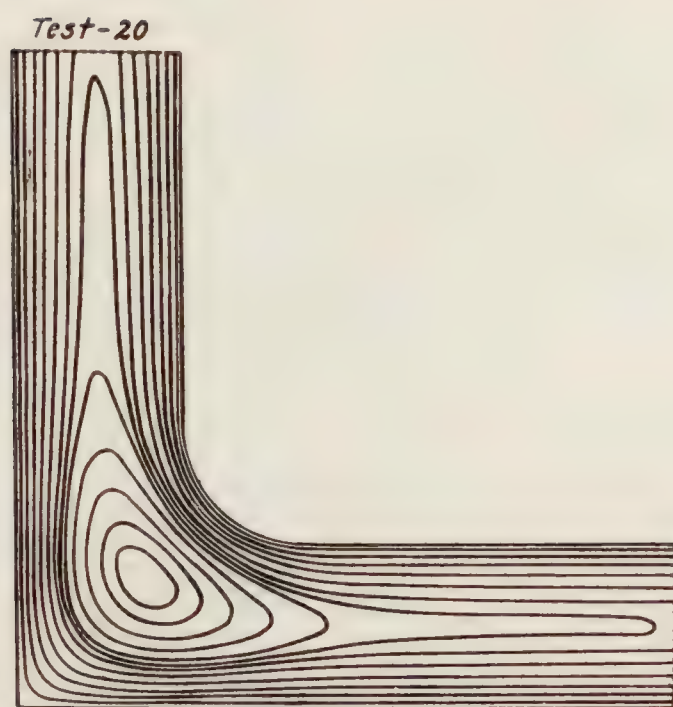


Contour Elevations
 .012-.037-.062-.087-.112-.137
 .187-.237-.287-.337-.357-.377
 Top of Bubble .387

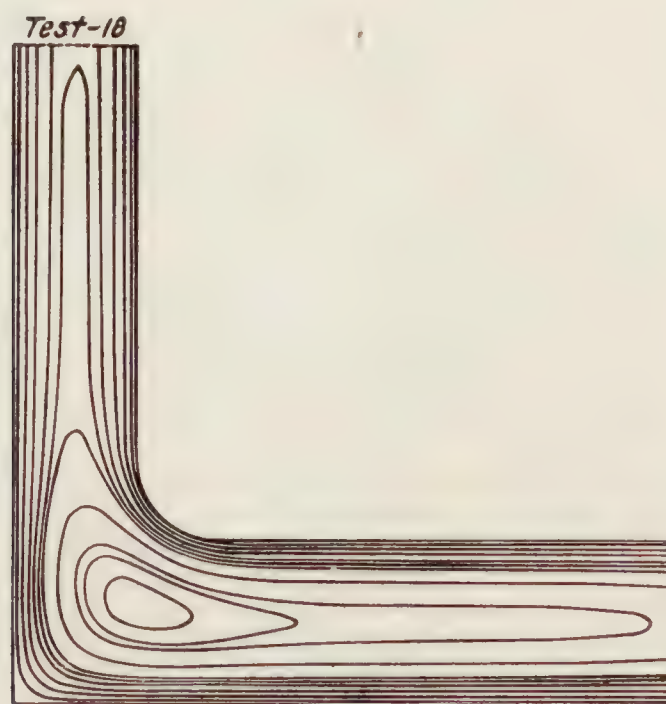


Contour Elevations
 .003-.017-.057-.087-.117
 .128-.167-.187-.212
 Top of Bubble .237

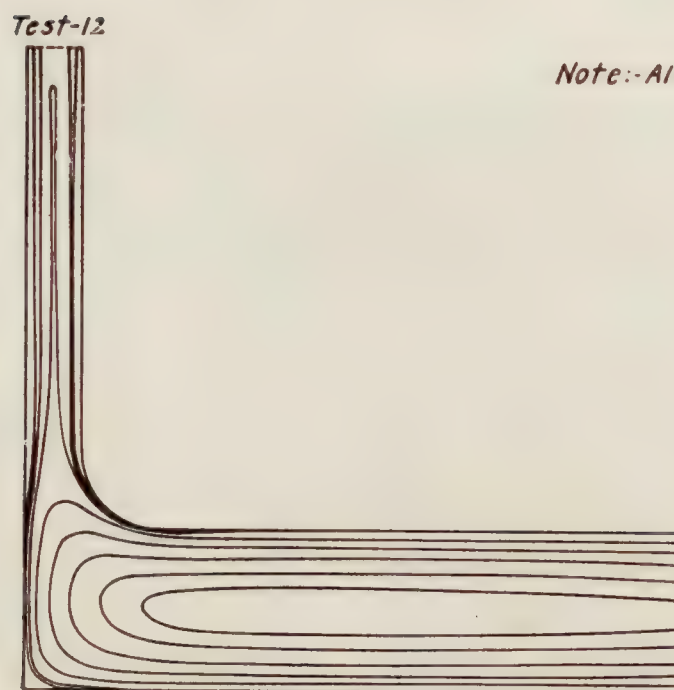
FIGURE 9.—Lines of shearing stress for I beams in torsion. (From soap-film tests on half sections)



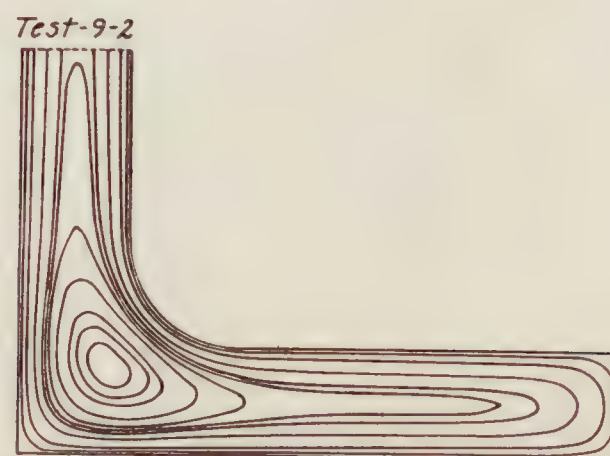
Contour Elevations
.013-.038-.063-.088-.113-.133
.145-.156-.178-.198-.218-.230
Top of Bubble-.238



Contour Elevations
.014-.039-.064-.089-.104
.119-.159-.197-.209-.229
Top of Bubble-.239



Contour Elevations
.005-.011-.019-.053
.103-.153-.203-.233
Top of Bubble-.253



Contour Elevations
.008-.028-.058-.078-.085
.098-.118-.138-.148-.158
Top of Bubble-.163

Note:-All Dimensions are in Inches

FIGURE 10.—Lines of shearing stress for U and Z[beams]in torsion. (From soap-film tests on half sections)

at the junction of the two component rectangles and α is a factor to be determined. We then have

$$K = 2K_1 + K_2 + 2\alpha D^4.$$

An examination of Figure 9 will show that the bubble tapers down at the ends of the flanges, as it normally would in a rectangle, while in the web it behaves more like a part of a long rectangle. For this reason, we shall calculate K_1 by the normal formula for the rectangle

$$K_1 = a_1 b_1^3 \mu \text{ or } K_1 = a_1 b_1^3 \left(\frac{16}{3} - \lambda \frac{b_1}{a_1} \right),$$

and K_2 by the formula

$$K_2 = \frac{16}{3} a_2 b_2^3.$$

The factor α for any section depends upon two things; the ratio of the radius of the fillet to the thickness of the flange and the ratio of the thickness of the narrower component rectangle to

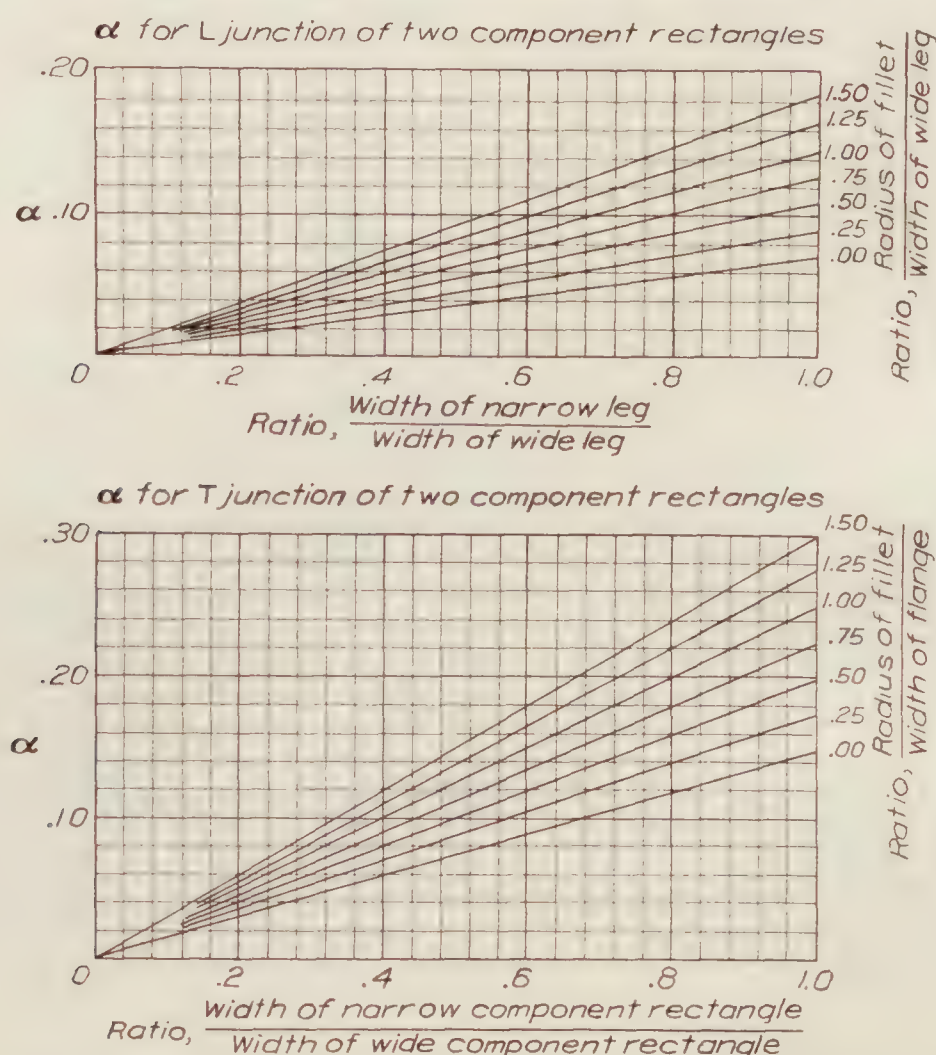


FIGURE 11.—Values of α for computing torsional rigidity of sections whose component parts are rectangles

the thickness of the wider component rectangle. The values of α for different combinations of these two factors, which were obtained through a variety of experiments with soap films and torsion tests of actual beams, are shown graphically in Figure 11. While our experiments were not extensive enough to prove conclusively that for a given ratio of radius of fillet to thickness of flange the variation in α is linear for varying ratios of the thicknesses of the two component rectangles, we feel that such a variation is close enough to the truth to warrant its use. Table IV shows how K calculated by this simple method for I sections agrees with results obtained by actual beam tests and soap-film tests.

TABLE IV.—Values of torsion constant K for I-beams

[Dimensions are in inches]

ACTUAL TORSION TESTS

Test	Thickness		Total height	Total width	Fillet radius R	D	D^4	$2K_1+K_2$	2α	Test K	Proposed formula K	Difference	G. and T. formula K	Difference
	Web	Flange												
I-7-----	0.500	0.500	3.46	2.240	0	0.625	0.153	0.263	0.300	0.300	0.309	Per cent +3.0	0.321	Per cent +7.0
I-8-----	.498	.498	3.46	2.230	0	.622	.150	.259	.300	.296	.304	+2.7	.317	+7.1
I-9-----	.501	.501	3.48	2.250	0	.626	.154	.266	.300	.301	.312	+3.7	.325	+8.0
I-10-----	.624	.876	4.00	2.740	0	.987	.947	1.164	.214	1.457	1.367	-6.1	1.416	-2.8
I-11-----	.624	.875	4.01	2.740	0.250	1.106	1.500	1.161	.255	1.600	1.543	-3.6	1.634	+2.1
I-12-----	.625	.874	4.00	2.740	0	.986	.945	1.158	.214	1.475	1.360	-7.8	1.412	-4.3
I-13-----	.624	.874	4.00	2.740	.250	1.104	1.485	1.157	.255	1.620	1.536	-5.2	1.631	+0.7
I-14-----	.623	.872	3.97	2.744	0	.990	.961	1.149	.214	1.355	1.355	0.0	1.404	+3.6
I-15-----	.624	.873	3.97	2.745	.250	1.103	1.481	1.153	.255	1.490	1.531	+2.7	1.625	+9.0
I-16-----	.622	.872	3.98	2.745	.500	1.224	2.245	1.149	.296	1.822	1.814	-0.5	1.920	+5.4
I-17-----	.622	.873	3.97	2.746	.750	1.340	3.305	1.152	.335	2.255	2.258	+0.1	2.356	+4.5
I-18-----	.507	1.045	4.49	2.750	.875	1.502	5.085	1.695	.227	2.720	2.850	+4.7	3.132	+15.2
I-19-----	.503	1.045	4.50	2.750	.875	1.498	5.040	1.693	.225	2.695	2.827	+4.9	3.078	+14.2
I-22-----	.498	1.039	4.48	2.760	.875	1.492	4.950	1.670	.224	2.734	2.779	+1.6	3.076	+12.5
I-23-----	.497	1.043	4.49	2.760	.875	1.492	4.950	1.689	.223	2.571	2.792	+8.6	3.096	+20.4
SOAP-FILM TESTS														
3-----	1.260	1.760	7.94	5.510	1.000	2.466	36.95	18.95	0.296	29.30	29.89	+2.0	31.57	+7.7
14-----	1.755	1.255	10.03	5.517	.875	2.276	26.84	19.78	.315	27.48	28.24	+2.8	29.17	+6.1
14-C2-----	1.650	1.100	9.92	5.160	.950	2.150	21.38	15.30	.315	23.22	22.04	-5.1	22.90	-1.4
15-----	2.507	1.260	10.03	5.512	1.250	2.929	73.55	45.71	.251	66.06	64.18	-2.8	64.45	-2.4
15-C2-----	2.390	1.050	9.90	5.050	1.390	2.820	63.20	38.92	.248	54.60	54.60	0.0	54.24	-0.7
16-2-----	1.260	1.257	10.00	5.510	.625	1.885	12.63	11.24	.400	13.74	16.29	+18.5	16.52	+20.3
16-2-C1-----	1.180	1.180	9.96	5.390	.640	1.793	10.45	9.26	.408	12.76	13.52	+6.0	13.69	+7.2
16-2-C2-----	1.105	1.105	9.98	5.260	.670	1.718	8.71	7.56	.420	10.84	11.22	+3.5	11.38	+5.0

All calculations were made with a 20-inch slide rule.

C1 and C2 indicate that first or second contour of the plate was used as the boundary of the cross section.

 D =Diameter of largest inscribed circle at junction of component rectangles. $K=2K_1+K_2+2\alpha D^4$. K_1 =torsion constant of flange. K_2 =torsion constant of web.

Results in column headed "G. and T. formula" were calculated by the Griffith and Taylor method.

Differences are expressed in per cent of test values.

An examination of the formula discloses the fact that the formula still holds at the limit where the web approaches zero thickness, since α will also approach zero. At the other limit, where the flange approaches zero thickness, α again approaches zero, but the value $K_2 = \frac{16}{3} a_2 b_2^3$ is somewhat in error because the web can no longer be considered a part of a long rectangle.

From the relations holding for an I beam, we obtain results for a T beam directly. The T beam has only one junction of component rectangles and consequently only αD^4 in the formula. Also K_2 must be modified slightly. The web now closes at one end, as it would normally in a rectangle, and therefore K_2 is one-half the K of a rectangle twice as long or

$$K_2 = a_2 b_2^3 \mu,$$

the value of μ corresponding to the ratio $2a \div b$. Our final result is

$$K = K_1 + K_2 + \alpha D^4.$$

For sections such as an L, we proceed in the same way. The wider leg is considered as the normal rectangle and the narrower leg as a part of a long rectangle. An examination of Figure 10 will show why this is done. Figure 11 gives the proper values for α . For sections made up of L junctions, such as U and Z sections, we proceed in the same way and add a correction for each junction.

In applying the soap-film method to U and Z sections, advantage was taken of the symmetry of these sections with respect to a line perpendicular to the bar at its middle point; L-shaped openings in the test plate, having a vertical septum at the ends of one or both legs, were used. When the legs of the L were of unequal thickness, it was desirable to have a septum at the end of each leg in order to be able to calculate two types of U or Z sections from a single test. By means of a simple calculation the effect of the septum at the end, when one is not desired,

can be removed. Values of the torsion constant given in Table V for U and Z sections were obtained in this way from L-shaped openings.

The actual torsion tests on wooden beams with L, T, U, and Z sections (Table VI) yielded apparent values of the torsion constant that were considerably greater than those given by the soap-film method for the same sections. The excesses in the values thus determined are attributable to two causes:

(1) The stiffening effect of the blocks that were glued to the ends of all beams tested to make the end sections rectangular. These blocks hindered the warping of the cross sections that takes place in the twisting of all cylinders or prisms not of circular section. (Fig. 4.)

TABLE V.—Values of torsion constant K for U or Z beams

[All dimensions are in inches]

Test	End of legs	Thickness		Overall		Fillet radius R	D	D^4	$2K_1+K_2$	$2a$	Soap film K	Pro- posed form- ula K	Differ- ence	G. and T. form- ula K	Differ- ence
		Legs	Bar	Length leg	Width bar										
5-1	Without septum	1.498	1.495	5.51	7.50	0	1.755	9.49	15.26	0.140	16.68	16.59	Per cent -0.5	17.71	Per cent +6.1
5-1-C1	do	1.390	1.390	5.30	7.34	0	1.630	7.06	12.08	.140	13.34	13.07	-2.0	13.85	+3.9
7-2	do	1.263	1.256	5.51	7.56	0	1.478	4.77	9.62	.140	10.12	10.29	+1.7	10.90	+5.9
7-2-C1	do	1.225	1.225	5.44	7.52	0	1.435	4.24	8.86	.140	9.39	9.45	+0.6	9.94	+5.9
7-2-C2	do	1.160	1.160	5.36	7.48	0	1.360	3.42	7.48	.140	8.06	7.96	-1.2	8.40	+4.2
9-2	do	1.006	1.008	5.51	7.54	1.00	1.515	5.27	5.20	.290	5.98	6.73	+12.5	7.49	+25.4
9-2-C1	do	.930	.940	5.41	7.48	1.04	1.451	4.43	4.12	.305	5.31	5.47	+3.0	6.14	+15.7
9-2-C2	do	.800	.810	5.26	7.38	1.14	1.339	3.21	2.65	.358	3.78	3.80	+0.5	4.18	+10.6
10	With septum	1.508	.752	6.00	11.98	.75	1.660	7.59	13.88	.107	14.94	14.69	-1.7	15.41	+3.1
10-C1	do	.710	1.470	5.97	11.96	.80	1.640	7.24	13.48	.108	14.46	14.26	-1.4	14.16	-2.1
10-C2	do	.580	1.450	5.96	11.90	.90	1.600	6.55	11.76	.093	12.78	12.37	-3.2	12.82	+0.3
11	do	1.506	1.507	6.00	12.06	.75	2.016	16.50	22.90	.215	26.18	26.45	+1.0	28.77	+9.9
11-C1	do	1.450	1.470	5.96	12.00	.79	1.980	15.38	20.80	.220	24.98	24.18	-3.2	26.39	+5.6
11-C2	do	1.353	1.373	5.96	11.98	.90	1.905	13.17	17.10	.240	20.60	20.26	-1.6	22.15	+7.5
12	do	.505	1.508	6.02	12.00	.75	1.586	6.32	13.07	.072	13.80	13.53	-1.9	13.57	-1.6
13	do	1.503	1.511	6.00	12.02	1.50	2.280	27.02	22.91	.290	30.72	30.74	0.0	34.56	+12.5
13-C1	do	1.450	1.460	5.98	11.96	1.52	2.220	24.28	20.62	.300	28.40	27.90	-1.7	31.35	+10.4
13-C2	do	1.380	1.380	5.94	11.88	1.56	2.153	21.50	17.64	.310	25.22	24.31	-3.6	27.25	+8.1
18	do	1.133	1.506	6.08	12.08	.75	1.820	10.97	17.11	.162	18.32	18.88	+3.0	20.53	+12.0
18-C1	do	1.040	1.460	6.02	12.00	.78	1.760	9.60	14.92	.157	16.16	16.42	+1.5	17.87	+10.6
18-C2	do	.900	1.370	5.98	11.86	.86	1.660	7.59	11.66	.154	12.58	12.83	+2.0	14.00	+11.3
19	do	1.506	1.507	6.01	12.00	.38	1.896	12.92	22.84	.177	23.74	25.13	+5.8	26.91	+13.4
19-C1	do	1.430	1.440	5.93	11.96	.39	1.815	10.86	19.88	.178	21.60	21.81	+1.0	23.13	+7.1
19-C2	do	1.330	1.330	5.91	11.82	.49	1.734	9.04	15.96	.193	17.16	17.70	+3.1	18.75	+9.3
20	do	1.504	1.504	6.00	12.00	1.12	2.149	21.32	22.75	.252	26.34	28.12	+6.8	31.20	+18.4
20-C1	do	1.420	1.440	5.94	11.86	1.15	2.069	18.32	19.50	.261	23.36	24.28	+4.0	26.90	+15.2
20-C2	do	1.280	1.310	5.88	11.74	1.25	1.944	14.30	14.56	.285	18.08	18.64	+3.0	20.65	+14.2

All calculations were made with a 20-inch slide rule.

Legs with septums at ends must be treated as parts of long rectangles.

C1 and C2 indicate that first or second contour of plate was used as the boundary of the cross section.

D =diameter of largest inscribed circle at the junction of component rectangles.

$K=2K_1+K_2+2aD^4$.

K_1 =torsion constant of one leg.

K_2 =torsion constant of bar.

Differences are expressed in per cent of soap-film values.

Results headed G. and T. formula were calculated by the Griffith and Taylor method.

TABLE VI.—Values of torsion constant *K* for L, T, U, and Z beams obtained by actual test

[All dimensions are in inches]

L-BEAMS

Test	Thickness		Overall		Fillet radius <i>R</i>	<i>D</i>	<i>D</i> ⁴	<i>K</i> ₁ + <i>K</i> ₂	α	<i>K</i>		
	Long leg	Short leg	Long leg	Short leg						Test	Proposed formula	G. and T formula
L 1.....	0.502	0.502	3.249	2.738	0.25	0.674	0.206	0.211	0.108	0.275	0.234	0.247
L 2.....	.502	.502	3.245	2.750	.25	.674	.206	.212	.108	.275	.234	.247
L 3.....	.500	.500	3.247	2.738	0	.586	.118	.209	.070	.272	.217	.224
L 4.....	.500	.500	3.242	2.745	0	.586	.118	.209	.070	.265	.217	.224
L 5.....	.312	.496	3.250	2.740	.25	.574	.109	.126	.068	.218	.133	.140
L 6.....	.313	.494	3.232	2.732	.25	.572	.107	.124	.068	.190	.132	.139
L 7.....	.504	.493	3.243	2.727	.25	.672	.204	.207	.108	.284	.229	.242
L 8.....	.502	.496	3.246	2.737	.25	.668	.199	.208	.108	.307	.221	.243

T BEAMS

Test	Thickness		Total height	Total width	Fillet radius <i>R</i>	<i>D</i>	<i>D</i> ⁴	<i>K</i> ₁ + <i>K</i> ₂	α	<i>K</i>			
	Flange	Web								Test	Proposed formula	G. and T. formula	Weber formula
T 1.....	0.504	0.504	3.240	2.755	0	0.630	0.158	0.214	0.15	0.274	0.238	0.243	-----
T 2.....	.503	.503	3.240	2.754	0.25	.754	.323	.213	.20	.318	.278	.289	-----
T 3.....	.503	.503	3.250	2.752	0	.629	.156	.213	.15	.275	.236	.242	-----
T 4.....	.503	.503	3.240	2.753	.25	.754	.323	.213	.20	.312	.277	.289	-----
T 5.....	.500	.500	3.234	2.740	0	.625	.152	.208	.15	.261	.231	.237	-----
T 6.....	.504	.504	3.231	2.740	.25	.754	.323	.213	.20	.294	.278	.290	-----
T 7.....	.501	.501	3.229	2.740	.50	.876	.589	.218	.25	.396	.365	.345	0.231
T 8.....	.502	.502	3.230	2.730	.75	.936	.768	.210	.30	.473	.460	.413	-----
T 9.....	.504	.504	3.250	2.750	0	-----	-----	.208	-----	.252	-----	-----	-----
T 10.....	.506	.506	3.250	2.750	0	.632	.160	.217	.15	.287	.240	.247	-----
T 11.....	.504	.504	3.250	2.750	0	-----	-----	.208	-----	.242	-----	-----	-----
T 12.....	.504	.504	3.250	2.750	0	.630	.158	.214	.15	.285	.238	.244	-----

U AND Z BEAMS

Test	Thickness		Overall		Fillet radius <i>R</i>	<i>D</i>	<i>D</i> ⁴	2 <i>K</i> ₁ + <i>K</i> ₂	2 α	<i>K</i>			
	Legs	Bar	Length leg	Width bar						Test	Proposed formula	G. and T. formula	Weber formula
U 1.....	0.502	0.502	2.750	3.750	0	0.588	0.120	0.321	0.140	0.408	0.338	0.350	-----
U 2.....	.501	.501	2.750	3.730	0.25	.672	.204	.319	.215	.444	.363	.390	-----
U 3.....	.502	.502	2.750	3.740	0	.588	.120	.321	.140	.436	.338	.349	-----
U 4.....	.501	.501	2.740	3.750	.25	.672	.204	.319	.215	.448	.363	.390	-----
U 5.....	.380	.379	2.749	3.499	.25	.530	.079	.142	.240	.251	.161	.172	-----
U 6.....	.377	.492	2.743	3.513	.25	.600	.130	.203	.165	.324	.224	.245	-----
U 7.....	.377	.623	2.741	3.514	.25	.692	.229	.323	.121	.452	.351	.376	-----
U 8.....	.377	.747	2.737	3.516	.25	.790	.390	.490	.096	.634	.527	.552	-----
U 9.....	.495	.495	2.743	3.752	0	.580	.113	.308	.140	.404	.324	.338	-----
U 10.....	.496	.496	2.738	3.740	.25	.666	.197	.309	.215	.423	.351	.379	-----
U 11.....	.495	.495	2.743	3.753	.50	.751	.318	.308	.290	.468	.400	.446	0.321
U 12.....	.496	.496	2.734	3.743	.75	.838	.493	.309	.365	.514	.489	.550	-----
Z 1.....	.498	.498	2.735	3.715	0	.669	.200	.311	.215	.498	.354	.381	-----
Z 2.....	.499	.499	2.736	3.718	0	.585	.117	.314	.140	.466	.330	.345	-----
Z 3.....	.501	.501	2.734	3.708	0	.672	.204	.316	.215	.488	.360	.388	-----
Z 4.....	.497	.497	2.736	3.714	0	.582	.115	.316	.140	.461	.326	.340	-----
Z 5.....	.375	.375	2.750	3.750	.50	.610	.138	.141	.345	.285	.189	.208	-----
Z 6.....	.375	.375	2.750	3.750	.50	.610	.138	.141	.345	.290	.189	.208	-----
Z 7.....	.375	.375	2.750	3.750	.25	.525	.076	.141	.240	.248	.159	.170	-----
Z 8.....	.376	.376	2.750	3.750	.25	.526	.077	.142	.240	.254	.161	.171	-----

All calculations were made with a 20-inch slide rule.
Weber formula assumes a radius of fillet equal to the thickness of the narrower component rectangle.
T 9 and T 11 did not have web glued to flange. They act, therefore, as two separate pieces except for additional stiffness resulting from filler blocks glued at ends to make end section rectangular.
For a discussion of the discrepancy between calculated and test values of *K*, see concluding remarks under "Formulas for Irregular Solid Sections."

(2) The combination of bending and torsion caused by the fact that in many instances the axis of twist did not coincide with the axis of the figure.

Neither of these causes would be as effective with **I** beams as with the sections just mentioned.

The soap-film method furnishes the value of the torsion constant K associated with pure torsion under ideal conditions as to the application of torque at the ends. Usually an actual beam will have a margin of safety as regards torsional rigidity because of the fixity of its ends.

CONCLUSIONS

The soap-film method proved to be a valuable aid in the solution of the torsion problem for cylinders and prisms for which no rigorous mathematical solution has been found. Not only is the method capable of furnishing the torsional rigidities and the stresses with considerable accuracy but it also gives a visual representation of the actual situation as regards torsional stresses, a representation that can be readily interpreted by the observer.

From a study of the soap-film tests and the actual torsion tests, it has been possible to conclude that the torsional rigidity of prisms with sections such as **I**, **T**, **L**, **U**, and **Z**, which are composed of rectangles, is equal to the sum of the torsional rigidities of prisms whose sections are the component rectangles, corrected by a simple additive term to take account of the increased stiffness resulting from the junctions of the rectangles.

The formulas developed by C. Weber for such sections were found to be fairly accurate when the widths of the component rectangles are extremely small in comparison with their lengths, as with many rolled-steel sections. (Reference 11.) For sections of wooden beams for which the component rectangles are wider (say the width greater than one-fifth the length), Weber's formulas give torsional rigidities that are much too low. His formulas always assume the presence of fillets, the radii of which are equal to the width of the narrower component rectangle. With thicker sections, such as those that we have tested, the variation of the torsional rigidity with the radii of the fillets can not be neglected. In our opinion, the reasoning employed by Weber in deriving his formulas is open to objections. The errors introduced, however, are negligible for very thin sections.

Griffith and Taylor developed rules for calculating the torsional rigidities of prisms of any section. The application of these rules to sections of the kind that we are considering is rather an intricate process as compared with the simple computation required by our proposed formula. The results obtained by Griffith and Taylor's rules are good for fairly compact sections. For sections made up of component rectangles, the results calculated by their rules appear to be somewhat too high.

Our tests show that the torsional stiffness of a beam may be materially increased by the way in which it is fastened at the ends. Two other factors are important in connection with the torsional behavior of wooden beams. They are rate of fiber strain and moisture content. Corrections for their influence on torsional properties were determined. We have concluded that a third factor, which has to do with the difference between the moduli of rigidity of wood referred to planes radial and tangential to the annual rings, may, in general, be neglected in design and a mean modulus used. For Sitka spruce this mean modulus is between one-fifteenth and one-sixteenth of Young's modulus parallel to the grain.

SUMMARY

This report reviews briefly the fundamental theory of torsion and shows how the more common torsion formulas have been developed from that theory. Formulas for solid and tubular sections that have yielded to mathematical treatment are given, and empirical formulas are developed for irregular sections whose component parts are rectangles. The empirical formulas are a result both of direct torsion tests of wooden specimens and of the application of the soap-film method of investigation to the sections in question. The mathematical analogy upon which the soap-film method is based is explained.

The effect of a lack of isotropy in wood, caused by the presence of the annual growth rings, is discussed and is shown to be relatively unimportant.

REFERENCES

- Reference 1. Love: Theory of Elasticity, art. 8.
 Reference 2. Love: Op. cit., art. 69.
 Reference 3. Love: Op. cit., art. 224.
 Reference 4. Love: Op. cit., art. 222.
 Reference 5. St. Venant: De la Torsion des Prismes, chap. IX, 1855.
 Reference 6. St. Venant: *In* Navier, Résumé de Lecons — third edition with notes and appendices by St. Venant.
 Reference 7. Prescott: Applied Elasticity, arts. 117 and 118.
 Reference 8. Prescott: Op. cit., art. 120.
 Reference 9. Prandtl, L.: Phys. Zeitschr. Bd. 4, 1903, p. 758.
 Reference 10. Griffith, A. A., and Taylor, G. I.: Technical Reports of the (British) Advisory Committee for Aeronautics, No. 333, June, 1917.
 Reference 11. Weber, Constantin: Forschungsarbeiten auf dem Gebiete des Ingenieurwesens, Heft 249.

BIBLIOGRAPHY

ARTICLES

1855. St. Venant: De la Torsion des Prismes—Extrait du Tome XIV des Mémoires Présentés par divers Savants a l'Académie des Sciences.
 1882. Voigt, W.: Allgemeine Formeln für die Bestimmung der Elasticitätskonstanten von Krystallen durch die Beobachtung der Biegung und Drillung von Prismen. Ann. der Physik u. Chemie (3) 16, (1882), p. 294.
 1886. Voigt, W.: Ueber die Torsion eines rechteckigen Prismas aus homogener krystallinischer Substanz. Ann. der Physik u. Chemie (3) 29 (1886), p. 604.
 1896. Bredt: Kritische Bemerkungen zur Drehungselastizität. Zeitschrift des Vereins deutscher Ingenieure, 1896, pp. 785–813.
 1899. Schulz, Bruno: Beitrag zur Torsionsfestigkeit. Zeitschrift für Architektur und Ingenieurwesen, 1899, p. 202.
 1901. Autenrieth: Beitrag zur Bestimmung der grössten Schubspannung im Querschnitt eines geraden, auf Drehung beanspruchten Stabes. Zeitschrift des Vereines deutscher Ingenieure, pp. 1099, 1901, part 2.
 1903. Prandtl, L.: Zur Torsion von prismatischen Stäben. Physikalische Zeitschrift, 4 (1903), p. 758.
 1904. Prandtl, L.: Eine neue Darstellung der Torsionsspannungen bei prismatischen Stäben von beliebigen Querschnitt. Jahresbericht des Deutschen Mathematiker-Vereinigung, 13 (1904), p. 31.
 1906. Anthes, Hugo: Versuchsmethode zur Ermittlung der Spannungsverteilung bei Torsion prismatischer Stäbe. Dinglers Polytechnisches Journal, Bd. 321, pp. 342, 356, 388, 443, 455, 471.
 1908. Kotter, Fritz: Ueber die Torsion des Winkeleisens. Sitzungsberichte der Königlich Preussischen Akademie der Wissenschaften, 1908, p. 935.
 1914. Gibson, A. H., and Ritchie, E. G.: A Study of the Circular-Arc Bow-Girder. Constable & Co., Ltd., London.
 1914. Kommers, J. B.: Torsion Tests of Cast Iron. American Machinist, May 28, 1914, vol. 40, p. 941.
 1915. Batho, Cyril: Torsional Stresses in Framed Structures. The calculation of torsion stresses in framed structures and thin-walled prisms. Engineering, October 15; with discussion by Ernest G. Ritchie, November 5, and a reply by Batho, December 17.
 1916. Batho, Cyril: The Torsion of Solid and Hollow Prisms and Cylinders. Engineering, Nov. 24, 1916.
 1917. Foppl, A.: Ueber den elastischen Verdrehungswinkel eines Stabs. Sitzungsberichte der Königl. Akademie München.
 1917. Griffith and Taylor: The Use of Soap Films in Solving Torsion Problems. Reports and Memoranda (New Series), No. 333, June, 1917. Presented by the Superintendent, Royal Aircraft Factory. Technical Report of the Advisory Committee for Aeronautics (British) for 1917–18, vol. 3, Strength of Const., etc.
 1917. Griffith, A. A.: The Determination of the Torsional Stiffness and Strength of Cylindrical Bars of any Sections. Reports and Memoranda (New Series), No. 334, June, 1917. Presented by Superintendent, Royal Aircraft Factory. Technical Report of the Advisory Committee for Aeronautics (British) for 1917–18, vol. 3, Strength of Const., etc.
 1917. Griffith and Taylor: The Problem of Flexure and Its Solution by the Soap-Film Method. R. & M., No. 399, November, 1917. Presented by the Superintendent, Royal Aircraft Factory. Technical Report of the Advisory Committee for Aeronautics (British) for 1917–18, vol. 3, Strength of Const., etc.
 1919. Elmendorf, A., and Grenoble, H. S.: Torsion Tests of Built-Up Spruce and Wrapped Veneer Tubes. Forest Products Laboratory Report.
 1921. Trefftz, E.: Ueber die Torsion prismatischer Stäbe von polygonalem Querschnitt. Mathematische Annalen, 1921, Band 82.

1921. The Moduli of Rigidity of Spruce. *Philosophical Magazine*, vol. 41, June, 1921, No. 246.
1921. Weber, C.: Die Lehre der Drehungsfestigkeit. *Forschungsarbeiten auf dem Gebiete des Ingenieurwesens* Heft. 249.
- 1921-22. Bairstow, L., and Pippard, A. J. Sutton: The Determination of Torsional Stresses in a Shaft of any Cross Section. *Proc. Inst. C. E.*, 1921-22, Part 2, vol. 214.
1921. Southwell: On the Determination of the Stresses in Braced Frameworks: Part I, The Effect of Axial Loading, Flexure, and Torsion Upon a Framework of Uniform Rectangular Cross Sections. *Reports and Memoranda No. 737 (British)*. Technical Report of the Advisory Committee for Aeronautics.
1922. Southwell: On the Determination of the Stresses in Braced Frameworks. Part II, The Effect of Shear Upon a Framework of Uniform Rectangular Cross Section. *Reports and Memoranda No. 790*. Technical Report of the Advisory Committee of Aeronautics (British).
1922. Southwell: On the Determination of Stresses in Braced Frameworks. Part III, The Effect of Axial Loading, Torsion, Flexure, and Shear Upon a Braced Tube of any Cross Sections. *Reports and Memoranda No. 791*. Technical Report of Advisory Committee for Aeronautics (British).
1922. Southwell: On the Determination of Stresses in Braced Frameworks. Part IV, The Effects of Axial Loading, Flexure, Torsion, and Shear Upon a Tubular Cross Section with Taper. *Reports and Memoranda No. 819*. Technical Report of Advisory Committee for Aeronautics (British).
1922. Weber, C.: Die Drehungsfestigkeit von Stäben. *Zeitschrift des Vereines Deutscher Ingenieure*, vol. 66, pp. 764-769, August, 1922.
1923. Weber, C.: The Torsional Strength of Bars. *Mechanical Engineering*, vol. 45, January, 1923.
1923. Young, C. R., Sager, W. L., and Hughes, C. A.: Torsional Strength of Rectangular Sections of Concrete, Plain and Reinforced. *Bul. No. 3*, 1922, University of Toronto.
1923. Wilson, T. R. C.: Torsion Tests of Box Beams. *Forest Products Laboratory Report*.
1924. Young, C. R., and Hughes, C. A.: Torsional Strength of Steel I Sections, *Bul. No. 4*, Section No. 3, 1924, University of Toronto.
1927. Dewar, Sir James. *Collected Papers of Sir James Dewar*. Cambridge University Press, 1927, vol. 11. Soap Bubbles of Long Duration, p. 1176; Studies of Liquid Films, p. 1206; Soap Films and Molecular Forces, p. 1333; Soap Films as Detectors, Stream Lines and Sound, p. 1334.
1928. Huber, Karl. Verdrehungselastizität und Festigkeit von Hölzern. *Zeitschrift des Vereines deutscher Ingenieure*, Band 72, Berlin, 14, April, 1928, Nr. 15.

BOOKS

- Aufgaben zur Theorie elastischer Körper. J. J. Weyrauch.
- Soap Bubbles and the Forces Which Mould Them. Society for Promoting Christian Knowledge, Lond. (1890), C. V. Boys.
- Elastizität und Festigkeit. Bach, C.
- Drang und Zwang: Eine höhere Festigkeitslehre für Ingenieure. Foppl, A., and Foppl, L.
- Theory of Elasticity. Love.
- The Mechanical Properties of Fluids, Collective Work. Van Nostrand, 1924.
- Résumé des leçons sur l'application de la mécanique à l'établissement des constructions et de machines. 3. éd. avec des notes et des appendices de St. Venant. 1864. Navier.

APPENDIX A

PRISMS OF NONISOTROPIC MATERIAL

In order to solve the torsion problem for a wooden beam, we shall consider a prism of non-isotropic material in which there are three mutually perpendicular planes of elastic symmetry, one of which is perpendicular to the direction of length of the prism. It will be shown that the solution of the torsion problem for such a prism can be reduced to the solution of the same problem for an isotropic prism whose section is obtained by transforming the boundaries of the original section through a linear transformation and whose modulus of rigidity is expressed in terms of the moduli of the original material.

Let the axis of Z lie along the direction of the length of the prism and the axes of X and Y be axes to which the boundary of the section is conveniently referred. (Fig. 12.) Let the planes ZX' and ZY' be the longitudinal planes of elastic symmetry and let G_1 and G_2 be the

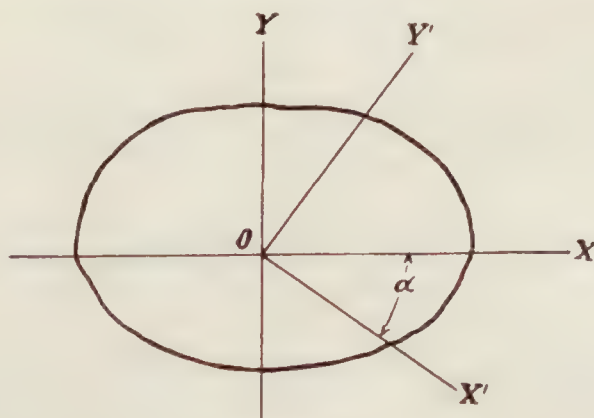


FIGURE 12

moduli of rigidity associated with shearing strains corresponding to the pairs of directions of the axes of Z and X' and of Z and Y' , respectively.

We form the same general picture of the state of stress and strain as for the isotropic prism (p. 10) and accordingly we again assume that the components of the displacement parallel to the X' , Y' , and Z axes, respectively, are expressed as follows:

$$u = -\tau y' z, \quad v = \tau z x', \quad w = \tau \phi(x', y'), \quad (1)$$

where τ is the angle of twist per unit length and ϕ is a function of x' and y' only, which is to be determined.

As a consequence of the type of displacement given by (1), all of the components of strain vanish except

$$\begin{aligned} e_{y'z} &= \frac{\partial w}{\partial y'} + \frac{\partial v}{\partial z} = \tau \left(\frac{\partial \phi}{\partial y'} + x' \right), \\ e_{zx'} &= \frac{\partial u}{\partial z} + \frac{\partial w}{\partial x'} = \tau \left(\frac{\partial \phi}{\partial x'} - y' \right). \end{aligned} \quad (2)$$

(Reference 1.) These are shearing strains corresponding to the pair of directions zy' and zx' , respectively. Then all stress components vanish except the components X'_z and Y'_z of shearing stress and these are given by

$$X'_z = G_1 e_{zx'}, \quad Y'_z = G_2 e_{y'z}. \quad (3)$$

(Reference 2.) Referred to the axes X and Y , which make an angle α with the axes X' and Y' , the stress components are

$$\begin{aligned} X_z &= G_2 e_{y'z} \sin \alpha - G_1 e_{zx'} \cos \alpha, \\ Y_z &= G_2 e_{y'z} \cos \alpha - G_1 e_{zx'} \sin \alpha. \end{aligned} \quad (4)$$

Entering the values of $e_{y'z}$ and $e_{zx'}$ from (2), noting that

$$x' = x \cos \alpha - y \sin \alpha, \quad y' = x \sin \alpha + y \cos \alpha,$$

and using the abbreviations

$$\begin{aligned} \kappa &= G_2 \sin^2 \alpha + G_1 \cos^2 \alpha, \\ \lambda &= (G_2 - G_1) \sin \alpha \cos \alpha, \\ \mu &= G_2 \cos^2 \alpha + G_1 \sin^2 \alpha, \end{aligned} \quad (5)$$

we find that equations (4) become

$$\begin{aligned} X_z &= \tau \left(\kappa \frac{\partial \phi}{\partial x} + \lambda \frac{\partial \phi}{\partial y} + \lambda x - \kappa y \right), \\ Y_z &= \tau \left(\lambda \frac{\partial \phi}{\partial x} + \mu \frac{\partial \phi}{\partial y} + \mu x - \lambda y \right). \end{aligned} \quad (6)$$

From the equations of equilibrium and equations (6), we obtain the differential equation which the unknown function ϕ must satisfy; namely,

$$\kappa \frac{\partial^2 \phi}{\partial x^2} + 2\lambda \frac{\partial^2 \phi}{\partial x \partial y} + \mu \frac{\partial^2 \phi}{\partial y^2} = 0. \quad (7)$$

This equation for the determination of ϕ corresponds to equation (3), page 11, for an isotropic prism.

The requirement that the lateral surface of the prism shall be free from traction leads to the following condition, which ϕ must satisfy on the curve $f(x, y) = 0$, the boundary of the cross section:

$$\begin{aligned} &\left(\kappa \frac{\partial \phi}{\partial x} + \lambda \frac{\partial \phi}{\partial y} \right) \frac{\partial f}{\partial x} + \left(\lambda \frac{\partial \phi}{\partial x} + \mu \frac{\partial \phi}{\partial y} \right) \frac{\partial f}{\partial y} \\ &= (\kappa y - \lambda x) \frac{\partial f}{\partial x} + (\lambda y - \mu x) \frac{\partial f}{\partial y}. \end{aligned} \quad (8)$$

After the change of independent variables

$$\xi = \delta x, \quad \eta = y - \gamma x, \quad (9)$$

where

$$\delta = \frac{\sqrt{G_1 G_2}}{\kappa}, \quad \gamma = \frac{\lambda}{\kappa}, \quad (10)$$

the differential equation (7) becomes

$$\frac{\partial^2 \phi}{\partial \xi^2} + \frac{\partial^2 \phi}{\partial \eta^2} = 0. \quad (11)$$

If the equation of the boundary $f(x, y) = 0$ is transformed into

$$F(\xi, \eta) = 0 \quad (12)$$

by the change of variables (9) the boundary condition on ϕ in equation (8) becomes

$$\delta \left(\frac{\partial \phi}{\partial \xi} \frac{\partial F}{\partial \xi} + \frac{\partial \phi}{\partial \eta} \frac{\partial F}{\partial \eta} \right) = \eta \frac{\partial F}{\partial \xi} - \xi \frac{\partial F}{\partial \eta}. \quad (13)$$

If we let

$$\phi' = \delta\phi, \quad (14)$$

this condition reduces further to

$$\frac{\partial\phi'}{\partial\xi} \frac{\partial F}{\partial\xi} + \frac{\partial\phi'}{\partial\eta} \frac{\partial F}{\partial\eta} = \eta \frac{\partial F}{\partial\xi} - \xi \frac{\partial F}{\partial\eta}, \quad (15)$$

or

$$\frac{\partial\phi'}{\partial v} = \eta \cos(\xi, v) - \xi \cos(\eta, v), \quad (16)$$

where v denotes the normal to the new boundary.

From (12) and (14)

$$\frac{\partial^2\phi'}{\partial\xi^2} + \frac{\partial^2\phi'}{\partial\eta^2} = 0. \quad (17)$$

The solution of (17) subject to the boundary condition (16) corresponds to the solution of the torsion problem for a prism whose section has the new boundary (12) and which is composed of isotropic material.

It will now be shown that the torsional rigidity of the original prism can be expressed in terms of the torsional rigidity of the transformed prism. For the couple T we have

$$T = \iint (Y_z x - X_z y) dx dy.$$

Entering for X_z and Y_z their expressions in terms of ϕ (equation 6) and changing the variables of integration to ξ and η by equations (9) we obtain

$$T = \frac{\tau}{\delta} \iint \left\{ \sqrt{G_1 G_2} \left(\xi \frac{\partial\phi}{\partial\eta} - \eta \frac{\partial\phi}{\partial\xi} \right) + \kappa(\xi^2 + \eta^2) \right\} d\xi d\eta, \quad (18)$$

where the integration is now extended over the area of the transformed cross section. It follows at once from equations (18) and (10) that the torsional rigidity C of the original prism is given by

$$C = \frac{\kappa}{\delta} \iint \left(\xi \frac{\partial\phi'}{\partial\eta} - \eta \frac{\partial\phi'}{\partial\xi} + \xi^2 + \eta^2 \right) d\xi d\eta. \quad (19)$$

The right-hand member of this equation is the torsional rigidity of an isotropic prism whose cross section is obtained from that of the original prism by the transformation (9) and whose modulus of rigidity is

$$\overline{G} = \frac{\kappa}{\delta} = \frac{(G_2 \sin^2 \alpha + G_1 \cos^2 \alpha)^2}{\sqrt{G_1 G_2}}. \quad (20)$$

LINES OF SHEARING STRESS AND INTENSITY OF SHEARING STRESS IN A NONISOTROPIC PRISM

Let Ψ' be a function associated with the transformed isotropic prism as the function Ψ was with such a prism in equation (10), page 12, that is, let

$$\Psi' = \psi' - \frac{1}{2}(\xi^2 + \eta^2),$$

where ψ' is a function conjugate to ϕ' . It follows that

$$X_z = \tau\kappa \frac{\partial\Psi'}{\partial\eta},$$

$$Y_z = \tau\kappa \left(\gamma \frac{\partial\Psi'}{\partial\eta} - \delta \frac{\partial\Psi'}{\partial\xi} \right).$$

If we now express these components in terms of the variables x and y , using equations (9), and let

$$\Psi'(\xi, \eta) = \Psi'(\delta x, y - \gamma x) = \Psi(x, y),$$

we obtain simply

$$X_z = \tau\kappa \frac{\partial \Psi}{\partial y}, \quad Y_z = -\tau\kappa \frac{\partial \Psi}{\partial x}. \quad (21)$$

It follows that the curves, $\Psi(x, y) = \text{constant}$, are lines of shearing stress and that the intensity of the shearing stress at any point is equal to

$$\tau\kappa \frac{\partial \Psi}{\partial v}, \quad (22)$$

v denoting the normal at the point in question to the curve $\Psi(x, y) = \text{constant}$, which passes through that point.

Applications to certain nonisotropic prisms with simple cross sections.

To take a typical example, let us suppose that the material is wood. It will be assumed that the plane $X'OZ$, Figure 12, is parallel to the annual rings which are considered to lie in planes. The moduli G_1 and G_2 (equations (3)) are sometimes called the tangential and the radial moduli, respectively.

(a) THE CIRCLE:

Let the axes OX' and OX coincide so that $\alpha = 0$. After the transformation (9) the circle becomes an ellipse with the semi-axes

$$a\sqrt{\frac{G_2}{G_1}} \text{ and } a.$$

On letting $\alpha = 0$ in equation (20) the modulus of rigidity of the transformed elliptic section is found to be

$$\bar{G} = G_1 \sqrt{\frac{G_1}{G_2}}.$$

The torsional rigidity of the original circular cylinder is equal to that of the transformed isotropic elliptic cylinder. We find (p. 15).

$$C = \pi \frac{G_1 G_2}{G_1 + G_2} a^4. \quad (23)$$

On comparing this result (equation (23)) with that on page 21, we see that the torsional rigidity of the given nonisotropic circular cylinder with moduli G_1 and G_2 is equal to the torsional rigidity of an equal isotropic circular cylinder with the modulus,

$$\frac{2G_1 G_2}{G_1 + G_2}.$$

It has sometimes been erroneously assumed that this quantity is the mean modulus for a section of any shape.

(b) THE ELLIPSE:

The annual rings make an angle α with the X -axis. The section of the transformed cylinder is obtained by using equations (9). The transformed section is an ellipse whose axis can be found. Entering these axes and the modulus as given by (20) in the expression for the torque of an elliptic cylinder, page 15, we find as the torsional rigidity of the transformed section and consequently that of the original section

$$C = \frac{m^3 G_1 G_2}{\kappa + m^2 \mu} \pi b^4, \quad (24)$$

where $m = \frac{a}{b}$ and κ and μ are given by equation (5). If

$$\frac{a}{b} = 2 \text{ and } G_1 = 0.9G_2,$$

we obtain

$$C = \frac{7.2\pi b^4 G_2}{4.6 \sin^2 \alpha + 4.9 \cos^2 \alpha}.$$

Denote by C_0 and C_{90} , respectively, the values of C when $\alpha = 0^\circ$ and 90° , respectively. Then

$$\frac{C_{90}}{C_0} = 1.065$$

and if

$$\frac{a}{b} = 3, \quad \frac{C_{90}}{C_0} = 1.087.$$

If

$G_1 = 0.8G_2$, we find that

$$\frac{C_{90}}{C_0} = 1.142 \text{ when } \frac{a}{b} = 2,$$

and

$$\frac{C_{90}}{C_0} = 1.195 \text{ when } \frac{a}{b} = 3.$$

The torsional rigidity of an elliptic cylinder in which the annual rings are perpendicular to the major axis is greater than that of an equal cylinder of the same material with the rings parallel to the major axis.

(c) THE RECTANGLE:

Let α , the angle between the annual rings and the X -axis, equal zero.

The equations of transformation (9) become

$$\xi = \sqrt{\frac{G_2}{G_1}} x,$$

$$\eta = y.$$

The rectangle with sides $2a$ and $2b$ is transformed into another rectangle with sides

$$2a\sqrt{\frac{G_2}{G_1}} \text{ and } 2b.$$

The modulus of rigidity of the transformed isotropic rectangular prism is, in accordance with (20)

$$G_1\sqrt{\frac{G_1}{G_2}}.$$

Then by the formula on page 15 the torsional rigidity of the transformed section is

$$C = G_1 ab^3 \left\{ \frac{16}{3} - \lambda \frac{b}{a} \sqrt{\frac{G_1}{G_2}} \right\}, \quad (25)$$

in which λ is to be taken from Table I by replacing the ratio of the sides by

$$\frac{a}{b} \sqrt{\frac{G_2}{G_1}}.$$

This result is in direct agreement with that of St. Venant, who obtained formulas for the cases in which $\alpha = 0^\circ$ and $\alpha = 90^\circ$.

If $\alpha = 90^\circ$, we find that the rectangle is transformed into a rectangle with sides

$$2a\sqrt{\frac{G_1}{G_2}} \text{ and } 2b$$

and that the modulus of rigidity of the transformed isotropic prism is

$$G_2\sqrt{\frac{G_2}{G_1}}.$$

Entering these results in the formula for an isotropic rectangular prism on page 15, we again obtain St. Venant's result for this case.

If $G_1 = 0.8G_2$ the torsional rigidity of a quarter-sawn board whose sides are in the ratio 3 to 1 is 18 per cent greater than that of a plain-sawn board of the same dimensions.

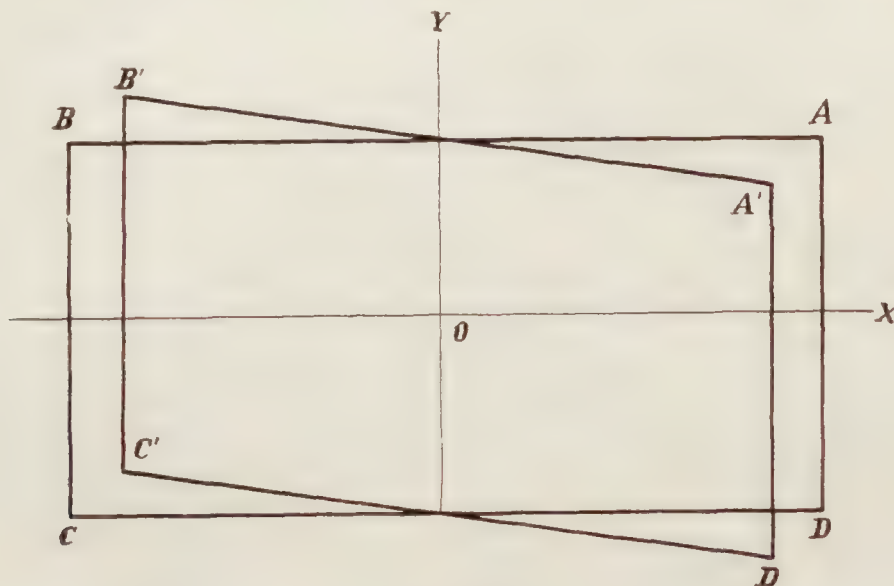


FIGURE 13

In general, the rectangle with sides $2a$ and $2b$ and vertices $ABCD$ is transformed into a parallelogram $A'B'C'D'$ whose vertices are at the points

$(\delta a, b - \gamma a)$, $(-\delta a, b + \gamma a)$, $(-\delta a, -b + \gamma a)$, and $(\delta a, -b - \gamma a)$ respectively.

(Fig. 13.) The sides are

$$A'B' = 2a\sqrt{\gamma^2 + \delta^2} \text{ and}$$

$$A'D' = 2b$$

The modulus of rigidity of the prism of transformed section is given by equation (20). The acute angle between adjacent sides of the parallelogram is found from the equation

$$\tan \theta = \frac{\delta}{\gamma}$$

The torsional rigidity of the transformed isotropic prism whose section is a parallelogram is calculated by the approximate formula

$$C = \frac{A^4}{41J} \bar{G}$$

where A is the area of the section and J is its polar moment of inertia. This formula is quite accurate at the extremes $\alpha = 0^\circ$ and $\alpha = 90^\circ$ if the ratio of the sides is 3 to 1. The use of this approximate formula to compute the torsional rigidity of the transformed prisms appears to be justified, since the angles of the parallelograms into which the rectangular sections are transformed differ but little from right angles. If the ratio of the sides of the rectangle is different from 3 to 1 the factor 41 in the denominator should be replaced by a different number so chosen that the formula gives results that agree well with the exact values for $\alpha = 0^\circ$ and $\alpha = 90^\circ$.

(d) THE EQUILATERAL TRIANGLE:

By the transformation (9) the equilateral triangle (fig. 14) with vertices A , B , and C at

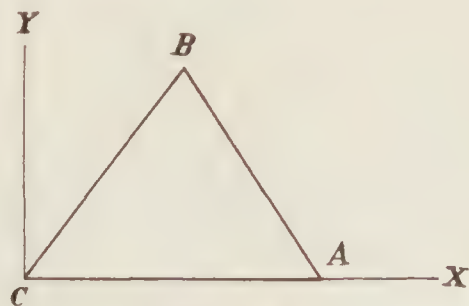


FIGURE 14

the points

$$(a, 0), \left(\frac{a}{2}, \frac{a}{2}\sqrt{3}\right), \text{ and } (0, 0)$$

is transformed into a triangle with vertices at

$$(\delta a, -\gamma a), \left[\frac{\delta a}{2}, (\sqrt{3} - \gamma)\frac{a}{2}\right], \text{ and } (0, 0),$$

respectively. Table VII gives the lengths of the new sides $C'B'$ and $C'A'$ and their included angle $C' = A'C'B'$ corresponding to various values of the angle α , α being the angle made by the planes of the annual rings with the X -axis, for wood. It was assumed that

$$G_1 = 0.8G_2$$

TABLE VII

α	δ	γ	Modulus	$C'B'/a$	$C'A'/a$	C'	C/K
0	1.118	0	$0.716G_2$	1.031	1.118	57 08	0.1928
$7\frac{1}{2}$	1.115	.032	$.719G_2$	1.016	1.116	58 25	.1937
15	1.101	.062	$.734G_2$	1.000	1.103	59 52	.192
$22\frac{1}{2}$	1.077	.085	$.772G_2$.984	1.080	61 21	.1924
30	1.052	.102	$.808G_2$.970	1.056	62 45	.1924
45	.994	.111	$.906G_2$.950	1.001	64 45	.1918

The torsional rigidity C used in the last column of Table VII was computed by the formula

$$C = \frac{A^4}{45J} \bar{G}, \quad (27)$$

where A , J and \bar{G} have the same meaning as on page 42. This formula, which is exact for the equilateral triangle, was thought to be sufficiently accurate for the computation of the rigidity of the slightly distorted transformed sections. According to the computed values the torsional rigidity does not vary appreciably with the angle α made by a plane of symmetry (the plane of the annual rings, for wood) with one of the bases. This result is not surprising in view of the symmetry of the section.

THE SOAP-FILM METHOD OF SOLVING THE TORSION PROBLEM FOR PRISMS OF NONISOTROPIC MATERIAL

The torsion problem for a prism of nonisotropic material having perpendicular longitudinal planes of elastic symmetry has been reduced by the linear transformation (9) to the torsion problem for an isotropic prism of a transformed section and a given modulus of elasticity. The soap-film method may accordingly be used when the transformed section is such that a rigorous mathematical solution of the torsion problem for this section is not available.

It follows from (19) in the way in which (15), page 12, was obtained from (6), page 11, that the torsional rigidity of the original prism, which is the same as that of the transformed prism, is given by

$$C = \frac{2\kappa}{\delta} \iint \Psi' \, d\xi \, d\eta. \quad (28)$$

This means that the torsional rigidity of the prism is proportional to the volume inclosed by the surface $z = \Psi'(\xi, \eta)$ and the plane $z = 0$, the function $\Psi'(\xi, \eta)$ vanishing on the boundary of the transformed section. Now $\Psi'(\xi, \eta)$ is proportional to the ordinates of a soap film stretched over an opening of the shape of the transformed section of the prism, the film being under a uniform excess pressure on one side. The proportionality factor can be determined from (28) and the previous discussion of the soap-film method.

The contour lines of the soap film stretched over the transformed section are the curves $\Psi'(\xi, \eta) = \text{constant}$. These curves when transformed by (9) become the curves $\Psi(x, y) = \text{constant}$, the lines of shearing stress of the original nonisotropic prism. This follows immediately from equations (21). From the distance between adjacent curves $\Psi(x, y) = \text{constant}$, we can, in accordance with (22), estimate the intensity of the shearing stress at a given point.

REFERENCES

- Reference 1. Love: Theory of Elasticity, art. 10.
 Reference 2. Love: Op. cit.; art. 62, equation (9); art. 105; and art. 110, equation (15).

APPENDIX B

THE GRIFFITH AND TAYLOR FORMULAS FOR TORQUE AND STRESS

Method of calculating torsional rigidity.

The method of Griffith and Taylor, which gives fairly accurate results for many sections, is summarized in this appendix. For a comparison with our results see the discussion in the body of the report.

We may write for any section

$$T = GK \frac{\theta}{L},$$

in which

T = the twisting moment.

G = the modulus of rigidity.

K = the torsion constant.

$\frac{\theta}{L}$ = the unit angle of twist.

For a circle

$$K = \frac{\pi r^4}{2},$$

which may be written

$$K = \frac{\pi r^2}{2} \times r^2 = \frac{A}{2} r^2,$$

in which A = the area. In general, then, let us assume that

$$K = \frac{A}{2} C^2,$$

in which C is called the equivalent torsional radius of the section. To determine the twist for a given moment, we must then find C for the section in question. Checking C for an equilateral triangle against C for its inscribed circle, we find that, while the area for the triangle is 65 per cent greater, C is only 10 per cent greater; this shows that projecting corners add but little to torsional stiffness. The first step, then, in getting the correct C for the section under consideration is to round off any projecting corners with an arc of suitable radius. The radius of such an arc depends upon the angle through which the tangent to the boundary turns in passing around such a corner, and also upon the radius of the largest circle that can be drawn in the section touching the boundary at more than two points. Let α be the angle through which the tangent passes in turning a corner; for the corner of a square it is 90 degrees, for the apex of an equilateral triangle it is 120 degrees, and so on. Let b equal the radius of the largest circle that can be drawn in the section and call r the radius of the arc for rounding off the corner. Table VIII gives the ratio of r to b .

TABLE VIII

$\frac{\alpha^\circ}{180^\circ}$	$\frac{r}{b}$	$\frac{\alpha^\circ}{180^\circ}$	$\frac{r}{b}$
0.0	1.000	0.6	0.375
.1	.930	.7	.270
.2	.850	.8	.210
.3	.750	.9	.170
.4	.625	1.0	.155
.5	.500		

In this way we make a new figure with all the outward corners rounded off.

Let

A_1 = the area of the new figure.

P_1 = the perimeter of the new figure.

Then our first approximation of C is

$$C_1 = \frac{2A_1}{P_1}.$$

Our second approximation is obtained as follows:

Let

A = the area of the original section.

P = the perimeter of the original section.

b = the radius of the largest inscribed circle.

$$= \frac{2A}{P}.$$

Then the square of C_1 as obtained by the first approximation must be multiplied by a factor λ taken from Table IX.

TABLE IX

$\frac{b}{h}$	λ	$\frac{b}{h}$	λ
1.00	1.000	0.70	0.897
.95	.998	.65	.848
.90	.994	.60	.793
.85	.984	.55	.732
.80	.966	.50	.667
.75	.938		

We have then

$$K = \frac{A}{2} \lambda C_1^2,$$

$$= \frac{A}{2} \lambda \left(\frac{2A_1}{P_1} \right)^2.$$

Sections in which more than one circle touching the boundary in three points can be drawn require special treatment. They must be divided into component sections. A value of C for each component is then calculated and the results added to obtain a C for the whole section. In dividing a section into component parts, the following rule is used: Imagine a circle of varying radius to move inside the section. There may be several positions where the circle and the boundary have three or more points of contact, and between each pair of such positions there will be a position of the circle where its radius is a minimum. Draw the division lines through the points of contact of these minimum circles. When the section includes long, narrow portions bounded by lines parallel or nearly so, such as the web of an I beam, the division lines should

Method of calculating stress.

Two formulas are given for calculating maximum stress. For compound sections, the formulas may be applied to each component part separately. Where there are no reentrant angles, the following formula is used:

$$q = \frac{2bG\tau}{1 + \frac{\pi^2 b^4}{A^2}} \left[1 + 0.15 \left(\frac{\pi^2 b^4}{A^2} - \frac{b}{\rho} \right) \right]$$

in which τ is the unit angle of twist $\frac{\theta}{L}$ and ρ is the radius of curvature of the boundary at the point in question. The maximum stress will usually occur at one of the points of contact of the largest inscribed circle. An exception may occur if the boundary is more concave at some other part than at these points of contact.

When the twisting moment is known and the angle of twist is not, τ may be obtained, of course, from—

$$T = KG\tau.$$

Where the boundary is concave, the following formula is recommended:

$$q = \frac{2bG\tau}{1 + \frac{\pi^2 b^4}{A^2}} \left[1 + \left\{ 0.118 \log_e \left(1 - \frac{b}{\rho} \right) - 0.238 \frac{b}{\rho} \right\} \tanh \frac{2\alpha}{\pi} \right]$$

in which α is the angle turned through by the tangent in turning around the reentrant portion. It must be remembered that for reentrant angles α is *negative*.

APPENDIX C

DESIGN VALUES FOR AIRPLANE MATERIAL

Recommended design values for wood for use in connection with the formulas of this report are given herewith. For metal, the allowable shearing stress values at present specified should be used for q except where better data are now available (as in Technical Note Number 189 of the National Advisory Committee for Aeronautics). For steels for which values are not now available, 10,000 pounds per square inch added to half the ultimate tensile strength gives a value that may be used for the ultimate shearing stress in torsion. The values for wood follow.

Spruce, $G = \frac{E}{15.5} = \frac{1,300,000}{15.5} = 84,000$ pounds per square inch.

Spruce, 45° plywood, $G_1 = 5G = 420,000$ pounds per square inch.

Spruce, $q = 1,000$ pounds per square inch.

Spruce, 45° plywood, $q = 2,370$ pounds per square inch.

REPORT No. 335

**AERODYNAMIC THEORY AND TEST
OF STRUT FORMS—II**

By R. H. SMITH

**Aerodynamical Laboratory
Bureau of Construction and Repair
U. S. Navy**

FOREWORD

The author wishes to express his sincere thanks to Dr. A. F. Zahm for his valuable advice and encouragement during the time this work was being accomplished and for his interest in the progress of the experimental results; also to the Bureau of Aeronautics and to the Bureau of Construction and Repair, United States Navy, whose interest and laboratory equipment in Washington, where the work was done, have made these studies possible.

REPORT No. 335

AERODYNAMIC THEORY AND TEST OF STRUT FORMS—PART II¹

By R. H. SMITH

S U M M A R Y

This report, submitted to the National Advisory Committee for Aeronautics for publication, presents the second of two studies under the same title. In this part five theoretical struts are developed from distributed sources and sinks and constructed for pressure and resistance tests in a wind tunnel. The surface pressures for symmetrical inviscid flow are computed for each strut from theory and compared with those found by experiment. The theoretical and experimental pressures are found to agree quantitatively near the bow, only qualitatively over the suction range, the experimental suction being uniformly a little low, and not at all near the stern.

This study is the strut sequel to Fuhrmann's research on airship forms, the one being a study in two dimensions, the other in three. A comparison of results indicates that the agreement between theory and experiment is somewhat better for bodies of revolution than for cylinders when both are shaped for slight resistance. The consistent deficiency of the experimental suction which is found in the case of struts was not found in the case of airships, for which the experimental suction was sometimes above sometimes below their theoretical values.

Along with these five theoretical struts were made three empirical struts of high repute, the British strut given in Reports and Memoranda Number 183, the German strut Number 53, and the United States Navy Number 2, and all eight tested for total resistance. Of the five theoretical struts, Number I excels as a fairing, Number V as a strut. Number V and the United States Navy Number 2 have about equal merit as struts, with the German Number 53 a close second and the British a poor third, the relative merits being 100, 103, and 112, respectively, of Reynolds Number 12×10^4 .

¹ This part was submitted in May, 1929, to the Johns Hopkins University as a doctor's dissertation. Part I was reported in Reference 10.

AERODYNAMIC THEORY AND TEST OF STRUT FORMS—PART II

By R. H. SMITH

INTRODUCTION¹

In Part I of this study we were concerned, among other things, with the inverse problem of finding a source-sink distribution whose flow boundary in a uniform stream was the surface of a given empirical strut of high service merit, and then of finding the theoretical pressure everywhere on the strut surface. We will now consider, in Part II, the direct problem of finding the flow boundaries, in a uniform stream, of a few balanced combinations of sources and sinks whose types of distribution are predetermined, and then of finding, as before, the theoretical pressure on the boundary surfaces. Strut models whose surfaces coincide with these flow boundaries will then be made and tested in a wind tunnel for surface pressure and total resistance.

The direct-problem study is analogous to that made by Fuhrmann on a series of surfaces of revolution resembling airships. (Ref. 1.) Part II may therefore be considered as the strut sequel to Fuhrmann's investigation, the one being a study in two dimensions, the other in three.² Before beginning the study, however, it may be well to consider, very briefly, a portion of the underlying mathematics leading to the basic equations of two-dimensional potential flow.

THE FUNDAMENTAL EQUATIONS

A general vector field, such as the distribution of velocity, V , throughout a moving mass of fluid, can always be resolved into two component fields, each present as if alone. One of these components, called the rotational field, arises from vortices and has curl but no divergence, the other, called the irrotational field, arises from sources and sinks and has divergence but no curl. The functional form of V for either component field is obviously fixed by the condition of absence of the other; that is, in the rotational field, V must be $\text{curl } F$, where F is a vector, in order to have no divergence, and in the irrotational field, V must be $\text{grad } \varphi$, where φ is a scalar, in order to have no curl. Accordingly the rotational component field has the equation

$$\text{curl } V = \text{curl curl } F \text{-----} (1)$$

and the irrotational component field has the equation

$$\text{div } V = \text{div grad } \varphi \text{-----} (2)$$

Vector fields whose rotational components are absent are always expressed in terms of scalar or potential fields as in equation (2) because of the great simplification of treatment which ensues.³ When this substitution can be made—that is, when the field is irrotational—it is susceptible to manageable treatment even when the sources and sinks which produce it are quite complex.

The present study includes an investigation of the velocity and pressure in a uniform stream of perfect fluid flowing symmetrically past each of five Rankine struts. The velocity field is therefore produced entirely by sources and sinks; hence is irrotational and susceptible to analysis

¹ See the general introduction, Part I, Reference 10.

² Part II was suggested to me by Dr. A. F. Zahm as suitable for a thesis.

³ It should be recalled that there are special circulatory fields which are irrotational and which are therefore expressible in terms of scalar fields. These fields are produced by line vortices which induce circumferential velocities inversely proportional to the radii.

by equation (2). If we assume the air to be incompressible,⁴ and if we allow for the strength of the sources and sinks enclosed by the closed path of integration, equation (2) becomes

$$\operatorname{div} V = \operatorname{div} \operatorname{grad} \varphi = \Delta^2 \varphi = 0 \quad (3)$$

Equation (3) is invariant to coordinate axes. If we choose cylindrical coordinates for the purpose of deriving the basic equations for this study, and if we assume for V axial symmetry about, and uniformity along z , equation (3) becomes,

$$\Delta^2 \varphi = \frac{1}{\rho} \frac{\partial}{\partial \rho} \left(\rho \frac{\partial \varphi}{\partial \rho} \right) = 0 \quad (4)$$

Since one is concerned with φ at finite distances, equation (4) may be written

$$\rho \frac{\partial \varphi}{\partial \rho} = C \quad (5)$$

from which clearly—

$$\varphi = C \ln \rho + A \quad (6)$$

In equation (6), $C \ln \rho$ is the potential due to a line source whose strength per unit length is $2 \pi C$ ⁵ and A is an added potential of a flow with no divergence such as the potential of a uniform superimposed stream. If this uniform stream has the velocity U along x normal to the source then $A = Ux$, because at great distances where the velocity of the flow from the source vanishes, A satisfies the boundary condition,

$$V_x = \frac{\partial \varphi}{\partial x} = \frac{\partial A}{\partial x} = U$$

Equation (6) then becomes

$$\varphi = C \ln \rho + Ux \quad (7)$$

Each term of equation (7), being a two-dimensional potential, must have a conjugate which satisfies the equation

$$\varphi + i\psi = f(z)$$

The conjugate to $C \ln \rho$ is seen to be $C\theta$ upon decomposing

$$\varphi + i\psi = C \ln z = C \ln (\rho e^{i\theta})$$

into its real and imaginary parts, and the conjugate to Ux is clearly Uy upon decomposing,

$$\varphi + i\psi = Uz = U(x + iy).$$

Accordingly the velocity potential, φ , and the stream function, ψ , of the flow from a line source along z and of a superimposed uniform stream normal to z , are given by the two equations—

$$\varphi = C \ln \rho + Ux \quad (8)$$

$$\psi = C\theta + Uy \quad (9)$$

THE RANKINE HALF STRUT

Preliminary to the treatment of the Rankine struts proper, a study of the half strut, which is produced by a line source normal to a uniform stream, will be made for two reasons; it will be useful in illustrating, in their simplest application, the analytics and the graphics which will be required in the strut development, and, secondly, it has considerable academic interest of its own.

⁴ The correction to divergence due to adiabatic compression is negligibly small in air flowing past a strut under ordinary flight conditions. (Ref. 8.)

⁵ The strength of a line source per unit length is $2 \pi \rho v_\rho$. From equation (5) $v_\rho = \frac{C}{\rho}$, hence the source strength per unit length is $2 \pi C$.

THEORETICAL TREATMENT

Let the contour of the half strut, which is the boundary surface between the source flow and the uniform stream, be $a b c d$, and let the source be at 0, Figure 1. Choose any point p inside, on or outside the boundary surface, and let pp_0 be its ordinate. We wish to express the stream function at p . Since the stream function may be considered physically as a flux across a line, a choice will be made at the outset between the arc pq and the ordinate pp_0 . Equation (9), of course, gives the flux across the arc, and mathematically this is the better choice. However, the equipotential diagram of flux across the ordinate (fig. 7) is more easily interpreted physically and has a symmetry lacking in the diagram of flux across the arc, due to a difference in those parts of the diagrams pertaining to the second quadrant of the field.⁶ On the other hand the ordinate interpretation requires that the half strength, πC , of the source be deducted from the stream function, ψ , at all points of the field. The deduction is required when θ is greater than $\frac{\pi}{2}$ to convert ψ from a flux across the arc to a flux across the ordinate, and when less than $\frac{\pi}{2}$

to compensate for the additional flux from the source across pp_0 as compared to that across rr_0 (fig. 1) when a uniform stream is superimposed.⁷ Hence the deduction, πC , while a simple constant mathematically, is two constants physically, each of which should be applied to different quadrants of the field, at different stages in the development and for different physical reasons.

Since even in the case of distributed sources both parts of the deduction are quite simple ones to compute, and since it seems best to clarify the interpretation of the diagrams, which have a certain value in themselves, the ordinate interpretation will be assumed and the deductions separated. This choice has also the important advantage of following the procedure of Fuhrmann.

Having made this choice we may write equation (9) in two parts corresponding to the two quadrants of the field,

$$\left. \begin{aligned} \frac{\psi}{C} &= -(\pi - \theta) + \frac{y}{a}, & x < 0 \\ \frac{\psi}{C} &= \theta + \frac{y}{a} - \pi, & x > 0 \end{aligned} \right\} \quad (10)$$

where $a = \frac{C}{U}$.

The equation of the half strut, given by letting $\psi = 0$ and $y = \rho \sin \theta$ in equation (10), is

$$\rho = a \frac{\pi - \theta}{\sin \theta} \quad (11)$$

From equation (11), the bow, b , is at $x_0 = -a$. (Fig. 1.) Going aft, the boundary surface intercepts the y axis at $y_0 = \pm \frac{\pi}{2}a$ and approaches asymptotically the two planes $y = \pm \pi a$. Since the parameter a is clearly a measure of the dimensions of the half strut, a series of values of a will give a series of similar contours with the source line as their common focus.

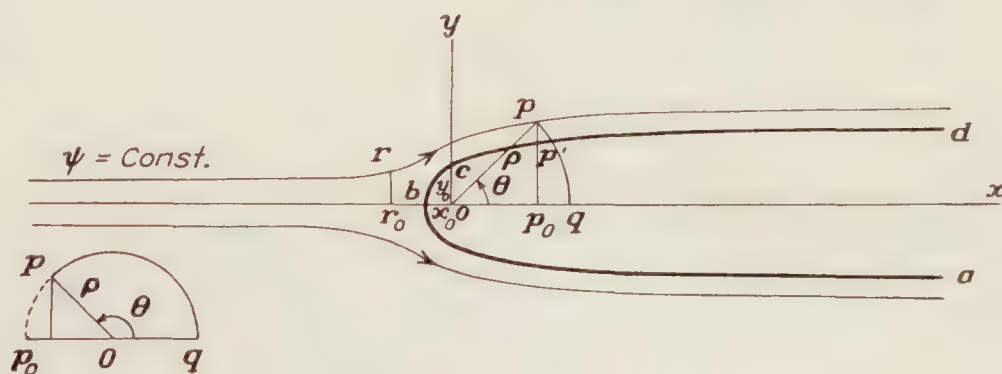


FIGURE 1

⁶ When the arc has second quadrant magnitude, θ for the arc diagram becomes $-(\pi - \theta)$ for the ordinate diagram, the minus sign indicating a right to left flux across the ordinate.

⁷ Since both rp and bcp' (fig. 1) are streamlines, no fluid crosses either and the flux across rr_0 is equal to that across pp' or to that across pp_0 decreased by πC , the half strength of the source.

⁸ Considered mathematically, equation (10) is simply equation (9) with the constant potential $-\pi C$ added in order that the body may have the equation $\psi = 0$ and then written in two forms so that only acute angles enter, which avoids ambiguity in the sign of the trigonometric functions.

Upon partial differentiation, equation (10) gives, at each point of the field, the component velocities

$$V_x = \frac{\partial \psi}{\partial y} = C \frac{x}{\rho^2} + U$$

$$V_y = -\frac{\partial \psi}{\partial x} = C \frac{y}{\rho^2}$$

whose resultant squared is,

$$V^2 = \frac{C^2}{\rho^2} \left(1 + 2 \frac{x}{a} \right) + U^2 \text{-----} (12)$$

If one defines p_n as the full impact pressure of the stream and p as the superstream pressure, or as the pressure above or below that of the distant stream, then, for steady flow,

$$\frac{p}{p_n} = 1 - \left(\frac{V}{U} \right)^2 \text{-----} (13)$$

or

$$\frac{p}{p_n} = - \left(\frac{a^2}{\rho^2} + 2 \frac{a}{\rho} \cos \theta \right) \text{-----} (14)$$

The curve of pressure $\frac{p}{p_n}$ versus the distance x aft the bow, plotted from equation (14) in Figure 5, shows that the pressure is a maximum at the nose, as usual, where it equals the full impact pressure of the uniform stream. Going aft, the pressure decreases rather sharply, passes through its zero value at $x = \frac{a}{2}$ and reaches a negative maximum from which it gradually subsides asymptotically to zero.

At any surface element of the half strut, the pressure exerts on the strut a drag, $p dy$ per unit length, whose integral over any zone or strip of the surface is the zonal pressural drag. (Ref. 2.) If D is the zonal drag per unit length,

$$D = 2 \int_{y_1}^{y_2} p \, dy,$$

$$\text{or} \quad D = -2a p_n \int_{\theta_1}^{\theta_2} \frac{1}{\rho^2} (a + 2\rho \cos \theta) (\rho \cos \theta \, d\theta + \sin \theta \, d\rho) \text{-----} (15)$$

After substituting for ρ its value $a \frac{\pi - \theta}{\sin \theta}$, and carrying through the integration,⁹ equation (15) reduces to the simple form,

$$D = 2a p_n \frac{\sin^2 \theta}{\pi - \theta} \Big|_{\theta_1}^{\theta_2} \text{-----} (16)$$

One observes from equation (16) that $D=0$, as it should, when the limits of θ are 0 and π , that is when the integration extends over the whole surface of the half strut. Going aft from the bow the zonal drag sharply increases from zero to its maximum value at $x = \frac{a}{2}$, where the pressure is zero, and thereafter vanishes asymptotically.

⁹ The step-by-step operations in this and subsequent integrations in this study are omitted. While for the most part the integrations are straightforward, they are nevertheless tediously long and distracting. They have been omitted everywhere, therefore, for uniformity and brevity, even though a certain amount of mathematical continuity is sacrificed.

Surfaces of constant speed or pressure in the field about the half strut are found by solving equation (12) when a series of values is assigned to V . If one lets $V = KU$ equation (12) becomes,

$$U^2 (K^2 - 1) = \left(\frac{C}{\rho}\right)^2 \left(1 + 2 \frac{\rho}{a} \cos \theta\right),$$

from which,

$$\rho^2 = \frac{a^2}{K^2 - 1} + \frac{2a\rho \cos \theta}{K^2 - 1} \quad (17)$$

If

$$\frac{a^2}{K^2 - 1} = r^2 - c^2, \text{ and } \frac{a}{K^2 - 1} = c,$$

equation (17) takes the form

$$\rho^2 = r^2 - c^2 + 2 \rho c \cos \theta$$

which one recognizes as the equation of a family of circles whose centers are at points $(c, 0)$ and whose radii are the values assigned to r . The radii of the circles and the abscissas of their centers are simply

$$\left. \begin{aligned} r &= Kc \\ c &= \frac{a}{K^2 - 1} \end{aligned} \right\} \quad (18)$$

It is interesting to note that the circle of infinite radius—that is the straight line—is the one for which $K = 1$, or for which V is the speed of the distant stream. This line crosses the bow at $x = \frac{a}{2}$ where the surface pressure is zero. The circles of constant speed or pressure are drawn from equations (18) in the upper half of Figure 6.

GRAPHICAL TREATMENT

Due to its simplicity, the whole treatment of the half strut has been carried through analytically. When one passes to the more complex distributions of sources and sinks, however, the analytical treatment becomes unmanageable, and graphical methods must be resorted to. For these more complicated cases the analytics can be carried without serious difficulty through the determination of the potential at any point of the flow field, but suddenly becomes unmanageable when the equation of the equipotential surfaces is required. Beginning therefore with the graphical determination of the streamlines, one of which is the strut surface, the determination of the velocity and pressure in such cases must be essentially graphical. In order to illustrate the method, it will be useful, to carry the simple case of the half strut through the first stages of the graphical treatment.

Beginning with equations (10), values of

$$\left. \begin{aligned} \frac{\psi_1'}{C} &= -(\pi - \theta) = \tan^{-1} \frac{y}{x} - \pi, & x < 0 \\ \frac{\psi_1'}{C} &= \theta = \tan^{-1} \frac{y}{x}, & x > 0 \end{aligned} \right\} \quad (19)$$

are computed for various values of x and y , as listed in Table I and plotted in Figure 7. For a series of values of x one reads from this figure the values of $\frac{\psi_1'}{C}$ corresponding to the values of y chosen, and deducts from each value of $\frac{\psi_1'}{C}$ the half strength of the source divided by C when x

¹⁰ The subscript, 1, indicates a source as distinguished from the subscript, 2, indicating a sink. The primes indicate that the stream function coefficients, $\frac{\psi}{C}$, have been reduced by the amount of the source-sink strength (divided by C) lying to the right, according to the first of equations (10), but not yet by the amount lying to the left, required by the second equation. When the latter deduction is made, the primes are omitted.

other, a distance U along x , so that the op set are in position $o'p'$ in Figure 2. The distances $qs = V$ are then read in succession simply by a scale, giving the resultant velocity along the stream-line in terms of the uniform stream speed U .

Finally knowing the velocity, the pressure for steady flow is given everywhere by equation (13). The pressures on the half-strut surface determined in this way agree with those given by equation (14).

FIVE RANKINE STRUTS

THEORETICAL DEVELOPMENT

In order to derive a series of Rankine struts whose shapes resemble the shape of struts used in aircraft, one needs a variety of distributed sources and sinks, particularly the latter. Following the treatment of the line source, the formulas for the stream function coefficient, $\frac{\psi_1}{C}$, and for the velocity potential coefficient, $\frac{\varphi_1}{C}$, will therefore be found for surface sources having three types of strength distribution, the uniform, the linear, and the parabolic.

The three distributed types of sources require treatments which are sufficiently similar to justify developing all three together. Accordingly the equations in the following development will appear in triplets, the first of which is always for the uniformly distributed source, the second for the linearly distributed one, and the third for the parabolic. They will be distinguished in the development by the subscripts a , b , and c respectively, added to the equation numbers.

Consider a strip of width, l , cut from an infinite plane and beset uniformly with line sources running lengthwise. If the elementary line sources are equal in strength the strip is a uniformly distributed source; if they have strengths proportional to their distance from one edge of the strip, the source is a linearly distributed one, and if their strengths are proportional to the square of this distance, the source is parabolically distributed.¹¹

Let the total strength of the strip source be $2\pi C$ per unit length along z . Then, clearly, an elementary strip, $d\xi$ (fig. 3) has the strengths, $2\pi C \frac{d\xi}{l}$, $2\pi C \frac{2\xi d\xi}{l^2}$, and $2\pi C \frac{3\xi^2 d\xi}{l^3}$, according as the distribution is uniform, linear or parabolic.

By equation (8) these elements at a distance ξ from the z axis, add to the velocity potential φ_1 at the point P , the values,

$$\begin{aligned}\frac{d\varphi_1}{C} &= \frac{1}{l} \ln \rho d\xi, \\ &= \frac{2}{l^2} \ln \rho \xi d\xi, \\ &= \frac{3}{l^3} \ln \rho \xi^2 d\xi,\end{aligned}$$

Substituting the value of ρ and writing in integral form, these equations become

$$\frac{\varphi_1}{C} = \frac{1}{2l} \int_0^l \ln [(x-\xi)^2 + y^2] d\xi \text{-----} (22a)$$

$$= \frac{2}{2l^2} \int_0^l \ln [(x-\xi)^2 + y^2] \xi d\xi \text{-----} (22b)$$

$$= \frac{3}{2l^3} \int_0^l \ln [(x-\xi)^2 + y^2] \xi^2 d\xi \text{-----} (22c)$$

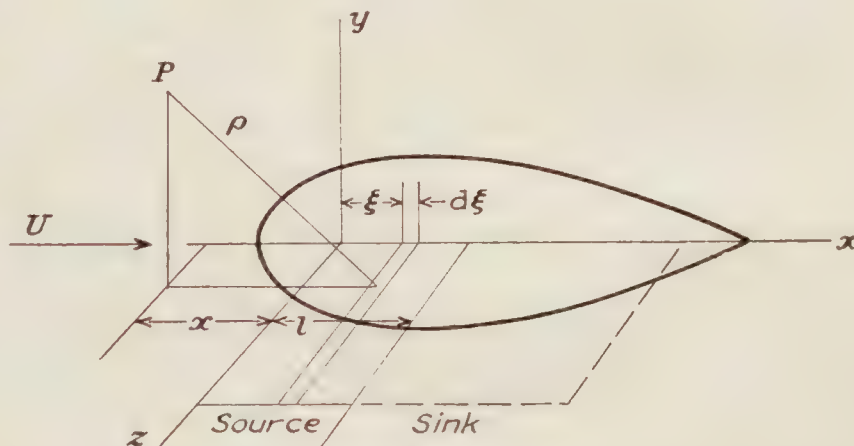


FIGURE 3

¹¹ Fuhrmann, Reference 1, used only the uniform and linear strength distribution.

Values of $\frac{\varphi_1}{C}$ will be required only for the determination of the bow and stern points of the boundary surfaces for which $y=0$. Letting $y=0$ in equations (22), and integrating, one obtains,¹²

$$\frac{\varphi_1}{C} = \frac{1}{l} [(l-x) \ln(x-l) + x \ln x - l] \text{-----} (23a)$$

$$= \frac{1}{l^2} \left[(l^2 - x^2) \ln(x-l) + x^2 \ln x - lx - \frac{l^2}{2} \right] \text{-----} (23b)$$

$$= \frac{1}{l^3} \left[(l^3 - x^3) \ln(x-l) + x^3 \ln x - lx^2 - \frac{l^2 x}{2} - \frac{l^3}{3} \right] \text{-----} (23c)$$

If equation (8) is differentiated partially with respect to x , we obtain the equation for the bow point,

$$V_x = \frac{\partial}{\partial x} \left(\frac{\varphi}{C} \right) = \frac{\partial}{\partial x} \left(\frac{\varphi_1}{C} \right) + \frac{U}{C} = 0 \text{-----} (24)$$

Differentiating equations (23) partially with respect to x and substituting in equation (24) one obtains,

$$\frac{U}{C} = \frac{1}{l} \left(\ln \frac{x-l}{x} \right) \text{-----} (25a)$$

$$= \frac{2}{l^2} \left(x \ln \frac{x-l}{x} + l \right) \text{-----} (25b)$$

$$= \frac{3}{l^3} \left(x^2 \ln \frac{x-l}{x} + xl + \frac{l^2}{2} \right) \text{-----} (25c)$$

These are the relations between the values of $\frac{U}{C}$ and the abscissas of the bow point, corresponding to equation (21) for the line source. The graphs of equation (25a), (25b), and (25c) are found in Figures 8, 9, and 10, respectively.

By equation (9) the elementary strip, $d\xi$, Figure 3, likewise adds to the stream function ψ_1' , at the point P the values,

$$\frac{d\psi_1'}{C} = \frac{1}{l} \left(\tan^{-1} \frac{y}{x-\xi} - n\pi \right) d\xi,$$

$$= \frac{2}{l^2} \left(\tan^{-1} \frac{y}{x-\xi} - n\pi \right) \xi d\xi,$$

$$= \frac{3}{l^3} \left(\tan^{-1} \frac{y}{x-\xi} - n\pi \right) \xi^2 d\xi,$$

where $n=1$ if $x < 0$ and $n=0$ if $x > 0$. The whole stream function at P due to the source is therefore,

$$\frac{\psi_1'}{C} = \frac{1}{l} \int_0 \tan^{-1} \frac{y}{x-\xi} d\xi - L \text{-----} (26a)$$

$$= \frac{2}{l^2} \int_0 \tan^{-1} \frac{y}{x-\xi} \xi d\xi - M \text{-----} (26b)$$

$$= \frac{3}{l^3} \int_0 \tan^{-1} \frac{y}{x-\xi} \xi^2 d\xi - N \text{-----} (26c)$$

¹² The integrated forms of equations (22a) and (22b), when y is retained, are

$$\frac{\varphi_1}{C} = \frac{1}{l} \left\{ \frac{1}{2} (l-x) \ln [(x-l)^2 + y^2] + \frac{x}{2} \ln (x^2 + y^2) - l - y \left(\tan^{-1} \frac{x-l}{y} - \tan^{-1} \frac{x}{y} \right) \right\} \text{-----} (23'a)$$

$$= \frac{1}{2l^2} \{ [(x-l)^2 + y^2] \ln [(x-l)^2 + y^2] - [(x-l)^2 + y^2] - (x^2 + y^2) \ln (x^2 + y^2) + (x^2 + y^2) \} + \frac{2x}{l} H \text{-----} (23'b)$$

where $H = \frac{\varphi_1}{C}$ for the uniform source given in equation (23'a).

The values chosen for y were, for all, +1, +2, +3, +4, +5, +6, +8, +10, +12, +14. The values chosen for x were in equation (28a), +5, +7, +9, +10, +11, +13, +16, +20, +25, +30, +35, +40, +50; in equation (28b), for $l=5$, -40, -35, -30, -25, -20, -16, -13, -10, -7, -5, -2, 0, +2, +4, +5, +6, +8, +11, +13, +16, +20, +25, +30, +35, +40, +50; for $l=20$, -40, -35, -30, -25, -20, -16, -13, -10, -3, -5, -2, 0, +2, +5, +7, +10, +13, +16, +18, +20, +22, +25, +30, +35, +40, +50; in equation (28c), -40, -35, -30, -25, -20, -16, -13, -10, -7, -5, -2, 0, +3, +5, +7, +9, +10, +11, +13, +16, +20, +25, +30, +35, +40, +50.

where,

$$L = \pi \left(1 - \frac{\xi}{l} \right) \text{-----} \quad (27a)$$

$$M = \pi \left(1 - \frac{\xi^2}{l^2} \right) \text{-----} \quad (27b)$$

$$N = \pi \left(1 - \frac{\xi^3}{l^3} \right) \text{-----} \quad (27c)$$

is the amount of the source half strength downstream, or to the right of ξ .

Equations (26) integrate to the equations,

$$\frac{\psi_1'}{C} = \frac{1}{l} \left[x \tan^{-1} \frac{y}{x} - (x-l) \tan^{-1} \frac{y}{x-l} + \frac{y}{2} \ln \frac{x^2+y^2}{(x-l)^2+y^2} \right] - L \text{-----} \quad (28a)$$

$$\frac{\psi_1'}{C} = \frac{1}{l^2} \left[(x^2-y^2) \tan^{-1} \frac{y}{x} - (x^2-y^2-l^2) \tan^{-1} \frac{y}{x-l} - ly + xy \ln \frac{x^2+y^2}{(x-l)^2+y^2} \right] - M \text{---} \quad (28b)$$

$$\frac{\psi_1'}{C} = \frac{1}{l^3} \left[3x^2 I_1 - 3x I_2 - (x-l)^3 \tan^{-1} \frac{y}{x-l} + x^3 \tan^{-1} \frac{y}{x} - \frac{yl}{2} (l-2x) \right. \\ \left. - \frac{y^3}{2} \ln \frac{x^2+y^2}{(x-l)^2+y^2} \right] - N \text{-----} \quad (28c)$$

where I_1 is the bracket term in equation (28a) and I_2 is the bracket term in equation (28b). Values of $\frac{\psi_1'}{C}$ have been computed from equations (28) for 10 values of y , for each of 13 values of x , in the case of the symmetrical distribution, (28a), and for each of 26 values of x in the case of (28b) and (28c), and all for $l=10$, in (28a) and (28c) and $l=5$ and $l=20$ in (28b).¹² The values of the stream function coefficients, $\frac{\psi_1'}{C}$, for the three distributed sources are given in Tables II, III, and IV and plotted in Figures 8, 9, and 10.

The corresponding sink strips produce potential coefficients of like magnitude but of opposite sign. One has therefore only to change the sign of C from positive to negative in equations (19) to (28) and in the corresponding figures to obtain the stream function coefficients and the values of $\frac{U}{C}$ for the four types of distributions when used as sinks. The stream function coefficient of a sink is denoted $\frac{\psi_2'}{C}$.

The combined coefficient of a source and sink, when both are equal in strength, is clearly $\frac{\psi_1' + \psi_2'}{C}$ which one obtains for any point in the flow field by simply adding the two stream function coefficients produced there by the two independent flows. By carefully adding coefficients taken from Figures 7 to 10 in a routine way, Figures 11 to 15 have been constructed, giving the stream function coefficients and the values of $\frac{U}{C}$ for the five source-sink combinations represented diagrammatically in Figure 4.

The five combinations contain two series of three each, one series has a common source combined with three types of sinks, the other has a common sink combined with three types of sources. Combinations I, II, III make up the first series, II, IV, V the second. It will be observed that no combinations are used giving vanishing source or sink strengths at the combined strip edges, such as would result, for example, by rotating the sink in combination III through an angle π about z at its mid-length. The edge of vanishing strength in such a combination produces a cusp at the bow or stern of the boundary surface. The surface then departs too far from forms of high merit to justify its study. This contrasts with the three dimensional case in which source-sink combinations having vanishing strengths at the ends produce boundary surfaces of revolution free of cusps and of good airship form. (Ref. 1.)

¹² See footnote on p. 732.

Equations (28) and their corresponding diagrams, Figures 8, 9, and 10, as well as the five combination diagrams, Figures 11 to 14, give the stream function coefficients corrected only for that part of the source-sink strength lying downstream. The physical interpretation of these diagrams is clear.

Upon superimposing a uniform field on these source-sink fields the second deduction must be made. The amount of the source-sink strength upstream (divided by C), must be deducted from each value of $\frac{\psi_1' + \psi_2'}{C}$ giving values of $\frac{\psi_1 + \psi_2}{C}$ as explained in connection with equation (10). These deductions, however, are very simple ones to make. If the ordinate to the point in the field, where the value of $\frac{\psi_1 + \psi_2}{C}$ is desired, stands on the source strip, the deduction may be read from graphs of equations (27). If the ordinate stands on the sink strip, one uses the relation that the strength upstream is the same as that downstream, with reversed sign, and obtains the deduction by reading the values as before from graphs of equations (27) but reversing the sign. After applying these deductions one obtains the same values of $\frac{\psi_1 + \psi_2}{C}$ as would have been obtained had equation (9) been used and no deductions made. From this point on, the developments proceeding from equations (9) and (10) are the same.

One next plots against y , the values of $\frac{\psi_1 + \psi_2}{C}$, just obtained, giving a family of curves of constant x , for each of the five combinations. The diagrams so obtained are shown in Figures 17 to 21 and correspond to Figure 16 for the half strut, whose use has already been explained. In each diagram, the straight line,

$$\frac{\psi}{C} = \frac{U}{C}y \text{-----} (29)$$

through the origin, is so sloped as to intersect the uppermost x curve at a value of y which is the desired half-thickness of the strut. To obtain the strut half thickness, the width and fineness ratio¹³ must be known. The width is known approximately from the total strip width of the source-sink combination. The fineness ratio was made approximately 3.5 which is common in practice.¹⁴ Having obtained the slopes, one draws across Figures 17 to 21 a series of parallels $\frac{\psi}{C} = \frac{U}{C}y + n\Delta\frac{\psi}{C}$ graded from the line $\frac{\psi}{C} = \frac{U}{C}y$ by integral multiples of $\Delta\frac{\psi}{C}$, just as was done in Figure 16 for the half strut.

Following the treatment of the half strut, the horizontals in Figures 17 to 21 give values of x, y which enable one to draw point by point the source-to-sink streamlines, $\frac{\psi_1 + \psi_2}{C} = \text{const.}$ These are drawn in the upper half of Figures 22 to 26. Similarly, the sloping parallels give values of x, y from which one draws the resultant flow streamlines $\frac{\psi}{C} = \text{const.}$, one being the strut form itself. These latter are drawn in the lower half of the figures. The values of x, y giving the strut surface and including the bow and stern points obtained from the $\frac{U}{C}$ curves of Figures 11 to 15 are given in Table V for each of the five struts.

¹³ The fineness ratio is the ratio of the strut width and maximum thickness.

¹⁴ If one changes the slope of the line by assigning a series of values to $\frac{U}{C}$ equation (29), a series of struts of varying fineness ratio is obtained.

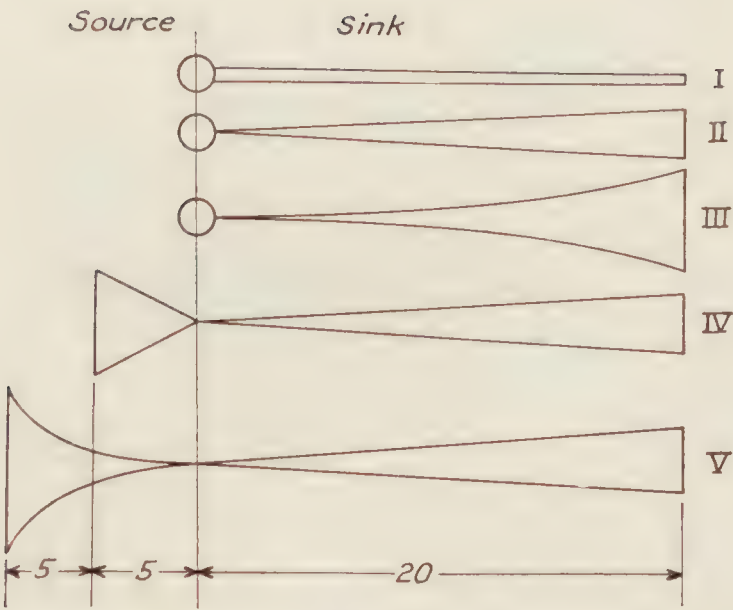


FIGURE 4

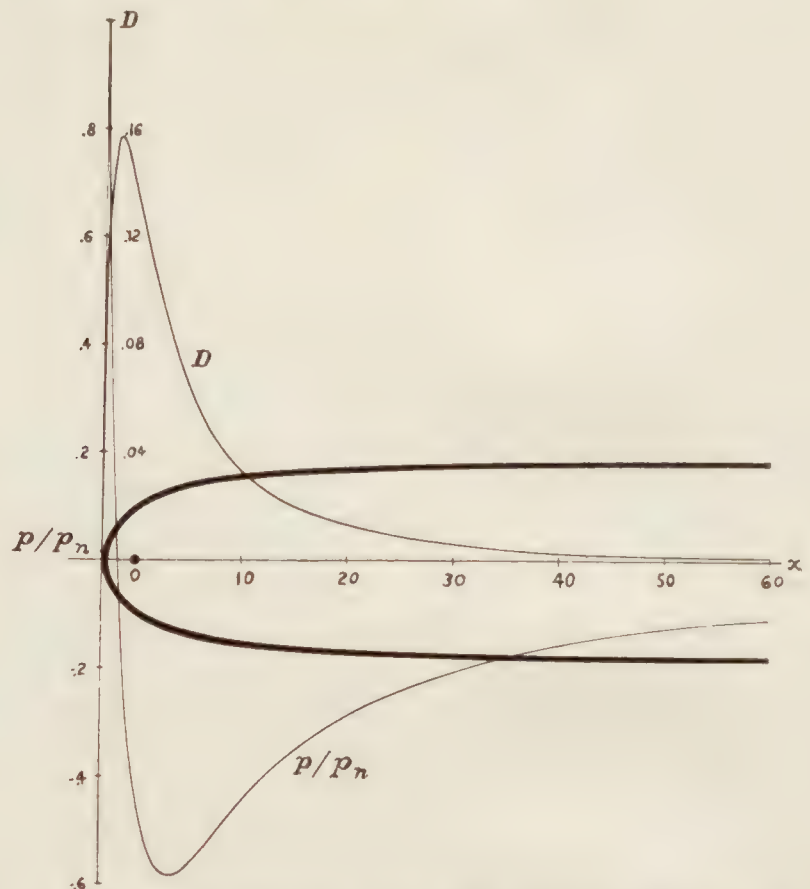


FIGURE 5.—Surface pressure and zonal drag of half strut formed by a line source in uniform stream. D in pounds per foot run at 40 miles per hour, standard inviscid air

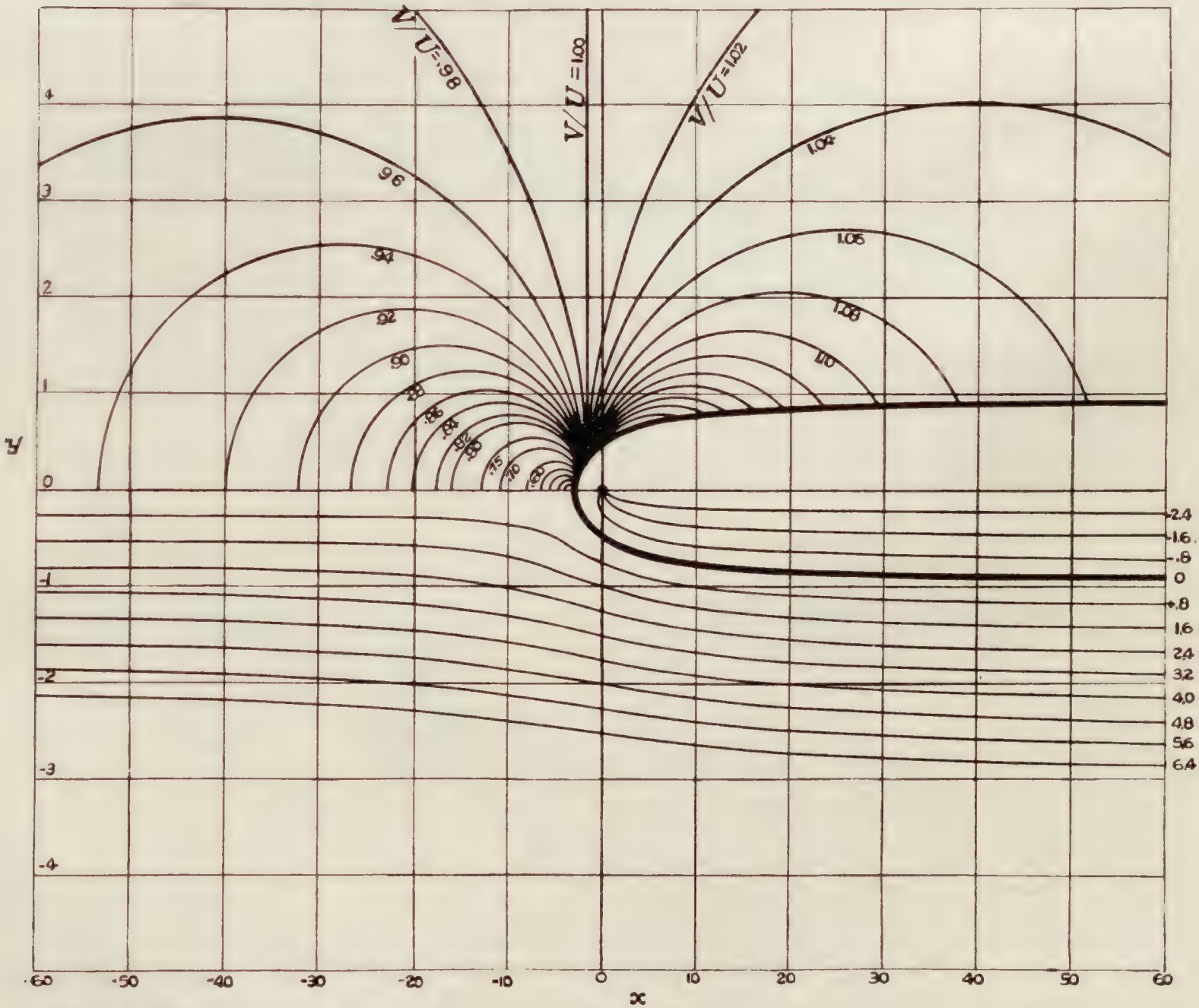
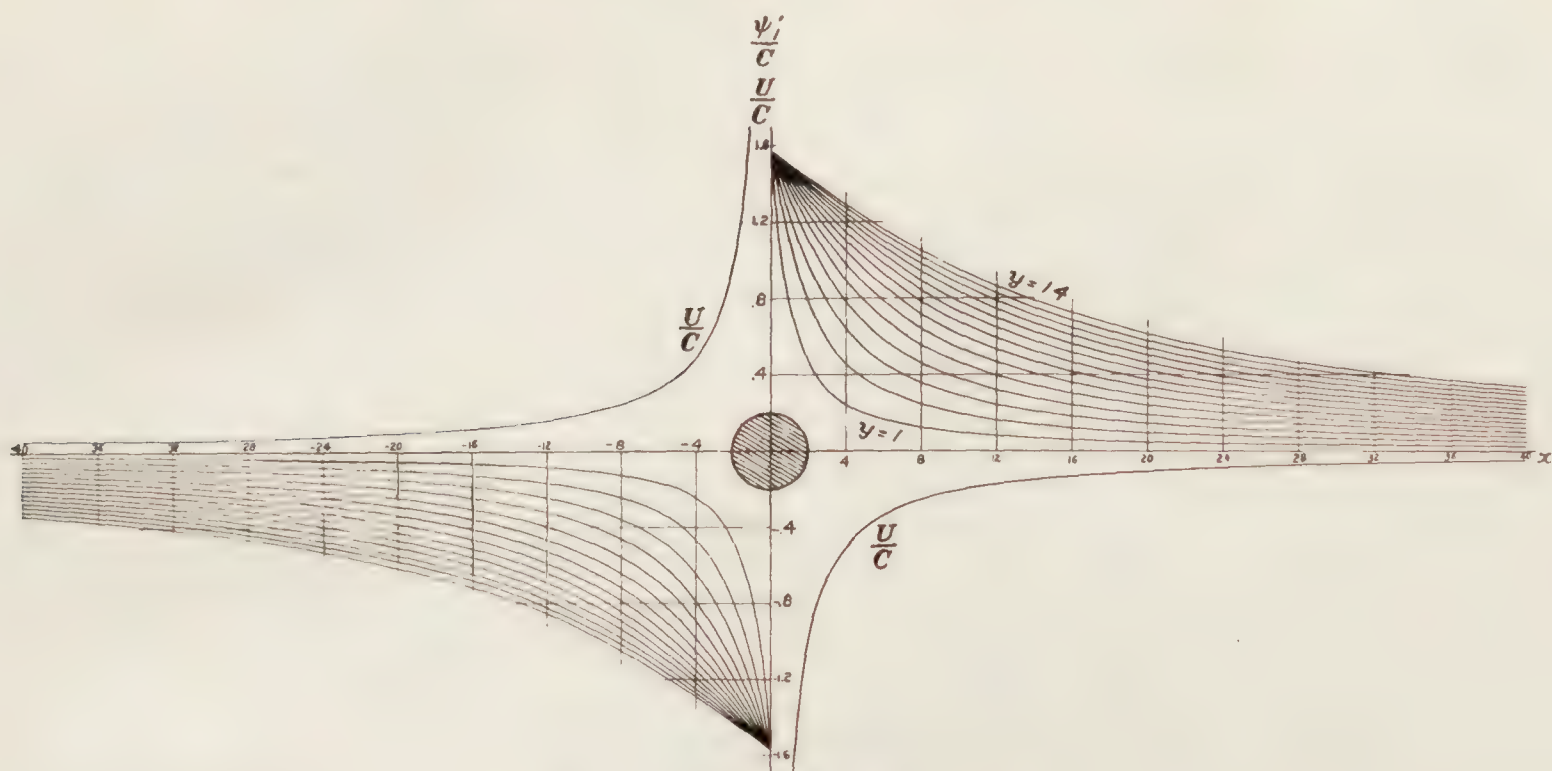
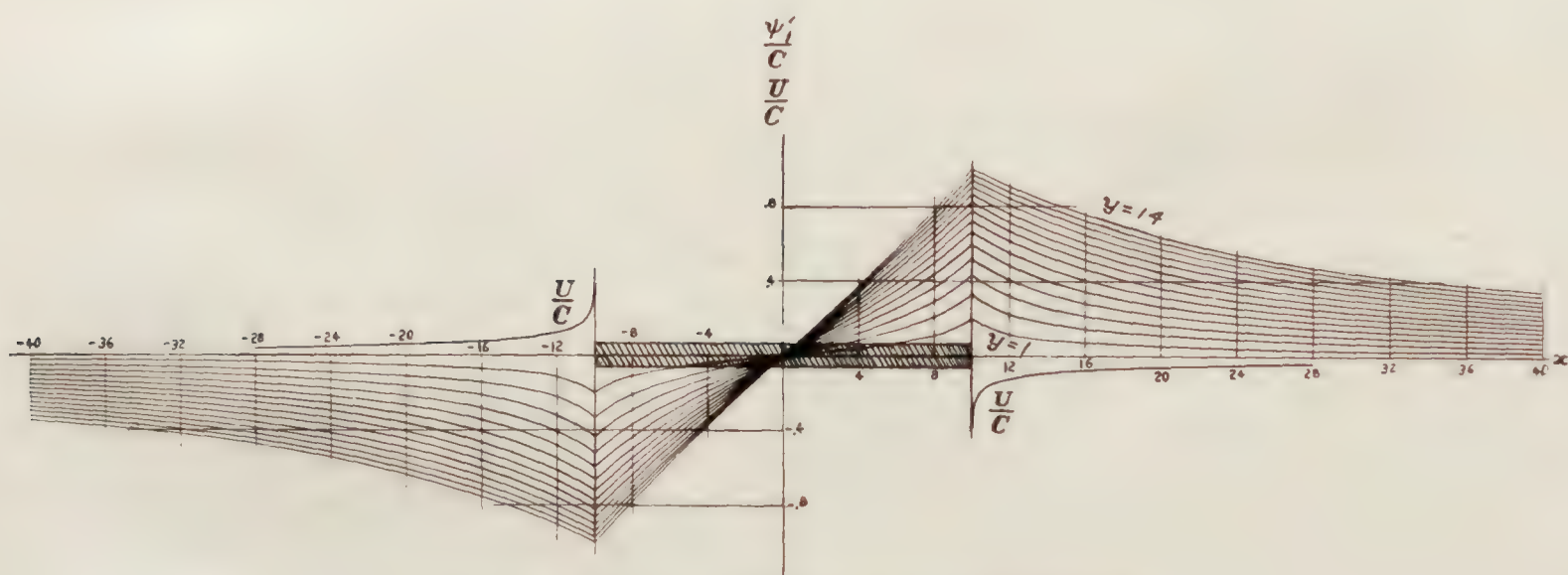
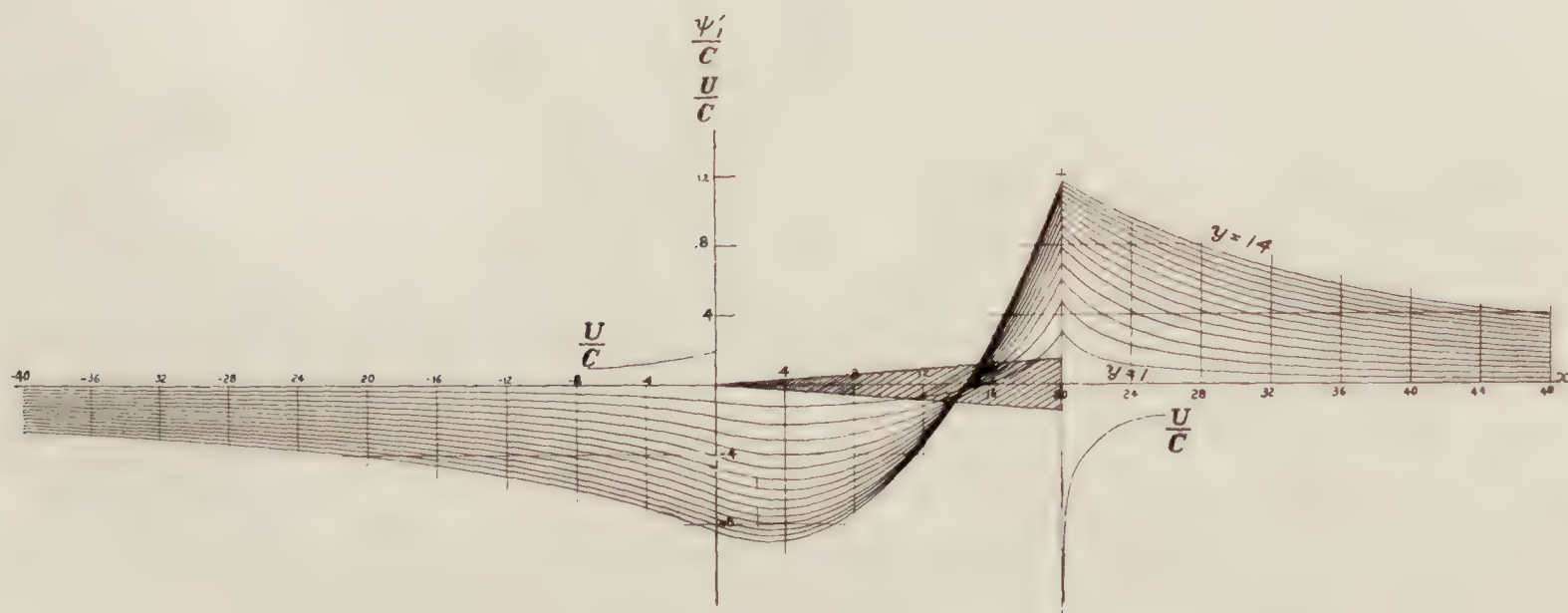


FIGURE 6.—Circles of constant speed and resultant streamlines for the half strut formed by a line source in a uniform inviscid stream

FIGURE 7.— $\frac{\psi'}{C}$ diagram for the line sourceFIGURE 8.— $\frac{\psi'}{C}$ diagram for the surface source of uniform intensityFIGURE 9.— $\frac{\psi'}{C}$ diagram for the surface source of linearly increasing intensity

Having constructed Figures 22 to 26, one obtains the velocity, and from the velocity the pressure along any streamline by the method explained in the treatment of the half strut. The velocity and pressure found at the surface of the five struts are listed in Tables VI to X. Finally

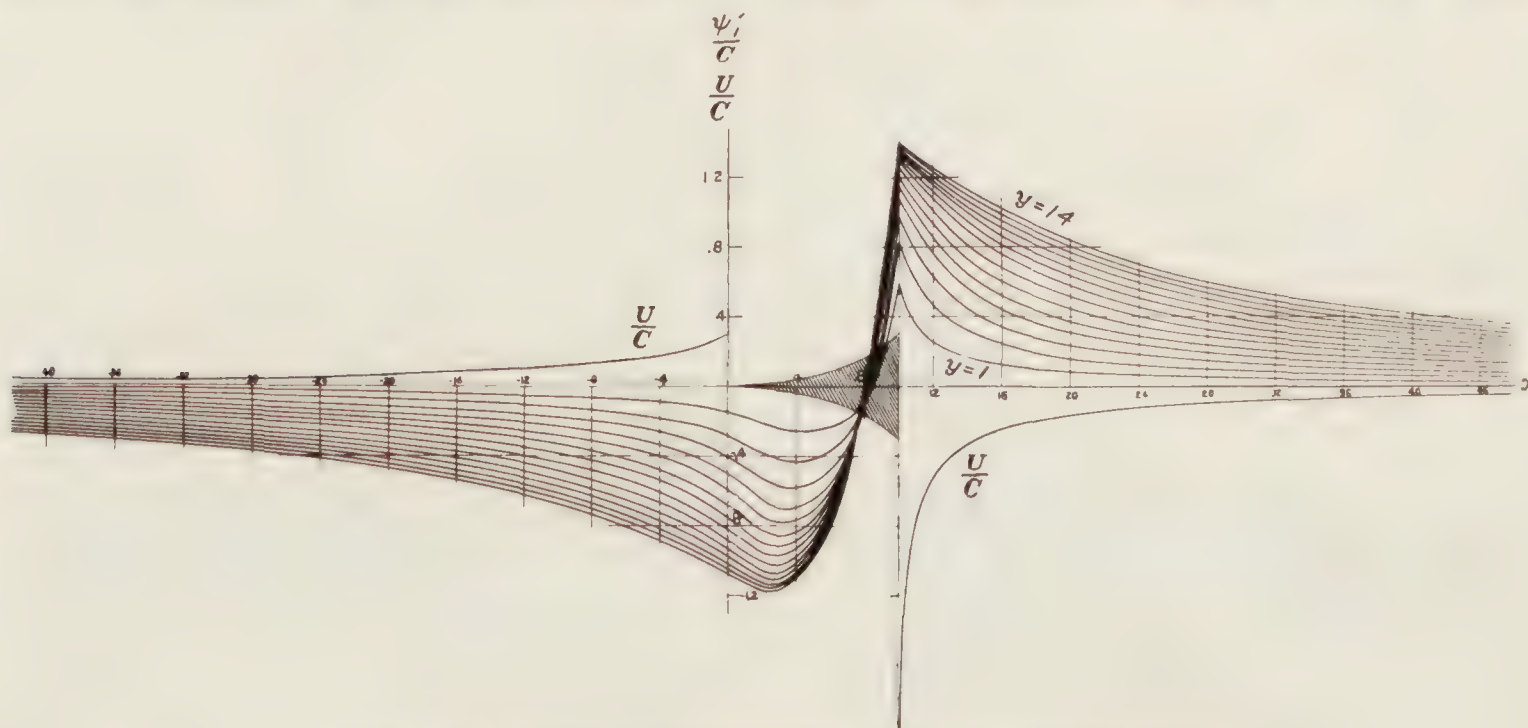


FIGURE 10.— $\frac{\psi'}{C}$ diagram for the surface source of parabolically increasing intensity

the pressures are plotted against strut width in Figures 27 to 31 and against strut half-thickness for integration in Figures 32 to 36.

The theoretical resistance of each strut in inviscid air is the integrated pressural drag which is proportional to the difference between the areas a , b , g , e , f , and g , c , g of the theoretical pres-

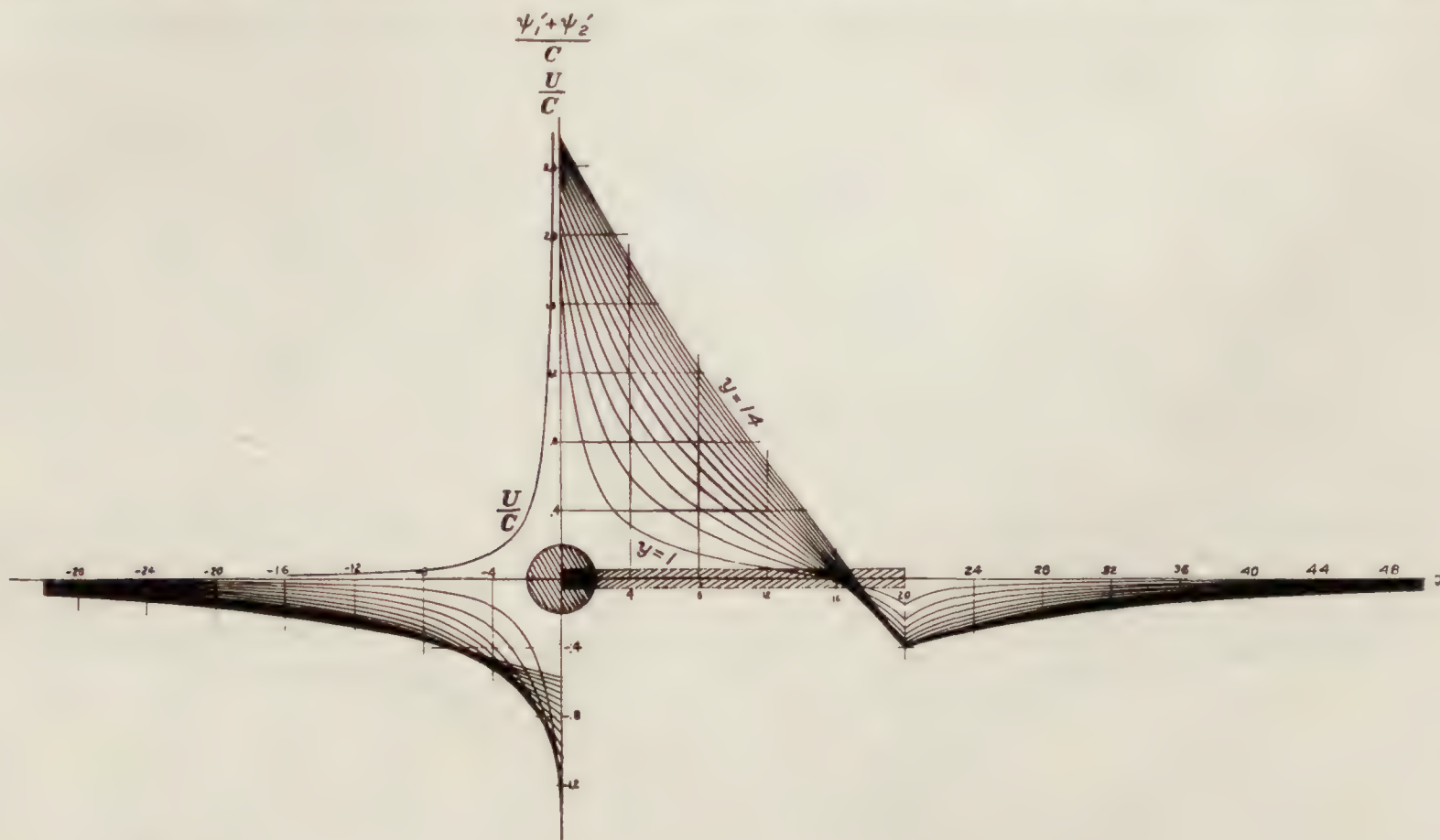


FIGURE 11.— $\frac{\psi'_1 + \psi'_2}{C}$ diagram for the source-sink combination No. I, Figure 4

sure curves in Figures 32 to 36. Since the theoretical resistance should be nothing, the areas should be equal. When the two areas for each strut are integrated they are found to be equal within the precision of the development. The magnitudes of the four components of pressure

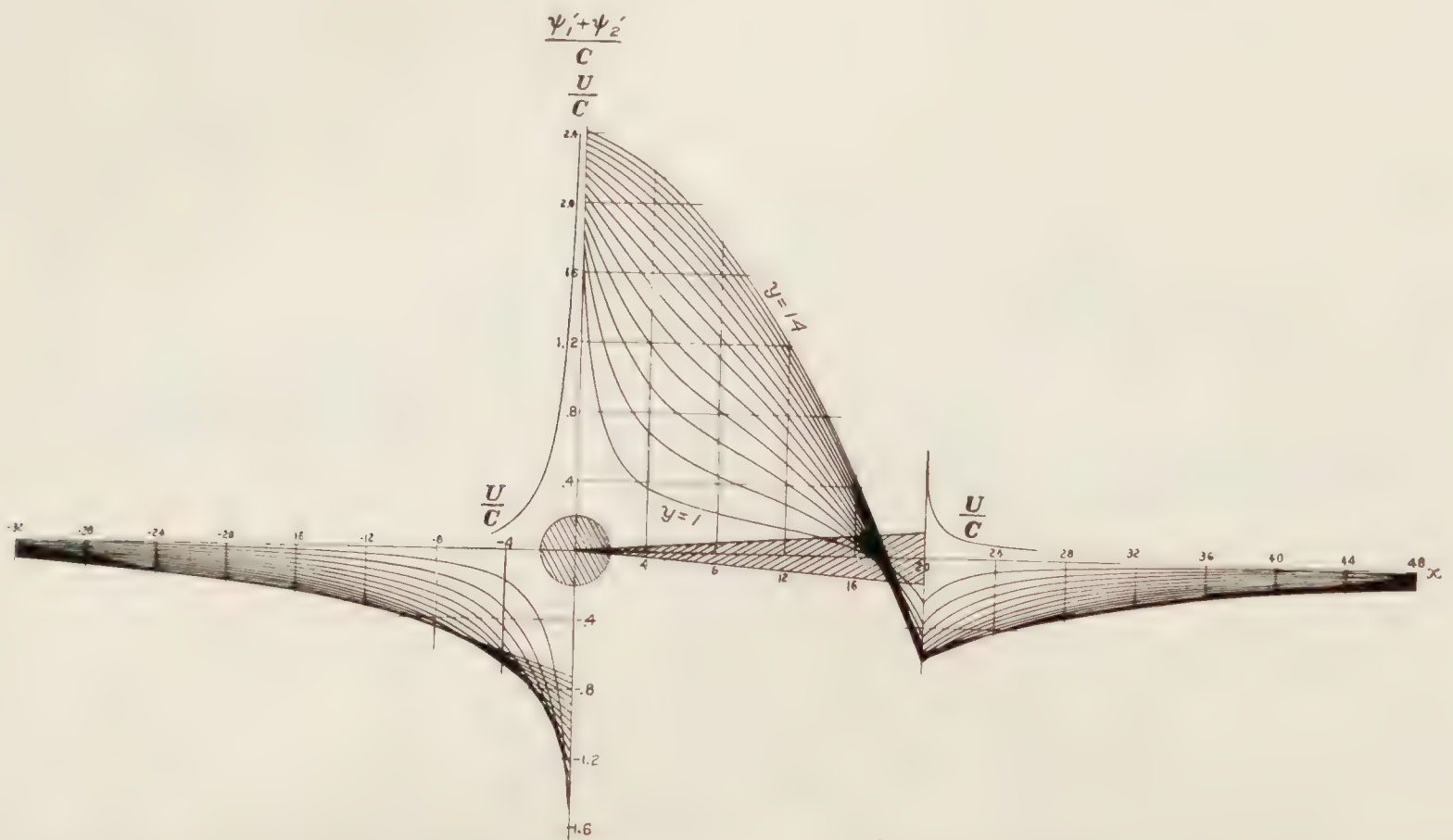


FIGURE 12.— $\frac{\psi'_1 + \psi'_2}{C}$ diagram for the source-sink combination No. II, Figure 4

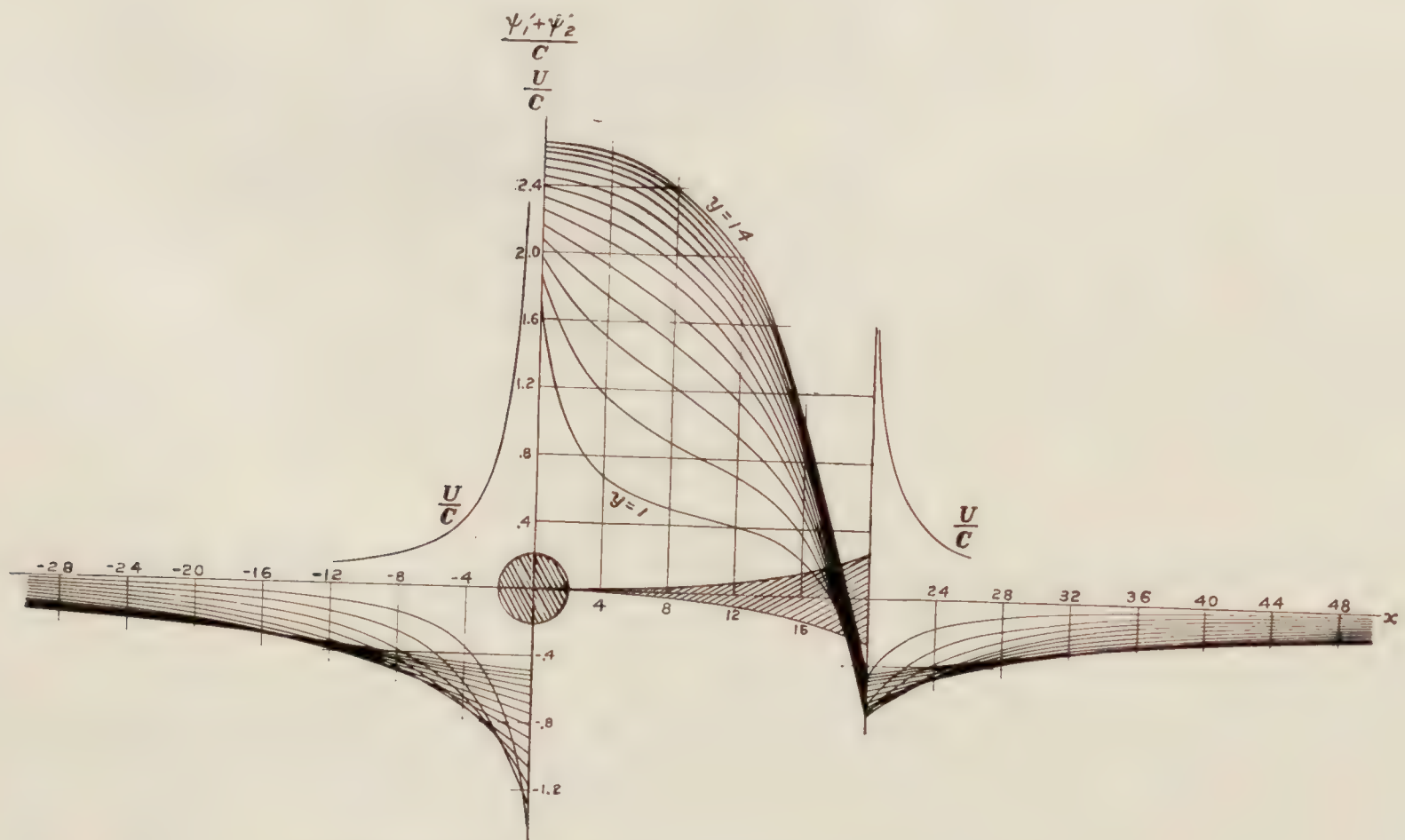


FIGURE 13.— $\frac{\psi'_1 + \psi'_2}{C}$ diagram for the source-sink combination No. III, Figure 4

drag alongstream, which are the upstream and downstream push and suction, are given for both theory and experiment in Table XII.¹⁵ The determination of the pressure distribution over the surface of the five struts completes the theoretical part of the study.

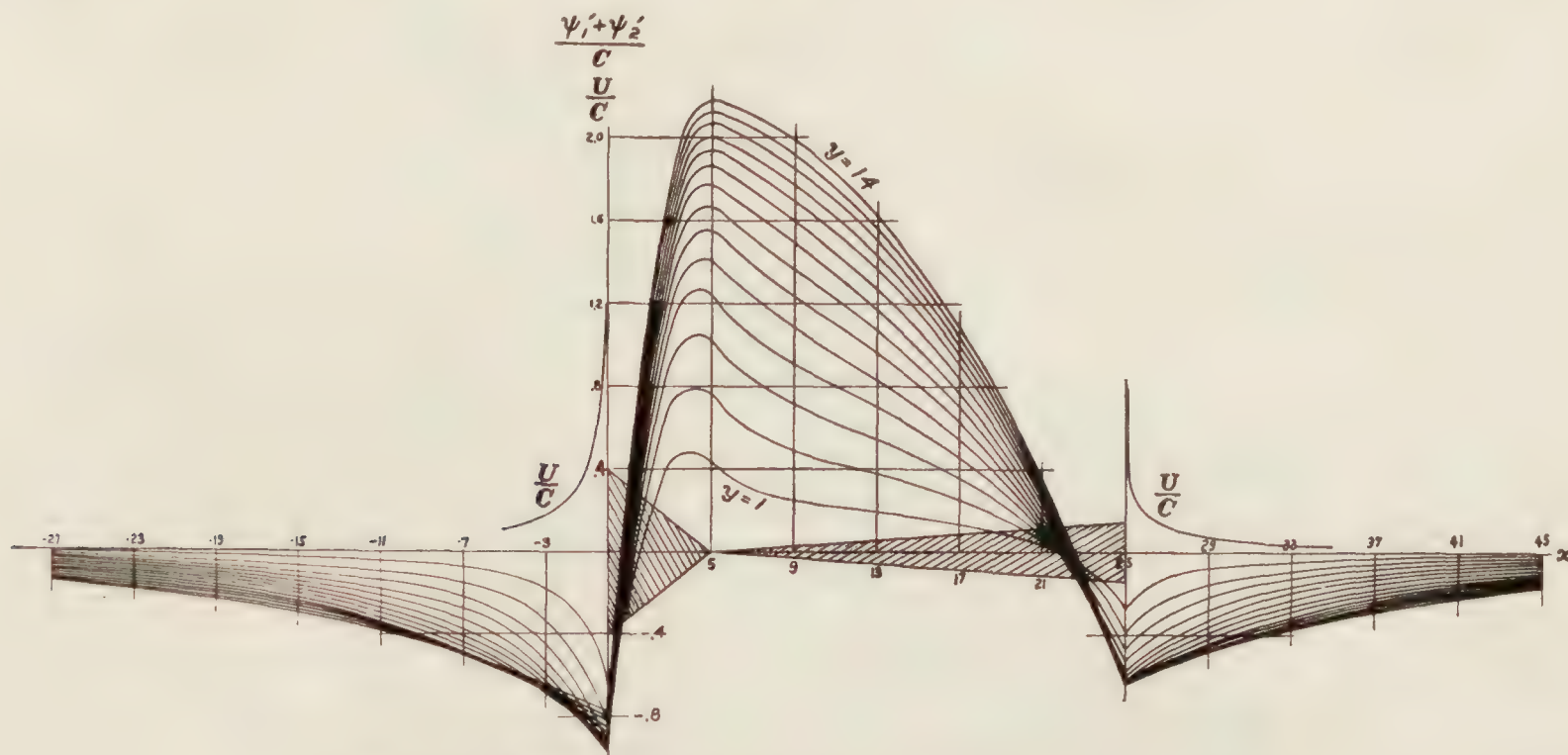


FIGURE 14.— $\frac{\psi'_1 + \psi'_2}{C}$ diagram for the source-sink combination No. IV, Figure 4

EXPERIMENTAL RESULTS¹⁶

In order to compare the theoretical surface speeds and pressures with the actual ones in the case of air, models of the five theoretical struts were made and each subjected to resistance and pressure distribution tests in a wind tunnel. Along with these five, three empirical struts

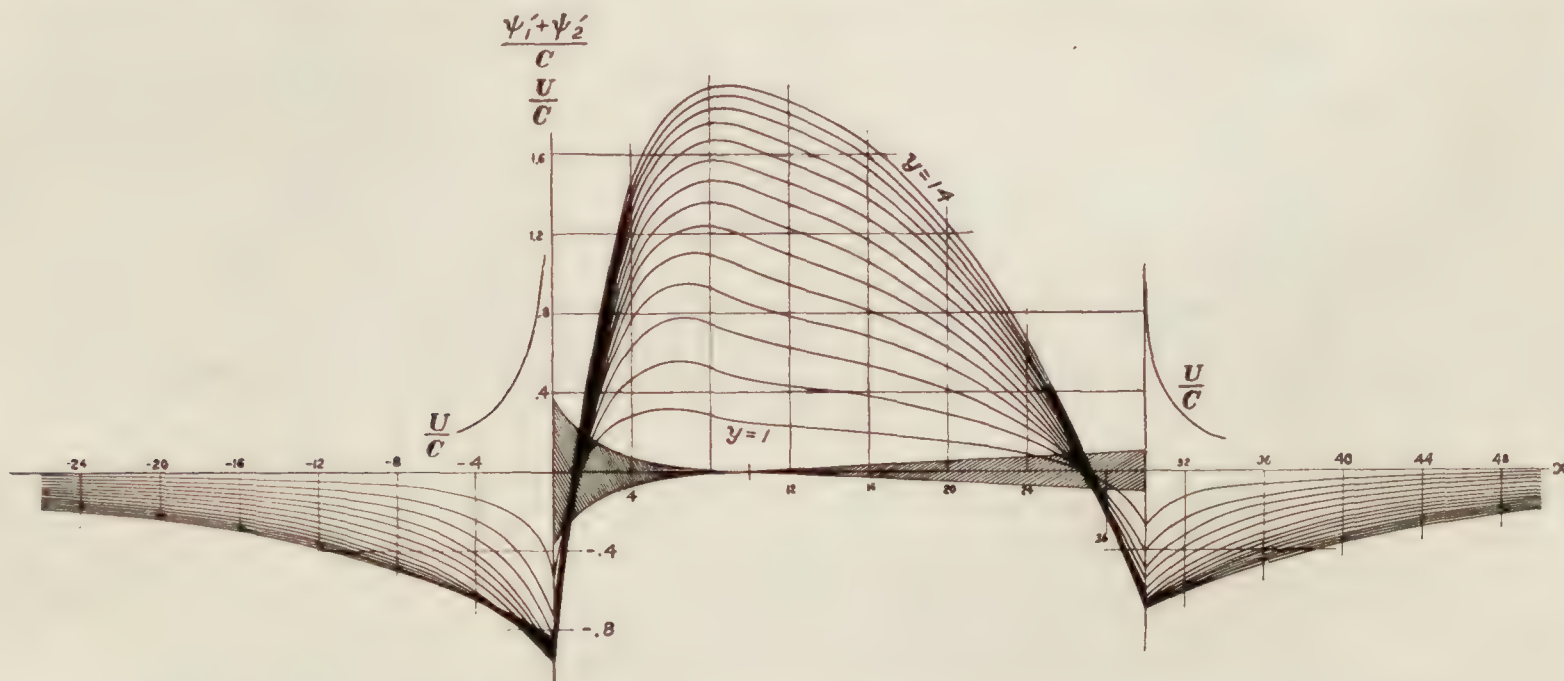


FIGURE 15.— $\frac{\psi'_1 + \psi'_2}{C}$ diagram for the source-sink combination No. V, Figure 4

of high repute were made, one British, one German, and one American, and their resistances determined for comparison. The remaining part of the study will be devoted to a description of the models and to an analysis of the experimental results.

¹⁵ The method used in Table XII of analyzing into its various components the resistance of a body moving through a fluid is due to Zahm. (Ref. 2.)

¹⁶ See opening paragraph under "Experimental investigation of U. S. Navy No. 2 strut," Part I. (Ref. 10.)

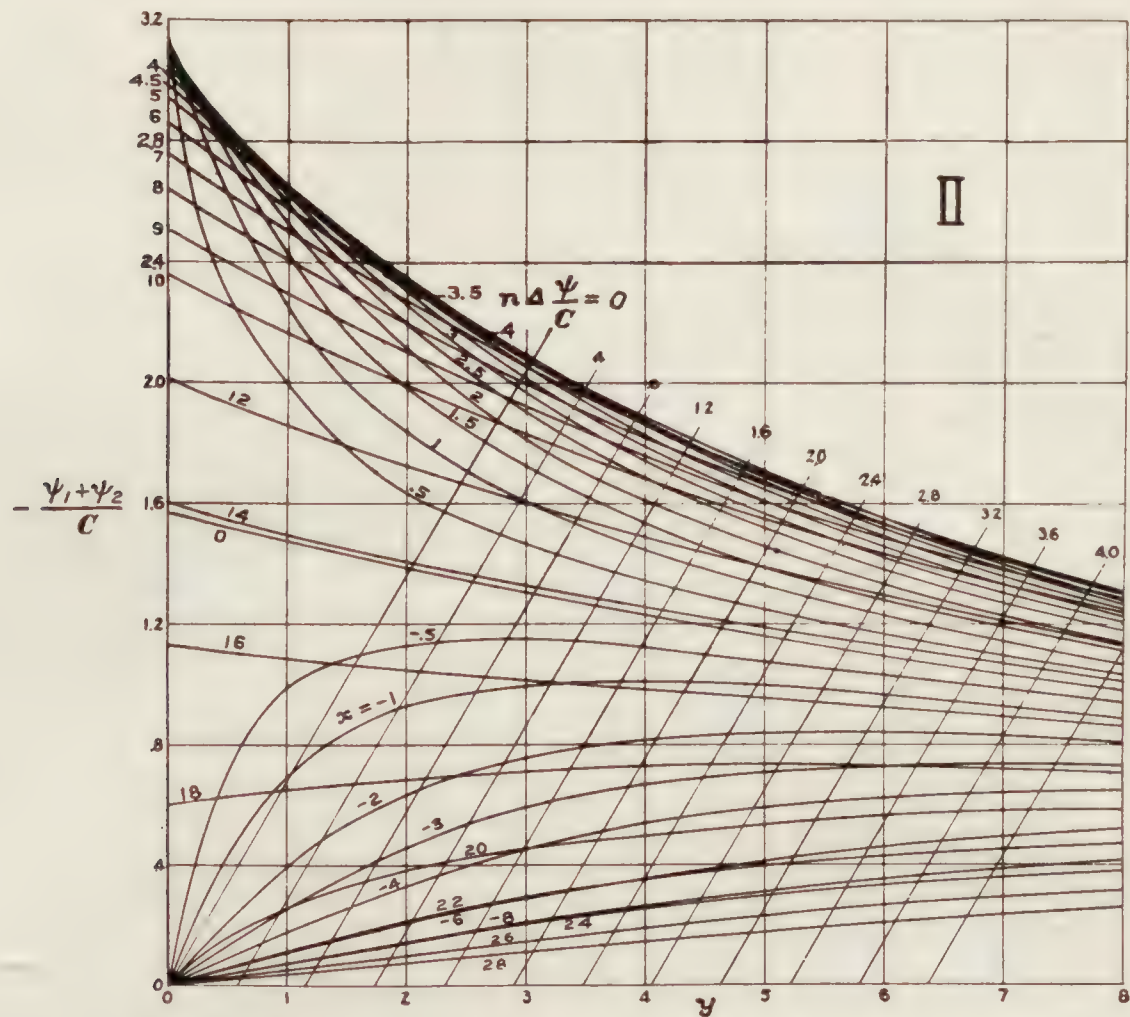


FIGURE 18.— $\frac{\psi_1 + \psi_2}{C}$ diagram for the source-sink combination No. II, Figure 4

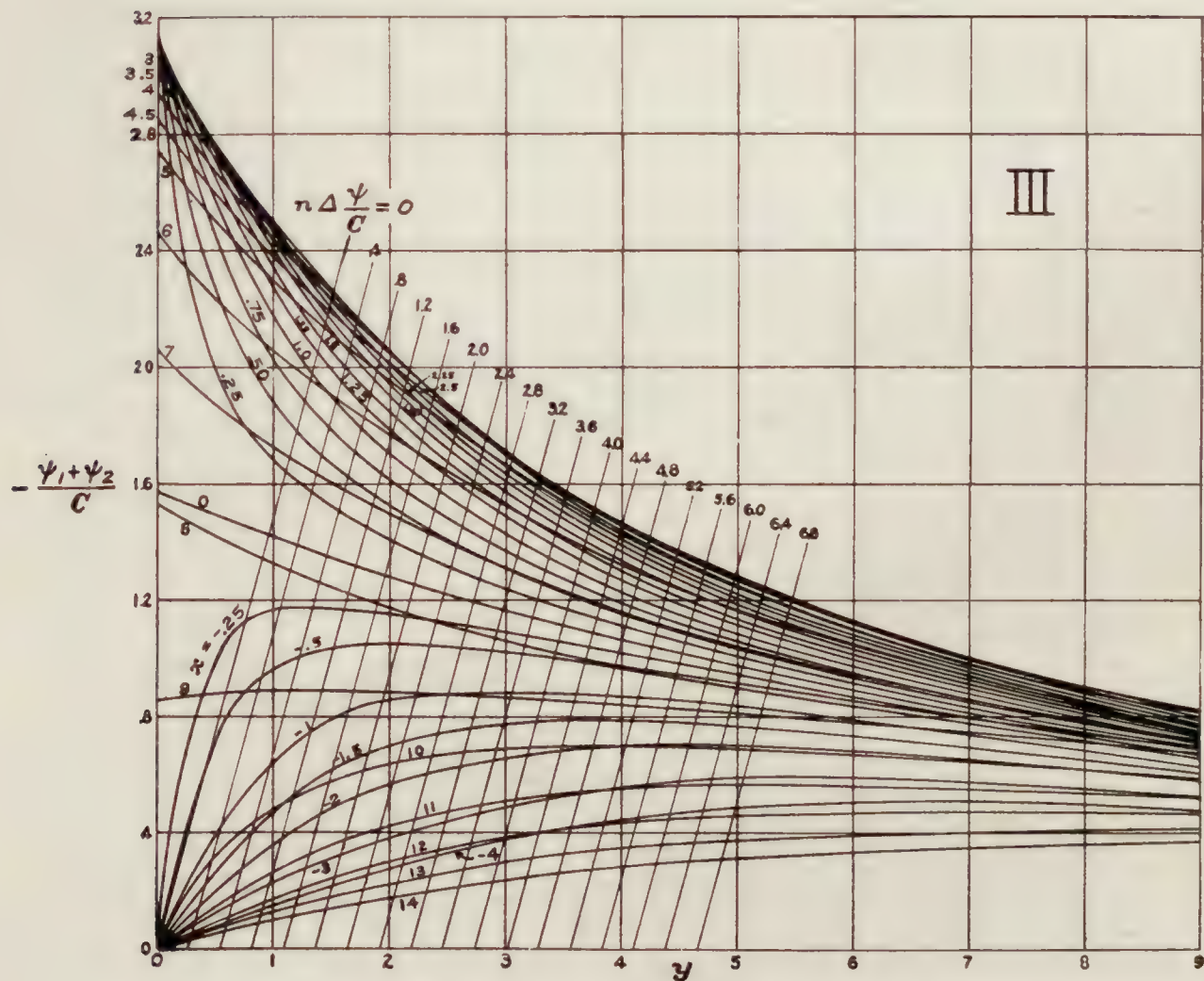
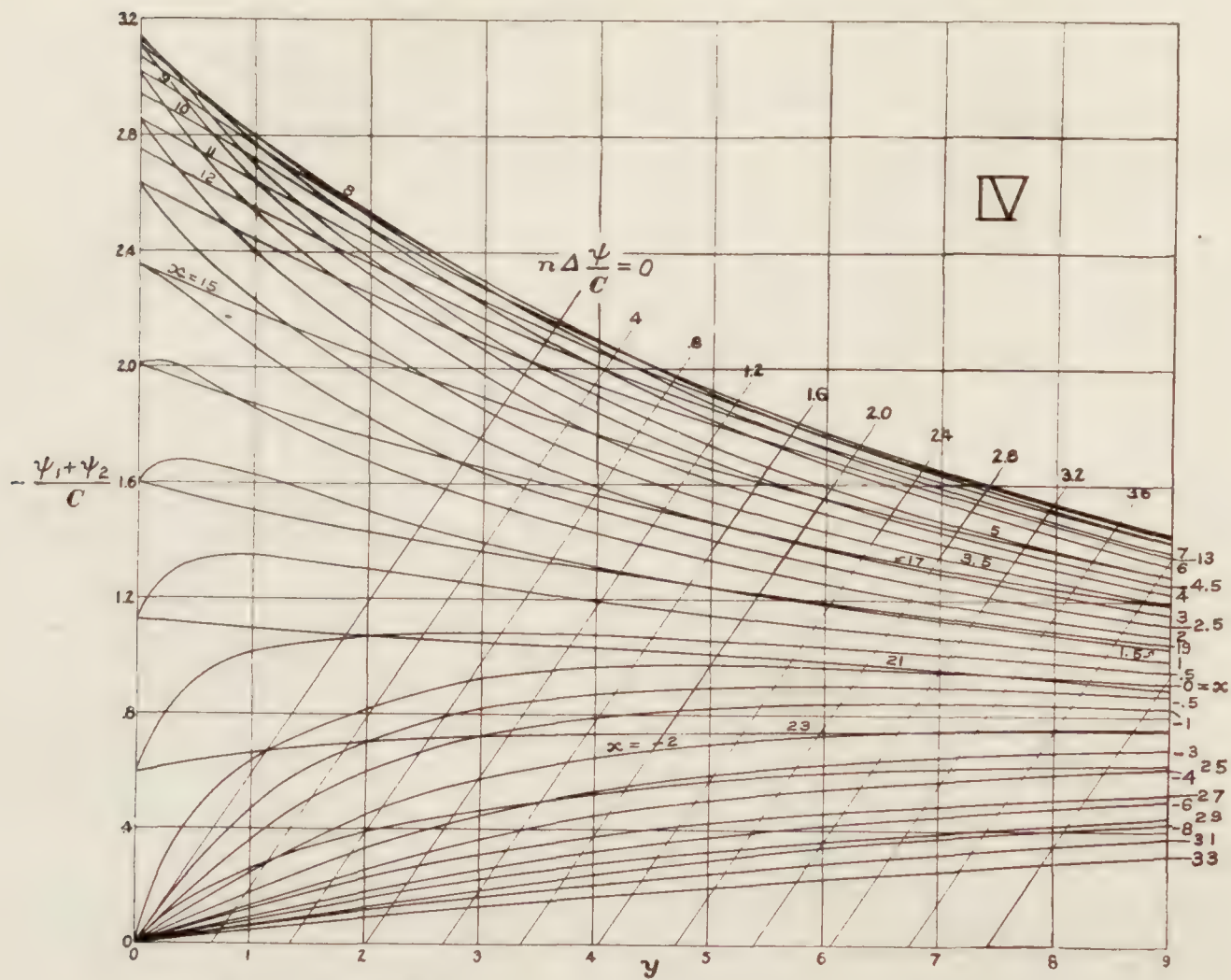
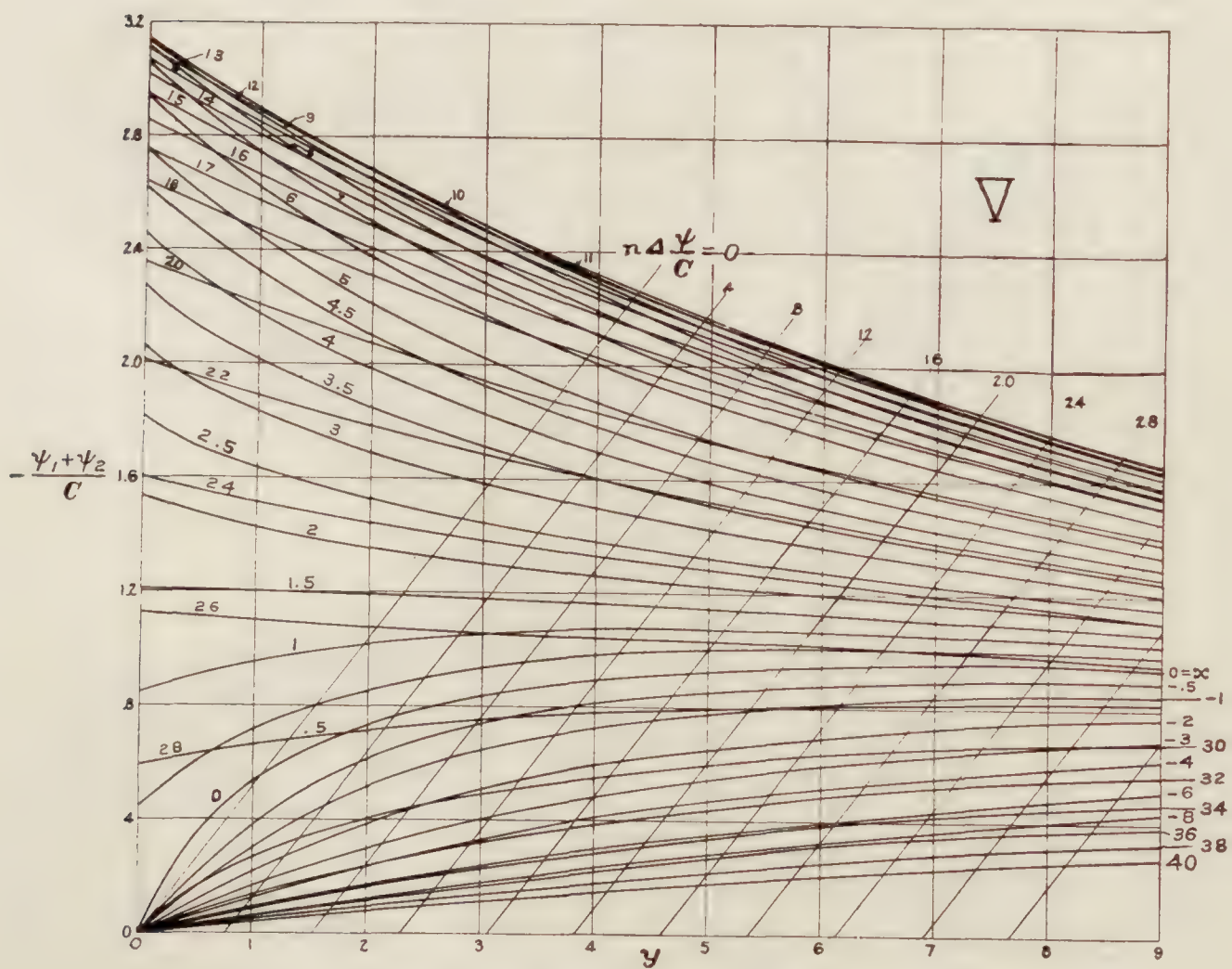


FIGURE 19.— $\frac{\psi_1 + \psi_2}{C}$ diagram for the source-sink combination No. III, Figure 4

FIGURE 20.— $\frac{\psi_1 + \psi_2}{C}$ diagram for the source-sink combination No. IV, Figure 4FIGURE 21.— $\frac{\psi_1 + \psi_2}{C}$ diagram for the source-sink combination No. V, Figure 4

APPARATUS AND EXPERIMENTAL METHOD

The wind tunnel used for these experiments was the United States Navy closed-circuit tunnel in Washington, which is equipped for force and moment measurement with Zahm's 6-component balance described in Reference 4. The test section of this tunnel is normally eight feet square and when so arranged the tunnel is capable of maintaining air speeds well

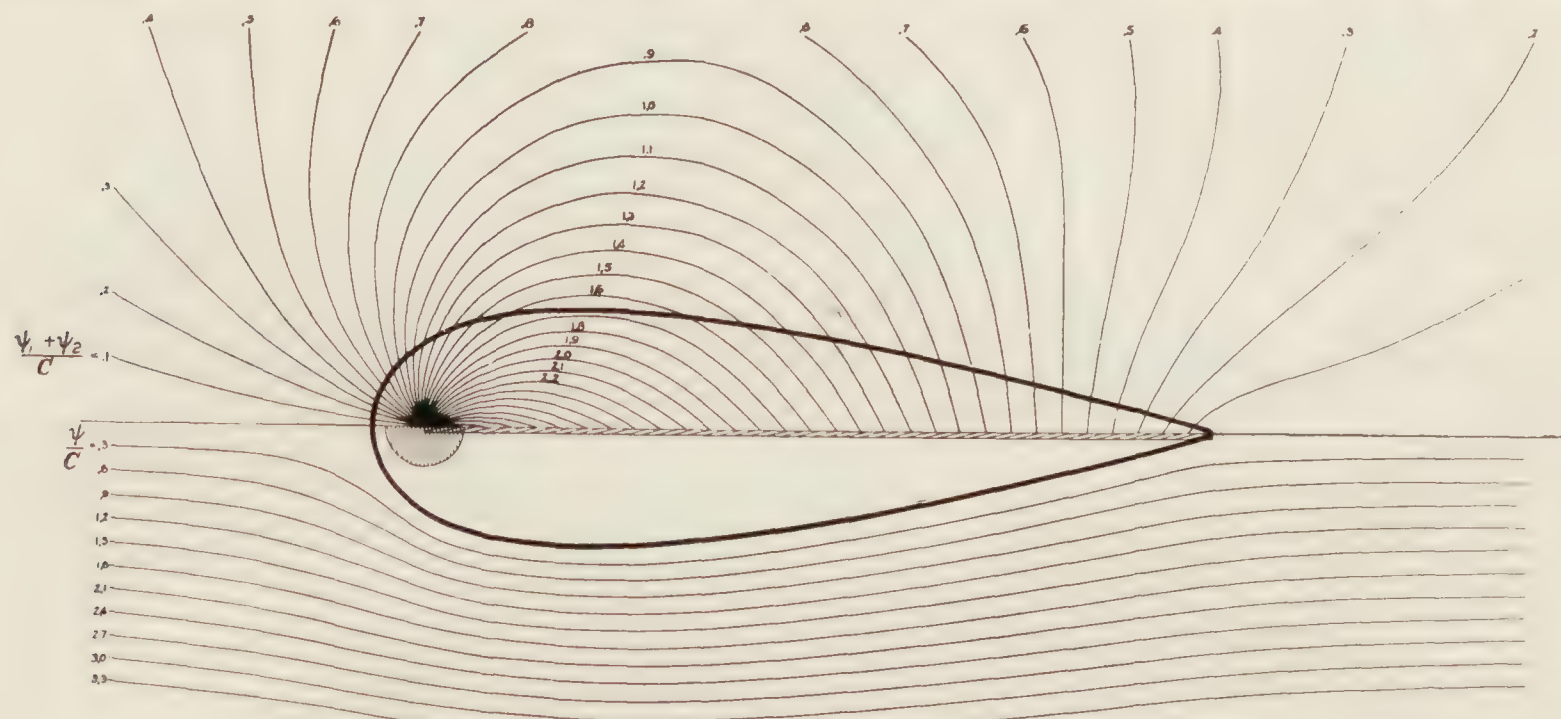


FIGURE 22.—Strut No. I, with source-to-sink and resultant streamlines

above 60 miles per hour whose mean values are controllable within one-half of 1 per cent. The balance is capable of measuring an air force or moment of a thousandth of a pound or pound-inch. The manometer from which the surface pressures were read was a single straight glass tube inclined approximately 1 to 10 and connected to an alcohol cistern. Its readings in vertical

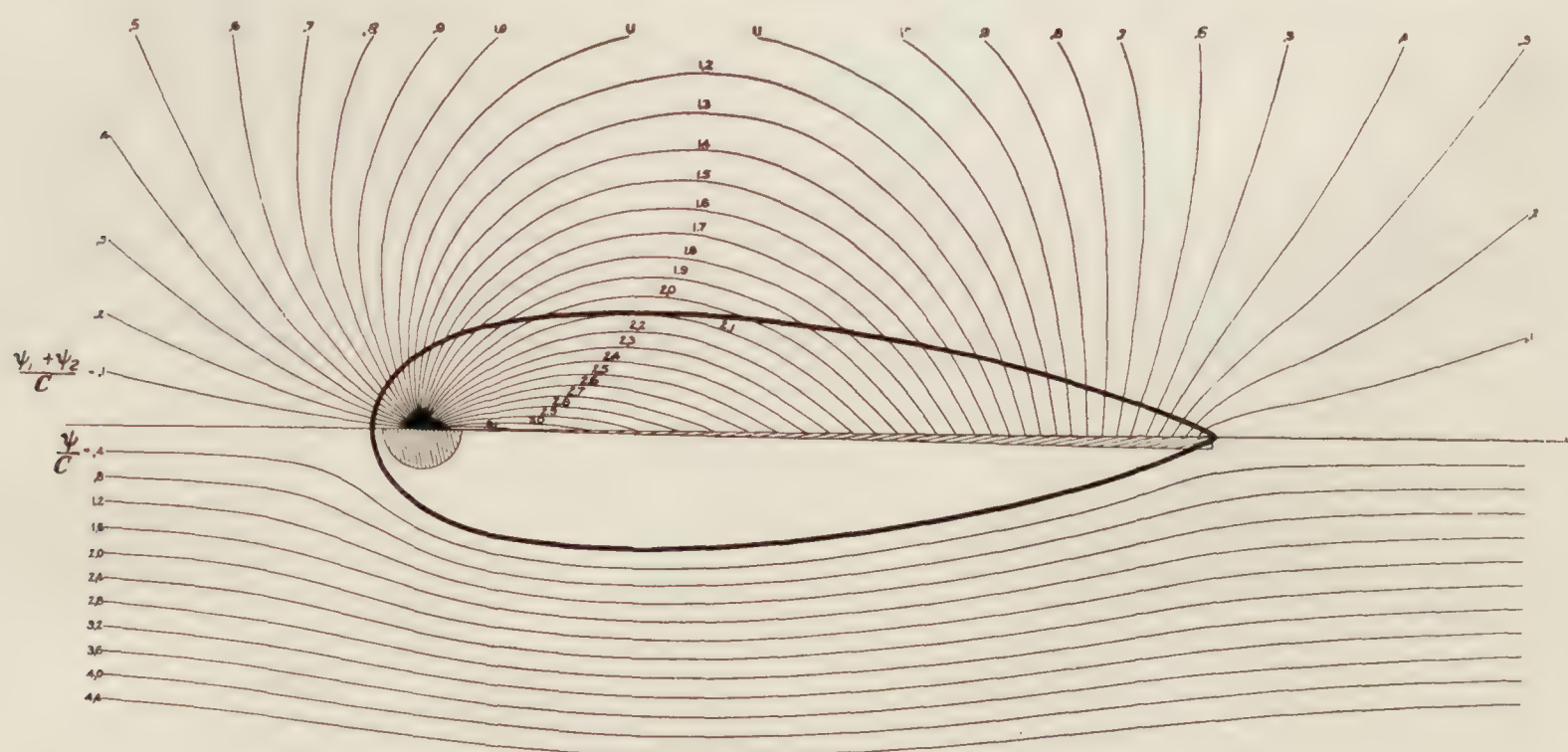


FIGURE 23.—Strut No. II, with source-to-sink and resultant streamlines

inches of water were carefully obtained by calibrating it against a water gauge capable of indicating pressures smaller than a thousandth inch of water.

The total resistance of each strut was obtained by attaching it to the 6-component balance which weighed its drag directly. The attaching holder was a thin 2-prong member whose

5-inch streamline prongs entered the strut at midspan as illustrated in Figure 37. Large separately supported end plates shielded the strut ends in both the resistance and the surface pressure tests as shown in Figures 37 and 38. These plates had the effect of making the strut a segment of a strut infinitely long and therefore of making the experimental conditions two

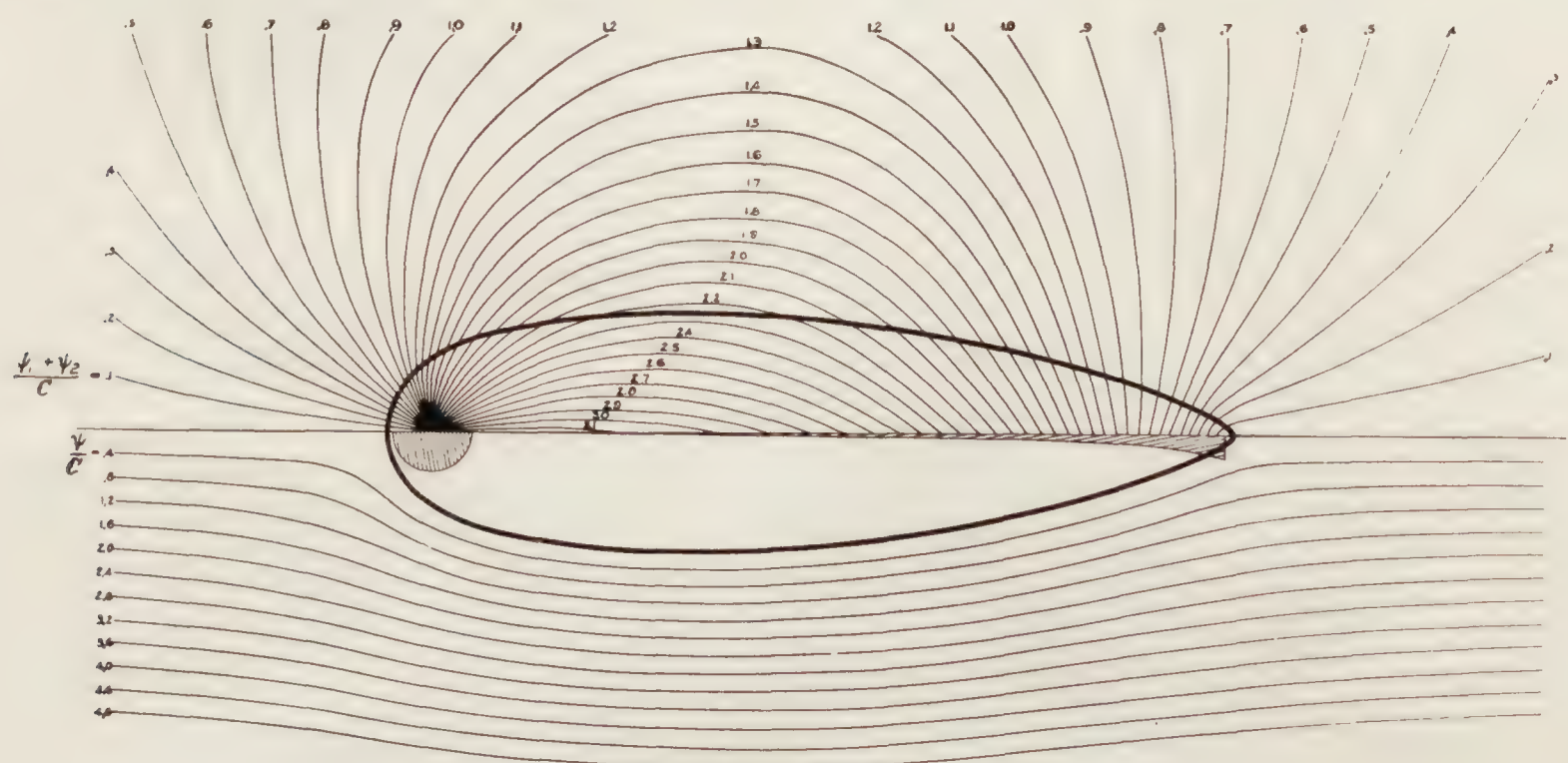


FIGURE 24.—Strut No. III, with source-to-sink and resultant streamlines

dimensional. No correction to the measured resistance was required, due to the pressure gradient along the tunnel, since the gradient is zero at the test section.

The pressure at each surface point was measured relative to the bow pressure by connecting the two differentially across the single-tube manometer.¹⁷ The air speed of the general air

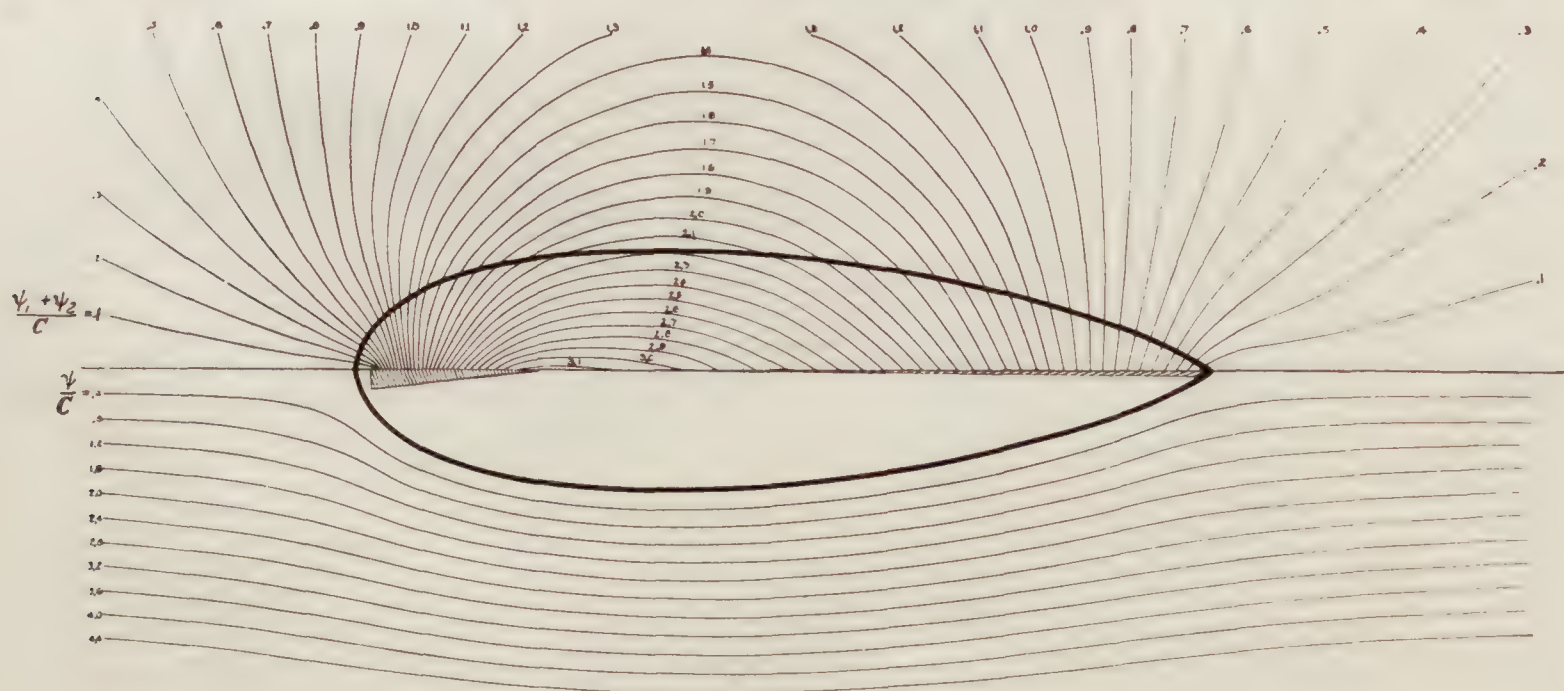


FIGURE 25.—Strut No. IV, with source-to-sink and resultant streamlines

stream was obtained by connecting the bow pressure and the static pressure of the distant air stream differentially across the speed indicating manometer. The static pressure of the stream was collected from the lateral perforations of a standard pitot-static tube placed sufficiently far abreast the bow of the strut to escape appreciable interference.

¹⁷ When the forward rest point is known it furnishes a convenient and accurate reference for pressure elsewhere on the surface, since the pressure there is always $\frac{1}{2}\rho V^2$.

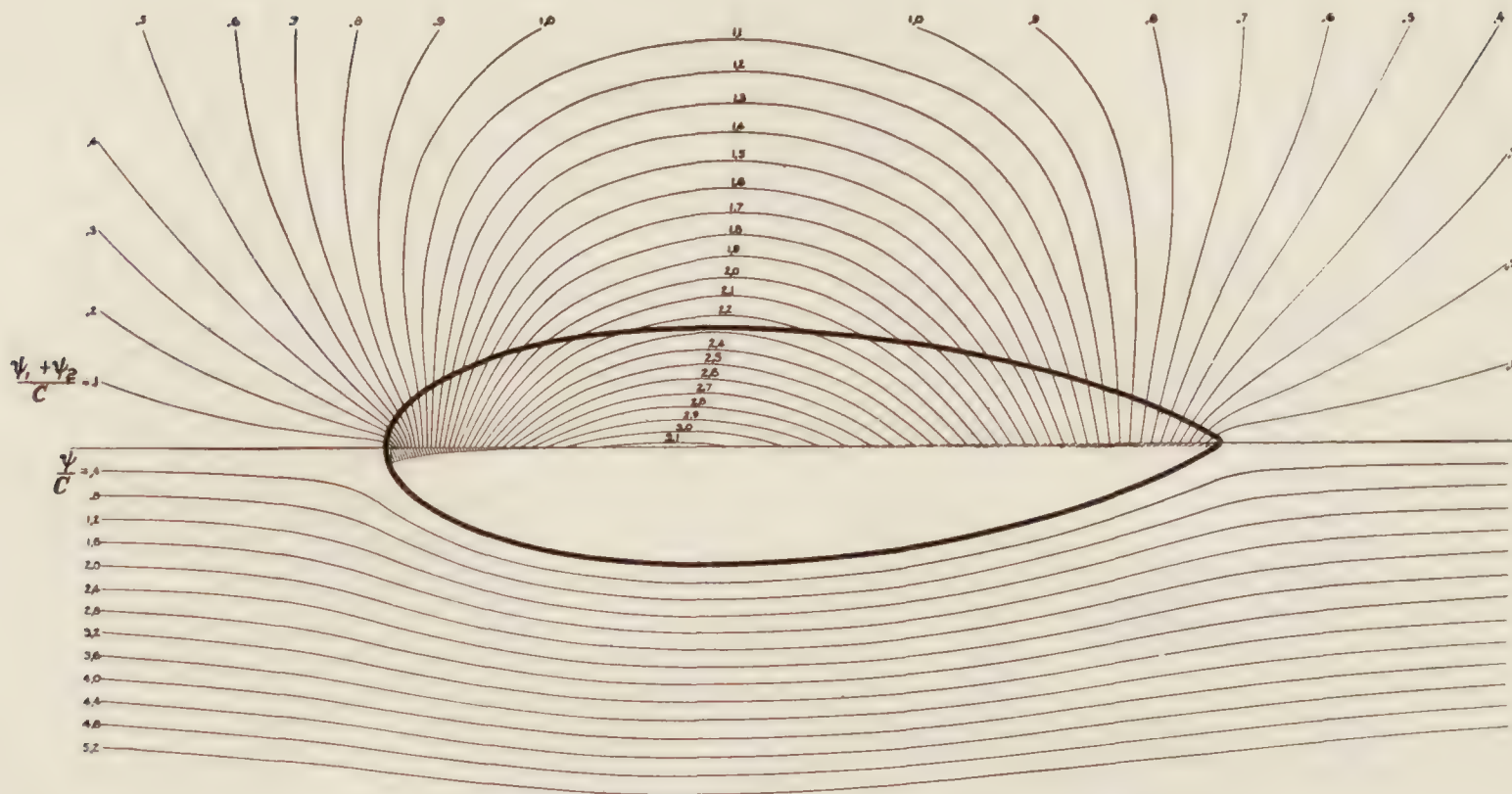
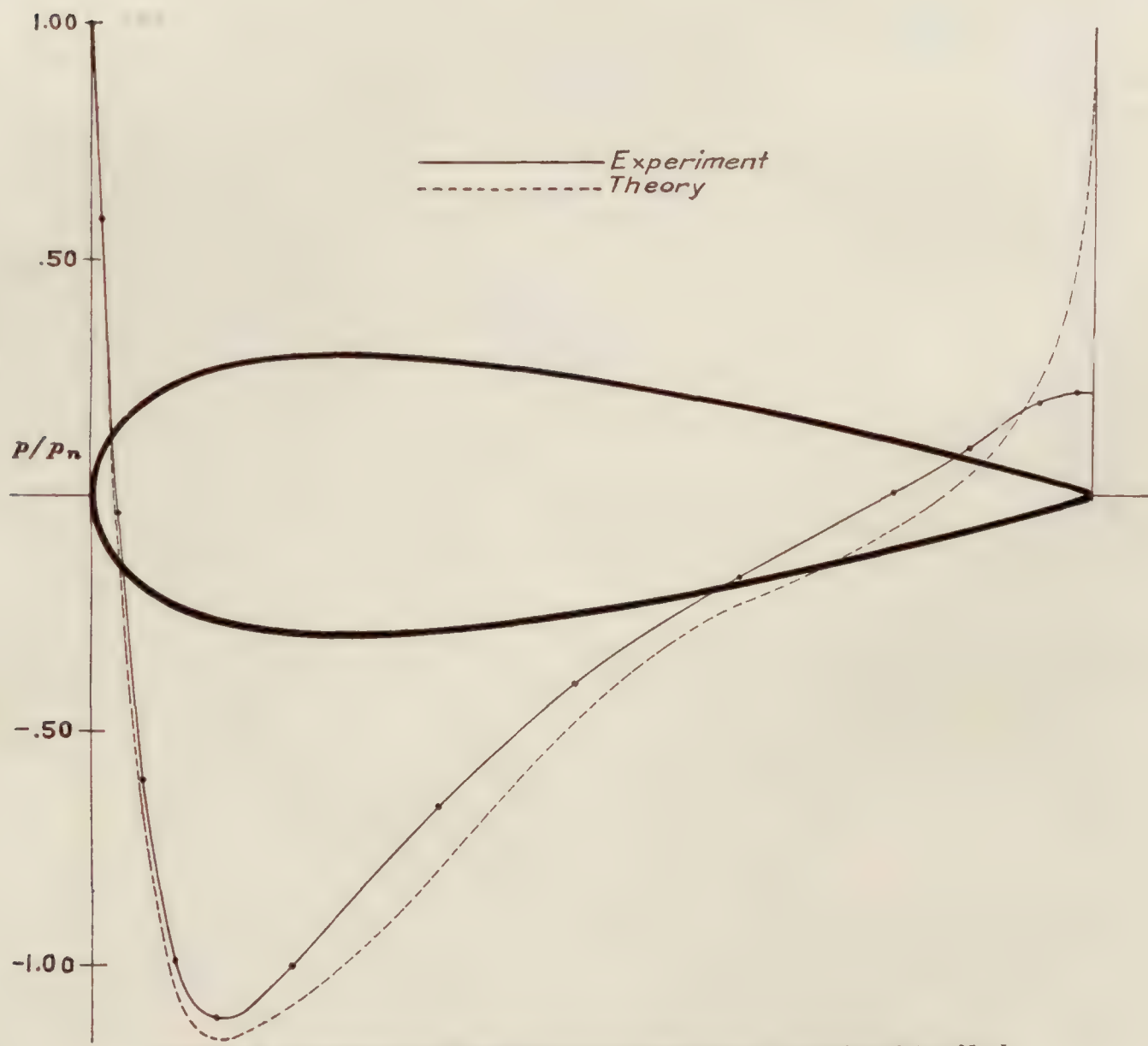
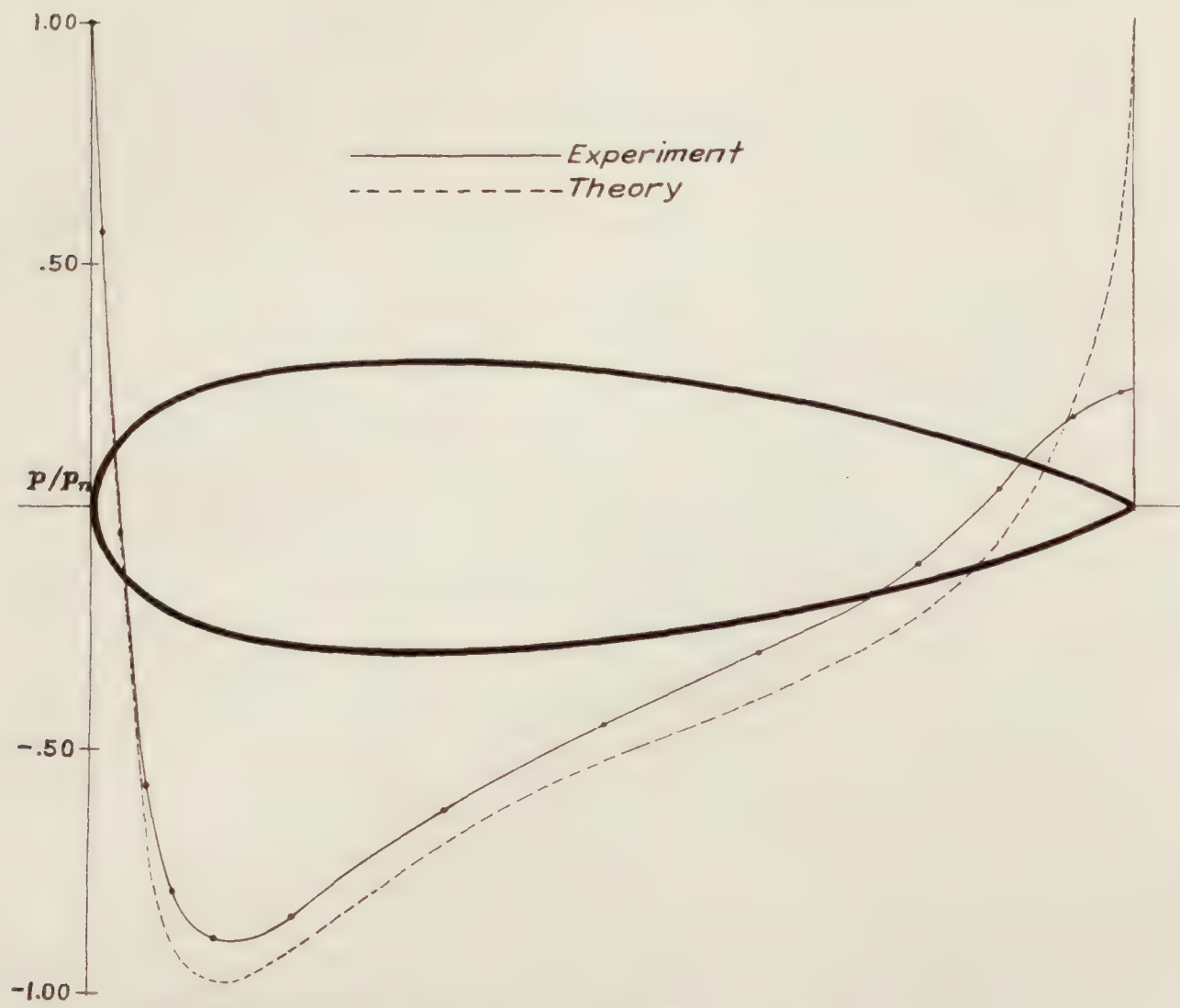
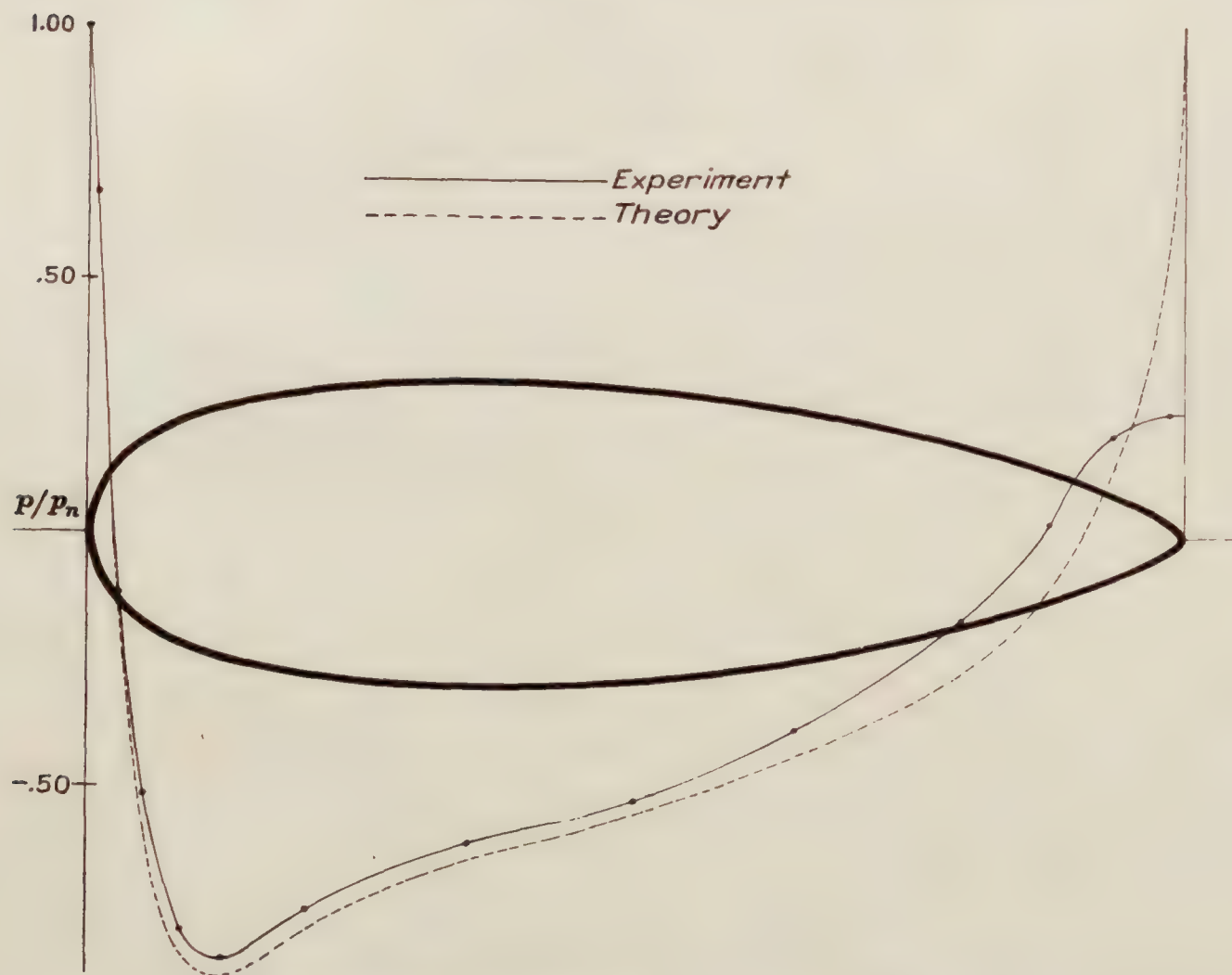
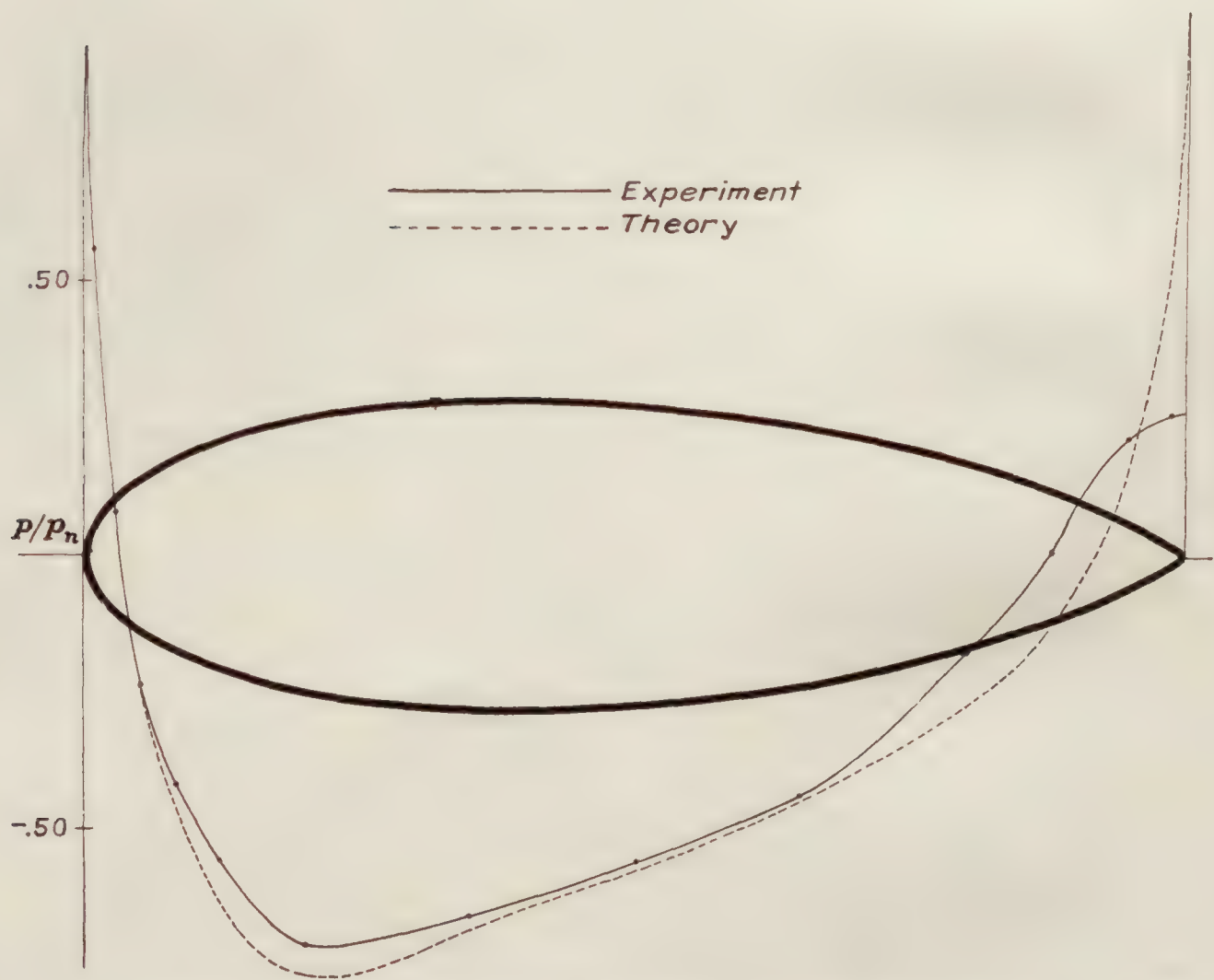
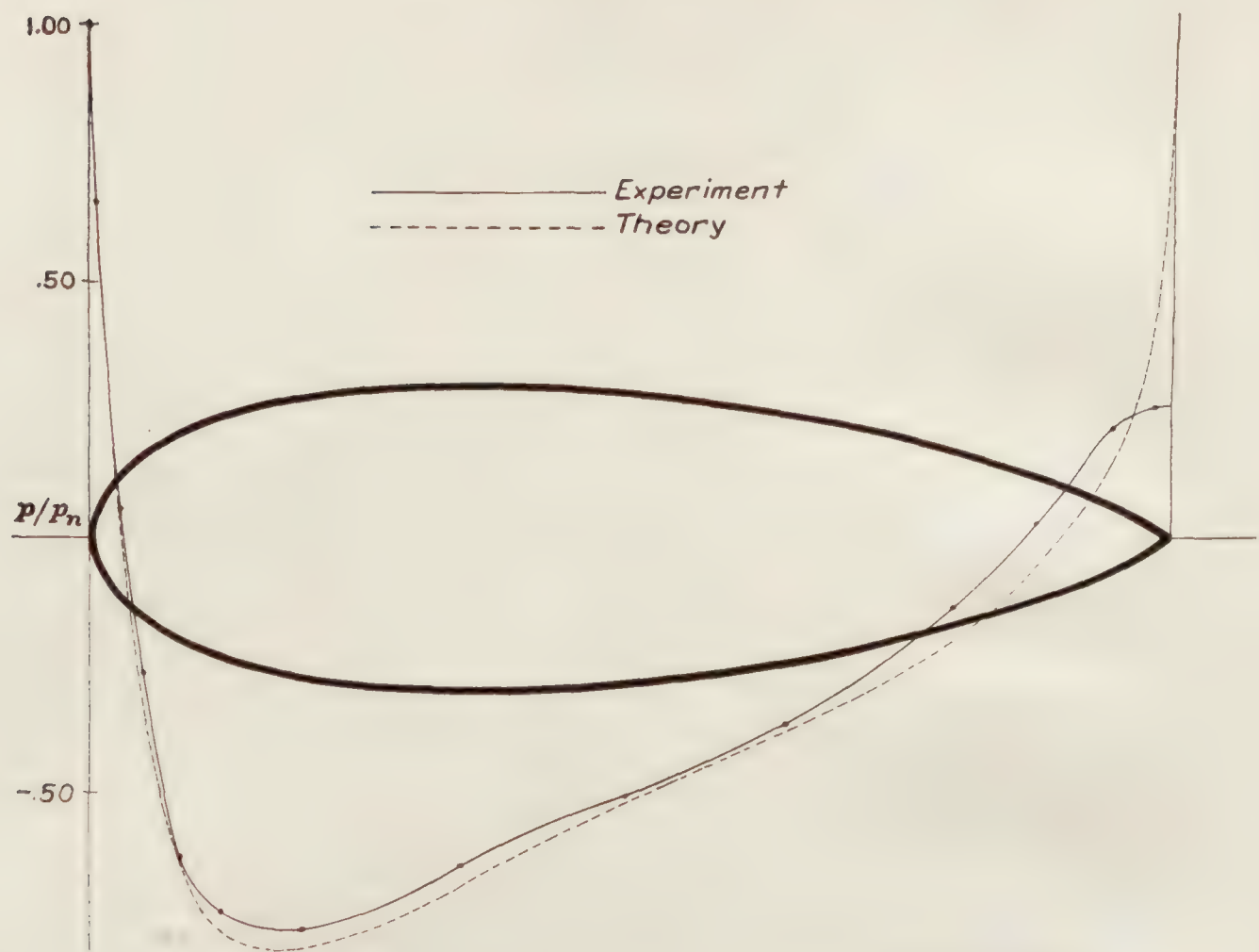


FIGURE 26.—Strut No. V, with source-to-sink and resultant streamlines

FIGURE 27.—Experimental and theoretical point pressure, p/p_n , over surface of strut No. I

FIGURE 28.—Experimental and theoretical point pressure, p/p_n , over surface of strut No. IIFIGURE 29.—Experimental and theoretical point pressure, p/p_n , over surface of strut No. II.



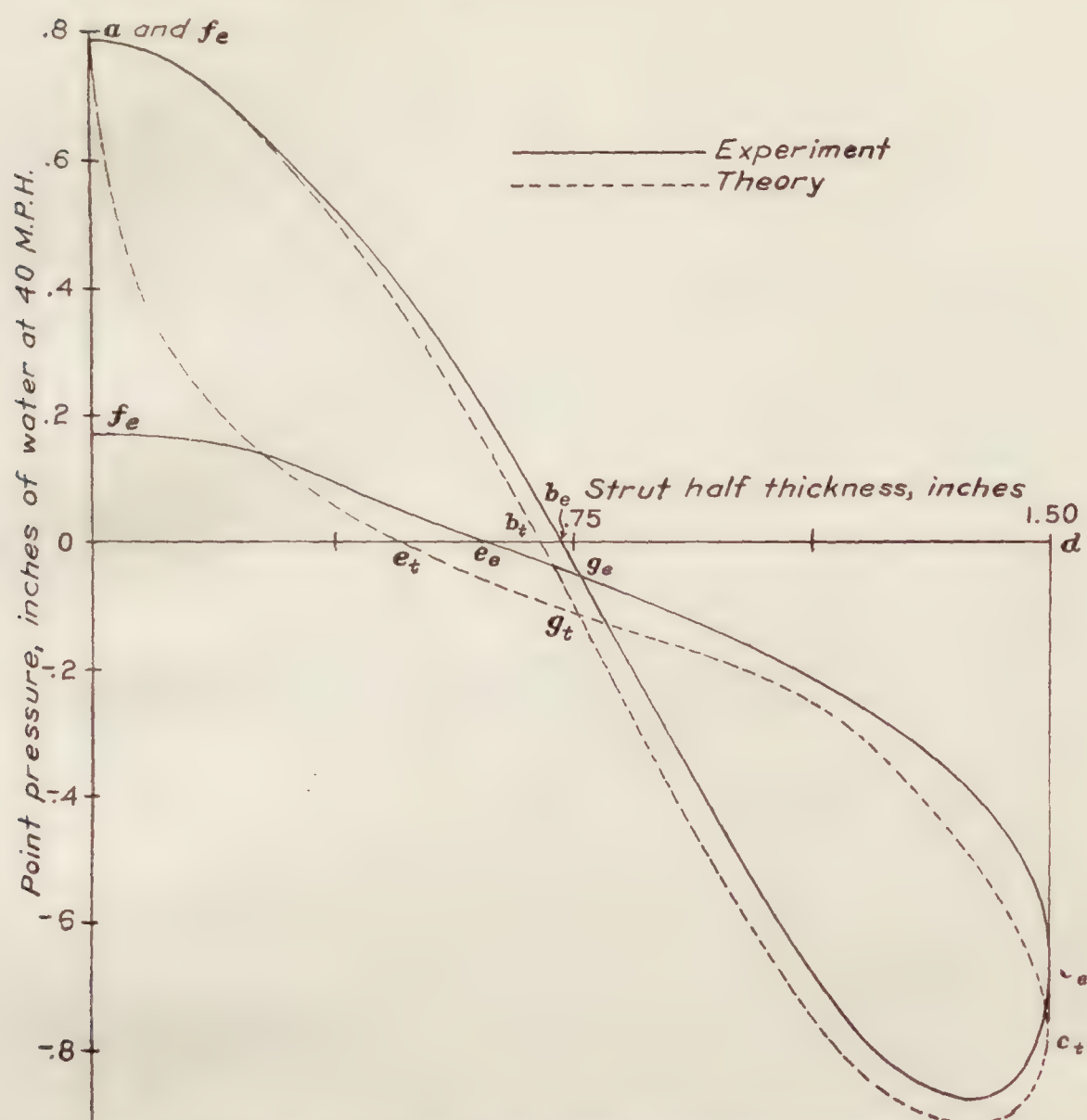


FIGURE 32.—Experimental and theoretical point pressure versus strut half thickness for strut No. I

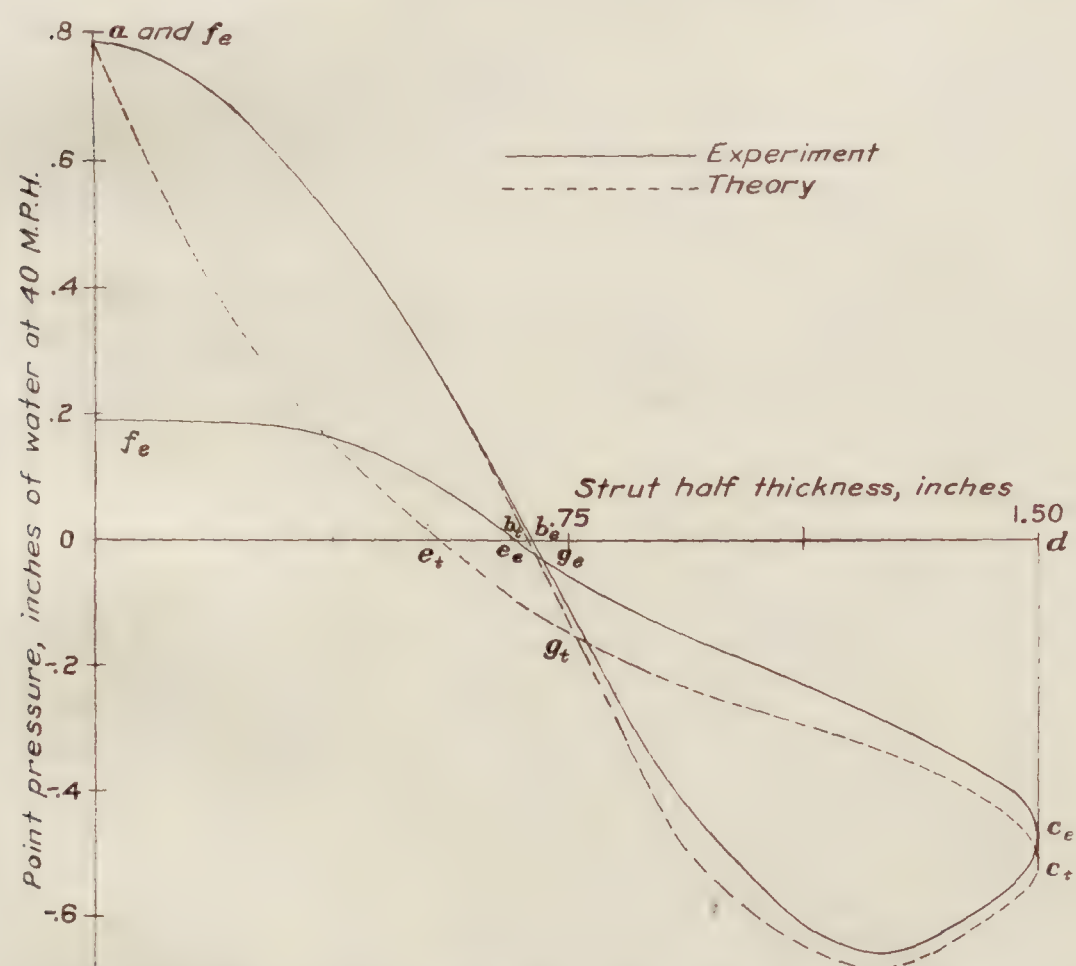


FIGURE 33.—Experimental and theoretical point pressure versus strut half thickness for strut No. II

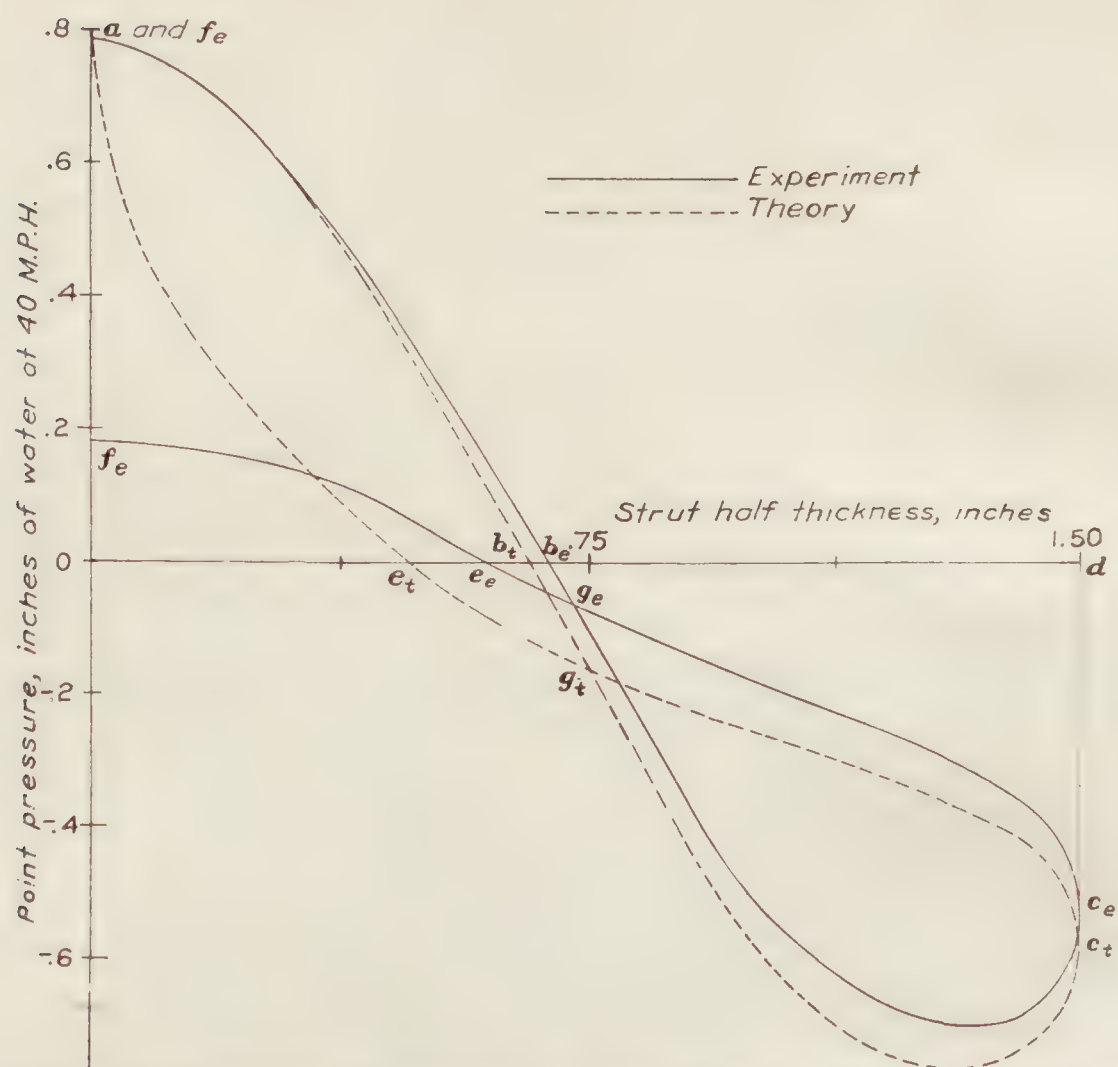


FIGURE 34.—Experimental and theoretical point pressure versus strut half thickness for strut No. III

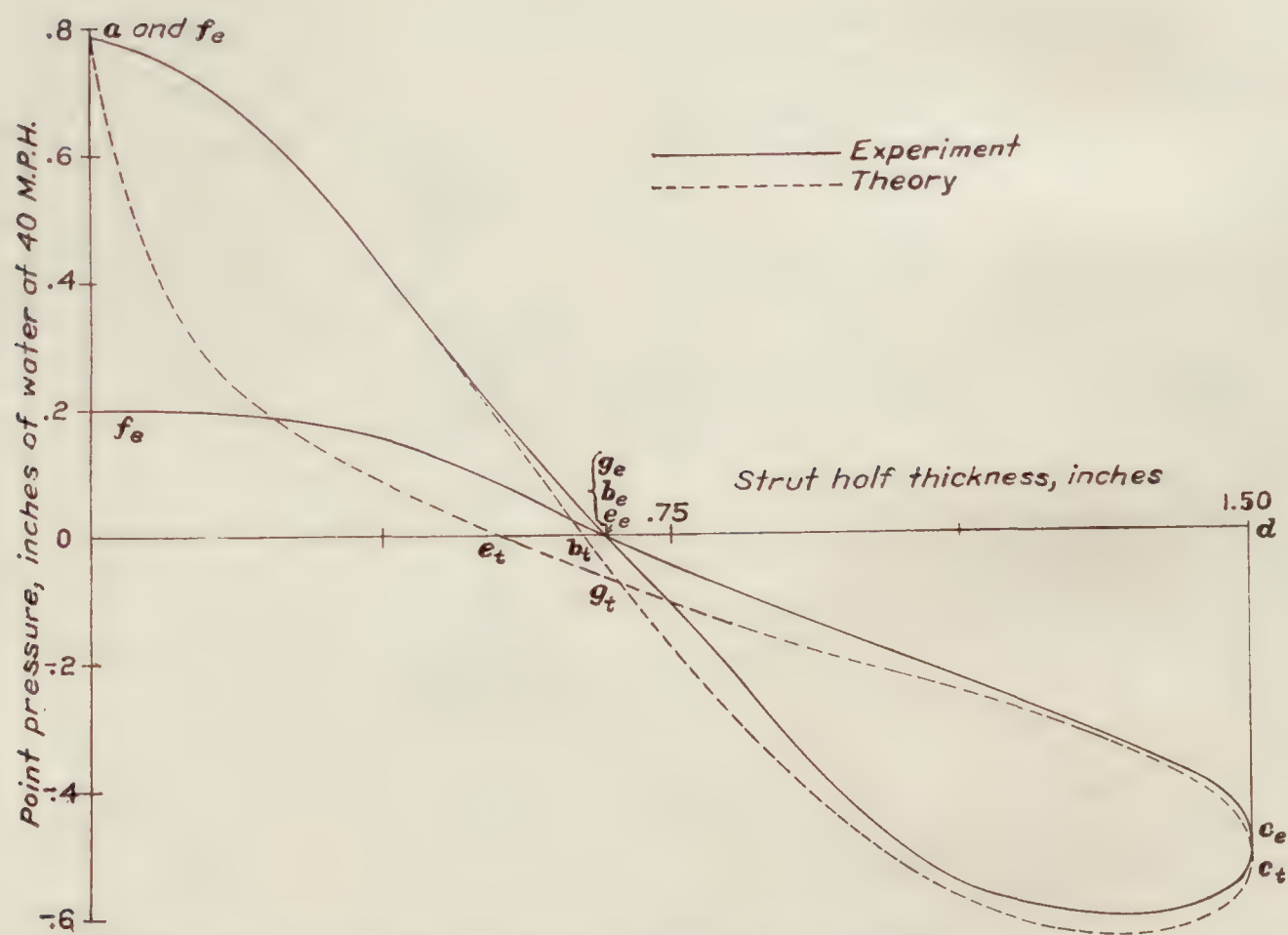


FIGURE 35.—Experimental and theoretical point pressure versus strut half thickness for strut No. IV

MODELS

The eight strut models were constructed of laminated wood and finished alike to a high polish. Strut Number I of the theoretical series of five was made of mahogany, the other four were of cherry at the bow and white pine at the stern. The three empirical struts were of white

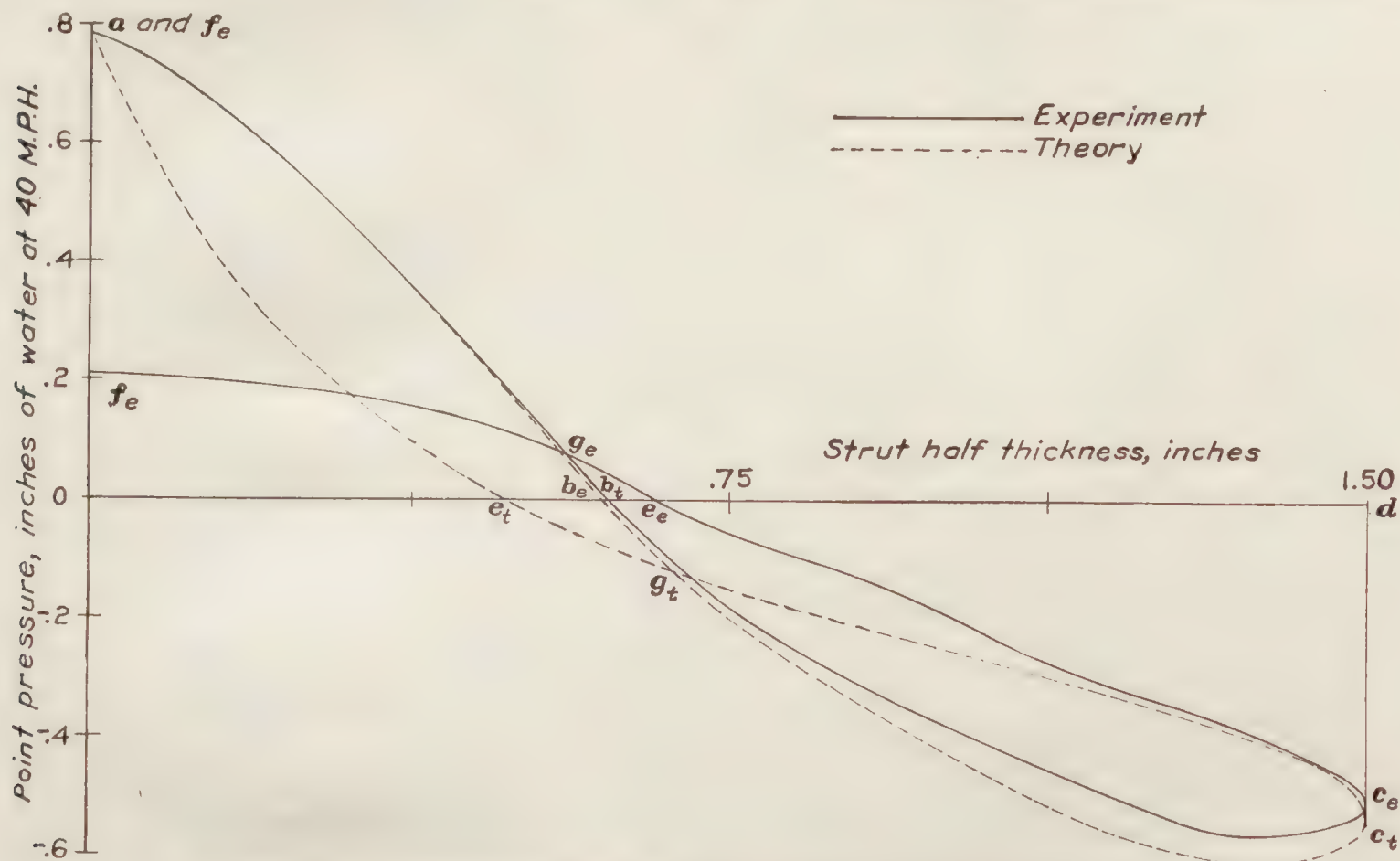


FIGURE 36.—Experimental and theoretical point pressure versus strut half thickness for strut No. V

pine only. The latter are designated R. & M. 183, being the British strut first given in R. & M. 183, but here changed from fineness-ratio 4 to 3.5 (ref. 7). Number 53 being the best German strut reported in Reference 5, and Navy Number 2 the best strut which has so far been developed in America. (Refs. 2 and 10.)

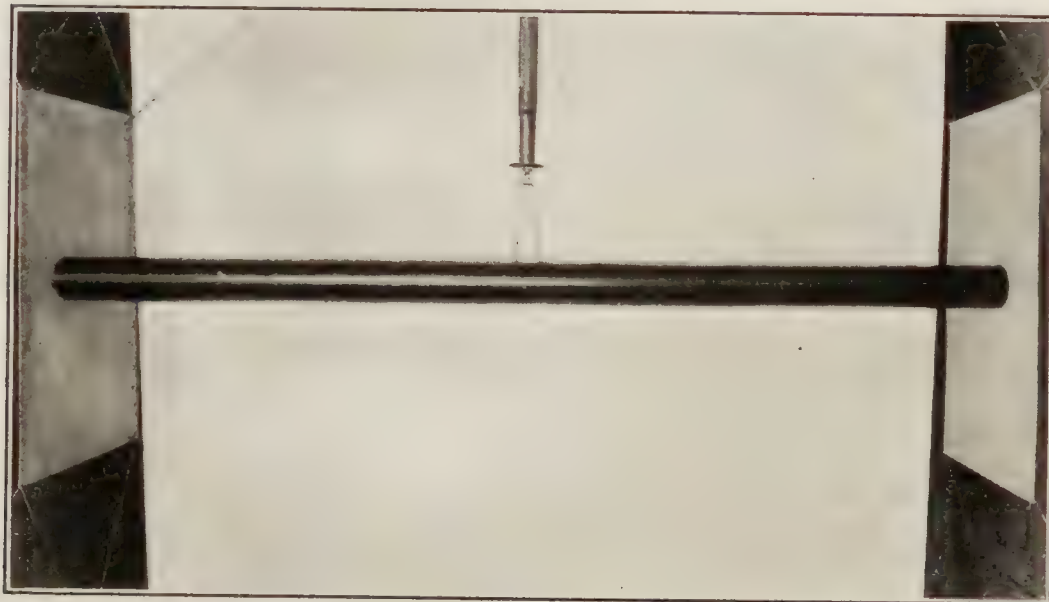


FIGURE 37

All eight were 60 by 10½ by 3 inches with sections conforming to accurate metal templates made from the ordinates in Table V. Final measurements of the struts agreed with the specified ordinates everywhere well within 0.02 inch, the average error of course being much less.

At an early stage in the construction of the five theoretical struts small copper tubes were inlaid running

near the surface from one end of the strut to its midsection, where they bent sharply and emerged at the surface points where pressures were to be measured. The ends of the tubes were then finished with the wood, and finally in the finished strut presented a row of pressure collectors 1 millimeter in diameter, accurately located and quite smooth. Care was taken to remove all roughness from the inner edge of the collectors. The location of the collectors is given in Tables VI to X. Figures 37 and 38, which are photographs of Strut Number V, illustrate the struts in finished form.

RESULTS

Table XI gives the results of the resistance tests in three forms—the resistance in pounds, the resistance coefficient based on frontal area, and the drag-strength ratio based on sectional moment of inertia. The two latter forms indicate merit of two kinds; the coefficient, C_D is a measure of merit of a strut form when its thickness is the major consideration; that is, when it is used as a fairing for round tubing or cable; the ratio D/I is a measure of merit when the strut is used in the usual way as a compression member of sufficient length to be susceptible to lateral failure as a column. Referring to Table XIa and Figure 39, Strut Number I has the greatest merit of the five as a fairing, but is poorest as a strut. Likewise Strut Number V has the greatest merit as a strut, but is only second best as a fairing. Furthermore, Table XIb and Figure 40 show that theoretical Strut Number V and the Navy Number 2 have about equal merit either as fairings or as struts and that Number 53 and R. & M. 183 follow in order of merit, the one having 3 per cent the other 12 per cent greater D/I than Number V or Navy Number 2 at R. N. 12×10^4 .

The results of the pressure-distribution tests on the five theoretical struts are given in Tables VI to X in four forms: First, the point pressures referred to the bow pressure as zero are given as read in inches of alcohol along the inclined manometer tube; second, the pressures given in the first form are converted to vertical inches of water; third, those in the second form are referred to the bow pressure as $\frac{1}{2}\rho V^2$; finally, those in the third form are referred to the bow pressure as unity. The pressures in the third form are plotted along with the theoretical pressures against the strut half-thickness, y , in Figures 32 to 36 for use in integrating graphically for the four elements of pressure drag. The elements of pressure drag are listed in Table XII for both theory and experiment.

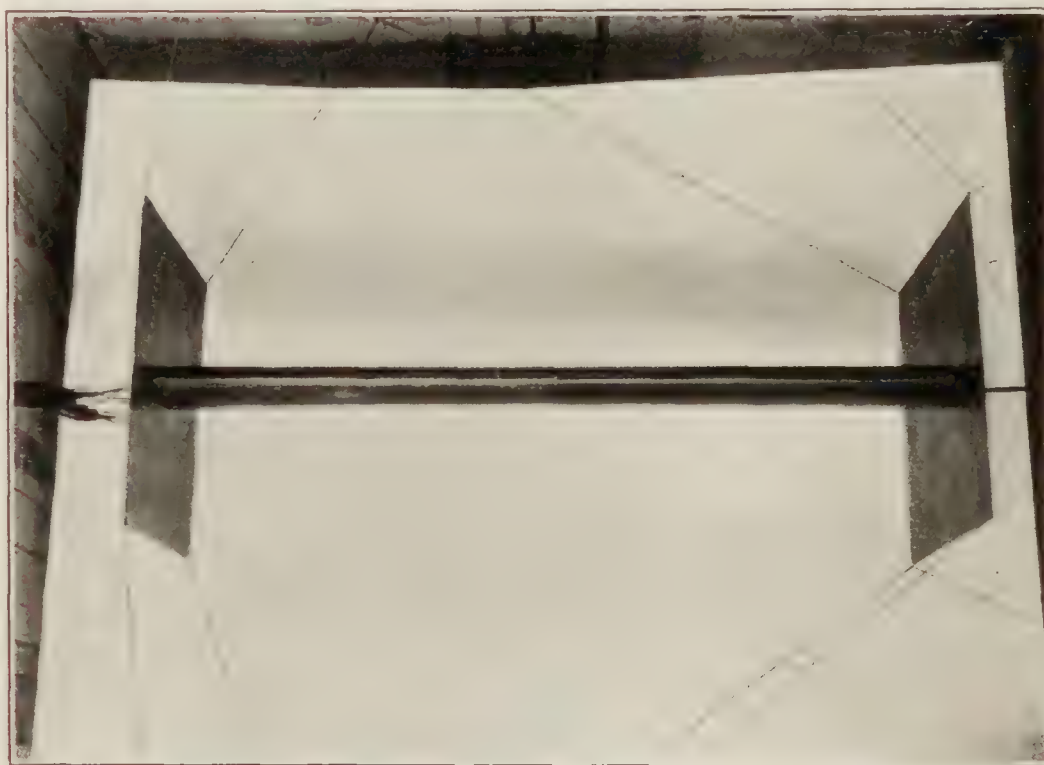


FIGURE 38

The values given show how small a residue the pressural drag is of the total upstream and the total downstream pressural forces acting and indicate the difficulty of such analyses. The table indicates that the whole drag contains from 40 to 50 per cent pressural and from 60 to 50 per cent frictional drag, when the air speed is 40 miles per hour.

The pressure coefficients, given in the fourth form in Table X, are plotted along with the theoretical pressure coefficients against the distance aft the bow in Figures 27 to 31 and show graphically the agreement between theory and experiment. In every case the experimental pressures were a little less than the theoretical over the suction range and rather uniformly so except near the stern, where the discrepancy increased and agreement became rather bad. As usual the pressures agreed near the bow and disagreed widely at the stern where the measured pressure is only one-fourth or one-fifth the theoretical value. For each strut the maximum suction occurred at the same position on the surface in both theory and experiment and moved aft and decreased in magnitude as the average strut ordinate shifted from strut to strut toward the stern.

CONCLUSIONS

Comparing Fuhrmann's results (ref. 1) with the results of this study, one finds the agreement between the theoretical and experimental pressures over the surface of low-resistance shapes rather better in three dimensional flow than in two. The consistent and uniform defi-

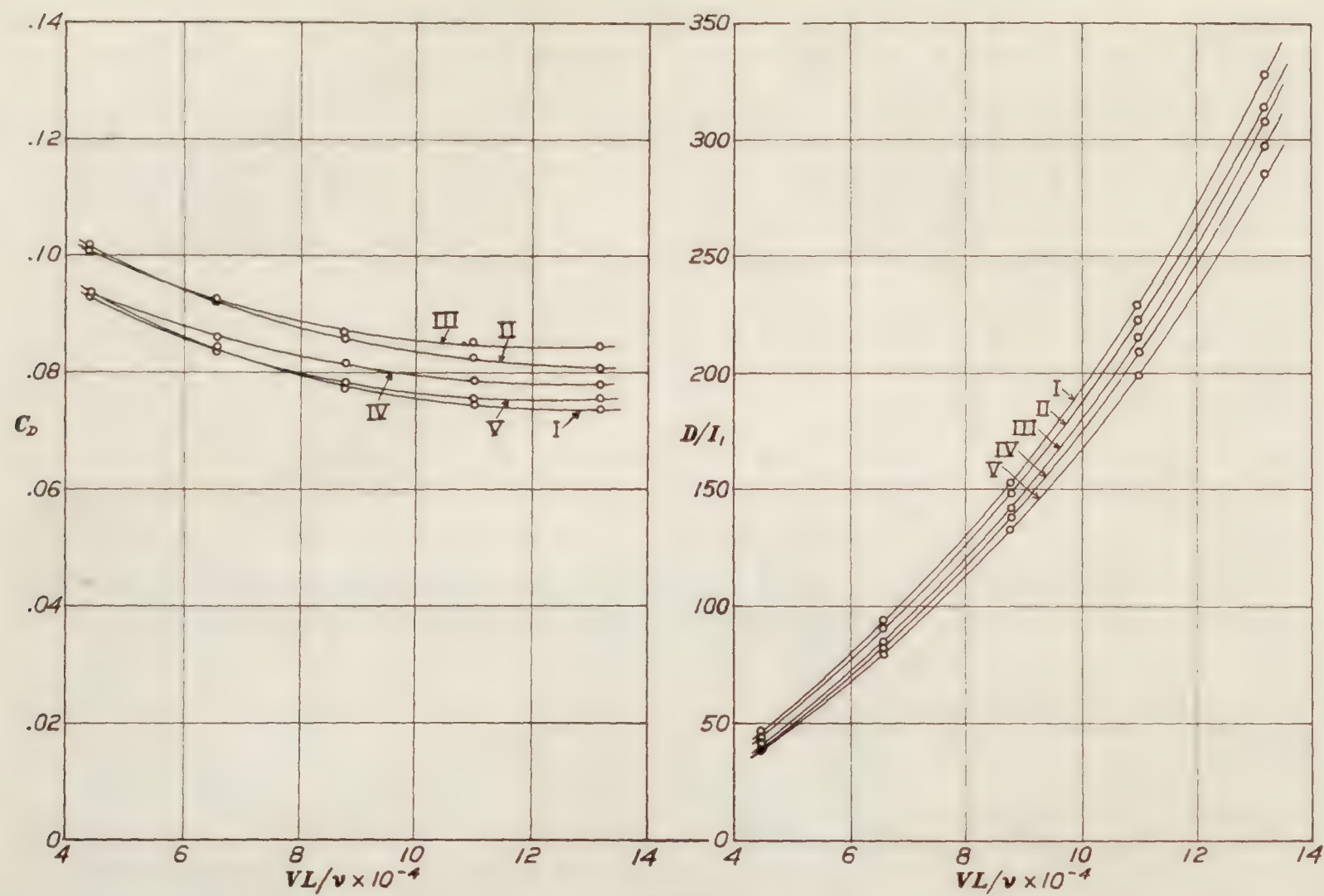


FIGURE 39

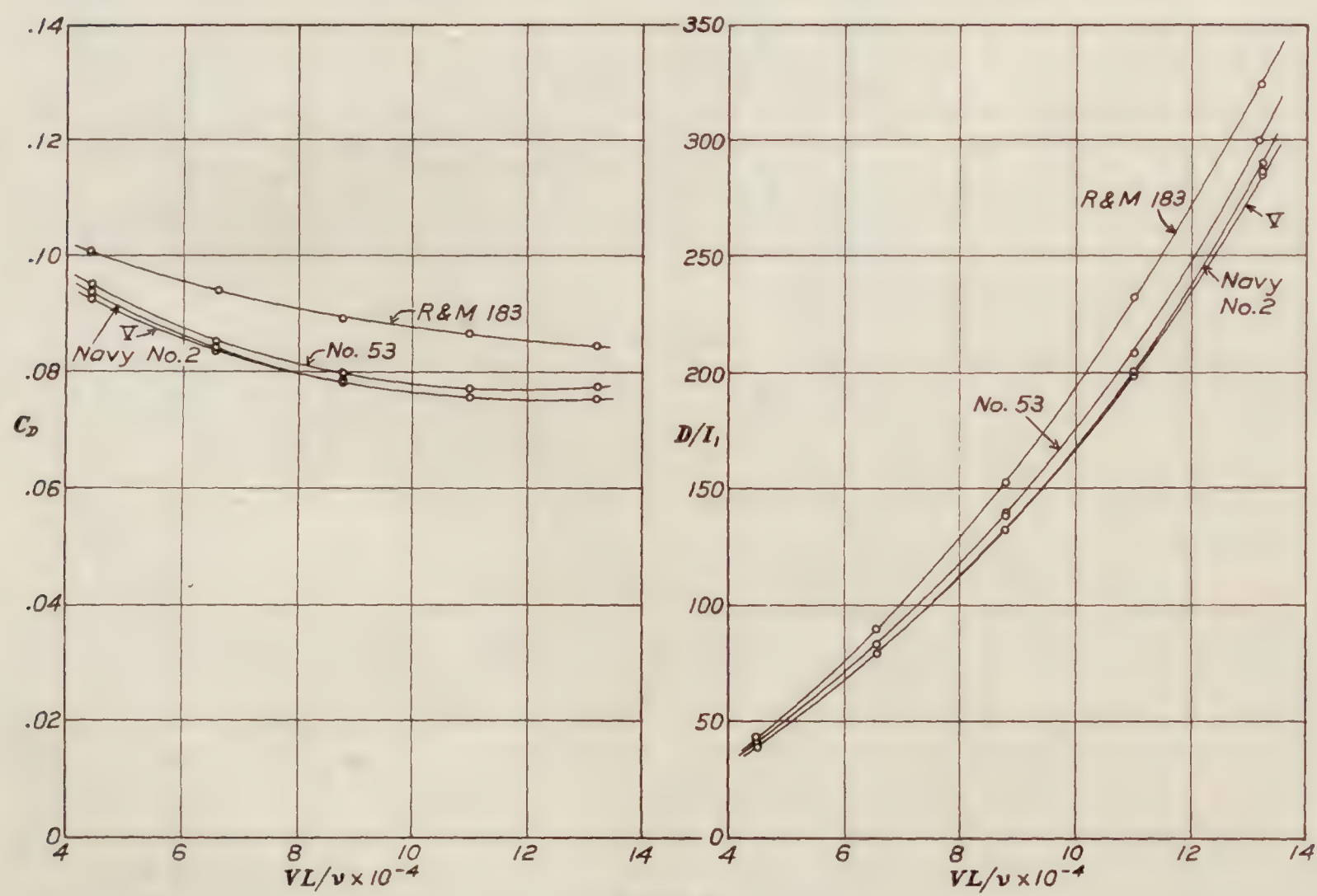


FIGURE 40

ciency of the experimental suction found for struts does not appear in the case of Fuhrmann's airships, for which the experimental pressures were sometimes above, sometimes below, their theoretical values. While the experimental pressures at the stern agree with theory better in the case of struts than in the case of airships, the defect may be less serious for airships, from the standpoint of pressural drag, because of the relatively smaller surface area affected. Also for airships the maximum suction by experiment came at a surface position aft that by theory, while for struts the two positions are found to coincide. In case of either airships or struts the functional character of the pressure distribution is strikingly similar in theory and experiment and leaves no doubt concerning the validity of the Rankine method.

From the standpoint of practical merit, Strut Number I seems to excel as an air fairing. For column use in aircraft, Strut Number V is equally as good as the Navy Number 2 which is the best empirical air strut so far developed. These two are found by comparative test to be followed closely in merit by the German Number 53 and to be considerably better than the British R. & M. 183, the relative order of resistances being 100, 103, and 112, respectively, at 12×10^4 R. N.

It may be well to point out that these strut studies leave the air strut in a rather unique position compared to the airship. In contrasting their aerodynamic status, one finds that no theoretical airship form of high merit has been found, while a theoretical strut has been found whose merit equals that of the best empirical strut. One finds further that the theoretical flow is known about no airship of good form, excepting the approximate flow about a rigid airship form found by v. Karman (ref. 9), while the theoretical flows about the two best struts are now known and about one of these by two wholly independent methods.

REFERENCES

1. A. Fuhrmann, on "Theoretische und Experimentelle Untersuchungen an Balloonmodellen, fahrbuch der Motorluftschiff-Studien-Gesellschaft Band V.
2. A. F. Zahm, R. H. Smith, and G. C. Hill. Point Drag and Total Drag of Navy Struts No. 1 Modified, Report No. 137, National Advisory Committee for Aeronautics, Washington, 1922.
3. D. W. Taylor, on Ship-Shaped Stream Forms, Transactions of the British Institution of Naval Architects, 1894.
4. A. F. Zahm, The Six-component Wind Balance, Report No. 146, National Advisory Committee for Aeronautics, Washington, 1922.
5. Max Munk. Weitere Widerstandsmessungen an Streben, Mitteilung 11 der Modell-Versuchsanstalt für Aerodynamik, Technische Berichte, Band II, 1918.
6. E. J. Gumbel, Englische Untersuchungen über den Widerstand von Streben. Technische Berichte, Band I, 1917.
7. C. H. Powell; The Resistance of Struts, Technical Report No. 416 of the Advisory Committee for Aeronautics for 1917-18.
8. A. F. Zahm; Pressure of Air on Coming to Rest from Various Speeds, Report No. 247, National Advisory Committee for Aeronautics, Washington, 1926.
9. Karman, Th. V., 1 Berechnung der Druckverteilung an Luftschiffkörpern. Abhandlungen aus dem Aerodynamischen Institut an der Technischen Hochschule, Aachen. 1927.
10. Smith, R. H., Aerodynamic Theory and Test of Strut Forms, National Advisory Committee for Aeronautics, Report No. 311. Washington, 1929.

AERODYNAMICAL LABORATORY,

BUREAU OF CONSTRUCTION AND REPAIR, U. S. NAVY,
WASHINGTON, D. C., April 3, 1929.

TABLE I.—STREAM FUNCTION COEFFICIENTS, $\frac{\psi_1'}{C}$, FOR A LINE SOURCE FROM EQUATION (19)

y	x											
	0	+1.0	+2.5	+5.0	+7.5	+10.0	+20.0	+30.0	+40.0	+50.0	+60.0	+90.0
0.2	+1.5708	+0.1970	+0.0800	+0.0401	+0.0267	+0.0201	+0.0102	+0.0067	+0.0050	+0.0041	+0.0034	+0.0022
0.5	1.5708	.4362	.1970	.0998	.0666	.0500	.0250	.0167	.0125	.0102	.0083	.0056
1.0	1.5708	.7854	.3804	.1975	.1326	.0998	.0497	.0333	.0250	.0201	.0166	.0110
2.0	1.5708	1.1071	.6777	.3805	.2606	.1975	.0998	.0666	.0497	.0401	.0334	.0222
3.0	1.5708	1.2488	.8761	.5405	.3805	.2915	.1486	.0998	.0747	.0599	.0490	.0333
4.0	1.5708	1.3259	1.0123	.6778	.4898	.3805	.1946	.1326	.0998	.0800	.0666	.0444
5.3	1.5708	1.3736	1.1071	.7854	.5882	.4637	.2449	.1652	.1245	.0998	.0832	.0555
6.0	1.5708	1.4056	1.1760	.8761	.6920	.5405	.2915	.1946	.1486	.1195	.0998	.0666
7.0	1.5708	1.4288	1.2278	.9803	.7511	.6109	.3336	.2292	.1733	.1390	.1160	.0777
8.0	1.5708	1.4466	1.2680	1.0123	.8177	.6749	.3804	.2606	.1946	.1588	.1326	.0887
9.0	1.5708	1.4602	1.2997	1.0635	.8761	.7298	.4227	.2915	.2213	.1780	.1489	.0998
10.0	1.5708	1.4713	1.3258	1.1071	.9273	.7854	.4637	.3217	.2449	.1975	.1652	.1108
11.0	1.5708	1.4800	1.3473	1.1440	.9721	.8331	.5029	.3514	.2685	.2167	.1812	.1216
12.0	1.5708	1.4876	1.3654	1.1761	1.0123	.8761	.5405	.3804	.2915	.2356	.1946	.1326
13.0	1.5708	1.4940	1.3808	1.2037	1.0474	.9151	.5765	.4090	.3142	.2545	.2132	.1434
14.0	1.5708	1.4995	1.3939	1.2278	1.0789	.9503	.6109	.4366	.3366	.2731	.2292	.1542
17.0	1.5708	1.5120	1.4250	1.2850	1.1550	1.0390	.7050	.5160	.4020	.3278	.2760	.1870
20.0	1.5708	1.5210	1.4460	1.3260	1.2121	1.1071	.7850	.5880	.4640	.3805	.3220	.2190
24.0	+1.5708	+1.5290	+1.4670	+1.3650	+1.2680	+1.1760	+.8760	+.6750	+.5400	+.4477	+.3800	+.2610

TABLE II.—STREAM FUNCTION COEFFICIENTS, $\frac{\psi_1'}{C}$, FOR A SURFACE SOURCE WHOSE STRENGTH IS UNIFORMLY DISTRIBUTED FROM EQUATION (28a)

$l=10$

x	y									
	1	2	3	4	5	6	8	10	12	14
+5	0	0	0	0	0	0	0	0	0	0
+7	+0.083	+0.158	+0.222	+0.277	+0.319	+0.354	+0.405	+0.435	+0.488	+0.492
+9	.207	.369	.496	.592	.670	.734	.830	.899	.950	.989
+10	.331	.523	.666	.777	.866	.939	1.051	1.132	1.192	1.239
+11	.227	.409	.554	.667	.763	.842	.966	1.057	1.125	1.179
+13	.145	.281	.403	.510	.604	.685	.817	.920	1.002	1.065
+16	.098	.193	.285	.369	.450	.522	.651	.759	.884	.918
+20	.061	.138	.205	.269	.332	.392	.502	.601	.687	.760
+25	.051	.102	.148	.202	.250	.296	.387	.469	.548	.616
+30	.040	.081	.121	.162	.200	.239	.314	.382	.452	.515
+35	.034	.067	.101	.134	.168	.198	.262	.324	.384	.440
+40	.029	.057	.086	.115	.143	.171	.226	.280	.330	.384
+50	+.022	+.045	+.067	+.089	+.111	+.134	.178	+.220	+.263	+.303

TABLE III.—STREAM FUNCTION COEFFICIENTS, $\frac{\psi_1'}{C}$, FOR A SURFACE SOURCE WHOSE STRENGTH INCREASES LINEARLY ALONG THE WIDTH FROM EQUATION (28b)

$l=5$

x	y									
	1	2	3	4	5	6	8	10	12	14
-40	-0.0249	-0.0497	-0.0702	-0.0948	-0.1152	-0.1390	-0.1850	-0.2364	-0.2789	-0.3204
-35	-.0276	-.0525	-.0800	-.1080	-.1323	-.1576	-.2005	-.2500	-.3010	-.3492
-30	-.0286	-.0600	-.0920	-.1250	-.1582	-.1800	-.2362	-.2862	-.3400	-.3972
-25	-.0389	-.0680	-.1066	-.1379	-.1714	-.2132	-.2720	-.3407	-.3992	-.4550
-20	-.0433	-.0804	-.1288	-.2279	-.2104	-.2478	-.3310	-.4063	-.4740	-.5399
-16	-.0515	-.1025	-.1549	-.2345	-.2592	-.3030	-.3938	-.4876	-.5560	-.6286
-13	-.0597	-.1226	-.1830	-.2394	-.2986	-.3527	-.4530	-.5630	-.6404	-.7099
-10	-.0760	-.1506	-.2247	-.2938	-.3615	-.4284	-.5430	-.6659	-.7365	-.8072
-7	-.0978	-.2030	-.2866	-.3716	-.4552	-.5305	-.6632	-.7729	-.8624	-.9376
-5	-.1222	-.2355	-.3518	-.4544	-.5474	-.6228	-.7724	-.8747	-.9680	-1.0376
-2	-.1962	-.3757	-.5227	-.6597	-.7670	-.8550	-.9883	-1.0885	-1.1543	-1.2091
0	-.3425	-.5901	-.7698	-.9012	-1.0000	-1.0758	-1.1818	-1.2528	-1.3036	-1.3365
+2	-.3572	-.5631	-.6861	-.7644	-.8168	-.8541	-.9051	-.9353	-.9572	-.9728
+4	+.4090	+.2277	+.0972	+.2895	+.3155	+.3342	+.3600	+.3746	+.3896	+.3980
+5	+.7040	+.9585	+1.1088	+1.2010	+1.2640	+1.3094	+1.3701	+1.4073	+1.4352	+1.4488
+6	+.4174	+.6999	+.8838	+1.0090	+1.0986	+1.1643	+1.2580	+1.3135	+1.3528	+1.3753
+8	+.2230	+.4241	+.5906	+.7260	+.8359	+.9209	+1.0496	+1.1382	+1.2028	+1.2450
+11	+.1328	+.2605	+.3798	+.4882	+.5750	+.6723	+.8113	+.9218	+1.0084	+1.0738
+13	+.1049	+.2071	+.3050	+.4000	+.4815	+.5682	+.6945	+.8043	+.9052	+.9685
+16	+.0790	+.1568	+.2348	+.3172	+.3895	+.4475	+.5678	+.6734	+.7608	+.8356
+20	+.0610	+.1201	+.2297	+.2428	+.2997	+.3474	+.4422	+.5425	+.6260	+.7080
+25	+.0482	+.0966	+.1390	+.1822	+.2194	+.2602	+.3471	+.4296	+.5027	+.5708
+30	+.0330	+.0769	+.0647	+.1485	+.1760	+.2096	+.2893	+.3481	+.4191	+.4837
+35	+.0306	+.0679	+.0900	+.1212	+.1577	+.1787	+.2438	+.3011	+.3606	+.4228
+40	+.0283	+.0561	+.0796	+.1313	+.1293	+.1565	+.2174	+.2626	+.3178	+.3751
+50	+.0202	+.0404	+.0618	+.0840	+.1050	+.1254	+.1657	+.2172	+.2569	+.2966

TABLE III.—STREAM FUNCTION COEFFICIENTS, $\frac{\psi_1'}{C}$, FOR A SURFACE SOURCE WHOSE STRENGTH INCREASES LINEARLY ALONG THE WIDTH FROM EQUATION (28b)—Con.

$$l=20$$

x	y									
	1	2	3	4	5	6	8	10	12	14
-40	-0.0189	-0.0380	-0.0588	-0.0747	-0.0948	-0.1120	-0.1497	-0.1867	-0.2209	-0.2591
-35	-0.0210	-0.0420	-0.0626	-0.0856	-0.1051	-0.1241	-0.1654	-0.2055	-0.2443	-0.2844
-30	-0.0233	-0.0470	-0.0699	-0.0909	-0.1165	-0.1379	-0.1835	-0.2294	-0.2691	-0.3181
-25	-0.0267	-0.0508	-0.0796	-0.1055	-0.1315	-0.1574	-0.2141	-0.2588	-0.3076	-0.3556
-20	-0.0307	-0.0610	-0.0918	-0.1231	-0.1520	-0.1817	-0.2404	-0.2961	-0.3519	-0.4042
-16	-0.0351	-0.0700	-0.1049	-0.1395	-0.1731	-0.2075	-0.2732	-0.3365	-0.4251	-0.4544
-13	-0.0394	-0.0788	-0.1177	-0.1562	-0.1981	-0.2318	-0.2505	-0.3701	-0.4375	-0.5001
-10	-0.0451	-0.0899	-0.1341	-0.1780	-0.2209	-0.2630	-0.3436	-0.4194	-0.4899	-0.5552
-7	-0.0529	-0.1029	-0.1565	-0.2065	-0.2562	-0.3039	-0.3941	-0.4772	-0.5529	-0.6219
-5	-0.0597	-0.1185	-0.1765	-0.2327	-0.2871	-0.3393	-0.4363	-0.5245	-0.6036	-0.6744
-2	-0.0757	-0.1495	-0.2204	-0.2857	-0.3512	-0.4107	-0.5188	-0.6133	-0.6952	-0.7672
0	-0.0962	-0.1849	-0.2669	-0.3425	-0.4122	-0.4764	-0.5901	-0.6869	-0.7696	-0.8403
+2	-0.1146	-0.2164	-0.3074	-0.3894	-0.4635	-0.5305	-0.6468	-0.7431	-0.8240	-0.8916
+4	-0.1199	-0.2261	-0.3195	-0.4024	-0.4759	-0.5413	-0.6514	-0.7400	-0.8114	-0.8700
+5	-0.1141	-0.1886	-0.3017	-0.3791	-0.4458	-0.5055	-0.5911	-0.6796	-0.7406	-0.7898
+6	-0.0924	-0.1712	-0.2383	-0.2950	-0.3435	-0.3848	-0.4756	-0.5000	-0.5377	-0.5674
+8	-0.0522	-0.0922	-0.1222	-0.1444	-0.1619	-0.1749	-0.1748	-0.1791	-0.2109	-0.2177
+11	+0.0426	+0.0603	+0.0724	+0.1009	+0.1269	+0.1522	+0.1819	+0.2165	+0.2433	+0.2726
+13	+0.1013	+0.1972	+0.2798	+0.3494	+0.4080	+0.4446	+0.5336	+0.5974	+0.6514	+0.6812
+16	+0.3035	+0.4755	+0.6033	+0.6960	+0.7860	+0.8546	+0.9633	+1.0451	+1.1087	+1.1596
+20	+0.1602	+0.3040	+0.4266	+0.5304	+0.6241	+0.6914	+0.8180	+0.9136	+0.9981	+1.0504
+25	+0.1008	+0.2046	+0.2889	+0.3763	+0.4543	+0.5259	+0.6573	+0.7519	+0.8363	+0.9065
+30	+0.0647	+0.1290	+0.1884	+0.2522	+0.3430	+0.3668	+0.4718	+0.5643	+0.6424	+0.7207
+35	+0.0483	+0.0967	+0.1435	+0.1901	+0.2369	+0.2809	+0.3666	+0.4462	+0.5230	+0.5879
+40	+0.0387	+0.0774	+0.0884	+0.1482	+0.1896	+0.2264	+0.2985	+0.3421	+0.4308	+0.4939
+50	+0.0277	+0.0549	+0.0837	+0.1116	+0.1361	+0.1650	+0.2170	+0.2709	+0.3208	+0.3681

TABLE IV.—STREAM FUNCTION COEFFICIENTS, $\frac{\psi_1'}{C}$, FOR A SURFACE SOURCE WHOSE STRENGTH INCREASES PARABOLICALLY ALONG THE WIDTH, FROM EQUATION (28c)

$$l=10$$

x	y									
	1	2	3	4	5	6	8	10	12	14
-40	-0.020	-0.060	-0.060	-0.080	-0.101	-0.121	-0.162	-0.205	-0.250	-0.288
-35	-0.021	-0.042	-0.066	-0.092	-0.118	-0.142	-0.190	-0.239	-0.281	-0.320
-30	-0.024	-0.048	-0.080	-0.112	-0.138	-0.160	-0.219	-0.268	-0.315	-0.356
-25	-0.030	-0.062	-0.095	-0.132	-0.158	-0.188	-0.252	-0.310	-0.358	-0.407
-20	-0.037	-0.072	-0.115	-0.155	-0.187	-0.221	-0.292	-0.360	-0.420	-0.475
-16	-0.046	-0.090	-0.140	-0.180	-0.218	-0.255	-0.337	-0.413	-0.482	-0.540
-13	-0.052	-0.102	-0.150	-0.200	-0.245	-0.288	-0.386	-0.468	-0.545	-0.602
-10	-0.060	-0.119	-0.177	-0.230	-0.279	-0.327	-0.436	-0.536	-0.611	-0.679
-7	-0.070	-0.143	-0.211	-0.272	-0.333	-0.392	-0.505	-0.622	-0.708	-0.769
-5	-0.083	-0.163	-0.238	-0.311	-0.379	-0.449	-0.568	-0.690	-0.780	-0.844
-2	-0.111	-0.216	-0.316	-0.404	-0.479	-0.566	-0.702	-0.817	-0.909	-0.976
0	-0.150	-0.284	-0.408	-0.505	-0.594	-0.683	-0.825	-0.932	-1.022	-1.084
+2	-0.217	-0.381	-0.527	-0.648	-0.744	-0.826	-0.953	-1.060	-1.129	-1.177
+5	-0.258	-0.416	-0.555	-0.647	-0.710	-0.767	-0.837	-0.900	-0.947	-0.977
+7	-0.192	-0.280	-0.353	-0.383	-0.398	-0.414	-0.446	-0.473	-0.487	-0.500
+9	+0.154	+0.218	+0.310	+0.399	+0.457	+0.480	+0.535	+0.581	+0.632	+0.662
+10	+0.580	+0.832	+0.975	+1.076	+1.151	+1.213	+1.298	+1.336	+1.368	+1.401
+11	+0.351	+0.605	+0.772	+0.909	+0.990	+1.056	+1.183	+1.243	+1.288	+1.320
+13	+0.204	+0.375	+0.525	+0.650	+0.738	+0.822	+0.988	+1.076	+1.130	+1.186
+16	+0.122	+0.242	+0.340	+0.437	+0.520	+0.601	+0.756	+0.863	+0.949	+1.021
+20	+0.082	+0.154	+0.233	+0.313	+0.370	+0.446	+0.577	+0.678	+0.770	+0.843
+25	+0.063	+0.118	+0.170	+0.228	+0.273	+0.325	+0.432	+0.525	+0.608	+0.668
+30	+0.045	+0.088	+0.132	+0.175	+0.217	+0.262	+0.340	+0.420	+0.490	+0.555
+35	+0.036	+0.072	+0.109	+0.142	+0.178	+0.219	+0.279	+0.352	+0.413	+0.475
+40	+0.030	+0.060	+0.089	+0.120	+0.151	+0.182	+0.243	+0.299	+0.353	+0.415
+50	+0.023	+0.046	+0.069	+0.092	+0.115	+0.137	+0.182	+0.230	+0.304	+0.320

TABLE Va.—ORDINATES GIVING THE SURFACES OF THE FIVE RANKINE STRUTS

Strut No. I		Strut No. II		Strut No. III		Strut No. IV		Strut No. V	
<i>x</i>	<i>y</i>	<i>x</i>	<i>y</i>	<i>x</i>	<i>y</i>	<i>x</i>	<i>y</i>	<i>x</i>	<i>y</i>
0	0	0	0	0	0	0	0	0	0
0.049	0.304	0.053	0.294	0.049	0.270	0.053	0.233	0.017	0.131
.098	.441	.152	.500	.098	.402	.217	.520	.052	.248
.196	.618	.250	.642	.196	.564	.422	.726	.086	.316
.294	.750	.348	.755	.294	.699	.627	.882	.189	.454
.392	.848	.495	.892	.441	.833	.832	.996	.292	.564
.539	.980	.642	.995	.588	.936	1.037	1.094	.430	.678
.686	1.080	.887	1.127	.833	1.073	1.446	1.233	.602	.791
.931	1.211	1.132	1.230	1.078	1.176	1.856	1.332	.774	.884
1.176	1.302	1.377	1.309	1.323	1.250	2.266	1.406	.946	.970
1.421	1.368	1.622	1.363	1.569	1.304	1.676	1.451	1.118	1.042
1.667	1.417	2.113	1.436	2.059	1.397	3.086	1.483	1.462	1.170
2.157	1.477	2.603	1.475	2.549	1.451	3.495	1.500	1.806	1.272
2.647	1.500	3.093	1.497	3.039	1.485	3.905	1.496	2.150	1.342
3.137	1.490	3.583	1.500	3.529	1.496	4.315	1.487	2.494	1.397
3.627	1.456	4.073	1.484	4.017	1.500	5.135	1.436	2.838	1.435
4.118	1.408	4.564	1.451	4.510	1.490	5.954	1.352	3.526	1.486
4.608	1.348	4.054	1.402	5.000	1.466	6.774	1.229	4.214	1.500
5.588	1.196	5.544	1.348	5.490	1.421	7.593	1.065	4.902	1.476
6.569	1.010	6.524	1.196	6.471	1.294	8.413	.861	5.590	1.428
7.549	.799	7.505	1.010	7.451	1.118	8.823	.746	6.278	1.352
8.529	.569	8.485	.770	8.431	.882	9.233	.615	6.967	1.249
9.020	.441	8.975	.627	8.922	.745	9.642	.467	7.655	1.101
9.510	.318	9.466	.470	9.412	.578	10.052	.287	8.343	.925
10.000	.186	9.711	.382	9.902	.387	10.257	.180	9.031	.712
10.245	.122	9.956	.284	10.147	.274	10.462	.061	9.375	.598
10.490	.029	10.201	.176	10.385	.147	10.519	0	9.719	.460
10.519	0	10.446	.056	10.455	.083			10.063	.275
		10.505	0	10.519	0			10.235	.186
								10.407	.072
								10.486	0

TABLE Vb.—ORDINATES GIVING THE SURFACES OF THE R. & M. 183 (BRITISH), NO. 53 (GERMAN), AND NAVY NO. 2 (AMERICAN) STRUTS

R. & M. 183		No. 53		Navy No. 2	
<i>x</i>	<i>y</i>	<i>x</i>	<i>y</i>	<i>x</i>	<i>y</i>
0	0	0	0	0	0
0.210	0.345	0.054	0.237	0.262	0.555
.525	.720	.189	.481	.525	.792
.788	.936	.378	.680	.787	.952
1.050	1.092	.607	.846	1.050	1.080
1.575	1.306	.905	1.022	1.312	1.180
2.100	1.440	1.215	1.164	1.575	1.260
2.625	1.487	1.592	1.298	1.837	1.320
3.150	1.500	2.119	1.416	2.100	1.375
3.675	1.495	2.632	1.477	2.625	1.440
4.200	1.475	3.361	1.500	3.150	1.480
4.725	1.443	4.192	1.498	3.675	1.500
5.250	1.404	4.860	1.457	4.200	1.500
5.775	1.344	5.540	1.380	4.725	1.498
6.300	1.272	6.273	1.275	5.250	1.440
6.825	1.187	6.900	1.151	5.775	1.378
7.350	1.092	7.588	1.004	6.300	1.290
7.875	.979	8.330	.810	6.825	1.207
8.400	.852	8.975	.620	7.350	1.107
8.925	.711	9.592	.413	7.875	.983
9.450	.564	10.000	.250	8.400	.852
9.975	.376	10.302	.102	8.925	.698
10.340	1.86	10.500	0	9.450	.510
10.500	0			9.975	.292
				10.500	0

TABLE VI.—THEORETICAL AND EXPERIMENTAL VELOCITIES AND PRESSURES ON THE SURFACE OF STRUT No. I AT 40 MILES PER HOUR

Hole No.	Hole position		Theoretical				Experimental				
			Velocity	Pressure			Pressure				Velocity
	<i>x</i>	<i>y</i>		<i>p</i>	<i>p/p_n</i>		(1)	(2)	<i>p</i>	<i>p/p_n</i>	
1	0	0	0	+0.787	+1.000		0	0	+0.787	+1.000	0
2	0.100	0.446	27.9	+0.412	+0.516		4.08	0	+0.464	+0.589	25.7
3	.300	.766	43.8	-.157	-.200		-10.89	-.323	-.857	-.030	40.8
4	.550	.997	52.1	-.546	-.694		-15.97	-1.261	-.474	-.602	50.7
5	.880	1.192	57.3	-.828	-1.053		-19.86	-1.567	-.780	-.991	56.5
6	1.300	1.348	58.9	-.913	-1.160		-21.10	-1.665	-.878	-1.117	58.2
7	2.100	1.472	57.8	-.853	-1.084		-20.00	-1.578	-.791	-1.005	56.7
8	3.640	1.461	53.8	-.635	-.807		-16.55	-1.314	-.527	-.669	51.7
9	5.240	1.255	48.3	-.358	-.455		-13.70	-1.081	-.294	-.374	46.9
10	6.800	.962	44.4	-.183	-.233		-11.75	-.927	-.140	-.178	43.4
11	8.400	.599	41.4	-.057	-.072		-9.91	-.781	+.006	+.008	39.8
12	9.220	.353	39.1	+.036	+.046		-8.95	-.706	+.081	+.103	37.9
13	9.950	.206	34.8	+.191	+.243		-7.98	-.629	+.158	+.201	35.8
14	10.350	.083	31.4	+.393	+.500		-7.81	-.616	+.171	+.218	35.4

¹ Inches of alcohol 1 to 10.

² Inches of water vertical.

TABLE VII.—THEORETICAL AND EXPERIMENTAL VELOCITIES AND PRESSURES ON THE SURFACE OF STRUT No. II AT 40 MILES PER HOUR

Hole No.	Hole position		Theoretical			Experimental				
			Velocity	Pressure		Pressure				Velocity
	<i>x</i>	<i>y</i>		<i>p</i>	<i>p/p_n</i>	(1)	(2)	<i>p</i>	<i>p/p_n</i>	
1	0	0	0	+0.787	+1.000	0	0	+0.787	+1.000	0
2	.100	0.432	26.4	+ .443	+ .563	-4.32	- .342	+ .446	+ .566	26.4
3	.300	.712	41.1	- .046	- .058	-10.55	- .831	- .044	- .056	41.1
4	.550	.938	50.5	- .465	- .592	-15.71	-1.239	- .452	- .575	50.2
5	.880	1.118	55.0	- .702	- .892	-17.81	-1.406	- .619	- .789	53.5
6	1.300	1.275	56.3	- .769	- .978	-18.79	-1.483	- .696	- .885	54.9
7	2.100	1.422	55.3	- .716	- .910	-18.36	-1.449	- .662	- .842	54.3
8	3.640	1.496	52.1	- .546	- .694	-16.19	-1.278	- .491	- .623	51.0
9	5.240	1.393	49.3	- .410	- .521	-14.45	-1.141	- .354	- .450	48.2
10	6.800	1.152	47.3	- .311	- .395	-12.96	-1.023	- .236	- .300	45.6
11	8.400	.800	44.3	- .178	- .227	-11.16	- .881	- .094	- .120	42.3
12	9.220	.564	41.4	- .055	- .070	-9.67	- .763	+ .024	+ .031	39.4
13	9.950	.309	35.7	+ .157	+ .200	-8.17	- .645	+ .142	+ .180	36.2
14	10.350	.108	27.4	+ .418	+ .532	-7.06	- .557	+ .230	+ .230	35.1

¹ Inches of alcohol 1 to 10.

² Inches of water vertical.

TABLE VIII.—THEORETICAL AND EXPERIMENTAL VELOCITIES AND PRESSURES ON THE SURFACE OF STRUT No. III AT 40 MILES PER HOUR

Hole No.	Hole position		Theoretical			Experimental				
			Velocity	Pressure		Pressure				Velocity
	<i>x</i>	<i>y</i>		<i>p</i>	<i>p/p_n</i>	(1)	(2)	<i>p</i>	<i>p/p_n</i>	
1	0	0	0	+0.787	+1.000	0	0	+0.787	+1.000	0
2	0.100	0.407	23.3	+ .519	+ .660	-3.28	- .258	+ .529	+ .672	22.9
3	.300	.711	42.7	- .110	- .140	-11.30	- .892	- .105	- .133	42.6
4	.550	.913	50.6	- .472	- .600	-15.10	-1.192	- .405	- .574	49.3
5	.880	1.108	54.1	- .650	- .826	-17.90	-1.413	- .626	- .796	53.6
6	1.300	1.240	54.8	- .686	- .872	-18.34	-1.447	- .660	- .839	54.3
7	2.100	1.393	53.4	- .614	- .781	-17.36	-1.368	- .581	- .739	52.8
8	3.640	1.500	51.3	- .506	- .643	-16.09	-1.267	- .480	- .610	50.7
9	5.240	1.437	49.8	- .431	- .548	-15.20	-1.200	- .413	- .525	49.4
10	6.800	1.230	47.9	- .341	- .434	-13.85	-1.091	- .304	- .386	47.1
11	8.400	.893	45.0	- .209	- .266	-11.43	- .902	- .211	- .166	43.2
12	9.220	.653	42.1	- .083	- .106	-9.77	- .770	+ .017	+ .022	39.6
13	9.950	.427	37.4	+ .099	+ .126	-8.02	- .632	+ .155	+ .197	35.8
14	10.350	.172	26.8	+ .433	+ .551	-7.58	- .598	+ .189	+ .240	34.9

¹ Inches of alcohol 1 to 10.

² Inches of water vertical.

TABLE IX.—THEORETICAL AND EXPERIMENTAL VELOCITIES AND PRESSURES ON THE SURFACE OF STRUT No. IV AT 40 MILES PER HOUR

Hole No.	Hole position		Theoretical			Experimental				
			Velocity	Pressure		Pressure				Velocity
	<i>x</i>	<i>y</i>		<i>p</i>	<i>p/p_n</i>	(1)	(2)	<i>p</i>	<i>p/p_n</i>	
1	0	0	0	+0.787	+1.000	0	0	+0.787	+1.000	0
2	.100	.323	23.6	+ .514	+ .653	-3.39	-0.268	+ .519	+ .659	23.4
3	.300	.606	39.0	+ .039	+ .050	-9.44	- .745	+ .042	+ .053	38.9
4	.550	.819	45.4	- .289	- .368	-12.64	- .998	- .211	- .268	45.1
5	.880	1.023	51.3	- .503	- .640	-16.32	-1.288	- .501	- .637	51.2
6	1.300	1.183	53.3	- .609	- .774	-17.38	-1.370	- .583	- .741	52.8
7	2.100	1.375	53.8	- .636	- .808	-17.72	-1.399	- .612	- .778	53.4
8	3.640	1.486	53.4	- .616	- .783	-16.46	-1.299	- .512	- .650	51.4
9	5.240	1.433	49.3	- .408	- .518	-15.03	-1.185	- .398	- .506	49.1
10	6.800	1.228	47.0	- .298	- .379	-13.60	-1.073	- .286	- .363	46.7
11	8.400	.868	44.0	- .163	- .208	-11.32	- .893	- .106	- .135	42.6
12	9.220	.623	41.2	- .047	- .060	-9.70	- .766	+ .021	+ .027	39.5
13	9.950	.336	37.0	+ .115	+ .147	-7.88	- .620	+ .167	+ .212	35.5
14	10.350	.128	32.7	+ .334	+ .425	-7.44	- .587	+ .200	+ .254	34.5

¹ Inches of alcohol 1 to 10.

² Inches of water vertical.

TABLE XIb.—RESISTANCE VALUES PER FOOT RUN FOR RANKINE STRUT NO. V COMPARED WITH THOSE FOR R. & M. 183 (BRITISH), No. 53 (GERMAN), NAVY No. 2 (AMERICAN)

Air speed V in miles per hour	Strut				$V_1 L_1$ (ft.) ² sec.	$\frac{V_1 L_1}{\nu}$ $\times 10^{-4}$
	R. & M. 183	No. 53	Navy 2	V		
	Drag, D , in pounds per foot run					
20	0. 0258	0. 0243	0. 0240	0. 0238	7. 34	4. 40
30	. 0544	. 0484	. 0472	. 0472	11. 00	6. 59
40	. 0912	. 0818	. 0796	. 0801	14. 67	8. 79
50	. 1390	. 1230	. 1206	. 1204	18. 34	10. 98
60	. 1938	. 1778	. 1748	. 1740	22. 00	13. 18
Drag coefficient $C_D = \frac{2 Dg}{\rho A V_1^2}$						
20	. 1010	. 0951	. 0940	. 0931	7. 34	4. 40
30	. 0945	. 0842	. 0821	. 0821	11. 00	6. 59
40	. 0893	. 0800	. 0779	. 0784	14. 67	8. 79
50	. 0870	. 0769	. 0755	. 0753	18. 34	10. 98
60	. 0844	. 0774	. 0761	. 0758	22. 00	13. 18
Drag-strength ratio, $\frac{D}{I_1}$, $\frac{\text{lb./foot}}{(\text{feet})^4}$						
20	43. 09	40. 99	39. 90	39. 09	7. 34	4. 40
30	90. 85	81. 65	78. 46	77. 53	11. 00	6. 59
40	152. 31	137. 99	132. 32	131. 57	14. 67	8. 79
50	232. 15	207. 50	200. 48	197. 77	18. 34	10. 98
60	323. 67	299. 94	290. 58	285. 81	22. 00	13. 18
Sectional moment of inertia I in. ⁴						
	12. 416	12. 292	12. 474	12. 624		

TABLE XII.—ALONG STREAM FORCES PER FOOT RUN OF STRUTS IN 40 MILES PER HOUR AIR SPEED

Theoretical	Strut No.	Downstream			Upstream			Pressural drag $D_p = P_1 - p^2$	Frictional drag D_f	Total drag $D = D_p + D_f$
		Push	Suction	Total p_1	Push	Suction	Total p_2			
	Pounds per foot run									
	I	0. 298	0. 214	0. 512	0. 086	0. 426	0. 512	0	0	0
	II	. 281	. 223	. 504	. 110	. 396	. 506	-. 002	0	0
	III	. 291	. 209	. 500	. 146	. 358	. 504	-. 004	0	0
	IV	. 256	. 181	. 437	. 099	. 338	. 437	0	0	0
	V	. 229	. 214	. 443	. 122	. 320	. 442	+. 001	0	0
	Pounds per foot run									
	Experimental	I	. 313	. 164	. 477	. 056	. 382	. 438	. 039	. 040
II		. 288	. 160	. 448	. 065	. 348	. 413	. 035	. 053	. 088
III		. 296	. 156	. 452	. 083	. 333	. 416	. 036	. 053	. 089
IV		. 264	. 157	. 421	. 080	. 308	. 388	. 033	. 050	. 083
V		. 232	. 172	. 404	. 084	. 289	. 373	. 031	. 049	. 080
Per cent of total measured drag, D										
I		391	205	596	70	477	547	49	51	100
II		327	182	509	74	395	469	40	60	100
III		332	175	507	93	374	467	39	61	100
IV		318	189	507	96	371	467	40	60	100
V		290	215	505	105	361	466	39	61	100

REPORT No. 336

**TESTS OF LARGE AIRFOILS
IN THE PROPELLER RESEARCH TUNNEL, INCLUDING
TWO WITH CORRUGATED SURFACES**

**By DONALD H. WOOD
Langley Memorial Aeronautical Laboratory**

REPORT No. 336

TESTS OF LARGE AIRFOILS IN THE PROPELLER RESEARCH TUNNEL, INCLUDING TWO WITH CORRUGATED SURFACES

By DONALD H. WOOD

SUMMARY

This report gives the results of the tests of seven 2 by 12 foot airfoils (Clark Y, smooth and corrugated, Göttingen 398, N. A. C. A. M-6, and N. A. C. A. 84). The tests were made in the Propeller Research Tunnel of the National Advisory Committee for Aeronautics at Reynolds Numbers up to 2,000,000. The Clark Y airfoil was tested with three degrees of surface smoothness.

The effect of small variations of smoothness of an airfoil is shown to be negligible. Corrugating the surface causes a flattening of the lift curve at the burble point and an increase in drag at small flying angles.

INTRODUCTION

At the annual conference of the National Advisory Committee for Aeronautics with aircraft manufacturers held at Langley Field, Va., in May, 1928, Col. V. E. Clark and others mentioned the lack of test data on corrugated wings and suggested that tests be made in the Committee's Propeller Research Tunnel. Here a comparatively high Reynolds number may be secured due to the large size of the models that can be used. It also seemed desirable to secure data on some representative wing sections with a view to the possible comparison with existing data from other tunnels.

In the Propeller Research Tunnel with its 20-foot diameter throat, airfoils of 2-foot chord and 12-foot span may be tested up to velocities of 100 M. P. H. This condition gives a Reynolds Number of about 2,000,000, which corresponds quite closely with that attained in the Variable Density Tunnel at 10 atmospheres pressure.

Four airfoils (Clark Y, Göttingen 398, N. A. C. A. M-6, and N. A. C. A. 84) were selected for the present tests. The Clark Y was tested with three degrees of surface smoothness. In addition, two corrugated metal covered Clark Y airfoils, one having Clark Y section at the top of the corrugations and the other Clark Y section under the metal covering, were tested.

Thus, eight separate tests were made at speeds of approximately 80 and 100 M. P. H. The average Reynolds Numbers were 1,575,000 and 1,940,000, respectively.

METHODS AND APPARATUS

SUPPORTS

The Propeller Research Tunnel, where this investigation was conducted, has been described in Reference 1. The regular tunnel equipment was employed so far as possible. Referring to Figure 1, the airfoil to be tested is supported on two heavy, braced bars and fitted to pivot about a point within the airfoil slightly above the chord at the quarter point. A "sting" attached to the center of the airfoil is carried back to a vertical tube to which it is pivoted. A rack and pinion operated by a crank serves to raise and lower this tube, thereby changing the angle of attack of the airfoil. These members are bolted to the floating frame of the balance. The lift and drag forces may then be read on the platform scales on the floor below.

To reduce the tare drag of the system all supporting members were surrounded with fairing attached to the fixed frame of the balance. To reduce interference with the airfoil the fairings were not carried up to the wing, the last 2 feet of the supports being streamlined instead. The effectiveness of this arrangement is indicated by the fact that the tare drag was only 3 pounds at 100 M. P. H. at most angles of attack. This was about 50 per cent of the gross minimum drag.

In measuring this tare drag the set-up was modified so that the wing was supported independently of the supports and sting; hence, the drag measured was that of the supports alone in the presence of the airfoil. This was accomplished by supporting the sting from a tube connecting the front supports within the wing, but not touching it. The wing was then supported by wires and pipes arranged at distances from the supports. This arrangement is shown in Figure 2. The angle of attack could then be easily changed by simply moving the wing and turning the regular crank to bring the sting parallel underneath. Readings on all the balances were taken at several angles and air velocities so that the proper corrections could be made to the lift and drag readings. A small correction to the balance readings was also necessary, due to the different distribution of the weight at the several angles of attack.

CONSTRUCTION OF AIRFOILS

Since the airfoils were to be of 12-foot span and 2-foot chord, the standard ordinates of the airfoil sections in per cent of the chord were reduced to inches on a 2-foot chord. The model

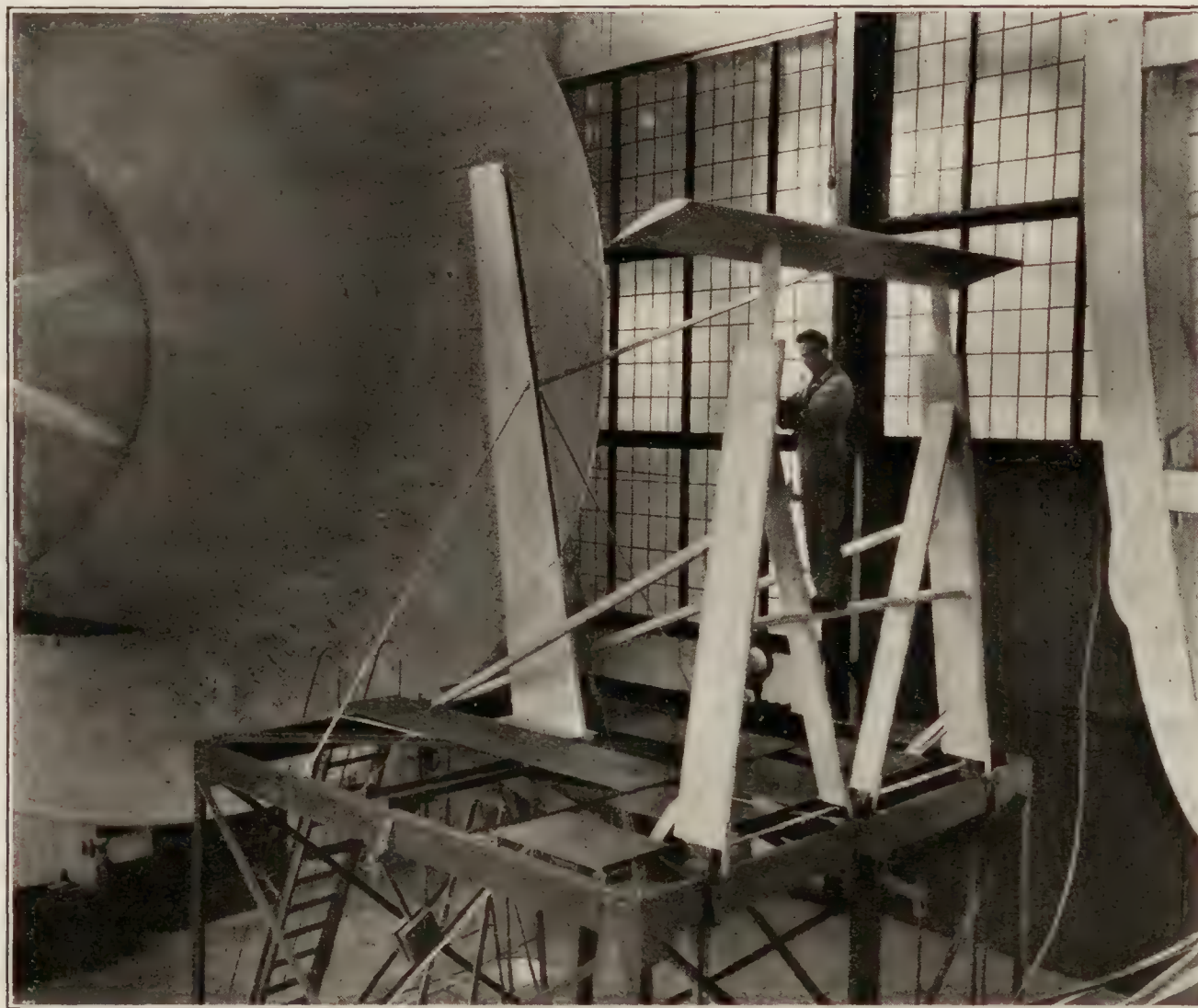


FIGURE 1.—Arrangement for wing tests

maker was given these ordinates to the nearest hundredth of an inch and was asked to work within $\frac{3}{100}$ or $\frac{1}{32}$ inch. Tables I-VI give the standard, specified, and measured ordinates. The measured values are the average of three measurements at the center span and halfway from the center to each tip. It will be noted that there are differences of as much as $\frac{3}{100}$ inch from the specified ordinates. They occur at the leading edge where the surface is well rounded. There is a considerably larger deviation for the thick corrugated airfoil which is accounted for by the difficulty of construction.

The leading and trailing edges were of laminated wood glued and formed to templates. At about the mid-chord a 3-inch wide beam was placed. These three members were spaced by solid ribs at 12-inch intervals along the span. The space between leading and trailing edges on the top and bottom surfaces was originally covered with $\frac{1}{16}$ -inch 3-ply plywood. After the first airfoil was completed examination showed considerable bowing and buckling of this thin covering. It was decided, however, before discarding this construction, to make a test, thereby

determining the effect of these small variations of surface contour. The plywood was then removed and $\frac{1}{16}$ -inch sheet aluminum substituted and a test made. The whole airfoil was then painted with two coats of brushing lacquer, sanding between coats. This gave a uniform smooth surface, although not as smooth as the bright sheet metal. All screw holes and cracks were filled with litharge and glycerin before painting. In Figure 3 are views of some of the airfoils.

The corrugated airfoils, one of which is illustrated at the bottom of Figure 3, were constructed in the same manner as the plywood airfoil, the corrugated metal covering being screwed to its surface. The metal sheet was of $\frac{1}{64}$ -inch thick aluminum with the corrugations rolled on a grooved wood form. The dimensions of these corrugations (fig. 4) were found by scaling down the average of several standard wings. Since it is impractical to run the corrugations completely around the leading edge, the sheet was left flat there, the corrugations starting a slight distance back on the top and bottom surfaces. In order to bring the corrugations into a scalloped edge at the rear, they were displaced one-half pitch on the top and bottom surfaces. This

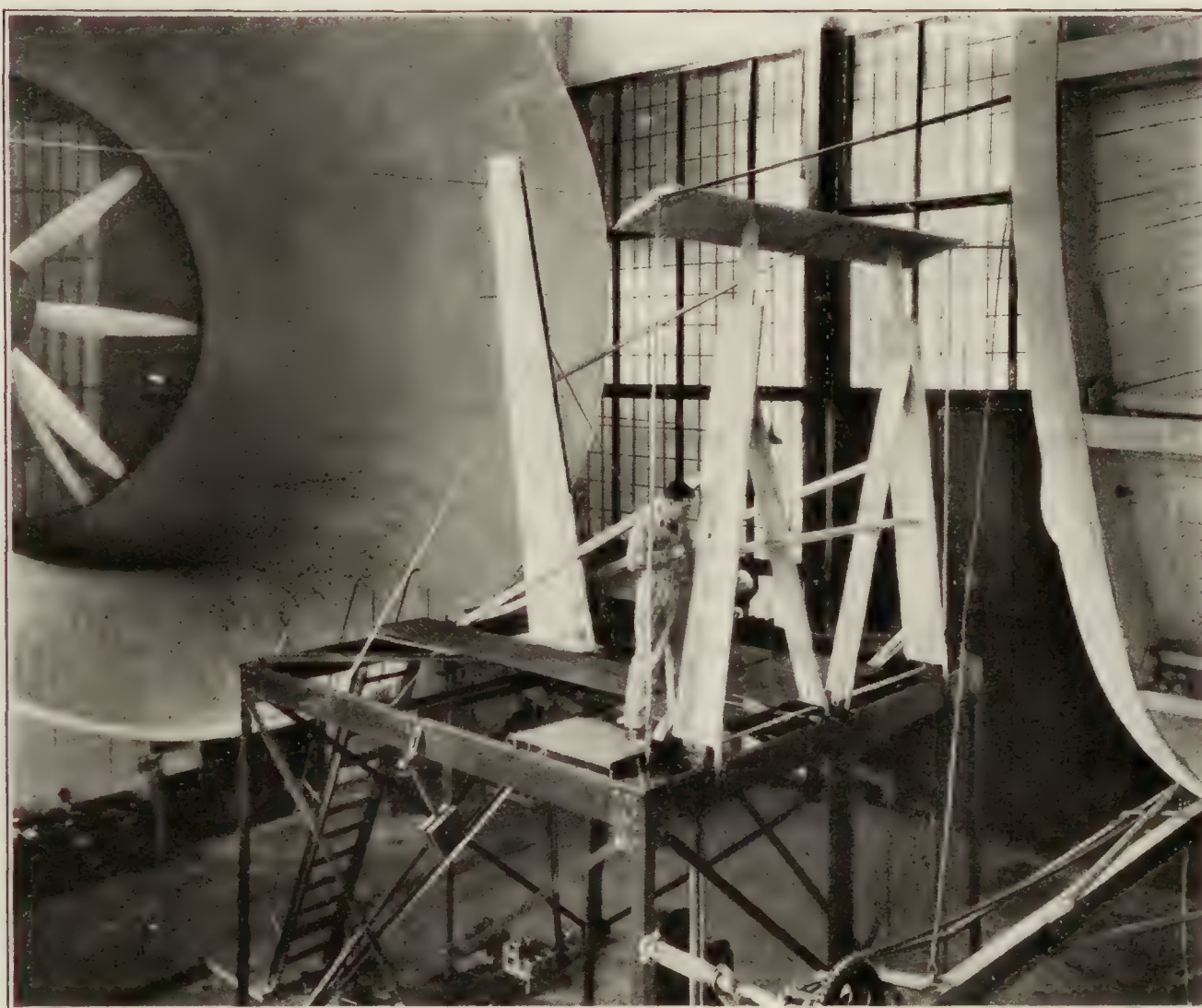


FIGURE 2.—Arrangement for tare drag test

and the leading edge construction necessitated slight departures from the basic Clark Y section. These are indicated in Figure 4.

TESTS

After mounting the airfoil a cover plate was screwed over the pivot-fitting opening, leaving only enough gap to allow the support to clear as the angle of attack was changed. Angles of attack indicated by a pointer on the moving rear support were checked against an inclinometer held on top of the sting just behind the airfoil.

Each test was run at tunnel air speeds of approximately 80 and 100 M. P. H. Air speeds were computed from the readings of a manometer connected to plates set in the walls of the tunnel passages calibrated against Pitot tubes suspended in the air stream at the position of the airfoil. Two readings were taken of front lift, rear lift, drag, and manometer at each angle of attack at each speed, one when the angles were successively increased from -9° to $+35^\circ$, and the second when decreased from $+35^\circ$ to -9° . This was done simply to secure two independent readings at each setting.

RESULTS

The results are given in the form of tables and curves of the absolute nondimensional coefficients C_L , C_D , C_M , C_p . From the observed readings these coefficients are computed in the usual manner from the equations

$$\begin{aligned} C_L &= \frac{\text{Lift}}{qS} & q &= \text{Dynamic pressure.} \\ C_D &= \frac{\text{Drag}}{qS} & S &= \text{Area of airfoil.} \\ C_{M_{c/4}} &= \frac{\text{Moment}_{c/4}}{qSc} & c &= \text{Chord of airfoil.} \\ C_p &= .25 - \frac{C_{M_{c/4}}}{C_L} \end{aligned}$$

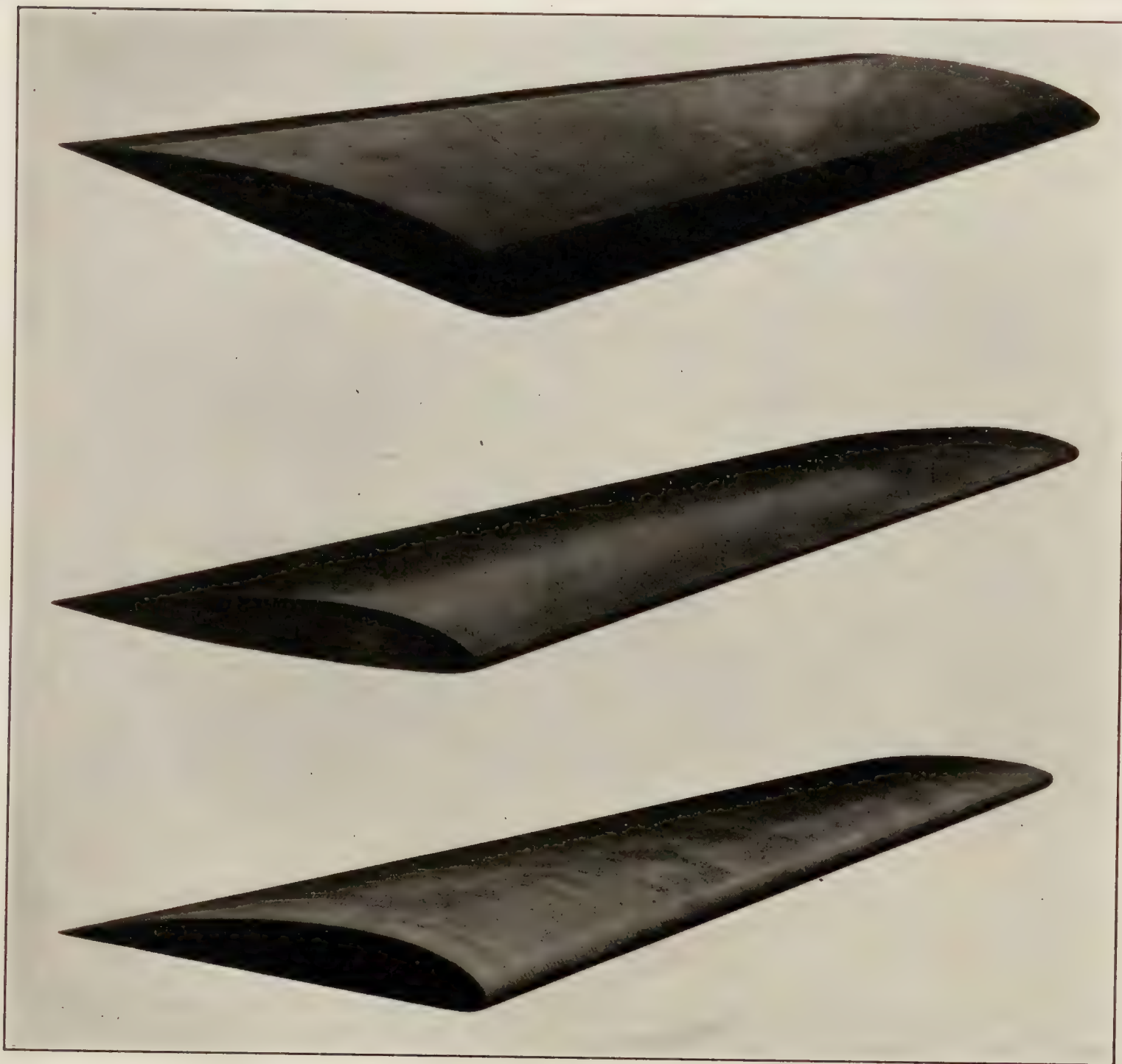


FIGURE 3.—Airfoils

The results have been corrected for boundary interference in accordance with the method given in References 2 and 3. For the open jet the interference amounts to an added downwash or an increase in the induced drag and induced angle of attack. The corrected test points as plotted, therefore, correspond to lower drag values and lower angles of attack than were measured. Since the airfoils were rectangular, the corrected results apply to rectangular wings rather than to elliptical.

The results are given in the form of curves (figs. 5-12) of C_L , C_D , L/D , and C_p against angle of attack, and apply directly to rectangular wings of aspect ratio 6 in free air. Numerical values are given in Tables VII-XIV.

In view of the established rules for aspect ratio correction, another type of diagram has come into quite extensive use, especially in England. In this diagram, Figures 13-18, profile drag C_{D_0} , $C_{M_{cl}}$ and angle of attack α_0 for infinite aspect ratio are plotted against lift coefficient. By simply adding the induced drag and induced angle of attack corresponding to any given aspect ratio to the values from the curves, the coefficients for that aspect ratio may be determined, thus eliminating the double computation required when converting from aspect ratio 6 to another aspect ratio. Only one curve is given for the Clark Y airfoils, that for the metal covered and painted, as this is comparable with the other airfoils of the series and there were negligible differences in the results for the several surfaces. For handy use the numerical values taken from the faired curves are given in Tables XV-XX. The induced drag for the loading corresponding to the particular wing shape should, of course, be used in deriving the coefficients for any finite aspect ratio.

Some of the characteristics of the airfoils are quite closely related, and, accordingly, the results for the Clark Y with various surfaces have been replotted in Figure 19. A set of points from a test in the old Variable Density Tunnel corrected for tunnel wall interference has been added for comparison. To compare the two corrugated wings with the smooth wing, Figure 20 is given. To aid in the selection of an airfoil for any given speed range, Figures 21 and 22 give $\frac{C_{D_0}}{C_{L_{max}}}$ against $\sqrt{\frac{C_{L_{max}}}{C_L}}$ or the speed ratio.

DISCUSSION

The reason for testing at two speeds was to determine the presence of scale effect. The differences were so slight that only one curve has been drawn through the points. The scattering of the points is, therefore, more an indication of the precision of the tests. The small forces at low angles of attack limit the precision of the minimum drag coefficient to ± 10 per cent.

On examination of the curves a few striking points will be noted. Some of the curves show breaks at the high angles (25° to 30°). It was noted during the tests that these breaks occurred at a higher angle when the angle of attack was being increased than when it was being decreased. The angles were not changed rapidly so the phenomena can not be charged to oscillation of the airfoil. There is probably some effect at these high angles, producing a condition which makes the flow tend to continue in a given way even though the new angle of attack dictates a change. These portions of the curves are mainly useful in discussion of rotary instability.

The N. A. C. A. M-6 shows consistently higher maximum lift at 100 M. P. H. than at 80. Experiments in the Variable Density Tunnel have shown that there is a variation of lift with Reynolds Number which may be quite rapid at certain values. It may be that for this airfoil the lift does increase rapidly at these Reynolds Numbers. The small center of pressure movement confirms other tests on this airfoil.

The effect of the different surfaces on the characteristics of the Clark Y airfoil is shown in Figure 19. Apparently reasonably small deviations from the true smooth surface have slight effect on the aerodynamic characteristics of this airfoil. While the range of surface smoothness was not large, the unpainted plywood was certainly rougher than the doped fabric of a wing as used on airplanes.

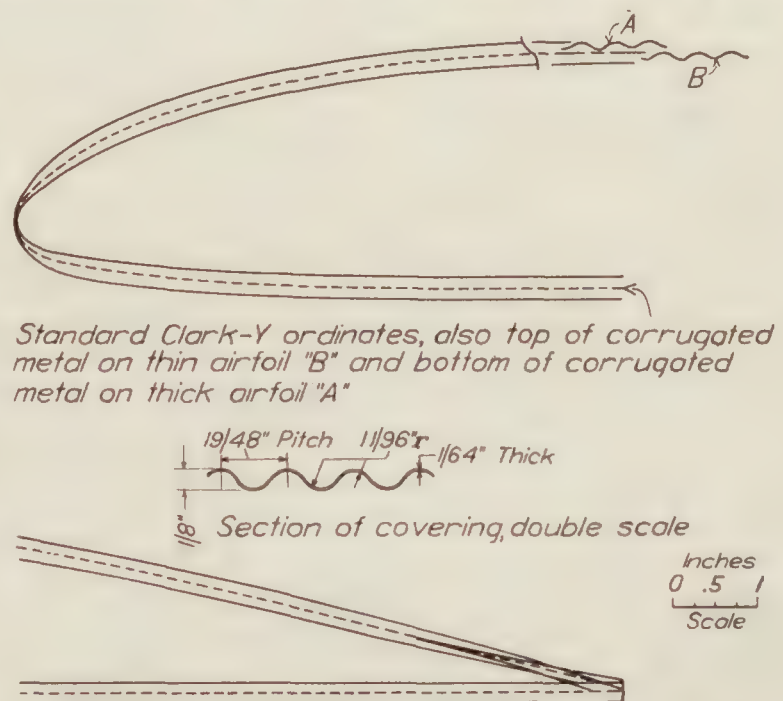


FIGURE 4.—Corrugated airfoils. Clark Y, basic section

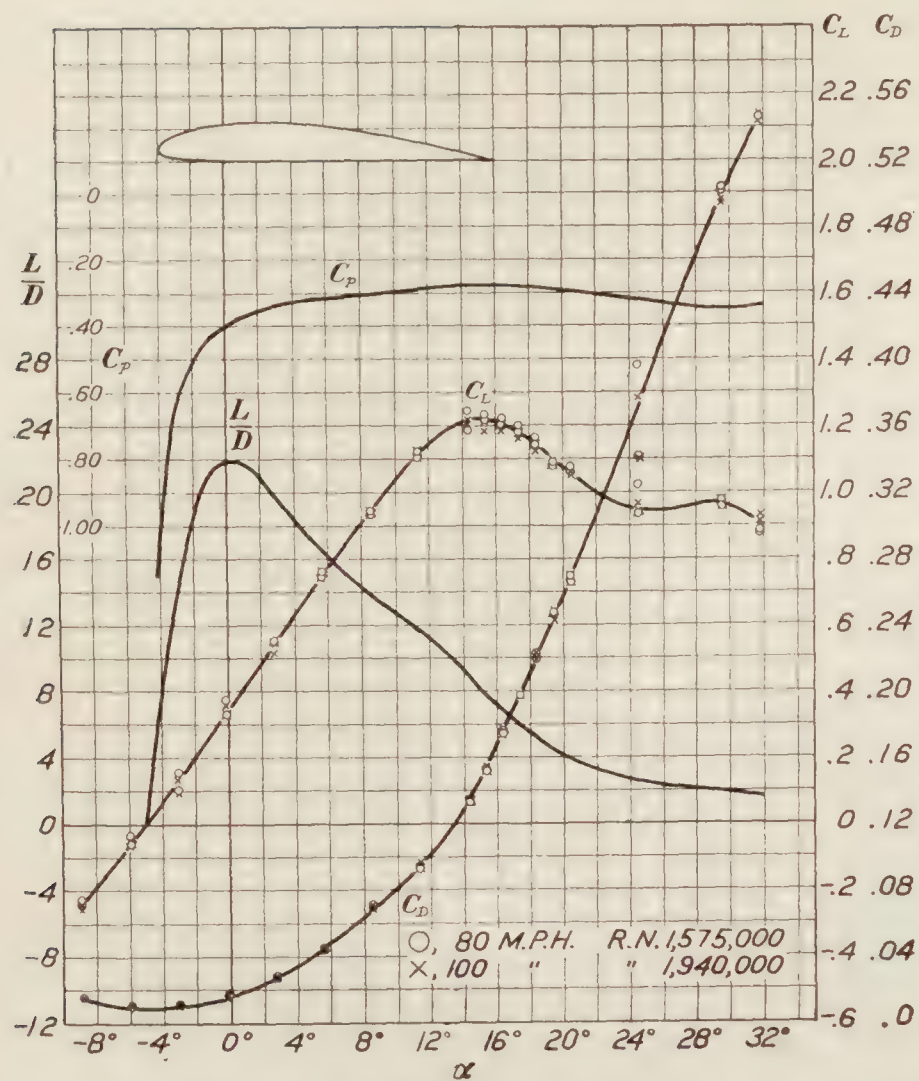


FIGURE 5.—Clark Y, plywood covered. Aspect ratio 6. Free air

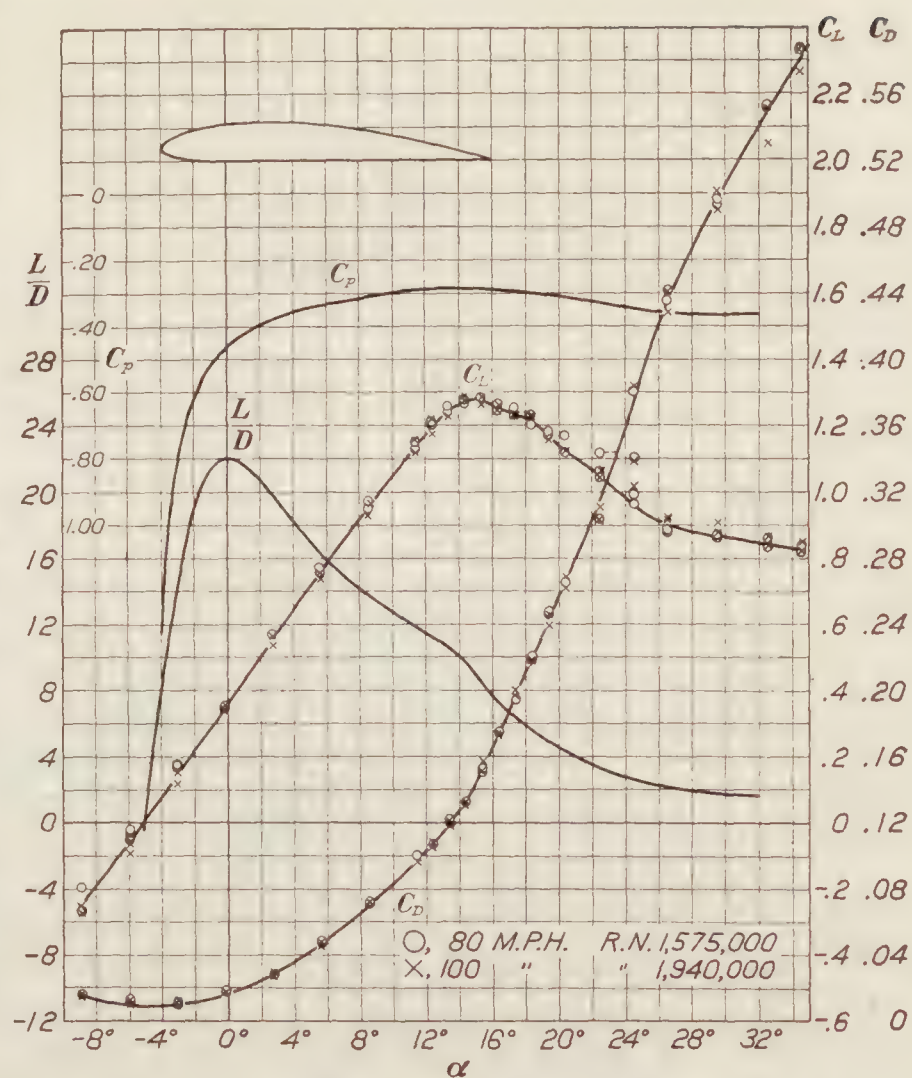


FIGURE 7.—Clark Y, metal covered, painted. Aspect ratio 6. Free air

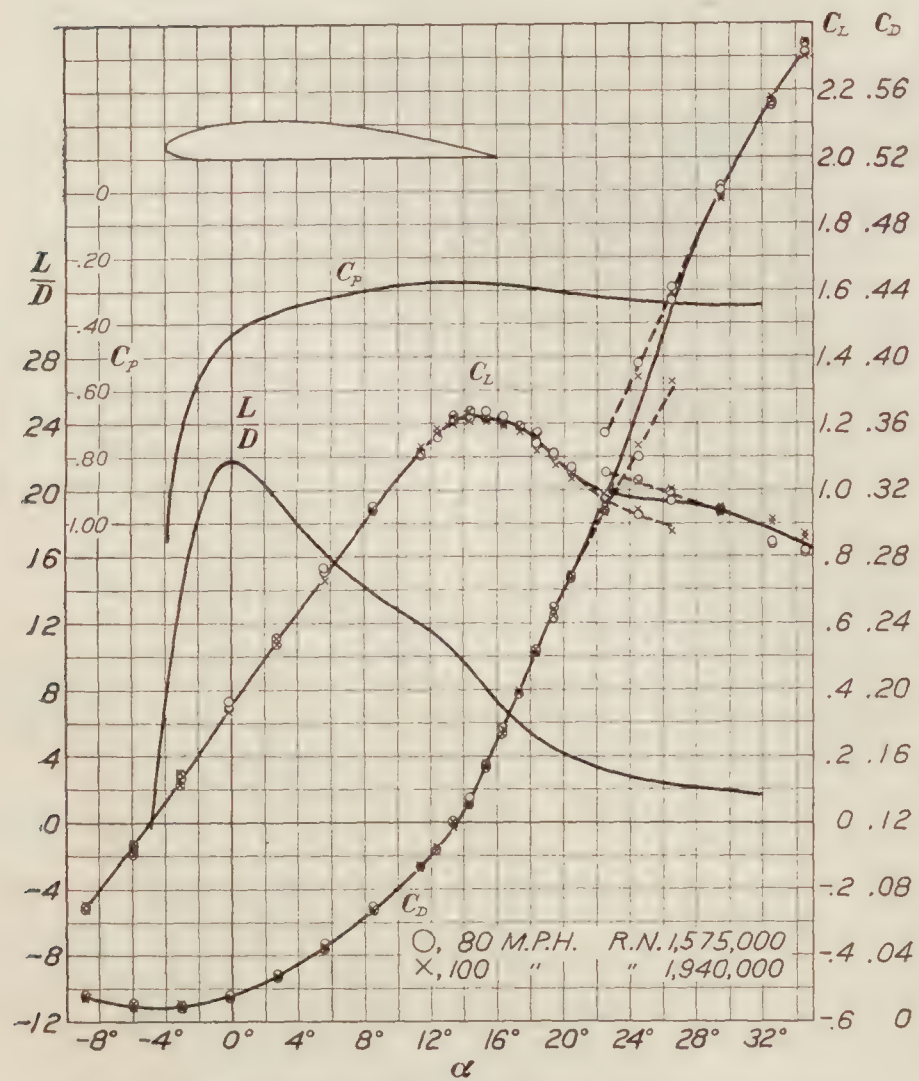


FIGURE 6.—Clark Y, metal covered, unpainted. Aspect ratio 6. Free air

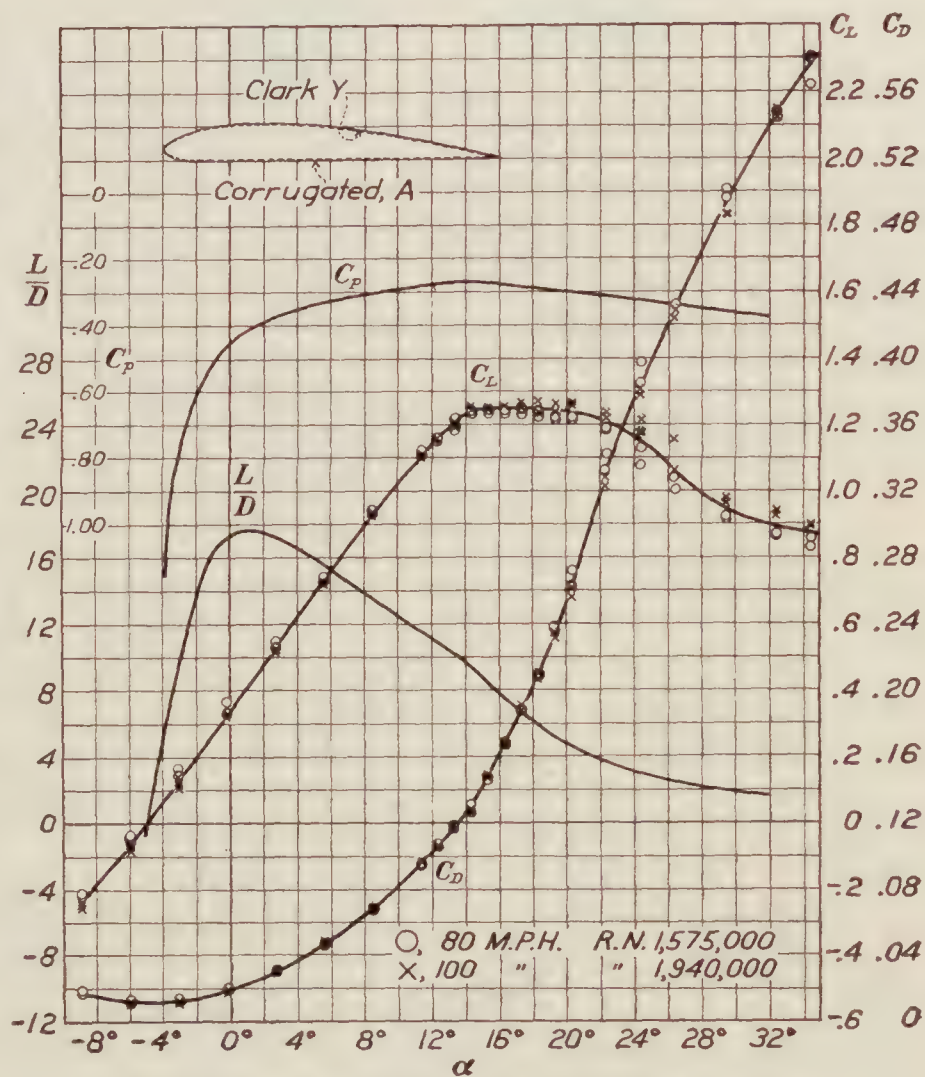


FIGURE 8.—Clark Y, corrugated, A. Aspect ratio 6. Free air

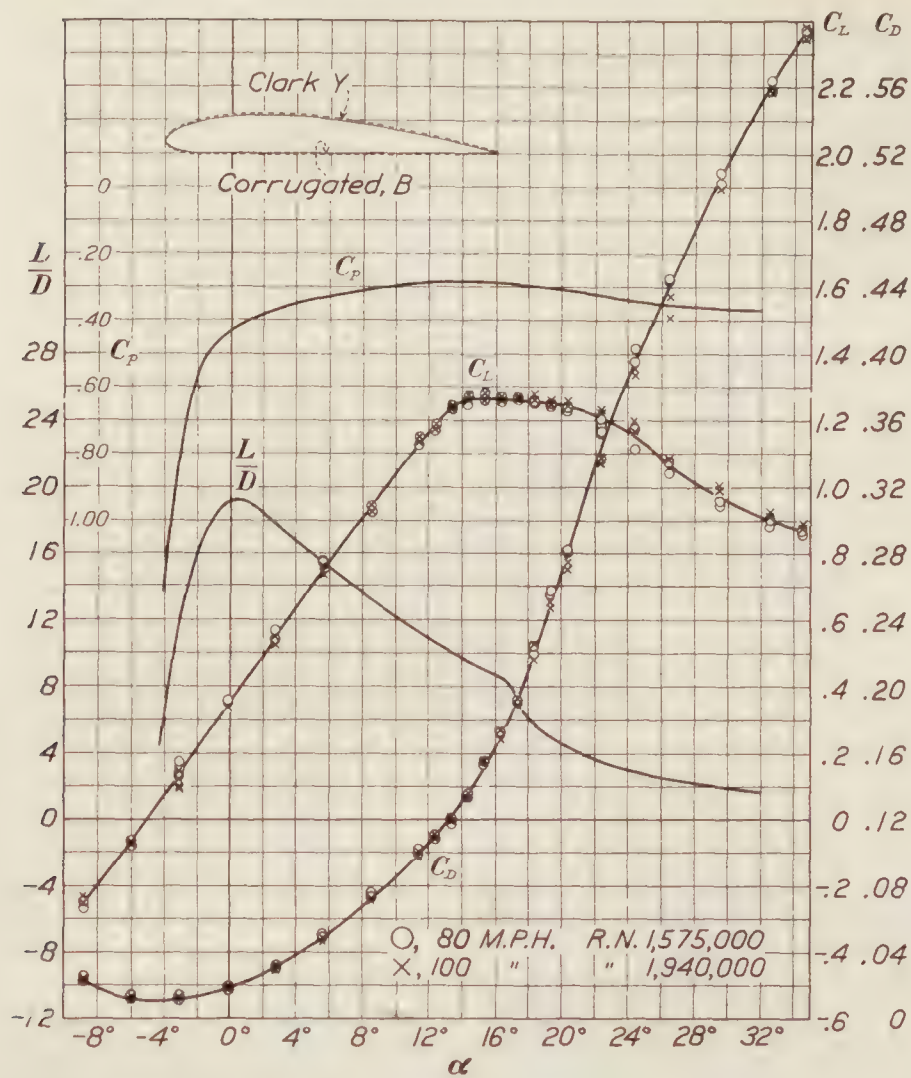


FIGURE 9.—Clark Y, corrugated, B. Aspect ratio 6. Free air

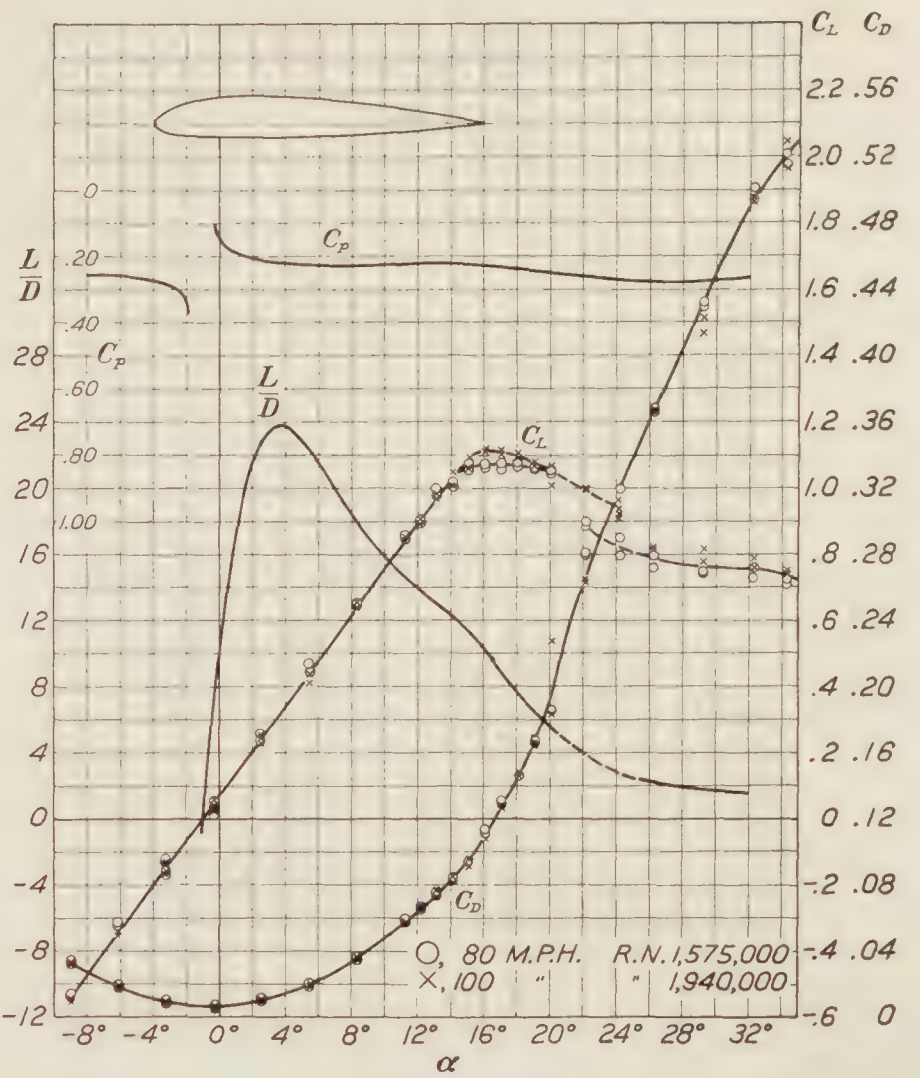


FIGURE 11.—N. A. C. A. M-6, metal covered, painted. Aspect ratio 6. Free air

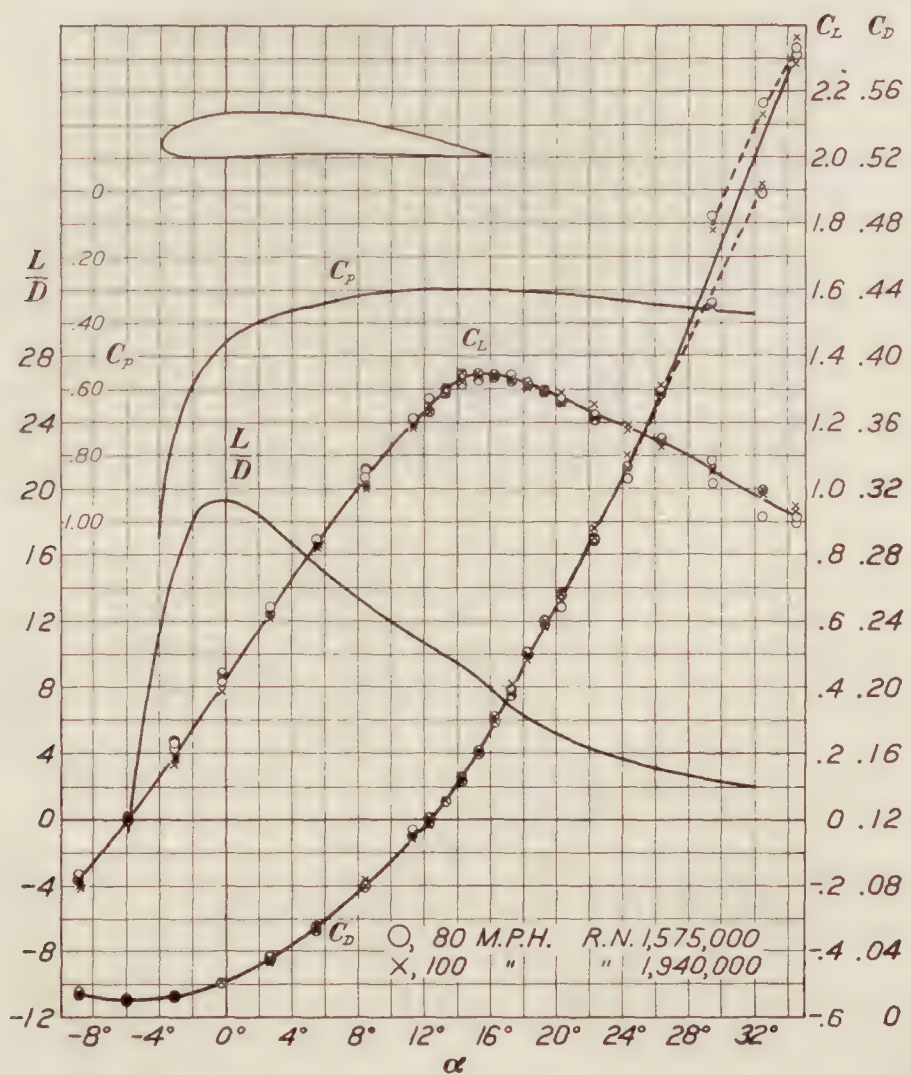


FIGURE 10.—Göttingen 398, metal covered, painted. Aspect ratio 6. Free air

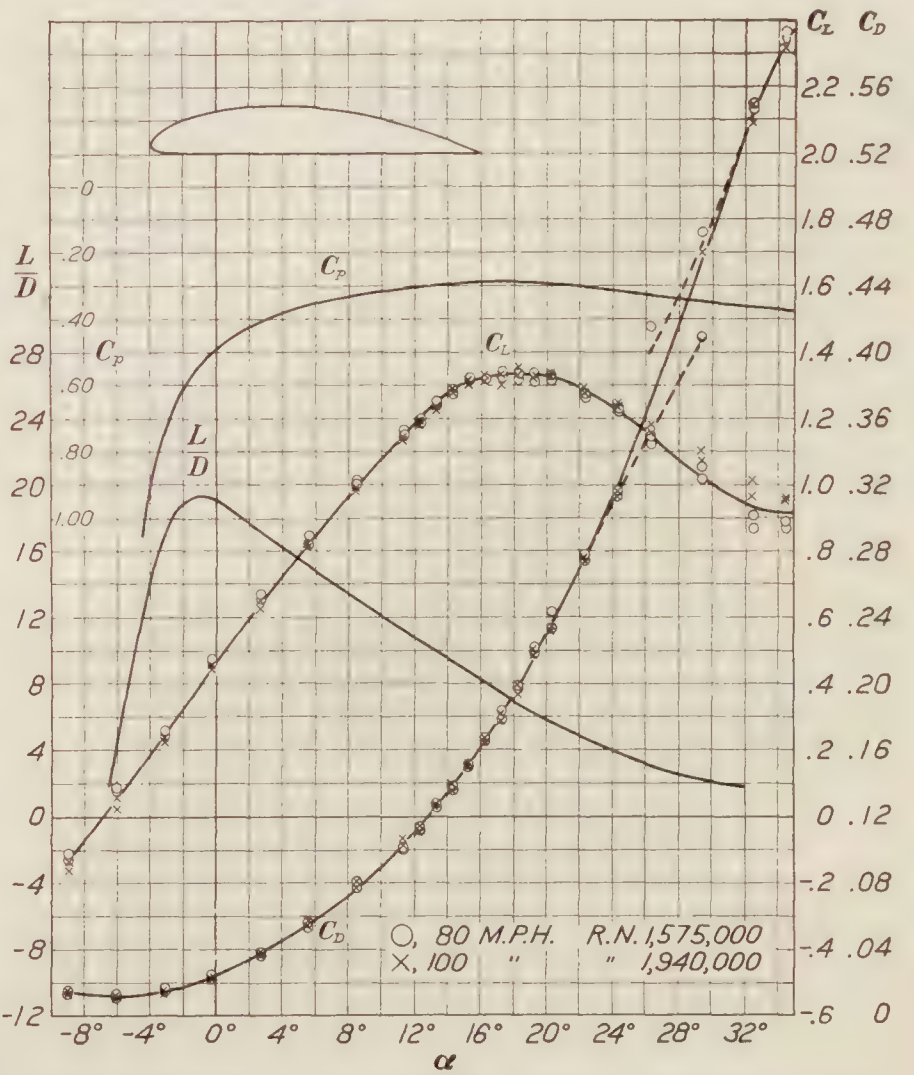


FIGURE 12.—N. A. C. A. 84, metal covered, painted. Aspect ratio 6. Free air

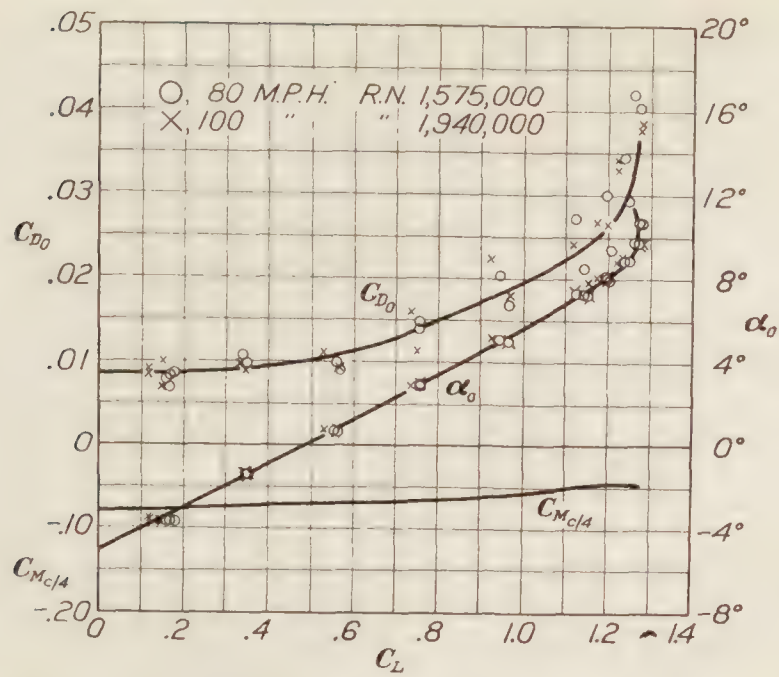


FIGURE 13.—Clark Y, metal covered, painted. Infinite aspect ratio. Free air

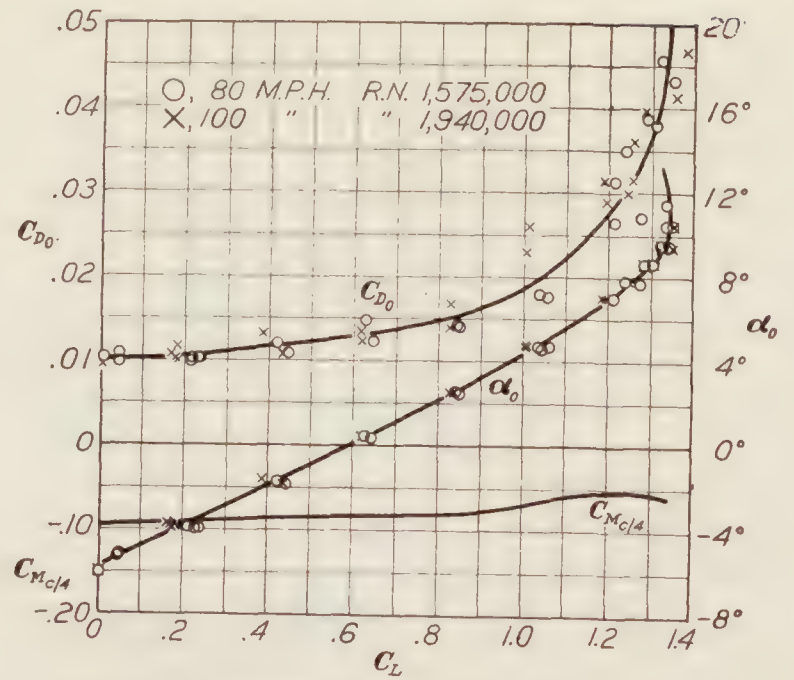


FIGURE 16.—Göttingen 398. Infinite aspect ratio. Free air

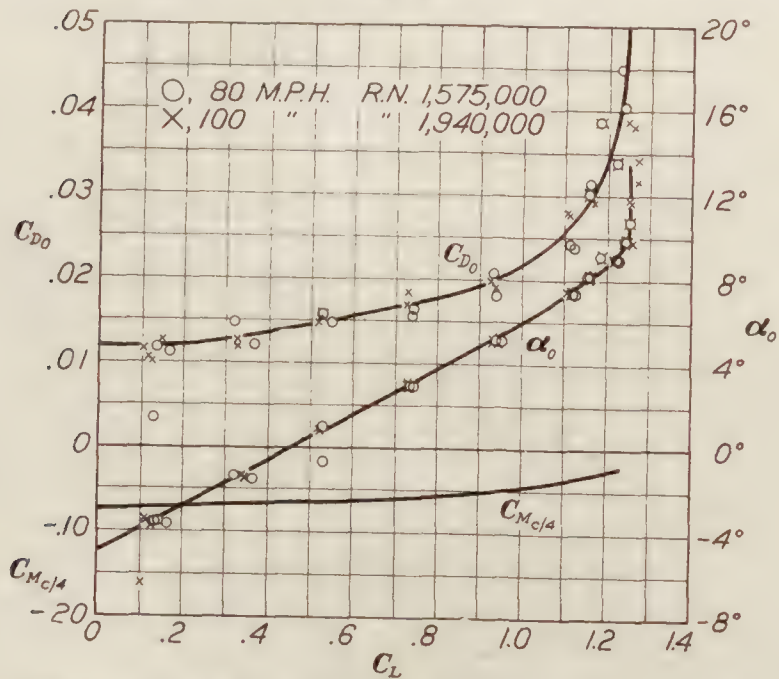


FIGURE 14.—Clark Y, corrugated, A. Infinite aspect ratio. Free air

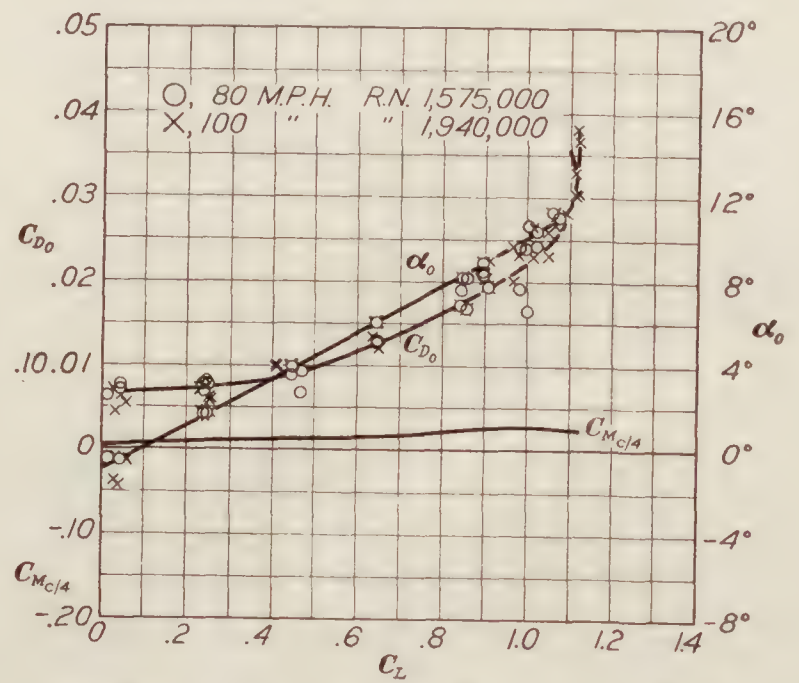


FIGURE 17.—N. A. C. A. M-6. Infinite aspect ratio. Free air

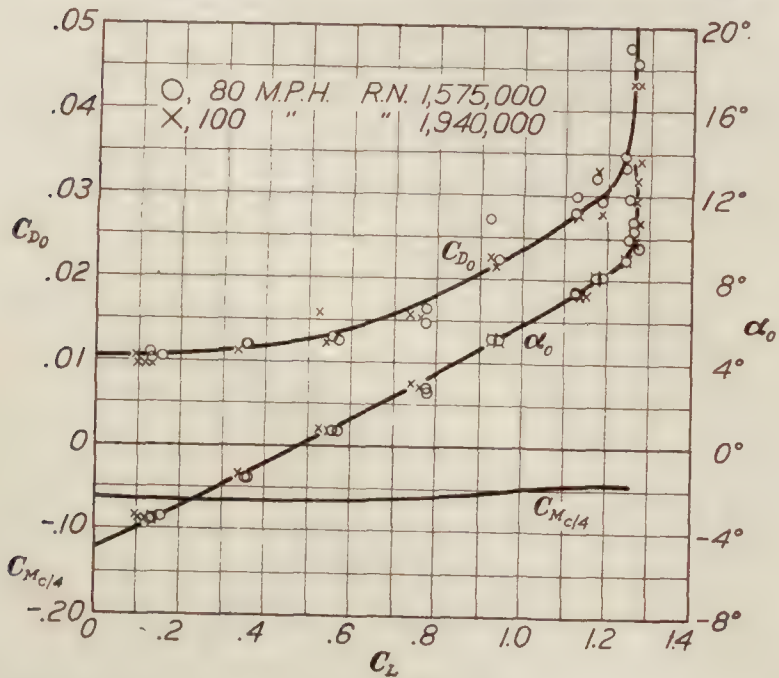


FIGURE 15.—Clark Y, corrugated, B. Infinite aspect ratio. Free air

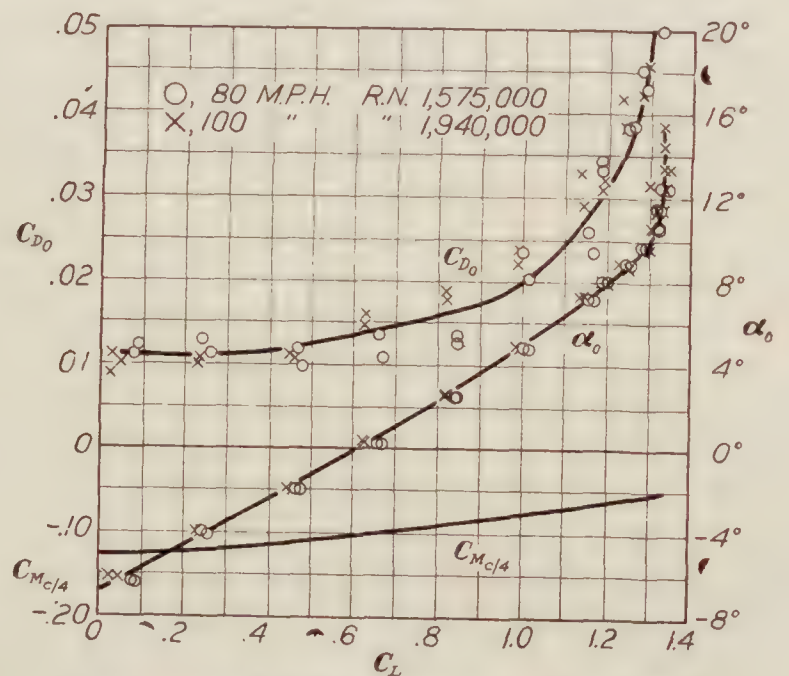


FIGURE 18.—N. A. C. A. 84. Infinite aspect ratio. Free air

Examination of the corrugated Clark Y airfoil in comparison with the smooth Clark Y (fig. 20) reveals a marked flattening of the lift curve for the corrugated sections at the burble point and a lower negative slope beyond the burble. Throughout the normal flying range the slope of the lift curve is unaffected. At any given angle the corrugated surface airfoil shows a

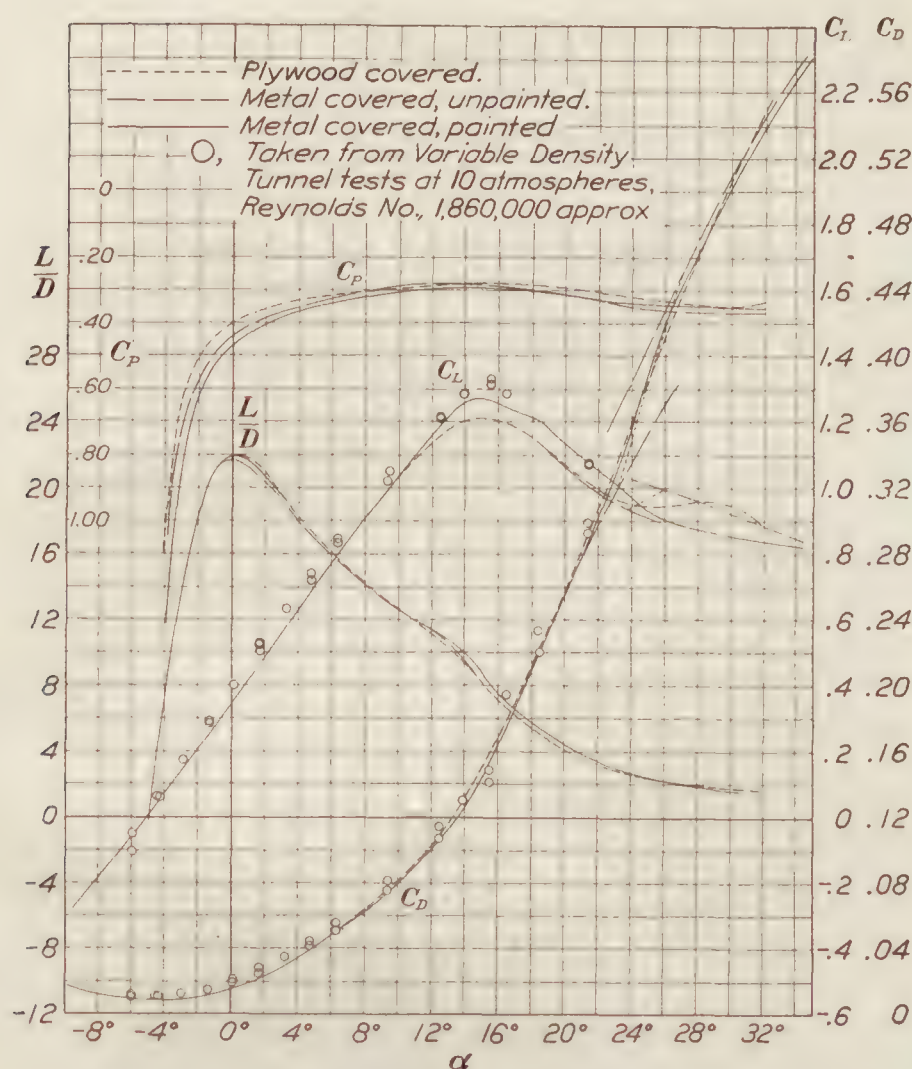


FIGURE 19.—Effect of different surfaces on characteristics of Clark Y. Plywood covered; metal covered, unpainted; metal covered, painted

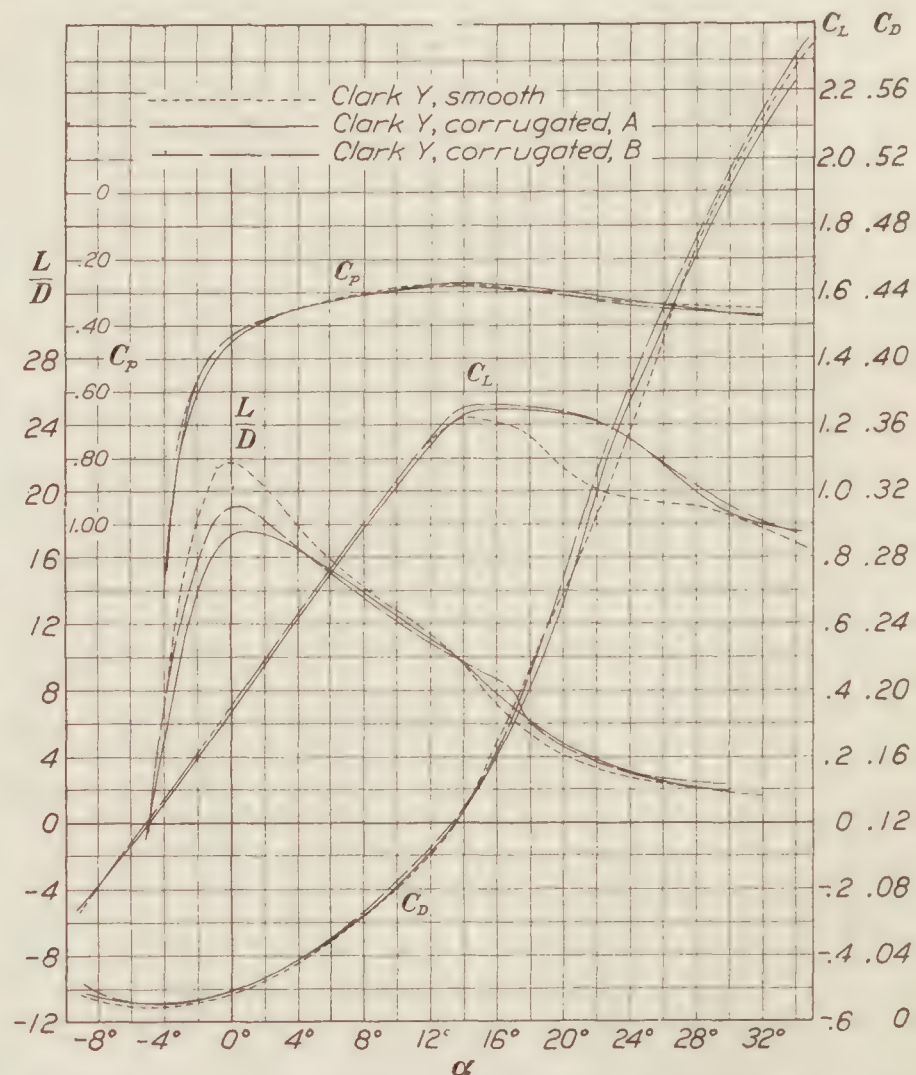


FIGURE 20.—Effect of corrugations in comparison with a smooth Clark Y. Corrugated, A; corrugated, B; metal covered, unpainted, smooth

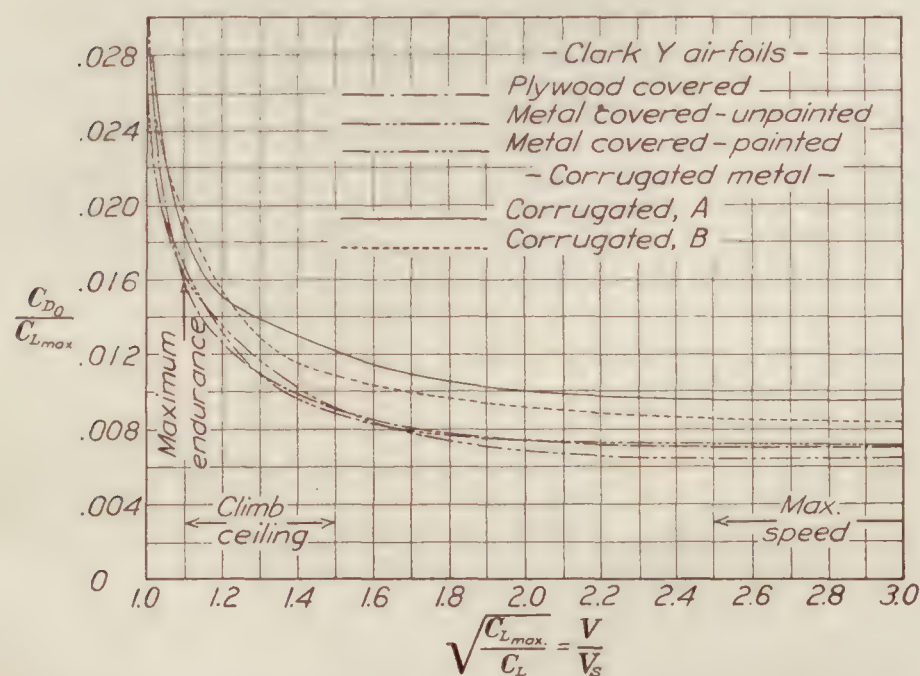


FIGURE 21.—Comparison curves. Profile drag for constant gross load and stalling speed. Clark Y airfoils

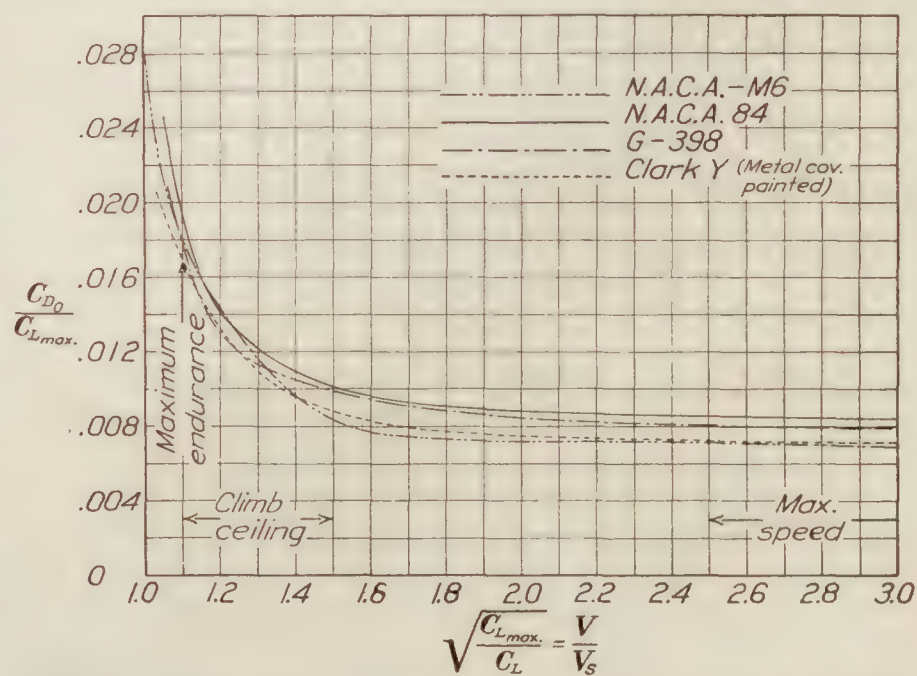


FIGURE 22.—Comparison curves. Profile drag for constant gross load and stalling speed. Different airfoils

slightly higher lift with considerably greater drag so that the Lift/Drag ratio is inferior to that of a smooth airfoil, although only slightly so at 6° and above.

A general flattening of the lift curve is to be noted for all of the airfoils near the burble in contrast to the sharp breaks often found from low-scale tests.

The variable density tunnel test points (fig. 19) indicate a slightly greater slope and a higher maximum lift. The minimum drag is also higher. A comparison with atmospheric tunnel tests on the same airfoil indicates the same scale effect as that predicted by the tests in the variable density tunnel. The agreement is quite in line with what would be expected in different tunnels.

Figures 21 and 22 have been prepared to place the selection or comparison on a common basis. It may be said, in general, that the best airfoil at any given speed is the one which has the lowest profile drag. The actual total drag will be greater by the amount of the induced drag which depends on the effective aspect ratio. It is desirable also to have a high maximum lift to reduce the required wing area. By plotting $\left(\frac{C_{D0}}{C_{L_{\max.}}}\right)$ against $\left(\frac{C_{L_{\max.}}}{C_L}\right)^{\frac{1}{2}} = \frac{V}{V_s}$, we secure a convenient diagram for comparing the sections on the basis of total profile drag for constant gross load and stalling speed. Since $\frac{C_{D0}}{C_{L_{\max.}}} = \left(\frac{D_0}{W}\right)$, the flying condition corresponding to any given speed ratio is indicated on the curves. The values of speed ratio for these conditions are taken from Reference 4. For general use the Clark Y appears the best, while the N. A. C. A. M-6 has the advantage at very high speeds; furthermore, the small center of pressure travel of the M-6 is also of value. The corrugated sections are inferior under all conditions. Too much dependence should not be placed on these diagrams, however, because the particular application may alter the relative position. Tests of a complete model should be the final criterion. Lacking other data, however, the comparison on this basis will be quite useful.

CONCLUSION

In the present tests Reynolds Numbers of 2,000,000 were attained by using large models. This is about 60 per cent of normal full scale.

1. The effect of small variations in the surface of an airfoil on the aerodynamic characteristics is shown to be negligible.

2. Corrugating the surface of an airfoil flattens out the lift curve at the burble point with a small increase of lift; but causes a reduction in effectiveness (L/D) throughout the normal flying range due to the increase of drag. Pressure distribution tests would probably indicate the nature of the holding off of the drop of the lift curve at the burble.

3. A general flattening of the lift curve at the burble is noted for all the airfoils tested rather than the sudden break found in low-scale tests.

4. The results appear to be in good agreement with those from other tests at the same Reynolds Numbers.

LANGLEY MEMORIAL AERONAUTICAL LABORATORY,
NATIONAL ADVISORY COMMITTEE FOR AERONAUTICS,
LANGLEY FIELD, VA., May 24, 1929.

REFERENCES

1. Weick, Fred E., and Wood, Donald H.: The Twenty-Foot Propeller Research Tunnel of the National Advisory Committee for Aeronautics. N. A. C. A. Technical Report No. 300, 1928.
2. Prandtl, L.: Applications of Modern Hydrodynamics to Aeronautics. N. A. C. A. Technical Report No. 116, 1925.
3. Glauert, H.: The Elements of Aerofoil and Airscrew Theory. Cambridge University Press, 1926.
4. Diehl, Walter S.: Engineering Aerodynamics. The Ronald Press, 1928.

TABLE I

Ordinates of Clark Y airfoil metal covered and painted
2-FOOT CHORD, 12-FOOT SPAN

Distance from leading edge in per cent of chord	Upper surface			Lower surface		
	Standard ordinate in per cent of chord	Specified ordinate for 2-foot chord in inches	Measured ordinate for 2-foot chord in inches	Standard ordinate in per cent of chord	Specified ordinate for 2-foot chord in inches	Measured ordinate for 2-foot chord in inches
0	3.50	0.84		3.50	0.84	
1.25	5.45	1.31	1.37	1.93	.46	0.52
2.5	6.50	1.56	1.62	1.47	.35	.37
5	7.90	1.90	1.94	.93	.22	.23
7.5	8.85	2.12	2.16	.63	.15	.15
10	9.60	2.30	2.33	.42	.10	.10
15	10.69	2.57	2.58	.15	.04	.02
20	11.36	2.73	2.71	.03	.01	.00
30	11.70	2.81	2.80	.00	.00	.00
40	11.40	2.74	2.73	.00	.00	.00
50	10.52	2.52	2.50	.00	.00	.00
60	9.15	2.20	2.16	.00	.00	.01
70	7.35	1.76	1.73	.00	.00	.01
80	5.22	1.25	1.23	.00	.00	.00
90	2.80	.67	.65	.00	.00	.00
95	1.49	.36	.33	.00	.00	.01
100	.12	.03	.03	.00	.00	.01

TABLE II

Ordinates of Clark Y airfoil corrugated metal
CLARK Y, CORRUGATED, A
2-FOOT CHORD, 12 FOOT SPAN

Distance from leading edge in per cent of chord	Upper surface				Lower surface			
	Top of corrugations		Bottom of corrugations		Top of corrugations		Bottom of corrugations	
	Specified ordinate for 2-foot chord in inches	Measured ordinate for 2-foot chord in inches	Specified ordinate for 2-foot chord in inches	Measured ordinate for 2-foot chord in inches	Specified ordinate for 2-foot chord in inches	Measured ordinate for 2-foot chord in inches	Specified ordinate for 2-foot chord in inches	Measured ordinate for 2-foot chord in inches
0	0.84		0.84		0.84		0.84	
1.25	1.58	1.59	1.47	1.51	.49	0.57	.57	0.66
2.5	1.84	1.84	1.71	1.74	.35	.40	.46	.49
5	2.16	2.18	2.04	2.08	.22	.25	.33	.34
7.5	2.39	2.41	2.27	2.32	.14	.18	.26	.27
10	2.57	2.60	2.45	2.50	.09	.13	.21	.23
15	2.82	2.85	2.71	2.74	.03	.07	.14	.16
20	2.98	3.01	2.87	2.92	.01	.04	.11	.14
30	3.07	3.11	2.96	3.01	.00	.05	.11	.14
40	3.00	3.02	2.89	2.92	.00	.04	.11	.13
50	2.78	2.83	2.67	2.73	.00	.01	.11	.10
60	2.46	2.49	2.35	2.40	.00	.00	.11	.10
70	2.02	2.06	1.91	1.96	.00	.00	.11	.09
80	1.51	1.53	1.40	1.43	.00	.02	.11	.11
90	.90	.92	.79	.83	.00	.05	.11	.14
95	.54	.59	.43	.49	.00	.07	.11	.16
100	.13	.29	.04	.20	.00	.11	.11	.20

TABLE III
Ordinates of Clark Y airfoil corrugated metal
CLARK Y, CORRUGATED, B
2-FOOT CHORD, 12-FOOT SPAN

Distance from leading edge in per cent of chord	Upper surface				Lower surface			
	Top of corrugations		Bottom of corrugations		Top of corrugations		Bottom of corrugations	
	Specified ordinate for 2-foot chord in inches	Measured ordinate for 2-foot chord in inches	Specified ordinate for 2-foot chord in inches	Measured ordinate for 2-foot chord in inches	Specified ordinate for 2-foot chord in inches	Measured ordinate for 2-foot chord in inches	Specified ordinate for 2-foot chord in inches	Measured ordinate for 2-foot chord in inches
0	0.84		0.84		0.84		0.84	
1.25	1.31	1.37	1.22	1.32	.46	0.50	.56	0.57
2.50	1.56	1.62	1.46	1.54	.35	.39	.48	.46
5	1.90	1.92	1.76	1.83	.22	.28	.35	.36
7.5	2.12	2.16	1.99	2.07	.15	.21	.28	.29
10	2.30	2.33	2.17	2.24	.10	.15	.22	.24
15	2.57	2.58	2.43	2.49	.04	.09	.16	.18
20	2.73	2.74	2.60	2.66	.01	.05	.13	.14
30	2.81	2.83	2.68	2.76	.00	.03	.11	.13
40	2.74	2.74	2.63	2.66	.00	.03	.11	.13
50	2.52	2.54	2.41	2.46	.00	.03	.11	.13
60	2.20	2.23	2.09	2.15	.00	.04	.11	.14
70	1.76	1.81	1.65	1.73	.00	.05	.11	.15
80	1.25	1.32	1.14	1.22	.00	.06	.11	.16
90	.67	.75	.56	.67	.00	.07	.11	.17
95	.36	.47	.25	.37	.00	.08	.11	.17
100	.13	.22	.02	.12	.00	.05	.11	.13

TABLE IV
Ordinates of Göttingen 398 airfoil, metal covered and painted
2-FOOT CHORD, 12-FOOT SPAN

Distance from leading edge in per cent of chord	Upper surface			Lower surface		
	Standard ordinate in per cent of chord	Specified ordinate for 2-foot chord in inches	Measured ordinate for 2-foot chord in inches	Standard ordinate in per cent of chord	Specified ordinate for 2-foot chord in inches	Measured ordinate for 2-foot chord in inches
0	3.74	0.90		3.74	0.90	
1.25	6.19	1.49	1.54	1.89	.45	0.48
2.5	7.40	1.78	1.83	1.28	.31	.34
5	8.86	2.13	2.20	.69	.17	.18
7.5	10.25	2.46	2.49	.35	.08	.10
10	11.25	2.70	2.71	.27	.06	.06
15	12.54	3.01	3.02	.05	.01	.02
20	13.34	3.20	3.19	.00	.00	.00
30	13.77	3.30	3.30	.05	.01	.01
40	13.34	3.20	3.19	.25	.06	.05
50	12.32	2.96	2.96	.27	.06	.07
60	10.56	2.53	2.55	.29	.07	.09
70	8.45	2.06	2.06	.28	.07	.09
80	6.08	1.46	1.45	.27	.06	.06
90	3.32	.80	.78	.13	.03	.02
95	1.87	.45	.43	.05	.01	.00
100	0.43	.10	.09	.00	.00	.00

TABLE V

Ordinates of N. A. C. A. M-6 airfoil, metal covered and painted
2-FOOT CHORD, 12-FOOT SPAN

Distance from leading edge in per cent of chord	Upper surface			Lower surface		
	Standard ordinate in per cent of chord	Specified ordinate for 2-foot chord in inches	Measured ordinate for 2-foot chord in inches	Standard ordinate in per cent of chord	Specified ordinate for 2-foot chord in inches	Measured ordinate for 2-foot chord in inches
0	0	0		0	0	
1.25	1.97	.47	0.52	-1.76	-.42	-0.38
2.5	2.81	.67	.72	-2.20	-.53	-.51
5.0	4.03	.97	1.00	-2.73	-.65	-.65
7.5	4.94	1.19	1.23	-3.03	-.73	-.74
10	5.71	1.37	1.41	-3.24	-.78	-.79
15	6.82	1.64	1.65	-3.47	-.83	-.84
20	7.55	1.81	1.81	-3.62	-.87	-.87
30	8.22	1.97	1.96	-3.79	-.91	-.92
40	8.05	1.93	1.90	-3.90	-.94	-.95
50	7.26	1.74	1.70	-3.94	-.95	-.95
60	6.03	1.45	1.43	-3.82	-.92	-.91
70	4.58	1.10	1.11	-3.48	-.84	-.82
80	3.06	.73	.75	-2.83	-.68	-.65
90	1.55	.37	.42	-1.77	-.42	-.38
95	.88	.21	.24	-1.08	-.26	-.20
100	.26	.06	.09	-.26	-.06	-.01

TABLE VI

Ordinates of N. A. C. A. 84 airfoil, metal covered and painted
2-FOOT CHORD, 12-FOOT SPAN

Distance from leading edge in per cent of chord	Upper surface			Lower surface		
	Standard ordinate in per cent of chord	Specified ordinate for 2-foot chord in inches	Measured ordinate for 2-foot chord in inches	Standard ordinate in per cent of chord	Specified ordinate for 2-foot chord in inches	Measured ordinate for 2-foot chord in inches
0	2.50	0.60		2.50	0.60	
1.25	4.85	1.16	1.22	.95	.23	0.28
2.5	6.05	1.45	1.49	.41	.10	.14
5	7.78	1.87	1.91	.10	.02	.05
7.5	9.03	2.17	2.19	.02	.01	.03
10	10.0	2.40	2.42	.00	.00	.01
15	11.5	2.76	2.78	.00	.00	.01
20	12.71	3.05	3.06	.00	.00	.01
30	14.0	3.36	3.35	.00	.00	.01
40	14.11	3.38	3.37	.00	.00	.00
50	13.50	3.24	3.22	.00	.00	.01
60	12.31	2.95	2.92	.00	.00	.01
70	10.32	2.47	2.44	.00	.00	.01
80	7.71	1.85	1.85	.00	.00	.01
90	4.39	1.05	1.08	.00	.00	.03
95	2.41	.58	.61	.00	.00	.04
100	.30	.07	.11	.00	.00	.05

TABLE VII

CLARK Y, PLYWOOD COVERED

Span, 12 feet. Chord, 2 feet. Area, 24 square feet.
Reynolds No. 1,940,000

ASPECT RATIO 6, FREE AIR

α	C_L	C_D	L/D	C_p	$C_{Mc/A}$
0					
-9	-0.245	0.0176	-----	0.046	-0.050
-8	-.184	.0127	-----	-.027	-.051
-6	-.060	.0093	-----	-.616	-.052
-4	.070	.0090	7.78	-1.01	-.053
-2	.209	.0111	18.83	.504	-.053
0	.350	.0160	21.92	.395	-.052
2	.493	.0237	20.80	.353	-.051
4	.637	.0348	18.30	.328	-.050
6	.781	.0485	16.10	.313	-.049
8	.917	.0642	14.28	.303	-.048
10	1.041	.0816	12.76	.292	-.044
12	1.148	.1023	11.21	.281	-.036
14	1.215	.1295	9.39	.275	-.031
16	1.214	.1690	7.19	.276	-.032
18	1.161	.2120	5.48	.281	-.036
20	1.078	.2585	4.17	.291	-.044
22	1.005	.3072	3.27	.303	-.053
24	.957	.3590	2.66	.317	-.064
26	.951	.4115	2.31	.330	-.076
28	.967	.4630	2.09	.340	-.087
30	.959	.5090	1.88	.343	-.089
32	.890	.550	1.62	.334	-.075

TABLE VIII

CLARK Y, METAL COVERED, UNPAINTED

Span 12 feet. Chord, 2 feet. Area, 24 square feet.
Reynolds No. 1,940,000

ASPECT RATIO 6, FREE AIR

α	C_L	C_D	L/D	C_p	$C_{Mc/A}$
0					
-9	-0.264	0.0160	-----	-0.015	-0.070
-8	-.204	.0129	-----	-.088	-.069
-6	-.073	.0093	-----	-.681	-.068
-4	.063	.0088	7.16	1.314	-.067
-2	.207	.0113	18.33	.564	-.065
0	.353	.0162	21.80	.434	-.065
2	.496	.0243	20.40	.377	-.064
4	.632	.0351	18.00	.350	-.063
6	.767	.0481	15.92	.327	-.059
8	.902	.0634	14.21	.303	-.048
10	1.035	.0801	12.90	.284	-.035
12	1.152	.1000	11.52	.274	-.028
14	1.220	.1266	9.65	.276	-.032
16	1.211	.1686	7.20	.281	-.038
18	1.164	.2136	5.45	.291	-.048
20	1.070	.2581	4.15	.306	-.060
22	1.003	.304	3.30	.322	-.072
24	.978	.356	2.75	.332	-.080
26	.964	.412	2.34	.338	-.085
28	.952	.469	2.03	.340	-.086
30	.928	.509	1.82	.343	-.086
32	.889	.545	1.63	.345	-.084
34	.845	.575	1.47	.339	-.075
35	.825	.589	1.40	.326	-.063

TABLE IX

CLARK Y, METAL COVERED AND PAINTED

Span, 12 feet. Chord, 2 feet. Area, 24 square feet.
Reynolds No. 1,940,000

ASPECT RATIO 6, FREE AIR

α	C_L	C_D	L/D	C_p	$C_{Mc/A}$
0					
-9	-0.255	0.0160	-----	-0.068	-0.081
-8	-.191	.0125	-----	-.179	-.082
-6	-.061	.0093	-----	-1.094	-.082
-4	.076	.0089	8.44	1.318	-.080
-2	.214	.0113	18.95	.614	-.078
0	.356	.0162	21.99	.461	-.075
2	.501	.0242	20.69	.394	-.072
4	.643	.0353	18.20	.357	-.069
6	.783	.0492	15.90	.334	-.066
8	.920	.0655	14.03	.318	-.063
10	1.050	.0828	12.69	.300	-.053
12	1.175	.1025	11.45	.289	-.046
14	1.268	.1266	10.01	.286	-.046
16	1.260	.1658	7.60	.290	-.050
18	1.221	.2101	5.81	.297	-.058
20	1.138	.257	4.43	.311	-.069
22	1.061	.303	3.51	.326	-.081
24	.978	.358	2.73	.343	-.091
26	.909	.422	2.15	.358	-.098
28	.877	.467	1.88	.366	-.102
30	.860	.505	1.70	.367	-.101
32	.842	.540	1.56	.363	-.095
34	.828	.573	1.44	.350	-.083
35	.822	.590	1.39	.341	-.075

TABLE X

CLARK Y, CORRUGATED METAL, A

Span, 12 feet. Chord, 2 feet. Area, 24 square feet.
Reynolds No. 1,940,000

ASPECT RATIO 6, FREE AIR

α	C_L	C_D	L/D	C_p	$C_{Mc/A}$
0					
-9	-0.246	0.0190	-----	-0.050	-0.074
-8	-.188	.0159	-----	-.143	-.074
-6	-.067	.0124	-----	-.84	-.073
-4	.062	.0120	5.17	1.41	-.072
-2	.197	.0142	13.89	.605	-.070
0	.338	.0195	17.33	.454	-.069
2	.480	.0274	17.51	.386	-.065
4	.620	.0375	16.53	.350	-.062
6	.761	.0498	15.28	.326	-.058
8	.896	.0643	13.93	.308	-.052
10	1.024	.0820	12.49	.293	-.044
12	1.143	.1024	11.18	.278	-.032
14	1.233	.1261	9.78	.268	-.022
16	1.250	.1610	7.75	.274	-.030
18	1.247	.2010	6.20	.288	-.047
20	1.239	.2545	4.85	.299	-.060
22	1.217	.3190	3.80	.310	-.073
24	1.163	.3750	3.10	.322	-.084
26	1.083	.4200	2.58	.339	-.096
28	.996	.4630	2.15	.356	-.105
30	.934	.5030	1.86	.369	-.111
32	.900	.539	1.67	.374	-.112
34	.879	.571	1.54	.375	-.110
35	.871	.583	1.50	.372	-.106

TABLE XI

CLARK Y, CORRUGATED METAL, B

Span, 12 feet. Chord, 2 feet. Area, 24 square feet.
Reynolds No. 1,940,000

ASPECT RATIO 6. FREE AIR

α	C_L	C_D	L/D	C_p	$C_{Mc/A}$
0					
-9	-0.261	0.0238	-----	-0.001	-0.065
-8	-.199	.0180	-----	-.076	-.065
-6	-.068	.0118	-----	-.706	-.065
-4	.070	.0107	6.54	1.179	-.065
-2	.212	.0134	15.82	.561	-.066
0	.354	.0186	19.03	.434	-.065
2	.495	.0269	18.39	.381	-.065
4	.636	.0379	16.77	.351	-.064
6	.778	.0514	15.13	.328	-.061
8	.910	.0673	13.52	.312	-.056
10	1.040	.0855	12.18	.297	-.049
12	1.166	.1060	11.00	.289	-.045
14	1.257	.1302	9.66	.284	-.043
16	1.263	.1635	7.73	.285	-.044
18	1.258	.2090	6.00	.294	-.055
20	1.247	.2682	4.65	.309	-.073
22	1.215	.3326	3.65	.326	-.092
24	1.163	.3860	3.02	.341	-.106
26	1.088	.4302	2.52	.350	-.109
28	1.017	.4735	2.15	.358	-.110
30	.960	.5140	1.87	.365	-.110
32	.910	.5515	1.65	.370	-.109
34	.871	.5838	1.49	.374	-.108
35	.868	.5980	1.45	.373	-.107

TABLE XII

GÖTTINGEN 398, METAL COVERED AND PAINTED

Span, 12 feet. Chord, 2 feet. Area, 24 square feet.
Reynolds No. 1,940,000

ASPECT RATIO 6, FREE AIR

α	C_L	C_D	L/D	C_p	$C_{Mc/A}$
0					
-9	-0.186	0.0150	-----	-0.261	-0.095
-8	-.129	.0128	-----	-.486	-.095
-6	-.003	.0103	-----	-31.15	-.094
-4	.131	.0113	11.60	.960	-.093
-2	.272	.0151	18.01	.581	-.090
0	.422	.0219	19.27	.458	-.088
2	.578	.0314	18.40	.397	-.085
4	.728	.0435	16.72	.363	-.082
6	.871	.0582	14.97	.340	-.078
8	1.005	.0755	13.31	.318	-.068
10	1.127	.0944	11.92	.301	-.057
12	1.234	.1153	10.69	.295	-.055
14	1.325	.1400	9.47	.293	-.057
16	1.347	.1725	7.82	.296	-.062
18	1.323	.2119	6.25	.302	-.069
20	1.281	.2481	5.16	.310	-.077
22	1.233	.2860	4.32	.320	-.086
24	1.190	.3270	3.64	.331	-.096
26	1.149	.370	3.10	.342	-.105
28	1.100	.419	2.62	.353	-.113
30	1.038	.469	2.21	.364	-.118
32	.979	.520	1.88	.375	-.122
34	.928	.570	1.63	.385	-.125
35	.909	.595	1.53	.388	-.125

TABLE XIII

N. A. C. A. M-6, METAL COVERED AND PAINTED

Span, 12 feet. Chord, 2 feet. Area, 24 square feet.
Reynolds No. 1,940,000

ASPECT RATIO 6. FREE AIR

α	C_L	C_D	L/D	C_p	$C_{Mc/A}$
0					
-9	-0.540	0.0330	-----	0.254	0.002
-8	-.471	.0277	-----	.256	.003
-6	-.337	.0182	-----	.262	.004
-4	-.202	.0115	-----	.275	.005
-2	-.067	.0079	-----	.340	.006
0	.068	.0070	9.85	.147	.007
2	.203	.0094	21.60	.206	.009
4	.338	.0142	23.80	.220	.010
6	.476	.0221	21.55	.225	.012
8	.618	.0336	18.40	.226	.015
10	.755	.0475	15.89	.226	.018
12	.893	.0638	13.99	.221	.026
14	1.023	.0824	12.41	.223	.028
16	1.113	.1082	10.28	.228	.024
18	1.094	.1441	7.60	.238	.013
20	1.054	.1912	5.50	.250	.000
22	.995	.262	3.80	.261	-.011
24	.948	.314	3.02	.270	-.019
26	.791	.361	2.19	.278	-.022
28	.770	.405	1.90	.277	-.021
30	.760	.448	1.70	.272	-.017
32	.756	.489	1.55	.263	-.010
34	.737	.518	1.42	.253	-.002
35	.720	.530	1.36	.244	.004

TABLE XIV

N. A. C. A. 84, METAL COVERED AND PAINTED

Span, 12 feet. Chord, 2 feet. Area, 24 square feet.
Reynolds No. 1,940,000

ASPECT RATIO 6, FREE AIR

α	C_L	C_D	L/D	C_p	$C_{Mc/A}$
0					
-9	-0.135	0.0140	-----	-0.675	-0.125
-8	-.070	.0126	-----	-1.54	-.126
-6	.054	.0116	4.55	2.59	-.126
-4	.187	.0131	14.29	.908	-.123
-2	.324	.0172	18.83	.614	-.118
0	.461	.0242	19.05	.493	-.112
2	.598	.0339	17.63	.426	-.105
4	.724	.0448	16.16	.384	-.097
6	.849	.0574	14.79	.355	-.089
8	.968	.0719	13.47	.333	-.080
10	1.080	.0896	12.06	.317	-.072
12	1.186	.1102	10.75	.303	-.063
14	1.278	.1341	9.53	.293	-.055
16	1.323	.1610	8.23	.289	-.051
18	1.333	.1928	6.92	.288	-.050
20	1.328	.2295	5.79	.292	-.055
22	1.291	.2698	4.79	.300	-.065
24	1.233	.3126	3.95	.312	-.077
26	1.161	.3610	3.22	.325	-.087
28	1.079	.4159	2.59	.336	-.093
30	1.000	.472	2.12	.349	-.099
32	.943	.530	1.78	.360	-.104
34	.917	.578	1.59	.369	-.109
35	.915	.595	1.54	.371	-.111

TABLE XV

CLARK Y, METAL COVERED AND PAINTED

Infinite aspect ratio characteristics. Computed from
A. R.=6 tests rectangular loading

$$C_{Di}=0.0563 C_L^2$$

$$\alpha_i=3.601 C_L$$

PLOTTED AS FIGURE 13

C_L	C_{D_0}	α_0	$C_{M_0/4}$
		°	
-0.061	0.0091	-5.78	-0.082
.076	.0086	-4.27	-.080
.214	.0087	-2.77	-.078
.356	.0091	-1.28	-.075
.501	.0101	.20	-.072
.643	.0121	1.69	-.069
.783	.0146	3.16	-.066
.920	.0179	4.69	-.063
1.050	.0207	6.22	-.053
1.175	.0249	7.77	-.046
1.268	.0361	9.44	-.046

TABLE XVI

CLARK Y, CORRUGATED METAL, A. CLARK Y, INSIDE
OF METALInfinite aspect ratio characteristics. Computed from
A. R.=6 tests rectangular loading

$$C_{Di}=0.0564 C_L^2$$

$$\alpha_i=3.612 C_L$$

PLOTTED AS FIGURE 14

C_L	C_{D_0}	α_0	$C_{M_0/4}$
		°	
-0.067	0.0121	-5.76	-0.073
.062	.0118	-4.22	-.072
.197	.0120	-2.71	-.070
.338	.0131	-1.22	-.069
.480	.0144	.27	-.065
.620	.0158	1.76	-.062
.761	.0171	3.26	-.058
.896	.0190	4.76	-.052
1.024	.0229	6.30	-.044
1.143	.0284	7.87	-.032
1.233	.0405	9.55	-.022
1.250	.0729	11.49	-.030

TABLE XVII

CLARK Y, CORRUGATED METAL, B

Infinite aspect ratio characteristics. Computed from
A. R.=6 tests rectangular loading

$$C_{Di}=0.0562 C_L^2$$

$$\alpha_i=3.594 C_L$$

PLOTTED AS FIGURE 15

C_L	C_{D_0}	α_0	$C_{M_0/4}$
		°	
-0.068	0.0115	-5.76	-0.065
.070	.0104	-4.25	-.065
.212	.0109	-2.76	-.066
.354	.0116	-1.27	-.065
.495	.0132	.22	-.065
.636	.0152	1.72	-.064
.778	.0174	3.20	-.061
.910	.0208	4.73	-.056
1.040	.0246	6.26	-.049
1.166	.0295	7.81	-.045
1.257	.0414	9.49	-.043
1.263	.0736	11.46	-.044

TABLE XVIII

GÖTTINGEN 398, METAL COVERED AND PAINTED

Infinite aspect ratio characteristics. Computed from
A. R.=6 tests rectangular loading

$$C_{Di}=0.0559 C_L^2$$

$$\alpha_i=3.575 C_L$$

PLOTTED AS FIGURE 16

C_L	C_{D_0}	α_0	$C_{M_0/4}$
		°	
-0.003	0.0103	-5.99	-0.094
.131	.0103	-4.47	-.093
.272	.0110	-2.97	-.090
.422	.0120	-1.51	-.088
.578	.0127	-.06	-.085
.728	.0139	1.40	-.082
.871	.0158	2.88	-.078
1.005	.0191	4.41	-.068
1.127	.0235	5.98	-.057
1.234	.0302	7.59	-.055
1.325	.0419	9.26	-.057
1.347	.0713	11.19	-.062

TABLE XIX

N. A. C. A. M-6, METAL COVERED AND PAINTED

Infinite aspect ratio characteristics. Computed from
A. R.=6 tests rectangular loading

$C_{Di}=0.0564\ C_L^2$

$\alpha_i=3.605\ C_L$

PLOTTED AS FIGURE 17

C_L	C_{Do}	α_o	$C_{Me}/4$
		n	
-0.067	0.0076	-1.76	0.006
.062	.0067	-.24	.007
.203	.0071	1.29	.009
.338	.0078	2.81	.010
.476	.0093	4.33	.012
.618	.0120	5.83	.015
.755	.0153	7.35	.018
.893	.0188	8.86	.026
1.023	.0233	10.40	.028
1.113	.0382	12.09	.024

TABLE XX

N. A. C. A. 84, METAL COVERED AND PAINTED

Infinite aspect ratio characteristics. Computed from
A. R.=6 tests rectangular loading

$C_{Di}=0.0566\ C_L^2$

$\alpha_i=3.600\ C_L$

PLOTTED AS FIGURE 18

C_L	C_{Do}	α_o	$C_{Me}/4$
		o	
-0.070	0.0123	-7.75	-0.126
.050	.0114	-6.19	-.126
.187	.0111	-4.67	-.123
.324	.0112	-3.17	-.118
.461	.0122	-1.66	-.112
.598	.0137	-.16	-.105
.724	.0152	1.40	-.097
.849	.0166	2.94	-.089
.968	.0188	4.52	-.080
1.080	.0236	6.11	-.072
1.186	.0307	7.73	-.063
1.278	.0417	9.40	-.055
1.323	.0618	11.23	-.051
1.333	.0920	13.20	-.050





SMITHSONIAN LIBRARIES



3 9088 01800 8607